

PAMPHLET BOX

Physics Abstracts

ISSN 0036-8091

Science Abstracts Series A
15th August 1983

Abstracts 74198-79041

UIC
AUG 24 1983
LIBRARY

inspec
The Institution of Electrical Engineers

Q
1
S3
V.86
1983
NO. 12-14
N/c

Sci.

PHYSICS ABSTRACTS

Physics Abstracts is one of a series of abstracts publications produced by INSPEC. Published twice monthly by the Institution of Electrical Engineers, it forms the world's major English-language abstracting service for the physics community.

SUBJECT SCOPE & COVERAGE

Physics Abstracts covers the whole field of physics. An impression of its scope can be gained from the classification scheme. The information contained in *Physics Abstracts* is derived from a wide range of sources including journals, reports, books, dissertations and conference papers published in all countries and languages of the world.

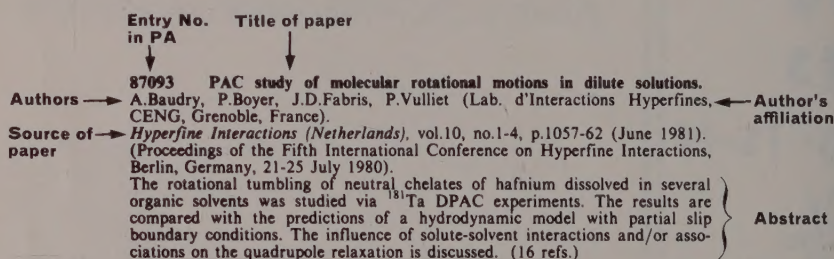
The number of items included is currently running at over 100,000 per year.

JOURNALS SCANNED

A list of the journals scanned for the INSPEC services is published with the twice-yearly author indexes to *Physics Abstracts*. Additions and amendments to this list are included in *Physics Abstracts* towards the end of the first issue for each month.

FORM OF ENTRY

All entries in *Physics Abstracts* follow the same basic pattern. The following example identifies the individual parts of a typical entry for an article from a journal.



Entries for other types of material differ mainly in the reference to the source, e.g., a report will refer to the report series and the number of the individual report. A conference paper on the other hand will normally refer to the title, place and date of the conference at which the paper was given.

SUBJECT ARRANGEMENT & SUBJECT GUIDE

The abstracts are arranged by subject in accordance with the scheme in the CLASSIFICATION and CONTENTS which appears opposite. The page number for the start of each subject section is given. An alphabetical index to the scheme—the SUBJECT GUIDE—follows the CLASSIFICATION and CONTENTS.

SUBJECT INDEXES

Detailed twice-yearly subject indexes to the individual entries are provided separately, covering the periods January-June and July-December. In these SUBJECT INDEXES each major concept occurring in each paper abstracted is indexed under headings drawn from the INSPEC Thesaurus.

AUTHOR INDEX

At the end of each issue, an alphabetical index of authors is provided showing the entry number of the items written by them. These indexes are cumulated every six months and, with the addition of the title of the individual papers, are published separately to cover the periods January-June and July-December of each year.

SUBSIDIARY INDEXES

Where appropriate, the following subsidiary indexes are included for the convenience of users:

Bibliography index of articles where a significant list of references or bibliography is contained.

Book index of books received and abstracted.

Corporate Author index where a corporate organisation rather than an individual is responsible for publication. This index includes all reports.

Conference index with reference to individual papers.

Subscription prices and ordering procedure are shown on the inside back cover.

PHYSICS ABSTRACTS is published twice monthly by the Institution of Electrical Engineers in association with the Institute of Electrical and Electronics Engineers Inc. Printed by Unwin Brothers Limited, The Gresham Press, Old Woking, Surrey. 2nd Class postage paid at Piscataway, N.J. 08854, USA. POSTMASTER: Send address changes to INSPEC/IEEE SERVICE CENTER, 445 Hoes Lane, Piscataway, N.J. 08854.

© 1983. THE INSTITUTION OF ELECTRICAL ENGINEERS. All rights reserved. No part of this publication may be reproduced, stored in a retrieval system, or transmitted, in any form or by any means, electronic, mechanical, photocopying, recording or otherwise without the prior permission of the Institution of Electrical Engineers.

Physics Abstracts

CLASSIFICATION AND CONTENTS

The abstracts are arranged by subject in accordance with the following scheme. The page number for each section is given. The CLASSIFICATION AND CONTENTS is followed by an alphabetical guide to the scheme, the SUBJECT GUIDE.

The classification scheme is the result of cooperation between INSPEC, the American Institute of Physics, the European Physical Society and the Physics Working Group of the ICSU-AB.

| | page | | page |
|---|------|---|------|
| 00 GENERAL | 5943 | 0620H Measurement standards and calibration | 5959 |
| 00 COMMUNICATION, EDUCATION, HISTORY, AND PHILOSOPHY | 5943 | 0620J Determination of fundamental constants | — |
| 10 Announcements, news, and organizational activities | — | 0630 Measurement of basic variables | 5959 |
| 30B Physics literature and publications | 5943 | 0630C Spatial variables measurement | 5959 |
| Publications of lectures (advanced institutes, summer schools, etc.) | — | 0630E Mass and density measurement | — |
| 30C Conference proceedings | 5943 | 0630F Time and frequency measurement | 5960 |
| 30E Monographs, and collections | 5944 | 0630G Velocity, acceleration and rotation measurement | 5960 |
| 30K Handbooks, dictionaries, tables and data compilation | — | 0630L Measurement of basic electromagnetic variables | 5960 |
| 30M Textbooks for graduates and researchers | 5945 | 0650 Data handling and computation | 5960 |
| 30P Textbooks for undergraduates | 5945 | 0660 Laboratory techniques | 5960 |
| 30R Surveys and tutorial papers; resource letters | 5945 | 0670 General instrumentation | 5961 |
| 30T Bibliographies | 5946 | 0690 Other topics in measurement science, general laboratory techniques and instrumentation systems | — |
| 40 Education | — | 0700 SPECIFIC INSTRUMENTATION AND TECHNIQUES OF GENERAL USE IN PHYSICS | 5961 |
| 50 Educational aids | 5946 | 0710 Mechanical instruments and measurement methods | 5961 |
| 55 General Physics | — | 0720 Thermal instruments and techniques | 5961 |
| 60 Biographical, historical, and personal notes | 5946 | 0720D Thermometry | 5962 |
| 65 History of science | 5946 | 0720F Calorimetry | 5962 |
| 70 Philosophy of science | — | 0720H Furnaces | 5962 |
| 75 Science and society | 5946 | 0720K High-temperature techniques and instrumentation; pyrometry | — |
| 90 Other topics of general interest | — | 0720M Cryogenics | 5962 |
| 00 MATHEMATICAL METHODS IN PHYSICS | 5946 | 0725 Hygrometry | 5963 |
| 10 Algebra, set theory, and graph theory | 5946 | 0730 Vacuum production and techniques | 5963 |
| 20 Group theory | 5947 | 0730C Vacuum pumps | — |
| 30 Function theory, analysis | 5947 | 0730D Vacuum meters | 5964 |
| 40 Geometry, differential geometry, and topology | 5947 | 0735 High pressure production and techniques | 5964 |
| 50 Probability theory, stochastic processes, and statistics | 5947 | 0750 Electrical instruments and techniques | 5964 |
| 60 Numerical approximation and analysis | 5947 | 0755 Magnetic instruments and techniques | 5964 |
| 70 Computational techniques | 5948 | 0758 Magnetic resonance spectrometers, auxiliary instruments and techniques | 5964 |
| 90 Other topics in mathematical methods in physics | — | 0760 Optical instruments and techniques | 5965 |
| 00 CLASSICAL AND QUANTUM PHYSICS; MECHANICS AND FIELDS | 5948 | 0760D Photometry and radiometry | 5965 |
| 20 Classical mechanics of discrete systems: general | — | 0760F Polarimetry and ellipsometry | 5965 |
| mathematical aspects | 5948 | 0760H Refractometry and reflectometry | 5965 |
| 30 Special relativity | 5949 | 0760L Interferometry | 5966 |
| 40 Classical mechanics of continuous media: general | — | 0760P Optical microscopy | 5966 |
| mathematical aspects | 5949 | 0762 Detection of radiation (bolometers, photoelectric cells, i.r. and submillimetre waves detection) | 5967 |
| 40D Mathematical theory of elasticity | — | 0765 Optical spectroscopy and spectrometers | 5967 |
| 40G Fluid dynamics: general mathematical aspects | 5949 | 0765E UV and visible spectroscopy and spectrometers | 5967 |
| 40K Waves and wave propagation: general mathematical aspects | 5949 | 0765G IR spectroscopy and spectrometers | 5968 |
| 50 Classical field theory | 5950 | 0768 Photography, photographic instruments and techniques | 5968 |
| 65 Quantum theory; quantum mechanics | 5950 | 0775 Mass spectrometers and mass spectrometry techniques | 5968 |
| 70 Theory of quantized fields | 5952 | 0777 Particle beam production and handling; targets | 5968 |
| 80 General theory of scattering | — | 0780 Electron and ion microscopes and techniques | 5968 |
| 00 RELATIVITY AND GRAVITATION | 5952 | 0785 X-ray, gamma-ray instruments and techniques | 5969 |
| 20 General relativity | 5952 | 0790 Other topics in specialised instrumentation | 5970 |
| 30 Gravitational waves and radiation: theory | 5952 | 1000 THE PHYSICS OF ELEMENTARY PARTICLES AND FIELDS | 5970 |
| 40 Continuous media; electromagnetic and other mixed gravitational systems | 5953 | 1100 GENERAL THEORY OF FIELDS AND PARTICLES | 5970 |
| 50 Unified field theories and other theories of gravitation | 5953 | 1110 Field theory | 5970 |
| 60 Quantum theory of gravitation | 5953 | 1120 S-matrix theory | 5974 |
| 65 Supergravity | 5954 | 1130 Symmetry and conservation laws | 5974 |
| 80 Experimental tests of general relativity and observations of gravitational radiation | 5954 | 1140 Currents and their properties | 5975 |
| 90 Other topics in relativity and gravitation | — | 1150 Dispersion relations and sum rules | 5975 |
| 00 STATISTICAL PHYSICS AND THERMODYNAMICS | 5954 | 1160 Complex angular momentum; Regge formalism | — |
| 20 Statistical mechanics | 5954 | 1180 Relativistic scattering theory | 5975 |
| 30 Quantum statistical mechanics | 5954 | 1190 Other topics in general field and particle theory | — |
| 40 Fluctuation phenomena, random processes, and Brownian motion | 5955 | 1200 SPECIFIC THEORIES AND INTERACTION MODELS; PARTICLE SYSTEMATICS | 5975 |
| 50 Lattice theory and statistics; Ising problems | 5956 | 1210 Unified field theories and models | 5975 |
| 60 Transport processes; theory | 5957 | 1220 Models of electromagnetic interactions | 5977 |
| 70 Thermodynamics | 5958 | 1220D Specific calculations and limits of quantum electrodynamics | 5977 |
| 90 Other topics in statistical physics and thermodynamics | — | 1220F Experimental tests of quantum electrodynamics | 5977 |
| 00 MEASUREMENT SCIENCE, GENERAL LABORATORY TECHNIQUES; AND INSTRUMENTATION SYSTEMS | 5959 | 1225 Models for gravitational interactions | 5978 |
| 20 Metrology | 5959 | 1230 Models of weak interactions | 5978 |
| 20D Measurement and error theory | 5959 | 1235 Composite models of particles | 5978 |
| 20F Units | 5959 | 1235C General properties of quantum chromodynamics (dynamics, confinement, etc.) | 5978 |
| | | 1235E Applications of quantum chromodynamics to particle properties and reactions | 5979 |
| | | 1235H Phenomenological composite models of particle structure and reactions (partons, bags, etc.) | 5979 |
| | | 1235K Other composite models | 5981 |

| | page | | page |
|---|------|---|------|
| 1240 Models of strong interactions | 5981 | 2360 alpha decay | 5996 |
| 1240E Statistical models | 5981 | 2390 Other topics in nuclear decay and radioactivity | 5996 |
| 1240F Bootstrap models | — | | |
| 1240H Duality and dual models | 5981 | 2400 NUCLEAR REACTIONS AND SCATTERING: GENERAL | 5996 |
| 1240K Hadron classification schemes | — | 2410 Nuclear reaction and scattering models and methods | 5996 |
| 1240M Complex angular momentum plane; Regge poles and cuts (Reggeons) | 5981 | 2410H Optical and diffraction models | 5998 |
| 1240P Absorptive, optical, and eikonal models | — | 2430 Resonance reactions and scattering | 5999 |
| 1240Q Potential models | 5981 | 2450 Direct reactions | 5999 |
| 1240R Peripheral models (one or more particle exchange) | 5981 | 2460 Statistical theory and fluctuations | 5999 |
| 1240S Multiperipheral and multi-Regge models | 5981 | 2470 Polarization in reactions and scattering | 6000 |
| 1240V Vector-meson dominance | 5981 | 2475 General properties of fission | 6000 |
| 1270 Hadron mass formulas | 5981 | 2490 Other topics in nuclear reactions and scattering, general | — |
| 1290 Miscellaneous theoretical ideas and models | 5981 | | |
| 1300 SPECIFIC REACTIONS AND PHENOMENOLOGY | 5981 | 2500 NUCLEAR REACTIONS AND SCATTERING: SPECIFIC REACTIONS | 6000 |
| 1310 Weak and electromagnetic interactions of leptons | 5981 | 2510 Nuclear reactions and scattering involving few-nucleon systems | 6000 |
| 1315 Neutrino interactions | 5982 | 2520 Photonic nuclear reactions and photon scattering | 6000 |
| 1320 Leptonic and semileptonic decays of mesons | 5982 | 2530 Lepton-induced reactions and scattering | 6000 |
| 1325 Hadronic decays of mesons | 5982 | 2540 Nucleon-induced reactions and scattering | 6000 |
| 1330 Decays of baryons | 5982 | 2550 ² H- and ³ H-induced reactions and scattering | 6003 |
| 1335 Decays of leptons | 5983 | 2560 ³ He- and ⁴ He-induced reactions and scattering | 6003 |
| 1340 Electromagnetic processes and properties | 5983 | 2570 Heavy ion induced reactions and scattering | 6004 |
| 1340D Electromagnetic mass differences | 5983 | 2580 Meson- and hyperon-induced reactions and scattering | 6006 |
| 1340F Electromagnetic form factors; electric and magnetic moments | 5983 | 2585 Fission reactions | 6007 |
| 1340H Electromagnetic decays | 5983 | 2588 Fusion reactions | 6008 |
| 1340K Electromagnetic corrections to strong and weak interaction processes | 5983 | 2590 Other topics in nuclear reactions and scattering: specific reactions | — |
| 1360 Photon and charged-lepton interactions with hadrons | 5983 | | |
| 1360F Elastic and Compton scattering | 5983 | 2700 PROPERTIES OF SPECIFIC NUCLEI LISTED BY MASS RANGES | 6008 |
| 1360H Total and inclusive cross sections | 5983 | 2710 A ≤ 5 | 6008 |
| 1360K Meson production | 5984 | 2720 6 ≤ A ≤ 19 | 6008 |
| 1360M Meson-resonance production | — | 2730 20 ≤ A ≤ 38 | 6009 |
| 1360P Baryon and baryon resonance production | 5984 | 2740 39 ≤ A ≤ 58 | 6009 |
| 1365 Hadron production by electron-positron collisions | 5984 | 2750 59 ≤ A ≤ 89 | 6009 |
| 1375 Hadron-induced low- and intermediate-energy reactions and scattering, energy ≤ 10 GeV | 5985 | 2760 90 ≤ A ≤ 149 | 6009 |
| 1375C Nucleon-nucleon interactions, including antinucleon, deuteron, etc. (energy ≤ 10 GeV) | 5985 | 2770 150 ≤ A ≤ 189 | 6009 |
| 1375E Hyperon-nucleon interactions (energy ≤ 10 GeV) | 5985 | 2780 190 ≤ A ≤ 219 | 6009 |
| 1375G Pion-baryon interactions (energy ≤ 10 GeV) | 5985 | 2790 220 ≤ A | 6009 |
| 1375J Kaon-baryon interactions (energy ≤ 10 GeV) | 5985 | | |
| 1375L Meson-meson interactions (energy ≤ 10 GeV) | 5985 | 2800 NUCLEAR ENGINEERING AND NUCLEAR POWER STUDIES | 6010 |
| 1385 Hadron-induced high- and super-high-energy interactions, energy > 10 GeV | 5985 | 2820 Neutron physics | 6010 |
| 1385D Elastic scattering (energy > 10 GeV) | 5986 | 2841 Fission reactor theory and design | 6010 |
| 1385F Inelastic scattering, two-particle final states (energy > 10 GeV) | — | 2842 Fission reactor materials | 6011 |
| 1385H Inelastic scattering, many-particle final states (energy > 10 GeV) | 5986 | 2842H Fuel preparation and reprocessing | 6016 |
| 1385K Inclusive reactions, including total cross sections, (energy > 10 GeV) | 5986 | 2843 Fission reactor operation | 6016 |
| 1385M Cosmic ray interactions | 5987 | 2844 Fission reactor protection systems, safety and accidents | 6018 |
| 1388 Polarisation in interactions and scattering | 5987 | 2850 Fission reactor types and applications | 6018 |
| 1390 Other topics in specific reactions and phenomenology of elementary particles | 5987 | 2852 Fusion reactors | 6019 |
| | | 2858 Integrated reactor systems | — |
| | | 2870 Nuclear explosions | 6020 |
| | | 2880 Radiation technology, including shielding | 6020 |
| | | 2890 Other topics in nuclear engineering and nuclear power studies | 6021 |
| 1400 PROPERTIES OF SPECIFIC PARTICLES AND RESONANCES | 5987 | | |
| 1420 Baryons and baryon resonances | 5987 | 2900 EXPERIMENTAL METHODS AND INSTRUMENTATION FOR ELEMENTARY-PARTICLE AND NUCLEAR PHYSICS | 6022 |
| 1440 Mesons and meson resonances | 5988 | 2910 Preacceleration (injection) | — |
| 1460 Leptons | 5988 | 2915 Electrostatic and linear particle accelerators | 6022 |
| 1480 Other and hypothetical particles | 5988 | 2920 Cyclic accelerators and storage facilities | 6022 |
| | | 2925 Particle sources and targets, preparation and technology | 6022 |
| 2000 NUCLEAR PHYSICS | 5988 | 2930 Radiation spectrometers and spectroscopic techniques | 6022 |
| 2100 NUCLEAR STRUCTURE | 5988 | 2940 Radiation detectors | 6023 |
| 2110 General and average properties of nuclei; properties of nuclear energy levels | 5988 | 2960 Counting circuits and nuclear electronics | 6024 |
| 2110D Binding energy and masses | 5989 | 2970 Radiation measurement, detection and counting | 6024 |
| 2110F Shape, charge, radius and form factors | 5989 | 2975 Polarization analysis | — |
| 2110H Spin, parity, and isobaric spin | 5989 | 2980 Nuclear information processing | 6024 |
| 2110J Spectroscopic factors | 5990 | 2990 Other topics in high-energy and nuclear experimental methods and instrumentation | 6024 |
| 2110K Electromagnetic moments | 5990 | | |
| 2110M Level density and structure | 5990 | 3000 ATOMIC AND MOLECULAR PHYSICS | 6025 |
| 2130 Nuclear forces | 5990 | | |
| 2140 Few-nucleon systems | 5992 | 3100 THEORY OF ATOMS AND MOLECULES | 6025 |
| 2160 Nuclear-structure models and methods | 5992 | 3110 General theory of structure, transitions and chemical binding | 6025 |
| 2160C Shell model | 5992 | 3115 General mathematical and computational developments | 6025 |
| 2160E Collective models | 5992 | 3120 Specific calculations and results | 6026 |
| 2160F Models based on group theory | 5993 | 3120D Complete ab initio calculations (exact or nearly exact calculations on small species) | — |
| 2160G Cluster models | 5993 | 3120E Ab initio LCAO and GO SCF calculations | 6027 |
| 2160J Hartree-Fock and random-phase approximations | 5993 | 3120G Other accurate, or nearly ab initio calculations (DIM method, SAMO method, etc.) | 6027 |
| 2165 Nuclear matter | 5993 | 3120L Statistical model calculations (Thomas-Fermi and Thomas-Fermi-Dirac models) | — |
| 2180 Hypernuclei | 5994 | 3120N Semi-empirical NDO calculations (CND0, INDO, MIND0, PCILO methods, etc.) | 6027 |
| 2190 Other topics in nuclear structure | — | | |
| 2300 RADIOACTIVITY AND ELECTROMAGNETIC TRANSITIONS | 5994 | | |
| 2320 Electromagnetic transitions | 5994 | | |
| 2320C Lifetimes and transition probabilities | 5995 | | |
| 2320N Internal conversion and extranuclear effects | 5995 | | |
| 2340 beta decay; electron and muon capture | 5995 | | |

| | page | | page |
|--|------|--|------|
| 120P Other semi-empirical calculations (Hückel, generalized Hückel, PPP methods, etc.) | 6028 | 3500 PROPERTIES OF ATOMS AND MOLECULES; INSTRUMENTS AND TECHNIQUES | 6046 |
| 120R Valence bond calculations (ab initio or not) | 6028 | Atoms | 6046 |
| 120T Electron correlation and CI calculations | 6028 | Atomic masses, mass spectra, abundances, and isotopes | 6046 |
| 120W Empirical methods (nonquantum methods for conformations, as Wiberg method, Westheimer method, etc.) | — | Electric and magnetic moments, polarizability | 6046 |
| 130 Corrections to electronic structure | 6029 | Relativistic corrections, fine- and hyperfine-structure constants | 6047 |
| 150 Excited states | 6029 | Ionization potentials, electron affinities | 6047 |
| 170 Effects of molecular interactions on electronic structure | 6030 | Weak Interactions | — |
| 170D Environmental and solvent effects | 6030 | Molecules | 6047 |
| 170F Potential-energy surfaces for collisions | 6030 | General molecular conformation and symmetry; stereochemistry | 6047 |
| 170H Time-dependent phenomena: excitation and relaxation processes, and reaction rates | 6030 | Interatomic distances and angles | 6047 |
| 170K Molecular solids | — | Bond strengths, dissociation energies, hydrogen bonding, etc | 6048 |
| 190 Other topics in the theory of atoms and molecules | 6030 | Barrier heights (internal rotation, inversion); rotational isomerism, conformational dynamics | 6048 |
| 200 ATOMIC SPECTRA AND INTERACTIONS WITH PHOTONS | 6030 | Electric and magnetic moments (and derivatives), polarizability, and magnetic susceptibility | 6048 |
| 220 Atomic spectra grouped by wavelength ranges | 6030 | Rotation, vibration, and vibration-rotation constants | 6048 |
| 220B Radiofrequency, microwave, and infrared spectra | 6030 | Hyperfine and fine-structure constants | 6048 |
| 220J Visible and ultraviolet spectra | 6031 | Ionization potentials, electron affinities, molecular core binding energy | 6049 |
| 220R X-ray spectra | 6031 | Weak interactions | — |
| 250 Fluorescence, phosphorescence | 6031 | Mass spectra | 6049 |
| 260 Zeeman and Stark effects | 6031 | Correlation times in molecular dynamics | — |
| 270 Spectral line shapes and intensities | 6031 | Atomic and molecular measurements and techniques | 6049 |
| 280 Photon interactions with atoms | 6032 | | |
| 280B Level crossing and optical pumping | 6032 | 3600 STUDIES OF SPECIAL ATOMS AND MOLECULES | 6049 |
| 280D Autoionization | 6032 | 3610 Exotic atoms and molecules (containing mesons, muons, and other abnormal particles) | 6049 |
| 280F Photoionization and photodetachment | 6032 | Macromolecules and polymer molecules | 6050 |
| 280H Auger effect and inner-shell ionization | 6032 | Atomic and molecular clusters | 6050 |
| 280K Multiphoton processes | 6032 | Other special atoms and molecules | — |
| 290 Other topics in atomic spectra and interactions with photons | 6032 | | |
| 300 MOLECULAR SPECTRA AND INTERACTIONS WITH PHOTONS | 6032 | 4000 CLASSICAL AREAS OF PHENOMENOLOGY | 6050 |
| 310 Calculation of molecular spectra | 6032 | | |
| 320 Molecular spectra grouped by wavelength ranges | 6033 | 4100 ELECTRICITY AND MAGNETISM; FIELDS AND CHARGED PARTICLES | 6050 |
| 320B Radiofrequency and microwave spectra | 6033 | Classical electromagnetism | 6050 |
| 320E Infrared spectra | 6034 | Electrostatics, magnetostatics | 6050 |
| 320F Raman and Rayleigh spectra | 6035 | Steady-state electromagnetic fields; electromagnetic induction | 6050 |
| 320K Visible spectra | 6035 | Electromagnetic waves: theory | 6050 |
| 320L Ultraviolet spectra | 6036 | Particles in electromagnetic fields: classical aspects | 6051 |
| 320N Vacuum ultraviolet spectra | 6036 | Particle beams and particle optics | 6051 |
| 320R X-ray spectra | — | Electron beams and electron optics | 6051 |
| 325 Nuclear magnetic resonance and relaxation; nuclear quadrupole resonance (NQR) | 6036 | Ion beams and ion optics | 6051 |
| 330 Electron paramagnetic resonance and relaxation | 6037 | Other topics in electricity and magnetism | — |
| 335 Double resonances and other multiple resonances | 6037 | | |
| 335H MODR and PMDR (microwave optical double resonance and phosphorescence microwave double resonance) | — | 4200 OPTICS | 6051 |
| 340 Mössbauer spectra | 6037 | 4210 Propagation and transmission in homogeneous media | 6051 |
| 345 Magneto-optical and electro-optical spectra; dichroism | 6037 | 4220 Propagation and transmission in inhomogeneous media | 6052 |
| 345B Zeeman and Stark effects | 6037 | 4230 Optical information, image formation and analysis | 6052 |
| 345C Magnetic circular dichroism | 6037 | Holography | 6053 |
| 350 Fluorescence, phosphorescence; radiationless transitions (intersystem crossing, internal conversion) | 6037 | Quantum optics | 6054 |
| 365 Photoelectron spectra | 6039 | Masers | 6054 |
| 370 Intensities and shapes of molecular spectral lines and bands | 6040 | Lasing processes | 6054 |
| 380 Photon interactions with molecules | 6040 | General theory of lasing action | 6054 |
| 380B Level crossing and optical pumping | 6040 | CO ₂ lasers | 6054 |
| 380E Autoionization, photoionization, and photodetachment | 6040 | Inert gas lasers | 6055 |
| 380G Diffuse spectra; predissociation, photodissociation | 6040 | Lasing action in other gas lasers | 6055 |
| 380K Multiphoton processes | 6041 | Chemical lasers | — |
| 390 Other topics in molecular spectra and interactions with photons | 6041 | Lasing action in liquids and organic dyes | 6055 |
| 400 ATOMIC AND MOLECULAR COLLISION PROCESSES AND INTERACTIONS | 6041 | Lasing action in semiconductors with junctions | 6055 |
| 410 General theories and models | 6041 | Lasing action in other solids | 6056 |
| 420 Interatomic and intermolecular potentials and forces | 6041 | Free electron lasers | 6056 |
| 440 Elastic scattering of atoms and molecules | 6042 | Laser systems and laser beam applications | 6058 |
| 450 Inelastic scattering of atoms and molecules | 6042 | Design of specific laser systems | 6058 |
| 450E Rotational and vibrational energy transfer | 6043 | Laser resonators and cavities | 6059 |
| 450H Electronic excitation and ionization (inc. beam-foil excitation and ionization) | 6043 | Laser beam modulation | 6060 |
| 450L Chemical reactions, energy disposal, and angular distribution, as studied by atomic and molecular beams | 6044 | Optical problems related to properties and interactions of laser beams | 6060 |
| 470 Charge transfer | 6044 | Optical problems related to applications of laser beams | 6060 |
| 480 Electron scattering | 6045 | Nonlinear optics | 6060 |
| 480B Elastic scattering of electrons by atoms and molecules | 6045 | General theory | — |
| 480D Atomic excitation and ionization by electron impact | 6045 | Stimulated Raman, Brillouin and Rayleigh scattering; parametric oscillations and harmonic generation | 6061 |
| 480G Molecular excitation, ionization, and dissociation by electron impact | 6046 | Phase conjugation | 6062 |
| 490 Other topics in atomic and molecular collision processes and interactions | — | Photon echoes, self-induced transparency, optical saturation and related effects | 6063 |
| | | Beam trapping, self focusing, thermal blooming, and related effects | 6064 |
| | | Optical materials | 6064 |
| | | Glass | 6064 |
| | | Light-sensitive materials | 6064 |
| | | Optical sources and standards | 6064 |
| | | Optical lens and mirror systems | 6064 |
| | | Coatings | 6065 |
| | | Optical devices, techniques and applications | 6065 |

| | | page | | | page |
|-------|--|------|-------|--|------|
| 4280B | Spatial filters, zone plates | 6065 | 4755K | Multiphase flows | 6087 |
| 4280C | Spectral and other filters | 6065 | 4755M | Flow through porous media | 6088 |
| 4280D | Monochromators | 6065 | 4760 | Flows in ducts, channels, and conduits | 6089 |
| 4280E | Shutters, windows, diaphragms, deflectors, choppers | 6066 | 4765 | Magnetohydrodynamics and electrohydrodynamics | 6089 |
| 4280F | Gratings, echelles | 6066 | 4770 | Reactive, radiative, or nonequilibrium flows | 6090 |
| 4280K | Optical beam modulators | 6066 | 4775 | Relativistic fluid dynamics | — |
| 4280L | Optical waveguides | 6066 | 4780 | Instrumentation for fluid dynamics | 6090 |
| 4280M | Fibre optics | 6066 | 4790 | Other topics in fluid dynamics | — |
| 4280Q | Image detectors, convertors, and intensifiers | 6069 | | | |
| 4280S | Optical communications devices | 6069 | 5000 | FLUIDS, PLASMAS AND ELECTRIC DISCHARGES | 6091 |
| 4282 | Integrated optics | 6069 | | | |
| 4285 | Optical testing and workshop techniques | 6069 | 5100 | KINETIC AND TRANSPORT THEORY OF FLUIDS; PHYSICAL PROPERTIES OF GASES | 6091 |
| 4290 | Other topics in optics | — | 5110 | Kinetic and transport theory | 6091 |
| | | | 5120 | Viscosity and diffusion: experimental | 6092 |
| 4300 | ACOUSTICS | 6069 | 5130 | Thermal properties of gases | 6092 |
| 4320 | General linear acoustics | 6069 | 5140 | Acoustical properties of gases; ultrasonic relaxation | — |
| 4325 | Nonlinear acoustics and macrosonics | 6070 | 5150 | Electrical phenomena in gases | 6092 |
| 4328 | Aeracoustics and atmospheric sound | — | 5160 | Magnetic phenomena in gases | — |
| 4330 | Underwater sound | 6070 | 5170 | Optical phenomena in gases | 6092 |
| 4335 | Ultrasonics, quantum acoustics, and physical effects of sound | 6071 | 5190 | Other topics in the physics of fluids | — |
| 4340 | Mechanical vibrations and shock | 6071 | | | |
| 4345 | Statistical studies of acoustical response | — | 5200 | THE PHYSICS OF PLASMAS AND ELECTRIC DISCHARGES | 6092 |
| 4350 | Noise, its effects and control | 6071 | 5220 | Elementary processes in plasma | 6092 |
| 4355 | Architectural acoustics | 6071 | 5220F | Electron collisions | 6092 |
| 4360 | Acoustic signal processing | 6071 | 5220H | Atomic, molecular, heavy-particle collisions | 6092 |
| 4363 | Acoustic holography | — | 5225 | Plasma basic properties | 6092 |
| 4370 | Speech communication | 6071 | 5225F | Transport properties | 6093 |
| 4375 | Music and musical instruments | 6072 | 5225P | Emission, absorption, and scattering of radiation | 6093 |
| 4385 | Acoustical measurements and instrumentation | 6072 | 5230 | Plasma flow; magnetohydrodynamics | 6094 |
| 4388 | Transduction; devices for the generation and reproduction of sound | 6073 | 5235 | Waves, oscillations, and instabilities in plasma | 6094 |
| 4390 | Other topics in acoustics | 6073 | 5235R | Plasma turbulence | 6095 |
| | | | 5235T | Shock waves | 6095 |
| 4400 | HEAT FLOW, THERMAL AND THERMODYNAMIC PROCESSES | 6073 | 5240 | Plasma interactions | 6095 |
| 4410 | Heat conduction (models, phenomenological description) | 6073 | 5240D | Electromagnetic wave propagation in plasma | 6095 |
| 4425 | Convective and constrained heat transfer | 6074 | 5240F | Antennas in plasma; plasma-filled wave guides | — |
| 4430 | Heat transfer in inhomogeneous media and through interfaces | 6074 | 5240H | Solid-plasma interactions | 6095 |
| 4440 | Radiative heat transfer | 6074 | 5240K | Sheaths | 6095 |
| 4450 | Thermal properties of matter (phenomenology, experimental techniques) | 6074 | 5240M | Beam interactions in plasma | 6095 |
| 4460 | Thermodynamic processes (phenomenology, experimental techniques) | 6075 | 5250 | Plasma production and heating | 6095 |
| 4490 | Other topics in heat flow, thermal and thermodynamic processes | — | 5250J | Plasma production and heating by laser beams | 6096 |
| | | | 5250L | Plasma production and heating by shock wave and wire explosion | 6096 |
| 4600 | MECHANICS, ELASTICITY, RHEOLOGY | 6075 | 5255 | Plasma equilibrium and confinement | 6096 |
| 4610 | Mechanics of discrete systems | 6075 | 5260 | Relativistic plasma | 6097 |
| 4620 | Continuum mechanics | 6075 | 5265 | Plasma simulation | — |
| 4630 | Mechanics of solids and rheology | 6075 | 5270 | Plasma diagnostic techniques and instrumentation | 6097 |
| 4630C | Static elasticity | 6075 | 5275 | Plasma devices and applications | 6097 |
| 4630J | Viscoelasticity, plasticity, viscoplasticity, creep, and stress relaxation | 6076 | 5280 | Electric discharges | 6098 |
| 4630L | Static buckling and instability | 6076 | 5290 | Other topics in plasma physics and electric discharges | — |
| 4630M | Vibrations, aeroelasticity, hydroelasticity, mechanical waves, and shocks | 6077 | | | |
| 4630N | Fracture mechanics, fatigue, and cracks | 6077 | 6000 | CONDENSED MATTER: STRUCTURE, THERMAL AND MECHANICAL PROPERTIES | 6098 |
| 4630P | Friction, wear, adherence, hardness, mechanical contacts | 6078 | | | |
| 4630R | Measurement methods and techniques | 6078 | 6100 | STRUCTURE OF LIQUIDS AND SOLIDS; CRYSTALLOGRAPHY | 6098 |
| 4660 | Rheology of fluids and pastes | 6079 | 6110 | X-ray determination of structures | 6099 |
| 4690 | Other topics in mechanics, elasticity, and rheology | — | 6110D | Theories of diffraction and scattering | 6099 |
| | | | 6110F | Experimental techniques | 6099 |
| 4700 | FLUID DYNAMICS | 6079 | 6112 | Neutron determination of structures | 6100 |
| 4710 | General theory | 6079 | 6114 | Electron determination of structures | 6100 |
| 4715 | Laminar flows | 6079 | 6114D | Theories of diffraction and scattering | 6100 |
| 4715C | Laminar boundary layers | 6079 | 6114F | Experimental diffraction and scattering | 6100 |
| 4715F | Stability of laminar flows | 6080 | 6114H | Low-energy electron diffraction (LEED) and reflection High-energy electron diffraction (RHEED) | — |
| 4720 | Hydrodynamic stability | 6080 | 6116 | Other determination of structures | 6100 |
| 4725 | Turbulent flows, convection, and heat transfer | 6080 | 6116D | Electron microscopy determinations | 6100 |
| 4725C | Isotropic turbulence | 6080 | 6116F | Field-ion microscopy determinations | — |
| 4725F | Boundary layer and shear turbulence | 6081 | 6116N | EPR and NMR determinations | — |
| 4725J | Turbulent diffusion | 6081 | 6120 | Classical, semiclassical, and quantum theories of liquid structure | 6101 |
| 4725M | Noise (turbulence generated) | 6081 | 6125 | Studies of specific liquid structures | 6101 |
| 4725Q | Convection and heat transfer | 6081 | 6125M | Liquid metals | 6102 |
| 4725R | Wakes | 6083 | 6130 | Liquid crystals | 6102 |
| 4730 | Rotational flow and vorticity | 6084 | 6140 | Amorphous and polymeric materials | 6104 |
| 4735 | Waves | 6085 | 6140D | Glasses | 6104 |
| 4740 | Compressible flows; shock and detonation phenomena | 6085 | 6140K | Polymers, elastomers, and plastics | 6105 |
| 4740D | General subsonic flows | 6085 | 6150 | Crystalline state | 6105 |
| 4740H | Transonic flows | 6085 | 6150C | Physics of crystal growth | 6105 |
| 4740K | Supersonic and hypersonic flows | 6086 | 6150E | Crystal symmetry; models and space groups, and crystalline systems and classes | 6106 |
| 4740N | Shock-wave interactions | 6086 | 6150J | Crystal morphology and orientation | 6107 |
| 4745 | Rarefied gas dynamics | 6086 | 6150K | Crystallographic aspects of polymorphic and order-disorder transformations | 6107 |
| 4750 | Non-Newtonian dynamics | 6086 | 6150L | Crystal binding | 6107 |
| 4755 | Nonhomogeneous flows | 6087 | 6155 | Specific structure of elements and alloys | 6108 |
| 4755B | Cavitation | — | 6155D | Nonmetallic elements | 6108 |
| 4755C | Jets | 6087 | 6155F | Metallic elements | 6108 |
| 4755E | Nozzles | — | 6155H | Alloys | 6108 |
| 4755H | Stratified flows | 6087 | 6160 | Specific structure of inorganic compounds | 6108 |
| | | | 6165 | Specific structure of organic compounds | 6111 |
| | | | 6170 | Defects in crystals | 6111 |

| | | | | | |
|------|---|------|-------|---|------|
| 170B | Interstitials and vacancies | 6112 | 6630D | Theory of diffusion and ionic conduction in solids | — |
| 170D | Colour centres | 6112 | 6630F | Self-diffusion in metals, semimetals, and alloys | 6139 |
| 170E | Other point defects | — | 6630H | Self-diffusion and ionic conduction in nonmetals | 6139 |
| 170G | Dislocations: theory | 6113 | 6630J | Diffusion, migration, and displacement of impurities | 6140 |
| 170J | Etch pits, decoration, transmission electron-microscopy and other direct observations of dislocations | 6113 | 6630L | Diffusion, migration, and displacement of other defects | 6141 |
| 170L | Slip, creep, internal friction and other indirect evidence of dislocations | 6114 | 6630N | Chemical interdiffusion | 6141 |
| 170N | Grain and twin boundaries | 6115 | 6630Q | Electromigration | 6141 |
| 170P | Stacking faults, stacking fault tetrahedra and other planar or extended defects | 6116 | 6660 | Thermal conduction in nonmetallic liquids | 6141 |
| 170R | Crystal impurities: general | 6116 | 6670 | Nonelectronic thermal conduction and heat-pulse propagation in nonmetallic solids | 6141 |
| 170T | Doping and implantation of impurities | 6116 | 6690 | Other topics in nonelectronic transport properties | 6142 |
| 170W | Impurity concentration, distribution, and gradients | 6118 | | | |
| 170Y | Interaction between different crystal structure defects | 6118 | 6700 | QUANTUM FLUIDS AND SOLIDS; LIQUID AND SOLID HELIUM | 6142 |
| 180 | Radiation damage and other irradiation effects | 6119 | 6720 | Quantum effects on the structure and dynamics of nondegenerate fluids | 6142 |
| 180B | Laser beams | 6119 | | | |
| 180C | X-rays | 6120 | 6740 | Boson degeneracy and superfluidity of helium-4 | 6142 |
| 180E | Gamma rays | 6120 | 6750 | Fermi fluids; liquid helium-3 | 6142 |
| 180F | Electrons and positrons | 6120 | 6760 | Mixed systems; liquid helium 3-4 mixtures | 6143 |
| 180H | Neutrons | 6121 | 6770 | Films | 6143 |
| 180J | Ions | 6122 | 6780 | Solid helium and related quantum crystals | 6143 |
| 180L | Atoms and molecules | 6122 | 6790 | Other topics in quantum fluids and solids (e.g. neutron-star matter) | 6143 |
| 180M | Channelling, blocking and energy loss of particles | 6123 | | | |
| 190 | Other topics in structure of liquids and solids | — | 6800 | SURFACES AND INTERFACES; THIN FILMS AND WHISKERS | 6144 |
| 200 | MECHANICAL AND ACOUSTIC PROPERTIES OF CONDENSED MATTER | 6124 | 6810 | Fluid surfaces and interfaces with fluids | 6144 |
| 210 | Mechanical properties of liquids | 6124 | 6815 | Liquid thin films | 6144 |
| 220 | Mechanical properties of solids (related to microscopic structure) | 6124 | 6820 | Solid surface structure | 6144 |
| 220D | Elastic constants | 6124 | 6825 | Mechanical and acoustical properties of solid surfaces and interfaces | 6145 |
| 220F | Deformation and plasticity | 6124 | 6830 | Dynamics of solid surfaces and interface vibrations | 6145 |
| 220H | Creep | 6125 | 6840 | Surface energy of solids; thermodynamic properties | 6145 |
| 220M | Fatigue, brittleness, fracture, and cracks | 6125 | 6845 | Solid-fluid interface processes | 6145 |
| 220P | Tribology | 6127 | 6848 | Solid-solid interfaces | 6147 |
| 230 | Mechanical and elastic waves | 6127 | 6855 | Thin film growth, structure, and epitaxy | 6147 |
| 240 | Anelasticity, internal friction, and damping | 6127 | 6860 | Physical properties of thin films, nonelectronic | 6149 |
| 250 | High-pressure and shock-wave effects in solids | 6127 | 6870 | Whiskers and dendrites: growth, structure, and nonelectronic properties | — |
| 260 | Acoustic properties of liquids | 6127 | 6890 | Other topics in the structure and nonelectronic properties of surfaces and thin films | 6149 |
| 265 | Acoustic properties of solids | 6127 | | | |
| 280 | Ultrasonic relaxation | 6128 | 7000 | CONDENSED MATTER: ELECTRONIC STRUCTURE, ELECTRICAL, MAGNETIC, AND OPTICAL PROPERTIES | 6149 |
| 290 | Other topics in mechanical and acoustical properties of condensed matter | — | | | |
| 300 | LATTICE DYNAMICS AND CRYSTAL STATISTICS | 6128 | | | |
| 310 | General theory | 6128 | 7100 | ELECTRON STATES | 6149 |
| 320 | Phonons and vibrations in crystal lattices | 6128 | 7110 | General theories and computational techniques | 6149 |
| 320D | Phonon states and bands, normal modes, and phonon dispersion | 6128 | 7120 | Electronic density of states determinations | 6150 |
| 320H | Phonon-phonon interactions | 6129 | 7125 | Nonlocalized single-particle electronic states | 6150 |
| 320K | Phonon-electron interactions | 6129 | 7125C | Techniques of band-structure calculation (general theory, applications of group theory, analytic continuation, etc) | 6150 |
| 320M | Phonon-defect interactions | — | 7125H | Measurement of Fermi surface parameters | 6151 |
| 320P | Localized modes | 6129 | 7125J | Effective mass and g-factors | — |
| 350 | Vibrational states in disordered systems | 6129 | 7125L | Electron energy states in liquid metals | — |
| 370 | Statistical mechanics of lattice vibrations | 6129 | 7125M | Electron energy states in amorphous and glassy solids | — |
| 375 | Statistical mechanics of displacive phase-transitions | 6129 | 7125P | Band structure of crystalline metals | 6151 |
| 390 | Other topics in lattice dynamics and crystal statistics | 6129 | 7125R | Band structure of crystalline elemental semiconductors | 6151 |
| 400 | EQUATIONS OF STATE, PHASE EQUILIBRIA, AND PHASE TRANSITIONS | 6129 | 7125T | Band structure of crystalline semiconductor compounds and insulators | 6151 |
| 410 | General theory of equations of state and phase equilibria | 6129 | 7130 | Metal-insulator transitions | 6152 |
| 430 | Equations of state of specific substances | 6129 | 7135 | Excitons and related phenomena | 6152 |
| 460 | General studies of phase transitions | 6130 | 7136 | Polaritons | 6153 |
| 470 | Phase equilibria, phase transitions, and critical points | 6130 | 7138 | Polarons and electron-phonon interactions | 6153 |
| 470D | Solid-liquid transitions | 6130 | 7145 | Collective effects | 6153 |
| 470F | Liquid-vapour transitions | 6131 | 7145G | Exchange, correlation, dielectric and magnetic functions, plasmons | 6153 |
| 470H | Solid-vapour transitions | 6131 | 7145J | Fermi-Thomas model | 6154 |
| 470J | Liquid-liquid transitions | — | 7145N | Calculations of total electronic binding energy | 6154 |
| 470K | Solid-solid transitions | 6131 | 7150 | Localized single-particle electronic states | 6154 |
| 470M | Transitions in liquid crystals | 6133 | 7155 | Impurity and defect levels | 6154 |
| 470P | Glass transitions | 6134 | 7155J | Localization in disordered structures | 6156 |
| 475 | Solubility, segregation, and mixing | 6134 | 7165 | Positron states | — |
| 480 | Other phase properties of systems | 6136 | 7170 | Level splitting and interactions | 6156 |
| 490 | Other topics in equations of state, phase equilibria, and phase transitions | — | 7170C | Crystal and ligand fields | 6157 |
| | | | 7170E | Spin-orbit coupling, Zeeman, Stark and strain splitting | 6158 |
| 500 | THERMAL PROPERTIES OF CONDENSED MATTER | 6136 | 7170G | Exchange interactions | 6158 |
| 520 | Heat capacities of liquids | 6136 | 7170J | Nuclear states and interactions | 6158 |
| 540 | Heat capacities of solids | 6136 | 7190 | Other topics in electron states | — |
| 550 | Thermodynamic properties and entropy | 6137 | | | |
| 570 | Thermal expansion and thermomechanical effects | 6138 | 7200 | ELECTRONIC TRANSPORT IN CONDENSED MATTER | 6158 |
| 590 | Other topics in thermal properties of condensed matter | 6138 | 7210 | Theory of electronic transport; scattering mechanisms | 6158 |
| | | | 7215 | Electronic conduction in metals and alloys | 6158 |
| 600 | TRANSPORT PROPERTIES OF CONDENSED MATTER (NONELECTRONIC) | 6138 | 7215C | Electrical and thermal conduction in amorphous and liquid metals and alloys | 6158 |
| 610 | Diffusion and ionic conduction in liquids | 6138 | 7215E | Electrical and thermal conduction in crystalline metals and alloys | 6159 |
| 620 | Diffusive momentum transport | 6139 | | | |
| 630 | Diffusion in solids | 6139 | | | |

| | | page | | | page |
|-------|--|------|-------|--|------|
| 7215G | Galvanomagnetic and other magnetotransport effects | 6159 | 7510J | Heisenberg and other quantized localized spin models | 6176 |
| 7215H | Thermomagnetic effects | — | 7510L | Band and itinerant models | 6177 |
| 7215J | Thermoelectric effects | 6159 | 7520 | Diamagnetism and paramagnetism | 6177 |
| 7215L | Relaxation times and mean free paths | 6159 | 7520C | Nonmetals | 6177 |
| 7215N | Collective modes, e.g. in one-dimensional conductors | 6159 | 7520E | Metals and alloys | 6177 |
| 7215Q | Scattering mechanisms and Kondo effect | 6160 | 7520H | Local moment in dilute alloys; Kondo effect | 6177 |
| 7220 | Conductivity phenomena in semiconductors and insulators | 6160 | 7525 | Spin arrangements in magnetically ordered materials (neutron studies, etc) | 6177 |
| 7220D | General theory, scattering mechanisms | 6160 | 7530 | Magnetically ordered materials, other intrinsic properties | 6178 |
| 7220F | Low-field transport and mobility; piezoresistance | 6160 | 7530C | Saturation moments and magnetic susceptibility | 6178 |
| 7220H | High-field and nonlinear effects | 6162 | 7530D | Spin waves | 6179 |
| 7220J | Charge carriers: generation, recombination, lifetime, and trapping | 6162 | 7530E | Exchange and superexchange interactions | 6180 |
| 7220M | Galvanomagnetic and other magnetotransport effects | 6163 | 7530G | Anisotropy | 6180 |
| 7220N | Thermomagnetic effects | — | 7530H | Magnetic impurity interactions | 6180 |
| 7220P | Thermoelectric effects | 6164 | 7530K | Magnetic phase boundaries | 6180 |
| 7230 | High-frequency effects; plasma effects | 6164 | 7530S | Magnetocaloric effect | — |
| 7240 | Photoconduction and photovoltaic effects; photodiode effects | 6164 | 7540 | Critical-point effects, specific heats, short-range order | 6181 |
| 7250 | Acoustoelectric effects | 6165 | 7540D | Ising and other classical spin models | 6182 |
| 7255 | Magnetoacoustic effects | 6166 | 7540F | Heisenberg and other quantized spin models | 6182 |
| 7260 | Mixed conductivity and conductivity transitions | 6166 | 7550 | Studies of specific magnetic materials | 6182 |
| 7270 | Noise processes and phenomena | 6166 | 7550B | Ferromagnetism of Fe and its alloys | 6182 |
| 7280 | Conductivity of specific semiconductors and insulators | 6166 | 7550C | Ferromagnetism of other metals | 6183 |
| 7280C | Elemental semiconductors | 6166 | 7550D | Ferromagnetism of nonmetals | 6183 |
| 7280E | III-V and II-VI semiconductors | 6166 | 7550E | Antiferromagnetics | 6183 |
| 7280G | Transition-metal compounds | 6167 | 7550G | Ferrimagnetics | 6183 |
| 7280J | Other crystalline inorganic semiconductors | 6167 | 7550K | Amorphous magnetic materials | 6184 |
| 7280L | Organic semiconductors | 6167 | 7550M | Magnetic liquids | 6184 |
| 7280N | Amorphous and glassy semiconductors | 6167 | 7560 | Domain effects, magnetization curves, and hysteresis | 6184 |
| 7280P | Liquid semiconductors | — | 7560C | Domain walls and domain structure | 6184 |
| 7290 | Other topics in electronic transport in condensed matter | — | 7560E | Magnetization curves, hysteresis, Barkhausen and related effects | 6184 |
| | | | 7560G | High coercivity materials | 6185 |
| | | | 7560J | Fine-particle systems | 6185 |
| | | | 7560L | Magnetic aftereffects | 6185 |
| | | | 7560N | Magnetic annealing and temperature-hysteresis effects | 6185 |
| 7300 | ELECTRONIC STRUCTURE AND ELECTRICAL PROPERTIES OF SURFACES, INTERFACES, AND THIN FILMS | 6167 | 7570 | Magnetic films and plates | 6185 |
| 7320 | Electronic surface states | 6167 | 7570K | Domain structure (magnetic bubbles) | 6186 |
| 7325 | Surface conductivity | 6168 | 7580 | Magnetomechanical and magnetoelectric effects, magnetostriction | 6186 |
| 7330 | Surface double layers, Schottky barriers, and work functions | 6168 | 7590 | Other topics in magnetic properties and materials | 6188 |
| 7340 | Interfaces | 6168 | 7600 | MAGNETIC RESONANCES AND RELAXATION IN CONDENSED MATTER; MÖSSBAUER EFFECT | 6188 |
| 7340B | Static electrification | — | 7620 | General theory of resonances and relaxation | — |
| 7340G | Tunnelling: general | — | 7630 | Electron paramagnetic resonance and relaxation | 6188 |
| 7340J | Metal-to-metal contacts | — | 7630D | Ions and impurities: general | 6188 |
| 7340L | Semiconductor-to-semiconductor contacts, p-n junctions, and heterojunctions | 6168 | 7630F | Iron group (3d) ions and impurities (Ti-Cu) | 6188 |
| 7340M | Semiconductor-electrolyte contacts | 6170 | 7630H | Platinum and palladium group (4d and 5d) ions and impurities (Zr-Ag and Hf-Au) | — |
| 7340N | Metal-nonmetal contacts | 6170 | 7630K | Rare-earth ions and impurities | 6188 |
| 7340Q | Metal-insulator-semiconductor structures | 6170 | 7630L | Other ions and impurities | 6188 |
| 7340R | Metal-insulator-metal structures | 6171 | 7630M | Colour centres and other defects | 6189 |
| 7340S | Metal-semiconductor-metal structures | — | 7630P | Conduction electrons | 6189 |
| 7360 | Electronic properties of thin films | 6171 | 7630R | Free radicals | 6189 |
| 7360D | Metallic thin films | 6171 | 7640 | Diamagnetic and cyclotron resonances | 6189 |
| 7360F | Semiconductor films | 6172 | 7650 | Ferromagnetic, antiferromagnetic, and ferrimagnetic resonances; spin wave resonance | 6189 |
| 7360H | Insulating thin films | 6172 | 7660 | Nuclear magnetic resonance and relaxation | 6189 |
| 7360K | Superconducting films | 6172 | 7660C | Chemical and Knight shifts | 6190 |
| 7390 | Other topics in electrical properties of surfaces, interfaces, and thin films | — | 7660E | Relaxation effects | 6190 |
| | | | 7660G | Quadrupole resonance | 6190 |
| 7400 | SUPERCONDUCTIVITY | 6172 | 7660L | Spin echoes | 6190 |
| 7410 | Occurrence, critical temperature | 6172 | 7670 | Magnetic double resonances and cross effects | 6191 |
| 7420 | Theory | 6173 | 7670D | Electron-nuclear double resonance (ENDOR) | 6191 |
| 7420F | BCS theory and its applications | 6173 | 7670E | Dynamical nuclear polarization | 6191 |
| 7430 | General properties | 6173 | 7670F | Double nuclear magnetic resonance (DNMR) | 6191 |
| 7430C | Magnetization curves, Meissner effect, penetration depth | 6173 | 7670H | Optical double magnetic resonance (ODMR) | 6191 |
| 7430E | Thermodynamic properties; thermal conductivity | 6173 | 7670K | Electron double resonance (ELDOR) | — |
| 7430G | Response to electromagnetic fields, nuclear magnetic resonance, ultrasonic attenuation | 6173 | 7680 | Mössbauer effect; other gamma-ray spectroscopy | 6191 |
| 7440 | Fluctuations and critical effects | 6174 | 7690 | Other topics in magnetic resonances and relaxation | 6193 |
| 7450 | Proximity effects, tunnelling phenomena, and Josephson effect | 6174 | 7700 | DIELECTRIC PROPERTIES AND MATERIALS | 6193 |
| 7455 | Type-I superconductivity | 6175 | 7720 | Permittivity | 6193 |
| 7460 | Type-II superconductivity | 6175 | 7730 | Polarization and depolarization effects | 6193 |
| 7460E | Mixed state, H_{c2} , surface sheath | 6175 | 7740 | Dielectric loss and relaxation | 6194 |
| 7460G | Flux pinning; fluxon-defect interactions | 6175 | 7750 | Dielectric breakdown and space-charge effects | 6194 |
| 7460J | Critical currents | 6175 | 7755 | Dielectric thin films | — |
| 7470 | Superconducting materials | 6175 | 7760 | Piezoelectricity and electrostriction | 6194 |
| 7470D | Material effects on T_c , K , critical currents | 6176 | 7770 | Pyroelectric and electrocaloric effects | 6194 |
| 7470G | Type-I superconductors (non transition metals) | 6176 | 7780 | Ferroelectricity and antiferroelectricity | 6194 |
| 7470L | Type-II superconductors (transition metals, alloys and compounds) | 6176 | 7780B | Transitions and Curie point | 6195 |
| 7470N | Dirty superconductors | 6176 | 7780D | Domain structure and effects; hysteresis | 6195 |
| 7470P | Materials for high-field applications | — | 7785 | Electrical resonances | 6195 |
| 7490 | Other topics in superconductivity | — | 7790 | Other topics in dielectric properties and materials | 6195 |
| | | | 7800 | OPTICAL PROPERTIES AND CONDENSED MATTER SPECTROSCOPY AND OTHER INTERACTIONS OF MATTER WITH PARTICLES AND RADIATION | 6195 |
| 7500 | MAGNETIC PROPERTIES AND MATERIALS | 6176 | 7820 | Optical properties and materials | 6195 |
| 7510 | General theory and models of magnetic ordering | 6176 | 7820B | General theory (for pure homogeneous materials) | 6195 |
| 7510D | Crystal-field theory and spin Hamiltonians | 6176 | | | |
| 7510H | Ising and other classical spin models | 6176 | | | |

| | page | | page | | |
|-------|--|------|-------|---|------|
| 7820D | Optical constants and parameters | 6196 | 8140E | Cold working, work hardening; annealing, recovery | 6221 |
| 7820E | Optical rotatory power | 6196 | | and recrystallisation; textures | 6222 |
| 7820F | Birefringence | 6196 | 8140G | Other heat and thermomechanical treatments | 6222 |
| 7820H | Piezo-, elasto- and acousto-optical effects | 6197 | 8140J | Elasticity and anelasticity | 6223 |
| 7820J | Electro-optical effects | 6197 | 8140L | Deformation, plasticity and creep | 6224 |
| 7820L | Magneto-optical effects | 6197 | 8140N | Fatigue, embrittlement, and fracture | 6226 |
| 7820N | Thermo-optical effects | 6197 | 8140P | Friction, lubrication, and wear | 6229 |
| 7830 | Infrared and Raman spectra and scattering | 6197 | 8140R | Electrical and magnetic properties (related to treatment conditions) | 6230 |
| 7835 | Brillouin and Rayleigh scattering | 6200 | 8140T | Optical properties (related to treatment conditions) | 6230 |
| 7840 | Visible and ultraviolet spectra | 6200 | 8160 | Corrosion, oxidation and surface treatments | 6230 |
| 7845 | Stimulated emission | 6201 | 8160B | Metals and alloys | 6231 |
| 7850 | Impurity and defect absorption in solids | 6201 | 8170 | Materials testing | 6233 |
| 7855 | Photoluminescence | 6201 | 8190 | Other topics in materials science | 6236 |
| 7860 | Other luminescence spectra and radiative recombination | 6204 | | | |
| | Electroluminescence | 6204 | 8200 | PHYSICAL CHEMISTRY | 6236 |
| 7860F | Cathodoluminescence, ionoluminescence | 6204 | 8220 | Chemical kinetics | 6236 |
| 7860K | Thermoluminescence | 6204 | 8220K | Potential energy surfaces for chemical reactions | 6236 |
| 7860M | Sonoluminescence, triboluminescence | 6205 | 8220M | Nonequilibrium kinetics | — |
| 7860P | Chemiluminescence | — | 8220R | Energy distribution and transfer, relaxation | 6237 |
| 7865 | Optical properties of thin films | 6205 | 8230 | Specific chemical reactions; reaction mechanisms | 6237 |
| 7870 | Other interactions of matter with particles and radiation | 6205 | 8235 | Polymer reactions and polymerization | 6238 |
| | Positron annihilation | 6205 | 8240 | Chemical kinetics and reactions; special regimes | 6239 |
| 7870B | X-ray scattering | 6206 | 8240D | Atomic and molecular beam reactions | — |
| 7870C | X-ray absorption and absorption edges | 6206 | 8240T | Chemiluminescence and chemical laser kinetics | 6239 |
| 7870D | X-ray emission threshold and fluorescence | 6206 | 8245 | Electrochemistry and electrophoresis | 6239 |
| 7870E | Microwave and radiofrequency interactions | 6206 | 8250 | Photochemistry and radiation chemistry | 6240 |
| 7870G | Other topics in optical properties of condensed matter and other interactions of matter with particles and radiation | 6206 | 8250E | Photodissociation, photoionization as studied by luminescence and radiationless transitions | — |
| | | | 8255 | Radiochemistry | 6241 |
| | | | 8260 | Chemical thermodynamics | 6241 |
| | | | 8265 | Surface processes | 6241 |
| | | | 8270 | Disperse systems | 6242 |
| | | | 8280 | Chemical analysis and related physical methods of analysis | 6242 |
| 7900 | ELECTRON AND ION EMISSION BY LIQUIDS AND SOLIDS; IMPACT PHENOMENA | 6206 | 8290 | Other topics in physical chemistry | — |
| 7920 | Impact phenomena | 6206 | | | |
| 7920D | Laser-light impact phenomena | 6206 | 8600 | ENERGY RESEARCH AND ENVIRONMENTAL SCIENCE | 6244 |
| 7920F | Electron impact: Auger emission | 6207 | 8610 | Energy resources and their utilisation | 6244 |
| 7920H | Electron impact: secondary emission | 6207 | 8610B | Fossil and other fuels | 6244 |
| 7920K | Other electron impact phenomena | 6207 | 8610D | Wind energy | 6244 |
| 7920N | Atom, molecule, and ion impact | 6207 | 8610F | Tidal and flow energy | — |
| 7920R | Atomic and molecular beam interactions | 6209 | 8610H | Geothermal energy | — |
| 7940 | Thermionic emission | 6209 | 8610K | Solar energy | 6245 |
| 7960 | Photoemission and photoelectron spectra | 6209 | 8610N | Nuclear energy | 6245 |
| 7970 | Field emission and field ionization | 6210 | 8610Z | Other topics | — |
| 7975 | Exoelectron emission | 6211 | 8630 | Energy conversion | 6245 |
| 7980 | Resonance tunnelling | — | 8630D | Electrochemical conversion: general | 6245 |
| 7990 | Other topics in emission and impact phenomena in condensed matter | — | 8630E | Primary cells | 6245 |
| | | | 8630F | Secondary cells | 6246 |
| 8000 | CROSS-DISCIPLINARY PHYSICS AND RELATED AREAS OF SCIENCE AND TECHNOLOGY | 6211 | 8630G | Fuel cells | 6247 |
| | | | 8630J | Photoelectric conversion: solar cells and arrays | 6247 |
| 8100 | MATERIALS SCIENCE | 6211 | 8630K | Photoelectrochemical conversion | 6254 |
| 8110 | Methods of crystal growth and purification | 6211 | 8630L | Electrodynamic and magnetohydrodynamic conversion | — |
| 8110B | Growth from vapour | 6211 | 8630M | Thermoelectric conversion | — |
| 8110D | Growth from solutions | 6211 | 8630N | Thermionic conversion | — |
| 8110F | Growth from melts | 6211 | 8630P | Photosynthesis | — |
| 8110H | Zone melting and zone refining | 6212 | 8630Q | Chemical energy conversion | 6254 |
| 8110J | Growth from solid phases | 6212 | 8630R | Thermal energy conversion (heat engines and heat pumps) | — |
| 8115 | Methods of thin film deposition | 6212 | 8630S | Photothermal conversion | 6254 |
| 8115C | Deposition by cathodic sputtering | 6213 | 8630Z | Other topics | 6255 |
| 8115G | Vacuum deposition | 6213 | 8640 | Energy storage (secondary energy) | 6255 |
| 8115H | Chemical vapour deposition | 6213 | 8640C | Storage in mechanical energy | — |
| 8115J | Ion plating and other vapour deposition | 6214 | 8640F | Storage in thermal energy | 6255 |
| 8115L | Deposition from liquid phases (melts and solutions) | 6214 | 8640H | Storage in chemical energy | 6255 |
| 8120 | Other methods of preparation of materials | 6215 | 8640K | Hydrogen storage and technology | 6255 |
| 8120C | Vacuum methods | — | 8640Z | Other topics | — |
| 8120E | Powder techniques, compaction and sintering | 6215 | 8660 | Requirement for energy: ecological aspects | — |
| 8120G | Specific metals and alloys (compacts, pseudoalloys) | 6215 | 8670 | Environmental science | 6255 |
| | | | 8670C | Soil | 6255 |
| 8120J | Dispersion-fibre-, and platelet-reinforced metal-based composites | 6216 | 8670E | Water | 6255 |
| 8120L | Ceramics and refractories | 6216 | 8670G | Atmosphere | 6256 |
| 8120N | Cermets, ceramic and refractory composites | 6217 | 8670J | Noise | 6256 |
| 8120P | Glasses | 6217 | 8670L | Measurement techniques in environmental science | 6256 |
| 8120Q | Glass-based composites, vitroceramics | — | 8670Z | Other topics | 6256 |
| 8120S | Polymers | — | 8690 | Other topics in energy research and environmental science | — |
| 8120T | Reinforced polymers and polymer-based composites | — | | | |
| 8130 | Phase diagrams and microstructures developed by solidification and solid-solid phase transformations | 6217 | 8700 | BIOPHYSICS, MEDICAL PHYSICS, AND BIOMEDICAL ENGINEERING | 6256 |
| 8130B | Phase diagrams of metals and alloys | 6217 | 8710 | General, theoretical, and mathematical biophysics | 6256 |
| 8130D | Phase diagrams of other materials | 6218 | 8715 | Molecular biophysics | 6257 |
| 8130F | Solidification | 6218 | 8715B | Structure, configuration, conformation, and active sites at the biomolecular level | 6257 |
| 8130H | Constant-composition solid-solid phase transformations: polymorphic, massive, and order-disorder | 6219 | 8715M | Interactions with radiations at the biomolecular level | 6258 |
| 8130K | Martensitic transformations | 6219 | 8716 | Biothermics | 6259 |
| 8130M | Precipitation | 6219 | 8720 | Membrane biophysics | 6259 |
| 8140 | Treatment of materials and its effects on microstructures and properties | 6220 | 8725 | Cellular biophysics | 6260 |
| 8140C | Solid solution hardening, precipitation hardening, dispersion hardening | 6221 | 8725D | Biological transport; cellular and subcellular transmembrane physics | 6260 |
| | | | 8730 | Biophysics of neurophysiological processes | 6261 |

| | | page | | page |
|-------|---|------|--|------|
| 8732 | Physiological optics, vision | 6262 | Interplanetary space | 6308 |
| 8732C | <i>Anatomy and optics of the eye</i> | 6262 | Aerospace facilities and techniques; space research | 6309 |
| 8732E | <i>Physiology of the eye; nerve structure and function</i> | 6262 | Other topics in space physics | — |
| 8732L | <i>Light detection; adaptation and discrimination</i> | 6262 | | |
| 8732N | <i>Colour detection; adaptation and discrimination</i> | 6262 | 9500 FUNDAMENTAL ASTRONOMY AND | |
| 8732S | <i>Psychophysics of vision, visual perception, binocular vision</i> | 6263 | ASTROPHYSICS, INSTRUMENTATION AND | |
| 8734 | Audition | 6263 | TECHNIQUES AND ASTRONOMICAL | 6310 |
| 8736 | Speech | 6263 | OBSERVATIONS | 6310 |
| 8738 | Mechano- and chemio-ceptions | 6264 | Fundamental astronomy | 6310 |
| 8740 | Biomagnetism | 6264 | <i>Celestial mechanics</i> | 6311 |
| 8745 | Biomechanics, biorheology, biological fluid dynamics | 6265 | 9510C | 6311 |
| 8750 | Biological effects of radiations | 6266 | 9530 Fundamental aspects of astrophysics | 6311 |
| 8750B | <i>Interactions of biosystems with radiations</i> | 6266 | 9545 Observatories | — |
| 8750C | <i>Bioacoustics (sonic and ultrasonic effects on living matter)</i> | — | 9555 Astronomical instruments | 6312 |
| 8750E | <i>Bio-optics (effects of microwaves, light, laser and other electromagnetic waves)</i> | 6266 | 9565 Auxiliary and recording instruments | — |
| 8750G | <i>Ionizing radiations (u.v., X-ray, gamma-ray; particle radiation effects)</i> | 6267 | 9570 Other instrumentation and techniques | 6312 |
| 8760 | Medical and biomedical uses of fields, radiations, and radioactivity | 6269 | 9575 Techniques of observation and reduction | 6312 |
| 8760B | <i>Sonic and ultrasonic radiation</i> | 6269 | 9580 Astronomical observations (listed by techniques of observation) | 6313 |
| 8760D | <i>Electric and magnetic fields (d.c. and pulsed)</i> | 6270 | 9580D | 6313 |
| 8760G | <i>Laser beams, microwaves, and other electromagnetic waves</i> | 6270 | 9580G | 6313 |
| 8760J | <i>Corpuscular radiation and radioisotopes</i> | 6270 | 9580J | 6313 |
| 8760L | <i>Preparation of radioactive materials for medical and biomedical uses</i> | — | 9580M | 6313 |
| 8760M | <i>Radiation dosimetry</i> | 6273 | 9580N | 6314 |
| 8760P | <i>Radiation protection</i> | 6275 | 9580Q | 6314 |
| 8760R | <i>Radioactive pollution</i> | 6275 | 9580S | 6314 |
| 8765 | Aerospace biophysics and medical physics (effects of accelerations, weightlessness and environment) | — | 9585 | 6314 |
| 8770 | Biomedical engineering | 6276 | 9590 Catalogues, atlases etc | 6314 |
| 8770E | <i>Diagnostic methods and instrumentation</i> | 6277 | 9590 Other topics in astronomy and astrophysics | 6314 |
| 8770G | <i>Patient care and treatment</i> | 6277 | 9600 SOLAR SYSTEM | 6314 |
| 8770J | <i>Prosthetics and other practical applications</i> | 6278 | 9610 General, solar nebula, and cosmogony | 6314 |
| 8780 | Biophysical instrumentation and techniques | 6278 | 9620 Moon | 6314 |
| 8790 | Other topics in biophysics, medical physics, and biomedical engineering | 6279 | 9630 Planets and satellites | 6314 |
| 9000 | GEOPHYSICS, ASTRONOMY AND ASTROPHYSICS | 6279 | 9630D | 6315 |
| 9100 | SOLID EARTH GEOPHYSICS | 6279 | 9630E | 6315 |
| 9110 | Geodesy and gravity | 6279 | 9630G | 6315 |
| 9125 | Geomagnetism and palaeomagnetism; geoelectricity | 6280 | 9630H | 6315 |
| 9130 | Seismology | 6282 | 9630J | 6315 |
| 9135 | Earth's interior structure and properties | 6284 | 9630K | 6315 |
| 9140 | Volcanology | 6286 | 9630M | 6315 |
| 9145 | Physics of plate tectonics | 6286 | 9630T | 6317 |
| 9150 | Marine geology and geophysics | 6288 | 9650 Other objects in the planetary system | 6317 |
| 9160 | Physical properties of rocks and minerals | 6288 | 9650D | 6317 |
| 9165 | Geophysical aspects of geology, mineralogy and petrology | 6289 | 9650G | 6317 |
| 9190 | Other topics in solid Earth geophysics | 6290 | 9650K | 6317 |
| 9200 | HYDROSPHERIC AND ATMOSPHERIC GEOPHYSICS | 6290 | 9650M | 6317 |
| 9210 | Physics of the oceans | 6290 | 9660 Solar physics | 6318 |
| 9220 | Interdisciplinary aspects of oceanography | 6291 | 9690 Other topics on the solar system | — |
| 9240 | Hydrology and glaciology | 6291 | 9700 STARS | 6319 |
| 9260 | Meteorology | 6292 | 9710 Stellar characteristics | 6319 |
| 9260S | <i>Climatology</i> | 6297 | 9720 Normal stars (by class): general or individual | 6320 |
| 9265 | Atmospheric optics | 6297 | 9730 Variable and peculiar stars | 6320 |
| 9290 | Other topics in hydrospheric and atmospheric geophysics | 6298 | 9760 Late stages of stellar evolution | 6322 |
| 9300 | GEOPHYSICAL OBSERVATIONS, INSTRUMENTATION, AND TECHNIQUES | 6299 | 9760B | 6322 |
| 9330 | Information related to geographical regions | 6299 | 9760G | 6322 |
| 9355 | International organizations, national and international programs | 6300 | 9760J | 6322 |
| 9365 | Data acquisition and storage | — | 9760L | 6322 |
| 9385 | Instrumentation and techniques for geophysical research | 6300 | 9780 Binary and multiple stars | 6322 |
| 9400 | AERONOMY AND SPACE PHYSICS | 6305 | 9790 Other topics in stellar astronomy | 6323 |
| 9410 | Physics of the neutral atmosphere | 6305 | 9800 STELLAR SYSTEMS; GALACTIC AND | |
| 9410Q | <i>Airglow and nightglow</i> | 6305 | EXTRAGALACTIC OBJECTS AND SYSTEMS; | |
| 9410S | <i>Aurora</i> | 6305 | THE UNIVERSE | 6323 |
| 9420 | Physics of the ionosphere | 6305 | 9810 Stellar dynamics | 6323 |
| 9430 | Physics of the magnetosphere | 6307 | 9820 Stellar clusters and associations | 6324 |
| 9440 | Cosmic rays | 6308 | 9840 Interstellar matter; and nebulae | 6324 |
| 9440C | <i>Origin and propagation outside the solar system</i> | 6308 | 9850 The Galaxy, extragalactic objects and systems | 6325 |
| 9440E | <i>Interplanetary propagation and effects</i> | — | 9850K | 6327 |
| 9440H | <i>Energetic solar particles and photons</i> | 6308 | 9870 Other objects and background radiations of unknown origin and distances | 6327 |
| 9440K | <i>Solar modulation and geophysical effects</i> | 6308 | 9870D | 6327 |
| 9440L | <i>Composition and energy spectra</i> | 6308 | 9870J | 6328 |
| 9440N | <i>Extensive air showers</i> | 6308 | 9870L | 6328 |
| 9440R | <i>High-energy interactions</i> | 6308 | 9870Q | 6328 |
| 9440T | <i>Muons and neutrinos</i> | 6308 | 9870S | 6328 |
| 9440V | <i>Cosmic-ray effects in meteorites and terrestrial matter</i> | 6308 | 9870V | 6329 |
| | | | 9880 Background radiations | 6329 |
| | | | 9890 Cosmology | 6329 |
| | | | 9890 Other topics in galactic and extragalactic astronomy | — |
| | | | AUTHOR INDEX | xvii |
| | | | followed by | |
| | | | SUBSIDIARY INDEXES | |

SUBJECT GUIDE

The SUBJECT GUIDE is an alphabetical index to subjects covered in the classification scheme, by which the abstracts are arranged. The numbers given are classification codes. The CLASSIFICATION AND CONTENTS, which precede the Guide, gives the page number for each section.

| | Classification | | Classification | | Classification |
|--|------------------------------|--|---------------------------------|--------------------------------------|--------------------------|
| A mesons | 1440 | Atomic polarisability | 3510D | Boson systems | 0530 |
| Ab initio calculations | 3120 | Atomic spectra | 32 | Boundary layer flow | 4715C, 4725F |
| Aberations | 4180, 4230, 4278 | Atomic structure | 31, 3510 | Boundary layer turbulence | 4725F |
| Abrasion | 4630P, 6220P, 8140P | Atomic transitions | 3110 | Brain | 87 |
| Absorptive models | 1240P | Atoms | 30 | Bremsstrahlung | 0350, 41, 7870 |
| Acceleration measurement | 0630Q | Audition | 8734 | Brillouin spectra | 3320F, 4265C, 5170, 7835 |
| Accumulation layers | 7320, 7340Q | Auger effect | | Brillouin zones | 6320, 7125 |
| Acoustic devices | 4385 | | 3280H, 7920F, 7920N, 7960, 8260 | Brink model | 2160G |
| Acoustic holography | 4363 | Aurora | 9410S | Brittleness | 4630N, 6220M, 8140N |
| Acoustic noise | 4350, 4360, 4388, 8670J | Autoionisation | 3280D, 3380E | Brownian motion | 0540 |
| Acoustic nuclear magnetic resonance | 7660 | Axial vector currents | 1140 | Bubble chambers | 2940 |
| Acoustic paramagnetic resonance | 7630 | Axiomatic field theory | 1110 | Buckling | 4630L, 6220F, 8140L |
| Acoustic properties of gases | 5140 | | | | |
| Acoustic properties of liquids | 6260 | | | | |
| Acoustic properties of solids | 6265 | | | | |
| Acoustic signal processing | 4360 | | | | |
| Acoustic wave propagation | 4320, 4325, 5140, 6260, 6265 | | | | |
| Acoustics | 43 | B mesons | 1440 | C invariance | 1130 |
| Acousto-optical effects | 5140, 5170, 7820H | Background radiation | 9870V | Calibration | 0620H |
| Acoustoelectric effects | 4388, 5140, 5150, 7250 | Band model of magnetism | 7510L | Calorimetry | 0720F |
| Adaptive optics | 42 | Band structure | 7125 | Cameras | 0768 |
| Adherence | 4630P | Barkhausen effect | 7560E | Capillarity | 6810 |
| Adhesion | 4630P, 6825, 8190 | Barrier heights | 3520J | Carbon dioxide lasers | 4255D, 4260 |
| Adsorption | 6845, 8265 | Baryon-baryon interactions | 1375C, 1375E, 1385 | Cardiology | 87 |
| Aerodynamics | 4740 | Baryon-baryon scattering | 1375C, 1375E, 1385 | Carrier density | 7220 |
| Aeroelasticity | 4630C, 4630M | Baryon decays | 1330 | Carrier lifetime | 7220J |
| Aeronomy | 94 | Baryon electric moment | 1340F, 1420 | Carrier mobility | 7220 |
| Aerosols | 4755K, 8270, 92 | Baryon-kaon interactions | 1375J, 1385 | Casting | 8120, 8130F |
| Aerospace | 9480, 9555 | Baryon-kaon scattering | 1375J, 1385 | Catalogues | 9585 |
| Aerospace biophysics | 8765 | Baryon magnetic moment | 1340F, 1420 | Cathodochromism | 7820 |
| Ageing | 8140Q | Baryon mass | 1420 | Cathodoluminescence | 7860H |
| Airglow | 9410Q | Baryon parity | 1420 | Cavitation | 4755B |
| Algebra | 0210 | Baryon-pion interactions | 1375G, 1385 | Celestial mechanics | 0320, 9510C |
| Alpha decay | 2360 | Baryon-pion scattering | 1375G, 1385 | Cells (electric) | 8630D |
| Alpha particle-nucleus reactions | 2560 | Baryon production | 1360P, 1365, 1375, 1385 | Cellular biophysics | 8725 |
| Alpha particle-nucleus scattering | 2560 | Baryon resonance production | 1360P, 1365, 1375, 1385 | Ceramic preparation | 8120L, 8120N |
| Alpha particle spectroscopy | 2930 | | | Ceramics | 81 |
| Alpha particles | 2140, 2710 | Baryon resonances | 1420 | Cermets | 81 |
| Amorphous semiconductors | 6140, 7125M, 7220, 7280N | Baryon spin | 1420 | CESR | 7630P |
| Amorphous state | 6140, 81 | Baryons | 1420 | Chalcogenide glasses | 6140D, 7280N |
| Anderson model | 7110, 7125M, 7155 | BCS theory | 2160, 7420F | Channel flow | 4760 |
| Anelasticity | 4630J, 6240, 8140J | Beam-foil excitation | 3450H | Channelling | 6180M |
| Anemometers | 4780, 9385 | Beam-foil ionisation | 3450H | Chaos | 0540 |
| Angular measurement | 0630C | Beam handling equipment | 2925 | Charge density waves | 7145, 7215N |
| Annealing | 8140E, 8140Q | Beam handling techniques | 2925 | Charge exchange | 3470 |
| Anodisation | 8160, 8245 | Bending | 4630J, 6220F, 8140L | Charge ordered states | 7145, 7150 |
| Antiferomagnetism | 7530 | Beta decay | 2340 | Charge transfer | 3470 |
| Antiferroelectric materials | 7780 | Beta ray spectroscopy | 2930 | Charge transfer reactions | 8230 |
| Antiferromagnetic properties of substances | 75, 7550E | Betatron | 2920 | Charge transfer states | 31, 7170C |
| Antiferromagnetic resonance | 7650 | Bethe-Salpeter equations | 1110 | Charm particles | 1420, 1440 |
| Antiphase boundaries | 81 | Bi-metric gravity theories | 0450 | Chemical analysis | 8280 |
| Antiphase domains | 81 | Bibliographies | 0130T | Chemical binding | 3110, 3520G |
| Antireflection coatings | 4270, 4278H, 4280 | Binary stars | 9780 | Chemical energy conversion | 8630Q |
| Appearance potential spectroscopy | 0785, 7870E | Binding energy | 31, 3520V, 6150L | Chemical energy storage | 8640H |
| APW calculations | 7110, 7125C | Bio-optics | 8750E, 8760G | Chemical kinetics | 8220 |
| Architectural acoustics | 4355 | Bioacoustics | 8738, 8750B, 8750C, 8760B | Chemical lasers | 4255K, 4260, 8240 |
| Artificial limbs | 8770J | Biocommunications | 87 | Chemical reactions | 3450L, 8230, 8235, 8240 |
| Artificial organs | 8770J | Biocontrol | 8710 | Chemical shifts | 3325, 7660C |
| Association | 6120, 6125, 8230 | Biocybernetics | 8710 | Chemical thermodynamics | 8260 |
| Asteroids | 9630H | Bioelectric phenomena | 8730, 8732E | Chemical vapour deposition | 6855, 8115H |
| Astroarchaeology | 9590 | Bioenergy conversion | 8630Z | Chemiluminescence | 5170, 7860P, 8240 |
| Astrometry | 95, 9555 | Biography | 0150 | Chemoception | 8738 |
| Astronomical instruments | 95 | Biological effects of radiation | 8750 | Chemisorption | 6845, 8265 |
| Astronomy and astrophysics | 95, 96, 97, 98 | Biological fluid dynamics | 8745 | Cherenkov detectors | 2940 |
| Atlases | 9585 | Biological techniques and instruments | 8780 | Cherenkov radiation | 41 |
| Atmospheric acoustics | 4328 | Biology | 87 | Chiral symmetries | 1130 |
| Atmospheric optics | 9265 | Biomagnetism | 8740, 8760D | Cholesteric liquid crystals | 6130, 6470M |
| Atmospherics | 9260, 94 | Biomass | 8630Z | CI calculations | 3120T |
| Atom beam reactions | 8240D | Biomechanics | 8745 | CIDEP | 3330 |
| Atom-surface impact | 34, 7920N, 7920R | Biomedical engineering | 8770 | CIDNP | 3325 |
| Atomic beams | 3440, 3450, 3580, 8240D | Biomedical equipment | 8770 | Cinematography | 0768 |
| Atomic clusters | 3640 | Biomedical measurement | 8770 | Claddings | 8160 |
| Atomic collisions | 34 | Biomedical ultrasonics | 8760G | Classical field theory | 0350 |
| Atomic electric moments | 3510D | Biomedical uses of radiation and radioactivity | 8760 | Classical mechanics | 0320, 0340 |
| Atomic electron correlations | 3120T | Biomembrane transport | 8720, 8725D | Classical statistical mechanics | 0520 |
| Atomic electron impact excitation | 3480 | Biomembranes | 8720 | Clebsch-Gordon coefficients | 0365 |
| Atomic electron impact ionization | 3480 | Biomolecular effects of radiation | 8715M, 8750 | Climatology | 9260 |
| Atomic excited states | 3150 | Biomolecular structure | 3620, 8715B | Cloud chambers | 2940 |
| Atomic fine structure | 3510F | Biophysical techniques and instruments | 8780 | Clouds | 9260 |
| Atomic fluorescence | 3250 | Biophysics | 87 | Cluster approximation | 7110, 7125M |
| Atomic forces | 3420 | Biorheology | 8745 | CND0 calculations | 3120N |
| Atomic hyperfine interactions | 3130 | Biothermics | 8716 | CO ₂ lasers | 4255D, 4260 |
| Atomic hyperfine structure | 3510F | Biotransport | 8725D, 8745 | Coal | 8610B |
| Atomic inelastic collisions | 3450 | Birefringence | 4210, 4220, 7820F | Coating techniques | 6855, 8115, 8160 |
| Atomic magnetic moments | 3510D | Black holes | 9760L | Coatings | 6855, 8115, 8160 |
| Atomic mass | 3510B | Blood | 87 | Coercivity | 7560, 7780 |
| Atomic orbital calculations | 3120 | Bolometers | 0720, 0762 | Coherent antiStokes Raman scattering | 3320F, 4265C, 7830 |
| Atomic orbitals | 3120 | Boltzmann equation | 0560 | Cold working | 8140E |
| Atomic phosphorescence | 3250 | Bond angles | 3520D | Collective accelerators | 2915 |
| Atomic physics | 30 | Bond lengths | 3520D | Colloids | 4755K, 8270 |
| | | Bond strength | 3520G | Colorimetry | 0760D |
| | | Bonds (chemical) | 31, 3520G, 6150L | Colour centre lasers | 4255R, 4260, 6170D |
| | | Bone | 87 | Colour centres | 6170D, 7155, 7630M, 7850 |
| | | Bootstrapping | 1150, 1240F | Colour model | 1235C |
| | | Bose-Einstein statistics | 0530 | Colour vision | 8732N |
| | | | | Comets | 9650G |

| Classification | | Classification | | Classification | |
|---|-------------------------------|-------------------------------------|---------------------------|--|----------------------------|
| Commensurate-incommensurate transformations | 0570, 6460, 6470K, 7780B | Dictionaries | 0130K | Electrojet | 94 |
| Compaction | 8120E | Dielectric function | 7145G, 7820D | Electroluminescence | 7860F |
| Complex angular momentum plane | 1160 | Dielectric hysteresis | 7780D | Electrolysis | 8245, 8630D |
| Composite material preparation | 8120J, 8120N, 8120Q, 8120T | Dielectric losses | 7740 | Electrolytic polishing | 8160, 8170 |
| Composite materials | 81 | Dielectric measurement | 0750 | Electromagnetic corrections | 1340H |
| Composite particle models | 1235 | Dielectric polarisation | 5150, 7730 | Electromagnetic decays | 1340H |
| Compressibility | 4630J, 51, 6210, 6220F, 8140L | Dielectric properties of substances | 77 | Electromagnetic fields | 4110 |
| Compressible flow | 4740 | Dielectric relaxation | 5150, 7740 | Electromagnetic induction | 4110F |
| Compton effect | 1360F, 6180C, 6180E, 7870 | Dielectric resonance | 7785 | Electromagnetic interaction models | 1220 |
| Computerised tomography | 8760J, 8770E | Dielectric thin films | 7755 | Electromagnetic wave propagation | 4110H |
| Configuration interactions | 3120T | Differential geometry | 0240 | Electromagnetic waves in plasma | 5240D |
| Conformational dynamics | 3520J | Diffraction gratings | 4280F | Electromagnetism | 0350, 4110 |
| Conservation laws | 1130 | Diffraction models | 1240S | Electromigration | 6610, 6630Q |
| Constrained heat transfer | 4425 | Diffuse spectra | 3380G | Electron affinity | 3510H, 3520V |
| Contact lenses | 8732, 8770J | Diffusion | 0560 | Electron beam deposition | 8115G |
| Continuous media mechanics | 4620, 4630 | Diffusion in gases | 5110, 5120 | Electron beam effects | 51, 6180F |
| Convection | 0560, 4425, 4725Q, 5130 | Diffusion in liquids | 6610 | Electron beams | 4180D |
| Conversion electron spectra | 2320N | Diffusion in solids | 6630 | Electron capture decay | 2340 |
| Correlation times | 3520Y | DIM method | 3120G | Electron diffraction crystallography | 6114 |
| Corrosion | 8160, 8160B | Dingle temperature | 7125, 7520 | Electron-electron interactions | 1310, 1365 |
| Corrosion protective coatings | 8160, 8160B | Diode lasers | 4255P, 4260 | Electron-electron scattering | 1310 |
| Corrosion testing | 8170 | Dirac equation | 0365 | Electron emission | 79 |
| Cosmic dust | 9840 | Direct nuclear reactions | 2450 | Electron energy states (condensed matter) | 71 |
| Cosmic ray interactions | 1385M, 9440 | Discharges (electric) | 5280 | Electron field emission | 7970 |
| Cosmic ray-nucleus reactions | 2590, 9440R | Disclinations | 6130, 6170G, 6170J, 6170L | Electron gas | 0530, 7145 |
| Cosmic rays | 9440, 9870S | Discrete system mechanics | 4610 | Electron-hadron interactions | 1360 |
| Cosmogony | 9610 | Dislocations | 6170G, 6170J, 6170L | Electron-hadron scattering | 1360F |
| Cosmology | 9880 | Disperse systems | 8270 | Electron-hole drops | 7135, 7855 |
| Cottrell atmospheres | 6170G, 6170J, 6170L | Dispersion hardening | 8140C | Electron-hole recombination | 7220J |
| Couette flow | 4730 | Dispersion relations | 0210, 1120, 1150 | Electron impact | 3480, 7920 |
| Coupled channel theory | 2410 | Displacive transformations | 6375, 6470K, 7780B | Electron lenses | 4180D |
| CP invariance | 1130 | Dissociation | 3380G, 3480G, 3520G | Electron microscopes | 0780 |
| CPA calculations | 6350, 7110, 7125 | Dissociation energies | 3520G | Electron microscopy | 0780, 6116D |
| CPT invariance | 1130 | Distorted wave Born approximations | 2410 | Electron-nucleus reactions | 2530 |
| Crack detection | 8170 | Distributed Bragg reflector lasers | 4260, 4282 | Electron-nucleus scattering | 2530 |
| Cracks | 4630N, 6220M, 8140N | Distributed feedback lasers | 4260, 4282 | Electron optics | 4180D |
| Crazing | 6220M, 8140N, 8160 | Domains | 8130, 8140 | Electron-phonon interactions | 6320K, 7138, 72, 7420 |
| Creep | 4630J, 6170L, 6220H, 8140L | Doping profiles | 6170W | Electron-positron interactions | 1310, 1365 |
| Creep testing | 8170 | Dosimeters | 2940, 2970 | Electron-positron scattering | 1310 |
| Critical points | 0570, 6460, 6470, 8260 | Dosimetry | 2880, 8760M | Electron probe analysis | 8280 |
| Crossing symmetries | 1150 | Double NMR | 3335, 7670F | Electron radiation | 41 |
| Cryogenics | 0720M | Double resonances | 3335, 7670 | Electron ring accelerators | 2915 |
| Crystal binding | 6150L | Drawing (mechanical) | 6220F, 8120, 8140L | Electron scattering | 3480 |
| Crystal defects | 6170 | Drift chambers | 2940 | Electron sources | 2925 |
| Crystal field theory | 7170C, 7510D | Dual models | 1240H | Electron spectra | 3365, 3480, 79 |
| Crystal growth | 6150C, 8110 | Duct flow | 4760 | Electron spectroscopy | 0780, 2930, 3365, 79, 8280 |
| Crystal growth from melt | 6150C, 8110F | Ductility | 4630J, 6220F, 8140L | Electron spin polarisation | 75 |
| Crystal growth from solution | 6150C, 8110D | Dye lasers | 4255M, 4260 | Electron traps | 7155, 7220J |
| Crystal growth from vapour | 6150C, 8110B | Dynamic nuclear polarisation | 3335, 7670E | Electronic conduction in thin films | 7360 |
| Crystal hyperfine field interactions | 7170, 7510D | Dynamic testing | 8170 | Electronic density of states | 7120 |
| Crystal inclusions | 6170, 8130, 8140 | Dynamical symmetries | 1130 | Electronic excitation | 3450H |
| Crystal microstructure | 6170, 6480, 8130, 8140 | Dynamics | 0320 | Electronic ionisation | 3450H |
| Crystal morphology | 6150J | Ear | 8734 | Electrons | 1460 |
| Crystal purification | 8110 | Earth | 90 | Electrophoresis | 8245 |
| Crystal structure | 61 | Earthquakes | 9130 | Electrophoretic coatings | 6855, 8115L, 8160 |
| Crystal structure of alloys | 6155H | ECG | 8730, 8770 | Electrophysiology | 8730, 8732E |
| Crystal structure of elements | 6155D, 6155F | Echelles | 4280F | Electroplating | 8115L, 8160 |
| Crystal structure of inorganic compounds | 6160 | Eclipses | 95, 9620, 9660 | Electropolishing | 8160, 8170 |
| Crystal structure of organic compounds | 6165 | Ecology | 8660 | Electrostatic accelerators | 2915 |
| Crystal surface and interface vibrations | 6830 | Education | 0140, 0150 | Electrostatic coatings | 8115, 8160 |
| Crystal symmetry | 6150E | Educational aids | 0150 | Electrostatic lenses | 4180 |
| Crystallisation | 6140, 6150C, 6470D | Educational computer use | 0150 | Electrostatics | 4110D |
| Crystallographic shear | 6170P | EEG | 8730, 8770 | Electrostriction | 7760 |
| Crystallography | 61 | Eikonal models | 1240P | Electroviscous effect | 6210, 6620, 8270 |
| Curie temperature | 7530K, 7540, 7780B | Einstein equation | 0420 | Elemental abundance | 3510B |
| Current algebra | 1140 | Einstein-Maxwell fields | 0440, 0450 | Elemental semiconductors | 7220, 7280C |
| CVD coatings | 6855, 8115H, 8160 | Elastic constants | 6220D | Elementary particle electric moments | 1340F |
| Cyclic accelerators | 2920 | Elastic deformation | 4630C, 6220F, 8140J | Elementary particle form factors | 1340F |
| Cyclotron resonance | 7125, 7640 | Elastic waves | 0340K, 4630M, 6230 | Elementary particle inclusive interactions | 1310, 1360H, 1365, 1385K |
| Cyclotrons | 2920 | Elasticity | 0340D, 4630C, 6220, 8140J | Elementary particle magnetic moments | 1340F |
| | | Elastomers | 3620, 6140K, 81 | Elementary particle polarisation | 1388 |
| | | ELDOR | 3335, 7670K | Elementary particle symmetries | 1130 |
| | | Election correlations | 3120T | Ellipsometry | 0760F |
| D mesons | 1440 | Electrets | 7730 | Embrittlement | 6220M, 8140N |
| De Haas-van Alphen effect | 7125 | Electric breakdown | 5280, 7750 | Emissivity | 6590 |
| Debye temperature | 6370 | Electric charge | 4110D | ENDOR | 3335, 7670D |
| Debye-Waller factors | 6370 | Electric discharges | 5280 | Energy conversion | 8630 |
| Decomposition | 6475, 8130 | Electric domains | 7780D | Energy gap | 7125, 74 |
| Deep levels | 7155 | Electric fields | 4110 | Energy loss of particles | 2970, 6180M |
| Defect electron energy states | 7155 | Electric moments | 2110K | Energy range relationships | 2970 |
| Defibrillators | 8770G, 8770J | Electrical conductivity of gases | 5150 | Energy research | 86 |
| Deformation | 0340, 4630, 6220F, 8140L | Electrical conductivity of liquids | 6610, 72 | Energy resources | 8610 |
| Degenerate semiconductors | 7220, 7280 | Electrical conductivity of solids | 72 | Energy storage | 8640 |
| Dendrites | 6870 | Electrical conductivity transitions | 7260 | Enthalpy | 0570, 6550, 8260 |
| Dendritic structure | 8130, 8140 | Electrical phenomena in gases | 5150 | Entropy | 0570, 5130, 6550 |
| Densitometry | 0768 | Electrical properties of substances | 5150, 72, 8140R | Epitaxial growth | 6855, 8115 |
| Density measurement | 0630E | Electrical variables measurement | 0750 | Epitaxial layers | 6855, 6860 |
| Density of liquids | 6210 | Electricity | 41 | EPR | 3330, 7630 |
| Density of solids | 6220, 8190 | Electro-optical effects | 3345, 5170, 7820J | Equations of state | 0570, 5110, 6410, 6430 |
| Desorption | 6845, 8265 | Electrocardiography | 8730, 8770 | Eta meson resonances | 1440 |
| Detonation | 4740, 8240 | Electrochemical analysis | 8280 | Eta mesons | 1440 |
| Deuteron-nucleon interactions | 1375C, 1385 | Electrochemical energy conversion | 8630D | Etching | 6170J, 8160, 8170 |
| Deuteron-nucleon scattering | 1375C, 1385 | Electrochemistry | 8245 | Euclidean field theory | 1110 |
| Deuteron-nucleus reactions | 2550 | Electrodeposition | 6855, 8115L, 8160, 8245 | Eutectic structure | 8130, 8140 |
| Deuteron-nucleus scattering | 2550 | Electrodynamics | 0350, 4170 | Evaporation | 6470F |
| Deuterons | 2140, 2710 | Electroencephalography | 8730, 8770 | Evolution (biological) | 8790 |
| Diamagnetic properties of substances | 5160, 7520 | Electroforming | 8120, 8245 | EXAFS | 3220R, 3320R, 7870D |
| Dibaryons | 1420 | Electrofluid dynamic conversion | 8630L | Exchange interactions (electron) | 7170G, 7530E |
| Dichroism | 3345, 7820F | Electrohydrodynamics | 4765 | Excimer lasers | 4255F, 4255H, 4260 |

| | Classification | | Classification | | Classification |
|---|-------------------------|---|---------------------------|--|---------------------|
| Excitons | 7135 | Gamma-ray sources | 2925 | Helium 3-nucleus reactions | 2560 |
| X-ray electron emission | 7975 | Gamma-ray sources (astronomical) | 9870Q | Helium 3-nucleus scattering | 2560 |
| X-ray sphere | 94 | Gamma-ray spectra | 2320, 7680 | Higgs bosons | 1480 |
| X-ray atoms | 3610 | Gamma-ray spectroscopy | 2930 | High-energy cosmic ray interactions | 1385M, 9440 |
| X-ray molecules | 3610 | Gamma ray transitions | 2320 | | |
| X-ray explosions | 4740, 4770, 8240 | Garnets | 7550G | High field effects | 7220H1 |
| Extraterrestrial life | 8790, 9590 | Gas lasers | 4255D, 4255F, 4255H, 4260 | High-frequency effects | 7230 |
| Eye | 8732 | Gases | 50 | High pressure effects in solids | 6250 |
| Eye anatomy and optics | 8732C | Gauge field theory | 1110 | High pressure techniques | 0735 |
| Eye physiology | 8732E | Gegenstein | 9650D | High temperature techniques | 0720K |
| | | Geiger counters | 2940 | History | 0160, 0165 |
| | | Gels | 8270 | Hodoscopes | 2970 |
| Mesons | 1440 | General relativity | 0420 | Hole traps | 7155, 7220J |
| Advection equation | 1180 | Generalised Huckel calculations | 3120P | Holography | 4240 |
| Alloy | 2870, 2880, 9260, 94 | Generator coordinate method | 2160E | Hopping conduction | 7220F |
| Arad ray effect | 7820L | Geodesy | 9110 | Hot carriers | 7220H, 7230 |
| Atmosphere | 4630N, 6220M, 8140N | Geoelectricity | 9125 | Hot working | 8140G |
| Atmosphere testing | 8170 | Geographical regions | 9330 | Hubbard model | 7110, 7510L |
| Dirac statistics | 0530 | Geology | 9165 | Huckel calculations | 3120P |
| Dirac level | 7125 | Geometrical optics | 42 | Humidity | 51, 9260 |
| Dirac surface | 7125H | Geometry | 0240 | Hybrid reactors | 2858 |
| Dirac systems | 0530 | Geophysical equipment | 9385 | Hydroelasticity | 4630C, 4630M |
| Dirac magnetic properties of substances | | Geophysics | 91, 92, 93 | Hydroelectric power | 8610F |
| | 75, 7550G | Geothermal energy | 8610H | Hydrogen bonds | 3520G |
| Dirac magnetic resonance | 7650 | Giant stars | 9720 | Hydrogen economy | 8640K |
| Diracites | 7550G | Ginzburg-Landau theory | 7420 | Hydrogen embrittlement | 6220M, 8140N, 8160 |
| Dirac acoustic resonance | 7125, 7255, 7580 | Glaciology | 9240 | Hydrogen power | 8640K |
| Dirac electric semiconductors | 7220, 7780 | Glass | 4270C, 6140D, 81 | Hydrogen production | 8640K |
| Dirac electricity | 7780 | Glass preparation | 8120P, 8120Q | Hydrogen storage | 8640K |
| Dirac magnetic properties of substances | | Glass transitions | 6470P | Hydrology | 9240 |
| | 75, 7550B, 7550C, 7550D | Glauber model | 2410H | Hydrosphere | 92 |
| Dirac magnetic resonance | 7650 | Glauber scattering | 1180 | Hygrometry | 0725 |
| Dirac nucleon systems | 2140 | Gluons | 1480 | Hypernuclei | 2180 |
| Dirac optics | 4280M | GO calculations | 3120 | Hyperon decays | 1330 |
| Dirac reinforced composites | 81 | Graded Lie algebras | 1130 | Hyperon-kaon interactions | 1375J, 1385 |
| Dirac emission electron microscopy | | Grain boundaries | 6170N, 8130, 8140 | Hyperon-kaon scattering | 1375J, 1385 |
| | 0780, 6116D | Grain size | 8130, 8140 | Hyperon-nucleon interactions | 1375E, 1385 |
| Dirac emission ion microscopy | 0780, 6116F | Granular structure | 81 | Hyperon-nucleon scattering | 1375E, 1385 |
| Dirac ion emission | 7970 | Graph theory | 0210 | Hyperon-nucleon reactions | 2580 |
| Dirac filtration | 4755M | Gravimeters | 9385 | Hyperon-nucleus scattering | 2580 |
| Dirac breeder reactors | 2850 | Gravitation | 04, 9530 | Hyperon-pion interactions | 1375G, 1385 |
| Dirac counters | 2940 | Gravitational collapse | 0440, 9530, 9760 | Hyperon-pion scattering | 1375G, 1385 |
| Dirac fusion reactor systems | 2858 | Gravitational constants | 0490 | Hyperon resonances | 1420 |
| Dirac power reactors | 2850 | Gravitational experiments | 0480 | Hyperons | 1420 |
| Dirac reactor design | 2841 | Gravitational interaction models | 1225 | Hypersonic flows | 4740K |
| Dirac reactor fuel | 2842 | Gravitational radiation | 0430, 0480 | Hypothetical particles | 1480 |
| Dirac reactor fuel preparation | 2842H | Gravitational waves | 0430, 0480 | | |
| Dirac reactor fuel reprocessing | 2842H | Gravity | 0320, 9110 | II-VI semiconductors | 7220, 7280E |
| Dirac reactor materials | 2842 | Grinding | 4285, 8120, 8160 | III-V semiconductors | 7220, 7280E |
| Dirac reactor operation | 2843 | Group theory | 0220, 0365, 1130 | III-VI semiconductors | 7220, 7280 |
| Dirac reactor safety | 2844 | Guided electromagnetic wave propagation | 0320, 4110H | Image convertors, detectors & intensifiers | 4280Q |
| Dirac reactor theory | 2841 | | 4280L | Image processing | 4230, 9575 |
| Dirac reactor waste | 2842 | Guided light propagation | 7220H | Impact ionisation | 7220H |
| Dirac research reactors | 2850 | Gunn effect | | Impurities | 6170R, 6170T, 6170W |
| Dirac flames | 8240 | | | Impurity and defect absorption spectra of solids | 7850 |
| Dirac electrostaticity | 6130, 7760 | H I regions | 9840 | Impurity electron states | 7155 |
| Dirac flow | 47 | H II regions | 9840 | Inclusions | 6170, 8130, 8140 |
| Dirac birefringence | 5170, 7820F | Hadron calorimeters | 2970 | Indeterminacy | 0365 |
| Dirac instrumentation | 4780 | Hadron classification schemes | 1240K | INDO calculations | 3120N |
| Dirac measurement | 4780 | Hadron-electron interactions | 1360 | INDOR | 3335 |
| Dirac separation | 4755 | Hadron-electron scattering | 1360F | Inert gas lasers | 4255F, 4260 |
| Dirac stability | 4720 | Hadron-hadron interactions | 1375, 1385 | Infrared astronomy | 95 |
| Dirac through porous media | 4755M | Hadron-hadron scattering | 1375, 1385 | Infrared detectors | 0730, 0762 |
| Dirac flowmeters | 4780 | Hadron-muon interactions | 1360 | Infrared imaging | 0720, 4280Q, 8760G |
| Dirac fluctuations | 0540 | Hadron-muon scattering | 1360F | Infrared sources (astronomical) | 9870L |
| Dirac fluid dynamics | 0340G, 47 | Hadron-nucleus reactions | 2540, 2580 | Infrared spectra | 3220B, 3320E, 7830 |
| Dirac fluid kinetic theory | 5110 | Hadron-nucleus scattering | 2540, 2580 | Injection lasers | 4255P, 4260 |
| Dirac fluid mechanics | 0340G, 47 | Hadron-photon interactions | 1360 | Injector acceleration | 2910 |
| Dirac fluid rheology | 4660 | Hadron-photon scattering | 1360F | Inner-shell ionisation | 3280H |
| Dirac fluid transport theory | 5110 | Hadronic decays | 1325, 1330 | Instrumentation | 06, 07 |
| Dirac fluorescence | 3250, 3350, 7855 | Haemodynamics | 8745 | Insulating thin films | 7360H |
| Dirac fluxmeters | 0755 | Half lives | 23 | Integral radiation detectors | 2970 |
| Dirac foams | 8270 | Hall effect | 7215G, 7220M | Integrated optics | 4282 |
| Dirac folding models | 2410H | Hardening | 8140C, 8140E, 8160 | Interacting boson model | 2160E, 2160F |
| Dirac forming processes | 8120 | Hardness | 4630P, 6220M, 6825, 8140N | Interatomic angles | 3520D |
| Dirac fossil fuels | 8610B | Hardness testing | 8170 | Interatomic distances | 3520D |
| Dirac Fourier transform optics | 4230 | Harmonic generation | 4265C, 4325, 4360 | Interatomic forces | 3420 |
| Dirac fracture | 4630N, 6220M, 8140N | Harmonic oscillators | 0365 | Interatomic potentials | 3420 |
| Dirac fracture toughness testing | 8170 | Hartree-Fock approximation | 2160J, 3120D, 3120G, 7110 | Interface phenomena | 68, 7340 |
| Dirac fragmentation reactions | 2450 | Hawking effects | 0460 | Interferometry | 0760L, 9575 |
| Dirac free-electron approximation | 7110, 7125C | Health hazards | 8750, 8760R, 8790 | Intergalactic matter | 9850 |
| Dirac free electron lasers | 4255T, 4260 | Health physics | 8760 | Intermediate boson decay | 1390 |
| Dirac free energy | 0570, 5130, 64, 6550 | Hearing | 8734 | Intermediate bosons | 1230, 1480 |
| Dirac free molecular flows | 4745 | Hearing aids | 8734, 8770J | Intermediate state | 7455 |
| Dirac free radicals | 30, 7630R, 8230, 8250 | Heat capacity | 4450 | Intermolecular forces | 3420 |
| Dirac Frenkel defects | 6170B | Heat conduction | 4410 | Intermolecular mechanics | 3420 |
| Dirac friction | 4630P, 6220P, 8140P | Heat engines | 8630R | Intermolecular potentials | 3420 |
| Dirac fuel cells | 8630G | Heat exchanges | 8630R | Internal conversion | 3250 |
| Dirac functional analysis | 0230 | Heat flow | 44 | Internal friction | 6170L, 6240, 8140J |
| Dirac functions | 0230 | Heat pumps | 8630R | Internal rotation | 3520J |
| Dirac fusion reactions | 2588 | Heat radiation | 4440 | Internal stresses | 4630, 6220, 8140 |
| Dirac fusion reactor plasma confinement | 5255 | Heat transfer | 44, 4725Q | Internal symmetries | 1130 |
| Dirac fusion reactors | 2852 | Heat treatment | 8140G | Interplanetary matter | 9460, 9650D |
| | | Heavily doped semiconductors | 7220, 7280 | Interstellar matter | 9840 |
| Galaxies | 9850 | Heavy ion-nucleus reactions | 2570 | Interstitials | 6170B |
| Galaxy | 9850 | Heavy ion-nucleus scattering | 2570 | Inversion | 3520J |
| Galvanomagnetic effects | 7215G, 7220M | Heavy leptons | 1460 | Inversion layers | 7320, 7340Q |
| Gamma ray angular distributions | 2320 | Heavy particle spectroscopy | 2930 | Ion-atom collisions | 34 |
| Gamma ray astronomy | 95 | Heisenberg model | 7510J, 7540F | Ion beam effects | 6180J |
| Gamma ray effects | 5170, 6180E | Helicity | 1130 | Ion beams | 4180G |
| Gamma-ray lasers | 4255 | Helicons | 7230 | | |
| Gamma ray mixing ratios | 2320 | | | | |

| | Classification | | Classification | | Classification |
|-------------------------------------|------------------------|--------------------------------------|------------------------------|---|------------------------------|
| Ion emission | 79 | Light interference | 4210, 4220 | Mass spectroscopic chemical analysis | 8280 |
| Ion implantation | 6170T, 6180J | Light interferometry | 0760L | Mass transfer | 0560 |
| Ion lasers | 4255F, 4255H, 4260 | Light modulation | 4260F, 4280K | Materials preparation | 8120 |
| Ion microscopes | 0780 | Light polarisation | 4210, 4220 | Materials science | 81 |
| Ion microscopy | 0780, 6116F | Light propagation | 4210, 4220 | Materials testing | 8170 |
| Ion-molecule collisions | 34 | Light scattering | 4210, 4220, 5170, 78 | Mathematical computing | 0270 |
| Ion optics | 4180G | Light sensitive materials | 4270G | Mathematics | 02 |
| Ion plating | 8115J, 8160 | Light sources | 4272 | Maxwell equations | 0350, 4110 |
| Ion pumps | 0730C | Light transmission | 4210, 4220 | MBE | 6855, 8115G |
| Ion recombination | 34 | Lightning | 9260 | Measurement | 06 |
| Ion sources | 0777, 2925 | Linear accelerators | 2915 | Mechanical birefringence | 4210, 7820F |
| Ion-surface impact | 7920N | Lipid bilayers | 8720, 8725 | Mechanical contact | 4630P |
| Ionic conduction in solids | 6630 | Liquid crystal phase transformations | 6130, 6470M | Mechanical energy storage | 8640C |
| Ionisation | 52, 5280, 79 | Liquid crystals | 6130 | Mechanical impact | 4630P |
| Ionisation counters | 2940 | Liquid helium 3-4 mixtures | 6760 | Mechanical properties of substances | 4630, 4660, 62, 8140 |
| Ionisation gauges | 0730D | Liquid helium-3 | 6750 | Mechanical property measurement | 4630R |
| Ionisation potentials | 3510H, 3520V | Liquid helium | 67 | Mechanical strength | 4630, 6220, 8140 |
| Ionoluminescence | 7860H | Liquid lasers | 4255M, 4260 | Mechanical testing | 8170 |
| Ionosphere | 9420 | Liquid metal embrittlement | 6220M, 8140N, 8160 | Mechanical waves | 4630M, 6230 |
| Irreversible thermodynamics | 0570 | Liquid phase epitaxial growth | 6855, 8115L | Mechanics | 0320, 0340, 46 |
| Ising lattices | 0550 | Liquid semiconductors | 6125, 7120, 7220, 7280P | Mechanoception | 8738 |
| Ising model | 7510H, 7540D | Liquid structure | 6120, 6125 | Medical diagnosis | 8770E |
| Isobaric analog resonances | 2430 | Liquid theory | 6120, 6130 | Medical effects of radiation | 8750 |
| Isobaric analog states | 2430 | Liquid-vapour transformations | 6470F | Medical physics | 87 |
| Isotope effects | 3130 | Liver | 87 | Medical uses of radiation and radioactivity | 8760 |
| Isotope enrichment | 2842H | Localized electron states | 7150 | Medicine | 87 |
| Isotope separation | 2842H, 3510B | Lorentz invariance | 1130 | Meissner effect | 7430C |
| Isotopes | 30, 3510B | Lorentz transformation | 0330 | Melting | 6470D |
| Isotropic turbulence | 4725C | Low energy electron diffraction | 6114H, 6820 | Membrane biophysics | 8720 |
| IV-VI semiconductors | 7220, 7280 | Low mass nuclear reactions | 2510 | Membranes | 5120, 6610, 8265, 8720, 8725 |
| | | Low temperature techniques | 0720M | Mercury (planet) | 9630D |
| Jahn-Teller effect | 3130, 7170C | LPE | 6855, 8115L | Meson absorption | 2580 |
| Jets | 4755C | Lubrication | 4630P, 6220P, 8140P | Meson capture | 2580 |
| Josephson effect | 7450 | Luminescence | 3250, 3350, 7855, 7860 | Meson decays | 1320, 1325 |
| Joule-Thomson effect | 5130 | Lung | 87 | Meson electric moments | 1340F, 1440 |
| Junction lasers | 4255P, 4260 | | | Meson magnetic moments | 1340F, 1440 |
| Jupiter | 9630K | | | Meson mass | 1440 |
| | | | | Meson-meson interactions | 1375L, 1385 |
| K-harmonics model | 2160G | Mach number | 4740 | Meson-meson scattering | 1375L, 1385 |
| Kaon absorption | 2580 | Macromolecules | 3620 | Meson-nucleon interactions | 1375, 1385 |
| Kaon-baryon interactions | 1375J, 1385 | Magnetic aftereffect | 7560L | Meson-nucleon scattering | 1375, 1385 |
| Kaon-baryon scattering | 1375J, 1385 | Magnetic anisotropy | 7530G | Meson-nucleus reactions | 2580 |
| Kaon capture | 2580 | Magnetic annealing | 7560N, 8140E | Meson-nucleus scattering | 2580 |
| Kaon decays | 1320, 1325 | Magnetic breakdown | 7125H | Meson parity | 1440 |
| Kaon-nucleus reactions | 2580 | Magnetic bubbles | 7570K | Meson production | 1360K, 1365, 1375, 1385 |
| Kaon-nucleus scattering | 2580 | Magnetic circular dichroism | 3345C, 7820L | Meson resonance production | 1360M, 1365, 1375, 1385 |
| Kaons | 1440 | Magnetic cooling | 0720M, 7530S | Meson resonances | 1440 |
| Kapitza resistance | 6740, 6830 | Magnetic domains | 7560C, 7570K | Meson spin | 1440 |
| Kidney | 87 | Magnetic fields | 4110 | Mesons | 1440 |
| Kinetic theory | 0520 | Magnetic hysteresis | 7560E | Mesosphere | 9260 |
| KKR calculations | 7110, 7125C | Magnetic lenses | 4180 | Metal corrosion | 8160B |
| Knight shift | 7660C | Magnetic materials | 75, 7550 | Metal-insulator boundaries | 7340N |
| Knock-on reactions | 2450 | Magnetic monopoles | 1480 | Metal-insulator-metal structures | 7340R |
| Knudsen flow | 4745 | Magnetic phenomena in gases | 5160 | Metal-insulator-semiconductor structures | 7340Q |
| Kondo effect | 7215Q, 7520H | Magnetic properties of substances | 5160, 75, 8140R | Metal-insulator transition | 7130 |
| Kronig-Penney model | 7110, 7125C | Magnetic relaxation | 5160, 76 | Metal oxidation | 8160B |
| | | Magnetic resonance | 3220B, 3325, 76 | Metal-semiconductor-metal structure | 7340S |
| Laboratory apparatus and techniques | 0150, 0660, 0670, 07 | Magnetic resonance spectrometers | 0758 | Metallography | 8170 |
| Laminar flows | 4715 | Magnetic semiconductors | 7220, 75 | Metallurgy | 81 |
| Laminates | 81 | Magnetic storms | 9430 | Metamagnetism | 7530K |
| Landau levels | 7145 | Magnetic thin films | 7570 | Meteorites | 9650M |
| Laser accessories | 4260 | Magnetic transitions | 7530K, 7540 | Meteorology | 9260 |
| Laser beam applications | 4260K | Magnetic traps | 5255 | Meteors | 9650K |
| Laser beam effects | 4260H, 6180B, 7920D | Magnetic variables measurement | 0755 | Microphones | 4385, 4388 |
| Laser beam modulation | 4260F | Magnetisation | 7430C, 7560 | Microscopes | 0760P |
| Laser beam properties | 4260H | Magnetism | 41, 5160, 75 | Microtomes | 2920 |
| Laser cavity resonators | 4260D | Magneto-optical effects | 3345, 5160, 5170, 7820L | Microwave-optical double resonance | 3335H, 7670H |
| Laser system design | 4260B | Magnetoacoustic effects | 5140, 5160, 7125, 7255, 7580 | Microwave spectra | 3220B, 3320B, 7870G |
| Laser theory | 4255B | Magnetocaloric effects | 7530S | Microwave spectrometers | 0758, 0765 |
| Laser velocimeters | 0630G, 4260K, 4780 | Magnetocardiography | 8740, 8760D | Mictomagnetism | 7540 |
| Lasers | 4255, 4260 | Magnetoelastic effects | 7580 | MINDO calculations | 3120N |
| Latent heat | 0570, 64, 6550, 8260 | Magnetolectric effects | 5150, 5160, 7580 | Mineralogy | 9160 |
| Lattice constants | 6150, 6155, 6160, 6165 | Magnetohydrodynamic conversion | 5230, 8630L | Mirrors | 4278 |
| Lattice dynamics | 63 | Magnetohydrodynamic waves | 4765, 5235, 7230 | Mixed conductivity | 7260 |
| Lattice energy | 6150L | Magnetohydrodynamics | 4765, 5230 | Mixed state | 7460E |
| Lattice field theory | 1110 | Magnetomechanical effects | 7580 | Mixed valence states | 7170C |
| Lattice localised modes | 6320P | Magnetometers | 0755, 9385 | Mixing | 6475 |
| Lattice phonons | 6320 | Magnetoresistance | 7215G, 7220M | Moderators | 2842 |
| Lattice theory and statistics | 0550 | Magnetosphere | 9430 | Moire fringes | 0760, 4210 |
| LCAO calculations | 3120, 7110 | Magnetostatic waves | 75 | Molecular beam epitaxial growth | 6855, 8115G |
| Least squares analysis | 0250 | Magnetostatics | 4110D | Molecular beam reactions | 8240D |
| Lee model | 1110 | Magnetostriiction | 7580 | Molecular beams | 3440, 3450, 3580, 8240D |
| Lenses | 4278 | Magnetotrons | 0750 | Molecular biophysics | 8715 |
| Lepton decays | 1335 | Magnons | 7530D, 7650 | Molecular clusters | 3640 |
| Lepton electromagnetic interactions | 1310 | Majorana-Weyl fields | 0450 | Molecular collisions | 34 |
| Lepton-lepton scattering | 1310 | Mandelstam representation | 1150 | Molecular configurations | 3520B |
| Lepton mass | 1460 | Many-body problems | 05, 9510C | Molecular dissociation | 3380G, 3480G |
| Lepton-nucleus reactions | 2530 | Many-body reaction theory | 2410 | Molecular dynamics | 3520Y |
| Lepton-nucleus scattering | 2530 | Marine geology | 9150 | Molecular electric moments | 3520M |
| Lepton parity | 1460 | Markov processes | 0540 | Molecular electron correlations | 3120T |
| Lepton spin | 1460 | Mars | 9630G | Molecular electron impact ionisation | 3480G |
| Lepton weak interactions | 1310 | Martensitic transformations | 6470K, 8130K | Molecular electronic states | 31 |
| Leptonic decays | 1320, 1330, 1335 | Masers | 4252 | Molecular fine structure | 3520S |
| Leptons | 1460 | Mass differences | 1340D | Molecular fluorescence | 3350 |
| Level crossing | 3280B, 3380B | Mass formulae | 1240K, 1270 | Molecular hyperfine interactions | 3130 |
| Light | 42 | Mass spectra | 3510B, 3520X | Molecular hyperfine structure | 3520S |
| Light absorption | 4210, 4220, 5170, 78 | Mass spectrometers | 0775 | Molecular inelastic collisions | 3450 |
| Light coherence | 4210, 4220, 4250 | | | Molecular magnetic moments | 3520M |

| | Classification | | Classification | | Classification |
|-----------------------------------|-------------------------|--|--------------------------|-----------------------------------|---------------------------|
| Molecular magnetic susceptibility | 3520M | Nonhomogeneous flows | 4755 | Oil | 8610B |
| Molecular moments | 3520M | Nonlinear acoustics | 4325 | Omega mesons | 1440 |
| Molecular nuclear coupling | 3325 | Nonlinear field theory | 1110 | One-dimensional conductivity | 7215N |
| Molecular orbitals | 3120 | Nonlinear optics | 4265 | One-meson exchange models | 1240R |
| Molecular orbitals calculations | 3120 | Nonlinear optics theory | 4265B | Opalescence | 7820 |
| Molecular phosphorescence | 3350 | Nonlinear symmetries | 1130 | Optical beam splitters | 4280 |
| Molecular photodissociation | 3380G | Nonlocal field theories | 1110 | Optical bistability | 4265, 4280 |
| Molecular physics | 30 | Normalising | 8140G | Optical choppers | 4280E |
| Molecular polarisability | 3520M | Novae | 9730 | Optical coatings | 4270, 4278H, 4280 |
| Molecular predissociation | 3380G | Nozzles | 4755E | Optical coherent transients | 4265G |
| Molecular rotation | 3310, 3520P | NQR | 3325, 7660G | Optical collimators | 4280 |
| Molecular rotation-vibration | | Nuclear backbending | 2110, 2110H | Optical communication devices | 4280S |
| | 3310, 3450E, 3520P | Nuclear binding energy | 2110D | Optical constants | 5170, 7820D |
| Molecular solids | 3170K | Nuclear bombardment target | 2925 | Optical couplers | 4280L, 4280M |
| Molecular spectra | 3320 | Nuclear charge | 2110F | Optical deflectors | 4280E |
| Molecular structure | 31, 3520B | Nuclear chemistry | 8255 | Optical design techniques | 4278, 4280 |
| Molecular symmetry | 3520B | Nuclear cluster model | 2160G | Optical diaphragms | 4280 |
| Molecular transitions | 3110 | Nuclear collective levels | 2110 | Optical dispersion | 4210, 4220, 5170, 7820 |
| Molecular vibration | 3310, 3520P, 6320, 7830 | Nuclear collective models | 2160E | Optical double resonance | 3335, 7670H |
| Molecule-surface impact | 34, 7920N, 7920R | Nuclear collective resonances | 2430 | Optical elements | 4278, 4280 |
| Molecules | 30 | Nuclear Coulomb effects | 2110 | Optical fabrication | 4285 |
| Monochromators | 0785, 4280D | Nuclear cranking model | 2160E | Optical fibres | 4280M |
| Monolayers | 6845, 8265 | Nuclear decay | 23 | Optical films | 4270, 4278, 4280, 7865 |
| Monte Carlo methods | 0250 | Nuclear deformation | 2110F | Optical filters | 4280B, 4280C |
| Moon | 9620 | Nuclear electric moments | 2110K | Optical frequency conversion | 4265C |
| Morin temperature | 7530K, 7540 | Nuclear electromagnetic transitions | 2320 | Optical glass | 4270C |
| Mossbauer effect | 2430, 2520, 3340, 7680 | Nuclear electronics | 2960 | Optical gratings | 4280F |
| Muffin-tin potential | 7110, 7125C | Nuclear emulsions | 2940 | Optical harmonic generation | 4265C |
| Multi-Regge models | 1240S | Nuclear energy | 8610N | Optical images | 4230 |
| Multiperipheral models | 1240S | Nuclear energy level lifetimes | 2320C | Optical information processing | 4230 |
| Multiphase flow | 4755K | Nuclear energy level schemes | 2110, 2110M | Optical instruments | 0760, 4278, 4280 |
| Multiphoton spectra | 3280K, 3380K | Nuclear energy level transitions | 2320 | Optical Kerr effect | 4265J |
| Multiple stars | 9780 | Nuclear energy levels | 2110, 2110M | Optical materials | 4270 |
| Multiwire proportional chambers | 2940 | Nuclear energy states | 2110, 2110M | Optical model | 1240P |
| Muon absorption | 2530 | Nuclear engineering | 28 | Optical modulation | 4260F, 4280K |
| Muon capture | 2340, 2530 | Nuclear engineering computing | 2841, 2980 | Optical monochromators | 4280D |
| Muon-hadron interactions | 1360 | Nuclear explosions | 2870 | Optical parametric devices | 4265C |
| Muon-hadron scattering | 1360F | Nuclear fireballs | 2460 | Optical phase conjugation | 4265F |
| Muon-nucleus reactions | 2530 | Nuclear fission | 2475, 2585 | Optical phenomena in gases | 5170 |
| Muon-nucleus scattering | 2530 | Nuclear forces | 2130 | Optical prisms | 4278, 4280 |
| Muon spin rotation | 7690 | Nuclear form factors | 2110F | Optical projectors | 4278 |
| Muons | 1460 | Nuclear g-factors | 2110K | Optical properties of substances | |
| Muscle | 87 | Nuclear giant resonances | 2430 | Optical pumping | 3280B, 3380B, 4255, 7845 |
| Musical acoustics | 4375 | Nuclear hole states | 2110 | Optical rangefinders | 4280 |
| | | Nuclear information processing | 2980 | Optical resolving power | 4230 |
| | | Nuclear instrument control | 2980 | Optical rotation | 4210, 7820E |
| | | Nuclear instrumentation | 2880, 29 | Optical saturable absorption | 4265G |
| | | Nuclear isobaric spin | 2110H | Optical saturation | 4265G |
| | | Nuclear magnetic moments | 2110K | Optical self-focusing | 4265J |
| | | Nuclear magnetic resonance | | Optical self-induced transparency | 4265G |
| | | | 3320B, 3325, 7430G, 7660 | Optical shutters | 4280E |
| | | Nuclear mass | 2110D | Optical sources | 4272 |
| | | Nuclear matrix elements | 2320 | Optical storage | 4230, 4240 |
| | | Nuclear matter | 2165 | Optical susceptibility | 77, 78 |
| | | Nuclear medicine | 8760J, 8770 | Optical systems | 0760, 4278, 4280 |
| | | Nuclear models | 2160 | Optical telescopes | 0760, 4278, 9555 |
| | | Nuclear optical model | 2410H | Optical testing | 4278, 4285 |
| | | Nuclear Overhauser effect | 3335 | Optical transfer function | 4230 |
| | | Nuclear parity | 2110H | Optical waveguide components | 4280L |
| | | Nuclear physics | 20 | Optical waveguides | 4280L |
| | | Nuclear polarisation in liquids and solids | 7660 | Optical windows | 4280E |
| | | Nuclear power | 28 | Optical workshop techniques | 4285 |
| | | Nuclear pumped lasers | 4255, 4260 | Optical zone plates | 4280B |
| | | Nuclear quadrupole resonance | 3325, 7660G | Optics | 0760, 0765, 42 |
| | | Nuclear radius | 2110F | OPW calculations | 7110, 7125C |
| | | Nuclear reaction models | 2410 | Orbital calculation methods | 3120 |
| | | Nuclear reactions | 24, 25 | Order-disorder transformations | |
| | | Nuclear resonance reactions | 2430 | | 6150K, 6460, 6470K, 8130H |
| | | Nuclear resonances | 2430 | Orthotics | 8770J |
| | | Nuclear rotational bands | 2110 | Otology | 8730 |
| | | Nuclear shape | 2110F | Overhauser effect | 3325 |
| | | Nuclear shell model | 2160C | Oxidation | 8160, 8160B, 8230 |
| | | Nuclear single particle levels | 2110 | Ozonosphere | 9260 |
| | | Nuclear size | 2110H | | |
| | | Nuclear spectroscopic factors | 2110J | | |
| | | Nuclear spin | 2110H | | |
| | | Nuclear statistical models | 2460 | | |
| | | Nuclear structure | 21 | | |
| | | Nuclear structure models | 2160 | | |
| | | Nuclear transition probabilities | 2320C | | |
| | | Nucleation | 6150C, 64, 6855, 8140 | | |
| | | Nucleon decays | 1330 | | |
| | | Nucleon-hyperon interactions | 1375E, 1385 | | |
| | | Nucleon-hyperon scattering | 1375E, 1385 | | |
| | | Nucleon-kaon interactions | 1375J, 1385 | | |
| | | Nucleon-kaon scattering | 1375J, 1385 | | |
| | | Nucleon-meson interactions | 1375, 1385 | | |
| | | Nucleon-meson scattering | 1375, 1385 | | |
| | | Nucleon-nucleon interactions | 1375C, 1385 | | |
| | | Nucleon-nucleon scattering | 1375C, 1385 | | |
| | | Nucleon-nucleus reactions | 2540 | | |
| | | Nucleon-nucleus scattering | 2540 | | |
| | | Nucleon-pion interactions | 1375G, 1385 | | |
| | | Nucleon-pion scattering | 1375G, 1385 | | |
| | | Nucleon-proton interactions | 1375C, 1385 | | |
| | | Nucleon-proton scattering | 1375C, 1385 | | |
| | | Nucleon radiative capture | 2540 | | |
| | | Nucleon radiography | 8170, 8760J | | |
| | | Nucleon scattering | 2820 | | |
| | | Nucleon sources | 2925 | | |
| | | Nucleon spectroscopy | 2930 | | |
| | | Nucleon stars | 9760J | | |
| | | Nucleon transport | 2820 | | |
| | | Neutrons | 1420 | | |
| | | Nightglow | 9410Q | | |
| | | Nilsson model | 2160C | | |
| | | NMR | 3220B, 3325, 7430G, 7660 | | |
| | | Nomenclature and symbols | 01 | | |
| | | Nomograms | 0260 | | |
| | | Non-Abelian fields | 1110 | | |
| | | Non-Newtonian dynamics | 4750 | | |
| | | Non-Newtonian flows | 4750 | | |
| | | Noncollisional ionisation | 3490 | | |
| | | Noncrystalline state structure | 6140 | | |
| | | Nondestructive testing | 8170 | | |
| | | Nonequilibrium flows | 4770 | | |
| | | Observatories | 9545 | | |
| | | Occultations | 9510 | | |
| | | Oceanography | 9210 | | |
| | | Ohmic contacts | 7340 | | |
| | | | | | |
| | | | | | |
| | | | | | |
| | | | | | |
| | | | | | |
| | | | | | |
| | | | | | |
| | | | | | |
| | | | | | |
| | | | | | |
| | | | | | |
| | | | | | |
| | | | | | |
| | | | | | |
| | | | | | |
| | | | | | |
| | | | | | |
| | | | | | |
| | | | | | |
| | | | | | |
| | | | | | |
| | | | | | |
| | | | | | |
| | | | | | |
| | | | | | |
| | | | | | |
| | | | | | |
| | | | | | |
| | | | | | |
| | | | | | |
| | | | | | |
| | | | | | |
| | | | | | |
| | | | | | |
| | | | | | |
| | | | | | |
| | | | | | |
| | | | | | |
| | | | | | |
| | | | | | |
| | | | | | |
| | | | | | |
| | | | | | |
| | | | | | |
| | | | | | |
| | | | | | |
| | | | | | |
| | | | | | |
| | | | | | |
| | | | | | |
| | | | | | |
| | | | | | |
| | | | | | |
| | | | | | |
| | | | | | |
| | | | | | |
| | | | | | |
| | | | | | |
| | | | | | |
| | | | | | |
| | | | | | |
| | | | | | |
| | | | | | |
| | | | | | |
| | | | | | |
| | | | | | |
| | | | | | |
| | | | | | |
| | | | | | |
| | | | | | |
| | | | | | |
| | | | | | |
| | | | | | |
| | | | | | |
| | | | | | |

| | Classification |
|--|----------------------------|
| Phase diagrams | 6470, 8130B, 8130D |
| Phase equilibrium | 0570, 64, 8130B, 8130D |
| Phase transformations | 0570, 64, 8130 |
| Phi mesons | 1440 |
| Philosophy of science | 0170 |
| Phonon interactions | 6320 |
| Phosphorescence | 3250, 3350, 7855 |
| Phosphorescence microwave double resonance | 3335H, 7670H |
| Photoacoustic effect | 4388, 6265 |
| Photocapacitance | 7240 |
| Photocathodes | 7960 |
| Photochemistry | 8250 |
| Photochromism | 7820 |
| Photoconductivity | 7240 |
| Photodetachment | 3280F, 3380E |
| Photodiodelectric effect | 7240 |
| Photodisintegration | 2520 |
| Photoelasticity | 4630C, 4630R, 7820F, 8140J |
| Photoelectric conversion | 8630J |
| Photoelectricity | 7240 |
| Photoelectrochemical conversion | 8630K |
| Photoelectromagnetic effects | 7240 |
| Photoelectron spectra | 3280F, 3365, 7960 |
| Photoemission | 7960 |
| Photofission | 2520, 2585 |
| Photography | 0768, 8250, 9575 |
| Photoionisation | 3280F, 3380E |
| Photoluminescence | 3250, 3350, 7855 |
| Photolysis | 8250 |
| Photomagnetic effect | 7520, 7590 |
| Photometry | 0760D, 9575 |
| Photomultipliers | 0760D, 2940 |
| Photon counting | 0762, 4250 |
| Photon echo | 4265G |
| Photon-hadron interactions | 1360 |
| Photon-hadron scattering | 1360F |
| Photon-nucleus scattering | 2520 |
| Photon sources | 2925 |
| Photons | 1480 |
| Photonuclear reactions | 2520 |
| Photoplasticity | 4630J, 6220F, 8140L |
| Photorefractive effect | 4240, 4270G, 7820 |
| Photosphere | 9660 |
| Photosynthesis | 8630P, 8725 |
| Photothermal conversion | 8630S |
| Photovoltaic effects | 7240 |
| Physical chemistry | 82 |
| Physical optics | 42 |
| Physiological models | 8710 |
| Physiological optics | 8732 |
| Physiology | 87 |
| Pick-up reactions | 2450 |
| Piezoelectricity | 7760 |
| Piezorefractance | 7820H |
| Piezoresistance | 7220F |
| Pinch effect | 5255 |
| Pion absorption | 2580 |
| Pion-baryon interactions | 1375G, 1385 |
| Pion-baryon scattering | 1375G, 1385 |
| Pion capture | 2580 |
| Pion decays | 1320, 1325 |
| Pion-nucleus reactions | 2580 |
| Pion-nucleus scattering | 2580 |
| Pions | 1440 |
| Pipe flow | 4760 |
| Plane wave Born approximations | 2410 |
| Planetary nebulae | 9840 |
| Planets | 9630, 9780 |
| Plasma | 52 |
| Plasma antennas | 5240F |
| Plasma applications | 5275 |
| Plasma arc spraying | 5275, 8115, 8160 |
| Plasma beam interactions | 5240M |
| Plasma collision processes | 5220F, 5220H |
| Plasma confinement | 5255 |
| Plasma deposited coatings | 6855, 8115J, 8160 |
| Plasma deposition | 8115J |
| Plasma devices | 5275 |
| Plasma diagnostics | 5270 |
| Plasma electromagnetic wave propagation | 5240D |
| Plasma elementary processes | 5220 |
| Plasma equilibrium | 5255 |
| Plasma-filled waveguides | 5240F |
| Plasma flow | 5230 |
| Plasma heating | 5250 |
| Plasma heating by laser beam | 5250J |
| Plasma heating by shock wave | 5250L |
| Plasma heating by wire explosion | 5250L |
| Plasma magnetohydrodynamics | 5230 |
| Plasma oscillations | 5235 |
| Plasma production by laser beam | 5250J |
| Plasma production by shock wave | 5250L |
| Plasma production by wire explosion | 5250L |
| Plasma radiation | 5225P |
| Plasma sheaths | 5240K |
| Plasma shock waves | 5235T |
| Plasma simulation | 5265 |
| Plasma sources | 5250 |
| Plasma transport processes | 5225F |
| Plasma turbulence | 5235R |
| Plasma-wall interactions | 5240H |

| | Classification |
|---|--------------------------------|
| Plasma waves | 5235 |
| Plasmons | 7145G, 7230 |
| Plastic crystals | 6150, 7660 |
| Plastic deformation | 4630J, 6220F, 8140L |
| Plastic detectors | 2940 |
| Plasticity | 4630J, 6220F, 8140L |
| Plastics | 6140K, 81 |
| Plate tectonics | 9145 |
| Pleochroism | 3345, 7820F |
| Pluto | 9630T |
| Pneumodynamics | 8745 |
| Poincare invariance | 1130 |
| Point contacts | 7340 |
| Point defects | 6170B, 6170D, 6170E, 7850 |
| Poiseuille flow | 4760 |
| Poisson ratio | 6220D, 8140J |
| Polar semiconductors | 7220, 7280 |
| Polarimeters | 0760F, 2975 |
| Polarimetry | 2975 |
| Polarised bombardment targets | 2925 |
| Polarised nuclear reactions | 2470 |
| Polarised sources | 2925 |
| Polaritons | 6320, 7136, 7830 |
| Polarography | 8280 |
| Polarons | 7138 |
| Polishing | 4285, 8160, 8170 |
| Pollution | 8670, 9220, 9260 |
| Polymer films | 6140K, 6855, 81 |
| Polymer melts | 4750, 6125 |
| Polymer molecules | 3620 |
| Polymer preparation | 8120S, 8120T |
| Polymer reactions | 8235 |
| Polymer solutions | 4750, 6125 |
| Polymerisation | 8235 |
| Polymers | 3620, 6140K, 81 |
| Polymorphic transformations | 6150K, 6470K, 8130H |
| Polymorphism | 6150K, 6155, 6160, 6165 |
| Pomeranchuk poles | 1240M |
| Population II stars | 9720 |
| Population inversion | 3280B, 3380B, 4250, 4255, 7845 |
| Porous materials | 4755M, 81 |
| Position sensitive detectors | 2940 |
| Positron annihilation in liquids and solids | 6180F, 7125, 7870B |
| Positron states | 7165 |
| Positrons | 1460 |
| Potential energy curves | 3190 |
| Potential energy surfaces | 3170F, 8220K |
| Potential models | 1240Q |
| Potts model | 0550 |
| Powder metallurgy | 8120E, 8120G |
| Powder spraying | 8115, 8160 |
| Powder technology | 8120E |
| Powders | 4755K, 8120 |
| PPP calculations | 3120P |
| Pre-equilibrium model | 2460 |
| Preacceleration | 2910 |
| Precipitation | 6475, 8130M, 8260 |
| Precipitation hardening | 8140C |
| Primary cells | 8630E |
| Probability theory | 0250 |
| Proportional counters | 2940 |
| Prosthetics | 8770J |
| Protective coatings | 8160 |
| Proteins | 3620, 8715 |
| Proton absorption | 2540 |
| Proton-hyperon interactions | 1375E, 1385 |
| Proton-hyperon scattering | 1375E, 1385 |
| Proton-kaon interactions | 1375J, 1385 |
| Proton-kaon scattering | 1375J, 1385 |
| Proton magnetic resonance | 3325, 7660 |
| Proton-meson interactions | 1375, 1385 |
| Proton-meson scattering | 1375, 1385 |
| Proton-neutron interactions | 1375C, 1385 |
| Proton-neutron scattering | 1375C, 1385 |
| Proton-nucleus reactions | 2540 |
| Proton-nucleus scattering | 2540 |
| Proton-pion interactions | 1375G, 1385 |
| Proton-pion scattering | 1375G, 1385 |
| Proton-proton interactions | 1375C, 1385 |
| Proton-proton scattering | 1375C, 1385 |
| Proton radiative capture | 2540 |
| Protons | 1420 |
| Pseudopotential methods | 7110, 7125C |
| Psi mesons | 1440 |
| Pulsars | 9760G |
| Pulsatile flow | 4760 |
| Pulse amplifiers | 2960 |
| Pulse counting | 2960 |
| Pulse height analysers | 2960 |
| Pulse shaping circuits | 2960 |
| Pyroelectricity | 7770 |
| Pyrometers | 0720, 0762 |
| Q-switching | 4260F |
| QCD | 1235C |
| QED | 1220 |
| Quadrupole moments | 2110K, 3520M, 7660 |
| Quantum electrodynamics | 1220 |
| Quantum field theory | 0370, 1110 |

| | Classification |
|---|--------------------------------|
| Quantum fluids | 0530, 67 |
| Quantum gravity | 0460 |
| Quantum measurement theory | 0365 |
| Quantum mechanics | 0365 |
| Quantum optics | 4250 |
| Quantum statistical mechanics | 0530 |
| Quark confinement | 1235C |
| Quark models | 1235 |
| Quarks | 1480 |
| Quasars | 9870J |
| Quenching (thermal) | 8140G |
| Radiation angular correlations | 2970 |
| Radiation belts | 9430 |
| Radiation chemistry | 8250 |
| Radiation coincidence measurements | 2970 |
| Radiation detectors | 0762, 2940, 2970 |
| Radiation effects | 5190, 6180 |
| Radiation gas dynamics | 4770 |
| Radiation hardening | 8140C |
| Radiation measurement | 2970 |
| Radiation monitoring | 2880, 2940, 2960, 2970, 8760P |
| Radiation monitoring electronics | 2960 |
| Radiation protection | 2880, 8760P |
| Radiation spectrometers | 2930 |
| Radiation spectroscopy | 2930 |
| Radiation therapy | 8760B, 8760G, 8760J, 8770G |
| Radiative effects | 3130 |
| Radiative flows | 4770 |
| Radiative transfer | 0560, 4440, 9265, 9530, 9710 |
| Radioactive dating | 0790, 9385 |
| Radioactive decay periods | 23 |
| Radioactive decay schemes | 23 |
| Radioactive pollution | 8670, 8760R |
| Radioactive sources | 2925 |
| Radioactive tracers | 2925, 8760J, 8760L |
| Radioactive waste | 2842 |
| Radioactivity | 23, 2880 |
| Radioactivity measurement | 2970 |
| Radioastronomy | 95 |
| Radiobiology | 8750G |
| Radiochemistry | 8255 |
| Radiofrequency spectra | 3220B, 3320B, 7870G |
| Radiofrequency spectrometers | 0758, 0765 |
| Radiography | 0785, 8170, 8760J, 8770E |
| Radioisotope scanning and imaging | 8760J, 8770E |
| Radiometry | 0760D |
| Radiosources (astronomical) | 9870D |
| Rain | 9260 |
| Raman lasers | 4255, 4260, 4265C |
| Raman spectra | 3320F, 7830 |
| Random noise | 0250, 7270 |
| Random phase approximations | 2160J, 7110, 7145 |
| Random processes | 0540 |
| Rarefied gas dynamics | 4745 |
| Rayleigh scattering | 3320F, 4265C, 7835 |
| Reaction kinetics | 8220, 8240 |
| Reactive flows | 4770 |
| Recrystallisation | 6150C, 8110J, 8140E |
| Reflection high energy electron diffraction | 6114H |
| Reflectivity | 42, 4210, 4220, 5170, 78 |
| Reflectometry | 0760H |
| Refractive index | 4110H, 4210, 4220, 5170, 7820D |
| Refractometers | 0760H |
| Refractories | 81 |
| Refractory preparation | 8120L, 8120N |
| Regge poles | 1160, 1240M |
| Relativistic band structure calculations | 7110, 7125C |
| Relativistic effects | 3130, 3510F |
| Relativistic field theory | 1110 |
| Relativistic flows | 4775 |
| Relativistic mechanics | 0330 |
| Relativistic plasmas | 5260 |
| Relativistic scattering theory | 1180 |
| Relativity | 04, 9530 |
| Remote sensing | 8670L, 9385 |
| Renormalisable fields | 1110 |
| Replica techniques | 0780, 6116, 68 |
| Resistance thermometers | 0720D |
| Resource letters | 0130R |
| Reverberation | 4355 |
| Reviews | 0130R |
| Rheopexy | 4660 |
| Rho mesons | 1440 |
| Ring lasers | 4260D |
| Rock magnetism | 9160 |
| Rotational energy transfer | 3450E |
| Rotational flow | 4730 |
| Rotational isomerism | 3520J |
| RPA calculations | 2160J, 7110, 7145 |
| S-matrix theory | 1120 |
| SAMO method | 3120G |

| | Classification |
|--|---------------------------|
| Vibrational energy transfer | 3450E |
| Vibrational states of disordered systems | 6350 |
| Vibrations | 0320, 0340K, 4340, 4630M |
| Viscoelasticity | 4630J, 4660, 6240, 8140J |
| Viscometers | 4780 |
| Viscoplasticity | 4630J, 6220F, 8140L |
| Viscosity | 5110, 5120, 6210, 6620 |
| Viscosity of gases | 5120 |
| Visible spectra | 3220J, 3320K, 7840 |
| Vision | 8732 |
| Visual perception | 8732S |
| Visual pigments | 8732L, 8732N |
| Vitreous state | 6140, 81 |
| Vlasov equation | 5220, 5225F |
| Voids (solid) | 6170, 6180 |
| Volcanology | 9140 |
| Volume measurement | 0630C |
| Vorticity | 4730, 6740 |
| VPE | 6855, 8115G, 8115H, 8115J |

| | |
|-------------------------|---------------------------|
| Wakes | 4725R |
| Water wave energy | 8610F |
| Wave energy | 8610F |
| Wave equations | 0340K, 0365 |
| Waves | 0340G, 0340K, 4735, 4740N |
| Weak interaction models | 1230 |

| | Classification |
|-------------------------------|---------------------|
| Weak interactions (atomic) | 3510W |
| Weak interactions (molecular) | 3520W |
| Wear | 4630P, 6220P, 8140P |
| Wear resistant coatings | 6220P, 8140P, 8160 |
| Weather analysis | 9260 |
| Weighing | 0630E |
| Weinberg-Salam model | 1210 |
| Westheimer method | 3120W |
| Wetting | 6810, 6845, 81 |
| Whiskers (crystal) | 6870 |
| White darfs | 9720 |
| Wiberg method | 3120W |
| Wigner functions | 0365 |
| Wind | 9260, 9410 |
| Wind energy | 8610D |
| Woods-Saxon potentials | 2160C |
| Work function | 7330, 7340, 79 |
| Work hardening | 8140E |

| | |
|--|------------------------|
| X-ray absorption spectra | 3220R, 3320R, 7870D |
| X-ray apparatus | 0785 |
| X-ray astronomy | 95 |
| X-ray crystallography | 6110 |
| X-ray diffraction | 6110 |
| X-ray diffraction examination of materials | 6155, 6160, 6165, 6170 |
| X-ray effects | 6180C |

| | Classification |
|------------------------------|----------------------------|
| X-ray emission spectra | 3220R, 3320R, 7870E |
| X-ray lasers | 4255 |
| X-ray monochromators | 0785, 6110F |
| X-ray scattering | 6110, 7870C |
| X-ray sources | 2925 |
| X-ray sources (astronomical) | 9870Q |
| X-ray spectra | 3220R, 3320R, 7870D, 7870E |
| X-ray spectroscopy | 2930 |
| Xalpha calculations | 3120G |

| | |
|-------------------|---------------------|
| Yang-Mills fields | 1110 |
| Yield point | 4630J, 6220F, 8140L |
| Young's modulus | 6220D, 8140J |
| Yrast states | 2110 |

| | |
|------------------|---------------------------------------|
| Zeeman effect | 3260, 3345B, 7170E, 7820L, 7830, 7840 |
| Zener effect | 7220H |
| Zener relaxation | 4630J, 6240, 8140J |
| Zero sound | 67 |
| Zodiacal light | 9460, 9650D |
| Zone melting | 8110H |
| Zone refining | 8110H |
| Zoology | 87 |

Physics Abstracts

15th AUGUST 1983

Volume 86

Number 1214

00.00 GENERAL

01.00 COMMUNICATION, EDUCATION, HISTORY, AND PHILOSOPHY

01.30 PHYSICS LITERATURE AND PUBLICATIONS

01.30C Conference proceedings

74198 Proceedings of the Hungarian-Austrian Health Physicists' Meeting. *Acta Phys. Acad. Sci. Hung. (Hungary)*, vol.52, no.3-4 (1982). [received: May 1983]

Conference held at: Győr, Hungary. Date 28 Sept.-1 Oct. 1981. The following topics were dealt with: dosimetry; environmental monitoring of radiation; radioactive pollution; medical effects of radiation exposure; radiation protection. Abstracts of individual papers can be found under the relevant classification codes in this or other issues.

74199 Workshop on Science Underground.

AIP Conf. Proc. (USA), no.96 (1982). [received: May 1983]

Conference held at: Los Alamos, CA, USA. Date 1982. The following topics were dealt with: underground science laboratories, solar neutrinos, proton decay, cosmic rays and apparatus, geophysics, astronomy, solar models, gravity waves, and double beta decay. Abstracts of individual papers can be found under the relevant classification codes in this or other issues.

74200 Proceedings of the Workshop on the Interaction Between Medium Energy Neutrons in Nuclei.

AIP Conf. Proc. (USA), no.97 (1982). [received: May 1983]

Conference held at: Bloomington, IN, USA. Date 28-30 Oct. 1982. Sponsors: NSF; DOE; Indiana Univ. The following topics were dealt with: nucleon-nucleon interaction; elastic scattering and optical model; NN interaction in nuclear reactions; macroscopic concepts; relativistic approaches; nucleus consists of more than nucleons, and experimental possibilities of the future. Abstracts of individual papers can be found under the relevant classification codes in this or other issues.

74201 Conference on Particles and Fields - 1982.

AIP Conf. Proc. (USA), no.98 (1982). [received: May 1983]

Conference held at: College Park, MD, USA. Date 28-30 Oct. 1982. The following topics were dealt with: grand unified theories; proton decay; magnetic monopoles; supergravity; accelerator technology; electron-positron physics; QCD; two-photon physics; glueballs; quark jets; proton-antiproton interactions; massive lepton production; Upsilon spectroscopy; B mesons; muon-hadron interactions. Abstracts of individual papers can be found under the relevant classification codes in this or other issues.

74202 Biomedical Engineering Society Symposia (papers in summary form only received).

Ann. Biomed. Eng. (USA), vol.11, no.1 (1983).

Conference held at: Chicago, IL, USA. Date 11-15 April 1983. The following topics were dealt with: bioengineering in exploration; recent advances in arterial wall research (physiology and bioengineering aspects); musculoskeletal mechanics; theoretical models of mass transport in the microcirculation; bioengineering aspects of noninvasive diagnosis of peripheral vascular disease; the interaction between the heart and vascular systems; mechanical behaviour of vascular smooth muscle; transport mechanisms of high frequency ventilation; single cell mechanics. 54 papers were presented.

74203 XX National Congress of the Italian Society for Nuclear Biology and Medicine held in association with the VI Annual Meeting of the Nuclear Medicine Section of the Italian Association for Radiology and Nuclear Medicine.

J. Nucl. Med. & Allied Sci. (Italy), vol.27, no.2 (April-June 1983).

Conference held at: Porto Cervo, Italy. Date 4-7 May 1983. The topics dealt with included: a double head rotating SPECT system; an electronic window for a gamma camera with variable zoom and centering; haemodynamic patterns in cirrhosis of the liver; a computer-assisted method for dactyoscintigraphy; first pass radionuclide angiocardiology using a ^{195m}Au generator; contemporary surface measurements of ^{59}Fe and ^{51}Cr using a multichannel analyser; radiometabolic therapy with ^{32}P in bone metastases; liver scintigraphy with radiocolloids; automatic analysis of scintigraphic dynamic series. 148 papers were presented, all of which are published in the present proceedings.

74204 Proceedings of the Topical Meeting of the COSPAR Interdisciplinary Scientific Commission A (Meetings A1 and A2) of the COSPAR Twenty-Fourth Plenary Meeting.

Adv. Space Res. (GB), vol.2, no.5 (1982). [received: April 1983]

Conference held at: Ottawa, Canada. Date 16 May-2 June 1982. The following topics were dealt with: the role of aerosols in climate, instrumentation and future measurement systems, retrieval procedures, measurements and observations, ground truth measurements, effects on remote sensing and on climate, and ozone variability in the middle atmosphere.

74205 NATO ASI on Atomic and Molecular Processes in Controlled Thermonuclear Fusion, Palermo, July 19-30, 1982. C.J. Joachain (Univ. Libre de Brussels, Brussels, Belgium), D.E. Post.

Comments At. & Mol. Phys. (GB), vol.13, no.2, p.85-94 (1983).

Atomic and molecular processes are proving to be key issues in the operation of controlled thermonuclear fusion experiments. The Comment reports on a recent NATO Advanced Study Institute conference devoted to this subject. (1 ref.)

74206 Collision topics at ESCAMP VI. J.B. Hasted (Birkbeck Coll., Univ. of London, London, England).

Comments At. & Mol. Phys. (GB), vol.13, no.2, p.95-101 (1983).

Plasma processes in fusion, in interstellar media, in ion sources, in hollow cathode discharges, in gas laser pumping, in laser breakdown of gases and in cryogenic systems were among the topics discussed at the sixth European Sectional Conference on Atomic and Molecular Processes in Ionized Gases, held in Oxford, September 1-3 1982. (12 refs.)

74207 Advanced Laser Technology and Applications.

Proc. SPIE Int. Soc. Opt. Eng. (USA), vol.335 (1982). [received: May 1983]

Conference held at: Arlington, VA, USA. Date 6-7 May 1982. The following topics were dealt with: laser performance of Nd:YLF; spectroscopic properties of TbP_2O_7 , $\text{TbLi}_2\text{P}_2\text{O}_7$ and $\text{TbAl}_2(\text{BO}_3)_4$; theoretical calculations of fluorescent branching ratios for $\text{YAlO}_3:\text{Er}^{3+}$ from the complete Judd-Ofelt theory; recent advances in coaxial flashlamp-pumped high energy dye lasers; wavelength selectivity with metal halide lasers; objective laser speckle method for 3-D displacement measurement on curved surfaces; frequency stabilisation of CO_2 lasers; 1 to 2 μm III-V compound detectors; miniature short-pulse Nd:YAG laser oscillator; 1.73 μm eyesafe laser rangefinder; unique applications of alexandrite lasers; CO_2 laser radar transmitters; progress in slab geometry solid state lasers and nuclear pumped $\text{O}_2(^1\Delta)-\text{I}_2$ lasers. 17 papers were presented, all of which are published in full in the present proceedings. Abstracts of individual papers can be found under the relevant classification codes in this or other issues.

74208 Fiber Optics: Short-Haul and Long-Haul Measurements and Applications.

Proc. SPIE Int. Soc. Opt. Eng. (USA), vol.355 (1982). [received: May 1983]

Conference held at: San Diego, CA, USA. Date 24-25 Aug. 1982. The conference included papers on the important subjects of short-haul systems and measurements. Attention was also given to the more popular subjects of long-haul systems and applications. Session 1 represents a potpourri of fiber optics: the papers address some of the more pressing topics of 1982. The work discussed is generally at the research level, in contrast to the more applications-oriented subjects on the other three sessions. The second session, on terminal devices, concentrates on those devices that allow full exploitation of the fiber capability. The third session addressed the subject of test and measurement and includes papers on component testing as well as system evaluation. The problems encountered in short-haul applications of fiber optics are unusual. Military applications of fibers, for example, are frequently over short distances. The problems, nevertheless, are severe. The last session addresses many of these short-haul problems.

74209 Proceedings of the Fourth International Workshop on Biomagnetism.

Nuovo Cimento D (Italy), vol.2D, ser.1, no.2 (March-April 1983).

Conference held at: Rome, Italy. Date 14-16 Sept. 1982. The following topics were dealt with: instrumentation; cardiomagnetism; neuromagnetism; bio susceptibility; magnetoplethysmography; other fields of the body. A brief appendix is given on the multiple expansion of a biomagnetic field. 46 papers were presented, all of which are published in full in the present proceedings. Abstracts of individual papers can be found under the relevant classification codes in this or other issues.

74210 2nd Annual Meeting of the Canadian Radiation Protection Association (papers in summary form only received).

Health Phys. (GB), vol.44, no.4 (April 1983).

Conference held at: Ottawa, Canada. Date 5-6 May 1981. The topics dealt with included: risk estimates for the induction of cancer due to low doses of low-LET radiation; potential health impacts of enhanced radiation levels in Port Hope, Ontario. UV radiation and suntanning; long term retention of a class Y uranium thorax burden; modification of a shadow shield whole body monitor for measurements of uranium lung burdens; internal dosimetry; evacuation during reactor incidents; dosimetric consideration of radioactive particle inhalation. 28 papers were presented.

74211 Saturn Conference.

Icarus (USA), vol.53, no.2 (Feb. 1983).

Conference held at: Tucson, AZ, USA. Date 11-15 May 1982. The following topics were dealt with: Saturn; A-ring; B-ring; ring bending waves; ring particles shepherding; spokes; micron-size particles; albedo; heat flux; energy balance; methane; Hyperion; Iapetus; Phoebe; Titan; NH_3 ice and clouds.

74212 Symposium on the Rise in Atmospheric Carbon Dioxide.

J. Geophys. Res. (USA), vol.88, no.C2 (20 Feb. 1983).

Conference held at: Bern, Switzerland. Date 14-18 Sept. 1981. Various aspects of the atmospheric carbon cycle were studied. In particular atmospheric chemistry changes due to industrial CO_2 release were studied. Several of the papers report actual CO_2 concentration observations recorded at various localities around the world.

74213 International Meeting on Lithium Batteries.

J. Power Sources (Switzerland), vol.9, no.3-4 (April-May 1983).

Conference held at: Rome, Italy. Date 27-29 April 1982. The following topics were dealt with: secondary cells, primary cells, Li-Al electrodes, electrolytes, diffusion in solids, corrosion, electrochemical electrodes, cathodes, anodes, electrochemistry, Li/SOCl_2 battery, Raman spectroscopy, liquid structure, Li/SO_2 cells, passivation, organic compounds, intercalation compounds, X-ray diffraction examination, cation glasses, NMR spectra, superionic conducting materials, viscoelasticity, scanning electron microscopy and viscosity of liquids. 25 papers were presented, of which all are published in full in the present proceedings.

74214 Bendor Free Electron Laser Conference.

J. Phys. Colloq. (France), vol.44, no.C-1 (Feb. 1983).

Conference held at: Bendor, France. Date 26 Sept.-1 Oct. 1982. Sponsors: CNRS; CENS; et al. The following topics were dealt with: preliminary results of the Adone storage ring FEL experiment; pulse propagation in free-electron lasers; status of the MSNW tapered-wiggler FEL experiment; high-efficiency free-electron laser results; the Brookhaven free-electron laser experiment; FEL quantum aspects; delay effect in laser amplifiers; free-electron laser oscillator

startup analysis; simulation of isochronous storage ring free-electron laser; helical undulator study; application of transverse gradient wigglers in high efficiency storage ring FELs; the UK free-electron laser; Linac technology for free-electron lasers; storage ring design optimisation for FEL operation; permanent magnet undulators; microtrons for free-electron lasers; tapered wigglers; optical klystrons; review of recent experimental results from the Stanford 3 μ m free-electron laser; the LELA undulator main features and performance; fully quantised many particle theory of a free-electron laser; one-dimensional numerical simulation of a free-electron laser-storage ring system; optical instabilities and coherence in the free-electron-laser; resonator cavity design for two-stage FEL experiment; far infrared free-electron laser; Cerenkov lasers and transverse mode structure of a tapered-wiggler FLE oscillator. 43 papers were presented, of which 32 are published in full in the present proceedings, and 11 as abstracts only. Abstracts of individual papers can be found under the relevant classification codes in this or other issues.

74215 International Workshop on Optical Phase Conjugation and Instabilities.

J. Phys. Colloq. (France), vol.44, no.C-2 (March 1983).

Conference held at: Cargèse, Corsica, France. Date: 20-24 Sept. 1982. Sponsors: CNRS. The following topics were dealt with: nonlinear propagation in degenerate four wave mixing; optical gratings; transients; pulse compression; spectroscopy and diagnostics; nonlinear polarisation and materials in degenerate four wave processes; strong optical excitations and nonlinearities; optical instabilities and chaos. Abstracts of individual papers can be found under the relevant classification codes in this or other issues.

74216 International Symposium on Theoretical Organic Chemistry.

Pure & Appl. Chem. (GB), vol.55, no.2 (Feb. 1983).

Conference held at: Dubrovnik, Croatia, Yugoslavia. Date: 30 Aug.-3 Sept. 1982. The following topics were dealt with: present-day problems in theoretical organic chemistry and their influence on preparative organic chemistry. 29 papers are published in full in the present proceedings. Abstracts of individual papers can be found under the relevant classification codes in this or other issues.

74217 Proceedings of the International Symposium on Magnetoelasticity in Transition Metals and Alloys.

Physica B & C (Netherlands), vol.119 B+C, no.1-2 (April 1983).

Conference held at: Nagoya, Japan. Date: 15-16 Sept. 1982. The following topics were dealt with: theory; phase transition; thermal expansion and Invar alloys; elastic constants; pressure dependence; magnetostriction; amorphous alloys. 33 papers are published in full in the present proceedings, and 4 as abstracts only. Abstracts of individual papers can be found under the relevant classification codes in this or other issues.

74218 VDE-Kongress '82 (VDE-Congress '82).

VDE Fachber. (Germany), vol.34 (1982).

Conference held at: Düsseldorf, Germany. Date: 4-6 Oct. 1982. The following topics were dealt with: electrical engineer's training, fibre optics engineering, optical fibres, telemetry, thermal power stations, solar power stations, nuclear power stations, water power reserves, power transmission and distribution, digital protection, HV switchgear, short-circuit currents, cable terminations, electric connectors, data networks, videodata, data communication systems, PCM, optical fibre cable systems, amorphous metals, electronic displays, radio paging, mobile radio systems and voice communication. 12 papers were presented, of which all are published in full in the present proceedings.

74219 Conference Record of the Sixteenth IEEE Photovoltaic Specialists Conference - 1982.

New York, USA: IEEE (1982), 1484 pp.

Conference held at: San Diego, CA, USA. Date: 27-30 Sept. 1982. The following topics were dealt with: space solar arrays, welded solar cell interconnection, silicon sheet materials, crystallisation techniques, directional solidification, crystal growth, non-destructive testing. Si solar cells, thin film cells, photovoltaic pumping systems, power supplies to apparatus, space vehicle power plants, III-V semiconductors, solar power stations, space radiation effects, high efficiency Si solar cells, polycrystalline Si impurities, grain boundaries, defect analysis, solar energy concentrators, CdS/Cu₂S solar cells, concentrating solar cells, CdS-based solar cells, terrestrial systems and economics, amorphous semiconductors, MIS/SIS solar cells, reliability testing and field experience and alternative solar cell materials. 278 papers were presented, of which 279 are published in full in the present proceedings, and 9 as abstracts only.

74220 Topical Meeting on Meteorological Optics. Technical Digest.

Washington, DC, USA: Opt. Soc. America (1983), 80 pp.

Conference held at: Incline Village, NV, USA. Date: 12-14 Jan. 1983. Sponsors: Opt. Soc. America; Air Force Office Sci. Res. The following topics were dealt with: green flash, red sunset, blue sky, snow colour, light scattering, droplet sizes, lunar corona, aerosols, rainbows, halos, polarised light, Ezekiel's wheels, singularities, light pillars, phase functions, mirages and air quality.

74221 Topical Meeting on Optical Techniques for Remote Probing of the Atmosphere. Technical Digest.

Washington, DC, USA: Opt. Soc. America (1983), 332 pp.

Conference held at: Incline Village, NV, USA. Date: 10-12 Jan. 1983. Sponsors: Opt. Soc. America; Air Force Office Sci. Res. The following topics were dealt with: optical radiation prospecting, laser remote sensing, aerosol, cloud, backscatter, Raman scattering, upper atmosphere wind, precipitation, atmosphere composition, chemical reaction, moisture, temperature, weather indicator, lidar system, radiometer, troposphere, spectrometer, interferometer, snow, Earthlimb emission, radiance, speckle phenomena, CO, NO, extinction coefficient, smoke, scintillation, evaporation, pressure, water content, optical pulses, densities, O₃, airflow, turbulence and stratosphere.

74222 Fourth International Ocean Disposal Symposium.

Plymouth, Devon, England: Plymouth Polytechnic (1983), ii+181 pp.

Conference held at: Plymouth, Devon, England. Date: 11-15 April 1983. The objective of this symposium is to provide a forum for the exchange of ideas and information among investigators involved in ocean disposal research; to enhance the scientific consideration of waste disposal in the marine environment with the production of a symposium volume; and to generate recommendations and guidelines for future studies on ocean disposal practices. Abstracts of individual papers can be found under the relevant classification codes in this or other issues.

74223 Proceedings of the Symposium on Low-Level Waste Disposal. Vol.3. Facility Design, Construction, and Operating Practices (NUREG/CP-0028).

Oak Ridge, TN, USA: Oak Ridge Nat. Lab (1982), ix+455 pp.

Conference held at: Washington, DC, USA. Date: 29-30 Sept. 1982. Sponsors: Office Nucl. Mater. Safety & Safeguards; U.S. Nucl. Regul. Comm.; Oak Ridge Nat. Lab. The following topics were dealt with: low level radioactive waste; radwaste disposal; waste facility design; operating practices; trench design; land disposal; health physics monitoring; environment protection; 24 papers were presented, all of which are published in full in the present proceedings.

74224 Proceedings of the Fifth Power Plant Dynamics, Control and Testing Symposium.

Knoxville, TN, USA: Univ. Knoxville (1983), 2 vol. vi+762 pp.

Conference held at: Knoxville, TN, USA. Date: 21-23 March 1983. Sponsors: Univ. Tennessee; IEEE; EPRI; et al. The following topics were dealt with: modeling and simulation of power systems; nuclear power system components; modeling and control of nonnuclear power systems; human factors and operator aids; power plant surveillance and diagnostics. Abstracts of individual papers can be found under the relevant classification codes in this or other issues.

74225 Fifteenth Annual Synchrotron Radiation Users Group Conference (papers in summary form only received).

Stoughton, WI, USA: Synchrotron Radiat. Center (1982), 80 pp.

Conference held at: Stoughton, WI, USA. Date: 18-19 Oct. 1982. The following topics were dealt with: applications of synchrotron radiation in photoemission and bandstructure determinations and synchrotron radiation sources. Abstracts of individual papers can be found under the relevant classification codes in this or other issues.

74226 Gallium Arsenide and Related Compounds, 1982. Tenth International Symposium on Gallium Arsenide and Related Compounds.

Bristol, England: IOP (1983), xvi+650 pp. [0 85498 156 X]

Conference held at: Albuquerque, NM, USA. Date: 19-22 Sept. 1982. Sponsors: Air Force Office Sci. Res. The volume contains eighty-five selected papers from those presented at the conference. The technical program of the conference included sessions on bulk and epitaxial crystal growth, optoelectronic devices, microwave devices, ion implantation, and characterization, and the chapters of this volume reflect these areas. Improvements in the preparation of high purity undoped semi-insulating GaAs were reported, along with considerable discussion of the EL2 electron trap in this material. Advances in bulk InP growth and the growth of bulk III-V alloys were presented. Research on GaAs, InP, and alloy high frequency and optoelectronic devices demonstrated increasingly sophisticated structures, including modulation-doped heterostructure charge-coupled devices. Readers will also detect greater sophistication in the techniques being used for characterizing defects, deep levels, and residual impurities in GaAs, InP and related alloys. The papers included reflect the current status of research in GaAs and related compound materials and devices. Abstracts of individual papers can be found under the relevant classification codes in this or other issues.

74227 Cloud Dynamics. Proceedings of a Symposium held at the Third General Assembly of IAMAP.

Dordrecht, Netherlands: Reidel (1982), vii+423 pp. [90 277 1458 4]

Conference held at: Hamburg, Germany. Date: 17-28 Aug. 1981. The following topics were dealt with: observation and models of shallow convective systems, and deep convective systems; the cloud phenomena considered range from cumulus and cloud streets to organised mesoscale cellular convection. Winter lake induced snow squalls, thunderstorms, hailstorms and tornadoes are discussed. Doppler radar observations and thunderstorm model results are discussed.

74228 Physics in Collision. High-Energy ee/pp Interactions. Proceedings of an International Conference.

New York, USA: Plenum (1983), x+432 pp. [0 306 40996 8]

Conference held at: Stockholm, Sweden. Date: 2-4 June 1982. The field of particle physics is developing very rapidly. During this past year, physicists added a new instrument to their arsenal for the study of quark-quark, quark-lepton, and lepton-lepton interactions. This machine, the PROTON-ANTI-PROTON COLLIDER, achieved the highest energy in the world. With its five detectors, it is beginning to explore hitherto inaccessible regions for new physics. Lepton-lepton machines with detectors at full efficiency are producing copious data of the very highest precision. The possibility of glueballs and the detailing of the properties of the upilon family have been of major importance this year. The particle jets which are believed to be direct manifestations of the quark structure of matter continue to provide valuable data against which we can test the ideas of QCD. With the advent of more and better data it is now possible to study in detail the formation evolution of hadronic states. Especially interesting are the properties of heavy quark states. A far-seeing look into the future development of any fecund scientific field is rarely accurate, but is always stimulating.

74229 The High-Energy Limit. Proceedings of the Eighteenth Course of the International School of Subnuclear Physics.

New York, USA: Plenum (1983), xi+1104 pp. [0 306 41036 2]

Conference held at: Erice, Italy. Date: 31 July-11 Aug. 1980. The following topics were dealt with: induced gravitation; gauge theories; unification; Lie algebras; electroweak physics; conservation laws; quark masses; high energy interactions; QCD; charmed particles; deep inelastic phenomena; QED; e⁺e⁻ physics. 26 papers were presented, all of which are published in full in the present proceedings. Abstracts of individual papers can be found under the relevant classification codes in this or other issues.

01.30E Monographs, and collections

74230 Magnetospheric plasma physics. A.Nishida [Ed.]

Dordrecht, Netherlands: Reidel (1982), xii+348 pp. [90 277 1345 6]

One of the six principal courses of the Autumn College of Plasma Physics, International Center for Theoretical Physics, Trieste, Italy, October 16-November 23, 1979, was devoted to space plasma physics. This monograph contains review articles drawn from the five lecture series comprising the space plasma physics course given on that occasion. The first, introductory chapter deals with the origin of the plasma that fills planetary magnetospheres. The means by which solar wind energy and momentum are communicated to the magnetosphere is discussed in the second chapter. The third chapter discusses a basic instability of magnetospheric tails that converts stored magnetic energy into flow kinetic energy and into accelerated particles. The fourth chapter presents results of advanced numerical simulation of auroral acceleration processes. The fifth chapter reviews the observations and theory of the electrostatic electron cyclotron harmonic waves responsible for the diffuse aurora.

74231 International advances in nondestructive testing. Vol.9. W.J.McGonagle [Ed.]

New York, USA: Gordon & Breach (1983), 363 pp. [0 677 16440 8]

The following topics were dealt with: light propagation in optical fibres; acoustical speckle interferometry; laser speckle interferometry; magnetic flux leakage inspection of wire rope; holographic nondestructive testing; Seebek effect in nondestructive evaluation of metals; electrostatic charge decay technique; digital nondestructive evaluation of composite materials; multi-directional eddy current coils; microencapsulated penetrant inspection.

- 74232 Annual review of nuclear and particle science. Vol.32.** J.D.Jackson, H.E.Gove, R.F.Schwitters [Ed.]
Palo Alto, CA, USA: Annual Reviews (1982), 595 pp. [0 8243 1532 4]
The book reviews developments in the following fields: beam foil and statistical spectroscopy; giant resonances; short lived nuclide identification; composite system interactions; QCD: particle electric-dipole moments; γ -ray astronomy; nuclear resonances; particle calorimetry; inertial confinement fusion; intermediate vector bosons; charged current neutrino interactions.
- 74233 Physico-Chemical Behaviour of Atmospheric Pollutants. Proceedings of the Second European Conference.**
Dordrecht, Netherlands: Reidel (1982), xvi+672 pp. [90 277 1349 9]
Conference held at: Varese, Italy. Date 29 Sept.-1 Oct. 1981. The following topics were dealt with: identification and analysis of pollutants, chemical and photochemical reactions, aerosols, pollutant cycles, and transport and modelling field experiments.

01.30M Textbooks for graduates and researchers

- 74234 Annual review of fluid mechanics. Vol.15.** M.Van Dyke, J.V.Wehausen, J.L.Lumley [Ed.]
Palo Alto, CA, USA: Annual Reviews (1983), 534 pp. [0 8243 0715 1]
The book, the annual review of fluid mechanics, contains 18 chapters and covers: Ernst Mach's contribution to fluid mechanism; fluid mechanics of green plants; snow avalanches; wind turbine; compressible liquid impact; autorotation; wave breaking; flames; turbulence; airfoils; two-phase flow; non-Newtonian fluid mechanics; magneto-atmospheric waves; Langmuir circulation; jets; pipe flow and freezing-melting interfaces.
- 74235 Microcomputer quantum mechanics.** J.P.Killingbeck.
Bristol, England: Adam Hilger (1983), x+177 pp. [0 85274 455 2]
Much of the book is about the wise use of microcomputers in scientific work, and so should be of interest to a wide group of students and research workers. The book has 12 chapters dealing with the following subjects: microcomputers and BASIC; tuning the instrument; iterative approach; finite-difference methods; numerical integration; Padé approximants; simple power series method; matrix calculation; hypervirial-perturbation methods; finite difference eigenvalue calculations; and one-dimensional model problems. Some case studies of quantum mechanics problems are given in the last chapter.
- 74236 Circulation in the coastal ocean.** G.T.Csanady.
Dordrecht, Netherlands: Reidel (1982), xi+279 pp. [90 277 1400 2]
The following topics were dealt with: fundamental equations and their simplification, inertial response to wind, the behaviour of the stratified sea, the subtle effects of topography, transient coastal currents, flow controlled by bottom friction, thermohaline circulation, and observed quasi-steady flow patterns in shallow seas.
- 74237 Gauge theory of dislocations and disclinations.** A.Kadic, D.G.B.Edelen.
Berlin, Germany: Springer-Verlag (1983), vii+290 pp. [3 540 11977 9]
Noting that the group $SO(3) \rightarrow T(3)$ may be viewed as a 6-parameter gauge group that leaves the Lagrangian of elasticity theory invariant, the Yang-Mills universal gauge theory construction is used to erect a complete continuum theory of material bodies with dislocation and disclination fields. Breaking of the homogeneity of the action of $SO(3)$ is shown to give rise to disclinations and rotational dislocations while homogeneity breaking of $T(3)$ gives rise to translational dislocations. A rigorous justification for replacing displacement gradients by the components of the distortion tensor and Newtonian kinematic velocity by distortional velocity is obtained. A complete analysis of the theory is made and an expansion in terms of a group scaling parameter is obtained. It is shown that in the first order approximation classical elasticity theory is recovered, while the second and third orders of approximation model theories of dislocations and disclinations, respectively. (45 refs.)

01.30P Textbooks for undergraduates

- 74238 Foundations of theoretical mechanics. II. Birkhoffian generalization of Hamiltonian mechanics.** R.M.Santilli.
Berlin, Germany: Springer-Verlag (1983), xix+370 pp. [3 540 09482 2]
The author of this volume shows that all sufficiently regular Newtonian systems, whether conservative or not, can be treated via conventional variational principles, Lie algebra techniques and methods from symplectic geometry. Contrary to the simpler systems usually described in textbooks on classical mechanics, these lead to a generalization of the usual Hamiltonian equations of analytic mechanics; the author calls them Birkhoffian. The author shows for the first time the most general and complete answer to the inverse problem, deals with the transformation theory, and gives numerous applications in physics, chemistry and engineering. The book was written not only for students of mechanics, but also for those who wish to apply the principles of mechanics to realistic and therefore typically nonconservative systems. (175 refs.)

- Annual review of fluid mechanics. Vol.15 See Entry 74234
Microcomputer quantum mechanics See Entry 74235

01.30R Surveys and tutorial papers; resource letters

- Annual review of fluid mechanics. Vol.15 See Entry 74234
Percolation. Models, analog and numerical simulations See Entry 74371
Continuous flow cryostats for experiments in the presence of appreciable heat influx to the specimen See Entry 74472
Highly sensitive polarimetric techniques (review) See Entry 74514
QCD, unification and the road to 'asymptopia' See Entry 74695
Physics of intermediate vector bosons See Entry 74701
A unified approach to QCD phenomenology See Entry 74702
Quantum chromodynamics: the modern theory of the strong interaction See Entry 74709
Hadronic physics of qq light quark mesons, quark molecules and glueballs See Entry 74714
Deep inelastic phenomena See Entry 74715
Exotic multi-quark states with charm See Entry 74740
Experimental e^+e^- physics See Entry 74752
Test of quantum electrodynamics and the study of heavy leptons See Entry 74754
 e^+e^- physics at PETRA See Entry 74755
Charged-current neutrino interactions See Entry 74757

- Electric-dipole moments of particles See Entry 74773
Lepton-hadron inclusive scattering and QCD See Entry 74778
Some recent results in e^+e^- physics in the US See Entry 74790
The free NN interaction, 50-1000 MeV See Entry 74792
Status of charmed particles See Entry 74822
Three-body forces See Entry 74855
Statistical spectroscopy See Entry 74872
The macroscopic approach to nuclear masses and deformations See Entry 74877
Theory of giant resonances See Entry 74883
Physics limitations of the optical model See Entry 74938
First order interpretation of optical potentials See Entry 74939
Coupling between low-lying nuclear states See Entry 74950
Proton and neutron elastic scattering between 80 and 1000 MeV See Entry 74965
Resonances in heavy-ion nuclear reactions See Entry 75021
An assessment of acoustic emission for nuclear pressure vessel monitoring See Entry 75099
Lessons learned about disposal design See Entry 75125
Overview of low-level radioactive waste disposal facilities subsidence See Entry 75136
Overview of design considerations for effective trench covers See Entry 75139
Alternatives to shallow land burial of low-level radioactive waste—an overview See Entry 75143
Inertial confinement fusion See Entry 75181
A brief survey on progress and trends in nuclear radiation detectors. I. Gas counters and liquid detectors See Entry 75241
ICRU recommendations on radiation quantities and units—a critical review See Entry 75248
Calorimetry in high-energy physics See Entry 75249
Evaluation of GTO molecular integrals See Entry 75273
Valence bond theory for conjugated hydrocarbons See Entry 75304
Beam-foil spectroscopy See Entry 75554
Current optics in Sweden See Entry 75574
A review of holographic nondestruction evaluation at Lawrence Livermore National Laboratory See Entry 75607
Holographic nondestructive evaluation: status and future See Entry 75608
Linac technology for free electron lasers See Entry 75663
High current limitations on storage ring FEL sources See Entry 75665
Stories of undulator light See Entry 75668
Quantum descriptions of free-electron lasers See Entry 75669
Nonlinear optics in fibers and near-infrared frequency conversion See Entry 75720
Degenerate four wave mixing in photorefractive BSO crystals and applications See Entry 75733
Laser beam critical behaviour and phase conjugation in the semiconductors, resonant media and electrooptic crystals See Entry 75734
Transport effects associated with turbulence with particular attention to the influence of helicity See Entry 75994
Autorotation See Entry 76047
Integrable, chaotic, and turbulent vortex motion in two-dimensional flows See Entry 76048
On the theory of the horizontal-axis wind turbine See Entry 76060
The impact of compressible liquids See Entry 76070
Numerical methods in non-Newtonian fluid mechanics See Entry 76079
The turbulent wall jet—measurements and modeling See Entry 76085
Two-phase flow patterns: a review of research results See Entry 76089
Mathematical modeling of two-phase flow See Entry 76097
Complex freezing-melting interfaces in fluid flow See Entry 76098
Flow in curved pipes See Entry 76116
Point defects in II-VI compounds See Entry 76420
Ion implantation in group II-VI compounds See Entry 76467
Shock crystallization of films See Entry 76812
Spin glasses. I See Entry 77184
Fluorescence of molecular crystals at high levels of optical pumping See Entry 77415
Vapour phase growth of some II-VI compounds See Entry 77545
Composite materials: some recent developments See Entry 77601
Rapid solidification of steels See Entry 77627
Effects of sodium and lithium environments on mechanical properties of ferrous alloys See Entry 77730
The ductile fracture of metals: a microstructural viewpoint See Entry 77742
Review of oxidation processes in plasmas See Entry 77778
Present status and problem of high temperature corrosion testing methods See Entry 77816
Quantum chemical and statistical-thermodynamic studies of equilibria and rates See Entry 77862
Instabilities, pattern formation, and turbulence in flames See Entry 77890
Rapid chemical methods for identification and study of short-lived nuclides See Entry 77946
Research on polycrystalline thin-film photovoltaic devices See Entry 78004
Theoretical and experimental studies of tandem or cascade solar cells: a review See Entry 78075
Aggregation and fusion of phospholipid vesicles See Entry 78155
Progress in phototransduction See Entry 78180
Inferences concerning anatomy and physiology of the human brain based on its magnetic field See Entry 78208
Microwaves and the blood-brain barrier: a review See Entry 78238
Biological signals processing: an application to ultrasonic echo signals sounding See Entry 78275

- High-resolution magnetic measurements of human cardiac electrophysiological events See Entry 78281
- Lung exploration by SPECT current status and perspectives See Entry 78326
- The radiation dose from coal burning: a review of pathways and data See Entry 78341
- Development of protection against radiation in Austria during the past decade See Entry 78357
- Automated analysis of abnormal electroencephalograms See Entry 78376
- Application of interferometry to the monitoring of sheep and cattle behaviour in arid zone paddocks See Entry 78387
- Instrumentation for biomagnetism See Entry 78393
- Characterization of the solid components of biological tissues by cross-polarization, magic angle NMR spectrometry See Entry 78402
- Health risks from electricity generation See Entry 78409
- On the localization of seismic events See Entry 78472
- The form and dynamics of Langmuir circulations See Entry 78556
- Snow avalanche motion and related phenomena See Entry 78574
- IRAS, the Infrared Astronomical Satellite See Entry 78783
- Magneto-atmospheric waves See Entry 78810
- Gamma-ray astronomy See Entry 78811
- Antiproton interactions with light elements as a test of GUT cosmology See Entry 79040

01.30T Bibliographies

- 74239 Heat and mass transfer bibliography—Soviet works. R.I.Soloukhin, O.G.Martynenko (Heat & Mass Transfer Inst., Minsk, Belorussian SSR). *Int. J. Heat & Mass Transfer (GB)*, vol.26, no.6, p.795-804 (June 1983). A bibliography of approximately 380 references is presented, covering Soviet works on thermodynamics, heat conduction, hydromechanics, phase changes, natural convection, forced convection, radiation, combined heat and mass transfer, high temperature thermophysics, rheophysics, and heat and mass transfer in technological processes. (380 refs.)
- The Coxeter-Todd lattice the Mitchell group and related sphere packings See Entry 74400

01.50 EDUCATIONAL AIDS

- 74240 Proposal for a national underground science facility. A.K.Mann (Dept. of Phys., Univ. of Pennsylvania, Philadelphia, PA, USA). *AIP Conf. Proc. (USA)*, no.96, p.16-36 (1982). [received: May 1983] (Workshop on Science Underground, Los Alamos, CA, USA, 1982). The idea is explored of establishing a laboratory complex shielded from the cosmic ray flux at the Earth's surface for the purpose of housing and providing technical support for experiments in particle physics, astrophysics, and other scientific disciplines. The scientific motivation for such an underground science facility is described, and the questions of location and desired properties of the facility are discussed. (9 refs.)
- 74241 Perspectives of fundamental research in the Gran Sasso Underground Laboratory. M.Conversi (Dept. of Phys., Univ. of Rome, Rome, Italy). *AIP Conf. Proc. (USA)*, no.96, p.37-51 (1982). [received: May 1983] (Workshop on Science Underground, Los Alamos, CA, USA, 1982). The installation of very massive and sophisticated particle detectors deep underground will provide a new way to attack frontier problems of subnuclear physics, astrophysics and cosmology. The author considers existing and future laboratories. (31 refs.)
- 74242 The Gran Sasso project. A.Zichichi (INFN, Rome, Italy). *AIP Conf. Proc. (USA)*, no.96, p.52-64 (1982). [received: May 1983] (Workshop on Science Underground, Los Alamos, CA, USA, 1982). The author presents the final solution adopted for the 'Gran Sasso' Underground Laboratory. (1 ref.)
- 74243 Particle physics below the Earth's surface, an overview of possibilities. J.G.Learned (Univ. of Hawaii, Manoa, Honolulu, HI, USA). *AIP Conf. Proc. (USA)*, no.96, p.236-47 (1982). [received: May 1983] (Workshop on Science Underground, Los Alamos, CA, USA, 1982). Potential subterranean cosmic ray and high energy particle physics experiments of current interest are reviewed. It is argued that most of the experiments may be attempted with instruments that fall generally into two classes: 1) detectors with greater than one thousand ton mass and MeV energy sensitivity, and 2) those with far greater mass, megatons or more, but much higher energy threshold, TeV. Those in class 1 are useful for nucleon decay searches, solar neutrino observations, and monitoring for supernovae in the Galaxy. Class 2 detectors are aimed at high energy neutrino astronomy and various cosmic ray muon studies and the nature of interactions at ultra high energies. Both types can do useful muon studies, depending particularly upon depth. Finally the prospects for second generation nucleon decay searches are discussed and it is concluded that a national underground laboratory may be justified sometime in the future, after the results of contemporary endeavors are available, but that at present it is not possible to define the characteristics required of such a national facility. However, it is suggested that studies be undertaken to evaluate the various options, including novel technology, such as TPC-like devices, and to evaluate location options, such as being near a surface cosmic ray installation, or being located in the ocean. (12 refs.)
- 74244 Microcomputer measurement of the velocity of sound in air. P.A.Bates (Div. of Phys. & Astron., Preston Polytech., Preston, England). *Phys. Educ. (GB)*, vol.18, no.3, p.128-33 (May 1983). The velocity of sound in air can be measured in a general physics laboratory using many well known methods such as Hebb's method, Kundt's tube, etc. The experiment described allows the velocity of sound in air to be determined relatively easily but it has really been developed to enable a student to use a microcomputer in a physical experiment. The intention has been for the student to become familiar with an Apple II microcomputer that is being used for data collection and to realise that data collected in this manner may be processed manually as well as with the aid of a computer. It is hoped that by using such techniques students may be instructed in the best use of computers in both the collection and handling of experimental results. (1 ref.)
- Workshop on Science Underground See Entry 74199
- Dose measurements in the teaching reactor of Budapest Technical University after the reconstruction See Entry 75192

01.60 BIOGRAPHICAL, HISTORICAL, AND PERSONAL NOTES

- 74245 Analysis of dust rain in the historic times of China. Zhang De'er (Chinese Acad. of Meteorological Sci., State Bur. of Meteorology, Beijing, China). *Kexue Tongbao (Foreign Lang. Ed.) (China)*, vol.28, no.3, p.361-6 (March 1983). The author has extracted 1156 historical writings of dust rain from local histories and history books written in biographical style. In this paper, some characteristics of dust rain and their climatic background are discussed. (5 refs.)
- 74246 Hauksbee's prototypical electrostatic generator. J.E.Senior. *Med. Instrum. (USA)*, vol.17, no.2, p.126-7 (March-April 1983). An event occurred in 1675 that proved to be of no little consequence in the history of electricity. The French astronomer Jean Picard observed a curious glow in the vacuum atop an oscillating column of mercury in a barometer. His observation set into motion a series of steps that 30 years later culminated in the construction of the prototype of the electrostatic generator by Francis Hauksbee (ca 1666-1713). The four essential components of the electrostatic generator—the rotating electric, cushion, collector, and prime conductor—were not to be incorporated into the design until the mid 18th century, but the device that the English scientific virtuoso designed to demonstrate the glow or 'mercurial phosphorus' of the barometer before members of the Royal Society of London was the 'phantom horse always runs before our modern locomotives', as Wells put it. (no refs.)
- 74247 Contributions of Ernst Mach to fluid mechanics. H.Reichenbach (Ernst-Mach-Inst., Freiburg, Germany). In book: *Annual review of fluid mechanics. Vol.15*, M.Van Dyke, J.V.Wehausen, J.L.Lumley [Ed.], p.1-28. Palo Alto, CA, USA: Annual Reviews (1983), 534 pp. [0 8243 0715 1] The author describes the contributions of Ernst Mach to experimental physics, especially to gas dynamics and ballistics, and thus not only explains the Institute's name but also serves a great physicist's reputation for noteworthy discoveries in natural science. (31 refs.)

01.65 HISTORY OF SCIENCE

- 74248 Correlation analysis in organic chemistry: retrospect. N.B.Chapman (Dept. of Chem., Univ. of Hull, Hull, England). *Indian J. Phys. Part B*, vol.56B, no.6, p.1-8 (Dec. 1982). [received: May 1983] The author traces the history of the subject, starting with Brønsted and Pedersen's famous paper of 1924. The treatment will have autobiographical and quasi-philosophic notes in it. It will highlight historically significant events: the publication in 1940 of the first edition of L.P. Hammett's *Physical Organic Chemistry*, the Faraday Society Discussion on Mechanism and Kinetics of organic reactions in liquid systems, 1941, H.H. Jaffe's chemical review, 1953, R.W. Taft's Chapter in Steric Effects in Organic Chemistry, ed. M.S. Newman, 1956, among others. The development of (a) the realisation of the importance of statistical methodology (and probity), (b) the separation of polar and steric effects, (c) the use of multiparameter equations, (d) extensions into biomedical chemical topics will be outlined. (15 refs.)
- 74249 The prediction and discovery of conical refraction by William Rowan Hamilton and Humphrey Lloyd (1832-1833). J.G.O'Hara (Historisches Inst., Univ. Stuttgart, Stuttgart, Germany). *Proc. R. Ir. Acad. Sect. A (Ireland)*, vol.82A, no.2, p.231-57 (Dec. 1982). [received: May 1983] The discovery of conical refraction in biaxial crystals by Humphrey Lloyd followed a brilliant mathematical prediction by William Rowan Hamilton, which was first announced at the Royal Irish Academy in October 1832. The importance of the discovery was entirely theoretical; it represented the completion of the theory of double refraction published by Huygens in 1690. Fresnel, who developed the received theory of double refraction in biaxial crystals, had inadequately described the form and properties of the wave surface which bears his name. Hamilton discovered four conoidal cusps on the wave surface, from which he predicted the phenomena of external and internal conical refraction. The discovery was a triumph for the view and methodology of optics presented by Hamilton in a series of memoirs on the 'Theory of systems of rays'. Hamilton's correspondence at the end of 1832 and in early 1833 reveals that the discovery was made possible by close collaboration with the experimentalist Lloyd. (23 refs.)

01.75 SCIENCE AND SOCIETY

- Accelerators—limitations of technology. A summary of the Snowmass accelerator working group reports See Entry 75212

02.00 MATHEMATICAL METHODS IN PHYSICS

02.10 ALGEBRA, SET THEORY, AND GRAPH THEORY

- 74250 Modular Jordan algebras of self-adjoint operators. Sh.A.Ayupov (Inst. of Math., Acad. of Sci., Tashkent, Uzbek SSR). *Theor. & Math. Phys. (USA)*, vol.53, no.1, p.994-7 (Oct. 1982). Translation of: *Theor. & Math. Fiz. (USSR)*, vol.53, no.1, p.77-82 (Oct. 1982). An investigation is made into the connection between the type of a JW algebra (i.e. a weakly closed Jordan algebra of self-adjoint operators on a Hilbert space) and the type of the enveloping von Neumann algebra. It is shown that every finite trace (faithful or normal) on a JW algebra A can be extended to a finite trace (faithful or normal, respectively) on the enveloping von Neumann algebra $u(A)$. Using this result, it is shown that the JW algebra A is modular if and only if $u(A)$ is a finite von Neumann algebra. If A is a reversible JW factor, then it has the type II₁; if and only if $u(A)$ has the type II₁. (12 refs.)
- Microcomputer quantum mechanics See Entry 74235
- Quaternion transformation and its application to the displacement analysis of spatial mechanisms See Entry 74255

- Irreducible tensors and their application in problems of the motion of a solid body in strong fields See Entry 74269
- The fundamental bordered matrix of linear estimation and the Duffin-Morley general linear electromechanical systems See Entry 74292
- Deformations of the algebra of functions on hermitian symmetric spaces resulting from quantization See Entry 74295
- Analysis of a bilinear relation for the six-vertex model See Entry 74323
- Differential rings used in Shirokov algebras See Entry 74324
- A procedure for generating realizations of Li-admissible and other nonassociative algebras See Entry 74652
- A unified algebraic approach to bound and continuum states of anharmonic potentials See Entry 75463
- Polynomial model for concentration and temperature dependence of excess thermodynamic functions See Entry 76670

02.20 GROUP THEORY

(for algebraic methods in quantum mechanics, see 03.65; for symmetries in elementary particle physics, see 11.30)

- 74251 Maximal symmetry in Banach spaces. G.V.Wood (Dept. of Maths., Univ. Coll., Swansea, Wales). *Proc. R. Ir. Acad. Sect. A (Ireland)*, vol.82A, no.2, p.176-86 (Dec. 1982). [received: May 1983]
- A Banach space X is convex-transitive if the orbit of any point on the unit sphere under the group of isometries has its convex hull dense in the unit ball. This implies that X is maximal i.e. no equivalent norm has a strictly larger group of isometries. The author characterizes real and complex $C_0(S)$ -spaces that are convex-transitive, and shows that there is a locally compact Hausdorff space S with no non-trivial homeomorphisms but with the complex space $S_0(S)$ maximal. (12 refs.)
- Use of $SU(n)$ Lie algebra in n level quantum system. I. Some general consequences See Entry 74306
- Use of $SU(n)$ Lie algebra in n level quantum system. II. Transformations in the state space, evolution problems See Entry 74307
- q -algebras without interaction See Entry 74316
- Generalizations of gravitational theory based on group covariance See Entry 74333
- Phenomenological renormalization and scaling fields See Entry 74408
- Algebraic construction of static axially symmetric self-dual fields See Entry 74625
- Recent developments in the theory of large N gauge fields See Entry 74637
- A procedure for generating realizations of Li-admissible and other nonassociative algebras See Entry 74652
- Krull dimension of factor rings of the enveloping algebra of a semi-simple Lie algebra See Entry 74655
- Simple Lie algebras and Dynkin diagrams See Entry 74662
- Group-theory analysis of coherent effects in multilevel systems See Entry 75611

02.30 FUNCTION THEORY, ANALYSIS

- 74252 Nonlinear boundary problem of a high order homogeneous elliptical equation. Huang Si-xun. *Fudan J. (China)*, vol.21, no.4, p.379-90 (Dec. 1982). In Chinese. [received: June 1983]
- Discusses the nonlinear boundary problem (A) of a high order homogeneous elliptical equation (E_0). First of all the author expresses the regular-solution $U(x,y)$ of equation (E_0) as the form of vector and then reduces the problem (A) to nonlinear general Riemann-Hilbert Poincaré problem. Finally the author uses the expression of a high order derivative of the homomorphic function which is analogous to Bekya's (1964) and considers the nonlinear general R-H-P problem as nonlinear Fredholm integral equations. When λ is sufficiently small and the linear Fredholm equations are solvable, by the help of Schauder's Fix-point theorem, the existence of the solution of problem (A) is proved. (5 refs.)
- 74253 On some linear integral equations generating solutions of nonlinear partial differential equations. F.W.Nijhoff, G.R.W. Quispel, J.van der Linden, H.W.Capel (Inst.-Lorentz voor Theoretische Natuurkunde, Leiden, Netherlands). *Physica A (Netherlands)*, vol.119A, no.1-2, p.101-42 (April 1983).
- Two types of linear inhomogeneous integral equations, which yield solutions of a broad class of nonlinear evolution equations, are investigated. One type is characterized by a two-fold integration with an arbitrary measure and contour over a complex variable k , and their complex conjugates, whereas the other one has a two-fold integration over one and the same contour. For special elements of the matrices closed partial differential equations can be derived, such as e.g. the nonlinear Schrödinger equation and the (real and complex) modified Korteweg-de Vries and sine-Gordon equations. The relations between the matrix elements are shown to lead to Miura transformations between the various partial differential equations. (32 refs.)
- 74254 Polynomial approximation of weakly differentiable functions on Banach spaces. J.Gomez Gil (Facultad de Matematicas, Univ. Complutense, Madrid, Spain), J.G.Llavona. *Proc. R. Ir. Acad. Sect. A (Ireland)*, vol.82A, no.2, p.141-50 (Dec. 1982). [received: May 1983]
- A characterization of dense polynomial algebras is obtained for a certain class of p -continuously differentiable Fechet functions between real Banach spaces. In order to study this result a new approximation property in Banach spaces, the bounded weak approximation property, is introduced and studied. (13 refs.)
- Foundations of theoretical mechanics. II. Birkhoffian generalization of Hamiltonian mechanics See Entry 74238
- Two new solutions to the problem of motion of a heavy gyrost See Entry 74268
- The influence of fluctuations on the hydrodynamic asymptotics of Green's functions See Entry 74284
- A one-parameter Backlund transformation for the Euclidean Liouville and wave equations See Entry 74288
- Nonlocal Korteweg-de Vries and Kadomtsev-Petviashvili equations See Entry 74322
- Stochastic transport in disordered systems See Entry 74374

- Generalized method of optimal identification and optimal estimation of non-linear dynamical systems See Entry 74389
- Geometric formulation of the indirect analytic representation of dynamical systems, exterior differential calculus on Banach spaces and variational selfadjointness See Entry 74592
- Generalized field theories and solutions See Entry 74602
- Path integration at the crossroad of stochastic and differential calculus See Entry 74642
- Generalized string amplitude and wave equation for hadrons See Entry 74747
- Exact calculations of the diffraction of s-polarized electromagnetic radiation from large-amplitude dielectric gratings See Entry 75579
- Mathematical modelling of the geometrical shape of polyhedral fibre-optic elements See Entry 75816
- On one method of solving problems in the nonstationary diffraction of acoustic waves by thin unclosed shells See Entry 75844
- Green's function of an elastic ring bounded by similar epitrochoids of class-2 and clamped along each boundary See Entry 75919
- The R-function method in solving problems on small elastoplastic deformations See Entry 75931
- On the validity of certain integro-differential equations for the density-orientation profile of molecular fluid interfaces See Entry 76749
- A generalized approximation of the Fermi-Dirac integrals See Entry 76820
- Correspondence analysis for describing the morphology of powders. Application to a commercial alumina powder See Entry 77539
- A nonlinear problem arising from combustion theory: Linan's problem See Entry 77889

02.40 GEOMETRY, DIFFERENTIAL GEOMETRY, AND TOPOLOGY

(see also 04. Relativity and gravitation)

- Space-time structure of gravitational solitons See Entry 74334
- Pregrometry See Entry 74335
- 'The gauge invariant effective action for quantum gravity and its semi-quantitative approximation' See Entry 74351
- Dimensional reduction See Entry 74360
- A justification for the scaling of the Thom-system See Entry 74417
- A micro-deSitter spacetime with constant torsion: a new vacuum solution of the Poincaré gauge field theory See Entry 74624
- Massive gauge theories in three dimensions at high temperature See Entry 74626
- Renormalization and scaling of non-abelian gauge fields in curved space-time See Entry 74631
- Two-point functions and renormalized observables See Entry 74632
- The geometry of the configuration space of non abelian gauge theories See Entry 74635

02.50 PROBABILITY THEORY, STOCHASTIC PROCESSES, AND STATISTICS

(see also 05. Statistical physics)

- Parametrization of open systems with effective quadratic Hamiltonians plus stochastic force See Entry 74319
- Stochastic transport in disordered systems See Entry 74374
- Modeling and analysis of dynamical systems subject to discontinuous noise processes See Entry 74377
- Hamiltonian model for the Brownian motion of a rigid rotor See Entry 74381
- Systematic elimination of fast variables in linear systems See Entry 74382
- Asymptotic properties of the Markovian master equations for multi-stationary systems See Entry 74385
- Fokker-Planck equation for a multiplicative stochastic process with a stationary Gaussian noise See Entry 74387
- Intrinsic randomness and intrinsic irreversibility in classical dynamical systems See Entry 74423
- Mechanism by which spatially homogeneous Yang-Mills fields become stochastic See Entry 74595
- Stochastic quantization and large N reduction See Entry 74627
- Stochastic quantization and Gribov problem See Entry 74634
- Path integration at the crossroad of stochastic and differential calculus See Entry 74642
- Matter from quark and gluon bits See Entry 74703
- Variational approach to dynamics of interfaces and quantized vortex lines See Entry 76725
- Markov analysis of alpha-helical, beta-sheet and random coil regions of proteins See Entry 78137

02.60 NUMERICAL APPROXIMATION AND ANALYSIS

- Microcomputer quantum mechanics See Entry 74235
- On one-dimensional stretching functions for finite-difference calculations See Entry 74281
- Application of the multigrid method to Poisson's equation in boundary-fitted coordinates See Entry 74282
- A numerical algorithm for solving inverse problems of two-dimensional wave equations See Entry 74287
- Self adjusting grid methods for one-dimensional hyperbolic conservation laws See Entry 74421
- Nonlinear regression least-squares method for determining relaxation time spectra for processes with first-order kinetics See Entry 74446
- A numerical method for two-dimensional Fokker-Planck equation See Entry 74954
- Efficient approach to designing linear combination filters See Entry 75780

- Eigenmode calculation of optical waveguides: finite elements versus other methods See Entry 75793
- Analysis of optical and microwave waveguide by finite elements See Entry 75794
- Design for minimum stress concentration by finite elements and linear programming See Entry 75920
- Some basic problems and engineering applications of boundary integral equation-boundary element method in elasticity See Entry 75924
- Use of the finite-element method in fracture mechanics See Entry 75961
- Modern methods of numerical investigation of rarefied gas phenomena See Entry 76073
- Application of the method of streams to one problem of the dynamics of a viscous stratified fluid See Entry 76088
- Numerical solution of equations of the dynamics of a viscous incompressible fluid containing dispersed particles See Entry 76096
- Algorithms for constructing spline regression polynomial models [material science data] See Entry 77659
- F-chart method applied to large-scale solar collector systems subject to a shadow effect of adjacent collectors See Entry 78093
- Performance of n forced circulation water heating systems in series See Entry 78097

02.70 COMPUTATIONAL TECHNIQUES

(for data handling and computation, see 06.50)

- Design for minimum stress concentration by finite elements and linear programming See Entry 75920

03.00 CLASSICAL AND QUANTUM PHYSICS; MECHANICS AND FIELDS

03.20 CLASSICAL MECHANICS OF DISCRETE SYSTEMS: GENERAL MATHEMATICAL ASPECTS

(for applied classical mechanics of discrete systems, see 46.10; for celestial mechanics, see 95.10)

- 74255** Quaternion transformation and its application to the displacement analysis of spatial mechanisms. W.Qingui (Peking Aeronaut. Inst., Peking, China). *Acta Mech. Sin. (China)*, no.1, p.54-61 (1983). In Chinese.
The quaternion component matrix is introduced first; it is shown that this matrix is a indication of the quaternion in a 4×4 matrix space. It is isomorphic to quaternion and this relation has been summarized into the Isomorphic Theorem 1. Secondly, a real number quaternion transformation is used to study the general motion of a rigid body and the relative motion of several rigid bodies; the attitude equations and the displacement equations in general motion of a rigid body in the form of the real number quaternions are derived. Lastly, the application of the derived formulae to the displacement analysis of spatial mechanisms is demonstrated. (9 refs.)
- 74256** Some classes of exact solutions of problems on the motions of two connected bodies. P.V.Kharlamov, M.Yu.Lesina. *Dopov. Akad. Nauk UkrSR, Ser. A (USSR)*, no.3, p.51-3 (1983). In Ukrainian.
A pair of rigid bodies with mass distribution the same as that of Lagrange gyroscopes are coupled by an ideal spherical hinge belonging to both symmetry axes. Such a system is a model for the so-called dual-spin satellite. The system is supposed to move in space without any external forces. Two classes of exact solutions are found for this problem. (8 refs.)
- 74257** Stability of gyro with harmonic nonlinearity in spinning vehicle. S.N.Singh (Dept. of Electrical Engng., Federal Univ. of Santa Catarina, Florianopolis, Brazil). *IEEE Trans. Aerosp. & Electron. Syst. (USA)*, vol.19, no.2, p.182-9 (March 1983).
A stability analysis of a single-axis rate gyroscope mounted in a space vehicle which is spinning with uncertain angular velocity ω_s about the spin axis of the gyro is presented. The complete nonlinear equation of motion, which includes the fundamental and second harmonic nonlinear terms, arising due to ω_s , is considered. For time-varying $\omega_s(t)$ using the circle criterion, it is shown that the gimbal motion is globally asymptotically stable if the Nyquist plot of the linear transfer function of the gyro lies in the interior of a certain disk. For the case of uncertain constant ω_s , using the Lyapunov approach, conditions for global asymptotic stability (GAS) and asymptotic stability are derived. Stable regions in parameter space of the gyro and state space are obtained. Analytical relations for the selection of gyro parameters are derived. (11 refs.)
- 74258** Supercritical behavior of an ordered trajectory. L.P.Kadanoff (James Franck Inst., Univ. of Chicago, Chicago, IL, USA). *J. Stat. Phys. (USA)*, vol.31, no.1, p.1-27 (April 1983).
The behavior of a particle undergoing a discrete, stepped motion around a circle is investigated for the case in which the average number of steps per revolution is the golden mean. The new features of this study are that the map in question is not invertible and that consequently the orbit is bunched into intervals within the circle. Because of this bunching, one can calculate the motion in some detail. (8 refs.)
- 74259** A delay induced bifurcation to oscillations. K.Gopalsamy (School of Maths., Flinders Univ., Bedford Park, Australia). *J. Math. & Phys. Sci. (India)*, vol.16, no.5, p.469-88 (Oct. 1982). [received: May 1983]
Hopf-bifurcation to oscillations in a time delayed logistic equation of the form $\dot{u}(t) = u(t)[a - \beta u(t) - \gamma u^2(t - \tau)]$ is considered with the delay τ as a bifurcation parameter. The stability of supercritically bifurcating periodic solutions and the instability of subcritically bifurcating solutions are established. (12 refs.)
- 74260** Inverse Feigenbaum bifurcations in Hamiltonian systems. G.Contopoulos (Dept. of Astron., Cornell Univ., Ithaca, NY, USA). *Lett. Nuovo Cimento (Italy)*, vol.37, ser.2, no.4, p.149-55 (28 May 1983).
The author presents cases of Feigenbaum sequences of infinite bifurcations followed by inverse sequences in a Hamiltonian system representing a rotating

galaxy. It seems that the reversal of the Feigenbaum sequences is a general property of rotating dynamical systems. Then it is seen how such infinite sequences are generated. (8 refs.)

- 74261** Zones of possible motion in the Klebsh problem. The critical case. T.I.Pogossyan. *Mekh. Tverd. Tela (USSR)*, no.15, p.3-23 (1983). In Russian.
The author gives a topological and geometrical analysis of the problem of the motion of a solid body for the case of Klebsh integrability. The bifurcation of three first integrals is studied and two quadratics according to velocity are obtained. The author describes the regions swept out in the body by the directional vector of the symmetry axis of a strong field for all critical values of the constants of the given integrals. (3 refs.)
- 74262** Concerning the conditions for the existence of one class of polynomial solutions of the equation of motion of a solid body having a point of rest. G.V.Mozalevskaya. *Mekh. Tverd. Tela (USSR)*, no.15, p.24-31 (1983). In Russian.
The author considers the motion of a gyrost at having its centre of gravity on the first major axis of an ellipsoid of inertia constructed for the point of rest of the gyrost at. (7 refs.)
- 74263** One particular case of motion of a C.V. Kovalevski gyroscope. I.N.Gashchenko, V.N.Kasyanik. *Mekh. Tverd. Tela (USSR)*, no.15, p.31-4 (1983). In Russian.
The author constructs a full solution to the problem of motion of a Kovalevski gyroscope in the case of an equation of a zero-point constant 4th integral and of integrals of the moment of momentum. An algorithm due to M.P. Kharlamov (1981) is employed. The motion in this case is shown to have a common characteristic with the motion of the Steklov gyroscope. (6 refs.)
- 74264** Motion of an A.I. Dokshevich gyroscope. A.P.Kharlamov, D.N.Kravchuk. *Mekh. Tverd. Tela (USSR)*, no.15, p.35-9 (1983). In Russian.
The authors construct a full solution to the problem of the motion of an A.I. Dokshevich gyroscope (1970). An algorithm due to M.P. Kharlamov (1981) is used. The motion appears to be of a type previously associated with a D.N. Goryacheva. Angular velocity hodographs are obtained. (5 refs.)
- 74265** Concerning the motion of a gyrost at in the case of A.I. Dokshevich. E.K.Sergeev. *Mekh. Tverd. Tela (USSR)*, no.15, p.39-47 (1983). In Russian.
The author uses the method of hodographs to investigate the double-parametric series of exact solutions of the motion of a symmetrical heavy gyrost at in the case of integrability as shown by A.I. Dokshevich (1970). Various curves of motion are constructed in the plane of the parameters. A class of periodic motions is identified and for this class an M.P. Kharlamov algorithm (1981), is realised. (4 refs.)
- 74266** Concerning one particular class of gyrost at motion. M.P.Kharlamov. *Mekh. Tverd. Tela (USSR)*, no.15, p.47-56 (1983). In Russian.
The author considers the motion of a gyrost at in the case of L.N. Sretenski (1963) ($A=B=4C$, centre of mass in the equatorial plane and gyrostatic moment directed along the axis of dynamic symmetry). A double-parametric series of periodic solutions of the Euler-Poisson equation is obtained. The motion is investigated by the method of hodographs. (8 refs.)
- 74267** The motion of an E.I. Kharlamov gyroscope in the A.I. Dokshevich case. L.N.Oreshkina, A.P.Kharlamov. *Mekh. Tverd. Tela (USSR)*, no.15, p.57-61 (1983). In Russian.
The authors use the method of hodographs for the qualitative investigation of the motion of a body in the case of A.I. Dokshevich (1970) in the works of P.M. Burlak and G.V. Gorr (Mekhanika Tverdogo Tela: 1978, vol.10, p.3-10; 1974, vol.7, p.7-9). More rigorous results are obtained on the basis of the algorithm due to M.P. Kharlamov (Mekhanika Tverdogo Tela: 1981, vol.13, p.10-14) for the construction of a full solution by computer methods. (8 refs.)
- 74268** Two new solutions to the problem of motion of a heavy gyrost at. E.I.Kharlamova, G.V.Mozalevskaya. *Mekh. Tverd. Tela (USSR)*, no.15, p.61-75 (1983). In Russian.
The authors obtain two new solutions to an integro-differential equation associated with the motion of a heavy gyrost at. In the first solution the gyrostatic moment is directed along the axis passing through the centre of gravity, while in the second solution it is directed along the orthogonal axis. (4 refs.)
- 74269** Irreducible tensors and their application in problems of the motion of a solid body in strong fields. Yu.M.Urman. *Mekh. Tverd. Tela (USSR)*, no.15, p.75-87 (1983). In Russian.
The author introduces the concept of the irreducible tensor as a physical value which during the rotation of space is transformed according to an irreducible representation of the group of rotation. The algebra and characteristics of these tensors are discussed. It is shown how the mathematical apparatus of irreducible tensors can be applied to the mechanics of cosmic flight and the theory of contactless gyroscopes. (7 refs.)
- 74270** Symmetry in systems with gyroscopic forces. M.P.Kharlamov. *Mekh. Tverd. Tela (USSR)*, no.15, p.87-93 (1983). In Russian.
The author introduces the concept of the symmetry group in the mechanics of systems with gyroscopic forces. Conditions are found for the existence in these systems of a linear inhomogeneous integral analogous to the integral of moment in natural mechanical systems with symmetry. The author demonstrates a general theorem which does not assume a global Lagrangian. The motion of a solid body with a stationary point is investigated. The most general form of the potential and gyroscopic forces is examined. (4 refs.)
- 74271** Asymptotic uniform motions of a gyrost at. Yu.P.Varkhalev. *Mekh. Tverd. Tela (USSR)*, no.15, p.93-8 (1983). In Russian.
The author examines the asymptotic uniform motion of a gyrost at in a central Newtonian force field. It is shown that the equation of motion permits a solution in the form of exponential functions of time depending on two arbitrary constant and representative classes of asymptotic uniform motions tending toward unstable uniform rotation. (9 refs.)
- 74272** Towards the construction of periodic solutions of Hamiltonian systems. V.S.Elfinov. *Mekh. Tverd. Tela (USSR)*, no.15, p.98-101 (1983). In Russian.
The author examines the problem of Pункare (Nauka, 1971, vol.1, p.771) and presents an algorithm for constructing periodic solutions for Hamiltonian systems without rotation towards a variable action-angle. (4 refs.)
- Foundations of theoretical mechanics. II. Birkhoffian generalization of Hamiltonian mechanics** See Entry 74238

43.30 SPECIAL RELATIVITY

4273 Theory of physical similarity. P.S.Gulati, S.Gulati (Cuttington Univ. Coll., Monrovia, Liberia).

Indian J. Theor. Phys., vol.29, no.3, p.209-26 (Sept. 1981).

Over the years many scientists have unsuccessfully proposed alternative theories to overcome the logical inconsistencies of Einstein's theory of special relativity. The authors have created an entirely new theory—called the 'Theory of physical similarity, based upon three fundamental postulates, the 'Motion-dependent time-unit', the 'Invariant length-unit', and the 'Principle of physical similarity'. Light velocity in this theory turns out to be 'motion-dependent' and the absolute frame is identifiable as the frame in which light velocity from a stationary source attains the absolute maximum, say c_0 . Again, as the invariant Crompton wavelengths of all fundamental particles are definable in this theory, the postulated basic invariant 'length-unit', say l_0 , can be identified with the Crompton wavelength of any fundamental particle, say the electron. Then the absolute rest 'time-unit' may be taken as l_0/c_0 . Applying this theory to mechanics, electromagnetism and optics, it is established that it overcomes all the epistemological problems of Einstein's theory and circumvents the drawbacks of all other theories. (58 refs.)

4274 Tachyonium, an action-at-a-distance model. P.Stephans (Dept. of Phys., Eastern Oregon State Coll., La Grande, OR, USA).

Nuovo Cimento A (Italy), vol.75A, ser.2, no.1, p.1-16 (1 May 1983).

A model is presented for a tachyon and a bradyon bound in circular orbits. They are taken to be charged point particles interacting through action-at-a-distance retarded potentials without radiation reaction. The superluminal Lorentz transformations used conform to the relativity principle in that it retains the constancy of the speed of light, the forms of Maxwell's equations and the Lorentz force equation, and requires electric charges to retain their electric character upon transformation from superluminal to subluminal frames. Interactions between a tachyon and a bradyon are restricted to regions within two interaction cones. Backward cones are related to retarded potentials and forward cones to advanced potentials; this should be taken into account in resolving causal paradoxes. The tachyonium atom consisting of a tachyon-bradyon pair interacting through retarded potentials has discrete values of total energy and angular momentum for a given mass ratio; it is shown that this discreteness does not occur for half-retarded-half-advanced potentials. Values for conserved quantities and other properties are presented. A model that might explain many of the features of quasars is suggested. (31 refs.)

4275 Local equilibrium axion for density flows in relativistic thermodynamics. J.Gariel (Univ. de Madagascar, Antsirana, Madagascar).

Nuovo Cimento B (Italy), vol.74B, ser.2, no.2, p.167-81 (11 April 1983). In French.

The author proposes a local-equilibrium axion for density flows in phenomenological relativistic thermodynamics of irreversible processes, so as to replace covariant form of the Gibbs relation suggested by Israel and Stewart (1979) which does not seem satisfactory. This axion enables one to find again the Eckart quasi-stationary state theory and fits in with the main results of the Israel-Stewart phenomenological theory for transient effects. The theory is limited to the typical case of a simple heat-conducting fluid. (16 refs.)

4276 The standard of length in the theory of relativity and Ehrenfest paradox. W.A.Rodrigues, Jr. (Inst. de Matematica, Estatística e Ciência da Computação, IMECC-UNICAMP, São Paulo, Brazil).

Nuovo Cimento B (Italy), vol.74B, ser.2, no.2, p.199-211 (11 April 1983).

The author investigates the physical systems which can be associated with the standard clocks and standard rulers of the theory of relativity. It is shown that, once the standard clock has been identified, the standard ruler is uniquely determined as being a 'light ruler'. The author investigates under what conditions material rods can be used as standard rulers. This shows the existence of two distinct contractions in the theory that are often confused: the Einstein and the Lorentz contractions. It is argued that the Lorentz contraction is a real phenomenon which results as a consequence of the interaction of material bodies with the ground-state vacuum of the Universe. These results permit one to give a definitive answer to the question 'do metric standards contract?' and also to solve Ehrenfest's paradox (1909) in an almost trivial way. (32 refs.)

4277 The relativistic problem of two identical bodies with an attractive force of constant magnitude. N.S.Shavokhina (Joint Inst. of Nuclear Res., Dubna, USSR).

Sov. Phys.-Dokl. (USA), vol.27, no.8, p.605-6 (Aug. 1982). Translation of: *Dokl. Akad. Nauk SSSR*, vol.265, no.4-6, p.852-6 (Aug. 1982). [received: May 1983]

The relativistic problem of two bodies attracting each other with a force constant in absolute magnitude can be represented as a boundary-value problem for a three-dimensional minimal surface in a pseudo-Euclidean space. In the case of identical bodies the problem simplifies greatly. (2 refs.)

On a three-body problem in relativistic quantum mechanics See Entry 74302

Localizability and coupling constants See Entry 74310

43.40 CLASSICAL MECHANICS OF CONTINUOUS MEDIA: GENERAL MATHEMATICAL ASPECTS

4278 The theorem of conservation of non-conservative field and the conservation laws for a certain class of continuum mechanics. Jin Fusheng (Changjiang River Shipping Sci. Res. Inst., Changjiang, China).

Acta Mech. Sin. (China), no.2, p.184-9 (1983). In Chinese.

The theorem of conservation of non-conservative fields has been derived using the differential variational principle, and the conservation laws of a certain class of continuum mechanics are given. (1 ref.)

Foundations of theoretical mechanics. II. Birkhoffian generalization of Hamiltonian mechanics See Entry 74238

43.40G Fluid dynamics: general mathematical aspects

(see also 47. Fluid dynamics)

4279 Improved difference methods for steady incompressible convective diffusion equations. Ye Jingtang (Fudan Univ., Shanghai, China).

Acta Mech. Sin. (China), no.2, p.111-18 (1983). In Chinese.

A group of difference schemes with self-adjusting ability is proposed; they can be utilized to solve steady incompressible convective diffusion problems. In the regions in which the local grid Reynolds number is small, the precisions of these schemes are equivalent to that of the centre difference scheme, whereas where the local grid Reynolds number is large the schemes are equivalent to the upwind difference scheme and ensure that the convergent solution can be

obtained. Therefore, when the centre difference scheme ceases to be effective, the schemes are still effective and their precisions are better than that of upwind scheme solution. The operation counts of these schemes are equivalent to that of centre difference scheme and upwind scheme, so these schemes are efficient and have wider applicability. (5 refs.)

4280 Mathematical model of population evolution in flowing liquid.

O.Ya.Olinik, V.S.Tkalich.

Dopov. Akad. Nauk UkrSR. Ser. A (USSR), no.3, p.47-51 (1983). In Ukrainian.

An extremal model is constructed which describes evolution of a set of populations in the given flow. A system of quasi-canonical equations is obtained which is reduced to a canonical system for an immovable fluid. An extremal model of sensitivity is constructed. The diffusion of populations and limiting components of the substrate are taken into account. (7 refs.)

4281 On one-dimensional stretching functions for finite-difference calculations. M.Vinokur (Mech. Engng. Res., Univ. of Santa Clara, Santa Clara, CA, USA).

J. Comput. Phys. (USA), vol.50, no.2, p.215-234 (May 1983).

The class of one-dimensional stretching functions used in finite-difference calculations is studied. For solutions containing a highly localized region of rapid variation, simple criteria for a stretching function are derived using a truncation error analysis. These criteria are used to investigate two types of stretching functions. One is an interior stretching function, for which the location and slope of an interior clustering region are specified. The simplest such function satisfying the criteria is found to be one based on the inverse hyperbolic sine, first employed by Thomas et al. (1972). The other type of function is a two-sided stretching function, for which the arbitrary slopes at the two ends of the one-dimensional interval are specified. The simplest such general function is found to be one based on the inverse tangent. The special case where the slopes were both equal and greater than one was first employed by Roberts (1971). The general two-sided function has many applications in the construction of finite-difference grids. (18 refs.)

4282 Application of the multigrid method to Poisson's equation in boundary-fitted coordinates. S.Ohring (David W. Taylor Naval Ship Res. & Dev. Centre, Bethesda, MD, USA).

J. Comput. Phys. (USA), vol.50, no.2, p.307-15 (May 1983).

The multigrid technique is a general strategy for solving partial differential equations, based on the elimination of error components. The author applies it to the solution of the Poisson equation in boundary-fitted coordinates; this gives an order of magnitude reduction in computer time. (11 refs.)

4283 Generation of boundary-fitted curvilinear coordinate systems for a two-dimensional axisymmetric flow problem. S.Uchikawa (Energy Res. Lab., Hitachi Ltd., Ibaraki, Japan).

J. Comput. Phys. (USA), vol.50, no.2, p.316-21 (May 1983).

The author considers two-dimensional axisymmetric flow; three different coordinate transformations are applied to the solution and compared for suitability. (4 refs.)

4284 The influence of fluctuations on the hydrodynamic asymptotics of Green's functions. Yu.V.Slyusarenko.

Ukr. Fiz. Zh. (USSR), vol.28, no.5, p.774-80 (May 1983). In Russian.

Hydrodynamic fluctuations are studied for their influence on the time asymptotics of Green's functions and correlation functions in a spatially inhomogeneous case. The behaviour of time asymptotics in the region of large and small wave vectors is also studied. (5 refs.)

Contributions of Ernst Mach to fluid mechanics See Entry 74247

On Brownian motion in fluids with spin See Entry 74383

Application of Pade approximation to turbulence problem See Entry 75987

03.40K Waves and wave propagation: general mathematical aspects

(see also 46.30M Mechanical and elastic waves, 43.20 General linear acoustics)

74285 Green's function method for periodic traveling wave solutions of the KdV equation. Liu Bao-Ping (Dept. of Math., Sichuan Univ., Chengdu, China), C.V.Pao.

Appl. Anal. (GB), vol.14, no.4, p.293-301 (1983).

The Green's function method is used for studying periodic traveling wave solutions of a generalized KdV equation. It is shown through the construction of an explicit Green's function that the periodic boundary-value problem for the traveling wave solution of the KdV equation is equivalent to an integral equation with a symmetrical kernel which generates a compact operator in the space of periodic functions. This integral representation also leads to the existence of a periodic traveling wave solution for an associated inhomogeneous KdV equation. (7 refs.)

74286 A new evaluation of the Goos-Hanchen shift and associated time delay. K.Yasumoto, Y.Oishi (Dept. of Computer Sci. & Communication Engng., Kyushu Univ., Fukuoka, Japan).

J. Appl. Phys. (USA), vol.54, no.5, p.2170-6 (May 1983).

A wave packet reflected totally at an interface between two media may undergo the Goos-Hanchen shift and associated time delay. Two different theoretical approaches have been presented so far to evaluate this phenomenon. One is the stationary-phase method and the other is the conventional energy-flux method. In this paper, a certain deficiency existing in the conventional energy-flux method is pointed out and a new energy-flux method is derived based on an accurate argument of the conservation of energy flux. The new energy-flux method confirms the consistency of the predictions by the stationary-phase method from the point of view of the conservation of energy. (14 refs.)

74287 A numerical algorithm for solving inverse problems of two-dimensional wave equations. Y.M.Chen (Dept. of Appl. Math. & Statistics, State Univ. of New York, Stony Brook, NY, USA), J.Q.Liu.

J. Comput. Phys. (USA), vol.50, no.2, p.193-208 (May 1983).

The new iterative numerical algorithm of the pulse-spectrum technique (PST) is extended and developed to solve inverse problems of two-dimensional linear wave equations. It has the practical advantages of having the necessary data measured on a portion of the boundary only and no geometric limitation on the testing objects. Numerical simulations on several simple examples are carried out to test the feasibility and to study the general characteristics of this technique without the real measurement data. It is found that PST does give excellent results even with a very coarse computational grid and it is as robust as in the one-dimensional case. (9 refs.)

74288 A one-parameter Backlund transformation for the Euclidean Liouville and wave equations. Huang Xun-Cheng (Shanghai Inst. of Computing Tech., Shanghai, China).

Phys. Scr. (Sweden), vol.27, no.5, p.321-2 (May 1983).

A Backlund transformation with an arbitrary parameter for the Euclidean Liouville equation and wave equation was obtained from the one without parameter. (5 refs.)

74289 Intensification of backscattering of waves by a body located near the irregular boundary of two media. V.U.Zavorotnyi, V.I.Tatarskii (Inst. of Atmospheric Phys., Acad. of Sci., Moscow, USSR).

Sov. Phys.-Dokl. (USA), vol.27, no.7, p.566-7 (July 1982). Translation of: *Dokl. Akad. Nauk SSSR*, vol.265, no.1-3, p.608-11 (July 1982). [received: April 1983]

The phenomenon of intensification of backscattering in media with large-scale spatial inhomogeneities has been described and experimentally observed. An analogous effect, but expressed to a much greater degree, can be observed in the scattering of waves by a body located near the irregular boundary of two media if the local coefficient of reflection of a wave from this boundary is close to unity. The theory describing the phenomenon of intensification of backscattering is the same in both cases and is very simple. The authors consider it with scalar waves as an example. The generalization to other cases is carried out in an obvious manner. (4 refs.)

74290 New results on the vibrating string with a continuous obstacle.

A.Bamberger, M.Schatzman (Centre de Maths. Appl., Ecole Polytech., Palaiseau, France).

SIAM J. Math. Anal. (USA), vol.14, no.3, p.560-95 (May 1983).

The authors give an explicit formula which describes the solution of the problem of the linear elastic string vibrating against a plane obstacle without loss of energy. This formula allows one to prove continuous dependence on the initial data; a regularity result in some bounded variation spaces is given. A numerical scheme is deduced from the explicit formula. Finally they prove the weak convergence of a subsequence of solutions of the penalized problem to a 'weak' solution (i.e. one which does not necessarily conserve energy) of the problem with an obstacle when the obstacle is arbitrary; when the obstacle is plane, all the sequence strongly converges to the solution of the obstacle problem which conserves the energy. (7 refs.)

74291 A new procedure for deriving shortened equations for parametrically interacting waves. N.P.Ivonchik, A.M.Fedorchenko.

Ukr. Fiz. Zh. (USSR), vol.28, no.4, p.620-2 (April 1983). In Russian.

Proposes a method of deriving shortened equations which ignores second amplitude derivatives. This method makes it possible to obtain more accurate approximations for parametric nonlinearity. (3 refs.) *V.G.P.*

Nonlocal Korteweg-de Vries and Kadomtsev-Petviashvili equations

See Entry 74322

Effects of topological solitons on autocorrelation functions for chains of coupled torsional oscillators

See Entry 74395

Vibrations of Mindlin's circular plates with variable thickness

See Entry 75949

03.50 CLASSICAL FIELD THEORY

74292 The fundamental bordered matrix of linear estimation and the Duffin-Morley general linear electromechanical systems. S.K.Mitra, M.L.Puri (Indian Statistical Inst., New Delhi, India).

Appl. Anal. (GB), vol.14, no.4, p.241-58 (1983). (16 refs.)

74293 Theoretical calculation of the anomalous Cerenkov radiation produced in the air. Zhang Ziping, Yang Bingxin, Xi Fuyun, Xu Kezun (Dept. of Modern Phys., Univ. of Sci. & Technol. of China, Hefei, China).

Kexue Tongbao (Foreign Lang. Ed.) (China), vol.28, no.2, p.184-9 (Feb. 1983).

Cerenkov radiation is produced when the velocity of charged particles passing through a medium is faster than the phase velocity of light in the same medium. You Junhan and Cheng Fuhua (1980) pointed out that the relativistic electrons moving through a considerable dense hydrogen gas will produce asymmetric line-emission-spectra corresponding to L_{α} and L_{β} lines. Using this phenomenon, the authors used a ^{90}Sr β radiative source with maximum energy of 2.2 MeV and activity of 22 mCi to measure the asymmetries of the angular distribution of the anomalous Cerenkov radiation produced by electrons when passing through the air. The resulting asymmetries at 21° , 30° and 40° are 1.069 ± 0.016 , 1.119 ± 0.016 and 1.048 ± 0.016 respectively, and the wavelengths of photons are near 2000 \AA . The aim of this paper is to give a theoretical calculation of the angular distribution of the anomalous Cerenkov radiation produced in the air through which the electrons pass and to make a comparison of the results with those from experiment. (5 refs.)

74294 Phase manifold geometry of Burgers hierarchy. S.De Filippo, M.Salerno, G.Vilasi (Istituto di Fisica, Univ. di Salerno, Salerno, Italy), G.Marmo.

Lett. Nuovo Cimento (Italy), vol.37, ser.2, no.3, p.105-10 (21 May 1983). (12 refs.)

Energy loss by slow magnetic monopoles

See Entry 74827

Transverse transport processes of charged particle systems in a strong magnetic field. II. Some discussions about the Boltzmann equation

See Entry 75572

03.65 QUANTUM THEORY; QUANTUM MECHANICS

(see also 05.30 Quantum statistical mechanics; for relativistic wave equations, see 11.10)

74295 Deformations of the algebra of functions on hermitian symmetric spaces resulting from quantization. C.Moreno (Chaire de Phys. Math., Coll. de France, Paris, France), P.Ortega-Navarro.

Ann. Inst. Henri Poincaré Sect. A (France), vol.38, no.3, p.215-41 (1983).

A*-product on a symplectic manifold, in the sense of A. Lichnerowicz (1977, 1980, 1981), is the first element in what should be called Weyl's quantization on the manifold. The covariant symbol $A \star B$ of the operator $A \cdot B$ is an exponential integral with positive phase and \hbar^{-1} as real parameter. The authors give an expression to find each term of the asymptotic development, as powers of \hbar , of this symbol. In this way they obtain a nontrivial formal deformation of the associative algebra $C^\infty(M)$. This deformation is not a Vey deformation at any order, just as in the Wick quantization on C^∞ . Each 2-cochain of the deformation is invariant by the group $\text{I}_0(M)$. Similarly they consider the contravariant Weyl's symbol $A^{\#} \cdot B$ of the operator $A \cdot B$. (In the Weyl's quantization on C^∞ this symbol is just the Moyal product of A and B .)

In this case the deformation obtained is a Vey deformation at the first order. It is no longer a Vey deformation at the second order. (31 refs.)

74296 Charged particles with short range interactions. S.Albeverio (Math. Inst., Ruhr-Univ. Bochum, Bochum, Germany), F.Gesztesy, R.Hoegh-Krohn, L.Streit.

Ann. Inst. Henri Poincaré Sect. A (France), vol.38, no.3, p.263-93 (1983).

Schrodinger Hamiltonians for charged particles with an additional force of very short range studied by scaling techniques and with a view towards low energy parameters. The authors present results for the zero range limit. In particular they give the leading terms for the S-matrix as the range parameter becomes small. As applications they compare the scattering lengths of charged particles and of their neutral counterparts and discuss the level shifts of mesic atoms. (47 refs.)

74297 Semiclassical analysis of low lying eigenvalues. I. Non-degenerate minima: asymptotic expansions. B.Simon (Dept. of Maths. & Phys., California Inst. of Technol., Pasadena, CA, USA).

Ann. Inst. Henri Poincaré Sect. A (France), vol.38, no.3, p.295-307 (1983).

Considers eigenvalues of Schrodinger operators of the form $-\Delta + \lambda^2 \hbar + \lambda g$ where $\hbar \geq 0$ has finitely many minima, each of which is non-degenerate. The author proves a folk theorem about the asymptotic behavior of the n th eigenvalue in the $\lambda \rightarrow \infty$ limit. The author concludes with a few remarks about the extension to Riemannian manifolds because of the significance to Witten's proof of the Morse inequalities. (22 refs.)

74298 Effect of intrinsic degrees of freedom on the quantum tunneling of a collective variable. D.M.Brink, M.C.Nemes, D.Vautherin (Div. de Phys. Theorique, Inst. de Phys. Nucleaire, Orsay, France).

Ann. Phys. (USA), vol.147, no.1, p.171-97 (15 April 1983).

The effect of intrinsic degrees of freedom on tunneling through a potential barrier is discussed using a BKW-like approximation. Intrinsic degrees of freedom are represented by a single harmonic oscillator. The theory leads to a formula for the effect of the coupling on the decay width Γ of a metastable state. When the frequency ω of the intrinsic degree of freedom is large, then $\Gamma \rightarrow \Gamma_{\text{ad}}$ where Γ_{ad} is the decay width calculated with the adiabatic barrier. An inequality $\Gamma \leq \Gamma_{\text{ad}}$ is proved for any form of the coupling Hamiltonian. Corrections are discussed and are shown to be of order $1/M$ where M is the mass of the tunneling coordinate. An application to fission is considered. The generalization of the formula for Γ for the case of many intrinsic degrees of freedom is given explicitly. (11 refs.)

74299 Finite difference method for initial-boundary problem on a class of nonlinear Schrodinger equations. Wu Xianghui.

Acta Sci. Nat. Univ. Sunyatseni (Zhongshandaxue Xuebao) (China), no.4, p.41-6 (1982). In Chinese.

The initial-boundary problem of a class nonlinear Schrodinger equation system is considered by using a finite difference method. It is proved that the four point implicit scheme and the six point implicit scheme for problem are convergent and stable. Finally, a numerical example is given. (2 refs.)

74300 Multi-instanton contributions in quantum mechanics. II. J.Zinn-Justin (CENS, Gif-sur-Yvette, France).

Nucl. Phys. B, Part. Phys. (Netherlands), vol.B218, no.2, p.333-48 (6 June 1983).

For pt.I see ibid., vol.192, p.125 (1981). The author presents a simplified derivation for the expression of the contribution of multi-instanton configurations in quantum mechanics in the semiclassical limit. The author shows that the expression one obtains is valid not only for the ground state energy but also for all excited states. The author illustrates the method on a few new examples. A relation between the various perturbative expansions of these multi-instanton contributions is conjectured. (7 refs.)

74301 Transverse transport processes of charged particle systems in a strong magnetic field. I. Quantum theory. Ho Yu-ping, Hu xi-wei, Chen Zheng-xiong (Inst. of Plasma Phys., Acad. Sinica, Hefei, China).

Commun. Theor. Phys. (China), vol.1, no.4, p.427-40 (1982).

The quantum theory of the transverse transport of charged particle systems in a strong, uniform magnetic field is reinvestigated. All such previous theories, based on the Kubo formula in the Landau representation, considered only the second-order term of the collisional expansion series. In the authors' theory, they still use the local representation. However, the macroscopic current operator corresponding to real measurements is used in the Kubo formula instead of the microscopically defined current operator. By applying the method of projection operators, they obtain formal expressions for the macroscopic current and then for various transport coefficients. (12 refs.)

74302 On a three-body problem in relativistic quantum mechanics. F.M.Lev (Inst. of Complex Sci. Res., Khabarovsk, USSR).

Fortschr. Phys. (Germany), vol.31, no.2, p.75-130 (1983).

Proceeding from the method of packing operators developed by Sokolov (1978) and from the 'light front variables' technique, the explicit formulae for packing operators and auxiliary mass operators for a system of three particles with arbitrary spins are derived. It is shown that for the packing operators there exists an infinite number of solutions yielding different physical consequences. The problem of the theory substantiation is discussed; the arguments in favour of a certain choice of packing operators are produced. (41 refs.)

74303 A review of recent developments in the theory and applications of geometric quantisation. P.Campbell (Dept. of Math., Univ. of Lancaster, Lancaster, England).

Hadronic J. (USA), vol.6, no.2, p.212-50 (March 1983).

Presents a review of the main elements of the standard Kostant-Souriau (KS)-theory. This takes as its starting point a discussion of the modern formulation of classical mechanical systems via symplectic geometry. The quantisation problem is then stated and the need for a global quantisation scheme is motivated. The (KS)-theory then proceeds through the conceptual levels of prequantisation, polarisation (real), and metaplectic frame bundle to give the construction of the representation space and the form of self-adjoint operators on it. The author deals with the modifications and enlargements of the standard (KS)-theory necessitated in certain cases. The main enlargement concerns the problem of dependence of the quantisation upon polarisation choice; the solution to this problem in terms of the so-called BKS-transformation is described for real and transverse polarisations. A related difficulty concerns the quantisation of a larger class of observables than can be dealt with via the standard (KS)-theory. The author outlines the main ideas behind this and the attempts at its solution. Other modifications deal with the possibility of trivial representation spaces and non-existence of components of the quantisation bundle. The review is concluded with some comments on recent applications of the (KS)-theory. (59 refs.)

74304 Classical and quantum mechanical Hamiltonians for velocity-dependent forces. M.Razavy (Theoretical Phys. Inst., Univ. of Alberta, Edmonton, Alberta, Canada).

Hadronic J. (USA), vol.6, no.2, p.406-39 (March 1983).

For velocity-dependent frictional or relativistic forces which do not depend explicitly on time, a direct non-Lagrangian method of constructing classical

Hamiltonians are given. These Hamiltonians are generally implicit functions of x and p , and only in certain cases can be given explicitly. They are all generators of motion in the coordinate space, and when this is their only required property, their number is infinite. In this method of construction, a generalization of the potential concept is obtained for velocity-dependent potentials, but this generalized potential function depends on the Hamiltonian itself. The problem of quantization is studied in detail for different types of Hamiltonians. It is argued that, while the Dirac rule of correspondence may lead to Heisenberg's equations of motion which are consistent with the canonical commutation relation, this consistency should not be viewed as the sole criterion for a satisfactory formulation of the problem since the results in most cases are unphysical, and the position-velocity uncertainty relation is violated. While an exact method of quantizing an implicit Hamiltonian is not known, for the cases where the momentum is an explicit function of the Hamiltonian and the coordinate, the classical-limit quantization may be used to find approximate wave functions and eigenvalues. (42 refs.)

74305 Bound s-state energies for superposed screened Coulomb potential in Eckert-Weizel approximation. A.P.Kajwadkar, L.K.Sharma (Dept. of Appl. Phys., Government Engng. Coll., Jabalpur, India).

Indian J. Pure & Appl. Phys., vol.21, no.2, p.103-6 (Feb. 1983).

Quantum defect, quantum number shift and bound s-state eigen energies for s states of a superposed screened Coulomb potential have been obtained. It is also observed that this potential possesses features similar to alkali atoms and alkali-like ions. (14 refs.)

74306 Use of $SU(n)$ Lie algebra in n level quantum system. I. Some general consequences. J.Tillieu, A.van Groenendaal (Lab. de Phys. Theorique, Univ. de Lille I, Villeneuve d'Ascq, France).

Int. J. Quantum Chem. (USA), vol.23, no.5, p.1807-16 (May 1983). In French.

In an n level quantum system there is a relation between each density operator and an element of $SU(n)$ Lie algebra. This relation is also established between Cartan's subalgebras and the complete sets of compatible observables. A scalar product is then defined in this algebra in order to introduce orthonormal bases and to simplify many calculations about expectation values of observables. Therefore simple general rules were established which show how to determine (completely or partly), from linearly independent observables, the density operator of the system. (13 refs.)

74307 Use of $SU(n)$ Lie algebra in n level quantum system. II. Transformations in the state space, evolution problems. J.Tillieu, A.van Groenendaal (Lab. de Phys. Theorique, Univ. de Lille I, Villeneuve d'Ascq, France).

Int. J. Quantum Chem. (USA), vol.23, no.5, p.1817-27 (May 1983).

For PT_1 , see *ibid.*, vol.23, p.1807 (1983). In the previous paper the authors examined, for a quantum system, the relation between its n -dimensional state space and the $SU(n)$ Lie algebra. The present paper is devoted to relations between unitary transformations in the state space and orthogonal transformations in Lie's algebra. Two cases can happen. First, the transformations are independently chosen in the two spaces; this amounts to changing the former relation. On the other hand, the relation is maintained and the unitary operators are then related to some of the orthogonal operators. This second case is used to study the evolution operators. (8 refs.)

74308 Relativistic quantum logic. P.Mittelstaedt (Inst. für Theoretische Phys., Univ. zu Köln, Köln, Germany).

Int. J. Theor. Phys. (USA), vol.22, no.4, p.293-314 (April 1983).

On the basis of the well-known quantum logic and quantum probability a formal language of relativistic quantum physics is developed. This language incorporates quantum logic as well as relativistic restrictions. It is shown that relativity imposes serious restrictions on the validity regions of propositions in space-time. By an additional postulate this relativistic quantum logic can be made consistent. The results are derived exclusively within the formal quantum language; they are, however, in accordance with well-known facts of relativistic quantum physics in Hilbert space. (29 refs.)

74309 Reflections on quantum logic. B.Z.Moroz (Dept. of Math., Hebrew Univ., Jerusalem, Israel).

Int. J. Theor. Phys. (USA), vol.22, no.4, p.329-40 (April 1983).

This is a short, self-contained summary of problems connected with the interpretation of state vectors in quantum mechanics. The author discusses the reconstruction of the ψ function from statistical data, some related mathematical questions, the classical 'paradoxes', the probability interpretation of the state vectors, and, finally, quantum logic in relation to hidden variable theories and Hilbert space formalism to build up a consistent framework for the indeterministic quantum picture of nature. (23 refs.)

74310 Localizability and coupling constants. A.J.Kalnay (Centro de Fisica, IVIC, Caracas, Venezuela).

Int. J. Theor. Phys. (USA), vol.22, no.4, p.359-61 (April 1983).

Considers for free elementary systems the postulates: (i) localizability of systems would not favor in a physical sense some inertial frames and (ii) standard quantum mechanics (or, at least, a skeleton of it) applies for localizability. It is known that, at least for the lower values of spin, (i) and (ii) imply a unique solution of the localization problem for the no-interaction case. Extrapolating the analysis to the case when interactions are present, the author offers arguments in favor of the conjecture that if elementary systems under interaction are localizable, then (i) and (ii) imply restrictions on the coupling constants, and probably their single-valuedness. (7 refs.)

74311 Minimal number of operators for observability of N -level quantum systems. A.Jamiołkowski (Inst. of Phys., Nicholas Copernicus Univ., Torun, Poland).

Int. J. Theor. Phys. (USA), vol.22, no.4, p.369-76 (April 1983).

Discusses the minimal number n_{\min} of operators A_1, \dots, A_n , whose expectation values at some instants determine the statistical state of an N -level quantum system. The author assumes that the macroscopic information about the system in question is given by the mean values $\text{Tr}[\rho(t_i)A_i] = m_i(t_i)$ of n self-adjoint operators A_1, \dots, A_n at some instants $t_1 < t_2 < \dots < t_n$, where $s < N^2 - 1$. (9 refs.)

74312 Bell's theorem and backwards-in-time causality. R.I.Sutherland (Dept. of Theoretical Phys., Univ. of New South Wales, Sydney, NSW, Australia).

Int. J. Theor. Phys. (USA), vol.22, no.4, p.377-84 (April 1983).

Bell (1964) has shown that quantum mechanics is incompatible with the notion of locality. The present author begins by considering the possibility of invoking backwards-in-time causality to explain this violation of locality. This then leads to an examination of the possible relevance of backwards-in-time causality to measurement outcomes in general. It is found that the situations in which it could be involved are limited owing to causality paradoxes. (8 refs.)

74313 Geometric dequantization and the correspondence problem. G.G.Emch (Dept. of Math. & Phys., Univ. of Rochester, Rochester, NY, USA).

Int. J. Theor. Phys. (USA), vol.22, no.5, p.397-420 (May 1983).

On the way to settle a conjecture proposed by Mackey. The author first presents in detail a complete solution to the correspondence problem for systems whose configuration space is \mathbb{R}^n . The author then indicates how this can be considered as a first step in the elaboration of a geometric dequantization program which would extend the results to more general manifold. (32 refs.)

74314 Critical dynamics and fluctuations for a mean-field model of cooperative behavior. D.A.Dawson (Dept. of Math. & Statistics, Carleton Univ., Ottawa, Canada).

J. Stat. Phys. (USA), vol.31, no.1, p.29-85 (April 1983).

The author examines in some detail the dynamics and fluctuations in the critical situation for a simple model exhibiting bistable macroscopic behavior. The model under consideration is a dynamic model of a collection of anharmonic oscillators in a two-well potential together with an attractive mean-field interaction. The system is studied in the limit as the number of oscillators goes to infinity. The limit is described by a nonlinear partial differential equation and the existence of a phase transition for this limiting system is established. The main result deals with the fluctuations at the critical point in the limit as the number of oscillators goes to infinity. It is established that these fluctuations are non-Gaussian and occur at a time scale slower than the noncritical fluctuations. The method used is based on the perturbation theory for Markov processes developed by Papanicolaou, Stroock, and Varadhan (1977) adapted to the context of probability-measure-valued processes. (58 refs.)

74315 The hydrogen atom as prototype of the large- N expansion. P.Du, P.duT.van der Merwe (Dept. of Phys., Brown Univ., Providence, RI, USA).

Lett. Nuovo Cimento (Italy), vol.37, ser.2, no.3, p.86-8 (21 May 1983).

The spectrum of the hydrogen atom in N -dimensions is considered as prototype of the semi-classical method and is shown to yield a closed-form expression for the excitation spectrum, which includes leading large- N quantum fluctuations. (7 refs.)

74316 q -algebras without interaction. P.Siafarikas (Dept. of Maths., Univ. of Patras, Patras, Greece), A.Jannussis, G.Brodimas, L.Papaloucas.

Lett. Nuovo Cimento (Italy), vol.37, ser.2, no.3, p.119-23 (21 May 1983).

(12 refs.)

74317 A connection between Borel and Pade summation techniques. M.F.Marziani (Istituto di Fisica, Univ. di Ferrara, Ferrara, Italy).

Lett. Nuovo Cimento (Italy), vol.37, ser.2, no.3, p.124-8 (21 May 1983).

The recently proposed combination of the Borel summability method with the first confluent form of the ϵ -algorithm of Wynn (1960) for summing the Born series of scattering integral equations, is shown to be equivalent, in a limiting case, to the construction of the sequence of $[n, n-1]$ Pade approximants to the same series. (8 refs.)

74318 Continual measurements for quantum open systems. A.Barchielli (Dipartimento di Fisica, Univ. di Milano, Milano, Italy).

Nuovo Cimento B (Italy), vol.74B, ser.2, no.2, p.113-38 (11 April 1983).

Starting from the recently introduced formalism of continual measurements in quantum mechanics, it is shown that, for the quantum open systems, it is possible to construct probability distributions for the values at all times of certain observables, without the continual measurement of such observables perturbing the dynamics of the system. More precisely, starting from the quantum description of an open system, a generalized stochastic process for certain observables is constructed, which is independent of the fact that these observables are actually measured or not. The example of the quantum Brownian motion is developed in detail. In such an example it is shown how the a priori arbitrary elements of the formalism are in reality determined by the dynamics of the system. (14 refs.)

74319 Parametrization of open systems with effective quadratic Hamiltonians plus stochastic force. E.S.Hernandez (Dept. de Fisica, Univ. de Buenos Aires, Buenos Aires, Argentina), S.S.Mizrahi.

Physica A (Netherlands), vol.119A, no.1-2, p.159-76 (April 1983).

The evolution generated by general dissipative Hamiltonians is analyzed when a stochastic force is included. Using a mapping technique, the equations of motion for the observables of interest can be given easily. A general dissipativity condition is extracted, whose fulfillment guarantees that thermal equilibrium is reached as the final stage of the evolution. Several existing frictional Hamiltonians are examined and it is seen that the correlation of the fluctuating force is essential to the destruction of a constant of motion inherent to pure quantal behaviour. (23 refs.)

74320 Quantization of the damped harmonic oscillator. H.Gzyl (Escuela de Fisica y Matematicas, Facultad de Ciencias, Univ. Central de Venezuela, Caracas, Venezuela).

Phys. Rev. A (USA), vol.27, no.5, p.2297-9 (May 1983).

By means of a canonical transformation that can be implemented as a unitary change of representation, the authors show how to quantize the damped harmonic oscillator. (5 refs.)

74321 Higher orders of perturbation theory for the screened Coulomb potential. S.P.Alliluev, V.M.Vainberg, V.S.Popov.

Sov. Phys.-Dokl. (USA), vol.27, no.7, p.560-2 (July 1982). Translation of: *Dokl. Akad. Nauk SSSR*, vol.265, no.1-3, p.597-601 (July 1982). [received: April 1983]

The calculation of the higher orders of perturbation theory in quantum mechanics has been significantly advanced recently by the development of logarithmic perturbation theory. The authors consider its application to the screen Coulomb potential. (9 refs.)

74322 Nonlocal Korteweg-de Vries and Kadomtsev-Petviashvili equations. A.I.Bobenko, V.B.Matveev, M.A.Sall' (A.A. Zhdanov State Univ., Leningrad, USSR).

Sov. Phys.-Dokl. (USA), vol.27, no.8, p.610-11 (Aug. 1982). Translation of: *Dokl. Akad. Nauk SSSR*, vol.265, no.4, p.1357-60 (Aug. 1982). [received: May 1983]

The authors fix a compact Riemann surface Γ of genus g with cut $[Q_1, Q_2]$, a basis of cycles $A_k, B_k, k=1, 2, \dots, g$, a nonspecial divisor $D=\sum_{i=1}^n p_i$, and a complex parameter α . They describe a consistent solution (the Baker-Akhiezer function) of a system of linear equations. The solution is real if $e=-i\theta/2-x_0$, x_0 is real, and the lattice of periods is self-adjoint. Then $\{\tilde{z}\}=\{\tilde{z}\}$. If it is assumed that ω_1 is real and ω_2 is purely imaginary with $\tilde{z}_2 \neq i\tilde{z}_1/2$, where n is an integer, one obtains a solution without singularities—the simple wave of the KdV equation. Degeneration of the solution (with $\omega_1 \rightarrow \infty, \omega_2 = i\pi$ fixed) gives solitons of the nonlocal KdV equation. The degeneration $\omega_2 \rightarrow \infty$, with ω_1 fixed gives the simplest periodic solution without singularities that is expressible in terms of the elementary functions. The double degeneration $\omega_1 \rightarrow \infty, \omega_2 \rightarrow \infty$ gives the simplest rational solutions. (6 refs.)

74323 Analysis of a bilinear relation for the six-vertex model. V.E.Korepin (V.A. Steklov Math. Inst., Acad. of Sci., USSR).

Sov. Phys.-Dokl. (USA), vol.27, no.8, p.612-13 (Aug. 1982). Translation of: *Dokl. Akad. Nauk SSSR*, vol.265, no.4-6, p.1361-4 (Aug. 1982). [received: May 1983]

The quantum method of the inverse scattering problem enables one to solve a wide class of two-dimensional models in statistical physics and quantum field theory. The most important quantity in this method is the monodromy matrix $T(\mu)$. The author considers the case when the dimensionality of this matrix is two. The matrix elements of $T(\mu)$ are quantum operators which depend on the spectral parameter μ . The authors construct a $T(\mu)$ which satisfies $R(\lambda, \mu)T(\lambda) \otimes T(\mu) = T(\mu) \otimes T(\lambda)R(\lambda, \mu)$, and $A(\mu)|0\rangle = a(\mu)|0\rangle$, $D(\mu)|0\rangle = d(\mu)|0\rangle$, $C(\mu)|0\rangle = 0$, $B(\mu)|0\rangle \neq 0$. A, B, C and D are the matrix elements of $T(\mu)$. (8 refs.)

74324 Differential rings used in Shirokov algebras. G.K.Tolokonnikov (V.A. Steklov Math. Inst., Acad. of Sci., USSR).

Theor. & Math. Phys. (USA), vol.53, no.1, p.952-4 (Oct. 1982). Translation of: *Theor. & Math. Fiz. (USSR)*, vol.53, no.1, p.16-19 (Oct. 1982).

A classification is given of differential algebras that include r^2 , $\delta(x)$, $x \in \mathbb{R}^n$, $\alpha=0$, ± 1 , $\pm 2, \dots$, and satisfy the condition $\phi\psi=0$ for elements ϕ, ψ : $\text{supp } \phi \subseteq \{0\}$, $\text{supp } \psi \subseteq \{0\}$. (10 refs.)

74325 Nonlinear Schrödinger equation with noncompact isogroup. V.G.Makhan'kov, O.K.Pashaev (Joint Inst. for Nuclear Res., Dubna, USSR). *Theor. & Math. Phys. (USA)*, vol.53, no.1, p.979-87 (Oct. 1982). Translation of: *Theor. & Math. Fiz. (USSR)*, vol.53, no.1, p.55-67 (Oct. 1982).

The properties of the nonlinear Schrödinger equation with noncompact isogroup are investigated. The example of the $U(1,1)$ nonlinear Schrödinger equation reveals the significant differences between this system and the previously considered vector nonlinear Schrödinger equation. The main feature—the large set of admissible boundary conditions on the field functions—leads to a rich spectrum of solutions of the system. Four types of boundary conditions and the corresponding soliton solutions are considered for the $U(1,1)$ model. Quasiclassical quantization of the solitons admits an interpretation in the language of 'drops' and 'bubbles' as bound states of a large number of bosons of the basic fields subject to the thermodynamic relations for a mixture of gases. The system is a continuous 'analog' of the Hubbard model for zero-value boundary conditions, and therefore the authors end with a discussion of this case. (16 refs.)

74326 WKB integrals for some central potentials and analytic expressions for energy eigenvalues. M.Seetharaman (Dept. of Theoretical Phys., Univ. of Madras, Madras, India).

Proceedings of the VI High Energy Physics Symposium (papers in summary form only received), Mysore, India, 6-11 Dec. 1982. (Bombay, India: Dept. Atomic Energy 1982), p.74

Summary form only given, as follows. The author carries out a direct evaluation of the integrals arising in the lowest order WKB quantization of the potentials: (i) $V(r) = 1/2\omega^2 r^2 + \lambda r^4$ (anharmonic oscillator), (ii) $V(r) = \mu r - \beta/r$ (charmonium potential). The implicit relation for the bound state energies is found to be expressible in terms of complete elliptic integrals. The author demonstrates how to carry out an approximate non-perturbative inversion of this implicit relation and arrives at explicit analytic expressions for E. These are in good agreement with known numerical results for these potentials.

Microcomputer quantum mechanics See Entry 74235

Confining potentials and analyticity of energy levels in angular momentum plane See Entry 74736

Nonlocal potentials and their exact and approximate local and velocity-dependent equivalents See Entry 74927

03.70 THEORY OF QUANTIZED FIELDS

(see also 11.10 Field theory)

74327 On the vanishing of correlation-connected diagrams in Hall's diagram technique. S.G.Tikhodeev (P.N. Lebedev Phys. Inst., Acad. of Sci., Moscow, USSR).

Sov. Phys.-Dokl. (USA), vol.27, no.8, p.624-5 (Aug. 1982). Translation of: *Dokl. Akad. Nauk SSSR*, vol.265, no.4-6, p.867-70 (Aug. 1982). [received: May 1983]

A diagram formalism for nonequilibrium processes which takes into account initial correlations was constructed by Hall (1975). In this graph method, a solid line on the graph corresponds to a matrix free Green function. The author generalizes the theorem proved by Hall about the vanishing of diagrams containing blocks $P^2 = \square$, and thus substantially decreases the number of nonvanishing diagrams. For instance, all connected diagrams which are obtained by adding correlation lines to a disconnected Keldysh diagram, as well as all diagrams in which all incoming and outgoing lines belong to correlators, are automatically correlation-connected and hence equal to zero. (3 refs.)

04.00 RELATIVITY AND GRAVITATION

(for special relativity, see 03.30; for relativistic astrophysics, see 93.30; for relativistic cosmology, see 98.80)

04.20 GENERAL RELATIVITY

(see also 02.40 Geometry and topology)

74328 Some solutions of the Einstein system of field equations corresponding to Taub metric. M.Bray.

Ann. Inst. Henri Poincaré Sect. A (France), vol.38, no.3, p.243-53 (1983). In French.

For several energy-momentum distributions (perfect fluid, thermodynamic dust, meson vector field) the integration of the complete Einstein system of field equations leads to some exact solutions possessing the plane symmetry defined by A.H. Taub (1951) (existence of a three parameter group of motions). (2 refs.)

74329 Rotational perturbations of Friedmann universes in Einstein zero mass scalar theory. K.D.Krori, J.C.Sarmah, D.Goswami (Math. Phys. Forum, Cotton Coll., Gauhati, India).

Can. J. Phys. (Canada), vol.61, no.5, p.744-7 (May 1983).

In an extension of a recent work by Bayin and Cooperstock (Phys. R&D, vol.22, p.2317, 1980) the authors investigate rotational perturbations of Friedmann universes in Einstein zero mass scalar theory. They find that except in

the case of 'perfect dragging', the zero mass scalar field has a damping effect on the rotation of matter. One of the three cases studied shows that the scalar field may exist only during a certain interval in the course of the evolution of the universe. The zero mass scalar field has acquired particular importance recently because of a suggestion by Weinberg and Wilczek (1978) that there should exist a pseudo-scalar boson, the so-called axion, of negligible mass. The work of Peccei and Quinn (1979) has lent further support to the idea of axions. (5 refs.)

74330 Viscous fluid in static spherically symmetric space-time. S.R.Maiti (Dept. of Phys., Midnapore Coll., Midnapore, India).

Int. J. Theor. Phys. (USA), vol.22, no.4, p.363-8 (April 1983).

Presents a static spherically symmetric viscous fluid solution of the Einstein field equation, assuming an equation of state $p = (\gamma - 1)\rho$. Though static, the solution has expansion, shear, and acceleration and can explain the cosmological red shift. Also it has a particle horizon. The singularity at the origin and larger viscosity make it unfit to represent a real universe. (4 refs.)

74331 Algebraic determination of the metric from the curvature in general relativity. G.S.Hall (Dept. of Math., Univ. of Aberdeen, Aberdeen, Scotland), C.B.G.McIntosh.

Int. J. Theor. Phys. (USA), vol.22, no.5, p.469-76 (May 1983).

The general solution for a symmetric second-order tensor X of the equation $X_{ab}R^{ab}_{cd} = 0$, where R is the Riemann tensor of a space-time manifold, and X is obtained in terms of the curvature 2-form structure of R by a straightforward geometrical technique, agrees with that given by McIntosh and Halford (1981, 1982) using a different procedure. Two results of earlier authors are derived as simple corollaries of the general theorem. (16 refs.)

74332 New general relativity—translation gauge theory. T.Shirafuji (Phys. Dept., Saitama Univ., Saitama, Japan).

Gauge Theory and Gravitation. Proceedings of the International Symposium, Nara, Japan, 20-24 Aug. 1982 (Berlin, Germany: Springer-Verlag 1983), p.16-25

In 1956 Utiyama proposed to introduce the gravitational fields as the gauge field of the Lorentz group. 24 fields were introduced by generalizing 6 constant parameters ω_{ij} ($= -\omega_{ji}$) for homogeneous Lorentz transformations to arbitrary functions $\omega_{ij}(x)$. The theory of gravitation based on the Weitzenböck space-time was called new general relativity. The author studies this translational gauge theory with reference to experimental tests. (14 refs.)

74333 Generalizations of gravitational theory based on group covariance. L.Halpern (Res. Inst. for Fundamental Phys., Kyoto, Japan).

Gauge Theory and Gravitation. Proceedings of the International Symposium, Nara, Japan, 20-24 Aug. 1982 (Berlin, Germany: Springer-Verlag 1983), p.26-30

The author develops a physical formalism of gravitation from symmetry group mathematics. The physics is dictated by mathematics based on semisimple Lie groups. (11 refs.)

74334 Space-time structure of gravitational solitons. A.Tomimatsu (Res. Inst. for Theoretical Phys., Hiroshima Univ., Hiroshima, Japan).

Gauge Theory and Gravitation. Proceedings of the International Symposium, Nara, Japan, 20-24 Aug. 1982 (Berlin, Germany: Springer-Verlag 1983), p.36-40

The axially symmetric and stationary soliton solution of Einstein's equations in a vacuum has been found by means of the inverse scattering problem technique. This solution has metric of the form $ds^2 = g_{ab}dx^a dx^b + h(dp^2 + dz^2)$, where $a, b = t, \phi$. (7 refs.)

74335 Pregelometry. K.Akama (Dept. of Phys., Saitama Medical Coll., Saitama, Japan).

Gauge Theory and Gravitation. Proceedings of the International Symposium, Nara, Japan, 20-24 Aug. 1982 (Berlin, Germany: Springer-Verlag 1983), p.267-71

The author adopts the dynamics of the Nielsen-Olesen vortex (1973) in a six-dimensional flat space-time, and shows that general relativity actually holds in four-spacetime. (5 refs.)

74336 The role of Newton's constant in Einstein's gravity. V.de Alfaro (Inst. di Fisica Teorica, Univ. di Torino, Torino, Italy).

The High-Energy Limit. Proceedings of the Eighteenth Course of the International School of Subnuclear Physics, Erice, Italy, 31 July-11 Aug. 1980 (New York, USA: Plenum 1983), p.149-75

Develops some remarks about the Einstein theory of gravity, called General Relativity after its invariance transformations. In particular the author addresses the role of the Newton constant according to the point of view that has been developed by Sergio Fubini, Giuseppe Furlan and the author (1979, 1980), and to the consequences of this point of view. (15 refs.)

Symmetries of the radiative Robinson-Trautman metrics See Entry 74338

Properties of a spin fluid in a Riemann-Cartan spacetime See Entry 74341

Self-gravitating null fluids See Entry 74342

Vanishing of the cosmological constant in non-Abelian Kaluza-Klein theories See Entry 74344

The stress-energy-momentum tensor of the Gauss map in the extended nonlinear σ -model See Entry 74608

Dyon black hole in the Tomimatsu-Sato-Yamazaki space-time See Entry 78812

Counterpart of the Kasner model in Brans-Dicke theory See Entry 79031

Large numbers hypothesis. IV. The cosmological constant and quantum physics See Entry 79034

04.30 GRAVITATIONAL WAVES AND RADIATION: THEORY

74337 On the Hawking radiation in a stationary Riemann space-time. Liu Liao (Dept. of Phys., Beijing Normal Univ., Beijing, China), Zhao Zheng.

Kexue Tongbao (Foreign Lang. Ed.) (China), vol.28, no.3, p.357-60 (March 1983).

It is well known that the thermal radiations from black holes, the Rindler radiations and the thermal radiations in de Sitter universe all come from the horizons. In a previous paper (1981), the authors put forth the conjecture, that the Hawking thermal radiation must exist in a stationary gravitational field, which has a horizon and the gravitational field on it is not zero. Now they prove the conjecture for a $1+1=2$ -dimensional static gravitational field. (7 refs.)

74338 Symmetries of the radiative Robinson-Trautman metrics. S.I.Tertychniy, V.V.Zhytnikov (Theoretical Phys. Dept., Moscow State Univ., Moscow, USSR).

Phys. Lett. A (Netherlands), vol.95A, no.8, p.419-21 (23 May 1983). The geometrical properties of radiative Robinson-Trautman metrics are presented. (5 refs.)

74339 Post-Newtonian gravitational radiation of a binary system of relatively extended bodies in the field theory of gravitation. A.A.Vlasov (Moscow State Univ., Moscow, USSR).

Theor. & Math. Phys. (USA), vol.53, no.1, p.998-1003 (Oct. 1982). Translation of: *Theor. & Math. Fiz. (USSR)*, vol.53, no.1, p.83-92 (Oct. 1982).

The post-Newtonian gravitational radiation of a binary system of relatively extended static spherically symmetric bodies in the field theory of gravitation is considered. (2 refs.)

74340 Absence of particle creation as an equilibrium condition. L.Parker (Dept. of Phys., Univ. of Wisconsin, Milwaukee, WI, USA).

Gauge Theory and Gravitation. Proceedings of the International Symposium, Nara, Japan, 20-24 Aug. 1982 (Berlin, Germany: Springer-Verlag 1983), p.89-95

From the observed range of validity of the Newtonian approximation, the cosmological constant Λ is known to be very small. In view of the fact that vacuum energy can contribute to the value of Λ , especially in conjunction with symmetry breaking, it is puzzling that the value of Λ is so small. The basic hypothesis is that the absence of particle creation, in particular, gravitons and minimally coupled massless scalar particles, is a kind of equilibrium condition toward which the evolution of the Universe tends, and that the classical Einstein equations must be consistent with that condition. (20 refs.)

On the phenomenon of rotation of the polarization vector of gravitational and neutrino waves in a strong neutrino radiation field See Entry 74343

Gravitational waves and their detection See Entry 74362

Gravitational waves See Entry 78808

04.40 CONTINUOUS MEDIA; ELECTROMAGNETIC AND OTHER MIXED GRAVITATIONAL SYSTEMS

74341 Properties of a spin fluid in a Riemann-Cartan spacetime. R.de Ritis (Istituto di Fisica Teorica, Univ. di Napoli, 19, Napoli, Italy), M.Lavorgna, G.Platania, C.Stornaiolo.

Phys. Lett. A (Netherlands), vol.95A, no.8, p.425-8 (23 May 1983).

The authors extend to the case of spin fluids in the Einstein-Cartan theory some results obtained by Taub (1959) and Lichnerowicz (1967) for a perfect fluid in general relativity. So doing they also give an extension of the Bernoulli theorem. They show a connection between torsion and a macroscopic quantity, the tensor $\Omega_{ij} = 2V[\gamma]_{ij}$. (7 refs.)

74342 Self-gravitating null fluids. P.S.Letelier (Dept. de Fisica, Univ. de Brasilia, Brasilia, Brazil).

Rev. Bras. Fis. (Brazil), vol.12, p.61-5 (March 1982). [received: April 1983]

An algorithm for generating solutions to the Einstein equations with a null fluid source, from vacuum solutions, is studied for space-times that admit an Abelian group of motions G_2 that act orthogonally transitively. (13 refs.)

74343 On the phenomenon of rotation of the polarization vector of gravitational and neutrino waves in a strong neutrino radiation field. L.Yu.Blazhenova-Mikulich, N.R.Sibgatullin (M.V. Lomonosov State Univ., Moscow, USSR).

Sov. Phys.-Dokl. (USA), vol.27, no.8, p.603-4 (Aug. 1982). Translation of: *Dokl. Akad. Nauk SSSR*, vol.265, no.4-6, p.849-52 (Aug. 1982). [received: May 1983]

considers the propagation of short gravitational and electromagnetic waves in an external field which is an arbitrary solution of the Einstein-Maxwell-Weyl equations. In this case there appears a small parameter, namely, the ratio of the characteristic scale of inhomogeneities of the perturbations to the characteristic scale of the space-time inhomogeneities of the background. One can look for a solution by expanding in powers of this small parameter. The presence of a background neutrino field leads to the result that the plane of polarization of a gravitational wave is rotated with the angular velocity defined by the expression $\omega = 8\pi G\hbar/c^2(n_+ - n_-)$, where n_+ and n_- are, respectively, the local densities of neutrinos and antineutrinos near the wave-front surface. The neutrinos and antineutrinos rotate the plane of polarization in opposite directions. The value of $G\hbar/c^2$ is of the order of 10^{-32} cm³.sec⁻¹, so that the phenomenon is weak and needs strong neutrino fields in order to be seen. (2 refs.)

Some solutions of the Einstein system of field equations corresponding to Taub metric See Entry 74328

Viscous fluid in static spherically symmetric space-time See Entry 74330

Symmetries of the radiative Robinson-Trautman metrics See Entry 74338

Larger numbers hypothesis. II. Electromagnetic radiation See Entry 79033

04.50 UNIFIED FIELD THEORIES AND OTHER THEORIES OF GRAVITATION

74344 Vanishing of the cosmological constant in non-Abelian Kaluza-Klein theories. M.W.Kalinowski (Inst. of Philosophy & Sociology, Polish Acad. of Sci., Warsaw, Poland).

Int. J. Theor. Phys. (USA), vol.22, no.5, p.385-96 (May 1983).

The author presents a new approach to the unification of gravity and non-Abelian gauge fields in the framework of Kaluza-Klein theory. It consists of introducing a new connection on the $(n+4)$ -dimensional manifold P (metrized principal fiber bundle). This connection is metrical, but with nonvanishing torsion. An enormous cosmological term in the Einstein equations vanishes due to this connection. The new connection simultaneously cancels Planck's mass term in the Dirac equation for the five-dimensional case. The usual interpretation of geodesic equations is still valid. (20 refs.)

74345 Perturbation of an exact strong-gravity solution. S.A.Baran (Internat. Centre for Theoretical Phys., Trieste, Italy).

Nuovo Cimento B (Italy), vol.74B, ser.2, no.2, p.121-20 (11 April 1983).

Perturbations of an exact strong-gravity solution are investigated. It is shown, by using the new multipole expansions previously presented, that this exact and static spherically symmetric solution is stable under odd-parity perturbations. (12 refs.)

74346 Extra space-time dimensions: towards a solution to the cosmological constant problem. V.A.Rubakov (Inst. for Nuclear Res., Acad. of Sci., Moscow, USSR), M.E.Shaposhnikov.

Phys. Lett. B (Netherlands), vol.125B, no.2-3, p.139-43 (26 May 1983).

The authors discuss the possibility that the cosmological constant problem is solved by raising the number of spatial dimensions a la Kaluza-Klein. In $(4+2)$ -dimensional pure gravity theory with the explicit Λ -term they find classical solutions with vanishing physical cosmological constant and compact 2-dimensions. However, there also exist solutions with the non-vanishing physical Λ -term, and the case $\Lambda_{\text{phys}}=0$ is not preferred at the classical level. They

conjecture that quantum corrections and/or additional interactions single out the solution with vanishing physical cosmological constant. (11 refs.)

74347 A geometrical foundation of a unified field theory. N.Rosen (Technion-Israel Inst. of Technol., Haifa, Israel), G.E.Tauber.

Gauge Theory and Gravitation. Proceedings of the International Symposium, Nara, Japan, 20-24 Aug. 1982 (Berlin, Germany: Springer-Verlag 1983), p.301-5

Einstein and Mayer (1931) proposed a formalism by which they were able to obtain a theory of gravitation and electro-magnetism similar to that of Kaluza and Klein. Instead of assuming, as these authors did, the existence of a five-dimensional continuum, they assumed that at each point of space-time, regarded as a Riemannian space, there exists a five-dimensional vector space. The authors generalize the approach of Einstein and Mayer to N-dimensions, and lay down the geometrical foundation of a possible unified field theory of gravitation with other fields. (6 refs.)

The High-Energy Limit. Proceedings of the Eighteenth Course of the International School of Subnuclear Physics See Entry 74229

Some solutions of the Einstein system of field equations corresponding to Taub metric See Entry 74328

Induced gravitation See Entry 74352

Cosmological phase transition in microcanonical gravity See Entry 74689

Kaluza-Klein type theory See Entry 74690

Scale invariant scalar-tensor theory and the origin of gravitational constant and particle masses See Entry 74691

Counterpart of the Kasner model in Brans-Dicke theory See Entry 79031

Quantization of a homogeneous isotropic cosmological model in five-dimensional field theory See Entry 79041

04.60 QUANTUM THEORY OF GRAVITATION

74348 Why is the cosmological constant small? S.G.Rajeev (Phys. Dept., Syracuse Univ., Syracuse, NY, USA).

Phys. Lett. B (Netherlands), vol.125B, no.2-3, p.144-6 (26 May 1983).

The author argues that singular metrics with finite action should be allowed in the path integral of quantum gravity. The path integral over such conformally flat configurations is studied. It is shown that the system is equivalent to a Coulomb gas. The cosmological constant acts as a charge density in this gas. Due to Debye screening, the effective cosmological constant at macroscopic distances is very small. Quantum gravity may thus explain the vanishing of the cosmological constant. (8 refs.)

74349 Manifestly covariant canonical formalism of quantum gravity—a brief survey. N.Nakanishi (Res. Inst. for Math. Sci., Kyoto Univ., Kyoto, Japan).

Gauge Theory and Gravitation. Proceedings of the International Symposium, Nara, Japan, 20-24 Aug. 1982 (Berlin, Germany: Springer-Verlag 1983), p.171-83

General relativity and quantum field are two successful fundamental theories of physics. It is, therefore, of very fundamental importance to unify both theories in a consistent manner. The author presents a quantum field-theoretical formalism of gravity. (37 refs.)

74350 A gauge invariant resummation of quantum gravity. A.Strominger (Inst. for Advanced Study, Princeton, NJ, USA).

Gauge Theory and Gravitation. Proceedings of the International Symposium, Nara, Japan, 20-24 Aug. 1982 (Berlin, Germany: Springer-Verlag 1983), p.184-8

Quantum gravity is expanded in powers of $1/D$, where D is the number of dimensions. The extra dimensions are highly compactified. The expansion is gauge invariant. The leading term is equivalent to the iterated one loop matter corrections due to a free, massless scalar field without the $1/6 R\phi^2$ term necessary for conformal invariance. The $1/D$ expansion is renormalizable. Flat space is found to be unstable under small fluctuations. (3 refs.)

74351 'The gauge invariant effective action for quantum gravity and its semi-quantitative approximation'. B.S.DeWitt (Univ. of Texas, Austin, TX, USA).

Gauge Theory and Gravitation. Proceedings of the International Symposium, Nara, Japan, 20-24 Aug. 1982 (Berlin, Germany: Springer-Verlag 1983), p.189-203

The author presents a configuration space of quantum gravity where the gauge transformed orbits comprise an infinite dimensional manifold. (no refs.)

74352 Induced gravitation. S.L.Adler (Inst. for Advanced study, Princeton, NJ, USA).

The High-Energy Limit. Proceedings of the Eighteenth Course of the International School of Subnuclear Physics, Erice, Italy, 31 July-11 Aug. 1980 (New York, USA: Plenum 1983), p.3-27

Describes some recent work which offers the possibility of both relating the gravitational and unification mass scales, and of permitting the formulation of a quantum theory of gravitation as a renormalizable field theory. The basic premise of what follows, first suggested by A.D. Sakharov (1967), is that the Einstein action is not a fundamental action at all, but rather is an induced effect—in Sakharov's words the 'metrical elasticity of space'—resulting from quantum fluctuations of the matter fields. (15 refs.)

74353 Induced gravity in quantum theory in a curved space. E.Etim (Dept. of Phys., Siegen Univ., Siegen, Germany).

The High-Energy Limit. Proceedings of the Eighteenth Course of the International School of Subnuclear Physics, Erice, Italy, 31 July-11 Aug. 1980 (New York, USA: Plenum 1983), p.367-86

The reason for interest in the unorthodox view of first order ($\sim R(x)$) gravity as a matter-induced quantum effect is really to find an argument not to quantise it. According to this view quantum gravity should be constructed with an action which is, at least, quadratic in the scalar curvature $R(x)$. Such a theory will not contain a dimensional parameter, like Newton's constant, and would probably be renormalisable. The author intends to acquaint the non-expert with the phenomenon of induction of the scalar curvature term in the matter Lagrangian in a curved space in both relativistic and non-relativistic quantum theories. (9 refs.)

Stability of gravitational merons See Entry 74357

One-loop divergences and β -functions in supergravity theories See Entry 74361

Charges from extra dimensions See Entry 74618

A micro-deSitter spacetime with constant torsion: a new vacuum solution of the Poincare gauge field theory See Entry 74624

The influence of neutrino rest mass on Dirac cosmology See Entry 79035

Quantization of a homogeneous isotropic cosmological model in five-dimensional field theory See Entry 79041

04.65 SUPERGRAVITY

74354 The stability of gauged supergravity. G.W.Gibbons, C.M.Hull, N.P.Warner (Univ. of Cambridge, Cambridge, England). *Nucl. Phys. B, Part. Phys. (Netherlands)*, vol.B218, no.1, p.173-90 (30 May 1983).

The authors establish classical positive energy theorems for the gauged supergravity models. These results show that the maximally supersymmetric vacuum states for these theories are supersymmetric anti-de Sitter space-times which, despite the presence of negative local energy densities are stable. They also discuss spontaneous symmetry breaking in these models. (22 refs.)

74355 The geometrical hierarchy model and $N=1$ supergravity. B.A.Ovrut (Dept. of Phys., Rockefeller Univ., New York, NY, USA), S.Raby.

Phys. Lett. B (Netherlands), vol.125B, no.4, p.270-4 (2 June 1983).

The authors incorporate the geometrical hierarchy model of Dimopoulos and Raby (1982) into $N=1$ supergravity. Supersymmetry is spontaneously broken at a scale of order 10^{11} GeV and the cosmological constant is fine tuned to zero. A grand unification mass of order M_{Planck} is induced at tree level. They discuss the low energy ($E \sim$ gravitino mass) theory and the ramifications of their model for proton decay. (9 refs.)

74356 Weak symmetry breaking by radiative corrections in broken supergravity. J.Ellis, J.S.Hagelin (Stanford Linear Accelerator Center, Stanford Univ., Stanford, CA, USA), D.V.Nanopoulos, K.Tamvakis.

Phys. Lett. B (Netherlands), vol.125B, no.4, p.275-81 (2 June 1983).

Weak interaction gauge symmetry breaking can be generated by radiative corrections in a spontaneously broken supergravity theory, provided the top quark is heavy enough. In one class of such theories the weak Higgs vacuum expectation values are determined by dimensional transmutation a la Coleman-Weinberg (1973), and may be considerably larger than the magnitudes of SUSY breaking mass parameters. In this scenario $m_t \geq 65$ GeV, the supersymmetric partners of known particles may have masses $\ll m_W$, the mass of the lighter neutral scalar Higgs boson is determined by radiative corrections, and there is some variant of a light pseudoscalar axion. In contrast to conventional Coleman-Weinberg models, the weak phase transition is second order and there is no likelihood of excess entropy production. (25 refs.)

74357 Stability of gravitational merons. K.G.Akdeniz (Dept. of Phys., Univ. of Istanbul, Istanbul, Turkey), A.Hacinliyan, J.Kalayci.

Phys. Lett. B (Netherlands), vol.125B, no.4, p.291-4 (2 June 1983).

The authors find that in gravitational models containing Yang-Mills fields merons are unstable. They use a model examined by de Alfaro, Fubini and Furlan (1980). In this model gravitation is coupled to matter fields as the effective (neglecting odd parity and spinorial fields) part of $N=4$ lagrangian for supergravity with $SU(2) \times SU(2)$ local invariance, where supersymmetry fixes uniquely the ratio between the cosmological constant and the color charge. (10 refs.)

74358 Grand unified theories with symmetry and local supersymmetry. R.Arnowitt, P.Nath, A.H.Chamseddine (Dept. of Phys., Northeastern Univ., Boston, MA, USA).

Gauge Theory and Gravitation. Proceedings of the International Symposium, Nara, Japan, 20-24 Aug. 1982 (Berlin, Germany: Springer-Verlag 1983), p.231-9

The properties of local supersymmetric (LS) grand unified models based on the gauge group $(N=1 \text{ supergravity}) \times SU(5)$ are described. The gravitational interactions of supergravity causes a dynamical symmetry breaking of both $SU(2) \times U(1)$ and supergravity at the mass $m_2 = km^2 \sim 300$ GeV where m is the scale of supersymmetry breaking. These results are maintained at the one loop level. The models described are relativistic in that they are in accord with low energy phenomenology. (20 refs.)

74359 Consistency of coupling in supergravity with propagating Lorentz connexion. H.Nishino (Inst. of Phys., Univ. of Tokyo, Tokyo, Japan).

Gauge Theory and Gravitation. Proceedings of the International Symposium, Nara, Japan, 20-24 Aug. 1982 (Berlin, Germany: Springer-Verlag 1983), p.249-53

Gauge principle is the most successful scheme in grand unifications of three kinds of interactions other than the gravitational interaction. The recent hierarchy problem of grand unification theories motivates consideration of supersymmetric extensions. Once supersymmetry is introduced in the description of nature, there is no theory other than supergravity which is consistent with the gravitational interaction. The author presents a supergravity theory with propagating Lorentz connexion. (9 refs.)

74360 Dimensional reduction. P.G.O.Freund (Dept. of Phys., Enrico Fermi Inst., Univ. of Chicago, Chicago, IL, USA).

Gauge Theory and Gravitation. Proceedings of the International Symposium, Nara, Japan, 20-24 Aug. 1982 (Berlin, Germany: Springer-Verlag 1983), p.259-61

The author considers cosmologies in which the effective space-dimensionality is time dependent. Starting with 11-dimensional supergravity, dimensional reduction gauge symmetries are applied. (14 refs.)

74361 One-loop divergences and β -functions in supergravity theories. E.S.Fradkin, A.A.Tseytlin (Dept. of Theoretical Phys., P.N. Lebedev Phys. Inst., Moscow, USSR).

Gauge Theory and Gravitation. Proceedings of the International Symposium, Nara, Japan, 20-24 Aug. 1982 (Berlin, Germany: Springer-Verlag 1983), p.293-300

The authors present results on explicit calculations (of counter-terms, β -functions, off shell and asymptotic behaviour) in quantum supergravity. (13 refs.)

Composite gauge bosons in sigma models and supergravitySee Entry 74611

Global and local supersymmetric grand unificationSee Entry 74670

Grand unification with local supersymmetrySee Entry 74674

04.80 EXPERIMENTAL TESTS OF GENERAL RELATIVITY AND OBSERVATIONS OF GRAVITATIONAL RADIATION

74362 Gravitational waves and their detection. J.Hough (Dept. of Natural Philosophy, Univ. of Glasgow, Glasgow, Scotland).

J. Br. Astron. Assoc. (GB), vol.93, no.3, p.101-4 (April 1983).

A short review of the problem of detecting gravity waves with special reference to the experiment being done at Glasgow University. The review summarizes the talk given to the Edinburgh meeting of the association in 1982 September. (no refs.)

Workshop on Science UndergroundSee Entry 74199

Direct observational upper limit to gravitational radiation from millisecond pulsar PSR 1937+214See Entry 78935

05.00 STATISTICAL PHYSICS AND THERMODYNAMICS

(see also 02.50 Probability theory, stochastic processes, and statistics)

05.20 STATISTICAL MECHANICS

74363 Cluster partition functions for a two-dimensional hard core square well gas. S.M.T.de la Selva, R.Dickman, W.C.Schieve, C.Canestaro (Center for Studies in Statistical Mech. & Thermodynamics, Univ. of Texas, Austin, TX, USA).

J. Chem. Phys. (USA), vol.78, no.11, p.6885-9 (1 June 1983).

The authors study physical (or Hill's) clusters in a two-dimensional hard core square well (HCSW) system. Partition functions for clusters of five or fewer particles have been determined, using both 'proximity' and 'negative energy' bond definitions. The cluster size distributions calculated on the basis of the partition functions are in good agreement with molecular dynamics simulations of the HCSW system. (7 refs.)

74364 Lower bounds for Wiener integrals. E.P.Gross (Dept. of Phys., Brandeis Univ., Waltham, MA, USA).

J. Stat. Phys. (USA), vol.31, no.1, p.115-28 (April 1983).

Techniques are developed to sharpen lower bounds for density matrices occurring in statistical mechanics. The Wiener integrals are treated by insertion of trial functionals and parametric representations of unity that involve functionals of the path. Jensen's inequality is applied to suitable parameter-dependent path measures. These yield stronger forms than the basic Feynman bound. The author also introduces trajectory insertions, and uses coupling constant integration and the hierarchy for correlation functions to improve the bounds. (10 refs.)

74365 Dynamics of a two-level system and estimate of the relaxation time. N.N.Bogolyubov, Jr., Fam Le Kien, A.S.Shumovskii (Joint Inst. for Nuclear Res., Dubna, USSR).

Theor. & Math. Phys. (USA), vol.53, no.1, p.1014-18 (Oct. 1982). Translation of: *Theor. & Mat. Fiz. (USSR)*, vol.53, no.1, p.108-13 (Oct. 1982).

The generalized kinetic equation for a system of two-level emitters interacting with the electromagnetic field obtained previously (1981) is used to find an equation for the single-particle distribution function and to investigate relaxation processes. (11 refs.)

On the Brownian motion of deformable particlesSee Entry 74386

The Boltzmann equation theory of charged particle transportSee Entry 74409

Large numbers hypothesis. III. Kinetic theory, statistical physics, and thermodynamicsSee Entry 74418

On information, negentropy and thermostaticsSee Entry 74424

On the theory of nonequilibrium processes in the projection operator methodSee Entry 74426

Semiclassical representation method in statistical physics of interacting molecules. I. General theorySee Entry 75468

Transverse transport processes of charged particle systems in a strong magnetic field. II. Some discussions about the Boltzmann equationSee Entry 75572

Expansion of single-particle distribution functions with respect to effective long-range potentialsSee Entry 76267

On the theory of nonequilibrium processes in the projection operator methodSee Entry 74426

Semiclassical representation method in statistical physics of interacting molecules. I. General theorySee Entry 75468

Transverse transport processes of charged particle systems in a strong magnetic field. II. Some discussions about the Boltzmann equationSee Entry 75572

Expansion of single-particle distribution functions with respect to effective long-range potentialsSee Entry 76267

On the theory of nonequilibrium processes in the projection operator methodSee Entry 74426

Semiclassical representation method in statistical physics of interacting molecules. I. General theorySee Entry 75468

Transverse transport processes of charged particle systems in a strong magnetic field. II. Some discussions about the Boltzmann equationSee Entry 75572

Expansion of single-particle distribution functions with respect to effective long-range potentialsSee Entry 76267

05.30 QUANTUM STATISTICAL MECHANICS

(see also 67. Quantum fluids, and 71. Electron states in condensed matter)

74366 On theory of the statistical generating functional for the order parameter. III. Effective action formalism for the order parameter. Zhou Guang-zhao, Su Zhao-bin, Hao Bai-jin, Yu Lu (Inst. of Theoretical Phys., Acad. Sinica, Beijing, China).

Commun. Theor. Phys. (China), vol.1, no.4, p.389-403 (1982).

For pt.II see *ibid.*, vol.1, no.3, p.307-18 (1982). A practical scheme is proposed to determine the quantum statistical properties of the order parameter in the framework of the closed time-path Green's functions (CTPGF). As a microscopic quantum theory, this formalism is applicable in principle to both equilibrium and nonequilibrium phenomena and is capable of dealing with statistical systems both above and below their phase transition point. This formalism can be used to discuss the statistical properties of simple as well as composite order parameters in either uniform or nonuniform systems. As simple illustrations and check for the theory, the proposed prescription is applied to the contact-interaction model for superconductivity and a unimode laser system coupled with two-energy level bound electrons. (11 refs.)

74367 Studies in the configuration interaction method. II. Generating functions and recurrence relations for the number of many-particle configurations. J.Katriel, R.Pauncz (Dept. of Chem., Technion-Israel Inst. of Technol., Haifa, Israel), J.J.C.Mulder.

Int. J. Quantum Chem. (USA), vol.23, no.5, p.1855-67 (May 1983).

For pt.I, see *Int. J. Quantum Chem. Quantum Chem. Symp.*, vol.15, p.101 (1981). Generating functions are constructed and recurrence relations are derived for the number of configurations of any number of particles with an arbitrary elementary spin for both fermions and bosons. Similar results are obtained for the number of configurations specified by the total weight and by the degree of excitation. (7 refs.)

74368 A set of 'ground hypotheses' for elementary-particle statistics. D.Costantini (Istituto di Statistica, Univ. di Bologna, Bologna, Italy), M.C.Galavotti, R.Rosa.

Nuovo Cimento B (Italy), vol.74B, ser.2, no.2, p.151-8 (11 April 1983).

A 'rational reconstruction' of the Maxwell-Boltzmann, Bose-Einstein and Fermi-Dirac statistics is proposed, that is a set of conditions (ground hypotheses) implying the probability functions which determine the above statistics. In order to accomplish this purpose, methods, language and results of inductive logic are adopted. (5 refs.)

74369 Exact ground states for a class of linear quantum spin systems. V.J. Caspers (Twente Univ. of Technol., Enschede, Netherlands), W. Magnus. *Physica A (Netherlands)*, vol.119A, no.1-2, p.291-4 (April 1983).
The singlet pair state (SPS) is shown to be the exact ground state for a class of linear quantum spin systems with anisotropic interactions. (4 refs.)

74370 Dynamics of classical and quantum spin systems with random fields. D. Boyanovsky, J.L. Cardy (Dept. of Phys., Univ. of California, Santa Barbara, CA, USA).

Phys. Rev. B (USA), vol.27, no.9, p.5557-69 (1 May 1983).

The authors study the effect of quenched time-independent random fields coupled linearly to the order parameter on the dynamical critical behavior of spin systems. They assume that the dynamics is described by a Langevin equation without conservation of the order parameter. It is shown that the dominant fluctuations are those induced by the random fields and, therefore, thermal fluctuations are irrelevant. This allows them to establish a relation between this model and a quantum spin system in the presence of a quenched random field. Moreover, they find that only static exponents in D dimensions are the same as those of the pure $(D-2)$ -dimensional theory, but the dynamical exponent z does not satisfy this relation. The quantum system in D dimensions is studied through its $(D+1)$ -dimensional equivalent model where the quenched random fields are totally correlated in the additional imaginary-time τ direction. The system is anisotropic, and there is a new exponent z_A associated with the scaling behavior in the τ direction. They find the relation $z_A = 2z_A$ to all orders in perturbation theory. For the zero-temperature quantum model they find that the static (zero-frequency) exponents are the same as those of the $(D-3)$ -dimensional pure quantum model. At finite temperature, when the classical system is finite in the τ direction, they predict a crossover to D -dimensional classical behavior in nonstatic response and correlation functions, with crossover exponent $(z_A \nu_{(D-2)})^{-1}$, where $\nu_{(D-2)}$ is the exponent ν for the $(D-2)$ -dimensional pure classical system. The static correlation functions do not have this crossover behavior and are the same as those of the $(D-3)$ -dimensional pure quantum model. The dimensional shift in static quantities for both quantum and classical dynamical systems is a consequence of a supersymmetry in the underlying field theory. The exponent $\lambda = 1 + \eta + O(1/N^2)$ in the large- N limit or $z_A = 1 + \eta + O(\epsilon^2)$ in the ϵ expansion where $\epsilon = 1 - d/(N+2)$ and η is the same as in the $(D-2)$ dimensional pure classical system. They also study the above classical random-field Ising problem using the interface approach, but are unable to draw any definite conclusion about the dynamics at the lower critical dimension $d=3$. (27 refs.)

Relativistic quantum logic See Entry 74308

Analysis of a bilinear relation for the six-vertex model See Entry 74323

A generalized approximation of the Fermi-Dirac integrals See Entry 76820

05.40 FLUCTUATION PHENOMENA, RANDOM PROCESSES, AND BROWNIAN MOTION

74371 Percolation. Models, analog and numerical simulations. J.P. Clerc, G. Giraud, J. Rousselle, R. Blanc (Dept. de Phys. des Systemes Desordones, Univ. de Provence, Marseille, France), J.P. Carton, E. Guyon, H. Ottavi, D. Stauffer.

Ann. Phys. (France), vol.8, no.1, p.5-105 (1983). In French.

This review article considers the problems in percolation using several complementary approaches: experimental simulations, numerical experiments, as well as statistical treatments and theoretical methods inherited from phase transition problems (such as scaling and real space renormalization). A simple introduction to the statistical concepts in percolation theory is given. The authors describe the results of numerical simulations, based on Monte Carlo methods, which also give a concrete grasp to the basic statistical definitions. Simulations are made in the critical regime around the percolation threshold p_c (where p is the probability that a given fraction of sites or bonds are active in a lattice) but also near $p=0$ or $p=1$ where the statistical characteristics of clusters can also be studied. The authors also discuss a method of exploration on incompletely connected networks, known as 'the ant on a labyrinth'. This random walk problem provides an intermediate situation between percolation and diffusion. They discuss in some detail the original contribution of percolation to the study of the electrical conductivity of a composite medium. The authors discuss two classes of problems in which different directions of space are not identical. Finally a first approach to the study of surface phenomena in percolation is given. (159 refs.)

74372 Zero-one law and asymptotic behaviour of transition probabilities of Markov processes. D. Revuz (Univ. Paris-VII, Paris, France).

Ann. Inst. Henri Poincaré Sect. B (France), vol.19, no.1, p.9-24 (1983). (15 refs.)

74373 Functional central-limit theorems for Markov processes. A. Tounti (Ecole Normale Supérieure, Bizerte, Tunisia).

Ann. Inst. Henri Poincaré Sect. B (France), vol.19, no.1, p.43-55 (1983). In French.

Extends the results of Maignet (1979), on Harris positive recurrent chains to positive recurrent Markov processes. (17 refs.)

74374 Stochastic transport in disordered systems. M. Sahimi, B.D. Hughes, L.E. Scriven, H.T. Davis (Dept. of Chem. Engng. & Materials Sci., Univ. of Minnesota, Minneapolis, MN, USA).

J. Chem. Phys. (USA), vol.78, no.11, p.6849-64 (1 June 1983).

The authors develop a theory of stochastic transport in disordered media, starting from a linear master equation with random transition rates. A Green function formalism is employed to reduce the basic equation to a form suitable for the construction of a class of effective medium approximations (EMAs). The lowest order EMA, developed in detail here, corresponds to recent approximations proposed by Odagaki and Lax (Phys. Rev. B 24, 5284, 1981), Summerfield (Solid State Commun. 39, 401, 1981), and Webman (Phys. Rev. Lett. 47, 1496, 1981). It yields an effective transition rate W_m which can be identified as the memory kernel of a generalized master equation, and used to define an associated continuous-time random walk on a uniform lattice. The long-time behavior of the mean-squared displacement arising from an initially localized state can be found from W_m as can diffusion constants in any case where the long-time behavior of the system is diffusive. Detailed calculations are presented for seven lattice systems in one, two, and three dimensions, and for a variety of probability density functions $f(w)$ for the transition rates. For percolation-type densities, i.e., those with only a fraction $p < 1$ of the bonds transmitting, the EMA predicts three distinct kinds of behavior: localization, 'fractal' transport with slower than linear growth of the mean-squared displacement, and diffusion in the cases $p < p_c$, $p = p_c$, $p > p_c$, respectively, where p_c is the bond percolation threshold of the lattice. Depending on the form of $f(w)$ near $w=0$, critical exponents may take values independent of $f(w)$ ('universality') or heavily dependent on $f(w)$ ('nonuniversality'). (73 refs.)

74375 A simple derivation of Langevin equations for nonequilibrium states. M. Ichihara (Dept. of Appl. Phys., Osaka Univ., Osaka, Japan).

J. Phys. Soc. Jpn. (Japan), vol.52, no.5, p.1541-8 (May 1983).

In the spirit of the linear response theory, a simple derivation is given of a Langevin equation for collective modes of a macroscopic system. Unlike the usual treatment, the author separates a weak interaction of individual particles with collective modes which is allowed to depend on time. In nonequilibrium cases, the author has shown that a damping constant of the collective modes can be expressed in terms of a time correlation function, in which its average is taken with respect to a nonequilibrium density matrix rather than a usual canonical density matrix. A microscopic expression for a Langevin random force is obtained in terms of fluctuations of a density matrix.

74376 Noise-induced order. K. Matsumoto, I. Tsuda (Dept. of Phys., Kyoto Univ., Kyoto, Japan).

J. Stat. Phys. (USA), vol.31, no.1, p.87-106 (April 1983).

A new noise effect on chaos in one-dimensional mappings is reported. The transition from chaotic behavior to ordered behavior induced by external noise is observed in a certain class of one-dimensional mappings. This transition is clearly shown in terms of the Lyapunov number, entropy, power spectrum, and the nature of orbits. (14 refs.)

74377 Modeling and analysis of dynamical systems subject to discontinuous noise processes. S.K. Srinivasan, S. Udayabhaskaran (Dept. of Math., Nat. Univ. of Singapore, Singapore).

J. Math. & Phys. Sci. (India), vol.16, no.5, p.415-30 (Oct. 1982). [received: May 1983]

The authors consider the problem of modelling and analysing systems driven by discontinuous Markov processes. The purely discontinuous Markov process of Feller-Kolmogorov type is described and its associated stochastic integral studied. Then a stochastic model of a dynamical system driven by such a process is presented. (18 refs.)

74378 Kinetic simulation of an aggregation process. C. Allain, B. Joughier (Lab. d'Hydrodynamique et de Mécanique Phys., ESPCI, Paris, France).

J. Phys. Lett. (France), vol.44, no.11, p.421-8 (1 June 1983). In French.

An experimental simulation in two dimensions has permitted the authors to study the growth of clusters during an aggregation process. The existence of a critical surface fraction and of self-similar geometrical properties of the cluster is demonstrated. (12 refs.)

74379 An analysis of Smoluchowski equation for sedimentation. H. Minowa (Phys. Dept., Numazu Nat. Coll. of Technol., Numazu-shi, Shizuoka, Japan).

Lett. Nuovo Cimento (Italy), vol.37, ser.2, no.3, p.99-104 (21 May 1983).

As an example of the theoretical analysis of the Smoluchowski equation, (S eq.), the collective motion of Brownian particles in sedimentation is studied here exactly. First, using the standard procedures the authors show that the general solution of the S eq., which is satisfied with some given boundary and initial conditions, can be expressed as a series expansion by a complete set of orthogonal functions. Next, letting the region tend to infinity, they reduce the solution in series form to an asymptotic solution in integral form. Further they prove that execution of the integration just results in the formula described in Chandrasekhar's review (1943). Nowadays, the Brownian motion under external force-field has become a big target of active research. The analysis given here is partially original and useful as a tool to solve the problems related to this motion such as the sedimentation, the surface kinetics of absorption or desorption, and the diffusion phenomena etc. (13 refs.)

74380 Two limit theorems for ergodically regenerated stochastic processes. J. Kupka (Monash Univ., Clayton, Victoria, Australia).

Math. Proc. Cambridge Philos. Soc. (GB), vol.93, pt.3, p.519-36 (May 1983).

There is a suitable difference between the recurrent event of Feller (1968) and the regenerative phenomenon of Kingman (1964). The former regenerates an entire ambient process, whereas the latter regenerates only itself. The author generalizes Feller's definition to a discrete regenerative phenomenon E in association with an arbitrary discrete-time stochastic process X . Two limit theorems of a general character are proved for the process X when it is regenerated by an ergodic phenomenon E . The first implies that X becomes strictly stationary at a uniform rate which is determined solely by the asymptotic behaviour of E . The second is essentially a mixing convergence theorem which implies the asymptotic independence of regenerating and regenerated events. Applications include (1) the outright independence of the regenerating events and the regenerated events which occur 'at the end of time', and (2) the identification of the transient features of X with the null sets of the stationary limiting probability. Numerous open questions are posed. (20 refs.)

74381 Hamiltonian model for the Brownian motion of a rigid rotor. K. Lindenberg, U. Kohanty (Dept. of Chem., Univ. of California, San Diego, La Jolla, CA, USA), V. Seshadri.

Physica A (Netherlands), vol.119A, no.1-2, p.1-16 (April 1983).

The authors derive stochastic equations for the motion of a rigid rotor in a linear heat bath starting from a fully dynamical (Hamiltonian) description. They obtain a generalized Langevin equation for the angular velocity of the rotor in which the fluctuations in the torque arise from the initial conditions of the heat bath. The dissipation is in general nonlinear and is related to the fluctuations via a fluctuation-dissipation relation that is a natural consequence of our description. In the Langevin limit we show that our equations are equivalent to the phenomenological Euler-Langevin equations. However, whereas the latter are necessarily expressed in components referred to a body-fixed coordinate system, our representation is valid in an arbitrary system of axes and is in that sense more general. Finally, we also examine the reduction of our model to the rotational diffusion equation in the high viscosity limit. We show that this reduction can be carried out via standard methods of adiabatic elimination if our representation of the rotor equations of motion is used. (26 refs.)

74382 Systematic elimination of fast variables in linear systems. U. Geigenmüller, U.M. Titulaer, B.U. Felderhof (Inst. für Theoretische Phys. A, RWTH Aachen, Aachen, Germany).

Physica A (Netherlands), vol.119A, no.1-2, p.41-52 (April 1983).

The authors consider linear systems in which some of the variables evolve on a much faster time scale than the remaining ones. By means of a systematic perturbation theory in the time-scale ratio they extract a reduced dynamics in terms of the slow variables only, valid after an initial transient period. The procedure provides a systematic extension of the usual adiabatic elimination scheme and gives corrections to it. They also find an expression for the long-time behavior of the correlation functions of the slow variables. These asymptotic expressions do not extrapolate back towards the equal-time correlations for t going to zero: the reason for this 'initial slip' is given and its magnitude calculated. Method and results are illustrated with a simple example of coupled oscillators. (15 refs.)

74383 On Brownian motion in fluids with spin. A.Perez-Madrid, J.M.Rubi, J.Casas-Vazquez (Dept. de Termologia, Univ. Autonoma de Barcelona, Barcelona, Spain).

Physica A (Netherlands), vol.119A, no.1-2, p.212-29 (April 1983).

A method of induced forces and torques is employed to study Brownian motion of a particle in a fluid with internal angular momentum (spin). One derives generalized Faxen theorems for the force and torque exerted on the particle. In the Landau-Lifshitz approach, one obtains fluctuation-dissipation theorems for the force and torque. The results are applied to quinoline and liquid nitrogen. (19 refs.)

74384 Brownian diffusion of a small particle in a suspension. II. Hydrodynamic effect in a random fixed bed. J.-P.Carton (Service de Phys. du Solide et de Resonance Magnetique, CENS, Gif sur Yvette, France), E.Dubois-Violette, J.Prost.

Physica A (Netherlands), vol.119A, no.1-2, p.307-16 (April 1983).

For pt.1 see *Phys. Lett.* vol.86A, p.401 (1981). The Brownian diffusion of a small particle in a fluid flowing through a random fixed bed of identical spheres is considered. To lowest order in the volume fraction ϕ of the suspension, the diffusion constant is shown to be renormalized in the direction transverse to the velocity as $D_{\perp} = D(1 + 3(\phi/2)^{1/2})$ provided the velocity is large enough. (6 refs.)

74385 Asymptotic properties of the Markovian master equations for multi-stationary systems. E.-J.Ding (Dept. of Phys., Liaoning Univ., Shenyang, Liaoning, China).

Physica A (Netherlands), vol.119A, no.1-2, p.317-26 (April 1983).

Asymptotic properties of the Markovian master equations for multi-stationary systems are discussed. It is proved that the convergence radii of the generating functions are greater than one in most cases. On this basis, the singular perturbation expansion method is generalized to include the case of multi-stationary systems beyond the bifurcation point. The properties of stationary states of the system in the thermodynamic limit are discussed, and the implications of multiplicity of states in the properties of the generating function are established. (6 refs.)

74386 On the Brownian motion of deformable particles. A.V.Zatovsky (Dept. of Theoretical Phys., Odessa State Univ., Odessa, USSR), V.Lisy.

Physica A (Netherlands), vol.119A, no.1-2, p.369-79 (April 1983).

The theory of the Brownian motion of deformable particles is presented taking into account the interaction between the rotational motion of the particle and vibrations of its form. The changes of the form of the Brownian particle are described by means of the coordinates used in the collective model of the atomic nuclei. The Einstein-Smoluchowski kinetic equation has been obtained in these coordinates. A canonical transformation of the variables is carried out into the space of the Eulerian angles and two deformation parameters. An approximate solution of the kinetic equation has been found using the new variables for particles which have an axially symmetrical shape in equilibrium. Simple time correlation functions of dynamic variables of the particle are calculated. (14 refs.)

74387 Fokker-Planck equation for a multiplicative stochastic process with a stationary Gaussian noise. J.Iwaniszewski (Inst. of Phys., Nicholas Copernicus Univ., Torun, Poland).

Phys. Lett. A (Netherlands), vol.95A, no.8, p.415-18 (23 May 1983).

Starting from a Langevin equation with stationary gaussian noise of arbitrary correlation time, a corresponding Fokker-Planck equation is derived under the condition of small noise strength. (11 refs.)

74388 Critical dimensionality and exponent of the 'true' self-avoiding walk. L.Pietronero (Inst. for Theoretical Phys., Univ. of California, Santa Barbara, CA, USA).

Phys. Rev. B (USA), vol.27, no.9, p.5887-9 (1 May 1983).

A simple, self-consistent method is formulated to compute the critical dimensionality d_c and the exponent ν of the 'true' self-avoiding walk as defined by Amit et al. (1983). There results $d_c=2$, in agreement with the renormalization analysis. In addition, the author obtains $\nu=2/(2+d)$ for $d<2$. The present method applied to the problem of the self-repelling chain reproduces the Flory exponent. (5 refs.)

74389 Generalized method of optimal identification and optimal estimation of nonlinear dynamical systems. V.V.Bek, V.P.Grigo'ev, A.R.Makhlin, I.S.Ukolov (Sci. Council on Complex Problem 'Cybernetics', Acad. of Sci., Moscow, USSR).

Sov. Phys.-Dokl. (USA), vol.27, no.8, p.589-90 (Aug. 1982). Translation of: *Dokl. Akad. Nauk SSSR*, vol.265, no.4-6, p.827-9 (Aug. 1982). [received: May 1983]

Examines the behavior of a dynamical object described by a stochastic equation of the form $dx/dt = f_1(x,u,t) + f_2(x,u,t)w(t)$. The equation of the measurements is of the form $z(t) = h(x,t) + v(t)$, where x is the n -dimensional extended parameter-and-state vector with the initial condition $x(t_0)$, which is a random vector with mathematical expectation $\mu_0(t_0)$ and covariance C_0 , u is the m -dimensional control vector, z is the r -dimensional measurement vector, $w(t)$ is the p -dimensional perturbation vector, and $v(t)$ is the r -dimensional vector of the random errors in the measurements. (2 refs.)

The influence of fluctuations on the hydrodynamic asymptotics of Green's functions See Entry 74284

Critical dynamics and fluctuations for a mean-field model of cooperative behavior See Entry 74314

Continual measurements for quantum open systems See Entry 74318

Dynamics of classical and quantum spin systems with random fields See Entry 74370

Probability estimates for symmetric simple exclusion random walks See Entry 74391

Random-walk theory for localization See Entry 74394

Effects of topological solitons on autocorrelation functions for chains of coupled torsional oscillators See Entry 74395

Attenuation of fluctuations by an external field in a correlated walk See Entry 74396

Comment on 'Canonical-ensemble results for the Ising model with random bonds in two dimensions' See Entry 74405

Reply to 'Comment on 'Canonical-ensemble results for the Ising model with random bonds in two dimensions'' See Entry 74406

On the solution of the Fokker-Planck equation for Brownian movement in a one-dimensional periodic potential See Entry 74413

Intrinsic randomness and intrinsic irreversibility in classical dynamical systems See Entry 74423

Optical turbulence: chaos in optical bistability See Entry 75712

Bifurcations to chaos in optical bistability See Entry 75713

Observation of periodic and chaotic instabilities in an all optical bistable system See Entry 75715

Optical chaos in second-harmonic generation See Entry 75723

On the logarithmic law and Karman's constant See Entry 75996

Complete devil's staircase, fractal dimension, and universality of mode-locking structure in the circle map See Entry 76583

Random walks and correlation factors in diffusion via the vacancy mechanism in hexagonal-close-packed lattices See Entry 76686

Variational approach to dynamics of interfaces and quantized vortex lines See Entry 76725

Markov analysis of alpha-helical, beta-sheet and random coil regions of proteins See Entry 78137

05.50 LATTICE THEORY AND STATISTICS; ISING PROBLEMS

(see also 75.10H Ising models)

74390 Block spin renormalization group for dipole gas and $(\phi)^4$. K.Gawedzki (IHES, Bures-sur-Yvette, France), A.Kupiainen.

Ann. Phys. (USA), vol.147, no.1, p.198-243 (15 April 1983).

A rigorous, non-perturbative analysis of the block spin (BS) renormalization group is performed for a large class of massless lattice models such as the dipole gas and $(\phi)^4$. Effective Hamiltonians are shown to be driven to the line of Gaussian fixed points by iteration of the BS-transformation. Analyticity of the pressure and the dielectric constant in the (weak) coupling is proven. In particular, the perturbative expansion in activity for the dipole gas is convergent. (10 refs.)

74391 Probability estimates for symmetric simple exclusion random walks. A.de Masi, E.Presutti (Istituto Matematico Univ. dell'Aquila, L'Aquila, Italy).

Ann. Inst. Henri Poincaré Sect. B (France), vol.19, no.1, p.71-85 (1983).

Finitely many symmetric random walks in \mathbb{Z} , interacting by simple exclusion are considered. It is assumed that $\sum_{i \in \mathbb{Z}} x_i^2 \rho(x) < \infty$ where $\rho(x)$ is the probability that a single random walk jumps by x . A coupling Q of this process and the corresponding free one (where the exclusion condition is dropped) is established so that $Q(\{|x_i(t) - x_i^{(0)}(t)| \leq t^{1/2} : i = 1, \dots, n\}) \geq 1 - AT^{-\alpha}$ $\alpha > 1/4$ $\gamma < \alpha \beta - 1/2$ $\beta = \sum_{i \in \mathbb{Z}} |x_i|^2 \rho(x) < \infty$ ($\beta \leq 2$) where n is the number of particles, $x_i(t)$ [$x_i^{(0)}(t)$] the position at time t of particle i in the interacting [free] process and A may depend on α , γ and n . (10 refs.)

74392 Statistical theory of the degree of polymerization. Lee Jingde.

Acta Sci. Nat. Univ. Sunyatseni (Zhongshandaxue Xuebao) (China), no.4, p.50-7 (1982). In Chinese.

Introducing the concepts of empty group and empty bond, the degree of polymerization of a molecule can be studied with the Ising model of metastable states, in which the statistical theory on thermal equilibrium can no longer be used. The system is stable when the free energy has a minimum in the appearance of activating agents. For a cyclic chain, since the lower temperature orbit can not reach the representation point of an ordering state in configuration space, then polymerization is impossible. But for a long chain containing N structural units, the theory gives the results that the ceiling temperature $T_c = 2J/k \ln N^{1/2}$. The results are in good agreement with experiments for polymerization and dissociation of polymers. (10 refs.)

74393 'l-relatively atomic and h-relatively atomic lattices'. S.H.Raza (Dept. of Maths., Univ. of Delhi, Delhi, India).

Indian J. Theor. Phys., vol.29, no.3, p.299-303 (Sept. 1981).

The author has obtained various properties of atoms. It is shown that the m -atomistic left complemented lattice is an l -relatively atomic lattice, and that if $p(L)$ is a complete atomic lattice, then $p(L)$ is h -relatively atomic lattice. (3 refs.)

74394 Random-walk theory for localization. M.Chaturvedi (Dept. of Phys. & Astrophys., Univ. of Delhi, Delhi, India), V.Srivastava.

Int. J. Quantum Chem. (USA), vol.23, no.4, p.1463-8 (April 1983).

A continuous-time random-walk theory has been developed for Anderson localization. On a continuous time scale random walks are performed along extended (i.e. propagating) and localized (i.e. trap) states. Complete information of disorder is contained in a distribution function called 'hopping time distribution function' $\psi_{nm}(t)$, which gives the probability per unit time for transition from state m to state n in time t . The 'stay-put' probability $P(t=\infty)$, which is the probability to rediscover an excitation at a site '0' at time $t=\infty$ if it was there at $t=0$, is obtained in terms of $\psi_{nm}(t)$. Appropriate forms for $\psi_{nm}(t)$ are constructed which are in conformity with the photoconductivity experiments on dispersive transport, and $P(\infty)$ are calculated. The results indicate that the entire spectrum consists of three regimes, namely those of (i) 'diffusion', (ii) 'weak diffusion', and (iii) 'no diffusion', which, respectively, designate the extension, the power-law localization, and the exponential localization of states. The results also shed light on the question of 'continuous or discontinuous (?) transition across the mobility edge. (9 refs.)

74395 Effects of topological solitons on autocorrelation functions for chains of coupled torsional oscillators. D.Perechak, R.Yaris, J.Skolnick (Dept. of Chem., Washington Univ., St. Louis, MO, USA).

J. Chem. Phys. (USA), vol.78, no.11, p.6914-27 (1 June 1983).

Brownian dynamics computer simulations were performed on chains of coupled torsional oscillators. The purpose was to observe the changes in autocorrelation functions, related to typical experimental measurements, caused by the introduction of topological solitons or kinks into the system. The authors considered three model systems: a chain of coupled torsional oscillators, a chain of coupled torsional oscillators with additional onefold rotational potentials acting on each oscillator, and a chain of coupled torsional oscillators with additional threefold rotational potentials. These models are of interest because of their application to torsional motions in polymeric systems, and, in particular, the system with onefold rotational potentials has been studied extensively as the sine-Gordon chain. They present simulation results for three autocorrelation functions of these three systems both with and without topological solitons. (26 refs.)

74396 Attenuation of fluctuations by an external field in a correlated walk. S.V.Godoy (Univ. Autonoma Metropolitana-Iztapalapa, Mexico City, Mexico).

J. Chem. Phys. (USA), vol.78, no.11, p.6940-6 (1 June 1983).

Correlated walk in the presence of an external field is applied to the study of diffusion coefficients in simple cubic lattices. A continuous time distribution is introduced with the aid of the pausing time distribution developed by Montroll (1965). An exact expression for the diffusion coefficient is derived for perfect cubic lattices. It is found that the external field attenuates the effects of the RMS deviations. These results are used to discuss the atomic diffusion in cubic lattices with impurities, which act as traps. Comparison with previous experimental and theoretical results is made and discussed. (14 refs.)

74397 Metastable states near the phase boundary: a finite-lattice study. C.J.Hamer (Dept. of Appl. Math. & Theoretical Phys., Univ. of Liverpool, Liverpool, England). *J. Phys. A (GB)*, vol.16, no.6, p.1247-55 (21 April 1983). The energy of the metastable vacuum in a complex magnetic field has been computed for the Hamiltonian field theory version of the Ising model in (1+1)D, using finite-lattice methods. Evidence is found for an essential singularity at the phase boundary, as predicted by the droplet model. (16 refs.)

74398 Finite-size scaling in the (2+1)D Ising model. C.J.Hamer (Dept. of Appl. Math. & Theoretical Phys., Univ. of Liverpool, Liverpool, England). *J. Phys. A (GB)*, vol.16, no.6, p.1257-66 (21 April 1983). Hamiltonian eigenvalues are calculated for the (2+1)D Ising model on lattices up to 5X5 sites. Finite-size scaling techniques are used to estimate the critical coupling $x_c=0.329\pm0.001$, and index $\nu=0.635\pm0.005$. The prospects are discussed for further applications of these methods in three and four dimensions. (29 refs.)

74399 High-temperature differentiability of lattice Gibbs states by Dobrushin uniqueness techniques. C.Prakash (Dept. of Math., Univ. of California, Irvine, CA, USA). *J. Stat. Phys. (USA)*, vol.31, no.1, p.169-228 (April 1983). The author establishes conditions for the differentiability, to any order, of the Gibbs states of classical lattice systems with arbitrary compact single-spin space and with interactions in the Dobrushin uniqueness region. The derivatives are expressed as series expansions and are shown to be continuous on the uniqueness region. The author also provides a procedure for estimating the size of the derivatives. These results verify a conjecture of L. Gross and extend his results (1981). (27 refs.)

74400 The Coxeter-Todd lattice the Mitchell group and related sphere packings. J.H.Conway (Univ. of Cambridge, Cambridge, England), N.J.A.Sloane. *Math. Proc. Cambridge Philos. Soc. (GB)*, vol.93, pt.3, p.421-40 (May 1983). The authors study the Coxeter-Todd lattice Λ_6^* , its automorphism group (which is Mitchell's reflection group 6.PSU(4,3).2), and the associated 12-dimensional real lattice K_{12} . They give several constructions for Λ_6^* , which is a $Z[\omega]$ -lattice where $\omega=e^{2\pi i/3}$; enumerate the congruence classes of $\Lambda_6^*/2\Lambda_6^*$ and $\Lambda_6^*/\theta\Lambda_6^*$, where $\theta=\omega-\bar{\omega}$; prove the lattice is unique; determine its covering radius and deep holes; and study its connections with the lattice E_6 and the Leech lattice. A number of new dense lattices in dimensions up to about 10^7 are constructed. They also given an explicit basis for the invariants of the Mitchell group. They conclude with an extensive bibliography. (61 refs.)

74401 Phase transitions for the Ising model on the closed Cayley tree. J.E.Krizan, P.F.Barth (Dept. of Phys., Univ. of Vermont, Burlington, VT, USA), M.L.Glasser. *Physica A (Netherlands)*, vol.119A, no.1-2, p.230-42 (April 1983). The closed Cayley tree with the Ising model which was defined by Jellitto for a branching ratio of two is here generalized to an arbitrary branching ratio. The occurrence of a discontinuity in the spin-spin correlation functions is demonstrated and the free energy is obtained. The topology of the network, with its interesting correlation results makes the model a candidate for further investigation. (10 refs.)

74402 Bond percolation on the square lattice: anisotropic systems. A.R.McGurn (Dept. of Phys., Western Michigan Univ., Kalamazoo, MI, USA). *Physica A (Netherlands)*, vol.119A, no.1-2, p.295-306 (April 1983). Bond percolation on the square lattice in which horizontal and vertical bonds can have different occupation probabilities is studied within the context of annealed model solutions for the zero-temperature bond-diluted Ising ferromagnet. The percolation probabilities and pair-connectedness functions for this percolation are obtained in terms of the concentration of horizontal and vertical bonds in the system. Also, the critical behavior of these properties near the critical bond concentrations is determined. The neutron scattering from the annealed isotropic bond-diluted Ising ferromagnet is then studied in bond concentration (percolation) and temperature variables near the critical bond concentration point. Comparison of the crossover from thermal to percolative behavior is made with recent experiments by Cowley et al. (1970) on $Rb_2Co_2Mg_{1-x}F_x$. Finally, certain exact results for anisotropic plaquette percolation on the square lattice are presented. (12 refs.)

74403 Connectivity constant of the kagome lattice. K.Bhadra, C.K.Majumdar (Phys. Dept., Calcutta Univ., Calcutta, India). *Pramana (India)*, vol.20, no.1, p.73-5 (Jan. 1983). [received: May 1983] From the computation of self-avoiding walks on the kagome lattice, its connectivity constant is found to be 2.569 ± 0.008 . (12 refs.)

74404 Probability density function of the double-Gaussian model. P.D.Beale (Lab. of Atomic & Solid State Phys., Cornell Univ., Ithaca, NY, USA). *Phys. Rev. B (USA)*, vol.27, no.9, p.5804-6 (1 May 1983). An exact factorization of the partition function of the double-Gaussian model into Gaussian and Ising components is exploited to derive an exact factorization of the block probability density function. The block probability density function factors into a Gaussian, which describes the phonons in the problem, and a block probability density function of a long-ranged Ising model. This quantity is shown to be consistent with scaling assumptions near criticality. As long as the correlation length and the block size are much larger than the phonon correlation length, the scaling assumptions are satisfied. (7 refs.)

74405 Comment on 'Canonical-ensemble results for the Ising model with random bonds in two dimensions. K.Binder (Inst. fur Festkörperforschung, Kernforschungsanlage Jülich, Jülich, Germany), I.Morgenstern. *Phys. Rev. B (USA)*, vol.27, no.9, p.5826-8 (1 May 1983). In numerical calculations of a quantity $A(T)=\partial \ln X_{EA}/\partial T$, where $X_{EA}=\sum \langle \sigma_i \sigma_j \rangle$, for finite LxL Edwards-Anderson (EA) models, Fernandez [Phys. Rev. B25, 417 (1982)] finds that $A(T)$ has a peak at $T_0\approx 0.6$ (Gaussian model) or $T_0\approx 1.0$, for $L=4, 6, 8, 10$, or 11, respectively. He finds that the peak height $\lambda_{max}=A(T_0)$ increases in direct proportion to L , and interprets his results in terms of a phase transition at T_0 , where the correlation length $\xi_{EA}\propto (T-T_0)^{-1}$. This conclusion is in disagreement with the authors' previous findings that ξ_{EA} is finite in this temperature range, although a (dynamic) 'freezing transition' of the spins occurs at $T_f\approx 1.0$ (Gaussian model) or $T_f\approx 1.3$ ($\pm J$ model), which lead us to suggest that the two-dimensional EA model has a phase transition at zero temperature only. (4 refs.)

74406 Reply to 'Comment on "Canonical-ensemble results for the Ising model with random bonds in two dimensions".' J.F.Fernandez (Centro de Física, Inst. Venezolano Investigaciones Científicas, Caracas, Venezuela). *Phys. Rev. B (USA)*, vol.27, no.9, p.5829-30 (1 May 1983). In the previous Comment, (see *ibid.*, vol.27, p.5826, 1983), Binder and Morgenstern use their previous result, $\langle S_i S_j \rangle^2 = c \exp(-r_{ij}/\xi)$ for small systems, plus their hypothesis that ξ and c depend weakly on L , to produce results

strongly similar to what the author has obtained previously (see *ibid.*, vol.25, p.417, 1982). They thus suggest that results, contrary to his own conclusion, do not indicate the existence of a critical point in the Edwards-Anderson model in two dimensions. He shows here that their claim is not well founded. (3 refs.)

74407 Renormalization groups for two- and three-dimensional kinetic Ising models. F.Haake, M.Lewenstein (Fachbereich Phys., Univ. Essen-Gesamthochschule, Essen, Germany). *Phys. Rev. B (USA)*, vol.27, no.9, p.5868-71 (1 May 1983). Presents a renormalization group for kinetic Ising models. Recursion relations for flip rates are established through double series in powers of the inverse temperature and a self-consistently determined time-scale ratio. A static transformation is obtained as a subset of recursion relations in which only the inverse temperature appears as expansion parameter. The best second-order value for $d=2$ is $z=2.2$ (with an uncertainty of roughly 10%), while for the simple cubic lattice in $d=3$ the authors find $z=1.98$ if T_c is adjusted to the known numerical value. (8 refs.)

74408 Phenomenological renormalization and scaling fields. M.N.Barber (Inst. for Theoretical Phys., Univ. of California, Santa Barbara, CA, USA). *Phys. Rev. B (USA)*, vol.27, no.9, p.5879-82 (1 May 1983). Two methods of obtaining the linear scaling fields and related exponents from a phenomenological renormalization group on a multiparameter system are presented. The methods are illustrated by application to the Baxter-Wu (triplet) and the anisotropic Ising models, yielding excellent agreement with all exact or conjectured results. (18 refs.)

Gauge theory of dislocations and disclinations See Entry 74237

Dynamics of classical and quantum spin systems with random fields See Entry 74370

Percolation. Models, analog and numerical simulations See Entry 74371

Substrate-strain effects on the Frenkel-Kontorova system See Entry 76582

Random walks and correlation factors in diffusion via the vacancy mechanism in hexagonal-close-packed lattices See Entry 76686

The localization transition on the Bethe lattice See Entry 76846

Monte Carlo study of a triangular Ising lattice. I See Entry 77122

Critical point estimates for the spin s Ising model from the high temperature series renormalisation group method See Entry 77194

Critical temperature for a random-bond Ising model with frustration on a square lattice See Entry 77195

Ising model with magnetic field and the Diophantine moment problem See Entry 77198

05.60 TRANSPORT PROCESSES: THEORY

74409 The Boltzmann equation theory of charged particle transport. D.R.A.McMahon (Res. School of Phys. Sci., Austrian Nat. Univ., Canberra, Australia). *Aust. J. Phys. (Australia)*, vol.36, no.2, p.163-83 (1983). It is shown how a formally exact Kubo-like response theory equivalent to the Boltzmann equation theory of charged particle transport can be constructed. The author's response theory gives the general wavevector and time-dependent velocity distribution at any time in terms of an initial distribution function, to which is added the 'response' induced by a generalized 'perturbation' over the intervening time. The usual Kubo linear response result for the distribution function is recovered by choosing the initial velocity distribution to be Maxwellian. For completeness the response theory introduces an exponential convergence function into the 'response' time integral. This is equivalent to using a modified Boltzmann equation but the general form of the transport theory is not changed. The modified transport theory can be used to advantage where possible convergence difficulties occur in numerical solutions of the Boltzmann equation. The paper gives a systematic development of the modified transport theory and shows how the author's response theory fits into the broader scheme of solving the Boltzmann equation. (30 refs.)

74410 Identification of the polyrelaxational nonlinear differential mass diffusion operator. A.G.Temkin (Polytech. Inst., Riga, USSR). *Int. J. Heat & Mass Transfer (GB)*, vol.26, no.5, p.741-5 (May 1983). Diffusion in a non-homogeneous mixture is described by a polyrelaxational equation involving the diffusion coefficient which depends on concentration and several physical parameters. A set of the relaxation time spectra and diffusion coefficients (as functions of concentration) form a polyrelaxational nonlinear differential operator of mass diffusion. The method presented for the identification of this operator consists of the experimental determination of the relaxation time spectrum and of all the diffusion coefficient parameters. As initial information, the time derivative of the mass moment of the diffusing substance, and a substantially nonhomogeneous initial distribution of concentrations in an insulated rod of any shape but constant cross section, are used. (5 refs.)

74411 One-dimensional Boltzmann equation with a three-body collision term. Shang-keng Ma (Dept. of Phys., Univ. of California, San Diego, La Jolla, CA, USA). *J. Stat. Phys. (USA)*, vol.31, no.1, p.107-14 (April 1983). It is shown that a linearized one-dimensional Boltzmann equation with a certain simple three-body collision term is trivially soluble. (5 refs.)

74412 On the higher derivatives of the H-function for a model Boltzmann equation. J.O.Vigfusson (Inst. fur Theoretische Phys., Univ. Zurich, Zurich, Switzerland). *Physica A (Netherlands)*, vol.119A, no.1-2, p.380-6 (April 1983). It is shown that, contrary to the current belief, the H-function for a discrete Boltzmann equation model in general does not satisfy the condition $(-1)^d d^d H/dt^d \geq 0$. (18 refs.)

74413 On the solution of the Fokker-Planck equation for Brownian movement in a one-dimensional periodic potential. W.T.Coffey (School of Engng., Trinity Coll., Dublin, Ireland), P.Grignolini, P.Marin. *Proc. R. Ir. Acad. Sect. A (Ireland)*, vol.82A, no.2, p.167-76 (Dec. 1982). [received: May 1983] The Fokker-Planck equation for the Brownian movement in a potential (commonly called the Kramers equation) has considerable application in (a) the diffusion of charge carriers, in semiconductors, (b) the Josephson tunnelling junction, (c) chemical reaction rates, (d) superionic conductors and (e) dielectric relaxation of dipoles with dipole-dipole interaction. In this paper it is shown how the problem of solving the Kramers equation (and hence calculating the number density of the diffusing particles) may be reduced to that of solving a set of differential-difference equations in the time domain only. A numerical solution of these equations is presented, and several ensemble averages are calculated. These show clearly the non-Gaussian behaviour of the distribution function. (14 refs.)

- 74414 Statistical thermodynamics of turbulent transport processes.** D.N.Zubarev (V.A. Steklov Math. Inst., Acad. of Sci., USSR). *Theor. & Math. Phys. (USA)*, vol.53, no.1, p.1004-14 (Oct. 1982). Translation of: *Theor. & Mat. Fiz. (USSR)*, vol.53, no.1, p.93-107 (Oct. 1982). The method of nonequilibrium statistical thermodynamics is applied to the theory of transport processes in a liquid in the presence of strong fluctuations. The distribution functional of the densities of the momentum, energy, and particle number satisfies a Fokker-Planck equation and determines the entropy of a state with strong fluctuations. This makes it possible to obtain not only a hierarchy of Reynolds equations but also an entropy production that gives expression to the second law of thermodynamics. (22 refs.)
- 74415 Nonequilibrium statistical thermodynamics of two diffusion processes: diffusion dechanneling of particles and diffusion migration of light impurities. II. 'Quasichemical reaction'.** Yu.A.Kashlev (A.A. Baikov Inst. of Metall., Acad. of Sci., Moscow, USSR). *Theor. & Math. Phys. (USA)*, vol.53, no.1, p.1029-34 (Oct. 1982). Translation of: *Theor. & Mat. Fiz. (USSR)*, vol.53, no.1, p.129-37 (Oct. 1982). For pt.I see *ibid.*, vol.51, p.289 (1982). Two typical diffusion processes—diffusion dechanneling of particles and diffusion migration of light impurities—are treated as a single 'quasichemical reaction'. The kinetic laws of this reaction are discussed. (27 refs.)
- Heat and mass transfer bibliography—Soviet works** See Entry 74239
- Improved difference methods for steady incompressible convective diffusion equations** See Entry 74279
- Transverse transport processes of charged particle systems in a strong magnetic field. I. Quantum theory** See Entry 74301
- Stochastic transport in disordered systems** See Entry 74374
- Attenuation of fluctuations by an external field in a correlated walk** See Entry 74396
- Transverse transport processes of charged particle systems in a strong magnetic field. II. Some discussions about the Boltzmann equation** See Entry 75572
- Modern methods of numerical investigation of rarefied gas phenomena** See Entry 76073
- Fluid flow and transfer behavior of a drop translating in an electric field at intermediate Reynolds numbers** See Entry 76119

05.70 THERMODYNAMICS

(see also 44.60 Thermodynamic processes, 64. Equations of state, phase equilibria and phase transitions, 65. Thermal properties of condensed matter; for chemical thermodynamics, see 82.60)

- 74416 Thermodynamics based on the Hahn-Banach theorem: the Clausius inequality.** M.Feinberg (Dept. of Chem. Engng., Univ. of Rochester, Rochester, NY, USA), R.Lavine. *Arch. Ration. Mech. & Anal. (Germany)*, vol.82, no.3, p.203-93 (1983). The authors' immediate concern is not with the Clausius-Duhem inequality in its full generality but rather with the form it takes for cyclic processes. This more limited statement, called the Clausius inequality, is usually deemed to be a logical precursor of the Clausius-Duhem inequality. They believe that most, if not all, special theories based upon consideration of cyclic processes share features which, when suitably abstracted, permit analysis of those theories within a common framework. In the spirit of work by Coleman and Owen (1974) they seek to develop a 'theory of theories' which, for example, makes possible isolation of precisely those attributes a particular theory must have so that within its framework one or another of the two statements takes on validity. They are especially interested in separating those aspects of the Clausius inequality that depend only on the force of the Second Law from those that depend upon additional structure that might or might not be present within a given theory. (31 refs.)
- 74417 A justification for the scaling of the Thom-system.** Liu Jian-min, Gong Chang-de (Dept. of Phys., Nanking Univ., Nanking, China). *Commun. Theor. Phys. (China)*, vol.1, no.4, p.405-12 (1982). Discusses the critical behavior Thom-system using catastrophe theory. The universal critical asymptotic form of the family of free energy functions for Thom-system with one order parameter and two field parameters is obtained. The expressions for critical exponents, the scaling laws, and the scaling hypotheses are all derived from this universal asymptotic form. (17 refs.)
- 74418 Large numbers hypothesis. III. Kinetic theory, statistical physics, and thermodynamics.** P.J.Adams (Phys. Dept., Univ. of Puget Sound, Tacoma, WA, USA). *Int. J. Theor. Phys. (USA)*, vol.22, no.5, p.437-60 (May 1983). For pt.II see *ibid.*, vol.22, no.5, p.421 (1983). Dirac's large numbers hypothesis (LNH) is incorporated into kinetic theory, statistical physics, and thermodynamics using the self-consistent formalism of units covariance. The incohesive equation and matter creation introduce modifications of the most fundamental laws of the subject. Liouville's theorem no longer holds, and the Boltzmann equation is modified, as is the *H*-theorem. This affects the second law of thermodynamics in that for canonical LNH neither reversible nor adiabatic processes are possible (as expected). A significant result is that the collision terms have the same form as in standard physics. This means that equilibrium distribution functions are identical to those of standard physics, as required for self-consistency with the precepts of LNH. The net effect of LNH is as though all matter in the Universe were weakly coupled to a large heat bath. (10 refs.)
- 74419 Some maximal thermodynamic efficiencies for the conversion of blackbody radiation.** P.T.Landsberg (Dept. of Electrical Engng., Univ. of Florida, Gainesville, FL, USA). *J. Appl. Phys. (USA)*, vol.54, no.5, p.2841-3 (May 1983). Two efficiency formulas are derived for the conversion of blackbody radiation and their relationship is briefly discussed. It enables one to give an analytical expression for the entropy generation rate obtained previously by microscopic considerations. (7 refs.)
- 74420 Relationship of the virial series to vapor condensation and the liquid state.** A.J.Yang, I.Pavlin, J.H.Gibbs (Dept. of Chem., Amherst Coll., Amherst, MA, USA). *J. Chem. Phys. (USA)*, vol.78, no.11, p.7005-6 (1 June 1983). Recent work, with Mayer's form for the canonical ensemble partition function *Q* for a system of *N* particles in volume *V* at temperature *T*, has yielded a mean cluster size distribution $\{n_i\}$ displaying a bimodality which arises first at the spinodal value for the density $\rho = N/V$. One might assume that discovery and use of correct volume-dependent cluster integrals $b_i(V)$, in place of $b_i(\infty)$ previously used, is all that is required to lower this first appearance of bimodality to the coexistence pressure. The authors adopt an alternative point of view and pressures that the equation for *Q* is subject to the same implicit

assumption of density homogeneity as, e.g., mean field theories, and that therefore it too requires generalization along the lines prescribed by van Hove. (8 refs.)

- 74421 Self adjusting grid methods for one-dimensional hyperbolic conservation laws.** A.Harten (School of Math. Sci., Tel-Aviv Univ., Tel-Aviv, Israel), J.M.Hyman. *J. Comput. Phys. (USA)*, vol.50, no.2, p.235-69 (May 1983). It is shown how to automatically adjust the grid to follow the dynamics of the numerical solution of hyperbolic conservation laws. The grid motion is determined by averaging the local characteristic velocities of the equations with respect to the amplitudes of the signals. The resulting algorithm is a simple extension of many currently popular Godunov-type methods. Computer codes using one of these methods can be easily modified to add the moving mesh as an option. Numerical examples are given that illustrate the improved accuracy of Godunov's (1959) and Roe's (1982) methods on a self-adjusting mesh. (14 refs.)
- 74422 The approximate nature of the Onsager-Casimir reciprocal relations.** U.Geigenmuller, U.M.Titulaer, B.U.Felderhof (Inst. fur Theoretische Phys. A, RWTH Aachen, Aachen, Germany). *Physica A (Netherlands)*, vol.119A, no.1-2, p.53-66 (April 1983). The authors study thermodynamic systems near equilibrium described by both slow and fast variables. A reduced relaxation matrix for the slow variables can be obtained from the full relaxation matrix by a systematic elimination of the fast variables. When the full-relaxation matrix possesses Onsager-Casimir symmetry, the reduced matrix has contributions that violate this symmetry. For a sensible choice of the variables they are in general of second order in the time-scale ratio relative to the dominant terms. The occurrence of such a symmetry violation is demonstrated for a simple example. The symmetry violation is related to initial slip in the correlation functions on the reduced level of description. They discuss a way to salvage the Onsager-Casimir relations by an appropriate modification of the thermodynamic potential, or rather of an associated function similar to the Lagrangian in mechanics. (10 refs.)
- 74423 Intrinsic randomness and intrinsic irreversibility in classical dynamical systems.** M.Courbage, I.Prigogine (Faculte des Sci., Univ. Libre de Bruxelles, Brussels, Belgium). *Proc. Natl. Acad. Sci. USA*, vol.80, no.8, p.2412-16 (April 1983). The authors continue their previous work (see *Physica* vol.98A, p.1-26, 1979) on dynamic 'intrinsically random' systems for which they can derive dissipative Markov processes through a one-to-one change of representation. For these systems, the unitary group of evolution can be transformed in this way into two distinct Markov processes leading to equilibrium for either $t \rightarrow +\infty$ or $t \rightarrow -\infty$. To lift the degeneracy, the authors first formulate the second principle as a selection rule that is meaningful in intrinsically random systems. For these systems, this excludes a set of unrealizable states. As a result of this exclusion, permitted initial conditions correspond to a set of states that is not invariant through velocity inversion. In this way, the time-reversal symmetry of dynamics is broken and these systems acquire a new feature one may call 'intrinsic irreversibility'. The set of admitted initial conditions can be characterized by an entropy displaying the amount of information necessary for their preparation. The initial conditions selected by the second law correspond to a finite amount of information, while the initial conditions that are rejected correspond to an infinite amount of information and are therefore 'impossible'. The authors believe that their formulation permits a microscopic formulation of the second law of thermodynamics for well-defined classes of dynamical systems. (11 refs.)
- 74424 On information, negentropy and thermostatics.** C.G.Chakrabarti (Dept. of Appl. Math., Univ. of Calcutta, Calcutta, India). *Pramana (India)*, vol.20, no.1, p.65-72 (Jan. 1983). [received: May 1983] The interrelation between some basic concepts of information, theory and thermodynamics has been studied on the basis of the statistical measures of entropy and information. The problems studied are the negentropy principle of information, a minimax information principle of thermal equilibrium and the role of information correlation in the derivation of a functional equation characterising the statistical equilibrium of a system. (30 refs.)
- 74425 Equilibrium phase interfaces.** L.M.Trushkinovskii (V.I. Vernadskii Inst. of Geochem. & Analytical Chem., Acad. of Sci., Moscow, USSR). *Sov. Phys.-Dokl. (USA)*, vol.27, no.7, p.551-3 (July 1982). Translation of: *Dokl. Akad. Nauk SSSR*, vol.265, no.1-3, p.306-10 (July 1982). [received: April 1983] The author obtains the complete set of conditions at a moving front of an equilibrium phase transition in a heat-conducting, nonlinearly elastic medium. To the usual conditions of continuity of the fluxes of mass, momentum, and energy, he adds a relation which is a generalization of the well known condition of continuity of the chemical potential and serves for determining the velocity of the front. The structure of the discontinuity is constructed on the basis of the nonlocal equation of state. (10 refs.)
- 74426 On the theory of nonequilibrium processes in the projection operator method.** M.Yu.Tseitlin. *Ukr. Fiz. Zh. (USSR)*, vol.28, no.5, p.748-52 (May 1983). In Russian. Local and nonlocal approaches to the theory of irreversible processes are studied on the basis of one and the same method. It is shown that in the limit of large times, it leads to similar results. (22 refs.)
- Local equilibrium axiom for density flows in relativistic thermodynamics** See Entry 74275
- Critical dynamics and fluctuations for a mean-field model of cooperative behavior** See Entry 74314
- Noise-induced order** See Entry 74376
- Critical dimensionality and exponent of the 'true' self-avoiding walk** See Entry 74388
- Phase transitions for the Ising model on the closed Cayley tree** See Entry 74401
- Comment on 'Canonical-ensemble results for the Ising model with random bonds in two dimensions** See Entry 74405
- Reply to 'Comment on "Canonical-ensemble results for the Ising model with random bonds in two dimensions"** See Entry 74406
- Statistical thermodynamics of turbulent transport processes** See Entry 74414
- Properties of the vacuum. I. Mechanical and thermodynamic** See Entry 74580
- Bicriticality in the polymerization of chains and rings** See Entry 77888

06.00 MEASUREMENT SCIENCE, GENERAL LABORATORY TECHNIQUES, AND INSTRUMENTATION SYSTEMS

06.20 METROLOGY

06.20D Measurement and error theory

- 74427** Expression of the uncertainties of final measurement results: Reprints. C.Eisenhart, H.H.Ku, R.Colle. Report NBS-SP-644, Nat. Bur. Stand., Washington, DC, USA (Jan. 1983), v+13 pp.
This publication reprints and collects in one convenient source three articles, by NBS authors, that present a philosophical basis, general guidelines, and specific recommendations for expressing the uncertainties of final measurement results. (8 refs.)
- Error determination for standards and limits to influencing factors in metrological certification of strain gauges** See Entry 74456
- Influence of statistical experimental errors on amplitude correlations in resonance spectroscopy** See Entry 75223
- Reduction of the random component in measuring pulse laser radiation intensity** See Entry 75703

06.20F Units

- ICRU recommendations on radiation quantities and units — a critical review** See Entry 75248

06.20H Measurement standards and calibration

- 74428** A new definition of a meter: analysis of presumption and consequences. S.Angelotti, P.Forcella. *Elettrotecnica (Italy)*, vol.70, no.2, p.145-9 (Feb. 1983). In Italian.
A new definition of a meter by the International Bureau for Weights and Measures (BIPM) Consultative Committee for the Definition of Meter (CCDM) based on the exact value of the speed of light (299,792,458 m/sec) is analysed. A detailed analysis of light propagation speed aspects is given arguing that identical concepts are used for other physical quantities, e.g. candle in the international system of units. Effects on other constants used (Avagardo, Planck, Boltzmann, etc.) are considered, arguing that a meter is defined as a unit of length, not a distance. Conceptual expansion to a distance would cause more profound conceptual changes. (no refs.) *T.H.*
- 74429** Cubic spline fit to the 1958 ⁴He scale of temperatures. C.F.Barenghi, R.J.Donnelly, R.N.Hills (Dept. of Phys., Univ. of Oregon, Eugene, OR, USA). *J. Low Temp. Phys. (USA)*, vol.51, no.3-4, p.319-27 (May 1983).
The authors present a fit to the T₉₀ scale of temperatures using a cubic spline representation of the vapor pressure as a function of temperature. A discussion of the use and accuracy of the fit is included. (5 refs.)
- Rugby clock** See Entry 74442
- Method of certifying digital transducers for strain gauges with inductive dividers** See Entry 74455
- Error determination for standards and limits to influencing factors in metrological certification of strain gauges** See Entry 74456
- The Rodnik-2VK standard humid-gas generator [hygrometer test facilities]** See Entry 74477
- Standard apparatus for checking and calibrating hygrometers at negative temperatures** See Entry 74478
- Electron-photon coincidence technique for the absolute calibration of VUV detectors** See Entry 74533
- System for measuring energy and peak power of low-level 1.064 μ m laser pulses** See Entry 75704
- Certification of Si powder diffraction standard reference material 640a** See Entry 76251
- Hungarian-Austrian co-operation in radiation dosimetry** See Entry 78332
- A secondary standard dosimetry system for calibration of radiation protection instruments** See Entry 78353
- Seismic transducers: calibration systems** See Entry 78687

06.30 MEASUREMENT OF BASIC VARIABLES

- 74430** On the sensitive and wide frequency range measurement of pressure. Y.Tanaka (Dept. of Appl. Mech., Okayama Univ., Okayama City, Japan), M.Masuda, Y.Shimamoto. *Bull. JSME (Japan)*, vol.26, no.213, p.364-71 (March 1983).
The authors present analysing methods of the response characteristics necessary for designing a miniature pressure detector of capacitance type and electronic methods for realizing a sensitive and wide-band measurement of pressure. Several detectors, a transducer and an amplifier are prepared with the object of examining the adaptability and practicality of these methods. Dynamic measurement and static comparative test between the present device and other high-sensitive pressure measuring methods show that the analysis can well express the detector response to pressure and that the present method enables measurements more sensitive than the resolution of 0.002 mmAq (0.02 Pa). (10 refs.)
- Test results of an integrated fiber-optics gyroscope brass board** See Entry 75825

06.30C Spatial variables measurement

- (inc. measurement of all variables extending in space e.g. diameter, height, thickness, displacement, surface topography, particle size, area of disperse systems)*
- 74431** Linear capacitive microdisplacement transduction using phase read-out. K.B.Klaassen, J.C.L.van Peppen (Dept. of Electrical Engng, Delft Univ. of Technol., Delft, Netherlands). *Sens. & Actuators (Switzerland)*, vol.3, no.3, p.209-20 (May 1983).
Describes a principle for capacitive transduction of microdisplacements. Transducers based on this principle achieve a fixed, built-in sensitivity which

is determined only by the transducer's electrode geometry. This geometry can be manufactured accurately by photolithographic processes. The principle renders the transducer immune to small movements in directions other than the main sensitivity axis and to a small rotation and tilt of the electrode planes. The transducers require only one active electrode plane to which wires must be connected. A realization of the principle in thin-film technology is described. This transducer achieves a resolution better than 25 nm, a measurement span of about 1 cm and a non-linearity smaller than 2 μ m peak deviation from linear. A large-scale printed-circuit board realization with an improved electrode geometry results in even better specifications when the scale factor is taken into account. (6 refs.)

- 74432** Piezoelectric subdivision method of multiple-beam interference for flatness measurement. Chien Shih-nan (Anhui Inst. of Optics & Fine Mech., Acad. of Sci., Peking, China). *Chin. J. Sci. Instrum. (China)*, vol.4, no.1, p.3-8 (Feb. 1983). In Chinese.
The flatness of a precise plane is generally measured by making use of fringes of equal thickness. A piezoelectric subdivision method of multiple-beam interference is described using a group of reference fringes. The original gap between two adjacent fringes is a, and the gap between the new reference fringe and the original one should be a/m. The flatness is tested by direct observation or photography by making use of a/m as a standard. (4 refs.)

- 74433** Cryogenic liquid level monitor using a frequency to voltage converter. S.J.Collocott (CSIRO Div. of Appl. Phys., Sydney, NSW, Australia). *Cryogenics (GB)*, vol.23, no.6, p.327-8 (June 1983).
A simple cryogenic liquid level monitor based on a frequency-to-voltage converter is described. The monitor is simple to construct and its design obviates the need for special techniques to eliminate the effects of stray capacitance. It has excellent linearity, high sensitivity, and uses a simple two-terminal capacitance probe. (5 refs.)

- 74434** Objective laser speckle method for 3-D displacement measurement on curved surfaces. C.C.Kin, F.P.Chiang (Dept. of Mech. Engng., State Univ. of New York, Stony Brook, NY, USA). *Proc. SPIE Int. Soc. Opt. Eng. (USA)*, vol.335, p.54-8 (1982). [received: May 1983] (Advanced Laser Technology and Applications, Arlington, VA, USA, 6-7 May 1982).
By illuminating a ground glass with a laser beam, a spatial field of speckles is created. These speckles are used as displacement gauging elements of curved 3-D objects whose surfaces are coated with photosensitive material. Equations are derived to show that all the three components of the surface displacement can be obtained from two specklegrams. (6 refs.)

- 74435** Image analysis on the cheap [microcomputer application]. J.Rodgers (Lombardy Sci. Ltd., Berkhamsted, England). *Lab. Microcomput. (GB)*, vol.1, no.1, p.15-19 (Spring 1982).
Describes how an Apple microcomputer and its 'Graphics Tablet' bit pad can be used to determine particle size distributions from micrographs. In the method particle shapes are digitised on the bit pad and standard software is used to calculate the particle size and compute the statistics. (no refs.)

- 74436** Laser interference method of measuring small taper angles in plates in the IR range. V.S.Sollogub. *Meas. Tech. (USA)*, vol.25, no.9, p.725-8 (Sept. 1982). Translation of: *Izmer. Tekh. (USSR)*, vol.25, no.9, p.16-18 (Sept. 1982). [received: May 1983]
The proposed method employs a collimated laser beam which passes through the test plate perpendicular to the surface, and a receiving device which measures the relative change in radiation power after passage through the plate. A characteristic feature of the method is that the plate is rotated slowly (deflected through a small angle) relative to the direction of the laser beam, e.g. with a screw rotation mechanism. One observes the changes in the transmission coefficient due to interference. One reads the output of the detecting device corresponding to extremal values of the transmission coefficient T_{max}, T_{min}; then the ratio T_{max}/T_{min} is used to determine the taper angle from a graph. The angle of deviation of the plate and the sense of the deviation play no part. (6 refs.)

- 74437** 3-D measurement by using a multiplex hologram. K.Okada, T.Honda, J.Tsujuchi (Imaging Sci. & Engng. Lab., Tokyo Inst. of Technol., Yokohama, Japan). *Opt. Commun. (Netherlands)*, vol.45, no.5, p.320-2 (1 May 1983).
A method for measuring three dimensional position by using a multiplex hologram is proposed with some examples of measurements. (8 refs.)

- 74438** Cantilever and capacitor technique for measuring dilatation. W.Primak, E.Monahan (Solid State Sci. Div., Argonne Nat. Lab., Argonne, IL, USA). *Rev. Sci. Instrum. (USA)*, vol.54, no.5, p.544-51 (May 1983).
The relationship of EerNisse's technique for measuring small dilatations caused by irradiation with short-range particles, which utilizes a metallized thin plate mounted as a cantilever below whose free end an electrode is placed (forming a capacitor), to a photoelastic technique and to an interferometric technique are derived. The effects of stray capacitance, the fringing field of the capacitor, the clamping stress on the cantilever plate, the electrical resistance of the metallic coating, the charging of the tank circuit of which the capacitor is an element, the flange bolting stress, and the beam heating are assessed, and examples of the manner in which they contaminate the data are given. (13 refs.)

- 74439** Accurate in situ measurement of near-surface volume dilatation in irradiated silica through capacitance monitoring of cantilever deflection. C.B.Norris (Sandia Nat. Labs., Albuquerque, NM, USA), E.P.EerNisse. *Rev. Sci. Instrum. (USA)*, vol.54, no.5, p.552-8 (May 1983).
Irradiating a solid with short-range particles often induces a net volume change in the range zone which results in a shallow layer of stressed material. Micron-depth volume dilatations in the part-per-million range can be studied using cantilever mounting of a long, thin, metallized specimen, whose stress-induced bending perturbs the capacitance between the cantilever and a small counterelectrode mounted close to the unirradiated face. This approach has been used successfully by many workers for more than 20 yrs. Elsewhere the authors have reported the construction of a highly sensitive cantilever/capacitor apparatus and its application in the first accurate measurements of ionization dilatation phenomena in fused silica and grown SiO₂ at low electron energies. In this paper they outline key details of apparatus design and experimental technique for successful cantilever/capacitor work. Many contrasts with the work of Primak and Monahan [Rev. Sci. Instrum. 54, 544 (1983), preceding paper] are pointed out. The authors also highlight previous short-term annealing results which make it clear that the compaction of silica will appear to be significantly less in optical measurements made hours after irradiation than in cantilever/capacitor measurements made minutes after irradiation. (19 refs.)

74440 Operating experience with the type UT-80B electromagnetic-acoustic thickness gauge. V.V.Klyuev, S.N.Shubaev, V.F.Muzhitskii (Sci.-Res. Inst. of Introscopy, Moscow, USSR).

Sov. J. Nondestr. Test. (USA), vol.18, no.9, p.700-5 (Sept. 1982). Translation of: *Defektoskopiya (USSR)*, vol.18, no.9, p.37-43 (Sept. 1982).

The type UT-80B electromagnetic-acoustic thickness gauge is described. The results of its tests and industrial operating experience are presented. (6 refs.)

74441 A family of grating sensors. R.T.Murray (Imperial Chem. Industries, Runcorn, England).

First International Conference on Optical Fibre Sensors, London, England, 26-28 April 1983 (London, England: IEE 1983), p.114-16

The author has examined a range of optical effects which could be used as the basis of a remote passive sensor with fibre optic links to the control point. In that most control situations require a number of variables to be reported to the intelligent centre it is important that the various sensors and transmission codes be compatible with one another. Conventionally in the industrial scene compatibility is achieved by supplying electrical power to a signal conditioner which then transmits the data as an analogue signal within the standard 4-20 m amp range. If however one attempts to design an optical system in which the sensors are entirely passive this approach is not open to one and the author has therefore obtained compatibility by seeking a universal parameter to which all important measurements can be transduced and which is then used to modulate the optical signal. The simplest quantity to measure optically is displacement to which the major physical variable, pressure, temperature, flow rate and level may readily be transduced. Many techniques exist for measuring displacement optically but for the sake of simplicity the author has chosen to use the properties of a pair of square wave gratings. (6 refs.)

Automated goniometer employing a ring laser See Entry 74510

Outlook for the use of the Michelson interferometer for measuring the physical parameters of nonuniform semiconductor structures See Entry 74524

Automated laser speckle interferometry displacement contour analyzer See Entry 74525

1.73 μm eyesafe laser rangefinder See Entry 75677

Fibre optics QC challenge See Entry 75802

Mathematical modelling of the geometrical shape of polyhedral fibre-optic elements See Entry 75816

Checking manufacturing accuracy for the axial system in an optical planometer See Entry 75837

Acoustical speckle interferometry See Entry 75888

A piezoelectric displacement transducer for use in a pulse-shape based analysis of acoustic emission See Entry 75889

Determination of the thickness of the information-carrying layer in the examination of the structure by the Barkhausen noise method See Entry 77844

06.30F Time and frequency measurement

(for astronomical aspects see 95.70)

74442 Rugby clock. S.Makumbi.

Electron. Today Int. (GB), vol.11, no.8, p.60-3 (Aug. 1982). [received: May 1983]

Describes a specialised receiver of the type required to demodulate and decode the Rugby time signals. The project clock displays the correct time of day, date, day of week with no need to ever correct it. Even when the signal completely disappears the clock senses this and automatically switches on to its own crystal timebase back-up clock. Included is a comprehensive alarm system comprising eight independent alarms. For each alarm setting there is a choice of a melody, altering the state of eight TTL-compatible lines. (no refs.)

Two-dimensional movements detected by optoelectronic means [cameras] See Entry 74547

06.30G Velocity, acceleration and rotation measurement

(for flow velocity measurement see 47.80)

74443 Some remarks on the selection of sensors for correlation velocity measurement systems. R.Massen (Inst. of Sci. & Technol., Konstanz, Germany).

Sens. & Actuators (Switzerland), vol.3, no.3, p.221-31 (May 1983).

Correlation is a very useful tool for measuring time-delays and velocities of moving surfaces and flows. As only the peak position of the sensor signal's cross-correlation function is evaluated, the d.c. parameters of the sensor and the analog preprocessing circuits play only a secondary role. The specific requirements for all sensors used in a correlation measurement system are related to the a.c. signal parameters: bandwidth, differential phase shift, spatial filtering. These requirements are discussed in general terms and a set of practical guide-lines for selecting and optimizing the sensors are presented. Two specific applications are covered. (14 refs.)

Harmonic feed-back approach to fiber gyro scale factor stabilization See Entry 75822

Analysis of noise and bias in the fibre optic gyroscope See Entry 75823

An integrated optic fibre gyroscope: performance and limitations See Entry 75824

Heterodyne optical fibre gyroscope See Entry 75826

Dispersion-induced non-reciprocal effects in phase-nulling fibre gyroscopes See Entry 75827

Laser diode frequency modulation for directional laser doppler velocimetry See Entry 76140

Differential Doppler velocimetry using polarization-preserving optical fiber See Entry 76141

06.30L Measurement of basic electromagnetic variables

(see also 07.50 Electrical instruments and techniques)

Peak sampled vibrating-reed for the measurement of electric fields in the presence of space charge See Entry 74493

Magnetostrictive fiber-optic sensor system for detecting DC magnetic fields See Entry 75812

A fibre optic electric field sensor using the electrooptic effect of $\text{Bi}_2\text{Ge}_2\text{O}_{12}$ See Entry 75829

06.50 DATA HANDLING AND COMPUTATION

(see also 02.70 Computational techniques; 29.80 Nuclear information processing; for optical data processing, storage and retrieval see 42.30; for geophysical data acquisition and storage see 93.65)

74444 A digital-to-digital interface for a laboratory microcomputer: hardware and software. G.H.Vickers, T.O.Trask, J.D.Parli, J.A.Wisman, B.Durham, R.B.Green (Dept. of Chem., Univ. of Arkansas, Fayetteville, AR, USA).

Chem. Biomed. & Environ. Instrum. (USA), vol.12, no.4, p.289-97 (1982-1983).

Describes the design and construction of a digital-to-digital interface for a laboratory microcomputer. In this application, signals from a laser-enhanced ionization experiment are processed with a boxcar signal averager which is interfaced to a Commodore PET 4032 microcomputer. Software has been developed for the microcomputer which performs various operations on the data and prints the values for the average analyte signal, average standard signal, analyte-to-standard ratio, average noise, and analyte signal-to-noise ratio. This interface is also applicable to other laboratory instruments with binary-coded decimal outputs. (6 refs.)

74445 Interfacing and operation of a Princeton Applied Research multi-channel detector controller with a Digital Equipment Corporation DECLA-B-11/MNC computer[spectroscopy application]. P.D.Smith (Biomedical Engng. & Instrumentation Branch, National Inst. of Health, Bethesda, MD, USA), G.W.Liesegang.

Interfaces Comput. (Switzerland), vol.1, no.2, p.161-70 (May 1983).

The hardware and software aspects of an interface between a Princeton Applied Research (PAR) model 1216 Vidicon controller and a Digital Equipment Corporation DECLA-B-11/MNC computer are described; the system is used to control parallel optoelectronic image detectors in spectroscopy. The interface permits complete control of the Vidicon scanning parameters and data gathering. A major advantage over the OMA series offered by PAR is that the computer is not dedicated to control of the Vidicon; its full capabilities are available for additional tasks such as experimental control. (5 refs.)

74446 Nonlinear regression least-squares method for determining relaxation time spectra for processes with first-order kinetics. J.R.Cost (Los Alamos Nat. Lab., Los Alamos, NM, USA).

J. Appl. Phys. (USA), vol.54, no.5, p.2137-46 (May 1983).

A simple method is shown for calculating the relaxation time spectrum which controls the rate at which a process following simple first-order kinetics takes place. The method involves unfolding a Fredholm equation of the first kind using least-squares and then using a modified nonlinear regression rather than a linear least-squares technique, thereby avoiding the highly oscillatory solutions which tend to occur with the latter with reduced mesh spacing or an increased number of bins. The validity and accuracy of the method for analyzing experimental data to reproduce various known input spectra are assessed and found to be excellent for data with no experimental error. For data with simulated experimental error with standard deviations up to $\sigma=0.05$ the method provides acceptable approximate solutions even though no exact solution is expected. Increasing the magnitude of the experimental error for a single lognormal input spectrum appears to have an increasing but nonsystematic affect upon the uncertainty of the approximate solution. Effects due to increasing the number of bins in the interval over which the spectrum is calculated are assessed and shown not to appreciably change the results, even for up to 60 bins. The method is shown to be applicable to a wide variety of input spectra, including single and double lognormal and box distributions. Importantly, in each of the cases studied the approximate solution appeared both to be unique and to converge toward the known input spectrum. Based upon this validation it is concluded that this method has applicability to a wide range of problems in which simple exponential decay is occurring with a spectrum of time constants. It may also be useful for problems with different kernels than that for first order kinetics; however, careful validation will be required. (10 refs.)

Image analysis on the cheap [microcomputer application] See Entry 74435

Analysis of shock data produced by a drop test See Entry 74458

Standard hygrometer facilities at the Promenergoremont cooperative See Entry 74479

An effective phase correction method in Fourier transform spectroscopy See Entry 74501

Automated laser speckle interferometry displacement contour analyzer See Entry 74525

An automated high resolution spectrometer with data system See Entry 74539

10-Hz coherence anti-Stokes Raman spectroscopy apparatus for turbulent combustion studies See Entry 74542

Automation of a gas analyser by personal computer See Entry 74554

Morphological SEM picture processing See Entry 74563

Computer generation of isomeric structures See Entry 75553

A method for automatic measurement of Brinell hardness using a microcomputer See Entry 75969

On-line Fourier analysis of the shapes of X-ray diffraction peaks See Entry 76253

06.60 LABORATORY TECHNIQUES

74447 The compensated reciprocating pump model BHB-1 for HPLC. Liu Chi-chia, Yu Yen-ching (Dalian Inst. of Chem. Phys., Acad. of Sci., Peking, China).

Chin. J. Sci. Instrum. (China), vol.4, no.1, p.57-65 (Feb. 1983). In Chinese.

The function, structure and design principle of a compensated reciprocating pump (Model BHB-1) used in liquid chromatography are described in detail. An equation for calculating the cam, the major driving part of the pump, has been derived. The used apparatus is described and the results of the pressure fluctuation and the pump operation are given. (no refs.)

74448 Welding parameter dependence of the shape of the channel formed during electron-beam welding. V.N.Rodigin.

Sov. Phys.-Dokl. (USA), vol.27, no.8, p.646-7 (Aug. 1982). Translation of: *Dokl. Akad. Nauk SSSR*, vol.265, no.4-6, p.1127-30 (Aug. 1982). [received: May 1983]

The shape of the vapor channel for electron-beam welding is a central question, since the shape of the channel determines the main parameters of the welded joint—its depth and width. When the beam moves along the surface of the metal, the metal melts at the forward wall of the channel and the molten metal is forced toward the rear wall of the channel. (7 refs.)

- Nonlinear interactions with intense femtosecond optical pulses See Entry 75710
- Amplitude and phase nonlinear response of bleachable dyes using picosecond excitation See Entry 75752
- Optical power limiter with picosecond response time See Entry 75756
- A simple method to cut a single crystal in any desired direction See Entry 76238

06.70 GENERAL INSTRUMENTATION

- 74449 Pd/a-Si:H metal-insulator-semiconductor Schottky barrier diode for hydrogen detection.** A.D'Amico, G.Fortunato, G.Petrocco (Istituto di Elettrotecnica dello Stato Solido, CNR, Roma, Italy), C.Colozza. *Appl. Phys. Lett. (USA)*, vol.42, no.11, p.964-5 (1 June 1983).
- Hydrogenated amorphous silicon (a-Si:H), produced by the glow-discharge technique, has been used to construct very low cost, high quality metal-insulator-semiconductor structures where palladium has been utilized as catalytic metal for hydrogen detection. With this device, hydrogen concentration in hydrogen-nitrogen mixture as low as 100 ppm has been detected. There is indication that the ultimate limit is much lower. (13 refs.)
- 74450 Characteristics of semiconductor gas sensors. I. Steady state gas response.** P.K.Clifford, D.T.Tuma (Electrical Engng. Dept., Carnegie-Mellon Univ., Pittsburgh, PA, USA).
- Sens. & Actuators (Switzerland)*, vol.3, no.3, p.233-54 (May 1983).
- The steady state gas sensing characteristics of SnO₂ gas sensors, as exemplified by the Taguchi Gas Sensor (TGS), are comprehensively studied. Resistance responses to hydrogen, methane, carbon monoxide and water vapor are experimentally characterized, with particular emphasis on multiple gas interactions. The presence of ambient oxygen is essential to the sensor's operation and the detection of combustible or reducing gas is mediated by reaction with adsorbed oxygen to the sensor surface. A quantitative model of device operation is constructed which unifies the diverse properties of the TGS and other semiconductor sensors. The model supplies the mathematical framework for meaningful comparisons of sensor performances of gas sensitivities. In addition, it provides for the intrinsic power law response of sensor electrical resistance to combustible gas concentrations, the competitive and synergistic interactions of several gas detected simultaneously, and the source of sensor unselectivity. (14 refs.)
- 74451 Characteristics of semiconductor gas sensors. II. Transient response to temperature change.** P.K.Clifford, D.T.Tuma (Electrical Engng. Dept., Carnegie-Mellon Univ., Pittsburgh, PA, USA).
- Sens. & Actuators (Switzerland)*, vol.3, no.3, p.255-81 (May 1983).
- For pt.1 see ibid., vol.3, no.3, p.233-54 (May 1983). Temperature-stimulated transient responses of the conductance of SnO₂ gas sensors, as exemplified by the Taguchi Gas Sensor (TGS) are comprehensively studied. These responses are derived at many temperatures for sensors exposed to several fixed concentrations of oxygen in nitrogen. The dynamic response of conductance exhibits complex kinetics characterized by time constants which range, depending on ambient conditions, from seconds to days. Measurement results are analyzed in the light of a proposed model of device behavior. This heuristic model is constructed by combining some fundamental experimental observations with kinetic predictions of the barrier layer theory of absorption. The analyses result in identification of the physical mechanisms responsible for the complex kinetics and long time constants. The authors find that sensor conductance is controlled by an intergranular potential barrier consequent to oxygen absorption. The barrier potential exhibits an Elovich-type rate kinetic and its functional dependences on sensor temperature for several oxygen partial pressures are determined. (28 refs.)
- 74452 Dummy stable bridge source digital strain indicator and the elimination of nonlinear errors.** Chang Yu-liang (Central Coal Mining Res. Inst., China).
- Chin. J. Sci. Instrum. (China)*, vol.4, no.1, p.25-31 (Feb. 1983). In Chinese.
- The dummy stable bridge source digital strain indicator proposed has a great advantage over traditional digital strain indicator. Its features are as follows: nonlinear errors inherent in strain indicator are eliminated; the structure is greatly simplified and the cost is reduced; system parametric errors of the instrument are reduced; the precision of the gage factor can be linearly adjusted to four-digit number by a multiple turn potentiometer, and the value can be read out directly from the dial of the potentiometer or from the display. Nonlinear errors and system parametric errors of both traditional and dummy stable bridge source are analysed in some detail. Nonlinear quantitative analysis of 45 applications is presented. (2 refs.)
- 74453 The design of an amperometric detector for FIA.** Ma Hui-chang Yen, Hui-yu (Inst. of Environmental Chem., Acad. of Sci., Peking, China).
- Chin. J. Sci. Instrum. (China)*, vol.4, no.1, p.44-8 (Feb. 1983). In Chinese.
- A new amperometric flow-through detector applied to flow injection analysis (FIA) and continuous flow analysis is designed. It is composed of an Au tubular working electrode, a stainless-steel tubular counter electrode, and AgCl reference electrode. By using the FIA technique, response is linear for levels from a few tenth of microgram to several milligrams per liter of solution. Analytical rates of 100 samples per hour can be achieved. (7 refs.)
- 74454 Metrological security of strain-gauge measurements in experimental studies.** A.I.Beklemishev, B.S.Dubov, N.P.Klokov, L.I.Kosov.
- Meas. Tech. (USA)*, vol.25, no.9, p.737-41 (Sept. 1982). Translation of: *Izmer. Tekh. (USSR)*, vol.25, no.9, p.32-5 (Sept. 1982). [received: May 1983]
- Strain-gauge measurements are the principal method of obtaining information in the course of various experimental studies. Strain-gauge systems are widely employed to measure forces, pressures, and displacements as well as to determine the strength of structural designs. These systems include the following elements: tensoresistors or tensoresistive transducers for nonelectrical quantities, measuring arrangement (equipment), and arrangements for recording and processing the information. The tensoresistors serve as primary transducers for determining strains in structures under various conditions in a strength experiment or as intermediate transducers in measuring arrangements. Metrological provisions for the tensoresistors are discussed. (24 refs.)
- 74455 Method of certifying digital transducers for strain gauges with inductive dividers.** M.L.Daichik, V.P.Silaev, A.R.Tsugba, M.M.Lupinski, L.M.Katanov.
- Meas. Tech. (USA)*, vol.25, no.9, p.742-4 (Sept. 1982). Translation of: *Izmer. Tekh. (USSR)*, vol.25, no.9, p.37-8 (Sept. 1982). [received: May 1983]
- The certification of a strain-gauge transducer requires the use of a simulator for the output signal of the strain-gauge resistor as the standard facility, this being a device that enables one to set the relative value $\Delta R/R$ with the required accuracy. This causes certain difficulties when one has to deal with transducers with wide limits of measurement and small errors. The authors consider checking the scale uniformity for a transducer with a four-digit inductive divider. In the coil for each digit, there are not only ten sections for

balancing the input signal but also a section equal in number of turns and therefore in induced EMF that transmits 1/10 of the voltage to the coil for the next digit. In the last digit, this section corresponds in induced EMF to one in the least-significant digit and does not participate in the automatic balancing. (no refs.)

74456 Error determination for standards and limits to influencing factors in metrological certification of strain gauges. L.I.Kosov.

Meas. Tech. (USA), vol.25, no.9, p.744-6 (Sept. 1982). Translation of: *Izmer. Tekh. (USSR)*, vol.25, no.9, p.38-9 (Sept. 1982). [received: May 1983]

Relations are derived for the permissible limit of the errors in standard facilities and for the influencing quantities for various characteristics of a strain gauge. These formulas enable one to use the characteristics laid down in the technical documentation to select measuring facilities having the required accuracy in testing samples of strain gauges, and also to establish the limits to the temperature variation in the time intervals. (6 refs.)

74457 Portable oscilloscope design. V.Foster (Hitachi Denshi (UK), Hendon Ltd., England).

New Electron. (GB), vol.16, no.8, p.56, 60 (19 April 1983).

Discusses the design of an Hitachi oscilloscope aimed at the field service market. The instrument had to be small and light, yet robust and easy to use, and due to these needs less obvious factors soon come into play. Since it had to have battery operation power consumption had to be kept to a minimum. The three areas where power could be saved: the DC converter; the cathode ray tube and the vertical output amplifier were all specially designed for maximum economy. (no refs.)

- On the sensitive and wide frequency range measurement of pressure See Entry 74430
- Linear capacitive microdisplacement transduction using phase read-out See Entry 74431
- Operating experience with the type UT-80B electromagnetic-acoustic thickness gauge See Entry 74440
- Some remarks on the selection of sensors for correlation velocity measurement systems See Entry 74443
- Continuous flow cryostats for experiments in the presence of appreciable heat influx to the specimen See Entry 74472
- Use of commercial metallic strain gauges as low temperature heaters See Entry 74473
- Peak sampled vibrating-reed for the measurement of electric fields in the presence of space charge See Entry 74493
- Cryostats for SQUID magnetometers See Entry 74496
- Installation to determine the index of the heterogeneity of glass See Entry 74540
- Automated fail-safe control system for independent operation of two radiation shutters on a rotating-anode X-ray source See Entry 76258
- A new transducer to monitor fatigue crack propagation See Entry 77822

07.00 SPECIFIC INSTRUMENTATION AND TECHNIQUES OF GENERAL USE IN PHYSICS

(see also within each subdiscipline for specialized instrumentation and techniques)

07.10 MECHANICAL INSTRUMENTS AND MEASUREMENT METHODS

(for measurement in the mechanics of solids and rheology, see 46.30R; for materials testing, see 81.70)

- 74458 Analysis of shock data produced by a drop test.** T.E.Lanham (IBM Corp., Armonk, NY, USA).
- IBM Tech. Disclosure Bull. (USA)*, vol.25, no.11A, p.5493-4 (April 1983).
- Shock data produced when an object under test is dropped from a predetermined height is analyzed by a program in order to determine a time profile of 'g'-levels and velocity changes experienced by the object. (no refs.)
- Stability of gyro with harmonic nonlinearity in spinning vehicle See Entry 74257
- Cantilever and capacitor technique for measuring dilatation See Entry 74438
- Accurate in situ measurement of near-surface volume dilatation in irradiated silica through capacitance monitoring of cantilever deflection See Entry 74439
- Simplified vibrating-reed technique for the measurement of the temperature dependence of Young's modulus of small samples See Entry 75970

07.20 THERMAL INSTRUMENTS AND TECHNIQUES

(see also 44.50 Thermal properties of matter, 44.60 Thermodynamic processes; for radiometry and detection of thermal radiation see 07.60D and 07.62)

- 74459 Detectors for thermal imaging.** J.A.Chiari, F.D.Morten (Mullard Ltd., Southampton, England).
- Electron. Components & Appl. (Netherlands)*, vol.4, no.4, p.242-52 (Aug. 1982). [received: April 1983]
- Using the natural infrared radiation of the environment, thermal imagers can see through fog and smoke, even in total darkness. They can also picture much that is otherwise invisible, such as heat loss and patterns of temperature distribution. Present developments in infrared detectors promise to simplify both the optics and electronics of tomorrow's thermal imagers. (6 refs.)
- 74460 Heat transfer performance of ceramic regenerator matrices with sine-duct shaped passages.** C.W.Rapley, A.I.C.Webb (Dept. of Mech. Engng., Sunderland Polytech., Sunderland, England).
- Int. J. Heat & Mass Transfer (GB)*, vol.26, no.6, p.805-14 (June 1983).
- Experimental data relating to the heat transfer performance of sine-duct type passages in laminar flow ceramic regenerator matrices are reported. In particular, the range of aspect ratio (ratio of passage height to base) for which data is available is extended and the influence of passage geometry is considered in a detailed comparison of the measurements with previously reported data. The results indicate that no clear advantage is likely to be obtained with

the higher aspect ratio matrices tested and overall the level of heat transfer is higher than may be expected from predictions with standard boundary conditions. (39 refs.)

74461 Observations on the stability of thermistors. T.J.Edwards (Phys. Dept., Univ. of Western Australia, Nedlands, Western Australia, Australia). *Rev. Sci. Instrum. (USA)*, vol.54, no.5, p.613-17 (May 1983). This paper investigates the long-term stability of three different types of thermistor with room-temperature resistances ranging from 80 to 150 k Ω . Precision measurements of thermistor resistance and temperature were made in a thermal environment controlled to ± 3 μ K. Measurements took place in between periods of limited thermal cycling and also during 100 days at constant temperature. Mechanical shock and strain appear to be the cause of the high drift rates observed in some thermistors; the majority of the thermistors were, however, very stable, with drift rates around 0.1 mK per 100 days and were unaffected by thermal cycling. Such low drift rates indicate that certain thermistors could be used as convenient temperature transfer standards with a reproducibility in the submillikelvin range. (17 refs.)

Signal-to-noise ratio analysis of a digital polarimeter application to thermal imaging See Entry 74516

Temperature-controlled microscope with millidegree stability .. See Entry 74532

Infrared optical constants of PtSi See Entry 77347

A universal heat source for active thermal inspection See Entry 77838

07.20D Thermometry

74462 Gate controlled amplifier for platinum NMR thermometry. Y.Jin-zaki (Dept. of Materials Sci., Hiroshima Univ., Hiroshima, Japan), Y.Okuda, A.J.Ikushima.

Cryogenics (GB), vol.23, no.6, p.321-3 (June 1983). A 250 kHz pulsed NMR circuit for measurement of platinum nuclear susceptibility is described. The nuclear free induction decay signal is detected using the single-coil method. Saturation of the amplifier is avoided by gating the RF pulse. This system is used for nuclear thermometry below 30 mK. (11 refs.)

74463 Fast neutron produced $^{54}\text{MnFe}$ nuclear orientation thermometers. H.Postma, H.Brouwer, H.C.Meijer (Dept. of Appl. Phys., Univ. of Technol., Delft, Netherlands).

Cryogenics (GB), vol.23, no.6, p.328-30 (June 1983). Fast-neutron irradiation of pure iron foils has been used to produce ^{54}Mn in iron for nuclear orientation thermometry instead of the commonly used diffusion technique. Compared with a $^{60}\text{CoCo}$ nuclear orientation thermometer good agreement was found. No deviations occurred if an externally magnetizing field of 0.2 T or larger was used. (10 refs.)

74464 Measurement of high gas-stream temperature using dynamic thermocouples. N.Venkatramani, P.Satyamurthy, N.S.Dixit, J.P.Lancelot, V.K.Rohatgi (Plasma Phys. Section, Bhabha Atomic Res. Centre, Bombay, India).

Int. J. Heat & Mass Transfer (GB), vol.26, no.5, p.663-9 (May 1983). The dynamic probe technique using the transient response of a thermocouple is one of the methods of measuring high temperature flowing gases. In this paper, the complete dynamic response of a thermocouple has been solved consisting of convective, conductive, and radiative terms. The solution has been used to arrive at correction factors for actual experimental data. The use of dynamic thermocouples in the measurement of temperature profiles has also been illustrated by experiment. The model is verified at lower temperatures using a bunsen flame. (9 refs.)

74465 New method for visualizing temperature distributions using thermochromism. O.Sano, R.Takaki (Faculty of General Education, Tokyo Univ. of Agriculture & Technol., Tokyo, Japan).

J. Phys. Soc. Jpn. (Japan), vol.52, no.5, p.1549-54 (May 1983). Thermochromism in aqueous solutions of cobalt chloride with sodium chloride was used to visualize temperature distributions in a liquid. Changes of color of the solution due to temperature variations were observed both by direct photography and by measurements of the transmittance of light. The advantage of the present method is that it visualizes the temperature itself (not its gradient) without giving any disturbance to the fluid. Several examples of applications to typical flows were shown.

74466 A temperature sensor using moire technique. S.F.Su, D.K.Hamrick (Dept. of Electrical Engng., Univ. of South Florida, Tampa, FL, USA). *IEEE SOUTHEASTCON '83 Conference Proceedings, Orlando, FL, USA*, 11-14 April 1983 (New York, USA: IEEE 1983), p.413-15

A sensitive temperature sensor based on moire pattern multiplication was experimentally simulated. The simulations showed that the sensor is capable of measuring a very small temperature variation of a medium in the liquid or vapor phase. The measuring system makes no physical contact with the medium which makes it suitable for contaminated environments that can not be directly contacted by the instruments. The sensitivity of the sensor (better than 0.01°C) is examined and some applications are discussed. (14 refs.)

A wide range low temperature digital display thermometer See Entry 74470

Automatic digital multichannel thermohygrometer See Entry 74481

Frequency-pulling superregenerator for observing NQR See Entry 74505

10-Hz coherence anti-Stokes Raman spectroscopy apparatus for turbulent combustion studies See Entry 74542

Computerized single mode temperature sensor See Entry 75797

Infrared measurement of specimen temperature profiles during fatigue crack propagation tests See Entry 77831

Investigation of the medium temperature at 11.7 GHz [microwave attenuation estimation] See Entry 78575

07.20F Calorimetry

74467 Photometric characteristics of calorimeters having conical cells of tantalum. S.A.Kaufman, A.A.Liberman, O.I.Yakovleva.

Meas. Tech. (USA), vol.25, no.9, p.729-31 (Sept. 1982). Translation of: *Izmer. Tekh. (USSR)*, vol.25, no.9, p.18-19 (Sept. 1982). [received: May 1983]

Standard measuring facilities for the impulsive energy of laser radiation must operate, in accord with the All-Union Checking Scheme, over wide spectral ($\Delta\lambda = 0.4$ to 12 μm) and dynamic (total energy in a pulse $W = 1 \cdot 10^{-2}$ to $1 \cdot 10^2$ J) ranges. Their total error δ_0 in this case is equal to 2-5%. In choosing material for the cavities used as receiving elements of measuring transducers for the standard units indicated it is necessary that it should have great resistance to the laser radiation (a power density $E > 10^5$ W/cm 2) and should provide a high value of the absorption coefficient for the cavities over the entire spectral

range. In view of this, the photometric characteristics of tantalum have been investigated and its possible application verified. (2 refs.)

74468 Chart for estimation of conduction heat leak from specimens used in the measurements of properties by the transient calorimetric technique. C.K.Hsieh, S.L.Yang (Mech. Engng. Dept., Univ. of Florida, Gainesville, FL, USA).

Rev. Sci. Instrum. (USA), vol.54, no.5, p.600-3 (May 1983).

In measuring thermophysical properties using the transient calorimetric method, conduction heat leak from test specimens can be a source of error if not properly accounted for. An analysis method is presented in this paper for determining the magnitude of this leak. The analysis consists of deriving the temperature profiles in the specimen support. These temperatures are then used to determine the heat leak using two different approaches. In the first approach, the heat penetration depth in the support is derived and used to obtain an added thermal capacitance to the specimen. In the second approach, the heat leak was considered to reduce the net heat input. Both small and large heat-leak cases were analyzed, with the latter estimated by means of two recurrence relations. A chart was also developed for a rapid estimation of this leak. In the absence of a reliable experiment to measure the heat leak, this paper provides a viable alternative for accurate leak determination. (13 refs.)

07.20H Furnaces

74469 Resistively heated high-temperature furnace for PES experiments on free atoms in the UHV with synchrotron radiation. K.-G.Wagner (D. Weinhagen mbH Co. KG, Elmshorn, Germany).

Vak.-Tech. (Germany), vol.32, no.3, p.67-9 (April 1983). In German.

Atomic spectroscopy with synchrotron (beam source of high intensity and continuous spectral distribution) makes it possible to prove the theoretical calculations for many-electron systems (momentaneous correlation of electron orbitals in the initial state, in the course of excitation and in the final state). The sample has to be converted in the vapour state to avoid interferences of neighbouring atoms. The high-temperature furnace developed and built for temperatures up to more than 1400°C for evaporation of transition elements and rare earths is described. (7 refs.)

07.20M Cryogenics

74470 A wide range low temperature digital display thermometer. Chen Shu-ch'i Fang, Chung-liang Ku, Shao-shan Sheng, Ling-hui (Shanghai Univ. of Sci. & Technol., Shanghai, China).

Chin. J. Sci. Instrum. (China), vol.4, no.1, p.37-43 (Feb. 1983). In Chinese.

The relationship between the forward voltage and temperature of Si switch diodes at the temperature range from liquid nitrogen temperature to room temperature under the conditions of different injection is discussed. The error due to approximating the nonlinear curve by a linear one is estimated. The design principle and operation of the sensor in a wide range low temperature digital display thermometer is discussed. It operates over the 70-300K range with an error below 0.5K. A conclusion is made that the V-T curve of the diode sensor at the whole temperature range can be approximated by a single straight line and that the contradiction between the high level injection and self-heat of the diode can be greatly reduced. The LT-1 low temperature thermometer is introduced. (10 refs.)

74471 Thermal design and tests of a subcooled superfluid helium refrigerator. Y.Hakuraku, H.Ogata (Mech. Engng. Res. Lab., Hitachi Ltd., Ibaraki, Japan).

Cryogenics (GB), vol.23, no.6, p.291-7 (June 1983).

Design methods for a subcooled superfluid helium refrigerator with high efficiency are studied. The design details are presented for a He I heat exchanger (perforated disk stack type), a He II heat exchanger (low fin tube type), an expansion valve, a safety valve, an initial filling valve and a pumping system. Heat loss, cooling capacity and cool-down time are also calculated. The test results for the trial-manufactured refrigeration system are presented in comparison with the designed values. (11 refs.)

74472 Continuous flow cryostats for experiments in the presence of appreciable heat influx to the specimen. A.I.Belyaeva, V.I.Silaev, Yu.N.Stelmakhov, Yu.E.Stetsenko (Phys.-Tech. Inst. of Low Temperatures, Acad. of Sci., Kharkov, USSR).

Cryogenics (GB), vol.23, no.6, p.303-8 (June 1983).

The review describes several cryostat designs for spectral and magneto-optical studies representing continuous flow systems with sample cooling by preset temperature vapour blow-over. The characteristic features and advantages are discussed. It is shown that among present-day heat transfer methods, this one is the most efficient for studies involving appreciable heat influx to the cooled sample. (20 refs.)

74473 Use of commercial metallic strain gauges as low temperature heaters. D.Moy, A.C.Anderson (Dept. of Phys., Univ. of Illinois, Urbana, IL, USA).

Cryogenics (GB), vol.23, no.6, p.330-1 (June 1983).

The heat capacity of a resistive strain gauge has been measured. Such gauges may be used as electrical heaters in low-temperature applications. The units are small, inexpensive, durable and reusable. (8 refs.)

Cryogenic liquid level monitor using a frequency to voltage converter See Entry 74433

Gate controlled amplifier for platinum NMR thermometry See Entry 74462

Fast neutron produced $^{54}\text{MnFe}$ nuclear orientation thermometers See Entry 74463

Method for measuring a vacuum in an environment at liquid helium temperatures See Entry 74489

Cryostats for SQUID magnetometers See Entry 74496

Infrared cryogenic studies. XV. Chloroalkanes in argon matrices See Entry 75387

Study of heat transfer in multilayer insulations based on composite spacer materials See Entry 75911

Stability and heat transfer of rotating cryogenics. I. Influence of rotation on the onset of convection in liquid ^4He See Entry 76040

07.25 HYGROMETRY

74474 Hygrometer classification and standardization models for static and dynamic characteristics. D. Heinze.

Meas. Tech. (USA), vol.25, no.9, p.758-63 (Sept. 1982). Translation of: *Izmer. Tekh. (USSR)*, vol.25, no.9, p.51-4 (Sept. 1982). [received: May 1983] Two completely different principles that can be distinguished on the basis of the physical process in the primary transducer and therefore the character of the energy interaction between the medium and the transducer are considered. The first is that the water in the medium attenuates an energy flux emitted by a source; the mass proportion of water is indicated by the flux reaching the detector. Examples are infrared, ultraviolet, UHF, and acoustic hygrometers. The second principle employs two-way energy transfer between the medium and the transducer. The state of thermodynamic equilibrium (stationary or static) is set up between the medium and the transducer. Relations are presented which enable one to describe various methods of humidity measurement. (6 refs.)

74475 Standard humid-air generator for checking high-temperature hygrometer. V.M.Belozhko, A.S.Gridnev, I.B.Kreps, V.F.Mandrokhlebov.

Meas. Tech. (USA), vol.25, no.9, p.767-71 (Sept. 1982). Translation of: *Izmer. Tekh. (USSR)*, vol.25, no.9, p.56-9 (Sept. 1982). [received: May 1983] Humid-air generators (HAG) for producing vapor-air mixtures with given parameters employ various methods in the Soviet Union and elsewhere, and the choice of these for a particular application is determined by technical and economic factors. The use of saturated salt solutions is the commonest, along with mixing of gas flows, and two-pressure and two-temperature methods. To choose a method corresponding best to the requirements for a high-temperature HAG, the authors evaluated the expected metrological characteristics of generators employing these methods. Using as the basic criterion (the expected overall error, the PSG-120 hygrometer test facility is described in some detail. (11 refs.)

74476 Salt-solution hygrometer generators [hygrometer test facilities]. A.S.Gridnev, V.F.Mandrokhlebov.

Meas. Tech. (USA), vol.25, no.9, p.772-6 (Sept. 1982). Translation of: *Izmer. Tekh. (USSR)*, vol.25, no.9, p.59-62 (Sept. 1982). [received: May 1983] The availability of special facilities for determining the static and dynamic characteristics of hygrometers is one of the most important factors characterizing the accuracy and unification of humidity measurements for vapor-gas media. The authors consider the salt-solution generators (SSG) produced in the Analitpribor cooperative on the basis of saturated salt solutions. The major error components involved in SSG are examined and a brief description of the stationary GST-510, the portable GPT-130 and the UPG-110 models is presented. (16 refs.)

74477 The Rodnik-2VK standard humid-gas generator [hygrometer test facilities]. I.A.Sokov, A.A.Zhilinskii, A.P.Beloshitskii, T.A.Satyr, N.P.Guzhva, E.P.Grokh.

Meas. Tech. (USA), vol.25, no.9, p.777-9 (Sept. 1982). Translation of: *Izmer. Tekh. (USSR)*, vol.25, no.9, p.63-5 (Sept. 1982). [received: May 1983]

To extend the working range in measuring relative humidity and to increase the number of transducers that can be checked simultaneously, the Kiev Automatics Institute has collaborated with Angarsk special designs office in designing the Rodnik-2VK humid-gas generator. This is a two-pressure and two-temperature generator. It consists of a Rodnik 2 generator and an external VK thermostatic chamber made by the experimental plant attached to the Kiev Automatics Institute. The Rodnik-2VK produces a vapor-gas mixture with a temperature of 5-60°C in the working volume of the outer chamber, which has an excess of 0.3-5 kPa and a relative humidity of 10-97%. The relative humidity is set by separate adjustment and stabilization of the pressure and temperature of the gas in the Rodnik 2 generator and in the working chamber. (5 refs.)

74478 Standard apparatus for checking and calibrating hygrometers at negative temperatures. E.A.Gershovich, L.D.Mchedlidze, N.D.Kol'shev.

Meas. Tech. (USA), vol.25, no.9, p.780-8 (Sept. 1982). Translation of: *Izmer. Tekh. (USSR)*, vol.25, no.9, p.67-8 (Sept. 1982). [received: May 1983]

A standard apparatus for calibrating, checking, and testing is described. It consists of the following major units: a Polys-1 standard dynamic moist-gas generator and a thermostatic test volume, in which the hygrometers to be tested or calibrated are installed. The generator supplies this volume continuously with a flow of vapor-gas mixture with a specified and accurately known humidity. The action of the Polys-1 generator is based on phase equilibrium at negative temperatures. The generator provides a vapor-gas mixture whose humidity corresponds to a dewpoint (ice point) in the range from -60 to +20°C with an error of $\pm 0.2^\circ\text{C}$ in the dewpoint. (8 refs.)

74479 Standard hygrometer facilities at the Promengoremont cooperative. G.V.Gorev, N.E.Osipova, R.L.Tarshish.

Meas. Tech. (USA), vol.25, no.9, p.783-5 (Sept. 1982). Translation of: *Izmer. Tekh. (USSR)*, vol.25, no.9, p.69-70 (Sept. 1982). [received: May 1983]

The Promengoremont production cooperative at Ivanovo operates relative-humidity transducers of EVCh type of its own manufacture in conjunction with various secondary instruments. The metrological equipment and standard facilities available at this cooperative are discussed. These include the PER-64 and PER-65 metrological chambers, a microchamber, a classification chamber and dynamic humid-gas generators operating on the two-pressure principle. A data acquisition system built for the parameters of the microclimate which is based on standardised humidity and temperature transducers is also described. (6 refs.)

74480 Standard facilities for measuring microconcentration of water in gases. A.P.Beloshitskii, Yu.A.Belousov, M.D.Simulik, L.Z.Savkun.

Meas. Tech. (USA), vol.25, no.9, p.785-7 (Sept. 1982). Translation of: *Izmer. Tekh. (USSR)*, vol.25, no.9, p.70-1 (Sept. 1982). [received: May 1983]

Discusses the Soviet development of methods and facilities for measuring volume proportions of water in the range 10^{-3} - $10^{-6}\%$. The Angarsk special designs office and the Irkutsk Etalon experimental plant in the period from 1963 to 1980 produced about 30000 hygrometers for measuring the volume proportion of water and relative humidity. It is suggested that there were only about 100 metrological facilities available in 1982 (the Lena hygrometers, the Angara apparatus, and the Rodnik and Rodnik-2 humid-gas generators) and that this is far from meeting the increasing demand for instrumentation in this field. (5 refs.)

74481 Automatic digital multichannel thermohygrometer. Yu.V.Arutyana, R.Sh.Gurgenidze, T.A.Gachechiladze, R.G.Gachechiladze, N.I.Narimanidze.

Meas. Tech. (USA), vol.25, no.10, p.844-5 (Oct. 1982). Translation of: *Izmer. Tekh. (USSR)*, vol.25, no.10, p.44 (Oct. 1982).

Describes the principle of a six-channel thermohygrometer with simultaneous measurement, transformation, display, and output of the relative humidity and temperature at each interrogated point. Microelectronic and hybrid circuits can be widely used in assembling the units to measure, display, and switch the signals in a single compact unit, and it is possible to combine rack-

mounting and desk-top forms. The instrument is suitable for laboratory or industrial applications. (no refs.)

74482 Automatic high-temperature psychrometers. G.V.Bauer, L.E.Murycheva, P.A.Pidzhimyan, T.Yu.Kharlamova.

Meas. Tech. (USA), vol.25, no.10, p.845-7 (Oct. 1982). Translation of: *Izmer. Tekh. (USSR)*, vol.25, no.10, p.45-6 (Oct. 1982).

Automation and acceleration of engineering processes have increased the demand for monitoring humidity on working gas mixtures at high temperatures. The operation and technical parameters of two hygrometers developed in the Soviet Union are described: the APV-201 automatic psychrometric humidity meter; and the APG-206 automatic psychrometric hygrometer. Both meters employ thermistors as the sensing elements and can be used for measuring humidity at the 30 to 100°C and 40 to 200°C ranges, respectively. (3 refs.)

74483 Piezoelectric sorption hygrometers. L.Z.Savkun, I.A.Rudykh, A.N.Dryanov, V.E.Ivashchenko.

Meas. Tech. (USA), vol.25, no.10, p.853-5 (Oct. 1982). Translation of: *Izmer. Tekh. (USSR)*, vol.25, no.10, p.52-3 (Oct. 1982).

One of the various sorption methods for measuring humidity is the so-called piezoelectric sorption kind based on the mass sensitivity of piezoelectric quartz resonators that utilize the thickness-shear type of vibrations. A single-channel sorption hygrometer developed on the basis of the humidity-sensitive piezoelectric sorption element with a film of silica-gel. The type Istok-1 hygrometer operates on the following principle: it converts simultaneously the relative humidity by means of a quartz thermal converter into discrete signals which are proportional to the relative humidity and the volumetric fraction of moisture of the saturated gas, and multiplies these signals by utilizing the relationship $B = \phi B_s$, where B is the volumetric fraction of moisture in the gas and B_s is the volumetric fraction of moisture in the saturated gas. (3 refs.)

74484 Heated hygrometer suite. A.M.Saradzhev, V.F.Mandrokhlebov, G.A.Nersesyan, R.Ya.Tiraspol'skaya, Z.F.Edzhubyan.

Meas. Tech. (USA), vol.25, no.10, p.862-4 (Oct. 1982). Translation of: *Izmer. Tekh. (USSR)*, vol.25, no.10, p.58-60 (Oct. 1982).

A system of heated hygrometers is described which is based on a unified transducer consisting of humidity and temperature transducers together with universal equipment providing measurement over wide ranges in the one-parameter humidity characteristics for air and gases under various working conditions (dewpoint and mass proportion of water), or two-parameter ones (relative humidity and heat content). The natural output characteristics of the humidity and temperature transducers are converted to unified electrical signals as a current (from 0 to 100 μA) and a voltage (from 0 to 10 mV) by means of various intermediate transducers based on standardized designs providing direct measurement of any of the above parameters on uniform (linear) scales in measuring or recording instruments. A high degree of unification has been attained by using the same circuit for all the intermediate transducers, which in each particular case differs only in the nominal values of the resistors. (no refs.)

74485 Improvements in thermoelectrolytic humidity transducers. A.M.Litvinov.

Meas. Tech. (USA), vol.25, no.10, p.867-70 (Oct. 1982). Translation of: *Izmer. Tekh. (USSR)*, vol.25, no.10, p.62-4 (Oct. 1982).

Describes the Soviet development of standard thermoelectric humidity transducers of LiCl type. Amongst the topics discussed are advancements of manufacturing technology, development of models which provide for explosion safety, protection from dust and spark safety in the power supply; and construction of the nominal static characteristic by means of nonuniform piecewise-linear approximation. The DV-1K model is considered in some detail. (13 refs.)

74486 Method of improving the accuracy of a thermoelectrolytic humidity transducer. Yu.G.Zav'yalov, A.M.Litvinov.

Meas. Tech. (USA), vol.25, no.10, p.870-3 (Oct. 1982). Translation of: *Izmer. Tekh. (USSR)*, vol.25, no.10, p.64-6 (Oct. 1982).

Heated thermoelectrolytic humidity transducers are widely used in measurement and control systems for gas humidity because of their high accuracy, reliability, and interchangeability. However, their use is held back to some extent by the fact that the readings are slightly dependent on the uninformative parameters. An analytical expression is derived that enables one to eliminate the dependence of the readings on the uninformative parameters. A test is proposed for remote checking of the reading reliability. The results can be used to improve the accuracy in measuring atmospheric humidity without altering the design of the device. (4 refs.)

Development trends in hygrometry See Entry 78702

Development prospects for dewpoint hygrometers See Entry 78703

Field differential hygrometer See Entry 78704

Ultraviolet hygrometer for measuring fluctuations in α atmospheric humidity ..

..... See Entry 78705

07.30 VACUUM PRODUCTION AND TECHNIQUES

(inc. pressures below 1 atmosphere; see also 47.45 Rarefied gas dynamics; 81.15G Vacuum deposition)

74487 UHV-compatible reaction cell for combined high-and low-pressure studies of surface reactions. K.-E.Keck, B.Kasemo (Phys. Dept., Chalmers Univ. of Technol., Göteborg, Sweden), A.Hoglund.

Rev. Sci. Instrum. (USA), vol.54, no.5, p.574-8 (May 1983).

The construction and performance of a combined reaction cell and sample exchange lock for studies of surface reactions at pressures up to a few atmospheres is described. In combination with a specially designed sample holder this construction allows simple and rapid transfer to the sample between the ultrahigh vacuum system and the reaction cell. The reaction cell is a self-contained unit that can be mounted on, e.g. a 2 $\frac{1}{2}$ -in. Con-Flat flange (or any other vacuum port with an ID ≥ 38 mm). The sample holder can be mounted on any commercial sample manipulator. In both the high- and low-pressure positions the sample can be heated and cooled. Results are presented for the times involved in moving the sample from high to low-pressure environments, pump-out times, etc. The use of this equipment in studies of the catalytic activity of Pt for the H_2 oxidation is briefly described. (6 refs.)

74488 Electromagnetic bearing for an epitaxy centrifuge in high vacuum. V.G.Schweitzer, A.Traxler, H.Bleuler (Inst. fur Mech., ETH, Zurich, Switzerland), E.Bauser, P.Koroknay.

Vak.-Tech. (Germany), vol.32, no.3, p.70-4 (April 1983). In German.

The principle of the contactless, electromagnetic suspension can be very well applied to vacuum techniques. This kind of bearing is used to suspend the rotor of an epitaxy centrifuge within a thin-walled vacuum tank. The bearing magnets and the rotor drive are outside the tank. The vertically hovering

rotor carriers on its lower end a heated crucible for the epitaxy experiments in the centrifugal field. These experiments require high vacuum conditions and an absolute absence of hydrocarbons. The authors describe the setup of the magnetic suspension, its dynamic behaviour. They describe the setup of the magnetic suspension, its dynamic behaviour, the vacuum-technical equipments of the construction, and its application to liquid phase epitaxy. (6 refs.)

07.30D Vacuum meters

74489 Method for measuring a vacuum in an environment at liquid helium temperatures. L.Cesnak, C.Schmidt (Kernforschungszentrum Karlsruhe, Inst. für Tech. Phys., Karlsruhe, Germany).

Cryogenics (GB), vol.23, no.6, p.317-19 (June 1983).

The experimental results of a new method to measure a vacuum in an environment at liquid helium temperatures are presented. The method uses a thin superconducting wire suspended in the vacuum vessel, the wire is heated by a current pulse $>I_c$. The cool down time, which depends on the heat transfer into the rest gas and on the axial heat conductance of the wire, is a measure of the vacuum and it is detected by the recovery of the wire to superconductivity. The results exhibit good resolution in the range of pressures from 5×10^{-3} to 5 Pa (5×10^{-5} to 5×10^{-2} mbar). (4 refs.)

07.35 HIGH PRESSURE PRODUCTION AND TECHNIQUES

(inc. pressures above 1 atmosphere)

UHV-compatible reaction cell for combined high-and low-pressure studies of surface reactions See Entry 74487

07.50 ELECTRICAL INSTRUMENTS AND TECHNIQUES

74490 A simple measurement method of pyroelectric coefficient for ferroelectric crystals. Shao Shi-ping.

Chin. J. Sci. Instrum. (China), vol.4, no.1, p.94-7 (Feb. 1983). In Chinese. (8 refs.)

74491 A new method of minority carrier lifetime measurement by the microwave photoconductive decay technique. Wang Zong-xin, Bao Zong-ming.

Fudan J. (China), vol.21, no.4, p.462-7 (Dec. 1982). In Chinese. [received: June 1983]

A new experimental method of contactless measurement of the minority carrier lifetime of a semiconductor using dielectric waveguides is introduced, and an analytical result is given. It has been proved that the decay process of minority carriers in the wafer can be determined from the decay curve proportional to the microwave transmission coefficient. By this, one can calculate the minority carrier lifetime of the semiconductor sample. The results coincide well with those of high frequency photoconductive decay method. Using this technique, one can also measure the distribution of minority carrier lifetimes in a wafer. This technique can be used as a monitor in semiconductor wafer processes. (7 refs.)

74492 Permittivity measurements of lossy liquids at millimeter-wave frequencies. L.Zanforline (Istituto di Elettrotecnica ed Elettronica, Univ. di Palermo, Palermo, Italy).

IEEE Trans. Microwave Theory & Tech. (USA), vol.MTT-31, no.5, p.417-19 (May 1983).

A measurement system is described which allows the determination of the complex permittivity of high-loss liquids at millimeter waves. Basically, the setup consists of a waveguide interferometer whose unknown arm embodies a liquid holder irradiated by an open-ended rectangular waveguide. The sample thickness is varied by means of a piston driven by a micrometer screw. The bridge output then is read as a function of the liquid thickness. Best fitting between experimental and computed data through a suitable model of the system enables the permittivity to be determined. The system can operate, with high sensitivity, over the whole frequency range of the dominant mode propagating in the waveguide setup employed. System performance is described through a set of experimental results obtained on ethanol, methanol, and pure water at 20°C and 70 GHz. (9 refs.)

74493 Peak sampled vibrating-reed for the measurement of electric fields in the presence of space charge. M.N.Horenstein (Dept. of Electrical Engng., Boston Univ., Boston, MA, USA).

Rev. Sci. Instrum. (USA), vol.54, no.5, p.591-3 (May 1983).

An electronically sampled vibrating-reed DC electric field sensor of the chopping field-mill variety is described. The compact, battery powered, self-contained sensor, which can be imbedded in any electrode surface, is capable of measuring true DC fields up to the 10^6 V/m range over an indefinite period of time; however, continuous peak sampling of the chopped periodic signal allows transients on the order of 10 ms to be monitored. Measurement in the presence of ionic space charge is made possible by keeping all structural components exposed to the field at a single equipotential. (8 refs.)

74494 A device for measuring the residual electrical conductivity of single crystals. V.A.Sandovskii, V.A.Romanov, Yu.I.Rebrin (Inst. of Metal Phys., Acad. of Sci., USSR).

Sov. J. Nondestr. Test. (USA), vol.18, no.9, p.745-7 (Sept. 1982). Translation of: *Defektoskopiya (USSR)*, vol.18, no.9, p.89-91 (Sept. 1982).

The authors have developed and constructed a device with an attached small eddy-current transducer for measuring the residual electrical conductivity of single crystals. (2 refs.)

74495 Evaluation of a synthetic time domain reflectometry system. M.R.Yeo (Marconi Electronic Devices, Lincoln, England).

Colloquium on 'Microwave Circuit CAD Techniques', London, England, 18 April 1983 (London, England: IEE 1983), p.2/1-4

Using Fast Fourier Transform (FFT) the accurate frequency domain measurements are converted into the time domain and a trace is produced which is similar to the sampling scope trace on a conventional TDR. This can then be used in the conventional way to study individual discontinuities. The difference between the synthetic TDR and the conventional TDR is that measurements made with the automatic network analyser are far more accurate than those from the sampling oscilloscope and more importantly, the practical difficulties of generating fast rise time pulses no longer limits the power available in high order harmonics (necessary for higher resolution measurements or discontinuities), since the synthetic TDR technique uses discrete frequency measurements with ample available power all the way through 18 GHz. A further advantage of the synthetic TDR technique is that the data can be manipulated. (4 refs.)

Hauksbee's prototypical electrostatic generator See Entry 74246

An RF bridge technique for contactless measurement of the carrier lifetime in silicon wafers See Entry 76989

A method of reducing the effect of the gap in eddy-current measurements of conductivity See Entry 77840

07.55 MAGNETIC INSTRUMENTS AND TECHNIQUES

74496 Cryostats for SQUID magnetometers. O.A.Testard (CENS, Gif-sur-Yvette, France), M.Locatelli.

Cryogenics (GB), vol.23, no.6, p.299-302 (June 1983).

A non-metallic and non-magnetic cryostat, with a very low thermal budget and a container type autonomy was developed, to condition SQUID magnetometers whose maximum sensitivity reaches $10^{-14} \text{ T Hz}^{-1/2}$. This instrumentation uses composite materials, thermal shock and vibration resistant, multilayer thermal radiative insulation, to detect vibrations with thermal equivalent emissivity lower than 10^{-3} . (11 refs.)

74497 Magnetic sensors with good signal-to-interference discrimination [biomagnetism application]. J.R.Storey (Dept. of Phys., Univ. of Auckland, Auckland, New Zealand).

Nuovo Cimento D (Italy), vol.2D, ser.1, no.2, p.153-65 (March-April 1983). (Proceedings of the Fourth International Workshop on Biomagnetism, Rome, Italy, 14-16 Sept. 1982).

Principles are established for the design of coil arrays which generate distant magnetic fields diminishing as a high inverse power of the distance. By a principle of reciprocity these arrays, when used as sensors in induction and SQUID magnetometers, have an inherently low sensitivity to distant sources of magnetic field. (8 refs.)

74498 Optimisation of the second-order gradiometer base length that has been designed for the measurement of weak inhomogeneous magnetic fields [biomagnetism application]. V.Zrubec, P.Vrabcek, P.Tekel (Inst. of Measurement & Measuring Tech., Slovak Acad. of Sci., Bratislava, Czechoslovakia).

Nuovo Cimento D (Italy), vol.2D, ser.1, no.2, p.175-83 (March-April 1983). (Proceedings of the Fourth International Workshop on Biomagnetism, Rome, Italy, 14-16 Sept. 1982).

Deals with an optimisation problem of the second-order superconducting gradiometer sensor systems that have been designed for measurement of the weak inhomogeneous magnetic fields in a magnetically disturbed environment. The conditions of maximum signal-to-noise ratio of the output of superconducting quantum magnetometers are considered. The influence of measured signal source parameters, of an outside disturbing source and of the own noise of the magnetometer on the gradiometer base length selection is analysed. (3 refs.)

74499 Flux quanta counting magnetometer using a thin-walled superconducting ring. D.S.McLachlan (IBM Corp., Armonk, NY, USA).

IBM Tech. Disclosure Bull. (USA), vol.25, no.11A, p.5532-3 (April 1983).

Describes a flux quanta counting magnetometer which can also be used as a digital voltmeter or ammeter. (no refs.)

74500 Permanent magnet undulators. K.Halbach (Lawrence Berkeley Lab., Univ. of California, Berkeley, CA, USA).

J. Phys. Colloq. (France), vol.44, no.C-1, p.211-16 (Feb. 1983). (Bendro Free Electron Laser Conference, Bendor, France, 26 Sept.-1 Oct. 1982).

Pure rare earth cobalt (REC) undulators and hybrid undulators, using both REC and steel, are described and compared with each other and with conventional and superconducting undulators. (5 refs.)

A symmetric third order gradiometer without external balancing for magneto-cardiography See Entry 78279

07.58 MAGNETIC RESONANCE SPECTROMETERS, AUXILIARY INSTRUMENTS AND TECHNIQUES

(see also 61.16N EPR and NMR determinations)

74501 An effective phase correction method in Fourier transform spectroscopy. Meng Ching-an (Inst. of Phys., Acad. of Sci., Peking, China).

Chin. J. Sci. Instrum. (China), vol.4, no.1, p.15-17 (Feb. 1983). In Chinese.

An effective method of correcting the first order phase shift resulting from the delayed sampling of time-domain signal of pulsed NMR is proposed. The correct shift time domain data are obtained by means of Fourier transforms with the aid of a computer. The method is especially effective in solid state NMR spectroscopy. (3 refs.)

74502 Trial-production of variable temperature equipment for ESR spectra instrument. Hsi Dan, Chao Pau-In, Wang Tah-hui (Inst. of Biophys., Acad. of Sci., Peking, China).

Chin. J. Sci. Instrum. (China), vol.4, no.1, p.72-6 (Feb. 1983). In Chinese.

With the development of electron spin resonance spectra technology, variable temperature equipment has become an important accessory. The authors describe the principle, construction and performance of a trial-produced variable temperature equipment and present some experimental results obtained with this equipment. (5 refs.)

74503 Computer simulation of NMR excited by synthesis frequencies. Wang Tung-sheng, Wu Hsueh-wen (East China Normal Univ., China).

Chin. J. Sci. Instrum. (China), vol.4, no.1, p.81-7 (Feb. 1983). In Chinese.

The synthesis frequency excited NMR is a novel method in high resolution Fourier transform NMR. In the synthesis frequency excitation, the intensity of the spectrum is not uniform and its distribution may be designed according to requirements. The synthesis frequency excitation may be performed with a modified continuous wave spectrometer. It has the same sensitivity as pulse Fourier transform NMR, but without the shortcomings of the latter. The principles of this novel method are described. For exploring its applications, a computer simulation of the experiment has been carried out using the DJ5-130 computer. It is shown that this method can be used to suppress strong solvent peak, to reduce the dynamic range of NMR signal, and to excite certain parts of the spectra. The method is not suitable for relaxation time measurements. (6 refs.)

74504 Phase shifter for the phase-detection scheme of magnetic resonance. S.Sanyal, A.K.Roy (Saha Inst. of Nuclear Phys., Calcutta, India), P.K.Nandi.

Indian J. Pure & Appl. Phys., vol.21, no.3, p.171-5 (March 1983).

A simple phase shifter for the reference signal is capable of handling the entire range of field modulation frequency used in magnetic resonance spectrometers. A discussion of the normally adopted technique for the reduction of the unavoidable switching spikes which arise when JFETs are used as analog switches in the phase-detector, is also given. (6 refs.)

74505 Frequency-pulling superregenerator for observing NQR. O.N.Bryukhanov, T.N.Rudakov (Kalininingrad Univ., Kaliningrad, USSR). *Instrum. & Exp. Tech. (USA)*, vol.25, no.4, pt.2, p.947-8 (July-Aug. 1982). Translation of: *Prib. & Tekh. Eksp. (USSR)*, vol.25, no.4, p.151-3 (July-Aug. 1982). [received: May 1983]

A description is given of a superregenerator with frequency pulling from an external source for the range 20-70 MHz. The design allows one to obtain the NQR absorption of dispersion signal at the output. The quenching frequency is 38 kHz, while the oscillation amplitude in the tuned circuit is 0.5 V, the modulation frequency is 30 Hz, and the frequency deviation in frequency modulation is 3 kHz. The superregenerator described can be used in an NQR spectrometer. It has been tested as a temperature transducer for the range 77-443K. (5 refs.)

74506 Use of a spiral fitting in observing nonstationary ESR signals. Yu.F.Panferov, O.Ya.Grinberg, A.A.Dubinskii, Ya.S.Lebedeve (Inst. of Chem. Phys., Acad. of Sci., Moscow, USSR). *Instrum. & Exp. Tech. (USA)*, vol.25, no.4, pt.2, p.949-50 (July-Aug. 1982). Translation of: *Prib. & Tekh. Eksp. (USSR)*, vol.25, no.4, p.153-4 (July-Aug. 1982). [received: May 1983]

A method is described for substantially increasing the amplitude of the magnitude UHF field at the specimen in a pulsed ESR spectrometer, which involves placing a spiral fitting on the ampul. (5 refs.)

74507 Extension of the lower limit of current measurements by the NMR method. A.I.Zhernovoi, N.M.Mel'nikov. *Meas. Tech. (USA)*, vol.25, no.10, p.879-80 (Oct. 1982). Translation of: *Izmer. Tekh. (USSR)*, vol.25, no.10, p.72-3 (Oct. 1982).

Describes the construction of a primary NMR converter for measuring both high and low DC currents. It uses a permanent magnet to obtain an additional uniform magnetic field, which produces the NMR signal, on which the field produced by the current being measured is superimposed. The permanent magnet produces in the air gap of the primary transducer, in which the NMR pickup is placed, a magnetic field with parameters which ensure a signal/noise ratio of not less than five when there is no current flowing in the conductor. (3 refs.)

Gate controlled amplifier for platinum NMR thermometrySee Entry 74462

Operator and algebraic methods for NMR spectroscopy. I. Generation of NMR spin speciesSee Entry 75408

Operator and algebraic methods for NMR spectroscopy. II. NMR projection operators and spin functionsSee Entry 75409

Beam-maser spectroscopy on cyanoacetylene-DSee Entry 75410

07.60 OPTICAL INSTRUMENTS AND TECHNIQUES

(for radiation detection, see 07.62; for spectroscopy and spectrometers, see 07.65; for holography, see 42.40; for optical sources and standards, see 42.72; for optical lens and mirror systems, see 42.78; for optical devices, techniques and applications, see 42.80; for optical testing and workshop techniques, see 42.85; for radiation spectrometers and spectroscopic techniques, see 29.30; for radiation measurement, detection and counting, see 29.70)

74508 A quasi-optical nulling method for material birefringence measurements at near-millimeter wavelengths. G.J.Simonis (Army Electronics Res. & Dev. Command, Harry Diamond Labs., Adelphi, MD, USA). *IEEE Trans. Microwave Theory & Tech. (USA)*, vol.MTT-31, no.4, p.356-8 (April 1983).

A quasi-optical technique for the measurement of birefringence is demonstrated at 245 GHz. The technique is applied to crystal quartz. The measured values are compared with values reported at nearby frequencies. The technique is used to determine the difference between the ordinary and extraordinary real indices of refraction directly, rather than by deducing the difference from separate measurements of the two indices. The technique is based on establishing a transmission null, thus providing appreciable sensitivity and precision for the measurement. (11 refs.)

74509 A Computer controlled time resolved optical intensity profile measurement system. I.H.White, J.E.Carroll (Dept. of Engng., Cambridge Univ. Engng., Cambridge, England). *Opt. Commun. (Netherlands)*, vol.45, no.5, p.289-94 (1 May 1983).

Describes a computer controlled system which provides data management and position control for time resolved measurement of near and far field, along with charge carrier concentration distributions of semiconductor lasers. Of particular interest is the manner in which microprocessor control of inexpensive motorised micrometers is used to provide accurate repeatable movements on submicron scales. Due to its noise reduction capability through computer averaging this system has been operated in conjunction with a 50 ps risetime photodiode, and thus is believed to allow time resolved measurement on the shortest reported timescales. The system provides a further advantage in that experimental data may be stored to give easy access for further processing. (6 refs.)

74510 Automated goniometer employing a ring laser. A.I.Vanyurikhin, I.I.Zaitsev.

Sov. J. Opt. Technol. (USA), vol.49, no.9, p.566-9 (Sept. 1982). Translation of: *Opt.-Mekh. Prom.-st. (USSR)*, vol.49, no.9, p.28-31 (Sept. 1982). This paper describes an automated ring-laser goniometer that exhibits high accuracy and excellent operating characteristics. The computation algorithms and the angle-measurement errors are given. (2 refs.)

Polarization-independent beam splitterSee Entry 75778

Optical probing of acoustic waves on rough surfacesSee Entry 75883

07.60D Photometry and radiometry

(inc. colorimetry; see also 07.62 Detection of radiation)

74511 Accuracy check for color CRTs. R.L.Donofrio, J.D.Ryan (Philips ECG Inc., Seneca Falls, NY, USA). *Electro-Opt. (USA)*, vol.15, no.3, p.43-6 (March 1983).

Presents a simple computer program, an amalgam of two colorimetric measurement techniques, which conveniently checks the accuracy of photometric and colorimetric CRT measurements. (5 refs.)

74512 Evaluation of accuracy of exposure-measuring system. V.A.Karpushin, R.B.Mitkin, A.A.Chernyak.

Sov. J. Opt. Technol. (USA), vol.49, no.9, p.545-8 (Sept. 1982). Translation of: *Opt.-Mekh. Prom.-st. (USSR)*, vol.49, no.9, p.10-13 (Sept. 1982).

A method for the comprehensive evaluation of the accuracy of the constituent elements of the circuit of exposure-measuring systems is examined with a calculation example. (12 refs.)

Photometric characteristics of calorimeters having conical cells of tantalumSee Entry 74467

Application of photon counting techniques to POTDRSee Entry 74519

Installation to determine the index of the heterogeneity of glassSee Entry 74540

Fibre optic colour sensors based on Fabry-Perot interferometrySee Entry 75820

Investigation of the medium temperature at 11.7 GHz [microwave attenuation estimation]See Entry 78575

07.60F Polarimetry and ellipsometry

74513 Measurement of Stokes parameters and their transformation matrices with the help of a magneto-optical cell. V.B.Karavanov, M.Yu.Sakhnovskii.

J. Appl. Spectrosc. (USA), vol.36, no.5, p.599-604 (May 1982). Translation of: *Zh. Prikl. Spektrosk. (USSR)*, vol.36, no.5, p.831-6 (May 1982). [received: Feb. 1983]

Examines a procedure for measuring the Stokes parameters with the help of a magneto-optical cell, separating the polarized (coherent) part of the beam, determining the difference in phases and ratio of the amplitudes of the linearly polarized components of radiation under conditions of specular reflection directly from intensity measurements. (11 refs.)

74514 Highly sensitive polarimetric techniques (review). V.S.Zapasskii. *J. Appl. Spectrosc. (USA)*, vol.37, no.2, p.857-69 (Aug. 1982). Translation of: *Zh. Prikl. Spektrosk. (USSR)*, vol.37, no.2, p.181-96 (Aug. 1982). [received: April 1983]

The author discusses existing methods of obtaining high sensitivity in polarimetric measurements. He concentrates his attention on measurement techniques that do not make particularly high demands on the optical quality of the investigated sample, i.e. the most practical schemes, which can be used in the design of commercial polarimeters and spectropolarimeters. He also briefly discusses the recently developed 'supersensitive' intracresonator methods, which can be used to detect the smallest values of optical anisotropy and are of particular promise for use in fundamental physical research. (28 refs.)

74515 Determination of the gain and absorption coefficients from Faraday rotation of the polarization plane of radiation. V.V.Mashko.

J. Appl. Spectrosc. (USA), vol.37, no.2, p.916-21 (Aug. 1982). Translation of: *Zh. Prikl. Spektrosk. (USSR)*, vol.37, no.2, p.250-6 (Aug. 1982). [received: April 1983]

The search for active laser media, the recording of low concentrations of materials, and other problems require the development of sensitive methods for the determination of the gain and absorption coefficients. One of these methods of determining optical densities is based on measurement of the phase anisotropy induced in a medium by an external field. Due to the high sensitivity of the measurement of the Faraday rotation angle of the polarization plane of radiation, the sensitivity of the determination of the optical densities by such measurements can attain a few times 10^{-8} even in the intracresonator version. Placement of the sample being investigated into a Fabry-Perot interferometer or a laser resonator permits increasing the sensitivity of one to two more orders of magnitude. The author considers the following measuring scheme: radiation of the probing source which is linearly polarized along the X axis passes through a cell containing the medium being investigated. A longitudinal magnetic field is imposed on the medium, as a result of which rotation of the polarization plane of the probing radiation occurs which is recorded with a scheme having a crossed polarizer, which consists of a polarizer and a photorecording system, or by a balance scheme which includes a Glan prism which splits the light beam incident on it into two orthogonally polarized beams (whose polarization planes make angles $\pm 45^\circ$ with the X axis), two photocells, and a balance amplifier. (9 refs.)

74516 Signal-to-noise ratio analysis of a digital polarimeter application to thermal imaging. B.F.Lamoureux, B.S.Prade (Lab. d'Optique Appl., Ecole Polytech.-ESTA, Palaiseau, France).

Rev. Sci. Instrum. (USA), vol.54, no.5, p.582-5 (May 1983). A digital scanning polarimeter is described. It measures the local variations of the rotatory power of a thin liquid crystal target. This device is used for thermal imaging purposes. The incident scanning beam is split after traversing the target in two parts and then analyzed with two analyzers and detectors. Taking into account the photon noise, the existence of an optimal angle of the analyzer azimuth is shown. A numerical example is given. (3 refs.)

74517 Polarimetric sensors: exploiting the axial stress in high birefringence fibers. S.C.Rashleigh (Naval Res. Lab., Washington, DC, USA).

First International Conference on Optical Fibre Sensors, London, England, 26-28 April 1983 (London, England: IEE 1983), p.210-13

An alternative configuration for polarimetric fiber-optic sensors has been proposed and demonstrated. It exploits the relationship between the axial stress and the transverse stress asymmetry in high birefringence fibers. Axially straining the fiber induces a large change in the fiber birefringence. In some applications, adequate sensitivity may be obtained by just axially stressing the birefringent fiber. This greatly simplifies the fabrication of polarimetric sensors as it may not be necessary to fabricate the sensor such that the field to be detected stresses the fiber asymmetrically. However, increased sensitivity can be obtained by fabricating the sensor such that the action of the physical field stresses that fiber both axially and transversely in the appropriate direction. For either configuration, sensitivities comparable to those of the Mach-Zehnder interferometric sensors can be expected. Also sensitivities up to ~ 20 times larger than those previously reported for polarimetric sensors have been demonstrated. (12 refs.)

07.60H Refractometry and reflectometry

74518 Heterodyne OTDR at 0.82 μ m. E.Bodtker, B.Tromborg (Telecommunication Res. Lab., Copenhagen, Denmark), J.Mark, C.J.Nielsen. *Electron. Lett. (GB)*, vol.19, no.10, p.361-2 (12 May 1983).

The authors report on a heterodyne OTDR measurement on a single-mode fibre at a wavelength of 0.82 μ m using a stabilised semiconductor laser. In the actual set-up the dynamic range is limited by polarisation noise. (4 refs.)

74519 Application of photon counting techniques to POTDR. J.N.Ross (CEGB, Bristol, England).

First International Conference on Optical Fibre Sensors, London, England, 26-28 April 1983 (London, England: IEE 1983), p.169-72.

Polarization optical time domain reflectometry (POTDR) is a technique for measuring the change in polarization state of light as it travels along a single mode optical fibre. The technique enables an optical fibre to be used as a distributed sensor which is able to make local measurements of stress, magnetic and possibly electric fields. The author reports the use of a photon correlation technique to process the signal from the detector and compares this method of signal processing with the analogue method used by Ross (see Appl. Optics, vol.21, p.3489, 1982). (5 refs.)

Optical fiber joint-loss measurement. Review of the causes of measurement inaccuracies and some proposals for meaningful measurements See Entry 75800

Two dimensional near-field contouring of optical fiber cores .. See Entry 75801

A sensitive technique for fibre profile characterization See Entry 75810

07.60L Interferometry

74520 Complex interferometry. L.Mertz (Phys. Sci. Lab., Lockheed Palo Alto Res. Lab., Palo Alto, CA, USA).

Appl. Opt. (USA), vol.22, no.10, p.1530-4 (15 May 1983).

An efficient device using a transparent grooved screen and three detector channels is described for measuring the complex coherence factor between two optical beams. The device statically provides both in-phase and quadrature fringe components, the same signals as are customarily available in radio interferometry. The deleterious effects of a nonplanarism in stellar interferometry are described along with a novel configuration for interferometrically combining two telescopes to provide simultaneously fringes anywhere in the field of view with the goal of optical aperture synthesis. Complex fringe detection also has certain applications in spectral interferometry, and a suitable interferometer with achromatized throughput is described. That interferometer may also be used for distance or thickness measurement. (17 refs.)

74521 Real-time fringe-pattern analysis. L.Mertz (Phys. Sci. Lab., Lockheed Palo Alto Res. Lab., Palo Alto, CA, USA).

Appl. Opt. (USA), vol.22, no.10, p.1535-9 (15 May 1983).

The task is to learn the phases of real positive intensity fringes from an optical testing interferometer. The introduction of substantial tilt into the interferometer establishes a field of finely spaced fringes that serve as a spatial heterodyne carrier. Sequential pixel values from a TV video signal of the picture are distributed among three separate signal channels, every third pixel going to the same channel. The distribution rate is set at ~ 3 pixels/fringe so that each channel senses one phase of a three-phase stroboscope or moiré. Complex weighting of the channel signals eliminates the common mode to provide an in-phase and quadrature analog fringe signals. A direct analog-to-digital arctangent converter, with that analog signal pair as input, provides 4-bit ($1/16$ -cycle resolution) fringe phase at a 5-MHz sampling rate. The converter is coupled to a turns counter that automatically registers unwrapped phase. The similarity of the signals to NTSC color TV encoding is noted along with certain other applications. (3 refs.)

74522 Talbot interferometry with a vibrating phase object. H.Kaijun, J.Jahns, A.W.Lohmann (Phys. Inst., Univ. Erlangen, Erlangen, Germany).

Opt. Commun. (Netherlands), vol.45, no.5, p.295-300 (1 May 1983).

Describes a Talbot interferometer for measuring a vibrating phase object. The time-average fringes are moiré patterns modulated by the zeroth-order Bessel function. They provide information about the tilt at every point of a vibrating plate, for example. The Talbot interferometer is robust (common path) and cheap (printers grids as beam-splitters). The experiments can be performed with laser illumination or with a collimated beam of white light. Some experimental results are shown. (9 refs.)

74523 Autocorrelation of ultrashort optical pulses using polarization interferometry. Pochi Yeh (Rockwell Internat. Sci. Center, Thousand Oaks, CA, USA).

Opt. Lett. (USA), vol.8, no.6, p.330-2 (June 1983).

A proposal and an analysis are presented for the autocorrelation of ultrashort optical pulses by using polarization interferometry in a birefringent crystal wedge. (8 refs.)

74524 Outlook for the use of the Michelson interferometer for measuring the physical parameters of nonuniform semiconductor structures. V.E.Kaminskii, A.A.Kokin.

Sov. Microelectron. (USA), vol.11, no.5, p.231-7 (Sept.-Oct. 1982). Translation of: *Mikroelektronika (USSR)*, vol.11, no.5, p.393-401 (Sept.-Oct. 1982). [received: May 1983]

The Michelson interferometer is a quite universal device which can be used for investigations, in particular of semiconductor structures. It allows one to determine the thickness of dielectric films, the refractive index and the profile of the carrier concentration distribution in semiconductors over a quite broad range of values. The Tikhonov regularization method with a stabilizer of the first order allows one to reproduce the carrier concentration distribution profile with good precision. The spatial resolution of the method described with the use of a Michelson interferometer is determined by the position of the short-wavelength edge of the spectrum from the radiation source. For semiconductor wafers, using the IR region of the spectrum, it turns out to be possible to achieve resolution of structural details even with submicron dimensions. Here the requirement of a large dynamic range of the detection apparatus is essential. (7 refs.)

74525 Automated laser speckle interferometry displacement contour analyzer. J.A.Schaeffel, Jr. (US Army Missile Command, Redstone Arsenal, AL, USA).

In book: *International advances in nondestructive testing. Vol.9*, W.J.McGonagle [Ed.], p.77-98. New York, USA: Gordon & Breach (1983), 363 pp. [0 677 16440 8]

The theory and an experimental configuration were developed for automated displacement contour analysis of laser speckle interferograms. The number of displacement contours available is proportional to the number of diffraction fringe orders n available throughout the offset distance x . The system was checked to determine how well fringe contours could be measured and found to be accurate to at least 4% of the measured distance by hand. System scanning speed is extremely important, and it was found that 5000 data points could be analyzed in about 4 min when the system was operating at about 20% of its maximum rated speed. This is very encouraging for systems in which as many as 10^6 data points would be analyzed. Advantages of the present system over those of the past include virtual operator-free scanning, high speed, low cost and full field displacement field mapping. (no refs.)

74526 Aperture analysis of laser speckle interferograms. J.A.Schaeffel, Jr. (US Army Missile Command, Redstone Arsenal, AL, USA).

In book: *International advances in nondestructive testing. Vol.9*, W.J.McGonagle [Ed.], p.99-111. New York, USA: Gordon & Breach (1983), 363 pp. [0 677 16440 8]

The aperture analysis of laser speckle interferograms is a simple direct approach to low-cost quantitative analysis. The process is simple to perform and provides a permanent record of the analysis. Basic advantages of this analysis include: low cost, simple optical alignment, simple system, permanent record of the data, excellent fringe contrast, high signal to noise ratio, real time inspection, and variable sensitivity. The specific disadvantage is that a slight amount of interpretation and formula usage is required. This is so insignificant that it is of little concern. (3 refs.)

74527 Partially coherent sources in interferometric sensors. S.A.Al-Chalabi, B.Culshaw, D.E.N.Davies (Dept. of Electronic & Electrical Engng., Univ. Coll. London, London, England).

First International Conference on Optical Fibre Sensors, London, England, 26-28 April 1983 (London, England: IEE 1983), p.132-5

Describes a system which is capable of measuring the state of remotely set interferometers which can be connected to the receiver via single mode optical fibres. The essence of the technique used is that a partially coherent optical source—such as a superluminescent diode—is used to illuminate the interferometer, which has to have a path length difference between its arms of at least one coherence length of the transmitted signal. The difference in the path lengths of the remote interferometer arms is measured at the receiver using another interferometer with a calibrated length (time) difference between its arms and the interferometric sensor system is configured such that all the transmitted power is utilized in the measurement. (3 refs.)

74528 Remote interferometric sensors using frequency modulated laser sources. D.Uttam, I.P.Gile, B.Culshaw, D.E.N.Davies (Dept. of Electronic & Electrical Engng., Univ. Coll. London, London, England).

First International Conference on Optical Fibre Sensors, London, England, 26-28 April 1983 (London, England: IEE 1983), p.182-4

Most interferometric sensors are designed to use highly coherent optical sources for measurement of small phase deviations. The authors describe the use of a frequency modulated source to excite an interferometer. It is shown that it is possible to read the state of a totally passive, remotely located interferometer with great accuracy. Further it is shown that multiplexing of several cascaded sensors is possible using saw-tooth FM. Initial experimental results, from an air-path Michelson interferometer, are presented. (8 refs.)

74529 Performance characteristics of a passively stabilized fiber interferometer using a (3x3) fiber directional coupler. K.P.Koo, A.Dandridge, A.B.Tveten (Naval Res. Lab., Washington, DC, USA).

First International Conference on Optical Fibre Sensors, London, England, 26-28 April 1983 (London, England: IEE 1983), p.200-4

In the field of fiber optic interferometry, there is increasing interest in passive stabilization schemes to overcome the signal fading problem inherent in the free running interferometer. The basic concept of the authors' passive detection schemes is to produce two optical signals from the interferometer with a $\pi/2$ phase difference, these may then be electronically processed to give a stable output. Recently, the authors have demonstrated such a passive stabilization scheme using a (3x3) fibre directional coupler (see Appl. Phys. Lett., vol.41, no.7, p.616, 1982). The authors now present additional results, relating the performance of such a passively stabilized system to the properties of the (3x3) fiber coupler and various parameters which govern the characteristics of the fiber interferometer. (3 refs.)

74530 Fiber-optic interferometric signal processor employing a differentiate and cross-multiply frequency discriminator. S.A.Kingsley (Batelle Columbus Labs., Columbus, OH, USA).

First International Conference on Optical Fibre Sensors, London, England, 26-28 April 1983 (London, England: IEE 1983), p.205-9

Describes two passive homodyne detection techniques and a compact signal processing unit which the author is developing for the Naval Research Laboratory (NRL). By passive, the author means a system which does not require feedback either to the interferometer via a PZT transducer or to the laser. Both the systems described employ a 'phase generated carrier' technique. The prototype brassboarded unit which the author is building for NRL uses a new type of phase detector which is called a differentiate and cross-multiply frequency discriminator. (12 refs.)

Piezoelectric subdivision method of multiple-beam interference for flatness measurement See Entry 74432

Laser interference method of measuring small taper angles in plates in the IR range See Entry 74436

A temperature sensor using moiré technique See Entry 74466

Small interferometer for Fourier spectrometry See Entry 74546

A review of holographic nondestructive evaluation at Lawrence Livermore National Laboratory See Entry 75607

Holographic nondestructive evaluation: status and future See Entry 75608

Optical bistability, regenerative pulsations, and transverse effects in room-temperature GaAs-AlGaAs superlattice etalons See Entry 75714

Computerized single mode temperature sensor See Entry 75797

Optical fiber interferometer desensitized to the environmental perturbation acting on the fiber probe See Entry 75798

Magnetostrictive fiber-optic sensor system for detecting DC magnetic fields See Entry 75812

Fibre optic colour sensors based on Fabry-Perot interferometry See Entry 75820

Reconstruction by multidirectional holographic interferometry of the concentration field in a supersaturated solution near a growing NaClO₃ crystal See Entry 77547

07.60P Optical microscopy

74531 Scanning optical microscope incorporating a digital framestore and microcomputer. I.J.Cox, C.J.R.Sheppard (Dept. of Engng. Sci., Univ. of Oxford, Oxford, England).

Appl. Opt. (USA), vol.22, no.10, p.1474-78 (15 May 1983).

A scanning optical microscope is particularly well suited for image digitization since the image is already in the form of an electronic signal. A mechanically scanned optical microscope is described, which is controlled by a microcomputer and the image displayed on a framestore. The results of several simple digital image-processing algorithms applied to the micrographs are presented. (6 refs.)

74532 Temperature-controlled microscope with millidegree stability. H.Yokoyama, S.Kobayashi, H.Kamei (Materials Div., Electrotech. Lab., Ibaraki, Japan).

Rev. Sci. Instrum. (USA), vol.54, no.5, p.611-12 (May 1983).

The authors constructed a simple polarizing microscope in which the sample temperature can be controlled with an accuracy of 10^{-3} °C from room temperature to about 60°C. The temperature stability at a sample was directly assessed using the temperature-dependent birefringence of a liquid-crystal sample. (5 refs.)

Net grating and the testing of magnification in the TEMSee Entry 74557

07.62 DETECTION OF RADIATION (BOLOMETERS, PHOTOELECTRIC CELLS, I.R. AND SUBMILLIMETRE WAVES DETECTION)

74533 Electron-photon coincidence technique for the absolute calibration of VUV detectors. R.McAdams (Chem. Dept., Univ. of Southern California, Los Angeles, CA, USA), S.K.Srivastava.

Appl. Opt. (USA), vol.22, no.10, p.1551-4 (15 May 1983).

A method is described whereby VUV photon detectors can be accurately calibrated. This method is illustrated by taking the 58.4-nm transition of He as an example. The technique consists of crossing a monoenergetic electron beam with a beam of He atoms. When inelastically scattered electrons which have excited the 2^1P state are detected in coincidence with the 58.4-nm photons emitted in the decay of the excited state, the interaction volume formed by the crossed beams constitutes a standard source of photons. By comparing the number of detected coincidences with the predicted number the calibration can be made. A total detector efficiency of 0.024 ± 0.003 is obtained for a Galileo 4830 channeltron. (15 refs.)

74534 Picosecond CdSe photodetector. W.Margulis, W.Sibbett (Blackett Lab., Imperial Coll., London, England).

Appl. Phys. Lett. (USA), vol.42, no.11, p.975-7 (1 June 1983).

The performance of a photoconductive device in which an evaporated CdSe film is used as the semiconductor medium is described. The results indicate an ultrafast response and a recovery time ~ 20 ps. (11 refs.)

74535 New devices and materials for ultrafast high speed photodetectors for the ultraviolet through to the infrared. B.K.Garside, F.L.Gouin (Opto-Electronics Ltd., Oakville, Ontario, Canada).

Proc. SPIE Int. Soc. Opt. Eng. (USA), vol.355, p.27-36 (1982). [received: May 1983] (Fiber Optics: Short-Haul and Long-Haul Measurements and Applications, San Diego, CA, USA, 24-25 Aug. 1982).

Recent developments in fiber optics and laser sources have emphasised the need for high efficiency semiconductor photodetectors responding at unprecedented speeds over an ever-expanding wavelength range. To meet these needs, new types of device structures and new materials are increasingly being explored. The influence of general device and material characteristics on device capability is discussed, and the limitations explained through the use of general, time-dependent detector models. Appropriate device structures and materials are discussed for the development of high quantum efficiency, fast detectors at wavelengths ranging from the ultraviolet through to the infrared region appropriate to future optical communications systems. Recent results using junction and modified Schottky barrier structures are described, and the development of new materials for detector applications in the visible and infrared spectral regions is discussed. (13 refs.)

74536 Pressure pulse in an infrared pneumatic detector: theory based on the Einstein coefficient for induced absorption. J.P.Gupta, R.N.Sachdev, K.G.Vohra (Air Monitoring Section, Bhabha Atomic Res. Centre, Bombay, India).

J. Appl. Phys. (USA), vol.54, no.5, p.2183-7 (May 1983).

The kinetics of gases due to absorption of infrared radiation on closed cells has been discussed with the use of the Einstein coefficient for emission and absorption of radiation. The expression derived for the magnitude of pressure pulse in the cell explains satisfactorily the observed characteristics of the pneumatic detector. (21 refs.)

Detectors for thermal imagingSee Entry 74459

Binary holographic LO beam multiplexer for IR imaging detector arraysSee Entry 75600

The heterojunction ZnSe-(Zn_{1-x}Cd_xTe)_{1-y}(In₂Te)_y having high sensitivity in the visible light range and its applicationsSee Entry 77024

Frequency properties of Ge-Si solid solution p-n junctionsSee Entry 77038

Photoresponse characteristics of thin-film nickel-nickel oxide-nickel tunneling junctionsSee Entry 77067

Infrared optical constants of PtSiSee Entry 77347

07.65 OPTICAL SPECTROSCOPY AND SPECTROMETERS

(inc. photoacoustic spectroscopy)

74537 System analysis and time delay spectrometry. I. H.Biering, O.Z.Pedersen.

Bruel & Kjaer Tech. Rev. (Denmark), no.1, p.3-51 (1983).

Time delay spectrometry (TDS) is a relatively new method for measurement of system response. Based on a linear sine sweep it optimizes measurement performance eliminating some earlier drawbacks of swept measurements. This method leads to adopting an identical complex description in the time and frequency domains. To fully utilize the benefits from this description it is essential to consider the general behaviour of two-port systems and the problems encountered in the measurement of these. The present part of the article is an overview of the theoretical foundation for analysis of linear and time invariant systems. (6 refs.)

74538 A broadband submillimeter wave spectrometer system with on-line microcomputer data analysis. E.Schafer, M.Winnewisser (Phys. Chem. Inst., Justus-Liebig-Universität, Giessen, Germany).

Ber. Bunsenges. Phys. Chem. (Germany), vol.87, no.4, p.327-34 (April 1983). A submillimeter wave spectrometer operating in the frequency range 100 to 800 GHz has been constructed for the study of transient molecules in the gas phase. The instrument employs harmonic generation of millimeter wave frequencies and a He-cooled InSb photoconducting detector. A high degree of flexibility is achieved using an exchangeable free-space Pyrex absorption cell and a microcomputer for on-line data analysis. The spectrometer can be operated in a free-running video mode together with a fast signal averager or phase-locked to a microwave reference with source modulation. It is shown that the reproducibility of line center frequency measurements up to 600 GHz is ± 10 kHz. Transitions with absorption coefficients of at least $3 \cdot 10^{-8}$ cm⁻¹

can be detected in the range from 150 to 250 GHz. Ground state rotational transitions of OCS between 200 and 690 GHz are reported and analysed. (35 refs.)

74539 An automated high resolution spectrometer with data system. L.Ramaley, S.C.Foster, J.A.Coxon (Dept. of Chem., Dalhousie Univ., Halifax, NS, Canada).

Chem. Biomed. & Environ. Instrum. (USA), vol.12, no.4, p.229-52 (1982-1983).

Describes a spectrometer used for recording rotationally-resolved spectra of small molecules. The spectrometer consists of a high resolution scanning monochromator and photon counting detector interfaced to a dedicated minicomputer. The interface is very versatile, providing operation in several modes with minimum demands on the computer. This allows the computer to run in a foreground-background mode in which data previously acquired can be analyzed or new software developed while simultaneously acquiring new data with almost complete invisibility. (12 refs.)

74540 Installation to determine the index of the heterogeneity of glass.

V.I.Shelyubskii, I.A.Megerdicheva.

Glass & Ceram. (USA), vol.39, no.5-6, p.271-4 (May-June 1982). Translation of: *Steklo & Keram. (USSR)*, vol.39, no.6, p.9-10 (June 1982). [received: March 1983]

A method of quantitative determination of the index of the heterogeneity of glass based on variation of scattering of a parallel beam of monochromatic light by fine glass powder in an immersion liquid with small temperature variations was proposed earlier (V.I. Shelyubskii 1969). To accelerate introduction of the method into plant practice, the authors developed a simple installation based on the standard SF-10 spectrophotometer, in which a considerable part of measuring the heterogeneity has been automated. The installation permits one to make measurements at any wavelengths. Similar auxiliary assemblies can be used in spectrophotometers of other types. (4 refs.)

74541 Anisotropy of nonresonant cubic susceptibility in three-frequency active spectroscopy of Raman scattering. V.V.Kvach, V.P.Kozich, V.A.Orlovich.

J. Appl. Spectrosc. (USA), vol.37, no.2, p.913-15 (Aug. 1982). Translation of: *Zh. Prikl. Spektrosk. (USSR)*, vol.37, no.2, p.247-9 (Aug. 1982). [received: April 1983]

The methods of active spectroscopy of Raman scattering (ASRS) permit investigating nonlinear cubic susceptibility $\chi_{ijk}^{(3)}$ ($\nu_1, \nu_2, -\nu_3$), which determines the generation of radiation of frequency $\nu_3 = \nu_1 + \nu_2 - \nu_3$ under the action on a medium of fluxes with frequencies ν_1, ν_2 , and ν_3 (ν_2 and ν_3 are the frequencies of biharmonic pumping, and ν_1 is the frequency of the probe wave). When these methods are used spectroscopically, the susceptibility consists, as a rule, of a resonant part $\chi_{ijk}^{(3)R}$, which takes into account the contribution of the vibration (transition) under investigation to the ASRS signal, and a nonresonant part $\chi_{ijk}^{(3)NR}$, which is caused by all the other processes in the medium and which forms an undesirable background signal. A simple method is proposed for the measurement of the anisotropy of nonresonant cubic susceptibility in a three-frequency ASRS scheme ($\nu_1 \neq \nu_2 \neq \nu_3$). (7 refs.)

74542 10-Hz coherence anti-Stokes Raman spectroscopy apparatus for turbulent combustion studies. L.P.Goss, D.D.Trump, B.G.MacDonald, G.L.Switzer (Systems Res. Labs. Inc., Dayton, OH, USA).

Rev. Sci. Instrum. (USA), vol.54, no.5, p.563-71 (May 1983).

A 10-Hz coherent anti-Stokes Raman spectroscopy (CARS) instrument capable of simultaneous thermometry and N_2 concentration measurements in a turbulent flame has been designed and constructed and is described in detail. The instrument employs the doubled output of a pulsed Nd:YAG laser for pumping a broadband dye laser and also for the CARS pump beam. The broadband dye laser is used to excite, during a single pulse, the entire Q Branch of N_2 , the CARS signal of which is recorded by a multichannel analyzer. Special problems which were encountered with the multichannel analyzer include signal retention and limited dynamic range. The former was greatly reduced by employing cleansing scans between laser firings, and the latter was circumvented by employing a multiple beamsplitter arrangement in which the CARS signal was divided into four separate intensity regions, each of which covered a specific temperature range. The 10-Hz operation of the instrument required the use of a mass storage device such as an 800-bits-per-inch tape. CARS data recorded and digitized by the multichannel analyzer were transferred via machine-coded instructions to a minicomputer for storage on tape. Analysis of the CARS data consisted of a nonlinear least-squares fit of the CARS bandshape for thermometry and integration of the CARS signal for N_2 concentrations. CARS measurements in a near-stoichiometric premixed propane flame and a turbulent diffusion flame are reported. Results of calibration measurements indicate that uncertainties of 4% in temperature and 6% in concentration are obtainable with this instrument. (28 refs.)

Interfacing and operation of a Princeton Applied Research multichannel detector controller with a Digital Equipment Corporation DECLAB-11/MNC computer[spectroscopy application]See Entry 74445

High-resolution synchronized-quantum-beat spectroscopy using modulation sidebands: measurement of pressure shifts of the hyperfine splitting in sodium $3^2S_{1/2}$ See Entry 75538

Repetitive scanning type self-modulation spectroscopy applied to a monitor of ambient air pollutionSee Entry 78118

07.65E UV and visible spectroscopy and spectrometers

74543 An automatic microcomputer-based system for measuring reaction rates by UV spectroscopy. H.Maskill, J.T.Thompson (Chem. Dept., Univ. of Stirling, Stirling, Scotland).

Lab. Microcomput. (GB), vol.1, no.1, p.11-14 (Spring 1982).

Describes a microcomputer-based system for analysing UV absorption spectra to give chemical reaction rates. The system is based on a Pye Unicam SP8-300 double beam UV spectrophotometer with cell-changer and an Apple II microcomputer fitted with a clock, single disc drive and Hitachi monitor. The cell changer can be controlled by the Apple. (no refs.)

74544 An electron-retardation device to improve the resolution of a Turner-type UV photoelectron spectrometer. R.Dressler, L.Neuhaus, M.Allan (Inst. de Chimie Phys., Univ. Perolles, Fribourg, Switzerland).

J. Electron Spectrosc. & Relat. Phenom. (Netherlands), vol.31, no.2, p.181-9 (May 1983).

A simple pre-retardation device without intermediate images that may be used to increase the resolution of Turner-type UV photoelectron spectrometers has been analyzed by means of electron trajectory calculations. A set of qualitative rules based on the calculations as well as performance tests of the actual device are presented. High-resolution spectra of naphthalene and anthracene are presented as an illustration and compared in detail with recent model calculations of Franck-Condon profiles by Ohno (1979). (11 refs.)

07.65G IR spectroscopy and spectrometers

- 74545** Tone-burst modulated color-center-laser spectroscopy. C.S.Gudem, M.H.Begemann, J.Pfaff, R.J.Saykally (Dept. of Chem., Univ. of California, Berkeley, CA, USA). *Opt. Lett. (USA)*, vol.8, no.6, p.310-12 (June 1983).
A new modulation technique useful for high-resolution spectroscopy with tunable infrared lasers is described. The high sensitivity of this method is demonstrated by measurements of NO $\nu=0$ to 2 overtone transitions and of transitions in the fundamental band of OH with a color-center laser operating near 2.7 μm . (11 refs.)
- 74546** Small interferometer for Fourier spectrometry. V.V.Arkhypov, T.B.Ezhevskaya. *Sov. J. Opt. Technol. (USA)*, vol.49, no.9, p.570-2 (Sept. 1982). Translation of: *Opt.-Mekh. Prom.-st. (USSR)*, vol.49, no.9, p.31-3 (Sept. 1982).
The optical schematic, construction and test results of a new small electro-dynamically driven interferometer unit for Fourier spectrometry that requires no adjustment are described. Areas for its possible application are discussed. (2 refs.)
- IR-spectroscopic investigation of molecular interactions in segmented polyurethanes See Entry 75561

07.68 PHOTOGRAPHY, PHOTOGRAPHIC INSTRUMENTS AND TECHNIQUES

(for light sensitive materials see also 42.70)

- 74547** Two-dimensional movements detected by optoelectronic means [cameras]. H.Komesker, U.Riss. *Elektronik (Germany)*, vol.32, no.8, p.57-60 (22 April 1983). In German.
A new kind of optoelectronic measuring technique, especially for measuring the travel and exposure times of camera shutters, is described. Even with fast shade speeds the measuring error can be $<1 \mu\text{s}$. The measurement points in the picture plane are the ends of plastic optical conductors. The signals of the transducers (PIN photodiodes) are processed by special trigger and amplifier circuits. The digital measured data can be either displayed immediately or stored on a digital cassette. (no refs.)
- 74548** Modernization of drum-type electrographic copiers. R.I.Darachyuna, G.Yu.Mitsyavichyus, G.A.Tarasov, V.G.Chepenko. *Sov. J. Opt. Technol. (USA)*, vol.49, no.9, p.585-7 (Sept. 1982). Translation of: *Opt.-Mekh. Prom.-st. (USSR)*, vol.49, no.9, p.46-7 (Sept. 1982).
This paper presents the parameters of a new electrographic printing process on arsenic triselenide layers with development by the magnetic brush method, used in the type ER-620 drum-type electrographic copiers, and shows its advantages over the traditional process of printing on selenium layers with image development by the cascade method. (no refs.)
- 74549** Sensitivity of methylmethacrylate-methacrylic acid X-ray photoresists measured using soft X-rays emitted from a laser plasma. V.A.Boiko, A.Ya.Vainer, K.M.Dymaev, S.A.Kireeva, V.F.Limanova, I.Yu.Skobelev, A.Ya.Faenov, S.Ya.Khakhalin (All-Union Sci.-Res. Inst. for Physicotech. & Radio Measurements, Mendelevov, USSR). *Sov. Phys.-Tech. Phys. (USA)*, vol.27, no.11, p.1416-17 (Nov. 1982). Translation of: *Zh. Tekh. Fiz. (USSR)*, vol.52, no.11, p.2300-2 (Nov. 1982). [received: May 1983]
The authors use heavy element doping and chemical structure alteration to increase the sensitivity of methylmethacrylate-methacrylic acid copolymers positive resists. (5 refs.)
- 74550** Reverse or negative bluescreen traveling matte process. J.Erland (Apogee Inc., Van Nuys, CA, USA). *SMPTE J. (USA)*, vol.92, no.3, p.268-75 (March 1983).
This article outlines a new approach to the production of motion picture traveling matte photography. A solution is demonstrated to overcome the problems encountered when photographing models, i.e. aircraft, space ships, etc., when these incorporate surface finishes such as specular metallic or glossy paint, or when they include thin sections such as struts or antennae. The process requires a sophisticated motion control system capable of multiple passes in registration. (no refs.)
- 74551** IMAX and OMNIMAX theatre design. W.C.Shaw, J.C.Douglas (Imax Systems Corp., Oakville, Ontario, Canada). *SMPTE J. (USA)*, vol.92, no.3, p.284-90 (March 1983).
Theatre design for both IMAX and OMNIMAX presentations opens up a variety of new possibilities and presents a host of problems, some old, and many new. Many traditional concepts of theatre design, such as clear sightlines to the bottom of the screen, are no longer justified, or even desirable. Conversely, because of the large included angles in the projection beam, projector light-ray clearances become critical at many points in the auditorium. Audience movement and safety are important factors, and several unusual concepts are discussed. Since most IMAX and OMNIMAX theatres are in new construction, there are unique opportunities to optimize the audience environment, including picture, sound, and acoustics. Existing IMAX theatres range in size from 120 to 980 seats, with 1400 seats projected. OMNIMAX theatres range from 94 to 380, with larger theatres in the planning stage. (6 refs.)
- 74552** The interface of color negative film and telecine. K.Staes, W.Markie. *SMPTE J. (USA)*, vol.92, no.3, p.303-7 (March 1983).
This article discusses the interface between color negative film and telecine systems, reviewing basic facts about the negative-positive process, and the spectral responses of telecines and color print film. Figures and equations are provided in a discussion of appropriate interface corrections in color reproduction using different films with different telecines. The article gives details of a telecine alignment that provides a reproducible, easy-handling method yielding excellent color reproduction quality. (2 refs.)
- Evaluation of accuracy of exposure-measuring system See Entry 74512
- Broad spectral band color image deblurring See Entry 75587
- Planar volume phase holograms formed in bleached photographic emulsions See Entry 75599
- Error in determining laser radiation divergence by the focal spot method See Entry 75702
- Coagulation of Ag in AgBr microcrystals See Entry 75761
- Digital image processing of flow visualization photographs See Entry 76127
- The design of an organic photoresistor with charge-acceptance memory. III. Electrical properties of PVK-diazonium salt system See Entry 76997
- Formation of metal images by a new peel-apart system See Entry 77906

- Gelatin-substituted cyanine dyes as spectral sensitizers for silver halide emulsions See Entry 77907
- Kinetics of silver cluster formation and trapped hole neutralization in silver halide emulsion grains digested with cadmium salts See Entry 77908
- A study of properties of clusters of photographic interest by means of a redox buffer solution See Entry 77909
- Image formation processes in concentric shell emulsions See Entry 77910
- Determination of the basic parameters of PER2-3-P xeroradiographic plate See Entry 78305

07.75 MASS SPECTROMETERS AND MASS SPECTROMETRY TECHNIQUES

(for mass spectroscopic chemical analysis, see 82.80)

- 74553** A combination field desorption/fast atom bombardment source for the MS-50 mass spectrometer. G.Hansen, D.Heller, J.Yergey, R.J.Cotter, C.Fensclau (Dept. of Pharmacology, Johns Hopkins Univ. School of Medicine, Baltimore, MD, USA). *Chem. Biomed. & Environ. Instrum. (USA)*, vol.12, no.4, p.275-88 (1982-1983).
Conversion of the combination EI/FD source supplied by Kratos for the MS-50 mass spectrometer to a combination FD/FAB source is described. Sensitivities in the combination source are equivalent to those of the stand alone FAB source supplied by Kratos and the EI/FD source. Some compounds could be analyzed by FAB only, others by FD only and a third group were susceptible to both techniques. The advantage of the combination source is that both techniques may be used without having to change ion sources or perform extensive instrumental manipulations. (11 refs.)
- 74554** Automation of a gas analyser by personal computer. J.Canteloup, J.P.Vassilakis (Lab. d'Etudes des Procédés d'Analyse Phys., IUT, Orsay, France). *Mes. Regul. Autom. (France)*, vol.48, no.8, p.29, 31-2 (16 May 1983). In French.
A microcomputer-controlled quadrupole mass spectrometer for quantitative analysis of the gaseous phase in modern vacuum treatment processes is presented. Its three main components (an ionisation chamber, an ion-separating quadrupole filter and an electron multiplier) are supplied and controlled from an electronics package. The automation of signal acquisition, digitised spectrum storage and restitution after processing, and spectral analysis is explained. Programs for spectrum acquisition and analysis, and monitoring of peripherals including calibration of converters and multiplexer and switching of relays, are mentioned. An example of an experiment with a Riber QX100 quadrupole spectrometer and Apple II Plus microcomputer is described, and spectra obtained for Ar in Ne are presented. (no refs.) M.B.D.
- Pulse shaper for time clamping to the rising edge of pulses in semiconductor detectors See Entry 75244
- Recent developments in ion mass spectrometers in the energy range below 100 keV See Entry 78665
- Ion mass spectrometer on ionosphere sounding satellite (ISS-b) See Entry 78788
- ## 07.77 PARTICLE BEAM PRODUCTION AND HANDLING; TARGETS
- (see also 29.25 in elementary-particle and nuclear physics, 41.80 Particle beams and particle optics)
- 74555** Apparatus for measurements on the fragmentation of MeV molecular-ion beams. B.J.Zabransky, P.J.Cooney, D.S.Gemmel, E.P.Kanter, Z.Vager (Phys. Div., Argonne Nat. Lab., Argonne, IL, USA). *Rev. Sci. Instrum. (USA)*, vol.54, no.5, p.531-40 (May 1983).
An apparatus for the study of the fragmentation of MeV molecular ions is described. The system permits high-resolution measurement of the joint distribution in energy and angle for fragment ions of selected charge and mass. Two movable detectors allow the study of spatial and temporal correlations among up to three fragments resulting from a single dissociation event. All experimental parameters are monitored, controlled, displayed, and recorded by a computer system that uses a linked network of four processors. Real-time, computer-generated color graphics, are employed to give a visual rendition of the relation between the detector positions and the trajectories of outgoing fragments. (23 refs.)
- 74556** Angular resolution in total cross-section measurements. I.Lazzizzera (Dept. of Phys., Univ. of Trento, Trento, Italy), A.Zecca. *Rev. Sci. Instrum. (USA)*, vol.54, no.5, p.541-3 (May 1983).
This paper deals with the calculation of the detection efficiency in total cross-section measurements for two geometries: rectangular beam-rectangular detector of equal (finite) dimensions and circular beam-circular detector. The solutions are given in analytical and graphical form. The use of the term 'angular resolution' is discussed and a new definition is proposed. (3 refs.)
- A combination field desorption/fast atom bombardment source for the MS-50 mass spectrometer See Entry 74553
- Dependence of the maximum magnetic induction and half-width of the field of electron-microscope lenses on the shape and material of the pole pieces See Entry 74566
- The application of adiabatic theorem to the beam dynamics in accelerators See Entry 75216
- Laser polarization of accelerated protons See Entry 75218
- Beam-foil spectroscopy See Entry 75554
- Foil/electron ion-beam lens See Entry 75573
- ## 07.80 ELECTRON AND ION MICROSCOPES AND TECHNIQUES
- (see also in condensed matter 61.16D Electron microscopy, 61.16F Field ion microscopy)
- 74557** Net grating and the testing of magnification in the TEM. Chen Hsiang-chen, Yin Sen-Yu (Shanghai Optical Instrument Res. Inst., Shanghai, China). *Chin. J. Sci. Instrum. (China)*, vol.4, no.1, p.9-14 (Feb. 1983). In Chinese.
The testing and determining of magnification for TEM is a fundamental testing technique in the transmission electron microscope (TEM). A simple

method of testing the groove-spacing of the gratings and replicas by means of a conventional microscope is described and errors encountered are statistically evaluated. (5 refs.)

74558 Clamping device for surface electron microscope samples with background neutralization. L.-A.Gang. *Feinwerktech. & Messtech. (Germany)*, vol.91, no.3, p.107-8 (April-May 1983). In German.

With the flexible clamping devices described, samples differing in structure, material and geometry can be quickly and simply placed in the beam path of the surface electron microscope. A screen attached to the clamping device permits neutralization of disturbing background appearances. (no refs.)

74559 AES investigation of silicon nitride film. Dai Dao-xuan, Ling Rong-fu, Wang Ji-tao, Wang De-xin, Dong Xi-wei, Luo Xing-hua. *Fudan J. (China)*, vol.21, no.4, p.468-73 (Dec. 1982). In Chinese. [received: June 1983]

The composition profiles of LPCVD silicon nitride films on silicon dioxide have been measured by AES using a PHI-550 type electron spectrometer. The Auger peak lines in nitride/silicon dioxide interface transition region have also been taken. The chemical compositions in the interface region have been analysed. (10 refs.)

74560 A modified bias-method for the determination of spectrometer functions. H.Ebel, G.Zuba, M.F.Ebel (Inst. für Angewandte und Tech. Phys., Tech. Univ. Wien, Wien, Austria). *J. Electron Spectrosc. & Relat. Phenom. (Netherlands)*, vol.31, no.2, p.123-30 (May 1983).

The results of quantitative surface analysis by means of X-ray photoelectron spectroscopy show a marked influence of the spectrometer function of the instrument employed. For an instrument without retardation and electron lenses the spectrometer function can be calculated, but for a more sophisticated type of instrument experimental determination of the spectrometer function is indispensable. In this paper a suitable method (variation of the bias) is described, which furthermore offers a possibility of checking the results. (3 refs.)

74561 Recent improvements to the Cambridge University 600 kV high resolution electron microscope. D.J.Smith, R.A.Camps, L.A.Freeman (High Resolution Electron Microscope, Univ. of Cambridge, Cambridge, England), R.Hill, W.C.Nixon, K.C.A.Smith.

J. Microsc. (GB), vol.130, pt.2, p.127-36 (May 1983). (MICRO 82: High Resolution Electron Microscopy, London, England, 12-16 July 1982). Several recent modifications to the Cambridge University 600 kV HREM have resulted in increased levels of performance and greater operating efficiency. Changes include new Permenur pole-pieces with a reduced gap leading to improved aberration coefficients, and an attachment to the tilt/shift supplies which facilitates accurate beam alignment. Resolution figures include: (a) an axial CTF extending, without zeros, beyond 1.8 Å at 575 kV; (b) tilted beam CTFs extending beyond 1.1 Å; and (c) lattice fringes of 0.72 Å spacing. (24 refs.)

74562 Procedures for focusing, stigmating and alignment in high resolution electron microscopy. W.O.Saxton, D.J.Smith (High Resolution Electron Microscope, Univ. of Cambridge, Cambridge, England), S.J.Erasmus.

J. Microsc. (GB), vol.130, pt.2, p.187-201 (May 1983). (MICRO 82: High Resolution Electron Microscopy, London, England, 12-16 July 1982). Several different approaches to the alignment, stigmating and focusing of a high resolution electron microscope are evaluated theoretically and experimentally. Ambiguities in the interpretation of diffractograms are pointed out which make it necessary to explore a range of incident beam directions before the correct alignment can be established. The variation of image contrast with the imaging conditions is examined in detail, and its global minimization is shown to be a reliable criteria for adjustment of all parameters. Recommendations are made as to the best procedures to adopt in various circumstances, and a computer-controlled procedure based on the image contrast is described which sets all parameters automatically in less than a minute. (37 refs.)

74563 Morphological SEM picture processing. D.Jeuin (Inst. de Recherches de la Siderurgie Française, Maizières-les-Metz, France).

J. Microsc. & Spectrosc. Electron. (France), vol.8, no.1, p.1-18 (Feb. 1983). A new system of quantitative image analysis of SEM images was developed in IRSID. It combines a SEM under the control of an EDS micro-analyzer with a scan generator, a microcomputer, and a texture analyzer. Morphological picture transformations are implemented on different kinds of data (digital or threshold electron images or X-ray maps) in order to make automatic image segmentation and to get quantitative morphological and chemical data on material microstructures. Position of the SEM beam on sample may be controlled by processed binary pictures for automatic local X-ray spectra or maps acquisitions. (39 refs.)

74564 Automatic electron probe microanalyser based on double measurement of dose. C.Marion, M.Vannier (Ecole des Mines de Paris, Centre de Géologie Générale et Minière, Fontainebleau, France).

J. Microsc. & Spectrosc. Electron. (France), vol.8, no.1, p.31-46 (Feb. 1983). In French. The automation of quantitative analysis using a wave dispersive spectrometer microprobe requires a high accuracy in the motions of the spectrometer. A new method, based on a double measurement of X-rays intensities on each side of the peak instead of one measurement on top is presented. This method allows a better analytical reproducibility and a permanent control of the working order of the spectrometers. (3 refs.)

74565 Electron microscope grid holders for a multipurpose specimen stage. C.E.Warble (CSIRO Div. of Chem. Phys., Clayton, Victoria, Australia).

Rev. Sci. Instrum. (USA), vol.54, no.5, p.607-10 (May 1983). In this article improved grid holders for use in a multipurpose electron microscope stage are described. Two models, made from copper, bronze, or brass, both allowing cooling and tilting, provide either (1) a heating capability with the grid in a strip configuration or (2) a full-circle grid without the heating facility. The mechanical stability, electrical, thermal, and anticontamination characteristics, and tilt movements are excellent. (3 refs.)

74566 Dependence of the maximum magnetic induction and half-width of the field of electron-microscope lenses on the shape and material of the pole pieces. S.F.Zelev.

Sov. J. Opt. Technol. (USA), vol.49, no.9, p.557-9 (Sept. 1982). Translation of: *Opt.-Mekh. Prom.-st. (USSR)*, vol.49, no.9, p.20-2 (Sept. 1982).

The dependence of the maximum magnetic induction B_0 and the half-width d of the field of electron-microscope electromagnetic lenses on the shape parameters $p=s/b$ of the pole pieces has been investigated, taking into account the materials that are usually used for them in Soviet electron microscopes (K50F2 Permenur, 50N and 79NM Permalloy). Graphs are presented that illustrate this dependence and are convenient to use for practical calculations of electromagnetic lenses. (3 refs.)

Resistively heated high-temperature furnace for PES experiments on free atoms in the UHV with synchrotron radiation See Entry 74469

Foil/electron ion-beam lens See Entry 75573

Prospects for improvement in EDX microanalysis See Entry 77938

Condenser aperture misalignment and solute profile asymmetries in STEM X-ray microanalysis See Entry 77939

Processing of noisy high resolution electron micrographs of crystalline biological membranes See Entry 78392

Combining accurate defocus with low-dose imaging in high resolution electron microscopy of biological material See Entry 78404

07.85 X-RAY, GAMMA-RAY INSTRUMENTS AND TECHNIQUES

74567 The cobalt 60 radiation equipment of Seibersdorf Research Centre. K.Mayr, G.Nezavdal, K.Spalek (Österreichisches Forschungszentrum Seibersdorf GmbH, Seibersdorf, Austria).

Acta Phys. Acad. Sci. Hung. (Hungary), vol.52, no.3-4, p.443-54 (1982). In German. [received: May 1983] (Proceedings of the Hungarian-Austrian Health Physicists' Meeting, Győr, Hungary, 28 Sept.-1 Oct. 1981). Describes the ^{60}Co irradiation equipment of Seibersdorf (Austria) Research Center, now expanded to 4.1 Peta-Becquerel (3.7 Peta-Becquerel for industrial purposes, 0.44 for scientific purposes: biology, radiation chemistry). The screening system, transport arrangements, controls and fire fighting system are described in detail. (no refs.) J.S.

74568 X-ray spectrograph design. M.P.Chrisp (Jet Propulsion Lab., California Inst. of Technol., Pasadena, CA, USA).

Appl. Opt. (USA), vol.22, no.10, p.1519-29 (15 May 1983). An aberration theory is applied to spectrograph design. The initial system considered has a toroidal mirror in front of a concave grating spectrograph giving spatial resolution perpendicular to the dispersion direction. The accuracy of the theory is shown by comparison of spot diagrams obtained from the aberrations with those produced by raytracing. The major aberrations affecting the vignetting at the intermediate slit and the spatial resolution are identified. A new system, using a holographic grating to give a flat focal plane, is then designed and optimized. It has increased spatial resolution over the wavelength range and is particularly suitable for microchannel array detectors. (8 refs.)

74569 Computer evaluation of real-time X-ray and acoustic images. M.H.Jacoby, R.S.Loe, P.A.Dondes (Lockheed Missiles & Space Co. Inc., Sunnyvale, CA, USA).

Proc. SPIE Int. Soc. Opt. Eng. (USA), vol.359, p.273-7 (1983). (Applications of Digital Image Processing IV, San Diego, CA, USA, 24-27 Aug. 1982). The weakest link in the inspection process is the subjective interpretation of data by inspectors. To overcome this troublesome fact computer based analysis systems have been developed. In the field of nondestructive evaluation (NDE) there is a large class of inspections that can benefit from computer analysis. X-ray images (both film and fluoroscopic) and acoustic images lend themselves to automatic analysis as do the one-dimensional signals associated with ultrasonic, eddy current and acoustic emission testing. Computer analysis can enhance and evaluate subtle details. Flaws can be located and measured, and acceptance decisions made by computer in a consistent and objective manner. The authors describe the interactive, computer-based analysis of real-time X-ray images and acoustic images of graphite/epoxy adhesively bonded structures. (11 refs.)

74570 Data acquisition and analysis in X-ray photoelectron spectroscopy using an Apple II microcomputer. A.F.Carley (Chem. Dept., Univ. Coll., Cardiff, Wales).

Lab. Microcomput. (GB), vol.1, no.2, p.8-13 (Summer 1982). Describes the author's system for automated X-ray photoelectron spectroscopy. Hardware described includes: Apple II microcomputer; 2 channel 12-bit D/A converter and 8-bit parallel port; 4 channel 12-bit A/D converter; parallel interface card; clock/calendar card; ROM+ card with keyboard filter ROM; disc drive interface. Also discussed is the software used for data acquisition and data analysis. (no refs.)

74571 An economical transfer vessel with detachable reactor for XPS studies. T.P.Debies, D.M.Schrall (Gulf Res. & Dev. Co., Pittsburgh, PA, USA).

J. Electron Spectrosc. & Relat. Phenom. (Netherlands), vol.31, no.2, p.191-6 (May 1983). The authors describe an economical transfer vessel with a detachable reactor for the performance of chemical reactions. The device was designed for use in combination with the Physical Electronics Model 550 ESCA/SAM/SIMS instrument, but can be modified for use with other spectrometers. (8 refs.)

74572 Gamma-reflection densitometer for the qualification of concrete shielding. B.Szepessy (Nuclear Training Reactor, Tech. Univ. Budapest, Budapest, Hungary).

Period. Polytech. Electr. Eng. (Hungary), vol.26, no.1-2, p.145-52 (1982). A gamma-reflection densitometer had been developed by the author. By analysis the gamma-spectra conclusions can be drawn about the inclusions in the concrete concerning their size and their depth. The device can be used in industry or other fields too. (5 refs.)

74573 Simple quasi-two-crystal X-ray spectrometer. K.Taniguchi (Dept. of Solid-State Electronics, Faculty of Engng., Osaka Electro-Communication Univ., Osaka, Japan).

Rev. Sci. Instrum. (USA), vol.54, no.5, p.559-62 (May 1983). A simple two-crystal spectrometer was constructed using a commercial single-crystal spectrometer, i.e. the second crystal and the detector were attached on the 2θ arm of a single-crystal spectrometer. The angle between the second crystal and the detector is preset to an optimum angle for the measurement region of interest. The condition for geometrically ideal analysis can be satisfied by rotating the θ axis and detector arm (2θ arm) at a rotation ratio of 1:3 using an external pair of gears whose ratio is 3:1. The wavelength can be directly read according to Bragg's diffraction law, like a commercial two-crystal spectrometer. The author measured sulphur-K β spectra for several sulphur compounds. It is concluded, from several measurements, that the spectra obtained with a high-resolution can be an important and powerful tool for the study of the valence band and can also be applied to chemical-state analysis. (4 refs.)

74574 Use of carbon felt as a cold cathode for a pulsed line X-ray source operated at high repetition rates. G.F.Erickson, P.N.Mace (Los Alamos Nat. Lab., Univ. of California, Los Alamos, NM, USA).

Rev. Sci. Instrum. (USA), vol.54, no.5, p.586-90 (May 1983). Tests to determine the usefulness of carbon felt as a cold cathode in high repetition rate X-ray systems are described. Application of these test results to design and operation of an X-ray preionizer for an excimer laser system

has resulted in a simple, reliable X-ray source which can be used at pulse rates up to 500 Hz for $>2 \times 10^7$ shots before the carbon felt must be replaced. (4 refs.)

74575 Radiation image converters for industrial introsopes. E.A.Gusev, B.I.Leonov, F.N.Novitskii (Sci.-Res. Inst. of Introscopy, Moscow, USSR). *Sov. J. Nondestr. Test. (USA)*, vol.18, no.9, p.669-71 (Sept. 1982). Translation of: *Defektoskopiya (USSR)*, vol.18, no.9, p.4-7 (Sept. 1982). Methods of visualizing the fields of penetrating radiations are examined and the advantages of converters with rare-earth elements and polycrystals of alkali-halogen compounds are pointed out. The possibilities of modern converters are shown and their comparative analysis is given. (8 refs.)

74576 X-ray lithography with a plasma-point source of soft X-radiation. V.A.Veretennikov, A.N.Dolgov, A.I.Isakov, V.L.Kantsyrev, O.N.Krokhin, A.P.Nekunde, O.V.Sagalovskaya, O.G.Semenov, Yu.V.Sidel'nikov, V.V.Ul'yanov (P.N. Lebedev Phys. Inst., Acad. of Sci., Moscow, USSR). *Sov. Tech. Phys. Lett. (USA)*, vol.8, no.9, p.448-9 (Sept. 1982). Translation of: *Pisma v Zh. Tekh. Fiz. (USSR)*, vol.8, no.17-18, p.1041-5 (Sept. 1982). [received: May 1983]

One of the major problems in the development of X-ray lithography is to produce a small, highly efficient, easily serviced source of soft X-radiation with an acceptable spectrum. Generally acknowledged as candidate sources for X-ray lithography are X-ray tubes with a rotating anode, synchrotron radiation sources, and laser-plasma sources. Each of these sources has its own advantages and disadvantages, which determine its practical value. The authors used a vacuum-spark apparatus as a plasma source. (15 refs.)

74577 Installation and commissioning of a Siemens SRS200 sequential X-ray-fluorescence spectrometer. A.M.E.Balacs, J.J.Jacobs. *Report M80*, Council for Miner. Technol., Randburg, S. Africa (25 Feb. 1983). 6 pp.

The operation of the Siemens SRS200 automatic X-ray spectrometer, which can also be operated manually, is described. Details of its application to routine analysis are given, and these demonstrate its high level of performance, even in the analysis of elements present in part-per-million concentrations. Modifications that were made to the sample cups and the installation of a nondedicated computer are discussed. (2 refs.)

74578 Nucleonic techniques for non-invasive, on-line measurement [industrial applications]. D.W.Neild (Salford Electrical Instruments Ltd., Eccles, England).

Colloquium on 'Non-Invasive On-Line Measurement in Industry', London, England, 13 April 1983 (London, England: IEE 1983), p.2/1-7

The word 'nucleonic' is intended to encompass gamma radiation in the energy range 40 KeV to 2.5 MeV (neutrons are not dealt with). The more conventional gamma absorption and 'back scatter' measurement systems are first considered and their disadvantages are outlined 'low-level' systems which are capable of replacing them in many applications are then discussed. 'Low level' gamma radiation is interpreted as implying a gamma flux rate of less than 0.75 milliroentgens/hour (7.5 μ Sv/hr). (no refs.)

Optics calculation: some new results on bent mirrors and ray-tracing See Entry 75773

A novel curved position-sensitive proportional counter for X-ray diffractometry See Entry 76256

Automated fail-safe control system for independent operation of two radiation shutters on a rotating-anode X-ray source See Entry 76258

Technique and method of bronchography See Entry 78290

Development prospects for power supplies for diagnostic X-ray sets See Entry 78300

Basic quality parameters of X-ray diagnostic equipments See Entry 78301

Effects of X-ray hardness on fluorogram informativeness See Entry 78302

Photographic recording conditions in a diagnostic X-ray system with an image intensifier See Entry 78303

Transmission of scattered radiation by X-ray grids See Entry 78304

Determination of the basic parameters of PER2-3-P xeroradiographic plate See Entry 78305

The GPR-1 longitudinal radioisotope gamma tomograph See Entry 78306

07.90 OTHER TOPICS IN SPECIALISED INSTRUMENTATION

74579 Analysis of precision in determination of diffusion coefficients by the isotope exchange technique. M.Nanba, Y.Oishi, K.Ando (Dept. of Nuclear Engng., Kyushu Univ., Fukuoka, Japan). *Mem. Fac. Eng. Kyushu Univ. (Japan)*, vol.42, no.4, p.245-50 (Dec. 1982). [received: May 1983]

The precision of diffusion coefficients determined by the gas-solid isotope exchange technique was analysed for the case where planar sheet diffusion is rate-controlled by the isotope exchange reaction. An objective function was employed to estimate the degree of fitting of the theoretical calculation to the experimental diffusion profile as a function of the sample size (l), the diffusion coefficient (D), the surface exchange coefficient (K), and the atoms in the gas and solid phases. The results indicated that the diffusion coefficient could be determined to a high degree of precision when (Kl/D) is greater than 1 and that with this condition satisfied, the precision of the determined diffusion coefficient increased with increased diffusion times. (6 refs.)

System for recording electron-atom collision cross sections using an AI-256-6 pulse analyzer See Entry 75551

Investigation of radiation induced aggregates by phonon techniques See Entry 76459

10.00 THE PHYSICS OF ELEMENTARY PARTICLES AND FIELDS

(for cosmic rays, see 94.40; for high energy-experimental techniques and instrumentation, see 29.)

11.00 GENERAL THEORY OF FIELDS AND PARTICLES

(see also 03.65 Quantum mechanics, 03.70 Theory of quantized fields, 03.80 General theory of scattering)

11.10 FIELD THEORY

74580 Properties of the vacuum. I. Mechanical and thermodynamic. J.Ambjorn, S.Wolfram (Dept. of Phys., California Inst. of Technol., Pasadena, CA, USA).

Ann. Phys. (USA), vol.147, no.1, p.1-32 (15 April 1983).

Casimir energies are calculated for quantized fields in cavities with a variety of forms. Consequences for models of the vacuum state are considered. The possibility of negative mass systems is discussed. Results on energy and entropy of finite quantum systems at non-zero temperature is given. (50 refs.)

74581 Fock space construction of the massless dipole field. A.Z.Capri, G.Grubl, R.Kobes (Theoretical Phys. Inst., Univ. of Alberta, Edmonton, Alberta, Canada).

Ann. Phys. (USA), vol.147, no.1, p.140-70 (15 April 1983).

The authors construct the Fock space representation of the free massless scalar dipole field in terms of creation and annihilation operators for the eigenvectors of the momentum operator. The Poincare group is implemented unitarily only on a subspace of the full (positive metric) Hilbert space. The subspace possess a Hermitean, local, irreducible scalar field constructed out of the (non-hermitean) dipole field. Thus this subspace is a perfect candidate for a physical subspace of observable particles. They show that this possibility is however excluded by the fact that these particles interact with an external c -number source in a manner that violates unitarity. They illustrate the construction by applying it to the linearized Higgs model with external c -number source and examine the (non-trivial) dynamics of the dipole degrees of freedom in this case. An explicit separation of the physical degrees of freedom from the unphysical ones is presented for this interacting model. (11 refs.)

74582 A microscopic theory of the Lambda transition. II. T.Toyoda (Inst. fur Theoretische Phys., Univ. Tübingen, Tübingen, Germany).

Ann. Phys. (USA), vol.147, no.1, p.244-66 (15 April 1983).

For pt.1 see *ibid.*, vol.141, p.154, (1982). The previously proposed finite temperature field theory of the lambda transition based on the Schwinger functional method is investigated further. A systematic method for calculating the higher-order loop terms is presented by introducing the one-loop Green's functions, which are found to be a natural finite temperature extension of the Beliaev-Hugenholtz-Pines-Gavoret-Noziers zero-temperature Green's functions. The application of the finite temperature loop expansion to the dynamical properties is presented by calculating the retarded density correlation functions at the one-loop level. The result gives a microscopic basis for the form of the dynamical structure factor recently proposed by Woods and Svensson (1978). From a general point of view, without using any approximations or model interactions. Goldstone's theorem for the lambda transition at finite temperature is presented. (24 refs.)

74583 A study of CP^{n-1} models on the sphere within the $1/n$ expansion. G.Munster (Inst. fur Theoretische Phys., Univ. Bern, Bern, Switzerland). *Nucl. Phys. B, Part. Phys. (Netherlands)*, vol.B218, no.1, p.1-31 (30 May 1983).

Two-dimensional CP^{n-1} models are considered within the $1/n$ expansion. Space-time is taken to be a sphere, which provides an infrared cut-off. In a sector with fixed topological charge the leading term of the $1/n$ expansion of the partition function is calculated exactly and its volume dependence is studied. In the limit of small volume it approaches the semiclassical instanton contribution. For large volumes it represents a flat Gaussian distribution of topological charge number. The large- n and large volume limits do not commute. (25 refs.)

74584 'Heating the quenched Eguchi-Kawai model. F.R.Klinkhamer (Leiden Obs., Leiden, Netherlands).

Nucl. Phys. B, Part. Phys. (Netherlands), vol.B218, no.1, p.32-42 (30 May 1983).

Considers the Eguchi-Kawai reduction, in the momentum-quenched prescription, of the $SU(N)$ lattice gauge theory for $N \rightarrow \infty$ and address the problem of how finite temperature might be incorporated. This is of interest in order to establish quark deconfinement at high temperatures. The author also shows that different procedures may be inequivalent. (33 refs.)

74585 A model regularizing gauge fields in the strong coupling region. J.M.Drouffe (CERN, Geneva, Switzerland).

Nucl. Phys. B, Part. Phys. (Netherlands), vol.B218, no.1, p.89-109 (30 May 1983).

Proposes a model using an effective lagrangian for bilocal gauge extended fields, looking somehow as an average over all open strings with fixed end points. The locality of the action is retrieved as a range parameter, which acts as a regulator, shrinks, and the Yang-Mills theory is recovered in this limit. The system is invariant by rotation and translation, generalizes lattice gauge theories and allows regularized strong coupling expansions for Yang-Mills field theory. (9 refs.)

74586 Superfield formalism for gauge theories with ghosts and gauge fixing terms from dynamics on superspace. J.Hoyos, M.Quiros, J.Ramirez Mittelbrunn, F.J.de Urries (Inst. de Estructura de la Materia, Madrid, Spain). *Nucl. Phys. B, Part. Phys. (Netherlands)*, vol.B218, no.1, p.159-72 (30 May 1983).

The geometrical condition of soul-flatness needed in the superfield approach to quantized gauge theories and extended BRS transformations, is derived from a lagrangian theory on a superspace $S^{4,2}$. Invariance of the superlagrangian and the lagrangian of quantized gauge theories under $Sp(2,R)$ and hermitian conjugation is discussed in different gauges. (18 refs.)

74587 Quantum meaning of classical (field) theory for Fermi systems. P.Garbaczewski (School of Theoretical Phys., Dublin Inst. for Advanced Studies, Dublin, Ireland).

Nucl. Phys. B, Part. Phys. (Netherlands), vol.B218, no.2, p.321-32 (6 June 1983).

The author gives a path integral reconstruction of two quantum problems: the Fermi oscillator and the chiral invariant Gross-Neveu model. Integrations are carried out with respect to genuine (i.e. c-number, non-Grassmann) paths, so that one is able to identify explicitly contributions of the c-number classical models to the transition amplitudes of their quantized Fermi partners. Stationarity 'points' of the respective actions are verified to coincide with the classical trajectories: of the classical oscillator and of the classical chiral invariant Gross-Neveu field. (21 refs.)

74588 Superspace formulation of supersymmetric gauge theories in 4 and 10 dimensions. M.Tonin (Istituto di Fisica, Univ. di Padova, Padova, Italy).

Nucl. Phys. B, Part. Phys. (Netherlands), vol.B218, no.2, p.366-80 (6 June 1983).

A first-order superspace Lagrangian formulation of supersymmetric Yang-Mills theories in 4 dimensions, proposed in a previous paper (1983) is extended to 10 dimensions. Moreover, a new Lagrangian density, obtained through the removal of some, but not all, of the auxiliary fields, is considered and investigated. In particular, its superconformal properties are discussed. (21 refs.)

74589 Dynamical symmetry breaking in models of spinor fields with quartic interactions in (1+1) dimensions. Wang Rhung-tai, Ni Guang-jiong (Dept. of Phys., Fudan Univ., China).

Commun. Theor. Phys. (China), vol.1, no.4, p.469-83 (1982).

A nonperturbative method, namely, variational method together with canonical transformations, is developed to study dynamical symmetry breaking. This method has been applied in the models of two dimensional massless fermion fields with quartic interactions. The results imply that the mechanism of dynamical symmetry breaking bears some analogy to the phenomenon of superconductivity. The new vacuum $|\bar{O}\rangle$ is just a relativistic BCS ground state. In this vacuum $|\bar{O}\rangle$, one can observe a quasi-particle with mass M_F . Furthermore, correlative vacuum $|\bar{O}\rangle$ exists and the mesons emerge with masses O and $2M_F$. It is also shown that dynamical symmetry breaking always occurs in the models with infrared slavery and asymptotic freedom, while it is meaningless to discuss dynamical symmetry breaking in infrared stable theory. (11 refs.)

74590 Noether analysis and infinitely conserved currents in super-chiral model. Feng Yuan-ping, Ge Mo-lin (Lanzhou Univ., Lanzhou, China).

Commun. Theor. Phys. (China), vol.1, no.4, p.485-93 (1982).

A systematic procedure in writing down the infinite set of nonlocal conserved currents for a super-chiral model is given via Noether analysis. The first three conserved currents are explicitly shown. (10 refs.)

74591 Connection theory of fibre bundle and prolongation structures of nonlinear evolution equations. Guo Han-ying, Hsiang Yan-yu, Wu Ke (Inst. of Theoretical Phys., Acad. Sinica, Beijing, China).

Commun. Theor. Phys. (China), vol.1, no.4, p.495-505 (1982).

It is shown that the proper geometrical framework for the nonlinear evolution equations (NEEs) and the soliton equations should be the fibre bundle theory, the principal bundle and its associated bundle and their connection theory. Based upon the requirement of covariance of the geometrical quantities, a covariant generic geometry theory for the prolongation structures of the NEEs is proposed and the fundamental equations for the prolongation structures are presented. The prolongation structure of the MKdV equation is concretely worked out by means of the covariant theory of the prolongation structure. (16 refs.)

74592 Geometric formulation of the indirect analytic representation of dynamical systems, exterior differential calculus on Banach spaces and variational selfadjointness. R.Trostel (Inst. fur Theoretische Phys., Tech. Univ. Berlin, Berlin, Germany).

Hadronic J. (USA), vol.6, no.2, p.305-405 (March 1983).

The exterior variational calculus is briefly reviewed and precised using, for example, Lang's exterior differential calculus on Banach spaces. Using this framework, a generalized Lemma of Poincare is proved and boundary terms are treated by using new equivalence relations compatible with the exterior differentiation and the respective Poincare-operator. Variational selfadjointness is defined using such equivalence relations comprising automatically Newtonian gauges. The most abstract way to define the indirect analytic representation is achieved by using another equivalence relation among physical 1-forms. As physics is primarily concerned with the solution of evolution equations, i.e. with finding the set of zeros of the physical 1-form, all those 1-forms of which the sets of zeros coincide are called equivalent. Within such an equivalence class, two physical 1-forms are called in genotopic (isotopic) relation to each other if one (both) of them is (are) variationally selfadjoint. The condition equations for isotopic or genotopic relations among 1-forms are derived and specified in the case of linear relationships. The author proves another theorem of the direct Lagrangian universality for all of those systems of which the evolution is C^n [t_0, t_1] ($n \geq 1$). (38 refs.)

74593 Decoupling theorem of quantum field theory in Minkowski space. E.B.Manoukian (Royal Military Coll. of Canada, Kingston, Ontario, Canada).

Int. J. Theor. Phys. (USA), vol.22, no.4, p.315-21 (April 1983).

The decoupling theorem of quantum field theory with massive particles is proved in Minkowski space when all the masses of the theory are led to go to infinity. The theorem establishes the vanishing property, in the distributional sense, of (absolutely convergent) Feynman amplitudes in a model independent way with subtractions performed at the origin. This extends previous efforts dealing with the proof of the theorem in the Euclidean region. (17 refs.)

74594 Dirac-Schwinger commutation relations on a lattice. A.Peres (Dept. of Phys., Technion-Israel Inst. of Technol., Haifa, Israel).

Int. J. Theor. Phys. (USA), vol.22, no.4, p.355-7 (April 1983).

Low-frequency excitations of a one-dimensional chain of oscillators propagate like waves with a uniform velocity. Therefore this lattice is Lorentz invariant on a macroscopic scale. The Dirac-Schwinger commutation relations are constructed explicitly and shown to have the correct limit for long wavelengths. A similar test could be used to check the Lorentz invariance of lattice field theories. (13 refs.)

74595 Mechanism by which spatially homogeneous Yang-Mills fields become stochastic. A.R.Avakyun, S.G.Arutyunyan, G.Z.Baseyan.

JETP Lett. (USA), vol.36, no.10, p.451-4 (20 Nov. 1982). Translation of: *Pis'ma v Zh. Eksp. & Teor. Fiz. (USSR)*, vol.36, no.10, p.372-4 (20 Nov. 1982). [received: June 1983]

A mechanical system with a nonzero angular momentum, corresponding to spatially homogeneous Yang-Mills fields, is analyzed. Numerical simulations have been carried out. A mechanism by which the fields become stochastic is found. (5 refs.)

74596 Renormalisation of the Fayet-Iliopoulos term in supersymmetric spontaneously broken U(1) gauge theories. T.R.Govindarajan (Phys. Dept., Indian Inst. of Technol., Kanpur, India), R.K.Kaul, B.Vijayalakshmi.

J. Phys. G (GB), vol.9, no.6, p.L103-6 (June 1983).

It is shown that the Fayet-Iliopoulos D term in $N=1$ supersymmetric spontaneously broken U(1) gauge theories may get one-loop corrections, even when trace U(1) charges are zero. However, these corrections are only logarithmically divergent and hence do not affect the naturalness of the theory. (9 refs.)

74597 On the covariant gauge parameter and the renormalisation group. R.D.C.Miller (CERN, Geneva, Switzerland).

J. Phys. G (GB), vol.9, no.6, p.595-603 (June 1983).

In a standard formulation of the renormalisation group (RG) a renormalised covariant gauge parameter is just as much a running parameter as are couplings and masses. In the past, by working in the Landau gauge, issues associated with a running covariant gauge parameter have largely been avoided. The present author looks at the main consequences of maintaining a general covariant gauge. He also reviews Gross' fixed gauge RG (1976) in which there has been renewed interest. For physical amplitudes this provides a simpler alternative to the standard RG. However, he shows that the fixed gauge RG invariants are in fact gauge dependent. Finally he points out that the Celmaster-Gonsalves relation (1979) is only true for the fixed gauge RG and not the standard RG. One may use this fact to extract the explicit gauge dependence of the fixed gauge RG invariants. (18 refs.)

74598 Non-Abelian gauge theories and Riemannian geometry on principal bundle with a scalar function or functional. An Ying, Chen Shi, Guo Hanying (Inst. of Theoretical Phys., Acad. Sinica, Beijing, China).

Kexue Tongbao (Foreign Lang. Ed.) (China), vol.28, no.1, p.34-9 (Jan. 1983). [received: June 1983]

It is shown that the non-Abelian gauge theories and their extension can be studied by means of the Riemannian geometry on principal bundles with an arbitrary scalar function or functional. The authors obtain the covariant conservation equations of gauge charges and the motion equations of test particles in the fields, based on the assumption that test particles move along the geodesics on the bundle space. They discuss the relationship between the Kaluza type actions and the usual Yang-Mills actions and suggest a kind of non-Abelian gauge theory with a scalar field. (7 refs.)

74599 Static and spherically symmetric dyon solutions in SU(N) gauge theory. Ma Zhongqi (Inst. of High Energy Phys., Acad. Sinica, Beijing, China).

Kexue Tonghao (Foreign Lang. Ed.) (China), vol.28, no.3, p.328-32 (March 1983). (13 refs.)

74600 Quantization of Galilean gauge theories. F.Palumbo (Istituto Nazionale di Fisica Nucleare, Frascati, Italy).

Lett. Nuovo Cimento (Italy), vol.37, ser.2, no.3, p.81-5 (21 May 1983).

Galilean gauge theories are quantized using Dirac's theory of canonical quantization of constrained systems. The infra-red sector for the Abelian case is exactly solved and shown to be analogous to that of the relativistic case. (7 refs.)

74601 Chiral property of the generalized Gross-Neveu model with $U_N \times U_N$ flavour chiral symmetry in 1+1 dimensions. S.Sakai (Inst. of Phys., Univ. of Tsukuba, Ibaraki, Japan).

Lett. Nuovo Cimento (Italy), vol.37, ser.2, no.3, p.95-8 (21 May 1983).

The generalized Gross-Neveu model with $U_N \times U_N$ flavour chiral symmetry in 1+1 dimensions is studied by means of boson-fermion metamorphosis. A more rigorous argument on the presence of the low-temperature phase of Berezinski-Kosterlitz-Thouless type is presented. Low-lying physical fermion masses are obtained. (13 refs.)

74602 Generalized field theories and solutions. J.L.Reid (Dept. of Phys. & Astron., Univ. of Georgia, Athens, GA, USA), P.B.Burt.

Lett. Nuovo Cimento (Italy), vol.37, ser.2, no.3, p.116-18 (21 May 1983).

By beginning with a special class of solutions of field equations, new field equations are derived. (8 refs.)

74603 Quantisation of spontaneously broken gauge theories in the unitary gauge through the Dirac-bracket formalism. H.O.Girotti, H.J.Rothe (Inst. de Fisica, Univ. Federal do Rio Grande do Sul, Porto Alegre, Brazil).

Nuovo Cimento A (Italy), vol.75A, ser.2, no.1, p.62-8 (1 May 1983).

The authors reconsider the quantisation of the Higgs model in the unitary gauge using the Dirac-bracket quantisation procedure. It is found that the structure of some of the equal-time commutators is quite abnormal. It is then shown in a very clear and systematic way that this anomalous structure is closely connected with the well-known quartically divergent contribution to the effective Higgs Lagrangian. This contribution has been shown to play an important role in the cancellation of nonrenormalisable divergences. (13 refs.)

74604 All the standard irreducible equations of spin $3/2$ without auxiliary spin $3/2$. G.Labonte (Inst. fur Theoretische Phys., Freie Univ. Berlin, Berlin, Germany).

Nuovo Cimento A (Italy), vol.75A, ser.2, no.1, p.69-79 (1 May 1983).

A construction is made of all the possible Γ -matrices for the standard relativistic wave equations of spin $3/2$, belonging to the family of those for which $3/2$ is not an auxiliary spin. The corresponding equations, which are irreducible when minimally coupled to an electromagnetic field, are obtained: some exist for any Harish-Chandra degree greater than or equal to four. (7 refs.)

74605 Remarks on Weyl's gauge field. M.Nishioka (Dept. of Phys., Faculty of Liberal Arts, Yamaguchi Univ., Yamaguchi, Japan).

Nuovo Cimento A (Italy), vol.75A, ser.2, no.1, p.80-6 (1 May 1983).

Using the manifestly gauge-invariant Lagrangian of the system in which a real scalar field (matter field) is interacting with itself and Weyl's gauge field, the author studies the equations of the matter field and Weyl's gauge field, and discusses the self-interacting term of the matter field. (9 refs.)

74606 Light spinor monopole. Li Xinzhou, Wang Kellin, Zhang Jianzu (Internat. Centre for Theoretical Phys., Trieste, Italy).

Nuovo Cimento A (Italy), vol.75A, ser.2, no.1, p.87-92 (1 May 1983).

Suggests that the monopole may have a light mass, which gives the possibility to avoid a conflict between cosmology and grand unification theory. (6 refs.)

74607 Gauge and nongauge curvature tensor copies. P.P.Srivastava (Internat. Centre for Theoretical Phys., Trieste, Italy).

Nuovo Cimento A (Italy), vol.75A, ser.2, no.1, p.93-9 (1 May 1983).

A procedure for constructing curvature tensor copies is discussed by using the anholonomic geometrical framework. The corresponding geometries are compared and the notion of gauge copy elucidated. An explicit calculation is also made. (10 refs.)

- 74608 The stress-energy-momentum tensor of the Gauss map in the extended nonlinear σ -model.** B.Nielsen (Math. Inst., Tech. Univ. of Denmark, Lyngby, Denmark). *Nuovo Cimento B (Italy)*, vol.74B, ser.2, no.2, p.159-66 (11 April 1983).
- By interpreting the nonlinear σ -model as the Gauss map associated to a certain immersion, the author derives an explicit connection between the energy-momentum tensor and the geometry of space-time. The author is then able to point out what follows: (i) the cosmological term is intimately connected with the mean curvature of the immersion, (ii) the possible space-times are restricted by a requirement on the associated immersions, (iii) the energy of the solution is given by the square of the mean curvature of the immersion. (12 refs.)
- 74609 Solutions to generalized double sine-Gordon equations.** K.Saermark (Phys. Lab. I, Tech. Univ. of Denmark, Lyngby, Denmark). *Phys. Lett. A (Netherlands)*, vol.95A, no.8, p.409-11 (23 May 1983).
- A non-linear differential equation, which encompasses the sine-Gordon and double sine-Gordon equations as special cases, is presented and a solution given in terms of Weierstrass' P functions. The equation is time independent, but a Lorentz transformation may in the usual way produce translational solutions. The special case of the double sine-Gordon equation is considered in some detail. (6 refs.)
- 74610 A reply to 'Gauge invariance and experimental processes'.** Y.Aharonov, C.K.Au (Dept. of Phys. & Astron., Univ. of South Carolina, Columbia, SC, USA). *Phys. Lett. A (Netherlands)*, vol.95A, no.8, p.412-14 (23 May 1983).
- For cited paper see *ibid.*, vol.92, p.71 (1982). The authors reply to the charges by K.H. Yang in his paper 'Gauge invariance and experimental processes'. (3 refs.)
- 74611 Composite gauge bosons in sigma models and supergravity.** A.C.Davis (Inst. for Advanced Study, Princeton, NJ, USA), A.J.Macfarlane, J.W.van Holten. *Phys. Lett. B (Netherlands)*, vol.125B, no.2-3, p.151-5 (26 May 1983).
- The authors discuss the non-compact $SU(n)_1/SU(n) \times U(1)$ sigma models and show there is no dynamical generation of the composite gauge boson in these models in two and three dimensions. They discuss some necessary conditions for the $SU(8)$ gauge boson in $N=8$ supergravity to become dynamical. (19 refs.)
- 74612 Dyon-axion dynamics.** W.Fischler (Dept. of Phys., Univ. of Pennsylvania, Philadelphia, PA, USA), J.Preskill. *Phys. Lett. B (Netherlands)*, vol.125B, no.2-3, p.165-70 (26 May 1983).
- The authors examine the coupling between magnetic monopoles and axions induced by the Witten effect, and discuss the cosmological implications of monopole-axion interactions. (14 refs.)
- 74613 Extended BRS symmetry in supersymmetric Yang-Mills theory.** N.K.Falck, A.C.Hirshfeld, J.Kubo (Inst. fur Phys., Univ. Dortmund, Dortmund, Germany). *Phys. Lett. B (Netherlands)*, vol.125B, no.2-3, p.175-7 (26 May 1983).
- The superspace formulation of pure Yang-Mills theory is extended to $N=1$ supersymmetric Yang-Mills. BRS and anti-BRS symmetry are incorporated in a natural way, and a compact expression for the Lagrangian including the gauge-fixing and Faddeev-Popov ghost terms, is easily derived. (14 refs.)
- 74614 Light composite supermultiplets.** T.R.Taylor (Fermi Nat. Accelerator Lab., Batavia, IL, USA). *Phys. Lett. B (Netherlands)*, vol.125B, no.2-3, p.185-9 (26 May 1983).
- It is argued that in a wide class of massless strongly interacting supersymmetric gauge theories there exist confining phases with unbroken supersymmetry. The author explains how to identify and interpret the light composite supermultiplet content of these phases. (12 refs.)
- 74615 Instantons on the lattice.** Y.Iwasaki, T.Yoshie (Inst. of Phys., Univ. of Tsukuba, Ibaraki, Japan). *Phys. Lett. B (Netherlands)*, vol.125B, no.2-3, p.197-200 (26 May 1983).
- The existence of instantons on the lattice is examined taking the two-dimensional CP^1 model as an example. Among theories which are identical in the naive continuum limit, some theories where short range fluctuations are suppressed possess stable instantons, while others do not. (11 refs.)
- 74616 Lattice actions and scaling properties.** Y.Iwasaki, T.Yoshie (Inst. of Phys., Univ. of Tsukuba, Ibaraki, Japan). *Phys. Lett. B (Netherlands)*, vol.125B, no.2-3, p.201-6 (26 May 1983).
- Scaling properties of the topological susceptibility and the magnetic susceptibility of the two-dimensional $O(3)$ σ model are studied by Monte Carlo simulations for various cases of lattice actions. It turns out that either the onset of the scaling law crucially depends on the form of lattice action, or that some physical quantities do not scale. (16 refs.)
- 74617 Gauge-invariant local fields in a gauge theory as interpolating fields for 'glueballs'.** M.Azam, P.P.Divakaran (Tata Inst. of Fundamental Res., Bombay, India). *Phys. Lett. B (Netherlands)*, vol.125B, no.2-3, p.207-10 (26 May 1983).
- A method of constructing all gauge-invariant local fields in a classical gauge theory, based on their being generated by a finite set of 'basic' invariants, is presented. A complete relativistic spin reduction of all two- and three-gluon basic invariant fields is given and their possible relevance to glueball classification indicated. (9 refs.)
- 74618 Charges from extra dimensions.** S.Weinberg (Dept. of Phys., Univ. of Texas, Austin, TX, USA). *Phys. Lett. B (Netherlands)*, vol.125B, no.4, p.265-9 (2 June 1983).
- A prescription is given for calculating gauge coupling constants in $(4+N)$ -dimensional models in which N dimensions form an arbitrary compact manifold: each coupling is given by the ratio of $2\pi(16\pi G)^{1/2}$ to an appropriate root-mean-square circumference of the manifold. It is speculated that these couplings will be of order $1/\sqrt{n}$, where n is the number of matter fields whose one-loop quantum energy density is responsible for the compactification. (7 refs.)
- 74619 A class of conformally invariant quantum theory theories.** E.Braaten, T.Curtright, G.Ghandour, C.Thorn (Dept. of Phys., Univ. of Florida, Gainesville, FL, USA). *Phys. Lett. B (Netherlands)*, vol.125B, no.4, p.301-4 (2 June 1983).
- A general family of two-dimensional field theories of the Liouville type, involving one or more scalar fields, is shown to be conformally invariant when quantized canonically over a large class of Fock space. (9 refs.)
- 74620 Unperturbed sine-Gordon solitons as Newtonian particles.** U.Enz (Philips Res. Labs., Eindhoven, Netherlands). *Phys. Rev. B (USA)*, vol.27, no.9, p.5815-16 (1 May 1983).
- The dynamics of the sine-Gordon soliton is studied by the consideration of the breather solution of the sine-Gordon equation in the limit of large soliton separation. It is found that in this limit the sine-Gordon soliton behaves as a Newtonian particle, i.e. the acceleration of the soliton is proportional to the force acting on it. The definition of the force acting on the soliton is scrutinized. (6 refs.)
- 74621 Sine-Gordon model for classical kink mechanics.** J.J.P.Leon (Lab. de Phys. Math., Univ. des Sci. et Tech. du Languedoc, Montpellier, France), G.Reinisch, J.C.Fernandez. *Phys. Rev. B (USA)*, vol.27, no.9, p.5817-18 (1 May 1983).
- To the extent that a sine-Gordon soliton may be viewed as a mass point in a given potential $V(x)$, the authors propose the resulting modified sine-Gordon equation which takes this potential into account and leads to a Newtonian dynamics of the kink in $V(x)$. (8 refs.)
- 74622 Relation between the classical Wilson loop and the angular parallel displacement.** V.Bezerra (Centro Brasileiro de Pesquisas Fisicas, Rio de Janeiro, Brazil). *Rev. Bras. Fis. (Brazil)*, vol.12, p.67-72 (March 1982). [received: April 1983]
- Investigates a simple relation between the classical Wilson loop and the angular parallel displacement along a closed path (circle) for the case of the instanton-like potentials. (9 refs.)
- 74623 Exact solution of covariant two-particle one-time equation with superposition of one-boson exchange quasipotentials.** V.N.Kapshai, N.B.Skachkov (Joint Inst. for Nuclear Res., Dubna, USSR). *Theor. & Math. Fiz. (USSR)*, vol.53, no.1, p.963-70 (Oct. 1982). Translation of: *Theor. & Math. Fiz. (USSR)*, vol.53, no.1, p.32-42 (Oct. 1982).
- The relativistic bound state of two scalar particles is considered in the Logunov-Tavkhelidze quasipotential approach in the case when the quasipotential is a superposition of a one-meson and a one-photon propagator. For the centrally symmetric case, a relativistic quantization condition for the energy levels is obtained and wave functions are constructed in the momentum representation and in the relativistic configuration representation. (11 refs.)
- 74624 A micro-deSitter spacetime with constant torsion: a new vacuum solution of the Poincare gauge field theory.** P.Baekler, F.W.Hehl (Inst. for Theoretical Phys., Univ. of Cologne, Cologne, Germany). *Gauge Theory and Gravitation. Proceedings of the International Symposium, Nara, Japan, 20-24 Aug. 1982* (Berlin, Germany: Springer-Verlag 1983), p.1-15.
- The authors study the Poincare gauge field theory with Lagrangians of the type (curvature scalar + torsion²)/ l^2 + curvature²/ \mathcal{M} . Here l is the Planck length and \mathcal{M} the coupling constant of the hypothetical Lorentz gauge bosons. They find a new vacuum solution with a deSitter metric and with constant microscopic torsion $\sim \sqrt{\mathcal{M}/l}$ and curvature $\sim \mathcal{M}/l^2$. Its curvature displays double duality properties. (82 refs.)
- 74625 Algebraic construction of static axially symmetric self-dual fields.** R.Sasaki (Res. Inst. for Theoretical Phys., Hiroshima Univ., Hiroshima, Japan). *Gauge Theory and Gravitation. Proceedings of the International Symposium, Nara, Japan, 20-24 Aug. 1982* (Berlin, Germany: Springer-Verlag 1983), p.31-5.
- The author presents the problem of solving self-dual gauge field equations for an arbitrary compact semisimple gauge group G . The discussion is mostly focused on the simple case of the static and axially symmetric configuration, in which the effective spacetime dimension is reduced to two. A main application is the construction of axially symmetric monopole solutions in gauge theories with an arbitrary group G and a single Higgs field in the adjoint representation. (7 refs.)
- 74626 Massive gauge theories in three dimensions at high temperature.** R.Jackiw (Center for Theoretical Phys., Dept. of Phys., MIT, Cambridge, MA, USA). *Gauge Theory and Gravitation. Proceedings of the International Symposium, Nara, Japan, 20-24 Aug. 1982* (Berlin, Germany: Springer-Verlag 1983), p.45-57.
- Gauge theories in three dimensions provide interesting case studies of gauge invariant quantum field theoretic phenomena. The special topological properties of odd-dimensional space allow the construction of a gauge invariant mass term in three dimensions. Moreover, for non-Abelian gauge groups, the configuration space of the quantum theory is not simply connected, and as a consequence the mass must be quantized. (7 refs.)
- 74627 Stochastic quantization and large N reduction.** J.Alfaro, B.Sakita (Dept. of Phys., City Coll., City Univ. of New York, New York, NY, USA). *Gauge Theory and Gravitation. Proceedings of the International Symposium, Nara, Japan, 20-24 Aug. 1982* (Berlin, Germany: Springer-Verlag 1983), p.65-74.
- The stochastic quantization method of Parisi and Wu is used in order to understand the quenched momentum prescription for large N theories. The Hermitian matrix field theory model is studied first and then the same method is applied to $SU(N)$ gauge theory. (5 refs.)
- 74628 Variational methods in the master field formulation for QCD_{3+1} .** M.Sato (Dept. of Phys., New York Univ., New York, NY, USA). *Gauge Theory and Gravitation. Proceedings of the International Symposium, Nara, Japan, 20-24 Aug. 1982* (Berlin, Germany: Springer-Verlag 1983), p.75-8.
- Master fields are formulated for finite N - QCD_{3+1} . They satisfy classical Yang-Mills equations with an infinite number of internal indices and an infinite number of constraints. Master fields and constraints on them in the large N limit are derived from the finite N master fields and constraints using vacuum dominance among color singlet states. The large N constraints can be explicitly solved and the solutions involve arbitrary functions which are used as trial functions in variational calculations. (5 refs.)
- 74629 Confinement by thick magnetic vortices.** T.Yoneya (Inst. of Phys., Univ. of Tokyo, Tokyo, Japan). *Gauge Theory and Gravitation. Proceedings of the International Symposium, Nara, Japan, 20-24 Aug. 1982* (Berlin, Germany: Springer-Verlag 1983), p.79-83.
- An argument is presented showing that the pure lattice gauge theories which are infrared unstable at the origin of the coupling constant are always in confining phase, provided that (i) the gauge group is compact and contains nontrivial center; (ii) Lagrangian does not contain long range interaction. The steps for an attempt at a proof of confinement are suggested. (4 refs.)
- 74630 Renormalizability of massive Yang-Mills theory.** T.Fukuda, H.Matsuda, Y.Seki, K.Yokoyama (Res. Inst. for Theoretical Phys., Hiroshima Univ., Hiroshima, Japan). *Gauge Theory and Gravitation. Proceedings of the International Symposium, Nara, Japan, 20-24 Aug. 1982* (Berlin, Germany: Springer-Verlag 1983), p.84-8.
- The authors aim to reveal the renormalizable structure of massive Yang-Mills (YM) theories on the basis of the formalism in the authors' previous work (1982), though there had so far been found several counter-observations. The formalism consists of four kinds of auxiliary scalar fields other than a massive gauge field A_μ ; a massless scalar fields ϕ^2 , in addition to the usual Lagrange

multiplier field η^a and a pair of Faddeev-Popov ghost fields C^a and \bar{C}^a . (8 refs.)

74631 Renormalization and scaling of non-abelian gauge fields in curved space-time. L.Parker (Dept. of Phys., Univ. of Wisconsin, Milwaukee, WI, USA).

Gauge Theory and Gravitation. Proceedings of the International Symposium, Nara, Japan, 20-24 Aug. 1982 (Berlin, Germany: Springer-Verlag 1983), p.96-100

Flat space-time non-abelian gauge field theories are renormalizable and asymptotically free. The author shows that non-abelian gauge fields in curved space-time are renormalizable at the one-loop level; and that the property of asymptotic freedom is preserved. (9 refs.)

74632 Two-point functions and renormalized observables. S.A.Fulling (Maths. Dept., Texas A&M Univ., College Station, TX, USA).

Gauge Theory and Gravitation. Proceedings of the International Symposium, Nara, Japan, 20-24 Aug. 1982 (Berlin, Germany: Springer-Verlag 1983), p.101-6

The author presents a theory of a quantized field propagating in a given curved background space-time. The theory is an unambiguous, internally consistent quantum theory of such a system, in which any physical quantity can in principle be calculated. Whether this kind of model is relevant to the real world is a separate question. The physical interpretation of a quantum field theory in curved space must be sought in the stress-energy-momentum tensor and other local field observables. (45 refs.)

74633 Vacuum energy in the bag model. P.Candelas (Center for Theoretical Phys., Univ. of Texas, Austin, TX, USA).

Gauge Theory and Gravitation. Proceedings of the International Symposium, Nara, Japan, 20-24 Aug. 1982 (Berlin, Germany: Springer-Verlag 1983), p.107-12

The vacuum energy of the Yang-Mills field is examined for the conditions of the bag model. The imposition of confining boundary conditions for all frequencies is shown to be inconsistent since this would result in the bag constant and certain of the shape tensions being infinite. (7 refs.)

74634 Stochastic quantization and Gribov problem. M.Horibe (Faculty of Education, Fukui Univ., Fukui, Japan), A.Hosoya, J.Sakamoto.

Gauge Theory and Gravitation. Proceedings of the International Symposium, Nara, Japan, 20-24 Aug. 1982 (Berlin, Germany: Springer-Verlag 1983), p.113-15

The authors report a modest progress in the Gribov problem in the framework of the stochastic quantization method. They present the Langevin equation for a gauge field without the necessity for gauge fixing. (5 refs.)

74635 The geometry of the configuration space of non abelian gauge theories. C.M.Viallet (Lab. de Phys. Theorique et Hautes Energies, Univ. Pierre et Marie Curie, Paris, France).

Gauge Theory and Gravitation. Proceedings of the International Symposium, Nara, Japan, 20-24 Aug. 1982 (Berlin, Germany: Springer-Verlag 1983), p.116-19

The author presents results on the geometry of the configuration space of non abelian gauge theories. It is on this space that a Schrodinger equation (or equivalently a path integral) is to be defined. The study of the geometry of the configuration space is a necessary step for a proper non perturbative quantization of the theory. (11 refs.)

74636 Lattice gauge theory—a progress report. J.Shigemitsu (Dept. of Phys., Brown Univ., Providence, RI, USA).

Gauge Theory and Gravitation. Proceedings of the International Symposium, Nara, Japan, 20-24 Aug. 1982 (Berlin, Germany: Springer-Verlag 1983), p.120-32

Some recent calculations in lattice gauge theory are reviewed. These include estimates of the heavy quark potential, the hadron spectrum, and scales of chiral symmetry breaking. (26 refs.)

74637 Recent developments in the theory of large N gauge fields. T.Eguchi, H.Kawai (Dept. of Phys., Univ. of Tokyo, Tokyo, Japan).

Gauge Theory and Gravitation. Proceedings of the International Symposium, Nara, Japan, 20-24 Aug. 1982 (Berlin, Germany: Springer-Verlag 1983), p.133-40

Quantum field theories with global or local symmetry greatly simplify in the limit $N \rightarrow \infty$. The authors discuss the effects of quenching reduction and twist in this limit. (11 refs.)

74638 Topological excitations on a lattice. Y.Iwasaki, T.Yoshie (Inst. of Phys., Univ. of Tsukuba, Ibaraki, Japan).

Gauge Theory and Gravitation. Proceedings of the International Symposium, Nara, Japan, 20-24 Aug. 1982 (Berlin, Germany: Springer-Verlag 1983), p.141-5

The authors study by numerical methods the existence of instantons and the role played by instantons on a lattice, by taking the CP model in two dimensions as an example. (11 refs.)

74639 Observation of Aharonov-Bohm effect by electron holography. A.Tonomura, T.Matsuda, R.Suzuki, A.Fukuhara, N.Osakabe, H.Umezaki, J.Endo, K.Shinagawa, Y.Sugita, H.Fujiwara (Central Res. Lab., Hitachi Ltd., Tokyo, Japan).

Gauge Theory and Gravitation. Proceedings of the International Symposium, Nara, Japan, 20-24 Aug. 1982 (Berlin, Germany: Springer-Verlag 1983), p.146-54

The authors discuss several experiments performed to observe the Aharonov-Bohm effect as evidence of gauge fields. (11 refs.)

74640 BRS transformation and color confinement. K.Nishijima (Dept. of Phys., Univ. of Tokyo, Tokyo, Japan).

Gauge Theory and Gravitation. Proceedings of the International Symposium, Nara, Japan, 20-24 Aug. 1982 (Berlin, Germany: Springer-Verlag 1983), p.155-60

Interpretation of hadrons in terms of quarks and antiquarks has been so successful that one can no longer think of its substitute. The hadron spectrum and high energy hadron reactions are believed to be described by means of quantum chromodynamics (QCD). In the lattice gauge theory the condition for quark confinement is given by the area law for the Wilson loop. The author looks for the corresponding condition within the framework of the conventional continuum field theory. (5 refs.)

74641 Covariant operator formalism of gauge theories and its extension to finite temperature. I.Ojima (Res. Inst. for Math. Sci., Kyoto Univ., Kyoto, Japan).

Gauge Theory and Gravitation. Proceedings of the International Symposium, Nara, Japan, 20-24 Aug. 1982 (Berlin, Germany: Springer-Verlag 1983), p.161-5

On the basis of 'thermo field dynamics' allowing the application of the Feynman diagram method to real-time Green's functions at $T \neq 0K$, a field-theoretical formulation of finite-temperature gauge theory is presented. It is an extension of the covariant operator formalism of gauge theory based upon

the BRS invariance: The subsidiary condition specifying physical states, the notion of observables, and the structure of the physical subspace at finite temperatures are clarified together with the key formula characterizing the temperature-dependent 'vacuum'. (12 refs.)

74642 Path integration at the crossroad of stochastic and differential calculus. C.DeWitt-Morette (Dept. of Astron. & Center for Relativity, Univ. of Texas, Austin, TX, USA).

Gauge Theory and Gravitation. Proceedings of the International Symposium, Nara, Japan, 20-24 Aug. 1982 (Berlin, Germany: Springer-Verlag 1983), p.166-70

Ever since Newton differential calculus has been a very successful language for the description of physical systems; stochastic calculus on the other hand has only recently become an instrument of thought but has already been used in challenging problems. The author presents some applications of stochastic calculus and differential calculus. (7 refs.)

74643 Background field method of gauge theory and the renormalization problem. S.Ichinohe, M.Motomoto (Inst. of Phys., Univ. of Tsukuba, Ibaraki, Japan).

Gauge Theory and Gravitation. Proceedings of the International Symposium, Nara, Japan, 20-24 Aug. 1982 (Berlin, Germany: Springer-Verlag 1983), p.204-7

The authors present the background field method proposed by DeWitt (1967) to quantize gauge theories without losing invariance. This is very important in discussing the renormalisation problem of non-abelian gauge theories. They discuss a systematic renormalisation procedure by using this method and by generalising the counter-term formula of 't Hooft to two loop processes. (4 refs.)

74644 The auxiliary field/ultraviolet finiteness connection. P.K.Townsend (Lab. de Phys. Theorique, Ecole Normale Supérieure, Paris, France).

Gauge Theory and Gravitation. Proceedings of the International Symposium, Nara, Japan, 20-24 Aug. 1982 (Berlin, Germany: Springer-Verlag 1983), p.240-8

The status of the auxiliary field program for supersymmetric field theories is reviewed, with emphasis on the implications for improved ultraviolet behaviour, and conversely on the implications of ultraviolet behaviour for auxiliary fields. (24 refs.)

74645 Non-local gauge theories. S.L.Adler (Inst. for Advanced Study, Princeton, NJ, USA).

The High-Energy Limit. Proceedings of the Eighteenth Course of the International School of Subnuclear Physics, Erice, Italy, 31 July-11 Aug. 1980 (New York, USA: Plenum 1983), p.29-123

The conventional quantum field theories describing the dynamics of flavor processes [such as the $SU(2) \otimes U(1)$ weak-electromagnetic model, or effective strong interaction field theories such as the σ -model or chiral Lagrangian models] are local field theories, in which all operators commute or anticommute for spacelike-separated arguments. The basic premise is that field theories describing color processes [such as $SU(3)$ quantum chromodynamics (QCD) for quark interactions, or heavy color models for possible quark-lepton constituents] should be constructed as non-local field theories, in which the gluon operators (and in the relativistic case, the fermion operators as well) contain components which do not simply commute or anticommute when the arguments are spacelike-separated. The author gives arguments to support this contention, and applications. (18 refs.)

74646 Bianchi-Backlund transformations, conservation laws, and linearization of various field theories. Ling-Lie Chau (Phys. Dept., Brookhaven Nat. Lab., Upton, NY, USA).

The High-Energy Limit. Proceedings of the Eighteenth Course of the International School of Subnuclear Physics, Erice, Italy, 31 July-11 Aug. 1980 (New York, USA: Plenum 1983), p.249-80

Discusses a possible future solution of non-Abelian gauge theories to help in the understanding of strong interactions. The author speculates whether the mathematical tools used to study two dimensional Yang-Mills theories can be used for four-dimensional non-Abelian gauge theories. (47 refs.)

Gauge theory of dislocations and disclinations See Entry 74237

Multi-instanton contributions in quantum mechanics. II See Entry 74300

New general relativity—translation gauge theory See Entry 74332

Vanishing of the cosmological constant in non-Abelian Kaluza-Klein theories ..

Manifestly covariant canonical formalism of quantum gravity—a brief survey—

..... See Entry 74344

A gauge invariant resummation of quantum gravity See Entry 74350

'The gauge invariant effective action for quantum gravity and its semi-

quantitative approximation' See Entry 74351

Induced gravitation See Entry 74352

Stability of gravitational merons See Entry 74357

Grand unified theories with symmetry and local supersymmetry ..

..... See Entry 74358

Consistency of coupling in supergravity with propagating Lorentz connexion ..

..... See Entry 74359

Dimensional reduction See Entry 74360

One-loop divergences and β -functions in supergravity theories ..

..... See Entry 74361

Metastable states near the phase boundary: a finite-lattice study ..

..... See Entry 74397

Finite-size scaling in the $(2+1)D$ Ising model See Entry 74398

Lepton-violating $\beta^- \beta^+$, $\beta^+ \beta^+$ decays, $(e^- e^+)$ conversion and double electron

capture in gauge theories See Entry 74648

Vacuum alignment and dynamical symmetry breaking in two-dimensional

models See Entry 74649

Fractional charges: global and local aspects See Entry 74650

Soft breaking of $N=4$ supersymmetry See Entry 74656

On the dynamic origin of the kinetic terms See Entry 74658

Testing the standard model See Entry 74669

Early unification and the Weinberg angle in the $SU(4)$ grand unified model ..

..... See Entry 74673

Grand unification with local supersymmetry See Entry 74674

An approach to gauge hierarchy in the minimal $SU(5)$ model of grand unifica-

tion See Entry 74675

Effective Lagrangian for $\Delta S=1$ and $\Delta S=2$ transition in the Higgs boson

exchange model of CP violation See Entry 74681

How supersymmetry makes neutron-antineutron oscillations more natural in

$SO(10)$ See Entry 74683

- Supersymmetric dipole mechanism and vacuum energy See Entry 74687
 Nonsymmetry of an inverted hierarchy model See Entry 74688
 How far we are in unifying the fundamental interactions See Entry 74692
 Electroweak physics of the 80s See Entry 74693
 QCD, unification and the road to 'asymptopia' See Entry 74695
 Properties of the vacuum. II. Electrodynamic See Entry 74696
 Wilson loop Langevin equations for U(1) lattice gauge theory See Entry 74698
 Electromagnetic vacuum and strong interactions See Entry 74699
 Deep inelastic scattering at small x : two- and three-loop calculations See Entry 74704
 Chemical potential on the lattice See Entry 74706
 Error estimate for the valence approximation to lattice QCD See Entry 74707
 Quaternionic formulation of fields associated with dyons See Entry 74710
 Gluon condensation and confinement of quarks See Entry 74713
 Deep inelastic phenomena See Entry 74715
 Higher dimensional renormalization group invariant vacuum condensates in quantum chromodynamics See Entry 74719
 Spectroscopy of hadrons: mesons See Entry 74723
 The de Broglie fusion method applied to quarks at the ends of strings See Entry 74726
 Instantons in the quark plasma See Entry 74728
 On scalar quark leakage in Klein-Gordon equation See Entry 74730
 Superstring interactions See Entry 74744
 The physics of dual vortices and static baryons in $2+1$ dimensions See Entry 74746
 Generalized string amplitude and wave equation for hadrons See Entry 74747
 Recent results from PETRA See Entry 74781
 Relativistic two-nucleon calculations on the light front See Entry 74860
 Pion dynamics in the relativistic nuclear many-body problem See Entry 74921
 Multiple scattering in the Lee model See Entry 74926
 Feynman diagram for reactive collisions See Entry 75481
 Large numbers hypothesis. IV. The cosmological constant and quantum physics See Entry 79034
 Do we live inside a domain wall? See Entry 79039

11.20 S-MATRIX THEORY

- Charged particles with short range interactions See Entry 74296
 Analysis of a bilinear relation for the six-vertex model See Entry 74323
 SU(5) without SU(5): why B-L is conserved and baryon number not in unified models of quarks and leptons See Entry 74694
 Scattering with absorptive interaction: energy-dependent potentials See Entry 74924

11.30 SYMMETRY AND CONSERVATION LAWS

(see also 02.20 Group theory)

- 74647 Shift operator approach of the spin-isospin supermultiplet state labelling problem: eigenvalue determination of the Ω and Φ labelling operators. J. Van der Jeugt, H.E. De Meyer, G. Vanden Bergh (Seminarie voor Wiskundige Natuurkunde, Rijksuniversiteit Gent, Gent, Belgium). *Ann. Phys. (USA)*, vol.147, no.1, p.85-139 (15 April 1983).
 The two missing labels problem which occurs in the reduction of SU(4) irreducible representation (irreps) into SU(2) \otimes SU(2), irreps has been solved by Moshinsky and Nagel (1963) who proposed a pair of commuting Hermitian labelling operators Ω and Φ . However, explicit and closed formulae expressing the eigenvalues and eigenvectors of Ω and Φ have not been found so far, except for a few particular and almost trivial cases. The authors find four sets of SU(2) \otimes SU(2) shift operators. Quite a number of relations connecting quadratic products of shift operators are constructed. On account of these, general formulae expressing the Ω - and Φ -eigenvalues for non-degenerate and twofold degenerate states are obtained. (38 refs.)
 74648 Lepton-violating $\beta^-\beta^+$, $\beta^+\beta^+$ decays, (e^-, e^+) conversion and double electron capture in gauge theories. J.D. Vergados (CERN, Geneva, Switzerland). *Nucl. Phys. B, Part. Phys. (Netherlands)*, vol.B218, no.1, p.109-44 (30 May 1983).
 The lepton violating processes $\beta^-\beta^+$, $\beta^+\beta^+$, (e^-, e^+) and double electron capture have been investigated in the context of modern gauge theories. Mechanisms involving light or heavy intermediate Majorana neutrinos, with or without right-handed currents, as well as Higgs particles, have been studied. The lepton-violating emission of light bosons, recently proposed by Georgi, Glashow and Nussinov (1981), has also been analyzed. From the analysis of the $^{48}\text{Ca} \rightarrow ^{48}\text{Ti}$ data the following limits emerge: $| \langle m_{\nu} \rangle | < 80 \text{ eV}$, $m_N > (2.20) \times 10^3 \text{ GeV}$, $m(W_R) > 400 \text{ GeV}$ and $g(\nu_{\tau}, 0) < 5 \times 10^{-3}$. The above limits are then used to predict the lifetimes for $\beta^+\beta^+$, (e^-, e^+) and double electron capture in the $A=58, 92$ and 96 systems employing realistic nuclear models. (38 refs.)
 74649 Vacuum alignment and dynamical symmetry breaking in two-dimensional models. A. d'Adda (Maths. Dept., Durham Univ., Durham, England), A.C. Davis, P. Vecchia. *Nucl. Phys. B, Part. Phys. (Netherlands)*, vol.B218, no.1, p.191-204 (30 May 1983).
 The authors discuss a class of two-dimensional models in which a non-Abelian gauge symmetry is dynamically broken by a fermion bilinear condensate. Using the $1/N$ expansion they examine the vacuum alignment of their models. For a chirally invariant model there is a vacuum degeneracy, when the chiral symmetry is explicitly broken the vacuum aligns. (8 refs.)
 74650 Fractional charges: global and local aspects. W.A. Bardeen (Fermilab, Batavia, IL, USA), S. Elitzur, Y. Frishman, E. Rabinovici. *Nucl. Phys. B, Part. Phys. (Netherlands)*, vol.B218, no.2, p.445-58 (6 June 1983).
 The properties of topological objects with fractional charge are studied. The authors first transform to new variables, in terms of which the lowest order contribution gives the fractional charge. They then gauge that fractional charge. Effects of the θ angle in two dimensions are studied. In particular arbitrary periods may be obtained. Induced extra charge due to θ turns out to

be proportional to $\sqrt{\theta}$. C and P violations due to θ may be arbitrarily small in some cases. (8 refs.)

- 74651 A note on supersymmetry breaking in $1+1$ dimensions. T. Murphy, L.O. Raifeartaigh (Dublin Inst. for Advanced Studies, Dublin, Ireland). *Nucl. Phys. B, Part. Phys. (Netherlands)*, vol.B218, no.2, p.484-92 (6 June 1983).
 The spontaneous breakdown of supersymmetry for a single chiral superfield in $1+1$ dimensions is investigated and a number of puzzling features are resolved by noting that the loop expansion is not always valid. It is found that both broken and unbroken supersymmetry are stable with respect to radiative corrections. (9 refs.)
 74652 A procedure for generating realizations of Li-admissible and other nonassociative algebras. A.J. Kalnay (Centro de Fisica, Inst. Venezolano de Investigaciones Cientificas, Caracas, Venezuela). *Hadronic J. (USA)*, vol.6, no.2, p.278-304 (March 1983).
 The author starts with an arbitrary nonassociative algebra β over a field F and arbitrarily selects two fixed elements $P, Q \in \beta^*$ and four fixed $\alpha_i \in F$. Then, generalizing Albert's quasiasociative algebras and Santilli's fundamental realization of the Lie-admissible algebras he constructs, in terms of β^* , P , Q and the α_i a new algebra β^{**} over the same field. After showing some formulae for the case of a general β^{**} , he restricts himself to the case in which P and Q belong to the center of β^* . He proves that, in such a case, if β^* is Lie-admissible, then β^{**} is also Lie-admissible. Moreover, if β^{**} is Lie-admissible and $P+$ has an inverse within β^* , then β^* is also Lie-admissible. The procedure $\beta^* \rightarrow \beta^{**}$ can, within certain limits, be iterated. Therefore he opens the possibility of an eventual significant enrichment of the set of available specific examples of Lie-admissible algebras. Theorems which resemble the above one are also obtained if, instead of Lie-admissible algebras, the following algebras are considered: commutative, power associative, flexible, Lie, commutative Jordan, Jordan-admissible, nil and Grassmann. Finally, a sufficient condition for the existence of a unit element within β^{**} is shown. (36 refs.)
 74653 Axions and supersymmetry. J.-M. Frere (Univ. Libre, Bruxelles, Belgium), J.-M. Gerard. *Lett. Nuovo Cimento (Italy)*, vol.37, ser.2, no.4, p.135-41 (28 May 1983).
 Most of the proposed supersymmetric low-energy models contain at least one accidental axial symmetry which at first sight could solve the strong CP problem. Unfortunately experimental, astrophysical and cosmological constraints on the one side and asymptotic freedom on the other are never simultaneously respected. The authors consider the supersymmetric realization of the Kim, Shifman, Vainshtein and Zakharov mechanism as a new guide for model building. (17 refs.)
 74654 Superconformal current multiplet. A. Smilagic (Internat. Centre for Theoretical Phys., Trieste, Italy). *Lett. Nuovo Cimento (Italy)*, vol.37, ser.2, no.4, p.156-60 (28 May 1983).
 The author considers a derivation of a superconformal current multiplet based directly on superconformal algebra. This gives the usual multiplet of currents without anomalies, directly in terms of 'improved' quantities and without reference to a particular Lagrangian model. (8 refs.)
 74655 Krull dimension of factor rings of the enveloping algebra of a semi-simple Lie algebra. S.P. Smith (Univ. of Southern California, Los Angeles, CA, USA). *Math. Proc. Cambridge Philos. Soc. (GB)*, vol.93, pt.3, p.459-66 (May 1983).
 Let \mathfrak{g} be a semi-simple complex Lie algebra with enveloping algebra $U(\mathfrak{g})$. It is shown that the Krull dimension of $U(\mathfrak{g})$ is bounded above by $\dim \mathfrak{g}^*$, where r is half the minimal dimension of a non-trivial G orbit in \mathfrak{g}^* (G is the adjoint group of \mathfrak{g}). (20 refs.)
 74656 Soft breaking of $N=4$ supersymmetry. J.J. van der Bij, York-Peng Yao (Dept. of Phys., Univ. of Michigan, Ann Arbor, MI, USA). *Phys. Lett. B (Netherlands)*, vol.125B, no.2-3, p.171-4 (26 May 1983).
 The authors consider the addition of soft breaking terms to the $N=4$ supersymmetric Yang-Mills Lagrangian. $N=1$ supersymmetric mass terms and mass terms of the form $(A^2 - B^2)$ do not give rise to any new divergence, which implies that in a gauge in which the massless theory is completely finite, this finiteness is preserved. All other soft terms give rise to at most logarithmic divergences. (7 refs.)
 74657 Mass spectrum of the W^\pm and Z supermultiplets. P. Fayet (Lab. de Phys. Theorique, Ecole Normale Supérieure, Paris, France). *Phys. Lett. B (Netherlands)*, vol.125B, no.2-3, p.178-84 (26 May 1983).
 In supersymmetric theories the W^\pm and Z may be associated with spin-1/2 and spin-0 partners, the latter being Higgs bosons. The author studies their mass matrix and shows that, in a class of theories with gravity-induced supersymmetry breaking, the spin-1/2 partners of the W^\pm and Z have masses $|m_{3/2} \pm m_W|$, $|m_{3/2} \pm m_Z|$, while spin-0 leptons and quarks have masses $|m_{3/2} \pm m_{l,q}|$, $|m_{3/2}|$ being the common mass of the gravitino, photino and gluinos. These new particles may all be heavier than the W^\pm . On the other hand, if the gravitino is lighter than $120 \text{ GeV}/c^2$ one expects to see, below a mass of $40 \text{ GeV}/c^2$, either spin-0 partners of leptons and quarks, or spin-1/2 partners of the W^\pm and Z . (16 refs.)
 74658 On the dynamic origin of the kinetic terms. A.V. Chizhov, M.V. Chizhov (Joint Inst. for Nuclear Res., Dubna, USSR). *Phys. Lett. B (Netherlands)*, vol.125B, no.2-3, p.190-2 (26 May 1983).
 In the one-loop approximation it is shown that the local self-interaction of the chiral spinor field gives rise to kinetic terms for collective fields in a self-consistent manner. (9 refs.)
 74659 On a self-consistent chiral doublet composite scheme. Y.F. Pirogov (Inst. for High Energy Phys., Serpukhov, USSR). *Phys. Lett. B (Netherlands)*, vol.125B, no.2-3, p.193-6 (26 May 1983).
 A composite scheme with a chiral doublet of charges $Q=(2/3, -1/3)$ is considered. The scheme is self-consistent in the sense that the constituent spectator chiral symmetry SU(2) \times U(1) coincides with the chiral electroweak symmetry. Due to the mirror fermions they both are anomaly free. The chiral colour symmetry arises as an effective symmetry of composite quarks. The scheme contains exotic composite fermions with isospin $I=3/2$. The common maximal effective symmetry of both ordinary and exotic composite fermions is the chiral SU(2) \times SU(4) one, the latter being a possible partial unified symmetry. (14 refs.)
 74660 The massless gluino and the pseudoscalar meson family. A.V. Smilga, M.I. Vysotsky (Inst. of Theoretical & Experimental Phys., Moscow, USSR). *Phys. Lett. B (Netherlands)*, vol.125B, no.2-3, p.227-9 (26 May 1983).
 It is shown that the masslessness of the gluino leads necessarily to the existence of a light isosinglet pseudoscalar boson which is not observed in experiment. Thus, any realistic supersymmetry model must include the mechanism for generating the gluino mass. (7 refs.)

74661 Algebra of nonlocal charges in two-dimensional chiral models. D.V.Volkov, V.D.Gershun, V.I.Tkach. *Ukr. Fiz. Zh. (USSR)*, vol.28, no.5, p.641-9 (May 1983). In Russian. Algebra of nonlocal charges is investigated in two-dimensional chiral models. It is shown that an infinite set of nonlocal charges can be derived by successively using the Poisson brackets for the first nonlocal charge. A general scheme is obtained for deriving the nonlocal charge algebra of the Poisson brackets. The algebra of the Poisson brackets is exactly computed for the first four nonlocal charges. It is shown that the Poisson brackets algebra of nonlocal charges generates an infinite-dimensional algebra different from the Kac-Moody algebra. (19 refs.)

74662 Simple Lie algebras and Dynkin diagrams. F.Buccella (Istituto di Fisica, Univ. di Roma, INFN, Roma, Italy). The High-Energy Limit. Proceedings of the Eighteenth Course of the International School of Subnuclear Physics, Erice, Italy, 31 July-11 Aug. 1980 (New York, USA: Plenum 1983), p.133-48 (2 refs.)

The High-Energy Limit. Proceedings of the Eighteenth Course of the International School of Subnuclear Physics See Entry 74229

Use of SU(n) Lie algebra in n level quantum system. I. Some general consequences See Entry 74306

Use of SU(n) Lie algebra in n level quantum system. II. Transformations in the state space, evolution problems See Entry 74307

Absence of particle creation as an equilibrium condition See Entry 74340

The stability of gauged supergravity See Entry 74354

The geometrical hierarchy model and N=1 supergravity See Entry 74355

Weak symmetry breaking by radiative corrections in broken supergravity See Entry 74356

Stability of gravitational merons See Entry 74357

Grand unified theories with symmetry and local supersymmetry See Entry 74358

Consistency of coupling in supergravity with propagating Lorentz connexion See Entry 74359

Heating the quenched Eguchi-Kawai model See Entry 74584

Superfield formalism for gauge theories with ghosts and gauge fixing terms from dynamics on superspace See Entry 74586

Quantum meaning of classical (field) theory for Fermi systems See Entry 74587

Superspace formulation of supersymmetric gauge theories in 4 and 10 dimensions See Entry 74588

Dynamical symmetry breaking in models of spinor fields with quartic interactions in (1+1) dimensions See Entry 74589

Noether analysis and infinitely conserved currents in super-chiral model See Entry 74590

Geometric formulation of the indirect analytic representation of dynamical systems, exterior differential calculus on Banach spaces and variational selfadjointness See Entry 74592

Renormalisation of the Fayet-Iliopoulos term in supersymmetric spontaneously broken U(1) gauge theories See Entry 74596

Static and spherically symmetric dyon solutions in SU(N) gauge theory See Entry 74599

Chiral property of the generalized Gross-Neveu model with $U_N \times U_N$ flavour chiral symmetry in 1+1 dimensions See Entry 74601

Quantisation of spontaneously broken gauge theories in the unitary gauge through the Dirac-bracket formalism See Entry 74603

Solutions to generalized double sine-Gordon equations See Entry 74609

Composite gauge bosons in sigma models and supergravity See Entry 74611

Extended BRS symmetry in supersymmetric Yang-Mills theory See Entry 74613

Light composite supermultiplets See Entry 74614

Stochastic quantization and large N reduction See Entry 74627

Lattice gauge theory—a progress report See Entry 74636

The auxiliary field/ultraviolet finiteness connection See Entry 74644

Non-local gauge theories See Entry 74645

Bianchi-Backlund transformations, conservation laws, and linearization of various field theories See Entry 74646

On the generality of the mass sum rule See Entry 74663

Theoretical predictions for baryon number violation See Entry 74666

Grand unification—a review See Entry 74667

Global and local supersymmetric grand unification See Entry 74670

Massless neutrinos in left-hand symmetric models See Entry 74671

Anomalous baryon number non-conservation in the presence of SU(5) monopoles See Entry 74672

Early unification and the Weinberg angle in the SU(4)⁴ grand unified model See Entry 74673

Grand unification with local supersymmetry See Entry 74674

An approach to gauge hierarchy in the minimal SU(5) model of grand unification See Entry 74675

Scalar loops and the Higgs mass in the Salam-Weinberg-Glashow model See Entry 74676

A supersymmetric preon model of particle physics See Entry 74679

Effective low energy custodial symmetry and Weinberg mixing See Entry 74682

How supersymmetry makes neutron-antineutron oscillations more natural in SO(10) See Entry 74683

Supersymmetric grand unification See Entry 74685

Aspects of grand unified models with softly broken supersymmetry See Entry 74686

Supersymmetric dipole mechanism and vacuum energy See Entry 74687

Nosonomy of an inverted hierarchy model See Entry 74688

How far we are in unifying the fundamental interactions See Entry 74692

SU(5) without SU(5): why B-L is conserved and baryon number not in unified models of quarks and leptons See Entry 74694

Supersymmetric QCD and its massless limit: an effective Lagrangian analysis See Entry 74705

On the low energy structure of QCD See Entry 74708

Use of final-energy sum rules to describe baryon properties in quantum chromodynamics and to estimate the proton lifetime in the SU(5) model See Entry 74718

Symmetry basis and physical basis for many-quark system See Entry 74729

Superstring interactions See Entry 74744

Spectrum of the supersymmetric Liouville theory See Entry 74745

The physics of dual vortices and static baryons in 2+1 dimensions See Entry 74746

Magnetic moments in quark-diquark model See Entry 74775

Prospects for polarized electrons at high energies See Entry 74825

Mesons and isobars See Entry 74854

Resonances in hyperon-hyperon systems See Entry 74896

Mechanisms for the enhancement of P- and T-invariant effects in neutron-nucleus reactions See Entry 74982

Particle physics and the new cosmology See Entry 79032

11.40 CURRENTS AND THEIR PROPERTIES

Noether analysis and infinitely conserved currents in super-chiral model See Entry 74590

Superconformal current multiplet See Entry 74654

Hadronic couplings of open beauty states See Entry 74735

Classification of exchange currents See Entry 74866

11.50 DISPERSION RELATIONS AND SUM RULES

74663 On the generality of the mass sum rule. J.Polchinski, M.B.Wise (Lyman Lab. of Phys., Harvard Univ., Cambridge, MA, USA). *Nucl. Phys. B, Part. Phys. (Netherlands)*, vol.B218, no.2, p.297-308 (6 June 1983). The sum rule, $\sum_i (-1)^{2J_i} (2J_i + 1) m_i^2 = 2\sum_a D^a \text{Tr} Q^a$, is studied to first order in supersymmetry breaking, treating the other interactions exactly. It is found to hold for spontaneous breaking and many types of explicit breaking. (15 refs.)

Use of final-energy sum rules to describe baryon properties in quantum chromodynamics and to estimate the proton lifetime in the SU(5) model See Entry 74718

Higher dimensional renormalization group invariant vacuum condensates in quantum chromodynamics See Entry 74719

What can we count on? A discussion of constituent-counting rules for interactions involving composite systems See Entry 74722

Hadronic couplings of open beauty states See Entry 74735

CFF-shell effects in VDM and the Compton sum rule See Entry 74749

11.80 RELATIVISTIC SCATTERING THEORY
(see also 03.80 General theory of scattering)

74664 Relativistic quantum states of a particle in an electromagnetic plane wave and a homogeneous magnetic field. J.Bergou (Central Res. Inst. for Phys., Budapest, Hungary), F.Ehlotzky. *Phys. Rev. A (USA)*, vol.27, no.5, p.2291-6 (May 1983). The exact solutions of the Klein-Gordon and Dirac equations are found by purely algebraic procedures for a charged particle embedded simultaneously in a plane-wave radiation field and in a uniform magnetic field which is directed parallel to the direction of propagation of the plane wave. Two cases of the solutions are considered: (i) the radiation field is a classical external plane wave and (ii) it is a quantized field. The connection with less explicit or more specific solutions of this problem known previously is established and possible applications are discussed. (12 refs.)

74665 New bounds for the total cross section and the zero free radius of the scattering amplitude. J.K.Mohapatra (Dept. of Phys., Regional Coll. of Education, Bhubaneswar, India), J.Maharana. Proceedings of the VI High Energy Physics Symposium (papers in summary form only received), Mysore, India, 6-11 Dec. 1982 (Bombay, India: Dept. Atomic Energy 1982), p.70. Summary form only given. Upper bounds on $\sigma_T(s)$ is deduced which seems to be an improvement over the existing ones if one supplements it with the behaviour of the slope parameter data. Bound, on the zero free radius of the scattering amplitude, is also obtained.

Optimised polynomial expansion and phase shift analysis of A-p scattering See Entry 74795

Scattering length in a system of three charged particles. See Entry 74922

12.00 SPECIFIC THEORIES AND INTERACTION MODELS; PARTICLE SYSTEMATICS

Annual review of nuclear and particle science. Vol.32 See Entry 74232

12.10 UNIFIED FIELD THEORIES AND MODELS

74666 Theoretical predictions for baryon number violation. P.Langacker (Univ. of Pennsylvania, Philadelphia, PA, USA). *AIP Conf. Proc. (USA)*, no.96, p.110-23 (1982). [received: May 1983] (Workshop on Science Underground, Los Alamos, CA, USA, 1982). The author describes the theoretical predictions for proton decay and other baryon number violating processes, emphasizing that there are many models and theories involving baryon number violation and that it is an experimental problem to distinguish between them. The author reviews the theoretical predictions for the unification mass M_X and for the weak angle $\sin^2 \theta_W$. It will be seen that the class of models involving an $SU_3 \times SU_2 \times U_1$ invariant descent between M_W and M_X are strongly favoured. The proton lifetime and branching ratio predictions for the SU_3 and other 3-2-1 desert models are reviewed, with emphasis on distinguishing between models and on the implications of the small value of the QCD parameter $\Lambda(\bar{u}s)$ that seems to be favoured by the data. The author discusses the consequences of low energy supersymmetry

for proton decay, nuclear effects, and models with low mass scales. Other topics, including the possibility of observing baryon number violation at accelerators, baryon number violation induced by magnetic monopoles, the violation of Lorentz invariance in proton decay, and antiproton cosmic rays are discussed. (26 refs.)

74667 Grand unification—a review. V.P.Nair, K.C.Wali (Phys. Dept., Syracuse Univ., Syracuse, NY, USA). *AIP Conf. Proc. (USA)*, no.98, p.1-18 (1982). [received: May 1983] (Conference on Particles and Fields - 1982, College Park, MD, USA, 28-30 Oct. 1982).

The authors emphasize the general ideas behind grand unification with special attention on the violation of well-known low energy conservation laws such as baryon and lepton number. They discuss the relevance of the grand unification ideas to astrophysics and some of the theoretical problems in model building, and the salient features of a few generic models. They conclude the review with some general remarks. (6 refs.)

74668 The proton decay—magnetic monopole connection. C.G.Callan, Jr. (Joseph Henry Labs., Princeton Univ., Princeton, NJ, USA). *AIP Conf. Proc. (USA)*, no.98, p.24-34 (1982). [received: May 1983] (Conference on Particles and Fields - 1982, College Park, MD, USA, 28-30 Oct. 1982).

It has been claimed that grand unification magnetic monopoles catalyze baryon decay at strong interaction rates. A qualitative discussion is given of the physical mechanisms underlying this process as well as a brief discussion of some of its phenomenological implications. (6 refs.)

74669 Testing the standard model. H.Gordon, W.Marciano (Brookhaven Nat. Lab., Upton, NY, USA), H.H.Williams, K.Abe, M.Chanowitz, R.Cool, M.Derrick, J.Friedman, B.Gittelman, M.Goldberg, K.Gottfried, P.Granis, I.Hinchcliffe, J.Jackson, H.Kagan, P.Lepage, A.Melissinos, T.O'Halloran, S.Olson, F.Paige, F.Pipkin, R.Ruchti, M.Samuel, K.Shinsky, R.Shrock, H.Siemann, H.Sticker, M.Tannenbaum, F.Taylor, M.Tuts, H.Tye, G.Tzanakos, H.Vogel, D.White, R.Wilson, J.Wiss. *AIP Conf. Proc. (USA)*, no.98, p.39-79 (1982). [received: May 1983] (Conference on Particles and Fields - 1982, College Park, MD, USA, 28-30 Oct. 1982).

The authors summarize the results of the standard model group which has studied the ways in which different facilities may be used to test in detail what we now call the standard model, that is $SU_c(3) \times SU(2) \times U(1)$. Shown below are the topics considered with the names of the individuals working on each topic. (36 refs.)

74670 Global and local supersymmetric grand unification. P.Nath (Dept. of Phys., Northeastern Univ., Boston, MA, USA), R.Arnowitz, A.H.Chamseddine. *AIP Conf. Proc. (USA)*, no.98, p.247-61 (1982). [received: May 1983] (Conference on Particles and Fields - 1982, College Park, MD, USA, 28-30 Oct. 1982).

A brief review of the globally supersymmetric grand unified theories is given. The new proposal of locally supersymmetric grand unification (supergravity GUTS) is discussed. Here the topics include construction of the Lagrangian which couples the $N=1$ supergravity multiplet with an arbitrary number of chiral multiplets and a gauge vector multiplet, super-Higgs phenomena and spontaneous breaking of supersymmetry and $SU(2) \times U(1)$ at a common weak interaction mass scale and phenomenological implications of supergravity GUTS. Questions relating to the ground state of the theory are also discussed. (34 refs.)

74671 Massless neutrinos in left-hand symmetric models. D.Wyler (CERN, Geneva, Switzerland), L.Wolfenstein. *Nucl. Phys. B, Part. Phys. (Netherlands)*, vol.B218, no.1, p.205-14 (30 May 1983).

Presents an alternative to the Yanagida-Gell-Mann-Ramond-Slansky method (1979) of obtaining small neutrino masses in spite of normal Dirac mass terms in left-right symmetric theories. In this scheme, the light neutrinos remain massless while there exist massive Dirac neutral leptons in each generation. The masses of these are determined by the scale of left-right symmetry breaking, which must be large enough to prevent flavour-changing processes such as $\mu \rightarrow e \gamma$. (25 refs.)

74672 Anomalous baryon number non-conservation in the presence of $SU(5)$ monopoles. V.A.Rubakov, M.S.Serebryakov (Inst. for Nuclear Res., Acad. of Sci., Moscow, USSR). *Nucl. Phys. B, Part. Phys. (Netherlands)*, vol.B218, no.1, p.240-68 (30 May 1983).

It is shown that the effects related to the Adler-Bell-Jackiw anomaly give rise to strong baryon number non-conservation in the presence of magnetic monopoles in the $SU(5)$ grand unified theory. The main assumption made is that, as long as distances of order 1 GeV^{-1} from the monopole center are considered, the masses of light fermions u, d, s, e, μ can be neglected, while heavy fermions decouple. Two types of the $SU(5)$ monopoles are studied, namely: (i) the fundamental monopole with a non-vanishing chromomagnetic charge (ii) the minimal purely electromagnetic monopole. In both cases the processes like $p + \text{monopole} \rightarrow e^+ + \text{monopole} + \text{everything}$ are allowed. It is argued that the cross sections of these processes are of order $1 \text{ GeV}^{-2} \beta^{-2}$, at least for sufficiently low monopole-proton relative velocities β . (37 refs.)

74673 Early unification and the Weinberg angle in the $SU(4)^4$ grand unified model. A.Yu.Ignatiev, N.G.Kozimirov, V.A.Kuzmin (Inst. for Nuclear Res., Acad. of Sci., Moscow, USSR). *Nucl. Phys. B, Part. Phys. (Netherlands)*, vol.B218, no.2, p.423-44 (6 June 1983).

In the framework of the grand unified gauge group $SU(4)^4$ the authors discuss possibilities to reconcile the low unification scale ($10^2\text{--}10^7 \text{ GeV}$) with the acceptable value of $\sin^2 \theta_W$. They consider various specific models which differ by the values of the intermediate mass scale, the choice of the fermion multiplets and by the embedding of the electroweak group $SU(2)$ into $SU(4)^4$. The class of theories with early unification and correct $\sin^2 \theta_W$ is constructed. They all predict new non-sequential fermions which are $SU(2)_{L,R}$ singlets and have unconventional electric charges. Cosmological implications of such theories are discussed and it is argued that new particles may well account for the positive results of searches for fractional charge in terrestrial matter. (19 refs.)

74674 Grand unification with local supersymmetry. L.E.Ibanez (Dept. de Fisica Teorica, Univ. Autonoma de Madrid, Madrid, Spain). *Nucl. Phys. B, Part. Phys. (Netherlands)*, vol.B218, no.2, p.514-44 (6 June 1983).

The author studies general conditions for obtaining spontaneous breaking of local supersymmetry in $N=1$ supergravity coupled to supersymmetric matter. The author considers in particular the coupling of $N=1$ supergravity to grand unified theories like $SU(5)$ and study the conditions which must be met in order to obtain a realistic model. Specific models are built in which local supersymmetry is broken at a scale $\sqrt{M_{\text{WMP}}} \sim 10^{10} \text{ GeV}$. This breaking of

supersymmetry is only detected at low energies through soft terms breaking explicitly the global supersymmetry. These soft terms (scalar masses, gaugino masses and trilinear scalar couplings) are renormalized at low energies according to the renormalization group. The $(\text{mass})^2$ of the Higgs doublet evolve towards negative values at low energies giving rise to $SU(2) \times U(1)$ breaking as a radiative effect of local supersymmetry breaking. The author finally points out the possible relevance of non-renormalizable superpotentials for the problem of fermion masses. (42 refs.)

74675 An approach to gauge hierarchy in the minimal $SU(5)$ model of grand unification. P.Ghose (Internat. Centre for Theoretical Phys., Trieste, Italy).

J. Phys. G (GB), vol.9, no.6, p.L107-10 (June 1983).

It is shown that if all mass generation through spontaneous symmetry breaking is predominantly caused by scalar loops in the minimal $SU(5)$ model of grand unification, it is possible to have an arbitrarily large gauge hierarchy $m_h \gg m_W$ with all Higgs bosons superheavy. No fine tuning is necessary in every order. (11 refs.)

74676 Scalar loops and the Higgs mass in the Salam-Weinberg-Glashow model. P.Ghose (Internat. Centre for Theoretical Phys., Trieste, Italy).

J. Phys. G (GB), vol.9, no.6, p.L111-14 (June 1983).

It is shown that spontaneous symmetry breaking is predominantly driven by scalar loops in the standard Salam-Weinberg-Glashow model if $\lambda \approx O(e^2)$. The Higgs mass is predicted to be $O(64 \text{ GeV})$, which is considerably higher than the Coleman-Weinberg prediction, (1973). (3 refs.)

74677 Space-time approach to the grand unified theory of the quarks and the leptons. O.Hara (Atomic Energy Res. Inst., Nihon Univ., Tokyo, Japan). *Nuovo Cimento A (Italy)*, vol.75A, ser.2, no.1, p.17-38 (1 May 1983).

A space-time approach to the grand unified theory of the quarks and leptons is given by starting from Weyl's tetrad formalism of the theory of general relativity. In this approach the lepton appears as a part of the space-time structure to prepare a local Lorentz frame which is indispensable for the description of the quark described by a Dirac spinor in conformity with the principle of general relativity, and the parallelism between the quark and the lepton is built in from the outset. The lepton thus introduced has a characteristic interaction with the gravitational field. So through this interaction this scheme can be tested experimentally, at least in principle. The discussion is restricted to the case in which only one kind of quark and lepton is included. In this respect it is still not realistic. (20 refs.)

74678 After the W particle, the Higgs. A.Watson.

New Sci. (GB), vol.98, no.1359, p.534-7 (26 May 1983).

Particle physicists feel certain they are on the right track in their attempts to develop a single unifying theory of nature's forces. Recent events have strengthened this opinion, but the theory contains a number of complex twists and there is plenty still for experimenters to discover—including a particle known as the Higgs. (no refs.)

74679 A supersymmetric preon model of particle physics. Y.J.Ng (Stanford Linear Accelerator Center, CA, USA), B.A.Ovrut. *Phys. Lett. B (Netherlands)*, vol.125B, no.2-3, p.147-50 (26 May 1983).

The authors present a supersymmetric preon model based on $SU(M)_{SC} \times SU(2)_L \times SU(3)_C \times U(1)$. Supersymmetry protects chiral symmetries from spontaneous breakdown and allows a solution to the strong CP problem. (11 refs.)

74680 On the S-wave interaction between massive fermions and a GUT magnetic monopole. M.A.Virasoro (Istituto di Fisica G. Marconi, Univ. di Roma, Rome, Italy).

Phys. Lett. B (Netherlands), vol.125B, no.2-3, p.161-4 (26 May 1983).

The author follows closely the line of analysis of Rubakov (1981, 1982) and Callan (1982) on the S-wave strong interaction between magnetic monopoles and fermions. The observation is that the inclusion of a bare mass term for the fermions modifies in a non-perturbative fashion the two dimensional action of the condensate field. It induces a repulsive barrier. The coefficient of transmission is not computed here. (7 refs.)

74681 Effective Lagrangian for $\Delta S=1$ and $\Delta S=2$ transition in the Higgs boson exchange model of CP violation. Y.Dupont (Centre de Phys. Theorique, Ecole Polytech., Palaiseau, France).

Phys. Lett. B (Netherlands), vol.125B, no.2-3, p.211-16 (26 May 1983).

Using standard renormalization group techniques, strong interaction corrections to $\Delta S=1$ and $\Delta S=2$ transitions are calculated in the Higgs-boson exchange model of CP violation. It is shown that the box diagram contribution to the ratio ϵ'/ϵ is not modified in any significant way with respect to lowest order calculation. (20 refs.)

74682 Effective low energy custodial symmetry and Weinberg mixing.

P.D.Mannheim (Dept. of Phys., Univ. of Connecticut, Storrs, CT, USA).

Phys. Lett. B (Netherlands), vol.125B, no.4, p.282-6 (2 June 1983).

The author presents a model of the weak interactions in which a custodial symmetry not present in the starting lagrangian emerges in the effective low energy sector of the theory. This symmetry maintains the relation $M_W = M_Z \cos \theta_W$ to any required degree of accuracy while leaving the quark mass spectrum completely unconstrained. (6 refs.)

74683 How supersymmetry makes neutron-antineutron oscillations more natural in $SO(10)$. D.Lust (Theoretische Phys., Univ. Muenchen, Munich, Germany).

Phys. Lett. B (Netherlands), vol.125B, no.4, p.295-300 (2 June 1983).

The author investigates the possibility of observable neutron-antineutron oscillations ($n\bar{n}$) in a supersymmetric $SO(10)$ -model. Since supersymmetry (SUSY) allows six-quark-operators with lower dimension than in the non-supersymmetric case and changes the renormalization group equations through the influence of the supersymmetric partners of the ordinary particles, the $n\bar{n}$ is indeed observable in this scheme. (17 refs.)

74684 Is there a desert beyond the mountains?. C.H.Llewellyn Smith (Dept. of Theoretical Phys., Univ. of Oxford, Oxford, England).

Physics in Collision. High-Energy $e e / p p$ Interactions. Proceedings of an International Conference, Stockholm, Sweden, 2-4 June 1982 (New York, USA: Plenum 1983), p.405-20

The author considers a few of the ways in which the desert may blossom. First he discusses the possibility that the W and Z are composite objects. Then he considers gauge theories, discussing expectations for the W and Z masses before describing the difficulties with the Higgs boson which have led theorists to espouse technicolour and supersymmetry. (53 refs.)

74685 Supersymmetric grand unification. N.Sakai (Nat. Lab. for High Energy Phys., Ibaraki, Japan).

Gauge Theory and Gravitation. Proceedings of the International Symposium, Nara, Japan, 20-24 Aug. 1982 (Berlin, Germany: Springer-Verlag 1983), p.208-16

After a brief discussion of motivations and prototype models, the author reviews recent studies of model building and of proton decay in supersymmetric grand unification. A new effect is mentioned for $\Delta B \neq 0$ four-scalar-inter-

reactions induced by an intermediate scale ($10^{10}\sim 10^{12}$ GeV) supersymmetry breaking. (28 refs.)

74686 Aspects of grand unified models with softly broken supersymmetry. K.Inoue (Dept. of Phys., Kyushu Univ., Fukuoka, Japan), A.Kakuto, H.Komatsu, S.Takeshita.

Gauge Theory and Gravitation. Proceedings of the International Symposium, Nara, Japan, 20-24 Aug. 1982 (Berlin, Germany: Springer-Verlag 1983), p.217-21

Supersymmetric theories have an outstanding property of no-renormalization for F-terms. This may give an important key to the solution of the gauge hierarchy problem in the grand unified theories (GUTs). If nature chooses a supersymmetric theory, the supersymmetry must be broken at low energies spontaneously or explicitly. In spontaneously broken supersymmetric theories, however, there is a severe constraint on masses of component fields in a given supermultiplet. The authors discuss explicit supersymmetry breaking in the $SU(3)\times SU(2)\times U(1)$ model with a minimal set of supermultiplets. (8 refs.)

74687 Supersymmetric dipole mechanism and vacuum energy. N.Ohta (Dept. of Phys., Faculty of Sci., Univ. of Tokyo, Tokyo, Japan).

Gauge Theory and Gravitation. Proceedings of the International Symposium, Nara, Japan, 20-24 Aug. 1982 (Berlin, Germany: Springer-Verlag 1983), p.222-6

The author discusses supersymmetric theories and the resolution of the gauge hierarchy problem in GUTs. The author also considers the non-renormalisation theorem and symmetry breaking in realistic supersymmetric models. (6 refs.)

74688 Nonomy of an inverted hierarchy model. T.Banks (Dept. of Phys. & Astron., Tel Aviv Univ., Ramat Aviv, Israel).

Gauge Theory and Gravitation. Proceedings of the International Symposium, Nara, Japan, 20-24 Aug. 1982 (Berlin, Germany: Springer-Verlag 1983), p.227-30

This is a report of an unsuccessful attempt to build a realistic grand unified model based on Witten's inverted hierarchy mechanism. Witten's phenomenon is a common property of supersymmetric gauge theories in which supersymmetry (SUSY) is spontaneously broken by the vacuum expectation value of an F term. (6 refs.)

74689 Cosmological phase transition in microcanonical gravity. G.Horowitz (Rishon LeTzion Inst. of Phys., Hebrew Univ., Jerusalem, Israel).

Gauge Theory and Gravitation. Proceedings of the International Symposium, Nara, Japan, 20-24 Aug. 1982 (Berlin, Germany: Springer-Verlag 1983), p.254-8

Phase transitions in cosmology, whether first or second order, spontaneous or dynamic, were first studied by methods which ignore or exclude gravitational effects (Linde, 1974). The basis for the exclusion was the assumption that the effects are local, and that since the relevant times are much larger than Planck times quantum gravity is unimportant and thus gravity enters only as a background metric which can be removed by studying results in a local inertial frame. The author presents realistic models in which there exists a non-quantum gravitation contribution to the entropy based on a microcanonical treatment of the statistical mechanics. (8 refs.)

74690 Kaluza-Klein type theory. H.Sugarwara (KEK, Tsukuba, Japan).

Gauge Theory and Gravitation. Proceedings of the International Symposium, Nara, Japan, 20-24 Aug. 1982 (Berlin, Germany: Springer-Verlag 1983), p.262-6

The author discusses two problems related to the recently proposed Kaluza-Klein type theory by T. Kaneko and the author (1983). One is Mach's principle and the other is a classical solution to Einstein's equation which has a $[6(X)]^2$ singularity. (3 refs.)

74691 Scale invariant scalar-tensor theory and the origin of gravitational constant and particle masses. Y.Fujii (Inst. of Phys., Univ. of Tokyo, Tokyo, Japan).

Gauge Theory and Gravitation. Proceedings of the International Symposium, Nara, Japan, 20-24 Aug. 1982 (Berlin, Germany: Springer-Verlag 1983), p.272-6

Scalar-tensor theory seems to offer a natural alternative to the standard theory of gravitation, especially in the unification of gravitation and elementary particles. The author presents a simple viable scalar-tensor theory the result of which is not a variable-G theory in the usual sense. (6 refs.)

74692 How far we are in unifying the fundamental interactions. F.Bucella (Istituto di Fisica, Univ. di Roma, INFN, Roma, Italy).

The High-Energy Limit. Proceedings of the Eighteenth Course of the International School of Subnuclear Physics, Erice, Italy, 31 July-11 Aug. 1980 (New York, USA: Plenum 1983), p.125-32

The author discusses unification and the enlargement of the underlying gauge group from $SU(3)_{\text{QCD}}\otimes U(1)_{\text{QED}}$ to $SU(4)$ and then to $SU(5)$. The effects on quark families are also discussed. (19 refs.)

74693 Electroweak physics of the 80s. J.J.Sakurai (Dept. of Phys., Univ. of California, Los Angeles, CA, USA).

The High-Energy Limit. Proceedings of the Eighteenth Course of the International School of Subnuclear Physics, Erice, Italy, 31 July-11 Aug. 1980 (New York, USA: Plenum 1983), p.177-247

Discusses electroweak gauge theories and quantum flavour dynamics for the 1980s. There were great successes in this field in the 1970s and the author speculates whether theorists can repeat this success. (93 refs.)

74694 $SU(5)$ without $SU(5)$: why B-L is conserved and baryon number not in unified models of quarks and leptons. H.J.Lipkin (Fermi Nat. Accelerator Lab., Batavia, IL, USA).

The High-Energy Limit. Proceedings of the Eighteenth Course of the International School of Subnuclear Physics, Erice, Italy, 31 July-11 Aug. 1980 (New York, USA: Plenum 1983), p.281-305

Discusses quark-lepton unification without assuming higher symmetries than $SU(3)$ and looks for properties generally attributed to $SU(5)$ models which are already present without the assumption of $SU(5)$. B-L conservation and baryon number violation is described. The author also discusses the search for model independent constraints on the S-matrix which are already present in view of known symmetries. (7 refs.)

74695 QCD, unification and the road to 'asymptopia'. S.J.Lindenbaum (Brookhaven Nat. Lab., Upton, NY, USA).

The High-Energy Limit. Proceedings of the Eighteenth Course of the International School of Subnuclear Physics, Erice, Italy, 31 July-11 Aug. 1980 (New York, USA: Plenum 1983), p.575-98

Discusses 'asymptopia', where asymptotic theorems come true, and the energy required for unification including the 'Great Desert' between 10^2 and 10^{12} GeV. QCD, hypercolour, technicolour and preons are also described. (35 refs.)

Conference on Particles and Fields - 1982 See Entry 74201

The High-Energy Limit. Proceedings of the Eighteenth Course of the International School of Subnuclear Physics See Entry 74229

A geometrical foundation of a unified field theory See Entry 74347

The geometrical hierarchy model and $N=1$ supergravity See Entry 74355

Weak symmetry breaking by radiative corrections in broken supergravity See Entry 74356

Renormalisation of the Fayet-Iliopoulos term in supersymmetric spontaneously broken $U(1)$ gauge theories See Entry 74596

Light spinor monopole See Entry 74606

Gauge and nongauge curvature tensor copies See Entry 74607

Vacuum alignment and dynamical symmetry breaking in two-dimensional models See Entry 74649

Physics of intermediate vector bosons See Entry 74701

Use of final-energy sum rules to describe baryon properties in quantum chromodynamics and to estimate the proton lifetime in the $SU(5)$ model See Entry 74718

e^+e^- physics at PETRA See Entry 74755

The effective proton lifetime and non-exponential decay See Entry 74767

Experiment to detect proton decay and neutrino oscillations (using cosmic ray neutrino events) See Entry 74770

Theoretical implications on ISABELLE physics See Entry 74820

Prospects for polarized electrons at high energies See Entry 74825

Particle physics and the new cosmology See Entry 79032

The influence of neutrino rest mass on Dirac cosmology See Entry 79035

Antiproton interactions with light elements as a test of GUT cosmology See Entry 79040

12.20 MODELS OF ELECTROMAGNETIC INTERACTIONS

Relativistic quantum states of a particle in an electromagnetic plane wave and a homogeneous magnetic field See Entry 74664

12.20D Specific calculations and limits of quantum electrodynamics

74696 Properties of the vacuum. II. Electrodynamics. J.Ambjorn, S.Wolfram (California Inst. of Technol., Pasadena, CA, USA).

Ann. Phys. (USA), vol.147, no.1, p.33-56 (15 April 1983).

For pt.1 see *ibid.*, vol.147, p.1-32 (1983). The behaviour of a charged scalar field in an external electric field is discussed. Vacuum polarization is calculated by explicit summation of modes. Instabilities encountered in the external field approximation are absent when back reaction effects are included through a self-consistent semiclassical procedure. (11 refs.)

74697 Does the electromagnetic mass of an electron depend on where it is? P.W.Milonni (Dept. of Phys., Univ. of Arkansas, Fayetteville, AR, USA).

Int. J. Theor. Phys. (USA), vol.22, no.4, p.323-8 (April 1983).

The question of whether the electromagnetic mass of the electron depends upon its electromagnetic environment is discussed in connection with previous theoretical and experimental work. When the quantization of the field in other than free space is properly understood, it is evident that the true electromagnetic mass of the electron is unaltered. (8 refs.)

74698 Wilson loop Langevin equations for $U(1)$ lattice gauge theory. G.Aldazabal, E.Dagotto, A.Gonzalez-Arroyo, N.Parga (Centro Atomico Bariloche, CNEA, Bariloche, Argentina).

Phys. Lett. B (Netherlands), vol.125B, no.4, p.305-7 (2 June 1983).

The authors study the stochastic quantization for lattice QED and derive the corresponding Langevin equations for the Wilson loops. The equivalence with the usual quantization procedure is established in the framework of strong coupling perturbation theory showing that the Wilson loop stochastic equations become the Schwinger-Dyson equations for the loops when the system reaches its equilibrium distribution. (4 refs.)

74699 Electromagnetic vacuum and strong interactions. Yu.A.Baurov, Yu.N.Banaev, V.K.Ablekov.

Sov. Phys.-Dokl. (USA), vol.27, no.8, p.607-9 (Aug. 1982). Translation of:

Dokl. Akad. Nauk SSSR, vol.265, no.4-6, p.1108-12 (Aug. 1982). [received: May 1983]

On the assumption that the elementary charge e is related through the properties of the vacuum state to the velocity c of propagation of the electromagnetic field by the dependence $e=e(c)$, then besides the observed value $c=c_0$, the velocity c can also take the value $c=-c_0$. The authors determine dependence of the strong-interaction constant on the nature of the interacting fields and develop the concepts of the structure of the electromagnetic vacuum. For this purpose, in 'empty space', the authors find the dependence $c=c(r,t)$ for $r>0$ and $r<0$ from the equation obtained for infinitely closely spaced events (i.e., when $d[c(r,t),t]=0$). (8 refs.)

74700 Confinement of light in a polarizable vacuum. A.Khare, T.Pradhan (Inst. of Phys., Bhubaneswar, India).

Proceedings of the VI High Energy Physics Symposium (papers in summary form only received), Mysore, India, 6-11 Dec. 1982 (Bombay, India: Dept. Atomic Energy 1982), p.76

Summary form only given. The authors show that an electrically polarizable vacuum with space-dependent permeability $\epsilon(r)=\mu^{-1}(r)=\exp(-\alpha r^2)$ can confine light whose quanta acquire a mass through interaction with this vacuum.

Quaternionic formulation of fields associated with dyons See Entry 74710

The physics of dual vortices and static baryons in 2+1 dimensions See Entry 74746

12.20F Experimental tests of quantum electrodynamics

The High-Energy Limit. Proceedings of the Eighteenth Course of the International School of Subnuclear Physics See Entry 74229

Recent results from PEP See Entry 74751

Test of quantum electrodynamics and the study of heavy leptons See Entry 74754

e^+e^- physics at PETRA See Entry 74755

12.25 MODELS FOR GRAVITATIONAL INTERACTIONS

(see also 04.60 Quantum theory of gravitation)

On the phenomenon of rotation of the polarization vector of gravitational and neutrino waves in a strong neutrino radiation field See Entry 74343

12.30 MODELS OF WEAK INTERACTIONS

74701 Physics of intermediate vector bosons. J.Ellis (CERN, Geneva, Switzerland), M.K.Gaillard, G.Girardi, P.Sorba.

In book: *Annual review of nuclear and particle science. Vol.32*, J.D.Jackson, H.E.Gove, R.F.Schwitters [Ed.], p.443-97. Palo Alto, CA, USA: Annual Reviews (1982), 595 pp. [0 8243 1532 4]

The authors describe the physics of weakly coupled vector bosons, their 'static' properties: mass, decay widths, and branching ratios and their production mechanisms: e^+e^- annihilation, lepton-induced reactions on nucleons, pp and pp collisions. The phenomenology of scalar particles associated with the clouded issue of symmetry breaking is reviewed and a conclusion that the best laboratory for their study may in fact be in associated production with vectors or in their decay is arrived at. (88 refs.)

Testing the standard model See Entry 74669

After the W particle, the Higgs See Entry 74678

Observation of neutrino and antineutrino induced coherent neutral pion production off Al^{27} See Entry 74756

12.35 COMPOSITE MODELS OF PARTICLES

Conference on Particles and Fields - 1982 See Entry 74201

How far we are in unifying the fundamental interactions See Entry 74692

Electroweak physics of the 80s See Entry 74693

Theoretical implications on ISABELLE physics See Entry 74820

12.35C General properties of quantum chromodynamics (dynamics, confinement, etc.)

74702 A unified approach to QCD phenomenology. S.J.Brodsky (Stanford Linear Accelerator Center, Stanford Univ., Stanford, CA, USA).

AIP Conf. Proc. (USA), no.98, p.146-75 (1982). [received: May 1983] (Conference on Particles and Fields - 1982, College Park, MD, USA, 28-30 Oct. 1982).

The Fock state wave functions of hadrons defined by quantizing quantum chromodynamics at equal time on the light-cone provides a unifying element in QCD predictions, from low to high momentum transfer. A number of novel QCD effects are reviewed, including heavy quark and higher twist phenomena, initial and final state interactions, direct processes, multiparticle collisions, color transparency, and nuclear target effects. A method for fixing the momentum scale in leading order QCD predictions is also briefly presented. (69 refs.)

74703 Matter from quark and gluon bits. J.Kuti (Inst. for Theoretical Phys., Univ. of California, Santa Barbara, CA, USA).

AIP Conf. Proc. (USA), no.98, p.199-217 (1982). [received: May 1983] (Conference on Particles and Fields - 1982, College Park, MD, USA, 28-30 Oct. 1982).

A powerful stochastic method is presented for the numerical evaluation of path integrals in quantum mechanics and quantum field theory. The method is directly applicable for the detailed numerical study of Quantum Chromodynamics (QCD) with lattice regularization. Important results on non-perturbative physical quantities, like the confining force between a heavy quark-antiquark pair, the critical temperature of thermal quark liberation and the mass gap are reviewed first within the pure gauge sector of the theory. The stochastic treatment of the complete fermionic problem is also described. (27 refs.)

74704 Deep inelastic scattering at small x : two- and three-loop calculations. N.Mitra (Dept. of Phys., Columbia Univ., New York, NY, USA).

Nucl. Phys. B, Part. Phys. (Netherlands), vol.B218, no.1, p.145-58 (30 May 1983).

The complete order g^4 and partial order g^6 calculation of deep inelastic scattering at small x is presented. The results agree with the conclusions of a theorem proved in an earlier paper that the total contribution to deep inelastic scattering at small x arises from a ladder diagram evaluated in a restricted region of phase. The subdominance of coupled constant renormalizations at small x is shown with the help of two- and three-loop examples. (10 refs.)

74705 Supersymmetric QCD and its massless limit: an effective Lagrangian analysis. T.R.Taylor (Fermilab, Batavia, IL, USA), G.Veneziano, S.Yankielowicz.

Nucl. Phys. B, Part. Phys. (Netherlands), vol.B218, no.2, p.493-513 (6 June 1983).

Supersymmetric QCD is studied by an effective Lagrangian method. When all flavours are massive supersymmetric vacua, reproducing the known value of Witten's index, then decoupling of heavy flavours occurs. When one or more flavours become massless, some chirality breaking order parameters run to infinity suggesting a non-smooth zero mass limit, in contrast with the case of ordinary QCD. Possible implications of these results on chiral and/or supersymmetry breaking patterns in the massless theory are briefly discussed. (14 refs.)

74706 Chemical potential on the lattice. P.Hasenfratz, F.Karsch (CERN, Geneva, Switzerland).

Phys. Lett. B (Netherlands), vol.125B, no.4, p.308-10 (2 June 1983).

The naive way of introducing chemical potential on the lattice leads to quadratic divergences even for free fermions. Starting from the analogy between the chemical potential and the fourth component of an abelian gauge field, a simple solution is proposed. For Wilson fermions it leads to a trivial modification of the hopping parameter of quarks propagating along the imaginary time direction. (8 refs.)

74707 Error estimate for the valence approximation to lattice QCD. W.Duffy (Dept. of Phys., Indiana Univ., Bloomington, IN, USA), G.Guralnik, D.Weingarten.

Phys. Lett. B (Netherlands), vol.125B, no.4, p.311-16 (2 June 1983).

A Monte Carlo algorithm is used to calculate m_N/m_p , m_Δ/m_p , m_Σ/m_p , m_π^2/f_π , f_π/m_p , f_π/m_π and Λ_{m}/m_p for lattice QCD with the number of flavors N_f of quarks contributing virtual loops given by zero, the valence approximation, and with N_f chosen, in effect to be -2 . The difference between corresponding

pairs of quantities with N_f of zero and N_f of -2 the authors take to be an estimate of the difference between the value for a realistic theory with N_f of $+2$ and for the approximate theory with N_f of zero. The changes in mass ratios and Λ_{m} are consistent with zero and typically $(20 \pm 20)\%$ while decay constant ratios change by as much as $(88 \pm 24)\%$. (10 refs.)

74708 On the low energy structure of QCD. J.Gasser, H.Leutwyler (Inst. für Theoretische Phys., Bern, Switzerland).

Phys. Lett. B (Netherlands), vol.125B, no.4, p.321-4 (2 June 1983).

The authors analyze the low energy structure of off-shell amplitudes in QCD. The method used automatically keeps track of the Ward identities associated with chiral symmetry. The infrared singularities generated by the Goldstone bosons are shown to lead to substantial deviations from the soft pion results. (15 refs.)

74709 Quantum chromodynamics: the modern theory of the strong interaction. F.Wilczek (Inst. for Theoretical Phys., Univ. of California, Santa Barbara, CA, USA).

In book: *Annual review of nuclear and particle science. Vol.32*, J.D.Jackson, H.E.Gove, R.F.Schwitters [Ed.], p.177-209. Palo Alto, CA, USA: Annual Reviews (1982), 595 pp. [0 8243 1532 4]

The nature of the strong interaction responsible for holding nuclei together and for a wealth of phenomena observed in high energy collisions has been a main concern of physics since the 1930s. It now appears that we have a precise microscopic theory that in principle solves the problem, in the same sense that quantum electrodynamics solves atomic spectroscopy and chemistry. The author reviews the nature of the theory, the evidence for it, and its implications for other parts of physics. (108 refs.)

74710 Quaternionic formulation of fields associated with dyons. S.Raj Kumar, B.S.Rajput (Dept. of Phys., Kumaun Univ., Naini Tal, India).

Proceedings of the VI High Energy Physics Symposium (papers in summary form only received), Mysore, India, 6-11 Dec. 1982 (Bombay, India: Dept. Atomic Energy 1982), p.54

Summary form only given. In order to make an attempt for the confinement problems of quantum chromodynamics (QCD) and the existing manifestly non-covariant as well as clumsy formalisms for the theory of monopoles in usual Hilbert space, the authors have developed the quaternionic formulation for generalized field equations of the fields associated with dyons. They have also developed the quaternionic formulation for generalized potential, current Lagrangian and field with their interrelationship in presence of dyons. It has been shown that these compact forms of generalized fields associated with dyons are unique, consistent and reproduce the usual electrodynamics in the absence of magnetic charge on dyons.

74711 Gluonium and QCD in the J/ψ region. E.D.Bloom (Stanford Linear Accelerator Center, Stanford Univ., Stanford, CA, USA).

Physics in Collision. High-Energy ee/pp Interactions. Proceedings of an International Conference, Stockholm, Sweden, 2-4 June 1982 (New York, USA: Plenum 1983), p.149-77

The existence of an extensive spectrum of colorless, flavorless bound states of two or more gluons has been firmly predicted by quantum chromodynamics (QCD). These gluonic bound states have been given the rather unattractive name 'glueballs.' It is expected that the lower lying 'glueball' states are bound states of mostly 2 gluons and in analogy to quarkonium, this system is called gluonium. It is also expected that gluonium states should be by far easier to observe than other 'glueballs' due to their relatively lower masses which are predicted to lie in the range 1 to 2 GeV. However, the experimental search for such states has proven to be a difficult and confusing one. The author reviews these elements of 'glueball fantasy' and concludes that there is no easy way of experimentally establishing the existence (or non existence) of gluonium states. What is necessary to determine the gluonium content of a candidate state is a detailed comparison with theory, particularly QCD. But can one presently trust QCD to guide correctly? To partially answer this question, experiment is compared to the predictions of QCD in the J/ψ region. (54 refs.)

74712 The Upsilon resonances—recent results. M.G.D.Gilchriese (Lab. of Nuclear Studies, Cornell Univ., Ithaca, NY, USA).

Physics in Collision. High-Energy ee/pp Interactions. Proceedings of an International Conference, Stockholm, Sweden, 2-4 June 1982 (New York, USA: Plenum 1983), p.179-211

The discovery of the Upsilon at Fermilab in 1977 and the subsequent confirmation at the DORIS e^+e^- storage ring began a new era in the study of heavy quark systems. The Upsilon states are composed of b and \bar{b} quarks bound by the strong force. The study of the spectroscopy of the $b\bar{b}$ 'atom' may be crucial to the understanding of the strong interaction and, in the continued absence of the top quark, may be the only way to make precise comparisons with Quantum Chromodynamics, the theory of the strong interaction. In addition, the Upsilon resonances below B meson threshold primarily decay into gluons which subsequently fragment into hadrons. One therefore has a rather pure sample of gluons, the properties of which can be studied. In particular, the comparison of gluon and quark hadronization is facilitated. (23 refs.)

74713 Gluon condensation and confinement of quarks. R.Fukuda (Res. Inst. for Fundamental Phys., Kyoto Univ., Kyoto, Japan).

Gauge Theory and Gravitation. Proceedings of the International Symposium, Nara, Japan, 20-24 Aug. 1982 (Berlin, Germany: Springer-Verlag 1983), p.58-61

The author considers if gluon condenses in the form of color singlet, then the dual variable becomes a good coordinate in the low energy region and acquires a mass gap. The vacuum of quantum chromodynamics will be filled with nontrivial configuration of gluonic fields $A_\mu^a(x)$; they condense in the vacuum in the form of color singlet and of Lorentz scalar. The author takes into account the effect of the gluon condensation and studies the vacuum state and excitation spectra. (4 refs.)

74714 Hadronic physics of qq light quark mesons, quark molecules and glueballs. S.J.Lindenbaum (Brookhaven Nat. Lab., Upton, NY, USA).

The High-Energy Limit. Proceedings of the Eighteenth Course of the International School of Subnuclear Physics, Erice, Italy, 31 July-11 Aug. 1980 (New York, USA: Plenum 1983), p.509-74 (30 refs.)

74715 Deep inelastic phenomena. C.Y.Prescott (Stanford Linear Accelerator Center, Stanford Univ., Stanford, CA, USA).

The High-Energy Limit. Proceedings of the Eighteenth Course of the International School of Subnuclear Physics, Erice, Italy, 31 July-11 Aug. 1980 (New York, USA: Plenum 1983), p.677-733

Reviews the picture of nucleon structure from deep inelastic scattering. The subjects discussed include the quark-parton model, scaling, QCD, Q^2 evolution, structure functions, and the R parameter. (16 refs.)

The High-Energy Limit. Proceedings of the Eighteenth Course of the International School of Subnuclear Physics See Entry 74729

Heating the quenched Eguchi-Kawai model See Entry 74584

- Variational methods in the master field formulation for QCD_{3+1} See Entry 74628
- Confinement by thick magnetic vortices See Entry 74629
- Vacuum energy in the bag model See Entry 74633
- Lattice gauge theory—a progress report See Entry 74636
- BRS transformation and color confinement See Entry 74640
- Non-local gauge theories See Entry 74645
- Testing the standard model See Entry 74669
- QCD, unification and the road to 'asymptopia' See Entry 74695
- The axial anomaly at finite temperature See Entry 74727
- The dynamics of a fragmentation model or a possible life after the parton stage See Entry 74738
- Exotic multi-quark states with charm See Entry 74740
- Quantized strings and QCD See Entry 74748
- e^+e^- physics at PETRA See Entry 74755
- Why most flavor dependence predictions for nonleptonic charm decays are wrong See Entry 74764
- Coupled channels and quarks in nucleon-nucleon scattering See Entry 74850
- Mesons and isobars See Entry 74854
- The nucleon-meson coupling vertex-structure and the process for the meson exchange in nuclear force See Entry 74859
- Hot dense nuclear matter and the transition to quark matter See Entry 74890

12.35E Applications of quantum chromodynamics to particle properties and reactions

- 74716 Massive lepton pair production—what has QCD done to the classical Drell-Yan model? E.L.Berger (High Energy Phys. Div., Argonne Nat. Lab., Argonne, IL, USA).
AIP Conf. Proc. (USA), no.98, p.312-42 (1982). [received: May 1983] (Conference on Particles and Fields - 1982, College Park, MD, USA, 28-30 Oct. 1982).
A report is presented of recent experimental and theoretical progress in studies of the production of massive lepton pairs in hadronic collisions. Among the topics discussed are deviations from scaling, the status of the proofs of factorization in the parton model, higher-order terms in the QCD expansion, the discrepancy between measured and predicted yields (K factor), high-twist terms, soft gluon effects, and transverse momentum distributions. (46 refs.)
- 74717 Muoproduction of J/ψ and the photon-gluon scattering process: $\gamma g \rightarrow J/\psi g$. R.Baier (Lab. de Phys. Theorique et Hautes Energies, Univ. Paris-Sud, Orsay, France), R.Ruckl.
Nucl. Phys. B, Part. Phys. (Netherlands), vol.B218, no.2, p.289-96 (6 June 1983).
Recent data on muoproduction of J/ψ reported by the European Muon Collaboration are used to examine the perturbative QCD subprocess $\gamma g \rightarrow J/\psi g$ as a possible production mechanism. The authors find that for sufficiently inelastic J/ψ s this process can account for the observed rates and distributions. They argue, however, that in total only about 10 to 20% of the observed J/ψ yield is due to this source. (12 refs.)
- 74718 Use of final-energy sum rules to describe baryon properties in quantum chromodynamics and to estimate the proton lifetime in the SU(5) model. N.V.Krasnikov, A.A.Pivovarov, N.N.Tavkhelidze (Inst. of Nuclear Res., Acad. of Sci., USSR).
JETP Lett. (USA), vol.36, no.7, p.333-7 (5 Oct. 1982). Translation of: *Pis'ma v Zh. Eksp. & Teor. Fiz. (USSR)*, vol.36, no.7, p.272-5 (5 Oct. 1982). [received: May 1983]
Final-energy sum rules are used to calculate the proton coupling constant λ_p with an interpolating proton current. The coupling constant λ_p can be used to calculate the matrix elements for proton decay in the grand unified SU(5) model. The proton lifetime is calculated to be $\tau_p = 10^{28} \times (M_X/10^{14} \text{ GeV})^4 \text{ yr}$, where M_X is the mass of the X boson. (12 refs.)
- 74719 Higher dimensional renormalization group invariant vacuum condensates in quantum chromodynamics. S.Narisson (CERN, Geneva, Switzerland), R.Tarrach.
Phys. Lett. B (Netherlands), vol.125B, no.2-3, p.217-22 (26 May 1983).
The renormalization of the five- and six-dimensional scalar gauge invariant composite operators is performed. The corresponding renormalization group invariant vacuum condensates are studied. The main results are that the six-dimensional gluon condensate does not mix with the quartic quark condensates nor the other way round. The authors also show that the factorization hypothesis of the four-quark operator does not lead to renormalization group invariant quark vacuum condensates. So, one has to be careful when keeping the six-dimensional operators in the QCD sum rule analysis. (6 refs.)
- 74720 No threshold-effects from QCD in deep inelastic lepton scattering. W.Kummer (Inst. für Theoretische Phys., Tech. Univ. Wien, Wien, Austria).
Phys. Lett. B (Netherlands), vol.125B, no.4, p.317-20 (2 June 1983).
Within the usual system of assumptions, QCD, even in the presence of quark masses, predicts no threshold effects to one-loop order. The author derives this result in an extremely simple manner using a gauge-independent, but threshold-dependent momentum subtraction prescription. (11 refs.)
- 74721 Low energy theorems as precision tests of QCD. J.Gasser, H.Leutwyler (Inst. für Theoretische Phys., Bern, Switzerland).
Phys. Lett. B (Netherlands), vol.125B, no.4, p.325-9 (2 June 1983).
The authors work out the low energy expansion of the $\pi\pi$ -scattering amplitude with a method proposed in a previous paper (Phys. Letts., vol. 125B, no.4, p.321, 1983). Using the measured D-waves as an input they predict the behaviour of the amplitude to order p^4 . The data agree with this prediction within the errors. (8 refs.)
- 74722 What can we count on? A discussion of constituent-counting rules for interactions involving composite systems. D.Sivers (Argonne Nat. Lab., Argonne, IL, USA).
In book: *Annual review of nuclear and particle science*. Vol.32, J.D.Jackson, H.E.Gove, R.F.Schwitters [Ed.], p.149-75. Palo Alto, CA, USA: Annual Reviews (1982), 595 pp. [0 8243 1532 4]
The author discusses QCD predictions for the hadronic form factors. The pion form factor is considered in some detail but he also looks at baryon form factors. Counting-rule predictions for the shape of deep inelastic structure functions are presented and QCD-based approaches to hadronic fixed-angle scattering are considered. (40 refs.)

- 74723 Spectroscopy of hadrons: mesons. S.P.Misra, A.R.Panda, S.Naik (Inst. of Phys., Bhubaneswar, India).
Proceedings of the VI High Energy Physics Symposium (papers in summary form only received), Mysore, India, 6-11 Dec. 1982 (Bombay, India: Dept. Atomic Energy 1982), p.69
Summary form only given. The authors consider the spectroscopy of hadrons with QCD inspired or other phenomenological potentials with a standard diagonalisation procedure using the oscillator basis. In the present model, they retain the four-component complete Dirac operator so that relativistic spin and orbital dependence as well as kinematics is fully retained. The energy eigenvalues are obtained by the optimisation of the energy expectation values, subject to the constraint of the appropriate normalisation of the wave functions. This enables one to retain the relativistic effects completely. The corrections to the wave functions within the same multiplet even in the 'nonrelativistic' case of the charmonium appear to be substantial.
- 74724 QCD and the space-time evolution of high-energy e^+e^- , $p\bar{p}$, and heavy ion collisions. J.D.Bjorken (Fermi Nat. Accelerator Lab., Batavia, IL, USA).
Physics in Collision. High-Energy ee/pp Interactions. Proceedings of an International Conference, Stockholm, Sweden, 2-4 June 1982 (New York, USA: Plenum 1983), p.343-68
The author concentrates on the space-time evolution of hadronic final states in various processes. It has been known for a long time that large distances are important at high energies, and that one therefore should be able to at least map out the basic space-time geography of the collision process. It must be admitted that so far, the space-time pictures have not led to very much in the way of practical (computational) insights, but given the present QCD ideology, it may be useful to look at the subject again. He begins with a discussion of e^+e^- annihilation into hadrons, a process blessed with well-known elements of simplicity. Then he considers the opposite extreme of highly relativistic nucleus-nucleus collisions. Here a space-time description has its own elements of simplicity, elements which might conceivably be applicable in hadron-hadron collisions. He then addresses the more immediate issues of how these ideas relate to present-day observations, especially high-energy hadron-hadron collisions. (40 refs.)
- 74725 Hadronic production of heavy flavours. L.Montanet (CERN, Geneva, Switzerland).
Physics in Collision. High-Energy ee/pp Interactions. Proceedings of an International Conference, Stockholm, Sweden, 2-4 June 1982 (New York, USA: Plenum 1983), p.369-86
Heavy quarks (i.e. charm c and Beauty b) turn out to be very useful probes to study hadron dynamics. There are good reasons to hope that the QCD perturbative theory can be applied to understand the production of heavy quarks in hadronic collisions, assuming the gluon-gluon fusion process $g\bar{g} \rightarrow Q\bar{Q}$ or the quark-quark fusion process $q\bar{q} \rightarrow Q\bar{Q}$. (26 refs.)
- On a self-consistent chiral doublet composite scheme See Entry 74659
- Theoretical predictions for baryon number violation See Entry 74666
- Effective Lagrangian for $\Delta S=1$ and $\Delta S=2$ transition in the Higgs boson exchange model of CP violation See Entry 74681
- On the low energy structure of QCD See Entry 74708
- Gluonium and QCD in the J/ψ region See Entry 74711
- The Upsilon resonances—recent results See Entry 74712
- Instantons in the quark plasma See Entry 74728
- An analysis of $(b\bar{b})$ -states in a static one-parameter potential model See Entry 74731
- The chromo-electromagnetic properties of a hadron See Entry 74743
- Charged-current neutrino interactions See Entry 74757
- Recent results from CLEO at the $\Upsilon(4s)$ See Entry 74760
- Analysis of scaling violation in nucleon structure functions See Entry 74771
- Deep inelastic muon hadron interactions See Entry 74776
- SPIN correlation in $ep \rightarrow eX$ scattering See Entry 74777
- Lepton-hadron inclusive scattering and QCD See Entry 74778
- Recent results from PETRA See Entry 74781
- Recent results in Υ spectroscopy from CESR See Entry 74782
- The influence of fragmentation models on the determination of the strong coupling constant in e^+e^- annihilation into hadrons See Entry 74783
- Analysis of the energy weighted angular correlations in hadronic annihilations at 22 and 34 GeV See Entry 74786
- Jets at Petra See Entry 74788
- Evidence for glueballs See Entry 74796
- Recent study of jets at the ISR See Entry 74805
- Analysis of inclusive particle ratios in π^+p interactions at 40 GeV/c See Entry 74815
- Some characteristics of secondary particles produced in pion-nucleus collisions in emulsion at 50 GeV/c See Entry 75053

12.35H Phenomenological composite models of particle structure and reactions (partons, bags, etc.)

- 74726 The de Broglie fusion method applied to quarks at the ends of strings. C.J.Burden, L.J.Tassie (Res. School of Phys. Sci., Australian Nat. Univ., Canberra, Australia).
Ann. Inst. Henri Poincaré Sect. A (France), vol.38, no.3, p.199-213 (1983).
Wave equations are found for diquarks restricted to a world line traced out by the end of a relativistic string. The method used involves combining two restricted Dirac equations using a variant of the de Broglie fusion method. The equation describing the spin 0 diquark is the Klein-Gordon equation restricted to the world line. However, the spin 1 diquark equation differs from the restricted Proca-de Broglie equation. (5 refs.)
- 74727 The axial anomaly at finite temperature. H.Itoyama, A.H.Mueller (Dept. of Phys., Columbia Univ., New York, NY, USA).
Nucl. Phys. B, Part. Phys. (Netherlands), vol.B218, no.2, p.349-65 (6 June 1983).
The axial anomaly and its constraints are examined at finite temperature. The axial anomaly is shown to be the same at $T \neq 0$ and $T=0$. When $T \ll \Lambda$ one is able to argue the existence of a narrow resonance in the QCD medium corresponding to pion propagation. However, when T is comparable to Λ one is unable to obtain any useful information from the axial anomaly. In particular, one is unable to see how $T_{\text{chiral}} \geq T_{\text{conf}}$ might follow from the anomaly constraint. (12 refs.)

74728 Instantons in the quark plasma. A.A.Abriksov, Jr. (Space Res. Inst., Moscow, USSR). *Nucl. Phys. B, Part. Phys. (Netherlands)*, vol.B218, no.2, p.459-83 (6 June 1983).

The thermodynamics of a dense plasma of light quarks is studied by means of exact Green functions. The author constructs the fermion propagator in a self-dual field at non-zero density and temperature. The fermion zero modes in the medium are considered with special attention. The non-diagonal elements of the density matrix generate an additional term in the instanton action in the one-loop approximations. Large pseudoparticles are suppressed by the medium and the instanton gas is dilute. The contribution to the thermodynamic functions is proportional to the total 4-volume occupied by pseudoparticles. Due to the product of the quark masses in the coefficient, the instanton density is small. Interaction of pseudoparticles with the 'quark condensate' $\langle 0|q\bar{q}|0\rangle$ in the physical vacuum of QCD enhances their influence and makes it quite notable. (15 refs.)

74729 Symmetry basis and physical basis for many-quark system. Shi Yi-jin (Inst. of Atomic Energy, Acad. Sinica, Beijing, China). *Commun. Theor. Phys. (China)*, vol.1, no.4, p.459-68 (1982).

A general expression for transformation coefficients between the symmetry basis and physical basis of the many-quark system has been given. For the channel with $(\text{TS})=(01)$ of a six-quark system, the transformation coefficients have been calculated. Interpreting again the fractional-parentage expansions of symmetry basis, the author pointed out that the fractional-parentage coefficients are essentially the Clebsch-Gordan coefficients for the corresponding SU_6 group. (4 refs.)

74730 On scalar quark leakage in Klein-Gordon equation. A.P.Kajwadkar, L.K.Sharma (Dept. of Appl. Phys., Government Engng. Coll., Jabalpur, India). *Indian J. Pure & Appl. Phys.*, vol.21, no.3, p.195-6 (March 1983).

A tunnelling phenomenon for two different confining potentials depicting the leakage of scalar quarks has been discussed. The transmission coefficients for these cases have been evaluated numerically and compared with those for the linear potential. (11 refs.)

74731 An analysis of (bb) -states in a static one-parameter potential model. A.Steiger (Lawrence Livermore Nat. Lab., Univ. of California, Livermore, CA, USA).

Phys. Lett. B (Netherlands), vol.125B, no.2-3, p.223-6 (26 May 1983). Masses and leptonic widths of (bb) -states are calculated with the potential $V(r)=[8\pi/(33-2N_f)](1-\lambda^2)/(r \log \lambda r)$. Particularly good agreement with recently published experimental results, including the average mass of the three observed P-wave states χ'_{bb} , is obtained for the constituent quark mass $m_b=4.735$ GeV, the OCD-parameter $\Lambda=\exp(-\gamma_E) \lambda=362.2$ MeV, and the number of active flavors $N_f=4$. (17 refs.)

74732 Can δ (980,0⁺) be a broad $qqqq$ state? N.N.Achasov, S.A.Devyanin, G.N.Shestakov (Dept. of Theoretical Phys., Inst. for Maths., Novosibirsk, USSR).

Phys. Scr. (Sweden), vol.27, no.5, p.330-3 (May 1983). It is shown that none of the arguments, presented by Bramon and Masso, against the possibility of interpreting the δ (980,0⁺)-resonance as a broad $qqqq$ -state and concerning (i) the $\eta \rightarrow \eta\pi\pi$ decay, (ii) the $D,E \rightarrow \delta\pi \rightarrow \pi\pi$ decays, (iii) the tadpole contributions to EM mass differences and mixings, is well founded, and some of them are plainly wrong. The authors discuss Tornqvist's resolution of the scalar mesons. (21 refs.)

74733 Antiquarks in a quark-gluon plasma. A.Mekjian (Dept. of Phys., Rutgers Univ., Piscataway, NJ, USA).

Proceedings of the International Conference on Nucleus-Nucleus Collisions (papers in summary form only received), East Lansing, MI, USA, 26 Sept.-1 Oct. 1982 (East Lansing, MI, USA: Michigan State Univ. 1982), p.138. Thermal properties of a heated system of quarks and gluons are investigated and compared to those of a system of nucleons and pions. Results are first given for a non-interacting system or asymptotically free system of quarks, antiquarks and gluons. Confinement is incorporated through the MIT Bag Model. The energy, density, pressure and entropy are calculated in an expansion in powers of μ_0/kT , where μ_0 is the quark chemical potential and T is the temperature of the system. The nuclear system is investigated using a density dependent effective interaction. The phase transition from nucleonic to quark matter is studied using the Gibbs' criteria. Specifically, phase equilibrium is established when the pressure and temperature of the two phases are equal and when the nucleon chemical potential is three times the quark chemical potential. (2 refs.)

74734 Baryon multiplicities in the (six quark) deuteron fragmentation. P.Pal (Uluberia Coll., Uluberia, India), P.Dasgupta, K.Dasgupta.

Proceedings of the VI High Energy Physics Symposium (papers in summary form only received), Mysore, India, 6-11 Dec. 1982 (Bombay, India: Dept. Atomic Energy 1982), p.62. Summary form only given. The multiplicities for various baryons produced in the deuteron fragmentation are studied on the basis of a six-quark picture of deuteron. Multiplicities of various types of baryons are expressed in terms of the probabilities A_{ij} , $i, j=0, 1, 2, 3$ with i indicating the number of valence quarks of the incident deuteron contained in any one of the two baryons produced in each collision and j denoting that in the other. Experimentally verifiable constraints on the multiplicities are shown to result from the positivity of A_{ij} . The possibility of determination of the quantities $v_i=\sum_j (\delta_{ij}+A_{ij})$ is also discussed. The results obtainable from the conventional two-nucleon picture of deuteron are also given and are compared with those obtained from the six-quark picture. It is shown how one can experimentally distinguish between the two pictures through a study of baryon multiplicities.

74735 Hadronic couplings of open beauty states. S.N.Ram (Dept. of Phys., Banaras Hindu Univ., Varanasi, India), C.P.Singh.

Proceedings of the VI High Energy Physics Symposium (papers in summary form only received), Mysore, India, 6-11 Dec. 1982 (Bombay, India: Dept. Atomic Energy 1982), p.66.

Summary form only given. Strong interaction coupling parameters of particles with beauty quantum number are obtained using dispersion sum rules in various forms, e.g. current algebra sum rules, superconvergence sum rules and finite energy sum rules, etc. These sum rules lead to a set of algebraic relations among masses and coupling constants. The authors compare the hadronic couplings of beautiful particles as obtained from various techniques and discuss their implications on the hadronic production of these states.

74736 Confining potentials and analyticity of energy levels in angular momentum plane. D.P.Datta, B.Mukherjee (Dept. of Phys., North Bengal Univ., Darjeeling, India).

Proceedings of the VI High Energy Physics Symposium (papers in summary form only received), Mysore, India, 6-11 Dec. 1982 (Bombay, India: Dept. Atomic Energy 1982), p.72.

Summary form only given, as follows. Analyticity of Schroedinger energy levels $E_n(l)$ in the half-plane $\text{Re } l > -1/2$ have been studied for confining

potentials of the type $V(r)=r+k\beta^{\beta}$, $-2<\beta<1$, k real or $r^{\alpha}+k\beta^{\beta}$, $0<\beta<\alpha$, k real, which reduce to the well-known charmonium potential for $\alpha=1$, $\beta=-1$. Use has been made of the Rellich-Kato theory for linear operators. It is first shown that the energy levels $E_n(\beta)$ are analytic in β in the interval (i) $-2<\beta<1$, $\alpha=1$; (ii) $0<\beta<\alpha$, $\alpha\neq 1$, for a fixed l in $\text{Re } l > -1/2$. The proof rests on the realization of a family of Schroedinger operators holomorphic in β in the specified interval for a fixed l in $\text{Re } l > -1/2$. Analyticity of $E_n(l)$ for pure power potential ($\beta=0$) is already known. A simple argument, based on the analyticity property in β , now proves the analyticity of $E_n(l)$ in $\text{Re } l > -1/2$ for a non-zero β , since it is known to be true for $\beta=0$.

74737 Gluonic and relativistic effects in harmonic oscillator model. A.Sharma, M.Gupta, M.P.Khanna (Dept. of Phys., Panjab Univ., Chandigarh, India).

Proceedings of the VI High Energy Physics Symposium (papers in summary form only received), Mysore, India, 6-11 Dec. 1982 (Bombay, India: Dept. Atomic Energy 1982), p.75.

Summary form only given, as follows. The harmonic oscillator quark model wherein Pauli spinors are replaced by Dirac spinors and quark masses are less than one-third of the nucleon mass, it studied in the spirit of the bag model. In particular, the authors have calculated G_A/G_V , μ_p , charge radius of proton, and their variation with quark mass and spring constant. They have also calculated certain gluon probability integrals. The trend of their result is the same as those of Golowich and Close et al., similarly the spatial matrix elements of non-leptonic decays are found to be of right order of magnitude. They demonstrate that the results of the standard bag model as well as those of non-relativistic HO model are reproducible in appropriate limits of the present scheme.

74738 The dynamics of a fragmentation model or a possible life after the parton stage. B.Andersson (Dept. of Theoretical Phys., Univ. of Lund, Lund, Sweden).

Physics in Collision. High-Energy $ee/ep/pp$ Interactions. Proceedings of an International Conference, Stockholm, Sweden, 2-4 June 1982 (New York, USA: Plenum 1983), p.303-26.

The author discusses how perturbative QCD works at distances much less than 1 fm. (24 refs.)

74739 Quark masses from the vector meson spectrum. E.Etim (Phys. Dept., Siegen Univ., Siegen, Germany).

The High-Energy Limit. Proceedings of the Eighteenth Course of the International School of Subnuclear Physics, Erice, Italy, 31 July-11 Aug. 1980 (New York, USA: Plenum 1983), p.343-65.

Considers the relationship between quark masses and the masses of their neutral vector meson bound states. This is done by studying the properties of the hadronic contribution to the photon propagator to second order in the electric charge. For low energies the corresponding vacuum polarisation amplitude is dominated by vector mesons while at high energies the quark structure of the current takes over. These two structures are required to match asymptotically. (13 refs.)

74740 Exotic multi-quark states with charm. H.J.Lipkin (Fermi Nat. Accelerator Lab., Batavia, IL, USA).

The High-Energy Limit. Proceedings of the Eighteenth Course of the International School of Subnuclear Physics, Erice, Italy, 31 July-11 Aug. 1980 (New York, USA: Plenum 1983), p.599-625.

The author describes some threshold exotics and multi-quark hadrons such as dimesons and dinucleons. This is then expanded to discuss multi-quark states which include charm, and models which describe the hadron structure. A nonrelativistic quark model is used. Mass formulae are given for mesons and baryons. (22 refs.)

WKB integrals for some central potentials and analytic expressions for energy eigenvalues See Entry 74326

Gauge-invariant local fields in a gauge theory as interpolating fields for 'glueballs' See Entry 74617

The massless gluino and the pseudoscalar meson family See Entry 74660

Deep inelastic phenomena See Entry 74715

Massive lepton pair production—what has QCD done to the classical Drell-Yan model? See Entry 74716

Higher dimensional renormalization group invariant vacuum condensates in quantum chromodynamics See Entry 74719

Superstring interactions See Entry 74744

The physics of dual vortices and static baryons in 2+1 dimensions See Entry 74746

On a mass formula of particles in $c\bar{c}$, $b\bar{b}$ and $t\bar{t}$ families See Entry 74750

The pion-quark coupling constant and the decay of vector mesons See Entry 74763

Why most flavor dependence predictions for nonleptonic charm decays are wrong See Entry 74764

Structure functions of relativistic systems composed of two spin $1/2$ particles See Entry 74772

Magnetic moments of the ground state baryons See Entry 74774

Magnetic moments in quark-diquark model See Entry 74775

Pion production at large p_T in photon-deuteron collisions See Entry 74779

Polarized single pion photoproductions test for various quark models See Entry 74780

The influence of fragmentation models on the determination of the strong coupling constant in e^+e^- annihilation into hadrons See Entry 74783

Jets at Petra See Entry 74788

Evidence for 'held-back' valence quarks from particle ratios in pp and $p\bar{p}$ collisions See Entry 74810

Coupled channels and quarks in nucleon-nucleon scattering See Entry 74850

Mesons and isobars See Entry 74854

Quarks, bags and the nucleon-nucleon interaction See Entry 74856

The nucleus consists of more than just nucleons, deltas and mesons See Entry 74857

Conventional approach to the problem of the deuteron smearing corrections See Entry 74869

Relativistic Brueckner-Hartree-Fock theory: theoretical foundations and empirical evidence See Entry 74880

12.35K Other composite models (inc. composite quarks and leptons)

- 74741** Generalized statistics and the rishon hypothesis. P.D.Jarvis (Dept. of Phys., Univ. of Tasmania, Hobart, Tasmania, Australia), H.S.Green. *Aust. J. Phys. (Australia)*, vol.36, no.2, p.123-6 (1983). It is pointed out that the proposal of Harari and others (1981), that leptons and quarks should be regarded as composites, consisting of rishons or quips, can be formulated as a field theory in terms of two fundamental spinor fields which satisfy a new generalization of quantum statistics. The requirement of macroscopic causality determines which of the many combinations of rishons may be observed as isolated particles. (14 refs.)
- 74742** A derivation of the Cabibbo angle and quark-lepton masses from a composite model. G.C.Yang (Hobei Inst. of Technol., Tianjin, China), H.C.Liu, L.F.Luo. *Lett. Nuovo Cimento (Italy)*, vol.37, ser.2, no.3, p.111-15 (21 May 1983). The Cabibbo angle and quark-lepton masses are derived from a composite model by taking into account the interaction between the internal degrees of freedom. (4 refs.)
- QCD, unification and the road to 'asymptopia'**See Entry 74695

12.40 MODELS OF STRONG INTERACTIONS

- On the S-wave interaction between massive fermions and a GUT magnetic monopole**See Entry 74680
- Electromagnetic vacuum and strong interactions**See Entry 74699
- Deep inelastic scattering at small x: two- and three-loop calculations**See Entry 74704
- New unitarity bounds and their near-saturation by ISR data** ..See Entry 74808
- Relativistic two-nucleon calculations on the light front**See Entry 74860

12.40E Statistical models

- 74743** The chromo-electromagnetic properties of a hadron. S.N.Banerjee, A.Chakraborty (Dept. of Phys., Jadavpur Univ., Calcutta, India). *Hadronic J. (USA)*, vol.6, no.2, p.251-8 (March 1983). The chromo-electromagnetic properties of a hadron, say a meson, have been investigated through the statistical model and some interesting properties emerge resulting in a phase transition. (5 refs.)
- On a mass formula of particles in $c\bar{c}$, $b\bar{b}$ and $t\bar{t}$ families**See Entry 74750
- The hydrodynamic model description of e^+e^- hadrons and the contribution of the simple wave regions**See Entry 74785
- Growth of $\langle p_t \rangle$ with multiplicity at the collider energy and a two-component model for pp collision**See Entry 74799

12.40H Duality and dual models

- 74744** Superstring interactions. M.B.Green, J.H.Schwarz (California Inst. of Technol., Pasadena, CA, USA). *Nucl. Phys. B, Part. Phys. (Netherlands)*, vol.B218, no.1, p.43-88 (30 May 1983). As a first step in the construction of a superstring field theory, the off-shell vertex for coupling three arbitrary open superstring states is constructed. A cubic interaction term in the supersymmetry charge is also obtained. Since the hamiltonian corresponds to the square of this supercharge, certain quartic interactions can be deduced as well. It appears likely, however, that the complete field theory of superstrings contains quartic and higher interactions in addition to those obtained here. (12 refs.)
- 74745** Spectrum of the supersymmetric Liouville theory. J.F.Arvis (Lab. de Phys. Theorique, Ecole Normale Supérieure, Paris, France). *Nucl. Phys. B, Part. Phys. (Netherlands)*, vol.B218, no.2, p.309-20 (6 June 1983). The author completes a previous paper (1983) on the supersymmetric Liouville theory in a box by explicitly working out the mode separation and obtaining the spectrum. The results are relevant for the theory of the spinning string in Polyakov's quantization. (7 refs.)
- 74746** The physics of dual vortices and static baryons in 2+1 dimensions. N.J.Snyderman (Lawrence Berkeley Lab., Univ. of California, Berkeley, CA, USA). *Nucl. Phys. B, Part. Phys. (Netherlands)*, vol.B218, no.2, p.381-422 (6 June 1983). The dual to Mandelstam $SU(N)$ models of magnetic confinement, which explicitly realize the superconducting phase of the $SU(N)$ gauge theory, are constructed and shown to explicitly realize 't Hooft's physical picture of the confining phase in 2+1 dimensions, in which electric vortices are Bloch walls between Z_N^* magnetic domains. These models generalize Polyakov's $SU(2) \rightarrow U(1)$ compact QED model to $SU(N) \rightarrow U(1)^{N-1}$. These models have also been considered by Wadia and Das (1981). Static baryons in $SU(3)$ are studied. A Hamiltonian analysis of the physics of confinement in these models is used to elucidate the beautiful correspondence of Hosotani (1977) that the electric vortex in the Polyakov model is related to the naive dual of a magnetic vortex in the insulating layer of a Josephson junction. (31 refs.)

- 74747** Generalized string amplitude and wave equation for hadrons. H.Suura (School of Phys. & Astron., Univ. of Minnesota, Minneapolis, MN, USA). *Gauge Theory and Gravitation. Proceedings of the International Symposium, Nara, Japan, 20-24 Aug. 1982* (Berlin, Germany: Springer-Verlag 1983), p.62-4. A gauge invariant Hamiltonian formulation of hadron dynamics involving a generalized string amplitude is proposed. Resulting partial integro-differential wave equations reflect the shielding of the long range potential and determine a universal logarithmic derivative of the hadronic wave functions. Because of this boundary condition, the new wave equation allows confined solutions without an explicit confinements potential in it. (2 refs.)
- 74748** Quantized strings and QCD. E.S.Fradkin, A.A.Tseytlin (Dept. of Theoretical Phys., P.N. Lebedev Phys. Inst., Moscow, USSR). *Gauge Theory and Gravitation. Proceedings of the International Symposium, Nara, Japan, 20-24 Aug. 1982* (Berlin, Germany: Springer-Verlag 1983), p.284-92. The authors present various quantised string models for $N_d = \infty$ QCD, the QCD strings having quarks at the ends. Meson scattering amplitudes are calculated, starting with the QCD path integral. (23 refs.)
- The de Broglie fusion method applied to quarks at the ends of strings**See Entry 74726

12.40M Complex angular momentum plane; Regge poles and cuts (Reggeons) (see also 11.60 for general theory)

- Kp and πp scattering in near forward directions**See Entry 74798

12.40Q Potential models

- Symmetry basis and physical basis for many-quark system**See Entry 74729

12.40R Peripheral models (one or more particle exchange)

- The nucleon-meson coupling vertex-structure and the process for the meson exchange in nuclear force**See Entry 74859

12.40S Multiperipheral and multi-Regge models (inc. diffraction and diffractive production models)

- Rapidity distribution of shower particles in proton-nucleus interactions in emulsions at 70 GeV**See Entry 74807

12.40V Vector-meson dominance

- 74749** CFF-shell effects in VDM and the Compton sum rule. A.Nandy. *Proceedings of the VI High Energy Physics Symposium (papers in summary form only received), Mysore, India, 6-11 Dec. 1982* (Bombay, India: Dept. Atomic Energy 1982), p.61. Summary form only given. It has been recognised for some time that the traditional attempts to compare Compton cross-section to vector meson nucleon scattering through VDM fall short of the experimental results by an overall normalization factor of around 2. The author has observed that similar problems in the case of radiative decays of vector mesons can be adequately explained by considering the off-shell effects in a generalised VDM and that this formalism also predicts the total VN cross-sections satisfactorily. The author applies the off-shell corrections to the Compton process and indicates that a closer fit can be obtained to the experimental results than in traditional VDM.

12.70 HADRON MASS FORMULAS

- 74750** On a mass formula of particles in $c\bar{c}$, $b\bar{b}$ and $t\bar{t}$ families. S.N.Banerjee, A.K.Sarker (Dept. of Phys., Jadavpur Univ., Calcutta, India). *Hadronic J. (USA)*, vol.6, no.2, p.440-54 (March 1983). A mass formula containing the masses of the constituent quarks, the radii of the particles and the potential parameters for the S-states of $c\bar{c}$, $b\bar{b}$ and $t\bar{t}$ families, has been suggested in the framework of the statistical model and the computed masses compare favourably with the corresponding experimental data. (11 refs.)
- Mass spectrum of the W^+ and Z supermultiplets**See Entry 74657
- Exotic multiquark states with charm**See Entry 74740

12.90 MISCELLANEOUS THEORETICAL IDEAS AND MODELS

- Is there a desert beyond the mountains?**See Entry 74684
- Deep inelastic phenomena**See Entry 74715

13.00 SPECIFIC REACTIONS AND PHENOMENOLOGY

13.10 WEAK AND ELECTROMAGNETIC INTERACTIONS OF LEPTONS

- 74751** Recent results from PEP. R.Weinstein (Univ. of Houston, Houston, TX, USA). *AIP Conf. Proc. (USA)*, no.98, p.126-45 (1982). [received: May 1983] (Conference on Particles and Fields - 1982, College Park, MD, USA, 28-30 Oct. 1982). Recent results from PEP are presented. In electroweak interactions the measured charge asymmetries for $e\bar{e} \rightarrow \mu\bar{\mu}$, $\tau\bar{\tau}$, and $e\bar{e} \rightarrow e\bar{e}$ are reported. Results are given for lifetime measurements of the τ lepton, D^0 meson, and b quark, and measured branching ratios for the τ are given. QED tests of the electron propagator and muon compton scattering are reported. In strong interactions, measurements are reported for R, and Energy-Energy Correlation measurements of α_s are given. Flavor tagging measurements are reported, including multiplicity and α_s for samples enriched in c and b, and fragmentation functions are reported for c and for b. The results of searches are also presented for 10 postulated particles. (12 refs.)
- 74752** Experimental e^+e^- physics. D.H.Saxon (Rutherford Appleton Lab., Didcot, England). *Hadronic J. (USA)*, vol.6, no.2, p.455-622 (March 1983). Electron-positron physics at high energies is reviewed, with particular emphasis on the physics underlying the experimental methods. This report is based on lectures given at the 12th British Summer School in Theoretical Physics, and is intended to be didactic rather than comprehensive. Results are included up to September 1982. (148 refs.)
- 74753** Nonlinear effects in colliding $\gamma\gamma$ beams. Ya.T.Grinchishin, M.P.Rekalo. *Ukr. Fiz. Zh. (USSR)*, vol.28, no.5, p.781-3 (May 1983). In Russian. When a low energy, high intensity photon beam interacts with a relativistic electron beam, there appear a number of qualitative properties characterised by nonlinear effects. The maximum energy of the created photons increases due to the absorption of two (or more) initial photons. Since the effective mass of an electron in an intense EM field is larger than that of a free electron, then the maximum energy of photons due to the reverse Compton effect decreases. (8 refs.) V.G.P.

74754 Test of quantum electrodynamics and the study of heavy leptons. S.C.C.Ting (MIT, Cambridge, MA, USA). The High-Energy Limit. Proceedings of the Eighteenth Course of the International School of Subnuclear Physics, Erice, Italy, 31 July-11 Aug. 1980 (New York, USA: Plenum 1983), p.735-79. In the last decade there have been many experiments designed to test the validity of quantum electrodynamics and to study heavy leptons. In earlier days one performed experiments of the type $\gamma + A \rightarrow A + e^+ + e^-$, whereby one checked the electron propagators at small distances. These types of experiments are limited to an accuracy of $\approx 5\%$ by the lack of precise knowledge of nuclear form factors and by the difficulty in monitoring the incident photon flux. With the construction of e^+e^- and e^-e^- colliding beams, one can by-pass most of these difficulties, as there is a purely electrodynamic system (to order α^2) and one can use the low-momentum-transfer part of the interaction (as in the small-angle $e^+e^- \rightarrow e^+e^-$ process) to monitor the interaction rate and compare the large-angle (with large-momentum transfer) part of the interaction with the prediction of QED, such as angular distributions, energy dependence, etc. (31 refs.)

74755 e^+e^- physics at PETRA. P.Duinker (Nat. Inst. for Nuclear & High Energy Phys., Amsterdam, Netherlands). The High-Energy Limit. Proceedings of the Eighteenth Course of the International School of Subnuclear Physics, Erice, Italy, 31 July-11 Aug. 1980 (New York, USA: Plenum 1983), p.873-1064. Reviews the PETRA e^+e^- collider and the experiments performed there. These include QED tests, electroweak model tests, two-photon interactions, hadron jets and QCD tests. (118 refs.)

Physics in Collision. High-Energy ee/pp Interactions. Proceedings of an International Conference See Entry 74228

Electroweak effects in e^+e^- annihilations See Entry 74787

Jets at Petra See Entry 74788

Recent results from the MAC and MARK II detectors at PEP See Entry 74789

13.15 NEUTRINO INTERACTIONS

(inc. interactions involving cosmic rays)

74756 Observation of neutrino and antineutrino induced coherent neutral pion production off Al^{27} . H.Faissner, E.Frenzel, M.Grimm, T.Hansl-Kozanecka, D.Hoffmann, E.Radermacher, D.Rein, H.Reithler, U.Samm, L.M.Schgal, H.Tuchscherer, H.de Witt (III Phys. Inst., Tech. Hochschule Aachen, Aachen, Germany), M.Baldo-Ceolin, F.Fobisut, H.Huzita, M.Loret, G.Puglieri.

Phys. Lett. B (Netherlands), vol.125B, no.2-3, p.230-6 (26 May 1983). The angular distribution of isolated π^0 s, produced by ν_μ s and $\bar{\nu}_\mu$ s in the Aachen-Padova spark chamber, shows a peak in the forward direction which is not explicable by resonance production. A similar effect is seen in the acoplanarity distribution of the decay photons, which shows an excess of nearly coplanar events. A control sample containing a recoil proton shows no such peaks and is well reproduced by a resonance model. The observed effects are consistent with neutral current (NC) induced coherent single π^0 production off the entire Al^{27} nucleus. The coherent cross sections are $\sigma^+ = (29 \pm 10) \times 10^{-40}$ cm²/nucleus and $\sigma^- = (25 \pm 7) \times 10^{-40}$ cm²/nucleus. They determine the isovector axial NC coupling constant $\beta = 0.93 \pm 0.12$. No η^0 mesons were observed, which limits the corresponding isoscalar coupling constant to $\delta < 0.7$ (with 90% confidence). (17 refs.)

74757 Charged-current neutrino interactions. H.E.Fisk (Fermilab, Batavia, IL, USA), F.Sciulli.

In book: *Annual review of nuclear and particle science*. Vol.32, J.D.Jackson, H.E.Gove, R.F.Schwitters [Ed.], p.499-573. Palo Alto, CA, USA: Annual Reviews (1982), 595 pp. [0 8243 1532 4].

This article is primarily intended to review the status of the deep inelastic, charged-current scattering of neutrinos from nucleons. Processes of the form, $\nu_\mu + N \rightarrow \mu^- + X$, have been an important subject for research since such processes were found to have the profound simplicity referred to as scaling. The authors show how the general features of the scaling hypothesis follow from the assumption of nearly free quarks inhabiting the nucleon, and derive the relevant formulae from a simple, physical picture. They also briefly review the relevant properties of the neutrino, its charged-current interactions with other elementary targets, the quark model of nucleon structure, and anticipated form of the inelastic cross section, and the tests and complications of the quark model using deep inelastic data. (174 refs.)

74758 Behaviour of charged particles multiplicities in deep inelastic processes. R.P.Bajpai, Yogesh (Dept. of Phys., Pradesh Univ., Simla, India). Proceedings of the VI High Energy Physics Symposium (papers in summary form only received), Mysore, India, 6-11 Dec. 1982 (Bombay, India: Dept. Atomic Energy 1982), p.68.

Summary form only given, as follows. The almost complete absence of any scaling violations in the total charged particles multiplicities observed in neutrino processes is sought to be understood in the framework of evolution equations. The recent data on charged pion production in e^+e^- annihilation are analysed and a parametrization of fragmentation function is obtained.

No threshold-effects from QCD in deep inelastic lepton scattering See Entry 74720

Analysis of scaling violation in nucleon structure functions See Entry 74771

13.20 LEPTONIC AND SEMILEPTONIC DECAYS OF MESONS

74759 Prompt neutrino results from Fermilab. R.C.Ball, C.T.Coffin, H.R.Gustafson, L.W.Jones, M.J.Longo, T.J.Roberts, B.P.Roe, E.Wang (Univ. of Michigan, Ann Arbor, MI, USA), M.E.Duffy, G.K.Fanourakis, R.J.Loveless, D.D.Reeder, D.L.Schumann, E.Smith, M.B.Crisler, J.S.Hoftun, T.Y.Ling, T.A.Romanowski, J.T.Volk, G.Conforto, C.Castoldi, S.Childress. *AIP Conf. Proc. (USA)*, no.98, p.262-73 (1982). [received: May 1983] (Conference on Particles and Fields - 1982, College Park, MD, USA, 28-30 Oct. 1982).

Results from a Fermilab experiment to study prompt neutrino production are presented. Assuming the prompt neutrinos come from the decay of charmed mesons a total DD production cross section of approximately $20 \mu\text{b}/\text{nucleon}$, is found in good agreement with previous CERN results. They find a $\bar{\nu}/\nu$ ratio and a ν_e/ν_μ of approximately 1.0. The energy and p_T spectra of the prompt neutrinos are consistent with those expected from DD production. Limits on the production of supersymmetric particles have also been obtained. (12 refs.)

74760 Recent results from CLEO at the $\Upsilon(4s)$. S.E.Csorna (Dept. of Phys. & Astron., Vanderbilt Univ., Nashville, TN, USA).

AIP Conf. Proc. (USA), no.98, p.358-80 (1982). [received: May 1983] (Conference on Particles and Fields - 1982, College Park, MD, USA, 28-30 Oct. 1982).

Inclusive properties of B meson decays, are studied. An upper limit is placed on $|b_{\bar{u}u}/b_{\bar{c}c}| < 0.2$ from semi-leptonic decays. Non-standard models are ruled out. (17 refs.)

74761 Manifestation of the axial photon in decays of charged $K[\pi]$ mesons. L.M.Slad' (Sci.-Res. Inst. of Nuclear Phys., M.V. Lomonosov State Univ., Moscow, USSR).

Sov. Phys.-Dokl. (USA), vol.27, no.7, p.570-2 (July 1982). Translation of: *Dokl. Akad. Nauk SSSR*, vol.265, no.1-3, p.615-18 (July 1982). [received: April 1983]

The author discusses the decay $K \rightarrow \mu \nu \gamma$. The background imitation of this mode of decay arises principally from the radiative decay $K \rightarrow \mu \gamma$ in connection with possible losses of a γ quantum (of course the equipment which records the γ must possess 4π -steradian geometry). Therefore, it is very important to measure the inefficiency L_γ of the detection of the γ quanta in the entire range of their permissible energies. He analyzes the region with muon kinetic energies T_μ from 60 to 100 MeV. (9 refs.)

74762 Detecting t-quark pairs at $\bar{p}p$ colliders using transverse dilepton masses and jets. V.Barger, A.D.Martin, R.J.N.Phillips.

Report RL-83-025, Rutherford Appleton Lab., Chilton, Oxon., England (March 1983), 14 pp.

Hadronic t production with semileptonic decays of either or both t and \bar{t} quarks gives distinctive transverse-momentum correlations of electrons (or muons) and neutrinos. Multiple semileptonic modes of the $t \rightarrow b c s$ decay cascades are statistically quite probable, but explicit calculations show that they scarcely affect the $\nu\nu$ correlations. Opposite sign dileptons, coming mainly from primary semileptonic decays of t and \bar{t} together, have correlations that also reflect the t quark mass but less decisively than the $\nu\nu$ correlations. Events with large missing p_T and no identified leptons are also expected, at a rate comparable to high p_T charged leptons. Distinctive broad jet signatures are also expected for all these events, with specific correlations of the trigger lepton and jet momenta. (18 refs.)

Conference on Particles and Fields - 1982 See Entry 74201

The decay of heavy flavor states in e^+e^- annihilations See Entry 74769

13.25 HADRONIC DECAYS OF MESONS

74763 The pion-quark coupling constant and the decay of vector mesons. A.Suzuki, R.K.Bhaduri (Dept. of Phys., McMaster Univ., Hamilton, Ontario, Canada).

Phys. Lett. B (Netherlands), vol.125B, no.4, p.347-50 (2 June 1983). The decay processes of vector mesons, like $\rho \rightarrow \pi\pi$ and $\rho \rightarrow \pi\gamma$, are considered in a model where the pions couple directly with the quarks. The coupling strength extracted from such decays is shown to be consistent with theoretical estimates. (15 refs.)

74764 Why most flavor dependence predictions for nonleptonic charm decays are wrong. H.J.Lipkin (Fermi Nat. Accelerator Lab., Batavia, IL, USA).

The High-Energy Limit. Proceedings of the Eighteenth Course of the International School of Subnuclear Physics, Erice, Italy, 31 July-11 Aug. 1980 (New York, USA: Plenum 1983), p.389-413.

The discovery of charmed particles with many open channels for nonleptonic decays has provided a new impetus for a theoretical understanding of these decay processes. The GIM current provides a well defined weak hamiltonian, which can justifiably be used to first order. The QCD approach to strong interactions gives flavor-independent couplings and flavor symmetry broken only by quark masses. In a model with n generations of quarks and $2n$ flavors, a flavor symmetry group $SU(2n)$ can be defined which is broken only by H_{weak} and the quark masses. Here again, the same two approaches of symmetry and dynamics have been used. However, both types of treatment tend to consider only the symmetry properties or dominant diagrams of the weak interaction, including some subtle effects, while overlooking rather obvious effects of strong interactions. This leads to incorrect predictions. (16 refs.)

Can $\delta(980,0^+)$ be a broad $qq\bar{q}\bar{q}$ state? See Entry 74732

Recent results from PEP See Entry 74751

13.30 DECAYS OF BARYONS

74765 Proton decay experiment in the Kolar Gold Fields. M.R.Krishnaswamy, M.G.K.Menon, N.K.Mondal, V.S.Narasimham, B.V.Sreekantan (Tata Inst. of Fundamental Res., Bombay, India), Y.Hayashi, N.Ito, S.Kawakami, S.Miyake.

AIP Conf. Proc. (USA), no.96, p.168-74 (1982). [received: May 1983] (Workshop on Science Underground, Los Alamos, CA, USA, 1982).

In total 6 events of special type have been recorded so far in the Kolar Gold Fields experiment. Out of them, three events are fully confined to the detector volume. It is shown that their characteristics are in conformity with the decay of bound nucleons and the background due to neutrino interactions is extremely small. Based on these events, it is suggested that a mean lifetime of protons is about 8×10^{30} years. (4 refs.)

74766 The Mont Blanc experiment on nucleon stability. G.Battistoni (Lab. Nazionali, INFN, Frascati, Italy), E.Bellotti, G.Bologna, P.Campagna, C.Castagnoli, V.Chiarella, D.C.Cundy, B.D'Ettorre Piazzoli, E.Fuorini, E.Iarocci, G.Mannocchi, G.P.Murtas, P.Negri, G.Nicoletti, G.Mannocchi, G.P.Murtas, P.Negri, G.Nicoletti, P.Picchi, M.Price, A.Pullia, S.Ragazzi, M.Rollier, O.Saavedra, L.Trasatti, L.Zanotti.

AIP Conf. Proc. (USA), no.98, p.19-23 (1982). [received: May 1983] (Conference on Particles and Fields - 1982, College Park, MD, USA, 28-30 Oct. 1982).

The Mont Blanc experiment has recorded four fully contained events with at least a 10 cm track in iron. Two events have a single track interpreted as a muon due to a quasi elastic neutrino interaction with a total visible energy around 400 MeV. The third one is a neutrino inelastic interaction of ~ 1.5 GeV energy. The fourth event, whose energy is around 1 GeV, cannot be easily identified as a neutrino. In order to study the possibility that this event is due to an inelastic interaction of a ν the authors have analysed 400 neutrino events collected in a calibration test performed at CERN, exposing a part of the final detector to an unfocused ν beam which simulated the expected spectrum of atmospheric neutrinos. (4 refs.)

74767 The effective proton lifetime and non-exponential decay. G.N.Fleming (Dept. of Phys., Pennsylvania State Univ., University Park, PA, USA).

Phys. Lett. B (Netherlands), vol.125B, no.4, p.287-90 (2 June 1983). Noting that in GUT models protons must be in the very early stage of the decay process. The author establishes a lower bound on the observable effective lifetime, depending on the ratio of the RMS deviation of the proton energy spectrum to the theoretically calculated width. He finds that if this ratio ranges from $10^{10 \pm 1}$ to 1, the lower bound on the effective lifetime climbs from $10^{30 \pm 2}$ yr to $10^{50 \pm 2}$ yr. He also argues that if protons are to avoid a form of kinematical fragmentation for one theoretical lifetime, then the effective lifetime for present-day protons is longer than 10^{36} yr. (9 refs.)

74768 Certain rare hypernuclear decays. V.A.Lyul'ka. *Ukr. Fiz. Zh. (USSR)*, vol.28, no.5, p.649-55 (May 1983). In Russian. Hypernuclear decays with production of γ -quanta as well as Dalitz pairs induced by the radiative and conversion decays of Λ -particles ($\Lambda \rightarrow n + \gamma$ and $\Lambda \rightarrow n + e^+ + e^-$, respectively) are discussed. The hypernuclei are considered to be useful for the investigation of these decays because in this case charged particles will take part in hypernuclear decays. Besides, nuclear spin selection rules are available restricting the number of form factors in a matrix element. Decays with production of several nuclei and nucleons can manifest an appreciable effect of the strong final-state interaction. The hypernuclear decays with production of leptons and π -mesons are briefly discussed as well. (19 refs.)

74769 The decay of heavy flavor states in e^+e^- annihilations. T.A.Ferguson (Lab. of Nuclear Studies, Cornell Univ., Ithaca, NY, USA). Physics in Collision. High-Energy $ee/pp/pp$ Interactions. Proceedings of an International Conference, Stockholm, Sweden, 2-4 June 1982 (New York, USA: Plenum 1983), p.387-403

The author reviews the recent results from e^+e^- experiments on the weak decays of particles containing charm or beauty. (35 refs.)

74770 Experiment to detect proton decay and neutrino oscillations (using cosmic ray neutrino events). D.B.Cline (Fermilab, Batavia, IL, USA). The High-Energy Limit. Proceedings of the Eighteenth Course of the International School of Subnuclear Physics, Erice, Italy, 31 July-11 Aug. 1980 (New York, USA: Plenum 1983), p.307-42

A large water Cherenkov detector is being constructed in a deep mine at Park City, Utah by a collaboration of Harvard, Purdue and Wisconsin physicists. The purpose of the detector is to observe proton or bound neutron decay to lifetimes of 0.7×10^{33} years. The detector is designed to be sensitive to several decay modes of the proton and to suppress the backgrounds that are naturally associated with cosmic ray muon and neutrino interactions in the walls of the mine or the overburden of the site. (8 refs.)

Theoretical predictions for baryon number violation See Entry 74666

The proton decay—magnetic monopole connection See Entry 74668

Supersymmetric grand unification See Entry 74685

Use of final-energy sum rules to describe baryon properties in quantum chromodynamics and to estimate the proton lifetime in the SU(5) model See Entry 74718

Nussex experiment and the future of the Mont Blanc laboratory See Entry 75225

IMB detector—the first 30 days See Entry 75226

The Harvard-Purdue-Wisconsin baryon decay experiment at Park City, Utah .. See Entry 75227

The Soudan nucleon decay experiments See Entry 75228

A proton decay and solar neutrino experiment with a liquid argon Time Protection Chamber See Entry 75230

13.35 DECAYS OF LEPTONS

Recent results from PEP See Entry 74751

13.40 ELECTROMAGNETIC PROCESSES AND PROPERTIES

13.40D Electromagnetic mass differences

Can $\delta(980, 0^+)$ be a broad $qq\bar{q}\bar{q}$ state? See Entry 74732

13.40F Electromagnetic form factors; electric and magnetic moments

74771 Analysis of scaling violation in nucleon structure functions. V.V.Ammosov, V.A.Gapienko, G.S.Gapienko, A.G.Denisov, V.G.Zaets, V.I.Klyukhin, V.I.Koreshev, P.V.Pitukhin, V.I.Sirotenko, E.A.Slobodyuk, Z.U.Usubov, P.A.Gorichev, V.I.Efremenko, S.P.Kruchinin, M.A.Kubantsev, I.V.Makhlyueva, A.V.Fedotov, V.I.Shekelyan, J.P.Berge, D.Bogert, J.Malko, F.A.Nezrick, R.Orava, R.Hanft, R.Endorf (Inst. of High-Energy Phys., USSR).

JETP Lett. (USA), vol.36, no.8, p.367-71 (20 Oct. 1982). Translation of: *Pis'ma v Zh. Eksp. & Teor. Fiz. (USSR)*, vol.36, no.8, p.300-4 (20 Oct. 1982). [received: June 1983]

Some new measurements of the nucleon structure functions F_2 and xF_3 have been carried out in an antineutrino experiment with a 15-foot bubble chamber. The structure functions are analyzed. The scaling violation in xF_3 can be described by quantum-chromodynamics effects with the scaling parameter $\Lambda_{QCD} \approx 0.3$ GeV and also by higher-twist effects. (10 refs.)

74772 Structure functions of relativistic systems composed of two spin $1/2$ particles. A.D.Linkevich, V.I.Savrin, N.B.Skachkov (Joint Inst. for Nuclear Res., Dubna, USSR).

Theor. & Math. Phys. (USA), vol.53, no.1, p.955-62 (Oct. 1982). Translation of: *Teor. & Mat. Fiz. (USSR)*, vol.53, no.1, p.20-31 (Oct. 1982).

Expressions are obtained for the structure functions of mesons in terms of the solutions of a covariant two-particle equation for the spin wave function of the system. (21 refs.)

74773 Electric-dipole moments of particles. N.F.Ramsey (Mount Holyoke Coll., South Hadley, MA, USA).

In book: *Annual review of nuclear and particle science*. Vol.32, J.D.Jackson, H.E.Gove, R.F.Schwitters [Ed.], p.211-33. Palo Alto, CA, USA: Annual Reviews (1982), 595 pp. [0 8243 1532 4]

Experimental measurements and theoretical predictions of electric-dipole moments are possible for many different particles, including neutrons, protons, electrons, muons, and hyperons, but the most sensitive tests of theories have

so far come from the neutron. The reason for this is the neutron's zero electric charge. (118 refs.)

74774 Magnetic moments of the ground state baryons. M.Gupta, N.Kaur (Dept. of Phys., Panjab Univ., Chandigarh, India). Proceedings of the VI High Energy Physics Symposium (papers in summary form only received), Mysore, India, 6-11 Dec. 1982 (Bombay, India: Dept. Atomic Energy 1982), p.55

Summary form only given, as follows. Baryon magnetic moments are calculated in the harmonic oscillator quark model incorporating: (i) a natural mass scale for quarks, taken as one-third of the nucleon mass for u and d quarks and the strange quark mass suggested by Lipkin's sum rule $m_u = m_d = m_{\Lambda} - m_p$, (ii) a minimal nontrivial mixing, viz., $|8^{1/2}_2\rangle = \cos\phi/(56.0^+)^{N=0} + \sin\phi/(70.0^+)^{N=2}$ and (iii) replacement of Pauli spinors by Dirac spinors for including relativistic corrections. In the parameter free non-relativistic limit, the authors find an excellent fit which gets further improved in the relativistic case.

74775 Magnetic moments in quark-diquark model. R.C.Verma (Dept. of Phys., Kumaun Univ., Naini Tal, India). Proceedings of the VI High Energy Physics Symposium (papers in summary form only received), Mysore, India, 6-11 Dec. 1982 (Bombay, India: Dept. Atomic Energy 1982), p.56

Summary form only given. In recent years, improved measurements of the hyperon moments have become available. The naive quark model does not yield complete agreement with the data. In particular low Σ^+ and large Ξ^- moments seem to require additional effects either in electromagnetic Hamiltonian or in the baryon wave functions. The author studies SU(6) breaking effects on baryon moments in the framework of quark-diquark model. SU(6) symmetry of the wave function is broken by assigning different probability to spin triplet and singlet diquarks, which can be controlled through a mixing angle. The author finds that such DH(6) breaking leads to nice agreement between theory and experiment. The author also observes that similar results also follow with wave functions modified due to quark-quark interaction mediated by gluon exchange.

Deep inelastic phenomena See Entry 74715

What can we count on? A discussion of constituent-counting rules for interactions involving composite systems See Entry 74722

Deep inelastic muon hadron interactions See Entry 74776

A review of two-photon physics See Entry 74829

13.40H Electromagnetic decays

CFF-shell effects in VDM and the Compton sum rule See Entry 74749

Observation of neutrino and antineutrino induced coherent neutral pion production off Al^{27} See Entry 74756

Manifestation of the axial photon in decays of charged $K[\pi]$ mesons See Entry 74761

The pion-quark coupling constant and the decay of vector mesons See Entry 74763

Certain rare hypernuclear decays See Entry 74768

13.40K Electromagnetic corrections to strong and weak interaction processes

Weak symmetry breaking by radiative corrections in broken supergravity See Entry 74356

A note on supersymmetry breaking in 1+1 dimensions See Entry 74651

Electroweak effects in e^+e^- annihilations See Entry 74787

13.60 PHOTON AND CHARGED-LEPTON INTERACTIONS WITH HADRONS

(for neutrino interactions, see 13.15)

Physics in Collision. High-Energy $ee/pp/pp$ Interactions. Proceedings of an International Conference See Entry 74228

High-energy hadrons produced by cosmic-ray muons in the earth as a source of background in proton-decay experiments See Entry 74823

13.60F Elastic and Compton scattering

CFF-shell effects in VDM and the Compton sum rule See Entry 74749

13.60H Total and inclusive cross sections

(inc. deep-inelastic processes)

74776 Deep inelastic muon hadron interactions.

AIP Conf. Proc. (USA), no.98, p.402-11 (1982). [received: May 1983] (Conference on Particles and Fields - 1982, College Park, MD, USA, 28-30 Oct. 1982).

Recent results in muon scattering from the EMC collaboration are presented on the fragmentation properties of quarks and the jet structure of deep inelastic interactions. The measurement of the structure function ratio $R = \sigma_L/\sigma_T$ is reported and also the new result of a measurement of the ratio $F_2^{(n)}(\text{Fe})/F_2^{(n)}(\text{D})$ which shows a totally unexpected behaviour as a function of x. (19 refs.)

74777 Spin correlation in $ep \rightarrow e\Lambda X$ scattering. M.Rafat, R.Ramachandran, I.I.T.Kanpur.

Proceedings of the VI High Energy Physics Symposium (papers in summary form only received), Mysore, India, 6-11 Dec. 1982 (Bombay, India: Dept. Atomic Energy 1982), p.73

Summary form only given. Perturbative ACD is used to predict the polarization of Λ produced in electron scattering from polarized proton. The asymmetry in valence and sea polarization inside polarized proton is estimated from constraints resulting from Altarelli-Parisi equations. Quark fragmentation into Λ is extracted from e^+e^- data. The authors' results indicate a definite and substantial correlation in proton and Λ polarizations.

74778 Lepton-hadron inclusive scattering and QCD. J.Steinberger (CERN, Geneva, Switzerland).

The High-Energy Limit. Proceedings of the Eighteenth Course of the International School of Subnuclear Physics, Erice, Italy, 31 July-11 Aug. 1980 (New York, USA: Plenum 1983), p.781-807

One of the most important developments in physics in the last decade is the evolution of a serious pretender to theory of strong interactions, Quantum Chromodynamics (QCD). In principle, the theory encompasses all strong interaction phenomena, however, at present, quantitative predictions are possible only for a limited number of experimental domains. The most quantitative predictions of QCD are still those for lepton-hadron inclusive scattering. The status of the comparison of the theory with experiment is reviewed. (17 refs.)

No threshold-effects from QCD in deep inelastic lepton scattering See Entry 74720

Polarized single pion photoproductions test for various quark models See Entry 74780

13.60K Meson production

74779 Pion production at large p_T in photon-deuteron collisions. T.Chandramohan (Dept. of Theoretical Phys., Univ. of Madras, Madras, India). Proceedings of the VI High Energy Physics Symposium (papers in summary form only received), Mysore, India, 6-11 Dec. 1982 (Bombay, India: Dept. Atomic Energy 1982), p.63

Summary form only given. Inclusive production of pions at large transverse momentum in photon-deuteron collisions is studied with an aim of revealing the six-quark content of the deuteron.

74780 Polarized single pion photoproductions test for various quark models. P.Nath, M.Gupta, M.P.Khanna (Dept. of Phys., Panjab Univ., Chandigarh, India).

Proceedings of the VI High Energy Physics Symposium (papers in summary form only received), Mysore, India, 6-11 Dec. 1982 (Bombay, India: Dept. Atomic Energy 1982), p.78

Summary form only given. The multipole analysis of resonance photocouplings of Babcock and Rosner is extended to the case of single-pion photoproduction by polarized photons. The various polarized cross-sections, polarized target asymmetry, polarized photon asymmetry, and recoil nucleon polarization are evaluated. The present analysis is exploited for discriminating different quark models which predict photocouplings of nonstrange baryon resonances. The analysis provides a viable approach for bringing out, in a fairly model independent manner, the finer distinctions of various models some of which incorporate relativistic and chromodynamic effects.

13.60P Baryon and baryon resonance production

S_{Pin} correlation in $ep \rightarrow e\Lambda X$ scattering See Entry 74777

Structure functions for the electrodisintegration of the deuteron at a momentum transfer of 1.8 GeV² See Entry 74963

13.65 HADRON PRODUCTION BY ELECTRON-POSITRON COLLISIONS

74781 Recent results from PETRA. A.Wagner (Phys. Inst., Univ. Heidelberg, Heidelberg, Germany).

AIP Conf. Proc. (USA), no.98, p.103-25 (1982). [received: May 1983] (Conference on Particles and Fields - 1982, College Park, MD, USA, 28-30 Oct. 1982).

Recent results from PETRA on the measurement of the total hadronic cross section of the strong coupling constant α_s and of the gluon spin are presented. The observation of a 4-jet structure is reported. Measurements of the interference of electromagnetic and weak interactions and of the parameters of the weak neutral current are reviewed. (31 refs.)

74782 Recent results in T spectroscopy from CESR. R.D.Schamberger, Jr. (State Univ. of New York, Stony Brook, NY, USA).

AIP Conf. Proc. (USA), no.98, p.381-401 (1982). [received: May 1983] (Conference on Particles and Fields - 1982, College Park, MD, USA, 28-30 Oct. 1982).

The author presents recent results in T spectroscopy from CESR. Primary emphasis in the past year in the area of spectroscopy has centered on the decay modes of the $T^*(3^3S_1)$. Hadronic transitions to both lower lying S states have been measured. Photon transitions to the 2^3P states have been observed in both inclusive and exclusive channels. Branching ratios and parameters of the 2^3P states will be presented. Limits on other states in the T system, accessible through e^+e^- annihilations, and results on an axion search are also reported. (45 refs.)

74783 The influence of fragmentation models on the determination of the strong coupling constant in e^+e^- annihilation into hadrons. H.J.Behrend, C.Chen, H.Fenner, M.J.Schachter, V.Schroder, H.Sindt (DESY, Hamburg, Germany), G.D'Agostini, W.D.Apel, S.Banerjee, J.Bodenkamp, D.Chrobaczek, J.Engler, G.Flugge, D.C.Fries, W.Fues, K.Gamerding, G.Hopp, H.Kuster, H.Muller, H.Randoll, G.Schmidt, H.Schneider, W.De Boer, G.Buschhorn, G.Grindhammer, P.Grosse-Wiesmann, B.Gunderson, C.Kiesling, R.Kotthaus, U.Kruse, H.Lierl, D.Luers, H.Oberlack, P.Schacht, P.Colas, A.Cordier, M.Davies, D.Fournier, J.F.Grivaz, J.Haissinski, V.Journe, A.Klarsfeld, F.Laplanche, F.Le Diberder, U.Mallik, J.J.Viellet, J.H.Field, R.George, M.Goldberg, B.Grossetete, O.Hamon, F.Kapusta, F.Kovacs, G.London, L.Poggioli, M.Rivoal, R.Aleksan, J.Bouchez, G.Carnesecchi, G.Cozzika, Y.Ducros, A.Gaidot, S.Jadach, Y.Lavagne, J.Pamela, J.P.Pansart, F.Pierre. Nucl. Phys. B, Part. Phys. (Netherlands), vol.B218, no.2, p.269-88 (6 June 1983).

Hadronic events obtained with the CELLO detector at PETRA were compared with first-order QCD predictions using two different models for the fragmentation of quarks and gluons, the Hoyer model and the Lund model. Both models are in reasonable agreement with the data, although they do not completely reproduce the details of many distributions. Several methods have been applied to determine the strong coupling constant α_s . Although within one model the value of α_s varies by 20% among the different methods, the values determined using the Lund model are 30% or more larger (depending on the method used) than the values determined with the Hoyer model. (21 refs.)

74784 Hadronic final states in e^+e^- annihilation. Recent results from TASSO. J.Proudfoot.

Report RL-83-031, Rutherford Appleton Lab., Chilton, Oxon., England (April 1983), 28 pp.

Measurements of charged and neutral hadron production in e^+e^- annihilation are presented. Some comparisons with theoretical predictions are given. (25 refs.)

74785 The hydrodynamic model description of e^+e^- hadrons and the contribution of the simple wave regions. A.Biswas, T.De (Saha Inst. of Nuclear Phys., Calcutta, India).

Proceedings of the VI High Energy Physics Symposium (papers in summary form only received), Mysore, India, 6-11 Dec. 1982 (Bombay, India: Dept. Atomic Energy 1982), p.60

Summary form only given. In the light of recent interest in and the success of hydro-dynamic model (Banerjee et al., 1981) in explaining the various features of hadronic e^+e^- annihilation, the contribution of the 'simple wave' regions which have been neglected in the previous works have been reanalysed. In the present work the authors have studied the number of particles and the amount of energy carried away by the 'simple wave' parts of the hadronic fireball system. They have also pointed out some errors in the earlier estimates. Their investigations show that the fraction of particle number contained in these regions is approximately 15-20% at the available range of c.m. energies in colliding beam machines. (2 refs.)

74786 Analysis of the energy weighted angular correlations in hadronic annihilations at 22 and 34 GeV.

Proceedings of the VI High Energy Physics Symposium (papers in summary form only received), Mysore, India, 6-11 Dec. 1982 (Bombay, India: Dept. Atomic Energy 1982), p.130

Measurements of energy weighted angular correlations in electron positron annihilations at cm energies of 22 GeV and 34 GeV are presented. The data are compared with perturbative QCD predictions. The theoretical predictions which refer to the partons describe the data reasonably well, depending on the approximations chosen. The effective strong coupling constant, α_s , has been determined with a method which is expected to be insensitive to fragmentation effects. Nonetheless, the values obtained shows a strong variation depending on the fragmentation model assumed. At large acollinearity angles QCD calculations going beyond the Leading Double Log approximation appear to be quite successful in describing the data. The agreement is improved when the smearing effect of heavy resonance decay is taken into account.

74787 Electroweak effects in e^+e^- annihilations. B.Naroska (DESY, Hamburg, Germany).

Physics in Collision. High-Energy ee/pp Interactions. Proceedings of an International Conference, Stockholm, Sweden, 2-4 June 1982 (New York, USA: Plenum 1983), p.213-31

The author reports on the evidence of electroweak interference effects in e^+e^- interactions. Data come mainly from 4 experiments at PETRA, namely CELLO, JADE, MARK J, and TASSO. (17 refs.)

74788 Jets at Petra. H.Oberlack (Max-Planck-Inst. fur Phys. & Astrophys., Werner-Heisenberg-Inst. fur Phys., München, Germany).

Physics in Collision. High-Energy ee/pp Interactions. Proceedings of an International Conference, Stockholm, Sweden, 2-4 June 1982 (New York, USA: Plenum 1983), p.233-72

The hadronic final state of e^+e^- reactions has provided a fruitful testing ground for QCD predictions, on quark pair production and colour radiative processes. In particular, the study of the topology of this final state in terms of jet production and their properties now leads to a certain amount of commonly accepted facts: quarks have spin 1/2, are pointlike down to distances of 10^{-16} cm, and are produced in oppositely charged pairs; coloured gluons are needed to reproduce the observed features of the data, are vector particles, and are produced according to a Bremsstrahlung spectrum. With increased statistics and improved experimental techniques, more refined studies are under way; and more and more detailed results become available. The author reviews result of analyses on parton formation and fragmentation in multi-hadronic final states which have become available very recently, from the five detectors at PETRA. (46 refs.)

74789 Recent results from the MAC and MARK II detectors at PEP. J.Dorfan (Stanford Linear Accelerator Center, Stanford Univ., Stanford, CA, USA).

Physics in Collision. High-Energy ee/pp Interactions. Proceedings of an International Conference, Stockholm, Sweden, 2-4 June 1982 (New York, USA: Plenum 1983), p.273-302

All the PEP data presented were taken at $E_{cm} = 29$ GeV. Topics covered are the total hadronic cross section, inclusive momentum distributions, energy-energy correlations and thereby a measure of α_s , the observation of D^* 's and a measurement of the charm fragmentation function, τ charged particle branching fractions, measurement of the τ lifetime and a search for charged, spin 0 scalars. (32 refs.)

74790 Some recent results in e^+e^- physics in the US. C.W.Peck (California Inst. of Technol., Pasadena, CA, USA).

The High-Energy Limit. Proceedings of the Eighteenth Course of the International School of Subnuclear Physics, Erice, Italy, 31 July-11 Aug. 1980 (New York, USA: Plenum 1983), p.809-38

Discusses several important results that have been reported from CESR and SPEAR. The author reports the recent results from Cornell on $b\bar{b}$ spectroscopy, those from SPEAR on $\bar{c}c$ spectroscopy, and only one new result from the Crystal Ball relating to charmed mesons. (30 refs.)

74791 A study of e^+e^- annihilation into hadrons in the 1400-2200 MeV energy range with the magnetic detector DM1 at DCI: observation and study of a ϕ' vector meson. J.Perez-y-Jorba (Lab. de l'Accelérateur Lineaire, Orsay, France).

The High-Energy Limit. Proceedings of the Eighteenth Course of the International School of Subnuclear Physics, Erice, Italy, 31 July-11 Aug. 1980 (New York, USA: Plenum 1983), p.839-71

The e^+e^- annihilation into hadrons has been studied for $1.4 < \sqrt{s} < 2.2$ GeV. The total integrated luminosity was 1500 nb^{-1} over the whole energy range. Accurate magnetic analysis of charged particle momenta allowed a constrained kinematical reconstruction of events with at most one neutral missing. Cross-sections are given for production of the following exclusive channels: $\pi^+\pi^+\pi^-\pi^-$ (including $\rho^0\pi^+\pi^-$), $\pi^+\pi^-\pi^+\pi^-\pi^0$ (including $\omega\pi^+\pi^-$), $K^+K^-, K_S^0K_L^0, K_S^0K^+\pi^-, K_S^0K^-\pi^+$ (including K^*K), $K^+K^-\pi^+\pi^-$ (including $K^*K\pi$). The only inclusive result concerns the production of K_S^0 . The $\rho'(1.55)$ is observed in the $4\pi^0$ channel with high statistics. A small bump in the $\omega\pi^+\pi^-$ channel is observed near 1.65 GeV with a height 6.7 standard deviation above background. The rather high cross-section $KK\pi$ production in the same region and the dynamics of this channel, exhibiting an $I=0, I=1$ interference, show that this bump is due to a new ϕ' vector meson rather than to an ω' . This new ϕ' (1.65 GeV) has a 150 MeV width and decays mainly in KK^* . (19 refs.)

| | |
|---|-----------------|
| Conference on Particles and Fields - 1982 | See Entry 74201 |
| Physics in Collision. High-Energy ee/ep/pp Interactions. Proceedings of an International Conference | See Entry 74228 |
| The High-Energy Limit. Proceedings of the Eighteenth Course of the International School of Subnuclear Physics | See Entry 74229 |
| QCD and the space-time evolution of high-energy e^+e^- , pp, and heavy ion collisions | See Entry 74724 |
| Experimental e^+e^- physics | See Entry 74752 |
| e^+e^- physics at PETRA | See Entry 74755 |
| Behaviour of charged particles multiplicities in deep inelastic processes | See Entry 74758 |
| Recent results from CLEO at the $\Upsilon(4s)$ | See Entry 74760 |
| Prospects for polarized electrons at high energies | See Entry 74825 |

13.75 HADRON-INDUCED LOW- AND INTERMEDIATE-ENERGY REACTIONS AND SCATTERING, ENERGY ≤ 10 GEV
(for higher energies, see 13.85)

| | |
|--|-----------------|
| Massive lepton pair production—what has QCD done to the classical Drell-Yan model? | See Entry 74716 |
| CFF-shell effects in VDM and the Compton sum rule | See Entry 74749 |

13.75C Nucleon-nucleon interactions, including antinucleon, deuteron, etc. (energy ≤ 10 GeV)
(for N-N interactions in nuclei, see 21.30)

| | |
|--|-----------------|
| 74792 The free NN interaction, 50-1000 MeV. D.V.Bugg (Queen Mary Coll., London, England). AIP Conf. Proc. (USA), no.97, p.1-19 (1982). [received: May 1983] (Proceedings of the Workshop on the Interaction Between Medium Energy Nucleons in Nuclei, Bloomington, IN, USA, 28-30 Oct. 1982). Phase shift solutions for pp elastic scattering are unique up to 800 MeV, and for np up to 500 MeV. There is excellent agreement between three analyses for all phase shifts δ and for elasticity parameters η of dominant inelastic partial waves (1D_2 , 3F_3 and 3P_2). For low partial waves, notably 3P_0 , 3P_1 and 3S_0 , there are some disagreements about η parameters, reflecting insensitivity of elastic data and some discrepancies amongst experiments. The need for further data is reviewed. Amplitudes for np—pn between 140 and 500 MeV are known accurately from phase shift analysis, and are almost purely real; they are useful for extracting nuclear matrix elements from (p,n) reactions. The Paris potential is the best potential model fit to data up to 425 MeV, but there are some small systematic discrepancies with data. (44 refs.) | |
| 74793 Energy dependence of spin-spin correlation parameters in large-angle pp-scattering. S.M.Troshin, N.E.Tyurin (Inst. for High Energy Phys., Moscow, USSR). Hadronic J. (USA), vol.6, no.2, p.259-77 (March 1983). A three-dimensional dynamic equation in quantum field theory for the scattering amplitude is used to analyse large-angle pp scattering with account for all spin components. The expressions are obtained for the spin-spin correlation parameters $A_{nn}(\pi/2)$ and $A_{ll}(\pi/2)$ which reveal oscillations with s. Such a behaviour allows one to understand the experimental results obtained at ZGS energies. The asymptotic values of the parameters $A_{nn}(\pi/2)$ and $A_{ll}(\pi/2)$ appear to be 1/3 and -1/3, respectively. (10 refs.) | |
| 74794 Charge asymmetry in the emission of direct electrons in pp interactions at 2.0 GeV/c. S.Banerjee, S.N.Ganguli, A.Gurtu, P.K.Malhotra, R.Raghavan, A.Subramanian, K.Sudhaker (Tata Inst. of Fundamental Res., Bombay, India). Proceedings of the VI High Energy Physics Symposium (papers in summary form only received), Mysore, India, 6-11 Dec. 1982 (Bombay, India: Dept. Atomic Energy 1982), p.132 A certain amount of charge asymmetry in the number of identified electrons and positrons seen to emerge from the reaction vertices of pp at 2.0 GeV/c in a hydrogen bubble chamber is reported. This charge asymmetry cannot be ascribed to any instrumental effect or the electromagnetic decays of known mesons. | |
| Proceedings of the Workshop on the Interaction Between Medium Energy Nucleons in Nuclei | See Entry 74200 |
| Coupled channels and quarks in nucleon-nucleon scattering | See Entry 74850 |
| Quarks, bags and the nucleon-nucleon interaction | See Entry 74856 |
| Relativistic Brueckner-Hartree-Fock theory: theoretical foundations and empirical evidence | See Entry 74880 |

13.75E Hyperon-nucleon interactions (energy ≤ 10 GeV)

| | |
|---|-----------------|
| 74795 Optimised polynomial expansion and phase shift analysis of Λ -p scattering. S.Mohanty (Dept. of Phys., Utkal Univ., Bhubaneswar, India), J.K.Mohapatra. Proceedings of the VI High Energy Physics Symposium (papers in summary form only received), Mysore, India, 6-11 Dec. 1982 (Bombay, India: Dept. Atomic Energy 1982), p.71 Summary form only given. The analytic cut t-plane of the helicity amplitudes of Λ -p scattering is mapped into the interior of an ellipse. The helicity amplitudes are then expressed as optimised polynomial expansions (OPE) in the mapped variable with the aim to exploit the capacity of OPE to store information. A fixed energy phase shift analysis is then performed using a few phase shifts and coupling constants as inputs to determine the parameters of the suitably truncated expansion. The parameters of the helicity amplitudes for higher j values, excited at that energy, are then reliably predicted, exhibiting a definite economy in the number of free parameters used by earlier workers for such phase shift analysis of Λ -p scattering. | |
| A-N interaction and the structure of ^4He , ^4H , ^3He and ^3H | See Entry 74894 |

13.75G Pion-baryon interactions (energy ≤ 10 GeV)

| | |
|--|-----------------|
| 74796 Evidence for glueballs. S.J.Lindenbaum (Brookhaven Nat. Lab., Upton, NY, USA). AIP Conf. Proc. (USA), no.98, p.218-46 (1982). [received: May 1983] (Conference on Particles and Fields - 1982, College Park, MD, USA, 28-30 Oct. 1982). This paper describes the observation and partial wave analysis of 1203 (22 GeV) $\pi^-p \rightarrow \phi\phi n$ events. This is an OZI suppressed channel in which the OZI suppression is found to be absent. Assuming QCD and the OZI rule as Ansatz, it is concluded that the breakdown of the OZI suppression is due to glueballs. The $g_{\pi}(2160)$ and the $g_{\pi}(2320)$ with $I^0J^{PC}=0^{++}2^{++}$ are two resonances determined from the partial wave analysis. It is concluded that one or two primary glueballs with the above quantum numbers are responsible for the observed two states. A brief discussion of other glueball candidates and some relevant phenomenology is also included. (34 refs.) | |
| 74797 Spin-rotation measurements in $\pi p \rightarrow K^0\Lambda$. K.W.Bell, J.A.Blissett, T.A.Broome, H.M.Daley, J.C.Hart, A.L.Lintern, R.Maybury, A.G.Parham, B.T.Payne, D.H.Saxon, T.G.Walker, J.B.Whittaker. Report RL-83-005, Rutherford Appleton Lab., Chilton, Oxon., England (March 1983), 39 pp. The first measurements of spin-rotation in meson-baryon scattering in the resonance region are presented. These measurements, for the reaction $\pi^-p \rightarrow K^0\Lambda$, confirm the main predictions of a previous partial-wave analysis. Comments are made on resonant couplings in the reaction $\pi^-p \rightarrow K^0\Lambda$. (26 refs.) | |
| Kp and πp scattering in near forward directions | See Entry 74798 |
| Off-energy shell scattering of pions on deuterons | See Entry 75054 |

13.75J Kaon-baryon interactions (energy ≤ 10 GeV)

| | |
|---|--|
| 74798 Kp and πp scattering in near forward directions. C.Savitri, P.K.Patnaik (Dept. of Phys., Sambalpur Univ., Sambalpur, India), R.C.Badatya. Proceedings of the VI High Energy Physics Symposium (papers in summary form only received), Mysore, India, 6-11 Dec. 1982 (Bombay, India: Dept. Atomic Energy 1982), p.68 Summary form only given. An analytic parametrisation procedure earlier applied to pp scattering is applied to Kp and πp scattering. In contrast to the pp case the procedure here is valid for non-forward directions also. Within the scope of P+f model and pomeron is assumed to be built out of s-channel branch cuts. The branch cuts are parametrised through conformal mapping and polynomial expansion methods. Theorems on high energy bounds are used to obtain the final result. The result is compared with experiment. | |
|---|--|

13.75L Meson-meson interactions (energy ≤ 10 GeV)

| | |
|---|-----------------|
| Low energy theorems as precision tests of QCD | See Entry 74721 |
|---|-----------------|

13.85 HADRON-INDUCED HIGH- AND SUPER-HIGH-ENERGY INTERACTIONS, ENERGY > 10 GEV
(for low energies, see 13.75)

| | |
|---|--|
| 74799 Growth of $\langle p_{\perp} \rangle$ with multiplicity at the collider energy and a two-component model for pp collision. H.Banerjee, T.De, D.Syam (Saha Inst. of Nuclear Phys., Calcutta, India). Proceedings of the VI High Energy Physics Symposium (papers in summary form only received), Mysore, India, 6-11 Dec. 1982 (Bombay, India: Dept. Atomic Energy 1982), p.59 Summary form only given. The recent observation (G. Arison et al., 1982) at the pp collider of the growth of $\langle p_{\perp} \rangle$ per particle with the multiplicity of secondaries in each event admits of a simple interpretation in the two-component model proposed by the authors (1982). According to this model events with large multiplicity correspond to the situation where more energy is pumped into the central fireball and less to the leading cluster. The $\langle p_{\perp} \rangle$ of secondaries emanating from the central fireball, which hadronizes hydrodynamically, grows with the energy of the fireball. The growth of multiplicity of secondaries from the central fireball has the typical power dependence $(W^{1/2})$ on the energy content of the fireball. Thus in this model there is direct correlation of the multiplicity of an event with $\langle p_{\perp} \rangle$ per particle. (2 refs.) | |
| 74800 Characteristics of high energy proton-deuteron interactions—an investigation of the space-time structure. D.Ghosh, L.Chatterjee, J.Roy, K.Basu Chowdhury, K.Sengupta, S.Nahan (Dept. of Phys., Jadavpur Univ., Calcutta, India). Proceedings of the VI High Energy Physics Symposium (papers in summary form only received), Mysore, India, 6-11 Dec. 1982 (Bombay, India: Dept. Atomic Energy 1982), p.134 The authors present the first detailed study on the multiplicity dependence of double scattered events in high energy proton-deuteron interaction rescattering probability and the even topology rescattering probe have been determined and the experimental data have been discussed in the context of conflicting theoretical estimates. | |
| 74801 A new approach to study of rescattering in pd interaction. D.Ghosh, L.Chatterjee, J.Roy, K.Basu Chowdhury, K.Sengupta, S.Naha, A.Roy Chowdhury, M.Basu, S.Nandy, D.Sural, A.Bhattacharyya, R.Banerjee, K.Roy Chowdhury, D.Mazumdar, S.Mondal, T.Roy (Dept. of Phys., Jadavpur Univ., Calcutta, India). Proceedings of the VI High Energy Physics Symposium (papers in summary form only received), Mysore, India, 6-11 Dec. 1982 (Bombay, India: Dept. Atomic Energy 1982), p.135 The authors present an estimation of the rescatter fraction f_{res} in proton-deuteron interaction at high energy using the wounded nucleon model of Bialas. The results are compared with those obtained by other methods. | |
| 74802 Hard scattering at ISR energies. N.A.McCubbin (Rutherford Appleton Lab., Chilton, Didcot, England). Physics in Collision. High-Energy ee/ep/pp Interactions. Proceedings of an International Conference, Stockholm, Sweden, 2-4 June 1982 (New York, USA: Plenum 1983), p.1-20 After giving a brief summary of the situation in hard scattering in hadron-hadron collisions, the author discusses in more detail some of the recent results from: di-lepton production (Drell-Yan); single photon production; experiments using a high p_T single particle trigger; experiments using a calorimeter trigger. (14 refs.) | |

74803 Proton-antiproton elastic scattering and total cross section at the CERN collider. B.Koene (NIKHEF-H, Amsterdam, Netherlands). Physics in Collision. High-Energy ee/ep/pp Interactions. Proceedings of an International Conference, Stockholm, Sweden, 2-4 June 1982 (New York, USA: Plenum 1983), p.85-97. Measurements of elastic scattering at low momentum transfer and of the total cross section were performed during the first physics run of the CERN proton-antiproton Collider at $\sqrt{s}=540$ GeV. Data were taken during about 15 h of running time with an antiproton bunch of $\sim 4 \times 10^9$ particles colliding against a proton bunch of $\sim 5 \times 10^{10}$ particles. The machine optics in the intersection region was the same as for normal SPS operation. The nominal luminosity was of the order of $10^{26} \text{ cm}^{-2} \text{ s}^{-1}$. (14 refs.)

Massive lepton pair production—what has QCD done to the classical Drell-Yan model? See Entry 74716

CFF-shell effects in VDM and the Compton sum rule See Entry 74749

Comparison of pp/pp interactions See Entry 74816

Off-energy shell scattering of pions on deuterons See Entry 75054

13.85D Elastic scattering (energy > 10 GeV)

74804 π^+p scattering at 65 to 140 MeV. B.G.Ritchie, R.S.Moore, B.M.Freedman (Univ. of South Carolina, Columbia, SC, USA), G.Das, R.C.Minehart, K.Gotow, W.J.Burger, H.J.Ziock. *Phys. Lett. B (Netherlands)*, vol.125B, no.2-3, p.128-32 (26 May 1983).

Differential cross sections for π^+p elastic scattering were measured for seven incident energies from 65 to 145 MeV at laboratory scattering angles between 93° and 165° . The results are compared with previous results of Bertin et al. (1976) and the phase-shift analysis of Arndt and Roper (1980). Agreement between the phase-shift analysis and the data is good. (13 refs.)

Energy dependence of spin-spin correlation parameters in large-angle pp-scattering See Entry 74793

Optimised polynomial expansion and phase shift analysis of Δ -p scattering See Entry 74795

Kp and πp scattering in near forward directions See Entry 74798

Proton-antiproton elastic scattering and total cross section at the CERN collider See Entry 74803

Antiproton-proton total and elastic cross-sections at the CERN ISR and the SPS collider See Entry 74806

13.85H Inelastic scattering, many-particle final states (energy > 10 GeV)

Muonproduction of J/ψ and the photon-gluon scattering process: $\gamma_g \rightarrow J/\psi g$ See Entry 74717

13.85K Inclusive reactions, including total cross sections, (energy > 10 GeV)

74805 Recent study of jets at the ISR. A.M.Segar (Dept. of Nuclear Phys., Univ. of Oxford, Oxford, England). *AIP Conf. Proc. (USA)*, no.98, p.274-92 (1982). [received: May 1983] (Conference on Particles and Fields - 1982, College Park, MD, USA, 28-30 Oct. 1982).

A review of results on jets is presented, with emphasis on recent data which are tending to support the interpretation of high transverse momentum phenomena in QCD. Calorimeter trigger results which show two-jet structure at high $E_T \geq 20$ GeV are presented. (13 refs.)

74806 Antiproton-proton total and elastic cross-sections at the CERN ISR and the SPS collider. D.L.Owen (CERN, Geneva, Switzerland). *AIP Conf. Proc. (USA)*, no.98, p.293-311 (1982). [received: May 1983] (Conference on Particles and Fields - 1982, College Park, MD, USA, 28-30 Oct. 1982).

Three experiments, currently running at CERN, are devoted to the measurement of total and elastic cross-sections in antiproton-proton collisions: experiments R210 and R211 at the ISR, and Experiment UA4 at the SPS Collider. The various experimental techniques and setups are briefly described, and the most recent results obtained are reported. The combined centre-of-mass energy range of the three experiments is $31 < \sqrt{s} < 540$ GeV. In this range the p_{\perp} total cross-section is found to rise approximately like $(\ln s)^2$, as does the pp total cross-section, and the difference, $\sigma_{\text{tot}}(pp) - \sigma_{\text{tot}}(p\bar{p})$, tends to zero as $s^{-1/2}$, with $\alpha \approx 1/2$. (no refs.)

74807 Rapidity distribution of shower particles in proton-nucleus interactions in emulsions at 70 GeV. G.C.Ghosh, B.K.Bandyopadhyay (Dept. of Phys., Presidency Coll., Calcutta, India). *Can. J. Phys. (Canada)*, vol.61, no.5, p.753-7 (May 1983).

Nuclear emulsion plates exposed to 70 GeV protons have been scanned for inelastic interactions. The rapidity distribution of the shower particles observed in 132 events are presented. The dependence of rapidity on the target nucleus mass number has been studied and compared with the results for other energies obtained by earlier workers. The individual rapidity of the shower particles observed in some high multiplicity events are also shown. The qualitative features of the observed rapidity distributions agree with the Glauber-Gribov multiperipheral model (1970). (14 refs.)

74808 New unitarity bounds and their near-saturation by ISR data. P.Valin (Dept. of Phys., McGill Univ., Montreal, Canada). *Nucl. Phys. B, Part. Phys. (Netherlands)*, vol.B218, no.1, p.215-39 (30 May 1983).

A new set of unitarity bounds supplemented by experimentally measured quantities is derived and tested against a recent compilation of ISR data to check the latter's internal consistency. These bounds are obtained by supplying one value of the absorptive elastic amplitude at a fixed non-zero t value. The general numerical technique is explicitly given in a simple form and some typical analytic results are displayed. The author also discusses as special cases some previously obtained bounds and points out the added usefulness of the newly derived bounds for experimentalists and their near-saturation by the existing data over an extended t interval. Applications include the relative normalization of different sets of data and tests for dubious data points; finally suggestions are made for pp collider measurement. (34 refs.)

74809 Observation of two-proton correlations in pNe interactions at 300 GeV/c. S.A.Azimov, M.L.Allaberdin, S.O.Edgorgov, Sh.V.Inogamov, E.A.Kosonovskii, V.D.Lipin, S.L.Lutpullaev, K.Olimov, Kh.A.Rizaev, T.P.Tarasova, K.T.Turdaliev, A.A.Yuldashev, B.S.Yuldashev (Physicotech. Inst., Acad. of Sci., Uzbek SSR). *JETP Lett. (USA)*, vol.36, no.9, p.428-31 (5 Nov. 1982). Translation of: *Pisma v Zh. Eksp. & Teor. Fiz. (USSR)*, vol.36, no.9, p.349-52 (5 Nov. 1982). [received: June 1983]

Experimental data reveal a correlation between protons with approximately equal momenta in the reactions $p\text{Ne} \rightarrow mp + X$, $m \geq 2$, at a primary momentum $p_0 = 300$ GeV/c. The correlation becomes closer as the momenta of the secondary protons increase. (9 refs.)

74810 Evidence for 'held-back' valence quarks from particle ratios in pp and pp collisions. A.Capella, Tran Thanh Van (Lab. de Phys. Theorique et Hautes Energies, Univ. de Paris XI, Orsay, France), U.P.Sukhatme. *Phys. Lett. B (Netherlands)*, vol.125B, no.4, p.330-4 (2 June 1983).

The authors show that recently measured particle ratios in the central region of pp and pp collisions give valuable information on the fate of valence quarks in a soft hadronic collision, indicating that the valence quark from each initial hadron is 'held back' with a small momentum fraction. This mechanism is a key feature of the dual parton fragmentation approach to low- p_T multiparticle production. (17 refs.)

74811 Evidence for the t-quark in pp collider data? V.Barger, A.D.Martin (Dept. of Phys., Univ. of Durham, Durham, England), R.J.N.Phillips. *Phys. Lett. B (Netherlands)*, vol.125B, no.4, p.339-42 (2 June 1983).

The authors propose a simple method to identify semileptonic weak decays $t \rightarrow b + \nu$ of any heavy particle t and to determine its mass independent of the production mechanism, using pp collider events that contain a single electron (or muon) and missing transverse momentum. Events with transverse mass $M_T(\nu) > 3$ GeV originate either from t-decays of mass $m_t > M_T(\nu) + m_b$, or from $W \rightarrow e \nu$ decays; the latter is a distinctive background that can be subtracted. The $M_T(\nu)$ distribution of electron events with jets recently observed in the UA1 experiment at CERN may be interpreted as being due to a t-quark with mass 25 to 40 GeV. (8 refs.)

74812 On the description of multiplicity distributions in multiple production processes in terms of combinatorics. J.Bartke (High Energy Lab., Joint Inst. for Nuclear Res., Moscow, USSR). *Phys. Scr. (Sweden)*, vol.27, no.4, p.225-7 (April 1983).

A new method of analysis of multiplicity distributions of secondary particles in multiple production processes is discussed and applied to high-energy proton-proton and nucleus-nucleus collisions. (26 refs.)

74813 $\phi\phi$ production in high-energy hadron-hadron collisions and enhancement near threshold. S.P.Misra (Inst. of Phys., Bhubaneswar, India). Proceedings of the VI High Energy Physics Symposium (papers in summary form only received), Mysore, India, 6-11 Dec. 1982 (Bombay, India: Dept. Atomic Energy 1982), p.58.

Summary form only given. Excessive $\phi\phi$ production has been seen in $\pi p \rightarrow \phi\phi x$ and $pp \rightarrow \phi\phi x$ with an enhancement near $\phi\phi$ threshold. The author interprets this as a direct evidence of gluon-gluon collisions and suggests that similar other reactions parallel to photon-photon collisions may be looked for. The phenomena observed again appear to indicate a subtle dynamical enhancement of some cross sections near threshold as a result of composite substructure.

74814 Study of inclusive γ -production in pp interactions at 12 GeV/c. S.Banerjee, S.Chakrabarti, S.N.Ganguli, A.Gurtu, P.K.Mahotra, R.Raghavan, A.Subramanian, K.Sudhakar (Tata Inst. of Fundamental Res., Bombay, India). Proceedings of the VI High Energy Physics Symposium (papers in summary form only received), Mysore, India, 6-11 Dec. 1982 (Bombay, India: Dept. Atomic Energy 1982), p.131.

The authors present a study of inclusive γ -production in pp interactions at 12 GeV/c. The data are obtained from the analysis of pictures taken in the BEBC at CERN. The inclusive γ cross-section and the average number of γ as a function of charged multiplicity are presented. Multiparticle correlation parameters are discussed and the 2γ mass distribution has been studied to obtain π^0 inclusive cross-section. x and p_T distributions of the γ s are compared with the distributions obtained from π^\pm assuming charge symmetry. The results have been compared with other inclusive γ studies.

74815 Analysis of inclusive particle ratios in π^-p interactions at 40 GeV/c. J.B.Singh (Dept. of Phys., Panjab Univ., Chandigarh, India). Proceedings of the VI High Energy Physics Symposium (papers in summary form only received), Mysore, India, 6-11 Dec. 1982 (Bombay, India: Dept. Atomic Energy 1982), p.123.

The results of inclusive study of particle production ratios in π^-p interactions at 40 GeV/c have been presented. The ratios π^+/π^- , π^0/π^- , π^-/π^- and π^-/π^+ as a function of the Feynman variable in the proton fragmentation region have been studied. The results obtained have been discussed in view of QCD theoretical models viz: quark-exchange, gluon-exchange, etc.

74816 Comparison of pp/pp interactions. M.Jacob (CERN, Geneva, Switzerland). Physics in Collision. High-Energy ee/ep/pp Interactions. Proceedings of an International Conference, Stockholm, Sweden, 2-4 June 1982 (New York, USA: Plenum 1983), p.21-41.

The use of the SPS as a pp collider is the driving force of the extensive pp programme at CERN. However, it was realized that, at a relatively low extra cost, one could also use the PS to inject the accumulated antiprotons either into a low-energy ring LEAR or into the ISR, even if injection and acceleration into the SPS remains the major part of the programme. The purpose of this note is to review the ISR part of the pp programme, presenting the physics results obtained so far. (22 refs.)

74817 First results of the UA1 experiment. M.Pimia (Helsinki Univ., Helsinki, Finland). Physics in Collision. High-Energy ee/ep/pp Interactions. Proceedings of an International Conference, Stockholm, Sweden, 2-4 June 1982 (New York, USA: Plenum 1983), p.43-66.

First results of the CERN SPS proton-antiproton collider which has short machine development and physics runs during autumn 1981 are described. (17 refs.)

74818 Status and first results from the UA2 experiment. P.Jenni (CERN, Geneva, Switzerland). Physics in Collision. High-Energy ee/ep/pp Interactions. Proceedings of an International Conference, Stockholm, Sweden, 2-4 June 1982 (New York, USA: Plenum 1983), p.67-83.

The UA2 detector was recently installed at the CERN Super Proton Synchrotron (SPS) pp Collider. The successful operation of the SPS pp Collider² allows the study of hadron interactions at a center of mass energy $\sqrt{s}=540$ GeV, one order of magnitude higher than previously available. The data

presented here were recorded with the UA2 detector during the first pp period in November-December 1981. (14 refs.)

74819 Results from the UA5 experiment. D.R.Ward (Cavendish Lab., Univ. of Cambridge, Cambridge, England). Physics in Collision. High-Energy ee/ep/pp Interactions. Proceedings of an International Conference, Stockholm, Sweden, 2-4 June 1982 (New York, USA: Plenum 1983), p.99-121. Presents a review of the results obtained using the UA5 streamer chamber detector in the early months since the successful operation of the CERN SPS pp collider at $\sqrt{s}=540$ GeV. The primary objective of the UA5 experiment was to carry out a rapid survey of hadronic interactions in this new energy regime. (21 refs.)

74820 Theoretical implications on ISABELLE physics. Ling-Lie Chau (Phys. Dept., Brookhaven Nat. Lab., Upton, NY, USA). The High-Energy Limit. Proceedings of the Eighteenth Course of the International School of Subnuclear Physics, Erice, Italy, 31 July-11 Aug. 1980 (New York, USA: Plenum 1983), p.447-93. Discusses theoretical work on unification, grand unification, quark models and intermediate bosons which lead to experimental work with pp and pp at ISABELLE. (48 refs.)

74821 Multiparticle hadronic systems produced in high-energy (pp) interactions, and comparison with (e^+e^-). M.Basile, C.Cara Romeo, L.Cifarelli, A.Contin, G.D'Alì, B.Esposito, P.Giusti, T.Massam, R.Nania, F.Palmonari, G.Sartorelli, G.Valenti, A.Zichichi (CERN, Geneva, Switzerland). The High-Energy Limit. Proceedings of the Eighteenth Course of the International School of Subnuclear Physics, Erice, Italy, 31 July-11 Aug. 1980 (New York, USA: Plenum 1983), p.495-507. Reports on a series of similarities between multiparticle hadronic systems produced in (pp) interactions and in (e^+e^-) annihilation. The new feature of this work is the fact that, in order to establish these similarities, the basic principle is to evaluate, for each (pp) interaction, the correct energy available for particle production. The old trend was to select high- p_T processes. The comparison of the multiparticle hadronic systems produced in (pp) interactions and (e^+e^-) annihilation is discussed in terms of the following five quantities: (i) the inclusive, single-particle, fractional momentum distribution of the produced particles; (ii) the inclusive transverse momentum distribution of the particles produced; (iii) the average charged particle multiplicity; (iv) the ratio of 'charged' to 'total' energy of the multiparticle hadronic systems produced; (v) the planarity of the multiparticle hadronic systems produced. (17 refs.)

74822 Status of charmed particles. F.Muller (CERN, Geneva, Switzerland). The High-Energy Limit. Proceedings of the Eighteenth Course of the International School of Subnuclear Physics, Erice, Italy, 31 July-11 Aug. 1980 (New York, USA: Plenum 1983), p.627-76. Summarizes the properties of known charmed particles (D , F and Λ_c) and then deal with production processes, mainly in hadronic interactions. (88 refs.)

Conference on Particles and Fields - 1982 See Entry 74201

Physics in Collision. High-Energy ee/ep/pp Interactions. Proceedings of an International Conference See Entry 74228

The High-Energy Limit. Proceedings of the Eighteenth Course of the International School of Subnuclear Physics See Entry 74229

QCD and the space-time evolution of high-energy e^+e^- , pp, and heavy ion collisions See Entry 74724

Hadronic couplings of open beauty states See Entry 74735

Detecting t-quark pairs at pp colliders using transverse dilepton masses and jets See Entry 74762

Event structure in collider and cosmic ray experiments See Entry 74824

Finding the t-quark in W boson decay debris See Entry 74828

Production of large P_T particles in p-nucleus and nucleus-nucleus collisions at high energies See Entry 75002

Some characteristics of secondary particles produced in pion-nucleus collisions in emulsion at 50 GeV/c See Entry 75053

13.85M Cosmic ray interactions
(see also 94.40 Cosmic rays)

74823 High-energy hadrons produced by cosmic-ray muons in the earth as a source of background in proton-decay experiments. A.S.Mal'gin, O.G.Ryazhskaya, V.G.Ryasnyi, F.F.Khal'chukov (Inst. of Nuclear Res., Acad. of Sci., USSR). JETP Lett. (USA), vol.36, no.8, p.376-9 (20 Oct. 1982). Translation of: Pis'ma v Zh. Eksp. & Teor. Fiz. (USSR), vol.36, no.8, p.308-10 (20 Oct. 1982). [received: June 1983] The flux density of neutrons with energies of 20-80 MeV produced by muons underground at a depth of 550 meters water-equivalent has been measured. The flux density of hadrons with energies above 0.7 GeV is estimated for various depths. The hadron background is important in experiments on the decay of the proton at depths down to 8000 meters water equivalent. (14 refs.)

74824 Event structure in collider and cosmic ray experiments. N.Yam-dagni (Inst. of Phys., Univ. of Stockholm, Stockholm, Sweden). Physics in Collision. High-Energy ee/ep/pp Interactions. Proceedings of an International Conference, Stockholm, Sweden, 2-4 June 1982 (New York, USA: Plenum 1983), p.327-41. The author compares some of the new collider results with the cosmic ray results from emulsion chamber experiments. The emulsion chamber data comes from three large emulsion chamber experiments. This data can be divided into two parts. The first part is one in which the incoming particle interacts in the target layer of a two-storeyed emulsion chamber (these events are called C-jets, as the target layer consists mainly of carbon). They are observed by the Brazil-Japan collaboration. The second part of the data consists of interactions taking place in air above the emulsion chamber (~1 km). These events are observed by all emulsion chamber experiments. (9 refs.)

13.88 POLARISATION IN INTERACTIONS AND SCATTERING

74825 Prospects for polarized electrons at high energies. C.Y.Prescott (Stanford Linear Accelerator Center, Stanford Univ., Stanford, CA, USA). The High-Energy Limit. Proceedings of the Eighteenth Course of the International School of Subnuclear Physics, Erice, Italy, 31 July-11 Aug. 1980 (New York, USA: Plenum 1983), p.415-46. Neutral current and electroweak processes at high energies are well known to have large spin-dependent components. Proven techniques for producing polarized beams at storage rings and linear accelerators are now available. It is argued that use of polarized electrons in e^+e^- annihilation at the Z^0 pole and above will provide the most precise tests of, and best experimental challenge to, the standard $SU(2)\times U(1)$ gauge theory model of electroweak interactions. (22 refs.)

SPin correlation in ep \rightarrow eAX scattering See Entry 74777

Polarized single pion photoproductions test for various quark models See Entry 74780

Energy dependence of spin-spin correlation parameters in large-angle pp-scattering See Entry 74793

13.90 OTHER TOPICS IN SPECIFIC REACTIONS AND PHENOMENOLOGY OF ELEMENTARY PARTICLES

74826 Two-photon physics. R.O.Polvado (Univ. of Maryland, College Park, MD, USA). AIP Conf. Proc. (USA), no.98, p.176-98 (1982). [received: May 1983] (Conference on Particles and Fields - 1982, College Park, MD, USA, 28-30 Oct. 1982).

A brief overview of $\gamma\gamma$ physics is presented. Two-body final states are considered and a preliminary result on non-resonant $\gamma\gamma\rightarrow h^+h^-$ ($h=\pi,K,p$) is given. The most recent results on the η' , ρ^0 , A_2 , and f' resonances are tabulated and the status of $\gamma\gamma\rightarrow\rho^0\rho^0$ is discussed. The measurements of F_2 and high P_T jets are summarized. (44 refs.)

74827 Energy loss by slow magnetic monopoles. J.Gea-Banacloche, K.Cahill, D.Rossbach (Dept. of Phys. & Astron., Univ. of New Mexico, Albuquerque, NM, USA), A.Comtet.

Let. Nuovo Cimento (Italy), vol.37, ser.2, no.4, p.145-8 (28 May 1983). Two approximate classical calculations of energy loss by very slow magnetic monopoles are described. It is shown that the energy loss per unit length to bound electrons varies as the square of the velocity of the monopole, while that to conduction electrons varies linearly. (6 refs.)

74828 Finding the t-quark in W boson decay debris. V.Barger, A.D.Martin (Dept. of Phys., Univ. of Durham, Durham, England), R.J.N.Phillips.

Phys. Lett. B (Netherlands), vol.125B, no.4, p.343-6 (2 June 1983). The authors point out a spectacular jet plus electron signature of t-quark production at pp colliders via W boson decay $W\rightarrow tb$ with subsequent $b\rightarrow jet$, and $t\rightarrow be\nu$ decays. The b jet momentum transverse to the beam has a jacobian peak near $p_T(b)=(M_W^2-m_t^2)/2M_W$; this jet is expected to be highly collimated. Electrons from t-decay occur with large momentum components normal to the b jet in the plane transverse to the beam. Both the b jacobian peak and transverse momenta of the t-decay fragments can be used in making further determinations of m_t . (7 refs.)

74829 A review of two-photon physics. S.Cooper (DESY, Hamburg, Germany).

Physics in Collision. High-Energy ee/ep/pp Interactions. Proceedings of an International Conference, Stockholm, Sweden, 2-4 June 1982 (New York, USA: Plenum 1983), p.123-48

This talk is intended as an introduction for those not yet expert in two-photon physics, especially those e^+e^- one-photon physicists who still think of two-photon events as background. The author concentrates on the physics questions involved, especially emphasizing the areas where she feels progress can be made in the near future. After a quick survey of the field and a few words about kinematics, she discusses in detail two major fields: the photon structure function and resonance production. (48 refs.)

Physics of intermediate vector bosons See Entry 74701

e^+e^- physics at PETRA See Entry 74755

14.00 PROPERTIES OF SPECIFIC PARTICLES AND RESONANCES

Workshop on Science Underground See Entry 74199

14.20 BARYONS AND BARYON RESONANCES
(inc. antiparticles)

Theoretical predictions for baryon number violation See Entry 74666

The proton decay-magnetic monopole connection See Entry 74668

How supersymmetry makes neutron-antineutron oscillations more natural in $SO(10)$ See Entry 74683

Supersymmetric grand unification See Entry 74685

A unified approach to QCD phenomenology See Entry 74702

Deep inelastic phenomena See Entry 74715

Use of final-energy sum rules to describe baryon properties in quantum chromodynamics and to estimate the proton lifetime in the $SU(5)$ model See Entry 74718

Exotic multiquark states with charm See Entry 74740

Proton decay experiment in the Kolar Gold Fields See Entry 74765

The Mont Blanc experiment on nucleon stability See Entry 74766

The effective proton lifetime and non-exponential decay See Entry 74767

Certain rare hypernuclear decays See Entry 74768

Experiment to detect proton decay and neutrino oscillations (using cosmic ray neutrino events) See Entry 74770

Analysis of scaling violation in nucleon structure functions See Entry 74771

- Magnetic moments of the ground state baryons See Entry 74774
 Magnetic moments in quark-diquark model See Entry 74775
 Status of charmed particles See Entry 74822
 Two-photon physics See Entry 74826
 Nusex experiment and the future of the Mont Blanc laboratory See Entry 75225
 IMB detector—the first 30 days See Entry 75226
 The Harvard-Purdue-Wisconsin baryon decay experiment at Park City, Utah See Entry 75227
 The Soudan nucleon decay experiments See Entry 75228
 The nucleon decay experiment in the Frejus tunnel See Entry 75229
 A proton decay and solar neutrino experiment with a liquid argon Time Protection Chamber See Entry 75230
 Magnetic monopoles, nucleon decay and DUMAND See Entry 75231

14.40 MESONS AND MESON RESONANCES

- Conference on Particles and Fields - 1982 See Entry 74201
 Testing the standard model See Entry 74669
 A unified approach to QCD phenomenology See Entry 74702
 The Upsilon resonances—recent results See Entry 74712
 Hadronic physics of $q\bar{q}$ light quark mesons, quark molecules and glueballs See Entry 74714
 Muoproduction of J/ψ and the photon-gluon scattering process: $\gamma, g \rightarrow J/\psi, g$ See Entry 74717
 Spectroscopy of hadrons: mesons See Entry 74723
 An analysis of $(b\bar{b})$ -states in a static one-parameter potential model See Entry 74731
 Can $\delta(980,0^+)$ be a broad $q\bar{q}q\bar{q}$ state? See Entry 74732
 Quark masses from the vector meson spectrum See Entry 74739
 Exotic multiquark states with charm See Entry 74740
 Quantized strings and QCD See Entry 74748
 On a mass formula of particles in $c\bar{c}$, $b\bar{b}$ and $t\bar{t}$ families See Entry 74750
 Recent results from PEP See Entry 74751
 Prompt neutrino results from Fermilab See Entry 74759
 Recent results from CLEO at the T(4s) See Entry 74760
 The pion-quark coupling constant and the decay of vector mesons See Entry 74763
 Why most flavor dependence predictions for nonleptonic charm decays are wrong See Entry 74764
 Structure functions of relativistic systems composed of two spin $1/2$ particles See Entry 74772
 Recent results in T spectroscopy from CESR See Entry 74782
 Some recent results in e^+e^- physics in the US See Entry 74790
 A study of e^+e^- annihilation into hadrons in the 1400-2200 MeV energy range with the magnetic detector DMI at DCI: observation and study of a ϕ' vector meson See Entry 74791
 Evidence for glueballs See Entry 74796
 Status of charmed particles See Entry 74822
 Two-photon physics See Entry 74826
 Some characteristics of secondary particles produced in pion-nucleus collisions in emulsion at 50 GeV/c See Entry 75053

14.60 LEPTONS

- On the phenomenon of rotation of the polarization vector of gravitational and neutrino waves in a strong neutrino radiation field See Entry 74343
 Massless neutrinos in left-hand symmetric models See Entry 74671
 Massive lepton pair production—what has QCD done to the classical Dreil-Yan model? See Entry 74716
 Generalized statistics and the rishon hypothesis See Entry 74741
 A derivation of the Cabibbo angle and quark-lepton masses from a composite model See Entry 74742
 Recent results from PEP See Entry 74751
 Test of quantum electrodynamics and the study of heavy leptons See Entry 74754
 Prompt neutrino results from Fermilab See Entry 74759
 Experiment to detect proton decay and neutrino oscillations (using cosmic ray neutrino events) See Entry 74770
 Effects of light and heavy Majorana neutrinos in neutrinoless double beta decay See Entry 74916
 The massive neutrino and clustering phenomena in the Universe See Entry 78806
 The influence of neutrino rest mass on Dirac cosmology See Entry 79035

14.80 OTHER AND HYPOTHETICAL PARTICLES

- 74830 Search for fractional charges. D.Liebowitz, M.Binder, K.O.H.Ziöck (Dept. of Phys., Univ. of Virginia, Charlottesville, VA, USA). *Phys. Rev. Lett. (USA)*, vol.50, no.21, p.1640-3 (23 May 1983).
 The results of a search for fractional charges on 24 steel spheres with a total mass of 720 μ g are reported. No fractional charges, spurious or otherwise, greater than 0.15 e were found. (5 refs.)
 Conference on Particles and Fields - 1982 See Entry 74201
 The High-Energy Limit. Proceedings of the Eighteenth Course of the International School of Subnuclear Physics See Entry 74229
 Weak symmetry breaking by radiative corrections in broken supergravity See Entry 74356
 Light spinor monopole See Entry 74606
 Composite gauge bosons in sigma models and supergravity See Entry 74611
 Dyon-axion dynamics See Entry 74612
 Algebraic construction of static axially symmetric self-dual fields See Entry 74625

- Lepton-violating $\beta^-\beta^-$, $\beta^+\beta^+$ decays, (e^-, e^+) conversion and double electron capture in gauge theories See Entry 74648
 Mass spectrum of the W^\pm and Z supermultiplets See Entry 74657
 The massless gluino and the pseudoscalar meson family See Entry 74660
 The proton decay—magnetic monopole connection See Entry 74668
 Testing the standard model See Entry 74669
 Anomalous baryon number non-conservation in the presence of SU(5) monopoles See Entry 74672
 Scalar loops and the Higgs mass in the Salam-Weinberg-Glashow model See Entry 74676
 After the W particle, the Higgs See Entry 74678
 A supersymmetric preon model of particle physics See Entry 74679
 On the S-wave interaction between massive fermions and a GUT magnetic monopole See Entry 74680
 Physics of intermediate vector bosons See Entry 74701
 Quaternionic formulation of fields associated with dyons See Entry 74710
 Instantons in the quark plasma See Entry 74728
 Quark masses from the vector meson spectrum See Entry 74739
 Generalized statistics and the rishon hypothesis See Entry 74741
 A derivation of the Cabibbo angle and quark-lepton masses from a composite model See Entry 74742
 Recent results from PEP See Entry 74751
 Manifestation of the axial photon in decays of charged $K[\pi]$ mesons See Entry 74761
 Detecting t-quark pairs at pp colliders using transverse dilepton masses and jets See Entry 74762
 Deep inelastic muon hadron interactions See Entry 74776
 Evidence for the t-quark in pp collider data? See Entry 74811
 Theoretical implications on ISABELLE physics See Entry 74820
 Energy loss by slow magnetic monopoles See Entry 74827
 Finding the t-quark in W boson decay debris See Entry 74828
 A review of two-photon physics See Entry 74829
 Magnetic monopoles, nucleon decay and DUMAND See Entry 75231
 Relativistic atomic level calculations with nuclei carrying additional fractional charges See Entry 75284
 Atomic excitation and ionization by slow magnetic monopoles See Entry 75489
 Circumvention of Parker's bound on galactic magnetic monopoles See Entry 78807

20.00 NUCLEAR PHYSICS

- Annual review of nuclear and particle science. Vol.32 See Entry 74232

21.00 NUCLEAR STRUCTURE

21.10 GENERAL AND AVERAGE PROPERTIES OF NUCLEI; PROPERTIES OF NUCLEAR ENERGY LEVELS

(for properties of specific nuclei listed by mass ranges, see 27.)

- 74831 Evidence concerning Δ -hole states. J.Rapaport (Ohio Univ., Athens, OH, USA). *AIP Conf. Proc. (USA)*, no.97, p.365-77 (1982). [received: May 1983]
 (Proceedings of the Workshop on the Interaction Between Medium Energy Nucleons in Nuclei, Bloomington, IN, USA, 28-30 Oct. 1982).
 Recent (p,n) experiments at intermediate energy at the Indiana University Cyclotron have been used to study the spin-isospin transfer response function of nuclei. In particular forward angle spectra are dominated by neutron peaks characterized with $\Delta L=0$ transfer, which have been identified as Gamow-Teller (GT) 1^+ states. The GT strength function in nuclei throughout the periodic table is presented. The sum of the total observed GT strength is compared to a model independent sum rule to obtain an A dependence of the quenching. General features of GT strength distributions are presented and discussed. A special effort is made to estimate how much of the GT strength resides at excitation energies between 20-40 MeV. The fact that less GT strength is observed than is expected may be associated with intrinsic nucleon degrees of freedom, in particular the excitation of Δ -hole states. (14 refs.)
 74832 Low lying yrast states of ^{32}S . R.M.Freeman, F.Haas, C.Beck, A.Niemeskern (Univ. Louis Pasteur, Strasbourg, France). *J. Phys. Lett. (France)*, vol.44, no.11, p.429-32 (1 June 1983).
 From angular correlation measurements with the $^{28}\text{Si}(\alpha, n\gamma)^{32}\text{S}$ reaction the 6762-keV level has been assigned $J^\pi=5^-$. Four new levels of ^{32}S have been observed at $E_x=7567$ -, 8345-, 9464 and 9637-keV. The 7567-keV level has been assigned $J^\pi=5^+$ and the 8345-keV level is a good candidate for the lowest 6^+ state. The two higher levels are probably negative parity high spin states. (3 refs.)
 74833 Level structure of the $N=88$ isotones ^{149}Pm , ^{151}Eu and ^{153}Tb . R.K.Guchhait (Dept. of Phys., Gurudas Coll., Calcutta, India), S.Bhattacharya, S.Sen. *J. Phys. G (GB)*, vol.9, no.6, p.631-42 (June 1983).
 The level structures of the $N=88$ isotones ^{149}Pm , ^{151}Eu and ^{153}Tb are studied in a version of the unified vibrational model which incorporates both pairing effects and anharmonicity in the core vibrations. The proton quasiparticle states in the $Z=50-82$ shell are coupled to anharmonic vibrations of the corresponding even cores. The calculated level energies, spectroscopic factor and E2 transition strengths are compared with available experimental data and predictions of other theoretical calculations. (40 refs.)

74834 High-spin states in ^{92}Tc . C.A.Fields, F.W.N.de Boer, B.J.Diana (Dept. of Phys., Univ. of Colorado, Boulder, CO, USA).

Nucl. Phys. A (Netherlands), vol.A401, no.1, p.117-23 (30 May 1983). High-spin states in ^{92}Tc have been studied using the 33 MeV $^{90}\text{Mo}(^3\text{He},p2n)^{92}\text{Tc}$ reaction. Levels up to $J=(13)$ are identified. The results are compared with various shell-model calculations. (9 refs.)

74835 Nuclear polarization and sign of the quadrupole moment of the $^{54}\text{Fe}(10^+)$ isomer. E.Davni, M.Hass, H.H.Bertschat, C.Broude, F.Davidovsky, G.Goldring, P.M.S.Lesser (Dept. of Nuclear Phys., Weizmann Inst. of Sci., Rehovot, Israel).

Phys. Rev. Lett. (USA), vol.50, no.21, p.1652-5 (23 May 1983). A novel approach to the determination of signs of quadrupole deformations of high-spin isomers is presented. Recoiling $^{54}\text{Fe}(10^+)$ isomers, populated by the reaction $^{45}\text{Sc}(^{12}\text{C}, p2n)$ are polarized by passage through an array of tilted carbon foils and stop in a Cd single crystal. The observation of a quadrupole precession serves to measure both the induced nuclear polarization and the sign of the quadrupole moment. A positive sign of $Q(^{54}\text{Fe}(10^+))$ has been deduced. (20 refs.)

74836 The $N=82$ isotones in the generalized seniority scheme. O.Scholten, H.Kruse (Nat. Superconducting Cyclotron Lab., Michigan State Univ., East Lansing, MI, USA).

Phys. Lett. B (Netherlands), vol.125B, no.2-3, p.113-15 (26 May 1983). A calculation for the $N=82$ isotones in the generalized seniority scheme is presented and compared with a shell model calculation. (9 refs.)

74837 Triaxial shapes of rotating nuclei with neutron numbers 88, 89, 90.

S.Frauentorf (Univ. of Tennessee, Knoxville, TN, USA), F.R.May, *Phys. Lett. B (Netherlands)*, vol.125B, no.4, p.245-50 (2 June 1983).

The tendency of high- j quasiparticles to drive rotating nuclei towards triaxial shapes is studied by means of the cranked shell model. Depending on the position of the chemical potential within the j -shell different γ -values are preferred by the quasiparticles, which may induce significant configuration dependent γ -deformations in γ -soft nuclei. As an example the rotational spectra of $Z=66, 67, N=88, 89, 90$ nuclides are studied. Equilibrium γ -values are found by minimizing the sum of phenomenological expressions for the ground state deformation- and rotational energies and the quasiparticle energies. The competition between $\nu_{1/2}$ (driving to $\gamma=0$) and $h_{11/2}$ (driving to $\gamma<0$) quasiparticles causes a γ -flip-flop between the configurations observed as changes of the signature splitting and E2-transition probabilities, which may be related to the prolate-oblate difference of the deformation energy. (21 refs.)

74838 Low-spin states in even Po and Rn isotopes and the interplay between collective and quasiparticle configurations. A.Zemel (Kernfysisch Versneller Inst., Rijksuniv. Groningen, Groningen, Netherlands), J.Dobes.

Phys. Rev. C (USA), vol.27, no.5, p.2311-16 (May 1983). Low-spin states in even Po and Rn isotopes are studied within the framework of the interacting-boson-approximation+two-quasiparticle model. The irregular behavior of the 4^+ levels is shown to result from an interplay between collective, quasiparticle, and quasineutron states. Some predictions are made for the corresponding Ra isotopes. (27 refs.)

74839 One- and three-quasiparticle states in $^{127,129,131,133}\text{Xe}$ and their coexistence with band structures. T.Lonnroth, J.Kumpulainen, C.Tuokko (Dept. of Phys., Univ. of Jyväskylä, Jyväskylä, Finland).

Phys. Scr. (Sweden), vol.27, no.4, p.228-40 (April 1983). Excited states in the nuclei $^{127,129,131,133}\text{Xe}$ were populated using the reactions $^{127}(p,n)^{127}\text{Xe}$ and $^{126,128,130}\text{Te}(\alpha,n)^{129,131,133}\text{Xe}$ and their de-excitation was studied using conventional γ -ray and conversion electron spectroscopy. A large number of new levels are identified, most of which are assigned a definite spin-parity. Shell-model arguments are used to identify one- and three-quasiparticle states. The competition between vibrational and quasiparticle excitations is studied, and it is found that quasiparticle excitations become yrast with the filling of the $N=82$ neutron shell. Notably, the $\nu_{11/2}$ band is cut by the three-quasi-particle excitations. (21 refs.)

74840 High-spin states in ^{97}Tc . D.Hippe, H.W.Schuh, U.Kaup, K.O.Zell, P.von Brentano (Inst. für Kernphys., Univ. zu Köln, Köln, Germany), D.B.Fossan.

Z. Phys. A (Germany), vol.311, no.4, p.329-37 (1983). The level scheme of ^{97}Tc was studied by gamma ray spectroscopy using the $^{96}\text{Zr}(^3\text{Li}, 3n)^{97}\text{Tc}$ reaction. New levels and spins and parities were established. ^{97}Tc is compared with the neighbouring even-even nucleus and with the results of an IBFM calculation. (30 refs.)

Variations of the gyromagnetic ratios of low-lying states in ^{192}Os See Entry 74844

Density-dependent charge asymmetry and the Coulomb energy anomaly See Entry 74851

The heavy-ion potential and its increasing transparency at intermediate energies See Entry 74865

The moments of strength functions See Entry 74902

Fast $\Delta I=0$ M1 transitions in the band crossing region See Entry 74903

Collective excitations of ^{82}Kr observed by in-beam and decay spectroscopy and their characterization by the interacting boson model See Entry 74906

A microscopically determined diabatic potential for heavy-ion collisions See Entry 74929

Quasimolecular and cluster states of light nuclei as examples of intermediate structure See Entry 74946

Fluid dynamics of giant resonances of high spin states See Entry 74949

Proton scattering to collective states: what we learn about the effective interaction in the nuclear medium See Entry 74970

Inelastic proton scattering to one-particle one-hole states See Entry 74971

Deformation effect in the fast neutron total cross section of aligned ^{59}Co See Entry 74992

$^{45}\text{Sc}(\alpha,\alpha n)^{44}\text{Sc}^{m+}$: a monitor reaction for alpha particle induced reactions See Entry 75005

21.10D Binding energy and masses

74841 Effect of the $\Delta(1236)$ isobar on the three-nucleon bound states. Ch.Hajduk, P.U.Sauer, W.Struive (Theoretical Phys., Univ. of Hannover, Hannover, Germany).

AIP Conf. Proc. (USA), no.97, p.404 (1982). [received: May 1983] (Proceedings of the Workshop on the Interaction Between Medium Energy Nucleons in Nuclei, Bloomington, IN, USA, 28-30 Oct. 1982).

Two-nucleon potentials are unable to account simultaneously for the binding energy and the EM form factors of the three-nucleon bound states. If the force is allowed to yield explicit Δ -isobar excitation, the two-nucleon interaction gets renormalized and a three-nucleon interaction and EM exchange-

currents (EC) arise, which are calculated. The single- Δ wave-function components are generated nonperturbatively in a coupled-channel approach by π - and p -exchange transition potentials in the isospin-triplet partial waves up to angular momentum $l=2$. In the model, the Δ improves the ^3H binding energy by 0.3 MeV and the ^3He charge form factor for momentum transfers $Q>4\text{ fm}^{-1}$. In order to improve the magnetic form factor, isovector π - and p -exchange mesonic EC between nucleonic configurations are added. (2 refs.)

Three-body forces See Entry 74855

Three-nucleon interaction in 3-, 4- and ∞ -body systems See Entry 74861

The macroscopic approach to nuclear masses and deformations See Entry 74877

Mass parameters for collective nuclear motion based on a diabatic single-particle basis See Entry 74879

Correlated basis theory of nucleon optical potential in nuclear matter See Entry 74886

Binding energy estimates for charmed few-body systems See Entry 74895

21.10F Shape, charge, radius and form factors

74842 Inelastic electron scattering to negative parity states of ^{28}Si . S.Yen, R.J.Sobie, T.E.Drake, H.Zarek (Dept. of Phys., Univ. of Toronto, Toronto, Ontario, Canada), C.F.Williamson, S.Kowalski, C.P.Sargent.

Phys. Rev. C (USA), vol.27, no.5, p.1939-56 (May 1983). Negative-parity states of ^{28}Si are studied by high-resolution inelastic electron scattering. The form factors of the 1^- (8.904), 5^- (9.702), 1^- , 2^- (9.929), 3_2^- (10.180), and 4^- $T=1$ (12.664) states are determined for the first time, for momentum transfers between 0.9 and 2.4 fm^{-1} . The 3_1^- (6.879) state is studied by subtracting off the theoretical contribution of the nearby 4^+ (6.889) state. An upper limit for the 5^- $T=1$ (13.248) is established. The 3^- $T=0/6^-$ $T=0$ complex (11.58) remains unresolved. The authors present evidence for oblate-prolate deformation changes in the 3^- $T=0$ states. The experimental data are compared with predictions of the open-shell random phase approximation of Rowe and Wong (1970). In ^{28}Si , the open-shell random phase approximation is demonstrated to be extremely sensitive to the ground state wave function used, and other possible limitations of the open-shell random phase approximation are discussed. (33 refs.)

Triaxial shapes of rotating nuclei with neutron numbers 88, 89, 90 See Entry 74837

Effect of the $\Delta(1236)$ isobar on the three-nucleon bound states See Entry 74841

Three-body forces See Entry 74855

Real part of the nuclear interaction potential between α or p and excited heavy nuclei See Entry 74864

Description of the neutron deficient Sr and Zr isotopes in the interacting boson model See Entry 74874

The macroscopic approach to nuclear masses and deformations See Entry 74877

Triaxial Hartree-Fock-Bogolyubov calculations with D1 effective interaction See Entry 74882

Shape transitions and isotope shifts of proton and neutron distributions in the samarium isotopes See Entry 74889

Anomaly in the optical potential for deformed nuclei See Entry 74966

Deformation effect in the fast neutron total cross section of aligned ^{59}Co See Entry 74992

Nuclear charge distribution in fission: fractional cumulative yields of isotopes of krypton and xenon in $^{249}\text{Cf}(n_{\text{th}},f)$ and $^{250}\text{Cf}(sp,f)$ See Entry 75057

21.10H Spin, parity, and isobaric spin

74843 An interacting boson-fermion model calculation for the odd-mass promethium isotopes. O.Scholten, T.Ozzello (Nat. Superconducting Cyclotron Lab., Michigan State Univ., East Lansing, MI, USA).

Phys. Lett. B (Netherlands), vol.125B, no.2-3, p.106-8 (26 May 1983). A calculation in the framework of the interacting boson-fermion model for the excitation energy and spectroscopic factors for the negative parity levels in the odd-mass promethium isotopes is presented. The parameters are compared with those obtained from an earlier calculation of the europium isotopes. (11 refs.)

Evidence concerning Δ -hole states See Entry 74831

Low lying yrast states of ^{32}S See Entry 74832

High-spin states in ^{97}Tc See Entry 74840

Inelastic electron scattering to negative parity states of ^{28}Si See Entry 74842

Proton occupancies in the even Se ground states via the $(d,^3\text{He})$ reaction See Entry 74847

Low-lying states in ^{109}In populated by the $(^3\text{He},d)$ reaction in ^{108}Cd See Entry 74849

Implication of the nonlocality in the effective N-N interaction: nuclear structure and spin observables See Entry 74853

Description of the neutron deficient Sr and Zr isotopes in the interacting boson model See Entry 74874

Levels in ^{204}Po from the decay of ^{204}At See Entry 74907

Average resonance capture studies of $^{162,164}\text{Dy}$ See Entry 74908

The decay of 56-s ^{148}Ce to levels of odd-odd ^{148}Pr See Entry 74913

Explicit representations of tensor spin orbit interactions for systems with maximum channel spin 3 See Entry 74936

$\Delta(1236)$ -isobar degrees of freedom and the strength of spin-isospin resonances See Entry 74945

Implications of the experimental results on the photodisintegration of ^4He See Entry 74959

$^{13}\text{C}(^3\text{p},p)$ cross section See Entry 74960

Parity violation and related effects in neutron-induced reactions See Entry 74986

Dirac-equation impulse approximation for intermediate-energy nucleon-nucleus scattering See Entry 74987

21.10J Spectroscopic factors

- Level structure of the $N=88$ isotones ^{149}Pm , ^{151}Eu and ^{153}Tb See Entry 74833
- An interacting boson-fermion model calculation for the odd-mass promethium isotopes See Entry 74843
- Proton occupancies in the even Se ground states via the $(d,^3\text{He})$ reaction See Entry 74847
- Low-lying states in ^{109}In populated by the $(^3\text{He},d)$ reaction in ^{108}Cd See Entry 74849
- Surface alpha clustering See Entry 74919
- Coulomb forces in the three-body problem with application to direct nuclear reactions See Entry 74953
- Elastic scattering of ^{20}Ne on ^{24}Mg See Entry 75019

21.10K Electromagnetic moments

- 74844 Variations of the gyromagnetic ratios of low-lying states in ^{192}Os .** H.H. Bolotin, I. Morrison, C.G. Ryan (School of Phys., Univ. of Melbourne, Parkville, Victoria, Australia), A.E. Stuchbery.
Nucl. Phys. A (Netherlands), vol. A401, no. 1, p.175-88 (30 May 1983).
The gyromagnetic ratios of the 2_1^+ and 4_1^+ states in ^{192}Os were measured relative to that of the 2_1^+ level. The thin foil perturbed γ -ray angular distribution technique was employed utilizing the transient hyperfine magnetic field present at the nuclei of these ions as they swiftly recoiled through a thin, magnetized Co foil. The states of interest were Coulomb excited using a beam of 220 MeV ^{38}Ni ions. The present measurements yielded ratios $g(2_1^+)/g(2_1^+)=0.68\pm 0.08$ and $g(4_1^+)/g(2_1^+)=1.00\pm 0.12$. The sizable disparity in the measured g -factors of the levels of the two low-lying bands is compared with interacting boson approximation model-based calculations, as well as with a Nilsson basis single-particle model description. (28 refs.)
- 74845 The effect of the $\Delta(1236)$ on the g -factor of nucleons.** R.D. Lawson (Argonne Nat. Lab., Argonne, IL, USA).
Phys. Lett. B (Netherlands), vol. 125B, no. 4, p.255-9 (2 June 1983).
The effect on M1 properties of including the Δ -degree of freedom is examined. In first order perturbation theory the main effect of including the Δ is to renormalize the g -factor of the valence nucleons. Formulas for this change are given for a central plus tensor (NN) \leftrightarrow (ND) transition potential. The effect on magnetic moments is small but $B(M1)$ between spin-orbit partners is decreased by 20-30%. Values for orbits near $A=16, 40, 90$ and 208 are given. (14 refs.)
- 74846 Nuclear orientation and NMR/ON of $^{205,207}\text{Po}$.** P. Herzog, H. Walitzki, K. Freitag, H. Hildebrand, K. Schlosser (Inst. für Strahlen- und Kernphys., Univ. Bonn, Bonn, Germany).
Z. Phys. A (Germany), vol. 311, no. 4, p.351-62 (1983).
 $^{205,207}\text{Po}$ have been implanted into cold host matrices of Fe, Ni, Zn and Be using an on-line isotope separator. Nuclear magnetic resonances of oriented ^{207}Po have been observed. The resonance frequencies for zero external field are $\nu_L(^{207}\text{PoFe})=575.08(20)\text{MHz}$, $\nu_L(^{207}\text{PoNi})=160.1(8)\text{MHz}$, $\nu_L(^{205}\text{PoFe})=551.7(8)\text{MHz}$. From the dependence of the resonance frequency on external magnetic field the g -factor of ^{207}Po is derived as $g(^{207}\text{Po})=+0.31(22)$. Using this value the magnetic hyperfine fields of Po in Fe and Ni are obtained as $B_{\text{hf}}(\text{PoFe})=+238(16)\text{T}$, $B_{\text{hf}}(\text{PoNi})=66.3(4.6)\text{T}$. The g -factor of ^{205}Po follows as $g(^{205}\text{Po})=+0.304(22)$. From the temperature dependence of the anisotropies of γ -lines in the decay of $^{205,207}\text{Po}$ the multipole mixing of several transitions is derived. The electric interaction frequencies in the hosts Zn and Be are also measured. (30 refs.)
- Nuclear polarization and sign of the quadrupole moment of the $^{54}\text{Fe}(1^+)$ isomer** See Entry 74835

21.10M Level density and structure

- 74847 Proton occupancies in the even Se ground states via the $(d,^3\text{He})$ reaction.** G. Rotbard, M. Vergnes, J. Verotte, G. Berrier-Ronsin, J. Kalifa, R. Tamisier (Inst. de Phys. Nucleaire, Orsay, France).
Nucl. Phys. A (Netherlands), vol. A401, no. 1, p.41-58 (30 May 1983).
The spectroscopic factors for the levels of $^{73,75,77,79,81}\text{As}$ has been measured in the $\text{Se}(d,^3\text{He})\text{As}$ reactions at 25.2 MeV. The proton occupation numbers deduced for the even Se isotopes show that the striking change in proton configuration, observed for the Fe isotopes between $N\leq 40$ and $N\geq 42$, does persist for the Se isotopes. This change is not reproduced, either by a model calculation using spectral distribution methods or by proton wave functions recently suggested for the Se isotopes to explain the results of the $\text{Se}(d,^3\text{Li})\text{Ge}$ reactions. (26 refs.)
- 74848 ^6Li levels excited by the $^9\text{Be}(p,\alpha)$ reaction at $E_p=30$ and 50 MeV.** T. Delbar, G. Gregoire (Inst. de Phys. Corpusculaire, Louvain-la-Neuve, Belgium), G. Paic.
Phys. Rev. C (USA), vol. 27, no. 5, p.1887-96 (May 1983).
The levels of the ^6Li nucleus were studied via the $^9\text{Be}(p,\alpha)$ reaction at incident proton energies of 30 and 50 MeV. Accurate excitation energies as well as some of the corresponding widths are extracted for the first few levels known. Marked differences with accepted values were found. The existence of higher excited states in the region $E_{\text{exc}}=8-12$ MeV cannot be ruled out. The aim is not study reaction mechanisms leading to ^6Li excited states but rather to establish their excitation energies and widths and to compare them to published values. The importance of understanding the continuum in the particle spectra is stressed as far as it influences the position and width of the excited states. (27 refs.)
- 74849 Low-lying states in ^{109}In populated by the $(^3\text{He},d)$ reaction in ^{108}Cd .** E.M. Takagui, F.C. Sampaio, O. Dietzsch (Inst. de Física, Univ. de São Paulo, São Paulo, Brazil).
Phys. Rev. C (USA), vol. 27, no. 5, p.1993-2002 (May 1983).
Nuclear levels in ^{109}In have been investigated by means of the $^{108}\text{Cd}(^3\text{He},d)^{109}\text{In}$ reaction, at incident energies of 19.5 and 21 MeV, using a magnetic spectrograph. Twenty-six levels, up to 3 MeV excitation, have been observed. The experimental angular distributions have been compared with distorted-wave Born approximation calculations to assign angular momentum transfers and to determine spectroscopic factors. Total spin assignments have tentatively been made with the help of shell-model predictions. The proton configuration for the ground state of ^{108}Cd has been deduced. The results are compared with previous data on ^{109}In and with $(^3\text{He},d)$ studies on other odd-mass indium isotopes. (28 refs.)
- One- and three-quasiparticle states in $^{127,129,131,133}\text{Xe}$ and their coexistence with band structures** See Entry 74839
- Inelastic electron scattering to negative parity states of ^{28}Si** See Entry 74842

- Variations of the gyromagnetic ratios of low-lying states in ^{192}Os** See Entry 74844
- Three-body forces in sd-shell nuclei** See Entry 74863
- Description of the neutron deficient Sr and Zr isotopes in the interacting boson model** See Entry 74874
- Population of ^{133}I from the beta decay of fission product ^{133}Te and the cluster-vibration model** See Entry 74905
- The decay of 56-s ^{148}Ce to levels of odd-odd ^{148}Pr** See Entry 74913
- Structure-dependent corrections to the parameters of resonant states in light nuclei** See Entry 74923
- Model study of intermediate state blocking in first-order optical potential theory** See Entry 74931
- The isoscalar quadrupole strength distribution above 10 MeV in ^{40}Ca** See Entry 74948
- Coupling between low-lying nuclear states** See Entry 74950
- Population of isomeric states in muonic atoms** See Entry 75557

21.30 NUCLEAR FORCES

(see also 13.75C Nucleon-nucleon interactions)

- 74850 Coupled channels and quarks in nucleon-nucleon scattering.** E.L. Lomon (MIT, Cambridge, MA, USA).
AIP Conf. Proc. (USA), no. 97, p.78-82 (1982). [received: May 1983]
(Proceedings of the Workshop on the Interaction Between Medium Energy Nucleons in Nuclei, Bloomington, IN, USA, 28-30 Oct. 1982).
In QCD hadron interactions are approximated by asymptotically free quarks at short range, and by exchange and production of confined hadrons at long range. The R-matrix formalism is introduced to match the exterior hadronic description to a complete set of internal q^6 states at an approximate radius expected to be smaller than the equilibrium bag radius. The long range interaction among NN, $N\Delta$, $\Delta\Delta$ and $NN^*(1440)$ channels is consistent with meson exchange potentials and scattering data up to 800 MeV laboratory kinetic energy. This predicts a deuteron with 4.0% D state and 2.3% total isobar component. The first $^3\text{S}_0$ and $^3\text{S}_1$, q^6 states, obtained from the standard MIT bag model parameters, satisfy the R-matrix condition of being at the energies of the $^3\text{S}_0$ and $^3\text{S}_1$ - $^3\text{D}_1$ wave function zeros for a quark boundary radius $R=1.10$ fm. A zero corresponds to a pole in the logarithmic derivative of a partial-wave function, whose residue is determined by the derivative of the q^6 state energy with respect to the boundary radius. (13 refs.)
- 74851 Density-dependent charge asymmetry and the Coulomb energy anomaly.** J.V. Noble (Dept. of Phys., Univ. of Virginia, Charlottesville, VA, USA).
AIP Conf. Proc. (USA), no. 97, p.83-6 (1982). [received: May 1983]
(Proceedings of the Workshop on the Interaction Between Medium Energy Nucleons in Nuclei, Bloomington, IN, USA, 28-30 Oct. 1982).
The 'discrepancy' between measured and calculated isodoublet mass splittings results from an overly optimistic view of the accuracy of present theory. In fact, charge symmetry breaking interactions are both sufficiently large and sufficiently uncertain that the 'best' theoretical estimates of the isodoublet splittings bracket the measured values within a fairly broad uncertainty. (11 refs.)
- 74852 Information from quasi-elastic scattering on the nucleon-nucleon interaction in nuclei.** N.S. Chant (Dept. of Phys. & Astron., Univ. of Maryland, College Park, MD, USA).
AIP Conf. Proc. (USA), no. 97, p.205-23 (1982). [received: May 1983]
(Proceedings of the Workshop on the Interaction Between Medium Energy Nucleons in Nuclei, Bloomington, IN, USA, 28-30 Oct. 1982).
Methods of obtaining information on the nucleon-nucleon interaction in nuclei by means of quasifree knockout reactions are discussed. Examples of off-shell effects are shown and information on the radial region probed is presented. Various possible measurement strategies are considered as well as the effects of spin orbit distortions. (22 refs.)
- 74853 Implication of the nonlocality in the effective N-N interaction: nuclear structure and spin observables.** W.G. Love (Dept. of Phys. & Astron., Univ. of Georgia, Athens, GA, USA), J.R. Comfort.
AIP Conf. Proc. (USA), no. 97, p.225 (1982). [received: May 1983]
(Proceedings of the Workshop on the Interaction Between Medium Energy Nucleons in Nuclei, Bloomington, IN, USA, 28-30 Oct. 1982).
Some consequences of nonlocal spin-dependent terms in the effective N-N interaction are considered for nucleon-nucleus scattering. In particular, these terms are shown to probe the poorly understood spin current modes of nuclear excitation. The simultaneous presence of this type of coupling together with appreciable spin \otimes current transition densities can be observed experimentally by measuring the differences between polarizations and analyzing powers. Schematic calculations are given for $0^+ \rightarrow 1^+$ and $0^+ \rightarrow 0^-$ transitions to illustrate the role of spin \otimes current couplings in calculations of P-A DWIA calculations have been made for the $^+1^+$ transition which support the more transparent schematic considerations. (4 refs.)
- 74854 Mesons and isobars.** M. Rho (Dept. of Phys., State Univ. of New York, Stony Brook, NY, USA).
AIP Conf. Proc. (USA), no. 97, p.350-64 (1982). [received: May 1983]
(Proceedings of the Workshop on the Interaction Between Medium Energy Nucleons in Nuclei, Bloomington, IN, USA, 28-30 Oct. 1982).
Meson and isobar degrees of freedom in nuclei are discussed in terms of the way chiral symmetry manifests itself in nuclear medium. A particular emphasis is placed on the role that pions (as the Goldstone bosons) play in enhancing and quenching the effective axial charge g_A^{eff} measured in some nuclear spin-isospin modes. (33 refs.)
- 74855 Three-body forces.** J.L. Friar (Los Alamos Nat. Lab., Los Alamos, NM, USA).
AIP Conf. Proc. (USA), no. 97, p.378-88 (1982). [received: May 1983]
(Proceedings of the Workshop on the Interaction Between Medium Energy Nucleons in Nuclei, Bloomington, IN, USA, 28-30 Oct. 1982).
Three-body forces are defined and their properties discussed. Evidence for such forces in the trinucleon bound states and scattering reactions is reviewed. The binding energy defects of the trinucleon bound states, the ^3He charge density, the Phillips line for doublet n-d scattering lengths, and three-nucleon breakup reactions are discussed, together with the possible influence of three-body forces on these observables. (23 refs.)

74856 Quarks, bags and the nucleon-nucleon interaction. G.E.Brown (State Univ. of New York, Stony Brook, NY, USA). *AIP Conf. Proc. (USA)*, no.97, p.389-97 (1982). [received: May 1983] (Proceedings of the Workshop on the Interaction Between Medium Energy Nucleons in Nuclei, Bloomington, IN, USA, 28-30 Oct. 1982). It is argued that pionic couplings have a greater influence on the short-range nucleon-nucleon interaction than the quark degrees of freedom. (20 refs.)

74857 The nucleus consists of more than just nucleons, deltas and mesons. G.A.Miller (CERN, Geneva, Switzerland). *AIP Conf. Proc. (USA)*, no.97, p.408-12 (1982). [received: May 1983] (Proceedings of the Workshop on the Interaction Between Medium Energy Nucleons in Nuclei, Bloomington, IN, USA, 28-30 Oct. 1982). The possibility that quark degrees of freedom have significant effects in nuclear physics is discussed. (24 refs.)

74858 Charge-dependent three-body force with isobar excitations. Shin Nan Yang (Dept. of Phys., Nat. Taiwan Univ., Taipei, Taiwan). *J. Phys. G (GB)*, vol.9, no.6, p.L115-18 (June 1983). The charge-dependent three-body force which involves the exchange of one photon and one pion together with the presence of one virtual-nucleon excited state (isobar) is considered. Its contribution toward the Coulomb energy difference of ^3He - ^3H is estimated to be negligible. (13 refs.)

74859 The nucleon-meson coupling vertex-structure and the process for the meson exchange in nuclear force. He Hanxin, Zhuo Yizhong, Sa Benhao (Inst. of Atomic Energy, Acad. Sinica, Beijing, China). *Kexue Tongbao (Foreign Lang. Ed.) (China)*, vol.28, no.3, p.321-4 (March 1983). Since the sixties the meson exchange theory has been so developed that it can explain the nuclear force quite well. The success of the quark model and the development of quantum chromodynamics (QCD) make one hope to understand the mechanism of the nuclear force more deeply. From the viewpoint of the quark model and QCD, the nuclear force appears as interactions caused by exchanging the colour-gluons among the quarks that constitute the nucleons. When the two nucleons come near enough to have an overlap, the exchange of the colour-gluons not only exists among the quarks inside a nucleon but also occurs between the quarks of two different nucleons. And the quarks of a nucleon can be scattered into the configuration of another nucleon, which gives a lowest order process of exchanging the gluons and quarks between the two nucleons. Due to the asymptotically-free and the confined properties of the QCD, this process of the one-gluon exchange comes about only in a very localized spacetime region and so it can be expected to make contribution to the short-range part of nuclear force. In addition, there exist the two-gluons exchange and the exchange of colour-singlet quark-antiquark ($q\bar{q}$)-pairs between two nucleons. One can thus expect these processes to be able to contribute to the intermediate-range and the long-range parts of nuclear force. (6 refs.)

74860 Relativistic two-nucleon calculations on the light front. L.Muller (Inst. fur Theoretische Phys. II, Ruhr-Univ., Bochum, Germany). *Nuovo Cimento A (Italy)*, vol.75A, ser.2, no.1, p.39-61 (1 May 1983). The relativistic theory for few-nucleon systems developed by Glockle and Muller (1981) is transformed into the light front formalism. For a model of scalar particles exchanging scalar mesons the 10 generators of the Poincare group are derived in pure particle space up to lowest order in the coupling. Because of the impossibility of a complete partial-wave decomposition on the light front, only bound states can be calculated numerically. This is done for the two-body system. The results differ from those at an instant because of the omission of higher-order terms. (15 refs.)

74861 Three-nucleon interaction in 3-, 4- and ∞ -body systems. J.Carolson, V.R.Pandharipande (Dept. of Phys., Univ. of Illinois, Urbana, IL, USA), R.B.Wiringa. *Nucl. Phys. A (Netherlands)*, vol.A401, no.1, p.59-85 (30 May 1983). The authors report results of variational calculations of ^3H , ^3He , ^4He and nuclear matter with the Urbana v_{14} two-nucleon interaction and realistic models of the three-nucleon interaction (TNI). These include the Tucson and isobar intermediate-state models of the two-pion exchange TNI. The latter is also studied with an intermediate-range three-nucleon repulsion. In general realistic TNI helps to bring the theory closer to experiment by giving extra binding energy to the $A=3$ and 4 nuclei and providing extra saturation to the nuclear matter binding energy. The Coulomb energy of ^3He and the r.m.s. radii of $Z=3,4$ nuclei are also well described. However, some problems remain unresolved. There is a slight overbinding of ^4He , an underbinding of nuclear matter, and the charge form factors of ^3He and ^4He , calculated with impulse approximation, deviate from the experimental at $q^2>5\text{ fm}^{-2}$. (35 refs.)

74862 Interplay between two- and three-body interaction in light nuclei and nuclear matter. R.B.Wiringa (Phys. Div., Argonne Nat. Lab., Argonne, IL, USA). *Nucl. Phys. A (Netherlands)*, vol.A401, no.1, p.86-92 (30 May 1983). A recent study of different models of three-nucleon interaction (TNI) in ^3He , ^3H , ^4He and nuclear matter is extended to study the influence of different choices of the accompanying two-body interaction. A new two-body potential, Argonne v_{14} , is coupled with both the Tucson and isobar intermediate-state models of two-pion-exchange TNI, with a phenomenological intermediate-range repulsive TNI added to the latter. Variational calculations are carried out for these systems, and compared to the earlier work. The author finds that a stronger tensor component in the two-body potential, as typified by a larger deuteron percentage, gives more attraction for the TNI, counteracting the saturation effect obtained when only two-body forces are considered. (17 refs.)

74863 Three-body forces in sd-shell nuclei. A.Polls, H.Muther, A.Faessler (Inst. fur Theoretische Phys., Univ. Tubingen, Tubingen, Germany), T.T.S.Kuo, E.Osnes. *Nucl. Phys. A (Netherlands)*, vol.A401, no.1, p.124-42 (30 May 1983). The influence of three-body forces on the excitation spectra of nuclei with 3 valence nucleons in the sd-shell is investigated. Three-body forces are considered, which arise from an intermediate excitation of the interacting nucleons to the $\Delta(3,3)$ resonance. Besides these real three-nucleon forces, effective three-body interactions are taken into account which are due to the restriction of the nuclear structure calculation to sd-shell configurations. Significant cancellations are observed between the different contributions to the effective three-nucleon force. The resulting three-body matrix elements yield only a small influence on the spectrum of the $A=19$ systems. The typical size of the matrix elements, however, is large enough to expect a serious influence on the results of shell-model calculations with more than three valence nucleons. (35 refs.)

74864 Real part of the nuclear interaction potential between α or p and excited heavy nuclei. X.S.Chen, C.Ngo, E.Tomasi (CENS, Gif-sur-Yvette, France), M.Barranco, X.Vinas, H.Ngo. *Nucl. Phys. A (Netherlands)*, vol.A401, no.1, p.143-56 (30 May 1983). The authors investigate, within a very simple double folding model, the nuclear interaction potential between α or p and excited heavy nuclei. The densities of the excited nuclei are calculated using a modified hot Thomas-Fermi model. Simple analytical expressions of the results are presented. The consequences of this calculation on evaporation probabilities is qualitatively discussed. (12 refs.)

74865 The heavy-ion potential and its increasing transparency at intermediate energies. A.Faessler, L.Rikus, S.B.Khadkikar (Inst. fur Theoretische Phys., Univ. Tubingen, Tubingen, Germany). *Nucl. Phys. A (Netherlands)*, vol.A401, no.1, p.157-74 (30 May 1983). Starting from the Reid soft-core potential and the collision of two nuclear matters the authors solve the Bethe-Goldstone equation for the complex reaction matrix. The local density approximation including a Bethe-Goldstone equation for the complex reaction matrix. The local density approximation including a finite range correction enables one to calculate the volume part of the optical potential between two heavy ions up to 100 MeV per nucleon. The surface contributions are calculated data for ^{16}O - ^{16}O are nicely reproduced including the reduction of the reaction cross section above 20 to 30 MeV per nucleon. The maximum of the reaction cross section at 10-20 MeV per nucleon is essentially due to the surface contributions. The description of the ^{12}C - ^{12}C data is not so satisfactory due to the assumption of weak coupling and the neglect of some rotational excitations. (26 refs.)

74866 Classification of exchange currents. J.L.Friar (Theoretical Div., Los Alamos Nat. Lab., Los Alamos, NM, USA). *Phys. Rev. C (USA)*, vol.27, no.5, p.2078-84 (May 1983). After expansion of the vector and axial vector currents in powers of (v/c) , a heretofore unremarked regularity results. Meson exchange currents can be classified into types I and II, according to the way they satisfy the constraints of special relativity. The archetypes of these two categories are the impulse approximation to the vector and axial vector currents. After a brief discussion of these constraints, the $(\rho\pi\gamma)$ and $(\omega\pi\gamma)$ exchange currents are constructed and classified, and used to illustrate a number of important points which are often overlooked. (29 refs.)

74867 Coupled bound and continuum eigenstates in momentum space. R.H.Landau (Dept. of Phys., Univ. of Surrey, Guildford, England). *Phys. Rev. C (USA)*, vol.27, no.5, p.2191-7 (May 1983). Described is a procedure for solving in momentum space the Coulomb plus nuclear problem for coupled bound and continuum eigenstates. The method is an extension of the Kwon-Tabakin (1978) formulation of the Lande subtraction technique. Complex eigenenergies are now determined after formulating and incorporating the correct momentum space 'boundary conditions' into the Schrodinger equation. This exact numerical procedure can be applied to local or nonlocal, complex or real potentials even with relativistic kinematics. Application to the K^-p problem and other systems with strongly coupled absorptive channels is indicated. (22 refs.)

| | |
|--|-----------------|
| Proceedings of the Workshop on the Interaction Between Medium Energy Nucleons in Nuclei | See Entry 74200 |
| Symmetry basis and physical basis for many-quark system | See Entry 74729 |
| The free NN interaction, 50-1000 MeV | See Entry 74792 |
| Effect of the $\Delta(1236)$ isobar on the three-nucleon bound states | See Entry 74841 |
| Mass dependence of the real optical model potential for light ions | See Entry 74868 |
| Conventional approach to the problem of the deuteron smearing corrections | See Entry 74869 |
| Relativistic Brueckner-Hartree-Fock theory: theoretical foundations and empirical evidence | See Entry 74880 |
| Effective interactions at low and intermediate energy | See Entry 74884 |
| Microscopic optical potentials | See Entry 74885 |
| The imaginary part of the relativistic optical potential | See Entry 74887 |
| A-N interaction and the structure of $^4_{{\Lambda}}\text{He}$, $^4_{{\Lambda}}\text{H}$, $^3_{{\Lambda}}\text{He}$ and $^3_{{\Lambda}}\text{H}$ | See Entry 74894 |
| Binding energy estimates for charmed few-body systems | See Entry 74895 |
| Isovector M1 transition matrix elements | See Entry 74899 |
| Gamow-Teller transition matrix elements | See Entry 74910 |
| Model study of intermediate state blocking in first-order optical potential theory | See Entry 74937 |
| First order interpretation of optical potentials | See Entry 74939 |
| Separable representation of the nonlocality of optical model potentials | See Entry 74940 |
| Implications of the experimental results on the photodisintegration of ^4He | See Entry 74959 |
| Proton and neutron elastic scattering between 80 and 1000 MeV | See Entry 74965 |
| Microscopic analysis of proton elastic scattering in the range 80-200 MeV | See Entry 74967 |
| Momentum-space optical potential and elastic scattering calculations | See Entry 74968 |
| A theory for proton- ^3He scattering | See Entry 74969 |
| Proton scattering to collective states: what we learn about the effective interaction in the nuclear medium | See Entry 74970 |
| Microscopic analysis of ^6Li ($\bar{p},p,g.s.$ and $^6\text{Li}(\bar{p},p')$ (2.18 MeV) analyzing powers at 25, 35, and 45 MeV | See Entry 74972 |
| Test of microscopic theory with data for simple transitions in the $^{90}\text{Zr}(\bar{p},p')$ and $^{89}\text{Y}(\bar{p},p')$ reactions | See Entry 74973 |
| The Schrodinger equivalent complex potential and the Dirac phenomenology | See Entry 74978 |
| Antiproton-nucleus interaction at low energy | See Entry 74989 |
| Impulse approximation NN amplitudes for proton-nucleus interactions | See Entry 74996 |
| Three-body model for p-wave pion- ^{16}O scattering | See Entry 75050 |

21.40 FEW-NUCLEON SYSTEMS

74768 Mass dependence of the real optical model potential for light ions. D.K.Srivastava, N.K.Ganguly, D.N.Basu (Variable Energy Cyclotron Centre, Calcutta, India).

Phys. Lett. B (Netherlands), vol.125B, no.4, p.260-4 (2 June 1983).

The observed target mass dependence of the volume integral per interacting nucleon pair of the real optical model potential for deuterons, helium-3 and alpha particles is explained in terms of the density dependence of the effective projectile-nucleon interaction. A mass dependence function for light ions is derived, which for density dependent forces consists of a volume, a surface, a curvature, and a higher order correction term. For non-saturating forces, this has only the volume term and fails to account for the observed mass dependence. (22 refs.)

74769 Conventional approach to the problem of the deuteron smearing corrections. D.Kusno (Dept. of Phys., Univ. of Indonesia, Jakarta, Indonesia), M.J.Moravcsik.

Phys. Rev. C (USA), vol.27, no.5, p.2173-90 (May 1983).

A comprehensive analysis of the problem of deuteron smearing corrections is given. Some problems of the usual approach (the conventional approach) are discussed. It is shown that the formalism adopted by this approach leads to (i) the existence of the so-called West β correction and (ii) the disagreement of the sum rules with the quark parton model expectations in leptonic scattering. It is also shown that in this formalism the electroproduction expression is not inconsistent. Following West for the identification of the wave function it is found that the smearing correction σ_e of the high-energy (50-370 GeV) pion and nucleon process is non-negligible and, hence, in contradiction with the usual expectations. Another test for this approach is suggested. (30 refs.)

74770 A radiochemical study on the existence of dineutron. K.Otozai (Dept. of Chem., Faculty of Sci., Osaka Univ., Osaka, Japan), T.Sekine, R.Arakawa, K.Hata, T.Saito, H.Baba.

Z. Phys. A (Germany), vol.311, no.4, p.303-9 (1983).

A radiochemical study has been made to search for dineutron 2n produced in the simultaneous two-neutron emission of the excited $^6\text{He}^*$ nuclei, $^6\text{He}^*$, induced in the reaction of $^9\text{Be} + n \rightarrow ^6\text{He}^* + \alpha$ with fast neutrons in a reactor. It was attempted to detect the radioactivity of ^{28}Mg as a product of the reaction $^2n + ^{27}\text{Al} \rightarrow ^{28}\text{Mg} + p$. The ^{28}Mg radioactivity observed in heterogeneous samples composed of the 2n -producing target Be and the 2n -detecting target Al separately was not found to be more than that of a side reaction, $^{27}\text{Al}(n,p)(n_{\text{th}},\gamma) + (n_{\text{th}},\gamma)(n,p)^{28}\text{Mg}$, whereas it clearly exceeded that of the side reaction in alloy samples made of Be and Al metals. The former experiment gives an upper limit of the production rate of the dineutron in the bound state 1×10^{-7} per event of the simultaneous two-neutron emission. A tentative explanation for the excessive ^{28}Mg radioactivity observed in the latter experiment is the following two-step process, $^9\text{Be} + n \rightarrow ^6\text{He} + \alpha$ and $^{27}\text{Al} + ^6\text{He} \rightarrow ^{28}\text{Mg} + \alpha + p$, rather than the process induced by the dineutron in a virtual state. (17 refs.)

Baryon multiplicities in the (six quark) deuteron fragmentation

See Entry 74734

Effect of the $\Delta(1236)$ isobar on the three-nucleon bound states

See Entry 74841

Coupled channels and quarks in nucleon-nucleon scattering

See Entry 74850

Three-body forces

See Entry 74855

Charge-dependent three-body force with isobar excitations

See Entry 74858

Relativistic two-nucleon calculations on the light front

See Entry 74860

Three-nucleon interaction in 3-, 4- and ∞ -body systems

See Entry 74861

Interplay between two- and three-body interaction in light nuclei and nuclear matter

See Entry 74862

21.60 NUCLEAR-STRUCTURE MODELS AND METHODS

(for hadronic atoms and molecules, see 36.10)

74771 Comparison of upper and lower bound methods using a soluble many-Fermion model. M.C.Cambiaggio, A.Klar, F.J.Margetan, A.Plastino, J.P.Vary (Phys. Dept., Iowa State Univ., Ames, IA, USA).

Phys. Rev. C (USA), vol.27, no.5, p.2340-55 (May 1983).

Upper bounds, lower bounds, and estimates based on moments are compared for the ground state energy of a soluble Hamiltonian due to Lipkin (1965). Several bounding methods based on variational approaches and one based on the method of moments are employed. The authors show that lower bounds are of comparable quality with upper bounds and are no more difficult to obtain. No single bounding method is found superior over the entire range of parameters they study for the soluble Hamiltonian. However, in one region they find an upper bound from one method which coincides with the lower bound of another method, thus yielding the exact ground state energy. They also show that estimation methods based on the easily calculated first and second moments of the eigenvalue distribution are surprisingly accurate for a wide range of coupling parameters and number of active particles. (19 refs.)

74772 Statistical spectroscopy. J.B.French, V.K.B.Kota (Dept. of Phys. & Astron., Univ. of Rochester, Rochester, NY, USA).

In book: *Annual review of nuclear and particle science*. Vol.32, J.D.Jackson, H.E.Gove, R.F.Schwitters [Ed.], p.35-64. Palo Alto, CA, USA: Annual Reviews (1982), 595 pp. [0 8243 1532 4]

The authors' aim in this article, which may serve as an introduction to more extensive reviews, is to make clear the principles and, without technical detail, something of the methods, results, possibilities, and limitations of statistical spectroscopy. (56 refs.)

Effect of the $\Delta(1236)$ isobar on the three-nucleon bound states

See Entry 74841

The effect of the $\Delta(1236)$ on the g-factor of nucleons

See Entry 74845

Density-dependent charge asymmetry and the Coulomb energy anomaly

See Entry 74851

Charge-dependent three-body force with isobar excitations

See Entry 74858

Relativistic two-nucleon calculations on the light front

See Entry 74860

Coupled bound and continuum eigenstates in momentum space

See Entry 74867

Effective interactions at low and intermediate energy

See Entry 74884

The imaginary part of the relativistic optical potential

See Entry 74887

Hot, dense matter in the bulk equilibrium approximation. II. Adiabats and alpha-particle effects

See Entry 74888

21.60C Shell model

74773 Temperature dependent shell corrections: numerical estimates for the lead region. O.Civitarese, A.L.De Paoli, A.Plastino (Dept. of Phys., Univ. of La Plata, La Plata, Argentina).

Z. Phys. A (Germany), vol.311, no.4, p.317-21 (1983).

Temperature dependent shell corrections are evaluated. The permanence of the shell structure and changes in the level density parameter are discussed for finite temperatures. Numerical estimates for ^{208}Pb are given. (17 refs.)

The $N=82$ isotones in the generalized seniority scheme

See Entry 74836

Triaxial shapes of rotating nuclei with neutron numbers 88, 89, 90

See Entry 74837

One- and three-quasiparticle states in $^{127,129,131,133}\text{Xe}$ and their coexistence with band structures

See Entry 74839

Inelastic electron scattering to negative parity states of ^{28}Si

See Entry 74842

Low-lying states in ^{109}In populated by the $(^3\text{He},d)$ reaction in ^{108}Cd

See Entry 74849

Three-body forces in sd-shell nuclei

See Entry 74863

Description of the neutron deficient Sr and Zr isotopes in the interacting boson model

See Entry 74874

Major shell centroids in the symplectic collective model

See Entry 74876

The macroscopic approach to nuclear masses and deformations

See Entry 74877

Proton capture to excited states of ^{16}O : $M1$, $E1$, and Gamow-Teller transitions and shell model calculations

See Entry 74904

Surface alpha clustering

See Entry 74919

Theory of heavy ion scattering on the basis of the two center shell model

See Entry 74934

Application of the microscopic $\text{sp}(3,\text{R})$ model to the giant monopole and quadrupole resonances in ^{16}O

See Entry 74947

Implications of the experimental results on the photodisintegration of ^4He

See Entry 74959

Three-body model for p -wave pion- ^{16}O scattering

See Entry 75050

21.60E Collective models

74774 Description of the neutron deficient Sr and Zr isotopes in the interacting boson model. D.Bucurescu, G.Cata, D.Cutoiu, G.Constantinescu, M.Ivascu, N.V.Zamfir (Central Inst. of Phys., Bucharest, Rumania).

Nucl. Phys. A (Netherlands), vol.A401, no.1, p.22-40 (30 May 1983).

The available experimental data for the neutron deficient isotopes of Sr (78 to 86) and Zr (80 to 86) are collected and compared to the predictions of IBA-1 model calculations. The variations of the collectivity along these two isotopic chains is well reproduced with a set of smoothly varying parameters of the model. The description of both the energy levels and the $B(E2)$ transition probabilities improves with decreasing N , the Hamiltonian evolving towards an $\text{SU}(3)$ dynamical symmetry. Both the large $B(E2)$ value of the $2_1^+ \rightarrow 0_{g.s.}^+$ transition and the predicted prolate shape for the very light isotopes, agree well with the recent findings of superdeformed nuclei around $Z, N \approx 38$. Transition strengths for the (p,t) reaction are calculated and compared to experimental observations for $0^+ \rightarrow 2^+$ states, and a discussion is made about the possible intruder character of the 0_2^+ state. The interacting boson-fermion approximation model is used to extend the calculations to some odd nuclei. Two shell $(1g_{7/2}, 2d_{5/2})$ calculations are performed for the positive-parity states in ^{83}Sr , ^{85}Sr and ^{85}Y and they compare well with the experimental level scheme of these nuclei below 3 MeV excitation. (46 refs.)

74775 Volume conservation in the liquid drop model. R.Gilmore, Da Hsuan Feng (Dept. of Phys. & Atmospheric Sci., Drexel Univ., Philadelphia, PA, USA).

Phys. Lett. B (Netherlands), vol.125B, no.2-3, p.99-102 (26 May 1983).

Although the $L=0$ (breathing) mode does not conserve volume and the $L=2$ (quadrupole) mode conserves volume only to first order, both modes together can conserve volume to second order when a certain interference relation among the six mode amplitudes is satisfied. The quantized versions of the liquid drop model with volume conservation imposed to first and to second order have different dynamical groups $[\text{U}(5), \text{U}(6)]$, respectively, different Hilbert spaces (infinite dimensional, finite dimensional, respectively), and different rotationally invariant operators from which Hamiltonians can be constructed. (8 refs.)

74776 Major shell centroids in the symplectic collective model. J.P.Draayer (Dept. of Phys. & Astron., Louisiana State Univ., Baton Rouge, LA, USA), G.Rosensteel.

Phys. Lett. B (Netherlands), vol.125B, no.4, p.237-9 (2 June 1983).

Analytic expressions are given for the major shell centroids of the collective potential $V(\beta,\gamma)$ and the shape observable β^2 in the $\text{Sp}(3,\text{R})$ symplectic model. The tools of statistical spectroscopy are shown to be useful, firstly, in translating a requirement that the underlying shell structure be preserved into constraints on the parameters of the collective potential and, secondly, in giving a reasonable estimate for a truncation of the infinite dimensional symplectic model space from experimental $\beta(E2)$ transition strengths. Results based on the centroid information are shown to compare favorably with results from exact calculations in the case of ^{20}Ne . (12 refs.)

74777 The macroscopic approach to nuclear masses and deformations. W.D.Myers, W.J.Swiatecki (Lawrence Berkeley Lab., Univ. of California, Berkeley, CA, USA).

In book: *Annual review of nuclear and particle science*. Vol.32, J.D.Jackson, H.E.Gove, R.F.Schwitters [Ed.], p.309-34. Palo Alto, CA, USA: Annual Reviews (1982), 595 pp. [0 8243 1532 4]

After approximately half a century of nuclear physics there is available today a large amount of experimental information on the masses and deformation energies of nuclei relatively close to the line of beta stability. The interpretation of these measurements has improved over the years and has been integrated into detailed theories of nuclear structure and deformabilities. The resulting understanding of both the gross features, as approximated by a liquid-drop or droplet model formula, and of the fine shell effect details, calculated using the Strutinsky method, is generally adequate to account for the binding energies with an accuracy that may be considerably better than 1 MeV (better than 0.1%) for short-range extrapolations, but becomes uncertain for more distant extrapolations. The relatively recent breakthrough in describing quantitatively the shell effects was associated with the indirect approach, in which shell corrections are added to a smooth background, provided by the liquid-drop model. In the future the direct approach of attacking the full many-body problem (in a suitable approximation) may become relatively more important. (126 refs.)

74878 Quantum mean-field theory of large-amplitude collective motion. F.E.Serr, J.W.Negele, G.Vichniac (Dept. of Phys., MIT, Cambridge, MA, USA).
Proceedings of the International Conference on Nucleus-Nucleus Collisions (papers in summary form only received), East Lansing, MI, USA, 26 Sept.-1 Oct. 1982 (East Lansing, MI, USA: Michigan State Univ. 1982), p.127.
A fundamental problem in nuclear physics is the formulation of a systematic quantum theory of collective motion for finite nuclei. The present work seeks insight on a set of time-dependent mean-field equations obtained by evaluating an appropriate functional integral representation of the evolution operator in the stationary phase approximation (SPA). Solutions to the SPA equations with real period correspond to eigenfunctions of large-amplitude collective motion. (2 refs.)

74879 Mass parameters for collective nuclear motion based on a diabatic single-particle basis. A.Lukasiak, W.Cassing, W.Norenberg (Gesellschaft für Schwerionenforschung, Darmstadt, Germany).
Proceedings of the International Conference on Nucleus-Nucleus Collisions (papers in summary form only received), East Lansing, MI, USA, 26 Sept.-1 Oct. 1982 (East Lansing, MI, USA: Michigan State Univ. 1982), p.128.
For collective kinetic energies per nucleon in the range 1/40 MeV $\leq E_{coll}/A \leq 40$ MeV adiabatic s.p. motion ceases to be valid because jump-probabilities at quasi-crossings of the adiabatic levels near the Fermi energy are close to 1. The authors include this type of transition in a quasi-static diabatic basis by a local transformation of the adiabatic states in which the nodal structure of the wavefunctions is preserved throughout the collective motion. First order perturbation theory with respect to $i\hbar q \partial/\partial q$ (q : parameter for the collective degree of freedom) then yields the 'diabatic' cranking model and corresponding expressions for the collective mass parameters are obtained. (2 refs.)

Level structure of the $N=88$ isotones ^{149}Pm , ^{151}Eu and ^{153}Tb See Entry 74833

Triaxial shapes of rotating nuclei with neutron numbers 88, 89, 90 See Entry 74837

Low-spin states in even Po and Rn isotopes and the interplay between collective and quasiparticle configurations See Entry 74838

High-spin states in ^{97}Tc See Entry 74840

An interacting boson-fermion model calculation for the odd-mass promethium isotopes See Entry 74843

Variations of the gyromagnetic ratios of low-lying states in ^{192}Os See Entry 74844

Shape transitions and isotope shifts of proton and neutron distributions in the samarium isotopes See Entry 74889

Collective excitations of ^{82}Kr observed by in-beam and decay spectroscopy and their characterization by the interacting boson model See Entry 74906

Average resonance capture studies of $^{162,164}\text{Dy}$ See Entry 74908

Boson number dependence of $E2$ transition rates in the rotational limit of the interacting boson model See Entry 74909

Quasimolecular and cluster states of light nuclei as examples of intermediate structure See Entry 74946

Application of the microscopic $\text{sp}(3,\text{R})$ model to the giant monopole and quadrupole resonances in ^{16}O See Entry 74947

Fluid dynamics of giant resonances of high spin states See Entry 74949

21.60F Models based on group theory

Low-spin states in even Po and Rn isotopes and the interplay between collective and quasiparticle configurations See Entry 74838

High-spin states in ^{97}Tc See Entry 74840

Variations of the gyromagnetic ratios of low-lying states in ^{192}Os See Entry 74844

Description of the neutron deficient Sr and Zr isotopes in the interacting boson model See Entry 74874

Major shell centroids in the symplectic collective model See Entry 74876

Quantum mean-field theory of large-amplitude collective motion See Entry 74878

Shape transitions and isotope shifts of proton and neutron distributions in the samarium isotopes See Entry 74889

Binding energy estimates for charmed few-body systems See Entry 74895

Collective excitations of ^{82}Kr observed by in-beam and decay spectroscopy and their characterization by the interacting boson model See Entry 74906

Average resonance capture studies of $^{162,164}\text{Dy}$ See Entry 74908

Boson number dependence of $E2$ transition rates in the rotational limit of the interacting boson model See Entry 74909

21.60G Cluster models

Population of ^{131}I from the beta decay of fission product $^{133}\text{Te}^g$ and the cluster-vibration model See Entry 74905

Surface alpha clustering See Entry 74919

Quasimolecular and cluster states of light nuclei as examples of intermediate structure See Entry 74946

Coulomb forces in the three-body problem with application to direct nuclear reactions See Entry 74953

21.60J Hartree-Fock and random-phase approximations

74880 Relativistic Brueckner-Hartree-Fock theory: theoretical foundations and empirical evidence. C.M.Shakin (Dept. of Phys., Brooklyn Coll., City Univ. of New York, New York, NY, USA).
AIP Conf. Proc. (USA), no.97, p.299-324 (1982). [received: May 1983]
(Proceedings of the Workshop on the Interaction Between Medium Energy Nucleons in Nuclei, Bloomington, IN, USA, 28-30 Oct. 1982).
It is suggested that the nucleon mass may be quite different in the interior of a large nucleus than in free space. The consequences of this assumption are explored using a model based on the one-boson-exchange model of the nuclear force. The author presents the results of parameter-free calculations of nuclear saturation curves, of the density and momentum-transfer dependence of the effective force in nuclei, and of the energy and density dependence of the nuclear optical potential. They also put forth some speculations concern-

ing the relation of boson-exchange models and quark models of the nucleon-nucleon interaction. (31 refs.)

74881 σ_+ strength in nuclei. D.Cha (Cyclotron Lab., Michigan State Univ., East Lansing, MI, USA).
Phys. Rev. C (USA), vol.27, no.5, p.2269-81 (May 1983).
The σ_+ strength function is studied with the quasiparticle random phase approximation. The residual interaction modifies the pairing theory strength function in two ways. The particle-hole interaction reduces the overall strength by about a factor of 2, without shifting strength between different levels. The particle-particle interaction does not affect the overall strength, but shifts part of the strength from the lowest excitation to a higher excitation energy region. By comparing the theory with the observed $\log(f_i)$ values of the β^+ decay in medium heavy nuclei, the author finds that an additional quenching is required for the σ_+ mode, similar in magnitude to the additional quenching present in other isovector-spin-flip transitions. Finally, the author predicts that there is a large concentration of the σ_+ strength at higher excitation energy which cannot be observed by the β^+ decay. (47 refs.)

74882 Triaxial Hartree-Fock-Bogolyubov calculations with $D1$ effective interaction. M.Girod (Service de Phys. Neutronique et Nucleaire, Centre d'Etudes de Bruyeres-le-Chatel, Montrouge, France), B.Grammaticos.
Phys. Rev. C (USA), vol.27, no.5, p.2317-39 (May 1983).
The Hartree-Fock and Hartree-Fock-Bogolyubov methods are used for the description of nuclei and triaxial (i.e. ellipsoidal) shapes. The Gogny $D1$ finite range density dependent interaction is employed. A comparison between various prescriptions for the calculation of pairing correlations in nuclei indicates the necessity for the self-consistent treatment of pairing. Using this last method the authors obtain results concerning nuclear shapes and deformation energy surfaces for nuclei ranging from the lightest ones to the fission barrier of ^{240}Pu . (34 refs.)

74883 Theory of giant resonances. K.Goeke, J.Speth (Inst. für Kernphys., Kernforschungsanlage Jülich, Jülich, Germany).
In book: *Annual review of nuclear and particle science*. Vol.32, J.D.Jackson, H.E.Gove, R.F.Schwitters [Ed.], p.65-115. Palo Alto, CA, USA: Annual Reviews (1982), 595 pp. [0 8243 1532 4]
The authors review the basic microscopic theories suitable for describing collective motion in finite Fermi systems. They view the nucleus as a system of independently moving quasi-particles in a way which allows an easy transition to infinite nuclear matter. First, they recall some basic concepts of time-dependent Hartree-Fock, Landau theory, and transport equations. Second, the resulting equations are considered in their small-amplitude limit, assuming the giant resonances to be harmonic vibrations around some static equilibrium state. This results basically in the random phase approximation and the corresponding zero-sound equation in nuclear matter. Various sum rules are formulated with respect to the RPA strength distribution associated with a given transition operator. These are used to relate other classical and semiclassical theories like the generator coordinate method or adiabatic time-dependent Hartree-Fock to RPA. In the last subsection, fluid dynamical and hydrodynamical approaches and their relationship to RPA and Landau's theory are reviewed and the concept of zero sound is discussed. (184 refs.)

Inelastic electron scattering to negative parity states of ^{28}Si See Entry 74842

Isovector $M1$ transition matrix elements See Entry 74899

Gamow-Teller transition matrix elements See Entry 74910

Pion dynamics in the relativistic nuclear many-body problem See Entry 74921

$\Delta(1236)$ -isobar degrees of freedom and the strength of spin-isospin resonances See Entry 74945

Fluid dynamics of giant resonances of high spin states See Entry 74949

Antiproton-nucleus interaction at low energy See Entry 74989

21.65 NUCLEAR MATTER

74884 Effective interactions at low and intermediate energy. C.Mahaux (Max-Planck-Inst. für Kernphys., Heidelberg, Germany).
AIP Conf. Proc. (USA), no.97, p.20-43 (1982). [received: May 1983]
(Proceedings of the Workshop on the Interaction Between Medium Energy Nucleons in Nuclei, Bloomington, IN, USA, 28-30 Oct. 1982).
Brueckner's reaction matrix g is an attractive candidate for the effective nucleon-nucleon interaction at positive as well as at negative energies. At positive energies, numerical calculations have been limited to nuclear matter; the results are then applied to finite nuclei with the help of local density approximations. Even in the case of nuclear matter, g is a complicated operator since it is nonlocal, state-dependent, nonhermitian and density-dependent. Further work is needed concerning the definition and the calculation of g in nuclear matter, its replacement by local operators, the local density approximation, the comparison with experimental data and with empirical effective interactions, and the relationship with the multiple scattering approach. (85 refs.)

74885 Microscopic optical potentials. H.V.von Geramb (Theoretische Kernphys., Univ. Hamburg, Hamburg, Germany).
AIP Conf. Proc. (USA), no.97, p.44-77 (1982). [received: May 1983]
(Proceedings of the Workshop on the Interaction Between Medium Energy Nucleons in Nuclei, Bloomington, IN, USA, 28-30 Oct. 1982).
Various versions of infinite nuclear matter reaction matrix elements (t -matrix elements) are generated from free NN potentials. Most emphasis is put on calculations with the momentum dependent Paris potential as input. A complex energy and density dependent interaction (25-500 MeV) is parameterised with convenient Yukawa-form factors to serve as effective interaction. Studies concentrate on elastic channel microscopic optical model potential and its general structure as compared to phenomenological potentials. Further detailed checks on the effective interactions are performed with exemplary studies of (p,p') transitions. (18 refs.)

74886 Correlated basis theory of nucleon optical potential in nuclear matter. S.Fantoni, B.L.Friman, V.R.Pandharipande (Dept. of Phys., Univ. of Illinois, Urbana, IL, USA).
AIP Conf. Proc. (USA), no.97, p.234-49 (1982). [received: May 1983]
(Proceedings of the Workshop on the Interaction Between Medium Energy Nucleons in Nuclei, Bloomington, IN, USA, 28-30 Oct. 1982).
The authors give a brief and simple outline of correlated basis perturbation theory and discuss the criterion for choosing the correlation operator. Next they discuss the choice of the nuclear Hamiltonian and give results obtained for nuclear binding energies, and the real and imaginary parts of the nucleon optical potential in nuclear matter. The effect of the nonlocality of the real part of the optical potential on the imaginary part is also discussed. (19 refs.)

74887 The imaginary part of the relativistic optical potential. C.J.Horowitz (Dept. of Phys., MIT, Cambridge, MA, USA). *AIP Conf. Proc. (USA)*, no.97, p.329-36 (1982). [received: May 1983] (Proceedings of the Workshop on the Interaction Between Medium Energy Nucleons in Nuclei, Bloomington, IN, USA, 28-30 Oct. 1982). The imaginary part of the relativistic optical potential is calculated in nuclear matter for the Walecka $\sigma + \omega$ model. Large Lorentz scalar and vector contributions are found in addition to an important three-vector potential. (9 refs.)

74888 Hot, dense matter in the bulk equilibrium approximation. II. Adiabats and alpha-particle effects. M.Pi, M.Barranco (Física Atomica y Nuclear, Facultad de Física, Univ. de Barcelona, Barcelona, Spain), S.Marcos. *Nuovo Cimento A (Italy)*, vol.75A, ser.2, no.1, p.100-12 (1 May 1983). The equation of state (EOS) of hot, dense matter is computed along two adiabats, $s=1$ and $s=1.5k$, neglecting effects associated with finite nuclear size. Detailed comparison with the results previously obtained from a more involved calculation which includes the effects here neglected shows how good the bulk approximation really is. Next, the authors have systematically included alpha-particles as free Boltzmann particles first, and finally they have taken into account the alpha-nucleon interaction in an approximated way via the virial expansion. In the range of temperatures and densities they are interested in, alpha-particles are very rare and their contribution to the equation of state is less important than plasma effects which are generally not considered in EOS calculations. (19 refs.)

74889 Shape transitions and isotope shifts of proton and neutron distributions in the samarium isotopes. J.Janecek, F.D.Becchetti (Dept. of Phys., Univ. of Michigan, Ann Arbor, MI, USA). *Phys. Rev. C (USA)*, vol.27, no.5, p.2282-91 (May 1983). The isotope shifts of the radii of the distributions of neutron and nucleon matter in the samarium isotopes are deduced by combining data from X-ray, muonic X-ray, and optical isotope shift measurements of charge (proton matter) radii with data for the isotope shifts of Coulomb displacement energies. The average isotope shifts from $A=144$ (spherical) to $A=154$ (deformed) are nearly the same for proton and neutron matter with $\gamma_N \approx 1.3$ or $(\rho_N)^{1/2} \propto A^{1/3}$. The neutron matter radii increase more rapidly than the proton matter radii in the region of the light transitional Sm isotopes. The transition from spherical to deformed ground states between $N=88$ and 90 is accompanied by a strong increase in the radius of the proton matter distribution ($\gamma_N \approx 1.9$), whereas the radius of the neutron-excess matter distribution remains almost constant ($\gamma_N \approx 0.0$). The data suggest strong even/odd staggering effects for both proton and neutron matter radii which are out of phase. The droplet model of the atomic nucleus when combined with experimental deformation parameters describes the isotope shift of the charge radii very well. The influence of zero-point vibrations in the light transitional Sm isotopes is apparent. The isotope shift of the neutron matter radii appears to be overestimated. The interacting boson model is found to describe the isotope shift of neutron matter radii satisfactorily but fails to reproduce the isotope shift of the charge radii. (44 refs.)

74890 Hot dense nuclear matter and the transition to quark matter. C.J.Horowitz, H.Schulz (Central Inst. for Nuclear Res., Rossendorf, Germany). Proceedings of the International Conference on Nucleus-Nucleus Collisions (papers in summary form only received), East Lansing, MI, USA, 26 Sept.-1 Oct. 1982 (East Lansing, MI, USA: Michigan State Univ. 1982), p.137. In order to calculate the phase transition of hot nuclear matter to quark matter the hot dense nuclear matter is described in relativistic Hartree and Hartree-Fock approximation under consideration of π -N interactions producing particle-hole and delta-hole excitations. The thermodynamic properties of the quark-gluon plasma are calculated in perturbative QCD in lowest non-trivial order of the quark-gluon coupling. For the nucleon degrees of freedom the authors obtain good agreement between relativistic Hartree and Hartree-Fock calculations as well as between these calculations and non-relativistic variational results. They find large increase in excitation energy and pressure due to pionic excitations which shift the baryon-quark matter phase transition to significantly higher temperatures where the sensitivity of the phase boundary to the values of the vacuum energy and the quark-gluon coupling constant is reduced. (4 refs.)

74891 First order phase transition in hot nuclear matter? H.Schulz, L.Munchow, G.Ropke, M.Schmidt (Central Inst. for Nuclear Res., Rossendorf, Germany). Proceedings of the International Conference on Nucleus-Nucleus Collisions (papers in summary form only received), East Lansing, MI, USA, 26 Sept.-1 Oct. 1982 (East Lansing, MI, USA: Michigan State Univ. 1982), p.139. Hot nuclear matter is considered in a quantum statistical approach taking into account the formation of clusters. The equation of state is obtained calculating the one-particle Green function in a ladder Hartree-Fock approximation. It shows a behaviour similar to that of a non-ideal gas with the characteristic van der Waals instabilities. Below the critical temperatures $T \approx 20$ MeV one reaches the phase unstable region. (4 refs.)

74892 Liquid gas phase instabilities in nuclear systems. M.W.Curtin, H.Toki, D.K.Scott (Nat. Superconducting Cyclotron Lab., Michigan State Univ., East Lansing, MI, USA), P.J.Siemens. Proceedings of the International Conference on Nucleus-Nucleus Collisions (papers in summary form only received), East Lansing, MI, USA, 26 Sept.-1 Oct. 1982 (East Lansing, MI, USA: Michigan State Univ. 1982), p.144. The conventional approach to composite fragment production in HI collisions from a single gaseous phase may require modification at temperatures below 20 MeV due to the onset of a liquid-gas phase instability. At high energies, corresponding to high temperatures, the yield of composite fragments falls off monotonically as a function of particle mass. This behavior is expected for emission of clusters from a high temperature, single gaseous phase where the composite production cross section can be related to a power of the nucleon cross section. In the region of $E_{\text{inc}} \approx 100$ MeV/u corresponding to $T \approx 20$ MeV, the distribution flattens and at still lower temperatures the trend reverses so that the alpha particle yield exceeds that of lighter particles. Due to the anomalously large binding energy of the α particle it is suggested that larger fragment masses be measured to determine if a liquid component exists during disassembly. A macroscopic approach is investigated using a Skyrme interaction with constants determined from $T=0$ nuclear matter considerations. Assuming these parameters are not temperature dependent, the pressure is calculated. Similarities with a Van der Waals system are observed. The coexistence region is mapped out and the critical temperature $T \approx 20$ MeV is extracted. (no refs.)

Antiquarks in a quark-gluon plasma See Entry 74733

Mesons and isobars See Entry 74854

Three-nucleon interaction in 3-, 4- and ∞ -body systems See Entry 74861

Interplay between two- and three-body interaction in light nuclei and nuclear matter See Entry 74862

Pion dynamics in the relativistic nuclear many-body problem . See Entry 74921
Model study of intermediate state blocking in first-order optical potential theory See Entry 74937

Proton scattering to collective states: what we learn about the effective interaction in the nuclear medium See Entry 74970

Antiproton-nucleus interaction at low energy See Entry 74989

Elastic scattering of heavy ions and the compressibility of nuclear matter See Entry 75009

Collective phenomenon in nucleus-nucleus interaction See Entry 75042

21.80 HYPERNUCLEI

74893 Weak decay of a hypernuclei. R.Grace (Carnegie-Mellon Univ., Pittsburgh, PA, USA). *AIP Conf. Proc. (USA)*, no.97, p.426 (1982). [received: May 1983] (Proceedings of the Workshop on the Interaction Between Medium Energy Nucleons in Nuclei, Bloomington, IN, USA, 28-30 Oct. 1982).

A hypernucleus must ultimately decay by a weak process after the more rapid strong and electromagnetic (strangeness conserving) processes are finished. There exists four weak decay modes for a hypernucleus: $\Lambda \rightarrow p + \pi^-$, $\Lambda \rightarrow n + \pi^0$ (mesonic decay); $\Lambda + p \rightarrow n + p$; $\Lambda + n \rightarrow n + n$ (nonmesonic decay). The mesonic decay modes are dominant in very light hypernuclei while the nonmesonic decay modes are dominant in heavier hypernuclei and depend on the four fermion weak interaction. This experiment is designed to test the understanding of this interaction. (no refs.)

74894 Λ -N interaction and the structure of ^4He , ^4H , ^3He and ^3H . Wu Hui-fang, Shen Jian-ping, Yu You-wen, Zhang Zong-ye (Inst. of High Energy Phys., Acad. Sinica, Beijing, China). *Commun. Theor. Phys. (China)*, vol.1, no.4, p.449-57 (1982).

The authors study the Λ -N interaction by using the meson exchange theory. They have considered four processes: (1) single K meson exchange, (2) single η and single ω meson exchange, (3) box diagrams of 2π and $\pi\rho$ exchanges with the intermediate states of ΣN , and (4) box diagrams of 2π and $\pi\rho$ exchanges with the intermediate states of $\Sigma\Delta$. For simplicity, the zero initial momentum approximation and the closure approximation have been taken in the calculation. The results are reasonable and consistent with experimental data. Especially for the cases of ^4He and ^4H , the theoretical spectra of ^4He and ^4H are in good agreement with the experimental data. (4 refs.)

74895 Binding energy estimates for charmed few-body systems. B.F.Gibson (Theoretical Div., Los Alamos Nat. Lab., Los Alamos, NM, USA), C.B.Dover, G.Bhamathi, D.R.Lehman. *Phys. Rev. C (USA)*, vol.27, no.5, p.2085-9 (May 1983).

By solving exact three- and four-body equations, the authors obtain estimates of the binding energies of light nuclei containing one charmed C_0^+ baryon. (20 refs.)

74896 Resonances in hyperon-hyperon systems. G.Bhamathi (Dept. of Theoretical Phys., Univ. of Madras, Madras, India).

Proceedings of the VI High Energy Physics Symposium (papers in summary form only received), Mysore, India, 6-11 Dec. 1982 (Bombay, India: Dept. Atomic Energy 1982), p.64.

Summary form only given, as follows. Recently elaborate theoretical studies have been made on the Σ and Ξ hypernuclei. Since the Ξ particle has strangeness -2 studies on (Ξ p) and other Ξ hypernuclei depend to a considerable degree on the exact knowledge of the interaction in other communicating channels such as $\Lambda\Lambda$, $\Lambda\Sigma$, $\Sigma\Sigma$, etc. One boson exchange models with the additional assumption of SU(3) symmetry have played a large role in determining the nature of the forces in these various systems. The author reports results on a detailed study of hyperon-hyperon interactions treated non-relativistically. Interesting resonance phenomena are found to be present in the singlet state, which are discussed in detail.

Certain rare hypernuclear decays See Entry 74768

23.00 RADIOACTIVITY AND ELECTROMAGNETIC TRANSITIONS

(see also 82.55 Radiochemistry)

23.20 ELECTROMAGNETIC TRANSITIONS

74897 Nuclear orientation of ^{152}Eu in gold. P.J.Blamey (Dept. of Otolaryngology, Univ. of Melbourne, Parkville, Victoria, Australia), D.Bingham, A.J.Barclay, J.D.Cashion. *Aust. J. Phys. (Australia)*, vol.36, no.2, p.127-33 (1983).

Nuclear orientation of ^{152}Eu in gold in the temperature range 9 mK—1 K has been used to determine the mixing ratios of a number of gamma transitions and the multipolarities of several beta transitions of the ^{152}Eu decay scheme. The results agree closely with those from γ - γ and γ - β angular correlation measurements where these have been done. The authors results on the hyperfine interaction of ^{152}Eu in gold contradicted those previously published. (20 refs.)

74898 Excitation of M1 strength in N=28 isotones by inelastic proton scattering at 200 MeV. N.Anantaraman, G.M.Crawley, A.Galonsky (Nat. Superconducting Cyclotron Lab., Michigan State Univ., East Lansing, MI, USA), C.Djalali, N.Marty, M.Morlet, A.Willis, J.-C.Jourdain. *AIP Conf. Proc. (USA)*, no.97, p.224 (1982). [received: May 1983] (Proceedings of the Workshop on the Interaction Between Medium Energy Nucleons in Nuclei, Bloomington, IN, USA, 28-30 Oct. 1982).

High-energy inelastic proton scattering at very forward angles has been found to selectively excite M1 states. The authors have used this reaction to study the M1 strength distribution in the N=28 isotones ^{48}Ca , ^{50}Ti , ^{51}V and ^{54}Fe . The measurements were performed with a beam of 201 MeV protons from the Orsay synchrocyclotron. (23 refs.)

74899 Isovector M1 transition matrix elements. I.S.Towner, F.C.Khanna (AECL, Chalk River Nuclear Labs., Chalk River, Ontario, Canada). *AIP Conf. Proc. (USA)*, no.97, p.405 (1982). [received: May 1983] (Proceedings of the Workshop on the Interaction Between Medium Energy Nucleons in Nuclei, Bloomington, IN, USA, 28-30 Oct. 1982).

Corrections to isovector M1 transition matrix elements are calculated in a model that incorporates the important dynamical aspects of nuclear structure (core polarisation, CP) meson exchange currents (MEC) and isobar currents (IC). The residual interaction is approximated by a one-boson-exchange potential and a short-range correlation function is introduced. (1 ref.)

74900 Low energy spectrum and directional correlation measurements in ^{187}Re . K.Singh, B.S.Grewal, R.Mittal, H.S.Sahota (Phys. Dept., Punjab Univ., Patiala, India).

Indian J. Pure & Appl. Phys., vol.21, no.2, p.107-11 (Feb. 1983).
The gamma ray spectrum of ^{187}Re in the low energy region 0-150 keV has been measured using a high resolution low energy intrinsic Ge detector. The controversial 7.1 keV transition has been confirmed. Also a new transition of energy 125.85 keV has been detected. Gamma-gamma directional correlations are measured for the 72-134 and 552-134 keV cascades. The multiple characters for 72, 134 and 552 keV have been assigned as $E1 + [2.7(7)\%M2, M1 + (2.9 \pm 0.3)\%E2]$ and $E1 + (4.75 \pm 0.75)\%M2$ respectively. (18 refs.)

74901 Gamma radiation from $^{50}\text{Cr}(p,p')^{50}\text{Cr}$ at $E=5.45-6.15$ MeV. M.Brenner, J.Nyberg (Dept. of Phys., Åbo Akad., Åbo, Finland), O.V.Chubinsky, Yu.F.Andronov.

J. Phys. G (GB), vol.9, no.6, p.683-9 (June 1983).
The gamma radiation due to the de-excitation of the 2_1^+ and 4_1^+ levels in ^{50}Cr was studied as a function of the energy, which was varied in 10 keV steps. In particular, strong peaks in the cross sections were observed for scattering to the 4_1^+ level. Using experimental data on spin-flip probability the contribution of the statistical mechanism to the excitation of the 2_1^+ level has been estimated. The estimated ratio $\Gamma_0/D_0 = 0.24$ was obtained for 11 MeV excitation of the compound nucleus. The contribution of direct reaction and isobaric analogue resonances to the cross section is discussed. (11 refs.)

74902 The moments of strength functions. G.G.Dussel, R.P.J.Perazzo, S.L.Reich, H.M.Sofia (Dept. de Física, Comisión Nacional de Energía Atómica, Buenos Aires, Argentina).

Nucl. Phys. A (Netherlands), vol.A401, no.1, p.1-21 (30 May 1983).
The authors show that moment of order n of the strength function is determined by the same order of the Brilloin-Wigner perturbative expansion. This fact is used to study the second moment for single-particle and collective excitations in the framework of nuclear field theory. They discuss the relationship of the second moment with the spreading width of the giant isovector $M1$ resonances in ^{208}Pb . (25 refs.)

74903 Fast $\Delta I=0$ M1 transitions in the band crossing region. P.Kennitz, J.Doring, L.Funke, E.Will, G.Winter (Zentralinstitut für Kernforschung Rosendorf, Dresden, Germany).

Phys. Lett. B (Netherlands), vol.125B, no.2-3, p.119-22 (26 May 1983).
Fast M1 transitions between states of equal spin have been found in $^{80,81,82}\text{Kr}$. They are interpreted as due to two-level mixings in connection with different alignment of particle angular momenta in the configurations involved. The large transition rates exclude a strong competition of proton and neutron components in the lowest $2q$ band. (10 refs.)

74904 Proton capture to excited states of ^{16}O : $M1$, $E1$, and Gamow-Teller transitions and shell model calculations. K.A.Snover, E.G.Adelberger (Nuclear Phys. Lab., Univ. of Washington, Seattle, WA, USA), P.G.Ikossi, B.A.Brown.

Phys. Rev. C (USA), vol.27, no.5, p.1837-65 (May 1983).
The authors have measured excitation functions of the γ rays resulting from the bombardment of ^{15}N by polarized and unpolarized protons in the energy range $E_p = 2.5-9.5$ MeV with emphasis on identifying dipole decays to the first (0^+) and second (3^-) excited states in ^{16}O . Resonances in γ_{12} are observed at $E_p = 16.21, 16.45, 16.82, 17.12, 18.03, 18.98, 19.90, 20.41$ MeV. The 16.21 and 17.12 MeV resonances in γ_{12} are identified as $M1$ decays of the $1^+ T=1$ states of the $6.05 \text{ MeV } 0^+$ state in ^{16}O . The measured ratio of reduced strengths $B(M1, \gamma_{12})/B(M1, \gamma_0)$ is 0.48 ± 0.03 for decays from the 16.21 MeV state and 0.55 ± 0.04 for decays from the 17.12 MeV state. The 18.03 MeV resonance is due to a $3^- T=1$ state in ^{16}O with a strength $\Gamma_{\gamma_{12}}/\Gamma = (1.96 \pm 0.27) \text{ eV}$ and the 18.98 MeV resonance is due to the $4^- T=1$ stretched particle-hole state with a strength of $(0.85 \pm 0.10) \text{ eV}$. They determine absolute particle and γ widths for these states. The $M1 \gamma_2$ width of the 18.98 MeV state ($7.1 \pm 3.1 \text{ eV}$), is in agreement with a shell-model calculation. Resonances in γ_3 are observed at 16.82 and 17.27 MeV and in γ_4 at 17.88 MeV. The excitation energies and widths of these levels as well as the strengths of the γ transitions suggest a $T=1$ character for all of the resonances for which capture γ rays are observed. Correspondences of their resonances to levels in ^{16}N are given. Strong α_1 branches for many of these states indicate isospin impurities. They compare γ widths, including ground-state $M1$ decays, and allowed β transition rates in $A=16$ nuclei with shell model calculations obtain rough agreement with the experimental results. Additional shell model calculations for $M1$ and Gamow-Teller decays in the $A=14, 15, 17$, and 18 nuclei are presented, which indicate that Gamow-Teller matrix elements are quenched by $\sim 20\%$ relative to shell model predictions and also relative to the spin part of the $M1$ matrix elements. (66 refs.)

74905 Population of ^{133}I from the beta decay of fission product ^{133}Te and the cluster-vibration model. H.G.Hicks, J.H.Landrum, E.A.Henry, R.A.Meyer (Lawrence Livermore Nat. Lab., Livermore, CA, USA), S.Brandt, V.Paar.

Phys. Rev. C (USA), vol.27, no.5, p.2203-16 (May 1983).
An automated rapid chemistry system has been used to isolate enriched sources of $12.4\text{-min } ^{133}\text{Te}$ from mixed fission products via the sequence $^{133}\text{Sb}(\beta)^{133}\text{Te}$. In addition, pure sources of ^{133}Te were obtained by using the reduction of Te^{VI} to Te^0 during the isomeric decay of $^{133}\text{Te}^m$. Singles, Compton suppression singles, and γ - γ coincidence $\text{Ge}(\text{Li})$ spectra were used to identify approximately 210 γ rays from the decay of ^{133}Te . This information was used to establish 38 levels below 3000 keV in ^{133}I . Cluster-vibration model calculations have been carried out for the $Z=53$ nucleus ^{133}I . The calculated level structure and transition probabilities are found to be in good agreement with the experimental results. (32 refs.)

74906 Collective excitations of ^{82}Kr observed by in-beam and decay spectroscopy and their characterization by the interacting boson model. R.A.Meyer, J.F.Wild (Lawrence Livermore Nat. Lab., Univ. of California, Livermore, CA, USA), K.Eskola, M.E.Leino, S.Vaisala, K.Forssten, U.Kaup, A.Gelberg.

Phys. Rev. C (USA), vol.27, no.5, p.2217-38 (May 1983).
A comprehensive investigation of the excited states of ^{82}Kr has been carried out through the γ -ray spectroscopy study of the radioactive decay of $^{82}\text{Br}^{\text{I}}$ ($t_{1/2} = 35.3 \text{ h}$, $J^\pi = 5^-$), $^{82}\text{Br}^{\text{II}}$ ($t_{1/2} = 6.1 \text{ min}$, $J^\pi = 2^-$), $^{82}\text{Rb}^{\text{I}}$ ($t_{1/2} = 1.273 \text{ min}$, $J^\pi = 1^+$), and $^{82}\text{Rb}^{\text{II}}$ ($t_{1/2} = 6.2 \text{ h}$, $J^\pi = 5^-$), and in-beam studies using the $^{80}\text{Se}(\alpha, 2n\gamma)^{82}\text{Kr}$ reaction. The authors use the ^{82}Kr level structure they determined, to test the interacting boson model. They show that the interacting boson model calculation can account for the observed levels below 3 MeV provided the underlying shell structure is taken into account. A low energy four quasiparticle $v_{1/2}(g_{7/2})^2_{1/2} 4^-$ band is proposed and its mixing with the octupole band is discussed. (38 refs.)

74907 Levels in ^{204}Po from the decay of ^{204}At . R.G.Helmer, C.W.Reich (Idaho Nat. Engng. Lab., EG&G Idaho Inc., Idaho Falls, ID, USA).

Phys. Rev. C (USA), vol.27, no.5, p.2248-60 (May 1983).
The electron-capture decay of ^{204}At (9 min) has been studied by means of γ and e^- multiscalar singles and γ - γ coincidence measurements with $\text{Ge}(\text{Li})$ and $\text{Si}(\text{Li})$ detector systems. The samples were produced by $\text{Ir}(^{16}\text{O}, xn)$ reactions and on-line isotope separation. About 50 γ -ray transitions have been assigned to the ^{204}Po decay, ~ 35 of which have been placed in a proposed level scheme for ^{204}Po . The energy of the $8^+ \rightarrow 6^+$ isomeric transition has been deduced to be 12.1 keV , and the half-life of the 8^+ isomer has been measured to be $150 \pm 10 \text{ ns}$. From these data, the $B(E2)$ value of this isomeric transition is found to be 3.7 Weisskopf units. The ^{204}At ground state is assigned an I^π value of 7^+ , which eliminates the need for some low-energy levels in ^{204}At and ^{200}Bi that were tentatively proposed in recent data evaluations, where a 5^+ assignment was made. (31 refs.)

74908 Average resonance capture studies of $^{162,164}\text{Dy}$. D.D.Warner, R.F.Casten, W.R.Kane (Brookhaven Nat. Lab., Upton, NY, USA), W.G.Gelley.

Phys. Rev. C (USA), vol.27, no.5, p.2292-310 (May 1983).
Primary γ -ray transitions in ^{162}Dy and ^{164}Dy have been studied following average resonance neutron capture with neutron beams of mean energy 2 and 24 keV . The averaging process guarantees the observation of the complete set of $J^\pi = 1^+(-), 2^+, 3^+, 4^+(-)$ states in ^{162}Dy (^{164}Dy) up to an excitation energy of 2 MeV . Use of the results of recent Monte Carlo calculations has been made to establish semiquantitative criteria for the J^π assignments. Further spin limitations have been imposed by the study of primary transitions following capture in the 2.72 and 3.68 eV resonances in ^{162}Dy and the 1.71 eV resonance in ^{164}Dy . The known completeness of the set of observed levels has been used to establish a correspondingly complete band structure in both nuclei. The results are discussed in the framework of both the interacting boson approximation and the geometrical model. (30 refs.)

74909 Boson number dependence of $E2$ transition rates in the rotational limit of the interacting boson model. P.Van Isacker (Centro de Estudios Nucleares, Univ. Nacional Autónoma de México, México City, México).

Phys. Rev. C (USA), vol.27, no.5, p.2447-50 (May 1983).
The author derives analytic expressions for $E2$ transition rates in the $\text{SU}(3)$ limit with a general $E2$ operator. With these expressions the influence of the boson number on the properties of a Michailov plot can be studied. (9 refs.)

Low lying yrast states of ^{32}S See Entry 74832

Level structure of the $N=88$ isotones ^{149}Pm , ^{151}Eu and ^{153}Tb See Entry 74833

One- and three-quasiparticle states in $^{127,129,131,133}\text{Xe}$ and their coexistence with band structures See Entry 74839

High-spin states in ^{97}Tc See Entry 74840

The effect of the $\Delta(1236)$ on the g -factor of nucleons See Entry 74845

Nuclear orientation and NMR/ON of $^{205,207}\text{Po}$ See Entry 74846

Description of the neutron deficient Sr and Zr isotopes in the interacting boson model See Entry 74874

Gamow-Teller transition matrix elements See Entry 74910

Identification of 26-minute Zr-84 See Entry 74912

The decay of $56\text{-s } ^{148}\text{Ce}$ to levels of odd-odd ^{148}Pr See Entry 74913

Study of inner bremsstrahlung accompanying non-unique second-forbidden β decay in ^{99}Tc See Entry 74914

Electron capture decay of ^{237}Pu , ^{235}Np , and ^{236}Np See Entry 74917

Electronic rearrangement on molecules accompanying β -decay investigated by nuclear resonance fluorescence See Entry 74918

Application of the microscopic $\text{sp}(3, \text{R})$ model to the giant monopole and quadrupole resonances in ^{16}O See Entry 74947

Yields of products in the spontaneous fission of ^{252}Cf by direct γ -ray spectroscopy See Entry 75056

23.20C Lifetimes and transition probabilities

The effect of the $\Delta(1236)$ on the g -factor of nucleons See Entry 74845

Description of the neutron deficient Sr and Zr isotopes in the interacting boson model See Entry 74874

Fast $\Delta I=0$ M1 transitions in the band crossing region See Entry 74903

Population of ^{133}I from the beta decay of fission product ^{133}Te and the cluster-vibration model See Entry 74905

Levels in ^{204}Po from the decay of ^{204}At See Entry 74907

23.20N Internal conversion and extranuclear effects

One- and three-quasiparticle states in $^{127,129,131,133}\text{Xe}$ and their coexistence with band structures See Entry 74839

Electron capture decay of ^{237}Pu , ^{235}Np , and ^{236}Np See Entry 74917

23.40 BETA DECAY; ELECTRON AND MUON CAPTURE

74910 Gamow-Teller transition matrix elements. F.C.Khanna, I.S.Towner (AECL, Chalk River Nuclear Labs., Chalk River, Ontario, Canada).
AIP Conf. Proc. (USA), no.97, p.406 (1982). [received: May 1983] (Proceedings of the Workshop on the Interaction Between Medium Energy Nucleons in Nuclei, Bloomington, IN, USA, 28-30 Oct. 1982).

Corrections to the off-diagonal Gamow-Teller (GT) transition matrix elements are calculated in a model similar to the one used (Towner and Khanna, 1979) to calculate the diagonal GT matrix elements. The residual interaction is approximated by a finite-range one-boson-exchange potential and a short-range correlation function is introduced. The calculation incorporates the effect of core polarisation (CP) to second order in perturbation theory, meson exchange currents (MEC) and isobar currents. Each of the MBB vertex (M is a meson and B is a nucleon or an isobar) has a monopole form factor. (1 ref.)

74911 Precise Q_β measurements for $A=91$ to 93 mass chains. R.Jafig-liola, M.Chatterjee, H.Dauter, J.K.P.Lee (Foster Radiation Lab., McGill Univ., Montreal, Quebec, Canada).

Can. J. Chem. (Canada), vol.61, no.4, p.694-6 (April 1983).
The Q_β values of $^{91-93}\text{Rb}$, $^{91-93}\text{Sr}$, and $^{92-93}\text{Y}$ were measured using mass-separated Rb sources obtained from an on line isotope separator. A ΔE -E

detector telescope consisting of a $300\text{ }\mu\text{m}\times 300\text{ mm}^2$ Si ΔE - and a $15\text{ mm}\times 500\text{ mm}^2$ Ge(HP) E detector was used. Results are in general agreement with recently published values but some discrepancies are indicated. (12 refs.)

74912 Identification of 26-minute Zr-84. S.Shibata, P.J.Karol (Dept. of Chem., Carnegie-Mellon Univ., Pittsburgh, PA, USA). *Can. J. Chem. (Canada)*, vol.61, no.4, p.754-6 (April 1983). An unknown γ -ray of energy 112.5 keV was found in zirconium fractions chemically extracted from isotopically enriched molybdenum targets bombarded with 500 and 800 MeV protons. All evidence suggests that the γ -ray is identifiable with the decay of ^{84}Zr to ^{84}Y . A half-life of $25.7\pm 0.5\text{ min}$ was obtained for ^{84}Zr , which is considerably longer than previously reported half-lives. The absolute abundance of the 112.5 keV γ -ray was also determined. Relative production cross sections for ^{84}Zr were calculated using these results and were consistent with the values interpolated from isotopic distribution curves for spallation reactions. (8 refs.)

74913 The decay of 56-s ^{148}Ce to levels of odd-odd ^{148}Pr . N.K.Aras, C.Chung, S.Faller, C.A.Stone, W.B.Walters (Dept. of Chem., Univ. of Maryland, College Park, MD, USA), R.L.Gill, M.Schmid, R.E.Chrien. *Can. J. Chem. (Canada)*, vol.61, no.4, p.780-5 (April 1983). The decay of ^{148}Ce to levels of ^{148}Pr has been studied using mass-separated sources. A half-life of $56\pm 1\text{ s}$ has been measured for the decay of ^{148}Ce . A level scheme containing 40 γ -rays and 15 excited levels is proposed for ^{148}Pr . Strongly β -fed 1^+ levels have been identified at 390 and 520 keV that are similar in position to 1^+ levels observed in isotonic ^{146}La and isotopic ^{146}Pr . (18 refs.)

74914 Study of inner bremsstrahlung accompanying non-unique second-forbidden β decay in ^{99}Tc . K.S.Gundu Rao, P.Venkataramiah, K.Gopala, H.Sanjeeviah (Dept. of Phys., Univ. of Mysore, Mysore, India). *J. Phys. G (GB)*, vol.9, no.6, p.691-5 (June 1983).

The inner bremsstrahlung spectrum accompanying non-unique second-forbidden β decay of ^{99}Tc has been measured in the energy region 50-280 keV using a $4.5\times 5.08\text{ cm}^2\text{NaI(Tl)}$ crystal scintillation spectrometer. The magnetic deflection method was employed to prevent β particles from the source reaching the detector. The measured spectrum was unfolded following the method of Liden and Starfelt (1954). The unfolded spectrum was compared with the theoretical distributions of Chang and Falkoff (1949), Lewis and Ford (1957) and Ford and Martin (1969). No agreement between theory and experiment is observed in any case. However, close proximity between experiment and the second-forbidden scalar theory of Chang and Falkoff exists in the energy region 50-150 keV. (19 refs.)

74915 ^{35}Na : a new neutron-rich sodium isotope. M.Langevin, C.Detraz, D.Guillemaud-Mueller (Inst. de Phys. Nucleaire, Orsay, France), A.C.Mueller, C.Thibault, F.Touchard, M.Epierre. *Phys. Lett. B (Netherlands)*, vol.125B, no.2-3, p.116-18 (26 May 1983). ^{35}Na produced by on-line isotope separation has been identified by the detection of β -delayed neutron emission. The measured half-life is $(1.5\pm 0.5)\text{ ms}$. (8 refs.)

74916 Effects of light and heavy Majorana neutrinos in neutrinoless double beta decay. A.Halprin, S.T.Petcov (Univ. of Delaware, Newark, DE, USA), S.P.Rosen.

Phys. Lett. B (Netherlands), vol.125B, no.4, p.335-8 (2 June 1983). The authors examine interference effects between the light neutrino and the heavy neutral lepton exchange amplitudes in neutrinoless double beta ($[\beta\beta]_0$) decay. Using the lower limit on the electron neutrino mass deduced from the tritium end point measurements and the most recent data on neutrinoless double beta decay of tellurium, they obtain an upper limit on the mass of the heavy neutral lepton of about 3 GeV. They also find that the effective Majorana mass parameter associated with the ($\beta\beta$)₀-decay exhibits a strong dependence on the parent nuclear species, and therefore searches for the ($\beta\beta$)₀-decay should be performed for several nuclei simultaneously and independently. (14 refs.)

74917 Electron capture decay of ^{237}Pu , ^{236}Np , and ^{236}Np . I.Ahmad, J.Hines, J.E.Gindler (Chem. Div., Argonne Nat. Lab., Argonne, IL, USA). *Phys. Rev. C (USA)*, vol.27, no.5, p.2239-47 (May 1983). Decay schemes of $45.3\text{-d }^{237}\text{Pu}$ and $1.55\times 10^5\text{ yr }^{236}\text{Np}$ have been investigated by measuring their γ ray and conversion electron spectra with a $5\text{-cm}^2\times 1\text{-cm}$ Ge detector and a cooled Si(Li) spectrometer, respectively. Intensities of γ rays, X-rays, and conversion electrons have been determined and these have been used to derive $\log ft$ values for EC and β^- transitions. In addition to confirming previously known level schemes in ^{237}Pu and ^{236}Np , the energies of the $4^+ \rightarrow 2^+$ and $6^+ \rightarrow 4^+$ transitions in the ^{236}Pu ground state band have been determined. Relative intensities of X-rays in the decay of ^{236}Np have also been measured. (16 refs.)

74918 Electronic rearrangement on molecules accompanying β -decay investigated by nuclear resonance fluorescence. G.Kehlenbeck, J.Ahlert, F.Wolf, L.Ziegler, F.Smend, M.Schumacher (II. Physikalisches Inst., Univ. Göttingen, Göttingen, Germany).

Z. Phys. A (Germany), vol.311, no.4, p.253-7 (1983). Using gaseous ^{60}Co sources, the velocity distribution of ^{60}Ni nuclei after β -decay of ^{60}Co has been measured by the nuclear-resonance-fluorescence coincidence (NRF-C) method. By comparison with model calculations, information is obtained on the rearrangement of electrons on the molecule as a consequence of the change of nuclear charge. In 42% of the rearrangement processes bound (NiL_2^+) or (NiL^+) molecule ions are formed. In 24% the molecule is singly charged but with the bonds between Ni and its molecular partners ruptured. In 34% the charging of more than one molecular partner leads to Coulomb explosion of the molecule. The probability of finding more than one charge on the molecule is larger by a factor of 2 as compared to the probability for electron shake-off on an isolated Ni atom. (22 refs.)

Workshop on Science Underground See Entry 74199

Lepton-violating $\beta^-\beta^-$, $\beta^+\beta^+$ decays, (e^-e^+) conversion and double electron capture in gauge theories See Entry 74648

Evidence concerning Δ -hole states See Entry 74831

σ_+ strength in nuclei See Entry 74881

Nuclear orientation of ^{152}Eu in gold See Entry 74897

Proton capture to excited states of ^{16}O : M1, E1, and Gamow-Teller transitions and shell model calculations See Entry 74904

Population of ^{131}I from the beta decay of fission product ^{133}Te and the cluster-vibration model See Entry 74905

Collective excitations of ^{82}Kr observed by in-beam and decay spectroscopy and their characterization by the interacting boson model See Entry 74906

Levels in ^{204}Po from the decay of ^{204}At See Entry 74907

$\Delta(1236)$ -isobar degrees of freedom and the strength of spin-isospin resonances See Entry 74945

Storage of ultracold neutrons in a vessel long enough for β decay See Entry 75217

An experimental investigation of the pressure and concentration dependence of muonic Coulomb capture and cascade in gases See Entry 75558

23.60 ALPHA DECAY

74919 Surface alpha clustering. I.Rotter (Zentralinst. für Kernforschung, Rossendorf, Germany).

Phys. Rev. C (USA), vol.27, no.5, p.2261-8 (May 1983). The problem of alpha decay is discussed on the basis of a theory which describes discrete and continuous states in a unified manner. A formula for numerical calculations is given in which configurational mixing as well as channel coupling is taken into account. The R -matrix approximation is shown to be justified if the width is spread over a small number of decay channels. Generally, renormalization of the wave function is necessary if a factorization of the width is assumed. The importance of channel coupling for the case of a small reduced width is discussed. (32 refs.)

The isoscalar quadrupole strength distribution above 10 MeV in ^{40}Ca See Entry 74948

23.90 OTHER TOPICS IN NUCLEAR DECAY AND RADIOACTIVITY

Certain rare hypernuclear decays See Entry 74768

24.00 NUCLEAR REACTIONS AND SCATTERING: GENERAL

24.10 NUCLEAR REACTION AND SCATTERING MODELS AND METHODS

74920 Dirac phenomenology for nuclear reactions. J.R.Shepard (Univ. of Colorado, Boulder, CO, USA).

AIP Conf. Proc. (USA), no.97, p.288-98 (1982). [received: May 1983] (Proceedings of the Workshop on the Interaction Between Medium Energy Nucleons in Nuclei, Bloomington, IN, USA, 28-30 Oct. 1982). The application of Dirac phenomenology to nuclear reactions is discussed. The large vector and scalar potentials necessary to describe the nucleon-nucleon spin-orbit interaction are found to enhance the small components of nuclear wavefunctions. This is found to have a potentially large effect on some electron- and nucleon-induced inelastic scattering amplitudes. (15 refs.)

74921 Pion dynamics in the relativistic nuclear many-body problem. B.D.Serot (Inst. for Theoretical Phys., Univ. of California, Santa Barbara, CA, USA).

AIP Conf. Proc. (USA), no.97, p.337-48 (1982). [received: May 1983] (Proceedings of the Workshop on the Interaction Between Medium Energy Nucleons in Nuclei, Bloomington, IN, USA, 28-30 Oct. 1982).

Pion interactions in the nuclear medium are studied using renormalizable relativistic quantum field theories. Previous studies using pseudoscalar πN coupling encountered difficulties due to the large strength of the πNN vertex. These difficulties may be avoided by formulating renormalizable field theories with pseudovector πN coupling using techniques introduced by Weinberg (1967, 1968, 1979) and Schwinger (1967). Calculations are performed for two specific models: the scalar-vector theory of Walecka (1974), extended to include π mesons in a non-chiral fashion, and the linear σ -model with an additional neutral vector meson. The pion propagator is evaluated in the one-nucleon-loop approximation, which corresponds to a relativistic random-phase approximation, which corresponds to a relativistic random-phase approximation built on the Hartree ground state. Virtual NN loops are included, and suitable renormalization techniques are employed. The local-density approximation is used to compare the threshold pion self-energy to the s -wave pion-nucleus optical potential. (18 refs.)

74922 Scattering length in a system of three charged particles. A.A.Kvitsinskii (A.A. Zhdanov Leningrad State Univ., Leningrad, USSR).

JETP Lett. (USA), vol.36, no.10, p.455-7 (20 Nov. 1982). Translation of: *Pis'ma v Zh. Eksp. & Teor. Fiz. (USSR)*, vol.36, no.10, p.375-7 (20 Nov. 1982). [received: June 1983] A modified definition is offered for the scattering length in a system of three charged particles. A correct method for calculating it is described. This method is used to calculate the scattering length for the scattering of the proton by the deuteron. (12 refs.)

74923 Structure-dependent corrections to the parameters of resonant states in light nuclei. T.Delbar, G.Gregoire (Inst. de Phys., Univ. Catholique de Louvain, Louvain-la-Neuve, Belgium), B.Antolkovic, G.Paic.

Phys. Rev. C (USA), vol.27, no.5, p.1897-900 (May 1983). It is shown that the position and width of resonant levels, as deduced from experimental spectra, are dependent upon their structure. The corresponding corrections to get true positions and widths may be considerable for light nuclei. (3 refs.)

74924 Scattering with absorptive interaction: energy-dependent potentials. W.Cassing (Gesellschaft für Schwerionenforschung, Darmstadt, Germany), M.Stingl, A.Weiguny.

Phys. Rev. C (USA), vol.27, no.5, p.1901-12 (May 1983). The energy dependence and analytic structure of the effective interaction for elastic scattering of composite particles are investigated using Feshbach's projection technique. A generalized Levinson theorem is established for complex, nonlocal, and energy-dependent interactions. The analytical results are illustrated by means of Argand diagrams for a solvable model and the effect of energy averaging is discussed. (12 refs.)

74925 Graphical analyses of connected-kernel scattering equations. A.Picklesimer (Dept. of Phys. & Astron., Univ. of Maryland, College Park, MD, USA).

Phys. Rev. C (USA), vol.27, no.5, p.1927-31 (May 1983). Simple graphical techniques are employed to obtain a new (simultaneous) derivation of a large class of connected-kernel scattering equations. This class includes the Rosenberger (1965), Benze-Redish-Sloan (1972, 1973, 1974), and connected-kernel multiple scattering equations as well as a host of generalizations of these and other equations. The basic result is the application of graphical methods to the derivation of interaction-set equations. This yields a

new, simplified form for some members of the class and elucidates the general structural features of the entire class. (19 refs.)

74926 Multiple scattering in the Lee model. M.G.Fuda (Dept. of Phys. & Astron., State Univ. of New York, Amherst, NY, USA). *Phys. Rev. C (USA)*, vol.27, no.5, p.2168-72 (May 1983). It is shown that the amplitude for the scattering of a θ particle from an arbitrary number of fixed N particles in the Lee model can be obtained from Watson's multiple scattering theory if the elementary interaction is taken to be the full θ - N T matrix, including the V -particle pole, and the propagator is taken to be a free particle propagator. (10 refs.)

74927 Nonlocal potentials and their exact and approximate local and velocity-dependent equivalents. H.Fiedeldey, S.A.Sofianos (Phys. Dept., Univ. of S Africa, Pretoria, S Africa). *Z. Phys. A (Germany)*, vol.311, no.4, p.339-49 (1983). The authors show that good approximations to the exact equivalent local potential (ELP) and damping factor of a nonlocal Perey-Buck potential can be calculated in the partial wave WKB approximation of Horiuchi (1980). The exact ELP and damping factor are obtained by means of a method previously given by Fiedeldey (1966, 1967). They also confirm that an approximate ELP proposed by Bauhoff et al. (1980) is of comparable accuracy as the Horiuchi approximation. These l -dependent ELP's exhibit reduced attraction in the interior and provide a test for higher order WKB approximations. They subsequently obtain an equivalent velocity dependent potential (EVDP) which is even exactly wave function equivalent to the original nonlocal potential. This almost local potential, unlike the trivial equivalent local potential, is smooth and well-behaved and is therefore particularly useful in nuclear reactions where the off-shell behaviour of the potential is important. (30 refs.)

74928 Further evidence for 'extra push'. W.Westmeier, R.A.Esterlund, A.Rox, P.Patzelt (Inst. fuer Kernchem., Marburg, Germany). Proceedings of the International Conference on Nucleus-Nucleus Collisions (papers in summary form only received), East Lansing, MI, USA, 26 Sept.-1 Oct. 1982 (East Lansing, MI, USA: Michigan State Univ. 1982), p.109. For massive heavy-ion systems, evidence has appeared which might be interpreted as a need for an extra inward radial velocity at contact for fusion to occur, a so-called 'extra push'. The amount of extra push is related to a parameter called the 'effective fissility' $(Z^2/A)_{\text{eff}}$, and systems with similar $(Z^2/A)_{\text{eff}}$ are expected to be dynamically equivalent. Hence, the systems $^{136}\text{Xe} + ^{208}\text{Pb}$ ($(Z^2/A)_{\text{eff}} = 32.3$) and $^{208}\text{Pb} + ^{48}\text{Ca}$ ($(Z^2/A)_{\text{eff}} = 31.9$) should exhibit equivalent amounts of extra push in their fusion excitation functions. Fusion model calculations based on this concept have been modified via scaling parameters fitted to experimental data, enabling one to calculate phenomenological fusion excitation functions for other heavy-ion reaction systems. The question remains open as to whether or not the scaling parameters derived from the data fits are universally valid as implied by the model. The authors present evidence favoring this thesis. (4 refs.)

74929 A microscopically determined diabatic potential for heavy-ion collisions. A.Lukasiak, W.Cassing, W.Norenberg (Gesellschaft fuer Schwerionenforschung, Darmstadt, Germany). Proceedings of the International Conference on Nucleus-Nucleus Collisions (papers in summary form only received), East Lansing, MI, USA, 26 Sept.-1 Oct. 1982 (East Lansing, MI, USA: Michigan State Univ. 1982), p.123. Heavy-ion collisions in the energy range of a few MeV/n above the Coulomb barrier imply collective velocities \dot{q} which are small compared to the Fermi-velocity ($\dot{q} \ll V_F$) but too large to allow for a description within the static diabatic single-particle representation. Dynamically this means that close to quasi-crossings of the adiabatic levels the nucleon likes to jump to the higher unoccupied level preserving the nodal structure of the wavefunction (Landau-Zener transition probability ≈ 1). In this way the symmetries of the collective motion are restored in the Hamiltonian, i.e. the coupling matrix element given by twice the spacing of the adiabatic levels at the quasi-crossing is neglected. The diabatic s.p. basis approximately corresponds to a basis transformation in which quasi-crossings of adiabatic s.p. motion thus leads to the creation of particle-hole excitations whenever a diabatic level crosses the Fermi-energy. With respect to the collective motion this excitation mechanism gives rise to a conservative potential which partially decays in time due to residual two-body collisions. This energy V_{diab} which can be temporarily stored in the s.p. motion is calculated within the 'diabatic' two-center shell model as a function of various collective degrees of freedom. (3 refs.)

74930 The influence of symmetries and nonadiabatic couplings on the diabatic potential for two colliding heavy ions. A.Lukasiak, W.Cassing, W.Norenberg (Gesellschaft fuer Schwerionenforschung, Darmstadt, Germany). Proceedings of the International Conference on Nucleus-Nucleus Collisions (papers in summary form only received), East Lansing, MI, USA, 26 Sept.-1 Oct. 1982 (East Lansing, MI, USA: Michigan State Univ. 1982), p.124. The concept of a diabatic s.p. representation $\{\phi_k\}$ (Zener 1932) is based on the assumption that the diabatic states smoothly follow changes of the nuclear mean field in contrast to adiabatic states which drastically change their structure in the vicinity of quasi-crossings. The symmetry properties and the nodal structure of these states therefore should be conserved. The radial nonadiabatic couplings $\langle \phi_k | -i\partial/\partial R | \phi_l \rangle$ describe the change of the diabatic states as a function of the collective coordinate and should be small for properly defined diabatic states. One way to achieve this is to assume maximum symmetry for the colliding system because the couplings vanish between states with different symmetries. The authors investigate this effect on the diabatic potential calculated within a representation (a) given by the symmetric two-center oscillator basis. In this case the parity, reflection through the collision plane, rotation and time reversal symmetries are conserved. For comparison also display the diabatic potential for an asymmetric system (b) where the parity and reflection symmetry is violated. The diabatic potential is significantly reduced in this case because the number of the nonadiabatic couplings have increased. (3 refs.)

74931 Scaling properties of hydrodynamical cross sections. N.Balazs, K.Dietrich, B.Schurmman (Phys. Dept., Tech. Univ. Munchen, Munchen, Germany). Proceedings of the International Conference on Nucleus-Nucleus Collisions (papers in summary form only received), East Lansing, MI, USA, 26 Sept.-1 Oct. 1982 (East Lansing, MI, USA: Michigan State Univ. 1982), p.129. Since numerical hydrodynamical calculations have shown that viscosity has little influence on the results the authors restrict themselves to non-viscous isentropic flow. For simplicity they only discuss collisions of equal nuclei. (4 refs.)

74932 Pineuts: a possible explanation for anomalous. W.C.McHarris, J.O.Rasmussen (Nuclear Sci. Div., Lawrence Berkeley Lab., Berkeley, CA, USA).

Proceedings of the International Conference on Nucleus-Nucleus Collisions (papers in summary form only received), East Lansing, MI, USA, 26 Sept.-1 Oct. 1982 (East Lansing, MI, USA: Michigan State Univ. 1982), p.130. A model that could explain the experimental properties of anomalous is the following: They could result from a nuclear halo of 'pineuts', hadronically bound states of a π^- and a few neutrons surrounding a nucleus. Although the s -wave π^-n interaction is repulsive, the p -wave is attractive. Thus, the possibility exists that neutron-rich nuclei (or nuclei with neutron-rich domains, such as the neck in a fissioning system) could have a sufficiently attractive velocity-dependent potential to allow π^-xn hadronically bound 'polynutron' systems. Relativistic heavy-ion collisions provide the best opportunity for forming such states, for it has been found that not only are π^- 's produced in copious quantities, but also they are Coulomb-focused near the same velocity as the projectile and target fragments, bathing the target in a localized, intense flux of π^- 's. Also, the excited nuclear fragments may likely have neutrons in barely-bound orbitals tailing out well beyond the normal nuclear radius. Whether or not free π^-xn clusters are bound, conditions are optimal for forming a nuclear stratospheric halo enriched in pineut clusters. (4 refs.)

74933 Classical limits of the multi-channel formalism via the Vlasov equation. M.J.Rhoades-Brown (Oak Ridge Nat. Lab., Oak Ridge, TN, USA), R.Y.Cusson, P.-G.Reinhardt.

Proceedings of the International Conference on Nucleus-Nucleus Collisions (papers in summary form only received), East Lansing, MI, USA, 26 Sept.-1 Oct. 1982 (East Lansing, MI, USA: Michigan State Univ. 1982), p.135. The authors have compared exact quantum-mechanical coupled-channels calculations of very heavy-ion inelastic scattering reactions with a formalism based on classical dynamical equations of motion plus the quantum-mechanical superposition principle. These studies have prompted further investigation into the classical limits of the quantum-mechanical multi-channel formalism and the role played by complex effective interactions in this limit. With these ideas in mind, the Vlasov equation for the case of a non-Hermitian Hamiltonian has been obtained from the Wigner representation of the density matrix. Solving this Vlasov equation within the classical limit shows that the corresponding classical equations of motion are the ones for a real potential augmented by a new equation for the time-dependent probability that the classical particle remains in its ground state. Classical elastic and absorption cross sections have also been worked out. (3 refs.)

74934 Theory of heavy ion scattering on the basis of the two center shell model. D.Hahn, W.Scheid, J.Y.Park (Justus-Liebig-Universität, Giessen, Germany).

Proceedings of the International Conference on Nucleus-Nucleus Collisions (papers in summary form only received), East Lansing, MI, USA, 26 Sept.-1 Oct. 1982 (East Lansing, MI, USA: Michigan State Univ. 1982), p.136. A model for the scattering of light nuclei is presented which describes the intrinsic nuclear structure on the basis of the two-center shell model (TCSM). The coordinates of this model are the relative coordinate between the nuclei and single-particle coordinates of the nucleons, which are referred to the center of mass of a rotating coordinate system. The basis set of wave functions for the nucleons is taken from the two-center shell model. In deriving the coupled channel equations the nonlocal potential terms are approximated by Taylor expansion. This semi-microscopic theory is applicable and suitable for the study of collective molecular resonance structures in the cross sections of light heavy ion scattering (e.g. $^{12}\text{C} + ^{12}\text{C}$). (2 refs.)

74935 Pauli spinor representations for spin 3/2 operators. G.J.Grube, J.Y.Park (Dept. of Phys., North Carolina State Univ., Raleigh, NC, USA).

Proceedings of the International Conference on Nucleus-Nucleus Collisions (papers in summary form only received), East Lansing, MI, USA, 26 Sept.-1 Oct. 1982 (East Lansing, MI, USA: Michigan State Univ. 1982), p.141. The authors present two types of representations for the spin 3/2 operators. The first representation has been constructed from Group Theoretic calculations. They present the second representations in the form of a generalized algorithm employing the Pauli spinors themselves, not just their elements. They are able to represent all orders of the 3/2 spin operators in terms of the Pauli spin 1/2 operators. Algorithms for the commutation and the anticommutation operators are also presented. (no refs.)

74936 Explicit representations of tensor spin orbit interactions for systems with maximum channel spin 3. G.J.Grube (Dept. of Phys., Illinois State Univ., Normal, IL, USA).

Proceedings of the International Conference on Nucleus-Nucleus Collisions (papers in summary form only received), East Lansing, MI, USA, 26 Sept.-1 Oct. 1982 (East Lansing, MI, USA: Michigan State Univ. 1982), p.142. One of the many interesting effects which may occur in nucleus-nucleus interactions is the spin orbit interaction. If one accepts the present wisdom, then the spin is averaged over the nucleus. For spin effects to be more readily discernible it is required that A be small and spin be large. The deuteron has been used for a long while to investigate spin effects. The representation of the deuteron wave function, which is $\psi_d = c_s \psi_s + c_d \psi_d$ requires that the coefficient c_d for the d state contribution be small. In particular contributions from terms with c_d^2 are usually ignored in calculations. However, there are several other nuclei which possess spins larger than 1/2 and which have quadrupole moments. While nuclei such as ^7Li , ^{10}B , ^{14}N do not possess the small mass, they do have larger d state contributions than the deuteron. In particular, the contribution from terms which contain c_d^2 should not be ignored in calculations. The author therefore, investigated several orders of the tensor spin orbit interactions among some of the nuclei. (no refs.)

Proceedings of the Workshop on the Interaction Between Medium Energy Nucleons in Nuclei See Entry 74200

Coupled channels and quarks in nucleon-nucleon scattering See Entry 74850

Information from quasi-elastic scattering on the nucleon-nucleon interaction in nuclei See Entry 74852

Implication of the nonlocality in the effective N-N interaction: nuclear structure and spin observables See Entry 74853

Three-body forces See Entry 74855

$\Delta(1236)$ -isobar degrees of freedom and the strength of spin-isospin resonances See Entry 74945

Coupling between low-lying nuclear states See Entry 74950

Heavy target fragment yields in the interaction of 28 GeV protons with ^{238}U See Entry 74952

Quantum approach to the nuclear collision process See Entry 74955

Nuclear pion photoproduction: a theory and the $^{16}\text{O}(\gamma, \pi^+)^{16}\text{N}$ (bound) example See Entry 74958

Implications of the experimental results on the photodisintegration of ^4He See Entry 74959

- An analytic distorted wave approximation for intermediate energy proton scattering See Entry 74964
- Proton scattering to collective states: what we learn about the effective interaction in the nuclear medium See Entry 74970
- Microscopic analysis of ^6Li (\bar{p},p), g.s. and ^6Li (\bar{p},p), (2.18 MeV) analyzing powers at 25, 35, and 45 MeV See Entry 74972
- Test of microscopic theory with data for simple transitions in the $^{90}\text{Zr}(\bar{p},p)$ and $^{89}\text{Y}(\bar{p},p)$ reactions See Entry 74973
- Energy dependence of the ratio of isovector effective interaction strengths $|J_{\pi-}/J_{\pi+}|$ from 0° (p,n) cross sections See Entry 74974
- Quasi-elastic scattering of polarised protons at 300 MeV See Entry 74975
- A pragmatic approach to the continuum spectrum in the quasifree scattering See Entry 74976
- The Schrodinger equivalent complex potential and the Dirac phenomenology See Entry 74978
- Nuclear mean free paths and transparency at intermediate energies See Entry 74980
- Low-energy n-p capture as a probe of two-nucleon dynamics See Entry 74984
- Parity violation and related effects in neutron-induced reactions See Entry 74986
- Dirac-equation impulse approximation for intermediate-energy nucleon-nucleus scattering See Entry 74987
- Microscopic formalism for intermediate energy transfer reactions: application to the (p,d) and (d,p) reactions See Entry 74991
- Deformation effect in the fast neutron total cross section of aligned ^{59}Co See Entry 74992
- Enhanced backward emission of heavy fragments in high-energy proton-nucleus collisions See Entry 74994
- Analysis of threshold (p,π^0) reactions See Entry 74995
- Impulse approximation NN amplitudes for proton-nucleus interactions See Entry 74996
- 800 MeV protons as probes of neutron transition densities See Entry 74997
- Measurements of analyzing power for $^2\text{H}(\bar{n},n)^2\text{H}$ scattering at 14.1 MeV and comparisons to $^2\text{H}(\bar{p},p)^2\text{H}$ See Entry 74999
- Double differential cross sections for (p, xn) reactions of ^{64}Zn , ^{65}Cu and ^{89}Y with 26 MeV protons See Entry 75000
- Production of large P_T particles in p-nucleus and nucleus-nucleus collisions at high energies See Entry 75002
- Complete set of first-order polarization observables in nucleon-deuteron elastic scattering near 20 MeV deuteron energy See Entry 75004
- Fragmentation spectra induced by light ions colliding with light nuclei See Entry 75006
- Separation of direct and compound nuclear contributions in inelastic α scattering See Entry 75007
- Phase shift analysis of alpha-particle elastic-scattering angular distributions on the ^{40}Ca target nucleus See Entry 75008
- Baryon rapidity distribution and stopping power of high-energy colliding nuclei See Entry 75014
- Orbiting phenomenon in $^{16}\text{O}, ^{28}\text{Si}$ scattering See Entry 75015
- Energy dependence of the production of pions, kaons and antikaons calculated in the hydrochemical model See Entry 75020
- A phenomenological formula for fusion cross section See Entry 75022
- Universal parametrization of fusion barrier See Entry 75023
- A new critical distance model for heavy-ion fusion reactions See Entry 75024
- Dynamical theory of incomplete fusion reactions See Entry 75028
- Experimental signatures for fast fission See Entry 75029
- A method for analytic evaluation of reaction rates for low energy nucleus-nucleus collisions in a hot gas of nuclei See Entry 75041
- The A dependence and threshold behaviour of the inclusive ($\pi, 2\pi$) reaction for T=0 nuclei See Entry 75049
- Three-body model for p-wave pion- ^{16}O scattering See Entry 75050
- Threshold estimates of ($\pi, 2\pi$) on nuclei in the Fermi gas model: one-body mechanism See Entry 75051
- Fermi motion and Pauli exclusion principle effects in $d(\pi^\pm, \pi^\pm p)n$ in the Δ -resonance region See Entry 75052
- A tool to study collective transitions between excited nuclear states See Entry 75066

24.10H Optical and diffraction models

- 74937 Model study of intermediate state blocking in first-order optical potential theory. Khin Maung Maung, P.C.Tandy (Dept. of Phys., Kent State Univ., Kent, OH, USA). *AIP Conf. Proc. (USA)*, no.97, p.87 (1982). [received: May 1983] (Proceedings of the Workshop on the Interaction Between Medium Energy Nucleons in Nuclei, Bloomington, IN, USA, 28-30 Oct. 1982). Restrictions on the intermediate states allowed for nucleon-nucleon scattering operators embedded in many-nucleon systems can arise in several circumstances. The most familiar is Pauli blocking of the occupied ground-state levels in the nucleon-nucleon G-matrix for nuclear matter. The corresponding projection operator is $Q_{NM} = \theta(p_1 - k_F)\theta(p_2 - k_F)$. The first-order optical potential from Watson multiple scattering theory involves a nucleon-nucleon scattering operator in which intermediate states of the struck nucleon corresponding to the target ground state are projected out. The corresponding projection operator is $Q = 1 - |\phi_0\rangle\langle\phi_0|$ where $|\phi_0\rangle$ is the target ground state. A simple model of the free NN t-matrix is employed to study and compare the effects of intermediate-state modifications through both these operators. Particular attention is paid to the unitarity properties of the resulting modified NN scattering operator for first-order optical potentials. (no refs.)
- 74938 Physics limitations of the optical model. N.Austern (Univ. of Pittsburgh, Pittsburgh, PA, USA). *AIP Conf. Proc. (USA)*, no.97, p.115-20 (1982). [received: May 1983] (Proceedings of the Workshop on the Interaction Between Medium Energy Nucleons in Nuclei, Bloomington, IN, USA, 28-30 Oct. 1982). Aspects of optical potential theory are discussed. The author tries to approach the OP from its applications. (15 refs.)

- 74939 First order interpretation of optical potentials. L.Ray (Dept. of Phys., Univ. of Texas, Austin, TX, USA). *AIP Conf. Proc. (USA)*, no.97, p.121-42 (1982). [received: May 1983] (Proceedings of the Workshop on the Interaction Between Medium Energy Nucleons in Nuclei, Bloomington, IN, USA, 28-30 Oct. 1982). The theoretical understanding of intermediate energy proton-nucleus observables in terms of nucleon-nucleon phenomenology and nonrelativistic multiple scattering theory is discussed. Specifically, the ability of local, second order, spin-dependent Kerman, McManus and Thaler (1959) optical potential models to describe proton-nucleus elastic scattering data from 300-800 MeV is reviewed. Calculations which rely on impulse approximation are fairly successful at 800 MeV but fail significantly for energies less than 500 MeV. Evidence is presented which indicates that medium effects are quite important in modifying the true proton-nucleon effective interaction from that given by the impulse approximation throughout the intermediate energy range, even at 800 MeV. It is concluded that the trends of the intermediate energy optical potentials can be accounted for qualitatively in terms of non-relativistic multiple scattering theory and medium modified effective interactions. The Glauber model and Dirac phenomenological approaches are briefly discussed. (49 refs.)
- 74940 Separable representation of the nonlocality of optical model potentials. G.Rawitscher (Univ. of Connecticut, Storrs, CT, USA). *AIP Conf. Proc. (USA)*, no.97, p.150 (1982). [received: May 1983] (Proceedings of the Workshop on the Interaction Between Medium Energy Nucleons in Nuclei, Bloomington, IN, USA, 28-30 Oct. 1982). Summary form only given, as follows. The nonlocality which is due to the coupling of the elastic channel to nuclear excited states is usually written in terms of Green's functions and inelastic transition potentials. The Green's functions can in turn be expanded in a sum of separable terms if positive energy Weinberg states are used as discrete basis sets in all channels, and the resulting expansion for the nonlocal optical potential becomes separable. If in addition a projection onto the elastic channel Weinberg states is performed, then the number of terms in the separable expansion is reduced to a practical number. Applications to nucleon-nucleus scattering at intermediate energies are envisaged. (1 ref.)
- 74941 Dirac phenomenology and the nuclear optical model. B.C.Clark, S.Hama (Dept. of Phys., Ohio State Univ., Columbus, OH, USA), R.L.Mercer. *AIP Conf. Proc. (USA)*, no.97, p.260-87 (1982). [received: May 1983] (Proceedings of the Workshop on the Interaction Between Medium Energy Nucleons in Nuclei, Bloomington, IN, USA, 28-30 Oct. 1982). A Dirac equation based optical model treatment of proton-nucleus scattering is discussed. Results obtained using a relativistic optical model consisting of Lorentz scalar and Lorentz four-vector components are given. The parameters in the model have been varied to obtain high quality fits to elastic differential cross section, analyzing power, and spin rotation function measurements. Features of these Dirac optical model potentials are compared with various theoretical relativistic calculations. (39 refs.)
- 74942 Diffraction scattering off strongly bound system. V.E.Kuzmichev (Phys. Inst., Univ. Bonn, Bonn, Germany). *Phys. Rev. C (USA)*, vol.27, no.5, p.2158-67 (May 1983). The scattering of a hadron on a strongly bound system of two hadrons (a dihadron) is considered in the high-energy limit for the relative hadron dihadron motion. The dihadron scatterer motion and the internal interaction are included in the author's consideration. It is shown that only small values of the internal transfer momentum of dihadron particles bring the principal contribution to the three-particle propagator in the eikonal approximation. On the basis of the exact analytical solution of the integral equation for the total Green's function the scattering amplitude is derived. It is shown that the scattering amplitude contains only single, double, and triple scattering terms. Three new terms to the Glauber formula for the total cross section are obtained. These terms decrease both the effective hadron-hadron cross section and the screening correction. (9 refs.)
- 74943 Selective transparency in the region of resonances. I.Rotter (Zentralinst. fur Kernforschung Rossendorf, Dresden, Germany). Proceedings of the International Conference on Nucleus-Nucleus Collisions (papers in summary form only received), East Lansing, MI, USA, 26 Sept.-1 Oct. 1982 (East Lansing, MI, USA: Michigan State Univ. 1982), p.126. The selective transparency in the region of resonances is a non-statistical effect. It should be taken into account in the analysis of the data by an imaginary part of the optical potential which has a resonance-like dependence on energy at the position of resonances. (3 refs.)
- 74944 Mean free path of a nucleon in nucleus-nucleus collision. B.Sinha (Nuclear Phys. Div., Bhabha Atomic Res. Centre, Bombay, India). Proceedings of the International Conference on Nucleus-Nucleus Collision (papers in summary form only received), East Lansing, MI, USA, 26 Sept.-1 Oct. 1982 (East Lansing, MI, USA: Michigan State Univ. 1982), p.131. The mean free path of a nucleon for two colliding nuclei has been calculated in terms of the imaginary part of the optical potential and the k effective mass. The nucleon belonging to a nucleus differs from the free nucleon in two substantial ways—the nucleon for colliding nuclei is dressed with internal Fermi motion and secondly, the Pauli blocking due to the occupied intrinsic states of the nuclei will tend to inhibit interaction between nucleons of the two nuclei unless the relative energy far exceeds the Fermi energy when Pauli blocking gets switched off. The internal motion energy of the nucleon is taken into account using a Fermi Gas model; Pauli blocking on the other hand is incorporated using a simple geometric model so that the distorted Fermi momentum is now expressed in terms of the undistorted momenta and the distortion factor F, the fractional volume of Fermi sphere which does not overlap with each other. An intrinsic 'temperature' dependence arising due to the diffuseness of the Fermi sphere is also taken into account. (2 refs.)
- Real part of the nuclear interaction potential between α or p and excited heavy nuclei See Entry 74864
- The heavy-ion potential and its increasing transparency at intermediate energies See Entry 74865
- Mass dependence of the real optical model potential for light ions See Entry 74868
- Relativistic Brueckner-Hartree-Fock theory: theoretical foundations and empirical evidence See Entry 74880
- Microscopic optical potentials See Entry 74885
- Correlated basis theory of nucleon optical potential in nuclear matter See Entry 74886
- The imaginary part of the relativistic optical potential See Entry 74887
- Pion dynamics in the relativistic nuclear many-body problem See Entry 74921
- Proton and neutron elastic scattering between 80 and 1000 MeV See Entry 74965

- Anomaly in the optical potential for deformed nuclei See Entry 74966
 Microscopic analysis of proton elastic scattering in the range 80-200 MeV See Entry 74967
 Momentum-space optical potential and elastic scattering calculations See Entry 74968
 A theory for proton-⁴He scattering See Entry 74969
 Quasi-elastic scattering of polarised protons at 300 MeV See Entry 74975
 1 GeV P-⁴⁰Ca elastic scattering See Entry 74985
 Antiproton-nucleus interaction at low energy See Entry 74989
 Calculation of the energy-averaged scattering function for high resolution low-energy neutron scattering data See Entry 74990
 Deformation effect in the fast neutron total cross section of aligned ⁵⁹Co See Entry 74992
 Neutron-nucleus spin-spin interaction in the low MeV range .. See Entry 74993
 800 MeV protons as probes of neutron transition densities See Entry 74997
 Proton isotonic density differences from 0.8 GeV proton-nucleus elastic scattering See Entry 74998
 Elastic scattering of ²⁰Ne on ²⁴Mg See Entry 75019

24.30 RESONANCE REACTIONS AND SCATTERING

74945 $\Delta(1236)$ -isobar degrees of freedom and the strength of spin-isospin resonances. J.Speth (Inst. fur Kernphys., KFA Julich, Julich, Germany). *AIP Conf. Proc. (USA)*, no.97, p.398-403 (1982). [received: May 1983] (Proceedings of the Workshop on the Interaction Between Medium Energy Nucleons in Nuclei, Bloomington, IN, USA, 28-30 Oct. 1982). The most interesting feature of the spin-isospin modes excited in charge-exchange reactions is the magnitude of the transition strength. In the case of the Gamow-Teller resonances (GTR) there exists a well established, model-independent, sum rule by Ikeda et al. (1961). So far only about 60% of this sum rule strength has been detected experimentally. Conventional nuclear structure effects seem to be unable to explain the 'missing' GT-strength. The Δ -isobar degrees of freedom play an important role in the quenching of the axial-vector coupling constant g_A . The author presents a consistent calculation of different experimental quantities in the 48 Ca-region which are all connected with the spin-isospin part of the particle-hole interaction. This part of the force is of crucial importance in connection with the 'quenching'. (9 refs.)

74946 Quasimolecular and cluster states of light nuclei as examples of intermediate structure. J.Cseh (Inst. of Nuclear Res., Hungarian Acad. of Sci., Debrecen, Hungary). *J. Phys. G (GB)*, vol.9, no.6, p.655-63 (June 1983). 4⁺, 6⁺ and 8⁺ resonances of the ¹²C+¹²C system, 5/2⁺ and 7/2⁺ cluster states of ¹⁹F and 0⁺ resonances from α scattering on ²⁴Mg and ²⁶Mg are analysed as intermediate structure data. Parameters of the underlying simple states and the couplings are deduced. (16 refs.)

74947 Application of the microscopic sp(3,R) model to the giant monopole and quadrupole resonances in ¹⁶O. M.G.Vassanji, D.J.Rowe (Dept. of Phys., Univ. of Toronto, Toronto, Ontario, Canada). *Phys. Lett. B (Netherlands)*, vol.125B, no.2-3, p.103-5 (26 May 1983). The microscopic sp(3,R) model is applied to the ground-state representation of ¹⁶O and the properties of the first few 0⁺ and 2⁺ states, including energies, RMS radii, and transition strengths, are calculated. The lowest excited 0⁺ and 2⁺ states are interpreted as giant resonances, the properties of the 2⁺ state are compared with experimental data in the resonance region. (11 refs.)

74948 The isoscalar quadrupole strength distribution above 10 MeV in ⁴⁰Ca. F.Zwarts, A.G.Drentje, M.N.Harakeh, A.van der Woude (Kernfysisch Versneller Inst., Groningen, Netherlands). *Phys. Lett. B (Netherlands)*, vol.125B, no.2-3, p.123-7 (26 May 1983). From angular correlation measurements of α_0 decay to the ³⁶Ar ground state, the isoscalar E2 strength distribution between 10 and 16 MeV in ⁴⁰Ca has been found to be concentrated in the interval $E_x=12.5-15.5$ MeV and to exhaust about 12% of the EWSR in the α_0 channel and about (45⁺¹⁰₋₁₅)% if extrapolated to all channels. (22 refs.)

74949 Fluid dynamics of giant resonances of high spin states. M.di Nardo, M.di Toro, G.Giansiracusa, U.Lombardo, G.Russo (Istituto Dipartimentale di Fisica, Univ. di Catania, Catania, Italy). *Phys. Lett. B (Netherlands)*, vol.125B, no.4, p.240-4 (2 June 1983). The authors describe giant resonances built on high spin states along the yrast line as scaling solutions of a linearized Vlasov equation in a rotating frame obtained from a TDHF theory in phase space. For oblate cranked solutions they get a shift and a splitting of the isoscalar giant resonances in terms of the angular velocity. Results are shown for ⁴⁰Ca and ¹⁶⁸Er. The relative CM strengths are also calculated. (20 refs.)

- Theory of giant resonances See Entry 74883
 Gamma radiation from ⁵⁰Cr(p,p')⁵⁰Cr at E=5.45-6.15 MeV .. See Entry 74901
 The moments of strength functions See Entry 74902
 Proton capture to excited states of ¹⁶O: M1, E1, and Gamow-Teller transitions and shell model calculations See Entry 74904
 Structure-dependent corrections to the parameters of resonant states in light nuclei See Entry 74923
¹³C(γ ,p) cross section See Entry 74960
 The concept of vibrational resonances associated with the secondary and tertiary wells of a multi-humped fission barrier See Entry 75060
 A tool to study collective transitions between excited nuclear states See Entry 75066
 Simulation of neutron transmission by fission nuclei in the region of unresolved resonances See Entry 75150

24.50 DIRECT REACTIONS

74950 Coupling between low-lying nuclear states. M.Ichimura (Inst. of Phys., Univ. of Tokyo, Tokyo, Japan). *AIP Conf. Proc. (USA)*, no.97, p.192-204 (1982). [received: May 1983] (Proceedings of the Workshop on the Interaction Between Medium Energy Nucleons in Nuclei, Bloomington, IN, USA, 28-30 Oct. 1982). Various treatments for nuclear direct reactions are briefly reviewed and some problems inherent to them are observed. Effects of coupling in deuteron breakup channels, discrete inelastic channels and rearrangement channels are discussed with the following examples: ⁵⁸Ni(d,p)⁵⁹Ni(p_{3/2}), ²⁴Mg(p,d)²³Mg(1/2⁺), and ²⁰⁸Pb(p,t)²⁰⁸Pb(3⁺). (40 refs.)

74951 Momentum transfer in the fragmentation of copper by 400-GeV protons. J.B.Cumming (Chem. Dept., Brookhaven Nat. Lab., Upton, NY, USA). *Can. J. Chem. (Canada)*, vol.61, no.4, p.697-700 (April 1983). Mean momenta transferred to products of the fragmentation of copper by 400-GeV protons have been determined by the thick-target thick-catcher technique. Comparison with data for incident protons and heavy ions indicates that the limiting fragmentation region has been reached and supports a simple relationship between momentum and energy transfers in peripheral reactions which had been proposed previously. (26 refs.)

74952 Heavy target fragment yields in the interaction of 28 GeV protons with ²³⁸U. B.V.Jacak, W.Loveland, D.J.Morrissey, P.L.McGaughey, G.T.Seborg (Lawrence Berkeley Lab., Univ. of California, Berkeley, CA, USA).

Can. J. Chem. (Canada), vol.61, no.4, p.701-7 (April 1983). The yields of target fragments from the interaction of 28 GeV protons with ²³⁸U have been measured, with special attention being given to those fragments with 160≤A≤200. From the measured fragment yields, isobaric production cross sections were calculated. Significant yields ($\sigma(A)\sim 1-10$ mb) of heavy target fragments (160≤A≤210) were found. These fragments are believed to be the non-fissioning survivors from the population of highly excited residual nuclei produced in the initial p-nucleus collision. A pedagogical calculation of the fission-particle emission competition shows how the initial highly excited heavy nuclei could evaporate ~20-50 particles while surviving fission competition. (42 refs.)

74953 Coulomb forces in the three-body problem with application to direct nuclear reactions. A.Osman (Internat. Centre for Theoretical Phys., Trieste, Italy).

Int. J. Theor. Phys. (USA), vol.22, no.4, p.341-53 (April 1983). Faddeev equations are considered in the case of three charged particles interacting with both separable nuclear two-body interactions and also including Coulomb forces. Modified Faddeev equations with Coulomb Green's functions are introduced. The three-body amplitudes are given into pure Coulomb and distorted-Coulomb amplitudes. Introducing a decomposition in the angular momentum states, a set of three-body integral equations is obtained. The effect of pure Coulomb amplitudes is studied in direct nuclear reactions and found to give a large contribution to the cross sections. The three-body integral equations obtained are applied for direct nuclear reactions. The angular distributions for ¹²C(⁶Li,d)¹⁶O, ¹⁶O(⁶Li,d)²⁰Ne, and ¹²C(⁶Li, α)¹⁴N transfer reactions are calculated as well as for the ⁶Li elastic scattering on ¹²C. From the good agreement between the theoretically calculated and experimental data, better spectroscopic factors are extracted. The effect of including Coulomb forces in the three-body problem is found to improve the results by about 16.26%. (27 refs.)

Information from quasi-elastic scattering on the nucleon-nucleon interaction in nuclei See Entry 74852

Gamma radiation from ⁵⁰Cr(p,p')⁵⁰Cr at E=5.45-6.15 MeV .. See Entry 74901

Quasi-elastic scattering of polarised protons at 300 MeV See Entry 74975

A pragmatic approach to the continuum spectrum in the quasifree scattering See Entry 74976

Microscopic formalism for intermediate energy transfer reactions: application to the (p,d) and (d,p) reactions See Entry 74991

Enhanced backward emission of heavy fragments in high-energy proton-nucleus collisions See Entry 74994

Separation of direct and compound nuclear contributions in inelastic α scattering See Entry 75007

24.60 STATISTICAL THEORY AND FLUCTUATIONS

74954 A numerical method for two-dimensional Fokker-Planck equation. Yang Ying-hui, Wu Xi-zhen, Peng Qing-quan (Inst. of Atomic Energy, Acad. Sinica, Beijing, China).

Commun. Theor. Phys. (China), vol.1, no.4, p.507-13 (1982). A general method for solving the two-dimensional F-P equation numerically is presented which can be applied to the study of the fission processes of systems with any forms of potentials and any viscosity as well as other processes, such as heavy ion collisions. (5 refs.)

74955 Quantum approach to the nuclear collision process. P.Danielewicz (Lawrence Berkeley Lab., Univ. of California, Berkeley, CA, USA). Proceedings of the International Conference on Nucleus-Nucleus Collisions (papers in summary form only received), East Lansing, MI, USA, 26 Sept.-1 Oct. 1982 (East Lansing, MI, USA: Michigan State Univ. 1982), p.132. Contrary to common belief nuclear collisions cannot be described classically at hundreds MeV/nucleon beam energies. At the initial stage of a (200-800) MeV/nucleon collision, the mean time τ between successive NN collisions is of the order of $1/(n_0\sigma v)\approx(1.7-3.5)$ fm/c. The value of τ implies uncertainties of nucleon energies in subsequent collisions $\hbar/\tau\approx(55-115)$ MeV. The uncertainties are comparable with values of nucleon energies in the mid-rapidity frame. The author has examined the role of quantum dynamics in high-energy nuclear collisions. He carries out numerical calculations of collisions in an interpreting nuclear-matter model. The quantum dynamics has been compared to a classical Markovian dynamics given by the Boltzmann equation. In quantum calculations, methods of nonequilibrium Green's functions have been employed. (3 refs.)

74956 Statistical generation of complete events in energetic nuclear collisions. G.Fai, J.Randrup (Lawrence Berkeley Lab., Univ. of California, Berkeley, CA, USA).

Proceedings of the International Conference on Nucleus-Nucleus Collisions (papers in summary form only received), East Lansing, MI, USA, 26 Sept.-1 Oct. 1982 (East Lansing, MI, USA: Michigan State Univ. 1982), p.133. While previous studies of medium and high-energy nuclear collisions were mostly focused on inclusive observables, recent improvements in instrumentation demand that nearly exclusive quantities be addressed. As a first step in this direction, the authors have developed a statistical model for complete multi-fragment events in energetic nuclear collisions. This model can provide a useful reference against which more refined models, as well as the bias introduced by specific detection systems, can be judged. (4 refs.)

74957 The 'Time-Dependent Hauser-Feshbach' equation for multi-step compound processes. K.W.McVoy, X.T.Tang (Phys. Dept., Univ. of Wisconsin, Madison, WI, USA).

Proceedings of the International Conference on Nucleus-Nucleus Collisions (papers in summary form only received), East Lansing, MI, USA, 26 Sept.-1 Oct. 1982 (East Lansing, MI, USA: Michigan State Univ. 1982), p.134. Although the exciton model of pre-compound reactions was proposed in 1966, full-scale analyses of the general 'multi-step compound' contribution to the

energy-averaged cross section have only been developed in recent years. These multi-doorway models assume the existence of (a) fine-structure levels which overlap, (b) a 'class' of doorway levels (e.g. $(n+1)$ -particle n -hole states) feeding them which (after 'spreading') overlap, (c) a class of broader doorways (e.g. n -particle, $(n-1)$ -hole states) feeding them which after spreading overlap, etc.—i.e. a hierarchy of doorway classes. Although these doorways are by definition not eigenstates of the full Hamiltonian, one of the important concepts to emerge from recent analyses is that of 'eigenclasses' σ , i.e. linear combinations of the doorway and fine-structure classes which diagonalize the matrix that couples the doorway classes and permit the multi-step compound cross section to be written as a sum of Hauser-Feshbach-type cross sections. (1 ref.)

- Real part of the nuclear interaction potential between α or p and excited heavy nuclei See Entry 74864
 Gamma radiation from $^{50}\text{Cr}(p,p'\gamma)^{50}\text{Cr}$ at $E=5.45\text{--}6.15$ MeV See Entry 74901
 Scattering with absorptive interaction: energy-dependent potentials See Entry 74924
 Pineuts: a possible explanation for anomalies See Entry 74932
 A pragmatic approach to the continuum spectrum in the quasifree scattering See Entry 74976
 A global study of the $p+^{27}\text{Al}$ reaction at 180 MeV See Entry 74977
 Enhanced backward emission of heavy fragments in high-energy proton-nucleus collisions See Entry 74994
 Double differential cross sections for (p, xn) reactions of ^{64}Zn , ^{65}Cu and ^{89}Y with 26 MeV protons See Entry 75000
 Separation of direct and compound nuclear contributions in inelastic α scattering See Entry 75007
 Elastic scattering of heavy ions and the compressibility of nuclear matter See Entry 75009
 Measurement of kinetic flow parameters for relativistic collisions of Ne on NaF and Ar on Pb_3O_4 See Entry 75017
 Energy dependence of the production of pions, kaons and antikaons calculated in the hadrochemical model See Entry 75020
 Threshold estimates of $(\pi, 2\pi)$ on nuclei in the Fermi gas model: one-body mechanism See Entry 75051
 Fission probability in the $^{232}\text{Th}(p,p'xn)$ reaction at low energy See Entry 75055
 Induced nuclear fission viewed as a diffusion process: transients See Entry 75062
 Simulation of neutron transmission by fission nuclei in the region of unresolved resonances See Entry 75150

24.70 POLARIZATION IN REACTIONS AND SCATTERING

- Nuclear polarization and sign of the quadrupole moment of the $^{54}\text{Fe}(10^+)$ isomer See Entry 74835
 Implication of the nonlocality in the effective N-N interaction: nuclear structure and spin observables See Entry 74853
 Proton capture to excited states of ^{16}O : $M1$, $E1$, and Gamow-Teller transitions and shell model calculations See Entry 74904
 Dirac phenomenology and the nuclear optical model See Entry 74941
 Anomaly in the optical potential for deformed nuclei See Entry 74966
 Microscopic analysis of proton elastic scattering in the range 80-200 MeV See Entry 74967
 Microscopic analysis of ^6Li ($\bar{p},p,g.s.$ and $^6\text{Li}(\bar{p},p')$ (2.18 MeV) analyzing powers at 25, 35, and 45 MeV See Entry 74972
 Quasi-elastic scattering of polarised protons at 300 MeV See Entry 74975
 Future prospects in N-nucleus interactions See Entry 74979
 Low-energy n-p capture as a probe of two-nucleon dynamics See Entry 74984
 Deformation effect in the fast neutron total cross section of aligned ^{59}Co See Entry 74992
 Neutron-nucleus spin-spin interaction in the low MeV range See Entry 74993
 Impulse approximation NN amplitudes for proton-nucleus interactions See Entry 74996
 Proton isotonic density differences from 0.8 GeV proton-nucleus elastic scattering See Entry 74998
 Measurements of analyzing power for $^2\text{H}(\bar{n},n^2)\text{H}$ scattering at 14.1 MeV and comparisons to $^2\text{H}(\bar{p},p^2)\text{H}$ See Entry 74999
 Polarization transfer in $A(\bar{d},pX)$ reactions See Entry 75003
 Complete set of first-order polarization observables in nucleon-deuteron elastic scattering near 20 MeV deuteron energy See Entry 75004
 Study of spin polarization of residual nuclei in heavy ion reactions by γ -ray circular polarization measurement See Entry 75018

24.75 GENERAL PROPERTIES OF FISSION

- Effect of intrinsic degrees of freedom on the quantum tunneling of a collective variable See Entry 74298
 Experimental signatures for fast fission See Entry 75029
 The concept of vibrational resonances associated with the secondary and tertiary wells of a multi-humped fission barrier See Entry 75060

25.00 NUCLEAR REACTIONS AND SCATTERING: SPECIFIC REACTIONS

25.10 NUCLEAR REACTIONS AND SCATTERING INVOLVING FEW-NUCLEON SYSTEMS

- Scattering length in a system of three charged particles. See Entry 74922
 A theory for proton- ^3He scattering See Entry 74969
 Low-energy n-p capture as a probe of two-nucleon dynamics See Entry 74984

Production of large P_T particles in p-nucleus and nucleus-nucleus collisions at high energies See Entry 75002

Complete set of first-order polarization observables in nucleon-deuteron elastic scattering near 20 MeV deuteron energy See Entry 75004

25.20 PHOTONUCLEAR REACTIONS AND PHOTON SCATTERING

74958 Nuclear pion photoproduction: a theory and the $^{16}\text{O}(\gamma,\pi^+)^{16}\text{N}(\text{bound})$ example. R.A.Eramzhyan (Inst. of Nuclear Res., Acad. of Sci., Moscow, USSR), M.Gmitro, S.S.Kamalov, R.Mach. *J. Phys. G (GB)*, vol.9, no.6, p.605-19 (June 1983).

A momentum-space expression for the nuclear pion photoproduction amplitude has been obtained and suitable approximations for it have been developed. Such a formulation naturally includes all pion-momentum-dependent terms of the amplitude and allows for an easy simultaneous treatment of several effects such as nucleon Fermi motion, relativistic and gauge invariance of the pion-nucleus photoproduction amplitude and multiple rescattering of pions. They all make important contributions to the photoproduction cross section. The $^{16}\text{O}(\gamma,\pi^+)$ reaction leading to the bound states of ^{16}N is analysed as an example. (27 refs.)

74959 Implications of the experimental results on the photodisintegration of ^4He . J.R.Calarco (Dept. of Phys., Univ. of New Hampshire, Durham, NH, USA), B.L.Berman, T.W.Donnelly. *Phys. Rev. C (USA)*, vol.27, no.5, p.1866-75 (May 1983).

The photoproton and photoneutron cross sections for ^4He are evaluated in the light of several recent measurements, and are found to be substantially different in the energy region below 30 MeV. Because these cross sections are dominated by $\Delta S=0$, $\Delta T=1$ E1 transitions, this result implies strong isospin mixing in the four-nucleon system. Furthermore, since available continuum shell-model calculations including Coulomb effects predict only small differences in the photoproton and photoneutron cross sections except near threshold, this result suggests that a nonzero charge asymmetry is present in the nuclear force. (53 refs.)

74960 $^{13}\text{C}(\gamma,p)$ cross section. D.Zubonov, R.A.Sutton, M.N.Thompson (School of Phys., Univ. of Melbourne, Parkville, Victoria, Australia), J.W.Jury. *Phys. Rev. C (USA)*, vol.27, no.5, p.1957-60 (May 1983).

A high resolution measurement of the $^{13}\text{C}(\gamma,p)$ cross section is presented from threshold to 28 MeV. In combination with the known $^{13}\text{C}(\gamma,n)$ cross section an estimate of the total absorption cross section is obtained and compared with current theoretical predictions. An estimate of the distribution of the isospin components in the giant dipole resonance shows the isospin splitting and the relative T_- and T_+ strengths are in agreement with predictions. (31 refs.)

74961 Measurement of the photoneutron yield in the irradiation of heavy materials in closed shells. E.G.Golikov, G.M.Vasnin, Yu.A.Koyazin (S.M. Kirov, Ural Polytech. Inst., Sverdlovsk, USSR). *Sov. J. Nondestr. Test. (USA)*, vol.18, no.9, p.682-4 (Sept. 1982). Translation of: *Defektoskopiya (USSR)*, vol.18, no.9, p.19-21 (Sept. 1982).

In the inspection of the technological parameters in the production of fissionable materials and nuclear fuel waste, it is necessary to place these materials behind a shielding shell (pipeline, fuel element, container, etc.). Because of the favorable nuclear physical properties of heavy materials, radiation methods with external radiation sources, particularly the high-energy beams of bremsstrahlung from electron accelerators appear highly suitable for this type of inspection. An all-wave counter was used to examine the dependence of the integral neutron yield in the irradiation of specimens of ^{238}U and ^{235}U in a flux of bremsstrahlung of a betatron with a spectrum endpoint energy of up to 25 MeV and of a combined object in a mixture of ^{238}U and ^{235}U isotopes in steel containers with a varying wall thickness. (8 refs.)

74962 Experimental investigation of the reaction $^{12}\text{C}(\gamma, \pi^0)X$ in the photon energy range between threshold and 450 MeV. J.Arends, N.Floss, A.Hege-rath, B.Mecking, G.Noldeke, R.Stenz (Physikalisches Inst., Univ. Bonn, Bonn, Germany).

Z. Phys. A (Germany), vol.311, no.4, p.367-74 (1983). The photoproduction of neutral pions on ^{12}C has been investigated between threshold and 450 MeV photon energy using a tagged photon beam at the Bonn 500 MeV synchrotron and a large acceptance detector. The π^0 detector consists of cylindrical wire chambers covering a solid angle of nearly 4π . Using a scintillation counter as an active ^{12}C target an attempt was made to separate coherent and incoherent π^0 photoproduction. The measured total and differential cross sections are compared to corresponding theoretical calculations. (20 refs.)

Yields of the photofission products of ^{237}Np See Entry 75063

25.30 LEPTON-INDUCED REACTIONS AND SCATTERING

74963 Structure functions for the electrodisintegration of the deuteron at a momentum transfer of 1.8 GeV^2 . Yu.I.Titov, A.S.Esaulov, E.V.Inopin, R.V.Akhmerov, E.M.Smelov (Physicotech. Inst., Acad. of Sci., Ukrainian SSR).

JETP Lett. (USA), vol.36, no.7, p.321-4 (5 Oct. 1982). Translation of: *Pis'ma v Zh. Eksp. & Teor. Fiz. (USSR)*, vol.36, no.7, p.262-5 (5 Oct. 1982). [received: May 1983]

Structure functions are found for the electrodisintegration of the deuteron near the threshold in the relativistic region with $q_{\text{max}}^2=1.8 \text{ GeV}^2$ and $\nu=0.5\text{--}0.65 \text{ GeV}$. (10 refs.)

Dirac phenomenology for nuclear reactions See Entry 74920

25.40 NUCLEON-INDUCED REACTIONS AND SCATTERING

(see also 28.20 Neutron physics)

74964 An analytic distorted wave approximation for intermediate energy proton scattering. F.di Marzio, K.Amos (School of Phys., Univ. of Melbourne, Parkville, Victoria, Australia).

Aust. J. Phys. (Australia), vol.36, no.2, p.135-53 (1983).

An analytic distorted wave approximation (ADWA) has been developed for use in analyses of intermediate energy inelastic proton scattering from nuclei. Applications are made to analyse 402 and 800 MeV data from the isoscalar and isovector 1^+ and 2^+ states in ^{12}C and to the 800 MeV data from the excitation of the $2^-(8.88 \text{ MeV})$ state in ^{16}O . Comparisons of predictions

made using different model two-nucleon t matrices and different models of nuclear structure are given. (13 refs.)

74965 Proton and neutron elastic scattering between 80 and 1000 MeV. P.Schwandt (Indiana Univ., Bloomington, IN, USA). *AIP Conf. Proc. (USA)*, no.97, p.89-109 (1982). [received: May 1983] (Proceedings of the Workshop on the Interaction Between Medium Energy Nucleons in Nuclei, Bloomington, IN, USA, 28-30 Oct. 1982). Reviews the available experimental data for nucleon-nucleus elastic scattering in the intermediate-energy regime (which, in nuclear physics, conventionally ranges from pion production threshold up to ~ 1 GeV; the author actually shows and discusses data for energies down to 80 MeV). The author discusses the description of these data in terms of conventional optical-model phenomenology, i.e. the 'standard' optical model based on Woods-Saxon potentials. The failures of the standard optical model and improvements of the phenomenology are described. (33 refs.)

74966 Anomaly in the optical potential for deformed nuclei. H.Sakaguchi, F.Ohtani, N.Nakamura, T.Noro, H.Sakamoto, H.Ogawa, T.Ichihara, M.Yoshi, S.Kobayashi (Dept. of Phys., Kyoto Univ., Kyoto, Japan). *AIP Conf. Proc. (USA)*, no.97, p.143-7 (1982). [received: May 1983] (Proceedings of the Workshop on the Interaction Between Medium Energy Nucleons in Nuclei, Bloomington, IN, USA, 28-30 Oct. 1982). Elastic scattering of 65 MeV polarized protons from rare earth nuclei has been measured. The volume integral of the real central part of the optical potential (J_0) and the volume integral of the spin orbit part of the potential (J_{ls}) show anomalous behaviors for these deformed nuclei. (3 refs.)

74967 Microscopic analysis of proton elastic scattering in the range 80-200 MeV. F.S.Dietrich (Lawrence Livermore Nat. Lab., Univ. of California, Livermore, CA, USA), F.Petrovich. *AIP Conf. Proc. (USA)*, no.97, p.148 (1982). [received: May 1983] (Proceedings of the Workshop on the Interaction Between Medium Energy Nucleons in Nuclei, Bloomington, IN, USA, 28-30 Oct. 1982). The authors have undertaken a systematic comparison of differential cross-section and analyzing-power data on ^{12}C , ^{28}Si , ^{40}Ca , ^{90}Zr , and ^{208}Pb at 80-200 MeV with calculations based on the single-step folding-model approach to the optical potential. In these calculations, proton densities have been inferred from electron scattering results, with neutron densities either the same as for protons (^{12}C , ^{28}Si , ^{40}Ca) or with a small neutron skin consistent with 800-MeV proton scattering results (^{90}Zr , ^{208}Pb). The effective two-body interactions that have been used are the Love-Franey t -matrix, a density-dependent interaction based on the Paris potential (calculated by von Geramb), and finally the Brieva-Rook density-dependent central interaction used with the spin-orbit part of the Love-Franey interaction. (no refs.)

74968 Momentum-space optical potential and elastic scattering calculations. D.H.Wolfe (Dept. of Phys., Kent State Univ., Kent, OH, USA), M.V.Hynes, A.Picklesimer, P.C.Tandy, R.M.Thaler. *AIP Conf. Proc. (USA)*, no.97, p.149 (1982). [received: May 1983] (Proceedings of the Workshop on the Interaction Between Medium Energy Nucleons in Nuclei, Bloomington, IN, USA, 28-30 Oct. 1982). Initial results are presented for proton-nucleus elastic scattering observables calculated with a newly developed microscopic momentum-space code. This is the first phase of a program to treat elastic and inelastic scattering consistently via an integral equation approach. A number of microscopic features which are often approximated or ignored are quite amenable to exact treatment within this approach, e.g. nonlocal effects in elastic scattering, and inelastic effects which are nonlinear in the NN t -matrix and target densities but nevertheless confined to one participating nucleon. (3 refs.)

74969 A theory for proton-He scattering. M.J.Paez, R.H.Landau (Dept. of Phys., Oregon State Univ., Corvallis, OR, USA). *AIP Conf. Proc. (USA)*, no.97, p.151 (1982). [received: May 1983] (Proceedings of the Workshop on the Interaction Between Medium Energy Nucleons in Nuclei, Bloomington, IN, USA, 28-30 Oct. 1982). The elastic scattering of proton from ^3He and ^4He is calculated with a microscopic momentum space optical potential. The theory is unique in its inclusion of the full structure of spin $1/2 \times 1/2$ scattering. It is equivalent to a co-ordinate space potential with central, spin-orbit and several tensor terms each described as non-local, and velocity dependent. Also included are nucleon recoil and binding, antisymmetrized NN amplitudes, a Lorentz invariant angle transformation (no small angle approximation), and realistic form factors for the matter and spin distributions of nucleons within the nucleus. (3 refs.)

74970 Proton scattering to collective states: what we learn about the effective interaction in the nuclear medium. J.J.Kelly (Dept. of Phys., MIT, Cambridge, MA, USA). *AIP Conf. Proc. (USA)*, no.97, p.153-75 (1982). [received: May 1983] (Proceedings of the Workshop on the Interaction Between Medium Energy Nucleons in Nuclei, Bloomington, IN, USA, 28-30 Oct. 1982). Electron scattering measurements of the normal parity isoscalar 'collective' excitations of $N=Z$ nuclei completely specify the nuclear structure information required for the analysis of complementary proton scattering experiments. The analysis of the proton scattering data is then interpreted as a study of the medium modifications of the two-nucleon effective interaction. It has been found that the isoscalar spin-independent central component of the effective interaction is strongly dependent upon density and is well described by the local density approximation based upon nuclear matter effective interactions. The results are sensitive to the difference between effective interactions based upon the Hamada-Johnston and Paris potentials, and favor an intermediate interaction. The qualitative features of the medium corrections can be adequately represented by a few physically motivated parameters, which can be chosen so as to reproduce either the Hamada-Johnston or Paris results. (20 refs.)

74971 Inelastic proton scattering to one-particle one-hole states. C.Olmer (Indiana Univ., Bloomington, IN, USA). *AIP Conf. Proc. (USA)*, no.97, p.176-9 (1982). [received: May 1983] (Proceedings of the Workshop on the Interaction Between Medium Energy Nucleons in Nuclei, Bloomington, IN, USA, 28-30 Oct. 1982). The study of intermediate-energy proton inelastic scattering to one-particle one-hole states has attracted considerable attention over the last few years. One primary purpose of these studies has been to exploit the structural simplicity of these excited states as a possible means of separating effects due to nuclear structure and those due to the reaction mechanism. The author concentrates on one particular area of investigation, namely the energy dependence of proton inelastic scattering. The author discusses the excitation of three high-spin, particle-hole states in ^{28}Si : the 5^- , $T=0$ state at 9.70 MeV, the 6^- , $T=0$ state at 11.58 MeV and the 5^- , $T=1$ state at 14.35 MeV. These states have been studied at proton energies between 65 MeV and 800 MeV. (17 refs.)

74972 Microscopic analysis of ^6Li (\bar{p},p) and $^6\text{Li}(\bar{p},p')$ (2.18 MeV) analyzing powers at 25, 35, and 45 MeV. C.H.Pope, F.S.Dietrich, D.Rowley (Lawrence Livermore Nat. Lab., Univ. of California, Livermore, CA, USA), H.E.Conzett, D.Eversheim, C.Rioux. *AIP Conf. Proc. (USA)*, no.97, p.226 (1982). [received: May 1983] (Proceedings of the Workshop on the Interaction Between Medium Energy Nucleons in Nuclei, Bloomington, IN, USA, 28-30 Oct. 1982). In the limit of the plane-wave Born approximation, analyzing powers for proton inelastic scattering result from interference between the central and spin-orbit parts of the effective nucleon-nucleon interaction. Because the real part of the effective spin-orbit interaction is generally much greater than its imaginary part, one expects that the analyzing powers should exhibit a sensitivity to the imaginary part of the effective central interaction. The presence of distortion in the entrance and exit channels modifies this conclusion somewhat, however for certain specific transitions this sensitivity is still maintained. To test this hypothesis the authors have measured analyzing powers for proton scattering to the ground state (1^+ ; $T=0$) and first excited state (3^+ ; $T=0$) of ^6Li at incident energies of 25, 35 and 45 MeV using the polarized beam of the LBL 88 in cyclotron. Agreement between the analyzing power data and the calculations is not very good for either the ground or first excited state, indicating some serious deficiency in the model. Possible improvements are discussed. (2 refs.)

74973 Test of microscopic theory with data for simple transitions in the $^{90}\text{Zr}(\bar{p},p')$ and $^{89}\text{Y}(\bar{p},p')$ reactions. A.Scott, W.G.Love (Univ. of Georgia, Athens, GA, USA), H.V.von Geramb. *AIP Conf. Proc. (USA)*, no.97, p.227 (1982). [received: May 1983] (Proceedings of the Workshop on the Interaction Between Medium Energy Nucleons in Nuclei, Bloomington, IN, USA, 28-30 Oct. 1982). Proton transition densities for simple (p,p') transitions in these nuclei have been 'calibrated' with (e,e') scattering results and two recent density-dependent (DD) N-N forces ($G1$ and $G4$) used in different types of microscopic calculations at 159.5 MeV. The 8^+ state in ^{90}Zr is a pure proton state and the 6^+ state is dominantly of the same configuration, so proton amplitudes were calculated with a $g_{9/2}^2$ density and Woods-Saxon potential agreeing with electron scattering; first with exact exchange and then using a pseudo potential for exchange amplitudes. The computed asymmetries (A_y) had small differences; both calculations are better fits to data than with a free N-N force, but fits are still not fully satisfactory. Other calculations (ALN), with direct input of (e,e') densities and a pseudo potential for exchange, produce A_y shapes differing from the exact calculations at larger angles. Similar ALN calculations for the 2_1^+ and 4_1^+ states in ^{90}Zr and simple transitions in ^{89}Y yield the same conclusion. (2 refs.)

74974 Energy dependence of the ratio of isovector effective interaction strengths $[J_{\pi\pi}/J_{\pi}]$ from 0° (p,n) cross sections. T.N.Taddeucci (Ohio Univ., Athens, OH, USA). *AIP Conf. Proc. (USA)*, no.97, p.228-31 (1982). [received: May 1983] (Proceedings of the Workshop on the Interaction Between Medium Energy Nucleons in Nuclei, Bloomington, IN, USA, 28-30 Oct. 1982). Ratios of 0° (p,n) cross sections indicate that the spin-flip to non-spin-flip interaction strength ratio $[J_{\pi\pi}/J_{\pi}]$ is approximately linear and target-mass independent for energies between 50 MeV and 200 MeV. To within a distortion-dependent factor of order unity, this latter ratio is well represented by $R(E_p) = E_p/(55.0 \pm 1.0 \text{ MeV})$. (6 refs.)

74975 Quasi-elastic scattering of polarised protons at 300 MeV. P.Kitching, P.W.Green, C.A.Miller, D.A.Hutchison, A.N.James, W.J.McDonald, K.Michaelian, G.C.Nelson, W.C.Olsen, D.M.Sheppard, J.Soukup, G.M.Stinson, I.J.van Heerden (TRIUMF, Univ. of Alberta, Edmonton, Alberta, Canada). *AIP Conf. Proc. (USA)*, no.97, p.232 (1982). [received: May 1983] (Proceedings of the Workshop on the Interaction Between Medium Energy Nucleons in Nuclei, Bloomington, IN, USA, 28-30 Oct. 1982). The authors' earlier measurements (1981) of the $^{40}\text{Ca}(\bar{p},2p)$ reaction at 200 MeV incident energy have been extended to 300 MeV using the TRIUMF polarised proton beam. Values of cross section and analysing powers for the knockout of protons for $1d_{3/2}$, $2s_{1/2}$ and $1d_{5/2}$ shells in ^{40}Ca are obtained and are compared to DWIA calculations incorporating spin orbit terms in the optical potentials, and also to calculations using optical potentials are derived from a relativistic approach based on the Dirac equation. The expected j -dependence of the analysing power is seen. The analyzing powers measured in the geometry where the angles of out going protons are very unequal are consistent with a value of zero for the two body polarization parameter, P , while its value is expected to be ~ 0.2 . Measurements for scattering from the $2s_{1/2}$ protons, which measure the value of P directly show no such effect. (1 ref.)

74976 A pragmatic approach to the continuum spectrum in the quasifree scattering. G.Ciungaru (Dept. of Phys. & Astron., Univ. of Maryland, College Park, MD, USA). *AIP Conf. Proc. (USA)*, no.97, p.250-3 (1982). [received: May 1983] (Proceedings of the Workshop on the Interaction Between Medium Energy Nucleons in Nuclei, Bloomington, IN, USA, 28-30 Oct. 1982). An expression for the continuum background in the quasifree scattering is given as the convolution of a number of rescattering steps of the quasifree particles on the residual nucleus. It is assumed that the rescattering probability can be expressed in terms of the inelastic scattering cross section of the quasifree particles. Comparison with the $^{58}\text{Ni}(p,2p)^{57}\text{Co}$ data at $E_0=198$ MeV supports the model prediction. (6 refs.)

74977 A global study of the $p+^{27}\text{Al}$ reaction at 180 MeV. S.-H.Zhou, K.Kwiatkowski, T.E.Ward, V.E.Viola, Jr. (Indiana Univ., Bloomington, IN, USA), H.Breuer, A.Gokmen, A.C.Mignerey, G.J.Mathews. *AIP Conf. Proc. (USA)*, no.97, p.254-9 (1982). [received: May 1983] (Proceedings of the Workshop on the Interaction Between Medium Energy Nucleons in Nuclei, Bloomington, IN, USA, 28-30 Oct. 1982). A global study of the mass, energy and angular distributions of all products formed in collisions of 180-MeV protons with ^{27}Al is reported. These data are compared with semiempirical and intranuclear-cascade-plus-evaporation calculations, as well as data from recent fission-fragment angular correlation studies with intermediate-energy light-ions incident on heavy target nuclei. It is found that there is substantial evidence for enhanced energy deposition in nucleon-nucleus collisions relative to the predictions of the intranuclear cascade calculation. (13 refs.)

74978 The Schrodinger equivalent complex potential and the Dirac phenomenology. M.Jaminon (Inst. de Phys., Univ. de Liege, Liege, Belgium). *AIP Conf. Proc. (USA)*, no.97, p.324-8 (1982). [received: May 1983] (Proceedings of the Workshop on the Interaction Between Medium Energy Nucleons in Nuclei, Bloomington, IN, USA, 28-30 Oct. 1982). The author shows that the phenomenological analyses of nucleon-nucleus elastic scattering data using a single-particle Dirac equation are not affected by the inclusion of a complex nuclear field that behaves like the space-like components of a vector. (7 refs.)

- 74979 Future prospects in N-nucleus interactions.** J.M. Moss (Los Alamos Nat. Lab., Los Alamos, NM, USA). *AIP Conf. Proc. (USA)*, no. 97, p.414-23 (1982). [received: May 1983] (Proceedings of the Workshop on the Interaction Between Medium Energy Nucleons in Nuclei, Bloomington, IN, USA, 28-30 Oct. 1982). The author examines in detail two research areas, polarization observables and antiproton-nucleus reactions, which should have near-term future impact on the understanding of the interaction of medium-energy nucleons in nuclei. More speculative future experiments employing cooled beams, double spectrometer systems, and large Q-value low momentum-transfer reactions are also discussed. (25 refs.)
- 74980 Nuclear mean free paths and transparency at intermediate energies.** P.J. Karol (Dept. of Chem., Carnegie-Mellon Univ., Pittsburgh, PA, USA). *Can. J. Chem. (Canada)*, vol. 61, no. 4, p.750-3 (April 1983). The soft-spheres model of nuclear reaction cross sections incorporating tapered density distributions is used to evaluate nucleon mean free paths and transparencies at intermediate energies. Comparison with similar calculations employing uniform density distributions shows the latter to give misleading results that nevertheless have been used in recent years as evidence that the physics of the nucleon-nucleon interaction within nuclei is incompletely understood. (19 refs.)
- 74981 Particle distribution around a copper beam stop for 72 MeV protons.** T.A. Broome, D.R. Perry, G.B. Stapleton (Rutherford Appleton Lab., Chilton, England), D. Duc. *Health Phys. (GB)*, vol. 44, no. 5, p.487-99 (May 1983). Results are presented of a nuclear reaction cross sections incorporating tapered density distributions is used to evaluate nucleon mean free paths and transparencies at intermediate energies. Comparison with similar calculations employing uniform density distributions shows the latter to give misleading results that nevertheless have been used in recent years as evidence that the physics of the nucleon-nucleon interaction within nuclei is incompletely understood. (19 refs.)
- 74982 Mechanisms for the enhancement of P- and T-invariant effects in neutron-nucleus reactions.** V.E. Bunakov, V.P. Gudkov (B.P. Konstantinov Inst. of Nuclear Phys., Acad. of Sci., USSR). *JETP Lett. (USA)*, vol. 36, no. 7, p.328-30 (5 Oct. 1982). Translation of: *Pis'ma v Zh. Eksp. & Teor. Fiz. (USSR)*, vol. 36, no. 7, p.268-70 (5 Oct. 1982). [received: May 1983] It is possible that T- and P-invariance effects are enhanced in the scattering of slow neutrons by compound nuclei. (7 refs.)
- 74983 Measurement of cumulative-neutron and cumulative-proton spectra in 1-GeV proton-nucleus interactions.** V.N. Baturin, V.V. Vikhrov, M.M. Makarov, V.V. Nelyubin, A.A. Naberezhnov, V.V. Sulimov, L.N. Uvarov (B.P. Konstantinov Inst. of Nuclear Phys., Acad. of Sci., USSR). *JETP Lett. (USA)*, vol. 36, no. 10, p.448-51 (20 Nov. 1982). Translation of: *Pis'ma v Zh. Eksp. & Teor. Fiz. (USSR)*, vol. 36, no. 10, p.370-2 (20 Nov. 1982). [received: June 1983] A comparative study has been made of the spectra of cumulative neutrons and protons produced at an angle of 114° in collisions of 1-GeV protons with ^9Be and ^{12}C nuclei. The slope parameters of the inclusive neutron spectra are similar to those of the proton spectra. (6 refs.)
- 74984 Low-energy n-p capture as a probe of two-nucleon dynamics.** J.M. Greben (Phys. Dept., Univ. of Alberta, Edmonton, Alberta, Canada), R.M. Woloshyn. *J. Phys. G (GB)*, vol. 9, no. 6, p.643-54 (June 1983). The authors examine the sensitivity of the cross section and polarisation observables in radiative neutron-proton capture to the uncertainty in the two-nucleon potential at short and intermediate range. These uncertainties are modelled by unitary phase-equivalent transformations of the Hamiltonian. They find that the photon linear polarisation is very sensitive to the resulting changes in the wavefunctions. The neutron analysing power is rather insensitive to these changes and could play a role in identifying effects not included in a potential model description. (30 refs.)
- 74985 1 GeV $P-^{40}\text{Ca}$ elastic scattering.** Lu Jifeng (Guangxi Teachers Training Coll., Xining, China), Liu Yuan, Wang Rulin. *Kexue Tongbao (Foreign Lang. Ed.) (China)*, vol. 28, no. 1, p.30-3 (Jan. 1983). [received: June 1983] 1 GeV proton elastic scattering on ^{40}Ca has been investigated by the optical limit approximation, and the nucleon-nucleon and alpha-nucleus amplitudes calculated. The results are discussed and compared with experimental data. (8 refs.)
- 74986 Parity violation and related effects in neutron-induced reactions.** V.E. Bunakov, V.P. Gudkov (Leningrad Inst. of Nuclear Phys., Gatchina, Leningrad, USSR). *Nucl. Phys. A (Netherlands)*, vol. A401, no. 1, p.93-116 (30 May 1983). The multi-channel multi-level nuclear reaction theory is used to give a general approach to various parity-violation effects observable in neutron-induced reactions on complex nuclei. The energy dependence and various enhancement factors of these effects are discussed and compared with experimental data on thermal and resonance neutrons. Special attention is paid to neutron-induced fission and to the information provided by these experiments. (48 refs.)
- 74987 Dirac-equation impulse approximation for intermediate-energy nucleon-nucleus scattering.** B.C. Clark, S. Hama (Dept. of Phys., Ohio State Univ., Columbus, OH, USA), R.L. Mercer, L. Ray, B.D. Serot. *Phys. Rev. Lett. (USA)*, vol. 50, no. 21, p.1644-7 (23 May 1983). In this application of Dirac phenomenology a relativistic impulse approximation is used to describe proton-nucleus elastic scattering at intermediate energies. The results demonstrate the superiority of this relativistic treatment over the nonrelativistic impulse approximation, especially with regard to spin observables. The method has important implications with respect to the extraction of neutron distributions. (16 refs.)
- 74988 Energy deposition in intermediate-energy nucleon-nucleus collisions.** K. Kwiatkowski, S.H. Zhou, T.E. Ward, V.E. Viola, Jr. (Dept. of Chem., Indiana Univ., Bloomington, IN, USA), H. Breuer, G.J. Mathews, A. Gokmen, A.C. Mignerey. *Phys. Rev. Lett. (USA)*, vol. 50, no. 21, p.1648-51 (23 May 1983). A global study of the mass, energy, and angular distributions of all products formed in collisions of 180-MeV protons with ^{27}Al is reported. These data are compared with calculations based on intranuclear-cascade-plus-evaporation, preequilibrium hybrid, and semiempirical models. It is found that there is evidence for enhanced energy deposition in nucleon-nucleus collisions relative to predictions of intranuclear cascade calculations. In contrast, preequilibrium calculations produce stronger energy damping, more consistent with observed data. (14 refs.)
- 74989 Antiproton-nucleus interaction at low energy.** T. Suzuki, H. Narumi (Dept. of Phys., Hiroshima Univ., Hiroshima, Japan). *Phys. Lett. B (Netherlands)*, vol. 125B, no. 4, p.251-4 (2 June 1983). On the basis of the Brueckner-Hartree-Fock theory, the self-energy of an antiproton in nuclear matter is evaluated with the static Bryan-Phillips (1968) potential, and the density-dependent effective NN interaction is estimated with this self-energy. Using the p-nucleus optical potential constructed by folding this effective NN interaction, one can predict the complex level shift of p-atoms. (12 refs.)
- 74990 Calculation of the energy-averaged scattering function for high resolution low-energy neutron scattering data.** C.H. Johnson, N.M. Larson (Oak Ridge Nat. Lab., Oak Ridge, TN, USA), C. Mahaux, R.R. Winters. *Phys. Rev. C (USA)*, vol. 27, no. 5, p.1913-26 (May 1983). The elastic scattering neutron cross section at low energy displays many narrow resonances. By definition, the optical-model scattering function is equal to a suitable energy average of the actual scattering function. This average should be independent of the particular representation chosen for parametrizing the actual scattering function and also fairly independent of the averaging weight function. In particular, it should be fairly independent of the width of the weight function, even though a sparsity of resonances might require the width to be comparable to the energy range of the measurements. It is shown by direct numerical calculations of the average that this holds in the example of the scattering of $p_{3/2}$ neutrons by ^{32}S . Attention is drawn to pitfalls which exist when this average is evaluated analytically from parametrized forms of the scattering function. Several ways of graphically representing or parametrizing the average scattering function are illustrated and discussed. (11 refs.)
- 74991 Microscopic formalism for intermediate energy transfer reactions: application to the (p,d) and (d,p) reactions.** L.D. Lukeking (Phys. Dept., Indiana Univ., Bloomington, IN, USA), J.P. Vary. *Phys. Rev. C (USA)*, vol. 27, no. 5, p.1967-87 (May 1983). Using a multiple scattering framework the authors construct a variant of the usual distorted-wave Born approximation transition matrix for stripping and pickup reactions. An alternative to the local energy approximation is derived which in the appropriate limit gives the commonly used zero range approximation for (p,d) and (d,p) reactions. Model calculations are developed in an eikonal framework and an examination of the sensitivity and energy dependence of the nuclear response function is made, using the $^{12}\text{C}(p,d)^{11}\text{C}(3/2^-)$ g.s.) process. (48 refs.)
- 74992 Deformation effect in the fast neutron total cross section of aligned ^{59}Co .** U. Fasoli, P. Pavan, D. Toniolo, G. Zago, R. Zannoni (Istituto di Fisica, Univ. degli Studi, Padova, Italy), G. Galeazzi. *Phys. Rev. C (USA)*, vol. 27, no. 5, p.2003-11 (May 1983). The variation of the total neutron cross section, $\Delta\sigma_{\text{align}}$, on ^{59}Co due to nuclear alignment of the target has been measured over the energy range from 0.8 to 20 MeV employing a cobalt single crystal with a 34% nuclear alignment. The results show that $\Delta\sigma_{\text{align}}$ oscillates from a minimum of -5% at about 2.5 MeV to a maximum of +1% at about 10 MeV. The data were successfully fitted by optical model coupled-channel calculations. The coupling terms were deduced from a model representing the ^{59}Co nucleus as a vibrational ^{60}Ni core coupled to a proton hole in a $(1/2_1^+)$ shell, without free parameters. The optical model parameters were determined by fitting the total cross section, which was independently measured. The theoretical calculations show that, at lower energies, $\Delta\sigma_{\text{align}}$ depends appreciably on the coupling with the low-lying levels. (47 refs.)
- 74993 Neutron-nucleus spin-spin interaction in the low MeV range.** W. Heeringa (Inst. fur Kernphys. und Teilchenphys., Kernforschungszentrum Karlsruhe, Karlsruhe, Germany), H. Postma. *Phys. Rev. C (USA)*, vol. 27, no. 5, p.2012-18 (May 1983). An attempt is made to find a satisfactory explanation for the average spin-spin cross section of ^{59}Co for neutrons between 0.3 and 2.9 MeV. Calculations with an optical model spin-spin potential obviously fail to reproduce these data. A hybrid model is developed containing elements of compound-nucleus formation and of the optical model. Partial waves with orbital momenta up to $l=4$ are taken into account: This model yields a good explanation of the ^{59}Co data. It also agrees with the spin-spin cross section of ^{16}O , the only other nucleus for which data exist above 0.1 MeV. (34 refs.)
- 74994 Enhanced backward emission of heavy fragments in high-energy proton-nucleus collisions.** J. Hufner (Inst. fur Theoretische Phys., Univ. Heidelberg, Heidelberg, Germany), H.M. Sommermann. *Phys. Rev. C (USA)*, vol. 27, no. 5, p.2090-5 (May 1983). The conventional description of high energy proton-nucleus collisions in terms of an intranuclear cascade and compound nuclear decay (the two-step model) breaks down at projectile energies $E_p > 10$ GeV. Unusual backward enhancements are found in the angular distribution of heavy fragments (Sc, Cu) from uranium targets. This effect is explained in a fast breakup model of deep spallation/cleavage processes. The observed backward emission originates in the competition between (backward-directed) Coulomb repulsion and (forward-directed) momentum components from recoiling nucleons. (10 refs.)
- 74995 Analysis of threshold (p,π^0) reactions.** D.A. Jenkins, M. Madden (Virginia Polytech. Inst. & State Univ., Blacksburg, VA, USA). *Phys. Rev. C (USA)*, vol. 27, no. 5, p.2096-103 (May 1983). A procedure is derived for analyzing (p,π^0) reactions near threshold where pions are present in only s- and p-wave states. The pions, which decay into two gammas, have an angular distribution in the center of mass which can be correlated to the angular distribution of its decay gammas in the laboratory. Functions are calculated which give the laboratory distribution of both gammas in terms of parameters describing the angular distribution of pions in the center of mass. By fitting these functions to the observed gamma distribution, the pion differential cross section is determined. (6 refs.)
- 74996 Impulse approximation NN amplitudes for proton-nucleus interactions.** J.A. McNeil (Dept. of Phys., Villanova Univ., Villanova, PA, USA), L. Ray, S.J. Wallace. *Phys. Rev. C (USA)*, vol. 27, no. 5, p.2123-32 (May 1983). Transformation of nucleon-nucleon amplitudes from the center of mass frame to the proton-nucleus Breit frame are developed for use in multiple scattering analyses. As a byproduct, a matrix equation is given for the invariant NN amplitudes in Dirac spinor representation. Based on recent NN phase shifts, Gaussian parametrization of the pp and np amplitudes are calculated and some proton-nucleus calculations are presented to illustrate the effects of the Breit frame amplitudes. For ^{40}Ca , these effects are quite small. (13 refs.)
- 74997 800 MeV protons as probes of neutron transition densities.** L. Ray, G.W. Hoffmann (Dept. of Phys., Univ. of Texas, Austin, TX, USA). *Phys. Rev. C (USA)*, vol. 27, no. 5, p.2133-42 (May 1983). Angular distribution data for 800 MeV $^{208}\text{Pb}(p,p')$ (2.61 MeV, 3^-) are analyzed to determine the sensitivity of the analysis to the neutron component of the transition density. The analysis employs the first order Kerman, McManus, and Thaler (1959) optical potential model (distorted wave Born approximation together with the impulse approximation). The total error in the multipole moment of the deduced transition density, $M_n(E3)$, is computed based on uncertainties in (1) the elastic and inelastic scattering data, (2) the geometry of the transition density, (3) the nucleon-nucleon amplitudes, (4) the proton transition density, (5) correlation corrections, and (6) medium modifications to the effective interactions. Under the presumption of an accu-

rate theoretical model, the minimal uncertainty in $M_n(E3)$ is $\pm 8.5\%$. Such accuracy permits meaningful comparisons with results from nuclear structure theory. (32 refs.)

74998 Proton isotonic density differences from 0.8 GeV proton-nucleus elastic scattering. L.Ray, G.W.Hoffmann (Dept. of Phys., Univ. of Texas, Austin, TX, USA).

Phys. Rev. C (USA), vol.27, no.5, p.2143-9 (May 1983).

Elastic differential cross sections and analyzing powers for 800 MeV $p+^{48}\text{Ca}$ and ^{54}Fe are analyzed to obtain the isotonic proton density difference. The calculations employ a local, spin-dependent, second order Kerman, McManus, and Thaler (1959) optical potential model; care is given to isovector, spin-unsaturated subshell, and phenomenological nuclear medium corrections. The results obtained here are compared with those from electron scattering experiments and theoretical expectations. The results of this analysis provide an overall consistency check on corresponding studies which start with known charge densities and determine neutron isotopic density differences. (28 refs.)

74999 Measurements of analyzing power for $^2\text{H}(\bar{n},n)^2\text{H}$ scattering at 14.1 MeV and comparisons to $^2\text{H}(\bar{p},p)^2\text{H}$. W.Tornow (Phys. Inst., Univ. Tübingen, Tübingen, Germany), R.C.Byrd, C.R.Howell, R.S.Pedroni, R.L.Walter.

Phys. Rev. C (USA), vol.27, no.5, p.2439-42 (May 1983).

Data for the analyzing power $A_y(\theta)$ for the elastic scattering of neutrons from deuterons have been measured at 14.1 MeV for the range from 30° to 153° (c.m.) to accuracies between ± 0.003 and ± 0.006 . The results are compared to previous n -d data at 14 MeV and are in significant disagreement with the most recent measurement. The present data are in excellent agreement with a Faddeev calculation by Doleschall (1982). The data are also very similar to p -d scattering data at 14.1 MeV, although systematic deviations are observed at forward angles and near the maximum of $A_y(\theta)$ at 130° . Recent calculations indicate that Coulomb effects can explain most of these differences, although some features will require further investigation. (11 refs.)

75000 Double differential cross sections for (p, xn) reactions of ^{64}Zn , ^{65}Cu and ^{89}Y with 26 MeV protons. W.Scobel, L.F.Hansen, B.A.Pohl, C.Wong, M.Blann (Lawrence Livermore Nat. Lab., Univ. of California, Livermore, CA, USA).

Z. Phys. A (Germany), vol.311, no.4, p.323-8 (1983).

Double differential cross sections for the inclusive production of neutrons from ^{64}Zn , ^{65}Cu and ^{89}Y bombarded with 26.0 MeV protons have been measured with time-of-flight techniques. The data reduction is discussed with respect to the influence of background corrections in the continuous part of the spectra, and a short comparison with preequilibrium model calculations is presented, showing good agreement with predictions of both, the hybrid and the geometry-dependent hybrid model including multiple particle emission. The question of how to treat pairing remains open. (19 refs.)

75001 Measurement of the average neutrons yield from 250 MeV protons absorbed in a lead target. Yu.V.Ryabov, G.K.Matushko, V.N.Slastnikov (Inst. for Nuclear Res., Acad. of Sci., Moscow, USSR).

Z. Phys. A (Germany), vol.311, no.4, p.363-5 (1983).

Neutron yield from 250 MeV protons accelerated by the ITEPh synchrotron is measured in a lead target 5 cm diameter and 10 cm long. The observed total yield is 2.56 ± 0.27 neutrons/proton, where the evaporation and cascade components are 2.30 ± 0.25 and 0.26 ± 0.11 neutrons/protons respectively. (12 refs.)

75002 Production of large P_T particles in p-nucleus and nucleus-nucleus collisions at high energies. D.S.Narayan (Tata Inst. of Fundamental Res., Bombay, India).

Proceedings of the VI High Energy Physics Symposium (papers in summary form only received), Mysore, India, 6-11 Dec. 1982 (Bombay, India: Dept. Atomic Energy 1982), p.57

Summary form only given. Recent results from ISR on the production of large P_T particles in p - α and α - α collisions and similar earlier results from Fermilab in P -nucleus collisions present a complex pattern. The results of these experiments are explained on the basis of the coherent tube model which implies collective interactions inside the nucleus.

Evidence concerning Δ -hole states See Entry 74831

^6Li levels excited by the $^9\text{Be}(p,\alpha)$ reaction at $E_p=30$ and 50 MeV See Entry 74848

Implication of the nonlocality in the effective N-N interaction: nuclear structure and spin observables See Entry 74853

Real part of the nuclear interaction potential between α or p and excited heavy nuclei See Entry 74864

A radiochemical study on the existence of dineutron See Entry 74870

Description of the neutron deficient Sr and Zr isotopes in the interacting boson model See Entry 74874

Microscopic optical potentials See Entry 74885

Gamma radiation from $^{50}\text{Cr}(p,p')^{50}\text{Cr}$ at $E=5.45$ -6.15 MeV See Entry 74901

Proton capture to excited states of ^{16}O : M1, E1, and Gamow-Teller transitions and shell model calculations See Entry 74904

Average resonance capture studies of $^{162,164}\text{Dy}$ See Entry 74908

Identification of 26-minute Zr-84 See Entry 74912

Dirac phenomenology for nuclear reactions See Entry 74920

First order interpretation of optical potentials See Entry 74939

Separable representation of the nonlocality of optical model potentials See Entry 74940

Dirac phenomenology and the nuclear optical model See Entry 74941

Diffraction scattering off strongly bound system See Entry 74942

$\Delta(1236)$ -isobar degrees of freedom and the strength of spin-isospin resonances See Entry 74945

Coupling between low-lying nuclear states See Entry 74950

Momentum transfer in the fragmentation of copper by 400-GeV protons See Entry 74951

Heavy target fragment yields in the interaction of 28 GeV protons with ^{238}U See Entry 74952

Complete set of first-order polarization observables in nucleon-deuteron elastic scattering near 20 MeV deuteron energy See Entry 75004

Fragmentation spectra induced by light ions colliding with light nuclei See Entry 75006

Fission probability in the $^{233}\text{Th}(p,p'xn)$ reaction at low energy See Entry 75055

Nuclear charge distribution in fission: fractional cumulative yields of isotopes of krypton and xenon in $^{235}\text{CF}(n_{\text{th}},f)$ and $^{250}\text{CF}(sp,n)$ See Entry 75057

Mass distributions in monoenergetic-neutron-induced fission of ^{239}Pu See Entry 75061

Simulation of neutron transmission by fission nuclei in the region of unresolved resonances See Entry 75150

Chemical effects of nuclear transformations in mixed potassium hexahalo-ogeno-metallates (IV), $\text{K}_2\text{MX}_6\cdot\text{Y}_{6-n}$. I. Chemical effects of the $^{81}\text{Br}(n,\gamma)^{82}\text{Br}$ nuclear process in mixed potassium hexabromochloro-osmates (IV), $\text{K}_2\text{OsBr}_6\text{Cl}_{6-n}$ See Entry 77912

Determining distribution and concentration of certain elements with the aid of a charged-particle beam See Entry 77944

Could ^7Be be destroyed by neutron absorption in the Sun? A note on the solar neutrino puzzle See Entry 78897

Antiproton interactions with light elements as a test of GUT cosmology See Entry 79040

25.50 ^2H - AND ^3H -INDUCED REACTIONS AND SCATTERING

75003 Polarization transfer in $\text{A}(\bar{d},\bar{p})\text{X}$ reactions. H.Sakamoto, M.Nakamura, H.Sakaguchi, H.Ogawa, S.Kobayashi (Dept. of Phys., Kyoto Univ., Kyoto, Japan), N.Matsuoka, K.Hatanaka, T.Noro, S.Kato.

AIP Conf. Proc. (USA), no.97, p.424 (1982). [received: May 1983] (Proceedings of the Workshop on the Interaction Between Medium Energy Nucleons in Nuclei, Bloomington, IN, USA, 28-30 Oct. 1982).

Summary form only given, as follows. Transverse polarization transfer coefficients (k_y') have been measured in the reactions ^{12}C , ^{58}Ni , $^{208}\text{Pb}(\bar{d},\bar{p})\text{X}$. The experiment was performed at RCNP AVF cyclotron laboratory using a 56 MeV vector-polarized deuteron beam. Emitted protons leaving the residuals in their continuum states were selected by Q-magnet pairs according to their momenta and were focused on the analyzer targets (Si-SSD) in the Si-Ge polarimeters located at 13.5° and 20.0° laboratory angles. The energy bins of the measured protons have been chosen to be 22, 26, 31 and 36 ± 2 MeV. (no refs.)

75004 Complete set of first-order polarization observables in nucleon-deuteron elastic scattering near 20 MeV deuteron energy. M.Sawada, S.Seki, K.Furuno, Y.Tagishi, Y.Nagashima, J.Schimizu, M.Ishikawa, T.Sugiyama, L.S.Chuang, W.Gruebler, J.Sanada (Inst. of Phys., Univ. of Tsukuba, Ibaraki, Japan), Y.Koike, Y.Taniguchi.

Phys. Rev. C (USA), vol.27, no.5, p.1932-8 (May 1983).

The authors have measured differential cross section and analyzing powers A_y , iT_{11} , T_{20} , T_{21} , and T_{22} for proton-deuteron elastic scattering near 20 MeV deuteron energy. The total error of the differential cross section was 1% or less. Each deuteron analyzing power was measured independently with the maximum efficiency. The total error of the analyzing power was less than 0.007. Faddeev calculations have been performed for three cases of nucleon-nucleon interaction. None of them gives an overall quantitative fit to the measured values. The effect of the Coulomb interaction is discussed. (23 refs.)

Proton occupancies in the even Se ground states via the $(d,^3\text{He})$ reaction See Entry 74847

Scattering length in a system of three charged particles. See Entry 74922

Coupling between low-lying nuclear states See Entry 74950

Nuclear mean free paths and transparency at intermediate energies See Entry 74980

Microscopic formalism for intermediate energy transfer reactions: application to the (p,d) and (d,p) reactions See Entry 74991

25.60 ^3He - AND ^4He -INDUCED REACTIONS AND SCATTERING

75005 $^{45}\text{Sc}(\alpha,\alpha')^{44}\text{Sc}^{m+g}$: a monitor reaction for alpha particle induced reactions. P.A.Beeley, J.Aaronson, K.Kokkas, J.J.Hogan (Dept. of Chem., McGill Univ., Montreal, Quebec, Canada).

Can. J. Chem. (Canada), vol.61, no.4, p.641-5 (April 1983).

The excitation function for the $^{45}\text{Sc}(\alpha,\alpha')^{44}\text{Sc}^{m+g}$ reactions have been measured at beam energies from 20 to 90 MeV. These provide a beam monitor for alpha particle induced reaction studies. The excitation functions and isomer ratios are discussed with particular reference to an apparent error in the decay scheme of $^{44}\text{Sc}^m$. (19 refs.)

75006 Fragmentation spectra induced by light ions colliding with light nuclei. T.Delbar, G.Gregoire, P.Belery (Inst. de Phys., Univ. Catholique de Louvain, Louvain-la-Neuve, Belgium), G.Paic.

Phys. Rev. C (USA), vol.27, no.5, p.1876-86 (May 1983).

Inclusive energy spectra of light charged particles from the $^6\text{Li}+^3\text{He}$, $^9\text{Be}+p$, and $^9\text{Be}+^3\text{He}$ reactions have been measured using beams of 30 to 75 MeV. The continuum parts have been studied in the framework of phase space calculations. The influence of other reaction mechanisms, such as final state interactions, sequential processes, and quasifree reactions is evaluated. The authors deduce the nontrivial angular dependence of the various phase spaces. (22 refs.)

75007 Separation of direct and compound nuclear contributions in inelastic α scattering. H.Ortner, W.Eyrich, A.Hofmann, U.Scheib (Phys. Inst., Univ. Erlangen-Nürnberg, Erlangen, Germany).

Phys. Rev. C (USA), vol.27, no.5, p.1988-92 (May 1983).

A method for separating direct and compound nuclear reaction contributions to inelastic α scattering on spin 0 targets is proposed. It is based on the characteristic behaviour of the parameters of the α - γ angular correlation function in a distorted-wave Born approximation and a Hauser-Feshbach model treatment. The method is applied to the reaction $^{28}\text{Si}(\alpha,\alpha')\gamma$. (16 refs.)

75008 Phase shift analysis of alpha-particle elastic-scattering angular distributions on the ^{40}Ca target nucleus. M.C.Mermaz (Dept. de Phys. Nucleaire, CENS, Gif-sur-Yvette, France).

Phys. Rev. C (USA), vol.27, no.5, p.2019-28 (May 1983).

A phase shift analysis of 15 alpha particle elastic scattering angular distributions measured accurately between 30° and 170° center of mass and between 26.13 and 47 MeV by the Basel group has been performed. Perfect agreement between experimental and the calculated differential cross sections is obtained over the full range of energy. The fluctuating behavior of the scattering matrix elements can possibly be explained by the presence of an intermediate-structure resonance phenomenon with contributions from many overlapping resonances. (26 refs.)

High-spin states in ^{92}Tc See Entry 74834

Real part of the nuclear interaction potential between α or p and excited heavy nuclei See Entry 74864

Quasimolecular and cluster states of light nuclei as examples of intermediate structure See Entry 74946

- Nuclear mean free paths and transparency at intermediate energies See Entry 74980
- Production of large P_T particles in p-nucleus and nucleus-nucleus collisions at high energies See Entry 75002
- Average transverse momenta of pions produced in nucleus-nucleus interactions at $p=4.5$ GeV/c per nucleon See Entry 75011
- Mass spectrometric determination of Rb fission yields from ^3He and ^4He induced fission of ^{238}U and ^{232}Th See Entry 75058
- Energy dependence of the probability for asymmetric fission of ^{213}At See Entry 75059
- Prompt light-ion emission in the $^{235}\text{U}+^4\text{He}$ reaction at 40 MeV/u^a See Entry 75064
- A tool to study collective transitions between excited nuclear states See Entry 75066
- Neutron yield of the (α, n) reaction for multicomponent media See Entry 75069

25.70 HEAVY ION INDUCED REACTIONS AND SCATTERING

- 75009** Elastic scattering of heavy ions and the compressibility of nuclear matter. K.A.Gridnev (NIIF, Leningrad State Univ., Leningrad, USSR), E.F.Hefter, K.Mikulas, V.M.Semjonov, V.B.Subbotin. *Aust. J. Phys. (Australia)*, vol.36, no.2, p.155-61 (1983). Analogies to hydrodynamics led recently to the derivation of a nonlinear Schrödinger equation for the elastic scattering of heavy ions (Delion et al., 1978). The numerical solution of this equation is shown to yield realistic values for the nuclear compressibility modulus $K=9C$, with very small uncertainties. (10 refs.)
- 75010** Fusion cross sections for $^{14}\text{N}+^{11}\text{B}$ at low energies. B.Dasmahapatra, B.Cujec, F.Lahlou (Dept. de Phys., Univ. Laval, Quebec, Canada). *Can. J. Phys. (Canada)*, vol.61, no.5, p.657-63 (May 1983). Fusion cross sections for the $^{14}\text{N}+^{11}\text{B}$ system have been measured from $E_{\text{cm}}=2.85$ to 8.53 MeV by the total γ -ray yield method. At energies just below the Coulomb barrier an enhancement similar to that present in the $^{12}\text{C}+^{12}\text{C}$ system, but less prominent, has been observed. A comparison of various ^{14}N -induced reactions shows that this enhancement is most prominent with an even-even target ($^{12}\text{C}, ^{16}\text{O}$), quite clear with an odd-even target (^{11}B), and almost disappears with an odd-odd target ($^{10}\text{B}, ^{14}\text{N}$). (13 refs.)
- 75011** Average transverse momenta of pions produced in nucleus-nucleus interactions at $p=4.5$ GeV/c per nucleon. M.Kh.Anikina, G.L.Vardenga, M.Gazdzitskii, A.I.Golokhvastov, T.D.Dzhobava, E.S.Kuznetsova, Yu.Lukstyn'sh, N.N.Nurgozhin, E.O.Okonov, T.G.Ostanevich, Yu.S.Pol', B.S.Suleimenov, G.G.Taran, S.A.Khorozov, E.K.Khusainov (Joint Inst. for Nuclear Res., USSR). *JETP Lett. (USA)*, vol.36, no.7, p.331-3 (5 Oct. 1982). Translation of: *Pis'ma v Zh. Eksp. & Teor. Fiz. (USSR)*, vol.36, no.7, p.270-2 (5 Oct. 1982). [received: May 1983]
- Analysis of $\langle p_{\perp} \rangle$ for the negative pions produced in the interactions $^4\text{He}+^6\text{Li}$, $\text{C}+\text{Al}$, $\text{Cu}+\text{Pb}$, $^{12}\text{C}+\text{C}$, $\text{Ne}+\text{Cu}$, and $^{20}\text{Ne}+\text{Ne}$ at projectile-nucleus momentum per nucleon of 4.5 GeV/c shows that $\langle p_{\perp} \rangle$ does not depend on the centrality of the interaction, on the mass of the projectile nucleus in the interval $A_p=4-20$, or on the mass of the target nucleus in the interval $A_T=6-64$. The values found for $\langle p_{\perp} \rangle$ are at odds with calculations from a thermodynamic model. (5 refs.)
- 75012** Heavy-ion elastic scattering and its connections with fusion and absorption processes. A.Scalia (Istituto Dipartimentale di Fisica, Univ. di Catania, Catania, Italy). *Lett. Nuovo Cimento (Italy)*, vol.37, ser.2, no.4, p.129-34 (28 May 1983). A simple expression for the heavy-ion elastic-scattering amplitude is presented. It reproduces the experimental values of the ratio of elastic scattering to Rutherford cross-sections and is suitable for a definition of the angles at which absorption and diffusion begin. The fusion and total reaction cross-sections are deduced from experimental elastic-scattering data. (6 refs.)
- 75013** Correlations between the alpha particles and ejectiles in the 208 MeV ^{14}N on ^{93}Nb reaction at three different ejectile angles. T.Fukuda (Dept. of Phys., Osaka Univ., Osaka, Japan), M.Ishihara, M.Tanaka, H.Ogata, I.Miura, M.Inoue, T.Shimoda, K.Katori, S.Nakayama. *Phys. Rev. C (USA)*, vol.27, no.5, p.2029-36 (May 1983). The in plane correlations between alpha particles and various ejectiles were investigated in the reaction of 208 MeV ^{14}N on ^{93}Nb at $\theta_{\text{H}}=+22^\circ$, $+50^\circ$, and $+80^\circ$. There were three sources of coincident alpha particles: (i) the sequential alpha decay of the excited ejectiles, (ii) the equilibrium alpha emission from the targetlike fragments, and (iii) the nonequilibrium process. Process (i) contributed mainly to the cross sections with the angular range of θ_{e} close to θ_{H} . Process (ii) contributed to the lowest part of the alpha energy spectra irrespectively of θ_{H} and θ_{e} . The remaining part was ascribed to process (iii). For this process the differential coincidence cross section of the lower energy part of the alpha particles was approximately factorized as $d^2\sigma/d\Omega_{\text{H}}d\Omega_{\text{e}}dE_{\text{H}}dE_{\text{e}}=K(d^2\sigma/d\Omega_{\text{H}}dE_{\text{H}})_{\text{single}}(d^2\sigma/d\Omega_{\text{e}}dE_{\text{e}})_{\text{single}}$ with $K\sim 0.4/b$, whereas the higher energy part of the alpha particles emitted at the forward angles had a tendency to coincide weakly with the ejectiles emitted at the backward angles ($\theta_{\text{H}}=+50^\circ$ and $+80^\circ$) as compared to the lower energy part of the alpha particles. (10 refs.)
- 75014** Baryon rapidity distribution and stopping power of high-energy colliding nuclei. J.Kapusta (School of Phys. & Astron., Univ. of Minnesota, Minneapolis, MN, USA). *Phys. Rev. C (USA)*, vol.27, no.5, p.2037-41 (May 1983). A very simple estimate is made of the baryon rapidity distribution to be expected from central collisions of high energy nuclei. This estimate is based upon straight-line trajectories and some average rapidity loss per nuclear-nucleon collision. It is found that U+U will become transparent at a beam energy of about 500 GeV/nucleon, or $15+15$ GeV/nucleon. (12 refs.)
- 75015** Orbiting phenomenon in $^{16}\text{O}, ^{28}\text{Si}$ scattering. C.S.Shastry (Groupe de Phys. Nucleaire Theorique, CRN, Strasbourg, France), I.Parjia. *Phys. Rev. C (USA)*, vol.27, no.5, p.2042-57 (May 1983). From an analysis of the effective potentials and the surface region behavior of quantum mechanical radial wave functions, the authors find that the most interesting physical phenomena taking place in $^{16}\text{O}+^{28}\text{Si}$ scattering at $E_{\text{lab}}=55$ MeV is the orbiting mechanism for $\ell=24, 25, 26$. They find that the orbital amplitude $A_0(\theta)$ generated by these partial waves acts coherently at large angles with the background amplitude $A_b(\theta)$ describing the remainder of the full amplitude. The enhanced large angle oscillations are caused by the almost, but not complete, destructive interference between $A_0(\theta)$ and $A_b(\theta)$. Using appropriate mathematical techniques, they show that at large angles $\theta\leq 180^\circ$, both $A_0(\theta)$ and $A_b(\theta)$ are dominated essentially by the same Legendre

polynomial. This explains the observation of Takemasa and Tamura (1978) that the cross sections generated by exact Regge pole terms behave quite similarly to that generated by the corresponding Regge background terms. Furthermore, their analysis clarifies the underlying reason for the success of the purely parametric Regge pole model at large angles. They also compare the infinite sequence of Regge poles generated by the barrier term in the Wentzel-Kramers-Brillouin formula for the 'nuclear' S matrix and the exact quantum mechanical orbiting Regge pole. The oscillatory behavior of the reflection function η_l of the $^{16}\text{O}+^{28}\text{Si}$ system at $E_{\text{lab}}=55$ MeV as a function of l for l below the orbiting regions is also explained. (13 refs.)

75016 Nuclear collisions of uranium nuclei up to ~ 1 GeV/nucleon. E.M.Friedlander, H.H.Heckman, Y.J.Karant (Lawrence Berkeley Lab., Univ. of California, Berkeley, CA, USA).

Phys. Rev. C (USA), vol.27, no.5, p.2436-8 (May 1983).

The authors report observations of inelastic interactions of uranium nuclei with energies up to ~ 1 GeV/nucleon in nuclear emulsions exposed on the occasion of the first successful acceleration of relativistic uranium ions. About one-half of the interactions lead to binary fission. With increasing primary energy, the relative frequency of violent nuclear interactions increases at the expense of binary fissions. Also reported is a range measurement of uranium nuclei in emulsion at 0.945 GeV/nucleon. (6 refs.)

75017 Measurement of kinetic flow parameters for relativistic collisions of Ne on NaF and Ar on Pb_3O_4 . D.Beavis, S.Y.Chu, S.Y.Fung, W.Gorn, A.Huie, D.Keane, J.J.Lu, R.T.Poe, B.C.Shen, G.VanDalen (Dept. of Phys., Univ. of California, Riverside, CA, USA).

Phys. Rev. C (USA), vol.27, no.5, p.2443-6 (May 1983).

The authors present kinetic flow parameters based on charged particle exclusive streamer chamber data for Ne on NaF at bombarding energies of 0.425 GeV/nucleon and 0.577 GeV/nucleon, and for Ar on Pb_3O_4 at 0.4 GeV/nucleon. Flow angles and aspect ratios are determined as functions of charged track multiplicity. The experimental findings are compared with predictions based on the intranuclear cascade model of Cugnon et al. (11 refs.)

75018 Study of spin polarization of residual nuclei in heavy ion reactions by γ -ray circular polarization measurement. K.Ikei.

Rep. Inst. Phys. & Chem. Res. (Japan), vol.59, no.1-2, p.20-47 (1983). In Japanese.

Fast light particles are emitted strongly at the forward direction in heavy ion reactions. To study the reaction mechanism of the phenomena, the authors measured circular polarization of coincident γ -rays emitted from the residual nucleus and deduced spin polarization. The experiments were performed using ^7Li and ^{14}N beams from the RIKEN cyclotron. The spin polarization for the $(^7\text{Li}, \alpha)$ reaction depends on α -particle energy and can be well explained as a recoil effect in the triton transfer process. The spin polarization for the $(^{14}\text{N}, \alpha)$ reaction, that also depends on α -particle energy, can be explained as a competition of massive-transfer process and deep-inelastic process. (41 refs.)

75019 Elastic scattering of ^{20}Ne on ^{24}Mg . W.J.Naude (Dept. of Phys., Univ. of Stellenbosch, Stellenbosch, S. Africa), H.S.Bradlow, O.Dietzsch, A.A.Pilt, W.D.M.Rae, D.Sinclair.

Z. Phys. A (Germany), vol.311, no.4, p.297-302 (1983).

Elastic scattering of ^{20}Ne on ^{24}Mg was studied at an incident ^{20}Ne energy of 40 MeV. Scattered ^{20}Ne and ^{24}Mg nuclei were observed in coincidence with a standard surface barrier and a position sensitive detector. The measured angular distribution shows periodic oscillations which are identified with the $^{24}\text{Mg}(^{20}\text{Ne}, ^{24}\text{Mg})^{20}\text{Ne}$ reaction. Taking interference between elastic scattering and transfer into account, an α -spectroscopic factor of $S=0.08\pm 0.02$ was deduced from the amplitude of the oscillations. (19 refs.)

75020 Energy dependence of the production of pions, kaons and antikaons calculated in the hydrochemical model. H.W.Barz (Zentralinst. für Kernforschung, Rossendorf, Germany), T.S.Biro, B.Lukacs, J.Zimanyi.

Z. Phys. A (Germany), vol.311, no.4, p.311-15 (1983).

Cross sections for the production of pions, kaons and antikaons in heavy ion reactions are calculated in the framework of the hydrochemical model. For the reaction Ne on NaF satisfactory agreement to the measured data is reached in a wide range of energies. The importance of consecutive hadron-hadron collisions for the mass dependence is shown. (23 refs.)

75021 Resonances in heavy-ion nuclear reactions. T.M.Cormier (Dept. of Phys. & Astron., Univ. of Rochester, Rochester, NY, USA).

In book: *Annual review of nuclear and particle science*. Vol.32, J.D.Jackson, H.E.Gove, R.F.Schwitters [Eds.], p.271-308. Palo Alto, CA, USA: Annual Reviews (1982), 595 pp. [0 8243 1532 4]

With the advent of tandem electrostatic accelerators in the early 1960s, nuclear physicists began the exploration of nuclear properties under extreme conditions of shape, angular momentum, temperature, density, and N/Z with heavy-ion reactions. This exploration continues today with ever-increasing vigor. The author examines some of the new and unexpected aspects of the nuclear structure of light nuclei that have been revealed in this exploration. He is primarily concerned with a new class of nuclear eigenstates observed experimentally in heavy-ion resonance reactions. These states are now known to exist in nuclei ranging from the s-d shell through the $f_{7/2}$ shell and are characterized by unexpectedly large partial decay widths for decay into fragments of comparable mass. These fission-like decays are usually taken as evidence for extreme deformations, and the term 'nuclear molecular state' has become almost universal in the literature. It should be pointed out, however, that the terminology, although universally accepted, implies more than is actually known about these states. (46 refs.)

75022 A phenomenological formula for fusion cross section. R.Giordano, F.Porto, S.Sambataro, A.Scalia (Istituto di Fisica, Univ. di Catania, Catania, Italy).

Proceedings of the International Conference on Nucleus-Nucleus Collisions (papers in summary form only received), East Lansing, MI, USA, 26 Sept.-1 Oct. 1982 (East Lansing, MI, USA: Michigan State Univ. 1982), p.101. The authors report on an empirical formula which reproduces the gross energy dependence for several heavy-ion systems and for different energy regimes. (2 refs.)

75023 Universal parametrization of fusion barrier. S.M.Lee, T.Nakagawa, W.Galster (Inst. of Phys., Univ. of Tsukuba, Ibaraki, Japan).

Proceedings of the International Conference on Nucleus-Nucleus Collisions (papers in summary form only received), East Lansing, MI, USA, 26 Sept.-1 Oct. 1982 (East Lansing, MI, USA: Michigan State Univ. 1982), p.103. The authors report on the unique parametrization of the heavy-ion fusion barrier $V_0(R_0)$ which is essentially universal and applicable for a wide mass range. Generally heavy-ion fusion cross sections at low energy are determined as follows: $\sigma_{\text{fus}}=\pi R_0^2(1-V_0(R_0)/E_{\text{cm}})$. By comparing experimental σ_{fus} with this equation one can determine R_0^{exp} and $V_0(R_0)^{\text{exp}}$ for a given system. The problem is, however, how to predict these quantities theoretically. Although many models have been proposed, usually based on the liquid drop model, none of them are really successful throughout a wide mass range covering from Light-Light to Heavy-Heavy systems. In order to evaluate

$V_B(r) = V_{Coul}(r) + V_N(r)$ at $r = R_B$, the authors choose the Woods-Saxon form for $V_N(r)$ in replacing R_1 range parameter, by R_B : $V_N(r) = V_0(1 + \exp((r - R_B)/a))^{-1}$. It should be noted that this potential gives the same value of $V_N(R_B)$ as another set of parameters of Woods-Saxon potential does, simply because of the 1 σ ambiguity. From the condition of $\partial V_B(r)/\partial r|_{r=R_B} = 0$, one finally gets $V_B(R_B) = Z_1 Z_2 e^2 (1 - 2a/R_B)/R_B$ where the following parameters are used: $R_B = R_1 + R_2 + \Delta R$, $R_1 = 1.12 A_1^{1/3} = 0.86 A_1^{-1/3}$, $1) \Delta R = 2.4$ fm and $a = 8.0/(A_1^{1/3} + A_2^{1/3})$ fm, the only empirically determined parameter. (1 ref.)

75024 A new critical distance model for heavy-ion fusion reactions. T.Matsuse, A.Arima (Dept. of Phys., Univ. of Tokyo, Bunkyo-ku, Japan), S.M.Lee.

Proceedings of the International Conference on Nucleus-Nucleus Collisions (papers in summary form only received), East Lansing, MI, USA, 26 Sept.-1 Oct. 1982 (East Lansing, MI, USA: Michigan State Univ. 1982), p.104

The rapid descent of the fusion cross section for lighter heavy-ion systems at higher energies (Region III) is interpreted in terms of a Fusion-Entry-Line based on a new concept of the critical distance between heavy ions. Taking into account the effect of Pauli exclusion principle between A_1 and A_2 , the critical distance $\sqrt{\langle d^2 \rangle}$ is expressed simply by using the mean square radius $\langle r^2 \rangle_A$. (1 ref.)

75025 Fusion-entry-line in fusion reactions for $^{12}C + ^{50}Cr$ and $^{32}S + ^{36}Si$. Y.Nagashima, S.M.Lee, T.Nakagawa, Y.Fukuchi, Y.Yokota, J.Schimizu, K.Furuno, T.Mikumo, N.X.Dai, T.Motobayashi, M.Yamanouchi (Inst. of Phys., Univ. of Tsukuba, Ibaraki, Japan).

Proceedings of the International Conference on Nucleus-Nucleus Collisions (papers in summary form only received), East Lansing, MI, USA, 26 Sept.-1 Oct. 1982 (East Lansing, MI, USA: Michigan State Univ. 1982), p.105

In spite of a great success of the Statistical-Yrast-Line Model to predict heavy-ion fusion cross sections for system $A < 80$ at higher energy, there is no good experimental data available up to now in which nearly symmetric- and very asymmetric systems, forming the same compound nucleus. The authors have chosen ^{62}Zn compound nucleus through two different entrance channels $^{32}S + ^{30}Si$ and $^{12}C + ^{50}Cr$ to study the former and the latter systems, respectively. (2 refs.)

75026 Incomplete fusion and nonequilibrium emission processes in the system $^{16}O + ^{93}Nb$ at 208 MeV. C.F.Maguire (Dept. of Phys. & Astron., Vanderbilt Univ., Nashville, TN, USA), R.L.Ferguson, B.Cheynis, I.-Y.Lee, R.Novotny, F.E.Obenshain, D.Pelte, F.Plasil, R.L.Robinson, G.R.Young.

Proceedings of the International Conference on Nucleus-Nucleus Collisions (papers in summary form only received), East Lansing, MI, USA, 26 Sept.-1 Oct. 1982 (East Lansing, MI, USA: Michigan State Univ. 1982), p.106

The authors have measured fusion-evaporation residue products from $^{16}O + ^{93}Nb$ reactions at 208 MeV incident energy both in singles and in coincidence with light-ions. Striking anomalies exist in the data relative to what is predicted assuming only complete fusion-evaporation occurs. The fusion singles experimental cross section at forward angles is a factor of two below that predicted by the code PACE. At larger angles the value is still several mb/sr while the predicted yield vanishes. To resolve this discrepancy they consider incomplete fusion in which deep-inelastic particle transfer scatters a highly excited target-like product in the forward quadrant where it is indistinguishable from an evaporation residue. (3 refs.)

75027 Incomplete fusion at low impact parameters with a ^{116}Sn target. C.Gerschel, N.Perrin, H.Tricoire, L.Valentin (Inst. de Phys. Nucleaire, Orsay, France).

Proceedings of the International Conference on Nucleus-Nucleus Collisions (papers in summary form only received), East Lansing, MI, USA, 26 Sept.-1 Oct. 1982 (East Lansing, MI, USA: Michigan State Univ. 1982), p.107

Gamma multiplicity measurements for given reaction channels following direct α particle emission confirm the low impact parameters observed with Sn targets in inclusive measurements. Mean γ multiplicities and variances σ of the Ω_γ distributions have been determined by the $P(x)$ method. On a ^{116}Sn target with 125 MeV ^{16}O projectiles the authors have measured $M_\gamma = 12 \pm 1$ and $\sigma = 6 \pm 1$ for the α 4n incomplete fusion channel. (Evaporation contribution is subtracted). They deduce $l_i/l_\alpha = 0.48$ where l_i is the entrance channel mean angular momentum and l_α the critical value for complete fusion. This low value is in agreement with other measurements on spherical targets and is lower than what is found with rare earth targets. (2 refs.)

75028 Dynamical theory of incomplete fusion reactions. T.Udagawa, T.Tamura (Dept. of Phys., Univ. of Texas, Austin, TX, USA).

Proceedings of the International Conference on Nucleus-Nucleus Collisions (papers in summary form only received), East Lansing, MI, USA, 26 Sept.-1 Oct. 1982 (East Lansing, MI, USA: Michigan State Univ. 1982), p.108

It is now well known that energetic light particles such as p, d, t and α are emitted copiously in reactions induced by heavy ions. An important feature there is that these emission processes are almost always accompanied by the fusion of the rest of the incident ion into the target nucleus. These processes have thus been called the massive transfer or incomplete fusion reactions. The authors have proposed a theory to describe such reactions as a two-step process involving a direct breakup as the first step, followed by the fusion of one of the breakup pair with the target nucleus (breakup-fusion process). (4 refs.)

75029 Experimental signatures for fast fission. B.B.Back, R.R.Betts, K.Cassidy, B.G.Glagola, J.E.Gindler, L.E.Glendenin, B.D.Wilkins (Chem. Div., Argonne Nat. Lab., Argonne, IL, USA).

Proceedings of the International Conference on Nucleus-Nucleus Collisions (papers in summary form only received), East Lansing, MI, USA, 26 Sept.-1 Oct. 1982 (East Lansing, MI, USA: Michigan State Univ. 1982), p.110

The extra push model of Swiatecki (1982) has been very successful in explaining the limitations for heavy ion fusion in terms of the dynamics of the reaction. One consequence of this model is the prediction of 'fast fission' reactions. These occur when the system is temporarily caught behind the conditional saddle, but reseparates again after a substantial mass transfer has taken place. If the time scale for mass equilibration is shorter than the reaction time, one may find that the emerging fragments are indistinguishable from true fission fragments in terms of mass, charge and kinetic energy. (2 refs.)

75030 Dissipative collisions with a fission-like exit channel in the $^{132}Xe + ^{56}Fe$ system. D.Bangert, F.Busch, B.Kohlmeier, F.Puhlhofer (Fachbereich Phys., Philipps-Univ. Marburg, Marburg, Germany), B.Heusch, K.D.Hildenbrand, W.F.W.Schneider, D.Schull.

Proceedings of the International Conference on Nucleus-Nucleus Collisions (papers in summary form only received), East Lansing, MI, USA, 26 Sept.-1 Oct. 1982 (East Lansing, MI, USA: Michigan State Univ. 1982), p.111

Using the ^{132}Xe -beam of the GSI-Unilac angular distributions of the reaction products have been measured by means of a ΔE -E ionization chamber at bombarding energies of 5, 5.7 and 8.5 MeV/u. At all incident energies fully relaxed fragments centered at $(Z + Z_f)/2 = 40$, are observed. These Z-distributions are symmetric and their width is independent of the scattering angle. The angular distribution for each element is consistent with an

1/sin θ -dependence. Very forward of the grazing angle, conventional deep inelastic processes are observed, too, they are clearly separated from symmetric fragments and represent a minor part of the total reaction cross section, at least for the lower bombarding energies. (3 refs.)

75031 Angular dependence of symmetric fragmentation for the $^{32}S + ^{59}Co$ reaction. G.Guillaume, A.Fahli, F.Rami, J.P.Coffin, P.Engelstein, B.Heusch, P.Wagner, P.Fintz, J.Richert (Univ. Louis Pasteur, Strasbourg, France).

Proceedings of the International Conference on Nucleus-Nucleus Collisions (papers in summary form only received), East Lansing, MI, USA, 26 Sept.-1 Oct. 1982 (East Lansing, MI, USA: Michigan State Univ. 1982), p.112

Attention has been devoted to the study of fission-like fragmentation for systems of mass around 100. This mechanism has been examined with respect to its dependence on the mass of the system, the energy and the angular momentum brought in. The results indicate that it proceeds partly through a timescale intermediate mechanism between true fission (compound nucleus formation) and deep inelastic collisions. Further investigation has been undertaken on the $^{32}S + ^{59}Co$ reaction which exhibits a different behavior (double peaked at projectile and target masses) for the $\sigma_{\text{fission}}/\sigma_{\text{total}}$ mass distribution that the one characterizing heavier systems like $^{32}S + ^{140}Ge$ (single peak at half mass of the compound nucleus). The experiment was conducted at the 16 MV-MP Tandem of Strasbourg by bombarding a $150 \mu\text{g}/\text{cm}^2$ ^{59}Co target with ^{32}S ions at laboratory incident energies equal to 128, 143, 158, 178 and 198 MeV. The fragments were identified with time of flight techniques. (4 refs.)

75032 Fission of Pb nuclei at high angular momenta. D.J.Hinde, J.O.Newton, J.R.Leigh, R.J.Charity (Dept. of Nuclear Phys., Australia Nat. Univ., Canberra, Australia).

Proceedings of the International Conference on Nucleus-Nucleus Collisions (papers in summary form only received), East Lansing, MI, USA, 26 Sept.-1 Oct. 1982 (East Lansing, MI, USA: Michigan State Univ. 1982), p.115

The surface asymmetry parameter K_s of the liquid drop model describing the dependence of the surface energy on neutron excess is important in determining the macroscopic part of fission barriers original 1.78 up to 3.0. By measuring fission probabilities for a series of nuclei with fixed Z and different N, information on the value of K_s may be gained. Fission and evaporation residue excitation functions have been measured after the nuclei $^{192,195,198,200}Pb$ were formed in the fusion of $^{28,30}Si$ with $^{164,167,170}Er$. The fission probabilities extracted were fitted using the rotation liquid drop/statistical model codes ORNL ALICE and MBII. (6 refs.)

75033 Fast Fourier component in fusion reactions with heavy ions. M.F.Rivet, B.Borderie, D.Gardes, H.Gauvin, F.Hanappe, J.Peter, B.Tamain, A.Zaric, Z.Zheng (Inst. de Phys. Nucleaire, Orsay, France).

Proceedings of the International Conference on Nucleus-Nucleus Collisions (papers in summary form only received), East Lansing, MI, USA, 26 Sept.-1 Oct. 1982 (East Lansing, MI, USA: Michigan State Univ. 1982), p.116

Recently some experimental observations and theoretical predictions suggested the existence of Fast Fission, an interaction mechanism intermediate between compound nucleus formation and deep inelastic collisions. Experimentally, the occurrence of Fast Fission was supported by two facts: the maximum l-value contribution to fusion l_{fus} can be substantially larger than the l-value for which the fission barrier vanishes $l_{\text{BG}} = 0$; the symmetric component mass distribution markedly broadens when $l_{\text{fus}} > l_{\text{BG}} = 0$. However, this broadening could be attributed to a lowering at high angular momenta of the mass asymmetry stiffness parameter rather than to the occurrence of a new mechanism. In order to rule out one of these hypothesis, the authors investigated the Ar+U system ($l_{\text{BG}} \approx 10h$) and compared it with the Ar+Bi and Ar+Au systems ($l_{\text{BG}} \approx 45$ to $70h$). Binary events mass distributions have been obtained using time of flight. Preliminary results are shown presenting the evolution of the FWHM of the symmetric component mass distribution as a function of the incident laboratory energy. As expected from earlier observations in the Ar+Ho system the FWHM for Ar+Au and Ar+Bi systems increases drastically when increasing the energy. Conversely for the Ar+U system, at the barrier, the FWHM has already reached a large value and no drastic evolution is seen as a function of the incident energy (and angular momentum). These observations emphasize the role played by the angular momentum dependent fission barrier and confirm the existence of the fast fission mechanism. (4 refs.)

75034 Enhanced fission probabilities observed in the $^{184}W + ^{184}W$ collision. G.Rudolf, J.C.Adloff, M.Dakowski, D.Disdier, A.Gobbi, U.Lyden, W.Muller, A.Olmi, V.Rauch, H.Sann, F.Scheibling (Univ. Louis Pasteur, Strasbourg, France).

Proceedings of the International Conference on Nucleus-Nucleus Collisions (papers in summary form only received), East Lansing, MI, USA, 26 Sept.-1 Oct. 1982 (East Lansing, MI, USA: Michigan State Univ. 1982), p.117

The $^{184}W + ^{184}W$ collision was measured at 8.2 MeV/u in order to correct for possible secondary effects in other ^{184}W -induced reaction studies. Surprisingly a negative drift attaining 3 charge units for $TKEL = 300$ MeV was observed in the measured (secondary) distributions. Such a drift can be explained either by light charged particle evaporation or by sequential fission. (1 ref.)

75035 Fission following capture reactions of $^{32}S + ^{208}Pb$. M.B.Tsang, D.Arduin (Cyclotron Lab., Michigan State Univ., Lansing, MI, USA), B.B.Back, P.A.Baisden, R.Betts, C.K.Gelbke, W.G.Lynch, M.A.McMahan, S.Saini, Z.Xu.

Proceedings of the International Conference on Nucleus-Nucleus Collisions (papers in summary form only received), East Lansing, MI, USA, 26 Sept.-1 Oct. 1982 (East Lansing, MI, USA: Michigan State Univ. 1982), p.118

Cross sections, angular and mass distributions were measured for the reaction $^{208}Pb(^{32}S, f)$ at incident energies between 180 and 270 MeV. At 250 and 266 MeV, a sizeable fraction of the capture cross section corresponds to angular momenta of vanishing liquid drop fission barrier. However, even at lower energies the observed large angular anisotropies cannot be reproduced by using average liquid drop model parameters. This fact has been taken as evidence for the occurrence of fast fission processes. This conclusion is corroborated by the observed rapid increase of the fission fragment mass distributions with incident energy. (4 refs.)

75036 Angular momentum dependence of fission barriers. J.vander Plicht, H.C.Britt, M.M.Fowler, Z.Fraenkel, A.Gavron, J.B.Wilhelmy (Los Alamos Nat. Lab., Univ. of California, Los Alamos, NM, USA), F.Plasil, T.Awes, G.R.Young, O.Hansen, C.Thorn, H.E.Wegner.

Proceedings of the International Conference on Nucleus-Nucleus Collisions (papers in summary form only received), East Lansing, MI, USA, 26 Sept.-1 Oct. 1982 (East Lansing, MI, USA: Michigan State Univ. 1982), p.119

The effect of angular momentum on fission barriers is investigated by studying excitation functions and angular distributions for various heavy-ion-induced-fission reactions. The authors obtained data on fission from the following reactions: $^{20}O + ^{142}Nd$, $^{14}Mg + ^{134}Ba$, $^{32}S + ^{126}Te$, $^{64}Ni + ^{94}Zr$, $^{96}Be + ^{177}Hf$, $^{12}C + ^{174}Yb$, $^{16}O + ^{170}Er$, $^{26}Mg + ^{160}Gd$, $^{32}S + ^{192}Os$, $^{12}C + ^{198}Pt$. (2 refs.)

75037 Potential pockets in the $^{238}\text{U} + ^{238}\text{U}$ system and their possible consequences. V.E.Oberacker (Phys. Dept., Vanderbilt Univ., Nashville, TN, USA), M.J.Rhodes-Brown, W.Greiner.

Proceedings of the International Conference on Nucleus-Nucleus Collisions (papers in summary form only received), East Lansing, MI, USA, 26 Sept.-1 Oct. 1982 (East Lansing, MI, USA: Michigan State Univ. 1982), p.120. Two experimental groups have recently studied positron emission in $^{238}\text{U} + ^{238}\text{U}$ reactions at $E_{\text{lab}} = 5.8 \text{ MeV/u}$ ($E_{\text{cm}} = 690 \text{ MeV}$). Positron energy spectra were measured in coincidence with ions scattered into various narrow angular windows. A preliminary analysis shows sharp maxima in the positron spectra located at 370 keV with a width $\Delta = 90 \text{ keV}$. The peak structure is not pronounced at ion scattering angles $\theta_{\text{lab}} = 45^\circ$ and vanishes around 209° . If the observed peaks are of atomic origin as expected theoretically (diving of the vacant quasi-molecular $1s$ -level into the lower continuum $E < -m_e c^2$), it must be produced in a very long-lasting U+U reaction ($T \approx 4 \times 10^{-20} \text{ s}$). The main problem with the above argument is the low beam energy which corresponds to only 95% of the 'spherical' Coulomb barrier height, using $R_{\text{int}} = 1.16(A_1^{1/3} + A_2^{1/3} + 2) \text{ fm}$. All conventional U+U interaction potential models predict dominant Rutherford scattering at this energy and hence much shorter times ($T \sim 2 \times 10^{-21} \text{ s}$). Greiner (1981) suggested that the prolonged nuclear sticking time might be caused by 'pockets' in the U+U interaction potential caused by the static β_2 and β_4 deformations of the nuclei. The authors have investigated the potential $U(r)$ within the framework of the double-folding model. $U(r)$ is obtained by averaging an appropriate nucleon-nucleon interaction over the matter distributions of the two colliding nuclei. (3 refs.)

75038 Possible sub-Coulomb resonances and fusion doorways in collisions of deformed heavy ions. W.T.Pinkston (Inst. for Theoretical Phys., Univ. of Frankfurt am Main, Frankfurt am Main, Germany).

Proceedings of the International Conference on Nucleus-Nucleus Collisions (papers in summary form only received), East Lansing, MI, USA, 26 Sept.-1 Oct. 1982 (East Lansing, MI, USA: Michigan State Univ. 1982), p.121. Calculations by Oberacker and Rhodes-Brown and by Seiwert predict 'pockets', i.e. secondary minima, in the interaction potentials of deformed heavy ions. These secondary minima occur for special relative orientations of the nuclear symmetry axes and for internuclear distances somewhat greater than conventional estimates of Coulomb barrier radii based on the assumption of spherical nuclei. Resonances resulting from trapping in these pockets could serve as doorways for sub-Coulomb fusion and might provide the 'sticking time' needed to explain the discrete structures in spectra of positrons produced in the collisions of very heavy ions (U-U, U-Cu). The resonant states, of angular momentum J , are special linear combinations of states of relative angular momentum L , and of the rotational momenta I_1, I_2 of the colliding nuclei. These linear combinations result in the preferred nuclear orientation. The results of calculations based on an oversimplified resonance model will be presented. The problems of obtaining a clear experimental signature of such resonances will be discussed. (no refs.)

75039 Energy dependence of ^{14}N mean free path in nuclear emulsions below 250 MeV per nucleon. N.Ashalata Devi, R.Bhanja, I.Dhar Ojha, R.R.Joseph, M.Shyam, S.K.Tuli (Dept. of Phys., Banaras Hindu Univ., Varanasi, India).

Proceedings of the International Conference on Nucleus-Nucleus Collisions (papers in summary form only received), East Lansing, MI, USA, 26 Sept.-1 Oct. 1982 (East Lansing, MI, USA: Michigan State Univ. 1982), p.122. Accurate information about the cross-sections of light nuclei with nuclear targets is of interest from several points of view. While detailed measurements are available at energies of a few MeV and also extensive work at the relativistic energies of a few GeV, the transition region of intermediate energies has comparatively limited data. The authors have measured the mean free path which is directly related to cross-sections in nuclear emulsions for the collisions produced by ^{14}N nuclei in an exposure at the Bevalac. (2 refs.)

75040 Direct measurement of reaction cross-section for ^{12}C projectiles at 1016 MeV. S.Kox, C.Perrin, N.Longueue, M.Buenerd, R.Cherkaoui, A.J.Cole, J.Menet, J.B.Viano (Inst. des Sci. Nucleaires, Grenoble, France), A.Gamp, R.Berthollet, C.Guet, J.Pinston.

Proceedings of the International Conference on Nucleus-Nucleus Collisions (papers in summary form only received), East Lansing, MI, USA, 26 Sept.-1 Oct. 1982 (East Lansing, MI, USA: Michigan State Univ. 1982), p.125. Considerable interest raised up recently in the experimental determination of reaction cross-section for heavy-ions. The variation of σ_r as a function of the incident energy the ion has been shown to follow the nucleon-nucleon cross-section rather than reaching the geometrical limit arising from a simple strong absorption picture. In order to investigate carefully this energy dependence, an experimental set-up has been designed, which allows a direct measurement of σ_r using beam attenuation method. Incident projectiles ($\sim 10^8 \text{ s}^{-1}$) are counted by a scintillator foil, whereas a scintillator frame is used to define the beam size on the target. Four meters downstream a scintillator slab of proper thickness allows counting the transmitted particles and provides a ΔE signal used for identification when combined with time of flight measurement. (4 refs.)

75041 A method for analytic evaluation of reaction rates for low energy nucleus-nucleus collisions in a hot gas of nuclei. H.J.Haubold, R.W.John (Zentralinst. für Astrophys., Akad. der Wissenschaften, Potsdam, Germany). Proceedings of the International Conference on Nucleus-Nucleus Collisions (papers in summary form only received), East Lansing, MI, USA, 26 Sept.-1 Oct. 1982 (East Lansing, MI, USA: Michigan State Univ. 1982), p.140 (3 refs.)

75042 Collective phenomenon in nucleus-nucleus interaction.

Proceedings of the VI High Energy Physics Symposium (papers in summary form only received), Mysore, India, 6-11 Dec. 1982 (Bombay, India: Dept. Atomic Energy 1982), p.136.

A lot of interest has been evoked in the possibility of the occurrence of collective phenomenon like nuclear shock waves in nucleus nucleus collisions at high energies. An experimental study of high energy nucleus-nucleus collisions offer a possibility to expose certain properties of nuclear matter at abnormally high densities due to these shock waves. In this experiment various experimental parameters like short range angular correlations, asymmetry and coplanarity parameters, etc. have been used which are sensitive to indicate emission of fragments from collective phenomenon in such interactions. The data used are from Fe-emulsion interactions at 1.77 GeV/A . About 400 events have been analysed for the effect. The data give some indication of the asymmetry in the emitted fragments.

75043 Fe-nucleus interactions at 1.8 GeV/nucleon.

Proceedings of the VI High Energy Physics Symposium (papers in summary form only received), Mysore, India, 6-11 Dec. 1982 (Bombay, India: Dept. Atomic Energy 1982), p.137.

Recently a lot of interest has been shown in the field of ion-ion interactions. In the present work the general characteristics of Fe-emulsion interactions at 1.77 GeV/nucleon have been studied. The result on mean free path, geometri-

cal cross-section, frequency distribution of black, grey and heavy fragments ($Z \geq 2$) are discussed and compared with the available data of others.

75044 Emission of α fragments in nucleus nucleus collision at high energy. R.Bhanja, N.A.L.Devi, R.R.Joseph, I.D.Ojha, M.Shyam, S.K.Tuli (Dept. of Phys., Banaras Hindu Univ., Varanasi, India).

Proceedings of the VI High Energy Physics Symposium (papers in summary form only received), Mysore, India, 6-11 Dec. 1982 (Bombay, India: Dept. Atomic Energy 1982), p.138.

The authors report on the α fragment emission in the interaction of ^{14}N with emulsion nuclei at 2.1 GeV/A . The identification of fragments has been done by taking into account the blob density B , gap density H > than a length $t(1.2 \text{ u})$ and gap length coefficient $G(B = \text{He}^{+4})$. (3 refs.)

75045 Search for anomalies in projectile fragments from Ar-emulsion interactions. R.R.Joseph, R.Bhanja, M.Shyam, S.K.Tuli (Dept. of Phys., Banaras Hindu Univ., Varanasi, India), S.B.Beri, V.S.Bhatia, G.Kaur, M.Kaur, I.S.Mitra, A.Bharti, K.B.Bhalla, M.Chaudhary, V.Kumar, S.Lokanathan, S.Satti, V.K.Gupta, G.L.Kaul, S.Kumar, L.K.Mangotra, Y.Prakash, N.K.Rao, S.Sankhyadhar.

Proceedings of the VI High Energy Physics Symposium (papers in summary form only received), Mysore, India, 6-11 Dec. 1982 (Bombay, India: Dept. Atomic Energy 1982), p.139.

The authors have collected more than 1500 Ar-emulsion interactions by line scanning. The projectile fragments ($Z \geq 2$) from these interactions are followed until they interact to give secondary, tertiary or higher generation interactions or leave the stack. Mean free path analysis of about 1200 such secondary or later generations is presented and possible evidence for the existence of anomalies will be discussed.

75046 Search for 'anomalons' in 4.5 A GeV ^{12}C -emulsion interaction. D.Ghosh, J.Roy, D.Banerjee, K.Sengupta, S.Naha (Dept. of Phys., Jadavpur Univ., Calcutta, India).

Proceedings of the VI High Energy Physics Symposium (papers in summary form only received), Mysore, India, 6-11 Dec. 1982 (Bombay, India: Dept. Atomic Energy 1982), p.140.

A stack of emulsion plates exposed to $4.5 \text{ A GeV } ^{12}\text{C}$ beam has been scanned to study whether the interaction mean free paths in nuclear emulsion of relativistic projectile fragments emitted are anomalously shorter for a fewer centimetres after their emission than at larger distances. The tracks were followed systematically through the stack, to search for these 'anomalons'.

75047 Pion laser study in relativistic nuclear collision. D.Ghosh, J.Roy, D.Banerjee, K.Sengupta, M.Basu, S.Naha (Dept. of Phys., Jadavpur Univ., Calcutta, India).

Proceedings of the VI High Energy Physics Symposium (papers in summary form only received), Mysore, India, 6-11 Dec. 1982 (Bombay, India: Dept. Atomic Energy 1982), p.141.

Presents an investigation on the coherent pion processes in relativistic heavy ion collision using data from emulsion plates exposed to ^{16}O beams at 2.1 GeV/nucleon . The inclusive pion distribution at different angular intervals has been compared with the chaotic and Poisson's distribution and information on coherent pion processes was obtained by looking for deviation from Poisson. The possible significance of the results has been discussed.

QCD and the space-time evolution of high-energy e^+e^- , $p\bar{p}$, and heavy ion collisions See Entry 74724

On the description of multiplicity distributions in multiple production processes in terms of combinatorics See Entry 74812

Nuclear polarization and sign of the quadrupole moment of the $^{54}\text{Fe}(10^+)$ isomer See Entry 74835

Variations of the gyromagnetic ratios of low-lying states in ^{192}Os See Entry 74844

The heavy-ion potential and its increasing transparency at intermediate energies See Entry 74865

Further evidence for 'extra push' See Entry 74928

A microscopically determined diabatic potential for heavy-ion collisions See Entry 74929

The influence of symmetries and nonadiabatic couplings on the diabatic potential for two colliding heavy ions See Entry 74930

Scaling properties of hydrodynamical cross sections See Entry 74931

Pineuts: a possible explanation for anomalons See Entry 74932

Classical limits of the multi-channel formalism via the Vlasov equation See Entry 74933

Theory of heavy ion scattering on the basis of the two center shell model See Entry 74934

Explicit representations of tensor spin orbit interactions for systems with maximum channel spin 3 See Entry 74936

Mean free path of a nucleon in nucleus-nucleus collision See Entry 74944

Quasimolecular and cluster states of light nuclei as examples of intermediate structure See Entry 74946

Coulomb forces in the three-body problem with application to direct nuclear reactions See Entry 74953

A numerical method for two-dimensional Fokker-Planck equation See Entry 74954

Statistical generation of complete events in energetic nuclear collisions See Entry 74956

Nuclear mean free paths and transparency at intermediate energies See Entry 74980

Study of fission-like products in the ^{84}Kr on ^{24}Mg reaction at 5.83 E/A (MeV) See Entry 75065

Low-density nuclear isomer and a possible explanation for the anomaly in the free path of nuclear fragments in photoemulsions See Entry 75247

25.80 MESON- AND HYPERON-INDUCED REACTIONS AND SCATTERING

75048 The scattering of positive kaons by nuclei. M.Krell (Dept. de Phys., Univ. de Sherbrooke, Sherbrooke, Quebec, Canada), A.W.Thomas. *Can. J. Phys. (Canada)*, vol.61, no.5, p.703-8 (May 1983).

The authors examine the sensitivity of low energy positive kaon (K^+)-nucleus scattering to the neutron distribution. By using the technique of isotope comparison which has worked well for low energy pions, they find that there seem to be 'windows' where one could already learn something quantitative about the neutron distribution despite the poorly known K^+ -nucleon phase shifts. (19 refs.)

75049 The A dependence and threshold behaviour of the inclusive ($\pi, 2\pi$) reaction for $T=0$ nuclei. J.Cohen (Dept. of Phys. & Astron., Tel Aviv Univ., Tel Aviv, Israel).

J. Phys. G (GB), vol.9, no.6, p.621-9 (June 1983).

The author calculates the dependence of the energy-differential inclusive cross section for the ($\pi, 2\pi$) reaction on the mass number A for $N=Z$ nuclei up to $A \sim 60$. He also calculates the variations of this cross section near threshold, where the outgoing pions have almost zero energy. He finds a significant A dependence resulting from the dominance of the increase in number of active particles over the decrease of matrix element squared. The threshold behaviour is strongly affected by Coulomb distortions of the outgoing pions, and he finds a large difference between the ($\pi^+, 2\pi^+$) and the ($\pi^-, \pi^+ \pi^-$) cases. The true absorption of final pions is also checked; and found to be of secondary importance. All cases are studied as a function of g' , the Migdal spin-isospin parameter. (22 refs.)

75050 Three-body model for p -wave pion- ^{16}O scattering. K.A.Kabir, M.Silver, N.Austern (Dept. of Phys. & Astron., Univ. of Pittsburgh, Pittsburgh, PA, USA).

Phys. Rev. C (USA), vol.27, no.5, p.2104-22 (May 1983).

A calculation of the elastic scattering of mesons from ^{16}O is performed, using a modification of the first-order multiple scattering theory of Kerman, McManus, and Thaler (1959), in which Pauli blocking effects are omitted from the τ operator. The modified τ operator is calculated in a three-body model, in which the struck nucleon is allowed to recoil in a Woods-Saxon nuclear shell model potential exerted by the remainder of the nucleus. The interaction between the meson and the struck nucleon is described by a separable potential. A set of coupled differential equations that describe the elastic and the excited channel wave functions is derived by approximating the shell model binding potential in the excited states of the nucleon as a potential for the meson-nucleon center of mass. This approximation is examined in detail. It is found that in the three-body model the bound states and the single particle resonances of the shell model potential alter the results significantly from those obtained in impulse approximation. (27 refs.)

75051 Threshold estimates of ($\pi, 2\pi$) on nuclei in the Fermi gas model: one-body mechanism. R.M.Rockmore (Dept. of Phys. & Astron., Rutgers State Univ., Piscataway, NJ, USA).

Phys. Rev. C (USA), vol.27, no.5, p.2150-7 (May 1983).

The one-nucleon contribution to threshold pion production in pion-nucleus collisions is calculated using a Fermi gas model of the nuclear excitation spectrum in order to carry out the sum over final nuclear states. For the one-body input a threshold approximant to the production amplitude from the phenomenological Lagrangian theory is used. The cross sections are found to have an η^4 dependence near threshold, where $\eta=(\omega_\pi-2m_\pi)/m_\pi$ for total incident pion energy ω_π . In a simple eikonal approach incident pion attenuation is found to lead to a reduction of threshold estimates by a factor of ~ 10 . (20 refs.)

75052 Fermi motion and Pauli exclusion principle effects in $d(\pi^\pm, \pi^\pm p)n$ in the Δ -resonance region. G.Ramachandran, R.S.Keshavamurthy, S.B.Patangi, V.Ravishanker (Dept. of Phys., Univ. of Mysore, Mysore, India).

Phys. Rev. C (USA), vol.27, no.5, p.2198-202 (May 1983).

An ab initio method of taking Fermi motion effects in pion scattering into account combined with proper antisymmetrization of the two nucleon final state in $d(\pi^\pm, \pi^\pm p)n$ shows that the reaction amplitude consists of not only a contribution from pion scattering on a proton but also pion scattering on a neutron, and that the two amplitudes differ considerably in their π - N c.m. energies. The neutron scattering contribution to the differential cross section exceeds 10% in as many as 51 out of 194 π^- events recorded in a recent kinematically complete experiment by Hofsteezer et al. (1981) in the Δ -resonance region. In several kinematical situations the neutron contribution exceeds 100% and could even be as high as $\sim 400\%$. (5 refs.)

75053 Some characteristics of secondary particles produced in pion-nucleus collisions in emulsion at 50 GeV/c. S.Ahmad, H.Ahrar, A.R.Khan, A.Ahmad, M.Irfan, M.Zafar, M.Shafi (Dept. of Phys., Aligarh Muslim Univ., Aligarh, India).

Phys. Scr. (Sweden), vol.27, no.5, p.323-9 (May 1983).

The authors report results on multiparticle production in 50 GeV/c π^- -interactions with emulsion nuclei. The general characteristics of heavy and shower particle multiplicity distributions are compared with the results from p -nucleus collisions at the same incident energy. The various experimental results have also been compared with the predictions of the existing theoretical models. They have observed that the mean normalized multiplicity (R_{A2}) in hadron-nucleus interactions as a function of the effective number of projectile encounters, $\langle \nu \rangle$, calculated by using the additive quark model suggests a new kind of scaling and R_{A2} vs. $\langle \nu \rangle$ is independent of nature of the projectile. (31 refs.)

75054 Off-energy shell scattering of pions on deuterons. G.Ramachandran, R.S.Keshavamurthy, S.B.Patangi, V.Ravishanker (Dept. of Phys., Univ. of Mysore, Mysore, India).

Proceedings of the VI High Energy Physics Symposium (papers in summary form only received), Mysore, India, 6-11 Dec. 1982 (Bombay, India: Dept. Atomic Energy 1982), p.67

Summary form only given, as follows. The authors analyse the recent experimental results of Hofsteezer et al. (1981) on $d(\pi^\pm, \pi^\pm p)n$ as a means to study the off-energy shell scattering of pions on nucleons. Their model takes ab initio into account the effects of Fermi motion and due consideration is also given to neutron scattering contributions arising out of the Pauli exclusion principle, which can even exceed 100% under appropriate kinematical situations. The present analysis reports preliminary results following some of the models for πN scattering suggested in recent years.

Pion dynamics in the relativistic nuclear many-body problem .See Entry 74921

Multiple scattering in the Lee modelSee Entry 74926

Diffraction scattering off strongly bound systemSee Entry 74942

The kaonic hydrogen atom in momentum spaceSee Entry 75555

25.85 FISSION REACTIONS

75055 Fission probability in the $^{232}\text{Th}(p,p'xfn)$ reaction at low energy. Chien Chung (Dept. of Chem., Univ. of Maryland, College Park, MD, USA), J.J.Hogan, H.H.Muller.

Can. J. Chem. (Canada), vol.61, no.4, p.646-8 (April 1983).

In recent works, a model was developed to calculate many of the features of $^{232}\text{Th}(p,x)$ reactions with incident proton energies to 100 MeV. The model reproduced many properties such as spallation excitation functions, total fission cross sections, the symmetric/asymmetric mass ratio, and fission charge dispersion data. In this work, the model approach is extended to consider the fission probability in $^{232}\text{Th}(p,p'xfn)$ fission channels. A comparison of the

results calculated from the model to the experimental data shows very good agreement, and again justified the approach of the model. (13 refs.)

75056 Yields of products in the spontaneous fission of ^{252}Cf by direct γ -ray spectroscopy. L.Toppare, H.N.Erten, N.K.Aras (Dept. of Chem., Middle East Tech. Univ., Ankara, Turkey).

Can. J. Chem. (Canada), vol.61, no.4, p.649-51 (April 1983).

Yields of products both in the light and heavy sides in the spontaneous fission of ^{252}Cf were measured by direct γ -ray spectroscopy technique. By suitably choosing collection, cooling, and counting times, it was possible to observe products with half-lives between 1 min and 1 h. A definite fine structure, as observed in the case of thermal neutron fission of ^{235}U and ^{239}Pu , was not observed. A graphical method was utilized to obtain the number of neutrons as a function of fragment mass using cumulative chain yields. (18 refs.)

75057 Nuclear charge distribution in fission: fractional cumulative yields of isotopes of krypton and xenon in $^{249}\text{Cf}(n_{\text{th}}, f)$ and $^{250}\text{Cf}(sp, f)$. H.-H.Meixler, K.Wolfsberg, H.O.Denschlag (Inst. für Kernchem., Univ. Mainz, Mainz, Germany).

Can. J. Chem. (Canada), vol.61, no.4, p.665-70 (April 1983).

The fractional cumulative yields (%) of the following rare gas isotopes were determined radiochemically in the thermal neutron induced fission of ^{249}Cf and in the spontaneous fission of ^{250}Cf and the following results were obtained for the two processes, respectively: ^{89}Kr : 77.6 ± 1.5 , —; ^{91}Kr : 31.0 ± 1.7 , ^{140}Xe : 12.5 ± 2.0 , ^{147}Xe : 4.0 ± 0.3 , ^{141}Xe : 32.0 ± 3.5 , ^{139}Xe : 32.0 ± 3.5 , ^{142}Xe : 0.9 ± 0.1 , <3.61 , and ^{143}Xe : 0.22 ± 0.08 , —. The results are discussed with respect to the systematics of nuclear charge distribution in fission. (24 refs.)

75058 Mass spectrometric determination of Rb fission yields from ^3He and ^4He induced fission of ^{238}U and ^{232}Th . P.L.Reeder (Pacific Northwest Lab., Richland, WA, USA).

Can. J. Chem. (Canada), vol.61, no.4, p.786-93 (April 1983).

Cumulative and independent fission yields of Rb isotopes have been measured for ^3He and ^4He induced fission of ^{232}Th and ^{238}U at bombarding energies slightly above the Coulomb barriers. The on line mass spectrometric technique provided yields for masses 89-97. Mean masses and widths of the Rb independent yield distributions were obtained and were compared to other fissioning systems with excitation energies up to 160 MeV. (31 refs.)

75059 Energy dependence of the probability for asymmetric fission of ^{213}At . E.N.Gruzintsev, M.G.Itkis, V.N.Okolovich, A.Ya.Rusanov, G.N.Smirenkin, V.N.Tolstikov (Inst. of Nuclear Phys., Acad. of Sci., Kazakh SSR).

JETP Lett. (USA), vol.36, no.8, p.372-6 (20 Oct. 1982). Translation of: *Pis'ma v Zh. Eksp. & Teor. Fiz. (USSR)*, vol.36, no.8, p.304-7 (20 Oct. 1982). [received: June 1983]

The mass distribution of the fragments of the fission of ^{213}At in the reaction $^{209}\text{Bi}(\alpha, f)$ has been measured for α energies in the range 34.7-50 MeV. Over the entire energy range studied, the asymmetric mode is an improbable, slightly energy-dependent mode for the ^{213}At fission. This property of the ^{213}At fission represents a qualitative distinction from the fission of heavy nuclei. (7 refs.)

75060 The concept of vibrational resonances associated with the secondary and tertiary wells of a multi-humped fission barrier. J.E.Lynn (Nuclear Phys. Div., AERE Harwell, England).

J. Phys. G (GB), vol.9, no.6, p.665-81 (June 1983).

Large-scale structures in the fission cross sections of the lower-charge actinides are commonly interpreted as pure vibrational (transmission) resonances associated with a well in the fission barrier. This well is often hypothesized to be a tertiary well, the secondary well of a double-humped barrier being too deep (according to most theoretical models) to allow undamped vibrational modes at the excitation energies involved. The author considers the possible width and strength ratios of low-lying states associated with secondary and tertiary wells, investigating the deviation, due to coupling of single-particle and vibrational motions, of these properties from the simple expectations of a simple transmission model. This deviation is found to be considerable. Comparison of the calculated resonance properties with experimental data is made; this slightly favours the tertiary well hypothesis. Overall, the results indicate that more detailed fission cross section and angular distribution measurements in conjunction with more realistic model calculations of the type outlined in this paper could help bring a definitive answer to the problem of the structure of the light actinide fission barriers. (11 refs.)

75061 Mass distributions in monoenergetic-neutron-induced fission of ^{239}Pu . J.E.Gindler, L.E.Glendenin, D.J.Henderson, J.W.Meadows (Argonne Nat. Lab., Argonne, IL, USA).

Phys. Rev. C (USA), vol.27, no.5, p.2058-62 (May 1983).

Fission product yields for 24 masses were determined for the fission of ^{239}Pu with essentially monoenergetic neutrons of 0.17, 1.0, 2.0, 3.4, 4.5, 6.1, and 7.9 MeV. Fission product activity were measured by Ge(Li) γ -ray spectrometry of irradiated ^{239}Pu targets and by chemical separation of the fission product elements followed by β counting. Yields of near symmetric (valley) fission products increase nearly monotonically with incident neutron energy and do not exhibit a break in the slope of the yield versus neutron energy curve in the energy region where second-change fission begins. This is in contrast to the curves for ^{232}Th , ^{235}U , and ^{238}U neutron-induced fission. (17 refs.)

75062 Induced nuclear fission viewed as a diffusion process: transients. P.Gränge (Univ. Louis Pasteur, Strasbourg, France), Li Jun-Qing, H.A.Weidenmüller.

Phys. Rev. C (USA), vol.27, no.5, p.2063-77 (May 1983).

Induced nuclear fission is viewed as a diffusion process of the fission degree of freedom over the fission barrier. The authors describe this process in terms of a Fokker-Planck equation which contains the fission variable and its canonically conjugate momentum. They solve this equation numerically for several energies (temperatures) of the fissioning nucleus neglecting changes of the fission barrier due to the temperature dependence of nuclear shell effects. They pay particular attention to the time τ needed for the system to build up the quasistationary probability flow over the fission barrier. The rate of the latter is approximated in terms of the Bohr-Wheeler formula or Kramers' transition state expression; the precise value of the quasistationary current depends on the nuclear friction constant β . Their results for τ are consistent with those obtained earlier in the framework of a simplified model. As long as $\beta \leq \beta_0$, the time τ is proportional to β^{-1} . This relationship exhibits the fact that with increasing friction β , the diffusion process is accelerated, so that it takes the system increasingly less time to attain the quasistationary distribution. The constant β_0 is roughly given by $2\omega_1$, where ω_1 is the frequency of a harmonic oscillator potential which oscillates the potential at the minimum corresponding to the initial configuration of the fissioning nucleus. The condition $\beta \leq \beta_0$ is roughly equivalent with the motion in that minimum being underdamped. The converse relationship τ increases with β is found for $\beta > \beta_0$. They ascribe this to the fact that now the fission variable executes an overdamped motion. Generalizing Kramers' original derivation, they obtain an analytical expression for the time dependence of the probability current

over the fission barrier. For $\beta \leq \beta_0$, this expression agrees well with their numerical results. They use it to calculate the energy dependence of the fission probability P_f and find that P_f grows much less rapidly with increasing excitation energy than would be predicted by the Bohr-Wheeler formula. This is in qualitative agreement with recent experimental findings and suggests that the energy dependence of P_f deserves further investigation and can be used to determine β experimentally. Their analysis does not yet include the additional time delay incurred by the system on its way from the saddle to the scission point. Clearly the time needed to establish the quasistationary situation at the scission point will be larger than τ . This would probably lead to additional modifications of the energy dependence of P_f . (16 refs.)

75063 Yields of the photofission products of ^{237}Np . M.Ya.Kondrat'ko, A.V.Mosov, K.A.Petzhak, O.A.Tedorovich. *Sov. At. Energy (USA)*, vol.53, no.3, p.629-32 (Sept. 1982). Translation of: *At. Energ. (USSR)*, vol.53, no.3, p.164-7 (Sept. 1982). [received: May 1983] The systematics of fission product yields and the possible application of these data for the nondestructive determination of fissile substances is considered. The authors investigate the mass and charge distributions of the photofission products of ^{237}Np in the region of the maximum bremsstrahlung energy of 22-28 MeV, using γ -spectrometric and radio-chemical methods. (7 refs.)

75064 Prompt light-ion emission in the $^{235}\text{U} + ^4\text{He}$ reaction at 40 MeV/u*. K.Kwiatkowski, V.E.Viola, Jr. (Indiana Univ., Bloomington, IN, USA).

Proceedings of the International Conference on Nucleus-Nucleus Collisions (papers in summary form only received), East Lansing, MI, USA, 26 Sept.-1 Oct. 1982 (East Lansing, MI, USA: Michigan State Univ. 1982), p.113. The spectra of H and He ions in coincidence with angle-correlated fission fragments have been measured for the $^{235}\text{U} + ^4\text{He}$ reaction at 40 MeV/u. These studies were performed at the University of Maryland cyclotron and employed a pair of $6 \times 46 \text{ mm}^2$ position-sensitive ion-implanted detectors to measure the angle between coincident fission fragments, θ_{AB} , along with an array of detector telescopes to detect coincident light ions. (2 refs.)

75065 Study of fission-like products in the $^{84}\text{Kr} + ^{24}\text{Mg}$ reaction at 5.83 E/A (MeV). B.Heusch, J.P.Coffin, P.Engelstein, G.Guillaume, F.Rami (Univ. Louis Pasteur, Strasbourg, France).

Proceedings of the International Conference on Nucleus-Nucleus Collisions (papers in summary form only received), East Lansing, MI, USA, 26 Sept.-1 Oct. 1982 (East Lansing, MI, USA: Michigan State Univ. 1982), p.114. The Kr+Mg reaction was carried out in the framework of a systematic to study the compound or composite system ^{108}Cd deexcitation dependence versus the asymmetry between different projectile and target mass combinations. Such results exist for the extreme entrance channels, p+Ag, $^{12}\text{C} + ^{98}\text{Mo}$, $^{19}\text{F} + ^{89}\text{Y}$ and the more symmetric channels $^{32}\text{S} + ^{74}\text{Ge}$. The present $^{84}\text{Kr} + ^{24}\text{Mg}$ study was undertaken because a clear separation of fission like contribution from deep inelastic processes was expected, similar to what has been observed for the neighbouring system $^{84}\text{Kr} + ^{27}\text{Al}$ at GSI. (2 refs.)

A numerical method for two-dimensional Fokker-Planck equation See Entry 74954

Parity violation and related effects in neutron-induced reactions See Entry 74986

Experimental signatures for fast fission See Entry 75029

Dissipative collisions with a fission-like exit channel in the $^{132}\text{Xe} + ^{56}\text{Fe}$ system See Entry 75030

Angular dependence of symmetric fragmentation for the $^{32}\text{S} + ^{59}\text{Co}$ reaction See Entry 75031

Fission of Pb nuclei at high angular momenta See Entry 75032

Fast Fourier component in fusion reactions with heavy ions See Entry 75033

Enhanced fission probabilities observed in the $^{184}\text{W} + ^{184}\text{W}$ collision See Entry 75034

Fission following capture reactions of $^{32}\text{S} + ^{208}\text{Pb}$ See Entry 75035

Angular momentum dependence of fission barriers See Entry 75036

Simulation of neutron transmission by fission nuclei in the region of unresolved resonances See Entry 75150

25.88 FUSION REACTIONS

75066 A tool to study collective transitions between excited nuclear states. W.Knupfer, M.G.Huber (Inst. for Theoretical Phys., Univ. Erlangen-Nurnberg, Erlangen, Germany). Proceedings of the International Conference on Nucleus-Nucleus Collisions (papers in summary form only received), East Lansing, MI, USA, 26 Sept.-1 Oct. 1982 (East Lansing, MI, USA: Michigan State Univ. 1982), p.102.

The radiative capture of two complex nuclei into a specific bound state 1ν of the united nucleus A (radiative fusion) $A_1(Z_1, N_1) + A_2(Z_2, N_2) \rightarrow A(Z_1 + Z_2, N_1 + N_2) + \gamma$ requires the coherent cooperation of all nucleons. This process can be used as an appropriate spectroscopic tool to investigate the existence of dinuclear substructures in the nuclear excitation spectrum and the possible existence of collective transitions between excited states. The authors present a microscopic model which allows one to convert completely the free energy of the entrance channel into a specific intermediate resonance A^* , which then is deexcited by a collective phototransition into an excited state 1ν of the united nucleus, A. This model has been applied to the $^{12}\text{C}(\alpha, \gamma)^{16}\text{O}(\mu - \nu)$ reaction. (3 refs.)

Further evidence for 'extra push' See Entry 74928

Fusion cross sections for $^{14}\text{N} + ^{11}\text{B}$ at low energies See Entry 75010

Heavy-ion elastic scattering and its connections with fusion and absorption processes See Entry 75012

A phenomenological formula for fusion cross section See Entry 75022

Universal parametrization of fusion barrier See Entry 75023

A new critical distance model for heavy-ion fusion reactions See Entry 75024

Fusion-entry-line in fusion reactions for $^{12}\text{C} + ^{50}\text{Cr}$ and $^{32}\text{S} + ^{30}\text{Si}$ See Entry 75025

Incomplete fusion and nonequilibrium emission processes in the system $^{16}\text{O} + ^{93}\text{Nb}$ at 200 MeV See Entry 75026

Incomplete fusion at low impact parameters with a ^{116}Sn target See Entry 75027

Dynamical theory of incomplete fusion reactions See Entry 75028

Fission of Pb nuclei at high angular momenta See Entry 75032

Fast Fourier component in fusion reactions with heavy ions See Entry 75033

Possible sub-Coulomb resonances and fusion doorways in collisions of deformed heavy ions See Entry 75038

27.00 PROPERTIES OF SPECIFIC NUCLEI LISTED BY MASS RANGES

27.10 $A \leq 5$

Effect of the $\Delta(1236)$ isobar on the three-nucleon bound states See Entry 74841

Coupled channels and quarks in nucleon-nucleon scattering See Entry 74850

Three-body forces See Entry 74855

Charge-dependent three-body force with isobar excitations See Entry 74858

Three-nucleon interaction in 3-, 4- and ∞ -body systems See Entry 74861

Interplay between two- and three-body interaction in light nuclei and nuclear matter See Entry 74862

Mass dependence of the real optical model potential for light ions See Entry 74868

Conventional approach to the problem of the deuteron smearing corrections See Entry 74869

A radiochemical study on the existence of dineutron See Entry 74870

A-N interaction and the structure of ^4He , ^4H , ^3He and ^3H See Entry 74894

Scattering length in a system of three charged particles See Entry 74922

Implications of the experimental results on the photodisintegration of ^4He See Entry 74959

Structure functions for the electrodisintegration of the deuteron at a momentum transfer of 1.8 GeV^2 See Entry 74963

A theory for proton- ^3He scattering See Entry 74969

Low-energy n-p capture as a probe of two-nucleon dynamics See Entry 74984

Measurements of analyzing power for $^2\text{H}(\bar{n}, n)^3\text{H}$ scattering at 14.1 MeV and comparisons to $^2\text{H}(\bar{p}, p)^3\text{H}$ See Entry 74999

Production of large P_T particles in p-nucleus and nucleus-nucleus collisions at high energies See Entry 75002

Complete set of first-order polarization observables in nucleon-deuteron elastic scattering near 20 MeV deuteron energy See Entry 75004

Fermi motion and Pauli exclusion principle effects in $d(\pi^\pm, \pi^\pm p)n$ in the Δ -resonance region See Entry 75052

Off-energy shell scattering of pions on deuterons See Entry 75054

The kaonic hydrogen atom in momentum space See Entry 75555

Biomedical applications of MWPC's for digital imaging of soft β emitters See Entry 78406

27.20 $6 \leq A \leq 19$

^6Li levels excited by the $^9\text{Be}(p, \alpha)$ reaction at $E_p = 30$ and 50 MeV See Entry 74848

The heavy-ion potential and its increasing transparency at intermediate energies See Entry 74865

A radiochemical study on the existence of dineutron See Entry 74870

Proton capture to excited states of ^{16}O : M1, E1, and Gamow-Teller transitions and shell model calculations See Entry 74904

Quasimolecular and cluster states of light nuclei as examples of intermediate structure See Entry 74946

Application of the microscopic $\text{sp}(3, \text{R})$ model to the giant monopole and quadrupole resonances in ^{16}O See Entry 74947

Coulomb forces in the three-body problem with application to direct nuclear reactions See Entry 74953

Nuclear pion photoproduction: a theory and the $^{16}\text{O}(\gamma, \pi^+)^{16}\text{N}(\text{bound})$ example See Entry 74958

$^{13}\text{C}(\gamma, p)$ cross section See Entry 74960

Experimental investigation of the reaction $^{12}\text{C}(\gamma, \pi^0)\text{X}$ in the photon energy range between threshold and 450 MeV See Entry 74962

An analytic distorted wave approximation for intermediate energy proton scattering See Entry 74964

Microscopic analysis of proton elastic scattering in the range 80-200 MeV See Entry 74967

Microscopic analysis of ^6Li (\bar{p}, p), g.s. and ^6Li (\bar{p}, p) (2.18 MeV) analyzing powers at 25, 35, and 45 MeV See Entry 74972

Measurement of cumulative-neutron and cumulative-proton spectra in 1-GeV proton-nucleus interactions See Entry 74983

Polarization transfer in $A(d, pX)$ reactions See Entry 75003

Fragmentation spectra induced by light ions colliding with light nuclei See Entry 75006

Fusion cross sections for $^{14}\text{N} + ^{11}\text{B}$ at low energies See Entry 75010

Energy dependence of the production of pions, kaons and antikaons calculated in the hadrochemical model See Entry 75020

Energy dependence of ^{14}N mean free path in nuclear emulsions below 250 MeV per nucleon See Entry 75039

Emission of α fragments in nucleus nucleus collision at high energy See Entry 75044

Search for 'anomalons' in 4.5 A GeV ^{12}C -emulsion interaction See Entry 75046

Pion laser study in relativistic nucleon collision See Entry 75047

Three-body model for p-wave pion- ^{16}O scattering See Entry 75050

Threshold estimates of $(\pi, 2n)$ on nuclei in the Fermi gas model: one-body mechanism See Entry 75051

A tool to study collective transitions between excited nuclear states See Entry 75066

Determining distribution and concentration of certain elements with the aid of a charged-particle beam See Entry 77944

Could ^7Be be destroyed by neutron absorption in the Sun? A note on the solar neutrino puzzle See Entry 78897

27.30 $20 \leq A \leq 38$

- Low lying yrast states of ^{32}S See Entry 74832
- Inelastic electron scattering to negative parity states of ^{28}Si See Entry 74842
- Major shell centroids in the symplectic collective model See Entry 74876
- ^{35}Na : a new neutron-rich sodium isotope See Entry 74915
- Quasimolecular and cluster states of light nuclei as examples of intermediate structure See Entry 74946
- Coupling between low-lying nuclear states See Entry 74950
- Microscopic analysis of proton elastic scattering in the range 80-200 MeV See Entry 74967
- Inelastic proton scattering to one-particle one-hole states See Entry 74971
- A global study of the $p+^{27}\text{Al}$ reaction at 180 MeV See Entry 74977
- Energy deposition in intermediate-energy nucleon-nucleus collisions See Entry 74988
- Calculation of the energy-averaged scattering function for high resolution low-energy neutron scattering data See Entry 74990
- Separation of direct and compound nuclear contributions in inelastic α scattering See Entry 75007
- Orbiting phenomenon in ^{16}O - ^{28}Si scattering See Entry 75015
- Measurement of kinetic flow parameters for relativistic collisions of Ne on NaF and Ar on Pb_3O_4 See Entry 75017
- Elastic scattering of ^{20}Ne on ^{24}Mg See Entry 75019
- Energy dependence of the production of pions, kaons and antikaons calculated in the hadrochemical model See Entry 75020
- Fusion-entry-line in fusion reactions for $^{12}\text{C}+^{50}\text{Cr}$ and $^{32}\text{S}+^{30}\text{Si}$ See Entry 75025
- Threshold estimates of $(\pi, 2\pi)$ on nuclei in the Fermi gas model: one-body mechanism See Entry 75051
- Study of fission-like products in the ^{84}Kr on ^{24}Mg reaction at 5.83 E/A (MeV) See Entry 75065

27.40 $39 \leq A \leq 58$

- Nuclear polarization and sign of the quadrupole moment of the $^{54}\text{Fe}(10^+)$ isomer See Entry 74835
- Excitation of M1 strength in $N=28$ isotones by inelastic proton scattering at 200 MeV See Entry 74898
- Gamma radiation from $^{50}\text{Cr}(p,p')^{50}\text{Cr}$ at $E=5.45\text{--}6.15$ MeV See Entry 74901
- $\Delta(1236)$ -isobar degrees of freedom and the strength of spin-isospin resonances See Entry 74945
- The isoscalar quadrupole strength distribution above 10 MeV in ^{40}Ca See Entry 74948
- Fluid dynamics of giant resonances of high spin states See Entry 74949
- Coupling between low-lying nuclear states See Entry 74950
- Microscopic analysis of proton elastic scattering in the range 80-200 MeV See Entry 74967
- A pragmatic approach to the continuum spectrum in the quasifree scattering See Entry 74976
- 1 GeV $\text{P-}^{40}\text{Ca}$ elastic scattering See Entry 74985
- Impulse approximation NN amplitudes for proton-nucleus interactions See Entry 74996
- Proton isotonic density differences from 0.8 GeV proton-nucleus elastic scattering See Entry 74998
- Polarization transfer in $\text{A}(\bar{d},p\text{X})$ reactions See Entry 75003
- $^{45}\text{Sc}(\alpha,\alpha n)^{44}\text{Sc}^m + \epsilon$: a monitor reaction for alpha particle induced reactions See Entry 75005
- Phase shift analysis of alpha-particle elastic-scattering angular distributions on the ^{40}Ca target nucleus See Entry 75008
- Fusion-entry-line in fusion reactions for $^{12}\text{C}+^{50}\text{Cr}$ and $^{32}\text{S}+^{30}\text{Si}$ See Entry 75025
- Dissipative collisions with a fission-like exit channel in the $^{132}\text{Xe}+^{56}\text{Fe}$ system See Entry 75030
- Fe-nucleus interactions at 1.8 GeV/nucleon See Entry 75043
- Search for anomalous in projectile fragments from Ar-emulsion, interactions See Entry 75045

27.50 $59 \leq A \leq 89$

- Proton occupancies in the even Se ground states via the $(d,^3\text{He})$ reaction See Entry 74847
- Description of the neutron deficient Sr and Zr isotopes in the interacting boson model See Entry 74874
- Fast $\Delta I=0$ M1 transitions in the band crossing region See Entry 74903
- Collective excitations of ^{82}Kr observed by in-beam and decay spectroscopy and their characterization by the interacting boson model See Entry 74906
- Identification of 26-minute Zr-84 See Entry 74912
- Momentum transfer in the fragmentation of copper by 400-GeV protons See Entry 74951
- Test of microscopic theory with data for simple transitions in the $^{90}\text{Zr}(p,p')$ and $^{89}\text{Y}(p,p')$ reactions See Entry 74973
- Particle distribution around a copper beam stop for 72 MeV protons See Entry 74981
- Deformation effect in the fast neutron total cross section of aligned ^{59}Co See Entry 74992
- Neutron-nucleus spin-spin interaction in the low MeV range See Entry 74993
- Double differential cross sections for (p, xn) reactions of ^{64}Zn , ^{65}Cu and ^{89}Y with 26 MeV protons See Entry 75000
- Fusion-entry-line in fusion reactions for $^{12}\text{C}+^{50}\text{Cr}$ and $^{32}\text{S}+^{30}\text{Si}$ See Entry 75025
- Angular dependence of symmetric fragmentation for the $^{32}\text{S}+^{59}\text{Co}$ reaction See Entry 75031
- Nuclear charge distribution in fission: fractional cumulative yields of isotopes of krypton and xenon in $^{249}\text{Cf}(n_{th},f)$ and $^{250}\text{Cf}(sp,f)$ See Entry 75057

Mass spectrometric determination of Rb fission yields from ^3He and ^4He induced fission of ^{238}U and ^{237}Th See Entry 75058

Chemical effects of nuclear transformations in mixed potassium hexahalo-oeno-metallates (IV), $\text{K}_2\text{MX}_6\text{V}_{6-n}$. I. Chemical effects of the $^{81}\text{Br}(n,\gamma)^{82}\text{Br}$ nuclear process in mixed potassium hexabromochloro-osmates (IV), $\text{K}_2\text{OsBr}_n\text{Cl}_{6-n}$ See Entry 77912

27.60 $90 \leq A \leq 149$

- Level structure of the $N=88$ isotones ^{149}Pm , ^{151}Eu and ^{153}Tb See Entry 74833
- High-spin states in ^{92}Tc See Entry 74834
- One- and three-quasiparticle states in $^{127,129,131,133}\text{Xe}$ and their coexistence with band structures See Entry 74839
- High-spin states in ^{97}Tc See Entry 74840
- An interacting boson-fermion model calculation for the odd-mass promethium isotopes See Entry 74843
- Low-lying states in ^{109}In populated by the $(^3\text{He},d)$ reaction in ^{108}Cd See Entry 74849
- Shape transitions and isotope shifts of proton and neutron distributions in the samarium isotopes See Entry 74889
- Population of ^{133}I from the beta decay of fission product ^{133}Te and the cluster-vibration model See Entry 74905
- Precise Q_β measurements for $A=91$ to 93 mass chains See Entry 74911
- The decay of 56-s ^{148}Ce to levels of odd-odd ^{148}Pr See Entry 74913
- Study of inner bremsstrahlung accompanying non-unique second-forbidden β decay in ^{99}Tc See Entry 74914
- Anomaly in the optical potential for deformed nuclei See Entry 74966
- Microscopic analysis of proton elastic scattering in the range 80-200 MeV See Entry 74967
- Test of microscopic theory with data for simple transitions in the $^{90}\text{Zr}(p,p')$ and $^{89}\text{Y}(p,p')$ reactions See Entry 74973
- Correlations between the alpha particles and ejectiles in the 208 MeV ^{14}N on ^{135}Nb reaction at three different ejectile angles See Entry 75013
- Incomplete fusion and nonequilibrium emission processes in the system $^{16}\text{O}+^{93}\text{Nb}$ at 208 MeV See Entry 75026
- Incomplete fusion at low impact parameters with a ^{116}Sn target See Entry 75027
- Angular momentum dependence of fission barriers See Entry 75036
- Nuclear charge distribution in fission: fractional cumulative yields of isotopes of krypton and xenon in $^{249}\text{Cf}(n_{th},f)$ and $^{250}\text{Cf}(sp,f)$ See Entry 75057

27.70 $150 \leq A \leq 189$

- Level structure of the $N=88$ isotones ^{149}Pm , ^{151}Eu and ^{153}Tb See Entry 74833
- Shape transitions and isotope shifts of proton and neutron distributions in the samarium isotopes See Entry 74889
- Nuclear orientation of ^{152}Eu in gold See Entry 74897
- Low energy spectrum and directional correlation measurements in ^{187}Re See Entry 74900
- Average resonance capture studies of $^{162,164}\text{Dy}$ See Entry 74908
- Fluid dynamics of giant resonances of high spin states See Entry 74949
- Anomaly in the optical potential for deformed nuclei See Entry 74966
- Fission of Pb nuclei at high angular momenta See Entry 75032
- Enhanced fission probabilities observed in the $^{184}\text{W}+^{184}\text{W}$ collision See Entry 75034
- Angular momentum dependence of fission barriers See Entry 75036

27.80 $190 \leq A \leq 219$

- Low-spin states in even Po and Rn isotopes and the interplay between collective and quasiparticle configurations See Entry 74838
- Variations of the gyromagnetic ratios of low-lying states in ^{192}Os See Entry 74844
- Nuclear orientation and NMR/ON of $^{205,207}\text{Po}$ See Entry 74846
- Temperature dependent shell corrections: numerical estimates for the lead region See Entry 74873
- The moments of strength functions See Entry 74902
- Levels in ^{204}Po from the decay of ^{204}At See Entry 74907
- Coupling between low-lying nuclear states See Entry 74950
- Microscopic analysis of proton elastic scattering in the range 80-200 MeV See Entry 74967
- 800 MeV protons as probes of neutron transition densities See Entry 74997
- Measurement of the average neutrons yield from 250 MeV protons absorbed in a lead target See Entry 75001
- Polarization transfer in $\text{A}(\bar{d},p\text{X})$ reactions See Entry 75003
- Fission of Pb nuclei at high angular momenta See Entry 75032
- Fission following capture reactions of $^{32}\text{S}+^{208}\text{Pb}$ See Entry 75035
- Angular momentum dependence of fission barriers See Entry 75036
- Energy dependence of the probability for asymmetric fission of ^{213}At See Entry 75059

27.90 $220 \leq A$

- Electron capture decay of ^{237}Pu , ^{235}Np , and ^{236}Np See Entry 74917
- Heavy target fragment yields in the interaction of 28 GeV protons with ^{238}U See Entry 74952
- Measurement of the photoneutron yield in the irradiation of heavy materials in closed shells See Entry 74961
- Baryon rapidity distribution and stopping power of high-energy colliding nuclei See Entry 75014
- Nuclear collisions of uranium nuclei up to ~ 1 GeV/nucleon See Entry 75016
- Fast Fourier component in fusion reactions with heavy ions See Entry 75033

- Potential pockets in the $^{238}\text{U} + ^{238}\text{U}$ system and their possible consequences See Entry 75037
- Possible sub-Coulomb resonances and fusion doorways in collisions of deformed heavy ions See Entry 75038
- Fission probability in the $^{232}\text{Th}(p,p'nf)$ reaction at low energy See Entry 75055
- Yields of products in the spontaneous fission of ^{252}Cf by direct γ -ray spectroscopy See Entry 75056
- Nuclear charge distribution in fission: fractional cumulative yields of isotopes of krypton and xenon in $^{249}\text{Cf}(n_{th},f)$ and $^{250}\text{Cf}(sp,f)$ See Entry 75057
- Mass spectrometric determination of Rb fission yields from ^3He and ^4He induced fission of ^{238}U and ^{232}Th See Entry 75058
- The concept of vibrational resonances associated with the secondary and tertiary wells of a multi-humped fission barrier See Entry 75060
- Mass distributions in monoenergetic-neutron-induced fission of ^{239}Pu See Entry 75061
- Yields of the photofission products of ^{237}Np See Entry 75063
- Prompt light-ion emission in the $^{235}\text{U} + ^4\text{He}$ reaction at 40 MeV/u^* See Entry 75064
- Neutronspektrum es doziszozsias vizsgalatok szamitassal es meressel elliptikus fantomban ^{252}Cf es nehveziviz moderalt ^{252}Cf neutron forrasokra (Neutron spectra and dose distribution calculations and measurements for a filled elliptical phantom using bare and heavy-water moderated ^{252}Cf neutron sources) See Entry 78352

28.00 NUCLEAR ENGINEERING AND NUCLEAR POWER STUDIES

(see also 86.10 Energy resources and their utilisation)

28.20 NEUTRON PHYSICS

(see also 25.40 Nucleon-induced reactions and scattering)

- 75067 Multislab multigroup transport theory with L th order anisotropic scattering. R.D.M.Garcia, C.E.Siewert (Dept. of Nuclear Engng. & Math., North Carolina State Univ., Raleigh, NC, USA). *J. Comput. Phys. (USA)*, vol.50, no.2, p.181-92 (May 1983). The special case of a triangular transfer matrix relevant to multigroup transport theory in multislabs with L th order anisotropic scattering is discussed, and the F_N method is used to establish accurate numerical results for a test problem. (5 refs.)
- 75068 Distribution of the flux density and hardness of the neutron spectrum with height and over the cross section of the heat-generating assemblies of VVER-365 and VVER-440 reactors. B.A.Bibichev, V.P.Maiorov, V.D.Sidorenko, P.I.Fedotov. *Sov. At. Energy (USA)*, vol.53, no.3, p.596-601 (Sept. 1982). Translation of: *At. Energy (USSR)*, vol.53, no.3, p.143-7 (Sept. 1982). [received: May 1983] The flux density and spectrum of the neutrons in the active zones of VVER-365 and VVER-440 reactors (water-cooled-water-modulated power reactors) can only be measured in special channels located in the central tubes of the heat-generating assemblies (HGA). The distribution of the flux density and spectrum of the neutrons with the HGA height is measured with the help of activation detectors in these channels. Experimental data on the distribution of these quantities over the HGA cross section are also necessary for checking and correcting the computational programs. Such information can be obtained from the concentration of certain fission products in the fuel after the HGA are unloaded from the reactor. (11 refs.)
- 75069 Neutron yield of the (α,n) reaction for multicomponent media. V.I.Bulanenko, V.V.Frolov, E.M.Tsenter. *Sov. At. Energy (USA)*, vol.53, no.3, p.622-8 (Sept. 1982). Translation of: *At. Energy (USSR)*, vol.53, no.3, p.160-4 (Sept. 1982). [received: May 1983] There has been a steady rise in the production and use of α -active nuclides in nuclear engineering, and it is necessary to know the accurate neutron yield Q for the solution of many practical problems, a detailed and reasoned list of which is given in the review. The components of Q are spontaneous nuclear fission and (α,n) reactions in light elements with $Z \leq 20$. The importance of taking (α,n) reactions accurately into account is illustrated. In view of the difference in composition of the set of materials and components actually used, it is preferable to obtain accurate information by calculational means. Whereas the calculation of the neutron yield of spontaneous fission with known nuclear data is not difficult, the calculation of the neutron yield of the (α,n) reaction $Q^{\alpha n}$ is far from obvious. Individual aspects of determining $Q^{\alpha n}$ and its dependence on the α -particle energy and composition of the medium have been considered. Systematic and critical analysis of these calculations, and also on the analysis of sources of error are discussed. (36 refs.)
- 75070 Research proposal for advanced diffractometer (US-Japan collaborative research in neutron scattering). M.Iizumi, S.Funahashi. Report JAERI-M-82-157, Japan Atomic Energy Res. Inst., Tokai, Ibaraki (Nov. 1982), 34 pp. This paper is the proposal submitted to the US-Japan meeting (1980) for the collaborative research in neutron scattering, in which it is proposed to carry out various kinds of new measurements by using the wide angle, curved linear position-sensitive counter. The time-division measurement of the diffraction patterns and the single-crystal diffractometry utilizing the inclination geometry are the principal research area proposed.
- A fast configuration with a conjugate flux independent of energy See Entry 75096
- Data evaluation on the absorption of neutrons by cadmium with the aid of integral experiments See Entry 75097
- Measurement of the effective cross-sections of absorption for fast reactor building materials using a fast configuration with a conjugated flux, independent of energy See Entry 75098
- Refinement of boundary conditions in the calculation of close-packed lattices by the surface pseudosources method See Entry 75105
- Control of the neutron distribution in a reactor by a liquid absorber See Entry 75161
- Storage of ultracold neutrons in a vessel long enough for β decay See Entry 75217

28.41 FISSION REACTOR THEORY AND DESIGN

- 75071 Nuclear data requirements for the design of fast neutron reactors. L.N.Usacev. *Yad. Energ. (Bulgaria)*, no.18, p.3-8 (1983). A survey of the basic requirements of nuclear data for fast neutron reactors is made with a view of present-day state of affairs in the data field. Particular emphasis is laid upon the areas developed within the framework of the cooperation among the CMEA member-countries. (9 refs.)
- 75072 Modification of the SUPERTOG program for operation with libraries containing tabulated densities of the elastic scattering anisotropy. G.K.Voykov, V.I.Gadjokov, K.D.Ilieva. *Yad. Energ. (Bulgaria)*, no.18, p.40-8 (1983). For the calculation of the group-to-group transfer matrix with the SUPERTOG program it is necessary to specify the data for the anisotropy of the elastic scattering with the coefficients of expansion of the density function into Legendre polynomials. For all materials of the ENDL library and for some materials from FND/FB-IV, the information for the scattering anisotropy is specified as tabulated values of the density function itself. For these materials the existing versions of SUPERTOG are inapplicable. The modification of the SUPERTOG program prepared by the authors makes the calculation of the elastic scattering matrix possible using the two ways of anisotropy setting. A method based on approximation with orthonormal polynomials is used for computing the required coefficients within the process of the program itself. This procedure takes up less than 15% of the SUPERTOG machine time. (6 refs.)
- 75073 Software for neutron physical calculations of fast neutron reactors. J.D.Jordanov, N.A.Antonov. *Yad. Energ. (Bulgaria)*, no.18, p.94-103 (1983). A set of programs has been developed for neutron physical calculations of fast neutron reactors. The set includes the PRIDAN program for calculating the effective cross-sections of the media, characteristic of the fast reactor systems, the MED program—a single dimension multigroup program for calculating fast reactors in the multigroup diffusion approximation and the ANALIT program for calculating the criticality in plane geometry. PRIDAN uses the formalism of the self-shielding factors and prepares the effective cross-sections using an iterative procedure. The values of the multigroup cross-sections obtained for different temperatures are used directly as input data for the other programs. MED calculates the critical dimensions, the coefficient of effective multiplication, the real and conjugated neutron flux, the integrated neutron fluxes for each energy group and each spatial zone, the distribution of the neutron fission sources. The ANALIT program solves under given conditions the diffusion multigroup equation analytically using a method proposed by the authors. The body of mathematic pertaining to the case is presented. (12 refs.)
- 75074 A FAST program for determining the neutron physical parameters of fast neutron reactors. J.D.Jordanov, N.A.Antonov. *Yad. Energ. (Bulgaria)*, no.18, p.104-9 (1983). The FAST program is part of the modulus developed at the Institute for Nuclear Research and Nuclear Energy in Sofia for calculating the neutron physical parameters of the fast neutron reactors. The program is written in FORTRAN IV. It calculates the normalized integral fluxes, the reaction rates, the leakages, the critical masses for the plutonium isotopes and the quantities characterizing the breeding of plutonium in the reactor. A test example is given for illustrating the program. (3 refs.)
- 75075 On-line fault diagnosis in a nuclear reactor by sequential testing. A.Ray, M.Desai, J.Deyst (Charles Stark Draper Lab. Inc., Cambridge, MA, USA). *IEEE Trans. Nucl. Sci. (USA)*, vol.ns-30, no.3, p.1850-5 (June 1983). A sequential test technique for on-line fault diagnosis of sensor signals has been developed and successfully demonstrated in an operating nuclear reactor. The methodology provides a systematic procedure for detection and isolation of sensor failures by taking into account consistencies among all available measurements of a given process variable. Fault diagnosis is accomplished on the basis of the cumulative information derived from the measurement history that includes the past and current observations. (10 refs.)
- 75076 Iconic displays, Rankine cycles and human factors for control rooms of nuclear power plants. L.Beltracchi. *IEEE Trans. Nucl. Sci. (USA)*, vol.ns-30, no.3, p.1856-61 (June 1983). This report discusses a concept for a nuclear power plants process iconic display to model the plant in the control room of a pressurized-water-reactor. The iconic display is based on the Rankine Cycle, a thermodynamic model for the power cycle. The display image contains coded information on the generation, transport, and removal of heat in the power plant process. (4 refs.)
- 75077 A pattern recognition method for nuclear reactor core surveillance. M.Invernizzi. *IEEE Trans. Nucl. Sci. (USA)*, vol.ns-30, no.3, p.1885-91 (June 1983). An automatic method for reactor core surveillance is described which employs pattern recognition techniques. A core vibration surveillance method for a pressurized water reactor has been developed which provides the early detection of failures. The sensors are eight ex-core ionization chambers. The algorithms used are heuristic but need only the definition of a small number of parameters. (16 refs.)
- 75078 Accreditation of qualification testing organizations the industry viewpoint. A.R.Roby (Northeast Utilities Service Co., Hartford, CT, USA). *IEEE Trans. Nucl. Sci. (USA)*, vol.ns-30, no.3, p.1917-19 (June 1983). The author presents the industry viewpoint on the program for the Accreditation of Qualification Testing Organizations, which has been proposed for rulemaking by the Nuclear Regulatory Commission. Presented is the industry perspective, developed and prepared through the AIF, identifying the serious concerns which the accreditation program has raised. Discussed are the disadvantages of the program and those present benefits which would be lost if the program was adopted. The value of greater emphasis on current regulation to improve the qualification processes is presented and details areas where the NRC proposals do not provide adequate justification for the accreditation program. (no refs.)
- 75079 Unbounded solutions of the nonlinear system of equations of nuclear-reactor kinetics. Yu.A.Kuznetsov, V.V.Shashkov (Sci.-Res. Inst. of Mech., N.I. Lobachevski State Univ., Gorki, USSR). *Sov. Phys.-Dokl. (USA)*, vol.27, no.7, p.545-7 (July 1982). Translation of: *Dokl. Akad. Nauk SSSR*, vol.265, no.1-3, p.587-92 (July 1982). [received: April 1983] The authors study the nonlinear integro-differential system of equations of reactor kinetics in the general form. The system of equations describes the evolution with time of the spatial and velocity distribution of neutrons and the spatial distributions of the precursors of delayed neutrons and the temperature of the medium in a nuclear reactor with allowance for feedback. (15 refs.)

75080 Harmonic simulation of a power reactor. P.T.Potapenko. *Sov. At. Energy (USSR)*, vol.53, no.3, p.608-13 (Sept. 1982). Translation of: *At. Energ. (USSR)*, vol.53, no.3, p.151-5 (Sept. 1982). [received: May 1983] The design of the control systems of contemporary power reactors is based on the distributed mathematical model of a reactor. The transfer matrix of a reactor relates the vector of the variation of the neutron distribution (ND) in individual zones or channels to the vector of the variation of the position of the regulating rods (the reactivity), and it is actually adopted as the mathematical model of a reactor. The difficulties in the experimental computational determination of the static transfer matrix are associated with the nonunique activation of a reactor to the critical steady state. The author presents an harmonic model of a power reactor. (14 refs.)

75081 WIMSCORE - A code for producing group constants for TDB, TRITON and CITATION codes from WIMS output. Y.Bartal, S.Yiftah. Report IA-1380, Israel Atomic Energy Comm., Yavne (Jan. 1983), 22 pp. A code was developed for producing group constants and other data needed for reactor core burnup calculations. The code named WIMSCORE gets its input from WIMS output files and evaluates it to be served as input to the diffusion-burnup codes TDB, TRITON and CITATION. The purpose of this code is to facilitate the automation of data transfer between codes which is otherwise a very time consuming and bound-to-error process. (11 refs.)

75082 Comparisons of energy dependent point-wise cross-section generation codes: RESEND, RESEND, RECENT. A.Hasegawa, T.Narita. Report JAERI-M-82-128, Japan Atomic Energy Res. Inst., Tokai, Ibaraki (Sept. 1982), 52 pp.

In order to improve the current situation for production of group cross-section sets, the authors performed intercomparison of energy dependent cross-section generation codes, i.e. RESEND, RESEND and RECENT which are currently used in the nuclear data community. And also the results were contributed to the international comparisons of energy dependent cross-section generation codes, organised by Dr. Cullen of IAEA. (7 refs.)

75083 A three-dimensional improved quasi-static core model for nuclear reactor control room simulators. S.G.Wagner, A.T.Shesler (Nuclear Power Systems, Combustion Engng. Inc., Windsor, CT, USA). Proceedings of the Fifth Power Plant Dynamics, Control and Testing Symposium, Knoxville, TN, USA, 21-23 March 1983 (Knoxville, TN, USA: Univ. Knoxville 1983), p.2/01-17 vol.1

With the availability of powerful modern mini-computers, more sophisticated and accurate modeling is now expected of nuclear reactor control room simulators. Today, such simulators must model a wide range of operational and accident conditions which place great demands on computers and models. The core model in Combustion Engineering Calvert Cliffs I full scope control room simulator illustrates this trend. It features a full core, three-dimensional space-time neutronic and thermal-hydraulic model and runs on one of the simulator's Perkin Elmer 3244 computers using a small fraction of that machine's computing capability. Addition of thermal-hydraulics and a new approach to the improved quasi-static method (IQSM) are described. The resulting model has successfully simulated operational and accident transients with a speed of 40 to 80 msec per reactor second. Thus, it fits easily into the real time requirements of the integrated simulator. (7 refs.)

75084 Interactive simulation of boiling water reactor systems using DARE P and VAX. K.Schwarzblat, M., D.Hetrick, J.Arellano G., J.M.Perez, A.Vilalobos, F.Mujica (Inst. de Investigaciones Electricas, Morelos, Mexico). Proceedings of the Fifth Power Plant Dynamics, Control and Testing Symposium, Knoxville, TN, USA, 21-23 March 1983 (Knoxville, TN, USA: Univ. Knoxville 1983), p.5/01-5 vol.1

A small engineering simulator for the Laguna Verde Nuclear Power Station in Mexico has been developed at the Instituto de Investigaciones Electricas (IIE) in Cuernavaca. The simulator is in the form of an input file for the DARE P Continuous System Simulation Language that was developed at the University of Arizona. Several new features have been added to interactive DARE for VAX by workers at IIE, including an optimization scheme for computing unknown initial conditions, a partitioning scheme to identify variables responsible for stiffness, and an optimization scheme for solving nonlinear algebraic equations that arise when fast variables are treated by the quasistatic approximation. The authors discuss the scheme for finding initial conditions, and present an example of a transient in the reactor and the recirculation flow controller. (4 refs.)

75085 Two phase flow simulator for a PWR nuclear power plants. M.A.Shinaishin (Reactors Dept., Atomic Energy Authority, Inshas, Egypt), M.N.Aly, Y.Abu-Shady. Proceedings of the Fifth Power Plant Dynamics, Control and Testing Symposium, Knoxville, TN, USA, 21-23 March 1983 (Knoxville, TN, USA: Univ. Knoxville 1983), p.14/01-23

The objective of this work is to develop a digital simulator of a complete Pressurized Water Reactor Nuclear Power Plant (PWRNPP) capable of simulating accidents in which vapor may be generated in the reactor core and transported along the primary loop. Extensive heat transfer correlations, two-phase friction multiplier and thermodynamic properties covering a wide range of pressure and temperature are included. Two models of the two phase flow, one of which has been adapted and the other has been developed, were implemented and responses were compared. In these models the void fraction, the heat transfer coefficients, and the two phase friction multiplier are defined differently. The results indicate negligible differences. (14 refs.)

75086 Whole-plant simulation for loop-type LMFBR dynamics. Y.Sagayama, M.Tanji (Advanced Reactors Engng. Dept., Mitsubishi Atomic Power Industries Inc., Saitama, Japan), H.Endo. Proceedings of the Fifth Power Plant Dynamics, Control and Testing Symposium, Knoxville, TN, USA, 21-23 March 1983 (Knoxville, TN, USA: Univ. Knoxville 1983), p.16/01-18 vol.1

A loop-type LMFBR of prototype plant is going to be developed in Japan. The whole-plant dynamic simulation program COPD (Code on Plant Dynamics) performs the basic tool of the characteristics analysis for control system design, evaluations of thermo-hydrodynamics for setting the design condition of components and accident analysis for explaining the validity of the reactor shutdown system of the plant. This paper describes the specifications of the model adapted to typical analysis items, verification of the model with the experimental results, reduction manner of the running cost and model improvement of the COPD program. (5 refs.)

75087 Application of real-time dynamic simulation of the analysis and design of large scale breeder reactor plants. F.J.Halfen, G.B.Kruger, R.A.Meyer (Advanced Reactor Systems Dept., General Electric Co., Sunnyvale, CA, USA).

Proceedings of the Fifth Power Plant Dynamics, Control and Testing Symposium, Knoxville, TN, USA, 21-23 March 1983 (Knoxville, TN, USA: Univ. Knoxville 1983), p.17/01-6 vol.1

Describes the approach being taken by GE-ARSD to the design of the Plant Control and Protection System (PCAPS) for a Large Scale Breeder Plant. The objective is to provide an approach to early 'front end' understanding of

the plant's transient, control and man-machine-interfaces using engineering simulation as a key design tool. This approach is intended to provide a superior PCAPS while minimizing the number of costly downstream design changes through more quantitative front-end analysis. The key element in the approach is the development of a minicomputer driven interactive engineering simulation facility using modern digital/CRT display hardware. This approach will also improve plant operability and facilitate safety reviews via plant operability validation testing while at the same time providing a focal point for PCAPS design integration. (1 ref.)

75088 A numerical integration approach suitable for simulating PWR dynamics using a microcomputer system. L.Zhiwei, T.W.Kerlin (Dept. of Nuclear Engng., Univ. of Tennessee, Knoxville, TN, USA). Proceedings of the Fifth Power Plant Dynamics, Control and Testing Symposium, Knoxville, TN, USA, 21-23 March 1983 (Knoxville, TN, USA: Univ. Knoxville 1983), p.18/01-25 vol.1

It is attractive to use microcomputer systems to simulate nuclear power plant dynamics for the purpose of teaching and/or control system design. An analysis and a comparison of feasibility of existing numerical integration methods have been made. The criteria for choosing the integration step using various numerical integration methods including the matrix exponential method are derived. (10 refs.)

Distribution of the flux density and hardness of the neutron spectrum with height and over the cross section of the heat-generating assemblies of VVER-365 and VVER-440 reactors See Entry 75068

Neutron yield of the (α, n) reaction for multicomponent media See Entry 75069

A fast configuration with a conjugate flux independent of energy See Entry 75096

Refinement of boundary conditions in the calculation of close-packed lattices by the surface pseudosources method See Entry 75105

A method of state equation decomposition and its application to the simulation of the dynamics of the active zone of the VVER reactor See Entry 75149

Simulation of neutron transmission by fission nuclei in the region of unresolved resonances See Entry 75150

Neutron-physical characteristics of a standard fast neutron reactor See Entry 75151

Investigation of the influence of some libraries of multigroup constants on the parameters of a standard fast neutron reactor See Entry 75152

Approximate noninteractive power regulation of a coupled-core nuclear reactor See Entry 75154

Digital computers in CANDU safety systems. I. History and concepts See Entry 75155

Neutron spectrum determination by multiple foil activation method See Entry 75159

Distributed microprocessor-based system for monitoring radiation in nuclear power plants See Entry 75160

Simulation of overcooling transients with the Modular Modeling System (MMS) See Entry 75164

Once through steam generator model See Entry 75165

Modeling and estimation applied to an AGR once-through boiler See Entry 75166

Dynamic computer simulation of the Fort St. Vrain steam turbines See Entry 75167

Simulation of recovery from a steam generator tube leak transient See Entry 75171

Temperature fields and thermal stress fields in radiation shieldings See Entry 75202

Role of sensitivity analysis in determining reactor quantities .. See Entry 75206

28.42 FISSION REACTOR MATERIALS

75089 Nomogram for determining the terminal activity and necessary decay time after the periodical filling of a container with short-lived radioactive materials. J.Krischan, H.Binder (Inst. fur Radiochem., Innsbruck, Austria).

Acta Phys. Acad. Sci. Hung. (Hungary), vol.52, no.3-4, p.455-67 (1982). In German. [received: May 1983] (Proceedings of the Hungarian-Austrian Health Physicists' Meeting, Gyor, Hungary, 28 Sept.-1 Oct. 1981). Describes a nomogram with auxiliary tables for determining the activity of radioactive waste in containers and the decay time required for activity to drop below legal limits. (5 refs.) J.S.

75090 Prediction of centrifugal pump cleaning ability in waste sludge. B.V.Churnetski (E.I. DuPont de Nemours & Co., Savannah River Lab., Aiken, SC, USA).

Nucl. & Chem. Waste Manage. (GB), vol.3, no.4, p.199-203 (1982). Radioactive waste at the Savannah River Plant (SRP) is being transferred from older waste tanks to new, stress-relieved tanks for more effective waste management. The technology developed for waste removal involves the use of long-shaft, recirculating, centrifugal pumps (slurry pumps). Testing completed at the Savannah River Laboratory's 30-meter-diameter mock-up waste tank related the effective cleaning radius (ECR) of a slurry pump to critical pump and material characteristics. Presently, this theory is being applied to radioactive waste at SRP. However, the technology can be applied to other remote handling situations where the slurry rheology can be determined. For SRP waste, an equation of the form $ECR \propto DV_0(\rho/\tau_0)^{1/2}$ was determined where D is the nozzle diameter, V_0 is the average initial velocity, ρ is the density of the slurry, and τ_0 is the yield stress of the slurry. Using this relationship, the cleaning performance of a pump operating in any SRP sludge environment can be predicted. Specifically, yield stress and density measurements on sludge samples can be used to predict the required number and effective location for slurry pumps in actual SRP waste tanks. (2 refs.)

75091 Current understanding of pitting and crevice corrosion and its application to test methods for determining the corrosion susceptibility of nuclear waste metallic containers. J.Kruger, K.Rhine (Center for Materials Sci., NBS, Washington, DC, USA).

Nucl. & Chem. Waste Manage. (GB), vol.3, no.4, p.205-27 (1982). A review of crevice and pitting corrosion mechanism and testing techniques is given to understand the fundamental problems involved in determining corrosion rates of alloys to be used as nuclear waste containers. The mechanisms are broken down into two sections, initiation and propagation of the crevice or pit. Theories of initiation include the absorbed ion displacement model, ion migration or penetration model and the breakdown-repair model. Experimental results concerning the initiation period include a discussion of the kinetics of initiation, the critical potential for breakdowns, and experimental factors

affecting the initiation. The theories of pit and crevice corrosion propagation are mentioned as well as factors affecting propagation. Several experimental techniques are discussed that are useful in determining the probability of pitting and/or crevice corrosion of alloys. In assessing the lifetime of the metallic container, accelerated tests are required. With this in mind the testing techniques concentrate on electrochemical techniques and various modifications of these basic techniques. Although susceptibility of alloys to pitting and crevice corrosion can be determined readily, initiation time and propagation rates are not as straightforward particularly over 1000 years. Nevertheless several testing techniques exist that may be used to determine these important values. (108 refs.)

75092 Incorporation of radionuclides in crystalline titanates. E.R.Vance, D.K.Agrawal (Materials Res. Lab., Pennsylvania State Univ., University Park, PA, USA).

Nucl. & Chem. Waste Manage. (GB), vol.3, no.4, p.229-34 (1982). The solid solubilities of some or all of Cs, Sr, Y, La, U, Th, and Na in each of barium hollandite, zirconolite and titanite were investigated by X-ray diffraction in samples prepared by ceramic techniques at 1100-1400°C. Various charge compensation schemes were used in attempts to incorporate aliovalent ions. Cs and Sr, but not the other ions, have extensive solid solubilities in barium hollandite. Zirconolite dissolves relatively large amounts of Na, as well as actinides and the smaller rare earths. Appreciable amounts of Sr, Na, rare earths, and actinides can be accommodated in titanite. Titanite is compatible with zirconolite but not with barium hollandite at ~1200°C. (24 refs.)

75093 Prediction of long-term leachability of a solidified radioactive waste from a short-term leachability test by a similitude law for leaching systems. C.Y.Hung (Office of Radiation Programs, US Environmental Protection Agency, Washington, DC, USA).

Nucl. & Chem. Waste Manage. (GB), vol.3, no.4, p.235-43 (1982). A similitude law for leaching systems has been developed on a one-dimensional mass transport theory which includes the processes of diffusion, sorption and radioactive decay. The similitude law can be used to determine the leaching characteristics of a solidified waste from a laboratory leaching test conducted for a similar test piece and to determine the long-term leaching characteristics of a test piece from the results of a short-term test. A leaching number developed from the similitude law was found to be the key parameter in characterizing leach test systems. A mathematical model based on one-dimensional transport theory was also developed to determine the general leaching characteristics of a solidified low-level radioactive waste in a test leachant. The results were normalized, based on the similitude law, in a leaching graph which uses the leaching number as a system parameter. The leaching number can be obtained through short-term leaching tests. The normalized leaching graph can be used to determine the leaching characteristics of a solidified waste without undergoing computer simulation or tedious numerical summations of infinite series. (16 refs.)

75094 Adsorption and stability prior to analysis of simulated nuclear waste leachate. H.M.Kingston, G.J.Lutz (Center for Analytical Chem., NBS, Washington, DC, USA).

Nucl. & Chem. Waste Manage. (GB), vol.3, no.4, p.245-9 (1982). Before analytical compositional analysis can be applied to the evaluation of the nuclear waste leachates, the credibility of the sample must be demonstrated. During the leaching in neutral to basic aqueous conditions the adsorption of metal ions onto the walls of the Teflon leach vessels was demonstrated. The adsorption was found to be variable for both zinc and neodymium. The resolubilization of zinc and neodymium using dilute nitric acid proved effective prior to analysis. Certain elemental groups represented by cesium, barium, and strontium demonstrated resistance to container adsorption during leaching under these conditions. The maintenance of a dissolved analytical sample was followed and demonstrated for at least seven weeks following the postleaching procedure. (8 refs.)

75095 Leachability of barium-radium sulphate sludges. P.M.Huck, B.Anderson (Dept. of Civil Engng., Univ. of Alberta, Edmonton, Alberta, Canada).

Nucl. & Chem. Waste Manage. (GB), vol.3, no.4, p.251-9 (1982). Presents results from the first phase of a research program designed to examine the leachability of radium-226 from barium-radium sulphate sludges. Bath leaching tests were performed. Results showed that liquid:solid contact time was relatively unimportant; radium in the sludge was stable in the presence of deionized water with a slight increase in the amount leached per gram of sludge occurring at higher liquid:solid ratios. Not unexpectedly, low and high values of leachant pH increased radium leaching. Both monovalent and divalent salt solutions also increased leaching; however, dissolved radium-226 activity levels in the leachate decreased as leachant molarity increased. For divalent salts this can be explained by the common ion effect; for monovalent salts it is opposite to results expected from solubility considerations. The interpretation of all results is complicated by the fact that in most tests, the amount of radium-226 present in the leachate was lower than the calculated contribution from the mother liquor present with the sludge. This apparent ability of the sludge to adsorb radium from solution may be related to dissolution and reprecipitation of the sludge during the leaching tests. (11 refs.)

75096 A fast configuration with a conjugate flux independent of energy. K.Fahrmann, E.Lehmann, G.Huttel, C.Reiche.

Yad. Energ. (Bulgaria), no.18, p.14-19 (1983). The existing configuration SEG-IV has been calculated to measure the effective cross-sections of absorption for structure-building materials. The configuration found in the ring reactor RRR is characterized with a conjugate flux, in the center, independent of energy. In this manner the absorption cross-sections of the different materials can be determined by the reactivities of small samples under identical conditions. (8 refs.)

75097 Data evaluation on the absorption of neutrons by cadmium with the aid of integral experiments. B.Bemer, K.Fahrmann, E.Lehmann.

Yad. Energ. (Bulgaria), no.18, p.20-6 (1983). A fast SEG-IV configuration containing Cadmium has been placed in the ring reactor at Rossendorf (RRR). The effects evaluated for the reactivity of pure scattering materials depend considerably on the cadmium data. In this manner by using comparisons with the respective experimental results, conclusions can be drawn for the existing group constants. Similar conclusions also follow from the determination of the energy dependence of the value function of the neutrons with the help of a neutron source. (8 refs.)

75098 Measurement of the effective cross-sections of absorption for fast reactor building materials using a fast configuration with a conjugated flux, independent of energy. K.Ditze, K.Fahrmann, D.Hedderich, G.Huttel, E.Lehmann.

Yad. Energ. (Bulgaria), no.18, p.27-33 (1983). The first measurements of the effective cross-sections of absorption for iron nickel and copper in the SEG-IV configuration have been described. Since in SEG-IV the spectrum of value (the separation potential) does not depend on the energy of the neutrons, the effects of the reactivity, measured with respect

to ^{10}B can be calculated as absorption cross-sections, averaged by the neutron spectrum. (15 refs.)

75099 An assessment of acoustic emission for nuclear pressure vessel monitoring. C.B.Scruby (Metall. Div., AERE, Harwell, England), H.N.G.Wadley.

Prog. Nucl. Energy (GB), vol.11, no.3, p.275-97 (1983). A critical review of the application of acoustic emission (AE) to the fabrication, proof testing and in-service monitoring of nuclear pressure vessels is presented. The detectability of deformation and fracture processes in pressure vessel steels is discussed, and recommendations made for improving source location accuracy and the development of quantitative source assessment techniques. Published data suggest that AE can make an important contribution to weld fabrication monitoring, and to the detection of defects in lower toughness materials during vessel proof testing. In high toughness materials, however, the signals generated during ductile crack growth may frequently be too weak for reliable detection. The feasibility of AE for continuous monitoring has not yet been adequately demonstrated because of high background noise levels and uncertainty about AE signal strengths from the defect growth processes that occur in service. In-service leak detection by AE shows considerable promise. (57 refs.)

75100 Tensile properties of 1.4970 austenitic stainless steel after corrosion caused by uranium dioxide and simulated fission products. L.Schafer, P.Hofmann (Inst. fur Material- und Festkörperforschung, Kernforschungszenstrum Karlsruhe, Karlsruhe, Germany).

J. Nucl. Mater. (Netherlands), vol.115, no.2-3, p.169-77 (April 1983). Flat tensile specimens of 1.4970 austenitic stainless steel were corroded at 650°C by UO_{2+x} to which the simulated fission products Cs, I and Te had been added. After corrosion, tensile tests were performed in air between 400 and 1000°C and strain rates between 0.005 and 50 mm/min. The different strengths of corroded specimens as compared to non-corroded specimens were correlated to the measured reaction zone thicknesses. To quantitatively describe the change in mechanical properties of the steel samples as a result of corrosion, a coefficient of effectiveness and a ductility factor were defined and determined as functions of the strain rate, the test temperature, the thermo-mechanical treatment, the simulated burnup, and the corrosion depth. It appears from the test results that the corrosion layer actually contributes to the strength of the corroded specimens. In some cases, however, an influence of the reaction zone on the uncorroded residual cross section of the specimens was observed. The ductility of the cladding material is always reduced by corrosion. (12 refs.)

75101 Irradiation effects on thermal conductivity of a light-water reactor pressure vessel steel. R.K.Williams, R.K.Nanstad, R.S.Graves, R.G.Berggren (Metals & Ceramics Div., Oak Ridge Nat. Lab., Oak Ridge, TN, USA).

J. Nucl. Mater. (Netherlands), vol.115, no.2-3, p.211-15 (April 1983). A Mn-1/2 Mo-1/2 Ni steel (ASTM A533 grade B class 1) similar to the material used for construction of early pressurized water reactors was examined for irradiation-induced changes in thermal conductivity. The mechanical properties of this steel have been shown to be sensitive to irradiation. Testing of a standard sample in the range 30 to 90°C showed that the thermal conductivity measurements had an absolute uncertainty of about $\pm 3\%$. Results on the control and irradiated samples showed a small (1.7%) increase in thermal conductivity after irradiation at about 290°C to fluences up to $2.4 \times 10^{23} \text{ n/m}^2$ ($E > 1 \text{ MeV}$). Thus, for the neutron irradiation conditions investigated, the thermal conductivity of this pressure vessel steel is not degraded. (15 refs.)

75102 Influence of nonmetallic elements on the compatibility of structural materials with liquid alkali metals. K.Natesan (Materials Sci. & Technol. Div., Argonne Nat. Lab., Argonne, IL, USA).

J. Nucl. Mater. (Netherlands), vol.115, no.2-3, p.251-62 (April 1983). Liquid alkali metals such as sodium and lithium are being considered as heat-transfer media in liquid-metal cooled fast-breeder reactors and a tritium-breeding blanket in fusion reactor, concepts, respectively. In these applications, the interaction(s) of nonmetallic impurity elements in the liquid alkali metals, such as oxygen, carbon, nitrogen, and hydrogen, with structural materials is of concern. The author discusses purification methods for control of nonmetallic impurity elements in liquid sodium and lithium, and the limitations of the various methods. Interactions between structural metals and nonmetallic elements in liquid alkali metals are analyzed in terms of equilibrium distribution coefficients and the concentrations of nonmetallic elements in liquid alkali metals that are sufficient for compound formation with the structural metals. A number of experimental observations that describe various types of interactions are presented, and major differences in material behavior in liquid sodium and lithium environments are identified. (42 refs.)

75103 Stability of unirradiated BISO-coated carbon-containing UO_2 particles at elevated temperatures. S.Kashimura, K.Ikawa, K.Iwamoto (JAERI, Ibaraki, Japan), K.Sakanishi.

J. Nucl. Mater. (Netherlands), vol.115, no.2-3, p.337-8 (April 1983). Presents the results of a similar out-of-pile heating experiment using BISO-coated C-containing UO_2 particles. Particles after heating were examined by means of X-ray microradiography and metallography. Description of BISO-coated particles used in the present experiment is given. Carbon content in the kernel measured by a coulometric method are also presented together with chemical phases detected by X-ray diffraction. (1 ref.)

75104 Computed tomographic methods for nuclear fuel characterization and safeguards. F.Levai (Nuclear Training Reactor, Tech. Univ. Budapest, Budapest, Hungary).

Period. Polytech. Electr. Eng. (Hungary), vol.26, no.1-2, p.153-69 (1982). A research project is going on to explore the technical feasibility of examining large bundles of nuclear fuel using computed tomographic methods. The methods offer capability of measuring three-dimensional distribution of important nuclear parameters inside the fuel bundle (burnup data, safeguarding information etc.). Computed tomography either transmission or emission allows complete exclusion of section not under study. The section under examination is described by a two-dimensional function which represents the linear absorption coefficient in the case of transmission imaging or radioisotope concentration in the case of emission imaging. To investigate the feasibility of the method for transmission imaging fuel bundles, experimental apparatuses have been constructed and rod shaped demonstration bundles of the Training Reactor of the Bp. Technical University have been imaged and are demonstrated. In the case of emission imaging the same scanning pattern can be used as in the case of transmission. Objectives of the gamma scanning, choice of fission products are outlined. A two-dimensional gamma scanning procedure is developed as a possible method for emission imaging irradiated fuel bundle on the station side. (9 refs.)

75105 Refinement of boundary conditions in the calculation of close-packed lattices by the surface pseudosources method. N.V.Sultanov, I.A.Zhokina.

Sov. At. Energy (USA), vol.53, no.3, p.614-18 (Sept. 1982). Translation of: *At. Energ. (USSR)*, vol.53, no.3, p.155-8 (Sept. 1982). [received: May 1983] In reactor calculations it is frequently necessary to solve the kinetic equations in square and hexahedral cells. As a rule these calculations are made in the Wigner-Seitz approximation, replacing the actual cell by a cylindricalized cell with an equal area. In close-packed lattices where the optical thickness of the moderator is less than one neutron mean free path, the details of the boundary conditions at the outside boundary of the cell begin to have a substantial effect on the integral characteristics of cells. By assuming isotropic reflection of neutrons at the outside boundary of a cell, the Wigner-Seitz approximation can be extended to the calculation of cells in close-packed lattices. (10 refs.)

75106 Gas release from uranium dioxide. V.Sh.Sulaberidze, A.V.Pershin. *Sov. At. Energy (USA)*, vol.53, no.3, p.619-21 (Sept. 1982). Translation of: *At. Energ. (USSR)*, vol.53, no.3, p.158-60 (Sept. 1982). [received: May 1983] The working parameters of nuclear reactor fuel elements are such that an appreciable part of the fuel does not reach the temperature at which columnar grains are formed (1900-2000K). Under such conditions the level of gas release is not determined by the volume diffusion of gaseous fission products (GFP) in the fuel, but by other mechanisms. This is manifested in the change of the temperature dependence of gas release, a complication of the dependence of the relative yield of GFP radionuclides from the fuel on the radioactive decay constant. The authors determine the temperature dependence of gas release from compact uranium dioxide in the range 770-1700K for a burnup of up to 1% of the uranium atoms. The GFP yield from a fuel sample was studied by an in-pile method. The experimental arrangement consisted of an irradiation device with the sample and an open helium loop. Gas samples were analyzed with standard spectrometric apparatus using a (Ge)Li detector. Gamma spectra of ^{87}Kr , ^{88}Kr , ^{85m}Kr , ^{135}Xe , ^{133}Xe , and ^{138}Xe were identified. (6 refs.)

75107 Study of the deactivation mechanisms for some constructional steels by secondary-ion mass spectrometry. Yu.G.Bobrov, S.M.Bashilov, G.M.Guryanov, A.P.Kovarskii.

Sov. At. Energy (USA), vol.53, no.3, p.638-41 (Sept. 1982). Translation of: *At. Energ. (USSR)*, vol.53, no.3, p.171-4 (Sept. 1982). [received: May 1983] Secondary-ion mass spectrometry SIMS has been used to examine the structure of the oxide films formed on 12Kh18N10T, 48TS, and 22K constructional steels under conditions simulating those in the first loop of boron-regulated pressurized water reactors type VVER-440, and also the changes in these films after processing with certain deactivating solutions. The concentration profiles were measured for the components of the alloys in the model films before and after chemical processing. (4 refs.)

75108 Preparation and certification of a uranium reference material. R.G.Hansen, E.J.Ring.

Report M84, Council for Miner. Technol., Randburg, S. Africa (25 Feb. 1983), 8 pp.

This report describes the preparation, analysis, and certification of a bulk sample of low-grade uranium ore for use as a reference material. An investigation into its state of radioactive equilibrium established that the material is suitable for the purpose for which it is primarily intended, i.e. the calibration of radiometric sorting equipment on mines. Eleven South African laboratories, using several well-established analytical techniques, contributed data on the uranium content of the material. (3 refs.)

75109 Investigation of inhomogeneity in ceramic reactor materials using laser-localized emission spectroscopy. R.Siechau, M.Mazurkiewicz, H.Nickel. **Report JUL-1834**, Kernforschungsanlage, Jülich, Germany (March 1983), 148 pp. In German.

Using laser-localized emission spectroscopy, a method has been developed for the determination of elemental inhomogeneity within the grains of three coarse-grained ceramic materials—the mullite-based Duritals M70 and E90 and the silica-based Masrock. The method had to be optimized to allow an acceptable detection of the elements to be analyzed in spite of the small quantities of evaporated material. A laser-produced crater of 100 μm diameter and depth was found to be necessary to produce the required amount of evaporated material, 0.5 to 0.7 μg depending on the material composition. (85 refs.)

75110 Fracture mechanics tests in static and cyclic loading conditions on structure graphite for high temperature reactor plants. W.Thiele, W.Delle, F.Schubert, H.Nickel.

Report JUL-1831, Kernforschungsanlage, Jülich, Germany (March 1983), 102 pp. In German.

Fracture mechanics tests have been carried out on nuclear reactor graphites manufactured by extrusion or by vibration moulding. In addition to the measurement of fracture toughness in static tests, cyclic tests with a sinusoidal load in the range for pulsating tensile stresses were carried out. The crack propagation rate was determined as a function of the stress intensity factor range. The anisotropic fracture behaviour observed in both static and cyclic tests was correlated with the anisometrical form of the pores identified during the investigation of the graphite morphology by means of the quantitative image analysis. (79 refs.)

75111 Problems in modelling the transport of material from deep-sea dumpsites. G.T.Needler (Bedford Inst. of Oceanography, Dartmouth, Nova Scotia, Canada).

Fourth International Ocean Disposal Symposium, Plymouth, Devon, England, 11-15 April 1983 (Plymouth, Devon, England: Plymouth Polytechnic 1983), p.33

The assessment of the hazard to man and the environment from deep-sea dumping requires estimates of the transport of contaminants from a dumpsite to a point of potential impact. Considering the nature of our knowledge of the marine environment, the construction of a single complex model for a wide variety of purposes is not only difficult but usually inappropriate. Simple models consistent with our knowledge of the dominant oceanic processes and tailored to particular needs will usually be more reliable. Selection of an appropriate simple model however requires considerable care. For example, collection dose assessments may require models giving accurate average distributions, but this may only be attainable at the expense of spatial and temporal resolution. On the other hand, critical path assessments require models maximizing specific pathways and such models in general yield inaccurate averages. Estimation of extreme but rare events is usually particularly difficult. (no refs.)

75112 The effects of radiation exposure on aquatic organisms. A.D.Woodhead, R.B.Setlow (Biology Dept., Brookhaven Nat. Lab., Upton, NY, USA).

Fourth International Ocean Disposal Symposium, Plymouth, Devon, England, 11-15 April 1983 (Plymouth, Devon, England: Plymouth Polytechnic 1983), p.135-6

The use of oceans as sinks for disposal of radioactive wastes involves risks to the marine biota, and indirectly to humans through the food chain. The present contribution is principally concerned with the first aspect of this problem, the somatic and genetic effects of accumulated radionuclides upon fish and other aquatic organisms. The authors begin by presenting a brief review of the information on radiation effects from a range of field and laboratory studies, including recent data from marine animals captured in the wild, which identify and estimate the accumulation of physiologically important radionuclides in different tissue and organs after exposure to low-level contamination for prolonged periods. Much of this information was derived from populations living in the vicinity of nuclear power stations located on ocean coasts, estuaries and rivers, although some data are available from fish living in the open sea. There are a few experimental studies in which fish have been kept in water containing radionuclides; some of these studies have shown changes in the distribution of radionuclides within fish during growth. (no refs.)

75113 Studies of the radiosensitivity of deep-sea bacteria. A.A.Yayanov (Scripps Inst. of Oceanography, Univ. of California, San Diego, La Jolla, CA, USA), L.S.Gomez, R.Van Bostel, A.S.Dietz.

Fourth International Ocean Disposal Symposium, Plymouth, Devon, England, 11-15 April 1983 (Plymouth, Devon, England: Plymouth Polytechnic 1983), p.137

Experiments on the sensitivity of the colony forming ability (CFA) of deep-sea bacteria to an external source of gamma rays from ^{60}Co are described. The bacteria were grown at 2°C and at the pressure of their depth of origin. The bacteria were irradiated either suspended in artificial seawater or immobilized in nutrient gels. The irradiations were done at 0°C either at atmospheric pressure or at the pressure of the depth of origin of the bacteria. The effect of irradiation was assessed by determining the ability of each cell in the irradiated population to form colonies in nutrient gels incubated at 2°C at the pressure of the depth of origin of the bacteria. The radiation dose was determined with the ferrous sulfate dosimeter. Among the conclusions are that the CFA of deep-sea bacteria is slightly more sensitive to gamma rays than is the CFA of shallow water bacteria; and, that this sensitivity is slightly correlated with depth of origin. The significance of the data on radiosensitivity to the disposal of radioactive wastes is discussed. (no refs.)

75114 Effect of radiation on sister chromatid exchanges and chromosomal deletions in the benthic worm *Neanthes arenaceodentata*. F.L.Harrison, D.W.Rice, M.E.Varela (Environmental Sci. Div., Lawrence Livermore Nat. Lab., Livermore, MA, USA).

Fourth International Ocean Disposal Symposium, Plymouth, Devon, England, 11-15 April 1983 (Plymouth, Devon, England: Plymouth Polytechnic 1983), p.138-9

Disposal of low-level, solid radioactive wastes in marine environments occurred on both the east and west coasts of the United States. Although these practices were discontinued by 1970, little effort was made until recently to determine the fate and distribution of the radionuclides released from these wastes. Information now available indicates that some leakage of radioactivity occurred, but the total impact of the releases on the ecosystems is not known. Traditional bioassay systems are unsuitable for assessing sublethal effects from ocean disposal of low-level radioactive waste, where mortality and phenotypic responses are not anticipated at the expected, low environmental disposal levels. The authors have examined the usefulness of SCE induction as a measure of low-level radiation effect in a sediment-dwelling marine worm, *Neanthes arenaceodentata*. This exchange does not alter the overall chromosome morphology and appears to be a sensitive indicator of DNA damage caused by environmental mutagens. (no refs.)

75115 Radioactive contamination of the marine environment, uptake and distribution of tritium and technetium in *Acetabularia* and other marine algae. G.Arapis, A.Bossus, G.Nuyts, P.Mathot, J.Collard, G.Gerber, R.Kirschmann, M.Cogneau, S.Bonotto (CEN/SCCK, Mol, Belgium).

Fourth International Ocean Disposal Symposium, Plymouth, Devon, England, 11-15 April 1983 (Plymouth, Devon, England: Plymouth Polytechnic 1983), p.140-2

The giant unicellular marine alga *Acetabularia acetabulum* has been used to study the fate of tritium administered in the form of tritiated water or of tritiated organic compounds. It has been found that tritiated water is rapidly taken up by the algae and is lost almost as rapidly. Three metabolic components can be discerned in release, one representing about 40% of the total with a half-life of a few seconds, a second one (about 50%) with a half life to about 1 min, representing probably water in the vacuole and a third (about 1.6%) with a half-life of about 5 hours. Incorporation of tritium into organic matter was studied by exposing the algae to tritiated water for a period of more than two weeks. Similar experiments have also been conducted using technetium as the pollutant. (no refs.)

75116 The role of biogenic debris in the vertical transport of transuranic wastes in the sea. N.S.Fisher, S.W.Fowler (IAEA, Lab. of Marine Radioactivity, Oceanographic Museum, Monaco).

Fourth International Ocean Disposal Symposium, Plymouth, Devon, England, 11-15 April 1983 (Plymouth, Devon, England: Plymouth Polytechnic 1983), p.143-4

Sinking biogenic particulate matter in the sea has been shown to contain elevated levels of various types of pollutants, including radionuclides, heavy metals, chlorinated hydrocarbons and other organic contaminants. Thus, fall-out levels of plutonium and americium, for example, in zooplankton fecal pellets (70-100 pCi kg^{-1} dry wt.) are significantly higher than that in either the organism that produced them (0.4 pCi kg^{-1} dry wt.) or the food which zooplankton ingest (3-4 pCi kg^{-1} dry wt.). Using transuranic elements as model pollutants it is possible to quantitatively describe biologically mediated processes which affect the distribution of wastes discharged to surface waters. (no refs.)

75117 Comparative behavior of plutonium and americium in the Equatorial Pacific. V.E.Noshkin, K.M.Wong, T.A.Jokela, J.L.Burnk, R.J.Eagle (Lawrence Livermore Nat. Labs., Univ. of California, Livermore, CA, USA).

Fourth International Ocean Disposal Symposium, Plymouth, Devon, England, 11-15 April 1983 (Plymouth, Devon, England: Plymouth Polytechnic 1983), p.145-8

To make reasonable predictions of the environmental behavior of disposed radioactive wastes in the deep ocean, it is useful to study contaminated sites where many of the processes, reactions, and rates that influence the fate of specific long-lived radionuclides can be identified and studied. The authors have previously studied the rate at which plutonium radionuclides are released from sedimentary deposits to the water column at Bikini and Eniwetak

Atolls. These atolls, site of the Pacific proving grounds, were contaminated with fission and activation products during nuclear device testing by the United States between 1946 and 1958. Long-lived radionuclides generated still persist in the atoll aquatic environment. Here they extend their description of the behavior of plutonium in the Equatorial Pacific (within and outside Bikini and Enewetak Atolls) and discuss the comparative chemistries and biological accumulation of plutonium and americium isotopes. Similarities exist among the aquatic characteristics and behavior of these transuranics at Enewetak and Bikini and at other sites contaminated by different sources. Unexplained differences are also noted, which indicates that one cannot yet confidently predict the universal aquatic behavior of the transuranics. (no refs.)

75118 The influence of diagenetic redox reactions on the distribution of $^{239,240}\text{Pu}$, ^{137}Cs , ^{241}Am and ^{55}Fe in sediments of the US continental margin. F.L.Sayles, H.D.Livingston (Woods Hole Oceanographic Instn., Woods Hole, MA, USA).

Fourth International Ocean Disposal Symposium, Plymouth, Devon, England, 11-15 April 1983 (Plymouth, Devon, England: Plymouth Polytechnic 1983), p.149-50

In view of the potential influence of diagenesis and redox state upon sediment-radioisotope associations, the authors have carried out a study of the relationship between the sedimentary distributions of several fallout nuclides and recognizable diagenetic redox reactions in marine sediments. The studies have taken place on transects of the eastern and western continental margins of the US distributions of $^{239,240}\text{Pu}$, ^{241}Am , ^{137}Cs and ^{55}Fe have been measured on a number of cores. The pore water chemistry of the sediments also has been characterized as regards trace metals, nutrients and other parameters required to define diagenetic redox zonation. (no refs.)

75119 Behavior of long-lived nuclides associated with radioactive wastes in the deep-sea. S.R.Aston, S.W.Fowler (IAEA, Lab. of Marine Radioactivity, Oceanographic Museum, Monaco).

Fourth International Ocean Disposal Symposium, Plymouth, Devon, England, 11-15 April 1983 (Plymouth, Devon, England: Plymouth Polytechnic 1983), p.151-2

Over the last two years a programme of research has been developed in relation to some aspects of the behavior of long-lived radionuclides associated with the deep-ocean disposal of radioactive wastes. Particular emphasis has been placed on the interactions of transuranic nuclides and technetium with sediments from existing or proposed dumpsites in the Atlantic and Pacific Oceans. Results are presented for experimental studies on the rate of adsorption, equilibrium K_d values and desorption of these radionuclides with sediments. Examples are shown of the experimental uptake of these nuclides by benthic infauna, and the transfer factors and tissue distributions reported. Comparative results for uptake from seawater and dumpsite sediments are presented and discussed. (no refs.)

75120 Development of an ocean model for use in radiological assessments of sea disposal of solid radioactive wastes. S.F.Mobbs (Nat. Radiological Protection Board, Chilton, England), P.A.Gurbutt, M.D.Hill, J.G.Shepherd, P.Killworth.

Fourth International Ocean Disposal Symposium, Plymouth, Devon, England, 11-15 April 1983 (Plymouth, Devon, England: Plymouth Polytechnic 1983), p.153-5

One of the principal objectives of a radiological assessment of a radioactive waste disposal practice is the calculation of the doses which may be received by man, both individually and collectively. Since these doses will, in the case of most disposal practices, be received over periods of the order of millions of years in the future it is necessary to develop models to predict the dispersion of radionuclides in the environment and their eventual pathways to man. In the case of disposal in the sea these models need to describe the important processes governing the distribution of radionuclides throughout the ocean, the sediments (both bed sediments and coastal sediments) and in marine biota. (no refs.)

75121 Equipment for 3-dimensional measurements of natural and artificial tracers in the sea. H.Appelquist, P.B.Nielsen (Danish Isotope Centre, Copenhagen, Denmark).

Fourth International Ocean Disposal Symposium, Plymouth, Devon, England, 11-15 April 1983 (Plymouth, Devon, England: Plymouth Polytechnic 1983), p.156-7

The Danish Isotope Centre has developed a data acquisition system to be used for dispersion and transport measurements in connection with waste disposal in the sea. The system consists of a preliminary computer developed by DIC, interfaced to the subsea detectors and the electronic navigation system. The primary computer has 8 digital input and output channels, 16 analog input channels and 10 output channels. It has a counter input for radioactivity detector and a RS-232 out/input for transmission to the HP 9825 desktop computer. The system for the moment is working with one radioactivity detector, two in-situ fluorimeters, thermistor and conductivity cells, echo sounder and Decca Navigator. Spare channels are applied for control of sensors in- and output voltages, but can be applied for alternative sensors as oxygen probes. (no refs.)

75122 Relationship between the distribution of radionuclides and the sedimentological and mineralogical traits of the coastal marine sediments (Gaeta, Latina, La Spezia, Italy). A.Broni, O.Ferretti, C.Papucci (Comitato Nazionale per l'Energia Nucleare, Rome, Italy).

Fourth International Ocean Disposal Symposium, Plymouth, Devon, England, 11-15 April 1983 (Plymouth, Devon, England: Plymouth Polytechnic 1983), p.158

Geomorphological, sedimentological and mineralogical studies are being conducted by the Comitato Nazionale per l'Energia Nucleare (CNEN) on the Italian coasts with the aim of finding possible correlations between the distribution of some radionuclides and these ground environmental parameters. Alluvial sediments have been examined and geological and cartographic data have been interpreted according to this framework. (no refs.)

75123 The NEA research and environmental surveillance program related to sea disposal of radioactive waste. P.Gurbutt (Fisheries Lab., Ministry of Agriculture, Lowestoft, England), W.Templeton, B.Ruegger.

Fourth International Ocean Disposal Symposium, Plymouth, Devon, England, 11-15 April 1983 (Plymouth, Devon, England: Plymouth Polytechnic 1983), p.159-60

Sea dumping operations of certain types of packaged low- and medium-level radioactive wastes have been carried out since 1967 in the North-East Atlantic under the auspices of the OECD nuclear energy agency. Since 1977 these operations are organised according to the requirements of the Multilateral Consultation and Surveillance Mechanism for Sea Dumping of Radioactive Waste established in conformity with the London Convention by the OECD Council. On the occasion of the 1980 review of the continued suitability of the North-East Atlantic site used for the disposal of radioactive waste, it was recommended that an effort should be made to increase the scientific data base relating to the oceanographic and biological characteristics of the dumping area. In particular, it was suggested that a site specific model of the

transfer of radionuclides in the marine environment be developed which would permit a better assessment of the potential radiation doses to man from the dumping of radioactive waste. To fulfil these objectives a research and environmental surveillance program related to sea disposal of radioactive waste was set up in 1981 with the participation of eleven member countries and the International Laboratory for Marine Radioactivity of the IAEA in Monaco. (no refs.)

75124 Proposed Department of Energy design and operations criteria for low-level radioactive waste disposal sites. H.D.Williams, K.L.Falconer, A.E.Grey (Nat. Low-Level Waste Management Program, EG&G Idaho, Idaho Falls, ID, USA).

Proceedings of the Symposium on Low-Level Waste Disposal. Vol.3. Facility Design, Construction, and Operating Practices (NUREG/CP-0028), Washington, DC, USA, 29-30 Sept. 1982 (Oak Ridge, TN, USA: Oak Ridge Nat. Lab 1982), p.15-26

It is the policy of the Department of Energy that operations under its authority which involve generation and disposal of low-level radioactive waste are conducted in a manner which assures that radiation exposure to employees and the public comply with the requirements of DOE Order 5480.1. To implement this policy, EG&G Idaho Inc., as the lead contractor to the Department of Energy's Low-Level Waste Management Program, initiated an effort in the fall of 1980 to develop criteria pertinent to the shallow land burial of low-level radioactive waste. Shallow land burial activities were divided into site selection, site design, site operation, waste acceptance, site closure/post-closure, and corrective actions. Criteria for each of the six areas were developed by a committee process. (no refs.)

75125 Lessons learned about disposal design. O.I.Oztunali (Dames & Moore, White Plains, NY, USA).

Proceedings of the Symposium on Low-Level Waste Disposal. Vol.3. Facility Design, Construction, and Operating Practices (NUREG/CP-0028), Washington, DC, USA, 29-30 Sept. 1982 (Oak Ridge, TN, USA: Oak Ridge Nat. Lab 1982), p.27-37

Presents a historical perspective on disposal facility design and its implementation (practices) in the US in view of the proposed 10 CFR Part 61 and the systems analysis approach recommended to achieve the performance objectives. Disposal facility design and practices are extremely important components of the systems approach to achieving the performance objectives since they can be controlled with a greater degree of confidence than some of the other components of the system. The predictability requirements of the proposed rule (i.e. the demonstration that the performance objectives are met) can most clearly be achieved if the license application relies heavily on components that can be controlled with confidence. An introduction amplifying the above concepts is presented first; this is followed by a recounting of several past disposal design related issues that influenced the formulation of 10 CFR Part 61 significantly. Lessons learned about disposal design and a discussion follow. (4 refs.)

75126 Trench design and construction techniques for low-level radioactive waste disposal. P.G.Tucker (Geotech. Lab., US Army Engineer Waterways Experiment Station, Vicksburg, MS, USA).

Proceedings of the Symposium on Low-Level Waste Disposal. Vol.3. Facility Design, Construction, and Operating Practices (NUREG/CP-0028), Washington, DC, USA, 29-30 Sept. 1982 (Oak Ridge, TN, USA: Oak Ridge Nat. Lab 1982), p.39-43

Problems encountered with the disposal of low-level radioactive waste by shallow land burial have brought about the realization that a reevaluation of disposal trench design and construction techniques is needed. Subsidence, the 'bathtub effect', and the infiltration of groundwater into the disposal trench are among the problems that have cast doubts on the ability of some facilities to control the movement of their buried radionuclides. They have also made the goal of total passive maintenance unattainable in the near future. The Nuclear Regulatory Commission and the US Army Corps of Engineers, Waterways Experiment Station (WES) have entered into an agreement whereby the WES is preparing a document which will detail the critical parameters involved with the design and construction of low-level radioactive waste disposal trenches. These parameters will include those which should be controlled through the issuance of specifications or license restrictions in order to ensure that the facility will function as expected. The author outlines the scope of the work, the work accomplished to date, the work remaining, and the basic philosophy behind the approaches taken in the preparation of this document. (no refs.)

75127 A conceptual facility designed for remedial action wastes. A.K.Phelps (Nuclear Fuel Operations, Bechtel Nat. Inc., Oak Ridge, TN, USA), M.G.White.

Proceedings of the Symposium on Low-Level Waste Disposal. Vol.3. Facility Design, Construction, and Operating Practices (NUREG/CP-0028), Washington, DC, USA, 29-30 Sept. 1982 (Oak Ridge, TN, USA: Oak Ridge Nat. Lab 1982), p.45-65

Presents two conceptual designs for below-grade land disposal in the Northeastern United States for remedial action wastes from the DOE Formerly Utilized Sites Remedial Action Program (FUSRAP). The wastes were generated by programs of the Manhattan Engineer District/Atomic Energy Commission (MED/AEC). These materials are largely trace-contaminated soils, sediments, and rubble resulting from a variety of activities, including research, processing, and storage of uranium and thorium ores and concentrates. The principal isotope of interest from a hazards control standpoint is radium-226. (5 refs.)

75128 Surface water considerations in facility design and operation. D.L.Schreiber (Schreiber Consultants Inc., Coeur d'Alene, ID, USA).

Proceedings of the Symposium on Low-Level Waste Disposal. Vol.3. Facility Design, Construction, and Operating Practices (NUREG/CP-0028), Washington, DC, USA, 29-30 Sept. 1982 (Oak Ridge, TN, USA: Oak Ridge Nat. Lab 1982), p.73-91

Surface water hydrology considerations are discussed for the design and operation of commercial low-level radioactive waste disposal facilities. Guidelines are recommended and bases presented for several hydrologic engineering factors, such as design flood flows, debris flows, erosion control, and water management, that must be accounted for in facility design and operation. Surface water hydrology practices at existing low-level radioactive waste disposal facilities are reviewed and compared with the recommended guidelines. Finally, the potential restrictiveness of the recommended guidelines is evaluated. (15 refs.)

75129 Operational practices to facilitate closure of low-level waste disposal facilities. G.L.DePoorter (Los Alamos Nat. Lab., Los Alamos, NM, USA).

Proceedings of the Symposium on Low-Level Waste Disposal. Vol.3. Facility Design, Construction, and Operating Practices (NUREG/CP-0028), Washington, DC, USA, 29-30 Sept. 1982 (Oak Ridge, TN, USA: Oak Ridge Nat. Lab 1982), p.93-100

Final closure of a low-level waste disposal facility must be considered during most of the phases in the life cycle of the facility. The author enumerates the

reasons for considering the closure of a low-level waste disposal facility during the operation, closure, and postclosure observation phases in the life of the cycle of the facility. Actions required during the preoperational, operational, and closure phases that will facilitate closure are discussed by using example trench configurations for an arid site and for a humid site. Performance criteria for the closed site are discussed in terms of the information required to predict site performance and the operating practices necessary to ensure that this desired and predicted performance is obtained. Activities that must be considered include initial site characterization, site design and lay out, site construction, waste from acceptance criteria, waste handling and trench capping and suitable vegetation. (no refs.)

75130 Land disposal technique for hazardous and low-level radioactive waste containment and encapsulation of hazardous waste disposal sites. A.A.Metry, M.H.Corbin (Roy F. Weston Inc., West Chester, PA, USA). Proceedings of the Symposium on Low-Level Waste Disposal. Vol.3. Facility Design, Construction, and Operating Practices (NUREG/CP-0028), Washington, DC, USA, 29-30 Sept. 1982 (Oak Ridge, TN, USA: Oak Ridge Nat. Lab 1982), p.101-30

This is based on several projects where hazardous waste and low-level radioactive waste was deposited on and below the surface. The primary objective of these projects was to develop stabilization and containment concepts for isolation of those waste materials and preventing potential migration of toxic and radioactive substances into the environment. Several concepts and control options are presented. These included: chemical fixation, grouting, bentonite slurry barrier, hydrogeologic isolation, impermeable covers and liners, ion exchange barrier, etc. A discussion of conceptual design methodology, modeling and simulation techniques, discussion of case history results, cost and economic information, and major program implementation features, is included. (10 refs.)

75131 Environmental monitoring considerations for low-level waste disposal sites. J.Sedlet (Argonne Nat. Lab., Argonne, IL, USA). Proceedings of the Symposium on Low-Level Waste Disposal. Vol.3. Facility Design, Construction, and Operating Practices (NUREG/CP-0028), Washington, DC, USA, 29-30 Sept. 1982 (Oak Ridge, TN, USA: Oak Ridge Nat. Lab 1982), p.131-50

An adequate monitoring program consists of measuring concentrations of radionuclides, chemically-toxic substances, and leachate indicators in environmental media and of evaluating specific physical properties of the site. In addition, the composition of the buried waste must be known. Methods for obtaining this information are discussed and monitoring programs are presented for the preoperational, operational, and postclosure phases of a disposal site. Environmental monitoring is considered in a broad context, since it includes monitoring burial trenches onsite, as well as surveillance in the offsite environment. Postclosure monitoring programs will be strongly influenced by the operational monitoring results. The results of the environmental monitoring program will be vital to successful site operation. These results should be used to determine if operational changes are needed and to predict future environmental impacts. (25 refs.)

75132 Health physics monitoring practices at commercial low-level waste disposal sites in light of 10 CFR 61 requirements. D.E.Hadlock, R.L.Gilchrist, C.D.Hooker, W.N.Herrington (Pacific Northwest Lab., Richland, WA, USA).

Proceedings of the Symposium on Low-Level Waste Disposal. Vol.3. Facility Design, Construction, and Operating Practices (NUREG/CP-0028), Washington, DC, USA, 29-30 Sept. 1982 (Oak Ridge, TN, USA: Oak Ridge Nat. Lab 1982), p.151-9

The importance of maintaining occupational radiation exposures 'As Low as Reasonably Achievable' (ALARA) is recognized and emphasized in 10 CFR 61 (Licensing Requirements for Land Disposal of Radioactive Waste) and the supporting implementing regulations. To ensure that current and future exposures are ALARA, the Nuclear Regulatory Commission contracted with the Pacific Northwest Laboratory (PNL) is operated for DOE by Battelle Memorial Institute) to: (1) evaluate current health physics practices at the low-level waste (LLW) sites of Barnwell, South Carolina, Beatty, Nevada, and Hanford, Washington; (2) write a manual of good practices for LLW sites; and (3) review the findings of the site appraisals as they apply to 10 CFR 61. (5 refs.)

75133 Light-water reactor low-level waste forms. B.D.Guilbeault (Engng. Div., NUS Corp., Gaithersburg, MD, USA).

Proceedings of the Symposium on Low-Level Waste Disposal. Vol.3. Facility Design, Construction, and Operating Practices (NUREG/CP-0028), Washington, DC, USA, 29-30 Sept. 1982 (Oak Ridge, TN, USA: Oak Ridge Nat. Lab 1982), p.161-75

In the proposed 10 CFR Part 61, 'Licensing Requirements for Land Disposal of Radioactive Waste', three waste-classification groups for low-level waste are identified. This classification system is based on the radionuclide inventory. The category into which a waste falls determines the requirements for its disposal. With light-water reactor waste, the concentration of some radionuclides can be easily determined through routine analytical methods; however, some radionuclides are impractical to measure. Numerous past studies have characterized the physical waste form and have looked at the easily determined radionuclides. The author reviews the physical waste forms, outlines where analytical information is currently available and/or easily obtainable, and discusses what further information on radionuclide concentrations is needed to meet the requirements of 10 CFR 61. The author also discusses the possible changes in the waste form due to the increased emphasis of volume reduction and finally, several areas that will need to be addressed in the future. (no refs.)

75134 12 years of experience of shallow land disposal of low and intermediate level radioactive waste in France. F.Van Kote (CEA, Paris, France).

Proceedings of the Symposium on Low-Level Waste Disposal. Vol.3. Facility Design, Construction, and Operating Practices (NUREG/CP-0028), Washington, DC, USA, 29-30 Sept. 1982 (Oak Ridge, TN, USA: Oak Ridge Nat. Lab 1982), p.177-200

In France, the long term industrial management of radioactive waste is handled by a national agency, the Agence Nationale pour la Gestion des Dechets Radioactifs (ANDRA) created in 1979 within the French Atomic Energy Commission (CEA). The French organization of radioactive waste management and ANDRA's work schedule and policy are briefly outlined. The solution adopted in France to dispose of low and intermediate activity level short lived waste (LLW and ILW) is shallow land burial at the Centre de la Manche which has been set in operation in 1969. The safety basic principles and technical options adopted for shallow land are reviewed then the different steps of waste management at the Centre de la Manche are described. Finally, the main conclusions drawn from the twelve years' experience gained at the Centre de la Manche are detailed. (no refs.)

75135 NRC's perspective on acceptability and approval of new techniques. E.F.Hawkins (US Nuclear Regulatory Comm., Washington, DC, USA).

Proceedings of the Symposium on Low-Level Waste Disposal. Vol.3. Facility Design, Construction, and Operating Practices (NUREG/CP-0028), Washington, DC, USA, 29-30 Sept. 1982 (Oak Ridge, TN, USA: Oak Ridge Nat. Lab 1982), p.211-22

Subpart D of the proposed 10 CFR Part 61 provides the technical requirements for land disposal of low-level radioactive wastes. Within the Subpart, the sections on site suitability (61.50), site design (61.51), and facility operation and site closure (61.52) have been oriented toward near-surface disposal, with subsections reserved for methods other than near-surface disposal. The orientations toward near-surface disposal reflects the current status and level of experience with low-level radioactive waste disposal and reflects the type of disposal facility the staff anticipates in most new license applications. The NRC's attitude towards alternative or new disposal techniques is discussed. (no refs.)

75136 Overview of low-level radioactive waste disposal facilities subsidence. R.L.Kahle, J.Rowlands (Ralph Stone & Co. Inc., Los Angeles, CA, USA).

Proceedings of the Symposium on Low-Level Waste Disposal. Vol.3. Facility Design, Construction, and Operating Practices (NUREG/CP-0028), Washington, DC, USA, 29-30 Sept. 1982 (Oak Ridge, TN, USA: Oak Ridge Nat. Lab 1982), p.223-52

The results of a case study of the Sheffield, Illinois, waste disposal facility, and literature reviews on problems at waste disposal facilities are presented. The types of problems, causes of the problems, and approaches to mitigate the problems are evaluated. The problems identified were surface subsidence, surface erosion, leachate and gas. Leachate resulted from water entry into trenches where subsidence occurred. Subsidence was attributed to random placement of waste containers into trenches leaving voids. The poorly compacted cover soil initially bridged the voids and subsequently collapsed and siphoned into the voids. Surface potholes and slumps resulted. Extensive potholing occurred during and after precipitation when the Sheffield loess soil piped into the voids. Long-term soil consolidation also resulted in area settlement. The approaches evaluated for trench stabilisation are discussed. (11 refs.)

75137 Waste form and its role in trench stability. D.G.Schweitzer (Dept. of Nuclear Energy, Brookhaven Nat. Lab., Upton, NY, USA).

Proceedings of the Symposium on Low-Level Waste Disposal. Vol.3. Facility Design, Construction, and Operating Practices (NUREG/CP-0028), Washington, DC, USA, 29-30 Sept. 1982 (Oak Ridge, TN, USA: Oak Ridge Nat. Lab 1982), p.253-60

NRC supported programs evaluating past and present performance of shallow land burial sites and programs developing technical criteria for disposal of low-level waste in shallow land burial facilities provide convincing evidence of the importance of the waste form in providing trench stability. A summary is given of past problems in shallow land burial sites resulting from degradable waste and resultant trench subsidence. Programs supporting the technical justification for the proposed requirements on waste, waste forms and high integrity containers carried out at BNL indicate the requirements necessary to assure safe isolation of low-level waste in shallow land burial sites. (9 refs.)

75138 Waste emplacement and closure techniques. L.W.White (Golder Associates, Ellicott City, MD, USA).

Proceedings of the Symposium on Low-Level Waste Disposal. Vol.3. Facility Design, Construction, and Operating Practices (NUREG/CP-0028), Washington, DC, USA, 29-30 Sept. 1982 (Oak Ridge, TN, USA: Oak Ridge Nat. Lab 1982), p.261-7

Past practices in the disposal of low level radioactive waste have been to randomly place waste packages into trenches to within one meter of the ground surface. The major factors that have determined past practices have been cost and the need to protect workmen from unacceptable radiation exposure. Experience has shown that such practices have led to expensive maintenance problems and difficulty in developing acceptable decommissioning schemes. There are a number of waste emplacement and closure techniques that could reduce long term institutional commitments to maintain the integrity of the site. Practical and relatively inexpensive ways of bounding the problem of trench fill subsidence and subsequent problems of trench cap and site stability are proposed. (no refs.)

75139 Overview of design considerations for effective trench covers. R.Skryness (Geotech. Div., Stone & Webster Engng. Corp., Boston, MA, USA).

Proceedings of the Symposium on Low-Level Waste Disposal. Vol.3. Facility Design, Construction, and Operating Practices (NUREG/CP-0028), Washington, DC, USA, 29-30 Sept. 1982 (Oak Ridge, TN, USA: Oak Ridge Nat. Lab 1982), p.277-88

The siting, design, and operation of low-level radioactive waste disposal facilities are directed toward the isolation of waste. Trench covers are an integral part of the site's surface water control plan and function with other elements of disposal site to reduce surface water infiltration, and contribute to overall isolation of the buried waste. Attributes of a good cover design include constructibility, utilization of readily available materials, cost effectiveness, long-term reliability, and low maintenance. Thorough knowledge of the site's environmental, geological, and hydrological conditions, and familiarity with the proposed site layout, site development sequence, and disposal operations are important prerequisites for effective trench cover design. In the final analysis, trench cover performance depends on the successful implementation of the construction design and the cover's compatibility with trench geometry, site conditions, disposal operations, and the overall surface water control plan. (no refs.)

75140 Biological intrusion barriers for large volume waste disposal sites. T.E.Hakonson (Los Alamos Nat. Lab., Los Alamos, NM, USA), J.F.Cline, W.H.Rickard.

Proceedings of the Symposium on Low-Level Waste Disposal. Vol.3. Facility Design, Construction, and Operating Practices (NUREG/CP-0028), Washington, DC, USA, 29-30 Sept. 1982 (Oak Ridge, TN, USA: Oak Ridge Nat. Lab 1982), p.289-308

Intrusion of plants and animals into shallow land burial sites with subsequent mobilization of toxic and radiotoxic materials has occurred. Based on recent pathway modeling studies, such intrusions can contribute to the dose received by man. The authors describe past work on developing biological intrusion barrier systems for application to large volume waste site stabilization. State-of-the-art concepts employing rock and chemical barriers are discussed relative to long term seviceability and cost of application. The interaction of bio-intrusion barrier systems with other processes affecting trench cover stability are discussed to ensure that trench cover designs minimize the potential dose to man. (29 refs.)

75141 An investigation of layered covers designed to limit infiltration at waste disposal sites. T.M.Johnson, B.L.Herzog, K.Cartwright, T.H.Larson (State Geological Survey Div., Illinois Dept. of Energy & Natural Resources, Champaign, IL, USA).

Proceedings of the Symposium on Low-Level Waste Disposal. Vol.3. Facility Design, Construction, and Operating Practices (NUREG/CP-0028), Washington, DC, USA, 29-30 Sept. 1982 (Oak Ridge, TN, USA: Oak Ridge Nat. Lab 1982), p.309-24.

Layered soils of highly contrasting texture have been shown to act as a barrier to infiltration because of differences in unsaturated hydraulic properties. Water infiltrating into a fine-grained soil overlying an unsaturated gravel will not enter the gravel until the overlying material is nearly saturated. As a result of what is commonly called the 'wick effect', moisture will flow laterally through the fine-grained soil above the gravel layer. Layered covers of compacted soil materials utilizing this phenomenon have been proposed to limit infiltration at waste disposal sites. Laboratory column experiments using a dual-gamma ray attenuation system to measure moisture content and density simultaneously have been used to observe the behavior of layered soils and to select materials for field testing. Currently underway are field-scale studies of alternative cover designs selected on the basis of two-dimensional modeling. (14 refs.)

75142 An application of soil arch and soil beam concepts to the construction of shallow land burial trench covers. E.A.Nowatzki, J.G.McCray (Univ. of Arizona, Tucson, AZ, USA).

Proceedings of the Symposium on Low-Level Waste Disposal. Vol.3. Facility Design, Construction, and Operating Practices (NUREG/CP-0028), Washington, DC, USA, 29-30 Sept. 1982 (Oak Ridge, TN, USA: Oak Ridge Nat. Lab 1982), p.325-42.

Reports on an investigation in which three different trench cap designs were developed and prototype trenches constructed in two different climatic environments to test the adequacy of the designs. The basic concept underlying each of the designs is that trench cap performance could be improved if the cap were stabilized in some way. In one design, controlled compaction alone was used to achieve high levels of in situ density. In another design, the emplacement of a strip of reinforcing geotextile in addition to controlled compaction was used. The third design incorporated a 'soil beam' into the cap in addition to controlled compaction. A soil beam is a structural member constructed of compacted soil surrounded by an overlapping sheet of geotextile. Underlying each of these designs is the concept of a 'soil arch'. Under proper conditions, soil has the ability to arch itself over small voids within the soil mass with little or no deformation at the surface. In order to test this concept and to evaluate the relative merits of the three designs, a system of settlement plates was installed at various levels in the caps. These settlement plates were monitored during and after construction so that absolute and relative displacements could be determined within a given trench. Difference in behavior among the three trenches could also be observed in this way. (5 refs.)

75143 Alternatives to shallow land burial of low-level radioactive waste—an overview. J.L.Ellis (Gilbert/Commonwealth, Reading, PA, USA).

Proceedings of the Symposium on Low-Level Waste Disposal. Vol.3. Facility Design, Construction, and Operating Practices (NUREG/CP-0028), Washington, DC, USA, 29-30 Sept. 1982 (Oak Ridge, TN, USA: Oak Ridge Nat. Lab 1982), p.347-64.

The alternatives to shallow land burial for disposal of low level radioactive waste are identified and a brief description of each concept is provided. The alternatives can be categorized as follows: near term isolation concepts, far term isolation concepts, dispersion concepts, and conversion concepts. The more promising near term isolation concepts are discussed in terms of advantages and disadvantages geological/environmental parameters, information/technology development requirements, and operational features. (24 refs.)

75144 Intermediate-depth burial of low-level wastes. V.C.Rogers, J.A.Adam (Rogers & Associates Engng. Corp., Salt Lake City, UT, USA).

Proceedings of the Symposium on Low-Level Waste Disposal. Vol.3. Facility Design, Construction, and Operating Practices (NUREG/CP-0028), Washington, DC, USA, 29-30 Sept. 1982 (Oak Ridge, TN, USA: Oak Ridge Nat. Lab 1982), p.365-77.

Intermediate depth burial is an alternative disposal method for those radioactive wastes that cannot be disposed in a traditional shallow land burial facility. In general, the environmental risks from surface intrusion events limit the radionuclide concentrations in wastes appropriate for near-surface disposal. The magnitude of these risks as well as the likelihood of a surface intrusion event are generally reduced as the depth of disposal increases. Therefore, many wastes exceeding Class C limits can be disposed safely at depths exceeding those for near-surface disposal, but which are significantly less than depths for deep geologic disposal. However, in considering intermediate depth burial, care should be taken to avoid significant increases in risks from other pathways such as migration in groundwater. Examples of intermediate depth burial are presented, along with cost comparisons to shallow land burial. (12 refs.)

75145 Predictability of solute transport in diffusion-controlled hydrogeologic regimes. R.W.Gillham, J.A.Cherry (Dept. of Earth Sci., Univ. of Waterloo, Waterloo, Ontario, Canada).

Proceedings of the Symposium on Low-Level Waste Disposal. Vol.3. Facility Design, Construction, and Operating Practices (NUREG/CP-0028), Washington, DC, USA, 29-30 Sept. 1982 (Oak Ridge, TN, USA: Oak Ridge Nat. Lab 1982), p.379-410.

Hydrogeologic regimes that are favourable for the subsurface management of low-level radioactive wastes must have transport properties that will limit the migration velocity of contaminants to some acceptably low value. Of equal importance, for the purpose of impact assessment and licensing, is the need to be able to predict, with reasonable degree of certainty and over long time periods, what the migration velocity of the various contaminants of interest will be. The authors present arguments to show that in addition to having favourable velocity characteristics, transport in saturated, diffusion-controlled hydrogeologic regimes is considerably more predictable than in the most common alternatives. The controlled and saturated-diffusion-controlled environments are compared, with particular consideration being given to the difficulties associated with the characterization of the respective transport parameters. (25 refs.)

75146 Canadian experience with the storage and disposal of low- and intermediate-level wastes. M.A.Feraday (Chalk River Nuclear Lab., AECL, Chalk River, Ontario, Canada).

Proceedings of the Symposium on Low-Level Waste Disposal. Vol.3. Facility Design, Construction, and Operating Practices (NUREG/CP-0028), Washington, DC, USA, 29-30 Sept. 1982 (Oak Ridge, TN, USA: Oak Ridge Nat. Lab 1982), p.411-29.

In Canada, large quantities of low- and intermediate-level radioactive solid waste arise from nuclear power reactors and research sites, fuel and radioiso-

tope production facilities and from many medical and industrial applications. Currently storage after volume reduction is being used as a safe way of managing these wastes for many years at a reasonable cost. Since permanent disposal has many advantages, disposal technologies including waste processing and characterization, site characterization, repository design and safety assessment are being developed. The preferred disposal strategy is one matching waste fractions, segregated according to hazardous life-time, with disposal concepts which can isolate wastes for the required period. Several possible disposal concepts are discussed. (18 refs.)

Fourth International Ocean Disposal Symposium See Entry 74222

Proceedings of the Symposium on Low-Level Waste Disposal. Vol.3. Facility Design, Construction, and Operating Practices (NUREG/CP-0028) See Entry 74223

Measurement of the photoneutron yield in the irradiation of heavy materials in closed shells See Entry 74961

Neutron yield of the (α, n) reaction for multicomponent media See Entry 75069

Activation and decay characteristics of radiation shielding heavy concretes See Entry 75201

Temperature fields and thermal stress fields in radiation shieldings See Entry 75202

Straight tube nests in concrete walls for radiation shielding See Entry 75203

Testing of radiation shielding concrete walls with portable betatrons See Entry 75204

Radiation damage in crystalline insulators, oxides and ceramic nuclear fuels See Entry 76488

A study on radiation-resistance of PIC (polymer-impregnated concrete) for container of conditioning and disposal of low and intermediate level radioactive wastes See Entry 76503

Electron damage in zirconium. I. Defect structure and loop character See Entry 76509

Electron damage in zirconium. II. Nucleation and growth of c-component loops See Entry 76510

A new calculation of thermal neutron damage and helium production in nickel See Entry 76518

The effect of He-irradiation on the fracture toughness of ThO₂ See Entry 76522

Computer simulation of collision cascades in monazite See Entry 76527

Thermodynamics on UO₂-ZrO₂-LnO₂-x solid solutions See Entry 76586

Mass spectrometric study on the vaporization of ternary compounds PuM₂(M=Fe, Co, Ni) See Entry 76603

Thermodynamic measurements and modeling of (UC_{1-x}O_x) See Entry 76669

The diffusion of uranium in U₃O₈ See Entry 76691

Diffusionless omega transformations in quenched and pressurized Zr-Mo alloys See Entry 77631

Life time calculations for LCF loading combined with tensional hold periods. Applications to Zircaloy-4 and AISI 304 See Entry 77728

Effects of sodium and lithium environments on mechanical properties of ferrous alloys See Entry 77730

The UO₂-Zircaloy chemical interaction See Entry 77787

Behaviour of alloying elements in high-temperature (1600°C-1800°C) transient oxidation of Zircaloy-4 LWR cladding tubes See Entry 77789

The role of the electrode potential control in corrosion research of stress corrosion crack growth propagation in austenite stainless steels for nuclear reactor components See Entry 77790

Comparison of chemical reactions in liquid lithium with those in liquid sodium See Entry 77880

Effects of recent neptunium studies on high-level waste hazard assessments See Entry 78368

28.42H Fuel preparation and reprocessing (inc. isotope separation and enrichment)

75147 Microwave-assisted solidification of free-falling radioactive droplets. E.Bonek (Inst. fur Nachrichtentech., Tech. Univ. Wien, Wien, Austria), K.Knotik, P.Leichter, G.Magerl, L.Rohrecker. Arch. Elektron. & Uebertragungstechnik. (Germany), vol.37, no.5-6, p.222-8 (May-June 1983).

Reports on the design and on the operation of a 14-GHz microwave system which heats droplets (2 to 4 mm diameter) of aqueous radioactive mixtures from 5°C to 100°C within 0.25 s during free fall. Additional, untreated free fall of 1 s turns the droplets to homogeneous, spherical particles of uniform size which are used in the production of high-temperature-reactor nuclear fuel. A square cross-section H₁₀₀ cavity, positioned vertically, with optimized dimensions is fed with 90 W CW power and serves as an applicator. The problem of nonuniform heating of high-loss spherical droplets is treated in depth. (9 refs.)

75148 Carbothermic synthesis of plutonium mononitride from the dioxide. Y.Suzuki, Y.Arai, T.Sasayama (Div. of Nuclear Fuel Res., JAERI, Ibaraki, Japan).

J. Nucl. Mater. (Netherlands), vol.115, no.2-3, p.331-3 (April 1983). A study was conducted in order to obtain detailed information on the carbothermic synthesis of pure PuN from PuO₂, for which only limited information is available. (7 refs.)

28.43 FISSION REACTOR OPERATION

75149 A method of state equation decomposition and its application to the simulation of the dynamics of the active zone of the VVER reactor. C.Karpeta, S.Roubal.

Automatizace (Czechoslovakia), vol.26, no.4, p.91-4 (April 1983). In Czech. Describes a method of numerical integration suitable for solving a system of nonlinear differential equations. The method is based on the decomposition of a linearised state equation into a fast and slow part. A program named ISSY for the decomposition and the numerical integration has been written in FORTRAN for the Odra computer. Application of the method described to the simulation of the dynamic properties of the active zone of the VVER reactor with the aim of carrying out nuclear power station analysis is described. In comparison with the classical Runge-Kutta method, the method described features higher speed and large range of numerical stability. (4 refs.) E.D.

75150 Simulation of neutron transmission by fission nuclei in the region of unresolved resonances. N.T.Kojumdzieva, N.B.Janeva. *Yad. Energ. (Bulgaria)*, no.18, p.34-9 (1983).

A procedure for the theoretical description of the transmission T_t and T_r for each energy and all thicknesses in the region of unresolved resonances in the interaction with S-neutrons has been presented on the basis of the statistical matrix of the collisions. The program of the procedure has been described. The program has been applied to the processing of the experimental results obtained in Dubna on the IBR-30. (6 refs.)

75151 Neutron-physical characteristics of a standard fast neutron reactor. J.D.Jordanov, N.A.Antonov.

Yad. Energ. (Bulgaria), no.18, p.49-56 (1983). The investigation of standard test reactors with fast neutrons makes possible the comparison of the different libraries of nuclear data and the various program set-ups for neutron physical analysis of fast neutron power reactors. Three versions of a model reactor of this type of sodium cooled power reactor, are considered. A program for the reliable calculation of the more important characteristics of such a reactor has been developed. The original library of multigroup constants in a 26 group approximation BNAB and the same library with reevaluated data for ^{239}Pu and ^{238}U (BNAB-M) have been used in the calculations. (7 refs.)

75152 Investigation of the influence of some libraries of multigroup constants on the parameters of a standard fast neutron reactor. J.D.Jordanov, N.A.Antonov.

Yad. Energ. (Bulgaria), no.18, p.57-62 (1983). Multigroup diffusion methods are usually used in the neutron physical analysis of fast neutron reactors. An important part in this analysis is the preparation of the effective multigroup cross-sections, characterizing a given reactor environment required for the solution of the multigroup diffusion equation and the solution itself of the diffusion equation in a multigroup approximation. Depending on the library of multigroup constants used, the errors in the determination of the neutron physical parameters of the fast neutron reactors vary. The calculations carried out make possible the evaluation of the influence of the neutron data from the various libraries on the parameters of a simplified model of a fast neutron power reactor. The results of the calculations are presented in tabular form. (9 refs.)

75153 Results of the measurement of the neutron noise in a reactor type WWER-440. II. A.T.Mikulski, G.Alexandrov, D.M.Bobrovski, N.Todorov, T.Zelinski.

Yad. Energ. (Bulgaria), no.18, p.63-9 (1983). For p.t. see Nukleonika vol.25, p.701 (1980). The results of the analysis of the fluctuating component of the signals obtained by neutron detectors, used in measurements of the WWER-440 reactor in the Kozloduj Atomic Power Station, have been presented. Signals from 8 rhodium SPN-detectors and 3 current ionization chambers have been processed. A TPA type computer is used for the calculations. Stochastic characteristics of the signals—correlation functions, spectrum densities, coherent functions, have been obtained. The results are presented in graphic form. Conclusion have been drawn as to the possibilities of using the results obtained for noise diagnostics of the condition of the reactor core. The results are of a preliminary nature. Work is proceeding on the theoretical explanation. (1 ref.)

75154 Approximate noninteractive power regulation of a coupled-core nuclear reactor. M.Tsuiji, Y.Ogawa (Dept. of Nuclear Engng., Faculty of Engng., Hokkaido Univ., Sapporo, Japan).

IEEE Trans. Nucl. Sci. (USA), vol.ns-30, no.3, p.1835-43 (June 1983). The authors describe an application of an approximate decoupling control to the noninteractive power regulation of each core in a coupled-core nuclear reactor model. A method for designing an approximate decoupling controller is presented. The controller consists of an output feedback compensator and a precompensator which is introduced to diagonalize an open-loop frequency response matrix approximately in the frequency range important to reactor dynamics. A 'multipoint diagonalization method' is adopted for the design of the precompensator. This method possesses some superiorities compared with the pseudo-diagonalization method. Digital simulations and graphical studies by the Gershgorin band demonstrate the usefulness of the multipoint diagonalization method as well as the effectiveness of the controller for power regulation. (12 refs.)

75155 Digital computers in CANDU safety systems. I. History and concepts. N.M.Ichiye (AECL, Mississauga, Ontario, Canada).

IEEE Trans. Nucl. Sci. (USA), vol.ns-30, no.3, p.1908-11 (June 1983). Digital computers have been used in CANDU (CANada Deuterium Uranium) reactors for direct digital control as well as control room functions such as alarm annunciation, data logging and the display of operating data on the control panels. However, until recently computers were not used in the special safety systems. The authors examine the increasing role computers are playing in CANDU safety systems, especially the two shutdown systems. The reasons for this strong trend toward increased use of computers are outlined and recent designs are described, with special emphasis on system concepts. (2 refs.)

75156 Digital computers in CANDU safety systems. II. Implementation and experience. R.S.Gilbert (AECL, Mississauga, Ontario, Canada).

IEEE Trans. Nucl. Sci. (USA), vol.ns-30, no.3, p.1912-16 (June 1983). For p.t. see *ibid.*, vol.ns-20, no.3, p.1908-1911 (1983). Microcomputer based systems have recently been applied to CANDU safety systems. The author describes three specific systems, a monitoring system, the programmable digital comparator (PDC) system, and a fully computerized shutdown system prototype. The system configurations, the hardware and the software used to implement these designs are discussed. Each of these systems uses commercial off-the-shelf hardware which has been modified and qualified when necessary to meet specific power plant requirements. (no refs.)

75157 Characteristics of linear induction electromagnetic pump with sodium side bars. T.Gotoh, M.Yamagata, A.Suzuoki (Energy Res. Lab., Hitachi Ltd., Ibaraki, Japan), Y.Kazawa. *J. At. Energy Soc. Jpn. (Japan)*, vol.25, no.3, p.196-200 (March 1983). In Japanese.

In order to develop an electromagnetic pump for high temperature use, a sodium side-bar type flat linear induction pump (FLIP) whose nominal operating conditions of flow rate and pump head are $1 \text{ m}^3/\text{min}$ and 226 kPa ($2.3 \text{ kg}/\text{cm}^2$) was fabricated. The performance tests were made in Na over the temperature range of 200–400°C and the following results were obtained. (1) The pump head at zero flow rate is in proportion to the square of the applied voltage and its proportional constant is $4.0 \times 10^{-3} \text{ kPa}/\text{V}^2$. (2) The temperature dependency of the pump head at zero flow rate is $4.7 \times 10^{-4} \text{ }^\circ\text{C}^{-1}$. (3) The overall pressure loss coefficient of this pump is 1.94 being 0.92 for the pump duct and 1.02 for the inlet and outlet reducers of the duct. (6 refs.)

75158 Experimental loop in the Nuclear Training Reactor Budapest. Gy.Csom, E.Kocsis, E.M.Zsolnay, E.J.Szondi, I.Szucs (Nuclear Training Reactor, Tech. Univ. Budapest, Budapest, Hungary).

Period. Polytech. Electr. Eng. (Hungary), vol.26, no.1-2, p.21-9 (1982). The in-pile loop built into the Nuclear Training Reactor of the Technical University Budapest is a common design carried out together with the specialists of the Moscow Energetic Institute. This experimental facility is serving for thermodynamic investigations of irradiated solutions under conditions of 20–300–°C temperature and max. 150 bar pressure. Therefore, the results of such experiments can provide valuable informations on the kinetics and mechanisms of chemical processes occurring in the primary and secondary circuits of WWER-type power reactors. (15 refs.)

75159 Neutron spectrum determination by multiple foil activation method. E.M.Zsolnay, E.J.Szondi (Nuclear Training Reactor, Tech. Univ. Budapest, Budapest, Hungary).

Period. Polytech. Electr. Eng. (Hungary), vol.26, no.1-2, p.31-46 (1982). The main features of the neutron spectrum unfolding code SANDBP are described and some results obtained using this code are presented. The program determines the neutron flux density spectrum from multiple foil activation measurements using an iterative method. Response functions deriving from the unfolded neutron spectrum can also be calculated, furthermore Monte-Carlo error analysis can be performed. The neutron spectrum in the centre of the core of the Budapest University's nuclear reactor was measured and unfolded with the aid of this program. (15 refs.)

75160 Distributed microprocessor-based system for monitoring radiation in nuclear power plants. A.A.Denisov, V.S.Zhernov, I.S.Krashennnikov, V.V.Matveev, N.V.Ryzhov, V.M.Skatkin.

Sov. At. Energy (USA), vol.53, no.3, p.577-86 (Sept. 1982). Translation of: *At. Energ. (USSR)*, vol.53, no.3, p.131-8 (Sept. 1982). [received: May 1983] Protection of the environment from anthropogenic actions is becoming a more urgent problem with each passing year. With the rapid growth of nuclear power, one of the complex and specific problems in this area is ecologically safe operation of nuclear electrical power plants, nuclear thermoelectrical power plants, AST, etc. The most important part of the problem is creating measuring and information gathering systems and control systems, which permit monitoring the changes in the environment due to the action of such objects. The authors examine the problems of constructing modern systems for radiation monitoring in nuclear power plants. (6 refs.)

75161 Control of the neutron distribution in a reactor by a liquid absorber. P.T.Potapenko.

Sov. At. Energy (USA), vol.53, no.3, p.601-7 (Sept. 1982). Translation of: *At. Energ. (USSR)*, vol.53, no.3, p.147-51 (Sept. 1982). [received: May 1983] The use of a liquid absorber of neutrons for control is one of the trends in the improvement of channel power reactors. Liquid regulation has been applied effectively on the reactors of Canadian nuclear power plants. An extensive program of the application of a liquid absorber on an RBMK has been carried out by Soviet scientists. Liquid regulating units (RU) for the three-dimensional control of the neutron distribution are discussed. (15 refs.)

75162 Technique for preparing microfilters with high specific capacity. G.N.Flerov, E.D.Vorob'ev, V.I.Kuznetsov, V.A.Shegolev, G.N.Akap'ev, P.Yu.Apel', T.I.Mamonova, L.I.Samolova.

Sov. At. Energy (USA), vol.53, no.3, p.652-4 (Sept. 1982). Translation of: *At. Energ. (USSR)*, vol.53, no.3, p.181-2 (Sept. 1982). [received: May 1983] As is well known, the rate of flow of a fluid or gas through a filter is inversely proportional to its thickness. The thickness of the usual nuclear microfilter is 10 μm , which does not always ensure high filter capacity, especially with small pore diameter. In order to increase the specific capacity of a filter, even thinner films can be used as the starting material, but it is extremely difficult to work with such filters, since their mechanical strength is inadequate. The authors investigated the possibility of obtaining microfilters with a thin filtering layer by irradiating a polymer film through a mask, consisting of a plate with openings, with accelerated ions with a free path in the bulk of the polymer less than the thickness of the film and with an irradiation dose that ensures complete subsequent etching of regions that are not protected by the mask to a depth equal to the path length of the ions. (4 refs.)

75163 Theoretische Beschreibung des Reaktorrauschens in einem stark gekoppelten reaktorphysikalisch-thermohydraulischen System (Theoretical determination of the reactor noise in a strongly coupled reactor kinetic-thermohydraulic system). L.Mesko, T.Katona.

Report KFKI-1983-36, Hungarian Acad. Sci., Budapest (1983), 20 pp. In German.

The coupled neutron-kinetic-thermohydraulic noise phenomena in a core of a PWR has been investigated. The theoretical model derived from the Markovian description of the multi-variable system enables the authors to calculate the auto- and cross power spectral densities and compare them with and without subcooled boiling. (8 refs.)

75164 Simulation of overcooling transients with the Modular Modeling System (MMS). P.K.Jain (Systems Control Inc., Palo Alto, CA, USA), S.Oh, S.M.Divakaruni.

Proceedings of the Fifth Power Plant Dynamics, Control and Testing Symposium, Knoxville, TN, USA, 21-23 March 1983 (Knoxville, TN, USA: Univ. Knoxville 1983), p.4/01-16 vol.1

The Modular Modeling System (MMS) code developed by the Electric Power Research Institute (EPRI) is an economical, dynamical simulation code for rapid and accurate analysis of operational transients and accidents in the PWRs. The key feature of the code is the user convenience in model adaptation to analyze series of transients for a given plant. Extended plant transients can be analyzed with sufficient accuracy and in faster-than real-time with proper choice of modules from the MMS library. However, when accuracy is not of primary concern and the modeling objective is to perform trend or scoping analyses, MMS offers simple modules that can be integrated into the plant model merely by replacing a few key modules. (5 refs.)

75165 Once through steam generator model. R.P.Broadwater, N.G.Demas (Tennessee Technol. Univ., Cookeville, TN USA).

Proceedings of the Fifth Power Plant Dynamics, Control and Testing Symposium, Knoxville, TN, USA, 21-23 March 1983 (Knoxville, TN, USA: Univ. Knoxville 1983), p.11/01-25 vol.1

Overfill transients can lead to rapid overcooling of the primary system in nuclear power plants. Such overcooling may result in excessive thermal stress of primary loop components, and is currently of considerable interest. This paper addresses modeling and simulation of a once through steam generator for overfill transients. In a computer simulation of this event, the simulation algorithm must switch from the normal operating mode for the steam generator to the overfill mode, and then be capable of switching back from the overfill mode to the normal mode. In transitioning between two different physical conditions in a simulation, major effects to avoid are jumps in state variables at the point of switching and oscillating back and forth across the switch boundary. The normal operating mode, the overfill mode, and the

switching between the modes are considered in this paper. The computer code used in the simulation is discussed and listed, and a brief description of the numerical techniques utilized is given. (3 refs.)

75166 Modeling and estimation applied to an AGR once-through boiler. C.Tye, W.J.Hill (Simon Engng. Lab., Univ. of Manchester, Manchester, England).

Proceedings of the Fifth Power Plant Dynamics, Control and Testing Symposium, Knoxville, TN, USA, 21-23 March 1983 (Knoxville, TN, USA: Univ. Knoxville 1983), p.13/01-19 vol.1

Nonlinear and linearised models of an AGR once-through serpentine boiler have been developed and used in studying the performance of a simple sub-optimal state estimation filter incorporating a nonlinear internal model. Uncertainties (biases) in the boiler inputs cause errors in the filter estimates, and these errors can be reduced somewhat by using a parallel bias estimation filter. The results obtained so far indicate that the state variables and outputs for the superheated steam region can be estimated with reasonable accuracy, but the estimates for the subcooled water and two phase regions can be poor if the biases are large. (14 refs.)

75167 Dynamic computer simulation of the Fort St. Vrain steam turbines. J.C.Conklin (Oak Ridge Nat. Lab., Oak Ridge, TN, USA).

Proceedings of the Fifth Power Plant Dynamics, Control and Testing Symposium, Knoxville, TN, USA, 21-23 March 1983 (Knoxville, TN, USA: Univ. Knoxville 1983), p.15/01-15

A computer simulation is described for the dynamic response of the Fort St. Vrain nuclear reactor regenerative intermediate- and low-pressure steam turbines. The fundamental computer modeling assumptions for the turbines and feedwater heaters are developed. A turbine heat balance specifying steam and feedwater conditions at a given generator load and the volumes of the feedwater heaters are all that are necessary as descriptive input parameters. Actual plant data for a generator load reduction from 100 to 50% power (which occurred as part of a plant transient on November 9, 1981) are compared with computer-generated predictions, with reasonably good agreement. (8 refs.)

Modification of the SUPERTOG program for operation with libraries containing tabulated densities of the elastic scattering anisotropy See Entry 75072

Software for neutron physical calculations of fast neutron reactors See Entry 75073

A FAST program for determining the neutron physical parameters of fast neutron reactors See Entry 75074

On-line fault diagnosis in a nuclear reactor by sequential testing See Entry 75075

Iconic displays, Rankine cycles and human factors for control rooms of nuclear power plants See Entry 75076

A pattern recognition method for nuclear reactor core surveillance See Entry 75077

Harmonic simulation of a power reactor See Entry 75080

A three-dimensional improved quasi-static core model for nuclear reactor control room simulators See Entry 75083

Interactive simulation of boiling water reactor systems using DARE P and VAX See Entry 75084

Two phase flow simulator for a PWR nuclear power plants See Entry 75085

Whole-plant simulation for loop-type LMFBR dynamics See Entry 75086

A fast configuration with a conjugate flux independent of energy See Entry 75096

Data evaluation on the absorption of neutrons by cadmium with the aid of integral experiments See Entry 75097

Measurement of the effective cross-sections of absorption for fast reactor building materials using a fast configuration with a conjugated flux, independent of energy See Entry 75098

An assessment of acoustic emission for nuclear pressure vessel monitoring See Entry 75099

Leakage detection by diagnostic analysis of oscillation See Entry 75168

Four-inch pipe whip test under BWR LOCA conditions: effect of overhang length See Entry 75169

Experimental verification of steam into sodium leak detection methods at the Czechoslovak modular steam generator 30 MW working at BOR 60 See Entry 75170

Simulation of recovery from a steam generator tube leak transient See Entry 75171

Two-phase flow patterns: a review of research results See Entry 76089

28.44 FISSION REACTOR PROTECTION SYSTEMS, SAFETY AND ACCIDENTS

75168 Leakage detection by diagnostic analysis of oscillation. P.Siklosy (VEIKI, Budapest, Hungary).

Energ. & Atomtech. (Hungary), vol.36, no.1, p.38-48 (Jan. 1983). In Hungarian.

The safe operation of nuclear power plants is based on controlling the stress cracking that precedes equipment failures in the primary circuit. Instrumental control of various effects caused by liquids flowing through ruptures is of great importance. Leakage detection based on noise analysis may be applied also. Interpretation, explanation and evaluation of measurement signals are, however, complex and preliminary experiments are necessary in which commissioning measurements play an important role. The question of special detectors and signal resolution are stressed. Trace transport, noise and ban filtering give rise to special problems. (13 refs.)

75169 Four-inch pipe whip test under BWR LOCA conditions: effect of overhang length. R.Kurihara, S.Ueda, T.Isozaki, N.Miyazaki, R.Kato (Japan Atomic Energy Res. Inst., Tokyo, Japan), K.Saito, S.Miyazono.

J. At. Energy Soc. Jpn. (Japan), vol.25, no.3, p.207-16 (March 1983). In Japanese.
Pipe whip tests or jet discharge tests have been performed at the Japan Atomic Energy Research Institute, which simulate the instantaneous guillotine break of primary coolant piping in nuclear power plants. The authors describe the results of the 4-inch pipe whip tests (RUN 5407, 5501, 5504, 5603), under the BWR LOCA conditions, which were performed from 1979 to 1981. The test pressure was 6.8 MPa and test temperature 285°C. In these tests, clearance was kept constant at the value of 100 mm and overhang lengths were 250, 400, 550 and 1000 mm, respectively. The main purpose of these tests is to investigate the effect of overhang length on pipe whip behavior. From the tests results, the pipe movement is effectively limited by the restraints if the overhang length is 250 mm or 400 mm. The deformation of

the test pipe and restraints becomes large with increasing overhang length. It is clarified that the test pipe collapses at the setting point of the restraints with the overhang length more than 900 mm. (11 refs.)

75170 Experimental verification of steam into sodium leak detection methods at the Czechoslovak modular steam generator 30 MW working at BOR 60. O.Matal, I.Sobotka, I.Banovets, M.Konarik, F.Varvarovski, K.Kafka, V.Makh, V.I.Kondrat'ev, V.V.Cernobrovkin, V.V.Golusko, V.S.Sroelov, Yu.V.Privalov, E.Pridehl, H.Mauersberger, K.I.Frohlich.

Jad. Energ. (Czechoslovakia), vol.29, no.5, p.183-9 (May 1983). In Russian.

Briefly describes leak detection methods checked-up by steam into sodium artificial leaks at the Czechoslovak modular steam generator 30 MW at the experimental power plant BOR 60. Further, chosen results of processed measurements, performed during operational verification of these methods are given and discussed, and attention is paid to some significant signal characteristics of sensors registering steam generator leakages. (23 refs.)

75171 Simulation of recovery from a steam generator tube leak transient. P.W.Wyatt (Westinghouse Electric Corp., Pittsburgh, PA, USA).

Proceedings of the Fifth Power Plant Dynamics, Control and Testing Symposium, Knoxville, TN, USA, 21-23 March 1983 (Knoxville, TN, USA: Univ. Knoxville 1983), p.3/01-9 vol.1

The importance attached to nuclear safety analysis has led to the development of many large, sophisticated thermal-hydraulics codes. These codes, however, are in general not suitable for use with the small computers used in reactor simulator application. They cannot operate in real time on such machines. But the need to respond to increasing demands for simulation fidelity and the upgrading of the simulator from a training device to an engineering tool necessitate a new approach to simulator modeling. The modeling is now required to increase in sophistication such that two-phase flow, reverse flow, stratification, condensation, evaporation, and natural circulation are described by incorporating a small thermal-hydraulics code in the simulator. Various analytical techniques are used to run in real time with a minimum of nodes. Such a drift-flux model of the reactor coolant system, steam generators and steam header, plus associated auxiliary systems, is described, and examples of typical training exercises are given. (7 refs.)

Gamma-reflection densitometer for the qualification of concrete shielding See Entry 74572

On-line fault diagnosis in a nuclear reactor by sequential testing See Entry 75075

Iconic displays, Rankine cycles and human factors for control rooms of nuclear power plants See Entry 75076

A pattern recognition method for nuclear reactor core surveillance See Entry 75077

Accreditation of qualification testing organizations the industry viewpoint See Entry 75078

WIMSCORE - A code for producing group constants for TDB, TRITON and CITATION codes from WIMS output See Entry 75081

A three-dimensional improved quasi-static core model for nuclear reactor control room simulators See Entry 75083

Interactive simulation of boiling water reactor systems using DARE P and VAX See Entry 75084

Whole-plant simulation for loop-type LMFBR dynamics See Entry 75086

Application of real-time dynamic simulation of the analysis and design of large scale breeder reactor plants See Entry 75087

A numerical integration approach suitable for simulating PWR dynamics using a microcomputer system See Entry 75088

Computed tomographic methods for nuclear fuel characterization and safeguards See Entry 75104

Digital computers in CANDU safety systems. I. History and concepts See Entry 75155

Digital computers in CANDU safety systems. II. Implementation and experience See Entry 75156

Theoretische Beschreibung des Reaktorausgangs in einem stark gekoppelten reaktorphysikalisch-thermohydraulischen System (Theoretical determination of the reactor noise in a strongly coupled reactor kinetic-thermohydraulic system) See Entry 75163

Simulation of overcooling transients with the Modular Modeling System (MMS) See Entry 75164

Once through steam generator model See Entry 75165

Activation and decay characteristics of radiation shielding heavy concretes See Entry 75201

Temperature fields and thermal stress fields in radiation shieldings See Entry 75202

Straight tube nests in concrete walls for radiation shielding See Entry 75203

Testing of radiation shielding concrete walls with portable betatrons See Entry 75204

Measuring apparatus for monitoring radioactive noble gas discharge in nuclear power plants See Entry 75205

Role of sensitivity analysis in determining reactor quantities See Entry 75206

Monitoring the distribution of radionuclides throughout the technological circuits of a nuclear power station See Entry 75207

28.50 FISSION REACTOR TYPES AND APPLICATIONS

Distribution of the flux density and hardness of the neutron spectrum with height and over the cross section of the heat-generating assemblies of VVER-365 and VVER-440 reactors See Entry 75068

Nuclear data requirements for the design of fast neutron reactors See Entry 75071

Software for neutron physical calculations of fast neutron reactors See Entry 75073

A FAST program for determining the neutron physical parameters of fast neutron reactors See Entry 75074

Iconic displays, Rankine cycles and human factors for control rooms of nuclear power plants See Entry 75076

A pattern recognition method for nuclear reactor core surveillance See Entry 75077

Interactive simulation of boiling water reactor systems using DARE P and VAX See Entry 75084

Two phase flow simulator for a PWR nuclear power plants See Entry 75085

- Whole-plant simulation for loop-type LMFBR dynamics See Entry 75086
- Application of real-time dynamic simulation of the analysis and design of large scale breeder reactor plants See Entry 75087
- A numerical integration approach suitable for simulating PWR dynamics using a microcomputer system See Entry 75088
- A fast configuration with a conjugate flux independent of energy See Entry 75096
- Data evaluation on the absorption of neutrons by cadmium with the aid of integral experiments See Entry 75097
- Measurement of the effective cross-sections of absorption for fast reactor building materials using a fast configuration with a conjugated flux, independent of energy See Entry 75098
- Irradiation effects on thermal conductivity of a light-water reactor pressure vessel steel See Entry 75101
- Study of the deactivation mechanisms for some constructional steels by secondary-ion mass spectrometry See Entry 75107
- Light-water reactor low-level waste forms See Entry 75133
- A method of state equation decomposition and its application to the simulation of the dynamics of the active zone of the VVER reactor See Entry 75149
- Neutron-physical characteristics of a standard fast neutron reactor See Entry 75151
- Investigation of the influence of some libraries of multigroup constants on the parameters of a standard fast neutron reactor See Entry 75152
- Results of the measurement of the neutron noise in a reactor type WWER-440, II See Entry 75153
- Digital computers in CANDU safety systems. I. History and concepts See Entry 75155
- Digital computers in CANDU safety systems. II. Implementation and experience See Entry 75156
- Characteristics of linear induction electromagnetic pump with sodium side bars See Entry 75157
- Experimental loop in the Nuclear Training Reactor Budapest See Entry 75158
- Theoretische Beschreibung des Reaktorrauschens in einem stark gekoppelten reaktorphysikalisch-thermohydraulischen System (Theoretical determination of the reactor noise in a strongly coupled reaktorkinetic-thermohydraulic system) See Entry 75163
- Modeling and estimation applied to an AGR once-through boiler See Entry 75166
- Dynamic computer simulation of the Fort St. Vrain steam turbines See Entry 75167
- Four-inch pipe whip test under BWR LOCA conditions: effect of overhang length See Entry 75169
- Experimental verification of steam into sodium leak detection methods at the Czechoslovak modular steam generator 30 MW working at BOR 60 See Entry 75170
- Dose measurements in the teaching reactor of Budapest Technical University after the reconstruction See Entry 75192
- Monitoring the distribution of radionuclides throughout the technological circuits of a nuclear power station See Entry 75207
- Two-phase flow patterns: a review of research results See Entry 76089

28.52 FUSION REACTORS

(for confinement, see 52.55)

- 75172 High power pulsed lasers. J.F.Holzrichter, D.Eimerl, E.V.George, J.B.Trenholme, W.W.Simmons, J.T.Hunt (Lawrence Livermore Nat. Lab., Univ. of California, Livermore, CA, USA). *J. Fusion Energy (USA)*, vol.2, no.1, p.5-45 (Feb. 1982). [received: June 1983]
- Pulsed high power lasers can deliver sufficient energy on inertial fusion time scales (0.1-10 ns) to heat and compress DT fuel to fusion reaction conditions. Several laser systems have been examined for application to the fusion problem. Examples are Nd:glass, CO₂, KrF, and I₂. A great deal of developmental effort has been applied to the Nd:glass laser and the CO₂ gas laser systems. These systems now deliver $>10^4$ J and $>20 \times 10^{12}$ W to inertial fusion targets. The Nova Nd:glass laser is being constructed to provide >200 kJ and $>200 \times 10^{12}$ W of 1 μ m radiation for fusion experimentation in the mid-1980s. For inertial fusion target gain, >100 times the laser input, it is expected that the laser must deliver $\sim 3-5$ MJ of energy on the 10-20 ns time scale. The authors review the developments in laser technology and outline approaches to construction of a 3-5 MJ driver. (83 refs.)
- 75173 Requirements for D-D tandem mirror reactors. F.Kantrowitz, R.W.Conn (School of Engng. & Appl. Sci., Univ. of California, Los Angeles, CA, USA). *J. Fusion Energy (USA)*, vol.2, no.1, p.59-70 (Feb. 1982). [received: June 1983]
- Requirements for D-D barrier tandem mirror reactors are calculated from an equilibrium power balance model. To obtain adequate plasma Q and reasonable power density, axisymmetric configurations are required to decrease barrier length and radial transport and to increase central cell beta. The authors find that for a reactor producing 900 MW net electric power from a $Q=6.5$ plasma, a central cell length of 225 m, maximum B of 15 T, and neutral beam injection energy of 700 keV are necessary. In addition to high central cell beta ($\sim 70\%$), high barrier beta ($\sim 40\%$) is needed to allow the ECRH power required to reduce the barrier potential. Using too much barrier ECRH power results in a decrease in Q . Nuclear elastic scattering of fusion products plays an important role in the overall plasma power balance. When nuclear scattering and coulomb scattering are included, the plasma Q value is increased by more than 40% compared to the case when coulomb scattering alone is considered. (29 refs.)
- 75174 Normal conducting steady-state toroidal magnet systems for ignited Tokamaks. K.Borrass, M.Soll (Max-Planck-Inst. für Plasmaphys., Garching, Germany). *J. Fusion Energy (USA)*, vol.2, no.1, p.71-82 (Feb. 1982). [received: June 1983]
- Normal conducting steady-state toroidal magnet systems are investigated, emphasis being placed on applications to large ignited next generation Tokamaks. The study is based on water-cooled tape wound D coils. The data for the TF magnet systems are calculated in a consistent manner with a computer program including the plasma, shield, ohmic heating coil system, and geometric requirements for blanket modules, beam ducts, etc. An opti-

mization procedure is used to find those TF coil systems which minimize cost-relevant quantities. The main results are that normal conducting TF coil systems of ignited next-generation Tokamaks (following JET, TFTR, etc.) can be operated in a stationary mode and fed from the grid. Cost for electricity is a relatively small portion of the investment cost even in the case of long integral burn times ($>10^7$ s). (12 refs.)

- 75175 Lower hybrid heating and current drive system for a Tokamak reactor. D.A.Ehst, C.D.Boley, K.Evans, Jr., Jungchung Jung, C.A.Trachsel, T.Hino (Fusion Power Program, Argonne Nat. Lab., Argonne, IL, USA). *J. Fusion Energy (USA)*, vol.2, no.1, p.83-109 (Feb. 1982). [received: June 1983]

A lower hybrid heating system has been designed for heating a Tokamak reactor to ignition and for sustaining steady-state operation by driving the toroidal plasma current. The power spectrum from an active/passive waveguide grill is computed, and the resulting equilibrium current density profile is computed from a full electromagnetic WKB analysis of wave propagation in a cylinder. The corresponding toroidal current profile is a low-current equilibrium which is stable to various ideal modes at an economically acceptable beta. The electronic circuitry is designed to minimize the electric power required for current drive, and the resulting design appears to provide reliable operation in a reactor environment. The same system can drive current during reactor startup if some of the waveguides are modified slightly. A typical sequence of startup equilibria is calculated. (51 refs.)

- 75176 Simulating field-reversed magnetic-mirror fusion devices. T.A.Brenge, B.I.Cohen, M.E.Stewart (Lawrence Livermore Nat. Lab., Livermore, CA, USA).

Computer (USA), vol.16, no.6, p.44-9 (June 1983).

Array processing techniques are allowing physicists to program in FORTRAN and generate fast machine code. The simulations show close agreement with theoretically predicted results. Nuclear energy research at Lawrence Livermore National Laboratory indicates that field-reversed magnetic mirror machines may offer greater efficiency and higher electrical yields than current reactor designs. Since theoretical analysis of the FRM is difficult, they are modelling the ion kinetics and electron physics of a fusion plasma to analyze the buildup and decay processes that might be characteristic of an actual machine. They have developed a simulation that accurately models the developing current distribution and use an array processor to obtain faster run times. (13 refs.)

- 75177 Lithium doping of candidate fusion reactor alloys to simulate simultaneous helium and damage production. J.Megusar, O.K.Harling, N.J.Grant (Dept. of Materials Sci. & Engng., MIT, Cambridge, MA, USA). *J. Nucl. Mater. (Netherlands)*, vol.115, no.2-3, p.192-6 (April 1983).

Lithium and boron doping techniques are possibilities for simulating simultaneous helium production and displacement damage in bulk specimens of non-nickel bearing materials in fast fission reactors. Rapid solidification processing and powder metallurgy salt decomposition were investigated for the preparation of lithium doped alloys. For convenience, austenitic stainless steel was doped rather than non-nickel bearing alloys for which this technique is ultimately designed. Neutron autoradiography verified a uniform distribution of lithium in the alloy. Although the same approach can be used to dope alloys uniformly with a stable boron compound, thus reducing the problem of grain boundary segregation and coarsening, the use of lithium doping should be an advantage because this dopant produces only helium and hydrogen when irradiated in a fast fission reactor. These elements are also produced in materials in the CTR environment. (15 refs.)

- 75178 Use of mercury to regenerate liquid-alloy tritium getters. D.H.W.Carstens, W.R.David (Los Alamos Nat. Lab., Los Alamos, NM, USA).

J. Nucl. Mater. (Netherlands), vol.115, no.2-3, p.203-5 (April 1983).

La₂Ni is investigated as a prototype alloy for the gettering of tritium in a fusion reactor. It is shown that it is possible to quantitatively regenerate the getter by first forming an intermediate mercury amalgam at relatively low temperatures. The gas-free amalgam is then thermally decomposed to obtain the original getter alloy. (6 refs.)

- 75179 Electron beam fusion, energy compression, and the absolute instability. R.Jones (Phys. Dept., Nat. Univ. of Singapore, Kent Ridge, Singapore). *Pramana (India)*, vol.20, no.1, p.47-54 (Jan. 1983). [received: May 1983]
- Absolute electron beam-plasma instability is suggested as a means of energy compression for pellet and linear inertial confinement fusion systems. (17 refs.)

- 75180 Fusion: towards reality [Tokamak experiment]. M.Abbott.

Pract. Electron. (GB), vol.19, no.6, p.30-4 (June 1983).

Discusses the project, based at Culham in Oxfordshire, known as the Joint European Torus (JET). The complex houses the most ambitious fusion venture of the European Atomic Energy Community (Eurotom). As far as the fusion alternative is concerned, only one mechanism has the potential to produce enough heat to generate commercially viable electric power. This toroidal machine is called a Tokamak. The objective of the JET project is to create a plasma with a size, density and temperature comparable to that required by a power producing reactor. This plasma will need to reach a temperature of 100 million degrees centigrade. The plasma column will be about two metres in diameter, and have a density 100 million million atoms per cubic centimetre. Although many other difficulties lie in the path towards an economic fusion power station, achieving these parameters on the JET is a quantum leap forward. (no refs.)

- 75181 Inertial confinement fusion. D.Keefe (Lawrence Berkeley Lab., Univ. of California, Berkeley, CA, USA).

In book: *Annual review of nuclear and particle science. Vol.32*, J.D.Jackson, H.E.Gove, R.F.Schwitters [Ed.], p.391-441. Palo Alto, CA, USA: Annual Reviews (1982), 595 pp. [0 8243 1532 4]

In future years inertial confinement fusion can offer an inviting alternative to magnetic confinement fusion for electricity generation. In particular, a much wider variety of choice in the design of the reaction containment vessel is allowed since this method of confinement does not require the vessel to be cocooned within intricate field windings. Furthermore, the overlap between reactor design and driver design is minimal. (48 refs.)

- 75182 Benchmark experiment on D-T neutrons and secondary gamma rays streaming through a concrete bent duct. S.Tanaka, Y.Oyama, N.Sasamoto, T.Nakamura.

Report JAERI-M-82-130, Japan Atomic Energy Res. Inst., Tokai, Ibaraki (Sept. 1982), 45 pp.

A streaming experiment was carried out to examine the behavior of D-T neutrons and secondary gamma rays in a concrete bent duct constructed as a personal access way in the Fusion Neutronics Source Facility (FNS). The distributions in the duct were measured for neutron and gamma-ray dose equivalents, fast neutron dose, and thermal neutron flux. The energy spectra of fast neutrons and gamma rays were also measured at four positions in the duct. This report describes in detail the experimental technique, the measured

data as well as the experimental conditions such as the configuration and the composition of the structural materials and the source conditions which are essential for the analysis of the measurements. (9 refs.)

75183 Japanese contributions to IAEA INTOR Workshop, Phase IIA. Chapters I, II, III: Summary and INTOR concept.

Report JAERI-M-82-170, Japan Atomic Energy Res. Inst., Tokai, Ibaraki (Nov. 1982), 102 pp.

Japanese contributions at INTOR Phase 2A are summarized. This report contains Introduction, Summary of the total report and INTOR Concepts.

75184 Japanese contributions to IAEA INTOR Workshop, Phase IIA. Chapter IV: Plasma confinement and control. K.Miyamoto, M.Sugihara, K.Ueda, S.Yamamoto, M.Maeno, S.Sengoku, N.Suzuki, S.Kasai, M.Nagami, T.Toda, K.Tani, M.Okamoto, N.Fujisawa.

Report JAERI-M-82-171, Japan Atomic Energy Res. Inst., Tokai, Ibaraki (Nov. 1982), 49 pp.

This report corresponds to Chapter IV of Japanese contribution report to IAEA INTOR workshop, Phase IIA. Studies are centered on confinement performance of INTOR core plasmas, losses induced by toroidal field ripples and discharge controls indispensable to long burn.

75185 Japanese contributions to IAEA INTOR Workshop, Phase IIA. Chapter V: RF heating and current drive. K.Miyamoto, M.Sugihara, H.Kimura, H.Matsumoto, K.Oadajima, T.Imai, A.Fukuyama, M.Okamoto, T.Nagashima, T.Yamamoto, T.Ohno, N.Kobayashi, T.Uchida, J.Ohmore, Y.Sawada, K.Ebisawa, K.Uchida, M.Yamauchi, N.Fujisawa.

Report JAERI-M-82-172, Japan Atomic Energy Res. Inst., Tokai, Ibaraki (Nov. 1982), 101 pp.

This report corresponds to Chapter V of Japanese contribution report to IAEA INTOR workshop, Phase IIA. Physics studies for radio frequency heating are concentrated on heating to ignition by means of ion cyclotron and lower hybrid ranges of frequencies, and discharge start-up assist and current drive by lower hybrid range. Their system design studies are also performed.

75186 Annual report of the Fusion Research and Development Center for the period of April 1, 1981 to March 31, 1982.

Report JAERI-M-82-154, Japan Atomic Energy Res. Inst., Tokai, Ibaraki (Nov. 1982), 211 pp.

Research and development activities of the Fusion Research and Development Centre (Division of Thermonuclear Fusion Research and Division of Large Tokamak Development) from April 1981 to March 1982 are described. Emphasis in the JFT-2 and Doublet III Tokamak programs was placed on high-power heating experiments. JFT-2M, which is to replace JFT-2, is in fabrication and will be operational in early 1983. Construction of JT-60 progressed as planned with its completion targeted in March 1985.

NATO ASI on Atomic and Molecular Processes in Controlled Thermonuclear Fusion, Palermo, July 19-30, 1982 See Entry 74205

Neutron yield of the (α, n) reaction for multicomponent media See Entry 75069

Nuclear pumped $O_x(\Delta_1)\Delta_2$ laser See Entry 75624

A new calculation of thermal neutron damage and helium production in nickel See Entry 76518

Vaporization study on the niobium-oxygen solid solution by mass-spectrometric method See Entry 76602

Diffusivity and permeability of hydrogen in neutron irradiated molybdenum and platinum See Entry 76701

Comparison of chemical reactions in liquid lithium with those in liquid sodium See Entry 77880

28.70 NUCLEAR EXPLOSIONS

(see also 47.40 Shock and detonation phenomena)

Examination of a hot particle from a recent atmospheric test See Entry 78111

28.80 RADIATION TECHNOLOGY, INCLUDING SHIELDING

(see also 87.60 Medical and biomedical uses of fields, radiations and radioactivity)

75187 Neutron sensitivity of SSNTD. L.Medveczky (Inst. of Nuclear Res. of the Hungarian Acad. of Sci., Debrecen, Hungary).

Acta Phys. Acad. Sci. Hung. (Hungary), vol.52, no.3-4, p.357-62 (1982). [received: May 1983] (Proceedings of the Hungarian-Austrian Health Physicists' Meeting, Gyor, Hungary, 28 Sept.-1 Oct. 1981).

Various types of solid state nuclear track detectors (SSNTDs) with and without converter radiators were irradiated with neutrons of different energy spectra in order to obtain information on their neutron sensitivity in beam dosimetry. Track revealing was performed by chemical etching. A manual track counting technique was chosen except for the case of thin plastic foils, where also automatic spark counting was used. (13 refs.)

75188 Environmental monitoring system at the Paks Nuclear Power Station. I.Feher, S.Deme, A.Andrasi (Health Phys. Dept., Central Res. Inst. for Phys., Budapest, Hungary).

Acta Phys. Acad. Sci. Hung. (Hungary), vol.52, no.3-4, p.373-9 (1982). [received: May 1983] (Proceedings of the Hungarian-Austrian Health Physicists' Meeting, Gyor, Hungary, 28 Sept.-1 Oct. 1981).

The environmental monitoring system of the Paks Nuclear Power Station (Hungary) has been designed with a dual aim: in normal operation: to check that the population's burden does not exceed the prescribed dose limit; under accidental conditions: to provide rapid information on the expected radiation burden of the population so that necessary steps can be taken. For assessing environmental doses the following parts of the monitoring system are used: telemetric stations to determine the time integral of ^{131}I concentration in air and the gamma dose rate; sampling stations and devices for sample measurement; mobile laboratories; a meteorological tower. The main principles and structure of the environmental monitoring system are discussed. (7 refs.)

75189 Telemetric and data acquisition system for environmental monitoring at the Paks Nuclear Power Station. S.Deme, I.Feher, M.Rovid (Health Phys. Dept., Central Res. Inst. for Phys., Budapest, Hungary).

Acta Phys. Acad. Sci. Hung. (Hungary), vol.52, no.3-4, p.381-7 (1982). [received: May 1983] (Proceedings of the Hungarian-Austrian Health Physicists' Meeting, Gyor, Hungary, 28 Sept.-1 Oct. 1981).

The telemetric and data acquisition system is an inherent part of the total environmental monitoring system of the Paks Nuclear Power Station (Hungary). The detectors of the telemetric system measure the following parameters: the gamma dose rates, the time integral of the ^{131}I activity concentration,

the water temperature, and the meteorological data needed for dispersion calculations. In the 48 channels of the central acquisition system the data mentioned above are stored in the form of pulses, with the exception of the wind direction, which is characterized by the most frequent direction during the measuring period (one hour or 6 minutes). The results are printed on a telex writer and punched on tape for further computer analysis. The characteristic features of the system and the possible uses of the data obtained, both for normal operation and emergency cases are discussed. (3 refs.)

75190 Gamma spectrometric measuring system for environmental sample analysis. A.Andrasi, P.Zombori (Health Phys. Dept., Central Res. Inst. for Phys., Budapest, Hungary).

Acta Phys. Acad. Sci. Hung. (Hungary), vol.52, no.3-4, p.389-95 (1982). [received: May 1983] (Proceedings of the Hungarian-Austrian Health Physicists' Meeting, Gyor, Hungary, 28 Sept.-1 Oct. 1981).

A desk calculator controlled gamma spectrometer was installed and calibrated for routine sample analysis in the environment of the first Hungarian nuclear power plant. A combined application of high efficiency NaI(Tl) and high resolution Ge(Li) spectrometry was elaborated to process the great number of measurements. Measurement is controlled and spectrum evaluation is performed by an on-line program (MEASSYSI) developed for the EMG-71666 desk calculator. The multi-step testing procedure proved the applicability and reliability of the system. (1 ref.)

75191 Comparison of field dose rate measurements and Monte Carlo calculations. L.Koblinger, I.Nemeth, P.Zombori, A.Andrasi (Health Phys. Dept., Central Res. Inst. for Phys., Budapest, Hungary).

Acta Phys. Acad. Sci. Hung. (Hungary), vol.52, no.3-4, p.397-404 (1982). [received: May 1983] (Proceedings of the Hungarian-Austrian Health Physicists' Meeting, Gyor, Hungary, 28 Sept.-1 Oct. 1981).

Dose rates from natural terrestrial gamma sources calculated by a Monte Carlo program and derived from NaI(Tl) scintillation measurements as well as calculated and measured count rates of G-M detectors are compared and show satisfactory agreement. (6 refs.)

75192 Dose measurements in the teaching reactor of Budapest Technical University after the reconstruction. E.Viragh (Tech. Univ., Budapest, Hungary).

Acta Phys. Acad. Sci. Hung. (Hungary), vol.52, no.3-4, p.347-52 (1982). In German. [received: May 1983] (Proceedings of the Hungarian-Austrian Health Physicists' Meeting, Gyor, Hungary, 28 Sept.-1 Oct. 1981).

Explains that the teaching reactor of Budapest Technical University has now been rebuilt to generate 100 kW. The fuel is enriched with 10% ^{235}U and the moderator is graphite+water. The measuring equipment comprises gamma dosimeters, neutron dosimeters and LiF and CaF_2 thermoluminescent detectors. Data of the reactor and some typical measurements are tabulated. (1 ref.) J.S.

75193 Monitoring external radiation in the environment: instruments and results of measurements. E.Tschirf, N.Vana (Univ. Wien, Wien, Austria).

Acta Phys. Acad. Sci. Hung. (Hungary), vol.52, no.3-4, p.363-72 (1982). In German. [received: May 1983] (Proceedings of the Hungarian-Austrian Health Physicists' Meeting, Gyor, Hungary, 28 Sept.-1 Oct. 1981).

Describes methods used for measuring radiation fields near the TRIGA reactor (Atomic Institute of Austrian Universities). Dose measurements are carried out with GM counter tubes and TL detectors (CaF_2/Dy and LiF/Mg, Ti). Results for 1979-81 are presented (graphs and tables). Results of counter tube measurements agreed with those of TL detectors. (3 refs.)

75194 Comparison between two thermoluminescence dosimeter materials. S.Babbout, C.Furetta (I Cattedra di Fisica Medica, Univ. degli Studi di Roma, Roma, Italy).

Radiat. Prot. Dosim. (GB), vol.4, no.1, p.37-42 (1983).

Comparison is made between the properties of two TL dosimetric materials, LiF and $\text{MgB}_2\text{O}_7\cdot\text{Dy}$. The results show that $\text{MgB}_2\text{O}_7\cdot\text{Dy}$ has promising properties for use as a personal dosimeter having better sensitivity and a lower dose threshold but providing less dosimetric information. (6 refs.)

75195 Large volume electret dosimeter for measurement of low level radiation. P.C.Gupta, P.Kotrappa, S.K.Dua (Health Phys. Div., Bhabha Atomic Res. Centre, Bombay, India).

Radiat. Prot. Dosim. (GB), vol.4, no.1, p.47-9 (1983).

An electret is a piece of dielectric carrying quasi-permanent electrostatic charge. A negatively charged electret loaded at the top centre of a 4.8 litre plastic chamber was observed to discharge exponentially with the cumulative dose. However, the dose required to bring the charge to half of its initial value $D_{1/2}$ depended on the dose rate (D). There was a systematic power function relationship between D and $D_{1/2}$ over certain ranges of electret charge. Such a relationship was used to calculate the unknown dose rate by knowing the ratio of initial to final charge and the time of exposure. There was a good agreement between the dose rates estimated to the dose rates expected from a standard radium source. The method was found to be sensitive enough to measure dose rates at environmental level ($10 \mu\text{R h}^{-1}$) within a period of 10 to 20 hrs. The method also provided an energy independent and time averaged dose rate measurement, an important factor in some cases. (4 refs.)

75196 Calculation of the activation energies for single TLD-900 glow-curve components. C.Bacci, R.Bernabei, S.d'Angelo (Inst. di Fisica 'G. Marconi', Univ. di Roma, Rome, Italy), C.Furetta.

Radiat. Eff. Lett. Sect. (GB), vol.76, no.3, p.55-9 (1983).

Presents the activation energies for $\text{CaSO}_4\cdot\text{Dy}$ (TLD-900) material as evaluated by a decomposition of the experimental glow-curve into single components. (9 refs.)

75197 SPICER: a sensitive radiation survey instrument. N.Latner, K.Miller, S.Watnick, R.T.Graveson (Environmental Measurements Lab., US Dept. of Energy, New York, NY, USA).

Health Phys. (GB), vol.44, no.4, p.379-86 (April 1983).

A compact, portable field instrument for measuring environmental γ -ray exposure rates has been developed. Based on an 18 cm diameter pressurized ionization chamber, a temperature compensated MOSFET electrometer and a digital readout with selectable integration times, it is a considerable improvement over previously used larger and bulkier instruments of this type. (6 refs.)

75198 A new phosphor $\text{Li}_2\text{B}_4\text{O}_7\cdot\text{Cu}$ for TLD. M.Takenaga, O.Yamamoto, T.Yamashita (Matsushita Electric Industrial Co. Ltd., Materials Res. Lab., Osaka, Japan).

Health Phys. (GB), vol.44, no.4, p.387-93 (April 1983).

The phosphor $\text{Li}_2\text{B}_4\text{O}_7\cdot\text{Cu}$ (0.03% by weight) has an effective atomic number of 7.3, which is very similar to that of tissue (7.4). This suggests that the phosphor should have excellent properties for thermoluminescent dosimetry. The phosphor prepared by a sintering method shows two glow peaks composed of a dosimetric peak at 205°C and a shoulder at 120°C , and a broad emission band peaking at 368 nm. The material based on the stoichiometric compound of $\text{Li}_2\text{O}\cdot 2\text{B}_2\text{O}_3$ has a good moisture resistant property. The dosime-

tric characteristics are as follows: (1) The sensitivity of γ rays is about 20 times higher than that of $\text{Li}_2\text{B}_4\text{O}_7\text{:Mn}$ prepared by the conventional melting method. (2) The dosimetry peak of 205°C fades less than 9% in intensity at 25°C after 60 days in dark. (3) The TL output is linear with exposure to about 10^4R , becoming sublinear above it. (4) The sensitivity loss caused by humidity is about 10-25% after 2-6 months of storage in air of 90% relative humidity at 25°C . (5) The energy dependence of TL output for photons is flat within the limit of 10% from 40 keV to 7 MeV. (6) The light induced fading is 10% after 3 h room lighting at 100 lux. (6 refs.)

75199 Multi-element dosimeters for radiation protection measurements. H.H.Rossi (Dept. of Radiology, Columbia Univ. Coll. of Physicians & Surgeons, New York, NY, USA).

Health Phys. (GB), vol.44, no.4, p.403-5 (April 1983).

A design for a multi-element tissue-equivalent proportional counter is presented, which should result in an instrument that is in several aspects superior to the single tissue equivalent proportional counters that have been applied for the determination of the dose equivalent, H. (8 refs.)

75200 New health physics perspectives affecting instrumentation technology. E.J.Vallario (Office of Nuclear Safety, US DOE, Washington, DC, USA).

IEEE Trans. Nucl. Sci. (USA), vol.ns-30, no.3, p.1905-7 (June 1983).

Measurements obtained from health physics instrumentation are basic to the radiation control process and are used by management to assure that radiation exposures are kept within limits specified by national-international authorities. Because of this inseparable relationship, health physics instrumentation must be keyed on a continuing basis to changes in radiation exposure standards. (11 refs.)

75201 Activation and decay characteristics of radiation shielding heavy concretes. E.M.Zsolnai, Gy.Csom, E.J.Szondi (Nuclear Training Reactor, Tech. Univ. Budapest, Budapest, Hungary).

Period. Polytech. Electr. Eng. (Hungary), vol.26, no.1-2, p.47-75 (1982).

Activation and decay characteristics of 4 different kinds of heavy concretes were studied. First the elementary composition of the concretes was determined, afterwards calculations were performed by the computer code CAP to determine the desired parameters. The results obtained for the different concretes were analysed and requirements of producing radiation shielding concretes with optimal activation characteristics were summarized. (26 refs.)

75202 Temperature fields and thermal stress fields in radiation shieldings. E.J.Szondi (Nuclear Training Reactor, Tech. Univ. Budapest, Budapest, Hungary).

Period. Polytech. Electr. Eng. (Hungary), vol.26, no.1-2, p.77-91 (1982).

The heat sources developing in the shieldings of radiation sources are presented. Approaching their locus dependence by a polynomial or by an exponential series, a differential equation for thermal conductivity will be obtained which can be solved analytically. In the knowledge of the temperature field the thermal stress field can be calculated. A computer program termed TESTRE ('thermal stress') was developed which provides a satisfactory approach of the thermal stress field. (15 refs.)

75203 Straight tube nests in concrete walls for radiation shielding. E.J.Szondi (Nuclear Training Reactor, Tech. Univ. Budapest, Budapest, Hungary).

Period. Polytech. Electr. Eng. (Hungary), vol.26, no.1-2, p.93-103 (1982).

Measuring cables, sampling pipelines etc. starting from the rooms of the primary circuit of the Paks Nuclear Power Plant are passed through concrete shielding walls in protective armatures made of straight tube nests. The confined area between the tubes affects the homogeneity of the concrete unfavourably. Because of the intricate geometry, the actual conditions can be followed only experimentally. In these experiments, the gamma-radiation field behind the protective armature has been investigated using both extended and point sources. The attenuating effect of wall armature specimen prepared under service conditions is inferior as compared with the specimen considered ideal, prepared in the laboratory. Local defects resulting from inhomogeneities in the concrete can be sufficiently detected. (8 refs.)

75204 Testing of radiation shielding concrete walls with portable betatrons. D.Bodizs (Nuclear Training Reactor, Tech. Univ. Budapest, Budapest, Hungary).

Period. Polytech. Electr. Eng. (Hungary), vol.26, no.1-2, p.105-12 (1982).

With high-intensity radiation sources, when the walls serving for radiation shielding simultaneously perform the function of structural elements of the building housing the source, the thickness of the walls is defined primarily by the required radiation shielding and not by statistical aspects, since from the construction view thinner walls would usually do as well. It is preferable to test the serviceability of such walls with respect to radiation shielding before the installation of the source, since the reinforcement of shielding, if found necessary after the installation of the accelerator or nuclear reactor, will be inconvenient and costly. On the other hand, in thick (60 to 120 cm) concrete walls the probability of the formation of cavities and of non-uniform density distribution will be higher, and these factors largely impair the radiation-shielding characteristics of the wall. For such tests, inspection with gamma rays is in general use. However, with increasing wall thicknesses, higher energies and intensities of the radiation will be required. The author therefore studied the serviceability of a transportable betatron providing 6 MeV X-ray radiation for testing the gamma ray attenuation power of concrete walls with thicknesses exceeding 60 cm. In the experiments discussed the author studied the detectability of defects (cavities) in concrete for various wall thicknesses and for the case of the cavities being located at various depths within the wall. (10 refs.)

75205 Measuring apparatus for monitoring radioactive noble gas discharge in nuclear power plants. S.Desi (Nuclear Training Reactor, Tech. Univ. Budapest, Budapest, Hungary).

Period. Polytech. Electr. Eng. (Hungary), vol.26, no.1-2, p.139-44 (1982).

An apparatus for measuring radioactive noble gases emitted through the ventilation stacks of nuclear power plants is described. The apparatus uses a semiconductor detector accommodated in a low-background measuring chamber. The data measured are processed with a CAMAC type multichannel analyzer and a microprocessor. Both sampling and measuring are fully automated. The results are shown on a colour display and recorded on punched tape. (no refs.)

75206 Role of sensitivity analysis in determining reactor quantities. K.Mihaly (Nuclear Training Reactor, Tech. Univ. Budapest, Budapest, Hungary).

Period. Polytech. Electr. Eng. (Hungary), vol.26, no.1-2, p.193-213 (1982).

The approach of the sensitivity analysis problem described here is shown to be an effective method for biological shield calculation to determine reactor quantities obtained from integral experiments. However, it must be borne in mind that in this case the integral experiments that can be carried out are more limited than in the case of core measurements. It is obviously somewhat risky to extrapolate the obtained results for all shield-designing requirements,

based on the sensitivity analysis of a particular data set, since sensitivities are extremely problem-dependent in shield calculations. This notwithstanding, the results presented here prove that at a certain stage of shield design, reliable and relatively rapid information can be obtained on the accuracy of a reactor quantity measured in a relatively undemanding integral experiment and calculated by a well-tested code, based on a semi-empirical calculation procedure using the method of cross section sensitivity analysis proposed here. (26 refs.)

75207 Monitoring the distribution of radionuclides throughout the technological circuits of a nuclear power station. V.L.Antonov, A.A.Gruzdeva, V.S.Zhernov, S.K.Kozlov, O.B.Lapshchev, V.V.Matveev, V.V.Pushkin, M.K.Romanichev, A.E.Shermakov, E.P.Vargin, L.P.Drozdoza.

Sov. At. Energy (USA), vol.53, no.3, p.587-95 (Sept. 1982). Translation of: *At. Energ. (USSR)*, vol.53, no.3, p.138-43 (Sept. 1982). [received: May 1983]

In recent years, the demands on the operating safety of nuclear power stations and the protection of the environment have been increased. Because of this, in modern radiation safety monitoring systems an important role is being assigned to the prediction of a possible deterioration of the radiation environment. For nuclear power stations with water-cooled-water-modulated power reactors (VVER), the most probable entry of radioactive substances into the outside medium is a result of breakdown of the turbogenerator hermetic sealing. The authors discuss the monitoring of radionuclides in the primary circuits. (4 refs.)

75208 A LiF es a CaSO_4 termolumineszcens detektorok neutronerzékenysége vizsgálatára (Thermal neutron sensitivity of LiF and CaSO_4 thermoluminescent detectors). P.P.Szabo, J.Palfalvi.

Report KFKI-1983-45, Hungarian Acad. Sci., Budapest (1983), 22 pp. In Hungarian.

The neutron sensitivity of LiF discs, ^7LiF , $\text{CaSO}_4\text{:Dy}$ and $\text{CaSO}_4\text{:Tm}$ powder was investigated at the neutron energies of 2 keV, 24 keV and 144 keV and with thermal neutrons. The neutron irradiations were carried out at the NBS reactor, Washington, DC, USA. (8 refs.)

75209 Application of optical fiber waveguides in radiation dosimetry. W.Gaebler, D.Braunig (Hahn-Meitner-Inst. für Kernforschung Berlin GmbH, Berlin, Germany).

First International Conference on Optical Fibre Sensors, London, England, 26-28 April 1983 (London, England: IEE 1983), p.185-9

It is shown that currently available optical fibers used for optical communication purposes exhibit properties, which are well suited for their application as radiation detectors. The sensitivity is adequate and the potential of a reset operation is presented. The annealing behavior has to be investigated by further research work. (14 refs.)

Proceedings of the Hungarian-Austrian Health Physicists' Meeting See Entry 74198

2nd Annual Meeting of the Canadian Radiation Protection Association (papers in summary form only received) See Entry 74210

Proceedings of the Symposium on Low-Level Waste Disposal, Vol.3. Facility Design, Construction, and Operating Practices (NUREG/CP-0028) See Entry 74223

Gamma-reflection densitometer for the qualification of concrete shielding See Entry 74572

Development of an ocean model for use in radiological assessments of sea disposal of solid radioactive wastes See Entry 75120

Environmental monitoring considerations for low-level waste disposal sites See Entry 75131

Health physics monitoring practices at commercial low-level waste disposal sites in light of 10 CFR 61 requirements See Entry 75132

Distributed microprocessor-based system for monitoring radiation in nuclear power plants See Entry 75160

Benchmark experiment on D-T neutrons and secondary gamma rays streaming through a concrete bent duct See Entry 75182

Examination of a hot particle from a recent atmospheric test See Entry 78111

An exact solution to the Gaussian cloud approximation for γ absorbed dose due to a ground-level release See Entry 78113

Detection and identification of emission sources on the basis of the trace element composition of aerosols See Entry 78116

Hungarian-Austrian co-operation in radiation dosimetry See Entry 78332

Determination of the energy response of dosimeters with a Bragg-monochromatized beam See Entry 78337

Measurement of the energy response of LiF-, CaF_2 - and CaSO_4 -TL-dosimeters See Entry 78338

Lithium drifted beryllium oxide high sensitivity thermoluminescent dosimeter See Entry 78339

Estimation of shallow-dose equivalent using a two-element dosimeter See Entry 78346

Depth-dose curves for ^{90}Sr and natural and depleted uranium in Mylar See Entry 78347

RADOK: an integrating, passive radon monitor See Entry 78349

A secondary standard dosimetry system for calibration of radiation protection instruments See Entry 78353

The role of radioactivity standard reference materials in Hungarian health physics practice See Entry 78354

TLD measurements with LiF and $\text{CaSO}_4\text{:Tm}$ See Entry 78355

Development of protection against radiation in Austria during the past decade See Entry 78357

Radioactive contamination of filamentous green algae in the Hungarian reach of the River Danube See Entry 78363

Radioactivity of fish in the Hungarian reach of the River Danube See Entry 78364

28.90 OTHER TOPICS IN NUCLEAR ENGINEERING AND NUCLEAR POWER STUDIES

75210 The nuclear export policy of the Reagan administration. J.F.Pilat, W.H.Donnelly, A.Verbruggen.

Energy Policy (GB), vol.11, no.2, p.168-76 (June 1983).

The Reagan Administration maintains the Carter Administration's objective of non-proliferation of nuclear weapons as being fundamental to US nuclear export policy. However, it sees the USA as having another important role to play in influencing the use of nuclear power and the trading of related goods

and technologies in other countries. While the Administration believes its policies will prove beneficial to the USA, there is concern that trade considerations are being given priority over preventing the proliferation of nuclear weapons. (37 refs.)

75211 Annual report of the division of high temperature engineering (April 1, 1981-March 31, 1982). Report JAERI-M-82-133, Japan Atomic Energy Res. Inst., Tokai, Ibaraki (Oct. 1982), 131 pp.
Research activities conducted in the Division of High Temperature Engineering during fiscal 1981 are described. R&D works of this division are mainly related to a multi-purpose very high-temperature gas-cooled reactor (VHTR) and a fusion reactor. This report deals with the main results obtained on material tests, development of computer codes, heat transfer, fluid-dynamics, structural mechanics and the construction of an M+A (Mother and Adapter) section of a HENDEL (Helium Engineering Demonstration Loop) as well.

29.00 EXPERIMENTAL METHODS AND INSTRUMENTATION FOR ELEMENTARY-PARTICLE AND NUCLEAR PHYSICS

29.15 ELECTROSTATIC AND LINEAR PARTICLE ACCELERATORS

The application of adiabatic theorem to the beam dynamics in accelerators See Entry 75216
The UK free electron laser See Entry 75662
Linac technology for free electron lasers See Entry 75663

29.20 CYCLIC ACCELERATORS AND STORAGE FACILITIES

(for plasma accelerators, see 52.75)

75212 Accelerators—limitations of technology. A summary of the Snow-mass accelerator working group reports. M.Tigner (Cornell Univ., Ithaca, NY, USA). *AIP Conf. Proc. (USA)*, no.98, p.80-8 (1982). [received: May 1983] (Conference on Particles and Fields - 1982, College Park, MD, USA, 28-30 Oct. 1982).
Hadron colliders and accelerators in the 20 TeV energy range turned out to be the majority interest among active members of the Accelerator Row Group. While other types of accelerator and other energy ranges were discussed, largely on the basis of work done elsewhere, the primary creative activities at this summer study focused on the hadron facility. Examining both the economic and accelerator physics dimensions of such a facility, some hope was given to the idea that a well designed and concentrated R/D program, elaborating much further on technologies, might bring a 20 TeV facility within the national reach. The central challenges for this R/D program appear to be (1) Achievement of virtual automation of superconducting magnet, accelerator housing and other accelerator component manufacture and installation. (2) Achievement of a thorough understanding in the field vs. cost relation for superconducting magnets. (3) Achievement of a thorough understanding of the luminosity-aperture-energy relation. (8 refs.)

75213 Detectors and luminosity for hadron colliders. R.Diebold (Argonne Nat. Lab., Argonne, IL, USA). *AIP Conf. Proc. (USA)*, no.98, p.89-102 (1982). [received: May 1983] (Conference on Particles and Fields - 1982, College Park, MD, USA, 28-30 Oct. 1982).
Three types of very high energy hadron-hadron colliders are discussed in terms of the trade-off between energy and luminosity. The usable luminosity depends both on the physics under study and the rate capabilities of the detector. (9 refs.)

75214 Charge oscillations in orbitrons. M.Porto Pato (Inst. de Fisica, Univ. de Sao Paulo, Sao Paulo, Brazil), L.C.Gomes. *Rev. Bras. Fis. (Brazil)*, vol.12, p.93-113 (March 1982). In Portuguese. [received: April 1983]
A statistical model for the electron distribution in orbitrons is constructed where the effect of the end plates is considered. A comparison is made with the measured density of charge. The electromagnetic oscillations generated by orbitrons are calculated as pressure waves and the results obtained are compared with the data. (9 refs.)

75215 Pions storage rings. G.Andlauer.
Proceedings of the International Conference on Nucleus-Nucleus Collisions (papers in summary form only received), East Lansing, MI, USA, 26 Sept.-1 Oct. 1982 (East Lansing, MI, USA: Michigan State Univ. 1982), p.143
The purpose of the paper is the project of pions storage rings that allow the direct collision between secondary particles. The linac injects the protons as projectiles in the synchrotron in order to obtain relativistic speeds. The projectiles react in the targets and drive secondary particles. The pions will be focussed and directed in storage rings so as to interfere at collision points that will provide a rich yield of unexpected results. (no refs.)

Bendro Free Electron Laser Conference See Entry 74214
The application of adiabatic theorem to the beam dynamics in accelerators See Entry 75216
SSRL Beam Line Wunder: Design and planning See Entry 75221
Preliminary results of the Adone storage ring FEL experiment, LELA See Entry 75648
Recent results of the ACO storage ring FEL experiment See Entry 75650
Theory of gain expanded free electron lasers See Entry 75652
Simulation of isochronous storage ring free electron laser See Entry 75658
Application of transverse gradient wigglers in high efficiency storage ring FELs See Entry 75661
Storage ring design optimization for FEL operation See Entry 75664
High current limitations on storage ring FEL sources See Entry 75665
Microtrons for free electron lasers See Entry 75666

29.25 PARTICLE SOURCES AND TARGETS, PREPARATION AND TECHNOLOGY

(see also 07.77 Particle production and handling; targets)

75216 The application of adiabatic theorem to the beam dynamics in accelerators. Fang Shouxian, Guo Zhiyuan, Wu Yingzhi (Inst. of High Energy Phys., Acad. Sinica, Beijing, China). *Commun. Theor. Phys. (China)*, vol.1, no.4, p.515-25 (1982).

The adiabatic criterion and the formulae for calculating the increment of adiabatic invariant due to the nonadiabatic change of parameters in Hamiltonian are derived. The authors have found that this increment is quite small, even in the case where the Landau's adiabatic criterion is violated. (4 refs.)

75217 Storage of ultracold neutrons in a vessel long enough for β decay. Yu.Yu.Kosvintsev, V.I.Morozov, G.I.Terekhov. *JETP Lett. (USA)*, vol.36, no.9, p.424-7 (5 Nov. 1982). Translation of: *Pis'ma v Zh. Eksp. & Teor. Fiz. (USSR)*, vol.36, no.9, p.346-9 (5 Nov. 1982). [received: June 1983]
Cooling a hermetically sealed aluminum vessel to 80K lowers the probability for the loss of ultracold neutrons to a level near the theoretical level. The additional loss in aluminum vessels is shown to be caused by a heating of the ultracold neutrons, for which the probability depends strongly on the temperature. A 'clean' vessel in which ultracold neutrons can be stored for a time equal to their lifetime with respect to β decay can be produced by freezing heavy ice on the surface of an aluminum vessel. (7 refs.)

75218 Laser polarization of accelerated protons. A.N.Zelenskii, S.A.Kokhanovskii, V.M.Lobashev, N.M.Sobolevskii (Inst. of Nuclear Res., Acad. of Sci., USSR). *JETP Lett. (USA)*, vol.36, no.10, p.433-5 (20 Nov. 1982). Translation of: *Pis'ma v Zh. Eksp. & Teor. Fiz. (USSR)*, vol.36, no.10, p.357-9 (20 Nov. 1982). [received: June 1983]

A method is proposed for using laser beams to polarize protons in a beam of fast hydrogen atoms. An intense atomic beam with an energy in the range 160-3000 MeV can be produced by neutralizing accelerated negative hydrogen ions. The implementation of this method would make it possible to produce a pulsed proton current two orders of magnitude higher than that obtainable by other methods. (3 refs.)

75219 Phase space cooling. S.van der Meer. *Phys. Bl. (Germany)*, vol.39, no.5, p.117-19 (May 1983). In German.
Cooling in particle beams is described as a process where oscillatory amplitude, beam cross section and breadth of the energy distribution curve are reduced by the subtraction of energy, for example by synchrotron radiation or by means of a spatially coincident energy absorbing beam. Models are drawn, energy distribution in an anti-proton beam is shown experimentally and the competition between energy gain from adjacent particles, at a rate proportional to amplification to the fourth power, and cooling at a rate linearly proportional to amplification, is illustrated. Stochastic cooling is mentioned and experimental work at CERN is illustrated. Particle storage of the order of 36000 pulses per day is claimed. Uses of beam cooling in Boson identification are reported. (3 refs.) G.M.E.

75220 Neutron yield from lead targets under radiation of electrons interacting with a single crystal. A.F.Antipenko, V.I.Kasilov, N.I.Lapin, S.F.Scherbak. *Ukr. Fiz. Zh. (USSR)*, vol.28, no.5, p.655-7 (May 1983). In Russian.
Photoneutron yield from amorphous lead targets of various thickness is measured. An oriented or misoriented Si crystal and an amorphous Au target have been used as a photon converter. It is shown possible to increase the neutron yield from amorphous targets using a single crystal as a photon target. (12 refs.)

75221 SSRL Beam Line Wunder: Design and planning. R.Z.Bachrach (Xerox Palo Alto Res. Center, Palo Alto, CA, USA), I.Lindau, M.H.Hecht, W.E.Spicer, L.E.Swartz, S.B.Hagstrom.
Fifteenth Annual Synchrotron Radiation Users Group Conference (papers in summary form only received), Stoughton, WI, USA, 18-19 Oct. 1982 (Stoughton, WI, USA: Synchrotron Radiat. Center 1982), p.3
The results of a design study and current planning are presented for a soft X-ray Synchrotron Radiation Beam Line utilizing a permanent magnet undulator insertion on SPEAR at the Stanford Synchrotron Radiation Laboratory. Modeling studies have shown that significant advantages can be obtained in the desired energy range 10-1000 eV using such a device rather than a bending magnet. The parameters which achieve this energy range best characterize the device as between a wiggler and an undulator. The authors have named this device a Wunder and are pursuing its implementation. Relative to a bending magnet, one gains approximately two orders of magnitude of useful flux and in addition, the horizontal beam divergence is reduced by approximately one order of magnitudes. (no refs.)

Fifteenth Annual Synchrotron Radiation Users Group Conference (papers in summary form only received) See Entry 74225
Angular resolution in total cross-section measurements See Entry 74556
Particle distribution around a copper beam stop for 72 MeV protons See Entry 74981
Electron laser facility (ELF) at the LLNL ETA See Entry 75660
Rate of polarization of electrons during resonant tunneling from W-EuS See Entry 77052

29.30 RADIATION SPECTROMETERS AND SPECTROSCOPIC TECHNIQUES

75222 The polarization spectrograph 'DUMAS'. M.Nakamura, H.Sakaguchi, H.Sakamoto, H.Ogawa, T.Ichihara, M.Yosoi, S.Kobayashi (Dept. of Phys., Kyoto Univ., Kyoto, Japan). *AIP Conf. Proc. (USA)*, no.97, p.425 (1982). [received: May 1983] (Proceedings of the Workshop on the Interaction Between Medium Energy Nucleons in Nuclei, Bloomington, IN, USA, 28-30 Oct. 1982).
The polarization measurement of emitted particles in nuclear reaction may play a significant role in the exploration of nuclear reaction mechanism, where the reaction may be induced by either polarized or unpolarized beam and even heavy ion beam. The polarization measurement should cover not only the emitted particles leading to the low-lying states but also those leading to the highly excited states of residual nuclei simultaneously. The authors have succeeded in design of a new separate function type polarization spectrograph with excellent performance characteristics, by introducing combined multipole fields into the system besides the separate field elements. The spectrograph named DUMAS (dual magnetic spectrograph) is now being installed in the experimental area for polarization measurement at RCNP. (no refs.)

75223 Influence of statistical experimental errors on amplitude correlations in resonance spectroscopy. H.M.Hofmann, T.Mertelmeier (Inst. für Theoretische Phys., Univ. Erlangen-Nürnberg, Erlangen, Germany), H.A.Weidenmüller. *Z. Phys. A (Germany)*, vol.311, no.4, p.289-95 (1983). Measurements taken at Triangle Universities on a running sequence of 53 d-wave resonances in ^{45}Sc strongly suggest that the reduced partial width amplitudes have a probability distribution which is not a multivariate Gaussian. The authors investigate whether this result could be caused by experimental statistical errors and find strong indications that this might indeed be the case. (6 refs.)

75224 Detection of radiation in the energy range 0.1 to 10 MeV by use of a nuclear gamma-ray spectrometer. W.M.Summers. Univ. Durham, England thesis, Feb. 1983.

An 86 cm², actively shielded Ge(Hp), nuclear gamma-ray spectrometer was flown from Palestine, Texas, USA, in August 1979, to a residual atmospheric pressure of 4.3 g cm⁻², by means of a high altitude balloon. The design, construction and response characteristics of the instrument, which has (a) an energy resolution of 2.5 keV at 1.33 MeV, (b) an opening angle of 5.2° (FWHM) and (c) a measured efficiency of 23% relative to a 3"×3" NaI(Tl) crystal, is described. Also presented are measurements of the gamma-ray lines which were detected at various atmospheric depths during the ascent phase of the flight. These features originate from secondary gamma production in the shield and Ge(Hp) crystal from atmospheric radiation 'leaking' through it.

Gamma spectrometric measuring system for environmental sample analysis See Entry 75190

Time dependence of the induced charge in closed ended HP Ge detectors See Entry 75239

Pulse shaper for time clamping to the rising edge of pulses in semiconductor detectors See Entry 75244

29.40 RADIATION DETECTORS

(for mass spectrometers, see 07.75)

75225 Nutex experiment and the future of the Mont Blanc laboratory. G.Battistoni (Lab. Nazionali, INFN, Frascati, Italy), E.Bellotti, G.Bologna, P.Campagna, C.Castagnoli, V.Chiarella, D.C.Cundy, B.D'Ettore, Piazzioli, E.Fiorini, E.Iarocci, G.Mannocchi, G.O.Murtas, P.Negri, G.Nicoletti, P.Picchi, M.Price, A.Pullia, S.Ragazzi, M.Rollier, O.Saavedra, L.Trasatti, L.Zanotti. *AIP Conf. Proc. (USA)*, no.96, p.124-37 (1982). [received: May 1983] (Workshop on Science Underground, Los Alamos, CA, USA, 1982).

For 20 years garages in the Mont Blanc road tunnel have been used as cosmic-ray underground laboratories. In 1973 in one of these laboratories the authors carried out a proton decay experiment using one ton of liquid scintillator surrounded by a 4π anticoincidence shield. Of course no proton decays were found and gave a lifetime limit of $>10^{25}$ years. However, at the same time no background events were found, and it was clear that the Mont Blanc laboratory was ideal for this type of experiment. The laboratory is located deep underground; the minimum depth is ~5000 m.w.e. There is only one problem: the typical size of the garages is (8.6×8×6.5) m³, which limits the mass of the detector. Actual proton decay detectors fall into two classes: totally active water Cherenkov detectors, and tracking calorimeters. In October 1979, during a new proton decay experiment, Nutex, a digital calorimeter was made for several reasons: small laboratory size; experience in digital tracking calorimeter techniques; and the desire to get quick and good results. (5 refs.)

75226 IMB detector—the first 30 days. R.M.Bionta (Univ. of Michigan, Ann Arbor, MI, USA), G.Blewitt, C.B.Brattin, B.G.Cortez, S.Errede, G.W.Foster, W.Gajewski, M.Goldhaber, J.Greenberg, T.J.Haines, T.W.Jones, D.Kielczewski, W.R.Kropp, J.G.Learned, E.Lehmann, J.M.LoSecco, P.V.Ramana Murthy, H.Park, F.Reines, J.Schultz, E.Shumard, D.Sinclair, D.W.Smith, H.Sobel, J.L.Stone, L.R.Sulak, R.Svoboda, J.C.van der Velde, C.Wuest. *AIP Conf. Proc. (USA)*, no.96, p.138-42 (1982). [received: May 1983] (Workshop on Science Underground, Los Alamos, CA, USA, 1982).

A large water Cherenkov detector, located 2000 feet below ground, has recently been turned on. The primary purpose of the device is to measure nucleon stability to limits 100 times better than previous measurements. The properties of the detector are described along with its operating characteristics. (no refs.)

75227 The Harvard-Purdue-Wisconsin baryon decay experiment at Park City, Utah. D.B.Cline (CERN, Geneva, Switzerland).

AIP Conf. Proc. (USA), no.96, p.143-60 (1982). [received: May 1983] (Workshop on Science Underground, Los Alamos, CA, USA, 1982).

A large tank of water, instrumented with photomultipliers and surrounded by an active shield using proportional wire tubes is being constructed in an underground laboratory at Park City, Utah. Baryon decay can be separated from background using the Cherenkov light pattern to a lifetime of approximately 4×10^{32} years in three years of running time. The status of the experiment is reported here. (4 refs.)

75228 The Soudan nucleon decay experiments. L.E.Price (Argonne Nat. Lab., Argonne, IL, USA).

AIP Conf. Proc. (USA), no.96, p.161-7 (1982). [received: May 1983] (Workshop on Science Underground, Los Alamos, CA, USA, 1982).

Two nucleon decay experiments using the Soudan mine are discussed. Soudan 1 is currently taking data: It contains 31 tons, and is based on proportional tubes. It has set an upper limit of 1.0×10^{30} years on the lifetime of the nucleon. Soudan 2 is a proposal based on long drift chambers with an initial mass of 1000 tons, to be expanded to 5000 tons. (5 refs.)

75229 The nucleon decay experiment in the Frejus tunnel. J.Ernwein (CENS, Gif-sur-Yvette, France).

AIP Conf. Proc. (USA), no.96, p.175-81 (1982). [received: May 1983] (Workshop on Science Underground, Los Alamos, CA, USA, 1982).

The author describes a 1.5 kiloton fine grained flash chamber detector which will be installed in an underground laboratory in the Frejus tunnel near Modane, France. It will be dedicated to the search for nucleon decay. It will also be possible to search for monopoles and study multimions. (8 refs.)

75230 A proton decay and solar neutrino experiment with a liquid argon Time Projection Chamber. H.H.Chen, P.J.Doe, H.-J.Mahler (Univ. of California, Irvine, CA, USA).

AIP Conf. Proc. (USA), no.96, p.182-5 (1982). [received: May 1983] (Workshop on Science Underground, Los Alamos, CA, USA, 1982).

Recent progress in development of the liquid argon Time Projection Chamber is reviewed. Application of this technique to a search for proton decay and ^8B solar neutrinos with directional sensitivity is considered. The steps necessary for a large scale application of this technique deep underground are described. (9 refs.)

75231 Magnetic monopoles, nucleon decay and DUMAND. P.C.Bosetti (Phys. Inst., Tech. Hochschule Aachen, Aachen, Germany).

AIP Conf. Proc. (USA), no.96, p.186-9 (1982). [received: May 1983] (Workshop on Science Underground, Los Alamos, CA, USA, 1982).

A search for magnetic monopoles catalyzing baryon decay has been performed. The detector—a water filled tank equipped with photomultiplier tubes—was most sensitive for monopoles with velocities less than 0.001c and interaction lengths less than 50 cm. No monopole has been found leading to an upper limit of $F(M) < 1.6 \times 10^{-2} \text{ m}^{-2} \text{ sr}^{-1} \text{ d}^{-1}$.

75232 Apparatus for automatic track etching of SSNTDs. G.Streubel, C.Meide (Sektion Physik., Tech. Univ. Dresden, Dresden, Germany).

Radiat. Prot. Dosim. (GB), vol.4, no.1, p.43-5 (1983).

The apparatus for automatic track etching of SSNTDs described is an apparatus for carrying out the complete treatment from detector etching to detectors drying in one tank. This tank is connected with the containers for the different liquids necessary by pipes. The control of the etching treatment is performed electronically. The apparatus permits simultaneous etching of about 105 detectors and allows good reproducibility. (5 refs.)

75233 Some aspects and results of the electrochemical etching of a thin-film track detector. J.Olszewski, T.Domanski, M.Hawrynski, W.Chruscielowski (Inst. of Occupational Medicine, Lodz, Poland).

Nucl. Tracks & Radiat. Meas. (GB), vol.6, no.4, p.161-74 (1982).

The authors report the effects for the commercially available cellulose nitrate foil, namely Kodak LR-115 type 2. This foil was irradiated with alpha particles (from a ^{239}Pu source) and then treated electrochemically. They find that the maximums of the frequency resonance curves are located between 0.5-1.5 kHz and depend on the electric field strength, applied on the Kodak foil; whereas the field-strength-resonance curves have their maximums between 0.5-1.2 kV and also depend on the frequency. The 'appearance' (or emergence) effect of the latent tracks was used as a criterion of track-enhancement in the electrochemical etching. The results obtained, especially the shapes of frequency resonance curves, are in very good agreement with those curves that can be predicted from a theoretical consideration of the mechanisms of the electrochemical etching phenomenon. In the theory presented the authors consider the foil as a dielectric between two plates of a capacitor. It vibrates mechanically in the alternating electric field. This vibration increases the probability of the interaction between ions and the material to be etched. Also, the effect of an additional flux of the ions of electrolyte, due to the action of the alternating field in the etchant, is considered. Both the assumptions permit one to predict the shape of resonance curves and to find some of the characteristic parameters of track detector material. (33 refs.)

75234 Development of a new EPL-free etchant for soda-glass nuclear track detectors. M.Farid, A.P.Sharma (Dept. of Phys., Kurukshetra Univ., Kurukshetra, India).

Nucl. Tracks & Radiat. Meas. (GB), vol.6, no.4, p.175-84 (1982).

When soda-glass track detectors are etched in hydrofluoric acid (48 vol.%), the common etchant, an etch product layer (EPL) is formed on the detector surface which interferes with further etching. The authors report a new three-component etchant consisting of HF (12 vol.%), H_2SO_4 (24%) and H_2O in the ratio 12:2:9 for soda-glass detectors to overcome the adverse effects of EPL. They have studied bulk-etch rate, track-etch rate, etch-pit diameter, etching efficiency and energy resolution of soda glass detectors for fission-fragment tracks of ^{252}Cf by using this new etchant. A comparison of the results with those reported by earlier workers shows the superiority of the new etchant over the etchants used earlier. (13 refs.)

75235 Neutron-sensitivity calculations for simple albedo track detectors.

J.Palfalvi (Central Res. Inst. for Phys., Budapest, Hungary).

Nucl. Tracks & Radiat. Meas. (GB), vol.6, no.4, p.185-8 (1982).

The neutron sensitivity of Kodak-Pathe LR 115 type II cellulose nitrate track detector, with LiF , $\text{Li}_2\text{B}_4\text{O}_7$ and B_4C (n,α) radiators was investigated by calculations. (1 ref.)

75236 Relocating tracks and projection measurements at different stages of development in plastic detectors. M.Debauvais, J.Ralarosy, J.Tripier, M.Meyer, L.Oberle (Centre de Recherches Nucleaires, Strasbourg, France).

Nucl. Tracks & Radiat. Meas. (GB), vol.6, no.4, p.189-92 (1982).

The authors present a procedure for relocating correlated track segments at various stages during the chemical treatment of a plastic track detector. This is done with the aid of a millimetric grid fixed to the detector. Photographs show the effect for the $\text{Au}(u,x)$ interaction at 10 MeV/amu with a Makropol sheet detector. (2 refs.)

75237 A new track etchant for plastic detectors. T.Singh, M.Singh, S.Singh, H.S.Virk (Dept. of Phys., Guru Nanak Dev Univ., Amritsar, India).

Nucl. Tracks & Radiat. Meas. (GB), vol.6, no.4, p.197-9 (1982).

The authors investigate the etching ability of alkaline earth metal hydroxides on ^{252}Cf -irradiated Lexan. Successful results were obtained for $\text{Ba}(\text{OH})_2 \cdot 8\text{H}_2\text{O}$. (10 refs.)

75238 A simple system for rapid assessment of etch pits. J.R.Harvey, A.R.Weeks (CEGB, Berkeley Nuclear Labs., Berkeley, England).

Nucl. Tracks & Radiat. Meas. (GB), vol.6, no.4, p.201-6 (1982).

A technique which gives information on the size and number of alpha-induced etch pits in CR39 plastic is described. The pits, produced by etching the CR39 in hot sodium hydroxide, are filled with a paste composed of fine particles of a scintillator (ZnS:Ag) in ethylene glycol. The light pulses produced when samples of CR39, treated in this way, are exposed to a high-intensity alpha particle source, are detected and counted. The technique is likely to be simpler and less time-consuming than existing alternative methods. (3 refs.)

75239 Time dependence of the induced charge in closed ended HP Ge detectors. A.Alberigi Quaranta, A.Catellani (Univ. of Modena, Modena, Italy), M.Cuzzilla, G.Zanarini.

IEEE Trans. Nucl. Sci. (USA), vol.ns-30, no.3, p.1862-9 (June 1983).

Starting from energy balance considerations, the time dependence of the induced charge in closed ended HPGe gamma detectors is numerically determined as a function of detectors geometry, applied voltage and coordinates of created e-h pairs. These data can support the choice of geometry and applied voltage for the optimal use of closed ended detectors. (11 refs.)

75240 Carrier surface recombination in Hgl_2 photon detectors. A.Levi, M.M.Schieber (School of Appl. Sci. & Technol., Hebrew Univ. of Jerusalem, Jerusalem, Israel), Z.Burshtein.

J. Appl. Phys. (USA), vol.54, no.5, p.2472-6 (May 1983).

Carrier collection efficiency versus voltage characteristics were studied in detail in Hgl_2 photon detectors of various thicknesses for the 5.9 keV X-ray emission of ^{55}Fe . The results prove the important role of carrier surface recombination in limiting the carrier collection, and its consequences on the detector performances. Electron and hole surface recombination velocities in the samples were about 10^4 cm/sec. Hole trapping times were about 10^{-6} s.

sec, while electron trapping times were much longer than $\sim 10^{-5}$ sec. (23 refs.)

75241 A brief survey on progress and trends in nuclear radiation detectors. **I. Gas counters and liquid detectors.** E.Sakai (Div. of Reactor Engng., JAERI, Ibaraki, Japan). *Radioisotopes (Japan)*, vol.32, no.3, p.135-42 (March 1983). In Japanese. Detection of nuclear radiation requires transducers using a variety of physical principles. The interactions of nuclear radiations with matter produce phenomena which can be measured as electrical pulses and currents. All nuclear radiations produce ionization in matter, either directly or indirectly through secondary radiation. It is this characteristic ionization which forms the basis of almost all nuclear radiation detectors. Detectors may be divided into those which collect and measure the primary and secondary ions produced by the nuclear radiation, and those which observe and measure some secondary effect produced by this ionization. This paper briefly describes liquid ion collection devices and gaseous ion collection devices which include multiwire proportional counters, self-geunched streamer counters, gas scintillation counters and gas scintillation proportional counters. (32 refs.) *K.B.*

75242 (Neutron, α) magreakcion alapulo szilardtest nyomozométer hatásfokának elemleti és kísérleti vizsgálata ((Neutron, α) nuclear reaction solid track detector efficiency: Theoretical and experimental studies). J.Pál-falvi.

Report KFKI-1983-46, Hungarian Acad. Sci., Budapest (1983), 23 pp. In Hungarian.

The neutron sensitivity of Kodak-Pathe LR 115 II type cellulose nitrate track detectors with different (n, α) radiators was investigated by calculations and measurements. The α counting efficiency using an optical microscope is 95% for α particles with maximum energy of 2 MeV. When using an image analyser the etched through-tracks (holes) with diameter greater than 2 μ m are counted. The efficiency then depends only on the original and removed layer thickness but not on the etching temperature within the range of 40 to 60°C and the 2.5 to 6 N normality of the NaOH etchant. Efficiency varies from about 3 to 20% for alphas from the $^6\text{Li}(n, \alpha)\text{T}$ reaction if the removed layer lies in the range of ~ 7 to 10 μ m, and varies from ~ 2 to 10% for $^{10}\text{B}(n, \alpha)^7\text{Li}$ reaction alphas when the layer removal is ~ 8 to 10 μ m. (8 refs.)

Workshop on Science Underground See Entry 74199

Proposal for a national underground science facility See Entry 74240

Perspectives of fundamental research in the Gran Sasso Underground Laboratory See Entry 74241

The Gran Sasso project See Entry 74242

Proton decay experiment in the Kolar Gold Fields See Entry 74765

The Mont Blanc experiment on nucleon stability See Entry 74766

Experiment to detect proton decay and neutrino oscillations (using cosmic ray neutrino events) See Entry 74770

Neutron sensitivity of SSNTD See Entry 75187

A LiF es a CaSO₄ termolumineszcens detektorok neutronerzekenysegenek vizsgálata (Thermal neutron sensitivity of LiF and CaSO₄ thermoluminescent detectors) See Entry 75208

Detectors and luminosity for hadron colliders See Entry 75213

Detection of radiation in the energy range 0.1 to 10 MeV by use of a nuclear gamma-ray spectrometer See Entry 75224

Electronic units for experimental investigations with the multisection detector 'Romashka' on the IRT-2000 reactor in Sofia See Entry 75243

Pulse shaper for time clamping to the rising edge of pulses in semiconductor detectors See Entry 75244

Activity determination in samples of isotope mixtures by using sum peaks in Ge(Li) spectra See Entry 75245

Low-density nuclear isomer and a possible explanation for the anomaly in the free path of nuclear fragments in photoemulsions See Entry 75247

Calorimetry in high-energy physics See Entry 75249

The use of solid-state nuclear track detectors in radiation dosimetry, medicine and biology See Entry 78344

Biomedical applications of MWPC's for digital imaging of soft β^- emitters See Entry 78406

The Fly's Eye See Entry 78817

29.60 COUNTING CIRCUITS AND NUCLEAR ELECTRONICS

75243 Electronic units for experimental investigations with the multisection detector 'Romashka' on the IRT-2000 reactor in Sofia. T.J.Grigorov, H.F.Muning, Ts.Ts.Pantelev. *Yad. Energ. (Bulgaria)*, no.18, p.70-4 (1983).

The general experimental set-up on the multiplicity spectrum measurements of the γ -rays from a single act of thermal neutron capture by the investigated nuclei has been described. The experiment is carried out with the aid of the twelve-sector scintillation detector 'Romashka'. A description of the signal level discriminator circuit with delay shaping and the duration of the output signals setting is given. The circuit of the accumulation, decoding and information display unit for the data from the 'Romashka' detector is presented. (4 refs.)

75244 Pulse shaper for time clamping to the rising edge of pulses in semiconductor detectors. A.A.Aleksandrov, V.A.Mokrousov, Yu.V.Pyatkov. *Instrum. & Exp. Tech. (USA)*, vol.25, no.4, pt.2, p.915-17 (July-Aug. 1982). Translation of: *Prib. & Tekh. Eksp. (USSR)*, vol.25, no.4, p.122-4 (July-Aug. 1982). [received: May 1983]

A pulse shaper is described for time clamping to the leading edge of preamplified current or voltage pulses in semiconductor detectors. Clamping is to the 0.5-0.9 amplitude level over a 4-100 nsec time range. For generator pulses with 5-nsec fronts, the error in time clamping is due to the dynamically changing amplitude and is ± 30 psec for a 6:1 dynamic range. The pulse shaper can be used to measure the rise times of pulses from surface-barrier or Ge(Li) detectors, or in time-of-flight spectrometers as a time marker. The pulse shaper is designed to conform to CAMAC standards and fits in a module of unit width. (5 refs.)

29.70 RADIATION MEASUREMENT, DETECTION AND COUNTING

(see also 29.30 Radiation spectrometers and spectroscopy, 29.40 Radiation detectors; for dosimetry, see 87.60M)

75245 Activity determination in samples of isotope mixtures by using sum peaks in Ge(Li) spectra. I.Uray, I.Torok, E.Gyarmati (Inst. of Nuclear Res. of the Hungarian Acad. of Sci., Debrecen, Hungary). *Acta Phys. Acad. Sci. Hung. (Hungary)*, vol.52, no.3-4, p.469-73 (1982). [received: May 1983] (Proceedings of the Hungarian-Austrian Health Physicists' Meeting, Gyor, Hungary, 28 Sept.-1 Oct. 1981).

The basic concept of the absolute activity determination based on sum peaks are briefly discussed. A possible extension of the method to measure the absolute activities of monoenergetic gamma sources is also given. (4 refs.)

75246 Calculation of radon and thoron daughters concentration by least squares. Zhang Chunzhang, Luo Daling. *Acta Sci. Nat. Univ. Sunyatseni (Zhongshandaxue Xuebao) (China)*, no.4, p.58-64 (1982). In Chinese.

The method of measuring radon and thoron daughters concentration during and after sampling is discussed and a versatile computer program for analyzing observed data of random and thoron daughters is written on the basis of the mathematical method of matrix and weighted least squares calculations. The program is suitable to calculate the concentration of radon and thoron, daughters from the total alpha counts and alpha spectroscopy data during and after sampling. The results of measurements show that greater accuracy of the concentration of radon and thoron daughters can be obtained by the weighted least squares calculation. (10 refs.)

75247 Low-density nuclear isomer and a possible explanation for the anomaly in the free path of nuclear fragments in photoemulsions. V.A.Khodel (I.V. Kurchatov Inst. of Atomic Energy, Acad. of Sci., Moscow, USSR). *JETP Lett. (USA)*, vol.36, no.7, p.325-7 (5 Oct. 1982). Translation of: *Pis'ma v Zh. Eksp. & Teor. Fiz. (USSR)*, vol.36, no.7, p.265-7 (5 Oct. 1982). [received: May 1983]

An explanation is proposed for the anomalous behavior of the free path of nuclear fragments in photoemulsions. (10 refs.)

75248 ICRU recommendations on radiation quantities and units — a critical review. K.Katoh (Nat. Lab. for High Energy Phys., Ibaraki, Japan). *Radioisotopes (Japan)*, vol.32, no.3, p.127-34 (March 1983). In Japanese. This review paper comments on ICRU (International Commission on Radiation Units and Measurements) recommendations for radiation quantities and units. The ICRU's proposed relation for $d\epsilon/dm$ (given) is not trivial, although the relationship between the non-stochastic quantity D and the stochastic quantity z is formulated. The probability distribution $f(z)$ of z may vary with matter system size. (34 refs.) *K.B.*

75249 Calorimetry in high-energy physics. C.W.Fabjan (CERN, Geneva, Switzerland), T.Ludlam.

In book: *Annual review of nuclear and particle science*, Vol.32, J.D.Jackson, H.E.Gove, R.F.Schwitters [Ed.], p.335-89. Palo Alto, CA, USA: Annual Reviews (1982), 595 pp. [0 8243 1532 4]

The detection of particles is the experimental tool of high-energy physics research, and the evolution of the field has been closely coupled to the development of improved methods for detecting and measuring an ever-widening spectrum of particle properties. Much of our present knowledge about the physics of elementary particles has been the result of a continuing refinement of techniques for measuring the trajectories of individual charged particles—from the early hodoscopes, cloud chambers, and emulsion stacks, to today's extraordinarily precise bubble and streamer chambers and sophisticated magnetic spectrometers, equipped with multiwire proportional or drift chambers (Charpak et al. 1978, Fabjan and Fischer 1980). The authors examine an intrinsically different class of detector that has come to the fore over the past decade and promises to greatly influence the scope of future experiments—total absorption detectors or calorimeters. (146 refs.)

Angular resolution in total cross-section measurements See Entry 74556

Nucleonic techniques for non-invasive, on-line measurement [industrial applications] See Entry 74578

The Mont Blanc experiment on nucleon stability See Entry 74766

Energy loss by slow magnetic monopoles See Entry 74827

Measuring apparatus for monitoring radioactive noble gas discharge in nuclear power plants See Entry 75205

Influence of statistical experimental errors on amplitude correlations in resonance spectroscopy See Entry 75223

Nusex experiment and the future of the Mont Blanc laboratory See Entry 75225

Dust concentration measurement probe using beta attenuation See Entry 77925

29.80 NUCLEAR INFORMATION PROCESSING

75250 A multicrate link system for use with CAMAC auxiliary controllers designed at Daresbury Laboratory. J.Alexander, J.Howson (Daresbury Lab., Sci. & Engng. Res. Council, Warrington, England). *Interfaces Comput. (Switzerland)*, vol.1, no.2, p.171-9 (May 1983).

Many CAMAC systems using auxiliary controllers need to access more modules than will fit into a single CAMAC crate. The Daresbury Link enables several auxiliary controllers to access modules in up to seven crates almost as quickly and simply as though they were in a single crate. The link is processor independent. (3 refs.)

29.90 OTHER TOPICS IN HIGH-ENERGY AND NUCLEAR EXPERIMENTAL METHODS AND INSTRUMENTATION

Proposal for a national underground science facility See Entry 74240

Perspectives of fundamental research in the Gran Sasso Underground Laboratory See Entry 74241

The Gran Sasso project See Entry 74242

30.00 ATOMIC AND MOLECULAR PHYSICS

(for physical chemistry, see 82.)

International Symposium on Theoretical Organic ChemistrySee Entry 74216

31.00 THEORY OF ATOMS AND MOLECULES

(see also 71. Electron states in condensed matter)

31.10 GENERAL THEORY OF STRUCTURE, TRANSITIONS AND CHEMICAL BINDING

75251 The hydrogen atom in strong magnetic fields: summation of the weak field series expansion. J.C. Le Guillou (Lab. de Phys. Theorique et Hautes Energies, Univ. Paris VI, Paris, France), J. Zinn-Justin. *Ann. Phys. (USA)*, vol.147, no.1, p.57-84 (15 April 1983).

Using the weak field expansion, the authors have calculated the ground-state energy of the hydrogen atom in a magnetic field for values of the field up to about 10^{13} G. The perturbative expansion has been summed by an order-dependent mapping method. The authors compare the results with previous calculations. The method allows one to obtain, first, more accurate values of the binding energy for a field up to 10^{10} G, then good results in the transition region between the two sets of accurate calculations of the literature, and finally still reasonably accurate values up to 10^{13} G. (42 refs.)

75252 On total π -electron energy of benzenoid hydrocarbons. I. Gutman, S. Petrovic (Faculty of Sci., Kragujevac, Yugoslavia). *Chem. Phys. Lett. (Netherlands)*, vol.97, no.3, p.292-4 (20 May 1983).

Hall's observation that the total π -electron energy E of benzenoid hydrocarbons is a linear function of the number of Kekule structures is supported by theoretical arguments and extensive numerical work. A rather accurate topological formula for E is obtained. (4 refs.)

75253 Reduction of the excited state into the ground state of a super-Hamiltonian. J. Katriel (Dept. of Chem., Technion-Israel Inst. of Technol., Haifa, Israel).

Int. J. Quantum Chem. (USA), vol.23, no.5, p.1767-80 (May 1983). A reformulation of the Hylleraas-Undheim-MacDonald variational procedure for excited states, involving the application of Lowdin's supersecular equation to a variational problem concerning the ground state of an appropriate super-Hamiltonian, is proposed. Some formal applications are presented. (17 refs.)

75254 A formula for calculating molecular energy differences from electrostatic potentials at nuclei. P. Politzer, P. Sjöberg (Dept. of Chem., Univ. of New Orleans, New Orleans, LA, USA).

J. Chem. Phys. (USA), vol.78, no.11, p.7008-10 (1 June 1983). Presents an accurate procedure for predicting energy differences for certain types of isoelectronic molecules. It can be used to obtain reasonable estimates of molecular electron affinities; these are often difficult to evaluate by experimental or other theoretical approaches. The authors have shown that electrostatic potentials at nuclei computed with Hartree-Fock wave functions can indeed be used to obtain energy-related quantities that are consistently more accurate than if they have been determined directly from the Hartree-Fock energies. (11 refs.)

75255 Hyperspherical coordinates in four particle systems. Y. Ohn (Dept. of Chem. & Phys., Univ. of Florida, Gainesville, FL, USA), J. Linderberg.

Mol. Phys. (GB), vol.49, no.1, p.53-64 (May 1983). Explicit formulae are provided for the kinetic energy functional in hyperspherical coordinates for a four particle system in a parametrization where the total angular momentum and the moments of inertia are exhibited. Asymptotically linear states are seen to correspond to specific axes in a three dimensional space. (9 refs.)

75256 Topological indices based on topological distances in molecular graphs. A.T. Balaban (Organic Chem. Dept., Polytech. of Bucharest, Bucharest, Rumania).

Pure & Appl. Chem. (GB), vol.55, no.2, p.199-206 (Feb. 1983). (International Symposium on Theoretical Organic Chemistry, Dubrovnik, Croatia, Yugoslavia, 30 Aug.-3 Sept. 1982).

Three new distance-based topological indices are described; two of them, D and D_1 (mean distance topological indices, for any graphs, and for acyclic graphs, respectively) have a modest discriminating ability but may be useful for correlations, e.g. with octane numbers. The third index, J (average distance sum connectivity) is the least degenerate single topological index proposed till now. The properties of this promising index J are discussed in more detail. (34 refs.)

Symmetry determined orbital and group overlapSee Entry 75274

Simultaneous relaxation of nuclear geometries and electric charge densities in electronic structure theoriesSee Entry 76822

Topological determinants in organic chemistrySee Entry 77873

31.15 GENERAL MATHEMATICAL AND COMPUTATIONAL DEVELOPMENTS

75257 Preparation of small atomic Gaussian basis sets for molecular calculations. J. Andzelm, E. Radzio-Andzelm, M. Klobukowski (Dept. of Chem., Univ. of Alberta, Edmonton, Alberta, Canada).

THEOCHEM (Netherlands), vol.11, no.1-2, p.197-9 (June 1983). The atomic basis sets developed by Pople and co-workers [1980] have been examined and compared with those obtained by the authors, using the same idea of transferring the valence parts of the basis from a larger basis set to a smaller one. In the authors' basis sets, denoted as $(K21/21)$, no common exponents for s and p valence PGF were assumed. The basis set parameters were optimized using the RHF method as described by Huzinaga and co-workers. (5 refs.)

75258 A possible resurrection of the ab initio maximum overlap (MOM) method. M.A. Whitehead, G.D. Zeiss (Dept. of Chem., McGill Univ., Montreal, Quebec, Canada).

Can. J. Chem. (Canada), vol.61, no.4, p.675-9 (April 1983).

A constrained variational theory is applied to the ab initio maximum overlap (MOM) method. The results for N_2 , HF, CO, and LiH, in which MOM wavefunctions satisfy constraints based on RHF, experimental or theoretical values, are discussed. The numerical results show that constraining the MOM wavefunctions with one or more constraints corrects the worst deficiencies in accuracy in the wavefunctions. (40 refs.)

75259 Integral evaluation algorithms and their implementation. D. Hegarty (Univ. of Groningen, Groningen, Netherlands), G. van der Velde.

Int. J. Quantum Chem. (USA), vol.23, no.4, p.1135-53 (April 1983).

Three different algorithms for the calculations of many center electron-repulsion integrals are discussed, all of which are considered to be economic in terms of the number of arithmetic operations. The common features of the algorithms are as follows: Cartesian Gaussian functions are used, integrals are calculated by blocks (a block being defined as the set of integrals obtainable from four given exponents on four given centers), and functions may be adopted to $R(3)$. Adaptation to molecular point group symmetry is not considered. Tables are given showing the minimum number of operations for a selection of block types allowing one to identify the theoretically most economic, and the corresponding salient features. Comments concerning the computer implementations are also given both on scalar and vector processors. In particular, the Cyber 205 is considered, a vector processor on which the authors have implemented what they believe to be the most efficient algorithm. (19 refs.)

75260 Rayleigh-Schrodinger perturbation theory for many-electron systems with partitioning of configurations by orders of excitation. W.J. Taylor (Dept. of Chem., Ohio State Univ., Columbus, OH, USA).

Int. J. Quantum Chem. (USA), vol.23, no.4, p.1653-65 (April 1983).

Rayleigh-Schrodinger perturbation theory for many-electron systems has been rederived by an extension of Lowdin's partitioning method in which excited configurations are further partitioned by their orders (two equivalent definitions of the order of a configuration are given). The resulting equations show explicitly how first-, second-, and third-order configurations contribute to the first three orders of perturbative corrections to the ground-state wave function, and the first six orders of corrections to the energy. Because the partitioning is by orders of configurations (rather than level, i.e. single, double, etc., excitations) the formalism is unaffected by the applicability, or nonapplicability, of Brillouin's theorem. (14 refs.)

75261 Chemical graph theory. IV. On the cyclic polynomial. J. Seibert, N. Trinajstić (Rugjer Boskovic Inst., Zagreb, Yugoslavia).

Int. J. Quantum Chem. (USA), vol.23, no.5, p.1829-41 (May 1983).

For pt.III, see Chem. Acta, vol.54, p.309 (1981). The definition of the cyclic polynomial of conjugated hydrocarbons is offered. The combinatorial characteristics of this polynomial are investigated. The most important property of the cyclic polynomial is that it can be used for enumeration of conjugated circuits. (30 refs.)

75262 The constrained variational formulation of energy functionals. P. Westhaus (Dept. of Phys., Oklahoma State Univ., Stillwater, OK, USA).

J. Chem. Phys. (USA), vol.78, no.11, p.6833-40 (1 June 1983).

Presents a generalization of the density functional formalism based upon constrained variations of the expectation value $\mathcal{E} = \langle \Psi | \hat{H} | \Psi \rangle$. The essential idea is to find the minimum value of \mathcal{E} with respect to a set of state vectors $S_a = \{ |\Psi_a\rangle \}$, each member of which yields the specified expectation values $q_i = \langle \Psi_a | \hat{A}_i | \Psi_a \rangle$ of set of observables \hat{A}_i , $i = 1 \dots M$. a denotes the collection of M expectation values q_i , $i = 1 \dots M$. If one or more N -electron vectors exist yielding the given M expectation values, a is said to be N representable. One thus obtains this minimum expectation value $E(a) = \min \mathcal{E}$ over S_a as a function of the assigned expectation values. In terms of the function $E(a)$, the exact ground state energy may be obtained by seeking its minimum value over all possible (N -representable) expectation values a . The traditional density functional formalism of Hohenberg and Kohn is seen to be a special case where the constraints are expressed by the expectation values of an indenumerable set of charge density operators, the members of which are indexed by the continuum of eigenvalues of the single particle position operator. The general ideas are illustrated by computing a function based upon constraining $(1/r)$ and $(1/r^2)$ for a one-electron atom. In this example, the formalism is carried out by solving a modified Schrodinger equation which includes Lagrange multipliers in order to take into account the constraints. The authors conclude, however, with an outline of how the unitary transformation formalism can be used to obtain the function $E(a)$ in a systematic fashion. (10 refs.)

75263 On the reliability of semi-empirical pseudopotentials: simulation of Hartree-Fock and Dirac-Fock results. P. Fuentealba, H. Stoll, L. von Szentpaly, P. Schwerdtfeger, H. Preuss (Inst. für Theoretische Chem., Univ. Stuttgart, Stuttgart, Germany).

J. Phys. B (GB), vol.16, no.11, p.L323-8 (14 June 1983).

Semi-empirical pseudopotentials can be modified in a simple way so as to reproduce frozen-core Hartree-Fock or Dirac-Fock results, respectively. The influence of relativistic effects is quantitatively discussed (i) for (r^4) expectation values and dipole polarisabilities of group IA and IB atoms, and (ii) for the bond lengths of K_2^+ and Cu_2 . (24 refs.)

75264 On the evaluation of the geometrical factors utilized in ligand polarization calculations. T. Meruane, R. Acevedo (Dept. of Chem. Engng., Univ. of Chile, Santiago, Chile).

Theor. Chim. Acta (Germany), vol.62, no.4, p.301-17 (1983).

Taking advantage of the irreducible tensor method put forward by T.S. Griffith (1962) in the case of molecular symmetry groups, both the molecular states and relevant operators can be classified in terms of irreducible representations of the molecular group in question, and therefore it is most convenient to express the relevant operators involved in any specific calculation in a symmetry adapted form. The authors deal with $d-d$ and $f-f$ type of transitions, and hence the 2^2 (electric quadrupole), 2^4 (electric hexadecapole) and the 2^6 -multipoles are considered in some detail. (14 refs.)

75265 Molecular orbital resonance theory: a new approach to the treatment of quantum chemical problems. T.P. Živković (Inst. 'Rudjer Boskovic', Zagreb, Yugoslavia).

Theor. Chim. Acta (Germany), vol.62, no.4, p.335-50 (1983).

An alternative approach to the treatment of the quantum chemical problems combining both, the MO and VB theory, is proposed. This approach retains the concept of resonance from the VB method, but it treats each particular bond in the MO sense. The method is illustrated with a few examples. Relative stabilities of benzene, pentalene and cyclobutadiene are derived. A Huckel $(4m+2)$ rule is derived for the annulenes. The charge polarisation in the case of the pentalene molecule is explained. A distortion of the pentalene molecule is considered and it is shown that within this approach the distortion depends on the charge polarisation. (23 refs.)

- Evaluation of GTO molecular integrals See Entry 75273
Computer generation of isomeric structures See Entry 75553

31.20 SPECIFIC CALCULATIONS AND RESULTS

- 75266** On the electronic structure of planar fluorinated amines and phosphines. D.S.Marynick (Dept. of Chem., Univ. of Texas, Arlington, TX, USA), D.C.Rosen, J.F.Liebman. *THEOCHEM (Netherlands)*, vol.11, no.1-2, p.47-50 (June 1983). The lowest closed-shell singlet state of planar PF_3 has recently been shown to have a highest occupied molecular orbital of a_1' symmetry, rather than the normally expected a_2'' symmetry found in planar NF_3 and related species. A simple orbital interaction diagram is presented to rationalize this unusual state. The effects of HOMO-LUMO mixing on the inversion barriers of NF_3 , NCl_3 , PF_3 , PCl_3 , and AsF_3 are also investigated, and it is found that such mixing significantly reduces the calculated inversion barriers for most of these species. (9 refs.)
- 75267** Stabilities of isomeric bromonium ions $\text{C}_2\text{H}_5\text{Br}^+$. R.A.Poirier (Phys. Sci. Div., Scarborough Coll., Univ. of Toronto, Toronto, Ontario, Canada), G.R.Demare, K.Yates, I.G.Csizmadia. *THEOCHEM (Netherlands)*, vol.11, no.1-2, p.137-41 (June 1983). Molecular orbital calculations are performed to determine the relative stability of the three isomeric or valence tautomeric structures of $\text{C}_2\text{H}_5\text{Br}^+$. A hydrogen bridged structure was also considered. (3 refs.)
- 75268** SCF and localized orbitals in ethylene: MBPT/CC results and comparison with one-million configuration CI. W.D.Laidig, G.D.Purvis, III, R.J.Bartlett (Univ. of Florida, Gainesville, FL, USA). *Chem. Phys. Lett. (Netherlands)*, vol.97, no.2, p.209-14 (13 May 1983). Many-body perturbation theory (MBPT) and coupled-cluster (CC) calculations are performed on the ethylene molecule employing canonical SCF and simple bond-orbital localized orbitals (LO). Full fourth-order MBPT [i.e. SDTQ MBPT(4)], CC doubles (CCD) and CC singles and doubles (CCSD) energies are compared with the over one-million configuration 'benchmark' CI calculation of Saxe et al. Though the SCF and LO reference determinant energies differ by 0.29706 hartree, the CCSD energy difference is only 1.7 mhartrees (mh). The authors' most extensive SCF orbital calculation, CCSD plus fourth-order triples, is found to be lower in energy than the CI result by 5.3 mh. (19 refs.)
- 75269** Molecular structure of orthosilicic acid and importance of (p-d) π bonding. An ab initio molecular orbital study. J.Saucer (Central Inst. of Phys. Chem., Acad. of Sci., Berlin, Germany). *Chem. Phys. Lett. (Netherlands)*, vol.97, no.3, p.275-8 (20 May 1983). OH and SiO bond lengths, the SiOH bond angle, favoured conformations of the protons and rotational barriers are obtained from 6-31G* calculations (assuming a tetrahedral SiO_4 structure). The role of d orbitals on silicon and/or oxygen atoms is assessed and the origin of the rotational barriers for silanol protons is discussed. (17 refs.)
- 75270** Ab initio study of structure and stability of the dimer $(\text{LiBeH}_2)_2$. Alternative configurations with mono- and bi-nuclear anions. L.P.Sukhanov, A.I.Boldyrev, O.P.Charkin (Inst. of New Chem. Problems, Acad. of Sci., Ghermogolovka, USSR). *Chem. Phys. Lett. (Netherlands)*, vol.97, no.4-5, p.373-7 (27 May 1983). The structure and stability of different configurations of the $(\text{LiBeH}_2)_2$ dimer are calculated within the Hartree-Fock-Roothaan method using STO-3G and double-zeta basis sets. The structure with a diboron-like anion $[\text{Be}_2\text{H}_2]^{2-}$ and two bridge Li^+ cations is favoured. The four nearest configurations are ≈ 10 -15 kcal/mole higher. A possible intramolecular rearrangement is discussed. (21 refs.)
- 75271** An improved two parameter omega technique for molecular orbital calculations. VI. Calculations on methyl substituted polycyclic aromatic hydrocarbons. H.O.Villar, E.A.Castro, F.M.Fernandez (Inst. de Investigaciones Fisicoquimicas Teoricas y Aplicadas, La Plata, Argentina). *Chem. Scr. (Sweden)*, vol.22, no.1, p.49-50 (1983). The improved two parameter omega technique is applied to calculate the pi-delocalization energies of the nearest positions to a single substrate ring fusion site in various polycyclic aromatic hydrocarbons. The PMO approximation is used and results are correlated with carcinogenic activity. Improvements with respect to simple Hückel results are noted. (12 refs.)
- 75272** Energy-band structure and charge distribution for BaC_6 . N.A.W.Holzwarth (Corporate Res.-Sci. Labs., Exxon Res. & Engng. Co., Linden, NJ, USA), D.P.Divincenzo, R.C.Tatar, S.Rabii. *Int. J. Quantum Chem. (USA)*, vol.23, no.4, p.1223-30 (April 1983). An ab initio self-consistent calculation has been carried out for the electronic properties of BaC_6 . Energy bands and charge densities are presented for BaC_6 and compared with those of LiC_6 . The results show that the band originating from Ba states has a mixture of s and d character and the d component hybridizes appreciably with the π bands of graphite. The Fermi level intersects this band as well as the graphite π bands, giving rise to a complicated Fermi surface with several types of carriers. Depending on the type of volumetric partitioning, the charge transfer from Ba to graphite layers is determined to be between 0.7 and 1.0 electron per Ba atom. The calculated results are consistent with available transport and optical measurements. (14 refs.)
- 75273** Evaluation of GTO molecular integrals. F.E.Harris (Dept. of Phys., Univ. of Utah, Salt Lake City, UT, USA). *Int. J. Quantum Chem. (USA)*, vol.23, no.4, p.1469-78 (April 1983). Methods for evaluating the function $F_m(r)$ occurring in molecular integrals over Gaussian-type orbitals are reviewed and extended. Formulas based on Bessel function and continued-fraction expansions are analyzed. The recommended evaluation procedures, embodied in a portable computer program, involve Pade approximations for various argument intervals and use recursion in m . The program is economical in storage requirements and faster than those in current use. (14 refs.)
- 75274** Symmetry determined orbital and group overlap. Z.Qianer (Dept. of Chem., Xiamen Univ., Xiamen, China). *Int. J. Quantum Chem. (USA)*, vol.23, no.4, p.1479-92 (April 1983). The MO theory of structural polyhedrons is one of the basic subjects closely related to the bonding theory of complex compounds and clusters. A series of valuable papers on this subject have been contributed by Hoffman (1977), Wade (1976), King (1977) and Lauher et al. (1977). A method called 'group overlap method' for constructing the symmetry orbitals and for calculating the group overlap integrals is proposed. It is hoped that the group overlap method may be used for the qualitative and quantitative MO study of structural polyhedrons. (13 refs.)
- 75275** Quantum chemical structure-activity relationships on β -carbolines as natural monoamine oxidase inhibitors. M.Martin, F.Sanz, M.Campillo, L.Pardo, J.Perez, J.Turmo (Dept. Bioestadística, Univ. Autónoma de Barcelona, Barcelona, Spain), J.M.Aullo. *Int. J. Quantum Chem. (USA)*, vol.23, no.4, p.1643-52 (April 1983). The electron density and the molecular electrostatic potential of the β -carbolines are studied using ab initio STO-3G wave functions. The analysis was done from the point of view of a previous model built with monoamine oxidase substrates and irreversible inhibitors. The results confirm the usefulness of the model and make it possible to propose new precision to the molecular electrostatic potential patterns needed to have monoamine oxidase inhibitory activity. (10 refs.)
- 75276** One-electron properties at the SCF ab initio level. G.De Brouckere (Van Der Waals Lab., Univ. of Amsterdam, Amsterdam, Netherlands). *Int. J. Quantum Chem. (USA)*, vol.23, no.4, p.1677 (April 1983). Summary form only given. The extent to which the Hartree-Fock single configuration model is capable of predicting the expectation values of a broad variety of one-electron observables measured in a wide range of organic molecules involving first and second row atoms is explored. An answer to this problem has been obtained through extended basis set calculations (p-type and d-type polarization functions used) of definite one-electron observables: electric dipole, and quadrupole moments, diamagnetic susceptibilities, second moment charge distribution anisotropies, ionization potential, nuclear (^{14}N , ^{17}O , ^{33}S) quadrupole coupling constants and deuteron coupling constants. (4 refs.)
- 75277** Ab initio MO calculations of benzene+TCNE and naphthalene+TCNE complexes with STO-3G π -split basis set. Y.Watanabe (Dept. of Chem., Faculty of Sci., Osaka City Univ., Osaka, Japan), H.Kashiwagi. *Int. J. Quantum Chem. (USA)*, vol.23, no.5, p.1339-52 (May 1983). Ab initio SCF MO calculations have been carried out on benzene+TCNE (tetracyanoethylene) and naphthalene+TCNE complexes with the STO-3G, STO-3G π -split (STO-3G for σ orbitals and a split basis for π orbitals), and 4-31G basis sets. The interaction energy, gross charges, dipole moment, and the electron density in the middle plane of the complexes have also been evaluated. The STO-3G π -split basis set is appropriate for the calculation of large π - π stacking complexes from two points of view, production of reliable results and ease of computations. The approximation scheme based on the semiorthogonalized orbitals is revealed to be very efficient to save CPU time and storage in such calculations. The stable conformation and the charge-transfer interaction of the two complexes are discussed on the basis of the calculated quantities. (16 refs.)
- 75278** Applicability of non-degenerate many-body perturbation theory to quasidegenerate electronic states: a model study. S.Wilson (Dept. of Theoretical Chem., Univ. of Oxford, Oxford, England), K.Jankowski, J.Paldus. *Int. J. Quantum Chem. (USA)*, vol.23, no.5, p.1781-802 (May 1983). The nondegenerate finite-order many-body perturbation theory is applied to simple model systems in which the degree of quasidegeneracy can be continuously varied over a wide range. Three ab initio minimum basis set models involving four hydrogen atoms in various spatial arrangements are considered. The results are compared with the exact full configuration-interaction approach, double-excitation configuration-interaction and the coupled-pair many-electron theory. (56 refs.)
- 75279** Ab initio calculation of the $X^1\Sigma^+$ state of CsH . B.C.Laskowski (Analatom Inc., Sunnyvale, CA, USA), S.P.Walch, P.A.Christiansen. *J. Chem. Phys. (USA)*, vol.78, no.11, p.6824-32 (1 June 1983). Relativistic effective core potential (RECP) and nonrelativistic all electron (NRAE) calculations are reported for the $X^1\Sigma^+$ state of CsH . The calculations are based on GVB plus single and double excitation CI wave functions with the $\text{Cs}(5s, 5p)$ as well as the two valence electrons correlated. The bonding in CsH is found to involve a $\text{Cs}(6s)\text{-H}(1s)$ bond but with a significant ionic (Cs^+H^-) component. Correlating the $\text{Cs}(5s, 5p)$ electrons leads to a significant bond shortening effect ($\sim 0.15a_0$). The effect is attributed to a contraction of the $\text{Cs}(6s)$ orbital and a shift toward higher energy of the Cs^+H^- asymptote upon correlating the $5s, 5p$ shell. Bond shortening due to relativistic contraction of the $\text{Cs}(6s)$ is only $\sim 0.05a_0$ in agreement with the small amount of $\text{Cs}(6s)$ character in the ionic bond orbital. The NRAE and RECP potential curves are very similar except for the shorter R_e for the RECP case (due to relativistic bond contraction). (26 refs.)
- 75280** Hyperfine structure in 6snd Rydberg configurations in barium. E.R.Eliel, W.Hogervorst (Natuurkundig Lab., Vrije Univ., Amsterdam, Netherlands). *J. Phys. B (GB)*, vol.16, no.11, p.1881-93 (14 June 1983). The hyperfine structure of the 6snd Rydberg configurations of barium has been investigated using a two-step excitation process and an atomic beam. Accurate hyperfine energies have been obtained on both the ^1D and ^3D levels, which are analysed in terms of singlet-triplet mixing. The mixing coefficients extracted for the $^1\text{D}_2$ and $^3\text{D}_2$ levels are shown to be internally consistent, to agree with known Landé factors and can well be predicted with existing multichannel quantum defect analyses. Finally the asymptotic behaviour of the singlet-triplet mixing coefficient is discussed in the framework of simple atomic theory. (26 refs.)
- 75281** Characteristic and matching polynomials of benzenoid hydrocarbons. I.Gutman (Faculty of Sci., Univ. of Kragujevac, Kragujevac, Yugoslavia). *J. Chem. Soc. Faraday Trans. II (GB)*, vol.79, pt.3, p.337-45 (March 1983). The characteristic and matching polynomials of the molecular graph of a benzenoid hydrocarbon are examined and a number of results proved for their coefficients. These results are then applied to the theory of topological resonance energy (TRE). It is demonstrated that all benzenoid hydrocarbons have positive TRE values and that the TRE model leads to absurd results in the case of polycyclic benzenoid systems. (10 refs.)
- 75282** Bicyclo(6.2.0)decapentaene [Molecular mechanics calculations]. N.L.Allinger, Y.H.Yuh (Dept. of Chem., Univ. of Georgia, Athens, GA, USA). *Pure & Appl. Chem. (GB)*, vol.55, no.2, p.191-7 (Feb. 1983). (International Symposium on Theoretical Organic Chemistry, Dubrovnik, Croatia, Yugoslavia, 30 Aug.-3 Sept. 1982). Molecular mechanics calculations (MMP2) on the title compound and related molecules, cyclobutadiene, cyclodecapentaene and others are described. Heats of formation, resonance energies and molecular structures were obtained, and where experimental comparisons are possible, the agreement is good. (19 refs.)

75283 On the role of Kekule valence structures. M.Randic (Dept. of Math. & Computer Sci., Drake Univ., Des Moines, IA, USA). *Pure & Appl. Chem. (GB)*, vol.55, no.2, p.347-54 (Feb. 1983). (International Symposium on Theoretical Organic Chemistry, Dubrovnik, Croatia, Yugoslavia, 30 Aug.-3 Sept. 1982).

Individual Kekule valence structures of conjugated hydrocarbons are examined and the relative role of the opposing 'aromatic' and 'antiaromatic' contributions scrutinized. The work follows previously proposed classifications of conjugated systems based on the enumeration of $4n+2$ and $4n$ conjugated circuits. In the present work attention is drawn to molecular formulae obtained by a partial superposition of selected Kekule valence structures and the situations in which they may play the dominant role and represent molecules adequately. (18 refs.)

75284 Relativistic atomic level calculations with nuclei carrying additional fractional charges. K.Rashid (Nuclear Phys. Div., Pakistan Inst. of Nuclear Sci. & Technol., Rawalpindi, Pakistan), B.Fricke. *Z. Phys. A (Germany)*, vol.311, no.4, p.283-7 (1983).

One-electron energy levels and wavelengths have been calculated for Na-like ions whose nuclei carry quarks with additional charges $\pm e/3$, $\pm 2e/3$. The calculations are based on relativistic self-consistent field procedures. The deviations from experimental values exhibit regularities which allow an extrapolation for the wavelengths of $3s-3p$, $3s-4p$, $3p-3d$, and $3p-4s$ transitions for the nuclear charge $Z=11\pm 1/3$, $\pm 2/3$. A number of transitions are found in the region of visible light which could be used in an optical search for quark atoms. (7 refs.)

Chemical graph theory. IV. On the cyclic polynomial See Entry 75261

Calculation of the diamagnetic shielding of the nuclei by the point-charge approximation See Entry 75320

Charge transfer transition for symmetry-forbidden charge transfer interaction. Theory and experimental verification See Entry 75325

Spectra of the ironlike ions from YXIV to Ag XXII See Entry 75338

Minima and maxima in the generalized oscillator strengths for the lithium isoelectronic sequence See Entry 75344

Microwave spectrum, dipole moment and ab initio molecular structure of 2-aminopropenenitrile ($\text{CH}_2=\text{C}(\text{NH}_2)\text{CN}$) See Entry 75368

The importance of the localization of the π -electron system on its ability to transmit the Fermi contact term of H-H coupling constants. A theoretical and experimental study See Entry 75403

The mechanism of carbonyl reduction by LiBH_4 : an ab initio investigation with inclusion of solvent effects See Entry 77867

Quantum chemical study of the molecular patterns of MAO inhibitors and substrates See Entry 78135

31.20E Ab initio LCAO and GO SCF calculations

75285 Charge, bond order and valence in the ab initio SCF theory. I.Mayer (Central Res. Inst. for Chem., Acad. of Sci., Budapest, Hungary). *Chem. Phys. Lett. (Netherlands)*, vol.97, no.3, p.270-4 (20 May 1983).

An operator of atomic charge is introduced, the expectation values of which are Mulliken's gross atomic populations on the individual atoms. Suitable definitions of the bond order (multiplicity) index and of the valence number of an atom in a molecule are also proposed for the SCF LCAO MO method. (The results apply also in the extended Hückel method). (6 refs.)

75286 Electronic structure of small copper clusters. E.Miyoshi (Fukuoka Dental Coll., Fukuoka, Japan), H.Tatewaki, T.Nakamura.

Int. J. Quantum Chem. (USA), vol.23, no.4, p.1201-7 (April 1983).

An all-electron ab initio LCAO-MO SCF calculation has been carried out for the electronic structure of small copper clusters (Cu_n , $n=2-6$). The basis set superposition error occurring in the calculation, the equilibrium configuration of Cu_3 , the bond energy in the clusters, and the localized d -hole in excited and ionized states of Cu_2 are closely examined. (14 refs.)

75287 Three-body nonadditive effects for hydrogen bonded water molecules: SCF study of hydrated species including H_2S and various metal ions. O.Novaro (Inst. de Física, Univ. Nacional Autónoma de México, México City, México).

Int. J. Quantum Chem. (USA), vol.23, no.4, p.1611-25 (April 1983).

The relative importance of purely nonadditive three-body terms in solvated systems is assessed through ab initio LCAO-MO-SCF studies of hydrogen bonded structures containing two or more water molecules plus a solvate species. Among the latter the cases of Li^+ , Ca^{2+} , and Mg^{2+} ions (of biological interest for aminoacid release processes in membrane transport) and of HDS molecules (of industrial importance in processes for the production of heavy water) are studied. (25 refs.)

75288 Theoretical study of degree of covalency in some $\text{CoF}_6^{(n-)} \text{ complexes}$ ($n=4,3$, and 2). E.Miyoshi, S.Obata, T.Takada, H.Kashiwagi, K.Ohno (Dept. of Chem., Faculty of Sci., Hokkaido Univ., Sapporo, Japan).

Int. J. Quantum Chem. (USA), vol.23, no.5, p.1753-65 (May 1983).

On the basis of a high-quality LCAO MO SCF calculation, covalency versus ionicity of a Co-F bond in the $\text{CoF}_6^{(n-)} \text{ complexes}$, where $n=4,3$, and 2, is discussed. The overlap and gross atomic populations, delocalization of certain MOS, and the charge densities in the bond region as well as around Fs all indicate that the covalency increases as n decreases or the valency of Co increases in these complexes. (12 refs.)

31.20G Other accurate, or nearly ab initio calculations (DIM method, SAMO method, etc.)

75289 Relativistic MS $X\alpha$ calculations of the electronic structure and related properties of PtCl_6^{2-} . A.Goursot, E.Penigault (Lab. de Photochimie Generale, Ecole Nat. Supérieure de Chimie de Mulhouse, Mulhouse, France), H.Chermette.

Chem. Phys. Lett. (Netherlands), vol.97, no.2, p.215-20 (13 May 1983).

Relativistic MS $X\alpha$ calculations have been performed on a PtCl_6^{2-} cluster in O_h symmetry. The electronic structure is discussed and compared with the electronic structure obtained recently for IrCl_6^{3-} . The theoretical photoionization and optical spectra are in very good agreement with experiment. (25 refs.)

75290 Revisit to the electron density, bond order, and aromaticity. H.Hosoya, M.Shobu, K.Takano, Y.Fujii (Dept. of Chem., Ochanomizu Univ., Tokyo, Japan).

Pure & Appl. Chem. (GB), vol.55, no.2, p.269-76 (Feb. 1983). (International Symposium on Theoretical Organic Chemistry, Dubrovnik, Croatia, Yugoslavia, 30 Aug.-3 Sept. 1982).

Spatial distribution of electrons in a molecule is analyzed by several different approaches, i.e., MO, VB, and graph-theoretical methods. Quantum chemical

interpretation of the concept of the oxidation number was obtained by ab initio MO calculation. The concepts of the local structure character and partial electron density are proposed and discussed. (42 refs.)

The Cooper minimum in Cl_2 See Entry 75446

31.20N Semi-empirical NDO calculations (CNDO, INDO, MINDO, PCILO methods, etc.)

75291 Dipole moments of fluorobenzenes by CNDO and INDO methods. S.Doraiswamy (Chem. Phys. Group, Tata Inst. of Fundamental Res., Bombay, India), S.D.Sharma.

THEOCHEM (Netherlands), vol.11, no.1-2, p.63-71 (June 1983).

The dipole moments of fluorobenzenes are evaluated by CNDO/2 and INDO molecular orbital calculations from reasonably assumed geometries. The results are compared with experimentally obtained values. It is found that both methods overestimate the dipole moments, the overestimation being more for INDO calculations. The disparity between the observed and calculated values of dipole moments increases with the addition of fluorines. To a good approximation, the charge densities at different positions in monofluorobenzene are sufficient to generate the electronic distribution pattern in higher members of the series. (20 refs.)

75292 Theoretical investigations of the interaction of but-2-ene with a sodium ion. R.Lochmann, W.Meiler, Th.Weller (Sektion Phys., Karl-Marx-Universität, Leipzig, Germany).

THEOCHEM (Netherlands), vol.11, no.1-2, p.73-7 (June 1983).

Investigation of the conformational behaviour of but-2-ene (cis and trans) and the interaction with a sodium ion is carried out by ab initio STO-3G, CNDO/2, and PCILO methods. Unlike the semiempirical results, the ab initio calculations predict that the isolated trans conformer is more stable than the cis form, in agreement with experimental data. All methods indicate a nearly free methyl group rotation. The interaction energy of a but-2-ene molecule with a sodium ion calculated by these methods shows different minima corresponding to different stable arrangements of the sodium ion in the but-2-ene/ Na^+ complex. In contrast to isobutene and but-1-ene, electrostatic effects are not important. An arrangement with the cation above the double bond seems to be most favoured owing to the dominating transfer interaction. (17 refs.)

75293 A theoretical study of the structure, charge distribution and gas-phase basicity of 1H-indazole and its N -methyl derivatives. J.Catalan, O.Mo, P.Perez, M.Yanez (Dept. de Química Física y Química Cuántica, Univ. Autónoma de Madrid, Madrid, Spain).

THEOCHEM (Netherlands), vol.11, no.1-2, p.143-53 (June 1983).

The authors have done ab initio calculations, using an STO-3G minimal basis set, for 1H-indazole and its N -methyl derivatives, to illustrate that important structural differences exist between the two tautomers and that appreciable geometrical changes take place upon methyl substitution. Theoretical geometries, fully optimized at INDO level, are reported. The variations observed in the structures of the two tautomers are explained in terms of σ -valence-shell electron-pair repulsions and of changes in the π -densities of the HOMOs of these compounds. It was also found that the tricoordinated nitrogen atom in 2-methylindazole (N_2) is a much stronger π -donor center than N_1 in the 1-methyl derivative, explaining some of the properties of these species. The calculated PAs indicate that these compounds are nitrogen bases and that the 2-methyl derivative is a much stronger base than the 1-methyl analog. The authors' calculated charge densities reproduce well the most important features of the ^{13}C and ^{14}N NMR spectra of these molecules. (30 refs.)

75294 On the stability of [furan] $^+$ and [vinylketene] $^+$. E.Canadell, J.P.Sarasa (Facultat de Química, Univ. de Barcelona, Tarragona, Spain).

THEOCHEM (Netherlands), vol.11, no.1-2, p.193-5 (June 1983).

Both the furan and the vinylketene structures have been proposed for the nonfragmenting $[\text{C}_4\text{H}_4\text{O}]^+$ ions generated by loss of CO from 2- and 4-pyrone molecular ions. Holmes and Terlouw [1979] reported on the thermochemistry of the neutral and ionic structures and concluded that [vinylketene] $^+$ was more stable than [furan] $^+$ by 3 kcal mol $^{-1}$. As part of a general theoretical study of the $[\text{C}_4\text{H}_4\text{O}]^+$ potential energy surface, the authors present some evidence in favor of the thermochemical estimation. The calculations reported are of the MINDO/3 type and the geometries were determined by minimization of the energy with respect to all the geometrical variables. (5 refs.)

75295 Conformational and MO studies of hydroxy-2-aminotetralins. D.Kocjan, T.Solmajer, M.Hodoscek, D.Hadzi (LED-Chem. & Pharmaceutical Works, Ljubljana, Yugoslavia).

Int. J. Quantum Chem. (USA), vol.23, no.4, p.1121-33 (April 1983).

Attempting to explain the differences in the pharmacological profiles of the isomeric monohydroxy- and dihydroxy-2-aminotetralins (DHAT) which are potent dopaminergic agonists the authors have calculated the conformational energies of 2-aminotetralin and its N,N -dipropyl derivative using the QCFF/PI and PCILO methods. Molecular electrostatic potential (MEP) maps based on ab initio (STO-3G) wave functions were computed for both dihydroxytetralins. Root-mean-square (RMS) deviations from steric congruence between the enantiomeric 5,6- and 6,7-DHAT based either on atomic centers or on the minima in MEP near the putative points of attachment to the receptor are small, but may nevertheless be sufficient to cause differences in activity on subtypes of the dopamine receptor. N,N -dipropyl substitution influences of conformational energies of the skeleton and the preferences in the orientation of the propyl groups in the isomeric DHAT may be important for the interaction with the receptor. The HOMO energies of the isomeric HAT and DHAT do not correlate with their potencies. (30 refs.)

75296 INDO studies on the electronic structure of lanthanoid compounds. Li Le-min, Ren Jing-ong, Xu Guang-xian, Wang Xiu-zhen (Dept. of Chem., Peking Univ., Beijing, China).

Int. J. Quantum Chem. (USA), vol.23, no.4, p.1305-16 (April 1983).

Expressions needed in INDO calculations for compounds containing 4f elements were derived and an INDO program suitable for lanthanoid compounds was written and tested. Electronic structure of LnF_3 and paramagnetic shift of NMR spectra of LnF_6^{3-} were studied. (24 refs.)

75297 Conformational studies of the $\beta(1\rightarrow3)$ linked disaccharide component of the immunologically active pentasaccharide of the Forssman antigen. J.S.Yadav, P.Luger (Inst. of Crystallography, Free Univ. Berlin, Berlin, Germany).

Int. J. Quantum Chem. (USA), vol.23, no.4, p.1433-9 (April 1983).

Conformational energy calculations of the PCILO level of approximation were performed on $\beta(1\rightarrow3)$ linked disaccharide consisting of N -acetylglucosamine and galactose of the Forssman antigen to examine the side group conformations and their influence on the mutual orientations of the two pyranosyl rings. Two low energy regions for the glycosidic bond conformations have been located in the grid search using classical potential functions. The PCILO

energy minimizations were then carried out in each of these regions. The preferred orientations of the nonreducing pyranosyl ring relative to the reducing ring were found to be in agreement with the available X-ray results. Moreover, the orientations of groups attached to the anomeric carbons were in good accordance with the requirements of the *exo*-anomeric effect. (13 refs.)

75298 Quantum chemical studies on the conformational structure of bacterial peptidoglycan. V. PCILO calculations on $\beta(1\rightarrow4)$ linked disaccharide of N-acetylglucosamine and N-acetyl muramic acid. J.S.Yadav (Inst. of Crystallography, Free Univ. Berlin, Berlin, Germany). *Int. J. Quantum Chem. (USA)*, vol.23, no.4, p.1441-50 (April 1983). For pt.IB see J. Theor Biol., vol.95, p.285 (1982). The glycan moiety of the bacterial peptidoglycan consists of alternatingly $\beta(1\rightarrow4)$ linked disaccharides of N-acetylglucosamine (NAG) and its 3-O-D lactic derivative, N-acetyl β -D-muramic acid (NAM). PCILO conformational energy calculations have been carried out for NAG-NAM and NAM-NAG disaccharides to see whether or not the glycan strands possess a chitinlike structure as suggested by earlier workers. In agreement with recent experimental findings, the present results also suggest that the chitinlike structure is energetically disallowed. Furthermore, the bulky N-acetyl substituents at C₂ positions of the two sugar molecules are found to be relatively less important in stabilizing mutual orientations of the two pyranosyl rings. (12 refs.)

75299 Ab initio MODPOT/VRDDO/MERGE calculations on energetic compounds. III. Nitroexplosives: polyanilinopolynitrobenzenes (including DATB, TATB, and Tetryl). P.C.Hariharan, W.S.Koski, J.J.Kaufman. *Int. J. Quantum Chem. (USA)*, vol.23, no.4, p.1493-504 (April 1983). Quantum chemical ab initio MODPOT/VRDDO calculations have been carried out on the following aminonitrobenzenes for which crystal structures had been determined experimentally: 4-nitroaniline; N,N-dimethyl-p-nitroaniline; 2,4,6-trinitroaniline; 1,3-diamino-2,4,6-trinitrobenzene (DATB-Form I); 1,3,5-triamino-2,4,6-trinitrobenzene (TATB); 2,3,4,6-tetranitroaniline; N-methyl-N,2,4,6-tetranitroaniline (Tetryl); and N-(β,β -trifluoroethyl)-N,2,4,5-tetranitrobenzene. These quantum chemical calculations were performed on the molecules in their conformations as found in their crystal structures. The calculations were carried out with ab initio programs which also incorporate as options several desirable features for calculations on large molecules: ab initio effective core model potentials (MODPOT) which enable calculations of valence electrons only explicitly, yet accurately, and a charge conserving integral prescreening evaluation (named VRDDO-variable retention of diatomic differential overlap) especially effective for spatially extended molecules. Aminonitrobenzenes are especially interesting since there are inherent intramolecular ring distortions and deviations from planarity and intramolecular hydrogen bonds as well as intermolecular hydrogen bonds causing further deviations from planarity. The theoretical indices resulting from the quantum chemical calculations are relevant to a number of properties and behavior characteristics of these molecules, both intramolecular and intermolecular. (29 refs.)

75300 Molecular orbital study of the relationship between the electronic structure and toxicity of silatranes. Liu Ruo-Zhuang, Zheng Shi-Jin, Yu Jian-Guo (Dept. of Chem., Beijing Normal Univ., Beijing, China). *Int. J. Quantum Chem. (USA)*, vol.23, no.4, p.1609-10 (April 1983). Silatranes are a class of heterocyclic derivatives of 5-coordinate silicon with general formula $\text{XSi}(\text{OCH}_2\text{CH}_2)_3\text{N}$. They are characterized by the unusual valency of the silicon atom and toxicity. The toxicity of this series of compounds varies mainly with the nature of the substituents at the silicon atom. The authors study the relationship between the electronic structure and toxicity of silatranes using semiempirical SCF MO calculations using the CNDO/2 method. (5 refs.)

75301 Calculation of excited-state properties of some small molecules: comparative study of the CNDO/S and CNDO/2- V_{N-1} potential methods. A.B.Sannigrahi (Dept. of Chem., India Inst. of Technol., Kharagpur, India), D.C.Mukherjee, B.R.De.

Int. J. Quantum Chem. (USA), vol.23, no.5, p.1695-705 (May 1983). The transition energy and geometry of the lowest excited ($\pi\pi^*$) singlet and triplet states of CO, CS, HNO, H₂CO, HFCO, and F₂CO molecules are calculated by CNDO/S and CNDO/2- V_{N-1} potential methods, and the results are compared with those of experimental and ab initio theoretical studies, wherever available. In the calculation of the vertical transition energy, the performance of the CNDO/S method is seen to be generally more satisfactory than that of the CNDO/2- V_{N-1} potential method, while the reverse is true for the excited-state geometry. The CNDO/S method as such fails to describe the geometry of the excited state, but a combined version (CNDO/S-2) of CNDO/S and CNDO/2, as well as the CNDO/2- V_{N-1} potential method is fairly successful in this regard. (40 refs.)

Force field for in-plane vibrations of trans-cis-diacetamide. Use of CNDO/Force method See Entry 75356

Electronic spectra and excited state dipole moments of heterocyclic pentaatomic systems and their benzo and dibenzo derivatives See Entry 75398

A MINDO/3 approach to the chemisorption of hydrogen on graphite See Entry 76769

A MINDO/3 approach to the chemisorption on graphite of electrophilic adsorbates See Entry 76770

CNDO/S parameters of C, O, and Si for solid state calculations See Entry 76839

A comparison of various MO methods for predicting regioselectivity in Diels-Alder reactions See Entry 77863

Catalytic effect on the selectivity of the Diels-Alder reaction See Entry 77869

Structure-activity relationship and the mechanism of analgesia of the analgesic drug 3-methyl-fentanyl and its analogs See Entry 78134

31.20P Other semi-empirical calculations (Hückel, generalized Hückel, PPP methods, etc.)

75302 Evaluation of HOMO-LUMO separation and homologous linearity of conjugated molecules. Yuan-sun Kiang, Er-ting Chen (Inst. of Theoretical Chem., Jilin Univ., Changchun, China). *Pure & Appl. Chem. (GB)*, vol.55, no.2, p.283-8 (Feb. 1983). (International Symposium on Theoretical Organic Chemistry, Dubrovnik, Croatia, Yugoslavia, 30 Aug.-3 Sept. 1982).

A variational method for calculating the HOMO and LUMO energies in the framework of Hückel theory is proposed. Graphical technique is employed for the evaluation of inverse adjacency matrix and collection of Dewar numbers is selected as a trial vector. Closed formulae for a few homologous series of conjugated hydrocarbons are deduced, which offer approximate HOMO (or LUMO) values with an average deviation less than 0.003. These formulae can

be used as 'homologous linearity' functions for rationalizing some of physico-chemical behaviours of conjugated homologs. (14 refs.)

A comparison of various MO methods for predicting regioselectivity in Diels-Alder reactions See Entry 77863

31.20R Valence bond calculations (ab initio or not)

75303 Applications of molecular orbital-valence bond theory in chemistry. N.D.Epiotis (Dept. of Chem., Univ. of Washington, Seattle, WA, USA). *Pure & Appl. Chem. (GB)*, vol.55, no.2, p.299-306 (Feb. 1983). (International Symposium on Theoretical Organic Chemistry, Dubrovnik, Croatia, Yugoslavia, 30 Aug.-3 Sept. 1982).

According to molecular orbital-valence bond (MOVB) theory, ground state organic molecules can be viewed as the result of 'forbidden' union of two fragments. Consequently, the stability of a molecule is a function of the fragment excitation requirement for its formation and chemical stereoselection a manifestation of fragment excitation reduction. The π electronic structure of benzene and the conformational isomerism of N₂H₄ and its derivatives are two simple illustrators of how and why MOVB theory has revolutionized the thinking about the structure and reactivity of molecules. (7 refs.)

75304 Valence bond theory for conjugated hydrocarbons. D.J.Klein (Dept. of Marine Sci., Texas A&M Univ., Galveston, TX, USA). *Pure & Appl. Chem. (GB)*, vol.55, no.2, p.299-306 (Feb. 1983). (International Symposium on Theoretical Organic Chemistry, Dubrovnik, Croatia, Yugoslavia, 30 Aug.-3 Sept. 1982).

Semiempirical valence bond theory for conjugated π -electron systems is reconsidered, with special attention being directed to common criticisms of the theory. Especially in light of recent results, flaws in the criticisms are revealed. (69 refs.)

Molecular orbital resonance theory: a new approach to the treatment of quantum chemical problems See Entry 75265

Revisit to the electron density, bond order, and aromaticity See Entry 75290

31.20T Electron correlation and CI calculations

75305 The dissociation energy of Cu₂: do we want to perform multi-reference singles and doubles CI's on many-electron systems? C.W.Bauschlicher, Jr. (NASA Ames Res. Center, Moffett Field, CA, USA). *Chem. Phys. Lett. (Netherlands)*, vol.97, no.2, p.204-8 (13 May 1983).

SDCI and restricted POLCI calculations are reported for Cu₂ using a CAS SCF reference space with the 4s and 4p orbitals defined as active. D₀ at the POLCI level is substantially better than for SDCI. The difference is attributed to size-consistency problems associated with including the 3d correlation in SDCI. A modification to either standard POLCI or SDCI is suggested. (18 refs.)

75306 Nature and location of excited charge-transfer states in the porphine-magnesium porphine dimer. J.D.Petke, G.M.Maggiora (Dept. of Chem., Univ. of Kansas, Lawrence, US, USA). *Chem. Phys. Lett. (Netherlands)*, vol.97, no.2, p.231-5 (13 May 1983).

The ground and excited states of a cofacial porphine-magnesium porphine dimer with a ring separation of 5.35 Å are investigated by ab initio configuration interaction calculations, using a floating Gaussian basis. A pair of charge-transfer states are found $\approx 23000\text{ cm}^{-1}$ above the ground state, but are lowered by $\approx 7400\text{ cm}^{-1}$ upon coordination of the Mg atom with chloride ion. (12 refs.)

75307 CNDO calculations of halogen-substituted diformamides. G.Ramana Rao, V.Venkata Chalapathi (Dept. of Phys., Univ. Coll., Kakatiya Univ., Warangal, India).

Indian J. Pure & Appl. Phys., vol.21, no.3, p.188-9 (March 1983). CNDO/2 calculations are made for diformamide C-fluorodiformamide and C-chlorodiformamide in trans-trans, trans-cis and cis-cis configurations. The charges, bond orders and dipole moments are discussed. (10 refs.)

75308 Electron correlation in linear hydrogen chains. J.G.Fripiat, J.Dehalle, J.M.Andre (Lab. de Chimie Theorique Appliquee, Facultes Univ. N.D. de la Paix, Namur, Belgium).

Int. J. Quantum Chem. (USA), vol.23, no.4, p.1179-89 (April 1983). The Moller-Plesset perturbation technique and configuration interaction methods are applied to linear chains of hydrogens in order to analyze the role of electron correlation on equilibrium geometries and binding energies of these systems. (17 refs.)

75309 Coordinate rotation studies of H⁻, He⁻, Be⁻, Mg⁻ resonances: basis set and configuration list dependence. D.T.Chuljian, J.Simons (Chem Dept., Univ. of Utah, Salt Lake City, UT, USA).

Int. J. Quantum Chem. (USA), vol.23, no.5, p.1723-38 (May 1983). The authors have performed coordinate rotated configuration interaction calculations on well-studied Feshbach resonances of H⁻ and He⁻ and on ²P shape resonances of Be⁻ and Mg⁻. The focus of the authors effort was the dependence of computed resonance energies on both the quality of the atomic-orbital basis and the level of treatment of electron correlation. Their results indicate that great care must be taken to guarantee that a basis is adequate; commonly used quantum-chemistry bases are probably far from satisfactory. Their findings also indicate that a proper treatment of inner-shell orbitals within coordinate rotation calculations is a formidable task. The authors are therefore encouraged to look carefully for modified coordinate rotation techniques that focus on the active valence-level orbitals and may avoid spurious complex energies arising from improper treatment of inner shells. (17 refs.)

75310 Electronic correlation contribution to the three-body potentials for water trimers. P.Habitz, P.Bagus, P.Siegbahn, E.Clementi (IBM Corp., Poughkeepsie, NY, USA).

Int. J. Quantum Chem. (USA), vol.23, no.5, p.1803-6 (May 1983). A number of trimers of water molecules have been computed with an extended basis set in the Hartree-Fock and in the direct CI approximations. It has been verified that the three-body interaction energy can be calculated within the Hartree-Fock method. Therefore, the correlation corrections to the Hartree-Fock level are essentially additive and do not contribute significantly to three-body effects. (26 refs.)

75311 Force field calculations for in-plane vibrations of oxamide: use of CNDO/force method. A.Annamalai, S.Singh (Dept. of Chem., Indian Inst. of Technol., Madras, India).

Indian J. Chem. A, vol.21A, no.10, p.949-52 (Oct. 1982). [received: April 1983] The theoretical force field for in-plane vibrations of oxamide has been evaluated using CNDO/force calculations. The initial force field is set up by taking the interaction and bending force constants of the CNDO/force field, and transferring the stretching force constants from force fields of chemically

related molecules. The experimental force field is then obtained by least squares refinement method considering the vibrational frequencies of $\text{H}_2\text{NCOCONH}_2$ and $\text{D}_2\text{NCOCOND}_2$. The band assignments are proposed on the basis of potential energy distributions. (16 refs.)

75312 Ab initio MRD-CI study of the electronic spectrum of SiH. M.Lewerenz, P.J.Bruna, S.D.Peyerimhoff (Lehrstuhl für Theoretische Chem., Univ. Bonn, Bonn, Germany), R.J.Buenker. *Mol. Phys. (GB)*, vol.49, no.1, p.1-24 (May 1983). Potential curves and other properties of the ground and excited states of SiH are calculated at close to full CI accuracy in DZP AO basis sets including f functions. The C^{2+} state of this system is shown to correspond to a second potential minimum of the $B^2\Sigma^+$ species which occurs because of an avoided crossing with a dissociative state of the same symmetry. The $D^2\Delta$ and $E^2\Sigma^+$ states are assigned as members of Rydberg series involving upper orbitals of $d\sigma$ and $d\pi$ symmetry respectively. In addition, a number of quartet states have been computed including the $^4\Pi$ and two $^4\Sigma^-$ species which have apparently not yet been characterized experimentally. The $^4\Pi$ state is found to be strongly repulsive, causing predissociation of the $4s$ and $4p$ members of the lowest Rydberg series; this observation is consistent with the fact that transitions to such upper states have yet to be observed experimentally. Computed spectroscopic constants, dipole and transition moments and dissociation energies are all found to agree quite well with experiment wherever comparison is possible, including results for spin-orbit constants as a function of vibrational level in the $X^2\Pi$ ground state. Comparison is also made with results for the isovalent systems PH^+ , CH and NH^+ at various levels and it is noted that NH^+ exhibits a number of unusual features because of the relatively high value of the nitrogen atom IP. (42 refs.)

75313 Virial partitioning analysis of electron correlation and nuclear motion in diatomic molecules. M.E.Stephens, P.J.Becker (Univ. Pierre et Marie Curie, Paris, France). *Mol. Phys. (GB)*, vol.49, no.1, p.65-89 (May 1983). Studies the influence of correlation and thermal motion on the electron distribution in several diatomic molecules. The influence of electron correlation is shown to be of the order of 10 per cent of the deformation density function and it tends to reduce the redistribution features due to bond formation. Vibrations are shown to play an important role in the thermally averaged charge density function but the influence of the deformation density is fairly small in the examples that are discussed (BeH and CO). The effect of anharmonicity can be quite significant. Further similar studies are needed in order to understand better the detailed balance in electron redistribution in molecules and solids, especially when interpreting experimental data from accurate diffraction experiments. (45 refs.)

75314 Energy levels of atomic nitrogen calculated in a multiconfiguration optimized potential model. K.Aashamar (Inst. of Phys., Univ. of Oslo, Oslo, Norway), T.M.Luke, J.D.Talman. *Phys. Scr. (Sweden)*, vol.27, no.4, p.267-74 (April 1983). The method of carrying out configuration interaction calculations using orbitals that are derived from variationally optimized potential [K. Aashamar, T.M. Luke, J.D. Talman, *J. Phys. B: Atom. Molec. Phys.* 12, p.3455 (1979), and vol.14, p.803 (1981)] is studied by applying it to the ground state and a considerable number of excited states of the nitrogen atom. The results of applying the method, using several correlation configurations, to the ground state multiplet are only slightly less satisfactory than the corresponding multiconfiguration Hartree-Fock results. It is shown furthermore that it is possible to obtain a unified description of a larger number of excited states within the model using quite restricted configuration sets which are chosen in a reasonable way. Wavelengths and oscillator strengths for a large number of transitions are calculated and compared with experiment. (21 refs.)

On avoided crossing between molecular excited states; photochemical implications See Entry 75324

Theoretical study of the lithium dimer and its anion See Entry 75330

Photophysics of aryl substituted 1,3,4-oxadiazoles: the triplet state of 2,5-diphenyl-1,3,4-oxadiazole See Entry 75365

Theoretical photoelectron spectroscopy of the nitrite ion See Entry 75435

Electron-correlation effects in electron-scattering cross-section calculations of N_2 See Entry 75528

Stability of small copper clusters: Cu_3 and Cu_4 See Entry 75562

On the reaction $\text{Mg} + \text{N}_2\text{O} \rightarrow \text{MgO} + \text{N}_2$ See Entry 77877

31.30 CORRECTIONS TO ELECTRONIC STRUCTURE

75315 Exact relation between the spectrum and the eigenfunctions of a generalized Jahn-Teller hamiltonian for different parameter values. H.G.Reik, F.Kaspar (Fakultät für Phys., Univ. Freiburg, Freiburg, Germany). *Chem. Phys. Lett. (Netherlands)*, vol.97, no.3, p.253-5 (20 May 1983). A generalized $E \otimes e$ Jahn-Teller hamiltonian with a parameter δ ($\delta = -1/4$ in the JT case) is studied. As in the Jahn-Teller case, the angular momentum is a constant of the motion with the eigenvalues $j+1/2$ where j is a non-negative integer. For j fixed, consider two values $\delta_1 = -j/2-1/2$ and $\delta_2 = -\delta_1-1/2$. The spectrum and the eigenfunctions for δ_2 are completely determined by the spectrum and the eigenfunctions for δ_1 . (12 refs.)

75316 On the momentum representation of the relativistic Hartree-Fock-Roothaan wavefunctions. T.Mukoyama (Inst. for Chem. Res., Kyoto Univ., Kyoto, Japan), T.Kagawa. *J. Phys. B (GB)*, vol.16, no.11, p.1875-80 (14 June 1983). Analytical expressions for the momentum representation of the relativistic Hartree-Fock-Roothaan wavefunctions are obtained by means of the Fourier-Bessel transformation. The momentum distributions are calculated by the use of these expressions and the results are compared with the corresponding distributions of the nonrelativistic and relativistic hydrogenic wavefunctions as well as the nonrelativistic Hartree-Fock-Roothaan wavefunctions. (14 refs.)

75317 Note on the spin-orbit radial integrals. A.J.Savukynas (Inst. of Phys., Acad. of Sci., Vilnius, Lithuanian SSR). *J. Phys. B (GB)*, vol.16, no.11, p.2063 (14 June 1983). In a recently published paper (Godefroid, 1982) the relations between the radial integrals of the mutual electronic spin-orbit interaction are derived. These and the other required relations were presented in the author's book (Jucys and Savukynas 1973) and in the references cited therein. These relations are also given there for the spin-spin and orbit-orbit interactions. (2 refs.)

75318 Vacuum polarization for an electron in a strong Coulomb field. A.R.Neghabian (Inst. für Theoretische Phys., Ruhr-Univ. Bochum, Bochum, Germany). *Phys. Rev. A (USA)*, vol.27, no.5, p.2311-20 (May 1983). The electronic energy shifts due to the vacuum polarization are calculated to all orders $\alpha(Z\alpha)^n$, $n \geq 1$, and $100 \leq Z \leq 174$. The calculations are carried through in momentum space and the results are generally in good agreement with coordinate-space results. The momentum-space method is discussed in detail. (17 refs.)

75319 Relativistic calculations of core-polarization effects on the hyperfine structure in the alkalis. J.-L.Heully, A.M.Martensson-Pendrill (Dept. of Phys., Chalmers Univ. of Technol., Goteborg, Sweden). *Phys. Scr. (Sweden)*, vol.27, no.4, p.291-6 (April 1983). A method for relativistic calculations of the hyperfine structure in the alkalis including core-polarisation effects is presented. The infinite summations over excited states is performed by using the inhomogeneous differential equation technique. By solving the equations recursively, the core-polarisation effects can be included to all orders. The relation of this method to the unrestricted Dirac-Fock approach and to the method used by Das and co-workers is discussed and numerical results are presented for the ground states of the alkalis from Na to Fr. (25 refs.)

75320 Calculation of the diamagnetic shielding of the nuclei by the point-charge approximation. Z.B.Maksic, K.Rupnik (Theoretical Chem. Group, 'Rudjer Boskovic' Inst., Zagreb, Yugoslavia). *Theor. Chim. Acta (Germany)*, vol.62, no.4, p.397-401 (1983). It is shown that the diamagnetic shielding of the nuclei can be calculated to a good accuracy by using point-charge approximation. Very good results were obtained by the semiempirical SCC-MO method employing Clementi-Raimondi AO basis set. (16 refs.)

On the reliability of semi-empirical pseudopotentials: simulation of Hartree-Fock and Dirac-Fock results See Entry 75263

Relativistic MS X α calculations of the electronic structure and related properties of PtCl_6^{2-} See Entry 75289

Exact solution of the Dirac-Coulomb equation and its application to bound-state problems. I. External fields See Entry 75343

K α^h hypersatellite spectrum and K shell double photoionization cross-section for Ar See Entry 75352

Relativistic calculation of atomic M-shell ionization by protons See Entry 75504

31.50 EXCITED STATES

75321 Lifetime, triplet-triplet absorption spectrum and relaxation energy of an acyclic conjugated triene triplet: a pulse radiolysis study. A.A.Gorman, I.Hamblett (Chem. Dept., Univ. of Manchester, Manchester, England). *Chem. Phys. Lett. (Netherlands)*, vol.97, no.4-5, p.42-6 (27 May 1983). The triplet state of neo-allocimene ($\tau = 333$ ns; $\lambda_{\text{max}} = 315$ nm) has been produced in toluene by pulse radiolysis. The establishment of a transient stationary position for reversible triplet energy transfer between this triene and anthracene has placed the equilibrium energy of the triene triplet at 169 ± 2 kJ mol $^{-1}$, 28 ± 2 kJ mol $^{-1}$ less than that of the Franck-Condon state. (23 refs.)

75322 On Rydberg series of autoionising resonances. J.P.Connerade (Blackett Lab., Imperial Coll., London, England). *J. Phys. B (GB)*, vol.16, no.11, p.L329-35 (14 June 1983). A recent formula due to Dubau and Seaton (1983) for the parametrisation of a Rydberg series of autoionising resonances is discussed and related to expressions given by other authors. A simple method of finding the four parameters is described and illustrated by an application to the autoionising spectrum of Xe I. (13 refs.)

75323 Variation of fine structure along atomic Rydberg series. L.R.Pendrill (Dept. of Phys., Chalmers Univ. of Technol., Goteborg, Sweden). *Phys. Scr. (Sweden)*, vol.27, no.5, p.371-3 (May 1983). Recent improvements in the accuracy of measurement of optical light wavelengths have enabled absolute atomic energy levels to be determined over long Rydberg series with comparable precision to that of the direct fine structure measurements of the series. An expression describing the variation of the fine structure along a Rydberg series in terms of Rydberg-Ritz parameters is derived and a check of consistency with experimental data is performed. (19 refs.)

75324 On avoided crossing between molecular excited states; photochemical implications. V.Bonacic-Koutecky (Inst. für Phys. Chem., Freie Univ. Berlin, Berlin, Germany). *Pure & Appl. Chem. (GB)*, vol.55, no.2, p.213-20 (Feb. 1983). (International Symposium on Theoretical Organic Chemistry, Dubrovnik, Croatia, Yugoslavia, 30 Aug.-3 Sept. 1982). The consequences of geometrical relaxation in butadiene and in unprotonated Schiff base-allylideneimine (torsion around $\text{C}=\text{C}$, $\text{C}=\text{N}$ and $\text{C}-\text{C}$ bonds) for low lying singlet and triplet states have been investigated employing large scale CI treatments. The analysis of the correlated wavefunctions in terms of the VB-like ionic and covalent structures has been carried out. The importance of zwitterionic highly polar states of dienes as well as of the low lying covalent excited state has been discussed. Photochemical implications of different minima on the energy surfaces of excited states with contrasting features of the wavefunctions have been proposed. (37 refs.)

75325 Charge transfer transition for symmetry-forbidden charge transfer interaction. Theory and experimental verification. I.Murata (Dept. of Chem., Faculty of Sci., Osaka Univ., Osaka, Japan). *Pure & Appl. Chem. (GB)*, vol.55, no.2, p.323-30 (Feb. 1983). (International Symposium on Theoretical Organic Chemistry, Dubrovnik, Croatia, Yugoslavia, 30 Aug.-3 Sept. 1982). The group theoretical analysis of the electronic structure of 1,4-dihydro-1,4-bis (dicyanomethylene) triptycene leads to an interesting but rarely documented notion, 'charge transfer transition for symmetry forbidden charge transfer interactions', which was supported by the substituent effects on the charge transfer band shifts. The substituent effects on the charge transfer band shifts were also observed in a series of 9,10-dihydro-9,10-o-benzoanthracene-1,4-diones. These results provide decisive evidence for the fact that the orbitals involved in the ground state charge transfer interaction need not be the same as those involved in the charge transfer transition. (24 refs.)

Reduction of the excited state into the ground state of a super-Hamiltonian See Entry 75253

Calculation of excited-state properties of some small molecules: comparative study of the CNDO/S and CNDO/2- $V_{\text{NC}+1}$ potential methods See Entry 75301

- Coordinate rotation studies of H^- , He^- , Be^- , Mg^- resonances: basis set and configuration list dependence See Entry 75309
- Energy levels of atomic nitrogen calculated in a multiconfiguration optimized potential model See Entry 75314
- Relativistic calculations of core-polarisation effects on the hyperfine structure in the alkalis See Entry 75319
- Laser spectroscopy of Rydberg states of two-electron atoms See Entry 75332
- Broadening of level-crossing signals in the $5^2P_{3/2}$ state of rubidium due to resonant collisions See Entry 75350
- Photophysics of aryl substituted 1,3,4-oxadiazoles: the triplet state of 2,5-diphenyl-1,3,4-oxadiazole See Entry 75365
- Rydberg series in the absorption spectrum of Te I limiting on $5s^25p^4g_{7/2}^0$ ionization limit See Entry 75402
- Observation of a metastable $^2\Delta$ state in BaCl See Entry 75418
- Spectroscopic and picosecond time-resolved studies of vibrational relaxation in naphthazarine in solid neon See Entry 75419
- Room-temperature rate constants for the gas-phase quenching of metastable molecular oxygen, $O_2(a^1\Delta_g)$ and $O_2(b^1\Sigma_g^+)$, by CO_2 , N_2O , NO , NH_3 , HCl and SO_2 See Entry 75423
- Spectroscopy and dynamics of jet-cooled 1,1'-binaphthyl See Entry 75424
- Photophysical anomalies of acridine in n-hexane See Entry 75432
- Twisted intramolecular charge transfer (TICT) excited states: energy and molecular structure See Entry 75433
- Energy-dependent energy transfer: deactivation of azulene (S_0 , E_{vib}) by 17 collider gases See Entry 75483
- Quasielastic state-changing collisions of high-Rydberg atoms with rare-gas atoms* See Entry 75491
- Electron impact investigation of the molecules $SeS(g)$ and $TeSe(g)$ under high-temperature equilibrium conditions See Entry 75527

31.70 EFFECTS OF MOLECULAR INTERACTIONS ON ELECTRONIC STRUCTURE

(see also 34. Atomic and molecular collision processes and interactions)

- 75326 Theoretical study of the potential energy curves of the series of diatomic radicals MeX , II. Application to $BeCl$ and MgF radicals. R. Montagnani, P. Riani, O. Salvetti (Istituto di Chimica Quantistica ed Energetica Molecolare, CNR, Pisa, Italy). *Theor. Chim. Acta (Germany)*, vol.62, no.4, p.329-34 (1983). For pt. I see *ibid.*, vol.60, p.399 (1982). The potential energy curves of some low lying electronic states of the diatomic radicals $BeCl$ and MgF have been calculated. The calculation has been performed according to a stepwise procedure. The potential energy curves are very similar to those of the mercury halide radicals, the electronic transitions of which can be employed for efficient laser apparatus. (11 refs.)

31.70D Environmental and solvent effects

- Solvent effects on the infrared active CO stretching frequencies of some metal carbonyl complexes. I. Dimanganese decarbonyl and dirhenium decarbonyl See Entry 75392
- Photophysical anomalies of acridine in n-hexane See Entry 75432
- The mechanism of carbonyl reduction by $LiBH_4$: an ab initio investigation with inclusion of solvent effects See Entry 77867
- Solvent effects in organic chemistry studied by correlation analysis See Entry 77874

31.70F Potential-energy surfaces for collisions

(see also 82.20K in chemical kinetics, 34.20 Intermolecular forces, 34.50L in beam studies)

- Quantum chemical and statistical-thermodynamic studies of equilibria and rates See Entry 77862
- Topography of potential energy surfaces See Entry 77864
- Potential surfaces for simple rearrangements See Entry 77885

31.70H Time-dependent phenomena: excitation and relaxation processes, and reaction rates

(see also 34. Atomic and molecular collisions)

- 75327 Time-resolved study of the subpicosecond dynamics of molecular rotations in liquids. J.M. Halbout, C.L. Tang (Cornell Univ., Ithaca, NY, USA). *J. Phys. Colloq. (France)*, vol.44, no.C-2, p.135-40 (March 1983). (International Workshop on Optical Phase Conjugation and Instabilities, Cargèse, Corsica, France, 20-24 Sept. 1982). Time resolved results on the relaxation of molecular rotations in liquids are reported. In CS_2 , in addition to the 2 picosecond Debye relaxation time, a 330-femtosecond short relaxation time is observed for the first time. This short relaxation time is interpreted as due to the relaxation of the molecules within the librational wells in the liquid. A similar short relaxation time on the order of 150 femtoseconds is also observed in neat liquid nitrobenzene. (11 refs.)
- Spectroscopic and picosecond time-resolved studies of vibrational relaxation in naphthazarine in solid neon See Entry 75419

31.90 OTHER TOPICS IN THE THEORY OF ATOMS AND MOLECULES

(inc. properties other than energy)

- 75328 The physical significance of multiple refinement minima in harmonic force field calculations. M. Lacy (Dept. of Phys. Chem., Univ. of Newcastle upon Tyne, Newcastle upon Tyne, England). *THEOCHEM (Netherlands)*, vol.11, no.1-2, p.1-9 (June 1983). The technique of comparing potential energy surfaces, introduced previously to study anharmonic force fields, is applied to the examination of multiple refinement minima in harmonic force field calculations. Although the varia-

tion of the potential surface caused by different data and weighting schemes is substantially larger than in the anharmonic case, the multiple refinement minima examined represent surfaces which are significantly different from each other. The approach is suggested as a first useful step in the appreciation of the physical significance of this and other features in molecular potential energy surfaces. (18 refs.)

- 75329 Topological properties of conformational potential energy surfaces. M.R. Peterson, I.G. Csizmadia (Dept. of Chem., Univ. of Toronto, Toronto, Ontario, Canada), R.W. Sharpe. *THEOCHEM (Netherlands)*, vol.11, no.1-2, p.127-35 (June 1983). Topological relations among the number of critical points of various orders (zero order are minima, first order are saddle points, etc.) are presented, which are invariants of the actual periodic (hyper)surfaces considered. The principal results involve the Betti numbers, the minimum number of critical points of given order that must be present, and the Euler characteristic, based on an alternating sum rule involving the number of critical points of each order. Several conformational potential energy (hyper)surfaces are analyzed in terms of these relationships, including two containing lines of degeneracy and degenerate critical points. (19 refs.)
- 75330 Theoretical study of the lithium dimer and its anion. H. Partridge (Univ. of Southern California, University Park, Los Angeles, CA, USA), C.W. Bauschlicher, Jr., P.E.M. Siegbahn. *Chem. Phys. Lett. (Netherlands)*, vol.97, no.2, p.198-203 (13 May 1983). Theoretical potential energy curves are reported for the $X^1\Sigma_g^+$ state of Li_2 and the $X^2\Sigma_u^+$ state of Li_2^- . The electron affinity of Li_2 is estimated to be 0.43 ± 0.02 eV. In addition, the authors show that for Li_2 and Li_2^- core correlation effects are small but shorten R_e of Li_2 by $0.04 a_0$ and slightly skew the potential curves. (21 refs.)
- 75331 Dissociation energy of aluminium monoselenide molecule. P. Sambasiva Rao (Dept. of Phys., J.N. Technol. Univ., Coll. of Engng., Anantapur, India), R. Ramakrishna Reddy, T.V. Ramakrishna Rao. *Indian J. Phys. Part B*, vol.56B, no.6, p.353-7 (Dec. 1982). [received: May 1983] The experimental potential energy curves for $X^2\Sigma^+$ and $A^2\Sigma^+$ states of $AlSe$ have been constructed using the method of Lakshman and Rao (1971). The dissociation energy for the ground state has been estimated to be 2.23 ± 0.08 eV, using the curve fitting procedure. (14 refs.)
- On the stability of [furan] $^+$ and [vinylketene] $^+$ See Entry 75294
- Conformational and MO studies of hydroxy-2-aminotetralins See Entry 75295
- New predissociations in GeH affecting all the $A^2\Delta$ state levels See Entry 75457

32.00 ATOMIC SPECTRA AND INTERACTIONS WITH PHOTONS

32.20 ATOMIC SPECTRA GROUPED BY WAVELENGTH RANGES

- 75332 Laser spectroscopy of Rydberg states of two-electron atoms. W. Hogervorst (Vrije Univ., Amsterdam, Holland). *Comments At. & Mol. Phys. (GB)*, vol.13, no.2, p.69-81 (1983). Recent progress in the study of the structure of Rydberg levels in two-electron atoms with narrow-band CW dye lasers is reviewed. New and accurate data have resulted in an assessment of the importance of two-body effects and in a critical test of multichannel quantum defect analyses. (38 refs.)
- 75333 Quantum defects of the $n^2P_{1/2,3/2}$ levels in ^{39}K and ^{85}Rb . C.-J. Lorenzen, K. Niemann (Inst. für Experimentalphys., Univ. Kiel, Kiel, Germany). *Phys. Scr. (Sweden)*, vol.27, no.4, p.300-5 (April 1983). The energies of the $n^2P_{1/2,3/2}$ level series in ^{39}K ($9 \leq n \leq 21$) and ^{85}Rb ($13 \leq n \leq 68$) have been measured using frequency-doubled CW dye laser radiation, a thermionic detector and a high-precision vacuum-wavemeter. By means of a Rydberg-Ritz fitting procedure accurate quantum defect data and ionization limits are given. The ionization limits are in agreement with the limits derived from energy data of other l -series which have been measured recently with laser spectroscopy techniques. The compact Rydberg-Ritz coefficient of all alkali term series with $l \leq 3$ is presented and the present status of alkali quantum defect data is discussed. This set of data includes also recent measurements of ^{133}Cs $n^2S_{1/2}$ and $n^2D_{3/2,5/2}$ levels and of some low-lying 7Li levels. (22 refs.)

Minima and maxima in the generalized oscillator strengths for the lithium isoelectronic sequence See Entry 75344

Electron double ionization cross section in sodium obtained from $K\alpha^b$ hypersatellite spectra See Entry 75525

32.20B Radiofrequency, microwave, and infrared spectra

(inc. magnetic resonance spectra)

- 75334 Nonlinear resonances which arise during the interaction of atoms with spaced powerful standing waves. B.Ya. Dubetskii (Inst. of Thermal Phys., Acad. of Sci., USSR). *Bull. Acad. Sci. USSR, Phys. Ser. (USA)*, vol.46, no.5, p.155-60 (1982). Translation of: *Izv. Akad. Nauk SSSR Ser. Fiz.*, vol.46, no.5, p.990-6 (1982). [received: May 1983] (Proceedings of the All-Union Conference on Luminescence Commemorating the Ninetieth Anniversary of the Birth of the Academician S.I. Vavilov, Leningrad, USSR, 21-24 April 1981). In 1974 the author began theoretical and then also experimental investigations of the possibilities of narrowing optical lines by means of the method of spaced fields (MSF) on the initiative of F.P. Chebotayev. In optics the use of the MSF is made difficult due to the large Doppler broadening of the line. The author advanced methods for eliminating the influence of the Doppler effect and for obtaining narrow lines on one-photon transitions for two-photon absorption in stimulated-Raman-scattering (SRS) spectroscopy. The results of the theory of the MSF are given. (32 refs.)

75335 Photoionization Raman spectroscopy. I.M.Beterov, N.V.Fateev, V.P.Chebotaev (Inst. of Thermal Phys., Acad. of Sci., USSR).

JETP Lett. (USA), vol.36, no.7, p.307-10 (5 Oct. 1982). Translation of: *Pis'ma v Zh. Eksp. & Teor. Fiz. (USSR)*, vol.36, no.7, p.251-3 (5 Oct. 1982). [received: May 1983]

Experiments are reported on the photoionization detection of stimulated Raman scattering by electronic transitions of sodium in an atomic beam. There is a dip in the signal corresponding to the nonresonant two-photon ionization of sodium by electromagnetic radiation at $\lambda_1=284.5$ nm and $\lambda_2=1.06$ μ m. The dip is due to a Raman resonance at the forbidden 3s-4s transition. (8 refs.)

75336 FO_2 radical and LMR spectra in reactions of fluorine atoms. P.B.Davies, F.Temps, H.G.Wagner, D.P.Stern.

Report 19/1982, Max-Planck-Inst. Stromungsforschung, Gottingen, Germany (Dec. 1982), 19 pp.

Far Infrared Laser Magnetic Resonance spectra of the FO_2 radical have been detected at eleven laser frequencies. The assignment is based on chemical and kinetic results and on a qualitative spectroscopic investigation. It is suggested that this radical may be responsible for many unassigned 5 and 10 μ m Laser Magnetic Resonance spectra. (26 refs.)

The spectrum of singly ionized phosphorus, P II See Entry 75339

High-resolution synchronized-quantum-beam spectroscopy using modulation sidebands: measurement of pressure shifts of the hyperfine splitting in sodium $3^2S_{1/2}$ See Entry 75538

32.20J Visible and ultraviolet spectra

(for fluorescence and phosphorescence spectra, see 32.50)

75337 Identification of the $4d^{10}5p^61S_0$ level in Xe III using optical spectroscopy. J.E.Hansen, F.G.Meijer (Zeeman Lab., Univ. of Amsterdam, Amsterdam, Netherlands), M.Outerd, W.Persson, H.O.Di Rocco.

Phys. Scr. (Sweden), vol.27, no.4, p.254-5 (April 1983).

Two different proposals for the identification of the $4d^{10}5p^61S_0$ level in Xe III are examined using the methods of optical spectroscopy. The proposal by Hertz [*Z. Phys.*, vol.A274, p.289, (1975)] is confirmed. The $5p^61S_0$ level is located 210 857.55 cm^{-1} above the Xe III ground state. (16 refs.)

75338 Spectra of the ironlike ions from YXIV to Ag XXII. J.-F.Wyart (Lab. Aime Cotton, CNRS II, Orsay, France), M.Klapisch, J.-L.Schwob, N.Schweitzer, P.Mandelbaum.

Phys. Scr. (Sweden), vol.27, no.4, p.275-90 (April 1983).

The spectra of the ironlike ions Y XIV, Zr XV, Nb XVI, Mo XVII, Ru XIX, Rh XX, Pd XXI and Ag XXII emitted by low inductance vacuum sparks have been observed in the range 25-90 Å. More than 440 lines have been identified for the first time as $3p^63d^8-3p^53d^9$ and $3p^63d^8-3p^63d^44p$ transitions. Three parametric interpretations of the whole isoelectronic sequence of energy levels have been performed for $3d^8$, $3p^63d^8$ and $3d^44p$ respectively. This has led to an accurate determination of scaling factors for the Slater and spin-orbit integrals calculated by the Hartree-Fock method. Predicted wavelengths and line strengths are given for Sr XIII. (17 refs.)

75339 The spectrum of singly ionized phosphorus, P II. N.Svendenius, C.E.Magnusson, P.O.Zetterberg (Phys. Dept., Lund Univ., Lund, Sweden).

Phys. Scr. (Sweden), vol.27, no.5, p.339-63 (May 1983).

New observations in the P II spectrum have been made in the wavelength region 500-12000 Å. The spectrum was excited in two different ways, using a high-frequency lamp and a sliding spark in vacuum. The term system now includes 159 levels and about 900 identified lines, which means a doubling of the number of levels and identified transitions. The energy of the lowest limit, $3s^23p^2P$, is derived from *ng*-series, which are all new. A linear Ritz formula gives the value 160010.6 cm^{-1} for the $2^3P_{3/2}$ component of the limit, and the ground term splitting 559.14 cm^{-1} in P III then gives 159451.5 cm^{-1} for the $2^1P_{1/2}$ limit level. (10 refs.)

75340 The configurations $3s^23p^53d$ and $3s3p^63d$ in Mn VIII and Fe IX. R.Smít, L.A.Svensson (Dept. of Phys., Univ. of Lund, Lund, Sweden).

Phys. Scr. (Sweden), vol.27, no.5, p.364-6 (May 1983).

The astrophysically important configuration $3s^23p^53d$ has been determined for Mn VIII and Fe IX by means of about 60 lines, classified as combinations $3s^23p^6-3s^23p^53d$ and $3s^23p^63d-3s3p^63d$. The authors also introduce a sensitive method for isoelectronic comparison of energy parameters. By this method the configuration $3s^23p^53d$ is studied through the Ar I sequence, thus supporting the reported Mn VIII and Fe IX identifications. (9 refs.)

Resistively heated high-temperature furnace for PES experiments on free atoms in the UHV with synchrotron radiation See Entry 74469

Relativistic atomic level calculations with nuclei carrying additional fractional charges See Entry 75284

State-selective single-electron capture by 80 keV C^{4+} ions from He, H₂ and Li See Entry 75498

Density of uranium ions in the $^4I_{9/2}$ ground state in a hollow-cathode type discharge See Entry 76223

32.20R X-ray spectra

Resistively heated high-temperature furnace for PES experiments on free atoms in the UHV with synchrotron radiation See Entry 74469

$K\alpha^h$ hypersatellite spectrum and K shell double photoionization cross-section for Ar See Entry 75352

Ionisation cross sections of Cd, Sn, Te, I and Ba for protons and alpha particles See Entry 75488

32.50 FLUORESCENCE, PHOSPHORESCENCE

(inc. quenching)

75341 Time-resolved two-dimensional imaging of ground-state species using laser-induced fluorescence. R.A.Dougal, P.F.Williams, D.C.Pease (Dept. of Electrical Engng., Texas Tech. Univ., Lubbock, TX, USA).

Rev. Sci. Instrum. (USA), vol.54, no.5, p.572-3 (May 1983).

Laser-induced fluorescence has been employed to obtain two-dimensional images of the spatial distribution of a vapor in the ground state with nanosecond resolution. The method has a wide range of potential applications, as it can be used to observe any species which has energy levels accessible to tunable laser systems. In the application described, aluminum vapor was observed jetting from spark gap electrodes and diffusing throughout the gap volume. (2 refs.)

Lifetimes of the Ne 2p fine structure states by measurements of linewidths of the laser induced fluorescence of an atomic beam See Entry 75347

Doppler-free laser spectroscopy measurements on a Ne discharge for determination of ^{22}Ne - ^{20}Ne isotope shifts See Entry 75349

Energy distribution of sputtered metastable Ca atoms See Entry 77504

32.60 ZEEMAN AND STARK EFFECTS

75342 Comment on 'Plasma satellites in the presence of nonresonant, coherent and polarised radiation'. N.J.Wiegart, U.Rebhan (Inst. für Experimentalphys. V, Ruhr-Universität, Bochum, Germany).

J. Phys. B (GB), vol.16, no.11, p.L367-8 (14 June 1983).

A recently published calculation by Drawin and Truong-Bach (ibid., vol.15, p.4477, 1982) concerning the high-frequency Stark effect is shown to be in error. 'Negative intensities' of satellite lines result from an incorrect mathematical treatment of the problem. (5 refs.)

75343 Exact solution of the Dirac-Coulomb equation and its application to bound-state problems. I. External fields. M.K.F.Wong (Dept. of Math., Fairfield Univ., Fairfield, CT, USA), Hsin-Yang Yeh.

Phys. Rev. A (USA), vol.27, no.5, p.2300-4 (May 1983).

An exact treatment of relativistic effects in bound-state problems in hydrogen-like atoms is given. In this paper the authors discuss the Zeeman effect and the Stark effect for relativistically bound electrons in a Coulomb field. For the Zeeman effect, the exact solution obtained by Darwin (1928) is used, and results of Crubellier and Feneuille (1971) for the Breit-Margenau correction are obtained in a simple way. For the Stark effect, the solution of Wong and Yeh (1982) is used. The exact expression can be readily compared with that of the Pauli approximation, and all correction terms can be identified. In the following paper they discuss interaction of the bound electron with radiation in an exact relativistic way. In the evaluation of the radial r^k matrix elements with $n' \neq n$, the authors present a closed-form expression as a sum over three parameters, derived from the method of the generating function of Laguerre polynomials. (14 refs.)

Lifetimes of the Ne 2p fine structure states by measurements of linewidths of the laser induced fluorescence of an atomic beam See Entry 75347

Observation of magnetically induced optical self-pulsing in a Fabry-Perot resonator See Entry 75717

32.70 SPECTRAL LINE SHAPES AND INTENSITIES

75344 Minima and maxima in the generalized oscillator strengths for the lithium isoelectronic sequence. S.N.Tiwary, C.A.Nicolaides (Inst. of Theoretical & Phys. Chem., Nat. Hellenic Res. Foundation, Athens, Greece).

Chem. Phys. Lett. (Netherlands), vol.97, no.3, p.283-4 (20 May 1983).

The authors have calculated the ionization generalized oscillator strengths (GOS) $f(K,k)$ as a function of the momentum transfer K for the followed dipole transitions $ns-kp$ (with $n=2$) in the lithium isoelectronic sequence through $Z=10$, in the Hartree-Fock (HF) approximation. The results clearly show (i) the regular and systematic trends of the occurrence of the extrema, (ii) the shift of their positions towards the higher values of K with increase of K , and finally; the gradual decrease of the magnitude of $f(K,k)$ with increase of atomic number Z . The results are discussed qualitatively. (7 refs.)

75345 Determination of the oscillator strengths of the $6D-6^1P_1$ atomic energy mercury transitions. P.van de Weijer, R.M.Cremers (Philips Res. Labs., Eindhoven, Netherlands).

J. Appl. Phys. (USA), vol.54, no.5, p.2835-6 (May 1983).

The magnitude of the oscillator strengths (f values) of the $6D-6^1P_1$ transitions of atomic mercury is of interest, e.g. for the determination of the 6^1P_1 mercury density in gas discharges by optical methods. However, contradictory results for these f values have been reported in the literature. Using the accurately known radiative lifetime of the 7^3S_1 level as a starting point, the authors performed combined emission and hook measurements. As a result they found $f=0.28 \pm 0.04$ and $f=0.25 \pm 0.05$ for the 577.0 nm ($6^3D_2-6^1P_1$) and 579.1 nm ($6^1D_2-6^1P_1$) line, respectively. (11 refs.)

75346 Collisional broadening of intra-Doppler resonances of selective reflection on the D_2 line of cesium. A.M.Akul'shin, V.L.Velichanski, A.S.Zibrov, V.V.Nikitin, V.V.Sautenkov, E.K.Yurkin, N.V.Senkov (P.N. Lebedev Phys. Inst., Acad. of Sci., Moscow, USSR).

JETP Lett. (USA), vol.36, no.7, p.303-7 (5 Oct. 1982). Translation of: *Pis'ma v Zh. Eksp. & Teor. Fiz. (USSR)*, vol.36, no.7, p.247-50 (5 Oct. 1982).

[received: May 1983]

The broadening of selective reflection resonances for cesium atom concentrations N such that collisional resonance broadening γ_c is less than the Doppler broadening is investigated. A method is proposed for measuring γ_c at the center of the atomic line. It is found that the N -dependence of the reflection resonance width for the D_2 line is $\gamma_c=(1.15 \pm 1.12) \times 10^{11} N$ Hz. (10 refs.)

75347 Lifetimes of the Ne 2p fine structure states by measurements of linewidths of the laser induced fluorescence of an atomic beam. M.J.Verheijen, H.C.W.Beijerinck, P.J.Eenshuistra, J.P.C.Kroon, N.F.Verster (Dept. of Phys., Eindhoven Univ. of Technol., Eindhoven, Netherlands).

Opt. Commun. (Netherlands), vol.45, no.5, p.336-41 (1 May 1983).

The laser induced fluorescence signal of a crossed atomic beam-photon beam is used to measure the natural lifetimes of six of the 2p fine structure states of Ne I. The excitation profiles are analysed with a model function consisting of an unbroadened Lorentzian lineshape with the full-width at half-maximum $\Delta\nu$ (natural lineshape) as a free parameter, which is then fully convoluted with the experimental conditions as Doppler effect, Zeeman splitting and saturation. The broadening due to these effects is typically 3 MHz. To avoid strong correlations of the value of $\Delta\nu$ with an incorrect shape of the model function, the authors only use the datapoints that are most sensitive to $\Delta\nu$, i.e. at the maximum and at half height. The resulting lifetimes lie all within the 1σ error bound (5%) from other experimental results. The results add an independent set of data to these well investigated lifetimes. (12 refs.)

75348 General dressed Hamiltonian for a composite particle in a medium. R.Fleckinger, Y.Soulet (Lab. de Phys. Quantique, Univ. Paul Sabatier, Toulouse, France).

Physica A (Netherlands), vol.119A, no.1-2, p.243-73 (April 1983).

The general dressed hamiltonian for a composite particle in a medium is obtained by using joined Fock-Tani representation for composite particles, causal Green's function method and Balescu's kinetic theory formulation. An explicit calculation of this dressed hamiltonian is presented within the frame of the medium-composite weak coupling approximation and tested on the hydrogen Ly_α -line broadening. (11 refs.)

75349 Doppler-free laser spectroscopy measurements on a Ne discharge for determination of ^{22}Ne , ^{20}Ne isotope shifts. C.Bellfrage, P.Grafstrom, S.Kroll, S.Svanberg (Dept. of Phys., Lund Inst. of Technol., Lund, Sweden). *Phys. Scr. (Sweden)*, vol.27, no.5, p.367-70 (May 1983). The authors have used Doppler-free polarization spectroscopy, intermodulated fluorescence and intermodulated optogalvanic spectroscopy for measuring isotope shifts in 6 Ne lines connecting the $2p^3s$ and $2p^3p$ configurations. The measurements were performed on two different hollow cathodes. For the 5852, 5882, 5945, 5976, 6143 and 6164 Å lines the ^{22}Ne isotope shift was found to be 2300(15), 1740(2), 1717(3), 1728(5), 1669(4) and 1663(5) MHz, respectively. These results are in fair agreement with previous optical spectroscopy data. (25 refs.)

Shape transitions and isotope shifts of proton and neutron distributions in the samarium isotopes See Entry 74889

Energy levels of atomic nitrogen calculated in a multiconfiguration optimized potential model See Entry 75314

Vacuum polarization for an electron in a strong Coulomb field See Entry 75318

Nonlinear resonances which arise during the interaction of atoms with spaced powerful standing waves See Entry 75334

An improved model for post-collision interaction (PCI) and high resolution Ar LMM Auger spectra revealing new PCI effects See Entry 75353

Excitation of Be^+ by electron impact See Entry 75515

Electron double ionization cross section in sodium obtained from $K\alpha^h$ hypersatellite spectra See Entry 75525

Polarization dependent properties of backward four-wave mixing See Entry 75743

Doppler-free conjugate emission in resonant gas media: lineshape, polarization properties and saturation See Entry 75744

Optogalvanic studies of neon glow discharge in magnetic fields: ion mobility measurements and detection of atomic alignment See Entry 76228

32.80 PHOTON INTERACTIONS WITH ATOMS

FO_2 radical and LMR spectra in reactions of fluorine atoms ..See Entry 75336

4f-ionization of atomic cerium See Entry 75493

32.80B Level crossing and optical pumping

75350 Broadening of level-crossing signals in the $5^2P_{3/2}$ state of rubidium due to resonant collisions. M.Lukaszewski, I.Jackowska (Inst. of Phys., Polish Acad. of Sci., Warsaw, Poland). *Phys. Lett. A (Netherlands)*, vol.95A, no.8, p.429-31 (23 May 1983).

Broadening of three isolated level-crossing signals in the resonance $5^2P_{3/2}$ state of ^{87}Rb due to resonant Rb-Rb collisions is investigated experimentally. The results confirm the interpretation of the experiments on collisional broadening of level-crossing signals in excited $P_{3/2}$ states of heavy alkali-metal atoms presented in the authors' recent paper (ref. unobtainable). The present work provides also additional experimental evidence that the description of resonant collisional depolarization of the $5^2P_{3/2}$ state of rubidium by the R^{-3} dipole-dipole potential is very satisfactory. (10 refs.)

Relaxation rate of atomic orientation See Entry 75537

Error optimization in the detection of level crossing through the measurement of $n^{(2)}(T)$ See Entry 75609

Observation of magnetically induced optical self-pulsing in a Fabry-Perot resonator See Entry 75717

32.80D Autoionization

Electron-impact excitation-autoionization in the cadmium isoelectronic sequence: a case of target term dependence in scattering theory See Entry 75521

Measurement of the cross section for electron-impact ionization of Xe^{6+} ions See Entry 75522

32.80F Photoionization and photodetachment

75351 Photoionisation cross section calculations using Dyson amplitudes: results for Ne. I.Cacelli (Istituto di Chimica Fisica, Univ. di Pisa, Pisa, Italy), V.Carravetta, R.Moccia. *J. Phys. B (GB)*, vol.16, no.11, p.1895-906 (14 June 1983).

Photoionisation cross sections of the main ionisation process of neon have been calculated for a wide range of photon energies. The partial cross sections were computed as a sum of a contribution expressible in terms of the Dyson amplitude corresponding to the ionisation processes considered plus a correction term. The numerical results obtained, in satisfactory agreement with the experiment, show, as expected, that for outer-shell ionisation the correction term decreases rapidly with the photon energy. For inner-shell ionisation, however, the correction term appears to be still important at relevant (~ 100 eV) energies of the photoelectron. Results given by different choices of the photoelectron waves are also presented. (20 refs.)

75352 $K\alpha^h$ hypersatellite spectrum and K shell double photoionization cross-section for Ar. E.Mikkola, J.Ahopelto (Lab. of Phys., Helsinki Univ. of Technol., Espoo, Finland). *Phys. Scr. (Sweden)*, vol.27, no.4, p.297-9 (April 1983).

The $K\alpha^h$ hypersatellite spectrum of gaseous Ar has been measured in photon excitation with a plane crystal Bragg spectrometer. The experimental energy of $K\alpha^h$ line is obtained. The result is in good agreement with available theoretical calculations. The K shell double photoionization cross-section is estimated from the measured hypersatellite intensity and it is compared with existing theoretical calculations based on the shake theory and correlated wave functions. (29 refs.)

Photoionization Raman spectroscopy See Entry 75335

32.80H Auger effect and inner-shell ionization

75353 An improved model for post-collision interaction (PCI) and high resolution Ar LMM Auger spectra revealing new PCI effects. K.Helenelund, S.Hedman, L.Asplund, U.Gelius, K.Siegbahn (Inst. of Phys., Univ. of Uppsala, Uppsala, Sweden). *Phys. Scr. (Sweden)*, vol.27, no.4, p.245-53 (April 1983).

An improved semi-classical model for post-collision interaction (PCI) in photo-excited Auger decay is presented. A simple analytical expression is obtained by using complex WKB wave functions for the slow electron. The model gives the right asymptotic line-shape at high excess energies and the energy shift of the peak maximum is in agreement with experimental results. New high resolution argon LMM Auger spectra excited by electrons at different excess energies (4.5-2751.0 eV) relative to the L_3 level in Ar are presented. Extra structures are observed at low excess energies and are tentatively interpreted to be caused by 'shake-down' processes of the slow electron. The relative shifts between Kr $M_5N_{23}N_{23}(^1S_0)$ and Ar $L_3M_{23}M_{23}(^1D_2)$ lines are measured and tabulated. The full widths and the asymmetry parameters at half and quarter maximum are also given. (68 refs.)

$K\alpha^h$ hypersatellite spectrum and K shell double photoionization cross-section for Ar See Entry 75352

32.80K Multiphoton processes

Nonlinear resonances which arise during the interaction of atoms with spaced powerful standing waves See Entry 75334

Photoionization Raman spectroscopy See Entry 75335

32.90 OTHER TOPICS IN ATOMIC SPECTRA AND INTERACTIONS WITH PHOTONS

Superradiation of extended systems See Entry 75610

33.00 MOLECULAR SPECTRA AND INTERACTIONS WITH PHOTONS

33.10 CALCULATION OF MOLECULAR SPECTRA

75354 Iterative methods for calculation of displacements of normal coordinates from observed vibrational intensities. F.T.Chau (Pentecostal School, Hong Kong, Hong Kong). *THEOCHEM (Netherlands)*, vol.11, no.1-2, p.155-61 (June 1983).

Three one-dimensional search techniques, namely the dichotomous search (or symmetrical two-point search), the Fibonacci search and the golden-ratio search are used to calculate the value of γ (the displacement in normal coordinates of a particular vibrational mode in an electronic transition) which gives the best agreement between the observed and the calculated vibrational intensities. All the methods are found to be powerful and converge rapidly to the desired result. The golden-ratio search method is preferred because of its speed and simplicity in programming. (6 refs.)

75355 Electron relaxation during strong electron-vibration coupling. V.N.Kharkyanen. *Dopov. Akad. Nauk UkrSR. Ser. A (USSR)*, no.1, p.58-61 (1983). In Ukrainian.

A kinetic description of the evolution of an electronic system placed in a thermostat is constructed for the case of a strong electron-vibration coupling when the usual perturbation theory parameter is not small. Necessary kinetic equations and their applicability limits are found by double reduction of the initial Liouville equation for the whole system. (5 refs.)

75356 Force field for in-plane vibrations of trans-cis-diacetamide. Use of CNDO/Force method. A.Annamalai, Surjit Singh (Dept. of Chem., Indian Inst. of Technol., Madras, India). *Indian J. Pure & Appl. Phys.*, vol.21, no.2, p.82-6 (Feb. 1983).

Using the CNDO/Force and the least squares refinement calculations, the redundancy-free internal valence force field is evaluated for the in-plane vibrations of trans-cis-diacetamide. The initial force field considered is based on the bending and interaction force constants obtained from the CNDO/Force calculations, and the stretching force constants transferred from chemically related molecules. The vibrational frequencies of $\text{CH}_3\text{CONHCOCH}_3$, $\text{CH}_3\text{CONDCOCH}_3$, $\text{CD}_3\text{CONHCOCD}_3$ and $\text{CD}_3\text{CONDCOCD}_3$ are employed in refining the force field. The refined force field obtained is found to be reasonable. (20 refs.)

75357 Force field study of some nonlinear XY₂ type molecules. S.Mohan, S.Gunasekaran, K.G.Ravikumar (Div. of Appl. Sci., Anna Univ., Madras Inst. of Technol., Madras, India). *Indian J. Pure & Appl. Phys.*, vol.21, no.2, p.121-2 (Feb. 1983).

The most probable force fields of the nonlinear XY₂-type molecules like SO_2 , ClO_2 and CF_2 have been fixed by a parametric method. The centrifugal distortion constants are used as additional data to fix the potential constants unambiguously. (17 refs.)

75358 Halogen-substituted amides. V. Modified valence force field for N,N-dichloroacetamide. K.Sree Ramulu, E.Krishna Murthy, G.Ramana Rao (Dept. of Phys., Univ. Coll., Kakatiya Univ., Warangal, India). *Indian J. Pure & Appl. Phys.*, vol.21, no.3, p.185-7 (March 1983).

For pt.IV see ibid., vol.20, no.10, p.787 (1982). A modified valence force field has been derived for N,N-dichloroacetamide from vibrational frequencies using a damped least-squares method. The nature of the normal vibrations has been investigated with the help of potential energy distributions. Arguments have been presented to revise the assignment of stretching mode of C-C to 1001 cm^{-1} . (10 refs.)

75359 Algebraic approach to molecular rotation-vibration spectra. F.Iachello (Wright Nuclear Structure Lab., Yale Univ., New Haven, CT, USA), R.D.Levine. *Int. J. Quantum Chem. (USA)*, vol.23, no.4, p.1679-81 (April 1983).

A summary of the recent progress in the algebraic approach to molecular spectra and dynamics is presented, with references. Particular attention is given to rotating diatomic molecules where not only the Morse but other anharmonic potentials can be discussed. (18 refs.)

- 75360 Binding energies and spectroscopic constants of the first-row and second-row diatomic hydrides.** P.C.Jain, A.J.Kaur, P.S.Bakshi, J.Shanker (Dept. of Phys., Agra Coll., Agra, India). *Indian J. Chem. A*, vol.21A, no.10, p.945-8 (Oct. 1982). [received: April 1983]
The phenomenological method recently used by Pandey and Pandey [ibid., vol.20A, p.592 (1981)] for calculating rotational constant (α_e), vibrational constant ($\omega_e X_e$) and binding energy (D_0) of the first-row and second-row diatomic hydrides has been revised by considering improved potential functions for interatomic energies. The potential function which considers the inverse power dependence of the repulsive energy on inter-nuclear distance and a modified value of ionic charge, produces best agreement with experiment. An explanation for the modified ionic charge has been provided in terms of electronegativity difference for constituent atoms forming the bond. (11 refs.)
- 75361 Evaluation of molecular properties of diatomic alkali halides.** Raj K. Gupta, A.J.Kaur, P.S.Bakshi, J.Shanker (Dept. of Phys., Agra Coll., Agra, India). *Indian J. Phys. Part B*, vol.56B, no.6, p.344-52 (Dec. 1982). [received: May 1983]
Values of rotation-vibration coupling constant α_e , vibrational anharmonicity constant $\omega_e X_e$ and higher order molecular spectroscopic constants β_e and γ_e of diatomic alkali halides have been calculated using the Hellmann potential. It is shown that the results obtained in the present study are in much better agreement with the corresponding experimental data than those obtained recently by Hasan, Pathak and Thakur (1981). (11 refs.)
- 75362 Vibrational spectra of fundamental tone of spontaneous emission of CO molecules under nonequilibrium conditions.** V.A.Dudkin, S.P.Sannikov. *J. Appl. Spectrosc. (USA)*, vol.36, no.5, p.550-2 (May 1982). Translation of: *Zh. Prikl. Spektrosk. (USSR)*, vol.36, no.5, p.780-3 (May 1982). [received: Feb. 1983]
Uses the calculated data to show that from the spectra of the fundamental tone it is possible to obtain information which is more limited, but for practical applications is more important, on the presence of a difference between the vibrational temperature of CO and that of the gas. (5 refs.)
- 75363 Force constants and vibrational spectra of methylphosphine, dimethylphosphine, and trimethylphosphine.** S.A.Katsyuba, I.S.Pominov, B.P.Khalepp. *J. Appl. Spectrosc. (USA)*, vol.36, no.5, p.553-6 (May 1982). Translation of: *Zh. Prikl. Spektrosk. (USSR)*, vol.36, no.5, p.783-7 (May 1982). [received: Feb. 1983] (12 refs.)
- Force field calculations for in-plane vibrations of oxamide: use of CNDO/force method** See Entry 75311
- Virial partitioning analysis of electron correlation and nuclear motion in diatomic molecules** See Entry 75313
- Microwave spectrum, dipole moment and ab initio molecular structure of 2-aminopropenitrile ($\text{CH}_2=\text{C}(\text{NH}_2)\text{CN}$)** See Entry 75368
- Selective dynamical coupling in the d-d spectra of octahedral d^3 complexes** See Entry 75374
- Vibrational spectra of phosphotungstate ion— $\text{PW}_{12}\text{O}_{40}^{3-}$** See Entry 75375
- Vibrational spectra of 2,5- and 2,6-dimethylanilines** See Entry 75376
- Spectra of substituted N-heterocyclic molecules. I. Spectra of substituted pyrimidines** See Entry 75377
- Experimental and theoretical determination of the fundamental vibrations of 2-halo ethanols. I. Gauche conformers** See Entry 75382
- Vibrational studies on conformational equilibrium in dimethylmethylphosphonate and methylmethylphosphinate** See Entry 75385
- Assignment of the M-C stretching and M-C-O deformation modes of some trigonal bipyramidal metal carbonyls** See Entry 75386
- Infrared cryogenic studies. XV. Chloroalkanes in argon matrices** See Entry 75387
- Rotational analysis of the $A''^1\text{X}^1\Sigma^+$ bands of $^{28}\text{Si}^{34}\text{S}$: perturbation studies in the A''^1 state** See Entry 75399
- Ultraviolet bands in diatomic mercury bromide** See Entry 75400
- ^1H and ^{13}C NMR and infrared spectroscopic study of the conformational equilibrium in S-methyl dithiocarbazate** See Entry 75411
- Observation of a metastable $^2\Delta$ state in BaCl** See Entry 75418
- Spectroscopic and picosecond time-resolved studies of vibrational relaxation in naphthazarine in solid neon** See Entry 75419
- Spectroscopy and dynamics of jet-cooled 1,1'-binaphthyl** See Entry 75424
- Study of optical relaxation of polyatomic molecules in the condensed phase by site-selective laser spectroscopy** See Entry 75426
- Irreversibility, time, and fluctuations in quantum statistical theory of dissipative molecule systems. II. Application to fluorescence spectroscopy** See Entry 75429
- Laser-induced fluorescence spectrum of the CCN radical with an Ar^+ laser** See Entry 75430
- Breakdown of dynamic equilibrium between the symmetric and deformation mode levels in CO_2 caused by excitation in an electrical discharge** See Entry 75453
- Experimental determination of the m_j distribution in inelastic scattering of Na_2 by He** See Entry 75495
- Out-of-plane force field for cyclic pentaatomic molecules with an OC-X-CO grouping ($\text{X}=\text{O}, \text{NH}, \text{CH}_2$)** See Entry 75546
- Applicability of R-K potential function for calculating molecular parameters of diatomic molecules** See Entry 75547
- Alignment of diatomic molecules by gaseous transport** See Entry 76142
- Collisional vibrational quenching of $\text{O}_2^+(v)$ and other molecular ions in planetary atmospheres** See Entry 78809

33.20 MOLECULAR SPECTRA GROUPED BY WAVELENGTH RANGES

(for magneto-optical and electro-optical spectra, see 33.45; for fluorescence and phosphorescence spectra, see 33.50; for photoelectron spectra, see 33.65)

- 75364 Peculiarities of dip (hole) burning in the spectra of organic molecules in vitreous matrices.** A.A.Gorokhovskii, Ya.V.Kikas, V.V.Pal'm, L.A.Rebane (Phys. Inst., Acad. of Sci., Estonian SSR). *Bull. Acad. Sci. USSR, Phys. Ser. (USA)*, vol.46, no.5, p.116-20 (1982). Translation of: *Izv. Akad. Nauk SSSR Ser. Fiz.*, vol.46, no.5, p.952-6 (1982). [received: May 1983] (Proceedings of the All-Union Conference on Luminescence Commemorating the Ninetieth Anniversary of the Birth of the Academician S.I. Vavilov, Leningrad, USSR, 21-24 April 1981).
The authors determine the homogeneous widths of the spectral lines using the method of photochemical hole burning. The impurity molecule of H_2 -tetra-4-tertiary-butylphthalocyanine (H_2Pc) was introduced into matrices of three types: organic glass (a mixture of isopropyl alcohol and ether in the ratio 2:5 by volume), a polycrystal having a large inhomogeneous broadening (nonane) and a Shpol'skii matrix (tetradecane). The inhomogeneous band in nonane is similar to the band in glass (it has a maximum at 697 nm and a width of 150 cm^{-1}), which ensures comparable excitation conditions. The hole was burned by means of a scanned oxazine laser which was pumped synchronously by a pulsed krypton laser operating in a mode-locking regime. By varying the degree of locking one could obtain a smooth contour of the oxazine lasing line with a width of from 0.2 to 1 cm^{-1} . In order to obtain a spectrally narrow hole-burning, the line was additionally monochromatized by means of an RC-110 interferometer.
- 75365 Photophysics of aryl substituted 1,3,4-oxadiazoles: the triplet state of 2,5-diphenyl-1,3,4-oxadiazole.** C.Rulliere (Centre de Phys., Moleculaire Optique et Hertzienne, Univ. de Bordeaux I, Talence, France), P.C.Roberge. *Chem. Phys. Lett. (Netherlands)*, vol.97, no.2, p.247-52 (13 May 1983).
A theoretical approach using a SCF CI method has been used to analyse the T_1-T_0 absorption spectrum of 2,5-diphenyl-1,3,4-oxadiazole. In its first triplet state in a non-polar solvent, this molecule is strongly non-planar. The conclusion is corroborated by comparison of the fluorescence and phosphorescence spectra. A change of geometry, towards a more planar conformation, appears to occur in an alcoholic solution. It is suggested that $n\pi$ autocomplexes are formed in the triplet state. Conflicting results published for the T-T absorption must be attributed to an impurity. (19 refs.)
- 75366 The hypersensitive $\Delta_g(\sigma_u\delta_u)-\Sigma_g$ transition of the uranyl ion.** C.D.Flint (Dept. of Chem., Birkbeck Coll., London, England). *Chem. Phys. Lett. (Netherlands)*, vol.97, no.3, p.317-18 (20 May 1983).
The $\Delta_g(\sigma_u\delta_u)-\Sigma_g(\sigma_u)^2$ transition of the uranyl ion which corresponds to an electron transfer for a weakly bonding oxygen orbital to a non-bonding uranium $5f_{z^2}$ orbital has characteristics similar to the so-called hypersensitive 4f-4f transitions of the lanthanide ions. (18 refs.)
- 75367 Some notes on exciplex emission from aromatic hydrocarbon-aromatic triarylamines.** A.K.Purkayastha, S.Basu (Dept. of Chem., Univ. Coll. of Sci., Calcutta, India). *Indian J. Phys. Part B*, vol.56B, no.6, p.375-8 (Dec. 1982). [received: May 1983]
Shows that if the one electron-one orbital energy level scheme for exciplex emission from aromatic hydrocarbon-aromatic triamine as proposed by Basu (1979) is accepted, then it is to be concluded that the hydrocarbon excited states involved are of α -parentage. (8 refs.)
- Algebraic approach to molecular rotation-vibration spectra** See Entry 75359
- Alignment of diatomic molecules by gaseous transport** See Entry 76142
- ### 33.20B Radiofrequency and microwave spectra
- (for NMR spectra, see 33.25; for EPR spectra, see 33.30)
- 75368 Microwave spectrum, dipole moment and ab initio molecular structure of 2-aminopropenitrile ($\text{CH}_2=\text{C}(\text{NH}_2)\text{CN}$).** A.Bauder, T.-K.Ha (Lab. fur Phys. Chem., Eidgenossische Tech. Hochschule, Zurich, Switzerland). *Chem. Phys. Lett. (Netherlands)*, vol.97, no.2, p.135-40 (13 May 1983).
The microwave spectrum of 2-aminopropenitrile has been investigated from 18 to 58 GHz. More than 70 rotational transitions have been assigned for the ground and one excited vibrational state. Rotational constants and centrifugal distortion constants were determined for these states. The electric dipole components $\mu_a=3.76(2)$, $\mu_b=0.71(9)$ and $\mu_{\text{total}}=3.83(8)\text{ D}$ were deduced from Stark splittings. The molecular structures of the almost planar stable conformer and a $90^\circ\text{ C}=\text{C}$ twisted conformer were optimized by ab initio calculations. Additional information was obtained on the lower excited electronic states. (12 refs.)
- 75369 The microwave spectrum of the SiN ($^2\Sigma^+$) radical.** S.Saito, Y.Endo, E.Hirota (Inst. for Molecular Sci., Ozakazi, Japan). *J. Chem. Phys. (USA)*, vol.78, no.11, p.6447-50 (1 June 1983).
The microwave absorption spectrum of the SiN radical has been detected in a DC glow discharge in a SiCl_4 or SiH_4/N_2 mixture. The three rotational transitions $N=2-1$, $3-2$, and $4-3$, have been observed in the frequency region 87 to 175 GHz by using a source-frequency modulation microwave spectrometer. The rotational constant, the centrifugal distortion constant, the spin-rotation coupling constant, and the magnetic hyperfine coupling constants b and c and the electric quadrupole coupling constant of the nitrogen nucleus have been precisely determined. The electronic structure of the SiN molecule has been briefly discussed using the magnetic hyperfine constants and also the quadrupole coupling constant $[3.05(23)\text{ MHz}]$ of ^{14}N . (18 refs.)
- The microwave and far-infrared spectra of the CH radical** See Entry 75371
- Beam-maser spectroscopy on cyanoacetylene-D** See Entry 75410
- Rotational Zeeman effect in ArHCl and ArDF** See Entry 75417
- Molecular g values, magnetic susceptibility anisotropies, and molecular quadrupole moments in $^{15}\text{N}_2\text{-HF}$, $^{15}\text{N}_2\text{-DF}$, OC-HF , OC-DF , and OC-HC van der Waals complexes** See Entry 75544
- Dielectric relaxation and dipole moment measurements of n -methylacetamide in benzene and dioxane solutions at different temperatures from microwave absorption studies** See Entry 77325

33.20E Infrared spectra

75370 Infrared heterodyne spectroscopy of seven gases in the vicinity of chlorine monoxide lines. H.A. Weaver, M.J. Mumma, J.L. Faris, T. Kostiuik, J.J. Hillman (Infrared & Radio Astron. Branch, NASA Goddard Space Flight Center, Greenbelt, MD, USA).

Appl. Opt. (USA), vol.22, no.10, p.1562-7 (15 May 1983).

Chlorine monoxide (ClO) is thought to play an important role in a photochemical cycle which causes the destruction of ozone in the Earth's stratosphere. Since lines of the (1,0) fundamental of ClO lie near $^{14}\text{C}^{16}\text{O}_2$ laser lines, IR heterodyne spectroscopy is potentially an important technique for monitoring the ClO abundance. However, due to the presence of lines from other trace atmospheric gases in this spectral range, the interpretation of such observations is ambiguous unless high-resolution laboratory measurements support the identifications. The authors report here measured frequencies for spectral lines of seven trace atmospheric gases which absorb near the $^{14}\text{C}^{16}\text{O}_2$ laser transitions relevant to the detection of ClO by IR heterodyne spectroscopy. (18 refs.)

75371 The microwave and far-infrared spectra of the CH radical. J.M. Brown (Dept. of Chem., Southampton Univ., Southampton, England), K.M. Evenson.

Astrophys. J. Lett. Ed. (USA), vol.268, no.1, pt.2, p.L51-6 (1 May 1983).

The frequencies, wavelengths, and line strengths for transitions of the CH molecule at microwave and far-infrared wavelengths have been calculated from an analysis of the laser magnetic resonance spectrum. The low-frequency transitions are between lambda-doublet type doublets, while the higher frequency transitions are between different spin-rotation levels. (17 refs.)

75372 IR dimer spectroscopy and Fermi resonance. J. Geraedts, S. Stolte, J. Reuss (Fysisch Lab., Katholieke Univ., Nijmegen, Nijmegen, Netherlands).

Chem. Phys. Lett. (Netherlands), vol.97, no.2, p.152-4 (13 May 1983).

A careful discussion of Fermi resonances is shown to explain qualitatively the many observed line shifts from molecular-beam infrared predissociation experiments. (14 refs.)

75373 Matrix spectroscopy in the gas phase: IR spectroscopy of argon clusters containing SF_6 or CH_3F . T.E. Gough, D.G. Knight, G. Scoles (Chem. Dept., Univ. of Waterloo, Waterloo, Ontario, Canada).

Chem. Phys. Lett. (Netherlands), vol.97, no.2, p.155-60 (13 May 1983).

Optothermal (bolometric) detection and a line-tunable CO_2 laser have been used, in conjunction with supersonic beams of dilute mixtures of SF_6 or CH_3F in Ar, to obtain the infrared spectra of Ar clusters containing these molecules. The spectra obtained at the limit of large clusters are remarkably similar to the infrared Ar matrix deposition spectra of the same molecules. (24 refs.)

75374 Selective dynamical coupling in the d-d spectra of octahedral d^3 complexes. A. Ceulemans (Dept. of Chem., Univ. of Leuven, Leuven, Belgium).

Chem. Phys. Lett. (Netherlands), vol.97, no.4-5, p.365-8 (27 May 1983).

The odd-parity vibrational modes which induce intensity in the $^4A_{2g} \rightarrow ^2E_g$ electronic d-d transition in octahedral d^3 complexes, are subdivided from octupolar parent modes, whereas the infrared spectrum is clearly dominated by dipolar terms. These complementary selection rules reflect the hexadecapolar character of the first $t_{2g} \rightarrow e_g$ orbital transition. (25 refs.)

75375 Vibrational spectra of phosphotungstate ion- $\text{PW}_{12}\text{O}_{40}^{3-}$. S.S. Saleem, G. Aruldas (Dept. of Phys., Univ. of Kerala, Kariavattom, India).

Indian J. Pure & Appl. Phys., vol.21, no.2, p.112-15 (Feb. 1983).

The infrared and Raman spectra of phosphotungstic acid have been recorded. The factor group analysis has been carried out using the site group approach for the phosphotungstate ion $\text{PW}_{12}\text{O}_{40}^{3-}$ of T_d symmetry. Based on group vibrations and factor group analysis a vibrational assignment has been proposed for the $\text{PW}_{12}\text{O}_{40}^{3-}$ ion. (23 refs.)

75376 Vibrational spectra of 2,5- and 2,6-dimethylanilines. S.K. Singh, R.N. Singh (Dept. of Phys. LS Coll., Bihar Univ., Muzaffarpur, India).

Indian J. Pure & Appl. Phys., vol.21, no.3, p.163-7 (March 1983).

The far infrared (200-500 cm^{-1}), infrared (200-4000 cm^{-1}) and laser Raman (100-3500 cm^{-1}) spectra of 2,5- and 2,6-dimethylanilines have been recorded using a Fourier far IR spectrometer, a Perkin Elmer grating spectrophotometer and a He-Ne laser Raman spectrometer respectively. The vibrational spectra have been analyzed assuming C_s and C_{2v} point groups respectively for these two compounds. The assignments for the fundamental vibrations, combination and overtone frequencies and the internal modes of vibrations of methyl groups as well as amino groups have been proposed. The vibration number in Wilson's notations for each mode of fundamental vibration has been indicated. (21 refs.)

75377 Spectra of substituted N-heterocyclic molecules. I. Spectra of substituted pyrimidines. S.L. Srivastava (Dept. of Phys., Univ. of Gorakhpur, Gorakhpur, India), M. Prasad.

Indian J. Phys. Part B, vol.56B, no.6, p.358-66 (Dec. 1982). [received: May 1983]

The author's work contains the electronic absorption spectra of 2 amino 4 methyl, 4,5 diamino, 2,4,6 triamino and 2,4 diamino 6 hydroxy pyrimidine in liquid state on Carl Zeiss UV VIS spectrophotometer in the region (50000-28000 cm^{-1}) and infrared absorption spectra of 2,4,6 triamino pyrimidine and 2,4 diamino 6 hydroxy pyrimidine dispersed in KBr disc on Carl Zeiss Specord 751R in the region 4000-4000 cm^{-1} . In view of the positions of the bands in the electronic spectra both $\pi-\pi^*$ and $n-\pi^*$ transitions were identified and on the basis of the positions of the typical infrared bands, tautomeric structures for 2,4,6 triamino and 2,4 diamino 6 hydroxy pyrimidine have been proposed. Probable modes of vibrations of the fundamentals have also been discussed. (9 refs.)

75378 Infrared spectra of OC-HX hydrogen-bonded complexes in solid argon. L. Andrews, R.T. Arlinghaus, G.L. Johnson (Dept. of Chem., Univ. of Virginia, Charlottesville, VA, USA).

J. Chem. Phys. (USA), vol.78, no.11, p.6347-52 (1 June 1983).

The hydrogen-bonded complexes OC-HX (X=F, Cl, Br) have been prepared by condensing Ar/HX and Ar/CO reagent mixtures at 12K. FTIR spectra of the complexes are characterized by strong H-X absorptions (ν_X) displaced below the isolated HX fundamental, strong C-O absorptions displaced above the isolated CO fundamental, and sharp degenerate librational modes (ν_L) in the far infrared. Observation of a single degenerate ν_L mode indicates linear structures for the complexes. The displacements $\Delta\nu_X$ and $\Delta\nu_{CO}$ for the complexes decrease in magnitude in the series $\text{HF} > \text{HCl} > \text{HBr}$ in direct relationship with the trend in hydrogen bonding strength for the hydrohalic acids. (23 refs.)

75379 Infrared spectrum of the CO_2 -HCl complex in solid argon at 12K. L. Andrews, R.T. Arlinghaus, G.L. Johnson (Dept. of Chem., Univ. of Virginia, Charlottesville, VA, USA).

J. Chem. Phys. (USA), vol.78, no.11, p.6353-7 (1 June 1983).

Co-condensation of CO_2 and HCl in excess argon at 12K produced the CO_2 -HCl hydrogen-bonded complex. Small shifts in the ν_X and ν_L modes, the low ν_L fundamental, and a very weak infrared Fermi doublet indicate a weakly bound complex. The more strongly bound CO_2 -HF and C^{18}O_2 -HF complexes gave more intense infrared Fermi doublets. The infrared intensity ratio ν_L/ν_X is 200/1 for the CO_2 -HF complex demonstrating that the HF ligand induces finite electrical asymmetry in the CO_2 submolecule. (12 refs.)

75380 Atomic charges and charge flows from infrared intensities: C-H bonds. M. Gussoni (Istituto di Chimica Industriale del Politecnico, Milano, Italy), P. Jona, G. Zerbi.

J. Chem. Phys. (USA), vol.78, no.11, p.6802-7 (1 June 1983).

Use is made of experimental infrared absorption intensities for calculating atomic charges and charge flows for a class of simple organic molecules. Various methods are discussed. Correlations of the calculated quantities with other independent structural parameters shed some new light on the peculiarities of the electrical properties of CH bonds. (26 refs.)

75381 Absolute band strengths of haloalkanes F-11 and F-12 in the 8-to-16- μm region. R.H. Kagann, J.W. Elkins (Gas and Particulate Sci. Div., NBS, Washington, DC, USA), R.L. Sams.

J. Geophys. Res. (USA), vol.88, no.C2, p.1427-32 (20 Feb. 1983).

The infrared strengths of three vibrational band systems of haloalkane F-11 and four vibrational band systems of haloalkane F-12 in the 'atmospheric window' between 8 and 16 μm were measured at $296 \pm 1\text{K}$ using a Fourier transform infrared spectrometer. These results were obtained at a maximum instrumental resolution of 0.06 cm^{-1} . The measurements of the total infrared band strengths for F-11 and F-12 would indicate approximately 17% and 5% greater absorbance, respectively, than those strengths used in recent greenhouse warming calculations by Ramanathan (1975). Wang et al. (1976), and Lalic et al. (1981), and consequently, a corresponding increase in the possible atmospheric warming effect by these haloalkanes. (28 refs.)

75382 Experimental and theoretical determination of the fundamental vibrations of 2-halo ethanol. I. Gauche conformers. G. Davidovics, J. Pourcin, M. Carles, L. Pizzala, H. Bodot (Centre de Saint-Jerome, Univ. de Provence, Marseille, France), L. Abouaf-Marguin, B. Gauthier-Roy.

J. Mol. Struct. (Netherlands), vol.99, no.3-4, p.165-78 (June 1983). In French.

From the Raman spectral study of X-CH₂-CH₂-OH and X-CH₂-CH₂-OD, X=F, Cl (liquid, solution, crystal) and from their IR spectra (4000 to 50 cm^{-1}) at different concentrations in CCl₄, CS₂ and C₆H₁₂ solutions, a coherent assignment of the fundamental vibrations was established for the gauche conformers of these molecules as auto-associated or monomeric species. The experimental and theoretical (GVFF calculations) results are shown to be consistent with a C₂ pseudosymmetry for the gauche conformer of 2-fluoroethanol. (27 refs.)

75383 N-H... π hydrogen bonding: infrared study of N-cyclohexylformamide-aromatic donor systems. A.D. Nikolic, N.L. Kobilarov, A.N. Brzic (Inst. of Chem., Univ. of Novi Sad, Novi Sad, Yugoslavia).

J. Mol. Struct. (Netherlands), vol.99, no.3-4, p.179-88 (June 1983).

Hydrogen bonding of N-cyclohexylformamide with benzene, toluene, ethylbenzene, n-propylbenzene and n-butylbenzene in CCl₄ solutions has been studied in the fundamental NH stretching vibration region. The formation constants for hydrogen bonded complexes are determined over the temperature range 25-60°C. The corresponding thermodynamic parameters are obtained and it is concluded that a weak hydrogen bond is formed. IR spectral and thermodynamic data are correlated and n-alkyl substituent effects considered. The results are also compared with GLC data obtained for the same systems. (28 refs.)

75384 IR and ^1H NMR studies on the hydrogen bond in homoconjugated cations of some pyridine N-oxides in nitromethane and acetonitrile. M. Szafar, Z. Dega-Szafar (Dept. of Chem., A. Mickiewicz Univ., Poznan, Poland).

J. Mol. Struct. (Netherlands), vol.99, no.3-4, p.189-95 (June 1983).

The IR spectra of seven hemiperchlorates of substituted pyridine N-oxides, which contain crystallographically symmetric and very short hydrogen bonds, have been investigated in dry nitromethane and acetonitrile- d_3 , and the following parameters obtained: $\nu_{\text{H}} \sim 1180 \text{ cm}^{-1}$, $A^{\text{H}}/A^{\text{D}} \sim 1.67$ and $\nu_{\text{H}}/\nu_{\text{D}} \sim 1.14$. The centre of gravity, ν_{H} , of the broad and strong absorption is, within experimental error, independent of the strength of the base used. The values of $\nu_{\text{H}}/\nu_{\text{D}}$ obtained suggest either a single asymmetrical minimum (as) or two unequal minima (ad) potential function. The chemical shift of the H-bonded protons of the investigated hemiperchlorates have been measured in dry nitromethane and acetonitrile and the values obtained (δ varies from 18.3 to 18.7 ppm) are lower than those observed in acid salts of carboxylic acid with a similar O...O distance. It is shown that the observed ca. 1 ppm upfield shift in hemiperchlorates relative to acid salts is caused by the diamagnetic anisotropy of the pyridine ring and not by the hydrogen bond strength. (25 refs.)

75385 Vibrational studies on conformational equilibrium in dimethylmethylphosphonate and methylidimethylphosphinate. B.J. Van Der Veken, M.A. Herman (Lab. voor Anorganische Scheikunde, Rijksuniv. Centrum Antwerpen, Antwerp, Belgium), A.J. Barnes.

J. Mol. Struct. (Netherlands), vol.99, no.3-4, p.197-206 (June 1983).

Low temperature Raman data, supplemented with Raman and IR solution spectra are used to assess and quantify the presence of two conformers in the liquid phase of both $\text{CH}_3\text{PO}(\text{OCH}_3)_2$ and $(\text{CH}_3)_2\text{PO}(\text{OCH}_3)$. From profile analysis of the $\nu(\text{P}=\text{O})$ region at different temperatures a liquid phase ΔH value of $3.3 \pm 0.4 \text{ kJ mol}^{-1}$ is established for $\text{CH}_3\text{PO}(\text{OCH}_3)_2$, while it is shown that a Fermi resonance in this mode prevents the abstraction of the corresponding ΔH value in $(\text{CH}_3)_2\text{PO}(\text{OCH}_3)$. (9 refs.)

75386 Assignment of the M-C stretching and M-C-O deformation modes of some trigonal bipyramidal metal carbonyls. M. Van Rentergem, E.G. Claeys, G.P. Van Der Kelen (Lab. for General & Inorganic Chem., Univ. of Ghent, Ghent, Belgium).

J. Mol. Struct. (Netherlands), vol.99, no.3-4, p.207-16 (June 1983).

A novel assignment of the $\nu(\text{Co})$ and $\delta(\text{CoO})$ modes of the compounds $\text{ClHgCo}(\text{Co})_4$, $\text{Hg}(\text{Co}(\text{Co})_4)_2$, $\text{Co}_2(\text{Co})_8$ and their axially substituted derivatives is presented. This assignment is based on a comparison of the frequency shifts due to substitution with the shifts observed in the spectra of the corresponding iron carbonyl compounds. The $\nu(\text{Fe})$ and $\delta(\text{FeO})$ vibrations are assigned unambiguously. (22 refs.)

75387 Infrared cryogenic studies. XV. Chloroalkanes in argon matrices. A.J. Barnes, M.L. Evans, H.E. Hallam (Dept. of Chem., Univ. Coll. of Swansea, Swansea, Wales).

J. Mol. Struct. (Netherlands), vol.99, no.3-4, p.235-45 (June 1983).

Infrared spectra are reported for chloroethane, chloropropane and chlorobutanes trapped in argon matrices at 10K. The spectra obtained are consistent

with the gas-phase conformational equilibrium having been trapped out in the matrices, both conformers of the primary chloropropane and chlorobutanes and all three conformers of the secondary 2-chlorobutane being observed. (15 refs.)

75388 Chloroacetyltriphenylphosphonium and the corresponding phosphorane. Physical chemistry and conformation study. J.P.Henichart (INSERM U-16, Lille, France), R.Houssin, C.Vaccher, M.Foulon, F.Baert. *J. Mol. Struct. (Netherlands)*, vol.99, no.3-4, p.283-93 (June 1983). In French.

The structures of chloroacetyltriphenylphosphonium and the corresponding phosphorane have been studied by IR, NMR (^1H , ^{13}C , ^{31}P) and X-ray crystallography. The compounds have analogous conformations, especially when an enolic form of the phosphonium last is considered. The molecules are nearly planar with phosphorus, oxygen and chlorine atoms being cis-cis with each other. This arrangement explains the ability of the phosphorane to undergo reactions in which these reactive centers are involved. (17 refs.)

75389 Shape of the $\nu(\text{OH})$ band in the IR spectra of H-complexes of pentachlorophenol. S.E.Odinkov, A.A.Mashkovskii, Z.A.Tarankova. *J. Appl. Spectrosc. (USA)*, vol.37, no.2, p.947-52 (Aug. 1982). Translation of: *Zh. Prikl. Spektrosk. (USSR)*, vol.37, no.2, p.284-90 (Aug. 1982). [received: April 1983]

The main attention in this work was paid to the investigation of changes in the shape of the $\nu(\text{OH})$ band in the H-complex depending on the strength of the bases. The changes in the $\nu(\text{OH})$ band were followed beginning with the weak H-complex of PCP (pentachlorophenol)-hexane up to the strongest complex of PCP-2,4,6-collidine (beginning of protonation of the base). The Fermi resonance nature of the appearance of a multiplet character in the structure of the $\nu(\text{OH})$ band in the entire series of variation of the strength of H-complexes was demonstrated. Strong Fermi resonance interactions of the stretching vibration $\nu(\text{OH})$ with combinations of deformational $\delta(\text{OH})$ and low frequency O-H...B vibrations were detected. This interaction leads to the appearance of two intense bands (D and E) in the IR spectra of strong H-complexes in the region of 400-1600 cm^{-1} . (13 refs.)

75390 The Q branch of 21^0-01^0 band of N_2O . Shen Zhiye, Liu Hui-fang (Dalian Inst. of Chem. Phys., Acad. Sinica, Beijing, China). *Kexue Tongbao (Foreign Lang. Ed.) (China)*, vol.28, no.2, p.213-15 (Feb. 1983).

The vibration-rotation spectra of N_2O are among the most thoroughly investigated IR spectra in the literature. Recently, the observation made by C. Amiot et al. (1976) gave molecular constants with great precision. There is, however, no information yet on the Q branch of the 21^0-01^0 band. The authors measurements were made by using a Laser Analytics model LS-3 tunable diode laser source IR spectrometer. The resulting spectra is shown. The whole spectra obtained are composed of 4 regions. Between 2577.1 and 2578.8 cm^{-1} , 37 lines of the Q branch were observed, most of which were well separated, while a few lines were mutually overlapping. The half-width of any single line, about 0.006 cm^{-1} , was somewhat broader than the Doppler width. (2 refs.)

75391 Highly strained single and double bonds. J.Michl, G.J.Radziszewski, J.W.Downing (Dept. of Chem., Univ. of Utah, Salt Lake City, UT, USA), R.D.Miller, P.Kovacic, M.Jawdosiuik, V.Bonacic-Koutecky. *Pure & Appl. Chem. (GBC)*, vol.55, no.2, p.315-21 (Feb. 1983). (International Symposium on Theoretical Organic Chemistry, Dubrovnik, Croatia, Yugoslavia, 30 Aug.-3 Sept. 1982).

The infrared spectra of the strained single bond compounds, [2.2.1]propellane, [2.1.1]propellane and [1.1.1]propellane, and the vibrational and electronic spectra of the strained bridgehead double bond compounds, adamantene and azahomoadamantene, are reported and discussed. (24 refs.)

75392 Solvent effects on the infrared active CO stretching frequencies of some metal carbonyl complexes. I. Dimanganese decarbonyl and dirhenium decarbonyl. D.J.Parker (Chem. Section, South London Coll., London, England). *Spectrochim. Acta Part A (GB)*, vol.39A, no.5, p.463-76 (1983).

The infrared spectra of $\text{Mn}_2(\text{CO})_{10}$ and $\text{Re}_2(\text{CO})_{10}$ have been measured in the CO stretching region in the gas phase and in each of seventy four solvents and solvent shifts related to the parameter δ_ν . Using straight chained hydrocarbon solvents, there is a linear relationship between band frequency and δ_ν for all three $\nu(\text{CO})$ modes for both compounds. While effects on $\nu_2(b)$ and ν_1 modes are similar for each compound a much larger effect occurs on the $\nu_3(a)$ mode of $\text{Re}_2(\text{CO})_{10}$ than that on the same mode of $\text{Mn}_2(\text{CO})_{10}$. It is suggested that this is associated with greater double bond character in the axial CO groups reflected in the stronger Re-Re bond for $\text{Re}_2(\text{CO})_{10}$. Deviations that are both positive and negative are observed for all other solvents. Usually positive deviations occur with the highest frequency $\nu_3(b)$ modes and negative deviations with the other modes. For polar solvents this has been explained in terms of the relative contribution of triple and double bond character to the CO groups involved and hence the sign of μ' (the change in dipole moment with respect to the vibrational coordinate of the solute bond). As the alkyl chain is lengthened deviations become less positive (or more negative). This is explained from increase in +I effect of the alkyl group causing more polarity in the functional group which leads to a more negative value for μ' . Trends in solvent effect for branch chain hydrocarbons, alkenes and alkyl benzenes are also discussed. (12 refs.)

Tone-burst modulated color-center-laser spectroscopy See Entry 74545

Vibrational spectra of fundamental tone of spontaneous emission of CO molecules under nonequilibrium conditions See Entry 75362

Vibrational and conformational studies of cyclopropylcarbonyl chloride See Entry 75394

Synthesis and structural study of N-ethylnorbornane-3-spiro-5'-oxazolidine-2,4'-dione and its hydrochloride See Entry 75395

^1H and ^{13}C NMR and infrared spectroscopic study of the conformational equilibrium in S-methyl diethiocarbamate See Entry 75411

Stark-tuned Lamb-dip spectroscopy of the ν_4 and $2\nu_2$ bands of $^{14}\text{NH}_3$ See Entry 75450

Breakdown of dynamic equilibrium between the symmetric and deformation mode levels in CO_2 caused by excitation in an electrical discharge See Entry 75453

Energy-dependent energy transfer: deactivation of azulene (S_0 , E_{vib}) by 17 collider gases See Entry 75483

Applications of degenerate four-wave mixing to high resolution molecular spectroscopy at 10.6 μm See Entry 75745

Spectra and structure of asymmetric carboxylic acid dimers in solution See Entry 77387

Study of complexes of hydrogen halides with diethyl ether in aprotic solvents by the method of IR spectroscopy See Entry 77389

The interaction induced spectra of liquid CS_2 . A computer simulation study See Entry 77392

The Brownian rotational motion and shape of IR-absorption lines See Entry 77401

Vibrational excitation of the allene-fluorine reaction in cryogenic matrices: possible mode selectivity See Entry 77878

33.20F Raman and Rayleigh spectra (inc. scattering)

75393 Surface enhanced Raman scattering (SERS) from pyridine on silver-UHV interfaces: excitation spectra. I.Pockrand, J.Billmann, A.Otto (Phys. Inst. III, Univ. Dusseldorf, Dusseldorf, Germany).

J. Chem. Phys. (USA), vol.78, no.11, p.6384-90 (1 June 1983). Excitation spectra of various surface enhanced Raman lines of pyridine adsorbed to evaporated silver films (1 L exposure) in UHV have been measured. Relative to ordinary scattering from thick pyridine layers on SERS inactive Ag films, every vibration exhibits a resonance profile which peaks at the same Stokes frequency corresponding to 2.0 eV independent of vibration. This value is shifted to the red after additional adsorption of 10^{-1} L of pyridine on the SERS active film. The ratio of corresponding Raman line intensities from 'bulk' and 'surface' pyridine varies differently for different vibrations with exciting frequency. The results are discussed with respect to various proposed enhancement mechanisms. (44 refs.)

75394 Vibrational and conformational studies of cyclopropylcarbonyl chloride. J.R.Durig, H.D.Bist, S.V.Saari, J.A.Smoother Smith, T.S.Little (Dept. of Chem., Univ. of South Carolina, Columbia, SC, USA).

J. Mol. Struct. (Netherlands), vol.99, no.3-4, p.217-33 (June 1983). The infrared (3500 to 20 cm^{-1}) and Raman (3200 to 10 cm^{-1}) spectra have been recorded for gaseous and solid cyclopropylcarbonyl chloride, $\text{C}_3\text{H}_5\text{CClO}$. Additionally, the Raman spectrum of the liquid has been recorded and qualitative depolarization values have been obtained. It has been determined that the conformer with the oxygen atom cis to the three-membered ring is the predominant form at ambient temperature in both the gaseous and liquid states but only the trans conformer is present in the spectra of the solid. The observed changes in ΔH in going from the gas to the liquid state indicates strong intermolecular association in the condensed phases which can account for the existence of the trans conformer in the solid state. The torsional mode has been tentatively assigned at 72 cm^{-1} in the far infrared spectrum of the vapor for the cis conformer, and for the trans conformer at $\sim 50 \text{ cm}^{-1}$. From these frequencies and the ΔH for the gas, estimates are given for the values of the coefficients of the Fourier expansion of the potential function for internal rotation. (22 refs.)

75395 Synthesis and structural study of N-ethylnorbornane-3-spiro-5'-oxazolidine-2,4'-dione and its hydrochloride. E.Galvez (Dept. de Química Orgánica, Univ. de Alcalá de Henares, Madrid, Spain), M.Martínez, G.G.Trigo, M.V.López, F.Florencio, P.Smith-Verdier, S.García-Blanco. *J. Mol. Struct. (Netherlands)*, vol.99, no.3-4, p.247-58 (June 1983).

N(8)-Ethylnorbornane-3-spiro-5'-oxazolidine-2,4'-dione hydrochloride has been synthesized and its crystal and molecular structures determined by X-ray diffraction, IR, Raman, ^1H NMR and ^{13}C NMR methods. It is found that the crystalline structure is maintained in D_2O solution. In D_2O solution a protonation equilibrium takes place and the percentages of the two isomers are calculated. In order to correlate the results, analogous spectroscopic measurements have also been made for the N-ethylnorbornane-3-spiro-5'-oxazolidine-2,4'-dione, for which a zwitterionic structure is deduced. (22 refs.)

75396 Two-photon Raman excitation and coherent anti-Stokes Raman spectroscopy probing of population changes in polyatomic molecules: a novel nonlinear optical technique for vibrational-relaxation studies. S.M.Gladkov, M.G.Karimov, N.I.Koroteev (Dept. of Phys., Moscow State Univ., Moscow, USSR). *Opt. Lett. (USA)*, vol.8, no.6, p.298-300 (June 1983).

Two-photon Raman excitation is used to populate selectively vibrational states in CO_2 and SF_6 . The collisional population of 01^0 , 02^0 , 03^0 , etc. by means of 10^0 and 02^0 states in CO_2 gas is studied by coherent anti-Stokes Raman spectroscopy. No population transfer is observed between Fermi-resonant $\text{CO}_2(10^0)$ and $\text{CO}_2(02^0)$ states with the rate constant $K \approx 7 \cdot 10^4 \text{ sec}^{-1} \text{ Torr}^{-1}$. The lifetime of the $\text{SF}_6(100000)$ state is found to be $\tau \approx 15 \mu\text{sec}$ Torr. (14 refs.)

Vibrational spectra of phosphotungstate ion- $\text{PW}_{12}\text{O}_{40}^{3-}$ See Entry 75375

Vibrational spectra of 2,5- and 2,6-dimethylanilines See Entry 75376

Experimental and theoretical determination of the fundamental vibrations of 2-halo ethanol. I. Gauche conformers See Entry 75382

Vibrational studies on conformational equilibrium in dimethylmethylphosphonate and methylmethylphosphonate See Entry 75385

Line displacement and line width in the binary collision theory of the vibrational phase relaxation See Entry 75486

Raman scattering by optically absorbing molecules adsorbed on 'smooth' Ag and Au surfaces: crystal violet See Entry 76784

The interaction induced spectra of liquid CS_2 . A computer simulation study See Entry 77392

RECLAS: resonant-enhanced CARS from C_2 produced by laser ablation of soot particles See Entry 77926

33.20K Visible spectra

75397 Electronic structure of model chlorophyll systems. W.D.Edwards, M.C.Zerner (Dept. of Chem., Univ. of Guelph, Guelph, Ontario, Canada).

Int. J. Quantum Chem. (USA), vol.23, no.4, p.1407-32 (April 1983). An examination of the ground and excited states of magnesium porphine and pheophorine and their positive and negative ions using the intermediate neglect of differential overlap/spectroscopic method is reported. It is found that rather large changes in the Mg out-of-plane coordinate can be attained at very little cost in energy. These geometric changes alone can be used to explain the large range of spectroscopic shifts observed in the visible band of chlorophyll that are site dependent. These calculations also show a porphyrin to Mg charge transfer excitation at about 20000 cm^{-1} , which, if populated and allowed to relax, becomes the lowest excited singlet. This suggests that the initial photochemical event in photosynthesis may be excitation to the visible Q band followed by internal conversion to the charge transfer state accompanied by movement of the Mg atom out of the plane of the ring. This movement could result in intermolecular charge transfer, and relaxation of the Mg atom back to the plane of the ring. The nature of the positive and negative ions of these model chlorophylls is discussed in light of their role as

the electron donor and their potential role as initial electron acceptor in photosynthesis. (49 refs.)

Relativistic MS X α calculations of the electronic structure and related properties of PtCl $_6^{2-}$ See Entry 75289

Charge transfer transition for symmetry-forbidden charge transfer interaction. Theory and experimental verification See Entry 75325

He(I) photoelectron and UV/visible absorption spectra of N $_3^-$, NO $_2^-$ and NO $_3^-$ in solution See Entry 75436

High-accuracy wave-number measurements in molecular iodine See Entry 75548

33.20L Ultraviolet spectra

75398 Electronic spectra and excited state dipole moments of heterocyclic pentaatomic systems and their benzo and dibenzo derivatives. G.Buemi, F.Zuccarello, G.Romeo (Istituto Dipartimentale di Chimica e Chimica Industriale, Univ. di Catania, Catania, Italy).

THEOCHEM (Netherlands), vol.11, no.1-2, p.115-26 (June 1983).

The heterocyclic systems furan, pyrrole and thiophene, as well as their benzo and dibenzo derivatives, have been studied by INDO/S and CINDO/SHIFT/UV methods in order to rationalize their electronic structure and UV spectra, and to calculate the excited state dipole moments. The importance of the doubly excited configurations was tested by means of the CINDV99 program. It is found that the biexcited configurations strongly influence the lowest energy weak band at about 5 eV, which is always predicted to arise from a singlet-singlet transition. The triplet states are not well calculated but it is not to be excluded that a singlet-triplet transition is overlapping with the previous singlet-singlet one. The optical UV spectrum of the sulphurated compounds is well interpreted without *d* orbital inclusion since the MOs involved in the transitions occurring below 7 eV arise nearly exclusively from *p* atomic orbitals. The small variations of dipole moments on passing from the ground to the lowest excited states suggest negligible solvent effect in the molecules examined. (39 refs.)

75399 Rotational analysis of the $A''\Pi-X''\Sigma^+$ bands of $^{28}\text{Si}^{34}\text{S}$: perturbation studies in the $A''\Pi$ state. G.Krishnamurthy, S.Gopal, P.Saraswathy, G.Lakshminarayana (Spectroscopy Div., Bhabha Atomic Res. Centre, Bombay, India).

Can. J. Phys. (Canada), vol.61, no.5, p.714-24 (May 1983).

The ultraviolet bands of the $A''\Pi-X''\Sigma^+$ system of a $^{28}\text{Si}^{34}\text{S}$ molecule were excited in emission in an electrodeless discharge tube and photographed in the fourth order of a 10.6 m Ebert grating spectrograph. Rotational analysis of thirteen bands lying in the region 2600-3000 Å was carried out. Perturbations observed in the $v=0-7$ levels of $A''\Pi$ were attributed to the perturbing states $e''\Sigma^-$, $d''\Delta$, $C''\Sigma^-$, and $D''\Delta$. Origins of the bands involving $v''=2, 6$, and 7 were found to have shifted from their expected positions, presumably due to perturbations. (9 refs.)

75400 Ultraviolet bands in diatomic mercury bromide. A.K.Rai, S.B.Rai, D.K.Rai (Dept. of Phys., Banaras Hindu Univ., Varanasi, India).

J. Phys. B (GB), vol.16, no.11, p.1907-13 (14 June 1983). The emission bands of diatomic mercury bromide molecule lying in the ultraviolet region have been reinvestigated under moderately high resolution. The bands observed in the wavelength range 2770-2700 Å (previously identified as a new D'-X system) simply form an extension (to high $|\Delta v|$ values) of the well known C-X system. The vibrational assignment of the bands has been confirmed by measuring the well resolved bromine isotope shift. In some bands structure due to mercury isotopes is also resolved. Precise vibrational constants for the X, C, D and E states and approximate rotational constants for the X, C and D states are reported. The E-X transition is shown to consist of two subsystems indicating that the E state is a $^2\Pi$ state. (6 refs.)

75401 Nature of deformation of ultraviolet absorption spectra of complex organic molecules. O.N.Glagoleva, M.G.Reva, V.D.Ryzhikov.

J. Appl. Spectrosc. (USA), vol.36, no.5, p.546-9 (May 1982). Translation of: *Zh. Prikl. Spektrosk. (USSR)*, vol.36, no.5, p.776-80 (May 1982). [received: Feb. 1983]

Clarifies the nature of the deformations of the electronic absorption spectra during association of complex organic molecules in the UV part of the spectrum, and outlines the possibility of explaining them according to concepts developed for the visible region. The examples used are potassium cosine and rhodamine 6Zh. (7 refs.)

Relativistic MS X α calculations of the electronic structure and related properties of PtCl $_6^{2-}$ See Entry 75289

Rydberg series in the absorption spectrum of Te I limiting on $5s^2 5p^4 S_{3/2}^0$ ionization limit See Entry 75402

UF $_6$ relaxation dynamics following near-ultraviolet excitation See Entry 75425

Photophysical anomalies of acridine in n-hexane See Entry 75432

He(I) photoelectron and UV/visible absorption spectra of N $_3^-$, NO $_2^-$ and NO $_3^-$ in solution See Entry 75436

New predissociations in GeH affecting all the $A^2\Delta$ state levels See Entry 75457

Two-photon excitation spectroscopy of phenanthrene singlet states below 50000 cm $^{-1}$ See Entry 75458

Collisional deactivation of vibrationally highly excited polyatomic molecules. II. Direct observations for excited toluene See Entry 75484

Collisional deactivation of vibrationally highly excited polyatomic molecules. III. Direct observations for substituted cycloheptatrienes See Entry 75485

33.20N Vacuum ultraviolet spectra

75402 Rydberg series in the absorption spectrum of Te I limiting on $5s^2 5p^4 S_{3/2}^0$ ionization limit. A.M.Catnu, M.Mazzoni (Osservatorio Astrofisico di Arcetri, Firenze, Italy), Y.N.Joshi.

Phys. Scr. (Sweden), vol.27, no.4, p.261-6 (April 1983).

The absorption spectrum of tellurium was photographed in the region 1000-2260 Å on a variety of spectrographs ranges in dispersion from 1.245 to 4.17 Å mm $^{-1}$. The absorption cell consisted of a flash pyrolysis system and the background continuum source consisted of a BRV source or a Garton flash lamp. The new observations have led to great extensions in eight Rydberg series limiting on $5p^3 \ ^4S_{3/2}^0$. One hundred and seventy five lines are classified in the region 1380-2260 Å quadrupling the number of classified lines previously reported in the literature. (21 refs.)

Measurement of absorption line intensities with VUV monochromators See Entry 75782

O $_2$ absorption cross sections (187-225 nm) from stratospheric solar flux measurements See Entry 78652

33.25 NUCLEAR MAGNETIC RESONANCE AND RELAXATION; NUCLEAR QUADRUPOLE RESONANCE (NQR)

75403 The importance of the localization of the π -electron system on its ability to transmit the Fermi contact term of H-H coupling constants. A theoretical and experimental study. J.C.Facelli, R.H.Contreras, D.G.de Kowalewski, V.J.Kowalewski, R.N.Piegaia (Dept. de Fisica, Univ. de Buenos Aires, Buenos Aires, Argentina).

THEOCHEM (Netherlands), vol.11, no.1-2, p.163-72 (June 1983).

Semiquantitative relationships between the localization of a π -electron system and its capacity to contribute to the spin-spin coupling constants are found theoretically and experimentally. Theoretically, enlargements of the INDO basis set and the tautomeric structures of 2-hydroxypyridine are used. Experimentally, the long-range H-H coupling constants in 6-methyl-2-pyridone are compared with the corresponding couplings in 2-X-6-methylpyridines (X=amino, formyl, cyano). Evidence shows that the π -contribution to the H-H coupling constants is greater when the localization of this electron system is increased: $-(39 \text{ refs.})$

75404 Intermolecular potentials from NMR data: H $_2$ -N $_2$ O and H $_2$ -CO $_2$. Lakshman Pandey, C.P.K.Reddy, K.Lalita Sarkar (Dept. of Phys., Indian of Technol., Kanpur, India).

Can. J. Phys. (Canada), vol.61, no.5, p.664-70 (May 1983).

Proton spin-lattice relaxation times T_1 were measured in mixtures of H $_2$ with N $_2$ O as a function of density, composition, and temperature (200-400K) in the region where $T_1 \propto \rho$. These data, along with the data obtained by Lalita and Bloom (1969) for H $_2$ -CO $_2$, were interpreted, using Bloem-Oppenheim theory (1967), to obtain the anisotropic intermolecular potential parameters. Two models, (i) the Lennard-Jones (12-6) potential (LJP) and (ii) the modified Buckingham (exp-2) potential (MBP), were used to represent the isotropic part of the intermolecular potential. The relative anisotropy in the attractive r^{-6} term and the quadrupole moments of N $_2$ O and CO $_2$ as obtained from MBP model are in better agreement with the values obtained from the polarizability data and the reported values, respectively, than those obtained from the LJP model. (14 refs.)

75405 ^{77}Se NMR studies of organoselenium compounds. VI. Substituent effects in 2-substituted selenolo[2,3-b]selenophenes studied by ^1H , ^{13}C and ^{77}Se NMR spectroscopy. A.Konar (Div. of Organic Chem., Univ. of Lund, Lund, Sweden), V.P.Litvinov.

Chem. Scr. (Sweden), vol.22, no.1, p.22-9 (1983).

For pt.1 see *ibid.*, vol.19, p.5 (1982). ^1H , ^{13}C and ^{77}Se NMR spectra of a series of 2-substituted selenolo[2,3-b]selenophenes have been determined. Derivatives containing both strongly electron-attracting and electron-donating substituents, as well as substituents of intermediate character, were chosen. Comparison with the shifts of the corresponding thieno[2,3-b]thiophenes and with selenophenes showed great similarities and good linear correlations were obtained. The influence of substituents on the selenium atoms in both the substituent-bearing and neighbouring rings is discussed. Regression equations for some of the shifts and dual and triple substituent parameters are also given. Comparison of the results obtained with those for 2-substituted selenolo[3,2-b]selenophenes revealed certain differences in the transmittance of substituent effects to similar positions in the two systems. (26 refs.)

75406 Survey of structural regularities in molecular properties. I. Carbon-13 chemical shifts in alkanes. M.Randic (Dept. of Math. & Computer Sci., Drake Univ., Des Moines, IA, USA).

Int. J. Quantum Chem. (USA), vol.23, no.5, p.1707-22 (May 1983).

Many regularities in properties among structurally related compounds are known but a systematic approach to investigate all such cases is rare. A plan is outlined for a systematic study of structural regularities that is based on use of selected graph invariants as prime auxiliary quantities. In this paper carbon-13 chemical shifts in alkanes are examined. Since NMR spectra of paraffins are well understood, the example provides a useful illustration of the approach, introduces basic concepts, and illustrates the kind of results that the graph-theoretical scheme generates. Differences and similarities between graph-theoretical viewing of the problem of structural regularities and customary direct use of additives are discussed in some detail. (18 refs.)

75407 High resolution proton magnetic resonance study on metal-free porphyrins. D.V.Behere, S.Mitra (Chem. Phys. Group, Tata Inst. of Fundamental Res., Bombay, India).

Indian J. Chem. A, vol.21A, no.10, p.966-9 (Oct. 1982). [received: April 1983]

High resolution (270 MHz) PMR spectra of metal-free tetraphenylporphyrin (I), *p*-methyltetraphenylporphyrin and octaethylporphyrin (II) have been recorded. Fine structure multiplets due to spin-spin coupling have been observed in their spectra. The dynamical effect of inner N-H proton tautomerism on the peripheral porphyrin protons has also been investigated through variable temperature measurements. (10 refs.)

75408 Operator and algebraic methods for NMR spectroscopy. I. Generation of NMR spin species. K.Balasubramanian (Dept. of Chem., Univ. of California, Berkeley, CA, USA).

J. Chem. Phys. (USA), vol.78, no.11, p.6358-68 (1 June 1983).

Algebraic methods are developed for generating NMR spin species and irreducible representations spanned by spin functions. These methods use generalized character cycle indices (S function when NMR groups are symmetric groups). A correspondence between the unitary group approach and the permutation group method for NMR is established by generating NMR Gel'fand states using Schur functions. The generalized character cycle indices of molecules whose NMR groups are expressible as generalized wreath products are shown to be generalized NMR plethysms of Schur functions. These techniques enable generation of spin species without the knowledge of the character tables of NMR groups. The author illustrates the methods developed here with several examples. The use of these techniques in generating symmetry-adapted NMR spin functions can be found in the accompanying paper. (18 refs.)

75409 Operator and algebraic methods for NMR spectroscopy. II. NMR projection operators and spin functions. K.Balasubramanian (Dept. of Chem., Univ. of California, Berkeley, CA, USA).

J. Chem. Phys. (USA), vol.78, no.11, p.6369-76 (1 June 1983).

For pt.1 see *ibid.*, vol.78, no.11, p.6358-68 (1983). The author outlines double coset and restricted character cycle index methods which generate the equivalence classes of NMR spin functions and the irreducible representations in the representation spanned by spin functions in any equivalence class. Elegant

operator methods are developed by which the projection operators of NMR groups can be obtained in terms of the projection operators of composing groups. Thus, the projection operators of NMR groups of many molecules can be obtained without the knowledge of their character tables. Projection operators thus obtained are applied on the set of spin functions in an equivalence class of NMR spin functions (rather than the whole set of spin functions) which are generated by double coset methods to obtain symmetry-adapted NMR spin functions in the composite particle representation. Methods are illustrated with several examples of molecules containing as many as 2^{30} NMR spin functions. The methods developed here are quite general so that they can be applied to NMR of nuclei with multipin states and they do not require the character tables of NMR groups. The techniques outlined here are illustrated with 2,2,3,3-tetramethyl butane for which the symmetry-adapted NMR spin couplings are obtained in the composite particle representation. The NMR Hamiltonian matrix of this molecule which is of order $2^{18} \times 2^{18}$ is factored into $2^9 \times 2^9$ matrix by the composite particle treatment. This is further factored into 8 1×1 matrices and 6 4×4 , 4 2×2 , and 3 8×8 matrices in the symmetry-adapted basis. (7 refs.)

75410 Beam-maser spectroscopy on cyanoacetylene-D. L.M.Tack, S.G.Kukulich (Dept. of Chem., Univ. of Arizona, Tucson, AZ, USA). *J. Chem. Phys. (USA)*, vol.78, no.11, p.6512-14 (1 June 1983). The $J=1-0$ transition frequencies were measured for NCCD using a beam-maser spectrometer. Hyperfine structure from ^{14}N and D was completely resolved. Analysis of the data directly gives the ^{14}N and deuterium quadrupole coupling constant along the internuclear axis $eqQ(^{14}\text{N}) = -4318.0 \pm 0.1$ kHz, $eqQ(\text{D}) = 203.5 \pm 1.5$ kHz. From the data the spin-rotation constant on ^{14}N was also measured: $C(^{14}\text{N}) = 1.1 \pm 0.2$ kHz. The spin-rotation data were used to calculate paramagnetic chemical shift tensor components $\sigma_{xx} = \sigma_{yy} = -593 \pm 40$ ppm. These experimentally determined tensor components were combined with calculated diamagnetic tensor components to give the isotropic shift $\sigma_{av} = 18 \pm 27$ ppm. (16 refs.)

75411 ^1H and ^{13}C NMR and infrared spectroscopic study of the conformational equilibrium in S-methyl dithiocarbamate. S.Manogaran, D.N.Sathyanarayana (Dept. of Inorganic & Phys. Chem., Indian Inst. of Sci., Bangalore, India).

J. Mol. Struct. (Netherlands), vol.99, no.3-4, p.267-73 (June 1983). Analysis of the variable temperature ^1H and ^{13}C and ambient temperature ^2H NMR spectra coupled with IR spectra of S-methyl dithiocarbamate shows that the results can be best rationalized in terms of a mixture of cis-cis and trans-cis conformers. The assignment of the proton chemical shifts has been supported by utilizing lanthanide induced shifts. The torsional barrier about the C-N bond has been determined; a full line shape analysis of the ^1H spectra at different temperatures has been made. The rotational behaviour in the N-protonated form relative to the free base is also noted. (20 refs.)

One-electron properties at the SCF ab initio level See Entry 75276
INDO studies on the electronic structure of lanthanoid compounds See Entry 75296

IR and ^1H NMR studies on the hydrogen bond in homoconjugated cations of some pyridine N-oxides in nitromethane and acetonitrile See Entry 75384
Chloroacetyltriphenylphosphonium and the corresponding phosphorane. Physical chemistry and conformation study See Entry 75388

Synthesis and structural study of N-ethylnortropane-3-spiro-5'-oxazolidine-2,4'-dione and its hydrochloride See Entry 75395

Stark-tuned Lamb-dip spectroscopy of the ν_4 and $2\nu_2$ bands of $^{14}\text{NH}_3$ See Entry 75450

Spectra and structure of asymmetric carboxylic acid dimers in solution See Entry 77387

33.30 ELECTRON PARAMAGNETIC RESONANCE AND RELAXATION

75412 An electron bombardment procedure for generating cation and neutral radicals in solid neon matrices at 4K: ESR study of $^{14}\text{N}_2^+$ and $^{15}\text{N}_2^+$. L.B.Knight, Jr., J.M.Bostick, R.W.Woodward, J.Steadman (Chem. Dept., Furman Univ., Greenville, SC, USA).

J. Chem. Phys. (USA), vol.78, no.11, p.6415-21 (1 June 1983). A new generation technique for matrix isolated cations and neutrals involving the electron bombardment of the matrix sample during deposition is presented. Use of the method for the study of ion-neutral reactions and other types of matrix experiments is discussed. Results for the gas phase electron bombardment of $(\text{CH}_3)_2\text{O}$ are compared with electron bombardment of $(\text{CH}_3)_2\text{O}$ conducted during neon deposition. The relative amounts of N and N_2^+ radicals trapped in neon matrices have been measured as a function of electron energies. An ESR analysis of $^{14}\text{N}_2^+$ and $^{15}\text{N}_2^+$ generated by electron bombardment in neon matrices at 4K yields: $g_{\text{iso}} = 2.0004(2)$; $A_{\text{iso}}(^{14}\text{N}) = 104.1(6)$ MHz and $A_{\text{iso}}(^{15}\text{N}) = 146.1(6)$ MHz. The ESR results are used to estimate the extent of s-p hybridization of N_2^+ and a comparison with theoretical calculations and several other 13 electron diatomic radicals is made. (40 refs.)

75413 The laser magnetic resonance spectrum of the ν_3 band of HSO at 10 μm . T.J.Sears, A.R.W.McKellar (Herzberg Inst. of Astrophys. Nat. Res. Council of Canada, Ottawa, Ontario, Canada).

Mol. Phys. (GB), vol.49, no.1, p.25-32 (May 1983). The ν_3 (SO stretching) fundamental band of the HSO radical in the 10 μm region has been studied using the technique of intracavity CO₂ laser magnetic resonance. HSO was produced in a flow system by reacting the products of a microwave discharge in an $\text{O}_2 + \text{Ar}$ mixture with CH_3SH . Spectra in the 998 to 1016 cm^{-1} region were assigned to transitions with $N' \leq 7$ and $K' \leq 3$; their analysis yielded values of the ν_3 band origin, and the rotational and spin-rotational parameters for the (001) state. The authors were not able to assign any transitions to the ν_2 (bending) band, which should lie at somewhat higher frequencies, and these (010) state levels may perturb ν_3 band transitions with $K_a \geq 4$ through Coriolis interactions. (20 refs.)

The microwave and far-infrared spectra of the CH radical See Entry 75371

33.35 DOUBLE RESONANCES AND OTHER MULTIPLE RESONANCES

75414 Sub-Doppler infrared-infrared double resonance spectroscopy of NH_3 using Stark tuning and a diode laser. W.H.Weber, R.W.Terhune (Ford Motor Co., Dearborn, MI, USA).

J. Chem. Phys. (USA), vol.78, no.11, p.6437-46 (1 June 1983). Double resonance experiments on NH_3 are described in which a CO laser pumps a 6 μm ν_4 transition while a tunable diode laser probes a 10 μm ν_2 transition having a common lower level. Four different combinations of

pump-probe transitions are studied. The CO laser is Lamb-dip stabilized on the pump transitions, which are tuned into coincidence with it using a precision intracavity Stark cell. The pump and probe beams overlap colinearly in the Stark cell. The double resonance signals appear as narrow transmission peaks on the diode laser scans. The narrowest observed widths are ≈ 3 MHz (FWHM), a large portion of which is due to unresolved hyperfine structure. An analysis of the various broadening mechanisms indicates that the diode laser contributes less than 1 MHz to the widths. Resonances due to velocity-preserving but state-changing collisions are seen. Asymmetries between co- and counterpropagating linewidths are shown to arise from a combination of field inhomogeneity and coherent narrowing effects. The data are recorded using a computer-aided, rapid-scan, digital signal averaging technique. (28 refs.)

33.40 MÖSSBAUER SPECTRA

75415 Mossbauer studies of after effects of Auger ionization following internal conversion in organo- $^{129\text{m}}$ tellurium compounds. A.Nath, C.Sauer, A.Halpern (Inst. für Festkörperforschung, KFA Jülich GmbH, Jülich, Germany).

J. Chem. Phys. (USA), vol.78, no.8, p.5125-8 (15 April 1983). The after effects of Auger ionization of diphenyl- $^{129\text{m}}\text{Te}$ -telluride, dibenzyl- $^{129\text{m}}\text{Te}$ telluride, and their dispersions in a solvent at 4.2K, were compared with the same systems labeled with tellurium in the ground state, viz ^{127}Te . The Mossbauer emission, in the former case is preceded by an Auger event and β decay, while in the latter case, it is preceded only by β decay. Three species were observed in the two compounds, I^- , C_6H_5 or $\text{C}_6\text{H}_5\text{CH}_2$, and the third one has tentatively been identified as $(\text{C}_6\text{H}_5)_2\text{I}^+$ or $(\text{C}_6\text{H}_5\text{CH}_2)_2\text{I}^+$. The formation of I^- represents rupture of both bonds, i.e., complete fragmentation of the molecule. The probability of fragmentation was estimated with the help of matrix isolation experiments, as the electronically excited tellurium-129 ion formed by fragmentation of the molecule, following the Auger ionization, may interact with a neighboring organo-tellurium molecule in neat compounds, and enter combination. In about 85% of the events in case of diphenyl telluride and 55% in the case of dibenzyl telluride, molecules escape complete fragmentation despite the fact that about 100 eV excitation energy may be deposited during charge neutralization. A novel mode for rapid disposal of energy is discussed. (29 refs.)

33.45 MAGNETO-OPTICAL AND ELECTRO-OPTICAL SPECTRA; DICHROISM

75416 Electric birefringences and molecular conformations of 2-aryloxirans in solution. M.J.Aroney, K.E.Calderbank, H.J.Stootman (Dept. of Inorganic Chem., Univ. of Sydney, Sydney, NSW, Australia).

J. Mol. Struct. (Netherlands), vol.99, no.3-4, p.259-65 (June 1983). Electric birefringence and dipole moment measurements have been made for five aryloxirans as solutes at 298K. The data are analysed to obtain information on the preferred solution-state conformations taking into account electronic and steric interactions between the aryl and oxiran ring systems. (33 refs.)

33.45B Zeeman and Stark effects

75417 Rotational Zeeman effect in ArHCl and ArDF . E.J.Campbell, W.G.Read (Noyes Chem. Lab., Univ. of Illinois, Urbana, IL, USA).

J. Chem. Phys. (USA), vol.78, no.11, p.6490-501 (1 June 1983). The molecular g values and magnetic susceptibility anisotropies of ArH^{35}Cl , ArH^{37}Cl , and ArDF have been measured using pulsed Fourier transform microwave spectroscopy carried out in a Fabry-Perot cavity located in the bore of a superconducting solenoid magnet. The measured magnetic parameters for these three molecules, obtained from rotational Zeeman splittings of $K=0$ R-branch transitions are given. The relationship between these measurements and the signs of the electric dipole moments, the molecular quadrupole moments, and the anisotropy in the second moments of the electronic charge distribution is discussed in detail, with particular emphasis on the effects of the large zero point bending motions present in these molecules. The relationships between the measured Zeeman parameters and the properties of the individual rare gas and hydrogen halide subunits is treated. The authors conclude that the contribution of the rare gas atom to the measured g_{\perp} values is negligibly small, but that the rare gas atom apparently does make a measurable contribution to the magnetic susceptibility anisotropies of at least the HF containing systems. (40 refs.)

Microwave spectrum, dipole moment and ab initio molecular structure of 2-aminopropenenitrile ($\text{CH}_2=\text{C}(\text{NH}_2)\text{CN}$) See Entry 75368

Sub-Doppler infrared-infrared double resonance spectroscopy of NH_3 using Stark tuning and a diode laser See Entry 75414

Quantum interference phenomena in the radiative decay of the $\tilde{\text{C}}(^1\text{B}_2)$ state of SO_2 See Entry 75431

Stark-tuned Lamb-dip spectroscopy of the ν_4 and $2\nu_2$ bands of $^{14}\text{NH}_3$ See Entry 75450

Molecular g values, magnetic susceptibility anisotropies, and molecular quadrupole moments in $^{15}\text{N}_2$ -HF, $^{15}\text{N}_2$ -DF, OC-HF, OC-DF, and OC-HC van der Waals complexes See Entry 75544

33.45C Magnetic circular dichroism

Anomalies in the magnetic circular dichroism of benzene in cyclohexane See Entry 77366

33.50 FLUORESCENCE, PHOSPHORESCENCE; RADIATIONLESS TRANSITIONS (INTERSYSTEM CROSSING, INTERNAL CONVERSION)

75418 Observation of a metastable $^2\Delta$ state in BaCl. H.Martin, P.Royen (Inst. of Phys., Univ. of Stockholm, Stockholm, Sweden).

Chem. Phys. Lett. (Netherlands), vol.97, no.2, p.127-9 (13 May 1983). Laser-induced fluorescence of gaseous BaCl was studied in the 0.5-2.0 μm spectral region. Transitions to a metastable $^2\Delta$ electronic state were observed which made a rotational and vibrational analysis possible of the $\Omega=5/2$ component of this state. (12 refs.)

75419 Spectroscopic and picosecond time-resolved studies of vibrational relaxation in naphthazarine in solid neon. V.E.Bondybey, S.V.Milton, J.H.English, P.M.Rentzepis (Bell Labs., Murray Hill, NJ, USA). *Chem. Phys. Lett. (Netherlands)*, vol.97, no.2, p.130-4 (13 May 1983). Very extensive vibrationally unrelaxed fluorescence is observed following dye-laser excitation of single vibronic levels of naphthazarine. The rates and pathways of its vibrational relaxation are examined by means of picosecond emission spectroscopy. Analysis of its vibrational and electronic spectra establishes a C_{2v} symmetry for free naphthazarine. (12 refs.)

75420 Vibrational redistribution in jet-cooled perylene. Intermediate coupling case. C.Bouzou, C.Jouvet, J.B.Lebland, P.Millie, A.Tramer (CENS, Gif-sur-Yvette, France), M.Sulkes. *Chem. Phys. Lett. (Netherlands)*, vol.97, no.2, p.161-6 (13 May 1983). Fluorescence excitation spectra (FES) and fluorescence spectra (FS) under single vibronic level excitation of perylene in a supersonic jet are reported. The fluorescence from the lowest vibronic levels of the S_1 state is purely resonant while for $\delta E_{vib} > 1600 \text{ cm}^{-1}$ broad-band emission spectra weakly dependent on ν_{exc} are explained by vibrational redistribution with a characteristic time $5 < \tau_{red} < 100 \text{ ps}$. In the intermediate δE_{vib} range ($700\text{--}1600 \text{ cm}^{-1}$) complex emission spectra correspond to a strong coupling between the doorway state and a small number of 'dark' states. The data are discussed in terms of a model assuming a rapid variation of the anharmonic coupling constant with the overall change of the vibrational quantum number between interacting levels. (8 refs.)

75421 Photosensitized luminescence of singlet oxygen in polymeric films. I.M.Bytva, G.P.Gurinovich, O.L.Golomb, V.V.Karpov (Inst. of Phys., Acad. of Sci., Minsk, USSR). *Chem. Phys. Lett. (Netherlands)*, vol.97, no.2, p.167-9 (13 May 1983). Singlet oxygen luminescence has been discovered in polymeric polyethyleneterephthalate and triacetate films coloured by porphyrin, triipallavine and anthraquinone dyes. Quantum yield of porphyrin-sensitized O_2 emission in a polyethyleneterephthalate film has been estimated to be 10^{-6} . The experimental evidence supports the fact that oxygen dissolved in a polymer matrix luminesces. (10 refs.)

75422 Oscillator strength of the $CN A^2\Pi_u \rightarrow B^2\Sigma^+ (0,0)$ transition. J.B.Halpern, Xiao Tang (Dept. of Chem., Howard Univ., Washington, DC, USA). *Chem. Phys. Lett. (Netherlands)*, vol.97, no.2, p.170-4 (13 May 1983). The relative oscillator strength of the $A^2\Pi_u \rightarrow B^2\Sigma^+$ transition has been measured by comparing the laser-induced fluorescence signal from excitation of a known distribution of $CN A^2\Pi_u$ and $CN B^2\Sigma^+$ produced by the photodissociation of cyanogen at 158 nm . The oscillator strength of the $A^2\Pi_u \rightarrow B^2\Sigma^+$ transition is 0.011 ± 0.006 times that of the $X^2\Sigma^+ \rightarrow B^2\Sigma^+$ system. This leads to a value of $(4.0 \pm 2.2) \times 10^{-4}$ for the band oscillator strength. (15 refs.)

75423 Room-temperature rate constants for the gas-phase quenching of metastable molecular oxygen, $O_2(a^1\Delta_g)$ and $O_2(b^1\Sigma_g^+)$, by CO_2 , N_2O , NO , NH_3 , HCl and SO_2 . R.B.Boodaghians, P.M.Borrell, P.Borrell (Dept. of Chem., Keele Univ., Keele, England). *Chem. Phys. Lett. (Netherlands)*, vol.97, no.2, p.193-7 (13 May 1983). The rate constants for collisional quenching of $O_2(b^1\Sigma_g^+)$ by CO_2 , N_2O , NO , NH_3 , HCl and SO_2 , and $O_2(a^1\Delta_g)$ by NO , NH_3 and HCl have been measured at room temperature by studying the emissions of singlet molecular oxygen at 762 and 634 nm in a flowing discharge. The rate constant for deactivation of $O_2(a^1\Delta_g)$ by SO_2 , determined from extrapolation of high-temperature data, is also reported. A comparison is made with previous results. (24 refs.)

75424 Spectroscopy and dynamics of jet-cooled 1,1'-binaphthyl. H.T.Jonkman, D.A.Wiersma (Chem. Dept., Univ. of Groningen, Groningen, Netherlands). *Chem. Phys. Lett. (Netherlands)*, vol.97, no.3, p.261-4 (20 May 1983). Fluorescence excitation and dispersed fluorescence spectra of jet-cooled 1,1'-binaphthyl are reported and analysed. The spectra indicate that in the ground and excited state the naphthalene rings are perpendicular to one another. The spectra can be further interpreted in terms of an exciton model with an exciton splitting of 21 cm^{-1} in the origin. From the structureless emission spectrum and lifetime it is concluded that, in the isolated molecule, efficient vibrational relaxation occurs through conversion of vibrational into librational energy. (17 refs.)

75425 UF_6 relaxation dynamics following near-ultraviolet excitation. S.Castiglione, G.Freddi, P.Morales (Lab. Tecn. Spec. ENEA, Rome, Italy). *Chem. Phys. Lett. (Netherlands)*, vol.97, no.3, p.319-23 (20 May 1983). Collisional relaxation dynamics of UF_6 following excitation in the first electronic absorption band is studied by an investigation of the red-shifted emission. A comparison with dissociation data is made and a simple kinetic model proposed previously is improved. (13 refs.)

75426 Study of optical relaxation of polyatomic molecules in the condensed phase by site-selective laser spectroscopy. M.N.Sapozhnikov, V.I.Alekseev (Laser Spectroscopy Lab., Inst. for Biological Tests of Chem. Compounds, Moscow, USSR). *Chem. Phys. Lett. (Netherlands)*, vol.97, no.3, p.331-6 (20 May 1983). Fluorescence line narrowing and hole burning in absorption spectra have been used for a study of electronic and vibrational relaxations and inhomogeneous distribution function for coporphyrin III molecules in solid ethanol and *n*-octane matrices in the temperature range from 3.2 to 26 K . (18 refs.)

75427 Intramolecular charge-transfer fluorescence from 9,9'-bianthryl absorbed on porous glass. N.Nakashima, D.Phillips (Davy Faraday Res. Lab., Royal Inst., London, England). *Chem. Phys. Lett. (Netherlands)*, vol.97, no.3, p.337-41 (20 May 1983). 9,9'-bianthryl (BA) absorbed on porous glass exhibits both intramolecular charge-transfer (CT) and anthracene-like fluorescence. The CT fluorescence exhibits no temperature dependence, suggesting that orientational relaxation on the time scale of fluorescence decay is absent. Complex fluorescence decay characteristics from BA and 9,10-diphenyl anthracene (DA) absorbed on the glass are interpreted in terms of absorption on a variety of sites. (18 refs.)

75428 Fluorescence excitation and multiphoton ionization spectroscopy of 3-methylindole in a supersonic jet. T.R.Hays, W.E.Henke, H.L.Selzle, E.W.Schlag (Inst. for Phys. & Theoretical Chem., Tech. Univ. of Munich, Garching, Germany). *Chem. Phys. Lett. (Netherlands)*, vol.97, no.4-5, p.347-51 (27 May 1983). The fluorescence excitation and multiphoton ionization spectroscopy of 3-methylindole (skatole) is reported. One electronic origin (1L_b) is assigned at 34875 cm^{-1} , the second (1L_a) suspected at 35483 cm^{-1} . Some 1L_a vibrational assignments are also made. Complex formation between skatole and some small molecules is indicated but not directly observed. (13 refs.)

75429 Irreversibility, time, and fluctuations in quantum statistical theory of dissipative molecule systems. II. Application to fluorescence spectroscopy. C.A.Chatzidimitriou-Dreismann (Iwan N. Stranski-Inst. for Phys. & Theoretical Chem., Tech. Univ. of Berlin, Berlin, Germany). *Int. J. Quantum Chem. (USA)*, vol.23, no.4, p.1505-16 (April 1983). For pt.I see Int. J. Quantum Chem. Quantum Chem. Symp., vol.16, p.195 (1982). Some basic concepts of the Prigogine quantum statistical theory of irreversible processes are discussed in connection with a previous paper by Chatzidimitriou-Dreismann and Lippert (1982). The removal of the 'dual role' that the Hamiltonian plays within conventional quantum theory corresponds to the introduction of a star-unitary operator \mathcal{U} called 'intrinsic time'. The formalism of the previous paper is extended to systems that interact with external fields. A formal specification of \mathcal{U} furthermore, follows from the Li invariance of the basic equations of motion and its connection with the intrinsic time. As an application to fluorescence spectroscopy, a photon counting experiment is presented. It allows the authors to detect certain predicted 'dynamical' fluctuations in emission spectra. Some current experimental results are reported concerning the resolution of the broad fluorescence band of fluoranthene (dissolved in ethanol) through detection of the underlying finer vibrational structure. (15 refs.)

75430 Laser-induced fluorescence spectrum of the CCN radical with an Ar^+ laser. K.Hakuta, H.Uehara (Sagami Chem. Res. Center Nishi-Ohnuma, Kanagawa, Japan). *J. Chem. Phys. (USA)*, vol.78, no.11, p.6484-9 (1 June 1983). The laser-induced fluorescence (LIF) spectrum of the CCN radical was observed with an Ar^+ laser. The laser line of 465.8 nm coincided with two rovibronic transitions: R_1 (23.5) and R_{21} (12.5) for $A^2\Delta_2(010)\Phi \rightarrow X^2\Pi_2(010)\Delta$. The LIF spectrum consisted of the resonant series: $A^2\Delta_2(010)\Phi \rightarrow X^2\Pi_2(v_1v_2v_3)\Delta$, and the collision-induced bands: $A^2\Delta_2(010)\Pi \rightarrow X^2\Pi_2(v_1v_2v_3)\Sigma^+$, Σ^- . The analysis yielded the vibrational and the vibronic parameters of the ground electronic state $X^2\Pi_2$. (18 refs.)

75431 Quantum interference phenomena in the radiative decay of the $\tilde{C}(^1B_2)$ state of SO_2 . M.Ivanco, J.Hager, W.Sharfin, S.C.Wallace (Dept. of Chem., Univ. of Toronto, Toronto, Ontario, Canada). *J. Chem. Phys. (USA)*, vol.78, no.11, p.6531-40 (1 June 1983). Quantum beat effects in the fluorescence decay of the $\tilde{C}(^1B_2)$ state of SO_2 have been analyzed in detail and the coupling mechanism, which gives rise to the quantum interference phenomena identified as vibronic mixing with the ground state. The use of transform-limited dye laser pulses for excitation permitted both the sensitive detection of weakly modulated quantum beats and a direct quantitative analysis of the magnitude of the interstate coupling. Small Zeeman shifts were also observed to be present, but because these are less than $1/20$ of those observed for singlet-triplet interactions in SO_2 and other molecules, they are attributed to indirect coupling effects via the ground state. The onset for predissociation at 218 nm is marked by the disappearance of the quantum beats and both confirms the vibronic coupling model and yields a spectroscopic measure of the ground state dissociation energy. Thus the dynamical behavior of the $\tilde{C}(^1B_2)$ state of SO_2 has been uniquely characterized through analysis of the quantum interference effects arising through interstate coupling and is the first such example in the limit of a sparse density of states in a polyatomic molecule. (30 refs.)

75432 Photophysical anomalies of acridine in *n*-hexane. W.S.Struve, J.H.Hedstrom, C.G.Morgante (Dept. of Chem., Iowa State Univ., Ames, IA, USA), A.K.Jameson, E.C.Lim. *J. Chem. Phys. (USA)*, vol.78, no.11, p.7006-8 (1 June 1983). The photophysics of acridine excited in its lowest-lying π, π^* state in various solvents has remained problematic despite several recent picosecond transient absorption and fluorescence studies. Room temperature risetimes of the 432 nm $T_0 \rightarrow T_1$ transient absorption of acridine exhibit wide solvent variations, ranging from $\sim 40 \text{ ps}$ in *n*-hexane to $\sim 200 \text{ ps}$ in ethanol. The authors present evidence that the $T_0 \rightarrow T_1$ transition absorption risetime of acridine in *n*-hexane is much more weakly temperature dependent than the reported fluorescence decay time. The fluorescing state and T_1 are therefore not directly coupled. Acceleration of $S_1 \rightarrow S_0$ internal conversion by the proximity effect does not appear to dominate the photophysics of acridine. (12 refs.)

75433 Twisted intramolecular charge transfer (TICT) excited states: energy and molecular structure. Z.R.Grabowski, J.Dobkowski (Inst. of Phys. Chem., Polish Acad. of Sci., Warsaw, Poland). *Pure & Appl. Chem. (GB)*, vol.55, no.2, p.245-52 (Feb. 1983). (International Symposium on Theoretical Organic Chemistry, Dubrovnik, Croatia, Yugoslavia, 30 Aug.-3 Sept. 1982). Numerous compounds of donor (D)-acceptor (A) type, in the excited singlet state undergo a relaxation to a highly polar state, preferentially in fluid polar solvents. Study of the rigid model molecules revealed the polar state to correspond to the D and A moieties mutually twisted by 90° . To find another proof for the structure of the TICT states, the energies of their emission were calculated for 18 molecules starting from the TICT model. The calculated values are compared to the 'polar' fluorescence maxima. The correlation may serve as a structural proof for the TICT states. (57 refs.)

Photophysics of aryl substituted 1,3,4-oxadiazoles: the triplet state of 2,5-diphenyl-1,3,4-oxadiazole See Entry 75365

Mossbauer studies of after effects of Auger ionization following internal conversion in organo- $^{129m}\text{tellurium}$ compounds See Entry 75415

Energy-dependent energy transfer: deactivation of azulene (S_0 , E_{vib}) by 17 collider gases See Entry 75483

A theoretical study of the effects of inhomogeneous level broadening on the spectral kinetic characteristics of the delayed emission from solid polar solutions of complex compounds See Entry 77439

Dynamics of $O(^1D_2)$ reactions with bifunctional substrates: alcohols and thiols See Entry 77875

Determination of product population and alignment using laser-induced fluorescence See Entry 77876

Proton phototransfer and nonradiative deactivation in hydrogen-bonded complexes of 2-anthrol See Entry 77882

Solute-solvent exciplex versus twisted intramolecular charge-transfer state in anomalous fluorescence of 4-NN-dimethylaminobenzonitrile See Entry 77902

Photophysics of derivatives of all-trans-1,6-diphenyl-1,3,5-hexatriene (DPH). I. Model involving fluorescence from S_2 and S_1 excited states See Entry 77903

Collisional vibrational quenching of $O_2(^1v)$ and other molecular ions in planetary atmospheres See Entry 77809

33.65 PHOTOELECTRON SPECTRA

75434 Theoretical study of electron transmission through N_2 . H.Estrada, M.Berman, L.S.Cederbaum, W.Domecke (Inst. fur Phys. Chem., Univ. Heidelberg, Heidelberg, Germany).

Chem. Phys. Lett. (Netherlands), vol.97, no.4-5, p.352-6 (27 May 1983).

The objective of the present work is to unfold the population of the vibrational levels from the experimental electron transmission spectra of N_2 . This is accomplished by comparing these spectra with theoretical spectra which have been obtained using computed resonant vibrational excitation cross sections and assuming a Boltzmann distribution for the population of the vibrational levels of the N_2 target molecule. The cross sections are calculated using an accurate non-local energy-dependent complex potential for the vibrational motion in the resonance state. These 'non-local cross sections' are compared with 'local cross sections' (obtained with the so-called boomerang model). It is shown that the two types of cross sections may differ from each other and that non-local cross sections are needed to unfold accurately the vibrational populations from experimental spectra. (22 refs.)

75435 Theoretical photoelectron spectroscopy of the nitrite ion. R.J.Harrison, N.C.Handy (Univ. Chem. Lab., Univ. of Cambridge, Cambridge, England).

Chem. Phys. Lett. (Netherlands), vol.97, no.4-5, p.410-12 (27 May 1983).

In the accompanying paper by Ballard et al. (1982) vertical ionisation energies of NO_2^- have been observed at 8.6 and 7.0 eV, from the photoelectron spectra of salts in adiponitrile. Large-scale configuration interaction calculations are reported on the ground and excited states of NO_2^- and NO_2 . The first three vertical ionisation energies are calculated to be 2.5, 3.9 and 4.0 eV. (15 refs.)

75436 He(I) photoelectron and UV/visible absorption spectra of N_3^- , NO_2^- and NO_3^- in solution. R.E.Ballard, J.Jones, E.Sutherland, Chun Bae Lee (School of Chemical Sci., Univ. of East Anglia, Norwich, England).

Chem. Phys. Lett. (Netherlands), vol.97, no.4-5, p.413-18 (27 May 1983).

The He(I) photoelectron spectra have been measured of tetra-N-butylammonium salts of N_3^- , NO_2^- and NO_3^- in adiponitrile solution; there are peaks or shoulders for N_3^- at 6.9 eV (π_g^-), for NO_2^- at 7.0 eV ($6a_1^-$) and 8.6 eV ($4b_2^-$), and for NO_3^- at ≈ 8.0 eV ($1a_2^-$) and ≈ 9.0 eV. Also measured are energies of electron-transfer processes in solution, such as $N_3^- + N\text{-methylpyridinium}^+ \rightarrow N_3 + N\text{-methylpyridinium}$. Analysis of the results enables the distinction to be made between electron transfer and internal transitions, e.g. the near UV absorption bands of N_3^- in solution, of controversial assignment, are undoubtedly due to electron transfer to solvent. (30 refs.)

75437 Photoelectron spectra of anions in solutions and the ionisation energy of the solvated electron. R.E.Ballard, J.Jones, E.Sutherland, Chun Bae Lee (School of Chem. Sci., Univ. of East Anglia, Norwich, England).

Chem. Phys. Lett. (Netherlands), vol.97, no.4-5, p.419-21 (27 May 1983).

The ionisation energy of the solvated electron in water and acetonitrile is calculated to be 1.73 (0.3) eV, this value being the mean difference between the vertical ionisation energy and $h\nu(\max)$ for the electron-transfer-to-solvent band of seven anions in solution. (21 refs.)

75438 Application of photoelectron spectroscopy to biologically active molecules and their constituent parts. IX. 1,4-benzodiazepin-2-ones. L.Klasinc, B.Ruscic, A.Sabljic, N.Trinajstic (Rugjer Boskovic Inst., Zagreb, Yugoslavia).

Int. J. Quantum Chem. (USA), vol.23, no.4, p.1667-76 (April 1983).

For pt.VIII see Int. J. Quantum Chem., Quantum Biol. Symp. vol.7, p.403. The HeI photoelectron (PE) spectra of desmethyldiazepam, diazepam, oxazepam, temazepam, 3-(S)-methyldesmethyldiazepam, 3-(S)-methyldiazepam, 5-methyl-2H-1,4-benzodiazepin-2-one, and benzo-phenothymine have been measured and analyzed. Their low-energy regions (up to 12.0 eV) have been completely assigned by the composite molecule method using the PE spectra of diphenylmethane, benzophenonemethylimine, acetamide, chlorobenzene, and acetophenonemethylimine to compare the electronic structure of equivalent parts. (38 refs.)

75439 Photoelectron spectroscopy of NHO^- and DNO^- . H.B.Ellis, Jr., G.B.Ellison (Dept. of Chem., Univ. of Colorado, Boulder, CO, USA).

J. Chem. Phys. (USA), vol.78, no.11, p.6541-58 (1 June 1983).

The authors obtained the photoelectron spectra of HNO^- and DNO^- using a recently constructed negative ion photoelectron spectrometer. They observe detachment to three different electronic states of HNO and DNO , namely the X^1A' , \bar{a}^2A' , and A^4A' states. The electron affinity of HNO is determined to be 0.338 ± 0.015 eV while that of DNO is 0.330 ± 0.015 eV. The \bar{a}^2A' state, which has not been observed directly before, is found to lie 0.778 ± 0.020 eV above the X^1A' state in HNO and 0.785 ± 0.020 eV in DNO . The authors see vibrational excitation up to $v_2=3$ of the $\nu_2(N-O)$ stretch) HNO and DNO X^1A' state. In the \bar{a}^2A' and A^4A' states, they see excitation of both ν_2 and $\nu_3(H-N-O)$ bend modes. The fundamental frequencies for the \bar{a}^2A' state are $\nu_2=1468 \pm 140$ cm^{-1} and $\nu_3=992 \pm 150$ cm^{-1} for HNO and $\nu_2=1452 \pm 140$ cm^{-1} and $\nu_3=750 \pm 140$ cm^{-1} for DNO . Analysis of transitions from vibrationally excited ions gives a ν_2 fundamental frequency of 1153 ± 170 cm^{-1} in HNO^- and 1113 ± 170 cm^{-1} in DNO^- . A study of the angular distribution of the photodetached electrons yields the values of β , the anisotropy parameter, for the various transitions in the spectrum. A Franck-Condon factor analysis of the HNO X^1A' band results in an estimate of the N-O bond length in the negative ion of 1.33 ± 0.02 Å. (62 refs.)

75440 Photoelectron spectra of adsorbed carbonates. M.A.Bartea, R.J.Madix (Dept. of Chem. Engng., Stanford Univ., Stanford, CA, USA).

J. Electron Spectrosc. & Relat. Phenom. (Netherlands), vol.31, no.2, p.101-8 (May 1983).

In order to provide photoelectron spectra for analytical purposes, X-ray and ultraviolet photoelectron spectra for known surface species have been measured. The surface carbonate on Ag(110), formed by reacting gaseous CO_2 with pre-adsorbed atomic oxygen, yields C 1s and O 1s peaks at 287.7 and 529.9 eV, respectively. The UPS results show features due to surface CO_3 which scale well with those for bulk carbonates. These observations, coupled with the increase in work function that accompanies carbonate formation, suggest strongly that this surface species is negatively charged. (13 refs.)

75441 X-ray and UV photoelectron-spectroscopic studies of pyridine adsorbed on evaporated nickel and palladium in the temperature range 140-385K. Y.Inoue, K.Kishi, S.Ikeda (Dept. of Chem., Osaka Univ., Osaka, Japan).

J. Electron Spectrosc. & Relat. Phenom. (Netherlands), vol.31, no.2, p.109-21 (May 1983).

The states of pyridine adsorbed on evaporated nickel and palladium films have been investigated as a function of temperature in the range 140-385K by means of X-ray and UV photoelectron spectroscopy. At $\sim 140K$, pyridine 'N-bonded' on the metal surfaces gives C 1s and N 1s peaks whose binding

energies are very close to those for condensed pyridine and 'N-bonded' pyridine on pre-oxidized nickel. The high-lying valence orbitals, $2b_1$ (π) and $1a_2$ (π) + $7a_1$ (π), of pyridine show shifts similar to those for the 'N-bonded' molecule on pre-oxidized nickel. At $\sim 290K$, π -bonded pyridine shows large shifts in the C 1s and N 1s peaks and in the high-lying valence orbitals, as observed for π -bonded benzene on nickel. The assignments of the adsorbed states are supported by work-function change data. A large proportion of pyridine converts from the 'N-bonded' to the π -bonded form between 220 and 290K. Formation of α -pyridyl is suggested at $\sim 375K$ on nickel. (22 refs.)

75442 Ionisation of cyanate ions in solution. R.E.Ballard, J.Jones, E.Sutherland (School of Chem. Sci., Univ. of East Anglia, Norwich, England).

J. Electron Spectrosc. & Relat. Phenom. (Netherlands), vol.31, no.2, p.145-50 (May 1983).

The He(I) photoelectron spectra of the ions OCN^- and SCN^- in adiponitrile solution have sharp bands peaking at 8.3 and 7.1 eV. In acetonitrile solution, the N-methylpyridinium salts possess UV/visible absorption bands at 4.16 (OCN^-), 3.64 (SCN^-) and 3.37 eV (SCN^-); these are assigned as electron transfers from anion to cation. The conclusion is drawn that the near-UV absorption bands of the anions are caused by electron transfers to the solvent. (22 refs.)

75443 He(I)/He(II) photoelectron band intensity ratios for simple organic molecules. P.H.Cannington, N.S.Ham (Div. of Chem. Phys., CSIRO, Clayton, Victoria, Australia).

J. Electron Spectrosc. & Relat. Phenom. (Netherlands), vol.31, no.2, p.175-9 (May 1983).

Band intensities in the He(I) and He(II) photoelectron spectra of some simple organic molecules (methanol, methylamine, formaldehyde, acetaldehyde, formic acid, acetic acid, methyl formate, ethylene, butadiene and methyl isothiocyanate) have been measured. The relative band intensity ratios for a number of ionizations from n and π orbitals are presented. (14 refs.)

75444 Study of the ionization process $BF^+(X^2\Sigma^+) \leftarrow BF(X^1\Sigma^+)$ by high-temperature photoelectron spectroscopy. J.M.Dyke, C.Kirby, A.Morris (Dept. of Chem., Univ. of Southampton, Southampton, England).

J. Chem. Soc. Faraday Trans. II (GB), vol.79, pt.3, p.483-90 (March 1983).

The He I photoelectron spectrum of the BF molecule, produced by passing BF_3 over heated boron, has been recorded. Only one band was observed and it was assigned to the ionization $BF^+(X^2\Sigma^+) \leftarrow BF(X^1\Sigma^+)$. For this band the adiabatic and vertical ionization potentials were coincident at 11.12 ± 0.01 eV and analysis of the observed vibrational structure gave $\omega_e = 1765 \pm 20$ cm^{-1} and $r_e = 1.208 \pm 0.005$ Å for the $BF^+(X^2\Sigma^+)$ state. Estimates of the first and higher vertical ionization potentials of BF are made by ab initio ΔSCF and Hartree-Fock-Slater calculations. (38 refs.)

75445 Photoelectron spectra of acenes. Electronic structure and substituent effects. L.Klasinc, B.Kovac (Rudjer Boskovic Inst., Zagreb, Croatia, Yugoslavia), H.Gusten.

Pure & Appl. Chem. (GB), vol.55, no.2, p.289-98 (Feb. 1983). (International Symposium on Theoretical Organic Chemistry, Dubrovnik, Croatia, Yugoslavia, 30 Aug.-3 Sept. 1982).

The valence-electronic structure of the first three members of the acene series, benzene, naphthalene and anthracene, is confirmed by their photoelectron (PE) spectra. This especially held for the π -ionizations which, according to their specific behaviour, could be assigned to different ionization modes. The vibrational fine structure of the observed systems is discussed. The effects of a series of substituents on the electronic structure of the parent molecules were traced in their PE spectra and compared. The results for methyl, chloro, methoxy and cyano substitution are described in detail. (31 refs.)

75446 The Cooper minimum in Cl_2 . T.A.Carlson, M.O.Krause (Chem. Div., Oak Ridge Nat. Lab., Oak Ridge, TN, USA), F.A.Grimm, T.A.Whitley.

Fifteenth Annual Synchrotron Radiation Users Group Conference (papers in summary form only received), Stoughton, WI, USA, 18-19 Oct. 1982 (Stoughton, WI, USA: Synchrotron Radiat. Center 1982), p.8-9.

Angle-resolved photoelectron spectroscopy using synchrotron radiation has been carried out on gaseous chlorine as a function of photon energy from 18 eV to 70 eV. From these data the partial cross sections and angular distribution parameter β have been derived for the first three orbitals. For the lone pair orbitals $2\pi_g$ and $2\pi_u$, distinct minima are found in both the partial cross sections and β values in the region of photoelectron energies from 30 to 40 eV. Less well-defined minima are also seen in the case of photoionization for the non-lone pair orbital, $5\sigma_g$. These features are believed related to the Cooper minimum that arises from an atomic 3p subshell. Calculations have also been carried out on the partial cross sections and β values using the multiple scattering $X\alpha$ method. Excellent agreement is obtained between experiment and theory. (no refs.)

75447 Excitation energy dependence in the photoemission satellite structures of CO and N_2 . W.Eberhardt, H.-J.Freund (Brookhaven Nat. Lab., Upton, NY, USA).

Fifteenth Annual Synchrotron Radiation Users Group Conference (papers in summary form only received), Stoughton, WI, USA, 18-19 Oct. 1982 (Stoughton, WI, USA: Synchrotron Radiat. Center 1982), p.13-14.

The photoemission spectrum of gaseous CO and N_2 is well known to exhibit structure which are not explainable in the independent particle picture of photoemission. These satellite lines correspond to ejection of a photoelectron with simultaneous electronic excitation of the remaining ion. The energetic distance of the satellite to the 'main' photoemission line reflects the ionic excitation energy. In principle it is now possible, based on energy and intensity, to assign the observed shake-up peaks to excited ionic configurations. In practice however this task becomes almost impossible; at least for higher energy states where many excited ionic states are almost degenerate in energy. The authors use the relative intensity of photoemission satellites in the outer core, inner valence region measured as a function of photon energy to identify the main contribution or parentage for each individual satellite. (no refs.)

Resistively heated high-temperature furnace for PES experiments on free atoms in the UHV with synchrotron radiation See Entry 74469

An electron-retardation device to improve the resolution of a Turner-type UV photoelectron spectrometer See Entry 74544

An economical transfer vessel with detachable reactor for XPS studies See Entry 74571

Angular distribution of Xe 5s-cp photoelectrons: a sensitive test of theory See Entry 75454

Characterization of resonances in photoionization See Entry 75455

33.70 INTENSITIES AND SHAPES OF MOLECULAR SPECTRAL LINES AND BANDS

75448 Thermal broadening of optical homogeneous linewidths in organic glasses and polymers studied via photochemical hole-burning. H.P.H.Thijssen, R.Van Den Berg, S.Volker (Gorlaeus & Huygens Labs, Univ. of Leyden, Leyden, Netherlands).

Chem. Phys. Lett. (Netherlands), vol.97, no.3, p.295-302 (20 May 1983). Photochemical hole-burning was used to study optical dephasing in the $S_1 \rightarrow S_0$ transitions of dimethyl-s-tetrazine, chlorin and free-base porphyrin in several organic glasses and polymers. The homogeneous width (Γ_{hom}) seems to follow a $T^{-1.3 \pm 0.1}$ law between 0.4 and 20 K for all guest-host pairs, and extrapolates the lifetime-limited values of each guest for $T \rightarrow 0$. For a given temperature, Γ_{hom} appears to be related to the number of OH groups in the glass, and to the size of side-groups on the polymer chain. (32 refs.)

75449 Electronic spectral study of praseodymium(III) complexes with cysteine and diols. A.Kothari, S.N.Misra, M.P.Bhutra (Dept. of Chem., Univ. of Jodhpur, Jodhpur, India).

Indian J. Pure & Appl. Phys., vol.21, no.2, p.127-9 (Feb. 1983). The electronic spectra of the complexes of praseodymium(III) with cysteine and diols have been studied and the values of Slater-Condon (F_2), Lande spin-orbit interaction (ζ_d), oscillator strength (P) and Judd-Ofelt intensity parameter (T_2) have been calculated. The calculated values of the nephelauxetic ratio β and bonding parameter $b^{1/2}$ suggest covalent character of these complexes. (11 refs.)

75450 Stark-tuned Lamb-dip spectroscopy of the ν_4 and $2\nu_2$ bands of $^{14}\text{NH}_3$. W.H.Weber, R.W.Terhune (Ford Motor Co., Dearborn, MI, USA). *J. Chem. Phys. (USA)*, vol.78, no.11, p.6422-36 (1 June 1983). Results are presented of Stark-tuned Lamb-dip measurements in the $6 \mu\text{m}$ ν_4 and $2\nu_2$ bands of $^{14}\text{NH}_3$ obtained using an isotopic CO laser with an intracavity Stark cell. Some 230 lines from the isotopes $^{12}\text{C}^{16}\text{O}$, $^{13}\text{C}^{16}\text{O}$, $^{12}\text{C}^{18}\text{O}$, and $^{13}\text{C}^{18}\text{O}$ were investigated with fields up to 30 kV/cm. 71 coincidences with Stark-tuned NH_3 lines, involving several hundred Lamb dips, were assigned and analyzed. The positions of these lines relative to the CO laser lines are reported with a typical accuracy of 5-20 MHz. Model calculations of Lamb-dip spectra are also given that include power and pressure broadening and the collisionally transferred resonances. These are directly compared with observed spectra, from which the authors deduce values for the pressure broadening coefficients and the collisional transfer efficiency. Nuclear hyperfine structure is resolved on several lines, and from fitting one of these the authors obtained the value $eqQ = -4.83 \pm 0.3$ MHz for the nuclear quadrupole coupling constant in the $s2\nu_2$ ($J=10$, $K=9$) state. The authors see numerous examples of weak 'forbidden' transitions $\Delta M_J = 0, \pm 2$. These arise from the nuclear quadrupole coupling, which mixes M_J states. (40 refs.)

75451 Oscillator strengths corresponding to hypersensitive transitions of Nd^{3+} , Ho^{3+} , and Er^{3+} ions in solutions of complexes with certain amino polycarboxylic acids and their relation to the polarizability of the molecule. S.V.Bel'tyukova, N.S.Poluektov, T.B.Kravchenko, N.A.Nazarenko. *J. Appl. Spectrosc. (USA)*, vol.37, no.2, p.937-40 (Aug. 1982). Translation of: *Zh. Prikl. Spektrosk. (USSR)*, vol.37, no.2, p.272-5 (Aug. 1982). [received: April 1983]

The intensity of the absorption bands corresponding to hypersensitive transitions of lanthanide ions in solutions of complexes with amino polycarboxylic acids is shown to be directly proportional to the polarizability of the residue of the ligand molecules coordinated with the lanthanide ion. In the case of ligands containing the o-hydroxyphenyl or hydroxynaphthalene residue, whose oxygen atom is coordinated with the lanthanide ion, the values of oscillator strengths corresponding to hypersensitive transitions are proportionally related to the polarizability of the residue to the whole ligand molecule. (14 refs.)

75452 Exact solution of the Dirac-Coulomb equation and its application to bound-state problems. II. Interaction with radiation. M.K.F.Wong (Dept. of Math., Fairfield Univ., Fairfield, CT, USA), Hsin-Yang Yeh. *Phys. Rev. A (USA)*, vol.27, no.5, p.2305-10 (May 1983). For pt.1, see *ibid.*, vol.27, no.5, p.2300 (1983). An exact treatment of relativistically bound electrons in hydrogenlike atoms interacting with radiation is given. The simplified solution of the Dirac-Coulomb equation obtained by Wong and Yeh (1982) is used in the calculation. Transition probabilities and sum rules are obtained. The authors' results can be readily compared with those of the Pauli approximation, and all correction terms can be identified. New sum rules have been obtained for the relativistic case which can be compared side by side with the corresponding ones in the nonrelativistic case. (7 refs.)

75453 Breakdown of dynamic equilibrium between the symmetric and deformation mode levels in CO_2 caused by excitation in an electrical discharge. I.M.Bertel', V.O.Petukhov, A.S.Solodukhin, S.A.Trushin, V.V.Churakov (Phys. Inst., Acad. of Sci., Minsk, Belorussian SSR). *Sov. Phys.-Tech. Phys. (USA)*, vol.27, no.11, p.1429-30 (Nov. 1982). Translation of: *Zh. Tekh. Fiz. (USSR)*, vol.52, no.11, p.2317-19 (Nov. 1982). [received: May 1983]

Theories predicting the relative populations of low-lying levels in CO_2 molecules during excitation in an electric discharge are based on the assumption that dynamic equilibrium holds between and within the symmetric ν_1 and deformation ν_2 mode levels. The authors report experimental results which show that dynamic equilibrium may not hold between the group 01^0 , 02^0 , and 03^0 and the remaining levels for these modes when CO_2 molecules are excited in either a pulse or a steady-state electrical discharge. The authors reached this conclusion by analyzing the populations of the 10^0 , 02^0 , 01^0 , and 00^1 levels. The effective vibrational temperatures corresponding to the relative population of the levels 10^0 (T_1), 01^0 (T_2), 02^0 (T_2), and 00^1 (T_3) in CO_2 were determined by measuring the ratios K_i of the gains of a weak signal corresponding to individual vibrational-rotational lines in the 00^1 - 10^0 ($i=1$), 00^1 - 02^0 ($i=2$), 00^1 - 10^1 ($i=3$), and 01^0 - 11^0 ($i=4$) bands. In finding the temperatures, it was assumed that the levels 10^0 and 02^0 , which are coupled by a Fermi resonance, are in dynamic equilibrium. (5 refs.)

Ab initio MRD-CI study of the electronic spectrum of SiH ...See Entry 75312
Lifetime, triplet-triplet absorption spectrum and relaxation energy of an acyclic conjugated triene triplet: a pulse radiolysis study ...See Entry 75321

The microwave and far-infrared spectra of the CH radical ...See Entry 75371
IR dimer spectroscopy and Fermi resonance ...See Entry 75372

Spectra of substituted N-heterocyclic molecules. I. Spectra of substituted pyrimidines ...See Entry 75377

Absolute band strengths of halocarbons F-11 and F-12 in the 8-to 16- μm region ...See Entry 75381

Assignment of the M-C stretching and M-C-O deformation modes of some trigonal bipyramidal metal carbonyls ...See Entry 75386

Shape of the $\nu(\text{OH})$ band in the IR spectra of H-complexes of pentachlorophenol ...See Entry 75389

Two-photon Raman excitation and coherent anti-Stokes Raman spectroscopy probing of population changes in polyatomic molecules: a novel nonlinear optical technique for vibrational-relaxation studies ...See Entry 75396

Sub-Doppler infrared-infrared double resonance spectroscopy of NH_3 using Stark tuning and a diode laser ...See Entry 75414

Vibrational redistribution in jet-cooled perylene. Intermediate coupling case ...See Entry 75420

Oscillator strength of the $\text{CN A } ^2\Pi_{1/2} \rightarrow \text{B } ^2\Sigma^+ (0,0)$ transition ...See Entry 75422

UF_6 relaxation dynamics following near-ultraviolet excitation ...See Entry 75425

Study of optical relaxation of polyatomic molecules in the condensed phase by site-selective laser spectroscopy ...See Entry 75426

Photoelectron spectroscopy of NHO^- and DNO^- ...See Entry 75439

Characterization of resonances in photoionization ...See Entry 75455

New predissociations in GeH affecting all the $A^2\Delta$ state levels ...See Entry 75457

Line displacement and line width in the binary collision theory of the vibrational phase relaxation ...See Entry 75486

The lasing characteristics of solutions of rhodamine 6G and coumarin 47 with inhomogeneously broadened spectra ...See Entry 75631

Measurement of absorption line intensities with VUV monochromators ...See Entry 75782

The interaction induced spectra of liquid CS_2 . A computer simulation study ...See Entry 77392

The Brownian rotational motion and shape of IR-absorption lines ...See Entry 77401

33.80 PHOTON INTERACTIONS WITH MOLECULES

Proton phototransfer and nonradiative deactivation in hydrogen-bonded complexes of 2-anthrol ...See Entry 77882

The mechanism of the photochemical oxidation of water to oxygen with silver chloride colloids ...See Entry 77999

33.80B Level crossing and optical pumping

Ab initio MRD-CI study of the electronic spectrum of SiH ...See Entry 75312

Error optimization in the detection of level crossing through the measurement of $n^2(T)$...See Entry 75609

33.80E Autoionization, photoionization, and photodetachment

75454 Angular distribution of Xe 5s- σp photoelectrons: a sensitive test of theory. H.Derenbach, V.Schmidt (Fakultat fur Phys., Univ. Freiburg, Freiburg, Germany).

J. Phys. B (GB), vol.16, no.11, p.L337-42 (14 June 1983). The angular asymmetry parameter β for 5s photoionisation in xenon has been measured in the energy range where the relativistic random-phase approximation (RPPA) including 5s, 5p and 4d interchannel couplings predicts a strong deviation from the nonrelativistic value of two. The authors' data clearly show a deviation from the value two but not as pronounced as predicted by the RPPA calculation. This indicates that the theory has to be further improved in this case. (23 refs.)

75455 Characterization of resonances in photoionization. W.Thiel (Fachbereich Phys. Chem., Univ. Marburg, Marburg, Germany).

J. Electron Spectrosc. & Relat. Phenom. (Netherlands), vol.31, no.2, p.151-60 (May 1983). Multiple-scattering calculations are used to characterize the σ_u resonances in the N_2 $X^2\Sigma_u^+$ and CO_2 $X^2\Sigma_u^+$ ionizations by means of radial density plots and to identify the resonant components in the corresponding continuum wavefunctions and cross-sections. (23 refs.)

Relativistic MS X α calculations of the electronic structure and related properties of PtCl_6^{2-} ...See Entry 75289

Mossbauer studies of after effects of Auger ionization following internal conversion in organo- $^{129\text{m}}$ tellurium compounds ...See Entry 75415

Fluorescence excitation and multiphoton ionization spectroscopy of 3-methylindole in a supersonic jet ...See Entry 75428

Ionisation of cyanate ions in solution ...See Entry 75442

Direct observation of the local-field-enhanced surface photochemical reactions ...See Entry 77905

33.80G Diffuse spectra; predissociation, photodissociation

75456 Observation of the $1^2\Pi_u \leftarrow X^2\Sigma_u^+$ system in Cs_2^+ . H.Helm, P.C.Cosby, D.L.Huestis (Molecular Phys. Lab., SRI Internat., Menlo Park, CA, USA).

J. Chem. Phys. (USA), vol.78, no.11, p.6451-4 (1 June 1983). Predissociation of vibrational levels in the $1^2\Pi_u$ state of Cs_2^+ has been observed by monitoring Cs^+ photofragments resulting from absorption of laser radiation by the $X^2\Sigma_u^+$ ground state. Predissociation of the $1^2\Pi_u$ state is induced by interaction with the repulsive $1^2\Sigma_u^+$ state and leads to the production of photofragments $\text{Cs}^+ + \text{Cs}$ in their ground electronic state with center-of-mass separation energies around 1 eV. The dominant features of the $1^2\Pi_u \leftarrow X^2\Sigma_u^+$ band system are confined to the wavelength range between 7700 and 8700 Å. A lower limit for the bond energy of the $1^2\Pi_u$ state, measured relative to its dissociation limit $\text{Cs}^+(^1S_0) + \text{Cs}(^2P_{1/2})$ is found to be 0.39 ± 0.1 eV. The spin-orbit splitting in the $1^2\Pi_u$ state is measured to be 280 cm^{-1} . (13 refs.)

75457 New predissociations in GeH affecting all the $A^2\Delta$ state levels. P.Erman, O.Gustafsson, M.Larsson (Phys. Dept. Royal Inst. of Technol., Stockholm, Sweden).

Phys. Scr. (Sweden), vol.27, no.4, p.256-60 (April 1983). Lifetimes have been measured of the rotational levels $N'=2-18$ of the $\text{GeH } A^2\Delta \leftarrow X^2\Pi (0,0)$ band yielding results in the range 75-85 ns. These are much shorter values than the authors had found earlier for the radiative lifetimes of

the same system in the analogous molecules CH and SiH (≈ 500 ns) suggesting that all α -state levels in GeH are subjected to predissociations in the same way as in CH and SiH, i.e. through direct interactions with the continuum of the ground state. This conclusion is also supported by *ab initio* calculations which give a lower limit of 200 ns for the radiative lifetime of the GeH α state. (19 refs.)

IR dimer spectroscopy and Fermi resonance See Entry 75372

Oscillator strength of the CN $A^2\Pi_1-B^2\Sigma^+$ (0,0) transition See Entry 75422

Quantum interference phenomena in the radiative decay of the \tilde{C}^1B_2 state of SO_2 See Entry 75431

He(I)/He(II) photoelectron band intensity ratios for simple organic molecules See Entry 75443

Two-frequency multiphoton absorption in UF_6 See Entry 75459

Direct observation of the local-field-enhanced surface photochemical reactions See Entry 77905

33.80K Multiphoton processes

75458 Two-photon excitation spectroscopy of phenanthrene singlet states below 50000 cm^{-1} . B.Dick, G.Hohlneicher (Lehrstuhl für Theoretische Chem., Univ. zu Köln, Cologne, Germany).

Chem. Phys. Lett. (Netherlands), vol.97, no.3, p.324-30 (20 May 1983). The two-photon excitation spectrum of phenanthrene in liquid solution is reported in the energy range $29000\text{--}49000\text{ cm}^{-1}$. Comparison with the one-photon spectrum and extended CNDO/S calculations allows assignment of eight singlet states. The strongest two-photon band is assigned to the B_0 state not seen directly in the UV spectrum. This high intensity and other features of the spectrum are in sharp contrast to the pairing selection rules which forbid two-photon transitions to 'plus' states in alternant hydrocarbons. (45 refs.)

75459 Two-frequency multiphoton absorption in UF_6 . G.Koren (Phys. Dept., Technion, Israel Inst. of Technol., Haifa, Israel).

J. Appl. Phys. (USA), vol.54, no.5, p.2827-9 (May 1983). The multiphoton absorption of $9.3\text{-}\mu\text{m}$ CO_2 laser radiation induced by multiphoton absorption of $16\text{-}\mu\text{m}$ CF_4 laser radiation in UF_6 is reported. An average vibrational energy deposition in the range of 1 to 2.8 eV per molecule is found, which is sufficient to cause the observed dissociation either by collision-assisted or unimolecular decomposition processes. (9 refs.)

75460 A theory of visible/UV multiphoton processes in molecules. I. Resonance effect on three-photon absorption. Y.Fujimura (Dept. of Chem., Faculty of Sci., Tohoku Univ., Sendai, Japan), S.H.Lin.

J. Chem. Phys. (USA), vol.78, no.11, p.6468-76 (1 June 1983). Using a transition operator formalism, an expression for three-photon transitions is derived. The transition operator formalism makes it possible to take into account the effects of population decays and pure dephasings occurring in the relevant vibronic states on the cross sections of the resonance multiphoton processes. It is shown that for a two-photon resonant ($2+1$) process, the cross section can approximately be divided into two terms; one is called sequential term which cannot be taken into account by using the lowest order time-dependent perturbation theory, and the other which can be derived from simultaneous three-photon cross section under constraint of a resonant condition for the second photon absorption. Assuming the adiabatic approximation for the molecular states, analytical expressions for the cross sections for the three-photon absorptions are derived in the displaced harmonic oscillator model of the molecules. An analytical expression taking into account the temperature effect is given for the simultaneous three-photon absorption cross section. (18 refs.)

75461 New experimental information from two-photon spectroscopy and comparison with theory. G.Hohlneicher, B.Dick (Lehrstuhl für Theoretische Chem., Univ. zu Köln, Köln, Germany).

Pure & Appl. Chem. (GB), vol.55, no.2, p.261-8 (Feb. 1983). (International Symposium on Theoretical Organic Chemistry, Dubrovnik, Croatia, Yugoslavia, 30 Aug.-3 Sept. 1982).

From a specially designed experiment, allowing the measurement of two-photon absorption spectra and two-photon polarization parameters over a wide spectral range new experimental information is obtained on the location of electronically excited states usually not seen in the UV-spectrum. By comparison with theory it is shown that in most of the examples investigated the ordering of the low lying excited states is different from what is usually expected. Correlation strongly influences the ordering especially in those systems which consist of loosely coupled π -systems. (31 refs.)

Two-photon Raman excitation and coherent anti-Stokes Raman spectroscopy probing of population changes in polyatomic molecules: a novel nonlinear optical technique for vibrational-relaxation studies See Entry 75396

Fluorescence excitation and multiphoton ionization spectroscopy of 3-methylindole in a supersonic jet See Entry 75428

33.90 OTHER TOPICS IN MOLECULAR SPECTRA AND INTERACTIONS WITH PHOTONS

Beam-maser spectroscopy on cyanoacetylene-D See Entry 75410

34.00 ATOMIC AND MOLECULAR COLLISION PROCESSES AND INTERACTIONS

34.10 GENERAL THEORIES AND MODELS

(inc. statistical theories, transition state, stochastic and trajectory models, etc; see also 82.20)

75462 Semiclassical theory for diatom-diatom collisions. G.D.Billing (Panum Inst., Univ. of Copenhagen, Copenhagen, Denmark).

Chem. Phys. Lett. (Netherlands), vol.97, no.2, p.188-92 (13 May 1983). A semiclassical approach to diatom-diatom collisions is presented. The method involves a classical treatment of the translational and rotational motion of both molecules. The vibrational degrees of freedom are quantized using a Monte oscillator approximation. The method is used to evaluate the accuracy of previous calculations based upon the energy-corrected harmonic-oscillator approach. (13 refs.)

Diffusional-drift-influenced chemical reactions at all gas densities See Entry 77884

34.20 INTERATOMIC AND INTERMOLECULAR POTENTIALS AND FORCES

(for molecular solids, see 31.70K)

75463 A unified algebraic approach to bound and continuum states of anharmonic potentials. C.E.Wulfman, R.D.Levine (Fritz Habere Molecular Dynamics Res. Center, Hebrew Univ., Jerusalem, Israel).

Chem. Phys. Lett. (Netherlands), vol.97, no.4-5, p.361-4 (27 May 1983). A general procedure for an algebraic formulation of the eigenvalue problem for hamiltonians which have both a discrete and a continuum spectrum is introduced. The one-dimensional Morse potential is used as an example, but more complex types of spectra can also be handled. (12 refs.)

75464 Calculation of van der Waals co-efficients in alkaline-earth chalcogenides. A.K.Kapur (Dept. of Phys., V.S.S.D. Coll., Kanpur, India), J.K.Jain.

Indian J. Theor. Phys., vol.29, no.3, p.291-8 (Sept. 1981). The van der Waals dipole-dipole and dipole-quadrupole interaction coefficients in alkaline-earth chalcogenides crystals have been estimated using the appropriate values of the crystalline state electronic polarizabilities of the ions obtained by using the polarizability radius cube relation. These values of electronic polarizabilities are in close agreement with the experimental values of Tessmann et al. (1953). Appropriate values of the effective number of electrons in the ion necessary to account for the actual polarizability of the ion have been used in these calculations. (16 refs.)

75465 Molecular electrostatic potential of a triple stranded helix: poly(dT).poly(dA).poly(dT). S.Corbin, R.Lavery, B.Pullman (Lab. de Biochimie Théorique, Inst. de Biologie Phys.-Chimique, Paris, France).

Int. J. Quantum Chem. (USA), vol.23, no.4, p.1451-61 (April 1983). The molecular electrostatic potential of the triple helix poly(dT).poly(dA).poly(dT) is calculated, and the results are examined in relation to those obtained for its component double and single helical parts. For the double helix presenting the standard Watson-Crick hydrogen bonds, the deepest potentials are formed on the side of the major groove, a situation similar to that observed in the A-DNA duplex. For the double helix presenting Hoogsteen-type hydrogen bonds the deepest potentials lie in the major groove, on the side of the pyrimidine strand. In the triple helix the deepest potentials are located in the major groove in a narrow zone over the thymine bases of the Watson-Crick pair. (13 refs.)

75466 Induction and dispersion energies including charge overlap effects: Green's-function-type methods. P.Claverie (Lab. de Chimie Quantique, Inst. de Biologie Phys.-Chimique, Paris, France).

Int. J. Quantum Chem. (USA), vol.23, no.4, p.1687-8 (April 1983). The evaluation of intermolecular interaction energies may now be based with sufficient accuracy upon the first and second order terms common to the exchange perturbation treatments symmetrized Rayleigh-Schrodinger (SRS), Murrell-Shaw and Musher-Amos (MSMA), Jezorski-Kolos (KJ). The author considers the Rayleigh-Schrodinger terms, namely, induction and dispersion, since the second-order exchange terms appear relatively much less important than the first-order exchange term. In contradistinction with the situation encountered for the electrostatic term, the multipolar expansion is now divergent, making it impossible to define a long range 'exact multipolar part' and a short-range 'penetration part' (which would have represented the so-called 'charge overlap effect'). He deals with the problem of representing the induction and dispersion terms directly without introducing any multipolar expansion of the matrix elements involving the interaction operator V . (23 refs.)

75467 An RKR-like inversion procedure for bound-continuum transition intensities. M.S.Child, H.Essen, R.J.Le Roy (Dept. of Theoretical Chem., Univ. of Oxford, Oxford, England).

J. Chem. Phys. (USA), vol.78, no.11, p.6732-40 (1 June 1983). A semiclassical RKR-like inversion procedure for determining a repulsive diatomic molecule potential energy curve from structured bound-continuum transition intensity data is derived and tested. The method presumes a knowledge of the (attractive), initial state potential well and of the energy and vibrational assignment of the absorbing or emitting level. Its application to a structured emission continuum of NaK observed by Breford and Engelke (*Chem. Phys. Lett.* 53, 282, 1979) yields a potential energy curve which is incompatible with other known properties of this system, a result which confirms the suggestion of Kato and Noda (*J. Chem. Phys.* 73, 4940, 1980) that the original assignment of the initial state for this spectrum is in error. (35 refs.)

75468 Semiclassical representation method in statistical physics of interacting molecules. I. General theory. E.P.Gordov, S.D.Tvorogov (Inst. of Atmospheric Optics, Acad. of Sci., Tomsk, USSR).

Physica A (Netherlands), vol.119A, no.1-2, p.339-55 (April 1983). The description of the method of transition from the quantum-statistical theory of interacting subsystems to a semi-classical one is given, using interacting molecules as an example. The kinetic equation for the distribution function of the classical subsystem, i.e. a translational motion of molecules which interacts with a quantum subsystem, namely, the internal motions of the molecules, is derived. The physical interpretation of the classical intermolecular potential and the origin of irreversibility of translational motion of molecules are discussed. (15 refs.)

A formula for calculating molecular energy differences from electrostatic potentials at nuclei See Entry 75254

Ab initio calculation of the $X^1\Sigma^+$ state of CsH See Entry 75279

Electronic correlation contribution to the three-body potentials for water trimers See Entry 75310

Force field study of some nonlinear XY_2 -type molecules See Entry 75357

Algebraic approach to molecular rotation-vibration spectra See Entry 75359

Binding energies and spectroscopic constants of the first-row and second-row diatomic hydrides See Entry 75360

Vibrational and conformational studies of cyclopropylcarbonyl chloride See Entry 75394

Intermolecular potentials from NMR data: H_2-N_2O and H_2-CO_2 See Entry 75404

Use of V^{N-1} potentials in Green's function calculations See Entry 75507

The geometry of the tert-butyl group: statistical analysis and model calculations See Entry 75540

Applicability of R-K potential function for calculating molecular parameters of diatomic molecules See Entry 75547

- Bound states in a classical gas See Entry 76147
 Ultrasonic study of molecular interaction in carbon tetrachloride-toluoline mixtures See Entry 76564
 Importance of exchange effects in the deformation of interacting ions See Entry 76914
 Dielectric relaxation and dipole moment measurements of *n*-methylacetamide in benzene and dioxane solutions at different temperatures from microwave absorption studies See Entry 77325
 Quantum chemical study of the molecular patterns of MAO inhibitors and substrates See Entry 78135

34.40 ELASTIC SCATTERING OF ATOMS AND MOLECULES

- 75469 An extended corresponding states model for the elastic collision rate in a real gas. J.W.Root, D.Bookin (Dept. of Chem., Univ. of California, Davis, CA, USA). *Chem. Phys. Lett. (Netherlands)*, vol.97, no.4-5, p.392-6 (27 May 1983).
 An extended corresponding states kinetic theory is proposed for the estimation of elastic collision rates in real gases under equilibrium conditions. The collision rates are obtained by combining the $\Omega^{(1,0)}$ reduced collision integral with the hard-sphere kinetic model. (14 refs.)
 Absolute determination of the differential elastic cross section and total inelastic cross sections for the collision He^+-He between 3 and 50 keV and between 0.25 and 3 degrees. Elaboration of a simple theoretical model See Entry 75475

34.50 INELASTIC SCATTERING OF ATOMS AND MOLECULES

- 75470 *M* dependence in rotationally inelastic collisions in cell experiments: implications of an irreducible tensor expansion for molecules in Σ electronic states. M.H.Alexander (Dept. of Chem., Univ. of Maryland, College Park, MD, USA), S.L.Davis. *J. Chem. Phys. (USA)*, vol.78, no.11, p.6754-62 (1 June 1983).
 The tensorial coupling of initial and final angular momenta, commonly used in atomic collisions and attributed to Grawert (1969), is here applied to *M* dependent collisions of molecules in Σ electronic states under conditions where the relative velocity vectors of the collision partners are uniformly distributed with respect to a laboratory fixed *z* axis. The integral inelastic cross sections are given by sums over tensor opacities, weighted by squares of vector coupling coefficients. The resulting expressions differ from those obtained within the tensorial treatment usually applied to molecular collisions. One can rigorously show that strict *M* conservation will not occur and, furthermore, that the complete matrix of $M \rightarrow M'$ cross sections can be related to the smaller set of tensor opacities. In the energy sudden limit the $JM \rightarrow JM'$ cross sections can be related to the degeneracy-averaged $J'' \rightarrow J'$ cross sections. Accurate close-coupling cross sections for the He- CO system due to Green are used to obtain the relevant tensor opacities and to demonstrate how degeneracy averaged $J'' \rightarrow J'$ cross sections can be extracted from the fully resolved $JM \rightarrow JM'$ cross sections. Finally, the sudden scaling relation is used to analyze rotational relaxation in the $\text{Na}_2(\text{A}^2\Sigma_u^+)+\text{He}$ system. The authors show that θ conservation, where $\theta = \cos^{-1}(\hat{j}_2)$, is a more appropriate dynamical model than *M* conservation. (62 refs.)
 75471 Semiclassical decoupling schemes in molecular collisions. K.Sakimoto (Inst. of Space & Astronaut. Sci., Tokyo, Japan). *J. Phys. Soc. Jpn. (Japan)*, vol.52, no.5, p.1563-71 (May 1983).
 Several decoupling schemes are discussed for the semiclassical impact parameter treatment of collisions between atoms and linear rigid rotors. First, a decoupling method analogous to the quantum mechanical one originating from the conservation of parity is found in the semiclassical treatment. Next, presently derived semiclassical versions of *l*-dominance and decoupled *l*-dominance approximations provide the author with an intuitive understanding of the physical meaning of these approximations. Numerical approximations are performed for the H^+-CO collision system. (18 refs.)
 75472 Fine-structure transitions in collisions of $\text{Kr}^+(\text{P})$ with rare gases. N.Kobayashi, T.Nakamura, Y.Kaneko (Dept. of Phys., Tokyo Metropolitan Univ., Tokyo, Japan). *J. Phys. Soc. Jpn. (Japan)*, vol.52, no.5, p.1581-4 (May 1983).
 Fine-structure transitions, $j=3/2 \rightarrow 1/2$ and $1/2 \rightarrow 3/2$, in the collisions of $\text{Kr}^+(\text{P})$ with rare gases were studied with an ion energy-loss spectrometer in the energy range from 500 eV to 1300 eV. The ions were produced with an electron-impact type ion-source. The fractional ratios of $j=1/2$ to $j=3/2$ states, $N(1/2)/N(3/2)$, contained in the primary beam were determined as a function of the electron energy in the ion source from 20 eV to 150 eV. The values were almost constant above the electron energy of 40 eV, and the average value of 0.479 ± 0.002 which is close but not exactly equal to the statistical value, 0.5, was obtained. The cross sections for the fine-structure transitions in the collisions of Kr^+ with He were also obtained.
 75473 Semiclassical complex angular momentum analysis of low-energy H^+-He differential cross sections. K.-E.Thylwe (Fachbereich Phys., Univ. Kaiserslautern, Kaiserslautern, Germany). *J. Phys. B (GB)*, vol.16, no.11, p.1915-30 (14 June 1983).
 A semiclassical complex angular momentum (CAM) description of low-energy elastic collisions is presented. The scattering amplitude is divided into two parts: the direct part is described by non-orbiting semiclassical trajectories, while the orbiting part is described by a small number of poles of the *S* matrix. The system H^+-He was studied in some detail. (31 refs.)
 75474 Collisional de-excitation of KrF^* excimer by simultaneous ionisation of excited neutrals. M.Matsuzawa, S.Kitaji (Dept. of Engng. Phys., Univ. of Electro-Communications, Tokyo, Japan). *J. Phys. B (GB)*, vol.16, no.11, p.1931-6 (14 June 1983).
 Dipole-dipole energy transfer is one of the major mechanisms in the collisional deexcitation of excimers by simultaneous ionisation of excited neutrals. Based on this mechanism, the cross sections for collisional de-excitation of KrF^* with several excited species are calculated to be 110-170 Å² at thermal energies. (20 refs.)
 75475 Absolute determination of the differential elastic cross section and total inelastic cross sections for the collision He^+-He between 3 and 50 keV and between 0.25 and 3 degrees. Elaboration of a simple theoretical model. D.Bordenave-Montesquieu, A.Boutonnet, C.Berges, R.Dagnac (Centre de Phys. Atomique, Univ. Paul Sabatier, Toulouse, France). *J. Phys. B (GB)*, vol.16, no.11, p.1937-55 (14 June 1983). In French.
 The authors studied, by energy loss spectrometry, the direct elastic and inelastic processes and measured their differential cross sections (DCS), with vary-

ing energy and scattering angle, for the He^+-He collision; the energies range from 3 to 50 keV (laboratory) and the scattering angles are varied from 0.25 to 3° (laboratory). To explain the elastic DCS behaviour, they elaborated a simple theoretical model which gives a good agreement with the experiment, chiefly at high energies. It also allows them to calibrate the experimental results and gives absolute values of the DCS. Further, by integration of the DCS over all scattering angles, they obtained total cross sections (TCS) for the inelastic processes. (17 refs.)

75476 Solution of the time-dependent Dirac equation by the finite difference method and application for $\text{Ca}^{20+}+\text{U}^{91+}$. U.Becker, N.Grun, W.Scheid (Inst. für Theoretische Phys., Justus-Leibig-Univ., Giessen, Germany). *J. Phys. B (GB)*, vol.16, no.11, p.1967-81 (14 June 1983).

The Dirac equation for an electron moving in time-dependent electromagnetic fields is solved by the method of finite differences. For simplicity the solution is restricted to problems with a rotational symmetry about an axis. The method is applied to the scattering of Cs^{20+} on a hydrogen-like U^{91+} ion at relativistic incident energies. Excitation and ionisation probabilities and the K-shell vacancy production probability are calculated. (27 refs.)

75477 Ionic-covalent problem in the $\text{H}^++\text{H}^+ \rightleftharpoons \text{H}^+\text{H}^+$ collisional system. V.Sidis, C.Kubach (Lab. des Collisions Atomiques et Moléculaires, Univ. de Paris-Sud, Orsay, France), D.Fussen. *Phys. Rev. A (USA)*, vol.27, no.5, p.2431-46 (May 1983).

A detailed theoretical study of $\text{H}^++\text{H}^+ \rightleftharpoons \text{H}^+\text{H}^+$ collisions in the $0.02 < E_{\text{cm}} < 10$ keV energy range is reported. Calculations of the relevant states of the quasimolecular system are carried out at large internuclear distances ($5a_0 < R < 100a_0$) with a model involving only the loosely bound electron of the system. The authors calculated adiabatic states agree well with the available accurate ab initio results. Diabatic states are found not only to differ from the conventionally invoked pure ionic and covalent states, but also to depend dramatically on the choice of the fixed electron coordinate origin. Such differences show up in the cross-section calculations when $\text{H}^*(n=3)+\text{H}$ channels are taken into account and demonstrate the need for considering the problem of the electron translation factor. Cross-section calculations are finally calculated in a 12-state projected valence-bond diabatic basis incorporating a common translation factor of the Schneiderman-Russek type. The results demonstrate the important contribution of $\text{H}^*(n=3)+\text{H}$ channels to the mutual neutralization process. Good agreement is obtained with the experimental data on neutralization and detachment in H^++H^+ and on H^+ formation in $\text{H}^*(s)+\text{H}$, for collision energies $E_{\text{cm}} \geq 200$ eV. At lower energies no explanation of the structures and magnitude of the experimental neutralization cross section is found. (57 refs.)

75478 A study of adiabaticity in the case of target degeneracy. E.R.A.Segre (Dept. de Física do Inst. Tecnol. de Aeronautica, Centro Tecnico Aeronautico, Sao Jose dos Campos, Brazil). *Rev. Bras. Fis. (Brazil)*, vol.12, p.115-22 (March 1982). In Portuguese. [received: April 1983]

The validity of the adiabatic approximation in the case of the collision of a semi-classical charged projectile and a target atom in a degenerate state is examined. The target is hydrogen atom in the first excited state, which allows calculations to be performed analytically, within the dipolar interaction and 'no-quenching' assumptions. It is confirmed, in a precisely quantitative way, that the adiabatic approximation breaks down for impact parameters larger than the Weisskopf radius, and the exact wave function describing the collision is given. (7 refs.)

75479 Stosse laserangeregter Atome zur Potentialbestimmung für die Systeme K (4S₀2P)-Ne, Ar, Kr, Xe (Laser-stimulated atomic collisions for potential determination for the system K (4S₀2P)-Ne, Ar, Kr, Xe). H.Tischer.

Report 16/1982, Max-Planck-Inst. Stromungsforschung, Gottingen, Germany (Dec. 1982), 89 pp. In German.

Gives the results and evaluations of total differential distributed cross section measurements for $\text{K}(4\text{P}_{3/2})-\text{Ar}$, Kr , Xe , Ne systems at thermal collision energies. First an introduction is given, then the theory behind the experiment is explained. The apparatus is described. Finally, the measurements are made for each system and these are described. (49 refs.)

75480 Messung feinstrukturauflösender differentieller Streuquerschnitte für Stosse von Kalium an Quecksilber mittels teilchen-Photon-Koinzidenz (Measurement of fine structure perturbed differential scattering cross-sections for the collision of potassium and mercury by particle-photon coincidence). H.Hubner.

Report 15/1982, Max-Planck-Inst. Stromungsforschung, Gottingen, Germany (Dec. 1982), 89 pp. In German.

Describes an experiment which is a continuation of measurements made by Schädlich (1978), Strunck (1976) and Kracht, who measured the differential excitation cross sections for the dominant first resonance levels of alkali-mercury systems. First the author gives a general introduction to the experiment. The aim of the experiment is to determine the time structure cross sections for the potassium-mercury collision system. A fast potassium beam is crossed with a thermal quick-silver beam, and the dispersed particles collide with the emitted photons. The system is controlled by computers and the typical measurement times are between 5 and 70 hours per angle. The construction of the experimental apparatus is described in some detail followed by measurement and evaluation methods. The results of the measurements are given. (60 refs.)

75481 Feynman diagram for reactive collisions. B.C.Mishra (Dept. of Phys., RDW Coll., Bhubaneswar, India), T.Pradhan.

Proceedings of the VI High Energy Physics Symposium (papers in summary form only received), Mysore, India, 6-11 Dec. 1982 (Bombay, India: Dept. Atomic Energy 1982), p.77

On the basis of a quantum field theoretic formulation of atomic collision phenomena involving nonrelativistic free and bound systems developed by the authors, they have drawn the Feynman diagram for the reactive collisions between the alkali atoms and halogen molecules and have calculated the cross section for the production of alkali halide molecules. Their result shows an excellent agreement with the experimental observations.

Apparatus for measurements on the fragmentation of MeV molecular-ion beams See Entry 74555

Broadening of level-crossing signals in the $5^2\text{P}_{3/2}$ state of rubidium due to resonant collisions See Entry 75350

K-shell excitation by K- to L-shell charge transfer in slow $\text{Kr}^{4+}-\text{Kr}$ and $\text{Xe}^{4+}-\text{Xe}$ collisions See Entry 75502

Theory of electron capture from a hydrogenlike ion by a bare ion; intermediate-state contributions to the amplitude See Entry 75503

Relativistic calculation of atomic M-shell ionization by protons See Entry 75504

Charge transfer of doubly charged and trebly charged ions with atomic hydrogen at thermal energies See Entry 75505

Electron capture in small-angle $\text{Ar}^{2+} + \text{Ar}$ collisions See Entry 75506
 Collisional vibrational quenching of $\text{O}_2^+(\nu)$ and other molecular ions in planetary atmospheres See Entry 78809

34.50E Rotational and vibrational energy transfer

75482 Vibrational energy transfer in $\text{A}^{2\Sigma^+}$ OH in flames. G.P. Smith, D.R. Crosley (SRI Internat., Menlo Park, CA, USA). *Appl. Opt. (USA)*, vol.22, no.10, p.1428-30 (15 May 1983). Measurements have been made of the collisional vibrational energy transfer from $\nu=1$ to $\nu=0$ within the $\text{A}^{2\Sigma^+}$ electronically excited state of the OH molecule present in the burnt gases of a methane-air flame. The results show that the transfer rate decreases with increasing initial rotational quantum number N' in $\nu=1$. This has implications for laser-induced fluorescence thermometry and concentration measurements in flames and for the understanding of the formation of A-state OH in flame reactions. (9 refs.)

75483 Energy-dependent energy transfer: deactivation of azulene (S_0 , E_{vib}) by 17 collider gases. M.J. Rossi, J.R. Pladziec, J.R. Barker (Dept. of Chem. Kinetics, SRI Internat., Menlo Park, CA, USA). *J. Chem. Phys. (USA)*, vol.78, no.11, p.6695-708 (1 June 1983). Collisional deactivation of highly vibrationally excited azulene in the electronic ground state was investigated using infrared fluorescence detection. Azulene (S_0 , E) was prepared with $E \approx 17500 \text{ cm}^{-1}$ and $E \approx 30600 \text{ cm}^{-1}$ by laser excitation at 600 and 337 nm, respectively. Advantage was taken of the fast integral conversion rate to S_0 azulene from $\text{S}_1(600 \text{ nm})$ and $\text{S}_2(337 \text{ nm})$ electronic states. The collider gases investigated are He, Ne, Ar, Kr, Xe, H_2 , D_2 , N_2 , CO , O_2 , CO_2 , H_2O , NH_3 , CH_4 , SF_6 , $n\text{-C}_4\text{H}_{10}$, and unexcited azulene. The results are expressed in terms of $\langle \Delta E(E) \rangle$, the average energy transferred per collision, which can depend on the vibrational excitation energy E of the azulene. Using previously obtained knowledge of the dependence of infrared fluorescence intensity on E (M.J. Rossi and J.R. Barker, *Chem. Phys. Lett.* 85, 21, 1982), two methods were used to obtain $\langle \Delta E(E) \rangle$ values from the fluorescence decay curves: (1) an approximate method that considered only the average energy, and (2) solution of the full collisional master equation. Both methods gave $\langle \Delta E(E) \rangle$ values that depend strongly on E . The limited experimental information on the identity of the energy-transfer processes operative in the deactivation of azulene is discussed. Additional experimental results on vibration-to-vibration energy transfer from azulene to CO_2 are presented, which indicate that the emission at $4.3 \mu\text{m}$ observed previously (J.R. Barker, M.J. Rossi, and J.R. Pladziec, *Chem. Phys. Lett.* 90, 99, 1982) originates not only from $\text{CO}_2(001)$, but from other states with one quantum of excitation in ν_3 . The experimental results are discussed in terms of models for energy transfer, which have appeared in the literature. It is concluded that only a superficial understanding exists and theory has lagged far behind experiments on energy transfer. (50 refs.)

75484 Collisional deactivation of vibrationally highly excited polyatomic molecules. II. Direct observations for excited toluene. H. Hippler, J. Troe, H.J. Wendelken (Inst. fur Phys. Chem., Univ. Gottingen, Gottingen, Germany). *J. Chem. Phys. (USA)*, vol.78, no.11, p.6709-17 (1 June 1983). Vibrationally highly excited toluene molecules with 52000 cm^{-1} of vibrational energy have been prepared by UV laser excitation of the isomer cycloheptatriene and subsequent isomerization. The collisional loss of energy from the excited toluene molecules has been observed directly by monitoring hot UV absorption spectra. Direct measurements of the average energies (ΔE) transferred per collision have been made for about 60 different bath gases. For complex bath gases, $\langle \Delta E \rangle$ values appear to be considerably smaller than those derived from earlier indirect measurements. $\langle \Delta E \rangle$ was found not (or only slightly) to depend on the excitation energy. (31 refs.)

75485 Collisional deactivation of vibrationally highly excited polyatomic molecules. III. Direct observations for substituted cycloheptatrienes. H.J. Hippler, J. Troe, H.J. Wendelken (Inst. fur Phys. Chem., Univ. Gottingen, Gottingen, Germany). *J. Chem. Phys. (USA)*, vol.78, no.11, p.6718-24 (1 June 1983). For pt.II see *ibid.*, vol.78, no.11, p.6709-17 (1983). Vibrationally highly excited ethyl-cycloheptatriene (41600 cm^{-1}) and isopropyl-cycloheptatriene (41800 cm^{-1}) molecules in the electronic ground state have been prepared by UV laser excitation inducing one-photon absorption and subsequent internal conversion. Collisional energy loss of these molecules has been followed directly by hot UV absorption spectroscopy. Average energies transferred per collision (ΔE) have been determined for a series of bath gases. $\langle \Delta E \rangle$ values were found, for a given bath gas, to increase very slightly with the size of the excited molecule. (31 refs.)

75486 Line displacement and line width in the binary collision theory of the vibrational phase relaxation. R. Ouilion (Dept. de Recherches Phys., Univ. Pierre et Marie Curie, Paris, France), V. Sergiescu, R. Tascou D'Leon. *Mol. Phys. (GB)*, vol.49, no.1, p.151-8 (May 1983). The authors present an elementary kinetic calculation of the displacement and width of a Raman line due to vibrational phase relaxation. The binary collision model is used and the relation between the two effects is stressed. The calculated values are compared with the experimental ones for gaseous (H_2/H_2 , H_2/He , H_2/Ar) and liquid (H_2/SF_6 , N_2/SF_6 , N_2/CCl_4) systems. A repulsive potential is used. (8 refs.)

75487 Streuquerschnitte für die Rotationsanregung von N_2 , O_2 und CH_4 durch Stöße mit He-Atomen (Scattering cross-section for the rotational excitation of N_2 , O_2 and CH_4 by collisions with the atoms). K.-H. Kohl. Report 17/1982, Max-Planck-Inst. Stromungsforschung, Gottingen, Germany (Dec. 1982), 116 pp. In German. Describes the experiment by first giving it an introduction, and the reasons behind the experiment. Measurement methods are given (principle construction of the scattering experiment, kinematics of the experiment and demands on the solution possibilities of the measurement apparatus) and then details of the measurement apparatus are given. Measurements results are given and graphs drawn where appropriate. An absolute total and inelastic differential effective cross section is evaluated, and finally the author presents a discussion. (54 refs.)

Time-resolved study of the subpicosecond dynamics of molecular rotations in liquids See Entry 75327

IR and ^1H NMR studies on the hydrogen bond in homoconjugated cations of some pyridine N-oxides in nitromethane and acetonitrile See Entry 75384

Two-photon Raman excitation and coherent anti-Stokes Raman spectroscopy probing of population changes in polyatomic molecules: a novel nonlinear optical technique for vibrational-relaxation studies See Entry 75396

Symmetric charge exchange between negative ions and atoms See Entry 75497

Heterogeneous vibrational relaxation upon free molecular flow of diatomic gas past concave bodies See Entry 76072

Energy redistribution among internal states of nitric oxide molecules upon scattering from Pt(111) crystal surface See Entry 77503

34.50H Electronic excitation and ionization (inc. beam-foil excitation and ionization)

75488 Ionisation cross sections of Cd, Sn, Te, I and Ba for protons and alpha particles. L. Avaldi, M. Milazzo, G. Trivita (Istituto di Fisica Generale Applicata, Univ. degli Studi di Milano, Milano, Italy), I.V. Mitchell. *J. Phys. B (GB)*, vol.16, no.11, p.1957-65 (14 June 1983).

K-shell X-ray production cross sections of ^{48}Cd , ^{50}Sn , ^{52}Te , ^{53}I and ^{56}Ba have been measured for alpha particles with energies between 2.2 and 2.8 MeV. In addition, production cross sections for ^{52}Te have been measured for protons between 1.6 and 3 MeV. The values have been compared with the earlier experiments and with the theoretical predictions given by four different approaches: the perturbed stationary state model corrected for relativistic, projectile Coulomb deflection, and energy-loss effects, the plane-wave Born approximation (PWBA) with corrections for relativistic effects, effective binding and Coulomb deflection, the semiclassical approximation corrected for the same effects as the PWBA in its most recent formulation and, lastly, the binary model corrected for effective energy and relativistic effects. The different degrees of agreement for each theory in the cases examined are discussed. (27 refs.)

75489 Atomic excitation and ionization by slow magnetic monopoles. G. Tiktopoulos (Phys. Dept., Nat. Tech. Univ., Athens, Greece). *Phys. Lett. B (Netherlands)*, vol.125B, no.2-3, p.156-60 (26 May 1983). Cross sections are calculated for transitions of atomic electrons induced by the close passage of very massive Dirac monopoles for monopole velocities small compared to the characteristic electron orbital velocity. (9 refs.)

75490 Detailed analysis of the scope of the modified Firsov model. S.A. Cruz, C. Vargas-Aburto (Inst. de Fisica, Univ. Nacional Autonoma de Mexico, Mexico City, Mexico), D.K. Brice, E.V. Alonso, D.G. Armour. *Phys. Rev. A (USA)*, vol.27, no.5, p.2403-20 (May 1983).

A detailed and systematic analysis of the scope of the Firsov model (1959) as modified by Cheshire (1969) when no adjustable parameters are included in the calculations of the low-velocity electronic-stopping cross section is presented. For this purpose the authors summarize and extend their previously reported [Radiat. Eff. Lett. 43, 79 (1979); Nucl. Instrum. Methods 170, 205 (1980)] preliminary results on the role of all computational degrees of freedom that influence the outcome of the calculations, namely, (a) inclusion of trajectory, (b) accuracy of wave functions and speed of atomic electrons, (c) motion of Firsov's plane, and (d) consideration of experimental conditions. The authors find that the Firsov theory is accurate only within a factor of 2; therefore, at least a scale factor is necessary in order to get reasonable agreement with experiment. (53 refs.)

75491 Quasielastic state-changing collisions of high-Rydberg atoms with rare-gas atoms*. K. Sasano, Y. Sato (Dept. of Engng. Phys., Univ. of Electro-Communications, Tokyo, Japan), M. Matsuzawa. *Phys. Rev. A (USA)*, vol.27, no.5, p.2421-30 (May 1983).

For $20 \leq n \leq 45$, two types of quasielastic state-changing-collisional (QESCC) processes, i.e., (i) l-changing and (ii) n- and l-changing processes, have been theoretically investigated based on the free-electron model in which an excited Rydberg electron behaves as if it were 'free' and slow with its interaction with a rare-gas atom playing a decisive role. It is shown that a parameter $u_{\text{min}} = \nu \Delta E a_0 / (hV)$ is quite useful for characterizing both of these QESCC processes in a unified way where $\nu (\approx \nu')$ is an effective principal quantum number of the initial (final) state, ΔE is an energy defect, and V is a relative velocity. It is theoretically found that higher-angular-momentum states are dominantly populated in the final channel of these QESCC processes with $1 < u_{\text{min}} \leq \nu$ such as in the n- and l-changing collision of $\text{Rb}^{**}(ns) + \text{He}$. This is in contrast with the uniform distribution over the final angular-momentum states for the usual l-changing processes, i.e., $u_{\text{min}} \leq 1$. The calculated cross sections of these QESCC processes with $1 < u_{\text{min}} \leq \nu$ are found to be in reasonable agreement with experimental findings available at present. (32 refs.)

75492 Semiclassical approach to trajectory effects on the anisotropy coefficient of L_3 -subshell X-rays induced by slow heavy particles collisions. E.C. Montenegro, A.C. De Pinho (Dept. de Fisica, PUC/RJ, Rio de Janeiro, Brazil). *Rev. Bras. Fis. (Brazil)*, vol.12, p.29-49 (March 1982). In Portuguese. [received: April 1983]

The deflection and the retardation of a slow bare heavy particle by the repulsive Coulomb field of the target nucleus are known to modify the ionization cross sections of inner shells. It is shown how to calculate these effects in the magnetic substates of the $2p$ -subshell in the frame of the impact parameter picture. These corrections are essential to understand the energy dependence of the anisotropy coefficient of X-rays emitted in transitions filling an L_3 -subshell vacancy produced by massive particle bombardment. (15 refs.)

75493 4f-ionization of atomic cerium. A. Bringer (Inst. fur Festkörperforschung, KFA Jülich, Jülich, Germany). *Solid State Commun. (USA)*, vol.46, no.8, p.591-3 (May 1983).

The binding of the 4f electron in a cerium atom is investigated for general shapes of the 4f wave function. There is no activation barrier for 4f-ionization, in contradiction to earlier calculation by Schluter and Varma (1982), who assumed a hydrogenic form. The existence of a second stationary electronic structure with extended 4f electrons and the 'bistability model' developed from it to explain spectroscopic data in Ce compounds can be ruled out on energetic grounds. (11 refs.)

75494 Transitions between excited states with mixed coupling $\text{Ne } 2p^4 4p$ N levels. V.M. Baran, G.L. Kononchuk, A.V. Yakunov. *Ukr. Fiz. Zh. (USSR)*, vol.28, no.5, p.658-60 (May 1983). In Russian.

Effective cross-sections are discussed for transitions between the fine structure components of the neon $2p^4 4p$ group levels. The results are obtained by two-frequency laser sounding of a discharge plasma. The total deactivation cross-section of the $4p[3/2]_2$ state is in good agreement with results of other authors. A possible dependence on the degree of degeneracy is discussed for probability of transition between the fine structure components. (10 refs.)

An improved model for post-collision interaction (PCI) and high resolution Ar LMM Auger spectra revealing new PCI effects See Entry 75353

Room-temperature rate constants for the gas-phase quenching of metastable molecular oxygen, $\text{O}_2(a^1\Delta_g)$ and $\text{O}_2(b^1\Sigma_g^+)$, by CO_2 , N_2O , NO , NH_3 , HCl and SO_2 See Entry 75423

UF_6 relaxation dynamics following near-ultraviolet excitation See Entry 75425

Study of the ionization process $\text{BF}^+(\text{X } 2\Sigma^+) \rightarrow \text{BF}(\text{X } 1\Sigma^+)$ by high-temperature photoelectron spectroscopy See Entry 75444

Charge transfer and ionisation processes involving multiply charged ions in collision with atomic hydrogen See Entry 75499

Transfer ionisation in slow collisions of multiply-charged ions with atoms See Entry 75500

34.50L Chemical reactions, energy disposal, and angular distribution, as studied by atomic and molecular beams

(see also 31.70F and 82.20K Potential-energy surfaces, 82.40D Beam reactions)

75495 Experimental determination of the m_J distribution in inelastic scattering of Na_2 by He. M.A. Treffers, J. Korving (Huygens Lab., Rijksuniv., Leyden, Netherlands).

Chem. Phys. Lett. (Netherlands), vol.97, no.3, p.342-5 (20 May 1983). The orientational distribution of Na_2 molecules scattered by He has been determined in a molecular beam experiment. At large angle scattering, where inelastic collisions are dominant, a high degree of alignment has been observed. This alignment depends strongly on the rotational quantum number J after scattering. The J dependence can be explained by assuming that during collisions m_J is conserved when the quantization axis is chosen parallel with the geometric apse. (9 refs.)

Energy redistribution among internal states of nitric oxide molecules upon scattering from Pt(111) crystal surface See Entry 77503

D_2O product angular and translational energy distributions from the oxidation of deuterium on Pt(111) See Entry 77919

34.70 CHARGE TRANSFER

(see also 82.30 Charge transfer reactions)

75496 Asymptotic theories of charge transfer at low energies. J.N. Bardsley (Univ. of Pittsburgh, Pittsburgh, PA, USA).

Comments At. & Mol. Phys. (GB), vol.13, no.2, p.51-7 (1983). Theories have been developed to treat charge exchange in ion-atom collision at large impact parameters that are based on asymptotic expressions for electron orbitals, JWKB treatment of orbital distortion and simple classical models for the nuclear motion. These methods, which can be applied without the use of a computer, have been remarkably successful for symmetric charge transfer. The basic elements of the asymptotic theories are reviewed and the problems associated with the application of asymmetric charge exchange are discussed. (17 refs.)

75497 Symmetric charge exchange between negative ions and atoms. S. Kundu, S.B. Karmahapatro (Saha Inst. of Nuclear Phys., Calcutta, India). *Indian J. Phys. Part B*, vol.56B, no.6, p.369-74 (Dec. 1982). [received: May 1983]

The authors have calculated the cross sections of symmetric charge exchange reactions: $\text{H}^- + \text{H} \rightarrow \text{H} + \text{H}^-$ (1) and $\text{Cl}^- + \text{Cl} \rightarrow \text{Cl} + \text{Cl}^-$ (2) in the energy range 1-20 keV using a method similar to that described by Karmahapatro (1965) with an assumption of one electron model of an atom. The wave function for H^- (i.e. the first two terms given by Lowdin and Appel (1953)) and for Cl^- (Lowdin and Appel 1956) have been used in calculating the cross section of the reactions (1) and (2). The transition probability of symmetric charge exchange is calculated with the usual approximation of the first-order time-dependent perturbation theory, while the relative motion of the reactants is considered classically. (18 refs.)

75498 State-selective single-electron capture by 80 keV C^{4+} ions from He, H_2 and Li. D. Dijkkamp (FOM Inst. for Atomic & Molecular Physics, Amsterdam, Netherlands), A. Brazuk, A.G. Drentje, F.J. de Heer, H. Winter. *J. Phys. B (GB)*, vol.16, no.11, p.1343-6 (14 June 1983).

Absolute excitation cross sections for single-electron capture into selected n, l states have been determined by VUV spectroscopy for impact of 80 keV C^{4+} on He, H_2 and Li. For all three collision systems the predominant final ion states belong to one or two electronic shells only. Within such shells a preferential population of higher l sublevels is found. (13 refs.)

75499 Charge transfer and ionisation processes involving multiply charged ions in collision with atomic hydrogen. D.J.W. Hardie, R.E. Olson (Dept. of Phys., Univ. of Missouri-Rolla, Rolla, MO, USA).

J. Phys. B (GB), vol.16, no.11, p.1983-96 (14 June 1983). Total cross sections are presented for the charge transfer reaction $\text{X}^{q+} + \text{H}(1s) \rightarrow \text{X}^{(q-1)+} + \text{H}^+$ and ionisation process $\text{X}^{q+} + \text{H}(1s) \rightarrow \text{X}^{q+} + \text{H}^+ + e^-$. Here X^{q+} is a fully or partially stripped ion. The collision energy range lies between 25-200 keV amu^{-1} . Cross sections are also given for charge transfer into particular ionic n states and n, l states for energies of 25 and 50 keV amu^{-1} , where $\text{X}^{q+} = \text{H}^+, \text{He}^{2+}, \text{C}^{6+}, \text{O}^{8+}$. The calculations were performed by the classical trajectory Monte Carlo method of Olson and Salop (1977), modified to allow for a better representation of the $\text{H}(1s)$ electronic radial distribution. Good agreement is seen with previous classical calculations and with quantum calculations performed by Ryufuku and Watanabe (1979) and others. The authors' results exhibit excellent accord (within 20%) with the measurements of Shah and Gilbody (1981). (13 refs.)

75500 Transfer ionisation in slow collisions of multiply-charged ions with atoms. W. Groh, A. Müller, A.S. Schlachter, E. Salzborn (Inst. für Kernphys., Univ. Giessen, Giessen, Germany).

J. Phys. B (GB), vol.16, no.11, p.1997-2015 (14 June 1983). Systematic experiments on transfer ionisation processes $\text{A}^{q+} + \text{B} \rightarrow \text{A}^{(q-k)+} + \text{B}^+(i-k) + e + \Delta E$ have been performed where A and B are rare-gas atoms, q is the charge state of the incident ions (up to 7 for Ne, 9 for Ar, 12 for Kr and 15 for Xe), k is the number of captured electrons found with the projectile long after the collision ($k=1, 2$ or 3) and i is the charge state of the slow recoil ion (measured by a time-of-flight coincidence technique). The projectile energies range from 3q keV to 15q keV; however, with very few exceptions, the charge-state fractions F_i of recoil ions were found to be independent of the energy in the energy range studied. The ionisation of five additional target electrons in 7% of the two-electron-capture collisions of Xe^{15+} ions with Xe atoms shows the importance of transfer ionisation in such collisions. The observed charge-state fractions of the recoil ions strongly depend on k , the number of electrons captured, and on q , the charge state of the projectile; the mean charge state $\langle i \rangle = \sum_i i F_i / \sum_i F_i$ increases strongly with increasing k and q . In general, the investigated processes are exoergic, and the charge states of the recoil ions produced are correlated with the potential energy available in the collision system. When the charge-state fractions F_i observed for a given target atom are plotted as a function of the maximum potential energy ΔE calculated for transitions between ground

states they fall on common curves which are only specified by the charge state i and the number of electrons k captured indicating that F_i depend explicitly neither upon the projectile species nor upon the incident charge state. (37 refs.)

75501 Single charge exchange in Ar^{6+} -He collisions. L. Opradolce, P. Valiron, R. McCarroll (Lab. d'Astrophys., Univ. de Bordeaux I, Talence, France).

J. Phys. B (GB), vol.16, no.11, p.2017-28 (14 June 1983). Cross sections for single charge exchange from Ar^{6+} incident on He have been calculated for ion energies in the range 1 to 200 keV (0.025 to 5 keV amu^{-1}). The adiabatic potential energies and the relevant radial and rotational coupling matrix elements of the system $\text{Ar}-\text{He}^{6+}$ are first calculated using a model potential method. The collision dynamics are then treated in the framework of the semiclassical (impact parameter) approximation. The cross sections for electron capture into a specific excited state of Ar^{5+} are compared with experiment. The validity of the theoretical model and the possible influence of translation effects are discussed. (21 refs.)

75502 K-shell excitation by K- to L-shell charge transfer in slow Kr^{4+} -Kr and Xe^{4+} -Xe collisions. R. Schuch, E. Justiniano, R. Hoffmann (Phys. Inst., Univ. Heidelberg, Heidelberg, Germany), W. Schadt, H. Schmidt-Bocking, P.H. Mokler, F. Bosch, W.A. Schonfeldt, Z. Stachura.

J. Phys. B (GB), vol.16, no.11, p.2029-37 (14 June 1983). The authors have measured K vacancy production probabilities with decelerated highly-charged Kr^{4+} (2.8 MeV u^{-1}) on Kr and Xe^{4+} (3.6 MeV u^{-1}) on Xe, by particle-photon coincidences. The impact-parameter-dependent probabilities reveal a dramatic change in shape and absolute height as soon as the projectile bears L-shell vacancies. From a comparison with calculations they conclude that K- to L-shell charge transfer can be described, even in the heavy collision system Xe on Xe, by the $2p\pi-2p\sigma$ rotational coupling mechanism when the relativistic energy splitting is taken into account. Deviations from a statistical distribution of the projectile L vacancies between the molecular levels are found. (18 refs.)

75503 Theory of electron capture from a hydrogenlike ion by a bare ion: intermediate-state contributions to the amplitude. S. Alston (Behlen Lab. of Phys., Univ. of Nebraska-Lincoln, Lincoln, NE, USA).

Phys. Rev. A (USA), vol.27, no.5, p.2342-57 (May 1983). Electro capture from a hydrogenlike ion of large nuclear charge Z_p by a bare ion of charge Z_e moving with speed v has been studied using the strong-potential Born approximation to the amplitude. Under the conditions $Z_e \ll Z_T$ and $Z_e v^2 \ll \hbar v$, it is shown that, in comparison with the impulse approximation, the correct weighting of the target spectrum of intermediate states in the strong-potential Born theory significantly alters the $1s \rightarrow 1s$ cross section and at the same time makes peaking approximations to the amplitude more realistic, even for low v . The specific cases of $Z_T = 6, 10$, and 18 are treated over the velocity range $Z_T/3 \leq \hbar v / e^2 \leq Z_T/10$. Instituting a one-electron model, K-shell capture cross sections and probabilities for protons on carbon, neon, and argon are calculated and compared with experiment. The strong-potential Born theory is seen to give a good representation of the data. Total cross sections for $1s \rightarrow 1s$ capture for $Z_p = Z_T = 1$ are also presented. (41 refs.)

75504 Relativistic calculation of atomic M-shell ionization by protons. Mau Hsiung Chen, B. Crasemann (Dept. of Phys. & Chem. Phys. Inst., Univ. of Oregon, Eugene, OR, USA), H. Mark.

Phys. Rev. A (USA), vol.27, no.5, p.2358-64 (May 1983). Relativistic plane-wave Born-approximation calculations of cross sections for M-shell ionization of ^{67}Zn , ^{79}Au , and ^{92}U by protons with incident energies from 0.05 to 1 MeV are reported. Dirac-Hartree-Slater wave functions were employed and binding-energy change and Coulomb deflection were taken into account. Associated X-ray production cross sections were also computed. Results are compared with previous theoretical predictions and with experimental data. Definite improvement in the theory has been attained by the use of realistic wave functions and consistent inclusion of the effects of relativity. (30 refs.)

75505 Charge transfer of doubly charged and trebly charged ions with atomic hydrogen at thermal energies. T.G. Heil (Dept. of Phys. & Astron., Univ. of Georgia, Athens, GA, USA), S.E. Butler, A. Dalgarno.

Phys. Rev. A (USA), vol.27, no.5, p.2365-83 (May 1983). The charge transfer of doubly charged and trebly charged ions of C, N, O, and Ne with atomic hydrogen at thermal energies is studied. Adiabatic potential-energy curves and radial coupling matrix elements are presented. The collision cross sections are calculated after transforming to a diabatic basis. For the trebly charged ions, there exists at least one exit channel into which charge transfer is highly probable. Cross sections for doubly charged ions are sensitive to the energy-level structure of the ionic species. (10 refs.)

75506 Electron capture in small-angle Ar^{2+} -Ar collisions. J. Stevens, R.S. Peterson, E. Pollack (Dept. of Phys., Univ. of Connecticut, Storrs, CT, USA).

Phys. Rev. A (USA), vol.27, no.5, p.2396-402 (May 1983). Electron capture in Ar^{2+} -Ar is studied at low keV energies. Using Ar^{2+} -He collisions as an energy reference the authors show that the dominant single-electron-capture process is endothermic and of the type $\text{Ar}^{2+} + \text{P} + \text{Ar} \rightarrow \text{Ar}^{2+} + \text{P} + \text{Ar}^{3+} + 3p^4 n l$. Detailed studies at 2.4 keV show $n l$ to be predominantly $3d$ and $4p$. Weaker exothermic processes are found and due mainly to long-lived, highly excited states of Ar^{2+} . The direct scattering and double-electron-capture channels are also studied. The direct scattering occurs with no Ar-target excitation. Differential cross sections are presented for the collision processes. The single-electron-capture results are interpreted with the use of a simple model in which a strongly attractive intermediate state couples the incident and outgoing channels. (21 refs.)

Energy-band structure and charge distribution for BaC_6 See Entry 75272

Ab initio MO calculations of benzene+TCNE and naphthalene+TCNE complexes with STO-3G π -split basis set See Entry 75277

Theoretical investigations of the interaction of but-2-ene with a sodium ion See Entry 75292

Atomic charges and charge flows from infrared intensities: C-H bonds See Entry 75380

He(I) photoelectron and UV/visible absorption spectra of N_3^- , NO_2^- and NO_3^- in solution See Entry 75436

Isolation of Fe charge states by ion implantation and their study by Mossbauer spectroscopy See Entry 76468

34.80 ELECTRON SCATTERING

75507 Use of V^{-1} potentials in Green's function calculations. P.Winkler (Dept. of Phys., Univ. of Nevada, Reno, NV, USA). *Int. J. Quantum Chem. (USA)*, vol.23, no.4, p.1571-7 (April 1983). An analysis of the leading effects of a propagator approach to the calculation of resonance energies is presented. By comparison with Δ SCF results, a simple approximation formula has been developed which contains the main features of the V^{-1} potential option and the diagonal Tamm-Dancoff approximation. This result is expected to be a useful guide for further refinements of the many-body aspects of the theory. (9 refs.)

34.80B Elastic scattering of electrons by atoms and molecules

75508 Application of HHOB approximation to e^{-} -Li elastic scattering. N.S.Rao, H.S.Desai (Phys. Dept., Faculty of Sci., MS Univ. of Baroda, Baroda, India).

Indian J. Pure & Appl. Phys., vol.21, no.3, p.159-62 (March 1983). High energy higher-order Born (HHOB) approximation is proposed by Yates (1979) is applied to calculate the elastic differential cross-sections and total cross-sections for e^{-} -Li elastic scattering at intermediate energies. Results of the calculations are compared with recent theoretical results of Byron and Joachain (1981) and the experimental data of Williams et al. (1976). (17 refs.)

75509 The $6s6p^2$ resonances in e -Hg scattering. N.S.Scott, P.G.Burke (Dept. of Appl. Math. & Theoretical Phys., Queen's Univ. of Belfast, Belfast, N Ireland), K.Bartschat.

J. Phys. B (GB), vol.16, no.11, p.L361-6 (14 June 1983). The elastic scattering and excitation cross sections for the $(6s6p)^3P_{0,1,2}$ states in e -Hg scattering are calculated from 4-7 eV using the relativistic R -matrix method. Resonances corresponding to the $6s6p^2$ configuration are found and their effect on the cross sections is discussed. In most cases good agreement with experiment is obtained, and certain features have been clarified. (24 refs.)

75510 The molecular structure of gaseous bis(trimethylsilyl)methane, $CH_3Si(CH_3)_2$, as determined by electron diffraction: an unusually large SiCISi angle. T.Fjelberg (Dept. of Chem., Univ. of Trondheim, Dragvoll, Norway), R.Seip, M.F.Lappert, A.Thorne.

J. Mol. Struct. (Netherlands), vol.99, no.3-4, p.295-302 (June 1983). Steric interaction between trimethylsilyl groups in the title compound is relieved by opening the SiCISi angle ($123.2^\circ(9)$), by stretching the central C-Si bonds slightly ($1.889(4)$ Å) and by a torsional displacement of the methyl groups from staggered positions ($25^\circ(5)$). The compound is compared to other strained *t*-butyl or trimethylsilyl substituted methanes and silanes. (14 refs.)

75511 The molecular structure of tetramethylhydrazine: a gas phase electron diffraction study. V.A.Naumov, O.A.Litvinov (Inst. of Organic & Phys. Chem., Acad. of Sci., Kazan Branch, Kazan, USSR), H.J.Geise, J.Dillen.

J. Mol. Struct. (Netherlands), vol.99, no.3-4, p.303-7 (June 1983). The molecular structure of tetramethylhydrazine, $(CH_3)_2NN(CH_3)_2$, has been investigated by electron diffraction in the gas phase. Diffraction intensities can be explained by a mixture of gauche and trans conformations in a 70:30% ratio. The r_g structure is characterized by $r(CH) = 1.096$ Å, $r(CN) = 1.463$ Å, $r(NN) = 1.410$ Å, $\angle NCH = 108.6^\circ$, $\angle CNC = 110.8^\circ$ and $\angle NNC = 113.5^\circ$. For the gauche conformation, the dihedral angle between two vicinal methyl groups is 78.5° . (6 refs.)

75512 An electron-diffraction investigation of the molecular structure and thermal dissociation of gaseous PCl_3 at $90^\circ C$. B.W.McClelland, L.Hedberg, K.Hedberg (Dept. of Chem., Oregon State Univ., Corvallis, OR, USA).

J. Mol. Struct. (Netherlands), vol.99, no.3-4, p.309-13 (June 1983). Interest in the structure of PCl_3 arose in the course of some other work which involved the equilibrium $PCl_3 = PCl_2 + Cl_2$. A part of the work comprised essentially a repeat of Adams and Bartell's experiment *ibid.*, vol.8, p.23 (1971). The authors discovered that under these experimental conditions appreciable amounts of PCl_3 and Cl_2 are generated by shift of the equilibrium—more, apparently, than had been assumed in previous electron-diffraction studies. Since the analysis takes into account the dissociation products, and since the sample was free from components other than those involved in the equilibrium, the authors thought it worthwhile to report the results. (14 refs.)

Electron-correlation effects in electron-scattering cross-section calculations of N_2 See Entry 75528
System for recording electron-atom collision cross sections using an AI-256-6 pulse analyzer See Entry 75551

34.80D Atomic excitation and ionization by electron impact

75513 $2S$ excitation of atomic hydrogen by electron impact at high energies. N.Saha (Dept. of Appl. Math., Univ. Coll. of Sci., Calcutta, India).

Can. J. Phys. (Canada), vol.61, no.5, p.748-52 (May 1983). The $2S$ excitation cross section of atomic hydrogen by electron impact at high energies has been calculated following the method of Das (1979). Comparison of the results for the differential cross section with other theoretical results, and comparison of the results for the total cross section with those of other the results of the present calculations are fairly accurate. (10 refs.)

75514 Low-energy electron impact excitation of the lowest-lying autoionizing level in Li. S.N.Tiwary (Dept. of Appl. Math. & Theoretical Phys., Queen's Univ. of Belfast, Belfast, Ireland).

Chem. Phys. Lett. (Netherlands), vol.97, no.2, p.221-3 (13 May 1983). The authors have calculated the electron impact total cross sections for the excitation of the lowest-lying autoionizing level generated due to the core-excitation $1s^2 2s^2 S^+ \rightarrow 1s2s^2 S^+$ transition in the lithium atomic system using Hartree-Fock wavefunctions for both initial and final states within the R -matrix method in the low bombarding energy region. The authors' results show that the energy dependence of cross sections is significantly different in nature from all earlier theoretical predictions. (11 refs.)

75515 Excitation of Be^+ by electron impact. P.S.Ganas, L.P.Gately (California State Univ., Los Angeles, CA, USA).

J. Appl. Phys. (USA), vol.54, no.5, p.2167-9 (May 1983). A realistic analytic central potential is used to generate wavefunctions for the ground and excited states of singly-ionized beryllium. Generalized oscillator strengths and integrated cross sections from threshold to 5 keV are calculated in the Born approximation for $2s$ - ns , $2s$ - np and $2s$ - nd excitations. Comparison of the cross sections with experimental and theoretical data is discussed for the $2s$ - $2p$ transition. (16 refs.)

75516 Excitation of helium-like ions by electron impact in the first-order exchange Coulomb approximation. S.Nakazaki (Dept. of Appl. Phys., Miyazaki Univ., Miyazaki, Japan).

J. Phys. Soc. Jpn. (Japan), vol.52, no.5, p.1555-62 (May 1983). Usefulness of the first-order exchange of Coulomb approximation has been examined by applying it to the electron impact excitation processes of helium-like ions. Collision strengths for the excitation from the ground state to the $n=2$ states (2^1S , 2^3S , 2^1P and 2^3P) for Li^+ , C^{4+} , O^{5+} and Si^{13+} have been calculated at energies up to five times the threshold energies. It is found that the present approximation improves the Coulomb-Born-Oppenheimer approximation remarkably and gives results comparable with the five-state close-coupling calculation of Wyngaarden et al. (1979). It is also found that the short range distortion effect is largely taken care of in the present first-order approximation.

75517 Eikonal approach to break-up processes of hydrogen-like ions by electron impact; exchange of electrons. H.Kotegawa (Dept. of Phys., Hiroshima Univ., Hiroshima, Japan).

J. Phys. Soc. Jpn. (Japan), vol.52, no.5, p.1572-80 (May 1983). The Coulomb-eikonal approximation is applied to evaluate the electron exchange amplitude in the ionization of hydrogen-like ions by an electron impact. This amplitude is reduced to a three-dimensional integral expression suitable for numerical calculations. The cross section including the contribution of the electron exchange is calculated for the ionization of He^+ , whose results show a reasonable agreement with experimental results. The exchange effect is found to be important in the ionization process in the intermediate as well as in the low energy region.

75518 Electron impact double-ionisation of Xe II. M.S.Pindzola (Dept. of Phys., Auburn Univ., Auburn, AL, USA), D.C.Griffin, C.Botcher.

J. Phys. B (GB), vol.16, no.11, p.L355-60 (14 June 1983). Electron impact inner-shell ionisation followed by autoionisation can dominate the total double-ionisation cross section for certain atomic ions. For Xe^{2+} the indirect contribution from the $4d^{10} 5s^2 5p^2 \rightarrow 4d^9 5s^2 5p^3$ ionisation followed by Auger decay is calculated to be three times the direct 'double-knockout' contribution. The distorted-wave inner-shell ionisation cross section is found to be strongly influenced by both ground-state correlations and term dependence in the ejected-electron continuum. The authors' Xe^{2+} results are in reasonable agreement with the recent experimental crossed-beam measurements of Achenbach et al. (1983). (13 refs.)

75519 Production of multiply charged rare-gas ions by relativistic electrons. A.Müller, W.Groh, U.Kneissl, R.Heil, H.Stroher, E.Salzborn (Inst. für Kernphys., Univ. Giessen, Giessen, Germany).

J. Phys. B (GB), vol.16, no.11, p.2039-52 (14 June 1983). Charge state spectra of ions generated in single collisions of 20 to 50 MeV electrons with rare-gas atoms have been measured by a time-of-flight technique. Relative abundances of ions in charge states up to $2+$ for He, $3+$ for Ne, $5+$ for Ar, $7+$ for Kr and $8+$ for Xe were deduced from the experiment. Higher charge states, e.g. $12+$ for Xe, could also be observed; however their quantitative fractions could not be determined. The relative abundances F_i of the different ion charge states i are constant in the investigated energy range; however they rapidly decrease with increasing i —strongly dependent on the atomic number of the bombarded target. The experimental results are in good agreement with calculations based on inner-shell ionisation cross sections folded with charge state distributions which result from the decay of the corresponding initial vacancies. The capability of fast electrons for efficient production of slow highly charged ions in single collisions with atoms is discussed. (21 refs.)

75520 Excitation cross sections of the vanadium atom. A.Yu.Krasavin, A.N.Kuchenev, Yu.M.Smirnov.

J. Appl. Spectrosc. (USA), vol.36, no.5, p.575-80 (May 1982). Translation of: *Zh. Prikl. Spektrosk. (USSR)*, vol.36, no.5, p.805-11 (May 1982). [received: Feb. 1983]

The ground state of the vanadium atom $4^4F_{3/2}$ refers to the configuration $3d^4 4s^1$, as a rule, the state of one, and sometimes both, s -electrons is altered upon the excitation of this atom by electron impact. The states of the excited vanadium atom can have a multiplicity which differs from the multiplicity of the ground state, i.e. they can be doublet or sextet. The investigation of the excitation processes of such states is of appreciable interest for the physics of atomic collisions and atomic spectroscopy. The authors investigated the excitation of the vanadium atom with an apparatus intended for measurement of the excitation cross sections of atoms of the refractory metals by electron impact. The application of the method of intersecting electron and atomic beams with recording of the photons emitted by the excited atoms from the beam intersection region forms the basis for the experiment. (2 refs.)

75521 Electron-impact excitation-autoionization in the cadmium isoelectronic sequence: a case of target term dependence in scattering theory. M.S.Pindzola (Dept. of Phys., Auburn Univ., Auburn, AL, USA), D.C.Griffin, C.Botcher.

Phys. Rev. A (USA), vol.27, no.5, p.2331-7 (May 1983).

Excitation-autoionization contributions to electron-impact ionization are calculated for several atomic ions in the cadmium isoelectronic sequence. The authors calculate excitation cross sections in the distorted-wave approximation and compare them in one case to a calculation in the close-coupling approximation. They focus attention on the $4d^{10} 5s^2 \rightarrow 4d^9 5s^2 nf$ inner-shell excitations in ln^+ , Sb^+ , and Xe^+ . Hartree-Fock atomic structure calculations for the $4d^9 5s^2 nf$ configurations are found to be highly term dependent. Thus the authors' predictions for the total ionization cross section from the $5s$ subshell for these ions exhibit strong target term dependence. The authors' Xe^+ results are found to be in excellent agreement with the recent experimental crossed-beam measurements of Gregory and Crandall (1983). (26 refs.)

75522 Measurement of the cross section for electron-impact ionization of Be^{4+} ions. D.C.Gregory, D.H.Crandall (Phys. Div., Oak Ridge Nat. Lab., Oak Ridge, TN, USA).

Phys. Rev. A (USA), vol.27, no.5, p.2338-41 (May 1983). The absolute cross section for electron-impact ionization of Be^{4+} has been measured from below threshold to 1500 eV with the Oak Ridge National Laboratory crossed-beams apparatus. Excitation of inner-shell electrons to autoionizing states is found to contribute up to a factor of 10 more than direct processes to the single-ionization cross section, and indirect effects dominate the measurement over the entire energy range studied. Good agreement is found with distorted-wave excitation calculations added to Lotz direct-ionization predictions. (17 refs.)

75523 Subshell formula for the Bethe-Born stopping approximation. J.M.Peek (Sandia Nat. Lab., Albuquerque, NM, USA).

Phys. Rev. A (USA), vol.27, no.5, p.2384-7 (May 1983). It is known that the subshell contributions to the coefficient of the $O(\ln E)$ asymptotic term of the Bethe-Born stopping-number formula are not given correctly by partitioning the squared matrix element defining this coefficient into a simple sum of its subshell contributions. This interesting result is extended to the second, or $O(1)$, asymptotic term in the stopping number. In

this case, the subshell decomposition results in a sum of two expressions. One is simply the subshell decomposition of the squared matrix element defining the $O(1)$ coefficient for the total system. The second term is more complex in form but sums to zero, as it must, when summed over all subshells in the target. It is pointed out that this second term and its summation requirement can be used to impose a useful restriction on the construction of theoretical subshell corrections for the Bethe-Born formula. (12 refs.)

75524 Excitation of hydrogenlike ions from ground state to arbitrary p state by electron impact. N.C.Deb, C.Sinha, N.C.Sil (Dept. of Theoretical Phys., Indian Association for the Cultivation of Sci., Calcutta, India). *Phys. Rev. A (USA)*, vol.27, no.5, p.2447-55 (May 1983).

The authors have formulated a generalized method for the evaluation of the cross sections for $1s\text{-}np$ excitation of hydrogenlike ions by electron impact both in Coulomb-Born and Coulomb-Born-Oppenheimer (CBO) approximations. In this formulation they have replaced the associated Laguerre polynomial for the final-state wave function by an integral representation. The main advantage of the authors' method is that the higher-order parametric differentiations usually adopted in order to obtain the amplitudes for the higher values of the principal quantum number n are avoided by one-dimensional integration. To the authors' knowledge, this is the first attempt to calculate the electron-ion excitation cross section in the CBO approximation for an arbitrary p state without any recourse to partial-wave analysis. They have also calculated asymptotic scaled cross sections for the limit $n \rightarrow \infty$ at different energies. The direct-excitation results are in good agreement with the existing theoretical findings of Tully for different n values in the intermediate- and high-energy regions. (26 refs.)

75525 Electron double ionization cross section in sodium obtained from $K\alpha$ hypersatellite spectra. J.Lahtinen, O.Keski-Rahkonen (Lab. of Phys., Helsinki Univ. of Technol., Espoo, Finland). *Phys. Scr. (Sweden)*, vol.27, no.5, p.334-8 (May 1983).

The $K\alpha$ hypersatellite spectrum of Na metal has been measured in electron excitation with voltages from 4 to 25 kV. The spectrum shows lines with initial $K^{-2}(K\alpha)^n$ and $K^{-2}L^{-1}$ holes. The energies of these lines as well as the K^2 binding energy have been determined and compared with theoretical calculations. The intensity of the line group with $K^{-2}L^{-1}$ initial configuration relative to the K^{-2} group has been measured and found to be in agreement with simple shake-off calculation. The electron double ionization cross section (EDC) of the K -shell has been determined from both thick and thin target measurements using the method developed by Saijonmaa and Keski-Rahkonen, and found to yield equivalent results. The EDC has also been calculated theoretically using classical and quantum mechanical binary encounter approximations as devised by Saijonmaa. Theory reproduces fairly well the magnitude and the atomic number dependence of the EDC whereas the shape of the EDC-curve as function of energy deviates clearly from observed values. (43 refs.)

Electron-photon coincidence technique for the absolute calibration of VUV detectors See Entry 74533

The $6s6p^2$ resonances in e-Hg scattering See Entry 75509

System for recording electron-atom collision cross sections using an AI-256-6 pulse analyzer See Entry 75551

Short wavelength laser calculations for electron pumping in neon-like krypton (Kr XXVII) See Entry 75621

34.80G Molecular excitation, ionization, and dissociation by electron impact

75526 Calculation of relative electron impact total ionization cross sections for organic molecules. W.L.Fitch (Zoecon Corp., Palo Alto, CA, USA), A.D.Sauter.

Anal. Chem. (USA), vol.55, no.6, p.832-5 (May 1983). A scheme is presented for the calculation of electron impact total ionization ratios for organic molecules. The scheme is based on the additivity of atomic ionization cross sections. The coefficients for the calculation are determined by a linear regression using 179 total ionization cross section measurements taken from the literature. The average error in the prediction of relative total ionization cross section for the 179 molecules was 4.69% by this approach. Other approaches employing diamagnetic susceptibility and molecular volume are shown to be inferior to the atomic additivity scheme. (23 refs.)

75527 Electron impact investigation of the molecules SeS(g) and TeSe(g) under high-temperature equilibrium conditions. M.Grade, J.Wiencke, W.Rosinger, W.Hirschwald (Inst. für Phys. Chem., Freie Univ. Berlin, Berlin, Germany).

Ber. Bunsenges. Phys. Chem. (Germany), vol.87, no.4, p.355-61 (April 1983). SeS(g) and TeSe(g) molecules, produced by Knudsen-cell vaporization of the mixed IIB/VIA-systems ZnS/ZnSe and CdSe/CdTe , were studied by energy-dispersive electron impact ionization. Analysis of ionization efficiency curves yields energy levels of excited ionic states of the molecule ions $\text{SeS}^+(g)$ and $\text{TeSe}^+(g)$. The energy levels correlate with corresponding states of $\text{S}_2^+(g)$, $\text{Se}_2^+(g)$ and $\text{Te}_2^+(g)$ derived from independent photoelectron spectroscopic data. (49 refs.)

75528 Electron-correlation effects in electron-scattering cross-section calculations of N_2 . M.Breitenstein, A.Endesfelder, H.Meyer, A.Schweig, W.Zittlau (Fachbereich Phys. Chem., Univ. Marburg, Marburg, Germany). *Chem. Phys. Lett. (Netherlands)*, vol.97, no.4-5, p.403-9 (27 May 1983). Total differential high-energy electron-scattering cross sections for N_2 have been calculated in the first Born approximation and compared with available experimental data. The importance of including electron correlation is demonstrated. (28 refs.)

75529 Wave packet formulation of the boomerang model for resonant electron-molecule scattering. C.W.McCurdy, J.L.Turner (Dept. of Chem., Ohio State Univ., Columbus, OH, USA).

J. Chem. Phys. (USA), vol.78, no.11, p.6773-9 (1 June 1983). A time-dependent formulation of the boomerang model for resonant electron-molecule scattering is presented in terms of a wave packet propagating on the complex potential surface of the metastable anion. The results of calculations using efficient semiclassical techniques for propagating the wave packet are found to be in excellent agreement with full quantum-mechanical calculations of vibrational excitation cross sections in $e^-\text{N}_2$ scattering. The application of the wave packet formulation is a computational and conceptual approach to the problem of resonant collisions with polyatomic molecules is discussed in the light of recent wave packet calculations on polyatomic photo-dissociation and Raman spectra. (27 refs.)

75530 Effect of gravity on density distributions and orthopositronium annihilation rates in ethane and methane near the critical point. S.C.Sharma, S.R.S.Kalle (Dept. of Phys., Univ. of Texas, Arlington, TX, USA).

J. Chem. Phys. (USA), vol.78, no.11, p.6897-900 (1 June 1983). The effect of gravity on density distributions has been studied in ethane and methane near the critical points using the linear-model parametric equation of state. The results obtained from this study are used to further understand the sensitivity of orthopositronium annihilation rates to density fluctuations in molecular gases. It is shown that the influence of gravity is too small to account for the recently observed dependence of orthopositronium annihilation rates on the density of ethane gas at 306.4K. However, a significant variation in local density vs. height is calculated at temperatures closer to the gas-liquid critical point. The density and temperature dependencies of the annihilation rates of orthopositronium atoms, recently observed in ethane and methane gases, are discussed in terms of the findings of this study. (19 refs.)

75531 Vibrational excitation of symmetric and bending modes of H_2O by slow electron impact. A.Jain, D.G.Thompson (Dept. of Appl. Math. & Theoretical Phys., Queen's Univ. of Belfast, Belfast, N Ireland).

J. Phys. B (GB), vol.16, no.11, p.1347-54 (14 June 1983). Electron impact vibrational excitation cross sections (differential, integral and momentum transfer) for the symmetric (100) and the bending (010) modes of the H_2O molecule are calculated in the fixed-nuclei and the impulse approximations from threshold to 10 eV. The normal coordinate dependent K -matrix elements are augmented with the laboratory frame first Born matrix elements for higher angular momenta in order to obtain converged cross sections via a closure formula. A sharp threshold peak and a broad resonance structure is seen around 6-8 eV in the integral cross section in agreement with the recent observations: while the A_1 scattering state plays a not unimportant role, the major contribution to this broad feature is due to the B_2 state. All results compare well with the crossed-beam experimental results of Seng and Linder (1974). (24 refs.)

75532 Doubly differential cross sections of secondary electrons ejected from gases by electron impact: 50-400 eV on N_2 . T.W.Shyn (Space Phys. Res. Lab., Univ. of Michigan, Ann Arbor, MI, USA).

Phys. Rev. A (USA), vol.27, no.5, p.2388-95 (May 1983). Doubly differential cross sections of secondary electrons ejected from N_2 by electron impact have been measured by a crossed-beam method. The incident energies used were 50, 70, 100, 200, and 400 eV. The energy and angular range of secondary electrons measured were from 1.0 eV to one-half of the difference between the incident energy and ionization potential and 12° to 156° , respectively. The present results have been compared with two previous measurements and considerable discrepancies were found. (13 refs.)

An electron bombardment procedure for generating cation and neutral radicals in solid neon matrices at 4K: ESR study of $^{14}\text{N}_2^+$ and $^{15}\text{N}_2^+$ See Entry 75412

Ionization effects in a system of a free electron laser and a molecular medium See Entry 75674

Proton phototransfer and nonradiative deactivation in hydrogen-bonded complexes of 2-anthrol See Entry 77882

35.00 PROPERTIES OF ATOMS AND MOLECULES; INSTRUMENTS AND TECHNIQUES

35.10 ATOMS

35.10B Atomic masses, mass spectra, abundances, and isotopes

(inc. isotope separation; for mass spectrometry, see also 07.75; for radioisotope separation see 28.42H or 82.55)

75533 A method for the numerical investigation of nonstationary processes in multisectinal installations for separating multicomponent isotope mixtures. E.V.Levin, N.I.Lagutsov, G.A.Sulaberidze.

J. Eng. Phys. (USA), vol.43, no.3, p.1027-31 (Sept. 1982). Translation of: *Inzh.-Fiz. Zh. (USSR)*, vol.43, no.3, p.456-62 (Sept. 1982). On the basis of the Dufort-Frankel method for the integration of differential equations of parabolic type, the authors develop a method for the numerical calculation of nonstationary processes. (9 refs.)

75534 Optimization of isotope-separation processes in columns. V.A.Kaminskii, V.M.Vetsko, G.A.Tevzadze, O.A.Devdariani, G.A.Sulaberidze. *Sov. At. Energy (USA)*, vol.53, no.3, p.642-7 (Sept. 1982). Translation of: *At. Energ. (USSR)*, vol.53, no.3, p.174-8 (Sept. 1982). [received: May 1983]

The production of stable isotopes requires large material expenditures, and therefore the optimization of separating installations has a decisive effect on the economics of production. The authors propose a general method for the multiparameter optimization of cascade installations consisting of packed columns. As the target function for the optimization, they selected the cost of the isotope product, which provides a comprehensive characterization of the total expenditures required for the production process and also determines the choice of the most efficient lines of capital investment and the rational limits of improving the quality of production. (8 refs.)

35.10D Electric and magnetic moments, polarizability

75535 Measurement of polarization and optical alignment of ^4He atoms in the 2^3S state. B.N.Sevast'yanov (A.F. Ioffe Physicotech. Inst., Acad. of Sci., Leningrad, USSR).

Sov. Phys.-Tech. Phys. (USA), vol.27, no.11, p.1411-13 (Nov. 1982). Translation of: *Zh. Tekh. Fiz. (USSR)*, vol.52, no.11, p.2294-7 (Nov. 1982). [received: May 1983] The author notes that Happer (1972), Daniels and Timsit (1971), and Scheerer (1974) measured the polarisation P of ^4He under assumptions which are valid only for optically thin layers. The author's present work is concerned with measuring P and the alignment A for optically oriented 2^3S ^4He atoms for both optically thin and optically thick layers. (11 refs.)

75536 Threshold for suppression of light fluctuations in a shock-heated plasma consisting of monatomic gases (M~9-11). G.K.Tumakayev, Z.A.Stepanova (A.F. Ioffe Physicotech. Inst., Acad. of Sci., Leningrad, USSR). *Sov. Phys.-Tech. Phys. (USA)*, vol.27, no.11, p.1420-1 (Nov. 1982). Translation of: *Zh. Tekh. Fiz. (USSR)*, vol.52, no.11, p.2305-7 (Nov. 1982). [received: May 1983]

The authors observe the emission from the plasma stream behind a shock wave front at Mach numbers M~8-9 and M~10-11 for Xe and Ar, respectively, and point out that for the development of flow instability, a necessary condition for fluctuation damping is that the electron collision efficiency (L) and the radiative decay (R), $L/R > 1$, i.e. the excited states must be depopulated more rapidly by collisions than by radiative decay. (8 refs.)

75537 Relaxation rate of atomic orientation. B.G.Matisov (M.I. Kalinin Polytech. Inst., Leningrad, USSR). *Sov. Phys.-Tech. Phys. (USA)*, vol.27, no.11, p.1421-2 (Nov. 1982). Translation of: *Zh. Tekh. Fiz. (USSR)*, vol.52, no.11, p.2307-8 (Nov. 1982). [received: May 1983]

One of the main experimental methods for gaining information on atomic diffusion coefficients or longitudinal collision relaxation times is by studying orientation relaxation of optically oriented atoms in the dark. The author solves the pumping equation analytically to determine the atomic orientation relaxation rate Γ at the initial time $t=0$ just after the optical pumping is discontinued. Exact allowance is made for all of the diffusion modes in the calculation of Γ . The authors found that Γ depends strongly on the pumping rate W. At first sight it seems strange that Γ , which describes relaxation 'in the dark', should depend on W; however, this behavior can be traced to the fact that the spatial distribution of the oriented atoms is determined by W. (5 refs.)

Determination of electric and magnetic magnitudes of atoms and molecules for optical frequencies See Entry 75545

35.10F Relativistic corrections, fine- and hyperfine-structure constants

75538 High-resolution synchronized-quantum-beat spectroscopy using modulation sidebands: measurement of pressure shifts of the hyperfine splitting in sodium $3^2S_{1/2}$. Y.Fukuda, M.Tanigawa, T.Hashi (Dept. of Phys., Kyoto Univ., Kyoto, Japan), K.Kondo. *Opt. Lett. (USA)*, vol.8, no.6, p.301-3 (June 1983).

Pressure shifts of the hyperfine splitting in Na $3^2S_{1/2}$ that are due to buffer gases have been measured for the first time to the authors' knowledge by all-optical means using the method of synchronized-quantum-beat spectroscopy reported previously (Y. Fukuda et al., *Opt. Commun.*, vol.38, p.357, 1981). The substrate coherence is excited and detected with amplitude-modulated mode-locked laser pulses tuned to the D_1 line (pulse-repetition frequency, f_p ; modulation frequency, f_m), and the resonances observed at $f_0 = n f_p + n' f_m$ (n and n' are integers) are used for the measurement. The pressure-shift coefficients obtained at 210°C are 82, 61, -1, and -47 Hz/Torr for He, N₂, Ar, and Kr, respectively, within an accuracy of ± 3 Hz/Torr. (7 refs.)

Hyperfine structure in 6snd Rydberg configurations in barium See Entry 75280

Relativistic calculations of core-polarisation effects on the hyperfine structure in the alkalis See Entry 75319

Variation of fine structure along atomic Rydberg series See Entry 75323

Lifetimes of the Ne 2p fine structure states by measurements of linewidths of the laser induced fluorescence of an atomic beam See Entry 75347

Fine-structure transitions in collisions of Kr⁺(²P_j) with rare gases See Entry 75472

Transitions between excited states with mixed coupling Ne 2p⁵4p Ne levels See Entry 75494

35.10H Ionization potentials, electron affinities

The hydrogen atom in strong magnetic fields: summation of the weak field series expansion See Entry 75251

Electron double ionization cross section in sodium obtained from K α^h hypersatellite spectra See Entry 75525

35.20 MOLECULES

(see also 61.55, 61.60, and 61.65 Specific structures of metals and alloys, of other inorganic materials, and of organic materials, respectively)

35.20B General molecular conformation and symmetry; stereochemistry

75539 Molecular mechanics of organic halides. VII. Iodides. A.Y.Meyer (Dept. of Organic Chem., Hebrew Univ., Jerusalem, Israel).

THEOCHEM (Netherlands), vol.11, no.1-2, p.95-106 (June 1983). For pt.VI see J. Chem. Soc. Perkin Trans., vol.2, p.1199 (1982). The molecular-mechanical force field is extended to encompass saturated organic iodides, including non-germinal diiodides. Calculations produce molecular geometry, dipole moment, conformer energies, solvation energies and barriers to internal rotation. Results are reported for 25 molecules, acyclic and cyclic, representing altogether 60 structural variants. Trends in structure and conformational tendency along series of analogous halides are discussed. (70 refs.)

75540 The geometry of the tert-butyl group: statistical analysis and model calculations. A.M.de Vos, A.M.M.Schreurs, J.Kroon (Structural Chem. Group, Rijksuniv., Utrecht, Netherlands), F.B.van Duijneveldt. *THEOCHEM (Netherlands)*, vol.11, no.1-2, p.107-13 (June 1983). A statistical analysis of the geometry of tertiary butoxy groups in molecular crystals reveals a significant departure from C_{3v} symmetry. The optimum geometry obtained by model calculations is in excellent agreement with the mean values of the bond parameters found in this analysis. The loss of three-fold symmetry and the flexibility of the tertiary butoxy group is discussed in terms of intra and intermolecular interactions. (15 refs.)

75541 An answer to the spiro versus ansa dilemma in cyclophosphazenes. III. N₃P₃Cl₃[HN-(CH₂)₄-NH]Cl₂P₃N₃. A serendipitous two-ring bridged-ansa phosphazene. G.Guerch, J.-F.Labarre, R.Lahana, R.Rouques, F.Sournies (Lab. Structure et Vie, Univ. Paul Sabatier, Toulouse, France).

J. Mol. Struct. (Netherlands), vol.99, no.3-4, p.275-82 (June 1983). For pt.II see ibid., vol.96, p.113 (1982). Reaction of N₃P₃Cl₆ with butylene-diamine (1:1) leads to a mixture of the expected monospiro compound as the major product and of two by-products (A) and (B). Mass spectrometry and X-ray analysis prove that (A) has a two-ring assembly structure in which two N₃P₃Cl₃ moieties are bridged through a [HN-(CH₂)₄-NH] entity. (14 refs.)

Electronic rearrangement on molecules accompanying β -decay investigated by nuclear resonance fluorescence See Entry 74918

Molecular structure of orthosilicic acid and importance of (p-d) π bonding. An ab initio molecular orbital study See Entry 75269

Ab initio study of structure and stability of the dimer (LiBeH₃)₂. Alternative configurations with mono- and bi-nuclear anions See Entry 75270

Ab initio MO calculations of benzene+TCNE and naphthalene+TCNE complexes with STO-3G π -split basis set See Entry 75277

Electronic structure of small copper clusters See Entry 75286

Theoretical investigations of the interaction of but-2-ene with a sodium ion See Entry 75292

A theoretical study of the structure, charge distribution and gas-phase basicity of 1H-indazole and its N-methyl derivatives See Entry 75293

On the stability of [furan]⁺ and [vinylketene]⁺ See Entry 75294

Conformational and MO studies of hydroxy-2-aminotetralins See Entry 75295

INDO studies on the electronic structure of lanthanoid compounds See Entry 75296

Conformational studies of the β (1-3) linked disaccharide component of the immunologically active pentasaccharide of the Forssman antigen See Entry 75297

Calculation of excited-state properties of some small molecules: comparative study of the CNDO/S and CNDO/2- V_{NA+1} potential methods See Entry 75301

CNDO calculations of halogen-substituted diformamides See Entry 75307

Virial partitioning analysis of electron correlation and nuclear motion in diatomic molecules See Entry 75313

Microwave spectrum, dipole moment and ab initio molecular structure of 2-aminopropenenitrile (CH₂=C(NH₂)CN) See Entry 75368

Vibrational studies on conformational equilibrium in dimethylmethylphosphonate and methylmethylphosphinate See Entry 75385

Infrared cryogenic studies. XV. Chloroalkanes in argon matrices See Entry 75387

Chloroacetyltriphenylphosphonium and the corresponding phosphorane. Physical chemistry and conformation study See Entry 75388

Vibrational and conformational studies of cyclopropylcarbonyl chloride See Entry 75394

Synthesis and structural study of N-ethylnortropane-3-spiro-5'-oxazolidine-2,4'-dione and its hydrochloride See Entry 75395

Survey of structural regularities in molecular properties. I. Carbon-13 chemical shifts in alkanes See Entry 75406

¹H and ¹³C NMR and infrared spectroscopic study of the conformational equilibrium in S-methyl dithiocarbamate See Entry 75411

Electric birefringences and molecular conformations of 2-aryloxiranes in solution See Entry 75416

Electronic spectral study of praseodymium(III) complexes with cysteine and diols See Entry 75449

The molecular structure of gaseous bis(trimethylsilyl)methane, CH₂(Si(CH₃)₃)₂, as determined by electron diffraction: an unusually large SiCSi angle See Entry 75510

The molecular structure of tetramethylhydrazine: a gas phase electron diffraction study See Entry 75511

An electron-diffraction investigation of the molecular structure and thermal dissociation of gaseous PCl₅ at 90°C See Entry 75512

Computer generation of isomeric structures See Entry 75553

The crystal and molecular structure of dihydroxy (malonato)-diammine platinum (II) See Entry 76386

CNDO/S parameters of C, O, and Si for solid state calculations See Entry 76839

Quantum chemical study of the molecular patterns of MAO inhibitors and substrates See Entry 78135

35.20D Interatomic distances and angles

75542 Isoelectronic molecules: the 13 and 22 electron sequences of diatomics. B.J.Laurenzi, C.Liitto (Dept. of Chem., State Univ. of New York, Albany, NY, USA).

J. Chem. Phys. (USA), vol.78, no.11, p.6808-23 (1 June 1983). A theory of isoelectronic molecules (J. Chem. Phys. 74, 1840, 1981) has been applied to the ground state of an even (22) electron and an odd (13) electron sequence of diatomics. Each of these is compared to the 14 electron sequence which had been studied previously. In the first instance, a striking correspondence in the dissociation energy $D_e(Z,Z')$, bond distance $R(Z,Z')$, and force constant $E''(Z,Z')$ surfaces for isovalent molecules from the 14 and 22 electron systems has become apparent. For the second, gross differences which arise in these surfaces when one electron is removed from 14 electron molecules are explicable in terms of the nature of the electron-pair bond as opposed to the one-electron bond. A stability rule which excludes ions with charges greater than plus or minus two units is found to hold for these sequences as well as the 14 electron one. (18 refs.)

Molecular structure of orthosilicic acid and importance of (p-d) π bonding. An ab initio molecular orbital study See Entry 75269

Highly strained single and double bonds See Entry 75391

Photoelectron spectroscopy of NHO⁻ and DNO⁻ See Entry 75439

The molecular structure of gaseous bis(trimethylsilyl)methane, CH₂(Si(CH₃)₃)₂, as determined by electron diffraction: an unusually large SiCSi angle See Entry 75510

35.20G Bond strengths, dissociation energies, hydrogen bonding, etc

- Charge, bond order and valence in the *ab initio* SCF theory ... See Entry 75285
- Three-body nonadditive effects for hydrogen bonded water molecules: SCF study of hydrated species including H_2S and various metal ions See Entry 75287
- Theoretical study of degree of covalency in some $\text{CoF}_6^{(n-1)-}$ complexes ($n=4,3$, and 2) See Entry 75288
- The dissociation energy of Cu_2 : do we want to perform multi-reference singles and doubles CIs on many-electron systems? See Entry 75305
- CNDO calculations of halogen-substituted diformamides See Entry 75307
- Ab initio* MRD-CI study of the electronic spectrum of SiH See Entry 75312
- Dissociation energy of aluminium monoselenide molecule See Entry 75331
- Binding energies and spectroscopic constants of the first-row and second-row diatomic hydrides See Entry 75360
- Infrared spectra of OC-HX hydrogen-bonded complexes in solid argon See Entry 75378
- Infrared spectrum of the $\text{CO}_2\text{-HCl}$ complex in solid argon at 12K See Entry 75379
- Atomic charges and charge flows from infrared intensities: C-H bonds See Entry 75380
- N-H... π hydrogen bonding: infrared study of *N*-cyclohexylformamide-aromatic donor systems See Entry 75383
- Quantum interference phenomena in the radiative decay of the $\tilde{\text{C}}(^1\text{B}_2)$ state of SO_2 See Entry 75431
- Molecular electrostatic potential of a triple stranded helix: poly(dT).poly(dA).poly(dT) See Entry 75465
- The geometry of the *tert*-butyl group: statistical analysis and model calculations See Entry 75540
- Isoelectronic molecules: the 13 and 22 electron sequences of diatomics See Entry 75542
- Rates of molecular desorption from solid surfaces: adsorption site dependence for CO on Ni(100) See Entry 76771

35.20J Barrier heights (internal rotation, inversion); rotational isomerism, conformational dynamics

- On the electronic structure of planar fluorinated amines and phosphines See Entry 75266
- Stabilities of isomeric bromonium ions $\text{C}_2\text{H}_4\text{Br}^+$ See Entry 75267
- Molecular structure of orthosilicic acid and importance of (p-d) π bonding. An *ab initio* molecular orbital study See Entry 75269
- Vibrational and conformational studies of cyclopropylcarbonyl chloride See Entry 75394
- ^1H and ^{13}C NMR and infrared spectroscopic study of the conformational equilibrium in *S*-methyl dithiocarbamate See Entry 75411
- Molecular mechanics of organic halides. VII. Iodides See Entry 75539
- Computer generation of isomeric structures See Entry 75553

35.20M Electric and magnetic moments (and derivatives), polarizability, and magnetic susceptibility

- 75543 Dipole moments of dichlorotoluenes in benzene solution. J.Prakash, B.Rai, Rahul (Dept. of Phys., Univ. of Gorakhpur, Gorakhpur, India). *Indian J. Pure & Appl. Phys.*, vol.21, no.2, p.123-4 (Feb. 1983).
- Dielectric constant, density and refractive index of 2,4; 2,6- and 3,4-dichlorotoluenes have been determined at 35°C using benzene as a non-polar solvent. These data have been utilized for evaluating their respective dipole moments using Palit's (1952) method. The dipole moment has been found to be 1.78, 0.65 and 2.29 D respectively for 2,4; 2,6- and 3,4-dichlorotoluenes. (15 refs.)
- 75544 Molecular *g* values, magnetic susceptibility anisotropies, and molecular quadrupole moments in $^{15}\text{N}_2\text{-HF}$, $^{15}\text{N}_2\text{-DF}$, OC-HF, OC-DF, and OC-HC van der Waals complexes. W.G.Read, E.J.Campbell (Noyes Chem. Lab., Univ. of Illinois, Urbana, IL, USA). *J. Chem. Phys. (USA)*, vol.78, no.11, p.6515-30 (1 June 1983).
- The rotational spectrum of $^{15}\text{N}_2\text{-DF}$, the rotational Stark effect in $^{15}\text{N}_2\text{-HF}$, and the rotational Zeeman effect in OC-HF, OC-DF, $^{15}\text{N}_2\text{-HF}$, $^{15}\text{N}_2\text{-DF}$, and OC-HCl van der Waals complexes have been studied using pulsed Fourier transform microwave spectroscopy carried out in a Fabry-Perot cavity. The Zeeman parameters are used to obtain the molecular quadrupole moments. The bulk magnetic susceptibility is estimated and the diamagnetic susceptibilities are calculated. The relationships between the Zeeman parameters measured for the complex and those of the free monomers are discussed. The authors observe that a simple zero order projection equation for g_{\perp} and χ_{\perp}^{HF} is reproducing the experimental values quite well. (32 refs.)
- 75545 Determination of electric and magnetic magnitudes of atoms and molecules for optical frequencies. P.Anastasovski (Faculty of Phys., Univ. 'Kiril i Metodij' vo Skopje, Skopje, Yugoslavia). *Opt. Acta (GB)*, vol.30, no.5, p.563-9 (May 1983).
- Presents results of an analysis, whose main task is to find the methods and equations for determining magnetic and electric magnitudes of atoms and substances for optical frequency fields. An original approach for the interpretation of the Pauli-Langevin and Van Vleck equations for molar magnetic susceptibility and molar polarizability of atoms gives very interesting results, which can be used to specify the magnitudes for magnetic and electric properties of atoms in the optical frequency region. The analysis starts with the assumption that magnetic and electric properties of atoms and compounds in the optical frequency region correlate with those for static fields. (4 refs.)
- One-electron properties at the SCF *ab initio* level See Entry 75276
- Ab initio* MO calculations of benzene+TCNE and naphthalene+TCNE complexes with STO-3G π -split basis set See Entry 75277
- Dipole moments of fluorobenzenes by CNDO and INDO methods See Entry 75291
- CNDO calculations of halogen-substituted diformamides See Entry 75307
- Ab initio* MRD-CI study of the electronic spectrum of SiH See Entry 75312
- Microwave spectrum, dipole moment and *ab initio* molecular structure of 2-aminopropenenitrile ($\text{CH}_2=\text{C}(\text{NH}_2)\text{CN}$) See Entry 75368

- Electronic spectra and excited state dipole moments of heterocyclic pentaatomic systems and their benzo and dibenzo derivatives See Entry 75398
- Electric birefringences and molecular conformations of 2-aryloxirans in solution See Entry 75416
- Rotational Zeeman effect in ArHCl and ArDF See Entry 75417
- Oscillator strengths corresponding to hypersensitive transitions of Nd^{3+} , Ho^{3+} , and Er^{3+} ions in solutions of complexes with certain amino polycarboxylic acids and their relation to the polarizability of the molecule See Entry 75451
- Calculation of van der Waals co-efficients in alkaline-earth chalcogenides See Entry 75464
- Molecular mechanics of organic halides. VII. Iodides See Entry 75539
- Dielectric relaxation and dipole moment measurements of *n*-methylacetamide in benzene and dioxane solutions at different temperatures from microwave absorption studies See Entry 77325
- Electric birefringence and molecular polarisability of $\text{CF}_3\text{Cl.CF}_3\text{Cl}$ See Entry 77356
- The interaction induced spectra of liquid CS_2 . A computer simulation study See Entry 77392

35.20P Rotation, vibration, and vibration-rotation constants

- 75546 Out-of-plane force field for cyclic pentaatomic molecules with an OC-X-CO grouping (X=O, NH, CH_2). M.G.Giorgini (Centro Studi Interfacolta sulla Spettroscopia Raman, Univ. di Bologna, Bologna, Italy). *THEOCHEM (Netherlands)*, vol.11, no.1-2, p.37-45 (June 1983).
- An out-of-plane force field common to maleic anhydride and imide has been worked out, emphasis being laid on the CC torsional force constants. The transferability of the calculated force field has been checked in a normal coordinate analysis for 4-cyclopentene-1,3-dione. (19 refs.)
- 75547 Applicability of R-K potential function for calculating molecular parameters of diatomic molecules. N.B.Ishwar, M.P.Varma, B.L.Jha (Dept. of Phys. & Maths., Indian School of Mines, Dhanbad, India). *Indian J. Phys. Part B*, vol.56B, no.6, p.367-8 (Dec. 1982). [received: May 1983]
- Varma and Jha (1981) have proposed a new potential energy function satisfying the necessary criteria of a suitable potential function for diatomic molecules. They have given an expression for calculating the rotational constant (α_e) and have used this expression for estimating the rotational constant (α_e) of alkaline earth halides and hydrides only. However according to Varshni (1957) an acceptable potential energy function should be capable of yielding correct (as far as practicable) values of both the molecular constants α_e and $\omega_e x_e$. The authors note deals with the calculation of α_e and $\omega_e x_e$ for a number of diatomic molecules as a complimentary part of their (Varma and Jha 1981) earlier paper. (7 refs.)
- Time-resolved study of the subpicosecond dynamics of molecular rotations in liquids See Entry 75327
- Vibrational spectra of fundamental tone of spontaneous emission of CO molecules under nonequilibrium conditions See Entry 75362
- Force constants and vibrational spectra of methylphosphine, dimethylphosphine, and trimethylphosphine See Entry 75363
- Microwave spectrum, dipole moment and *ab initio* molecular structure of 2-aminopropenenitrile ($\text{CH}_2=\text{C}(\text{NH}_2)\text{CN}$) See Entry 75368
- The microwave spectrum of the $\text{SiN} (^2\Sigma^+)$ radical See Entry 75369
- Vibrational spectra of phosphotungstate ion- $\text{PW}_{12}\text{O}_{40}^{3-}$ See Entry 75375
- Infrared spectra of OC-HX hydrogen-bonded complexes in solid argon See Entry 75378
- Infrared spectrum of the $\text{CO}_2\text{-HCl}$ complex in solid argon at 12K See Entry 75379
- Experimental and theoretical determination of the fundamental vibrations of 2-halo ethanolos. I. Gauche conformers See Entry 75382
- Laser-induced fluorescence spectrum of the CCN radical with an Ar^+ laser See Entry 75430
- Theoretical study of electron transmission through N_2 See Entry 75434
- Photoelectron spectroscopy of NHO^- and DNO^- See Entry 75439
- Stark-tuned Lamb-dip spectroscopy of the ν_4 and $2\nu_2$ bands of $^{14}\text{NH}_3$ See Entry 75450
- Breakdown of dynamic equilibrium between the symmetric and deformation mode levels in CO_2 caused by excitation in an electrical discharge See Entry 75453
- Observation of the $1^1\Pi_u\text{-X}^2\Sigma_g^+$ system in Cs_2^+ See Entry 75456
- Isoelectronic molecules: the 13 and 22 electron sequences of diatomics See Entry 75542
- Molecular *g* values, magnetic susceptibility anisotropies, and molecular quadrupole moments in $^{15}\text{N}_2\text{-HF}$, $^{15}\text{N}_2\text{-DF}$, OC-HF, OC-DF, and OC-HC van der Waals complexes See Entry 75544
- Dynamics of the CO_2 upper laser level as measured with a tunable diode laser See Entry 75619
- Picosecond molecular dynamics in liquids via degenerate four-wave mixing See Entry 75731
- Applications of degenerate four-wave mixing to high resolution molecular spectroscopy at 10.6 μm See Entry 75745

35.20S Hyperfine and fine-structure constants

- 75548 High-accuracy wave-number measurements in molecular iodine. L.Housek, W.M.Fairbank, Jr. (Dept. of Phys., Colorado State Univ., Fort Collins, CO, USA). *Opt. Lett. (USA)*, vol.8, no.6, p.322-3 (June 1983).
- Absolute wave-number measurements, with an accuracy of 2-11 parts in 10^9 , are presented for 27 $^{127}\text{I}_2$ hyperfine-structure lines in the range 5763-6563 Å. Individual components were resolved by saturation spectroscopy and their wave numbers measured by a comparison with wavelength standards made using a temperature-stabilized Fabry-Perot interferometer. Good consistency is found among the four accepted $^{127}\text{I}_2$ wavelength standards. The result of a previous measurement at 6563 Å, which was used as the basis for a Rydberg-constant determination, is also confirmed. (7 refs.)
- The microwave spectrum of the $\text{SiN} (^2\Sigma^+)$ radical See Entry 75369
- High resolution proton magnetic resonance study on metal-free porphyrins See Entry 75407

- Sub-Doppler infrared-infrared double resonance spectroscopy of NH_3 using Stark tuning and a diode laser See Entry 75414
- Photoelectron spectra of acenes. Electronic structure and substituent effects See Entry 75445

35.20V Ionization potentials, electron affinities, molecular core binding energy

- A formula for calculating molecular energy differences from electrostatic potentials at nuclei See Entry 75254
- One-electron properties at the SCF ab initio level See Entry 75276
- Electron correlation in linear hydrogen chains See Entry 75308
- Theoretical study of the lithium dimer and its anion See Entry 75330
- Highly strained single and double bonds See Entry 75391
- Theoretical photoelectron spectroscopy of the nitrite ion See Entry 75435
- Photoelectron spectra of anions in solutions and the ionisation energy of the solvated electron See Entry 75437
- Photoelectron spectroscopy of NHO^- and DNO^- See Entry 75439
- X-ray and UV photoelectron-spectroscopic studies of pyridine adsorbed on evaporated nickel and palladium in the temperature range 140-385K See Entry 75441
- Study of the ionization process $\text{BF}^+(\text{X}^{2+}) \rightarrow \text{BF}(\text{X}^{1+})$ by high-temperature photoelectron spectroscopy See Entry 75444
- Photoelectron spectra of acenes. Electronic structure and substituent effects See Entry 75445
- Stability of small copper clusters: Cu_3 and Cu_4 See Entry 75562
- Rates of molecular desorption from solid surfaces: adsorption site dependence for CO on Ni(100) See Entry 76771
- CNDO/S parameters of C, O, and Si for solid state calculations See Entry 76839
- On the measurement of binding energies in liquid ESCA and the relation to electrochemical half-cell EMFs See Entry 77943
- Effect of screening due to free mobile charges on the binding energy of an H^- ion See Entry 78803

35.20X Mass spectra

- 75549 Mass spectra of some substituted methylcyclodioxanes. E.Pelletier, J.F.Harrod (Chem. Dept., McGill Univ., Montreal, Quebec, Canada). *Can. J. Chem. (Canada)*, vol.61, no.4, p.762-8 (April 1983).
- The mass spectra of the substituted methylcyclodioxanes ($\text{Si}(\text{CH}_3)_2(\text{X})\text{O}_n$, where $\text{X}=\text{H}$ ($n=4, 5$ and 6), $\text{X}=\text{C}_6\text{H}_5$ ($n=3$ and 4), $\text{X}=\text{Br}$ ($n=3$ and 4), $\text{X}=\text{Co}(\text{CO})_4$ ($n=4$ and 5) have been measured. The compounds $\text{X}=\text{H}$ fragment by the same kinds of substituent loss and ring contraction mechanisms as previously reported for the compounds $\text{X}=\text{CH}_3$ but also by the loss of methylhydrogensilane. The compounds $\text{X}=\text{Ph}$ fragment by loss of benzene from an intramolecularly bridging benzenonium ion, formed from $[\text{M}-\text{CH}_3]^+$ and by losses of the phenylmethylsilane fragments. The compounds $\text{X}=\text{Br}$ only undergo substituent loss without ring fragmentation. The compounds $\text{X}=\text{Co}(\text{CO})_4$ show stepwise loss of all CO groups from $[\text{M}]^+$, $[\text{M}-\text{Co}(\text{CO})_4]^+$, and $[\text{M}]^{2+}$. (10 refs.)
- 75550 HOC^+ : laboratory observation of a proposed interstellar species. P.C.Burgers, J.L.Holmes (Chem. Dept., Univ. of Ottawa, Ottawa, Ontario, Canada). *Chem. Phys. Lett. (Netherlands)*, vol.97, no.2, p.236-8 (13 May 1983).
- The ion $[\text{HOC}^+]$ together with some $[\text{HC}^+\text{O}]$ is generated by the dissociative ionisation of CD_3OH . Collisional activation mass spectral characteristics of the two isomers are reported. $\Delta H_f([\text{HOC}^+])$ is estimated to be 930 ± 20 kJ mol^{-1} . (21 refs.)
- An answer to the spiro versus ansa dilemma in cyclophosphazenes. III. $\text{N}_3\text{P}_3\text{Cl}_6\text{HN}-(\text{CH}_2)_4-\text{NH}[\text{Cl}_2\text{P}_3\text{N}_3]$. A serendipitous two-ring bridged-assembly phosphazene See Entry 75541

35.80 ATOMIC AND MOLECULAR MEASUREMENTS AND TECHNIQUES

- 75551 System for recording electron-atom collision cross sections using an AI-256-6 pulse analyzer. Yu.I.Malakhov, M.B.Shapochkin (Moscow Power Inst., Moscow, USSR). *Instrum. & Exp. Tech. (USA)*, vol.25, no.4, pt.2, p.962-4 (July-Aug. 1982). Translation of: *Prib. & Tekh. Eksp. (USSR)*, vol.25, no.4, p.164-6 (July-Aug. 1982). [received: May 1983]
- A block diagram is given for a signal-analyzing system based on an AI-256-6 pulse analyzer. The system is used to measure spectral line intensities and determine how they depend on the electron energy. The basic circuits are given for the stepper motor actuator and for the unit interfacing the Ch3-38 frequency meter with the BS-50 DC power source. (3 refs.)
- 75552 Time resolved polarization spectroscopy: level kinetics and rotational diffusion. A.J.Cross, D.H.Waldeck, G.R.Fleming (Dept. of Chem., Univ. of Chicago, Chicago, IL, USA). *J. Chem. Phys. (USA)*, vol.78, no.11, p.6455-67 (1 June 1983).
- Time resolved polarization spectroscopy is a powerful and sensitive technique for the study of dynamics in the liquid phase. Using this technique, it is possible to obtain information about various relaxation processes in solution, including the motions of molecules in different electronic states, and the transitions between these states. Since the experiment typically measures both electronic relaxation and molecular reorientation, the observed signal can have a complicated form which represents a coupling of these two effects in a way that depends on the particular scheme of decay processes which are present in a given system. The authors present a general algorithm for deriving the form of the experimental signal for an arbitrary scheme for systems exhibiting these phenomena, assuming that the molecular motion is described by asymmetric rotational diffusion. Several examples are presented and experimental results interpreted using the derived formulas, including cases where (1) the excited state diffusion tensor differs from that of the ground state, (2) decay of the excited state occurs to levels that do not return to the ground state, (3) the principal contribution to the signal results from birefringence, (4) there are several intermediate excited states which undergo rapid relaxation, and (5) two overlapping absorption bands create an initial condition with more than one excited state populated. Application of this formalism to fluorescence depolarization experiments is also discussed. (38 refs.)

- 75553 Computer generation of isomeric structures. N.Trinajstic, Z.Jericevic (Rugjer Boskovic Inst., Zagreb, Yugoslavia), J.V.Knop, W.R.Muller, K.Szymanski. *Pure & Appl. Chem. (GB)*, vol.55, no.2, p.379-90 (Feb. 1983). (International Symposium on Theoretical Organic Chemistry, Dubrovnik, Croatia, Yugoslavia, 30 Aug.-3 Sept. 1982).
- The algorithms are developed for computer enumeration and generation of isomeric acyclic structures (alkanes, alkenes, alkynes, alkanols, alkanals, alkanones, etc.), benzenoid hydrocarbons, and aza-benzenoids. They are based on the common strategy which consists of representing a given structure by an integers sequence and the use of the induced order notion. (69 refs.)
- 75554 Beam-foil spectroscopy. H.G.Berry (Phys. Div., Argonne Nat. Lab., Argonne, IL, USA), M.Hass. In book: *Annual review of nuclear and particle science*. Vol.32, J.D.Jackson, H.E.Gove, R.F.Schwitters [Ed.], p.1-34. Palo Alto, CA, USA: Annual Reviews (1982), 595 pp. [0 8243 1532 4]
- The authors briefly summarize lifetime and spectroscopy measurements. They treat in more detail the alignment and excitation aspects of the beam-foil source, particularly in the applications to nuclear magnetic moment measurements. (132 refs.)

- An automated high resolution spectrometer with data system See Entry 74539
- Time-resolved study of the subpicosecond dynamics of molecular rotations in liquids See Entry 75327
- New experimental information from two-photon spectroscopy and comparison with theory See Entry 75461

36.00 STUDIES OF SPECIAL ATOMS AND MOLECULES

36.10 EXOTIC ATOMS AND MOLECULES (CONTAINING MESONS, MUONS, AND OTHER ABNORMAL PARTICLES)

- 75555 The kaonic hydrogen atom in momentum space. R.H.Landau (Dept. of Phys., Univ. of Surrey, Guildford, England). *AIP Conf. Proc. (USA)*, no.97, p.407 (1982). [received: May 1983] (Proceedings of the Workshop on the Interaction Between Medium Energy Nucleons in Nuclei, Bloomington, IN, USA, 28-30 Oct. 1982).
- It is well known that the strong absorption by a heavy nucleus of a negative kaon in a bound atomic state leads to unusual and sometimes unexpected dependence on the nuclear potential. In order to obtain a theoretical understanding of this problem, and try to understand recent experimental results. The author has studied kaonic hydrogen (K^-p), a conceptually simpler system which nonetheless displays much of the same physics. To do this, the author has applied new momentum space methods to solve the combined Coulomb plus nuclear interactions problem. The author's procedure is an extension of the Kwon-Tabakin (1978) technique of removing the logarithmic singularity of the Coulomb potential via a subtraction procedure suggested by Lande. (3 refs.)
- 75556 Muonium atoms in liquid and solid neopentane. B.W.Ng, J.M.Stadlbauer, Y.C.Jean, D.C.Walker (Chem. Dept., Univ. of British Columbia, Vancouver, British Columbia, Canada). *Can. J. Chem. (Canada)*, vol.61, no.4, p.671-4 (April 1983).
- Relatively long-lived muonium atoms have been observed in neopentane (dimethylpropane). The yields of all muon states are found to be essentially the same in liquid and solid neopentane and the same as those in water. These results have bearings on three matters of current interest in muonium chemistry: the origin of the 'background' spin relaxation; the formation mechanism; and the change in yields at the liquid-solid phase transition. These data were obtained by the μSR technique (muon spin rotation) at the TRIUMF accelerator. (16 refs.)
- 75557 Population of isomeric states in muonic atoms. J.De Kam, G.Wolschin (Inst. fur Theoretische Phys., Univ. of Heidelberg, Heidelberg, Germany). *Phys. Lett. B (Netherlands)*, vol.125B, no.2-3, p.109-12 (26 May 1983).
- The probability to populate the isomeric state in radiationless muonic transitions is calculated. The authors find that for muon induced reactions the population ratio isomeric state to ground state is larger by an order of magnitude as compared to nucleon induced reactions at the corresponding energy. (14 refs.)
- 75558 An experimental investigation of the pressure and concentration dependence of muonic Coulomb capture and cascade in gases. P.Ehrhart, F.J.Hartmann, E.Kohler, H.Daniel (Phys.-Dept., Tech. Univ. Munchen, Garching, Germany). *Z. Phys. A (Germany)*, vol.311, no.4, p.259-66 (1983).
- Muonic Coulomb capture ratios and X-ray intensity patterns in four binary mixtures of the gases N_2 , Ne, Ar, Kr, and Xe have been measured at three atomic ratios. An influence of the concentration has been established. The Lyman series intensity patterns of pure N_2 , Ne, Ar, Kr, and Xe were measured at pressures between 0.4 and 51 bar and found to depend on the pressure. Possible explanations are discussed. (49 refs.)

- Charged particles with short range interactions See Entry 74296
- Coupled bound and continuum eigenstates in momentum space See Entry 74867
- Antiproton-nucleus interaction at low energy See Entry 74989
- Temperature effects on positronium formation and inhibition: a contribution to the elucidation of early spur processes. IV. Methanol and ethanol solutions See Entry 77913

36.20 MACROMOLECULES AND POLYMER MOLECULES

(for biological macromolecules, see also 87.15; for polymer reactions and polymerization, see 82.35)

75559 Tri-axial ellipsoids as models for macromolecules in solution: procedures for numerical inversion of the shape functions leading to a stable unique solution. S.E.Harding (Dept. of Biochem., Univ. of Bristol Medical School, Bristol, England).

Comput. Biol. & Med. (GB), vol.13, no.2, p.89-97 (1983).

Two FORTRAN IV algorithms are given for determining the two axial ratios of a macromolecule (as modelled by a tri-axial ellipsoid) from its hydrodynamic parameters. The first involves a simple graphical inversion procedure of the volume independent A and R functions but can only be applied to a restricted range of macromolecules. The second algorithm is more general and involves an R -function constrained non-linear least squares fit to birefringence decay data. (9 refs.)

75560 Photon correlation spectroscopy of polymer solutions. C.Y.Chai, K.W.Min (Calgon Res. Labs., Calgon Corp., Pittsburgh, PA, USA).

J. Polym. Sci. Polym. Phys. Ed. (USA), vol.21, no.5, p.807-20 (May 1983).

A polynomial subdistribution method for analyzing the correlation profile in photon correlation spectroscopy of polymer solutions is described. This method generates a continuous distribution function from the measured photoelectron time-correlation function, which can be related to particle size or molecular weight distribution of solute. The method is tested using simulated data for unimodal and bimodal distributions and compared with cumulant and histogram methods, respectively. The polynomial subdistribution method has an advantage in that it not only generates a continuous distribution curve but also works well for bimodal distributions whose peaks are close together. (14 refs.)

75561 IR-spectroscopic investigation of molecular interactions in segmented polyurethanes. V.P.Volkov, K.V.Nel'son, E.N.Sotnikova, N.P.Apukhina, L.I.Potepun.

J. Appl. Spectrosc. (USA), vol.36, no.5, p.557-61 (May 1982). Translation of: *Zh. Prikl. Spektrosk. (USSR)*, vol.36, no.5, p.787-92 (May 1982). [received: Feb. 1983]

Experiments were conducted on polytetramethylene oxide (PTMO) elastomers and polybutadiene (PBD) elastomers i.e. two series of urethane elastomers differing in the nature both of the flexible and of the rigid segments. The elastomers were studied in the form of thin films and the spectra were recorded on a Perkin-Elmer two-beam spectrophotometer. The absorption bands in the region of NH and amide I were separated using integral equations of the first kind, with dispersive regularisation. (12 refs.)

Quantum chemical studies on the conformational structure of bacterial peptidoglycan. V. PCIO calculations on $\beta(1\rightarrow4)$ linked disaccharide of N-acetylglucosamine and N-acetyl muramic acid See Entry 75298

Determination of the weight-average molecular weight of polyamide-6 on the basis of melt viscosity See Entry 75976

Welding of polymers of nonuniform molecular weight See Entry 77727

Transient kinetics of chemical reactions with bounded diffusion perpendicular to the reaction coordinate: intermolecular processes with slow conformational changes See Entry 77879

Comparison of theoretical and thermodynamic values of interconsequent interactions in DNA See Entry 78121

Evidence for coherent excitation in biological systems See Entry 78123

The structure of bovine rhodopsin See Entry 78126

The structure of Panulirus interruptus hemocyanin at 4.0 Å resolution and a preliminary description of the copper-containing oxygen binding site See Entry 78127

Three-dimensional structure of membrane-bound cytochrome c oxidase See Entry 78128

The metal centers of cytochrome c oxidase: structures and interactions See Entry 78129

Structural studies of a bacteriochlorophyll-containing protein. See Entry 78130

Possible incorporation of the purine-purine mispairs in the DNA helix and the interpretation of the transversion-type point mutations See Entry 78132

Theory of living state. VII. Bose-Einstein-like ordering in temperature and time domain See Entry 78133

36.40 ATOMIC AND MOLECULAR CLUSTERS

75562 Stability of small copper clusters: Cu_3 and Cu_4 . G.H.Jeung, M.Pelissier, J.C.Barthelat (Lab. de Phys. Quantique, Univ. Paul Sabatier, Toulouse, France).

Chem. Phys. Lett. (Netherlands), vol.97, no.4-5, p.369-72 (27 May 1983).

The ground states of small clusters of copper atoms (Cu_2 , Cu_3 , and Cu_4) have been studied at the CI level using a small basis set and an effective core potential to describe the copper atom. A near degeneracy of three stable conformations is found for Cu_3 in accordance with the experimental result. The rhombus and T-form are stable for Cu_4 . The binding energy per atom is nearly constant for these clusters. (24 refs.)

75563 Theoretical aspects of cluster formation by keV bombardment of rare-gas solids. B.J.Garrison, N.Wingrad (Dept. of Chem., Pennsylvania State Univ., University Park, PA, USA).

Chem. Phys. Lett. (Netherlands), vol.97, no.4-5, p.381-6 (27 May 1983).

The mechanism of energy dissipation in argon crystals bombarded by 100 and 500 eV Ar^+ has been examined using classical dynamics. The study indicates that very high yields may be expected and that large molecular Ar clusters, Ar_n , may form via recombination in the near surface region. The results are compared qualitatively to recent matrix-isolation SIMS experiments on a variety of inert-gas solids. (16 refs.)

75564 Understanding the middle atmosphere via the laboratory: ion cluster investigations. R.G.Keesee, A.W.Castleman, Jr. (Dept. of Chem., Pennsylvania State Univ., University Park, PA, USA).

Ann. Geophys. (France), vol.1, no.1, p.75-80 (Jan.-Feb. 1983).

Ion clusters can be formed in the laboratory by either of two basic methods. One involves the generation of primary ions, followed by the clustering of neutrals onto these ions, while the second commences with the formation of neutral clusters which are subsequently ionized. Through both approaches, requisite thermochemical and reaction rate data are being acquired which are enabling a more complete understanding of the nature and processes of the middle atmosphere including its composition, electrical conductivity, and aerosol formation mechanisms. Laboratory methods and measurements concerning the formation, structure, and stability of small clusters are reviewed, with

emphasis on the manner in which these results can be and have been applied to problems related to the middle atmosphere. (37 refs.)

Electronic structure of small copper clusters See Entry 75286

40.00 CLASSICAL AREAS OF PHENOMENOLOGY

(inc. applications)

41.00 ELECTRICITY AND MAGNETISM; FIELDS AND CHARGED PARTICLES

(see also 03.50 Maxwell theory: general mathematical aspects)

41.10 CLASSICAL ELECTROMAGNETISM

41.10D Electrostatics, magnetostatics

Peak sampled vibrating-reed for the measurement of electric fields in the presence of space charge See Entry 74493

41.10F Steady-state electromagnetic fields; electromagnetic induction

75565 Electromagnetic field of an oscillating point dipole in the presence of spherical interfaces. M.T.Hirvonen (Acta Polytech. Scandinavica, Helsinki, Finland).

Acta Polytech. Scand. Math. & Comput. Sci. Ser. (Finland), no.Ma39, p.1-37 (1983).

The electromagnetic field of a sinusoidally oscillating electric or magnetic point dipole is calculated in the presence of spherical inhomogeneities. An analytical series solution of the Helmholtz equation in a space containing one sphere is first derived on the basis of the spherical wave expansion of the retarded vector potential of a dipole. The solution is completely general with respect to the frequency and the values of the constant permittivity, permeability and conductivity of the sphere and its surroundings. A system of two concentric spheres is next treated in a similar way. Finally, an analytical formula for the translatory transformation of the vector wave functions is applied to derive a precise solution to the problem of the scattering of dipolar waves from a system of two nonconcentric spheres. A number of numerical examples chosen to represent practical situations in geophysical mineral exploration are given. (5 refs.)

Determination of electromagnetic field scattered by small defects and influence of boundary between media See Entry 75571

41.10H Electromagnetic waves: theory

75566 Energy and power of nonperiodic fields in nonlinear lossy media. P.Proksch (Inst. für Nachrichtentechn., Tech. Univ. Wien, Wien, Austria).

Arch. Elektron. & Übertragungstechn. (Germany), vol.37, no.5-6, p.165-70 (May-June 1983).

General relations for the energy and power of nonperiodic electromagnetic fields in nonlinear lossy media are derived. They are inequalities and can be considered as a generalization of relaxations for the power of sinusoidal fields discovered by P. Penfield (1960). With the relations derived it is possible to determine limiting values for the energy levels in the different frequency bands and the conversion efficiency for various cases of frequency conversion. (5 refs.)

75567 Electromagnetic plane wave diffraction by a body of revolution. A.Ciarkowski (Lab. of Appl. Math. Phys., Tech. Univ. of Denmark, Lyngby, Denmark).

Bull. Acad. Pol. Sci. Ser. Sci. Tech. (Poland), vol.30, no.1-2, p.21-30 (1982).

The problem of electromagnetic plane wave diffraction by a perfectly conducting, convex body of revolution with a rim is considered. The analysis is based on Ufimtsev's method (1962) of edge waves. A high-frequency approximation to the scattered field is constructed. (1 ref.)

75568 A coordinate-free approach to wave reflection from a uniaxially anisotropic medium. H.C.Chen (Dept. of Electrical & Computer Engng., Ohio Univ., Athens, OH, USA).

IEEE Trans. Microwave Theory & Tech. (USA), vol.MTT-31, no.4, p.331-6 (April 1983).

Presents a coordinate-free method of solving the problem of electromagnetic wave reflection from the surface of uniaxially anisotropic medium. Based on the direct manipulation of vectors, dyadics, and their invariants, the method eliminates the use of coordinate systems. It facilitates solutions and provides results in a greater generality. The paper contains the following results in coordinate-free forms: (a) the dispersion equations; (b) the directions of field vectors; (c) the Poynting vectors (ray vectors) and group velocities; (d) the laws of reflection and refraction; and (e) the transmission and reflection coefficients. The results are valid for the incident wave having any polarization, and the optic axis of the uniaxial medium being arbitrarily oriented with respect to the interface and the plane of incidence. (20 refs.)

75569 Random non-linear electromagnetic waves in vacuo. P.H.Roberts (School of Math., Univ. of Newcastle upon Tyne, Newcastle upon Tyne, England).

Physica A (Netherlands), vol.119A, no.1-2, p.274-90 (April 1983).

The attempt made by Einstein and Stern to deduce Planck's law by classical reasoning, invoking only the zero-point background radiation, is reconsidered for a sea of electromagnetic waves, the interactions necessary for thermalization being provided by non-linearities in the wave equations rather than by, as in their case, charged particles. It is shown that, when the Cabot-Putterman ansatz is invoked, the resulting Wave-Boltzmann equation possesses Planck's law as steady-state solution. (17 refs.)

75570 Wave excitation of an oscillator having a discrete series of stable amplitudes. D.B.Duboshinski, Ya.B.Duboshinski. *Sov. Phys.-Dokl. (USA)*, vol.27, no.7, p.564-5 (July 1982). Translation of: *Dokl. Akad. Nauk SSSR*, vol.265, no.1-3, p.605-7 (July 1982). [received: April 1983]

Examines the excitation of a nonlinear oscillator by a wave. It is shown that under certain conditions undamped oscillations are excited at a frequency close to the natural frequency. The possible amplitudes of the oscillations form a discrete spectrum, with the amplitudes remaining practically constant over a wide range of wave intensities. (5 refs.)

75571 Determination of electromagnetic field scattered by small defects and influence of boundary between media. A.A.Orlovskii (Physicomech. Inst., Acad. of Sci., Ukrainian SSR).

Sov. J. Nondestr. Test. (USA), vol.18, no.9, p.705-12 (Sept. 1982). Translation of: *Defektoskopiya (USSR)*, vol.18, no.9, p.43-51 (Sept. 1982).

An analytical solution is obtained to the problem of electric and magnetic dipole moments equivalent to an ellipsoidal defect in space, for an arbitrary source of primary field and for a defect of dimensions much smaller than the wavelength, taking into account the effect of the boundary between media on determining the moments of equivalent dipoles. The derived equations for the field vectors are extended to the case of plane-layer media. (17 refs.)

41.70 PARTICLES IN ELECTROMAGNETIC FIELDS: CLASSICAL ASPECTS

(inc. synchrotron radiation)

75572 Transverse transport processes of charged particle systems in a strong magnetic field. II. Some discussions about the Boltzmann equation. Ho Yu-ping (Inst. of Plasma Phys., Acad. Sinica, Hefei, China). *Commun. Theor. Phys. (China)*, vol.1, no.4, p.441-8 (1982).

For pt.1 see *ibid.*, vol.1, no.4, p.441-8 (1982). It is pointed out that in a strong magnetic field the usual Boltzmann equation with Lorentz force term is inconsistent with the fundamental requirements of the general theory of non-equilibrium statistical mechanics. Furthermore, if a collision term corresponding to particles in different gyroorbits is used, the author finds that all the transport coefficients are exactly zero. General expressions for the transport coefficients in classical systems are then obtained by introducing the macroscopic velocities. A comparison between the author's results and those of the usual Boltzmann equation indicates that in the case of short range force, the lowest order terms are the same and the results of the Boltzmann equation become increasingly worse as more higher order terms are kept. (4 refs.)

Permanent magnet undulators See Entry 74500
Pulse propagation in free electron lasers See Entry 75649
Theory of gain expanded free electron lasers See Entry 75652
Free electron laser oscillator startup analysis See Entry 75657
Tapered wigglers See Entry 75667
Stories of undulator light See Entry 75668
Optical klystrons See Entry 75671

41.80 PARTICLE BEAMS AND PARTICLE OPTICS

(see also 07.80 Electron and ion microscopy, 07.77 Beam handling equipment)

41.80D Electron beams and electron optics

Procedures for focusing, stigmating and alignment in high resolution electron microscopy See Entry 74562

41.80G Ion beams and ion optics

75573 Foil/electron ion-beam lens. R.A.McCorkle (IBM Corp., Armonk, NY, USA).

IBM Tech. Disclosure Bull. (USA), vol.25, no.11A, p.5508-9 (April 1983). Describes a technique for a focused ion-beam system in which the ion beam is passed through a thin metal foil after it passes through the final focussing lens and before it strikes a target in order to electrically neutralize the beam and enable a sharper focus to be obtained at the target. (4 refs.)

42.00 OPTICS

(for properties of gases and of liquids and solids, see 51.70 and 78. respectively; for atmospheric optics, see 92.65; for physiology of the eye, see 87.32)

75574 Current optics in Sweden. E.Engelstam (Inst. of Optical Res., Royal Inst. of Technol., Stockholm, Sweden).

J. Opt. (France), vol.14, no.2, p.61-8 (March-April 1983). Reviews the current state of optical research and optics-optronics industrial activity in Sweden. (6 refs.)

42.10 PROPAGATION AND TRANSMISSION IN HOMOGENEOUS MEDIA

75575 Diffraction of the Hermite-Gaussian waves on opaque semi-infinite plane. L.Janicijevic (Fakultet za Fiziku, Univ. 'Kiril i Metodij' vo Skopje, Skopje, Yugoslavia).

J. Opt. (France), vol.14, no.2, p.83-92 (March-April 1983). The diffracted wave amplitude and the irradiance distribution are found for the case of an m, n -mode incident Hermite-Gaussian wave on an opaque semi-infinite plane. It is done by the method prescribed by Miyamoto and Wolf (see *Journ. Optic. Soc. Am.*, vol.52, p.615 and 636, 1962), which is based on Young's idea for interpretation of diffraction phenomena. The results obtained by this method are expressed in a form which allows a suitable qualitative interpretation of the diffraction pattern. The results of the general mode theory, are specialised to the case of the fundamental mode and the first few modes of the Hermite-Gaussian incident wave beam. (9 refs.)

75576 Generalized reciprocity for gratings of finite conductivity. A.Roger (Lab. d'Optique Electromagnetique, Faculte des Sci. et Tech., Centre de Saint-Jerome, Marseille, France).

Opt. Acta (GB), vol.30, no.5, p.575-85 (May 1983). Demonstrates generalized reciprocity relations in the two fundamental cases of polarization for gratings of finite conductivity. These relations are the analogues of those described in a previous paper for infinitely conducting gratings (see *ibid.*, vol.29, p.1427, 1982). The classical expressions of energy conservation and the reciprocity theorem are then derived, as well as the linear relations (i.e. functional derivatives) between small variations of the groove profile and of the complex coefficients describing the diffracted field. Moreover, the author shows that the relations for finite conductivity tend towards the relations already found for infinite conductivity when the index of the material tends towards infinity. Several numerical examples are then given to make clear the usefulness of the functional derivatives. (10 refs.)

75577 Centro-symmetry in Fraunhofer diffraction patterns. A.W.Lohmann, J.Ojeda-Castaneda (Phys. Inst., Erlangen, Germany).

Opt. Acta (GB), vol.30, no.5, p.629-37 (May 1983). Most of the known Fraunhofer diffraction patterns are centro-symmetrical. The cause of this symmetry is usually a real object transmittance, but complex objects with phase factors can also cause diffraction patterns with centro-symmetry. Actually, the set of real objects is only a small sub-set of the set of all those objects that produce diffraction patterns with centro-symmetry. (5 refs.)

75578 Fraunhofer diffraction patterns of tilted planar objects. K.Patorski (Warsaw Tech. Univ., Inst. of Design of Precise & Optical Instruments, Warsaw, Poland).

Opt. Acta (GB), vol.30, no.5, p.673-9 (May 1983). Attention is drawn to the changes in the Fraunhofer diffraction patterns encountered when the planar objects become tilted with respect to the optical axis. The differences between the far-field images observed in the well-known untitled case and the one investigated are shown and discussed using examples of familiar objects, such as square or rectangular apertures and linear diffraction gratings. (3 refs.)

75579 Exact calculations of the diffraction of s-polarized electromagnetic radiation from large-amplitude dielectric gratings. N.Garcia (Dept. de Fisica, Univ. Autonoma de Madrid, Madrid, Spain), A.A.Maradudin.

Opt. Commun. (Netherlands), vol.45, no.5, p.301-6 (1 May 1983). On the basis of the extinction theorem form of Green's theorem the authors have calculated the diffraction of s-polarized electromagnetic radiation from large amplitude, dielectric gratings of several different profiles. The authors demonstrate the existence of Wood 'anomalies' for gratings of sufficiently large amplitude, and identify them as threshold singularities. No evidence of resonance singularities due to the excitation of leaky surface waves supported by the grating is obtained for the grating profiles and corrugation strengths considered here, in contrast with earlier interpretations of analogous results. Rainbow scattering is predicted. Finally, no significant enhancement of the scattered field by the grating surface is found. (17 refs.)

75580 Exact calculations of p-polarized electromagnetic fields incident on grating surfaces: surface polariton resonances. N.Garcia (Dept. de Fisica Fundamental, Univ. Autonoma de Madrid, Madrid, Spain).

Opt. Commun. (Netherlands), vol.45, no.5, p.307-10 (1 May 1983). Exact calculations of the interaction of p-polarized light from grating surfaces are presented by using the theory of Toigo, Marvin, Celli and Hill (see *Phys. Rev.*, vol.B15, p.5618, 1977). New features for the scattered field are found for light resonating with surface plasmon polaritons; the reflectivity present maxima for large amplitude gratings. The electromagnetic field is calculated on a fine grid near the grating. The author finds enhancements of the order of 200 to 300 for the square of the field that could partly explain SERS. (13 refs.)

75581 Reflection of ultrashort pulses from layered media. S.A.Shakir, N.A.Yusuf, M.C.Mirzaa (Dept. of Phys., Yarmouk Univ., Irbid, Jordan).

Opt. Commun. (Netherlands), vol.45, no.5, p.317-19 (1 May 1983). The reflection of very short pulses from optical systems composed of planar layers is solved in terms of a simple finite series. The series correspond to the superposition of the pulses reflected from all the boundaries. Each term in the series is the scaled and time-shifted replica of the incident pulse. The case of a single film (Fabry-Perot interferometer) is solved exactly in terms of an infinite series similar to the series found for the more general system. (4 refs.)

75582 Marechal intensity formula for small-Fresnel-number systems. S.Szapiel (Inst. of Design of Precise & Optical Instruments, Warsaw Tech. Univ., Warsaw, Poland).

Opt. Lett. (USA), vol.8, no.6, p.327-9 (June 1983). A simple modification of the known Marechal intensity formula is proposed. It enables one to evaluate the near-the-diffraction-focus intensity distribution for well-corrected optical systems with small Fresnel numbers of the focusing geometry. As an example, the focal-shift effect in perfect systems is briefly reexamined. (22 refs.)

75583 Electromagnetic formulation for treating optical reflections from graded-material surfaces. A.G.Lieberman.

Report NBS-TN-1171, Nat. Bur. Stand., Washington, DC, USA (Dec. 1982), 32 pp.

The reflection of a monochromatic plane wave falling obliquely upon the surface of an arbitrary, flat, depth-dependent material is investigated theoretically. The complex reflection coefficient for either principal (s or p) polarization of the field is shown to satisfy a nonlinear differential equation of the Riccati type. An alternate formulation based on the wave impedance (i.e., impedance or admittance) functions is also presented. The impedance functions are shown to satisfy Riccati differential equations of their own. The reflection coefficient formulation and the wave impedance formulations are related via a bilinear algebraic transformation. Singularities appearing in the reflection coefficient formulation may be suppressed in the impedance formulation, and vice-versa. The advantage of either formulation is that the reflection coefficients for an arbitrary, depth-dependent medium can be obtained directly without having to solve Maxwell's equations for the internal field configurations.

The prediction and discovery of conical refraction by William Rowan Hamilton and Humphrey Lloyd (1832-1833) See Entry 74249

Complex interferometry See Entry 74520

Real-time fringe-pattern analysis See Entry 74521

Autocorrelation of ultrashort optical pulses using polarization interferometry See Entry 74523

Achromatic system for far-field diffraction with broadband illumination See Entry 75590

Ray tracing in a planar lens with spherically symmetric quadratic index profile See Entry 75763

- Performance evaluation of an apodized optical system with polarization masks See Entry 75766
- Realization of 90°- and 180° hybrids for optical frequencies See Entry 75777
- Calculation of the light transmission coefficient of a hollow combination light-guide See Entry 75789
- Development of fabrication technology and measurement systems for multimode, single-mode and polarization maintaining optical fibers See Entry 75796
- The influence of mode-coupling on the degree of coherence in an optical fiber See Entry 75811
- Measurement of fiber birefringence by wavelength scanning: effect of dispersion See Entry 75813
- Analysis of noise and bias in the fibre optic gyroscope See Entry 75823

42.20 PROPAGATION AND TRANSMISSION IN INHOMOGENEOUS MEDIA

- 75584 On stochastic models of light absorption. J.E.Mann (Dept. of Statistics, Virginia Polytech. Inst. & State Univ., Blacksburg, VA, USA). *Bull. Math. Biol. (GB)*, vol.45, no.2, p.229-37 (1983).
Previously developed light absorption models have treated the effective quantity of light-absorbing material within the experimental environment as a constant, i.e. a parameter. These models are, however, probabilistic in nature and are properly applied and interpreted only in statistical sense. Thus, it is clearly logical to regard the effective quantity of light-absorbing material to be a random variable. In this paper an asymptotic distribution is derived for this random quantity, and it is shown how this distribution may be incorporated into present models. These results may be applied to light absorption by plant and crop canopies as well as to liquid or solid media. Furthermore, previous models are based upon the assumption that light is parallel, or effectively so, as for solar light. Such models may be inadequate for an artificial (laboratory) environment which utilizes point source light. Present models for estimating light interception and radiation intensity are modified so as to accommodate a proximate point source of light. Numerical examples are included to illustrate the theory. (11 refs.)
- 75585 The a priori calculation of the diffuse reflectance of a turbid medium. H.G.Hecht (Dept. of Chem., South Dakota State Univ., Brookings, SD, USA). *Opt. Acta (GB)*, vol.30, no.5, p.659-68 (May 1983).
A derivation has been given by Hartel (see Licht., vol.10, p.141, 1940) which relates the angular distribution of multiple scatter to that of single scatter, as determined by the Mie theory. Hartel's result is used to generalize Thiesing's equations for a medium which both scatters and absorbs radiation. The result is similar to the two-parameter theories used by numerous other workers, the difference being that the formulation given here constitutes an a priori method which relates the multiple scattering characteristics to the single scatter problem, whose solution is well known. Reflectance properties are calculated by numerically solving the equations for two illustrative cases. (14 refs.)
- Objective laser speckle method for 3-D displacement measurement on curved surfaces See Entry 74434
- Optical turbulence: chaos in optical bistability See Entry 75712
- Raman scattering from metal smokes See Entry 75794
- The effectiveness of astronomical speckle transfer function reweighting algorithms See Entry 78825

42.30 OPTICAL INFORMATION, IMAGE FORMATION AND ANALYSIS

- 75586 Analytical tools for nonlinear image restoration. W.A.Porter, P.D.Oliver (Dept. of Electrical & Computer Engng., Louisiana State Univ., Baton Rouge, LA, USA). *Appl. Opt. (USA)*, vol.22, no.10, p.1424-6 (15 May 1983).
The authors point out a common interest between the optical processing and the system theory communities. Study of the work of Saleh et al. (see ibid., vol.20, p.4089, 1981) is taken as a case in point. The image retrieval algorithm of Saleh et al. is shown to be a special case of a more general algorithm available in the work of Rall (see Rendiconti del Circolo Matematico di Palermo Ser.2, vol.10, 1961). The authors also summarise some selected results from the system theory literature that may be of interest to the optical processing community. (12 refs.)
- 75587 Broad spectral band color image deblurring. T.H.Chao, S.L.Zhuang, S.Z.Mao, F.T.S.Yu (Electrical Engng. Dept., Pennsylvania State Univ., University Park, PA, USA). *Appl. Opt. (USA)*, vol.22, no.10, p.1439-44 (15 May 1983).
A broadband white-light processing technique for smeared color photographic image deblurring is described. The technique utilizes a diffraction grating method to disperse the smeared image spectra in the Fourier plane so that the entire spectral band of the white-light source can be utilized for the deblurring. In this paper the technique of synthesizing a fan-shape type complex deblurring filter to accommodate wavelength variation is presented. Experimental results showed that this broad spectral band processing technique offers an excellent coherent artificial noise suppression, and the technique is particularly suitable for color image deblurring. Experimental demonstrations and comparisons with the narrowband and coherent deblurring are also provided. (12 refs.)
- 75588 Image processing for extended depth of field. R.J.Pieper, A.Korpe (Dept. of Electrical & Computing Engng., Univ. of Iowa, Iowa City, IA, USA). *Appl. Opt. (USA)*, vol.22, no.10, p.1449-53 (15 May 1983).
Improvement in the depth of field is demonstrated by properly processing a succession of image samples. Due to the limited depth of field each image sample has in-focus as well as out-of-focus segments. By setting criteria for selecting the in-focus segments, an improved composite image is formed. Three algorithms for implementing this construction are discussed. (9 refs.)
- 75589 Transforming images into block stationary behavior. R.N.Strickland (Electrical Engng. Dept., Univ. of Arizona, Tucson, AZ, USA). *Appl. Opt. (USA)*, vol.22, no.10, p.1462-73 (15 May 1983).
The statistical behavior of images is inherently nonstationary. Unfortunately, most image processing algorithms assume stationary image models. Spatially adaptive algorithms have been developed which take into account local image statistics. In this paper the author derives radiometric and geometric transforms which generate nearly stationary (block stationary) images in the first and second moments. The author shows that true stationarity is impossible to realize. The aim of these transformations is to enhance the performance of nonadaptive processing techniques in particular data compression. (17 refs.)
- 75590 Achromatic system for far-field diffraction with broadband illumination. R.Ferriere, J.P.Goedebuer (Lab. de Phys. Generale et Optique, Univ. de France-Comte, Besancon, France). *Appl. Opt. (USA)*, vol.22, no.10, p.1540-5 (15 May 1983).
An achromatic Fourier transformer working with spatially coherent but temporally incoherent light is described both theoretically and experimentally. The achromatic Fraunhofer diffraction pattern results from the incoherent superposition of the monochromatic diffraction patterns generated by every spectral component of light. Wavelength compensation is achieved by a specific configuration combining airspaced zone plates and lenses. Several parameters, such as the spectral resolution of the setup or the spectral broadness of the source, govern the accuracy of coincidence of the various monochromatic patterns. Experimental results demonstrate the broadband operation of the system; the error on the achromatic Fourier transformation is 2% over the visible spectrum. Applications in colored image processing are also reported. (15 refs.)
- 75591 Coherent optical fiber communication potential and problems. E.E.Basch, H.A.Carnes (Communications Products Lab., GTE Labs. Inc., Waltham, MA, USA). *Proc. SPIE Int. Soc. Opt. Eng. (USA)*, vol.355, p.43-8 (1982). [received: May 1983] (Fiber Optics: Short-Haul and Long-Haul Measurements and Applications, San Diego, CA, USA, 24-25 Aug. 1982).
Optical guided wave transmission has provided both economic and technical advantages for an array of telecommunication applications. The advances in capability of optical transmission have been the result of dramatic improvements in fiber and other opto-electronic devices. What has not changed significantly is the technique of superimposing information onto the optical carrier. As a result, the information carrying capacity and also the repeater free operation of guided optical wave systems have not reached their full potential. Coherent optical communications is an approach whereby information is carried out by either the amplitude, frequency or phase of an optical carrier. Heterodyne detection would increase receiver sensitivity and permit closer optical carrier spacing and thus increase information carrying capacity. This would be achieved by IF filtering with highly selective electrical networks. There are several implementation difficulties that must be overcome to achieve the advantages of optical coherent communications. (6 refs.)
- 75592 Gray level pseudocolouring with three primary colours by a diffraction grating modulation method. J.A.Mendez, J.Bescos (Inst. de Optica, Madrid, Spain). *J. Opt. (France)*, vol.14, no.2, p.69-73 (March-April 1983).
Presents a two step procedure which encodes the object intensity transmittance, the contrast reversal transmittance and the product of both transmittances in three primary colours from a grey tone object transparency. First, a diffraction grating is used to generate and modulate the three transmittances in different orientations. Then, the pseudocoloured image is obtained through selective colour filtering of the diffraction orders in the Fourier plane of a white light partially coherent system. The theoretical analysis, method and some experimental results are provided. (15 refs.)
- 75593 On some explicit deconvolution formulas. C.A.Berenstein (Univ. of Maryland, College Park, MD, USA), B.A.Taylor, A.Yger. *J. Opt. (France)*, vol.14, no.2, p.75-82 (March-April 1983). In French.
The aim is to solve the following problem: given several measuring devices defined by a convolution with distributions μ_1, \dots, μ_m of compact support in R^n one would like to construct explicitly deconvolutors, i.e. distributions ν_1, \dots, ν_m , also of compact support, such that: $\mu_1 * \nu_1 + \dots + \mu_m * \nu_m = \delta$ where δ designs the convolution operation; such distributions ν_1, \dots, ν_m define measuring devices which, as soon as they have been constructed, allow one to reconstruct exactly an arbitrary signal $f \in C^\infty(R^n)$ which was measured through the original devices defined by convolution, with distributions μ_1, \dots, μ_m . By explicit, the authors mean that ν_1, \dots, ν_m are given by formulas involving the μ_i, \dots, μ_m , convolution, differentiation, integration and sums. The authors try to solve that kind of problem under particular hypothesis on μ_1, \dots, μ_m , so as to include all examples where the question has arisen and specially the case of the use of two optical devices whose transfer functions are $1/\pi R_1(J_1(r_1)/r)$ and $1/\pi R_2(J_1(r_2)/r)$ with distinct R_1 and R_2 . (16 refs.)
- 75594 A new method for noncoherent image processing by using an astigmatic system. N.G.Gaggioli, P.Bouchaud (Dept. de Fisica, Inst. Nacional de Tecnologia Industrial, Buenos Aires, Argentina). *J. Opt. (France)*, vol.14, no.2, p.93-105 (March-April 1983). In French.
When a point on a uniform background is observed through an astigmatic system (for instance, cylindrical lenses), the image will be a segment which is perpendicular to the cylinder. A line parallel to the cylinder would give an almost invisible image after traversing the system; on the other hand a line parallel to the astigmatic segment will give an enhanced image. By using such a simple device, spatial filtering could easily be performed by rotating the astigmatic system. This method allows one to perform optical processing, giving highly luminous images. It is thus possible to work in real-time using noncoherent light. (3 refs.)
- 75595 Optical pseudocolor encoding using adaptive electronic halftoning. C.Billotet-Hoffmann, O.Bryngdahl (Dept. of Phys., Univ. of Essen, Essen, Germany). *Opt. Commun. (Netherlands)*, vol.45, no.5, p.327-30 (1 May 1983).
Conversion of density to pseudocolor may be achieved using halftone recordings in optical filtering setups. The authors show and point out the possibility of applying object dependent electronic halftoning techniques for this purpose. (5 refs.)
- 75596 Formation of fine-structure image by corner reflectors, operating on the basis of the total internal reflection effect. G.V.Denisuk, V.I.Korneev. *Sov. J. Opt. Technol. (USA)*, vol.49, no.9, p.535-7 (Sept. 1982). Translation of: *Opt.-Mekh. Prom.-st. (USSR)*, vol.49, no.9, p.1-3 (Sept. 1982).
It is shown analytically and experimentally that the light wave, reflected by an ideal corner reflector, operating on the basis of the total internal reflection effect, is split into six elementary light waves that are not in phase with each other. The energy distribution in the diffraction image of a point in the form of six nuclei, located at the joints of the reflector sectors symmetrically with respect to the seventh central nucleus. All the nuclei have approximately equal intensity, and the pattern is limited by the diffraction in an individual sector. (12 refs.)

75597 Image formation in electron-beam-charged (001)- and (110)-cut $\text{Bi}_{12}\text{SiO}_{20}$ and $\text{Bi}_{12}\text{GeO}_{20}$ slices. V.N.Astratov, A.V.II'inskiĭ, S.N.Reznikov, O.M.Rysakov (A.F. Ioffe Physicstechn. Inst., Acad. of Sci., Leningrad, USSR).

Sov. Tech. Phys. Lett. (USA), vol.8, no.9, p.455-6 (Sept. 1982). Translation of: *Pis'ma v Zh. Tekh. Fiz. (USSR)*, vol.8, no.17-18, p.1056-9 (Sept. 1982). [received: May 1983]

Room-temperature-operating spatial-temporal light modulators made from $\text{Bi}_{12}\text{SiO}_{20}$ and $\text{Bi}_{12}\text{GeO}_{20}$ crystals, with electron-beam addressing, have recently attracted interest. The authors used crystalline slices cut in two orientations: with the (001) cut and with the (110) cut. The slices were covered with an insulating film and had dimensions of $30 \times 30 \times 0.8$ mm. In the (001) case the electron beam produces a positive image with a large-detail contrast of 40:1. In the (110) case the spatial-frequency spectrum does not contain a zero component, and the image obtained is contoured. In both cases the electron-beam energy was 7 keV. The complete brightening of the slice in the (001) case and the maximum image contrast in the (110) case were achieved at electron-beam currents below $30 \mu\text{A}$. (8 refs.)

75598 Fingerprint identification by matched filtering using photorefractive crystals. S.F.Su, D.K.Hamrick (Dept. of Electrical Engng., Univ. of South Florida, Tampa, FL, USA).

IEEE SOUTHEASTCON '83 Conference Proceedings, Orlando, FL, USA, 11-14 April 1983 (New York, USA: IEEE 1983), p.322-4

Fingerprint identification by matched filtering using photorefractive crystals (lithium niobate) is investigated. This technique has several advantages over the conventional methods. With lithium niobate as the matched filter recording medium the authors have obtained a signal-to-noise ratio several db higher than that with photographic films. This technique utilizes photorefractive effect to produce Fourier transform holograms inside the crystal. This approach has shown better separation of the output signals. The possibility of the performance of parallel filtering with a large number of fingerprints, based on the angular selectivity property of volume holograms, is also investigated. (24 refs.)

Scanning optical microscope incorporating a digital framestore and microcomputer See Entry 74531

Aberrations of holographic toroidal grating systems See Entry 75601

Laser plate storage See Entry 75759

Nonisothermal relaxation during photorecording in AsSe layers See Entry 75760

Confocal optical feedback processing system: an improved optical design See Entry 75762

Performance evaluation of an apodized optical system with polarization masks See Entry 75766

Automated calculation of two-lens and three-lens components See Entry 75769

Efficient approach to designing linear combination filters See Entry 75780

Optimized amplitude filtering for superresolution over a restricted field. III. Effects due to variation of the field extent See Entry 75781

Digital image processing of flow visualization photographs See Entry 76127

The effectiveness of astronomical speckle transfer function reweighting algorithms See Entry 78825

42.40 HOLOGRAPHY

(for acoustic holography, see 43.63)

75599 Planar volume phase holograms formed in bleached photographic emulsions. R.R.A.Syms, L.Solymer (Dept. of Engng. Sci., Univ. of Oxford, Oxford, England).

Appl. Opt. (USA), vol.22, no.10, p.1479-96 (15 May 1983).

Volume phase holograms are formed by a standard process in commercially available photographic emulsion. The material is characterized before recording, and initial experimental results are presented for reconstruction under index-matched conditions. An initial comparison is made using two-wave coupled-wave theory and a technique of curve fitting with experimental measurements of transmission and diffraction efficiency. The model works well close to the Bragg condition, but several differences are noted between theory and experiment away from the Bragg condition. An anomalous absorptive effect is noted in transmission. An improved model is then formulated, again using coupled-wave theory, and capable of analytic solution, taking into account phase and absorption modulation, a second harmonic in the grating profile and the appearance of some higher diffraction orders. Using this model, all the initial experimental results are satisfactorily explained, and the effect of spurious gratings in the hologram response is noted. The model is then used with an extensive set of experimental results to deduce the major characteristics of the material, including saturation of the modulation with exposure. The formulation of a mixed grating and possible dispersion of the modulation are also investigated. Suggestions are made for the design of more complicated components using this material and for material improvement. (50 refs.)

75600 Binary holographic LO beam multiplexer for IR imaging detector arrays. W.B.Veldkamp, E.J.Van Allen (MIT Lincoln Lab., Lexington, MA, USA).

Appl. Opt. (USA), vol.22, no.10, p.1497-507 (15 May 1983).

A binary holographic technique for infrared laser beam multiplexing is described. The technique was used to generate amplitude distribution matched and phase matched local oscillators for a heterodyne IR imaging detector array. It uses a high accuracy interlaced binary diffraction grating to multiplex single LO wave fronts. (26 refs.)

75601 Aberrations of holographic toroidal grating systems. M.P.Chrisp (Jet Propulsion Lab., California Inst. of Technol., Pasadena, CA, USA).

Appl. Opt. (USA), vol.22, no.10, p.1508-18 (15 May 1983).

Expressions are derived for the sixteen wave front aberration coefficients of a single grating. These give the wave aberration to the fourth order for a plane symmetric grating system. The contributions from each mirror and grating can be added to give the aberrations in the final image. Problems encountered with intermediate astigmatic images are overcome by defining the wave front aberration with respect to an astigmatic reference surface. There is one field variable describing displacement of the object point from the symmetry plane. The aperture stop may be placed anywhere in the system, and equations are given for the aberration changes produced by shifting this position. (13 refs.)

75602 Fabrication of PMMA holographic grating by KrF excimer laser. M.Murahara, Y.Kawamura, K.Tooyoda, S.Namba (Inst. of Phys. & Chem. Res., Wako, Japan).

Oyo Buturi (Japan), vol.52, no.1, p.83-9 (Jan. 1983). In Japanese.

Preparation, sensitization and developing procedures to fabricate holographic gratings with groove spacing between $2.7 \mu\text{m}$ and $0.19 \mu\text{m}$ on a thin PMMA film are described. Polymethyl methacrylate (PMMA) sensitized by 4~7% anthracene at the KrF laser wavelength (249 nm) was used as the photosensitizer. A sensitivity about one hundred times larger as compared with pure PMMA was realized. This sensitization made it possible to obtain the grating by a single exposure of the short KrF laser pulse (12 ns). As recording equipment, a new interferometer was designed. Using this optical system, the authors were able to change the grating pitch over a wide range without readjustment of the optical axis. (18 refs.)

75603 Contra-directional two-wave mixing in photorefractive media. P.Yeh (Rockwell Internat. Sci. Center, Thousand Oaks, CA, USA).

Opt. Commun. (Netherlands), vol.45, no.5, p.323-6 (1 May 1983).

The energy transfer between two counter-propagating beams in photorefractive media is analyzed. A solution of a nonlinear model of holographic two-wave mixing is presented. Expressions for the transmissivity are obtained and discussed. (14 refs.)

75604 Wave amplification and parametric generation by dynamic holograms on surfaces. N.F.Pilipetskii, A.N.Sudarkin, V.V.Shkunov (Inst. of Problems in Mech., Acad. of Sci., Moscow, USSR).

Sov. Phys.-Dokl. (USA), vol.27, no.7, p.558-60 (July 1982). Translation of: *Dokl. Akad. Nauk SSSR*, vol.265, no.1-3, p.324-7 (July 1982). [received: April 1983]

Recent papers on phase conjugation (or 'wavefront reversal') at an interface have drawn attention to the problem of converting light and sound beams by means of dynamic holograms recorded on a reflecting surface. The authors discuss the problems of dynamic correction and amplification of beams by means of holograms of this type, and also the possibility of using such holograms to create a parametric generator of sound or light waves having a high degree of directionality. (12 refs.)

75605 Polarisation control of tone transmission brightness in holographic image of light scattering surfaces and layers. O.V.Angelskii, A.G.Uschenko, V.V.Tkach, V.V.Yatsenko.

Ukr. Fiz. Zh. (USSR), vol.28, no.4, p.603-5 (April 1983). In Russian.

It is shown that the tone transmission brightness in images of planar inhomogeneous optical objects depends on the polarisations of the illuminating and reference fields as well as on the angular characteristics of the holographic recording. A matrix method is proposed for the calculation of the reconstructed holographic image brightness and the optimum polarisation of the reference field. By varying the polarisation and angular characteristics of the recording, it is possible to increase or decrease the image brightness by 5-15 times. (2 refs.) V.G.P.

75606 Properties of holographic gratings in silicon crystals under ultrashort light pulse recording. I. Theory. L.V.Mizrukhin, I.I.Peshko, M.S.Soskin, A.I.Khizhnyak.

Ukr. Fiz. Zh. (USSR), vol.28, no.5, p.675-83 (May 1983). In Russian.

Dynamic characteristics of the diffraction grating in Si are investigated theoretically in case of ultrashort light pulse recording. The main physical mechanisms affecting the refractive index variation are analyzed for a Si crystal. The behaviour of diffraction efficiency for a single picosecond pulse and a train gives information on the change in the refractive index due to one electron-hole pair, absorption cross-section, Auger-recombination coefficient and temperature derivative of the refractive index. (20 refs.)

75607 A review of holographic nondestructive evaluation at Lawrence Livermore National Laboratory. D.M.Boyd (Engng. Sci. Div., Lawrence Livermore Nat. Lab., California Univ., Livermore, CA, USA).

In book: *International advances in nondestructive testing*. Vol.9, W.J.McGonagle [Ed.], p.159-76. New York, USA: Gordon & Breach (1983), 363 pp. [0 677 16440 8]

At Lawrence Livermore National Laboratory two holographic facilities have been established for the technology transfer of holographic interferometry. A review is presented of the principles of holographic interferometry (HI) and the application of this technique to nondestructive evaluation. Simplified quantitative analysis using a coincident viewing and illumination optical arrangement is described. (18 refs.)

75608 Holographic nondestructive evaluation: status and future. G.Birnbaum (Office of Nondestructive Evaluation, NBS, Washington, DC, USA), C.M.Vest.

In book: *International advances in nondestructive testing*. Vol.9, W.J.McGonagle [Ed.], p.257-82. New York, USA: Gordon & Breach (1983), 363 pp. [0 677 16440 8]

The results and conclusions of an extensive review of the literature and practice of holographic nondestructive evaluation are reported. Although this technique has several technically unique features, and has been shown to be a feasible nondestructive testing technique in a very large number of laboratory investigations, its commercial application is rare. A counter example is its prevalent use in testing of aircraft and heavy equipment tires. The status of the technique is reviewed, recent and potential technical advances are enumerated, and suggestions of activities which would enable full realization and evaluation of the potential of holographic NDE in the future are made. (18 refs.)

3-D measurement by using a multiplex hologram See Entry 74437

X-ray spectrograph design See Entry 74568

Fingerprint identification by matched filtering using photorefractive crystals See Entry 75598

Laser beam critical behaviour and phase conjugation in the semiconductors, resonant media and electrooptic crystals See Entry 75734

Coherent light amplification and optical phase conjugation with photorefractive materials See Entry 75747

Diffraction gyration and reversal of the laser beam wave front in electrooptic crystals See Entry 75750

Nonisothermal relaxation during photorecording in AsSe layers See Entry 75760

Reconstruction by multidirectional holographic interferometry of the concentration field in a supersaturated solution near a growing NaClO_3 crystal See Entry 77547

Dispersive concentrating (DISCO) systems based on transmission phase holograms for solar applications See Entry 78045

Technique and method of bronchography See Entry 78290

42.50 QUANTUM OPTICS

75609 Error optimization in the detection of level crossing through the measurement of $n^2(T)$. J.J.Sanz, M.A.Rebolledo (Dept. de Óptica y Estructura de la Materia, Univ. de Santander, Santander, Spain). *Appl. Opt. (USA)*, vol.22, no.10, p.1555-61 (15 May 1983).

Equations for calculation of the crossing point determination error and the signal width error in level-crossing experiments are generalized when the normalized second-order factorial moment of the fluorescence obtained is measured. To minimize the magnitude of these errors the authors study the behavior of these values on varying the magnetic field sweep interval, the counting time and the mean fluorescence intensity. (1 ref.)

75610 Superradiation of extended systems. A.V.Andreev, Yu.A.II'inskiĭ (M.V. Lomonosov Moscow State Univ., Moscow, USSR). *Bull. Acad. Sci. USSR, Phys. Ser. (USA)*, vol.46, no.5, p.150-4 (1982). Translation of: *Izv. Akad. Nauk SSSR Ser. Fiz.*, vol.46, no.5, p.985-9 (1982). [received: May 1983] (Proceedings of the All-Union Conference on Luminescence Commemorating the Ninetieth Anniversary of the Birth of the Academician S.I. Vavilov, Leningrad, USSR, 21-24 April 1981).

The effect of collective spontaneous emission or superradiation (SR) is currently described chiefly within the framework of two approaches: quantum and semiclassical. The semiclassical theories take account of the field nonuniformity along the length of the sample, but they do not describe the process of SR avalanche production and therefore require the introduction of extraneous sources of spontaneous noise or the stipulation of nonzero initial and boundary conditions. In [1981] the authors developed a quantum theory of SR, which takes account of the spatial variations of the field density. In the present work, a comparison is made between the results of the mode theory and space theory of SR. (6 refs.)

75611 Group-theory analysis of coherent effects in multilevel systems. V.P.Karasev, L.A.Shelenin (P.N. Lebedev Phys. Inst., Acad. of Sci., USSR). *Bull. Acad. Sci. USSR, Phys. Ser. (USA)*, vol.46, no.5, p.161-7 (1982). Translation of: *Izv. Akad. Nauk SSSR Ser. Fiz.*, vol.46, no.5, p.997-1003 (1982). [received: May 1983] (Proceedings of the All-Union Conference on Luminescence Commemorating the Ninetieth Anniversary of the Birth of the Academician S.I. Vavilov, Leningrad, USSR, 21-24 April 1981).

A brief exposition is given of the foundations of a consistent group treatment of various generalizations of the Dicke model which take account of the multilevel nature and degeneration of the levels of individual radiators, as well as the relaxation processes along with the radiation processes. The results obtained allow on the one hand a generalization of the 'two-level' procedures to the n -level case, and on the other hand the substantial simplification of the calculations of the characteristic quantities of cooperative processes: the intensities, radiation-field correlation functions, various averages, etc. Note likewise that the proposed treatment is suitable not only for studying the interaction of matter with an electromagnetic field, but also the interaction of matter with boson fields (for example, acoustic fields). (30 refs.)

Bendor Free Electron Laser Conference See Entry 74214

Generation of electromagnetic waves during photochemical reactions See Entry 75613

Photon statistics of an m -photon laser with k -photon losses ... See Entry 75617

Asymptotically exact equations for the averages in the theory of laser systems See Entry 75618

FEL quantum aspects See Entry 75656

Quantum descriptions of free-electron lasers See Entry 75669

Non-linear optical mixing of frequencies of a strong bichromatic field interacting with a two-level atom at high proton densities See Entry 75722

Radiation generation by collective phenomena in semiconductors See Entry 77414

42.52 MASERS

75612 Electron cyclotron maser interaction in an open resonator with slowly varying cross-section. Zhou Lezhu, Xu Chenghe (Dept. of Radio Electronics, Peking Univ., Peking, China). *Acta Sci. Nat. Univ. Pekin. (China)*, no.6, p.67-76 (1982). In Chinese.

On the basis of theory previously presented, the authors studied the cyclotron maser interaction between a cyclotron electron beam and the RF field in an open resonator with slowly varying cross-sections. Firstly, the general expressions for RF field in this open resonator are given and it is considered that the axial wave number of the RF field is variable. Then starting from the relativistic Vlasov equation of plasma dynamics, some analytical expressions for the beam-wave interaction have been derived. For arbitrary resonator geometry these results can be used to determine cyclotron maser interaction power, starting condition and other parameters. For the special longitudinal field profile, such as sine-profile they are in good agreement with the previous results. (10 refs.)

75613 Generation of electromagnetic waves during photochemical reactions. Yu.V.Glazkov, G.P.Shpen'kov, L.A.Khil'manovich. *J. Appl. Spectrosc. (USA)*, vol.36, no.5, p.569-72 (May 1982). Translation of: *Zh. Prikl. Spektrosk. (USSR)*, vol.36, no.5, p.800-3 (May 1982). [received: Feb. 1983]

Reports a successful attempt to generate electromagnetic waves via the nuclear polarization effect using a resonance profile with an enhanced Q. (7 refs.)

Electron laser facility (ELF) at the LLNL ETA See Entry 75660

42.55 LASING PROCESSES

75614 'Tunnel' locking stimulated Raman radiation components in an optical resonator. V.N.Lugovoi, A.L.Dyshko (P.N. Lebedev Phys. Inst., Acad. of Sci., Moscow, USSR). *Opt. Acta (GB)*, vol.30, no.5, p.587-605 (May 1983).

Stimulated Raman radiation is considered in an optical resonator excited by an external light beam. It is assumed that the resonator is filled with a dispersive (condensed) medium for a length of the medium (along the resonator axis) close to several 'tunnel' lengths. A Raman-active medium is assumed to fill part of the resonator length along the resonator axis. Numerical calculations are presented of tunnel locking stimulated Raman radiation components. The shape of light pulses is calculated, and the band of locking Stokes components is derived. The feasibility of generating a light pulse of duration $3 \times 10^{-14} \times 10^{-15}$ s in a frequency region close to the point $\partial^2 n_{\text{eff}} / \partial \omega^2 = 0$, located usually in the infrared spectral region (n_{eff} is the effective refractive index of the substance inside the resonator) is discussed. Also

discussed is the feasibility of correcting the refractive-index dispersion and generating femtosecond light pulses in the visible spectral region. (36 refs.)

Advanced Laser Technology and Applications See Entry 74207

Bendor Free Electron Laser Conference See Entry 74214

42.55B General theory of lasing action

75615 Space-time and space-averaged equations for a two-mirror laser: theory and numerical results. M.Baer, I.Last (Chem. Div., Soreq Nuclear Res. Centre, Yavne, Israel). *Appl. Opt. (USA)*, vol.22, no.10, p.1578-91 (15 May 1983).

A theoretical model is considered for an unsteady three-level (single-mode) laser. By use of the rotating wave approximation, the usual semiclassical equations are transformed into a system of first-order spacetime (ST) equations. The space oscillations of the population difference (hole-burning effects) and the motion of the atoms are included in the treatment. After the introduction of several assumptions, the ST equations are transformed to a set of time-dependent space-averaged (SA) equations. The numerical calculations were performed for a pulsed two-mirror laser with a finite phase memory decay constant and for resonance and nonresonance frequencies. The calculations show that the SA equations give almost the same results as the much more complicated ST equations. (25 refs.)

75616 Delay effect in laser amplifiers. F.Hopf (Optical Sci. Center, Univ. of Arizona, Tucson, AZ, USA). *J. Phys. Colloq. (France)*, vol.44, no.C-1, p.137-44 (Feb. 1983). (Bendor Free Electron Laser Conference, Bendor, France, 26 Sept.-1 Oct. 1982).

In the Stanford Free Electron Laser it is necessary to desynchronize the electron pulses from the accelerator with the light pulses. This effect is a major complication in the data analysis of the FEL. The author considers the desynchronization effect for a laser amplifier. The equations are substantially simpler than the FEL, and most of the results can be obtained analytically. Both the gain (linear) and saturation (nonlinear) regimes are investigated. (7 refs.)

75617 Photon statistics of an m -photon laser with k -photon losses. U.Herzog (Zentralinst. für Optik und Spektroskopie, Akad. der Wissenschaften, Berlin, Germany). *Opt. Acta (GB)*, vol.30, no.5, p.639-52 (May 1983).

With the help of an approximation scheme valid for $\bar{n} \gg 1$ and $\Delta n^2 \ll \bar{n}^2$ (where \bar{n} is the mean value and Δn^2 the variance of the photon number), the photon statistics of an m -photon laser with k -photon losses ($m, k = 1, 2, \dots$) is studied theoretically for arbitrary values of the atomic population inversion s produced by an external pumping source. For $m > k$, $m = k$ and $m < k$, the dependences of the steady-state values of the mean photon number and of the quantity $\Delta n^2 / \bar{n}$ on gain and saturation are investigated. In the limit of strong saturation (well above the threshold for $m > k$) the photon statistics are characterized by the steady-state value $\Delta n^2 / \bar{n} = (1/2)(1 + m/k)$. (23 refs.)

75618 Asymptotically exact equations for the averages in the theory of laser systems. G.O.Balabanyan (Electronic Engng. Inst., Moscow, USSR). *Sov. Phys.-Dokl. (USA)*, vol.27, no.7, p.543-4 (July 1982). Translation of: *Dokl. Akad. Nauk SSSR*, vol.265, no.1-3, p.314-17 (July 1982). [received: April 1983]

For laser models of the Dicke type, the author gives asymptotically exact (in the sense of the thermodynamic limit) equations, obtained by the method of ordered operators, for the averages of operators which depend only on the radiation variables. For two concrete models, he considers the solutions of these equations and their physical consequences. (10 refs.)

On theory of the statistical generating functional for the order parameter. III. Effective action formalism for the order parameter See Entry 74366

42.55D CO₂ lasers

75619 Dynamics of the CO₂ upper laser level as measured with a tunable diode laser. C.Dang, J.Reid, B.K.Garside (Dept. of Engng. Phys. & Phys., McMaster Univ., Hamilton, Ontario, Canada). *IEEE J. Quantum Electron. (USA)*, vol.QE-19, no.4, p.755-64 (April 1983).

A tunable diode laser (TDL) operating in the 2140-2310 cm⁻¹ wavenumber region is used to probe a conventional CW CO₂ laser discharge. Detailed vibrational populations in CO₂ are measured under lasing conditions, i.e., in the presence of an intense 10 μ m field. The TDL is also used to investigate the rate of recovery of the populations in a variety of vibrational levels after the passage of an intense 10 μ m pulse. The authors deal mainly with the behavior of the upper laser level, and the associated ν_3 mode. The authors show that electron deexcitation of the ν_3 mode is very important, and is responsible for the limitation of the ν_3 mode temperature observed previously. In typical gas mixtures, the ratio of the ν_3 mode electron deexcitation rate constant to the electron excitation rate constant is $\sim 3.5:1$. (30 refs.)

75620 Simultaneous quasisteady oscillation on 10.6 and 18.4- μ m transitions in a gasdynamic CO₂ laser. D.G.Bakanov, L.S.Kornienko, A.I.Odintsov, A.I.Fedoseev. *J. Appl. Spectrosc. (USA)*, vol.37, no.2, p.901-4 (Aug. 1982). Translation of: *Zh. Prikl. Spektrosk. (USSR)*, vol.37, no.2, p.233-6 (Aug. 1982). [received: April 1983]

Resonant action of laser IR emission is an effective means of selectively exciting vibrational levels and energy transfer between different modes of polyatomic molecules. In inverted media it is possible to use induced 'dropping' of molecules from excited levels to low levels, with the concomitant amplification or generation of radiation. In a system of anharmonic oscillators in which the time of interaction of the molecules with the radiation greatly exceeds the characteristic V-V exchange time, but is less than the V-T relaxation time, the 'warming up' of the vibrational mode can lead to the formation of quasi-equilibrium distributions with inversion between particular vibrational-rotational levels. In this case the optical pumping channel need not be directly connected with the upper level of the inverted transition. The authors report the observation of simultaneous oscillation on the 00⁰1-10⁰0 ($\lambda = 10.6 \mu$ m) and 03⁰10-10⁰0 ($\lambda = 18.4 \mu$ m) transitions in a quasisteady gasdynamic CO₂ laser. The role of 10.6- μ m emission in pumping the coupled modes (ν_1 and ν_2) of the CO₂ molecule and the formation of inversion on the 18.4- μ m transition is discussed. (9 refs.)

Improved discharge uniformity for transverse radio frequency waveguide CO₂ lasers See Entry 75684

Frequency stabilization of CO₂ lasers: some applications See Entry 75701

42.55F Inert gas lasers

75621 Short wavelength laser calculations for electron pumping in neon-like krypton (Kr XXVII). U.Feldman (E.O. Hulburt Center for Space Res., Naval Res. Lab., Washington, DC, USA), A.K.Bhatia, S.Suckewer. *J. Appl. Phys. (USA)*, vol.54, no.5, p.2188-97 (May 1983). The authors present calculations of electron impact collision strengths and spontaneous radiative decay rates for neon-like krypton (Kr XXVII) for the $2s^2 2p^6$, $2s^2 2p^5 3s$, $ss^2 2p^3 3p$, and $2s^2 2p^5 3d$ configurations. From these atomic data the level populations as a function of the electron density were calculated at two temperatures ($T_e = 1 \times 10^4$ K and $T_e = 3 \times 10^4$ K). The analysis of level populations shows that a volume of krypton in which a significant number of the ions are in the Kr XXVII degree of ionization can produce a significant gain in transitions between the $2s^2 2p^5 3s$ and $2s^2 2p^5 3p$ configurations. At an electron density of 1×10^{19} cm⁻³ the plasma length has to be on the order of 1 m; at a density of 1×10^{21} cm⁻³ the length is reduced to about 0.5 cm; and at an electron density of 1×10^{22} cm⁻³ the length of the plasma is further reduced to about 1 mm. (18 refs.)

42.55H Lasing action in other gas lasers

75622 Parameter regimes for X-ray lasing in plasmas. R.C.Elton (Naval Res. Lab., Washington, DC, USA). *Comments At. & Mol. Phys. (GB)*, vol.13, no.2, p.59-67 (1983). A straightforward physical analysis is used to define the limiting electron density as a function of temperature, concentration and dimensions for generating population inversion and gain in a hydrogenic plasma of varying nuclear charge Z . A suitable parameter regime bounded by electron collisional mixing and radiative trapping of resonance radiation is defined. Good agreement is found with an established rate equation numerical model. The importance of a minimal ground state density is emphasized by the results. (23 refs.)

75623 Wavelength selectivity with metal halide lasers. I.Liberman, S.G.Leslie (Westinghouse Res. & Dev. Center, Pittsburgh, PA, USA). *Proc. SPIE Int. Soc. Opt. Eng. (USA)*, vol.335, p.48-51 (1982). [received: May 1983] (Advanced Laser Technology and Applications, Arlington, VA, USA, 6-7 May 1982).

Metal halide excimer lasers promise to be an efficient source of high power laser energy in the visible and near infrared. Based on extensive work on the HgBr laser one can expect that the nine lasers based on the group 2B metals (Zn, Cd, Hg) and the halides (Cl, Br, I) can each be tuned over a 100 Å region. By using these lasers to pump hydrogen isotope Raman cells, a significant portion of the visible and near infrared can be accessed with practical gas laser sources. (6 refs.)

75624 Nuclear pumped $O_2(^1\Delta)$ -I₂ laser. G.H.Miley, M.S.Zediker (Fusion Studies Lab., Univ. of Illinois, Urbana, IL, USA). *Proc. SPIE Int. Soc. Opt. Eng. (USA)*, vol.335, p.109-15 (1982). [received: May 1983] (Advanced Laser Technology and Applications, Arlington, VA, USA, 6-7 May 1982).

Neutrons from a pulsed Training Research Isotope Products General Atomics (TRIGA) research reactor are used to create nuclear reactions in a boron coating on the wall of an irradiation chamber that surrounds flowing oxygen. This generates high-energy ions that interact with the oxygen, producing the long-lived metastable, $O_2(^1\Delta)$. Current experiments use 1 to 5 Torr of O_2 in 100 to 200 Torr of Ar carrier gas. The 1.27-μm emission from $O_2(^1\Delta)$ is monitored 8 meters from the excitation region and nearly 1 second after the reactor pulse (—10 msec wide). Results to date indicate $O_2(^1\Delta)/O_2(^3\Sigma)$ fractions obtained are well above the 17% required to invert iodine in a flowing transfer laser. The $O_2(^1\Delta)$ -I₂ laser is of particular interest as a candidate driver for an inertial-confinement fusion reactor. Since energy coupling between the pellet and driver occurs directly through neutrons, relatively high system efficiencies appear possible. Further, the long-lived $O_2(^1\Delta)$ state provides the energy storage time (fractions of a second) needed between pellet implosions. (13 refs.)

75625 Laser based on vapors of complex molecules with self-pumping of the active medium. N.A.Borisovich, V.A.Tolkachev, V.Ya.Tulach, M.K.Khitrun. *J. Appl. Spectrosc. (USA)*, vol.37, no.2, p.881-5 (Aug. 1982). Translation of: *Zh. Prikl. Spektrosk. (USSR)*, vol.37, no.2, p.209-14 (Aug. 1982). [received: April 1983]

One of the favorable qualities of lasers based on vapors of complex molecules is the low density of the active medium and the concomitant small thermooptic losses and the low viscosity. Measurements of the rate of mode scanning in frequency caused by variation of the optical cavity length due to changes in the properties of the active medium with laser pumping as well as the efficiency of diffraction and self-diffraction by the optically induced spatially periodic grating have shown that the refraction effects in vapor lasers are an order of magnitude smaller than in lasers based on solutions, and have a resonant nonthermo-optic nature. The authors have carried out a comparison of the beam divergence of vapor and solution lasers. (12 refs.)

75626 Optimizing the lasing efficiency of a POPOP vapor laser. V.A.Povedailo. *J. Appl. Spectrosc. (USA)*, vol.37, no.2, p.888-92 (Aug. 1982). Translation of: *Zh. Prikl. Spektrosk. (USSR)*, vol.37, no.2, p.217-23 (Aug. 1982). [received: April 1983]

The author has carried out calculations and experiments relative to optimization of the output power and pulse duration of a POPOP vapor laser. The calculation is based on a model developed previously, taking into account the temperature dependence of the vibrational heat capacity of the active molecules and the buffer gas. In the numerical solution, the temperature dependence of the heat capacity was approximated by a simplified expression based on a model of identical vibrational oscillators. (14 refs.)

75627 Single-mode operation of Doppler-broadened lasers by injection locking. R.W.Dunn, S.T.Hendow, W.W.Chow, J.G.Small (Inst. for Modern Optics, Univ. of New Mexico, Albuquerque, NM, USA). *Opt. Lett. (USA)*, vol.8, no.6, p.319-21 (June 1983). A multimode He-Ne laser can be forced to oscillate in a single mode by injecting a narrow-band signal into the resonator. The authors show experimentally that the minimum injected intensity required for single-mode operation occurs at an injection frequency detuned from line center. This is in agreement with the results from a semiclassical theory of an inhomogeneously broadened injection-locked laser. (6 refs.)

75628 New applications of CO lasers. E.A.Gavronskaya, M.I.Zinchenko, S.N.Leonov, R.A.Liukonen. *Sov. Phys.-Tech. Phys. (USA)*, vol.27, no.11, p.1409-10 (Nov. 1982). Translation of: *Zh. Tekh. Fiz. (USSR)*, vol.52, no.11, p.2292-4 (Nov. 1982). [received: May 1983] Reports findings concerning simultaneous lasing from a CO laser in the 5 and 10 μm regions achieved by suitably selecting the components in the active medium. Simultaneous lasing was first unsuccessfully attempted by Sequin et al. (1972); however, it was found that the CW lasing power at 5 or 10 μm depends on the amount of CO and CO₂ in the active medium. (6 refs.)

Simultaneous quasisteady oscillation on 10.6 and 18.4-μm transitions in a gas-dynamic CO₂ laser See Entry 75620
Sensitivity of the intracavity method of determination of small optical losses in a continuously operating gas laser See Entry 75693
Phase conjugation of KrF laser radiation See Entry 75736

42.55M Lasing action in liquids and organic dyes

75629 Coherence effects in synchronously pumped mode-locked dye lasers. L.W.Casperson (School of Engng. & Appl. Sci., Univ. of California, Los Angeles, CA, USA).

J. Appl. Phys. (USA), vol.54, no.5, p.2198-208 (May 1983). A formalism is developed for describing the evolution of picosecond mode-locked pulses in synchronously pumped dye lasers. The finite phase memory of the molecular wave functions is included, and it is found that the resultant coherence effects can be dominant for operation close to exact synchrony. Considerations of the isotropic molecular orientational distribution and the finite vibrational relaxation times are also essential in obtaining quantitative agreement with experimental results. (25 refs.)

75630 Effect of a thermal lattice on the generated line width of a dye laser with distributed feedback. A.A.Afanasyev, V.A.Batyrev, M.V.Korol'kov. *J. Appl. Spectrosc. (USA)*, vol.37, no.2, p.899-901 (Aug. 1982). Translation of: *Zh. Prikl. Spektrosk. (USSR)*, vol.37, no.2, p.230-3 (Aug. 1982). [received: April 1983]

The paper is concerned with estimating the contribution of a nonstationary thermal grating to the width of a DF laser line. The authors examine a laser with dynamic DF formed in the active medium by an interference coherent pumping field. In the active medium of such a laser, together with the resonance grating, thermal and nonresonance gratings of another type can be efficiently excited. The time for establishing the thermal grating τ_T is usually much greater than the resonant time and can be comparable to the pumping pulse duration. For this reason, the contribution of the thermal grating to DF can vary during the generation process, which according to linear theory must be accompanied by a change in the characteristic frequencies and threshold pumping powers of the DF laser. They estimate the change in frequency related to the development of the thermal grating from the conditions of self excitation of the DF laser, assuming that the time τ_T is much greater than the time for establishing the generation process. With this assumption, the generation process is quasistationary and, therefore, the spectrum of characteristic frequencies and the threshold pumping power of the DF laser can be determined. (10 refs.)

75631 The lasing characteristics of solutions of rhodamine 6G and coumarin 47 with inhomogeneously broadened spectra. A.I.Akimov, L.V.Levshin, A.M.Saetskii, V.I.Yuzhakov.

J. Appl. Spectrosc. (USA), vol.37, no.2, p.904-8 (Aug. 1982). Translation of: *Zh. Prikl. Spektrosk. (USSR)*, vol.37, no.2, p.236-41 (Aug. 1982). [received: April 1983]

The lasing efficiency of dyes depends not only on the structure of their molecules, but also on the addition to the solutions of substances that affect their spectral and luminescent properties, particularly additives that enhance the inhomogeneous broadening (IB) of the electronic spectra. The authors study the effect of such additives on the spectral and power characteristics of the lasing of alcoholic solutions of the dyes rhodamine 6G and coumarin 47. (11 refs.)

Generation of ultrashort pulses in a dye laser with light-induced distributed feedback and a high repetition rate See Entry 75681

Recent technical advances in coaxial flashlamp-pumped high energy dye lasers See Entry 75683

42.55P Lasing action in semiconductors with junctions

75632 Longitudinal mode characteristics for 1.3 μm GaInAsP/InP DFB lasers just below the threshold current. H.Okuda, J.Kinoshita, Y.Hirayama, Y.Uematsu (Toshiba Corp., Kawasaki, Japan).

Electron. Lett. (GB), vol.19, no.10, p.362-3 (12 May 1983). The stopband and the Bragg wavelength in a DFB laser clearly observed by measuring longitudinal mode characteristics just below the threshold current. It became clear that the first-order longitudinal mode oscillation did not always occur. Coupling coefficients K for the DFB laser were deduced to be 10 to 40 cm⁻¹ from the stopband width. (5 refs.)

75633 Simple formulas giving temperature profiles in active layer of stripe geometry laser diode without oxide barriers. W.Nakwaski (Inst. of Phys., Tech. Univ. of Lodz, Lodz, Poland).

Electron. Lett. (GB), vol.19, no.10, p.368-709 (12 May 1983). The simple, approximated formulas describing the temperature distribution in the active layer of the stripe geometry laser diode without oxide barriers have been derived by the author. (7 refs.)

75634 Degradation mechanism in 1.3 μm InGaAsP/InP buried crescent laser diode at a high temperature. E.Oomura, H.Higuchi, R.Hirano, Y.Sakakibara, H.Namizaki, W.Susaki.

Electron. Lett. (GB), vol.19, no.11, p.407-8 (26 May 1983). A leakage current flowing through a junction between a p-InP current blocking layer and an n-InP cladding layer is examined in connection with a degradation of a buried crescent laser diode at a high temperature. The degradation characteristics have been successfully explained by a theoretical model proposed in this study. (4 refs.)

75635 1.5 μm wavelength GaInAsP C³ lasers: single frequency operation and wideband frequency tuning. W.Tsang, N.A.Olsson (Bell Labs., Murray Hill, NJ, USA), R.A.Linke, R.A.Logan.

Electron. Lett. (GB), vol.19, no.11, p.415-17 (26 May 1983). The authors have characterised the temporal-spectral behaviour of 1.5 μm wavelength cleaved-coupled-cavity (C³) lasers. Single longitudinal mode discrimination ratios in excess of 300:1 are obtained under high bit rate modulation. Bit error rate of less than $\leq 10^{-7}$ are obtained under single-frequency operation with direct modulation up to 1 Gbit/s. Averaged frequency tuning rates as large as 26 Å/ma and frequency tuning excursion of 300 Å are

achieved when the C^3 laser is operated in a frequency modulation mode. (5 refs.)

75636 High-output room-temperature pulsed operation for broad contact InP/In_{0.53}Ga_{0.47}As/InP lasers grown by molecular beam epitaxy. R.K. DeFreez, R.A. Elliott, J.S. Blakemore (Oregon Graduate Center, Beaverton, OR, USA), B.I. Miller, J.H. McFee, R.J. Martin. *J. Appl. Phys. (USA)*, vol.54, no.5, p.2177-82 (May 1983). Operating characteristics are described for broad contact double-heterostructure (DH) lasers grown by molecular beam epitaxy (MBE), with In_{0.53}Ga_{0.47}As active layers lattice matched to InP. These were operated at $T \approx 293K$, with (low duty cycle) pulses of current from 1.5 to $3I_0$. The lowest threshold current density, $J_{th} \approx 2800 A/cm^2$, is some 40% higher than an ideal cavity expectation. Under these strong pulse conditions, a multimode output was observed, with pronounced spatially filamentary characteristics. The output was plane polarized perpendicular to the active layer, indicative of TM mode dominance. This nontypical polarization, considered in conjunction with an indicated trend of external differential quantum efficiency increasing with length, is consistent with polarization-selective internal losses or polarization-dependent gain as the mode-controlling feature, rather than facet reflection losses. (51 refs.)

75637 Low-current-threshold (GaAl)As visible lasers with emission wavelengths below 750 nm. T. Hayakawa, S. Yamamoto, H. Hayashi, N. Miyauchi, S. Yano, T. Hijikata (Central Res. Labs., Sharp Corp., Nara, Japan). *J. Appl. Phys. (USA)*, vol.54, no.5, p.2209-13 (May 1983). Low-current-threshold behaviour of (GaAl)As v -channeled substrate inner stripe lasers emitting below 750 nm is presented. The variation of the threshold current of these devices with the lasing wavelength agrees with that of $1/\eta$, calculated using the energy-band parameters where the indirect-direct crossover is assigned at the AlAs mole fraction of 0.45. CW operation was achieved at as short as 688 nm. These performances result from the improved laser properties by growing the Te-doped cladding layer on top of the active layer using the p -type GaAs as a substrate. (32 refs.)

75638 Majority carrier concentration and quasi-Fermi level for Pb_{1-x}Sn_xTe DH diode lasers. D. Dadarlat, R.M. Candea, M. Barlea (State Committee for Nuclear Energy, Inst. of Isotopic & Molecular Technol., Cluj-Napoca, Rumania). *Phys. Status Solidi a (Germany)*, vol.76, no.1, p.K61-5 (16 March 1983). The authors make some quantitative considerations on the majority carrier concentration and on the quasi-Fermi level for PbSnTe DH diode lasers, assuming a degenerate regime for the holes. The case of a very small energy gap, $E_g < Q_p$, is also analysed. (4 refs.)

75639 Pressure induced polarization ellipticity in injection lasers. N.B. Patel, M.B.Z. Morosini, T.J.B. Serra, J.E. Ripper (Inst. de Fisica 'Gleb Wataghin', Univ. Estadual de Campinas, Campinas, Brazil). *Rev. Bras. Fis. (Brazil)*, vol.12, p.51-9 (March 1982). [received: April 1983] Departure from linear polarization of laser modes was observed to be induced by applied uniaxial stress. The induced polarization ellipticity was observed to be independent of injection current but a function of applied stress and of the individual laser. Nonzero ellipticity was observed in some lasers even at threshold. (8 refs.)

75640 Interface states and current threshold of GaAs/Al_xGa_{1-x}As double-heterostructure lasers grown by molecular beam epitaxy. C.S. Hong, W.I. Wang (Rockwell Internat., Microelectronics Res. & Dev. Center, Thousand Oaks, CA, USA). Gallium Arsenide and Related Compounds, 1982. Tenth International Symposium on Gallium Arsenide and Related Compounds, Albuquerque, NM, USA, 19-22 Sept. 1982 (Bristol, England: IOP 1983), p.297-302. A comparative study of the luminescence efficiency of Al_xGa_{1-x}As, GaAs, and GaAs/Al_xGa_{1-x}As heterojunctions grown at different temperatures has been performed to determine the factors that influence the current threshold of GaAs/Al_xGa_{1-x}As double heterostructure lasers grown by molecular beam epitaxy (MBE). The quality of Al_xGa_{1-x}As confinement layers is found not to influence the threshold current density of MBE-grown lasers. The mechanism that influences the current threshold is found to be the traps at the GaAs/Al_xGa_{1-x}As interface as resulted from the irregular surface of the low temperature grown Al_xGa_{1-x}As. The possible influence of the results on the role of MBE in integrated optics is discussed. (10 refs.)

75641 AM and FM quantum noise in InGaAsP lasers. Y. Yamamoto, T. Mukai (Mushashino Electrical Communication Lab., NTT, Tokyo, Japan). Gallium Arsenide and Related Compounds, 1982. Tenth International Symposium on Gallium Arsenide and Related Compounds, Albuquerque, NM, USA, 19-22 Sept. 1982 (Bristol, England: IOP 1983), p.311-16. Four different theoretical formulations for AM and FM quantum noise properties in semiconductor lasers are compared with each other for InGaAsP lasers. These formulations are based on van der Pol, Fokker-Planck, rate, and photon density matrix equations. Experimental AM and FM quantum noise properties for InGaAsP BH laser emitting at 1.3 μ m show good agreement with theoretical predictions. (11 refs.)

A Computer controlled time resolved optical intensity profile measurement system See Entry 74509

0.81 μ m band AlGaAs/GaAs double channel planar buried heterostructure laser with large optical cavity See Entry 75687

New approach to the manufacture of low-threshold 1.5 μ m distributed feedback lasers See Entry 75688

Low threshold photopumped Al_xGa_{1-x}As quantum-well heterostructure lasers See Entry 75689

Spectrum studies on a GaAs-AlGaAs multi-quantum-well laser diode grown by molecular beam epitaxy See Entry 75690

Passive mode locking of buried heterostructure lasers with nonuniform current injection See Entry 75696

Study and application of the mass transport phenomenon in InP See Entry 76719

Hot carrier relaxation processes in 1.3 μ m quaternary InGaAsP: analysis and application to temperature dependence of laser threshold See Entry 76973

Low pressure metalorganic chemical vapor deposition on InP and related compounds See Entry 77577

MOCVD growth and characterization of high luminescence efficiency Al_xGa_{1-x}As See Entry 77583

42.55R Lasing action in other solids (inc. solid Raman lasers)

75642 Luminescence of laser crystals. Yu.K. Voron'ko, V.V. Osiko, I.A. Shcherbakov (P.N. Lebedev Phys. Inst., Acad. of Sci., USSR). *Bull. Acad. Sci. USSR, Phys. Ser. (USA)*, vol.46, no.5, p.134-43 (1982). Translation of: *Izv. Akad. Nauk SSSR Ser. Fiz.*, vol.46, no.5, p.970-8 (1982). [received: May 1983] (Proceedings of the All-Union Conference on Luminescence Commemorating the Ninetieth Anniversary of the Birth of the Academician S.I. Vavilov, Leningrad, USSR, 21-24 April 1981). A method is developed for performing quantitative investigations of the processes of the transformation of the electron-excitation energy into a group of optically active centers which interact with one another and with a field of external radiation. As an example of the experimental verification of this method, the authors present results obtained for a YAG-Cr³⁺, Nd³⁺ crystal. The Cr³⁺ ions served as energy donors, and the Nd³⁺ ions served as acceptors. The concentration of the former amounted to 1.2 at.% ($1.7 \times 10^{20} \text{ cm}^{-3}$); the concentration of the latter amounted to 0.63 at.% ($0.9 \times 10^{20} \text{ cm}^{-3}$). Energy transfer, according to the data of Kiss et al. [1964], is accomplished from the ²E state of the chromium ions to the ⁴F_{3/2} state of the neodymium ions. The times for relaxation from the absorption bands of Cr³⁺ to the metastable state ²E and from the absorption bands of the Nd³⁺ ions to the metastable state ⁴F_{3/2} greatly exceed all other characteristic times. (23 refs.)

75643 Transition rates of Tb³⁺ in TbP₃O₁₄, TbLiP₄O₁₂, and TbAl₃(BO₃)₄: an evaluation for laser applications. S. Colak, W.K. Swicker (Philips Labs., Briarcliff Manor, NY, USA). *J. Appl. Phys. (USA)*, vol.54, no.5, p.2156-66 (May 1983).

The properties of Tb³⁺ in crystals of three stoichiometric Tb compounds, namely TbP₃O₁₄, TbLiP₄O₁₂, and TbAl₃(BO₃)₄ have been studied by spectroscopic absorption and emission methods to evaluate these materials as hosts for Tb³⁺ laser applications. The absorption spectra between 50000 and 2000 cm^{-1} at 300K, the emission spectra between 27000 and 14000 cm^{-1} at 300K, and the fluorescence decay characteristics of ³D₄ emission at 300 and 5K are given. Because of cross relaxation, the ³D₃ and ³G₅ emissions in all three materials were concentration-quenched strongly with a similar behavior observed in other hosts. Quenching in the ³D₄ states was negligible except for TbAl₃(BO₃)₄ where moderate quenching was observed due to energy transfer to nonradiative traps. Transition rates between various states were calculated by using the Judd-Oftel approach and a first order wavefunction set, and good fit was obtained between the calculated and experimental parameters. The transition rates were then used to find the emission cross sections of various lines. (72 refs.)

75644 Evaluation of the thermal focal length produced in a repetitively pulsed solid-state laser. Hou Jing-ya (Laser Lab., HuaZhong Inst. of Technol., Wuhan, China). *J. Appl. Phys. (USA)*, vol.54, no.5, p.2214-18 (May 1983).

An approximate expression for the focal length of the thermal lens produced in a repetitively pulsed laser rod is presented. Numerical evaluations reveal relations between thermal focusing and the rod radius, cooling conditions, pulse repetition rate, and nonuniformity of pumping. The aberration produced under different operating conditions is also discussed. A critical rod radius is identified for which the thermal lens effect is most sensitive to cooling and nonuniformity of pumping. (5 refs.)

75645 Crystalline KGd(WO₄)₂ laser with a semiconductor pump system. I.S. Galkin, A.L. Zakegim, V.M. Markonov, V.M. Nikolaev, A.A. Pavlyuk, I.P. Petrovich, V.Yu. Petrun'kin, A.P. Shkadarevich, V.D. Yarzhenkovskii. *J. Appl. Spectrosc. (USA)*, vol.37, no.2, p.886-8 (Aug. 1982). Translation of: *Zh. Prikl. Spektrosk. (USSR)*, vol.37, no.2, p.215-17 (Aug. 1982). [received: April 1983]

The authors report a study of a model of a laser with light diode pumping based on a crystal of KGd(WO₄)₂:Nd³⁺. KGd(WO₄)₂ crystals may be produced with rather large dimensions (close to YAG) and attain activator concentrations (up to 10 at.%) higher than those attainable in YAG. (6 refs.)

75646 A ruby laser in an electron beam field. M.R. Bedilov, Kh.B. Beisembayeva, P.K. Khabibullaev, R.P. Saidov. *Ukr. Fiz. Zh. (USSR)*, vol.28, no.4, p.607-8 (April 1983). In Russian. Studies the working of ruby lasers and lasers based on glass: Nd³⁺ in electron beam fields with doses of $D = 10^{11}$ - 10^{14} electron/cm². It is found that the changes in the laser generating characteristics strongly depend on D and irradiation conditions, as well as on the nature of the active elements. (4 refs.) V.G.P.

Progress in glass components for neodymium lasers See Entry 75676

1.73 μ m eyesafe laser rangefinder See Entry 75677

Progress in slab geometry solid state lasers See Entry 75678

Optimizing the efficiency of lasers with passive shutters See Entry 75679

Laser performance of Nd:YLF See Entry 75682

Miniature short-pulse Nd:YAG laser oscillator See Entry 75685

Unique applications of alexandrite lasers See Entry 75686

Passively mode-locked Nd:YAG and ruby lasers with high brightness per unit active volume See Entry 75692

The dynamics of a mode locked and frequency-doubled laser See Entry 75698

Q-switching of the YAG laser by coloured KCl crystals See Entry 75699

System for measuring energy and peak power of low-level 1.064 μ m laser pulses See Entry 75704

Analysis of valence-electron structures of Y₃Al₅O₁₂(YAG) and Al₂O₃, Cr₂O₃ (ruby)—study of certain properties of these laser materials related to their valence-electron structures See Entry 76901

Spectroscopic properties of TbP₃O₁₄, TbLiP₄O₁₂, and TbAl₃(BO₃)₄ See Entry 77426

Theoretical calculations of fluorescent branching ratios for YAlO₃:Er³⁺ from the complete Judd-Oftel theory See Entry 77427

Quantum efficiency of alexandrite See Entry 77430

Physicochemical and spectral luminescence properties of a glass based on the SiO₂-Al₂O₃-La₂O₃-Nd₂O₃ system See Entry 77438

42.55T Free electron lasers

75647 Effects of space charge on the performance of an orotron. R.P. Leavitt, D.E. Wortman (US Army Electronics Res. & Dev. Command, Harry Diamond Labs., Adelphi, MD, USA). *J. Appl. Phys. (USA)*, vol.54, no.5, p.2830-1 (May 1983).

The authors consider the effects of mutual electronic repulsion in the electron beam in the orotron, based on the general analysis of Gover and Sprangle

- [IEEE J. Quantum Electron. QE-17, 1196 (1981)]. The theory of orotron operation is extended to include space-charge effects, and calculations are made to determine starting current, output power, and efficiency. Results of the calculations are in good agreement with available experimental results at low (~ 6.7 A/cm²) beam current densities. The theory predicts that an output power of 264 W CW may be obtainable at 75 GHz with a beam current density of 50 A/cm². (9 refs.)
- 75648 Preliminary results of the Adone storage ring FEL experiment.** LELA. R.Barbini (Lab. Nazionali di Frascati, INFN, Frascati, Italy), G.Vignola, S.Trillo, R.Boni, S.De Simone, S.Faini, S.Guiducci, M.Pregger, M.Serio, B.Spataro, S.Tazzari, F.Tazzioli, M.Vescovi, A.Cattoni, C.Sanelli, M.Castellano, N.Cavallo, F.Cevenini, M.R.Masullo, P.Patteri, R.Rinzivillo, A.Cutolo, S.Solimeno. *J. Phys. Colloq. (France)*, vol.44, no.C-1, p.1-10 (Feb. 1983). (Bendor Free Electron Laser Conference, Bendor, France, 26 Sept.-1 Oct. 1982). Gives a short description of the LELA (Free Electron Laser on Adone) experiment. Results on the spontaneous radiation angle and energy spectra and preliminary results on optical gain measurements are also discussed. (8 refs.)
- 75649 Pulse propagation in free electron lasers.** W.B.Colson (Quantum Inst., Univ. of California, Santa Barbara, CA, USA), A.Renieri. *J. Phys. Colloq. (France)*, vol.44, no.C-1, p.11-27 (Feb. 1983). (Bendor Free Electron Laser Conference, Bendor, France, 26 Sept.-1 Oct. 1982). The main features relevant to pulse propagation in free electron lasers are discussed, together with a comparison to the Stanford oscillator experimental data. (37 refs.)
- 75650 Recent results of the ACO storage ring FEL experiment.** M.Billardon (Ecole Supérieure de Phys. et Chimie, Paris, France), D.A.G.Deacon, P.Elleau, J.M.Ortega, K.E.Robinson, C.Bazin, M.Bergher, J.M.J.Madey, Y.Petroff, M.Velghe. *J. Phys. Colloq. (France)*, vol.44, no.C-1, p.29-71 (Feb. 1983). (Bendor Free Electron Laser Conference, Bendor, France, 26 Sept.-1 Oct. 1982). A permanent magnet undulator has been built and installed on the ACO Storage Ring. The undulator design, the spontaneous emission and gain of the system, as well as the laser induced bunch lengthening of the electron bunch, are presented. A low-loss optical cavity has recently also been built and operated on the ring. Its performance and the degradation problems of the mirrors are discussed. Amplification of the spontaneous emission stored in the optical cavity has been observed. Also, preliminary results on the operation of an optical klystron are reported and interpreted. (29 refs.)
- 75651 Status of the MSNW tapered-wiggler FEL experiment.** J.M.Slater (Math. Sci. Northwest Inc., Bellevue, WA, USA), J.Adamski, D.C.Quimby, T.L.Churchill, L.Y.Nelson, R.E.Center. *J. Phys. Colloq. (France)*, vol.44, no.C-1, p.73-83 (Feb. 1983). (Bendor Free Electron Laser Conference, Bendor, France, 26 Sept.-1 Oct. 1982). Describes an experimental investigation of basic aspects of the tapered-wiggler free-electron laser. The effect of the FEL interaction on the electron energy distribution has been measured in a simple single pass amplifier configuration, with electrons and photons making a single pass through the tapered wiggler. A peak electron energy loss of about 9 percent and a net loss of 2.5 percent have been observed. (10 refs.)
- 75652 Theory of gain expanded free electron lasers.** N.M.Kroll, M.N.Rosenbluth (Univ. of California, San Diego, CA, USA). *J. Phys. Colloq. (France)*, vol.44, no.C-1, p.85-107 (Feb. 1983). (Bendor Free Electron Laser Conference, Bendor, France, 26 Sept.-1 Oct. 1982). A linearized theory for two dimensional wigglers of a general form is developed, and an extension of the Madey gain-spread theorem is obtained to include transverse excitation. The storage ring operation of such structures in the quasi-linear regime is analyzed. For the gain expanded case it is found that the laser radiation is subject to the same limitation as has been found in the one dimensional case, namely that it is at most of the order of the product of the synchrotron radiation and the fractional energy aperture. (16 refs.)
- 75653 High-efficiency free-electron laser results.** K.Boyer, C.A.Brau, B.E.Newnam, W.E.Stein, R.W.Warren, J.G.Winston, L.M.Young (Los Alamos Nat. Lab., Univ. of California, Los Alamos, NM, USA). *J. Phys. Colloq. (France)*, vol.44, no.C-1, p.109-117 (Feb. 1983). (Bendor Free Electron Laser Conference, Bendor, France, 26 Sept.-1 Oct. 1982). Results obtained with a tapered-wiggler free-electron laser show deceleration of electrons by as much as 7%, and extraction of more than 3% of the total electron-beam energy as laser energy. (3 refs.)
- 75654 The Brookhaven free electron laser experiment.** S.Krinsky, A.Lucio, C.Pellegrini, A.van Steenberg, L.H.Yu (Nat. Synchrotron Light Source, Brookhaven Nat. Lab., Upton, NY, USA). *J. Phys. Colloq. (France)*, vol.44, no.C-1, p.113-14 (Feb. 1983). (Bendor Free Electron Laser Conference, Bendor, France, 26 Sept.-1 Oct. 1982). Summary form only given, as follows. Reports on the status of the free electron laser experiment at Brookhaven with a description of the permanent undulator already built and ready to be installed on the VUV storage ring. (no refs.)
- 75655 TRW free electron laser experiment.** C.Shih, G.R.Neil, J.Munch, S.Fornaca, J.A.Edighoffer, M.Z.Caponi, H.E.Boehmer (TRW, One Space Park, Redondo Beach, CA, USA). *J. Phys. Colloq. (France)*, vol.44, no.C-1, p.115-23 (Feb. 1983). (Bendor Free Electron Laser Conference, Bendor, France, 26 Sept.-1 Oct. 1982). The details of the TRW free electron laser experiment at Stanford are presented. (no refs.)
- 75656 FEL quantum aspects.** G.Dattoli, A.Renieri (ENEA, Dipartimento Tecnologie Intersectoriali di Base, Centro Ricerche Energia Frascati, Frascati, Roma, Italy). *J. Phys. Colloq. (France)*, vol.44, no.C-1, p.125-36 (Feb. 1983). (Bendor Free Electron Laser Conference, Bendor, France, 26 Sept.-1 Oct. 1982). Reviews the main aspects of FEL quantum analysis in the framework of the Hamiltonian representation, both from the group theory point of view and from the dynamical one. Finally the authors point out how the formalism must be implemented in order to obtain results useful for future experimental tests. (20 refs.)
- 75657 Free electron laser oscillator startup analysis.** P.Sprangle, C.M.Tang, I.Bernstein (Naval Res. Lab., Washington, DC, USA). *J. Phys. Colloq. (France)*, vol.44, no.C-1, p.145 (Feb. 1983). (Bendor Free Electron Laser Conference, Bendor, France, 26 Sept.-1 Oct. 1982). Summary form only given, as follows. An analysis of the free electron laser (FEL) oscillator startup problem is presented. The model is spatially one-dimensional though many important three-dimensional effects are heuristically included. The electron beam consists of pulses of arbitrary shape and are mono-energetic with no spread in either the longitudinal or transverse velocities. The wiggler parameters are taken to be fixed. Finally the analysis is carried out in the low gain, small signal regime. (no refs.)

- 75658 Simulation of isochronous storage ring free electron laser.** A.Gaupp (Freie Univ. Berlin, Berlin, Germany). *J. Phys. Colloq. (France)*, vol.44, no.C-1, p.147-51 (Feb. 1983). (Bendor Free Electron Laser Conference, Bendor, France, 26 Sept.-1 Oct. 1982). A one dimensional simulation of a free electron laser in a storage ring operating close to isochronism is performed for a set of parameters to match the free electron laser proposal for the Berlin storage ring BESSY. (9 refs.)
- 75659 Transverse optical klystrons: a feasibility experiment on harmonic generation.** R.Coisson (Istituto di Fisica, Univ. di Parma, Parma, Italy), F.De Martini. *J. Phys. Colloq. (France)*, vol.44, no.C-1, p.163-6 (Feb. 1983). (Bendor Free Electron Laser Conference, Bendor, France, 26 Sept.-1 Oct. 1982). The authors indicate some measurements proposed to study (in the visible and near UV) the possibility of producing harmonics by a '(transverse) optical klystron'. (11 refs.)
- 75660 Electron laser facility (ELF) at the LLNL ETA.** D.Prosnitz (Lawrence Livermore Nat. Lab., Livermore, CA, USA), A.M.Sessler, K.Halbach, D.B.Hopkins, A.C.Paul, G.D.Stover, J.T.Tanabe, J.S.Wurtele. *J. Phys. Colloq. (France)*, vol.44, no.C-1, p.167 (Feb. 1983). (Bendor Free Electron Laser Conference, Bendor, France, 26 Sept.-1 Oct. 1982). Summary form only given, as follows. A high gain MM wave tapered wiggler free electron laser (FEL) amplifier has been designed and is under construction at Lawrence Livermore National Laboratory. The 5 MeV experimental test accelerator (ETA) is used as the electron source. The ELF design is presented, along with predicted performance, at 2, 4 and 8 mm. (no refs.)
- 75661 Application of transverse gradient wigglers in high efficiency storage ring FELs.** J.M.J.Madey (High Energy Phys. Lab., Stanford Univ., Stanford, CA, USA). *J. Phys. Colloq. (France)*, vol.44, no.C-1, p.169-78 (Feb. 1983). (Bendor Free Electron Laser Conference, Bendor, France, 26 Sept.-1 Oct. 1982). A significant improvement in the power output, efficiency, and gain of storage ring free electron lasers (FELs) can be realized through the use of a gain-expanded wiggler. The design of such systems must emphasize energy acceptance, peak current, and emittance. Long (10 m) interaction lengths must also be provided. (11 refs.)
- 75662 The UK free electron laser.** M.W.Poole (SERC, Daresbury Lab., Daresbury, England), S.D.Smith. *J. Phys. Colloq. (France)*, vol.44, no.C-1, p.179-83 (Feb. 1983). (Bendor Free Electron Laser Conference, Bendor, France, 26 Sept.-1 Oct. 1982). A UK free electron laser project has now been formally approved, based on the high power linear accelerator of the Kelvin Laboratory at East Kilbride, Scotland. Detailed design parameters of the system, centred on 10.6 μ m output radiation, are presented. The proposed experimental programme is briefly summarised and possible research applications are mentioned. (8 refs.)
- 75663 Linac technology for free electron lasers.** R.K.Cooper (Los Alamos Nat. Lab., Los Alamos, NM, USA), P.L.Morton, P.B.Wilson, D.Keefe, A.Faltens. *J. Phys. Colloq. (France)*, vol.44, no.C-1, p.185-200 (Feb. 1983). (Bendor Free Electron Laser Conference, Bendor, France, 26 Sept.-1 Oct. 1982). Electron linear accelerator technology for high-power, short-wavelength free-electron lasers reviewed. The authors concentrate on the properties of high-energy electron linear accelerators for use in free-electron lasers operating principally in the Compton regime. To fix the focus somewhat, they consider electron energies in the 20- to 200-MeV range and consider requirements for high-power free-electron lasers operating in the 0.5- to 10- μ m range. Thus neither Cockcroft-Walton type accelerators nor pulsed-diode machines are discussed. (20 refs.)
- 75664 Storage ring design optimization for FEL operation.** H.Wiedemann (Stanford Linear Accelerator Center, Stanford Univ., Stanford, CA, USA). *J. Phys. Colloq. (France)*, vol.44, no.C-1, p.201-9 (Feb. 1983). (Bendor Free Electron Laser Conference, Bendor, France, 26 Sept.-1 Oct. 1982). The basic physics of electron storage rings and some limitations are discussed. For high beam current density and short damping times, the main limitation comes from the Touschek effect. However, peak currents of a few hundred amperes per bunch can be expected at a beam energy of 1 GeV, and more than one bunch should be filled in order to maximize the total free electron laser (FEL) power. (8 refs.)
- 75665 High current limitations on storage ring FEL sources.** J.L.Duff (Lab. de l'Accélérateur Linéaire, Univ. de Paris-Sud, Orsay, France). *J. Phys. Colloq. (France)*, vol.44, no.C-1, p.217-32 (Feb. 1983). (Bendor Free Electron Laser Conference, Bendor, France, 26 Sept.-1 Oct. 1982). Storage rings dedicated to free electron laser (FEL) sources must show good beam performances in order to obtain high gains. In particular bunch length, energy spread, beam intensity and transverse emittance have to satisfy special requirements. In order to appreciate the storage ring problems, the author briefly overviews twenty years of experience obtained with small and medium energy storage rings which were initially built as high energy physics facilities. The limiting effects and possible means to remedy the inconveniences are discussed. (29 refs.)
- 75666 Microtrons for free electron lasers.** S.Rosander (Dept. of Electron Phys., Royal Inst. of Technol., Stockholm, Sweden). *J. Phys. Colloq. (France)*, vol.44, no.C-1, p.233-7 (Feb. 1983). (Bendor Free Electron Laser Conference, Bendor, France, 26 Sept.-1 Oct. 1982). The various microtron types are shortly described and electron beam characteristics, relevant to FEL operation, of existing machines are given. Some possible lines of development are indicated. (12 refs.)
- 75667 Tapered wigglers.** S.A.Mani (W.J. Schafer Associates Inc., Wakefield, MA, USA). *J. Phys. Colloq. (France)*, vol.44, no.C-1, p.239-53 (Feb. 1983). (Bendor Free Electron Laser Conference, Bendor, France, 26 Sept.-1 Oct. 1982). The theory of the tapered wiggler free electron laser is reviewed. The analysis is based upon a one-dimensional Hamiltonian. The effects of finite beam emittance are discussed. Practical issues connected with realizing a tapered wiggler oscillator are enumerated with some proposed solutions. Finally, the operation of the tapered FEL as a high current, high gain amplifier is analyzed with implications of using an electron storage ring or induction accelerator as an electron beam source. (19 refs.)
- 75668 Stories of undulator light.** C.J.Elliott (Los Alamos Nat. Lab., Los Alamos, NM, USA). *J. Phys. Colloq. (France)*, vol.44, no.C-1, p.255-87 (Feb. 1983). (Bendor Free Electron Laser Conference, Bendor, France, 26 Sept.-1 Oct. 1982). Optical details of free-electron lasers are reviewed including a layman's account of many of the ideas; a historical account of work over the last two years; a mathematical characterization of various schemes; a formulation of the mathematical problem as a non-linear fixed-point problem; and a description of computational techniques. (28 refs.)

75669 Quantum descriptions of free-electron lasers. W.Becker, J.K.McIver (Dept. of Phys. & Astron., Univ. of New Mexico, Albuquerque, NM, USA).

J. Phys. Colloq. (France), vol.44, no.C-1, p.289-311 (Feb. 1983). (Bendor Free Electron Laser Conference, Bendor, France, 26 Sept.-1 Oct. 1982). The various quantum mechanical descriptions of the free-electron laser are reviewed: (1) calculating the gain from the mismatch between the matrix elements for emission and absorption of a single photon, derived from the Dirac- or Klein-Gordon equation; (2) a multiphoton description based on the model of a constant current interacting with a quantized electromagnetic field; (3) solving the Klein-Gordon equation in the presence of both the laser and the wiggler taken as classical external fields, which gives a unified description of all operating regimes but spontaneous emission; (4) a fully quantized small-signal solution of the nonrelativistic many particle Bambi-Renieri Hamiltonian defined in a moving frame. This approach displays the difference between classical and quantum-mechanical fluctuations in the start up. (43 refs.)

75670 Free electron laser in the infrared: the experimental activity at the ENEA Frascati Centre. U.Bizzarri, F.Cioci, G.Dattoli, A.De Angelis, M.Ercolani, E.Florentino, G.P.Gallerano, T.Letardi, A.Marino, G.Messina, A.Renieri, E.Sabia, A.Vignati (ENEA, Dipartimento Tecnologie Intersettoriali di Base, CRE, Frascati, Roma, Italy).

J. Phys. Colloq. (France), vol.44, no.C-1, p.313-32 (Feb. 1983). (Bendor Free Electron Laser Conference, Bendor, France, 26 Sept.-1 Oct. 1982). Describes the experimental activity aimed at the realization of a free electron laser operating in the spectral region 10 to 30 μm . The ENEA experimental activity is developing through three main stages: 1. Amplification experiment of a CW CO₂ laser beam, which will concern the analysis of the spontaneous and stimulated emission in a helical wiggler at $\lambda=10.6 \mu\text{m}$. 2. Oscillation experiment at $\lambda=32 \mu\text{m}$ and at higher harmonics, employing a variable gap linear wiggler. 3. Tunable operation of the FEL in the wavelength range 10 to 30 μm , employing the same wiggler and a new microtron with 35 MeV maximum energy. (7 refs.)

75671 Optical klystrons. P.Elleau (Dept. de Physico-Chimie, CENS, Gif-sur-Yvette, France).

J. Phys. Colloq. (France), vol.44, no.C-1, p.333-52 (Feb. 1983). (Bendor Free Electron Laser Conference, Bendor, France, 26 Sept.-1 Oct. 1982). The optical klystron is a modification of the undulator which can be used to improve the gain in a free electron laser. Spontaneous emission and gain are theoretically studied as functions of electron energy and wavelength. Several effects limiting the gain enhancement are calculated: energy spread, angular spread, beam dimensions. The author briefly discusses how one can use the electron beam bunching generated by the optical klystron to emit coherent synchrotron radiation. (49 refs.)

75672 Review of recent experimental results from the Stanford 3 μm free electron laser. S.Benson, D.A.G.Deacon, J.N.Eckstein, J.M.J.Madey, K.Robinson, T.I.Smith, R.Taber (High Energy Phys. Lab., Stanford Univ., Stanford, CA, USA).

J. Phys. Colloq. (France), vol.44, no.C-1, p.353-62 (Feb. 1983). (Bendor Free Electron Laser Conference, Bendor, France, 26 Sept.-1 Oct. 1982). New data has been taken on the Stanford free electron laser (FEL) with improved electron beam characteristics. For the first time the temporal structure of the optical pulses has been studied using optical autocorrelation techniques. The new data are compared and contrasted with earlier data. Several puzzling aspects of the previous data appear correlated with drifts in the spectrum and current of the electron beam. Autocorrelation results indicate nearly transform limited pulses which are shorter than expected at large values of the cavity length detuning. Experiments carried out to study the intrinsic second harmonic radiation and the effects of the superimposed solenoidal magnetic field on laser operation are also reported. (6 refs.)

75673 The nonlinear gain in the free-electron laser with a long wiggler. M.V.Fedorov (P.N. Lebedev Phys. Inst., Moscow, USSR). *Opt. Acta (GB)*, vol.30, no.5, p.669-72 (May 1983). The nonlinear gain of the free-electron laser with a long wiggler is derived, and the regimes of weak and strong saturation are investigated. (3 refs.)

75674 Ionization effects in a system of a free electron laser and a molecular medium. J.Guillory (Jaycor, Alexandria, VA, USA), H.Wilhelmsen. *Phys. Scr. (Sweden)*, vol.27, no.5, p.374-5 (May 1983). It is estimated that ionization of molecules by the electron beam is insufficient to cause background plasma densities that would dominate the beam effects. The pressure of molecular gas for optimum coupling of FEL and molecular medium is of the order of 10^{-6} torr for beam densities of 10^9 cm^{-3} . (5 refs.)

75675 A new mechanism of excitation of a diffraction-radiation generator (free-electron laser). Yu.I.Evdokimenko, K.A.Lukin, I.D.Revin, B.K.Skrýnnik, A.V.Shestopalov (Sci.-Res. Inst. of Radiophys. & Electronics, Acad. of Sci., Kharkov, Ukrainian SSR). *Sov. Phys.-Dokl. (USA)*, vol.27, no.7, p.554-6 (July 1982). Translation of: *Dokl. Akad. Nauk SSSR*, vol.265, no.1-3, p.318-21 (July 1982). [received: April 1983]

The authors consider the case of excitation of the TEM_{01q} mode in the open resonator; this mode is called the first mode of the open resonator of the diffraction-radiation generator-free-electron laser. The spatial structure of the mode is such that there are two field spots along the direction of electron motion and the total phase of the oscillations at these spots differ by π . (5 refs.)

Permanent magnet undulators See Entry 74500

Delay effect in laser amplifiers See Entry 75616

Mirrors that are electron transparent for use in free-electron-laser oscillators See Entry 75680

Helical undulator study See Entry 75691

42.60 LASER SYSTEMS AND LASER BEAM APPLICATIONS

75676 Progress in glass components for neodymium lasers. G.Dube (Schott Optical Glass Inc., Duryea, PA, USA).

Proc. SPIE Int. Soc. Opt. Eng. (USA), vol.335, p.10-14 (1982). [received: May 1983] (Advanced Laser Technology and Applications, Arlington, VA, USA, 6-7 May 1982). Describes some of the recent progress in glass materials used to generate, control, and attenuate Nd: laser light. Technical and manufacturing developments for phosphate laser glasses, large monolithic apodizers, high damage threshold AR treated glasses, filters, and other elements will be presented. (5 refs.)

75677 1.73 μm eyesafe laser rangefinder. M.Knights, J.Kuppenheimer, E.Chicklis (Defensive Systems Div., Sanders Associates Inc., Nashua, NH, USA).

Proc. SPIE Int. Soc. Opt. Eng. (USA), vol.335, p.83-4 (1982). [received: May 1983] (Advanced Laser Technology and Applications, Arlington, VA, USA, 6-7 May 1982). The ocular hazards associated with high peak power laser rangefinders can be avoided in systems which emit in the spectral range $\lambda > 1.4 \mu\text{m}$. The authors describe the operation of a 1.73 μm laser in erbium-doped lithium yttrium fluoride (Er³⁺:YLF) and discuss two ranging systems which utilize this 1.73 μm laser source. (no refs.)

75678 Progress in slab geometry solid state lasers. J.M.Eggleson, T.Kane, K.Kuhn, R.L.Byer (Appl. Phys. Dept., Stanford Univ., Stanford, CA, USA).

Proc. SPIE Int. Soc. Opt. Eng. (USA), vol.335, p.104-8 (1982). [received: May 1983] (Advanced Laser Technology and Applications, Arlington, VA, USA, 6-7 May 1982). A slab geometry, with a zigzag totally internally reflected optical path, significantly reduces thermal focusing, stress induced biaxial focusing and birefringence in a solid state laser host. The authors present results of a theoretical and experimental study of slab geometry Nd:Glass and Nd:YAG laser systems. (12 refs.)

75679 Optimizing the efficiency of lasers with passive shutters. S.A.Mikhonov, A.N.Khodinskii, V.A.Kononov.

J. Appl. Spectrosc. (USA), vol.37, no.2, p.896-9 (Aug. 1982). Translation of: *Zh. Prikl. Spektrosk. (USSR)*, vol.37, no.2, p.227-30 (Aug. 1982). [received: April 1983] Starting from the principles for calculating laser parameters, the authors propose simple approximate expressions for calculating the optimal transmission of the output reflector and shutter, corresponding to maximum laser efficiency. The results of the calculations are experimentally checked for lasers based on neodymium ions with shutters based on F₂⁻ color centers in lithium fluoride. (5 refs.)

75680 Mirrors that are electron transparent for use in free-electron-laser oscillators. J.H.McAdoo (Sachs/Freeman Associates Inc., Bowie, MD, USA), V.L.Granatstein.

Opt. Lett. (USA), vol.8, no.6, p.316-18 (June 1983). The surface motion of gold-coated Mylar pellicle was measured interferometrically while the pellicle was subjected to bombardment from a 15-MeV, 40-mA pulsed electron beam. No surface motion as large as 0.3 μm was observed during the electron pulse. A radiation dose of 5×10^7 rad did not damage the surface. The results show that this foil can be used as an end mirror in free-electron-laser oscillators. (13 refs.)

75681 Generation of ultrashort pulses in a dye laser with light-induced distributed feedback and a high repetition rate. A.N.Rubinov, Yu.Slovenas, I.Chesnulavichyus, T.Sh.Efendiev (Phys. Inst., Acad. of Sci., Minsk, Belorussian SSR).

Sov. Phys.-Tech. Phys. (USA), vol.27, no.11, p.1408-9 (Nov. 1982). Translation of: *Zh. Tekh. Fiz. (USSR)*, vol.52, no.11, p.2290-2 (Nov. 1982). [received: May 1983] Tunable ultrashort laser pulses can be used to directly study the time behavior of ultrafast light-induced processes in materials. The authors' method for obtaining ultrashort laser pulses with an adjustable spectrum involves using light-induced distributed feedback. Such lasers are simpler, more stable, and easier to work with than other types of mode-locked dye lasers. The authors report measurements of the emission characteristics of a dye laser with light-induced distributed feedback operating at a high duty cycle with pulse durations in the picosecond range. They show that the pulse duration from a distributed feedback laser can be reduced by decreasing the total length of the periodic structure and by delaying the interfering pump pulses relative to one another. The authors also report generation of unprecedentedly short pulses (of picosecond duration) using a distributed feedback dye laser. (3 refs.)

Advanced Laser Technology and Applications See Entry 74207

Bendor Free Electron Laser Conference See Entry 74214

Use of carbon felt as a cold cathode for a pulsed line X-ray source operated at high repetition rates See Entry 74574

High power pulsed lasers See Entry 75172

Preliminary results of the Adone storage ring FEL experiment, LELA See Entry 75648

Recent results of the ACO storage ring FEL experiment See Entry 75650

Status of the MSNW tapered-wiggler FEL experiment See Entry 75651

High-efficiency free-electron laser results See Entry 75653

The Brookhaven free electron laser experiment See Entry 75654

TRW free electron laser experiment See Entry 75655

High-efficiency laser-pulse compression by stimulated Brillouin scattering See Entry 75727

Evaluation of electrode shape and nondestructive evaluation method for welded solar cell interconnects See Entry 77858

Nondestructive testing of interconnect welds using the Scanning Laser Acoustic Microscope (SLAM) See Entry 77859

42.60B Design of specific laser systems

75682 Laser performance of Nd:YLF. J.C.McCarthy, M.G.Knights, E.P.Chicklis (Defensive Systems Div., Sanders Associates Inc., Nashua, NH, USA).

Proc. SPIE Int. Soc. Opt. Eng. (USA), vol.335, p.2-4 (1982). [received: May 1983] (Advanced Laser Technology and Applications, Arlington, VA, USA, 6-7 May 1982). Flashpumped, Q-switched performance of Nd:YLF is reported in both single and multimode operation. Approximately 400 mJ was extracted from a $1/4 \times 3.0$ inch Nd:YLF rod in a single, Q-switched pulse. (5 refs.)

75683 Recent technical advances in coaxial flashlamp-pumped high energy dye lasers. S.E.Neister (Phase-R Corp., New Durham, NH, USA). *Proc. SPIE Int. Soc. Opt. Eng. (USA)*, vol.335, p.36-47 (1982). [received: May 1983] (Advanced Laser Technology and Applications, Arlington, VA, USA, 6-7 May 1982). (11 refs.)

75684 Improved discharge uniformity for transverse radio frequency waveguide CO₂ lasers. G.A.Griffith (Teledyne Electronics, Newbury Park, CA, USA). *Proc. SPIE Int. Soc. Opt. Eng. (USA)*, vol.335, p.69-71 (1982). [received: May 1983] (Advanced Laser Technology and Applications, Arlington, VA, USA, 6-7 May 1982).

Transverse RF waveguide lasers have demonstrated an undesirable nonuniform gas discharge related to the electrical transmission line properties of the optical waveguide structure. Laser efficiency has been increased over 4 times to 11% for a laser of electrical length in excess of $2/3 \lambda$ at 200 MHz by correcting the voltage standing wave pattern with periodic inductor shunts. Peak outputs of 8 Watts at 10% efficiency and peak efficiencies of 1% at 4.4 Watt output have been attained with sealed operation for a 21.6 cm device. (3 refs.)

75685 Miniature short-pulse Nd:YAG laser oscillator. E.D.Reed, E.G.Erickson (GTE Products Corp., Sylvania Systems Group-Western Div., Mountain View, CA, USA).

Proc. SPIE Int. Soc. Opt. Eng. (USA), vol.335, p.78-82 (1982). [received: May 1983] (Advanced Laser Technology and Applications, Arlington, VA, USA, 6-7 May 1982).

A miniature Nd:YAG laser oscillator has been demonstrated which uses pulse-slice cavity dumping to achieve optical pulses of 425 ± 50 picoseconds FWHM. (no refs.)

75686 Unique applications of alexandrite lasers. H.Samelson, J.C.Walling, D.F.Heller (Allied Corp., Electro-Optical Products, Mt. Bethel, NJ, USA).

Proc. SPIE Int. Soc. Opt. Eng. (USA), vol.335, p.85-94 (1982). [received: May 1983] (Advanced Laser Technology and Applications, Arlington, VA, USA, 6-7 May 1982).

The fundamental principles underlying the 3- and 4-level laser operation of alexandrite are discussed and recent performance highlights are given. Applications in the fields of hole drilling, semiconductor processing, photochemistry and lidar are described. (9 refs.)

75687 0.81 μ m band AlGaAs/GaAs double channel planar buried heterostructure laser with large optical cavity. M.Ueno, H.Kawano, T.Furuse, I.Sakuma (Opto-Electronics Res. Labs., Nippon Electric Co. Ltd., Kawasaki-City, Japan).

Electron. Lett. (GB), vol.19, no.10, p.370-1 (12 May 1983).

0.81 μ m band AlGaAs/GaAs double channel planar buried heterostructure laser diodes with large optical cavity have been developed as light sources for use in analogue optical fibre communication systems. Linear light-output/current characteristics in a single longitudinal-mode spectrum at a modulation frequency $f=100$ MHz with modulation index $m=0.9$ have been attained. (9 refs.)

75688 New approach to the manufacture of low-threshold 1.5 μ m distributed feedback lasers. L.D.Westbrook, A.W.Nelson, C.Dix (British Telecom Res. Labs., Ipswich, England).

Electron. Lett. (GB), vol.19, no.11, p.423-4 (26 May 1983).

Low-threshold-current (85 mA), oxide isolated InGaAsP/InP distributed feedback (DFB) lasers operating at a wavelength of $\lambda=1.5 \mu$ m have been produced for the first time using electron-beam-written DFB corrugations overgrown by MOCVD. The control and flexibility afforded by these techniques considerably ease the complexity of DFB laser manufacture. (7 refs.)

75689 Low threshold photopumped AlGa_xAs quantum-well heterostructure lasers. R.D.Burnham, W.Streifer, D.R.Scifres (Xerox Palo Alto Res. Center, Palo Alto, CA, USA), N.Holonyak, Jr., K.Hess, M.D.Camras. *J. Appl. Phys. (USA)*, vol.54, no.5, p.2618-22 (May 1983).

Data are presented on very low threshold photopumped separate-confinement quantum-well heterostructure (SC QWH) lasers grown by metalorganic chemical vapor deposition (MOCVD). An unusually thin single quantum well (size $L_z \leq 60 \text{ \AA}$) is employed in the QWH with the carriers confined ('trapped') in the interior 'cladding' region, which serves also as the optical waveguide. Excess carriers, which are photogenerated (or injected), are confined in the thin interior cladding region (size $L_z \sim 1000 \text{ \AA}$) and, in this charge reservoir and waveguide region, are thermionically 'emitted' back and forth across the well until scattered to lower energy in the well ($\Delta E \sim \hbar\omega_0$) and collected. Continuous (CW) 300K photopumped laser operation of these QWHs is demonstrated for very short cavities. For one QWH wafer laser operation occurs at $\lambda \sim 7730 \text{ \AA}$ with a photopumping threshold of 380 W/cm^2 ($J_{th} \sim 160 \text{ A/cm}^2$) and for another wafer at $\lambda \sim 7000 \text{ \AA}$ with threshold 10^3 W/cm^2 ($J_{th} \sim 410 \text{ A/cm}^2$). The photopumped samples are as small as $20 \times 40 \mu\text{m}$, thus making these laser thresholds (for such short cavity lengths) a factor of 3-10 better than the lowest previously reported. (11 refs.)

75690 Spectrum studies on a GaAs-AlGaAs multi-quantum-well laser diode grown by molecular beam epitaxy. H.Iwamura, T.Saku, H.Kobayashi, Y.Horikoshi (Musashino Electrical Communication Lab., Nippon Telegraph & Telephone Public Co., Tokyo, Japan).

J. Appl. Phys. (USA), vol.54, no.5, p.2692-5 (May 1983).

Spontaneous and stimulated emission spectrum and the different characteristics between TE and TM polarizations were investigated on a GaAs-AlGaAs multi-quantum-well (MQW) laser diode grown by molecular beam epitaxy. The MQW laser lases at 38 meV below the photoluminescence peak energy corresponding to the lowest confined electron to heavy hole recombination energy E_{hh} , calculated using the Kronig-Penney model. However, this energy separation cannot be interpreted in terms of the LO-phonon assisted recombination which is usually accepted. The LO-phonon assisted recombination model can be ruled out by comparing the spontaneous emission and the stimulated emission for various injection current levels. The emission energy of the TE polarization was lower than that of the TM polarization. The intensity of the TE is much larger than the TM polarization. These differences can be interpreted in terms of the selection rule for the dipole recombination between confined electron to heavy hole and electron to light hole bands. (14 refs.)

75691 Helical undulator study. E.D.Shaw (Bell Telephone Labs., Murray Hill, NJ, USA), R.M.Emanuelson, G.A.Herbst.

J. Phys. Colloq. (France), vol.44, no.C-1, p.153-61 (Feb. 1983). (Bendor Free Electron Laser Conference, Bendor, France, 26 Sept.-1 Oct. 1982).

A five period helical undulator prototype of novel design has been constructed and tested. Magnetic field measurements indicate this design to be satisfactory for the construction of a fifty period undulator for a free electron laser designed to provide an output tunable from 100 μ m to 400 μ m. (16 refs.)

75692 Passively mode-locked Nd:YAG and ruby lasers with high brightness per unit active volume. O.P.Varnavsky, A.N.Kirkin, A.M.Leontovich, R.G.Mirzoyan, A.M.Mozharovsky, I.I.Solomatina (P.N. Lebedev Phys. Inst., Acad. of Sci., Moscow, USSR).

Opt. Commun. (Netherlands), vol.45, no.5, p.342-5 (1 May 1983).

Passively mode-locked Nd:YAG (at room temperature) and ruby (at $\approx 100\text{K}$) lasers with unstable confocal resonators are described. They generated ultra-short pulses with a single pulse energy up to 50 mJ (Nd:YAG) and 50-100 mJ (ruby) and duration ≈ 40 ps. The active volume was only 5-10 cm³. A beam divergence $\approx 3 \times 10^{-4}$ rad close to the diffraction limit and high brightness of radiation $\approx 10^{17} \text{ W cm}^{-2} \text{ srad}^{-1}$ were obtained. (4 refs.)

Simultaneous quasisteady oscillation on 10.6 and 18.4- μ m transitions in a gas-dynamic CO₂ laser See Entry 75620

Effect of a thermal lattice on the generated line width of a dye laser with distributed feedback See Entry 75630

High-output room-temperature pulsed operation for broad contact InP/In_{0.53}Ga_{0.47}As/InP lasers grown by molecular beam epitaxy See Entry 75636

Low-current-threshold (GaAl)As visible lasers with emission wavelengths below 750 nm See Entry 75637

Electron laser facility (ELF) at the LLNL ETA See Entry 75660

Application of transverse gradient wigglers in high efficiency storage ring FELs See Entry 75661

The UK free electron laser See Entry 75662

Linac technology for free electron lasers See Entry 75663

Storage ring design optimization for FEL operation See Entry 75664

Passive mode locking of buried heterostructure lasers with nonuniform current injection See Entry 75696

System for measuring energy and peak power of low-level 1.064 μ m laser pulses See Entry 75704

Low pressure metalorganic chemical vapor deposition on InP and related compounds See Entry 75757

42.60D Laser resonators and cavities

75693 Sensitivity of the intracavity method of determination of small optical losses in a continuously operating gas laser. A.S.Burmistrov, A.I.Popov.

J. Appl. Spectrosc. (USA), vol.37, no.2, p.877-81 (Aug. 1982). Translation of: *Zh. Prikl. Spektrosk. (USSR)*, vol.37, no.2, p.205-9 (Aug. 1982). [received: April 1983]

In order to measure small optical losses, in particular, in order to determine faint absorption lines of gases and the concentrations of the latter, intracavity resonator procedures (IRP) are used in which the sample being investigated is placed inside the laser resonator. Significantly, the peculiarities of IRP with continuously operating lasers having a narrow laser transition line—such that one can neglect within its limits the spectral dependence of the optical density of the sample under investigation—have been studied to a lesser extent. Since this form of IRP is also of practical interest, it was the subject of the authors' investigation. Specifically, the authors have investigated the case in which a gas laser with a qualitatively homogeneous type of broadening of the generating transition is used for the IRP. A typical example is a helium-neon laser with $\lambda=3.39 \mu\text{m}$ used for the analysis of microconcentrations of hydrocarbons. (7 refs.)

75694 Some properties of phase-matched resonators. Ya.Z.Virnik, V.B.Gerasimov, M.V.Zakharov, V.K.Orlov, A.Ya.Sagalovich.

Sov. Phys.-Tech. Phys. (USA), vol.27, no.11, p.1424-5 (Nov. 1982). Translation of: *Zh. Tekh. Fiz. (USSR)*, vol.52, no.11, p.2310-12 (Nov. 1982). [received: May 1983]

Both rotating mirrors and pass resonators are widely used today as phase-matching devices in laser setups. Resonators with rotating mirrors are always stable, and in most cases the fields oscillations are similar to the fields produced in confocal resonators. The authors show that the properties of pass-type phase-matched resonators are much more diverse. (5 refs.)

75695 Derivation of the coupling coefficients for the eigenfunctions of a spherical, optical resonator in the case of mismatching and misalignment of the incident wave. F.Bayer-Helms.

Report PTB-Me-43, Phys.-Tech. Bundesanstalt, Braunschweig, Germany (Feb. 1983), 61 pp. In German.

A Gaussian beam is characterized by a structural parameter, e.g. the waist radius, and the coordinate of its waist. The transverse modes derived from a Gaussian beam may form complete functional systems such as the S_z system with the Hermitean polynomials $H_m(x) H_n(y)$ which refers to Cartesian coordinates, and the S_r system with the generalized Laguerre polynomials $L_p^{(0)}(r^2)$ which refers to cylinder coordinates. Each transverse mode of a Gaussian beam considered as an incident wave, e.g. m,n from the S_z system, can be represented with the aid of the functions of a complete system of another Gaussian beam, \bar{S}_z or \bar{S}_r , which at the same time, furnishes the eigenfunctions of a spherical, optical resonator. In compliance with this conception, the series coefficients become coupling coefficients which are given by coupling integrals. These integrals formed by one each function from the S_z and \bar{S}_z systems, are evaluated for the general case of their geometric arrangement in relation to each other, i.e. for mismatching-the structural parameters and/or the position of the waists differ-as well for misalignment—the axes of both systems do not coincide. (8 refs.)

'Tunnel' locking stimulated Raman radiation components in an optical resonator See Entry 75614

Single-mode operation of Doppler-broadened lasers by injection locking See Entry 75627

A new mechanism of excitation of a diffraction-radiation generator (free-electron laser) See Entry 75675

Passively mode-locked Nd:YAG and ruby lasers with high brightness per unit active volume See Entry 75692

Theory of mode locking at coherent Brillouin interaction See Entry 75697

Optical chaos in second-harmonic generation See Entry 75723

Optical phase conjugation in laser resonators See Entry 75740

Misalignment sensitivity of optical resonators with phase-conjugate mirrors See Entry 75749

42.60F Laser beam modulation

75696 Passive mode locking of buried heterostructure lasers with nonuniform current injection. C.Harder, J.S.Smith, K.Y.Lau, A.Yariv (California Inst. of Technol., Pasadena, CA, USA).

Appl. Phys. Lett. (USA), vol.42, no.9, p.772-4 (1 May 1983). In this letter the authors report on a novel method to passively mode lock a semiconductor laser. They present experimental results of GaAlAs buried heterostructure semiconductor lasers with a split contact coupled to an external cavity. The split contact structure is used to introduce a controllable amount of saturable absorption which is necessary to initiate passive mode locking. Unlike previous passive mode locking techniques, the method presented does not rely on absorption introduced by damaging the crystal and is consequently inherently more reliable. They have obtained pulses with a full width at half-maximum of 35 ps at repetition frequencies between 500 MHz and 1.5 GHz. (25 refs.)

75697 Theory of mode locking at coherent Brillouin interaction. V.N.Lugovoi (P.N. Lebedev Phys. Inst., Acad. of Sci., Moscow, USSR).

IEEE J. Quantum Electron. (USA), vol.QE-19, no.4, p.764-9 (April 1983). Locking different components of stimulated Brillouin radiation is considered in an optical resonator for a partial filling of the resonator with a Brillouin-active medium exhibiting a coherent (parametric) interaction between the components. The dependence of the type of stable locking on the form of the longitudinal filling of the resonator with the Brillouin-active medium is shown and investigated. In particular, the possibility of the formation of single (over the period $T = 2\pi/\omega_B$, where ω_B is the Brillouin shift) light pulses is shown, provided the length of the medium ranges in intervals spaced by a characteristic 'Brillouin' length $L_B = \pi c/\omega_B n$ (where n is the medium refractive index). A new mechanism of mode locking in lasers is proposed and considered, owing to the coherent interaction between modes in the Brillouin-active medium (which partly fills the laser resonator), the effect being achieved, in particular, for the intensities of the modes generated less than the threshold of stimulated Brillouin radiation in the resonator. The conditions are elucidated of the formation of single (over the period T) light pulses. (30 refs.)

75698 The dynamics of a mode locked and frequency-doubled laser. R.M.Vasu (Central Instruments & Services Lab., Indian Inst. of Sci., Bangalore, India), K.P.J.Reddy.

Pramana (India), vol.20, no.1, p.55-64 (Jan. 1983). [received: May 1983] The theory for the transient build-up of mode locked pulses in a mode-locked and frequency-doubled laser is presented. The time required for the mode-locked pulsewidth to reach a steady-state value is computed. It is found that steady state is reached faster in the presence of internal frequency doubling because of the broadening effect of the doubling crystal. The effects of different conversion efficiencies and modulation depths on the mode-locked pulsewidth are investigated and the results are graphically presented. (14 refs.)

75699 Q-switching of the YAG laser by coloured KCl crystals. V.A.Antonov, V.M.Bezruchko, V.L.Strizhevskii, I.N.Khalimonova, A.B.Sharafutdinov, Yu.N.Yashkir.

Ukr. Fiz. Zh. (USSR), vol.28, no.4, p.609-10 (April 1983). In Russian. Investigates the Q-switching of a YAG laser by KCl crystals with colour centres. The best Q-switching energy characteristics are achieved by choosing the output mirror with an optimal reflection coefficient during initial transmission of the coloured KCl crystal equal to 0.40 ± 0.05 . (9 refs.) V.G.P.

Remote interferometric sensors using frequency modulated laser sources See Entry 74528

Single-mode operation of Doppler-broadened lasers by injection locking See Entry 75627

Coherence effects in synchronously pumped mode-locked dye lasers See Entry 75629

Electrooptic interaction in oversized waveguide modulators See Entry 75784

A single-block hexagonal electrooptical Q-switch See Entry 75785

Acousto-optical modulator of a laser beam See Entry 75786

Laser diode frequency modulation for directional laser doppler velocimetry See Entry 76140

42.60H Optical problems related to properties and interactions of laser beams

75700 Synchronisation of laser modes by amplitude modulation: linear analysis in the spectral domain. M.Piche (Inst. Nat. de la Recherche Sci., Varennes, Quebec, Canada).

Can. J. Phys. (Canada), vol.61, no.5, p.725-35 (May 1983). In French. A theoretical study of homogeneous gain laser mode-locking by means of loss modulation is presented. A linear and causal mathematical formulation is used to describe the interaction between the laser field and the homogeneous medium. The frequency spectrum generated by the laser field is shown to satisfy a difference equation whose order is fixed by the Fourier expansion of the modulation function. Three types of solutions have been found to this equation: a family of uncoupled solutions called supermodes, a single solution, and a continuum of solutions. Unstable laser emission associated with a detuned modulation frequency is attributed to the onset of a continuum of solutions. A frequency filter with a small bandwidth suppresses such a continuum. As a result, the laser field quickly converges towards a stable profile over a broad band of modulation frequencies. (28 refs.)

75701 Frequency stabilization of CO₂ lasers: some applications. C.Freed (Lincoln Lab., MIT, Lexington, MA, USA).

Proc. SPIE Int. Soc. Opt. Eng. (USA), vol.335, p.59-68 (1982). [received: May 1983] (Advanced Laser Technology and Applications, Arlington, VA, USA, 6-7 May 1982).

Reviews the frequency stabilization and selected application of CO₂ lasers at MIT Lincoln Laboratory. Unsurpassed spectral purity and short-term stability was achieved. A long-term stabilization technique, which was used to line-center lock any regular or hot-band CO₂ isotope laser transition, is also described. (12 refs.)

75702 Error in determining laser radiation divergence by the focal spot method. Yu.A.Drozhdin, V.E.Prokopenko, V.B.Semenov.

Meas. Tech. (USA), vol.25, no.9, p.732-4 (Sept. 1982). Translation of: *Izmer. Tekh. (USSR)*, vol.25, no.9, p.19-21 (Sept. 1982). [received: May 1983]

The focal spot method using a mirror wedge is dealt with and the characteristics of the photographic paper as the radiation recorder are examined. The results indicate that the method considered is sufficiently convenient for practical utilisation. Compared to the focal spot method without a mirror wedge, it assumes a commensurate measurement error and requires 10-20 times less time for processing the results. (6 refs.)

75703 Reduction of the random component in measuring pulse laser radiation intensity. V.M.Rubinshtein, A.F.Kotlyuk, A.P.Romashkov.

Meas. Tech. (USA), vol.25, no.9, p.734-7 (Sept. 1982). Translation of: *Izmer. Tekh. (USSR)*, vol.25, no.9, p.21-2 (Sept. 1982). [received: May 1983]

In reproducing and transmitting the dimension of the pulse laser radiation power unit, the measurements are performed for the regime of a periodic pulse train by using two stroboscopic transducers, the first of which measures the value of the maximum power, and the second the running value of the pulse power. A result of the measurements is a set (realization) of ratios of the powers mentioned which permits determination of the amplitude-time relationship of the optical pulse measured and a description of its shape. An estimate of the random component of the error in measuring pulse laser radiation power is given and a numerical method to reduce it based on an interpolation procedure is proposed. (5 refs.)

75704 System for measuring energy and peak power of low-level 1.064 μ m laser pulses. A.A.Sanders, A.L.Rasmussen.

Report NB-NT-1058, Nat. Bur. Stand., Washington, DC, USA (Oct. 1982) iii+39 pp.

Transfer standards have been developed for measuring 1.064 μ m laser pulses of duration about 10-100 ns, peak irradiance of about 10^{-8} - 10^{-4} W/cm², and fluences of about 10^{-10} - 10^{-3} J/cm². These energy and power measurement devices use PIN and APD silicon detectors, respectively, and can be used as stable transfer standards with total uncertainties (random errors computed at the 95 percent confidence level) of 10 to 15 percent. The system for calibrating these transfer standards is also described and consists of a CW Nd:YAG laser beam acousto-optically modulated to provide low-level laser pulses of known peak power and energy. A detailed evaluation of systematic and random errors is also shown. (4 refs.)

Photometric characteristics of calorimeters having conical cells of tantalum See Entry 74467

Evaluation of the thermal focal length produced in a repetitively pulsed solid-state laser See Entry 75644

Picosecond transient orientational and concentration gratings in germanium See Entry 75708

Diffraction gyration and reversal of the laser beam wave front in electrooptic crystals See Entry 75750

Realization of 90° and 180° hybrids for optical frequencies See Entry 75777

Effects of semiconducting oxide films on the reflectivity change in a metal on radiation heating See Entry 77344

42.60K Optical problems related to applications of laser beams

75705 CO₂ laser radar transmitters. G.R.Osche, C.E.Harris, R.S.Eng (Electro-Optics Systems Lab., Raytheon Co., Sudbury, MA, USA).

Proc. SPIE Int. Soc. Opt. Eng. (USA), vol.335, p.95-103 (1982). [received: May 1983] (Advanced Laser Technology and Applications, Arlington, VA, USA, 6-7 May 1982).

The advent of multifunctional CO₂ laser radars has led to the development of a variety of transmitter modules suitable for both coherent and noncoherent applications. Development trends in CO₂ TEA and modulated waveguide lasers, the principal laser radar transmitter technologies, are reviewed. (10 refs.)

Objective laser speckle method for 3-D displacement measurement on curved surfaces See Entry 74434

Laser interference method of measuring small taper angles in plates in the IR range See Entry 74436

Automated goniometer employing a ring laser See Entry 74510

Remote interferometric sensors using frequency modulated laser sources See Entry 74528

10-Hz coherence anti-Stokes Raman spectroscopy apparatus for turbulent combustion studies See Entry 74542

Tone-burst modulated color-center-laser spectroscopy See Entry 74545

Unique applications of alexandrite lasers See Entry 75686

Frequency stabilization of CO₂ lasers: some applications See Entry 75701

Laser plate storage See Entry 75759

Optical systems of laser scanners See Entry 75766

Acousto-optical modulator of a laser beam See Entry 75786

A method for automatic measurement of Brinell hardness using a microcomputer See Entry 75969

Laser diode frequency modulation for directional laser doppler velocimetry See Entry 76140

Differential Doppler velocimetry using polarization-preserving optical fiber See Entry 76141

Medical laser equipment for continuous operation See Entry 78289

42.65 NONLINEAR OPTICS

75706 Method of quasi-energy states in nonlinear optics. A.O.Melikyan, M.L.Ter-Mikaelyan (Inst. of Phys. Res., Acad. of Sci., USSR).

Bull. Acad. Sci. USSR, Phys. Ser. (USA), vol.46, no.5, p.168-72 (1982). Translation of: *Izv. Akad. Nauk SSSR Ser. Fiz.*, vol.46, no.5, p.1004-6 (1982). [received: May 1983] (Proceedings of the All-Union Conference on Luminescence Commemorating the Ninetieth Anniversary of the Birth of the Academician S.I. Vavilov, Leningrad, USSR, 21-24 April 1981).

Many important results, a significant portion of which has already been included in textbooks and monographs, have been obtained in the theory of the interaction of coherent electromagnetic radiation with atoms. The authors discuss the relationship of the method of quasi-energy states (QES) with the 'first principles' of radiation theory. The QES themselves were introduced independently of quantum radiation theory and only certain of their properties were interpreted in the spirit of the latter. The authors have demonstrated that the clarification of this relationship allows on the one hand the establishment of the applicability boundary of the classical description of an electromagnetic field interacting with atoms, and on the other hand a new physical interpretation of intensity effects during spontaneous emission from atoms in a powerful light field. (15 refs.)

75707 Fabrication of GaAs bistable optical devices. J.L.Jewell, H.M.Gibbs (Optical Sci. Center, Univ. of Arizona, Tucson, AZ, USA), A.C.Gossard, A.Passner, W.Wiegmann. *Mater. Lett. (Netherlands)*, vol.1, no.5-6, p.148-51 (April 1983). Techniques for the construction of flat etalons containing GaAs are presented including: an arrangement of GaAs and AlGaAs layers on top of a GaAs substrate which results in successful substrate removal, a procedure for etching away the substrate, and a technique for mounting the remaining sample between dielectric mirrors. Experimental results from such devices are also presented. (10 refs.)

75708 Picosecond transient orientational and concentration gratings in germanium. A.L.Smiri, T.F.Boggess (Dept. of Phys., Center for Appl. Quantum Electronics, North Texas State Univ., Denton, TX, USA), B.S.Wherrett, G.P.Perryman, A.Miller. *IEEE J. Quantum Electron. (USA)*, vol.QE-19, no.4, p.690-700 (April 1983).

Presents and discusses the results of picosecond transient grating self-diffraction measurements in germanium that can be understood in terms of an orientational grating produced by anisotropic (in k space) state-filling. Although there have been predictions and indirect experimental evidence for isotropic state-filling in germanium, this is the first direct experimental indication of anisotropic state-filling in a semiconductor. The authors compare the self-diffracted signals from orientational gratings with those from band-filling induced concentration gratings and find several distinctions, all of which can be explained in terms of the theory developed in the preceding paper (1980). In addition, the authors have performed three-pulse transient lifetime measurements which indicate that the concentration grating decay is tens of picoseconds, while the orientational grating decay is too rapid to resolve with 8 ps pulses. (19 refs.)

75709 Nonphotochemical hole burning in a hydrogen bonding glass: dependence on deuteration. B.L.Fearey, R.P.Stout, J.M.Hayes, G.J.Small (Dept. of Chem., Iowa State Univ., Ames, IA, USA). *J. Chem. Phys. (USA)*, vol.78, no.11, p.7013-15 (1 June 1983). The authors conducted a study to ascertain whether hydrogen bond modes are instrumental for nonphotochemical hole burning in polar organic glasses. Spectra were obtained in the photoexcitation (fluorescence) mode. The dependence of zero-phonon hole width on burn temperature was also studied. (21 refs.)

75710 Nonlinear interactions with intense femtosecond optical pulses. C.V.Shank (Bell Telephone Labs., Holmdel, NJ, USA). *J. Phys. Colloq. (France)*, vol.44, no.C-2, p.69 (March 1983). (International Workshop on Optical Phase Conjugation and Instabilities, Cargèse, Corsica, France, 20-24 Sept. 1982). Summary form only given, as follows. Recent advances in optical pulse generation techniques have led to the production of short optical pulses in the femtosecond time domain. The author discusses the interaction of intense femtosecond optical pulses in solids and liquids. The use of nonlinear interactions to generate a compressed optical pulse as short as 30 femtoseconds is described. In addition, the generation of a white light continuum in the femtosecond domain is discussed.

75711 Highly nonlinear optical effects in liquid crystals. S.D.Durbin, S.M.Arakelian, M.M.Cheung, Y.R.Shen (Dept. of Phys., Univ. of California, Berkeley, CA, USA). *J. Phys. Colloq. (France)*, vol.44, no.C-2, p.161-9 (March 1983). (International Workshop on Optical Phase Conjugation and Instabilities, Cargèse, Corsica, France, 20-24 Sept. 1982). CW laser fields are strong enough to induce a large refractive index change in a liquid crystal. Optical-field-induced structural transition can occur. The large optical nonlinearity can lead to some unusual highly nonlinear optical phenomena. (21 refs.)

75712 Optical turbulence: chaos in optical bistability. K.Ikeda (Dept. of Phys., Kyoto Univ., Kyoto, Japan). *J. Phys. Colloq. (France)*, vol.44, no.C-2, p.183-92 (March 1983). (International Workshop on Optical Phase Conjugation and Instabilities, Cargèse, Corsica, France, 20-24 Sept. 1982). The transmitted light from a bistable optical cavity can exhibit a variety of bifurcation phenomena, passing from a stationary state, through successive periodic and chaotic states to a final fully developed chaotic state, as the intensity of incident laser light is increased. Recent studies on these phenomena are reviewed from a theoretical point of view. (16 refs.)

75713 Bifurcations to chaos in optical bistability. F.A.Hopf (Optical Sci. Center, Univ. of Arizona, Tucson, AZ, USA). *J. Phys. Colloq. (France)*, vol.44, no.C-2, p.193 (March 1983). (International Workshop on Optical Phase Conjugation and Instabilities, Cargèse, Corsica, France, 20-24 Sept. 1982). Summary form only given, as follows. Recent predictions by Ikeda show novel instabilities in optically bistable devices which can give chaotic behavior. Experiments confirming this prediction are presented. A discussion of the nature of chaos and the rationale for its study is also given.

75714 Optical bistability, regenerative pulsations, and transverse effects in room-temperature GaAs-AlGaAs superlattice etalons. H.M.Gibbs, J.L.Jewell, J.V.Moloney, K.Tai, S.S.Tarnag, D.A.Weinberger (Optical Sci. Center, Univ. of Arizona, Tucson, AZ, USA), A.C.Gossard, S.L.McCall, A.Passner, W.Wiegmann. *J. Phys. Colloq. (France)*, vol.44, no.C-2, p.195-204 (March 1983). (International Workshop on Optical Phase Conjugation and Instabilities, Cargèse, Corsica, France, 20-24 Sept. 1982). The quantum wells provided by a superlattice increase the binding energy of free excitons in GaAs, permitting 300K bistable operation. Thermal and excitonic refractive index effects compete, resulting in regenerative pulsations. Transverse observations and simulations provide other interesting effects. (21 refs.)

75715 Observation of periodic and chaotic instabilities in an all optical bistable system. H.Nakatsuka, S.Asaka, H.Ito, M.Matsuoka (Dept. of Phys., Kyoto Univ., Kyoto, Japan). *J. Phys. Colloq. (France)*, vol.44, no.C-2, p.205-6 (March 1983). (International Workshop on Optical Phase Conjugation and Instabilities, Cargèse, Corsica, France, 20-24 Sept. 1982). Summary form only given, as follows. Bifurcations to periodic and chaotic states have been observed in an all optical ring cavity. A mode-locked pulse train was used as a strong quasi-CW light source. The ring cavity consisted of a single-mode optical fiber allowing a propagation of a quasi-plane wave. The results are in good agreement with the theory of Ikeda et al. (see Phys. Rev. Lett., vol.45, p.709, 1980). (4 refs.)

75716 Optical bistability in the frustrated-total-reflection optical cavity. B.Bosacchi (Western Electric Engng. Res. Center, Princeton, NJ, USA), L.M.Narducci. *Opt. Lett. (USA)*, vol.8, no.6, p.324-6 (June 1983). The nonlinear behavior of a frustrated-total-reflection (FTR) optical cavity containing a nonlinear Kerr medium is considered. It is shown that optical bistability may occur at lower incident power than in the nonlinear interface system. Other potential advantages of the resonant FTR configuration over other geometries are also briefly discussed. (11 refs.)

75717 Observation of magnetically induced optical self-pulsing in a Fabry-Perot resonator. F.Mitschke, J.Mlynek, W.Lange (Inst. für Quantenoptik, Univ. Hannover, Hannover, Germany). *Phys. Rev. Lett. (USA)*, vol.50, no.21, p.1660-3 (23 May 1983). Magnetically induced optical self-pulsing has been observed in a Fabry-Perot resonator containing sodium vapor. Experiments are performed on optically pumped Zeeman sublevels of the Na ground state in the presence of a static transverse magnetic field B . When B exceeds a critical value B_{cr} , self-sustained spin precession occurs, and the transmitted light is found to be modulated at about the Larmor frequency. The use of this tunable current-controlled oscillator in optical FM signal transmission is demonstrated. (8 refs.)

Nonlinear resonances which arise during the interaction of atoms with spaced powerful standing waves See Entry 75334

Peculiarities of dip (hole) burning in the spectra of organic molecules in vitreous matrices See Entry 75364

Study of optical relaxation of polyatomic molecules in the condensed phase by site-selective laser spectroscopy See Entry 75426

Thermal broadening of optical homogeneous linewidths in organic glasses and polymers studied via photochemical hole-burning See Entry 75448

Analytical tools for nonlinear image restoration See Entry 75586

Contra-directional two-wave mixing in photorefractive media See Entry 75603

The nonlinear gain in the free-electron laser with a long wiggler See Entry 75673

Ferroelectric liquid crystal electro-optics using the surface stabilized structure See Entry 77362

42.65C Stimulated Raman, Brillouin and Rayleigh scattering; parametric oscillations and harmonic generation

75718 Amplification by stimulated Raman scattering in low-loss optical fibers. G.A.Koepp (Comsat Labs., Clarksburg, MD, USA). *Arch. Elektron. & Übertragungstechnik. (Germany)*, vol.37, no.5-6, p.145-52 (May-June 1983).

The feasibility of amplifying optical signals in low-loss fibers via stimulated Raman scattering in the infrared spectral region is discussed. After the theoretical and experimental work is reviewed, numerical results are given that predict gain values in excess of 50 dB and conversion efficiency up to 90 percent in a low-loss fiber for an 1-W pump laser. The concurrence of stimulated Brillouin scattering is shown to drastically reduce the fiber length that can be utilized in such an amplifier. Several methods are presented for reducing this limitation. (57 refs.)

75719 Picosecond time-resolved CARS in isotopically mixed crystals of benzene. F.Ho, W.-S.Tsay, J.Trout, S.Velsko, R.M.Hochstrasser (Dept. of Chem., Univ. of Pennsylvania, Philadelphia, PA, USA). *Chem. Phys. Lett. (Netherlands)*, vol.97, no.2, p.141-6 (13 May 1983). Time-resolved coherent anti-Stokes Raman experiments are reported for the benzene crystal 991 cm^{-1} mode and in mixed $\text{C}_6\text{H}_6/\text{C}_6\text{D}_6$ crystals. Addition of C_6D_6 results in an increase in the rate at which the excitation is trapped. This is explained by the recent theory of Velsko and Hochstrasser which predicts that the trapping rate should undergo a maximum at some isotopic impurity concentration, consistent with observations from time and frequency domain studies. A proper convolution procedure for CARS experiments in the time domain is presented. (21 refs.)

75720 Nonlinear optics in fibers and near-infrared frequency conversion. Chnlon Lin (Bell Labs., Holmdel, NJ, USA). *Proc. SPIE Int. Soc. Opt. Eng. (USA)*, vol.355, p.17-26 (1982). [received: May 1983] (Fiber Optics: Short-Haul and Long-Haul Measurements and Applications, San Diego, CA, USA, 24-25 Aug. 1982).

Nonlinear optical effects in fibers can affect the intensity and spectral characteristics of an optical signal and thus present power transmission limitations. On the other hand, one can make use of nonlinear optics in fibers for efficient frequency conversion and generation of new frequencies which are important for fiber-optics studies and measurements. In this paper the author reviews the use of single-mode fibers for near-infrared frequency conversion in the 1.1-1.7 μm spectral region by stimulated Raman scattering, tunable Raman oscillation, and stimulated, phase-matched four-photon parametric mixing, and discuss their applications. (34 refs.)

75721 Frequency-angular diffusion of intense quiresonant radiation. A.I.Plekhanov, S.G.Rautian, V.P.Safonov, B.M.Chernobrod (Inst. of Automation & Electrometry, Acad. of Sci., Novosibirsk, USSR). *JETP Lett. (USA)*, vol.36, no.7, p.284-7 (5 Oct. 1982). Translation of: *Pis'ma v Zh. Eksp. & Teor. Fiz. (USSR)*, vol.36, no.7, p.232-4 (5 Oct. 1982). [received: May 1983]

It is established experimentally, using the probing field method, that frequency-angular diffusion of intense quasi-resonant radiation is due to four-photon resonant parametric scattering of light under conditions of large amplification in a narrow channel of one of the scattering components. (5 refs.)

75722 Non-linear optical mixing of frequencies of a strong bichromatic field interacting with a two-level atom at high proton densities. C.Mavroyannis (Div. of Chem., Nat. Res. Council of Canada, Ottawa, Ontario, Canada). *Mol. Phys. (GB)*, vol.49, no.1, p.171-91 (May 1983).

The author studied the excitation spectrum arising from the interaction of a two-level atom with two strong electromagnetic fields whose initially populated modes ω_a and ω_b are near resonance with the atomic transition frequency. In the limit of high photon densities the Green's function of the system describing the electronic transition in question has been derived in a closed form and includes processes arising from the interaction of seven photon modes of both laser fields. The spectral function of the system is calculated when the frequency ω_a of the one laser field is in resonance with the atomic transition frequency while the frequency ω_b of the other field is varied. The probability amplitudes describing the relative intensities of the peaks in question are expressed as functions of the parameters $\eta_a = \Omega_a/\Delta$ and $\eta_b = \Omega_b/\Delta$, where Ω_a and Ω_b are the Rabi frequencies of the two laser fields, respectively.

It is found that when $\eta_a \geq 1$ and $\eta_b \geq 1$ the expression for the relative intensities of the bands in question are remarkably enhanced and take extremely large positive or negative values. Results of numerical calculations for a wide range of values of η_a and η_b when $\eta_a = \eta_b \geq 1$ are presented graphically and the complete excitation spectrum is discussed in detail. (22 refs.)

75723 Optical chaos in second-harmonic generation. C.M.Savage, D.F.Walls (Phys. Dept., Univ. of Waikato, Hamilton, New Zealand). *Opt. Acta (GB)*, vol.30, no.5, p.557-61 (May 1983). Instabilities leading to self-pulsing, period doubling and chaos are predicted to occur in two simple systems in nonlinear optics. Namely, second-harmonic generation, inside a coherently driven optical cavity, and subharmonic generation internal to the laser cavity. (19 refs.)

75724 Continuous-wave, single frequency, second harmonic generation in sodium vapour. M.H.Dunn (Dept. of Phys., Univ. of St. Andrews, Fife, Scotland).

Opt. Commun. (Netherlands), vol.45, no.5, p.346-50 (1 May 1983). Single frequency, second harmonic radiation has been generated continuously in sodium vapour using resonant enhancement provided by the two photon transition 3S-4D at 578.7 nm, and a transverse magnetic field to remove the isotropy of the vapour. Phase matching and linewidth effects have been studied. The generation profile of the vapour is shown to be Doppler limited. (24 refs.)

75725 Stimulated Raman oscillation in capillary waveguide resonators. A.J.Berry, D.C.Hanna (Dept. of Phys., Univ. of Southampton, Southampton, England).

Opt. Commun. (Netherlands), vol.45, no.5, p.357-60 (1 May 1983). The threshold for stimulated Raman scattering in H_2 gas using a 1.06 μ m pump has been reduced by a factor of 30 (to ~ 40 kW in a 35 ns pulse) by the combined use of a capillary waveguide and a resonator providing Stokes feedback. Similar enhancement has been observed in CH_4 where, in addition, the use of a dispersive resonator has allowed suppression of stimulated Brillouin scattering even with single mode pumping. (15 refs.)

75726 Coherent anti-Stokes Raman scattering in thin-film dielectric waveguides. G.I.Stegeman, R.Fortenberry, C.Karagulleff, R.Moshrefzadeh (Arizona Res. Labs., Univ. of Arizona, Tucson, AZ, USA), W.M.Hetherington, III, N.E.Van Wyck, J.E.Sipe.

Opt. Lett. (USA), vol.8, no.6, p.295-7 (June 1983). The authors analyze coherent anti-Stokes Raman scattering in thin-film dielectric waveguides. Extraordinary large signal levels are predicted, and two applications of this phenomenon are discussed. (12 refs.)

75727 High-efficiency laser-pulse compression by stimulated Brillouin scattering. M.J.Damzen, M.H.R.Hutchinson (Blackett Lab., Imperial Coll., London, England).

Opt. Lett. (USA), vol.8, no.6, p.313-15 (June 1983). Highly efficient compression of laser pulses down to 1 nsec in duration by stimulated Brillouin scattering has been demonstrated. Compression ratios of ~ 10 and energy-conversion efficiencies $> 70\%$ have been produced. Several compressor systems have been investigated, including the use of tapered waveguides, long-focal-length geometries, and generator-amplifier systems. (11 refs.)

75728 Parametric generation of submillimeter radiation in semiconductors in the field of a bichromatic pulse. S.K.Avetissian, E.M.Kazarian, A.O.Melikian, H.R.Minasian (Polytech. Inst., Erevan, USSR).

Phys. Status Solidi b (Germany), vol.116, no.2, p.455-63 (1 April 1983). The self-consistent problem of the interaction of three collinear laser pulses with frequencies ω_1 , ω_2 , ω_3 , propagating in a semiconductor, is discussed. The quasi-energy spectrum of the semiconductor is determined for the excitation frequencies ω_1 , $\omega_2 \leq E_g/\hbar$, where E_g is the forbidden band width, and $\omega_3 = \omega_2 - \omega_1 \leq E_g/\hbar$. The problem of resonance parametric generation of the difference frequency ω_3 is considered on the basis of an exact expression for the semiconductor polarization. The possibility of submillimeter radiation generation in semiconductors with $E_g \approx 0.1$ eV is shown. The efficiency of a conversion of the corresponding process is determined. (15 refs.)

75729 Resonant upversion of light at wavelength $\lambda = 1.06 \mu$ m in rubidium vapor. V.A.Kiyashko, A.K.Popov, V.P.Timofeev, G.V.Yurov (L.V. Kirenskiy Phys. Inst., Acad. of Sci., Krasnoyarsk, USSR). *Sov. Phys.-Tech. Phys. (USA)*, vol.27, no.11, p.1405-6 (Nov. 1982). Translation of: *Zh. Tekh. Fiz. (USSR)*, vol.52, no.11, p.2286-8 (Nov. 1982). [received: May 1983]

One promising method for frequency conversion of weak IR radiation into visible and near UV light involves using resonant four-wave parametric processes of the type $\omega_4 = \omega_1 + \omega_2 + \omega_{IR}$ in gaseous media. In this method, two types of experimental setup are usually used—some atomic transition ω_{IR} in the nonlinear medium which is forbidden in the electric dipole approximation is chosen so that it is in resonance with pumping light at frequencies ω_1 and ω_2 from an intense two-photon source, or else the frequency ω_{IR} of the transition is taken equal to the sum $\omega_{IR} = \omega_1 + \omega_2$ of the weak IR signal frequency ω_{IR} and a single strong pumping frequency ω_1 . The authors consider a scheme of the second type. The interacting waves are assumed to be monochromatic plane waves and the pumping fields E_1 and E_2 are assumed given over the length of the nonlinear medium. (6 refs.)

75730 Maximum time compression of light pulses in stimulated Brillouin scattering. V.A.Gorbanov (All-Union Sci.-Res. Inst. for Electric Welding Equipment Design & Technol., Leningrad, USSR).

Sov. Phys.-Tech. Phys. (USA), vol.27, no.11, p.1418-19 (Nov. 1982). Translation of: *Zh. Tekh. Fiz. (USSR)*, vol.52, no.11, p.2302-5 (Nov. 1982). [received: May 1983]

Studies stimulated Brillouin scattering in a focused pumping beam from a theoretical viewpoint. The author shows that if the focusing geometry is optimal and the threshold is suitably exceeded, twenty- to thirtyfold compression is possible with an energy reflection coefficient nearly equal to unity; moreover, the duration of the reflected pulse can be made shorter than the hyper-sonic relaxation time by a factor of ten. The author studies the energy and time parameters of a Stokes pulse in stimulated Brillouin scattering using the plane wave approximation with allowance for axial amplitude nonuniformity caused by focusing. (6 refs.)

Photoionization Raman spectroscopy See Entry 75335

Two-photon Raman excitation and coherent anti-Stokes Raman spectroscopy probing of population changes in polyatomic molecules: a novel nonlinear optical technique for vibrational-relaxation studies See Entry 75396

'Tunnel' locking stimulated Raman radiation components in an optical resonator See Entry 75614

Transverse optical klystrons: a feasibility experiment on harmonic generation See Entry 75659

Theory of mode locking at coherent Brillouin interaction See Entry 75697

The dynamics of a mode locked and frequency-doubled laser See Entry 75698

Efficient phase conjugation under parametric-feedback conditions See Entry 75732

Some thoughts and observations of phase conjugation in the ultraviolet See Entry 75735

Phase conjugation of KrF laser radiation See Entry 75736

Relation between degenerate four-wave mixing and coherent anti-Stokes Raman scattering See Entry 75738

Optical phase conjugation in laser resonators See Entry 75740

Phase conjugation in liquids in the picosecond range See Entry 75742

RECLAS: resonant-enhanced CARS from C_2 produced by laser ablation of soot particles See Entry 77926

42.65F Phase conjugation

75731 Picosecond molecular dynamics in liquids via degenerate four-wave mixing. G.A.Kenney-Wallace, S.C.Wallace (Univ. of Toronto, Toronto, Ontario, Canada).

IEEE J. Quantum Electron. (USA), vol.QE-19, no.4, p.719-23 (April 1983). Reports measurements of degenerate four-wave mixing in liquids to study the picosecond orientational dynamics of molecules and the transition of a probe molecule from many-particle to single-particle rotational behavior as a function of dilution. Data for C_2 in pure and dilute alkane systems are presented, in which the molecular motion is characterized as diffusion, rather than impulsive, at times ≥ 0.9 ps, the limiting single-particle orientational correlation time in n-pentane at 300K. (27 refs.)

75732 Efficient phase conjugation under parametric-feedback conditions. V.I.Odintsov, L.F.Rogacheva (M.V. Lomonosov Moscow State Univ., Moscow, USSR).

JETP Lett. (USA), vol.36, no.8, p.344-7 (20 Oct. 1982). Translation of: *Pis'ma v Zh. Eksp. & Teor. Fiz. (USSR)*, vol.36, no.8, p.281-4 (20 Oct. 1982). [received: June 1983]

A new method is proposed for exciting stimulated Brillouin scattering under generation conditions in a system with parametric feedback. Phase conjugation of the pump beam can be achieved at a considerably lower threshold intensity by this new method. (2 refs.)

75733 Degenerate four wave mixing in photorefractive BSO crystals and applications. J.P.Huignard (Lab. Central de Recherches, Thomson-CSF, Orsay, France).

J. Phys. Colloq. (France), vol.44, no.C-2, p.3-4 (March 1983). (International Workshop on Optical Phase Conjugation and Instabilities, Cargèse, Corsica, France, 20-24 Sept. 1982).

Over the past few years a new field of interest has emerged in coherent optics: nonlinear optical phase conjugation. The field includes the possibility of operating in real time on the phase and amplitude of optical wavefronts. The use of such nonlinear interactions has resulted in numerous new applications such as adaptive optics, image transmission and amplification and nonlinear spectroscopy. The author reviews the basic properties of phase conjugate mirrors and the applications of wave mixing experiments in photorefractive crystals to: optical processing, dynamic holography, interferometry, and phase conjugation. (no refs.)

75734 Laser beam critical behaviour and phase conjugation in the semiconductors, resonant media and electrooptic crystals. N.Kukhtarev, A.Borshch, M.Brodin, V.Volkov, T.Semenets (Inst. of Phys., Acad. of Sci., Kiev, Ukrainian SSR).

J. Phys. Colloq. (France), vol.44, no.C-2, p.5-14 (March 1983). (International Workshop on Optical Phase Conjugation and Instabilities, Cargèse, Corsica, France, 20-24 Sept. 1982).

A brief review of the authors' studies of optical hysteresis and holographic phase conjugation in semiconductors, resonant media and electrooptic crystals is given together with some new results. (16 refs.)

75735 Some thoughts and observations of phase conjugation in the ultraviolet. B.J.Feldman, I.Bigio, R.A.Fisher, M.Slatkine (Los Alamos Nat. Lab., Los Alamos, NM, USA).

J. Phys. Colloq. (France), vol.44, no.C-2, p.17 (March 1983). (International Workshop on Optical Phase Conjugation and Instabilities, Cargèse, Corsica, France, 20-24 Sept. 1982).

Summary form only given, as follows. Reports on ultraviolet phase conjugation studies using KrF, XeF, and quadrupled Nd:YAG lasers. Processes studied include stimulated Brillouin scattering, stimulated Raman scattering, and degenerate four-wave mixing. In some cases phase conjugate efficiencies of greater than 80% are observed. Implications and applications of these phenomena are discussed.

75736 Phase conjugation of KrF laser radiation. M.C.Gower, R.G.Caro (Laser Div., SERC Rutherford Appleton Lab., Chilton, Didcot, England).

J. Phys. Colloq. (France), vol.44, no.C-2, p.19-25 (March 1983). (International Workshop on Optical Phase Conjugation and Instabilities, Cargèse, Corsica, France, 20-24 Sept. 1982).

Reports observations of phase conjugate reflection of KrF laser radiation using both degenerate four-wave mixing (DFWM) and stimulated Brillouin scattering (SBS). Using DFWM the authors have measured reflectivities of $\sim 300\%$ and the results are in good agreement with a theory for a thermally induced mechanism in the medium. The SBS phase conjugate mirror has been used in a variety of applications which are of interest to the development of high energy rare-gas halide lasers. (10 refs.)

75737 Degenerate frequency mixing in saturable amplifiers. J.Reintjes, B.L.Wexler, N.Dieu, J.L.Walsh (Laser Phys. Branch, US Naval Res. Lab., Washington, DC, USA).

J. Phys. Colloq. (France), vol.44, no.C-2, p.27-37 (March 1983). (International Workshop on Optical Phase Conjugation and Instabilities, Cargèse, Corsica, France, 20-24 Sept. 1982).

Phase conjugation by degenerate frequency mixing has been studied in saturable amplifiers for various interaction geometries and polarization combinations. Theoretical results are compared with measurements in a XeCl amplifier. Experimental reflectivities as high as 100 are observed. (19 refs.)

75738 Relation between degenerate four-wave mixing and coherent anti-Stokes Raman scattering. S.Chandra (Sci. Applications Inc., McLean, VA, USA).

J. Phys. Colloq. (France), vol.44, no.C-2, p.39-40 (March 1983). (International Workshop on Optical Phase Conjugation and Instabilities, Cargèse, Corsica, France, 20-24 Sept. 1982).

Attempts to establish a connection between DFWM and CARS using Lorentz transformations. It is shown that a Lorentz transformed DFWM (at least in optically rare media) appears indistinguishable from CARS. Conversely, no matter how complex a CARS geometry, a simple Lorentz transformation will render it looking like a DFWM. (1 ref.)

- 75739 Phase conjugate oscillators.** A.Siegman (Edward L. Ginzton Lab., Stanford Univ., Stanford, CA, USA). *J. Phys. Colloq. (France)*, vol.44, no.C-2, p.43 (March 1983). (International Workshop on Optical Phase Conjugation and Instabilities, Cargèse, Corsica, France, 20-24 Sept. 1982).
Summary form only given as follows. Considers the various aspects of oscillating devices using optical phase conjugation: resonant modes in phase conjugate devices, 'self-pumped' phase conjugation effects in conventional lasers.
- 75740 Optical phase conjugation in laser resonators.** C.R.Giuliano, R.C.Lind, T.R.O'Meara, G.C.Valley (Hughes Res. Labs., Malibu, CA, USA). *J. Phys. Colloq. (France)*, vol.44, no.C-2, p.45-58 (March 1983). (International Workshop on Optical Phase Conjugation and Instabilities, Cargèse, Corsica, France, 20-24 Sept. 1982).
The use of phase conjugating 'mirrors' in oscillating optical structures has been a subject of recent interest, both experimentally and theoretically. One of the attractive features of a phase conjugate resonator, PCR, is its ability to provide an output wave whose wavefront depends only on the quality of the output coupler and is essentially independent of intracavity aberrations. Several concepts for PCRs are presented in which either degenerate four-wave mixing or stimulated Brillouin scattering is employed as the phase conjugate mirror; advantages and drawbacks of each are discussed. (22 refs.)
- 75741 New study and application of phase conjugation with photorefractive crystals.** B.Fischer (California Inst. of Technol., Pasadena, CA, USA). *J. Phys. Colloq. (France)*, vol.44, no.C-2, p.59 (March 1983). (International Workshop on Optical Phase Conjugation and Instabilities, Cargèse, Corsica, France, 20-24 Sept. 1982).
Summary form only given, as follows. A theoretical and experimental study of four-wave mixing in photorefractive crystals like SBN and BaTiO₃ is presented. A detailed theoretical analysis of the beam coupling as well as new experiments and applications are described through a distortion; among them, one-way optical field imaging, a passive (no external pumps) phase conjugate mirror which is pumped by the signal and its use in a laser resonator.
- 75742 Phase conjugation in liquids in the picosecond range.** G.Rivoire, J.L.Ferrier, J.Gazengel, N.Phu Xuan (Lab. d'Optique des Fluides, Univ. d'Angers, Angers, France). *J. Phys. Colloq. (France)*, vol.44, no.C-2, p.81-90 (March 1983). (International Workshop on Optical Phase Conjugation and Instabilities, Cargèse, Corsica, France, 20-24 Sept. 1982).
Phase conjugation is produced in the picosecond range, in different liquids, by degenerate four wave mixing, and by stimulated backward Rayleigh and Raman scatterings. The intensities and efficiencies are measured, and the influences of the exciting power and the nonlinear medium length are studied. The feasibility of image reconstruction, even with a change in the wavelength due to Raman scattering, is proved and analysed theoretically and experimentally. Temporal applications are proposed. (15 refs.)
- 75743 Polarization dependent properties of backward four-wave mixing.** S.Saikan (Dept. of Phys., Osaka Univ., Osaka, Japan). *J. Phys. Colloq. (France)*, vol.44, no.C-2, p.93-100 (March 1983). (International Workshop on Optical Phase Conjugation and Instabilities, Cargèse, Corsica, France, 20-24 Sept. 1982).
Theoretical analyses have been made of polarization- and angular momentum-dependences of backward four-wave mixing in atomic lines. These results were also applied to the problem of 'vectorial' phase-conjugation in atomic vapours. Experimental demonstration of the vectorial phase-conjugation was carried out in D₂ resonance line of sodium. Concerning the phase-conjugation spectroscopy in condensed matter, it has been proposed to detect X₁₂₂₁⁽³⁾ component to eliminate thermal grating effect. (11 refs.)
- 75744 Doppler-free conjugate emission in resonant gas media: lineshape, polarization properties and saturation.** D.Bloch, R.K.Raj, K.S.Peng, M.Ducloy (Lab. de Phys. des Lasers, Univ. Paris-Nord, Villetaneuse, France). *J. Phys. Colloq. (France)*, vol.44, no.C-2, p.101-11 (March 1983). (International Workshop on Optical Phase Conjugation and Instabilities, Cargèse, Corsica, France, 20-24 Sept. 1982).
Analyses some specific features of degenerate four-wave mixing in resonant gas media. One shows that the polarization of the phase conjugate emission is strongly affected by the residual Doppler effect. With saturating intensities, very peculiar emission lineshapes are observed and are shown to be typical effects of the velocity distribution. (18 refs.)
- 75745 Applications of degenerate four-wave mixing to high resolution molecular spectroscopy at 10.6 μm .** J.L.Boulnois (QUANTEL, les Ulis, France). *J. Phys. Colloq. (France)*, vol.44, no.C-2, p.113-24 (March 1983). (International Workshop on Optical Phase Conjugation and Instabilities, Cargèse, Corsica, France, 20-24 Sept. 1982).
CW phase conjugation on the ν_3 vibrational bands of SF₆ and OsO₄ is demonstrated as a means of investigation in high resolution spectroscopy through resonant degenerate four-wave mixing at 10.6 μm by using a stable low power CO₂ laser operating on the P(18), P(16), P(12) lines respectively. Peak reflectivities of 3.8 $\times 10^{-3}$ are measured in SF₆. They only reach 0.34 $\times 10^{-3}$ in OsO₄. Phase conjugate spectra with 2 MHz, namely sub-Doppler resolutions, are compared with simultaneous recordings of the saturated-absorption spectra over a 80 MHz bandwidth. The saturation splitting encountered on a one-photon transition in SF₆ is also analysed in terms of pressure broadening and pump imbalance. (35 refs.)
- 75746 Resonant intracavity phase conjugation in two and three-level systems.** G.P.Agrawal (Dept. of Phys., City Univ. of New York, New York, NY, USA). *J. Phys. Colloq. (France)*, vol.44, no.C-2, p.125-31 (March 1983). (International Workshop on Optical Phase Conjugation and Instabilities, Cargèse, Corsica, France, 20-24 Sept. 1982).
A general theory of intracavity phase conjugation, applicable to any resonance situation, is developed. It is applied to discuss the cases of two-level and A-type three-level systems. The phase-conjugate reflectivity exhibits bistability and hysteresis in both cases. (22 refs.)
- 75747 Coherent light amplification and optical phase conjugation with photorefractive materials.** P.Gunter (Lab. of Solid State Phys., Swiss Federal Inst. of Technol., Zurich, Switzerland). *J. Phys. Colloq. (France)*, vol.44, no.C-2, p.141-7 (March 1983). (International Workshop on Optical Phase Conjugation and Instabilities, Cargèse, Corsica, France, 20-24 Sept. 1982).
The electric field and fringe spacing dependence of the stationary energy transfer between two writing beams in volume phase-hologram formation with photoconductive electro-optic materials (KNbO₃:Fe²⁺, Bi₁₂(Si, Ge)O₂₀,...) has been studied. Experimental results are compared with the theoretical expressions describing the influence of the different photoinduced space-charge fields in photorefractive media. A peak exponential gain of $\Gamma = 15 \text{ cm}^{-1}$ has been reached in KNbO₃:Fe²⁺ for the proper choice of experimental parameters (such as recording wavelength, fringe spacing, applied electric field, etc.).

Results of the electric field dependence of the wavefront reflectivity p in degenerate four-wave mixing experiments are reported and discussed in terms of a similar theoretical treatment as the two-wave mixing experiments. It is shown, that peak reflectivities of $\rho = 25$ percent have been reached for KNbO₃:Fe²⁺, that conjugate complex wavefronts can be generated and that distorted optical wave fronts can be effectively corrected by four-wave mixing experiments in KNbO₃:Fe²⁺. (12 refs.)

75748 Degenerate four-wave mixing in semiconductors and ferroelectrics. M.B.Klein, R.K.Jain, G.C.Valley (Hughes Res. Labs., Malibu, CA, USA). *J. Phys. Colloq. (France)*, vol.44, no.C-2, p.149-58 (March 1983). (International Workshop on Optical Phase Conjugation and Instabilities, Cargèse, Corsica, France, 20-24 Sept. 1982).

Semiconductors and ferroelectrics are promising candidate materials for a variety of applications of degenerate four-wave mixing. The authors review nonlinear mechanisms in each material and compare the performance of both types of materials for degenerate four-wave mixing applications. (27 refs.)

75749 Misalignment sensitivity of optical resonators with phase-conjugate mirrors. Wang Shaomin (Dept. of Phys., Hangzhou Univ., Hangzhou, China).

Kexue Tongbao (Foreign Lang. Ed.) (China), vol.28, no.2, p.173-7 (Feb. 1983).

Although the phase-conjugate resonator (PCR) has a series of good characteristics, e.g. it is unconditionally stable, and it can compensate intracavity distortions; yet the misalignment phenomenon has already been observed experimentally. In the present paper, an augmented 4X4 ray transfer matrix formalism is used to describe the operation of the PCR, and a misalignment sensitivity is worked out theoretically. (6 refs.)

75750 Diffraction gyration and reversal of the laser beam wave front in electrooptic crystals. N.V.Kukhtarev.

Ukr. Fiz. Zh. (USSR), vol.28, no.4, p.612-14 (April 1983). In Russian.

Theoretically investigates a new effect—the diffraction gyration of light waves and describes the process of polarisation wavefront reversal during the recording of dynamic holograms in electrooptic crystals. (7 refs.) V.G.P.

International Workshop on Optical Phase Conjugation and Instabilities See Entry 74215

Wave amplification and parametric generation by dynamic holograms on surfaces See Entry 75604

42.65G Photon echoes, self-induced transparency, optical saturation and related effects

75751 Direct free-hole absorption induced in germanium by 1.06 μm picosecond pulses. R.B.James (Solid State Div., Oak Ridge Nat. Lab., Oak Ridge, TN, USA).

IEEE J. Quantum Electron. (USA), vol.QE-19, no.4, p.701-10 (April 1983).

The intervalence-band absorption coefficient in germanium is calculated as a function of the hole density and temperature for light with a wavelength of 1.06 μm . At this wavelength, the direct free-hole transitions in germanium occur between the heavy- and split-off hole bands, and between the light- and split-off hole bands. This absorption mechanism is normally negligible compared to the interband absorption; however, for a sufficiently dense electron-hole plasma, the free hole intervalence-band absorption can become comparable to the interband absorption. Furthermore, the interaction of the intense 1.06 μm light alters the distribution of resonantly coupled hole states, and leads to an intensity dependence in the intervalence-band absorption cross section. For a fixed hole density, the intervalence-band cross sections due to free-hole transitions between the heavy- and split-off hole bands and between the light- and split-off hole bands are found to decrease with increasing intensity in a manner closely approximated by an inhomogeneously broadened two-level model. Values for the saturation intensity of each resonant transition are calculated as a function of the hole density and temperature. The intensities required to begin to saturate the direct free-hole transitions are easily attainable using picosecond pulses. (42 refs.)

75752 Amplitude and phase nonlinear response of bleachable dyes using picosecond excitation. M.A.Vasil'eva (Lebedev Phys. Inst., Moscow, USSR), J.Vishchak, V.Gulbinas, V.I.Malyshov, A.V.Masalov, V.Kabelka, V.Syrus.

IEEE J. Quantum Electron. (USA), vol.QE-19, no.4, p.724-30 (April 1983).

Amplitude and phase responses of bleachable dyes are experimentally investigated using a picosecond pump and probe pulse technique combined with light polarization measurements. In the measurements, the amplitude response appears in the form of induced birefringence. The method of measurement is adapted for dyes with fast relaxation of the excited state; these dyes are used for mode locking in ultrashort pulse lasers. Experimental results of phase response contribution and mutual relaxation time of amplitude and phase responses are presented for some polymethine dyes. (18 refs.)

75753 Picosecond interband saturation and intraband relaxation in germanium. A.L.Smiri, B.S.Wherrett, T.F.Boggess (Dept. of Phys., North Texas State Univ., Denton, TX, USA).

J. Phys. Colloq. (France), vol.44, no.C-2, p.71-80 (March 1983). (International Workshop on Optical Phase Conjugation and Instabilities, Cargèse, Corsica, France, 20-24 Sept. 1982).

Picosecond techniques have been used to identify and investigate two sources for the saturation of interband transitions in germanium: the usual band-filling and a previously unobserved contribution from anisotropic state-filling. (15 refs.)

75754 Nonlinear real index of refraction variations of a gas medium due to a monochromatic radiation near resonance. J.I.Cotrim Vasconcellos (Inst. de Física 'Gleb Wataghin', Univ. Estadual de Campinas, Campinas, Brazil). *Rev. Bras. Fis. (Brazil)*, vol.12, p.15-27 (March 1982). In Portuguese. [received: April 1983]

The author has calculated the nonlinear real index of refraction variations of a gas medium due to a strong monochromatic radiation causing saturation effects. The gas is supposed to be composed of two-level molecules with which the external field is nearly resonant. He assumes homogeneous (hard collisions, spontaneous decay) and inhomogeneous (Doppler effect) broadening mechanisms acting on the real index of refraction of the medium. The nonlinear dispersion of the medium is studied as a function of the detuning frequencies, saturation conditions and for various ratios between the homogeneous and inhomogeneous linewidths. In particular, the modification of the index of refraction due to saturation effects are emphasized. (15 refs.)

Photon statistics of an m -photon laser with k -photon losses See Entry 75617

Passive mode locking of buried heterostructure lasers with nonuniform current injection See Entry 75696

Degenerate frequency mixing in saturable amplifiers See Entry 75737

Doppler-free conjugate emission in resonant gas media: lineshape, polarization properties and saturation See Entry 75744

- Applications of degenerate four-wave mixing to high resolution molecular spectroscopy at 10.6 μm See Entry 75745
- Resonant intracavity phase conjugation in two and three-level systems See Entry 75746
- Photon-echo studies of collisional relaxation in weakly ionized noble-gas mixtures See Entry 76219
- Measurement of the hyperfine structure of Pr^{3+} :YAG by quantum-beat free-induction decay, hole burning, and optically detected nuclear quadrupole resonance See Entry 77291

42.65J Beam trapping, self focusing, thermal blooming, and related effects

- 75755 Coherent phenomena involved in the time-resolved optical Kerr effect. J.-L. Oudar (CNET, Bagneux, France). *IEEE J. Quantum Electron. (USA)*, vol. QE-19, no. 4, p.713-18 (April 1983). The effect of parametric coupling between pump and probe beams in time-resolved optical Kerr effect is theoretically discussed for various experimental configurations. It is shown that with a circularly polarized pump beam, the polarization changes induced on a nearly collinear probe beam are due to this coherence effect only. In other configurations, this parametric coupling can appear as an additional contribution to the observed signal, especially when pump and probe are derived from the same laser beam. It is pointed out that this coupling can occur not only when the pump and probe beams are at the same wavelength, but also when the difference or the sum of their frequencies can excite a Raman or a two-photon resonance in the medium. (17 refs.)
- 75756 Optical power limiter with picosecond response time. M.J. Soileau, W.E. Williams, E.W. Van Stryland (Dept. of Phys., Center for Appl. Quantum Electronics, North Texas State Univ., Denton, TX, USA). *IEEE J. Quantum Electron. (USA)*, vol. QE-19, no. 4, p.731-5 (April 1983). Optical self-action in CS_2 and other liquids was used to make a power-limiting device having a picosecond response time. This device uses self-focusing in liquids to produce phase aberrations and laser-induced breakdown, which in turn limit the transmitted power. This device has near-unity transmission for input power below P_c , which is of the order of the critical power for self-focusing, and limits the transmitted power to a nearly constant value for input power greater than P_c . The onset of nonlinear transmission was adjusted by mixing various liquids to adjust the nonlinear refractive index. Experimental results using linearly and circularly polarized 40 ps (FWHM) pulses at 1.06 μm are presented. (26 refs.)
- 75757 Self-squeezing of light propagating through nonlinear optically isotropic media. R. Tanas, S. Kielich (Inst. of Phys., A. Mickiewicz Univ., Poznan, Poland). *Opt. Commun. (Netherlands)*, vol. 45, no. 5, p.351-6 (1 May 1983). In an isotropic medium in which light self-induces a cubic optical nonlinearity, the light is shown to be in squeezed states on traversal of the medium. The dependence of the squeezing effect on the polarization state of the field and the nonlinear molecular parameters is derived explicitly. A comparison is made to the photon antibunching effect in the same phenomenon. (14 refs.)
- 75758 Self-focusing of light in a laser plasma. V.L. Artsimovich, L.M. Gorbunov, V.S. Kas'yanov, V.V. Korobkin (P.N. Lebedev Phys. Inst., Acad. of Sci., Moscow, USSR). *Sov. Phys.-Dokl. (USA)*, vol. 27, no. 8, p.618-19 (Aug. 1982). Translation of: *Dokl. Akad. Nauk SSSR*, vol. 265, no. 4-6, p.857-9 (Aug. 1982). [received: May 1983] Observations of self-focusing in the investigation of the space-time structure of the scattered radiation at the fundamental frequency ω_0 at an angle of 90° to the incident beam and to the normal to the target are reported. The experiments were carried out with the radiation of a single-frequency neodymium laser focused onto the surfaces of flat aluminum, polyethylene, and polished-glass targets at normal and oblique (20°) incidence. The spatial and time resolutions in the investigation of the scattering characteristics amounted to 5 μm and 40 psec, respectively. (9 refs.)

42.70 OPTICAL MATERIALS

- 75759 Laser plate storage. R.F. Marks, R.A. Pollak (IBM Corp., Armonk, NY, USA). *IBM Tech. Disclosure Bull. (USA)*, vol. 25, no. 11A, p.5547-8 (April 1983). Some thin films, such as Nb_2O_5 , can be selectively grown or removed in a controlled chemical environment by applying laser illumination of suitable intensity. The authors show that an optical information storage system having an erase capability is a possible application of the phenomenon. (no refs.)
- 75760 Nonisothermal relaxation during photorecording in AsSe layers. A.A. Kikineshi, V.I. Mikla, D.G. Semak, M.M. Shpiyak. *Ukr. Fiz. Zh. (USSR)*, vol. 28, no. 5, p.786-8 (May 1983). In Russian. Presents the results of an experimental investigation into the electron-hole processes and structural changes during reverse photorecording. The localised states taking part in photoinduced changes are identified by measuring the thermally stimulated conduction currents. It is found that the diffraction effectiveness of elementary holograms, recorded at $T=80\text{K}$ by the light of a He-Ne laser, increases in the interval 210 to 230K. (7 refs.) V.G.P.
- Properties of holographic gratings in silicon crystals under ultrashort light pulse recording. I. Theory See Entry 75606
- Restoration of spectral transmission of magnesium fluoride windows in the VUV region See Entry 75783
- Infrared optical constants of PISI See Entry 77347
- Production methods and properties of diamond-like carbon films See Entry 75766
- Variation of optical inhomogeneity of ruby crystals See Entry 77771
- Ge-Al thin films for selective solar absorbers See Entry 78099

42.70C Glass

- Progress in glass components for neodymium lasers See Entry 75676
- Physicochemical and spectral luminescence properties of a glass based on the $\text{SiO}_2\text{-Al}_2\text{O}_3\text{-La}_2\text{O}_3\text{-Nd}_2\text{O}_3$ system See Entry 77438
- Variation of lighting engineering characteristics of selenium-cadmium glass during hardening See Entry 77613
- Multicomponent glasses of GeO_2 and Sb_2O_3 with Bi_2O_3 , TiO_2 , and/or PbO See Entry 77620

42.70G Light-sensitive materials

- 75761 Coagulation of Ag in AgBr microcrystals. M.V. Kurik, B.T. Piven'. *Ukr. Fiz. Zh. (USSR)*, vol. 28, no. 5, p.788-9 (May 1983). In Russian. Using electron microscopy of latent image centres in AgBr microcrystals, the authors found a new effect: that the coalescence of latent image centres under the action of laser radiation occurs on the surface of microcrystals in places with determined symmetry with the formation of symmetrically distributed regions of Ag coalescence. A possible explanation for this effect is given. (4 refs.) V.G.P.
- Modernization of drum-type electrographic copiers See Entry 74548
- Fingerprint identification by matched filtering using photorefractive crystals See Entry 75598
- Degenerate four wave mixing in photorefractive BSO crystals and applications See Entry 75733
- New study and application of phase conjugation with photorefractive crystals See Entry 75741
- Coherent light amplification and optical phase conjugation with photorefractive materials See Entry 75747

42.72 OPTICAL SOURCES AND STANDARDS

(for spectroscopic light sources, see also 07.65)

- Partially coherent sources in interferometric sensors See Entry 74527
- Bright light sources from shock deceleration of hypersonic plasma streams in dense gases See Entry 76169

42.78 OPTICAL LENS AND MIRROR SYSTEMS

(for microscopes, see 07.60P; for photographic instruments, see 07.68; for astronomical telescopes, see 95.55)

- 75762 Confocal optical feedback processing system: an improved optical design. S. Johnston, S.H. Lee (Dept. of Electrical Engng. & Computer Sci., Univ. of California, San Diego, La Jolla, CA, USA). *Appl. Opt. (USA)*, vol. 22, no. 10, p.1431-8 (15 May 1983). Coherent optical feedback in the form of a simple confocal resonator has been used to solve partial differential and integral equations. However, due to aberrations, the simple feedback system has a limited space-bandwidth product. An attempt is made here to increase the space-bandwidth product and the accuracy of the optical solution by introducing optical elements with spherical surfaces and negative lens effects into the simple confocal system. (5 refs.)
- 75763 Ray tracing in a planar lens with spherically symmetric quadratic index profile. T. Sakamoto (Industrial Lab., Hyogo Prefecture, Kobe, Japan). *Appl. Opt. (USA)*, vol. 22, no. 10, p.1598-600 (15 May 1983). Some formulas of importance in lens design and evaluation have been derived on a planar lens with spherically symmetric quadratic index profile. Also a nondestructive evaluation method of the focusing constant in the index profile has been developed by the method of least squares. (9 refs.)
- 75764 Examination of plastic focusing fiber lens. S. Otake, S. Kawawa, K. Takasugi. *Anritsu Tech. Bull. (Japan)*, no. 44, p.106-12 (March 1983). In Japanese. Estimating and manufacturing of plastic focusing fiber lenses which have a nearly parabolic refractive index distribution were examined, and then performances and problems were expressed. Performances of plastic focusing fiber lenses for optical communication can be estimated by measuring of a distortion of the image, a curve of the refractive index distribution, a diameter of the focal point, and a transmission loss. The best transmission loss of test samples is -3.2 dB , so improvements will be required for use in optical communication. The method of manufacturing plastic focusing fiber lenses needs further reexamination, because of the problems awaiting solution, such as impurities, reappearance and working efficiency. (3 refs.)
- 75765 Deficient spline and the method of vignetting determination. Loh Rong, Sha Cunxian (Dept. of Computer Sci. & Technol., Peking Univ., Peking, China). *Acta Sci. Nat. Univ. Pekin. (China)*, no. 5, p.14-25 (1982). In Chinese. Suggests a cubic deficient spline method. This method is constructed on local procedures, and can combat unnatural wiggles in the interpolant. A specific lens is taken as an example. The authors determine its pupil shape by this cubic deficient spline method. (8 refs.)
- 75766 Performance evaluation of an apodized optical system with polarization masks. S.D. Gupta (Instrument Res. & Dev. Establ., Dehra Dun, India). *Opt. Acta (GB)*, vol. 30, no. 5, p.607-21 (May 1983). It sometimes becomes necessary to modify the imaging characteristics of an optical system to achieve better performance for certain applications. The modification can be achieved by various means, and the usual practice has been to modify the amplitude and phase transmissions over different zones of the pupil of the optical system; such a modification is called apodization. The author reports a method of apodization in which three polarization masks are placed at different orientations over the pupil of the optical system, which is illuminated with an elliptically polarized light beam. The performance of this apodized optical system has been investigated in terms of diffraction patterns and optical transfer functions by making use of the Jones matrix approach. It has been shown that, by suitably choosing the state of polarization of the illuminating beam and the orientation of the polarization masks, the performance of the optical system can be effectively modified. Further, with an analyser in the image plane, the diffraction pattern as well as the optical transfer function can be continuously modified for required roles. (11 refs.)
- 75767 First results of two-coordinate computer treatment of an optical surface. E.A. Vitrichenko, V.V. Gorelik, O.A. Evseev, Sh.Sh. Irtuganov, V.A. Malykhin, V.V. Nekrasov, A.M. Prokhorov, A.V. Rebrov, A.V. Savel'ev, E.V. Trushin (Inst. for Space Res., Acad. of Sci., Moscow, USSR). *Sov. Phys.-Dokl. (USA)*, vol. 27, no. 7, p.579-80 (July 1982). Translation of: *Dokl. Akad. Nauk SSSR*, vol. 265, no. 1-3, p.328-30 (July 1982). [received: April 1983] The most typical errors of large optical surfaces, such as astronomical mirrors, are local errors. The elimination of such errors by means of classical technology involves certain difficulties. Automated technological systems have been developed for the solution of this problem which permit the improvement of an optical surface using computer control. The authors present the results of the first factory trials of the ZEBRA-2 system in the fabrication of real optical components. (5 refs.)

75768 Optical systems of laser scanners. L.A.Markova, V.P.Mikheev, B.S.Rozov, P.I.Savostin.

Sov. J. Opt. Technol. (USA), vol.49, no.9, p.548-50 (Sept. 1982). Translation of: *Opt.-Mekh. Prom.-st. (USSR)*, vol.49, no.9, p.13-15 (Sept. 1982). The capabilities of optical light-beam scanning systems are analysed from the viewpoint of achieving the maximum resolution in devices for processing graphical information. The three most widely used scanning systems and the basic relations for analysing each of them are examined. (8 refs.)

75769 Automated calculation of two-lens and three-lens components. N.I.Kutsenko, T.I.Lushchik, M.Yu.Maulik.

Sov. J. Opt. Technol. (USA), vol.49, no.9, p.559-61 (Sept. 1982). Translation of: *Opt.-Mekh. Prom.-st. (USSR)*, vol.49, no.9, p.23-4 (Sept. 1982). A program is described for the automated calculation of two-lens and three-lens cemented components, having the same outer glasses, for given basic parameters P, W, C with the structural features of the component and higher order aberrations taken into account. (7 refs.)

75770 Basic parameters of an infinitely thin component. S.N.Bezdid'ko.

Sov. J. Opt. Technol. (USA), vol.49, no.9, p.561-2 (Sept. 1982). Translation of: *Opt.-Mekh. Prom.-st. (USSR)*, vol.49, no.9, p.24-5 (Sept. 1982). The basic parameters of infinitely thin components for a symmetrical arrangement of object and image are determined. A number of the relations in the basic parameter theory acquire a simpler form in this case, and the modified parameter W takes on a direct physical meaning. (2 refs.)

75771 Algorithm for the automated calculation of the tolerances on the structural elements of optical systems. A.P.Grammatin, N.E.Kundeleva.

Sov. J. Opt. Technol. (USA), vol.49, no.9, p.563-6 (Sept. 1982). Translation of: *Opt.-Mekh. Prom.-st. (USSR)*, vol.49, no.9, p.25-8 (Sept. 1982). An algorithm is proposed that is based on a determination of the tolerances on the structural elements of optical systems in terms of a given deviation of the wave or geometrical aberration, taking into account their technological limits and the discreteness of the values used. An example is given, involving the calculation of the tolerances on a telescope objective by using the proposed method. (7 refs.)

75772 Full field-of-view zone of optical sights for target and hunting guns. N.I.Kutnyakova.

Sov. J. Opt. Technol. (USA), vol.49, no.9, p.583-5 (Sept. 1982). Translation of: *Opt.-Mekh. Prom.-st. (USSR)*, vol.49, no.9, p.43-6 (Sept. 1982). An important performance characteristic of optical sights for target and hunting guns—the full field-of-view zone, which supplements and expands the concept of exit pupil relief—is defined. A method for measuring this characteristic has been developed. (3 refs.)

75773 Optics calculation: some new results on bent mirrors and ray-tracing. F.Cerrina (Synchrotron Radiation Center, Stoughton, WI, USA). Fifteenth Annual Synchrotron Radiation Users Group Conference (papers in summary form only received), Stoughton, WI, USA, 18-19 Oct. 1982 (Stoughton, WI, USA: Synchrotron Radiat. Center 1982), p.10-11. A possible solution to the high cost of grind-and-polish optical elements for the soft X-rays in some applications may reside in the use of cylindrical 'bent mirrors', where the required profile is obtained by bending a flat with a suitable edge contour. The author presents the results of further studies on this subject, where he tries to elucidate the advantages and limitations of the method. (no refs.)

75774 Lenses for microlithography; state-of-the-art and future developments. C.Babolat (CERCO, Les Ulis, France). Microcircuit Engineering 82. International Conference on Microlithography, Grenoble, France, 5-8 Oct. 1982 (Grenoble, France: Comité du Colloque International sur la Microlithographie 1982), p.65-8. In French. States that direct stepping on wafers needs better reduction lenses. The author shows the characteristics of the lenses of recent years and of up-to-date products. Future performances of near and deep UV lenses are examined. (no refs.)

Formation of fine-structure image by corner reflectors, operating on the basis of the total internal reflection effect See Entry 75596

Mirrors that are electron transparent for use in free-electron-laser oscillators See Entry 75680

Some properties of phase-matched resonators See Entry 75694

Derivation of the coupling coefficients for the eigenfunctions of a spherical, optical resonator in the case of mismatching and misalignment of the incident wave See Entry 75695

Optical phase conjugation in laser resonators See Entry 75740

Misalignment sensitivity of optical resonators with phase-conjugate mirrors See Entry 75749

Fabrication of a grid on a non-flat substrate by e-beam lithography [telescope lens fabrication] See Entry 75841

Engineering design for a photovoltaic central station power plant using tracking concentrator photovoltaic arrays See Entry 78030

Radiation heat exchange in a solar cavity-type receiver at various times See Entry 78094

Mechanical model of the insect eye See Entry 78391

42.78H Coatings

75775 Application of a continuous monitoring technique for the deposition of multilayer dielectric films with reproducible characteristics over a wide spectral region. A.P.Ovcharenko, E.A.Lupashko, A.P.Sulka.

J. Appl. Spectrosc. (USA), vol.36, no.5, p.604-6 (May 1982). Translation of: *Zh. Prikl. Spektrosk. (USSR)*, vol.36, no.5, p.837-9 (May 1982). [received: Feb. 1983]

Proposes a variation of the continuous control technique, which enables the production of a multilayer dielectric coating with optical characteristics in the region of transparency close to those calculated and which guarantees reproducibility of the results. (13 refs.)

75776 Antistatic and abrasion-resistant coating on polymer optical components having a complicated surface profile. G.A.Aleksandrov, N.Z.Khaliulina, V.V.Polezhaev, N.P.Anokhina.

Sov. J. Opt. Technol. (USA), vol.49, no.9, p.578-9 (Sept. 1982). Translation of: *Opt.-Mekh. Prom.-st. (USSR)*, vol.49, no.9, p.38-9 (Sept. 1982). It is shown that silicon oxide coatings, obtained by thermal evaporation in vacuum on polymer optical components having a complicated surface profile, considerably improve their antistatic, abrasion-resistance and operational properties. (5 refs.)

42.80 OPTICAL DEVICES, TECHNIQUES AND APPLICATIONS

[for optical instruments and techniques, see 07.60; for optical spectroscopy, see 07.65; for photography, see 07.68; for holography, see 42.40; for lasers, see 42.55 and 42.60; for masers, see 42.52]

75777 Realization of 90°- and 180° hybrids for optical frequencies. W.R.Leeb (Inst. für Nachrichtentechnik, Tech. Univ. Wien, Wien, Austria). *Arch. Elektron. & Übertragungstechnik. (Germany)*, vol.37, no.5-6, p.203-6 (May-June 1983).

A method to realise optical hybrids for freely propagating laser beams is presented. It is based on the phase shift that can be introduced between orthogonally polarized beam components by the use of polarizers and quarter-wave plates. For mathematical treatment of a 90°- and a 180° hybrid the Jones matrix algebra is employed. Design and successful testing of a 90° hybrid for the 10 μ m wavelength of a CO₂ laser is reported. (2 refs.)

75778 Polarization-independent beam splitter. E.E.Bergmann (Lehigh Univ., Bethlehem, PA, USA).

Rev. Sci. Instrum. (USA), vol.54, no.5, p.579-81 (May 1983). The author reports a new type of beam splitter capable of producing a division of light in a polarization-independent manner. Most off-axis beam splitter have a pronounced polarization dependence. An experimental device with a splitting ratio of about 7 dB varied less than ± 0.1 dB as a function of incident linear polarization. The device is fabricated from a thin plate of suitably oriented, uncoated, crystalline quartz. (3 refs.)

75779 Evaluation of parameters of schlieren instruments having a photoelectric information converter. A.S.Avrachenko, T.M.Bezudnyaya, E.Yu.Durovich, E.I.Krasovskii.

Sov. J. Opt. Technol. (USA), vol.49, no.9, p.538-9 (Sept. 1982). Translation of: *Opt.-Mekh. Prom.-st. (USSR)*, vol.49, no.9, p.4-5 (Sept. 1982). This paper examines the basic relationships and construction principle of an ultrasonic simulator of density inhomogeneities for the evaluation of the sensitivity, dynamic range and frequency characteristics of schlieren instruments. (10 refs.)

Automated goniometer employing a ring laser See Entry 74510

1.73 μ m eyesafe laser rangefinder See Entry 75677

Confocal optical feedback processing system: an improved optical design See Entry 75762

Basic parameters of an infinitely thin component See Entry 75770

42.80B Spatial filters, zone plates

75780 Efficient approach to designing linear combination filters. B.V.K.Vijaya Kumar (Dept. of Electrical Engng., Carnegie-Mellon Univ., Pittsburgh, PA, USA).

Appl. Opt. (USA), vol.22, no.10, p.1445-8 (15 May 1983). Various linear combinations of simple matched spatial filters have been proposed in the literature to improve the discrimination in multiclass pattern recognition. It has been shown that all such approaches based on deterministic constraints can be modeled as similar matrix/vector problems, the only differences arising in the individual constraint vectors. Since the design of any of these linear combination filters (LCF) can be posed as a common matrix/vector problem, efficient iterative methods can be used to determine the LCFs. The application of one such method called the modified hyperplane (MHP) method for determining the LCF is described and its convergence behavior is numerically investigated for a set of seven patterns. It is shown that the MHP method yields correct LCFs (with rms error $< 0.1\%$) in less than ten iterations. (11 refs.)

A new method for noncoherent image processing by using an astigmatic system See Entry 75594

Fingerprint identification by matched filtering using photorefractive crystals See Entry 75598

42.80C Spectral and other filters

75781 Optimized amplitude filtering for superresolution over a restricted field. III. Effects due to variation of the field extent. R.Boivin, A.Boivin (Dept. de Phys., Univ. Laval, Quebec, Canada).

Opt. Acta (GB), vol.30, no.5, p.681-98 (May 1983). For pt.II see *ibid.*, vol.27, p.1641 (1980). In the application of Frieden's impulse-generating filter to superresolution, the characteristics of the point response as well as those of the filter are seen to depend on the extent of the restricted field. The authors present curves that show how the filter and its diffraction pattern change with field extent, and the behaviour of some pertinent figures of merit is examined under various conditions. For a given field extent it is found that (1) the resolution gain eventually increases linearly with the order M to which the point response approximates the delta function, (2) the filter transmission ratio exhibits a maximum for a certain value of M and eventually settles to the levels characteristic of the Zernike polynomials and (3) the Strehl central-irradiance ratio and the encircled-energy ratio for the restricted field drop without limit once M exceeds the superresolution threshold. The trade-off between resolution gain, central irradiance and field extent is also investigated. (13 refs.)

Broad spectral band color image deblurring See Entry 75587

Optical pseudocolor encoding using adaptive electronic halftoning See Entry 75595

Acousto-optical modulator of a laser beam See Entry 75786

Variation of lighting engineering characteristics of selenium-cadmium glass during hardening See Entry 77613

42.80D Monochromators

75782 Measurement of absorption line intensities with VUV monochromators. B.R.Lewis (Res. School of Phys. Sci., Australian Nat. Univ., Canberra, Australia).

Appl. Opt. (USA), vol.22, no.10, p.1546-50 (15 May 1983). Problems involved with the use of VUV scanning monochromators in the measurement of absorption line intensities are discussed. Instrumental modifications enabling the accurate determination of equivalent widths at maximum wavelength resolution are described. (14 refs.)

42.80E Shutters, windows, diaphragms, deflectors, choppers

75783 Restoration of spectral transmission of magnesium fluoride windows in the VUV region. N.E.Budina, V.M.Reiterov, L.P.Shishatskaya. *Sov. J. Opt. Technol. (USA)*, vol.49, no.9, p.587-9 (Sept. 1982). Translation of: *Opt.-Mekh. Prom.-st. (USSR)*, vol.49, no.9, p.48-50 (Sept. 1982). It is shown that the VUV-absorbing oxide film on the surface of windows, which has usually been removed only by means of mechanical polishing, can be dissolved completely by boiling in water; the window transmission is then restored by a subsequent heat treatment. (12 refs.)

Optimizing the efficiency of lasers with passive shutters See Entry 75679
Performance evaluation of an apodized optical system with polarization masks See Entry 75766

42.80F Gratings, echelles

A family of grating sensors See Entry 74441
X-ray spectrograph design See Entry 74568
Generalized reciprocity for gratings of finite conductivity See Entry 75576
Exact calculations of the diffraction of s-polarized electromagnetic radiation from large-amplitude dielectric gratings See Entry 75579
Exact calculations of p-polarized electromagnetic fields incident on grating surfaces: surface polariton resonances See Entry 75580
Broad spectral band color image deblurring See Entry 75587
Gray level pseudocolouring with three primary colours by a diffraction grating modulation method See Entry 75592
Aberrations of holographic toroidal grating systems See Entry 75601
Fabrication of PMMA holographic grating by KrF excimer laser See Entry 75602
E-beam fabrication of devices for optical communication systems See Entry 75840
Periodic structure formed during the action of high-power coherent radiation on a semiconductor surface See Entry 76495

42.80K Optical beam modulators

75784 Electrooptic interaction in oversized waveguide modulators. A.L.Scholtz (Inst. für Nachrichtentechnik, Tech. Univ. Wien, Wien, Austria). *Arch. Elektron. & Übertragungstechnik. (Germany)*, vol.37, no.5-6, p.207-10 (May-June 1983).
 The coupled-mode formalism is employed to analyze oversized waveguide electrooptic modulators. The author takes into account the orientation of the electrooptic tensor with respect to the waveguide coordinates as well as the different, nonuniform distribution of the interacting optical and electrical fields. Numerical results for the modulation efficiency of a CO₂ laser modulator agree well with published experimental data. (11 refs.)
75785 A single-block hexagonal electrooptical Q-switch. C.Shaohuo (Shanghai Inst. of Optics & Fine Mech., Acad. Sinica, Shanghai, China). *IEEE J. Quantum Electron. (USA)*, vol.QE-19, no.4, p.736-42 (April 1983).
 A single-block hexagonal LiNbO₃ electrooptical switch was developed. It has the advantages of easy operation, an integrated polarizer, a modulator, and an analyzer, low loss, and a high extinction ratio. It can be used as an intracavity electrooptical Q-switch for lasers, and as a switch for pulse selection in mode-locked lasers. (7 refs.)
75786 Acousto-optical modulator of a laser beam. M.Klima. *Sdelovaci Tech. (Czechoslovakia)*, vol.31, no.4, p.137-9 (April 1983). In Czech.
 The physical properties and technological preparation of calomel (Hg₂Cl₂) monocrystalline material are first outlined. The principle of applying this material to an acousto-optical modulator is described and experimental results obtained are discussed. Application possibilities envisaged are discussed which include laser recorders of TV signals and laser printers. Other acousto-optical elements considered include optical filters and signal processors. (15 refs.)
E.D.
Tone-burst modulated color-center-laser spectroscopy See Entry 74545
Image formation in electron-beam-charged (001)- and (110)-cut Bi₂SiO₅ and Bi₂GeO₂₀ slices See Entry 75597
Dark-field microbend-modulated fibreoptic sensor system (DFMMFSS) See Entry 75821
Harmonic feed-back approach to fiber gyro scale factor stabilization See Entry 75822

42.80L Optical waveguides

(for fibre optical waveguides, see 42.80M)

75787 Dispersion and luminescence measurements of optical waveguides. A.Faik, L.Allen, C.Eicher, A.Gagola, P.D.Townsend (School of Math. & Phys. Sci., Univ. of Sussex, Brighton, England), C.W.Pitt. *J. Appl. Phys. (USA)*, vol.54, no.5, p.2597-601 (May 1983).
 Measurements are reported for the dispersion curves in the visible wavelength range of a variety of optical waveguides. Waveguides were formed in LiNbO₃ and LiTaO₃ by the implantation of helium ions. The radiation damage reduces the refractive index in both materials by about 12% throughout the visible region. This is thought to result from amorphization of the lattice. Waveguides formed by impurity enhancement of the refractive index were measured in soda lime glass doped by ion exchange of Li, K, Rb, Cs, or Ag. In each case the percentage increase in index was wavelength dependent. In particular, the Ag ion exchange waveguides have features attributed to colloidal silver metal. The metal colloids give both dispersion anomalies and a red luminescence. The luminescence was used to measure the losses in the waveguide. (22 refs.)
75788 Nonuniqueness of the determination of the dielectric constant profile of a planar optical waveguide from the spectrum of waveguide mode refractive indices. V.N.Mogilevich. *J. Appl. Spectrosc. (USA)*, vol.36, no.5, p.595-8 (May 1982). Translation of: *Zh. Prikl. Spektrosk. (USSR)*, vol.36, no.5, p.827-31 (May 1982). [received: Feb. 1983]
 An important problem in studying planar optical waveguides is establishing the profiles of their dielectric constant $\epsilon(x)$. A direct experimental determination of the distribution $\epsilon(x)$ is difficult. In this connection, methods for reproducing profiles from easily accessible measurements of the spectrum of the

refractive indices of waveguides modes, confined by the waveguide at one or several wavelengths, are being developed. In so doing, preference is given to single-wave methods, which do not require the dispersion of the material of the waveguide layer to be accounted for. However, the uniqueness of the solution of the waveguide problem does not yet indicate that a single dielectric constant profile can be associated with a given spectrum of waveguide refractive indices. Based on an analysis of exact dispersion equations, the author shows that different distributions $\epsilon(x)$ can be associated with a single spectrum of waveguide refractive indices. (5 refs.)

75789 Calculation of the light transmission coefficient of a hollow combination lightguide. I.N.Kalinchuk. *Sov. J. Opt. Technol. (USA)*, vol.49, no.9, p.540-2 (Sept. 1982). Translation of: *Opt.-Mekh. Prom.-st. (USSR)*, vol.49, no.9, p.5-8 (Sept. 1982).
 Questions dealing with the passage of light flux through a hollow combination lightguide are examined. Analytical expressions are obtained for calculating the light transmission coefficients of combination and slotted lightguides. The results of an experimental study of the light transmission coefficients of lightguides are presented. (8 refs.)

75790 Fabrication of optical waveguides in LiNbO₃ and LiTaO₃ crystals by ion irradiation. L.M.Shteingart (Phys. Inst., Acad. of Sci., Belorussian SSR). *Sov. Phys.-Tech. Phys. (USA)*, vol.27, no.11, p.1414-15 (Nov. 1982). Translation of: *Zh. Tekh. Fiz. (USSR)*, vol.52, no.11, p.2297-300 (Nov. 1982). [received: May 1983]
 The author reports test results of optical waveguides in various LiNbO₃ and LiTaO₃ crystals fabricated by ion bombardment. When LiNbO₃ and LiTaO₃ are irradiated with ions, the refractive indices for the ordinary and extraordinary waves decrease, so that only S-type waveguides can be produced in these materials. (7 refs.)

75791 The manufacture of optical fibres. P.Allias. *Toute Electron. (France)*, no.484, p.18-21 (May 1983). In French.
 The process of fabrication of optical fibres for communications purposes, as carried out by the Lyons Optical Transmission Co. under licence from Corning and improved by work done at the Marcoussis laboratories, is described, the various stages being illustrated very effectively by photographs and diagrams. The process is in two stages, preparation of the 'preform' which can then be used for the second stage, which is drawing into a filament of 20 km length, and reeling. (no refs.) J.S.

75792 Characterization of insert molded single optical-fiber connectors using ceramic balls. H.Murata (Ibaraki Electrical Communication Lab., NTT, Ibaraki, Japan). *Trans. Inst. Electron. & Commun. Eng. Jpn. Sect. E (Japan)*, vol.E66, no.3, p.179-85 (March 1983).
 Molded demountable single fiber connectors have been constructed, which contain precision balls within the plug moldings to locate the fiber and to align a pair of plugs. Transmission loss characteristics are examined and fiber placement precision investigated. The samples tested have exhibited less than 0.2 dB losses with index matching and less than 2 μ m fiber displacements on an average for ordinary multimode fibers. For practical application, arbitrary diameter plugs using two sorts of balls and premolding plug ferrules are also investigated. The results exhibit high precision and low losses corresponding to the design condition. The molding procedure is simple and needs no complicated alignment mechanisms. These connectors are low in cost and possible to assemble in the field. (8 refs.)

75793 Eigenmode calculation of optical waveguides: finite elements versus other methods. P.E.Lagasse (Lab. for Electromagnetism & Acoustics, State Univ. Ghent, Ghent, Belgium).
 Colloquium on 'Recent Developments in High Frequency Electromagnetic Field Analysis by Finite Element Methods', London, England, 16 May 1983 (London, England: IEE 1983), p.1/1-3
 The author briefly reviews the use of the finite element method (FEM) for the eigenmode analysis of optical waveguides. A number of eigenmode calculation methods are enumerated and compared to the FEM. (13 refs.)
75794 Analysis of optical and microwave waveguide by finite elements. B.M.Azizur Rahman (Dept. of Electronics & Electrical Engng., Univ. Coll., London, England).
 Colloquium on 'Recent Developments in High Frequency Electromagnetic Field Analysis by Finite Element Methods', London, England, 16 May 1983 (London, England: IEE 1983), p.2/1-4
 The finite element method has emerged as one of the most successful numerical methods for the analysis of high frequency microwave and optical waveguide problems. With the development of communication technology, the concept of waveguide has broadened. In most cases closed form analytic solutions for the practical waveguiding structures are not available. The optical waveguides are inherently inhomogeneous, and in many cases the dielectric material may be anisotropic. For the analysis of these types of problems vector H field finite-element method may be extremely powerful. (3 refs.)

Stimulated Raman oscillation in capillary waveguide resonators See Entry 75725
Coherent anti-Stokes Raman scattering in thin-film dielectric waveguides See Entry 75726
Electrooptic interaction in oversized waveguide modulators See Entry 75784
E-beam fabrication of devices for optical communication systems See Entry 75840
Multicomponent glasses of GeO₂ and Sb₂O₃ with Bi₂O₃, Ti₂O, and/or PbO See Entry 77620

42.80M Fibre optics

75795 Analysis of thermally induced loss in fiber-optic ribbons. G.S.Brockway (Plastics Engng. Consultants Inc., Lawrenceville, GA, USA), M.R.Santana. *Bell Syst. Tech. J. (USA)*, vol.62, no.4, pt.1, p.993-1018 (April 1983).
 Added loss during temperature cycling in a given ribboned fiber is shown to be caused by thermally induced axial compressive strain imparted to the fiber. A microbending-sensitivity parameter δ is introduced which reduces all loss-strain curves corresponding to different fibers to one characteristic master curve. Thermoviscoelasticity theory is used to calculate the time- and temperature-dependent compressive strain imparted to a ribboned fiber during a standard environmental cycle. Combining these analytical results with environmental data, the functional relationship between fiber-compressive strain and the added loss for a fiber of any given δ in an adhesive sandwich ribbon (ASR) with urethane-acrylate (UA) coated fibers has been determined. Using this analysis, the added loss for a UA ASR can now be predicted for any environmental cycle. The critical material properties that dominate the environmental performance of ASRs are the tape shrinkback at elevated temperatures and the product αEA of the coefficient α of thermal expansion, the

time- and temperature-dependent relaxation modulus E , and the area A of the coating. (9 refs.)

75796 Development of fabrication technology and measurement systems for multimode, single-mode and polarization maintaining optical fibers. J.A.Kurki (Semiconductor Lab., Tech. Res. Centre of Finland, Espoo, Finland). *Commentat. Phys.-Math. (Finland)*, no.56, p.1-110 (1983). Describes an optical fiber fabrication system consisting of a MCDV-system and a fiber drawing tower. Attenuation and bandwidth were studied in multimode and single-mode fibers in relation to material compositions and process parameters. Backscattering measurements for conical fibers are reported. A new technique for fabricating polarization maintaining fibers and preliminary measurement results are presented. (79 refs.)

75797 Computerized single mode temperature sensor. M.Essemli, J.Fontaine (Univ. Louis Pasteur, Strasbourg, France), P.Meyrueis. *Proc. SPIE Int. Soc. Opt. Eng. (USA)*, vol.355, p.2-5 (1982). [received: May 1983] (Fiber Optics: Short-Haul and Long-Haul Measurements and Applications, San Diego, CA, USA, 24-25 Aug. 1982). A computerized single mode fiber interferometer has been designed and built. The authors describe the design of this system and discuss the results. Polarisation problems are optimised, and a very high temperature sensitivity is obtained. (9 refs.)

75798 Optical fiber interferometer sensitized to the environmental perturbation acting on the fiber probe. M.Martinelli (CISE SpA, Milano, Italy). *Proc. SPIE Int. Soc. Opt. Eng. (USA)*, vol.355, p.6-10 (1982). [received: May 1983] (Fiber Optics: Short-Haul and Long-Haul Measurements and Applications, San Diego, CA, USA, 24-25 Aug. 1982). The passage of the reference and sensing beam through the same path in a single-mode optical fiber constitutes the basis of the new interferometer. Two main applications are suggested: Michelson-type interferometer for vibrating target measurements (FOMI) and fiber-optic link noise-free for fiber-optic sensor applications (FOIL). The experimental results point out the high noise-rejection operated by the new scheme compared with a conventional fiber-optic interferometer. (14 refs.)

75799 Modal noise in multimode optical fibers. E.G.Rawson (Xerox Palo Alto Res. Centers, Palo Alto, CA, USA), J.W.Goodman. *Proc. SPIE Int. Soc. Opt. Eng. (USA)*, vol.355, p.37-42 (1982). [received: May 1983] (Fiber Optics: Short-Haul and Long-Haul Measurements and Applications, San Diego, CA, USA, 24-25 Aug. 1982). A changing speckle pattern exists at the output of a multimode optical fiber if the optical source is sufficiently coherent. When spatial filtration (for example, at a misaligned connector) or polarization filtration (for example, in certain access couplers) occurs in the presence of such speckle, the optical signal power fluctuates; such fluctuations are called 'modal noise'. The authors review modal noise theory and experiment, including the prediction and measurement of the modal noise signal-to-noise ratio in the presence of spatial filtration and constrained total guided power. It also presents new results relating to modal noise effects in fiber branching devices such as star couplers, access couplers, and power dividers. (13 refs.)

75800 Optical fiber joint-loss measurement. Review of the causes of measurement inaccuracies and some proposals for meaningful measurements. F.M.E.Sladen (Thomas & Betts Corp., Raritan, NJ, USA). *Proc. SPIE Int. Soc. Opt. Eng. (USA)*, vol.355, p.57-60 (1982). [received: May 1983] (Fiber Optics: Short-Haul and Long-Haul Measurements and Applications, San Diego, CA, USA, 24-25 Aug. 1982). Splices and demountable connectors are a necessary component in optical-fiber systems as they allow for flexibility in both the installation and maintenance of optical-fiber links. Permanent joints (i.e., splices) tend to have less effect on system performance than remountable connectors; however, they are both capable of profoundly influencing system performance. Joints generally affect both the attenuation and bandwidth of an optical fiber link and thus require careful study. The four factors affecting joint loss are mechanical misalignments, fiber parameter mismatch, the physical properties of the medium separating the fiber ends and the excitation conditions existing in the fiber immediately prior to the joint. Some of the difficulties in measuring optical fiber joint loss are outlined and some examples of experimental test sets presented. The optical time domain reflectometry technique for loss estimation has many advantages for measurements in the field, although there still seems to be some doubts about obtaining quantitative results. (7 refs.)

75801 Two dimensional near-field contouring of optical fiber cores. E.M.Kim, D.L.Franzen (Electromagnetic Technol. Div., NBS, Boulder, CO, USA). *Proc. SPIE Int. Soc. Opt. Eng. (USA)*, vol.355, p.76-83 (1982). [received: May 1983] (Fiber Optics: Short-Haul and Long-Haul Measurements and Applications, San Diego, CA, USA, 24-25 Aug. 1982). A microcomputer controlled system is described for measuring the two dimensional nearfield radiation pattern from optical fibers. Because radiation measurements may be made in two dimensions, a novel method has been devised whereby a constant intensity contour of the core is mapped. A modified left-most-looking (LML) digital image encoding algorithm is used to map the contour of the fiber core. The iso-intensity map provides information about the tolerance field, in which all of the measured iso-intensity points lie, and core connector joints, and terminal points. The authors discuss the measurement apparatus, accuracy, precision, stability, and method of analysis of the NBS system. In addition, results are presented on measurements of core diameters, the length dependence of such measurements, wavelength dependence of the radiation patterns, power law fits to the patterns, calibration apparatus, and iso-intensity contours of telecommunications-grade fibers. (18 refs.)

75802 Fibre optics QC challenge. *Qual. Today (GB)*, p.9 (May 1983). The accurate measurement of optical fibres is essential both for quality control and to aid accurate splicing. The Fibercheck system from Vickers Instruments which has been designed to make fast, inexpensive and extremely precise measurement of optical fibres, is described. (no refs.)

75803 Novel polarisation phenomena on anisotropic multimoded fibers. A.W.Snyder, F.Ruhl (Inst. of Advanced Studies, Australian Nat. Univ., Canberra, Australia). *Electron. Lett. (GB)*, vol.19, no.11, p.401-2 (26 May 1983). The lowest-order modes of multimoded fibers composed of birefringent material can differ radically from the familiar modes of multimoded isotropic fibers. In general, the modal fields are neither uniformly polarised nor circularly symmetric as they would be on circularly symmetric isotropic fibers that are weakly guiding. Thus multimoded anisotropic fibers can exhibit dramatic polarisation effects which may have important practical applications. These effects are investigated by the authors. (5 refs.)

75804 Multiquartic approximation in single-mode optical fibres. G.Coppa, P.Di Vita (Centro StudiLab., Telecomunicazioni SpA, Torino, Italy). *Electron. Lett. (GB)*, vol.19, no.11, p.430-2 (26 May 1983). A new stratification method based on the approximation of the actual index profile of the fibre by means of a set of quartic curves is proposed. The method permits one to deduce accurately the propagation characteristics in the least calculation time, particularly on fibres with nonmonotonic index profiles. (6 refs.)

75805 Hybrid modes in circular cylindrical optical fibers. K.Morishita (Dept. of Precision Engng., Osaka Electro-Communication Univ., Osaka, Japan). *IEEE Trans. Microwave Theory & Tech. (USA)*, vol.MTT-31, no.4, p.344-50 (April 1983). The classification of hybrid modes in circular optical fibers is studied. It is shown that problems of the mode classifications, i.e. the crossover of the dispersion characteristics and the remarkable changes of the polarization states and the field configurations, are caused by the coupling of the HE-type modes. (16 refs.)

75806 Comments on 'The dynamical behavior of a single-mode optical fiber strain gage' [and reply]. P.A.A.Laura, J.L.Pombo (Inst. of Appl. Mech., Puerto Belgrano Naval Base, Argentina). *IEEE Trans. Microwave Theory & Tech. (USA)*, vol.MTT-31, no.4, p.364-6 (April 1983).

The frequency spectrum of the phase change signal and the resistive strain gage signal are in very good agreement. The authors discuss two points which need further clarification: (a) the validity of the mechanical analysis with special reference to the single-mode approximation; and (b) the effect of an axial force which may be present if the mechanical boundary conditions restrain the axial displacements of the structural element. (6 refs.)

75807 Silicon optical fiber splice. M.J.Brady, L.D.Comerford (IBM Corp., Armonk, NY, USA).

IBM Tech. Disclosure Bull. (USA), vol.25, no.11A, p.5518-19 (April 1983). Describes a splice connector for optical fibres which is formed by joining Si slabs having aligned anisotropically etched apparatus forming a sleeve which self-aligns the fibres as they are fully inserted. (no refs.)

75808 Safe optical connector. J.D.Crow (IBM Corp., Armonk, NY, USA).

IBM Tech. Disclosure Bull. (USA), vol.25, no.11A, p.5520-2 (April 1983). Fiber-optic connectors are described which are safe to view when disconnected even when powered by a semiconductor laser. (no refs.)

75809 Cast connector for fiber-optic modules. M.J.Brady, C.B.Burstell, L.D.Comerford (IBM Corp., Armonk, NY, USA).

IBM Tech. Disclosure Bull. (USA), vol.25, no.11A, p.5525-7 (April 1983). A miniature optical fiber connector is described for providing fiber-optic connection through a sidewall of an integrated circuit module. (no refs.)

75810 A sensitive technique for fibre profile characterization. B.Grossman (Centro de Pesquisa da Telebras-CPqD, São Paulo, Brazil). *Opt. Acta (GB)*, vol.30, no.5, p.623-7 (May 1983).

A technique has been developed that permits the detection of fluctuations as small as 1 part in 10^5 in the refractive index of graded index fibres. It consists of measuring the derivative of the profile rather than the profile itself. The procedure enables small defects on the profile to be emphasized in a smooth background. (4 refs.)

75811 The influence of mode-coupling on the degree of coherence in an optical fiber. M.Imai, Y.Ohtsuka (Dept. of Engng. Sci., Hokkaido Univ., Sapporo, Japan).

Opt. Commun. (Netherlands), vol.45, no.5, p.331-5 (1 May 1983). The modulus of the complex degree of coherence across the exit face of a coherently excited optical fiber is investigated by taking account of coupling effects between propagating modes. The authors also discuss the results of numerical calculations for a quasi-single mode fiber. The modulus exhibits an oscillatory behaviour along the fiber length if coupling or beating is present. The oscillatory modulus is found to be large compared with the value it would assume if the cross-terms were neglected. (10 refs.)

75812 Magnetostrictive fiber-optic sensor system for detecting DC magnetic fields. J.P.Willson, R.E.Jones (Standard Telecommunication Labs. Ltd., Harlow, England).

Opt. Lett. (USA), vol.8, no.6, p.333-5 (June 1983). A magnetostrictive fiber-optic sensor system employing a thin film of amorphous $\text{Fe}_{80}\text{B}_{20}$ alloy coated directly onto the fiber cladding is reported. A novel detection system to facilitate measurement of DC magnetic fields is described, and results presented show the advantages of amorphous alloys compared with nickel for sensing purposes. (8 refs.)

75813 Measurement of fiber birefringence by wavelength scanning: effect of dispersion. S.C.Rashleigh (Naval Res. Lab., Washington, DC, USA). *Opt. Lett. (USA)*, vol.8, no.6, p.336-8 (June 1983).

Scanning the wavelength in high-birefringence fibers inherently measures the group delay difference, and not the phase delay difference between the two polarization modes. Dispersion of the birefringence will result in a 10-20% error in fiber beat lengths interpolated from such measurements, even if only stress birefringence is present. Geometrical dispersion can introduce even larger errors in some fibers. (9 refs.)

75814 Modal-noise evaluation in multimode-fiber transmission. T.Kanada, K.Aoyama (Yokosuka Electrical Communication Lab., Nippon Telegraph & Telephone Public Corp., Kanagawa, Japan).

Opt. Lett. (USA), vol.8, no.6, p.339-41 (June 1983). Modal noise that occurs at fiber connecting points has been investigated theoretically and experimentally. Visibility, an important factor that determines the modal-noise power has been obtained as a function of laser-diode (LD) coherency and fiber bandwidth. Modal-noise formulas, with such parameters as visibility, fiber-connection loss, and the number of modes that the fiber supports, are presented. Modal noise that is due to LD mode-partition noise is also discussed. The analytical results agree well with the experimental ones. (8 refs.)

75815 Amplification and reshaping of optical solitons in glass fiber. III. Amplifiers with random gain. Y.Kodama (Dept. of Maths., Ohio State Univ., Columbus, OH, USA), A.Hasegawa.

Opt. Lett. (USA), vol.8, no.6, p.332-4 (June 1983). For pt.II, see *ibid.*, vol.7, p.339 (1982). The optical solitons in a glass fiber with dissipation can be reshaped by periodic amplifications and thereby can be stably transmitted for a sufficiently large distance. The authors show that the solitons retain this basic property even when the amplifiers have gains with random variation. (2 refs.)

75816 Mathematical modelling of the geometrical shape of polyhedral fibre-optic elements. N.I. Isaev, I.A. Shirkova.

Sov. J. Opt. Technol. (USA), vol.49, no.9, p.543-4 (Sept. 1982). Translation of: *Opt.-Mekh. Prom.-st. (USSR)*, vol.49, no.9, p.8-10 (Sept. 1982). The question of mathematical modelling of the cross section of polyhedral elements is examined. The results of a harmonic analysis of the given and actual contours are given. (2 refs.)

75817 The propagation of light in optical fibers. M.D. Feit (Lawrence Livermore Nat. Lab., Univ. of California, Livermore, CA, USA). In book: *International advances in nondestructive testing, Vol.9*, W.J. McGonagle [Ed.], p.1-16. New York, USA: Gordon & Breach (1983), 363 pp. [0 677 16440 8]

A very complete theoretical model of light propagation in optical fibers has been developed which treats the total transmitted beam rather than individual modes of the system. The model enables the study of important aspects of light propagation in realistic fibers: spatial and angular confinement of the transmitted light, power losses due to absorbing jackets and splices, and bandwidth restrictions that result because the individual modes propagate energy with differing group velocities. In addition, a complete modal description of the light, i.e. find all the mode shapes and their corresponding wavenumbers, can be retrieved. The model enables the treatment of fibers with arbitrary refractive index profiles, with finite core and cladding regions, and with lossy components. It also serves as a check on more approximate theoretical methods. Excellent agreement with experimental results gives one confidence in the applicability of the model to real situations. (6 refs.)

75818 Intelligent turbidity monitoring using fibre optics. P. Exanté, G.D. Pitt, B.J. Scott, M.V. Verrells (Stand. Telecommunication Labs. Ltd., Harlow, England).

First International Conference on Optical Fibre Sensors, London, England, 26-28 April 1983 (London, England: IEE 1983), p.109-13

The development of oil in water measuring equipment has been used to illustrate the pros and cons of fibre optic sensors. Following a wholly fibre optic solution, a more robust system was chosen where fibre optics were retained to transmit radiation to and from the measurement cell because of stringent hazardous space requirements. Where these were not necessary, and the cost of the instrument was a prime factor, the fibre optics were discarded. However, the development has come full circle in that several purely technical advantages of optical fibres have been identified such that entirely new on-line measurement techniques now seem to be feasible. These may succeed since new areas are being opened up which will provide new information and where there is no cost-sensitive or already entrenched technology available that will act as competition. The development of intelligent turbidity metering which provides a new approach to three-phase flow and concentration measurement has been discussed. (3 refs.)

75819 Stabilization of single and multimode fiber optical microbend sensors. G.F. Lipscomb, S.K. Yao, C.K. Asawa (TRW Technol. Res. Center, Redondo Beach, CA, USA).

First International Conference on Optical Fibre Sensors, London, England, 26-28 April 1983 (London, England: IEE 1983), p.117-21

Stability and reproducibility problems in single and multimode fiber optic microbend strain sensors are found to be due to interference between the core mode and cladding modes in the bend region. The authors have observed strong oscillatory behavior in the core mode of a bent single mode fiber. The origin of such oscillations is due to coupling between the guided core-mode and the guided cladding-modes as verified experimentally. Application of this information to multimode fiber microbending devices has resulted in significant improvement in microbending loss sensitivity and response stability, which is very important for microbend fiber optical sensors, modulators/switches and power tap applications. Furthermore, the strong oscillation in a bent single-mode fiber may be utilized as an extremely high sensitivity microbend sensor or acoustic hydrophone. (6 refs.)

75820 Fibre optic colour sensors based on Fabry-Perot interferometry. E.R. Cox, B.E. Jones (Dept. of Instrumentation & Analytical Sci., Univ. of Manchester Inst. of Sci. & Technol., Manchester, England).

First International Conference on Optical Fibre Sensors, London, England, 26-28 April 1983 (London, England: IEE 1983), p.122-6

Describes the construction of simple and rugged wavelength sensors based on the Fabry-Perot white light interferometer. A changing physical parameter such as temperature or pressure can be translated into the mirror displacements. Two completely different approaches to sensor construction are considered, the air-spaced and solid spacer sensors, which allow for a variety of applications. An important aspect of the work has been to investigate techniques for assembly which require minimal alignment of components, hence reducing production costs. (3 refs.)

75821 Dark-field microbend-modulated fibreoptic sensor system (DFMMFSS). C.M. Davis (Optical Technol. Inc., McLean, VA, USA), T.A. Litovitz, Macedo, P.B.

First International Conference on Optical Fibre Sensors, London, England, 26-28 April 1983 (London, England: IEE 1983), p.127-31

Shows that dark-field microbend-modulated (DFMM) fiber optic sensors exhibiting a large linear range can be operated in array configurations employing one source, a source optical fiber bus, one or more detection fibers and photodetectors. When operated in a time division multiplexed mode only a single detection fiber and photodetector are required. Arrays such as these may be used to obtain data from a number of sensors deployed over a large area. (5 refs.)

75822 Harmonic feed-back approach to fiber gyro scale factor stabilization. B.Y. Kim, H.C. Lefevre, R.A. Bergh, H.J. Shaw (Edward L. Ginzton Lab., Stanford Univ., Stanford, CA, USA).

First International Conference on Optical Fibre Sensors, London, England, 26-28 April 1983 (London, England: IEE 1983), p.136-7

A second harmonic phase modulation technique is studied which can be used for the closed-loop operation of dynamically biased fiber gyroscopes. This has a dynamic range that is limited only by that of the phase modulator. Also, the dependence of scale factor on the source wavelength is greatly suppressed. (5 refs.)

75823 Analysis of noise and bias in the fibre optic gyroscope. E. Jones (Stand. Telecommunication Labs. Ltd., Harlow, England).

First International Conference on Optical Fibre Sensors, London, England, 26-28 April 1983 (London, England: IEE 1983), p.138-42

The noise due to fibre end reflections has been computed, and a rigorous derivation has been given of backscatter noise. The noise equivalent rotation rates (NERRs) due to these sources have been compared with that due to source noise. The minimum architecture has been shown to be immune to fourth port reflections and finite isolation in the beam splitter or directional coupler, therefore the design of this component is not critical. The bias due to fibre birefringence has been shown to decrease indefinitely when polarizers are cascaded, in contrast with the extinction ratio of the cascade. The com-

puter model has confirmed this analytical result in the presence of an extended range of fibre optic gyroscope (FOG) effects. (9 refs.)

75824 An integrated optic fibre gyroscope: performance and limitations. M.C. Bone, J.W. Parker (Stand. Telecommunication Labs. Ltd., Harlow, England).

First International Conference on Optical Fibre Sensors, London, England, 26-28 April 1983 (London, England: IEE 1983), p.143-6

Considers the design of the components for an integrated optics (IO) gyro, and the limitations imposed by their performance. The authors examine in detail those features which differ from a bulk or all-fibre gyro and are unique to an IO implementation, and conclude by describing the design of a practical gyro chip. (10 refs.)

75825 Test results of an integrated fiber-optics gyroscope brass board. H.J. Arditty (Lab. Central de Recherches, Thomson-CSF, Orsay, France), J.P. Bettini, Ph. Graindorge, H.C. Lefevre, M. Papuchon, Y. Bourbin, S. Vatoux, D. Berard, J.Y. Colombin.

First International Conference on Optical Fibre Sensors, London, England, 26-28 April 1983 (London, England: IEE 1983), p.147-50

Describes the design of a brass-board single axis fiber gyroscope using an optical integrated multifunction circuit and reports its test results. (29 refs.)

75826 Heterodyne optical fibre gyroscope. I.P. Giles, B. Culshaw, D.E.N. Davies (Dept. of Electronic & Electrical Engng., Univ. Coll. London, London, England).

First International Conference on Optical Fibre Sensors, London, England, 26-28 April 1983 (London, England: IEE 1983), p.151-4

The optical fibre gyroscope is potentially a useful navigation instrument, but it is probably the case that an ideal system architecture remains to be defined. The authors assess the potential of a heterodyne gyroscope in terms of both sensitivity and stability. (9 refs.)

75827 Dispersion-induced non-reciprocal effects in phase-nulling fibre gyroscopes. A.J. Barlow, M.S. Dye, B.T. Trayner (British Aerospace plc, Bristol, England).

First International Conference on Optical Fibre Sensors, London, England, 26-28 April 1983 (London, England: IEE 1983), p.155-8

Evaluates the magnitude of the dispersive effects and the variation with temperature, wavelength and axial fibre tension. The results are then applied to the phase-nulling gyro to show the effect of dispersion on the output-versus-rate curve. It is found that the non-linearity and scale factor changes introduced by dispersion are too small to significantly effect gyro performance over a wide operating range. However, a large zero bias which varies with temperature arises from gyro operation at high fringe orders. By inserting a second modulator driven at the centre frequency, zero-order fringe operation is possible thereby substantially reducing the zero bias drift introduced by dispersion. (10 refs.)

75828 Multimode fiber optic sensors. W.B. Spillman, Jr., D.H. McMahon (Sperry Res. Center, Sudbury, MA, USA).

First International Conference on Optical Fibre Sensors, London, England, 26-28 April 1983 (London, England: IEE 1983), p.160-3

Multimode fiber optic sensor research carried out at the Sperry Research Center is discussed. Emphasis is placed upon a description of a generic technique based upon the photoelastic effect, for the creation of a whole class of multimode fiber optic sensors. A presentation of recent results is also given. (8 refs.)

75829 A fibre optic electric field sensor using the electrooptic effect of $\text{Bi}_2\text{Ge}_2\text{O}_{12}$. K. Shibata (Fuji Electric Corporate Res. & Dev. Ltd., Tokyo, Japan).

First International Conference on Optical Fibre Sensors, London, England, 26-28 April 1983 (London, England: IEE 1983), p.164-8

Describes the electric field sensor using $\text{Bi}_2\text{Ge}_2\text{O}_{12}$, outlining its characteristics and giving an example of measuring a real electric field using this sensor. (7 refs.)

75830 Photoelastic pressure sensor with optical fibre links using wavelength characterization. B.E. Jones, R.C. Spooner (Dept. of Instrumentation & Analytical Sci., Univ. of Manchester Inst. of Sci. & Technol., Manchester, England).

First International Conference on Optical Fibre Sensors, London, England, 26-28 April 1983 (London, England: IEE 1983), p.173-7

A bulk-sensitive pressure sensor based on the photoelastic effect with multimode optical fibre transmission links is described. Inaccuracies caused by adventitious changes in light intensity or system attenuation may be overcome by employing wavelength characterization so that the pressure is related to the wavelengths at which intensity peaks occur in a spectral scan of the transmitted light. Proposals are made for an improved sensor using programmable instrumentation. (15 refs.)

Fiber Optics: Short-Haul and Long-Haul Measurements and Applications See Entry 74208

A family of grating sensors See Entry 74441

Polarimetric sensors: exploiting the axial stress in high birefringence fibers See Entry 74517

Heterodyne OTDR at 0.82 μm See Entry 74518

Application of photon counting techniques to POTDR See Entry 74519

Partially coherent sources in interferometric sensors See Entry 74527

Performance characteristics of a passively stabilized fiber interferometer using a (3x3) fiber directional coupler See Entry 74529

Fiber-optic interferometric signal processor employing a differentiate and cross-multiply frequency discriminator See Entry 74530

Application of optical fiber waveguides in radiation dosimetry See Entry 75209

Coherent optical fiber communication potential and problems See Entry 75591

Amplification by stimulated Raman scattering in low-loss optical fibers See Entry 75718

Nonlinear optics in fibers and near-infrared frequency conversion See Entry 75720

Examination of plastic focusing fiber lens See Entry 75764

Fluctuation phenomena setting principal and practical limits to the performance of optical communication systems See Entry 75833

Uniform evaluation of multichannel, hermaphroditic fiber optic connectors for tactical applications See Entry 75835

A second generation of optical fiber component from HP See Entry 75836

Optical probing of acoustic waves on rough surfaces See Entry 75883

Pressure and pressure gradient fiber-optic lever hydrophones See Entry 75892

Laser diode frequency modulation for directional laser doppler velocimetry See Entry 76140

- Differential Doppler velocimetry using polarization-preserving optical fiber See Entry 76141
- Fiber-optic absorption/fluorescence probes for combustion measurements See Entry 77927
- Limitations of a single optical fibre fluorimeter system due to background fluorescence See Entry 77947
- A fiber optics fluorimeter for algae detection and mapping See Entry 78408

42.80Q Image detectors, convertors, and intensifiers

- 75831 Study of the gain coefficient of the electron flow in a microchannel plate.** E.P.Semenov.
Sov. J. Opt. Technol. (USA), vol.49, no.9, p.554-6 (Sept. 1982). Translation of: *Opt.-Mekh. Prom.-st. (USSR)*, vol.49, no.9, p.18-20 (Sept. 1982).
It is shown that by specifying the gain coefficient of the electron flow of a microchannel plate and the electrostatic field intensity in the channel, one can select the optimum values of the secondary electron emission coefficient of the emitter and the secondary electron emission coefficient for the first collision which make it possible to reduce the noise factor of the device. (15 refs.)
- 75832 Equipment and method for objective evaluation of characteristics of electron-optical converters.** Yu.Z.Matskovskaya, Yu.G.Edel'shtein, N.A.Savenchuk, V.E.Kolesnikov.
Sov. J. Opt. Technol. (USA), vol.49, no.9, p.572-4 (Sept. 1982). Translation of: *Opt.-Mekh. Prom.-st. (USSR)*, vol.49, no.9, p.33-5 (Sept. 1982).
Equipment for measuring the signal/noise ratio of electron-optical converters and a method of grading converters by means of a generalized characteristic, obtained on the basis of a determination of the signal/noise ratio and the modulation transfer function are described. (6 refs.)
- Infrared optical constants of PISI See Entry 77347

42.80S Optical communications devices

- 75833 Fluctuation phenomena setting principal and practical limits to the performance of optical communication systems.** G.Grau (Inst. fur Hochfrequenztech. und Quantenelektronik, Univ. Karlsruhe, Karlsruhe, Germany).
Arch. Elektron. & Uebertragungstechnik. (Germany), vol.37, no.5-6, p.137-45 (May-June 1983).
Optical communication systems show fluctuation phenomena which are not familiar to the classical communications engineer. These phenomena may set limits to the performance of optical systems. The most important noise sources are discussed. (16 refs.)
- 75834 Optoelectronic broadband switches.** R.I.MacDonald, R.H.Hum, E.H.Hara (Dept. of Communications, Communications Res. Centre, Ottawa, Ontario, Canada).
Proc. SPIE Int. Soc. Opt. Eng. (USA), vol.355, p.11-16 (1982). [received: May 1983] (Fiber Optics: Short-Haul and Long-Haul Measurements and Applications, San Diego, CA, USA, 24-25 Aug. 1982).
Progress in optoelectronic broadband switch matrices is reviewed. An experimental integrated 2X2 matrix based on photoconductive optical detectors is described. Isolation greater than 50 dB at frequencies up to 100 MHz is observed in this matrix, which is contained in a single TO-5 package. (9 refs.)
- 75835 Uniform evaluation of multichannel, hermaphroditic fiber optic connectors for tactical applications.** M.D.Drake, F.Gomes, M.Lesnick, G.W.Styskal (MITRE Corp., Bedford, MA, USA), V.E.Kalomiris.
Proc. SPIE Int. Soc. Opt. Eng. (USA), vol.355, p.61-9 (1982). [received: May 1983] (Fiber Optics: Short-Haul and Long-Haul Measurements and Applications, San Diego, CA, USA, 24-25 Aug. 1982).
Describes an evaluation of candidate multichannel, hermaphroditic fiber optic connectors under uniform, and where possible, standard conditions. Connectors manufactured by TRW, Bell-Northern, Hughes, ITT-STL (Ptmargan) and ITT-Cannon were tested. The optical insertion loss was measured while the connectors underwent (1) normal mating, (2) repetitive mating, (3) strain relief flexing, (4) temperature cycling, (5) connector-to-cable tensile stress and, (6) connector-to-connector tensile stress. In addition, the candidate connectors were rated by attributes for (1) mating forces, (2) alignment ease, (3) cleaning, (4) handling damage, and (5) human factors. (3 refs.)
- 75836 A second generation of optical fibre component from HP.** S.Mello-Grand.
Elettron. Oggi (Italy), no.3, p.223-4 (March 1983). In Italian.
Second-generation components described include a short distance transmitter (HFBR 1501) and receiver (HFBR 2500) using integrated circuits in small plastic packages and plastic material optical fibres. A 'snap-in' connectors (SMA) range allows easy interfacing. The new range of transmitters (1502) and receivers (2502), allows transmission speeds of 1 m bit/sec at a distance of 22 metres to be attained. New connectors extend transmission speed to 5M bits/sec at 500 metres. (no refs.) T.H.
- Fiber Optics: Short-Haul and Long-Haul Measurements and Applications See Entry 74208
- New devices and materials for ultrafast high speed photodetectors for the ultraviolet through to the infrared See Entry 74535
- Binary holographic LO beam multiplexer for IR imaging detector arrays See Entry 75600
- Examination of plastic focusing fiber lens See Entry 75764
- Dark-field microbend-modulated fibreoptic sensor system (DFMMFSS) See Entry 75821
- E-beam fabrication of devices for optical communication systems See Entry 75840

42.82 INTEGRATED OPTICS

(for optical waveguides see also 42.80L)

- Effect of a thermal lattice on the generated line width of a dye laser with distributed feedback See Entry 75630
- Interface states and current threshold of GaAs/Al_xGa_{1-x}As double-heterostructure lasers grown by molecular beam epitaxy See Entry 75640
- An integrated optic fibre gyroscope: performance and limitations See Entry 75824
- Test results of an integrated fiber-optics gyroscope brass board See Entry 75825
- E-beam fabrication of devices for optical communication systems See Entry 75840

42.85 OPTICAL TESTING AND WORKSHOP TECHNIQUES

- 75837 Checking manufacturing accuracy for the axial system in an optical planometer.** A.I.Sergeeva.
Meas. Tech. (USA), vol.25, no.9, p.723-4 (Sept. 1982). Translation of: *Izmer. Tekh. (USSR)*, vol.25, no.9, p.15-16 (Sept. 1982). [received: May 1983]
Several types of planometer are in production whose working principle involves defining an initial plane by means of three base points lying at three widely separated points on the surface and measuring the distances of points on the test surface to this surface. The accuracy of manufacture for the axial system is checked by optical means, but the tolerances in the manufacture mean that the axis of rotation is not unambiguously oriented with respect to the base element. A test method is described which enables one to determine the error caused by lack of parallelism between the sighting line and the base element. The method also enables one to adjust the orientation of the axis of rotation for various angular positions of the sighting tube. (6 refs.)
- 75838 Design of cylindrical ring springs.** N.A.Lobedev, A.V.Matveev.
Sov. J. Opt. Technol. (USA), vol.49, no.9, p.579-83 (Sept. 1982). Translation of: *Opt.-Mekh. Prom.-st. (USSR)*, vol.49, no.9, p.39-43 (Sept. 1982).
The types of cylindrical ring springs having an arbitrary number of slots are examined. The results, obtained from an evaluation of the spring stiffness and strength, are presented in dimensionless tabulated form, convenient for optical instrument designers. (7 refs.)
- 75839 Modernization of 2ShP-200M and ShPS-350M lathes.** N.M.Vorontsova, L.I.Mastyugin.
Sov. J. Opt. Technol. (USA), vol.49, no.9, p.589-91 (Sept. 1982). Translation of: *Opt.-Mekh. Prom.-st. (USSR)*, vol.49, no.9, p.50-2 (Sept. 1982).
The modernization of the 2ShP-200M and ShPS-350M lathes for the purpose of using them in fine diamond grinding and preliminary diamond polishing operations is described. (5 refs.)
- 75840 E-beam fabrication of devices for optical communication systems.** P.G.Flavin, C.Dix, M.E.Jones (British Telecommunications Res. Labs., Ipswich, England).
Microcircuit Engineering 82. International Conference on Microlithography, Grenoble, France, 5-8 Oct. 1982 (Grenoble, France: Comité du Colloque International sur la Microlithographie 1982), p.50-5
Electron beam lithography has been used in the fabrication of waveguides and gratings for optical communication devices. Software has been developed which extends the pattern data input format of a Cambridge Instruments EBMF and allows the easy specification of curved structures. It has been used to define waveguides with widths 2-5 µm and radii 75-500 µm, for both mask making and direct writing applications. Curved rib waveguides in GaAs/GaAlAs with an edge roughness <20 nm have been fabricated by ion beam milling, using a Ti mask defined by the lift-off technique. Gratings for distributed feedback laser structures have been defined in resist with periods down to 0.23 µm. Patterns with 0.46 µm period have been etched into the InP substrates. (15 refs.)
- 75841 Fabrication of a grid on a non-flat substrate by e-beam lithography [telescope lens fabrication].** M.E.Roulet, L.Stauffer, H.W.Luginbuhl.
Microcircuit Engineering 82. International Conference on Microlithography, Grenoble, France, 5-8 Oct. 1982 (Grenoble, France: Comité du Colloque International sur la Microlithographie 1982), p.61-4
The Hipparcos satellite will be launched in 1986 by the European Space Agency to perform an astrometrical mission. A key part of the telescope is a lens with a grid pattern on it. It is proposed to realize this structure using a vector scan pattern generator (Philips Beamwriter) in conjunction with conventional chrome mask fabrication techniques. This approach takes advantage of the accurate registration and high resolution of e-beam pattern generators and of the flexibility and the programmable beam focus and beam deflection control of vector scan systems. The authors demonstrate that the application of electron beam lithography is suitable for writing high-resolution patterns on non-flat substrates and that microlithography can be used successfully in other applications. (no refs.)
- Lenses for microlithography; state-of-the-art and future developments See Entry 75774
- Application of a continuous monitoring technique for the deposition of multi-layer dielectric films with reproducible characteristics over a wide spectral region See Entry 75775
- Restoration of spectral transmission of magnesium fluoride windows in the VUV region See Entry 75783
- Development of fabrication technology and measurement systems for multi-mode, single-mode and polarization maintaining optical fibers See Entry 75796
- Optical fiber joint-loss measurement. Review of the causes of measurement inaccuracies and some proposals for meaningful measurements See Entry 75800
- Two dimensional near-field contouring of optical fiber cores See Entry 75801
- Fibre optics QC challenge See Entry 75802
- Uniform evaluation of multichannel, hermaphroditic fiber optic connectors for tactical applications See Entry 75835

43.00 ACOUSTICS

(for audition, see 87.34; for speech, see 87.36; for sound effects on living matter, see 87.50C)

43.20 GENERAL LINEAR ACOUSTICS

(see also 03.40K Mathematical problems in waves and wave propagation)

- 75842 Transfer functions and impulse responses of rigid and elastic spheres.** C.Gazanhes, J.P.Sessarego, J.P.Herauld, J.Leandre (Lab. de Mécanique et d'Acoustique, CNRS, Marseille, France).
Acustica (Germany), vol.52, no.5, p.265-72 (April 1983). In French.
The transfer functions and the impulse responses of rigid and elastic spheres are investigated for values of the reduced parameter ka from 0.2 up to 28. These functions are calculated initially from modal theory and then verified experimentally from back-scattering measurements. For rigid spheres some examples are given of impulse responses derived by different techniques and the influence of creeping waves is discussed. For elastic spheres a smoothed impulse response is computed by taking the inverse Fourier transform of the

transfer function. The authors show that the impulse response is a combination of numerous discrete impulses due to multiple internal reflections in the sphere. (11 refs.)

75843 On the structure of the directivity for scattering by a rigid strip. W. Poppe (Max-Planck-Inst. für Stromungsforschung, Göttingen, Germany). *Acustica (Germany)*, vol.52, no.5, p.273-8 (April 1983). Recent studies on scattering problems lead to the result that for scattering of a plane wave by a rigid strip the directivity, which is a function of the angle of incidence and the angle of observation, may be expressed in terms of a function of one variable only. This feature is not obviously shown by the classical representations of the directivity. In this paper the relation between the long-known solutions and the recent results is investigated. Furthermore the asymptotic behaviour of the function of one variable characterizing the far-field for low and high frequencies is dealt with. A graphical representation of this function is shown for the case when the wavelength is of same order of magnitude as the width of the strip. (6 refs.)

75844 On one method of solving problems in the nonstationary diffraction of acoustic waves by thin unclosed shells. V.V.Dikhta. *Dopov. Akad. Nauk UkrSR. Ser. A (USSR)*, no.1, p.42-5 (1983). In Ukrainian. Presents a general solution of a nonstationary diffraction problem based on linear acoustics for unclosed shells of arbitrary geometric shape. The method worked out to solve the boundary value problems is based on a specific algebraization of boundary conditions and allows one to obtain exact expressions for the Laplace transformants of the solutions. (1 ref.)

75845 Observation of diffraction caustics for ultrasound. Rui-qi Dong, L.Adler (Dept. of Welding Engng., Ohio State Univ., Columbus, OH, USA), P.A.Doyle. *J. Appl. Phys. (USA)*, vol.54, no.5, p.2832-4 (May 1983). The formation of caustics due to the diffraction of ultrasound is observed by scanning in the shadow region close behind an elliptical obstacle in water. Good agreement is obtained between experiment and the theoretical geometry of the caustic, which is an astroid centered in that shadow region. (9 refs.)

75846 Series of waves transmitted by fluid and hollow cylinders. An exact solution. A.Derem. *Rev. Cethedec (France)*, vol.19, no.73, p.1-27 (1982). In French. For the plane acoustic wave scattering by an infinite circular fluid cylinder, the exact solution of the problem may be rewritten in the form of a series which, after the Sommerfeld-Watson transformation has been applied, appears to be naturally associated with the reflected wave and the set of the transmitted waves. As the cylindrical fluid scatterer becomes an infinite fluid cylindrical shell, immersed in an external fluid and filled itself by a third internal fluid, the exact solution may again be developed into a series, which is still associated with the reflected wave and the totality of the transmitted waves. More precisely, one shows that, so to speak, the division of two determinants of order 4 may be carried out exactly, if working in the frame of an appropriate algebra whose variables are the reflection and transmission coefficients, and then relying on simple rules which one tries to formulate. The mechanism which is encountered, when considered from the mathematical point of view, is that of the limited continued fraction. Formally, the interactions at the two successive interfaces are separated in a clear-cut fashion. At each interface, it is supposed, that the interactions are purely local. (18 refs.)

75847 Transmission of a bounded acoustic beam in the 'far field' case. I. Transmission across a dioptr. M.Rousseau (Lab. de Mecanique Theorique, Univ. Pierre-et-Marie-Curie, Paris, France). *Rev. Cethedec (France)*, vol.19, no.73, p.53-67 (1982). In French. Theoretical aspects of bounded-beam transmission or reflection on interfaces introduce some new effects with respect to the plane-wave theory. J. and S. Tjøtta (1981) have developed an analytical model to describe in three dimensions, the refracted field through a water/sediment interface. They have also shown that, in two dimensions, and if dissipation is neglected, the deviation effects are still present. Their method is based upon a Green representation of the ultrasonic field. Using a Fourier-transform technique, the author has discarded some of their hypothesis. The two dimensional solution for the very far field is therefore more accurately described. In particular, she does not necessarily suppose the wavelength to be smaller than the beam width or the emitter-interface distance. Different incident-beam shapes are considered and a numerical study is proposed for each of them. (7 refs.)

75848 Transmission of a bounded acoustic beam in the 'far field' case. II. Transmission across a fluid film. M.Rousseau (Lab. de Mecanique Theorique, Univ. Pierre-et-Marie-Curie, Paris, France). *Rev. Cethedec (France)*, vol.19, no.73, p.69-90 (1982). In French. For pt.I see ibid., vol.68, p.53 (1982). The transmission of an ultrasonic bounded beam does not follow the classical laws of geometrical acoustics. In a first part, the author derived an approximate analytical solution to describe the very far field transmitted through a fluid/fluid interface. In this second part, she extends the method to a fluid layer immersed in a liquid. He obtains approximate expressions of the very far field transmitted through the layer. It again yields angular-beam-deviation effects, but these effects depend strongly on the modes in the layer. Several incident beam shapes are considered and a numerical study is proposed for each of them. (6 refs.)

75849 Diffraction of an acoustic wave by a plate moving near a plane. E.A.Krasil'shchikova (M.V. Lomonosov State Univ., Moscow, USSR). *Sov. Phys.-Dokl. (USA)*, vol.27, no.8, p.600-2 (Aug. 1982). Translation of: *Dokl. Akad. Nauk SSSR*, vol.265, no.4-6, p.1345-9 (Aug. 1982). [received: May 1983] In an ideal compressible medium with a stationary plane H, a plate AB moves translationally in a straight line at an angle γ , $-\pi/2 \leq \gamma \leq \pi/2$ relative to this plane; the angle of attack of the plate is zero. At time t_0 , the plate encounters an acoustic wave propagating along the plane H. The wave front is a plane inclined at an angle β , $0 < \beta \leq \pi$ relative to the plane H and moving with the velocity of sound c. The author considers plane-parallel flows of a gas in a fixed coordinate system Oxz. The origin O is situated at the point occupied by the boundary A of the plate at the time t_0 . Starting at the time when the wave reaches the boundary B of the plate, a vortex line, i.e., a line of discontinuity of the horizontal velocities, descends from the surface of the plate. (7 refs.)

Computer simulation of acoustic intensity in a rectangular enclosure See Entry 75863

Computer simulation of sound in polygonoidal shaped enclosures See Entry 75864

A geometric approach to the filtered backpropagation algorithm See Entry 75865

43.25 NONLINEAR ACOUSTICS AND MACROSONICS

(see also 43.60 Acoustic signal processing; 43.88 Transduction; devices for generation and production of sound)

75850 Multimode interference mechanism in $V(z)$ curves obtained by acoustic line focus beam. J.Kushibiki, K.Horii, N.Chubachi (Dept. of Electrical Engng., Tohoku Univ., Sendai, Japan). *Electron. Lett. (GB)*, vol.19, no.10, p.359-61 (12 May 1983). The multimode interference mechanism in the acoustic material signatures of $V(z)$ curves, which generally deforms the dip intervals and the shape, is investigated theoretically and experimentally for the acoustic line focus beam. It is shown, taking a (111)-Si substrate as an example, that $V(z)$ curves associated with multiple leaky waves are represented as a superposition of elemental $V(z)$ curves with different characteristic dip intervals corresponding to the respective velocities of the leaky waves. (9 refs.)

75851 Phase conjugation in acoustics. A.Levelut (Lab. d'Ultrasons, Univ. Pierre et Marie Curie, Paris, France). *J. Phys. Colloq. (France)*, vol.44, no.C-2, p.61-6 (March 1983). (International Workshop on Optical Phase Conjugation and Instabilities, Cargese, Corsica, France, 20-24 Sept. 1982). Coupling between the elastic strain ϵ and the electric field E of the forms $B\epsilon E$ or $\gamma\epsilon^2 E$ make phase conjugation possible in acoustics. The simple case of a single acoustic wave and its-conjugated wave is first given. Then the more complicated case of phonon echoes is presented. Some examples of applications are given. (14 refs.)

75852 Influence of relaxation on the acoustic self-induced transparency. G.T.Adamashvili (Tbilisi State Univ., Tbilisi, USSR). *Phys. Lett. A (Netherlands)*, vol.95A, no.8, p.439-42 (23 May 1983). Using a singular perturbation theory for the method of the inverse scattering transform, the influence of transverse relaxation of the acoustic self-induced transparency is considered. It is shown that account of the relaxation improves the quantitative agreement of the theory with experiment. (7 refs.)

75853 Concentration mechanism for acoustic self-effects in stratifying liquid solutions. F.V.Bunkin, G.A.Lyakhov, O.B.Shuman (P.N. Lebedev Phys. Inst., Acad. of Sci., Moscow, USSR). *Sov. Tech. Phys. Lett. (USA)*, vol.8, no.9, p.451-2 (Sept. 1982). Translation of: *Pis'ma v Zh. Tekh. Fiz. (USSR)*, vol.8, no.17-18, p.1048-51 (Sept. 1982). [received: May 1983]

A natural direction in the development of nonlinear acoustics is to make use of some inelastic nonlinearity mechanisms (by selecting appropriate media): 1) universal nonlinearity mechanisms, e.g. the thermal mechanisms and the acoustic-streaming mechanism; and 2) mechanisms which are specific to a particular class of liquids. Particularly interesting in the second group are mechanisms associated with acoustically induced changes in physical quantities X which are order parameters for phase transitions. (6 refs.)

75854 A closed form method for the measurement of attenuation in nonlinearly dispersive media. P.A.Narayana, J.Ophir (Dept. of Radiology, Univ. of Texas Medical School, Houston, TX, USA). *Ultrason. Imaging (USA)*, vol.5, no.1, p.17-21 (Jan. 1983). A closed form solution of the equation describing the spectrum of a Gaussian pulse propagating in a medium with nonlinear frequency dependence of attenuation is presented. This solution suggests that in general the spectrum remains Gaussian, subject only to center frequency downshift and bandwidth reduction. The possibility of experimentally determining the two nonlinear material parameters from the measurement of the center frequency downshift and the reduced bandwidth is proposed. (11 refs.)

75855 Spectral shifts of ultrasonic propagation: a study of theoretical and experimental laws. P.A.Narayana, J.Ophir (Dept. of Radiology, Univ. of Texas Medical School, Houston, TX, USA). *Ultrason. Imaging (USA)*, vol.5, no.1, p.22-9 (Jan. 1983). The theoretical relationship between center frequency downshift and the spectral bandwidth was investigated for pulses with a sinc(x) spectrum propagating through lossy media. Power law and exponential models for frequency dependence of attenuation were used. Six target materials encompassing a range of attenuation parameters were used to verify the theoretical model. The frequency downshift data from these materials was used to calculate their respective attenuation parameters. It was shown theoretically and verified experimentally that for small frequency downshifts, the sinc(x) model yields the same material parameters as the Gaussian model. The choice of the model for the attenuation of the material was found to be inconsequential. (7 refs.)

Acoustic streaming, dimensional analysis of nonlinearities, and tone hole mutual interactions in woodwinds See Entry 75877

Application of the mixed representation to the study of acoustic-gravity waves See Entry 76057

Interaction of resonant particles with acoustic solitons in metals See Entry 77008

Nonlinear effects in hypersound propagation within the $\text{Ni}^{2+}:\text{Al}_2\text{O}_3$ system See Entry 77259

43.30 UNDERWATER SOUND

(see also 92.10 Physics of the ocean)

75856 Error rates for M-ary noncoherent FSK in impulsive reverberation noise. A.M.Maras, H.Davidson, A.G.J.Holt (Dept. of Electrical & Electronic Engng., Newcastle upon Tyne Univ., Newcastle upon Tyne, England). *Electron. Lett. (GB)*, vol.19, no.11, p.405-6 (26 May 1983).

It is shown that reverberation noise for primary acoustic scattering in the ocean has an integral representation and that a canonical model for its analysis can be found. Exact values of error rates for M-ary noncoherent FSK for correlation receivers in such noise are given. Comparison with the well known Gaussian case is also made. (8 refs.)

75857 Applications of adaptive signal processing to the reduction of flow-induced noise in small underwater vehicles. R.N.Carpenter, T.J.Curry, D.Pearson (Ocean Systems Div., Gould Inc., Middletown, RI, USA). Proceedings of ICASSP 83. IEEE International Conference on Acoustics, Speech and Signal Processing, Boston, MA, USA, 14-16 April 1983 (New York, USA: IEEE 1983), p.969-72 vol.3

The authors investigate analytically and experimentally the effectiveness of adaptive filtering for reducing flow induced sonar interference. Noise and signal fields are modeled and applied to an array whose beamformer is designed to maximize signal to noise ratio. The beamformer output is applied to an adaptive processing system with two auxiliary channels, one for a spatial sample, and one for a temporal sample of interference. Noise, signal, and

adaptive filter parameters are examined analytically to define design guidelines for the system and assess performance in a variety of realistic signal and noise situations. The hardware implementation emphasizes architectures that meet the performance requirements and are responsive to the physical constraints of small underwater vehicles. A digital high speed, pipelined transversal filter is used to produce the noise cancelling signal, and computations for error signal and filter weights are performed in parallel by high speed microprocessors. (3 refs.)

75858 A detector for acoustic directionality. P.G.Harper, S.I.Jardine, A.J.Quinn, D.M.Treherne (Dept. of Phys., Heriot-Watt Univ., Edinburgh, Scotland).

Proceedings of ICASSP 83. IEEE International Conference on Acoustics, Speech and Signal Processing, Boston, MA, USA, 14-16 April 1983 (New York, USA: IEEE 1983), p.977-80 vol.3

Describes the principles, construction and performance of a new type of acoustic directional detecting instrument intended for borehole operation and adapted to a circularly confined space. The operating principle lies in the orientational pinning of resonator vibrational modes to the pressure gradient of the sound source. In its simplest form, a pair of antinodes lines up with the source direction. The resonator consists of a metal hemispherical shell suspended at its apex and equipped with semiconductor strain gauges. The encapsulated device has been tested in water and achieves an accuracy of 2°. (5 refs.)

75859 The impact of refraction on time-delay estimation. E.R.Robinson, A.H.Qazi (Naval Underwater Systems Center, New London Lab., New London, CT, USA).

Proceedings of ICASSP 83. IEEE International Conference on Acoustics, Speech and Signal Processing, Boston, MA, USA, 14-16 April 1983 (New York, USA: IEEE 1983), p.981-4 vol.3

The objective is to investigate the sensitivity of correlograms to various sound velocity profiles, using the Generic Sonar Model to compute the cross-correlation function for an array of two separated receivers situated in realistic ocean environments. The results were compared with those predicted assuming isovelocity profiles. The influence of the target range and bearing, as well as the vertical separations of the receivers, is demonstrated for each environment considered. (2 refs.)

43.35 ULTRASONICS, QUANTUM ACOUSTICS, AND PHYSICAL EFFECTS OF SOUND

(for phonons in crystal lattices, see 63.; for plasma acoustics, see 52.35; for low-temperature acoustics and sound in liquid helium, see 67.; for acoustic properties of liquids, see 62.60; for acoustical properties of solids, see 62.65; for ultrasonic relaxation, see 62.80; for acoustic properties of thin films, see 68.60; for surface waves in solids, see 68.25; for acoustoelectric effects and acoustic wave amplification, see 72.50; for magnetoacoustic effects, oscillations and resonance, see 72.55; for acousto-optical effects and acoustic holography, see 78.20H and 43.63; for sound effects on living matter, see 87.50)

A piezoelectric displacement transducer for use in a pulse-shape based analysis of acoustic emission See Entry 75889

An ultrasonic viscometer for the measurement of dynamic shear viscosity of liquids See Entry 76131

43.40 MECHANICAL VIBRATIONS AND SHOCK

(see also 46.30M Vibrations, aeroelasticity, hydroelasticity, mechanical waves and shocks)

Measurement of vibration velocity distributions and mode analysis in thick disks of Pb (Zr,Ti)O₃ See Entry 75891

43.50 NOISE, ITS EFFECTS AND CONTROL

(see also 86.70J Environmental science)

75860 Airborne sound insulation index of double walls: application of two simplified methods for estimating transmission loss. G.Pagliarini, R.Pompili (Istituto di Fisica Tecnica, Univ. di Bologna, Bologna, Italy).

Acustica (Germany), vol.52, no.5, p.296-9 (April 1983).

Two simplified methods have been applied to a considerable number of cases for different values of the surface masses and the distance between the two panels: the transmission loss curves so calculated have been compared with the reference curve of ISO/R 717 in order to obtain the sound insulation index I_a . The results have been correlated towards a single equation (one for each method) which provides, for a given value of $\sigma_1 = \sigma_2$ and d , the corresponding value of I_a . (11 refs.)

75861 Modular system for reducing the noise of tube-cooled HV motors. W.Amey (Standard Products Div., Siemens AG, Erlangen, Germany), M.Tikvicki.

Siemens Power Eng. (Germany), vol.5, no.2, p.77-81 (March-April 1983). Various demands are placed on electric motors with respect to noise emission. For Siemens tube-cooled HV motors, which are in themselves quiet running, sound-reducing elements have been developed as a modular system for still greater individual reduction of aerodynamic, magnetic and bearing noise. (5 refs.)

Physical parameters at the valuation of the annoyance of industrial noises See Entry 78117

43.55 ARCHITECTURAL ACOUSTICS

75862 Videotape editing suite design. D.M.Winkler (Teletronics, New York, NY, USA).

SMPTE J. (USA), vol.92, no.3, p.276-83 (March 1983).

Two problems traditionally ignored in the design of videotape post-production editing suites are room acoustics and overall system integration with an editing computer. This paper offers a solution to each of these problems. A method of system design, used to create Teletronics's Editing Suite B, is presented. A physical overview of the editing suite is described, including acoustic requirements and a system control and integration scheme. (8 refs.)

75863 Computer simulation of acoustic intensity in a rectangular enclosure. D.Allen-Booth, G.J.McNulty (Sheffield City Polytech., Sheffield, England).

10th IMACS World Congress on System Simulation and Scientific Computation, Montreal, Canada, 8-13 Aug. 1982 (New Brunswick, NJ, USA: IMACS 1982), p.287-9 vol.3

The paper is concerned with the prediction of omnidirectional sound intensity in an enclosed area. The main feature of the work is the estimation of sound intensity at a receiving point for a given number of reflections. This is highlighted by the fact that for a hard walled enclosure or one of low absorption coefficient then the effect of reflection is high. In such a case the number of reflections is computed to indicate the additional sound intensity required. Thus the acoustics of the area can be planned to suit a given requirement. (3 refs.)

75864 Computer simulation of sound in polygonal shaped enclosures. G.J.McNulty, D.Allen-Booth, R.Gunson, A.Tanchou (Sheffield City Polytech., Sheffield, England).

10th IMACS World Congress on System Simulation and Scientific Computation, Montreal, Canada, 8-13 Aug. 1982 (New Brunswick, NJ, USA: IMACS 1982), p.290-2 vol.3

The predicted and experimental investigation of sound pressure levels in an irregular planform area is presented. A feature of the work is the computer mapping of the area and the consideration of images and reflection orders for a given area. (4 refs.)

IMAX and OMNIMAX theatre design See Entry 74551

43.60 ACOUSTIC SIGNAL PROCESSING

75865 A geometric approach to the filtered backpropagation algorithm.

M.L.Oristaglio (Schlumberger-Doll Res., Ridgefield, CT, USA).

Ultrason. Imaging (USA), vol.5, no.1, p.30-7 (Jan. 1983).

Shows how the filtered backpropagation algorithm for parallel-beam diffraction tomography can be implemented geometrically by weighted straight-line projections. The resulting algorithm is formally equivalent to the original approach using Fourier transforms, but reorganizes the calculations to separately backpropagate each plane-wave component of the filtered data. In principle, at least, the projection method also suggests the design of an ultrasound scanner that records the wavefield with line detectors. (6 refs.)

75866 Lateral inverse filtering of ultrasonic B-scan images. H.Schomberg, W.Vollman, G.Mahnke (Philips Forschungslab. Hamburg, Hamburg, Germany).

Ultrason. Imaging (USA), vol.5, no.1, p.38-54 (Jan. 1983).

The formation of ultrasonic B-scan images using parallel beams may be modelled as a lateral, one-dimensional convolution of the beam profile and an unknown but wanted reflection coefficient. Lateral inverse filtering, or deconvolution, might therefore be used to improve the image quality. Two different deconvolution techniques are applied to both an image of a tissue mimicking phantom and a human liver. An enhancement of the resolution (defined as the reciprocal of the half-width of the image of a point reflector) of about 1.4 is achieved. This is in good agreement with the previously derived formula $R = \sqrt{\ln \text{SNR}}$, which relates the signal-to-noise ratio, SNR, to the resolution enhancement, R. However, each method also creates artifacts, and despite the slight resolution enhancement, the deconvolved liver images do not exhibit more information nor are they more appealing. So it is felt that the computational effort is wasted. This failure is not a fault of the special deconvolution techniques tried, but rather caused by the logarithmic dependence of R on SNR and by the noise level, which is largely due to macro- and microscopic inhomogeneities of the tissue and cannot be made arbitrarily small. (14 refs.)

75867 Modal dispersion effects on coherent signal processing parameters.

K.D.Flowers (Naval Res. Lab., Washington, DC, USA).

Proceedings of ICASSP 83. IEEE International Conference on Acoustics, Speech and Signal Processing, Boston, MA, USA, 14-16 April 1983 (New York, USA: IEEE 1983), p.973-6 vol.3

Acoustic signals propagated in deep ocean ducts are geometrically (or modally) dispersed. Using a model, which for long range deep ocean propagation has been shown adequately to predict dispersion measures, the author determines that the effect of dispersion on the bandwidth of the signal is small. However, in coherently correlating spectrally separated but related signals the effect on the allowable integration time is significant. Curves relating the allowable integration time as functions of frequency and range rate between the source and receiver are presented. (5 refs.)

75868 Pitch translation of trumpet tones. F.Cahn (New England Digital Corp., White River Junction, VT, USA).

Proceedings of ICASSP 83. IEEE International Conference on Acoustics, Speech and Signal Processing, Boston, MA, USA, 14-16 April 1983 (New York, USA: IEEE 1983), p.1380-3 vol.3

In an attempt to design trumpet timbres for digital music synthesis, notes of a trumpet were digitally recorded. Spectral analysis at high resolution showed both a harmonic line spectrum and a weak continuous spectrum. The continuous spectrum did not appear to contribute to the tone. Shifting the pitch by sample rate conversion (interpolation or decimation) caused serious changes in tone unless the spectral envelope was deconvolved from the signal before pitch shifting and reconvolved with the shifted signal. This procedure can be used to simulate the spectral envelope of a trumpet, which remains roughly constant as the pitch is changed. (4 refs.)

Computer evaluation of real-time X-ray and acoustic images .. See Entry 74569

Applications of adaptive signal processing to the reduction of flow-induced noise in small underwater vehicles See Entry 75857

A new wire phantom for accurate measurement of acoustic resolution See Entry 75887

43.70 SPEECH COMMUNICATION

(inc. speech perception, speech intelligibility, and speech synthesis; see also 87.36 Speech)

75869 Intelligibility of consonants in CVC utterances produced by dyadic rule synthesis. L.C.W.Pols (Inst. for Perception TNO, Soesterberg, Netherlands), J.P.Olive.

Speech Commun. (Netherlands), vol.2, no.1, p.3-13 (May 1983).

The intelligibility of initial and final consonants in monosyllabic CVC utterances was measured for rule-synthesized speech (dyadic concatenation). In order to evaluate the intelligibility results, two additional speech conditions were tested: PCM-coded speech (12 bits, 10 kHz sampling rate), and LPC-resynthesized speech (12 coefficients). The stimulus set consisted of all possible initial and final consonants appearing in nine different CVC contexts,

namely with three vowels and with three nonneighboring consonants. The subjects had to identify the initial or final consonant in each word and could choose any single consonant as a response. The overall percentage correct scores, averaged over 33 listeners, for the initial and final consonants, were 93% and 92.8% for PCM-coded speech, 86.7% and 85.4% for LPC-synthesis, and 58.2% and 73.5% for rule-synthesized speech. Apart from these scores also the actual confusions are discussed in some detail. More important than the scores achieved for this particular, meanwhile improved, version of the rule-synthesis system, was the insight gained in how to evaluate and improve such systems. (24 refs.)

75870 Categorical or continuous speech perception: a new test. D.W. Masaro, M.M. Cohen (Univ. of California, Santa Cruz, CA, USA). *Speech Commun. (Netherlands)*, vol.2, no.1, p.15-35 (May 1983). An important question in speech perception is whether listeners have continuous or categorical information about the acoustic signal in speech. Most traditional experimental studies have been interpreted as evidence for categorical perception. It is argued in this paper that more recent results taken as evidence against categorical perception are not unequivocally negative. Accordingly, further tests between continuous and categorical views of speech perception are necessary. In the present experiments, listeners were asked for continuous rather than discrete judgements in order to provide a more direct answer to this question. Subjects were asked to rate speech sounds according to where they fell on a particular speech continuum. The continua consisted of stop consonants varying in place (/b/ to /d/) or voicing (/b/ to /p/) or a vowel continuum varying from /i/ to /I/. The distributions of rating responses of individual subjects were used to test quantitative models of categorical and continuous perception of acoustic features in speech. The results provide strong evidence against the categorical perception of speech contrasts, and contribute additional evidence for the role of continuous acoustic feature information in speech processing. (45 refs.)

75871 A synthesis-based method for pitch extraction. K.K. Paliwal, P.V.S. Rao (Speech & Digital Systems Group, Tata Inst. of Fundamental Res., Bombay, India). *Speech Commun. (Netherlands)*, vol.2, no.1, p.37-45 (May 1983). A synthesis-based method for pitch extraction of the speech signal is proposed. The method synthesizes a number of log power spectra for different values of fundamental frequency and compares them with the log power spectrum of the input speech segment. The average magnitude (AM) difference between the two spectra is used for comparison. The value of fundamental frequency that gives the minimum AM difference between the synthesized spectrum and the input spectrum is chosen as the estimated value of fundamental frequency. The voiced/unvoiced decision is made on the basis of the value of the AM difference at the minimum. For synthesizing the log power spectrum, the speech signal is assumed to be the output of an all-pole filter. The transfer function of the all-pole filter is estimated from the input speech segment by using the autocorrelation method of linear prediction. The synthesis-based method is tried out on real speech data and the results are discussed. (18 refs.)

75872 An analysis of the diplophonia phenomenon. P.H. Dejonckere, J. Lebacqz. *Speech Commun. (Netherlands)*, vol.2, no.1, p.47-56 (May 1983). Diplophonia is the simultaneous presence in the voice of two separate tones, heard as distinctly different in pitch. While permanent diplophonia is a somewhat rare phenomenon, transient bitonality is frequently noticed in patients either with lesional or functional hoarseness. Diplophonia was observed in 72 patients, and various acoustical, visual and glottographical techniques of investigation were performed. Acoustically, diplophonia is due to the addition of a second subharmonic series to the normal F_0 harmonic structure. Mechanically, diplophonia is always associated with abnormal oscillatory movements of the vocal folds involving a double or multiple phased closing or opening movement of the glottis, or a beating phenomenon of the two folds oscillating at different frequencies. As a general rule, diplophonia is associated with excessive air escape through the glottis, which is a cause of hoarseness. Diplophonia is not a specific characteristic of a particular aetiology of dysphonia. (15 refs.)

75873 Time domain properties of the two-pole model of the glottal waveform and implications for LPC. J.R. Deller, Jr. (Dept. of Electrical Engng., Illinois Inst. of Technol., Chicago, IL, USA). *Speech Commun. (Netherlands)*, vol.2, no.1, p.57-63 (May 1983). LPC speech production models often assume a two real pole function for the glottal volume velocity waveform. This paper discusses the properties of this glottal model with respect to key time domain features and concludes that it is physiologically unrealistic for normal waveform representation. Implications for the performance of LPC analysis schemes, and the perceptual quality of vowel sounds synthesized using this model, are discussed. (27 refs.)

75874 Helium speech processor using linear prediction. S.W. Beet, C.C. Goodyear (Dept. of Electrical Engng., Univ. of Liverpool, Liverpool, England). *Electron. Lett. (GB)*, vol.19, no.11, p.408-10 (26 May 1983). Currently available helium speech processors provide a linear frequency scaling but, at the greater depths encountered in recent years, a nonlinear shift is desirable. The authors suggest a method based on linear prediction, which will produce such a shift, while retaining a reasonably low computational cost. (6 refs.)

75875 Theoretical model for the Speech Input Device SID3. I. Filters. D. Schofield, D.R. Manning. *Report NPL-DITC-20/83*, Nat. Phys. Lab., Teddington, England (April 1983), 17 pp. SID3 is a hardware preprocessor used in the NPL work on speech recognition. This is part 1 of a set of reports in which the operation of SID3 is described, giving a mathematical model of its operations as far as practicable. This model is used to answer questions on the dynamic response of SID3 and its ability to measure the frequency and level of correlation when the input is a pure tone, and to resolve pairs of pure tones. The current report studies the filters used in the three voiced correlation channels and derives their static and dynamic characteristics. (4 refs.)

A preliminary model of subjective voice quality See Entry 78200
Vibrotactile identification of vowels See Entry 78201

43.75 MUSIC AND MUSICAL INSTRUMENTS

75876 Oboe normal mode adjustment via reed and staple proportioning. A.H. Benade (Dept. of Phys., Case Western Reserve Univ., Cleveland, OH, USA), W.B. Richards. *J. Acoust. Soc. Am. (USA)*, vol.73, no.5, p.1794-803 (May 1983). The authors have analyzed a simple theoretical model of an oboe, having a truncated conical air column of variable length and a reed assembly consisting of a tapered neck leading to a closed, cylindrical cavity. Proportions are

chosen for this assembly so that its input admittance at the bottom of the neck is very closely the same function of frequency as the admittance of the missing conical segment at the apex of the air column for frequencies below the tone-hole cutoff. The most important requirements are that the reed assembly by itself possess the same volume and lowest-mode frequency as the missing apex. The intervals between the first-mode frequency and the below-cutoff frequencies of the second, third, and fourth modes of the model instrument can be made harmonic to within five cents as the length of the air column is varied to sweep the first mode through an octave range. The authors have investigated the effects of small variations in the proportions of the reed assembly on the natural frequencies of the model instrument. The results provide practical guidance for adjustment of the reed structure of a real oboe to special features of its own not-quite-conical acoustical behavior. (18 refs.)

75877 Acoustic streaming, dimensional analysis of nonlinearities, and tone hole mutual interactions in woodwinds. D.H. Keefe (Dept. of Phys., Case Western Reserve Univ., Cleveland, OH, USA). *J. Acoust. Soc. Am. (USA)*, vol.73, no.5, p.1804-20 (May 1983). The transmission line description of a woodwind assumes that the linearized wave equation of acoustics is accurate, and that the woodwind tone holes are independently represented in the transmission line by shunt and series impedances. Additional interactions exist between the tone holes when the inter-hole separation becomes small relative to the main bore diameter. Internal hole interactions, expressed via the main bore evanescent modes, are most important in woodwinds with large diameter holes such as the saxophone and Boehm flute. Tone holes interact externally to a lesser degree when the radiated sound field from one hole modifies the near field of neighboring holes. Acoustic streaming and convective nonlinearities are components of the sound field in woodwinds under playing conditions. The presence of the nonlinear sound field is correlated with changes in timbre and the stability of oscillation, and is more pronounced for tone holes whose height is much smaller than the hole diameter. Dimensional analysis, using the Reynolds number associated with the steady streaming velocity and the Strouhal number associated with the strength of the convective nonlinearity along the streamlines near the tone hole edges, is used to estimate the importance of sound field nonlinearities in various woodwinds. Observation and dimensional analysis are in agreement that nonlinearities are most important for the low register tones of a woodwind. The tone hole geometries of woodwind families are tabulated and discussed. (29 refs.)

75878 Flue organ pipes: adjustments affecting steady waveform. A.W. Nolle (Dept. of Phys., Univ. of Texas, Austin, TX, USA). *J. Acoust. Soc. Am. (USA)*, vol.73, no.5, p.1821-32 (May 1983). Adjustable flue organ pipes are used in studying the phase and amplitudes of harmonics relative to the fundamental for various horizontal positions of the upper lip, and the behavior of the spectrum as the mean jet velocity is changed in the range 5 to 39 m/s. An analog-digital electrical oscillator with two resonant circuits and a switchlike feedback characteristic resembling that suggested by Fletcher for flue pipes is also studied; biasing in the feedback circuit is analogous to displacing the pipe lip relative to the jet. Phase of a pipe harmonic relative to the fundamental changes approximately 180° at the amplitude minimum of the harmonic, as the lip is displaced horizontally, and slowly elsewhere. The electrical analog gives similar results. For each pipe model there is a 'saturation' value of supply pressure (jet velocity) above which the fundamental amplitude is nearly constant. Evidence of phase locking of free-edge signals to the pipe oscillation is found. With a broad beveled lip, pipe oscillation can occur without the jet entering the pipe. (20 refs.)

Pitch translation of trumpet tones See Entry 75868
Music perception and elementary auditory sensations. II See Entry 78190

43.85 ACOUSTICAL MEASUREMENTS AND INSTRUMENTATION

[for acoustic noise measurement, see also 43.50; for photoacoustic spectroscopy, see 07.65]

75879 Quality control of round or elliptical objects by detecting multiply reflected and refocused photoacoustic signal. H. Coufal, S.T. Lam, A.C. Tam (IBM Corp., Armonk, NY, USA). *IBM Tech. Disclosure Bull. (USA)*, vol.25, no.11A, p.5446-7 (April 1983). The technique of detecting multiply reflected and self-refocused pulsed photoacoustic signals (generated and detected at the center of the disk) provides an unsurpassed quality-control method, being non-destructive, non-contact and non-contaminating, reliable and fast. (1 ref.)

75880 Acoustic testing. T.E. Lanham (IBM Corp., Armonk, NY, USA). *IBM Tech. Disclosure Bull. (USA)*, vol.25, no.11A, p.5495-6 (April 1983). Describes a technique to measure the nuisance value of noise to a human operator by using a program which operates on the constant bandwidth data stored in an analyzer to generate a modified frequency spectrum of the noise levels representing the output from an ideal analyzer with swept filter of constant percentage bandwidth. (no refs.)

75881 Automatic sound power measurement. T.E. Lanham (IBM Corp., Armonk, NY, USA). *IBM Tech. Disclosure Bull. (USA)*, vol.25, no.11A, p.5497-8 (April 1983). Describes a technique by which sound power of apparatus under test is automatically measured under computer control by means of a rotating boom carrying a number of microphones supplying sound data to a digital analyzer. (no refs.)

75882 The optimization of electronic precision in ultrasonic velocity measurements. A comparison of the time interval averaging and sing around methods. J.D. Aindow, R.C. Chivers (Phys. Dept., Univ. of Surrey, Guildford, England). *J. Acoust. Soc. Am. (USA)*, vol.73, no.5, p.1833-7 (May 1983). Measurement of ultrasonic velocity is of importance in fluids for physical chemistry and in solids for both fundamental and applied investigations. In fluids, the sing around technique is most widely advocated as a single measurement principle with calculated high precision. Time interval averaging has also been used for some time, but its potential has been greatly increased by recent developments in instrumentation. The purpose of this paper is to define a criterion, based upon confirmatory experimental evidence, for the preferential use of one technique or the other in a given experimental situation. (11 refs.)

75883 Optical probing of acoustic waves on rough surfaces. R.L. Jungerman, B.T. Khuri-Yakub, G.S. Kino (Edward L. Ginzton Lab., W.W. Hansen Lab. of Phys., Stanford Univ., Stanford, CA, USA). *J. Acoust. Soc. Am. (USA)*, vol.73, no.5, p.1838-41 (May 1983). The problem of optically measuring acoustic displacements on samples with rough surface texture is examined. A focusing lens system which increases the amount of scattered light collected from a rough surface is presented. A

computer-controlled scanning system for an all-fiber-optic acoustic surface wave probe is described which electronically divides out surface reflectance changes encountered while measuring rough samples. The probe demonstrates the ability to optically measure acoustic displacements on surfaces with a roughness comparable to that produced by most common manufacturing processes. An image of the acoustic field surrounding a defect in an aluminum test sample is presented. (11 refs.)

75884 Doppler time mapping. A.R.Gondeck (Dept. of Electrical Engng., Univ. of South Florida, Tampa, FL, USA).

J. Acoust. Soc. Am. (USA), vol.73, no.5, p.1863-4 (May 1983).

The algorithm presented by D.W. Ricker ['Echo waveform synthesis in a rapidly varying geometry', *ibid.*, vol.72, p.1321-1323 (1982)] for describing time-mapping when the trajectories of both a moving target and the projector are known contained the problem that some of the vehicle motion is transparent and error is introduced. An alternative algorithm, described in this letter, avoids this problem, is computationally more efficient, with no accumulative error, and is simple to program. (2 refs.)

75885 Comments on 'Doppler time mapping' [J. Acoust. Soc. Am. 73, 1863-1864 (1983)]. D.W.Ricker (Appl. Res. Lab., Pennsylvania State Univ., State College, PA, USA).

J. Acoust. Soc. Am. (USA), vol.73, no.5, p.1864-5 (May 1983).

The subject paper presents an algorithm which compensates for transit time errors due to motion induced wave-front distortion which arises from motion normal to the line of sight between a projector and scatterer. This error is small in most practical applications and may, if necessary, be compensated for by a redefinition of the line of sight vector utilized by D.W. Ricker ['Echo waveform synthesis in a rapidly varying geometry', *ibid.*, vol. 72, p.1321-1323 (1982)]. (2 refs.)

75886 A novel electron beam recording material—poly(pentene-2 sulfone)—for real time display of acoustical frequency. Tang Keguang, Yang Yongyuan, Gao Zhimin, Feng Shujing, Wu Shikang (Inst. of Photographic Chem., Acad. Sinica, Beijing, China).

Kexue Tongbao (Foreign Lang. Ed.) (China), vol.28, no.2, p.206-8 (Feb. 1983).

The authors report that poly(pentene-2 sulfone) films containing a photosensitive agent is a good electron beam recording material for real time acoustics. (6 refs.)

75887 A new wire phantom for accurate measurement of acoustic resolution. W.S.N. Trimmer, D.Vilkomerson (Technicare/Special Res. Group, Somerset, NJ, USA).

Ultrason. Imaging (USA), vol.5, no.1, p.87-93 (Jan. 1983).

Describes a phantom which is easier to use and gives more accurate results than a phantom made from several pairs of solid wires. This phantom employs two concepts: spatially modulated wires and diverging wires. Spatially modulated wires, such as helically twisted wires, reflect the sound into a broad range of angles. This has two advantages: (1) it is easier to align the transducer with the reflected beam, (2) the diffuse reflection is similar to the scattering from tissue, and the system gain need not be turned abnormally low. Diverging wires improve the accuracy and convenience of the measurement. Rather than many pairs of parallel wires, a single pair of wires which diverge from an apex is used. By scanning across this pair until the wires are just resolved, the resolution can be easily calculated. (3 refs.)

75888 Acoustical speckle interferometry. J.A.Schaeff, Jr. (US Army Missile Res. & Dev. Command, Redstone Arsenal, AL, USA).

In book: *International advances in nondestructive testing*. Vol.9, W.J.McGonagle [Ed.], p.17-76. New York, USA: Gordon & Breach (1983), 363 pp. [0 677 16440 8]

The basic theory for pulse-echo and continuous wave acoustical speckle interferometry was presented. This theory included the propagation of sound in an LSL interface with a scattering-reflecting layer below the interface. Also the method of scanning and cross-correlation using the square of the difference of two signals was presented. Two separate hardware systems were developed to make displacement predictions using the pulse-echo and continuous wave modes. These systems are very accurate and can make displacement measurements to within ± 0.001 inch using an XY-table with a 0.001 inch step increment. XY-tables with a smaller increment could improve these measurements by at least one order of magnitude. Pulse-echo acoustical interferometry was found to be sensitive to motion in three dimensions which may limit its usefulness since it requires scanning over an area to predict two-dimensional motion. Continuous wave acoustical speckle interferometry in contrast to pulse-echo scanning was found to be sensitive mainly to motion in two dimensions. (10 refs.)

Microcomputer measurement of the velocity of sound in air ... See Entry 74244

A closed form method for the measurement of attenuation in nonlinearly dispersive media ... See Entry 75854

A detector for acoustic directionality ... See Entry 75858

Pressure and pressure gradient fiber-optic lever hydrophones ... See Entry 75892

Annular arrays for quantitative pulsed Doppler ultrasonic flowmeters ... See Entry 76138

Some results on the resolution of small inclusions in ultrasonic immersion testing of steel with focused probes ... See Entry 77829

Samples for determining the point of exit and the angle of entry of the ultrasonic beam in pipe inspection ... See Entry 77834

Maximum attainable sensitivity of inspection by 'multiple shadows' method ... See Entry 77835

Use of oblique wide-beam probe for inspection of strips with normal waves ... See Entry 77836

Digital nondestructive evaluation of composite materials [ultrasonic inspection] ... See Entry 77854

Evaluation of electrode shape and nondestructive evaluation method for welded solar cell interconnects ... See Entry 77858

Nondestructive testing of interconnect welds using the Scanning Laser Acoustic Microscope (SLAM) ... See Entry 77859

Airflow resistivity instrument for in situ measurement on the Earth's ground surface ... See Entry 78708

43.88 TRANSDUCTION; DEVICES FOR THE GENERATION AND REPRODUCTION OF SOUND

75889 A piezoelectric displacement transducer for use in a pulse-shape based analysis of acoustic emission. J.Niewisch, P.Krammer (Siemens AG, Erlangen, Germany).

Sens. & Actuators (Switzerland), vol.3, no.3, p.187-93 (May 1983).

In order to assess the quality of the transducer, a measuring procedure is presented based on the comparison of the responses expected from theory with those actually measured. To a good approximation the transducer fulfills the requirements of a displacement transducer. (6 refs.)

75890 Development of a high intensity acoustic source. Ch'i Po-chun (Peking Inst. of Strength & Environment Engng., Peking, China).

Chin. J. Sci. Instrum. (China), vol.4, no.1, p.66-71 (Feb. 1983). In Chinese. Describes an acoustic generator with high power and wide bandwidth. The electropneumatic loudspeaker has power output up to 6000 acoustic watts. It can meet the needs for high intensity sound environmental test in astronautic and aeronautic engineering and is also suitable for long-distance music or speech transmission. The operational principle of the DQY-6000S electropneumatic loudspeaker is presented together with the elementary design theory and the characteristics of the vibration system. The method and data regarding the generator adjustments are given. (5 refs.)

75891 Measurement of vibration velocity distributions and mode analysis in thick disks of Pb (Zr,Ti)O₃. S.Ueha, S.Sakuma, E.Mori (Research Lab. of Precision Machinery Electronics, Tokyo Inst. of Technol., Yokohama, Japan).

J. Acoust. Soc. Am. (USA), vol.73, no.5, p.1842-7 (May 1983). The vertical vibration velocity distributions and the frequency spectra of disk-type transducers with bevelled and unbevelled edges are measured as a function of the diameter-to-thickness ratio. In this experiment, transducers of Pb(Zr,Ti)O₃ are used and the diameter-to-thickness ratios are changed from 2 to 12. The frequency spectra are measured in the band from 1-700 kHz, and the velocity distributions are measured along the radial direction with an optical heterodyne technique. The theoretical frequency spectra are analytically derived from the wave equation of the disk-type transducer and compared to the experimental results. The theoretical velocity distributions are also proven to be true and to agree with the measured ones. (7 refs.)

75892 Pressure and pressure gradient fiber-optic lever hydrophones. F.W.Cuomo (Dept. of Physics, Univ. of Rhode Island, Kingston, RI, USA).

J. Acoust. Soc. Am. (USA), vol.73, no.5, p.1848-57 (May 1983).

Fiber-optic levers have been found useful in the design of intracardiac pressure transducers, low-displacement biological measurements, and more generally as noncontact optical proximity detectors. In this paper the utilization of a bifurcated fiber-optical lever in the design of hydrophones of the pressure and pressure gradient types has been considered. This approach leads to simplicity, low cost, and relative ease in implementation. Some optical and acoustical considerations are given to establish the validity of the experimental data presented. It is shown that, with little effort, these devices can provide acoustic sensitivities at least equivalent to those of piezoceramic elements within the same frequency range and can generate acceptable directivity patterns in the pressure and pressure gradient modes. (18 refs.)

75893 Flexural disk hydrophones using polyvinylidene fluoride (PVDF) piezoelectric film: desensitization with increasing hydrostatic pressure. A.J.Holten, A.D.Parsons, A.E.J.Wilson (Plessey Res. (Caswell), AllenClarkRes.Centre.Ltd., Caswell, Towcester, England).

J. Acoust. Soc. Am. (USA), vol.73, no.5, p.1858-62 (May 1983).

A piezoelectric polymer polyvinylidene fluoride hydrophone was developed which shows significant desensitization as the hydrostatic pressure is increased from 0 to 0.62 MPa. The authors show theoretically and experimentally that this is due to the boundary of the disk changing from 'simply supported' to 'clamped'. They investigate ways in which this problem can be overcome using a profiled disk with rounded supports. (8 refs.)

75894 Variable amplitude, phase, and field shape ultrasonic transducers. J.W.Gray, R.O.Claus (Dept. of Electrical Engng., Virginia Polytech. Inst. & State Univ., Blacksburg, VA, USA).

IEEE SOUTHEASTCON '83 Conference Proceedings, Orlando, FL, USA, 11-14 April 1983 (New York, USA: IEEE 1983), p.416-20

A piezoelectric ultrasonic transducer with multiple electrodes is described. Control of both the amplitude and the phase of the signals applied to the individual electrodes of the transducer with variable spatial amplitude profiles. The specific example of a transducer with a two-dimensional Gaussian field profile that may be focused to a spot at a selected distance from the transducer surface is discussed. Both theoretical design criteria and experimental results are presented. (7 refs.)

43.90 OTHER TOPICS IN ACOUSTICS

A piezoelectric displacement transducer for use in a pulse-shape based analysis of acoustic emission ... See Entry 75889

44.00 HEAT FLOW, THERMAL AND THERMODYNAMIC PROCESSES

44.10 HEAT CONDUCTION (MODELS, PHENOMENOLOGICAL DESCRIPTION)

75895 Regularisation of solutions of inverse heat conduction problem. V.M.Vigak.

Dopov. Akad. Nauk UkrSR. Ser. A (USSR), no.3, p.31-4 (1983). In Ukrainian.

One method of solution regularization is proposed for an inverse incorrect heat conduction problem. The question of constructing a stable solution is discussed. (6 refs.)

75896 Thermal effects in a long rotating cylindrical shaft of piezo-electric material with a concentric circular axial hole. K.K.Kundu (Ramakrishna Mission Sikshanamandira, Howrah, West Bengal, India).

Indian J. Theor. Phys., vol.29, no.3, p.281-9 (Sept. 1981).

A problem of thermal effects in a rotating cylindrical shaft with concentric circular hole has been considered. To solve such a problem the author makes use of the equation of elasticity, Maxwell's equations, and the equation of heat conduction in the steady state simultaneously and the other relevant constitutive relations have also been used. Finally, displacements in the r and z directions have been found. (8 refs.)

75897 Effective macroscopic description for heat conduction in periodic composites. J.L.Auriault (Inst. de Mecanique de Grenoble, Grenoble, France).

Int. J. Heat & Mass Transfer (GB), vol.26, no.6, p.861-9 (June 1983).

Effective parameters for the macroscopic behaviour of periodic composites are determined, concerning static or transient heat conduction, when the wavelength is large compared to the length of the period. Different situations are analysed using the homogenization method, which lead to different macroscopic descriptions: single classical partial differential equations, single integral partial differential equations with memory effect, systems of partial differential equations, etc. Some simple examples are given where analytical results are possible. (20 refs.)

75898 Heat flow through fiber-reinforced composite layer. V.T.Golovchan, V.I.Kushch (Inst. of Superhard Materials, Acad. of Sci., Kiev, Ukrainian SSR).

J. Eng. Phys. (USA), vol.43, no.3, p.995-1000 (Sept. 1982). Translation of: *Inzh.-Fiz. Zh. (USSR)*, vol.43, no.3, p.417-24 (Sept. 1982).

The problem of heat flow through a layer with a finite number of rows of periodically positioned fibers all oriented along the same direction is solved.

75899 Numerical method for solving the coupled problem radiative-convective and conductive heat transfer. Yu.K.Malikov, V.G.Lisienko, V.V.Volkov (S.M. Kirov Ural Polytech. Inst., Sverdlovsk, USSR).

J. Eng. Phys. (USA), vol.43, no.3, p.1035-41 (Sept. 1982). Translation of: *Inzh.-Fiz. Zh. (USSR)*, vol.43, no.3, p.467-74 (Sept. 1982).

The solution of the problem of complex heat transfer is reduced to a systematic solution of a system of nonlinear equations and the heat-conduction equations. A rapid iterative method is proposed for solving the system of equations. (5 refs.)

A second law analysis of the concentric tube heat exchanger: optimisation of wall conductivity See Entry 75904

Heating of a thin wire by a constant current with density sufficient for the appearance of thermoplasticity See Entry 77683

44.25 CONVECTIVE AND CONSTRAINED HEAT TRANSFER

(see also 47.25Q Convection and heat transfer)

75900 Effect of evaporation on convective heat exchange of a porous plate in a rarefied medium. P.A.Novikov, V.S.Yalovets, Z.M.Yudovin (A.V. Lykov Inst. of Heat & Mass Transfer, Acad. of Sci., Minsk, Belorussian SSR).

J. Eng. Phys. (USA), vol.43, no.3, p.966-9 (Sept. 1982). Translation of: *Inzh.-Fiz. Zh. (USSR)*, vol.43, no.3, p.379-84 (Sept. 1982).

Two heat-exchange regimes are experimentally observed for a horizontal porous plate as liquid evaporates from the plate into a rarefied medium. In one of these regimes mass transfer of vapor completely determines the convective heat exchange. (14 refs.)

75901 Heat transfer in enclosures with programmed heat release. V.K.Aver'yanov, S.I.Bykov.

J. Eng. Phys. (USA), vol.43, no.3, p.987-92 (Sept. 1982). Translation of: *Inzh.-Fiz. Zh. (USSR)*, vol.43, no.3, p.406-12 (Sept. 1982).

The problems of calculating the indoor air temperature, heat consumption, and room temperatures with arbitrary thermal perturbations are examined. (10 refs.)

Heat flow through fiber-reinforced composite layer See Entry 75898

Numerical method for solving the coupled problem radiative-convective and conductive heat transfer See Entry 75899

Free convection about a sphere at small Grashof number See Entry 76010

Nonlinear convection in a porous layer with finite conducting boundaries See Entry 76024

Heat transfer and horizontally averaged temperature of convection with large viscosity variations See Entry 76025

Radiation heat exchange in a solar cavity-type receiver at various times See Entry 78094

44.30 HEAT TRANSFER IN INHOMOGENEOUS MEDIA AND THROUGH INTERFACES

75902 Stefan problem with initial heat shock. I.I.Danilyuk.

Dopov. Akad. Nauk UkrSR. Ser. A (USSR), no.3, p.9-14 (1983). In Ukrainian.

The two-phase Stefan problem with a discontinuous initial temperature ('heat shock') is considered and reduced to three nonlinear equations. Three stages of a crystallization process are described—initial, middle and final. The existence theorem for small time values is also proved. (4 refs.)

75903 On the mechanism of macrolayer formation in nucleate pool boiling at high heat flux. A.M.Bhat (Mech. Engng. Dept., Regional Engng. Coll., Srinagar, India), R.Prakash, J.S.Saini.

Int. J. Heat & Mass Transfer (GB), vol.26, no.5, p.735-40 (May 1983).

In nucleate boiling at high heat flux, a liquid layer, known as the 'macrolayer', is trapped between the heating surface and the vapour masses. An analysis of the mechanism of formation of this macrolayer is presented. Based on the analysis, a theoretical expression has been derived for the initial thickness of the macrolayer. The agreement between the theoretical values of the initial macrolayer thickness and the experimental values published in the literature is reasonably good. (11 refs.)

75904 A second law analysis of the concentric tube heat exchanger: optimisation of wall conductivity. K.Chowdhury, S.Sarangi (Advanced Centre for Cryogenic Engng., Indian Inst. of Technol., Kharagpur, India).

Int. J. Heat & Mass Transfer (GB), vol.26, no.5, p.783-6 (May 1983).

Investigates the effect of axial heat conduction on the performance of concentric tube counterflow heat exchanger and derive an expression for the optimum thermal conductivity of the partition wall. (10 refs.)

75905 An analysis of substrate heat losses in Stefan's problem with a constant flux. B.Jayaram, W.Strieder (Univ. of Notre Dame, Notre Dame, IN, USA).

Int. J. Heat & Mass Transfer (GB), vol.26, no.5, p.786-90 (May 1983).

In the present study the heat balance integral method is used to obtain melting rates and heat losses into the substrate for the melting of a semi-infinite solid on a conducting substrate, both initially at the solid melting temperature, by a constant uniform heat source at the substrate interface. Results show that in many cases the latent heat sink will significantly reduce substrate heat losses on melting. (10 refs.)

75906 Boiling on a finned tube and a finned tube bundle. E.Hahne, J.Muller (Inst. fur Thermodynamik und Warmetech., Univ. Stuttgart, Stuttgart, Germany).

Int. J. Heat & Mass Transfer (GB), vol.26, no.6, p.849-59 (June 1983).

An experimental investigation was carried out in a 151 dm³ container in R 11, at saturation state of 1 bar and 23.3°C. The heat transfer coefficients measured on a single tube in the container, resembled approximately results for the case that only one tube is heated within an in-line 18 tube bundle. For a twin tube arrangement, the heat transfer coefficient of the upper tube is up to 80% higher than that of the lower tube. The heat transfer curve of this upper tube represents quite well the heat transfer coefficients of tubes enclosed in the bundle. Only for the bottom and top tubes of the bundle differences do occur. The possibility to obtain tube bundle data, at least to some extent, by much simpler twin-tube or triple-tube experiments would facilitate experimental investigations. (20 refs.)

75907 Heat liberation during vapor condensation in a thermosiphon. N.I.Mirmov, I.G.Velyakova (V.V. Kuibyshev Arkhangel' Forest Technol. Inst., USSR).

J. Eng. Phys. (USA), vol.43, no.3, p.970-4 (Sept. 1982). Translation of: *Inzh.-Fiz. Zh. (USSR)*, vol.43, no.3, p.385-90 (Sept. 1982).

A method is described for calculation of the heat-transfer coefficient during condensation of vapor of single component and binary heat-transfer agents in a thermosiphon. Results of processing experimental data are presented. (10 refs.)

Effective macroscopic description for heat conduction in periodic composites See Entry 75897

The effect of thermal boundary conditions on the heat transport in vertical channels heated from below See Entry 76004

Theoretical prediction of maximum heat flux in power transients See Entry 76019

Overhanging interfacial gravity waves of large amplitude See Entry 76053

Simplified nonlinear descriptions of two-phase flow instabilities in vertical boiling channel See Entry 76091

Drop-to-filmwise condensation transition: heat transfer measurements for ethanediol See Entry 76601

Radiation heat exchange in a solar cavity-type receiver at various times See Entry 78094

A simplified theory for a matrix solar collector See Entry 78096

Seasonal thermal inventory See Entry 78105

44.40 RADIATIVE HEAT TRANSFER

75908 Thermal performance of radiative cooling panels. P.Berdahl, M.Martin, F.Sakkal (Lawrence Berkeley Lab., Univ. of California, Berkeley, CA, USA).

Int. J. Heat & Mass Transfer (GB), vol.26, no.6, p.871-80 (June 1983).

The performance of panels which cool by means of thermal infrared heat transfer to the sky is calculated from basic principles. The efficiency of a radiative cooling panel is defined. Computer calculations with the full heat transfer equations are performed for horizontal surface with infrared-transparent covers. Plots of efficiency versus a dimensionless temperature difference are shown to be insensitive to variations in air temperature, wind speed, and sky radiance resulting in plots analogous to standard efficiency curves for solar panels. Experimental measurements show that, for most applications, white paint is a better radiator than aluminized polyvinyl fluoride film. (38 refs.)

75909 Source function expansion for radiative transfer in an anisotropically scattering slab with reflecting boundaries. S.M.Shouman, M.N.Ozisik (Dept. of Nuclear & Mech. Engng., North Carolina State Univ., Raleigh, NC, USA).

Int. J. Heat & Mass Transfer (GB), vol.26, no.6, p.951-3 (June 1983).

The source function expansion method is applied for the solution of radiation transfer in an anisotropically scattering plane parallel slab. The authors consider radiative heat transfer for azimuthally symmetric, gray, absorbing, emitting, anisotropically scattering, plane-parallel slab with specularly reflecting boundaries confined to a medium $-L \leq x \leq L$ measured in the optical variable x . (5 refs.)

75910 A calorimetric method for the measurement of the Stefan-Boltzmann constant. D.Giulietti, M.Lucchesi (Istituto di Fisica, Univ. di Pisa, Pisa, Italy), L.Galgani.

Nuovo Cimento B (Italy), vol.74B, ser.2, no.2, p.187-98 (11 April 1983).

Presents a new calorimetric method for the determination of the Stefan-Boltzmann constant σ at the melting point of ice. The method is completely unaffected by problems related to diffraction effects, which limited the accuracy of most previous experiments in σ determinations. (17 refs.)

Numerical method for solving the coupled problem radiative-convective and conductive heat transfer See Entry 75899

Radiation heat exchange in a solar cavity-type receiver at various times See Entry 78094

Seasonal thermal inventory See Entry 78105

44.50 THERMAL PROPERTIES OF MATTER (PHENOMENOLOGY, EXPERIMENTAL TECHNIQUES)

(see also 07.20 Thermal instruments and techniques)

75911 Study of heat transfer in multilayer insulations based on composite spacer materials. R.S.Mikhalkenko, V.F.Getmanets, N.P.Pershin, Yu.V.Batozskii (Phys.-Tech. Inst. of Low Temperatures, Acad. of Sci., Khar'kov, USSR).

Cryogenics (GB), vol.23, no.6, p.309-11 (June 1983).

A calorimeter was developed to study the heat conduction coefficient of multilayer insulations and optical characteristics of their shields and spacers. Data on heat conduction of insulation with spacers of various compositions were obtained. Experimental and theoretical analyses were carried out on radiation and contact components of heat transfer. (1 ref.)

Measurement of high gas-stream temperature using dynamic thermocouples See Entry 74464

Influence of thermoelastic bending on photoacoustic experiments related to measurements of thermal diffusivity of metals See Entry 76675

44.60 THERMODYNAMIC PROCESSES (PHENOMENOLOGY, EXPERIMENTAL TECHNIQUES)

(see also 05.70 Thermodynamics, 07.20 Thermal instruments and techniques)

75912 Local heat exchange in the film condensation of a stationary vapor on a vertical surface. G.I.Gimbutis (Antanas Sneckus Kaunas Polytech. Inst., Kaunas, USSR).

J. Eng. Phys. (USA), vol.43, no.3, p.974-9 (Sept. 1982). Translation of: *Inzh.-Fiz. Zh. (USSR)*, vol.43, no.3, p.390-7 (Sept. 1982).

A method is described for calculating the distributions of the heat-transfer coefficient and heat flux over the height of a condensation surface under all regimes of condensate film flow. Data on these distributions are also presented. (13 refs.)

75913 Design of cooling channels with improved thermohydraulic characteristics. G.N.Dul'nev, V.A.Korablev, A.V.Sharkov (Leningrad Inst. of Precision Mech. & Optics, Leningrad, USSR).

J. Eng. Phys. (USA), vol.43, no.3, p.983-7 (Sept. 1982). Translation of: *Inzh.-Fiz. Zh. (USSR)*, vol.43, no.3, p.401-6 (Sept. 1982).

A method is proposed for designing the profile of a slot channel so as to ensure a uniform temperature field in the cooled object. (4 refs.)

75914 A method of calculating the temperature field in multilayer media. O.D.Reshetin (Agrophys. Sci.-Res. Inst., Leningrad, USSR).

J. Eng. Phys. (USA), vol.43, no.3, p.1048-54 (Sept. 1982). Translation of: *Inzh.-Fiz. Zh. (USSR)*, vol.43, no.3, p.483-92 (Sept. 1982).

An approximate method is developed for calculating the temperature field in composite bodies for arbitrary boundary conditions on the outer and inner boundaries. (14 refs.)

75915 Evaporation and condensation on two parallel plates at finite Reynolds numbers. K.Aoki, C.Cercignani (Dipartimento di Matematica, Politecnico di Milano, Milano, Italy).

Phys. Fluids (USA), vol.26, no.5, p.1163-4 (May 1983). A kinetic theory analysis of the problem described in the title indicates that the disagreement with the continuum solution of Plesset can be less severe than it is usually assumed. (19 refs.)

Measurement of high gas-stream temperature using dynamic thermocouples See Entry 74464

New method for visualizing temperature distributions using thermochromism See Entry 74465

Effect of evaporation on convective heat exchange of a porous plate in a rarefied medium See Entry 75900

Heat transfer in enclosures with programmed heat release See Entry 75901

Complex freezing-melting interfaces in fluid flow See Entry 76098

A class of systems with a large autocorrelation coefficient See Entry 76152

Drop-to-filmwise condensation transition: heat transfer measurements for ethanediol See Entry 76601

46.00 MECHANICS, ELASTICITY, RHEOLOGY

46.10 MECHANICS OF DISCRETE SYSTEMS

(see also 03.20 General mathematical aspects)

Some classes of exact solutions of problems on the motions of two connected bodies See Entry 74256

46.20 CONTINUUM MECHANICS

(see also 03.40 General mathematical aspects)

75916 The balanced form laminate. Liu Xi-li (Harbin Civil Engng. Inst., Harbin, China).

Acta Mech. Solida Sin. (China), no.1, p.23-33 (1982). In Chinese.

The balanced form of laminate is discussed on the basis of classical lamination theory. The generalized balanced form conditions applicable to the laminate theory as well as the netting theory are derived. The mechanism of the balanced form is explained. The balanced form is the ply form for which the relative stretches in all directions in the plane of the laminate are equal. The method for calculating stress and strain of balanced form laminate is discussed. By introducing the concept of balanced strain, the balanced form of laminates composited with metal lamina is treated. The balanced form formulas for the netting theory are given in tables. Results of the study can be applied to laminates reinforced by one kind of fiber as well as to the hybrid laminates reinforced by many kinds of fiber. (4 refs.)

75917 Experimental determination of the critical pressure for a shallow elliptically paraboloidal shell. V.I.Babenko, M.M.Pugolovok.

Dopov. Akad. Nauk UkrSR. Ser. A (USSR), no.1, p.32-5 (1983). In Ukrainian.

Presents results of an experimental check of theoretical formulas obtained earlier for critical loads. (7 refs.)

75918 Solution of problems on the stressed state of an inhomogeneous hollow cone. Ya.M.Grigorenko, A.T.Vasilenko, N.D.Pankratova.

Dopov. Akad. Nauk UkrSR. Ser. A (USSR), no.1, p.38-42 (1983). In Ukrainian.

Suggests an approach to determine the stressed state of an infinite multilayer hollow cone affected by symmetric and asymmetric loads changing according to the polynomial laws. (7 refs.)

75919 Green's function of an elastic ring bounded by similar epitrochoids of class-2 and clamped along each boundary. R.S.Dube (Dept. of Math., Ranchi Univ., Ranchi, India).

Indian J. Pure & Appl. Math., vol.14, no.3, p.362-76 (March 1983).

An expression is found for the transverse displacement due to an isolated load in a thin elastic ring bounded by similar epitrochoids of class-2 and clamped along each boundary. The displacement is found as an infinite convergent series and the unknown coefficients are determined by applying a condition of convergence (Singh 1960). (4 refs.)

75920 Design for minimum stress concentration by finite elements and linear programming. P.Pedersen, C.L.Laursen (Dept. of Solid Mech., Tech. Univ. of Denmark, Lyngby, Denmark).

J. Struct. Mech. (USA), vol.10, no.4, p.375-91 (1982-1983).

The problem of design for minimum stress concentration is highly nonlinear and must be solved iteratively. Each iteration (redesign) involves three steps: an analysis of the stresses for a design, a sensitivity analysis corresponding to possible changes in this design, and the decision of redesign. For stress analysis, the FEM is a unified approach which is applied to axisymmetric solids that are also subjected to nonaxisymmetric loads. The decision of redesign is a linear programming problem and can thus be solved with the Simplex algorithm. The introduction of move-limits to the formulation is of major importance. The optimization approach is described in general, but most of the paper concentrates on a specific example and shows optimum shapes of a shoulder fillet in a stepped bar. Loads are bending, tension, or torsion, and the stress concentrations are considerably reduced. (7 refs.)

75921 A set of strain-displacement relations in nonlinear theories of rods and shells. A.Maewal (Dept. of Mech. Engng., Yale Univ., New Haven, CT, USA).

J. Struct. Mech. (USA), vol.10, no.4, p.393-401 (1982-1983).

The direct approach of Reissner (1973, 1974) and of Simmonds and Danielson (1972) is used to derive polynomial approximations to the strain-displacement relations in nonlinear theories of rods and shells via the representation of the finite rotational displacement matrix in terms of the exponential of an antisymmetric matrix. (8 refs.)

46.30 MECHANICS OF SOLIDS AND RHEOLOGY

(see also 62.20 Mechanical properties of solids, as related to microscopic structure)

75922 Singularity of contact-edge stress in laminated composites under uniform extension. R.I.Zwiers, T.C.T.Ting (Dept. of Civil Engng. & Metall., Univ. of Illinois, Chicago, IL, USA).

J. Compos. Mater. (USA), vol.17, no.1, p.49-63 (Jan. 1983). [received: June 1983]

The unusually large and possibly infinite stress at the contact-edge is one of the factors responsible for delamination when the composite is subjected to external loading. The authors study the stress singularities at the contact-edge of an interface between two adjacent layers in a laminated composite. Each layer of the composite is assumed to be of the same orthotropic material with one of the principal axes being the fiber direction. However, the angle θ which is the fiber orientation varies from layer to layer. The composite is subjected to uniform extension in the plane of the layers. It is shown that a singularity of the type $k r^{\delta}$ ($\delta < 0$) may exist, but that it depends on the stacking sequence of the layers and the complete boundary conditions. (12 refs.)

46.30C Static elasticity

75923 Variational principles of finite deformation of elasticity in nonconservative systems. Xiong Yaoxi (Peking Inst. of Aeronaut. & Astronautics, Peking, China).

Acta Mech. Sin. (China), no.1, p.86-90 (1983). In Chinese.

Starting from the theorem of virtual work in finite elastic deformation, the author establishes and proves quasi-variational principles of finite elasticity suitable for general nonconservative systems. (4 refs.)

75924 Some basic problems and engineering applications of boundary integral equation-boundary element method in elasticity. Du Qing-hua, Yao Zhen-han (Dept. of Engng. Mech., Qinghua Univ., China).

Acta Mech. Solida Sin. (China), no.1, p.1-22 (1982). In Chinese.

The direct boundary integral equation-boundary element method in elasticity is developed by inner product forms of weighted residual processes. The formulations are first established for potential problems, elastostatic problems and Kirchhoff's plate problems with the restriction of Liapunov boundary regular surfaces. The variational functionals are also given and the corner conditions are discussed. By proper treatment of the specific fundamental solutions and numerical discretizations a series of concrete problems are solved. The results of the investigation include: torsional problem of shafts with variable diameter, axial loading of axial symmetric bodies, bending of axial symmetric bodies and the plate bending problems. The investigation also showed that such numerical results are necessary for improving and increasing the accuracy of the useful engineering data on stress concentration and plate problems (including the cases of free boundaries and corner points). (39 refs.)

75925 On the problem of a ribbon-like rigid inclusion in a micropolar elastic space. M.Kaciewicz, S.Matysiak (Acad. Polonaise des Sci., Warsaw, Poland).

Bull. Acad. Pol. Sci. Ser. Sci. Tech. (Poland), vol.30, no.1-2, p.11-20 (1982).

The problem of a ribbon-like inclusion in a micropolar elastic space is considered. Singularities of stresses at the ends of the inclusion are investigated and compared with results for the problem of a crack. (12 refs.)

75926 Local stress-deformed state near sharp elastic inclusions in an isotropic plate. L.T.Berezhnitskii, I.T.Denisyuk.

Dopov. Akad. Nauk UkrSR. Ser. A (USSR), no.3, p.27-31 (1983). In Ukrainian.

An elastic equilibrium problem solution is presented for an anisotropic plate containing a sharp-pointed anisotropic elastic inclusion. The stress tensor and displacement vector asymptotic representation for the matrix is established in the vicinity of the inclusion tip. It is shown that the local stress field consists of hard and soft components. (7 refs.)

75927 Elastic equilibrium of channel shells with planar curvilinear centre lines. Ya.M.Grigorenko, V.I.Gulyaev, E.A.Gotsulyak, K.Ashuri.

Dopov. Akad. Nauk UkrSR. Ser. A (USSR), no.3, p.38-41 (1983). In Ukrainian.

Methods of differential geometry were used to analyze geometric properties of cyclic surfaces determining tube shells. The effect of geometric parameters on the stress-strain state of the tubes is investigated on the basis of the moment theory of shells. It is shown that deformation of the line of centres results in a considerable increase in the maximum values of stress and strain fields. (8 refs.)

Multimode fiber optic sensors See Entry 75828

Photoelastic pressure sensor with optical fibre links using wavelength characterization See Entry 75830

Thermal effects in a long rotating cylindrical shaft of piezo-electric material with a concentric circular axial hole See Entry 75896

- Green's function of an elastic ring bounded by similar epitrochoids of class-2 and clamped along each boundary See Entry 75919
- Design for minimum stress concentration by finite elements and linear programming See Entry 75920
- A set of strain-displacement relations in nonlinear theories of rods and shells ..
..... See Entry 75921
- On the cyclic differential auxiliary function of longitudinal-transverse bending of beam on the elastic foundation See Entry 75929
- Ultimate strength of sandwich panels with a honeycomb core
..... See Entry 75939
- Ponding instability of cylindrical air-supported membranes under nonsymmetrical loadings See Entry 75943
- The effect of multiple buckling modes on the postbuckling behavior of plane elastic frames. I. Symmetric frames See Entry 75944
- The effect of multiple buckling modes on the postbuckling behavior of plane elastic frames. II. Asymmetric frames See Entry 75945
- A correct Taylor series methods in determining the mixed mode SIF using photoelastic field data See Entry 75953
- Two coplanar Griffith cracks in an orthotropic semi-infinite medium
..... See Entry 75958
- Distribution of stresses and displacements near a crack in a homogeneous body with straight-line anisotropy of general form See Entry 75963
- Contact stresses in two elastic bodies. (Elastic bodies are rectangular plates) ...
..... See Entry 75966

46.30J Viscoelasticity, plasticity, viscoplasticity, creep, and stress relaxation (inc. rheology of solids)

- 75928 Bending of square plates supported only at middle points of the edges under uniformly distributed load. Li Ding-kun (Fuzhou Univ., China). *Acta Mech. Solida Sin. (China)*, no.1, p.99-105 (1982). In Chinese. (5 refs.)
- 75929 On the cyclic differential auxiliary function of longitudinal-transverse bending of beam on the elastic foundation. Lin Yan-tian (Huazhong Inst. of Technol., China). *Acta Mech. Solida Sin. (China)*, no.1, p.127-36 (1982). In Chinese. (no refs.)
- 75930 Simple methods of estimating the stress and strain at the notch root. N.Miki (Faculty of Engng., Ehime Univ., Ehime, Japan), K.Ohji, K.Ogura. *Bull. JSME (Japan)*, vol.26, no.213, p.331-9 (March 1983).
An elastic-plastic analysis of notched plates subjected to tension force or bending moment was made. Based on this analysis, methods of evaluating approximately the stress and strain at the notch root were proposed. Dimensionless master curves were proposed for estimating the stress and strain concentration factors under small-scale yielding condition and the stress and strain at the notch root under large-scale yielding condition. A simple formula was further developed by which the stress and strain at the notch root could approximately be calculated under load conditions below and above the gross yield stress by using the J-integral, together with a formula for estimating the J-integral. (10 refs.)
- 75931 The R-function method in solving problems on small elastoplastic deformations. V.L.Rvachov, M.S.Sinekop, L.K.Kravchenko. *Dopov. Akad. Nauk UkrSR. Ser. A (USSR)*, no.1, p.48-52 (1983). In Ukrainian.
An approach is given to solving an elastoplastic problem based on the methods of elastic solution, R-functions and the variational method. (6 refs.)
- 75932 Creep transition of transversely isotropic cylinder under internal pressure. S.K.Gupta, V.D.Rana (Dept. of Math., Himachal Pradesh Univ., Simla, India). *J. Math. & Phys. Sci. (India)*, vol.16, no.5, p.499-505 (Oct. 1982). [received: May 1983]
Derives the transitional stresses for a transversely isotropic thick-walled cylinder under internal pressure for three stages of creep. It has been shown that for vanishing anisotropy, the creep stresses are the same as those given by Gupta and Dharmani (1979) for a compressible material and by Bailey (1951) and Odqvist (1974) for an incompressible material. Numerical results for a thick-walled cylinder made of beryl have been depicted graphically. For elastic material, the curves obtained are the same as given by Marin (1966). (15 refs.)
- 75933 On dynamical description of fiber reinforced composites. G.Tolf (Dept. of Mech., Royal Inst. of Technol., Stockholm, Sweden). *J. Compos. Mater. (USA)*, vol.17, no.1, p.77-90 (Jan. 1983). [received: June 1983]
In the attempts to describe the dynamical behaviour of fiber reinforced composites, various models have been proposed. Most of these make the assumption that on the microlevel either the fibers can be regarded as rigid or the displacements vary in a prescribed way, mostly linear, so that the composite on the macrolevel can be described by fields that represent rigid translations and rotations of the midpoint of the fiber. A model of quadratic, linearly elastic fibers in a quadratic array of a linearly elastic matrix is proposed to find out when these assumptions are made legitimate. Comparison is made to the models mentioned above. It is found that the difference in stiffness can be rather small for these assumptions to be valid, but the dispersion in the lowest mode, i.e. the translational mode of the fiber, is due not to coupling with a rotational mode but to a deformation of the fiber. Also, as seen in the models assuming rigid fibers, it is found that the constants in the power expansion of the dispersion relation depend linearly on the stiffness ratio between fiber and matrix. (10 refs.)
- 75934 Bounds on displacements for elastoplastic structures by the application of energy methods. M.Capurso (Univ. di Bologna, Istituto di Sci. delle Costruzioni, Bologna, Italy). *J. Struct. Mech. (USA)*, vol.10, no.4, p.403-17 (1982-1983).
Structures composed of an elastoplastic rate-insensitive material subjected to high intensity dynamic transient disturbance are considered. A general inequality which bounds displacements from above is presented. This property allows for a meaningful approach to the problem by means of a 'holonomic' solution of the structure subjected to static fictitious loads. A simple application is presented. (14 refs.)

- 75935 Development of the concept of slip in the theory of plasticity. M.Ya.Leonov, B.A.Rychkov (Inst. of Automation, Acad. of Sci., Frunze, USSR). *Sov. Mater. Sci. (USA)*, vol.18, no.4, p.291-9 (July-Aug. 1982). Translation of: *Fiz.-Khim. Mekh. Mater. (USSR)*, vol.18, no.4, p.3-12 (July-Aug. 1982). [received: May 1983]
In formulating the basic positions of the theory of plasticity it is more natural to start not from the conditions of plasticity (the surface of loading) but from the relationships between stresses and deformations, which are provided by an experiment. The authors supplement such an approach, developed by A.A. Il'yushin, by construction of a simplified mechanism of plastic deformation (slip). The concept of slip leads to the understanding of the resistance to shear, an alternative to the understanding of the surface of loading. (12 refs.)
- 75936 Inelastic deformation of materials. K.N.Rusinko (Lenin Komsomol L'vov Polytech. Inst., Lvov, Ukrainian SSR). *Sov. Mater. Sci. (USA)*, vol.18, no.4, p.315-19 (July-Aug. 1982). Translation of: *Fiz.-Khim. Mekh. Mater. (USSR)*, vol.18, no.4, p.30-5 (July-Aug. 1982). [received: May 1983]
On the basis of physical concepts variations of the theory of inelastic deformation occurring with time are considered. If fulfillment of the Drucker postulate is taken as the criterion of truth of the variant of the tensor of plasticity, then the theory of slip and the theory of flow (with a regular surface of loading) lead to opposite results. According to the theory of flow, the difference in resistance may be determined only by the level of stresses, and according to the theory of slip, it may not be determined only by the value of stresses. (11 refs.)
- 75937 An asymptotic of a bend of a thin ligament under small loads. T.Ya.Ershova. *Vestn. Mosk. Univ. Ser. 1 (USSR)*, no.2, p.83-7 (March-April 1983). In Russian.
The behaviour of a thin ligament is studied considering geometric nonlinearity. It is shown that the stress concentration factor depends on the tensile load N . When the load is small enough ($N \sim \delta^2$, $\alpha > 2$) the value of the stress concentration factor in the first approximation is the same as in the linear case. (5 refs.)
- Analysis of thermally induced loss in fiber-optic ribbons See Entry 75795
- Some basic problems and engineering applications of boundary integral equation-boundary element method in elasticity See Entry 75924
- The near-tip displacement fields for a mode-III crack in steady growth in an elastic perfectly-plastic medium See Entry 75952
- Plastic flow of shallow shells interacting with rigid dies See Entry 75967
- Analysis on plasticity in materials with strain hardening and strain-rate sensitivity under uniaxial tension See Entry 76548
- A viscous shell formulation for the analysis of thin sheet metal forming
..... See Entry 77704
- Rectangular tubular steel columns loaded biaxially See Entry 77709
- ## 46.30L Static buckling and instability
- 75938 Note on the optimal design to the stability of clamped column under axial compression. Chueng Kengtung, Zhong Wanxie (Res. Inst. of Engng. Mech., Dalian Inst. of Technol., China). *Acta Mech. Sin. (China)*, no.1, p.45-53 (1983). In Chinese.
The optimal design of clamped column under axial compression is a classical problem. Instead of the single buckling mode criterion, as Olhoff and Rasmussen (1976) pointed out that therein two buckling modes associated with the criterion of the degenerate case must be considered. Olhoff has also deduced the necessary condition for this criterion and solved the clamped optimum column problem. But one can find that the Olhoff condition is somewhat vague. According to the theory of eigenvalue problems, if eigenvectors y_1 and y_2 correspond to the same eigenvalue λ , then any linear combination of them $\tau y_1 + \beta y_2$ is also an eigenvector. But if $y_{1a} = y_1$ and $y_{2a} = \tau y_1 + \beta y_2$ are substituted into the criterion it is found that the equality will be violated in some cases. The sensitivity analysis of the optimal degenerate design is carried out first. (5 refs.)
- 75939 Ultimate strength of sandwich panels with a honeycomb core. Zhou Zhulin (Shuanghai GRP Res. Inst., Shanghai, China). *Acta Mech. Sin. (China)*, no.1, p.62-9 (1983). In Chinese.
Sandwich panels with a honeycomb core are structural members composed of thin plates. Local instabilities of sandwich panels with honeycomb core may be classified into three types: wrinkling, shear buckling, and intra-cellular buckling. The theoretical analysis of wrinkling is based on the assumption that the compressive faces can be treated as the local instability of a plate attached to an elastic medium. Considering initial irregularities and shear deformation of the faces, the author calculates the stress in the cores and the adhesive layers; then uses Mohr's strength theory to get the ultimate strength of the faces when cores or adhesive layers are destroyed. (11 refs.)
- 75940 Bifurcation of an obliquely fiber-reinforced elastic slab under axial loads. M.Kurashige (Dept. of Mech. Engng. II, Tohoku Univ., Sendai, Japan). *Bull. JSME (Japan)*, vol.26, no.213, p.347-50 (March 1983).
In the framework of the theory of continua with kinematical constraint of inextensibility, bifurcation from homogeneous finite deformation of an obliquely fiber-reinforced elastic slab under axial loads, both tensile and compressive, is studied. The matrix is assumed to be Blatz-Ko foam rubber. In spite of the uniform axial stress loading, the initial homogeneous deformation consists not only of axial extension or contraction but also of pure shear deformation owing to the oblique reinforcement. The bifurcation is analyzed on the basis of the incremental deformation theory. For various wavelength-to-thickness ratios, the critical loads are shown in the form of curves as a function of fiber inclination. (8 refs.)
- 75941 Buckle pattern of biaxially compressed simply supported orthotropic rectangular plates. C.Libove (Dept. of Mech. & Aerospace Engng., Syracuse Univ., Syracuse, NY, USA). *J. Compos. Mater. (USA)*, vol.17, no.1, p.45-8 (Jan. 1983). [received: June 1983]
Simply supported orthotropic elastic rectangular plates in biaxial compression are considered, and it is proved that such plates will buckle with m or n (or both) equal to 1, where m and n are the number of half waves in the two principal directions. While this theorem may be known to many as an empirical computational fact, it does not appear to have been explicitly stated or proved heretofore in the literature on orthotropic plates. (3 refs.)

75942 Study on failure of pipes with multiple thinned parts by external pressure. T.Shibata, T.Nomi, H.Nakai (Faculty of Engng., Kyoto Univ., Kyoto, Japan). *J. Soc. Mater. Sci. Jpn. (Japan)*, vol.32, no.354, p.298-303 (March 1983). In Japanese.

The buckling strength of a thin pipe under external pressure has been theoretically analyzed by von Mises. However, the strength of a thin pipe with locally thinned parts has not been studied. It was shown previously (1979) that the buckling strength for such a pipe decreases when compared with a pipe having no thinned part. Also it was suggested that a specimen having two thinned parts may show lower strength than a specimen with a single thinned part. Experiments were carried out in order to check the above suggestion by using the specimens having no pipe end restriction to deformation. The experimental results did not show any dependence of strength of the number of thinned parts, and this was explained by the stress distribution in the pipe. (4 refs.)

75943 Ponding instability of cylindrical air-supported membranes under nonsymmetrical loadings. S.Lukasiewicz, P.G.Glockner (Dept. of Mech. Engng., Univ. of Calgary, Calgary, Alberta, Canada). *J. Struct. Mech. (USA)*, vol.10, no.4, p.419-35 (1982-1983).

Deals with the stability of a cylindrical air-supported membrane subjected to an eccentric line load and an accumulating ponding fluid in the depression caused by the load. A critical value of the load is calculated by solving the equations of equilibrium for the structure. Results of the analysis indicate that the eccentricity causes a significant increase in the value of the critical load. The elastic properties of the membrane are included in the analysis which leads to slightly lower critical loads than the corresponding 'inextensional' membrane case. (3 refs.)

75944 The effect of multiple buckling modes on the postbuckling behavior of plane elastic frames. I. Symmetric frames. M.Pignataro, N.Rizzi (Istituto di Sci. delle Costruzioni, Univ. di Roma, Rome, Italy). *J. Struct. Mech. (USA)*, vol.10, no.4, p.437-58 (1982-1983).

The postbuckling behavior of a one-bay, two-storey frame with built-in edges and symmetric with respect to midspan is analyzed. Columns are assumed to be inextensible and shear-undeformable, and beams are rigid. Then two buckling modes are possible, that is, sideways of the lower floor with rigid horizontal displacement of the top floor and sideways of the top floor with the lower floor undergoing no displacement. Obviously, the two buckling modes occur simultaneously if the ratios EI/h^2 (EI being the bending stiffness of a column and h its length) are properly selected. Within the framework of a Koiter-type energy approach a suitable perturbation formulation is derived from a 'hybrid' functional which is obtained by adding to the potential energy certain extra terms which account for the nonlinear energy associated with the internal forces applied to the beam at the joints. Results show that the postbuckling behavior of a single buckling mode can be stable or unstable according to the value of the ratio h/l , where l is the frame span. (25 refs.)

75945 The effect of multiple buckling modes on the postbuckling behavior of plane elastic frames. II. Asymmetric frames. N.Rizzi, M.Pignataro (Istituto di Sci. delle Costruzioni, Univ. di Roma, Rome, Italy). *J. Struct. Mech. (USA)*, vol.10, no.4, p.459-74 (1982-1983).

For pt.1 see *ibid.*, vol.10, no.4, p.437-58 (1982-83). The postbuckling behavior of an asymmetric one-bay, two-storey frame with clamped edges is analyzed. Columns have different bending stiffnesses and are pairwise of the same length. By assuming columns to be inextensible and shear undeformable, and beams to be rigid, two buckling modes are possible which are described by the sideways of the lower floor with a rigid horizontal displacement of the upper floor and a sideways of the upper floor, the lower floor undergoing no displacement. By properly selecting the ratios EI/h^2 (EI being the bending stiffness of a column and h its length) the two buckling modes may occur simultaneously. A third buckling mode is also possible but this third case is not considered. The Koiter general nonlinear theory of elastic stability recast in a form convenient for the development of finite element models has been employed. Column constraints on the field variable ϕ (ϕ being the cross-section rotation) are accounted for by means of Lagrangian multipliers. Results show that the postbuckling behavior of a single buckling mode is always asymmetric unstable and depends both on the degree of asymmetry of the structure and on the ratio h/l , l being the frame span. (19 refs.)

75946 Local buckling of thin tensioned plate with a crack. T.Fujimoto, S.Sumi (Dept. of Aeronaut. Engng., Kyushu Univ., Fukuoka, Japan). *Mem. Fac. Eng. Kyushu Univ. (Japan)*, vol.42, no.4, p.355-70 (Dec. 1982). [received: May 1983]

The local buckling characteristics of elastic plates with a central crack subjected to uniaxial tensile load are analysed by the finite element method based on the linear bifurcation theory. The boundary element method is applied to the analysis of the two dimensional stress field in the pre-buckling state, associated with the buckling analysis. The predicted buckling loads and modes are compared with the experimental results. The accuracy of analysis of the in-plane stress distribution near a crack is also discussed in conjunction with the behavior of local buckling. (25 refs.)

75947 Stability of strengthened toroidal shell segments under the uniform external pressure. A.V.Netrebko. *Vestn. Mosk. Univ. Ser. I (USSR)*, no.2, p.100-3 (March-April 1983). In Russian.

In considering the stability, the author uses the Newton-Raffson method for solving the nonlinear stability equations for a toroidal shell. The influence of the support on the magnitude of the critical load and the shape of the deflection is also studied. (4 refs.)

46.30M Vibrations, aeroelasticity, hydroelasticity, mechanical waves, and shocks

(see also 43.40 Mechanical vibrations and shock)

75948 Dynamical characteristics of structures with eccentricity and lateral transmission effect under forced vibration. Wang Yun-jian (Inst. of Engng. Mech., Acad. Sinica, Beijing, China). *Acta Mech. Solida Sin. (China)*, no.1, p.53-63 (1982). In Chinese.

Discusses the effects of eccentric structure, mass center position vibration in the direction of the inertial major axis on the dynamical characteristics. The author also investigates the effect of lateral response under forced vibration. (2 refs.)

75949 Vibrations of Mindlin's circular plates with variable thickness. K.Suzuki (Faculty of Engng., Yamagata Univ., Yonezawa, Japan), T.Yamaguchi, Y.Hirano, T.Kosawada, S.Takahashi. *Bull. JSME (Japan)*, vol.26, no.213, p.424-31 (March 1983).

The vibrations of circular plates with variable thicknesses are studied by the method of Mindlin's thick plate theory. An exact solution of circular plates with a hole is obtained. The effects of some parameters on frequencies are

discussed and the present theory is compared with the classical theory. (17 refs.)

75950 Radial vibration of a thin circular composite plate of variable modulus of elasticity and variable density with a central hole. S.Bhaduri (Inst. of Theoretical Phys., Calcutta, India), B.R.Pal. *Indian J. Theor. Phys.*, vol.29, no.3, p.239-45 (Sept. 1981).

The extensional vibration of a thin circular composite annulus plate of nonhomogeneous isotropic material, in which both the density and the modulus of elasticity are variable, has been considered here. (8 refs.)

75951 Vibrations of cantilevered circular cylindrical shells: shallow versus deep shell theory. J.K.Lee, A.W.Leissa, A.J.Wang (Dept. of Engng. Mech., Ohio State Univ., Columbus, OH, USA). *Int. J. Mech. Sci. (GB)*, vol.25, no.5, p.361-83 (1983).

Free vibrations of cantilevered circular cylindrical shells having rectangular plan forms are studied by means of the Ritz method. The deep shell theory of V.V. Novozhilov (1964) and A.L. Goldenveizer (1961) is used and compared with the usual shallow shell theory for a wide range of shell parameters. A thorough convergence study is presented along with comparisons to previously published finite element solutions and experimental results. Accurately computed frequency parameters and mode shapes for various shell configurations are presented. The present paper appears to be the first comprehensive study presenting rigorous comparisons between the two shell theories in dealing with free vibrations of cantilevered cylindrical shells. (23 refs.)

Stability loss of detonation waves in lengthened charges of heterogeneous explosives See Entry 76066

Distribution of axisymmetric waves in a piezoceramic planar cylinder See Entry 77328

46.30N Fracture mechanics, fatigue, and cracks

75952 The near-tip displacement fields for a mode-III crack in steady growth in an elastic perfectly-plastic medium. Hwang Kehchih, Dai Yao (Tsinghua Univ., China). *Acta Mech. Sin. (China)*, no.1, p.77-80 (1983). In Chinese.

Chitaley and McClintock (1971) have given the asymptotic near-tip stress field expressions for strains in integrals and a numerical solution for small-scale yielding for a mode-III crack growing steadily in an elastic perfectly-plastic medium. As pointed out by Rice (1975), the numerical results for the crack-opening displacements, equal to $0.15 k_{III}^2/kG$ at the tip (k_{III} —stress intensity factor, k —shear yield stress, G —shearing modulus), are questionable. Here, the asymptotic expressions for the plastic strains γ_x^p , γ_y^p and W are given for the active loading zone ($0 \leq \theta \leq \theta_0$), for the unloading zone ($\theta_0 \leq \theta \leq \pi - \theta_0$) and for the reloading zone ($\pi - \theta_0 \leq \theta \leq \pi$). (3 refs.)

75953 A correct Taylor series methods in determining the mixed mode SIF using photoelastic field data. Du Jiaji, Jia Youquan (Tianjin Univ., Tianjin, China). *Acta Mech. Sin. (China)*, no.2, p.185-96 (1983). In Chinese.

When considering the mixed-mode condition where both K_I and K_{II} occur together the photoelastic fringe loops are not always symmetrical at the tip of crack. The Taylor series correction method was applied to mixed-mode problems. The data used to determine stress intensity factors were measured simultaneously at several rays which intersected the fringe loops and originated from the crack tip. The least squares method was employed to reduce the errors. (8 refs.)

75954 Some problems in the combined fracture criterion of cracks. Kuang Zhen-bang (Xi'an Jiaotong Univ., China). *Acta Mech. Solida Sin. (China)*, no.1, p.91-8 (1982). In Chinese. (9 refs.)

75955 A procedure for evaluating the stress intensity factor at crack tip in a finite internally cracked tensile plate. Chen Yi-zhou, Guan Zhong-xin (North-western Polytech. Univ., China). *Acta Mech. Solida Sin. (China)*, no.1, p.120-6 (1982). In Chinese. (6 refs.)

75956 Effect of combined stresses on contact fatigue. Wen Shizhu. *Chin. J. Mech. Eng. (China)*, vol.18, no.4, p.1-7 (Dec. 1982). In Chinese. [received: May 1983]

By using the statistical technique of experiment and treating data, the effect of combined stresses on contact fatigue is investigated. The superimposed tensile bending stress markedly shortens the process of fatigue, but the effect of compressive stress is dependent on its magnitude. A small superimposed compressive bending stress can increase the fatigue life, while a large compressive bending stress decreases it. There is a critical compressive bending stress at which the fatigue life becomes maximum. According to the experimental results, the author attempts to analyze the availability of some hypotheses of decisive stress for estimation of contact fatigue, and indicates that taking the maximum surface shear stress as the decisive stress is more suitable than others. It seems that the initiation of combined stressed contact fatigue takes place at the surface. (8 refs.)

75957 Distribution of pressure necessary to produce Griffith cracks of prescribed shape in an orthotropic medium. A.K.Das, B.Behera (Dept. of Maths., Regional Engng. Coll., Rourkela, India). *Indian J. Technol.*, vol.20, no.11, p.419-26 (Nov. 1982). [received: May 1983]

The author considers the problems of determining the distribution of surface stresses necessary to produce Griffith cracks of prescribed shape in (i) an infinite orthotropic plane, and (ii) an infinite orthotropic strip of finite width. The analytical expression for crack energy necessary to produce Griffith cracks of prescribed shape has been determined. The numerical calculations of the required pressure have been made taking into account the values of constants for boron-epoxy composite and some isotropic material. (9 refs.)

75958 Two coplanar Griffith cracks in an orthotropic semi-infinite medium. R.B.Mohapatra, H.Parhi (Regional Engng. Coll., Rourkela, India). *J. Math. & Phys. Sci. (India)*, vol.16, no.6, p.545-63 (Dec. 1982). [received: May 1983]

The authors consider the problem of determining the stress-intensity factors in a semi-infinite orthotropic elastic medium containing two coplanar cracks, parallel to the boundary. They assume that the cracks are opened by constant internal pressure and that the free edge of the medium is rigidly clamped. The mixed boundary conditions lead to two sets of triple integral equations, which are solved by using Finite Hilbert transform technique. Analytical expressions up to h^{-8} are derived for stress-intensity factors where h , which is much greater than 1, is the distance of the cracks from the free boundary. Numerical calculations for a fibre-reinforced composite material and an isotropic material are carried out and the effect of orthotropy on the stress intensity factors is reported. (10 refs.)

75959 Finite element analysis of surface crack configuration obtained by electrical potential method. S.Sakata, M.Hayashi, T.Shimizu, S.Shida (Mech. Engng. Res. Lab., Hitachi Ltd., Hitachi, Japan). *J. Soc. Mater. Sci. Jpn. (Japan)*, vol.32, no.354, p.334-9 (March 1983). In Japanese.

Finite element procedures were used to discuss the practicality of the electrical potential technique for monitoring the surface crack of a plate. The analysis applied to solve the potential field problems involves the solution of the Laplace equation. Analytical figures were modeled as three-dimensional bodies using eight-nodes isoparametric elements. A computer program ADI-NAT was employed in the study. From finite element analyses, the following method of determining surface crack configurations was proposed. The electrical potential ratio is determined first at several positions from a crack center and the relationship between electric potential ratio and distance from a crack center is obtained. By assuming that a surface crack takes a half elliptical configuration, the crack length c at the surface can be estimated from the relation between the crack area ratio and the distribution of electrical potential ratio from a crack center. The crack depth a can then be determined from the distribution of the normalized electrical potential ratio. (4 refs.)

75960 Fatigue and fracture mechanics. T.V.Duggan (Mech. Behaviour of Materials Lab., Portsmouth Polytech., Portsmouth, England). *Phys. Technol. (GB)*, vol.14, no.3, p.126-32 (May 1983). The formation and behaviour of cracks are first examined and their influence on the mechanical integrity of components is stressed. A wide variety of physical and environmental factors which affect modern design methods are discussed. (9 refs.)

75961 Use of the finite-element method in fracture mechanics. E.M.Morozov, G.P.Nikishkov (Moscow Engng. Phys. Inst., Moscow, USSR). *Sov. Mater. Sci. (USA)*, vol.18, no.4, p.299-314 (July-Aug. 1982). Translation of: *Fiz.-Khim. Mekh. Mater. (USSR)*, vol.18, no.4, p.13-29 (July-Aug. 1982). [received: May 1983]

It is possible to distinguish various aspects of the use of the finite-element method in problems of fracture mechanics. First, calculation of the parameters controlling fracture (stress intensity factors, the contour J-integral, etc.) for areas of different form. Second, simulation of the processes of fracture or of the behavior of bodies with a stationary crack under conditions for which adequate mathematical models have not yet been constructed. Calculation experiments in combination with full-scale ones are especially successful. Third, analysis of the strength of actual structures from the point of view of the resistance to brittle fracture on the basis of the finite-element method is extremely important for practical purposes. (80 refs.)

75962 Mathematical models of fatigue crack growth. S.Ya.Yarema, L.S.Mel'nichok (G.V. Karpenko Physicomech. Inst., Acad. of Sci., Lvov, Ukrainian SSR). *Sov. Mater. Sci. (USA)*, vol.18, no.4, p.337-43 (July-Aug. 1982). Translation of: *Fiz.-Khim. Mekh. Mater. (USSR)*, vol.18, no.4, p.55-61 (July-Aug. 1982). [received: May 1983]

Cyclic crack resistance tests of materials include measurements of the crack length l_i in the sample and of the corresponding number of load cycles N_i with a specified periodically changing load. The set of data $\{l_i, N_i\}_{i=1}^m$ is subjected to primary treatment to determine the pairs of values: the crack growth rate $v = \Delta l / N$ and the maximum stress intensity factor K_{\max} or its range ΔK . The block of data obtained $\{v_i, K_i\}_{i=1}^m$ is represented in a system of coordinates with logarithmic scales ($\log v$ vs. $\log K$) by points, the combination of which is called the experimental fatigue failure curve. In the second stage of treatment the $\{v_i, K_i\}_{i=1}^m$ block is described by an analytical expression of the specified form $v = f(\alpha_1 v_m, \dots, \alpha_m, K)$, which is a mathematical model of fatigue crack growth. (12 refs.)

75963 Distribution of stresses and displacements near a crack in a homogeneous body with straight-line anisotropy of general form. V.V.Panas-yuk, L.T.Berezhnitskii, M.E.Chaplya (G.V. Karpenko Physicomech. Inst., Acad. of Sci., Lvov, Ukrainian SSR). *Sov. Mater. Sci. (USA)*, vol.18, no.4, p.343-9 (July-Aug. 1982). Translation of: *Fiz.-Khim. Mekh. Mater. (USSR)*, vol.18, no.4, p.61-9 (July-Aug. 1982). [received: May 1983]

Many constructional composite materials are considered as a first approximation as homogeneous with anisotropy of the elastic and strength properties. In the case of straight-line anisotropy it is possible to obtain condition of boundary problems of the theory of elasticity with the use of methods of the theory of functions of a complex variable. (11 refs.)

75964 Plane problems of finite regions containing multiple cracks. M.Isida, H.Tsuru.

Technol. Rep. Kyushu Univ. (Japan), vol.55, no.6, p.649-56 (Dec. 1982). In Japanese. [received: May 1983]

Deals with the analysis of the crack tip stress intensity factors of the following problems: (1) An infinite row of edge cracks on the side of a strip under tension. (2) Infinite rows of edge cracks on both sides of a strip under tension. (3) Edge cracks on both sides of a plate under tensions of stress, displacement and concentrated loading types. (4) An infinite row of collinear cracks in the middle of a strip under tensions of stress and displacement types. The stress function is based on the eigenfunction expansions of the complex potentials satisfying the traction free conditions along the crack edges. The unknown coefficients are determined with the modified boundary collocation technique in which the stress resultant or displacement of each segment is required to take assigned values, and the stress intensity factor is calculated from the obtained stress function. The accuracy of the proposed method is shown to be excellent by checking the convergence of the numerical values with increasing values of the number of the segments. (8 refs.)

75965 Behaviour of cracks in a plate considering residual stresses. R.Wille.

Vestn. Mosk. Univ. Ser. 1 (USSR), no.2, p.91-5 (March-April 1983). In Russian.

A plate of finite breadth with one surface crack is considered. There are some residual stresses distributed in the plate. The author computes the intensity coefficient for different depths of the crack and different distributions of residual stresses. The position of the closed crack is found in the zone of pressing stresses. The results of the computation are analyzed and compared with analytical solutions for a half-plane with a crack perpendicular to the boundary. (3 refs.)

Local buckling of thin tensioned plate with a crack See Entry 75946

Thermal-activation interpretation of splitting fracture See Entry 76559

Mechanism of fatigue crack propagation in metallic materials See Entry 76561

Theoretical prediction of the cracking stress of three-dimensional randomly distributed steel fibre reinforced concrete See Entry 77721

X-ray fractographic study on fatigue fracture surface of SM50A steel See Entry 77739

On the stability of shear cracks and the calculation of compressive strength See Entry 78531

The dynamic tensile strength of ice and ice-silicate mixtures .. See Entry 78833

46.30P Friction, wear, adherence, hardness, mechanical contacts

75966 Contact stresses in two elastic bodies. (Elastic bodies are rectangular plates). Y.Minakuchi (Faculty of Engng., Yamanashi Univ., Takeda, Kofu, Japan), T.Sawa, K.Yoshimine, T.Koizumi. *Bull. JSME (Japan)*, vol.26, no.213, p.340-6 (March 1983).

The contact problem of two laminated dissimilar rectangular plates subject to an arbitrary symmetric loading is considered. The two dimensional theory of elasticity is used to analyse the contact stress and the deformation between the rectangular plates. By neglecting shearing stress on the contact surface, an exact solution satisfying the remaining boundary conditions is obtained. Numerical calculations are carried out for various rigidities and thicknesses of the plates under various loading conditions. In order to examine the results of the theoretical analysis the contact stress is measured experimentally by using pressure-sensitive pins attached to a rectangular plate. (11 refs.)

75967 Plastic flow of shallow shells interacting with rigid dies. G.I.L'vov. *Dopov. Akad. Nauk UkrSR. Ser. A (USSR)*, no.3, p.44-7 (1983). In Ukrainian.

Deals with a variational statement of contact problems of elastoplastic deformation of shallow shells interacting with rigid dies. The solution existence and uniqueness are proved for flow equations which are regularized. The control of regularization is given in terms of the theory of variational inequalities. (5 refs.)

75968 Variational methods of investigating certain classes of three-dimensional problems of contact between elastic bodies in the presence of friction. A.A.Spektor (All-Union Sci.-Res. Construction-Technol. Inst. of Bearing Industry, Moscow, USSR). *Sov. Phys.-Dokl. (USA)*, vol.27, no.7, p.548-50 (July 1982). Translation of: *Dokl. Akad. Nauk SSSR*, vol.265, no.1-3, p.592-6 (July 1982). [received: April 1983]

Three-dimensional static problems of contact between an elastic body and an elastic base in the presence of friction, when the coefficient of friction depends on the pressure and the local slippage of the body relative to the base, are discussed. The formation of slippage and cohesion regions at the contact surface is assumed. (13 refs.)

Effect of combined stresses on contact fatigue See Entry 75956

Solution of the steady-state problem of heat exchange and flow of lubricant in radial sliding bearings with self-aligning segments See Entry 76028

Means of plastic self-indentation of solids in contact See Entry 76765

Wear analysis See Entry 77767

46.30R Measurement methods and techniques (see also 07.10 Mechanical instruments and techniques, 81.70 Materials testing)

75969 A method for automatic measurement of Brinell hardness using a microcomputer. H.An (Faculty of Engng., Osaka Electro-Communication Univ., Osaka, Japan).

Bull. Jpn. Soc. Precis. Eng. (Japan), vol.16, no.4, p.261-2 (Dec. 1982).

An inexpensive and simple automated method of non-contact type using a laser has been developed. Comparison examination of the observed results on the Brinell hardness value using a conventional measuring microscope method and those of this automated method is reported. (4 refs.)

75970 Simplified vibrating-reed technique for the measurement of the temperature dependence of Young's modulus of small samples. W.A.Aiello, C.R.Wolfe, W.A.Little (Dept. of Phys., Stanford Univ., Stanford, CA, USA). *Rev. Sci. Instrum. (USA)*, vol.54, no.5, p.594-6 (May 1983).

A simplified vibrating-reed technique for the measurement of the temperature dependence of Young's modulus of small thin samples is described. The vibration of the reed is detected optically rather than with a capacitively coupled electrode as has been used by previous investigators. The optical coupling greatly simplifies the sample stage and electronic circuitry. It is made possible by the use of a microminiature Joule-Thomson-effect refrigerator which mounts directly onto the X-Y stage of a metallurgical microscope. Because of the refrigerator's small size and lack of mechanical vibrations, the high-quality room temperature optics of the microscope can be used to detect the small amplitude vibration of the reed over a wide temperature range. The authors have observed the Curie and Neel points of the magnetic phase transitions of terbium at $T_C = 221K$ and $T_N = 233K$, respectively. In addition, they have measured Young's modulus at 280K to be 5.90×10^{11} dyn/cm². (10 refs.)

Dummy stable bridge source digital strain indicator and the elimination of nonlinear errors See Entry 74452

Talbot interferometry with a vibrating phase object See Entry 74522

Determination of electromagnetic field scattered by small defects and influence of boundary between media See Entry 75571

Stabilization of single and multimode fiber optical microbend sensors See Entry 75819

Acoustical speckle interferometry See Entry 75888

A correct Taylor series methods in determining the mixed mode SIF using photoelastic field data See Entry 75953

Finite element analysis of surface crack configuration obtained by electrical potential method See Entry 75959

Wear analysis See Entry 77767

Numerical analysis of ductile fracture experiments using single-edge notched tension specimens See Entry 77819

Measurement of crack profile of semi-elliptical surface cracks using the AC potential technique See Entry 77827

Infrared measurement of specimen temperature profiles during fatigue crack propagation tests See Entry 77831

46.60 RHEOLOGY OF FLUIDS AND PASTES

75971 The rheology of the fiber-forming process in melts of incompatible polymers at highly uniform shear. M.P.Zabugina, E.P.Plotnikova, G.V.Vinogradov, V.E.Dreval (Inst. of Petrochem. Synthesis, Acad. of Sci., Moscow, USSR).

Int. J. Polym. Mater. (GB), vol.10, no.1, p.1-12 (1983).

The viscoelastic properties of polymer mixtures were investigated over a wide range of component concentrations and viscosities in a field of relatively low shear rates and highly uniform shear stresses. Mixtures of polyethylene and polystyrene were studied. (22 refs.)

75972 Linear and nonlinear viscoelastic functions for polymer melts and concentrated solutions. G.A.Alvarez, H.-J.Cantow (Inst. für Makromolekulare Chem., Univ.-Freiburg, Freiburg, Germany).

Int. J. Polym. Mater. (GB), vol.10, no.1, p.53-76 (1983).

Recent modifications of the Rouse theory for polymer melts and concentrated solutions are presented and compared with measurements of dynamic modulus and oscillatory first normal stress coefficients for cis-1,4-polybutadiene (PB). Measurements of finite-amplitude storage modulus and second normal stress coefficient are given along with current theories to explain these effects. Non-linear transient measurements for PB melts, although in some cases impeded by instrument compliance, provide critical tests for theory. The procedure of extending results of the network theory to nonlinear behaviour, as exemplified by Carreau's model, is shortly reviewed. It is concluded that molecular theories based on clear, independently testable assumptions of molecular architecture, are likely to be better guides for progress in polymer dynamics, than empirical theories. (21 refs.)

75973 Explanation for the 3.4-power law for viscosity of polymeric liquids on the basis of the tube model. M.Doi (Dept. of Phys., Tokyo Metropolitan Univ., Tokyo, Japan).

J. Polym. Sci. Polym. Phys. Ed. (USA), vol.21, no.5, p.667-84 (May 1983).

The viscosity $\eta_0(M)$ of polymeric liquids of molecular weight M is calculated on the basis of the tube model formulated by Doi and Edwards (see *J. Chem. Soc. Faraday Trans. II*, vol.74, p.1789, 1978). The contour length fluctuation of polymers along the tube, which was neglected in ref.3, is now explicitly taken into account. The result is $\eta_0(M) = 9.6\eta_0(M_c)(M/M_c)^3[1 - 1.04(M_c/M)^{1/2}]^{1/2}$ ($M \geq 10M_c$) where $M_c = 2M_e$ and M_e is the molecular weight between the entanglement points. This result is numerically close to the empirical 3.4-power law, $\eta_0(M) = \eta_0(M_c)(M/M_c)^{3.4}$, for $10M_c \leq M \leq 100M_c$. It is concluded that the 3.4-power law is actually an approximate expression for the real curve which slowly approaches the asymptotic form. (11 refs.)

75974 Positive hole pressures and negative exit pressures generated by molten polyethylene flowing through a slit die. A.S.Lodge, L.de Vargas (Rheology Res. Center, Univ. of Wisconsin, Madison, WI, USA).

Rheol. Acta (Germany), vol.22, no.2, p.151-70 (March-April 1983).

A new slit die rheometer has been constructed to measure elastic and viscous properties of molten polymers at low shear rates. The wall shear stress σ and the extrapolated exit pressure P_x are determined by means of two pressure transducers mounted flush with a die wall. The hole pressure P^* is obtained from one of the flush-mounted transducers and a third transducer mounted in a transverse slot opposite the flush-mounted transducer. The wall shear rate $\dot{\gamma}$ is obtained from a metering pump. Electrical heaters give melt temperatures that are uniform to within $\pm 0.1^\circ\text{C}$ at 150°C . For two low-density polyethylene samples of Melt Index 2 and 50, at shear rates in the range 0.1 to 8 s^{-1} , it is found that (a) viscosity values agree with those obtained using two Weissenberg Rheogoniometers (WRGs); (b) hole pressure data agree with the predictions of the 'HPB' transverse-slot equation $N_1 = 2\delta dP^*/d\sigma$ when WRG data are used for the first normal stress difference N_1 ; and (c) exit pressures are large and negative, in marked disagreement with certain published equations relating P_x , N_1 and σ . An error analysis shows that P_x values can contain significant negative contributions arising from the pressure dependence of viscosity, even at low shear rates. As a means for in-line measurement of melt elasticity at low shear rates, the results favor the use of the hole pressure, but raise serious questions about the use of the exit pressure. (66 refs.)

75975 Polymer melt rheology with a slit die. H.M.Laun (Kunststofflab., BASF Aktiengesellschaft, Ludwigshafen/Rhein, Germany).

Rheol. Acta (Germany), vol.22, no.2, p.171-85 (March-April 1983).

A piston drive high pressure slit die rheometer with three pressure holes along the die and one in the barrel was used to investigate viscosity, entrance and exit pressure losses, and pressure coefficient of viscosity of a LDPE (low density polyethylene) melt. Hydrostatic calibration of melt pressure transducers can be performed in the rheometer. The slit die results are compared with measurements on circular dies assuming linear and parabolic pressure profiles in both cases. A simplified conversion from apparent to true viscosity, applicable for single point measurements, has been used. In spite of the different symmetries the Bagley correction from the linear pressure profile of circular dies was found to be equal to the sum of exit and entrance pressure losses in the slit. The magnitude and sign of the exit pressure loss depend on the type of pressure profile used. The influence of a pressure dependent viscosity and a temperature gradient along the die on the curvature of the pressure profile is discussed. To directly investigate the effect of pressure the pressure level at constant flow rate was increased stepwise by means of a valve attached to the exit of the slit die. (18 refs.)

75976 Determination of the weight-average molecular weight of polyamide-6 on the basis of melt viscosity. Z.Kembski, J.Torzecki (Inst. of Chem. Engng., Lodz Tech. Univ., Lodz, Poland).

Rheol. Acta (Germany), vol.22, no.2, p.186-96 (March-April 1983).

A theory of a two-point rheometrical method of determination of the weight-average molecular weight M_w of polyamide-6 is presented. The method is based on the measurement of the instantaneous values of zero-shear-rate viscosity of the degrading polymer melt, and a formula is derived which enables the calculation of the initial value of M_w (i.e. at zero-residence-time in molten state) of the investigated sample. The experimental verification of the method proves its applicability. The considerations carried out may be regarded as a first step towards developing a theory of an in-line rheometer for a continuous determination of M_w . (39 refs.)

75977 The rheological behaviour of HDPE/LDPE blends. I. End effects and shear viscosity. D.Curto, F.P.La Mantia, D.Acierno (Istituto di Ingegneria Chimica, Univ. of Palermo, Palermo, Italy).

Rheol. Acta (Germany), vol.22, no.2, p.197-208 (March-April 1983).

The rheological behaviour of three types of HDPE/LDPE (high density polyethylene/low density polyethylene) blends at several compositions (various weight percentages of LDPE) has been studied with the aid of a capillary rheometer and three different capillaries. In particular, entrance effects and shear viscosities have been determined over a wide shear rate region and at different temperatures. Thus activation energies could also be evaluated.

Synergistic effects are evidenced when the relevant properties of the homopolymers parents are not too different from one another. (14 refs.)

75978 Rheograms for engineering thermoplastics from melt flow index. A.V.Shenoy, D.R.Saini, V.M.Nadkarni (Chem. Engng. Div., Nat. Chem. Lab., Pune, India).

Rheol. Acta (Germany), vol.22, no.2, p.209-22 (March-April 1983).

A method proposed earlier has been extended to estimate complete flow curves or rheograms of engineering plastics. Master curves that are independent of the grade and temperature have been generated and presented for acrylics, polyacetal, nylons, polyethylene terephthalate, polycarbonate and polysulfone. The influence of the various molecular parameters on the viscosity behaviour of polymer melts have been explained rationally. More specifically, the effects of chain branching and of chain rigidity on the master curve of a resin type have been elucidated with reference to polyacetal and polysulfone, respectively. The method presented can be used effectively by processors of engineering plastics. (21 refs.)

Viscoelastic squeeze-film flows—Maxwell fluids See Entry 76075

Plane and axis-symmetric stagnation flow of a Maxwellian fluid See Entry 76076

On nonlinear effects in the extensional flow of polymeric liquids See Entry 76077

47.00 FLUID DYNAMICS

(for fluid dynamics of quantum fluids, see 67.; for geophysical fluid dynamics, see 92.10; for astrophysical gas dynamics, see 95.30; for biological fluid dynamics, see 87.45)

47.10 GENERAL THEORY

(see also 03.40G Mathematical aspects)

75979 On mean residence times in flow systems. R.C.Awasthi, K.Vasudeva (Dept. of Chem. Technol., Univ. of Bombay, Bombay, India).

Chem. Eng. Sci. (GB), vol.38, no.2, p.313-19 (1983).

A widely accepted result of residence time theory states that mean residence time is equal to the system volume divided by the flow rate. Taking a two section system it is argued and experimentally demonstrated that the above theoretical result is not universal. A possible implication of this result is that even for a single section system the above result may not hold in all the cases. This is also supported by experimental data on a single section system. (15 refs.)

Contributions of Ernst Mach to fluid mechanics See Entry 74247

On one-dimensional stretching functions for finite-difference calculations See Entry 74281

Application of the multigrid method to Poisson's equation in boundary-fitted coordinates See Entry 74282

Generation of boundary-fitted curvilinear coordinate systems for a two-dimensional axisymmetric flow problem See Entry 74283

On Brownian motion in fluids with spin See Entry 74383

A theoretical study of laminar mixed convection from a horizontal cylinder in a cross stream See Entry 75982

Drag of a vaporizing spherical particle in a slow flow of a binary mixture of gases See Entry 76058

Application of the triple-deck theory of viscous-inviscid interaction to bodies of revolution See Entry 76064

Simplified nonlinear descriptions of two-phase flow instabilities in vertical boiling channel See Entry 76091

47.15 LAMINAR FLOWS

75980 Analysis of the Couette flow by means of the new direct-simulation method. K.Nambu (Inst. of High Speed Mech., Tohoku Univ., Sendai, Japan).

J. Phys. Soc. Jpn. (Japan), vol.52, no.5, p.1602-8 (May 1983).

By use of the new direct-simulation method, the exact numerical solution of the Couette-flow problem is obtained over the whole range of the Knudsen number. (The wall Mach number is 3.0.) By comparing the obtained solution, with the approximate six-moment solution, the accuracy of the latter is examined in detail. For the flow velocity and shearing stress, the six-moment solution shows reasonable agreement with the simulation solution. For the temperature, density, and heat flux, the error of the six-moment solution is fairly large in all flow regimes except the near-continuum one. The pressure is not uniform in the transition-flow regime, which is different from the prediction of the six-moment solution.

Analysis of transient natural convection flow at high Prandtl number using a matched asymptotic expansion technique See Entry 76018

Laminar natural convection from a horizontal plate and the influence of plate-edge extensions See Entry 76023

Unsteady flow of a viscous fluid in a porous elliptic tube See Entry 76101

Multiple solutions and hysteresis in steady parallel viscous flows See Entry 76114

Flow in curved pipes See Entry 76116

Theory of capillary viscometer for gases See Entry 76135

A volume flow measuring device employing pseudonoise heat impulses See Entry 76137

Barodiffusion in a binary mixture due to rotation of a circular cylinder See Entry 76143

47.15C Laminar boundary layers

75981 Action of an elastic boundary on a boundary layer. L.P.Kozlov, V.I.Korobov, V.V.Babenko.

Dopov. Akad. Nauk UkrSR. Ser. A (USSR), no.1, p.45-7 (1983). In Ukrainian.

Establishes the fact that the selective character of elastic plates affects the boundary layer. It was found that the magnitude of the effect and the range of Reynolds numbers corresponding to the maximum efficiency are associated with the mechanical parameters of the surfaces. (6 refs.)

75982 A theoretical study of laminar mixed convection from a horizontal cylinder in a cross stream. H.M.Badr (Mech. Engng. Dept., Univ. of Petroleum & Minerals, Dhahran, Saudi Arabia). *Int. J. Heat & Mass Transfer (GB)*, vol.26, no.5, p.639-53 (May 1983).

The problem of laminar mixed convection from a horizontal isothermal cylinder is considered. The free stream direction is assumed to be horizontal and perpendicular to the cylinder axis. The study is based on the solution of the full Navier-Stokes and energy equations for 2-dim. flow of a Boussinesq fluid. The free stream is assumed to start impulsively from rest and the velocity and thermal boundary layers are developed in time until reaching steady conditions. The investigation covered the ranges of Reynolds number $1 < Re < 40$ and Grashof numbers up to $Gr = 5Re^2$ while keeping Prandtl number at a constant value of 0.7. Comparison of results with previous experimental correlations shows a good agreement. The streamline and isotherm patterns are plotted and different aspects of the phenomenon are discussed. (21 refs.)

75983 Turbulent spots, wave packets, and growth. F.W.Chambers, A.S.W.Thomas (Advanced Res. Organization, Lockheed-Georgia Co., Marietta, GA, USA).

Phys. Fluids (USA), vol.26, no.5, p.1160-2 (May 1983). The smoke wire technique was used to study initial formation and growth of turbulent spots in a laminar boundary layer. The spots were observed to result not from the breakdown of wave packets arising at the spot generator but from longitudinal structures which preceded the wave packets. The original wave packet in turn was observed to ultimately take the form of oblique waves trailing the spot. These waves had little apparent involvement in the growth of the spot and did not appear to be associated with the formation of new spots within the region visualized. (4 refs.)

75984 Approximate determination of the boundary of a lubricating layer. M.A.Galakhov, V.P.Kovalev (Physicotech. Inst., Moscow, USSR). *Sov. Phys.-Dokl. (USA)*, vol.27, no.7, p.535-7 (July 1982). Translation of: *Dokl. Akad. Nauk SSSR*, vol.265, no.1-3, p.560-4 (July 1982). [received: April 1983]

The authors consider the flow of a thin layer of a viscous incompressible liquid between two rigid smooth bodies which are steadily rocking and (or) sliding. They attach a coordinate system to the axes of the bodies in such a way that the region occupied by the liquid is time-independent. They position the x and y axes in the plane tangent to one of the bodies at the point located at the shortest distance from the other body. Let a bounded contact region ω exist in which the liquid occupies the entire interval in z between the surfaces, and let a Reynolds-type equation $\text{div}(h^3 \text{grad } p) = 12 \mu h \dot{h} = 0$, be valid in this region, where $h(x,y)$ is the distance in z between the surfaces, μ is the viscosity of the liquid, $p(x,y)$ is the pressure on it, and $u = u(x,y) = 2^{-1} [u_1(x,y) + u_2(x,y)]$ is the rocking velocity (one-half the sum of the surface velocities). (2 refs.)

The cancellation of a sound-excited Tollmien-Schlichting wave with plate vibration See Entry 75985

A novel property of the displacement thickness in three-dimensional boundary-layer theory See Entry 75999

A class of backward free-convective boundary-layer similarity solutions See Entry 76003

On the effects of viscous dissipation and pressure work in free convection loops See Entry 76008

Convective diffusion toward rotating polar spherical electrode See Entry 76027

Plane and axis-symmetric stagnation flow of a Maxwellian fluid See Entry 76076

Regular flow around a flat plate set between two parallel walls with different permeabilities See Entry 76100

The evolution of Tollmien-Schlichting waves near a leading edge. II. Numerical determination of amplitudes See Entry 76111

Unsteady laminar flow of a viscous liquid in a symmetrical porous-walled channel of varying width See Entry 76112

47.15F Stability of laminar flows

75985 The cancellation of a sound-excited Tollmien-Schlichting wave with plate vibration. C.J.Gedney (Dept. of Mech. Engng., MIT, Cambridge, MA, USA).

Phys. Fluids (USA), vol.26, no.5, p.1158-60 (May 1983). An experiment is conducted in which plate vibration is used to successfully cancel a sound-excited Tollmien-Schlichting wave. With sound excitation, transition to turbulence in the boundary layer occurs at a streamwise Reynolds number (R_x) of 1.2×10^6 . The addition of plate vibration delays the transition to $R_x = 1.8 \times 10^6$. In the laminar region of the boundary layer (at $R_x = 0.97 \times 10^6$) the addition of plate vibration reduces the level of streamwise velocity fluctuations from more than 100 times to only two times the particle velocity of the sound excitation. (8 refs.)

47.20 HYDRODYNAMIC STABILITY

75986 Unsteady flow of viscous incompressible liquid around cylinder at small Reynolds numbers. N.A.Gumerov.

Vestn. Mosk. Univ. Ser. I (USSR), no.2, p.79-83 (March-April 1983). In Russian.

The asymptotic behaviour of the resistance force is studied. It is shown that, for the case in question, the stationary solution of the approximate Stokes equation does not exist. (2 refs.)

Viscous-inviscid interactions in cascades See Entry 75997

Symmetry analysis of convection patterns See Entry 76002

Monotonic and oscillatory instabilities of a two-layer system of immiscible liquids heated from below See Entry 76029

Stability and heat transfer of rotating cryogenics. I. Influence of rotation on the onset of convection in liquid ^4He See Entry 76040

On the unsteady motion of a profile in a heavy fluid bounded by a free line See Entry 76051

Unsteady flow of a dusty viscous liquid through confocal elliptical ducts See Entry 76090

Axisymmetrical two-dimensional steady and unsteady flow through porous media See Entry 76099

Convective instabilities in binary mixtures in a porous medium See Entry 76106

Unsteady laminar flow of a viscous liquid in a symmetrical porous-walled channel of varying width See Entry 76112

Nonlinear electrohydrodynamic Rayleigh-Taylor instability. I. A perpendicular field in the absence of surface charges See Entry 76120

Measurements of pressure fluctuation in turbulent flow See Entry 76136

Instabilities, pattern formation, and turbulence in flames See Entry 77890

47.25 TURBULENT FLOWS, CONVECTION, AND HEAT TRANSFER

75987 Application of Pade approximation to turbulence problem. A.Fukuyu (Dept. of Math. Sci., Tokyo Denki Univ., Saitama, Japan).

J. Phys. Soc. Jpn. (Japan), vol.52, no.5, p.1593-601 (May 1983). The energy spectrum function $E(k,t)$ for one-dimensional Burgers' turbulence is defined as a Taylor series expansion in time variable t . Assuming a multivariate Gaussian distribution of velocity field at an initial instant, the first six coefficients of this Taylor series are calculated explicitly in terms of the initial energy spectrum. To approximate to $E(k,t)$ the Pade approximation is adopted. The numerical results show that a Pade approximant is much better than a partial sum of Taylor series as an approximation to $E(k,t)$ for wave numbers which are not large compared with a representative wave number. (9 refs.)

Statistical thermodynamics of turbulent transport processes See Entry 74414

47.25C Isotropic turbulence

75988 Technical improvements for direct numerical simulation of homogeneous three-dimensional turbulence. C.Basdevant (Lab. de Meteorologie Dynamique, Ecole Normale Supérieure, Paris, France).

J. Comput. Phys. (USA), vol.50, no.2, p.209-214 (May 1983). Several equivalent forms of incompressible Navier-Stokes equations in three dimensions are presented. The required number of Fourier transforms and input/output passes are discussed for spectral simulation of periodic flow. (2 refs.)

75989 Turbulent bores and hydraulic jumps. P.A.Madsen, I.A.Svendsen (Inst. of Hydrodynamics & Hydraulic Engng., Tech. Univ. of Denmark, Lyngby, Denmark).

J. Fluid Mech. (GB), vol.129, p.1-25 (April 1983). A theoretical model for the velocity field and the surface profile of bores and hydraulic jumps is developed. The turbulence is assumed to be concentrated in a wedge that originates at the toe of the front and spreads towards the bottom, and the turbulent closure used is a simplified $k-\epsilon$ model allowing for non-equilibrium in the turbulent kinetic energy. The flow equations are satisfied in depth-integrated form (method of weighted residuals), and measured deviations from static pressure are analysed and shown to have a negligible effect on the results. Comparison with measurements shows good agreement, but there is a clear need for further experimental results in the highly turbulent region near the free surface. Some basic mechanisms of the flow are discussed and explained from the theory. (31 refs.)

75990 A statistical model of fluid-element motions and vertical diffusion in a homogeneous stratified turbulent flow. H.J.Pearson (Dept. of Appl. Maths. & Theoretical Phys., Univ. of Cambridge, Cambridge, England), J.S.Puttock, J.C.R.Hunt.

J. Fluid Mech. (GB), vol.129, p.219-49 (April 1983). The vertical displacements $Z(t)$ of fluid elements passing through a source $z=0$ at $t=0$ in a horizontal mean flow with stably stratified statistically stationary turbulence (with buoyancy frequency N and velocity time-scale T), under the action of random pressure gradients and damping by internal wave motions, are investigated by a model Langevin-like equation, and by a general Lagrangian analysis of the displacements, of the density flux and of the energy of fluid elements. Solutions for the mean-square displacement $\overline{Z^2(t)}$, the mean-square velocity $\overline{w^2}$, and the autocorrelation of the velocity are calculated in terms of the spectrum $\Phi(s)$ of the pressure gradient. The authors use model equations for the momentum of fluid elements and for the exchange of density fluctuations between fluid elements, taking the elements' diffusion timescale to be γ^{-1} times the buoyancy timescale N^{-1} , where γ is a measurable parameter. (39 refs.)

75991 Asymptotic near-wall stress dissipation rates in a turbulent flow. B.E.Laund, W.C.Reynolds (Centre d'Etudes, Le Breau, France).

Phys. Fluids (USA), vol.26, no.5, p.1157-8 (May 1983). Provides an analysis for the correct behavior of the dissipation tensor in the Reynolds-stress transport equation in the limit as a wall is approached. This differs from what is used conventionally, and hence is important for turbulence models that include the near-wall region. (2 refs.)

75992 The spatial derivative of temperature in a turbulent flow and Taylor's hypothesis. L.W.B.Browne, R.A.Antonia, S.Rajagopalan (Dept. of Mech. Engng., Univ. of Newcastle, Newcastle, New South Wales, Australia).

Phys. Fluids (USA), vol.26, no.5, p.1222-7 (May 1983). Statistics of the streamwise derivative of temperature fluctuations on the centerline and at one streamwise station in the self-preserving region of a turbulent plane jet have been obtained by two techniques. In one, the derivative is approximated by the difference between the signals from two cold wires separated in the streamwise direction. In the other, the streamwise derivative is inferred from the temporal derivative and different convection velocities. Instantaneous values, root-mean-square values, skewness, and flatness factors are in reasonable agreement for a sufficiently large range of separations regardless of whether the mean velocity (Taylor's hypothesis) or the instantaneous velocity are used as the convection velocity. Corrections for turbulence intensity, that are often applied to Taylor's hypothesis, do not seem warranted. The difference between spectra of the temperature difference and temporal derivative spectra cannot be resolved by identifying the convection velocity with a frequency-dependent phase velocity of the temperature fluctuation. (13 refs.)

75993 A model for the turbulent energy spectrum. R.J.Driscoll, L.A.Kennedy (Dept. of Mech. & Aerospace Engng., State Univ. of New York, Amherst, NY, USA).

Phys. Fluids (USA), vol.26, no.5, p.1228-33 (May 1983). A simple empirical model is developed for the isotropic kinetic energy spectrum. The model can define the spectral distribution as a function of Reynolds number at all wavenumbers. It is compared with spectral data from different types of flows over the $13 \leq Re_\lambda \leq 7000$ range. (18 refs.)

75994 Transport effects associated with turbulence with particular attention to the influence of helicity. H.K.Moffatt (Dept. of Appl. Math. & Theoretical Phys., Univ. of Cambridge, Cambridge, England). *Rep. Prog. Phys. (GB)*, vol.46, no.5, p.621-64 (May 1983). The action of turbulence on a passive convected scalar field (e.g. temperature) or vector field (e.g. the magnetic field in an electrically conducting fluid) is reviewed, with particular attention paid to anomalous effects that can arise through the influence of Coriolis forces in a rotating system on the statistics of the turbulence. The simplest such effect (which corresponds to a breaking of the Onsager symmetry relations) is a 'skew-diffusion' effect, i.e. the appearance of a component of turbulent heat flux perpendicular to the local mean temperature gradient. The famous α effect of magnetohydrodynamic dynamo theory is also in this category, as is the more subtle Radler effect (the appearance of a mean electromotive force perpendicular to the mean current in a plasma). These effects are all associated with the helicity of a turbulent flow, i.e. the correlation between the velocity field $u(x,t)$ and the vorticity field $\omega(x,t) = \text{curl } u$. (41 refs.)

75995 Homogeneous turbulence. J.N.Gence (Ecole Centrale de Lyon, Univ. Claude Bernard Lyon, Ecully, France). In book: *Annual review of fluid mechanics. Vol.15*, M.Van Dyke, J.V.Wehausen, J.L.Lumley [Ed.], p.201-22. Palo Alto, CA, USA: Annual Reviews (1983), 534 pp. [0 8243 0715 1] When studying turbulent flows, it is customary to split all instantaneous random quantities into an averaged and a fluctuating part. Accordingly, the understanding of such flows implies the analysis of the different interactions between the mean and the fluctuating motion. The mean flow field and the statistical moments associated with the fluctuating motion satisfy an infinite set of equations. In order to simplify the equations and to make it easier to understand the physics of the phenomena, different homogeneous turbulent flow models have been proposed. (39 refs.)

Annual review of fluid mechanics. Vol.15 See Entry 74234
Turbulent spots, wave packets, and growth See Entry 75983
The turbulence measurement in a two-dimensional wake flow of a cylinder See Entry 76033
Integrable, chaotic, and turbulent vortex motion in two-dimensional flows See Entry 76048
Structure and behavior of a turbulent ring vortex See Entry 76049
The turbulent wall jet—measurements and modeling See Entry 76085
An experimental study of entraining, stress-driven, stratified flow in an annulus See Entry 76087
Functional formulation of magnetohydrodynamic turbulence in a rotating frame of reference See Entry 76121
Measurements of pressure fluctuation in turbulent flow See Entry 76136
Instabilities, pattern formation, and turbulence in flames See Entry 77890

47.25F Boundary layer and shear turbulence

75996 On the logarithmic law and Karman's constant. Chou Zuwei (Fu Dan Univ., Shanghai, China). *Acta Mech. Sin. (China)*, no.1, p.27-33 (1983). In Chinese. Starting from the stochastic motion of small spherical vortices, the flow feature of a fully turbulent region of wall turbulence was studied and the differential equation describing this stochastic process was set up. By solving the above equation, the famous logarithmic law was obtained again and Karman's constant was theoretically determined. (11 refs.)

75997 Viscous-inviscid interactions in cascades. C.Hirsch, P.Janssens (Dept. of Fluid Mech., Vrije Univ. Brussel, Brussel, Belgium). *Isr. J. Technol. (Israel)*, vol.20, no.3, p.109-26 (1982). A method has been developed to predict turning and loss coefficients for axial and centrifugal turbomachines in the context of a viscous-inviscid interaction scheme. The procedure computes the blade-to-blade flow field around an arbitrary blade and takes into account the blade boundary layers, eventual separation of these boundary layers and the wake downstream of the trailing edge. The interaction is expressed by the wake displacement body method. The potential flow is solved in a finite-element Galerkin approximation with mixed boundary values. The separation line between the inviscid flow and separated boundary layers and the wake is iteratively searched using a free streamline method. The outlet angle is corrected with a Kutta-Joukowski condition and zero loading is ensured on the wake downstream of the trailing edge. Results are presented and discussed for axial and radial bladings. (29 refs.)

75998 The characteristics of low-speed streaks in the near-wall region of a turbulent boundary layer. C.R.Smith, S.P.Metzler (Dept. of Mech. Engrg. & Mech., Lehigh Univ., Bethlehem, PA, USA). *J. Fluid Mech. (GB)*, vol.129, p.27-54 (April 1983). Employing a high-speed video system and hydrogen bubble-wire flow visualization, the characteristics of the low-speed streaks which occur in the near-wall region of turbulent boundary layers have been examined for a Reynolds-number range of $740 < Re_\tau < 5830$. The results indicate that the statistics of non-dimensional spanwise streak spacing are essentially invariant with Reynolds number, exhibiting consistent values of $\lambda^+ \approx 100$ and remarkably similar probability distributions conforming to lognormal behaviour. Further studies show that streak spacing increases with distance from the wall owing to a merging and intermittency process which occurs for $y^+ \geq 5$. An additional observation is that, although low-speed streaks are not fixed in time and space, they demonstrate a tremendous persistence, often maintaining their integrity and reinforcing themselves for time periods up to an order of magnitude longer than the observed bursting times associated with wall region turbulence production. A mechanism for the formation of low-speed streaks is suggested which may explain both the observed merging behaviour and the streak persistence. (37 refs.)

75999 A novel property of the displacement thickness in three-dimensional boundary-layer theory. T.Cebeci, G.L.Keller, H.Unt (Dept. of Mech. Engrg., California State Univ., Long Beach, CA, USA), K.Stewartson. *Phys. Fluids (USA)*, vol.26, no.5, p.1192-7 (May 1983). It is shown that the equivalent blowing velocity of a three-dimensional boundary layer can be either positive or negative near separation depending on the geometry of the flow. The situation is illustrated by a computation of the boundary layer in the planes of symmetry of a thin ellipsoid moving in the direction of its major axis. This result is of importance in estimating the effect of the boundary layer on the external flow and is distinct from the two-dimensional problem where the blowing velocity always appears to be positive near separation. (8 refs.)

The cancellation of a sound-excited Tollmien-Schlichting wave with plate vibration See Entry 75985
Convective diffusion toward rotating polar spherical electrode See Entry 76027
Turbulent boundary layer associated with periodic rotating wakes See Entry 76035
Plane and axis-symmetric stagnation flow of a Maxwellian fluid See Entry 76076
Regular flow around a flat plate set between two parallel walls with different permeabilities See Entry 76100
The evolution of Tollmien-Schlichting waves near a leading edge. II. Numerical determination of amplitudes See Entry 76111
Thermal structure of a flat plate turbulent boundary layer diffusion flame See Entry 76125

47.25J Turbulent diffusion

A statistical model of fluid-element motions and vertical diffusion in a homogeneous stratified turbulent flow See Entry 75990
Parametrization of air pollution in the surface layer of a complex of transforming and interacting admixtures See Entry 78112

47.25M Noise (turbulence generated)

Effect of sound absorbing wall linings on aerodynamic forces of a subsonic vibrating cascade See Entry 76062

47.25Q Convection and heat transfer

(see also 44.25 Convective and constrained heat transfer)

76000 Temperature field produced in a flowing gas by a cylinder with modulated temperature. J.Kielbasa (Acad. Polonaise des Sci., Warsaw, Poland). *Bull. Acad. Pol. Sci. Ser. Sci. Tech. (Poland)*, vol.30, no.1-2, p.31-6 (1982). The solution of the temperature field produced in flowing gas by a cylinder whose surface periodically changes temperature is given. It is demonstrated that the relations in this case are similar to those in the case of temperature distribution around a linear heat source periodic in time placed in a gas flow. (4 refs.)

76001 Breakup of a thin liquid layer heated from below. E.Hasegawa (Keio Univ., Yokohama, Japan), J.Kojima. *Bull. JSME (Japan)*, vol.26, no.213, p.380-6 (March 1983). When a thin liquid layer, which is at rest under the action of gravity on a horizontal wall, is locally heated from below, a flow is induced in the layer by the surface-tension force. The flow in such a case is studied theoretically by using the Stokes approximation and the thin film approximation. This flow is governed by two dimensionless parameters, Nusselt number N and thermal Weber number M . When the liquid layer is heated from below, the free surface is always depressed. When the heating is strong, the liquid layer breaks up. The critical value of the thermal Weber number, above which the liquid layer breaks up, is found as a function of N . The shapes of the surface just when a breakup occurs are calculated. The critical thermal Weber numbers are experimentally found for the case of an oil sheet. (8 refs.)

76002 Symmetry analysis of convection patterns. Chen Shi-gang (Inst. of Phys., Acad. Sinica, Beijing, China). *Commun. Theor. Phys. (China)*, vol.1, no.4, p.413-26 (1982). Carries out a symmetry analysis of convection patterns of Newton-Boussinesq fluid in some finite containers. The author also discusses, from the viewpoint of symmetry analysis, the behaviour of infinitely extended fluid layer, as a limit of that in finite container, near convection threshold. (10 refs.)

76003 A class of backward free-convective boundary-layer similarity solutions. H.K.Kuiken (Philips Res. Labs., Eindhoven, Netherlands). *Int. J. Heat & Mass Transfer (GB)*, vol.26, no.5, p.655-61 (May 1983). Presents a class of backward free-convective boundary-layer similarity solutions. It is shown that these boundary layers can be produced along slender downward-projecting slabs of prescribed thickness variation, which are infinitely long. It is pointed out that these solutions can be used to describe free-convective flows along vertical fins which have received attention in the literature before. An important result is that the temperature along a downward-projecting fin of constant thickness varies in proportion to the inverse of the seventh power of the shifted longitudinal coordinate. (8 refs.)

76004 The effect of thermal boundary conditions on the heat transport in vertical channels heated from below. H.Frick (Inst. fur Reaktorbauelemente, Kernforschungszentrum Karlsruhe, Karlsruhe, Germany). *Int. J. Heat & Mass Transfer (GB)*, vol.26, no.5, p.681-8 (May 1983). A numerical analysis is carried out of the effect of perfectly conducting and adiabatic vertical walls on the heat transport by convection in a fluid heated from below. The equations of motion for a high Prandtl number fluid and the heat equation have been solved by the Galerkin method. Because of the side walls, the convection velocity field has three velocity components and depends on all three spatial coordinates. A two velocity component approximation, as well as the full three component representation of the velocity field, is employed in the numerical analysis. The results indicate the surprising accuracy of the two component approximation. Converged solutions are determined for a range of aspect ratios A between $A=0$ (Benard convection) and $A=20$ (Hele-Shaw convection). (25 refs.)

76005 Enhanced and local heat transfer, pressure drop, and flow visualization for arrays of block-like electronic components. E.M.Sparrow, S.B.Vemuri, D.S.Kadle (Dept. of Mech. Engrg., Univ. of Minnesota, Minneapolis, MN, USA). *Int. J. Heat & Mass Transfer (GB)*, vol.26, no.5, p.689-99 (May 1983). Experiments were performed to investigate the heat transfer and fluid flow characteristics of arrays of heat-generating, block-like modules affixed to one wall of a parallel-plate channel and cooled by forced convection airflow. Heat transfer enhancements exceeding a factor of two were achieved by the use of multiple fence-like barriers, with the interbarrier spacing and the barrier height being varied parametrically along with the Reynolds number. The barrier-related pressure drop for a multi-barrier system was found to be less than the corresponding multiple of the pressure drop for a single-barrier system when the interbarrier spacing is small. When the barriers are separated by six or more rows of modules, the direct multiple is applicable. The heat transfer coefficients at individual surfaces of the various modules were measured in fully populated arrays without barriers, in arrays with barriers, and in arrays in which there was a missing module. Perspectives on

the heat transfer and pressure drop results were provided by flow visualizations performed using the oil-lampblack technique. (1 ref.)

76006 Thermal convection in a cavity filled with a porous medium: a classification of limiting behaviours. P.A.Blythe (Center for the Application of Math., Lehigh Univ., Bethlehem, PA, USA), P.G.Simpkins, P.G.Daniels. *Int. J. Heat & Mass Transfer (GB)*, vol.26, no.5, p.701-8 (May 1983). Thermally driven flows in a 2-dim. rectangular cavity filled with a fluid-saturated porous medium are considered in the large Rayleigh number limit when the applied temperature gradient is perpendicular to the gravity vector. The standard boundary layer description of these flows is shown to be valid only for $R \gg 10^4 L^2$, where R is the Rayleigh number based on the cavity height and L is the cavity aspect ratio (length/depth). For flows in which $R = O(L^2)$, $L \rightarrow \infty$, the horizontal layers merge and a different solution regime exists. A discussion of the relationship between the merged layer limit (R/L^2 fixed, $L \rightarrow \infty$) and the classical Hadley cell limit (R fixed, $L \rightarrow \infty$) is given. It is found that the intermediate regime R/L fixed, $L \rightarrow \infty$, provides the necessary bridge between the merged layer and the Hadley solutions. Bounds on the extent of the various regimes in the (R, L) parameter space are deduced. The scaling suggested by the merged layer regime gives rise to an alternative correlation of heat transfer data. Existing theories for the Nusselt number are reviewed and shown to be consistent with the new scaling law. (16 refs.)

76007 A correlation for heat transfer by natural convection from horizontal cylinders that accounts for viscous dissipation. R.M.Fand (Dept. of Mech. Engng., Univ. of Hawaii, Honolulu, HI, USA), J.Brucker. *Int. J. Heat & Mass Transfer (GB)*, vol.26, no.5, p.709-16 (May 1983). Eight previously published correlation equations plus one new correlation for heat transfer by natural convection from horizontal isothermal cylinders are tested against a fairly extensive body of experimental data culled from the literature for $10^{-8} < Ra < 10^8$ and $0.7 < Pr < 4 \times 10^4$. The new equation, which represents the Nusselt number as a function of the Prandtl and Rayleigh numbers plus an additional dimensionless parameter that accounts for viscous dissipation, is shown to correlate the experimental data more accurately than does any one of the eight previously published equations. It is concluded that viscous dissipation may not be neglected in all cases of natural convection horizontal cylinders, and further, that the inclusion of a viscous dissipation term in certain related problems, such as natural convection in porous media, may lead to more accurate correlation equations. (28 refs.)

76008 On the effects of viscous dissipation and pressure work in free convection loops. H.H.Bau (Dept. of Mech. Engng. & Appl. Mech., Univ. of Pennsylvania, Philadelphia, PA, USA), K.E.Torrance. *Int. J. Heat & Mass Transfer (GB)*, vol.26, no.5, p.727-34 (May 1983). The effects of viscous dissipation and pressure work are examined theoretically for laminar free convection loops. The appropriate governing equations are derived. Whereas previous work has considered only dissipation effects, the present paper shows that dissipation and pressure work effects are of comparable magnitude and must be considered together. Analytical solutions are presented for several open and closed loops. Both constant flux and constant temperature heating conditions are examined. Viscous dissipation and pressure work effects are found to have opposing influences on the flow in a loop. The former can enhance a flow for certain heating orientations, but the latter is usually dominant and retards a flow. (14 refs.)

76009 Thermal convection in a porous medium composed of alternating thick and thin layers. R.McKibbin (Dept. of Theoretical & Appl. Mech., Univ. of Auckland, Auckland, New Zealand), P.A.Tyvand. *Int. J. Heat & Mass Transfer (GB)*, vol.26, no.5, p.761-80 (May 1983). This paper is a continuation of a recent work by the present authors [J. Fluid Mech. 118, 315-339 (1982)]. The previous paper concentrated on buoyancy-driven convection in a porous medium composed of alternating material layers of equal thicknesses. The present work is a study of the limit case where every alternate layer is very thin and has very small permeability. The onset of convection in such a system and the heat flux at slightly supercritical Rayleigh numbers is studied. As in the earlier work, an investigation of the convergence to homogeneous anisotropy is made. Furthermore, emphasis is placed on applications in insulation techniques and convection in snow layers. (12 refs.)

76010 Free convection about a sphere at small Grashof number. S.N.Singh (Dept. of Mech. Engng., Univ. of Kentucky, Lexington, KY, USA), M.M.Hasan. *Int. J. Heat & Mass Transfer (GB)*, vol.26, no.5, p.781-3 (May 1983).

The authors numerically calculate the flow properties of a free convection problem about an isothermally heated sphere by the series truncation method when the Grashof number is of order unity. In fact, the series truncation method is used to solve the free convection between concentric spheres. A method similar to that used by Dennis and Singh (1978) for the flow between two rotating spheres and Singh and Chen (1980) for free convection problem is used in the present paper. The stream function and the temperature distribution are expanded as series of orthogonal Gegenbauer functions and Legendre polynomials, respectively, in terms of the angle θ of spherical polar coordinates (r, θ, ϕ). The finite set of equations which results from a certain level of truncation is solved numerically for $Pr=0.7$ and Grashof numbers in the range 0.01-1. (10 refs.)

76011 The influence of sound on natural convection from vertical flat plates. H.Matsumura (Dept. of Mech. Engng., Univ. of Akita, Akita, Japan).

Int. J. Heat & Mass Transfer (GB), vol.26, no.5, p.790-2 (May 1983). The author investigates experimentally the influence of a sound field on the natural convective heat transfer from vertical flat plates by means of flat plates of various width. (6 refs.)

76012 Natural convection heat transfer in a porous layer with internal flow obstructions. A.Bejan (Dept. of Mech. Engng., Univ. of Colorado, Boulder, CO, USA).

Int. J. Heat & Mass Transfer (GB), vol.26, no.6, p.815-22 (June 1983). Documents the effect of internal flow obstructions on heat transfer through a 2-dim. porous layer heated from the side. Three types of flow obstructions have been considered. Horizontal diathermal partitions were found to decrease the heat transfer rate in cases where the overall heat transfer was dominated by convection. In the conduction-dominated regime, horizontal diathermal partitions were found to increase the heat transfer rate slightly. Horizontal adiabatic partitions, on the other hand, were found to increase the heat transfer rate when the dominating mechanism is convection. Finally, vertical diathermal partitions were shown to reduce the heat transfer rate by roughly 50% in the convection-dominated regime. Numerical heat transfer results are reported in the domain $0.1 < L/H < 2$ and $50 < Ra_H < 1000$, where L/H is the length/height ratio and Ra_H is the Darcy-modified Rayleigh number based on height. (17 refs.)

76013 Heat transfer in nucleate pool boiling at high heat flux. A.M.Bhat (Dept. of Mech. Engng., Regional Engng. Coll., Srinagar, India), R.Prakash, J.S.Saini.

Int. J. Heat & Mass Transfer (GB), vol.26, no.6, p.833-40 (June 1983). An analytical model for heat transfer in nucleate pool boiling at high heat flux, near the critical value, is proposed. It is hypothesized that the heat transfer in this region takes place mainly due to the heat conduction through the liquid macrolayer formed on the heating surface. The results of the analysis have been compared with some experimental results and the agreement is found to be reasonably good. (14 refs.)

76014 Pool boiling heat transfer in a confined space. Shi-Chune Yao (Dept. of Mech. Engng., Carnegie-Mellon Univ., Pittsburgh, PA, USA).

Int. J. Heat & Mass Transfer (GB), vol.26, no.6, p.841-8 (June 1983). Pool boiling heat transfer in a confined space has been studied for vertical narrow annuli with closed bottoms. Experiments were performed for Freon-113, acetone, and water at 1 atm. for annuli with heights of 25.4 and 76.2 mm, and gap sizes of 0.32, 0.80 and 2.58 mm. Three boiling regimes are identified through visual observation. The importance of the Bond number is also demonstrated. When the Bond number is less than unity, the isolated deformed bubble regime occurs at low heat flux and the coalesced deformed bubble regime is observed at high heat flux. For Bond numbers slightly larger than unity at high heat flux, nucleation on the heated surface has been observed. The general behavior of the boiling curves and the heat transfer mechanisms of these boiling regimes are presented and discussed. (11 refs.)

76015 Duct-flow versus external-flow natural convection at a short, wall-attached horizontal cylinder. E.M.Sparrow, P.Souza Mendes, M.A.Ansari, A.T.Prata (Dept. of Mech. Engng., Univ. of Minnesota, Minneapolis, MN, USA).

Int. J. Heat & Mass Transfer (GB), vol.26, no.6, p.881-9 (June 1983). Natural convection heat transfer coefficients were measured at a short horizontal cylinder affixed to an equi-temperature vertical plate for the condition that the plate and the cylinder form one wall of a vertical duct. The duct was open to the ambient at the top and bottom and, aside from the plate and cylinder, its other walls were not directly heated. Substantially higher cylinder heat transfer coefficients could be attained in the duct-flow mode than in the external-flow mode (i.e. where the plate and cylinder face a large open space). Duct-flow-related enhancements of up to 60% were measured. The enhancement is maximized when the duct is as narrow as possible and when the cylinder is positioned near the lower end of the plate. The radiation surface properties of the unheated walls of the duct also affect the degree of enhancement, with black surfaces bringing about greater enhancement by virtue of their higher buoyancy-creating temperature. (8 refs.)

76016 A method of heat exchangers calculation. J.Lach, W.Pieczka (Inst. de Recherches Nucleaires, Service du Genie des Piles, Swierk-Otwock, Poland).

Int. J. Heat & Mass Transfer (GB), vol.26, no.6, p.891-9 (June 1983). A heat transfer analysis of a type of heat exchanger is presented. The conservation laws are limited to the energy balance equations expressed by first order partial differential equations system. Similar problems have been considered in the past but the exact solution has not been presented. The analytical solution of the equation system is given. The heat exchanger equations are the particular case of this equation system. A similar analysis method can be applied in the theory of recuperators and regenerators. Obtaining the general solution for the extension of the heat exchanger problem increases the number of the physical phenomena which can be analyzed with the aid of the method presented. Numerous conservation laws can be described by the differential equations systems discussed, while the method used allows the analysis of various problems described by this type of equation to be simplified. (10 refs.)

76017 An investigation of transient boiling heat transfer with conjugate nature. Shi-Chune Yao (Dept. of Mech. Engng., Carnegie-Mellon Univ., Pittsburgh, PA, USA), A.Salehpour.

Int. J. Heat & Mass Transfer (GB), vol.26, no.6, p.901-9 (June 1983). Temperature controlled transient boiling experiments have been performed to study the effects of mass flux on boiling of F-113 in a vertical annular channel. At higher velocities transient effects have been suppressed. Quenching may start from both ends of the heated tube and quenching starting at the downstream end may result in a lower critical heat flux. Transient convective boiling heat transfer could be of conjugate nature with respect to the solid wall. However, the behavior of a transient conjugate heat transfer problem can be primarily characterized by the parameter: dT_i/dt (the interface temperature rate). This is confirmed by the analysis of a conduction problem, a single phase convection problem, and the data of the present experiments. The transient critical heat flux increases as dT_i/dt increases for heat-up processes but decreases as $|dT_i/dt|$ increases for cool-down processes. (11 refs.)

76018 Analysis of transient natural convection flow at high Prandtl number using a matched asymptotic expansion technique. V.P.Carey (Dept. of Mech. Engng., Univ. of California, Berkeley, CA, USA).

Int. J. Heat & Mass Transfer (GB), vol.26, no.6, p.911-19 (June 1983). The method of matched asymptotic expansions, which has been used in previous studies of steady natural convection flow, is extended to transient natural convection flows at high Prandtl number (σ). Expansion solutions, valid for large σ , are presented for the transient natural convection flow near a vertical surface which undergoes a step change in temperature. Throughout the transient, the flow is found to have the same dual-layer structure which is characteristic of steady flow at high Prandtl number. For large σ , the time to steady state is shown to increase proportional to $\sigma^{1/2}$. The temperature and velocity overshoot, which occurs during the transient at moderate σ , is shown to disappear as $\sigma \rightarrow \infty$. Uniformly valid expansions for the velocity and temperature profiles near the surface are in good agreement with the calculated solution of the full governing equations for σ as low as 16. For large σ , a simple relation for the propagation of the leading edge effect is also obtained which is consistent with the results of past studies for $\sigma=10$ and $\sigma=100$. (18 refs.)

76019 Theoretical prediction of maximum heat flux in power transients. A.Serizawa (Dept. of Nuclear Engng., Kyoto Univ., Kyoto, Japan).

Int. J. Heat & Mass Transfer (GB), vol.26, no.6, p.921-32 (June 1983). A model has been formulated to predict the burnout characteristics during a power increase. The analytical description of the model is built upon visual and photographic observations of the vapour-liquid configuration near the maximum heat flux reported by other investigators. The broad conclusion is that the maximum heat flux occurs because of a balance between the consumption of a thin liquid layer formed between a vapour blanket and a heated surface and the supply of liquid during the postulated transient. It is also found that the liquid layer thickness is a primary influence on the transient burnout behaviour as well as the liquid supply to the layer. (26 refs.)

76020 The geyser effect in a two-phase thermosyphon. C.Casarosa, E.Latrofa (Istituto di Fisica Generale ed Applicata, Univ. di Pisa, Pisa, Italy), A.Shelginski.

Int. J. Heat & Mass Transfer (GB), vol.26, no.6, p.933-41 (June 1983).

A phenomenon which was observed during experimental research work carried out on a two-phase thermosyphon with water as the working fluid is described. The phenomenon is a pulsed boiling at low pressure and was called the 'geyser effect'. The heat transfer coefficient at the thermosyphon evaporator has been measured and a functional law, which links this coefficient with the pressure and the specific thermal flux, is proposed; a correlation of the type $Nu = CRe^{0.8}Pr^b$ is also shown to represent satisfactorily the experimental data. (24 refs.)

76021 Combined influence of dissipation and Hall effects on free convective flow in a rotating fluid. H.L.Agrawal, P.C.Ram, V.Singh (Dept. of Appl. Math., Banaras Hindu Univ., Varanasi, India).

Indian J. Pure & Appl. Math., vol.14, no.3, p.314-21 (March 1983).

The present analysis is made to investigate the effects of Hall currents and viscous dissipation on the hydromagnetic free convective flow in the Ekman layer of a conducting liquid past an infinite porous plate. The problem is solved analytically. The velocity and temperature profiles are shown on graphs and the numerical values of τ_w and skin-friction at the plate in x - and y -directions have been tabulated. It is found that primary shear-stress increases and the secondary shear-stress decreases with the increase of magnetic and Hall parameters, whereas the rate of heat transfer from the plate decreases with it. (7 refs.)

76022 Pressure drop during forced convection boiling of binary refrigerant mixtures. L.C.Singal, C.P.Sharma, H.K.Varma (Mech. & Industrial Engng. Dept., Univ. of Roorkee, Roorkee, India).

Int. J. Multiphase Flow (GB), vol.9, no.3, p.309-23 (June 1983).

An experimental investigation was carried out in an electrically heated horizontal tube to measure pressure drop for various flow rates and heat fluxes during forced convection boiling of pure refrigerant 12 and four compositions of refrigerants 13 and 12 mixtures. The Martinelli-Nelson correlation, using the properties of the flowing refrigerant mixture, could not predict satisfactorily the pressure drop data. Total, as well as frictional pressure drops were found to be function of concentration. Two separate models each for total, as well as frictional pressure drop were developed for predicting the corresponding pressure drop. In each case, the maximum per cent deviation between predicted and measured pressure drop was within $\pm 30\%$. (18 refs.)

76023 Laminar natural convection from a horizontal plate and the influence of plate-edge extensions. R.J.Goldstein, K.-S.Lau (Dept. of Mech. Engng., Univ. of Minnesota, Minneapolis, MN, USA).

J. Fluid Mech. (GB), vol.129, p.55-75 (April 1983).

Laminar natural convection from a horizontal plate is studied by a finite-difference analysis and by experiments for Rayleigh numbers from 10 to 10^4 . The plate with uniform surface temperature or concentration on one side and insulated on the other is situated in an 'infinite' fluid medium. The buoyancy near the surface is directed either outward or inward normal to the active surface—equivalent to a heated plate facing upward or downward. The effect of insulated vertical and horizontal extensions to the plate are also examined. Finite-difference solutions are obtained for a heated strip in a two-dimensional domain for a Prandtl number of 0.7. Mass-transfer experiments are performed with square naphthalene plates in air. Both numerical and experimental results justify a $1/5$ -power law in the present range of Rayleigh number—i.e. Nusselt number or Sherwood number proportional to the Rayleigh number raised to the $1/5$ power. (30 refs.)

76024 Nonlinear convection in a porous layer with finite conducting boundaries. N.Riahi (Dept. of Theoretical & Appl. Mech., Univ. of Illinois, Urbana, IL, USA).

J. Fluid Mech. (GB), vol.129, p.153-71 (April 1983).

The problem of finite-amplitude thermal convection in a porous layer with finite conducting boundaries is investigated. The nonlinear problem of three-dimensional convection is solved by expanding the dependent variables in terms of powers of the amplitude of convection. The preferred mode of convection is determined by a stability analysis in which arbitrary infinitesimal disturbances are superimposed on the steady solutions. Square-flow-pattern convection is found to be preferred in a bounded region Γ in the (γ_b, γ_t) -space, where γ_b and γ_t are the ratios of the thermal conductivities of the lower and upper boundaries to that of the fluid. Two-dimensional rolls are found to be the preferred pattern outside Γ . The qualitative features of the convection problem appear to be essentially symmetric with respect to γ_b and γ_t . The dependence of the heat transported by convection on γ_b and γ_t is computed for the various solutions analysed in the paper. (13 refs.)

76025 Heat transfer and horizontally averaged temperature of convection with large viscosity variations. F.M.Richter (Dept. of Earth Sci., Cambridge Univ., Cambridge, England), H.-C.Nataf, S.F.Daly.

J. Fluid Mech. (GB), vol.129, p.173-92 (April 1983).

Experiments with fluids whose viscosity depends strongly on temperature are used to study the effect of viscosity variations in the range 10^{-10} on the heat transfer and horizontally averaged temperature of a convecting layer between horizontal isothermal boundaries. At large viscosity variations (3×10^3 and 10^5) and Rayleigh numbers less than the critical value given by linear theory, the system can be either conductive or convective depending on whether the Rayleigh number is increased from an earlier conductive state or decreased from a preexisting convective state. At higher Rayleigh numbers and for the entire range of viscosity variation studied the heat transfer differs little ($< 20\%$) from that of a uniform-viscosity fluid when the Rayleigh number is defined in terms of the viscosity corresponding to a temperature equal to the average of the boundary temperatures. The relationship between Nusselt number and supercriticality (R_a/R_c) is even more remarkable being independent of viscosity variation and indistinguishable from that of a uniform-viscosity fluid with appropriate Prandtl number. The horizontally averaged temperature becomes increasingly asymmetrical with increasing viscosity variation due to the relatively large temperature change across the cold, more-viscous boundary layer, and results in an isothermal interior temperature significantly hotter than the average of the boundary temperatures. (17 refs.)

76026 Applicability of boundary-layer theory to calculation of heat transfer under separation conditions. Yu.F.Gortyshev, I.M.Varfolomeev ('A.N. Tupolev' Kazan Inst. of Aviation, Kazan, USSR).

J. Eng. Phys. (USA), vol.43, no.3, p.979-82 (Sept. 1982). Translation of: *Inzh.-Fiz. Zh. (USSR)*, vol.43, no.3, p.397-401 (Sept. 1982).

The conditions are examined under which methods and relations developed for attachment flow are applicable to regions of separation flow. (10 refs.)

76027 Convective diffusion toward rotating polar spherical electrode. O.Vain, N.A.Pokryvailo (Inst. of Theoretical Foundations of Chem. Processes, Prague, Czechoslovakia).

J. Eng. Phys. (USA), vol.43, no.3, p.1020-6 (Sept. 1982). Translation of: *Inzh.-Fiz. Zh. (USSR)*, vol.43, no.3, p.448-56 (Sept. 1982).

Results are given of a theoretical and experimental study of a concave mass exchange in the regime of limiting diffusion current toward the polar surface of a rotating sphere, for a creeping and boundary-layer type of flow near the surface. (15 refs.)

76028 Solution of the steady-state problem of heat exchange and flow of lubricant in radial sliding bearings with self-aligning segments. V.V.Rukhlinskii, L.A.Gura, O.M.Borisenko (Kharkov Polytech. Inst., Kharkov, Ukrainian SSR).

J. Eng. Phys. (USA), vol.43, no.3, p.1041-7 (Sept. 1982). Translation of: *Inzh.-Fiz. Zh. (USSR)*, vol.43, no.3, p.475-83 (Sept. 1982).

Describes a method based on the use of implicit finite-difference schemes, and it presents the results of the numerical solution of the problem of heat exchange and flow of lubricant in multisegment radial sliding bearings. (3 refs.)

76029 Monotonic and oscillatory instabilities of a two-layer system of immiscible liquids heated from below. G.Z.Gershuni, E.M.Zhukhovitskii (A.M. Gorki State Univ., Perm, USSR).

Sov. Phys.-Dokl. (USA), vol.27, no.7, p.531-3 (July 1982). Translation of: *Dokl. Akad. Nauk SSSR*, vol.265, no.1-3, p.302-5 (July 1982). [received: April 1983]

The authors consider the convective stability of the mechanical equilibrium of a system of two plane horizontal layers of immiscible liquids heated from below. They show that hydrodynamic and thermal interaction of the interface, in contrast with the situation in a homogeneous liquid induces oscillatory modes in the spectrum of the convective perturbations. Under definite conditions the mechanical equilibrium of a layered system heated from below is unstable against oscillatory perturbations. (3 refs.)

76030 Accuracy of analytical computational methods in thermohydrodynamics of two-phase systems. G.M.Arutyunyan, S.T.Ovsepian.

Sov. Phys.-Dokl. (USA), vol.27, no.8, p.631-3 (Aug. 1982). Translation of: *Dokl. Akad. Nauk SSSR*, vol.265, no.4-6, p.1367-70 (Aug. 1982). [received: May 1983]

The authors assert that the general analytical methods developed by G.M. Arutyunyan and S.T. Ovsepian [Izv. Akad. Nauk SSSR, Mekh. Zhidk. Gaza, No.5, p.81 (1977)] for calculating thermohydrodynamic processes in two-phase liquid-vapor systems are accurate enough for practical applications. (8 refs.)

76031 Heat transfer in toroidal pipes when the Prandtl number is large. S.I.Chernyschenko.

Vestn. Mosk. Univ. Ser. 1 (USSR), no.2, p.87-90 (March-April 1983). In Russian.

Discusses the temperature distribution in a toroidal pipe in the limit case $Pr \rightarrow \infty$. The temperature is constant along the streamlines of the secondary flow. The temperature distribution on the streamlines is governed by an equation which is derived from the primary equation ($Pr \neq \infty$) by integration along closed streamlines. The boundary condition for this equation follows from the existence of the closed boundary layer near the wall and the symmetry plane of the pipe. (4 refs.)

76032 Non-stationary dissipative structures in a non-linear heat-conducting medium. G.G.Elenin, S.P.Kurdyumov, A.A.Samarskii.

Zh. Vychisl. Mat. & Mat. Fiz. (USSR), vol.23, no.2, p.380-90 (March-April 1983). In Russian. English translation in: *USSR Comput. Math. & Math. Phys. (GB)*

A study is made of dissipative structures arising in a nonlinear heat-conducting medium from a nonlinear source. In relation to the characteristics of the medium examined, heating occurs either by a propagating thermal wave or by thermal structures localized at fundamental lengths. The emergence of the structures in an initially uniform cold medium leads to a definite space-time ordering. The space-time order in the medium is determined by the eigenfunctions of a non-linear boundary problem. The eigenfunctions are analysed and the stability of the dissipative structures is studied. (55 refs.) A.J.B.

Heat and mass transfer bibliography—Soviet works See Entry 74239

Heat transfer performance of ceramic regenerator matrices with sine-duct shaped passages See Entry 74460

Effect of evaporation on convective heat exchange of a porous plate in a rarefied medium See Entry 75900

Local heat exchange in the film condensation of a stationary vapor on a vertical surface See Entry 75912

A theoretical study of laminar mixed convection from a horizontal cylinder in a cross stream See Entry 75982

Transport effects associated with turbulence with particular attention to the influence of helicity See Entry 75994

Experiments on a rotating fluid heated from below See Entry 76038

Stability and heat transfer of rotating cryogenics. I. Influence of rotation on the onset of convection in liquid ^4He See Entry 76040

Heat transfer of a swirled flow of gas suspension in a short channel See Entry 76043

The transport from a drop in an alternating electric field See Entry 76080

Complex freezing-melting interfaces in fluid flow See Entry 76098

Heat transfer in a fluidized bed with allowance for the filtration component See Entry 76105

Convective instabilities in binary mixtures in a porous medium See Entry 76106

Unsteady natural convection in a porous layer See Entry 76107

Magnetohydrodynamic flow of liquid metals in curved channels See Entry 76113

Radiation heat exchange in a solar cavity-type receiver at various times See Entry 78094

47.25R Wakes

76033 The turbulence measurement in a two-dimensional wake flow of a cylinder. Wei Zhonglei, Niu Zhennan (Dept. of Mech., Peking Univ., Peking, China).

Acta Mech. Sin. (China), no.1, p.70-6 (1983). In Chinese.

Presents some experimental results of the turbulence quantities in a two-dimensional wake of a cylinder and compares these data with Chou's theoretical computational results (1959). (4 refs.)

76034 The structure of a turbulent wake behind a cruciform circular cylinder. I. The mean velocity field. H.Osaka (Faculty of Engng., Yamaguchi Univ., Tokiwadai, Ube, Japan), I.Nakamura, H.Yamada, Y.Kuwata, Y.Kageyama.

Bull. JSME (Japan), vol.26, no.213, p.356-63 (March 1983).

The mean velocity field of a turbulent wake behind a cruciform circular cylinder which is composed of two sufficiently long circular cylinders is examined experimentally. The measurements were performed for the surface pressure distributions on the cruciform circular cylinder and the mean velocity profiles in the wake at a number of downstream stations in a wide range of $x/d=3$ to 594. It is revealed that the decay rate of centerline velocity defect is considerably slower, while the rate of growth of the half-width for the $y=z$ plane of the present wake is very close to that of a two-dimensional wake. In the center region of the wake of the cruciform shape, secondary flows are observed and the magnitude of the flow is measured. (14 refs.)

76035 Turbulent boundary layer associated with periodic rotating wakes. F.A.E.Abd-Elkhalek, Y.Yamamoto, M.Inoue, T.Ikui (Dept. of Mech. Engng., Kyushu Univ., Fukuoka, Japan).

Mem. Fac. Eng. Kyushu Univ. (Japan), vol.42, no.4, p.279-316 (Dec. 1982). [received: May 1983]

The authors attempt to develop a better understanding of the nature of the annulus wall boundary layer that is influenced by periodic disturbances of rotor wakes in an axial flow turbomachine. The mean and phase-locked measurements were made in the turbulent boundary layer on the hub wall behind a rotor with circular cross-section blades. It was found that the periodic disturbances imposed by the rotor wakes cause a considerable deviation of the mean flow properties of the boundary layer from those of undisturbed boundary layer (natural turbulent boundary layer). This phenomenon is caused by interaction of the rotor wakes and the boundary layer which results in a secondary flow associated with re-distribution process of kinematic energy. Introducing the periodic disturbances into the mean boundary layer equation, a term of unsteady force was included in the momentum integral equation. (12 refs.)

Structure and behavior of a turbulent ring vortex See Entry 76049

47.30 ROTATIONAL FLOW AND VORTICITY

76036 One-dimensional mathematical model on peculiar gathering behaviour of particles in a rotating loop. Xu Jianjun (Inst. of Mech., Acad. Sinica, Peking, China).

Acta Mech. Sin. (China), no.1, p.91-4 (1983). In Chinese.

The gathering behaviour of the particles embedded in the fluid of a rotating loop such as the Chandler loop (1958) is discussed theoretically. A simplified model is given and the character of the integral curves of the basic equation is discussed on the phase plane. The result shows that for a certain condition a stable spiral point near the front crescent surface of the loop exists and particle gathering occurs. (14 refs.)

76037 Experimental studies of the flow past a circular cylinder in homogeneous rotating fluid. Liu Yinian, Jia Fu (Inst. of Mech., Chinese Acad. of Sci., Peking, China).

Acta Mech. Sin. (China), no.2, p.119-25 (1983). In Chinese.

The flow past an isolated topography in a rotating system of significance to many geophysical problems. The authors describe experiments on the flow past a circular cylinder in homogeneous rotating fluid. Measurements are given of the block coefficient (which characterizes the flow pattern), the Rossby number, the relative height of the cylinder etc., and their variations along the rotating axis. (8 refs.)

76038 Experiments on a rotating fluid heated from below. D.Tang (Dept. of Chem. Engng., Univ. of Illinois, Urbana-Champaign, IL, USA), J.L.Hudson.

Int. J. Heat & Mass Transfer (GB), vol.26, no.6, p.943-9 (June 1983).

Heat transfer measurements have been made in a right circular cylinder which is heated from below and rotated steadily about its vertical axis. The range of rotational rates was chosen such that both the gravitational and centrifugal acceleration influenced the convection. Two silicon oils having Prandtl numbers $\sigma=3100$ and $\sigma=7.2$ were used in the experiments. The influence of rotation on heat transfer and on the onset of gravitational instabilities was determined. (18 refs.)

76039 Drag on eccentrically positioned spheres translating and rotating in tubes. H.Tozeren (Dept. of Engng. Sci., Middle East Tech. Univ., Ankara, Turkey).

J. Fluid Mech. (GB), vol.129, p.77-90 (April 1983).

The steady motion of an eccentrically positioned sphere in a circular cylindrical tube filled with viscous fluid is considered as a regular perturbation of the axisymmetric problem. A sequence of boundary-value problems is formulated involving Stokes equations and some linear boundary conditions. Solutions of the first- and second-order problems yield the leading terms in the perturbation series of the additional drag and the torque on the spheres. The results are found to be in good agreement with the previous off-axis solutions. (7 refs.)

76040 Stability and heat transfer of rotating cryogenics. I. Influence of rotation on the onset of convection in liquid ^4He . P.G.J.Lucas, J.M.Potenhauer, R.J.Donnely (Dept. of Phys., Univ. of Oregon, Eugene, OR, USA).

J. Fluid Mech. (GB), vol.129, p.251-64 (April 1983).

Equipment is described for performing measurements of the Rayleigh-Benard instability in a sample of rotating liquid ^4He . Data are presented on the dependence of the critical Rayleigh number for the onset of convection on Prandtl number in the range $0.49 < Pr < 0.76$ and over a range of dimensionless angular velocities $0 < \Omega < 200$. Evidence for the existence of subcritical convection is presented. (30 refs.)

76041 Numerical processing of flow-visualization pictures—measurement of two-dimensional vortex flow. K.Imachi, K.Ohmi (Faculty of Engng. Sci., Osaka Univ., Toyonaka, Japan).

J. Fluid Mech. (GB), vol.129, p.283-311 (April 1983).

A new system has been developed for estimating experimentally some of the principal physical variables of fluid flows, through flow-visualization and image-processing techniques. Distributions of stream function, vorticity and pressure are calculated by this system with reasonable accuracy for two examples of two-dimensional flow: namely unsteady twin-vortex flow behind a circular cylinder accelerated impulsively to constant speed, and Karman vortices behind a circular cylinder moving at constant speed. A detailed explanation of the image-processing technique and the numerical calculation process is given first, and then some consideration is given to calculated results in these two types of flow. Comparison shows that some results of the unsteady twin-vortex experiment coincide well with those of previously published experimental investigations and theoretical calculations. Errors introduced at each stage of this system are estimated in some detail. (11 refs.)

76042 A viscous vortex pair in ground effect. A.J.Peace, N.Riley (School of Maths. & Phys., Univ. of East Anglia, Norwich, England).

J. Fluid Mech. (GB), vol.129, p.409-26 (April 1983).

The authors calculate the flow induced by a vortex pair in a viscous fluid, which is otherwise at rest, in the presence of a plane boundary. This may be either a no-slip or a stress-free boundary. The phenomenon of rebound of the vortices from the boundary occurs for either type of boundary, and an explanation for this is offered in terms of viscous effects. (13 refs.)

76043 Heat transfer of a swirled flow of gas suspension in a short channel. A.I.Mironov, F.I.Sharafutdinov, V.A.Filin, V.K.Shchukin (Tupolev Kazan Aviation Inst., USSR).

J. Eng. Phys. (USA), vol.43, no.3, p.955-60 (Sept. 1982). Translation of: *Inzh.-Fiz. Zh. (USSR)*, vol.43, no.3, p.365-70 (Sept. 1982).

On the basis of generalized experimental data obtained by the method of local modeling, the authors suggest a method of calculating the heat transfer of a swirled flow of gas suspension in a short channel. (5 refs.)

76044 Numerical analysis of an axisymmetric viscous flow. Mya Oou, T.Kambe (Kyushu Univ., Fukuoka, Japan).

Mem. Fac. Eng. Kyushu Univ. (Japan), vol.42, no.4, p.371-88 (Dec. 1982). [received: May 1983]

The head-on collision of two coaxial viscous vortex rings is simulated by numerical integration of the Navier-Stokes equation for a viscous incompressible fluid. Numerical results are employed to examine the behaviors of time dependent flow quantities and confirm the importance of viscosity when the cores of the two vortex rings come into contact. Sudden decrease of the total energy and circulation, subsequent to the period of their apparent conservation, is observed to be similar to the energy catastrophe known in the turbulence theory. (6 refs.)

76045 Low Reynolds number flow in a rotating tank with barriers. B.R.Munson, L.D.Sturges (Dept. of Engng. Sci. & Mech., Iowa State Univ., Ames, IA, USA).

Phys. Fluids (USA), vol.26, no.5, p.1173-6 (May 1983).

Experimental and theoretical results are presented for two-dimensional creeping flow in a rotating circular tank that has stationary barriers against its wall. The type of flow pattern obtained depends on the number and size of the barriers. (4 refs.)

76046 Weissenberg effect and its dependence upon the experimental geometry. G.Eitelberg (Inst. fur Experimentelle Stromungsmech., DFVLR, Gottingen, Germany).

Rheol. Acta (Germany), vol.22, no.2, p.131-6 (March-April 1983).

The flow of a second-order fluid with a free surface between two coaxially mounted cylinders of finite length, the inner one of which is rotating, is being studied. In the case of slow flow and small shear rates the flow can be divided into a primary flow in the plane perpendicular to the axis of rotation and a secondary flow in the meridional plane. These flow components are numerically calculated and the results are compared with the analytical results for the semi-infinite cylinder approximation. The influence of the finiteness of the cylinders (end effect) upon the free surface deformation is analysed. The numerical results for the secondary flow are compared with results obtained by flow visualisation. (8 refs.)

76047 Autorotation. H.J.Lugt (David W. Taylor Naval Ship Res. & Dev. Center, Bethesda, MD, USA).

In book: *Annual review of fluid mechanics. Vol.15*, M.Van Dyke, J.V.Wehausen, J.L.Lumley [Ed.], p.123-47. Palo Alto, CA, USA: Annual Reviews (1983), 534 pp. [0 8243 0715 1]

The subject of autorotation has been a stepchild in fluid dynamics. It is barely mentioned in textbooks and considered more a curiosity than a topic for serious study. Some people have even labeled autorotation as 'toy aerodynamics', a notion that is certainly not justified. The theoretical difficulties are indicated by the fact that autorotation is essentially a nonlinear phenomenon associated with vortex shedding. Analogies exist to vortex-induced vibrations of bodies, a subject area that has attracted more attention in the past than autorotation. All of these problems are addressed in this review. (64 refs.)

76048 Integrable, chaotic, and turbulent vortex motion in two-dimensional flows. H.Aref (Div. of Engng., Brown Univ., Providence, RI, USA).

In book: *Annual review of fluid mechanics. Vol.15*, M.Van Dyke, J.V.Wehausen, J.L.Lumley [Ed.], p.345-89. Palo Alto, CA, USA: Annual Reviews (1983), 534 pp. [0 8243 0715 1]

The author discusses the restricted subject of two-dimensional vortex motion according to the program indicated by the title. Even with this restriction the spectrum of necessary analytical techniques and possible physical applications is remarkably broad. (204 refs.)

76049 Structure and behavior of a turbulent ring vortex. P.E.M.Schneider.

Report 12/1982, Max-Planck-Inst. Stromungsforschung, Gottingen, Germany (Oct. 1982), i+42 pp.

Of the three flow phases which an unstable ring vortex can take, the turbulent condition is described. A dyed turbulent water ring vortex moving in otherwise stationary water has a warmer shell than its surroundings; a cooler core than its shell; and produces secondary vortices. Parts of these unstable secondary vortices go to form the wake of the turbulent vortex. This production of secondary vortices seems to be responsible for parts of the sound spectra, both of single turbulent vortex, and of jets. The mixing of vortex core and vortex shell material in the secondary vortices is described. The core of the primary vortex controls the frequency of the series of secondary vortices by means of this mixing process. (22 refs.)

Diffraction of an acoustic wave by a plate moving near a plane See Entry 75849

Transport effects associated with turbulence with particular attention to the influence of helicity See Entry 75994

On the logarithmic law and Karman's constant See Entry 75996

Combined influence of dissipation and Hall effects on free convective flow in a rotating fluid See Entry 76021

Convective diffusion toward rotating polar spherical electrode See Entry 76027

Turbulent boundary layer associated with periodic rotating wakes See Entry 76035

Non-equilibrium flow of a vibrationally relaxing gas behind three-dimensional unsteady curved shock wave See Entry 76065

The magnetic analogue of Ertel's potential vorticity theorem See Entry 76118

Functional formulation of magnetohydrodynamic turbulence in a rotating frame of reference See Entry 76121

Barodiffusion in a binary mixture due to rotation of a circular cylinder See Entry 76143

47.35 WAVES

- 76050** Analysis of run up height of surface waves in a liquid body excited by the seismological effect. Ni Haoqing (Inst. of Water Conservancy & Hydroelectric Power Res., China). *Acta Mech. Sin. (China)*, no.2, p.144-55 (1983). In Chinese.
From the viewpoint of finite wave height the author derives an analytic solution for the forced oscillation of a liquid body against the surface of a dam excited by seismological effects. A formulae for the run up height of the surface waves is obtained, and can be used in the design of that part of the dam above the highest water level, and to determine its elevation. (11 refs.)
- 76051** On the unsteady motion of a profile in a heavy fluid bounded by a free line. P.Capodanno (Acad. Polonaise des Sci., Warsaw, Poland). *Bull. Acad. Pol. Sci. Ser. Sci. Tech. (Poland)*, vol.30, no.1-2, p.121-34 (1982). In French.
The unsteady motion about a horizontal show translation of an arbitrary profile in an inviscid incompressible heavy fluid in irrotational motion bounded by a free line is studied. In the first part it is proved, using the conformal mapping of the linearized fluid domain into a circular ring, that the ordinate of the free line satisfies a singular integro-differential equation. In the second part, having supposed that the profile is a circle, its harmonic vertical oscillations are studied. An explicit solution for the ordinate of the free line, the complex potential and the aerodynamic forces is obtained. In a more general case it is shown using Fourier's transform, that the problem can be reduced to Fredholm's equation of the third kind. (9 refs.)
- 76052** The contraction of contaminant distributions in reversing flows. R.Smith (Dept. of Appl. Math. & Theoretical Phys., Univ. of Cambridge, Cambridge, England). *J. Fluid Mech. (GB)*, vol.129, p.137-51 (April 1983).
Exact expressions are derived for the centroid and variance as functions across the flow when there has been an initially uniform contaminant release in an oscillatory flow. Two examples are given to demonstrate that there can be a substantial region of the flow (where the velocity shear is relatively large) in which the contaminant distribution exhibits contraction after flow reversal. This effect, and the sensitivity of the variance to the precise time of discharge, is most marked when the flow oscillations are rapid relative to the timescale for cross-sectional mixing. (14 refs.)
- 76053** Overhanging interfacial gravity waves of large amplitude. D.I.Meiron, P.G.Saffman (Appl. Maths, California Inst. of Technol., Pasadena, CA, USA). *J. Fluid Mech. (GB)*, vol.129, p.213-18 (April 1983).
Methods to investigate the existence of overhanging gravity waves of permanent form at the interface between two uniform fluids of different density are discussed. Numerical results which demonstrate their existence are presented. (4 refs.)
- 76054** Scale effects in a wave-refraction experiment. T.Sprinks (Dept. of Maths., Univ. of Essex, Colchester, England), R.Smith. *J. Fluid Mech. (GB)*, vol.129, p.455-71 (April 1983).
The experimental results of Provis (1975, 1976) for wave amplification at a conical island bear little resemblance to the theoretical predictions of Smith & Sprinks (1975). Here Provis's suggestion is confirmed: that his experiments were dominated by viscous damping and by standing waves between the island and the wavemaker. Estimates are given as to how large an experiment needs to be to avoid these important scale effects. (16 refs.)
- 76055** Effect of water-current interaction on the wave parameter. Li Yucheng (Res. Inst. of Ocean Engng., Dalian Inst. of Technol., Dalian, China). *J. Dalian Inst. Technol. (Dalian Gongxueyuan Xuebao) (China)*, vol.21, no.4, p.81-9 (Dec. 1982). In Chinese. [received: June 1983]
The interaction of a gravity wave with a steady uniform current is discussed. Analysis indicates there is no dominant difference between the results derived from the equation of conservation of wave energy flux and those derived from the equation of conservation of wave action flux. Numerical calculations of wavelength change by different non-linear wave theories show that errors in the results computed by the linear wave theory are less than 10 percent within the range of $0.15 \leq d/L \leq 0.40$, $0.01 \leq H/L \leq 0.07$ and $-0.15 \leq U/C \leq 0.30$, where d is the water depth, H is the wave height in still water, L is the wave length in still water, C is the wave celerity in still water and U is the surface current velocity. Numerical calculations of wave height change employing different wave theories show that errors in the results obtained by the linear wave theory in comparison with the non-linear theories are greater when the opposing relative current and wave steepness become larger. However, within the range of the following currents such errors are not significant. These results were verified by model tests. (7 refs.)
- 76056** Energy flux in capillary-gravity waves. S.J.Hogan (Dept. of Appl. Math. & Theoretical Phys., Univ. of Cambridge, Cambridge, England). *Phys. Fluids (USA)*, vol.26, no.5, p.1206-9 (May 1983).
The relative energy flux F_{rel} of capillary-gravity waves on a moving stream is calculated for various wavelengths, as a function of wave amplitude. In some cases, abrupt changes in the sign of F_{rel} are found to occur for a small increase in wave amplitude. The way in which the phenomena might be observed experimentally is indicated. (10 refs.)
- 76057** Application of the mixed representation to the study of acoustic-gravity waves. B.Poiree (DRET, Paris-Armees, France). *Rev. Cethedec (France)*, vol.19, no.73, p.29-54 (1982). In French.
It is easier to use a mixed representation (Lagrangian perturbations, Eulerian variables) rather than a pure Eulerian representation in order to deduce the dispersion equation for acoustic-gravity waves in a stratified flow of heterogeneous perfect fluid. The dispersion equation is looked for on the basis of the two representations and advantages of the first representation over the second one are thus placed in evidence: (1) Applying small perturbation equations written down in the mixed representation allows one to get rid of hypotheses usually considered in a fluid at rest (homogeneity and isothermal atmosphere). Hines' equation is thus generalized. (2) The use of the Eulerian representation brings up two important points. The first of these concerns the writing of the perturbed state equation in this representation. The second one concerns ambiguities which appear in the search for a solution in the form of an inhomogeneous harmonic plane wave in a system of partial differential equations with variable coefficients whenever no orders of magnitude are accounted for. To end with, the energy equation is given in both representations. (34 refs.)

Annual review of fluid mechanics. Vol.15 See Entry 74234
Turbulent spots, wave packets, and growth See Entry 75983
The cancellation of a sound-excited Tollmien-Schlichting wave with plate vibration See Entry 75985
Compressibility effects on waves in stratified two-phase flow ..See Entry 76086

Breaking waves on beaches See Entry 78555
Magneto-atmospheric waves See Entry 78810

47.40 COMPRESSIBLE FLOWS; SHOCK AND DETONATION PHENOMENA

(see also 28.70 Nuclear explosions, 52.35T Plasma shock waves)

- 76058** Drag of a vaporizing spherical particle in a slow flow of a binary mixture of gases. A.Yu.Boris. *Sov. Phys.-Dokl. (USA)*, vol.27, no.7, p.507-8 (July 1982). Translation of: *Dokl. Akad. Nauk SSSR*, vol.265, no.1-3, p.553-5 (July 1982). [received: April 1983]
Taking into account the Barnett concentration stresses the author proposes to solve the problem of the influence of vaporization (condensation) on the force acting on a sphere in a slow flow of a binary mixture of gases. He shows that the concentration stresses can exert a significant influence on the drag of the sphere. He discusses the quasi-steady vaporization of a spherical particle situated in a mixture of its own vapor with a gaseous component that is insoluble in the sphere. (6 refs.)
- 76059** Calculation of gas flow in a zone of energy release in a cylindrically-symmetrical explosion. V.G.Grudnitskii, V.N.Rygalin. *Zh. Vychisl. Mat. & Mat. Fiz. (USSR)*, vol.23, no.2, p.413-22 (March-April 1983). In Russian. English translation in: *USSR Comput. Math. & Math. Phys. (GB)*
The problem of a cylindrically-symmetrical explosion in a quiescent gas was investigated numerically. Energy is liberated in the medium in accordance with the equation of state of a polytropic gas. The instantaneous and continuous liberation of energy in the course of a certain time was investigated, together with the different types of distribution of the emitted energy along the radius. On the basis of the theory of dimensionality, laws of similarity are derived, characterizing the rate of development of the gasdynamic processes in the region of action of the source. (12 refs.) A.J.B.
- 76060** On the theory of the horizontal-axis wind turbine. O.De Vries (Nat. Aerospace Lab., NLR, Amsterdam, Netherlands).
In book: *Annual review of fluid mechanics. Vol.15*, M.Van Dyke, J.V.Wehausen, J.L.Lumley [Ed.], p.77-96. Palo Alto, CA, USA: Annual Reviews (1983), 534 pp. [0 8243 0715 1]
The extraction of energy from the wind is an old idea, one used by sailing ships and windmills for many centuries. The development of ancient windmills was based on empiricism and engineering skill. The development of the fluid mechanics, or more specifically the aerodynamics, of windmills (wind turbines in modern usage) is more recent. The study of the aerodynamics of wind turbines was begun after World War I by Betz (1926) and Glauert (1935) and got a new impulse after the 'energy crisis' of 1973-74. Nowadays, it is a worldwide field of research, stimulated and guided by national research programs in the US, Sweden, Denmark, The Netherlands, Great Britain, and many other countries. (39 refs.)
- 76061** Low-Reynolds-number airfoils. P.B.S.Lissaman (AeroVironment Inc., Pasadena, CA, USA).
In book: *Annual review of fluid mechanics. Vol.15*, M.Van Dyke, J.V.Wehausen, J.L.Lumley [Ed.], p.223-39. Palo Alto, CA, USA: Annual Reviews (1983), 534 pp. [0 8243 0715 1]
The airfoil section is the quintessence of a wing or lifting surface and, as such, occupies a central position in any design discipline relating to fluid mechanics, from animal flight through marine propellers to aircraft. The proper functioning of the airfoil is the prerequisite to the satisfactory performance of the lifting surface itself, and thus the airfoil is of fundamental technical importance. The author describes the fluid mechanics, performance, and design of low-Reynolds-number airfoils, which he takes to include the range between Reynolds numbers of about 10^4 and 10^6 . (9 refs.)
- Annual review of fluid mechanics. Vol.15 See Entry 74234
Compressibility effects on waves in stratified two-phase flow ..See Entry 76086

47.40D General subsonic flows

- 76062** Effect of sound absorbing wall linings on aerodynamic forces of a subsonic vibrating cascade. N.Yamasaki, M.Namba (Dept. of Aeronautical Engng., Kyushu Univ., Fukuoka, Japan). *Mem. Fac. Eng. Kyushu Univ. (Japan)*, vol.42, no.4, p.251-78 (Dec. 1982). [received: May 1983]
A method of singularity is developed to predict the effect of sound absorbing wall liners on the unsteady aerodynamic forces for a linear cascade vibrating in a subsonic uniform flow between parallel walls. A side wall of the model is partially composed of a sound absorbing liner with uniform acoustic admittance. The lined section of the wall is confined to the portion swept by blades. Substantial variation of the total aerodynamic work with change in the wall admittance is found to occur only in a confined range of the admittance magnitude. The functional form of the aerodynamic work as a function of the admittance magnitude is heavily dependent on the admittance phase. (12 refs.)

Diffraction of an acoustic wave by a plate moving near a plane See Entry 75849

47.40H Transonic flows

- 76063** A mixed direct-inverse problem of the transonic plane cascade. Shen Mengyu, Ma Yuanle (Qinghua Univ., China). *Acta Mech. Sin. (China)*, no.1, p.1-6 (1983). In Chinese.
A mixed direct-inverse problem of the transonic plane cascade is presented, and a general solution procedure is given. By using a computer code based upon the described mixed direct-inverse scheme, the flow field through a given plane cascade can be analyzed, the transonic plane cascade can be designed with desirable aerodynamic performance and reasonable strength characteristics, and a desirable local correction of the transonic plane cascade profile can also be made. The formulation of this mixed direct-inverse problem and its solution procedure have been tested by application to the example of Hobson's impulse cascade (1977). The result is satisfactory. (8 refs.)

47.40K Supersonic and hypersonic flows

76064 Application of the triple-deck theory of viscous-inviscid interaction to bodies of revolution. Ming-ke Huang, G.R.Inger (Dept. of Aerospace Engng. Sci., Univ. of Colorado, Boulder, CO, USA). *J. Fluid Mech. (GB)*, vol.129, p.427-41 (April 1983).
The general triple-deck theory of laminar viscous-inviscid interaction is extended to axisymmetric bodies. With body radius/length ratios scaled in terms of Reynolds number as $Re^{-1/8}$ ($\beta > 0$), it is found that for $\beta < 3$ the only three-dimensional effect is that on the incoming undisturbed boundary-layer profile as accounted for by the Mangler transformation. When $\beta = 3$, however, an explicit axisymmetric effect on the interaction equations also enters: the upper-deck flow is governed by the equation of axisymmetric potential disturbance flow, whereas the middle and lower decks are still governed by equations of two-dimensional form. When $\beta > 3$, the body is so slender that transverse curvature effects become important and the lower decks too are explicitly influenced by three-dimensional effects. A detailed example application of this theory is given for weak interactions on a flared cylinder and cone in supersonic flow with $\beta \leq 3$. The three-dimensional effects on the interactive pressure and shear-stress distributions are shown to relieve the strength of the interaction and reduce its upstream influence, as expected. (24 refs.)

Hypersonic flow behavior in magnetohydrodynamic channel See Entry 76117

47.40N Shock-wave interactions

76065 Non-equilibrium flow of a vibrationally relaxing gas behind three-dimensional unsteady curved shock wave. V.D.Sharma, R.Shyam (Acad. Polonaise des Sci., Warsaw, Poland). *Bull. Acad. Pol. Sci. Ser. Sci. Tech. (Poland)*, vol.30, no.1-2, p.1-9 (1982).
A shock wave is assumed to exist in a three-dimensional unsteady flow of a vibrationally relaxing gas. The variation of flow parameters at any point on the streak lines behind the shock surface is determined in terms of the shock geometry and the upstream flow conditions. The expressions for the vorticity and the curvature of a streak line at the rear of the shock surface are also determined in terms of the known quantities. (7 refs.)

76066 Stability loss of detonation waves in lengthened charges of heterogeneous explosives. V.A.Danilenko, V.M.Kudinov. *Dopov. Akad. Nauk UkrSR. Ser. A (USSR)*, no.3, p.41-4 (1983). In Ukrainian.
It is shown that stationary detonation waves of heterogeneous explosives lose their stability at distances from the initiation place exceeding those specified by stationary and stable conditions. The stability loss results in formation of detonation waves with a pulsating front. Two stationary conditions with different detonation rates in the explosive length were found for the detonation of explosives of a solid oxidizer-liquid fuel type. (4 refs.)

76067 Two-point implicit scheme for the Euler equations. S.Obayashi (Inst. of Engng. Mech., Tsukuba Univ., Ibaraki, Japan), K.Kuwahara. *J. Phys. Soc. Jpn. (Japan)*, vol.52, no.5, p.1525-30 (May 1983).
A new two-point implicit scheme for solving the Euler equations was developed, which is second-order accurate in space and time. This is an extension of the MacCormack implicit scheme, and takes account of the following points: 1. solving for the physical quantity itself at a new time-step, not for change of the physical quantity in time, 2. modifying the implicit operators for stability so as not to decrease accuracy of the approximation of the first derivative. The resulting method is efficient and easy to program. This scheme was compared with various other schemes for a shock tube problem. No physically irrelevant pressure distributions of the shock wave obtained by the present method were observed. It was confirmed that the present one produced good results for a large CFL number.

76068 On the propagation of weak and moderately strong, curved shock waves. F.Obermeier (Max-Planck-Inst. für Stromungsforschung, Göttingen, Germany). *J. Fluid Mech. (GB)*, vol.129, p.123-36 (April 1983).
The author studies the theoretical description of curved converging shock waves, where nonlinear interaction effects, between the shock fronts and the flow behind them, and refraction effects are equally important. In a non-viscous, isenergetic and isentropic flow the problem can be described by a nonlinear wave equation for the pressure field. This equation then admits an analytical solution with the help of the method of strained coordinates provided that the nonlinear terms contain only derivatives with respect to two independent variables. This restrictive condition is approximately fulfilled if the incoming wave is only slightly curved. (18 refs.)

76069 Analysis of self-similar problems of imploding shock waves by the method of characteristics. Y.Nakamura (Faculty of Engng., Kumamoto Univ., Kumamoto, Japan). *Phys. Fluids (USA)*, vol.26, no.5, p.1234-9 (May 1983).
The asymptotic self-similar form of cylindrically or spherically imploding shock waves is extracted by numerically solving non-self-similar problems. The shock wave is generated by a contracting piston with finite initial velocity. For the initial shock motion, a perturbation method is used to determine the starting condition for the numerical calculation. Propagation of the shock wave and flow field properties are obtained and the transition of the non-self-similar motion of the shock wave into the self-similar one is presented. Good agreement between self-similar exponents determined from the variation of the shock strength and those calculated by Guderley is obtained. (21 refs.)

76070 The impact of compressible liquids. M.B.Lesser (Univ. of Lulea, Lulea, Sweden), J.E.Field.
In book: *Annual review of fluid mechanics. Vol.15*, M.Van Dyke, J.V.Wehausen, J.L.Lumley [Ed.], p.97-122. Palo Alto, CA, USA: Annual Reviews (1983), 534 pp. [0 8243 0715 1]
The authors' review concentrates on determining the maximum pressure-loading and other possible damage mechanisms that will erode a solid target. This implies that the early stages of the impact process are studied, during which the shock waves signaling a collision are spreading out through both the liquid and solid. Compressible behavior of the liquid and the motion of the solid target have to be taken into account. The problem involves, in general, free surfaces and the constitutive behavior of both liquid and target. The approach has been analytical, numerical, and experimental, with perhaps the largest gains made experimentally. (94 refs.)

A study of the steady-state reaction-zone structure of a homogeneous and a heterogeneous explosive See Entry 76126

47.45 RAREFIED GAS DYNAMICS

(see also 07.30 Vacuum production and techniques)

76071 Thermophoresis of spherical particles and the dependence of the jump coefficients on the accommodation coefficient. Shen Ching (Inst. of Mech., Acad. Sinica, Peking, China). *Acta Mech. Sin. (China)*, no.1, p.5-15 (1983). In Chinese.
The problem of thermophoretic force exerted on a sphere held in a rarefied gas ($K_n \ll 1$) with a temperature gradient is considered. In the inner region the Boltzmann-Krook-Welander equation is solved under Maxwell-type boundary conditions in the wall, and this solution is matched with the solution of the Stokes and Laplace equations. The slip coefficient C_m , the thermal creep coefficient C_s , and the temperature jump coefficient C_t are determined from the first approximation of the inner solution. The thermophoretic force thus obtained is in good agreement with experimental data, and the values of C_m , C_s , C_t thus calculated and their dependence on the thermal accommodation coefficient a are also in good agreement with the results of solution of the planar problem obtained by using variational and other methods. (14 refs.)

76072 Heterogeneous vibrational relaxation upon free molecular flow of diatomic gas past concave bodies. L.P.Gashtol'd (N.A. Voznesenskii Leningrad Inst. of Finance & Economics, Leningrad, USSR). *J. Eng. Phys. (USA)*, vol.43, no.3, p.1012-16 (Sept. 1982). Translation of: *Inzh.-Fiz. Zh. (USSR)*, vol.43, no.3, p.438-43 (Sept. 1982).
The method of successive calculation of multiple reflections is used for investigating heterogeneous vibrational relaxation when a free molecular stream of diatomic gas flows past a concave body. (4 refs.)

76073 Modern methods of numerical investigation of rarefied gas phenomena. F.G.Tcheremissine (Dept. of Aeronautical Engng., Indian Inst. of Sci., Bangalore, India). *Proc. Indian Acad. Sci. Eng. Sci.*, vol.5, pt.2, p.159-67 (July 1982). [received: April 1983]

It is well-known that an adequate description of a dilute gas is given by the Boltzmann equation of the kinetic theory of gases. To meet today's technological needs, different attempts to obtain numerical solutions of this equation have been made. These attempts can be divided into two main groups; stochastic simulation of gas phenomena, and numerical methods to solve the Boltzmann equation itself. The first approach arose from purely intuitive considerations; later some theoretical analysis followed and the relation to the Boltzmann equation became more evident. Thus the direct stochastic simulation of molecular motion received theoretical approval. The second approach did not need any theoretical justification; here the problem of prime importance was that of its practical efficiency. The way to improve the accuracy of this method lay in the application of economical numerical algorithms based on recent advances in computational fluid mechanics and in numerical methods in general. Further sophistication of computers will provide technological support for more accurate investigations of rarefied gas phenomena. (19 refs.)

Effect of evaporation on convective heat exchange of a porous plate in a rarefied medium See Entry 75900

47.50 NON-NEWTONIAN DYNAMICS

76074 Some constitutive equations for non-Newtonian fluids. C.F.Chan, Man Fong (Dept. of Mech., Peking Univ., Peking, China). *Acta Mech. Sin. (China)*, no.1, p.16-26 (1983). In Chinese.
Non-Newtonian fluids may be classified as (i) inelastic fluids, fluids whose viscosity is not a constant, (ii) fluids with yield stress, (iii) fluids with elastic properties, (iv) thixotropic fluids. Some constitutive equations of the above four types of fluids have been considered. Their usefulness and conditions under which they may be used have also been discussed. Numerical values of some of the parameters occurring in these constitutive equations have been given. (12 refs.)

76075 Viscoelastic squeeze-film flows—Maxwell fluids. N.Phan-Thien, R.I.Tanner (Dept. of Mech. Engng., Univ. of Sydney, Sydney, Australia). *J. Fluid Mech. (GB)*, vol.129, p.265-81 (April 1983).
An exact solution for the squeeze-film motion in an upper convected Maxwell fluid is given for both the plane and axisymmetric cases. Inertia and viscoelastic effects are included, and it is shown that the solution depends only on the product of the Weissenberg and Reynolds numbers. Solutions are generated for values of this product up to 500 without numerical problems. The solutions show wave propagation and show a reduced load capacity relative to the Newtonian case. (20 refs.)

76076 Plane and axis-symmetric stagnation flow of a Maxwellian fluid. N.Phan-Thien (Dept. of Mech. Engng., Univ. of Sydney, Sydney, NSW, Australia). *Rheol. Acta (Germany)*, vol.22, no.2, p.127-30 (March-April 1983).
Exact solutions to the plane and axis-symmetric stagnation flows of a Maxwellian fluid including inertia are reported. It is found that the fluid elasticity decreases the boundary layer thickness. (6 refs.)

76077 On nonlinear effects in the extensional flow of polymeric liquids. A.I.Leonov, A.N.Prokunin (Inst. for Problems in Mech., Acad. of Sci., Moscow, USSR). *Rheol. Acta (Germany)*, vol.22, no.2, p.137-50 (March-April 1983).
The problems of uniform extension of liquids under constant strain rate and constant stretching force have been studied using a nonlinear rheological theory that describes the effects of finite elastic strains in viscoelastic liquids, with provision for the influence of deformative orientation on a scalar relaxation time. It has been shown that the predictions of the theory are in rather good agreement with numerous data for the extensional flow of polyisobutylene, even without taking the deformative orientation into account, (however, in cases where the latter was important it was considered in detail). Some new results for the extensional properties of polyethylene melts, as well as those from the literature, show that its behaviour is qualitatively different from that of polyisobutylene. The mathematical description of the extensional flow of polyethylene has to take into consideration the mechanism of flow thermoactivation and, apparently, an accumulation of ruptures of macromolecules in addition to the deformative orientation phenomenon. (25 refs.)

76078 Injection moulding of thermoplastics: freezing during mould filling. S.M.Richardson (Dept. of Chem. Engng. & Chem. Technol., Imperial Coll. London, London, England). *Rheol. Acta (Germany)*, vol.22, no.2, p.223-36 (March-April 1983).
The injection moulding of thermoplastic polymers involves, during mould filling, flows of hot melts into mould networks, the walls of which are so cold that frozen layers form on them. Theoretical analyses of such flows are presented. (8 refs.)

76079 Numerical methods in non-Newtonian fluid mechanics. M.J.Crochet (Univ. Catholique de Louvain, Louvain-la Neuve, Belgium), K.Walters. In book: *Annual review of fluid mechanics*. Vol.15, M.Van Dyke, J.V.Wehausen, J.L.Lumley [Ed.], p.241-60. Palo Alto, CA, USA: Annual Reviews (1983), 534 pp. [0 8243 0715 1]
The authors introduce a flow classification (Crochet et al. 1983) and consider briefly the numerical methods required in each flow type. They then concentrate on one subject, namely the flow of highly elastic liquids in complex geometries. The reasons for this emphasis are twofold. First, the related flow problems have a different structure from that found in the corresponding Newtonian situation, and second, much of the worthwhile research effort in non-Newtonian fluid mechanics in the last decade has been expended in this direction. (89 refs.)

Positive hole pressures and negative exit pressures generated by molten polyethylene flowing through a slit die See Entry 75974

The rheological behaviour of HDPE/LDPE blends. I. End effects and shear viscosity See Entry 75977

Flow in curved pipes See Entry 76116

Oriental effect of the extensional flow field on solutions of rigid rodlike macromolecule—disappearance of the isotropic to nematic phase transitions See Entry 76628

47.55 NONHOMOGENEOUS FLOWS

76080 The transport from a drop in an alternating electric field. S.K.Griffiths (Sandia Nat. Labs., Albuquerque, NM, USA), F.A.Morrison, Jr.

Int. J. Heat & Mass Transfer (GB), vol.26, no.5, p.717-26 (May 1983).
Analyses of heat and mass transfer from a drop in an electric field have, to date, dealt only with steady electric fields. This study presents both high and low Peclet number solutions for transport in an alternating electric field. The low Peclet number transport is investigated analytically using a composite, double perturbation expansion. Special analytic methods are developed to consider the previously untreated transport problem where the steady and time-dependent components of the fluid motion are of equal magnitude. A digital computer is employed to obtain exact solutions to the recursive governing equations. These solutions yield accurate results for Peclet number in the range 0-30 and thermal vibration number above 200. (23 refs.)

76081 Settling of encapsulated droplets at low Reynolds numbers. E.Rushton, G.A.Davies (Dept. of Chem. Engng., Univ. of Manchester Inst. of Sci. & Technol., Manchester, England).

Int. J. Multiphase Flow (GB), vol.9, no.3, p.337-42 (June 1983).
Deals with some interesting problems associated with translation of liquid droplets which have not previously been considered and which have some importance in defining process conditions in their application. The problems relate to translation and settling of encapsulated droplets in viscous liquids and arise in membrane separation processes which are now the subject of much research and development work, Li (1971), Li and Asher (1973), Martin and Davies (1976). In these processes, the overall objective is to selectively extract compound(s) from a liquid into a second immiscible liquid. This is accomplished by separating the two miscible phases, donor and receptor, by a membrane through which the solids may diffuse. One such process uses a liquid membrane phase so that there are three fluid phases; the membrane phase has to be immiscible with the other two. (10 refs.)

76082 Field-flow fractionation. R.Smith (Dept. of Appl. Maths. & Theoretical Phys., Univ. of Cambridge, Cambridge, England).

J. Fluid Mech. (GB), vol.129, p.347-64 (April 1983).
If different contaminant species are subject to different transverse drift rates (e.g. gravitational settling), then there is a tendency for the species to separate out. The efficiency of this separation depends upon the relative shapes of the longitudinal concentration distributions. Jayaraj & Subramanian (1978) have drawn attention to the disparity between their computed skew concentration distributions and the symmetric Gaussian distributions predicted by one-dimensional diffusion models. Here it is shown that a one-dimensional delay-diffusion model yields suitably skew predictions. The model equation is used to investigate the extent to which the separation of different contaminant species can be improved by pre-treating the sample (i.e. allowing differential drift) in a stationary fluid before being eluted into the shear flow. Pretreatment is found to be very effective for plane Poiseuille flow but not for the thermogravitational columns. (10 refs.)

Viscous-inviscid interactions in cascades See Entry 75997

47.55C Jets

76083 Velocity distribution in turbulent cross jets. K.Subramanya (Civil Engng. Dept., Indian Inst. of Technol., Kanpur, India), P.D.Porey.

Indian J. Technol., vol.20, no.11, p.427-33 (Nov. 1982). [received: May 1983]
An experimental study of the velocity distribution of a round turbulent jet penetrating into a cross flow fluid with the same properties as the jet is reported. The axial component of the jet velocity vector at various transverse locations of a cross section are found to be distributed according to a similarity law. In two mutually perpendicular transverse directions the similarity profiles are found to have identical functional form. Their length scales also have identical functional form. The maximum axial velocity of the jet is found to decay exponentially with a penetration length parameter. The potential length of the jet is shown to be a function ratio of the cross jet. (10 refs.)

76084 Effect of initial velocity difference between phases on evolution of two-phase jet. A.I.Kartushinskii, V.A.Leonov, A.S.Mul'gi ('Sergo Ordzhonikidze' Moscow Inst. of Aviation, Moscow, USSR).

J. Eng. Phys. (USA), vol.43, no.3, p.960-2 (Sept. 1982). Translation of: *Inzh.-Fiz. Zh. (USSR)*, vol.43, no.3, p.371-4 (Sept. 1982).
Results of an experimental study are presented concerning the effect which the initial difference between the velocity of the gas and the velocity of the pollutant particles have on the characteristics of an inundated air jet carrying a pollutant in the form of spherical particles of high-density material. (4 refs.)

76085 The turbulent wall jet—measurements and modeling. B.E.Launder (Dept. of Mech. Engng., Univ. of Manchester Inst. of Sci. & Technol., Manchester, England), W.Rodi.

In book: *Annual review of fluid mechanics*. Vol.15, M.Van Dyke, J.V.Wehausen, J.L.Lumley [Ed.], p.429-59. Palo Alto, CA, USA: Annual Reviews (1983), 534 pp. [0 8243 0715 1]
The turbulent wall jet, even limiting attention to the topographically simple cases beloved of academics, arguably provides more puzzles for those seeking an ordered set of rules to describe turbulence than any other class of turbulent shear layer. One can regard a wall jet as a boundary layer in

which, by virtue of the initially supplied momentum, the velocity over some region in the shear layer exceeds that in the free stream. The authors extend a previous review on turbulent wall jets. They consider physical processes in more detail, radial wall jets and examines how well current calculation schemes succeed in mimicking the measured behaviour of wall jets. (69 refs.)

The spatial derivative of temperature in a turbulent flow and Taylor's hypothesis See Entry 75992

The impact of compressible liquids See Entry 76070

Gas jets in fluidized beds: the influence of particle size, shape and density of gas and solids entrainment See Entry 76103

47.55H Stratified flows

76086 Compressibility effects on waves in stratified two-phase flow. G.B.Wallis, B.J.Hutchings (Thayer School of Engng., Dartmouth Coll., Hanover, NH, USA).

Int. J. Multiphase Flow (GB), vol.9, no.3, p.325-36 (June 1983).
Ardron (1980) presented both one-dimensional and two-dimensional analyses of wave propagation in horizontal stratified two-phase flow. He compared the two approaches and concluded that the comparison helped to improve confidence in the use of one-dimensional approximations for the analysis of complex systems such as nuclear reactors. There are several assumptions in Ardron's developments. When alternative assumptions are made the results change. By examining the consequences of several possible assumptions the authors have learned from this example that considerable care may be necessary in the reduction of a mini-dimensional two-phase flow problem to a simpler form. The authors present a more complete two-dimensional solution of this problem and discusses the limitations of the approximate solutions. (2 refs.)

76087 An experimental study of entraining, stress-driven, stratified flow in an annulus. D.R.Scranton, W.R.Lindberg (Dept. of Mech. Engng., Univ. of Wyoming, Laramie, WY, USA).

Phys. Fluids (USA), vol.26, no.5, p.1198-205 (May 1983).
An experimental study of turbulent, two-layer stratified entrainment in an annular, surface stress driven geometry is described. Density and velocity probes were used to determine interfacial locations and flow patterns. Annular geometry effects were examined using three channel widths. The entire flow system was constructed of clear plastic to facilitate observations. The measurements and observations of these flows over a wide range of Richardson number indicate a strong secondary circulation, radial interfacial tilt, and a dominant dependence of flow parameters on the annular radius. It is concluded that the entrainment results in annuli such as the one used in this study may not be directly applicable to one-dimensional entrainment processes. (15 refs.)

76088 Application of the method of streams to one problem of the dynamics of a viscous stratified fluid. A.V.Babakov.

Zh. Vychisl. Mat. & Mat. Fiz. (USSR), vol.23, no.2, p.432-9 (March-April 1983). In Russian. English translation in: *USSR Comput. Math. & Math. Phys. (GB)*

A difference scheme based on the method of streams is proposed for the numerical investigation of problems of the dynamics of a viscous incompressible stratified fluid. The results are presented of a systematic study of the problem of collapse of a uniform 'spot' situated in a fluid with stable stratifications obtained on the basis of this difference scheme. The results are compared with existing numerical and experimental data, and a conclusion is made regarding the parameters of a calculating grid necessary for numerical investigation of the problem. (10 refs.) A.J.B.

A statistical model of fluid-element motions and vertical diffusion in a homogeneous stratified turbulent flow See Entry 75990

47.55K Multiphase flows

76089 Two-phase flow patterns: a review of research results. S.Z.Rouhani, M.S.Sohal (EG&G Idaho Inc., Idaho Falls, ID, USA).

Prog. Nucl. Energy (GB), vol.11, no.3, p.219-59 (1983).
Presents a literature review covering various aspects of two-phase flow patterns. After a description of commonly observed flow regimes in horizontal and vertical pipes, some different types of flow pattern maps are discussed. Experimental techniques for direct and indirect determination of flow regimes are reviewed. These include direct viewing, photography, X-ray and statistical analysis of fluctuations in measured pressure or void fraction which yield power spectral density and probability density functions. The recent advances in the use of neutron noise analysis are also discussed. Flow regime transition criteria based on correlations and theoretical derivations are covered next. Finally, the effects of wall roughness, heat flux and flow acceleration on flow regime transitions are discussed. Throughout the paper an attempt has been made to identify the areas where new development work is needed. (69 refs.)

76090 Unsteady flow of a dusty viscous liquid through confocal elliptical ducts. M.Gupta, H.S.Sharma (Dept. of Maths., Agra Coll., Agra, India).

Indian J. Theor. Phys., vol.29, no.3, p.227-37 (Sept. 1981).
The unsteady flow of a dusty viscous liquid through long confocal elliptical ducts when the axial pressure gradient is an arbitrary function of time have been investigated by repeated use of the finite Mathieu transform and the Laplace transform. The cases when this pressure gradient is impulsive, exponential, and periodic have been discussed as particular examples. The results for unsteady flow of a dusty viscous liquid when the confocal elliptic cylinders transit to co-axial circular cylinders have been deduced. (13 refs.)

76091 Simplified nonlinear descriptions of two-phase flow instabilities in vertical boiling channel. H.Gurgenci, T.N.Veziroglu, S.Kakac (Dept. of Mech. Engng., Univ. of Miami, Coral Gables, FL, USA).

Int. J. Heat & Mass Transfer (GB), vol.26, no.5, p.671-9 (May 1983).
A constant-property homogeneous-flow model is developed to generate the limit cycles of pressure-drop and density-wave oscillations in a single-channel upflow boiling system operating between constant pressures, with upstream compressibility introduced through a surge tank. In the model, thermodynamic equilibrium conditions are assumed and the effects of the wall heat storage and the variation of the fluid properties are neglected. Satisfactory agreement with the experimental cycles is noted for the pressure-drop oscillations. As for the density-wave oscillations, the agreement with the experiments is reasonably good regarding the periods of the oscillations, but not so good for the amplitudes. (8 refs.)

76092 Gas particulate flow through a tube of varying cross-section. S.Prabha, R.K.Jain (Dept. of Math., Indian Inst. of Technol., Kanpur, India).

Indian J. Pure & Appl. Math., vol.14, no.3, p.377-94 (March 1983).
Gas-particulate flow with incompressible gas phase and compressible particle phase is considered through a tube of varying cross-section. Series solution for small Reynolds number is developed in terms of the small parameter ϵ which

gives the rate of variation of the cross-section of the tube with the axial distance. Expressions for the stream functions and velocity components for gas and particle phases, pressure distribution and shear stress at the tube wall are obtained correct up to the order of ϵ^2 . It is shown that the particulate density increases in the radial direction and becomes large at the tube wall. It is further indicated that the shear stress at the tube wall for gas-particulate flow is less as compared to the shear stress for the gas-phase only. (13 refs.)

76093 On the slow translation of a solid submerged in a fluid with a surfactant surface film. II. R.Shail, D.K.Gooden (Dept. of Maths., Univ. of Surrey, Guildford, England).

Int. J. Multiphase Flow (GB), vol.9, no.3, p.227-50 (June 1983).
For pt.1 see *ibid.*, vol.8, p.627-639 (1982). In Shail and Gooden (1982) the problem of a solid particle translating in a semi-infinite fluid, whose surface is contaminated with a surfactant film, was examined in the quasi-steady Stokes flow regime. Various linearised models governing the variation of film concentration were considered, but the analysis was approximate in that the fluid motion generated was represented by that due to Stokeslet situated at the center of the particle. In this paper the authors remove the latter restriction and treat two specific solids, namely a rigid flat circular disk and a sphere, which move axisymmetrically perpendicular to the fluid surface. This surface is assumed to remain plane throughout the motion. The velocity field in the translating-disk problem is represented in terms of harmonic functions, and the resulting mixed boundary-value problems are reduced, for each of the film behaviours examined, to the solution of sets of simultaneous Fredholm integral equations of the second kind. These equations are solved both iteratively and numerically, and the drag on the disk is computed. For the sphere a stream-function formulation in bispherical coordinates is used. Application of the boundary conditions at the sphere and film results in infinite sets of simultaneous linear equations for the coefficients in the eigenfunction expansion of the stream function. These equations are solved by the method of truncation, and the drag on the sphere is determined. (14 refs.)

76094 Two-phase flow in a vertical pipe and the phenomenon of choking: homogeneous diffusion model. I. Homogeneous flow models. Z.Bilicki, J.Kestin (Brown Univ., Providence, RI, USA).

Int. J. Multiphase Flow (GB), vol.9, no.3, p.269-88 (June 1983).
Examines the topological structure of all possible solutions which can exist in flows through adiabatic constant-area ducts for which the homogeneous diffusion model has been assumed. The conservation equations are one-dimensional with the single space variable z , but gravity effects are included. The conservation equations are coupled with three equations of state: a pure substance, a perfect gas with constant specific heats, and a homogeneous two-phase system in thermodynamic equilibrium. The preferred state variables are pressure P , enthalpy h , and mass flux G^2 . The topological characteristics of the solutions allow one to study all flow patterns which can, and which cannot, occur in a pipe of given length L into which fluid is discharged through a rounded entrance from a stagnation reservoir and whose back-pressure is slowly lowered. The set of flow patterns is analogous to that which occurs with a perfect gas, except that the characteristic numerical values are different. They must be obtained by numerical integration and the influence of gravity must be allowed for. The preceding conclusions are valid for all assumptions concerning the shearing stress at the wall which make it dependent on the state parameters only, but not on their derivatives with respect to z . However, the study is limited to upward flows for which the shearing stress at the wall and the gravitational acceleration are codirectional. (17 refs.)

76095 Particle fraction and velocity measurement in gas-powder streams by capacitance transducers. G.A.Irons, J.S.Chang (McMaster Univ., Hamilton, Ontario, Canada).

Int. J. Multiphase Flow (GB), vol.9, no.3, p.289-97 (June 1983).
A simple, economical and accurate technique, based on the different dielectric constants of solids and gases, has been developed to determine instantaneous, in-situ void fractions and particle velocities in gas-powder streams. Two different electrode configurations, were investigated for sensitivity and flow-regime dependency. Stationary, as well as high speed cinematographic, calibrations were performed. The technique is suitable for process control. (12 refs.)

76096 Numerical solution of equations of the dynamics of a viscous incompressible fluid containing dispersed particles. A.L.Dorfman.

Zh. Vychisl. Mat. & Mat. Fiz. (USSR), vol.23, no.2, p.423-31 (March-April 1983). In Russian. English translation in: *USSR Comput. Math. & Math. Phys. (GB)*

The author presents a numerical finite-difference algorithm, based on the method of decomposition, for solving equations of the movement of heterogeneous mixtures, represented with the aid of an ensemble of mutually-penetrating and mutually-interacting continuous media occupying one and the same volume. (8 refs.) A.J.B.

76097 Mathematical modeling of two-phase flow. D.A.Drew (Dept. of Math. Sci., Rensselaer Polytech. Inst., Troy, NY, USA).

In book: *Annual review of fluid mechanics. Vol.15*, M.Van Dyke, J.V.Wehausen, J.L.Lumley [Ed.], p.261-91. Palo Alto, CA, USA: Annual Reviews (1983), 534 pp. [0 8243 0715 1]

Examines the common features of dispersed two-phase flows from a continuum-mechanical approach. Since it is not universally accepted that such an approach is valid, the author discusses some philosophical reasons for taking such an approach. The approach is based on the view that it is sufficient to describe each material as a continuum, occupying the same region in space. This new 'material' consists of two interacting materials (called phases, even though they often are not different phases of the same material). The author reviews the connection with the exact, or microscopic description, through the application of an averaging process to the continuum mechanical equations describing the exact motion of each material at each point. (71 refs.)

76098 Complex freezing-melting interfaces in fluid flow. M.Epstein (West Coast Office, Fauske & Associates Inc., Encino, CA, USA), F.B.Cheung.

In book: *Annual review of fluid mechanics. Vol.15*, M.Van Dyke, J.V.Wehausen, J.L.Lumley [Ed.], p.293-319. Palo Alto, CA, USA: Annual Reviews (1983), 534 pp. [0 8243 0715 1]

The authors present an overall view of the subject of solid-liquid phase change in fluid flow with major emphasis on situations in which there are strong interactions among the flow and the motion as well as the shape of the solid-liquid interface. They discuss the problems and phenomena of solid-liquid phase change in a flowing melt in three main groups. These are (a) phase change in external forced flow, (b) phase change in internal forced flow and (c) phase change in natural convection flow. (82 refs.)

Intelligent turbidity monitoring using fibre optics See Entry 75818

Evaporation and condensation on two parallel plates at finite Reynolds numbers See Entry 75915

Accuracy of analytical computational methods in thermohydrodynamics of two-phase systems See Entry 76030

Heat transfer of a swirled flow of gas suspension in a short channel See Entry 76043

Compressibility effects on waves in stratified two-phase flow See Entry 76086

Flow in curved pipes See Entry 76116

Role of hydrodynamic interaction of dispersed particles in structuration processes in alternating electric field See Entry 76123

Use of the electromagnetic flowmeter in a two-phase flow See Entry 76132

47.55M Flow through porous media

76099 Axisymmetrical two-dimensional steady and unsteady flow through porous media. Liu Ciqun (Lanchou Res. Div. of Mech. of Flow Through Porous Media, Acad. Sinica, Lanchou, China).

Acta Mech. Sin. (China), no.2, p.103-10 (1983). In Chinese.
The author studies the axisymmetrical two-dimensional steady and unsteady flow of homogeneous liquids in carbonate reservoirs. A formula for limiting producing rate is given for a balanced state of injection and production that can be used to estimate maximum output. Line source solutions are sought for the unsteady flow of a slightly compressible liquid doubleporous media that can be used to analyse data for partially penetrating well testing. (11 refs.)

76100 Regular flow around a flat plate set between two parallel walls with different permeabilities. P.Capodanno (Acad. Polonaise des Sci., Warsaw, Poland).

Bull. Acad. Pol. Sci. Ser. Sci. Tech. (Poland), vol.30, no.1-2, p.115-20 (1982).

It is shown that if the permeabilities and the plenum-chamber pressures satisfy suitable conditions, there is one regular flow, with finite velocity at the sharp trailing edge, around a flat plate set between two parallel walls with different permeabilities. (4 refs.)

76101 Unsteady flow of a viscous fluid in a porous elliptic tube. P.C.Gupta, R.G.Sharma (Dept. of Maths., Agra Coll., Agra, India).

Indian J. Theor. Phys., vol.29, no.3, p.271-9 (Sept. 1981).

Unsteady laminar flow of a viscous incompressible fluid through porous media in a long uniform elliptic tube with impermeable boundary has been studied by using Mathieu functions and the technique of Laplace transforms. The axial pressure gradient has been taken as any function of time. A few particular cases, i.e. flow under constant pressure gradient and harmonically oscillating pressure gradient have been discussed. Flow of ordinary viscous fluid with no resistancy of media has been deduced. It is observed that if one puts $\rho(\tau)=0$, the result coincides with that obtained by Narasimhacharyulu and Pattabhiramacharyulu (1978). (5 refs.)

76102 Residence time distribution in annular packed and fluidized beds. K.Kasthuri, G.S.Laddha (AC Coll. of Technol., Madras, India).

Indian J. Technol., vol.20, no.11, p.438-40 (Nov. 1982). [received: May 1983]

Residence time distribution studies are presented for flow through annular packed and fluidized beds. A generalized correlation for predicting the axial dispersion coefficient, applicable for both fixed and expanded beds is proposed. (6 refs.)

76103 Gas jets in fluidized beds: the influence of particle size, shape and density of gas and solids entrainment. M.Filla, L.Massimilla, S.Vaccaro (Istituto di Chimica Industriale e Impianti Chimici, Univ. di Napoli, Napoli, Italy).

Int. J. Multiphase Flow (GB), vol.9, no.3, p.259-67 (June 1983).

Gas has been injected in two-dimensional fluidized beds of solids different in size, density and shape. The ranges of solids sizes and bed heights were such as to produce relatively steady permanent jets. The mechanics of dispersion of these jets has been studied measuring jet angles, jet gas and solids velocity profiles, and particle entrainment velocities. The proportions of total mass and momentum flowrates pertaining to gas and solids have been calculated from these data. (16 refs.)

76104 Statistical study of fluctuation of gas flow rate in caps in fluidized-bed processing units. A.P.Baskakov, V.G.Tuponogov, N.F.Filippovskii (S.M. Kirov Ural Polytech. Inst., Sverdlovsk, USSR).

J. Eng. Phys. (USA), vol.43, no.3, p.949-51 (Sept. 1982). Translation of: *Inzh.-Fiz. Zh. (USSR)*, vol.43, no.3, p.357-60 (Sept. 1982).

Results are presented from correlational and spectral analysis of gas flow rate fluctuations in caps in fluidized-bed processing units with bed depths up to 0.8 m. (5 refs.)

76105 Heat transfer in a fluidized bed with allowance for the filtration component. N.V.Antonishin, M.A.Geller, V.I.Ivanyutenko (A.V. Lykov Inst. of Heat & Mass Transfer, Acad. of Sci., Minsk, Belorussian SSR).

J. Eng. Phys. (USA), vol.43, no.3, p.952-5 (Sept. 1982). Translation of: *Inzh.-Fiz. Zh. (USSR)*, vol.43, no.3, p.360-4 (Sept. 1982).

A two-phase model of surface-to-pseudoturbulent dispersed bed heat transfer is applied for calculating temperature fields in a fluidized bed. Calculation results are compared with experimental data. (6 refs.)

76106 Convective instabilities in binary mixtures in a porous medium. H.Brand (Inst. for Theoretical Phys., Univ. of California, Santa Barbara, CA, USA), V.Steinberg.

Physica A (Netherlands), vol.119A, no.1-2, p.327-38 (April 1983).

The authors investigate the instabilities which can occur when a layer of a mixture of two miscible fluids in a porous medium is heated from below or from above. They find that either a stationary instability or an oscillatory instability can occur as the first bifurcation depending on the sign and the magnitude of the Soret coefficient. The possibility of an oscillatory convective instability when heating is done from above is pointed out for the first time. They discuss the mechanism of these instabilities using energy balance considerations. (27 refs.)

76107 Unsteady natural convection in a porous layer. D.Poulidakos, A.Bejan (Dept. of Mech. Engng., Univ. of Colorado, Boulder, CO, USA).

Phys. Fluids (USA), vol.26, no.5, p.1183-91 (May 1983).

The focus of this paper is on the functionals of the transient mechanism responsible for the establishment of natural convection in a two-dimensional porous layer confined between isothermal vertical walls and insulated horizontal walls. In the first part of the paper, pure scaling arguments are used to identify the characteristic time scales of the phenomenon and, based on these scales, the evolution of the porous system to steady state. The type of steady state is shown to depend on the relative order of magnitude of the characteristic time scales. Distinct vertical boundary layers are shown to be possible if $(L/H)Ra^{1/2} > 1$, and distinct horizontal layers if $(H/L)^{1/2}Ra^{1/4} > 1$. In the second part of the paper, these and other scaling laws of the transient evolution to steady state are successfully tested against a series of transient numerical experiments conducted in the range $H/L=0.2-5$ and $Ra=10-50$. (24 refs.)

- Thermal convection in a cavity filled with a porous medium: a classification of limiting behaviours See Entry 76006
- Thermal convection in a porous medium composed of alternating thick and thin layers See Entry 76009
- Natural convection heat transfer in a porous layer with internal flow obstructions See Entry 76012
- Nonlinear convection in a porous layer with finite conducting boundaries See Entry 76024
- Unsteady laminar flow of a viscous liquid in a symmetrical porous-walled channel of varying width See Entry 76112
- Modelling of flow phenomena in porous media See Entry 78545
- The transient flow in naturally fractured reservoirs with three-porosity systems See Entry 78563

47.60 FLOWS IN DUCTS, CHANNELS, AND CONDUITS

(for biological fluid dynamics, see 87.45)

- 76108 The flow of granular materials. III. Rapid shear flows.** S.B.Savage (Dept. of Civil Engng. & Appl. Mech., McGill Univ., West Montreal, Quebec, Canada), R.M.Nedderman, U.Tuzun, G.T.Houlsby. *Chem. Eng. Sci. (GB)*, vol.38, no.2, p.189-206 (1983). The authors consider the case of the rapid flows that occur in chutes and open channels. (48 refs.)
- 76109 Axisymmetric meniscus formation: a viscous-fluid model for cones.** P.T.Squire (School of Phys., Univ. of Bath, Bath, England). *J. Fluid Mech. (GB)*, vol.129, p.91-108 (April 1983). The dynamics of the formation of the axisymmetric meniscus around a cone contacting a free liquid surface are discussed. An approximate phenomenological model is set up. In the case considered, where $Re \ll 1$ and viscosity dominates the retarding forces, this leads to a differential equation relating the height of the circle of contact to time. Solutions are derived, involving one or more unknown parameters, which describe the time dependence of the height of the circle of contact. Experimental data, obtained from delayed flash photographs of the meniscus profiles of silicone fluid climbing over the surface of glass cones, provide general support for the model. The agreement between the predicted and observed height as a function of time is sufficiently close to justify the model as a useful description. (16 refs.)
- 76110 Shear layers in converging flow of fluid of non-uniform density and viscosity.** B.R.Duffy (Dept. of Appl. Maths. & Theoretical Phys., Univ. of Cambridge, Cambridge, England). *J. Fluid Mech. (GB)*, vol.129, p.109-21 (April 1983). The authors present an asymptotic study of steady two-dimensional radial flow between converging plane walls (Jeffery-Hamel flow) when the viscosity μ and density ρ vary with the angular coordinate θ . Two representative situations are considered, the first being a two-layer system (in which μ and ρ are uniform except for discontinuities at an interface $\theta = \theta_0$), and the other involving a fluid for which μ and ρ vary continuously with θ . The flow is analysed in the asymptotic limit when a parameter c related to the wall pressure gradient is large; this corresponds to converging flow at large Reynolds number. Solutions are derived for the boundary layers at the walls and for the shear layer at the interface; the results are shown to agree well with some exact (numerical) profiles. (4 refs.)
- 76111 The evolution of Tollmien-Schlichting waves near a leading edge. II. Numerical determination of amplitudes.** M.E.Goldstein, P.M.Sockol, J.Sanz (NASA, Lewis Res. Center, Cleveland, OH, USA). *J. Fluid Mech. (GB)*, vol.129, p.443-53 (April 1983). For pt.1 see ibid., vol.127, p.59 (1983). It was shown in Part 1 (1983) that the amplitude of the spatially growing Tollmien-Schlichting wave generated by a time-harmonic free-stream disturbance is related to the coefficient multiplying the lowest-order Lam & Rott asymptotic eigensolution of the unsteady boundary-layer equation. In this part the authors use a numerical solution of the unsteady boundary-layer equation to determine that coefficient for the case of a uniformly pulsating stream. (10 refs.)
- 76112 Unsteady laminar flow of a viscous liquid in a symmetrical porous-walled channel of varying width.** O.Prakash (Government Coll., Sambharlake, Rajasthan, India). *J. Math. & Phys. Sci. (India)*, vol.16, no.6, p.605-17 (Dec. 1982). [received: May 1983] The fully developed unsteady flow of a Newtonian incompressible fluid through a symmetrical porous-walled channel of varying width is considered. The flux across a representative section is viewed as composed of a pulsatile part superposed on a steady part and the flow downstream of this section is investigated by expanding vorticity and stream functions in series of powers of the small ratio of the mean channel width to a characteristic length along its axis over which significant changes in flow variables take place. The inertia terms in the equations of motion are retained and their first order effects are estimated. Numerical results computed for a channel having sinusoidal boundary and also for a tapering channel are presented graphically. It is observed that the inertia terms have considerable unsymmetrical effect on skin friction before and after the maximum constriction in the channel, the effect being greatest just at the time of the onset of fresh pulse. This effect is aggravated by increase in the frequency parameter. (11 refs.)
- 76113 Magneto-hydrodynamic flow of liquid metals in curved channels.** K.Sudo (Faculty of Engng., Hiroshima Univ., Hiroshima, Japan), K.Ueda, S.Oshima. *Mem. Fac. Eng. Hiroshima Univ. (Japan)*, vol.8, no.2, p.61-9 (1983). The steady flow of liquid metals in curved channels of rectangular cross-section in the presence of magnetic fields which are applied radially, transversely and axially, is analyzed numerically. The internal mechanism of the flow is made clear and the resistance coefficient which is significant from the engineering standpoint is calculated. Numerical results are obtained and the effects of the magnetic field on the flow are examined. It is found from the results that an applied magnetic field suppresses the secondary flow. Under a radial and a transverse magnetic field, electric currents flow in the direction of a channel axis as well as in the cross sectional plane of the channel. And under an axial magnetic field, three eddies of an electric current appear in the cross sectional plane of the channel. (11 refs.)
- 76114 Multiple solutions and hysteresis in steady parallel viscous flows.** S.H.Davis, G.A.Kriegsmann (Dept. of Engng. Sci. & Appl. Math., Northwestern University, Evanston, IL, USA), R.L.Laurence, S.Rosenblat. *Phys. Fluids (USA)*, vol.26, no.5, p.1177-82 (May 1983). A study is made of flows of viscous fluids when viscosity varies with temperature according to an Arrhenius law, and when viscous dissipation is taken into account. It is shown that for fluids with highly temperature-sensitive viscosity the graph of shear rate against shear stress is an S-shaped curve,

with either one or three values of shear rate for given shear stress. In this situation hysteresis can occur if steady unidirectional flow is maintained. The velocity and temperature profiles are calculated, and the manner in which the temperature-sensitivity parameter affects the conclusions is discussed. The calculations serve as criteria for evaluating the importance of viscous-heating effects in applications. (7 refs.)

- 76115 Free oscillations of a viscous incompressible fluid at the entrance to a pipe with an annular cross section of small curvature.** E.V.Bogdanova (Computing Center, Acad. of Sci., Moscow, USSR). *Sov. Phys.-Dokl. (USA)*, vol.27, no.7, p.533-5 (July 1982). Translation of: *Dokl. Akad. Nauk SSSR*, vol.265, no.1-3, p.556-60 (July 1982). [received: April 1983] Suppose a uniform stream of an incompressible fluid with velocity U_0^* and kinematic viscosity ν^* enters a semi-infinite circular pipe of radius $b^* = 1/2 L^*$ which contains a concentric inner pipe of radius $b^* = 1/2 L^*$ ($L^* \ll b^*$). The author introduces the Reynolds number $Re = U_0^* L^* \nu^{*-1}$, and assumes that it is much larger than unity. Using the basic ideas of the theory of the free interaction of a boundary layer for internal flows, she traces the development of free perturbations at gradually increasing distances from the pipe entrance to steady-state viscous flow. (4 refs.)
- 76116 Flow in curved pipes.** S.A.Berger, L.Talbot (Dept. of Mech. Engng., Univ. of California, Berkeley, CA, USA), L.-S.Yao. In book: *Annual review of fluid mechanics*. Vol.15, M.Van Dyke, J.V.Wehausen, J.L.Lumley [Ed.], p.461-512. Palo Alto, CA, USA: Annual Reviews (1983), 534 pp. [0 8243 0715 1] Reviews as comprehensively as possible what is known about the flow in curved tubes and pipes. The authors discuss developing and fully developed flows, both steady and unsteady, in rigid infinitely coiled pipes; the flow in finite bends; thermal effects; and more briefly multiphase flow, the flow of non-Newtonian fluids, and the effect of flexible walls. Laminar incompressible flows is their primary concern. They do not consider curved open-channel flows, since they differ enough in analysis and application to receive separate attention. The main emphasis is on tubes or pipes with circular cross sections. (168 refs.)
- Heat transfer performance of ceramic regenerator matrices with sine-duct shaped passages See Entry 74460
- Positive hole pressures and negative exit pressures generated by molten polyethylene flowing through a slit die See Entry 75974
- The effect of thermal boundary conditions on the heat transport in vertical channels heated from below See Entry 76004
- Enhanced and local heat transfer, pressure drop, and flow visualization for arrays of block-like electronic components See Entry 76005
- An investigation of transient boiling heat transfer with conjugate nature See Entry 76017
- Pressure drop during forced convection boiling of binary refrigerant mixtures .. See Entry 76022
- Heat transfer in toroidal pipes when the Prandtl number is large See Entry 76031
- Drag on eccentrically positioned spheres translating and rotating in tubes See Entry 76039
- Heat transfer of a swirled flow of gas suspension in a short channel See Entry 76043
- An experimental study of entraining, stress-driven, stratified flow in an annulus See Entry 76087
- Two-phase flow patterns: a review of research results See Entry 76089
- Simplified nonlinear descriptions of two-phase flow instabilities in vertical boiling channel See Entry 76091
- Gas particulate flow through a tube of varying cross-section .. See Entry 76092
- Two-phase flow in a vertical pipe and the phenomenon of choking: homogeneous diffusion model. I. Homogeneous flow models See Entry 76094
- Theory of capillary viscometer for gases See Entry 76135
- Flow distribution in parallel connected manifolds for evacuated tubular solar collectors See Entry 78092
- A theoretical model of absorption of gases by the bronchial wall See Entry 78221

47.65 MAGNETOHYDRODYNAMICS AND ELECTROHYDRODYNAMICS

(for MHD in plasma, see 52.30)

- 76117 Hypersonic flow behavior in magnetohydrodynamic channel.** E.Xuequan (Inst. of Mech. Acad. Sinica, Peking, China). *Acta Mech. Sin. (China)*, no.2, p.133-43 (1983). In Chinese. For small magnetic Reynolds number and small magnetic interaction parameter the effects of a continuous magnetic field on the hypersonic flow of an inviscid compressible electrical conducting fluid are considered at the entrance region of the channel. Analytical expressions for the electric current density and Lorentz force are obtained by solving the Laplace equation with the complex variable function theory. The conditions for circular electric current are found, and the perturbation equations and the integral formulae of the perturbation parameters derived. The digital solutions of the perturbation equations show that the hypersonic flow has a flow behavior analogous to that of an incompressible fluid. The characteristics of the flow near the specific points are discussed. (5 refs.)
- 76118 The magnetic analogue of Ertel's potential vorticity theorem.** R.Hide (Geophys. Fluid Dynamics Lab., Meteorological Office, Bracknell, England). *Ann. Geophys. (France)*, vol.1, no.1, p.59-60 (Jan.-Feb. 1983). A magnetic field B pervading an electrically-conducting fluid of density ρ moving with Eulerian flow velocity u is shown to satisfy $D\Gamma/Dt = 0$ when Ohm's law holds and the electrical conductivity is infinite. Γ is the 'potential magnetic field', defined as $\nabla \Lambda / \rho$ where Λ is any scalar function satisfying $\Delta \Lambda / Dt \equiv \partial \Lambda / \partial t + u \cdot \nabla \Lambda = 0$ if t denotes time. This result is analogous to Ertel's potential vorticity theorem for an inviscid fluid, namely $D\Pi/Dt = 0$ where $\Pi \equiv \omega \cdot \nabla \Lambda / \rho$ if ω is the absolute vorticity (equal to $\nabla \times u + 2\Omega$ if u is measured in a system that rotates with angular velocity relative to an inertial frame). It is also shown that $D(\rho^{-1} \xi \cdot \nabla G(Z))/Dt = 0$ where $\xi = B$ or ω , $Z = \Gamma$ or Π , and G is any differentiable function of Z . (3 refs.)

76119 Fluid flow and transfer behavior of a drop translating in an electric field at intermediate Reynolds numbers. L.S.Chang, J.C.Berg (Dept. of Chem. Engng., Univ. of Washington, Seattle, WA, USA).

Int. J. Heat & Mass Transfer (GB), vol.26, no.6, p.823-32 (June 1983). Approximate solutions for fluid motion in and around a drop translating in an electric field at an intermediate Reynolds number are obtained using the Galerkin method. Separation angles wake lengths and drag coefficients all vary as a function of the applied field strength. Continuous-phase mass transfer rates for the case of high Peclet numbers are obtained for various values of Reynolds number, viscosity ratio, and a dimensionless parameter W_1 , characterizing the relative importance of electrical and gravitational effects. Only when W_1 is substantially greater than unity is the rate of transport enhanced significantly by the imposed electric field. (13 refs.)

76120 Nonlinear electrohydrodynamic Rayleigh-Taylor instability. I. A perpendicular shear flow in the absence of surface charges. A.el.M.A.Mohamed, E.I.S.El Shehawey (Dept. of Maths., Ain Shams Univ., Heliopolis, Cairo, Egypt).

J. Fluid Mech. (GB), vol.129, p.473-94 (April 1983). Nonlinear electrohydrodynamic Rayleigh-Taylor instability is investigated. A charge-free surface separating two semi-infinite dielectric fluids influenced by a normal electric field is subjected to nonlinear deformations. The authors use the method of multiple-scale perturbations in order to obtain uniformly valid expansions near the cutoff wavenumber separating stable from unstable flows. They obtain two nonlinear Schrodinger equations by means of which one can deduce the cutoff wavenumber and analyse the stability of the system. It is found that if a finite-amplitude wave exists then its small modulation is stable. The authors also obtain the surface elevation for such waves. The electric field plays a dual role in the stability criterion and the dielectric constant plays a distinctive role in this analysis. If the dielectric constant of the upper fluid is smaller than that of the lower fluid the field has a destabilizing effect for large wavenumbers. For relatively smaller wavenumbers the electric field stabilizes considerable parts of the first and second subharmonic regions in the stability diagrams; a result which is in contrast with the linear theory. (29 refs.)

76121 Functional formulation of magnetohydrodynamic turbulence in a rotating frame of reference. Goodarz Ahmadi (Dept. of Mech. & Industrial Engng., Clarkson Coll., Potsdam, NY, USA).

J. Math. & Phys. Sci. (India), vol.16, no.5, p.453-61 (Oct. 1982). [received: May 1983] The functional formulation of magnetohydrodynamic turbulence in a rotating frame of reference is considered. The joint characteristic functional is introduced and Hopf's functional equation is obtained. The reformulation in terms of probability density functional is derived and the generalized Lewis-Krishnan functional formulation is also discussed. (24 refs.)

76122 Steady constantly-inclined MHD flow. O.P.Chandna, H.Toews (Univ. of Windsor, Windsor, Ontario, Canada).

J. Math. & Phys. Sci. (India), vol.16, no.6, p.565-74 (Dec. 1982). [received: May 1983] The authors determine the solutions and the geometries of steady constantly inclined plane flows of a viscous, infinitely conducting fluid when the magnetic lines and their orthogonal trajectories, coincide with the curves that form an isometric curvilinear net. They recapitulate the basic equations governing the motion and derive from these an alternate set of equations suitable for this work. (5 refs.)

76123 Role of hydrodynamic interaction of dispersed particles in structuring processes in alternating electric field. N.I.Gamayunov, V.A.Murtsovkin (Kalinin Polytech. Inst., Kalinin, USSR).

J. Eng. Phys. (USA), vol.43, no.3, p.963-5 (Sept. 1982). Translation of: *Inzh.-Fiz. Zh. (USSR)*, vol.43, no.3, p.375-8 (Sept. 1982). A study is made of the process involved in forming of one-dimensional periodic structures as a result of hydrodynamic interaction of dispersed particles and the dependence of this process on the parameters of the external electric field in which it occurs. (5 refs.)

76124 Controlling the oscillations of an inhomogeneous liquid by means of an electric field. S.V.Nesterov, S.Ya.Sekerzh-Zenkovich (Inst. of Problems in Mech., Acad. of Sci., Moscow, USSR).

Sov. Phys.-Dokl. (USA), vol.27, no.7, p.538-9 (July 1982). Translation of: *Dokl. Akad. Nauk SSSR*, vol.265, no.1-3, p.564-6 (July 1982). [received: April 1983]

It has been noted that regular self-oscillations can be excited at an interface between a dielectric liquid and a conducting liquid by means of a constant electric field. These regular oscillations can be converted to stochastic oscillations by varying the intensity of the electric field. Inasmuch as the natural oscillations depend explicitly on the electric-field intensity, it is natural to assume that an electric field could be used to control the oscillations of an interface between two liquids excited mechanically. To test this assumption the authors have carried out an experiment. (4 refs.)

Transport effects associated with turbulence with particular attention to the influence of helicity See Entry 75994

Magnetohydrodynamic flow of liquid metals in curved channels See Entry 76113

47.70 REACTIVE, RADIATIVE, OR NONEQUILIBRIUM FLOWS

76125 Thermal structure of a flat plate turbulent boundary layer diffusion flame. T.Ueda (Faculty of Sci. & Technol., Keio Univ., Yokohama, Japan), M.Mizomoto, S.Ikai.

Bull. JSME (Japan), vol.26, no.213, p.399-405 (March 1983). Measurements of fluctuating temperature and fluctuating velocity have been made. Results show that a profile of turbulent intensity of temperature fluctuation has two maxima and one minimum. The minimum is located at the station where the gradient of mean temperature is zero. On the other hand, gradients of mean temperature at stations of two maxima are very high. In the region between the flat plate and the flame, the thermal structure is characterized by low frequency fluctuations. In the region between the flame and the edge of the thermal boundary layer, the thermal structure is characterized by high amplitude and high frequency temperature fluctuations. (12 refs.)

76126 A study of the steady-state reaction-zone structure of a homogeneous and a heterogeneous explosive. R.Engelke, J.B.Bdzil (Univ. of California, Los Alamos Nat. Lab., Los Alamos, NM, USA).

Phys. Fluids (USA), vol.26, no.5, p.1210-21 (May 1983). The two-dimensional steady-state reaction-zone structure of a homogeneous and a heterogeneous explosive is studied. To do this theoretical results obtained from the Euler equations of compressible flow are combined with experimental data on steady-state detonation shock-wave speed and shape as a

function of the explosive charge size. The theoretical results, constrained by the experiments, define an inverse problem for the chemical heat-release function in the reaction zone which follows the shock wave; this problem is solved. The heterogeneous explosive is made from the homogeneous one by adding small quantities of other materials. Because of this, the two explosives were closely related in many respects. In spite of this, quite large differences in the detonation characteristics are observed between the two explosives, both in the wave speed as a function of charge size and in the shape of shock-wave loci near the explosive edge. It is found that a single forward rate exponentially dependent on the inverse of the local shock pressure can 'explain' the homogeneous case observations, but that a rate with much less state dependence near the explosive edge is necessary to understand the observations for the heterogeneous material. Near the failure diameter of both materials, prominent structures are found on the experimental shock-wave loci. These structures would seem to be incompatible with a steady flow and call into question whether two-dimensional steady-state detonations occur at all in condensed explosives near their failure diameter. (16 refs.)

Non-equilibrium flow of a vibrationally relaxing gas behind three-dimensional unsteady curved shock wave See Entry 76065

Shear flow induced cholesteric-nematic transition See Entry 76625

Instabilities, pattern formation, and turbulence in flames See Entry 77890

47.80 INSTRUMENTATION FOR FLUID DYNAMICS

76127 Digital image processing of flow visualization photographs. L.Hes-selink (Dept. of Aeronautics & Astronautics, Stanford Univ., Stanford, CA, USA), B.S.White.

Appl. Opt. (USA), vol.22, no.10, p.1454-61 (15 May 1983). This paper is concerned with the propagation of laser light through a slab of randomly varying medium. A theoretical analysis is presented which relates the spectrum of the recorded-intensity field some distance downstream of the medium to the spectrum of the index-of-refraction field. For a homogeneous and isotropic random field, the 3-D spectrum of the medium is obtained from the 2-D spectrum of the photograph by dividing each component of the spectrum by the frequency raised to the fourth power. Free-space propagation outside the random medium is accounted for by a scaling factor. Experimental results are presented which support the theoretical analysis. The nonintrusive diagnostic technique presented here is applicable to photographs which contain partially developed caustic networks. (19 refs.)

76128 Dynamic behaviour and stability of thermistor air flowmeters. A.Catellani, R.Stacchiotti, A.Taroni (Istituto di Fisica, Univ. di Modena, Modena, Italy), C.Canali.

Sens. & Actuators (Switzerland), vol.3, no.3, p.195-202 (May 1983). Experimental measurements of the response time of air flowmeters using both PTC silicon and NTC oxide thermistors as self-heated elements are reported. The dependence of the response time on the thermistor bias conditions and the flow parameters is measured and discussed. Two simple configurations are tested: in the first, the self-heated thermistor is inserted as an active arm of a Wheatstone bridge, with constant voltage bias; in the second (constant temperature difference), a differential amplifier keeps the Wheatstone bridge balanced. The last configuration gives a response time of less than 1 s. Finally, experimental results on the long-term stability of the complete flowmeters and the two types of thermistors are presented. (5 refs.)

76129 Directional gas-flow measurement with pyroelectric anemometers (PA). H.Rahnamai, J.N.Zemel (Moore School of Electrical Engng., Univ. of Pennsylvania, Philadelphia, PA, USA).

Sens. & Actuators (Switzerland), vol.3, no.3, p.203-7 (May 1983). The directional flow characteristics of pyroelectric anemometers, fabricated using z-cut LiTaO₃ plates are studied. The heater resistor and the two sensor electrodes were evaporated NiCr films. The ratios of the lengths of the charge-sensing electrodes to the electrode-heater separation distance β , were 32 and 54. The flow-angle dependence of the difference pyroelectric response was measured. The results yield a $\cos^2 \alpha$ flow-angle dependence, where α is the fluid flow angle normal to the electrode length. Because of the large value of β , this angular dependence is in close agreement with the empirical formula often used for the hot wire anemometer. (7 refs.)

76130 Dynamic particle sizing in suspension by laser anemometry technique. S.L.Lee (Dept. of Mech. Engng., State Univ. of New York, Stony Brook, NY, USA).

Mater. Lett. (Netherlands), vol.1, no.5-6, p.189-93 (April 1983). A new optical particle sizing technique is presented by which in situ local measurements can be made in a suspension of particulates in flow by laser-Doppler anemometry. This technique is unintrusive and produces far more accurate results than conventional collection sizing technique. It is also fast due to the use of digital electronics and real-time data processing and analysis in a minicomputer. Some sample measurement results are also presented. (10 refs.)

76131 An ultrasonic viscometer for the measurement of dynamic shear viscosity of liquids. V.N.Bindal, Mukesh Chandra, J.N.Som (Nat. Phys. Lab., New Delhi, India).

Indian J. Pure & Appl. Phys., vol.21, no.3, p.176-9 (March 1983). An ultrasonic viscometer for the measurement of dynamic shear viscosity of liquids at 10 MHz frequency over a wide range of temperature has been described. A shear wave reflectance technique at normal incidence has been adopted. A BT-cut quartz crystal along with a fused quartz delay line has been used for generating shear waves. The viscosity measurements performed on glycerine reveal that the results are in good agreement with known accepted values. The viscometer has been found to be capable of measuring viscosity with comparable accuracy under temperature-controlled conditions. The system is reliable and offers potential applications for studying viscoelastic behaviour of liquids in the frequency range (3 to 50 MHz) by incorporating some minor modifications. (14 refs.)

76132 Use of the electromagnetic flowmeter in a two-phase flow. R.N.Bernier, C.E.Brennen (California Inst. of Technol., Pasadena, CA, USA).

Int. J. Multiphase Flow (GB), vol.9, no.3, p.251-7 (June 1983). The use of the transverse field electromagnetic meter for two-phase flows is investigated. It is shown both experimentally and theoretically that this device measures the average velocity of the continuous liquid phase provided this has some minimum electrical conductivity. The calibration is quite independent of void fraction, flow regime, axisymmetric velocity profile, or the electrical conductivity of the continuous liquid phase. The dynamic capability of the meter for use in measuring unsteady two-phase flows is also demonstrated to be considerable. (7 refs.)

- 76133 Cross-correlation flow measurement—a history and the state of the art.** J.Coulthard (Dept. of Electrical Instrumentation & Control Engng., Teesside Polytech., Middlesbrough, England). *Meas. & Control (GB)*, vol.16, no.6, p.214-18 (June 1983). Since the early 1970s, conferences and articles dealing with advances in flow measurement techniques have usually contained a section describing flowmeters which measure the time of flight of fluid disturbances between various types of sensors, using cross-correlation techniques. Up to the present time, no large instrument manufacturer has brought a complete cross-section flowmeter to the market, but current developments may change this situation in the near future. This article summarises the research and development carried out in the recent past, highlights the main problems and indicates the present state of the art. (12 refs.)
- 76134 The instrumentation of a modern fluid mechanics research laboratory.** L. M.P.Escudier (Brown Boveri Res. Centre, Baden-Dattwil, Switzerland). *Meas. & Control (GB)*, vol.16, no.6, p.231-5 (June 1983). Describes the instrumentation to be found in the fluid mechanics research laboratory of the Brown Boveri Research Centre, Switzerland. The article indicates the physical principles of instrumentation intended for the measurement of velocity, pressure, flow rate and shear stress in gas and liquid flows primarily using automated data-acquisition systems. The sensors discussed range from extremely simple in both construction and use (e.g. the total-head tube) to highly complex (e.g. the laser Doppler anemometer). (6 refs.)
- 76135 Theory of capillary viscometer for gases.** K.Shiba, T.Ichinohe, J.Kitamura (Faculty of Engng., Toyo Univ., Kawagoe, Japan). *Oyo Buturi (Japan)*, vol.52, no.1, p.69-74 (Jan. 1983). In Japanese. The correct theory of the capillary viscometer for gases is not yet established, as the customary theory assumes that the increase of volume and the decrease of density of the flowing gas due to the decrease of pressure are negligible, in spite of the decrease of the pressure itself not being negligible. In this paper, at first a differential equation to express Hagen-Poiseuille's law for gases is obtained on the basis that the mass flow rate of gas in the capillary tube, in a steady state, is a function of the distance from the axis of the capillary tube. Then some approximate solutions of the differential equation are obtained which represent approximately the measuring principle of the capillary viscometer for gases. (2 refs.)
- 76136 Measurements of pressure fluctuation in turbulent flow.** T.Komatsu, T.Shibata, M.Ura. *Technol. Rep. Kyushu Univ. (Japan)*, vol.55, no.6, p.569-75 (Dec. 1982). In Japanese. [received: May 1983] The study is concerned with the measurements of pressure in nonsteady three-dimensional water flow. A total head tube is connected to a small semiconductor pressure transducer, which has a high frequency response. Experiments on the directional characteristics of the total head tube are carried out and the results are formulated. Because the pressure detected by the tube is always affected by the dynamic pressure and the inertial effect in the case of nonsteady flow, it is vital to eliminate the effect from the pressure readings. Two dual-sensor hot film probes and the total head tube are put together as closely as possible in order to obtain simultaneous data on the three components of velocity and pressure at almost the same point. The dynamic pressure and the inertial effect are evaluated, so that the latter is neglected because of its smallness. The spectra of pressure fluctuations in the viscous subrange are given by a $-1/3$ power-law. (8 refs.)
- 76137 A volume flow measuring device employing pseudonoise heat impulses.** W.Witte (Univ. Kaiserslautern, Kaiserslautern, Germany). *Tech. Mess. (Germany)*, vol.50, no.4, p.135-41 (April 1983). In German. For the determination of the volume flow rate of a homogeneous fluid the transit time of thermally tagged fluid particles is measured. The tagged fluid particles are low intensity heat impulses constituting a binary pseudonoise sequence. If appropriate sequences are employed and the measuring signals are processed by correlation, the thermal stress of the fluid can easily be limited to about 1K. The applicability of this principle of flow measurement is proved by the determination of the flow rate of diesel oil. (17 refs.)
- 76138 Annular arrays for quantitative pulsed Doppler ultrasonic flowmeters.** Chong-Cheng Fu, L.Gertzberg (Dept. of Electrical Engng., Stanford Univ., Stanford, CA, USA). *Ultrason. Imaging (USA)*, vol.5, no.1, p.1-16 (Jan. 1983). A theory, based on the Fourier-Bessel series expansion, is developed to synthesize circularly symmetric field patterns by means of concentric annular arrays. The application of this theory to the formation of variable-width uniform sector beams is studied in detail and results in a canonical design procedure. Calculated beam patterns are compared to the actual measured patterns obtained from a prototype array suitable for transcutaneous investigation of the central blood-flow system and are observed to be in good agreement. The implementation of such arrays in the compensated-first-moment flowmeter is described. Methods of beam-pattern improvement are also discussed. (14 refs.)
- 76139 Electromagnetic non invasive measurement: application to flow measurement.** M.L.Sanderson (Dept. of Electronic & Electrical Engng., Univ. of Salford, Salford, England). Colloquium on 'Non-Invasive On-Line Measurement in Industry', London, England, 13 April 1983 (London, England: IEE 1983), p.6/1-4 Describes the development of a capacitively coupled electromagnetic flowmeter which is suitable for non-intrusive industrial measurements. Problems associated with the electronic detection system and spurious signals picked-up by the high impedance levels are discussed. It is suggested that the flowmeter can be modified for use with dielectric liquids using the displacement current rather than the conduction current. (3 refs.)
- 76140 Laser diode frequency modulation for directional laser doppler velocimetry.** J.D.C.Jones, M.Corke, A.D.Kersey, D.A.Jackson (Univ. of Kent, Canterbury, England). First International Conference on Optical Fibre Sensors, London, England, 26-28 April 1983 (London, England: IEE 1983), p.178-81 The phenomenon of current induced frequency modulation in laser diodes has been exploited to produce a compact solid state LDV system, which provides the frequency shifting required for direction sensing by electronic means, and without additional components. A simple modification of the apparatus to produce an optical fibre launched LDV system is described. (5 refs.)
- 76141 Differential Doppler velocimetry using polarization-preserving optical fiber.** A.A.Boiarski, S.A.Kingsley (Battelle Columbus Labs., Columbus, OH, USA). First International Conference on Optical Fibre Sensors, London, England, 26-28 April 1983 (London, England: IEE 1983), p.214-16 Describes a unique fibre optic laser Doppler anemometer (FOLDA) device which employs two single-mode input fibers and a single multimode collecting fiber. This device uses a differential backscattering LDA configuration. The

authors also present velocity measurement results for a case of practical interest. (9 refs.)

- On the sensitive and wide frequency range measurement of pressure See Entry 74430
- Some remarks on the selection of sensors for correlation velocity measurement systems See Entry 74443
- Intelligent turbidity monitoring using fibre optics See Entry 75818
- Turbulent spots, wave packets, and growth See Entry 75983
- The characteristics of low-speed streaks in the near-wall region of a turbulent boundary layer See Entry 75998
- Enhanced and local heat transfer, pressure drop, and flow visualization for arrays of block-like electronic components See Entry 76005
- Numerical processing of flow-visualization pictures—measurement of two-dimensional vortex flow See Entry 76041
- Low Reynolds number flow in a rotating tank with barriers See Entry 76045
- An experimental study of entraining, stress-driven, stratified flow in an annulus See Entry 76087
- Two-phase flow patterns: a review of research results See Entry 76089
- Particle fraction and velocity measurement in gas-powder streams by capacitance transducers See Entry 76095
- Limitations of a single optical fibre fluorimeter system due to background fluorescence See Entry 77947
- Airflow resistivity instrument for in situ measurement on the Earth's ground surface See Entry 78708

50.00 FLUIDS, PLASMAS AND ELECTRIC DISCHARGES

[for fluid dynamics, see 47.; for the physics of condensed matter, see 60. and 70.]

51.00 KINETIC AND TRANSPORT THEORY OF FLUIDS; PHYSICAL PROPERTIES OF GASES

51.10 KINETIC AND TRANSPORT THEORY

- 76142 Alignment of diatomic molecules by gaseous transport.** A.J.Bain, A.J.McCaffery (School of Chem. & Molecular Sci., Univ. of Sussex, Brighton, England). *Chem. Phys. Lett. (Netherlands)*, vol.97, no.2, p.239-42 (13 May 1983). Iodine molecules in a flow cell containing helium as a carrier gas appear to be partially aligned. This has been determined by comparison of circular polarisation ratios of rotationally resolved emission lines in the flow cell with those obtained from a similar cell containing I_2 in an isotropic environment. After all other possibilities have been eliminated, two experimental indicators of alignment remain. One is the reduction of the absolute value of the circular polarisation ratio and the other is the differential reduction of one of the P,R-doublet emission lines. (16 refs.)
- 76143 Barodiffusion in a binary mixture due to rotation of a circular cylinder.** A.C.Srivastava (Dept. of Math., Dibrugarh Univ., Dibrugarh, India). *J. Math. & Phys. Sci. (India)*, vol.16, no.5, p.463-7 (Oct. 1982). [received: May 1983] The diffusion effect in a binary mixture of incompressible viscous fluids filling the space outside a circular cylinder rotating with a constant angular velocity has been discussed. The case when the mixture is bounded by another stationary circular cylinder has also been discussed. In both the cases it is assumed that the flow is laminar and stable. It has been found that the effect of the pressure gradient created by the rotation of the cylinder is to separate the mixture because of their different densities; the lighter component gets collected near the rotating cylinder. (3 refs.)
- 76144 Measurements of the mutual diffusion coefficients of a nonideal gas mixture of helium and carbon dioxide.** A.G.Karpushin, Sh.K.Bibolov (S.M. Kirov Kazakh State Univ., Alma-Ata, USSR). *J. Eng. Phys. (USA)*, vol.43, no.3, p.1017-19 (Sept. 1982). Translation of: *Inzh.-Fiz. Zh. (USSR)*, vol.43, no.3, p.443-7 (Sept. 1982). The authors consider a method for the calculation of the mutual diffusion coefficient of nonideal gases. A formula is presented for the barometric dependence of the helium-carbon dioxide system. (12 refs.)
- 76145 Time correlation functions for the one-dimensional Lorentz gas.** R.M.Mazo, H.van Beijeren (Inst. für Theoretische Phys. A & B, RWTH Aachen, Aachen, Germany). *Physica A (Netherlands)*, vol.119A, no.1-2, p.197-211 (April 1983). The velocity autocorrelation function and related quantities are investigated for the one-dimensional deterministic Lorentz gas, consisting of randomly distributed fixed scatterers and light particles moving back and forth between two of these at a constant given speed. An expansion for the velocity autocorrelation function given by Grassberger, which is useful for short times, is reconstructed. The long time behavior is investigated by Fourier transform techniques. (22 refs.)
- 76146 Computed energy and spatial statistical properties of stored ions cooled by a buffer gas.** F.Vedel, J.Andre, M.Vedel, G.Brincourt (Univ. de Provence, Phys. des Interactions Ioniques et Moléculaires, Marseille, France). *Phys. Rev. A (USA)*, vol.27, no.5, p.2321-30 (May 1983). The authors describe a three-dimensional model, based on the temporal invariance of the statistical properties, which allows one to calculate the spatial and energy probability densities of strongly confined ions in the presence of a buffer gas. This model is then applied to a population of Cs^+ ions for which the authors compute these densities within the whole stability diagram and for various gases. In the case of helium, in particular, the authors show that these laws can be described by Gaussian functions, and they present the evolution of the temporal average of the spatial dispersions and ionic temperatures at the working point. (27 refs.)

- 76147 Bound states in a classical gas.** N.B.Gorev, A.I.Sokolovskii. *Ukr. Fiz. Zh. (USSR)*, vol.28, no.4, p.617-18 (April 1983). In Russian. On the basis of the theory for density excitations for the case of a classical gas of particles interacting by way of a pair potential of the rectangular well type with a solid core, the authors have obtained expressions for the number of connected pairs (molecules) as well as for the high temperature asymptotics. (5 refs.) V.G.P.
- Heterogeneous vibrational relaxation upon free molecular flow of diatomic gas past concave bodies** See Entry 76072
- Modern methods of numerical investigation of rarefied gas phenomena** See Entry 76073
- Calculation of vapour-liquid equilibria with equations of state from the extended van-der-Waals theory. II. Application of the equation to mixtures** See Entry 76600
- Diffusional-drift-influenced chemical reactions at all gas densities** See Entry 77884

51.20 VISCOSITY AND DIFFUSION: EXPERIMENTAL

- 76148 The viscosity and diffusion coefficient of binary mixtures of nitrous oxide with He, Ne and CO.** J.Kestin (Div. of Engng., Brown Univ., Providence, RI, USA), W.A.Wakeham. *Ber. Bunsenges. Phys. Chem. (Germany)*, vol.87, no.4, p.309-11 (April 1983). Absolute measurements are reported of the low-density viscosity of binary mixtures of nitrous oxide with helium, neon and carbon monoxide in the temperature range 25 to 200°C. The viscosity data, which have an accuracy of $\pm 0.3\%$, are employed to confirm that the three systems, involving a weakly polar component, may be incorporated into the correlation scheme of the KRW law of corresponding states. The scaling parameters σ_{ij} and ϵ_{ij} which secure the optimum representation of the data by means of the universal collision integral Ω_{22} are derived. The internally consistent binary diffusion coefficients, calculated from the mixture viscosity, may themselves be successfully represented with the aid of the universal collision integral Ω_{11} . (16 refs.)
- 76149 Measurements of the viscosity of compressed gaseous and liquid nitrogen.** D.E.Diller (Nat. Engng. Lab., NBS, Boulder, CO, USA). *Physica A (Netherlands)*, vol.119A, no.1-2, p.92-100 (April 1983). The shear viscosity coefficients of compressed gaseous and liquid nitrogen have been measured with a torsional piezoelectric quartz crystal viscometer at temperatures between 90 and 300K and at pressures up to 30 MPa (4350 psia). The measurements have been compared with other measurements; with a correlating equation, previously proposed for calculating the viscosities of pure compressed gaseous and liquid nitrogen; and with an extended corresponding states model, previously proposed for calculating the viscosities of fluid mixtures. (14 refs.)

Aero-diffusion method of estimating evaporation in a non-stratified atmosphere See Entry 78565

51.30 THERMAL PROPERTIES OF GASES

- 76150 Parametric scaled equation of state of restricted cubic model.** Zhou Xuehua (Inst. of Mech., Acad. Sinica, Peking, China). *Acta Mech. Sin. (China)*, no.2, p.173-8 (1983). In Chinese. A new method of calculating specific heat at constant volume near the critical point of a fluid is presented. The calculated specific heat of CO_2 agrees well with the measured value. (12 refs.)
- 76151 New values for the thermodynamic parameters of water vapor.** D.Sonnag. *Meas. Tech. (USA)*, vol.25, no.9, p.764-7 (Sept. 1982). Translation of: *Izmer. Tekh. (USSR)*, vol.25, no.9, p.54-6 (Sept. 1982). [received: May 1983] Unification of physical quantities in international practice extends both to the numerical values and to the units of measurement. The revision of these quantities has required reconsideration of the data on the thermodynamic parameters of water vapor. A method of obtaining the new thermodynamic parameters based on the use of the Clausius-Clapeyron equation is described and the resulting formulas are discussed with regard to the accuracy obtained. (16 refs.)
- 76152 A class of systems with a large autorecuperation coefficient.** V.A.Namiot. *Sov. Phys.-Tech. Phys. (USA)*, vol.27, no.11, p.1430-1 (Nov. 1982). Translation of: *Zh. Tekh. Fiz. (USSR)*, vol.52, no.11, p.2319-20 (Nov. 1982). [received: May 1983] The phenomenon of autorecuperation may be observed whenever a modulated beam of charged particles is incident at an appropriate angle on a plasma or gas target. When autorecuperation takes place, some of the energy lost by the beam in collisions with the particles in the medium is returned to the beam. Since the number of nuclear reactions occurring in the target is proportional to the number of collisions, the effective energy loss per nuclear reaction is thus reduced. The decrease in the energy loss is described by the autorecuperation factor η_{arc} , which is defined as the ratio of the energy returned to the beam divided by the total energy lost in collisions with particles in the target. The closer η_{arc} is to unity, the more efficiently the beam energy is utilized. The processes responsible for autorecuperation was studied by the author (1982) in the linear approximation, which is only applicable when $\eta_{arc} \ll 1$. It therefore remains unclear if it is possible to have a situation with $\eta_{arc} \sim 1$. Indeed, when nonlinear effects are included qualitatively new behavior may occur, such as shock wave formation or breakage of the target material, which greatly increase the energy dissipation inside the target and hence reduce η_{arc} . The author now considers a very simple example which is easily treated analytically and involves indirect autorecuperation in a nonideal gas (i.e. autorecuperation when an intermediate system is present). For this example, values $\eta_{arc} \sim 1$ can be achieved. (2 refs.)

Bound states in a classical gas See Entry 76147

51.50 ELECTRICAL PHENOMENA IN GASES

(see also 52. Plasma and electric discharges)

- 76153 Dielectric strength of gas mixtures comprising SF_6 , CO_2 , C_2F_6 and SF_6/N_2 , C_2F_6 .** Y.Qiu (Xi'an Jiaotong Univ., Xi'an, China), E.Kuffel. *IEEE Trans. Power Appar. & Syst. (USA)*, vol.PAS-102, no.5, p.1445-51 (May 1983). In a previous paper breakdown strengths of $\text{C}_2\text{F}_6/\text{SF}_6/\text{CO}_2$ gas mixtures in various proportions were reported for a 30 mm rod-sphere gap under AC and impulse voltages. A mixture of 1% C_2F_6 + 59% SF_6 + 40% CO_2 exhibited higher dielectric strength than pure SF_6 in the pressure range between 350

and 400 kPa. The present paper compares CO_2 and N_2 as a buffer in gas mixtures and extends the studies to a nearly uniform field gap and a highly non-uniform field gap. Additional experiments confirmed that the use of CO_2 as a buffer in gas mixtures is superior to N_2 and that some $\text{C}_2\text{F}_6/\text{SF}_6/\text{CO}_2$ gas mixtures have higher dielectric strength and are cheaper than pure SF_6 . (17 refs.)

Optogalvanic studies of neon glow discharge in magnetic fields: ion mobility measurements and detection of atomic alignment See Entry 76228

Stratification of a glow discharge in a gas stream at enhanced power inputs See Entry 76229

51.70 OPTICAL PHENOMENA IN GASES

(for liquids, see 78.)

- Theoretical calculation of the anomalous Cerenkov radiation produced in the air** See Entry 7429
- Resonant upconversion of light at wavelength $\lambda = 1.06 \mu\text{m}$ in rubidium vapor** See Entry 75729
- Nonlinear real index of refraction variations of a gas medium due to a monochromatic radiation near resonance** See Entry 75754
- Bright light sources from shock deceleration of hypersonic plasma streams in dense gases** See Entry 76169

52.00 THE PHYSICS OF PLASMAS AND ELECTRIC DISCHARGES

(for solid-state plasma, see 72.30)

52.20 ELEMENTARY PROCESSES IN PLASMA

- 76154 Hamiltonian formulation of the second-order drift equations of motion.** G.V.Stupakov (Inst. of Nuclear Phys., Acad. of Sci., USSR). *JETP Lett. (USA)*, vol.36, no.9, p.387-90 (5 Nov. 1982). Translation of: *Pis'ma v Zh. Eksp. & Teor. Fiz. (USSR)*, vol.36, no.9, p.318-20 (5 Nov. 1982). [received: June 1983] An expression is obtained for the Hamiltonian describing drift motion up to terms quadratic in the Larmor radius. (8 refs.)
- Transmission of sonics through ionised medium: damping considerations** See Entry 76187
- Radial guiding center drifts and omnigenity in bumpy torus confinement systems** See Entry 76205
- Slowing down of ion rings** See Entry 76213
- Photon-echo studies of collisional relaxation in weakly ionized noble-gas mixtures** See Entry 76219

52.20F Electron collisions

- 76155 Effects of a constant magnetic field on electron-electron collisions.** K.Matsuda (GA Technol. Inc., San Diego, CA, USA). *Phys. Fluids (USA)*, vol.26, no.5, p.1247-51 (May 1983). The Rostoker equation has been numerically compared with the Fokker-Planck equation for a plasma with axially symmetric velocity distributions by computing electron slowing-down rates and velocity-space diffusion rates due to collisions with background electrons. The results in a case of $\Omega_e \sim \omega_{pe}$ agree well with the corresponding quantities obtained from the Fokker-Planck operator. In the case of a strongly magnetized plasma ($\Omega_e \gg \omega_{pe}$), the results indicate corrections to the Fokker-Planck coefficients which are different from the one suggested by a previous work. (6 refs.)
- Screening effect of degenerate electron background in high density plasmas. III. Local field correction due to electron interaction** See Entry 76161

52.20H Atomic, molecular, heavy-particle collisions

- NATO ASI on Atomic and Molecular Processes in Controlled Thermonuclear Fusion, Palermo, July 19-30, 1982** See Entry 74205
- Collision topics at ESCAMPIG VI** See Entry 74206
- Threshold for suppression of light fluctuations in a shock-heated plasma consisting of monatomic gases ($M \sim 9-11$)** See Entry 75536
- Screening effect of degenerate electron background in high density plasmas. III. Local field correction due to electron interaction** See Entry 76161
- Transport and re-deposition of limiter-released metal impurities** See Entry 76163
- Observations of magnetized plasma flow through stationary background plasma** See Entry 76173

52.25 PLASMA BASIC PROPERTIES

- 76156 The two-dimensional one-component plasma at $\Gamma=2$: behavior of correlation functions in strip geometry.** P.J.Forrester (Dept. of Math., Univ. of Melbourne, Parkville, Victoria, Australia), B.Jancovici, E.R.Smith. *J. Stat. Phys. (USA)*, vol.31, no.1, p.129-40 (April 1983). The authors consider a strip of two-dimensional one-component plasma of particles of charge q at a temperature T such that the coupling constant be $\Gamma = q^2/k_B T = 2$. The strip is of finite width and infinite length and bears charge densities on either edge. Inside the strip and on one side, the dielectric constant is 1; on the other side of the strip, it may be either 1 or 0 (in the latter case, image forces play an important role). The free energy as well as the one-particle and two-particle distribution functions can be exactly computed. They obey a variety of sum rules reflecting the Coulombic behavior of the system. At large separations the truncated two-particle distribution function behaves with algebraically decaying oscillations. The strip of finite width in fact is correlated along the strip much as a one-dimensional system is correlated. (17 refs.)
- 76157 Parameter optimizations of multiple-mirror reactors.** F.Najmabadi, A.J.Lichtenberg, M.A.Lieberman (Univ. of California, Berkeley, CA, USA). *Nucl. Fusion (Austria)*, vol.23, no.5, p.609-31 (May 1983). The diffusion density profile model for multiple-mirror devices is limited to machines with a large number of cells and high mirror ratios. A new discrete staircase density profile model, without those limitations, has been developed.

This model, along with the diffusion model, has been used to study the parameters of steady-state multiple-mirror reactors. A linear fusion device consisting of a central solenoid and multiple mirrors at each end has been considered. The magnetic field is taken to be produced by a solenoid and mirror-quadrupole assemblies which produce an average-minimum-B stable configuration. Different means of supplying the re-circulating power, including high-energy neutral-D injectors, are considered. Distribution functions of alpha particles and beam particles in this machine have been calculated. Trade-offs among the length of the machine, Q =fusion power/beam power, and other machine parameters in two different operating modes; wetwood burner (pure-T plasma background) and conventional (T and D background plasma), have been studied. It is found that the staircase density profile results in shorter reactors with a larger number of cells, compared to those of the diffusion-determined density profile. (14 refs.)

76158 Generalized Klimontovich theory for fluctuations and correlations in plasmas. A.J.D.Lambert (Dept. of Appl. Phys., Tech Hogeschool, Eindhoven, Netherlands).

Physica A (Netherlands), vol.119A, no.1-2, p.177-96 (April 1983).

In order to deal with a non-ideal plasma a method is developed that gives a microscopic hierarchy of equations for the fluctuation in density of a classical plasma, existing of pointlike particles. Starting from the evolution equations of a Fourier-transformed one-particle distribution function, expressions for every correlation function can be found in a straightforward way. Results like the Landau- and the Lenard-Balescu collision integral and the time-dependent correlation functions of Rostoker are recovered when the hierarchy in the lowest significant order is cut off. (11 refs.)

76159 Surface density profile and surface tension of the one-component classical plasma. P.Ballone (Scuola Internazionale Superiore di Studi Avanzati, Trieste, Italy), G.Senatore, M.P.Tosi.

Physica A (Netherlands), vol.119A, no.1-2, p.356-68 (April 1983).

The density profile and the interfacial tension of two classical plasmas in equilibrium at different densities are evaluated in the square-density-gradient approximation. For equilibrium in the absence of applied external voltage, the profile is oscillatory in the higher-density plasma and the interfacial tension is positive. The amplitude and phase of these oscillations and the magnitude of the interfacial tension are related to the width of the background profile. Approximate representations of the equilibrium profile by matching of its asymptotic forms are analyzed. A comparison with computer simulation data and a critical discussion of a local density theory are also presented. (13 refs.)

Screening effect of degenerate electron background in high density plasmas. III. Local field correction due to electron interaction See Entry 76161

Transport and re-deposition of limiter-released metal impurities See Entry 76163

Enhanced diffusion in strongly magnetized plasmas See Entry 76165

Effect of self absorption on emitted intensity of Na-5890 Å line in water gas combustion plasma See Entry 76167

Spectroscopic observation of MeV-range multiply charged ions in a laser plasma See Entry 76168

Approximations in magnetoionic theory See Entry 76170

Transmission of sonics through ionised medium: damping considerations See Entry 76187

Self-consistent calculation of the α -effect and turbulent magnetic diffusion See Entry 76191

Plasmon spontaneous emission and entropy in Kaufman and Morrison's formalism for the quasilinear equations of plasma physics See Entry 76194

A numerical analysis of flute modes in the ELMO Bumpy Torus See Entry 76211

Slowing down of ion rings See Entry 76213

Operation of the tandem-mirror plasma experiment with skew neutral-beam injection See Entry 76214

Tonks-Datner diagnostics of electron density profiles See Entry 76220

Density of uranium ions in the $^4I_{9/2}$ ground state in a hollow-cathode type discharge See Entry 76223

Influence of plasma composition in a low-inductance vacuum spark on the parameters of a microchip region See Entry 76231

52.25F Transport properties

76160 A one-dimensional study of Tokamak current reversal. L.R.O.Storey (Inst. Nat. de Recherche Sci., Varennes, Quebec, Canada).

Can. J. Phys. (Canada), vol.61, no.5, p.671-9 (May 1983).

The possibility of being able to reverse the toroidal current in a Tokamak, without undue loss of plasma, is studied using diffusive magnetohydrodynamics (MHD), together with a one-dimensional model in which the torus is represented by a long cylindrical slab. For a plasma with free surfaces, it predicts that the entire plasma will expand outwards and be lost before the current even changes sign. However, interaction of the outer surface with conducting limiters can impede the expansion, and other ways of preserving the plasma may exist in two dimensions, so current reversal may be feasible after all. (16 refs.)

76161 Screening effect of degenerate electron background in high density plasmas. III. Local field correction due to electron interaction. S.Chimaru, H.Iyetomi (Dept. of Phys., Univ. of Tokyo, Tokyo, Japan).

J. Phys. Soc. Jpn. (Japan), vol.52, no.5, p.1730-3 (May 1983).

For pt.II see ibid., vol.50, p.3778 (1981). Local-field correction due to the exchange and correlation effects between electrons introduces the screening function for the electron-ion interaction different from that for the ion-ion interaction. The resulting corrections to the calculation of the electric resistivity are numerically investigated. It is found that the corrections are substantial in magnitude even at the electron density ($n_e \approx 1$) of relatively weak coupling. (16 refs.)

76162 Heavy-impurity transport in the TFR Tokamak—comparison of line emission with numerical simulations.

Nucl. Fusion (Austria), vol.23, no.5, p.559-69 (May 1983).

Heavy-element ion line emissions are simulated with a numerical code using two adjustable, radius-independent parameters in the flux density expression: an anomalous diffusion coefficient D_A and an inward convective velocity V_A . Previously reported results on the laser blow-off injection of V, Cr, and Ni are, thus, interpreted. The quasi-stationary phase of Ohmically heated high-density ($n_0 \approx 1.5 \times 10^{14}$ cm $^{-3}$) discharges is also simulated, thus allowing the plasma impurity content and the radiated power to be calculated. The necessary numerical values of D_A and V_A are in the range of 2000-4000 cm 2 s $^{-1}$ and 400-800 cm.s $^{-1}$, respectively. (18 refs.)

76163 Transport and re-deposition of limiter-released metal impurities. H.A.Claassen, H.Repp (Inst. für Plasmaphys., KFA Jülich GmbH, Jülich, Germany).

Nucl. Fusion (Austria), vol.23, no.5, p.597-607 (May 1983).

The transport and re-deposition of limiter- (or divertor-target)-released metal impurities in a given counter-streaming scrape-off layer plasma is studied analytically by using a kinetic approach. Electron impact ionization, Coulomb collisions with the hydrogen ions, and impurity ion acceleration in a pre-sheath electric field are accounted for. The friction and electric-field forces provide the driving forces for impurity re-cycling in front of the limiter. Both hydrogen ion sputtering and self-sputtering are included (the latter for impurity emission perpendicular to the limiter surface). The analytical formulas are numerically evaluated for the example of sputtered iron impurities, assuming a simple model for a scrape-off layer plasma in contact with a stainless-steel poloidal ring limiter. (10 refs.)

76164 Ripple loss of suprathermal alpha particles during slowing-down in a Tokamak reactor. K.Tani, T.Takizuka, M.Azumi, H.Kishimoto (JAERI, Ibaraki, Japan).

Nucl. Fusion (Austria), vol.23, no.5, p.657-65 (May 1983).

The slowing-down process of suprathermal alpha particles in a rippled toroidal field is investigated by means of an orbit-following Monte Carlo code. It is found that numerical results on the collisionless ripple loss agree fairly well with the theoretical predictions. The collisional diffusion coefficient for non-ergodic banana particles in a field ripple is derived. The ripple-enhanced power loss of alpha particles during slowing-down amounts to 10% of their total power in a reactor-grade Tokamak with a toroidal-field ripple of $\delta \sim 1\%$. The fraction of particle loss is 1.5 to 1.8 times as large as that of power loss. The ripple-enhanced banana drift dominates the alpha-particle loss process. (22 refs.)

76165 Enhanced diffusion in strongly magnetized plasmas. G.Fromling (Inst. für Theoretische Phys., Ruhr-Univ. Bochum, Bochum, Germany).

Phys. Fluids (USA), vol.26, no.5, p.1240-6 (May 1983).

Particle diffusion transverse to a strong uniform magnetic field is studied within a three-dimensional electrostatic guiding-center model in which particle streaming along the magnetic field lines is admitted as well as transverse $E \times B$ drifting. Only the randomizing influence of thermal fluctuations excited by particle discreteness is considered. The electric field autocorrelation coefficient is obtained in the form of a modified fluctuation-dissipation theorem. It is shown that because of the competition between the parallel and perpendicular decorrelation mechanisms, the divergence of the diffusion coefficient in the previous finite-volume theories disappears. The diffusion coefficient is Bohm like (proportional to $1/B$) for magnetic fields which are not too strong, and goes over to a classical variation (proportional to $1/B^2$) in the limit $B \rightarrow \infty$. (29 refs.)

76166 Effect of impurities on heat and particle transport in Tokamaks. A.V.Nedospasov (Inst. of High Temperatures, Acad. of Sci., USSR).

Sov. Tech. Phys. Lett. (USA), vol.8, no.9, p.450-1 (Sept. 1982). Translation of: *Pis'ma v Zh. Tekh. Fiz. (USSR)*, vol.8, no.17-18, p.1045-8 (Sept. 1982).

[received: May 1983]

The plasma diffusion coefficients and the electronic thermal conductivities observed in tokamaks have yet to be convincingly explained. The authors discuss the hypothesis that transport in a tokamak is affected by a current-driven turbulent convection caused by impurities. (6 refs.)

Effects of a constant magnetic field on electron-electron collisions See Entry 76155

Parameter optimizations of multiple-mirror reactors See Entry 76157

Inertial and viscous effects in the nonlinear growth of the tearing mode See Entry 76172

Drift motion of a charged particle in a homogeneous magnetic field and in the electric field of the rotating potential wave See Entry 76189

Cyclotron loss of fast particles from a bumpy Tokamak See Entry 76203

Radial guiding center drifts and omnigenity in bumpy torus confinement systems See Entry 76205

Models for the development of the discharge in a Tokamak See Entry 76227

52.25P Emission, absorption, and scattering of radiation

76167 Effect of self absorption on emitted intensity of Na-5890 Å line in water gas combustion plasma. N.K.Joshi, V.K.Rohatgi (Plasma Phys. Section, Bhabha Atomic Res. Centre, Bombay, India).

Int. J. Energy Res. (GB), vol.7, no.2, p.155-61 (April-June 1983).

Numerical calculations have been carried out to explain the effect of self absorption on the nature of the emitted intensity of the Na-5890 Å line of the sodium doublet in water gas combustion plasma. The self absorption is purely an effect caused by the presence of cold wall boundary layers in an MHD duct. The effect of seed concentration, core temperature, wall temperature, boundary layer thickness and profile parameters on line shapes has been studied. It has been found that seed percentage is the major factor influencing the line shape parameters and core temperature is the major factor affecting the maximum radiated monochromatic line intensity. (7 refs.)

76168 Spectroscopic observation of MeV-range multiply charged ions in a laser plasma. N.G.Basov, S.V.Bobashev, K.Gotz, M.P.Kalashnikov, A.P.Meshcherkin, Yu.A.Mikhailov, A.V.Rode, G.V.Sklizkov, S.I.Fedotov, E.Forster, H.Endert (P.N. Lebedev Phys. Inst., Acad. of Sci., Moscow, USSR).

JETP Lett. (USA), vol.36, no.7, p.281-4 (5 Oct. 1982). Translation of: *Pis'ma v Zh. Eksp. & Teor. Fiz. (USSR)*, vol.36, no.7, p.229-32 (5 Oct. 1982).

[received: May 1983]

The broadening of the resonance line of the helium-like ion of phosphorus emitted by a laser plasma is discussed. The broadening is interpreted as a Doppler frequency shift of the emission of high-energy P^{+13} ions. The energy spectrum of these fast ions is determined. The temperature of the electrons responsible for the ion acceleration is estimated. (10 refs.)

76169 Bright light sources from shock deceleration of hypersonic plasma streams in dense gases. A.S.Kamrukov, N.P.Kozlov, Yu.S.Protasov, A.M.Semenov (N.E. Bauman Higher Tech. Coll., Moscow, USSR).

Sov. Phys.-Tech. Phys. (USA), vol.27, no.11, p.1427-8 (Nov. 1982). Translation of: *Zh. Tekh. Fiz. (USSR)*, vol.52, no.11, p.2314-17 (Nov. 1982).

[received: May 1983]

The authors study the possibility of designing a light source with brightness characteristics comparing favorably with the most intense shock wave sources but without the disadvantages of explosive sources. Such a light source can be achieved by shock deceleration of hypersonic plasma streams in dense gases. (5 refs.)

- Threshold for suppression of light fluctuations in a shock-heated plasma consisting of monatomic gases ($M \sim 9-11$) See Entry 75536
- Self-focusing of light in a laser plasma See Entry 75758
- Observations of magnetized plasma flow through stationary background plasma See Entry 76173
- Spectroscopic investigation of laser-initiated low-pressure plasmas in atmospheric gases See Entry 76200
- Steady-state laser deflagration sustained by a resonant laser beam, and possibilities for exciting laser deflagration waves See Entry 76201

52.30 PLASMA FLOW; MAGNETOHYDRODYNAMICS

(see also 47.65 Fluid dynamics)

- 76170** Approximations in magnetoionic theory. K.G.Budden (Cavendish Lab., Univ. of Cambridge, Cambridge, England). *J. Atmos. & Terr. Phys. (GB)*, vol.45, no.4, p.213-18 (April 1983). Approximate formulae exist for the two refractive indices and the two wave polarizations in a cold magnetoplasma, known as the quasi-longitudinal and quasi-transverse approximations. Some of the commonly used forms of these formulae are wrong. The correct versions are given and the range of their validity is examined. (7 refs.)
- 76171** Finite-aspect-ratio MHD equations for Tokamaks. H.R.Strauss (Courant Inst. of Math. Sci., New York Univ., New York, NY, USA). *Nucl. Fusion (Austria)*, vol.23, no.5, p.649-55 (May 1983). A consistently ordered set of reduced MHD equations is derived for finite-aspect-ratio Tokamaks. The equations correctly reproduce Merier's low-beta interchange stability criterion. A numerical application to Tokamak ballooning stability is given. Finite-aspect-ratio effects tend to be stabilizing at low beta and destabilizing at high beta. (18 refs.)
- 76172** Inertial and viscous effects in the nonlinear growth of the tearing mode. D.Edery, M.Frey, J.P.Somon, M.Taggar, J.L.Soule (CEA, Centre d'Etudes Nucleaires, Fontenay-aux-Roses, France), R.Pellat, M.N.Bussac. *Phys. Fluids (USA)*, vol.26, no.5, p.1165-7 (May 1983). The nonlinear self-similar tearing-mode solution of Rutherford (1973) is revisited. The stream function for the plasma flow including inertia, convection, and viscosity is explicitly computed. In all cases Rutherford's solution is asymptotically valid. (7 refs.)
- 76173** Observations of magnetized plasma flow through stationary background plasma. G.Jellison, C.R.Parsons (Inst. for Phys. Sci. & Technol., Univ. of Maryland, College Park, MD, USA). *Phys. Fluids (USA)*, vol.26, no.5, p.1171-2 (May 1983). The collisionless flow of a laser-produced barium plasma through low-pressure photoionized xenon in the presence of a uniform, transverse magnetic field is studied. Deceleration of the barium is observed, and attributed to magnetically induced instabilities. Interaction close (4 cm) to the target is observed. The front thickness is observed to vary inversely with field strength. Spontaneous emission of 4554.03 Å radiation increases by more than an order of magnitude when the B field and background gas are both present, indicating significant electron heating. Theory shows that these observations can be explained by the modified two-stream instability and the magnetized ion-ion instability. (10 refs.)
- 76174** Magnetohydrodynamic equilibrium and stability of field-reversed configurations. J.L.Schwarzmeier, D.C.Barnes, D.W.Hewett, C.E.Seyler, A.I.Shestakov, R.L.Spencer (Los Alamos Nat. Lab., Univ. of California, Los Alamos, NM, USA). *Phys. Fluids (USA)*, vol.26, no.5, p.1295-8 (May 1983). Magnetohydrodynamic equilibrium and stability studies of field-reversed configurations are presented. Experimentally realistic equilibria are calculated numerically for a plasma inside a conducting cylinder. Stability studies indicate that equilibria ranging from elliptical to highly racetrack-shaped are all unstable to the internal tilting mode. (15 refs.)
- Effect of self absorption on emitted intensity of Na-5890 Å line in water gas combustion plasma See Entry 76167
- Bright light sources from shock deceleration of hypersonic plasma streams in dense gases See Entry 76169
- Field saturation for arbitrary temperature in resonance absorption See Entry 76183
- Slowing down of ion rings See Entry 76213

52.35 WAVES, OSCILLATIONS, AND INSTABILITIES IN PLASMA

- 76175** Comment on 'Electromagnetic decay into a surface plasma wave and an ion acoustic surface wave in a semi-infinite plasma'. E.Mateev, I.Zhelyazkov (Faculty of Phys., Sofia Univ., Sofia, Bulgaria). *J. Appl. Phys. (USA)*, vol.54, no.5, p.2837 (May 1983). For original paper see K. Yasumoto, *ibid.*, vol.52, p.3238 (1981). It is pointed out that the parametric instability of surface modes in a semi-infinite plasma is a four-wave process and the threshold should be $\sim 0.7(m_i/m_e)^{1/2}$ times larger than that found by Yasumoto [*J. Appl. Phys.* 52, 3238 (1981)]. (4 refs.)
- 76176** Buneman instability and Pierce instability in a collisionless bounded plasma. S.Iizuka, K.Saeki, N.Sato, Y.Hatta (Dept. of Electronic Engng., Tohoku Univ., Sendai, Japan). *J. Phys. Soc. Jpn. (Japan)*, vol.52, no.5, p.1618-28 (May 1983). A systematic experiment is performed on the Buneman instability and the Pierce instability in a bounded plasma consisting of beam electrons and stationary ions. Current fluctuations are confirmed to be induced by the Buneman instability. On the other hand, the Pierce instability gives rise to a current limitation. The phenomena are well explained by Mikhailovskii's theory taking account of ion motion in a bounded plasma.
- 76177** Influence of external helical field on the tearing mode. Ma Tengcai, Long Yongxing (Southwestern Inst. of Phys., Acad. Sinica, Leshan, China). *Kexue Tongbao (Foreign Lang. Ed.) (China)*, vol.28, no.3, p.316-20 (March 1983). It has been found that in many Tokamak discharges a strong correlation exists between the tearing modes and the current disruption. The disruption is initiated by the current in helical windings, and a small resonant helical field will exert a stabilizing effect on the disruptive instability if it is not too large. Thus, in a Tokamak and in systems with external windings, such as stellarators, analyses of the influence of the helical field on the 2/1 mode have been considered important. The authors attempt to explain the behaviour of the

2/1 mode on the basis of the nonlinear theory of tearing modes, and take into consideration the effect of the external helical field and the resonant interaction between plasma and helical field. (7 refs.)

- 76178** A kinetic cross-field streaming instability. C.S.Wu, Y.M.Zhou, S.T.Tsai, S.C.Guo (Inst. for Phys. Sci. & Technol., Univ. of Maryland, College Park, MD, USA), D.Winske, K.Papadopoulos. *Phys. Fluids (USA)*, vol.26, no.5, p.1259-67 (May 1983). In a high-beta plasma, the so-called modified two-stream instability, which results from strongly magnetized electrons drifting relative to unmagnetized ions across a homogeneous magnetic field, is misnamed because the mode is highly kinetic, particularly when the relative streaming velocity exceeds the Alfvén speed of the plasma. This kinetic cross-field streaming instability is investigated in detail, examining the effect of the electromagnetic terms and the stability boundaries in both low- and high-beta plasmas. An approximate dispersion relation showing the relation of this mode to the whistler is derived and solutions of it are compared with those obtained from the exact dispersion relation. The kinetic mode, unlike the usual modified two-stream instability, is not stabilized by electromagnetic effects when the relative electron-ion drift speed exceeds the Alfvén speed. (31 refs.)
- 76179** Linear analysis of the coalescence instability. A.Bondeson (Inst. for Electromagnetic Field Theory, Chalmers Univ. of Technol., Goteborg, Sweden). *Phys. Fluids (USA)*, vol.26, no.5, p.1275-8 (May 1983). The linear instability of pairwise-coalescing magnetic islands is studied analytically and numerically using incompressible ideal magnetohydrodynamics. An energy principle calculation shows that for small values of the island width w , the growth rate of the instability is proportional to $w^{3/2}$. Numerical simulations are presented giving detailed information about the mode structure. (11 refs.)
- 76180** Nonlinear evolution of the transverse instability of plane-envelope solitons. P.A.E.M.Janssen (Dept. of Oceanography, Royal Netherlands Meteorological Inst., De Bilt, Netherlands), J.J.Rasmussen. *Phys. Fluids (USA)*, vol.26, no.5, p.1279-87 (May 1983). The nonlinear evolution of the transverse instability of plane envelope soliton solutions of the nonlinear Schrödinger equation is investigated. For the case where the spatial derivatives in the two-dimensional nonlinear Schrödinger equation are elliptic a critical transverse wavenumber is found above which the soliton is stable. Application of the multiple time scale method near this critical transverse wavenumber gives a dynamical equation for the nonlinear evolution of the transverse instability. Nonlinearity is found to enhance the growth of the linearly unstable mode. The results are discussed in connection with soliton collapse. (25 refs.)
- 76181** Suppression of magnetic islands by RF driven currents. A.H.Reiman (Dept. of Phys. & Astron., Univ. of Maryland, College Park, MD, USA). *Phys. Fluids (USA)*, vol.26, no.5, p.1338-40 (May 1983). The quasilinear theory for the saturation of nonlinear tearing modes is modified to include RF driven currents. It is shown that the presence of lower hybrid driven currents can strongly suppress the growth of magnetic islands. (4 refs.)
- 76182** Zero-frequency cyclotron wave on an intense relativistic-electron beam. T.P.Starke, H.V.Wong, W.W.Rienstra, B.N.Moore, E.Cornet, H.A.Davis (Austin Res. Associates, Austin, TX, USA). *Phys. Fluids (USA)*, vol.26, no.5, p.1349-58 (May 1983). The zero-frequency cyclotron wave is studied on an unneutralized, magnetized relativistic-electron beam. This stationary mode occurs where the Doppler-shifted beam-cyclotron dispersion branch crosses the wavenumber axis. In this experiment zero-frequency-cyclotron waves have been generated by the injection of foil (and foilless) diode beams into a drift tube. A linear-cyclotron wave-dissipation theory is presented, which includes the radial electron-energy variation $\gamma(r)$ due to beam space charge. The $\gamma(r)$ variation causes only one propagating eigenmode to exist for each azimuthal-mode number. Numerical simulations of the beam and the cyclotron wave are described. Experimental measurements of the mode radial dependence, the wavelength scaling with magnetic field, and the wavelength scaling with beam energy are also presented. (15 refs.)
- 76183** Field saturation for arbitrary temperature in resonance absorption. B.Bezzerides, S.J.Gitomer (Los Alamos Nat. Lab., Univ. of California, Los Alamos, NM, USA). *Phys. Fluids (USA)*, vol.26, no.5, p.1359-63 (May 1983). A nonlinear theory of a driven, inhomogeneous, one-dimensional plasma of arbitrary temperature is presented. The model is solved numerically and analytically and detailed expressions are given for the saturated electric field excited at critical density. The results of the calculation are valid for arbitrary temperature and connect in a continuous manner the limits of cold wavebreaking and linear convective saturation. Comparison of the results of the calculation with particle simulations is made and good agreement is obtained. (7 refs.)
- 76184** Growth and saturation of the two-plasmon decay instability. H.A.Baldis, C.J.Walsh (Div. of Phys., Nat. Res. Council, Ottawa, Ontario, Canada). *Phys. Fluids (USA)*, vol.26, no.5, p.1364-75 (May 1983). An experimental study of the two-plasmon decay instability is reported. An intense CO₂ laser (10.6 μ m) was used to generate the instability in a long scale length, preformed plasma. The principal experimental diagnostic measurement was time-resolved Thomson scattering, with resolution in either ω or k space. The results show that the instability evolves basically in agreement with linear theories, then saturates by the nonlinear process of mode coupling to short-wavelength ion fluctuations. At saturation, density fluctuations close to 20% are observed in both the electron and ion waves. (27 refs.)
- 76185** Nonlinear saturation of the Pierce instability. D.Jovanovic (Inst. of Phys., Beograd, Yugoslavia). *Phys. Scr. (Sweden)*, vol.27, no.5, p.376-9 (May 1983). The early stage in the saturation of the Pierce instability is investigated assuming weak nonlinearities. It is demonstrated that the energy transfer to the growing electric potential causes a deceleration of the electron beam, leading to enhancement of the potential and decrease of the wavelength close to the beam inlet boundary. The possible relationship between this effect and the formation of double layers is discussed. (10 refs.)
- 76186** Low frequency surface waves in the presence of an external high frequency electric field [plasma]. N.Gopalaswamy, S.Krishan (Dept. of Phys., Indian Inst. of Sci., Bangalore, India). *Pramana (India)*, vol.20, no.1, p.23-40 (Jan. 1983). [received: May 1983] The problem of surface sound propagation in the presence of external high frequency dipole electric field is investigated using Vlasov-Poisson equations. The structure of the electric field of these surface waves is also determined. It has been found that the ion sound waves that exist in the presence of external high frequency waves are true surface waves while those without the external

field are quasisurface waves as the former waves decay within one wavelength away from the surface. (12 refs.)

76187 Transmission of sonics through ionised medium: damping considerations. A.P.Saxena, N.S.Suryanarayana (Ravishankar Univ., Raipur, India). *Pramana (India)*, vol.20, no.1, p.41-6 (Jan. 1983). [received: May 1983] The various energy loss mechanisms in ion acoustic wave propagation in a gas discharge plasma have been discussed. The relative characteristic acoustic impedance of the plasma has also been experimentally determined which would help to measure the electron temperature of the plasma. (14 refs.)

76188 Self-excited oscillations in the parameters of a laser plasma near the target surface in gases at high pressure. N.N.Rykalin, A.A.Uglov, M.B.Ignat'ev (A.A. Baikov Inst. of Metall., Acad. of Sci., Moscow, USSR). *Sov. Phys.-Dokl. (USA)*, vol.27, no.8, p.628-9 (Aug. 1982). Translation of: *Dokl. Akad. Nauk SSSR*, vol.265, no.4-6, p.1117-19 (Aug. 1982). [received: May 1983]

Reports an experimental study of the spatial inhomogeneity of a laser plasma in gases at high pressure, based on the use of probe measurements. A pulsed neodymium laser was used in the experiments; it emitted pulses of length $\tau \sim 0.5$ -1.0 msec with maximum energy of 30 J at wavelength $\lambda = 1.06 \mu\text{m}$. (9 refs.)

76189 Drift motion of a charged particle in a homogeneous magnetic field and in the electric field of the rotating potential wave. Yu.N.Eliseev, K.N.Stepanov.

Ukr. Fiz. Zh. (USSR), vol.28, no.5, p.683-92 (May 1983). In Russian. Drift equations describing the motion of a nonrelativistic charged particle in the homogeneous magnetic field and in the electric field of a rotating potential wave under the Cherenkov and cyclotron resonance conditions are obtained by means of the averaging method. The drift motion integrals are found and the drift trajectory being a part of an ellipse or a hyperbola is determined on the phase plane. Time integration of the drift equations is performed for a monochromatic wave, the motion being periodic. The oscillation period approaches infinity in the separatrix. The possibility of particle accumulation near singular points on the phase plane is pointed out which may lead to a resonant particle concentration in the respective radius. (6 refs.)

Electron beam fusion, energy compression, and the absolute instability See Entry 75179

Threshold for suppression of light fluctuations in a shock-heated plasma consisting of monatomic gases ($M \sim 9$ -11) See Entry 75536

Surface density profile and surface tension of the one-component classical plasma See Entry 76159

Ripple loss of suprathermal alpha particles during slowing-down in a Tokamak reactor See Entry 76164

Approximations in magnetoionic theory See Entry 76170

Finite-aspect-ratio MHD equations for Tokamaks See Entry 76171

Inertial and viscous effects in the nonlinear growth of the tearing mode See Entry 76172

Observations of magnetized plasma flow through stationary background plasma See Entry 76173

Magnetohydrodynamic equilibrium and stability of field-reversed configurations See Entry 76174

Instabilities induced by resonant absorption of an electromagnetic wave in an inhomogeneous plasma See Entry 76192

Resonant resistive instability of a relativistic electron beam in a plasma See Entry 76193

Plasmon spontaneous emission and entropy in Kaufman and Morrison's formalism for the quasilinear equations of plasma physics See Entry 76194

Parametric excitation of a drift wave and associated ion heating by a modulated ion beam See Entry 76196

The classical theory of the bumpy torus relativistic annulus See Entry 76197

Stable equilibria having arbitrary q profile See Entry 76207

Rotational instabilities in the field-reversed configuration: results of hybrid simulations See Entry 76210

A numerical analysis of flute modes in the ELMO Bumpy Torus See Entry 76211

52.35R Plasma turbulence

76190 Model of Burgers turbulence for turbulent ionization waves. N.Bekki (Dept. of Phys., Nagoya Univ., Nagoya, Japan). *J. Phys. Soc. Jpn. (Japan)*, vol.52, no.5, p.1505-8 (May 1983).

Turbulent ionization waves in the positive column of a glow discharge are investigated theoretically. It is shown that the turbulent ionization waves can be described by a model of Burgers turbulence. The closed equation by means of the modified cumulant approximation is solved numerically for a typically initial condition. The squared density spectrum is shown to agree with the experimental results.

76191 Self-consistent calculation of the α -effect and turbulent magnetic diffusion. I.T.Drummond (Dept. of Appl. Maths. & Theoretical Phys., Univ. of Cambridge, Cambridge, England).

J. Fluid Mech. (GB), vol.129, p.337-45 (April 1983). The author uses the method of Phythian & Curtis (1978) to obtain a self-consistent calculation in lowest order of perturbation theory, for the α -coefficient and effective diffusivity of a magnetic field in a plasma with Gaussian turbulence. (9 refs.)

52.35T Shock waves

Bright light sources from shock deceleration of hypersonic plasma streams in dense gases See Entry 76169

52.40 PLASMA INTERACTIONS

52.40D Electromagnetic wave propagation in plasma

76192 Instabilities induced by resonant absorption of an electromagnetic wave in an inhomogeneous plasma. J.C.Adam, A.G.Serveniére, G.Laval (Centre de Phys. Théorique, Ecole Polytech., Palaiseau, France).

J. Phys. Colloq. (France), vol.44, no.C-2, p.171-9 (March 1983). (International Workshop on Optical Phase Conjugation and Instabilities, Cargèse, Corsica, France, 20-24 Sept. 1982).

For oblique incidence and appropriate polarization, a coherent electromagnetic wave generates longitudinal Langmuir waves in an inhomogeneous plasma. These longitudinal waves propagate nonlinearly through the plasma even for rather low incident energy flux. This nonlinearity induces instabilities by coupling with two other Langmuir waves and an ion sound wave. For weak nonlinearity or strong damping, periodic time dependent solutions are found. They correspond to periodic emissions of soliton-like perturbations. For stronger nonlinearity, the solitons are emitted in a chaotic way. The consequence of this behaviour on the reflected electromagnetic wave and the plasma will be discussed. (4 refs.)

Self-focusing of light in a laser plasma See Entry 75758

52.40H Solid-plasma interactions

A one-dimensional study of Tokamak current reversal See Entry 76160

Effect of self absorption on emitted intensity of Na-5890 Å line in water gas combustion plasma See Entry 76167

Low frequency surface waves in the presence of an external high frequency electric field [plasma] See Entry 76186

52.40K Sheaths

Nonlinear saturation of the Pierce instability See Entry 76185

52.40M Beam interactions in plasma

76193 Resonant resistive instability of a relativistic electron beam in a plasma. L.E.Aranchuk, V.D.Vikharev, V.V.Gorev, S.F.Zhandarov, S.V.Zakharov, V.D.Korolev, L.I.Rudakov, V.P.Smirnov, L.I.Urutskov (I.V. Kurchatov Inst. of Atomic Energy, Moscow, USSR).

JETP Lett. (USA), vol.36, no.9, p.405-8 (5 Nov. 1982). Translation of: *Pisma v Zh. Eksp. & Teor. Fiz. (USSR)*, vol.36, no.9, p.331-4 (5 Nov. 1982). [received: June 1983]

An instability of a relativistic electron beam in a plasma has been observed. This instability occurs in a time shorter than the scale time for changes in the magnetic field, $\tau_d = 4\pi\sigma^2/c^2$, and results in a displacement of the beam as a whole to the side wall of the drift chamber. (3 refs.)

76194 Plasmon spontaneous emission and entropy in Kaufman and Morrison's formalism for the quasilinear equations of plasma physics. R.J.-M.Grognard (Div. of Radiophys., CSIRO, Sydney, Australia).

Phys. Lett. A (Netherlands), vol.95A, no.8, p.432-5 (23 May 1983).

The Poisson bracket defined by Kaufman and Morrison (see *ibid.*, vol.88, p.405, 1982) to derive the standard quasilinear equations of plasma physics is slightly modified to account for the spontaneous emission of plasma waves. A more satisfying 'H theorem' results from this modification. (4 refs.)

76195 BIRTH: A beam deposition code for non-circular tokamak plasmas. M.Otsuka, M.Nagami, T.Matsuda.

Report JAERI-M-82-129, Japan Atomic Energy Res. Inst., Tokai, Ibaraki (Sept. 1982), 35 pp.

A new beam deposition code has been developed which is capable of calculating fast ion deposition profiles including the orbit correction. The code incorporates any injection geometry and a noncircular cross section plasma with a variable elongation and an outward shift of the magnetic flux surface. Typical c.p.u. time on a DEC-10 computer is 10-20 seconds and 5-10 seconds with and without the orbit correction, respectively. This is shorter by an order of magnitude than that of other codes, e.g. Monte Carlo codes. The power deposition profile calculated by this code is in good agreement with that calculated by a Monte Carlo code. (13 refs.)

Electron beam fusion, energy compression, and the absolute instability See Entry 75179

A kinetic cross-field streaming instability See Entry 76178

Zero-frequency cyclotron wave on an intense relativistic-electron beam See Entry 76182

Nonlinear saturation of the Pierce instability See Entry 76185

Operation of the tandem-mirror plasma experiment with skew neutral-beam injection See Entry 76214

52.50 PLASMA PRODUCTION AND HEATING

76196 Parametric excitation of a drift wave and associated ion heating by a modulated ion beam. M.Yatsuzuka, K.Satoh, S.Nobuhara (Dept. of Electrical Engng., Himeji Inst. of Technol., Hyogo, Japan), K.Yatsui, M.Yokoyama.

J. Phys. Soc. Jpn. (Japan), vol.52, no.5, p.1609-17 (May 1983).

An ion beam modulated near the low-hybrid frequency is injected into a low- β plasma immersed in a longitudinal magnetic field. Parametric excitation of a drift wave and a lower-hybrid wave is observed. From the measurement of the threshold electric field, an RF field parallel to the magnetic field is found to play an important role in the excitation of the instability. Substantial increase of the ion and electron temperatures has been observed with the growth of the instability. Such a rapid heating may be principally due to the drift wave instability driven parametrically. (20 refs.)

76197 The classical theory of the bumpy torus relativistic annulus. S.Hamasaki, N.A.Krall, J.L.Sperling (JAYCOR, San Diego, CA, USA).

Nucl. Fusion (Austria), vol.23, no.5, p.571-96 (May 1983).

The relativistic electron annulus is a critical component of the bumpy torus magnetic fusion concept. An analysis of the annulus is presented in which the ring steady state is determined by the explicit balance of quasi-linear heating and classical losses, i.e. collisions and synchrotron radiation. Both anisotropy and loss-cone effects are included in the formalism. It is demonstrated that a large number of electron cyclotron harmonics, not just the first and second, contribute in an appreciable way to annulus steady state and power balance. Without a loss cone, the analysis reproduces the relativistic passing electron population observed in bumpy tori on confined drift surfaces near the centre

of the bumpy torus cross-section. Loss-cone effects permit an annulus population with large perpendicular pressure to exist. It is shown that the balance between quasi-linear heating and the classical losses cannot account for the experimental scaling of bumpy torus annulus temperature; therefore, processes not included in the classical ring power balance model must contribute in a non-trivial way to observed annulus properties. (18 refs.)

76198 A unified theory of a class of mode conversion problems. R.A.Cairns (Dept. of Appl. Maths., Univ. of St. Andrews, St. Andrews, Scotland), C.N.Lashmore-Davies.

Phys. Fluids (USA), vol.26, no.5, p.1268-74 (May 1983).

Many radio-frequency heating methods involve conversion of an incoming wave to another mode which only propagates within the plasma and is ultimately damped. A method previously used to consider electron cyclotron heating by the O mode is extended to other mode conversion phenomena. From the properties of the dispersion relation in the neighborhood of the mode conversion point, differential equations for the mode amplitudes are constructed, in a well-defined way, which give energy conservation in the absence of damping. An analytic solution gives the transmission and conversion coefficients in terms of parameters defining the local behavior of the dispersion relation. The technique is applied to a number of problems, showing that they can all be solved by elementary algebraic manipulations of the local dispersion relation. The phenomenon of electron cyclotron emission also falls rather naturally into this mode conversion picture. It is also suggested that the method of dealing with cyclotron emission may have some relevance to the more general problem of energy transport across a magnetic field. The technique, therefore, brings together into a unified theory a number of problems which have been treated by diverse, and usually more complicated, mathematical techniques in the existing literature. (16 refs.)

76199 Direct measurement of anisotropy of hot electron rings using synchrotron emission. S.Tamor (Sci. Appl. Inc., La Jolla, CA, USA).

Phys. Fluids (USA), vol.26, no.5, p.1335-7 (May 1983).

It is pointed out that velocity-space anisotropy of a relativistic electron ring is reflected in the angular distribution of the intensity and polarization of the synchrotron emission, and it is suggested that this effect may be useful for direct measurement of the anisotropy. Results of sample computations for a loss-cone type of distribution are presented. (7 refs.)

NATO ASI on Atomic and Molecular Processes in Controlled Thermonuclear Fusion, Palermo, July 19-30, 1982 See Entry 74205

Steady-state radial heat conduction in a Z pinch See Entry 76212

52.50J Plasma production and heating by laser beams

76200 Spectroscopic investigation of laser-initiated low-pressure plasmas in atmospheric gases. R.A.Armstrong (US Air Force Geophysics Lab., Hanscom Air Force Base, MA, USA), R.A.Lucht, W.T.Rawlins.

Appl. Opt. (USA), vol.22, no.10, p.1573-7 (15 May 1983).

Laser-initiated breakdown of N_2 , O_2 , and Ar has been investigated at sub-atmospheric pressures using a pulsed (10-nsec) Nd:yttrium aluminum garnet (Nd:YAG) laser at 1.06 μ m. Breakdown thresholds have been determined from 3 to 760 Torr, and spectral analysis of the plasma emission has been carried out at 10 and 125 Torr over the 300-600-nm range. Sharp spectral features arising from highly excited singly and multiply charged ions are reported as well as an underlying continuum at intermediate pressure. Time-resolved measurements indicate a complex kinetic dynamic optical behavior. (14 refs.)

76201 Steady-state laser deflagration sustained by a resonant laser beam, and possibilities for exciting laser deflagration waves. G.I.Kozlov, V.A.Kuznetsov (Inst. of Problems in Mech., Acad. of Sci., Moscow, USSR).

Sov. Tech. Phys. Lett. (USA), vol.8, no.9, p.458-9 (Sept. 1982). Translation of: *Pis'ma v Zh. Tekh. Fiz. (USSR)*, vol.8, no.17-18, p.1063-7 (Sept. 1982). [received: May 1983]

An intense laser deflagration has been observed for the first time in a resonant laser beam in carbon dioxide. The authors used a 1.5-kW CW CO_2 laser to produce and sustain steady-state laser deflagration. A vertical laser beam enters the cooled chamber through a salt-lens window. The chamber is filled with carbon dioxide. The laser beam is focused to a spot 0.5 mm in diameter at the exit of a nozzle. At atmospheric pressure they observe no significant emission near the spot, but as the gas pressure is raised to 5-10 atm, intense blue emission of a steady-state flame appears near the neck of the caustic. (no refs.)

76202 Self-focusing of laser beam crossing a laser plasma. J.S.Bakos, I.B.Foldes, P.N.Ignacz, Z.Sorlei.

Report KFKI-1983-12, Hungarian Acad. Sci., Budapest (1983), 10 pp.

A crossed beam experiment was performed to clarify the mechanism of self-focusing in a laser produced spark. The plasma was created by one beam and self-focusing was observed in the weak probe beam which crossed the plasma. Experimental results show that the cause of self-focusing is the nonuniform heating mechanism. (9 refs.)

Ionization effects in a system of a free electron laser and a molecular medium See Entry 75674

Self-focusing of light in a laser plasma See Entry 75758

Spectroscopic observation of MeV-range multiply charged ions in a laser plasma See Entry 76168

Observations of magnetized plasma flow through stationary background plasma See Entry 76173

Self-excited oscillations in the parameters of a laser plasma near the target surface in gases at high pressure See Entry 76188

52.50L Plasma production and heating by shock wave and wire explosion

Threshold for suppression of light fluctuations in a shock-heated plasma consisting of monatomic gases ($M \sim 9-11$) See Entry 75536

52.55 PLASMA EQUILIBRIUM AND CONFINEMENT

76203 Cyclotron loss of fast particles from a bumpy Tokamak. S.V.Putinskii (I.V. Kurchatov Inst. of Atomic Energy, Moscow, USSR).

JETP Lett. (USA), vol.36, no.9, p.397-400 (5 Nov. 1982). Translation of: *Pis'ma v Zh. Eksp. & Teor. Fiz. (USSR)*, vol.36, no.9, p.326-8 (5 Nov. 1982). [received: June 1983]

A possible mechanism for the loss of fast particles from a Tokamak is examined: a cyclotron resonance of the particles with the bumpiness perturbations

of the toroidal magnetic field. The radial diffusion coefficient of the particles is estimated. (5 refs.)

76204 Sawteeth, magnetic disturbances, and magnetic flux regeneration in the reversed-field pinch. R.G.Watt, R.A.Nebel (Los Alamos Nat. Lab., Los Alamos, NM, USA).

Phys. Fluids (USA), vol.26, no.5, p.1168-70 (May 1983).

A comparison of experimental data and theoretical results is presented that may help to explain the underlying causes of the flux regeneration mechanism ('dynamo') in the reversed-field pinch (RFP). Discrete events are seen on many diagnostic measurements which are coincident with observable increases in toroidal magnetic flux in discharges where the pinch parameter θ ($\theta \equiv B_{\theta\text{wall}}/(B_z)$) exceeds the value 1.6. By observing the relative timing and the θ dependence of these events as the discharge is returned to lower values of θ , a case may be made for associating the $m=1$ tearing mode with the RFP dynamo. (12 refs.)

76205 Radial guiding center drifts and omnigenity in bumpy torus confinement systems. R.D.Hazeltine, P.J.Catto (Plasma Res. Inst., Sci. Applications Inc., Boulder, CO, USA).

Phys. Fluids (USA), vol.26, no.5, p.1252-8 (May 1983).

Collisional transport of a high-temperature plasma across the confining field of a bumpy torus magnetic confinement system depends sensitively upon the functional form of the radial guiding center drift, and thus upon details of the confinement geometry. A general and relatively explicit formula for the radial drift is derived, using the large aspect ratio results of a previous equilibrium study. Allowance is made for (i) arbitrary toroidal variation of the confining field; (ii) field distortion due to plasma currents; (iii) noncircular deformation of the toroidal field coils. However, the analysis pertains only to the plasma core, and not to the high-beta annuli (electron rings) which are usually present in experiments. The question of bumpy torus omnigenity—whether any bumpy torus field configuration is consistent with a vanishing, or nearly vanishing, radial drift—is also investigated. It is found that omnigenity cannot occur, at least in the vicinity of the magnetic axis. (10 refs.)

76206 Evaluation of the structure of ergodic fields. A.H.Boozer (Plasma Phys. Lab., Princeton Univ., Princeton, NJ, USA).

Phys. Fluids (USA), vol.26, no.5, p.1288-91 (May 1983).

A method of analyzing ergodic magnetic fields is given, including a generalization of magnetic coordinates to such fields. The results of this analysis can be used in existing Monte Carlo codes to assess the enhanced transport associated with imperfect surfaces. The Hamiltonian for a general magnetic field is given as part of this analysis. (12 refs.)

76207 Stable equilibria having arbitrary q profile. A.Reiman (Lab. for Plasma & Fusion Energy Studies, Univ. of Maryland, College Park, MD, USA), A.Boozer.

Phys. Fluids (USA), vol.26, no.5, p.1292-4 (May 1983).

It is shown that minimum energy equilibria can be constructed with any q (inverse rotational transform) profile such that $1/q$ is continuous. These equilibria are stable to both ideal magnetohydrodynamic (MHD) and tearing modes. In particular, explicit equilibria are presented which have a local minimum in q but are nevertheless stable. (11 refs.)

76208 Two-dimensional equilibria of field-reversed configurations in a perfectly conducting cylindrical shell. D.W.Hewett, R.L.Spencer (Los Alamos Nat. Lab., Los Alamos, NM, USA).

Phys. Fluids (USA), vol.26, no.5, p.1299-304 (May 1983).

Two-dimensional field-reversed equilibria bounded by a conducting cylinder are computed. The computation is made possible by using a global constraint and by using a computational algorithm that is protective of the initial guess. A pressure profile is used that has sufficient generality to match experimentally produced configurations. It is found that for some choices of separatrix radius and separatrix beta, no equilibria exist. The reasons for loss of equilibrium are discussed and an example of a configuration near loss of equilibrium conditions is given. (14 refs.)

76209 Nonlinear, single-helicity magnetic reconnection in the reversed-field pinch. E.J.Caramana, R.A.Nebel, D.D.Schnack (Los Alamos Nat. Lab., Los Alamos, NM, USA).

Phys. Fluids (USA), vol.26, no.5, p.1305-19 (May 1983).

A computational and analytical study of the nonlinear evolution of single-helicity, resistive, current-driven modes in the reversed-field pinch utilizing the single-fluid magnetohydrodynamic approximation is presented. In the start-up phase it is found that an off-axis current peak can be anomalously dissipated by globally reconnecting current-driven modes. The reconnection is seen to be well described by the Kadomtsev reconnection model, which is directly applied to the reversed-field-pinch regime. During the sustainment phase of the discharge, stable profiles are driven unstable by transport processes and destabilized by the resulting current-driven instabilities. The dynamics of the toroidal field is of fundamental importance in the evolution of these modes. The reversed-field-pinch profile is restabilized by two successive global reconstructions: the first removes the rational surface; the second restores it. It is also found that magnetic reconnection can occur in the reversed-field pinch without a linear phase. Although the interaction of instabilities with different helicities is not directly investigated, the importance of this phenomenon in the reversed-field pinch is discussed. (49 refs.)

76210 Rotational instabilities in the field-reversed configuration: results of hybrid simulations. D.S.Harned (Coll. of Engng., Univ. of California, Berkeley, CA, USA).

Phys. Fluids (USA), vol.26, no.5, p.1320-6 (May 1983).

Rotational instabilities in rigidly rotating field-reversed configuration (FRC) equilibria are studied using a quasineutral hybrid simulation code. The authors observe unstable $m=2$ modes at levels of ion rotation below instability thresholds predicted by finite-Larmor-radius fluid theory. Nonlinear effects are found to reduce the growth rate and lower the real frequency of the $m=2$ mode at large amplitude. Instabilities with $m>2$ have been observed for strongly reversed cases. It is also found that growth rates for these instabilities can be reduced by increasing the ratio of the plasma radius to the ion Larmor radius. (20 refs.)

76211 A numerical analysis of flute modes in the ELMO Bumpy Torus. A.M.El Nadi, J.C.Whitson (Fusion Energy Div., Oak Ridge Nat. Lab., Oak Ridge, TN, USA).

Phys. Fluids (USA), vol.26, no.5, p.1327-9 (May 1983).

Allowing for realistic magnetic field and plasma density profiles, a radial eigenvalue computer code was used to investigate flute modes in the ELMO Bumpy Torus (EBT). (8 refs.)

76212 Steady-state radial heat conduction in a Z pinch. D.W.Schudder (Los Alamos Nat. Lab., Univ. of California, Los Alamos, NM, USA).

Phys. Fluids (USA), vol.26, no.5, p.1330-4 (May 1983).

One-dimensional steady-state radial profiles of a classical Z pinch are calculated. The effects of ion thermal conduction and bremsstrahlung radiation losses are induced self-consistently, as are Ohmic heating, pressure balance, and an equation of state. It is shown that the upper current limit of approxi-

mately 1.4 MA for an equilibrium pinch found when only bremsstrahlung losses are allowed is virtually unaffected by the inclusion of ion thermal conduction. However, solutions with lower currents are now allowed. The profile-smoothing effect of ion thermal conduction is not sufficient to produce a pressure profile stable to $m=0$ modes. Total losses due to radial conduction are shown to be small for a thermonuclear plasma. (17 refs.)

76213 Slowing down of ion rings. C.B.Ruchti, R.V.Lovell (Dept. of Appl. Phys., Cornell Univ., Ithaca, NY, USA). *Phys. Fluids (USA)*, vol.26, no.5, p.1341-8 (May 1983).

A study is made of the slowing down of self-consistent, large-orbit ion rings due to small-angle Coulomb scattering in a dense, low-temperature plasma. A kinetic equation is derived for the ion-ring distribution function $f(P, I, t)$, where P is the canonical angular momentum, and I is an adiabatic invariant which is an implicit function of P and the particle energy. The ratio of the time scale for the perpendicular momentum change (diffusion) to that for the parallel momentum change (drag) is m/M , with M the ion mass and m the electron mass. Therefore, drag is the dominant collisional effect, and the slowing down corresponds to incompressible flow in the (P, I) plane. This flow is calculated numerically by computing sequences of equilibria. Initially well-trapped distribution functions are found to have essentially no particle loss during the first slowing-down time τ , which is defined as the time it would take a single ring particle to slow down to zero energy. In most of the cases studied, the rings shrink in both radius and in axial length, with the field reversal increasing by $\approx 10\%$ within one τ . The rate of loss of toroidal kinetic energy exceeds the loss of poloidal energy by a factor of typically 1.5-2.0. The self-consistent toroidal electric field opposes the slowing down, increasing the ring lifetime by 20%-50% over the single-particle slowing-down time. (16 refs.)

76214 Operation of the tandem-mirror plasma experiment with skew neutral-beam injection. T.C.Simonen, S.L.Allen, T.A.Casper, J.F.Clauser, C.A.Clover, F.H.Coensgen, D.L.Cornell, W.F.Cummins, C.C.Damm, M.Flammer, J.H.Foote, R.K.Goodman, D.P.Grubbs, E.B.Hooper, R.S.Hornady, A.L.Hunt, R.G.Kerr, A.W.Molvik, R.H.Munger, W.E.Nexsen, T.J.Orzechowski, W.L.Pickles, P.Poulsen, M.E.Rensink, B.W.Stallard, W.C.Turner, W.L.Hsu, W.Bauer (Lawrence Livermore Nat. Lab., Univ. of California, Livermore, CA, USA), T.L.Yu, D.Zimmermann. *Phys. Rev. Lett. (USA)*, vol.50, no.21, p.1668-71 (23 May 1983).

Tandem-mirror plasma with sloshing-ion end plugs has been produced. Ion-velocity distribution functions are peaked at 47° to the magnetic field lines. Low-level ion-cyclotron fluctuations were detected at 1.8 times the plug-midplane frequency and with properties predicted by theory; they did not degrade plasma confinement in the plugs or central cell. (21 refs.)

76215 Relaxation calculation of the electrostatic properties of compensated Penning traps with hyperbolic electrodes. G.Gabrielse (Dept. of Phys., Univ. of Washington, Seattle, WA, USA).

Phys. Rev. A (USA), vol.27, no.5, p.2277-90 (May 1983). Spectacular accuracies have been achieved with single elementary particles trapped in hyperbolic Penning traps, but only after anharmonicities have been tuned out of these traps by varying the potential of extra compensation electrodes introduced into the traps. The relaxation calculation reported is the first theoretical study of the electrostatic properties of such compensated Penning traps. Enough computations have been completed to clarify the basic physics involved in anharmonicity compensation and to provide useful, quantitative information for experiments in progress (especially for testing of anharmonicity systematics). The clearer picture of anharmonicity compensation which emerges suggests that the design of existing Penning traps could be significantly improved. An optimal electrode configuration is proposed which, in principle, makes the harmonic oscillation frequency of a trapped particle independent of changes in the compensation potential. (17 refs.)

76216 Wire X pinch in a high-current diode. S.M.Zakharov, G.V.Ivanenkov, A.A.Kolomenskii, S.A.Pikuz, A.I.Samokhin, I.U.Shmid (P.N. Lebedev Phys. Inst., Acad. of Sci., Moscow, USSR). *Sov. Tech. Phys. Lett. (USA)*, vol.8, no.9, p.456-7 (Sept. 1982). Translation of: *Pis'ma v Zh. Tekh. Fiz. (USSR)*, vol.8, no.17-18, p.1060-3 (Sept. 1982). [received: May 1983]

In the present experiments, wire X pinches were produced in the diode of the Don high-current accelerator with a forming line having parameters of 400 kV, 1.5 kJ, and 30 ns. The dynamics of the pinch were studied by five-frame high-speed interference and shadow photography in the beam from a ruby laser. The time interval between frames was 10 ns, and the exposure time was 3 ns. (2 refs.)

Fusion: towards reality [Tokamak experiment] See Entry 75180

Parameter optimizations of multiple-mirror reactors See Entry 76157

A one-dimensional study of Tokamak current reversal See Entry 76160

Heavy-impurity transport in the TFR Tokamak—comparison of line emission with numerical simulations See Entry 76162

Transport and re-deposition of limiter-released metal impurities See Entry 76163

Ripple loss of suprathermal alpha particles during slowing-down in a Tokamak reactor See Entry 76164

Effect of impurities on heat and particle transport in Tokamaks See Entry 76166

Finite-aspect-ratio MHD equations for Tokamaks See Entry 76171

Magnetohydrodynamic equilibrium and stability of field-reversed configurations See Entry 76174

The classical theory of the bumpy torus relativistic annulus See Entry 76197

Measurement of ionisation rate coefficients of nitrogen ions .. See Entry 76218

Design of a helical-axis stellarator See Entry 76221

Models for the development of the discharge in a Tokamak See Entry 76227

52.60 RELATIVISTIC PLASMA

Zero-frequency cyclotron wave on an intense relativistic-electron beam See Entry 76182

The classical theory of the bumpy torus relativistic annulus See Entry 76197

52.70 PLASMA DIAGNOSTIC TECHNIQUES AND INSTRUMENTATION

76217 Application of the method of resonance fluorescence for diagnostics of a high-temperature plasma. V.S.Burakov, G.T.Razdobarin (Phys. Inst., Acad. of Sci., Belorussian SSR).

Bull. Acad. Sci. USSR, Phys. Ser. (USA), vol.46, no.5, p.121-7 (1982). Translation of: *Izv. Akad. Nauk SSSR Ser. Fiz.*, vol.46, no.5, p.957-63 (1982). [received: May 1983] (Proceedings of the All-Union Conference on Luminescence Commemorating the Ninetieth Anniversary of the Birth of the Academician S.I. Vavilov, Leningrad, USSR, 21-24 April 1981).

The authors interpret the results obtained in the joint investigations performed by the Leningrad and Belorussian physicists which were directed at developing the method of resonance fluorescence for the diagnostics of high-temperature plasma. (46 refs.)

76218 Measurement of ionisation rate coefficients of nitrogen ions. R.Brown, W.M.Deuchars, D.E.Kidd, H.P.Summers, L.Wood (Dept. of Natural Philosophy, Univ. of Strathclyde, Glasgow, Scotland). *J. Phys. B (GB)*, vol.16, no.11, p.2053-62 (14 June 1983).

Time histories of the emission of a number of spectrum lines of the ions N^{+} to N^{3+} have been measured in a theta-pinch discharge of maximum axial electron temperature 100 eV and electron density $8 \times 10^{15} \text{ cm}^{-3}$. The lines observed in the discharge are subordinate lines in the quartz UV region and the observations were made both end on and side on to the discharge axis. Ionisation rate coefficients have been inferred from comparison with a theoretical model of the transient ionisation. The rates are conveniently expressed as scaling factors of an empirical ionisation rate expression due to Kunze (1971). These factors are 1.5 and 0.55 for N^{3+} and N^{4+} and the electron temperatures at the times of maximum abundance of these ions are 32 eV and 68 eV respectively. The result N^{4+} agrees well with the measurements of Kunze. (21 refs.)

76219 Photon-echo studies of collisional relaxation in weakly ionized noble-gas mixtures. M.R.Woodworth (Dept. of Phys., Univ. of Chicago, Chicago, IL, USA).

Opt. Lett. (USA), vol.8, no.6, p.307-9 (June 1983). Photon-echo relaxation rates are measured in weakly ionized plasmas of binary mixtures of noble gases in which the photon echo generated on a transition in one noble-gas species is damped primarily by atoms of the second species. The special cases of pure krypton and xenon are extensions of previous work in pure helium, neon, and argon. With the exception of mixtures with helium as the perturber, measured relaxation rates are consistent with collisional line-broadening calculations. (12 refs.)

76220 Tonks-Dattner diagnostics of electron density profiles. M.Mentzoni (Inst. of Phys., Univ. of Oslo, Oslo, Norway). *Phys. Scr. (Sweden)*, vol.27, no.4, p.311-13 (April 1983).

The uniqueness of Tonks-Dattner-diagnostics for determining the spatial electron density profile, $N_e(R)$, across a plasma column has been investigated. By choosing $N_e(R)$ either parabolic or linear it was found that the solutions yielded approximately overlapping profiles in the R -region for which the resonances occur. The whole profile enters into the equation for the average electron density, a quantity which is measured by microwave cavity techniques. The two profiles yielded thermal electron velocities which differed by about 15%. (8 refs.)

NATO ASI on Atomic and Molecular Processes in Controlled Thermonuclear Fusion, Palermo, July 19-30, 1982 See Entry 74205

Doppler-free laser spectroscopy measurements on a Ne discharge for determination of ^{22}Ne , ^{20}Ne isotope shifts See Entry 75349

Observations of magnetized plasma flow through stationary background plasma See Entry 76173

Self-excited oscillations in the parameters of a laser plasma near the target surface in gases at high pressure See Entry 76188

Spectroscopic investigation of laser-initiated low-pressure plasmas in atmospheric gases See Entry 76200

Sawtooth, magnetic disturbances, and magnetic flux regeneration in the reversed-field pinch See Entry 76204

Density of uranium ions in the $^4f_{7/2}^0$ ground state in a hollow-cathode type discharge See Entry 76223

Optogalvanic studies of neon glow discharge in magnetic fields: ion mobility measurements and detection of atomic alignment See Entry 76228

Real-time etch plasma monitor system See Entry 77775

Ionospheric plasma parameters measurement instrument for satellite experiment with SIT See Entry 78680

An instrument for rapidly measuring plasma distribution functions with high resolution See Entry 78775

Sond-R, an instrument for vertical probing of ionospheric plasma by means of CLP on board of a geophysical rocket See Entry 78781

52.75 PLASMA DEVICES AND APPLICATIONS

(see also 28.52 Fusion reactors, 86.30L Electrogasdynamic and magnetohydrodynamic conversion; for ion sources, see 29.25 Particle sources and targets)

76221 Design of a helical-axis stellarator. S.Yoshikawa (Princeton Plasma Phys. Lab., Princeton, NJ, USA). *Nucl. Fusion (Austria)*, vol.23, no.5, p.667-9 (May 1983).

A simple coil system is found to be sufficient for providing a helical-axis stellarator configuration with a deep vacuum magnetic well and short connection length. A system similar to the one reported here may provide good confinement for thermonuclear plasmas. (3 refs.)

76222 Directions of electrical engineering development. Z.Ciok. *Wiad. Elektrotech. (Poland)*, vol.51, no.1-2, p.18-22 (1-15 Jan. 1983). In Polish. [received: May 1983]

This article presents basic directions of electrical engineering development, and discusses perspectives of electric power generation development with particular attention focused on new sources of energy such as controlled thermonuclear reactions, and on its transmission, distribution, and use. (15 refs.)

A one-dimensional study of Tokamak current reversal See Entry 76160

Nonlinear saturation of the Pierce instability See Entry 76185

Wire X pinch in a high-current diode See Entry 76216

52.80 ELECTRIC DISCHARGES

(see also 51.50 Electrical phenomena in gases)

76223 Density of uranium ions in the $4f_{7/2}^0$ ground state in a hollow-cathode type discharge. P.Pianarosa, P.Bouchard, J.P.Saint-Dizier, J.M.Gagne (Dept. de Genie Phys., Ecole Polytech., Montreal, Quebec, Canada).

Appl. Opt. (USA), vol.22, no.10, p.1568-72 (15 May 1983).

A hollow-cathode type discharge cell as generator of uranium ions is investigated. The $4f_{7/2}^0$ ground-state ion density has been obtained by absorption spectroscopy of 5493 and 4244 Å. The absorption measurements have been performed using two identical hollow-cathode lamps: one acting as a light source, the other as a reservoir of free ions. Neon and xenon have been used as discharge sustaining gases. In the author's experimental conditions the measured ion ground-state density is of the order of 10^{12} ions cm^{-3} . Absorption measurements performed at 5915 and 4246 Å of U I give a density of the order of 10^{12} atoms cm^{-3} . This latter value is in excellent agreement with a previously measured value obtained by laser-absorption spectroscopy. (18 refs.)

76224 Thermal behavior of a solid particle in an arc discharge during transient cooling conditions. P.Meubus, M.Elayoubi (Centre de Recherche du Moyen Nord, Univ. du Quebec a Chicoutimi, Chicoutimi, Quebec, Canada). *Can. J. Phys. (Canada)*, vol.61, no.5, p.683-90 (May 1983).

The thermal behavior of a tungsten particle has been studied in an argon arc discharge during transient extinction conditions. At the beginning of the transient process, the particle is electrically neutral and is at the cathode voltage. During this period of time, it is observed that the thermionic cooling effect plays a major role in the heat transfer mechanisms. Within the limits of the solid surface and surrounding gas temperatures investigated, which varied between 3600 and 3300K for the surface and between 8000 and 6000K for the argon gas, the heat transfer rates by convection and radiation are of the same magnitude but opposite in sign. Each of them amounts to less than 10% of the heat loss rate induced by thermionic emission. Besides the theoretical aspect of the study, the cooling effect observed (about $6 \times 10^4 \text{ K s}^{-1}$) may be of interest for improving solid surface properties, provided that the solid particle possesses characteristic thermionic emission properties. (19 refs.)

76225 Partial discharge by high AC and DC voltages. H.Duarte-Ramos. *Electr. Energ.-Electron. (Portugal)*, no.185, p.107-11 (March 1983). In Portuguese.

Compares the influence of some factors on partial discharges in solid dielectrics with voids by high AC and DC voltages, such as permittivity, conductivity, time, applied voltage, temperature and space charge. (4 refs.)

76226 One particular aspect of the influence of the support electrode material upon the intensity of the lines in a spark discharge. V.D.Kurochkin. *J. Appl. Spectrosc. (USA)*, vol.37, no.2, p.872-6 (Aug. 1982). Translation of: *Zh. Prikl. Spektrosk. (USSR)*, vol.37, no.2, p.200-5 (Aug. 1982). [received: April 1983]

Electron levels are excited in collisions with fast electrons of the tail of the distribution function. The author determined experimentally the importance of the atoms of the support electrode in collision processes of this type, which occur in the plasma of a capacitor-supplied spark discharge. The investigations were made on W, Ta, Hf, Zr, Ir, Pt, Al, Cu, Zn, Mg, and Ag electrodes the active portions of which were cylinders with a diameter of 2 mm and a length of 5 mm. These metals are distinguished by both their thermophysical characteristics and their ability to oxidize. (10 refs.)

76227 Models for the development of the discharge in a Tokamak. Yu.N.Dnestrovskij, G.V.Pereverzev (I.V. Kurchatov Atomic Energy Inst., Moscow, USSR).

Nucl. Fusion (Austria), vol.23, no.5, p.633-48 (May 1983).

Numerical models for the development of the discharge in a Tokamak are considered. A hybrid model which describes the diffusion and convective processes and also the impurity radiation is used as the basis for a detailed study of the filling-gas ionization stage, the formation of the hot plasma column during the period of total current rise and the energy balance in the quasi-steady-state stage of the discharge. The model shows reasonable agreement with experiment at all stages of the discharge in a Tokamak. (29 refs.)

76228 Optogalvanic studies of neon glow discharge in magnetic fields: ion mobility measurements and detection of atomic alignment. L.R.Pendrill, M.Pettersson, U.Osterberg (Dept. of Phys., Chalmers Tekniska Hogskola, Goteborg, Sweden).

Phys. Scr. (Sweden), vol.27, no.4, p.306-10 (April 1983).

Studies have been made of optogalvanic signals when a glow discharge of neon, irradiated with light from a highly monochromatic dye laser, is subject to externally applied magnetic fields. The slow response of the discharge to an abrupt change in laser intensity is affected by varying magnetic field and discharge voltage in a way to suggest that positive Ne ions play an important role in the production of optogalvanic signals. A novel sub-Doppler spectral profile is observed, and an interpretation based on a discussion of the time-dependence of the optogalvanic signal as a sensitivity monitor of ionic velocities is presented. This effect is also a function of the atomic alignment. (18 refs.)

76229 Stratification of a glow discharge in a gas stream at enhanced power inputs. A.A.Besshaposhnikov, V.I.Blokhin, V.B.Voronin, S.V.Dvurechenskii, V.A.Mysin, S.V.Pashkin, N.A.Sokolov (I.V. Kurchatov Inst. of Atomic Energy, Moscow, USSR).

Sov. Phys.-Dokl. (USA), vol.27, no.8, p.633-5 (Aug. 1982). Translation of: *Dokl. Akad. Nauk SSSR*, vol.265, no.4-6, p.1371-4 (Aug. 1982). [received: May 1983]

The authors have discovered a mechanism of excitation of striations that is connected with the nonstationary process of accumulation of chemically active particles (radicals and metastable molecules) in a gas-discharge plasma. (14 refs.)

76230 Movement of an arc spot in a magnetic field. S.A.Yukhimchuk, O.M.Sviderskaya (V.Ya. Chubar' Mech. Engng. Inst., Zaporozh'e, USSR).

Sov. Phys.-Tech. Phys. (USA), vol.27, no.11, p.1393-6 (Nov. 1982). Translation of: *Zh. Tekh. Fiz. (USSR)*, vol.52, no.11, p.2270-5 (Nov. 1982). [received: May 1983]

A device is described for studying arc spot motion in magnetic field. Experimental curves are reported for the average velocity, and the results are analyzed statistically and presented as histograms which reveal a nearly Gaussian distribution. The factors responsible for irregular arc spot jumping and the effects this has on electrode erosion are discussed. (7 refs.)

76231 Influence of plasma composition in a low-inductance vacuum spark on the parameters of a micropinch region. Yu.V.Sidel'nikov (Inst. of Spectroscopy, Acad. of Sci., USSR).

Sov. Phys.-Tech. Phys. (USA), vol.27, no.11, p.1402-3 (Nov. 1982). Translation of: *Zh. Tekh. Fiz. (USSR)*, vol.52, no.11, p.2283-4 (Nov. 1982). [received: May 1983]

The anodes in the author's low-inductance vacuum spark setup ($V_0=16 \text{ kV}$, $C_0=10 \text{ μF}$, $I_m=200 \text{ kA}$) consisted of pure titanium or of the alloys 50% Ti+50% Mo, Nb, or 80% Ti+20% Mo, Nb. The plasma parameters in the micropinch regions were found from resonance line spectra of helium-like ions and their satellites. The X-ray spectra were recorded using a focusing quartz spectrograph ($2d=6.67 \text{ Å}$) with spectral resolution $7 \times 10^{-4} \text{ Å}$. The author recorded Ti XX-XXI spectra for different plasma compositions under identical exposure conditions (100 discharges were used for each spectrum). The findings indicate that the electron temperature and plasma density in a low-inductance vacuum spark micropinch can both be increased by adding heavy elements. (9 refs.)

Doppler-free laser spectroscopy measurements on a Ne discharge for determination of ^{22}Ne - ^{20}Ne isotope shifts See Entry 75349

Breakdown of dynamic equilibrium between the symmetric and deformation mode levels in CO_2 caused by excitation in an electrical discharge See Entry 75453

Self-focusing of light in a laser plasma See Entry 75758

Dielectric strength of gas mixtures comprising SF_6 , CO , C_2F_8 and SF_6 , N_2 , C_2F_8 See Entry 76153

Model of Burgers turbulence for turbulent ionization waves See Entry 76190

Self-focusing of laser beam crossing a laser plasma See Entry 76202

On the analytic description of the process of electric-discharge sintering of metal powders See Entry 77594

60.00 CONDENSED MATTER: STRUCTURE, THERMAL AND MECHANICAL PROPERTIES

61.00 STRUCTURE OF LIQUIDS AND SOLIDS; CRYSTALLOGRAPHY

(see also 68.20 Solid surface structure, 71. Electron states)

76232 Anisotropic scaling of three-dimensional intensity data. Z.Shakked (Dept. of Structural Chem., Weizmann Inst. of Sci., Rehovot, Israel).

Acta Crystallogr. Sect. A (Denmark), vol.A39, pt.3, p.278-9 (1 May 1983).

Three-dimensional diffractometer data collected from single crystals of large and anisotropic mosaic spread were shown to suffer from severe systematic errors. The application of anisotropic scaling of the structure factors in the refinement process proved to be very useful in correcting these errors, yielding more accurate parameters, comparable to those obtained from high-quality crystals. (7 refs.)

76233 A technique for the calculation of multislice transmission functions for crystals with large (or infinite) repeat distances in the beam direction. A.R.Wilson (Electron Microscope Unit, Univ. of Sydney, Sydney, NSW, Australia).

Acta Crystallogr. Sect. A (Denmark), vol.A39, pt.3, p.282-6 (1 May 1983).

A partially analytic technique for the calculation of electron transmission functions used in multislice calculations is developed. This development utilizes the fact that atomic scattering amplitudes are generally available as fitting parameters to four Gaussians. The result is especially applicable to calculations with a large or infinite repeat distance in the incident-beam direction and initial test calculations give a time saving of a factor of four. Sample results are given for the calculation of images from an inclined stacking fault in gold. (11 refs.)

76234 Secondary extinction factor for spherical crystals. T.Kawamura, N.Kato (Dept. of Crystalline Materials Sci., Nagoya Univ., Nagoya, Japan).

Acta Crystallogr. Sect. A (Denmark), vol.A39, pt.3, p.305-10 (1 May 1983).

The extinction factor η was numerically calculated for spherical crystals based on the new statistical dynamical theory [Kato (1976)]. The optical paths in the Bragg case and other geometrical cases such as the Laue-Bragg-Laue are properly treated, so that the accuracy is estimated to be 0.1% for $\mu_0 R \leq 3.0$, $\sigma R \leq 2.0$ and $\theta_B \leq 30^\circ$ (μ_0 absorption coefficient, σ is the coupling constant of the energy transfer equations, θ_B the Bragg angle). Based on these calculations a universal fitting function $\eta(\mu_0 R, \sigma R, \theta_B)$ is proposed in the above-mentioned domains. The accuracy is better than 0.4% if η is larger than 10%. The difference between the present and the conventional theories is significant if the extinction exceeds 20%. (9 refs.)

76235 Absorption and secondary extinction. F.R.Thornley (Dept. of Appl. Phys., Univ. of Strathclyde, Glasgow, Scotland).

Acta Crystallogr. Sect. A (Denmark), vol.A39, pt.3, p.326-32 (1 May 1983).

A comparison is made of the treatment of absorption in the theories of secondary extinction by Werner (1974) and by Becker & Coppens (1974). The Werner approach treats absorption and extinction together, whereas Becker & Coppens assume a prior correction for absorption, and make an approximate allowance for the effect of absorption on the extinction by modifying the parameter representing the effective crystal dimension. By consideration of the form of the corrections for a specially simple crystal shape, it is shown that the Becker & Coppens method predicts slightly greater extinction than does the unified treatment of Werner. However, the difference is small, and likely to be unimportant in practice. The Werner solution of the Hamilton-Zachariasen transfer equations is exact, but not easy to use. The Becker & Coppens results are approximate, but they are presented in a form convenient for computation. (12 refs.)

76236 Crystallographic applications of the elementary divisor theorem. M.A.Fortes (Dept. de Metalurgia, Univ. Tecnica de Lisboa, Lisboa, Portugal).

Acta Crystallogr. Sect. A (Denmark), vol.A39, pt.3, p.348-50 (1 May 1983).

A crystallographic interpretation of the elementary divisor theorem applied to square integral matrices is presented. The concept of a least multiplier of a

rational square matrix is introduced and its properties are derived from the theorem. These topics are relevant in the formulation of a general theory of coincidence-site lattices. (3 refs.)

76237 A test of a robust/resistant refinement procedure on synthetic data sets. E.Prince (Nat. Measurement Lab., NBS, Washington, DC, USA), W.L.Nicholson.

Acta Crystallogr. Sect. A (Denmark), vol.A39, pt.3, p.407-10 (1 May 1983). The conventional crystallographic least-squares procedure has been compared with a robust/resistant modification in which the weight of each reflection is multiplied by a function of the ratio of its residual to a resistant measure of the width of the residual distribution on the previous cycle. Three synthetic data sets were created by adding random errors, according to various probability distributions, to the calculated structure factors for a known crystal structure. A set with a Gaussian error distribution was refined with two sets of weights: one assigned correctly in proportion to the reciprocals of the variances of the data points, the other using unit weights throughout. The second error distribution was Gaussian contaminated by 10% drawn from another Gaussian distribution with its variance nine times greater. The third distribution was a long-tailed distribution derived by dividing a random variable with a Gaussian distribution by an independent random variable with a uniform distribution. Each of the first three cases was refined to convergence using both conventional and robust/resistant procedures, with the modified procedure leading to a result at least as close to the known structure as the conventional procedure. In the fourth case, the conventional procedure gave a poor fit, but the robust/resistant procedure converged to a reasonable approximation to the correct structure. (9 refs.)

76238 A simple method to cut a single crystal in any desired direction. C.Campos, L.P.Cardoso, S.Caticha-Ellis (Crystallographic Lab., Inst. de Física, UNICAMP, Sao Paulo, Brazil).

J. Appl. Crystallogr. (Denmark), vol.16, pt.3, p.360 (1 June 1983). A simple and efficient method to cut a single crystal of any shape along any desired crystallographic direction with a disk diamond saw without angular adjustments has been developed. The basic idea of the method is to align the crystal accurately and to transfer it to a saw without the goniometer head whose grip would not stand the cutting pressure of the saw. As in this method of alignment the crystal can be rotated through 360° around the normal to the reflecting plane and independently around the ω axis, it is easy to align it to be cut along any prescribed non-crystallographic direction. (2 refs.)

61.10 X-RAY DETERMINATION OF STRUCTURES

(see also 61.80 Radiation damage and other irradiation effects; for specific determinations, see 61.55 to 61.80)

76239 Patterson derivation of structure invariants: a numerical test. S.Bruckner, G.Allegre (Dipartimento di Chimica, Politecnico di Milano, Milano, Italy).

Acta Crystallogr. Sect. A (Denmark), vol.A39, pt.3, p.273-7 (1 May 1983). A numerical test is carried out on the theory proposed by one of the authors [Allegre (1979)], which derives three-phase invariants from the Patterson function. The method is checked with two structures already solved (P1 space group). For the strong Sayre triples the calculated cosine invariants are generally positive; the negative invariants arise from relatively minor features of the Patterson background, and so are more difficult to obtain. With a suitable choice both of the error standard deviation and of the degree of sharpening of the Patterson function, the average value of the calculated cosine invariants within small subsets of Sayre triples is reasonably close to +1, while that of the negative invariants is either smaller and positive or slight negative. The agreement between the test calculations and the results obtained after structural refinement is much improved if the calculated amplitudes and an extended limiting sphere are used instead of the experimental data. (12 refs.)

61.10D Theories of diffraction and scattering

76240 Dynamical X-ray propagation: a theoretical approach to the creation of new wave fields. F.Balibar (Lab. de Mineralogie-Cristallographie, Univ. Pierre et Marie Curie, Paris, France), F.N.Chukhovskii, C.Malgrange.

Acta Crystallogr. Sect. A (Denmark), vol.A39, pt.3, p.387-99 (1 May 1983). Although it is commonly invoked, the phenomenon of 'creation of new wave fields', which is responsible for some of the features visible on topographic images, has never been really explained in theoretical terms. This is done here in the case of a crystal deformed by a uniform strain gradient. The appropriate Green function is expanded in reciprocal space as a wave packet of non-plane waves, each component corresponding to a single value of the deviation parameter at the entrance surface. It is then shown that each component of this wave packet is made up of four parts, two of which can be identified as 'normal' wave fields (i.e. those predicted by the Eikonal theory); the two others are the so-called 'created wave fields'; it is shown that they correspond to interbranch scattering from one branch of the dispersion surface to the other and give rise to two extra beams. These created wave fields extract a fraction $e^{-2\pi|\nu|}$ out of the normal energy flow ($|\nu|$ being inversely proportional to the strain gradient), in full agreement with previous computer experiments. (21 refs.)

76241 On the X-ray-reflectivity of elastically bent perfect crystals. Z.H.Kalman (Racah Inst. of Phys., Hebrew Univ., Jerusalem, Israel), S.Weissmann.

J. Appl. Crystallogr. (Denmark), vol.16, pt.3, p.295-303 (1 June 1983). The integrated X-ray reflectivity of elastically bent, but otherwise perfect, crystals are calculated for Laue-type reflections covering the entire curvature range. Anomalous transmission and elastic anisotropy are taken into account, and it is shown that both these effects affect appreciably the reflected intensities for both weakly and strongly bent crystals. The validity of the reflectivity vs. curvature relation thus obtained is experimentally confirmed for a number of reflections from silicon crystals. The implications of the experimental results to brittle fracture are discussed. (13 refs.)

76242 Determination of lattice parameters of non-cubic systems from pairs of X-ray diffraction lines. Guo Changlin, Ma Litai (Shanghai Inst. of Ceramics, Acad. Sinica, Shanghai, China).

Kexue Tongbao (Foreign Lang. Ed.) (China), vol.28, no.3, p.346-51 (March 1983). To calculate the lattice parameters by measuring the difference of angles δ_{ij} between two diffraction lines of polycrystalline materials has many advantages. Comparatively speaking, it is rather simple and convenient technically to measure the difference of angles or the relative distance between two diffraction lines. Moreover, the precision requirement is not high for the X-ray apparatus and the measuring device. So it is easy to obtain accurate results. Popovic (1971) and Halliwell (1972) suggested a method for precise

determination of lattice parameters from pairs of X-ray diffraction lines. But it is applicable only to the simplest cubic system. In this paper, the equations of the pair-method applicable to all crystal systems regardless of their complexity have been derived. A procedure for measuring lattice parameters by processing is also provided. In addition, some practical examples are given. (6 refs.)

76243 Analysis of the inclination method for the investigation of Pendellosing interference of neutrons and X-rays. N.E.Belova (Inst. fur Atomenergie 'I.V. Kurchatov', Moscow, USSR), F.Eichhorn, V.A.Somenkov, K.Utemisov, S.Sh.Shilshtein.

Phys. Status Solidi a (Germany), vol.76, no.1, p.257-65 (16 March 1983). In German.

Pendellosing interferences in a wide range of crystal thicknesses and extinction lengths can be measured by the inclination method. The positions of the extrema of intensity coincide well with the calculated ones but the observed contrast of the oscillations is considerably weaker than the theoretical one. A mathematical model is given, taking into account the influence of several factors which characterize as well the incident radiation as the crystal examined. From this follows, that the inclination method is insensitive to many disturbing factors, and therefore it can be used for metrological purposes. (10 refs.)

76244 On the theory of X-ray diffraction in a perfect crystal with distorted surface layer. Yu.N.Belyaev, A.V.Kolpakov (Dept. of Phys., Moscow State Univ., Moscow, USSR).

Phys. Status Solidi a (Germany), vol.76, no.2, p.641-6 (16 April 1983). X-ray diffraction in a perfect crystal with distorted surface layer is considered on the basis of the recurrence relations for amplitude reflection and transmission coefficients of X-rays in a multilayer crystal. It is shown that such parameters of a distorted layer as its thickness and change in the interplanar spacing can be determined directly from diffraction curves of different orders. (15 refs.)

76245 X-ray diffraction by mixed-layer structures with a random distribution of stacking faults. B.A.Sakharov, A.S.Naumov, V.A.Drits (Geological Inst., Acad. of Sci., Moscow, USSR).

Sov. Phys.-Dokl. (USA), vol.27, no.7, p.523-5 (July 1982). Translation of: *Dokl. Akad. Nauk SSSR*, vol.265, no.1-3, p.339-43 (July 1982). [received: April 1983]

The authors generalize the mathematical formalism for the general case of diffraction from model layered systems which contain, at the same time, both layers of different types and different types of stacking faults, whose distribution in the bulk of the crystal can be characterized by a different degree of order-disorder and is described by a particular choice of probability factors. (8 refs.)

76246 Intensity of X-rays scattered by layered structures with short-range order factors $S \geq 1$, $G \geq 1$. B.A.Sakharov, A.S.Naumov, V.A.Drits (Geology Inst., Acad. of Sci., Moscow, USSR).

Sov. Phys.-Dokl. (USA), vol.27, no.8, p.583-4 (Aug. 1982). Translation of: *Dokl. Akad. Nauk SSSR*, vol.265, no.4-6, p.871-4 (Aug. 1982). [received: May 1983]

The goal of the work reported by the authors was to generalize the matrix method of calculating the intensity of X-ray scattering for layered structures containing at the same time layers of different types and stacking faults whose distribution in the bulk of the crystal is specified with the aid of arbitrary values of S and G. (4 refs.)

61.10F Experimental techniques

(inc. apparatus, techniques and calculation methods for analyzing experimental results; see also 07.85 X-ray, gamma-ray instruments and techniques)

76247 Recovery of concentration spectra of binary solids from diffraction profiles by means of band matrices. P.Schattschneider, A.Wagendristel (Inst. für Angewandte und Tech. Phys., Tech. Univ. Vienna, Vienna, Austria).

Appl. Phys. A (Germany), vol.A31, no.2, p.81-6 (June 1983). A method for the retrieval of concentration spectra of crystalline mixtures from X-ray diffraction profiles is described. Both spectra are associated with an integral equation which can be simplified to yield a set of linear equations. Solutions are readily obtained by triangular decomposition since the equations are typically described by band matrices. The method has been tested with simulated diffraction profiles to allow for a variety of options concerning the concentration spectra. The procedure is well suited for binary alloys containing crystals of different structure and lattice parameters. The time consumption of the calculations is significantly reduced as compared to hitherto available methods. (16 refs.)

76248 The short-range structure of Ti and Zr BCC solid solutions containing the ω phase. III. Extension of the diffraction theory to partially transformed systems. B.Borie, H.L.Yakel (Metals & Ceramics Div., Oak Ridge Nat. Lab., Oak Ridge, TN, USA).

Acta Crystallogr. Sect. A (Denmark), vol.A39, pt.3, p.287-97 (1 May 1983). A refinement of earlier models used to compute intensity distributions for the diffuse ω phase is described. The model includes both faulted ω regions and untransformed BCC regions. The diffuse intensity generated by this model is compared with experiment. A result of this calculation is that, unlike its predecessors, it causes the observed diffuse maxima under the sharp fundamental Bragg reflections. The model is shown to be compatible with measurements of the integrated intensities of the fundamental reflections. A correction to the single-variant intensity calculation to account for interference effects among the variants is displayed. The result is compared with those of other structural models for the diffuse ω phase, and the implications of its details are discussed. (11 refs.)

76249 Strengthened translation functions. An automated method for the positioning of a correctly oriented fragment by translation functions in DIRDIF Fourier space. H.M.Doesburg, P.T.Beurskens (Crystallography Lab., Univ. of Nijmegen, Nijmegen, Netherlands).

Acta Crystallogr. Sect. A (Denmark), vol.A39, pt.3, p.368-76 (1 May 1983). Translation functions are used to determine the position of a correctly oriented molecular fragment. Usually, translation functions are defined for the Patterson space. A new translation function is presented, which is defined as a convolution in electron-density space, and expressed as a Fourier synthesis. After expansion of the reflection data to space group P1, coefficients for the synthesis are obtained by direct methods on difference structure factors (the DIRDIF procedures). From the position of the maximum in the translation function, the position of the known fragment relative to symmetry elements can be obtained. The new translation function provides a fast and reliable method for the positioning of a correctly oriented fragment, if the fragment constitutes at least about 10% of the total scattering power of the primitive unit cell. The procedure has been automated in the computer program

TRADIR. Examples of applications on known and unknown structures are given. (38 refs.)

76250 Generalized relations between *d*-orbital occupancies of transition-metal atoms and electron-density multipole population parameters from X-ray diffraction data. A.Holladay, P.Leung, P.Coppens (Dept. of Chem., State Univ. of New York, Buffalo, NY, USA).

Acta Crystallogr. Sect. A (Denmark), vol.16, pt.3, p.377-87 (1 May 1983). Generalized relations relating multipole population parameters to *d*-orbital occupancies of transition-metal atoms are presented. The relations are cast in the form of a 15×15 matrix which reduces to smaller size for site symmetries higher than 1. The matrix takes into account differences in normalization of density functions and atomic orbitals. The expressions are applied to diffraction data on $\text{Cr}(\text{CO})_6$, $\text{Mn}_2(\text{CO})_{10}$, $\text{Co}_2(\text{CO})_8$, $\text{Co}_3(\text{CO})_9\text{CH}_3$, $\text{Co}(\text{NH}_3)_6\text{Cr}(\text{CN})_6$ and $\text{Co}(\text{NH}_3)_6\text{Co}(\text{CN})_6$. In all cases crystal-field destabilized orbitals are depopulated relative to stabilized orbitals. Results are in almost quantitative agreement with theoretical populations; small remaining discrepancies are to be analyzed further for their possible significance. (29 refs.)

76251 Certification of Si powder diffraction standard reference material 640a. C.R.Hubbard (Center for Materials Sci., NBS, Washington, DC, USA).

J. Appl. Crystallogr. (Denmark), vol.16, pt.3, p.285-8 (1 June 1983). A new lot of high-purity silicon powder with mean crystallite size of about 6 μm has been certified as Standard Reference Material 640a. This SRM can be used as both an external and an internal 2θ calibration standard. The lattice parameter, uncorrected for refraction, is $a = 5.430825(11)$ for $\lambda(\text{Cu K}\alpha_1) = 1.5405981 \text{ \AA}$ at 298.1K. (13 refs.)

76252 Rational functions as profile models in powder diffraction. N.P.Pyrros (JCPDS-Internat. Center for Diffraction Data, NBS, Washington, DC, USA), C.R.Hubbard.

J. Appl. Crystallogr. (Denmark), vol.16, pt.3, p.289-94 (1 June 1983). Rational functions, the ratio of two polynomials, are shown to be good approximations to powder diffraction profiles. These functions are generalizations of the Lorentzian, the modified Lorentzian, and the profile model of Parrish (Parrish, Huang and Ayers (1976). *Trans. Am. Crystallogr. Assoc.* 12, 55-73). The simplest of these functions is of the form $f(x) = 1/(1 + A_1x^2 + A_2x^4)$ with constants A_1 and A_2 that describe the shape of the peak, $x = 2\theta - 2\theta_0$, and $2\theta_0$ the position of the peak maximum. This function approximates very well Pearson VII distributions with exponents between 1 and 3. An asymmetric profile model with different A_1 , A_2 parameters for the two halves of the peaks was fitted to silicon X-ray powder diffraction profiles and gave unweighted agreement factors from $R_2 = 0.02$ to 0.04 for peaks varying from 28 to $137^\circ 2\theta$. (12 refs.)

76253 On-line Fourier analysis of the shapes of X-ray diffraction peaks. W.H.Schlossberg (Bendix Corp., Kansas City, MO, USA), J.B.Cohen.

J. Appl. Crystallogr. (Denmark), vol.16, pt.3, p.304-8 (1 June 1983). A technique for on-line data collection and Fourier analysis of diffraction profiles is described to obtain information on particle size and microstrain from multiple orders of a reflection or from a single peak. Equations are given for errors in these quantities due to counting statistics. Their use in determining these parameters to operator-specified limits reduces the usual time required for data collection. (15 refs.)

76254 The determination of crystallite-size and lattice-strain parameters in conjunction with the profile-refinement method for the determination of crystal structures. Th.H.De Keijser, E.J.Mitteemeijer, H.C.F.Rozendaal (Lab. of Metall., Delft Univ. of Technol., Delft, Netherlands).

J. Appl. Crystallogr. (Denmark), vol.16, pt.3, p.309-16 (1 June 1983). It is shown that the current status of the least-squares profile-refinement method, for the determination of crystal structures from X-ray and neutron powder diagrams, allows the simultaneous determination of crystallite-size and lattice-strain parameters. As profile-shape functions the Voigt, pseudo-Voigt and Pearson VII functions are considered. Formulae are obtained enabling structure refinement and size-strain analysis in the same computer run. (35 refs.)

76255 Residual stresses in cubic materials with orthorhombic or monoclinic specimen symmetry: influence of texture on ψ splitting and non-linear behaviour. C.M.Brakman (Lab. of Metall., Delft Univ. of Technol., Delft, Netherlands).

J. Appl. Crystallogr. (Denmark), vol.16, pt.3, p.325-40 (1 June 1983). A quantitative formulation is given of the X-ray diffraction determination of (elastic) lattice deformation in a direction determined by two angles ψ and ϕ with respect to the specimen frame: the so-called $\sin^2\psi$ method giving full credit now to crystallographic texture. In most cases of practical X-ray stress analysis (residual) stresses are evaluated by the traditional $\sin^2\psi$ method using quasi-isotropic X-ray elastic constants depending on the lattice plane $\{hkl\}$ chosen for the measurement but not on the directions ϕ and ψ . For the case of a textured specimen, however, the single-crystal elastic tensor components should be coupled to the orientation distribution function (ODF). At variance with most papers published on this subject, which describe the texture using ideal texture components, a general method is developed making full use of relevant ODF theory. It is demonstrated that for orthorhombic specimen symmetry no ψ splitting occurs in contrast with the case of monoclinic specimen symmetry. The theory developed is used to explain some experimental results published previously. All calculations use Reuss's theory of elasticity which neglects the mutual coupling of the crystallites. (46 refs.)

76256 A novel curved position-sensitive proportional counter for X-ray diffractometry. E.R.Wolfel (STOE Appl. Lab., Darmstadt, Germany).

J. Appl. Crystallogr. (Denmark), vol.16, pt.3, p.341-8 (1 June 1983). A novel position-sensitive detector (PSD) is described which has been used on the STOE focusing monochromatic-beam diffractometer. The anode wire of the PSD coincides with the focusing circle of the diffractometer and covers a range of $\Delta 2\theta = 60^\circ$. Within a few minutes, data were collected from polycrystalline transmission samples and capillaries, and with a furnace as an attachment to the diffractometer phase transitions and solid-state reactions were studied. Some of the results are discussed, the characteristics of the PSD are described and compared with conventional counters. (5 refs.)

76257 PROMETHEUS. A program system for investigation of anharmonic thermal vibrations in crystals. U.H.Zucker, E.Perenthaler, W.F.Kuhs, R.Bachmann, H.Schulz (Max-Planck-Inst. für Festkörperforschung, Stuttgart, Germany).

J. Appl. Crystallogr. (Denmark), vol.16, pt.3, p.358 (1 June 1983). PROMETHEUS is a Fortran IV program system for investigation of anharmonic thermal vibrations in crystals, using elastic X-ray or neutron data. Three different anharmonic-temperature-factor equations can be used, one of them up to sixth-order terms. The corresponding probability densities and mean effective atomic potentials can be calculated. Programs for correction of isotropic thermal diffuse scattering and of isotropic and anisotropic extinction are included. Fast averaging of symmetrically equivalent reflections combined

with extended reflection statistics is possible. Calculations of Fourier syntheses and their errors and of Patterson functions can be carried out and the corresponding contour maps can be plotted. (14 refs.)

76258 Automated fail-safe control system for independent operation of two radiation shutters on a rotating-anode X-ray source. M.T.Short, W.J.Eisler Jr., F.J.Stevens (Argonne Nat. Lab., Argonne, IL, USA).

J. Appl. Crystallogr. (Denmark), vol.16, pt.3, p.359-60 (1 June 1983). The design of certain X-ray-generating rotating-anode devices enables the use of multiple ports through which X-rays can exit for experimental use. However, use of additional ports in such devices raises radiation safety concerns, and all attempts should be made to reduce to a minimum the amount of X-ray exposure. The authors present the design of a safety system which is used with equipment which consists of an Elliott GX-20 rotating anode and two Huber precession cameras (models 200 and 206), to allow the simultaneous operation of both precession cameras with operator safety. (no refs.)

76259 A new method for determining the lattice parameters from powder patterns of orthorhombic crystals. The influence of systematic errors and its partial elimination. A.Lutts (Lab. de Metall. Phys., Univ. Catholique de Louvain, Louvain-la-Neuve, Belgium).

Z. Kristallogr. (Germany), vol.161, no.3-4, p.195-207 (1982). The author describes a new method by which it is possible to calculate easily and rapidly the three lattice parameters from the angular position of each diffracted line. Also described is a procedure whereby it is possible to eliminate partially the influence of systematic errors in the square of the axial ratios used for these parameter determinations. This method and procedure is illustrated by an actual example. (8 refs.)

Standard X-ray diffraction powder patterns. Section 19 - Data for 51 substances See Entry 76407

The correct rules for determining the sign of fault vectors in X-ray topography See Entry 76458

61.12 NEUTRON DETERMINATION OF STRUCTURES

(for specific determinations, see 61.55 to 61.80)

Research proposal for advanced diffractometer (US-Japan collaborative research in neutron scattering) See Entry 75070

Analysis of the inclination method for the investigation of Pendellosung interference of neutrons and X-rays See Entry 76243

The determination of crystallite-size and lattice-strain parameters in conjunction with the profile-refinement method for the determination of crystal structures See Entry 76254

PROMETHEUS. A program system for investigation of anharmonic thermal vibrations in crystals See Entry 76257

Peak-shape analysis for protein neutron crystallography with position-sensitive detectors See Entry 78401

61.14 ELECTRON DETERMINATION OF STRUCTURES

(for specific determinations, see 61.55 to 61.80)

61.14D Theories of diffraction and scattering

Use of an overlay-film configuration to improve contrast of low-angle electron diffraction in thin films with columnar microstructure See Entry 76799

61.14F Experimental diffraction and scattering

76260 Use of high-symmetry zone axes in electron diffraction in determining crystal point and space groups. J.W.Steeds, R.Vincent (Dept. of Phys., Univ. of Bristol, Bristol, England).

J. Appl. Crystallogr. (Denmark), vol.16, pt.3, p.317-24 (1 June 1983). A sequence of steps is given for making use of the information available on convergent-beam electron diffraction patterns from high-symmetry zone axes for crystal point- and space-group determination. (15 refs.)

The measurement of inner potential for diamond, germanium and silicon See Entry 76358

61.16 OTHER DETERMINATION OF STRUCTURES

(for specific determinations, see 61.55 to 61.80)

61.16D Electron microscopy determinations

76261 ALCHEMI: a new technique for locating atoms in small crystals. J.C.H.Spence, J.Taft (Dept. of Phys., Arizona State Univ., Tempe, AZ, USA).

J. Microsc. (GB), vol.130, pt.2, p.147-54 (May 1983). (MICRO 82: High Resolution Electron Microscopy, London, England, 12-16 July 1982).

Atom location by channelling enhanced microanalysis (ALCHEMI) is a quantitative technique for identifying the crystallographic sites, distribution and types of substitutional impurities in many crystals. The method involves no adjustable parameters, can be applied to areas as small as a few hundred angstroms and to impurity concentrations down to about 0.1 atomic per cent. It is capable of distinguishing neighbours in the periodic table. The method uses the incident electron beam orientation dependence of characteristic X-ray emission and uses an energy dispersive X-ray microanalyser fitted to a transmission electron microscope. The method does not require the specimen thickness or precise orientation to be known, and makes few assumptions about the form of the dynamical electron wavefunction, which need not be calculated or predicted. The classical problems of cation ordering in spinels, feldspars and olivine have now been studied by this method. (16 refs.)

76262 The relative accuracy of axial and non-axial methods for the measurement of lattice spacings. D.J.Hall, P.G.Self, W.M.Stobbs (Dept. of Metall. & Materials Sci., Univ. of Cambridge, Cambridge, England).

J. Microsc. (GB), vol.130, pt.2, p.215-24 (May 1983). (MICRO 82: High Resolution Electron Microscopy, London, England, 12-16 July 1982).

The various different transmission electron microscopical techniques available for the measurement of lattice spacings are discussed, and the limited situations under which lattice fringe spacing measurement is the most appropriate approach are considered. The relative accuracy of measurements on images obtained under axial and non-axial conditions is further considered, and the

generally greater accuracy of the latter technique demonstrated. Further results on the use of the method for the measurement of the carbon content of retained austenite in a dual phase steel are included. (18 refs.)

76263 Direct surface imaging in small metal particles. L.D.Marks (Cavendish Lab., Univ. of Cambridge, Cambridge, England), D.J.Smith. *Nature (GB)*, vol.303, no.5915, p.316-17 (26 May 1983). Atomic-level information about the surfaces of small metal particles has been recorded directly with a 600-kV high-resolution electron microscope. The authors have studied small polycrystalline particles of silver and gold tilted to bring their surfaces parallel to the electron beam. However, unlike previous workers using this normal reflection electron microscopy configuration, they have used conventional bright field axial imaging thereby considerably facilitating image interpretation. As well as clean, sharp surface images, morphological details of catalytic significance, such as the distribution of surface steps, particle faceting and the nature of surface reconstructions, have been obtained. Moreover, detailed computer simulations confirmed that the electron micrographs can be interpreted in terms of atomic columns and, in particular, established that some micrographs showed, for the first time in a transmission electron microscope direct atomic-scale imaging of a reconstructed metal surface. (20 refs.)

76264 Extinction contours by inelastic scattering of electrons. P.Duval, H.Peyre, J.-C.Malaurent, L.Henry (Lab. de Phys. des Solides, Univ. Paris-Sud, Orsay, France). *Philos. Mag. A (GB)*, vol.47, no.5, p.741-51 (May 1983). In French.

By shifting the objective aperture of the electron microscope from the bright-field position to the Bragg reflection dark-field position, Hashimoto (1974) observed that the extinction contour fringes split into two. He concluded that the electrons are inelastically scattered either before or after Bragg reflection. However, the experiments reported show that the splitting is due to the sample parasitic layers. These results can be interpreted using a divergent illumination model of the scattered beam. (5 refs.)

Recent improvements to the Cambridge University 600 kV high resolution electron microscope See Entry 74561

Morphological SEM picture processing See Entry 74563

A high-resolution electron microscopic study of defects in sodium β'' -alumina See Entry 76414

HREM and STEM of defects in multiply-twinned particles See Entry 76456

Surface crystallography of thin films by electron diffraction in the STEM See Entry 76760

High resolution imaging of the interfacial region in metal-insulator-semiconductor and Schottky diodes See Entry 76798

Use of an overlay-film configuration to improve contrast of low-angle electron diffraction in thin films with columnar microstructure See Entry 76799

The transmission electron microscopy of 1 to 2 nm rhodium particles dispersed on γ - Al_2O_3 See Entry 76818

61.20 CLASSICAL, SEMICLASSICAL, AND QUANTUM THEORIES OF LIQUID STRUCTURE (for kinetic and transport theory, see 51.10; for electronic states, see 71.; for liquid helium, see 67.)

76265 Low density properties of a two dimensional dipolar fluid. C.G.Joslin (Dept. of Chem., MIT, Cambridge, MA, USA). *Mol. Phys. (GB)*, vol.49, no.1, p.129-49 (May 1983).

Second and third pressure and dielectric virial coefficients are calculated for a two dimensional fluid of hard discs with embedded central point dipoles. These exact results are compared with the predictions of various integral equation theories based upon the hypernetted chain (HNC) approximation. The linearized (LHNC) equation gives poor pressure virial coefficients B_2^* and C_2^* , but good results for the dielectric coefficients B_2^* and C_2^* . The quadratic (QHNC) equation gives a good approximation to B_2^* and C_2^* , even for large values of the dipole moment μ^* , but C_2^* is very poor and is of the wrong sign for $\mu^* \geq 2.5$. This failure is traced to the arbitrary neglect of rotational invariants other than J_1 , $\Delta(12)$ and $D(12)$ in the eigenfunction expansion of the pair correlation functions $h(12)$ and $c(12)$ of the fluid. The author also computes the critical point of the fluid. The critical constants are very different from those previously calculated in the mean spherical approximation (MSA). (31 refs.)

76266 The extension of pure fluid thermodynamic properties to supercritical mixtures. A comparison of current theories with computer data over a large region of states. C.Hoheisel, U.Deiters (Ruhr-Univ. Bochum, Bochum, Germany), K.Lucas.

Mol. Phys. (GB), vol.49, no.1, p.159-70 (May 1983). Current theories to extend pure fluid thermodynamic properties to supercritical mixtures have been examined by comparison with computer data. Emphasis is placed on a large variation of potential parameter ratios and density. It is found that, while the VDWI approximation is generally the best, its predictions are considerably poorer at supercritical conditions than in the normal liquid range. (20 refs.)

76267 Expansion of single-particle distribution functions with respect to effective long-range potentials. V.L.Kuz'min (Leningrad State Univ., Leningrad, USSR).

Theor. & Math. Phys. (USA), vol.53, no.1, p.988-73 (Oct. 1982). Translation of: *Theor. & Mat. Fiz. (USSR)*, vol.53, no.1, p.68-76 (Oct. 1982). For a classical system of interacting particles with charges and rigid dipole moments an expansion is constructed with respect to irreducible diagrams for the single-particle distribution function by resummation of the functional series with respect to the electrostatic part of the interaction. This expansion is a series in an effective 'dressed' potential, and in contrast to the original expansion does not contain long-range Coulomb divergences. As an illustration, the asymptotic behavior of the single-particle distribution function in the surface layer of a polar liquid is obtained on the basis of the direct selection and summation of the important diagrams. (25 refs.)

A theoretical simulation of bulk water See Entry 76268

Molecular dynamics simulation of liquid water between two walls See Entry 76269

Reference interaction site model (RISM) for the liquid structure of oxygen, chlorine and iodine See Entry 76271

Molecular dynamics studies of molten NaI. I. Quasi-elastic neutron scattering See Entry 76280

Molecular dynamics studies of molten NaI. II. Mass-, charge- and number density fluctuations See Entry 76281

Hard discs with embedded three dimensional quadrupoles See Entry 76587

A study of solid and liquid carbon tetrafluoride using the constant pressure molecular dynamics technique See Entry 76606

Viscosity of binary liquid mixtures in hard-sphere approximation See Entry 76682

Low temperature expansions for the second and third cluster integrals of a two dimensional quantum system of hard discs See Entry 76720

Interacting bosons and properties of liquid ^4He II See Entry 76721

Effect of molecular ordering in thin water films See Entry 76751

61.25 STUDIES OF SPECIFIC LIQUID STRUCTURES

(see also 61.40 Amorphous and polymeric materials)

76268 A theoretical simulation of bulk water. S.Fraga (Dept. of Chem., Univ. of Alberta, Edmonton, Alberta, Canada).

Can. J. Phys. (Canada), vol.61, no.5, p.680-2 (May 1983). A new formulation has been used in the study of a water cluster with 65 molecules. The fact that the calculated average potential energy per molecule agrees with the Monte Carlo result at 300K suggests that this method, which is fast and inexpensive, might be used to obtain estimates of such energies for other systems as well as in generating starting configurations for Monte Carlo calculation. (6 refs.)

76269 Molecular dynamics simulation of liquid water between two walls. M.Marchesi (Istituto per i Circuiti Elettronici, CNR, Genoa, Italy). *Chem. Phys. Lett. (Netherlands)*, vol.97, no.2, p.224-30 (13 May 1983).

A molecular dynamics simulation, lasting ≈ 25 ps, has been performed with 150 ST2 water molecules between two quasihard repulsive walls, at a temperature of 302K. A number of static and dynamic properties have been computed as a function of the distance from the walls, showing that water near the walls is in general more 'ordered' than in the bulk, and that this bulk water behaves like ordinary liquid ST2 water. (31 refs.)

76270 Spherical non-draining Boc-poly(α,ϵ -L-lysine) macromolecules: SAXS and viscosity studies. S.M.Aharoni, N.S.Murphy (Corporate Res. & Dev., Allied Corp., Morristown, NJ, USA).

Polym. Commun. (GB), vol.24, no.5, p.132-6 (May 1983). Homologues of t-butyloxycarbonyl blocked poly(α,ϵ -L-lysine) were studied by SAXS and viscosity measurements in DMF. It was found that under rigorously anhydrous conditions no polyelectrolyte effects exist. Macromolecular sizes obtained from both techniques showed a linear dependence on $M^{1/3}$, indicating the macromolecules to be non-draining and spherical in shape. Comparison with calculated sizes indicates the molecules in solution to contain substantial amounts of solvent within their non-draining volumes. The ratio of radius of gyration to hydrodynamic radius, and shape analysis of some SAXS data, indicate that these spherical macromolecules may be somewhat less dense on the surface than their non-draining core. The results are in general agreement with previous results obtained by other techniques. (6 refs.)

76271 Reference interaction site model (RISM) for the liquid structure of oxygen, chlorine and iodine. R.V.Gopala Rao, B.M.Satpathy (Dept. of Chem., Jadavpur Univ., Calcutta, India). *Indian J. Pure & Appl. Phys.*, vol.21, no.2, p.92-6 (Feb. 1983).

The reference interaction site model (RISM) equations have been used for fused hard spheres as well as Lennard-Jones (LJ) interaction sites fluids to obtain the site-site distribution functions and the structure function of liquid oxygen, chlorine and iodine. The use of LJ interaction sites improves the result over that of hard sphere calculations of Hsu et al. [Chem Phys (Netherlands), 14 (1976) 213] for oxygen. In chlorine a three (hard sphere interaction)-site model with an auxiliary site at the centre of the molecule works better than a two (LJ)-site model. Liquid iodine has been studied with a three-site model. In the case of oxygen, the agreement is excellent and in the other two cases the RISM theory fails to give a good account of the experimental results and the agreement is only qualitative. The intermolecular potential functions have been obtained for these liquids from the RISM structure function. (11 refs.)

76272 Structure of liquid hydrogen fluoride studied by infrared and Raman spectroscopy. B.Desbat, P.V.Huon (Lab. de Spectroscopie Infrarouge et Raman, Univ. de Bordeaux I, Talence, France).

J. Chem. Phys. (USA), vol.78, no.11, p.6377-83 (1 June 1983). Infrared and Raman spectra of hydrogen fluoride, deuterium fluoride, and their isotopic mixtures at various temperatures from 293 to 77K have been recorded and analyzed in comparison with calculated data obtained from the classical G.F. matrix method applied to hypothetical structures chosen a priori. The best fit lead to the most probable structure of HF at 293K which is a zig-zag chain with six or seven molecules having an angle of 42° with the average axis. At a lower temperature (190K), just before solidification, the chains become longer, $n=8$ with an angle $\theta \approx 35^\circ$. These structures fit well with the high dielectric constant of liquid hydrogen fluoride and lead to a calculated Kirkwood factor $g_1=3.65$ at 293K and $g_1=5.36$ at 190K which are in perfect agreement with known experimental values. (22 refs.)

76273 The HCl-HCl interaction: from quantum mechanical calculations to properties of the liquid. C.Votava, R.Ahlrichs, A.Geiger (Inst. fur Phys. Chem. und Elektrochem., Univ. Karlsruhe, Karlsruhe, Germany).

J. Chem. Phys. (USA), vol.78, no.11, p.6841-8 (1 June 1983). Analytical HCl-HCl pair potentials are derived from large quantum mechanical calculations at CEPA-(SD) level. The computed well depth for the dimer is 1.9 kcal/mol. Those pair potentials are used in molecular dynamics simulation studies at $T=297\text{K}$ and $\rho=0.8354\text{ g/cm}^3$. The results for the static (e.g. pair distribution functions) and dynamic properties are compared with experimental and other molecular dynamics results. Comparison of the results from different simulation runs allows a check on their sensitivity with respect to the pair potential employed. It turns out that the potential yielding the best fit to the computed interaction energies gives a good representation of properties of liquid HCl. However, a readjustment of this potential—in order to account for well-known deficiencies of the quantum mechanical calculations—results in a slight improvement especially in the mean potential energy and the pressure. Finally, the authors used the computed pair potential to determine the structure and association energy of $(\text{HCl})_n$ clusters with cyclic and chain structure. (29 refs.)

76274 Experimental measurements of solvation forces in nonpolar liquids. H.K.Christenson (Dept. of Appl. Math., Inst. of Advanced Studies, Australian Nat. Univ., Canberra, Australia).

J. Chem. Phys. (USA), vol.78, no.11, p.6906-13 (1 June 1983). Forces between molecularly smooth mica surfaces immersed in tetrachloromethane, benzene, and 2,2,4-trimethylpentane have been measured. In tetrachloromethane and benzene the force law is an oscillatory function of the separation between the mica surfaces, with a periodicity equal to the mean molec-

cular diameter and a measurable range of approximately ten periods, or about 5 nm. Beyond this separation, the oscillations merge into a purely attractive 'tail'. In 2,2,2-trimethylpentane the force law shows only short-range oscillatory behavior, below 2 nm; at larger separations the force is everywhere attractive. The results are compared with measurements on cyclohexane, octamethylcyclotetrasiloxane and *n*-octane, including some repeat measurements. When the distance scale is normalized by the mean periodicity of the force curve for each liquid, the results for the four fairly rigid molecules benzene, tetracloromethane, cyclohexane, and octamethylcyclotetrasiloxane are very similar; minor differences possibly being due to varying trace amounts of water in the liquids. In the above systems the force laws are oscillatory functions of the surface separation, with a periodicity roughly equal to the molecular diameter and a measurable range of about ten periods. The peak-to-peak amplitude shows an essentially exponential decay. By contrast, the existence of free intramolecular rotation in the two flexible molecules 2,2,4-trimethylpentane and *n*-octane is sufficient to reduce the solvation forces to 2 nm or less. The results indicate that the amount of liquid structuring for inert liquids depends mainly on the internal rigidity of the molecules, while the effect of molecular shape, size, and temperature is of secondary importance. (40 refs.)

76275 The structure of liquid neon: an anomaly resolved. J.G.Powles, J.L.Abasal (Phys. Labs., Univ. of Kent, Canterbury, England). *J. Phys. C (GB)*, vol.16, no.14, p.L441-4 (20 May 1983).

It is shown that the structure $g(r)$ of liquid neon can be regarded as resulting from an effective interatomic pair-potential of Lennard-Jones 12-6 form with parameters from thermodynamics, provided due account is taken of quantum corrections. Liquid neon therefore 'corresponds' with liquid argon and is not anomalous, as appeared previously to be the case. The novel and useful observation is made that the quantum corrections to $g(r)$ tend to be small for large r . (19 refs.)

76276 One-dimensional models of polymer dynamics. I. Dashpot-spring models applied to a single rotor. M.L.Mansfield (Dept. of Chem., Dartmouth Coll., Hanover, NH, USA).

J. Polym. Sci. Polym. Phys. Ed. (USA), vol.21, no.5, p.773-86 (May 1983). The proposition of Clark and Zimm (1972) that a dashpot and a spring can be used in place of a set of rotational barriers in polymer dynamics is studied. The simplest possible case is examined here, that of a single rotor. Reasons for altering the Clark-Zimm diffusion equation are presented and an alternative diffusion equation is proposed. The results of both diffusion equations for the correlation function $\langle \exp[-i\theta(t)] \exp[i\theta(t)] \rangle$ (θ is the angular position of the rotor) are compared with the correlation function for a rotor in an n -fold cosine potential. Although the two diffusion equations differ, both agree well with the n -fold cosine model for barriers above a few $k_B T$. This agreement is obtained in the absence of adjustable parameters, and motivates the application of these two diffusion equations to polymeric systems. (38 refs.)

76277 One-dimensional models of polymer dynamics. II. A dashpot-spring model. M.L.Mansfield (Dept. of Chem., Dartmouth Coll., Hanover, NH, USA).

J. Polym. Sci. Polym. Phys. Ed. (USA), vol.21, no.5, p.787-806 (May 1983). For pt.I see *ibid.*, vol.21, no.5, p.773-86 (1983). The assumption of Clark and Zimm (1972) that coupled dashpots and springs can be used to model the dynamics of polymer molecules is applied to a model different from that of Clark and Zimm. The dielectric relaxation spectrum of the model is computed in time and frequency domains. The relaxation spectrum can be fitted reasonably well by the empirical Williams-Watts (1970) and Havriliak-Negami functions (1966). The best-fit Williams-Watts and Havriliak-Negami parameters are given as functions of the parameters of the model. The model is compared with several related models found in the literature and possible interpretations are given. (17 refs.)

76278 The melt anisotropy of ultrahigh-molecular-weight polyethylene. A.E.Zachariades, J.A.Logan (IBM Res. Lab., San Jose, CA, USA).

J. Polym. Sci. Polym. Phys. Ed. (USA), vol.21, no.5, p.821-30 (May 1983). In the course of melt-flow crystallization studies with ultrahigh-molecular-weight polyethylene (UHMWPE), it was observed that the melt of UHMWPE is highly anisotropic above its equilibrium melting point and has a tendency to fibrillate. An examination of the melt anisotropy of UHMWPE by optical, thermal, and X-ray analysis indicates that the melt anisotropy persists at 345°C, i.e. the temperature at which the polymer degrades under nitrogen, and appears similar to a smectic liquid-crystalline phase. (11 refs.)

76279 X-ray diffraction analysis of molten potassium bromide. H.Ohno, K.Furukawa (Molten Materials Lab., JAERI, Ibaraki, Japan), R.Takagi, K.Igarashi, J.Mochinaga.

J. Chem. Soc. Faraday Trans. II (GB), vol.79, pt.3, p.463-71 (March 1983). The radial distribution function of molten KBr has been determined by the X-ray diffraction method and numerical values of the structure, $Q_i(Q)$, $S(Q)$ and $g(r)$ are given. (27 refs.)

76280 Molecular dynamics studies of molten NaI. I. Quasi-elastic neutron scattering. M.Dixon (Dept. of Theoretical Phys., Oxford, England).

Philos. Mag. B (GB), vol.47, no.5, p.509-30 (May 1983). The quasi-elastic neutron scattering spectrum of molten NaI has been calculated using molecular dynamics simulation. The wave-vector dependences of the coherent and incoherent partial contributions to the spectrum are reported. A comparison is made between the spectra obtained from rigid-ion and polarisable-ion model simulations. The spectra are contrasted with those obtained by neutron scattering. (22 refs.)

76281 Molecular dynamics studies of molten NaI. II. Mass-, charge- and number density fluctuations. M.Dixon (Dept. of Theoretical Phys., Oxford, England).

Philos. Mag. B (GB), vol.47, no.5, p.531-54 (May 1983). For pt.I see *ibid.*, vol.47, no.5, p.509 (1983). Molecular dynamics simulations of molten NaI have been performed using both rigid-ion and polarisable-ion models. The mass-, charge- and number-density autocorrelation functions have been calculated together with their frequency spectra. The liquid-state analogues of longitudinal optic and acoustic phonons are identified at longer wavelengths. The acoustic modes are weak and broad. The major differences between the rigid-ion model and the polarisable-ion model are that: (1) there is a substantial difference between their static charge-charge structure factors, $S_{QQ}(q)$, and (2) the normalised charge-charge dynamical structure spectra at longer wavelengths differ in intensity and frequency of the optic mode. The mode for the polarisable-ion model occurs at a lower frequency and is less well resolved. (29 refs.)

The structural analysis of Li₂O.2SiO₂ glass and melt by Raman spectroscopy ..

.....See Entry 76311

Ultrasonic studies of N-formylmorpholine + water mixtures ..

.....See Entry 76570

A study of solid and liquid carbon tetrafluoride using the constant pressure molecular dynamics technique ..

.....See Entry 76606

Modified Gruneisen and Anderson-Gruneisen relations for quasi-spherical molecular liquids ..

.....See Entry 76654

Spectra and structure of asymmetric carboxylic acid dimers in solution ..

.....See Entry 77387

Study of structure of copolymers of ethylene tetrasulfide and vinyl cyanide ..

.....See Entry 77390

Raman spectroscopic studies of the structure of electrolytes used in the Li/SOCl₂ battery ..

.....See Entry 77978

61.25M Liquid metals

76282 Structure and thermodynamics of liquid Bi. R.N.Joarder, S.Palchoudhury, R.V.Gopala Rao (Faculty of Sci., Jadavpur Univ., Calcutta, India).

Indian J. Pure & Appl. Phys., vol.21, no.3, p.151-4 (March 1983).

A thermodynamic perturbation method based on the Gibbs-Bogoliubov inequality has been applied to a nonsimple liquid metal, namely Bi through the Heine-Abarenkov-Animalu pseudopotential and this procedure yields the possibility of two packing densities. A static structure-factor calculation with two packings yields the shoulder characteristics quite reasonably. Calculations of the close packing of the liquid yield satisfactory results. (20 refs.)

76283 Excess enthalpies of liquid (copper+tellurium) alloys. R.Blachnik, B.Gather (Anorganische Chem., FB Chem. Biologie, Univ.-GH-Siegen, Siegen, Germany).

J. Chem. Thermodyn. (GB), vol.15, no.4, p.401-2 (April 1983).

Reports measurements of the excess molar enthalpies H_m^E of liquid copper and tellurium alloy mixtures. The thermal effects measured were those of consecutive additions of small amounts of solid Cu at room temperature (298K) to the calorimetric cell containing liquid tellurium at 727 and 1005K respectively. The small influence of temperature on H_m^E for $\{(1-x)\text{Cu}+x\text{Te}\}$ indicates that the chemical interactions in these melts are of mixed ionic and metallic character. (5 refs.)

76284 The structure of liquid Fe₇₅B₂₅ by neutron scattering. W.Matz (Zentralinst. fur Kernforschung, Akad. der Wissenschaften, Rossendorf, Germany), B.Kunsch, E.Wieser.

Phys. Status Solidi a (Germany), vol.76, no.1, p.K17-20 (16 March 1983).

The authors report the measurement of the structure factor $S(Q)$ of liquid Fe₇₅B₂₅ at temperatures of 1600, 1700, and 1800K by neutron diffraction. In order to avoid the strong neutron absorption by natural boron, boron of 97.2% purity enriched to 99.2% ¹⁰B was used. The neutron diffraction pattern were recorded from $Q=2.5 \text{ nm}^{-1}$ to $Q=89 \text{ nm}^{-1}$ using a neutron wavelength of $\lambda=0.1038 \text{ nm}$. For low values of Q they included the magnetic scattering from spin fluctuations into the paramagnetic cross section. (11 refs.)

²³Na Knight shift of liquid Na-Sn alloys ..

.....See Entry 77276

61.30 LIQUID CRYSTALS

(see also 64.70M Transitions in liquid crystals)

76285 Optical microstructure of oriented liquid crystal polymers. C.Viney, G.R.Mitchell, A.H.Windle (Dept. of Metall. & Materials Sci., Univ. of Cambridge, Cambridge, England).

Polym. Commun. (GB), vol.24, no.5, p.145-6 (May 1983).

Optical microstructures of two thermotropic liquid copolyester samples are presented. Although the samples exhibit pronounced molecular orientation as measured by X-ray diffraction, the optical patterns show no preferred orientation when viewed using crossed polars. These apparently contradictory results suggest that the optical indicatrix is either not uniaxial or that its unique axis is not aligned with the local chain axis, or both. In either case, the structural implication is that there is rotational correlation about the long axes of adjacent molecules. (15 refs.)

76286 Measurement of the surface-tension anisotropy of a nematic liquid crystal. S.R.Nersisyan, V.O.Oganesyan, V.B.Pakhalov, N.V.Tabiryan, Yu.S.Chilingaryan (Erevan State Univ., Erevan, USSR).

JETP Lett. (USA), vol.36, no.8, p.358-61 (20 Oct. 1982). Translation of: *JETP* in Zh. Eksp. & Teor. Fiz. (USSR), vol.36, no.8, p.292-5 (20 Oct. 1982). [received: June 1983]

The surface tension anisotropy factor of the nematic liquid crystal MBBA σ_a is determined experimentally. The magnitude of σ_a , which is measured for the first time, is $\sigma_a \approx 10^{-3} \text{ erg/cm}^2$. (8 refs.)

76287 The mean spherical model (and other approximations) for nematics. T.J.Sluckin (Faculty of Math. Studies, Univ. of Southampton, Southampton, England).

Mol. Phys. (GB), vol.49, no.1, p.221-31 (May 1983).

Kloczkowski and Stecki (1982) have recently found an exact mean spherical approximation (MSA) solution to a simple liquid crystal model. The dependence of the nematic-isotropic transition temperature on potential range and molecular packing fraction is examined using MSA and some other alternative tractable approximations for this model. Some comparison is made with computer simulation results. All the simple approximation schemes, all of which have been used in serious liquid crystal calculations, are heavily deficient. (13 refs.)

76288 Surface anchoring of liquid crystal molecules on various substrates. J.A.Castellano (Stanford Resources Inc., San Jose, CA, USA).

Mol. Cryst. & Liq. Cryst. (GB), vol.94, no.1-2, p.33-41 (1983).

Ever since Mauguin (1911) described the fabrication of liquid crystal cells by rubbing glass plates with paper to obtain uniform homogeneous alignment, scientists have been attempting to study and understand the mechanism of anchoring and the subsequent alignment of these materials on various substrates. More than 35 different methods for creating surface alignment have been reported using both organic and inorganic films as well as various mechanical treatments. Many of these methods are reviewed and categorized. The mechanism of surface anchoring involves not one but several mechanisms. The nature of the surface material, the liquid crystal structure, and the past history of the surface all play major roles in determining the mechanism for a specific technique. (23 refs.)

76289 2,3-dicyanohydroquinone derivative liquid crystals having strong negative dielectric anisotropy. T.Inukai, K.Furukawa, H.Inoue, K.Terashima (Liquid Crystals Div., Chisso Corp., Yokohama, Japan).

Mol. Cryst. & Liq. Cryst. (GB), vol.94, no.1-2, p.109-18 (1983).

Three groups of liquid crystalline derivatives of 2,3-dicyanohydroquinone were synthesized. The dielectric anisotropy values, $\Delta\epsilon$, for these compounds were estimated to be around -20 by extrapolation. Some basic evaluations of these compounds, in view of their application as component materials for the practically usable nematic mixtures of highly negative $\Delta\epsilon$, were made using their solution in a substituted phenyl cyclohexanecarboxylate nematic mixture; $\Delta\epsilon$, viscosity, dichroic ratio of dyes, driving voltages and response times are

described in relation to their molecular length. By use of several selected members of these compounds, one can make practical nematic compositions having $\Delta\epsilon$ of -5 and viscosity of 40 cp at 20° . The guest-host display device can be driven with 3 volts at acceptable response times of $100\sim 200$ milliseconds at room temperatures, to give positive color contrast, i.e. colored in on-state. (7 refs.)

76290 Low viscous compounds of highly nematic character. R.Eidenschink (E. Merck, Zentrallab. fur Industriechemikalien, Darmstadt, Germany). *Mol. Cryst. & Liq. Cryst. (GB)*, vol.94, no.1-2, p.119-25 (1983). Mixtures of broad nematic temperature ranges that permit acceptably short switching times of electro-optical displays at -40°C can be composed of compounds of relatively low polarity and high transition temperatures from the nematic to the isotropic state (T_N). Structures combining 1,4-phenylene and trans-1,4-cyclohexylene rings are particularly suited for this purpose. (30 refs.)

76291 Total internal reflection—a method for determining of LC anchoring and orientation on various substrates. A.I.Derzhanski, H.P.Hinov (Inst. of Solid State Phys., Sofia, Bulgaria), D.Riviere. *Mol. Cryst. & Liq. Cryst. (GB)*, vol.94, no.1-2, p.127-38 (1983). The general problems being important for the determination of the liquid crystal surface anchoring and liquid crystal surface orientation of nematics, large-pitch cholesterics, and some smectics by means of attenuated total internal reflection (ATR) of a visible light beam have been outlined. The advantages and disadvantages of ATR for measuring of the surface energy have been discussed and compared with those of other well-known methods. The possible influence of additional orienting and/or conducting layers on the reflectivity and polarization of the incident wave are also briefly discussed. (88 refs.)

76292 New liquid crystal materials; physical properties and performance in displays for automobile, high information density and guest-host applications. M.Schadt, M.Petrzlik, P.R.Gerber, A.Villiger, G.Tricks (Central Res. Units, F. Hoffmann-La Roche & Co. Ltd., Basel, Switzerland). *Mol. Cryst. & Liq. Cryst. (GB)*, vol.94, no.1-2, p.139-53 (1983). Four novel liquid crystal classes are presented, namely bi-, tri-, and tetracyclic ethanes, pyridazines, and tetracyclic chloro-dieters. Each class exhibits distinct physical characteristics, such as low viscosities $\eta\sim 12$ cP, low elastic ratios $k_{33}/k_{11}\sim 1$, large mesomorphic ranges $\sim 40^\circ\text{C}\dots 250^\circ\text{C}$, large negative dielectric anisotropies $\Delta\epsilon\sim -9$ and/or low dielectric relaxation frequencies $f_c\sim 1$ kHz. It is shown that the dielectric Debye relaxation time τ characterizing the hindered rotation of polar nematic molecules around their short axes is much more affected by molecular structural factors than by their rotational viscosity η . The material and electro-optical properties of mixtures for twisted nematic and guest-host LCDs comprising the new compounds are presented. The mixtures cover a wide range of applications such as high contrast, fast and multiplexable automotive TN-LCDs; positive and negative contrast guest-host LCDs; high-information density matrix, and dual-frequency addressable LCDs. (20 refs.)

76293 Relation between TN-cell response time and transition temperatures of liquid crystal materials. A.Mukoh, H.Abe, T.Kitamura, N.Kamezawa, M.Satoh (Hitachi Res. Lab., Hitachi Ltd., Ibaraki, Japan). *Mol. Cryst. & Liq. Cryst. (GB)*, vol.94, no.1-2, p.155-65 (1983). The relation between the transition temperature of typical nematic liquid crystal mixtures and the dynamic properties of twisted nematic (TN) cells are presented. The extrapolated response time at the nematic-isotropic transition temperature is of use as a relative response time in the comparison of liquid crystal materials with each other. The glass transition temperature of liquid crystal mixtures is one of the best indicators of the dynamic properties of TN-cells. The linear relation between the reciprocal ΔT , and the logarithm of the reciprocal response time led the authors to believe that they could improve the response time of TN-cells by producing liquid crystal materials with lower T_g s. They assumed that the lower limit for the response time of TN-cells at 25°C is about $10\sim 20$ ms from the above relation. (10 refs.)

76294 Thermal behavior of two polar A-smectics. D.Guillon, G.Poeti, A.Skoulies (Centre de Recherches sur les Macromolécules, Strasbourg, France). *Mol. Cryst. & Liq. Cryst. Lett. (GB)*, vol.92, no.2, p.35-9 (1983). The experimental X-ray diffraction data reported recently in the literature for a cyano and a nitro smectogen are used to calculate some parameters of the smectic A phase, such as the molecular area of the paraffin tails and the degree of head to head association of the molecules. It is shown that the presence of a lateral methyl group on the aromatic cores enhances the head to head association of the molecules. It is, finally, suggested that the slight interruption observed in the temperature variation of the layer spacing could be related to a poor miscibility of the head to head and the side by side associated molecules. (6 refs.)

76295 Dynamics of a Fredericks transition in side chain nematic polymers: determination of the viscoelastic coefficients K_1 and γ_1 . C.Casagrande, M.Veyssie, C.Weill (Lab. de Phys. de la Matière Condensée, Coll. de France, Paris, France), H.Finkelmann. *Mol. Cryst. & Liq. Cryst. Lett. (GB)*, vol.92, no.2, p.49-55 (1983). Reports measurements of the splay elastic constant, K_1 , and the twist viscosity coefficient, γ_1 , of side chain mesomorphic polymers; they compare them to the values obtained for certain low molecular weight compounds, similar to the nematic moiety of the polymers. (4 refs.)

76296 Stable liquid crystals with large negative dielectric anisotropy. II. M.A.Osman, T.Huynh-ba (Brown Boveri Res. Center, Baden, Switzerland). *Mol. Cryst. & Liq. Cryst. Lett. (GB)*, vol.92, no.2, p.57-62 (1983). 2,3-Dicyano-4-n-pentyl phenol was synthesized. The mesomorphic properties of its benzoic and cyclohexane carboxylic acid esters are described. The effect of lateral substituents on the thermodynamic stability of the mesophase is discussed. The esters of this phenol are photochemically stable LCs with large negative $\Delta\epsilon$. Their clearing points are relatively high but their viscosities are expected to be also relatively high. (10 refs.)

76297 Orientational fluctuations of a lyotropic nematic liquid crystal measured by quasielastic light scattering. S.Kumar, L.J.Yu, J.D.Litster (Dept. of Phys., MIT, Cambridge, MA, USA). *Phys. Rev. Lett. (USA)*, vol.50, no.21, p.1672-5 (23 May 1983). The nematic-isotropic and the nematic-to-lamellar phase changes in the lyotropic liquid crystal formed by decylammonium chloride micelles in a water-ammonium chloride solution have been studied by light scattering. The former transition shows behavior identical to that observed in thermotropic liquid crystals. The nematic-lamellar transition appears closely similar to a thermotropic nematic-smectic-A change and the elastic constants diverge according to the analogy to superfluid helium and the three-dimensional xy model. (12 refs.)

76298 Optical method for determination of anchoring energy of tilted nematic layers. L.Komitov, A.G.Petrov (Inst. of Solid State Phys., Bulgarian Acad. of Sci., Sofia, Bulgaria). *Phys. Status Solidi a (Germany)*, vol.76, no.1, p.137-43 (16 March 1983). By measuring the surface tilt angles in a hybrid nematic layer with homogeneously tilted and reversely tilted (splayed) parts, the strength of anchoring can be obtained. The theory and some experimental demonstrations of the method are presented. For SiO_2 coating and MBBA liquid crystal, the measured anchoring energy is 4×10^{-6} J/m². (12 refs.)

76299 X-ray diffraction studies on the mesophases of n-p-cyanobenzylidene-p-octyloxy aniline in magnetic field. B.Jha, B.Bhattacharjee, S.Paul, R.Paul (Phys. Dept., North Bengal Univ., Darjeeling, India). *Phys. Status Solidi a (Germany)*, vol.76, no.2, p.461-6 (16 April 1983). X-ray diffraction is studied for n-p-cyanobenzylidene-p-octyloxy aniline in both, nematic and smectic phases ordered by a magnetic field. The orientational distribution function and the order parameters at different temperatures are calculated. From the temperature variation of the distribution function, an approximate expression for the potential of the molecular field is obtained. The layer spacings in the smectic phase and intermolecular distances at different temperatures and different magnetic fields are determined. The average intermolecular distances are found to be dependent on the magnetic field strength. (25 refs.)

76300 Microdiffraction applied to thermotropic liquid crystalline polymers. A.M.Donald (Dept. of Metall. & Materials Sci., Univ. of Cambridge, Cambridge, England). *Philos. Mag. A (GB)*, vol.47, no.5, p.L13-17 (May 1983). The usefulness of electron 'microdiffraction' techniques for studying orientation in sheared films of a thermotropic liquid crystalline polymer is demonstrated. Patterns recorded from regions ~ 150 nm in diameter exhibit much higher degrees of orientation than is apparent in conventional selected-area diffraction patterns. Local variations in the micro-orientation axis can be detected as the specimen is traversed. (8 refs.)

76301 Mean-field model for antiferroelectric smectic-A liquid crystals. L.Longa, W.H.de Jeu (Solid State Phys. Lab., Univ. of Groningen, Groningen, Netherlands). *Solid State Commun. (USA)*, vol.46, no.9, p.693-6 (June 1983). A theoretical description is proposed for recently observed antiferroelectric smectic-A phases. Order parameters are introduced that retain information on the head-tail asymmetry of the constituent molecules and minimum ingredients are given for an averaged model potential. The calculations show that for high orientational order the antiferroelectric smectic-A structure is the best compromise between dipole repulsion and dispersive attraction. The resulting phase diagrams compare favorably with the experimental situation. (9 refs.)

76302 'Nonclassical' temperature dependence of the order parameter of nematic liquid crystals. E.M.Aver'yanov, V.A.Zhukov, V.Ya.Zrnyanov, Yu.I.Ruolene, V.F.Shabanov (L.V. Kirenski Inst. of Phys., Acad. of Sci., Krasnoyarsk, USSR). *Sov. Phys.-Solid State (USA)*, vol.24, no.11, p.1861-3 (Nov. 1982). Translation of: *Fiz. Tverd. Tela (USSR)*, vol.24, no.11, p.3279-82 (Nov. 1982). [received: May 1983] Infrared polarization spectroscopy was used to determine the absolute values of the orientational order parameter s of four liquid crystals belonging to the homologous series of alkoxycyanobiphenyls. The Landau theory is used to justify the familiar empirical approximation $s=s_0(1-T/T_c)^{\beta}$ and a qualitative interpretation is given of the 'nonclassical' values of the parameters $s_0\neq 1$ and $\beta=0.18\pm 0.04$. (13 refs.)

76303 Induced cholesteric systems with negative temperature dependences of the helical pitch. N.L.Kramarenko, L.N.Lisetskii, L.G.Derkach (A.M. Gorki State Univ., Kharkov, Ukrainian SSR). *Sov. Phys.-Solid State (USA)*, vol.24, no.11, p.1863-5 (Nov. 1982). Translation of: *Fiz. Tverd. Tela (USSR)*, vol.24, no.11, p.3283-5 (Nov. 1982). [received: May 1983] It is shown that a negative temperature dependence of the helical pitch p may occur in the case of liquid-crystal systems formed by a nonsmectogenic nematic with small admixtures of cholesteryl esters. The sign and value of dp/dT are governed by the degree of anharmonicity of the rotational vibrations of molecules associated with the characteristic features of their geometric shape. (13 refs.)

76304 Translational order in smectic liquid crystals. Allowance for features of the intermolecular forces. L.N.Lisetskii. *Sov. Phys.-Solid State (USA)*, vol.24, no.11, p.1909-12 (Nov. 1982). Translation of: *Fiz. Tverd. Tela (USSR)*, vol.24, no.11, p.3361-5 (Nov. 1982). [received: May 1983] The mean molecular field approximation is used to discuss translational ordering in smectic mesophases. Qualitative features arising from the inclusion of successive terms in the Fourier expansion of the model potential are noted. The model developed can be used to describe not only the phase transition but also smectic, A-nematic transitions between different smectic mesophases, as well as translational melting of molecular crystals of mesogenic substances. (12 refs.)

76305 Second-sound soliton in a liquid crystal. I.V.Ioffe, B.I.Lembrikov. *Sov. Phys.-Solid State (USA)*, vol.24, no.11, p.1958-9 (Nov. 1982). Translation of: *Fiz. Tverd. Tela (USSR)*, vol.24, no.11, p.3446-8 (Nov. 1982). [received: May 1983] Influence of nonlinear effects during propagation of wave packets in dispersive media results in the appearance of solitons. The authors show that a second-sound soliton can be excited by a modulated electromagnetic wave propagating in a smectic A liquid crystal along a direction inclined to the layers. Such a soliton can be observed in the same way as second-sound waves. (8 refs.)

76306 Nature of the flexoelectric effect in MBBA. A.S.Vasilevskaya, A.V.Kaznacheev, A.S.Sonin. *Sov. Phys.-Solid State (USA)*, vol.24, no.12, p.2118 (Dec. 1983). Translation of: *Fiz. Tverd. Tela (USSR)*, vol.24, no.12, p.3714-15 (Dec. 1983). A comparison of the temperature dependences of the flexoelectric coefficient and of the order parameter should make it possible to determine the contribution of particular multiples to the flexoelectric polarization. The authors have investigated the temperature dependence of the flexoelectric coefficient e_2 in a nematic liquid crystal of MBBA with a negative dielectric anisotropy. (7 refs.)

76307 Orientational effects in the mesophase under short laser pulses; nonlinearity buildup. S.M.Arakelyan, O.V.Garibyan, A.S.Karayan, Yu.S.Chilligaryan (State Univ., Erevan, USSR). *Sov. Tech. Phys. Lett. (USA)*, vol.8, no.9, p.452-4 (Sept. 1982). Translation of: *Pisma v Zh. Tekh. Fiz. (USSR)*, vol.8, no.17-18, p.1051-6 (Sept. 1982). [received: May 1983] Strong orientational effects in the mesophase are believed to be extremely slow and are taken into account only for the case of CW (or quasi-CW) laser

beams. On the other hand, it was noted experimentally a long time ago that even nanosecond-pulse lasers of sufficiently high power ($p \geq 1$ MW) can cause light-induced (orientational) macroscopic structural distortions in nematic liquid crystals. The authors report the first theoretical and experimental study of this effect. (9 refs.)

- Highly nonlinear optical effects in liquid crystals See Entry 75711
 Reentrant phase transition of chiral smectic C liquid crystal in electric field See Entry 76623
 Crossover between two- and three-dimensional melting in a smectic-B-smectic-A phase transition in BBOA See Entry 76624
 Shear flow induced cholesteric-nematic transition See Entry 76625
 Phase characterization and enthalpies of selected disubstituted biphenylcyclohexanes See Entry 76626
 Ferroelectric liquid crystal electro-optics using the surface stabilized structure See Entry 77362
 Raman spectra and molecular orientation statistics for nematic liquid crystals See Entry 77391
 Determination of the ratios K_{11}/K_{22} and γ_1/K_{11} in nematic liquid crystals by correlation spectroscopy See Entry 77403

61.40 AMORPHOUS AND POLYMERIC MATERIALS

(see also 64.70P Glass transitions 81.20P to 81.20T, and 81.60 Materials science)

- 76308 Preparation and study of the structure development of amorphous Pb-Sb alloys. M.Kamal (Dept. de Phys., Univ. de Mansourah, Mansourah, Egypt), J.C.Pieri, R.Jouty. *Mem. & Etud. Sci. Rev. Metall. (France)*, vol.80, no.3, p.143-8 (March 1983). In French.
 An investigation is described, using electron diffraction and X-ray diffraction, of the structure and growth properties of Pb-Sb alloys obtained by superquenching from the molten condition. (9 refs.)
 76309 Structural changes in amorphous Fe_3B_{17} by neutron irradiation. J.Weis, I.Cerven (Dept. of Phys., Slovak Techn. Univ., Bratislava, Czechoslovakia). *Phys. Status Solidi a (Germany)*, vol.76, no.1, p.K49-51 (16 March 1983).
 The authors study the neutron irradiation effects on amorphous Fe_3B_{17} . They study the structural changes using X-ray diffraction. Ribbons of amorphous metals were prepared by rapid quenching from the melt. (7 refs.)
 International Meeting on Lithium Batteries See Entry 74213
 Nanosecond optical transmission studies of laser annealing in ion-implanted silicon-on-sapphire See Entry 76494
 Investigations of two-level tunneling systems in n-irradiated quartz by diffuse X-ray scattering See Entry 76520
 Assessment of damage ranges by measurements of the refractive index in ion implanted LiNbO_3 and LiTaO_3 See Entry 76526
 The importance of ionization and displacement damage to the crystalline-amorphous transformation observed in quartz See Entry 76540
 Phonon lifetime and thermal conductivity in amorphous solids See Entry 76716
 Shock crystallization of films See Entry 76812
 Effect of heat treatment on the conduction and structure of Ge-Se-Te amorphous alloys See Entry 76950
 Thermal-relaxation studies of the stability of amorphous structures in zirconium-based superconducting alloys See Entry 77082
 Mossbauer spectroscopy of amorphous silicon-tin-hydrogen alloys See Entry 77296
 Amorphous problem in EXAFS data analysis See Entry 77479
 Crystallization of amorphous mercury selenide films See Entry 77569

61.40D Glasses

- 76310 Non-isothermal analysis of the crystallization of the amorphous germanium dioxide. A.Montenero, E.Baiocchi (Istituto di Chimica Fisica, Parma, Italy), M.Bettinelli, L.Di Sipio, A.Sotgiu. *Mater. Chem. & Phys. (Switzerland)*, vol.8, no.4, p.379-86 (April 1983).
 The amorphous germanium dioxide devitrification has been investigated, with particular regard to the kinetic aspects and to the crystallization mechanism. The amorphous material transforms into the hexagonal dioxide modification, which is metastable at the considered temperatures. This fact is in accordance with the presence of tetrahedrally coordinated Ge in both the glass and the devitrified material. The crystallization kinetics are investigated by means of the DTA technique; a rigorous method of analysis enables the determination of the activation energy E_{act} , the Arrhenius preexponential factor A and the morphological index n characteristic of the devitrification reaction. (17 refs.)
 76311 The structural analysis of $\text{Li}_2\text{O} \cdot 2\text{SiO}_2$ glass and melt by Raman spectroscopy. N.Iwamoto, N.Umesaki (Welding Res. Inst., Osaka Univ., Ibaraki, Japan), K.Dohi. *J. Jpn. Inst. Met. (Japan)*, vol.47, no.5, p.382-9 (1983). In Japanese.
 Raman spectra for $\text{Li}_2\text{O} \cdot 2\text{SiO}_2$ glass and melt at different temperatures were measured by using the high temperature Raman spectroscopic technique. Raman spectra observed in the frequency range from 800 to 1200 cm^{-1} consist of three Raman bands near 940-50, 1000-10 and $1050-80 \text{ cm}^{-1}$. These bands are attributed to the Si-O stretching vibrations of SiO_3^{2-} chain, SiO_2 three-dimensional network and $\text{Si}_2\text{O}_7^{2-}$ sheet silicate anions with two, zero and one non-bridging oxygens per silicon atom, respectively. The fractions of the three silicate anions in $\text{Li}_2\text{O} \cdot 2\text{SiO}_2$ glass and melt were calculated from the area intensities of the three bands. Above the glass transition temperature T_g increased. However, there is only little difference between the Raman spectra of glass and melt, so that it is suggested that the glass structure is roughly similar to the corresponding melt structure. Furthermore, the coordination numbers of the nearest neighbour correlations Si-Si, O-Si and O-O in $\text{Li}_2\text{O} \cdot 2\text{SiO}_2$ glass and melt were estimated from the fractions of the three silicate anions, and were in good agreement with the values in $\text{Li}_2\text{O} \cdot 2\text{SiO}_2$ crystal. (28 refs.)

76312 Glass formation in the system of $(\text{CaO}, \text{Na}_2\text{O})\text{-Fe}_2\text{O}_3\text{-(SiO}_2, \text{B}_2\text{O}_3, \text{GeO}_2)$ and some physical properties of $\text{CaO-Fe}_2\text{O}_3\text{-SiO}_2$ glasses. N.Soga, H.Nasu, R.Ota (Faculty of Engng., Kyoto Univ., Kyoto, Japan). *J. Soc. Mater. Sci. Jpn. (Japan)*, vol.32, no.354, p.322-6 (March 1983). In Japanese.

The glass forming regions in the systems of $\text{Na}_2\text{O-Fe}_2\text{O}_3\text{-Fe}_2\text{O}_3\text{-(SiO}_2 \text{ or } \text{B}_2\text{O}_3)$ and $\text{CaO-Fe}_2\text{O}_3\text{-(SiO}_2, \text{B}_2\text{O}_3 \text{ or } \text{GeO}_2)$ were determined. (Na_2O or $\text{CaO-Fe}_2\text{O}_3\text{-SiO}_2$ glasses were found to be capable of containing up to 30 mole% Fe_2O_3 , while (Na_2O or $\text{CaO-Fe}_2\text{O}_3\text{-(B}_2\text{O}_3 \text{ or } \text{GeO}_2)$ glasses up to 20 mole% Fe_2O_3). The glass forming region in the system (Na_2O or $\text{CaO-Fe}_2\text{O}_3\text{-(SiO}_2 \text{ or } \text{B}_2\text{O}_3)$ was narrower than that in the system (Na_2O or $\text{CaO-Fe}_2\text{O}_3\text{-(SiO}_2 \text{ or } \text{B}_2\text{O}_3)$). Although the density of the $\text{CaO-Fe}_2\text{O}_3\text{-SiO}_2$ glasses increased linearly with Fe_2O_3 content when CaO/SiO_2 ratio was kept constant, the molar volume increased with Fe_2O_3 content. On the other hand at constant Fe_2O_3 content, the molar volume decreased with increasing CaO/SiO_2 ratio. This implies that Fe_2O_3 tends to loosen the glass structure and CaO to tighten the glass structure in the systems containing less than 40 mole% SiO_2 . (10 refs.)

76313 Influence of directed chemical bonding on the structure of metallic glasses. Two-dimensional model. H.Hermann (Zentralinst. für Festkörperphys. und Werkstofforschung, Akad. der Wissenschaften, Dresden, Germany). *Phys. Status Solidi b (Germany)*, vol.117, no.1, p.185-95 (1 May 1983).
 Non-central potentials are used to describe directed chemical bonding due to metalloids in amorphous metal-metalloid systems. Average atomic volume, partial pair distribution functions, local symmetries, and correlation functions of symmetry coefficients are calculated for two-dimensional model systems produced numerically by simultaneously carrying out density variation and energy relaxation. The model reproduces qualitatively essential experimental results. (13 refs.)

76314 Neutron diffraction study of 2 $\text{TeO}_2 \cdot \text{V}_2\text{O}_5$ glass. S.Neov, I.Gerassimova, B.Sydzhimov (Inst. of Nuclear Res. & Nuclear Energy, Bulgarian Acad. of Sci., Sofia, Bulgaria).

Phys. Status Solidi a (Germany), vol.76, no.1, p.297-301 (16 March 1983).
 The short-range atomic order is investigated in a glass composed of 66.7 mol% TeO_2 and 33.3 mol% V_2O_5 using the neutron diffraction method. It is established that the coordination state of the Te atom changes at the transition into the glassy state—in 65% of the cases the TeO_4 groups pass into TeO_3 pyramids with an averaged Te-O distance of 0.196 nm. On the basis of the structural data obtained, the results of X-ray diffraction and IR-spectroscopy, a plausible model of the glass structure is proposed. (14 refs.)

76315 Electron microscopy and electron diffraction study on crystallization of metastable phases in amorphous Fe-B alloys. P.Duhaj (Inst. of Phys., Electro-Phys. Res. Centre, Slovakian Acad. of Sci., Bratislava, Czechoslovakia), F.Hanic. *Phys. Status Solidi a (Germany)*, vol.76, no.2, p.467-77 (16 April 1983).

Crystallization is investigated of amorphous $\text{Fe}_{100-x}\text{B}_x$ where $x=14, 16, 18, 20$ at.% alloys using electron microscopy and electron diffraction. Above the eutectical composition, the crystallization in the alloys begins with the tetragonal metastable Fe_3B and the ordered cubic Fe_2B phases. Below the eutectical composition besides the Fe_3B phase an orthorhombic supersaturated solid solution $\alpha\text{-Fe}_{23}$ with an order-disorder arrangement of B-atoms is formed. Both instable supersaturated solid solution ($\alpha\text{-Fe}_{23}$), Fe_3B , and tetragonal Fe_2B contain similar short range order arrangements of Fe-B atoms in the form of bridging groups. (20 refs.)

76316 On nucleation of crystallization in CoB_{30} glasses. U.Koster, H.Blank (Univ. Dortmund, Dortmund, Germany). *Scr. Metall. (USA)*, vol.17, no.4, p.495-9 (April 1983).

Presents results of an investigation on the nucleation behaviour in CoB_{30} glasses, which have been found to form spherical eutectic cells during crystallization. Such an isotropic shape is the prerequisite for deriving a relation between the diameter distribution of these cells embedded in the amorphous matrix and the distribution of their circular intersections revealed in an arbitrary plane through the partially crystallized ribbon. (9 refs.)

76317 Molecular dynamics studies of the structures and properties for halide glasses. K.Hirao, N.Soga (Dept. of Industrial Chem., Kyoto Univ., Kyoto, Japan).

Yogyo-Kyokai-Shi (Japan), vol.91, no.1, p.11-17 (1983).
 The molecular dynamics calculations on halide glasses assuming ionic potential functions were made in order to obtain the correlation between the structure and properties. The results of computations on the metastable liquid and glassy state of AgI and ZnCl₂ are presented. The statistical mechanics of the glasses and the glass transition were obtained. The volume and enthalpy as functions of temperature showed that sudden changes in the derivative of the volume-temperature and the enthalpy-temperature plot occurred in the region of 0.6 T_m . (16 refs.)

76318 Calculation of the crystallization behaviour of metallic glasses. H.W.Bergmann, H.U.Fritsch (Inst. für Werkstoffkunde und Werkstofftech., Univ. Clausthal, Clausthal, Germany).

Rapidly Solidified Amorphous and Crystalline Alloys. Proceedings of the Materials Research Society Annual Meeting, Boston, MA, USA, Nov. 1981 (New York, USA: North-Holland 1982), p.225-8
 A method is proposed to calculate the crystallization behaviour of multicomponent metallic glasses with several phases. Various geometric shapes of precipitate can be considered. The model also takes into account changes in concentration which arise during precipitation. (5 refs.)

76319 Influence of Cr, Mn, Co and Ni on the crystallization behaviour of $(\text{Fe}_{1-x}\text{M}_x)_2$ metalloids, metallic glasses. H.W.Bergmann, U.Brokmeyer (Inst. für Werkstoffkunde und Werkstofftech., Univ. of Clausthal, Clausthal, Germany).

Rapidly Solidified Amorphous and Crystalline Alloys. Proceedings of the Materials Research Society Annual Meeting, Boston, MA, USA, Nov. 1981 (New York, USA: North-Holland 1982), p.235-41

The influence of Cr, Mn, Co and Ni on the thermodynamic properties (molar heat of fusion, heat of crystallization and melting temperature), crystallization behaviour and hardness was studied in $(\text{Fe}_{1-x}\text{M}_x)_2\text{B}_{17}$ as a function of the x content. The crystallization behaviour can be described by three parameters which enables an extrapolation to longer times. (5 refs.)

76320 Crystallization behavior and properties of rapidly solidified Ni-Mo-B alloys. C.C.Wan (AiRes. Casting Co., Torrance, CA, USA).

Rapidly Solidified Amorphous and Crystalline Alloys. Proceedings of the Materials Research Society Annual Meeting, Boston, MA, USA, Nov. 1981 (New York, USA: North-Holland 1982), p.441-7
 The crystallization phenomena of certain ternary glass Ni-Mo-B alloys and their consolidated bulk properties, including age hardening effects after proper heat treatment, are investigated. Within the composition range studied, the glassy alloys crystallize by a two-stage process—first by forming a metastable microcrystalline structure of Ni solid solution at temperature around 490-530°C followed by boride precipitation at temperatures around 700-770°C.

The boride, which is identified by X-ray diffraction as Mo_2NiB_3 , grows to submicron size after the alloys have been thermally treated at 1000°C and above for certain periods of time. Microstructural analysis shows borides isolated and well dispersed in Ni-Mo alloy matrix. Age hardening is achieved by precipitating the Ni/Mo intermetallic compound(s) in Ni-Mo matrix at an intermediate temperature of previously solutionized samples. Another characteristic is the high eutectic temperature. This allows the alloys to be hot consolidated to full density by certain commercially available processes, such as hot isostatic pressing, while still maintaining the unique microstructure inherited from rapid solidification process. Hardness, hot hardness and hot tensile properties of some consolidated alloys are discussed. (9 refs.)

76321 Micromechanisms of crystallization in (Fe,Co,Ni)-Zr metallic glasses. H.-G.Franke, U.Koster, H.-W.Schroeder (Abteilung Chemietechnik, Univ. Dortmund, Dortmund, Germany), J.Muller. Rapidly Solidified Amorphous and Crystalline Alloys. Proceedings of the Materials Research Society Annual Meeting, Boston, MA, USA, Nov. 1981 (New York, USA: North-Holland 1982), p.455-60. Depending on the Zr-concentration crystallization of (Fe,Co,Ni)-Zr glasses has been found by TEM studies to occur by primary and polymorphic crystallization but not by eutectic crystallization reactions. Nucleation and growth rates of these reactions have been analyzed systematically. Thermal stability as indicated by growth as well as nucleation rates decreases with increasing Zr-content and atomic number of the late transition metal. Using this knowledge on nucleation and growth rates, conditions for designing particular microstructures by crystallization reactions can be predicted. (10 refs.)

Helium bubble growth during 1 MeV electron irradiation at 300K in 5 keV-He⁺ pre-implanted nickel and an amorphous Fe-Ni-Mo-B alloy See Entry 76505

Modifications of sodium concentration profiles after electron and proton irradiation of glasses See Entry 76513

Localized shear deformation of amorphous metals See Entry 76551

Kinetic study on glass formation and crystallization behavior in a continuously cooling melt See Entry 76597

Constant-pressure simulation of silica See Entry 76629

Microstructural study of devitrified amorphous alloys See Entry 76651

Thermal expansion of amorphous iron-chromium-boron alloys See Entry 76678

(Ag₂O)_x(Li₂O)_{1-x}·2B₂O₃ mixed cation glasses See Entry 76694

Spin coated amorphous chalcogenide films: structural characterization See Entry 76802

Multiple phase transitions in GeTe films. Dynamics and film structure See Entry 76814

Electrical and Raman study of lithium borotungstate and boromolybdate glasses See Entry 77011

⁵⁷Fe Mossbauer study of amorphous Fe₈₁B_{13.5}Si_{3.5}C₂ See Entry 77301

A structural interpretation of the vibrational spectra of binary fluorohafnate glasses See Entry 77378

Raman scattering spectra and structural properties of the chalcogenide glasses Sb₂As_{1-x}SI See Entry 77384

Physicochemical and spectral luminescence properties of a glass based on the SiO₂-Al₂O₃-La₂O₃-Nd₂O₃ system See Entry 77438

Hot consolidation/devitrification metallic glasses—novel multiphase crystalline alloys in bulk shapes with technological potentials See Entry 77600

The fining of glass. A Raman-spectrometric investigation into the action of arsenic oxides See Entry 77615

Multicomponent glasses of GeO₂ and Sb₂O₃ with Bi₂O₃, Ti₂O, and/or PbO See Entry 77620

Mechanical properties of (Fe_{100-x}M_x)₈₃B₁₇ metallic glasses See Entry 77760

Deformation induced dilatations and new observations on fracture in compression in metallic glasses at low temperatures See Entry 77761

The effect of hydrogen on an iron based amorphous alloy See Entry 77762

61.40K Polymers, elastomers, and plastics

76322 On the problem of cross links in trans-polyacetylene: normal-coordinate calculations. G.Zannoni, G.Zerbi (Dipartimento di Chimica Industriale e Ingegneria Chimica, Politecnico di Milano, Milan, Italy).

Chem. Phys. Lett. (Netherlands), vol.97, no.2, p.147-51 (13 May 1983).

Normal-coordinate calculations are carried out on a simple model of a cross link in trans-polyacetylene (PA). The results indicate the need for a reanalysis of the presently accepted vibrational assignment of trans-PA and suggest the need for a more thorough chemical study of purposely cross-linked PA. The authors consider vibrational spectra as a possible tool for the molecular characterisation of PA. The analysis of the infrared and Raman spectra of trans-PA indicates that some medium-weak lines were left unexplained by the various author who focused their attention on the contributions to the spectra of a perfect chain. (26 refs.)

76323 Modified two-phase model for the mechanical properties of the semicrystalline polymer—polyethylene. P.K.Biswas, S.Sengupta (Phys. Dept., Presidency Coll., Calcutta, India), A.N.Basu.

Indian J. Pure & Appl. Phys., vol.21, no.2, p.73-7 (Feb. 1983).

A phenomenological model for semicrystalline polymer is proposed which takes into account both variation of crystallinity and orientation of the molecular chains with the direction of draw. The elastic properties of the polymer are calculated in terms of those of the constituent phases as in Takayanagi's (1973) model. At the drawn state it has been shown that a partially oriented crystalline phase may be considered as a superposition of a perfectly aligned crystalline portion on a polycrystalline phase. The model contains only two adjustable parameters. The model is applied in the case of high density polyethylene and the agreement of the predicted values of the elastic moduli along the direction of draw and perpendicular to it and shear modulus are in close agreement with the experimental values. (16 refs.)

76324 Structure property relationship in unsaturated polyamides. A.Ray, M.M.Maiti, S.Maiti (Materials Sci. Centre, Indian Inst. of Technol., Kharagpur, India).

Int. J. Polym. Mater. (GB), vol.10, no.1, p.21-37 (1983).

Unsaturated polyamides from fumaric acid and ortho-, meta- and para-phenylene diamine were prepared by thionyl chloride activated low temperature polycondensation in polar solvents. The polymers were found to be soluble in highly polar solvents. The solubility parameter of the polymers was calculated from Small's group contribution, which agreed well with the experimental values. X-ray diffraction study revealed that the polymers were amor-

phous. The isomeric effect on the thermal and electrical properties of polymers was discussed. (24 refs.)

76325 Relaxation function of linear polymers. G.M.Bartenev, Z.P.Shul'man, B.M.Khusid (Inst. of Phys. Chem., Acad. of Sci., Moscow, USSR).

J. Eng. Phys. (USA), vol.43, no.3, p.1002-6 (Sept. 1982). Translation of: *Inzh.-Fiz. Zh. (USSR)*, vol.43, no.3, p.425-30 (Sept. 1982).

The relaxation function of linear polymers possessing a discrete relaxation time spectrum is analysed. (11 refs.)

76326 Preoriented poly(ethylene terephthalate) yarns: influence of the gauche-trans transformation on crystallization. R.Galli, M.Canetti, P.Sadocco, A.Seves, L.Vicini (Stazione Sperimentale per la Cellulosa, Carta e Fibre Tessili, Vegetali ed Artificiali, Milano, Italy).

J. Polym. Sci. Polym. Phys. Ed. (USA), vol.21, no.5, p.717-23 (May 1983).

Effects of macromolecular orientation on the crystallization of preoriented poly(ethylene terephthalate) filaments were studied. Infrared spectrophotometry and differential scanning calorimetry analyses showed that macromolecular segments in the trans conformation begin to crystallize below the glass transition temperature. Since filaments prepared by stretching at room temperature have different degrees of orientation, it is possible to evidence correlations between crystallization from an anisotropic matrix and the resulting morphology. (8 refs.)

Microdiffraction applied to thermotropic liquid crystalline polymers See Entry 76300

Mechanism of high ionic conductivity in elastomeric networks See Entry 76696

Raman spectra and physical structure of cellulose triacetate See Entry 77388

Study of structure of copolymers of ethylene tetrasulfide and vinyl cyanide See Entry 77390

61.50 CRYSTALLINE STATE

(inc. molecular motions in solids; for magnetic structure and spin systems, see 75.25)

76327 Crystal structures containing five atoms per primitive cell. M.Hosoya (Dept. of Phys., Univ. of the Ryukyus, Okinawa, Japan).

Bull. Coll. Sci. Univ. Ryukyus (Japan), no.35, p.9-52 (March 1983).

Enumeration of the species in genus ABCDE, ABCD₂, ABC₂, AB₂C₂, AB₄, A₂B₃, and A₅ is carried out. Their numbers are 52, 236, 356, 484, 520, 642, and 373 respectively. New notation of the species is proposed. (4 refs.)

76328 Line profiles for a collection of identical crystals: effect of a linear transformation of shape. G.Allegre (Istituto di Chimica, Politecnico di Milano, Milano, Italy), A.J.C.Wilson.

Acta Crystallogr. Sect. A (Denmark), vol.A39, pt.3, p.280-2 (1 May 1983).

A linear transformation is defined as a distortion of the unit lengths along three Cartesian axes and of their angles, preserving the same covariant coordinates of the corresponding points. The mathematical relationship between the line profiles of two mutually transformed crystals is proposed. It makes it possible, for example, to get the line profiles for ellipsoids, parallelepipeds, distorted tetrahedra and octahedra from the exact results reported by Langford & Wilson (1978) for spheres, cubes, regular tetrahedra and octahedra. (9 refs.)

76329 N-dimensional coincidence-site-lattice theory. M.A.Fortes (Dept. de Metalurgia, Univ. Tecnica de Lisboa, Lisboa, Portugal).

Acta Crystallogr. Sect. A (Denmark), vol.A39, pt.3, p.351-7 (1 May 1983).

A matricial theory of coincidence-site and displacement-shift-complete (DSC) lattices of arbitrary dimension is developed. Vector bases for these lattices can easily be determined from particular factorizations of the matrix defining the relative orientation. Various properties of the two lattices are derived, including the reciprocity relations. The general conditions for coincidence and the problem of coincidence in sublattices of lower dimension are also discussed. (27 refs.)

76330 CO/N₂ solid solutions: head-tail reorientations. Shang-Bin Liu, M.S.Conradi (Dept. of Phys., Coll. of William and Mary, Williamsburg, VA, USA).

J. Chem. Phys. (USA), vol.78, no.11, p.6901-5 (1 June 1983).

The rates of CO reorientation in α -phase solid solutions of CO/N₂ were determined with dielectric spectroscopy. The activation energy is found to be an increasing and approximately linear function of the CO concentration x , similar to the transition temperature T_{tr} . The extrapolated activation energy for CO reorientation in α -N₂ is compared to that in pure α -CO: the transition temperatures and libration frequencies of α -N₂ and α -CO are also compared. Evidently, the same interactions control T_{tr} , the librations, and the energy barriers to reorientation. The CO dipole moment magnitudes determined from the dielectric data are all about 30% below the free molecule value. Not all of this discrepancy is ascribable to incomplete filling of the cell to the solid sample and librational reduction of the effective moment. (28 refs.)

Strengthened translation functions. An automated method for the positioning of a correctly oriented fragment by translation functions in DIRDIF Fourier space See Entry 76249

Peculiarities of phase transitions and physical properties in (NH₄)₂SbF₆ See Entry 76613

Heat capacity study of the phase transitions in As₄S₃ and As₄S₄ See Entry 76661

Barriers to rotation of the cyclopentadienyl ligand: spin-lattice relaxation time measurements and atom-atom potential calculations on cyclopentadienyl manganese and rhenium tricarbonyl and vanadium tetracarbonyl complexes See Entry 77278

Structure and dipole relaxation mechanisms in the cyclic alcohols cyclopentanol to cyclo-octanol See Entry 77326

61.50C Physics of crystal growth

(for techniques of crystal growth and film deposition, see 81.10 and 81.15; for epitaxy, thin films, see 68.55; for whiskers, see 68.70)

76331 Ice crystal morphology and growth rates at low supersaturations and high temperatures. S.C.Colbeck (US Army Cold Regions Res. & Engng. Lab., Hanover, NH, USA).

J. Appl. Phys. (USA), vol.54, no.5, p.2677-82 (May 1983).

At an excess vapor density (supersaturation of about 10^{-4}) adjacent to the ice crystal surface of 5.6×10^{-10} g/cc, there is a transition between the high faceted kinetic growth form and the rounded equilibrium form at temperatures above -6°C . At lower temperatures there is a transition in the equilibrium form to hexagonal prisms because of a reduction in the disordered

surface layer. The growth rate of ice crystals from the vapor is analyzed by a simple model which accounts for vapor flow and surface processes separately. The conditions for highly temperature sensitive growth are identified from the model. (17 refs.)

76332 The effect of Soret diffusion on the morphological stability of a binary alloy crystal. D.T.J.Hurle (Royal Signals & Radar Establ., Great Malvern, England).

J. Cryst. Growth (Netherlands), vol.61, no.3, p.463-72 (April-May 1983).

The classic Mullins-Sekerka analysis (1964) of the morphological stability of the interface of a crystal growing from a dilute binary alloy melt is reworked with inclusion of Soret diffusion. As expected, for reasonable values of the Soret coefficient, the criterion for interface breakdown is not significantly altered. However, it is found that for solutes having small segregation coefficients ($k < 1$), the critical wavelength, at which the breakdown first occurs, is markedly altered both under conventional growth conditions and for the extreme conditions encountered with pulsed laser beam annealing. The physical reasons for the effect are elucidated. (10 refs.)

76333 Interface shape studies for silicon ribbon growth by the EFG technique. I. Transport phenomena modeling. J.P.Kalejs (Mobil Solar Energy Corp., Waltham, MA, USA), L.-Y.Chin, F.M.Carlsion.

J. Cryst. Growth (Netherlands), vol.61, no.3, p.473-84 (April-May 1983).

The influence of process parameters on the interface shape of silicon ribbon grown by the edge-defined film-fed growth (EFG) technique has been studied with the help of finite element solutions of the heat and mass transport equations. The interface shape is calculated to be convex toward the melt for a wide range of growth parameters. Significant inhomogeneities of segregated impurities through the ribbon thickness are associated with this interface shape for impurities with segregation coefficients much less than unity. The influence of asymmetry in the geometry and temperature fields on interface configuration and solute segregation is examined. Interface tilt produced by this asymmetry is shown to lead to deviations from normal segregation behavior at large tilt angles. (11 refs.)

76334 Interface shape studies for silicon ribbon growth by the EFG technique. II. Effect of die asymmetry. J.P.Kalejs (Mobil Solar Energy Corp., Waltham, MA, USA).

J. Cryst. Growth (Netherlands), vol.61, no.3, p.485-93 (April-May 1983).

For p.t.I see *ibid.*, vol.61, no.3, p.473-84 (1983). Interface shapes in silicon ribbon EFG (edge-defined film-fed growth) have been investigated experimentally with the examination of ribbon grown with asymmetry in the interface environment created by modifying die geometry in the ribbon thickness dimension. Changes in ribbon properties are examined in view of the predictions for interface configuration and impurity segregation behavior obtained from finite element modeling of heat and mass transport processes. (8 refs.)

76335 Crystal growth and temperature variation of the lattice parameters in LaF_3 , CeF_3 , PrF_3 and NdF_3 . W.Korczak, P.Mikolajczak (Experimental Phys. Dept., Inst. of Phys., Marie Curie-Skłodowska Univ., Lublin, Poland).

J. Cryst. Growth (Netherlands), vol.61, no.3, p.601-5 (April-May 1983).

The growth of REF_3 ($\text{RE} = \text{La, Ce, Pr, Nd}$) single crystals by the Bridgman-Stockbarger method is described. The temperature dependence of the lattice parameters a and c and the thermal expansion coefficients α of these materials in the range of 87-291K are reported. (7 refs.)

76336 Mathematical model for corundum single crystal growth by Verneuil method. R.Grzymkowski, B.Mochnacki, J.Suchy (Silesian Polytech. School, Gliwice, Poland).

J. Cryst. Growth (Netherlands), vol.61, no.3, p.629-36 (April-May 1983).

A mathematical model which is an attempt to describe the complex process of monocrystallization by the Verneuil method is presented. The problem has been solved through the method of finite differences and at the same time making use of a certain modification of the mathematical description of Stefan's problem called the alternating phase truncation method. The elaborated algorithm and the examples of solutions given at the end of the present study point at the usefulness of the presented method of numerical simulation for modern designing and controlling the processes of crystal production. (10 refs.)

76337 Segregation during directional melting and its implications on seeded crystal growth: a theoretical analysis. E.D.Bourret, J.J.Favier, A.F.Witt (Dept. of Materials Sci. & Engng., MIT, Cambridge, MA, USA).

J. Cryst. Growth (Netherlands), vol.61, no.3, p.681-8 (April-May 1983).

Directional melting of binary systems in the absence of convection is analyzed for concurrent compositional changes at the crystal-melt interface. It is shown that steady-state conditions cannot normally be reached during seeding and that the growth interface temperature during the ensuing initial stages of growth is a function of backmelt conditions. The theoretical treatment is numerically applied to $\text{Hg}_{1-x}\text{Cd}_x\text{Te}$ and Ga-doped Ge. (10 refs.)

76338 Polarity identification of CdTe crystallites. H.Iwanaga, T.Yoshiie (Faculty of Liberal Arts, Nagasaki Univ., Nagasaki, Japan), S.Takeuchi, K.Mochizuki.

J. Cryst. Growth (Netherlands), vol.61, no.3, p.691-4 (April-May 1983).

The crystal polarity of CdTe with the zincblende structure has been shown to be identifiable by triangular etch pits developed on the {110} plane which is easy to obtain as the cleavage plane or the growth habit plane. Examples are given of identifying the growth polarity of as-grown crystallites. (9 refs.)

76339 On the influence of natural convection on mass transfer process in gallium phosphide crystal growth from solution. L.L.Regel, Nguyen Thanh Nghi (Space Res. Inst., Acad. of Sci., Moscow, USSR).

Mater. Res. Bull. (USA), vol.18, no.4, p.499-506 (April 1983).

Mass transfer process under various (space and terrestrial) conditions of crystal growing from solution have been considered. Dimensionless criteria from the reduced mass transport equation for the boundary layer approximation have been used to estimate the conditions at which natural convection occurs and how large its effect is. The data of the on-ground and Salyut-6 orbital station experiments have helped to determine the phosphorus diffusion coefficients in the liquid gallium in the temperature range 1000-1100°C and to give possible reasons for deviation of some parameters from experimental data given by other authors. Comparison of crystal growth results on Earth and in space was used to reveal a quantitative relationship between the growth rate and convection intensity. (20 refs.)

76340 Theoretical and experimental study of growth sector boundaries in deuterated potassium dihydrogen phosphate single crystals. S.Grosswig, J.Hartwig, U.Schellenberger, W.-D.Zimmer (Friedrich-Schiller-Univ., Jena, Germany).

Phys. Status Solidi a (Germany), vol.76, no.1, p.241-7 (16 March 1983).

An analytical model is applied to describe the lattice deformation of a growth sector boundary. The theoretical results are compared with precision lattice parameter measurements and with contrast distributions in double crystal topographs. A good qualitative agreement can be stated. The width of the area where a strong lattice parameter change appears can be estimated. (18 refs.)

76341 LEC growth of InP(Mn) for p-type and semi-insulating materials. R.E.Nahory, A.A.Ballman, H.Brown, M.R.Wilson (Bell Labs, Holmdel, NJ, USA).

Gallium Arsenide and Related Compounds, 1982. Tenth International Symposium on Gallium Arsenide and Related Compounds, Albuquerque, NM, USA, 19-22 Sept. 1982 (Bristol, England: IOP 1983), p.7-14.

Both p-type and semi-insulating InP bulk crystals have been grown with the use of Mn impurities, which are found to be deep acceptors with ionization energy near 0.3 eV. Several 200-gram ingots were prepared with $p = 3 \times 10^{14}$ to $5 \times 10^{16} \text{ cm}^{-3}$ at 300K. Under the proper conditions, semi-insulating material was also grown, with resistivity of 10^7 ohm-cm at 300K. (6 refs.)

76342 Reproducibility and uniformity considerations in LEC growth of undoped, semi-insulating GaAs for large-area, direct implantation technology. L.B.Ta, R.N.Thomas, G.W.Eldridge, H.M.Hobgood (Westinghouse R&D Center, Pittsburgh, PA, USA).

Gallium Arsenide and Related Compounds, 1982. Tenth International Symposium on Gallium Arsenide and Related Compounds, Albuquerque, NM, USA, 19-22 Sept. 1982 (Bristol, England: IOP 1983), p.31-9.

Large diameter ($\leq 75 \text{ mm}$) undoped GaAs crystals grown by the LEC technique from As-rich melts exhibit reproducible high resistivity, thermal stability and predictable implantation characteristics in contrast to semi-insulating Ga-rich material which exhibits a p-type conversion after prolonged annealing at 860°C, resulting from the outdiffusion of EL2 deep donors revealing uncompensated residual carbon acceptors at the wafer surface. It has been found empirically that factors such as crystal-crucible rotation and pull speed in LEC growth affect the radial and slice-to-slice uniformity during implantation. Crystals grown under conditions of co-rotation of seed and crucible often exhibit significant radial variations in measured sheet resistance and mobility with characteristic p-type cores in the wafer centers after 860°C/15 minute annealing. Counter-rotation and slow pull rates are found to be beneficial in the growth of GaAs substrates with radially uniform semi-insulating behavior and thermal stability. (11 refs.)

Gallium Arsenide and Related Compounds, 1982. Tenth International Symposium on Gallium Arsenide and Related Compounds See Entry 74226

A series of rare earth silicates $\text{RE}_2^{3+}\text{M}^{3+}[\text{SiO}_4]_2(\text{OH})$ [synthesis and crystal structure] See Entry 76394

The theoretical shape of sucrose crystals from energy calculations See Entry 76410

Point defects in II-VI compounds See Entry 76420

X-ray investigation of crystal defects in Czochralski grown InP single crystals See Entry 76435

Characterization of defects in InP substrates See Entry 76436

Double doped low dislocation density InP with low optical absorption See Entry 76474

Preferred crystallographic orientation for crystallisation under nonhydrostatic stress See Entry 76593

On the solvability of the two-phase quasistationary crystallization problem See Entry 76595

Vapour phase growth of some II-VI compounds See Entry 77545

Hydrogen uranyl arsenate hydrate single crystals: $\text{H}_2(\text{UO}_2)_2(\text{AsO}_4)_2 \cdot 8\text{H}_2\text{O}$: gel growth and characterization See Entry 77546

Reconstruction by multidirectional holographic interferometry of the concentration field in a supersaturated solution near a growing NaClO_3 crystal See Entry 77547

Growth of single crystals of hexagonal boron nitride See Entry 77548

Characterization of flux-grown $\text{Ca}(\text{WO}_4)_x(\text{MoO}_4)_{1-x}$ crystals See Entry 77550

Temperature profile and thermal stress calculations in GaAs crystals growing from the melt See Entry 77551

Effect of variable thermal conductivity on isotherms in Bridgman growth See Entry 77552

Crystal growth of solid solutions $\text{La}_{1-x}\text{Ba}_x\text{F}_{3-x}$ See Entry 77553

In situ purification growth of undoped semi-insulating GaAs single crystals See Entry 77558

A new method for the growth of circular nickel crystals by zone melting See Entry 77560

Preparation of bulk alloys of III-V compounds See Entry 77561

Chemical transport of MnS and MnSe using HCl as a transporting agent See Entry 77883

61.50E Crystal symmetry; models and space groups, and crystalline systems and classes

76343 Space-group symmetry and the joint probability distribution of the magnitude and phase of a triple product: an unexpected result in the eleven pairs of chiral spacegroups. W.M.G.F.Pontenagel, H.Krabbandam (Lab. voor Struikturechem., Rijksuniv., Utrecht, Netherlands).

Acta Crystallogr. Sect. A (Denmark), vol.A39, pt.3, p.333-40 (1 May 1983).

The main term of the probability distribution of a triple product in an arbitrary space group is derived via the central limit theorem. The results are in general identical to those obtained by Giacovazzo (1980) i.e. in any space group the well known distribution functions for P_1 and P_1 are valid for general triple products and triple products with restricted phase angles, respectively, provided a suitable weight is applied. However, in the eleven pairs of enantiomorphously related space groups it is found that there are triple products for which the most probable phase angle assumes a value different from zero. As an example, in P_4 , the most probable phase for the triple product $E_{221}E_{401}E_{223}$, given its magnitude, appears to be -45° . (11 refs.)

76344 Point-group determination by convergent-beam electron diffraction. M.Tanaka, R.Saito, H.Sekii (Dept. of Phys., Tohoku Univ., Sendai, Japan).

Acta Crystallogr. Sect. A (Denmark), vol.A39, pt.3, p.357-68 (1 May 1983).

The method of point-group determination from convergent-beam electron diffraction patterns has been established by Buxton et al. (1976). However, Table 2 given by them is inconvenient for practical purposes, since many symmetries of the dark-field and $\pm G$ dark-field patterns are not given and are left for the reader's consideration. The table is improved and completed with the help of some new symmetry symbols and illustration of symmetries. The new table makes the point-group determination easy and quick. The symmetries of the symmetrical many-beam convergent-beam electron diffraction patterns have been studied by Tinnappel (1975) using group theory. It is shown that the graphical method used by Buxton et al. can reveal the symmetries of these patterns. A method of point-group determination which uses three types of symmetrical many-beam patterns, the hexagonal six-beam,

square four-beam and rectangular four-beam patterns, is described. This method requires only one photograph in determining most diffraction groups. This fact means that the method is more convenient and reliable than that of Buxton et al., since their method requires two or three photographs for most cases. Experimental results which verify the theoretical ones are given. The characteristic features of the symmetrical many-beam method are discussed. (12 refs.)

76345 Geometric units in tetragonal crystal structures. C.Chieh (Guelph-Waterloo Centre for Graduate Work in Chem., Univ. of Waterloo, Waterloo, Ontario, Canada).

Acta Crystallogr. Sect. A (Denmark), vol.A39, pt.3, p.415-21 (1 May 1983). Tetragonal space groups are classified from the geometric-unit view point by considering crystal structures as a result of combinations and permutations of some basic polyhedral units. There are nine patterns among two categories represented by four units packed on the (110) and (100) planes. Category (I) consists of five types with four units packed on the (110) plane. The centers of these units are $0,0,0$; $0,0,1/2$; $1/2,1/2,0$ and $1/2,1/2,1/2$. In that order, the patterns can be represented by $ABCD$, $AA'BB'$, $ABA'B'$, $ABBA'$ and $AA'A'A'$. Each letter represents an independent unit; primes are used to indicate one of the following orientation relationships: identity, fourfold rotation, mirror plane parallel to (110), and mirror plane parallel to (100). These units have the shape of tetragonal prisms and they stack in the same way as the crystallographic unit cells. Category (II) has four types packed on the (100) plane and the centers of these units are at $0,0,0$; $0,1/2,1/4$; $0,0,1/2$ and $0,1/2,3/4$. In that order, the patterns can be represented by $ACBD$, $ABA'B'$, $AA'BB'$ and $AA'A'A'$. The ideal polyhedra for category (II) are truncated tetragonal prisms or flattened truncated octahedra depending on the axial ratio c/a . For simplicity, these polyhedra are transformed into tetragonal prisms so that all geometric units have the same shape. Units in category (II) stack in an interlocking fashion, like the work of a bricklayer. The overlap displacements for the interlocking are in the (001) direction. The symmetries of the geometric units in some space groups depend on the choice of origin, but a shift to equivalent origins changes neither the packing patterns nor the symmetries of the geometric units. (19 refs.)

76346 Application of an algebraic method to isolate a basic system from a vector system. V.A.Lebedev, E.A.Soldatov, E.A.Kuz'min, N.V.Belov (Physicotech. Res. Inst., N.I. Lobachevskii State Univ., Gorki, USSR). *Sov. Phys.-Dokl. (USA)*, vol.27, no.7, p.509-11 (July 1982). Translation of: *Dokl. Akad. Nauk SSSR*, vol.265, no.1-3, p.73-6 (July 1982). [received: April 1983]

The authors have developed an algorithm which is executed on a BESM-6 computer in the form of a program written in FORTRAN. The operation of the program can be arbitrarily divided into the following states: 1) Calculation of the coefficients $b_i(hkl)$ from individual experimental structure factors $|U(hkl)|^2$; 2) location of the interatomic function with storage of the coordinates of the points and their weights; 3) construction, from the modified coefficients $b_i(hkl)$, of superposition functions of rank M with the aid of the solution of the system of polynomials; 4) calculation of the weights of the points on the superposition function as the sum of the weights of the interatomic vectors from the given atom to the other atoms. (3 refs.)

76347 Criterion for a structure to belong to a homometric set. V.G.Rau, T.F.Rau, V.V.Ilyukhin, N.V.Belov (P.I. Lebedev-Polyanskii State Pedagogical Inst., Vladimir, USSR).

Sov. Phys.-Dokl. (USA), vol.27, no.7, p.513-15 (July 1982). Translation of: *Dokl. Akad. Nauk SSSR*, vol.265, no.1-3, p.80-3 (July 1982). [received: April 1983]

The authors find a broader criterion for belonging in those cases when the vector system is not a grid system. One should expect that in this case as well the criterion may prove to be based on the VS pseudosymmetry, which arises as the composition of local symmetry elements of the subsystem. (4 refs.)

76348 On some distinctive features of cyclotomic Patterson sets. V.G.Rau, L.G.Parkhomov, V.V.Ilyukhin, N.V.Belov (P.I. Lebedev-Polyanskii State Pedagogical Inst., Vladimir, USSR).

Sov. Phys.-Dokl. (USA), vol.27, no.7, p.521-3 (July 1982). Translation of: *Dokl. Akad. Nauk SSSR*, vol.265, no.1-3, p.336-9 (July 1982). [received: April 1983]

In previous publications, (see *ibid.*, vol.25, p.960, 1980) using combinatorial methods of number theory the authors have obtained formulas for calculating the number of cyclotomic Patterson sets. An investigation of the relation between the sets of coordinates of these sets discloses a number of distinctive features typical of linear basic systems. In the present paper they attempt an analysis of these features, within the framework of the general problem of seeking the conditions of existence of homometric sets and calculating and constructing them. (5 refs.)

76349 Special cases of symmetry of reciprocal phase space. E.V.Chuprunov, T.N.Tarkhova, N.V.Belov (Physicotech. Res. Inst., N.I. Lobachevskii State Univ., Gorki, USSR).

Sov. Phys.-Dokl. (USA), vol.27, no.8, p.585-6 (Aug. 1982). Translation of: *Dokl. Akad. Nauk SSSR*, vol.265, no.4-6, p.874-7 (Aug. 1982). [received: May 1983]

In a number of cases associated with the solution of the phase problem, it is necessary to know and take account of the symmetry of the distribution of the phases of the structure amplitudes, independently of their absolute values. For a given crystal structure, the authors assign to each site of its reciprocal lattice a real number ϕ , $0 \leq \phi \leq \pi$, equal to the phase of the corresponding structure amplitude. The resulting space is called the reciprocal phase space (RPS). The group of motions which transform into themselves when the phase relations of the RPS are taken into account are called the symmetry group of the RPS. Symmetry groups of RPS are supergroups of the symmetry groups of the Fourier space. (5 refs.)

76350 On the characteristic equations of crystallographic matrices. E.A.Soldatov, A.E.Kuz'min, N.V.Belov (Physicotech. Res. Inst., N.I. Lobachevskii State Univ., Gorki, USSR).

Sov. Phys.-Dokl. (USA), vol.27, no.8, p.587-8 (Aug. 1982). Translation of: *Dokl. Akad. Nauk SSSR*, vol.265, no.4-6, p.1390-2 (Aug. 1982). [received: May 1983]

Symmetry transformations in N -dimensional space can be represented by a group of matrices. If the matrices of this group are integral, then such a group is crystallographic, i.e., for certain lattices in their primitive basis the group expresses rotations of these lattices into themselves. The integrality of a finite group of (unimodular) matrices is a sufficient condition for the existence of such lattices. It is shown that the 'crystallographic nature' of the matrices is associated with more general properties than their integrality and unimodularity; to be precise it consists in distinctive features of the spectrum of eigenvalues of these matrices. (3 refs.)

Use of high-symmetry zone axes in electron diffraction in determining crystal point and space groups See Entry 76260

Ordering in orthorhombic crystals See Entry 76584

61.50J Crystal morphology and orientation

Fracture mechanics tests in static and cyclic loading conditions on structure graphite for high temperature reactor plants See Entry 75110

The effect of Soret diffusion on the morphological stability of a binary alloy crystal See Entry 76332

Polarity identification of CdTe crystallites See Entry 76338

Geometric units in tetragonal crystal structures See Entry 76345

Development of morphological instability and cells during rapid solidification of laser annealed silicon alloys See Entry 76598

Orientation of particles of a new phase appearing in crystals See Entry 76645

Li/SOCl₂ cells for high temperature applications See Entry 77971

61.50K Crystallographic aspects of polymorphic and order-disorder transformations

High-pressure and high-temperature crystallographic study of the gillespite I-II phase transition See Entry 76604

Structural changes of a piezoelectric crystal BaZnGeO₄ on thermal phase transition See Entry 76621

Influence of the crystallography of the grain boundary/grain system on the α - γ phase shift in Fe-4% Ni alloys See Entry 77633

Nature of the anomalous spontaneous deformation of iron in the presence of hydrogen See Entry 77701

61.50L Crystal binding

76351 Packing analysis and calculation of sublimation energies of borane crystals. T.Beringhelli (Istituto di Chimica Generale ed Inorganica, Univ. di Milano, Milano, Italy), G.Filippini, A.Gavezotti, M.Simonetta. *THEOCHEM (Netherlands)*, vol.11, no.1-2, p.51-61 (June 1983).

Using known X-ray crystal structures of boranes, some indices related to crystal stability and close-packing are obtained. An examination of possible non-bonded potential functions for boron atoms in crystals is carried out, and by using suitably rescaled hydrocarbon functions, the sublimation energies of boranes are calculated. Correlations with the number of boron atoms in the molecule and molecular volumes are found. Potential energy barriers for large-amplitude molecular reorientations are also calculated and are found to be of the same order of magnitude as lattice energies for many borane crystals. (9 refs.)

76352 A cusp-constrained scattering factor for bonded hydrogen atoms. R.Van Der Wal, R.F.Stewart (Dept. of Chem. Phys., Univ. of Groningen, Groningen, Netherlands).

Acta Crystallogr. Sect. A (Denmark), vol.A39, pt.3, p.422-4 (1 May 1983). A simple one-parameter form factor that satisfies a cusp condition has been developed. A one-parameter form factor, based on a 1s-type density function, is more tractable in a least-squares analysis than the corresponding cusp-constrained form factor. Application of both form factors for bonded hydrogen atoms to X-ray diffraction data of sucrose revealed a more contracted density for H bonded to C compared to H bonded to O. (11 refs.)

76353 On the logarithmic potential potential form for the short-range interactions in alkali halide crystals. R.K.Gupta, P.S.Bakhshi, J.Shanker (Dept. of Phys., Agra Coll., Agra, India), A.J.Kaur.

Indian J. Pure & Appl. Phys., vol.21, no.3, p.180-1 (March 1983). The logarithmic potential for short-range repulsive interactions in alkali halides used by recent workers does not give good account of the cohesive energy. The suitability of this potential with and without including van der Waals interactions has been examined. The potential parameters and from them the cohesive energies are calculated and compared with the experimental values. The logarithmic potential form is inferior to the already known and frequently used exponential potential form. (11 refs.)

76354 A polynomial relationship for lattice energy in crystals. A.P.Kajwadkar, L.K.Sharma (Dept. of Appl. Phys., Government Engng. Coll., Jabalpur, India).

Indian J. Pure & Appl. Phys., vol.21, no.3, p.193-4 (March 1983). The generalized form of Born-Mayer equation without compressibility term has been modified and a polynomial of the type

$U_L = U_{ELBC}[k - 0.3729x + 0.0695x^2 + \dots]$ has been suggested for rapid and easy calculation of lattice energy in crystals. The relation is applied to calculate lattice energy in more than 40 different crystals. The results obtained show marked improvement over those reported by earlier workers. (10 refs.)

76355 On the mechanical stability of BCC transition elements and alloys. E.S.Machlin, J.Shao (Henry Krumb School of Mines, Columbia Univ., New York, NY, USA).

J. Phys. & Chem. Solids (GB), vol.44, no.5, p.435-44 (1983). A volume independent and a volume dependent lattice energy function involving short-range interatomic potentials were able to be fitted to the elastic constants, cohesive energy, lattice parameter and for the latter function to the vacancy formation energy and BCC-FCC lattice stability energy, as well, for FCC metals and BCC alkali metals, but not to the cohesive energy and C elastic constant of BCC transition metals. The assumption that directional, but partial, covalent bonds exist between nearest-neighbours in the BCC transition elements provides an explanation for the latter results and in addition explains the identical dependence of C' and the BCC-FCC lattice stability upon N_d , where N_d is the average number of d electrons, for the BCC transition metals and alloys. Both the mechanical and thermodynamic stability of the BCC structure for transition metals and all transition metal alloys disappears for $5-N_d \geq 2$ and < -1 . (19 refs.)

76356 Expansion of electrostatic multipole interaction energies of tetragonal, hexagonal and trigonal crystals in terms of strain tensor components. P.Herzig (Inst. fur Phys. Chem., Univ. Wien, Wien, Austria).

Solid State Commun. (USA), vol.46, no.9, p.685-8 (June 1983). The electrostatic multipole interaction energy of a crystal formulated within the spherical tensor rotation in a previous paper is expanded in terms of strain components. The method by Nijboer and de Wette (1957) can be used to calculate the required lattice sums. Expansions of this type are particularly useful to evaluate lattice energies by a minimization procedure, but other possible applications are also suggested. As examples, the electrostatic energies of tetragonal $\text{CaCl}_2 \cdot 6\text{H}_2\text{O}$ and of compounds with the chalcopyrite structure are expanded as functions of the axial ratio c/a , and, in the second case, also in terms of the internal parameter u . (15 refs.)

76357 The calculation of the electrostatic lattice energy of polar crystals by slice-wise summation, with an application to BeO. P.Hartman (Inst. voor Aardwetenschappen, Rijksuniversiteit Utrecht, Utrecht, Netherlands). *Z. Kristallogr. (Germany)*, vol.161, no.3-4, p.259-63 (1982). In the calculation of the electrostatic part of the lattice energy of polar crystals by slice-wise summation, as occurs in the Madelung method, an extra energy term, E_{corr} , is needed. This term is due to a double limit to infinity, one parallel to the slices, the other perpendicular to them. It was found that $E_{\text{corr}} = -2\pi\mu^2/V$, where μ is the dipole moment of the slice and V the unit cell volume. The method is applied to BeO. (10 refs.)

Possible equilibrium states of the zirconium-hydrogen system in the low temperature limit See Entry 76365

Study of sodium-nitrogen bonds in the oxynitrides NaSiO and NaGeON with normal tetrahedral structure See Entry 76397

Hybridization and surface relaxation in diamond-like crystals See Entry 76752

Electron densities and chemical bonding in TiC, TiN, and TiO derived from energy band calculations See Entry 76841

Electronic and cohesive properties of small sodium particles See Entry 76869

Infrared and Raman spectra of barium nitrite monohydrate See Entry 77381

Distinction between 'free' CS_3^{2-} in ionic compounds and coordinated CS_3^{2-} in metallic complexes by the means of IR spectroscopy of solids See Entry 77396

Nuclear magnetic resonance of silica polymorphs See Entry 78537

61.55 SPECIFIC STRUCTURE OF ELEMENTS AND ALLOYS

61.55D Nonmetallic elements

76358 The measurement of inner potential for diamond, germanium and silicon. D.E.Ashenford, N.D.Lisgarten (Phys. Dept., Imperial Coll., London, England).

Acta Crystallogr. Sect. A (Denmark), vol.A39, pt.3, p.311-14 (1 May 1983). Measurements of the inner potentials for diamond, germanium and silicon have been made using the Shinohara method and Kikuchi lines. In the case of germanium, a method has been derived which allows the use of crystals appreciably off-cut from nominal $\{hkl\}$ artificially prepared faces. The mean values obtained are 18.2 V for diamond, 13.4 V for germanium and 10.9 V for silicon. Comparisons are made with previous experimental results and theoretical calculations. (11 refs.)

76359 The recursion method and the electronic charge density in diamond and silicon. R.Jones, T.King (Dept. of Phys., Univ. of Exeter, Exeter, England).

Philos. Mag. B (GB), vol.47, no.5, p.491-3 (May 1983). A method for calculating the electronic charge density in a small region at the centre of a cluster of atoms by means of the recursion method is presented. The results of the application of this technique to diamond and silicon are discussed. (4 refs.)

61.55F Metallic elements

Oriented crystallization of metals in the presence of electric current See Entry 76596

61.55H Alloys

76360 Compounds with the structural type of ThMn_{12} in rare earth metal-gallium-iron systems. I.A.Griniv, O.I.Godovanets, R.V.Lapunova, Yu.M.Grin, Ya.P.Yarmolyuk.

Dopov. Akad. Nauk UkrSR. Ser. A (USSR), no.1, p.74-7 (1983). In Ukrainian.

Crystal structure of $\text{SmGa}_{0.5}\text{Fe}_{1.5}$ has been studied by the X-ray powder method: structure type ThMn_{12} , space group $14/mmm$, $a=0.8671(6)$, $c=0.5090(3)$ nm; 2 Sm in $2(a) 000$, 8 Fe in $8(f) 1/4 1/4 1/4$; $8\text{Ga}_{0.86}\text{Fe}_{0.14}$ in $8(i) x 00$, $x=0.336$; $8\text{Ga}_{0.86}\text{Fe}_{0.14}$ in $8(j) x 1/20$, $x=0.285$; R_1 -value is 0.116 for 40 reflections. Coordination numbers of atoms are: 20 for Sm; 12 for Fe; 12, 14 for Ga. Homogeneity ranges of compounds with ThMn_{12} type structure have been studied at 600°C for systems of Ce, Pr, Nd, Gd, Tb, Dy, Ho, Er, Tm, Yb, Y and lattice parameters have been determined. (8 refs.)

76361 Intermediate phases of vanadium-rhenium system. V.N.Eremenko, A.M.Kharkova, T.Ya.Velikanova.

Dopov. Akad. Nauk UkrSR. Ser. A (USSR), no.1, p.77-80 (1983). In Ukrainian.

The structure of vanadium-rhenium alloys and intermediate phases are studied by X-ray (Debye, diffractometric), optical microscopy, microdurometry and determination of the superconducting transition temperatures in a range of 69-86 at.% Re. The σ -phase is formed at the AB_3 composition. Its lattice constants are: $a=0.944\pm0.001$ nm, $c=0.489\pm0.001$ nm in the alloy containing 76 at.% Re, space group D_{4h}^{14} , structural type D8_h . The lower temperature limit of the σ -phase existence ranges between 1723 and 1773K. At the composition 71 at.% Re A -phase is formed, its structural type is $A-15$ (Cr_3Si), space group $\text{Pm}\bar{3}\text{n}$, $a=0.48783\pm0.00007$ nm. It is formed in peritectoid reaction $\alpha+\epsilon=A$ at the temperature range of 2223 and 2473K and undergoes the eutectoid disintegration $A\rightleftharpoons\alpha+\epsilon_1$ at about 1373K. (8 refs.)

76362 Crystal structure and magnetic susceptibility of RCuSn system. L.P.Komarova, R.V.Skolozdra, I.V.Filatova.

Dopov. Akad. Nauk UkrSR. Ser. A (USSR), no.1, p.81-3 (1983). In Ukrainian.

Crystal structure of LaCuSn and YCuSn was determined and magnetic susceptibility of RCuSn compounds ($R=\text{Y, La, Ce, Pr, Nd, Sm, Gd, Tb, Dy, Ho, Er, Tm, Lu}$) in a temperature range of 78-293K was measured. The structure of LaCuSn is isotypic of AlB_2 -type, the structure of other compounds belongs to CaIn_2 -type. Compounds with Y, La, Lu are Pauli paramagnetics, magnetic susceptibility of the other compounds, except SmCuSn , is described by the Curie-Weiss law. Effective magnetic moments of these compounds are in good agreement with the theoretical values for free R^{2+} ions; the moment of SmCuSn is 0.78 μ_B . (4 refs.)

76363 Allowance for a three-body potential in a theory of short-range order of dilute binary alloys. L.A.Bol'shov (Polytech. Inst., Vologda, USSR). *Fiz. Met. & Metalloved. (USSR)*, vol.55, no.4, p.636-42 (April 1983). In Russian. English translation in: *Phys. Met. & Metallogr. (GB)*.

The pair and three-body potentials are used to obtain an expression for the pair correlation function of a binary alloy in an approximation which is linear in the solute concentration. (14 refs.) A.T.

76364 Parametrized functionals of the local electron density in transition metals. Yu.A.Khon (Inst. of Atmospheric Optics, Acad. of Sci., Tomsk, USSR).

Fiz. Met. & Metalloved. (USSR), vol.55, no.4, p.643-8 (April 1983). In Russian. English translation in: *Phys. Met. & Metallogr. (GB)*.

An expression is obtained for the total energy of transition metals in the form of a functional of the local electron density containing parameters. An analysis of the correctness of the functionals obtained in this way is verified by calculating the atomic properties of some 3d-metals. (17 refs.) A.T.

76365 Possible equilibrium states of the zirconium-hydrogen system in the low temperature limit. I.G.Ratishvili (Inst. of Phys., Acad. of Sci., Tbilisi, Georgian SSR).

Fiz. Met. & Metalloved. (USSR), vol.55, no.4, p.665-75 (April 1983). In Russian. English translation in: *Phys. Met. & Metallogr. (GB)*.

The published experimental data are used to study the likely nature of ordering of hydrogen in the Zr-H system and the results are then used to identify the states of the system which should correspond to the lowest energy of the hydrogen atom subsystem at $T=0\text{K}$. (21 refs.) A.T.

76366 Structural changes in martensite observed in high-nickel steel as a result of low-temperature heating. L.I.Lysak, V.E.Danil'chenko, Ya.N.Vovk, V.A.Okhrimenko (Inst. of Metal Phys., Acad. of Sci., Kiev, Ukrainian SSR).

Fiz. Met. & Metalloved. (USSR), vol.55, no.4, p.717-23 (April 1983). In Russian. English translation in: *Phys. Met. & Metallogr. (GB)*.

The X-ray diffraction method was used to study structural changes in α -martensite during heating of high-nickel steel single crystals. The study was carried out between liquid nitrogen temperature and 100°C. Changes in the diffraction spots and diffuse fringes of α -martensite led to the conclusion of formation of twins in the $\{011\}\{011\}$ system and of precipitation of carbon in these twins and in the matrix martensite. (13 refs.) A.T.

76367 Short-range ordering in nickel-chromium thermocouple alloys. D.D.Pollock (Dept. of Mech. & Aerospace Engng., State Univ. of New York, Buffalo, NY, USA).

J. Test. & Eval. (USA), vol.11, no.3, p.225-6 (May 1983).

A short-range, lattice-ordering mechanism has been used extensively to explain the anomalous thermoelectric properties of such alloys as Chromel and Nicrosil. This concept appears to have had its origin in early crystallographic work that postulated this mechanism to explain experimentally observed changes in the relative electrical resistance of nickel-chromium alloys. Later crystallographic work, confirmed by several additional investigators, shows no evidence for the existence of short-range order in nickel-chromium alloys containing less than 25 at.% Cr. Since short-range ordering has not been established as being responsible for the thermoelectric properties of nickel-chromium alloys, this mechanism may not arbitrarily be considered as the sole rationale for their behaviors. (17 refs.)

76368 Electron microscopy study of two new long period structures in Pt_3Ti alloys ($3\leq x\leq 8$). D.Schryvers, J.van Landuyt, G.van Tendeloo, S.Amelinck (Rijksuniversiteit Antwerpen, Antwerp, Belgium).

Phys. Status Solidi a (Germany), vol.76, no.2, p.575-93 (16 April 1983).

Alloys with compositions varying between Pt_3Ti and Pt_3Ti are studied by means of electron diffraction and high resolution electron microscopy. The Pt_3Ti superstructure is confirmed and it is found that also in this case the light minority atoms can be revealed in high resolution images as bright dots under suitably chosen imaging conditions. Two new long period antiphase boundary structures based on the face centered cubic structure are determined: (a) an orthorhombic one-dimensional superstructure with composition $\text{Pt}_{13}\text{Ti}_2$ and (b) a tetragonal two-dimensional superstructure with composition $\text{Pt}_{21}\text{Ti}_4$. Descriptions of several faults in the microtexture of these superstructures are given. (9 refs.)

76369 Neutron diffraction study of the $\text{Ni}_2\text{Mn}_{1-x}\text{Cr}_x\text{Sn}$ system. W.Bazela-Wrobel, A.Szytula (Inst. of Phys., Tech. Univ. of Cracow, Cracow, Poland).

Phys. Status Solidi a (Germany), vol.76, no.2, p.K117-20 (16 April 1983).

Reports on structural and magnetic properties of cubic $\text{Ni}_2\text{Mn}_{1-x}\text{Cr}_x\text{Sn}$ obtained by means of X-ray and neutron diffraction as well as magnetometric methods. (8 refs.)

The short-range structure of Ti and Zr BCC solid solutions containing the α phase. III. Extension of the diffraction theory to partially transformed systems See Entry 76248

Microstructure and properties of fine grained supersaturated Fe-C alloys See Entry 76650

Note on the magnetic and magneto-optical properties of Ni_2In type 3d transition metal compounds See Entry 77156

On the change in the austenite lattice parameter due to the martensitic transformation in an Fe-32Ni alloy See Entry 77636

Martensitic transformations in low-carbon nickel-molybdenum steels See Entry 77638

61.60 SPECIFIC STRUCTURE OF INORGANIC COMPOUNDS

76370 The crystal structure of $\text{K}_2\text{Si}^{\text{IV}}\text{Si}^{\text{IV}}\text{O}_6$. D.K.Swanson, C.T.Prewitt (Dept. of Earth & Space Sci., State Univ. of New York, Stony Brook, NY, USA).

Am. Mineral. (USA), vol.68, p.581-5 (May-June 1983).

The crystal structure of $\text{K}_2\text{Si}^{\text{IV}}\text{Si}^{\text{IV}}\text{O}_6$ has been refined in space group $\text{P6}_3/\text{m}$ to an $R=2.02\%$ and is confirmed to be isotypic with wadeite ($\text{K}_2\text{ZrSi}_2\text{O}_6$). The atomic charges of $\text{Si}^{\text{IV}}\text{O}_4$, $\text{O}(1)_{\text{br}}$ and $\text{O}(2)_{\text{br}}$ are +3.3, +2.5, -1.4 and -1.4, respectively, and suggest that an increase in the coordination number of a Si atom from 4 to 6 significantly increases the ionic character of that atom. The mean octahedral Si-O distance, 1.778 Å, compares well with that predicted by an empirical equation, 1.781 Å.

76371 Unusual cell volume behavior in the $\text{LaNb}_{1-x}\text{V}_x\text{O}_4$ system. A.T.Aldred (Materials Sci. Div., Argonne Nat. Lab., Argonne, IL, USA).

Mater. Lett. (Netherlands), vol.1, no.5-6, p.197-9 (April 1983).

The crystal structures and lattice constants of the $\text{LaNb}_{1-x}\text{V}_x\text{O}_4$ system have been determined at room temperature. The system undergoes a monoclinic to tetragonal phase transformation with an increase in x analogous to the transition as a function of temperature in pure LaNbO_4 . The unit cell volume increases with an increase in x in the monoclinic phase despite the fact that

vanadium is a smaller ion than niobium. A more normal contraction of the cell volume is observed in the tetragonal phase. The origin of this unusual behavior is unclear at present. (12 refs.)

76372 On the crystal structure of some non-stoichiometric mixed lead oxide halides and their relation to the minerals 'Loretoite' and 'Sundiusite'. B. Aurivillius (Div. of Inorganic Chem., Lund Inst. of Technol., Lund, Sweden). *Chem. Scr. (Sweden)*, vol.22, no.1, p.5-11 (1983).

Synthetic lead oxychloride, $\alpha\text{-Pb}_2\text{O}_6\text{Cl}_2$, isotypic to the now discredited mineral loretoite, has previously been assigned a pseudo-tetragonal unit cell, ASTM Card 6-0393. It is shown here that a phase with this metrics can not be obtained on melting pure PbO and pure PbCl₂ in inert crucibles. Phases with the metrics of $\alpha\text{-Pb}_2\text{O}_6\text{Cl}_2$ have previously been obtained by the present author on contaminating compounds $7\text{PbO}\cdot\text{PbX}_2$, $\text{X}=\text{Cl}$, Br or I, with oxides of the elements R: Si, Ge, P, V, As, Mo and W. The general idealized formula of these compounds is $(7-n)\text{PbO}\cdot n\text{RO}_3\cdot\text{PbX}_2$. Their crystal structures are disordered but their subcells are found to consist of $(\text{Pb}, \text{R})_4\text{O}_4\pm\epsilon^+$ blocks and X^- layers. Ideally the unit cells contain $10(\text{Pb}+\text{R}+\text{X})$ layers. The present work deals with chlorides and bromides where $\text{R}=\text{Ti}$, Nb, Ta, S and Cr. Single crystal diffractometer data were collected for $6\text{PbO}\cdot\text{NbO}_3\cdot\text{PbBr}_2$, $6.5\text{PbO}\cdot0.5\text{SO}_3\cdot\text{PbCl}_2$ and $6.5\text{PbO}\cdot0.5\text{CrO}_3\cdot\text{PbCl}_2$. The data could be interpreted by means of the above structure. The R -factors and number of observed reflections are in turn: 0.1237, 192 independent; 0.0589, 195 independent and 0.0774, 495 ($hkl\pm hkl$). Synthetic $8\text{PbO}\cdot\text{PbSO}_4\cdot\text{PbCl}_2$ prepared on reacting the components in platinum crucibles at 640 or 780°C is poly-phasic with an observed density of 8.0 Mg m^{-3} . (6 refs.)

76373 X-ray diffraction study of basal (ab)-plane structure and diffuse scattering from silver atoms in disordered stage-2 $\text{Ag}_{0.18}\text{TiS}_2$. K.-I. Ohshima, S.C. Moss (Dept. of Phys., Univ. of Houston, Houston, TX, USA). *Acta Crystallogr. Sect. A (Denmark)*, vol.A39, pt.3, p.298-305 (1 May 1983). X-ray results are presented on the crystallographic parameters in the basal (ab) plane and the short-range order diffuse scattering from intercalated silver atoms in disordered stage-2 $\text{Ag}_{0.18}\text{TiS}_2$ at room temperature. The silver atoms in the intercalated plane occupy the octahedral sites and the in-plane temperature parameter of the silver atoms has a value of $B=3.0\pm0.1\text{ Å}^2$, suggesting both weak bonding and correspondingly rapid diffusion. Rodlike diffuse scattering parallel to c^* at $1/3, 2/3, 0$ and their equivalent positions is observed and reveals the three-dimensional (2D) feature of the disordered state. From analyzing this 2D diffuse intensity by the method of Borie & Sparks (1971), the planar short-range order parameters were determined. A comparison of this planar short-range order with the 2D Ornstein-Zernike correlation function demonstrates the long-range nature of the 2D short-range order with a correlation range κ^{-1} of $4.88\pm0.4\text{ Å}$. Using a linearized mean-field approximation for the correlation functions of a binary Ising system well above T_c developed by Clapp & Moss (1966), a set of oscillatory atomic-pair interaction potential ratios was obtained where the direct interactions were significant out to at least four to five neighbors. (21 refs.)

76374 Electron density in NaF and KCl crystals in the self-consistent local-density-functional approximation (LDA). G. Bobel, P. Cortona (Istituto di Sci. Fisiche, Univ. di Genova, Genova, Italy), C. Sommers, F.G. Fumi. *Acta Crystallogr. Sect. A (Denmark)*, vol.A39, pt.3, p.400-7 (1 May 1983). The electron density $\rho(r)$ in NaF and KCl crystals—composed of 'isoelectronic' alkali and halogen ions—has been computed self-consistently by the method of augmented spherical waves in the local-density-functional approximation (LDA). Calculations were also carried out of the heat of formation of the salts from the alkali metal and the halogen molecule from the pertinent total energies as well as the diamagnetic susceptibility of the solid. The structure factors were then calculated for the low-order 'difference' and 'sum' reflections, the former of which are particularly sensitive to ionic deformations. The computed structure factors are compared with the structure factors obtained from experiment. The latter are also compared with the structure factors calculated from the Hartree-Fock free-ion atomic factors. The conclusion is that in the NaF and KCl crystals the anion 'contracts' and the cation 'expands' in passing from the free-ion state to the state of the ion in the crystal. Independent evidence of this type of effect is provided by the Tessman et al. (1953) 'ionic polarizabilities' and by the Fumi & Tosi, Tosi & Fumi (1964) 'crystal ionic radii'. (77 refs.)

76375 X-ray, crystal data, magnetic susceptibility and electrical conductivity of hydrated trnickel pentasulphide. J.P. Mishra, Lakshmi (Dept. of Chem., Univ. of Gorakhpur, Gorakhpur, India). *Indian J. Pure & Appl. Phys.*, vol.21, no.3, p.69-72 (Feb. 1983). The compound, hydrated trnickel pentasulphide, has been prepared in solid state condition. X-ray powder diffraction pattern of the compound shows cubic structures with $a=8.503\text{ Å}$ and $Z=3$. The magnetic susceptibility measurement shows that the compound is paramagnetic in the temperature range 305-715K with Curie constant $C=1.62\text{ K emu/mol}$ and effective magnetic moment $p=3.60\text{ } \mu_B$ (Bohr magnetron). The electrical conductivity measurement explains the impurity levels and intrinsic semiconducting behaviour in the temperature range 313-433K and 533-713K with activation energy 0.05 and 0.60 eV respectively. Above 713K, the compound becomes metallic. Thermogravimetric analysis and differential analysis data indicate the presence of nonstoichiometric compound and dehydration step. The density of the compound is found to be $3.20\pm0.10\text{ g/cc}$. (8 refs.)

76376 Cation distribution from Cu²⁺ temperatures in slow cooled and quenched copper ferrite samples. S.A. Patil (Phys. Dept., Shivaji Univ., Kolhapur, India).

Indian J. Pure & Appl. Phys., vol.21, no.3, p.182-3 (March 1983). Curie temperatures for slow cooled and quenched copper ferrite samples are used to compute cation distribution using Gillet's formula. Cation distribution is discussed on the basis of oxygen nonstoichiometry and square bond formation of Cu^{2+} in copper ferrite. The deviation in theoretical and experimental magnetic moment values may be due to randomly distributed Cu^{2+} ions in oxygen interstices and formation of Fe^{3+} ions on B sites. (14 refs.)

76377 Fe_3PO_7 , a case of Fe^{3+} fivefold coordination. Structural and magnetic studies. A. Modaresi, A. Courtois (Lab. de Chimie du Solide Mineral, Univ. de Nancy, Nancy, France), R. Gerardin, B. Malman, C. Gleitzer. *J. Solid State Chem. (USA)*, vol.47, no.3, p.245-55 (May 1983). In French. The structure of Fe_3PO_7 is established from a single crystal. The cell is trigonal $R\bar{3}m$, with, in hexagonal reference $a=8.006(5)$, $c=6.863(5)\text{ Å}$, $Z=3$. The structure is determined with the direct method and refined to $R=0.027$. The PO_4 tetrahedra are isolated; the iron atoms are in a five coordinated site constituted of trigonal bipyramids sharing 2 edges and forming groups of 3 hexahedra; through these shared edges the iron atoms are at 3.13 Å a distance rather short which brings a repulsion causing the off centering of the cation along the pseudo axis of the bipyramid. The magnetic measurements and the Mossbauer spectroscopy show antiferromagnetic behaviour and, in the paramagnetic state, outstanding parameters ($\mu=6.45\text{ } \mu_B$, $\theta_p=-1707\text{ K}$) recalling however $\text{Ca}_2\text{Fe}_2\text{O}_5$ or LaFeO_3 . The Mossbauer spectroscopy gives, at room temperature, parameters classical for trivalent

iron; through cooling, it points to a magnetic transition temperature of $160\pm3\text{ K}$ below which the spectrum displays at least 2 hyperfine patterns. The magnetic interactions are discussed. (44 refs.)

76378 Crystal structure of $\text{Fe}_2\text{P}_2\text{O}_7$. J.T. Higgins (Ventures Res. Div., Ashland Chem. Co., Dublin, OH, USA), J.S. Swinnea, H. Steinfink. *J. Solid State Chem. (USA)*, vol.47, no.3, p.278-83 (May 1983). $\text{Fe}_2\text{P}_2\text{O}_7$ crystallizes in the $C1$ space group with lattice parameters $a=6.649(2)\text{ Å}$, $b=8.484(2)\text{ Å}$, $c=4.488(1)\text{ Å}$, $\alpha=90.04^\circ$, $\beta=103.89(3)^\circ$, $\gamma=92.82(3)^\circ$, and $\rho_{\text{calc}}=3.86\text{ g/cc}$. It is essentially isostructural with $\beta\text{-Zn}_2\text{P}_2\text{O}_7$. As in the Zn compound, the bridging oxygen atom in the P_2O_7 group shows a high anisotropic thermal motion. It appears that the P-O-P bond angle is linear as a result of extensive p bonding with the p orbitals on the bridging oxygen atom. The high thermal motion is vibration of the atom into cavities in the structure. (10 refs.)

76379 Preparation and properties of the systems $\text{Fe}_{2-x}\text{Cr}_x\text{WO}_6$, $\text{Fe}_{2-x}\text{Rh}_x\text{WO}_6$, and $\text{Cr}_{2-x}\text{Rh}_x\text{WO}_6$. H. Leiva, R. Kershaw, K. Dwight, A. Wold (Dept. of Chem., Brown Univ., Providence, RI, USA). *J. Solid State Chem. (USA)*, vol.47, no.3, p.293-300 (May 1983). Solid solutions of the end members Fe_2WO_6 , Cr_2WO_6 , and Rh_2WO_6 have been prepared and their crystallographic and magnetic properties studied. All solid solutions crystallize with the trirutile structure, and their magnetic behavior is characterized by the existence of antiferromagnetic interactions and effective molar Curie constants corresponding to those expected from contributions of the spin only moments of high-spin Fe^{3+} , Cr^{3+} , and diamagnetic low-spin Rh^{3+} ions. Fe_2WO_6 crystallizes with the tri- α - PbO_2 structure and is antiferromagnetic and conducting. The random rutile Rh_2WO_6 is conducting, and the difference between its magnetic and electric properties and those of the inverse trirutile Cr_2WO_6 are discussed in terms of possible interactions between $\text{Cr}^{3+}(3d)$ or $\text{Rh}^{3+}(4d)$ orbitals and $\text{W}^{6+}(5d)$ orbitals. (17 refs.)

76380 Preparation and crystal structure of $\text{Na}_2\text{Mn}_2\text{S}_3$. K. Klepp, P. Bottcher, W. Bronger (Inst. für Anorganische Chem., RWTH Aachen, Aachen, Germany). *J. Solid State Chem. (USA)*, vol.47, no.3, p.301-6 (May 1983). $\text{Na}_2\text{Mn}_2\text{S}_3$ was prepared by reacting manganese powder with an excess of anhydrous sodium carbonate and elemental sulfur at 870K. Extraction of the solidified melt with water and alcohol yielded well developed, bright red crystals. $\text{Na}_2\text{Mn}_2\text{S}_3$ crystallizes with a new monoclinic structure type, space group $C2/c$, $Z=8$, with $a=14.942(2)\text{ Å}$, $b=13.276(2)\text{ Å}$, $c=6.851(2)\text{ Å}$, and $\beta=116.50(1)^\circ$. The crystal structure was determined from single crystal diffractometer data and refined to a conventional R value of 0.026 for 1613 observed reflections. The atomic arrangement shows sulfur-manganese-sulfur slabs which are separated from each other by corrugated layers of sodium atoms. A prominent feature of the crystal structure is the formation of short, four-membered zigzag chains built up by MnS_4 tetrahedra sharing edges. These chains are further connected by the remaining apices to form an infinite sheet. Short Mn-Mn distances (3.02 and 3.05 Å, respectively) are found within the four membered chains. Susceptibility measurements show antiferromagnetic interactions between the Mn atoms. (11 refs.)

76381 Preparation and structure of fluorite-type $(\text{Sr}_x\text{Y}_{1-x})\text{Cl}_{2.05}$. E. Mason, H.A. Fick (Dept. of Chem., Michigan State Univ., East Lansing, MI, USA). *J. Solid State Chem. (USA)*, vol.47, no.3, p.314-21 (May 1983). Anion excess colorless fluorite-type strontium-yttrium chloride has been prepared. Single crystals of the Sr-Y compound exhibit a primitive cubic lattice with $a=6.967(1)\text{ Å}$. Two mutually exclusive structural models for solutions, neither of which is exact, are discussed. The first is a vacancy model in which the extra charge which results from substitution of Y^{3+} for Sr^{2+} is balanced by the simultaneous removal of a $\text{Sr}^{2+}\text{-Cl}^-$ ion pair. This model requires individual ion sites to be partially occupied and nonequivalent and is strongly suggestive of vacancy ordering. Refinement in space group $P1$, with sites refined independently, led to $R=0.1096$. The second model describes the structure in terms of a Willis cluster of defects and includes both anion vacancies and interstitial anions. Full-matrix least squares refinement in space group $Fm\bar{3}m$, with positions analogous to those in UO_2 and $(\text{Ca}_x\text{Y}_{1-x})\text{F}_{2.10}$, converged at $R=0.0633$ for the 114 face-centered parent structure reflections whose $|F|^2 > \sigma(F^2)$. This second model is discussed in relation to a probable true solution which involves long range order. (37 refs.)

76382 The oxysulfide anion $[\text{NbS}_2\text{O}]^{3-}$: synthesis and crystal structure of $\text{Ba}_2(\text{NbS}_2\text{O})(\text{NbS}_2\text{O})_3$. L.E. Rendon-Diazmirion (Inst. de Investigaciones en Materiales, Univ. Nacional Autonoma de Mexico, Mexico City, Mexico), C.F. Campana, H. Steinfink. *J. Solid State Chem. (USA)*, vol.47, no.3, p.322-7 (May 1983). The authors report on the preparation and crystal structure of $\text{Ba}_2(\text{NbS}_2\text{O})(\text{NbS}_2\text{O})_3$ using X-ray diffraction techniques. The structure was solved using the direct method which provided Ba and Nb positions. Three-dimensional electron density maps calculated from amplitudes phased with the heavy atoms revealed the S positions. The conventional R remained around 7%, the temperature factors for two S atoms were anomalously high, and bond lengths to Nb were very short. Replacing these atoms with oxygen permitted refinement of the data to a conventional R of 4.02% and $\omega R=4.19\%$ for the observed 1599 independent reflections. (21 refs.)

76383 A structure refinement of the high pressure modification Ba_2II . H.P. Beck (Inst. für Anorganische Chem., Erlangen, Erlangen, Germany). *J. Solid State Chem. (USA)*, vol.47, no.3, p.328-32 (May 1983). A high pressure phase Ba_2II , which can be quenched and retained as a metastable form at ambient conditions, is reported. The structure has been determined by X-ray investigations using single crystals. Ba_2II crystallizes in an anti- Fe_2P -type arrangement, space group $P6_2m$, $a=9.142(6)\text{ Å}$, $c=5.173(3)\text{ Å}$, which is slightly denser than the PbCl_2 -type structure found at normal pressure. Structural features of the two phases are discussed in comparison. (11 refs.)

76384 Aluminum distribution in the boron framework of $\gamma\text{-AlB}_{12}$. I. Higashi (Inst. of Phys. & Chem. Res., Saitama, Japan). *J. Solid State Chem. (USA)*, vol.47, no.3, p.333-49 (May 1983). The crystal structure of $\gamma\text{-AlB}_{12}$ ($P2_12_1$), $a=16.573(4)\text{ Å}$, $b=17.510(3)\text{ Å}$, $c=10.144(1)\text{ Å}$ was reinvestigated by single-crystal X-ray diffractometry and the nature of the metal distribution in the boron framework examined. Starting from the structure data published by Hughes et al. (1977), 458 independent parameters, including the occupancies of 11 Al sites, were finally refined to a conventional R value of 2.9%. A total of 5282 observed unique reflections ($\text{MoK}\alpha$ radiation; $2\theta < 64^\circ$) were used. Although distributed in an apparently complicated manner, the aluminum atoms occur in the boron framework according to a simple rule as in the crystals of the $\alpha\text{-AlB}_{12}$ structure type. The numbers of the valence electrons of Al, allotted to the six boron subunits, $\text{B}_{12}(\text{i-iv})$, $\text{B}_{20}(\text{C}_2\text{C}_3)$, proportionately to the contact frequencies of Al with the units, are 2.2, 1.9, 2.2, 1.9, 5.3, and 5.2, respectively. The charge assignment is compatible with the ionic formula $20/3\text{ Al}^{+2.4}\text{B}_{12}^{2-}\cdot 2\text{B}_{20}^{2-}$, proposed from preliminary molecular orbital calculations. A negative charge balance among the six boron units at about 1:1:1:1:3:3

seems to be essential for making up the stable boron framework of $\gamma\text{-AlB}_{12}$. (17 refs.)

76385 Structural aspect of a $\text{Zn}_{0.25}\text{Mn}_{0.12}\text{Fe}_{0.13}\text{S}_{0.5}$ crystal. Zhen-Chuan Kang (Dept. of Phys., Arizona State Univ., Tempe, AZ, USA). *J. Microsc. & Spectrosc. Electron. (France)*, vol.8, no.1, p.19-24 (Feb. 1983). The structure and composition of a crystal of $\text{Zn}_{0.25}\text{Mn}_{0.12}\text{Fe}_{0.13}\text{S}_{0.5}$, found in a sample of the mineral frankite, have been determined by electron microscopy and microanalysis. It is a polytype of the form ...ABABABACACA... with composition in weight per cent determined by X-ray spectroscopy as 34.9 ± 0.1 Zn, 15.5 ± 0.1 Fe, 14.8 ± 0.1 Mn, 34.7 ± 0.1 S. (4 refs.)

76386 The crystal and molecular structure of dihydroxy (malonato)-diammine platinum (II). Li Genpei, Tang Youqi (Inst. of Phys. Chem., Peking Univ., Peking, China), Guan Yintong, Tang Wenxia, Dai Anbang. *Kexue Tongbao (Foreign Lang. Ed.) (China)*, vol.28, no.2, p.200-5 (Feb. 1983).

A few platinum complexes having antitumor properties have attracted much interest in recent years. The authors have synthesized and tested the Pt(IV) malonato complex, which appears to exhibit significant activity on W-256 cancer. For this reason and in order to obtain more interesting information on the Pt(IV) malonato complex, they have determined the crystal and molecular structure. (10 refs.)

76387 Plane $[\text{Te}_6]^{4-}$ ions connected in chains in K_2SnTe_6 . B.Eisenmann, H.Schwerer, H.E.Schafer (Abteilung II für Anorganische Chem., Tech. Hochschule Darmstadt, Darmstadt, Germany).

The new compound K_2SnTe_6 crystallizes in the tetragonal system (space group: 14cm , Nr.108) with $a=848.1(3)$ pm, $c=1536.9(7)$ pm, $c/a=1.812$, $z=4$. In the structure there are plane $[\text{Te}_6]^{4-}$ anions, which are connected to chains by tetrahedrally coordinated Sn-atoms. (3 refs.)

76388 Synthesis and crystal structure of the inter-alkali-metal chloride RbLiCl_2 . H.-C.Gaebell, G.Meyer, R.Hoppe (Inst. für Anorganische und Analytische Chem., Univ. Giessen, Giessen, Germany).

The crystal structure of RbLiCl_2 [$a=1441.3(3)$, $b=412.57(8)$, $c=720.9(1)$ pm, Guinier-Simon data, orthorhombic, Ccmn, No.63, $Z=4$] was determined and refined from single crystal data, with $R=0.074$, $R_w=0.062$. The coordination polyhedron of Rb^+ is a bicapped trigonal prism, since Li^+ is tetrahedrally coordinated. $[\text{LiCl}_4]^-$ tetrahedra are connected via common corners to undulated layers $\text{O}_2^-[\text{LiCl}_4]^-$ parallel to (100). The structure is closely related to that of SrZnO_3 . (16 refs.)

76389 $\text{Ti}_x\text{Ti}_6\text{Se}_8$ and $\text{Ti}_x\text{Nb}_6\text{Se}_8$, two phases with filled up Nb_3Te_4 type of structure showing pronounced cation disorder. H.Boller (Inst. für Phys. Chem., Univ. Wien, Wien, Austria), K.Klepp.

The new ternary chalcogenides $\text{Ti}_x\text{Ti}_6\text{Se}_8$ ($x=0.76$) and $\text{Ti}_x\text{Nb}_6\text{Se}_8$ ($x=0.70$) crystallize with a partially filled up Nb_3Te_4 structure: space group $P6_3/m$, $Z=1$ with $a=9.882(1)$, $c=3.590(1)$ Å ($\text{Ti}_{0.76}\text{Ti}_6\text{Se}_8$); $a=10.033(2)$, $c=3.475(1)$ Å ($\text{Ti}_{0.70}\text{Nb}_6\text{Se}_8$). The crystal structures were determined from single crystal diffractometer data and refined to conventional R-values of 0.077 and 0.055 respectively. The Ti atoms in the octahedral channels cannot be localized. In $\text{Ti}_x\text{Ti}_6\text{Se}_8$ diffuse scattering indicates one-dimensional short range order. A model of the cation distribution in $\text{Ti}_{0.76}\text{Ti}_6\text{Se}_8$ is discussed. (8 refs.)

76390 Refinement of the crystal structure of CeO_2Si_2 (ThCr $_2\text{Si}_2$ -type).

C.Horvath, P.Rogl (Inst. für Phys. Chem., Univ. Wien, Wien, Austria). *Mater. Res. Bull. (USA)*, vol.18, no.4, p.443-8 (April 1983). The crystal structure of CeO_2Si_2 has been determined from single crystal X-ray counter data. CeO_2Si_2 is tetragonal, $14/mmm$, $Z=2$; the cell parameters are $a=0.41617(5)$ and $c=0.98481(28)$ nm. The final reliability factor $R=\Sigma|\Delta F|/\Sigma|F_0|$ is 0.027 for 129 observed reflections ($|F_0|>2\sigma$). CeO_2Si_2 is isotypic with the ordered structure type of ThCr_2Si_2 (BaAl $_4$ -derivative type). (15 refs.)

76391 Lithium insertion into manganese spinels. M.M.Thackeray, W.I.F.David, P.G.Bruce, J.B.Goodenough (Inorganic Chem. Lab., Univ. of Oxford, Oxford, England).

Lithium has been inserted chemically and electrochemically into Mn_2O_4 and $[\text{LiMn}_2]\text{O}_4$ at room temperature. From X-ray diffraction, it is shown that the $[\text{Mn}_2]\text{O}_4$ subarray of the $\text{A}[\text{B}_2]\text{X}_4$ spinels remains unperturbed and that the electrons compensating for the Li^+ -ion charge reduce Mn^{3+} to Mn^{2+} in Mn_2O_4 and Mn^{3+} to Mn^{2+} in $[\text{LiMn}_2]\text{O}_4$. In $\text{Li}_x\text{Mn}_2\text{O}_4$, the tetragonal distortion due to a cooperative Jahn-Teller distortion by octahedral-site Mn^{3+} ions decreases with x from $c/a=1.157$ for $x=0$ to $c/a=1.054$ for $x=1$. The system $\text{Li}_{1+x}[\text{Mn}_2]\text{O}_4$ is cubic at $x=0$ and tetragonal ($c/a=1.161$) at $x=1.2$. Electrochemical data reveal a two-phase region in the $\text{Li}_{1+x}\text{Mn}_2\text{O}_4$ system and a maximum $x_m=1.25$. X-ray diffraction confirms the coexistence of a cubic and a tetragonal phase in the compositional range $0.1 \leq x \leq 0.8$. The X-ray data also show that the inserted Li^+ ions occupy the interstitial octahedral positions of the spinel structure. However, in $\text{Li}_x\text{Mn}_2\text{O}_4$ the tetrahedral-site Mn^{2+} ions are displaced from the A positions to the interstitial octahedral positions, as in $\text{Li}_x\text{Fe}_2\text{O}_4$, whereas the tetrahedral-site Li^+ ions in $[\text{LiMn}_2]\text{O}_4$ remain on the A sites. (7 refs.)

76392 Study of the structure and the conditions of stability of a new arsenide of iron: $\text{Fe}_{12}\text{As}_5$. S.Maaref, R.Madar (ENIG, Gabes, Tunisia).

The crystal structure determination of the new phase $\text{Fe}_{12}\text{As}_5$, like the isostructural phase $(\text{RuFe})_{12}\text{As}_5$, gives a rhombohedral cell with space group $R\bar{3}$. The metallic atoms are for one part inserted in square pyramidal and triangular bipyramidal sites and for the other part gathered in a metallic bipyramidal cluster. This description makes clear the relation between the structures of M_2X and M_3X phases. This new structural type appears as an intermediate case resulting from the increase of metallic interactions leading to the formation of metallic clusters. (8 refs.)

76393 Crystalline structure and magnetic properties of the low temperature variation of $\beta\text{-TiFeBr}_3$. N.Jouini, L.Guen, M.Tournoux (Lab. de Chimie des Solides, UER de Chimie, Nantes, France).

DTA and X-ray studies of TiFeBr_3 show a transition at 384°C . The low temperature phase $\beta\text{-TiFeBr}_3$ is related to NH_4CdCl_3 and crystallizes in the orthorhombic system with $a=9.279(4)$ Å, $b=3.984(3)$ Å, $c=15.070(7)$ Å, $Z=4$. The crystal structure has been determined from 564 independent reflections. The structure contains FeBr_6 octahedra in which each Fe atom is coordinated to six Br atoms. The FeBr_6 octahedra share vertices to form infinite double chains along the b axis. This compound behaves paramagnetically above 40K , with a Curie-Weiss temperature of $\theta=12\text{K}$ and a magnetic moment of $\mu=5.59 \mu_B$, but becomes antiferromagnetic below 14K . (22 refs.)

76394 A series of rare earth silicates $\text{RE}_2^{3+}\text{M}^{3+}[\text{SiO}_4]_2(\text{OH})$ [synthesis and crystal structure]. P.Bettermann, J.Lexow, F.Liebau, F.Seifert (Mineralogisches Inst., Univ. Kiel, Kiel, Germany).

A series of isotypic silicates of composition $\text{RE}_2\text{M}[\text{SiO}_4]_2(\text{OH})$ with $\text{RE}=\text{La}^{3+}$, Ce^{3+} , Pr^{3+} , Nd^{3+} , Sm^{3+} , Eu^{3+} , and $\text{M}=\text{Al}^{3+}$, Fe^{3+} has been synthesized under hydrothermal conditions. Lattice constants of two members as determined from single crystal X-ray diffraction data are: $\text{La}_2\text{Al}[\text{SiO}_4]_2(\text{OH})$ ($\text{La}_2\text{Fe}[\text{SiO}_4]_2(\text{OH})$) $a_0=7.401$ (7.346) Å, $b_0=5.702$ (5.862) Å, $c_0=17.072$ (17.196) Å, $\beta=112.4^\circ$ (112.5°), $P2_1/c$, $Z=4$. (10 refs.)

76395 Fluorinated compounds $\text{A}^{\text{I}}\text{BaM}_2^{\text{III}}\text{F}_9$ ($\text{A}^{\text{I}}=\text{Na}, \text{K}$; $\text{M}^{\text{III}}=\text{Ga}, \text{Cr}, \text{V}, \text{Fe}$). A.de Kozak, M.Samouel (Univ. Pierre et Marie Curie, Paris, France), M.Lebland, G.Ferey.

Rev. Chim. Miner. (France), vol.19, no.6, p.668-72 (1982). In French. Solid state synthesis, crystallochemical and magnetic investigations are presented of a new fluoride series of formula $\text{A}^{\text{I}}\text{BaM}_2^{\text{III}}\text{F}_9$, isotypical with monocline $\text{Ba}_2\text{CoFeF}_9$. (5 refs.)

76396 Crystal structure of $\text{Nd}_2\text{AlO}_3\text{N}$. Determination of the oxygen-nitrogen order by neutron diffraction. R.Marchand, R.Pastuszak, Y.Laurent, G.Roult.

Rev. Chim. Miner. (France), vol.19, no.6, p.684-9 (1982). In French. Oxynitride $\text{Nd}_2\text{AlO}_3\text{N}$ crystallizes in the tetragonal system with $a=3.7046(2)$ and $c=12.5301(13)$ Å. It possesses a structure which is related to the K_2NiF_6 type which can be described as a two-dimensional perovskite. The ordered arrangement between oxygen and nitrogen has been determined by time-of-flight neutron diffraction and profile analysis. This order leads to a loss of symmetry and the space group is 14mm . The aluminum atoms are at the centre of octahedra built up by five oxygen and one nitrogen. The two independent neodymium atoms have a coordination number of 9 but their environment is quite different. (7 refs.)

76397 Study of sodium-nitrogen bonds in the oxynitrides NaSiO and NaGeON with normal tetrahedral structure. J.Guyader, J.-M.Malhaire, Y.Laurent (UER, 'Structure et Propriétés de la Matière', Rennes, France).

Rev. Chim. Miner. (France), vol.19, no.6, p.701-6 (1982). By heating Na_2SiO_3 at $900-950^\circ\text{C}$ and Na_2GeO_3 at 750°C under an ammonia flow, two new oxynitrides NaSiON and NaGeON have been prepared. They are isotypic with LiSiON and possess a normal tetrahedral structure related to the wurtzite-type. The unit cells are orthorhombic with parameters $a=5.346$ (2), $b=7.186$ (3), $c=4.823$ (2) Å for NaSiON and $a=5.584$ (3), $b=7.403$ (3), $c=5.037$ (2) Å for NaGeON . The space group is $P2_1$. They are the first compounds showing tetrahedra $\text{Na}(\text{O}_3\text{N})$ with Na-N stable bonds. (9 refs.)

76398 Refinement of the crystal structures of two manganese silicates $\text{Na}_2\text{Mn}_2\text{Si}_2\text{O}_7$ and $\text{Na}_5(\text{Mn}, \text{Na})_3\text{MnSi}_2\text{O}_{18}$. L.P.Otoshchenko, V.I.Simonov, N.V.Belov (A.V. Shubnikov Inst. of Crystallography, Acad. of Sci., Moscow, USSR).

Sov. Phys.-Dokl. (USA), vol.27, no.7, p.511-13 (July 1982). Translation of: Dokl. Akad. Nauk SSSR, vol.265, no.1-3, p.76-9 (July 1982). [received: April 1983] The structures of two manganese silicates, $\text{Na}_2\text{Mn}_2\text{Si}_2\text{O}_7$ and $\text{Na}_5(\text{Mn}, \text{Na})_3\text{MnSi}_2\text{O}_{18}$ have been refined, using diffractometric data in the anisotropic approximation for the amplitudes of the thermal vibrations of the atoms, to discrepancy factors $R=6.1$ and 5.9% respectively, from 1319 to 1675 independent structure amplitudes. In the diorthosilicate $\text{Na}_2\text{Mn}_2\text{Si}_2\text{O}_7$ one of the basal Mn^{2+} cations was located in a fairly regular MnO_4 tetrahedron while the other was located in a trigonal MnO_3 bipyramid with a substantial scatter of Mn-O distances (2.05-2.46 Å). The metasilicate $\text{Na}_5(\text{Mn}, \text{Na})_3\text{MnSi}_2\text{O}_{18}$ is characterized by the fact that, along with purely Na and Mn polyhedra, polyhedra which are randomly occupied by Na^+ and Mn^{2+} cations jointly are also present in its structure. (11 refs.)

76399 Crystal structure of a new Na, Fe^{3+} orthophosphate $(\text{Fe}_9\text{O}_{15}[\text{H}_{1.5}\text{O}_{0.5}]\text{Na}_5[\text{PO}_4]_2=\text{Fe}_9\text{O}_{15}^{3+}\text{Na}_5[\text{PO}_4]_2\text{F}_{0.5}\text{SHF}$. O.V.Yakubovich, E.N.Matvienko, M.A.Simonov, N.V.Belov (M.V. Lomonosov State Univ., Moscow, USSR).

Sov. Phys.-Dokl. (USA), vol.27, no.7, p.516-18 (July 1982). Translation of: Dokl. Akad. Nauk SSSR, vol.265, no.1-3, p.83-8 (July 1982). [received: April 1983]

The unit-cell parameters were determined by the oscillating-crystal method (X-ray powder camera, Mo radiation). The trigonal symmetry of the crystals was established from X-ray goniometric scans of $h0k$ and $hk1$. The parameters of the trigonal cell were refined on a PI Syntex four-circle automatic diffractometer: $a=10.463(7)$ and $c=6.596(4)$ Å. The intensities of 1136 independent nonzero reflections ($I \geq 1.96\sigma$) were recorded by the $2\theta\theta$ method at a variable scanning rate of $6-24^\circ/\text{min}$ on the same diffractometer (MoK α radiation, $\max \sin \theta/\lambda=1.0 \text{ Å}^{-1}$). The absence of regular extinctions among the reflections points to the possible symmetry groups $P3$ and $P3_1$. (2 refs.)

76400 The cation distribution of tin-doped magnetites. E.Yu.Aksenova, E.L.Arinkina, Yu.A.Mamalyu.

Ukr. Fiz. Zh. (USSR), vol.28, no.5, p.704-7 (May 1983). In Russian. The cation distribution of tin-doped magnetite has been studied by two independent methods: magnetic and crystallochemical. The Sn^{4+} ions are localized both in the octahedral and tetrahedral sites. Discrepancy of magnetic and crystallographic data can be explained by participation of Sn^{4+} ions in formation of the magnetic moment of ferrite. (6 refs.)

76401 The crystal structure of simonite, $\text{TiHfAs}_2\text{S}_6$. P.Engel, W.Nowacki (Lab. für Kristallographie, Univ. Bern, Bern, Switzerland), T.Balic-Zunic, S.Scavnicar.

Z. Kristallogr. (Germany), vol.161, no.3-4, p.159-66 (1982). The crystal structure of a new sulfosalt, $\text{TiHfAs}_2\text{S}_6$, has been determined. The crystal is monoclinic with space group $P2_1/\text{m}$. Four formula units are contained in a unit cell of dimensions $a_0=5.948(2)$ Å, $b_0=11.404(6)$ Å, $c_0=15.979(5)$ Å, $\beta=90.15(1)^\circ$. The structure was determined by direct methods and refined to a final R-value of 0.05 for 2462 observed reflections. The AsS_3 pyramids form infinite AsS_2 -chains parallel [101]. The Hg atom has a deformed octahedral coordination by 3+3S atoms. The octahedra form a double chain parallel to [100]. The Ti atom is coordinated by 7+2S atoms. The coordination polyhedra form layers parallel to (001). The mean Ti-S, Hg-S and As-S distances are 3.43, 2.86, 2.27 Å, respectively. (11 refs.)

76402 The distribution of Fe^{3+} and Ga^{3+} between octahedral and tetrahedral sites in garnets, $\text{Y}_3(\text{Fe}, \text{Ga})_5\text{O}_{12}$, at different temperatures. G.Amthauer, V.Gunzler, S.S.Hafner, D.Reinen (Univ. Marburg, Marburg, Germany).

Z. Kristallogr. (Germany), vol.161, no.3-4, p.167-86 (1982). The distribution of Fe^{3+} and Ga^{3+} between the octahedral and tetrahedral sites in two garnets with the compositions $\text{Y}_3\text{Fe}_4\text{GaO}_{12}$ and $\text{Y}_3\text{Fe}_3\text{Ga}_2\text{O}_{12}$ was studied after heating at temperatures between 1000°C and 1500°C using

Mossbauer and electronic absorption spectroscopy. Fe^{3+} shows preference for the octahedral sites and Ga^{3+} for the tetrahedral sites. At elevated temperatures, a more disordered distribution is observed. The standard Gibbs free energy change ΔG° per exchange pair according to the reaction $\text{Fe}^{2+}(\text{oct}) + \text{Ga}^{3+}(\text{tet}) \rightleftharpoons \text{Ga}^{2+}(\text{oct}) + \text{Fe}^{3+}(\text{tet})$ is 4.7–5.3 kcal and the enthalpy change ΔH° is of the same magnitude. ΔH° may be correlated with the d -electron site preference for the tetrahedral coordination, which is considerably larger for d^{10} than for d^2 configured cations. The rather slow kinetics of the cation exchange between octahedral and tetrahedral sites at temperatures below 1200°C is probably due to the corner-sharing topology of the coordination polyhedra. (24 refs.)

76403 Cation distributions in $(\text{Fe}_{1-x}\text{Me}_x)(\text{PO}_4)_2$ graftonite-type solid solutions determined by Mossbauer spectroscopy. A.G.Nord (Swedish Museum of Natural History, Stockholm, Sweden), T.Ericsson.
Z. Kristallogr. (Germany), vol.161, no.3-4, p.209-24 (1982). Solid solutions of $\text{Me}_2(\text{PO}_4)_2$ in $\text{Fe}_2(\text{PO}_4)_2$, with the graftonite-type structure, have been prepared and equilibrated at 1070K ($\text{Me} = \text{Mg}, \text{Ca}, \text{Co}, \text{Ni}, \text{Zn}, \text{or Cd}$). The $(\text{Fe}_{1-x}\text{Me}_x)_2(\text{PO}_4)_2$ phases are isomorphous with $\text{Fe}_2(\text{PO}_4)_2$, as well as with the mineral graftonite. Accurate unit cell dimensions ($P2_1/c$) have been obtained from Guinier-Hagg photographic data. The unit cell volume is strongly correlated with the amount and size of the incorporated Me^{2+} cation. Mossbauer spectroscopy (^{57}Fe) has been used to determine the cation distribution of Fe^{2+} and Me^{2+} between the three distinct cationic environments in the structure: one octahedron and two five-coordinated polyhedra, all distorted. (29 refs.)

76404 The crystal structure of $\text{Tl}_6\text{Cd}_3(\text{N}_3)_{14}$. H.Krischner, C.Kratky, H.E.Maier (Univ. Graz, Graz, Austria).
Z. Kristallogr. (Germany), vol.161, no.3-4, p.225-9 (1982). In German. $\text{Tl}_6\text{Cd}_3(\text{N}_3)_{14}$ was prepared by the reaction of aqueous solutions of cadmium azide with thallium azide. The lattice parameters are at 298K (100K): $a = 8.603$ (8.552), $b = 10.532$ (10.487), $c = 11.767$ (11.614) Å, $\alpha = 99.92$ (100.31), $\beta = 107.68$ (107.50), $\gamma = 113.51$ (113.47)°, space group $P1$, $Z = 1$. The crystal structure was determined by the Patterson method using 6198 independent low temperature MoK α diffractometer data and refined to $R = 0.087$. The structure consists of $\text{Cd}(\text{N}_3)_6$ -octahedra which share two nitrogen corners. The thallium ions are surrounded by eight azide groups. The azide groups are linear with N-N distances of 1.17(5) Å. (6 refs.)

76405 Crystal structure of synthetic $\text{K}_2\text{Mg}(\text{CO}_3)_2$. K.-F.Hesse, B.Simons (Mineralogisches Inst., Univ. Kiel, Kiel, Germany).
Z. Kristallogr. (Germany), vol.161, no.3-4, p.289-92 (1982). The structure of synthetic $\text{K}_2\text{Mg}(\text{CO}_3)_2$ is trigonal with space group $R\bar{3}m$, $a_0 = 5.150(1)$, $c_0 = 17.290(3)$ Å, $Z = 3$ and $D_x = 2.79$ g cm $^{-3}$, and was refined to R (unweighted) = 0.057 and R (weighted) = 0.036 using 280 non-equivalent reflections. The compound is isostructural with buetschelite, $\text{K}_2\text{Ca}(\text{CO}_3)_2$. The structure consists of isolated $[\text{CO}_3]_2$ polyhedra (C-O distance 1.283 Å), $[\text{MgO}_6]$ octahedra (Mg-O distance 2.093 Å) and $[\text{KO}_6]$ polyhedra (K-O mean distance 2.801 Å). The $[\text{CO}_3]_2$ group is non-planar and the distance of the carbon atom from the plane of the three oxygen atoms is 0.014(3) Å. (19 refs.)

76406 The crystal structure of $\text{KCd}(\text{N}_3)_3 \cdot \text{H}_2\text{O}$ and $\text{K}_2\text{Cd}(\text{N}_3)_4$. W.Clegg (Inst. fur Anorganische Chem., Univ. Gottingen, Gottingen, Germany), H.Krischner, A.I.Saracoglu, G.M.Sheldrick.
Z. Kristallogr. (Germany), vol.161, no.3-4, p.307-13 (1982). $\text{KCd}(\text{N}_3)_3 \cdot \text{H}_2\text{O}$ crystallizes in space group $Pnma$ with $a = 11.991(2)$, $b = 3.712(1)$, $c = 17.292(2)$ Å and $Z = 4$. $\text{K}_2\text{Cd}(\text{N}_3)_4$ crystallizes in space group $C2/m$ with $a = 14.272(2)$, $b = 3.787(1)$, $c = 8.887(2)$, $\beta = 92.83(2)^\circ$ and $Z = 2$. The structures have been determined from single crystal X-ray data. The final R -values are 0.074 and 0.063 respectively. In both structures cadmium is surrounded octahedrally by six azide groups; the $\text{Cd}(\text{N}_3)_6$ -octahedra share edges. Potassium is coordinated by seven azide groups and two water molecules in $\text{KCd}(\text{N}_3)_3 \cdot \text{H}_2\text{O}$ and by eight azide groups in $\text{K}_2\text{Cd}(\text{N}_3)_4$. In both structures all azide groups are approximately parallel, with mean N-N = 1.17(5) Å. (9 refs.)

76407 Standard X-ray diffraction powder patterns. Section 19 - Data for 51 substances. M.C.Morris, H.F.McMurdie, E.H.Evans, B.Paretzkin, H.S.Parker, N.P.Pyrrors, C.R.Hubbard.
Report NBS-MN-25-19, Nat. Bur. Stand., Washington, DC, USA (Dec. 1982), iv + 114 pp.
The standard X-ray powder diffraction patterns, useful for identification, were obtained by manual or automated diffractometer methods, or were calculated from published crystal structure data. The lattice constants from the experimental work were refined by least-squares methods, and reflections were assigned Miller indices consistent with space group extinctions. Relative intensities, calculated densities, literature references, and other relevant data are included.

Crystal growth and temperature variation of the lattice parameters in LaF_3 , CeF_3 , PrF_3 and NdF_3 See Entry 76335

Theoretical and experimental study of growth sector boundaries in deuterated potassium dihydrogen phosphate single crystals See Entry 76340

Study of the solid-liquid equilibria of pseudo-binary systems $\text{MPO}_3\text{-Ca}(\text{PO}_3)_3$ ($\text{M} = \text{Rb}, \text{Cs}$) See Entry 76590

Multilayered polytypes in boron nitride See Entry 76616

Phase transitions in tetragonal CdP_2 See Entry 76619

High pressure reactions of oxometallics. VI. High pressure synthesis of mixed valence compounds $\text{VO}_{2-x}(\text{OH})_x$ with CaCl_2 -structure See Entry 76636

Solid state studies on substituted CuCr_2O_4 spinel See Entry 76946

Preparation and properties of substituted iron tungstates See Entry 76947

Optical phonons and structure of TlGaS_2 , TlGaSe_2 , and TlInS_2 layer single crystals See Entry 77393

X-ray K-absorption fine structure study of $\text{Cu}_x\text{Zn}_{1-x}\text{Fe}_2\text{O}_4$ ($x = 0.2, 0.4, 0.6$ and 0.8) See Entry 77480

Crystal structure and electrical resistivity of $\text{MoS}_2\text{-NbS}_2$ alloys produced by self-propagating high-temperature synthesis See Entry 77595

Preparation and investigation of solid solutions with a perovskite structure See Entry 77604

Mechanistic studies of oxide electrodes reversibly incorporating Li^+ ions See Entry 77893

Nuclear magnetic resonance of silica polymorphs See Entry 78537

61.65 SPECIFIC STRUCTURE OF ORGANIC COMPOUNDS

76408 Modeling the phase change in crystalline biphenyl by using a temperature-dependent potential. W.R.Busing (Chem. Div., Oak Ridge Nat. Lab., Oak Ridge, TN, USA).
Acta Crystallogr. Sect. A (Denmark), vol.A39, pt.3, p.340-7 (1 May 1983).

The structures of two crystalline phases of biphenyl ($\text{C}_{12}\text{H}_{10}$) were modeled using an exp-6-1 nonbonded potential and $(1 - \cos^2 \phi)$ terms for the phenyl-phenyl conjugation energy. Preliminary calculations were made by minimizing the energy of a model starting from the 110K structure, space group $P2_1/a$, with planar molecules. Doubling the b axis and relaxing all symmetry caused the model to transform to a structure with twisted molecules, space group Pn , essentially the same as the approximate structure reported from neutron diffraction studies at 22K. Increasing the contribution of the conjugation energy reversed the transformation, and calculations show that the potential that produces planar molecules in the crystal predicts twisted molecules in the gas phase, in agreement with experiment. A new temperature-dependent potential is described in which the nonbonded terms are modified according to the thermal motions of the atoms involved. Ways of combining the motions of the two atoms involved are considered. This new potential was applied to biphenyl to calculate successfully the observed unit-cell volumes and thermal expansion. The model reproduces the torsion angles in the 22K structure, and increasing temperature produces the experimental phase change, although the predicted transition temperature is higher than that observed. (41 refs.)

76409 Preliminary X-ray study of heratomin and Hg-derivative of geraniol. D.Rauth, K.N.Goswami (Dept. of Phys., Univ. of Jammu, Jammu, India).

Indian J. Pure & Appl. Phys., vol.21, no.3, p.184 (March 1983).

The unit cell and space group of heratomin and the Hg-derivative of geraniol have been determined by X-ray diffraction. The compounds are monoclinic with space groups $P2_1/m$ and $P2_1/c$ respectively. (2 refs.)

76410 The theoretical shape of sucrose crystals from energy calculations. M.Saska, A.S.Myrson (School of Chem. Engng., Georgia Inst. of Technol., Atlanta, GA, USA).

J. Cryst. Growth (Netherlands), vol.61, no.3, p.546-55 (April-May 1983).

The surface energies of individual crystallographic faces of crystalline sucrose were calculated using two forms of the 6-exp (Buckingham) potential. Hydrogen bond energies were calculated as a sum of O-H, O...H and O...O interactions where the Lippincott-Schroeder short-range potential was used for O-H and O...H pairs and the 6-exp potential for the non-bonded O...O interactions. Assuming that the surface energy equals half of the cohesive energy of the crystal, the attachment and surface energies of most of the faces found on as sucrose crystal were calculated. A computer program was written to draw the theoretical shape of crystals given the positions (central distances) of its faces. The resulting sucrose shapes are elongated along the c -axis. It is argued that the c -axis elongated habit is an intrinsic shape for vapor grown sucrose crystals (if realizable) and it is suggested that the usual shapes of solution growth sucrose crystals can be explained in terms of solvent (water) adsorption. (18 refs.)

76411 Crystal structure of N -m-tolyl phthalimide. K.Chandrasekhar, V.Pattabhi, S.Swaminathan (Dept. of Crystallography & Biophys., Univ. of Madras, Madras, India).

Pramana (India), vol.20, no.1, p.19-22 (Jan. 1983). [received: May 1983]
 N -m-tolyl phthalimide, $\text{C}_{15}\text{H}_9\text{NO}_2$, crystallizes in the space group Cc with unit cell dimensions, $a = 8.54(1)$, $b = 19.89(2)$, $c = 7.59(1)$ Å, $\beta = 114.53(1)^\circ$ and $Z = 4$. $V_c = 1173(2)$ Å 3 , $D_m = 1.35(1)$, $D_c = 1.344$ mg.m $^{-3}$, $M_r = 237$ Å CoK α = 1.7903 Å. The structure was solved by MULTAN and refined to an R -factor of 0.116 for 632 counter reflections. The molecules are held together by van der Waal's forces. The angle between the tolyl plane and the plane through the phthalimide group is $53.4(4)^\circ$. (11 refs.)

76412 Crystal structure of triphenylantimony dibenzoate, $\text{C}_{39}\text{H}_{27}\text{O}_4\text{Sb}$. V.A.Lbedev, R.I.Bochkova, L.F.Kuzubova, E.A.Kuz'min, V.V.Sharutin, N.V.Belov (Physicotech. Res. Inst., N.I. Lobachevskii State Univ., Gorki, USSR).

Sov. Phys.-Dokl. (USA), vol.27, no.7, p.519-21 (July 1982). Translation of: *Dokl. Akad. Nauk SSSR*, vol.265, no.1-3, p.332-5 (July 1982). [received: April 1983]

Crystals of triphenylantimony dibenzoate were subjected to a comprehensive X-ray structure analysis. The specimen chosen for the investigations was a transparent, slightly yellowish, rectangular plate measuring $0.46 \times 0.32 \times 0.28$ mm. The unit cell was rhombic with $a = 15.834(7)$, $b = 19.584(1)$, $c = 16.827(7)$ Å. (4 refs.)

Chloroacetyltriphenylphosphonium and the corresponding phosphorane. Physical chemistry and conformation study See Entry 75388

Synthesis and structural study of N -ethylnortropane-3-spiro-5'-oxazolidine-2,4'-dione and its hydrochloride See Entry 75395

An answer to the spiro versus ansa dilemma in cyclophosphazenes. III. $\text{N}_3\text{P}_3\text{Cl}_3[\text{HN}-(\text{CH}_2)_4-\text{NH}]\text{Cl}_3\text{P}_3\text{N}_3$. A serendipitous two-ring bridged-assembly phosphazene See Entry 75541

Standard X-ray diffraction powder patterns. Section 19 - Data for 51 substances See Entry 76407

Structure and dipole relaxation mechanisms in the cyclic alcohols cyclopentanol to cyclo-octanol See Entry 77326

61.70 DEFECTS IN CRYSTALS

(see also 61.80 Radiation damage, 62. Mechanical and acoustic properties, 71.55 Impurity and defect levels, 76.30M EPR of colour centres and other defects, 78.50 Impurity and defect absorption in solids, 81.40 Treatment of materials)

76413 The onset temperature for void formation in extremely pure iron. L.de Schepper, G.Knuyt, L.M.Stals, P.Moser (Limburgs Univ. Centrum, Diepenbeek, Belgium).

Radiat. Eff. Lett. Sect. (GB), vol.76, no.1-2, p.43-54 (1983).

The onset temperature for void formation in extremely pure iron is measured in a simulation study by 1 MeV electron microscopy. It is found to be between 430 and 470K; this is substantially lower than reported earlier in the literature. It is shown that the observed onset temperature is consistent with vacancy migration in stage III (200-220K) in α -iron, provided that the interaction between interstitial carbon atoms and vacancies is taken into account. (29 refs.)

76414 A high-resolution electron microscopic study of defects in sodium β'' -alumina. R.Hull (Dept. of Metall. & Sci. of Materials, Univ. of Oxford, Oxford, England), D.J.Smith, C.J.Humphreys. *J. Microsc. (GB)*, vol.130, pt.2, p.203-14 (May 1983). (MICRO 82: High Resolution Electron Microscopy, London, England, 12-16 July 1982). A high-resolution electron-microscopic study of sodium β'' -alumina, a polytype of the more-widely-studied sodium β - and β' -alumina, has been undertaken using the 600 kV instrument at Cambridge University. Images revealed the loss of sodium-containing planes, which had caused crystals to collapse and shear into defect layers. A model for the structure of these defects is proposed, based on the use of computed images and by comparison with high-resolution images of silver β'' -alumina. (18 refs.)

The recursion method and a first-principles tight-binding calculation of the band structures of diamond and silicon See Entry 76837

ODMR investigation of recombination in μ -Si:H See Entry 77293

I. The emission spectra of TL produced by ion implanted CaF_2 See Entry 77465

II. Thermally induced changes in the TL of ion implanted CaF_2 See Entry 77466

Investigation of the structure and phase composition of a stainless steel wire after electroplastic drawing See Entry 77667

Diffusive intergranular cavity growth in creep in tension and torsion See Entry 77696

61.70B Interstitials and vacancies

(exc. colour centres)

76415 A determination of vacancy properties in Au-Ni solid solutions, via analysis of stress-induced and short range ordering kinetics. E.Balanat, M.Halbwachs, J.Hillairet, C.Mairy (Dept. de Recherche Fondamentale, CENG, Grenoble, France), P.Guyot, J.P.Simon. *Acta Metall. (USA)*, vol.31, no.6, p.883-92 (June 1983).

Vacancy properties were studied in an α -Au-30 at.% Ni solid solution, with use of electrical resistivity and mechanical after-effect measurements, for the monitoring or short-range and stress-induced ordering kinetics, respectively. It is shown that, due to the inherent sensitivity of the methods used, valuable information about the vacancy parameters and related atomic mobility can be inferred from analysis of the ordering rate at low temperatures, that is in conditions of non-equilibrium for the α -phase. The respective activation energies for self-diffusion, and vacancy migration which were derived from the rate temperature dependence are 1.85 and 1.10 eV, respectively. These values yield a consistent fit to the ordering pattern observed during quench and isochronal anneal cycles. Information about vacancy sink densities and lifetimes were inferred also. The salient feature of the results is that, while the atom jump rate is not substantially modified by alloying, vacancy mobility is markedly slowed down; conversely the vacancy formation energy appears to be strongly decreased. A Au-5 at.% Ni alloy for which the α -phase is stable at all temperatures was studied also. (23 refs.)

76416 On the nature of point defects and the effect of oxidation on substitutional dopant diffusion in silicon. T.Y.Tan, U.Gosele, F.F.Morehead (IBM Thomas J. Watson Res. Center, Yorktown Heights, NY, USA).

Appl. Phys. A (Germany), vol.A31, no.2, p.97-108 (June 1983). An extensive analysis of the substitutional dopant diffusion phenomena in silicon during oxidation is presented. The analysis covers qualitative as well as quantitative aspects of the oxidation-enhanced and -retarded diffusion (OED and ORD) phenomena, and examines three different possible assumptions that can be made on the nature of the silicon thermal equilibrium point defect species: silicon self-interstitials (I) only, vacancies (V) only, coexistence of I and V. The only consistent way to interpret all properly documented OED/ORD data is to assume that I and V coexist under oxidation as well as under thermal equilibrium conditions at high temperatures. (58 refs.)

76417 Boundary conditions in computer simulations of point defects. H.R.Schober (Inst. für Festkörperforschung KFA, Jülich, Jülich, Germany). *Radiat. Eff. Lett. Sect. (GB)*, vol.76, no.1-2, p.19-24 (1983). In computer simulations of metals, volume dependent contributions to the energy are often introduced. It is shown how such volume terms affect calculations with different boundary conditions. (10 refs.)

76418 Theory of annealing of vacancy pores in thin metal foils. N.A.Demin, Yu.V.Konobeev.

Fiz. Met. & Metalloved. (USSR), vol.55, no.4, p.701-6 (April 1983). In Russian. English translation in: *Phys. Met. & Metallogr. (GB)*. A theoretical analysis is made of the influence of free surfaces on the kinetics of isothermal annealing of vacancy pores in a thin metal foil. It is shown that in the case of pores located close to the surface the rate of dissolution may be considerably higher than for isolated pores in the bulk of a metal. (6 refs.) A.T.

76419 Some physical properties and point defects in $\text{Bi}_{2-x}\text{In}_x\text{Te}_3$ mixed crystals. P.Lostak, J.Horak, L.Koudelka (Univ. of Chem. Technol., Pardubice, Czechoslovakia).

Phys. Status Solidi A (Germany), vol.76, no.1, p.K71-5 (16 March 1983). The authors report for the first time the preparation of single crystals of $\text{Bi}_{2-x}\text{In}_x\text{Te}_3$ ($x=0$ to 0.04) and the results of a study of their optical parameters (transmission and the index of refraction) which they have correlated with some transport parameters of the crystals (electric conductivity and Hall coefficient). From the analysis of the physical parameters they have evaluated point defects formed in the mixed crystals due to the incorporation of indium atoms into the Bi_2Te_3 crystal lattice. (9 refs.)

76420 Point defects in II-VI compounds. T.Taguchi, B.Ray (Faculty of Engng., Osaka Univ., Osaka, Japan).

Prog. Cryst. Growth & Charact. (GB), vol.6, no.2, p.103-62 (1983). An extensive survey is made of recent developments in the study and characterisation of lattice defects in II-VI compounds, including both point defects and complex-defect centres. Point defect generation during crystal growth and by bombardment of crystals with high energy electrons or light ions is considered in detail and the different vacancy and interstitial atomic configurations are elucidated. The formation and character of complex-defect centres are examined and linked to the low temperature photoluminescent emission spectra observed in these materials. The stability at room temperature of both isolated and other centres associated with vacancies is discussed in relation to lattice distortions and energy levels in the forbidden energy gap. The application of Rutherford backscattering, deep-level-transient spectroscopic and photo-acoustic spectroscopic techniques is shown to have advanced the understanding of lattice defects in II-VI compounds. Some possible future developments in defect studies are identified and of them the use of particular lower temperature, crystal growth techniques is seen as an important early step in reducing intrinsic defect levels. (195 refs.)

76421 Mechanism of electron-excitation-induced defect creation in alkali halides. N.Itoh (Dept. of Crystalline Material Sci., Nagoya Univ., Nagoya, Japan).

Radiat. Eff. (GB), vol.64, no.1-4, p.161-9 (1982). [received: May 1983] (Proceedings of the First International Conference on 'Radiation Effects in Insulators', Arco, Largo di Garda, Italy, 1981).

Mechanisms of the defect creation in alkali halides induced by electronic excitation, suggested within these three decades, are surveyed, emphasizing how they are related to the overall yield of defect creation in solids. The experimental and theoretical studies which are critical check points for proposed mechanisms are discussed in detail. It is pointed out that the processes of localization of the wave functions of the electrons and holes and the conversion of localized electronic energy to the motion of the lattice atoms should be understood. The mechanisms of the dynamic motion of atoms to which the electronic energy is imparted and of the stabilization of the primary products, the neutral interstitials and vacancies in the halogen sublattice, are also discussed. (61 refs.)

On the mechanical stability of BCC transition elements and alloys See Entry 76355

Preparation and structure of fluorite-type $(\text{Sr},\text{Y})\text{Cl}_{2.05}$ See Entry 76381

Crystal structure of a new $\text{Na}_2\text{Fe}^{3+}$ orthophosphate $(\text{Fe}_{0.5}\square_{0.5}(\text{H}_{1.5}\square_{0.5})\text{Na}_2\text{PO}_4)_2 = \text{Fe}_{0.5}^{3+}\text{Na}_2\text{PO}_4\cdot 1.5\text{HF}$ See Entry 76399

On the nature, characterisation and applications of point defects in insulators See Entry 76424

Theory of strongly relaxed point defects in oxides See Entry 76425

Exact solutions to a model for the growth of radiation damage during progressive ion implantation See Entry 76462

Photo-chemical reaction and photo-induced polarization studies in sulphur-doped potassium bromide See Entry 76482

The inhomogeneity effect in the vacancy-dislocation interaction for α -iron See Entry 76483

Observation of impurity-interstitial interaction in irradiated niobium See Entry 76485

Irradiation induced order-disorder in Ni_3Al and NiAl See Entry 76504

Microstructural transitions in Pt-C alloys during high-voltage-electron-microscope irradiation See Entry 76508

Electron damage in zirconium. I. Defect structure and loop character See Entry 76509

Electron damage in zirconium. II. Nucleation and growth of c-component loops See Entry 76510

Temperature dependence of the threshold energy for atom displacement in irradiated molybdenum See Entry 76511

The temperature dependence of the threshold displacement energy in MgO See Entry 76512

Effect of 5.5-MeV electron bombardment on the high-temperature mechanical properties of nickel See Entry 76516

Anomalous defect interaction and amorphization during self-irradiation of Si crystals at 450K See Entry 76524

Dynamical behaviour of interstitials in elemental semiconductors See Entry 76576

Thermal vibrations and static displacements of atoms in nonstoichiometric titanium carbide See Entry 76579

Vacancy pump as a mechanism of growth of precipitates during precipitation of solid solutions See Entry 76630

Random walks and correlation factors in diffusion via the vacancy mechanism in hexagonal-close-packed lattices See Entry 76686

Oxygen self-diffusion in Fe-doped MgO single crystals See Entry 76690

Computer simulation of the correlation factors in vacancy-pair diffusion in NaCl-type lattices See Entry 76698

Diffusion of iron in aluminum studied by Mossbauer spectroscopy See Entry 76705

The role of volume diffusion in DIGM, a reappraisal See Entry 76709

Kinetics of self-interstitials generated at the Si/SiO₂ interface See Entry 76796

Microscopic model of the EL2 level in GaAs See Entry 76889

Effect of vacancies and foreign metal ions on the valent state of samarium in SmB_6 See Entry 76904

The DC resistivity of modified PZT ceramics See Entry 76944

EPR study of ordering in stoichiometric β -aluminate See Entry 77256

Dielectric properties of modified PZT ceramics See Entry 77318

Piezoelectric properties of modified PZT ceramics See Entry 77330

Formation of lattice defects in CdS crystals by nitrogen laser radiation See Entry 77450

Positron annihilation on pure and carbon-doped α -iron in thermal equilibrium See Entry 77477

Electrical conductivity and infrared absorption spectrometry study of hematite precipitation from defective ferrites See Entry 77647

Annealing behaviour of dilute FeTi, FeCu, and FeMn alloys in the temperature range above stage III following low-temperature electron irradiation See Entry 77682

61.70D Colour centres

76422 Neutron induced colour and luminescence centres in yttrium-aluminium garnet single crystals. A.F.Rakov (Inst. of Nuclear Phys., Acad. of Sci., Tashkent, Uzbek SSR).

Phys. Status Solidi A (Germany), vol.76, no.1, p.K57-60 (16 March 1983). The nature of colour (CC) and luminescence (LC) centres occurring in yttrium-aluminium garnet (YAG) crystals is discussed on the basis of optical absorption (OA) and photoluminescence (PL) spectra. YAG crystals, grown by Czochralski and horizontal directed crystallization methods, were examined. The samples have been irradiated by neutrons of energy $E>0.2$ MeV, creating defect structures in crystals. The neutron doses were 10^{16} to 10^{19} n/cm². (7 refs.)

76423 On production of Z_1 centres in NaCl:Sm^{2+} crystals. K.N.Reddy, M.D.Iqbal Ahmed (Dept. of Phys., Osmania Univ., Secunderabad, India), V.H.Babu.

Phys. Status Solidi a (Germany), vol.76, no.2, p.K167-70 (16 April 1983). The authors study the formation of Z_1 centres in NaCl:Sm^{2+} crystals and the effect of deformation on Z_1 centres with the help of optical absorption and thermoluminescence (TL) measurements. The results lead to the conclusion that a small concentration of Z_1 centres is formed during irradiation without optical bleaching, confirming the earlier optical absorption work of Marat-Mendes and Comins (1975). TL measurements suggest that the concentration of Z_1 centres is greatly increased by deformation as previously noted by Radhakrishna and Chowdary (1972) and Kamavisdar and Deshmukh (1981). (6 refs.)

76424 On the nature, characterisation and applications of point defects in insulators. B.Henderson (Phys. Lab., Trinity Coll., Dublin, Ireland). *Radiat. Eff. (GB)*, vol.64, no.1-4, p.35-47 (1982). [received: May 1983] (Proceedings of the First International Conference on 'Radiation Effects in Insulators', Arco, Largo di Garda, Italy, 1981).

Outlines some basic properties of defects in insulators and describes experimental techniques by which these defects may be characterized. The production of defects by various types of particle irradiation is discussed. Finally, some discussion is presented of the potential device application of defective crystals, including tunable colour centre lasers, miniaturised optical circuitry and neuron dosimetry. (25 refs.)

76425 Theory of strongly relaxed point defects in oxides. W.B.Fowler (Dept. of Phys., Lehigh Univ., Bethlehem, PA, USA). *Radiat. Eff. (GB)*, vol.64, no.1-4, p.63-9 (1982). [received: May 1983] (Proceedings of the First International Conference on 'Radiation Effects in Insulators', Arco, Largo di Garda, Italy, 1981).

Experimental and theoretical efforts during recent years have led to structural models for several of the fundamental point defects in oxide materials. In many of these cases it has become apparent that asymmetric relaxations of neighboring atoms play a key role in the detailed structure and properties of these defects. Such effects are not as common in prototype insulators such as alkali halides (a notable exception being the Type II F_A center). Strong relaxations in a number of oxides have been treated theoretically by Schirmer using a 'bound small polaron model'. Similar ideas had been incorporated into a treatment of the E'_1 center in SiO_2 by Yip and Fowler (1975), and more recently by Griscom and Fowler (1980). Extensive computations on the E'_1 , E'_2 , and peroxy-radical centers using MNDO and MINDO/3 quantum-chemistry approaches indicate that the defect geometries and properties are strongly related to atomic relaxations about them. It is likely that these effects are important in other insulating materials as well. (44 refs.)

Effects of gamma-ray irradiation on OH^- doped KBr crystals See Entry 76501

Metallic alloy precipitates in high dose indium implanted MgO See Entry 76642

The electronic structure of F-centres in alkali halide crystals See Entry 76887

Electronic structure of thallous centres and $\text{Ti}^{3+}-V_L$ recombination in KCl crystal See Entry 76888

Li tunneling effects on spin-lattice relaxation rates of a color center in CaO:Li See Entry 77262

Optical properties of the $\text{Ti}^{3+}(1)$ center in KCl See Entry 77419

Colour centre luminescence of $\alpha\text{-Al}_2\text{O}_3$ See Entry 77455

Thermoluminescence and optical absorption studies. Rubidium bromide doped with barium See Entry 77463

On the mechanisms of thermoluminescence and deformation luminescence in gamma-irradiated KCl See Entry 77464

61.70G Dislocations: theory

76426 The temperature dependence of the line tensions of dislocations in several b.c.c. metals. H.G.Schmid (Max-Planck-Inst. für Metall., Inst. für Werkstoffwissenschaften, Stuttgart, Germany).

Mater. Sci. & Eng. (Switzerland), vol.59, no.1, p.L7-9 (May 1983). The line tensions of dislocations in molybdenum, niobium, tantalum and $\alpha\text{-Fe}$ have been computed as a function of temperature over ranges of several hundred kelvins, using published data on the elastic constants and their dependence on temperature. (14 refs.)

76427 Low-temperature fluctuational motion of dislocations in crystals. I. Quantum and dissipative effects. A.I.Osetskii (Inst. for Problem of Cryobiology & Cryomedicine, Acad. of Sci., Kharkov, Ukrainian SSR).

Phys. Status Solidi b (Germany), vol.117, no.1, p.355-65 (1 May 1983). A mechanism underlying fluctuational bending of dislocation segments is considered which is based on periodical ordering in the thermal motion of atoms near the dislocation core. Basic principles of calculating the probability of dislocation unpinning from local obstacles due to the fluctuations are formulated. As found, the interaction of dislocation segments experiencing fluctuational bending with phonons and/or conduction electrons, described in the framework of the usual dissipation model, can result in a reduction of the energy of atoms near the dislocation core during the fluctuation. Consequently, the effective activation energy of the dislocation unpinning from local obstacles is increased, i.e. the mean velocity of the activated dislocation motion drops. Activated dislocation motion at low temperatures is analysed with an account of the possible quantum mechanical fluctuations which can arise in condensed structures owing to the correlation of atomic zero point vibrations. An expression is derived for the probability of low temperature fluctuational dislocation with allowance for quantum mechanical effects. (11 refs.)

76428 Analytical calculation of parameters of thermally activated dislocation motion through a random array of point obstacles. A.I.Landau (Phys. Tech. Inst. of Low Temperatures, Acad. of Sci., Kharkov, Ukrainian SSR). *Phys. Status Solidi a (Germany)*, vol.76, no.1, p.207-16 (16 March 1983). A method is proposed which enables the calculation of the velocity of the thermally activated dislocation motion through a random array of similar-type point obstacles, based entirely on analytical relations, without recourse to computer simulation. The method enables also the calculation of the probability densities of attack angles and dislocation segment lengths which describe the probability-geometric characteristics of a dislocation in the physical system. (23 refs.)

76429 The effect of the crystal anisotropy on the energy of the dislocation-impurity atmosphere elastic interaction in silicon. G.N.Gaidukov, S.K.Maksimov, A.A.Podrezov (Inst. of Electronic Technol., Moscow, USSR). *Phys. Status Solidi a (Germany)*, vol.76, no.2, p.453-9 (16 April 1983). The energy of the system: straight dislocation-impurity atmosphere, is investigated within the framework of the linear anisotropic theory of elasticity. A

numerical calculation is performed for the edge dislocations oriented along the directions (110) and (112), with the Burgers vectors $1/2(110)$ and $1/3(111)$, and for impurity atoms presented as point spherical defects in Si. It is shown that for certain impurity concentrations separating the domains where the preferable orientation of the dislocation line is along the direction (112) L , from that where the preferable direction is (110). (13 refs.)

76430 Dynamic dislocation pile-ups. H.Ockendon (Somerville Coll., Oxford Univ., Oxford, England).

Philos. Mag. A (GB), vol.47, no.5, p.707-19 (May 1983). The motion of a continuous distribution of dislocations moving under a constant imposed stress towards a small locked dislocation is considered. This problem can be modelled as a non-linear partial differential equation for a complex stress function if a linear-stress-velocity law is assumed. If the initial density of the distribution is sufficiently small, the dynamic pile-up that occurs can be described using matched asymptotic expansions. In particular, the force on the locked dislocation is derived as a function of time. It is further shown that the solution remains valid when the velocity is proportional to any positive power of the stress. (5 refs.)

76431 Model of formation of lined-up-dipole slip bands with a predominant screw component. V.G.Kurdyumov (Inst. of High-Pressure Phys., Acad. of Sci., Moscow, USSR).

Sov. Phys.-Dokl. (USA), vol.27, no.8, p.650-2 (Aug. 1982). Translation of: *Dokl. Akad. Nauk SSSR*, vol.265, no.4-6, p.1382-5 (Aug. 1982). [received: May 1983]

Proposes a model of longitudinal development of a slip band of the lined-up-dipole type. The main idea of the model is the hypothesis that loops are nucleated successively under the action of stresses, at the end of a lined-up-dipole configuration of screw dislocations. (6 refs.)

76432 Computer simulation of an edge dislocation in a naphthalene crystal. N.N.Mokichev, L.G.Pakhomov (Sci.-Res. Inst. of Chem., Lobachevski State Univ., Gorki, USSR).

Sov. Phys.-Solid State (USA), vol.24, no.11, p.1925-7 (Nov. 1982). Translation of: *Fiz. Tverd. Tela (USSR)*, vol.24, no.11, p.3389-93 (Nov. 1982). [received: May 1983]

The equilibrium configuration is found for the core of a [010] (001) edge dislocation in a naphthalene crystal. The change in the binding energy of molecules in the core is determined, relative to a perfect crystal; the radius and elastic energy of the core are estimated. The change in the polarization energy of the crystal due to a free carrier in the core is determined. The range of action of a dislocation as regards the electron and hole conduction levels is found. (23 refs.)

Gauge theory of dislocations and disclinations See Entry 74237

The inhomogeneity effect in the vacancy-dislocation interaction for α -iron See Entry 76483

An acoustic emission source model for both continuous and burst-type emission analysis. I. Theory See Entry 76568

Accommodation of misfit in heterostructures with continuous and islands films See Entry 76813

61.70J Etch pits, decoration, transmission electron-microscopy and other direct observations of dislocations

76433 Generation of dislocations introduced by bending stress in a Si wafer. R.Sawada, T.Karaki, J.Watanabe (Musashino Electrical Communication Lab., Nippon Telegraph & Telephone Public Corp., Musashino, Tokyo, Japan).

Appl. Phys. A (Germany), vol.A31, no.2, p.109-14 (June 1983). Distribution and morphology for dislocations introduced in (001) Si wafers subjected to bending stress at 800°, 900°, and 1100°C were investigated. For wafers bent around a [110] axis at 900° and 1100°C, straight dislocations appeared along the [110] direction only near the neutral plane, and were absent at the surfaces where bending stress is greatest. However, for wafers bent at 800°C, such straight dislocations were not formed. Dependence of the dislocation distribution and morphology on heat treatment temperature is explained on the basis of interaction between bending stress and SiO_2 precipitates introduced in bulk. Also, it was found that the straight [110] dislocations remained still near the neutral plane, even when additional reverse bending stress was applied around an axis parallel to the dislocations, but were transferred toward the tensile surface by bending around an axis normal to the dislocation direction. (24 refs.)

76434 Evaluation of misfit dislocations in planar, zinc-diffused $\text{In}_{0.53}\text{Ga}_{0.47}\text{As}$ PIN photodiodes. A.K.Chin, B.V.Dutt, W.S.Trimmer, J.R.Zuber, T.Boone, K.D.Trapp (Bell Labs., Murray Hill, NJ, USA).

Mater. Lett. (Netherlands), vol.1, no.5-6, p.152-6 (April 1983). Misfit dislocations in planar, zinc-diffused $\text{In}_{0.53}\text{Ga}_{0.47}\text{As}$ PIN photodiodes were analyzed using defect etching, cathodoluminescence, and electron-beam-induced current (EBIC). It was found that the misfit dislocations in wafers grown by liquid-phase epitaxy are present only in the InP buffer layer and they act as nonradiative recombination centers. These dislocations also affect the p-n junction since the misfit stress locally increases the diffusion depth by 80-400 Å. EBIC examination of the photodiodes under reverse bias shows that the misfit dislocations do not cause localized breakdown of the p-n junction. (26 refs.)

76435 X-ray investigation of crystal defects in Czochralski grown InP single crystals. P.Franzosi (Istituto MASPEC, Parma, Italy), C.Ghezzi.

J. Cryst. Growth (Netherlands), vol.61, no.3, p.591-600 (April-May 1983). X-ray diffraction topography was employed to study extended crystal defects in InP single crystals grown by the Czochralski liquid-encapsulation technique. Semi-insulating iron-doped, p-type and n-type crystals were investigated and two main defects, dislocation lines and large precipitate-like defects, were evidenced. The generation mechanism for the dislocations and the nature of the large defects were analyzed. (26 refs.)

76436 Characterization of defects in InP substrates. D.J.Stirland, D.G.Hart, S.Clark (Allen Clark Res. Centre, Plessey Res. (Caswell), Caswell Ltd., England), J.C.Regnaud, C.R.Elliott.

J. Cryst. Growth (Netherlands), vol.61, no.3, p.645-57 (April-May 1983). Unusual inclusion-like defects (grappes) which occur in many LEC InP ingots have been studied in an [001] Ge-doped wafer by optical microscopy of the etched wafer surface, reflection and transmission X-ray topography, and transmission polarised infra-red microscopy. The defects produced a variety of different contrast features on reflection X-ray topographs. By using all the techniques in combination to examine individual defects it was deduced that the observed contrast effects were consistent with previous postulates regarding the structures of these defects. Essentially, all the defects are similar in structure but vary in diameter from 5-200 μm , and consist of central core

regions surrounded by prismatic dislocation loop arrays. It was also established that the majority of defects are situated on line dislocations, and they possess effective Burgers vectors which differ from those of the dislocations on which they are located. (17 refs.)

76437 Interstitial loop growth in HVEM-irradiated nickel foils. K.M.Miller (Berkeley Nuclear Labs., CEBG, Berkeley, England). *J. Nucl. Mater. (Netherlands)*, vol.115, no.2-3, p.216-22 (April 1983). A recently presented model (see *ibid.*, vol.110, p.265, 1982) for the development of a dislocation density in HVEM-irradiated thin foils has been applied to nickel. From matching the results to previously reported experimental measurements of loop radius growth as a function of position in the foil, the dislocation bias and vacancy migration energy in nickel have been determined. A comparison has been carried out of the effect on the results of using two distinct sink strengths to model the flow of defects to the dislocation loops. Equally good fits to the experimental data have been obtained with either sink strength and consequently it has not proved possible to select a preferable representation for the loops. (8 refs.)

76438 First observations of defects in α -gallium at room temperature. N.Durbec, B.Pichaud, F.Minari (Lab. de Phys. Cristalline, Univ. Aix-Marseille III, Marseille, France). *J. Microsc. & Spectrosc. Electron. (France)*, vol.8, no.1, p.47-52 (Feb. 1983). The authors have been able to examine some crystals of gallium near the melting point by TEM. They show that good images can be obtained but indexing the diffraction patterns offers some difficulties, because several sections of the reciprocal lattice are almost identical. This study allows some previous results (obtained by X-ray transmission topography) about dislocations in Ga to be checked and reveals the existence of stacking faults. Furthermore, at such temperatures, one can observe the climbing of these defects. (6 refs.)

76439 The effect of annealing on the dislocation dissociation in plastically deformed silicon. V.V.Aristov, M.N.Zolotukhin, V.V.Kveder, Yu.A.Osipyan, I.I.Snighireva, I.I.Khodov (Inst. of Solid State Phys., Acad. of Sci., Chernogolovka, USSR). *Phys. Status Solidi a (Germany)*, vol.76, no.2, p.485-91 (16 April 1983). The dissociation of dislocations in deformed and annealed silicon samples is studied using the weak beam method of electron microscopy. It is shown that the annealing of samples may result in a significant decrease of the dissociation widths of dislocations with a predominant screw component. In samples deformed without annealing a major portion of such dislocations is split anomalously widely as compared to those with a predominant edge component, whereas after annealing the dissociation widths of dislocations of all orientations agree with the theoretical dependence. A possible relationship between the change in the dislocation dissociation after annealing and the behaviour of the EPR signal from dislocations is discussed. (25 refs.)

76440 Transmission electron microscopy of dislocation structures in V_3Si single crystals after deformation at high temperatures. U.Kramer (Sektion Phys., Tech. Univ. Dresden, Dresden, Germany). *Philos. Mag. A (GB)*, vol.47, no.5, p.721-40 (May 1983). The plastic deformation of the intermetallic compound V_3Si at 1280 to 1500°C takes place by gliding and climbing of dislocations. The Burgers vector of single dislocations is (100). Occasionally a dislocation with Burgers vector (110) is observed in nodes. The slip plane of indirectly heated samples is {001}. Straight dislocations preferentially run along (100) and (110) directions. The absence of screw dislocations is explained by their higher mobility compared with edge and 45° dislocations and the presence of two slip planes for each screw dislocation. Sub-grain boundaries in deformed crystals are mostly formed by two sets of dislocations with different Burgers vectors of type (100). During dynamic recovery, elongated prismatic dislocation loops are generated in (100) directions. (26 refs.)

76441 Optical damping of dislocations in KCl crystals. M.A.Golosovskii, Ya.M.Soifer (Inst. of Solid-State Phys., Acad. of Sci., Chernogolovka, USSR). *Sov. Phys.-Solid State (USA)*, vol.24, no.11, p.1890-3 (Nov. 1982). Translation of: *Fiz. Tverd. Tela (USSR)*, vol.24, no.11, p.3327-32 (Nov. 1982). [received: May 1983] A study was made of the influence of the F light on the dislocation damping of ultrasound (optical damping of dislocations) and on the dislocation charge of additively colored and γ -irradiated KCl crystals of different purity. It was found that optical damping of dislocations occurred in all the investigated crystals and this was due to the appearance of new pinning points under the influence of light. The conditions of formation of such pinning points depended on the dislocation charge, purity of a crystal, and the method of introduction of the F centers. An analysis was made of binary systems in which the phenomenon of optical damping of dislocations could be observed. (5 refs.)

Determination of the atomic configuration of twin boundaries in tungsten by field-ion microscopy See Entry 76455

Interaction of dislocations with impurities in silicon crystals studied by in situ X-ray topography See Entry 76484

Electron damage in zirconium. I. Defect structure and loop character See Entry 76509

Electron damage in zirconium. II. Nucleation and growth of c-component loops See Entry 76510

Temperature dependence of the threshold energy for atom displacement in irradiated molybdenum See Entry 76511

The temperature dependence of the threshold displacement energy in MgO See Entry 76512

Anomalous defect interaction and amorphization during self-irradiation of Si crystals at 450K See Entry 76524

Mechanism of fatigue crack propagation in metallic materials See Entry 76561

Defect evaluation of Si MBE film See Entry 76803

Bloch wall arrangement and Barkhausen noise in steels 22 NiMoCr 3 7 and 15 MnMoNiV 5 3 See Entry 77201

Birefringence and structural defects in Cu_2O crystals See Entry 77355

Characterization of flux-grown $Ca(WO_4)_x(MoO_4)_{1-x}$ crystals See Entry 77550

Growth of high quality Ge MBE film See Entry 77571

Phase transformation studies of laser-processed Fe-0.2%C-Cr surface alloys See Entry 77635

The analysis of dislocation networks formed in Zircaloy-4 during high temperature creep See Entry 77707

Thermal stability in microstructure and rupture strength of directionally solidified Ni-Al-Ti eutectic alloys See Entry 77736

Effect of prior deformation on the cleavage of zinc single crystals See Entry 77747

61.70L Slip, creep, internal friction and other indirect evidence of dislocations

(see also 62.20H Creep, 62.40 Internal friction)

76442 Temperature dependence of the resistance to motion of edge dislocations in Fe-Co solid solutions. E.F.Dudarev, V.V.Rudchenko, V.A.Brovkov (V.D. Kuznetsov Siberian Physicotech. Sci.-Res. Inst., State Univ., Tomsk, USSR). *Fiz. Met. & Metalloved. (USSR)*, vol.55, no.4, p.811-13 (April 1983). In Russian. English translation in: *Phys. Met. & Metallogr. (GB)* An investigation was made of the composition and temperature dependences of the stress at which dislocations began to overcome the drag caused by substitutional and interstitial atoms. This was done for Fe-Co solid solutions with different amounts of interstitial impurities in order to determine the influence of cobalt and of these impurities on the resistance to motion of edge dislocations. The stress in question was deduced from the amplitude dependences of the internal friction of the investigated solid solutions. The results indicated that atoms of the alloying element and the interstitial impurity atoms contributed to the resistance to the motion of edge dislocations. (8 refs.) A.T.

76443 Stress relaxation experiments for proving the existence of an obstacle spectrum for thermally activated dislocation motion. F.Appel, U.Messerschmidt (Inst. of Solid State Phys. & Electron Microscopy, Acad. of Sci., Halle/Saale, Germany), Yu.Z.Estrin. *Mater. Sci. & Eng. (Switzerland)*, vol.59, no.1, p.41-7 (May 1983). The decrease in the activation volume of thermally activated dislocation motion observed in a constant-strain-rate test is often attributed to the generation of additional short-range obstacles in the deformation process. The alternative explanation is that the dislocation velocity increases with increase in strain if the structure of the short-range obstacles is constant. The activation volume is then decreased by a related decrease in the activation distance. By means of the stress relaxation tests at attempt was made to decide between these two possibilities by comparing the interaction potential of the short-range defects present at small strains with that at large strains. The investigations were performed on calcium-doped NaCl crystals. The results suggest that new short-range obstacles are produced during the deformation in addition to the impurity defects present in the undeformed material. (25 refs.)

76444 Low-temperature dislocation pinning and breakaway observed in Ta containing H. H.Mizubayashi, T.Arai, S.Okuda (Inst. of Materials Sci., Univ. of Tsukuba, Ibaraki, Japan). *Phys. Status Solidi a (Germany)*, vol.76, no.1, p.165-77 (16 March 1983). Internal friction (IF) and modulus below 100K in high purity Ta polycrystalline specimens containing very low concentration of H (RRR=2600 to 5000, $C_H \approx 8$ to 20 at. ppm) are studied after various treatments, i.e. quenching into liquid He, high amplitude vibration ($\epsilon_s \approx 2$ to 5×10^{-5}) at 5K (HAV(5K)) and the slow cool-down with or without vibration at low amplitude ($\epsilon_s \approx 2 \times 10^{-6}$) (the ON- or OFF-cool-down). During warm-up after the OFF-cool-down from $\approx 60K$, an anomalous softening is observed to occur below 60K, but during the ON-cool-down from $\approx 60K$, this decreased modulus is almost remained but not recovered. This observation is reproducible repeatedly. Detailed observations suggest that there are at least two types of H pinners in this temperature range; the one is responsible for an appearance of the anomalous softening through the breakaway of dislocations from them, the weak H pinners and the other, responsible for the remaining part of the pinning, the strong H pinners. (12 refs.)

76445 X-ray topographic in-situ observation of slip band propagation in MgO single crystals. U.Messerschmidt, Y.Nishino, T.Imura, H.Saka (Dept. of Metall., Nagoya Univ., Nagoya, Japan). *Phys. Status Solidi a (Germany)*, vol.76, no.1, p.277-84 (16 March 1983). Magnesium oxide single crystals are deformed in a Lang camera attached to a high intensity X-ray source. The development of the slip band structure is monitored by a video recording system. The specimens deform by localized slip bands. The slip band structures can partly be related to peculiarities in the stress-strain curves. A small size effects is observed in the macroscopic yield stress as well as in the stress for the initiation of the first slip band. The size effect may explain the discrepancy between the yield stresses measured macroscopically and by in-situ deformation experiments in the high-voltage electron microscope. In some specimens which deform by screw dislocation slip bands, plastic instabilities occur due to the sudden generation and spreading of edge type slip bands. (22 refs.)

76446 The investigation of heat release in slip bands in alkali halide crystals. N.L.Sizova (Inst. of Crystallography, Acad. of Sci., Moscow, USSR), V.D.Natsik, I.I.Gorina, V.R.Regel. *Phys. Status Solidi a (Germany)*, vol.76, no.2, p.447-51 (16 April 1983). An evaluation is made of the temperature rise in slip bands consisting of edge and screw dislocations during deformation of LiF single crystals by compression and the experimental data are compared with those calculated. It is shown using thermosensitive CLC layers that a local temperature rise from 0.1 to 1K is observed in slip bands during the deformation of LiF single crystal specimen. The measured and calculated temperature rises in slip bands are in reasonable agreement. (11 refs.)

76447 Pinning of dislocations on the departure side of strengthening dispersoids. V.C.Nardone, J.K.Tien (Henry Krumb School of Mines, Columbia Univ., New York, NY, USA). *Scr. Metall. (USA)*, vol.17, no.4, p.467-70 (April 1983). Two alternative explanations for the phenomenon observed during creep of oxide dispersion strengthened alloys involving the dislocation/particle configuration. It appears that the dislocations are being pinned even though they are already on the departure side of the oxide dispersoids. It can be proposed that dislocation/particle association leads to a lower energy configuration relative to the case when the dislocation and dispersoid are not in contact. On the other hand, the dislocation/particle configuration may be explained by the local climb of dislocations over particles as proposed by Ham and Brown (1975). (7 refs.)

76448 Dislocation internal friction in crystalline silicon whiskers. S.A.Antipov, V.I.Belyavskii, A.I.Drozhdin (Polytech. Inst., Voronezh, USSR).

Sov. Phys.-Solid State (USA), vol.24, no.11, p.1854-6 (Nov. 1982). Translation of: *Fiz. Tverd. Tela (USSR)*, vol.24, no.11, p.3268-72 (Nov. 1982). [received: May 1983]

An investigation was made of the relaxation spectrum of the internal friction in plastically deformed silicon whisker crystals. A study was made of the influence of doping with electrically active B, P, and As impurities on the activation energy of the Bordoni relaxation mechanism. The dependence of the activation energy on the degree of doping was attributed to changes in the electron spectrum resulting from the formation and motion of kinks in 60° and screw dislocations. (19 refs.)

76449 Nature of dislocation hysteresis losses and nonlinear effect in lead at high vibration amplitudes. V.V.Lomakin, L.N.Pal'-Val', V.Ya.Platkov, A.M.Roshchupkin (Physicotech. Inst. of Low Temperatures, Acad. of Sci., Kharkov, Ukrainian SSR).

Sov. Phys.-Solid State (USA), vol.24, no.11, p.1915-18 (Nov. 1982). Translation of: *Fiz. Tverd. Tela (USSR)*, vol.24, no.11, p.3370-6 (Nov. 1982). [received: May 1983]

The nature of the dislocation hysteresis was established and changes in this hysteresis were determined by investigating the dependence of the dislocation-induced absorption of ultrasound (coefficient α) on the amplitude of ultrasound ϵ_0 in single crystals of pure lead and of lead containing Ti and Sn impurities. The investigation was carried out in a wide range of ϵ_0 under superconducting transition conditions. In the superconducting (*s*) state both pure Pb and that doped with Ti exhibited a maximum in the dependence $\alpha(\epsilon_0)$ at high values of ϵ_0 on transition to the normal (*n*) state this maximum changed to a plateau. This provided a direct proof of a change in the static nature of the dislocation hysteresis to the dynamic process because of an increase in the coefficient of the electron drag of dislocations. Estimates were obtained of the range of lengths of dislocation loops: 2.4×10^{-4} cm $< L_N < 10.4 \times 10^{-4}$ cm. In the case of lead containing Sn the dynamic hysteresis occurred in both the normal and superconducting states. In the range of amplitudes above that of the maximum and at the beginning of the plateau all single crystals exhibited a rise of α on increase of ϵ_0 in the superconducting and normal states; this rise was due to nonlinear effects observed in the case of strong bending of L_N loops. An analysis was made of the amplitude dependence of the losses associated with this effect. The results were in good agreement with the experimental data. (24 refs.)

76450 Investigation of the distributions of distances traveled by short dislocation segments in Ge. V.A.Makara, B.V.Petukhov (A.V. Shubnikov Inst. of Crystallography, Acad. of Sci., Moscow, USSR).

Sov. Phys.-Solid State (USA), vol.24, no.11 (Nov. 1982). Translation of: *Fiz. Tverd. Tela (USSR)*, vol.24, no.11, p.6170L1 a6170Yp (Nov. 1982). [received: May 1983]

The authors report the results of an experimental investigation of the distribution of distances traveled by short dislocation segments in Ge crystals and propose a simple model which makes it possible to explain satisfactorily the results obtained and to derive from them some parameters of the interaction between dislocations and defects. (6 refs.)

Transmission electron microscopy of dislocation structures in V_3Si single crystals after deformation at high temperatures See Entry 76440

The effect of implanted helium on the high temperature mechanical properties of a model austenitic Fe-17% Cr-17% Ni alloy See Entry 76521

Dependence of the rate of intrareactor creep on the stress See Entry 76552

A quantitative approach to the cell shuffling model See Entry 76557

Internal friction in cold-worked nickel-carbon See Entry 76563

An acoustic emission source model for both continuous and burst-type emission analysis. II. Experiments See Entry 76569

Means of plastic self-indentation of solids in contact See Entry 76765

Simultaneous effect of UV-irradiation and deformation See Entry 76999

Strain dependence of the low-frequency dielectric constants of a few alkali halides See Entry 77316

Changes in the polarization and diffraction of light at dislocations with screw components in plastically deformed cadmium sulfide See Entry 77351

Birefringence and structural defects in Cu_2O crystals See Entry 77355

Raman light scattering in semiconductors containing dislocations See Entry 77399

Preparation and properties of Fe-1.65 wt.% Cr single crystals See Entry 77542

Influence of a high pressure on the kinetics of formation of lath (packet) martensite See Entry 77637

Influence of the temperature and rate of deformation on the dynamic recrystallization of $KhN77TYuR$ alloy single crystals See Entry 77668

Static and dynamic strain aging in a Ni(C) solid solution See Entry 77676

High-temperature creep and dislocation structure of vanadium See Entry 77700

The analysis of dislocation networks formed in Zircaloy-4 during high temperature creep See Entry 77707

Mechanical properties and structural stability of alloys See Entry 77711

The activation area and the activation enthalpy of cadmium single crystals determined during creep See Entry 77712

Thermal activation analysis by stress relaxation in some FCC metals See Entry 77713

Ion implantation effect on fatigue crack initiation in Ti-24V .. See Entry 77750

The effect of pre-existing epsilon martensite on the hydrogen induced fracture of austenitic stainless steel See Entry 77752

61.70N Grain and twin boundaries

76451 Effects of triaxial stressing on creep cavitation of grain boundaries. T.-L.Sham, A.Needleman (Div. of Engng., Brown Univ., Providence, RI, USA).

Acta Metall. (USA), vol.31, no.6, p.919-26 (June 1983). Investigates the influence of triaxial stressing on the growth of cavities on grain boundaries by the combined processes of plastic creep flow and grain boundary diffusion. The coupling arises from local accommodation of matter on the grain boundary near the cavity tip due to plastic creep deformability of the grains. This has the effect of shortening the diffusion path length on the grain boundary and increasing the cavity volumetric growth rate. An increase in triaxiality is found to accelerate the matter flux flowing from the cavity surfaces onto the grain boundaries and thus increase the cavity volume-

tric growth rate. This occurs at attainable levels of triaxiality. However, the enhancement in the triaxial stress state does not affect the effective diffusion path length very significantly. A simple formula for the volumetric growth rate of the cavity is suggested and it is found to give a good approximation to the numerically computed results. (13 refs.)

76452 Modified Wulff constructions for twinned particles. L.D.Marks (Dept. of Phys., Univ. of Cambridge, Cambridge, England).

J. Cryst. Growth (Netherlands), vol.61, no.3, p.556-66 (April-May 1983). Reports the application of a modified form of the Wulff construction to derive theoretical shapes and total surface energies for twinned particles. It is proposed that the incorporation of twin boundaries in faceted particles leads to a number of constrained local minimum in the total surface energy (at constant volume), in addition to the minimum of a single crystal Wulff polyhedron. A procedure for generating these constrained local minima is described. The model is then applied to determine the structures of twinned particles in face-centred materials. Two possible configurations are examined, an arrangement where the crystals are symmetric about the twin boundaries, and an asymmetric configuration. Shapes and total surface energies for a large number of twinned structures are given using a simple model which includes only (111) and (100) surface facets. Excellent agreement is obtained between the theoretical model and experimental results. (22 refs.)

76453 Lattice fringe imaging studies of the twin structures in electrocrystallized nickel coatings. N.Atanassov, M.Pasemann (Inst. of Phys. Chem., Bulgarian Acad. of Sci., Sofia, Bulgaria).

J. Microsc. & Spectrosc. Electron. (France), vol.8, no.1, p.25-30 (Feb. 1983). The twin structure of electrocrystallized nickel layers has been examined by means of the lattice fringe imaging method with a tilted incident beam. The results show different kinds of inhomogeneities, as e.g. an intermediate layer of about 1 nm thickness or an agglomeration of impurities inside the twin boundary. (9 refs.)

76454 Investigation of asymmetrical grain boundaries and their coincidence site lattices. An.Nguyen, R.Herrmann, G.Worm (Sektion Phys., Humboldt-Univ. zu Berlin, Berlin, Germany).

Phys. Status Solidi b (Germany), vol.116, no.2, p.501-10 (1 April 1983). A method for the examination of asymmetrical grain boundaries with randomly directed axes of rotation is presented. In so far as the axis of rotation lies in a plane of symmetry of the crystal the geometrical relation between symmetrical and asymmetrical grain boundaries is shown. The CSL Bravais cells corresponding to asymmetrical grain boundaries and the facet angles for the considered grain boundaries are calculated. (7 refs.)

76455 Determination of the atomic configuration of twin boundaries in tungsten by field-ion microscopy. I.M.Mikhailovskii (Physicotech. Inst., Acad. of Sci., Kharkov, Ukrainian SSR).

Sov. Phys.-Solid State (USA), vol.24, no.11, p.1822-4 (Nov. 1982). Translation of: *Fiz. Tverd. Tela (USSR)*, vol.24, no.11, p.3210-15 (Nov. 1982). [received: May 1983]

Field-ion microscopy was used to study the structure of twin boundaries in deformed and recrystallized tungsten. An analysis of the atomic topography of the surface near twin boundaries showed that twins in tungsten are of the reflection type without rigid translation of lattices. It was established that those dislocations at twin boundaries which compensate the lattice misorientation from the special case are perfect lattice dislocations with the Burgers vector $1/2 [111]$. The core radius of such dislocations is 0.3-0.7 nm in deformed tungsten and 0.3-0.5 nm in recrystallized samples. Lattice and twinning dislocations at twin boundaries do not split into partial and zonal dislocations. (17 refs.)

Structural changes in martensite observed in high-nickel steel as a result of low-temperature heating See Entry 76366

Electron microscopy study of two new long period structures in Pt_3Ti alloys ($3 \leq x \leq 8$) See Entry 76368

HREM and STEM of defects in multiply-twinned particles See Entry 76456

Furnace annealing of ion implanted polycrystalline silicon See Entry 76473

The effect of implanted helium on the high temperature mechanical properties of a model austenitic Fe-17% Cr-17% Ni alloy See Entry 76521

High-angle grain-boundary premelting transition: A molecular-dynamics study See Entry 76615

Multilayered polytypes in boron nitride See Entry 76616

The role of volume diffusion in DIGM, a reappraisal See Entry 76709

Evidence of the formation of twins by deformation and 'growth-accidents' in evaporated thin films of gold See Entry 76815

Kink deformation of $(TMTSF)_2ClO_4$ single crystal and its influence on electrical resistivity See Entry 76932

Grain boundaries as possible origin of flicker noise in GaP polycrystalline material See Entry 77013

Influence of the crystallography of the grain boundary/grain system on the $\alpha \rightarrow \gamma$ phase shift in Fe-4% Ni alloys See Entry 77633

Phase transformation studies of laser-processed Fe-0.2% C-Cr surface alloys See Entry 77635

The investigation of dissolution and precipitation kinetics of secondary phases in a $Cr15Ni70W10MoAlTiB$ alloy See Entry 77649

Grain-coarsening resistance and the stability of second-phase dispersions in rapidly solidified steels See Entry 77654

Influence of aging on secondary recrystallization and mechanical properties of polycrystalline NaCl samples prepared by hot pressing See Entry 77678

Pseudo-elastic behaviour in rapidly-quenched dilute tin alloys See Entry 77695

A study of intergranular cavity growth controlled by the coupling of diffusion and power law creep See Entry 77697

Creep of 0.6Cr-0.6Mo-0.3V steel at low stresses See Entry 77710

Cyclic grain boundary migration during high temperature fatigue. I. Microstructural observations See Entry 77718

Cyclic grain boundary migration during high temperature fatigue. II. Measurements of grain boundary sliding See Entry 77719

Effects of segregated phosphorus on stress corrosion cracking susceptibility of 3Cr-0.5Mo steel See Entry 77799

Polycrystal X-ray topography (PXT) of a cast silicon photovoltaic cell See Entry 77988

Improved efficiencies of semiconductor and metallurgical grade cast silicon solar cells by hydrogen plasma treatment See Entry 78058

Grain boundary effects and Li passivation in polycrystalline silicon See Entry 78059

Enhanced diffusion of phosphorus at grain boundaries [Si solar cells] See Entry 78061

- Grain boundary structure and properties in polycrystalline silicon See Entry 78069
- Grain boundaries in silicon solar cells See Entry 78070
- Evaluation of EBIC images at grain boundaries See Entry 78071
- Carrier transport at grain boundaries in silicon See Entry 78072
- Grain boundary effects in polycrystalline silicon solar cells See Entry 78073

61.70P Stacking faults, stacking fault tetrahedra and other planar or extended defects

76456 HREM and STEM of defects in multiply-twinned particles. L.D.Marks (Cavendish Lab., Univ. of Cambridge, Cambridge, England), D.J.Smith. *J. Microsc. (GB)*, vol.130, pt.2, p.249-61 (May 1983). (MICRO 82: High Resolution Electron Microscopy, London, England, 12-16 July 1982). The structure of defects in multiply-twinned particles has been studied in detail using high-resolution lattice imaging, dark field and microdiffraction techniques. Icosahedral particles with sizes greater than about 15 nm were found to contain defects, in the form of stacking fault loops parallel with the external surface, which were extremely difficult to detect by conventional amplitude contrast techniques. Microdiffraction mappings correlated with these results showing large rotations of the face-centred cubic segments. Results for decahedral particles indicated the presence of stacking faults running adjacent to, and parallel with, the twin boundaries. Microdiffraction maps confirmed that the particle structure was face-centred cubic, and also verified that the apparent epitaxy of these particles was highly variable. Models for the defects are proposed and discussed, and the relative merits of HREM and STEM for elucidating structural details in small particles is briefly considered. Finally, the potential for direct imaging at surfaces, as demonstrated by some recent images, is discussed. (29 refs.)

76457 Orientation dependence of oxidation stacking fault density in silicon. A.I.Pekarev, G.F.Krasnova, G.Z.Nemtsev (Moscow Inst. of Electronic Tech., Moscow, USSR). *Phys. Status Solidi a (Germany)*, vol.76, no.1, p.327-30 (16 March 1983). Cylindrical silicon samples are oxidized in wet atmosphere at 1150°C. The dependences of the oxidation-induced stacking fault (OSF) density on the cylindrical surface orientation are obtained for the zones {001} and {111}. The 'shallow' minima are located on the planes {100} and {110} and the 'deep' minima on high-index atomic-rough planes. A model is proposed, according to which OSF are formed on surface mechanical damages and on point defect clusters and precipitates. The calculated and experimental curves behave identically. (7 refs.)

76458 The correct rules for determining the sign of fault vectors in X-ray topography. A.R.Lang (H.H. Wills Phys. Lab., Univ. of Bristol, Bristol, England). *Phys. Status Solidi a (Germany)*, vol.76, no.2, p.595-9 (16 April 1983). The sign conventions employed in electron and X-ray diffraction contrast theories of stacking faults are discussed with reference to their predictions concerning the dependence of first-fringe contrast upon the sign of the fault vector under diffraction conditions when anomalous transmission is significant. It is pointed out that since 1975 error has appeared in papers dealing with the X-ray case. Guidance for the correct interpretation of X-ray topographs is given. (20 refs.)

76459 Investigation of radiation induced aggregates by phonon techniques. J.M.Grimshaw, M.Locatell (CENG-SBT/LCP, Grenoble, France). *Radiat. Eff. (GB)*, vol.64, no.1-4, p.119-23 (1982). [received: May 1983] (Proceedings of the First International Conference on 'Radiation Effects in Insulators', Arco, Largo di Garda, Italy, 1981). The authors discuss the determination of the size of extended defects in solids using phonon scattering, a method which has the advantage that it does not create further damage in the crystal during the investigation. They describe the principle of the method as it has been developed using thermal conductivity, then discuss the operation and applicability of the superconducting tunnel junction phonon spectrometer, and finally consider the phonon microscope. (5 refs.)

X-ray diffraction by mixed-layer structures with a random distribution of stacking faults See Entry 76245

Intensity of X-rays scattered by layered structures with short-range order factors $S \geq 1$, $G \geq 1$ See Entry 76246

First observations of defects in α -gallium at room temperature See Entry 76438

Compound synthesis in TiO_2 implanted with rubidium See Entry 76471

Anomalous defect interaction and amorphization during self-irradiation of Si crystals at 450K See Entry 76524

Kinetics of self-interstitials generated at the Si/SiO₂ interface See Entry 76796

Effect of one-dimensional disorder on exciton states in semiconductors See Entry 76852

61.70R Crystal impurities: general

(see also 71.55 Impurity and defect levels; 81.10 Purification techniques)

76460 Binding energy of an impurity atom in a transition metal. S.M.Dunaevskii. *Sov. Phys.-Solid State (USA)*, vol.24, no.12, p.2110-11 (Dec. 1983). Translation of: *Fiz. Tverd. Tela (USSR)*, vol.24, no.12, p.3701-3 (Dec. 1983). The author obtains an expression for the impurity atom binding energy in transition metals which is equivalent to the Varma-Wilson expression (1980) but which does not include the direct Coulomb interaction between the impurity and the transition metal matrix. (6 refs.)

The effect of the crystal anisotropy on the energy of the dislocation-impurity atmosphere elastic interaction in silicon See Entry 76429

Influence of an impurity ion on the geometry of its immediate environment See Entry 76912

61.70T Doping and implantation of impurities

76461 Modulation doping structures in silicon by molecular beam epitaxy and off-line ion implantation. T.De Jong, W.A.S.Douma, S.Doorn, F.W.Saris (FOM-Inst. for Atomic & Molecular Phys., Amsterdam, Netherlands). *Mater. Lett. (Netherlands)*, vol.1, no.5-6, p.157-62 (April 1983).

The authors have made buried layers and modulation doping profiles in Si by combining ultrahigh vacuum Si molecular beam epitaxy with off-line ion implantation. Abrupt doping profiles were obtained by using low implantation energy and a low temperature substrate preparation step prior to growth. (16 refs.)

76462 Exact solutions to a model for the growth of radiation damage during progressive ion implantation. C.H.J.Johnson (Div. of Chem. Phys., CSIRO, Clayton, Victoria, Australia). *Radiat. Eff. Lett. Sect. (GB)*, vol.76, no.3, p.73-8 (1983).

A kinetic model for the growth of radiation damage based on different types of scattering center is discussed and the exact (implicit) solution is given for the concentrations of trapped interstitials as functions of the fluence. (2 refs.)

76463 Ion implantation damage and annealing in germanium. O.W.Holland, B.R.Appleton, J.Narayan (Solid State Div., Oak Ridge Nat. Lab., Oak Ridge, TN, USA).

J. Appl. Phys. (USA), vol.54, no.5, p.2295-301 (May 1983). The authors have observed a unique damage structure, which forms within the amorphous phase, in ion-implanted Ge above a certain ion dose. This structure, which represents a drastic alteration of the near-surface morphology, is responsible for the adsorption of large quantities of C and O onto the surface of the implanted area. Results are presented of a systematic study of this effect and possible mechanisms for its information are discussed. Ion implantation conditions desirable for device applications are established and deleterious effects due to the presence of this damage upon both solid- and liquid-phase epitaxial growth of the implanted layers are discussed. (19 refs.)

76464 Pulsed thermal annealing of ion-implanted silicon. P.D.Scovell, E.J.Spurgin (Standard Telecommunication Labs. Ltd., Harlow, England). *J. Appl. Phys. (USA)*, vol.54, no.5, p.2413-18 (May 1983).

The use of a graphite strip heater to anneal implanted silicon has been investigated. The good electrical activity of an arsenic implanted layer obtained after annealing in this way is shown to degrade after simulated low temperature processing and lead to highly resistive layers. The annealing system has been used to reactivate such layers by employing high temperature thermal pulses of short duration which avoids excessive inter-diffusion. The same annealing schedule has been used successfully to activate highly doped antimony, boron, and phosphorous layers. The importance of controlling the ambient has also been studied and it is concluded that annealing in nitrogen avoids out-diffusion of dopant from the surface. (7 refs.)

76465 Radiation damage in ion-implanted quartz crystals. II. Annealing behaviour. H.Fischer, G.Gotz, H.Karge (Sektion Phys., Friedrich-Schiller-Universität, Jena, Germany). *Phys. Status Solidi a (Germany)*, vol.76, no.2, p.493-8 (16 April 1983).

For pt.1 see ibid., vol.76, p.249 (1983). Quartz crystals (Z-cuts) are implanted with Ar⁺ (150 keV) and He⁺ (35 keV) ions at room temperature. The annealing behaviour of the radiation damage between 300 and 1370K is investigated by Rutherford backscattering spectrometry (RBS). Three stages with different thermal stability of the defects are found: 1. Simple defects produced at nuclear deposited energy densities $G_n \approx 1 \times 10^{20}$ keV cm⁻³ can be completely annealed at 770K. 2. Amorphized microregions generated between $G_n = 1 \times 10^{20}$ keV cm⁻³ and 2.5×10^{20} keV cm⁻³ fully recrystallize at 1270K. 3. RBS-amorphous layers formed at $G_n \geq 2.5 \times 10^{20}$ keV cm⁻³ cannot be annealed. (12 refs.)

76466 Recoil implantation yields and depth profiles. Analytical expressions for primary and cascade contributions. A.Gras-Marti (Dept. de Física, Univ. de Alicante, Alicante, Spain).

Phys. Status Solidi a (Germany), vol.76, no.2, p.621-7 (16 April 1983). Recoil implantation of thin layers into the underlying substrate material is described within multiple scattering theory. Simple analytical expressions are derived for both primary and cascade recoil implantation yields and depth profiles. Predictions are compared with those of other models. (20 refs.)

76467 Ion implantation in group II-VI compounds. F.J.Bryant (Dept. of Phys., Univ. of Hull, Hull, England). *Prog. Cryst. Growth & Charact. (GB)*, vol.6, no.2, p.191-263 (1983).

A brief survey of possible experimental arrangements for ion implantation, with particular reference to those in the author's laboratory, is followed by a discussion of implantation parameters which have been shown to be important in the implantation doping of group II-VI compounds. There follows an illustration of the value of implantation in providing samples suitable for monitoring electron radiation damage and determining atomic displacement threshold energies in II-VI lattices. The potentialities of laser annealing and electron beam annealing are considered briefly. Optically-detected magnetic resonance is shown to be an important new technique in the study of radiation damage and the identification of defects in ion-implanted layers. Experimentally-observed changes in the energy splittings of implanted rare earth ions have been observed after various post-implantation isochronal annealing treatments and they have been compared with theoretical calculations based on simple crystal field models to give lattice site locations of the implanted ions. A review of published implantation work on II-VI compounds is followed by some thoughts on the future of ion implantation studies in II-VI compounds. (100 refs.)

76468 Isolation of Fe charge states by ion implantation and their study by Mossbauer spectroscopy. M.van Rossum, E.Verbiest, H.Pattyn, R.Coussement (Inst. voor Kern- en Stralingsfysika, Leuven, Belgium), S.Bukhsan. *Radiat. Eff. (GB)*, vol.64, no.1-4, p.77 (1982). [received: May 1983] (Proceedings of the First International Conference on 'Radiation Effects in Insulators', Arco, Largo di Garda, Italy, 1981).

Summary form only given, as follows. Matrix isolation of impurity atoms in a frozen rare-gas lattice is a well-known technique for the study of atoms in quasi-free states. The usual procedure consists of co-evaporating these atoms together with the matrix atoms and depositing them simultaneously on a cold substrate. Subsequently, the frozen samples can be studied by optical spectroscopy or, as has been proved more recently, by Mossbauer spectroscopy. The technical limitations of the co-evaporation procedure narrow the application range of this method. The authors have therefore tried to develop the ion implantation technique as a suitable alternative to the co-evaporation. Ion implantation does not put any limitation on the species and the concentration of the isolated atoms; moreover, it is particularly suited for the isolation of radioactive impurities, which may be investigated by Mossbauer spectroscopy. In a first series of experiments, ⁵⁷Co has been implanted into a frozen Xe matrix, thereby producing isolated Fe²⁺ and Fe⁰ states by the electron capture decay of the implanted nuclei. A second experiment was devoted to the study of ⁵⁷Fe implanted in solid O₂. Due to the high reactivity of oxygen, it would

have been impossible to produce this sample by co-evaporation. Mossbauer data show some evidence that in this case Fe^{2+} states have been produced. The results of these experiments will be discussed and further perspectives will be sketched. (2 refs.)

76469 Ion implantation in insulators. P.Thevenard (Dept. de Phys. des Matériaux, Univ. Claude Bernard Lyon I, Villeurbanne, France). *Radiat. Eff. (GB)*, vol.64, no.1-4, p.117 (1982). [received: May 1983] (Proceedings of the First International Conference on 'Radiation Effects in Insulators', Arco, Largo di Garda, Italy, 1981). The modifications of insulating materials by ion implantation can be of considerable interest for many applications. The main parameters which determine the charge state and site location of the implanted atoms in insulating targets are: ionicity of the chemical bond of the lattice, electronegativity, thermal or radiation enhanced diffusion processes, and intrinsic defects. For heavily implanted insulators, phase changes of compositional type can occur which can lead to strong modifications of the physical properties of the implanted layer. In order to obtain information of the relative extent of the critical parameters of chemical implantation in insulators it is necessary to combine analysis with different techniques such as, nuclear techniques, TEM, ESR, optical spectroscopy, X-ray diffraction at glancing analogue, etc. To illustrate the effects of these parameters, typical experimental results obtained in implanted binary or ternary compounds are reported (alkali halides, silver halides, alkaline earth oxides or fluorides, transition metal oxides, natural minerals, etc.). (no refs.)

76470 Chemical effects of carbon ion implantation into alkali halides. K.Rossler, A.Wolthuis, R.K.Bera (Inst. für Chemie I, KFA Jülich GmbH, Jülich, Germany). *Radiat. Eff. (GB)*, vol.64, no.1-4, p.181 (1982). [received: May 1983] (Proceedings of the First International Conference on 'Radiation Effects in Insulators', Arco, Largo di Garda, Italy, 1981). The implantation of 230 keV carbon ions into alkali halide single crystals AX (A=Na, K, Rb, Cs; X=F, Cl, Br, I) at temperatures $T \leq 77\text{K}$ gives rise to intensive, highly resolved, optical absorption bands in the visible regions (2.3-2.8 eV, peak half width ~ 0.004 eV). They resemble very much the Swan band system of matrix isolated C_2 . The influence of the matrix on the fine structure of the absorption bands is discussed. These carbon-centres are formed to a lesser extent or not at all when implanting at 200K and 300K, respectively. They bleach out at room temperature. Radiochemical experiments at room temperature with carbon atoms stemming from the $^{14}\text{C}(\text{p},\alpha)^{11}\text{C}$ -nuclear reaction in BN/AX mixtures show the formation of carbon compounds such as CX_4 , CX_3H , CX_2H_2 , CXH_3 and CH_4 . Thus, the primarily formed C_2 -aggregate or C-X intermediates which are stable at $T \leq 77\text{K}$, at higher temperature are gradually transformed to stable carbon-halogen compounds. The reactions of matrix isolated carbon upon dissolving the ionic crystals are of interest for the labelling of organic compounds with ^{11}C . (no refs.)

76471 Compound synthesis in TiO_2 implanted with rubidium. M.Guer-mazi, P.Thevenard, C.Dupuy (Dept. de Phys. des Matériaux, Univ. Claude Bernard Lyon I, Villeurbanne, France). *Radiat. Eff. (GB)*, vol.64, no.1-4, p.197 (1982). [received: May 1983] (Proceedings of the First International Conference on 'Radiation Effects in Insulators', Arco, Largo di Garda, Italy, 1981). Rubidium ions, with energy in the range 0.1 MeV, 2.0 MeV have been implanted in TiO_2 single crystals at RT and LNT. Defects induced by implantation have been studied by optical spectroscopy, X-ray diffraction, RBS, TEM and electrical conductivity. During implantation, the implanted samples are blue colored after irradiation. This coloration is due to an optical absorption band localized at 900 nm which corresponds to optical transition of intrinsic defects identified at Ti^{3+} . These defects are induced by a chemical reaction between the implanted ions and the oxygen of the lattice. The synthesis of a new phase in heavily implanted rutile is exhibited by using a thermal treatment and by combining techniques such as RBS, TEM and X-ray diffraction at glancing angle in the temperature range 300°C-700°C. Planar defects have been observed in the implanted area. A correlation is exhibited between these defects and the precipitates of the new phase. From X-ray diffraction measurements and TEM observations, the composition of the synthesized compound is likely Rb_2TiO_3 . (3 refs.)

76472 Study of ytterbium implanted calcia stabilized zirconia thin films and yttria stabilized zirconia single crystals. C.Cohen, J.Siejka (Univ. Paris VII, Paris, France), M.Berti, A.V.Drigo, M.Croset, M.M.Tosic. *Radiat. Eff. (GB)*, vol.64, no.1-4, p.221-31 (1982). [received: May 1983] (Proceedings of the First International Conference on 'Radiation Effects in Insulators', Arco, Largo di Garda, Italy, 1981). Calcia stabilized zirconia thin films and yttria stabilized zirconia single crystals were Yb implanted at 150 and 210 keV, and at various doses up to 1.3×10^{17} ions/cm² in order to modify locally the oxygen transport properties. Rutherford backscattering and nuclear microanalysis on the implanted thin films give information about the implantation profiles and sputtering yields. The results show that the ratio of the sputtering rates of two elements of the film is equal to their concentration ratio. At high implantation doses the Yb profile is nearly flat in the surface region with $[\text{Yb}]/[\text{Zr}] = 1.1$. ^{18}O tracing experiments demonstrate that a significant oxidation of the implanted samples occurs in air at room temperature. Further oxidation takes place during a 500°C annealing in air which does not modify the Yb profile and leads to a final mean composition. For the YSZ single crystals, channelling measurements demonstrated that the implanted region is highly damaged. As YSZ and Yb stabilized zirconia have the same lattice parameters, after high temperature annealing (1000 to 1300°C), a good crystalline quality and a full epitaxy with the YSZ substrate is achieved in this region even for the highest implantation dose. The annealings do not modify markedly the Yb profiles. (14 refs.)

76473 Furnace annealing of ion implanted polycrystalline silicon. J.L.Tandon, H.B.Harrison, C.L.Neoh, K.T.Short, J.S.Williams (Dept. of Communication & Electronic Engng., RMIT, Melbourne, Australia). Grain Boundaries in Semiconductors. Proceedings of the Materials Research Society Annual Meeting, Boston, MA, USA, Nov. 1981 (New York, USA: North-Holland 1982), p.317-23. Rutherford backscattering, Van der Pauw and TEM measurements were used to characterise the annealing behaviour of antimony implanted LPCVD polysilicon. High electrical activity without dopant redistribution was obtained for 600°C annealing of 1×10^{15} cm⁻² and 3×10^{15} cm⁻² antimony implanted samples. Subsequent annealing at temperatures $\geq 900^\circ\text{C}$ resulted in considerable grain-boundary-assisted redistribution of antimony within the polycrystalline layers and associated changes in sheet resistance. The authors' results suggest that the sheet resistance of the films is controlled by dopant segregation at grain boundaries and the fraction of antimony distributed on active sites within individual grains. (20 refs.)

76474 Double doped low dislocation density InP with low optical absorption. A.A.Ballman, A.M.Glass, R.E.Nahory, H.Brown (Bell Labs., Holmdel, NJ, USA). Gallium Arsenide and Related Compounds, 1982. Tenth International Symposium on Gallium Arsenide and Related Compounds, Albuquerque, NM, USA, 19-22 Sept. 1982 (Bristol, England: IOP 1983), p.15-21. Liquid encapsulated Czochralski growth of low dislocation density, low optical absorption InP single crystals has been achieved by double doping with sulfur (donor) and zinc (acceptor) impurities. The dislocation density is controlled by the total impurity content $N_A + N_D$ while the free carrier concentration, which determines the optical absorption, is controlled by the difference $N_D - N_A$ of the active sulfur and zinc concentrations. The authors demonstrate that the technique gives the degree of freedom to grow crystals with low dislocation densities and with independent control of free carrier concentrations. Optical absorption coefficients as low as 1 cm^{-1} at $1.3 \mu\text{m}$ have been measured on crystals with dislocation densities from 10^2 to 10^3 cm^{-2} . (9 refs.)

76475 Incorporation of amphoteric impurities in high purity GaAs. T.S.Low, B.J.Skromme, G.E.Stillman (Electrical Engng. Res. Lab., Univ. of Illinois, Urbana, IL, USA). Gallium Arsenide and Related Compounds, 1982. Tenth International Symposium on Gallium Arsenide and Related Compounds, Albuquerque, NM, USA, 19-22 Sept. 1982 (Bristol, England: IOP 1983), p.515-22. The incorporation of Group IV impurities as donors and as acceptors in high purity epitaxial GaAs has been investigated using photothermal ionization spectroscopy and variable temperature photoluminescence to detect donors and acceptors respectively. Samples from several sources of high purity LPE, AsCl_3 -VPE, AsH_3 -VPE, MOCVD, and MBE, grown GaAs were measured to establish the typical residual impurities present and their relative concentrations. For AsH_3 -VPE, MOCVD and MBE GaAs, impurity incorporation data are presented as a function of III/V ratio. The relative incorporation of amphoteric impurities as donors and acceptors is compared with the model of Teramoto (1972) for LPE and its extension to AsCl_3 -VPE by Ashen et al. (1975). (16 refs.)

76476 Effects of relative damage, Fermi energy and annealing technique in ion implanted GaAs. H.Kanber, M.Feng (Torrance Res. Center, Hughes Aircraft Co., Torrance, CA, USA), J.M.Wheeler. Gallium Arsenide and Related Compounds, 1982. Tenth International Symposium on Gallium Arsenide and Related Compounds, Albuquerque, NM, USA, 19-22 Sept. 1982 (Bristol, England: IOP 1983), p.605-12. Be and Cd were implanted into Cr-O doped horizontal Bridgman, undoped LEC and undoped VPE GaAs substrates and capless annealed in an As_4/H_2 atmosphere. Low dose Be implants upon annealing had concentration depth profiles which strongly depended on the GaAs origin. Cr and Mn redistribute quite differently for acceptor and donor implants. A model is proposed to describe the observations which incorporates the effects of relative damage due to the implant, the effect of Fermi energy on impurity migration and the effect of the arsine overpressure and anneal temperature on the diffusion profiles. (11 refs.)

76477 Implantation annealing in GaAs by incoherent light. D.E.Davies (Rome Air Dev. Center, Hanscom AFB, MA, USA), P.J.McNally, T.G.Ryan, K.J.Soda, J.J.Comer. Gallium Arsenide and Related Compounds, 1982. Tenth International Symposium on Gallium Arsenide and Related Compounds, Albuquerque, NM, USA, 19-22 Sept. 1982 (Bristol, England: IOP 1983), p.619-25. Implanted GaAs has been successfully activated through concentrating the output of quartz halogen lamps to anneal in times ~ 1 sec. The resulting layers are not restricted by the reduced mobilities and thermal instabilities of laser annealed GaAs. Better activation can be obtained than with furnace annealing but this generally requires maximum temperatures $\geq 1050^\circ\text{C}$. (12 refs.)

Lithium doping of candidate fusion reactor alloys to simulate simultaneous helium and damage production See Entry 75177

LEC growth of InP(Mn) for p-type and semi-insulating materials See Entry 76341

Reproducibility and uniformity considerations in LEC growth of undoped, semi-insulating GaAs for large-area, direct implantation technology See Entry 76342

Annealing of arsenic- and antimony-implanted silicon single crystals using a CW xenon arc lamp See Entry 76486

Incorporation of oxygen atoms into As^+ implanted silicon during CW CO_2 laser annealing in O_2 See Entry 76490

Nanosecond optical transmission studies of laser annealing in ion-implanted silicon-on-sapphire See Entry 76494

Radiation damage in ion-implanted quartz crystals. Part I: Nuclear and electronic energy deposition See Entry 76523

Assessment of damage ranges by measurements of the refractive index in ion implanted LiNbO_3 and LiTaO_3 See Entry 76526

Acoustic emission initiated by ion implantation in bubble garnet films See Entry 76567

Development of morphological instability and cells during rapid solidification of laser annealed silicon alloys See Entry 76598

AgCl intrinsic properties modifications by ion implantation See Entry 76640

Thermal evolution of precipitated phases in Au implanted MgO single crystal .. See Entry 76641

Metallic alloy precipitates in high dose indium implanted MgO See Entry 76642

On the nature of the phases formed when metals are implanted with oxygen or nitrogen See Entry 76643

XPS studies of SiO_2 surface layers formed by oxygen ion implantation into silicon See Entry 76757

High temperature annealing defects of high resistivity Si doped by neutron transmutation See Entry 76876

Behavior of shallow acceptors following neutron transmutation doping See Entry 76894

Electrical resistance of diamond implanted at liquid nitrogen temperature with carbon ions See Entry 76941

A direct comparison of LEC GaAs grown using low- and high-pressure techniques See Entry 76942

Isolation characteristics in selectivity O^+ and Cr^+ implanted GaAs See Entry 76953

Influence of nitrogen ion implantation on the electrical transport properties of InTe and InSe thin films See Entry 77076

- Mossbauer study of iron hydride formation by low temperature ion implantation See Entry 77311
- Refractive index changes of ion-implanted quartz See Entry 77350
- Raman spectroscopy for characterization of annealing of ion-implanted InP See Entry 77402
- I. The emission spectra of TL produced by ion implanted CaF_2 See Entry 77465
- II. Thermally induced changes in the TL of ion implanted CaF_2 See Entry 77466
- The growth of helium bubbles in stainless steel at high temperatures See Entry 77677
- Nitrogen migration during wear in an implanted steel See Entry 77768
- Ion nitriding behavior of several low alloy steels See Entry 77798
- Deep level defects and annealing studies in one-MeV electron irradiated (AlGa)As-GaAs solar cells See Entry 78032
- Radiation damage in front and back illuminated high resistivity silicon solar cells See Entry 78033
- End-of-life aspects of BSF technology for thin silicon solar cells See Entry 78037
- Improved efficiencies of semiconductor and metallurgical grade cast silicon solar cells by hydrogen plasma treatment See Entry 78058
- Enhanced diffusion of phosphorus at grain boundaries [Si solar cells] See Entry 78061

61.70W Impurity concentration, distribution, and gradients

(see also 66.30J Diffusion, migration and displacement of impurities)

- 76478 A new profiling technique applicable to the measurements sensitive to the free-carrier concentration rather than the depletion-layer thickness. B.Davari, P.Das (Electrical, Computer & Systems Engng. Dept., Rensselaer Polytech. Inst., Troy, NY, USA). *IEEE Electron Device Lett. (USA)*, vol.EDL-4, no.6, p.169-72 (June 1983). A novel profiling procedure, where the free-carrier concentration is the primary measured quantity, is demonstrated. This method allows the depth profiling of the dopant concentration and other properties such as trap energy levels and generation lifetime by measurements monitoring such parameters as surface conductivity, surface photovoltage, reflectance, transverse acoustoelectric voltage (TAV), and Hall voltage. Nondestructive profiling is also possible by contactless methods, e.g. TAV measurements. The distinct difference between the pulsed capacitance-voltage (C-V) measurement and the proposed procedure is that in the former the measurable physical quantity is the depletion-layer width which is modulated by an external field. In the technique proposed here, the carrier concentration as a function of bias field is monitored and the depletion-layer width is then calculated. The theoretical analysis leading to the evaluation of the depletion width as a function of bias field is presented along with an experimental example, utilizing the nondestructive TAV measurement. (14 refs.)
- 76479 Matrix effect and surface oxidation in depth profiling of $\text{AlGa}_{1-x}\text{As}$ by secondary ion mass spectrometry using O_2^+ primary ions. C.Meyer, M.Maier (Inst. für Halbleitertechnik, RWTH Aachen, Aachen, Germany), D.Bimberg. *J. Appl. Phys. (USA)*, vol.54, no.5, p.2672-6 (May 1983). The dependence of the ionization probability in secondary ion mass spectrometry experiments of the dopants Be, Ge, and Sn and the matrix atoms Ga and As in $\text{AlGa}_{1-x}\text{As}$ with $0 \leq x \leq 0.83$ on the matrix composition is determined using O_2^+ primary ions. The composition of the surface is analyzed for the first time by Auger electron spectrometry during O_2^+ bombardment. The ionization probability shows an approximately linear increase with increasing Al content ranging from a factor of 2.5 (for Ga^+) to 7.5 (for Ge^+). The variation of the ionization probability is a function of the degree of oxidation which depends on the metal-oxygen bond energy and on the availability of oxygen. The availability of oxygen is controlled by the implantation sputtering process during O_2^+ bombardment. (17 refs.)
- 76480 Measuring the density distribution of a charged impurity in thin silicon films by electron reflection. G.V.Galiev, V.V.Kapaev, V.G.Mokrov. *Sov. Phys.-Tech. Phys. (USA)*, vol.27, no.11, p.1400-1 (Nov. 1982). Translation of: *Zh. Tekh. Fiz. (USSR)*, vol.52, no.11, p.2281-2 (Nov. 1982). [received: May 1983]
- The trend toward thinner active regions in micro- and optoelectronic devices requires the development of precise methods for controlling the spatial density distribution N of charged impurity in thin (submicron) semiconductor layers. The authors promising method for monitoring the density of activated impurities in semiconductors involves electron reflection. The authors report for the first time data obtained by electron reflection combined with successive etching of semiconductor layers. The authors recorded the charged impurity density distribution as a function of depth in silicon wafers. The low-field electron reflection spectra were recorded using standard electrolytic methods for photon energies in the range $h\nu = 3.1\text{--}3.8$ eV. The thin surface regions of the wafer samples were doped with ions to form regions with widely differing impurity densities as a function of depth. The authors studied $\text{n}^+\text{-n}$ and $\text{p}^+\text{-p}$ structures. (6 refs.)
- 76481 Coulomb potential fluctuations in high-purity n-type III-V semiconductors. P.A.Fedders (Dept. of Phys., Washington Univ., St. Louis, MO, USA). Gallium Arsenide and Related Compounds, 1982. Tenth International Symposium on Gallium Arsenide and Related Compounds, Albuquerque, NM, USA, 19-22 Sept. 1982 (Bristol, England: IOP 1983), p.545-52. Investigates the effects of fluctuations in the Coulomb potential due to charged impurities in high-purity n-type III-V semiconductors at low temperatures. Assuming that charged donors and acceptors are randomly distributed at high temperatures, the author concludes that the donors are selectively filled at low temperatures leaving nonrandom distributions of charged and filled donors. The potential fluctuations from these distributions can approximately account for a number of experimental observations on low-temperature high-purity GaAs. (10 refs.)
- Lithium doping of candidate fusion reactor alloys to simulate simultaneous helium and damage production See Entry 75177
- ALCHEMI: a new technique for locating atoms in small crystals See Entry 76261
- Recoil implantation yields and depth profiles. Analytical expressions for primary and cascade contributions See Entry 76466

- Ion implantation in group II-VI compounds See Entry 76467
- Study of ytterbium implanted calcia stabilized zirconia thin films and yttria stabilized zirconia single crystals See Entry 76472
- Effects of relative damage, Fermi energy and annealing technique in ion implanted GaAs See Entry 76476
- Incorporation of oxygen atoms into As^+ implanted silicon during CW CO_2 laser annealing in O_2 See Entry 76490
- Effect of 5.5-MeV electron bombardment on the high-temperature mechanical properties of nickel See Entry 76516
- Dissolution of vanadium carbide in steel, in the case of formation of a ferrite layer at the interface See Entry 76631
- Solvus of $\text{KCl}:\text{Ca}^{2+}$ solid solution by flotation measurements of density of single crystals See Entry 76638
- Orientation of particles of a new phase appearing in crystals See Entry 76645
- Concentration dependence of the boron diffusion coefficient in silicon See Entry 76703
- Ti-W alloy interaction with silicon in the presence of PtSi See Entry 76711
- Mechanism of graphite baffle gettering in organometallic vapor phase epitaxy; adsorption of trimethylaluminum on graphite See Entry 76809
- Capacitance/voltage characteristics of semiconductor-insulator-semiconductor (SIS) structure See Entry 77020
- Angle-lapping and staining observations of Si doping superlattice structures See Entry 77025
- The variation of the p/n junction position in GaAs/GaAlAs double heterostructures grown by low pressure MO VPE See Entry 77027
- Flash-lamp annealing of ion-implanted silicon and its application to solar cells See Entry 78000

61.70Y Interaction between different crystal structure defects

- 76482 Photo-chemical reaction and photo-induced polarization studies in sulphur-doped potassium bromide. J.Prakash (Dept. of Phys., Univ. of Gorakhpur, Gorakhpur, India). *Phys. Status Solidi b (Germany)*, vol.117, no.1, p.161-9 (1 May 1983). The absorption bands of Sn^{2+} -anion vacancy dipoles in KBr lie in the ultraviolet range. Irradiation in the short-wavelength absorption bands results in a photochemical reaction. It is observed that the irradiation in the presence of an electric field in the long-wavelength absorption band creates a situation in which more dipoles are aligned along the electric field direction. Irradiation in the absence of the electric field in the long-wavelength absorption band is found to destroy the frozen-in alignment of polarized dipoles. (27 refs.)
- 76483 The inhomogeneity effect in the vacancy-dislocation interaction for α -iron. G.Knuyt, L.M.Stals, L.de Schepper, H.van Swyngenhoven (Materials Phys. Group, Limburgs Univ. Centrum, Diepenbeek, Belgium). *Phys. Status Solidi a (Germany)*, vol.76, no.2, p.K175-8 (16 April 1983). The authors investigate the inhomogeneity effect between a vacancy and a dislocation line in α -iron. They consider the physical consequences of this interaction in creep, void swelling, positron annihilation and pre-vacancy effects. (8 refs.)
- 76484 Interaction of dislocations with impurities in silicon crystals studied by in situ X-ray topography. K.Sumino, M.Imai (Res. Inst. for Iron, Steel & Other Metals, Tohoku Univ., Sendai, Japan). *Philos. Mag. A (GB)*, vol.47, no.5, p.753-66 (May 1983). The characteristics of dislocation locking due to the development of an impurity atmosphere have been investigated by the in situ X-ray topographic technique for silicon crystals doped with various types of impurities. Oxygen, nitrogen and phosphorus atoms are found to be effective in locking dislocations while carbon atoms are not. The dependence of the locking behaviour on the impurity concentration is investigated in detail for oxygen-doped crystals. It is known that the magnitude of the locking force is determined uniquely by the number of impurity atoms congregated on a unit length of dislocations if the species and concentration of the impurity atoms in the crystal are specified. Individual nitrogen atoms exhibit the strongest locking effect among the impurity atoms investigated. However, locking proceeds most pronouncedly in oxygen-doped crystals owing to a high diffusion rate and a higher solubility of oxygen atoms in silicon. The origins of the strong locking effects at various impurity atoms are discussed. (21 refs.)
- 76485 Observation of impurity-interstitial interaction in irradiated niobium. A.K.Zhetbaev, Sh.Sh.Ibragimov, A.K.Shokanov, A.N.Ozernoi (Inst. of Nuclear Phys., Acad. of Sci., Alma-Ata, Kazakhstan SSR). *Sov. Phys.-Dokl. (USA)*, vol.27, no.7, p.556-7 (July 1982). Translation of: *Dokl. Akad. Nauk SSSR*, vol.265, no.1-3, p.321-3 (July 1982). [received: April 1983]
- Presents the results of an investigation that uses the Mossbauer effect to study the interaction of radiation-induced point defects with impurities in the form of cobalt (iron) atoms. (7 refs.)
- The effect of the crystal anisotropy on the energy of the dislocation-impurity atmosphere elastic interaction in silicon See Entry 76429
- Pinning of dislocations on the departure side of strengthening dispersoids See Entry 76447
- Nature of dislocation hysteresis losses and nonlinear effect in lead at high vibration amplitudes See Entry 76449
- Investigation of the distributions of distances traveled by short dislocation segments in Ge See Entry 76450
- Lattice fringe imaging studies of the twin structures in electro-crystallized nickel coatings See Entry 76453
- Internal friction in cold-worked nickel-carbon See Entry 76563
- Diffusion of iron in aluminum studied by Mossbauer spectroscopy See Entry 76705
- Static and dynamic strain aging in a Ni(C) solid solution See Entry 77676
- Annealing behaviour of dilute FeTi, FeCu, and FeMn alloys in the temperature range above stage III following low-temperature electron irradiation See Entry 77682

61.80 RADIATION DAMAGE AND OTHER IRRADIATION EFFECTS

[for techniques of structure determination, see 61.10 to 61.16; for electron and ion impact phenomena, see 79.20]

76486 Annealing of arsenic- and antimony-implanted silicon single crystals using a CW xenon arc lamp. A.Nylandsted Larsen (Inst. of Phys., Univ. of Aarhus, Aarhus, Denmark), L.Correra. *Radiat. Eff. Lett. Sect. (GB)*, vol.76, no.3, p.67-72 (1983). Continuous, incoherent light from a xenon arc lamp has been used to anneal radiation damage in (100) silicon single crystals produced by implantation of 30-keV arsenic or antimony ions to doses between 1×10^{15} cm⁻² and 1×10^{16} cm⁻². The recrystallized layers have been characterized by Rutherford-backscattering spectroscopy, ion-channeling, transmission electron microscopy, and sheet-resistivity measurements. (16 refs.)

76487 Calculation of temperature fields in a silicon film during an optical anneal. N.I.Sterzhanov, V.I.Pilipenko, V.N.Topchii, L.S.Slobodkin, G.N.Pshenichnaya, P.A.Vakul'chik (A.V. Lykov Inst. of Heat & Mass Transfer, Acad. of Sci., Minsk, Belorussian SSR). *J. Eng. Phys. (USA)*, vol.43, no.3, p.1032-5 (Sept. 1982). Translation of: *Inzh.-Fiz. Zh. (USSR)*, vol.43, no.3, p.463-7 (Sept. 1982). The authors consider a theoretical method for the calculation of temperature fields in silicon films during a pulsed optical anneal. (9 refs.)

76488 Radiation damage in crystalline insulators, oxides and ceramic nuclear fuels. Hj.Matzke (Commission of the European Communities, Joint Res. Centre, Karlsruhe Establ., Karlsruhe, Germany). *Radiat. Eff. (GB)*, vol.64, no.1-4, p.3-33 (1982). [received: May 1983]. (Proceedings of the First International Conference on 'Radiation Effects in Insulators', Arco, Largo di Garda, Italy, 1981). Studies of radiation damage in crystalline insulators usually originate from problems connected with heavy ion impact during ion bombardment, from neutron irradiation with and without fission in nuclear reactors, or from α -decay with the resulting damage due to recoil daughter atoms of the decaying nuclei of actinide compounds. The materials involved cover a broad range of compounds, e.g. from BeO to CmO₂ for oxides, for which most work has been done. The damage studied ranges from production of isolated Frenkel pairs to complete amorphization of the crystalline compound (metamictization). The available knowledge is discussed. Emphasis is put on simple binary oxides and on ceramic nuclear fuel materials, i.e. oxides carbides and nitrides of U and Pu. Recent work on irradiated glasses is also briefly discussed since these glasses are considered as promising media for safe storage of radioactive waste for long periods of time. (181 refs.)

On the nature, characterisation and applications of point defects in insulators See Entry 76424

Photo-chemical reaction and photo-induced polarization studies in sulphur-doped potassium bromide See Entry 76482

Light-induced ESR centres in single crystal rutile See Entry 77254

61.80B Laser beams

76489 Optical transmission at 3.39 μ m during pulsed laser annealing of silicon. S.A.Lyon, Y.H.Chen, J.F.Lin (Dept. of Electrical Engng. & Computer Sci., Princeton Univ., Princeton, NJ, USA). *Appl. Phys. Lett. (USA)*, vol.42, no.11, p.978-80 (1 June 1983). The authors have measured the infrared transmission at 3.39 μ m, for bulk Si and Si:Al and for silicon on sapphire during pulsed laser annealing. The transmission drops sharply and remains near zero for approximately 100 ns in all samples. The infrared transmission in bulk Si requires milliseconds to completely recover. They attribute this effect to a thermally induced change in the index of refraction of the silicon and associated tuning of the Fabry-Perot cavity formed by the faces of the Si wafers. Their experiments yield no evidence for an optical gap as expected for a Bose condensed exciton phase, and thus are supportive of the thermal melting model of laser annealing. (21 refs.)

76490 Incorporation of oxygen atoms into As⁺ implanted silicon during CW CO₂ laser annealing in O₂. I.W.Boyd (Phys. Dept., Heriot-Watt Univ., Edinburgh, Scotland). *Appl. Phys. A (Germany)*, vol.A31, no.2, p.71-4 (June 1983). By annealing Si layers amorphised by ion-implantation with a CW CO₂ laser beam in oxygen rich environments, it has been possible to incorporate O atoms into the recrystallized lattice. Absorption measurements on such regrown layers by infrared spectrometry have shown that the impurities are preferentially bonded into substitutional lattice sites, rather than existing interstitially. Supplementary RHEED studies have indicated that β -cristobalite, a crystalline form of SiO₂, has been formed. These investigations highlight the importance of the ambient during CW laser annealing. (15 refs.)

76491 Bubble growth in laser irradiated glass. D.E.Hastings (Phys. Sci. Inc., Woburn, MA, USA). *J. Appl. Phys. (USA)*, vol.54, no.5, p.2223-9 (May 1983). The authors have considered the problem of the growth of a bubble from a preexisting nucleation site in laser irradiated glass. They show that thermal expansion of gases inside the bubble will not give significant growth. For glass temperatures below the vaporization temperature they show that a bubble can grow by CO₂ diffusion for glasses with a soda content. For glass temperatures above the vaporization temperature they examine the growth of vapor bubbles. They conclude that bubbles of several microns in size can be obtained in laser irradiated glass. (19 refs.)

76492 Temperature evolutions in silicon induced by a scanned CW laser, pulsed laser, or an electron beam. F.Ferrieu, G.Auvert (CNET-CNS, Meylan, France). *J. Appl. Phys. (USA)*, vol.54, no.5, p.2646-9 (May 1983). A self-consistent time procedure for solving a nonlinear heat diffusion equation is proposed. This paper addresses three-dimensional time dependent heat equations with nonlinear sources and diffusivity. The semianalytical model of the static regime is thereby extended to transient treatment. The advantage of this method is that it allows handling of nonlinearity in the heat diffusion equation, while keeping calculations simple. The method may be applied to either a CW laser beam or a pulsed beam. In the latter case, the method applies for any spot size, since the problem remains three-dimensional. Different deposited energy penetrations are reviewed, among them the Gaussian-shaped deposited energy corresponding to the case of the scanned electron beam. Using this method, temperatures are calculated and compared with the high speed melting isotherm for silicon under CW laser irradiation. (12 refs.)

76493 Laser-stimulated mass transfer in metals. M.E.Gurevich, L.N.J.arikov, V.G.Novitskii, A.E.Pogorelov, A.F.Zhuravlev (Inst. of Metal Phys., Acad. of Sci., Kiev, Ukrainian SSR). *Phys. Status Solidi a (Germany)*, vol.76, no.2, p.479-84 (16 April 1983). Mass transfer in iron and nickel stimulated by pulsed laser radiation is studied by the radioactive isotope method. New experimental results are obtained and an analysis in terms of kinetic equations is given. It is shown: (a) exposure of the metal surface to high intensity pulsed laser radiation leads to an accelerated atomic migration into the sample; (b) an effective retardation, the value of which depends upon the presence of crystalline defects in metals has an essential influence on the atomic migration rate stimulated by the laser; (c) multiple laser loading results in a concentration maximum formed inside the sample, the depth displacement of which depends upon the energy of light flux and the number of pulsed loadings. (14 refs.)

76494 Nanosecond optical transmission studies of laser annealing in ion-implanted silicon-on-sapphire. M.C.Lee, H.W.Lo, A.Aydinli, G.J.Trott, A.Compaan (Dept. of Phys., Kansas State Univ., Manhattan, KS, USA), E.B.Hale. *Solid State Commun. (USA)*, vol.46, no.9, p.677-80 (June 1983). Time-resolved optical transmission has been studied using 633 and 514 nm CW probes on ion-implantation-amorphized silicon-on-sapphire during annealing by a 10 nsec, ~ 1 J/cm² pulse at either 532 nm or 485 nm. As recrystallization sets in the transmitted signal at 514 nm rises by $\sim 10^3$ in ~ 60 nsec and provides a measure of regrowth velocity. Beyond 200 nsec the much slower transmission rise is used to provide an estimate of the Si cooling rate. The difference in transmission observed between initially crystalline and initially amorphous Si provide an estimate of the latent heat of recrystallization of the amorphous phase. (17 refs.)

76495 Periodic structure formed during the action of high-power coherent radiation on a semiconductor surface. V.P.Aksenov, B.G.Zhurkin (P.N. Lebedev Phys. Inst., Acad. of Sci., Moscow, USSR). *Sov. Phys.-Dokl. (USA)*, vol.27, no.8, p.630-1 (Aug. 1982). Translation of: *Dokl. Akad. Nauk SSSR*, vol.265, no.4-6, p.1365-6 (Aug. 1982). [received: May 1983]. Reports the results of a study of the parameters of the diffraction gratings which are formed on the surface of germanium and silicon under intense optical radiation. Unpolarized Nd:YAG-laser radiation was focused on the surface of the germanium. The Q-switched Nd:YAG laser ($\lambda=1.06 \mu$ m) had a power of 100 kW at a pulse length of around 100 nsec and a pulse-repetition frequency of 400 Hz. The formation of structure on the surface of the sample was monitored by observing the intensity of the diffracted rays of the second harmonic of the Nd:YAG laser ($\lambda=0.53 \mu$ m). (6 refs.)

76496 Critical factors in laser and electron beam glazing of materials. P.R.Strutt, B.G.Lewis (Univ. of Connecticut, Storrs, CT, USA), B.H.Kear. Rapidly Solidified Amorphous and Crystalline Alloys. Proceedings of the Materials Research Society Annual Meeting, Boston, MA, USA, Nov. 1981 (New York, USA: North-Holland 1982), p.485-95. The major effects of laser and electron beam glazing on solidification microstructure and melt zone geometry are described. It is shown that under comparable processing conditions, i.e. absorbed power density and interaction time, the glazed microstructures are similar. Some variations in microstructure of laser and electron beam glazed M2 steel have been noted, which seem to be related to fluid flow effects in the melt zone and possible interactions with the environment. (8 refs.)

76497 Characterization and properties of laser quenched aluminum bronzes. C.W.Draper (Western Electric, Princeton, NJ, USA), J.M.Vandenberg, C.M.Preece, C.R.Clayton. Rapidly Solidified Amorphous and Crystalline Alloys. Proceedings of the Materials Research Society Annual Meeting, Boston, MA, USA, Nov. 1981 (New York, USA: North-Holland 1982), p.529-33. Commercial aluminum bronze (Cu-Al-Fe) alloys have been laser quenched with both continuous and pulsed CO₂ laser sources. Metastable near surface regions of approximately 10 μ m thickness have been produced. The quenched surfaces have been characterized by optical microscopy, SEM, EDX, AES and glancing angle XRD. The behavior of both laser quenched and 'as received' conventional surfaces have been tested in both cavitation erosion and corrosion environments. In some cases significant differences are observed and can be rationalized from the microstructural changes accompanying the self quenching. (19 refs.)

Nonisothermal relaxation during photorecording in AsSe layers See Entry 75760

Coagulation of Ag in AgBr microcrystals See Entry 75761

The effect of Soret diffusion on the morphological stability of a binary alloy crystal See Entry 76332

Ion implantation in group II-VI compounds See Entry 76467

Development of morphological instability and cells during rapid solidification of laser annealed silicon alloys See Entry 76598

Critical point of isostructural phase transition in photomodified anthracene See Entry 76612

Microstructure and mechanical properties of laser-processed Ni-Al-Mo base alloys See Entry 76652

Rapidly solidified microstructure in surface layers of laser-alloyed Mo on Fe-C substrates See Entry 76763

An analysis of the process of recrystallization of silicon thin films with either a scanning laser or strip heater See Entry 76801

Peculiarities of photoelectric phenomena in glassy As₂S₃ See Entry 77005

Effect of laser irradiation on the electrical properties of polycrystalline thin films of tellurium See Entry 77077

Determination of thermal variation of the refractive index of cubic crystals and measurement of their light absorption coefficient See Entry 77349

Raman microprobe study of recrystallization in ion-implanted and laser-annealed polycrystalline silicon See Entry 77374

Laser formation of a 'cold liquid' See Entry 77487

Fabrication of GaAs-Mo-Si structures by metalorganic chemical vapor deposition and laser annealing See Entry 77572

Phase transformation studies of laser-processed Fe-0.2% C-Cr surface alloys See Entry 77635

Surface alloying of iron alloys by laser beam melting See Entry 77807

Production and properties of amorphous layers on metal substrates by laser and electron beam melting See Entry 77808

Laser surface treatment of aerospace steels See Entry 77809

Surface melting of cast iron with a high power laser beam See Entry 77810

61.80C X-rays

76498 Radiation effects in CaWO_4 crystals. E.Ekpo Eno, R.Grasser, A.Schermann (I. Phys. Inst., Justus-Liebig-Universität, Giessen, Germany). *Phys. Status Solidi a (Germany)*, vol.76, no.2, p.113-16 (16 April 1983). The authors report results on CaWO_4 single crystals under irradiation with X-rays or 1 MeV protons that include luminescence and optical transmission measurements at temperatures ranging from LNT (liquid nitrogen temperature) to RT (room temperature). The X-rays were produced in a 150 kV, 20 mA tube. The 1 MeV protons came from a high voltage 1.3 MeV Van-de-Graaff accelerator. (9 refs.)

76499 Radiation damage in polyacrylonitrile. M.R.Murthy (Dept. of Phys., Kakatiya Univ., Warangal, India), S.Radhakrishna. *Pramana (India)*, vol.20, no.1, p.85-90 (Jan. 1983). [received: May 1983] Radiation damage in polyacrylonitrile (PAN) has been studied in the temperature range 273 to 420 K using thermoluminescence, electron spin resonance and optical absorption techniques. A TL glow peak has been observed with maximum at 362 K. The species responsible for the TL glow peak has been identified to be due to the free radical $-\text{CH}_2\cdot\text{CH}(\text{CN})\text{CH}_2\cdot\text{CH}(\text{CN})\text{CH}_2\cdot$ by correlation with the data obtained by the temperature variation of ESR and optical absorption spectra of the x-irradiated, pre- and post-x-irradiated and thermally-treated samples. A mechanism of formation of network structures accelerated by the free radicals formed on irradiation has been investigated to explain the optical absorption spectra. The TL glow peak is analysed by various methods and corresponds to an activation energy of 1 eV, following second order kinetics. (14 refs.)

76500 Annealing of defects in X-ray and electron irradiated $\text{Cd}_x\text{Hg}_{1-x}\text{Te}$ single crystals. O.A.Kramchenko, M.V.Pashkovskii, N.A.Chutskii. *Ukr. Fiz. Zh. (USSR)*, vol.28, no.5, p.717-20 (May 1983). In Russian. X-ray irradiation at 77 K induces formation of defects in $\text{Cd}_x\text{Hg}_{1-x}\text{Te}$ single crystals. These defects cause changes in the conductivity and Hall constant. Annealing of the formed defects occurs at one state in a 130-220 K range. The value is obtained for the annealing activation energy $-E = 0.05 \pm 0.02$ eV. Annealing data are in good agreement with those for the temperature dependence of conductivity before and after irradiation. On the basis of the results obtained Te vacancies are supposed to form due to X-ray irradiation in $\text{Cd}_x\text{Hg}_{1-x}\text{Te}$. (7 refs.)

On production of Zr_1 centres in NaCl:Sm^{2+} crystals See Entry 76423
Optical damping of dislocations in KCl crystals See Entry 76441
Conductivity of ionic dielectrics under pulsed bombardment by electron and X-ray beams of medium density See Entry 76962

61.80E Gamma rays

76501 Effects of gamma-ray irradiation on OH^- doped KBr crystals. A.Scacco, F.Somma (Istituto di Fisica, Univ. di Roma, Roma, Italy). *Radiat. Eff. Lett. Sect. (GB)*, vol.76, no.1-2, p.7-12 (1983). Crystals of undoped and OH^- doped KBr have been γ -ray irradiated at room temperature. Colouring curves of doped samples show bleaching effects with highly absorbed energy doses. This result is interpreted in terms of a reaction between the OH^- impurities and the formed F-centres which predominate on the enhancement of the colouration due to the excess of anion vacancies induced by the OH^- defects. (15 refs.)

76502 Gamma radiation effects on the strength of a borosilicate glass. W.A.Zdaniewski, T.E.Easler, R.C.Bratt (Dept. of Materials Sci. & Engng., Pennsylvania State Univ., University Park, PA, USA). *J. Am. Ceram. Soc. (USA)*, vol.66, no.5, p.311-13 (May 1983). The effects of ^{60}Co gamma radiation on the strength-related mechanical properties of a borosilicate glass were examined. Although the glass darkened considerably, only a very slight densification was observed after irradiation to levels of 10^6 rads. The strength distributions were not appreciably changed by the irradiation, nor was the calculated slow crack growth parameter, or N value. Neither did radiation affect the elastic modulus or the fracture toughness of the glass. Gamma radiation does not affect the strength below 10^6 rads. (27 refs.)

76503 A study on radiation-resistance of PIC (polymer-impregnated concrete) for container of conditioning and disposal of low and intermediate level radioactive wastes. K.Ishizaki (Central Lab., Chichibu Cement Co. Ltd., Kumagaya, Japan), K.Araki, Y.Kasahara, G.Sudoh. *J. Soc. Mater. Sci. Jpn. (Japan)*, vol.32, no.354, p.327-33 (March 1983). In Japanese.

The application of PIC (polymer-impregnated concrete) to the container for conditioning and disposal of low and intermediate level radioactive wastes have been investigated, because the PIC has excellent characteristics such as high mechanical strength, high water impermeability, good corrosion resistance and good durability. It is necessary to evaluate the resistance to gamma-rays when considering the PIC-container for radioactive wastes. The radiation-resistance of PIC with test piece was evaluated by irradiation with gamma-rays. The specimens impregnated by MMA (methylmethacrylate) monomer and a solution of 10% of PS (polystyrene) in MMA monomer (MMA:PS) were polymerized by irradiating for 5 hr at the dose rate of 1 MR (1×10^6 Roentgen)/hr. PIC specimens were exposed up to maximum 1000 MR to ^{60}Co gamma-rays in air and under water. This simulates shallow land disposal and deep sea dumping conditions, respectively. (14 refs.)

Observation of impurity-interstitial interaction in irradiated niobium See Entry 76485

Radiation effects on MOS devices: dosimetry, annealing, irradiation sequence, and sources See Entry 76506

Microhardness of glassy chalcogenides in the $(\text{As}_2\text{Se}_3)_x(\text{Bi}_2\text{Se}_3)_{1-x}$ system See Entry 76553

Effect of γ -irradiation on viscosity-temperature characteristics of blended oils See Entry 76683

Photoelectric spectroscopy of radiation defects in germanium See Entry 77002

Thermoluminescence and optical absorption studies. Rubidium bromide doped with barium See Entry 77463

On the mechanisms of thermoluminescence and deformation luminescence in gamma-irradiated KCl See Entry 77464

The effect of radiation and cryogenic temperature on the fatigue resistance of G-11 CR glass-cloth/epoxy laminates See Entry 77729

61.80F Electrons and positrons

76504 Irradiation induced order-disorder in Ni_3Al and NiAl . H.C.Liu, T.E.Mitchell (Dept. of Metall. & Materials Sci., Case Western Reserve Univ., Cleveland, OH, USA).

Acta Metall. (USA), vol.31, no.6, p.863-72 (June 1983). Irradiation induced order-disorder phenomena in $\gamma\text{-Ni}_3\text{Al}$ and $\beta\text{-NiAl}$ have been investigated by high voltage electron irradiation at temperatures from 10 to 470 K. In Ni_3Al , at $T \leq 190$ K irradiation creates a completely disordered structure by 1 dpa. At $T \approx 200$ -240 K, a residual state of order with $S \approx 0.1$ -0.15 is created by about 2 dpa, and disordering rates are found to be temperature dependent. Irradiation-enhanced re-ordering through an interstitial mechanism is a likely explanation in this temperature regime. At $T \geq 250$ K, intermediate degrees of order with $S \geq 0.2$ are produced by irradiation. The degree of order in Ni_3Al increases with increasing irradiation temperature and re-ordering through the migration of vacancies is apparently more effective than the migration of interstitials. NiAl , CoAl and NiGa still maintain partially-ordered states even after irradiation at 10 K (150 K for NiGa) to 3 dpa. The effect of crystallographic orientation on disordering rates suggests that 'wrong' recombination of point defects is the more likely disordering mechanism at lower voltage irradiations and the replacement collision sequence mechanism becomes important at higher voltage irradiations. (38 refs.)

76505 Helium bubble growth during 1 MeV electron irradiation at 300 K in 5 keV- He^+ pre-implanted nickel and an amorphous Fe-Ni-Mo-B alloy. H.van Swygenhoven, L.M.Stals, G.Knuyt (Limburgs Univ. Centrum, Diepenbeek, Belgium).

Radiat. Eff. Lett. Sect. (GB), vol.76, no.1-2, p.29-41 (1983). The influence of 1 MeV electron irradiation at 300 K on the diameter distribution of helium bubbles after 5 keV He^+ implantation in nickel and in Metglas 2826 MB ($\text{Fe}_{40}\text{Ni}_{30}\text{Mo}_4\text{B}_{26}$) is investigated. Electron irradiation induces additional bubble growth in both materials. Helium bubble growth in nickel as a function of damage dose (2-18 dpa) is as effective during e^- irradiation of a He^+ pre-implanted specimen as it is during further He^+ implantation. This indicates that a significant proportion of the implanted helium resides outside the bubbles after He^+ implantation and that this helium precipitates into the bubbles during electron irradiation. In the amorphous alloy, the helium bubbles grow less during electron irradiation than during further He^+ implantation. (14 refs.)

76506 Radiation effects on MOS devices: dosimetry, annealing, irradiation sequence, and sources. E.G.Stassinopoulos, G.J.Brucker (NASA/Goddard Space Flight Center, Greenbelt, MD, USA), O.Van Gunten, A.R.Knudson, T.M.Jordan.

IEEE Trans. Nucl. Sci. (USA), vol.ns-30, no.3, p.1880-4 (June 1983). The authors report investigations of dosimetry, annealing, irradiation sequences, and radioactive sources, involved in the determination of radiation effects on MOS devices. Results show that agreement in the experimental and theoretical surface to average doses support the use of thermo-luminescent dosimeters (manganese activated calcium fluoride) in specifying the surface dose delivered to thin gate insulators of MOS devices. Annealing measurements indicate the existence of at least two energy levels, or activation energies, for recovery of soft oxide MOS devices after irradiation by electrons, protons, and gammas. (12 refs.)

76507 Megavolt electron irradiation induced regrowth of amorphous zones in silicon. J.Washburn, D.K.Sadana (Dept. of Materials Sci. & Mineral Engng., Univ. of California, Berkeley, CA, USA).

J. Appl. Phys. (USA), vol.54, no.5, p.2380-2 (May 1983). Deep buried amorphous layers were created in (100)Si by 11-MeV As^+ implantation. The effect of 1.2-MeV electron irradiation at the upper and lower surfaces of the buried layer was investigated in thin cross-section specimens prepared for transmission electron microscopy. It was found that in partially amorphous silicon amorphous zones (≤ 100 Å) imbedded in crystalline matrix shrank during the irradiation. On the basis of these results and earlier published data, the mechanism of the crystal to amorphous transformation has been discussed. (10 refs.)

76508 Microstructural transitions in Pt-C alloys during high-voltage-electron-microscope irradiation. P.G.Regnier, N.Q.Lam (Materials Sci. & Technol. Div., Argonne Nat. Lab., Argonne, IL, USA), K.H.Westmacott. *J. Nucl. Mater. (Netherlands)*, vol.115, no.2-3, p.286-96 (April 1983).

Radiation-induced microstructural changes in Pt-C alloys under irradiation inside a high-voltage electron microscope were investigated as a function of energy and temperature. Electrons of energy > 380 keV can displace C atoms from the monolayer carbon platelets previously created by co-precipitation of C and vacancies on {100} planes. The collapsed vacant sites left behind in the platelets by this direct displacement process amalgamate after a certain incubation dose. At higher energies, > 560 keV, the electrons can impart a considerable energy to the C atoms, which, in turn, become sufficiently energetic to displace the Pt atoms via secondary C-Pt collisions. Consequently, in these energy regimes, significant changes in the alloy microstructure, such as stimulated precipitate coarsening and formation of interstitial loops in the matrix, take place, even though the incident electrons have energies far below the displacement threshold of the matrix element (~ 1.3 MeV). The incubation doses for the formation of visible defect clusters inside the C precipitates and in the matrix were measured and fitted to simple analytical formalisms. The present work indicates the importance of accounting for secondary-collision processes in the assessment of radiation damage in alloys in which the alloying elements are drastically different in atomic mass. (26 refs.)

76509 Electron damage in zirconium. I. Defect structure and loop character. M.Griffiths, M.H.Loretto, R.E.Smallman (Dept. of Metall. & Materials, Univ. of Birmingham, Birmingham, England).

J. Nucl. Mater. (Netherlands), vol.115, no.2-3, p.313-22 (April 1983). Zirconium ($\geq 99.95\%$ Zr) has been irradiated using 1 MeV electrons at temperatures between 273 and 773 K in a high-voltage electron microscope and the nature of the clustered damage assessed. It has been shown that both interstitial and vacancy loops of $b = \frac{1}{2}(1120)$ nucleate and grow during electron irradiation within this temperature range. Some loops of $b = \frac{1}{2}(1123)$ and $\frac{1}{6}(2023)$ are also observed. The significance of the observation of vacancy loops is discussed in terms of current theories of defect clustering during irradiation and it is concluded that the presence of imposed stress influences the clustering. (21 refs.)

76510 Electron damage in zirconium. II. Nucleation and growth of c-component loops. M.Griffiths, M.H.Loretto, R.E.Smallman (Dept. of Metall. & Materials, Univ. of Birmingham, Birmingham, England).

J. Nucl. Mater. (Netherlands), vol.115, no.2-3, p.323-30 (April 1983). For Pt-I see *ibid.*, vol.115, p.313-22 (1983). Interstitial loops of $b = \frac{1}{2}(1123)$ have been observed to nucleate and grow during HVEM electron irradiation of Zr at temperatures ~ 650 K. Observations suggest that nucleation and early growth of these loops takes place on a combination of {1011} and {1010}

planes. Subsequent glide of the glissile $\frac{1}{3}(11\bar{2}3)$ dislocations produces irregular loops which lie on irrational planes and are frequently chair-shaped. Of the six possible $\{1011\}$ planes there are only two for which nucleation of these loops is observed in foils having normals close to (1210) . These observations and observations of perfect (a) type vacancy and interstitial loops have been interpreted in terms of the stress imposed in the Zr foil by the oxide formed during in situ irradiation at high temperature. The observations are discussed in terms of radiation-induced growth. (18 refs.)

76511 Temperature dependence of the threshold energy for atom displacement in irradiated molybdenum. W.Zag, K.Urban (Inst. fur Phys., Max-Planck-Inst. fur Metall., Stuttgart, Germany). *Phys. Status Solidi A (Germany)*, vol.76, no.1, p.285-95 (16 March 1983). The effective threshold energy for atom displacement is measured in molybdenum single crystals in a high-voltage electron microscope. Displacement is monitored at $70\text{K} \leq T \leq 300\text{K}$ by observing the nucleation of interstitial dislocation loops and at $500\text{K} \leq T \leq 800\text{K}$ by measuring the growth rate of previously induced loops. By use of reference irradiations the results of both methods may be calibrated to allow comparison over the whole temperature range covered. At $70\text{K} \leq T \leq 150\text{K}$ the effective threshold energy for irradiation along a $\langle 100 \rangle$ -direction is found to have a constant value of (34.5 ± 0.5) eV. Above this range the threshold energy decreases continuously with temperature to (26.5 ± 0.5) eV at 800K . The role of subthreshold processes is discussed. It is found that such processes contribute little to the displacement cross section. The observed temperature dependence of the displacement threshold energy is explained in terms of the effect of thermal vibrations on the production of stable Frenkel pairs. (32 refs.)

76512 The temperature dependence of the threshold displacement energy in MgO. G.P.Pells (Metall. Div., AERE Harwell, Didcot, England). *Radiat. Eff. (GB)*, vol.64, no.1-4, p.71-5 (1982). [received: May 1983] (Proceedings of the First International Conference on 'Radiation Effects in Insulators', Arco, Largo di Garda, Italy, 1981). The threshold voltage at which visible defects could be produced in MgO by electron irradiation in a HVEM has been determined over a wide range of temperature for the $\langle 001 \rangle$ and $\langle 111 \rangle$ directions. In a separate experiment, the growth of oxygen vacancy centres produced by electron irradiation along $\langle 001 \rangle$ at 90K was followed by optical absorption measurements for several energies between 325 kV and 500 kV . The oxygen vacancy growth measurements gave an upper limit to the threshold voltage of 300 kV which is equivalent to a value of the threshold displacement energy E_d for oxygen of 53 eV . The HVEM measurements over the temperature range $125\text{--}1070\text{K}$ gave an effective threshold voltage which varied considerably with temperature. The effective threshold at room temperature and below occurred at 460 kV which is considerably higher than the optically determined oxygen threshold and must therefore correspond to the magnesium threshold. This gives a value of E_d for magnesium of $60 \pm 3\text{ eV}$ for all three directions. At higher temperatures the effective threshold voltage fell to give minima at $\sim 700\text{K}$ for each of the three orientations. Comparison with the optical measurements suggests that the minima are the thresholds for oxygen displacement. It is proposed that the decrease in the effective threshold is a defect mobility effect which allows dislocation loops to be formed from the displaced oxygen ions only. The minima at 700K would therefore correspond to values of E_d for oxygen of $44 \pm 3\text{ eV}$ for $\langle 001 \rangle$, $64 \pm 3\text{ eV}$ for $\langle 011 \rangle$ and $46 \pm 3\text{ eV}$ for $\langle 111 \rangle$. At higher temperatures for $\langle 001 \rangle$ and $\langle 011 \rangle$ the effective thresholds rose to a peak at $\sim 900\text{K}$ of 340 kV and 410 kV respectively. (12 refs.)

76513 Modifications of sodium concentration profiles after electron and proton irradiation of glasses. G.Battaglin, G.Della Mea, G.de Marchi, P.Mazzoldi (Istituto di Fisica, GNSM-CNR, Padova, Italy), O.Puglisi. *Radiat. Eff. (GB)*, vol.64, no.1-4, p.99-102 (1982). [received: May 1983] (Proceedings of the First International Conference on 'Radiation Effects in Insulators', Arco, Largo di Garda, Italy, 1981). The authors studied the effect of electron and proton irradiation on the depth distribution of sodium in commercial soda-lime glasses. Samples have been irradiated at different energies and fluences. The ^{23}Na (p, α) ^{20}Ne nuclear reaction has been used to determine the sodium profiles. No detectable changes in the sodium concentration profiles have been introduced during the measurements, the proton fluences and doses needed in this type of analysis being very low. The obtained results support the hypothesis that the driving force for Na diffusion is mainly connected to the build-up of an electric field whose direction is determined by the projectile charge, while Na mobility changes because of the local temperature increase due to the beam power dissipation. (17 refs.)

76514 Electron and ion beam effects in Auger electron spectroscopy. G.Pignatelli, G.Queirolo (SGS/ATES Componenti Elettronici SpA, Milan, Italy). *Radiat. Eff. (GB)*, vol.64, no.1-4, p.109 (1982). [received: May 1983] (Proceedings of the First International Conference on 'Radiation Effects in Insulators', Arco, Largo di Garda, Italy, 1981). Summary form only given. Reports some observations on the electron and ion beam interactions on some of the insulating and conducting films used in silicon device technology. Among the materials considered, silicon nitride and P-doped silicon dioxide are of primary interest, and will be treated in some detail; results on other films, both insulating (Al_2O_3 , B-doped SiO_2 , etc.) and conducting (Al-Si alloys) will also be reported. The results show that much care has to be taken when performing or interpreting the AES data, and how to use, in some cases, the electron beam irradiation effects to increase the sensitivity of the method. (no refs.)

76515 Electric field effects on radiation defects annealing in p-InP. A.Sibille (CNET, Bagnex, France). *Solid State Commun. (USA)*, vol.46, no.9, p.673-5 (June 1983). The author has performed annealing experiments on electron irradiated Schottky diodes on p-InP. They show a strong influence of the applied reverse bias during annealing on the recovery of the free hole concentration, as well as on the disappearance of the dominant radiation induced hole traps detected by deep level transient spectroscopy (DLTS). Compensating defects are observed to drift under the action of the electric field and accumulate at the edge of the depleted zone, while the main hole traps created by the irradiation anneal faster when empty of holes or subjected to an electric field. (10 refs.)

76516 Effect of 5.5-MeV electron bombardment on the high-temperature mechanical properties of nickel. V.L.Arbuzov, S.N.Votinov, A.A.Grigor'yan, S.E.Danilov, S.M.Klotsman (Inst. of Metall. Phys., Acad. of Sci., Sverdlovsk, USSR). *Sov. Phys.-Dokl. (USA)*, vol.27, no.8, p.641-2 (Aug. 1982). Translation of: *Dokl. Akad. Nauk SSSR*, vol.265, no.4-6, p.1120-1 (Aug. 1982). [received: May 1983] Reports a study of the high-temperature radiation embrittlement of nickel-based alloys under conditions such that the production of helium due to nuclear reactions is eliminated, and the redistribution of impurities under

bombardment results from macroscopic flows of point defects (inclusions and vacancies) into sinks of the dislocation and grain-boundary type. (4 refs.)

76517 Swelling in cold-deformed OKh16N15M3B steel on irradiation in a high-voltage electron microscope. M.M.Kantor, V.N.Kolotinskii, I.I.Novikov, A.G.Ioltukhovskii, V.K.Vasil'ev, N.Yu.Zav'yalova. *Sov. At. Energy (USA)*, vol.53, no.3, p.633-7 (Sept. 1982). Translation of: *At. Energy. (USSR)*, vol.53, no.3, p.167-71 (Sept. 1982). [received: May 1983] Previous cold deformation greatly reduces the swelling of austenitic steel on neutron irradiation at $400\text{--}650^\circ\text{C}$. It has been found that the reduced swelling in cold-deformed steels of types 316 and OKh16N15M3B is due to reduction in the growth rates of the pores, whose mean size decreases as the degree of deformation rises. The authors study the effects of cold deformation in OKh16N15M3B and outline experimental methods used. (13 refs.)

| | |
|---|-----------------|
| A ruby laser in an electron beam field | See Entry 75646 |
| Point defects in II-VI compounds | See Entry 76420 |
| Interstitial loop growth in HVEM-irradiated nickel foils | See Entry 76437 |
| Ion implantation in group II-VI compounds | See Entry 76467 |
| Temperature evolutions in silicon induced by a scanned CW laser, pulsed laser, or an electron beam | See Entry 76492 |
| Critical factors in laser and electron beam glazing of materials | See Entry 76496 |
| Annealing of defects in X-ray and electron irradiated $\text{Cd}_{1-x}\text{Hg}_x\text{Te}$ single crystals | See Entry 76500 |
| The influence of the planar potential form on the channelling radiation spectrum | See Entry 76529 |
| Electromagnetic radiation of quasicannelling positrons | See Entry 76530 |
| Undulator radiation of relativistic electrons in a polydomain ferromagnetic | See Entry 76531 |
| Molecular-type channeling of relativistic electrons in crystals | See Entry 76535 |
| Study of various approximations for the continuum planar potentials at channelling. I. Monoatomic crystals | See Entry 76536 |
| The importance of ionization and displacement damage to the crystalline-amorphous transformation observed in quartz | See Entry 76540 |
| Transmission electron microscopy of RSP Fe/Cr/Mn/Mo/C alloy | See Entry 76653 |
| Multiple phase transitions in GeTe films. Dynamics and film structure | See Entry 76814 |
| Defects induced by electron irradiation in InP | See Entry 76878 |
| Electron bombardment induced defect states in p-InP | See Entry 76882 |
| Conductivity of ionic dielectrics under pulsed bombardment by electron and X-ray beams of medium density | See Entry 76962 |
| Electron-beam-induced conduction in fluorinated ethylene propylene copolymer and its acrylonitrile graft copolymer | See Entry 76969 |
| Multiple scattering of relativistic particles in crystals | See Entry 77496 |
| Annealing behaviour of dilute FeTi, FeCu, and FeMn alloys in the temperature range above stage III following low-temperature electron irradiation | See Entry 77682 |
| Production and properties of amorphous layers on metal substrates by laser and electron beam melting | See Entry 77808 |
| Property enhancement in rapidly quenched alloy surfaces | See Entry 77811 |
| Deep level defects and annealing studies in one-MeV electron irradiated (AlGa)As-GaAs solar cells | See Entry 78032 |
| Radiation damage in front and back illuminated high resistivity silicon solar cells | See Entry 78033 |
| End-of-life aspects of BSF technology for thin silicon solar cells | See Entry 78037 |

61.80H Neutrons

76518 A new calculation of thermal neutron damage and helium production in nickel. L.R.Greenwood (Chem. Engng. Div., Argonne Nat. Lab., Argonne, IL, USA).

J. Nucl. Mater. (Netherlands), vol.115, no.2-3, p.137-42 (April 1983). It has long been recognized that thermal neutron irradiations of nickel-bearing materials generate high levels of helium from the sequential $^{58}\text{Ni}(n, \gamma)^{59}\text{Ni}(n, \alpha)^{56}\text{Fe}$ nuclear reactions. This process is used to simulate fusion reactor helium-to-displacement damage rates in stainless steel during fission reactor irradiations. However, it has not previously been recognized that the ^{56}Fe recoils will also cause significant displacement damage. At thermal neutron energies the $340\text{ keV } ^{56}\text{Fe}$ recoil event will displace 1762 atoms in nickel. The helium (appm)-to-displacement ratio from this process will be 567, a value that can be used to correct previous displacement calculations in nickel-bearing materials. This effect can nearly double the displacement damage in nickel in HFIR at high neutron fluences. (7 refs.)

76519 Effect of neutron irradiation on the deformation of copper and internally oxidized copper-aluminium alloy. H.R.Higgy (Hot Lab., Atomic Energy Establ., Cairo, Egypt).

J. Nucl. Mater. (Netherlands), vol.115, no.2-3, p.307-12 (April 1983). The effect of neutron irradiation on the deformation of pure copper and of internally oxidized Cu-0.09 wt.% Al alloy was studied. Single crystals of different orientation were grown from pure copper and Cu-0.09 wt.% Al rods, and the alloy crystals were internally oxidized. Tensile specimens were prepared from the crystals, and were irradiated to a neutron fluence of $5.5 \times 10^{19}\text{ n/cm}^2$ ($E > 1\text{ MeV}$) at a temperature below 70°C . All control and irradiated specimens were tensile-tested. The addition of second-phase particles was found to have considerable effect on the deformation of irradiated copper. The increase in critical resolved shear stress was less in internally oxidized Cu-0.09 wt.% Al (Cu- Al_2O_3) than in pure copper, while the change in ultimate shear stress and shear strain was much less. Yield point phenomena appeared in all crystals, but the drop in shear stress at the yield point was less in Cu- Al_2O_3 . Two values of work-hardening coefficient (n) appeared in all unirradiated crystals, the first, a slightly larger one, was substantially decreased by irradiation, while the second was nearly unchanged. The decrease in n by irradiation was considerably larger in Cu- Al_2O_3 . (18 refs.)

- 76520** Investigations of two-level tunneling systems in n-irradiated quartz by diffuse X-ray scattering. D.Grasse, O.Kocar, J.Piesl (Sektion Phys., Univ. der Munchen, Munchen, Germany), S.C.Moss. *Radiat. Eff. (GB)*, vol.64, no.1-4, p.233 (1982). [received: May 1983] (Proceedings of the First International Conference on 'Radiation Effects in Insulators', Arco, Largo di Garda, Italy, 1981). Recent observation of the acoustic saturation and of phonon echoes in crystalline quartz after light irradiation with fast neutrons indicates that there are the same low-energy atomic tunnelling systems as in SiO₂ glass. The authors report measurements of the diffuse X-ray scattering and of the lattice parameter change from neutron irradiated quartz single crystals studying the strength and symmetry of strain defects and their local correlations. For dose 3×10^{18} n/cm² the diffuse scattering close to the Bragg peaks together with the lattice parameters change shows that the neutrons create defective regions with a volume change of 29 mean atomic volumes. The distortion field of these regions shows no high symmetry. The radius of the heavily strained region is ~ 10 Å. For higher doses the regions grow a little bit but mainly new defective regions are built. According to the various volume fractions of defective regions at various doses the first strong amorphous halo at about $K \approx 1.5 \text{ Å}^{-1}$ was detected. Since this amorphous scattering is isotropic and during annealing the regions disappear mainly without changing their size they are led to the conclusion that the defective regions are glass-like in nature. So the size of the tunnelling system has to be smaller than 20 Å. (no refs.)
- Irradiation effects on thermal conductivity of a light-water reactor pressure vessel steel See Entry 75101
- Lithium doping of candidate fusion reactor alloys to simulate simultaneous helium and damage production See Entry 75177
- Structural changes in amorphous Fe₃B₁₇ by neutron irradiation See Entry 76309
- Neutron induced colour and luminescence centres in yttrium-aluminium garnet single crystals See Entry 76422
- Swelling in cold-deformed OKh16N15M3B steel on irradiation in a high-voltage electron microscope See Entry 76517
- The importance of ionization and displacement damage to the crystalline-amorphous transformation observed in quartz See Entry 76540
- Diffusivity and permeability of hydrogen in neutron irradiated molybdenum and platinum See Entry 76701
- High temperature annealing defects of high resistivity Si doped by neutron transmutation See Entry 76876
- Behavior of shallow acceptors following neutron transmutation doping See Entry 76894
- The Lorenz function for aluminium of different chemical purity, neutron irradiated or plastically deformed See Entry 76928
- Low-temperature-irradiation study of flux-line pinning in type-II superconductors See Entry 77118
- Colour centre luminescence of α -Al₂O₃ See Entry 77455
- Helium embrittlement of iron-chromium alloys See Entry 77723

61.80J Ions

(for ion implantation, see 61.70T)

- 76521** The effect of implanted helium on the high temperature mechanical properties of a model austenitic Fe-17% Cr-17% Ni alloy. H.Schroeder (Inst. fur Festkörperforschung, KFA Jülich, Jülich, Germany), D.N.Braski. *J. Nucl. Mater. (Netherlands)*, vol.115, no.2-3, p.297-306 (April 1983). Foils of the ternary alloy Fe-17 wt% Cr-17 wt% Ni were cyclotron-implanted with 160 appm helium and then creep rupture tested at 1023K together with unimplanted controls. The range of the applied stress was 9.8 MPa till 39.2 MPa. In addition, a few tensile tests ($\dot{\epsilon} = 1.5 \times 10^{-3}$ /s) were performed with implanted and unimplanted specimens at the same temperature. The mechanical properties of the material are changed by the presence of helium—characteristically for high temperature helium embrittlement: reduced ductility, reduced creep rupture time, increased yield stress (matrix hardening) and intergranular fracture. The changes in the mechanical properties are accompanied by a change in the deformation mode from 'climb and glide' (mixed with some grain boundary sliding) in the unimplanted samples to predominantly grain boundary sliding in the helium implanted ones. This can be correlated with high densities of helium bubbles in grain boundaries. Initiation of grain boundary cracks seems to be strongly influenced by very large helium bubbles at grain boundary triple point junctions. (14 refs.)
- 76522** The effect of He-irradiation on the fracture toughness of ThO₂. H.Matzke, J.L.Routbort (Joint Res. Centre, Karlsruhe Establ., Karlsruhe, Germany). *J. Nucl. Mater. (Netherlands)*, vol.115, no.2-3, p.334-6 (April 1983). The effect of irradiation with doubly charged He²⁺ ions (α -particles) is reported. The results show that the irradiation of ThO₂ with high energy He-ions does not cause premature fracture, as reported by Clinard and Rohr (1981) for self-irradiated PuO₂, but rather causes radiation hardening. The fracture toughness increases by up to 25%. (19 refs.)
- 76523** Radiation damage in ion-implanted quartz crystals. Part I: Nuclear and electronic energy deposition. H.Fischer, G.Gotz, H.Karge (Sektion Phys., Friedrich-Schiller-Univ., Jena, Germany). *Phys. Status Solidi a (Germany)*, vol.76, no.1, p.249-56 (16 March 1983). The disorder formation in quartz crystals by implantation of He⁺, B⁺, and Ar⁺ ions at room temperature is investigated by Rutherford-backscattering spectrometry (RBS). The efficiency of the process of damage production is strongly dependent on the energy deposition mechanism and the degree of disorder. Three characteristic stages of defect formation are found in dependence on nuclear deposited energy density G_n : (I) Point defects are produced at $G_n \leq 1 \times 10^{20}$ keV/cm³. (II) Amorphous microregions are generated up to the formation of a quasi amorphous layer (termed 'RBS-amorphous') at $G_n \approx 2.5 \times 10^{20}$ keV/cm³. (III) Further structural changes occur in RBS-amorphous layers at larger G_n values. Disorder formation due to electronic processes is possible, but only in predamaged quartz, and at a very low efficiency. (16 refs.)
- 76524** Anomalous defect interaction and amorphization during self-irradiation of Si crystals at 450K. J.Belz, K.F.Heidemann, H.F.Kappert, E.Te Kaat (Inst. fur Phys., Univ. Dortmund, Dortmund, Germany). *Phys. Status Solidi a (Germany)*, vol.76, no.1, p.K81-4 (16 March 1983). 2 MeV Si²⁺ irradiation of silicon crystals with sufficiently high doses leads to amorphization at temperatures up to 400K. The authors report the results of optical and electron microscopical investigations which show that the dose dependence of the defect production at irradiation temperatures above 400K is determined by extreme defect interaction processes resulting in recombina-

tion and cluster formation of point defects (5×10^{13} to 5×10^{15} cm⁻²) and formation of stacking faults and dislocations (5×10^{15} to 3×10^{17} cm⁻²). The final amorphization represents a new mechanism originating from a dense dislocation network. (7 refs.)

- 76525** Repulsive potentials and nuclear stopping in ionic insulators. J.P.Biersack (Hahn-Meitner-Inst. fur Kernforschung Berlin GmbH, Berlin, Germany), M.Stadele. *Radiat. Eff. (GB)*, vol.64, no.1-4, p.51-60 (1982). [received: May 1983] (Proceedings of the First International Conference on 'Radiation Effects in Insulators', Arco, Largo di Garda, Italy, 1981). In ionic crystals or other insulators with partial ionic binding, the ion-target interaction differs from that of neutral atoms due to different electronic distributions and overall electrical charges. Consequently, the nuclear stopping power and defect production by recoiling atoms will deviate from standard values, obtained from e.g. Moliere potentials. Realistic potentials between the projectile ion and target ion are determined by the free electron gas model of overlapping Hartree-Fock-Slater or Lenz-Jensen ions (and neutral atoms for comparison). With the new potentials, the transferred energies T and the range of interaction are determined for either damage production ($T > E_d$) and for nuclear stopping ($T > h\nu$ for bound ions). In addition the excitation of optical phonons is taken into account which are excited by the transient electrical field of the charged projectile. (12 refs.)
- 76526** Assessment of damage ranges by measurements of the refractive index in ion implanted LiNbO₃ and LiTaO₃. A.Faik, P.G.Dawber, D.J.O'Connor, P.D.Townsend (School of Math. & Phys. Sci., Univ. of Sussex, Falmer, Brighton, England). *Radiat. Eff. (GB)*, vol.64, no.1-4, p.235-40 (1982). [received: May 1983] (Proceedings of the First International Conference on 'Radiation Effects in Insulators', Arco, Largo di Garda, Italy, 1981). Ion implantation in LiNbO₃ and LiTaO₃ produces radiation damage by nuclear collisions. The amorphisation of the lattice reduces the refractive index of the material. In the case of fast ion bombardment with helium this damage layer is buried below the surface. The refractive index profile which then exists a suitable for an optical waveguide on the surface which supports several modes. Analysis of the refractive index profile yields the damage distribution in the crystal and this in turn can be compared with theoretical estimates of the damage production and ion ranges. The analyses show that in the high energy range from 0.5 to 2.0 MeV the depth of the damage is predominantly controlled by the electronic stopping. (16 refs.)
- Dispersion and luminescence measurements of optical waveguides See Entry 75787
- Point defects in II-VI compounds See Entry 76420
- Exact solutions to a model for the growth of radiation damage during progressive ion implantation See Entry 76462
- Ion implantation damage and annealing in germanium See Entry 76463
- Pulsed thermal annealing of ion-implanted silicon See Entry 76464
- Ion implantation in insulators See Entry 76469
- Effects of relative damage, Fermi energy and annealing technique in ion implanted GaAs See Entry 76476
- Annealing of arsenic- and antimony-implanted silicon single crystals using a CW xenon arc lamp See Entry 76486
- Radiation effects in CaWO₄ crystals See Entry 76498
- Radiation effects on MOS devices: dosimetry, annealing, irradiation sequence, and sources See Entry 76506
- Megavolt electron irradiation induced regrowth of amorphous zones in silicon See Entry 76507
- Modifications of sodium concentration profiles after electron and proton irradiation of glasses See Entry 76513
- Electron and ion beam effects in Auger electron spectrometry See Entry 76514
- The importance of ionization and displacement damage to the crystalline-amorphous transformation observed in quartz See Entry 76540
- Lateral stress-induced blistering of aluminium films under helium irradiation See Entry 76753
- High resistivity in p-type InP by deuteron bombardment See Entry 76937
- Raman microprobe study of recrystallization in ion-implanted and laser-annealed polycrystalline silicon See Entry 77374
- The growth of helium bubbles in stainless steel at high temperatures See Entry 77677
- Radiation damage enhancement of the penetration of water into silica glass See Entry 77917
- The influence of hydrogen ion bombardment on the photovoltaic properties of Cu/Cu₂O Schottky barrier solar cells See Entry 77993

61.80L Atoms and molecules

- 76527** Computer simulation of collision cascades in monazite. M.T.Robinson (Solid State Div., Oak Ridge Nat. Lab., Oak Ridge, TN, USA). *Phys. Rev. B (USA)*, vol.27, no.9, p.5347-59 (1 May 1983). Collision cascades in the monoclinic mineral monazite have been studied with a modified version of the computer-simulation program MARLOWE. Most of the calculations were made for the irradiation of polycrystalline CePO₄ by normally incident 50-eV to 100-keV Ar atoms. A few calculations were made for 1-keV Cu atoms recoiling from lattice sites in a hypothetical form of Cu with the monazite structure. Although there are many fewer replacements and substantially more channeling in the mineral, collision cascades in monazite are generally similar to those in metals in size and shape. The dimensions of the calculated cascades suggest that the amorphization of monazite by Ar-ion irradiation probably commences when collision cascades begin to overlap. The calculations give a detailed view of the structure of the cascades in monazite that should be useful in interpreting radiation effects in proposed nuclear-waste isolation media. (41 refs.)

61.80M Channelling, blocking and energy loss of particles

(see also 29.70 Energy loss and range relations)

76528 On anomalies in the ionization probability of the fast atomic particles in crystals. V.A.Bazylev, A.V.Demura (I.V. Kurchatov Inst. of Atomic Energy, Moscow, USSR). *Radiat. Eff. Lett. Sect. (GB)*, vol.76, no.1-2, p.13-17 (1983). The anomalous dependence of the ionization probability of fast atomic particles during channelling in crystals on the angle between the direction of the particle momentum and crystallographic axes is predicted. (3 refs.)

76529 The influence of the planar potential form on the channelling radiation spectrum. Yu.I.Dudchik, F.F.Komarov (Inst. of Appl. Phys. Problems, Belorussian Univ., Minsk, Belorussian SSR). *Radiat. Eff. Lett. Sect. (GB)*, vol.76, no.3, p.61-5 (1983). Energies for transitions between bound states for planar-channeled electrons are calculated. The continuum planar potential constructed from atomic ones in the Molier and Hartree-Fock-Slater approximation are used. It is shown that the H-F-S line energies calculations are in a good agreement with the experimental data for diamond. (14 refs.)

76530 Electromagnetic radiation of quasicchannelling positrons. V.V.Beloshitsky, Yu.A.Bykovsky, M.H.Kumekhov (Moscow Engng. Phys. Inst., Moscow, USSR). *Radiat. Eff. Lett. Sect. (GB)*, vol.76, no.3, p.93-100 (1983). The contribution of quasicchannelling positrons to the channelling radiation spectrum is studied in the general case with the account of the dechannelling and nondipole character of the radiation at high energies. Limits of the dipole approximation are studied depending on the positron energy and the tilt angle of the crystal. Theoretical results show good agreement with experiments on diamond and silicon for 10-GeV positrons at different tilt angles. (10 refs.)

76531 Undulator radiation of relativistic electrons in a polydomain ferro-magnetic. G.M.Genkin, V.V.Zil'berberg (Inst. of Appl. Phys., Acad. of Sci., USSR). *JETP Lett. (USA)*, vol.36, no.9, p.408-11 (5 Nov. 1982). Translation of: *Pis'ma v Zh. Eksp. & Teor. Fiz. (USSR)*, vol.36, no.9, p.334-6 (5 Nov. 1982). [received: June 1983] The radiation emitted by a relativistic electron moving in a ferromagnet perpendicular to the magnetization axis is studied. Some possibilities for controlling the radiation frequency are examined. Under certain conditions this radiation has both a higher power and a higher photon energy than the radiation of a channeled particle. (6 refs.)

76532 Experimental observation of volume capture by a curved single crystal in the channelling regime. V.A.Andreev, V.V.Baublis, E.A.Damaskinski, A.G.Krivishch, L.G.Kudin, V.V.Marchenkov, V.F.Morozov, V.V.Nelyubin, E.M.Orishchin, G.E.Petrov, G.A.Ryabov, V.M.Samsonov, L.E.Samsonov, E.M.Spiridenkov, V.V.Sulimov, O.I.Sumbayev, V.A.Shechel'skii (B.P. Konstantinov Inst. of Nuclear Phys., Acad. of Sci., Moscow, USSR). *JETP Lett. (USA)*, vol.36, no.9, p.415-19 (5 Nov. 1982). Translation of: *Pis'ma v Zh. Eksp. & Teor. Fiz. (USSR)*, vol.36, no.9, p.340-3 (5 Nov. 1982). [received: June 1983] It is shown for the first time that a curved single crystal can capture particles in the channelling regime for angles exceeding the Lindhard angle. 1-GeV protons were captured during channelling by (111) and (110) planes and by (110) axis along the entire length of a 1-cm silicon single-crystal curved along a radius of 46 cm in the entire angular range up to 20 mrad. (4 refs.)

76533 Computer simulations of slowing down of heavy ions in polycrystalline materials. M.Hautala (Dept. of Phys., Univ. of Helsinki, Helsinki, Finland). *Phys. Lett. A (Netherlands)*, vol.95A, no.8, p.436-8 (23 May 1983). A fast computer code is constructed to simulate the slowing down of ions in crystalline materials. The programme is used to study the range distributions of 120 keV Pb in polycrystalline Al and 60 keV Al in polycrystalline Ta. Good agreement with experiment is found, when partial preferred orientation of the microcrystals is assumed. (9 refs.)

76534 Energy losses in crystalline and amorphous solids in the intermediate energy region. E.Kuhrt, R.Wedell (Sektion Phys., Humboldt-Univ. zu Berlin, Berlin, Germany). *Phys. Status Solidi b (Germany)*, vol.116, no.2, p.585-95 (1 April 1983). Using the classical theory for two moving charged particles the electronic stopping power of amorphous and random oriented crystalline solids is calculated. It is shown that in the intermediate energy region, where the stopping is maximized, motion of the target electrons must be considered. The specific problems of energy losses in crystals are discussed and directional effects are taken into account. Calculated values of the stopping power agree well with experimental results for protons in the random as well as in the channelling regime. (38 refs.)

76535 Molecular-type channelling of relativistic electrons in crystals. E.G.Vyatkin, Yu.M.Filimonov, A.M.Taratin, S.A.Vorobiev (Inst. of Nuclear Phys., Tomsk Polytech. Inst., Tomsk, USSR). *Phys. Status Solidi b (Germany)*, vol.117, no.1, p.41-50 (1 May 1983). Channelling of relativistic electrons in (110) direction in a diamond crystal and the channelling radiation spectra are investigated using computer simulation by the binary collision model and using the model of a continuum potential of the atomic rows. In a computer experiment the atomic- and molecular-type states of channeled electrons are revealed, and the orientational dependence of the electron trapping probability in these states is obtained. The peculiarities revealed of the angular distributions and radiation spectra of electrons in the molecular-type states should make it possible to discover these states experimentally. (9 refs.)

76536 Study of various approximations for the continuum planar potentials at channelling. I. Monoatomic crystals. G.V.Dedkov (Phys. Dept., Karbadio-Balkarian State Univ., Nalchik, USSR). *Phys. Status Solidi b (Germany)*, vol.117, no.1, p.57-66 (1 May 1983). A detailed analysis of different approximations for the continuum planar potentials under channelling conditions is given. The continuum potentials for positrons (electrons) channeled in (110) and (100) planes in crystals of diamond silicon, and tungsten are calculated in different approximations to the screening function. The model of an atom with a piecewise exponentially decaying electron density is discussed. The influence of the thermal vibrations and the atomic shell structure on the potentials is investigated. Some estimates of the photon energy radiated at channelling of 56 MeV electrons in (110) planes of C are given. (14 refs.)

76537 Experimental energy-loss function, $\text{Im}[-1/\epsilon(q,\omega)]$, for aluminium. P.E.Batson, J.Silcox (School of Appl. & Engng. Phys., Cornell Univ., Ithaca, NY, USA). *Phys. Rev. B (USA)*, vol.27, no.9, p.5224-39 (1 May 1983). The authors describe highly accurate (0.2-1%) intensity measurements for the inelastic scattering of 75-keV electrons in $\sim 1000\text{-\AA}$ -thick polycrystalline aluminum films in the region of $(0.0\text{-}3.1)\text{-\AA}^{-1}$ transferred wave vector and (0-100)-eV energy loss. The work was performed on the Cornell University electron spectrometer-microscope-computer system. These measurements clarify some experimental problem associated with multiple scattering which obscure the single scattering distribution. They present a new method for eliminating the distribution of intensity attributable to multiple scattering involving quasielastic events. This subtraction method is accurate to $\sim 0.01\%$ of the single-bulk-plasmon intensity. Next, they extend an earlier correction method to obtain the single scattering energy-loss function $\text{Im}[-1/\epsilon]$ from the residue to the first process, which consists of multiple plasmons and quasiparticle transitions. Details of the specific procedures are included. They point out several features in the result—the bulk-plasmon intensity, dispersion, and width, the quasi-particle continuum, and a simultaneous two-plasmon scattering. The latter is, for the first time, characterized completely as to intensity, dispersion, and energy width. Finally, they present a comparison of the measured bulk-plasmon dispersion with some recent model calculations. (50 refs.)

76538 Range calculations for high-energy heavy atoms in complex media. W.Westmeier, K.Rossler (Inst. für Kernchemie, Lahnberge, Marburg, Germany). *Radiat. Eff. (GB)*, vol.64, no.1-4, p.61 (1982). [received: May 1983] (Proceedings of the First International Conference on 'Radiation Effects in Insulators', Arco, Largo di Garda, Italy, 1981). Summary form only given, as follows. The computer code MARLOWE was used to evaluate energy vs. range curves in the binary collision approximation. The program was extended to the high-energy regime taking into account the stripping of electrons from the projectile and the concomitant changes in the interaction potentials especially for the inelastic part of the collisions. A complementary computer code LATTIC was developed for the parameterization of the lattice description. This code enables the application of MARLOWE to target materials with complicated crystallographic structure, such as, e.g. ThF_4 , KClO_4 and NH_4Cl . Test calculations for a series of projectile/target combinations showed a reasonable agreement with experimental recoil ranges of Pd, Ag, Os, and Ir isotopes from proton induced spallation in different targets. These calculations also indicate that density effects, i.e. the reduction in the ionization loss of fast charged particles due to the dielectric polarization of the medium, seem to be of minor importance for particle velocities below $\beta=0.01$. (no refs.)

76539 Interaction of charged particles and local modes. J.Janszky (Res. Lab. for Crystal Phys., Budapest, Hungary), Yu.Ya.Yushin. *Radiat. Eff. (GB)*, vol.64, no.1-4, p.171-3 (1982). [received: May 1983] (Proceedings of the First International Conference on 'Radiation Effects in Insulators', Arco, Largo di Garda, Italy, 1981). By means of the coherent states technique the interaction of local modes of imperfections in alkali halide crystals with charged particles emerging from an ion avalanche is investigated. The energy obtained by an imperfection and that lost by a particle on unit way due to the interaction are evaluated. Part of the excess energy of the mode relaxes through phonon processes, a smaller part of the energy is emitted by the crystal on the local mode frequency. This way during the interaction the local mode emits infrared radiation; an estimate is given concerning the intensity of this radiation. This intensity has a well-defined peak at the velocity of particles being in resonance with the local mode frequency. Using different local centres some information can be obtained about the velocity distribution of particles inside the crystal during irradiation. (4 refs.)

76540 The importance of ionization and displacement damage to the crystalline-amorphous transformation observed in quartz. D.G.Howitz, J.F.DeNatale (Dept. of Mech. Engng., Univ. of California, Davis, CA, USA). *Radiat. Phys. & Chem. (GB)*, vol.21, no.5, p.445-9 (1983). A radiolytic yield and an average displacement damage cross section are calculated for quartz based upon recent ion, neutron and electron irradiation studies. (27 refs.)

76541 Stimulated emission by charged particles in natural hollow crystalline channels. V.I.Vysotskii, R.N.Kuz'min (T.G. Shevchenko State Univ., Kiev, Ukrainian SSR). *Sov. Phys.-Solid State (USA)*, vol.24, no.12, p.2120-1 (Dec. 1983). Translation of: *Fiz. Tverd. Tela (USSR)*, vol.24, no.12, p.3718-20 (Dec. 1983). It has been conjectured that stimulated emission of X-rays and gamma rays can occur due to resonance transitions of relativistic electrons between levels of the transverse motion of electrons during their channelling in crystals. The authors propose a qualitatively new model of coherent amplification in the interval $\lambda \approx 1\text{-}10\text{ \AA}$ based on the quantum motion of relativistic positrons in natural hollow rectilinear cylindrical channels of radius $R \approx 4\text{-}40\text{ \AA}$. The required system of such channels can be found in aluminosilicate crystals (zeolites such as mordenite, gmelinite, offretite, etc.) with $R \approx 4\text{ \AA}$ and asbestochrysotile packets with $R \approx 40\text{ \AA}$. (5 refs.)

76542 Scaling of the band structure of channelized particles. I.D.Feranchuk, B.A.Chevganov (V.I. Lenin State Univ., Minsk, Belorussian SSR). *Sov. Phys.-Tech. Phys. (USA)*, vol.27, no.11, p.1397-8 (Nov. 1982). Translation of: *Zh. Tekh. Fiz. (USSR)*, vol.52, no.11, p.2276-8 (Nov. 1982). [received: May 1983] The authors show that the dependence of the energy band spectrum of relativistic channeling particles on the longitudinal energy and on the amplitude and period of the interplane potential is of a universal character. It is therefore possible to find the particle energy levels for different potential parameters and longitudinal energies using a single 'standard' band spectrum. The authors describe an effective method for calculating energy bands for particles channelling in a plane and construct some 'standard' spectra. (5 refs.)

| | |
|--|-----------------|
| ALCHEMI: a new technique for locating atoms in small crystals | See Entry 76261 |
| Assessment of damage ranges by measurements of the refractive index in ion implanted LiNbO_3 and LiTaO_3 | See Entry 76526 |
| Computer simulation of collision cascades in monazite | See Entry 76527 |
| The relative importance of multiple inelastic scattering in the quantification of EELS | See Entry 77490 |

62.00 MECHANICAL AND ACOUSTIC PROPERTIES OF CONDENSED MATTER

(see also 46.30 *Mechanics of solids and rheology*, 61.70 *Defects in crystals*, 68.25 *Surfaces and interfaces*, 81. *Materials science; for thermomechanical effects*, see 65.70; for magnetomechanical effects, see 75.80; for piezoelectric effects, see 77.60; for elasto-optical effects, see 78.20H)

62.10 MECHANICAL PROPERTIES OF LIQUIDS

(for viscosity of liquids, see 66.20)

- Dipole moments of dichlorotoluenes in benzene solution See Entry 75543
- Linear and nonlinear viscoelastic functions for polymer melts and concentrated solutions See Entry 75972
- New liquid crystal materials; physical properties and performance in displays for automobile, high information density and guest-host applications See Entry 76292
- Dynamics of a Fredericks transition in side chain nematic polymers: determination of the viscoelastic coefficients K_1 and γ_1 See Entry 76295
- Oriental fluctuations of a lyotropic nematic liquid crystal measured by quasielastic light scattering See Entry 76297
- Ultrasonic study of two-component systems See Entry 76565
- Modified Gruneisen and Anderson-Gruneisen relations for quasi-spherical molecular liquids See Entry 76654
- Experimental determination of diffusion coefficients, viscosities, densities and refractive indexes of 11 binary liquid systems See Entry 76679
- Electric birefringence and molecular polarisability of $\text{CF}_2\text{Cl.CF}_2\text{Cl}$ See Entry 77356
- Determination of the ratios K_{11}/K_{22} and γ_1/K_{11} in nematic liquid crystals by correlation spectroscopy See Entry 77403

62.20 MECHANICAL PROPERTIES OF SOLIDS (RELATED TO MICROSCOPIC STRUCTURE)

(see also 81.40 *Treatment of materials and its effects on microstructures and properties*, 81.70 *Materials testing*)

- Temperature fields and thermal stress fields in radiation shieldings See Entry 75202
- Thermal expansion of amorphous iron-chromium-boron alloys See Entry 76678
- Structure/property relationships and applications of rapidly solidified aluminum alloys See Entry 77661

62.20D Elastic constants

(see also 03.40D *Mathematical theory of elasticity*, 81.40J *Elasticity and anelasticity*)

- 76543 Temperature dependence of elastic stiffness C_{11} in LiNbO_3 . I.Tomeno, S.Matsumura (Toshiba Res. & Dev. Center, Toshiba Corp., Kawasaki, Japan). *J. Phys. Soc. Jpn. (Japan)*, vol.52, no.5, p.1515-17 (May 1983). The elastic stiffness C_{11} of a single domain LiNbO_3 crystal (C_{11}^E) and that of a multidomain crystal (C_{11}^D) were measured by the ultrasonic phase comparison method in the temperature range between 300 and 1223K. The stiffness C_{11}^D was about 2% larger than C_{11}^E at room temperature and both decreased linearly with increasing temperature. The results indicated that the spontaneous polarization P_3 was approximately constant in the temperature range described. (19 refs.)
- 76544 The variation of elastic constants of nickel-iron single crystal alloys from 78.76 to 300K. A.Kanrar, U.S.Ghosh (Dept. of Magnetism, Indian Assoc. for the Cultivation of Sci., Calcutta, India). *J. Phys. & Chem. Solids (GB)*, vol.44, no.5, p.457-62 (1983). The temperature dependences of three independent adiabatic elastic stiffness coefficients C_{11} , C_{12} and C_{44} of four Ni-Fe single crystal alloys with compositions from 50 to 90 wt.% of Ni have been studied by the ultrasonic pulse superposition technique from 78.76 to 300K. The elastic constants of the alloys exhibit normal temperature dependencies in the range of temperature investigated. A good fit of the experimental data to Lakkad's phenomenological model (1971) for the temperature dependence of elastic constants was obtained. (14 refs.)
- 76545 Dependence of the Poisson ratio on the electron-phonon interaction constant. A.S.Balankin (Engng.-Phys. Inst., Moscow, USSR). *Sov. Phys.-Solid State (USA)*, vol.24, no.12, p.2102-3 (Dec. 1983). Translation of: *Fiz. Tverd. Tela (USSR)*, vol.24, no.12, p.3689-90 (Dec. 1983). The interaction of electrons with lattice vibrations via the deformation potential leads to a renormalization of the elastic moduli which must clearly give rise to a dependence of the Poisson ratio on the electron-phonon interaction constant. The author studies this dependence by solving the elasticity equations, including the deformation interaction of electrons with lattice vibrations, in conjunction with the Maxwell equations and the transport equation for conduction electrons for the case of an isotropic metal and using the Frohlich model of the electron-phonon interaction. (9 refs.)
- 76546 Temperature dependence of the elastic modulus of polymer glasses. A.B.Sinani, V.A.Stepanov, I.I.Timoshenko (A.F. Ioffe Physicotech. Inst., Acad. of Sci., Leningrad, USSR). *Sov. Tech. Phys. Lett. (USA)*, vol.8, no.9, p.441-2 (Sept. 1982). Translation of: *Pis'ma v Zh. Tekh. Fiz. (USSR)*, vol.8, no.17-18, p.1025-9 (Sept. 1982). [received: May 1983] The authors show that the temperature dependence of the elastic moduli of polymer glasses has a twofold nature: On the one hand, a relaxation of the modulus associated with a change in the mobility of the various molecular groupings. On the other hand, the modulus is affected by anharmonic effects, characteristic of any condensed system and particularly strong in the case of a weak intermolecular interaction. The contribution of the second mechanism is extremely important in polymer glasses, indicating that the forces determining the elastic behavior are of an intermolecular nature. (6 refs.)

- 76547 Measurement of elastic moduli of small specimen by means of rectangular parallel piped resonance method. T.Goto (Dental Material & Technol., Gifu Coll. of Dentistry, Gifu, Japan), N.Soga. *Yogyo-Kyokai-Shi (Japan)*, vol.91, no.1, p.24-31 (1983). The rectangular parallelepiped resonance method was used for measurements of the elastic constants and their temperature dependences for SiO_2 glass and MgO single crystals with about 2 mm in edge length. It was found that (1) even a small specimen of 2 mm size could be used, (2) sample preparation was quite easy as compared with the ultrasonic technique, (3) the resonant frequency necessary for the measurement was low, and (4) the temperature dependences of elastic constants on both isotropic and nonisotropic solid could be obtained accurately by measuring the relative changes of resonant frequencies from the room temperature values, if the force imparted to the specimens was kept constant during the measurement of temperature variation. (11 refs.)
- Modified two-phase model for the mechanical properties of the semicrystalline polymer—polyethylene See Entry 7632
- On the mechanical stability of BCC transition elements and alloys See Entry 76355
- Gamma radiation effects on the strength of a borosilicate glass See Entry 76502
- Computation of Debye temperatures of some cubic and hexagonal crystals from the elastic constant data near 0K See Entry 76578
- Phase diagram of ZrV_2 See Entry 76589
- Structural phase transition of layer compound $(\text{C}_2\text{H}_5\text{NH}_3)_2\text{FeCl}_4$ See Entry 76609
- ΔE effect of a Mn ferrite single crystal at temperatures between 150 and 300K See Entry 77230
- Elastic anomaly in an itinerant-electron antiferromagnet See Entry 77245
- Low-temperature elastic-constant anomalies in Fe-Cr-Ni-Mn alloys See Entry 77247
- Magnetoelastic effect in dilute Fe-Co alloys See Entry 77248
- Elastic, dielectric, and piezoelectric properties of cancrinite carbonate single crystals See Entry 77332
- Effects of interlaminar forces on longitudinal acoustic modes of *n*-alkanes See Entry 77375
- Physicochemical and spectral luminescence properties of a glass based on the $\text{SiO}_2\text{-Al}_2\text{O}_3\text{-La}_2\text{O}_3\text{-Nd}_2\text{O}_3$ system See Entry 77438
- Influence of the composition of the particles contained in austenite on the characteristics of the $\gamma \rightarrow \alpha$ transformation See Entry 77639
- Bulk modulus and martensitic transformation in Mn-Cu alloys See Entry 77642
- Precipitation studies in lead-tin alloys See Entry 77644
- Studies of epoxy resin systems. II. Effect of crosslinking on the physical properties of an epoxy resin See Entry 77656
- X-ray stress measurement of high manganese austenitic steels See Entry 77687
- X-ray stress measurement of coarse grained 18-8 stainless steel by complex oscillation technique See Entry 77688
- The elastic constants of ultradrawn polypropylene See Entry 77689
- Effect of porosity on the mechanical properties of nitrogen ceramics See Entry 77690
- Elastic moduli, hardness and thermal expansion of some metaphosphate glasses See Entry 77693
- Elastic properties of alkali silicate glasses See Entry 77694
- X-ray investigation of stress measurement of heat resisting materials (on the X-ray elastic constants and the residual stresses of nickel base alloy) See Entry 77817

62.20F Deformation and plasticity

(inc. yield, ductility and superplasticity; see also 81.40L *Deformation, plasticity and creep*)

- 76548 Analysis on plasticity in materials with strain hardening and strain-rate sensitivity under uniaxial tension. Lian Jianshe. *Chin. J. Mech. Eng. (China)*, vol.18, no.4, p.21-30 (Dec. 1982). In Chinese. [received: May 1983] For the analysis of plastic flow and necking development of materials with both work hardening and strain-rate sensitivity under uniaxial tension, it is proved that the basis of Hart's analysis (1967) is the same as Hutchinson et al.'s analysis (1977) based on the constitutive law ($\sigma = K\dot{\epsilon}^m$). Based on Hart's analysis, the flow-stability and the criterion of stability of Hart and Jonas et al. (1976, 1977) are discussed. Also, considering the initial geometric imperfection ($\alpha(0)$), the incremental and the integral analysis are given for necking development respectively. From the incremental analysis, both relations between the total elongation δ and m as well as n are given as: $\delta = (1/\alpha(0))^{m-1}$; $\delta = (1/\alpha(0))^{m+n-1}$. The result of the integral analysis is the same as the integral expressions (when $n=0$) derived by Hutchinson et al. Comparing these theoretical results with experimental results, the coincidence is good. In addition, a load analysis is made and two load expressions are given. (11 refs.)
- 76549 Cross-slip in the high-temperature deformation of germanium, silicon and indium antimonide. H.Siethoff (Phys. Inst., Univ. Wurzburg, Wurzburg, Germany). *Philos. Mag. A (GB)*, vol.47, no.5, p.657-69 (May 1983). In most materials, steady-state creep at high temperatures is governed by diffusion-controlled recovery processes. Exceptions to this rule are silicon and germanium, where the measured activation energies are distinctly higher than those of self-diffusion, an effect which has not been understood until now. It is shown that a cross-slip mechanism is most probably working in the steady-state regime of these semiconductor elements, and that Escaig's model (1968) can describe fairly well the published data. In the light of these results, the recently discovered second recovery stage (stage V) in the stress-strain curves of germanium, silicon and indium antimonide may be caused by cross-slip rather than by a diffusion-controlled recovery process, as proposed earlier. (38 refs.)
- 76550 Identification of slip systems in cubic boron nitride. C.A.Brookes, R.M.Hooper, W.A.Lambert (Dept. of Engng. Sci., Univ. of Exeter, Exeter, England). *Philos. Mag. A (GB)*, vol.47, no.5, p.19-12 (May 1983). Knoop indentation hardness measurements have been made at room temperature, on (001) and (111) surfaces of cubic boron nitride crystals. Subsequent

heat treatment of the crystals, in air at temperatures of 900°C and above, caused a rapid expansion of the dislocated volume beneath the indentation and the formation of etched slip traces. Observations on the nature of anisotropy in hardness and the geometry of the slip traces have been used to identify {111}{110} as the active slip system in cubic boron nitride. (11 refs.)

76551 Localized shear deformation of amorphous metals. J.C.M.Li (Dept. of Mech. Engng., Univ. of Rochester, Rochester, NY, USA). Rapidly Solidified Amorphous and Crystalline Alloys. Proceedings of the Materials Research Society Annual Meeting, Boston, MA, USA, Nov. 1981 (New York, USA: North-Holland 1982), p.267-76

The characteristics of localized deformation in amorphous metals are reviewed. All the available evidence seems to suggest that dislocations are responsible for shear localization. These dislocations seem to require a stress concentration for their nucleation. Once nucleated, they are capable of producing both forward and reverse shear in a narrow band, much like the dislocations in crystalline materials. (27 refs.)

Tensile properties of 1.4970 austenitic stainless steel after corrosion caused by uranium dioxide and simulated fission products See Entry 75100

Residual stresses in cubic materials with orthorhombic or monoclinic specimen symmetry: influence of texture on ψ splitting and non-linear behaviour See Entry 76255

On production of Z_1 centres in NaCl:Sm²⁺ crystals See Entry 76423

The effect of annealing on the dislocation dissociation in plastically deformed silicon See Entry 76439

Transmission electron microscopy of dislocation structures in V₃Si single crystals after deformation at high temperatures See Entry 76440

Stress relaxation experiments for proving the existence of an obstacle spectrum for thermally activated dislocation motion See Entry 76443

X-ray topographic in-situ observation of slip band propagation in MgO single crystals See Entry 76445

Effects of triaxial stressing on creep cavitation of grain boundaries See Entry 76451

Swelling in cold-deformed OKh16N15M3B steel on irradiation in a high-voltage electron microscope See Entry 76517

Effect of neutron irradiation on the deformation of copper and internally oxidized copper-aluminium alloy See Entry 76519

The effect of implanted helium on the high temperature mechanical properties of a model austenitic Fe-17% Cr-17% Ni alloy See Entry 76521

Dependence of the rate of intrareactor creep on the stress See Entry 76552

Microhardness of β -alumina single crystals See Entry 76556

Influence of the concentration of chemical sites on the strength of solid polymers See Entry 76560

Physical model of plasticity of a transition See Entry 76605

Structural phase transition of layer compound (C₂H₅NH₃)₂FeCl₄ See Entry 76609

Microstructure and properties of fine grained supersaturated Fe-C alloys See Entry 76650

Microstructural study of devitrified amorphous alloys See Entry 76651

Means of plastic self-indentation of solids in contact See Entry 76765

Evidence of the formation of twins by deformation and 'growth-accidents' in evaporated thin films of gold See Entry 76815

The Lorenz function for aluminium of different chemical purity, neutron irradiated or plastically deformed See Entry 76928

Simultaneous effect of UV-irradiation and deformation See Entry 76999

Preparing conditions and magnetic properties of rapidly quenched high silicon iron ribbons See Entry 77212

Changes in the polarization and diffraction of light at dislocations with screw components in plastically deformed cadmium sulfide See Entry 77351

Birefringence and structural defects in Cu₂O crystals See Entry 77355

Preparation and properties of Fe-1.65 wt.%Cr single crystals See Entry 77542

Deceleration of relaxation in a Cu-Si alloy See Entry 77653

Studies of epoxy resin systems. II. Effect of crosslinking on the physical properties of an epoxy resin See Entry 77656

Studies of epoxy resin systems. III. Effect of sub-T_g aging on the physical properties of a fully cured epoxy resin See Entry 77657

Studies of epoxy resin systems. IV. Fracture toughness of an epoxy resin: a study of the effect of crosslinking and sub-T_g aging See Entry 77658

Strengthening mechanisms in Inconel 718 superalloy See Entry 77665

Influence of the temperature and rate of deformation on the dynamic recrystallization of KhN77TYuR alloy single crystals See Entry 77668

Austenitising process of steels and effect of plastic deformation on the process See Entry 77671

Structural dependence of microscopic residual shear stress at worked surface See Entry 77672

Relative work hardening rates See Entry 77675

Influence of heat treatment on the structure and long-term strength of γ/γ' -MeC nickel eutectic. Length memory effect See Entry 77680

Characteristics of formation of the structure during deformation of low-alloy chromium by rolling at temperatures 1400-1450K See Entry 77681

Heating of a thin wire by a constant current with density sufficient for the appearance of thermoplasticity See Entry 77683

X-ray stress measurement of high manganese austenitic steels See Entry 77687

Pseudo-elastic behaviour in rapidly-quenched dilute tin alloys See Entry 77695

Modified method for determination of energy stored in metal during its deformation See Entry 77698

Tensile strength of ultra high modulus linear polyethylene filaments See Entry 77699

Nature of the anomalous spontaneous deformation of iron in the presence of hydrogen See Entry 77701

High-temperature shape memory in titanium nickelide See Entry 77702

Influence of plastic deformation on the properties of chromium bronze See Entry 77703

A viscous shell formulation for the analysis of thin sheet metal forming See Entry 77704

Measuring temperature dependence of secondary forming behavior of cellular polystyrene sheets See Entry 77705

Thermal stress measurements of tungsten fiber-copper composites See Entry 77708

Rectangular tubular steel columns loaded biaxially See Entry 77709

Mechanical properties and structural stability of alloys See Entry 77711

Thermal activation analysis by stress relaxation in some FCC metals See Entry 77713

Cold deformation of a nickel-base superalloy See Entry 77714

Composition and processing effects on the properties of one-component polyurethanes See Entry 77715

A recommended procedure for determining the strain rate sensitivity in superplasticity See Entry 77716

Tensile strength of hot-pressed ZrO₂-Y₂O₃ at high temperature See Entry 77717

Laws connecting viscous fracture with the flow limit See Entry 77720

The mechanical properties and tensile fracture characteristics of partially annealed low carbon mild steel sheet See Entry 77743

Effect of prior deformation on the cleavage of zinc single crystals See Entry 77747

Fractography of polyethylene glycol dimethacrylate doped with polymethyl methacrylate See Entry 77748

Strain localization and hydrogen embrittlement See Entry 77749

Ion implantation effect on fatigue crack initiation in Ti-24V See Entry 77750

The effect of pre-existing epsilon martensite on the hydrogen induced fracture of austenitic stainless steel See Entry 77752

A brittle to ductile transition in NiAl of a critical grain size See Entry 77753

Deformation induced dilatations and new observations on fracture in compression in metallic glasses at low temperatures See Entry 77761

On the yield loads of plates with array of holes See Entry 77823

Density change of glassy Pd₇Si_{16.5}Cu_{4.5} alloy during cold drawing See Entry 77860

62.20H Creep
(see also 81.40L Deformation, plasticity and creep)

76552 Dependence of the rate of intrareactor creep on the stress. Yu.S.Patiletyov, O.G.Tyupkina (Inst. of Nuclear Phys., Acad. of Sci., Alma-Ata, Kazakh SSR). *Fiz. Met. & Metalloved. (USSR)*, vol.55, no.4, p.792-7 (April 1983). In Russian. English translation in: *Phys. Met. & Metallogr. (GB)*

The mechanism of radiation creep, based on the combined motion of dislocations including glide and climb, is used to calculate the rate of deformation $\dot{\epsilon}_{rad}$ on the stress σ . It is shown that at low stresses the rate of rise of $\dot{\epsilon}_{rad}$ on increase in σ follows a nearly linear law, whereas at high values of σ there is a considerable deviation from linearity. These theoretical predictions are in agreement with the experimentally observed nonlinear dependence of the rate of intrareactor creep on the applied stress. (22 refs.) A.T.

Creep transition of transversely isotropic cylinder under internal pressure See Entry 75932

Pinning of dislocations on the departure side of strengthening dispersoids See Entry 76447

Effects of triaxial stressing on creep cavitation of grain boundaries See Entry 76451

The inhomogeneity effect in the vacancy-dislocation interaction for α -iron See Entry 76483

Cross-slip in the high-temperature deformation of germanium, silicon and indium antimonide See Entry 76549

Influence of the concentration of chemical sites on the strength of solid polymers See Entry 76560

Diffusive intergranular cavity growth in creep in tension and torsion See Entry 77696

A study of intergranular cavity growth controlled by the coupling of diffusion and power law creep See Entry 77697

High-temperature creep and dislocation structure of vanadium See Entry 77700

The analysis of dislocation networks formed in Zircaloy-4 during high temperature creep See Entry 77707

Creep of 0.6Cr-0.6Mo-0.3V steel at low stresses See Entry 77710

The activation area and the activation enthalpy of cadmium single crystals determined during creep See Entry 77712

Life time calculations for LCF loading combined with tensional hold periods. Applications to Zircaloy-4 and AISI 304 See Entry 77728

Thermal stability in microstructure and rupture strength of directionally solidified Ni-Al-Ti eutectic alloys See Entry 77736

Intergranular creep embrittlement by non-soluble impurity: Pb in precipitation hardened Al-Mg-Si alloys See Entry 77746

62.20M Fatigue, brittleness, fracture, and cracks
(inc. hardness; see also 81.40N Fatigue, embrittlement and fracture)

76553 Microhardness of glassy chalcogenides in the (As₂Se₃)_x(Bi₂Se₃)_{1-x} system. A.O.Matkov's'kii, O.I.Shpotyuk, I.V.Savits'kii, V.A.Kayushkii, L.V.Kraev's'ka. *Dopov. Akad. Nauk UkrSR. Ser. A (USSR)*, no.1, p.83-6 (1983). In Ukrainian.

It is established that reduction of Bi₂Se₃ content in the (As₂Se₃)_x(Bi₂Se₃)_{1-x} (0.88 $\leq x \leq 1.00$) system increases microhardness values of glass. The character of chemical bonds varies essentially under γ -irradiation. However, heat treatment at 80 and 120°C does not restore the initial values of microhardness. (6 refs.)

76554 A theoretical study of acoustic emission from a crack extension event. I.M.Boswarva (Joint Inst. for Advancement of Flight Sci., George Washington Univ., Hampton, VA, USA). *J. Phys. & Chem. Solids (GB)*, vol.44, no.5, p.379-88 (1983).

The acoustic emission signals resulting from a small extension of an existing crack in a body under tensile stress are calculated using a particular model of

the crack extension event. The dependence of the signal on the duration of the event is evaluated; and it is shown that the signal strength depends markedly on the position and characteristics of the transducer and on the crack orientation. Simultaneous measurements with an array of transducers on the surface of the specimen could therefore provide additional information about the nature of the crack extension event. (11 refs.)

76555 Theory of fatigue for brittle flaws originating from residual stress concentrations. E.R.Fuller, B.R.Lawn (Fracture & Deformation Div., NBS, Washington, DC, USA), R.F.Cook. *J. Am. Ceram. Soc. (USA)*, vol.66, no.5, p.314-21 (May 1983).

A theory is formulated for the general fatigue response of brittle flaws which experience residual stress concentrations. The indentation crack is taken as a model flaw system for the purpose of setting up the basic fracture mechanics equations, but the essential results are expected to have a wider range of applicability in the strength characterization of ceramics. A starting fatigue differential equation is first set up by combining an appropriate stress intensity factor for point- or line-contact flaws with a power-law crack velocity function. Analytical solutions are then obtained for the case of static fatigue. The resulting relation between lifetime and failure stress is shown to have exactly the same power-law form as the conventional solution for Griffith (residual-stress-free) flaws. This 'equivalence' is used as a basis for extending the results to dynamic fatigue. A comparison of these analytical solutions with numerical counterparts defines the limits of accuracy of the theoretical procedure. However, while the form of the life-time relation remains invariant, the values of the exponent and coefficient differ significantly for flaws with and without residual stress. (20 refs.)

76556 Microhardness of β -alumina single crystals. J.Thery, A.M.Lejus (Lab. de Chimie Appliquée de l'Etat Solide, ENSCP, Paris, France).

Mater. Res. Bull. (USA), vol.18, no.4, p.481-90 (April 1983). In French. Knoop microhardness is investigated as a function of indenter orientation on the $\{1120\}$ and $\{0001\}$ planes of β_{M+} alumina single crystals ($M^+ = Na^+$, Ag^+ , K^+ , Tl^+ , NH_4^+). For the prismatic planes, maximum hardness values are always obtained along the $[0001]$ direction. For the basal plane the direction corresponding to the maximum hardness depends upon the nature of the M^+ ion. For β_{Na} alumina the maximum hardness value is found along the $\{1120\}$ directions; in this case microhardness anisotropy analysis suggests that the active slip systems are $\{0001\}$ $\{1120\}$. For β_{Ag} , β_K , β_{Tl} the maximum hardness value is along the $\{1010\}$ directions. This difference of mechanical behaviour might be in relation with the structural differences in these β -aluminas (variations in the local structure of the conduction planes). The temperature dependence of the microhardness for β_{Na} and β_{Ag} single crystals is reported between 20° and $700^\circ C$. (27 refs.)

76557 A quantitative approach to the cell shuttling model. D.J.Quesnel, J.C.Tsou (Mech. Engng. Dept., Univ. of Rochester, Rochester, NY, USA).

Mater. Sci. & Eng. (Switzerland), vol.59, no.1, p.91-8 (May 1983). A quantitative treatment of the cell shuttling model for strain accommodation in cellular microstructures during low cycle fatigue is developed. Based on the fraction of dislocation interactions with repulsive character, the functional form for the distribution of mesh lengths available for reversed deformations is determined explicitly and is used to evaluate the contribution of the cell shuttling model to the hysteretic stress-strain behavior. It is shown analytically that the cell shuttling model leads to a linear relationship between cell size and critical mesh length when the dislocation configuration and hence the stress-strain behavior is required to be reproduced on each consecutive cycle. (15 refs.)

76558 On the contrast between mode I and mode III fatigue crack propagation under variable-amplitude loading conditions. H.Nayeb-Hashemi (Dept. of Mech. Engng., Northeastern Univ., Boston, MA, USA), S.Suresh, R.O.Ritchie.

Mater. Sci. & Eng. (Switzerland), vol.59, no.1, p.L1-5 (May 1983). From the perspective of defect-tolerant life prediction procedures, the mode III fatigue crack subjected to variable-amplitude loading presents a less complex problem than the mode I crack. In the absence of loading sequence interaction effects, crack growth rates and hence fatigue lifetimes should be predictable from mere constant-amplitude data simply by summing the damage (in the form of Coffin-Manson damage or in terms of the relevant crack tip characterizing parameter, i.e. ΔK , the crack tip displacement ΔCTD etc.) for each load reversal in the loading history. Preliminary attempts at such simple modelling approaches for mode III cracks subjected to single overload cycling and arbitrary loading histories in fact appear promising for the prediction of variable-amplitude crack growth behavior. (16 refs.)

76559 Thermal-activation interpretation of splitting fracture. A.M.Molodets, A.N.Dremin (Inst. of Chem. Phys., Acad. of Sci., Chernogolovka, USSR).

Sov. Phys.-Dokl. (USA), vol.27, no.8, p.652-4 (Aug. 1982). Translation of: *Dokl. Akad. Nauk SSSR*, vol.265, no.4-6, p.1385-9 (Aug. 1982). [received: May 1983]

When solids are loaded under quasistatic conditions the main part of the durability is accounted for by the duration τ of the stage of accumulation of fracture nuclei. In this case τ and the applied stress σ are related in a manner characteristic of thermally activated processes: $\tau = \tau_0 \exp((U_0 - \gamma\sigma)/RT)$, where R is the gas constant, T is the absolute temperature, τ_0 is a universal coefficient for solids (equal to 10^{-13} sec), U_0 is the activation energy, which is determined by interatomic interaction and is a constant of the material, and γ is a coefficient which is determined by the superatomic structure and reflects the role of local stresses in the process of formation of incipient discontinuities. The authors give a functional relation between the local stresses and average stresses which enables the dependence of the splitting-fracture strength on the time of the subcritical stage to be described on the basis of this equation. (8 refs.)

76560 Influence of the concentration of chemical sites on the strength of solid polymers. N.N.Peschanskaya, V.A.Stepanov, E.M.Filyanov (A.F. Ioffe Physicotech. Inst., Acad. of Sci., Leningrad, USSR).

Sov. Phys.-Solid State (USA), vol.24, no.11, p.1851-4 (Nov. 1982). Translation of: *Fiz. Tverd. Tela (USSR)*, vol.24, no.11, p.3272-7 (Nov. 1982). [received: May 1983]

An investigation was made of the resistance to deformation and the kinetic parameters of creep of epoxy resins with different degrees of cross-linking. A full analysis was found between the deformation and relaxation properties of cross-linked and linear polymers below the glass-transition temperature. (15 refs.)

76561 Mechanism of fatigue crack propagation in metallic materials. M.N.Georgiev, V.Yu.Dogadushkin, N.Ya.Mezhova, V.N.Minaev, L.P.Strok (All-Union Sci.-Res. Inst. for Railroad Transportation, Moscow, USSR).

Sov. Mater. Sci. (USA), vol.18, no.4, p.319-25 (July-Aug. 1982). Translation of: *Fiz.-Khim. Mekh. Mater. (USSR)*, vol.18, no.4, p.35-42 (July-Aug. 1982). [received: May 1983]

On the basis of dislocation concepts and linear fracture mechanics and taking into consideration the results of X-ray and electron fractography an attempt is made to explain the mechanism of fatigue crack growth. (23 refs.)

Distribution of pressure necessary to produce Griffith cracks of prescribed shape in an orthotropic medium See Entry 75957

Fatigue and fracture mechanics See Entry 75960

Influence of Cr, Mn, Co and Ni on the crystallization behaviour of $(Fe_{1-x}M_x)$ metalloid- $_{1-x}$ metallic glasses See Entry 7632

Crystallization behavior and properties of rapidly solidified Ni-Mo-B alloys See Entry 76320

Gamma radiation effects on the strength of a borosilicate glass See Entry 76502

Effect of 5.5-MeV electron bombardment on the high-temperature mechanical properties of nickel See Entry 76516

The effect of implanted helium on the high temperature mechanical properties of a model austenitic Fe-17% Cr-17% Ni alloy See Entry 76521

The effect of He-irradiation on the fracture toughness of ThO_2 See Entry 76522

Identification of slip systems in cubic boron nitride See Entry 76550

Microstructure and properties of fine grained supersaturated Fe-C alloys See Entry 76650

Microstructure and mechanical properties of laser-processed Ni-Al-Mo base alloys See Entry 76652

Transmission electron microscopy of RSP Fe/Cr/Mn/Mo/C alloy See Entry 76653

Characterization of flux-grown $Ca(WO_4)_x(MoO_4)_{1-x}$ crystals See Entry 77550

Fabrication and characterization of $TiC_{1-x}N_x$ ($0 \leq x \leq 1$) and $Mo_2B_{2-x}C_x$ ($x=0, 1.0, 2.0$) by high-pressure hot-pressing See Entry 77602

Formation of a nickel-clad titanium carbide coating and effect of spraying conditions on its structure and properties See Entry 77612

Melt processing and properties of barium-Sialon glasses See Entry 77614

Martensitic transformations in low-carbon nickel-molybdenum steels See Entry 77638

Studies of epoxy resin systems. IV. Fracture toughness of an epoxy resin: a study of the effect of crosslinking and sub- T_g aging See Entry 77658

Strengthening mechanisms in hot-rolled magnesium and magnesium alloys See Entry 77662

Toughening by monoclinic zirconia See Entry 77663

Influence of aging on secondary recrystallization and mechanical properties of polycrystalline NaCl samples prepared by hot pressing See Entry 77678

Influence of heat treatment on the structure and long-term strength of γ/α MeC nickel eutectic. Length memory effect See Entry 77680

Elastic moduli, hardness and thermal expansion of some metaphosphate glasses See Entry 77693

Tensile strength of ultra high modulus linear polyethylene filaments See Entry 77699

Influence of plastic deformation on the properties of chromium bronze See Entry 77703

Measuring temperature dependence of secondary forming behavior of cellular polystyrene sheets See Entry 77705

Cyclic grain boundary migration during high temperature fatigue. I. Microstructural observations See Entry 77718

Cyclic grain boundary migration during high temperature fatigue. II. Measurements of grain boundary sliding See Entry 77719

Laws connecting viscous fracture with the flow limit See Entry 77720

Theoretical prediction of the cracking stress of three-dimensional randomly distributed steel fibre reinforced concrete See Entry 77721

Polymer-filler interaction in polystyrene filled with coated glass spheres. I. Interfacial adhesion control See Entry 77722

Helium embrittlement of iron-chromium alloys See Entry 77723

Investigation of structural changes during fracture of $\gamma + \epsilon$ steel See Entry 77724

Electron magnetic spectrometer investigation of fracture surfaces formed in vacuum and in air See Entry 77725

Effect of two-phase solidification on fracture toughness of aluminium alloys See Entry 77726

Welding of polymers of nonuniform molecular weight See Entry 77727

Life time calculations for LCF loading combined with tensional load periods. Applications to Zircaloy-4 and AISI 304 See Entry 77728

The effect of radiation and cryogenic temperature on the fatigue resistance of G-11 CR glass-cloth/epoxy laminates See Entry 77729

Effects of sodium and lithium environments on mechanical properties of ferrous alloys See Entry 77730

Determination of threshold stress intensity for crack growth at high temperature in silicon carbide ceramics See Entry 77731

Influence of thermal decomposition on the mechanical properties of magnesia-stabilized cubic zirconia See Entry 77732

Fracture toughness of unidirectional glass/carbon hybrid composites See Entry 77733

Enhancement of strength in composites reinforced with previously stressed fibers See Entry 77734

Distributions of fatigue life and fatigue strength in notched specimens of a carbon eight-harness-satin laminate See Entry 77735

Thermal stability in microstructure and rupture strength of directionally solidified Ni-Al-Ti eutectic alloys See Entry 77736

Effects of thickness and compressive residual stress of boronized layer on bending fatigue strength properties of boronized steels See Entry 77737

X-ray fractography on fatigue fractured surface See Entry 77738

X-ray fractographic study on fatigue fracture surface of SM50A steel See Entry 77739

Effect of specimen size and configuration of fatigue crack growth behavior of mild steel butt welded joints See Entry 77740

Impact fracture mechanisms in polymer blends: rubber-toughened nylon See Entry 77741

The ductile fracture of metals: a microstructural viewpoint See Entry 77742

The mechanical properties and tensile fracture characteristics of partially annealed low carbon mild steel sheet See Entry 77743

Low cycle fatigue of aluminum at elevated temperatures See Entry 77744

The influence of the static I load mode and R ratio on mode III fatigue crack growth behaviour in mild steel See Entry 77745

Intergranular creep embrittlement by non-soluble impurity: Pb in precipitation hardened Al-Mg-Si alloys See Entry 77746

Effect of prior deformation on the cleavage of zinc single crystals See Entry 77747

Fractography of polyethylene glycol dimethacrylate doped with polymethyl methacrylate See Entry 77748

Strain localization and hydrogen embrittlement See Entry 77749

Ion implantation effect on fatigue crack initiation in Ti-24V See Entry 77750

Effect of multiple crack propagation on the high temperature low cycle fatigue of a cast nickel-base alloy See Entry 77751

The effect of pre-existing epsilon martensite on the hydrogen induced fracture of austenitic stainless steel See Entry 77752

A brittle to ductile transition in NiAl of a critical grain size See Entry 77753

High-temperature transgranular fracture in an austenitic stainless steel See Entry 77754

Crack resistance of pearlitic eutectoid steels. I. Fracture of steels in short-term loading See Entry 77755

Influence of vacuum and low temperature on fatigue crack growth rate in magnesium alloy sheets See Entry 77756

Cyclic strength of magnesium-base reinforced composites See Entry 77757

Microstructure and mechanical strength of aluminum titanate ceramic prepared from mixture of alumina and titania See Entry 77758

Prediction of intergranular failure in Ni-Cr based alloys in low cycle fatigue at high temperatures - UK16 See Entry 77759

Mechanical properties of (Fe_{100-x}Mn_x)₈₃B₁₇ metallic glasses See Entry 77760

Deformation induced dilatations and new observations on fracture in compression in metallic glasses at low temperatures See Entry 77761

The effect of hydrogen on an iron based amorphous alloy See Entry 77762

Environmental cracking of amorphous alloys See Entry 77763

Mechanisms of material removal during erosion of a stainless steel See Entry 77764

The role of the electrode potential control in corrosion research of stress corrosion crack growth propagation in austenite stainless steels for nuclear reactor components See Entry 77790

The effect of molybdenum addition on the mechanical metallurgy and corrosion properties of the 13%Cr4%Ni steel See Entry 77797

Fatigue corrosion behaviour of various metallic materials in chloride environment See Entry 77800

Surface melting of cast iron with a high power laser beam See Entry 77810

Property enhancement in rapidly quenched alloy surfaces See Entry 77811

Technique to predict specimen failure in cyclic fatigue tests See Entry 77812

Assessment of critical temperature of embrittlement and transverse widening of the test piece in impact bend test See Entry 77826

62.20P Tribology

(see also 81.40P Friction, lubrication and wear)

Transmission electron microscopy of RSP Fe/Cr/Mn/Mo/C alloy See Entry 76653

Determining the frictional properties of thin films of lubricants See Entry 76817

Mechanisms of material removal during erosion of a stainless steel See Entry 77764

Geometrical aspects of the tribological properties of graphite fiber reinforced polyimide composites See Entry 77765

Scuffing under cyclic loading—unexpected effect of frequency See Entry 77766

Wear analysis See Entry 77767

Nitrogen migration during wear in an implanted steel See Entry 77768

Fretting of amorphous alloys See Entry 77769

Wear of transition metal rich glassy alloys See Entry 77770

62.30 MECHANICAL AND ELASTIC WAVES

(see also 03.40K Mathematical aspects)

Distribution of axisymmetric waves in a piezoceramic planar cylinder See Entry 77328

62.40 ANELASTICITY, INTERNAL FRICTION, AND DAMPING

(see also 81.40J Elasticity and anelasticity)

76562 Anelastic relaxation phenomena in plasma-sprayed (Al₂O₃)₃MgO spinel with reference to diffusion process. M.Halbachs (Ecole Nat. Supérieure de Ceramique Industrielle, Limoges, France), P.Mazot, J.Woirgard. *Phys. Status Solidi a (Germany)*, vol.76, no.1, p.157-64 (16 March 1983). Internal friction experiments are performed on a plasma-sprayed (Al₂O₃)₃MgO non-stoichiometric spinel. Isothermal damping spectra are obtained between 650 and 850°C. They revealed a high isolated peak for forced torsional vibration frequencies ranging between 10⁻⁵ and 30 Hz. The temperature dependence of the relaxation rate follows a Boltzmann law over more than four decades: $\tau^{-1}(s^{-1}) = 10^{19}(s^{-1}) \exp(-3.96(eV)/kT)$. The corresponding activation energy appears to be in rather good agreement with cationic diffusion data for the same material. A point defect migration mechanism is inferred for the observed damping and the relaxation rate is assigned to the mean cationic jump frequency. The present results show that

internal friction is a promising approach for the kinetic and structural study of ionic mobility in oxide compounds. (20 refs.)

76563 Internal friction in cold-worked nickel-carbon. B.Purniah, R.Ranganathan (Materials Sci. Lab., Reactor Res. Centre, Tamil Nadu, India). *Philos. Mag. A (GB)*, vol.47, no.5, p.L23-7 (May 1983). An experimental investigation of relaxation in the cold-worked Ni-C system reveals an internal friction maximum at ~430°C at a frequency of ~1 Hz. The peak is thought to be due to the dislocation-carbon interaction analogues to the cold-work peak in b.c.c. metals. This peak found in f.c.c. metals seems to illustrate the Seeger model (1979) for the 'Snoek-Koster' relaxation or the cold-work peak. (7 refs.)

Temperature dependence of the resistance to motion of edge dislocations in Fe-Co solid solutions See Entry 76442

Low-frequency current noise and internal friction in solids See Entry 77014

Piezoelectric properties of modified PZT ceramics See Entry 77330

Precipitation studies in lead-tin alloys See Entry 77644

Deceleration of relaxation in a Cu-Si alloy See Entry 77653

Studies of epoxy resin systems. I. A study of the origins of the secondary relaxations of epoxy resins by thermally stimulated depolarization See Entry 77655

Nonlinear resonance in Cu₃Au See Entry 77691

Elasticity and anelasticity of a 304 stainless steel at below room temperature See Entry 77692

Damping capacity and pitting corrosion resistance of Fe-Mo-Cr alloys See Entry 77793

Investigation of internal friction in fused quartz, steel, Plexiglass, and Westerly granite from 0.01 to 1.00 Hertz at 10⁻⁸ to 10⁻⁷ strain amplitude See Entry 78533

62.50 HIGH-PRESSURE AND SHOCK-WAVE EFFECTS IN SOLIDS

High-pressure and high-temperature crystallographic study of the gillespite I-II phase transition See Entry 76604

Orientation relation in the pressure-induced transition B1—B2 of RbCl observed by an X-ray four-circle diffractometer See Entry 76608

Shock crystallization of films See Entry 76812

Phenomenological theory of shock-induced polarisation. II. Mathematical treatment of the oscillogram See Entry 77322

Diffusionless omega transformations in quenched and pressurized Zr-Mo alloys See Entry 77631

Spall studies of differently treated 2024Al specimens See Entry 77706

Shock temperatures of SiO₂ and their geophysical implications See Entry 78536

62.60 ACOUSTIC PROPERTIES OF LIQUIDS

(see also 62.80 Ultrasonic relaxation; for sound propagation, see 43.; for second sound in quantum fluids, see 67.40, 67.50 and 67.60)

76564 Ultrasonic study of molecular interaction in carbon tetrachloride-toluidine mixtures. V.A.Tabhane, B.A.Patki (Dept. of Phys., Inst. of Sci., Nagpur, India). *Indian J. Pure & Appl. Phys.*, vol.21, no.3, p.155-8 (March 1983). The velocity of ultrasonic waves (2 MHz) for different compositions of mixtures of CCl₄+o-toluidine and CCl₄+p-toluidine has been measured in the temperature range 10-50°C and 30-55°C respectively. The velocity (c) versus composition (C_m) plots exhibit peak at X_A:X_B=8:2 in CCl₄+p-toluidine. The excess compressibility β_a^E , excess van der Waals' parameter b^E and (dc/dT)^E have been discussed in the light of intermolecular AB interaction and resulting disorder in these mixtures. The strength of AB interaction depends not only upon the nature of the groups but also on their relative positions in the ring. (26 refs.)

76565 Ultrasonic study of two-component systems. P.Pande, B.P.Pandey (Dept. of Petroleum Engng., Indian School of Mines, Dhanbad, India). *Indian J. Phys. Part B*, vol.56B, no.6, p.325-33 (Dec. 1982). [received: May 1983]

Adiabatic compressibility (β), molar volume (V), intermolecular free length (L_f), available volume (V_a), free volume (V_f), and Raos number (R) has been calculated from ultrasonic velocity and density measurements in two binary systems, viz., carbon tetrachloride+benzene and carbon tetrachloride+acetone at 25°C. Non-linear behaviour in these properties show presence of molecular interaction, which is weak in the first system while strong in the second one. Rao's (1940, 1941) equation has been discussed in light of recent studies. (38 refs.)

Ultrasonic studies of N-formylmorpholine+water mixtures See Entry 76570

62.65 ACOUSTIC PROPERTIES OF SOLIDS

(see also 62.80 Ultrasonic relaxation; for sound propagation, see 43.; for lattice dynamics and phonons, see 63.; for magnetoacoustic effects, see 72.55; for acoustoelectric effects, see 72.50; for acousto-optical effects, see 78.20H)

76566 Temperature dependence of the velocity of ultrasound and electrical conductivity of an epoxy composite with a carbon filler. I.N.Ermolenko, V.I.Krylovich, V.I.Alekseenko, V.I.Dubkova, P.N.Logvinovich, I.P.Lyubliner (Inst. of Appl. Phys., Acad. of Sci., Minsk, Belorussian SSR). *J. Eng. Phys. (USA)*, vol.43, no.3, p.992-5 (Sept. 1982). Translation of: *Inzh.-Fiz. Zh. (USSR)*, vol.43, no.3, p.413-17 (Sept. 1982). Experimental data are given on the behavior of the velocity of ultrasound and electrical conductivity as a function of the temperature in an epoxy composite material filled with carbon fiber. (12 refs.)

76567 Acoustic emission initiated by ion implantation in bubble garnet films. D.Adiene, L.Pranevicius, G.Zubauskas (Phys. Dept., Kaunas Polytech. Inst., Kaunas, USSR). *Phys. Status Solidi a (Germany)*, vol.76, no.1, p.K35-7 (16 March 1983). The authors present the results of the acoustic emission (AE) from bubble garnet films during implantation for H⁺ and Ne⁺ at 100 keV energy. These results are compared with static bubble parameters in Ne⁺ implanted films. AE detection was carried out by the means of a bulk LiNbO₃ crystal of 1.2

MHz resonance frequency. Acoustic contact with the garnet film was provided. Garnet films with composition $(\text{YSmCa})_2(\text{FeGe})_5\text{O}_{12}$ grown by LPE on (111) GGG substrates were investigated. (4 refs.)

76568 An acoustic emission source model for both continuous and burst-type emission analysis. I. Theory. D.Rouby, P.Fleischmann, C.Duvergier (Inst. Nat. des Sci. Appl. de Lyon, Villeurbanne, France). *Philos. Mag. A (GB)*, vol.47, no.5, p.671-87 (May 1983).

An acoustic emission model is presented. The source is described by a dislocation which moves between two steady positions. By using dynamic Green functions, expressions for the displacement waves emitted by the creation of a small dislocation loop are given, as a function of the orientation between the Burgers vector, propagation path and the loop area. The elastic wave emitted by a source event is obtained, in time and frequency domains, by considering the dislocation movement over the whole source area. For frequencies higher than 2 MHz, the displacement, which is pulse shaped, bears a close relation with source area and dislocation velocity; this accounts for burst-type acoustic emission analysis in a quantitative way. The signal produced by very numerous and randomly activated sources is analysed; this analysis permits the interpretation of continuous emission. (17 refs.)

76569 An acoustic emission source model for both continuous and burst-type emission analysis. II. Experiments. D.Rouby, P.Fleischmann, C.Duvergier (Inst. Nat. des Sci. Appl. de Lyon, Villeurbanne, France). *Philos. Mag. A (GB)*, vol.47, no.5, p.689-705 (May 1983).

For pt.I see *ibid.*, vol.47, no.5, p.671 (1983). In part I, an acoustic emission source model has been proposed. In the second part, the source model is used to interpret both continuous emission and burst-type emission. The acoustic emission is recorded by using broad-band piezoelectric transducers which are described. In the case of continuous emission, linked to homogeneous plastic deformation, spectral analysis gives access to the dislocation mean flight time. For Al-Mg solid solutions, evidence is found for thermally activated obstacle passing: the flight time decreases if the test temperature increases and if the Mg content decreases. In the case of burst-type emission, observed during tensile testing of 2024 T351 aluminium alloy, examples of recorded signals are given. The signal contains numerous echoes which are analysed: these echoes result from reflections and mode conversions inside the specimen and permit source localization. The direct recording of the displacement wave predicted by the source model using a 'thick' piezoelectric transducer is described. The shape of the displacement impulse leads to the source event time and to the source size. (14 refs.)

Nature of dislocation hysteresis losses and nonlinear effect in lead at high vibration amplitudes See Entry 76449

The variation of elastic constants of nickel-iron single crystal alloys from 78.76 to 300K See Entry 76544

A theoretical study of acoustic emission from a crack extension event See Entry 76554

Structural phase transition of layer compound $(\text{C}_2\text{H}_5\text{NH}_3)_2\text{FeCl}_4$ See Entry 76609

Influence of thermoelastic bending on photoacoustic experiments related to measurements of thermal diffusivity of metals See Entry 76675

Parametric amplification of sound and magnetoacoustic echo in concentrated rare-earth paramagnets of the Van Vleck type See Entry 77009

Longitudinal ultrasonic attenuation in normal and superconducting lead at low temperatures See Entry 77092

Nonlinear effects in hypersound propagation within the $\text{Ni}^{2+}:\text{Al}_2\text{O}_3$ system See Entry 77259

Acoustic phonon absorption and dispersion in hydroxyl-doped KCl crystals at low temperatures [Brillouin scattering] See Entry 77404

Quantum efficiency of alexandrite See Entry 77430

Precipitation studies in lead-tin alloys See Entry 77644

Elastic properties of alkali silicate glasses See Entry 77694

Evaluation of acoustic properties of 'thin' laminations and one-line nonmetallic inclusions in steel sheets See Entry 77833

62.80 ULTRASONIC RELAXATION

(see also 74.30G Ultrasonic attenuation in superconductors, 43.35 Ultrasonics)

76570 Ultrasonic studies of N-formylmorpholine+water mixtures. A.M.Awad, A.M.North, R.A.Petrick (Dept. of Pure & Appl. Chem., Univ. of Strathclyde, Glasgow, Scotland). *J. Chem. Soc. Faraday Trans. II (GB)*, vol.79, pt.3, p.449-61 (March 1983).

N-formylmorpholine (NFM)+water mixtures are used to extract aromatics from petroleum feedstocks. Possible conformational and structural causes of this specific solvation are investigated using ultrasonic attenuation and velocity measurement complemented by ^{13}C NMR, density and viscosity observations. The conformational studies suggest that gross rearrangements of the morpholine ring are relatively slow (below 60 MHz) but that inversion at the nitrogen atom is faster, with lower activation energy, than in other morpholine analogues. Structural information is inferred mainly from excess volumes and adiabatic compressibilities of mixing. The observations suggest that when NFM is added to water it first introduces hydrogen bonding and ordering of water molecules not bound into an extended ice I tetrahedral structure; then at higher concentrations it disrupts this structure to a less open, but no less compressible, hydrogen-bonded array of 'quasi-planar' NFM capable of absorbing aromatic rings. (31 refs.)

Acoustic phonon absorption and dispersion in hydroxyl-doped KCl crystals at low temperatures [Brillouin scattering] See Entry 77404

63.00 LATTICE DYNAMICS AND CRYSTAL STATISTICS

(see also 05.50 Lattice theory, 65. Thermal properties, 66.70 Thermal conduction, 68.30 Dynamics of surface and interface vibrations, 78.30 Infrared and Raman spectra)

63.10 GENERAL THEORY

76571 Generator coordinate treatment of some model periodic systems. L.R.Kauder, A.K.Ray, S.B.Trickey (Dept. of Phys., Univ. of Florida, Gainesville, FL, USA). *Int. J. Quantum Chem. (USA)*, vol.23, no.4, p.1355-61 (April 1983).

The generator coordinate method (GCM) is a powerful variational technique invented for studying nuclear collective motion and extended in recent times by Lathouwers, Van Leuven, and Laskowski et al. to problems of molecular electronic structure and vibrations. In preparation for the application of GCM to electron correlation, and lattice dynamical problems in solids, the authors have studied linear periodically bounded systems consisting of one- and two-mass anharmonic chains of both finite and infinite length. Preliminary results for the variational energy and vibrational spectra from some simple intrinsic functions are presented. (7 refs.)

76572 A quantum field theory of crystals. IV. T.Kitamura (Dept. of Phys., Univ. of Alberta, Edmonton, Alberta, Canada). *Physica A (Netherlands)*, vol.119A, no.1-2, p.67-77 (April 1983).

For pt.III see *ibid.*, vol.110A, p.282 (1982). One-dimensional boson and fermion systems are investigated for which the ground state expectation value of a molecule field does not exist; the assumptions on the energy bands and the two-body potential are the same for both systems. The systems behave essentially in the same fashion; they have particle-hole pairs, gapless phonons, energy dispersions with a linear momentum etc. It is shown that the coefficient of the momentum in the boson energy spectrum is larger than that in the fermion one. (5 refs.)

63.20 PHONONS AND VIBRATIONS IN CRYSTAL LATTICES

Probability density function of the double-Gaussian model See Entry 74404

PROMETHEUS. A program system for investigation of anharmonic thermal vibrations in crystals See Entry 76257

CO/N_2 solid solutions: head-tail reorientations See Entry 76330

Crystal structure of $\text{Fe}_2\text{P}_2\text{O}_7$ See Entry 76378

Thermal vibrations and static displacements of atoms in nonstoichiometric titanium carbide See Entry 76579

A quantum field theoretic approach to the calculation of reduction factors in Jahn-Teller systems. I. General theory See Entry 76908

A quantum field theoretic approach to the calculation of reduction factors in Jahn-Teller systems. II. $E\otimes(\sum(\alpha_1+e))$ in octahedral symmetry See Entry 76909

A quantum field theoretic approach to the calculation of reduction factors in Jahn-Teller systems. III. $\Gamma_{8g} \otimes (\sum(\alpha_1+e+\tau_2))$ in octahedral symmetry See Entry 76910

Influence of external electric field on incommensurate-commensurate phase transition in K_2SeO_4 and $(\text{NH}_4)_2\text{BeF}_4$ crystals. II. Dynamic properties See Entry 77336

Calculated lifetime and decay mechanism of the 991 cm^{-1} mode in crystalline benzene at 1.6K See Entry 77371

The far-infrared spectrum of ice Ih in the range $8\text{--}25\text{ cm}^{-1}$. Sound waves and difference bands, with application to Saturn's rings See Entry 77376

Raman scattering by soft plasmon-LO phonon modes in ferroelectric semiconductors See Entry 77380

Infrared and Raman spectra of barium nitrite monohydrate See Entry 77381

Infrared absorption spectra of hydrogen complexes in type I diamonds See Entry 77382

Distinction between 'free' CS_2^{2-} in ionic compounds and coordinated CS_2^{2-} in metallic complexes by the means of IR spectroscopy of solids See Entry 77396

Raman light scattering in semiconductors containing dislocations See Entry 77399

Acoustic phonon absorption and dispersion in hydroxyl-doped KCl crystals at low temperatures [Brillouin scattering] See Entry 77404

63.20D Phonon states and bands, normal modes, and phonon dispersion

76573 Lattice dynamics of isotopic alloys with applications to ^{67}Zn Mossbauer spectroscopy. W.T.Vetterling, D.Candela (Lyman Lab. of Phys., Harvard Univ., Cambridge, MA, USA). *Phys. Rev. B (USA)*, vol.27, no.9, p.5394-403 (1 May 1983).

The 'recursion method' is applied to the dynamics of disordered lattices, and is used explicitly to calculate properties of isotopically disordered zinc. The specific heat and atomic motion are calculated for the special case of an isotopically pure lattice and compared to previous experimental and theoretical results. Then Mossbauer-effect calculations for the high-resolution ^{67}Zn isotope are presented, including evaluations of the Mossbauer line shift with temperature, the anisotropic recoil-free fraction, and the Goldanskii-Karyagin effect. In addition, the effect of zero-point motion on the Mossbauer line position and linewidth in isotopically disordered zinc is discussed. (61 refs.)

76574 Vibrational properties of silver iodide at high frequencies. A.P.Kovalenko. *Ukr. Fiz. Zh. (USSR)*, vol.28, no.5, p.696-704 (May 1983). In Russian.

Vibrational properties of AgI at high frequencies are considered by means of a model admitting an existence of slightly centre-displaced tetrahedral positions of Ag^+ in the wurtzite structure. Such displaced positions lead directly to an appearance of two 'impurity' bands in the vibrational crystal spectrum according to experimental results. (12 refs.)

Model calculations of local electron and phonon densities of states in bimetallic superlattices See Entry 76827

Two dimensional magnetophonon resonance in GaInAs-InP superlattices See Entry 77037

- Effects of interlaminar forces on longitudinal acoustic modes of *n*-alkanes See Entry 77375
- Optical phonons and structure of TiGaSe_2 , TiGaSe_2 , and TlInS_2 layer single crystals See Entry 77393
- A comparison of the Raman spectra of ZnGa_2Se_4 and other gallium defect chalcopyrites See Entry 77397
- Nonequilibrium phonons in ZnSe single crystals See Entry 77400

63.20H Phonon-phonon interactions

- Infrared optical absorption due to one and two phonon processes in black phosphorus See Entry 77379

63.20K Phonon-electron interactions

- 76575 Influence of electron relaxation on the damping of long-wavelength optical phonons in metals heavily doped semiconductors. I.P.Ipatova, A.V.Subashiev, V.A.Shchukin (A.F. Ioffe Physicotech. Inst., Acad. of Sci., Leningrad, USSR). *Sov. Phys.-Solid State (USA)*, vol.24, no.11, p.1932-6 (Nov. 1982). Translation of: *Fiz. Tverd. Tela (USSR)*, vol.24, no.11, p.3401-9 (Nov. 1982). [received: May 1983]

It is shown that the electronic contribution to the damping of optical phonons with small wave numbers, when the interaction of the phonons with free electrons (the Landau mechanism) is ineffective, is due to the finite lifetime of the electrons. As this decreases, the phonon damping variation is not monotonic, which may cause the Raman lines to become narrower with increasing temperature and impurity concentration. There is experimental evidence of such behavior. In many-valley semiconductors, there is a contribution to the phonon damping from unscreened diffusion of electrons in particular valleys, as well as from the relaxation mechanism. The diffusion mechanism also gives a strong dispersion of the optical branch at small wave numbers. The applicability of a single linearized transport equation in the limits of both fast and slow relaxation is elucidated. (19 refs.)

- Dependence of the Poisson ratio on the electron-phonon interaction constant See Entry 76545

- Theory of the Verwey transition in the mixed valence compound Eu_2S_4 See Entry 76847

- Electromagnetic wave absorption by an electron-phonon system under parametric resonance See Entry 76862

- Transverse magnetophonon resonance in *n*-GaAs under pulsed high magnetic fields See Entry 76974

- Two dimensional magnetophonon resonance in GaInAs-InP superlattices See Entry 77037

- Electron-phonon interaction model for the relation between magnetic and elastic properties in itinerant electron ferromagnets See Entry 77237

- Theory of cyclotron resonance width for electrons inelastically scattered by phonons See Entry 77264

- Raman light scattering in semiconductors containing dislocations See Entry 77399

- Enhanced excitation transfer during vibrational relaxation after pumping and generalized Forster's formula See Entry 77440

- Low-frequency secondary radiation in polar semiconductors at finite temperatures See Entry 77441

- Multiphonon effects in field electron emission See Entry 77537

63.20P Localized modes

- 76576 Dynamical behaviour of interstitials in elemental semiconductors. D.N.Talwar (Dept. of Marine Sci., Texas A&M Univ., Galveston, TX, USA).

J. Appl. Phys. (USA), vol.54, no.5, p.2366-71 (May 1983).

The dynamical behaviour of isolated interstitials in elemental semiconductors has been described using the well-known Green's function theory. Assuming the defect to be at the tetrahedral site, the author has exploited the symmetry properties of the point group $\{T_d\}$ so as to make the problem amenable to calculations. The conditions for the occurrence of impurity modes and IR absorption have been derived in terms of the mass of interstitial and the impurity-host interactions. All the involved lattice Green's functions are calculated by incorporating the phonons obtained from a simplified second-neighbour force model fitted to neutron scattering experiments on silicon. Numerical calculations are made for the localised vibrational modes and the impurity-induced IR absorption for different interstitials in Si. The calculated results are compared with existing theoretical and experimental data. (33 refs.)

- 76577 Solitary waves in one-dimensional hydrogen-bonded systems. S.Yomosa (Dept. of Phys., Nagoya Univ., Nagoya, Japan).

J. Phys. Soc. Jpn. (Japan), vol.52, no.5, p.1866-73 (May 1983).

The author has studied again the dynamical properties of protons in one-dimensional H-bonded system, taking account of the coupling between the proton motion and the lattice deformation. It is found that the solitary waves of the proton-polarization are accompanied by the local lattice-deformations. Kink and antikink solutions correspond to ionic D_i default (H_2O^+ ion) and I_i default (OH^- ion), respectively. Two modes of solitary waves and two modes of phonons are found in the four respective regions of wave velocities.

- Interaction of charged particles and local modes See Entry 76539

- Ultrafast vibrational relaxation and hot luminescence of Ti^{3+} centers in KI See Entry 77435

63.50 VIBRATIONAL STATES IN DISORDERED SYSTEMS

- On the problem of cross links in trans-polyacetylene: normal-coordinate calculations See Entry 76322

- Phonon lifetime and thermal conductivity in amorphous solids See Entry 76716

- A structural interpretation of the vibrational spectra of binary fluorohafnate glasses See Entry 77378

63.70 STATISTICAL MECHANICS OF LATTICE VIBRATIONS

(see also 65. Thermal properties of condensed matter, 66.70 Thermal conduction)

- 76578 Computation of Debye temperatures of some cubic and hexagonal crystals from the elastic constant data near 0K. Madhusudan Singh (Dept. of Phys., Bihar Inst. of Technol., Sindri, India), S.Tolpadi. *Indian J. Pure & Appl. Phys.*, vol.21, no.3, p.140-4 (March 1983).

A numerical integration method using Weddle's rule has been applied to compute the limiting Debye temperature (θ_D^∞) of 47 cubic and 14 hexagonal crystals from the elastic constant data near 0K. These computed values are in very good agreement with the calorimetric Debye temperatures (θ_D^c) confirming the equivalence of θ_D^∞ and θ_D^c in low temperature regions. (42 refs.)

- 76579 Thermal vibrations and static displacements of atoms in nonstoichiometric titanium carbide. P.Capkova, R.Kuzel, J.Sedivy (Dept. of Semiconductor Phys., Charles Univ., Prague, Czechoslovakia). *Phys. Status Solidi a (Germany)*, vol.76, no.1, p.383-90 (16 March 1983).

By X-ray diffraction measurements made in the temperature range 293 to 1173K following properties of $\text{TiC}_{0.967}$ are investigated: amplitudes of thermal vibrations of Ti and C atoms, Debye characteristic temperature, and static displacement of Ti atoms around a vacancy in the carbon sublattice. (14 refs.)

- Lattice dynamics of isotopic alloys with applications to ^{67}Zn Mossbauer spectroscopy See Entry 76573

- Changes in the electron structure of Fe-Ni alloys with the FCC lattice as a result of a magnetic phase transition See Entry 76836

- Lattice temperature and hyperfine interactions of $\text{Pb}_{1-x}\text{Sn}_x\text{Te}$ ($0.21 \leq x \leq 0.75$) See Entry 77300

63.75 STATISTICAL MECHANICS OF DISPLACIVE PHASE-TRANSITIONS

(for order-disorder and statistical mechanics of model systems, see 64.60; for crystallographic aspects of polymorphic and order-disorder transformations, see 61.50K)

- Peierls instability and charge density waves at the surface of a metal with a quasione-dimensional electron spectrum See Entry 76935

- Raman scattering by soft plasmon-LO phonon modes in ferroelectric semiconductors See Entry 77380

63.90 OTHER TOPICS IN LATTICE DYNAMICS AND CRYSTAL STATISTICS

- Rb_2ZnCl_4 : three heat-capacity anomalies due to soft-mode and commensurate-incommensurate transitions See Entry 76658

- Amplitude-fluctuation effects on magnetic-resonance line shape and soliton density in incommensurate systems See Entry 77272

- Influence of external electric field on incommensurate-commensurate phase transition in K_2SeO_4 and $(\text{NH}_4)_2\text{BeF}_4$ crystals. II. Dynamic properties See Entry 77336

64.00 EQUATIONS OF STATE, PHASE EQUILIBRIA, AND PHASE TRANSITIONS

(see also 82.60 Chemical thermodynamics)

64.10 GENERAL THEORY OF EQUATIONS OF STATE AND PHASE EQUILIBRIA

- Low density properties of a two dimensional dipolar fluid See Entry 76265

- Calculation of vapour-liquid equilibria with equations of state from the extended van-der-Waals theory. II. Application of the equation to mixtures See Entry 76600

64.30 EQUATIONS OF STATE OF SPECIFIC SUBSTANCES

(see also 65.70 Thermal expansion)

- 76580 Construction of a wide-range tabular equation of state for copper. K.S.Trainor (Lawrence Livermore Nat. Lab., Univ. of California, Livermore, CA, USA).

J. Appl. Phys. (USA), vol.54, no.5, p.2372-9 (May 1983).

A global equation of state (EOS) for copper has been constructed, ranging from densities of 10^{-3} - 10^3 Mg/m^3 and from ambient temperatures to $5 \times 10^4 \text{ eV}$ ($1 \text{ eV} = 11604.5 \text{ K}$). Six different theoretical models were used: a soft sphere liquid model at low temperatures below melt density; an ionisation equilibrium model based on a modified Saha method at moderate temperatures in expansion; a nonideal plasma theory for high temperatures; a modified Thomas-Fermi-Kirzhnits model in compression; rigorous electron band theory for the zero degree isotherm; and a semiempirical model in the solid-liquid-vapour region. Assembly of the EOS will be described. Agreement with existing experimental data is good. (32 refs.)

- 76581 Equation of state of sodium at pressures up to 30 GPa. I.V.Aleksandrov, V.N.Kachinskii, I.N.Makarenko, S.M.Stishov (Inst. of Crystallography, Acad. of Sci., USSR).

JETP Lett. (USA), vol.36, no.9, p.411-15 (5 Nov. 1982). Translation of: *Pisma v Zh. Eksp. & Teor. Fiz. (USSR)*, vol.36, no.9, p.336-9 (5 Nov. 1982). [received: June 1983]

The equation of state of sodium has been studied by an X-ray method at pressures up to 30 GPa at 303K for the first time, through the use of a diamond-anvil technique. The possibility of using this equation of state to construct a high-pressure scale is discussed. (14 refs.)

Calculation of vapour-liquid equilibria with equations of state from the extended van-der-Waals theory. II. Application of the equation to mixtures See Entry 76600

64.60 GENERAL STUDIES OF PHASE TRANSITIONS

(for critical phenomena in quantum fluids, superconductors, magnetic materials and ferroelectrics, see 67., 74.40, 75.40 and 77.80 respectively)

76582 Substrate-strain effects on the Frenkel-Kontorova system. T. Munakata (Dept. of Appl. Math. & Phys., Kyoto Univ., Kyoto, Japan). *J. Phys. Soc. Jpn. (Japan)*, vol.52, no.5, p.1635-40 (May 1983). Substrate-strain effects on the Frenkel-Kontorova system are investigated under the continuum approximation. The long-wavelength component of the strain field is shown to give rise to an extra biharmonic potential, modifying the basic equation from the sine-Gordon to the double sine-Gordon equation. A kink propagates accompanied by a local strain field, thus behaving like a kind of polaron. Implications for the commensurate-incommensurate transition studied by Frank and van der Merwe and others are also given.

76583 Complete devil's staircase, fractal dimension, and universality of mode-locking structure in the circle map. M.H. Jensen, P. Bak, T. Bohr (H.C. Ørsted Inst., Copenhagen, Denmark). *Phys. Rev. Lett. (USA)*, vol.50, no.21, p.1637-9 (23 May 1983). It is shown numerically that the stability intervals for limit cycles of the circle map form a complete devil's staircase at the onset of chaos. The complementary set to the stability intervals is a Cantor set of fractal dimension $D=0.87$. This exponent is found to be universal for a large class of functions. (10 refs.)

76584 Ordering in orthorhombic crystals. A. Ya. Mitus', A.Z. Patashinskii. *Sov. Phys.-Solid State (USA)*, vol.24, no.11, p.1900-4 (Nov. 1982). Translation of: *Fiz. Tverd. Tela (USSR)*, vol.24, no.11, p.3344-52 (Nov. 1982). [received: May 1983]

An effective Hamiltonian describing spatial ordering and a local crystal order parameter of orthorhombic symmetry (a tensor of rank four) are proposed. Simple models are used to study a sequence of phase transitions involving a change in the symmetry in a crystal. The absence of biaxial nematic liquid crystals is discussed. The behaviour of thermodynamic and elastic properties of crystals in the neighborhood of their phase transitions is investigated. The region of existence of a metastable low-temperature phase in first-order phase transitions is found to be small: $\tau \leq 0.01$. The proposed theory predicts premelting anomalies in crystals. (10 refs.)

Equilibrium phase interfaces See Entry 74425

Low density properties of a two dimensional dipolar fluid See Entry 76265

Translational order in smectic liquid crystals. Allowance for features of the intermolecular forces See Entry 76304

Micromechanisms of crystallization in (Fe,Co,Ni)-Zr metallic glasses See Entry 76321

Spontaneous radiative coupling of atomic energy levels See Entry 76588

Phase equilibria in the H_2/C_2H_4 system at temperatures from 114.1 to 247.1K and pressures to 600 MPa See Entry 76599

Discontinuities of the order parameter in system of mutually interacting single-level particles See Entry 77191

Amplitude-fluctuation effects on magnetic-resonance line shape and soliton density in incommensurate systems See Entry 77272

64.70 PHASE EQUILIBRIA, PHASE TRANSITIONS, AND CRITICAL POINTS

(see also 81.30 Phase diagrams and microstructures developed by solidification and solid-solid phase transformations)

76585 Solid+liquid equilibrium diagram of acetanilide+phenacetine mixtures determined by differential scanning calorimetry. M. Antonietti Macip (Dept. of Materials Engng., Drexel Univ., Philadelphia, PA, USA), M. Antonia Valerdi.

Mater. Chem. & Phys. (Switzerland), vol.8, no.3, p.259-64 (March 1983). Experiments for the title system are described and results reported in tabular form. The system forms solid solutions with a minimum. Location of the acrostallotropic point has been determined. (5 refs.)

76586 Thermodynamics on UO_2 - ZrO_2 - LnO_2 -x solid solutions. F. Schleifer, A. Naoumidis, H. Nickel (Inst. fur Reaktorwerkstoffe, KFA Julich GmbH, Julich, Germany).

J. Nucl. Mater. (Netherlands), vol.115, no.2-3, p.143-58 (April 1983).

The stability and the equilibrium oxygen partial pressure of solid solutions between UO_2 , ZrO_2 and the oxides of the lanthanides (LnO_{2-x}) were studied. The oxygen potential of the mixed oxides was determined by the EMF-method. Both solid Fe+FeO and dry air electrodes were used as reference. The results indicate that the uranium substitution by zirconium and the lanthanides in the U-Zr-Ln mixed oxides stabilizes the higher 'uranium valencies' by increasing the oxygen solubility in these solid solutions under a given oxygen partial pressure. The strength of this stabilization increases in the order of Zr, Nd, Ce, La substitutions. The difference in the stabilization of mean uranium vacancies can also be interpreted in terms of the difference in the lattice parameter of the solid solutions. (43 refs.)

76587 Hard discs with embedded three dimensional quadrupoles. P.N. Kusalik, S.F.O'Shea (Dept. of Chem., Univ. of Lethbridge, Lethbridge, Alberta, Canada).

Mol. Phys. (GB), vol.49, no.1, p.33-52 (May 1983).

A survey of the structural and thermodynamic behaviour of hard discs with embedded three dimensional quadrupoles of linear symmetry has been made using Monte Carlo methods. The results for dilute samples at high temperatures (small quadrupole moments) are consistent with thermodynamic perturbation theory. Those for higher density or lower temperatures (larger quadrupole moments) indicate the existence of two solid phases, one a high density hexagonal solid and the other a lower density square structure. No convincing evidence was found for the existence of a distinct liquid phase, but the data are not sufficiently detailed to provide a reliable determination of the phase diagram. Structural evidence has been found for the coexistence of the two solids, and the interface between the two structures seems to lead to relatively little disruption in either phase, at least for small 'domain' sizes. The stability of the square structure is easily understood in terms of the large quadrupole energy it achieves, in spite of being about 15 per cent less dense

than the hexagonal solid, which has approximately the same energy. (32 refs.)

76588 Spontaneous radiative coupling of atomic energy levels. D.A. Cardimona, C.R. Stroud, Jr. (Inst. of Optics, Univ. of Rochester, Rochester, NY, USA).

Phys. Rev. A (USA), vol.27, no.5, p.2456-61 (May 1983). Density-matrix equations of motion derived from Heisenberg picture source-field quantum electrodynamics contain damping constants and frequency shifts which are not associated with a single radiative transition but which instead couple two separate transitions together. In the absence of degeneracies in the atomic levels, these coupling terms are normally neglected when the rotating-wave approximation is invoked. These terms cannot be neglected when there are degeneracies or near degeneracies. In this paper the authors interpret the generalized frequency shifts, show how they can be renormalized, and included in shifts of atomic energy levels and altered damping constants and discuss their experimental significance. (12 refs.)

76589 Phase diagram of ZrV_2 . A.S. Balankin (Engng. Phys. Inst., Moscow, USSR).

Sov. Phys.-Solid State (USA), vol.24, no.11, p.1777-8 (Nov. 1982). Translation of: *Fiz. Tverd. Tela (USSR)*, vol.24, no.11, p.3475-7 (Nov. 1982). [received: May 1983]

A complete phase diagram of ZrV_2 corresponding to the thermodynamic potential is a set of intersecting hypersurfaces in a nine-dimensional space of the coefficients a_i , d_i , and α_i ($i=1,2$) and b_i , C_i , and A_i . The main features of the phase transitions in ZrV_2 can be described by considering a phase diagram using the coordinates $\alpha_2/d_1 = 1/2 C_{44}$. (9 refs.)

Potentiometric study of the thermodynamic properties of intermetallic compounds Ca_2Ni_7 . Structural interpretation See Entry 76667

Thermodynamics of ternary Fe-Co-Ni austenites See Entry 76668

Thermodynamic measurements and modeling of $(UC_{1-x}O_x)$ See Entry 76669

Thermodynamic properties of liquid silver-thallium alloys See Entry 77616

Determination of thermodynamic activities of components in the sections $x_{Cr}=0.11$ and $x_{Cr}=0.33$ of γ -solid solution Cr-Fe-Ni at 1500K See Entry 77617

Bi-In system See Entry 77618

Decomposition of sigma phase in a Ni-Cr-W system See Entry 77619

On the formation of Fe-carbides in Cu-Fe and Cu-Au-Fe alloys See Entry 77652

Application of neutron diffraction to a study of phases in Type 316 stainless steel weld metals See Entry 77685

64.70D Solid-liquid transitions

(see also 81.30F Solidification)

76590 Study of the solid-liquid equilibria of pseudo-binary systems $MPbO_3$ - $Ce(PO_3)_3$ ($M=Rb, Cs$). M. Rzaigui, N. Kbir Arigui (Lab. de Phys.-Chimie Minérale, Ecole Normale Supérieure, Tunis, Tunisia).

Mater. Chem. & Phys. (Switzerland), vol.8, no.4, p.365-78 (April 1983). In French.

The establishment of solid-liquid phase equilibrium diagrams of the system $MPbO_3$ - $Ce(PO_3)_3$ with $M=Rb$ and Cs , provides evidence of condensed phosphates of different compositions: $M_2Ce(PO_3)_4$ and $M_2Ce(PO_3)_5$. The chemical preparation and the main crystallographic features established by X-ray diffraction and IR spectroscopy are discussed. (13 refs.)

76591 Theoretical derivation of Lindemann constant for Mie's potential using Sharan and Prakash's criterion for melting. S. Prakash (Dept. of Phys., Inst. of Technol., New Delhi, India).

Indian J. Pure & Appl. Phys., vol.21, no.3, p.148-50 (March 1983).

Sharan and Prakash (1967) from their study on alkali halides using Born and Born Mayer's potentials concluded that the ratio of the interatomic separation at the point of inflection to that at absolute zero is approximately constant. The same has been used for getting the ratio U_0/kT_m (where U_0 is the interaction energy per particle at absolute zero of temperature and T_m the melting temperature) and also the Sutherland-Lindemann empirical melting point equations from Mie's potential. It has been concluded that the Sutherland-Lindemann constant is structure dependent. The agreement between the theory and experiment for U_0/kT_m is good for alkali halides. The theory has been extended to include the order-disorder effect in binary systems. (4 refs.)

76592 Oscillatory morphological instabilities due to non-equilibrium segregation. S.R. Coriell (NBS, Washington, DC, USA), R.F. Sekerka.

J. Cryst. Growth (Netherlands), vol.61, no.3, p.499-508 (April-May 1983).

Linear perturbation theory is used to study morphological instability for rapid directional solidification at constant velocity under conditions where there is significant departure from local equilibrium at an initially planar solid-liquid interface. Under conditions where the segregation coefficient k depends significantly on velocity v , the stability criterion depends explicitly on both k and $\partial k/\partial v$ and instabilities that are oscillatory in time can occur for solute concentrations that are much smaller than those that would be necessary to cause non-oscillatory instability for the same k if $\partial k/\partial v$ were simply neglected. Such oscillatory instabilities seem to be related to a 'solute pump' mechanism according to which local changes in k , due to periodic changes in local interface velocity v , can occur out of phase with local interface position, thus resulting in lateral inhomogeneity of concentration on a length scale large enough that the resulting instabilities will not be suppressed by capillarity. Such instabilities can, however, be suppressed by a sufficiently large dependence of interface undercooling on v . (11 refs.)

76593 Preferred crystallographic orientation for crystallisation under non-hydrostatic stress. M.E. Fleet (Dept. of Geology, Univ. of Western Ontario, London, Ontario, Canada).

Phys. Status Solidi A (Germany), vol.76, no.1, p.151-6 (16 March 1983).

The equation of Gibbs for the chemical potential of a nonhydrostatically-stressed solid in an adjacent fluid is revised to $\mu = A + pV - \sigma'_{ij} \epsilon'_{ij} V_0$ (where, V_0 is the molar volume at a reference state of zero stress, σ'_{ij} is the deviatoric stress tensor, ϵ'_{ij} is the deviatoric strain tensor, and p is the pressure of the hydrostatic component of the nonhydrostatic stress field). μ is equated with the Gibbs free energy of the pure phase and is independent of the fluid pressure. Preferred crystallographic orientation of a crystalline phase deformed through crystallisation under nonhydrostatic stress is indicated by minimisation of $-1/2\sigma'_{ij}\epsilon'_{ij}$ (where, σ'_{ij} is the stress tensor, and ϵ'_{ij} is the strain tensor). (13 refs.)

76594 Pressure effect on the melting point of alkali metals. T.Soma, H.Matsuo Kagaya, J.Sato (Dept. of Appl. Phys. & Math., Mining Coll., Akita Univ., Akita, Japan).

Solid State Commun. (USA), vol.46, no.8, p.661-3 (May 1983).

The mean-square displacement of alkali metals is studied theoretically using the authors local Heine-Abarenkov-type model potential in the perturbational scheme. The temperature-dependent mean-square displacement of alkali metals decreases as a function of the compressed volume. Lindemann's criterion for melting x_m , which is defined as the ratio of two times the root-mean-square displacement to the nearest-neighbour distance, is found to be nearly constant for five alkali metals. The volume effect on the melting temperature of alkali metals is studied by keeping x_m constant. The obtained melting curve increases as function of the compressed volume and are qualitatively in good agreement with the observed tendency for alkali metals. (12 refs.)

76595 On the solvability of the two-phase quasistationary crystallization problem. E.V.Radkevich, A.S.Melikulov.

Sov. Phys.-Dokl. (USA), vol.27, no.7, p.540-2 (July 1982). Translation of: *Dokl. Akad. Nauk SSSR*, vol.265, no.1-3, p.58-62 (July 1982). [received: April 1983]

Using the boundary-variation method, the authors prove that the two-phase elliptical boundary-value problem with a free boundary and adjoining fixed boundary is solvable in the class of Lipschitz free boundaries. (3 refs.)

76596 Oriented crystallization of metals in the presence of electric current. V.F.Gordeev, A.V.Pustogarov, Ya.R.Kuchero, V.A.Sukhinin. *Sov. Tech. Phys. Lett. (USA)*, vol.8, no.9, p.465-7 (Sept. 1982). Translation of: *Pis'ma v Zh. Tekh. Fiz. (USSR)*, vol.8, no.17-18, p.1079-81 (Sept. 1982). [received: May 1983]

The authors report a study of the effect of current flow on the crystallization of metals. The metal was melted at the electrodes of an arc and by the heating of conductors through which a high current was passed. In both cases, the crystallization of the metals occurred after the current flow was stopped. The surface temperature of the liquid metal was measured with a fast PFM-315 micropyrometer. The structure of the materials was studied by the LAU method with URS-60 and DRON-1 X-ray diffraction cameras. (6 refs.)

76597 Kinetic study on glass formation and crystallization behavior in a continuously cooling melt. R.Ota, T.Kato, N.Soga (Dept. of Industrial Chem., Kyoto Univ., Kyoto-shi, Japan).

Yogyo-Kyokai-Shi (Japan), vol.91, no.2, p.73-81 (1983). In Japanese.

An equation has been derived which gives the fraction $X(t)$ of a crystallized phase in a continuously cooling melt assuming homogeneous nucleation and isotropic crystal growth. From this equation a tentative and simple expression for $X(t)$ has been constructed in terms of liquid parameters which enables the essential roles of liquid parameters involved in the glass formation of a supercooled liquid to be understood. Assuming a minimal constant value for $X(t)$ the critical cooling rate Q^* of a given melt can be estimated from the liquid parameters by, $\log Q^* = -\log \eta_L - 0.06 E_a/T_L - 3 T_0/T_L + 2 \log T_L - \log V - 38 \alpha^2 \Delta S_f - 0.25 \log X(t) + 5 \pm 0.5$ where Q^* is critical cooling rate (K/s), η_L is the liquid viscosity (poise), E_a is the activation energy for viscous flow (cal/mol) at the liquidus temperature T_L (K), T_0 is a constant in the Fulcher type viscosity (K), V is the molar volume (cm³/mol), ΔS_f is the fusion entropy per flow unit (cal/K.mol) and α is the dimensionless surface tension in the range 0.3-0.5. Although the equation has been derived for one-component liquid, it may be valid also for multi-component liquid in a semi-quantitative way as has been tested in the B₂O₃-Na₂O system. (27 refs.)

76598 Development of morphological instability and cells during rapid solidification of laser annealed silicon alloys. J.Narayan, C.W.White (Solid State Div., Oak Ridge Nat. Lab., Oak Ridge, TN, USA).

Rapidly Solidified Amorphous and Crystalline Alloys. Proceedings of the Materials Research Society Annual Meeting, Boston, MA, USA, Nov. 1981 (New York, USA: North-Holland 1982), p.553-8

The details of morphological instability occurring during rapid solidification have been studied in In⁺, Ga⁺, Sb⁺, Bi⁺, Ge⁺, Fe⁺ and Cr⁺ implanted silicon specimens after pulsed laser annealing. The average cell sizes were determined at the onset of instability and in the region of well-developed instability using electron microscopy. The total and substitutional solute concentration profiles were determined using Rutherford backscattering and channeling techniques. The formation of cells and the critical solute concentrations associated with instability were studied as a function of velocity of solidification. The results were compared with the predictions of the perturbation theory which took into account the dependence of distribution coefficients on the velocity of solidification. A good agreement between the calculations and the experimental results was obtained. The authors also examined theoretically the effect of reduction in surface tension due to segregation of impurities on cell sizes and critical solute concentrations associated with instability. (6 refs.)

Stefan problem with initial heat shock See Entry 75902

An analysis of substrate heat losses in Stefan's problem with a constant flux See Entry 75905

Influence of Cr, Mn, Co and Ni on the crystallization behaviour of (Fe_{1-x}M_x)₂ metalloid_{1-y} metallic glasses See Entry 76319

Segregation during directional melting and its implications on seeded crystal growth: a theoretical analysis See Entry 76337

Transmission electron microscopy of RSP Fe/Cr/Mn/Mo/C alloy See Entry 76653

Heat capacity study of the phase transitions in As₄S₃ and As₄S₄ See Entry 76661

Supercooling of liquid H₂ and the possible production of superfluid H₂ See Entry 76746

Orientational ordering of commensurate Fe(CO)₅ monolayers on graphite See Entry 76783

Laser formation of a 'cold liquid' See Entry 77487

Effect of variable thermal conductivity on isotherms in Bridgman growth See Entry 77552

Oscillatory crystallization of a stratifying alloy See Entry 77621

Direct observation of the coarsening of solidification structure in Sn-Pb alloy See Entry 77622

Simplified determination of cooling conditions of aluminium-silicon alloys See Entry 77623

Ferrite morphology in rapidly solidified ferritic Fe-Cr-C steels See Entry 77624

Structure of Fe-40 at.%Al obtained by rapid quenching from melt See Entry 77625

Rapid solidification of steels See Entry 77627

FCC and BCC solidification products in a rapidly solidified austenitic steel See Entry 77628

Effect of two-phase solidification on fracture toughness of aluminium alloys See Entry 77726

Surface alloying of iron alloys by laser beam melting See Entry 77807

Shock temperatures of SiO₂ and their geophysical implications See Entry 78536

64.70F Liquid-vapour transitions

76599 Phase equilibria in the H₂/C₂H₄ system at temperatures from 114.1 to 247.1K and pressures to 600 MPa. A.Heintz, W.B.Streett (School of Chem. Engng., Cornell Univ., Ithaca, NY, USA).

Ber. Bunsenges. Phys. Chem. (Germany), vol.87, no.4, p.298-303 (April 1983). Experimental data for liquid-vapor phase compositions of hydrogen+ethylene are reported for 14 temperatures in the range 114.1 to 247.1K and pressures up to 600 MPa. The data have been obtained using a vapor-recirculating apparatus suitable for measurement up to 1000 MPa. The entire region of liquid-vapor coexistence has been explored. The mixture critical line and the pressure temperature trace of the 3-phase line solid-liquid-vapor have been located. These lines intersect at 153K and 675 MPa to form an upper critical end point. Results obtained up to 52 MPa have been compared with published data. (14 refs.)

76600 Calculation of vapour-liquid equilibria with equations of state from the extended van-der-Waals theory. II. Application of the equation to mixtures. G.Hecht, J.Kaiser, M.Walter.

Chem. Tech. (Germany), vol.35, no.4, p.209-11 (April 1983). In German. For pt.I see ibid., vol.35, p.37, (1983). For an equation of state derived from an extended van der Waals theory a set of mixing rules for multicomponent mixture constants is introduced. This enables the prediction of vapour liquid equilibria, as tested for some binary mixtures. For mixtures of n-alkanes and of H₂ with n-alkanes two correlations are proposed for the binary interaction parameters. The results of boiling pressure calculations show a degree of accuracy that would be sufficient for most technological cases. (53 refs.)

76601 Drop-to-filmwise condensation transition: heat transfer measurements for ethanediol. S.A.Stylianou, J.W.Rose (Dept. of Mech. Engng., Queen Mary Coll., Univ. of London, London, England).

Int. J. Heat & Mass Transfer (GB), vol.26, no.5, p.747-60 (May 1983). Measurements of vapour-to-surface temperature difference and heat flux are reported for dropwise, mixed and film condensation of ethanediol on an oleic acid-promoted copper surface and on a pte-coated surface. Tests were carried out at seven vapour temperatures (pressures) in the range 386K (3.8 kPa) to 440K (35.6 kPa). Air, ethanediol and water were used as coolants. At low and moderate cooling intensities dropwise condensation was observed for both surfaces and the $\Delta T-Q$ data for the two surfaces were in good agreement with each other and with dropwise condensation theory. At higher cooling intensities transition to mixed condensation was observed in the case of the pte surface. This was accompanied by departure from the theoretical $\Delta T-Q$ curve and the heat flux passed through a maximum with increasing cooling intensity. In the case of the oleic acid-promoted copper surface, ideal dropwise behaviour persisted to somewhat higher values of ΔT and Q before abrupt transition to film condensation occurred. The post transition filmwise data were in good agreement with the Nusselt theory. For both surfaces, reversion to ideal dropwise condensation occurred as the cooling intensity was reduced. Two possible mechanisms for the transition process are suggested. (9 refs.)

The extension of pure fluid thermodynamic properties to supercritical mixtures. A comparison of current theories with computer data over a large region of states See Entry 76266

64.70H Solid-vapour transitions

76602 Vaporization study on the niobium-oxygen solid solution by mass-spectrometric method. T.Matsui, K.Naito (Dept. of Nuclear Engng., Nagoya Univ., Nagoya, Japan).

J. Nucl. Mater. (Netherlands), vol.115, no.2-3, p.178-86 (April 1983). The vapor pressures over the niobium-oxygen solid solution were measured by mass-spectrometric method in the temperature range 2091-2379K. The main vapor species were observed to be NbO(g) and NbO₂(g). The solidus line of the niobium-oxygen solid solution and the solubility limit of oxygen in niobium metal at high temperatures were determined from the vaporization behavior. The partial pressure of oxygen was calculated as a function of temperature and O/Nb composition from the partial pressures of NbO(g) and NbO₂(g), from which the partial molar enthalpy and entropy of oxygen in the niobium-oxygen solid solution were determined. The compositional dependence of the partial pressure of oxygen was observed to obey the Henry's law at low oxygen concentrations in niobium metal less than about 5 at.%. (32 refs.)

76603 Mass spectrometric study on the vaporization of ternary compounds PuM₂C(M=Fe, Co, Ni). Y.Suzuki, Y.Arai, T.Ohmichi, T.Sasayama (Div. of Nuclear Fuel Res., JAERI, Ibaraki, Japan).

J. Nucl. Mater. (Netherlands), vol.115, no.2-3, p.187-91 (April 1983). The thermochemical properties of ternary compounds PuFeC₂, PuCoC₂ and PuNiC₂ were investigated in the temperature range 1420-1853K by means of the Knudsen effusion mass spectrometric technique. The peritectic reactions at 1650, 1610 and 1670K were suggested for these three compounds, respectively. Below the peritectic temperature, their vaporization process was incongruent, as the vapor pressures of Fe, Co and Ni were much higher than that of Pu. The free energies of formation of PuFeC₂, PuCoC₂ and PuNiC₂ have been determined from the vapor pressure data. (11 refs.)

Packing analysis and calculation of sublimation energies of borane crystals See Entry 76351

Study and application of the mass transport phenomenon in InP See Entry 76719

64.70K Solid-solid transitions

(see also 61.50K Crystallographic aspects of polymorphic and order-disorder transformations, 81.30H, 81.30K, 81.30M
Microstructures developed by solid-solid phase transformations)

76604 High-pressure and high-temperature crystallographic study of the gillespite I-II phase transition. R.M.Hazen, L.W.Finger (Geophys. Lab., Carnegie Instn. of Washington, Washington, DC, USA).

Am. Mineral. (USA), vol.68, p.595-603 (May-June 1983). Crystal structures of gillespite, BaFeSi₄O₁₀ which has a reversible first-order phase transition at 18 kbar, were refined from data collected at 1 bar and 9, 21, and 45 kbar. Silicate-layer topology is constant through the transition, but

coordination of barium increases from 8 to 10. The almost perfect square-planar coordination group of iron in gillespite I ($\text{Fe-O}=1.98 \text{ \AA}$) changes to a flattened tetrahedron with two additional long Fe-O bonds ($\sim 3 \text{ \AA}$) in gillespite II. The volume discontinuity at the gillespite I-II transition is best described as a consequence of the increased coordination of barium and iron. Unit-cell parameters of gillespite were measured under nine high-pressure and fourteen combined high-pressure, high-temperature (PT) conditions. The Clausius-Clapeyron slope of the transition is $27 \pm 9 \text{ bar/}^\circ\text{C}$, which is similar to the slope of gillespite-I isochores. On the basis of these observations, the behaviour of the gillespite I-II transition is consistent with a geometrically controlled phase transformation, in which the size of the barium site is the critical dimensional factor.

76605 Physical model of plasticity of a transition. V.A.Ermolaev, V.A.Likhachev (A.A. Zhdanov State Univ., Leningrad, USSR). *Fiz. Met. & Metalloved. (USSR)*, vol.55, no.4, p.693-700 (April 1983). In Russian. English translation in: *Phys. Met. & Metallogr. (GB)*. A model is proposed to account for the plasticity of a phase transition. Expressions are obtained for the macroscopic distortion as a function of the applied stresses. An allowance is made for the contribution to the macroscopic accommodation effect at the transition front. The results are compared with the published experimental data. (17 refs.) A.T.

76606 A study of solid and liquid carbon tetrafluoride using the constant pressure molecular dynamics technique. S.Nose, M.L.Klein (Chem. Div., Nat. Res. Council of Canada, Ottawa, Ontario, Canada). *J. Chem. Phys. (USA)*, vol.78, no.11, p.6928-39 (1 June 1983). The constant pressure molecular dynamics technique originally proposed by Andersen to study fluids and subsequently generalized by Parrinello and Rahman (1980-82) to deal with crystals of arbitrary symmetry has been further extended to treat molecular systems. As a pedagogical example designed to illustrate the utility of this approach, the authors have investigated the properties of carbon tetrafluoride in its condensed phases using an intermolecular potential based upon atom-atom interactions. In particular, they have explored the effect of changes in temperature and pressure on the orientationally ordered low temperature monoclinic solid. As in the real crystal, isobaric heating to sufficiently high temperature causes the ordered phase to transform spontaneously to a noncubic orientationally disordered phase. The properties of this disordered phase are also examined along with those of the liquid. The atom-atom potential appears to correlate a wide range of experimental data. The possible role of the electrostatic octopole-octopole interactions is also discussed briefly. (44 refs.)

76607 Jahn-Teller phase transitions in RbCuCl_3 . M.Harada (Res. Reactor Inst., Kyoto Univ., Osaka, Japan). *J. Phys. Soc. Jpn. (Japan)*, vol.52, no.5, p.1646-57 (May 1983). The phase transition at 66°C in RbCuCl_3 has been investigated by X-ray diffraction methods. Structure analyses have been carried out using the topographic data. For high-temperature structure, three equally plausible space groups $P6_3/\text{mmc}$, $P6_2c$ and $P6_1mc$ have been examined by a block diagonal least squares refinement. The room-temperature structure has the superstructure with the lattice parameter doubled along the b -axis and the space group is Pbcn . The mode analysis of the Jahn-Teller active mode was carried out and the intensity distribution of the superlattice reflections was consistent with the atomic shifts corresponding to the zone boundary M_4^+ -mode. There exists the second-order piezodistortive coupling between the antiferrodistortive static displacements and the homogeneous strains. From this coupling, the precise temperature dependence of the superlattice reflection is derived. (19 refs.)

76608 Orientation relation in the pressure-induced transition $\text{B1} \rightarrow \text{B2}$ of RbCl observed by an X-ray four-circle diffractometer. H.Fujiwara, N.Nakagiri, M.Nomura (Dept. of Materials Sci., Hiroshima Univ., Hiroshima, Japan). *J. Phys. Soc. Jpn. (Japan)*, vol.52, no.5, p.1665-8 (May 1983). The orientation distribution of the $\{110\}$ diffracted line of the pressure-induced B2 phase of RbCl after $\text{B1} \rightarrow \text{B2}$ transition was measured with an X-ray four-circle diffractometer on which the Merrill-Bassett type diamond anvil pressure cell was mounted. Judging from the $\{110\}$ pole figure of the B2 phase, the center of which is the $[100]$ axis of the B1 phase, the orientation relation was $[111](\text{B2})//[100](\text{B1})$ and $[100](\text{B2})//[111](\text{B1})$. The result agreed with that obtained by Okai from X-ray diffraction photograph.

76609 Structural phase transition of layer compound $(\text{C}_2\text{H}_5\text{NH}_3)_2\text{FeCl}_4$. T.Suzuki, M.Yoshizawa, T.Goto, T.Yamakami, M.Takahashi, T.Fujimura (Res. Inst. for Sci. Measurements, Tohoku Univ., Sendai, Japan). *J. Phys. Soc. Jpn. (Japan)*, vol.52, no.5, p.1669-75 (May 1983). The sequence of the structural phase transitions of the layer compound $(\text{C}_2\text{H}_5\text{NH}_3)_2\text{FeCl}_4$ has been determined with the ultrasonic, dielectric and polarized microscope measurements as following: Phase I (D_{6h}^{17})-(378.8K)-Phase II (D_{2h}^{18})-(203.5K)-Phase III-(133.7K)-Phase IV. The set of the critical exponents obtained with ultrasonic methods are explained by the results of the renormalization group theory on the three dimensional XY model. The ferroelastic domains are observed in the phase II and phase III. The anomaly of the dielectric constant is found near the II-III phase transition point. (17 refs.)

76610 Observations on the phase transition in quartz by synchrotron-radiation X-ray topography. A.Zarka (Lab. de Mineralogie-Cristallographie, Univ. Pierre et Marie Curie, Paris, France). *J. Appl. Crystallogr. (Denmark)*, vol.16, pt.3, p.354-6 (1 June 1983). By use of a high-temperature camera designed for in situ synchrotron-radiation X-ray topography the α - β transition was investigated in a Z-cut synthetic-quartz sample. Preliminary dynamical observations on movement of the boundaries between α and β phases and α_1 and α_2 domains are reported. (11 refs.)

76611 On 'forbidden' reflections in calcia- and yttria-stabilized zirconia (CSZ and YSZ). L.H.Schoenlein, A.H.Heuer (Dept. of Metall. & Materials Sci., Case Western Reserve Univ., Cleveland, OH, USA). *J. Appl. Crystallogr. (Denmark)*, vol.16, pt.3, p.357 (1 June 1983). In an earlier paper (see Schoenlein, Hobbs & Heuer, vol.13, p.375-9, 1980, henceforth referred to as SHH), the authors suggested that reflections 'forbidden' for both cubic (c) and tetragonal (t) ZrO_2 but occasionally present in diffraction patterns from stabilized ZrO_2 crystals containing t precipitates (CSZ and YSZ), e.g. Fig.5 (CSZ) of SHH, could be attributed to transformation of the t precipitates to monoclinic (m) symmetry. They now consider the monoclinic symmetry of the transformed particles unlikely and suggest that transformation to a new polymorph of ZrO_2 with orthorhombic (o) symmetry had occurred; o - ZrO_2 can form from t - ZrO_2 by a stress-induced diffusionless transformation (Schoenlein, 1982; Schoenlein, Ruhle & Heuer, 1983). (3 refs.)

76612 Critical point of isostructural phase transition in photomodified anthracene. I.L.Aptekar', A.E.Galashin (Inst. of Solid State Phys., Acad. of Sci., Moscow, USSR). *JETP Lett. (USA)*, vol.36, no.7, p.314-18 (5 Oct. 1982). Translation of: *Pis'ma v Zh. Eksp. & Teor. Fiz. (USSR)*, vol.36, no.7, p.256-9 (5 Oct. 1982). [received: May 1983] An isostructural phase transition (IPT) is observed under certain temperatures and UV radiation intensities in a photomodified anthracene (dianthracene) crystal. The IPT curve, which ends at the critical point, and the coordinates of this point ($T_c=620 \pm 20\text{K}$, $I_c=70^{+9.0}_{-5.3}$ photons/ cm^2s) are calculated from the experimental data. (5 refs.)

76613 Peculiarities of phase transitions and physical properties in $(\text{NH}_4)_2\text{SbF}_6$. L.M.Avkhshtem', R.L.Davidovich, L.A.Zemnukhova, P.S.Gordienko (Inst. of Chem., Acad. of Sci., Vladivostok, USSR), V.Urbonavičius, J.Grigas. *Phys. Status Solidi b (Germany)*, vol.116, no.2, p.483-8 (1 April 1983). The dynamics of the $(\text{NH}_4)_2\text{SbF}_6$ crystal lattice showing the superionic phase transition is studied in a broad temperature interval by NMR and NQR methods, together with electrophysical and calorimetric properties. The investigations establish the ionic state of the axial fluorine atom in relation to equatorial atoms in the $[\text{SbF}_6]^{2-}$ complex. The successive phase transitions are revealed and the mechanism of the phase transitions is elucidated. The phase transitions are caused by the reorientation movements of NH_4 and $[\text{SbF}_6]^{2-}$ groups. The authors also describe the influence of water solution inclusions in the crystal on the superionic phase transition. (9 refs.)

76614 Jahn-Teller transition in NdMnO_3 . N.Kamegashira, Y.Miyazaki (Dept. of Materials Sci., Toyohashi Univ. of Technol., Toyohashi, Japan). *Phys. Status Solidi a (Germany)*, vol.76, no.1, p.K39-42 (16 March 1983). The Jahn-Teller type phase transition is firstly identified in neodymium manganite near 1100K based on the results of measurements of electrical conductivity, high temperature X-ray diffractometry, and differential thermal analysis (DTA). (14 refs.)

76615 High-angle grain-boundary premelting transition: A molecular-dynamics study. G.Ciccotti, M.Guillope, V.Pontikis (Section de Recherches de Metall. Phys., CENS, Gif-sur-Yvette, France). *Phys. Rev. B (USA)*, vol.27, no.9, p.5576-85 (1 May 1983). The authors studied the structure and self-diffusion in the FCC $[001](310)2=5$ coincidence high-angle tilt grain boundary by molecular-dynamics simulation. The calculations have been performed at various temperatures and fixed reduced number density, $\rho=0.984$, using Lennard-Jones (12-6) pair-interaction potential. The temperature dependence of the local thermodynamic properties in a small region around the grain boundary clearly points out that a structural transition occurs well below the melting point ($T_{\text{trans}} < 0.5T_m$, with T_m the melting-point temperature). This transition appears to be very smooth and indicates the onset of a partially disordered structure inside the boundary which goes continuously to the liquid at the melting temperature. The thickness of the region affected by the transition grows very slowly with increasing temperature and finally, due to the finite size of the simulated system, causes the migration of the grain boundary. In their simulation this happens for $T \sim 0.9T_m$. The self-diffusion coefficient, D_{GB} , in the grain boundary has a value comparable to, although definitely lower than, that of the quenched liquid at the corresponding temperature and density. Like the structural properties, D_{GB} goes continuously to the liquid value at $T=T_m$. (27 refs.)

76616 Multilayered polytypes in boron nitride. A.V.Kurdyumov, G.S.Oleinik, N.F.Östrovskaya, A.N.Pilyankevich, S.N.Gromyko, I.N.Frantsevich (Inst. of Problems in Materials Sci., Acad. of Sci., Kiev, Ukrainian SSR). *Sov. Phys.-Dokl. (USA)*, vol.27, no.7, p.575-6 (July 1982). Translation of: *Dokl. Akad. Nauk SSSR*, vol.265, no.1-3, p.66-8 (July 1982). [received: April 1983] In the present work, in which the authors have investigated the structural features of the wurtzite-sphalerite transformation, they discovered for the first time, the formation of multilayered polytypes of boron nitride. For the investigation they used transmission electron microscopy of thin chips of particles removed from the fracture surface of polycrystalline sinter cakes on a carbon replica. A dispersed powder of wurtzite boron nitride, was subjected to sintering at a pressure of 77 kbar and temperatures of 1400-1800 $^\circ\text{C}$ to produce only a partial phase transition of the wurtzite-sphalerite type. (5 refs.)

76617 Surface second-order phase transitions conserving the number of atoms in a unit cell. I.P.Ipatova, Yu.E.Kitaev, A.V.Subashiev (A.F. Ioffe Physicotech. Inst., Acad. of Sci., Leningrad, USSR). *Sov. Phys.-Solid State (USA)*, vol.24, no.11, p.1880-4 (Nov. 1982). Translation of: *Fiz. Tverd. Tela (USSR)*, vol.24, no.11, p.3311-17 (Nov. 1982). [received: May 1983] A group-theory analysis is given of the possible changes in the lattice symmetry in second-order phase transitions on an atomically clean surface, which conserve the number of atoms in a unit cell. Eighty two period groups in three-dimensional space were used to describe the symmetry of the surface layer affected by the change in structure. For comparison, an analysis was also made of the possible changes in symmetry in second-order phase transitions in purely two-dimensional systems. Phase transitions occurring in the Potts model were identified. (18 refs.)

76618 Influence of isotopic substitution on the $\text{T} \rightarrow \text{M2}$ phase transition in $\text{V}_{1-x}\text{Fe}_x\text{O}_2$ single crystals. E.I.Terukov, M.Wolf, W.Reichelt, H.-P.Bruckner, W.Bruckner, H.Oppermann (Central Inst. of Solid State Phys. & Materials Sci., Acad. of Sci., Dresden, Germany). *Sov. Phys.-Solid State (USA)*, vol.24, no.11, p.1946-7 (Nov. 1982). Translation of: *Fiz. Tverd. Tela (USSR)*, vol.24, no.11, p.3426-8 (Nov. 1982). [received: May 1983] The authors carried out an experimental study of the isotopic replacement of ^{16}O with ^{18}O in iron-doped VO_2 single crystals, and attempted to carry out a critical analysis of the experimental results associated with the $\text{T} \rightarrow \text{M2}$ phase transition. The $\text{V}_{1-x}\text{Fe}_x\text{O}_2$ crystals were prepared by the method of chemical transport reactions in a closed chamber using TeCl_4 as the transport gas. The temperature of the $\text{T} \rightarrow \text{M2}$ phase transition was determined by measuring the temperature dependence of the magnetic susceptibility. The absolute values of this susceptibility at 223 and 173K were used to find the concentration of iron in $\text{V}_{1-x}\text{Fe}_x\text{O}_2$ samples. The results obtained were confirmed by the results of an activation analysis. The authors report that the observations militate strongly against the spin Peierls model for the explanation of the $\text{T} \rightarrow \text{M2}$ phase transition. (7 refs.)

- 76619 Phase transitions in tetragonal CdP₂.** A.U.Sheleg, V.P.Novikov (Inst. of Solid-State & Semiconductor Phys., Acad. of Sci., Minsk, Belorussian SSR). *Sov. Phys-Solid State (USA)*, vol.24, no.11, p.2000-1 (Nov. 1982). Translation of: *Fiz. Tverd. Tela (USSR)*, vol.24, no.11, p.3508-11 (Nov. 1982). [received: May 1983]
X-ray diffraction is employed to study the phase transitions in CdP₂. The investigation reveals five complex anomalies, the most characteristic feature of which is a plateau in temperature dependences of the lattice parameters. These features are manifested by the temperature dependences of the thermal expansion coefficients in the form of doubled λ -like peaks. The studies lead to the conclusion that the phase transitions occur as a single process associated with a cascade of superstructures which are separated by intermediate incommensurate phases. (18 refs.)
- 76620 Role of the surface energy in phase transitions with two order parameters.** A.N.Semenov, F.M.Terent'ev, A.V.Chubukov (M.V. Lomonosov State Univ., Moscow, USSR). *Sov. Phys-Solid State (USA)*, vol.24, no.12, p.2111-12 (Dec. 1983). Translation of: *Fiz. Tverd. Tela (USSR)*, vol.24, no.12, p.3704-6 (Dec. 1983). The authors consider the simplest model with two order parameters, i.e. the Lifshitz model, and take into account the spatial inhomogeneity of the order parameters related to the bounded nature of the sample and the surface energy. They show that such conditions may compensate for the shortcomings of this simple model and may yield a description of a wider class of effects without even inclusion of higher powers in the free energy expansion in terms of the order parameters. (9 refs.)
- 76621 Structural changes of a piezoelectric crystal BaZnGeO₄ on thermal phase transition.** K.Iijima, F.Marumo (Res. Lab. of Engng. Materials, Tokyo Inst. of Technol., Yokohama-shi, Japan), H.Takei. *Yogyo-Kyokai-Shi (Japan)*, vol.91, no.2, p.67-72 (1983). In Japanese.
Structural changes on thermal phase transition have been investigated by X-ray diffraction technique, on a piezoelectric crystal BaZnGeO₄. Space groups and cell dimensions are: $P6_322$, $a=5.407(2)$ Å and $c=8.975(5)$ Å (at 900°C) for phase I, and $P6_3$, $a=9.320(1)$ Å and $c=8.866(5)$ Å (at 420°C) for phase II. The lattice vectors of phase I and phase II are in the relations, $a_1=(2a_{11}+b_{11})/3$, $b_1=(b_{11}-a_{11})/3$ and $c_1=c_{II}$. The change in intensities of superlattice reflections with temperature indicates an abrupt change of the structure at the phase transition point between the two phases. At 420°C, 710°C, 800°C and 900°C, the crystal structures were refined with single-crystal X-ray diffraction data to the final R values of 0.076, 0.062, 0.052 and 0.061 for 575, 417, 138 and 132 observed reflections, respectively. The crystal has a stuffed structure derived from the high tridymite frame-work with Ba²⁺ ions at the large interstices between the six-membered rings of ZnO₄ and GeO₄ tetrahedra. (14 refs.)
- 76622 The β - α transition in rapidly quenched Sn-Ge alloys.** W.M.Galleneault, R.W.Smith (Dept. of Metall. Engng., Queen's Univ., Kingston, Ontario, Canada).
Rapidly Solidified Amorphous and Crystalline Alloys. Proceedings of the Materials Research Society Annual Meeting, Boston, MA, USA, Nov. 1981 (New York, USA: North-Holland 1982), p.387-96
Dilute Sn-Ge alloys were prepared as ribbons by melt-spinning using a 4" copper drum. They were then transformed into grey tin at 242K in the as-cast-condition, and after annealing. It is shown that germanium: (1) when in solid solution impedes the β - α transformation; (2) when in solid solution cannot effect nucleation; and (3) has a solubility in α -Sn in excess of 1 wt.% Ge. In addition it is proposed that β - α transformation is restricted because the presence of germanium strengthens the β -Sn matrix. (12 refs.)
- CO/N₂ solid solutions: head-tail reorientations** See Entry 76330
- Short-range ordering in nickel-chromium thermocouple alloys** See Entry 76367
- Unusual cell volume behavior in the LaNb_{1-x}V_xO₄ system** See Entry 76371
- Modeling the phase change in crystalline biphenyl by using a temperature-dependent potential** See Entry 76408
- Irradiation induced order-disorder in Ni₃Al and NiAl** See Entry 76504
- Ordering in orthorhombic crystals** See Entry 76584
- Phase diagram of ZrV₂** See Entry 76589
- Microstructure and properties of fine grained supersaturated Fe-C alloys** See Entry 76650
- Rb₂ZnCl₄: three heat-capacity anomalies due to soft-mode and commensurate-incommensurate transitions** See Entry 76658
- Heat capacity of tetramethylammonium trichloromanganate(II) from 1.5 to 300K** See Entry 76659
- K₂SeO₄: calorimetric studies of two successive phase transitions** See Entry 76660
- Heat capacity study of the phase transitions in As₂S₃ and As₂S₄** See Entry 76661
- Schottky anomaly and phase transition in the specific heat and in the spectra of KdY(MoO₄)₂** See Entry 76664
- Thermal properties of Cu₃SnS₆** See Entry 76665
- Phase transition on stepped silicon surfaces** See Entry 76754
- On the stability of surface martensite in β -phase Cu-Zn alloys** See Entry 76758
- Transitions of adsorbates on random substrates** See Entry 76781
- Multiple phase transitions in GeTe films. Dynamics and film structure** See Entry 76814
- Peierls instability and charge density waves at the surface of a metal with a quasideimensional electron spectrum** See Entry 76935
- Solid state studies on substituted CuCr₂O₄ spinel** See Entry 76946
- Effect of heat treatment on the conduction and structure of Ge-Se-Te amorphous alloys** See Entry 76950
- Electrical transport and phase stability in silver iodide-cadmium iodide** See Entry 76952
- Microwave transport properties around the structural phase transition of MnSe** See Entry 76954
- Neutron diffraction effects of the distorted structure of Ni-67.7 at.% Fe alloy in the magnetic ordered state** See Entry 77147
- Magnetic properties and crystal distortion of hexagonal Mn₃Ga** See Entry 77152
- EPR study of ordering in stoichiometric β -aluminate** See Entry 77256
- Temperature-dependent nuclear magnetic resonance in CuInX₂ (X=S,Se,Te) chalcopyrite-structure compounds** See Entry 77271
- ⁵⁷Fe Mossbauer spectroscopy on FePt Invar alloys** See Entry 77312

- The isomeric shift anomaly near phase transition temperature** See Entry 77314
- Order-disorder phase transition and dielectric constant of ice Ic** See Entry 77317
- Structure and dipole relaxation mechanisms in the cyclic alcohols cyclopentanol to cyclo-octanol** See Entry 77326
- High-temperature phase transitions in pure and deuterated ammonium dihydrogen phosphate: conductivity and dielectric measurements** See Entry 77334
- Influence of external electric field on incommensurate-commensurate phase transition in K₂SeO₄ and (NH₄)₂BeF₄ crystals. I. Static properties** See Entry 77335
- Influence of external electric field on incommensurate-commensurate phase transition in K₂SeO₄ and (NH₄)₂BeF₄ crystals. II. Dynamic properties** See Entry 77336
- Integrated scattering of light in lead magnoniobate, which is a ferroelectric with a diffuse phase transition** See Entry 77405
- Temperature dependence of optical absorption near the order-disorder phase transition of sodium nitrate** See Entry 77408
- Effect of pressure on the absorption spectra of solid O₂** See Entry 77412
- Study of positron lifetimes in α , β and γ cerium at high pressures** See Entry 77476
- Rapid solidification of steels** See Entry 77627
- Diffusionless omega transformations in quenched and pressurized Zr-Mo alloys** See Entry 77631
- Order-disorder transformation study in 25-35 at.% Cd-Mg alloys by energy dispersive X-ray diffraction (EDXD)** See Entry 77632
- Influence of the crystallography of the grain boundary/grain system on the α - γ phase shift in Fe-4%Ni alloys** See Entry 77633
- TTT curves for the formation of austenite** See Entry 77634
- Phase transformation studies of laser-processed Fe-0.2% C-Cr surface alloys** See Entry 77635
- On the change in the austenite lattice parameter due to the martensitic transformation in an Fe-32Ni alloy** See Entry 77636
- Influence of a high pressure on the kinetics of formation of lath (packet) martensite** See Entry 77637
- Martensitic transformations in low-carbon nickel-molybdenum steels** See Entry 77638
- Influence of the composition of the particles contained in austenite on the characteristics of the γ - α transformation** See Entry 77639
- Thermodynamics of the martensitic transformation in high-nickel iron alloys. Thermal effect** See Entry 77640
- Structure mechanics connected with the martensitic transformation of steels. Consequences for industry** See Entry 77641
- Bulk modulus and martensitic transformation in Mn-Cu alloys** See Entry 77642
- Landau theory for a cubic to tetragonal structural phase transformation** See Entry 77643
- Carbon content of retained austenite in quenched steels** See Entry 77666
- Nonlinear resonance in Cu₃Au** See Entry 77691
- Elasticity and anelasticity of a 304 stainless steel at below room temperature** See Entry 77692
- Nature of the anomalous spontaneous deformation of iron in the presence of hydrogen** See Entry 77701
- High-temperature shape memory in titanium nickelide** See Entry 77702
- Shock temperatures of SiO₂ and their geophysical implications** See Entry 77836
- Olivine to spinel transformation in Mg₂SiO₄ via faulted structures** See Entry 77838

64.70M Transitions in liquid crystals

- 76623 Reentrant phase transition of chiral smectic C liquid crystal in electric field.** M.Yamashita, H.Kimura (Dept. of Appl. Phys., Nagoya Univ., Nagoya, Japan). *J. Phys. Soc. Jpn. (Japan)*, vol.52, no.5, p.1509-11 (May 1983).
The reentrant behaviour (Sm C-Sm C*-Sm C-Sm C*) observed experimentally in an electric field near the chiral smectic C to smectic A phase transition point is investigated. That curious phenomenon is attributed to the non-linear excitation of the turn of the director field in the smectic C phase. Similar behaviour near the Lifshitz point in the magnetic field versus temperature plane is also explained by that excitation. (11 refs.)
- 76624 Crossover between two- and three-dimensional melting in a smectic-B-smectic-A phase transition in BBOA.** S.M.Stishov, S.N.Nefedov, A.N.Zisman (Inst. of Crystallography, Acad. of Sci., Moscow, USSR). *JETP Lett. (USA)*, vol.36, no.8, p.348-52 (20 Oct. 1982). Translation of: *Pis'ma v Zh. Eksp. i Teor. Fiz. (USSR)*, vol.36, no.8, p.284-7 (20 Oct. 1982). [received: June 1983]
It is established that the curve of the first-order of phase transition smectic-B(S_B)-smectic-A(S_A) in *N*-(4-*n*-butyloxybenzylidene)-4-*n*-octylaniline (BBOA or 40.8) terminates at the end critical point (ECP), coalescing with the curve of the second-order phase transition smectic-A-nematic (N). An increase in the volume ΔV and entropy ΔS jumps on the S_B-S_A transition line with an increase in pressure is attributed to the crossover between two- and three-dimensional melting. (9 refs.)
- 76625 Shear flow induced cholesteric-nematic transition.** G.Derfel (Inst. of Phys., Tech. Univ. of Lodz, Lodz, Poland). *Mol. Cryst. & Liq. Cryst. Lett. (GB)*, vol.92, no.2, p.41-7 (1983).
It is shown that the shear flow induced cholesteric-nematic transition occurs if the helix axis is normal to the shear plane and the shear rate exceeds a critical value. (3 refs.)
- 76626 Phase characterization and enthalpies of selected disubstituted biphenylcyclohexanes.** H.J.Muller, W.Haase (Inst. fur Phys. Chem., Tech. Hochschule Darmstadt, Darmstadt, Germany). *Mol. Cryst. & Liq. Cryst. Lett. (GB)*, vol.92, no.2, p.63-8 (1983).
The data from DSC-thermal analysis of a selected number of disubstituted biphenylcyclohexanes is reported. All nonpolar compounds in the series exhibit smectic B-phases, whereas the polar members with e.g. halogenes or cyano groups either only occur in the nematic phase or nematic and smectic A-phase. The phase behaviour and the enthalpies of transition are discussed. (6 refs.)

- The mean spherical model (and other approximations) for nematogens See Entry 76287
- Low viscous compounds of highly nematic character See Entry 76290
- New liquid crystal materials; physical properties and performance in displays for automobile, high information density and guest-host applications See Entry 76292
- Relation between TN-cell response time and transition temperatures of liquid crystal materials See Entry 76293
- Dynamics of a Fredericks transition in side chain nematic polymers: determination of the viscoelastic coefficients K_1 and γ_1 See Entry 76295
- Stable liquid crystals with large negative dielectric anisotropy. II. See Entry 76296
- Orientational fluctuations of a lyotropic nematic liquid crystal measured by quasielastic light scattering See Entry 76297
- Mean-field model for antiferroelectric smectic-A liquid crystals See Entry 76301
- Translational order in smectic liquid crystals. Allowance for features of the intermolecular forces See Entry 76304
- Orientational effects in the mesophase under short laser pulses; nonlinearity buildup See Entry 76307

64.70P Glass transitions

- 76627 The influence of thermodynamic interactions on the glass transition of poly(vinyl chloride)-benzylbutylphthalate mixtures. S.K.Roy, G.R.Brown, L.E.St.-Pierre (Dept. of Chem., McGill Univ., Montreal, Quebec, Canada). *Int. J. Polym. Mater. (GB)*, vol.10, no.1, p.13-20 (1983).
- The glass transition temperature and the interaction parameters, χ , for poly(vinyl chloride) plasticized with benzylbutylphthalate have been determined over a wide range of concentrations. The classical iso-free volume theory of the glass transition fails to explain the experimental results. However, Kovacs' modified iso-free volume theory with the addition to the free volume of an excess volume of mixing based on the χ parameter suitably rationalizes the experimental values. (15 refs.)
- 76628 Orientational effect of the extensional flow field on solutions of rigid rodlike macromolecule—disappearance of the isotropic to nematic phase transitions. M.Mansuripur (Xerox Corp., Palo Alto Res. Centre, Palo Alto, CA, USA). *Int. J. Multiphase Flow (GB)*, vol.9, no.3, p.299-307 (June 1983).
- The effect of steady state uniaxial extensional flow on a solution of rigid rodlike macromolecules is theoretically studied. The mean field theory of Maier and Saupe is extended to cover situations in which the macromolecular solution is subjected to an extensional flow field. It is found that for a given solution a critical flow gradient exists beyond which the first order nematic-isotropic phase transition, which is typical of such solutions in the absence of flow, disappears. A similar result is obtained when the theory of Onsager is applied to the problem. Order parameter as a function of flow gradient is calculated and it is shown that the contribution of flow to the ordering of macromolecules is most significant when the stationary solution is isotropic but close to the transition point. (17 refs.)
- 76629 Constant-pressure simulation of silica. S.K.Mitra (Dept. of Computer Sci., Univ. of Reading, Reading, England). *Philos. Mag. B (GB)*, vol.47, no.5, p.L63-7 (May 1983).
- The results of molecular dynamics simulations of silica at different constant pressures are reported. These are compared with the constant-volume simulation results of the same system. The thermodynamic properties of these simulations were found to be dependent on the condition imposed on the system. The lowering of constant pressure on the system decreases its fictive glass-transition temperature. The structural properties of the simulated glasses were found to be less sensitive to these external conditions. (3 refs.)
- Molecular dynamics studies of the structures and properties for halide glasses See Entry 76317
- Mechanism of high ionic conductivity in elastomeric networks See Entry 76696
- Dielectric and dynamic-mechanical behaviour of ethylene-vinyl alcohol copolymers See Entry 77324
- A structural interpretation of the vibrational spectra of binary fluoroborate glasses See Entry 77378
- Multicomponent glasses of GeO_2 and Sb_2O_3 with Bi_2O_3 , Ti_2O_3 , and/or PbO See Entry 77620
- Studies of epoxy resin systems. III. Effect of sub- T_g aging on the physical properties of a fully cured epoxy resin See Entry 77657
- Studies of epoxy resin systems. IV. Fracture toughness of an epoxy resin: a study of the effect of crosslinking and sub- T_g aging See Entry 77658

64.75 SOLUBILITY, SEGREGATION, AND MIXING

- 76630 Vacancy pump as a mechanism of growth of precipitates during precipitation of solid solutions. G.G.Samsonide, A.N.Orlov, Yu.V.Trushin (A.F. Ioffe Physicotech. Inst., Acad. of Sci., Leningrad, USSR). *Fiz. Met. & Metalloved. (USSR)*, vol.55, no.4, p.676-84 (April 1983). In Russian. English translation in: *Phys. Met. & Metallogr. (GB)*
- An analysis is made of the growth of spherically symmetric precipitates of a new phase in a substitutional solid solution. This is done using a vacancy pump model in which vacancy-impurity complexes are the agents which carry mass to precipitates. A method is suggested for solving the balance equations for impurity atoms, vacancies, and complexes in the absence of a local equilibrium of their concentrations. The dependences of the concentrations of complexes and vacancies on the coordinate r and on the time t are found in two limiting cases of long and short precipitate formation times. An expression is obtained for the rate of growth of a precipitate valid over periods of practical interest. (6 refs.) A.T.
- 76631 Dissolution of vanadium carbide in steel, in the case of formation of a ferrite layer at the interface. V.V.Popov, D.A.Emel'yanov (S.M. Kirov Ural Polytech. Inst., Sverdlovsk, USSR). *Fiz. Met. & Metalloved. (USSR)*, vol.55, no.4, p.685-92 (April 1983). In Russian. English translation in: *Phys. Met. & Metallogr. (GB)*
- A theoretical analysis is made of the process of multicomponent diffusion during dissolution of vanadium carbide in steel in the case of formation of a ferrite layer at the interface. Expressions are obtained for the distributions of the concentrations of the components in the matrix and of the amounts of the diffused matter, as well as for the kinetics of dissolution of the precipitate.

The values of the interface concentrations are found by a method involving simultaneous solution of thermodynamics equations and of the mass balance equations. A theoretical calculation is made of the distributions of the concentrations in the diffusion zone and the results of calculations and experiments are compared. (17 refs.) A.T.

- 76632 Investigation of the precipitation of supersaturated solid solutions in alloys of magnesium with dysprosium. L.L.Rokhlin (A.A. Baikov Inst. of Metall., Acad. of Sci., Moscow, USSR). *Fiz. Met. & Metalloved. (USSR)*, vol.55, no.4, p.733-8 (April 1983). In Russian. English translation in: *Phys. Met. & Metallogr. (GB)*
- Precipitation of supersaturated solid solutions of dysprosium in magnesium was found to occur in three stages corresponding to ordering, formation of platelet crystals of a nonequilibrium phase with the orthorhombic lattice, and formation of large platelet crystals of the equilibrium phase. (4 refs.) A.T.
- 76633 The role of solitons and the kinetics of precipitate growth in boron doped silicon-germanium alloys. N.Savides (School of Phys., Univ. of Sydney, Sydney, NSW, Australia). *J. Appl. Phys. (USA)*, vol.54, no.5, p.2402-6 (May 1983).
- The time dependence of the thermoelectric transport properties of boron doped $\text{Si}_{10}\text{Ge}_{90}$ alloys has been investigated for times between 1 and 8700 h at an isothermal heat treatment temperature of 1100 K. Changes in the Seebeck coefficient, electrical resistivity, and carrier concentration which result from the precipitation of boron are reported. Three distinct stages are observed in the precipitation process: (a) an initial stage of precipitate zone growth lasting for about 1000 h characterised by a parabolic rate law, (b) a final stage commencing after about 4000 h and obeying the conventional Lifshitz-Slyozov post nucleation rate law, and (c) a lengthy intermediate stage lasting for about 3000 h in which the transition from initial to final stage takes place. A recently proposed soliton model for the kinetics of precipitate growth in binary phase systems is found to correctly reproduce the experimental observations. It is also reported that the precipitation process is reversible and the precipitated boron can be put back into solid solution by high temperature annealing. (16 refs.)
- 76634 Liquid immiscibility in the systems $\text{X}_2\text{O}-\text{MO}-\text{B}_2\text{O}_3-\text{SiO}_2$ ($\text{X}=\text{Na}, \text{K}; \text{M}=\text{Mg}, \text{Ca}, \text{Ba}$) and $\text{Na}_2\text{O}-\text{MgO}-\text{BaO}-\text{B}_2\text{O}_3-\text{SiO}_2$. P.Taylor, A.B.Campbell, D.G.Owen (Atomic Energy of Canada Ltd., Whiteshell Nuclear Res. Establish., Pinawa, Manitoba, Canada). *J. Am. Ceram. Soc. (USA)*, vol.66, no.5, p.347-51 (May 1983).
- The limits of miscibility at 650°C were determined for compositions with the mole ratio $\text{SiO}_2/\text{B}_2\text{O}_3=1.07$ in the systems $\text{X}_2\text{O}-\text{MO}-\text{B}_2\text{O}_3-\text{SiO}_2$ ($\text{X}=\text{Na}, \text{K}; \text{M}=\text{Mg}, \text{Ca}, \text{Ba}$) and $\text{Na}_2\text{O}-\text{MgO}-\text{BaO}-\text{B}_2\text{O}_3-\text{SiO}_2$. The form of the miscibility gaps in the quaternary systems is similar to that previously described for the system $\text{Na}_2\text{O}-\text{ZnO}-\text{B}_2\text{O}_3-\text{SiO}_2$. The topography of miscibility gaps in systems of this type is discussed in detail. The extent of the miscibility gap is correlated with the polarizing power of each cation, X and M ($\text{Na} > \text{K}$ and $\text{Zn} > \text{Mg} > \text{Ca} > \text{Ba}$) both among the seven quaternary systems and within the single five-component system examined. The possibility of using empirical correlations observed among the quaternary systems to predict the behavior of other compositions, or of more complex systems, is explored. (23 refs.)
- 76635 Study on the formation of ternary compounds in titanium-nitrogen-hydrogen system. K.Uchida, B.Kyoh, K.Fuji (Dept. of Nuclear Engng., Kinki Univ., Higashiosaka, Japan), S.Imoto. *J. Jpn. Inst. Met. (Japan)*, vol.47, no.5, p.445-9 (1983). In Japanese.
- The titanium-nitrogen-hydrogen system has been studied by X-ray diffraction analysis and hydrogen analysis of specimens prepared by the reaction of non-stoichiometric titanium nitrides with hydrogen under a pressure of 6 mPa at 873K. In the specimens with nitrogen to titanium ratio less than 0.5, a ternary hcp compound was formed by absorption of hydrogen. The ternary compound had a wide range in both hydrogen and nitrogen contents and is considered as $\alpha\text{-Ti}$ dissolving hydrogen and nitrogen. It is concluded that the solubility of hydrogen in Ti is much increased by nitrogen dissolution. For the specimens with nitrogen to titanium ratio more than 0.6, the crystal structure remained unchanged after the hydrogenation, and the amount of hydrogen absorbed was considerably lower than that in the hcp ternary compound. The maximum solubility of hydrogen was found to be limited by $(\text{N}+\text{H})/\text{Ti}=0.9$, approximately. The enthalpy of the reaction producing the hcp ternary compound from hypostoichiometric TiN was determined by measuring hydrogen equilibrium pressures at various temperatures. The value was -66.15 kJ/mol. (10 refs.)
- 76636 High pressure reactions of oxometallics. VI. High pressure synthesis of mixed valence compounds $\text{VO}_{2-x}(\text{OH})_x$ with CaCl_2 -structure. K.-J.Range, R.Zintl (Inst. fur Anorganische Chem., Univ. Regensburg, Regensburg, Germany). *Mater. Res. Bull. (USA)*, vol.18, no.4, p.411-19 (April 1983). In German.
- Mixed valence compounds $\text{VO}_{2-x}(\text{OH})_x$ ($0.13 < x < 0.37$) were synthesized by high pressure-high temperature decomposition on ammonium metavanadate, NH_4VO_3 , at $p > 20$ kbar and $T = 700\text{--}800^\circ\text{C}$. The blue-black substances crystallize in the orthorhombic system, space group Pnmm. Single crystal data for $\text{VO}_{1.7}(\text{OH})_{0.3}$ ($a=4.5113(7)$ Å, $b=4.6303(8)$ Å, $c=2.8652(5)$ Å) confirmed the structure to be CaCl_2 type, a distorted variant of the rutile structure. On heating in air to about 250°C , $\text{VO}_{2-x}(\text{OH})_x$ is oxidized to VO_2 , which can conveniently be prepared from NH_4VO_3 in this way. (5 refs.)
- 76637 Relevance of the Cahn-Hilliard-Cook theory at early times in spinodal decomposition. J.Marro, J.L.Valles (Dept. de Fisica Teorica, Univ. de Barcelona, Barcelona, Spain). *Phys. Lett. A (Netherlands)*, vol.95A, no.8, p.443-6 (23 May 1983).
- The authors analyse Cook's equation for spinodal decomposition and compare its predictions with computer-simulation data to conclude its formal consistency with the observations at early times. They thus provide a simple reference for the analysis of experiments at early, observable times and for the development of theory at late times. (10 refs.)
- 76638 Solvus of $\text{KCl}:\text{Ca}^{2+}$ solid solution by flotation measurements of density of single crystals. V.B.Dudnikova, V.S.Urusov (Inst. of Geochem. & Analytical Chem., Moscow, USSR). *Phys. Status Solidi A (Germany)*, vol.76, no.1, p.217-21 (16 March 1983).
- Solvus of the system $\text{KCl}:\text{Ca}^{2+}$ is plotted within the concentration range from 3×10^{-2} to 2.5×10^{-1} mol.% at temperatures from 400 to 550°C . The decomposition of the solid solution after different regimes of thermal treatment is fixed by a change in density with the aid of the flotation procedure. A thermodynamic analysis of the experimental data evaluates the dissolution energy of the impurity, (1.37 ± 0.14) eV, and vibration entropy $(\Delta S_v/k = 7.7 \pm 2.3)$. (9 refs.)
- 76639 TEM precipitation studies in Te-rich as-grown PbTe single crystals. M.Muhlberg (Sektion Phys., Humboldt-Univ. zu Berlin, Berlin, Germany), D.Hesse. *Phys. Status Solidi A (Germany)*, vol.76, no.2, p.513-24 (16 April 1983).
- In Te-rich as-grown PbTe single crystals small homogeneously distributed inhomogeneities are detected by TEM. They are identified as tellurium precipi-

piates. The largest of them permit the determination of their orientation: (001) Te||[111] PbTe, [110] Te||[110] PbTe. An estimation of the number of Te atoms absorbed by the precipitates results in values which are comparable with the maximum deviation from stoichiometry. The results allow a detailed comparison with literature data on precipitates in $A^{14}B^{VI}$ semiconductors. They support the idea of a diffusion-determined precipitation due to the retrograde course of the solidus line. (30 refs.)

76640 AgCl intrinsic properties modifications by ion implantation. J.Gisclon (Dept. de Phys. des Materiaux, Univ. Claude Bernard Lyon I, Villeurbanne, France), J.Bert, L.Vignal, Ch.Diane, J.Dupuy. *Radiat. Eff. (GB)*, vol.64, no.1-4, p.125-34 (1982). [received: May 1983] (Proceedings of the First International Conference on 'Radiation Effects in Insulators', Arco, Largo di Garda, Italy, 1981). The damage produced by energetic ion implantation (100 keV < E < 1 MeV) in AgCl (single crystals or thin films) is mainly due to the Ag⁺ sublattice. At liquid nitrogen temperature (LNT), the photographic process being blocked, the main defects created are identified as silver clusters. Their formation is analysed by means of the study of optical absorption spectra; this method permits cluster characterization with respect to elastic collision-energy. After a computer deconvolution of optical spectra, the authors are able to give some detail about intrinsic and extrinsic colloids. They then point out the formation conditions and the characterization of a metallic phase in the silver chloride matrix. (14 refs.)

76641 Thermal evolution of precipitated phases in Au implanted MgO single crystal. G.Aouchacra, G.Chassagne, J.Serughetti (Dept. de Phys. des Materiaux, Univ. Claude Bernard, Lyon I, Villeurbanne, France). *Radiat. Eff. (GB)*, vol.64, no.1-4, p.189-96 (1982). [received: May 1983] (Proceedings of the First International Conference on 'Radiation Effects in Insulators', Arco, Largo di Garda, Italy, 1981). MgO single crystals implanted with Au⁺ ions (180 keV, $6.10 \cdot 10^{17}$ ions cm⁻²) and annealed at temperatures between 25°C and 1100°C, have been analysed—by optical spectrophotometry—Rutherford backscattering (to confirm the effective presence and to study the distribution profile of Au atoms), and by TEM and X-ray diffraction (to identify the phase precipitated by thermal treatment). Thermal annealing between 550°C and 1100°C produced an optical absorption band located between 565 nm and 600 nm. This band can be attributed to a FCC Au precipitate with diameter varying from 50 to 200 Å. Larger metallic colloids 1000 Å are in simple orientation with the matrix. Annealing at temperatures higher than 500°C produces a supplementary optical absorption located at 425 nm. This band can be attributed to Au plasma resonance. After annealing for 15 min at 1100°C, a new phase is detected by X-ray diffraction and TEM and identified as Au₃Mg alloy with hexagonal structure. (16 refs.)

76642 Metallic alloy precipitates in high dose indium implanted MgO. A.Perez, M.Treilleux, L.Fritsch (Dept. de Phys. des Materiaux, Univ. Claude Bernard Lyon I, Villeurbanne, France), G.Marest. *Radiat. Eff. (GB)*, vol.64, no.1-4, p.199-203 (1982). [received: May 1983] (Proceedings of the First International Conference on 'Radiation Effects in Insulators', Arco, Largo di Garda, Italy, 1981). MgO implanted at room temperature with 150 keV In⁺ ions and doses ranging from 10^{15} to 10^{17} ions cm⁻² was studied by optical absorption and transmission electron microscopy (TEM). Creation of defects in the anionic sublattice (F⁻, F²⁻, F₂-centers) and in the cationic sublattice (V⁻-centers) are observed. Subsequent annealings of the implanted crystals have shown different behaviours depending on the implanted dose. For medium dose (2×10^{16} ions cm⁻²), the formation of In³⁺ species seems to be the preponderant phenomenon. At higher dose (8×10^{16} ions cm⁻²), metallic precipitates are formed between 400 and 700°C. The identification of these precipitates has been achieved using TEM: they are formed of a metallic alloy Mg₃In with a hexagonal structure and their orientation relationship with respect to the MgO matrix is: (001)_{Mg3In}//(111)_{MgO} and $[1120]_{Mg3In} // [111]_{MgO}$. (14 refs.)

76643 On the nature of the phases formed when metals are implanted with oxygen or nitrogen. R.Kelly (IBM Thomas J. Watson Res. Center, Yorktown Heights, NY, USA). *Radiat. Eff. (GB)*, vol.64, no.1-4, p.205-20 (1982). [received: May 1983] (Proceedings of the First International Conference on 'Radiation Effects in Insulators', Arco, Largo di Garda, Italy, 1981). Although the average composition change resulting from O or N implantation in a metal is small up to a dose of about 3×10^{16} ions/cm², the implanted atoms tend to be atomically mobile under the conditions used for bombardments and precipitation of an oxide or nitride can be expected. The object of this work is to explain what phases are formed. One model is based on the postulate that the precipitates are at the surface and have a high anion-to-cation ratio. The resultant phase therefore tends to be that which arises from the impact of any heavy particle on the surface of a high oxide or nitride. An alternative model is based on the postulate that the precipitates tend, independently of where they form, to be in qualified thermodynamic equilibrium with the metal. A consideration of the known examples of O or N implantation suggests that qualified thermodynamic equilibrium is the better guide to which phases are formed. (119 refs.)

76644 Accuracy of calculation of the heat of dissolution of hydrogen in nontransition metals. V.G.Orlov. *Sov. Phys.-Solid State (USA)*, vol.24, no.11, p.1865-9 (Nov. 1982). Translation of: *Fiz. Tverd. Tela (USSR)*, vol.24, no.11, p.3286-92 (Nov. 1982). [received: May 1983] The pseudopotential model of a metal is used to discuss the various contributions to the heat of dissolution Q of a hydrogen impurity in nontransition metals. The sensitivity of the results of the form of screening and the type of pseudopotential is investigated. The experimental values of Q for a solid solution phase of hydrogen in aluminum and magnesium are compared with the values calculated using various models. (26 refs.)

76645 Orientation of particles of a new phase appearing in crystals. A.B.Vasil'ev, S.F.Chernov (A.V. Shubnikov Inst. of Crystallography, Acad. of Sci., Moscow, USSR). *Sov. Phys.-Solid State (USA)*, vol.24, no.12, p.2103-5 (Dec. 1983). Translation of: *Fiz. Tverd. Tela (USSR)*, vol.24, no.12, p.3691-3 (Dec. 1983). The authors describe an investigation of the process of formation and orientation of particles of a new impurity phase in an anteprecipitate and in the matrix proper in the case of KCl (with 0.1 wt.% of SnBr₂ in the charge) and ZnO crystals. They determine the topography of the impurity distribution by vacuum decoration (with gold) and electron-microscopic examination; they also determined the orientation of the particles of the new phase by electron diffraction. (17 refs.)

76646 Interface spinodal decomposition in LPE In₂Ga_{1-x}As₂P_{1-y} lattice-matched to InP. H.Launois, M.Quillec, F.Glas, M.J.Treacy (CNET, Bagneux, France).

Gallium Arsenide and Related Compounds, 1982. Tenth International Symposium on Gallium Arsenide and Related Compounds, Albuquerque, NM, USA, 19-22 Sept. 1982 (Bristol, England: IOP 1983), p.537-44. Concentration modulations are presented in some LPE In₂Ga_{1-x}As₂P_{1-y} layers grown by liquid phase epitaxy on (001) InP. On the basis of thermal treatments and of different temperature growths, the authors show that this latter parameter determines the existence of the composition modulations. They propose an interpretation of these effects on the basis of liquid-solid interface spinodal decomposition. As a consequence, they have obtained homogeneous high mobility quaternary alloys ($\lambda = 1.3 \mu\text{m}$). (11 refs.)

Incorporation of radionuclides in crystalline titanates See Entry 75092

Calculation of the crystallization behaviour of metallic glasses See Entry 76318

Structure property relationship in unsaturated polyamides See Entry 76324

The effect of Soret diffusion on the morphological stability of a binary alloy crystal See Entry 76332

Segregation during directional melting and its implications on seeded crystal growth: a theoretical analysis See Entry 76337

Structural changes in martensite observed in high-nickel steel as a result of low-temperature heating See Entry 76366

Theory of annealing of vacancy pores in thin metal foils See Entry 76418

Chemical effects of carbon ion implantation into alkali halides See Entry 76470

Compound synthesis in TiO₂ implanted with rubidium See Entry 76471

Solid-liquid equilibrium diagram of acetanilide+phenacetin mixtures determined by differential scanning calorimetry See Entry 76585

Thermodynamics on UO₂-ZrO₂-LnO₂-x solid solutions See Entry 76586

Oscillatory morphological instabilities due to non-equilibrium segregation See Entry 76592

Phase equilibria in the H₂/C₂H₄ system at temperatures from 114.1 to 247.1 K and pressures to 600 MPa See Entry 76599

Calculation of vapour-liquid equilibria with equations of state from the extended van-der-Waals theory. II. Application of the equation to mixtures See Entry 76600

On 'forbidden' reflections in calcia- and yttria-stabilized zirconia (CSZ and YSZ) See Entry 76611

The influence of thermodynamic interactions on the glass transition of poly(vinyl chloride)-benzylbutylphthalate mixtures See Entry 76627

Microstructures of rapidly solidified Fe-Al-Zr alloys See Entry 76649

Microstructural study of devitrified amorphous alloys See Entry 76651

Investigation of redistribution of the alloying elements during diffusion annealing of titanium alloys See Entry 76687

Thermal-relaxation studies of the stability of amorphous structures in zirconium-based superconducting alloys See Entry 77082

Spin waves in ageing ferromagnetic alloys with isostructural precipitates of a new phase See Entry 77161

Anomalous elastic properties of Fe-Ni (FCC) alloys and their Invar properties See Entry 77246

Electron localization on defects and optical nuclear polarization in disordered and semimagnetic semiconductors See Entry 77270

Birefringence and structural defects in Cu₂O crystals See Entry 77355

Decay behaviour of high-excitation luminescence in GaP:N. II. Experimental results on the densities of the coexisting phases and the relevant recombination processes See Entry 77443

Crystal growth of solid solutions La_{1-x}Ba_xF_{3-x} See Entry 77553

Thermodynamic properties of liquid silver-thallium alloys See Entry 77616

FCC and BCC solidification products in a rapidly solidified austenitic steel See Entry 77628

Influence of the composition of the particles contained in austenite on the characteristics of the $\gamma \rightarrow \alpha$ transformation See Entry 77639

Precipitation studies in lead-tin alloys See Entry 77644

The formation of discrete precipitate dispersions on mobile interphase boundaries in iron-base alloys See Entry 77645

A TEM investigation of the structure of nitrogen-implanted Ti-6Al-4V See Entry 77646

Electrical conductivity and infrared absorption spectrometry study of hematite precipitation from defective ferrites See Entry 77647

On the precipitation of Laves phase in 12 Cr-Mo-V-W steel heated for a long time See Entry 77648

The investigation of dissolution and precipitation kinetics of secondary phases in a Cr15Ni70W10MoAlTiB alloy See Entry 77649

VC coarsening in 0.5Cr-0.5Mo-0.25V steel See Entry 77650

Carbide transformations in microstructurally unstable low alloy ferritic steel See Entry 77651

On the formation of Fe-carbides in Cu-Fe and Cu-Au-Fe alloys See Entry 77652

Deceleration of relaxation in a Cu-Si alloy See Entry 77653

Grain-coarsening resistance and the stability of second-phase dispersions in rapidly solidified steels See Entry 77654

Analysis of a rapidly solidified high-phosphorus austenitic steel containing an amorphous phase See Entry 77660

Effects of the quenching conditions on the growth of GP zones in Al-Zn alloys See Entry 77664

Electron magnetic spectrometer investigation of fracture surfaces formed in vacuum and in air See Entry 77725

Intergranular creep embrittlement by non-soluble impurity: Pb in precipitation hardened Al-Mg-Si alloys See Entry 77746

The effect of hydrogen on an iron based amorphous alloy See Entry 77762

The oxidation behaviour of hot pressed aluminium nitride See Entry 77781

The selective dissolution of SUS04 and SUS16 austenitic stainless steels in a hydrochloric acid solution See Entry 77792

- Effects of segregated phosphorus on stress corrosion cracking susceptibility of 3Cr-0.5Mo steel See Entry 77799
 Comparison of chemical reactions in liquid lithium with those in liquid sodium See Entry 77880

64.80 OTHER PHASE PROPERTIES OF SYSTEMS

- 76647 Morphology of residual austenite in structural steels.** L.M.Utevskii, T.V.Eterashvili, R.I.Entin (Republican Centre of Electron Microscopy, Georgian Polytech. Inst., Tbilisi, USSR). *Fiz. Met. & Metalloved. (USSR)*, vol.55, no.4, p.816-18 (April 1983). In Russian. English translation in: *Phys. Met. & Metallogr. (GB)*
 The morphology and distribution of residual austenite were investigated in structural steels 10Kh2G3M, 38KhS, and 33Kh3N2M. The study was carried out by electron microscopy and microdiffraction methods. The results indicated formation of layers of the residual austenite located in certain preferred positions (such as the boundaries of martensitic laths and packets). (8 refs.) A.T.
- 76648 Lattice-fringe imaging of precipitation-hardened cobalt rare-earth magnets.** J.Fidler (Inst. of Appl. & Tech. Phys., Tech. Univ. Wien, Wien, Austria). *Philos. Mag. A (GB)*, vol.47, no.5, p.L19-22 (May 1983).
 The different microphases of high coercivity (Co, Fe, Cu, Zr)₇Sm permanent magnets have been studied and characterized by means of high-resolution electron microscopy. From lattice-fringe images of the cellular microstructure the misfit of the crystal lattice parameter between the coherent cell boundary phase and the cell interior phase is determined. It is shown that the platelet phase within the cell interiors consists of a hexagonal Co₁₂Sm₂ layer. (7 refs.)
- 76649 Microstructures of rapidly solidified Fe-Al-Zr alloys.** A.N.Patel, L.F.Vassamillet, A.H.Clauer (Battelle Columbus Labs., Columbus, OH, USA).
 Rapidly Solidified Amorphous and Crystalline Alloys. Proceedings of the Materials Research Society Annual Meeting, Boston, MA, USA, Nov. 1981 (New York, USA: North-Holland 1982), p.259-63
 Rapidly quenched short fibers of FeAl and Fe-8Al-XZr (X=0.1,0.2,0.4, and 1) alloys were produced by the pendant drop melt extraction process, (PDME) to explore the feasibility of producing intermediate temperature, oxidation resistant iron base alloys. The fibers had a diameter of 20 to 50 μ m and ranged in length from 2-5 mm. The cooling rate was insufficient to retain zirconium in solution in the Zr-containing alloys, resulting in precipitates of the type Fe₃(Zr,Al) having differing compositions at the grain boundaries and within the matrix. No precipitates were observed in the FeAl alloys. The precipitates were uniform in distribution and size. Grain boundary precipitation and precipitate size both decreased with decreasing Zr contents. (3 refs.)
- 76650 Microstructure and properties of fine grained supersaturated Fe-C alloys.** B.L.Mordike, H.W.Bergmann (Inst. für Werkstoffkunde und Werkstofftech., Univ. of Clausthal, Clausthal, Germany).
 Rapidly Solidified Amorphous and Crystalline Alloys. Proceedings of the Materials Research Society Annual Meeting, Boston, MA, USA, Nov. 1981 (New York, USA: North-Holland 1982), p.423-7
 Rapidly quenched tapes of Fe-C-X alloys (X=Cr, Mn, Ni, Co, Al, Si) were produced by melt spinning. The hardness, ductility, grain size and micro and lattice structure were determined. The system Fe-2.1C-13Cr was chosen for further study. The transformation (isothermal and continuous) characteristics were determined for the as quenched and reannealed states. The results can be presented in the form of TTT diagrams and hardness measurements. (4 refs.)
- 76651 Microstructural study of devitrified amorphous alloys.** L.Vassamillet, R.Maringer, R.Carbonara, J.McCall (Battelle-Columbus, Columbus, OH, USA).
 Rapidly Solidified Amorphous and Crystalline Alloys. Proceedings of the Materials Research Society Annual Meeting, Boston, MA, USA, Nov. 1981 (New York, USA: North-Holland 1982), p.449-53
 Several amorphous alloys were subjected to thermal processing subsequent to their rapid solidification. These alloys have been characterized utilizing metallographic (optical, TEM, and SEM) and X-ray methods. Also, mechanical property evaluations have been made. The alloys exhibit extremely fine grain size; some have a high degree of preferred orientation and second-phase precipitates in the submicron size range. Most have good modulus, high yield and ultimate strength, high reduction in area but limited percent elongation. (no refs.)
- 76652 Microstructure and mechanical properties of laser-processed Ni-Al-Mo base alloys.** D.B.Snow (United Technol. Res. Center, East Hartford, CT, USA).
 Rapidly Solidified Amorphous and Crystalline Alloys. Proceedings of the Materials Research Society Annual Meeting, Boston, MA, USA, Nov. 1981 (New York, USA: North-Holland 1982), p.523-7
 The addition of molybdenum to nickel base superalloys which contain a γ' volume fraction of ≤ 0.35 allows them to be consolidated from powder by laser processing at solidification rates of $\sim 10^4$ C/s. The as-solidified microstructure of these alloys is dendritic, and consists of a fine dispersion ~ 20 nm cuboidal γ' in a supersaturated FCC γ matrix. When annealed at 500-700°C, additional age hardening occurs via the precipitation of ≤ 10 nm, Dia-structure Ni₃Mo, DO₂₂-structure Ni₃Mo and/or Pt₂Mo-structure Ni₃Mo. This combined strengthening by very fine γ' and Ni₃Mo dispersions in laser-processed material makes alloys of this type attractive for potential turbine disk applications. However, the 6-15 at% molybdenum required to prevent cracking during laser consolidation renders many of these alloys prone to an embrittling cellular phase transformation, $\gamma + \gamma' + \text{Ni}_3\text{Mo} \rightarrow \gamma + \text{orthorhombic Ni}_3\text{Mo}$, at temperatures of $\leq 900^\circ\text{C}$. (12 refs.)
- 76653 Transmission electron microscopy of RSP Fe/Cr/Mn/Mo/C alloy.** J.J.Rayment, G.Thomas (Materials & Molecular Res. Div., Univ. of California, Berkeley, CA, USA).
 Rapidly Solidified Amorphous and Crystalline Alloys. Proceedings of the Materials Research Society Annual Meeting, Boston, MA, USA, Nov. 1981 (New York, USA: North-Holland 1982), p.547-52
 Rapid solidification processing (RSP) has been carried out on an Fe/Cr/Mn/Mo/C alloy using both electron-beam melting and piston-and-anvil techniques. Preliminary TEM results show RSP produces a refined duplex microstructure of ferrite and martensite, with a typical ferrite grain size of 0.50-3.0 microns. This RSP microstructure is significantly different from that observed in the conventionally austenitized and quenched alloys—a lath martensitic microstructure with thin films of retained interlath austenite. The morphological change produced by RSP is accompanied by an increase in hardness from 48 R_c to 61 R_c (~ 480 to 720 VHN). It is intended to use electron-beam specimens to examine the potential beneficial effect of RSP upon sliding wear resistance and, by careful TEM studies, it will be possible

to characterize the microstructure and its role in the hardness and wear behavior of the RSP alloy. (10 refs.)

- Critical factors in laser and electron beam glazing of materials See Entry 76496
 Characterization and properties of laser quenched aluminum bronzes See Entry 76497
 Development of morphological instability and cells during rapid solidification of laser annealed silicon alloys See Entry 76598
 Magnetically hard Alnico 5 alloy with a mischmetal addition See Entry 77213
 Rapid solidification of steels See Entry 77627
 FCC and BCC solidification products in a rapidly solidified austenitic steel See Entry 77628
 Microstructure of a rapidly solidified Al-Fe-Co-Ni alloy See Entry 77629
 Rapidly solidified long range ordered alloys See Entry 77630
 A TEM investigation of the structure of nitrogen-implanted Ti-6Al-4V See Entry 77646
 Analysis of a rapidly solidified high-phosphorus austenitic steel containing an amorphous phase See Entry 77660
 Structure/property relationships and applications of rapidly solidified aluminum alloys See Entry 77661
 Investigation of the structure and phase composition of a stainless steel wire after electroplastic drawing See Entry 77667
 Influence of heat treatment on the structure and long-term strength of γ/γ' -MeC nickel eutectic. Length memory effect See Entry 77680
 Characteristics of formation of the structure during deformation of low-alloy chromium by rolling at temperatures 1400-1450K See Entry 77681
 Investigation of structural changes during fracture of $\gamma + \sigma$ steel See Entry 77724

65.00 THERMAL PROPERTIES OF CONDENSED MATTER

(see also 05.70 Thermodynamics, 63. Lattice dynamics; for thermal conduction in nonmetallic liquids, see 66.60; for thermal conduction in nonmetallic solids, see 66.70; for electronic thermal conduction, see 72.15, 72.20 and 74.30E; for thermodynamic properties of quantum fluids, see 67.40, 67.50, and 67.60; for thermal properties of solid helium, see 67.80)

65.20 HEAT CAPACITIES OF LIQUIDS

- 76654 Modified Gruneisen and Anderson-Gruneisen relations for quasi-spherical molecular liquids.** B.K.Sharma (Dept. of Phys., Regional Coll. of Education, Bhubaneswar, India). *Pramana (India)*, vol.20, no.1, p.91-103 (Jan. 1983). [received: May 1983]
 The validity of the expression for the Gruneisen parameter of liquids has been tested by obtaining expressions for the heat capacity ratio, isothermal and adiabatic Anderson-Gruneisen parameters, C_p -parameter, Rao's (1941) acoustic parameter, Beyer's nonlinearity parameter, and relate them to the Gruneisen parameter. The calculated values for five liquefied gases comprising of quasi-spherical molecules are reasonably satisfactory and explain the experimental results for the variation of heat capacity ratio, Beyer's nonlinearity parameter and C_p -parameter with temperature for liquid state. It is shown that the isochoric temperature derivative of the sound speed, specified heat ratio and the compressibility are dominant factors with significant contribution for influencing the thermo-acoustic properties of liquids. (32 refs.)

65.40 HEAT CAPACITIES OF SOLIDS

(for specific heat of superconductors, see 74.30E; for specific heat of magnetic systems, see 75.40)

- 76655 Heat capacity, relative enthalpy, and calorimetric entropy of silicate minerals: an empirical method of prediction.** G.R.Robinson, Jr., J.L.Haas, Jr. (Nat. Center for the Thermodynamic Data of Minerals, US Geological Survey, Reston, VA, USA). *Am. Mineral. (USA)*, vol.68, p.541-53 (May-June 1983).
 A procedure to estimate the standard molar heat capacity, relative enthalpy, and calorimetric entropy of silicate minerals has been devised and evaluated. These are estimated by summing, in appropriate proportions, fictive molar isobaric heat capacities, relative enthalpies, and entropies evaluated for structural components of the mineral phases such as MgO-4, MgO-6 or MgO-8 where the Mg is in 4-, 6-, or 8-fold coordination, respectively. The fictive molar heat capacities and entropies were obtained from a large body of experimental calorimetric data on heat capacity, entropy, and relative enthalpy for minerals. The summation technique has a precision better than 2% for heat capacity and relative enthalpy, and 5% for entropy, relative to the data base, between 298 and 1500K. The accuracy of prediction of molar heat capacity and relative enthalpy for mineral phases and specific heat for rocks is expected to be within 3% using this technique. The accuracy of prediction of molar calorimetric entropy is expected to be within 5% using this technique.
- 76656 Lattice and Schottky contributions to the morphology of lanthanide heat capacities.** E.F.Westrum, Jr. (Dept. of Chem., Univ. of Michigan, Ann Arbor, MI, USA). *J. Chem. Thermodyn. (GB)*, vol.15, no.4, p.305-25 (April 1983).
 In this lecture paper the author focusses mainly on the Schottky contribution to heat capacity, mostly for its inherent interest, but also in a nontrivial way to utilize it as a tool to deduce the reliability of a scheme for the evaluation of the lattice contribution of the heat capacity, the latter step is seen as being essential in analyzing the morphology of the heat capacity curve. (54 refs.)
- 76657 Heat capacity and thermodynamic properties of molybdenum from 5 to 302K.** L.M.Khrilovich, I.E.Paukov (Inst. of Inorganic Chem., Novosibirsk, USSR). *J. Chem. Thermodyn. (GB)*, vol.15, no.4, p.333-7 (April 1983).
 The heat capacity of pure molybdenum was measured by adiabatic-shield calorimetry in the temperature range 5 to 302K; no transitions or thermal anomalies were found. At 298.15K, the heat capacity at constant pressure C_p , the entropy S° , and the function $[(G^\circ(T) - H^\circ(0))/T]$ have values (23.86 ± 0.03) , (28.56 ± 0.08) , and $-(13.16 \pm 0.03)$ J.K⁻¹.mol⁻¹ respectively.

The results are compared with earlier by other investigators values found. (5 refs.)

76658 Rb₂ZnCl₄: three heat-capacity anomalies due to soft-mode and commensurate-incommensurate transitions. T.Atake, K.Nomoto, B.K.Chaudhuri, H.Chihara (Dept. of Chem., Faculty of Sci., Osaka Univ., Osaka, Japan). *J. Chem. Thermodyn. (GB)*, vol.15, no.4, p.339-50 (April 1983). There are three phase transitions shown by Rb₂ZnCl₄. The transition temperatures, the enthalpies of transition, and the entropies of transition are (74.6±0.15)K, (30±1) J.mol⁻¹, (0.42±0.01) J.K⁻¹.mol⁻¹; (195.2±0.02)K, (6.2±0.9) J.mol⁻¹, (0.032±0.005) J.K⁻¹.mol⁻¹; (303.2±0.3)K, (222±7) J.mol⁻¹, (0.66±0.14) J.K⁻¹.mol⁻¹. The second transition shows a very sharp heat-capacity peak but the other two are much broader, being consistent with the soft-mode mechanism. Thermodynamic functions of Rb₂ZnCl₄ are tabulated. A comparison is made with the behaviour of ferroelectrics of the same type: K₂SeO₄ and Rb₂ZnBr₄. (45 refs.)

76659 Heat capacity of tetramethylammonium trichloromanganate(II) from 1.5 to 300K. A.G.Dunn, M.Jewess, L.A.K.Staveley, R.D.Worswick (Inorganic Chem. Lab., Univ. of Oxford, Oxford, England). *J. Chem. Thermodyn. (GB)*, vol.15, no.4, p.351-6 (April 1983). The heat capacity of tetramethylammonium trichloromanganate(II), N(CH₃)₄MnCl₃, from 1.5 to 300K, is reported. The principal novelty of the results is in the region above 52K, for which only a very small-scale plot has previously been published. From the results the authors estimate the anomalous molar entropy gain associated with the monoclinic-to-hexagonal transition (T_h=126K) as R is 2.8. (19 refs.)

76660 K₂SeO₄: calorimetric studies of two successive phase transitions. T.Atake, K.Nomoto, B.K.Chaudhuri, H.Chihara (Dept. of Chem., Faculty of Sci., Osaka Univ., Osaka, Japan). *J. Chem. Thermodyn. (GB)*, vol.15, no.4, p.383-94 (April 1983). The heat capacity of K₂SeO₄ was measured from 3 to 300K. The commensurate-incommensurate transition (so-called lock-in transition) showed a rather broad anomaly at (95.1±0.1)K. The enthalpy and entropy of transition are (1.1±0.2) J.mol⁻¹ and (0.012±0.002) J.K⁻¹.mol⁻¹, respectively. The incommensurate-normal transition has a heat-capacity maximum at (127.7±0.1)K and appears to be of second order; its enthalpy and entropy changes are (110±5) J.mol⁻¹ and (0.88±0.05) J.K⁻¹.mol⁻¹. Some thermodynamic functions are derived. (56 refs.)

76661 Heat capacity study of the phase transitions in As₂S₃ and As₄S₄. T.K.Chattopadhyay, E.Gmelin, H.G.von Schnering (Max-Planck-Inst. fur Festkörperforschung, Stuttgart, Germany). *Phys. Status Solidi a (Germany)*, vol.76, no.2, p.543-51 (16 April 1983). Heat capacity of As₂S₃ is measured in the range 100 to 500K. The structural phase transition (β to α) and the crystalline-to-plastic phase transition (α to γ) are investigated and these phase transition temperatures are determined to be (422±0.5) and (432±0.5)K, respectively. The results are compared with those of P₂S₅ which are recently studied. There is a strong similarity in the thermodynamic properties between the two compounds. The plastic phase of As₂S₃ can be retained down to (391±2)K with a hysteresis in the specific heat-temperature curve. Heat capacity of As₄S₄ is also measured in the range 100 to 600K. The structural phase transition temperature (α to β) and melting temperature are determined to be (340±2) and (582±1)K, respectively. As₄S₄ does not transform to a plastic state, and therefore, the melting entropy (54.32 J mol⁻¹ K⁻¹) is very high compared to the melting entropy (3.34 J mol⁻¹ K⁻¹) of As₂S₃. (15 refs.)

76662 Heat-capacity studies of crystal-field effects in dilute RRh₂B₄ compounds. H.B.Radousky, B.D.Dunlap, G.S.Knapp, D.G.Niarchos (Argonne Nat. Lab., Argonne, IL, USA). *Phys. Rev. B (USA)*, vol.27, no.9, p.5526-9 (1 May 1983). Specific-heat data are presented for a number of compounds of the form R₂Y_{1-x}Rh₂B₄, where R=(Dy, Ho, Er, and Tm) is a rare-earth element and x=0.1. Schottky anomalies arising from crystal-field splittings of the rare-earth ions are analyzed using crystal-field parameters recently determined for ErRh₂B₄. Utilizing simple scaling arguments for the crystal-field parameters as the rare-earth ion is changed, a satisfactory explanation of the specific-heat data is obtained. (8 refs.)

76663 Magnetic field dependence of the electronic specific heat of TiBe₂: an estimate from magnetization data. F.Acker, R.Huguenin (Inst. de Phys. Experimentale, Univ. de Lausanne, Lausanne, Switzerland), J.L.Smith, G.R.Stewart. *Phys. Rev. B (USA)*, vol.27, no.9, p.5883-6 (1 May 1983). An estimate of the variation with magnetic field in the electronic specific heat of TiBe₂ is given. From the thermodynamic relationship $\partial S/\partial H = \partial M/\partial T$ and from M-vs-T data it follows that C/T (at T<2K) should remain constant within 0.2% for 0≤H≤40 kOe. A further increase in H up to 70 kOe should cause C/T to drop by about 10%. This is in fair agreement with recent experimental results for C/T (70 kOe)-C/T(0). The origin of the drop in C/T is still uncertain. Paramagnon theory gives no satisfactory fit of the high-field data. (18 refs.)

76664 Schottky anomaly and phase transition in the specific heat and in the spectra of K Dy(MoO₄)₂. I.E.Paukov, L.E.Reznik, G.I.Frolova (Inst. of Inorganic Chem., Acad. of Sci., Novosibirsk, USSR). *Sov. Phys.-Solid State (USA)*, vol.24, no.11, p.1976-7 (Nov. 1982). Translation of: *Fiz. Tverd. Tela (USSR)*, vol.24, no.11, p.3473-5 (Nov. 1982). [received: May 1983] Reports a continuation of the study of the effects of the crystal field on the specific heat and spectra of KLn(MoO₄)₂ compounds. This crystal is interesting because a unique phase transition of the Jahn-Teller type to an antiferro-distortion phase at ~14K was discovered in this compound. The authors determined the energies of all eight Stark components (Kramers doublets) of the ground state ⁶H_{15/2} of the Dy³⁺ ion in the crystal field of this material. This was done by investigating the ⁶F_{9/2}-⁶H_{15/2} transition using the absorption and luminescence spectra. The specific heat of a K Dy(MoO₄)₂ crystal was determined. A Schottky anomaly C_S(T) was found in the specific heat and attributed to the thermal population of the Stark levels. (8 refs.)

76665 Thermal properties of Cu₂SnS₄. M.I.Aliev, D.G.Arasly, T.G.Dzhabrailov (Inst. of Phys., Acad. of Sci., Baku, Azerbaijan SSR). *Sov. Phys.-Solid State (USA)*, vol.24, no.11, p.1978-9 (Nov. 1982). Translation of: *Fiz. Tverd. Tela (USSR)*, vol.24, no.11, p.3477-8 (Nov. 1982). [received: May 1983] The authors give the results of an experimental study of the thermal diffusivity α, specific heat C_p, thermal conductivity κ, and electrical conductivity σ of Cu₂SnS₄ in the temperature range 80-400K, which includes a phase transition point. (3 refs.)

76666 Specific heat of Co(Si_{1-x}Se_x)₂ and magnetic properties in weak fields. G.A.Petrakovskii, A.G.Klimenko, S.S.Aplesnin, F.S.Rakhmenkulov, A.V.Baranov (L.V. Kirenski Inst. of Phys., Acad. of Sci., Krasnoyarsk, USSR). *Sov. Phys.-Solid State (USA)*, vol.24, no.12, p.2095-9 (Dec. 1983). Translation of: *Fiz. Tverd. Tela (USSR)*, vol.24, no.12, p.3676-83 (Dec. 1983). The temperature dependences of the specific heat and weak-field magnetic properties were determined in the range of compositions 0≤x≤0.15. Structural and magnetic anomalies of the specific heat were determined. Low-temperature hysteresis and relaxation of the magnetization were studied. A comparison was made of the phase diagrams obtained experimentally and also theoretically by the Monte Carlo method. (16 refs.)

Peculiarities of phase transitions and physical properties in (NH₄)₂SbF₇
..... See Entry 76613

Constant-pressure simulation of silica See Entry 76629

Polynomial model for concentration and temperature dependence of excess thermodynamic functions See Entry 76670

Thermodynamical and structural properties of amorphous Fe₈₀B₂₀ and Fe₈₀P₁₃C₇ alloys See Entry 76922

65.50 THERMODYNAMIC PROPERTIES AND ENTROPY

76667 Potentiometric study of the thermodynamic properties of intermetallic compounds Ca₂Ni₅. Structural interpretation. M.Notin, J.Hertz (Lab. de Thermodynamique Metall., Univ. de Nancy I, Vandœuvre-les-Nancy, France).

Acta Metall. (USA), vol.31, no.6, p.903-8 (June 1983). In French. The calcium activity was studied in the Ca₂Ni₅ alloys until the equilibrium with pure nickel in the range 1000-1350K by means of a (pure Ca) ||CaF₂|| (alloyed Ca) solid electrolyte cell. The nickel activity was deduced by Gibbs-Duhem integration and the integral quantities of formation of the CaNi₅, Ca₂Ni₇, CaNi₃, CaNi₂ intermetallic compounds were obtained. The structures of these phases have the same general formula N₅M_{2n-1}N_n^{*}. The change of the thermodynamic data with n is discussed. (15 refs.)

76668 Thermodynamics of ternary Fe-Co-N austenites. C.Ko, R.B.McLellan (Dept. of Mech. Engng. & Materials Sci., William Marsh Rice Univ., Houston, TX, USA).

J. Phys. & Chem. Solids (GB), vol.44, no.5, p.467-70 (1983). Gas-solid equilibrium measurements have been used to determine the variation with cobalt concentration in the range 0-9 at.% Co of the partial molar enthalpies and excess entropies in ternary Fe-Co-N austenites in the temperature range 1173-1503K. The resulting thermodynamic data show a relative invariance in these thermodynamic functions in excellent accord with the cell model for ternary solid solutions containing a substitutional and an interstitial species in which the presence of the substitutional species creates 'antitrapping' sites for interstitial atoms. (11 refs.)

76669 Thermodynamic measurements and modeling of (UC_{1-x}O_x). T.M.Besmann (Chem. Technol. Div., Oak Ridge Nat. Lab., Oak Ridge, TN, USA).

J. Am. Ceram. Soc. (USA), vol.66, no.5, p.353-5 (May 1983). Measurements were made of (CO) pressure over (UC_{1-x}O_x) at 1823, 1773, 1673, 1573, and 1473K for various values of x, in the presence of (UC_{1.86}). The data were used to model (UC_{1-x}O_x) as a solid solution of (UC) and (UO₂), where ΔG²⁸ is represented by an expansion in two terms, the first of which is temperature-dependent. The model allows for the accurate prediction of chemical activities and phase equilibria in regions also containing (UC_{1.86}), (UO_{2-y}), (UC_{1.86})-(UO₂), and (UO_{2-y})-{U}. (24 refs.)

76670 Polynomial model for concentration and temperature dependence of excess thermodynamic functions. J.Velisek (Inst. of Phys. Metall., Czechoslovak Acad. of Sci., Brno, Czechoslovakia).

Kovove Mater. (Czechoslovakia), vol.21, no.2, p.105-14 (1983). A polynomial model has been developed which retains the simplicity of features of models based on the Newmann-Kopp's rule but which expresses more rigorously the temperature dependence of the excess thermodynamic data. For the metallic phases with high values of excess heat capacity their contribution to the temperature dependence of the excess enthalpy, entropy and free enthalpy data should be considered whenever it is possible. As shown by examples, the proposed model makes it possible to express the excess heat capacity (and therefore the excess enthalpy, entropy and free enthalpy) on temperature and concentration in a simple analytical form at least for ordinary binary systems. It gives a better approximation over the Neumann-Kopp's approach. (10 refs.)

76671 Calculation of activity coefficients of conduction electrons in metals and in semiconductors. A.G.Guy (Dept. of Phys. & Space Sci., Florida Inst. of Technol., Melbourne, FL, USA).

Solid-State Electron. (GB), vol.26, no.5, p.433-6 (May 1983). Previous work has demonstrated that an important thermodynamic property of the conduction electrons, their partial enthalpy h, can be calculated from experimental data on thermopower. It is shown here that useful approximate values of the activity coefficient, f_c, can be deduced for both metals and semiconductors from data on h. The validity of this deduction is verified by comparison with published experimental data on the variation of electrical potential with the amount of doping of n-type silicon. These data are also employed to estimate that the partial excess entropy makes a contribution of about 15% (compared to h) to the value of f_c. (17 refs.)

76672 Thermodynamic properties of dilute solutions of hydrogen in glassy Pd₈₀Si₂₀. R.S.Finocchio, C.L.Tsai, B.C.Giessen (Dept. of Chem., Northeastern Univ., Boston, MA, USA).

Rapidly Solidified Amorphous and Crystalline Alloys. Proceedings of the Materials Research Society Annual Meeting, Boston, MA, USA, Nov. 1981 (New York, USA: North-Holland 1982), p.243-8. Equilibrium vapor pressures of dilute solutions of hydrogen in glassy Pd₈₀Si₂₀ have been measured from 10-90°C and at hydrogen pressures P of 1-100 torr. Under these conditions the ratio of hydrogen to alloy, x, as determined by a volumetric method, reaches a maximum value of 0.0070. Over this range of x, the system exhibits a positive deviation from Sieverts' law; isotherms were analyzed in terms of Lacher's modified statistical mechanical theory of hydrogen in palladium. The data were used to calculate relative partial molar enthalpies, excess entropies, and excess free energies for the formation of the solid solutions. The thermodynamic properties were found to vary with hydrogen content over the composition range studied. (11 refs.)

Structure and thermodynamics of liquid Bi See Entry 76282

Molecular dynamics studies of the structures and properties for halide glasses See Entry 76317

- The distribution of Fe^{3+} and Ga^{3+} between octahedral and tetrahedral sites in garnets, $\text{Y}_3(\text{Fe,Ga})_5\text{O}_{12}$, at different temperatures See Entry 76402
- Thermodynamics on $\text{UO}_2\text{-ZrO}_2\text{-LnO}_{2-x}$ solid solutions See Entry 76586
- Preferred crystallographic orientation for crystallisation under nonhydrostatic stress See Entry 76593
- Vaporization study on the niobium-oxygen solid solution by mass-spectrometric method See Entry 76602
- Mass spectrometric study on the vaporization of ternary compounds $\text{PuMC}_2(\text{M}=\text{Fe, Co, Ni})$ See Entry 76603
- Crossover between two- and three-dimensional melting in a smectic-B-smectic-A phase transition in BBOA See Entry 76624
- The influence of thermodynamic interactions on the glass transition of poly(vinyl chloride)-benzylbutylphthalate mixtures See Entry 76627
- Study on the formation of ternary compounds in titanium-nitrogen-hydrogen system See Entry 76635
- Heat capacity, relative enthalpy, and calorimetric entropy of silicate minerals: an empirical method of prediction See Entry 76655
- Heat capacity and thermodynamic properties of molybdenum from 5 to 302K See Entry 76657
- K_2SeO_4 : calorimetric studies of two successive phase transitions See Entry 76660
- The method of thermodynamic perturbation in the intermediate valence problem See Entry 76902
- Thermodynamic properties of liquid silver-thallium alloys See Entry 77616
- Determination of thermodynamic activities of components in the sections $x_{\text{Cr}}=0.11$ and $x_{\text{Cr}}=0.33$ of γ -solid solution Cr-Fe-Ni at 1500K See Entry 77617
- Thermodynamics of the martensitic transformation in high-nickel iron alloys. Thermal effect See Entry 77640
- Properties of $\gamma/\gamma\text{-}\delta$ eutectic composite material See Entry 77673
- The activation area and the activation enthalpy of cadmium single crystals determined during creep See Entry 77712
- Strain localization and hydrogen embrittlement See Entry 77749

65.70 THERMAL EXPANSION AND THERMOMECHANICAL EFFECTS

(see also 64.30 Equations of state; for electronic thermal conduction, see 72.15 and 72.20; for thermal conductivity of superconductors, see 74.30E; for pyroelectric and electrocaloric effects, see 77.70)

- 76673 Thermal expansion of high-silica glass. M.L.Mironova, G.L.Chernysheva, N.G.Oreshnikova, O.K.Botvinkin, E.A.Abramyan (State Sci.-Res. Inst. of Glass, USSR). *Glass & Ceram. (USA)*, vol.39, no.5-6, p.229-3 (May-June 1982). Translation of: *Steklo & Keram. (USSR)*, vol.39, no.5, p.11-12 (May 1982). [received: March 1983]
- Data are presented on the dependence of the temperature coefficient of linear expansion of $\text{B}_2\text{O}_3\text{-SiO}_2$ glass on composition (92 to 96% SiO_2 content). (2 refs.)
- 76674 Calculating the temperature coefficient of linear expansion of glazes and calcined ceramic masses. A.A.Novopashin, D.A.Romanyuk (Kuibyshev Construction Engng. Inst., Kuibyshev, USSR). *Glass & Ceram. (USA)*, vol.39, no.5-6, p.257-8 (May-June 1982). Translation of: *Steklo & Keram. (USSR)*, vol.39, no.5, p.27 (May 1982). [received: March 1983]
- A new method was developed for calculating the temperature coefficient of linear expansion α_t of silicate glass by structural and energy indices. The calculating formula has the following form: $\alpha_t = 0.31[2.21 + (106 - E_{av})F_{av}]T^{1/3}$, where E_{av} is the average value of the energy of the single cation-oxygen bond, F_{av} is the structural factor that characterizes the effect of the size and number of modifying cations in the glass on its properties, and T is absolute temperature. An example of calculating α_t of glaze and porcelain is given. (1 ref.)
- 76675 Influence of thermoelastic bending on photoacoustic experiments related to measurements of thermal diffusivity of metals. G.Rousset, F.Lepoutre (CNRS, Ecole Centrale des Arts et Manufactures, Chatenay-Malabry, France), L.Bertrand. *J. Appl. Phys. (USA)*, vol.54, no.5, p.2383-91 (May 1983).
- In some photoacoustic experiments, thermoelastic bendings of solid samples produce strong signals which cannot be analysed by usual photoacoustic calculations. The authors propose a model that, using the thermoelastic equations, analytically explains the effect of this bending. It is found that the model agrees well with data obtained from an experiment sensitive to thermoelastic deformations only. Furthermore, the model is also consistent with previous piezoelectric-photoacoustic calculations. This experiment also leads to measurements of thermal diffusivities. (19 refs.)
- 76676 Thermal expansivity measurements below 300K on a copper-beryllium alloy. R.L.Holtz, C.A.Swenson (Ames Lab., USDOE, Ames, IA, USA). *J. Appl. Phys. (USA)*, vol.54, no.5, p.2844-6 (May 1983).
- High accuracy (0.1%) linear thermal expansivity results are given for a copper-1.8 wt.% beryllium alloy in both the half-hard and precipitation-hardened conditions. These results, which are of technical importance for low temperature experiments, also show a small anomaly near 25K in the temperature dependence of the ratio of the alloy expansivity to that of copper. (7 refs.)
- 76677 Two numerical schemes for thermoelasticity equations. A.Bermudez, J.M.Viano (Dept. de Ecuaciones Funcionales, Univ. de Santiago, Santiago, Spain). *RAIRO Anal. Numer. (France)*, vol.17, no.2, p.121-36 (1983).
- The authors study two semidiscrete schemes for approximating the equations of linear thermoelasticity and obtain error estimates. For solving the semidiscrete problems at each time step, they give an iterative method. At each iteration, one must solve an elasticity problem and a thermal problem. (9 refs.)

- 76678 Thermal expansion of amorphous iron-chromium-boron alloys. G.Hunger, H.W.Bergmann, B.L.Mordike (Inst. für Werkstoffkunde und Werkstofftech., Univ. of Clausthal, Clausthal, Germany). *Rapidly Solidified Amorphous and Crystalline Alloys. Proceedings of the Materials Research Society Annual Meeting, Boston, MA, USA, Nov. 1981* (New York, USA: North-Holland 1982), p.231-4.
- In amorphous iron-chromium alloys, magnetic contraction is superimposed on the thermal expansion. Depending on the proportion of antiferromagnetic chromium, the resultant coefficient of expansion is either positive, negative or zero. The chromium content also changes the Curie temperature. Relaxation processes have a marked effect on the thermal expansion. Long term and short term expansion behaviour is compared and discussed. In addition the crystallization behaviour and mechanical properties of the alloys are reported. (6 refs.)
- Crystal growth and temperature variation of the lattice parameters in LaF_3 , CeF_3 , PrF_3 and NdF_3 See Entry 76335
- Modeling the phase change in crystalline biphenyl by using a temperature-dependent potential See Entry 76408
- Phase transitions in tetragonal CdP_2 See Entry 76619
- Constant-pressure simulation of silica See Entry 76629
- Thermal expansion of Cr and Cr-V alloys See Entry 77239
- Thermal expansion of ZrZn_2 See Entry 77240
- Thermal expansion and specific heat anomalies in UPt below the ferromagnetic ordering temperature See Entry 77241
- Thermal expansion measurements in Fe-base Invar alloys See Entry 77242
- Invar anomalies of Fe-Pd alloys See Entry 77243
- Contribution of the temperature change in the local magnetic moment to the Invar effect See Entry 77244
- Physicochemical and spectral luminescence properties of a glass based on the $\text{SiO}_2\text{-Al}_2\text{O}_3\text{-La}_2\text{O}_3\text{-Nd}_2\text{O}_3$ system See Entry 77438
- Melt processing and properties of barium-Sialon glasses See Entry 77614
- Multicomponent glasses of GeO_2 and Sb_2O_3 with Bi_2O_3 , Ti_2O_3 , and/or PbO See Entry 77620
- Heating of a thin wire by a constant current with density sufficient for the appearance of thermoplasticity See Entry 77683
- Elastic moduli, hardness and thermal expansion of some metaphosphate glasses See Entry 77693
- Thermal stress measurements of tungsten fiber-copper composites See Entry 77708

65.90 OTHER TOPICS IN THERMAL PROPERTIES OF CONDENSED MATTER

- Thermal-activation interpretation of splitting fracture See Entry 76559

66.00 TRANSPORT PROPERTIES OF CONDENSED MATTER (NONELECTRONIC)

66.10 DIFFUSION AND IONIC CONDUCTION IN LIQUIDS

- 76679 Experimental determination of diffusion coefficients, viscosities, densities and refractive indexes of 11 binary liquid systems. W.Baldauf, H.Knapp (Inst. für Thermodynamik und Anlagentechnik, Tech. Univ. Berlin, Berlin, Germany). *Ber. Bunsenges. Phys. Chem. (Germany)*, vol.87, no.4, p.304-9 (April 1983).
- Diffusion coefficients in 11 binary liquid mixtures were determined as a function of temperature and composition with the dispersion method. Simultaneously the density, the kinematic viscosity and the refraction index were measured. The mixtures investigated were acetone-water, acetone-toluene, acetone-n-butylacetate, succinic acid-water, succinic acid-n-butylalcohol, n-butylalcohol-water, phenol-water, phenol-toluene, phenol-n-butylacetate, phenol-diisopropylether, and phenol-4-methyl-2-pentanone. (12 refs.)
- 76680 The ^2H thermal diffusion isotope effect in benzene and methanol. Ning-Yuan Richard Ma, A.L.Beyerlein (Dept. of Chem. & Geology, Clemson Univ., Clemson, SC, USA). *J. Chem. Phys. (USA)*, vol.78, no.11, p.7010-11 (1 June 1983).
- Investigates the contribution of isotope mass distribution to the ^2H thermal diffusion isotope effect by measuring α (thermal diffusion factor) for the mixtures: benzene-benzene d_4 , benzene-*o* deuterobenzene, benzene-*p* deuterobenzene, methanol d_1 (CH_3OD)-methanol d_4 , and methanol-methanol d_1 (CH_3OD). There is a possibility that the interpretation of α for methanol d_1 mixtures may be complicated by hydrogen-deuterium exchange. However, the good agreement between the ^{13}C and ^2H self-diffusion coefficients for methanol indicate such isotope exchange does not contribute significantly to diffusion processes. (18 refs.)
- 76681 A concentration dependence of diffusion coefficients in Sn-Pb and In-Zn melts. G.P.Grinevich, V.I.Oglobyla, V.I.Loizovoi, L.P.Golovinski. *Ukr. Fiz. Zh. (USSR)*, vol.28, no.5, p.692-6 (May 1983). In Russian.
- Concentration dependences of diffusion coefficients D of atoms are studied for ^{119}Sn , ^{125}Sb and ^{110m}Ag , ^{65}Zn in melts of Sn-Pb (400°C) and In-Zn (500°C), respectively, using simultaneous diffusion of several radioactive impurities in a vertical capillary specimen. An effect of a continuous decrease of D is found when the second component concentration increases. The experimental values of D are in good agreement with those calculated from the solid sphere liquid model. The statistic distribution of atoms relative to their sort is, probably, the most possible. (14 refs.)
- International Meeting on Lithium Batteries See Entry 74213
- Brownian diffusion of a small particle in a suspension. II. Hydrodynamic effect in a random fixed bed See Entry 74384
- One-dimensional models of polymer dynamics. I. Dashpot-spring models applied to a single rotor See Entry 76276
- On the influence of natural convection on mass transfer process in gallium phosphide crystal growth from solution See Entry 76339
- The electrical conductivity of solid and molten cesium hydroxide—a contribution to solid proton conductors See Entry 76688

- A conductance equation for binary liquid systems consisting of an electrolyte component and an indifferent solvent See Entry 77897
- Lithium-cupric sulfide cells See Entry 77968

66.20 DIFFUSIVE MOMENTUM TRANSPORT

(inc. viscosity of liquids)

- 76682** Viscosity of binary liquid mixtures in hard-sphere approximation. Harminder (Phys. Dept., Coll. of Home Sci., Punjab Agricultural Univ., Kaoni, Punjab, India). *Indian J. Pure & Appl. Phys.*, vol.21, no.2, p.119-20 (Feb. 1983). Argon-krypton binary liquid mixture has been simulated as a hypothetical hard-sphere fluid, for its viscosity through conformal solution theory. The agreement between the experimental data and calculated values using Enskog theory is found to be excellent. (7 refs.)
- 76683** Effect of γ -irradiation on viscosity-temperature characteristics of blended oils. V.G.Thomas, S.B.Srivastava (Chem. Div., Bhabha Atomic Res. Centre, Bombay, India). *Indian J. Technol.*, vol.20, no.12, p.502-3 (Dec. 1982). [received: May 1983] The effect of γ -irradiation on the viscosity-temperature behaviour of two polymer-blended oils is studied. The irradiated blends have poorer viscosity-temperature characteristics than the unirradiated blends. (2 refs.)
- 76684** Viscosity of a mixture of *n*-butyl and isobutyl alcohols at different temperatures and pressures. R.A.Mustafaev, D.K.Ganiev (Ch. Il'drym Polytech. Inst., Baku, Azerbaidzhan SSR). *J. Eng. Phys. (USA)*, vol.43, no.3, p.1001 (Sept. 1982). Translation of: *Inzh.-Fiz. Zh. (USSR)*, vol.43, no.3, p.424-5 (Sept. 1982). The results of an experimental investigation of the dynamic viscosity of binary mixtures of *n*-butyl and isobutyl alcohols are given. In preparing the mixtures the authors paid particular attention to the purity of the components. After drying they were repeatedly distilled under vacuum. Results of chromatographic analysis showed that the purity of the individual substances was 99.9%; the concentration error in the determination of the composition of the mixture was less than 0.1%. (3 refs.)
- 76685** Viscosity behaviour of binary mixtures of non-polar solvents. M.Chauhan, R.Misra, A.Singh, J.P.Shukla, M.C.Saxena (Phys. Dept., Lucknow Univ., Lucknow, India). *Pramana (India)*, vol.20, no.1, p.77-84 (Jan. 1983). [received: May 1983] The viscous nature of binary liquid solutions of non-polar solvents, viz. *n*-heptane, benzene, carbon tetrachloride and paraffin oil has been studied in terms of the deviation from the ideal law. The ideal law is supposed to take the form of (weighted) geometric mean. The viscous behaviour has been observed over a range of temperatures (298-322°K). The relative excess volume and relative excess enthalpy of activation have been evaluated to study the increase in viscosity associated with the shrinkage in mixing of its components. (11 refs.)
- Explanation for the 3.4-power law for viscosity of polymeric liquids on the basis of the tube model See Entry 75973
- Measurements of the viscosity of compressed gaseous and liquid nitrogen See Entry 76149
- Spherical non-draining Boc-poly(α -L-lysine) macromolecules: SAXS and viscosity studies See Entry 76270
- 2,3-dicyanohydroquinone derivative liquid crystals having strong negative dielectric anisotropy See Entry 76289
- Low viscous compounds of highly nematic character See Entry 76290
- New liquid crystal materials; physical properties and performance in displays for automobile, high information density and guest-host applications See Entry 76292
- Dynamics of a Fredericks transition in side chain nematic polymers: determination of the viscoelastic coefficients K_1 and γ_1 See Entry 76295
- Stable liquid crystals with large negative dielectric anisotropy. II. See Entry 76296
- Experimental determination of diffusion coefficients, viscosities, densities and refractive indexes of 11 binary liquid systems See Entry 76679
- Lithium-cupric sulfide cells See Entry 77968

66.30 DIFFUSION IN SOLIDS

- 76686** Random walks and correlation factors in diffusion via the vacancy mechanism in hexagonal-close-packed lattices. M.Koiwa, S.Ishioka (Res. Inst. for Iron, Steel & Other Metals, Tohoku Univ., Sendai, Japan). *Philos. Mag. A (GB)*, vol.47, no.5, p.767-74 (May 1983). Random walks on hexagonal-close-packed lattices are considered. By decreasing the probability of inter-plane jumps relative to that of intra-plane jumps, random-walk properties exhibit features characteristic of a two-dimensional lattice. For a given set of jump probabilities, the number of distinct lattice points visited in an *n*-step walk $S_n \sim n/\log n$, to a three-dimensional trend, $S_n \sim n$. Correlation factors for self-diffusion via the vacancy mechanism are also calculated exactly for various sets of two-jump frequencies; a previous approximate evaluation by Mullen (1961) is confirmed. (5 refs.)
- International Meeting on Lithium Batteries See Entry 74213
- Analysis of precision in determination of diffusion coefficients by the isotope exchange technique See Entry 74579
- Nitrogen migration during wear in an implanted steel See Entry 77768

66.30F Self-diffusion in metals, semimetals, and alloys

- 76687** Investigation of redistribution of the alloying elements during diffusion annealing of titanium alloys. A.A.Popov, L.I.Anisimova, A.L.Vinit'skiy, Yu.P.Denisov, O.G.Lapin (S.M. Kirov Ural Polytech. Inst., Sverdlovsk, USSR). *Fiz. Met. & Metalloved. (USSR)*, vol.55, no.4, p.749-53 (April 1983). In Russian. English translation in: *Phys. Met. & Metallogr. (GB)* Methods of X-ray microspectroscopic analysis and metallography were used to study the diffusion of alloying elements (chromium, aluminium, and molybdenum) during annealing of diffusion pairs composed of an alloy with additives and unalloyed titanium (VT1-0) at temperatures 800-1000°C. The high-temperature distribution of the alloying elements was determined by cooling a sample in water after annealing. It was found that the motion of the phase boundary during annealing at 800-850°C was due to the diffusion of chromium and aluminium, and was not controlled by the boundary processes. The depth of penetration of chromium into the α -phase was practically independent

- of the annealing duration, whereas aluminium became segregated at the interphase boundaries. (6 refs.) *A.T.*
- The onset temperature for void formation in extremely pure iron See Entry 76413
- Nuclear magnetic resonance study of atomic motions in vanadium See Entry 77277
- Positron annihilation on pure and carbon-doped α -iron in thermal equilibrium See Entry 77477
- On the processes responsible for the degradation of the aluminium-lithium electrode used as anode material in lithium aprotic electrolyte batteries See Entry 77892

66.30H Self-diffusion and ionic conduction in nonmetals

- 76688** The electrical conductivity of solid and molten cesium hydroxide—a contribution to solid proton conductors. K.-H.Haas (Inst. für Neutronenphys. und Reaktortech., Kernforschungszentrums Karlsruhe, Karlsruhe, Germany), U.Schindewolf. *Ber. Bunsenges. Phys. Chem. (Germany)*, vol.87, no.4, p.346-8 (April 1983). The electrical conductivity of solid cesium hydroxide was by several powers of ten larger, its activation energy by a factor of two to three lower than those of normal solid salts. A steep tenfold increase of the conductivity was observed at the α - β phase transition temperature of solid cesium hydroxide (220°C), above which the OH⁻ ions can rotate freely (rotator phase). A further increase by three powers of ten occurred between 280°C and the melting point (335°C), above which the conductivity was that of a normal molten salt. (23 refs.)
- 76689** Diffusion of cobalt in KCl single crystals. D.Damien, K.V.Reddy (Dept. of Phys., Indian Inst. of Technol., Madras, India). *Indian J. Pure & Appl. Phys.*, vol.21, no.3, p.133-6 (March 1983). Results of the studies on the diffusion of the cobalt in KCl are reported. Annealing was restricted to the temperature range 700-760°C, due to the poor solubility of cobalt. While profiles of crystals annealed for short durations exhibit only one region, long-time annealed samples show up a region of slow diffusion near the surface, in addition to the region of normal diffusion. This anomalous character is explained as due to the poor solubility of CoCl₂²⁻ ions formed in alkali halide lattices. The region of normal diffusion is treated as due to the migration of this complex ion by vacancy mechanism. Values of the activation energy for CoCl₂²⁻ ion diffusion and the enthalpy of migration, obtained from the present study are 1.71 eV and 1.12 eV respectively. (16 refs.)
- 76690** Oxygen self-diffusion in Fe-doped MgO single crystals. K.Ando, Y.Kurokawa, Y.Oishi (Dept. of Nuclear Engng., Kyushu Univ., Fukuoka, Japan). *J. Chem. Phys. (USA)*, vol.78, no.11, p.6890-2 (1 June 1983). Oxygen self-diffusion coefficients in Fe-doped MgO single crystals were determined by an isotope exchange technique. The results indicated dopant-insensitive diffusion, which was interpreted as due to the vacancy pair mechanism. (13 refs.)
- 76691** The diffusion of uranium in U₃O₈. D.Glasser Leme, H.J.Matzke (Karlsruhe Establ., European Inst. for Transuranium Elements, Karlsruhe, Germany). *J. Nucl. Mater. (Netherlands)*, vol.115, no.2-3, p.350-3 (April 1983). The self-diffusion of uranium was measured using U-233 as a tracer. It was found that diffusion in orthorhombic U₃O_{8(-x)} proceeds at rates similar to those in cubic UO_{2.2}. It is thus much faster than U diffusion in UO₂, but not fast enough to explain the observed segregation of metal atoms during the oxidation of (U, Pu)C or (U, Pu)O₂ to MO₂ and M₂O₈ for temperatures below 800°C. Though no enhanced diffusion was observed while reducing U₃O₈ to UO_{2+x}, the mechanical and chemical processes taking place during the oxidation of MO_{2+x} to M₂O₈ might enhance metal atom diffusion. Tracer experiments with the thin layer condition are not suitable to verify this hypothesis because of disintegration of the diffusion specimens into powder under oxidizing conditions. (18 refs.)
- 76692** Ionic conductivity of AlN containing Y₂O₃ or Al₂O₃ at 1173–1773K. M.Yahagi, K.S.Goto (Tokyo Inst. of Technol., Tokyo, Japan). *J. Jpn. Inst. Met. (Japan)*, vol.47, no.5, p.419-25 (1983). In Japanese. The electrical conductivity has been measured at temperatures of 1173K to 1773K on the sintered AlN-Y₂O₃ and AlN-Al₂O₃ systems. The electrical conductivity was independent of nitrogen pressure of 5×10⁻³-10⁻⁵ Pa at 1473K and 1673K. The results on the DC polarization and the EMF of the galvanic cell using AlN as the solid electrolyte are suggesting the predominant ionic conduction. In the experimental temperature range, the specific conductivity can be expressed as follows: for AlN-2 mass%Y₂O₃, $\sigma(\text{S.m}^{-1}) = 1.07(\pm 0.56) \times 10^5 \exp(-E/RT)$, where the activation energy is 169±5 kJ/mol.; AlN-2 mass%Al₂O₃, $\sigma(\text{S.m}^{-1}) = 5.52(\pm 1.67) \times 10^5 \exp(-E/RT)$, where the activation energy is 200±3 kJ/mol. (24 refs.)
- 76693** Interfacial conduction in lithium iodide containing inert oxides. J.B.Phipps, D.H.Whitmore (Dept. of Materials Sci. & Engng., Northwestern Univ., Evanston, IL, USA). *J. Power Sources (Switzerland)*, vol.9, no.3-4, p.373-8 (April-May 1983). (International Meeting on Lithium Batteries, Rome, Italy, 27-29 April 1982). Temperature-dependent conductivities are reported for a lithium iodide sample sandwiched between two fused silica plates and for an LiI film deposited on a silica plate. The existence of an Li-SiO₂ interfacial conduction path possessing a conductivity of about 5 ohm⁻¹ at 25°C is confirmed. In addition, an infiltration technique for the preparation of LiI-ceramic particle composites is discussed. (8 refs.)
- 76694** (Ag₂O)_x(Li₂O)_{1-x}2B₂O₃ mixed cation glasses. A.Magistris, G.Chiodelli (Centro di Studio per la Termodinamica ed Elettrochimica, CNR, Pavia, Italy), M.Villa. *J. Power Sources (Switzerland)*, vol.9, no.3-4, p.379-82 (April-May 1983). (International Meeting on Lithium Batteries, Rome, Italy, 27-29 April 1982). An analysis of the ¹¹B NMR spectra in the (Ag₂O)_x(Li₂O)_{1-x}2B₂O₃ glasses shows that the glass network consists of an equal number of BO₂ and BO₃ units and that it does not undergo major changes when a cation is totally or partially substituted by another. The ¹¹B NMR spectra reveal the existence of cation pairs and suggest that Li-Li pairs are more stable than Li-Ag pairs. The ¹¹B spin-lattice relaxation times at 117K display a kind of mixed alkali behavior. These findings suggest that a relationship exists between the increased resistivity of the mixed glasses and the spectra of the low-lying excitations. (7 refs.)

76695 Mechanism of ion conduction in alkali metal-polymer complexes. D.F.Shriver, R.Dupon, M.Stainer (Dept. of Chem., Northwestern Univ., Evanston, IL, USA).

J. Power Sources (Switzerland), vol.9, no.3-4, p.383-8 (April-May 1983). (International Meeting on Lithium Batteries, Rome, Italy, 27-29 April 1982). Polymer electrolytes have many materials properties which are attractive for applications in advanced electrochemical devices. However the ionic conductivities are still too low for widespread utilization. One avenue for the improvement of the conductivity is the delineation of the factors which influence ion transport in polymers. The most successful models for alkali metal ion transport in polymers are based on the concept that ions are passed between polymer segments by large amplitude polymer motions, and that relatively few interactions between the ion and polar polymer groups are broken in the transition state. Evidence for the contribution of polymer segmental motion to ion transport is obtained from the form of the temperature-dependent conductivity, from the higher conductivity for amorphous than for crystalline polymers, from the decrease in conductivity with increasing pressure, and from doping experiments. Simple energy estimates indicate that the ion motion probably occurs with the breaking of at most one or two cation-polar group interactions, rather than the hop of an ion from one polymer chain to the next. (19 refs.)

76696 Mechanism of high ionic conductivity in elastomeric networks. H.Cheradame, A.Gandini, A.Killis, J.F.Le Nest (Lab. de Chimie des Polymères, Ecole Française de Papeterie, St. Martin d'Hères, France). *J. Power Sources (Switzerland)*, vol.9, no.3-4, p.389-95 (April-May 1983). (International Meeting on Lithium Batteries, Rome, Italy, 27-29 April 1982). The viscoelastic properties and the ionic conductivity of polyether-polyurethane networks containing alkali metal salts have been studied at various temperatures, salt concentrations and network structures. The reduced temperature, $T-T_g$, is the predominant parameter which governs the viscoelastic behaviour and the ionic conductivity of these networks. Using the free volume concept an expression is derived for the ionic conductivity, irrespective of the macrostructure involved. The logarithm of the reduced conductivity, σ_r/σ_{TR} (which is the ratio of the conductivity at a given temperature to that at the reference temperature), is a linear function of the shift factor, $\log a_T$, given by the dynamic mechanical properties. A comparison is made between the WLF parameters C_1 and C_2 , obtained from conductivity and viscoelastic measurements. (13 refs.)

76697 Ionic conductivity of BaFCl. K.Somaiah (Dept. of Phys., Post-Graduate Coll. of Sci., Osmania Univ., Saifabad, Hyderabad, India), V.Hari Babu.

Phys. Status Solidi b (Germany), vol.117, no.1, p.75-9 (1 May 1983). The ionic conductivity of undoped and doped BaFCl, single crystals is measured. In BaFCl, the measurements are performed parallel and perpendicular to the crystallographic c -axis. Incorporation of monovalent impurities (Tl, Na) enhances the conductivity while it decreases by doping with trivalent impurities (Gd). The results indicate that BaFCl exhibits anionic conduction via halide ion vacancies and that the thermally generated lattice defects are of Schottky type. The probable mechanism for the conduction process in these crystals is discussed on the basis of structural considerations of the unit cell. (9 refs.)

76698 Computer simulation of the correlation factors in vacancy-pair diffusion in NaCl-type lattices. R.-L.Lindstrom, R.Lindstrom (Dept. of Math. & Phys., Univ. of Joensuu, Joensuu, Finland).

Philos. Mag. A (GB), vol.47, no.5, p.627-33 (May 1983). Monte Carlo methods have been used to calculate the correlation factors of ions and vacancies when the diffusion proceeds via a bound vacancy-pair mechanism in NaCl-type lattices. The estimator proposed to Stolwijk and Bakker (1977) and the authors' moment estimator both give slightly smaller correlation factors for the ions in comparison to those deduced analytically. However, the correlation factors of the vacancies are in good agreement with theory. (10 refs.)

76699 Proton conductivity of a hydrogen bond chain in a strong electric field. P.M.Tomchuk, V.V.Krasnogolovets, N.A.Protsenko. *Ukr. Fiz. Zh. (USSR)*, vol.28, no.5, p.767-74 (May 1983). In Russian. Proton conductivity of a hydrogen bond chain is considered in a small-radius polaron model. An expression is given for the density of a space-charge limited current caused by the proton polaron (proton holes) transport. The criterion for the jumping mechanism regime is given. (23 refs.)

A high-resolution electron microscopic study of defects in sodium β'' -alumina See Entry 76414

Peculiarities of phase transitions and physical properties in $(\text{NH}_4)_2\text{SbF}_6$ See Entry 76613

Kinetics of self-interstitials generated at the Si/SiO₂ interface See Entry 76796

High-temperature phase transitions in pure and deuterated ammonium dihydrogen phosphate: conductivity and dielectric measurements See Entry 77334

Sintering kinetics of tantalum carbide See Entry 77606

The oxidation behaviour of hot pressed aluminium nitride See Entry 77781

Introduction to the scaling properties in electrochemistry: from the 'TEISI' model to the lithium fractal ordering in Li_xFeS_2 layered structure See Entry 77894

Mechanistic studies of reversible layer-type electrodes See Entry 77984

Study of ^{18}O diffusion in magnesium orthosilicate by nuclear microanalysis See Entry 78529

66.30J Diffusion, migration, and displacement of impurities

76700 Kinetics and mechanism of hydrogen diffusion in hydrides of titanium, zirconium and TiNi_3 . E.Brauer, R.Gruener (Inst. für Phys. Chem., Univ. Frankfurt, Frankfurt/Main, Germany), F.Rauch. *Ber. Bunsenges. Phys. Chem. (Germany)*, vol.87, no.4, p.341-5 (April 1983). Hydrides of titanium and zirconium formed during cathodic polarization in acid solutions were investigated by the ^{15}N nuclear reaction method. Hydrogen depth profiles obtained in this way give informations about the hydrogen concentration in the metal, allowing to determine diffusion coefficients and to study the absorption of hydrogen by the metal lattice and the kinetics of the hydride layer growth. The mechanism was studied using Ti single crystals. The hydrogen diffusion was found to depend on the crystal orientation. (19 refs.)

76701 Diffusivity and permeability of hydrogen in neutron irradiated molybdenum and platinum. H.Katsuta, T.Iwai, H.Ohno (Molten Materials Lab., JAERI, Ibaraki, Japan).

J. Nucl. Mater. (Netherlands), vol.115, no.2-3, p.206-10 (April 1983). Hydrogen permeability and diffusivity were measured in neutron irradiated (3.0×10^{15} or 1.2×10^{16} n/cm²) metals of pure molybdenum of BCC structure and platinum of FCC. Although hydrogen permeability in molybdenum was decreased by 10% to 20% by the irradiation, in platinum it was increased by about 10%. X-ray diffraction analysis of the irradiated metals was also performed to study the relation between hydrogen behaviour in the metals and its neutron irradiated structures. (12 refs.)

76702 Reversible isopentane-induced depression of carbon dioxide permeation through polycarbonate. R.T.Chern, W.J.Koros, H.B.Hopfenberg, V.T.Stannett (Dept. of Chem. Engng., North Carolina State Univ., Raleigh, NC, USA).

J. Polym. Sci. Polym. Phys. Ed. (USA), vol.21, no.5, p.753-63 (May 1983). Permeability data are reported for carbon dioxide in Lexan polycarbonate at 35°C. Measurements were made for both pure carbon dioxide and for a mixed feed consisting of carbon dioxide with a 117.8-torr (0.155-atm) partial pressure of isopentane. The effects of varying upstream CO_2 driving pressure from 1 up to 20 atm were studied. The permeability to CO_2 is reduced significantly in the presence of isopentane; however, the fractional depression of the CO_2 permeability due to the isopentane at low driving pressures is much more significant than at high CO_2 driving pressures. The well-known pressure dependence of carbon dioxide permeabilities in glassy polymers, therefore, is largely diminished by introducing isopentane to the pure carbon dioxide feed. These observations are consistent with a model for transport in glassy polymers which explains the observed trends in terms of competition between the two penetrants for microvoid sorption sites existing in the nonequilibrium glassy polymer. (13 refs.)

76703 Concentration dependence of the boron diffusion coefficient in silicon. Dao Khac An, Le Hoang Mai, Pham Hoi (Dept. of Phys. & Technol. of Semiconductor Devices, Inst. of Phys., Hanoi, Vietnam).

Phys. Status Solidi a (Germany), vol.76, no.1, p.K85-8 (16 March 1983). Describes some experimental results of boron diffusion in silicon using boron nitride and BBr_3 liquid sources in the temperature range 900 to 1050°C in nitrogen ambient. Profiles of boron impurities were obtained from the differential resistivity technique. The diffusion coefficient versus impurity concentration was determined by the Boltzmann-Mantano analysis method. (10 refs.)

76704 Co tracer diffusion in Al. G.M.Hood, R.J.Schultz, J.Armstrong (Chalk River Nuclear Lab., AECL, Chalk River, Ontario, Canada).

Philos. Mag. A (GB), vol.47, no.5, p.775-9 (May 1983). Measurements of ^{60}Co diffusion in Al single crystals have been made at 930-, 913, 804 and 724K. The results support previous work on this system by Peterson and Rothman (1970). Analysis of the combined results yields the equation $D = 5.06 \times 10^{-2} \exp(-1.82 \text{ eV}/k_B T) \text{ m}^2 \text{ s}^{-1}$. (6 refs.)

76705 Diffusion of iron in aluminum studied by Mossbauer spectroscopy. S.Mantl (Inst. für Festkörperforschung, Kernforschungsanlage Jülich GmbH, Jülich, Germany), W.Petry, K.Schroeder, G.Vogl.

Phys. Rev. B (USA), vol.27, no.9, p.5313-31 (1 May 1983). The broadening of the ^{57}Fe Mossbauer line due to diffusion jumps of the Fe atoms in an Al single crystal has been measured as a function of crystal orientation. The broadening is strongly anisotropic. Theoretical calculations for the broadening using the five-frequency model for the motion of an Fe atom via vacancies show that the following information about the geometry and perturbed jump frequencies of the Fe-vacancy complex can be obtained: (i) The anisotropy of the broadening yields information about the jump geometry and jump-frequency ratios, (ii) the absolute value and the temperature dependence of the broadening yield the diffusion coefficient and the activation energy for Fe diffusion, and (iii) the anomalous decrease of the Mossbauer intensity in the vicinity of the melting point yields information about the binding energy of the Fe-vacancy complex. The results are consistent with the following interpretation: Fe in Al moves by exchanging sites with nearest-neighbor vacancies. The binding energy of an Fe-vacancy complex is $E_b = 0.29 \text{ eV}$. The diffusion coefficient of Fe in Al is $D_{Fe} = 1.1 \times 10^{14} \exp[-(2.3 \pm 0.2 \text{ eV})/k_B T] \text{ cm}^2 \text{ s}^{-1}$ in reasonable agreement with results from tracer experiments. Values are obtained for different jump frequencies of a vacancy in the vicinity of an Fe atom. (61 refs.)

76706 Method approach to investigating the high-temperature hydrogen permeability of metals. V.I.Pokhmurskiy, I.I.Sidorak, R.G.Parkheta (G.V. Karpenko Physicomech. Inst., Acad. of Sci., Lvov, Ukrainian SSR). *Sov. Mater. Sci. (USA)*, vol.18, no.4, p.363-6 (July-Aug. 1982). Translation of: *Fiz.-Khim. Mekh. Mater. (USSR)*, vol.18, no.4, p.81-5 (July-Aug. 1982). [received May 1983]

Presents the basic principles of a method approach to conducting investigations of high-temperature hydrogen permeability of metals. The use of these principles would make it possible to critically evaluate the published results obtained, would provide the possibility of correct comparison and appropriate analysis of them, and also would ease their theoretical and practical use. (15 refs.)

76707 The concentrated profile of photostimulated Ag diffusion in thin As_2S_3 layers. M.T.Kostyshyn, O.P.Kasyarum, A.A.Kudryavtsev.

Ukr. Fiz. Zh. (USSR), vol.28, no.5, p.710-13 (May 1983). In Russian. The influence of Ag-doping degree in the interface region of As_2S_3 on the kinetics of Ag photostimulated diffusion (PSD) into thin As_2S_3 layers is investigated in a two-layer semiconductor-metal structure. It is discovered that an increase of the PSD rate at the initial stage is related to formation of a particular Ag-doped semiconductor region at the As_2S_3 -Ag interface. The initial stage of Ag PSD is completed when the depth of such region reaches about 11.6 nm. The spread of the Ag-doped region onto the whole semiconductor volume takes place at the stationary Ag-concentration behind the diffusion front (about 80% from the maximum concentration which may be reached by the PSD-method in such a semiconductor). (4 refs.)

76708 The Cd-diffusion in InP. W.Kuebart, O.Hildebrand, H.W.Marten (Phys. Inst., Univ. Stuttgart, Stuttgart, Germany), N.Arnold. Gallium Arsenide and Related Compounds, 1982. Tenth International Symposium on Gallium Arsenide and Related Compounds, Albuquerque, NM, USA, 19-22 Sept. 1982 (Bristol, England: IOP 1983), p.597-604. Cd diffusion profiles in InP have been measured using a BPO profile plotter. These profiles are explained with a new, local equilibrium diffusion theory: the diffusing Cd atoms appear as singly and doubly ionized acceptors, the latter one having a considerably higher diffusion coefficient. With a new EBIC theory and from the correlation between EBIC and etching lines, the authors can explain the observed EBIC linescans and the origin of the etch lines. (8 refs.)

On the nature of point defects and the effect of oxidation on substitutional dopant diffusion in siliconSee Entry 76416

Ion implantation in insulatorsSee Entry 76469

Effects of relative damage, Fermi energy and annealing technique in ion implanted GaAsSee Entry 76476

Dissolution of vanadium carbide in steel, in the case of formation of a ferrite layer at the interfaceSee Entry 76631

Enhanced diffusion of phosphorus at grain boundaries [Si solar cells]See Entry 78061

66.30L Diffusion, migration, and displacement of other defects

76709 The role of volume diffusion in DIGM, a reappraisal. K.Tashiro, G.R.Purdy (McMaster Univ., Hamilton, Ontario, Canada). *Ser. Metall. (USA)*, vol.17, no.4, p.455-8 (April 1983). Presents results of some current experiments on high temperature diffusion induced grain boundary migration (DIGM), and suggests that the role of volume diffusion in the process needs to be reassessed. (14 refs.)

Mechanism of fatigue crack propagation in metallic materialsSee Entry 76561

Anelastic relaxation phenomena in plasma-sprayed (Al₂O₃)₃MgO spinel with reference to diffusion processSee Entry 76562

High-angle grain-boundary premelting transition: A molecular-dynamics studySee Entry 76615

66.30N Chemical interdiffusion

76710 The effect of interposed silicide thickness on growth rate in bilayer silicide thin-film structures: the Si(111)/Pd₂Si/Cr system. E.C.Zingu (Dept. of Phys., Univ. of the Western Cape, Bellville, S Africa), C.Comrie, R.Pretorius. *J. Appl. Phys. (USA)*, vol.54, no.5, p.2392-401 (May 1983). A model has been developed, using Fick's diffusion equations, to describe the effect of interposed silicide thickness on the growth rate of the outer silicide layer in bilayer metal-silicon thin film system. The model is based on diffusion-limited transport of silicon through the interposed silicide layer and predicts that the growth rate of the outer silicide layer will be inversely proportional to the thickness of the interposed layer, if the interposed thickness exceeds a certain critical value. To test the model, the growth rate of CrSi₂ formation in the Si(111)/Pd₂Si/Cr system was studied as a function of Pd₂Si thickness. The CrSi₂ thickness was always found to increase linearly with annealing time, indicating a reaction-limited process. For thin epitaxial Pd₂Si layers the CrSi₂ growth rate was equal to that of CrSi₂ grown directly on Si. However, for epitaxial Pd₂Si layers thicker than the critical thickness, CrSi₂ growth was inhibited causing the growth rate to be inversely proportional to Pd₂Si thickness, in contrast to that found for CrSi₂ formation on nonepitaxial Pd₂Si where no thickness effects were found. The thickness effect of the epitaxial Pd₂Si layer is believed to be due to its microstructure, which inhibits silicon diffusion. (12 refs.)

76711 Ti-W alloy interaction with silicon in the presence of PtSi. F.Nava, C.Nobili (Istituto di Fisica, Univ. di Modena, Modena, Italy), G.Ferla, G.Iannuzzi, G.Queirolo, G.Celotti. *J. Appl. Phys. (USA)*, vol.54, no.5, p.2434-40 (May 1983). Ti-W alloy film was deposited by conventional DC sputtering on a PtSi film grown on a (100) silicon substrate. Two sets of samples were prepared with different oxygen content in the Ti-W film. MeV "He" backscattering analysis shows, after vacuum annealing, the formation of a ternary mixture (Ti_{1-x}W_x)Si₂(x=0.24). The Ti:W ratio in the mixture is the same as in the as-deposited film. The growth in the 625-775°C temperature range is directly proportional to the time and the process is thermally activated with an activation energy of 3.3±0.1 eV. During the thermal annealing the platinum silicide is always located between the ternary mixture and the Si substrate. X-ray diffraction indicates the formation of a pseudobinary solid solution with an hexagonal structure with a=4.61±0.01 Å and c=6.47±0.02 Å. The presence of the oxygen slows down the reaction but does not change the mechanism of the compound formation. The content and distribution of impurities was measured using Auger technique combined with Ar sputtering. In the two sets of samples the average oxygen concentration is 1% and about 5%, respectively. The oxygen is mainly located at the Ti-W/PtSi interface. During the compound formation the oxygen distribution is not modified. (28 refs.)

Electrical characteristics of thin Ni₂Si, and NiSi₂ layers grown on siliconSee Entry 77071

66.30Q Electromigration

76712 Effects of annealing and electromigration on surface morphology of polycrystalline films. Chi-Yang Chang (Kaoshiung Inst. of Technol., Kaoshiung, Taiwan), Huei-Li Huang. *J. Appl. Phys. (USA)*, vol.54, no.5, p.2287-94 (May 1983). The capillary-induced surface mass transport has been extended to cases where there is a notch and/or a ridge on a bicrystal system. Changes in the surface morphology caused by capillary-induced and electromigration-induced surface diffusions and grain boundary diffusions have been analyzed. Thermal grooving is shown to develop only when the initial slope of a notch on the crystal surface is less than γ_b/2γ_s(γ_b and γ_s are, respectively, the grain boundary and the surface Gibbs free energy) or when the initial surface contains a ridge at the grain boundary. The slope of the grooving profile is invariant with time but its depth develops as the one fourth power of time. Surface fluxes due to the electromigration origin change the morphology in an asymmetric manner, biased in the direction of the electron flow. When combined with fluxes from grain boundary diffusion, severe mass depletion and accumulation can occur, giving rise to characteristic electromigration damage of open circuit failures. Finally, the concept of an optimum annealing time in relation to electromigration is explored. (23 refs.)

76713 New insights on the reversal of the site of electromigration failure in gold films doped with alkali. R.E.Hummel, S.Matts-Goho, R.T.DeHoff (Dept. of Materials Sci. & Engng., Univ. of Florida, Gainesville, FL, USA). *J. Appl. Phys. (USA)*, vol.54, no.5, p.2855-6 (May 1983). The description of current-induced failures in thin film metallizations used in microelectronic devices should not be limited to electron wind arguments. Several failure mechanisms such as grain boundary grooving, thermotransport and electrotransport, may contribute to matter transport under conditions normally encountered in service. Grain boundary grooving is accelerated by

doping thin gold films with alkali ions. Pure thin gold stripes which are subjected to a direct current of high density fail near the cathode, whereas similar gold films doped with alkali ions fail near the anode. Experiments utilizing Auger electron spectroscopy show an enrichment of alkali metal near the anode after current stressing. The accumulation of alkali metal at the anode promotes grain boundary grooving and void formation there. (17 refs.)

76714 Temperature-ramp resistance analysis to characterize electromigration [of IC conductors]. R.W.Pasco, J.A.Schwarz (Dept. of Chem. Engng. & Materials Sci., Syracuse Univ., Syracuse, NY, USA). *Solid-State Electron. (GB)*, vol.26, no.5, p.445-52 (May 1983). A temperature-ramp technique is presented that enables determination of the kinetic parameters for electromigration processes. With this method, pre-exponentials and activation energies can be measured in a single experiment requiring a few hours. The technique is applicable to both practical and fundamental studies of electromigration. For example, in terms of the former, reliability factors for conductor lifetimes can be readily determined. As far as the latter, new conductor compositions can be rapidly screened to ascertain their electromigration behavior. To demonstrate the application of the method, Temperature-ramp Resistance Analysis to Characterize Electromigration (TRACE) has been applied to thin-film aluminum conductors. Results have yielded activation energies in agreement with literature values. Furthermore, TRACE results have been used, along with resistivity results from the literature, to determine the current density effect on the pre-exponential factor. The value of the current density exponent thus determined is in accord with the range reported in the literature for Mean Time to Failure (MTF) experiments. (18 refs.)

66.60 THERMAL CONDUCTION IN NONMETALLIC LIQUIDS

[for thermal conduction in liquid metals, see 72.15C]

76715 Theory of thermal waves. V.A.Bubnov (Moscow Machine-Tool Inst., Moscow, USSR). *J. Eng. Phys. (USA)*, vol.43, no.3, p.1006-12 (Sept. 1982). Translation of: *Inzh.-Fiz. Zh. (USSR)*, vol.43, no.3, p.431-8 (Sept. 1982). An analogy between thermal and electromagnetic waves is established. The conditions under which thermal oscillations can give rise to acoustical oscillations are derived. The coefficients of thermal conductivity in liquid helium are calculated as a function of the temperature below the lambda point. (13 refs.)

66.70 NONELECTRONIC THERMAL CONDUCTION AND HEAT-PULSE PROPAGATION IN NONMETALLIC SOLIDS

[for thermal conduction in solid metals, see 72.15C and 72.15E; for statistical mechanics of lattice vibrations, see 63.70]

76716 Phonon lifetime and thermal conductivity in amorphous solids. K.Handrich (Sektion Phys., Tech. Hochschule Leuna-Merseburg, Merseburg, Germany). *Phys. Status Solidi b (Germany)*, vol.116, no.2, p.533-8 (1 April 1983). After a short discussion of the static structure factor S(k) in the small angle region and the low-temperature thermal conductivity K(T) of amorphous solids, a perturbation theory is developed, which yields the phonon lifetime τ_k and the thermal conductivity K of a weakly and randomly inhomogeneous solid. It is shown that the strong increase of S(k) for k≤10⁻² Å⁻¹ leads to τ_k~k and K~T² for T≤1 K. From S(k)≈const. for k≥10⁻² Å⁻¹ it follows that τ_k~k⁴ (Rayleigh scattering). Thus phonons with wave vectors k≥10⁻² Å⁻¹ will be strongly scattered and will not contribute to the thermal conductivity. This is the reason for the plateau of K for T≥1 K. (15 refs.)

76717 Thermal conductivity of amorphous silicon. H.J.Goldsmid, M.M.Kaila, G.L.Paul (School of Phys., Univ. of New South Wales, Kensington, NSW, Australia). *Phys. Status Solidi a (Germany)*, vol.76, no.1, p.K31-3 (16 March 1983). The authors have recently developed a new steady state method for the measurement of the thermal conductivity of thin layers of poorly conducting materials. Here they describe the technique and report its application to the determination of the thermal conductivity of amorphous silicon. (1 ref.)

76718 Theory of heat conduction in solids. L.P.Bulat, V.G.Yatsyuk (Lvov Polytech. Inst., Ternopol, USSR). *Sov. Phys.-Solid State (USA)*, vol.24, no.11, p.1994-5 (Nov. 1982). Translation of: *Fiz. Tverd. Tela (USSR)*, vol.24, no.11, p.3499-501 (Nov. 1982). [received: May 1983]

The authors study the influence of the temperature dependence of the thermal conductivity on the temperatures of quasiparticle subsystems participating in heat transport. They are interested mainly in internal (bulk) effects in fairly large samples. They consider the specific case of an isotropic technologically homogeneous semiconductor containing one type of carrier (electrons). It is assumed that the electron (T_e) and lattice (T_l) temperatures can be introduced independently. They ignore the influence of the electron-phonon drag on heat conduction, and carry out an analysis in the one-dimensional geometry of heat conduction across an infinite layer. (5 refs.)

Investigation of radiation induced aggregates by phonon techniquesSee Entry 76459

Temperature evolutions in silicon induced by a scanned CW laser, pulsed laser, or an electron beamSee Entry 76492

Thermal properties of Cu₈SnS₆See Entry 76665

Transport properties of thermoelectric materials for coolers ...See Entry 76983

Physicochemical and spectral luminescence properties of a glass based on the SiO₂-Al₂O₃-La₂O₃-Nd₂O₃ systemSee Entry 77438

Fabrication and characterization of TiC_{1-x}N_x (0≤x≤1) and Mo₂B_{1-x}C_x (x=0, 1.0, 2.0) by high-pressure hot-pressingSee Entry 77602

Heating of a thin wire by a constant current with density sufficient for the appearance of thermoplasticitySee Entry 77683

66.90 OTHER TOPICS IN NONELECTRONIC TRANSPORT PROPERTIES

76719 Study and application of the mass transport phenomenon in InP. T.R.Chen, L.C.Chiu, A.Hasson, K.L.Yu, U.Koren, S.Margalit, A.Yariv (California Inst. of Technol., Pasadena, CA, USA). *J. Appl. Phys. (USA)*, vol.54, no.5, p.2407-12 (May 1983). A study of the mass transport phenomenon in InP is presented. Conditions and possible explanation for the transport process are discussed. Characteristics of the mass transported InP homojunctions are described and compared with those in the InP-InGaAsP heterojunctions. Effects of the mass transported junction on laser performance are discussed. (8 refs.)

67.00 QUANTUM FLUIDS AND SOLIDS; LIQUID AND SOLID HELIUM

(see also 05.30 Quantum statistical mechanics)

67.20 QUANTUM EFFECTS ON THE STRUCTURE AND DYNAMICS OF NONDEGENERATE FLUIDS

76720 Low temperature expansions for the second and third cluster integrals of a two dimensional quantum system of hard discs. W.G.Gibson (Lab. de Phys. Theorique et Hautes Energies, Univ. de Paris Sud, Orsay, France). *Mol. Phys. (GB)*, vol.49, no.1, p.103-28 (May 1983). Low temperature series are derived for the second and third cluster integrals of a quantum mechanical, two dimensional gas of hard discs. The methods used are similar to those previously employed for the three dimensional, hard sphere gas, but the presence of logarithmic terms makes both the derivations and the results more complicated in the present case. The corresponding contributions to the density expansion of the specific heat are calculated. The three body contribution is large and negative, thus leading to a downturn in the specific heat at low temperature, in accordance with a prediction of Siddon and Schick (1974). (31 refs.)

67.40 BOSON DEGENERACY AND SUPERFLUIDITY OF HELIUM-4

76721 Interacting bosons and properties of liquid ^4He II. K.M.Khanna, S.Chaubha Singh (Dept. of Materials Sci., Nat. Inst. of Foundry & Forge Technol., Ranchi, India), O.P.Sinha. *Indian J. Pure & Appl. Phys.*, vol.21, no.2, p.97-102 (Feb. 1983). Properties of interacting bosons have been studied using the Hamiltonian written in terms of the density fluctuation operator ρ_k and the velocity operator v_k . Calculations carried out for the excitation spectrum, structure factor and velocity of sound for a dilute system of bosons using Gaussian potential and Lennard-Jones potential show a marked agreement with the corresponding values obtained experimentally for liquid ^4He for only some definite values of wave number k only. The calculations show that if the transition temperature is large, the depletion is small and vice versa. (12 refs.)

76722 Sound conversion phenomena at the free surface of liquid helium. II. Experimental determination of acoustic coefficients and surface absorption coefficients. H.Wiechert, F.I.Buchholz (Inst. für Phys., Johannes-Gutenberg Univ., Mainz, Mainz, Germany). *J. Low Temp. Phys. (USA)*, vol.51, no.3-4, p.291-318 (May 1983). For pt.I see *ibid.*, vol.39, p.623 (1980). The acoustic coefficients of reflection, transmission, and transformation of first-, second-, and gas sound waves incident normally on the free surface of liquid helium have been determined. It is shown that equilibrium theories of boundary conditions disagree with the experiments. Nonequilibrium theories, however, which take into account that mass and energy transport processes occur at the liquid-vapor interface of helium II, lead to a very good description of the experimental data below 2K. Within experimental accuracy the measurements fully confirm several kinetic models of evaporation and energy transport processes. Near the λ point, deviations from the theory have been found which might be attributed to influences of critical phenomena. The surface absorption coefficients of first-, second-, and gas sound waves could be deduced from the experimental data on the acoustic coefficients, and it is shown that, in agreement with the theory, appreciable energy dissipation occurs at the free surface of helium II when a second-sound or a gas sound wave is incident. (55 refs.)

76723 Measurements of the Kapitza resistance and Onsager cross-coefficient for the ^4He crystal-superfluid interface. P.E.Wolf, D.O.Edwards, S.Balibar (Groupe de Phys. des Solides, Ecole Normale Supérieure, Paris, France). *J. Low Temp. Phys. (USA)*, vol.51, no.5-6, p.489-504 (June 1983). The effect of a heat current across the atomically rough crystal-superfluid interface in ^4He has been studied below 1K. The chemical potential difference $\Delta\mu$ and temperature difference ΔT were measured simultaneously, the ΔT by means of a 'superfluid melting-curve thermometer'. The results give the mean phonon transmission coefficient across the interface $\bar{\tau}$ and a dimensionless quantity β that determines the Onsager coefficient linking $\Delta\mu$ with the heat current. The transmission probability $\bar{\tau}$ is proportional to T^2 below 0.2K, in agreement with other experiments and with various theories, and it depends slightly on the crystal orientation, increasing near the c axis. The coefficient β , which is roughly independent of temperature and orientation, agrees with a recent theory of Bowley and Edwards. (20 refs.)

76724 Mutual friction and vortex motion near the superfluid transition. A.Onuki (Dept. of Phys., Kyushu Univ., Fukuoka, Japan). *J. Low Temp. Phys. (USA)*, vol.51, no.5-6, p.601-32 (June 1983). The mutual friction parameters B and B' for a moving vortex are calculated near the superfluid transition. They are proportional to the kinetic coefficient associated with the order parameter and, as $T \rightarrow T_\lambda$, diverge as $(T_\lambda - T)^{-1/3}$, in agreement with experiment. The nonlinear couplings between the order parameter ψ and the entropy m , both the reversible one and the one in the free energy, are found to be crucial in the mutual friction near the λ point. First, the reversible coupling in the dynamic equations makes the chemical potential deviation long-ranged and causes the dissipation to take place only near the vortex core. Second, B' can diverge as $T \rightarrow T_\lambda$ only in the presence of the coupling of the form $m|\psi|^2$ in the free energy. Thus the E model of Halperin et al. (1976) where the latter coupling is absent cannot explain the critical anomaly of B' . The helical mode of a single vortex line is also investigated and its dispersion relation is found to be quite different from that at

low temperatures. This mode has the same time scale as that of the second-sound mode when the wave vectors are of the order of the inverse correlation length, thus obeying the usual dynamic scaling law. The time correlation functions of the displacement fluctuations of a vortex line are also obtained. The force acting on a moving vortex is calculated and is found to be equal to the classical Magnus force. (48 refs.)

76725 Variational approach to dynamics of interfaces and quantized vortex lines. K.Kawasaki (Dept. of Phys., Kyushu Univ., Fukuoka, Japan). *Physica A (Netherlands)*, vol.119A, no.1-2, p.17-40 (April 1983). A variational formulation is presented for deriving equations of motion of topological singularities of stochastic nonlinear field equations which permits a clear separation of static and kinetic interactions that enter the problem. The method is used to obtain stochastic equations of motion of interfaces of binary critical fluids and also of quantized vortex lines of superfluid Helium with thermal noise. (19 refs.)

76726 Calculations of ground-state properties of liquid ^4He droplets. V.R.Pandharipande (Univ. of Illinois, Urbana, IL, USA), J.G.Zabolitzky, S.C.Pieper, R.B.Wiringa, U.Helmreich. *Phys. Rev. Lett. (USA)*, vol.50, no.21, p.1676-9 (23 May 1983). Quantum mechanical calculations of the ground states of droplets of N atoms of ^4He are reported. The calculations have been made by the variational Monte Carlo method for $3 \leq N \leq 728$ and by the Green's function Monte Carlo method for $3 \leq N \leq 112$. The energies, RMS radii, and density distributions are reported; liquid-drop fits to the energies and radii are discussed. (10 refs.)

76727 Damping of second sound in superfluid helium near T_λ . M.J.Crooks, B.J.Robinson (Dept. of Phys., Univ. of British Columbia, Vancouver, British Columbia, Canada). *Phys. Rev. B (USA)*, vol.27, no.9, p.5433-9 (1 May 1983). The damping coefficient of second sound has been measured in liquid helium at saturated vapor pressure near T_λ . The results cover the temperature range $40 \text{ mK} > T - T_\lambda > 40 \text{ } \mu\text{K}$, and were obtained by the measurement of decay rates in a high- Q second-sound resonant cavity. These values are in good agreement with the predictions of nonlinear renormalization-group analysis applied to the asymmetric planar spin model for liquid helium in the 'crossover' and precritical temperature ranges. (26 refs.)

76728 Experimental study of the flow of liquid ^4He through very small channels: Finite-size effects near T_λ . N.Giordano (Dept. of Phys., Purdue Univ., West Lafayette, IN, USA). *Phys. Rev. B (USA)*, vol.27, no.9, p.5447-59 (1 May 1983). The flow of liquid ^4He through the very small cylindrical channels present in Nucleopore filters has been studied. Filters with channel diameters in the range 100-3300 Å have been utilized, with emphasis on the behavior in the vicinity of the superfluid transition. As observed by many previous workers, the author finds that the onset of superfluid flow of the ^4He in the channels occurs at a temperature, $T_{\lambda c}$, which is below the transition temperature of bulk ^4He . The results for the variation of $T_{\lambda c}$ with channel size are in good quantitative agreement with the current theory. (47 refs.)

76729 Atomic impurities in liquid helium. K.E.Kurten (Courant Inst. of Math. Sci., New York Univ., New York, NY, USA), M.L.Ristig. *Phys. Rev. B (USA)*, vol.27, no.9, p.5479-85 (1 May 1983). Paired-phonon analysis is employed to determine the optimal ground-state wave function of Jastrow type for a binary boson mixture. The formalism is specialized and applied for studying the behavior of ^3He , ^4He , and Cs impurities in liquid ^4He at saturation density. The authors present numerical results on chemical potentials, volume coefficients, and related quantities and discuss the properties of the optimal radial distribution functions and static structure functions characterizing the atomic impurities. (25 refs.)

76730 Experimental study of the Kosterlitz-Thouless transition in ^4He films. J.Maps, R.B.Hallock (Dept. of Phys. & Astron., Univ. of Massachusetts, Amherst, MA, USA). *Phys. Rev. B (USA)*, vol.27, no.9, p.5491-507 (1 May 1983). Measurements of the effective thermal conductance of a ^4He film on a Mylar substrate are reported in the vicinity of the transition to superfluid behavior. Experiments have been conducted as a function of film thickness and are consistent with the expected exponential behavior of the free vortex number density as the transition is approached from the normal-fluid side. On the superfluid side of the transition the effective conductance is observed to be a power law in the applied thermal power. The connection between the exponent of the power law and the superfluid density is examined. The experiments reveal an apparent upper limit to the number density of velocity-induced free vortices. Preliminary results for ^3He - ^4He mixtures are reported as are nonlinear effects in the ^4He -vapor conductance. (42 refs.)

76731 Spatial structure changes in ^4He at fixed density as a function of temperature. F.W.Wirth, D.A.Ewen, R.B.Hallock (Dept. of Phys. & Astron., Univ. of Massachusetts, Amherst, MA, USA). *Phys. Rev. B (USA)*, vol.27, no.9, p.5848-51 (1 May 1983). X-ray scattering techniques have been used to determine changes in spatial order when cooling ^4He below T_λ at several fixed values of the density. The results show surprisingly little density dependence and are relevant to the discussion of condensate fraction determinations in ^4He . (20 refs.)

76732 Sound velocity in helium-filled porous Vycor glass. J.R.Beamish, A.Hikata, C.Elbaum (Metals Res. Lab., Brown Univ., Providence, RI, USA). *Phys. Rev. B (USA)*, vol.27, no.9, p.5848-51 (1 May 1983). The velocity of longitudinal and transverse sound in helium-filled porous Vycor glass was measured and analyzed with the use of the Biot theory of sound propagation in fluid-filled porous media. From transverse wave velocities, the superfluid fraction was determined and, from longitudinal velocities, the elastic properties of the helium were determined. (10 refs.)

Theory of thermal waves See Entry 76715

67.50 FERMION FLUIDS; LIQUID HELIUM-3

76733 Spectroscopy with sound on superfluid ^3He B. D.M.Lee (Lab. of Atomic & Solid State Phys., Cornell Univ., Ithaca, NY, USA). *Int. J. Quantum Chem. (USA)*, vol.23, no.4, p.1191-9 (April 1983). Collective modes of superfluid ^3He β have been studied by means of sound attenuation and sound velocity studies. A new sound attenuation peak has been observed in superfluid ^3He B at $\hbar\omega \approx \Delta(T)$. This peak has been identified with the real squashing mode. Pulse time of flight methods has been used in these studies. At high sound amplitudes, interesting transient effects have been observed which have been tentatively identified with solitonlike behavior. (18 refs.)

76734 History-dependent nonlinear dissipation in superfluid $^3\text{He-A}$. R.Gay, M.Bagley, J.R.Hook, D.J.Sandford, H.E.Hall (Phys. Dept., Univ. of Manchester, Manchester, England).

J. Low Temp. Phys. (USA), vol.51, no.3-4, p.227-48 (May 1983). The authors have studied nonlinear dissipation in oscillatory flow of $^3\text{He-A}$ through 49- μm and 17- μm -wide channels by means of torsion pendulum experiments at about 50 Hz. The observed effects are strongly history dependent; the dissipation at a given measuring amplitude is strongly increased if the sample is cooled through T_c while oscillating at large amplitude. Once a highly dissipative state has been created it does not noticeably decay below T_c , though a more dissipative state can be created below T_c by a period of sufficiently large-amplitude oscillation. The results are described semiquantitatively by a model based on the idea of superflow collapse by motion of the \vec{l} vector, with consequent orbital dissipation. This history dependence is introduced into this model by postulating the existence of surface singularities in the \vec{l} texture, the density of which is determined by the previous history of the helium. (16 refs.)

76735 Ground state of $^3\text{He-A}$ in a sphere. P.Hirschfeld, D.L.Stein (Joseph Henry Labs. of Phys., Princeton Univ., Princeton, NJ, USA).

J. Low Temp. Phys. (USA), vol.51, no.3-4, p.257-63 (May 1983). The authors compare the free energies and currents of four trial states of $^3\text{He-A}$ in spherical geometries. The spherical boojum texture is found to be energetically stable for all container radii down to $R \sim 46\xi$, where ξ is the superfluid coherence length. Textures with line defects in the bulk become energetically favorable below this radius. (7 refs.)

76736 Spin diffusion and spin echo in normal liquid ^3He . A.Pal, P.Bhat-tacharyya (Tata Inst. of Fundamental Res., Bombay, India).

J. Low Temp. Phys. (USA), vol.51, no.3-4, p.265-78 (May 1983). The problem of spin diffusion in normal liquid ^3He in the presence of precessional effects is reexamined taking into account the energy dependence of the quasiparticle relaxation time. This leads to a generalization of Leggett's relation (1970) for the successive height of the echoes in a ϕ -180°-180° experiment. Reanalyzing the experiment of Corricini et al. (1972) (including finite-temperature corrections) leads to almost exact and model-independent values of F_1^a and λ_D . (19 refs.)

76737 Evidence for nonsingular vorticity in the Helsinki experiments on rotating $^3\text{He-A}$. N.K.Seppala, G.E.Volovik (Low Temperature Lab., Helsinki Univ. of Technol., Espoo, Finland).

J. Low Temp. Phys. (USA), vol.51, no.3-4, p.279-90 (May 1983). A theory for the satellite peak in the NMR spectrum of rotating superfluid $^3\text{He-A}$ is presented. Absorption at the frequency of the satellite is produced by spin waves localized on vortex lines. The peak frequency and total intensity of the satellite are calculated for both singular and nonsingular vortices; a comparison with the Helsinki NMR data strongly suggests that nonsingular vorticity was actually observed in the experiments. (15 refs.)

76738 Quasiparticle scattering amplitude for normal liquid ^3He . M.Pfützner, P.Wolfe (Phys. Dept., Tech. Univ. München, Garching, Germany).

J. Low Temp. Phys. (USA), vol.51, no.5-6, p.535-59 (June 1983). The quasiparticle scattering amplitude is calculated from a semimicroscopic model by analytically solving a generalization of Landau's integral equation to momentum transfers up to $2p_F$. This solution in general does not obey exchange symmetry for a given particle-hole irreducible vertex part $f_{pp}(q)$. The authors establish conditions for and explicitly construct exchange-symmetric scattering amplitudes by adding higher angular momentum components. Results using certain models for $f_{pp}(q)$ are compared with transport properties of liquid ^3He . (34 refs.)

76739 Superfluidic ^3He . II. D.Vollhardt (Max-Planck-Inst. für Phys. und Astrophys., München, Germany).

Phys. Bl. (Germany), vol.39, no.5, p.120-4 (May 1983). In German. For pt.1 see *ibid.*, vol.39, p.41-5 (1983). This is the second of a series of three papers dealing with liquid ^3He where Cooper Pairs are generated at a temperature of 2.6 K. A Bose-Einstein system is postulated for quantum coherence and the effects of container walls and magnetic field are briefly discussed. Mass flows are calculated in the anisotropic fluid and, finally, superconductivity stability is examined, allowing for spin-path coupling. (20 refs.) *G.M.E.*

76740 Hydrodynamic sound experiments in normal and superfluid ^3He . G.Eska, K.Neumaier, W.Schoepe, K.Uhlir, W.Wiedemann (Zentralinst. für Tieftemperaturforschung, Garching, Germany).

Phys. Rev. B (USA), vol.27, no.9, p.5534-48 (1 May 1983). In a cylindrical resonator the attenuation and the velocity of first sound in normal and superfluid ^3He have been measured in the frequency range from 40 to 300 kHz and at pressures of 8, 18.8, and 28 bar. In the normal fluid the viscosity deduced from the authors' data agrees with previously reported values; the sound velocity in this regime can be explained by taking into account mean-free-path effects and zero-sound corrections. The results for the viscosity in the superfluid confirm the previous observations of a continuous decrease down to the lowest temperatures in contradiction to theoretical predictions. The sound-velocity data in the superfluid regime indicate that specular reflection of the quasiparticles may occur at the resonator walls. (37 refs.)

67.60 MIXED SYSTEMS; LIQUID HELIUM 3-4 MIXTURES

76741 Neutron scattering from liquid mixtures of ^3He and ^4He . K.S.Pedersen, R.A.Cowley (Dept. of Phys., Univ. of Edinburgh, Edinburgh, England).

J. Phys. C (GB), vol.16, no.14, p.2671-8 (20 May 1983). Calculations have been made of the dynamic structure factor $S(Q, \omega)$ of liquid mixtures of 6%, 12%, 25%, 50% and 75% of ^3He in ^4He using a polarisation potential theory. The resulting spectra contain two principal features: ^4He phonon-rotor excitations and ^3He quasiparticle-quasihole excitations. It is not however possible to describe the scattering quantitatively without taking account of the interference terms arising in the scattering. The frequencies of the well defined excitations are almost independent of concentration. (14 refs.)

76742 Dissociation of Abrikosov-Nielsen-Olesen vortices. L.G.Jensen, P.J.Steinhardt (Dept. of Phys., Univ. of Pennsylvania, Philadelphia, PA, USA).

Phys. Rev. B (USA), vol.27, no.9, p.5549-56 (1 May 1983). In this paper the authors discuss how Abrikosov-Nielsen-Olesen vortices can act as impurities that seed first-order phase transitions. The seeding mechanism comes about through dissociation of what is normally considered to be topologically stable defects. They discuss the conditions necessary for dissociation in which the core, which contains the seed of stable phase, becomes unstable and grows radially, converting the system from a metastable phase to

a stable phase. They also discuss some peculiar characteristics of vortices in superfluid $^3\text{He-}^4\text{He}$ and the vortex dissociation that occurs when the $^3\text{He-}^4\text{He}$ phase separates at low temperatures. (6 refs.)

Atomic impurities in liquid helium See Entry 76729

Experimental study of the Kosterlitz-Thouless transition in ^4He films See Entry 76730

67.70 FILMS

(inc. physical adsorption)

Experimental study of the Kosterlitz-Thouless transition in ^4He films See Entry 76730

67.80 SOLID HELIUM AND RELATED QUANTUM CRYSTALS

76743 Nuclear susceptibility and Zeeman-exchange relaxation time of solid ^3He along the melting curve below 15 mK. K.Ichikawa (Faculty of Sci. & Technol., Kinki Univ., Osaka, Japan), Y.Mori, T.Hata, C.Kanamori, H.Okamoto, T.Kodama, T.Shigi.

J. Phys. Soc. Jpn. (Japan), vol.52, no.5, p.1676-81 (May 1983). Nuclear magnetic susceptibility and Zeeman-exchange relaxation time T_{ZX} of solid ^3He have been measured by the pulsed NMR method using the Pomeranchuk cooling technique between 15 mK and 0.97 mK in a static field of about 70 gauss. A magnetic transition to the antiferromagnetic phase was observed at 1.00 mK where the susceptibility decreased to 42% of its maximum value. This drop in susceptibility coincides with the abrupt leveling of ^3He pressure in the cooling process which shows thermodynamically a phase transition due to abrupt decrease of solid ^3He entropy. The magnitude of T_{ZX} is consistent with the one estimated from BPP (Bloembergen-Purcell-Pound) theory, but the observed temperature dependence can not be explained on this basis. (14 refs.)

76744 Pulsed NMR studies in solid H_2 . I. Solid echoes and nuclear spin-spin relaxation times after a two-pulse sequence. I.Yu, S.Washburn, H.Meyer (Dept. of Phys., Duke Univ., Durham, NC, USA).

J. Low Temp. Phys. (USA), vol.51, no.3-4, p.369-400 (May 1983). Describes a systematic pulsed NMR study on several solid H_2 samples with ortho concentration X between 10% and 70% at temperatures between 0.08 and 2 K, where the intramolecular dipole-dipole interaction is the dominant spin-spin interaction. Nuclear spin echoes from a two-pulse sequence are studied using a RF phase-coherent spectrometer and they show the quasiquadrupolar nature of the echo formations. A density matrix method applied to the system of ortho- H_2 molecules can account for most of the observed properties of the echoes. From the decay of the echo envelope the authors obtain information on the static intermolecular nuclear interactions and the local inhomogeneous magnetic field distribution. (24 refs.)

76745 Pulsed NMR studies in solid H_2 . II. Stimulated echoes and cross relaxation times. I.Yu, S.Washburn, M.Calkins, H.Meyer (Dept. of Phys., Duke Univ., Durham, NC, USA).

J. Low Temp. Phys. (USA), vol.51, no.3-4, p.401-22 (May 1983). For pt.1 see *ibid.*, vol.51, p.369 (1983). A study of the stimulated echo following a three-pulse sequence is presented for solid H_2 samples with ortho concentrations X between 15% and 65%, and over the temperature range between $T = 0.1$ and 2 K. The stimulated echo decay time τ_E is found to increase sharply upon cooling through the transition into the long-range ordered phase for $X > 0.55$. However, the increase is only gradual during the progressive orientational ordering in the HCP phase for $X \leq 0.55$. The predictions of a density matrix method for the stimulated echo amplitude are used for comparison with the experiment. A phenomenological approach shows that the results for τ_E can be interpreted in terms of a combination of longitudinal relaxation times T_1 and cross relaxation times T_{12} , the latter expressing the flip-flop transitions between the spin states of neighboring ortho- H_2 molecules. These cross relaxation times are calculated from τ_E and T_1 data and found to increase with linewidth as the orientational ordering progresses. (21 refs.)

Measurements of the Kapitza resistance and Onsager cross-coefficient for the ^4He crystal-superfluid interface See Entry 76723

67.90 OTHER TOPICS IN QUANTUM FLUIDS AND SOLIDS (E.G. NEUTRON-STAR MATTER)

76746 Supercooling of liquid H_2 and the possible production of superfluid H_2 . H.J.Maris, G.M.Seidel, T.E.Huber (Dept. of Phys., Brown Univ., Providence, RI, USA).

J. Low Temp. Phys. (USA), vol.51, no.5-6, p.471-87 (June 1983). The authors discuss the extent to which it may be possible to supercool liquid H_2 below its normal freezing temperature. They show that there is a significant prospect that H_2 could be supercooled to arbitrarily low temperatures, and that in this way superfluid H_2 might be produced. A brief discussion is given of the properties of the anticipated superfluid phase. (38 refs.)

76747 Calculation of nuclear-spin-relaxation rate for spin-polarized atomic hydrogen. R.M.C.Ahn, J.P.H.W.Eijnde, B.J.Verhaar (Dept. of Phys., Tech. Hogeschool Eindhoven, Eindhoven, Netherlands).

Phys. Rev. B (USA), vol.27, no.9, p.5424-32 (1 May 1983). Approximations introduced in previous calculations of spin relaxation for spin-polarized atomic hydrogen are investigated by carrying out a more exact coupled-channel calculation. With the exception of the high-temperature approximation, the approximations turn out to be justified up to the 10^{-3} level of accuracy. It is shown that at the lowest temperatures for which experimental data are available, the high-temperature limit underestimates relaxation rates by a factor of up to 2. For a comparison with experimental data it is also of interest to pay attention to the expression for the atomic hydrogen relaxation rates in terms of transition amplitudes for two-particle collisions. Discrepancies by a factor of 2 among previous derivations of relaxation rates are pointed out. To shed light on these discrepancies the authors present two alternative derivations in which special attention is paid to identical-particle aspects. Comparing with experiment, they find their volume relaxation rate to be in better agreement with measured values than that obtained by other groups. The theoretical surface relaxation rate, however, still shows a discrepancy with experiment by a factor of order 50. (22 refs.)

68.00 SURFACES AND INTERFACES; THIN FILMS AND WHISKERS

[for impact phenomena, see 79.; for physics of crystal growth, see 61.50C; for corrosion, oxidation, and surface treatments, see 81.60]

68.10 FLUID SURFACES AND INTERFACES WITH FLUIDS

(inc. surface tension, capillarity, wetting and related phenomena)

76748 Surface tension measurements for the n-alcohols in the temperature range from -40°C to $+40^{\circ}\text{C}$. R.Strey, T.Schmeling (Max-Planck-Inst. für Biophys. Chem., Göttingen, Germany). *Ber. Bunsenges. Phys. Chem. (Germany)*, vol.87, no.4, p.324-7 (April 1983). The surface tension of the n-alcohols from methanol through n-octanol were measured between about -40°C and $+40^{\circ}\text{C}$. The surface tension data can be represented with $\pm 0.5\%$ by linear functions of temperature over the considered temperature range. The increase of surface tension with increasing chain length of the alcohol is in accord with the theorem of corresponding states. (18 refs.)

76749 On the validity of certain integro-differential equations for the density-orientation profile of molecular fluid interfaces. P.Tarazona, R.Evans (H.H. Wills Phys. Lab., Univ. of Bristol, Bristol, England). *Chem. Phys. Lett. (Netherlands)*, vol.97, no.3, p.279-82 (20 May 1983). The status of some recently proposed integro-differential equations for the density-orientation profiles, $\rho(r_i, \omega_i)$, of non-uniform molecular fluids is examined. Two of the equations derived by Gubbins (1980), which involve derivatives with respect to angular coordinates ω_i , are shown to be incorrect and corrected versions are proposed. The implications of the results for pairwise correlations and for the surface tension of the liquid-gas interface are discussed. (8 refs.)

76750 The surface tension of water. N.R.Pallas, B.A.Pethica (Clarkson Coll. Potsdam, NY, USA). *Colloids & Surf. (Netherlands)*, vol.6, no.3, p.221-7 (April 1983). The air-water interfacial tension has been redetermined by the capillary rise and Wilhelmy plate methods at 25°C . The drop-volume method, using the Harkins-Brown corrections, gives good values for glass tips if appropriate precautions are taken. The effect of replacing air with He or N_2 at 1 atm. was not measurable, but CO_2 at 1 atm. gives a significant lowering of the interfacial tension. Measurements over the range $20-45^{\circ}\text{C}$ are also reported. (21 refs.)

Measurement of the surface-tension anisotropy of a nematic liquid crystal See Entry 76286

Surface anchoring of liquid crystal molecules on various substrates See Entry 76288

Total internal reflection—a method for determining of LC anchoring and orientation on various substrates See Entry 76291

Optical method for determination of anchoring energy of tilted nematic layers See Entry 76298

68.15 LIQUID THIN FILMS

76751 Effect of molecular ordering in thin water films. V.Ya.Antonchenko, V.V.Ilin, M.M.Makovskii. *Dopov. Akad. Nauk UkrSR. Ser. A (USSR)*, no.1, p.53-5 (1983). In Ukrainian. Studies the properties of a thin water film by the Monte-Carlo method. It is shown that the translational inhomogeneity causes orientational ordering of water molecules. This allows one to interpret at a molecular level the notion of 'insoluble volume'. (6 refs.)

Transmission of a bounded acoustic beam in the 'far field' case. II. Transmission across a fluid film See Entry 75848

Breakup of a thin liquid layer heated from below See Entry 76001

Microdiffraction applied to thermotropic liquid crystalline polymers See Entry 76300

Determining the frictional properties of thin films of lubricants See Entry 76817

68.20 SOLID SURFACE STRUCTURE

76752 Hybridization and surface relaxation in diamond-like crystals. V.Barone, G.Dei (Cattedra di Chimica Teorica, Univ. di Napoli, Napoli, Italy). *THEOCHEM (Netherlands)*, vol.11, no.1-2, p.173-85 (June 1983).

The role of variable hybridization in the description of covalent solids is discussed. As an example the criterion of 'maximum overlap-straight bond' is applied to investigate changes in plane-to-plane spacings induced normal to a free (111) surface in diamond-like crystals. The simple model used appears to have general validity and suggests that formation of a free surface always determines a 'localized' pattern of perturbed lattice distances in the direction perpendicular to the surface. Numerical results are in agreement with previous cluster computations and indicate a heavily damped oscillation of interatomic distances around a mean value when proceeding inwards from the free (111) surface for both diamond and silicon. The results support the so-called H-model for the (111) surfaces of diamond-like crystals, and exclude the possibility of graphite-like delocalization. (53 refs.)

76753 Lateral stress-induced blistering of aluminium films under helium irradiation. H.J.Whitlow (Inst. of Phys., Univ. of Aarhus, Aarhus, Denmark), S.E.Donnelly, M.Renier, A.A.Lucas. *J. Nucl. Mater. (Netherlands)*, vol.115, no.2-3, p.347-9 (April 1983). Discusses the phenomena of blistering and flaking of surfaces irradiated with energetic He ions. The choice of appropriate models is far from clear. The authors' aim has been not to unambiguously resolve this problem, but rather to illustrate that under conditions where an easy fracture plane is clearly defined, blisters, seemingly identical to those observed under conventional conditions, can be found as a result of lateral stresses only. (12 refs.)

76754 Phase transition on stepped silicon surfaces. V.I.Mashanov, B.Z.Ol'shanetskii (Inst. of the Phys. of Semiconductors, Acad. Sci., Novosibirsk, USSR).

JETP Lett. (USA), vol.36, no.8, p.355-8 (20 Oct. 1982). Translation of: *Pis'ma v Zh. Eksp. & Teor. Fiz. (USSR)*, vol.36, no.8, p.290-2 (20 Oct. 1982). [received: June 1983]

Phase transitions are discovered on clean silicon surfaces inclined away from (111) toward [211] planes. At temperatures below 850°C , systems of ordered steps with height equal to three interplanar distances d_{111} , which reform reversibly into steps with height equal to a single interplanar distance above 850°C , form on such surfaces. (12 refs.)

76755 The concentration of surface $\text{V}=\text{O}$ species on oxidized vanadium oxide catalysts. A.Miyamoto, A.Hattori, Y.Murakami (Dept. of Synthetic Chem., Nagoya Univ., Nagoya, Japan). *J. Solid State Chem. (USA)*, vol.47, no.3, p.373-5 (May 1983).

On the basis of an oxidized surface state model of vanadium oxides, Andersson (1982) has theoretically shown that the concentration of surface $\text{V}=\text{O}$ species on oxidized V_2O_3 or V_2O_4 catalyst is higher than that on V_2O_5 catalyst. The authors confirm the validity of this inference experimentally. V_2O_5 was prepared by the thermal decomposition of ammonium metavanadate at 773K for 3 hr in a stream of O_2 . XPS spectra of the preoxidized catalysts were obtained Shimadzu ESCA 750 photoelectron spectrometer. (5 refs.)

76756 An X-ray photoelectron spectroscopy study of the surface segregation of LaNi_5 heated in H_2 -atmosphere. Hu Gang, Wu Yue (Changchun Inst. of Appl. Chem., Acad. Sinica, China). *Kexue Tongbao (Foreign Lang. Ed.) (China)*, vol.28, no.3, p.341-5 (March 1983).

Due to its ability to store large amount of reversible hydrogen—a promising energy carrier of the future— LaNi_5 has aroused much interest. Researches on its hydrogen-absorbing ability, the surface structures as well as the position of hydrogen in LaNi_5 hydride have been extensively carried out in the last few years. The authors report results obtained by XPS-study of the change of the surface composition of LaNi_5 heated in H_2 -atmosphere. (8 refs.)

76757 XPS studies of SiO_2 surface layers formed by oxygen ion implantation into silicon. D.Schulze, J.Finster (Sektion Chem., Karl-Marx-Univ. Leipzig, Leipzig, Germany), E.Hensel, W.Skorupa, U.Kreissig. *Phys. Status Solidi A (Germany)*, vol.76, no.1, p.K21-4 (16 March 1983). The authors report the examination of SiO_2 surface layers of 160 nm thickness formed by ion implantation into silicon. XPS measurements into the depth were done after a step-by-step chemical etch of the SiO_2 layer. The chemical nature and the thickness of the transition layer to the silicon were determined. For comparison the same measurements were done on thermal oxide. (9 refs.)

76758 On the stability of surface martensite in β -phase Cu-Zn alloys. F.C.Lovey (Centro Atomico Bariloche, Bariloche, Argentina), J.Ferron, L.S.Del Bernardez, M.Ahlers.

Scri. Metall. (USA), vol.17, no.4, p.501-4 (April 1983).

The subsurface layer composition has been investigated by combining Auger electron spectroscopy with ion beam bombardment. It can be concluded from the results that the most likely reason for the formation of a surface martensite is a compositional change of the near-surface region due to the oxide layer which acts as a sink for Zn atoms. (17 refs.)

76759 LEED studies of several structural models of the $\text{Si}(100)$ surface. G.J.R.Jones, B.W.Holland (Dept. of Phys., Univ. of Warwick, Coventry, England).

Solid State Commun. (USA), vol.46, no.8, p.651-5 (May 1983).

Dynamical LEED calculations are performed for the Poppendieck $c(4 \times 2)$ and the Chadi (2×1) , $c(2 \times 2)$, $p(2 \times 2)$ and (4×2) structures. All the non- (2×1) structures give forbidden beams that are far too intense, and comparison with experiment shows that none of the structures individually, nor any combination of the Chadi structures, can represent the $\text{Si}(100)$ surface. (16 refs.)

76760 Surface crystallography of thin films by electron diffraction in the STEM. K.Truszkowska, M.J.Yacamán (Inst. de Física, Univ. Nacional Autónoma de México, Mexico City, México).

Surf. Sci. (Netherlands), vol.127, no.3, p.L159-64 (May 1983).

It is shown that by using STEM microdiffraction it is possible to obtain surface reflections from thin metallic films. The technique is demonstrated for a gold film. Reflections from the surface reproduce the (23×1) superlattice for the (111) surface previously reported in the literature. It is also shown that the film surface consists of reconstructed (5×1) domains which when interlocking produce the (23×1) pattern. (12 refs.)

76761 Observation of superstructure formation on $\text{Rh}(001)$ by laser-pulse assisted field evaporation. Chi-fong Ai, T.T.Tsong (Phys. Dept., Pennsylvania State Univ., University Park, PA, USA).

Surf. Sci. (Netherlands), vol.127, no.3, p.L165-71 (May 1983).

Pulsed-laser assisted field evaporation of the $\text{Rh}(001)$ plane produces a $p(2 \times 2)$ structure. This structure can be destroyed by pulsed-laser heating the surface in the absence of an applied field, and can be restored to near perfection if the pulsed-laser heating is done in an applied field of 3 to 4 V/Å. The degree of order increases with the applied electric field. The observed $p(2 \times 2)$ surface is therefore a field stabilized structure. (14 refs.)

76762 Synthesis of cellular amorphous films on the surfaces of alloys with a periodic-pulse CO_2 laser. A.A.Katsnel'son, V.A.Alekseev, V.Yu.Baranov, A.A.Mezhevov, N.A.Khatanova, E.E.Kamzueva (M.V. Lomonosov State Univ., Moscow, USSR).

Sov. Tech. Phys. Lett. (USA), vol.8, no.9, p.462-3 (Sept. 1982). Translation of: *Pis'ma v Zh. Tekh. Fiz. (USSR)*, vol.8, no.17-18, p.1072-4 (Sept. 1982). [received: May 1983]

The authors report an attempt to synthesize an amorphous film with a uniform cellular structure on the surface of the alloy $\text{Fe}_{80}\text{P}_{10}\text{C}_7$. They used a periodic-pulse closed-loop CO_2 laser with a maximum pulse repetition frequency of 1 kHz. The $\text{Fe}_{80}\text{P}_{10}\text{C}_7$ alloy was produced in a vacuum furnace; the sample was a cylinder with a diameter ~ 9 mm. (7 refs.)

76763 Rapidly solidified microstructure in surface layers of laser-alloyed Mo on Fe-C substrates. T.R.Tucker, A.H.Clauer, S.L.Ream, C.T.Walters (Batelle Columbus Labs., Columbus, OH, USA).

Rapidly Solidified Amorphous and Crystalline Alloys. Proceedings of the Materials Research Society Annual Meeting, Boston, MA, USA, Nov. 1981 (New York, USA: North-Holland 1982), p.541-5. Shaped continuous-wave laser beams have been used to alloy molybdenum coatings into Fe-C substrates. The Mo overlay was first deposited by the plasma spray process in an inert gas environment. Slowly scanned laser radiation then melted a layer 2 to 5 times the thickness of the original coating causing the two metallic species to mix. Melt proceeded from the coating/substrate interface, the Mo melt temperatures being significantly higher than that of the base material. Fusion zone microstructures for indi-

dual melt passes appeared to be homogeneous, and molybdenum composition was found to be relatively uniform. With overlapping melt passes, the microstructures became more complex with heat effects apparent in the overlap regions. (4 refs.)

- Direct surface imaging in small metal particles See Entry 76263
Orientation dependence of oxidation stacking fault density in silicon See Entry 76457
Matrix effect and surface oxidation in depth profiling of $\text{AlGa}_{1-x}\text{As}$ by secondary ion mass spectrometry using O_2^+ primary ions See Entry 76479
Periodic structure formed during the action of high-power coherent radiation on a semiconductor surface See Entry 76495
Surface second-order phase transitions conserving the number of atoms in a unit cell See Entry 76617
Effects of annealing and electromigration on surface morphology of polycrystalline films See Entry 76712
Determination of the molecular symmetry of acetylene on Ni(001) by electron-impact scattering See Entry 76782
Effect of surface reconstruction on the adsorption of Ge on clean Si(111) See Entry 76785
Anodic bonding of imperfect surfaces See Entry 76797
Angular distributions of Au and Cu atoms sputtered from Au-Cu alloys by keV Ar^+ ion bombardment See Entry 77513
Structural dependence of microscopic residual shear stress at worked surface ... See Entry 77672
Wear of transition metal rich glassy alloys See Entry 77770
Changes of the surface composition of glass during reactive and argon ion etching See Entry 77772
Characterization of mechanochemically polished (111) surface of silicon crystal by diffuse X-ray scattering See Entry 77777

68.25 MECHANICAL AND ACOUSTICAL PROPERTIES OF SOLID SURFACES AND INTERFACES

(for tribology, see 62.20P and 81.40P)

76764 Velocity measurement of multiple leaky waves on germanium by line-focus-beam acoustic microscope using FFT. J.Kushibiki, K.Horii, N.Chubachi (Dept. of Electrical Engng., Tohoku Univ., Sendai, Japan). *Electron. Lett. (GB)*, vol.19, no.11, p.404-5 (26 May 1983). $V(z)$ curves obtained by the acoustic line-focus beam are deformed due to multiple leaky waves. A novel velocity measurement method with FFT is developed for a $V(z)$ curve analysis. Experiments are performed for a (111) Ge sample and two mode spectra are separately measured corresponding to two velocities for a leaky SAW and a leaky pseudo-SAW existing on the boundary of water/sample. (4 refs.)

76765 Means of plastic self-indentation of solids in contact. Ya.E.Geguzin, V.G.Kononenko (A.M. Gorki State Univ., Kharkov, Ukrainian SSR). *Sov. Phys.-Solid State (USA)*, vol.24, no.11, p.1997-8 (Nov. 1982). Translation of: *Fiz. Tverd. Tela (USSR)*, vol.24, no.11, p.3503-5 (Nov. 1982). [received: May 1983]

If an interaction at the molecular level takes place along the place of contact between two solids, i.e. if a specific energy $\Delta\alpha = 2\alpha - \alpha_0$ is evolved (α and α_0 are the surface and boundary energies, respectively), plastic deformation may occur in the contact zone because of the generation and motion of dislocation loops. Obviously, the extent of plasticity is limited because an increase in the contact area reduces the contact stresses to some limiting value below which the dislocation sources become inactive. The authors consider specifically this factor which limits the means and assume that the active relaxation mechanisms disperse dislocation pile-ups which might give rise to stresses counteracting the capillary stresses. (3 refs.)

- Transmission of a bounded acoustic beam in the 'far field' case. I. Transmission across a dioptr See Entry 75847
Transmission of a bounded acoustic beam in the 'far field' case. II. Transmission across a fluid film See Entry 75848
Multimode interference mechanism in $V(z)$ curves obtained by acoustic line focus beam See Entry 75850
Optical probing of acoustic waves on rough surfaces See Entry 75883
Propagation of surface acoustic waves in n-type GaAs films ... See Entry 77007

68.30 DYNAMICS OF SOLID SURFACES AND INTERFACE VIBRATIONS

76766 Vibrational interaction between hydrogen atoms adsorbed on Pd(100). C.Nyberg, C.G.Tengstall (Dept. of Phys., Chalmers Univ. of Technol., Goteborg, Sweden).

Phys. Rev. Lett. (USA), vol.50, no.21, p.1680-3 (23 May 1983). Vibrational energy shifts have been observed for the substitutionally disordered $p(1 \times 1)(\text{H}+\text{D})$ and $c(2 \times 2)(\text{H}+\text{D})$ structures on Pd(100). Between 0 and 1 hydrogen concentration the hydrogen vibrational energy shifts by 3.5 and 0.5 meV for the $p(1 \times 1)$ and $c(2 \times 2)$ structures, respectively. It is argued that the relatively large energy shift of the $p(1 \times 1)$ structure is mainly due to adatom-adatom interaction mediated by the metal electrons. (23 refs.)

- Diffusion of hydrogen on metal surfaces: strong coupling limit See Entry 76788
Model calculations of local electron and phonon densities of states in bimetallic superlattices See Entry 76827
Peierls instability and charge density waves at the surface of a metal with a quasideimensional electron spectrum See Entry 76935
A new scattering mechanism for EELS See Entry 77495
Multiphonon effects in field electron emission See Entry 77537

68.40 SURFACE ENERGY OF SOLIDS; THERMODYNAMIC PROPERTIES

76767 Surface free energy and stress of a Lennard-Jones crystal. J.Q.Broughton, G.H.Gilmer (Bell Labs., Murray Hill, NJ, USA). *Acta Metall. (USA)*, vol.31, no.6, p.845-51 (June 1983). Surface excess free energies and stresses have been calculated by molecular dynamics techniques for three low-index crystal faces. Properties of the (111),

(100) and (110) faces of a face centered cubic crystal composed of Lennard-Jones particles have been investigated. Large variations in the surface stress are present; the (111) and (100) exhibit compressive and tensile stress, respectively, over the temperature range from 0K to the triple point. The excess free energies of the three faces are approximately equal at temperatures within 10% of the triple point. The values obtained for the free energies of crystal-vapor, crystal-liquid and liquid-vapor interfaces are used to calculate the thickness of a quasi-liquid layer on the crystal-vapor interface at temperatures near the triple point. (35 refs.)

Role of the surface energy in phase transitions with two order parameters See Entry 76620

Electronic and cohesive properties of small sodium particles ... See Entry 76869

68.45 SOLID-FLUID INTERFACE PROCESSES

(see also 82.65 Sorption and accommodation coefficients)

76768 Strongly bound chemisorption state for benzene on silicon (111). M.N.Piancastelli (Dept. of Chem., Univ. of Wisconsin, Madison, WI, USA), F.Cerrina, G.Margaritondo, A.Franciosi, J.H.Weaver.

Appl. Phys. Lett. (USA), vol.42, no.11, p.990-1 (1 June 1983). Dramatic differences were observed between the room-temperature reactivity of benzene on cleaved Si and on cleaved Ge and GaAs with synchrotron-radiation photoemission. No evidence of benzene adsorption was observed on Ge or GaAs. On Si the authors unexpectedly observed a strongly bound state, probably due to the formation of phenylic-like C-Si bonds. (8 refs.)

76769 A MINDO/3 approach to the chemisorption of hydrogen on graphite. F.Illas, F.Sanz, J.Virgili (Dept. de Quimica-Fisica, Univ. de Barcelona, Barcelona, Spain).

THEOCHEM (Netherlands), vol.11, no.1-2, p.79-86 (June 1983). The MINDO/3 method is applied to the chemisorption of hydrogen on graphite using a finite model for the surface. Various cluster models are used in order to establish the influence of cluster size. Hydrogen atoms are used to avoid edge effects. The process appears to be endothermic and a potential barrier is found for adsorption over a carbon atom and over the bond connecting two nearest neighbours carbon atoms. Adsorption over the center of the hexagonal lattice appears to be unfavorable. Results suggest that a model having ten carbon atoms and eight hydrogen atoms is good enough as a graphite surface model. (31 refs.)

76770 A MINDO/3 approach to the chemisorption on graphite of electrophilic adsorbates. F.Illas, F.Sanz, J.Virgili (Dept. de Quimica-Fisica, Univ. de Barcelona, Barcelona, Spain).

THEOCHEM (Netherlands), vol.11, no.1-2, p.87-93 (June 1983). The MINDO/3 method has been applied to the chemisorption of atomic carbon and nitrogen on a finite cluster model of the graphite surface consisting of ten carbon atoms and eight hydrogen atoms. The process appears to be endothermic and potential barriers have been calculated for adsorption onto a carbon atom onto the bond connecting two nearest neighbour carbon atoms and onto the center of the hexagonal graphite ring. Chemisorption onto the center of the hexagonal ring involves cross-overs between different states in the region around the maximum. Results suggest that the UHF method is more appropriate than the RHF method in the case of atomic carbon chemisorption. (24 refs.)

76771 Rates of molecular desorption from solid surfaces: adsorption site dependence for CO on Ni(100). J.N.Allison, Y.Zeiri, A.Redondo, W.A.Goddard, III (Arthur Amos Noyes Lab. of Chem. Phys., California Inst. of Technol., Pasadena, CA, USA).

Chem. Phys. Lett. (Netherlands), vol.97, no.4-5, p.387-91 (27 May 1983). The role of different adsorption sites on the rate of desorption of CO from Ni(100) surfaces has been studied using the classical stochastic diffusion theory (CSDT) formulation. The microscopic parameters of the system (force constants and bond energies) have been obtained from ab initio cluster calculations (Ni_4 and Ni_{20} clusters) with generalized valence bond wavefunctions. In good agreement with experiment, the authors' calculations show that desorption occurs in two temperature ranges: 400-600K and 150-250K. In the higher-temperature range, the one-fold and two-fold sites are primarily responsible for the desorption rate, while for the lower-temperature range, the four-fold (weakest binding site) is dominant (experimentally achieved by poisoning the surface with S). (13 refs.)

76772 Quasiclassical trajectories study on the two-dimensional model of the dissociative chemisorption of H_2 on a lithium cluster surface. J.Vojtik, J.Savrdra (J. Heyrovsky Inst. of Phys. Chem. & Electrochem., Czechoslovak Acad. of Sci., Prague, Czechoslovakia), J.Fiser.

Chem. Phys. Lett. (Netherlands), vol.97, no.4-5, p.397-402 (27 May 1983). A two-dimensional $\text{H}_2\text{-Li}_8$ potential surface of 'diatomics-in-molecules' quality is constructed and used in a quasiclassical trajectory model study of dissociative adsorption of H_2 on the cluster surface. The effect of the translational and vibrational energy of H_2 on the outcome of the collision with the surface is discussed. (18 refs.)

76773 Properties of thermally modified controlled porous glasses (CPG). I. Influence of additional thermal treatment of CPG on adsorption processes on its surface. A.L.Dawidowicz, I.Choma (Dept. of Chem. Phys., Inst. of Chem., Maria Curie Sklodowska Univ., Lublin, Poland).

Mater. Chem. & Phys. (Switzerland), vol.8, no.4, p.323-36 (April 1983). Controlled porous glasses (CPG) are the sorbents and supports of chemically bonded phases very widely applied in chromatographic columns for the separation of polymers and biopolymers by means of gel permeation and affinity chromatography. The chemical structure of CPG surface can easily be changed by additional heating of porous glass. Such thermal modification leads to the enrichment of the surface in boron atoms. In consequence, the prepared materials possess specific surface properties. Some adsorption isotherms obtained for chemically different compounds on the CPG surfaces thermally treated in various ways are presented. (23 refs.)

76774 Cluster calculations of the $\text{H}_2\text{O}/\text{Pt}(111)$ system. J.Paul, A.Rosen (Dept. of Phys., Chalmers Univ. of Technol., Goteborg, Sweden).

Int. J. Quantum Chem. (USA), vol.23, no.4, p.1231-8 (April 1983). The electronic interaction between water and a Pt(111) surface as evaluated for different $\text{Pt}(\text{H}_2\text{O})_n$ clusters is discussed. Hartree-Fock-Slater (HFS) one-electron ground state energies, ionization potentials, partial densities of states, and Mulliken occupation numbers are related to bonding shifts, as well as initial and final state screening for different orientations of the molecule. The formation of $\text{Pt-H}_2\text{O}$ bonds are sensitive to the orientation since surface oriented H atoms bridge the spatial separation between O $2p$ and Pt $5d$ orbitals and thus increase the intermixing of metal and adsorbate orbitals. The dipole moment and the net charge of the H_2O molecule is also discussed. Finally, approximations of the metal- H_2O potential for use in statistical models of the liquid-metal interface are suggested. (21 refs.)

- 76775** A study on the orientation of imidazoles on copper as corrosion inhibitor and possible adhesion promoter for electric devices. S.Yoshida, H.Ishida (Dept. of Macromolecular Sci., Case Western Reserve Univ., Cleveland, OH, USA). *J. Chem. Phys. (USA)*, vol.78, no.11, p.6960-9 (1 June 1983). The structure of various imidazoles on the surfaces of copper and gold mirrors has been studied by Fourier transform infrared reflection-absorption spectroscopy in order to elucidate the molecular mechanisms of corrosion inhibition of metal surfaces by imidazoles. Heptadecylimidazole, undecylimidazole, phenylimidazole, and imidazole were used to investigate the orientation of the imidazole ring and the accompanying side groups. When a gold mirror was withdrawn slowly from an ethanol solution of undecylimidazole, the imidazole ring adsorbed onto the surface flatly and the C-C bond of the hydrocarbon chain became parallel to the surface. A similar trend was observed on all imidazole derivatives studied. The orientation of the outer layers was disturbed when the thickness was increased. With a copper mirror, the structure of the imidazole at room temperature depended on the method of adsorption. A slowly withdrawn sample showed a predominant complex formation whereby the solution placed dropwise on the copper surface showed a combination of complexes, randomly orientated layers, and oriented layers similar to gold. The heat treatment at 80°C eliminated the difference caused by the adsorption methods. Upon complex formation, the orientation of the imidazole became random. This complex is tentatively assigned to diundecylimidazolato copper(II), an inner complex with copper. Further heat treatment at 150°C yielded another complex. The structure of undecylimidazole adsorbed from an acidic aqueous solution on a copper mirror has also been studied. The imidazole adsorbed very rapidly to form a thick layer due to the acceleration of complex formation by the activated imidazole ring. A similar structure in the imidazole layers was obtained both from an ethanol solution and an acidic aqueous solution. However, coadsorption of the small amount of acid used remains to be a question. Again, the heat treatment at 150°C yielded the infrared spectrum similar to the complex obtained from the ethanol solution. (48 refs.)
- 76776** Effect of adsorption of vapours on the electrical conductivity of a series of some naphthyl polyenes: Adsorption and desorption kinetics. A.Sircar, B.Mallik, T.N.Misra (Optics Dept., Indian Assoc. for the Cultivation of Sci., Calcutta, India). *J. Phys. & Chem. Solids (GB)*, vol.44, no.5, p.401-5 (1983). Deals with the change in semiconductivity of a series of naphthyl polyenes of the type $R-(CH=CH)_n-R$, where R stands for the naphthyl group and $n=1-6$, on adsorption of vapours of some organic solvents at a constant sample temperature. Appreciable enhancement in the conductivity is observed. Such enhancement depends on the chemical nature of the solvent and also on the vapour pressure. The desorption is much slower than that of adsorption. Both the adsorption and desorption kinetics follow the modified Roginsky-Zeldovich relation. Kinetics for the compounds having odd- n is distinctly different from those with even- n . The results show that in all these vapour-semiconductor systems, the adsorption is a two-stage process. (9 refs.)
- 76777** The adsorption of ammonia on an Fe(110) single-crystal surface studied by high-resolution electron energy-loss spectroscopy (EELS). W.Erley, H.Ibach (Inst. für Grenzflächenforschung und Vakuumphys., KFA Jülich, Jülich, Germany). *J. Electron Spectrosc. & Relat. Phenom. (Netherlands)*, vol.31, no.2, p.161-74 (May 1983). The EELS spectra of ammonia adsorbed on an Fe(110) surface at 110K reveal four different adsorption states of molecular ammonia with increasing coverage: chemisorption at 'on-top' sites, chemisorption at multi-coordinated sites, adsorption in a second layer, and multilayer condensation. Thermal processing of an ammonia-covered sample to 155K causes desorption of both the condensed phase and the second layer without any fragmentation of ammonia. Further heating of the sample leads to a much weaker desorption of molecular ammonia up to a temperature of 260K. EELS spectra recorded after heating to 290K show only small amounts of atomic nitrogen and hydrogen present on the surface, indicating partial decomposition of ammonia. The formation of species such as NH_2 (ads) or NH (ads) during the thermal-processing experiments could not be observed. (17 refs.)
- 76778** Quantum chemical studies of chemisorption at anion or cation sites of the GaP (110) surface. Coverage dependence of adsorption energy and equilibrium in cases of positive and negative partial charge injection. W.Lorenz, C.Engler, A.Nechwatal, G.Adler (Sektion Chem., Karl-Marx-Univ. Leipzig, Leipzig, Germany). *Phys. Status Solidi b (Germany)*, vol.117, no.1, p.203-12 (1 May 1983). Chemisorption of electronegative or electropositive atoms at anion or cation sites of a relaxed GaP (110) surface is investigated in the TB approximation, with parameters corresponding to fluorine or lithium adsorption. Local densities of states and the dependence of the surface Fermi energy, partial charge injection, adsorption energy, and adsorption equilibrium upon the adsorption density are reported. (15 refs.)
- 76779** Modelling and illustration of a penetration mechanism for hydrogen into metal. C.Opitz, F.Dubler (Sektion Chem., Friedrich-Schiller-Univ., Jena, Germany). *Phys. Status Solidi a (Germany)*, vol.76, no.2, p.505-12 (16 April 1983). The insertion of hydrogen into metals is investigated in the system $H/Nb_3I_8^{3+}$ using the cluster-bulk analogy. Energies and charge distributions are calculated in the frame of EHT approach for some positions of the H atom along a possible penetration path. The insertion process is characterized by a small activation energy (50 kJ/mol) and negativation of hydrogen. The hydrogen atom is strongly bound in the centre of the $Nb_3I_8^{3+}$ -cluster. The bond energy is 260 kJ/mol. Furthermore, the charge distribution is drawn in some selected positions of the reaction path to give a qualitative survey on the penetration mechanism in an illustrative manner. (13 refs.)
- 76780** Adsorption of oxygen on GaAs(001) surfaces by UPS. D.Flamme (Sektion Chem., Karl-Marx-Univ. Leipzig, Leipzig, Germany), E.-H.Weber. *Phys. Status Solidi a (Germany)*, vol.76, no.2, p.K163-6 (16 April 1983). The authors have made adsorption experiments on clean GaAs (001) surfaces prepared by sputtering with 400 eV Ar^+ ions and annealing at 770K. They present the ultraviolet photoemission spectra of a clean GaAs (001) surface which was then exposed to dry oxygen (10^2 , 10^4 L) and finally annealed at 770K. Marked changes occur at ≈ 5 and ≈ 10 eV binding energy, and the emission at 10 eV disappears on annealing. (5 refs.)
- 76781** Transitions of adsorbates on random substrates. W.Kinzel (Inst. für Festkörperforschung der Kernforschungsanlage Jülich, Jülich, Germany). *Phys. Rev. B (USA)*, vol.27, no.9, p.5819-20 (1 May 1983). It is pointed out that impurities and defects destroy any order-disorder phase transition of adsorbates on surfaces. (11 refs.)

- 76782** Determination of the molecular symmetry of acetylene on Ni(001) by electron-impact scattering. N.J.DiNardo, J.E.Demuth, P.Avouris (IBM Thomas J. Watson Res. Center, Yorktown Heights, NY, USA). *Phys. Rev. B (USA)*, vol.27, no.9, p.5832-5 (1 May 1983). Angle-dependent electron-energy-loss measurements of acetylene on Ni(001) are used to deduce molecular symmetry on the surface by consideration of selection rules for vibrational excitation by impact scattering. Chemisorbed acetylene has C_{2v} symmetry with a mirror plane along (110) and a molecular plane tilted relative to the surface. (13 refs.)
- 76783** Orientational ordering of commensurate $Fe(CO)_5$ monolayers on graphite. R.Wang, H.Taub (Dept. of Phys., Univ. of Missouri, Columbia, MO, USA), H.Schechter, R.Brener, J.Suzanne, F.Y.Hansen. *Phys. Rev. B (USA)*, vol.27, no.9, p.5864-7 (1 May 1983). Elastic neutron diffraction and Mossbauer spectroscopy have been used to study the structure, orientational-disordering (OD) transition, and melting of an $Fe(CO)_5$ submonolayer adsorbed on Grafoil. The OD transition occurs between 150 and 167K from a two-sublattice ($\sqrt{7} \times \sqrt{21}$) structure to a nearly ($\sqrt{7} \times \sqrt{7}$) phase in which the molecules are believed to rotate about the surface normal. Mossbauer spectra exhibit a more abrupt variation with temperature near melting at 170K than through the OD transition. (18 refs.)
- 76784** Raman scattering by optically absorbing molecules adsorbed on 'smooth' Ag and Au surfaces: crystal violet. E.Burstein (Phys. Dept., Univ. of Pennsylvania, Philadelphia, PA, USA), G.Burns, F.H.Dacol. *Solid State Commun. (USA)*, vol.46, no.8, p.595-9 (May 1983). Reports data on the resonant Raman scattering (RS) by crystal violet (CV) adsorbed on Ag and Au surfaces. The data show that the RS and luminescence by CV on a smooth Au surface is greater by an order of magnitude than that on a smooth Ag surface. These results, which are contrary to what one expects from mechanisms that depend on the complex dielectric constant of the metal substrate, are attributed to contributions that depend on the chemical bonding of the CV molecules with the metal substrate. (9 refs.)
- 76785** Effect of surface reconstruction on the adsorption of Ge on clean $Si(111)$. P.Chen, D.Bolmont, C.A.Sebenne (Lab. de Phys. des Solides, Univ. Pierre & Marie Curie, Paris, France). *Solid State Commun. (USA)*, vol.46, no.9, p.689-91 (June 1983). The effect of ultrahigh vacuum deposition of Ge below and at monolayer (ML) coverage onto a 7×7 reconstructed clean $Si(111)$ surface held at room temperature is studied by low energy electron diffraction (LEED), Auger electron spectroscopy (AES) and photoemission yield spectroscopy (PYS). The results are compared to those obtained on 2×1 reconstructed clean $Si(111)$: (i) the Si dangling bond states are replaced by Ge dangling bond states at submonolayer coverages in both cases; (ii) the 7×7 reconstruction persists below 1 ML, it is not replaced by a $\sqrt{3} \times \sqrt{3}$ $R30^\circ$ at $1/3$ ML as it was on the 2×1 ; and (iii) the coverage below 1 ML is not homogeneous on the 7×7 reconstruction. This behaviour can be explained by the influence of the inhomogeneities associated with the 7×7 reconstruction. (17 refs.)
- 76786** Layer-dependent shifts in ionization potential and Auger energies for Kr/Cu (110). T.Mandel, G.Kaindl (Inst. für Atom- und Festkörperforschung, Freie Univ. Berlin, Berlin, Germany), K.Horn, M.Iwan, H.U.Middelmann, C.Mariani. *Solid State Commun. (USA)*, vol.46, no.9, p.713-16 (June 1983). Photoelectron spectra of the krypton 3d core-levels and MNN Auger spectra of krypton mono- and multilayers on Cu(110) have been recorded with synchrotron radiation. The Kr-3d line is found to shift to higher binding energies by 0.73 eV for first- and second-layer adsorption, respectively. This value is much larger than the work function decrease for Kr monolayer adsorption, $\Delta\phi = -0.29$ eV. The shift in Auger line energies is found to be about three times larger than the 3d line shift. These observations can be readily explained in terms of image-charge screening of the hole states. (16 refs.)
- 76787** The melting line for ethylene on graphite. J.Z.Larese, R.J.Rollefson (Phys. Dept., Wesleyan Univ., Middletown, CT, USA). *Surf. Sci. (Netherlands)*, vol.127, no.3, p.L172-8 (May 1983). Using the minimum in the nuclear magnetic spin-lattice relaxation time versus temperature as an indicator of melting the authors have mapped out the solid-fluid phase boundary for ethylene adsorbed on graphite. At low coverages the ethylene forms a self-bound monolayer solid with a melting temperature of about 68K. The molecules in the solid retain orientational mobility down to 55K, the lowest temperatures explored. (12 refs.)
- 76788** Diffusion of hydrogen on metal surfaces: strong coupling limit. M.D.Miller (James Franck Inst., Univ. of Chicago, Chicago, IL, USA). *Surf. Sci. (Netherlands)*, vol.127, no.3, p.383-402 (May 1983). Recently DiFoggio and Gomer (1980, 1982) measured diffusion coefficients for $^1H/W(110)$ and $^2H/W(110)$ using the field emission fluctuation method. Qualitatively, they found two temperature regimes: high temperature thermally activated behavior and a low temperature regime of temperature independent diffusivity. The present author examines in detail the possibility that the thermal regime is due to phonon assisted tunneling (small polarons). By means of a Kubo formulation, the high temperature real part of the frequency dependent diffusivity is calculated. It is concluded that for $H/W(110)$ a polaronic mechanism would require an implausibly large adatom-phonon coupling. (33 refs.)
- 76789** The formation of a surface iodide on Ni(100) and adsorption of I_2 at low temperatures. R.G.Jones, C.F.McConville, D.P.Woodruff (Dept. of Phys., Univ. of Warwick, Coventry, England). *Surf. Sci. (Netherlands)*, vol.127, no.3, p.424-40 (May 1983). Iodine adsorption on clean Ni(100) has been investigated using low energy electron diffraction (LEED) and Auger electron spectroscopy (AES). At temperatures below 340K a saturated surface of adsorbed iodine atoms in a $c(2 \times 2)$ structure is observed. Adsorption of iodine on clean Ni(100) at temperatures in excess of 370K forms a structure identified as a single layer of the layered compound NiI_2 on the metal substrate. Solid iodine is shown to grow epitaxially on both the $c(2 \times 2)$ chemisorbed surface and the surface iodide at temperatures less than 185K. Heating to $185 < T < 226$ K leaves a physisorbed molecular iodine layer, while on returning to room temperature the original $c(2 \times 2)$ or iodide is restored. (17 refs.)
- 76790** The temperature dependence of the interaction of oxygen with Pd(111): a study by photoemission and Auger spectroscopy. D.L.Weissman-Wenocur, M.L.Sheik, P.M.Stefan, I.Lindau, W.E.Spicer (Stanford Electronics Labs., Stanford Univ., Stanford, CA, USA). *Surf. Sci. (Netherlands)*, vol.127, no.3, p.513-25 (May 1983). The temperature dependence of the different binding states of oxygen on Pd(111) has been studied using photoemission spectroscopy and Auger spectroscopy. By examining the oxygen 2s binding energies, three distinct states are observed, which are identified as surface chemisorbed oxygen, oxygen incorporated into the first Pd layers, and subsurface oxygen. Changes in the relative oxygen Auger peak heights for 1000K exposure temperature are explained if the oxygen is assumed to become more negatively charged as it

penetrates the Pd surface. A model for the interaction of oxygen with the Pd(111) surface is proposed. (21 refs.)

76791 A LEED-AES study of the structure of sulfur monolayers on the Mo(100) crystal face. M.Salmeron, G.A.Somorjai (Dept. of Chem., Univ. of California, Berkeley, CA, USA), R.R.Chianelli. *Surf. Sci. (Netherlands)*, vol.127, no.3, p.526-40 (May 1983). The formation of ordered phases of sulfur on the molybdenum (100) crystal face has been studied by low energy electron diffraction (LEED), Auger electron spectroscopy (AES) and thermal desorption spectroscopy (TDS). Sulfur was deposited from a S₂ molecular flux streaming out of an Ag₂S containing electrochemical cell inside the UHV chamber. The use of a controlled flux of S₂ allowed the careful determination of saturation values for the monolayer, as well as the formation of multilayers of sulfur. This allowed the calibration of Auger intensities in terms of sulfur coverage. Various ordered structures were observed by LEED for different values of the S coverage. Real space models for these structures are proposed that satisfy the coverage values observed and place sulfur atoms only on high symmetry four-fold sites on the (100) molybdenum surface. (22 refs.)

76792 The role of sulfur in oxygen adsorption on niobium. A.P.Kazantsev (A.F. Ioffe Physicotech. Inst., Acad. of Sci., Leningrad, USSR). *Sov. Phys.-Tech. Phys. (USA)*, vol.27, no.11, p.1406-7 (Nov. 1982). Translation of: *Zh. Tekh. Fiz. (USSR)*, vol.52, no.11, p.2289-90 (Nov. 1982). [received: May 1983]

Surfaces are always purified of surface and bulk contaminants before metal surfaces are cleaned and purified. Sulfur atoms are very frequently observed on metal surfaces when samples are exposed to air or heated because sulfur atoms segregate out from the interior. In some cases these sulfur atoms may affect the adsorption properties. The author studied adsorption of oxygen on a pure polycrystalline niobium surface by Auger electron spectroscopy. The chemical bonding of oxygen to metal surfaces is known to be altered when the metal is oxidized or during adsorption and segregation of impurity atoms; as a result, both the shape and the energy shifts of the Auger peaks are changed. The author recorded the undifferentiated Auger peaks in order to use the changes in the area underneath the oxygen peak to follow the changes in oxygen concentration in the analyzed surface region. (9 refs.)

76793 Adsorption of O₂ and CO on thin films of palladium. V.D.Vankar, R.W.Vook, B.C.De Cooman (Dept. of Chem. Engng. & Materials Sci., Syracuse Univ., Syracuse, NY, USA). *Thin Solid Films (Switzerland)*, vol.102, no.4, p.313-26 (29 April 1983). The adsorption of O₂ and CO on polycrystalline and (111) monocrystalline thin palladium films formed by vapor deposition has been studied by means of Auger electron spectroscopy (AES), low energy electron diffraction (LEED) and mass spectrometry. The palladium film thicknesses ranged from 15 to approximately 1500 Å. The experiments were carried out at 298K. Surface topographical effects were studied in various ways, one of which was a method consisting of repeated alternating vapor deposition of palladium and gaseous exposure. In all cases studied, no LEED pattern other than the normal Pd(1×1) pattern was observed after gaseous exposures up to 6000 langmuir of O₂ or 7200 langmuir of CO. However, AES showed clearly that some O₂ and CO adsorbed on polycrystalline and monocrystalline surfaces that were either contaminated or rough. Thick (1500 Å) smooth Pd(111) films grown on mica showed no evidence of significant O₂ or CO adsorption, and in both cases the AES intensity ratio of the O(512 eV) line to the Pd(329 eV) line was near zero. (28 refs.)

76794 Photon stimulated ion desorption from Na₂WO₃. R.L.Benbow, M.R.Thuler, Z.Hurtych (Phys. Dept., Northern Illinois Univ., Dekalb, IL, USA). Fifteenth Annual Synchrotron Radiation Users Group Conference (papers in summary form only received), Stoughton, WI, USA, 18-19 Oct. 1982 (Stoughton, WI, USA: Synchrotron Radiat. Center 1982), p.6-7. The authors have studied photon-stimulated desorption (PSD) of O⁺ ions from Na₂WO₃ in the range 30 eV ≤ hν ≤ 85 eV. The results show the potential for using the Knotek-Feibelman interaction as a bonding-site sensitive probe of certain species on the surface. (2 refs.)

76795 Sorption of hydrogen and deuterium in a glassy Pd-Si alloy by a bending-cantilever method. B.S.Berry, W.C.Pritchett (IBM Thomas J. Watson Res. Center, Yorktown Heights, NY, USA). Rapidly Solidified Amorphous and Crystalline Alloys. Proceedings of the Materials Research Society Annual Meeting, Boston, MA, USA, Nov. 1981 (New York, USA: North-Holland 1982), p.249-53. The dilatation caused by the sorption of H and D in amorphous samples of melt-spun Pd₈₂Si₁₈ and sputter-deposited Pd₈₁Si₁₉ has been measured at room temperature for ambient charging pressures P up to 760 torr. By comparison with the strength of the Gorsky relaxation, it is concluded that (a) the dilatations per hydrogen and deuterium atom are identical and independent of concentration and (b) the non-linearity of the dilatation vs. P^{1/2} isotherms is due solely to a deviation from Sieverts' law. The isotherms exhibit a distinct isotope-dependence, of a similar nature to that for crystalline Pd. A sputter-deposited film is found to dissolve more H or D than a melt-spun ribbon, due possibly to a less structurally-relaxed configuration. (3 refs.)

Intramolecular charge-transfer fluorescence from 9,9'-bianthryl adsorbed on porous glass See Entry 75427

Photoelectron spectra of adsorbed carbonates See Entry 75440

X-ray and UV photoelectron-spectroscopic studies of pyridine adsorbed on evaporated nickel and palladium in the temperature range 140-385K See Entry 75441

Physical model of plasticity of a transition See Entry 76605

Vibrational interaction between hydrogen atoms adsorbed on Pd(100) See Entry 76766

Mechanism of graphite baffle gettering in organometallic vapor phase epitaxy; adsorption of trimethylaluminum on graphite See Entry 76809

Pieterls instability and charge density waves at the surface of a metal with a quasideimensional electron spectrum See Entry 76935

On the role of surface phenomena in the Staebler-Wronski effect See Entry 76994

A covalent model for the bonding of adsorbed hydrocarbon fragments on the (111) face of platinum See Entry 77018

Variation of the characteristic electron energy loss spectra of molybdenum, doped with Ba⁺ ions See Entry 77494

Scattering and surface recoiling TOF spectra of neutrals and ions from rare gas bombardment of Ge, GeO₂, and H₂O adsorbed n Ge See Entry 77498

Energy redistribution among internal states of nitric oxide molecules upon scattering from Pt(111) crystal surface See Entry 77503

Reply to 'Comment on 'X-ray photoelectron spectroscopic studies of oxygen chemisorption on thick films of photoconducting cadmium sulphide' See Entry 77519

Photoemission of Xe and Kr adsorbed on the W(110) plane See Entry 77524

Optical 4d excitation in a monolayer of Xe on Au See Entry 77527

Photoemission does not measure the energies of orbitals (or: Configurational model of adsorbate structure and excitations) See Entry 77528

The bandstructure of CO on Cu(111); breakdown of the single particle picture See Entry 77529

High-temperature adsorption of atmospheric oxygen on silicon nitride powders See Entry 77782

Photoreactions on finely divided semiconductors See Entry 77915

Adsorption-complex isomerism and quantum-chemical studies in heterogeneous catalysis See Entry 77916

Radiation damage enhancement of the penetration of water into silica glass See Entry 77917

The adsorption and dissociation of methyl isocyanide on Rh(111) See Entry 77918

D₂O product angular and translational energy distributions from the oxidation of deuterium on Pt(111) See Entry 77919

The mechanism of the CO₂ formation on Pt(111) and polycrystalline surfaces at low temperatures See Entry 77921

68.48 SOLID-SOLID INTERFACES

(inc. bicrystals; for grain boundaries, see 61.70N)

76796 Kinetics of self-interstitials generated at the Si/SiO₂ interface. K.Taniguchi, D.A.Antoniadis (Dept. of Electrical Engng. & Computer Sci., MIT, Cambridge, MA, USA), Y.Matsushita. *Appl. Phys. Lett. (USA)*, vol.42, no.11, p.961-3 (1 June 1983).

The kinetics of self-interstitials in silicon were investigated by monitoring oxidation stacking faults on backside oxidized silicon wafers in the temperature range 1100-1200°C in a wet O₂ ambient. The diffusion coefficient and thermal equilibrium concentration of self-interstitials were obtained by optimizing model parameters to match calculated and experimental observations of growth of oxidation stacking faults at the front surface of silicon wafers protected from oxidation by a composite SiO₂/poly Si/Si₃N₄ film. (22 refs.)

76797 Anodic bonding of imperfect surfaces. T.R.Anthony (General Electric Res. & Dev. Centre, Schenectady, NY, USA). *J. Appl. Phys. (USA)*, vol.54, no.5, p.2419-28 (May 1983).

The intimate surface contact necessary for anodic bonding of a metal to a glass is examined in terms of the electrostatic forces which promote this contact and surface imperfections which prevent this contact. Surface imperfections that are considered include foreign particles, isolated hillocks, and periodic curved and angular surfaces. With curved and angular surfaces, a critical voltage exists that causes spontaneous mating of the surfaces by elastic or plastic deformation. Below this voltage, intimate surface contact is achieved by viscous flow. For isolated hillocks and foreign particles, surface conformation generally occurs by viscous flow because of large stress concentrations at these imperfections. The resulting time required for intimate surface contact is a very sensitive function of the imperfection size. (25 refs.)

76798 High resolution imaging of the interfacial region in metal-insulator-semiconductor and Schottky diodes. M.A.Green, A.W.Blakers (Joint Microelectronics Res. Centre, Univ. of New South Wales, Kensington, Australia), O.L.Krivaneck. *J. Appl. Phys. (USA)*, vol.54, no.5, p.2885-7 (May 1983).

Interfacial oxides can greatly influence the properties of metal-semiconductor heterojunctions as demonstrated by recent work on metal-insulator-semiconductor solar cells. The physical structure of such interfacial regions is examined using high resolution electron microscopy. Simultaneous imaging of the lattice structure on both sides of the interfacial region is reported for the first time. (6 refs.)

Interface spinodal decomposition in LPE In_{0.5}Ga_{0.5}As_{0.5}P_{0.5} lattice-matched to InP See Entry 76646

The concentrated profile of photostimulated Ag diffusion in thin As₂S₃ layers See Entry 76707

Effects of annealing and electromigration on surface morphology of polycrystalline films See Entry 76712

Accommodation of misfit in heterostructures with continuous and islands films See Entry 76813

Tunnel barriers on Pb-In-Au alloy films See Entry 77050

Ion knock-on broadening effects in Auger sputter profiling studies of ultra-thin SiO₂ layers on Si See Entry 77502

The formation of discrete precipitate dispersions on mobile interphase boundaries in iron-base alloys See Entry 77645

68.55 THIN FILM GROWTH, STRUCTURE, AND EPITAXY

(for techniques of crystal growth and film deposition, see 81.10 and 81.15)

76799 Use of an overlay-film configuration to improve contrast of low-angle electron diffraction in thin films with columnar microstructure. S.Nakahara, A.F.Hebard (Bell Labs., Murray Hill, NJ, USA). *Mater. Lett. (Netherlands)*, vol.1, no.5-6, p.141-4 (April 1983).

Periodicities associated with columnar microstructure have been observed in the electron diffraction patterns obtained from a thin-film overlay structure. This structure consists of a copper/copper-oxide film containing a small regularly-spaced array of columns and covered by a polycrystalline gold film. Both the transmitted and diffracted beams within the gold film act as independent incident beams for the underlying copper film, the latter giving rise to the formation of sub-diffraction rings around strongly-diffracted spots of gold lines. These sub-rings, appearing only because of this double diffraction effect, were found to represent the spatially-periodic distribution of columns in the copper film. (7 refs.)

76800 Substrates for epitaxial growth of hexaferrite films. F.Licci, S.Rinaldi, T.Besagni (Istituto MASPEC, CNR, Parma, Italy). *Mater. Lett. (Netherlands)*, vol.1, no.5-6, p.163-5 (April 1983).

By suitable substitution of iron by nonmagnetic trivalent cations in hexagonal ferrites, the authors succeeded in obtaining compounds which are paramagnetic at room temperature, isomorphous with R-Fe₁₂O₁₉, where R=Ba, Sr or Pb, and have lattice parameters close to the hexaferrite ones. These materials

may be suitable substrates for epitaxial deposition of magnetic hexaferrite films. (4 refs.)

76801 An analysis of the process of recrystallization of silicon thin films with either a scanning laser or strip heater. H.E.Cline (General Electric Corporate Res. & Dev., Schenectady, NY, USA). *J. Appl. Phys. (USA)*, vol.54, no.5, p.2683-91 (May 1983).

An analysis of the temperature, stress distribution, and crystal growth was made to model the process of recrystallization of silicon thin films with either a scanning laser or strip heater. The temperature distribution of a wafer with one or more thin film layers was calculated using both Green's function and Fourier series methods. With increasing velocity, the temperature profile becomes asymmetric and the maximum temperature decreases. Heat flow is influenced by the applied heat profile, the layer thicknesses, thermal properties, heat transfer coefficient between the wafer and substrate, and the velocity of the heat zone. If the heat zone is wider than the wafer thickness the temperature profile may be approximated using a one-dimensional model. Thermal stresses are generated by either a nonuniform temperature or differential thermal expansion between layers. Temperature differences along the film that are greater than 10°C may plastically deform the silicon film. To crystallize cell-free single-crystal thin films a critical ratio of the thermal gradient to the solidification velocity must be exceeded. The criterion for the crystallization of defect-free material is derived in terms of the solidification rate, heat transfer, and stability of the planar solid-liquid interface during crystal growth. It is predicted that defect-free silicon films are possible at rates below 0.005 cm/sec from a comparison with conventional growth of silicon single crystals. (20 refs.)

76802 Spin coated amorphous chalcogenide films: structural characterization. G.C.Chern, I.Lauks (Dept. of Electrical Engng. & Sci., Univ. of Pennsylvania, Philadelphia, PA, USA).

J. Appl. Phys. (USA), vol.54, no.5, p.2701-5 (May 1983). Thin films that are substantially amorphous arsenic sulfide have been prepared by spin deposition from solutions of *n*-propylamine or *n*-butylamine. These materials have been investigated by nuclear magnetic resonance, infrared absorption, and elemental analysis. A structural model is suggested based on As_2S_3 clusters surrounded by amine as an amine salt. (58 refs.)

76803 Defect evaluation of Si MBE film. Y.Ota (Bell Labs., Reading, PA, USA).

J. Cryst. Growth (Netherlands), vol.61, no.3, p.439-48 (April-May 1983). Crystalline defects in (100) and (111) Si MBE films were evaluated by various chemical etching techniques. Although the defects and defect patterns in an MBE film were similar to those observed in a CVD film, they were generated by different mechanisms because of the vast difference in the growth conditions of the two epitaxial techniques. Furthermore, (111) Si MBE films contained a unique defect pattern which has not been observed in CVD films. Defect etch patterns in a Si MBE film are described in terms of the cause of the defects. (20 refs.)

76804 Morphology of organometallic CVD grown GaAs epitaxial layers.

D.H.Reep, S.K.Ghandhi (Rensselaer Polytech. Inst., Troy, NY, USA). *J. Cryst. Growth (Netherlands)*, vol.61, no.3, p.449-57 (April-May 1983). Growth conditions and resulting epitaxial layer morphology are presented for atmospheric pressure OM-CVD layers of GaAs, grown at 700°C on (100), (100)+ 3° , (110), (110), (111)Ga, and (111)As oriented substrates. The substrate orientation found most favorable for useable devices is either the (100) or misoriented (100). For these substrates, the epitaxial layer morphology is largely independent of reactant flux, in contrast to the results found for the other orientations. A simple model is presented to explain the morphology of layers grown on the (111)As and (111)Ga faces. Finally, impact of the morphology study on the electrical characteristics of the layers, and on the growth of polycrystalline layers, is discussed. (39 refs.)

76805 Interface reactions and grain growth processes in poly-GaAs deposited on molybdenum substrates by the organometallic process. S.K.Shastry, S.K.Ghandhi (Rensselaer Polytech. Inst., Troy, NY, USA).

J. Cryst. Growth (Netherlands), vol.61, no.3, p.458-62 (April-May 1983). Describes grain growth processes for polycrystalline gallium arsenide on molybdenum substrates. Growth was carried out by the pyrolytic decomposition of trimethylgallium and arsine in hydrogen. The ability of the organometallic process to allow the growth of gallium arsenide over a wide temperature range is exploited in the initial nucleation and growth phase to obtain full coverage of the substrate. A heat treatment step is used to provide grain expansion and results in a surface with a rippled character. It is proposed that this comes about by the dissociation of GaAs at the interface, due to strong Mo-As reactions at the annealing temperature, resulting in regrowth of GaAs from a liquid-like phase. Eventual growth of a device quality, active layer is accomplished by conventional CVD growth at $650\text{--}700^\circ\text{C}$, resulting in an average grain size of $6\text{ }\mu\text{m}$ for a $6\text{--}7\text{ }\mu\text{m}$ thick overall structure. (15 refs.)

76806 Influences of substrate surface structures and water vapor on the nucleation, epitaxy and graphoepitaxy of tin thin films grown on potassium chloride substrates. T.Osaka, T.Kawana, T.Noijima (Dept. of Metall. Engng., Waseda Univ., Tokyo, Japan), K.Heinemann.

J. Cryst. Growth (Netherlands), vol.61, no.3, p.509-24 (April-May 1983). Thin films of tin were prepared by vapor deposition on vacuum-cleaved potassium chloride substrates with and without exposure to water vapor, and on air-cleaved substrates. Examination by optical and electron microscopy revealed that the cleavage surface of the substrate had fine structures composed of six characteristic features. On clean substrates, {100} epitaxial films and graphoepitaxial films were produced, depending upon the surface structures of the substrate. For the case of air-cleaved and water-vapor-exposed substrates, a decrease of the {100} epitaxy and modifications of the substrate surfaces were observed. Possible mechanisms for these findings are discussed. (31 refs.)

76807 Growth kinetics of LPE $\text{Ga}_{0.83}\text{Al}_{0.17}\text{Sb}$ layers grown from supercooled solutions. M.Mebarki, P.Salsac, A.Jouille, G.Bougnat (Univ. des Sci. et Tech. du Languedoc, Montpellier, France).

J. Cryst. Growth (Netherlands), vol.61, no.3, p.637-40 (April-May 1983). GaSb and $\text{Ga}_{0.83}\text{Al}_{0.17}\text{Sb}$ alloys were grown by liquid phase epitaxy from supercooled solutions. The composition profiles were determined and the thicknesses of the layers were measured as a function of the growth time and the cooling rate. The data are quantitatively consistent with a simple diffusion limited growth model, available for binary and ternary compounds. The diffusivity of antimony was found to be $D_{\text{Sb}} = 7.1 \times 10^{-10}\text{ cm}^2\text{ s}^{-1}$ for GaSb (at 560°C) and $D_{\text{Sb}} = 6.7 \times 10^{-10}\text{ cm}^2\text{ s}^{-1}$ for $\text{Ga}_{0.83}\text{Al}_{0.17}\text{Sb}$ (at 550°C). (17 refs.)

76808 Electroepitaxy from a limited solution volume: growth kinetics calculations. Z.R.Zytikiewicz (Inst. of Phys., Polish Acad. of Sci., Warszawa, Poland).

J. Cryst. Growth (Netherlands), vol.61, no.3, p.665-74 (April-May 1983). The analytical expression for the growth rate is obtained and applied, as an example, to GaAs. The advantages of using thin solution layers in electroepi-

taxy of GaAs instead of the previously used systems are discussed. It is shown that limitation of the solution height causes a reduction of the influence of diffusion on the growth rate and results in better homogeneity of the grown layers. Moreover, elimination of convective mixing in the solution volume allows easier control of the growth process. (32 refs.)

76809 Mechanism of graphite baffle gettering in organometallic vapor phase epitaxy; adsorption of trimethylaluminum on graphite. D.W.Kisker, D.A.Stevenson (Dept. of Materials Sci. & Engng., Stanford Univ., Stanford, CA, USA).

J. Electron. Mater. (USA), vol.12, no.2, p.459-82 (March 1983). The adsorption of trimethylaluminum (TMA) on graphite surfaces was investigated using a controlled gas flow system and a molecular beam mass spectrometer. Values for the amount of TMA adsorbed on graphite surfaces under a variety of conditions were determined by analyzing the transient response attending abrupt changes in input gas composition. Significant adsorption of TMA was observed, with a heat of adsorption of 15.7 kcal/mole . When graphite baffles are used in organometallic vapor phase epitaxy, there are several important practical consequences of the adsorption: the gettering of impurities, the doping efficiency, and difficulties in establishing sharp junctions. (14 refs.)

76810 Auger and AC impedance studies of the RF sputter deposited Fe_2O_3 films. S.C.Tjong (Dept. of Chem. Engng., Univ. of Saskatchewan, Saskatoon, Saskatchewan, Canada).

Mater. Res. Bull. (USA), vol.18, no.4, p.421-7 (April 1983). Thin iron oxide films were prepared by RF sputtering techniques. X-ray diffraction and Auger electron spectroscopic techniques were used to determine the structure of the films. The results showed that the film prepared with such techniques has an $\alpha\text{-Fe}_2\text{O}_3$ structure. AC impedance techniques were also applied to determine the electrochemical properties of the films. It was found that the film exhibited semiconducting properties in the borate buffer solution at the anodic potentials below 0.73 V vs. RHE. (5 refs.)

76811 Formation of semiconductor epitaxial films by pulse heating crystallization or regrowth. L.N.Aleksandrov (Inst. of Semiconductor Phys., Acad. of Sci., Novosibirsk, USSR).

Phys. Status Solidi A (Germany), vol.76, no.1, p.179-90 (16 March 1983). The contemporary state and perspectives of methods used, namely thermodynamic and kinetic characteristics of amorphous film crystallization and regrowth processes by pulse (laser, electron beam etc.) heating are considered. On the base of experimental data thermodynamic diagrams of the processes of normal and accelerated, explosive or shock, crystallization of amorphous film (in the solid state) or regrowth (through the liquid phase) are given. An analysis of the acting mechanism by comparing the waiting time t_0 for the appearance of the first nucleus of the crystalline or liquid phase with the time Δt of heating pulse is made. Calculation of possible size of the crystalline blocks and of the time of their growth gives ≈ 1 to $100\text{ }\mu\text{m}$ by ≈ 1 to $100\text{ }\mu\text{s}$. The ways for improving the structure of polycrystalline epitaxial semiconductor films with large blocks are discussed. (51 refs.)

76812 Shock crystallization of films. L.N.Aleksandrov, F.L.Edelman (Inst. of Semiconductor Phys., Acad. of Sci., Novosibirsk, USSR).

Phys. Status Solidi A (Germany), vol.76, no.2, p.409-27 (16 April 1983). The phenomenon of shock (explosive) film crystallization with a rate several orders higher than the normal one at the transition of films from the amorphous to the crystalline state is considered. Experimental data for films of antimony, germanium, silicon, silicon dioxide, and silicon oxynitride, for the structure and mechanism of crystallization are discussed in detail. The connection has been established between the temperature and energy of the phase transition and elastic stresses and heat conduction of amorphous and crystalline phases with an energy of external effects and initial temperature. The model of the process of shock crystallization in films has been developed and the difficulties of the theory of this phenomenon have been revealed. The possible time of the self-sustaining shock crystallization has been estimated depending on the film temperature for structures on the basis of amorphous SiO_2 , Si films-Si, shock crystallization is required for its quantitative description. (39 refs.)

76813 Accommodation of misfit in heterostructures with continuous and islands films. E.M.Trukhanov (Inst. of Semiconductor Phys., Acad. of Sci., Novosibirsk, USSR).

Phys. Status Solidi A (Germany), vol.76, no.2, p.437-45 (16 April 1983). An equation is derived for the equilibrium dislocation configuration in a slip plane with a stress distribution depending on a single coordinate. The equation allows one to determine the critical film thickness at which dislocations are first formed in various heterostructures. Critical thicknesses are discussed for systems with a continuous film, with a semi-infinite film, bounded by a straight edge, and with a series of parallel strips on the substrate surface. The theoretical data are in agreement with the observed ones for continuous films. They are confirmed by experimental results for the heterostructure with a discontinuous film. The peculiarities of stable and unstable equilibrium dislocations are discussed for the mentioned heterostructures. (21 refs.)

76814 Multiple phase transitions in GeTe films. Dynamics and film structure. O.Bostanjoglo (Optisches Inst., Tech. Univ. Berlin, Berlin, Germany).

Phys. Status Solidi A (Germany), vol.76, no.2, p.525-31 (16 April 1983). Electron pulse-crystallization of amorphous $\text{Ge}_{0.8}\text{Te}_{0.2}$ films, serving as a model substance for multiple transitions, is investigated by 'time-resolved' TEM. Precipitation and amorphization of Te crystallites, and generation of different textures of crystalline GeTe successively occur during a μs annealing pulse, depositing 1.1 kW/cm^2 in the film. The growth velocities of the different GeTe textures range from 0.3 to 10 m/s at the beam centre, dropping by more than one order of magnitude beyond the irradiated area. The various phases spatially separate in concentric regions, fast transitions being characterized by a sharp demarcation between the participating phases. (17 refs.)

76815 Evidence of the formation of twins by deformation and 'growth-accidents' in evaporated thin films of gold. A.H.King (Dept. of Materials Sci. & Engng., State Univ. of New York, Stony Brook, NY, USA).

Phys. Status Solidi A (Germany), vol.76, no.2, p.629-36 (16 April 1983). Transmission electron microscope observations of twins in epitaxially grown gold single crystals are presented. It is demonstrated that most, though not all, of the twins found in such specimens arise from deformation of the material during handling. A mechanism for the formation of grown-in twins is proposed to explain some of the observed features. (8 refs.)

Lattice fringe imaging studies of the twin structures in electro-crystallized nickel coatings See Entry 76453

Modulation doping structures in silicon by molecular beam epitaxy and off-line ion implantation See Entry 76461

Ion implantation damage and annealing in germanium See Entry 76463

Interface spinodal decomposition in LPE $\text{In}_x\text{Ga}_{1-x}\text{As}_y\text{P}_{1-y}$ lattice-matched to InP See Entry 76464

- The effect of interposed silicide thickness on growth rate in bilayer silicide thin-film structures: the Si(111)/Pd₂Si/Cr systemSee Entry 76710
- Ti-W alloy interaction with silicon in the presence of PtSiSee Entry 76711
- Effects of annealing and electromigration on surface morphology of polycrystalline filmsSee Entry 76712
- Study and application of the mass transport phenomenon in InPSee Entry 76719
- Surface crystallography of thin films by electron diffraction in the STEMSee Entry 76760
- The formation of a surface iodide on Ni{100} and adsorption of I₂ at low temperaturesSee Entry 76789
- Residual donors and acceptors in high-purity GaAs and InP grown by hydride VPESee Entry 76883
- Some properties of amorphous Si thin films and their application to sensors. I. Power sensorSee Entry 76938
- The heterojunction ZnSe-(Zn_{1-x}Cd_xTe)_{1-y}(In₂Te)_{3y} having high sensitivity in the visible light range and its applicationsSee Entry 77024
- Angle-lapping and staining observations of Si doping superlattice structuresSee Entry 77025
- The variation of the p/n junction position in GaAs/GaAlAs double heterostructures grown by low pressure MO VPESee Entry 77027
- Electrical characteristics of thin Ni₂Si, and NiSi₂ layers grown on siliconSee Entry 77071
- Preparation, physical properties, and superconductivity of La_{3-x}S₄ filmsSee Entry 77085
- Effect of magnetic field in RF sputtering on the crystal orientation and magnetic properties of Co-Cr perpendicular anisotropy filmsSee Entry 77219
- Epitaxial growth and annealing control of EMR properties of thick homogeneous Ga substituted yttrium iron garnet filmsSee Entry 77267
- Mossbauer spectroscopy of amorphous silicon-tin-hydrogen alloysSee Entry 77296
- Raman microprobe study of recrystallization in ion-implanted and laser-annealed polycrystalline siliconSee Entry 77374
- Raman spectra and physical structure of cellulose triacetateSee Entry 77388
- Photoluminescence of molecular beam epitaxially grown Ge-doped GaAsSee Entry 77431
- Photoluminescent and electrical properties of InGaPAs mixed crystals liquid-phase-epitaxially grown on (100) GaAsSee Entry 77432
- Zero-phonon lines in electroluminescence and photoluminescence of ZnS:Mn thin films grown by atomic layer epitaxySee Entry 77459
- Refractive index of GaAs-AlAs superlattice grown by MBESee Entry 77470
- Picosecond reflectivity measurements on glow discharge a-Si:HSee Entry 77471
- Far ultraviolet photoelectric study of thin SnSe evaporated filmsSee Entry 77522
- Field emission fluctuation phenomena of potassium microcrystals on tungsten. I. Spectral density functions and flip-flopSee Entry 77535
- Field emission fluctuation phenomena of potassium microcrystals on tungsten. II. Temperature dependence and simulation of noise propertiesSee Entry 77536
- Solid-phase lateral epitaxy of chemical-vapor-deposited amorphous silicon by furnace annealingSee Entry 77562
- Structural and optical properties of sprayed CuInSe₂ filmsSee Entry 77564
- Microstructure trends in metal(aluminum, copper, indium, lead, tin)-metal oxide thin films prepared by reactive ion beam sputter depositionSee Entry 77567
- Thin film field effect transistors incorporating hydrogenated amorphous silicon produced by r.f. magnetron sputteringSee Entry 77568
- Crystallization of amorphous mercury selenide filmsSee Entry 77569
- Incorporation rates of gallium and aluminum on GaAs during molecular beam epitaxy at high substrate temperaturesSee Entry 77570
- Growth of high quality Ge MBE filmSee Entry 77571
- A comparison between InP films growth by the hydride and chloride techniquesSee Entry 77573
- Reactive pulse plasma crystallization of TiN layers on substrates at 500KSee Entry 77574
- The growth of epitaxial InP by the chloride process in nitrogen and in the presence of phosphineSee Entry 77575
- Modelling of GaAs growth in the low pressure halide transport systemSee Entry 77576
- Low pressure metalorganic chemical vapor deposition on InP and related compoundsSee Entry 77577
- Effect of deposition parameters on the microstructure of chemically vapour-deposited SnO₂ filmsSee Entry 77579
- Investigation of crystallographic properties of thin germanium crystals grown on silicon substrates by chemical vapor depositionSee Entry 77580
- Efficiency of the SiH₄ oxidation reaction in chemical vapour deposition of SiO₂ films at low temperatureSee Entry 77581
- MOCVD growth and characterization of high luminescence efficiency Al_{0.53}Ga_{0.47}AsSee Entry 77583
- LPE growth of InP/InGaAs/InP DH wafers on (100) InP substratesSee Entry 77584
- Direct liquid phase epitaxial growth of high-quality InP on (111)A oriented In_{0.53}Ga_{0.47}AsSee Entry 77585
- Gradient-free isothermal liquid-phase heteroepitaxy of A^{III}B^V compoundsSee Entry 77589
- Investigation of capless heat treatment of MBE n-GaAsSee Entry 77686
- Review of oxidation processes in plasmasSee Entry 77778
- Realisation et caracterisation de cellules solaires Cu₂S-CdZnS (Realisation and characterisation of Cu₂S-CdZnS solar cells)See Entry 78013
- The metal interconnected cascade solar cellSee Entry 78035

68.60 PHYSICAL PROPERTIES OF THIN FILMS, NONELECTRONIC

76816 Adhesion of aluminum films deposited on glass. F.Kobayashi, A.Nomura, T.Kano (Faculty of Engng., Shinshu Univ., Nagano, Japan). *J. Fac. Eng. Shinshu Univ. (Japan)*, no.53, p.45-53 (Dec. 1982). In Japanese. Adhesion of aluminum films deposited on glass substrate was experimentally studied for effects of the substrate temperature, substrate cleaning processes, and time lapse after deposition. Aluminum films were obtained at various substrate temperatures ranging from room temperature to 200°C and glass substrates were arranged by application of three different cleaning processes. The adhesion was measured by the scratch method. With rise in substrate temperature, the adhesion increases slightly in the range from room temperature to 100°C, but abruptly in the range 100-125°C, saturating above 150°C. Films obtained above 150°C exhibit a higher adhesion by a factor of 50 than those obtained at room temperature. As for the change in adhesion with time, at 312 hr films obtained at room temperature and those obtained at 200°C exhibit adhesions 10 and 1.5 times as high as those at 24 hr, respectively, with the latter films always kept higher in adhesion than the former. The three different cleaning processes applied on substrate had no effect on the adhesion. (10 refs.)

76817 Determining the frictional properties of thin films of lubricants. I.V.Kragel'skii, N.V.Gitis (A.A. Blagonravov Inst. of Mech. Engng., Acad. of Sci., Moscow, USSR). *Sov. Phys.-Dokl. (USA)*, vol.27, no.8, p.644-5 (Aug. 1982). Translation of: *Dokl. Akad. Nauk SSSR*, vol.265, no.4-6, p.1125-7 (Aug. 1982). [received: May 1983]

The tendency toward an increase in loading and heat stress at points of friction gives rise to the use of highly viscous and plastic lubricating materials and to a decrease in the roughness of rubbing surfaces, and leads to an increase in the danger of seizing and sticking as a result of the 'film starvation' effect. This effect consists of the fact that, under certain conditions, the thin films on the rubbing surfaces are worn away at the regions of actual contact and do not have time to be restored in the spaces between these regions. To investigate the effect in an actual frictional contact, the authors applied to the cylindrical surfaces of hardened steel rollers a regular microrelief of type IV by vibrational rolling. The profile of the rollers over the circumference was similar to the periodic profile of the packet of plates. (4 refs.)

Thermal modulation spectrum and electron structure of niobiumSee Entry 77474

Property enhancement in rapidly quenched alloy surfacesSee Entry 77811

68.90 OTHER TOPICS IN THE STRUCTURE AND NONELECTRONIC PROPERTIES OF SURFACES AND THIN FILMS

76818 The transmission electron microscopy of 1 to 2 nm rhodium particles dispersed on γ-Al₂O₃. S.B.Newcomb, W.M.Stobbs, J.A.Little (Dept. of Metall. & Materials Sci., Univ. of Cambridge, Cambridge, England). *Phys. Status Solidi a (Germany)*, vol.76, no.1, p.191-6 (16 March 1983). The primary problem in the transmission electron microscopical examination of small supported catalyst particles is differentiating them from their support. Methods for doing this using relatively low resolution dark field and bright field Fresnel techniques are described. High resolution images of rhodium particles, identified by this method, are discussed in relation to current models for their structure and morphology. (11 refs.)

70.00 CONDENSED MATTER: ELECTRONIC STRUCTURE, ELECTRICAL, MAGNETIC, AND OPTICAL PROPERTIES

(see also 81.40R Electrical and magnetic properties related to materials treatment, 81.40T Optical properties related to materials treatment)

71.00 ELECTRON STATES

(see also 63. Lattice dynamics, 73. Surfaces, interfaces, and thin films)

71.10 GENERAL THEORIES AND COMPUTATIONAL TECHNIQUES

76819 Some considerations on U_{eff} values entering the Hubbard Hamiltonian. J.Friedel, C.Noguera (Phys. des Solides, Univ. Paris XI, Orsay, France). *Int. J. Quantum Chem. (USA)*, vol.23, no.4, p.1209-21 (April 1983). One of the simplest ways to take into account correlations between electrons in solid state physics, beyond the usual one electron approximation, is to use the Hubbard Hamiltonian $H = \sum_{ij} \beta_{ij} C_i^\dagger C_j + U \sum_i n_{i\uparrow} n_{i\downarrow}$ ($1-\sigma_i$), $n_i = C_i^\dagger C_i$. Although it corresponds to very severe approximations, since intersite correlations are neglected, and since the whole problem is reduced to a single parameter U , it is already very difficult to solve, and exact solutions exist in only a few cases. It is thus not desired to introduce more complications in the Hamiltonian; but it could be interesting to understand, at least qualitatively, which processes influence the value taken by parameter U . The question arises in concrete cases, such as transition metals or organic molecules; comparing experiments and approximate solutions of the Hubbard Hamiltonian has been shown that, in most cases, the value of U that yields the best fit is very different from what would be expected from atomic considerations. For instance, if one wants to study correlation on atoms of type M , a pure atomic point of view would affect to U the change in energy U_{at} in the redox-type

equation $2M \rightleftharpoons M^+ + M^-$. However it seems that solid state effects plays an important role and the authors discuss three of them. (12 refs.)

76820 A generalized approximation of the Fermi-Dirac integrals. X.Aymerich-Humet, F.Serra-Mestres, J.Millan (Dept. d'Electricitat i Electronica, Univ. Autònoma de Barcelona, Barcelona, Spain). *J. Appl. Phys. (USA)*, vol.54, no.5, p.2850-1 (May 1983). An analytical approximation for the Fermi-Dirac integral $F_j(\eta)$ for real j is proposed. This approximation works for $-\infty < \eta < \infty$, with an error of 1.2% for $-1/2 < j < 1/2$ and 0.7% for $1/2 < j < 5/2$. The error increases with j for higher j values. (11 refs.)

76821 Relationship between the Kittler-Falicov method and the coherent potential approximation for disordered alloys. G.Gomez-Santos (Dept. de Física Fundamental, Univ. Autònoma, Madrid, Spain). *J. Phys. C (GB)*, vol.16, no.14, p.L453-8 (20 May 1983). The decoupling procedure involved in the configurational average of the Kittler-Falicov method for alloys is discussed. As a result of this analysis, a relationship between this method and the coherent potential approximation is established. (11 refs.)

76822 Simultaneous relaxation of nuclear geometries and electric charge densities in electronic structure theories. P.Bendt, A.Zunger (Solar Energy Res. Inst., Golden, CO, USA). *Phys. Rev. Lett. (USA)*, vol.50, no.21, p.1684-8 (23 May 1983).

A simple formalism is presented, within the density-functional approach, which constitutes a powerful scheme for directly calculating the ground-state energy of systems with arbitrarily located nuclei and their accompanying electrons. The method permits simultaneous relaxation of both the atomic geometries and the electronic charge densities of polyatomic systems towards equilibrium. It circumvents the far less efficient indirect (consecutive) approach in which the equilibrium geometry is determined after calculation of energies on the Born-Oppenheimer surface. (14 refs.)

76823 MO study of counter anions of TMTSF: electronic structure of NO_3^- , BF_4^- , ClO_4^- and FSO_3^- . H.Teramae, K.Tanaka, K.Shiotani, T.Yamabe (Dept. of Hydrocarbon Chem., Kyoto Univ., Kyoto Japan). *Solid State Commun. (USA)*, vol.46, no.8, p.633-7 (May 1983). The electronic structure and geometrical structure of NO_3^- , BF_4^- , ClO_4^- and FSO_3^- anions are studied by means of the ab initio molecular orbital method. According to the results obtained, the central atoms of these anions are all positively charged and the surrounding atoms negatively charged. The bonding nature of ClO_4^- and FSO_3^- is similar to that of XF_6^- ($X = \text{P, As}$ and Sb) previously studied, and has a coordination-like character. However, BF_4^- and NO_3^- show a covalent-like character. The ion radii of these anions are determined from the total density contour maps obtained by the calculation. (19 refs.)

76824 Density of unidimensional finite disordered system particles. L.A.Zil'berman.

Ukr. Fiz. Zh. (USSR), vol.28, no.5, p.752-60 (May 1983). In Russian. The structure of states is studied in one-dimensional finite disordered systems. The random potential $v(x)$ is considered as a Gaussian white noise. In a quasi-elastic region the energy particle density can be divided into two terms: the first is changed at distances of about a localization length and the second is a modulated standing wave with a period of π/ω . At negative energy $\omega = -q^2$ the boundary influence vanishes at a distance of about q^{-1} . (11 refs.)

71.20 ELECTRONIC DENSITY OF STATES DETERMINATIONS

(inc. energy states of liquid semiconductors; see also 65.40 Lattice and electronic heat capacity)

76825 Effects of energy dependence in the electronic density of states on some normal state properties. B.Mitrovic, J.P.Carbotte (Dept. of Phys., McMaster Univ., Hamilton, Ontario, Canada).

Can. J. Phys. (Canada), vol.61, no.5, p.758-83 (May 1983). The authors study the effects of energy dependence in the electronic density of states (EDOS) on the electron quasiparticle properties in the normal state. The Migdal-Eliashberg equations (1958, 1960) generalized to include a non-constant EDOS are derived in the isotropic approximation. By numerical solution of the electron self-energy equations in the normal state, they assess the effect of the interplay of the energy dependence in the EDOS, the electron-phonon interaction, and/or elastic impurity scattering on the electron quasiparticle properties. Self-consistency requirements are fully discussed. (55 refs.)

76826 Effects of energy dependence in the electronic density of states on some superconducting properties. B.Mitrovic, J.P.Carbotte (Dept. of Phys., McMaster Univ., Hamilton, Ontario, Canada).

Can. J. Phys. (Canada), vol.61, no.5, p.784-801 (May 1983). The authors study the influence of energy dependence in the electronic density of states (EDOS) on the single particle tunneling characteristics into a superconductor. The Migdal-Eliashberg equations (1958, 1960) generalized to the case of a nonconstant EDOS are derived. Three equations are involved, one for the gap, another for the renormalization function, and a new one for the chemical potential shift which does not appear in the conventional formulation. Numerical solutions of these equations are obtained, from which current voltage characteristics are calculated for a model EDOS. The 'inversion' of the calculated tunneling conductance shows that the effects of the peaks in the EDOS, on the scale of several Debye energies are important and cannot necessarily be reproduced within the usual Eliashberg theory by working with some effective value of electron-phonon spectral density $\alpha^2(\omega)F(\omega)$ and/or Coulomb parameter μ^* without introducing unphysical features to these parameters. (57 refs.)

76827 Model calculations of local electron and phonon densities of states in bimetallic superlattices. M.Menon, G.B.Arnold (Univ. of Notre Dame, Notre Dame, IN, USA).

Phys. Rev. B (USA), vol.27, no.9, p.5508-18 (1 May 1983). The authors have analytically obtained the exact Green's functions for electrons and phonons in a bimetallic superlattice. The electrons are treated in the tight-binding approximation, and the phonons are of one acoustic branch in a lattice with nearest-neighbor coupling. The most interesting effects arise near the interfaces when the acoustical or electronic coupling between layers is large compared to the intralayer coupling. In this large coupling case, the local phonon density of states at low frequency is enhanced by a linear contribution due to interface modes. The appearance of electronic interface states in the local density of states is discussed. The impact of the results on superconducting properties is considered. The influence of zone-folding effects is found to be small. (16 refs.)

Density of unidimensional finite disordered system particles ... See Entry 76824

Electronic states of disordered binary alloys with strong off-diagonal disorder ... See Entry 76829

The recursion method and a first-principles tight-binding calculation of the band structures of diamond and silicon ... See Entry 76837

Electron densities and chemical bonding in TiC, TiN, and TiO derived from energy band calculations ... See Entry 76841

Relativistic extended Huckel studies of cluster models of solid HgTe, CdTe, and PbTe: densities of states and nuclear spin-spin coupling ... See Entry 76842

Generation-annealing kinetics of the interface donor states at 0.25 eV above the midgap and the turn-around phenomena on oxidized silicon during avalanche electron injection ... See Entry 77017

Surface states at semiconductor-liquid junction ... See Entry 77045

The density of states in DC glow discharge deposited a-Si:H from Schottky barrier diode admittance measurements ... See Entry 77072

71.25 NONLOCALIZED SINGLE-PARTICLE ELECTRONIC STATES

76828 Interacting stereo-irregular chains: a model for conducting polymers. S.Stafstrom, R.Riklund, K.A.Chao (Dept. of Phys. & Measurement Technol., Univ. of Linköping, Linköping, Sweden).

Int. J. Quantum Chem. (USA), vol.23, no.4, p.1363-83 (April 1983). Interacting stereo-irregular chains of hydrogen atoms, which simulate the topological structure of many conducting polymers, are generated by a computer and solved numerically with the unrestricted Hartree-Fock method with a modified spin polarized potential. The electron localization is investigated, and a mechanism for the interchain tunneling is discovered. Local antiferromagnetic ordering is derived which may explain the AF behavior observed in some conducting polymers. (30 refs.)

76829 Electronic states of disordered binary alloys with strong off-diagonal disorder. S.Yoshino (Inst. of Materials Sci., Univ. of Tsukuba, Ibaraki, Japan), K.Hoshino, M.Goda.

J. Phys. Soc. Jpn. (Japan), vol.52, no.5, p.1687-91 (May 1983). The properties of eigenvalues and/or eigenfunctions of disordered binary alloys A_xB_{1-x} with off-diagonal disorder are investigated numerically in the two-dimensional square lattice with 50×50 lattice sites. Special attention is focused on the eigenfunctions near the band edges of A or B subbands when t_{AB} is much larger than t_{AA} and t_{BB} , where t_{ij} s ($i, j = A$ or B) are transfer energies between i and j sites. It is shown that the states near the inner band edges are highly localized within A or B atom clusters and the states near the outer band edges are localized within the clusters of atoms connected by AB bonds. The numerical results of the density of states as a function of t_{AB} are consistent with previous results and support the importance of the repulsive effect between bands. (9 refs.)

76830 A CNDO/INDO crystal orbital model for transition metal polymers of the 3d series-basis equations. M.C.Bohm (Inst. für Organische Chem., Univ. Heidelberg, Heidelberg, Germany).

Theor. Chim. Acta (Germany), vol.62, no.4, p.351-72 (1983). The crystal orbital formalism in the right-binding approximation is combined with a recently developed CNDO/INDO model for transition metal species of the 3d series in order to allow band structure calculations on the Hartree-Fock SCF level for one-dimensional (1D) chains with organometallic unit cells. The band structure approach based on the CNDO and INDO approximation can be used for any atom combination up to bromine under the inclusion of the 3d series. The matrix elements for the tight-binding Hamiltonian are derived for an improved CNDO and INDO framework. The total energy of the 1D chain is partitioned into one-center contributions and into two-center increments of the intracell and intercell type. (65 refs.)

76831 A CNDO/INDO crystal orbital model for transition metal polymers of the 3d series—the band structure of nickel(II)glyoximate. M.C.Bohm (Inst. für Organische Chem., Univ. Heidelberg, Heidelberg, Germany).

Theor. Chim. Acta (Germany), vol.62, no.4, p.373-96 (1983). The band structure of nickel(II)glyoximate has been studied by means of semiempirical INDO calculations implemented into the crystal orbital formalism of the tight-binding approximation. It has been shown that the crystal orbital approach allowed the rationalization of various experimental results. The theoretical model should be a suitable tool for the systematic investigation of the electronic structure of recently designed low-dimensional systems with organometallic stacking units. It can be expected that such an approach facilitates the formulation of general rules and principles that determine the physical and chemical properties of quasi one-dimensional conducting or semi-conducting polymers. (36 refs.)

Perturbation theoretical investigation of electron correlation effects in infinite metallic and semiconducting polymers ... See Entry 76865

Zero-gap type I semiconductor in a quantizing magnetic field ... See Entry 76977

The electronic structure of the Na_xWO_3 bronzes: a photoemission study ... See Entry 77530

71.25C Techniques of band-structure calculation (general theory, applications of group theory, analytic continuation, etc)

76832 A method for the calculation of improved band gaps in the crystal orbital formalism. M.C.Bohm (Inst. für Organische Chem., Univ. Heidelberg, Heidelberg, Germany).

Solid State Commun. (USA), vol.46, no.9, p.709-12 (June 1983). A computational method for the calculation of improved band gaps in the crystal orbital (CO) formalism based on the Hartree-Fock (HF) procedure is developed. The approach makes use of fractional k-averaged band occupation numbers in the band structure technique. An electron in the recalculated conduction band(s) feel the averaged potential of $(N-1)$ electrons. The method is applied to the LiH polymer. Semiempirical INDO CO calculations lead to an $\epsilon(k)$ lowering of nearly 3 eV for the improved conduction band in comparison to the dispersion curve of the standard variational approach. The two $\epsilon(k)$ curves are characterized due to slightly different dispersions. (22 refs.)

CNDO/S parameters of C, O, and Si for solid state calculations ... See Entry 76839

71.25H Measurement of Fermi surface parameters
(inc. dHvA, magnetoacoustic, position annihilation, and cyclotron resonance studies, etc.)

76833 Positron-annihilation measurements of the Fermi surface of copper-base solid solutions with gallium, germanium, and nickel. K.-H.Steinmetz, H.-P.Fischer (Inst. fur Metallforschung, Univ. Munster, Munster, Germany), M.Martin, E.Nembach.

Phys. Status Solidi b (Germany), vol.116, no.2, p.575-83 (1 April 1983). The [011] cross-section of the Fermi surface of Cu-rich solid solutions with Ga, Ge, and Ni is measured by positron annihilation. The 'rotating specimen' method is used. The concentrations of Ga and Ge cover the whole range of primary solid solutions; C_{Ni} extends up to 22 at.%. For all three solutes investigated, the neck radius of the Fermi surface increases monotonously with solute concentration. For a given electron per atom ratio e/a , Ga widens the neck 32% more than Ge does. All three solutes decrease the ratio of maximum to minimum diameter of the Fermi surface. The electronic structure of these solid solutions is not exclusively determined by the e/a ratio, but depends on the specific properties of the solute. The present experimental results do not support the view that the extent of primary solid solutions is mainly governed by the electron structure. (32 refs.)

76834 A theoretical investigation of the Fermi surfaces of bismuth and antimony. J.Rose, R.Schuchardt (Sektion Phys., Humboldt-Univ. zu Berlin, Berlin, Germany).

Phys. Status Solidi b (Germany), vol.117, no.1, p.213-24 (1 May 1983). The band structure and Fermi surfaces of Bi and Sb are studied with four different semiempirical pseudopotentials. By application of a Golin potential (1968) screened by the Heine-Abarankov form of dielectric function reasonable band structures are obtained. The calculated Fermi surfaces show very good agreement with the experimental data. Remaining discrepancies with respect to lower lying valence bands are analysed and compared with other calculations. (53 refs.)

76835 Electronic properties of dilute copper alloys. I. Theory. I.Mertig (Sektion Phys., Tech. Univ. Dresden, Dresden, Germany), E.Mrosan, R.Zeller, P.H.Dederichs, P.Ziesche.

Phys. Status Solidi b (Germany), vol.117, no.1, p.335-44 (1 May 1983). The electronic properties of 4d transition metal impurities and sp impurities of the third, fourth, and fifth rows of the periodic table in a Cu host are calculated self-consistently. The impurity is embedded in the perfect crystal environment and described by a single perturbed muffin-tin potential in the KKR-Green function scheme. The influence of the impurities on the de Haas-van Alphen effect (Dingle temperatures and changes in areas of the Fermi surface) and the residual resistivity are discussed. For the residual resistivity the linearized Boltzmann equation is solved taking into account the full anisotropic band structure of the host. (22 refs.)

Majority carrier concentration and quasi-Fermi level for $Pb_{1-x}Sn_xTe$ DH diode lasers See Entry 75638

Changes in the electron structure of Fe-Ni alloys with the FCC lattice as a result of a magnetic phase transition See Entry 76836

Theoretical aspects of magnetoelasticity in transition metals and alloys See Entry 77233

71.25P Band structure of crystalline metals

76836 Changes in the electron structure of Fe-Ni alloys with the FCC lattice as a result of a magnetic phase transition. V.V.Bukhalenkov (S.M. Kirov Ural Polytech. Inst., Sverdlovsk, USSR).

Fiz. Met. & Metalloved. (USSR), vol.55, no.4, p.826-9 (April 1983). In Russian. English translation in: *Phys. Met. & Metallogr. (GB)*

A study was made of a change in the isomeric shift in the Mossbauer effect of ^{57}Fe nuclei in Fe-Ni alloys. This was done in the critical range of compositions corresponding to the establishment of a ferromagnetic order under the influence of temperature. The increase in the isomeric shift as a result of ferromagnetic ordering was attributed to a shift of the absolute position of the Fermi level associated with the exchange splitting of the 3d band, magnetostriuctive changes in the atomic volume, and a possible discontinuity of the second-order Doppler shift because of a change in the Debye temperature and transformation of the vibration spectrum of the nuclei. (14 refs.) A.T.

Theoretical aspects of magnetoelasticity in transition metals and alloys See Entry 77233

Model for optical absorption in transition metals containing d impurities See Entry 77417

Thermal modulation spectrum and electron structure of niobium See Entry 77474

Soft X-ray emission spectra of aluminium in β -phase Cu-Ni-Al and Cu-Mn-Al alloys See Entry 77482

Resonant photoemission and f-band dispersion in Ulr_3 See Entry 77525

71.25R Band structure of crystalline elemental semiconductors

76837 The recursion method and a first-principles tight-binding calculation of the band structures of diamond and silicon. R.Jones, T.King (Dept. of Phys., Univ. of Exeter, Exeter, England).

Philos. Mag. B (GB), vol.47, no.5, p.481-90 (May 1983). A tight-binding first-principles calculation of the band structures of diamond and silicon is presented. The numerical crystal potential (including a local exchange-correlation term) is fitted to a superposition of simple analytic functions centred on each atom. A basis of localised s and p orbitals is calculated from this potential and fitted to a combination of Gaussians. All Hamiltonian and overlap matrix elements are then evaluated analytically, and the local density of states can be calculated by a recursion method modified to deal with overlap. An extension of the method to the study of crystal defects is discussed. (14 refs.)

76838 An operational method to model carrier degeneracy and band gap narrowing. M.S.Adler (General Electric Co., Corporate Res. & Dev. Center, Schenectady, NY, USA).

Solid-State Electron. (GB), vol.26, no.5, p.387-96 (May 1983).

An operational method of modeling heavily doped silicon to include effects of carrier degeneracy and band gap narrowing is presented. The issue of carrier degeneracy on majority carrier flow is discussed together with the question of the ambiguity in the electrostatic potential associated with identifying which band edge is narrowed. Using an exact numerical analysis of a bipolar transistor as an example it is shown that when modeling carrier flow in quasi-neutral regions, classical statistics can be used for the majority carrier and

the ambiguity in the electrostatic potential can be ignored. Overall, it is shown that for the same quasi-neutral heavily doped regions the effects of carrier degeneracy and band gap narrowing are accurately modeled within the context of classical statistics by adding the quasi field term to the minority carrier transport equation that is based on the commonly used 'band gap narrowing' data available from measurements of minority carrier transport in heavily doped regions. (15 refs.)

Picosecond interband saturation and intraband relaxation in germanium See Entry 75753

A theoretical investigation of the Fermi surfaces of bismuth and antimony See Entry 76834

A semi-empirical tight-binding theory of the electronic structure of semiconductors See Entry 76843

Photovoltaic measurement of bandgap narrowing in moderately doped silicon See Entry 77000

Resonant photoemission from Si See Entry 77521

71.25T Band structure of crystalline semiconductor compounds and insulators

76839 CNDO/S parameters of C, O, and Si for solid state calculations. P.Deak (Phys. Inst. Tech. Univ., Budapest, Budapest, Hungary).

Int. J. Quantum Chem. (USA), vol.23, no.4, p.1165-77 (April 1983).

Semiempirical methods used in cluster-type calculations must be applicable for calculating ionization potentials ('valence band') and electronic transitions ('gap'). CNDO/S seems to be an appropriate choice for this purpose. However, the solids of main interest (as, e.g. diamond and silica) contain saturated bonds for which the original parametrization does not work well. A new set of parameters was determined for C, O, and Si by fitting them to vertical ionization potentials and to singlet electronic transitions of their saturated molecules. The transferability of the parameters were also checked. By these parameters a successful description of the electronic structures of diamond and silica became possible. (63 refs.)

76840 Recent investigations on the electronic structure of the fourth and fifth group transition metal monocarbides, mononitrides, and monoxides. A.Neckel (Inst. fur Phys. Chem., Univ. Wien, Vienna, Austria).

Int. J. Quantum Chem. (USA), vol.23, no.4, p.1317-53 (April 1983).

An overview of band structure calculations on the fourth and fifth group transition metal monocarbides, mononitrides, and monoxides is given. Furthermore, the relations of three categories of experimental properties, which allow insight into the electronic structure of the above mentioned compounds, and the results of band structure calculations are discussed. Theoretical predictions are compared with experimental findings. The considered experimental properties are valence band photoemission spectra, valence band X-ray emission spectra, and optical properties. (100 refs.)

76841 Electron densities and chemical bonding in TiC, TiN, and TiO derived from energy band calculations. P.Blaha, K.Schwarz (Inst. fur Tech. Elektrochem., Tech. Univ. Wien, Vienna, Austria).

Int. J. Quantum Chem. (USA), vol.23, no.4, p.1535-52 (April 1983).

The chemical bonding in the interesting class of refractory transition metal compounds is illustrated for TiC, TiN, and TiO. Self-consistent augmented plane wave (APW) calculations are already available for these compounds. Using the respective potentials the author have repeated the band calculations on a finer k grid with the linearized APW method to obtain accurate densities of states (DOS). These DOS can be divided into local partial contributions to characterize the bonding. Further information can be obtained from a decomposition of the metal d DOS into dt_{2g} and eg symmetry components. These partial local DOS are compared into the LCAO counterpart and give a first picture of the chemical bonding in these compounds. The electron densities corresponding to the occupied valence states are obtained from the LAPW calculations. They provide further insight into characteristic trends in the series from TiC to TiO: around the nonmetal sit and density shows increasing localization; around the metal site the deviation from spherical symmetry changes from e_g to t_{2g} . These effects can be traced back to the three types of valence bands. Electron density plots of characteristic band states (all energies of a selected k point in the Brillouin zone) will be shown. These plots can describe the different types of bonding occurring in these systems. (15 refs.)

76842 Relativistic extended Huckel studies of cluster models of solid HgTe, CdTe, and PbTe: densities of states and nuclear spin-spin coupling. M.Hotokka, L.Laaksonen, P.Pyykko, A.Viste (Dept. of Phys. Chem., Abo Akad., Abo, Finland).

Int. J. Quantum Chem. (USA), vol.23, no.4, p.1685 (April 1983).

Summary form only given. Relativistic extended Huckel (REX) and EHT molecular orbital calculations have been carried out for a variety of cluster models of crystalline HgTe and CdTe. The local environment of each atom in the crystals and in the selected clusters is tetrahedral, and the largest clusters studied here are of formula $M_{10}Te_{10}$. Clusters $Hg_{10}Te_{10}$, $Hg_4Te_{13}^{18-}$, and $Hg_{13}Te_4^{18+}$, studied in wurtzite and zinc-blende isomeric forms, are found by REX double-zeta calculations to be more stable in the zinc-blende form, in agreement with the known crystal structure of HgTe and CdTe. For PbTe (NaCl structure), a cluster model Pb_6Te_6 is considered. Densities of states for clusters M_nTe_n are found to exhibit trends in reasonable qualitative agreement with available experimental data and earlier band structure calculations. For HgTe clusters there is very little difference between results for wurtzite and zinc-blende REX results, and the best overall correspondence with bulk properties occurs for the largest cluster models. Band gaps calculated by REX tend to increase in the order $PbTe < HgTe < CdTe$. Nuclear spin-spin coupling has been investigated by the REXNMR program. (5 refs.)

76843 A semi-empirical tight-binding theory of the electronic structure of semiconductors. P.Vogl (Inst. fur Theoretische Phys., Univ. Graz, Graz, Austria), H.P.Hjalmarson, J.D.Dow.

J. Phys. & Chem. Solids (GB), vol.44, no.5, p.365-78 (1983).

A nearest-neighbor semi-empirical tight-binding theory of energy bands in zincblende and diamond structure materials is developed and applied to the following sp^3 -bonded semiconductors: C, Si, Ge, Sn, SiC, GaP, GaAs, GaSb, InP, InAs, InSb, AlP, AlAs, AlSb, ZnSe, and ZnTe. For each of these materials the theory uses only thirteen parameters to reproduce the major features of conduction and valence bands. The matrix elements exhibit chemical trends, the differences in diagonal matrix elements are proportional to differences in free-atom orbital energies and the off-diagonal matrix elements obey the d^{-2} rule of Harrison et al. The lowest energy conduction bands are well described as a result of the introduction of an excited s state, s^* , on each atom. Examination of the chemical trends in this sp^3s^* model yields a crude but 'universal' sp^3s^* model whose parameters do not depend explicitly on band gaps, but rather are functions of atomic energies and bond lengths alone. The 'universal' model, although cruder than the sp^3s^* model for any

single semiconductor, can be employed to study relationships between the band structures of different semiconductors; the authors use it to predict band edge discontinuities of heterojunctions. (35 refs.)

76844 Self-consistent embedded-cluster calculations of the electronic structure of alkaline earth fluorides in the Hartree-Fock-Slater approximation. N.C.Amaral, B.Maffei, D.Guenzburger (Dept. de Física, Univ. Federal de Goiás, Goiânia, Brazil).

Phys. Status Solidi b (Germany), vol.117, no.1, p.141-53 (1 May 1983). Molecular orbital calculations are performed for clusters representing the CaF_2 , SrF_2 , and BaF_2 ionic crystals. The discrete variational method is employed, with the $\chi\alpha$ approximation for the exchange interaction; a detailed investigation of different models for embedding the clusters in the solids led to a realistic description of the effect of the neighbouring ions in the infinite crystal. The results obtained are used to interpret optical and photoelectron data reported in the literature. In the case of CaF_2 , comparisons are made with existing band structure calculations. (33 refs.)

76845 Instability of a heavily doped semiconductor near the band inversion point. M.A.Korzhuev (A.A. Baikov Inst. of Metall., Acad. of Sci., Moscow, USSR).

Sov. Phys.-Solid State (USA), vol.24, no.11, p.1961-2 (Nov. 1982). Translation of: *Fiz. Tverd. Tela (USSR)*, vol.24, no.11, p.3451-3 (Nov. 1982). [received: May 1983]

Inversion of the conduction and valence bands accompanied by vanishing of the band gap $E_g = E(L_g^-) - E(L_g^+)$ and a transition to a zero-gap state are exhibited by solid solutions of IV-VI semiconductors ($\text{Pb}_{1-x}\text{Sn}_x\text{Te}$, $\text{Pb}_{1-x}\text{Sn}_x\text{Se}$) when the pressure P , the temperature T , or the composition x are varied. The authors have used the energy band parameters of $\text{Pb}_{1-x}\text{Sn}_x\text{Se}$ solid solutions, which are typical of solutions of IV-VI semiconductors and which agree with the dependences $E_F(E_g)$ calculated using the six-band Dimmock model of the electron energy spectrum. The dependences $E(E_g)$ are recalculated on the P , T , and x scales. (7 refs.)

Effects of relative damage, Fermi energy and annealing technique in ion implanted GaAs See Entry 76476

A method for the calculation of improved band gaps in the crystal orbital formalism See Entry 76832

The electronic structure of GaP (110) and Cu-phthalocyanine overlayers studied by ellipsometry See Entry 77015

Electronic properties of InAs-GaSb superlattices See Entry 77032

Electronic structure of semiconductor superlattices See Entry 77035

High pressure photoelectric studies of semiconductor-electrolyte systems See Entry 77044

Temperature dependence of the electron permittivity of IV-VI semiconductors See Entry 77321

Spectral studies on new dioxouranium (VI) complexes of tridentate Schiff bases derived from salicylhydrazide and salicylaldehyde or substituted salicylaldehydes See Entry 77372

Spectroscopic studies of oxovanadium(IV) complexes of biguanide, dibiguanides and α -methyl-1-amidinourea See Entry 77373

Fundamental optical absorption and valence bands in alkali silver halide crystals See Entry 77406

Vacuum ultraviolet reflectance spectra and band structures of pyrites (FeS_2 , CoS_2 and NiS_2) and NiO measured with synchrotron radiation See Entry 77407

Reflectance and thermorefectance spectra and energy band structure of GeSe crystals See Entry 77410

Valence-band splitting of SrTiO_3 See Entry 77420

Far ultraviolet photoelectric study of thin SnSe evaporated films See Entry 77522

High-pressure growth of polycrystalline molybdenum disulphide See Entry 77591

71.30 METAL-INSULATOR TRANSITIONS

76846 The localization transition on the Bethe lattice. H.Kunz (Inst. de Phys. Théorique, EPFL, Lausanne, Switzerland), B.Souillard.

J. Phys. Lett. (France), vol.44, no.11, p.411-14 (1 June 1983). Presents exact results concerning the localization transition on the Bethe lattice. In a certain number of situations, the authors prove the existence of a transition from extended to localized regime when varying the energy or the disorder. The density of states is analytic at the mobility edges and the exponent ν governing the divergence of the localization length is found equal to 1. (5 refs.)

76847 Theory of the Verwey transition in the mixed valence compound EuS_2 . D.Ihle, B.Lorenz (Sektion Phys., Karl-Marx-Universität Leipzig, Leipzig, Germany).

Phys. Status Solidi b (Germany), vol.116, no.2, p.539-46 (1 April 1983). The Verwey transition in EuS_2 at $T_V = 186$ K is explained on the basis of a model which takes into account the Coulomb interaction of the extra $4f$ electrons at the Eu^{2+} ions and the formation of small polarons due to the interaction with phonons. This model is treated in the Hartree and cluster variation approximations. At T_V a first-order Verwey transition is obtained. The magnitude of the observed entropy change at T_V is explained. Above T_V the polarons are found to be considerably short-range ordered. (20 refs.)

X-ray scattering study of $2k_F$ and $4k_F$ CDW in TMTTF-TCNQ See Entry 76863

Perturbation theoretical investigation of electron correlation effects in infinite metallic and semiconducting polymers See Entry 76865

Quantum localization in one-dimensional quasi-random systems and magnetic breakdown See Entry 76871

On the role of the correlation length near the onset of non-metallic conduction See Entry 77010

Influence of Mn ion substitution by Fe on the electrical and magnetic properties of an $\text{La}_{0.6}\text{P}_{0.4}\text{MnO}_3$ crystal See Entry 77159

Reflection of light from a two-phase metal-insulator system See Entry 77398

71.35 EXCITONS AND RELATED PHENOMENA (inc. electron-hole drops)

76848 Anderson transition in the exciton-impurity band in silicon. P.D.Altukhov, A.V.Ivanov, A.A.Rogachev (A.F. Ioffe Physicotech. Inst., Acad. of Sci., Moscow, USSR).

JETP Lett. (USA), vol.36, no.9, p.401-4 (5 Nov. 1982). Translation of: *Pis'ma v Zh. Eksp. i Teor. Fiz. (USSR)*, vol.36, no.9, p.328-31 (5 Nov. 1982). [received: June 1983]

An Anderson transition is observed in the exciton-impurity band (EIB) in Si:P with donor concentration $n_D = n \approx 1.5 \times 10^{17} \text{ cm}^{-3}$. The transition is accompanied by a sharp rearrangement of the recombination-radiation spectrum of EIB with increasing n_D in the region $n_D \approx n^*$ due to increases exciton mobility and a change in the polarization of radiation in a magnetic field. (5 refs.)

76849 On the theory of singlet and triplet charge-transfer excitons. B.J.Schmid, P.Reineker (Abteilung für Theoretische Phys., Univ. Ulm, Ulm, Germany).

Phys. Status Solidi b (Germany), vol.117, no.1, p.117-26 (1 May 1983).

A many-particle Hamiltonian for electrons which takes into account their energy in a periodic potential and in an external magnetic field, as well as their Coulomb and spin-spin interaction energies is specialized for charge-transfer excitons on a linear chain with one donor and one acceptor molecule in the unit cell. The Hamiltonian decomposes into a part of singlet excitons, which is diagonalized exactly, and a part for triplet excitons, whose diagonalization is reduced to wave vector dependent eigenvalue problems of the dimension of the unit cell. The fine-structure tensor is expressed explicitly in terms of electronic matrix elements. (20 refs.)

76850 Emission of free and bound excitons in layered GaSe crystals. Yu.P.Gnatenko, Z.D.Kovalyuk, P.A.Skubenko, Yu.I.Zhirko (Inst. of Phys., Acad. of Sci., Kiev, Ukrainian SSR).

Phys. Status Solidi b (Germany), vol.117, no.1, p.283-7 (1 May 1983).

The emission spectra of GaSe single crystals of ϵ -modification doped with Co of 0.001 to 0.5 wt.% concentration are investigated at different temperatures ($T = 4.2$ to 35K) using polarized light. It is shown that the wide emission band with energy 2.031 eV is due to structural defects while the other wide bands of 2.039 and 2.008 eV are due to indirect exciton transitions with radiation of TO-phonons. The narrow emission lines correspond to the decay of direct excitons bound on different defects and to their phonon satellites involving phonons of $(14.5 \pm 0.5) \text{ meV}$. The temperature dependence of a doublet structure of the free exciton emission line, which is thought to be due to the peculiarities of the GaSe crystal band structure, namely the splitting of the valence band by interlayer interaction is investigated. (15 refs.)

76851 Excitonic correlations and a first-order phase transition in an excitonic dielectric. B.A.Volkov, V.V.Tugushev (P.N. Lebedev Phys. Inst., Acad. of Sci., Moscow, USSR).

Sov. Phys.-Dokl. (USA), vol.27, no.8, p.636-8 (Aug. 1982). Translation of: *Dokl. Akad. Nauk SSSR*, vol.265, no.4-6, p.1374-8 (Aug. 1982). [received: May 1983]

The influence of many-particle correlations on a dielectric phase transition, is considered in systems with electron-hole pairing. The most detailed discussion is devoted to results for a model of an isotropic semimetal, whose one-electron spectra of the conduction band, and of the valence band are connected by the relation $\epsilon_c(k) = -\epsilon_v(k)$, where k is the electron quasimomentum. As the temperature is lowered, a second-order phase transition takes place at the point $T = T_c$ into the 'excitonic-dielectric' state, i.e. a condensate of electron-hole pairs is formed. In the limit of large electron density ($na_0 \gg 1$, a_0 is exciton radius, n is the concentration of electrons and holes), all correlation corrections to the self-consistent field theory are small and of the order of the parameter $T_c/\epsilon_F \ll 1$ (ϵ_F is the Fermi energy). (4 refs.)

76852 Effect of one-dimensional disorder on exciton states in semiconductors. A.Yu.Maslov, L.G.Suslina (A.F. Ioffe Physicotech. Inst., Acad. of Sci., Leningrad, USSR).

Sov. Phys.-Solid State (USA), vol.24, no.11, p.1928-31 (Nov. 1982). Translation of: *Fiz. Tverd. Tela (USSR)*, vol.24, no.11, p.3394-400 (Nov. 1982). [received: May 1983]

A theoretical and experimental study of the effect of one-dimensional (structural) disorder on exciton states in semiconductors is reported. One-dimensional disorder is due to a random distribution of close-packed layers in the direction of the optic axis. Disorder in the stacking of layers leads to a random one-dimensional potential which localizes the motion of quasiparticles in the direction of stacking. It is shown that differences in the exciton localization energy at different points of a crystal lead to an inhomogeneous broadening of exciton states. The dependence of the broadening on the concentration of stacking faults is calculated in a model of uncorrelated distribution of close-packed layers. The results of an experimental study of the broadening of exciton states in ZnS crystals with stacking faults are reported. The measured results are quite well described by the proposed theoretical model. (16 refs.)

76853 Zeeman effect and diamagnetic shift of a free exciton in gallium arsenide crystals. L.P.Nikitin, I.B.Rusanov, R.P.Selsyan, T.V.Yezeva (A.F. Ioffe Physicotech. Inst., Acad. of Sci., Leningrad, USSR).

Sov. Phys.-Solid State (USA), vol.24, no.11, p.1962-4 (Nov. 1982). Translation of: *Fiz. Tverd. Tela (USSR)*, vol.24, no.11, p.3453-6 (Nov. 1982). [received: May 1983]

The authors consider the Zeeman effect and diamagnetic shift of Wannier-Mott excitons in GaAs. The perturbation treatment of these effects has previously been shown to be valid up to $\sim 12 \text{ KOe}$. The authors examine this validity by studying the absorption spectra of thin unstressed GaAs crystals. (10 refs.)

76854 Bound states in the presence of a screened Coulomb potential in a magnetic field. S.B.Anokhin, M.V.Ivanov (A.A. Zhdanov State Univ., Leningrad, USSR).

Sov. Phys.-Solid State (USA), vol.24, no.11, p.1979-80 (Nov. 1982). Translation of: *Fiz. Tverd. Tela (USSR)*, vol.24, no.11, p.3478-80 (Nov. 1982). [received: May 1983]

The use of high-power light sources can create carrier densities in semiconductor crystals sufficient for a detailed experimental investigation of the screening of excitons. The simplest theoretical model for the description of this effect is an analysis of the interaction of an electron and a hole via a screened Coulomb potential. The authors report the results of numerical calculations of the energy eigenvalues for a system with a Hamiltonian operator which has the form of a cylindrical coordinate system (ρ, ϕ, z) after separation of the motion over the angle ϕ . (10 refs.)

76855 Self-localized excitons in molecular crystals with allowance for anharmonicity of the lattice and dispersion. N.I.Kislukha, A.V.Karbovskii, V.I.Ponomarenko.
Ukr. Fiz. Zh. (USSR), vol.28, no.5, p.661-6 (May 1983). In Russian.
The possibility of self-localized exciton formation is studied in terms of the continuous approximation with allowance for anharmonicity of the lattice and dispersion. When the resonance interaction is weak and anharmonicity is strong, there, possibly, exist self-localized states alongside the exciton states. It is shown what role the crystal lattice dimensionality plays for two- and three-dimensional lattices. (5 refs.)

Optical bistability, regenerative pulsations, and transverse effects in room-temperature GaAs-AlGaAs superlattice etalons See Entry 75714

Two-photon transitions to exciton polaritons See Entry 76856

Photoconductivity of Y₂O₃ crystals with self-localized excitons See Entry 77003

Prediction of a resonance-enhanced laser-beam displacement at total internal reflection in semiconductors See Entry 77345

Magneto-optical study of the fundamental absorption edge in Cd_{1-x}Mn_xTe See Entry 77369

Raman light scattering in semiconductors containing dislocations See Entry 77399

Spectroscopic properties of triplet excited polyvinylcarbazoles and vinylcarbazole copolymers See Entry 77428

Time characteristics of secondary emissions in ZnTe under band-to-band excitation See Entry 77433

Electron-hole liquid in indium antimonide in a strong magnetic field See Entry 77436

Decay behaviour of high-excitation luminescence in GaP:N. II. Experimental results on the densities of the coexisting phases and the relevant recombination processes See Entry 77443

Extrinsic photoluminescence from GaAs quantum wells See Entry 77446

Localization of electronic states and cathodoluminescence of bound exciton complexes in ZnSe crystals See Entry 77462

Electron-hole drops in vanadium dioxide See Entry 77468

Faraday rotation in the exciton part of the spectrum of CuBr See Entry 77473

Resonant photoemission from Si See Entry 77521

71.36 POLARITONS
(inc. photon-phonon and photon-magnon interactions)

76856 Two-photon transitions to exciton polaritons. A.R.Hassan (Internat. Centre for Theoretical Phys., Trieste, Italy).
Indian J. Theor. Phys., vol.29, no.3, p.203-8 (Sept. 1981).
A semiclassical theory for the creation of excitonic polariton states by two-photon absorption, via an intermediate exciton state, is given. A band model has been introduced which gives the dominant contribution to this process. A numerical calculation is found to be in good agreement with a recent observation in CuCl. (15 refs.)

76857 Optical properties of polaritons in thin crystal films. V.N.Myasnikov, S.V.Marisova, A.N.Lipovchenko (Inst. of Phys., Acad. of Sci., Kiev, Ukrainian SSR).
Phys. Status Solidi b (Germany), vol.117, no.1, p.109-16 (1 May 1983).
The dispersion relation for polaritons in a crystal slab of an arbitrary thickness is derived by the quantum Green function method. The equation is reduced to the classical electrodynamics form with an effective dielectric function depending on the crystal thickness. The energy and the radiation damping of polariton modes in thin anthracene crystals are calculated and compared with the experimental values based on studies of low-temperature luminescence and refractive index dispersion. (14 refs.)

76858 Observation of dispersion on magnetic polaritons. K.M.Haussler (Sektion Phys., Univ. Munchen, Munchen, Germany), J.Brandmuller, L.Merten, H.Finsterholz, A.Lehmeyer.
Phys. Status Solidi b (Germany), vol.117, no.1, p.225-8 (1 May 1983).
Far-infrared reflectivity measurements on uniaxial antiferromagnetic CoF₂ display a characteristic dispersion of the magnetic reststrahlenbands if the wave vector components of the radiation are varied by choosing different angles of incidence. Thus the expected dispersion behaviour of the so-called magnetic polaritons is demonstrated experimentally in a direct manner for the first time. The simulation of the infrared reflectivity spectra based on a generalized formula for anisotropic magnetically ordered insulators shows good agreement with the experimental results and can be used to predict even weak polariton dispersion effects. (11 refs.)

76859 Effects of a transition layer on slab polaritons. L.Wendler (Sektion Phys., Friedrich-Schiller-Univ. Jena, Jena, Germany).
Phys. Status Solidi b (Germany), vol.117, no.1, p.241-6 (1 May 1983).
Dispersion relations are derived for polaritons in a dielectric slab, coated with a transition layer (thickness 20 to 150 Å), on a substrate. If $\tilde{\epsilon}(\omega)$ is the dielectric function of the transition layer a splitting of the dispersion curves occurs for resonances of the form $\tilde{\epsilon}(\omega_1)=\infty$ and $\tilde{\epsilon}(\omega_2)=0$ in the case of p-polarized polaritons. In the case of s-polarized polaritons the splitting is obtained only for resonances of the form $\tilde{\epsilon}(\omega_1)=\infty$. (6 refs.)

Prediction of a resonance-enhanced laser-beam displacement at total internal reflection in semiconductors See Entry 77345

Time characteristics of secondary emissions in ZnTe under band-to-band excitation See Entry 77433

71.38 POLARONS AND ELECTRON-PHONON INTERACTIONS
(for electron-phonon interactions in lattices, see also 63.20K)

76860 Theory of solitons in molecular chains. A.A.Eremko, A.I.Sergienko (Inst. of Theoretical Phys., Acad. of Sci., Kiev, Ukrainian SSR).
Sov. Phys.-Solid State (USA), vol.24, no.12, p.2122 (Dec. 1983). Translation of: *Fiz. Tverd. Tela (USSR)*, vol.24, no.12, p.3720-2 (Dec. 1983).
The authors have shown that collective excited states of the soliton type can occur in one-dimensional molecular chains irrespective of the sign of the resonant interaction. For dipole-dipole interactions $J>0$, the neighboring molecules near a soliton are excited in phase, whereas for $J<0$, they are in antiphase. The internal soliton energy is always lower than the bottom of the exciton band. This is one of the factors which determine large stability of solitons. (5 refs.)

76861 Intrinsic polaron energy with allowance for dynamic correlations. A.P.Popov.
Ukr. Fiz. Zh. (USSR), vol.28, no.4, p.623-4 (April 1983). In Russian.
To calculate the energy of the polaron ground state with zero full momentum, the author uses a method which is a logical development and extension of the Pekar-Buymistrov method. The calculations lead to energy values of the autolocalized state somewhat lower than those obtained using other calculation methods. (6 refs.) V.G.P.

76862 Electromagnetic wave absorption by an electron-phonon system under parametric resonance. Nguyen Van Trong.
Ukr. Fiz. Zh. (USSR), vol.28, no.5, p.760-7 (May 1983). In Russian.
A quantum kinetic equation is considered for an electron-phonon system exposed to an external radiation field under conditions of parametric resonance decay. The collision term obtained is used to calculate the dissipative conductivity. With the external field intensity being close to the threshold value corresponding to the parametric instability, the conductivity is shown to have a logarithmic singularity. (8 refs.)

Theory of the Verwey transition in the mixed valence compound Eu₂S₄ See Entry 76847

Perturbation theoretical investigation of electron correlation effects in infinite metallic and semiconducting polymers See Entry 76865

Ordering of localized electron pairs in crystals with varying valency See Entry 76874

Temperature dependence of the Wannier-Stark level width in a semiconductor in a strong electric field See Entry 76913

Cyclotron resonance and the role of polaron effects in surface layers on Hg_{1-x}Cd_xTe See Entry 77265

71.45 COLLECTIVE EFFECTS

76863 X-ray scattering study of 2k_F and 4k_F CDW in TMTTF-TCNQ. S.Kagoshima, J.P.Pouget (Lab. de Phys. des Solides, Univ. Paris Sud, Orsay, France), H.Anzai.
J. Phys. Soc. Jpn. (Japan), vol.52, no.5, p.1629-34 (May 1983).
In the organic one-dimensional conductor TMTTF-TCNQ, the 2k_F and the 4k_F CDW were found by the diffuse X-ray photographic method. The 2k_F CDW condenses at 36K, at which the metal-insulator transition occurs, and forms three-dimensionally ordered structures indicating the occurrence of the Peierls transition. A different and unusual temperature dependence is shown by the 4k_F CDW. The transverse ordering of CDW is easily destroyed by the X-ray irradiation. Observed wave number of the transverse ordering and the strong irradiation effect suggest that the 2k_F CDW grows on both TCNQ and TMTTF stacks. However the 4k_F CDW is expected to be present mostly on the TMTTF stack.

76864 Electron localization in a two-dimensional system in strong magnetic fields. I. Case of short-range scatterers. T.Ando (Inst. of Appl. Phys., Univ. of Tsukuba, Ibaraki, Japan).
J. Phys. Soc. Jpn. (Japan), vol.52, no.5, p.1740-9 (May 1983).
A computer simulation is performed to study localization of a two-dimensional electron system in strong magnetic fields. Scatterers with short-range δ -potentials are assumed, and the localization criterion based on the Thouless number $g(L)$ is employed. It is shown that states are localized exponentially except in the vicinity of the center of each Landau level. The decay rate of the localized wave function, i.e. the inverse localization length, approaches zero smoothly at the center. This suggests that only the states just at the center of the Landau level are not localized and all the other states are exponentially localized, although the localization length is extremely large near the center. The energy range where the localization length is extremely large becomes wider with the Landau level index. (28 refs.)

Theory of solitons in molecular chains See Entry 76860

Peierls instability and charge density waves at the surface of a metal with a quasideimensional electron spectrum See Entry 76935

Zero-gap type I semiconductor in a quantizing magnetic field See Entry 76977

Magnetostriction of bismuth and graphite in fields up to 40 Tesla See Entry 77227

⁷⁵Se nuclear magnetic resonance in di-tetramethyltetraselenafulvalene phosphorus hexafluoride [(TMTSF)₂PF₆] under pressure See Entry 77280

71.45G Exchange, correlation, dielectric and magnetic functions, plasmons

76865 Perturbation theoretical investigation of electron correlation effects in infinite metallic and semiconducting polymers. S.Suhai (Lehrstuhl fur Theoretische Chem., Friedrich-Alexander-Univ. Erlangen-Nurnberg, Erlangen, Germany).
Int. J. Quantum Chem. (USA), vol.23, no.4, p.1239-56 (April 1983).
Moller-Plesset-type perturbation theory is applied to calculate electron correlation effects in infinite, periodic, metallic, and semiconducting polymers. Different possible choices of the zeroth-order Hamiltonian (symmetry adapted Hartree-Fock, spin-, and charge-density waves), the influence of the size of the atomic basis sets, lattice and conduction band sums are investigated. In the case of semiconducting systems a very efficient version of the method using optimally localized Wannier functions has been worked out. Applications include model calculations for infinite atomic hydrogen chains, the investigation of the role of correlation effects in the bond alternation and metal-insulator phase transition in polyene, different one- and many-particle effects contributing to the single-particle gap in polyene, and the calculation of correlated quasiparticle band structures using the electronic polaron model. (23 refs.)

76866 De-correlation technique for separation of Drude parameters from wavelength modulation spectroscopy data. M.Burd, R.Stearns, R.Braunstein (Dept. of Phys., Univ. of California, Los Angeles, CA, USA).
Phys. Status Solidi b (Germany), vol.117, no.1, p.101-7 (1 May 1983).
Separation of bound- and free-electron contributions to the dielectric function is necessary for an accurate analysis of interband transitions. A technique for doing this separation which does not require low energy data is presented. The technique makes use of the fact that the functions which describe the contributions of each part are sufficiently uncorrelated, allowing the construction of a correlation function which uses the Drude effective mass and Drude relaxation time as adjustable parameters. The technique is shown to properly separate a test function and to yield reasonable results from experimental data. (22 refs.)

76867 Inverse dielectric function for a semi-infinite solid. F.Bechstedt, R.Enderlein, D.Reichardt (Sektion Phys., Humboldt-Univ. zu Berlin, Berlin, Germany).

Phys. Status Solidi b (Germany), vol.117, no.1, p.261-70 (1 May 1983).

An old problem is addressed here: the description of the dielectric response of electrons near the surface of an infinite half space to perturbing potentials and external charges. Taking into account spatial dispersion, expressions are derived for the screened potential and the inverse dielectric function within the approximation of specular electron reflection. The expressions generalize former results in a way that spatial symmetries of the problem are properly reflected. The boundary conditions are shown to follow from the definition of the screened potential. The inverse dielectric function obtained in the treatment fulfils the orthogonality relation to the dielectric function and the f -sum rule. (20 refs.)

Dynamics of classical and quantum spin systems with random fields

See Entry 74370

Direct free-hole absorption induced in germanium by 1.06 μ m picosecond pulses

See Entry 75751

Experimental energy-loss function, $\text{Im}[-1/\epsilon(q,\omega)]$, for aluminium

See Entry 76537

Generator coordinate treatment of some model periodic systems

See Entry 76571

Some considerations on U_{eff} values entering the Hubbard Hamiltonian

See Entry 76819

The recursion method and a first-principles tight-binding calculation of the band structures of diamond and silicon

See Entry 76837

Excitonic correlations and a first-order phase transition in an excitonic dielectric

See Entry 76851

Correlation correction to the Thomas-Fermi-Dirac statistical model of condensed matter

See Entry 76868

Fermi-liquid approach to a description of localized magnetic moments in transition metals

See Entry 77148

Raman scattering by soft plasmon-LO phonon modes in ferroelectric semiconductors

See Entry 77380

Radiation generation by collective phenomena in semiconductors

See Entry 77414

Inelastic electron scattering from small metal spheres

See Entry 77492

Energy loss measurements on Co_2Sm thin films

See Entry 77497

A new method for determining relaxation energies by means of AES and XPS and its application to silicon compounds

See Entry 77520

71.45J Fermi-Thomas model

76868 Correlation correction to the Thomas-Fermi-Dirac statistical model of condensed matter. K.Ebina, T.Nakamura (Dept. of Material Phys., Osaka Univ., Toyonaka, Japan).

J. Phys. Soc. Jpn. (Japan), vol.52, no.5, p.1658-64 (May 1983).

Effect of the correlation energy on the Thomas-Fermi-Dirac statistical model of condensed matter is studied systematically by means of a perturbation method. The pressure curves are obtained with main interest in the low pressure region where the correlation effect is appreciable. The instability of the statistical model occurring at a certain negative pressure is discussed in connection with the thermodynamical stability of electron gas in the outermost region of the Wigner-Seitz sphere; and with the binding problem for an aggregate of atoms at zero pressure.

71.45N Calculations of total electronic binding energy

(see also 61.50L Crystal binding)

76869 Electronic and cohesive properties of small sodium particles. M.P.Iniguez (Dept. de Optica, Univ. de Valladolid, Valladolid, Spain), C.Baladron, J.A.Alonso.

Surf. Sci. (Netherlands), vol.127, no.3, p.367-76 (May 1983).

The density functional formalism is used to study the variation with size of the electronic and cohesive properties of small sodium particles. The ionization potential, electron affinity, electronic chemical potential and the cohesive and surface energies have been calculated for microparticles containing up to 339 sodium atoms. (16 refs.)

Parametrized functionals of the local electron density in transition metals

See Entry 76364

71.50 LOCALIZED SINGLE-PARTICLE ELECTRONIC STATES

(exc. impurities; for localisation in disordered structures, see 71.55J)

76870 Local partial DOS and experimental Al K spectra of transition metal aluminides. Charge transfer trend. C.Muller (Sektion Phys., Tech. Univ. Dresden, Dresden, Germany), W.Blau, P.Ziesche.

Phys. Status Solidi b (Germany), vol.116, no.2, p.561-73 (1 April 1983).

For the B2-type compounds VAl, CrAl, MnAl, FeAl, CoAl, and NiAl the local partial DOS (densities of states) and the corresponding integrated DOS are determined on the basis of a linear KKR method. The calculated local partial DOS are directly compared to experimental SXE (soft X-ray emission)-spectra. The integrated local partial DOS provide the valence charge distributions per unit cell. The latter are used to estimate the charge transfer in the intermetallic compounds. The calculated results are in good agreement with the experimental observed trend. (28 refs.)

76871 Quantum localization in one-dimensional quasi-random systems and magnetic breakdown. A.A.Slutskin, L.Yu.Gorelik (Phys.-Tech. Inst. of Low Temperatures, Acad. of Sci., Kharkov, Ukrainian SSR).

Solid State Commun. (USA), vol.46, no.8, p.601-3 (May 1983).

The magnetic breakdown in metals is shown to cause the appearance of a new class of one-dimensional quasi-random 'incommensurable' systems where the electrons are localized due to quantum interference effects. At this time both absolute localization and phase transition of 'metal-dielectric' type can be realized. (5 refs.)

76872 Multichannel localization and magnetic impurities. O.N.Dorokhov (L.D. Landau Inst. for Theoretical Phys., Acad. of Sci., Moscow, USSR).

Solid State Commun. (USA), vol.46, no.8, p.605-8 (May 1983).

The behaviour of an electron in N -coupled conducting chains of length L is studied in the presence of magnetic impurities. The electron flow can be

expanded in an orthonormal set of $2N$ channels. Each channel has its own transmission coefficient $T_n(L)$. Spontaneous breaking of the symmetry between channels results in $2N$ different exponential dependences $T_n(L) \sim \exp(-L/l_n^*)$ where l_n^* is a localization length in the n th channel. Low frequency kinetic behaviour depends on the channel with the maximum localization length l_0^* . (16 refs.)

76873 Asymptotic behavior of the density of states of electrons interacting with critical fluctuations of the order parameter. M.I.Auslender, M.I.Katnelson (Inst. of Metal Phys., Acad. of Sci., Sverdlovsk, USSR).

Sov. Phys.-Dokl. (USA), vol.27, no.7, p.562-4 (July 1982). Translation of: *Dokl. Akad. Nauk SSSR*, vol.265, no.1-3, p.601-4 (July 1982). [received: April 1983]

The interaction of an electron with fluctuations of the order parameter (in magnetic semiconductors, solid and liquid solutions, liquid helium, etc.) may significantly alter the character of its motion, leading to the occurrence of self-localized states. In studying the self-localization of a single electron it is necessary to estimate its averaged partition function $Z(\beta) = (\text{Tr} \exp(-\beta H))$, where H is the Hamiltonian of the electron in the field ϕ of the fluctuations β is the temperature, and $\langle \dots \rangle$ denotes the operation of averaging over the ensemble of fluctuations. (10 refs.)

76874 Ordering of localized electron pairs in crystals with varying valency. L.A.Manakova, S.P.Ionov (Inst. of Physiologically Active Substances, Acad. of Sci., Chernogolovka, USSR).

Sov. Phys.-Dokl. (USA), vol.27, no.7, p.568-70 (July 1982). Translation of: *Dokl. Akad. Nauk SSSR*, vol.265, no.1-3, p.611-14 (July 1982). [received: April 1983]

Results of the analysis of various types of ordering of localized electron pairs (defined by Anderson as bipolarons) are given in terms of interaction parameters and the electron concentration. An important aspect of the work is that it takes into account the fact that the degree of lattice polarization due to the bipolaron-phonon interaction is related to the parameters of the ground state of the crystal in a self-consistent manner. (14 refs.)

76875 Localized centers in bismuth silicate crystals. M.G.Ermakov, A.V.Khomich, P.I.Perov, I.A.Gorn, V.V.Kucha (Inst. of Radio Engng. & Electronics, Acad. of Sci., USSR).

Sov. Microelectron. (USA), vol.11, no.5, p.250-4 (Sept.-Oct. 1982). Translation of: *Mikroelektronika (USSR)*, vol.11, no.5, p.424-9 (Sept.-Oct. 1982). [received: May 1983]

Bismuth silicate ($\text{Bi}_2\text{SiO}_{20}$) crystals, due to their electrooptic, piezoelectric, and elastooptic effects, have found broad application in quantum electronic and optoelectronic structures such as modulators, deflectors, spatial modulators, image converters, holographic memories, etc. The functioning of all of these structures is greatly affected by the presence of localized states in the forbidden band which influence the optical, electrical, and photoelectric properties of the crystals. In order to investigate the localized states the authors have measured the photoconductivity, EPR, and photo-EPR spectra in an electric field, the spectrum of the additional absorption of undoped $\text{Bi}_2\text{SiO}_{20}$ crystals due to the photochromic effect, and the photoconductivity and EPR spectra of bismuth silicate doped with aluminum and gallium (the Al_2O_3 and Ga_2O_3 doping in the melt was up to 0.5 wt.%). (16 refs.)

Electron localization in a two-dimensional system in strong magnetic fields.

Case of short-range scatterers

See Entry 76864

Effect of oxygen on the electrical properties of β -zinc phthalocyanine single crystals

See Entry 76961

Multiplet effects and breakdown of dipole selection rules in the $3d-4f$ core-electron-energy-loss spectra of La, Ce, and Gd

See Entry 77493

71.55 IMPURITY AND DEFECT LEVELS

76876 High temperature annealing defects of high resistivity Si doped by neutron transmutation. Wu Shuxiang, Yan Maoxun, Hua Zhongli, Zhang Yufeng, Du Yongchang (Dept. of Phys., Peking Univ., Peking, China).

Acta Sci. Nat. Univ. Pekin. (China), no.6, p.62-6 (1982). In Chinese.

Neutron transmutation doped silicon was studied with DLTS. After annealing in nitrogen at 850°C , three deep levels were found in the gap located at 0.2 eV, 0.23 eV and 0.49 eV respectively below the conduction band. It is suggested that they are related to the complex consisting of neutron irradiation damage and quenched-in defects, excited impurities, and the complex of excited impurities and defects of neutron irradiation, respectively. (7 refs.)

76877 Clustered hydrogenic centers in impure semiconductors. K.A.Chao, K.-F.Berggren (Dept. of Phys. & Measurement Technol., Univ. of Linköping, Linköping, Sweden).

Int. J. Quantum Chem. (USA), vol.23, no.4, p.1155-63 (April 1983).

Doped semiconductors with shallow impurities provide an ideal situation to study a collection of hydrogenlike atoms under controllable experimental conditions. The authors present the results of recent cluster calculation of the electronic properties of such systems. (19 refs.)

76878 Defects induced by electron irradiation in InP. J.Suski, J.C.Bourgoin (Groupe de Phys. des Solides, Univ. Paris VII, Paris, France), H.Lim.

J. Appl. Phys. (USA), vol.54, no.5, p.2852-4 (May 1983).

Schottky diodes made on n -type InP, containing $2 \times 10^{16} \text{ cm}^{-3}$ free carriers, have been irradiated at room temperature with $\sim 1 \text{ MeV}$ electrons. Using transient capacitance techniques, three electron traps situated at 0.14, 0.24, and 0.41 eV below the conduction band have been detected. Measurement of their introduction rates and comparison with the carrier removal rate measured at 80K indicate that these traps represent $\sim 20\%$ of the electrically active defects created by the irradiation. The capture cross section for electrons of the trap at $E_c - 0.24 \text{ eV}$ is $3 \times 10^{-20} \text{ cm}^2$. (8 refs.)

76879 Magnetic impurities in semiconductors. S.Fukuchi, Y.Kayanuma (Dept. of Phys., Tohoku Univ., Sendai, Japan).

J. Phys. Soc. Jpn. (Japan), vol.52, no.5, p.1682-6 (May 1983).

The magnetic-nonmagnetic transition of impurities in semiconductors is studied by a simple one-dimensional model. The model is a two-electron system in a linear chain with a short-range impurity potential v . The intra-site two-body repulsive energy U is assumed throughout the crystal. The phase boundary for the transition is calculated numerically exactly by the use of the Green's function formalism. In contrast with the model of Mattis and Lieb, the singlet ground state becomes degenerate with the lowest one-electron scattering state (magnetic) for practically all value of v as U exceeds a critical value U_c which is of the same order of magnitude as v .

76880 Stability of oxygen impurity in silicon and gallium phosphide. M.Jaros (Dept. of Theoretical Phys., Newcastle upon Tyne Univ., Newcastle upon Tyne, England). *J. Phys. C (GB)*, vol.16, no.14, p.1459-63 (20 May 1983). It is argued that the stable positions of the oxygen impurity in the lattice of silicon and gallium phosphide can be explained in terms of a simple first-order mechanism, without invoking a second-order process known as the pseudo Jahn-Teller effect. (10 refs.)

76881 Energy levels of an electron bound on a donor-acceptor pair. B.L.Gel'mont (A.F. Ioffe Physicotech. Inst., Acad. of Sci., Moscow, USSR). *JETP Lett. (USA)*, vol.36, no.10, p.443-5 (20 Nov. 1982). Translation of: *Pisma v Zh. Eksp. & Teor. Fiz. (USSR)*, vol.36, no.10, p.365-7 (20 Nov. 1982). [received: June 1983] The problem of the dependence of the binding energy of an electron in a donor-acceptor pair on the distance R between the donor and acceptor is examined. It is shown that the critical distance R_c is an essential singularity at which an infinite number of levels converge. (3 refs.)

76882 Electron bombardment induced defect states in p-InP. M.Levinson, H.Temkin, W.A.Bonner (Bell Labs., Murray Hill, NJ, USA). *J. Electron. Mater.* (USA), vol.12, no.2, p.423-32 (March 1983). A deep level transient spectroscopy (DLTS) study has been made of 1 MeV electron bombardment induced defect states in the lower half band gap of EC grown Zn doped p-InP. One state was observed in the unirradiated material with a hole emission activation energy H of 0.15 eV. Irradiation resulted in two new states with H of 0.34 and 0.58 eV, and introduction rates $dN_i/d\phi$ of 1 and 0.04 cm^{-2} , respectively. Annealing experiments revealed the appearance of an additional state with H (0.52 eV), and recovery of the 0.34 eV defect state above 150°C. The 0.52 eV and 0.58 eV states were found at the highest concentration near the metal-semiconductor interface. The implications of the large introduction rate of the 0.34 eV state are discussed. (17 refs.)

76883 Residual donors and acceptors in high-purity GaAs and InP grown by hydride VPE. B.J.Skromme, T.S.Low, T.J.Roth, G.E.Stillman (Dept. of Electrical Engng., Univ. of Illinois, Urbana, IL, USA), J.K.Kennedy, J.K.Abrokwhah. *J. Electron. Mater.* (USA), vol.12, no.2, p.433-57 (March 1983). Residual donors and acceptors in epitaxial films of GaAs and InP grown by the hydride vapor phase epitaxy technique were investigated using the complementary techniques of photothermal ionization spectroscopy and variable-temperature photoluminescence. High-purity samples of GaAs grown in three different laboratories were compared and high-purity InP samples were also measured. The dominant shallow acceptors in the GaAs samples were found to be C and Zn, and deep Cu and Mn acceptors were also observed. The donors Si, S, and Ge were observed in the GaAs with S being dominant. A clear correlation was observed between the gas phase stoichiometry during growth and the relative incorporation of column IV donors (Si and Ge) and column VI donors (S) in GaAs. Substrate quality, source purity, and atmospheric contamination of the growth system were found to influence the photoluminescence spectra of the GaAs samples. (41 refs.)

76884 Theory of interimpurity transitions in condensed medium. L.N.Christophorov, V.N.Kharkyanen (Inst. of Theoretical Phys., Acad. of Sci., Kiev, Ukrainian SSR). *Phys. Status Solidi b (Germany)*, vol.116, no.2, p.415-25 (1 April 1983). The problem investigated is the quantum particle transfer between impurities imbedded in a condensed medium via the states of the latter. The kinetic equation explicitly containing no medium indices (the role of the medium is taken into account by effective constants found from 'free' medium properties) is obtained. The two-impurity case (donor-acceptor transfer) is considered in detail for a one-dimensional model of a crystal. (18 refs.)

76885 Comparison of different approaches to the study of local defects in crystals. II. Substitutional impurities in the tight-binding approximation. C.Pisani, R.Dovesi, P.Ugliengo (Inst. of Theoretical Chem., Univ. of Turin, Turin, Italy). *Phys. Status Solidi b (Germany)*, vol.116, no.2, p.547-56 (1 April 1983). Different approaches to the study of local defects in perfect crystals are compared as applied to the classical problem of substitutional impurities in tight binding (TB) cubic metals. The standard embedding procedure proposed by Koster and Slater (KS) is perfectly suited for this problem and its results are taken as a reference. It is thus possible to evaluate the performance of isolated cluster (IC) calculations, and of those 'perturbed cluster' approaches which correct the cluster molecular solution by a suitable coupling operator (MLEC schemes). It is shown that while IC results are affected by enormous relative errors at small perturbations even with large clusters, the MLEC approach is very effective in accounting for the presence of the surrounding media and reproducing the correct electronic structure within the cluster. (14 refs.)

76886 Energy levels and binding energy of ion pairs in Si. H.Lemke (Zentralinst. für Elektronenphys., Akad. der Wissenschaften, Berlin, Germany). *Phys. Status Solidi a (Germany)*, vol.76, no.1, p.223-34 (16 March 1983). In German. The energy levels of the ion pairs between the acceptor Ga and the donors Fe, Mn, Cr are investigated by DLTS- and TSCA-techniques. The donor levels and capture coefficients for holes lie at $E_d+0.24\text{ eV}$, $E_d-0.36\text{ eV}$, $E_d+0.47\text{ eV}$ and $r_p=4\times10^{-8}$ ($T=120\text{K}$), 1×10^{-11} (90K), $2\times10^{-8}\text{ cm}^2\text{ s}^{-1}$ (240K) for FeGa, MnGa, CrGa. The binding energies for all neutral ion pairs between B, Al, Ga and Fe, Mn, Cr are determined. These energies lie between 0.3 and 0.7 eV and show a 'chemical shift' with both pairing atoms. Between the acceptor energy E_A , the energy E^{++} of the 'free' double charged donor and the donor energy E^{++}_p of the pair there exist an approximation $E^{++}_p \approx E^{++} + aE_A$ with $a=5$ (Fe), 6.5 (Mn), and 8 for Cr. In the case of Fe and Cr the level E^{++} must lie in the valence band ($\approx E_v-0.15\text{ eV}$). (11 refs.)

76887 The electronic structure of F-centres in alkali halide crystals. Z.S.Herman (Quantum Chem. Group, Univ. of Uppsala, Uppsala, Sweden), G.Barnett. *Rev. Bras. Fis. (Brazil)*, vol.12, p.73-91 (March 1982). [received: April 1983] A method is presented for estimating the number of bound states of different orbital angular momentum quantum number for an F-centre residing in an alkali halide crystal through the introduction of a spherically symmetric potential well of finite depth. The method is illustrated through its application to the F-centre in sodium chloride, and the results for F-centres in various alkali halide lattices are tabulated. The results provide a good account of the experimental features of the F-centre including the K-band which, it is suggested, is due to transitions from the $2p$ to excited levels. Values for the effective range of penetration of the defect electron with the neighbouring cation in different crystals are determined by requiring that the well depth be independent of orbital angular momentum quantum number. The technique is applied to estimate the Madelung constant and Madelung potential for the host crystals. (no refs.)

76888 Electronic structure of thallous centres and $\text{Ti}^{++}-\text{V}_k$ recombination in KCl crystal. E.Kotomin, A.Shluger, I.Tale (Latvian State Univ., Riga, Latvian SSR). *Solid State Commun. (USA)*, vol.46, no.8, p.625-9 (May 1983). Parameters of impurity Ti^{++} ion required for the calculation of different thallous centres in alkali halides are obtained for the semiempirical method of the intermediate neglect of differential overlap (INDO). The electronic structure of Ti^{++} , Ti^{++} , $(\text{Ti}_2)^{3+}$ centres in KCl is calculated. The potential energy curves for the recombination of nearest Ti^{++} , V_k centres against the breathing vibrational mode of the V_k centre are calculated. This recombination (hole trapping) is found to be nonradiative tunneling with small activation energy. Experimental data is also discussed in the light of the present calculations. (40 refs.)

76889 Microscopic model of the EL2 level in GaAs. J.Lagowski, M.Kaminska, J.M.Parsey, H.C.Gatos, W.Walukiewicz (MIT, Cambridge, MA, USA). Gallium Arsenide and Related Compounds, 1982. Tenth International Symposium on Gallium Arsenide and Related Compounds, Albuquerque, NM, USA, 19-22 Sept. 1982 (Bristol, England: IOP 1983), p.41-8. It was found that the defect responsible for the dominant deep donor $E_c-0.76\text{ eV}$ (EL2) in melt-grown GaAs also introduces a shallow donor level at $E_c-0.025\text{ eV}$. This finding makes possible the refinement of the authors' antisite defect As_{Ga} model of the EL2 formation in melt growth to a microscopic model which accounts for the, thus far, observed electronic behavior of EL2 (including its metastable state). In addition to the antisite defect As_{Ga} , the proposed defect center involves an arsenic vacancy V_{As} on a neighboring site. This complex is similar to a DX center exhibiting a large lattice relaxation energy. (24 refs.)

76890 Interactions among certain deep-level traps in GaAs. Zou Yuanxi, Zhou Jicheng, Mo Peigen, Lu Fengzheng, Li Liansheng, Shao Juan, Hong Lei (Shanghai Inst. of Metall., Acad. Sinica, Shanghai, China), Sun Henghui, Sheng Chi, Sun Qing. Gallium Arsenide and Related Compounds, 1982. Tenth International Symposium on Gallium Arsenide and Related Compounds, Albuquerque, NM, USA, 19-22 Sept. 1982 (Bristol, England: IOP 1983), p.49-56. The interactions among certain defects in GaAs including the deep levels A, B, C and EL2 as well as certain shallow donors are discussed on the basis of DLTS measurements on VPE and LPE grown bulk GaAs. The model proposed previously by one of the authors (Zou, 1974) to account for two predicted unknown acceptors in GaAs, which are expected to be equal in concentration but different in nature just like the A and B hole traps reported later by Lang and Logan (1975), is elaborated in the light of the present findings. (31 refs.)

76891 Thermal conversion of undoped GaAs and the outdiffusion of the main electron trap EL2. B.Hughes, C.Li (Santa Rosa Technol. Center, Hewlett-Packard, Santa Rosa, CA, USA). Gallium Arsenide and Related Compounds, 1982. Tenth International Symposium on Gallium Arsenide and Related Compounds, Albuquerque, NM, USA, 19-22 Sept. 1982 (Bristol, England: IOP 1983), p.57-64. The deep level donor EL2 compensates acceptors making undoped GaAs grown by the low-pressure LEC technique semi-insulating. Hall effect measurements vs. temperature were used to substantiate this model. The concentration of electrically active EL2 in the layer near the surface decreased during annealing at 850°C in a hydrogen atmosphere. The observed p-type thermal conversion of undoped semi-insulating GaAs is caused by the decrease in the EL2 concentration. EL2 did not decrease, however, during annealing in a nitrogen atmosphere; this suggests that the apparent EL2 loss is associated with indiffusion of hydrogen. (19 refs.)

76892 Re-examination of the mid-gap electron trap (EL2) in different GaAs wafers by photocapacitance, DLTS and photoluminescence spectra. M.Taniguchi, T.Ikoma (Inst. of Industrial Sci., Univ. of Tokyo, Tokyo, Japan). Gallium Arsenide and Related Compounds, 1982. Tenth International Symposium on Gallium Arsenide and Related Compounds, Albuquerque, NM, USA, 19-22 Sept. 1982 (Bristol, England: IOP 1983), p.65-70. Using DLTS, photocapacitance, and photoluminescence methods, the authors re-examined a mid-gap electron trap (EL2) in variously grown GaAs wafers; some were ion-implanted (O, As, Ga, Si and N) and annealed. All the samples contained EL2 as a major electron trap. From these results, a new mid-gap electron trap (EL2-O) was distinguished from EL2, which has the same emission rate but different photoionization energies. Results also suggest that the 0.64 eV PL band is not related to EL2 but to an oxygen-induced level. (16 refs.)

76893 Dependence of emission-capture properties of dominant traps and interface states on alloying in organometallic VPE $\text{Al}_x\text{Ga}_{1-x}\text{As}$. T.Matsumoto, P.K.Bhattacharya, J.Darmawan (Dept. of Electrical & Computer Engng., Oregon State Univ., Corvallis, OR, USA), M.J.Ludowise. Gallium Arsenide and Related Compounds, 1982. Tenth International Symposium on Gallium Arsenide and Related Compounds, Albuquerque, NM, USA, 19-22 Sept. 1982 (Bristol, England: IOP 1983), p.289-96. Thermal emission and capture and photoionization properties of three dominant electron traps in organometallic VPE $\text{Al}_x\text{Ga}_{1-x}\text{As}$ have been investigated. Some of the trends have been explained by a configuration coordinate model. New deep levels are not observed at the grown GaAs/ $\text{Al}_x\text{Ga}_{1-x}\text{As}$ heterointerface. Evidence is shown of transfer doping phenomena at the $\text{Al}_x\text{Ga}_{1-x}\text{As}$ -GaAs:Cr substrate interface for $x\geq 0.4$. (30 refs.)

76894 Behavior of shallow acceptors following neutron transmutation doping. A.T.Hunter, M.H.Young, R.Baron, J.P.Baukus, O.J.Marsh (Hughes Res. Lab., Malibu, CA, USA). Gallium Arsenide and Related Compounds, 1982. Tenth International Symposium on Gallium Arsenide and Related Compounds, Albuquerque, NM, USA, 19-22 Sept. 1982 (Bristol, England: IOP 1983), p.509-14. Neutron transmutation doping of p-type liquid encapsulated Czochralski (LEC) GaAs has been carried out. The concentrations of C, an 0.7 eV level, and an 0.2 eV level present in the starting material remain unchanged. All of the added Se is expected to incorporate as a donor. Approximately 50% of the added Ge is incorporated as an acceptor for samples with 1.5 and $3.4\times10^{15}\text{ cm}^{-3}$ added Ge. These studies confirm the authors' estimates of the activation energy of the 0.07 eV acceptor, as well as the total concentration of acceptors in the original material. (5 refs.)

- 76895 Deep levels in InP grown by SSD method.** C.H.Chung, S.K.Noh, S.C.Park, C.K.Kim (Dept. of Phys., Yonsei Univ., Seoul, Korea). Gallium Arsenide and Related Compounds, 1982. Tenth International Symposium on Gallium Arsenide and Related Compounds, Albuquerque, NM, USA, 19-22 Sept. 1982 (Bristol, England: IOP 1983), p.641-6.
- Six electron traps have been observed in InP bulk crystals by deep-level transient spectroscopy and photoluminescence measurements. The crystals were grown by the SSD (synthesis by solute diffusion) method. Three deep impurity levels induced by low-temperature heat treatment ($\leq 500^\circ\text{C}$) have the same activation energies of 0.43 eV but somewhat different cross sections. The origin of these deep impurity levels may be due to a specific complex which includes P vacancies and defects. (10 refs.)
- Reproducibility and uniformity considerations in LEC growth of undoped, semi-insulating GaAs for large-area, direct implantation technology** See Entry 76342
- Incorporation of amphoteric impurities in high purity GaAs** See Entry 76475
- Coulomb potential fluctuations in high-purity n-type III-V semiconductors** See Entry 76481
- Electric field effects on radiation defects annealing in p-InP** See Entry 76515
- Anderson transition in the exciton-impurity band in silicon** See Entry 76848
- Multichannel localization and magnetic impurities** See Entry 76872
- Quadrupole splitting of hydrogen-like atom levels in crystals** See Entry 76915
- Effect of temperature on the electrical transport properties of p-type polycrystalline indium antimonide** See Entry 76948
- Self quenching of extrinsic photoconductivity in GaAs:Cr** See Entry 76990
- The electric and photoelectric properties of TiSbSe_2 crystals in the region of impurity conduction** See Entry 76995
- Photoelectric spectroscopy of radiation defects in germanium** See Entry 77002
- Characterization of surface states in MOS capacitors by a modified DLTS technique** See Entry 77062
- Spin susceptibility of electrons and magnetic hyperfine interactions in a conductor with resonance levels** See Entry 77131
- Bethe-Ansatz solution of the Anderson model of a magnetic impurity with orbital degeneracy** See Entry 77138
- Electron localization on defects and optical nuclear polarization in disordered and semimagnetic semiconductors** See Entry 77270
- Photoluminescence of molecular beam epitaxially grown Ge-doped GaAs** See Entry 77431
- Enhanced excitation transfer during vibrational relaxation after pumping and generalized Forster's formula** See Entry 77440
- Radiative recombination in $\gamma\text{-La}_2\text{S}_3$ single crystals** See Entry 77444
- Extrinsic photoluminescence from GaAs quantum wells** See Entry 77446
- Impurity photoluminescence in GaAs/ $\text{Ga}_{1-x}\text{Al}_x$ As multiple quantum wells** See Entry 77447
- Deep acceptor photoluminescence in GaAs** See Entry 77456
- Photoluminescence of oxygen-induced states in $\text{GaAs}_{1-x}\text{P}_x$** See Entry 77457
- Localization of electronic states and cathodoluminescence of bound exciton complexes in ZnSe crystals** See Entry 77462
- Thermoluminescence and optical absorption studies. Rubidium bromide doped with barium** See Entry 77463
- I. The emission spectra of TL produced by ion implanted CaF_2** See Entry 77465
- Investigation of capless heat treatment of MBE n-GaAs** See Entry 77686
- Deep level defects and annealing studies in one-MeV electron irradiated (AlGa)As-GaAs solar cells** See Entry 78032

71.55J Localization in disordered structures

- 76896 Measurement of deep levels in hydrogenated amorphous silicon by transient voltage spectroscopy.** N.M.Johnson (Xerox Palo Alto Res. Center, Palo Alto, CA, USA). *Appl. Phys. Lett. (USA)*, vol.42, no.11, p.981-3 (1 June 1983).
- Electronic defect levels in amorphous silicon Schottky diodes have been measured by capacitance transient spectroscopy performed in the constant capacitance mode. In hydrogenated amorphous silicon deep levels are continuously distributed in energy and of sufficient density to dominate the electrical properties. The constant capacitance mode, applied for the first time to an amorphous semiconductor, offers significant advantages over the transient capacitance mode for measuring the bulk density of gap states. For example, numerical solution of Poisson's equation for only the steady-state charge distribution is required to analyze the transient response of a diode after a trap-filling voltage pulse. The technique has been used to record time-resolved transients, which saturate with respect to pulse width, and the analysis yields deep level distributions in the range of $10^{17} \text{ eV}^{-1} \text{ cm}^{-3}$ over the energy interval from 0.6 to 0.9 eV below the conduction-band mobility edge. (11 refs.)
- 76897 Defect states and donors in thermally annealed or post-hydrogenated chemically vapor-deposited amorphous Si_3N_4 alloy.** G.Sasaki, S.Fujita, A.Sasaki (Dept. of Electrical Eng., Kyoto Univ., Kyoto, Japan). *J. Appl. Phys. (USA)*, vol.54, no.5, p.2696-700 (May 1983).
- Thermal annealing and post-hydrogenation effects on the electrical properties of chemically vapor-deposited (CVD) amorphous silicon-nitrogen ($\text{a-Si}_3\text{N}_4$) alloys are studied. Annealing of CVD a-Si and a-SiN_x films causes the increases in the ESR centers, the hopping conduction, and the gap-state density evaluated by the field-effect method. The nitrogen incorporation reduces the number of ESR centers in a film. The Fermi level of CVD a-SiN_x films is shifted by post-hydrogenation, which suggests that the films include donors. The $n_{\text{H}}\tau$ products of CVD a-Si and a-SiN_x films are increased by post-hydrogenation, exceeding two orders of the magnitude. Post-hydrogenated CVD a-SiN_x films show larger $n_{\text{H}}\tau$ product than post-hydrogenated CVD a-Si . (30 refs.)
- 76898 On local density of states in Anderson localized systems.** F.J.Ohkawa (Inst. for Solid State Phys., Univ. of Tokyo, Tokyo, Japan). *J. Phys. Soc. Jpn. (Japan)*, vol.52, no.5, p.1710-17 (May 1983).
- The ensemble average of local densities of states defined by $g_2(\epsilon_1, \epsilon_2) = \langle \rho(\epsilon_1, \tau) \rho(\epsilon_2, \tau) \rangle$ is theoretically investigated, where $\rho(\epsilon, \tau)$ is the local density of states of disordered systems. It is shown by using the self-consistent theory due to Vollhardt and Wolfe and a physical picture of localization due to Mott, which includes the effect of 'level repulsion', that $g_2(\epsilon_1 - \epsilon_2)$ is non zero even if the states around ϵ_2 are localized. (14 refs.)

- 76899 Transmission coefficient and the localization length of an electron in N bound disordered chains.** O.N.Dorokhov (L.D. Landau Inst. of Theoretical Phys., Acad. of Sci., Chernogolovka, USSR). *JETP Lett. (USA)*, vol.36, no.7, p.318-21 (5 Oct. 1982). Translation of: *Pis'ma v Zh. Eksp. i Teor. Fiz. (USSR)*, vol.36, no.7, p.259-62 (5 Oct. 1982). [received: May 1983]
- A model of N-coupled chains with defects for which it is possible to prove rigorously the presence of localization with arbitrarily strong coupling between chains is examined. N different localization lengths arise under these conditions. (8 refs.)
- 76900 Self-consistent study of localisation.** A.Brezini (Internat. Centre for Theoretical Phys., Trieste, Italy), G.Olivier. *Philos. Mag. B (GB)*, vol.47, no.5, p.461-9 (May 1983).
- The localisation models of Abou-Chakra et al. (1973, 1974) and Kumar et al. (1975) are critically re-examined in the limit of weak disorder. By using an improved method of approximation, the displacement of the mobility edge is studied as a function of disorder. The results are compared to other theories in the light of the present approximation. (14 refs.)
- Electronic states of disordered binary alloys with strong off-diagonal disorder** See Entry 76829
- The localization transition on the Bethe lattice** See Entry 76846
- The method of thermodynamic perturbation in the intermediate valence problem** See Entry 76902
- Transient photoconductivity and thermalisation in amorphous semiconductors** See Entry 76998
- On the role of the correlation length near the onset of non-metallic conduction** See Entry 77010
- Kondo effect in disordered two-dimensional systems** See Entry 77136
- ## 71.70 LEVEL SPLITTING AND INTERACTIONS
- (see also 75.10 - in magnetic phenomena, 75.30E Exchange and superexchange interactions, 73.20 Electronic surface states)
- 76901 Analysis of valence-electron structures of $\text{Y}_3\text{Al}_5\text{O}_{12}$ (YAG) and Al_2O_3 , Cr_2O_3 (ruby) - study of certain properties of these laser materials related to their valence-electron structures.** S.H.Yu (Jinan Univ., Changchun, China), L.H.Yu. *Proc. SPIE Int. Soc. Opt. Eng. (USA)*, vol.335, p.16-30 (1982). [received: May 1983] (Advanced Laser Technology and Applications, Arlington, VA, USA, 6-7 May 1982).
- A direct method of determination of the valence-electron structure from its crystal structure has been presented by the writer at XIIth International Congress of Crystallography, at Ottawa, 1981. Here the method is applied to determine the valence-electron structures of $\text{Y}_3\text{Al}_5\text{O}_{12}$ (YAG) and Al_2O_3 , Cr_2O_3 (ruby) to see how certain properties of these laser materials are related to their valence-electron structures. The first point observed is the very strong, continuous, but zig-zag three-dimensional fractional covalent M-O bond nets (M=Al or Cr) being connected with the high melting points, the great resistance against the puncture by the strong laser beam. In the case of Nd-YAG, the distortion caused by the replacement of the Y atoms by almost the same size Nd atoms is small. On the other hand, because of the similarity of the valence-electron structures of $\alpha\text{-Al}_2\text{O}_3$ and Cr_2O_3 , the replacement of Al atoms by the little larger size Cr atoms in small amount is easily understood. The large atomic spins of magnetic moment $m_B = 2.76 \mu_B$ (=experiment value, the theoretical $m_B = 2.70 \mu_B$) of Cr atoms pointing parallel to the c axis of the hexagonal lattice, is found to be due to the direction of the spin situated in the space of lowest density space of the valence-electron cloud distribution. This agrees with the result of $\alpha\text{-Fe}$ disclosed in the paper 'Electron theory of the magnetic moment structures of $\alpha\text{-Fe}$, $\epsilon\text{-Co}$, Ni from neutron diffraction experiments' presented at the Symposium on Neutron Scattering, Argonne National Laboratory, 1981. (20 refs.)
- 76902 The method of thermodynamic perturbation in the intermediate valence problem.** M.E.Foglio (Inst. de Fisica 'Gleb Wataghin', Univ. Estadual de Campinas, Campinas, Brazil). *Rev. Bras. Fis. (Brazil)*, vol.12, p.123-60 (March 1982). [received: April 1983]
- The effect of hybridization on the free energy and the magnetic susceptibility χ of intermediate valence compounds is studied, employing the method of thermodynamic perturbation in the second order. The method is applied to a lattice with a variable concentration c of impurities that are described by the Anderson model. (24 refs.)
- 76903 X-ray L_{III} absorption spectroscopy of europium in intermetallics of the EuM_2Si_2 type.** N.D.Samsonova, L.D.Finkel'shtein, E.M.Levin (Inst. of Metal Phys., Acad. of Sci., Sverdlovsk, USSR). *Sov. Phys.-Solid State (USSR)*, vol.24, no.12, p.2116-17 (Dec. 1983). Translation of: *Fiz. Tverd. Tela (USA)*, vol.24, no.12, p.3711-14 (Dec. 1983).
- The valence state of Eu in EuM_2Si_2 (M=Fe, Co, Ni, Cu) is studied using X-ray absorption spectroscopy. Results are compared with the isomeric shift of the average NMR signal. (12 refs.)
- 76904 Effect of vacancies and foreign metal ions on the valent state of samarium in SmB_6 .** E.S.Konvalova, Yu.B.Paderno, T.Lundstrom, L.D.Finkel'shtein, N.N.Efremova, E.M.Dudnik (Inst. of Materials Sci., Acad. of Sci., Ukrainian SSR). *Sov. Powder Metall. & Met. Ceram. (USA)*, vol.21, no.10, p.820-3 (Oct. 1982). Translation of: *Poroshk. Metall. (USSR)*, vol.21, no.10, p.78-82 (Oct. 1982). [received: May 1983]
- A study was made of $\text{Sm}_2\text{M}_{1-x}\text{B}_6$ solid solutions, where M represents ions of di- and trivalent metals, and of metal-deficient Sm_2B_6 phases produced by synthesis. The mixed-configuration state of samarium in SmB_6 is stable and unaffected by defectiveness of structure and the presence of vacancies of metallic states in the lattice. The introduction of atoms of stable integral valence into the SmB_6 crystal lattice alters the valent state of the samarium atoms. The introduction of divalent atoms of atomic radius larger than that of samarium increases the lattice constant of the boride and results in the effective valence gradually growing to the integral value 3. The larger the atomic radius of the addition metal, the lower is the concentration of this addition at which a change in the valence of the samarium atoms is observed. The introduction of trivalent atoms shifts the mixed-configuration state of Sm ions toward smaller values of effective valence, but an integral value is not attained. The effect of substitution of magnetic elements (Eu and Gd) for samarium is the same as that of substitution of nonmagnetic elements (Yb and La). (9 refs.)
- Jahn-Teller transition in NdMnO_3** See Entry 76614
- High pressure reactions of oxometallics. VI. High pressure synthesis of mixed valence compounds $\text{VO}_{2-x}(\text{OH})_x$ with CaCl_2 -structure** See Entry 76636

| | |
|---|-----------------|
| Theory of the Verwey transition in the mixed valence compound Eu_2S_4 | See Entry 76847 |
| Ternary mixed valence oxygen deficient K_2NiF_4 type copper oxides. Progressive evolution of a semiconducting state from a semimetallic state in $\text{La}_{2-x}\text{Sr}_x\text{CuO}_{4-x/2-s}$ | See Entry 76945 |
| Characteristics of the magnetic susceptibility of films consisting of mixed-valence compounds | See Entry 77130 |
| Theory of magnetic susceptibility of mixed-valent $\text{Ce}_{0.76}\text{La}_{0.14}\text{Th}_{0.1}$ | See Entry 77133 |
| Bethe-Ansatz solution of the Anderson model of a magnetic impurity with orbital degeneracy | See Entry 77138 |
| ^{57}Fe Mossbauer study of amorphous $\text{Fe}_{81}\text{B}_{13.5}\text{Si}_{3.5}\text{C}_2$ | See Entry 77301 |
| Influence of isomer-shift distribution on Mossbauer quadrupole spectra in amorphous magnetic insulators | See Entry 77309 |
| Study of positron lifetimes in α , β and γ cerium at high pressures | See Entry 77476 |

71.70C Crystal and ligand fields

| | |
|--|--|
| 76905 Energy level diagrams for d^2 - d^8 configurations in a cubic field. Y. Sakunthalamma, K. Purandar, S.V.K. Lakshman (Dept. of Phys., SVU Coll., Tirupati, India). <i>Indian J. Pure & Appl. Phys.</i> , vol.21, no.3, p.190-2 (March 1983). Tanabe-Sugano diagrams are of great help to scientists working on the transition metal ions embedded in crystals in the optical absorption spectra. Since fixing the band positions with Racah parameter (C) involves a great amount of computer work, the cubic field energy matrices for d^2 , d^3 , d^4 , d^5 , d^6 , d^7 , and d^8 electronic configurations are diagonalized. A few typical energy level diagrams drawn between Dq/B and E/B for certain values of C/B are presented. (2 refs.) | |
| 76906 Comparative crystal-field analysis of Eu^{3+} : Y_2O_3 . B.M. Angelov (Dept. of Phys. Chem., Higher Inst. of Food Technol., Plovdiv, Bulgaria). <i>J. Phys. C (GB)</i> , vol.16, no.14, p.1437-9 (20 May 1983). The dependence of the crystal-field parameters for Eu^{3+} : Y_2O_3 upon four sets of radial expectation values $\langle r^n \rangle_{4f}$ has been examined. It is shown that the more extended wavefunctions reproduce better the available experimental data. The europium-oxygen overlap has been calculated and found to give parameters comparable to the experimental ones. The same trend is reflected on the variation of the crystal-field strength evaluated as an average parameter. (17 refs.) | |
| 76907 Anomalous linewidths of the crystal electric field excitations in $\text{La}_{0.997}\text{Tm}_{0.003}\text{Al}_2$ below the superconducting transition. R. Feile, K. Knorr (Inst. fur Phys., Johannes Gutenberg Univ. Mainz, Mainz, Germany), J.K. Kjems, B. Frick, M. Loewenhaupt. <i>J. Phys. C (GB)</i> , vol.16, no.14, p.1465-9 (20 May 1983). Inelastic neutron scattering experiments on $\text{La}_{0.997}\text{Tm}_{0.003}\text{Al}_2$ show an inelastic electric field transition at 0.75 meV. The width of this transition decreases monotonically in the temperature range from 9.5K down to the superconducting temperature at $T_c = 3.15\text{K}$. Below T_c a sudden decrease of the linewidth is observed levelling off at a finite value between 2.5K and 60 mK. (14 refs.) | |
| 76908 A quantum field theoretic approach to the calculation of reduction factors in Jahn-Teller systems. I. General theory. S.H. Payne, G.E. Stedman (Dept. of Phys., Univ. of Canterbury, Christchurch, New Zealand). <i>J. Phys. C (GB)</i> , vol.16, no.14, p.2679-703 (20 May 1983). Ham reduction factors are defined in the context of a field theoretic formalism and are thus generalised to cover arbitrary choices of electronic states, linear and nonlinear ion-lattice couplings, anharmonic lattice interactions, the mixing of electronic levels, second- and higher-order reduction factors and notably the effect of temperature in populating a distribution of vibronic states. Symmetry considerations are integrated with the field theoretic formalism in diagram form. Calculational techniques are described in some detail. Comparison is made with a similar generalisation of the standard definition of the reduction factor, which however implies the choice of particular vibronic states and does not include the effects of finite temperature. Symmetry considerations allow the first-order reduction factor to be written as a sum of products of $6j$ symbols (of the relevant symmetry group) and physical parameters. This in turn prescribes the form of sum rules linking the reduction factors in some approximation. The most important sum rules are exact at second order if the ion-lattice interaction contains only time-even operators. As a concrete illustration of the results, a simple tetragonal example is analysed in some detail. (21 refs.) | |
| 76909 A quantum field theoretic approach to the calculation of reduction factors in Jahn-Teller systems. II. $\text{E}_g(2\alpha_1 + e)$ in octahedral symmetry. S.H. Payne, G.E. Stedman (Dept. of Phys., Univ. of Canterbury, Christchurch, New Zealand). <i>J. Phys. C (GB)</i> , vol.16, no.14, p.2705-23 (20 May 1983). For pt.I see <i>ibid.</i> , vol.16, no.14, p.2679 (1983). The formalism of the preceding paper is applied to doublet levels in octahedral symmetry in interaction with many lattice modes of all frequencies through linear, nonlinear and anharmonic couplings. It is shown explicitly that when non-linear and anharmonic couplings are present, the interaction with symmetric modes (which have been ignored in the Jahn-Teller problem up till now) will contribute to reduction factors. The authors give the constraints upon the topology of any field theoretic diagram for it to contribute to a given reduction factor. These permit the generalisation of some results to all orders of perturbation. Explicit formulae are given for each reduction factor and for all temperatures and all fundamental interactions, up to fourth order and in some cases sixth order of perturbation. For example, at low temperatures the temperature-dependent part of a reduction factor varies as T^2 in second order, while at fourth order it will vary as T^4 , T^5 , T^6 or T^9 depending on whether linear, non-linear or both of these mixed with anharmonic effects are responsible. The conditions under which the sum rule $q = 1/2(1+p)$ breaks down are discussed in detail. For example, it is valid for all linear couplings at all temperatures if only one phonon frequency is chosen (Einstein lattice), while in a realistic (multifrequency) lattice contributions from nonlinear and anharmonic coupling violating the sum rule appear at sixth order. (22 refs.) | |
| 76910 A quantum field theoretic approach to the calculation of reduction factors in Jahn-Teller systems. III. $\text{E}_g(2\alpha_1 + e + \tau_2)$ in octahedral symmetry. S.H. Payne, G.E. Stedman (Dept. of Phys., Univ. of Canterbury, Christchurch, New Zealand). <i>J. Phys. C (GB)</i> , vol.16, no.14, p.2725-48 (20 May 1983). For pt.II see <i>ibid.</i> , vol.16, no.14, p.2705 (1983). The method and results of the two previous papers are extended to triplet and quartet electronic states in octahedral symmetry. Explicit expressions are given for all reduction factors to fourth order, including nonlinear, anharmonic and symmetric interactions. Sum rules for reduction factors, and the conditions under which they are | |

| | |
|--|-----------------|
| broken, are discussed in detail for each system, in the general coupling case, in the case where one coupling symmetry only is assumed, and in the case of equal coupling. A general proof is given for all Jahn-Teller systems, including tetrahedral and icosahedral systems, that sum rules associated with time-reversal considerations at second order are also valid at fourth order to the case of coupling to isoenergetic modes. For triplet systems weak τ_2 coupling together with nonlinear and anharmonic effects may be expected to have disproportionately large effects by inducing violations of sum rules and by introducing resonant terms. For quartet systems many novel sum rules are discussed. By testing such rules or by measuring the temperature dependence of a reduction factor it is possible in principle to determine whether either coupling symmetry is dominant and whether any of nonlinear, anharmonic and symmetric coupling effects are significant in practice. (29 refs.) | |
| 76911 Crystal-field calculation of the 3d multiplets of the binuclear Ni(II) monothiocarboxylates. J.A. Sordo, F. Gomez Beltran, L. Pueyo (Dept. de Quimica Fisica, Univ. de Oviedo, Oviedo, Spain). <i>J. Solid State Chem. (USA)</i> , vol.47, no.3, p.350-60 (May 1983). The electronic spectra of the dimers $(\text{Ni(R-COS)}_2)_2$ and $(\text{Ni(R-COS)}_2)_2 \cdot \text{C}_2\text{H}_5\text{OH}$ are calculated by crystal-field theory in terms of different polyhedra of coordination around the two Ni^{2+} ions. The necessary radial parameters are taken from other clusters of Ni^{2+} after a detailed study of their intercluster transferability. The calculations are organized in two blocks. In the first one, the Ni^{2+} - Ni^{2+} interaction is neglected and the clusters Ni^{2+} , Ni^{2+}O_4 and Ni^{2+}O_2 are considered. In the second block, this interaction is explicitly taken into account as a point-charge perturbation produced by one of the two metal ions on the 3d states of the other one. Accordingly, we deal with the $\text{Ni}^{2+}\text{Ni}^{2+}$ in which the Ni^{2+} acts as a pointlike ligand of charge q , and with the $\text{Ni}^{2+}\text{O}_4\text{Ni}^{2+}$ and the $\text{Ni}^{2+}\text{O}_2\text{Ni}^{2+}$, where the Ni^{2+} is the punctual ligand. The calculation shows that the optical spectra and magnetic moments of these dimers can be best reproduced if $q \approx 0$, i.e. when the metal-metal electrostatic interaction is negligible. The agreement with the experiments quickly disappears as q grows. This calculation supports the interpretation of Meljón et al. (1970) according to which the 3d electronic distribution of the Ni^{2+} ions in these dimers is probably controlled by their nearest neighbors rather than by the metal-metal interaction. (19 refs.) | |
| 76912 Influence of an impurity ion on the geometry of its immediate environment. V.N. Vasyukov, S.N. Lukin, G.A. Tsintsadze (Physicotech. Inst., Acad. of Sci., Donetsk, Ukrainian SSR). <i>Sov. Phys.-Solid State (USA)</i> , vol.24, no.11, p.1995-6 (Nov. 1982). <i>Translation of: Fiz. Tverd. Tela (USSR)</i> , vol.24, no.11, p.3501-3 (Nov. 1982). [received: May 1983] Demonstrates the active role of an impurity ion in the formation of the geometry of its immediate environment. A Co^{2+} paramagnetic impurity ion replacing isovalently an ion which does not exhibit orbital degeneracy of the ground state alters the existing trigonal distortion of the octahedral immediate environment. This is a special case of the pseudo-Jahn-Teller effect. (5 refs.) | |
| Generalized relations between d-orbital occupancies of transition-metal atoms and electron-density multipole population parameters from X-ray diffraction data | See Entry 76250 |
| Lithium insertion into manganese spinels | See Entry 76391 |
| Heat-capacity studies of crystal-field effects in dilute RRh_2B_4 compounds | See Entry 76662 |
| Schottky anomaly and phase transition in the specific heat and in the spectra of $\text{KdY(MoO}_4)_2$ | See Entry 76664 |
| Quadrupole splitting of hydrogen-like atom levels in crystals | See Entry 76915 |
| Spin susceptibility of electrons and magnetic hyperfine interactions in a conductor with resonance levels | See Entry 77131 |
| Theory of magnetic susceptibility of mixed-valent $\text{Ce}_{0.76}\text{La}_{0.14}\text{Th}_{0.1}$ | See Entry 77133 |
| Rare earth single-ion anisotropy and the magnetic structures of the RTiO_3 perovskites: $\text{R} = \text{Tb, Dy, Ho, Er}$ and Tm | See Entry 77142 |
| A binary ferromagnetic alloy with magnetic moments dependent on local environment. II. Neutron magnetic elastic scattering and hyperfine field distribution | See Entry 77146 |
| EPR study of Cu^{2+} ions in single crystal of strontium formate dihydrate | See Entry 77253 |
| EPR and luminescence of Mn^{2+} in distorted tetrahedral symmetry in CaZnF_4 crystals | See Entry 77255 |
| Electron-spin resonance study of spin dynamics in the one-dimensional magnetic crystal doped with diamagnetic impurities $(\text{CH}_3)_4\text{NMn}^{2+}\text{Cl}_3\text{Cd}^{2+}$ | See Entry 77257 |
| Electric field effect in the case of cubic Gd^{3+} centers in BaF_2 | See Entry 77260 |
| ^1H and ^{13}C NMR of the chloride of tricyclopentadienyluranium IV. Evolution of the contact shift | See Entry 77275 |
| Nuclear spin-lattice relaxation in doped silicon under optical pumping conditions | See Entry 77281 |
| Nuclear-quadrupole-resonance study of the ground state of praseodymium in lanthanum trifluoride | See Entry 77282 |
| Temperature dependences of the sublattice magnetizations in nickel ferrite | See Entry 77286 |
| Measurement of the hyperfine structure of Pr^{3+} :YAG by quantum-beat free-induction decay, hole burning, and optically detected nuclear quadrupole resonance | See Entry 77291 |
| Optical detection of cross relaxation between rare-earth ions in lanthanum trichloride crystals | See Entry 77294 |
| Giant hyperfine field on ^{151}Eu in EuFe_{12} [Mossbauer study] | See Entry 77297 |
| Lattice temperature and hyperfine interactions of $\text{Pb}_{1-x}\text{Sn}_x\text{Te}$ ($0.21 \leq x \leq 0.75$) | See Entry 77300 |
| The hyperfine interaction of gadolinium and holmium in cubic Ho: (Gd, Ce)Fe compounds | See Entry 77302 |
| Magnetic hyperfine splitting in Mossbauer spectra of microcrystals | See Entry 77303 |
| Magnetic order in isoelectronic Co(GaVFe) alloys | See Entry 77306 |
| Electric susceptibility of mixed cerium/lanthanum ethyl sulfate crystals | See Entry 77343 |
| Optical properties of the Ti^{3+} center in KCl | See Entry 77419 |
| Intensities of f - f transitions in the luminescence of ionic crystals activated by rare-earth elements | See Entry 77423 |
| Phosphorescent lifetime and quantum yield measurements of $\text{K}_4\text{Pt}_2(\text{H}_2\text{P}_2\text{O}_7)_4$ from 1.6 to 300K | See Entry 77425 |

- Theoretical calculations of fluorescent branching ratios for $\text{YAlO}_3\text{:Er}^{3+}$ from the complete Judd-Ofelt theory See Entry 77427
- Selective site excitation of europium-doped monoclinic Gd_2O_3 See Entry 77449

71.70E Spin-orbit coupling, Zeeman, Stark and strain splitting

- 76913 Temperature dependence of the Wannier-Stark level width in a semiconductor in a strong electric field. A.M.Berezhevskii, A.A.Ovchinnikov (L.Ya. Karpov Inst. of Phys. Chem., Moscow, USSR). *Phys. Status Solidi b (Germany)*, vol.117, no.1, p.289-99 (1 May 1983). Analytical expressions for the level width of the Wannier-Stark ladder caused by an electron-phonon interaction are derived. They allow to investigate the dependence of the width on temperature, external field, and semiconductor band parameters. It turns out that with increase in temperature the width associated with acoustic phonons is drastically increased whereas the width associated with optical phonons rises much more slowly. It seems that almost all experiments for finding the Wannier-Stark ladder had been carried out at too high temperatures when the interaction of an electron with acoustic phonons eliminates the ladder. (13 refs.)
- Schottky anomaly and phase transition in the specific heat and in the spectra of $\text{K Dy(MoO}_4)_2$ See Entry 76664
- Zeeman effect and diamagnetic shift of a free exciton in gallium arsenide crystals See Entry 76853
- Effect of the profile of an inhomogeneously broadened ESR line on the steady-state distribution of the Zeeman temperature under saturation conditions See Entry 77252
- Nuclear-quadrupole-resonance study of the ground state of praseodymium in lanthanum trifluoride See Entry 77282
- Selective site excitation of europium-doped monoclinic Gd_2O_3 See Entry 77449
- Multiplet effects and breakdown of dipole selection rules in the $3d-4f$ core-electron-energy-loss spectra of La, Ce, and Gd See Entry 77493

71.70G Exchange interactions

- 76914 Importance of exchange effects in the deformation of interacting ions. M.Gutowski, M.Kakol, L.Piela (Faculty of Chem., Univ. of Warsaw, Warsaw, Poland). *Int. J. Quantum Chem. (USA)*, vol.23, no.5, p.1843-53 (May 1983). In calculations for liquids or solids one often considers a limited cluster of atoms or molecules in the electrostatic field of their environment. In this paper possibilities of improving this model by inclusion of the exchange deformation potential are shown. The reported numerical results for the LiF and NaF molecules as well as for the LiF and NaF perfect crystals indicate the importance of the exchange deformation effects. (46 refs.)
- Exchange interactions between dimers of chromium(III). A cluster approach See Entry 77169
- Combined effects of exchange and g-value anisotropy in the conduction-electron spin resonance of metals See Entry 77263

71.70J Nuclear states and interactions

- 76915 Quadrupole splitting of hydrogen-like atom levels in crystals. V.G.Baryshevskii, S.A.Kuten, V.I.Rapoport (Dept. of Phys., Belorussian State Univ., Minsk, Belorussia SSR). *Phys. Status Solidi b (Germany)*, vol.116, no.2, p.489-500 (1 April 1983). The theory of the behaviour of a hydrogen-like impurity atom with a quadrupole moment in a crystal is presented. It is shown that available EPR data on atomic hydrogen trapped in crystalline SiO_2 testify to the fact that it has an electric quadrupole moment. Another proof is presented of atomic hydrogen and muonium (a light isotope of hydrogen) trapped at the same sites in the α -quartz lattice. (33 refs.)
- Fe_3PO_4 , a case of Fe^{3+} fivefold coordination. Structural and magnetic studies See Entry 76777
- Spin susceptibility of electrons and magnetic hyperfine interactions in a conductor with resonance levels See Entry 77131
- A binary ferromagnetic alloy with magnetic moments dependent on local environment. II. Neutron magnetic elastic scattering and hyperfine field distribution See Entry 77146
- EPR and luminescence of Mn^{2+} in distorted tetrahedral symmetry in CaZnF_4 crystals See Entry 77255
- EPR study of ordering in stoichiometric β -aluminate See Entry 77256
- Electron-spin resonance study of spin dynamics in the one-dimensional magnetic crystal doped with diamagnetic impurities $(\text{CH}_3)_4\text{NMn}^{2+}\text{Cl}_3\text{Cd}^{2+}$ See Entry 77257
- Temperature-dependent nuclear magnetic resonance in CuInX_2 ($\text{X}=\text{S,Se,Te}$) chalcopyrite-structure compounds See Entry 77271
- Nuclear spin-lattice relaxation in doped silicon under optical pumping conditions See Entry 77281
- Nuclear-quadrupole-resonance study of the ground state of praseodymium in lanthanum trifluoride See Entry 77282
- Temperature dependences of the sublattice magnetizations in nickel ferrite See Entry 77286
- Electron nuclear double resonance of ^{13}C nuclei with natural abundance in trissarcosine calcium chloride doped with Mn^{2+} ions See Entry 77287
- Giant hyperfine field on ^{151}Eu in EuFeP_{12} [Mossbauer study] See Entry 77297
- Lattice temperature and hyperfine interactions of $\text{Pb}_{1-x}\text{Sn}_x\text{Te}$ ($0.21 \leq x \leq 0.75$) See Entry 77300
- The hyperfine interaction of gadolinium and holmium in cubic Ho: (Gd, Ce/Fe_2) compounds See Entry 77302
- Magnetic hyperfine splitting in Mossbauer spectra of microcrystals See Entry 77303
- ^{57}Fe Mossbauer spectroscopy on FePt Invar alloys See Entry 77312

72.00 ELECTRONIC TRANSPORT IN CONDENSED MATTER

(for surfaces, interfaces, and thin films, see 73.)

Conference Record of the Sixteenth IEEE Photovoltaic Specialists Conference - 1982 See Entry 74219

72.10 THEORY OF ELECTRONIC TRANSPORT; SCATTERING MECHANISMS

- 76916 Quantum transport in quasi-one-dimensional systems. V.K.Arora (Dept. of Phys., Univ. of Riyadh, Riyadh, Saudi Arabia), M.Prasad. *Phys. Status Solidi b (Germany)*, vol.117, no.1, p.127-40 (1 May 1983). The results of quantum transport investigations in quasi-one-dimensional systems assumed to be of cylindrical geometry are presented. Quantum size effects become important when the de Broglie wavelength (λ_D) of confined electrons becomes comparable to the radius R_0 of the cylindrical geometry. In the extreme quantum limit, $\lambda_D > R_0$, the resistivity is found to be proportional to λ_D^2/A , where $A = \pi R_0^2$ is the area of cross-section. Similar behavior is found for electrons confined to a strong magnetic field, $\lambda_D \gg \lambda = (\hbar c/eB)^{1/2}$, when $A = \pi \lambda^2$ is the area of the cyclotron orbit or radius λ in a magnetic field of strength B . The quantum-transport behavior of electrons confined in thin wires is found to be analogous to that of electrons confined in a magnetic field. (51 refs.)
- 76917 Phase recurrences and metastability in a one-dimensional solid. C.J.Lambert, P.D.Beale, M.F.Thorpe (Dept. of Theoretical Phys., Univ. of Oxford, Oxford, England). *Phys. Rev. B (USA)*, vol.27, no.9, p.5860-3 (1 May 1983). The inverse localization length α (and hence resistance) of a one-dimensional disordered solid can be expressed in terms of a cumulative phase ϵ which obeys a nonlinear finite-difference equation. The authors examine this equation in the limit of zero disorder and obtain an expression for probability distribution $P(\epsilon)$. In the band-gap region, there is a stable fixed point leading to a nonzero α . At discrete points within a band there are metastable attractors with period ≥ 2 which for a small amount of disorder can lead to anomalies in α . (16 refs.)
- 76918 Ballistic passage of current carriers in crystals with a narrow allowed band. A.A.Ignatov (Inst. of Appl. Phys., Acad. of Sci., Gorki, USSR). *Sov. Phys.-Dokl. (USA)*, vol.27, no.8, p.619-21 (Aug. 1982). Translation of: *Dokl. Akad. Nauk SSSR*, vol.265, no.4-6, p.859-62 (Aug. 1982). [received: May 1983] Studies the volt-ampere characteristic of a crystal with a narrow allowed band under conditions of ballistic passage of current carriers through the sample ($x \ll v_0\tau$, where x is the thickness of the crystal, τ is the relaxation time of the particle momentum, and v_0 is the characteristic velocity acquired by the particles in the electric field). It is assumed that the current carriers are created in the sample by monopolar injection from one of the contacts (the 'cathode'). This formulation of the problem is fairly realistic in molecular crystals because of their characteristic long relaxation times of the momenta of the current carriers. (10 refs.)
- Percolation. Models, analog and numerical simulations See Entry 74371
- Electromagnetic wave absorption by an electron-phonon system under parametric resonance See Entry 76862
- Conductivity and Hall coefficient studies in plastically deformed CdTe single crystals See Entry 76975
- ## 72.15 ELECTRONIC CONDUCTION IN METALS AND ALLOYS
- 76919 Electron transport and magnetic properties of some mixed-valent alkalthiocuprates. B.P.Ghosh, M.Chaudhury, K.Nag (Dept. of Inorganic Chem., Indian Assoc. for the Cultivation of Sci., Calcutta, India). *J. Solid State Chem. (USA)*, vol.47, no.3, p.307-13 (May 1983). Electrical transport properties of some two-dimensional isostructural compounds KCuS_3 , RbCuS_3 , and CsCuS_3 and a one dimensional conductor $\text{Na}_2\text{Cu}_4\text{S}_4$ have been investigated. Conductivities have been measured on pelletized materials in the temperature range 300 to 150K. All of them behave as metallic conductors. The room temperature conductivities of these compounds are KCuS_3 , $1600 \Omega^{-1} \text{cm}^{-1}$; RbCuS_3 , $1400 \Omega^{-1} \text{cm}^{-1}$; CsCuS_3 , $1250 \Omega^{-1} \text{cm}^{-1}$; $\text{Na}_2\text{Cu}_4\text{S}_4$, $700 \Omega^{-1} \text{cm}^{-1}$. The observed trend in conductivities among the isostructural compounds may be rationalized either on the basis of shortest Cu-Cu distances or on the carrier charge concentrations per unit volume. All of these compounds behave as Pauli paramagnetic materials. (25 refs.)
- ## 72.15C Electrical and thermal conduction in amorphous and liquid metals and alloys
- 76920 Compound-forming effect in the resistivity of liquid Na-Pb alloys. S.Matsunaga, S.Tamaki (Dept. of Phys., Niigata Univ., Niigata, Japan). *J. Phys. Soc. Jpn. (Japan)*, vol.52, no.5, p.1725-9 (May 1983). The electrical resistivity of Na-Pb alloys has been measured as a function of temperature and concentration. The curve of the resistivity has a remarkable maximum around the composition of 75 at.%Na. The curve of temperature dependence of the resistivity has also a sharp maximum at 80 at.%Na. From these results and the thermodynamic properties of this system, it is inferred that there forms a grouping of Na_2Pb in liquid Na-Pb alloys. The resistivity isotherm was analysed in terms of compound-forming effect. (14 refs.)
- 76921 The pressure- and temperature dependence of the electrical resistivity of some amorphous Fe-B alloys. G.Fritsch (ZWE Phys., Hochschule der Bundeswehr Munchen, Neubiberg, Germany), J.Willer, H.Schink, A.Wildermuth, E.Luscher. *J. Magn. & Magn. Mater. (Netherlands)*, vol.37, no.1, p.30-8 (May 1983). Reports measurements of the electrical resistivity of the amorphous alloys $\text{Fe}_{40}\text{Ni}_{40}\text{P}_{14}\text{B}_6$ (Metglas 2826), $\text{Fe}_{32}\text{Ni}_{36}\text{Cr}_{14}\text{P}_{12}\text{B}_6$ (Metglas 2826A), $\text{Fe}_{80}\text{B}_{20}$ (Metglas 2605) and $\text{Fe}_{75}\text{B}_{25}$ as a function of pressure and temperature. The pressure is varied between 0 and 12 GPa, the temperature between 1.2 and 380K. At low temperatures the pressure dependence yields additional information on the scattering mechanism. (26 refs.)

76922 Thermodynamical and structural properties of amorphous $\text{Fe}_{80}\text{B}_{20}$ and $\text{Fe}_{80}\text{P}_{13}\text{C}_7$ alloys. V.M.Pan, I.Ya.Dekhtyar, M.E.Osinovskii, S.E.Litvin, B.G.Nikitin, M.M.Nishenko, M.P.Voronko (Inst. of Metal Phys., Acad. of Sci., Kiev, Ukrainian SSR). *Phys. Status Solidi a (Germany)*, vol.76, no.1, p.197-206 (16 March 1983). Such properties of amorphous $\text{Fe}_{80}\text{B}_{20}$ and $\text{Fe}_{80}\text{P}_{13}\text{C}_7$ alloys as heat capacity and electric resistivity in the temperature range 1.5 to 300K, magnetoresistance in perpendicular and parallel magnetic fields up to $\approx 4.78 \times 10^6$ A/m, magnetization, and the Mossbauer effect at 100 and 300K are investigated. The data obtained are interpreted in terms of the hypothesis of short-range order and weakly-coupled 'paramagnetic' centres in a ferromagnetic matrix. A phenomenological description of magnetoresistance data is given and a correlation with the Mossbauer data is discussed. (17 refs.)

76923 Influence of s-d hybridization on the electrical conductivity of liquid transition metals. V.T.Shvets (Odessa Technol. Inst. of Refrigeration Industry, Odessa, USSR). *Theor. & Math. Phys. (USSR)*, vol.53, no.1, p.1040-6 (Oct. 1982). Translation of: *Teor. & Mat. Fiz. (USSR)*, vol.53, no.1, p.146-55 (Oct. 1982). Retarded Green's functions are used to develop a theory of the electrical conductivity of liquid transition metals with systematic allowance for the hybridization of the s and d state of the conduction electrons. It is shown that the conductivity can be represented as a sum of three terms, one of which is due to the scattering of s electrons by ions, including resonance scattering by d states, the second is due to tunneling of d electrons through d states, and the third is due to transitions of almost localized d electrons to delocalized s states and reverse transitions from s to d states. Expressions for each of the contributions are obtained in the framework of perturbation theory with respect to the pseudopotential of the electron-ion interaction, the hybridization potential, and the resonance integral. (14 refs.)

72.15E Electrical and thermal conduction in crystalline metals and alloys

76924 Low-frequency electrical resistance of iron, cobalt, and nickel in the vicinity of their Curie temperatures. B.C.Sales, M.B.Maple (Inst. for Pure & Appl. Phys. Sci., Univ. of California, San Diego, CA, USA). *Appl. Phys. A (Germany)*, vol.A31, no.2, p.115-17 (June 1983). Alternating-current electrical resistance measurements between 17 Hz and 100 kHz were made on high purity Fe, Co, and Ni wires in the vicinity of their Curie temperatures (T_c). The electrical resistance was independent of frequency for temperatures (T) above T_c . As the temperature was lowered, however, there was an abrupt jump in the electrical resistance at T_c followed by a gradual decrease toward its DC value. The magnitude of the electrical resistance jump at T_c increased as the square root of the frequency. The enhancement of the electrical resistance for $T \leq T_c$ is produced by an abrupt decrease of the skin depth at T_c which, in turn, is due to the sudden increase in the initial magnetic permeability at T_c . Measurements of the AC electrical resistance in the vicinity of the Curie temperature of certain ferromagnetic metals can be utilized to 1) accurately determine the Curie temperature using frequencies as low as 17 Hz, and 2) quantitatively determine the initial magnetic permeability as a function of temperature and heat treatment. (2 refs.)

76925 Characteristics of the electrical resistivity of magnetically ordered Pd-base alloys. V.A.Matveev, G.V.Fedorov, N.V.Volkenshtein (Inst. of Metal Phys., Acad. of Sci., Sverdlovsk, USSR). *Fiz. Met. & Metalloved. (USSR)*, vol.55, no.4, p.707-10 (April 1983). In Russian. English translation in: *Phys. Met. & Metallogr. (GB)*. The electrical resistivity of Pd-Mn alloys with 1.25-10 at.%Mn was investigated in the temperature range 20-300K. The concentration and temperature dependences $\rho(c,T)$ obtained in the range 120-300K showed that $\rho(c,T)$ deviated from linearity in the direction of the temperature axis. The nature of this deviation made it possible to divide the investigated alloys into two groups with the following manganese concentrations $c < 5$ at.% and $c > 5$ at.%; these groups corresponded to a ferromagnetic state and to a spin glass state of Pd-Mn alloys. The behaviour of $\rho(c,T)$ observed in the investigated temperature range is explained on the basis of the s-d scattering model which leads to the conclusion that the transition of Pd-Mn alloys from the ferromagnetic to the spin glass state is accompanied by a change in the energy band structure. (11 refs.) A.T.

76926 Anomalous Hall effect in an antiferromagnetic metal. V.A.Volkov, S.I.Masharov, A.F.Rybalko (S.M. Kirov Ural Polytech. Inst., Sverdlovsk, USSR). *Fiz. Met. & Metalloved. (USSR)*, vol.55, no.4, p.818-20 (April 1983). In Russian. English translation in: *Phys. Met. & Metallogr. (GB)*. A theoretical study is made of this effect, which is associated with asymmetric scattering of conduction electrons by spin inhomogeneities. The s-d or s-f exchange model is used for the case of a two-sublattice antiferromagnet. The temperature dependence of the anomalous Hall coefficient is considered and its singularities due to antiferromagnetic ordering are discussed. (5 refs.) A.T.

76927 The electrical resistivity of short-range ordered alloys and its temperature dependence. J.Richter, G.Schubert (Wissenschaftsbereich Phys., Hochschule für Verkehrswesen Friedrich List, Dresden, Germany). *Phys. Status Solidi b (Germany)*, vol.116, no.2, p.597-605 (1 April 1983). The electrical resistivity R of short-range ordered binary alloys with BCC structure is calculated using the force-force correlation function scheme in the weak-scattering limit. For the description of short-range order for temperatures above the critical temperature, the theory of Clapp and Moss (1966, 1968) is applied yielding the Fourier transform of the Cowley short-range order parameters and their dependences on the interatomic potential, the concentration and the temperature. In AB ordering alloys the short-range order causes a decrease of the resistivity R in comparison with a totally stochastic alloy and a positive temperature coefficient $(1/R) dR/dT$. In clustering alloys the atomic short-range order increases the resistivity and yields negative $(1/R) dR/dT$. This qualitative relation between R and $(1/R) dR/dT$ is in agreement with Mooij's rule (1973). Furthermore, the short-range ordering causes characteristic deviations from the Nordheim behaviour. (29 refs.)

76928 The Lorenz function for aluminium of different chemical purity, neutron irradiated or plastically deformed. H.Misiorek, T.Zakrzewski, J.Rafalowicz (Inst. for Low Temperature & Structure Res., Polish Acad. of Sci., Wrocław, Poland). *Phys. Status Solidi a (Germany)*, vol.76, no.1, p.K25-6 (16 March 1983). The authors perform thermal and electric conductivity measurements in aluminium samples with chemical purity of 6N, 5N, 4N, and 3N. The samples were investigated in the temperature range 4.2 to 50 K in the non-deformed state, fast neutron irradiated state, and plastically deformed (elongated) state. Neutron irradiated (dose 10^{13} and 10^{16} n/cm²) or plastic deformation (3 to

16%) were performed in liquid N₂. From the results of the measurements they plot a family of L(T) curves for different purity Al. (3 refs.)

Irradiation effects on thermal conductivity of a light-water reactor pressure vessel steel See Entry 75101

Electronic properties of dilute copper alloys. I. Theory See Entry 76835

Low-frequency current noise and internal friction in solids See Entry 77014

Low-temperature transport properties of RERh_4B_4 compounds (RE=Sm, Ho, Er, Lu) See Entry 77078

Magnetic and electrical properties of CrGe and $\text{Cr}_{11}\text{Ge}_8$ See Entry 77132

Magnetic susceptibility and electrical resistivity of electrotransport purified scandium single crystals from ≈ 1 to 300K See Entry 77135

Study of the critical behaviour of the magnetization and electrical resistivity in cubic La(Fe, Si)_{13} compounds See Entry 77155

72.15G Galvanomagnetic and other magnetotransport effects

76929 Relaxation phenomena in amorphous $\text{Co}_{75-x}\text{Mn}_x\text{B}_{25}$ induced by stress annealing. A.Ehrhardt, R.Kern, U.Gonser (Fachbereich Angewandte Phys., Univ. des Saarlandes, Saarbrücken, Germany). *Appl. Phys. A (Germany)*, vol.A31, no.2, p.93-5 (June 1983). The change of the magnetization direction in amorphous ferromagnets by the application of a magnetic field and a tensile stress is investigated by magnetoresistivity measurements. Attention is focussed on permanently remaining influences on the domain structure induced by stress annealing treatments. To observe any dependence on the sign of the magnetostriction λ_s , the authors investigated the amorphous $\text{Co}_{75-x}\text{Mn}_x\text{B}_{25}$ system where the sign of λ_s changes from negative to positive values with increasing Mn content. Surprisingly the stress-annealed samples showed a similar behavior independent of the sign of the magnetostriction. (8 refs.)

76930 Transverse magnetoresistance of amorphous $\text{Fe}_{40-x}\text{Ni}_{40}\text{Cr}_x\text{B}_{20}$ alloys in magnetic fields up to 20 T. P.Czarnecki (Inst. of Phys., A. Mickiewicz Univ., Poznań, Poland), G.Fritzkowski. *Phys. Status Solidi a (Germany)*, vol.76, no.1, p.K93-6 (16 March 1983). Investigates the influence of chromium on the magnetoresistance of amorphous ferromagnetic $\text{Fe}_{40-x}\text{Ni}_{40}\text{Cr}_x\text{B}_{20}$ alloys both in low and strong magnetic fields up to 20 T. (9 refs.)

76931 Anomalies of the Hall coefficient in the region of a negative temperature coefficient of the resistance of disordered Ti-Cr alloys. A.S.Sherbakov, A.F.Prekul, N.V.Volkenshtein (Inst. of Metal Phys., Acad. of Sci., Sverdlovsk, USSR). *Sov. Phys.-Solid State (USA)*, vol.24, no.11, p.1982-3 (Nov. 1982). Translation of: *Fiz. Tverd. Tela (USSR)*, vol.24, no.11, p.3483-5 (Nov. 1982). [received: May 1983] Formation of a pseudogap at the Fermi level of alloys containing only metals is an unusual phenomenon, therefore, there is a natural interest in the behavior of the various physical properties of materials exhibiting a pseudogap near the critical composition x_c . The authors report the results of an investigation of the Hall coefficient of the alloy system $\text{Ti}_{1-x}\text{Cr}_x$ ($0 < x < 15$ at.% Cr), which is a typical representative of the investigated class of alloys (this system is characterized by $x_c \approx 7$ at.% Cr). (6 refs.)

Thermodynamical and structural properties of amorphous $\text{Fe}_{80}\text{B}_{20}$ and $\text{Fe}_{80}\text{P}_{13}\text{C}_7$ alloys See Entry 76922

Galvanomagnetic properties of thin inhomogeneous films See Entry 77069

Electrical characteristics of thin Ni_2Si and NiSi_2 layers grown on silicon See Entry 77071

Influence of Mn ion substitution by Fe on the electrical and magnetic properties of an $\text{La}_{0.6}\text{P}_{0.4}\text{MnO}_3$ crystal See Entry 77159

72.15J Thermoelectric effects

Short-range ordering in nickel-chromium thermocouple alloys See Entry 76367

Calculation of activity coefficients of conduction electrons in metals and in semiconductors See Entry 76671

The electronic properties of $[\text{CH}(\text{FeCl}_4)_{0.61}]_x$ See Entry 76934

Influence of Mn ion substitution by Fe on the electrical and magnetic properties of an $\text{La}_{0.6}\text{P}_{0.4}\text{MnO}_3$ crystal See Entry 77159

The Seebeck effect as used for the nondestructive evaluation of metals See Entry 77852

72.15L Relaxation times and mean free paths

Temperature coefficient of the resistance of chromium-copper alloy films See Entry 77070

72.15N Collective modes, e.g. in one-dimensional conductors

76932 Kink deformation of $(\text{TMTSF})_2\text{ClO}_4$ single crystal and its influence on electrical resistivity. T.Ishiguro, T.Ukachi (Electrotech. Lab., Ibaraki, Japan), K.Kato, K.Murata, K.Kajimura, M.Tokumoto, H.Tokumoto, H.Anzai, G.Saito. *J. Phys. Soc. Jpn. (Japan)*, vol.52, no.5, p.1585-92 (May 1983). Mechanical kinks are formed in a needle crystal of bis (tetramethyltetraselenafulvalenium) perchlorate, $(\text{TMTSF})_2\text{ClO}_4$, by applying stresses. The kink which has definite angle of 18.4° accompanies an antikink with the same angle in the opposite direction. By the X-ray precession photograph, the authors show that the kink is ascribed to the mechanical twinning with the boundary on the (210) plane. The electrical resistivity measurements in a deformed part, lying between the kink and antikink, and in a region including the kink, were carried out. They did not show substantial difference compared with those in the undeformed part. However, the kink which accompanies distortion in a molecular stack is considered to be one of the causes of the resistance jump (stepwise increase in resistance), which is frequently observed during cooling.

76933 Non-linear conductivity of one-dimensional charge density wave. S.E.Burkov, V.L.Pokrovsky (L.D. Landau Inst. for Theoretical Phys., Moscow, USSR). *Solid State Commun. (USA)*, vol.46, no.8, p.609-11 (May 1983). A pure system with one-dimensional CDW placed in a homogeneous electric field is considered. Non-linear effects are found to appear due to motion of a

soliton superstructure. The dependence of the differential conductivity on the electric field is calculated. (8 refs.)

76934 The electronic properties of $[\text{CH}(\text{FeCl}_4)_{0.61}]_x$ Y.W.Park, J.C.Woo, K.H.Yoo, W.K.Han, C.H.Choi (Dept. of Phys., Seoul Nat. Univ., Seoul, Korea), T.Kobayashi, H.Shirakawa. *Solid State Commun. (USA)*, vol.46, no.9, p.731-4 (June 1983). The temperature dependence of DC conductivity, thermopower and electron paramagnetic resonance (EPR) results on $[\text{CH}(\text{FeCl}_4)_{0.61}]_x$ are reported. The DC conductivity and thermopower measurements indicate metallic charge transport along the polyacetylene chain interrupted by the interfibril contact resistances and also 'dragged' primarily by the dopant ions. The initial measurements of EPR show Dysonian lineshape with very broad linewidth ($\Delta H \approx 600$ G at room temperature). The temperature dependence of EPR absorption intensity implies that there exist localized magnetic moments. The observed g value ($g \approx 2.03$) suggests the dopant anion is in a form of $(\text{FeCl}_4)^-$. (22 refs.)

76935 Peierls instability and charge density waves at the surface of a metal with a quasideimensional electron spectrum. O.M.Braun, E.A.Pashitskii (Inst. of Phys., Acad. of Sci., Kiev, Ukrainian SSR). *Sov. Phys.-Solid State (USA)*, vol.24, no.11, p.1893-6 (Nov. 1982). *Translation of: Fiz. Tverd. Tela (USSR)*, vol.24, no.11, p.3333-8 (Nov. 1982). [received: May 1983] It is shown that a displacive (Peierls) transition at an anisotropic surface of a quasideimensional metal should occur at a higher critical temperature than in the bulk. The existence of an adsorbed layer with an optical spectrum of adatom vibrations facilitates the formation of surface charge density waves. (22 refs.)

A CNDO/INDO crystal orbital model for transition metal polymers of the 3d series-basis equations See Entry 76830

A CNDO/INDO crystal orbital model for transition metal polymers of the 3d series—the band structure of nickel(II)glyoximate See Entry 76831

Electron transport and magnetic properties of some mixed-valent alkalthiocuprates See Entry 76919

High-pressure effects on the $2k_F$ and $4k_F$ transitions in the quasi-one-dimensional magnetic conductor $\text{MEM-}(\text{TCNQ})_2$ See Entry 77238

Electron-spin-echo experiments on the one-dimensional conductor $[(\text{fluoranthene})_2]^{+}[(\text{PF}_6)_x(\text{SbF}_6)_{1-x}]^{-}$ ($x \approx 0.5$) See Entry 77261

72.15Q Scattering mechanisms and Kondo effect

(see also 75.20H Local moments in dilute alloys)

On local density of states in Anderson localized systems See Entry 76898

Kondo effect in disordered two-dimensional systems See Entry 77136

Bethe-Ansatz solution of the Anderson model of a magnetic impurity with orbital degeneracy See Entry 77138

72.20 CONDUCTIVITY PHENOMENA IN SEMICONDUCTORS AND INSULATORS

(for nonelectronic thermal conduction, see 66.70)

Gallium Arsenide and Related Compounds, 1982. Tenth International Symposium on Gallium Arsenide and Related Compounds See Entry 74226

72.20D General theory, scattering mechanisms

76936 Anisotropy of transport properties due to direction-dependent band nonparabolicity. M.Storuder, H.T.Langhammer (Sektion Phys., Martin-Luther-Univ. Halle/Wittenberg, Halle, Germany). *Phys. Status Solidi b (Germany)*, vol.117, no.1, p.329-33 (1 May 1983). In addition to two-band conduction or the action of an anisotropic-mixed scattering mechanism a further possibility is proposed for the interpretation of the anisotropy of the Seebeck coefficient, the Hall coefficient, and the Lorenz number of semiconducting crystals with noncubic symmetry. In the band model a nonparabolicity is considered which depends on the crystal direction. For acoustic mode scattering the expected anisotropy of these effects is calculated in dependence on the reduced Fermi level with the nonparabolicity as the parameter. The numerical results show that in contrast to the isotropic nonparabolicity the model used here predicts distinct anisotropies. (13 refs.)

Screening of electrostatic fields in crystalline semiconductors by electrons hopping over defects See Entry 76949

Electron power loss in the (100) n channel of a Si metal-oxide-semiconductor field-effect transistor. I. Intrasubband phonon scattering See Entry 77057

Electron power loss in the (100) n channel of a Si metal-oxide-semiconductor field-effect transistor. II. Intrasubband phonon scattering See Entry 77058

72.20F Low-field transport and mobility; piezoresistance

76937 High resistivity in p -type InP by deuteron bombardment. M.W.Focht, B.Schwartz (Bell Labs., Murray Hill, NJ, USA). *Appl. Phys. Lett. (USA)*, vol.42, no.11, p.970-2 (1 June 1983). High resistivity layers have been achieved in p -type InP using deuteron bombardment. A curve of average resistivity versus bombardment dose has been determined for p -type InP with an initial background carrier concentration of $1 \times 10^{18} \text{ cm}^{-3}$. It has been shown that average resistivities of $10^9 \Omega \text{ cm}$ or higher can be attained reproducibly, over a dose range 3×10^{13} – 1×10^{14} deuterons/ cm^2 . (13 refs.)

76938 Some properties of amorphous Si thin films and their application to sensors. I. Power sensor. I.Sugiura, S.Kodato, K.Takahashi, M.Konagai. *Anriutsu Tech. Bull. (Japan)*, no.44, p.93-7 (March 1983). In Japanese. Because an amorphous Si thin film containing a microcrystalline phase has properties of a very high dark-conductivity, a large thermoelectric effect and piezoresistance effect, the film can be used as a new electronic material for thermocouple power sensors. The fabrication process of a device used for measurement of the thermoelectric power of the films is reported. The films were deposited on glass substrate, using $\text{SiF}_4 + \text{H}_2$ gases by a d.c. glow discharge. Experimental results on electrical and thermoelectric properties of the films are presented. They show that the Seebeck coefficient (S) is 150–220 $\mu\text{V/K}$, in the proximity of room temperature. The fabrication process and properties of the power sensor are given. The power sensitivity is 1500 $\mu\text{V/mW}$ and the linearity is better than 1%, when input power is 0.1–10 mW. (8 refs.)

76939 The conductivity and thermoelectric power of amorphous silicon. Chu Juehui, Zhang Guobing, Zhang Tianyi (Peking Univ., Peking, China). *Acta Sci. Nat. Univ. Pekin. (China)*, no.5, p.70-6 (1982). In Chinese. Deals with the measurement of conductivity and thermoelectric power of amorphous silicon in the temperature range from 77 to 470K. Specimens are prepared either by the glow discharge-deposition method (sample 1) or by the vacuum evaporation method (sample 2). The sign of the thermoelectric power S of these two samples are negative throughout the temperature range. Experimental results indicate that the conductivity activation energy of a -Si above 300K are 0.25 eV (sample 1) and 0.62 eV (sample 2) obtained by conductivity temperature dependence. These values are in good agreement with the values obtained directly by thermoelectric power measurement (0.24 eV for sample 1, 0.65 eV for sample 2) in the temperature range. The ranges of localized states ($E_C - E_A$) are equal to 0.09 eV and 0.25 eV, the hopping energy W for sample 1 and sample 2 are respectively 0.01 eV and 0.07 eV. (4 refs.)

76940 Electron transport in sub-micron GaAs channels at 300K. B.R.Na. (Centre of Advanced Study in Radio Phys. & Electronics, Calcutta Univ., Calcutta, India), M.Deb Roy. *Appl. Phys. A (Germany)*, vol.A31, no.2, p.65-70 (June 1983). Transient velocity-field characteristics have been computed for GaAs channels having lengths of 0.1, 0.2, 0.5, 1, and 20 μm for electric fields between 1 and 50 kV/cm at 300K. The results are compared with earlier calculations and the significant features of the computed results are discussed. It is found that the electron motion for all channel lengths and for all fields is significantly affected by collisions. The threshold field for negative differential mobility increases, and the magnitude of the differential mobility decreases with decrease in the length of the sample. The maximum steady-state velocity increases with decrease in the length and may be as high as $5.4 \times 10^7 \text{ cm/s}$ for 0.1 μm samples. (31 refs.)

76941 Electrical resistance of diamond implanted at liquid nitrogen temperature with carbon ions. J.F.Prins (Nuclear Phys. Res. Unit, Univ. of the Witwatersrand, Johannesburg, S Africa). *Radiat. Eff. Lett. Sect. (GB)*, vol.76, no.3, p.79-82 (1983). Carbon ion implantation of diamond to high fluence, below the temperature at which diamond growth can occur, usually leads to black layers of high conductivity. This study shows that for a low enough temperature of the diamond during implantation, a black layer with high electrical resistance can develop. In particular, carbon ion implantation at liquid nitrogen temperature, leads to an implanted layer with electrical resistance about one million times higher than the resistance obtained for implantation at temperatures above room temperature. (5 refs.)

76942 A direct comparison of LEC GaAs grown using low- and high-pressure techniques. W.M.Duncan, G.H.Westphal, J.B.Sherer (Central Res. Labs., Texas Instruments Inc., Dallas, TX, USA). *IEEE Electron Device Lett. (USA)*, vol.EDL-4, no.6, p.199-201 (June 1983). A direct comparison has been made between the properties and implant behavior of undoped semi-insulating (SI) low- and high-pressure liquid encapsulated Czochralski (LEC) GaAs. Although the properties of high-pressure LEC had previously been well characterized, this is the first detailed study of the quality of low-pressure LEC material. It is shown that both material types are similar in structural quality, purity, and in the characteristics of conducting layers formed by direct ion implantation. Arsenic-rich melts and B_2O_3 with greater than 500-ppm H_2O content are required for obtaining reproducible and stable SI behavior growing from quartz crucibles. (16 refs.)

76943 Electron and hole carrier mobilities for liquid phase epitaxially grown GaP in the temperature range 200–550K. Y.C.Kao, O.Eknoyan (Electrical Engng. Dept., Texas A&M Univ., College Station, TX, USA). *J. Appl. Phys. (USA)*, vol.54, no.5, p.2468-71 (May 1983). Mobility data for GaP in the temperature range 200–550K as a function of impurity concentration are presented. The data were determined from sheet Hall coefficient and resistivity measurements obtained using the van der Pauw method. The results are given for a wide range of concentrations ranging from unintentionally doped to degenerately doped conditions. The maximum values of the electron and hole mobilities at room temperature were found to be 160 and 135 cm^2/Vs , respectively. The observed average temperature dependence of the mobility is $T^{-1.7}$ for electrons and $T^{-2.3}$ for holes. (16 refs.)

76944 The DC resistivity of modified PZT ceramics. Long Wu, Tien-Shou Wu, Chung-Chuang Wei (Res. Inst. of Electronics & Electrical Engng., Nat. Cheng-Kung Univ., Tainan, Taiwan), Hsi-Chuan Liu. *J. Phys. C (GB)*, vol.16, no.14, p.2823-32 (20 May 1983). PZT ceramics with various impurities were prepared by the powder metal-lurgy method, in the temperature range 1150–1350°C. The electrical resistivity of each composition has been studied. Explanations based on the distribution model were given. Within the solubility limit, the impurities can produce A-site vacancies or produce O-site vacancies for the PZT ceramics, depending on the valence and the size of impurity ion. When the A-site vacancy produced was added, it acted as a donor, contributed electrons to the conduction process, and increased the resistivity of ceramics, owing to the p -type electrical conduction of undoped ceramics. But the O-site vacancy produced served as an acceptor, contributed holes to the conduction process and thus decreased the resistivity. (20 refs.)

76945 Ternary mixed valence oxygen deficient K_2NiF_4 type copper oxides. Progressive evolution of a semiconducting state from a semimetallic state in $\text{La}_{2-x}\text{Sr}_x\text{CuO}_{4-x/2-y}$. N.Nguyen, F.Studer, B.Raveau (Lab. de Cristallographie et Chimie du Solide, Univ. de Caen, Caen, France). *J. Phys. & Chem. Solids (GB)*, vol.44, no.5, p.389-400 (1983). In French. Magnetic and electron transport properties of the mixed valence copper oxides $\text{La}_{2-x}\text{Sr}_x\text{CuO}_{4-x/2-y}$ ($0 \leq x \leq 1.20$) have been investigated in the temperature range 120–650K. A progressive evolution of the conductivity from a semiconductor to a semi-metallic behavior, as the amount of trivalent copper increases, has been observed. The positive sign of the Seebeck coefficient and the evolution of the conductivity and magnetic properties have been interpreted. (13 refs.)

76946 Solid state studies on substituted CuCr_2O_4 spinel. K.S.De, J.Ghose, K.S.R.C.Murthy (Dept. of Chem., Indian Inst. of Technol., Kharagpur, India). *J. Solid State Chem. (USA)*, vol.47, no.3, p.264-77 (May 1983). Changes in crystallographic, electrical, and thermal properties of CuCr_2O_4 spinel were investigated by replacing Cu with Mg, i.e. $\text{Cu}_{1-x}\text{Mg}_x\text{Cr}_2\text{O}_4$ and Cr with Al, i.e. $\text{CuCr}_{2-x}\text{Al}_x\text{O}_4$. The tetragonal distortion in CuCr_2O_4 disappeared with 60% replacement of Cu by Mg ($x=0.6$) or 50% replacement of Cr by Al ($x=1.0$). The temperature variation of electrical resistivity for all the tetragonal samples was similar to that of CuCr_2O_4 . The first order, diffusionless phase transition was manifest in the hysteresis loops of $\log \rho$ vs. $1/T$ plots. The resistivity and activation energy for conduction changed sharply near the phase transition composition. With the replacement of Cr by Al, the conduction in CuCr_2O_4 was found to change from p type to n type. The low

thermal stability of the spinel was found to be due to a high concentration of tetrahedral Cu^{2+} ions (>80%) and compressed tetragonal distortion which strains the spinel lattice. This strain is removed by replacing either Cu with Mg or Cr with Al, whereby the spinel becomes stable. (32 refs.)

76947 Preparation and properties of substituted iron tungstates. K.Sieber, H.Leiva, K.Kourtakis, R.Kershaw, K.Dwight, A.Wold (Dept. of Chem., Brown Univ., Providence, RI, USA). *J. Solid State Chem. (USA)*, vol.47, no.3, p.361-7 (May 1983). Polycrystalline samples of members of the systems $\text{Fe}_{2-x}\text{Cr}_x\text{WO}_6$ and $\text{Fe}_{1-x}\text{Mn}_x\text{WO}_4$ were prepared and single crystals of $\text{Fe}_{1-x}\text{Mn}_x\text{WO}_4$ were grown by chemical vapor transport. Their crystallographic parameters and electrical properties were characterized. Fe_2WO_6 crystallizes with the tri- α - PbO_3 structure and is an n-type semiconductor. For $0.3 \leq x \leq 2$, the system $\text{Fe}_{2-x}\text{Cr}_x\text{WO}_6$ crystallizes with the inverse triurilite structure and is nonconducting due to blocking of iron(II)-iron(III) conduction paths by chromium(III). For $0 \leq x \leq 1$, the system $\text{Fe}_{1-x}\text{Mn}_x\text{WO}_4$ crystallizes with the wolframite structure and shows p-type semiconducting behavior. The nature of the variation of resistivity with x of $\text{Fe}_{1-x}\text{Mn}_x\text{WO}_4$ suggests that inter-chain electron transfer may occur in this structure. (15 refs.)

76948 Effect of temperature on the electrical transport properties of p-type polycrystalline indium antimonide. P.C.Mathur, A.K.Shukla, R.P.Sharma, P.K.Goyal (Dept. of Phys. & Astrophys., Univ. of Delhi, Delhi, India). *J. Electron. Mater.* (USA), vol.12, no.2, p.483-506 (March 1983). Measurements of Hall coefficient (R_H), DC conductivity and Hall mobility have been made on p-type polycrystalline indium antimonide in the temperature range ~77-450K. The average size of the grains in the sample was ~0.15 μm . It is found that Hall coefficient in the low temperature range is determined by the carrier concentration in the crystallites and n-type conduction predominates over p-type conduction above room temperature. Conductivity and Hall mobility were found to be thermally activated above 120K while the conduction near liquid nitrogen temperature is predominated by the variable range hopping. The effect of grain boundaries is found to be removed above ~370K. (52 refs.)

76949 Screening of electrostatic fields in crystalline semiconductors by electrons hopping over defects. N.A.Poklonski, V.F.Stelmakh (A.N. Sechenko Sci.-Res. Inst. of Appl. Phys. Problems, Minsk, USSR). *Phys. Status Solidi b (Germany)*, vol.117, no.1, p.93-9 (1 May 1983). The expression for the electrostatic field screening length is obtained and it is shown that the effective concentration of electrons hopping via defects is included both into the screening length and electrical conductivity. The ratio of the diffusion coefficient to the drift mobility for hopping electrons is found. (12 refs.)

76950 Effect of heat treatment on the conduction and structure of Ge-Se-Te amorphous alloys. M.M.Hafiz (Dept. of Phys., Assiut Univ., Assiut, Egypt), A.A.Ammar, A.I.Al-Adi, A.Mohamed. *Phys. Status Solidi a (Germany)*, vol.76, no.1, p.319-25 (16 March 1983). The effect of heat treatment on the structure and electrical resistivity of the amorphous alloys of the system $\text{Ge}_{20}\text{Se}_{70-x}\text{Te}_{10-x}$ where $x=15,30$, and 50 is studied. Irreversible resistivity changes are observed after heating above the glass transition temperature accompanied by the appearance of the dendritic Te crystalline phase. The amount of the crystalline phase increases with increasing the annealing temperature. The effect of heat treatment on the structure transformation is investigated using DTA, X-ray, and scanning microscopy. The amorphous to crystalline transformation and its effect on the resistivity is discussed. (23 refs.)

76951 Electrical conduction through anodic oxides on InP. G.Eftekhari, D.de Cogan, B.Tuck (Dept. of Electrical & Electronic Engng., Univ. of Nottingham, Nottingham, England). *Phys. Status Solidi a (Germany)*, vol.76, no.1, p.331-6 (16 March 1983). The results of measurements of a.c. and d.c. electrical properties in anodic oxides on n-type indium phosphide are reported. The d.c. current, which is polarity dependent, appears to be due to Schottky emission. The semiconductor surface is inverted at zero bias with a potential of ~0.9 V. An oxide and surface states charge density of 2.2×10^{11} electrons cm^{-2} is measured. The oxide relative permittivity decreases from 14.8 at 400 Hz to 4.5 at 10^6 Hz and the a.c. conductivity has a sublinear dependence on frequency. (16 refs.)

76952 Electrical transport and phase stability in silver iodide-cadmium iodide. J.W.Brightwell, C.N.Buckley, L.S.Miller, B.Ray (Faculty of Appl. Sci., Coventry Polytech., Coventry, England). *Phys. Status Solidi a (Germany)*, vol.76, no.1, p.391-9 (16 March 1983). A form of the equilibrium diagram for the system AgI-CdI₂ is proposed on the basis of thermal, X-ray diffractometer, and electrical conductivity data. Only one intermediate equilibrium phase, of composition Ag_2CdI_4 , of tetragonal form with $a_0=6.35$ Å and $c_0=12.7$ Å is apparent; the previously reported hexagonal form of this composition being metastable. Low levels of CdI₂ are found to enhance the formation of the cubic, γ -form, of AgI and to increase the electrical conductivity. For various levels of CdI₂ inclusion in AgI, the principal increase in conductivity occurs in the region of 110°C instead of at 146°C as in pure AgI. (15 refs.)

76953 Isolation characteristics in selectivity O^+ and Cr^+ implanted GaAs. S.Nojima (Musashino Electrical Communication Lab., Nippon Telegraph & Telephone Public Corp., Tokyo, Japan). *Phys. Status Solidi a (Germany)*, vol.76, no.1, p.K9-12 (16 March 1983). The author reports annealing behavior for isolation resistances in O^+ and Cr^+ implanted GaAs crystals. The isolation resistances between two terminals were measured in the darkness at room temperature. (5 refs.)

76954 Microwave transport properties around the structural phase transition of MnSe. Y.Watanabe, J.Takeuchi, M.Oka (Dept. of Phys., Shimane Univ., Matsue, Japan). *Phys. Status Solidi a (Germany)*, vol.76, no.1, p.K13-15 (16 March 1983). The authors report the measurement of the microwave (9.4 GHz) resistivities ϕ_m performed around the sharp structural transition in InMnSe. The microwave method, which requires no electrode in resistivity measurements, seems to provide an excellent tool for the investigation around the structural phase changes. Evaluation of ϕ_m was made on the basis of the eddy current loss method, by using a reference specimen to determine the cavity constant. The microwave skin depth estimated for the ϕ_m value obtained below was 0.4 to 1.2 mm, a comparable order of the grain size. They therefore assume that the effect of the boundary layer of coarse grains is small in the present case. (6 refs.)

76955 Dependence of electrical properties in iron-cobalt, iron-zinc ferrites near stoichiometry on firing temperature and atmosphere. B.Gillot, F.Jemmal (Lab. de Recherches sur la Reactivite des Solides, Faculte des Sci., Dijon, France). *Phys. Status Solidi a (Germany)*, vol.76, no.2, p.601-8 (16 April 1983). The electrical conductivity and the thermoelectric power of some finely-divided cobalt and zinc ferrites near stoichiometry are studied as a function of firing temperature and atmosphere. It is determined that iron-excess ferrites

obtained at low preparation temperature or firing in vacuum above 600°C are of n-type and of much higher conductivity than iron-deficient ferrites which are obtained by oxidation at 300°C or by firing in air with the development of vacancies on octahedral sites and exhibiting p-type conduction. Abrupt changes in conductivity and energy occur as the stoichiometry varies from an iron deficiency to an iron or zinc excess. (15 refs.)

76956 Effect of free carrier screening on the electron mobility of GaAs: a study by field-effect measurements. R.H.Wallis (Lab. Central de Recherche, Thomson-CSF, Orsay, France). *Physica B & C (Netherlands)*, vol.117-118 B+C, pt.2, p.756-8 (March 1983). (Proceedings of the 16th International Conference on the Physics of Semiconductors, Montpellier, France, 6-10 Sept. 1982). By using a field effect technique, the electron mobility in GaAs at 300K has been studied in two systems where the free electron concentration may be varied over a wide range while the density of ionized impurities is kept constant. These are (a) a thin, almost fully depleted n-type layer on a semi-insulating substrate and (b) a GaAs/Al_{0.3}Ga_{0.7}As modulation doped heterojunction. In both cases the mobility falls by more than a factor of two as the free electron concentration is reduced, due to loss of screening. (7 refs.)

76957 Time-dependent field effect in amorphous chalcogenides. C.Bullock, J.M.Marshall, C.Main (Dept. of Phys., Dundee Coll. of Technol., Dundee, Scotland). *Philos. Mag. B (GB)*, vol.47, no.5, p.L69-75 (May 1983).

Exploratory measurements of the transient decay of the field effect in amorphous films from the system $\text{As}_2\text{Te}_3\text{-As}_2\text{Se}_3$ are reported. The excess current is shown to exhibit a power-law dependence upon time over the range 5-5000 s. The rate of decay increases with increasing temperature for a given composition, and with increasing selenium concentration as the composition is varied. The data are discussed in terms of a mechanism of thermalisation of excess charge carriers with localised states which are distributed over a range of energy. The possibility that the decay of the field effect is related to that of the transient photoconductivity is examined. (9 refs.)

76958 The interpretation of drift mobility experiments on amorphous silicon. W.E.Spear, H.Steemers (Carnegie Lab. of Phys., Univ. of Dundee, Dundee, Scotland). *Philos. Mag. B (GB)*, vol.47, no.5, p.L77-82 (May 1983).

A simple analysis is given of the charge displacements expected in a drift mobility experiment from (a) the carrier generation and (b) the subsequent drift of the excess carriers across the specimen. It is then shown that the features of the observed pulses in experiments on a-Si are in quantitative agreement with the predicted behaviour and show a clear transition between events (a) and (b). On the basis of these and of other results it is concluded that, under the experimental conditions, the main component of the observed displacement is associated with the transit of excess electrons, leading to an extended state mobility of about $10 \text{ cm}^2 \text{ V}^{-1} \text{ s}^{-1}$. These conclusions disagree with the recent work of Silver and coworkers (1982, 1983) and throw considerable doubt on their estimated mobility of $10^3 \text{ cm}^2 \text{ V}^{-1} \text{ s}^{-1}$ for a-Si. (15 refs.)

Reproducibility and uniformity considerations in LEC growth of undoped, semi-insulating GaAs for large-area, direct implantation technology See Entry 76342

X-ray, crystal data, magnetic susceptibility and electrical conductivity of hydrated tririckel pentasulphide See Entry 76375

Preparation and properties of the systems $\text{Fe}_{2-x}\text{Cr}_x\text{WO}_6$, $\text{Fe}_{2-x}\text{Rh}_x\text{WO}_6$, and $\text{Cr}_{2-x}\text{Rh}_x\text{WO}_6$ See Entry 76379

Some physical properties and point defects in $\text{Bi}_{2-x}\text{In}_x\text{Te}_3$ mixed crystals See Entry 76419

Compound synthesis in TiO_2 implanted with rubidium See Entry 76471

Annealing of defects in X-ray and electron irradiated $\text{Cd,Hg}_{1-x}\text{Te}$ single crystals See Entry 76500

Temperature dependence of the velocity of ultrasound and electrical conductivity of an epoxy composite with a carbon filler See Entry 76566

Jahn-Teller transition in NdMnO_3 See Entry 76614

The role of solitons and the kinetics of precipitate growth in boron doped silicon-germanium alloys See Entry 76633

Thermal properties of Cu_6SnS_6 See Entry 76665

Effect of adsorption of vapours on the electrical conductivity of a series of some naphthyl polyenes: Adsorption and desorption kinetics See Entry 76776

Defect states and donors in thermally annealed or post-hydrogenated chemically vapor-deposited amorphous SiN_x alloy See Entry 76897

Effect of oxygen on the electrical properties of β -zinc phthalocyanine single crystals See Entry 76961

Conductivity and Hall coefficient studies in plastically deformed CdTe single crystals See Entry 76975

Conductivity and Hall effect in single crystals of CuCr_2Se_4 magnetic spinel See Entry 76978

Electrical conductivity, thermoelectric power and Hall effect in p-type molybdenite (MoS_2) crystal See Entry 76981

Electrical conduction in sintered α - Sb_2O_4 See Entry 76982

Transport properties of thermoelectric materials for coolers See Entry 76983

The electric and photoelectric properties of TlSbSe_2 crystals in the region of impurity conduction See Entry 76995

Some electrical properties of $\text{Au}_x\text{Te}/\text{CdTe}$ heterojunctions on CdTe thick films See Entry 77028

Interfacial electrical properties of ion-beam sputter deposited amorphous carbon on silicon See Entry 77055

Raman spectroscopy for characterization of annealing of ion-implanted InP See Entry 77402

Formation of lattice defects in CdS crystals by nitrogen laser radiation See Entry 77450

Localization of electronic states and cathodoluminescence of bound exciton complexes in ZnSe crystals See Entry 77462

In situ purification growth of undoped semi-insulating GaAs single crystals See Entry 77558

High-pressure growth of polycrystalline molybdenum disulphide See Entry 77591

Crystal structure and electrical resistivity of $\text{MoS}_2\text{-NbS}_2$ alloys produced by self-propagating high-temperature synthesis See Entry 77595

Electrical conductivity and infrared absorption spectrometry study of hematite precipitation from defective ferrites See Entry 77647

Thermal isomerization and degradation of polyacetylene See Entry 77887

72.20H High-field and nonlinear effects

76959 Ballistic transport in GaAs. C.K.Williams, T.H.Glisson, M.A.Littlejohn, J.R.Hauser (Dept. of Electrical Engng., North Carolina State Univ., Raleigh, NC, USA).

IEEE Electron Device Lett. (USA), vol.EDL-4, no.6, p.161-3 (June 1983). Ballistic transport in GaAs has been studied using an ensemble Monte Carlo simulation. Duration and spatial extent of ballistic transport for a hot electron distribution can be defined from such studies. Mean displacement of the ensemble increases quadratically with time for a specified interval. This observation provides a phenomenological definition of ensemble ballistic transport. This phenomenological definition is compared with a theoretical definition based on time at which a significant fraction of an ensemble have experienced at least one collision. From these studies, times and distances are given for which a single-particle ballistic equation and a Langevin equation accurately describe ensemble transport in GaAs. (9 refs.)

76960 Experimental determination of impact ionization coefficients in (100) GaAs. G.E.Bulman, V.M.Robbins, K.F.Brennan, K.Hess, G.E.Stillman (Electrical Engng. Res. Lab., Univ. of Illinois, Urbana, IL, USA).

IEEE Electron Device Lett. (USA), vol.EDL-4, no.6, p.181-5 (June 1983). The room-temperature electron and hole impact ionization coefficients, α and β , respectively, have been determined for (100)-GaAs using photocurrent multiplication measurements on specially fabricated p-n junction devices with active region net donor concentrations from $n=1.1 \times 10^{17}$ to $2.2 \times 10^{15} \text{ cm}^{-3}$. In contrast with many previous reports, the electron impact ionization coefficient is found to be greater than the hole impact ionization coefficient over the entire doping and electric field range studied. The ratio α/β decreases from 2.5 to 1.3 as the electric field is increased from 2.22 to $6.25 \times 10^5 \text{ V/cm}$. These results have been confirmed by avalanche noise measurements with both electron and hole injection on the same devices. (24 refs.)

76961 Effect of oxygen on the electrical properties of β -zinc phthalocyanine single crystals. T.G.Abel-Malik (Dept. of Phys., Univ. of El-Minia, El-Minia, Egypt).

Phys. Status Solidi a (Germany), vol.76, no.2, p.K159-62 (16 April 1983). The author reports measurements of ohmic and space charge limited (SCL) currents in β -zinc phthalocyanine (β -ZnPc) single crystals and determines both depth and concentration of localized levels in crystalline specimens of this material. (7 refs.)

76962 Conductivity of ionic dielectrics under pulsed bombardment by electron and X-ray beams of medium density. D.I.Vaisburd, G.A.Mesyats, V.L.Naminov, E.G.Tavanov (Inst. of High-Current Electronics, Acad. of Sci., Tomsk, USSR).

Sov. Phys.-Dokl. (USA), vol.27, no.8, p.625-8 (Aug. 1982). Translation of: *Dokl. Akad. Nauk SSSR*, vol.265, no.4-6, p.1113-16 (Aug. 1982). [received: May 1983]

To elucidate the mechanism for the conductivity of ionic dielectrics under pulsed bombardment by X-ray and electron beams of medium and high density, one must consider the wide energy range covered by the spectrum of nonequilibrium electrons and holes. The authors examine the region of medium beam densities, where the low-energy conductivity vanishes. The samples are thin wafers of alkali-halide crystals. The experiments show that at medium beam densities the fast conductivity is due in comparable measure to the intracenter, temperature-independent conductivity and the high-energy conductivity, which falls off with temperature with an activation energy equal to the energy of the short-wavelength phonon. The amplitude of the fast component therefore falls off more slowly with temperature than does the high-energy conductivity. (14 refs.)

2D hot electron transport in a modulation-doped GaAs/AlGaAs interface See Entry 77030

Electron transport in heterojunctions and superlattices See Entry 77031

Hot electron effects in heterolayers See Entry 77036

72.20J Charge carriers: generation, recombination, lifetime, and trapping

76963 Determination of diffusion length of electron beam induced minority carriers in polycrystalline GaAs. O.Paz (General Technol. Div., IBM East Fishkill, Hopewell Junction, NY, USA).

Appl. Phys. Lett. (USA), vol.42, no.11, p.958-60 (1 June 1983). A method of combining Schottky barrier electron beam induced current imaging of grain clusters with quantitative determination of diffusion length is demonstrated. This was achieved by comparing the measured number of collected carriers per incident electron, corrected for backscattered, and secondary electrons to a calculated value. A source function compensated for metal thickness was used. Diffusion lengths were measured in GaAs samples and ranged from $0.2 \mu\text{m}$ for polycrystalline and bulk single crystal material to $7.5 \mu\text{m}$ for chemical vapor deposition grown layers. These values were independently verified through a comparison with quantum efficiency data. (13 refs.)

76964 Electron diffusion lengths in Mn-doped InP. C.-L.Chiang, S.Wagner (Dept. of Electrical Engng. & Computer Sci., Princeton Univ., Princeton, NJ, USA), A.A.Ballman.

Mater. Lett. (Netherlands), vol.1, no.5-6, p.145-7 (April 1983). The minority carrier (electron) diffusion length L_n was measured in Mn-doped p-type single crystals of InP. The surface photovoltage technique on electrolyte/InP diodes was employed. For samples with hole densities p ranging from $4.1 \times 10^{14} \text{ cm}^{-3}$ to $5.3 \times 10^{16} \text{ cm}^{-3}$ (296K), $L_n = 2.20 \times 10^3 / p^{0.45} \mu\text{m}$. L_n does not appear to be affected by the high concentration of neutral Mn. (16 refs.)

76965 Determination of carrier lifetime in Si by optical modulation. D.L.Polla (Honeywell Electro-Optics Operation, Lexington, MA, USA).

IEEE Electron Device Lett. (USA), vol.EDL-4, no.6, p.185-7 (June 1983). A contactless optical modulation technique for the determination of photogenerated carrier lifetime in silicon is presented. The method is based on the measurement of the optically modulated free-carrier absorption in Si at $10.6 \mu\text{m}$. The fractional change in transmitted intensity of a DC below band-gap probe beam (with $\hbar\omega_p < E_g$) due to a modulated pump beam (with $\hbar\omega_p > E_g$) is proportional to the excess carrier lifetime. This optical modulation technique, which is relatively simple, contactless, and nondestructive, may have significant potential as a high-resolution high-sensitivity tool for Si wafer screening, crystal growth studies, and process evaluation. (9 refs.)

76966 Minority-carrier diffusion-length measurement and lifetime in $\text{Pb}_{0.8}\text{Sn}_{0.2}\text{Te}$ and indium-doped PbTe liquid phase epitaxy layers. A.Shahar, M.Oron, A.Zussman (Soreq Nuclear Res. Centre, Yavne, Israel).

J. Appl. Phys. (USA), vol.54, no.5, p.2477-82 (May 1983). Minority carrier diffusion length was measured between 10-110K, using a laser light spot scanning technique in $\text{Pb}_{0.8}\text{Sn}_{0.2}\text{Te}$ and In-doped PbTe layers,

grown by liquid phase epitaxy. A new method for fabricating diodes with a bevelled surface is described. Diffusion lengths L of about 10 and $1 \mu\text{m}$ were measured in $\text{Pb}_{0.8}\text{Sn}_{0.2}\text{Te}$ epilayers grown at 500 and 600°C , respectively. In indium-doped PbTe epilayers, L varies with temperature in the range 0.2 to $1.6 \mu\text{m}$. The measured diffusion length was used with available mobility data to derive the minority-carrier lifetime in these epilayers. Comparison of the experimental results with theory shows that in undoped $\text{Pb}_{0.8}\text{Sn}_{0.2}\text{Te}$, carrier lifetime is dominated by band-to-band radiative and Auger recombination mechanisms, while in In-doped PbTe, recombination takes place via nonradiative centres. The implications of the observed diffusion length and the derived lifetime values on the performance of optoelectronic devices are discussed. (28 refs.)

76967 Effect of reabsorbed recombination radiation on the diffusion length of minority carriers in wide-band-gap semiconductors. Ovon Roos (Jet Propulsion Lab., California Inst. of Technol., Pasadena, CA, USA).

J. Appl. Phys. (USA), vol.54, no.5, p.2495-8 (May 1983). The integrodifferential equation governing the diffusion of minority carriers under the influence of both recombination by flaws and multiple photon absorption and emission via band-band transitions recently developed by the author is solved by means of a variational principle. It is shown that for bulk material the effect of the reabsorbed recombination radiation (RRR) on carrier diffusion is negligible when the average mean free path of photons is larger than the diffusion length of the carriers. In the opposite case, this is not true and the results previously obtained by a different method are recovered. Applied to GaAs, these findings signify that if the diffusion length L due to flaws or recombination centres possesses a magnitude less than $1 \mu\text{m}$, the effect of the RRR may safely be ignored. But, on the other hand, if L is greater than $1 \mu\text{m}$, there exists an effective diffusion length L_{eff} always larger than L , which is engendered by the RRR and which enhances carrier transport. This enhancement becomes noticeable only at high doping levels. (6 refs.)

76968 Comments on 'Carrier recombination through shallow donor/acceptor levels in heavily doped silicon'. M.S.Tyagi (Dept. of Electrical Engng., Indian Inst. of Technol., Kanpur, India).

J. Appl. Phys. (USA), vol.54, no.5, p.2857-9 (May 1983). For original paper see Hu and Oldham, *Appl. Phys. Lett.*, vol.35, p.636 (1979). Carrier recombination through shallow donor/acceptor levels in heavily doped silicon is analyzed. It is found that the Shockley, Read, and Hall theory of recombination is unable to explain the sharp decrease in lifetime with increasing dopant concentrations. However, trap assisted Auger recombination through these levels satisfactorily explains the observed lifetimes as well as their temperature dependences. (18 refs.)

76969 Electron-beam-induced conduction in fluorinated ethylene propylene copolymer and its acrylonitrile graft copolymer. S.G.Joshi, N.D.Ghate (Nat. Chem. Lab., Poona, India), J.F.Jog, S.J.Walzade, S.V.Bhoraskar.

J. Polym. Sci. Polym. Phys. Ed. (USA), vol.21, no.5, p.685-97 (May 1983). Electron-beam-induced conductivity (EBIC) studies were carried out on fluorinated ethylene propylene copolymer (FEP) and its acrylonitrile graft copolymer (FEP-g-AN). The current transport parallel to the surface under the influence of an electron beam of medium energy (6-30 keV) is reported. The gain in EBIC is calculated and its characteristic variation as a function of beam energy is studied. Minima in the gain versus energy curves have been obtained around 21 keV for FEP, 12 and 18 keV for FEP-g-AN, and 12 keV for polyacrylonitrile (PAN). This behavior is explained by assuming the existence of electron trapping bands close to the surface, at characteristic distances below the surface of the polymeric film corresponding to the range of incident electrons. Gains of the order of 5, 12, and 30 have been obtained respectively for FEP, FEP-g-AN, and PAN for the maximum energy of incident electrons used. (21 refs.)

76970 Depolarization current in a dielectric with deep trapped charge layers. H.Sodolski (Inst. of Phys., Tech. Univ., Gdansk, Poland).

Phys. Status Solidi a (Germany), vol.76, no.1, p.303-9 (16 March 1983). The depolarization current in a dielectric with two bipolar, immobile charge layers is considered. Using simplifying assumptions, the depolarization current equations in the short-circuited system are obtained. Two cases are considered: the isothermal discharge and the thermally stimulated discharge. The influence of several parameters on the TSD current spectra is examined. The theoretical results and the experimental ρ peak for polyester polymer are compared. (8 refs.)

76971 Transfer mechanisms of nonequilibrium charge carriers in graded band-gap semiconductors. A.I.Basyk, V.F.Kovalenko, G.P.Peka (T.G. Shevchenko State Univ., Kiev, Ukrainian SSR).

Phys. Status Solidi a (Germany), vol.76, no.2, p.429-35 (16 April 1983). An analysis is made of carrier transfer in a graded band-gap semiconductor with allowance for both, the photon- and the diffusion-drift transfer mechanisms of the nonequilibrium charge carriers with linear radiative and nonradiative recombination. The conditions expressed in terms of the experimentally measured recombination parameters are obtained, under which one mechanism prevails over the other. The calculated dependences of the effective shift length L_{eff} of the nonequilibrium carrier on grad E_g for different absorption models are investigated. The derived dependences are supported by tests performed on the solid solutions $n\text{-Al}_x\text{Ga}_{1-x}\text{As}$ silicon doped at high levels of doping. (12 refs.)

76972 Photogeneration and geminate recombination in amorphous silicon. F.Carasco, W.E.Spear (Carnegie Lab. of Phys., Univ. of Dundee, Dundee, Scotland).

Philos. Mag. B (GB), vol.47, no.5, p.495-507 (May 1983). Photogeneration in undoped amorphous silicon (a-Si) has been investigated at photon energies ϵ_{ph} from 3.1 to 1.3 eV, lying above and below the optical gap of the material (1.65 eV). The measurements were carried out on p-i-n junctions, deposited by the glow-discharge technique, in which the saturated (primary) photocurrent J_p under reverse bias is a reliable measure of the quantum efficiency of photogeneration, η . It is shown both by direct measurement of η and from the field dependence of J_p that at photon energies above 1.5 eV η closely approaches unity. $J_p(E)$ is completely independent of the applied field for E between 20 and 150 kV cm^{-1} which, according to the Onsager theory, gives a thermalisation length $r_0 \approx 400 \text{ \AA}$ and $\eta(20 \text{ kV cm}^{-1}) \approx 0.95$. It is concluded that geminate recombination does not impose any fundamental limitation on photogeneration in a-Si at photon energies of interest in photovoltaic applications. At $\epsilon_{\text{ph}} < 1.5 \text{ eV}$, involving transitions into electron tail states, η decreases rapidly and $J_p(E)$ shows a field dependence in agreement with the Onsager theory; geminate recombination thus plays a predominant role in this spectral range. The temperature dependence of J_p has been investigated and shows a rapid rise in activation energy for $\epsilon_{\text{ph}} < 1.5 \text{ eV}$, suggesting that photogeneration involves a thermal activation step into the extended states. These results are discussed on the basis of a simple model. (16 refs.)

76973 Hot carrier relaxation processes in 1.3 μm quaternary InGaAsP: analysis and application to temperature dependence of laser threshold. J. Shah, B. Etienne, R.F. Leheny, R.E. Nahory (Bell Labs., Holmdel, NJ, USA). Gallium Arsenide and Related Compounds, 1982, Tenth International Symposium on Gallium Arsenide and Related Compounds, Albuquerque, NM, USA, 19-22 Sept. 1982 (Bristol, England: IOP 1983), p.303-10.

The authors discuss two aspects of carrier energy relaxation processes in 1.3 μm quaternary InGaAsP. They demonstrate that the combined effect of this alloy's four LO phonons on the carrier energy relaxation is well approximated by a single effective phonon with $\hbar\omega = 31.6$ meV for $35\text{K} < T_c < 160\text{K}$ and 33.5 meV for $160\text{K} < T_c < 500\text{K}$. Carrier heating effects are shown to contribute significantly to temperature sensitivity of threshold in 1.3 μm lasers. A single $T_c = 90\text{K}$ describes the data when T is taken to be the carrier temperature rather than the lattice temperature. (15 refs.)

A new method of minority carrier lifetime measurement by the microwave photoconductive decay technique See Entry 74491

Outlook for the use of the Michelson interferometer for measuring the physical parameters of nonuniform semiconductor structures See Entry 74524

Carrier surface recombination in HgI₂ photon detectors See Entry 75240

Majority carrier concentration and quasi-Fermi level for Pb_{1-x}Sn_xTe DH diode lasers See Entry 75638

A new profiling technique applicable to the measurements sensitive to the free-carrier concentration rather than the depletion-layer thickness See Entry 76478

The interpretation of drift mobility experiments on amorphous silicon See Entry 76958

An RF bridge technique for contactless measurement of the carrier lifetime in silicon wafers See Entry 76989

Self quenching of extrinsic photoconductivity in GaAs:Cr See Entry 76990

Photoconductivity, photovoltages, and photogenerated solitons in polyacetylene See Entry 76991

The electric and photoelectric properties of TiSbSe₂ crystals in the region of impurity conduction See Entry 76995

Transient photoconductivity and thermalisation in amorphous semiconductors See Entry 76998

Peculiarities of photoelectric phenomena in glassy As₂S₃ See Entry 77005

The thickness dependence of excess carrier lifetime and mobility in amorphous silicon junctions See Entry 77022

Heterolayer screening of an external ion field See Entry 77040

Effect of a static field on the parameters of a superlattice created in a semiconductor by a standing laser wave See Entry 77041

The effect of hydrogen on the electrical properties of n-type Pb_{0.9}Cd_{0.1}Te thin films See Entry 77074

Influence of nitrogen ion implantation on the electrical transport properties of InTe and InSe thin films See Entry 77076

Effect of laser irradiation on the electrical properties of polycrystalline thin films of tellurium See Entry 77077

Picosecond reflectivity measurements on glow discharge a-Si:H See Entry 77471

Determination of minority carrier lifetime and effective back surface recombination velocity in BSF silicon solar cells from transient measurements See Entry 77990

Model calculations for silicon inversion layer solar cells See Entry 78009

Deep level defects and annealing studies in one-MeV electron irradiated (AlGa)As-GaAs solar cells See Entry 78032

Effects of indirect bandgap top cells in a monolithic cascade cell structure See Entry 78036

Diffusion length and solar cell efficiency See Entry 78048

The flux method applied to excess carrier transport in solar cells See Entry 78049

Generalised boundary conditions for the minority carrier diffusion equation in solar cells See Entry 78050

Determination of silicon cell model parameters using a least-squares-fit to experimental spectral response and the V-I curve See Entry 78051

A new method of impurity gettering in polycrystalline solar cells See Entry 78057

The measurement of variations in minority carrier lifetime due to microstructural defects in large area polysilicon wafers See Entry 78060

Bifacial cells of p⁺In⁺ structure See Entry 78062

On the effective minority carrier diffusion length of polycrystalline silicon solar cells See Entry 78063

The V-groove silicon solar cell See Entry 78065

Carrier transport at grain boundaries in silicon See Entry 78072

Grain boundary effects in polycrystalline silicon solar cells See Entry 78073

72.20M Galvanomagnetic and other magnetotransport effects

76974 Transverse magnetophonon resonance in n-GaAs under pulsed high magnetic fields. G.Kido, N.Miura (Inst. for Solid State Phys., Univ. of Tokyo, Tokyo, Japan).

J. Phys. Soc. Jpn. (Japan), vol.52, no.5, p.1734-9 (May 1983). Magnetophonon resonance of high purity epitaxial n-type GaAs was investigated in the configuration of $j \perp B$ at various temperatures from 77 to 303K using pulsed high magnetic fields up to 30 T. In the high magnetic field and low temperature region, a nonlinear increase of the amplitude against the field was clearly observed in the resonant oscillation. A relation between the damping factor and the magnetic field was determined to be $\gamma \propto B^{2/3}$ from the experiment, which suggests that the electron-phonon scattering is the dominant process for the damping at high magnetic field according to the Barker's theory (1972). (12 refs.)

76975 Conductivity and Hall coefficient studies in plastically deformed CdTe single crystals. M.Nagabhooshanam, V.Hari Babu (Dept. of Phys., Osmania Univ., Hyderabad, India).

Phys. Status Solidi a (Germany), vol.76, no.1, p.K89-92 (16 March 1983). The authors investigate the nature of dislocations formed due to plastic deformation by indentations in CdTe crystals and their influence on transport properties (Hall effect, conductivity, and carrier mobility). A probable explanation of the experimental results is also given. (11 refs.)

76976 New type of quantum oscillation of the transverse magnetoresistance of semiconductors. V.M.Polyanovskii, Nguyen Hong Shon (V.I. Lenin State Univ., Kishinev, USSR).

Sov. Phys.-Solid State (USA), vol.24, no.11, p.1857-8 (Nov. 1982). Translation of: *Fiz. Tverd. Tela (USSR)*, vol.24, no.11, p.3273-5 (Nov. 1982). [received: May 1983]

A rigorous quantum-mechanical treatment of a quasirelativistic scattering mechanism is employed to predict maxima in the transverse magnetoresistance of nondegenerate semiconductors which occur when the separation between the Landau levels is equal to the width of the conduction band in the direction of the applied magnetic field. (6 refs.)

76977 Zero-gap type I semiconductor in a quantizing magnetic field. Yu.V.Petrov (All-Union Sci.-Res. & Planning Inst. of Mech. Processing of Minerals, Leningrad, USSR).

Sov. Phys.-Solid State (USA), vol.24, no.11, p.1939-41 (Nov. 1982). Translation of: *Fiz. Tverd. Tela (USSR)*, vol.24, no.11, p.3413-18 (Nov. 1982). [received: May 1983]

The conductivity of a semiconductor with a quasirelativistic electron energy spectrum in a quantizing magnetic field is calculated. The conductivity expressed in terms of the density of band states reduces formally to the expression obtained earlier by Skobov (1960) for a system with a one-band parabolic spectrum. The Shubnikov-de Haas effect is obtained in the quasi-classical approximation. The behavior of oscillation amplitudes for different occupancies of Landau subbands is discussed. It is shown that a dependence of the chemical potential μ on the magnetic field H leads to a shift of H in which the transverse conductivity is maximal compared with the usual maximum. (10 refs.)

76978 Conductivity and Hall effect in single crystals of CuCr₂Se₄ magnetic spinel. V.V.Tsurkan, K.M.Golant, I.M.Yurin, S.I.Radautsan, V.E.Tezlevan, V.G.Veselago (Inst. of Appl. Phys., Acad. of Sci., Kishinev, Moldavian SSR).

Sov. Phys.-Solid State (USA), vol.24, no.11, p.1970-1 (Nov. 1982). Translation of: *Fiz. Tverd. Tela (USSR)*, vol.24, no.11, p.3465-7 (Nov. 1982). [received: May 1983]

The authors have carried out an experimental study of the Hall effect and of the electrical conductivity of CuCr₂Se₄ single crystals at temperatures 4.2-300K in order to determine the influence of a phase transition on the kinetics of the electrical conductivity and also to obtain information on the mechanisms of carrier scattering. (8 refs.)

76979 Magnetoconcentration effect in the presence of transverse gradient of the thermal carrier generation. R.N.Litovskii, A.P.Medvid'. *Ukr. Fiz. Zh. (USSR)*, vol.28, no.5, p.731-6 (May 1983). In Russian.

The problem is solved for the bipolar drift of the current carriers in intrinsic semiconductor plates in the presence of transverse conductivity anisotropy or a magnetic field, deflecting the carriers to one of the surfaces, and a transverse thermal generation gradient. The saturation current is shown to depend on the sign and value of the transverse temperature difference ΔT on the lateral surfaces of the plate at the constant mean temperature of the sample. At low ΔT the saturation current shows a linear dependence on ΔT , while at a sufficiently high ΔT , change of the sign results in a significant variation of the saturation current. The effect considered is common for a wide range of problems concerning the bipolar drift of intrinsic and injected current carriers in the presence of the transverse anisotropy of conductivity, nonuniformity of doping or nonuniform generation. (7 refs.)

76980 Magnetic-field dependence of the Hall factor of gallium arsenide. D.L.Rode, C.M.Wolfe (Washington Univ., St. Louis, MO, UA), G.E.Stillman.

Gallium Arsenide and Related Compounds, 1982, Tenth International Symposium on Gallium Arsenide and Related Compounds, Albuquerque, NM, USA, 19-22 Sept. 1982 (Bristol, England: IOP 1983), p.569-72

The magnetic-field dependence of the Hall factor from 0.44 to 83 kG for electrons in n-GaAs at room temperature is examined experimentally and theoretically. Lateral uniformity of the moderately pure n-GaAs sample is determined from photoconductivity and infrared transmission measurements. Theoretical calculations include Kane bands, admixed wave functions, lattice scattering and Brooks-Herring scattering. Theoretical and experimental values of Hall factor agree to within 0.7 percent. (4 refs.)

LEC growth of InP(Mn) for p-type and semi-insulating materials See Entry 76341

Some physical properties and point defects in Bi_{2-x}In_xTe₃ mixed crystals See Entry 76419

Pulsed thermal annealing of ion-implanted silicon See Entry 76464

A new profiling technique applicable to the measurements sensitive to the free-carrier concentration rather than the depletion-layer thickness See Entry 76478

Annealing of defects in X-ray and electron irradiated Cd_xHg_{1-x}Te single crystals See Entry 76500

Microscopic model of the EL2 level in GaAs See Entry 76889

Thermal conversion of undoped GaAs and the outdiffusion of the main electron trap EL2 See Entry 76891

Anisotropy of transport properties due to direction-dependent band nonparabolicity See Entry 76936

Electron and hole carrier mobilities for liquid phase epitaxially grown GaP in the temperature range 200-550K See Entry 76943

Effect of temperature on the electrical transport properties of p-type polycrystalline indium antimonide See Entry 76948

Electrical conductivity, thermoelectric power and Hall effect in p-type molybdenite (MoS₂) crystal See Entry 76981

Transport properties of thermoelectric materials for coolers See Entry 76983

The electric and photoelectric properties of TiSbSe₂ crystals in the region of impurity conduction See Entry 76995

On the role of the correlation length near the onset of non-metallic conduction See Entry 77010

Magnetoresistance anisotropy due to the 2D-electron subsystem at a GaAs/AlGaAs interface See Entry 77026

Effect of tangential magnetic field on the two-dimensional electron transport in N-AlGaAs/GaAs superlattices and hetero-interfaces See Entry 77029

2D hot electron transport in a modulation-doped GaAs/AlGaAs interface See Entry 77030

Mobility in modulation doped GaAs-GaAlAs superlattices See Entry 77034

Two dimensional magnetophonon resonance in GaInAs-InP superlattices See Entry 77037

Quantized Hall and transverse resistivities in silicon MOS n-inversion layers See Entry 77063

- Galvanomagnetic properties of thin inhomogeneous films See Entry 77069
- The effect of hydrogen on the electrical properties of n-type $\text{Pb}_{0.9}\text{Cd}_{0.1}\text{Te}$ thin films See Entry 77074
- Effect of laser irradiation on the electrical properties of polycrystalline thin films of tellurium See Entry 77077
- Influence of Mn ion substitution by Fe on the electrical and magnetic properties of an $\text{La}_{0.6}\text{P}_{0.4}\text{MnO}_3$ crystal See Entry 77159
- Photoluminescent and electrical properties of InGaPAs mixed crystals liquid-phase-epitaxially grown on (100) GaAs See Entry 77432
- MOCVD growth and characterization of high luminescence efficiency $\text{Al}_x\text{Ga}_{1-x}\text{As}$ See Entry 77583
- Flash-lamp annealing of ion-implanted silicon and its application to solar cells See Entry 78000

72.20P Thermoelectric effects

- 76981 Electrical conductivity, thermoelectric power and Hall effect in p-type molybdenite (MoS_2) crystal. S.R.G.Thakurta, A.K.Dutta (Dept. of Magnetism, Indian Assoc. for the Cultivation of Sci., Calcutta, India). *J. Phys. & Chem. Solids (GB)*, vol.44, no.5, p.407-16 (1983).
- Principal electrical conductivities and Seebeck coefficients, as well as Hall effect, in p-type single crystals of natural molybdenite (MoS_2) have been investigated within the temperature range 100K to 850K. The results have been discussed and the values of different parameters of the charge carriers obtained. (18 refs.)
- 76982 Electrical conduction in sintered $\alpha\text{-Sb}_2\text{O}_3$. M.Miyayama, S.Ogi, H.Yanagida (Dept. of Industrial Chem., Faculty of Engng., Univ. of Tokyo, Tokyo, Japan). *J. Am. Ceram. Soc. (USA)*, vol.66, no.5, p.351-2 (May 1983).
- Electrical conductivity and thermoelectric power were measured on sintered $\alpha\text{-Sb}_2\text{O}_3$ at 250° to 780°C. Oxygen partial pressure dependence of the conductivity and sign of the Seebeck coefficient showed $\alpha\text{-Sb}_2\text{O}_3$ to be a p-type semiconductor above 600°C in the oxygen pressure range of 10^2 to 10^3 Pa. A hopping conduction was proposed from very small hole mobility with an activation energy of 18 kJ/mol. (9 refs.)
- 76983 Transport properties of thermoelectric materials for coolers. A.Sher, M.Shiloh, D.Ilycyer, D.Eger (Soreq Nuclear Res. Centre, Yavne, Israel). *J. Electron. Mater. (USA)*, vol.12, no.2, p.247-63 (March 1983).
- The Seebeck coefficient, thermal conductivity, electrical conductivity and Hall coefficient of cooler grade, p- and n-type ternary alloys of $\text{Bi}_2\text{Te}_3\text{-Sb}_2\text{Te}_3\text{-Sb}_2\text{Se}_3$ were measured between 10 and 300K. Between 300K and about 150K the temperature dependence of the transport properties can be explained by assuming nondegeneracy and a lattice scattering mechanism. The difference between the temperature dependence of the Hall effect in n- and p-type alloys can be explained by the presence of sub-bands of light and heavy holes in the valence band of p-type alloys. (15 refs.)
- 76984 Electrophysical properties of niobium carbide single crystals. V.S.Sinel'nikova, V.G.Grebenkina (Inst. of Materials Sci., Acad. of Sci., Ukrainian SSR). *Sov. Powder Metall. & Met. Ceram. (USA)*, vol.21, no.10, p.804-6 (Oct. 1982). Translation of: *Poroshk. Metall. (USSR)*, vol.21, no.10, p.59-62 (Oct. 1982). [received: May 1983]
- An investigation was carried out into the temperature dependence of the electrical resistivity, thermal conductivity, and coefficient of thermo-emf of single-crystal niobium carbide. It is shown that the electrical resistivity of single-crystal niobium carbide, a material of high purity and perfect structure, is higher than that of polycrystalline materials. (8 refs.)
- The role of solitons and the kinetics of precipitate growth in boron doped silicon-germanium alloys See Entry 76633
- Calculation of activity coefficients of conduction electrons in metals and in semiconductors See Entry 76671
- Anisotropy of transport properties due to direction-dependent band nonparabolicity See Entry 76936
- Some properties of amorphous Si thin films and their application to sensors. I. Power sensor See Entry 76938
- The conductivity and thermoelectric power of amorphous silicon See Entry 76939
- Ternary mixed valence oxygen deficient K_2NiF_4 type copper oxides. Progressive evolution of a semiconducting state from a semimetallic state in $\text{La}_{2-x}\text{Sr}_x\text{CuO}_{4-x/2-s}$ See Entry 76945
- Solid state studies on substituted CuCr_2O_4 spinel See Entry 76946
- Dependence of electrical properties in iron-cobalt, iron-zinc ferrites near stoichiometry on firing temperature and atmosphere See Entry 76955
- Influence of Mn ion substitution by Fe on the electrical and magnetic properties of an $\text{La}_{0.6}\text{P}_{0.4}\text{MnO}_3$ crystal See Entry 77159
- Cation distribution of the system $\text{Zn}_{1-x}\text{Co}_x\text{FeMnO}_4$ by X-ray, electrical conductivity and Mossbauer studies See Entry 77308

72.30 HIGH-FREQUENCY EFFECTS; PLASMA EFFECTS

- 76985 Excitation of ion cyclotron waves at the difference frequency of two microwave beams in a semiconductor. K.P.Maheshwari (Dept. of Phys., Government Coll., Rajasthan, India), G.Tarey. *J. Phys. & Chem. Solids (GB)*, vol.44, no.5, p.463-6 (1983).
- Presents an investigation of the resonant excitation of the electrostatic ion cyclotron wave at the difference frequency of two microwave beams propagating in a magnetoactive solid state plasma, viz. n InSb. The resonant excitation of the electrostatic ion cyclotron wave occurs when the difference frequency of the two microwave beams and the difference of their propagation vectors satisfy the dispersion relation corresponding to the electrostatic ion cyclotron wave. For typical plasma parameters of n InSb and microwave beams of power densities 1 MW cm^{-2} , the power density of the excited ion cyclotron wave is 0.40 kW cm^{-2} when external magnetic field is 1.46 kG ($\omega_c/\omega = 0.1$). The power density of the excited ion cyclotron wave increases with the magnetic field. This study may provide new means for the characterisation and diagnostic of semiconductors. (8 refs.)

- 76986 Multifilament and multidomain stationary states in a hot electron-hole plasma in GaAs. B.S.Kerner, V.F.Sinkevich. *JETP Lett. (USA)*, vol.36, no.10, p.436-9 (20 Nov. 1982). Translation of: *Pis'ma v Zh. Eksp. & Teor. Fiz. (USSR)*, vol.36, no.10, p.359-62 (20 Nov. 1982). [received: June 1983]
- An electron-hole plasma in GaAs which is heated by a field initially stratifies along the direction perpendicular to the field at room temperature. This stratification results in the formation of numerous current filaments. As the voltage across the sample is increased, these filaments become stratified along the field direction into domains (striations), and the sample becomes filled with plasma 'droplets'. (6 refs.)
- Radiation generation by collective phenomena in semiconductors See Entry 77414

72.40 PHOTOCONDUCTION AND PHOTOVOLTAIC EFFECTS; PHOTODIELECTRIC EFFECTS

- 76987 Electrochemical study of the thermal treatment effects on Cu_3S thin films. R.Duo, E.Fatas (Electrochem. Dept., Univ. Autonoma de Madrid, Madrid, Spain), F.Arjona, E.Garcia Camarero. *Mater. Chem. & Phys. (Switzerland)*, vol.8, no.3, p.203-6 (March 1983).
- The effects of thermal treatments on the stoichiometry and photovoltaic properties of Cu_3S thin films have been studied. It has been observed that the evaporation of a thin copper film on Cu_3S , followed by thermal treatment in vacuum, improves the $\text{Cu}_3\text{S}/\text{CdS}$ heterojunctions due to a rise in the stoichiometry and fill factor. (4 refs.)
- 76988 Negative photoelectric effects in p-TiGaSe₂. S.G.Abdullayeva, V.A.Aliyev (Inst. of Phys., Acad. of Sci., Baku, Azerbaidzhan SSR). *Mater. Chem. & Phys. (Switzerland)*, vol.8, no.3, p.279-87 (March 1983).
- Deals with the results obtained while studying the photoelectrical properties of p-TiGaSe₂ crystals at high injection levels. Two phenomena have been recorded and investigated, namely the negative photoconductivity and the negative remanent photoconductivity. The current-voltage, time, spectral, lux, and temperature dependences of the above phenomena have been studied and the mechanisms of these phenomena are suggested. The microprobe studies conducted have allowed one to establish the presence of selenium inclusions in the form of 200 μm -long cylinders with butt-end diameters from 3 to 10 μm . The effect of these inclusions on the photoelectrical properties of TiGaSe₂ is shown. (14 refs.)
- 76989 An RF bridge technique for contactless measurement of the carrier lifetime in silicon wafers. T.Tiedje, J.I.Haberman, R.W.Francis, A.K.Ghosh (Corporate Res. Lab., Exxon Res. & Engng. Co., Linden, NJ, USA). *J. Appl. Phys. (USA)*, vol.54, no.5, p.2499-503 (May 1983).
- A contactless RF technique has been developed for measurement of the photoconductivity induced in silicon wafers by a flash of light from GaAs laser diodes. The carrier lifetime inferred from the photoconductivity decay correlates well with diffusion length measurements made on solar cells fabricated from the same wafers. The technique has been applied successfully to silicon whose resistivity is as low as $0.1 \Omega \text{ cm}$ and lifetime as short as 0.2 μs . (7 refs.)
- 76990 Self quenching of extrinsic photoconductivity in GaAs:Cr. R.Masut, C.M.Penchina (Dept. of Phys. & Astron., Univ. of Massachusetts, Amherst, MA, USA). *J. Electron. Mater. (USA)*, vol.12, no.2, p.323-44 (March 1983).
- Results of a combination of phototransport measurements (including extrinsic photoconductivity (PC), optical absorption, and photo Hall experiments) are presented to characterize the deep levels introduced by Cr in semi-insulating GaAs. The extrinsic PC shows a spectrum which sharpens rapidly as the temperature is lowered, and is quenched by an additive infrared source. This is explained with the aid of the photo-Hall measurements. The results are interpreted in terms of a simple model of an electron-hole recombination mechanism which is present at low temperature. This recombination causes self-quenching of the PC signal via a drastic reduction of the photogenerated free carriers. (19 refs.)
- 76991 Photoconductivity, photovoltaics, and photogenerated solitons in polyacetylene. B.R.Weinberger (Corporate Res. Lab., Exxon Res. & Engng. Co., Linden, NJ, USA). *Phys. Rev. Lett. (USA)*, vol.50, no.21, p.1693-6 (23 May 1983).
- The nature of photogenerated charge carriers in $(\text{CH})_x$ is explored through the photoconductive and photovoltaic response of the polymer. Experimental results are discussed in the context of the soliton model of charge carriers. It is concluded that photogenerated charged soliton pairs may play a role in $(\text{CH})_x$ photoconductivity but cannot produce the observed photovoltaic response of $(\text{CH})_x$ devices. (24 refs.)
- 76992 Far-infrared photoconductivity spectroscopy of shallow acceptors in InSb. R.Meisels, F.Kuchar (Inst. fur Festkorperphys. Univ. Wien, Wien, Austria). *Phys. Status Solidi b (Germany)*, vol.116, no.2, p.557-60 (1 April 1983).
- Acceptor excitations as well as ionization spectra are observed in InSb doped with Ge and Cd using Fourier transform spectroscopy and photoconductivity techniques. Best agreement with theoretical results is obtained with the following values for the Luttinger parameters: $\gamma_1 = 36.13$, $\gamma_2 = 16.24$, and $\gamma_3 = 17.34$ which were recently deduced by Littler et al. (13 refs.)
- 76993 Optical conductivity in the impurity band of doped semiconductors. J.Gryko (Inst. of Phys. Chem., Polish Acad. of Sci., Warsaw, Poland). *Phys. Status Solidi b (Germany)*, vol.117, no.1, p.313-22 (1 May 1983).
- A formula for the optical conductivity is derived from the Kubo relation in a framework of tight-binding approximation using a method due to Matsubara and Toyozawa (1961). The derived formula is applied to the calculation of the optical conductivity and optical absorption in the far IR of doped semiconductors at low temperatures. The calculated values of the optical absorption obtained using different approximated Green's functions are compared with the experimental data for Sb doped germanium. (23 refs.)
- 76994 On the role of surface phenomena in the Staebler-Wronski effect. A.G.Kazanski, V.F.Kiselev, E.A.Silave, V.S.Vavilov (Dept. of Phys., Moscow State Univ., Moscow, USSR). *Phys. Status Solidi a (Germany)*, vol.76, no.1, p.337-43 (16 March 1983).
- The results concerning the influence of adsorption of water vapour ammonia, and diethylether on the Staebler-Wronski effect in amorphous silicon are presented. It is shown that the effect is not due to the surface charging after adsorption. The influence of adsorption on the 'dark' conductivity and photoconductivity is observed only after the adsorption of water in the region of rather high concentrations of adsorbed molecules. This is, most probably, due to the proton processes. The sources of protons on the surface seem to be the coordination-bound water molecules. (21 refs.)

76995 The electric and photoelectric properties of TlSbSe₂ crystals in the region of impurity conduction. D.V.Gitsu, I.N.Grincheshin, N.S.Popovich (Inst. of Appl. Phys., Acad. of Sci., Kishinev, Moldavian SSR). *Phys. Status Solidi a (Germany)*, vol.76, no.1, p.K5-7 (16 March 1983). Experimental results on the electric and photoelectric properties of p- and n-TlSbSe₂ crystals in the region of impurity conduction are presented. Measurements of the photoconductivity were made by the modulation method with spectral resolution of 40 to 60 Å. For clarifying the energetic position of local levels in the band gap of TlSbSe₂ crystals, the temperature dependence of the dark conductivity in the temperature interval 77 to 300 K was investigated. The temperature dependences of carrier concentration and Hall mobilities for n-TlSbSe₂ crystals are given. (2 refs.)

76996 Characteristic steps in the relaxation curves of field-quenched persistent photoconductivity of Pb_{0.75}Sn_{0.25}Te:In. K.H.Hermann, K.-P.Mollmann (Bereich Experimentelle Halbleiterphys., Humboldt-Univ. zu Berlin, Berlin, Germany).

Phys. Status Solidi a (Germany), vol.76, no.1, p.K67-70 (16 March 1983). The authors present further experimental facts concerning field-quenched persistent photoconductivity and to discuss how these results relate to the hypothesis of a ferroelectric state below T_c. In the experiments single-crystal bulk samples and epitaxial layers have been investigated. (8 refs.)

76997 The design of an organic photoreceptor with charge-acceptance memory. III. Electrical properties of PVK-diazonium salt system. J.Hanna, E.Inoue (Imaging Sci. & Engng. Lab., Tokyo Inst. of Technol., Yokohama, Japan).

Photogr. Sci. & Eng. (USA), vol.27, no.2, p.51-8 (March-April 1983).

For pt.II see ibid., vol.26, p.69 (1982). The electrical properties of a photoreceptor with a charge-acceptance memory consisting of PVK (poly-N-vinylcarbazole) diazonium salt, and TNF are investigated using several measurements and techniques. These include the dark and photo-induced discharge characteristics of the surface potential, the leakage current under corona charging and the photocurrent using a time of flight technique. It is concluded that the doping of diazonium salt introduces hole traps in PVK, and that the photo-induced reduction of charge-acceptance in the photoreceptor (the memory effect) is ascribed to the enhancement of the carrier injection efficiency from the conductive substrate into the organic layer. Based on these results, a possible explanation of the memory effect has been tested using the current-voltage characteristic of an insulator under a high electric field. (4 refs.)

76998 Transient photoconductivity and thermalisation in amorphous semiconductors. J.M.Marshall, C.Main (Dept. of Phys., Dundee Coll. of Technol., Dundee, Scotland).

Philos. Mag. B (GB), vol.47, no.5, p.471-80 (May 1983).

In a number of recent publications, transient photoconductivity data for amorphous semiconductors have been interpreted in terms of the thermalisation of excess charge carriers with localised states which are distributed over a range of energy. A central feature of the 'intuitive thermalisation' model, which has been applied in some such analyses, concerns the introduction of a demarcation energy separating 'shallow' from 'deep' traps. The position of this demarcation energy is defined solely in terms of localised state release time constants, and it is assumed that 'shallow' centres are in quasi-thermal equilibrium with extended states. The authors examine the validity of this approach, and the consequences of application of such a model in the analysis of localised state distributions. It is demonstrated that the thermalisation process is a complex function of trapping and release time constants, and that the influence of deep traps prevents the establishment of quasi-thermal equilibrium for shallower centres. They show that the model will, in the general case, yield erroneous results for the energy distribution of localised states. (13 refs.)

76999 Simultaneous effect of UV-irradiation and deformation. G.Turchanyi, J.Janszky, S.Racz, I.Tarjan (Res. Lab. of Crystal Phys., Budapest, Hungary).

Radiat. Eff. (GB), vol.64, no.1-4, p.175-9 (1982). [received: May 1983] (Proceedings of the First International Conference on 'Radiation Effects in Insulators', Arco, Largo di Garda, Italy, 1981).

Reports on experiments performed on X-ray coloured KCl single crystals by means of dislocation photoconduction. This method makes use of the internal electric field developing in ionic crystals due to charged dislocations during their deformation. The effect of previous illuminations in the visible region on the photocurrent produced by VUV-light was also investigated, a memory effect and changes of the sign of the photocurrents were found under suitable conditions. It was shown that using visible light of high enough intensity the direction of the photocurrent produced by it also changes sign. The problems involved in the dislocation photoconduction method are discussed. (6 refs.)

77000 Photovoltaic measurement of bandgap narrowing in moderately doped silicon. J.A.Del Alamo, R.M.Swanson, A.Lietoila (Stanford Electronics Labs., Stanford Univ., Stanford, CA, USA).

Solid-State Electron. (GB), vol.26, no.5, p.483-9 (May 1983).

Solar cells have been fabricated on n-type and p-type moderately doped Si. The shrinkage of the Si bandgap has been obtained by measuring the internal quantum efficiency in the near infrared spectrum ($h\nu = 1.00-1.25$ eV) around the fundamental absorption edge. The results agree with previous optical measurements of bandgap narrowing in Si. It is postulated that this optically-determined bandgap narrowing is the rigid shrinkage of the forbidden gap due to many-body effects. The 'device bandgap narrowing' obtained by measuring the pn product in bipolar devices leads to discrepant values because (i) the density of states in the conduction and valence band is modified due to the potential fluctuations originating in the variations in local impurity density, and (ii) the influence of Fermi-Dirac statistics. (38 refs.)

77001 Anomalous photo-emf in a model of a heavily doped and compensated ferroelectric. V.B.Sandomirskii, Sh.S.Khalilov, E.V.Chenskii (Inst. of Radio Engng. & Electronics, Acad. of Sci., Moscow, USSR). *Sov. Phys.-Solid State (USA)*, vol.24, no.11, p.1885-9 (Nov. 1982). Translation of: *Fiz. Tverd. Tela (USSR)*, vol.24, no.11, p.3318-26 (Nov. 1982). [received: May 1983]

A model of a heavily doped and compensated ferroelectric is proposed. The equilibrium properties of the fluctuation potential are discussed. It is shown that the influence of the spontaneous polarization P_s and the nonlinearity of the permittivity on the fluctuation potential gives rise to a nonequivalence of regions where the electric field is parallel and antiparallel to P_s . With uniform illumination, an uncompensated photo-EMF can occur, for example because of the nonequivalent recombination currents in space charge layers in these regions. The existence of a distinctive direction leads to a summation of elementary photovoltages along the c axis, resulting in an anomalously high photovoltage. Under strong illumination, the fluctuation potential is screened by carriers, and the photo-emf falls as the illumination becomes stronger. The intensity threshold corresponding to the onset of screening falls exponentially with decreasing temperature. The results from this model are compared with experiment. (22 refs.)

77002 Photoelectric spectroscopy of radiation defects in germanium. B.G.Golubev, V.I.Ivanov-Omskii, G.I.Kropotov (A.F. Ioffe Physicotech. Inst., Acad. of Sci., Leningrad, USSR).

Sov. Phys.-Solid State (USA), vol.24, no.11, p.1937-8 (Nov. 1982). Translation of: *Fiz. Tverd. Tela (USSR)*, vol.24, no.11, p.3410-12 (Nov. 1982). [received: May 1983]

An investigation was made of the influence of point defects created by γ rays on the spectrum of photothermal ionization of group V donors in Ge. An analysis of a defect-induced fine structure of lines due to optical transitions from the ground to excited states of Sb and P donors in a magnetic field demonstrated that point radiation defects are usually located at fixed positions in the vicinity of donor atoms. The energy separations between the peaks in the fine structure of the lines was used to estimate the degree of deformation near the central cell occupied by a donor. (7 refs.)

77003 Photoconductivity of Y₂O₃ crystals with self-localized excitons. V.N.Abramov, A.I.Kuznetsov (Inst. of Phys., Acad. of Sci., Tartu, Estonian SSR).

Sov. Phys.-Solid State (USA), vol.24, no.12, p.2108-9 (Dec. 1983). Translation of: *Fiz. Tverd. Tela (USSR)*, vol.24, no.12, p.3698-701 (Dec. 1983).

Yttrium oxide Y₂O₃ (T_1 , $E_g = 6.1$ eV) crystals are of great interest since they represent an example of the self-localization of excitons in metal oxides. It is of interest to obtain additional data on the exciton self-localization in Y₂O₃ from the excitation spectra of the photoconductivity in the exciton maximum region and in the region of the long-wavelength edge of interband transitions. The authors' measurements were made on Y₂O₃ crystals grown by the Verneuil method. They used plates of $6.0 \times 3.0 \times 3.5$ mm dimensions with a working surface represented by the cleavage plane {111}. (5 refs.)

77004 The role of defects in formation of the cadmium iodide photosensitivity. A.B.Lyskovich, O.B.Kushnir, A.V.Gal'chinskii.

Ukr. Fiz. Zh. (USSR), vol.28, no.5, p.707-9 (May 1983). In Russian.

The impurity photosensitivity of CdI₂ crystals has been investigated. It is shown that this photosensitivity is due to occupation of available trapping levels which are related to defects of the crystal structure. (8 refs.)

77005 Peculiarities of photoelectric phenomena in glassy As₂S₃.

N.G.D'yachenko, A.Yu.Popov, A.V.Tyurin, A.S.Sheveleva.

Ukr. Fiz. Zh. (USSR), vol.28, no.5, p.742-8 (May 1983). In Russian.

He-Ne-laser-induced a.c. photoconductivity of glassy As₂S₃ was studied and the results obtained were analyzed using the compensated semiconductor model. Exposure of light and heating is supposed to give rise to processes causing changes in the concentration and properties of defects that play the role of trapping and recombination centres for nonequilibrium carriers. (17 refs.)

77006 Low temperature persistent photoconductivity in two-dimensional electron gas FETs. J.F.Rochette, P.Delescluse, M.Laviron, D.Delagebeaudeuf, J.Chevrier, N.T.Linh (Thomson CSF Central Res. Lab., Orsay, France).

Gallium Arsenide and Related Compounds, 1982. Tenth International Symposium on Gallium Arsenide and Related Compounds, Albuquerque, NM, USA, 19-22 Sept. 1982 (Bristol, England: IOP 1983), p.385-92.

Persistent photoconductivity effect (PPC) has been studied in AlGaAs layers, selectively doped GaAs/AlGaAs heterostructures and two-dimensional electron gas FET (TEGFET). Using the adequate rate equation and some simplifying assumptions the dark and light stationary regimes and the transitory regime are perfectly fitted at all temperatures by adjusting the unknown parameters. It is shown that, while in AlGaAs and heterostructures the PPC effect is eliminated by heating, in short gate length TEGFETs it can also be removed by applying a large drain voltage. (15 refs.)

A new method of minority carrier lifetime measurement by the microwave photoconductive decay technique See Entry 74491

Nonisothermal relaxation during photorecording in AsSe layers See Entry 75760

A new profiling technique applicable to the measurements sensitive to the free-carrier concentration rather than the depletion-layer thickness See Entry 76478

Localized centers in bismuth silicate crystals See Entry 76875

Re-examination of the mid-gap electron trap (EL2) in different GaAs wafers by photocapacitance, DLTS and photoluminescence spectra See Entry 76892

Experimental determination of impact ionization coefficients in (100) GaAs See Entry 76960

Electron diffusion lengths in Mn-doped InP See Entry 76964

Effect of reabsorbed recombination radiation on the diffusion length of minority carriers in wide-band-gap semiconductors See Entry 76967

Magnetic-field dependence of the Hall factor of gallium arsenide See Entry 76980

The heterojunction ZnSe-(Zn_{1-x}Cd_x)Te_{1-y}(In₂Te)_y having high sensitivity in the visible light range and its applications See Entry 77024

Some electrical properties of Au_xTe/CdTe heterojunctions on CdTe thick films See Entry 77028

High pressure photoelectric studies of semiconductor-electrolyte systems See Entry 77044

Photoelectric fatigue of photoresistors based on polycrystalline CdS:Cu:Cl films See Entry 77075

Formation of lattice defects in CdS crystals by nitrogen laser radiation See Entry 77450

Energy position of luminescence (photosensitivity) centres in CdSe_{1-x}Te_x solid solutions See Entry 77453

Oxidized rare earth-iron compounds in photoassisted electrolysis of water See Entry 77896

The influence of hydrogen ion bombardment on the photovoltaic properties of Cu/Cu₂O Schottky barrier solar cells See Entry 77993

72.50 ACOUSTOELECTRIC EFFECTS

77007 Propagation of surface acoustic waves in n-type GaAs films. Chi-Chong Wu (Dept. of Appl. Math., Nat. Chiao Tung Univ., Hsinchu, Taiwan), Jensen Tsai.

J. Low Temp. Phys. (USA), vol.51, no.3-4, p.453-67 (May 1983).

The effect of nonparabolicity of the amplification of surface acoustic waves in n-type GaAs films is investigated quantum mechanically in the GHz-frequency region. Numerical results show that the amplification coefficient for the nonparabolic band structures is enhanced due to the nonlinear nature of the energy band in semiconductors. Moreover, the amplification coefficients in semiconductors depend on the temperature, the electronic screening effect, the

frequency of sound waves, the applied electric field, and the thickness of the semiconductor film. (12 refs.)

A new profiling technique applicable to the measurements sensitive to the free-carrier concentration rather than the depletion-layer thickness See Entry 76478

72.55 MAGNETOACOUSTIC EFFECTS

77008 Interaction of resonant particles with acoustic solitons in metals. V.Ya.Demikhovskii, G.M.Maksimova, V.E.Sautkin (Res. Physicotech. Inst., Gor'kii State Univ., Gor'kii, USSR). *JETP Lett. (USA)*, vol.36, no.7, p.299-303 (5 Oct. 1982). Translation of: *Pis'ma v Zh. Eksp. & Teor. Fiz. (USSR)*, vol.36, no.7, p.244-7 (5 Oct. 1982). [received: May 1983]

A theory is derived for acoustic solitons in a metal plate in a quantizing magnetic field with an electronic nonlinearity much greater than the lattice nonlinearity. The damping law for the soliton amplitude is found for collisionless and collisional damping. (5 refs.)

77009 Parametric amplification of sound and magnetoacoustic echo in concentrated rare-earth paramagnets of the Van Vleck type. S.L.Tsarevskii (V.I. Ul'yanov-Lenin State Univ., Kazan, USSR). *Sov. Phys.-Solid State (USA)*, vol.24, no.12, p.2107-8 (Dec. 1983). Translation of: *Fiz. Tverd. Tela (USSR)*, vol.24, no.12, p.3696-8 (Dec. 1983). The author shows that, in concentrated rare-earth paramagnets of the Van Vleck type in a static magnetic field $H \sim 50$ kOe, an elastic wave of frequency $\omega_1 (\sim 10^{10}$ Hz) may interact parametrically with the magnetic component of the electromagnetic pump field of frequency $2\omega_1$. This interaction may be used for parametric amplification of sound and should be observable as a 'magnetoacoustic echo' (an analog of the electroacoustic echo in nonlinear piezoelectric crystals). (7 refs.)

72.60 MIXED CONDUCTIVITY AND CONDUCTIVITY TRANSITIONS

77010 On the role of the correlation length near the onset of non-metallic conduction. Z.Ovadyahu (Brookhaven Nat. Lab., Upton, NY, USA). *Y. Imry*.

J. Phys. C (GB), vol.16, no.14, p.L471-6 (20 May 1983). The conductivity of indium oxide films was studied as a function of $k_F l$ (including $k_F l \leq 1$), film thickness, temperature and magnetic field. For sufficiently thin films the authors observe a change from logarithmic to faster temperature dependence below a temperature determined by R_D . The analogous crossover for thicker samples is shown to depend on $k_F l$. Whether a given system is 'thin' enough for R_D to be the relevant parameter in this respect is determined by the value of the correlation length ξ . (19 refs.)

77011 Electrical and Raman study of lithium boronate and boromolybdate glasses. A.Levasseur, M.Kbala, M.Sanz (Lab. de Chimie du Solide, CNRS, Talence, France), M.Couzi.

J. Solid State Chem. (USA), vol.47, no.3, p.256-63 (May 1983). In French. Conductivity studies of glasses obtained from the $B_2O_3-Li_2O-Li_2MoO_4$ and $B_2O_3-Li_2O-Li_2WO_4$ systems have been carried out. The presence of the transition element in tetrahedral coordination and with two different oxidation states is discussed. A Raman spectroscopy study shows that the MoO_4 or WO_4 tetrahedra are slightly compressed by the network forming lattice. (8 refs.)

Low-frequency electrical resistance of iron, cobalt, and nickel in the vicinity of their Curie temperatures See Entry 76924

Electron transport in heterojunctions and superlattices See Entry 77031

Electronic structure of semiconductor superlattices See Entry 77035

Influence of Mn ion substitution by Fe on the electrical and magnetic properties of a $La_{0.6}P_{0.4}MnO_3$ crystal See Entry 77159

72.70 NOISE PROCESSES AND PHENOMENA

77012 1/f noise in polycrystalline silicon resistors. H.C.de Graaff, M.T.M.Huybers (Philips Res. Labs., Eindhoven, Netherlands). *J. Appl. Phys. (USA)*, vol.54, no.5, p.2504-7 (May 1983).

The 1/f noise in polycrystalline silicon resistors has been measured at room temperature. The resistors were manufactured in low-pressure chemical vapor deposition films, implanted with B, P, and As and processed in two different technologies with different temperature cycles. The spectral density was essentially independent of the type of implantation and of the processing. The results can be described with Hooge's empirical law (1978) and Klempner's model (1979) for the 1/f noise in Schottky barriers. At low doping levels Hooge's constant turned out to be $\sim 4 \times 10^{-3}$ and it decreased with increasing doping concentration, more or less as $(\mu/\mu_{\text{lattice}})^2$. (16 refs.)

77013 Grain boundaries as possible origin of flicker noise in GaP polycrystalline material. A.D'Amico, G.Petrocco, G.Stochino (Istituto di Elettronica dello Stato Solido, CNR, Roma, Italy), A.Salsano, G.Luzzi.

Phys. Status Solidi a (Germany), vol.76, no.2, p.K125-9 (16 April 1983). The authors indicate that grain boundaries in GaP polycrystalline material give a substantial contribution to the total low frequency noise. In particular they report results concerning excess noise measurements in GaP for two cases: a) when the polarization current is applied across a single grain, b) when the same current is applied across two different grains separated by only one grain boundary. Moreover both n- and p-type GaP materials are taken into consideration at room temperature (295K) and close to liquid nitrogen temperature (81K). (4 refs.)

77014 Low-frequency current noise and internal friction in solids. Sh.M.Kogan, K.E.Nagaev (Inst. of Radio Engng. & Electronics, Acad. of Sci., Moscow, USSR).

Sov. Phys.-Solid State (USA), vol.24, no.11, p.1921-5 (Nov. 1982). Translation of: *Fiz. Tverd. Tela (USSR)*, vol.24, no.11, p.3381-8 (Nov. 1982). [received: May 1983]

A study is made of the carrier-mobility and resistivity fluctuations in a crystal which arise from the spontaneous movement of defects. These movements, in particular the reorientation of defects with a symmetry lower than the point symmetry of the perfect crystal, contribute to the internal friction, and this gives a relation between the current noise and the internal friction in solids. Conditions are derived under which the current noise due to defects exceeds that due to temperature fluctuations and the equilibrium current noise. It is shown that the current noise due to the spontaneous movement of defects is observable in metals. The 1/f low-frequency current noise intensity in metallic films estimated from the background in the internal friction spectra of metals is in agreement with the observed 1/f current noise. (18 refs.)

Field emission fluctuation phenomena of potassium microcrystals on tungsten. I. Spectral density functions and flip-flop See Entry 77535

Field emission fluctuation phenomena of potassium microcrystals on tungsten. II. Temperature dependence and simulation of noise properties See Entry 77536

72.80 CONDUCTIVITY OF SPECIFIC SEMICONDUCTORS AND INSULATORS

(see also 81.40R Electrical and magnetic properties related to materials treatment)

The role of defects in formation of the cadmium iodide photosensitivity See Entry 77004

72.80C Elemental semiconductors

Pulsed thermal annealing of ion-implanted silicon See Entry 76464

Furnace annealing of ion implanted polycrystalline silicon See Entry 76473

Some properties of amorphous Si thin films and their application to sensors. I. Power sensor See Entry 76938

The conductivity and thermoelectric power of amorphous silicon See Entry 76939

Electrical resistance of diamond implanted at liquid nitrogen temperature with carbon ions See Entry 76941

The interpretation of drift mobility experiments on amorphous silicon See Entry 76958

Determination of carrier lifetime in Si by optical modulation See Entry 76965

Comments on 'Carrier recombination through shallow donor/acceptor levels in heavily doped silicon' See Entry 76968

Photogeneration and geminate recombination in amorphous silicon See Entry 76972

An RF bridge technique for contactless measurement of the carrier lifetime in silicon wafers See Entry 76989

Optical conductivity in the impurity band of doped semiconductors See Entry 76993

Photoelectric spectroscopy of radiation defects in germanium See Entry 77002

1/f noise in polycrystalline silicon resistors See Entry 77012

Effect of laser irradiation on the electrical properties of polycrystalline thin films of tellurium See Entry 77077

Picosecond reflectivity measurements on glow discharge a-Si:H See Entry 77471

Growth of high quality Ge MBE film See Entry 77571

Determination of minority carrier lifetime and effective back surface recombination velocity in BSF silicon solar cells from transient measurements See Entry 77990

Flash-lamp annealing of ion-implanted silicon and its application to solar cells See Entry 78000

Model calculations for silicon inversion layer solar cells See Entry 78009

The measurement of variations in minority carrier lifetime due to microstructural defects in large area polysilicon wafers See Entry 78060

Grain boundary structure and properties in polycrystalline silicon See Entry 78069

72.80E III-V and II-VI semiconductors

Gallium Arsenide and Related Compounds, 1982. Tenth International Symposium on Gallium Arsenide and Related Compounds See Entry 74226

LEC growth of InP(Mn) for p-type and semi-insulating materials See Entry 76341

Reproducibility and uniformity considerations in LEC growth of undoped, semi-insulating GaAs for large-area, direct implantation technology See Entry 76342

Annealing of defects in X-ray and electron irradiated $Cd_{0.9}Hg_{0.1}Te$ single crystals See Entry 76500

Microscopic model of the EL2 level in GaAs See Entry 76889

Thermal conversion of undoped GaAs and the outdiffusion of the main electron trap EL2 See Entry 76891

Re-examination of the mid-gap electron trap (EL2) in different GaAs wafers by photocapacitance, DLTS and photoluminescence spectra See Entry 76892

High resistivity in p-type InP by deuteron bombardment See Entry 76937

Electron transport in sub-micron GaAs channels at 300K See Entry 76940

A direct comparison of LEC GaAs grown using low- and high-pressure techniques See Entry 76942

Electron and hole carrier mobilities for liquid phase epitaxially grown GaP in the temperature range 200-550K See Entry 76943

Effect of temperature on the electrical transport properties of p-type polycrystalline indium antimonide See Entry 76948

Isolation characteristics in selectivity O^+ and Cr^+ implanted GaAs See Entry 76953

Effect of free carrier screening on the electron mobility of GaAs: a study by field-effect measurements See Entry 76956

Ballistic transport in GaAs See Entry 76959

Experimental determination of impact ionization coefficients in (100) GaAs See Entry 76960

Determination of diffusion length of electron beam induced minority carriers in polycrystalline GaAs See Entry 76963

Electron diffusion lengths in Mn-doped InP See Entry 76964

Transverse magnetophonon resonance in n-GaAs under pulsed high magnetic fields See Entry 76974

Conductivity and Hall coefficient studies in plastically deformed CdTe single crystals See Entry 76975

Magnetic-field dependence of the Hall factor of gallium arsenide See Entry 76980

- Multifilament and multidomain stationary states in a hot electron-hole plasma in GaAs See Entry 76986
- Low temperature persistent photoconductivity in two-dimensional electron gas FETs See Entry 77006
- The heterojunction $\text{ZnSe}-(\text{Zn}_{1-x}\text{Cd}_x\text{Te})_{1-y}(\text{In}_y\text{Te})_y$ having high sensitivity in the visible light range and its applications See Entry 77024
- Photoelectric fatigue of photoresistors based on polycrystalline $\text{CdS}:\text{Cu}:\text{Cl}$ films See Entry 77075
- Raman spectroscopy for characterization of annealing of ion-implanted InP See Entry 77402
- Photoluminescent and electrical properties of InGaP As mixed crystals liquid-phase-epitaxially grown on (100) GaAs See Entry 77432
- Formation of lattice defects in CdS crystals by nitrogen laser radiation See Entry 77450
- Energy position of luminescence (photosensitivity) centres in $\text{CdSe}_{1-x}\text{Te}_x$ solid solutions See Entry 77453
- Localization of electronic states and cathodoluminescence of bound exciton complexes in ZnSe crystals See Entry 77462
- In situ purification growth of undoped semi-insulating GaAs single crystals See Entry 77558
- Low pressure metalorganic chemical vapor deposition on InP and related compounds See Entry 77577
- MOCVD growth and characterization of high luminescence efficiency $\text{Al}_x\text{Ga}_{1-x}\text{As}$ See Entry 77583
- Realisation et caractérisation de cellules solaires $\text{Cu}_2\text{S}-\text{CdZnS}$ (Realisation and characterisation of $\text{Cu}_2\text{S}-\text{CdZnS}$ solar cells) See Entry 78013
- Deep level defects and annealing studies in one-MeV electron irradiated $(\text{AlGa})\text{As}-\text{GaAs}$ solar cells See Entry 78032
- Effects of indirect bandgap top cells in a monolithic cascade cell structure See Entry 78036

72.80G Transition-metal compounds

- Auger and AC impedance studies of the RF sputter deposited Fe_2O_3 films See Entry 76810
- Preparation and properties of substituted iron tungstates See Entry 76947
- Dependence of electrical properties in iron-cobalt, iron-zinc ferrites near stoichiometry on firing temperature and atmosphere See Entry 76955
- Conductivity and Hall effect in single crystals of CuCr_2Se_4 magnetic spinel See Entry 76978
- Electrical conductivity, thermoelectric power and Hall effect in p-type molybdenite (MoS_2) crystal See Entry 76981
- Electrophysical properties of niobium carbide single crystals See Entry 76984
- High-pressure growth of polycrystalline molybdenum disulphide See Entry 77591
- Crystal structure and electrical resistivity of $\text{MoS}_2-\text{NbS}_2$ alloys produced by self-propagating high-temperature synthesis See Entry 77595

72.80J Other crystalline inorganic semiconductors

- The role of solitons and the kinetics of precipitate growth in boron doped silicon-germanium alloys See Entry 76633
- The DC resistivity of modified PZT ceramics See Entry 76944
- Ternary mixed valence oxygen deficient K_2NiF_4 type copper oxides. Progressive evolution of a semiconducting state from a semimetallic state in $\text{La}_{2-x}\text{Sr}_x\text{CuO}_{4-x/2-\delta}$ See Entry 76945
- Solid state studies on substituted CuCr_2O_4 spinel See Entry 76946
- Minority-carrier diffusion-length measurement and lifetime in $\text{Pb}_{0.9}\text{Sn}_{0.1}\text{Te}$ and indium-doped PbTe liquid phase epitaxy layers See Entry 76966
- Electrical conduction in sintered $\alpha\text{-Sb}_2\text{O}_4$ See Entry 76982
- Transport properties of thermoelectric materials for coolers See Entry 76983
- The electric and photoelectric properties of TlSbSe_2 crystals in the region of impurity conduction See Entry 76995
- Characteristic steps in the relaxation curves of field-quenched persistent photoconductivity of $\text{Pb}_{0.78}\text{Sn}_{0.22}\text{Te}:\text{In}$ See Entry 76996
- Electrical and optical properties of SnO_2 thin layers received using the method of oxidation of thermally vapoured Sn layers See Entry 77073
- The effect of hydrogen on the electrical properties of n-type $\text{Pb}_{0.9}\text{Cd}_{0.1}\text{Te}$ thin films See Entry 77074
- Electrical conductivity and infrared absorption spectrometry study of hematite precipitation from defective ferrites See Entry 77647

72.80L Organic semiconductors

- Effect of adsorption of vapours on the electrical conductivity of a series of some naphthyl polyenes: Adsorption and desorption kinetics See Entry 76776
- Effect of oxygen on the electrical properties of β -zinc phthalocyanine single crystals See Entry 76961
- Photoconductivity, photovoltages, and photogenerated solitons in polyacetylene See Entry 76991

72.80N Amorphous and glassy semiconductors

- Nonisothermal relaxation during photorecording in AsSe layers See Entry 75760
- Defect states and donors in thermally annealed or post-hydrogenated chemically vapor-deposited amorphous SiN_x alloy See Entry 76897
- Some properties of amorphous Si thin films and their application to sensors. I. Power sensor See Entry 76938
- The conductivity and thermoelectric power of amorphous silicon See Entry 76939
- Effect of heat treatment on the conduction and structure of Ge-Se-Te amorphous alloys See Entry 76950
- Time-dependent field effect in amorphous chalcogenides See Entry 76957
- The interpretation of drift mobility experiments on amorphous silicon See Entry 76958

- Photogeneration and geminate recombination in amorphous silicon See Entry 76972
- Peculiarities of photoelectric phenomena in glassy As_2S_3 See Entry 77005
- Picosecond reflectivity measurements on glow discharge a-Si:H See Entry 77471
- Design parameters of high efficiency a-SiC:H/a-Si:H heterojunction solar cells See Entry 78080

73.00 ELECTRONIC STRUCTURE AND ELECTRICAL PROPERTIES OF SURFACES, INTERFACES, AND THIN FILMS

- Conference Record of the Sixteenth IEEE Photovoltaic Specialists Conference - 1982 See Entry 74219

73.20 ELECTRONIC SURFACE STATES

(for emission and impact phenomena, see 79.)

- 77015 The electronic structure of GaP (110) and Cu-phthalocyanine overlayers studied by ellipsometry. A.Ritz, H.Luth (Physikalisches Inst., Rheinisch-Westfälische Tech. Hochschule Aachen, Aachen, Germany). *Appl. Phys. A (Germany)*, vol.A31, no.2, p.75-80 (June 1983). Ellipsometric spectroscopy in the spectral range $1.4\text{ eV} < \hbar\omega < 4\text{ eV}$ is used to study cleaved GaP (110) surfaces after adsorption of hydrogen and oxygen and after deposition of Cu-Phthalocyanine (CuPc) molecules. The adsorption of gases and of CuPc induces band bending changes which are derived from changes of the optical constants in the space charge layer due to an electric field effect. For the clean surface, furthermore, information is obtained about electronic surface states. CuPc overlayers with thicknesses below one monolayer exhibit an optical absorption which suggests a chemisorption interaction through the macrocyclic π -system of the Pc-molecules. (28 refs.)
- 77016 Interface trap generation in silicon dioxide when electrons are captured by trapped holes. S.K.Lai (IBM Thomas J. Watson Res. Center, Yorktown Heights, NY, USA). *J. Appl. Phys. (USA)*, vol.54, no.5, p.2540-6 (May 1983). A characteristic interface trap was observed in a hole trapping experiment when electrons were captured by trapped holes injected by an avalanche in the silicon. The observations could be explained by the generation of new electronic states through relaxation of strained bonds which were proposed to be the origin of hole traps. The result is either a weak bond in the network or two dangling bonds with no net charge. The weak bond or dangling bonds gives rise to neutral traps in the bulk and interface traps at the interface of the oxide. The presence of interface traps for such defects at the interface is predicted by theoretical calculations. (40 refs.)
- 77017 Generation-annealing kinetics of the interface donor states at 0.25 eV above the midgap and the turn-around phenomena on oxidized silicon during avalanche electron injection. C.-T.Sah, J.Y.-C.Sun, J.J.-T.Zou (Dept. of Electrical Engng., Univ. of Illinois, Illinois, IL, USA). *J. Appl. Phys. (USA)*, vol.54, no.5, p.2547-55 (May 1983). The generation and the annealing kinetics of the donorlike peaked interface density of states (DOSS) at 0.25 eV above the midgap and the turn-around phenomenon of the flat-band voltage generated by the avalanche electron injection are reported. The generation of the peaked interface DOS follows a first-order kinetics and it anneals out at 25 °C following a second-order kinetics. The devices with dry oxide show a small buildup of peaked DOS as well as a small turn-around phenomenon. However, after a deionized (DI) water rinse before gate metallization, a large buildup of peaked DOS and turn-around states were observed. After avalanche electron injection is terminated, in the devices with small peaked DOS, the midgap voltage slowly drifts in the negative voltage direction under negative gate bias. However, in the devices with large peaked DOS, the midgap voltage slowly drifts in the positive gate voltage direction even under negative gate bias. Detailed analyses of both the generation and annealing data suggest that the peaked DOS is a donor which can account for most of the turn-around phenomenon as well as the midgap voltage instability phenomenon after avalanche electron injection. DI water dependence suggests that the peaked DOS and the turn-around states may be related to hydroxyl species in the oxide. (28 refs.)
- 77018 A covalent model for the bonding of adsorbed hydrocarbon fragments on the (111) face of platinum. C.Minot, M.A.Van Hove, G.A.Somorjai (Lawrence Berkeley Lab., Univ. of California, Berkeley, CA, USA). *Surf. Sci. (Netherlands)*, vol.127, no.3, p.441-60 (May 1983). A systematic molecular orbital study of the location of CH_3 and C-CH_3 ($n=1, 2, 3$) species on a Pt(111) single-crystal surface has been performed by using both a cluster model and a band structure calculation within the framework of the Extended Huckel Theory (EHT). These species may be involved in the hydrogenation/dehydrogenation processes of hydrocarbons. The observed dependence of the adsorption site on the number of hydrogens in the CH_n fragments suggests that any C-H bond breaking in CH_n species must involve a change of adsorbate bonding site. The carbon is found to be located on the surface in such a way as to complete its tetravalency. Thus, CH occupies a three-fold coordinated hollow site, CH_2 a two-fold coordinated bridge site and CH_3 a one-fold coordinated top site, C-CH_3 is found to be perpendicular to the surface in a three-fold hollow site in agreement with experimental observations. It is also found that a displacement of $\text{C-CH}_2\text{-R}$ to a top site makes a β C-R cleavage easier. (61 refs.)
- Interface states and current threshold of $\text{GaAs}/\text{Al}_x\text{Ga}_{1-x}\text{As}$ double-heterostructure lasers grown by molecular beam epitaxy See Entry 75640
- Cluster calculations of the $\text{H}_2\text{O}/\text{Pt}(111)$ system See Entry 76774
- Quantum chemical studies of chemisorption at anion or cation sites of the GaP (110) surface. Coverage dependence of adsorption energy and equilibrium in cases of positive and negative partial charge injection See Entry 76878
- Model calculations of local electron and phonon densities of states in bimetallic superlattices See Entry 76827
- Electron localization in a two-dimensional system in strong magnetic fields. I. Case of short-range scatterers See Entry 76864
- Electronic and cohesive properties of small sodium particles See Entry 76869
- Dependence of emission-capture properties of dominant traps and interface states on alloying in organometallic VPE $\text{Al}_x\text{Ga}_{1-x}\text{As}$ See Entry 76893
- Electrical conduction through anodic oxides on InP See Entry 76951

- Electronic properties of InAs-GaSb superlattices See Entry 77032
- Electronic structure of semiconductor superlattices See Entry 77035
- Heterolayer screening of an external ion field See Entry 77040
- Surface states at semiconductor-liquid junction See Entry 77045
- Si-transition metal interface formation and bulk electronic structure of 3d metal disilicides See Entry 77053
- Interfacial electrical properties of ion-beam sputter deposited amorphous carbon on silicon See Entry 77055
- The electrical behavior of GaAs-insulator interfaces: a discrete energy interface state model See Entry 77060
- Quantization of photo-excited carriers in GaAs doping superlattices See Entry 77395
- Comments on 'Laser excitation of surface electronic states for a one-dimensional semiconductor' by W.C. Murphy and T.F. George See Entry 77485
- Reply to comments on 'Laser excitation of surface electronic states for a one-dimensional semiconductor' by G.W. Bryant See Entry 77486
- Excitations in charge-transfer atom scattering See Entry 77515
- Photoemission of Xe and Kr adsorbed on the W(110) plane See Entry 77524
- Photoemission does not measure the energies of orbitals (or: Configurational model of adsorbate structure and excitations) See Entry 77528
- The bandstructure of CO on Cu(111); breakdown of the single particle picture See Entry 77529
- Angle-resolved photoemission study of the GaAs(100) surface and the Ge-GaAs(100) interface See Entry 77534
- Exoelectron emission from surface states in a ferroelectric See Entry 77538
- Barrier height enhancement in semiconductor-insulator-semiconductor solar cells due to surface states and insulator charges See Entry 78010
- Grain boundary effects and Li passivation in polycrystalline silicon See Entry 78059

73.25 SURFACE CONDUCTIVITY

- A new profiling technique applicable to the measurements sensitive to the free-carrier concentration rather than the depletion-layer thickness See Entry 76478

73.30 SURFACE DOUBLE LAYERS, SCHOTTKY BARRIERS, AND WORK FUNCTIONS

- 77019 Invalidation of the scaling property of surface potential kinetics in HDPE. H.von Berlepsch, L.Brehmer (Inst. für Polymerenchem. 'Erich Correns', Akad. der Wissenschaften, Teltow-Seehof, Germany). *Phys. Status Solidi a (Germany)*, vol.76, no.1, p.K27-9 (16 March 1983). The study of the surface potential kinetics $V(t)$ has proved to be a powerful tool in investigating charge carrier transport processes for partially crystalline high-resistance polymer solids. The authors investigate in detail this problem from the experimental point of view on HDPE. Excess charge was introduced into the sample by exposure to a positive or negative point corona discharge (corona voltages up to 8 kV, air gap 10^{-2} m). After a corona charging for 10 s the isothermal potential decay was measured by the field mill technique. (11 refs.)
- Layer-dependent shifts in ionization potential and Auger energies for Kr/Cu (110) See Entry 76786
- Electrical conduction through anodic oxides on InP See Entry 76951
- Si-transition metal interface formation and bulk electronic structure of 3d metal disilicides See Entry 77053
- Fabrication of GaAs-Mo-Si structures by metalorganic chemical vapor deposition and laser annealing See Entry 77572

73.40 INTERFACES

- 77020 Capacitance/voltage characteristics of semiconductor-insulator-semiconductor (SIS) structure. K.Nagai, Y.Hayashi, T.Sekigawa (Electrotech. Lab., Ibaraki, Japan). *Electron. Lett. (GB)*, vol.19, no.10, p.376-7 (12 May 1983). Ideal capacitance/voltage curves of $\text{Si}(2)\text{-SiO}_2\text{-Si}(1)$ structure are computed in the absence of surface states and oxide changes with the SiO_2 thicknesses, conductivity types, impurity concentrations of $\text{Si}(1)$ and (2) as parameters. Impurity concentrations of $\text{Si}(1)$, (2) and SiO_2 thickness can be estimated from the measured capacitance/voltage curves by comparing them with the calculated ones as in the case with the conventional MOS structure. (5 refs.)
- 77021 Incomplete space-charge layers in semiconductors. D.Redfield (RCA Labs., Princeton, NJ, USA). *J. Appl. Phys. (USA)*, vol.54, no.5, p.2860-2 (May 1983). Analysis of the potential and field profiles in space-charge layers near semiconductor interfaces is extended to consider cases in which the thickness of the semiconductor layer is less than the conventional 'width' of the space-charge region that would exist if the semiconductor were very thick. It is shown that both electrostatic effects and possible Fermi-level changes are important in these cases. The apparent deficiency of charge that such thin layers present is found to be illusory; adequate charge is always available. However, the process which provides this charge may alter the work function of the semiconductor and therefore change the potential distribution. (5 refs.)
- 77022 The thickness dependence of excess carrier lifetime and mobility in amorphous silicon junctions. H.Steemers, W.E.Spear, P.G.Ie Comber (Carnegie Lab. of Phys., Univ. of Dundee, Dundee, Scotland). *Philos. Mag. B (GB)*, vol.47, no.5, p.L83-8 (May 1983). Fast transient methods have been used to determine the electron drift mobility μ_e and lifetime τ_e in a-Si p-i-n junctions ranging in thickness from $d \approx 0.4$ to $15 \mu\text{m}$. Similar data were obtained for holes on the thinner specimens. For $d < 4 \mu\text{m}$, $\mu_e \tau_e \approx \mu_h \tau_h$, and both are proportional to d^2 . It is shown that the thickness dependence of $\mu_e \tau_e$ arises almost entirely from that of τ_e . For $d \geq 10 \mu\text{m}$, τ_e tends towards a constant value of $1\text{-}2 \mu\text{s}$, which represents the true electron lifetime of the material with respect to deep centres. The free lifetime is about 100 ns. A possible explanation for the observed thickness dependence of $\mu_e \tau_e$ is given. (9 refs.)
- Barrier height enhancement in semiconductor-insulator-semiconductor solar cells due to surface states and insulator charges See Entry 78010

73.40L Semiconductor-to-semiconductor contacts, p-n junctions, and heterojunctions

- 77023 Empirical rule to predict heterojunction band discontinuities. A.D.Katnani, G.Margaritondo (Dept. of Phys., Univ. of Wisconsin, Madison, WI, USA). *J. Appl. Phys. (USA)*, vol.54, no.5, p.2522-5 (May 1983). The authors have developed an empirical table of valence-band-edge energy positions for group IV, III-V, and II-VI semiconductors, referred to the valence-band edge of germanium. The energy positions listed in the table were deduced from systematic photoemission measurements of heterojunction valence-band discontinuities performed on semiconducting substrates with Si or Ge overlayers. The table can be used to estimate the valence-band discontinuities of heterojunctions between compound semiconductors, with several advantages and better accuracy with respect to the widely used twenty-year-old electron-affinity rule and to other more recent theories. (32 refs.)
- 77024 The heterojunction $\text{ZnSe}(\text{Zn}_{1-x}\text{Cd}_x\text{Te})_{1-y}(\text{In}_y\text{Te}_3)_y$ having high sensitivity in the visible light range and its applications. S.Fujiwara, T.Chikamura, M.Fukai (Materials Res. Lab., Matsushita Electric Industrial Co. Ltd., Osaka, Japan). *J. Cryst. Growth (Netherlands)*, vol.61, no.3, p.567-75 (April-May 1983). The effect of a ZnSe film on the heterostructural $\text{ZnSe}(\text{Zn}_{1-x}\text{Cd}_x\text{Te})_{1-y}(\text{In}_y\text{Te}_3)_y$ film was studied from the standpoint of crystal growth. It is made clear that the ZnSe film improves the crystallinity of the $(\text{Zn}_{1-x}\text{Cd}_x\text{Te})_{1-y}(\text{In}_y\text{Te}_3)_y$ film evaporated on the ZnSe film and improves the spectral sensitivity of the heterostructure in the visible to the near-infrared light range. This heterostructure which consists of many elements can be fabricated by simple evaporation and anneal methods. One of the applications of this heterostructure is the photoconductive target in a camera tube. A camera tube with such a heterostructure is called 'Newvicon' and has excellent features such as high sensitivity, low dark current, no burn-in and small lag. This heterostructure can be also applied to illuminometers, photometers and solid state imagers. (10 refs.)
- 77025 Angle-lapping and staining observations of Si doping superlattice structures. T.Sakamoto (Electrotech. Lab., Ibaraki, Japan). *J. Cryst. Growth (Netherlands)*, vol.61, no.3, p.705-6 (April-May 1983). The angle-lapping and staining technique has been successfully used for the observation of a whole view of carrier profiles of Si doping superlattice structures with very thin multi-layered p/n junctions. The Si MBE films obtained are single crystalline and have very smooth surfaces. The carrier concentrations of the p-layers and the n-layers are estimated to be 3×10^{17} and 1×10^{16} atoms/cm³, respectively. Angle-lapping was done very slowly using silica powder on a polyacrylate plate of 5 mm thick for about 10-20 min. The angle-lapped surfaces are very smooth and flat. Staining was done using a solution of $\text{HF-HNO}_3\text{-HCHO}$ under a 100 W incandescent lamp for 10-20 s. (8 refs.)
- 77026 Magnetoresistance anisotropy due to the 2D-electron subsystem at a GaAs/AlGaAs interface. V.A.Volkov, D.V.Galchenkov, I.M.Grodnenski, K.V.Starostin (Inst. of Radio Engng. & Electronics, Acad. of Sci., USSR). *JETP Lett. (USA)*, vol.36, no.9, p.420-4 (5 Nov. 1982). Translation of: *Pisma v Zh. Eksp. & Teor. Fiz. (USSR)*, vol.36, no.9, p.343-6 (5 Nov. 1982). [received: June 1983] Effects of the coexistence of 2D and 3D electrons in the structure GaAs/n-AlGaAs have been studied for the first time over the temperature range $T = 4.2\text{-}300\text{K}$. The angular dependence of the magnetoresistance might be used as a new test of the two-dimensionality of an electron subsystem. This test would work over broad ranges of T and H , in contrast with the Shubnikov-de Haas effect. (4 refs.)
- 77027 The variation of the p/n junction position in GaAs/GaAlAs double heterostructures grown by low pressure MO VPE. S.D.Hersee, M.Baldy, J.P.Duchemin (Thomson-CSF, Domaine De Corbeville, Orsay, France). *J. Electron. Mater. (USA)*, vol.12, no.2, p.345-57 (March 1983). A modified contact resistance profiler has been used to determine the doping type of the active layer in GaAs/GaAlAs double heterostructure grown by low pressure metal-organic vapour phase epitaxy (LP-MO VPE). It was found that under normal growth conditions, the p/n junction is located inside the 'p-type' $\text{Ga}_{0.65}\text{Al}_{0.35}$ confinement layer. SIMS data show that this displacement of the p/n junction is due to electrical compensation of the zinc doping. (6 refs.)
- 77028 Some electrical properties of $\text{Au}_x\text{Te}/\text{CdTe}$ heterojunctions on CdTe thick films. J.Touskova, D.Kindl, J.Tousek, E.Klier (Dept. of Semiconductor Phys., Charles Univ., Prague, Czechoslovakia). *Phys. Status Solidi a (Germany)*, vol.76, no.1, p.365-74 (16 March 1983). Measurements of I - U characteristics at several temperatures, the voltage and frequency dependences of capacitance, and the photocurrent of samples are used for studying some electrical properties of heterojunctions formed on sintered layers of n-type CdTe. According to the geometrical arrangement, two types of samples are investigated: group A on an insulating substrate with planar electrodes, group B on a conducting substrate with sandwich electrodes. The p-n junctions are formed in both cases by chemical reaction with AuCl_3 solution. The transport of charge across the junction at both, A and B groups is controlled by some process of tunnelling through the barrier from one side and by thermal emission from the opposite side of the junction followed by recombination at interface states. The C - U characteristics of B-samples show the usual form typical for the abrupt junction, whereas the capacitance of A-samples is essentially influenced by the internal capacitance of the polycrystalline layer. An energy band model of the junction is suggested. (8 refs.)
- 77029 Effect of tangential magnetic field on the two-dimensional electron transport in N-AlGaAs/GaAs superlattices and hetero-interfaces. H.Sakaki, H.Ohno, S.Nishi, J.Yoshino (Inst. of Industrial Sci., Univ. of Tokyo, Tokyo, Japan). *Physica B & C (Netherlands)*, vol.117-118 B+C, pt.2, p.703-5 (March 1983). (Proceedings of the 16th International Conference on the Physics of Semiconductors, Montpellier, France, 6-10 Sept. 1982). Magnetoresistance $\Delta\rho/\rho$ of a two dimensional electron gas at N-AlGaAs/GaAs heterojunction interfaces and superlattices is studied for the magnetic field, B_y , parallel to heterojunctions. $\Delta\rho/\rho$ at the interface is found to contain a term having linear dependence both on B_y and on electric field parallel to the current, E_x . This is ascribed to the deformation of wavefunction by the Lorentz force, which affects the electron scattering by impurities distributed only on one side of the interface. Similar measurement on superlattices is found effective in evaluating the possible asymmetry of the structure and the spatial distribution of scatterers. (7 refs.)

- 77030** 2D hot electron transport in a modulation-doped GaAs/AlGaAs interface. M.Inoue, H.Hida, M.Inayama, Y.Inuishi (Dept. of Electrical Engng., Osaka Univ., Osaka, Japan), K.Nanbu, S.Hiyamizu. *Physica B & C (Netherlands)*, vol.117-118 B+C, pt.2, p.720-2 (March 1983). (Proceedings of the 16th International Conference on the Physics of Semiconductors, Montpellier, France, 6-10 Sept. 1982). Direct evidence of polar optical phonon emission and intersubband transfer of 2D electrons has been observed in GaAs/Al_xGa_{1-x}As ($x=0.3$) heterostructures. Magnetophonon resonance as well as SDH effect were observed simultaneously in magneto-resistance data at 4.2K. These electron scatterings are responsible for the cooling process of high mobility 2D electrons heated by applied electric fields. The electron temperature and velocity were also measured to reveal hot electron effects of the 2DEG. (14 refs.)
- 77031** Electron transport in heterojunctions and superlattices. K.Hess (Dept. of Electrical Engng., Univ. of Illinois, Urbana, IL, USA). *Physica B & C (Netherlands)*, vol.117-118 B+C, pt.2, p.723-8 (March 1983). (Proceedings of the 16th International Conference on the Physics of Semiconductors, Montpellier, France, 6-10 Sept. 1982). Theoretical and experimental results are presented for high field transport in heterojunction structures parallel to the layers. It is shown that these structures exhibit new transport effects with high potential for device applications. A novel oscillator principle and novel storage and switching phenomena are described. These effects are real-space analogies to well-known k-space effects such as the Gunn effect. (17 refs.)
- 77032** Electronic properties of InAs-GaSb superlattices. Y.Guldner (Groupe de Phys. des Solides, Ecole Normale Supérieure, Paris, France). *Physica B & C (Netherlands)*, vol.117-118 B+C, pt.2, p.735-40 (March 1983). (Proceedings of the 16th International Conference on the Physics of Semiconductors, Montpellier, France, 6-10 Sept. 1982). Transport and far-infrared magneto-absorption performed in InAs-GaSb superlattices covering the entire semimetallic regime are described. The sub-band parameters are determined, evidencing the semimetallic nature, the three-dimensional character of the superlattices and the confinement of both electrons and holes at the interfaces in the heterojunction limit. (18 refs.)
- 77033** GaSb-AlSb-InAs multi-heterojunctions. H.Takaoaka, Chin-An Chang, E.E.Mendez, L.L.Chang, L.Esaki (IBM Thomas J. Watson Res. Center, Yorktown Heights, NY, USA). *Physica B & C (Netherlands)*, vol.117-118 B+C, pt.2, p.741-3 (March 1983). (Proceedings of the 16th International Conference on the Physics of Semiconductors, Montpellier, France, 6-10 Sept. 1982). The authors have made transport measurements on GaSb-AlSb-InAs multi-heterojunctions prepared by MBE. The result has been analyzed on the basis of electron tunneling across thin AlSb layers. (7 refs.)
- 77034** Mobility in modulation doped GaAs-GaAlAs superlattices. G.Fishman, D.Calecki (Groupe de Phys. des Solides, Univ. de Paris VII, Paris, France). *Physica B & C (Netherlands)*, vol.117-118 B+C, pt.2, p.744-6 (March 1983). (Proceedings of the 16th International Conference on the Physics of Semiconductors, Montpellier, France, 6-10 Sept. 1982). The authors use an analytical approach to calculate the electron mobility parallel to the layers in modulation doped GaAs-GaAlAs superlattices; it allows comparison with recent experimental results. They take into account intersubband electron scattering that occurs when electron density becomes sufficiently high. Order of magnitude and variations of the Hall mobility with the undoped spacer of GaAlAs and with the electron density are explained and discussed. (6 refs.)
- 77035** Electronic structure of semiconductor superlattices. M.Altarelli (Max-Planck-Inst. für Festkörperforschung, Stuttgart, Germany). *Physica B & C (Netherlands)*, vol.117-118 B+C, pt.2, p.747-9 (March 1983). (Proceedings of the 16th International Conference on the Physics of Semiconductors, Montpellier, France, 6-10 Sept. 1982). A new approach to the calculation of the electronic structure of semiconductor superlattices in the envelope-function approximation is presented and applied to the type II InAs-GaSb system. The method allows a realistic description of the band edges of the constituent materials, and yields, therefore, accurate results for the sub-band dispersion in the direction parallel to the layers. Some novel aspects of the semiconductor-semimetal transition in InAs-GaSb are pointed out. (8 refs.)
- 77036** Hot electron effects in heterolayers. P.J.Price (IBM Thomas J. Watson Res. Center, Yorktown Heights, NY, USA). *Physica B & C (Netherlands)*, vol.117-118 B+C, pt.2, p.750-2 (March 1983). (Proceedings of the 16th International Conference on the Physics of Semiconductors, Montpellier, France, 6-10 Sept. 1982). Phenomena of interaction in the direction perpendicular to the layer planes, for hot electrons in heterolayer structures such as may be grown by molecular beam epitaxy, are discussed. In particular, energy transfer between electrons in neighboring heterolayers, due to mutual Coulomb scattering and escape of electrons from a heterolayer, due to phonon scattering processes, are analyzed; and it is shown that substantial rates are possible. (no refs.)
- 77037** Two dimensional magnetophonon resonance in GaInAs-InP superlattices. M.A.Brummell, R.J.Nicholas (Clarendon Lab., Univ. of Oxford, Oxford, England), J.C.Porter, M.Razeghi, M.A.Poisson. *Physica B & C (Netherlands)*, vol.117-118 B+C, pt.2, p.753-5 (March 1983). (Proceedings of the 16th International Conference on the Physics of Semiconductors, Montpellier, France, 6-10 Sept. 1982). Cyclotron resonance and magnetophonon resonance studies have been made of superlattices grown from thin layers of Ga_{0.47}In_{0.53}As and InP, which exhibit two dimensional behaviour at temperatures up to 250K. The electron effective mass varies with layer thickness in reasonable agreement with the calculated non-parabolicity. The LO phonon energies are calculated from magnetophonon oscillations and mass values obtained from cyclotron resonance. A strong series of oscillations results from the dominant 'GaAs-like' mode in GaInAs. A second, weaker series corresponds to the energy of the InP LO phonon. This is evidence for a long range phonon interaction, with the field of the phonons extending into the GaInAs to cause a significant coupling with the electrons bound in the quantum wells. (13 refs.)
- 77038** Frequency properties of Ge-Si solid solution p-n junctions. M.Ya.Bakirov, R.S.Madatov, Yu.M.Mustafayev. *Radio Eng. & Electron. Phys. (USA)*, vol.27, no.6, p.153-4 (June 1982). Translation of: *Radioekh. & Elektron. (USSR)*, vol.27, no.6, p.1239-40 (June 1982). [received: May 1983] Ge-Si solid solutions are promising materials for making visible and IR radiation detectors. There are a number of papers in the literature that are devoted to Ge-Si alloy photodetectors. The literature contains no information about the lag of these photodetectors. The authors present the results of tests of the frequency characteristics of Ge-Si solid solution p-n junctions, which were made by the diffusion of antimony into p-type crystals with initial carrier densities of 10^{15} cm^{-3} and had an area of $1-2.5 \text{ mm}^2$. The frequency charac-

teristics were measured in samples with a sensitivity of 0.3-0.5 A/W. An LG-126 laser with $\lambda=1.5 \mu\text{m}$ was used as the radiation source. The radiation was modulated with an ML-4 electrooptic modulator. The photocurrent in the load ($R_1=10^5 \text{ ohms}$) was measured by means of a U2-8 wide-band amplifier. (4 refs.)

- 77039** Actual turn-on voltage of microplasmas [p-n junctions]. V.P.Shapovalov. *Radio Eng. & Electron. Phys. (USA)*, vol.27, no.6, p.154-5 (June 1982). Translation of: *Radioekh. & Elektron. (USSR)*, vol.27, no.6, p.1240-2 (June 1982). [received: May 1983] The turn-on voltage (U_{on}) of microplasma centers in p-n junctions is a function of external factors that give rise to the carrier generation rate in the microplasma region. An investigation of the quantitative dependence of the microplasma U_{on} on the temperature and the overvoltage increment (dU/dt) through the p-n junction is discussed for increasing the operation reliability of semiconductor devices. (5 refs.)
- 77040** Heterolayer screening of an external ion field. P.J.Price (IBM Thomas J. Watson Res. Center, Yorktown Heights, NY, USA). *Surf. Sci. (Netherlands)*, vol.127, no.3, p.377-82 (May 1983). The theory of screening by heterolayer carriers, in their ground sub-band, is used to investigate the conditions in which the classical image charge applies to the polarization by an external ion field. An estimate of the field penetrating to the far side of the heterolayer is obtained. (5 refs.)
- 77041** Effect of a static field on the parameters of a superlattice created in a semiconductor by a standing laser wave. I.M.Dykman, P.M.Tomchuk (Inst. of Semiconductors, Acad. of Sci., Kiev, Ukrainian SSR). *Sov. Phys.-Solid State (USA)*, vol.24, no.11, p.1847-50 (Nov. 1982). Translation of: *Fiz. Tverd. Tela (USSR)*, vol.24, no.11, p.3255-61 (Nov. 1982). [received: May 1983] A quantum transport equation for the one-particle distribution function of electrons in a semiconductor subjected to a static field F_0 and to the field of a standing laser wave is derived. The parameters of the superlattices of the electron density, of the field strength, and of the electron temperature which are created by the laser wave are determined. Such lattices have the same spatial period but the dependences of their amplitudes on F_0 are different. By varying F_0 and the lattice temperature, it is possible to alter the relative magnitudes of the amplitudes of the sublattices and even to reduce the amplitude of any sublattice to zero. (12 refs.)
- 77042** The heterojunction parameters from a microscopic point of view: recent progress. A.D.Katnani, R.R.Daniels, Te-Xiu Zhao, G.Margaritondo (Dept. of Phys., Univ. of Wisconsin, Madison, WI, USA). Fifteenth Annual Synchrotron Radiation Users Group Conference (papers in summary form only received), Stoughton, WI, USA, 18-19 Oct. 1982 (Stoughton, WI, USA: Synchrotron Radiat. Center 1982), p.27 The use of surface-sensitive experimental techniques produced in the past year important advances in the understanding of the microscopic nature of heterojunction parameters. In particular, systematic valence band discontinuity measurements were extended to a large number of interfaces involving Si overlayers and the results confirmed that the LCAO approach by Harrison (1977) is the best first-order calculation of this parameter. Local effects, however, limit the accuracy of the estimate to 0.2-0.3 eV. Evidence was obtained to show that surface defects play an important role in the interface Fermi-level pinning for heterojunctions involving III-V compounds, and therefore in the establishment of the built-in potential. The authors found that the pinning position for GaAs-Si, 0.7(3) eV above the top of the GaAs valence band, is consistent within the experimental accuracy with that reported by Monch et al. (1982) for Ge on GaAs. Furthermore, the difference between the pinning positions of E_F for GaAs-Si and for GaP-Si qualitatively reproduces the theoretical predictions for surface antisite defects. (3 refs.)
- 77043** Electrical properties of ZnO-Bi₂O₃-metal oxide heterojunction—a clue of a role of intergranular layers in ZnO varistors. K.Eda (Wireless Res. Lab., Matsushita Electric Industrial Co. Ltd., Osaka, Japan). Grain Boundaries in Semiconductors. Proceedings of the Materials Research Society Annual Meeting, Boston, MA, USA, Nov. 1981 (New York, USA: North-Holland 1982), p.381-92 Zinc Oxide (ZnO) Ceramics-Bismuth Oxide (Bi₂O₃). Metal Oxide thin film heterojunction made by sputtering technique showed a highly non-Ohmic property. The voltage-current characteristics and the dielectric properties showed dependence on Bi₂O₃ metal oxide thin film thickness. In this paper after reviewing and discussing the electrical properties of ZnO varistors, the role of intergranular layers in the ZnO varistor is discussed based on experimental results with the heterojunction. (23 refs.)
- Evaluation of misfit dislocations in planar, zinc-diffused In_{0.53}Ga_{0.47}As PIN photodiodes** See Entry 76434
- Dependence of emission-capture properties of dominant traps and interface states on alloying in organometallic VPE Al_xGa_{1-x}As** See Entry 76893
- Effect of free carrier screening on the electron mobility of GaAs: a study by field-effect measurements** See Entry 76956
- Experimental determination of impact ionization coefficients in (100) GaAs** See Entry 76960
- Electrochemical study of the thermal treatment effects on Cu₂S thin films** See Entry 76987
- Low temperature persistent photoconductivity in two-dimensional electron gas FETs** See Entry 77006
- The thickness dependence of excess carrier lifetime and mobility in amorphous silicon junctions** See Entry 77022
- Double-injection currents and field effect in sapphire-base silicon p⁺nn⁺ diodes** See Entry 77066
- Quantization of photo-excited carriers in GaAs doping superlattices** See Entry 77395
- Synchrotron radiation photoemission as a probe for overlayers on compound semiconductor surfaces: Ge:GaAs (110)** See Entry 77533
- Angle-resolved photoemission study of the GaAs(100) surface and the Ge-GaAs(100) interface** See Entry 77534
- Flash-lamp annealing of ion-implanted silicon and its application to solar cells** See Entry 78000
- Efficient pAl_xGa_{1-x}As-pGaAs:Si-nGaAs photocells for use in intense sunlight** See Entry 78005
- The metal interconnected cascade solar cell** See Entry 78035
- Effects of indirect bandgap top cells in a monolithic cascade cell structure** See Entry 78036
- Recent developments for the AlGaAsSb cell** See Entry 78077
- Design parameters of high efficiency a-Si:H/a-Si:H heterojunction solar cells** See Entry 78080

73.40M Semiconductor-electrolyte contacts

77044 High pressure photoelectric studies of semiconductor-electrolyte systems. D.A.Gulino, L.R.Faulkner, H.G.Drickamer (Materials Res. Lab., Univ. of Illinois, Urbana, IL, USA). *J. Appl. Phys. (USA)*, vol.54, no.5, p.2483-8 (May 1983). Data are presented which show the behaviour of the valence and conduction band-edge energies (E_v and E_c , respectively) as a function of pressure for the n -type semiconductor electrodes TiO_2 , CdS , and CdSe . For TiO_2 , the 3 meV/kbar increase in the band-gap energy (E_g) is due entirely to an increase in E_c . For CdS , the 5.1 meV/kbar increase in E_g is the difference between the 9.5-11.5 meV/kbar increase in E_c and the (calculated) 4.5-6.5 meV/kbar increase in E_v . In the case of CdSe , both E_c and E_v move to lower energies with increasing pressure. Their behaviour is complex. (22 refs.)

77045 Surface states at semiconductor-liquid junction. K.Kobayashi, Y.Aikawa, M.Sukigara (Inst. of Industrial Sci., Univ. of Tokyo, Tokyo, Japan). *J. Appl. Phys. (USA)*, vol.54, no.5, p.2526-32 (May 1983). Surface states at a junction of n - TiO_2 and aqueous solution were studied by means of the capacitance measurement. It appeared that, from the relation between surface-state capacitance and electrode potential, surface states with state density of $8 \times 10^{-4} \text{ cm}^{-2}$ were located at 0.5 eV below the bottom of the conduction band. The electron capture cross section of $2.0 \times 10^{-19} \text{ cm}^2$ was obtained from the frequency dependence of surface-state capacitance. The effect of the UV irradiation of TiO_2 on the surface-state capacitance suggested that this surface state originated from adsorbates. (25 refs.)

77046 Light-induced recombination centers during pulse radiolysis of an electrolyte-semiconductor system. A.A.Revina (Inst. of Electrochem., Acad. of Sci., Moscow, USSR). *Sov. Electrochem. (USA)*, vol.18, no.8, p.989-91 (Aug. 1982). Translation of: *Elektrokhimiya (USSR)*, vol.18, no.8, p.1114-17 (Aug. 1982). [received: May 1983] Luminescence measurements were made during pulse radiolysis which were based on the recording of the emission of the excited species formed under the action of ionizing radiation. The radiolytic conversions were studied in an heterogeneous system of electrode (titanium oxide anode)-electrolyte, and in separate experiments TiO_2 -electrolyte-Pt. The electrolyte chosen was a saturated methanolic solution of magnesium chloride, hexahydrate. The results obtained for the spectral and kinetic characteristics of the luminescence signals for heterophase pulse radiolysis and the detection of a photoradiation effect permit the forward view that this method considerably widens the possibilities of studying the mechanism of reactions of intermediate species at an electrode/electrolyte interface. (6 refs.)

73.40N Metal-nonmetal contacts

77047 Electrical characteristics of amorphous iron-tungsten contacts on silicon. M.Finetti, E.-T.-S.Pan, I.Suni, M.-A.Nicolet (California Inst. of Technol., Pasadena, CA, USA). *Appl. Phys. Lett. (USA)*, vol.42, no.11, p.987-9 (1 June 1983). The electrical characteristics of amorphous Fe-W contacts have been determined on both p -type and n -type silicon. The amorphous films were obtained by cosputtering from a composite target. Contact resistivities, $\rho_c = 1 \times 10^{-7}$ and $\rho_c = 2.8 \times 10^{-6}$, were measured on n^+ and p^+ silicon, respectively. These values remain constant after thermal treatment up to at least 500°C. A barrier height, $\phi_{bn} = 0.61 \text{ V}$, was measured on n -type silicon. (18 refs.)

77048 Au-Mg improved ohmic contacts to p -GaAs. N.A.Papanislaou, N.Christou (Naval Res. Lab., Washington, DC, USA). *Electron. Lett. (GB)*, vol.19, no.11, p.418-20 (26 May 1983). A novel ohmic contact alloy to p -GaAs consisting of 96 weight % Au and 4 weight % Mg, a Mo barrier metal and Au overlay is described. Contact resistivities as low as $8 \times 10^{-5} \Omega \text{ cm}^2$ are achieved on heavily doped substrates. Auger sputter profiles show these contacts to be thermally stable up to 450°C. (7 refs.)

77049 Schottky barrier type diode with an electrochemically prepared copolymer having pyrrole and N -methylpyrrole units. H.Koezuka, S.Etoh (Materials Engng. Lab., Mitsubishi Electric Corp., Hyogo, Japan). *J. Appl. Phys. (USA)*, vol.54, no.5, p.2511-16 (May 1983). A Schottky type diode has been constructed with the electrochemically prepared copolymer having pyrrole and N -methylpyrrole units and a low work function metal (In). The heat treatment of the copolymer in air was performed in order to stabilize the electrical characteristics of the device before the deposition of a blocking electrode. The electrical properties have been investigated by means of I - V and C - V measurements. The diode quality factor and the barrier height have been obtained to be $n=1.2$ and $\phi_b=0.81 \text{ V}$ by applying a thermionic emission theory, respectively. At high current densities in the forward direction, a space-charge-limited current has been observed. This observation would be due to the charge-injection across the thin oxidized layer which would be formed during the heat treatment of the copolymer in air. Other junction parameters have been also determined by means of C - V measurements. (22 refs.)

77050 Tunnel barriers on Pb-In-Au alloy films. J.M.Baker, J.H.Magerlein (IBM Thomas J. Watson Res. Center, Yorktown Heights, NY, USA). *J. Appl. Phys. (USA)*, vol.54, no.5, p.2556-68 (May 1983). Tunnel barrier oxides consisting primarily of In_2O_3 formed on Pb-In-Au alloys by various thermal and RF-plasma oxidation techniques were characterized in situ using ellipsometry and Auger electron spectroscopy (AES). The results were compared to measurements of the Josephson critical current density j_c and the specific capacitance of tunnel junctions fabricated on the same wafers. It was found for junctions with oxides consisting entirely of In_2O_3 that j_c exceeded 3 KA/cm^2 and did not depend strongly on oxide thickness from about 3 nm (for thermally-grown oxides) to 4.5-7 nm (for RF-grown oxides). The addition of a thin layer of PbO_2 at the top of the barrier, either by backscattering during RF oxidation or by deposition onto a thermal oxide, caused by a substantial decrease in j_c , while the presence of PbO in the bulk of the oxide had little effect. The specific capacitance of the lower current density junctions was essentially the same for either 3- or 4.5-6 nm thick oxides and was consistent with a barrier thickness of order 2 nm. These results are interpreted as evidence that tunneling occurs through a Schottky barrier in the indium oxide at the interface with the counterelectrode. Such a barrier, which is consistent with the known behavior of In_2O_3 as a degenerately-doped semiconductor, would account for effective tunneling and capacitance thicknesses less than the physical oxide thickness. (42 refs.)

77051 Tunneling current density $j(V)$ for Pb-In-Au alloy junctions and tunnel barrier modeling. J.H.Magerlein (IBM Thomas J. Watson Res. Center, Yorktown Heights, NY, USA). *J. Appl. Phys. (USA)*, vol.54, no.5, p.2569-77 (May 1983). Tunnel barriers formed by RF oxidation of Pb-In-Au alloys and consisting largely of In_2O_3 have been studied by measuring the current density as a function of applied voltage $j(V)$ for voltages up to 1 V. The junctions studied here, which were oxidized on Pb- or photoresist-coated RF cathodes, showed no evidence of a barrier height below about 1 eV. A trapezoidal barrier with a height of at least 1 eV and a thickness equal to that of the oxide film, roughly 6 nm, would have a tunneling current far below that observed for these junctions. Furthermore, the measured $j(V)$ curves were inconsistent with those calculated for a trapezoidal barrier, even for a barrier thickness less than the physical oxide thickness. The $j(V)$ curves were, however, similar to those calculated for tunneling through a Schottky barrier in the indium oxide at the interface with the counterelectrode. Such a barrier, which is also suggested by recent measurements of oxide thickness and junction electrical properties at low voltages, might be expected to form between the metal electrodes and In_2O_3 , which can be a degenerately-doped n -type semiconductor. (33 refs.)

77052 Rate of polarization of electrons during resonant tunneling from W-EuS. R.A.Melikyan (State Univ., Erevan, USSR). *Sov. Phys.-Tech. Phys. (USA)*, vol.27, no.11, p.1422-3 (Nov. 1982). Translation of: *Zh. Tekh. Fiz. (USSR)*, vol.52, no.11, p.2308-10 (Nov. 1982). [received: May 1983] The acceleration of polarized electrons to GeV energies in ring accelerators requires a polarized electron source capable of producing electrons at 10^{11} - 10^{12} e/us with emittance 10^{-3} rad cm , and the beam polarization P should be high and the energy spread minimal. The author finds ways to increase the polarized electron current during resonant tunneling using the experimental data of Kisker et al. (1976 and 1978). The author shows that the increase in the internal barrier near the W-EuS interface may be attributed to the presence of surface ferromagnetic semiconductor states near the surface and to mirror-charge forces. (9 refs.)

77053 Si-transition metal interface formation and bulk electronic structure of 3d metal silicides. A.Francioci, D.G.O'Neill, J.H.Weaver (Synchrotron Radiation Center, Univ. of Wisconsin-Madison, Stoughton, WI, USA). Fifteenth Annual Synchrotron Radiation Users Group Conference (papers in summary form only received), Stoughton, WI, USA, 18-19 Oct. 1982 (Stoughton, WI, USA: Synchrotron Radiat. Center 1982), p.18 The authors have performed photoemission investigations of Si-Ca, Si-Ti, and Si-Cr interface formation through analysis of the interface electronic structure as a function of metal coverage on cleaved Si(111). To characterize Si-metal chemical bonding in general and to emphasize the effect of stoichiometry variations on the electronic structure, they have also conducted studies of bulk Ti, V, Cr, Co, and Ni silicides cleaved in situ. The bulk results reveal the Si- p /metal- d character of the bonding, the varying importance of the 'non-bonding' metal-derived d features, and the decoupling of Si- p and Si- s states predicted by recent calculations. Comparison of bulk silicides and the products of interface reaction show important differences both in the nonbonding d states and in the hybrid Si- p /metal- d orbitals. In all cases, interface reaction occurs after a first stage of interface formation in which the emission from intrinsic Si surface state is removed and the final value of the Schottky barrier height is reached. The fundamental parameters of the junction, therefore, are determined by microscopic reaction on a scale of 1-2 atomic layers rather than by the subsequent stages of Si-metal reaction when an interface region of complex morphology is created. (no refs.)

77054 Effects of surface layer defects and adsorbed oxygen on TiO_2 -rutile Schottky barriers. M.Levinson (Bell Labs, Murray Hill, NJ, USA). Grain Boundaries in Semiconductors. Proceedings of the Materials Research Society Annual Meeting, Boston, MA, USA, Nov. 1981 (New York, USA: North-Holland 1982), p.363-7 The electronic properties of TiO_2 surfaces are of interest to further understanding of grain boundary effects in TiO_2 and ZnO based varistor devices. Schottky barriers have been fabricated by Au or Al metallization on Nb doped TiO_2 -rutile [001] single crystal surfaces. Surface conditions included the presence or absence of either mechanical polishing induced surface defects and/or adsorbed oxygen. I-V measurements on Au samples indicate that surface defects yield ohmic behavior, but the defects may be electrically compensated by adsorbed oxygen to give non-ohmic I-V curves. All Al junctions show ohmic behavior which is interpreted in terms of reaction with surface oxygen. These results explain the necessity of firing varistor materials in an oxidizing atmosphere and suggest that the role of additives in these materials is to stabilize the oxygen concentration at the grain boundaries. (9 refs.)

Fabrication of GaAs-Mo-Si structures by metalorganic chemical vapor deposition and laser annealing See Entry 77572

73.40Q Metal-insulator-semiconductor structures (inc. semiconductor-to-insulator)

77055 Interfacial electrical properties of ion-beam sputter deposited amorphous carbon on silicon. A.A.Khan, J.A.Woolam (Dept. of Electrical Engng., Univ. of Nebraska, Lincoln, NE, USA), Y.Chung, B.Banks. *IEEE Electron Device Lett. (USA)*, vol.EDL-4, no.5, p.146-9 (May 1983). Amorphous, 'diamond-like' carbon films have been deposited on Si substrates, using ion-beam sputtering. The interfacial properties are studied for an Al/C/Si MIS system using capacitance and conductance measurements. Data are analyzed using existence theories for interfacial electrical properties. The density of electronic states at the interface along with corresponding time constants are determined, and the density of interface states is unusually low for an as yet unoptimized structure. (16 refs.)

77056 Radiation effects in nitrided oxides [MOS devices]. F.L.Terry, Jr., R.J.Aucoin, M.L.Naiman, P.W.Wyatt (Lincoln Lab., MIT, Lexington, MA, USA), S.D.Senturia. *IEEE Electron Device Lett. (USA)*, vol.EDL-4, no.6, p.191-3 (June 1983). Electron radiation effects on silicon dioxide films, before and after ammonia annealing (nitridation), have been studied. The most striking result is that the generation of radiation-induced interface states is nearly eliminated in the nitrided oxides. (8 refs.)

77057 Electron power loss in the (100) n channel of a Si metal-oxide-semiconductor field-effect transistor. I. Intrasubband phonon scattering. C.M.Krowne (Electronics Technol. Div., Naval Res. Lab., Washington, DC, USA). *J. Appl. Phys. (USA)*, vol.54, no.5, p.2441-54 (May 1983). The electron energy relaxation is studied as a function of the 'electron temperature' T_e in the n channel of a (100) surface silicon MOSFET (metal-oxide-semiconductor field-effect transistor) device by inspecting the phenomenological energy relaxation time $\tau_e(T_e)$ at 4.2K, 77K, and 300K lattice temper-

ratures. τ_i is theoretically calculated in order to determine the relative contributions of shear horizontal (SH), pressure-shear vertical (P-SV), shear vertical-pressure (SV-P), total reflection shear vertical pressure (TR), and Rayleigh (R) surface acoustic phonon modes to the electron energy relaxation at the interface. Two-dimensional electron transport is assumed and the effects of subbanding near the interface are included. Only electron scatter events within subbands are studied (intrasubband). This exhaustive study finds that surface modes do not dominate the electron energy relaxation at the Si-SiO₂ interface at $T_i=4.2\text{K}$. Some other mechanism(s) must predominate at $T_i=4.2\text{K}$. (18 refs.)

77058 Electron power loss in the (100) n channel of a Si metal-oxide-semiconductor field-effect transistor. II. Intrasubband phonon scattering. C.M.Krowne (Electronics Technol. Div., Naval Res. Lab., Washington, DC, USA).

J. Appl. Phys. (USA), vol.54, no.5, p.2455-67 (May 1983).

For pt.I see ibid., vol.54, no.5, p.2441 (1983). A simple matrix element is used to approximate electron-acoustic phonon scattering between different electron subbands i in the n channel of a (100) surface silicon MOSFET (metal-oxide-semiconductor field-effect transistor) device. This matrix element is used to determine the form of the electron power loss P_{ij} in a $i \rightarrow j$ intersubband transition. P_{10} is calculated for $T_i=4.2\text{K}$ lattice temperature and electron temperatures T_e between 4.4K and 18K when the electron inversion density $N_{\text{inv}}=(3.76-10.0)\times 10^{11}\text{cm}^{-2}$ and an acceptor density $N_A=10^{14}\text{cm}^{-3}$, and compared to Fang and Fowler's (1970) experimental data (which is put into the form of an experimental power loss P_{exp}). This is justified since the total power loss P due to intrasubband scattering as well as other P_{ij} terms besides P_{10} is small. It is found that good to excellent fits between P_{10} and P_{exp} occur by adjusting the separation Δ_{e10} between the lowest two circular subband edges. Δ_{e10} is between 5.2 and 9.4 meV, and the electron-phonon deformation coupling constant $D\approx 3.5\text{eV}$. The values of Δ_{e10} obtained in such a manner roughly agree with Stern's (1972) theoretical self-consistent results. P_{10} is very sensitive to both Δ_{e10} and to the effective mass for motion parallel to the surface m_i with the results implying that $m_i=0.19m_0$ (m_0 =free electron rest mass). If one wants to find the contribution of intersubband scattering to P at higher T_i , the formalism should still be applicable, although the approach could be much more complicated due to the addition of new P_{ij} terms coming from both higher subbands and new scattering agents such as optical modes. (22 refs.)

77059 Effect of silicon orientation and hydrogen anneal on tunneling from Si into SiO₂. Z.A.Weinberg, A.Hartstein (IBM Thomas J. Watson Res. Center, Yorktown Heights, NY, USA).

J. Appl. Phys. (USA), vol.54, no.5, p.2517-21 (May 1983).

The issue of transverse momentum conservation in tunneling is examined by photon-assisted-tunneling measurements on metal-oxide-silicon structures. Results are compared for tunneling from silicon of (100), (110), and (111) orientations. The results for (100) and (110) are almost identical. For (111) it is concluded that the interface barrier energy is higher by about 0.5 eV than for (100) samples. This difference exists only for unannealed samples and is almost eliminated by the 400°C standard forming gas (10% H₂, 90% N₂) anneal. The barrier for the (111) interface has therefore a greater sensitivity to hydrogen than for the other two orientations. The experiments and their consistency with the usual (dark) Fowler-Nordheim tunneling from silicon into SiO₂ show that transverse momentum (parallel to the interface) conservation is not observed. (12 refs.)

77060 The electrical behavior of GaAs-insulator interfaces: a discrete energy interface state model. T.E.Kazior, J.Lagowski, H.C.Gatos (MIT, Cambridge, MA, USA).

J. Appl. Phys. (USA), vol.54, no.5, p.2533-9 (May 1983).

The relationship between the electrical behavior of GaAs metal insulator semiconductor (MIS) structures and the high density discrete energy interface states (0.7 and 0.9 eV below the conduction band) was investigated utilizing photo- and thermal emission from the interface states in conjunction with capacitance measurements. It was found that all essential features of the anomalous behavior of GaAs MIS structures, such as the frequency dispersion and the C-V hysteresis, can be explained on the basis of nonequilibrium charging and discharging of the high density discrete energy interface states. (23 refs.)

77061 Metal/Insulator/Si structures with low interface state density fabricated by combined ion beam sputtering and atomic hydrogen beam treatment. M.Garrigues, R.Blanchet, C.Sibran, P.Viktorovitch (Lab. d'Electronique, Automatique et Mesures Electriques, Ecole Centrale de Lyon, Ecully, France).

J. Appl. Phys. (USA), vol.54, no.5, p.2863-5 (May 1983).

Ion beam techniques, combining insulator deposition and atomic hydrogen treatment, are used for the fabrication of metal-insulator-silicon (MIS) structures at low temperature (300°C). SiN_xO_y and AlN_xO_y insulating layers are deposited by reactively sputtering either a silicon or an aluminum target with a nitrogen ion beam. The y/x ratio is controlled by introducing pure molecular oxygen in the vicinity of the substrate. The resistivity and dielectric strength of the films increase with the y/x ratio and exceed typically $10^{16}\Omega\text{cm}$ and $2\times 10^8\text{V/cm}$, respectively. The electrical properties of the MIS devices were investigated by the capacitance/conductance method. The dramatic reduction of the interface state density (below $10^{11}\text{cm}^{-2}\text{eV}^{-1}$ with AlN_xO_y) consecutive to H treatment and annealing in nitrogen at 300°C, is interpreted on the basis of the formation, weakening, and strengthening of Si-H bonds. (6 refs.)

77062 Characterization of surface states in MOS capacitors by a modified DLTS technique. V.Kumar, S.B.Iyer (Dept. of Phys., Indian Inst. of Sci., Bangalore, India).

Phys. Status Solidi a (Germany), vol.76, no.2, p.637-40 (16 April 1983).

A modified DLTS technique for characterization of surface states in MOS structures is proposed. It involves scanning the bias while applying small filling pulses at constant temperature. The surface states behave as discrete levels when the pulses are small. Results on a Cu-SiO₂-p-Si tunnel diode are presented as example. (15 refs.)

77063 Quantized Hall and transverse resistivities in silicon MOS n -inversion layers. K.Yoshihiro, J.Kinoshita, K.Inagaki, C.Yamanouchi (Electrotech. Lab., Ibaraki, Japan), J.Moriyama, S.Kawaji, *Physica B & C (Netherlands)*, vol.117-118 B-Kwaj, pt.2, p.706-8 (March 1983). (Proceedings of the 16th International Conference on the Physics of Semiconductors, Montpellier, France, 6-10 Sept. 1982).

The results are reported of the quantized Hall and transverse resistivity measurements made on n -channel (100) inversion layers of Si-MOSFET devices at temperatures $T=1.6$ to 0.5K , magnetic fields $H=9.0$ and 10.5T for various excitation current densities. The Hall resistivity ρ_{xy} is found to be integral fractions of h/e^2 in precision better than 0.2ppm over the concentration of electrons $ieH/hc=1\times 10^{12}$ to $3\times 10^{12}/\text{cm}^2$ ($i=4, 8, 12$) at the lowest temperatures. When the transverse resistivity ρ_{xx} is finite in the Hall plateau regions, the deviation in ρ_{xy} is roughly given by $\Delta\rho_{xy}(i)=C\rho_{xx}^{\text{min}}(i)$ where

$C\approx -0.1$. This result is two orders of magnitude as large as that expected from existing theories. (15 refs.)

77064 Electrical characterization of Al-SiO₂-Si (N -type) tunnel structures. Influence of LPCVD and LPO₂ oxide growth technologies on the properties of the Si-SiO₂ interface. G.Pananakakis, G.Kamarinos, M.El-Sayed (Lab. de Phys. des Composants a Semiconducteurs ERA, CNRS, ENSERG, Grenoble, France), V.Le Goascoz.

Solid-State Electron. (GB), vol.26, no.5, p.415-26 (May 1983).

Metal-thin oxide-silicon tunnel diodes are studied. Two kinds of thin oxides (thickness $\delta < 30\text{\AA}$) are examined. The first fabricated by oxidation under low oxygen pressure (LPO₂) at $T\approx 950^\circ\text{C}$. The second fabricated by low pressure chemical vapor deposition (LPCVD) at $T\approx 880^\circ\text{C}$. The influence of thermal annealing of these devices has been studied. (I , V), $C(V, \omega)$ and $G(V, \omega)$ experimental characteristics are analysed and compared with theoretical (I , V) curves issued from a detailed and original model. Interface states energy distribution $N_{\text{SS}}(E)$, surface potential (V_s) vs. applied voltage (V_a), effective affinities (χ_n and χ_p) and oxide thickness homogeneity are deduced. The influence of pinholes is also discussed. It is worth noting the complementarity of experimental results and the theoretical (I , V) simulation. LPCVD oxides after annealing are found to be more homogeneous and provide a lower density $N_{\text{SS}}(E)$ of interface states than LPO₂ thin oxides. (37 refs.)

77065 Dark-capacitance transients in MIS tunnel diodes. W.E.Dahlke, J.A.Shimer (Sherman Fairchild Lab., Lehigh Univ., Bethlehem, PA, USA). *Solid-State Electron. (GB)*, vol.26, no.5, p.465-72 (May 1983).

Dark-capacitance transients in MIS tunnel diodes switched from accumulation to deep depletion depend on the interface state occupancy. This time dependent function is derived and its behavior described for electron emission and electron-hole pair generation with tunneling and thermally controlled occupancies. A new method of determining the tunneling relaxation time constant τ_T from the electron emission transient at low temperature is described. Measurements of MIS tunnel diodes with oxide thickness $d_{\text{ox}}=17$ to 80\AA agree with theory and the resultant values of τ_T compare with previously reported results from photocapacitance. (7 refs.)

77066 Double-injection currents and field effect in sapphire-base silicon p^+nn^+ diodes. V.S.Lysenko, R.N.Litovskii, M.M.Lokshin, M.F.Scherbakova.

Ukr. Fiz. Zh. (USSR), vol.28, no.5, p.736-41 (May 1983). In Russian.

Investigates current-voltage characteristics of double-injection currents in sapphire-base silicon diodes and estimates efficient lifetime and bipolar length of diffusion for electron-hole pairs. Transverse anisotropy of conduction is shown insignificant for double-injection currents. It is also experimentally proved possible to control double-injection currents by the field effect. Strong fields exhibit an injection break-down due to current carrier heating. (10 refs.)

Radiation effects on MOS devices: dosimetry, annealing, irradiation sequence, and sources See Entry 76506

Interface trap generation in silicon dioxide when electrons are captured by trapped holes See Entry 77016

Generation-annealing kinetics of the interface donor states at 0.25 eV above the midgap and the turn-around phenomena on oxidized silicon during avalanche electron injection See Entry 77017

Model calculations for silicon inversion layer solar cells See Entry 78009

73.40R Metal-insulator-metal structures

77067 Photoresponse characteristics of thin-film nickel-nickel oxide-nickel tunneling junctions. R.G.Marshalek (Dept. of Electrical Engng., & Computer Sci., Johns Hopkins Univ., Baltimore, MD, USA), F.M.Davidson.

IEEE J. Quantum Electron. (USA), vol.QE-19, no.4, p.743-54 (April 1983).

Photoinduced tunneling currents in thin-film Ni-NiO-Ni tunneling junctions were measured as a function of photon energy over the range $2.0\text{eV}\leq h\nu\leq 2.7\text{eV}$. The photoresponse mechanism was found to be consistent with a photon assisted tunneling mechanism. Inelastic electron-electron collisions were found to strongly influence the photoassisted tunneling currents. (53 refs.)

77068 Temperature dependence of voltage controlled negative resistance in an electroformed Cu-SiO₂-Cu structure. S.A.Y.Ali-Ismael, C.A.Hogarth (Dept. of Phys., Brunel Univ., Uxbridge, England).

Phys. Status Solidi a (Germany), vol.76, no.2, p.559-63 (16 April 1983).

Measurements of voltage-current characteristics as functions of temperature are described for electroformed thin film structures of Cu-SiO₂-Cu over the temperature range 24 to 95°C . The results are consistent with a model in which the filaments which bridge the insulator as a consequence of the forming process are essentially metallic in nature, the temperature coefficient of resistance being shown to be positive. (15 refs.)

73.60 ELECTRONIC PROPERTIES OF THIN FILMS

77069 Galvanomagnetic properties of thin inhomogeneous films. B.Ya.Balagurov.

Sov. Phys.-Solid State (USA), vol.24, no.11, p.1988-9 (Nov. 1982). Translation of: *Fiz. Tverd. Tela (USSR)*, vol.24, no.11, p.3492-4 (Nov. 1982).

[received: May 1983]

Applies the theory of an effective medium (TEM) to the galvanomagnetic properties of two-dimensional two-component media (thin films) in a transverse magnetic field H . The author finds an analytic solution of the equations by the TEM method, which has the same form as the exact solution. At a critical carrier density this solution reduces to the Dykne result (1970). The author also determines the conditions which restrict the application of the TEM method (for a sample with an arbitrary carrier density) to the problem under discussion: the first condition is that the conductivities of the two components should not differ too greatly and the second that the magnetic field H cannot exceed a certain maximum value. (5 refs.)

73.60D Metallic thin films

77070 Temperature coefficient of the resistance of chromium-copper alloy films. A.R.Patel, G.K.Shivakumar (Dept. of Phys., Sardar Patel Univ., Gujarat, India), N.C.Pandya, N.C.Chourasia.

Mater. Lett. (Netherlands), vol.1, no.5-6, p.181-3 (April 1983).

The temperature coefficient of the resistance of chromium-copper films has been measured in the thickness range 500-4900 \AA from 33 to 190°C . It is observed that the Fuchs-Sondheimer theory explains the observed thickness dependence satisfactorily. The mean free path of the conduction electrons and the TCR of an infinitely thick film have been computed as 363\AA and $2.886\times 10^{-3}\text{C}^{-1}$ respectively at 33°C . A linear variation of the reciprocal mean free path with temperature has also been established. (8 refs.)

77071 Electrical characteristics of thin Ni_2Si and NiSi_2 layers grown on silicon. E.G.Colgan, M.Maenpaa, M.Finetti, M.-A.Nicolet (California Inst. of Technol., Pasadena, CA, USA). *J. Electron. Mater.* (USA), vol.12, no.2, p.413-22 (March 1983). The authors have determined the resistivity, carrier concentration, and Hall mobility as a function of thickness (700-3000 Å) of Ni_2Si , NiSi and NiSi_2 layers formed by vacuum annealing at 270-300°C, $\approx 400^\circ\text{C}$ and $\approx 800^\circ\text{C}$, respectively, of nickel films vacuum-deposited on a silicon substrate ($\langle 111 \rangle$ n-type and $\langle 100 \rangle$ p-type Si $\rho \approx 1 \text{ K}\Omega$). The layer thicknesses were measured by 2 MeV $^4\text{He}^+$ backscattering spectrometry. The silicide phase was confirmed by X-ray measurements. The electrical measurements were carried out using the van der Pauw configuration. The electrical transport parameters are independent of the film thickness within the experimental uncertainty. The Hall factors were found to be unity. The majority carriers are electrons in NiSi and holes in Ni_2Si and NiSi_2 . (16 refs.)

73.60F Semiconductor films

77072 The density of states in DC glow discharge deposited a-Si:H from Schottky barrier diode admittance measurements. P.K.Jain, R.V.Kruzelecky, S.Zukotynski (Dept. of Electrical Engng., Univ. of Toronto, Toronto, Ontario, Canada).

Can. J. Phys. (Canada), vol.61, no.5, p.736-43 (May 1983).

An experimental and theoretical study of the admittance of a-Si:H Schottky barrier diodes versus frequency, temperature, and voltage is presented. A full numerical analysis of the admittance of the Schottky diode with an arbitrary density of states (DOS) distribution is given. It is based on a general model using an equivalent circuit of the devices. The analysis takes into account the thermal response time of gap states as well as the transport of carriers. The DOS distribution near the Fermi level is determined for diodes prepared using direct current glow discharge deposited a-Si:H. It is shown from the admittance study that the thermionic theory is appropriate to describe the transport of electrons across the junction. The occupancy of bulk states is controlled mainly by the interaction kinetics of these states with the electrons in the conduction band and not by transport of these electrons. (11 refs.)

77073 Electrical and optical properties of SnO_2 thin layers received using the method of oxidation of thermally vapoured Sn layers. A.Klos, M.Romanis, E.Zalewski.

Pr. Ośrodka Badańczo-Rozwojowego Przetwornikow Obrazu (Poland), no.2, p.29-38 (1982). In Polish.

The work includes description of electrical and optical properties of transparent, conductive SnO_2 thin layers. Thermally evaporated Sn layers were oxidized at temperature 300-350°C in the flow of oxygen under atmospheric pressure. SnO_2 layers of transmission 0.6-0.9 in the region of $\lambda = 300\text{-}360 \text{ nm}$ and resistance per square of approximately 250 Ω were obtained. (11 refs.)

77074 The effect of hydrogen on the electrical properties of n-type $\text{Pb}_{0.9}\text{Cd}_{0.1}\text{Te}$ thin films. A.L.Dawar, C.Jagadish, K.V.Ferdinand, P.Kumar, P.C.Mathur (Dept. of Phys. & Astrophys., Univ. of Delhi, Delhi, India).

J. Phys. & Chem. Solids (GB), vol.44, no.5, p.453-5 (1983).

Measurements of the Hall coefficient and the DC conductivity were made on flash evaporated n-type $\text{Pb}_{0.9}\text{Cd}_{0.1}\text{Te}$ epitaxial films exposed to molecular hydrogen gas at high pressures (up to 500 psi) in the temperature range 77-300K. It has been found that the effect of hydrogen on the films is to reduce the concentration of the extrinsic carriers and to increase their mobility. It is believed that hydrogen gas removes cadmium ions and neutral cadmium atoms from these films. (26 refs.)

77075 Photoelectric fatigue of photoresistors based on polycrystalline $\text{CdS}:\text{Cu}:\text{Cl}$ films. T.B.Torchinskaya, L.N.Baidokha, L.F.Zharovskii, M.Ya.Rakhlin.

J. Appl. Spectrosc. (USA), vol.36, no.5, p.589-95 (May 1982). Translation of: *Zh. Prikl. Spektrosk. (USSR)*, vol.36, no.5, p.821-7 (May 1982). [received: Feb. 1983]

In order to study further the phenomenon of photoelectric fatigue of polycrystalline photoresistors and to clarify its mechanism, the authors investigated the photoluminescence and excitation spectra, the photocurrent spectra at 77K, and the thermally stimulated conductivity (TSC) of photoresistors based on $\text{CdS}:\text{Cu}:\text{Cl}$ polycrystalline films in the range 4.2-400K. (22 refs.)

77076 Influence of nitrogen ion implantation on the electrical transport properties of InTe and InSe thin films. D.V.Krishna Sastry, P.Jayarama Reddy (Dept. of Phys., Sri Venkateswara Univ., Tirupati, India).

Phys. Status Solidi a (Germany), vol.76, no.1, p.345-50 (16 March 1983).

Amorphous and crystalline thin films of InTe and InSe are prepared by the discrete evaporation of the materials from a tantalum boat. Electrical conductivity and mobility are measured on these films. The films are implanted with nitrogen ions, with varying ion dosages and their electrical conductivity and mobility are measured again. The results show that the electrical conductivity and mobility are lowered on ion implantation, more so, when the ion dosage is high. This is explained in terms of the lattice damage caused by the bombardment of the energetic incident ion. The films are restored back partially to their original state by thermal annealing as observed from the conductivity and mobility data. (17 refs.)

77077 Effect of laser irradiation on the electrical properties of polycrystalline thin films of tellurium. G.P.Srivastava, K.N.Tripathi, N.K.Sengal (Dept. of Phys. & Astrophys., Univ. of Delhi, Delhi, India).

Phys. Status Solidi a (Germany), vol.76, no.2, p.K137-40 (16 April 1983). Polycrystalline thin films of tellurium have been irradiated with a pulsed Q-switched ruby laser. DC conductivity and Hall effect studies that the irradiated films have lower values of free carrier concentration and higher values of Hall mobility. (19 refs.)

Furnace annealing of ion implanted polycrystalline silicon See Entry 76473

Auger and AC impedance studies of the RF sputter deposited Fe_2O_3 films See Entry 76810

Defect states and donors in thermally annealed or post-hydrogenated chemically vapor-deposited amorphous SiN_x alloy See Entry 76897

Some properties of amorphous Si thin films and their application to sensors. I. Power sensor See Entry 76938

Electron and hole carrier mobilities for liquid phase epitaxially grown GaP in the temperature range 200-550K See Entry 76943

Effect of free carrier screening on the electron mobility of GaAs: a study by field-effect measurements See Entry 76956

Time-dependent field effect in amorphous chalcogenides See Entry 76957

Minority-carrier diffusion-length measurement and lifetime in $\text{Pb}_{0.9}\text{Sn}_{0.1}\text{Te}$ and indium-doped PbTe liquid phase epitaxy layers See Entry 76966

Transverse magnetophonon resonance in n-GaAs under pulsed high magnetic fields See Entry 76974

Low temperature persistent photoconductivity in two-dimensional electron gas FETs See Entry 77006

On the role of the correlation length near the onset of non-metallic conduction See Entry 77010

1/f noise in polycrystalline silicon resistors See Entry 77012

Angle-lapping and staining observations of Si doping superlattice structures See Entry 77025

Photoluminescent and electrical properties of InGaPAs mixed crystals liquid-phase-epitaxially grown on (100) GaAs See Entry 77432

Picosecond reflectivity measurements on glow discharge a-Si:H See Entry 77471

Growth of high quality Ge MBE film See Entry 77571

Low pressure metalorganic chemical vapor deposition on InP and related compounds See Entry 77577

MOCVD growth and characterization of high luminescence efficiency $\text{Al}_x\text{Ga}_{1-x}\text{As}$ See Entry 77583

Investigation of capless heat treatment of MBE n-GaAs See Entry 77686

Efficiency of the a-Si:H solar cell and grain size of SnO_2 transparent conductive film See Entry 77998

Realisation et caracterisation de cellules solaires $\text{Cu}_2\text{S}-\text{CdZnS}$ (Realisation and characterisation of $\text{Cu}_2\text{S}-\text{CdZnS}$ solar cells) See Entry 78013

73.60H Insulating thin films

Invalidity of the scaling property of surface potential kinetics in HDPE See Entry 77019

Interfacial electrical properties of ion-beam sputter deposited amorphous carbon on silicon See Entry 77055

Metal/Insulator/Si structures with low interface state density fabricated by combined ion beam sputtering and atomic hydrogen beam treatment See Entry 77061

73.60K Superconducting films

Preparation, physical properties, and superconductivity of $\text{La}_{1-x}\text{S}_x$ films See Entry 77085

Nonselective effect of electromagnetic radiation on a superconducting film in the resistive state See Entry 77093

Far-infrared conductivity and anomalous below-gap absorption in superconducting granular NBN See Entry 77094

Fluctuation conductivity of tin films below the superconducting transition temperature See Entry 77095

The superconductive energy gaps of thin-film AuAl_2 and AuIn_2 See Entry 77101

Switching process between bistable positions of multiquantum flux tubes in a thin-film type I superconductor See Entry 77105

74.00 SUPERCONDUCTIVITY

74.10 OCCURRENCE, CRITICAL TEMPERATURE

77078 Low-temperature transport properties of RERh_2B_4 compounds (RE=Sm, Ho, Er, Lu). W.Odoni, H.R.Ott (Lab. fur Festkorperphys., ETH-Honggerberg, Zurich, Switzerland), M.B.Maple.

J. Low Temp. Phys. (USA), vol.51, no.5-6, p.505-33 (June 1983).

The authors have measured the low-temperature electrical resistivity ρ and thermal conductivity λ of a selection of RERh_2B_4 compounds. The compound LuRh_2B_4 served as the standard material concerning superconductivity and HoRh_2B_4 as that for magnetic ordering. For ErRh_2B_4 they studied, in particular, the transition from the superconducting to the normal state with decreasing temperature. In SmRh_2B_4 both $\rho(T)$ and $\lambda(T)$ reveal the strong interaction between the magnetic moments of the Sm^{3+} ions and the conduction electrons, which is partly quenched at the transition to the antiferromagnetic state. Depending on the material considered, the thermal conductivity data are analyzed using theoretical calculations due to Bardeen et al. (1958); Kadanoff and Martin (1961); and Ambegaokar and Griffin (1964). (46 refs.)

77079 Influence of impurity scattering on the critical temperature of superconductors with a partial gap in the electron spectrum. A.M.Gabovich (Inst. of Phys., Acad. of Sci., Kiev, Ukrainian SSR), A.S.Shpigel.

J. Low Temp. Phys. (USA), vol.51, no.5-6, p.581-99 (June 1983).

The influence of the scattering potential of nonmagnetic and magnetic impurities on the critical superconducting transition temperature T_c is considered for superconductors with either a completely or partially dielectric electron spectrum. It is shown that T_c rises with increasing concentration of nonmagnetic impurities, i.e. the Anderson theorem is violated in such systems. Magnetic impurity scattering lowers T_c . However, this reduction is weakened compared to usual superconductors, due to the presence of the dielectric gap on the Fermi surface. (51 refs.)

77080 Superconductivity and magnetism in the pseudoternary system $\text{Dy}(\text{Ru}, \text{Rh}_{1-x})_2\text{B}_4$. H.C.Hamaker, M.B.Maple (Inst. for Pure & Appl. Phys. Sci., Univ. of California, San Diego, La Jolla, CA, USA).

J. Low Temp. Phys. (USA), vol.51, no.5-6, p.633-53 (June 1983).

The pseudoternary system $\text{Dy}(\text{Ru}, \text{Rh}_{1-x})_2\text{B}_4$ has been studied by means of AC magnetic susceptibility, electrical resistance, heat capacity, static magnetic susceptibility, and magnetization measurements. A low-temperature phase diagram was determined for the range of concentrations $0.1 < x \leq 1$. Superconductivity occurs for $x \leq 0.35$, with a sharp depression of the superconducting critical temperature near $x \approx 0.3$. Long-range magnetic order exists for all concentrations x ; the rhodium-rich compounds exhibit antiferromagnetism while the ruthenium-rich compounds are ferromagnetic. Pseudoternary compounds near the critical limit possibly exhibit reentrant antiferromagnetic superconductivity, a hitherto unobserved phenomenon. The competition between antiferromagnetism and ferromagnetism apparently leads to a mixed phase in a comparatively wide range of concentrations. (42 refs.)

77081 A new superconducting metal glass $\text{Mo}_{70}\text{Ge}_{20}\text{B}_{10}$. Liu Zhiyi, Zhao Zhongxian, Yang Dayu, Wang Chaoguo (Inst. of Phys., Acad. Sinica, Beijing, China).

Kexue Tongbao (Foreign Lang. Ed.) (China), vol.28, no.2, p.170-2 (Feb. 1983).

The authors use a rapid liquid quench method to prepare the amorphous transition metal-metalloid system, $\text{Mo}_{70}\text{Ge}_{20}\text{B}_{10}$. The samples were analyzed by X-ray, electron microscopy and differential thermal analysis. (9 refs.)

77082 Thermal-relaxation studies of the stability of amorphous structures in zirconium-based superconducting alloys. S.J.Poon (Dept. of Phys., Univ. of Virginia, Charlottesville, VA, USA).

Phys. Rev. B (USA), vol.27, no.9, p.5519-25 (1 May 1983).

The superconducting transition temperature T_c of amorphous $\text{Zr}_2\text{X}(\text{X}=\text{Co}, \text{Ni}, \text{Pd})$ and $\text{Zr}_3\text{X}(\text{X}=\text{Ni}, \text{Pd}, \text{Rh})$ alloys annealed isothermally below their crystallization temperatures is studied as a function of annealing time (up to ~ 20 -100 h). Upon annealing, T_c is always found to decrease below its value in the as-quenched state. The major portion of T_c depression is attributed to the relaxation of 'quenched-in' strains. Alloys of Zr_2Co , Zr_2Ni , Zr_2Pd , and Zr_3Rh which undergo polymorphous crystallization (P alloys) show trends of saturation in T_c . On the other hand, for Zr_3Ni and Zr_3Pd alloys which crystallize eutectically (E alloys), saturation in T_c is only observed at relatively low annealing temperatures over rather short intervals of annealing time. The results are attributed to the stability and instability of the 'equilibrium' amorphous structures in the P and E alloys, respectively. It is conjectured that instability in the E alloys leads to initial microscopic phase separation, the homogeneity of which is evidenced by results of transition width and flux pinning measurements. All homogeneous samples exhibit very weak flux-pinning force of about 10^4 N/m² at 1.5K. Prolonged annealing of E alloys leads to eutectic decomposition. Predictions derived from a simple 'proximity-effect' model are consistent with the present findings. (28 refs.)

77083 Critical fields of liquid superconducting metallic hydrogen. J.Jaffe, N.W.Ashcroft (Lab. of Atomic & Solid State Phys. & Materials Sci. Center, Cornell Univ., Ithaca, NY, USA).

Phys. Rev. B (USA), vol.27, no.9, p.5852-5 (1 May 1983).

Liquid metallic hydrogen, in a fully dissociated state, is predicted at certain densities to pass from dirty to clean and from type-II to type-I superconducting behavior as the temperature is lowered. (18 refs.)

77084 Superconducting properties of tellurium at high pressure. M.A.Irina (Inst. of Phys. of High Pressures, Acad. of Sci., Troitsk, USSR). *Sov. Phys.-Solid State (USA)*, vol.24, no.11, p.1954-5 (Nov. 1982). Translation of: *Fiz. Tverd. Tela (USSR)*, vol.24, no.11, p.3439-41 (Nov. 1982). [received: May 1983]

An investigation of the dependence $T_c(P)$ of tellurium revealed that in the range of pressures P from 15.0 to 30.0 GPa the value of T_c changed from 3K to 6.5 \pm 0.6K. The results reported indicated that, beginning from $P\sim 8.6$ GPa, the superconducting transition temperature T_c of tellurium measured at a given pressure, depended strongly on the initial carrier density. (15 refs.)

77085 Preparation, physical properties, and superconductivity of $\text{La}_{2-x}\text{S}_4$ films. L.V.Mel'nikova, D.P.Moisev, V.M.Postnikov (Inst. of Phys., Acad. of Sci., Kiev, Ukrainian SSR).

Sov. Phys.-Solid State (USA), vol.24, no.11, p.1985-6 (Nov. 1982). Translation of: *Fiz. Tverd. Tela (USSR)*, vol.24, no.11, p.3487-9 (Nov. 1982). [received: May 1983]

The evaporated layer deposition of $\text{La}_{2-x}\text{S}_4$ superconducting films is described. The optical absorption and the film structure are studied with electron diffraction. The films exhibited a superconducting transition at 6K. (10 refs.)

77086 Increasing the critical properties of superconducting molybdenum sulfides by hydrogen absorption. N.E.Alekseievskii, A.V.Mitin (Inst. of Phys. Problems, Acad. of Sci., Moscow, USSR).

Sov. Tech. Phys. Lett. (USA), vol.8, no.9, p.443-4 (Sept. 1982). Translation of: *Pisma v Zh. Tekh. Fiz. (USSR)*, vol.8, no.17-18, p.1029-32 (Sept. 1982). [received: May 1983]

Molybdenum sulfides of the composition $\text{A}_x\text{Mo}_{6-y}\text{S}_8$ ($\text{A}=\text{Pb}, \text{Sn}, \dots$) are among the most promising superconductors for applications. Some of them ($\text{Pb}_x\text{Mo}_{6-y}\text{S}_8$, for example) exhibit in addition to record high values of the second critical field, $H_{c2}(4.2\text{K})\approx 500$ kOe—high critical temperatures, $T_c\approx 14$ -15K, and high critical current densities, $J_c(T=1.7\text{K}, H=100$ kOe) $\approx 5\cdot 10^4$ A/m². The authors report data on the effect of hydrogen on the properties of ternary and multicomponent sulfides of molybdenum. The critical properties and the temperature dependence of the resistivity $\rho(T)$ were measured for bulk samples in the form of hollow cylinders with an outside diameter of 5 mm, an inside diameter of 2 mm, and a length of 16-18 mm. The values of J_c were determined by a contactless method, from the difference between the magnetic fields inside and outside the sample. Curves of the transition to the superconducting state were recorded by the standard four-contact potentiometer method from the change in the resistance. (7 refs.)

Anomalous linewidths of the crystal electric field excitations in $\text{La}_{0.997}\text{Tm}_{0.003}\text{Al}_2$ below the superconducting transition See Entry 76907

Equations of superconductivity for transition metals in the Wannier representation See Entry 77087

A new semiempirical formula for superconducting transition temperatures of metals and alloys See Entry 77088

Diamagnetic shielding magnetization in the intermediate state of the organic superconductor ditetramethyltetraselenafulvalenium perchlorate $(\text{TMTSF})_2\text{ClO}_4$ See Entry 77090

Specific heat jump for superconducting virtual bound state alloys See Entry 77091

Effect of a magnetic field on the specific heat jump of a superconducting alloy containing paramagnetic impurities with local states within the gap See Entry 77096

The superconductive energy gaps of thin-film AuAl_2 and AuIn_2 See Entry 77101

Specific heat discontinuity of a proximity-effect sandwich system containing Kondo impurities See Entry 77104

Multiple tunneling in granular three-dimensional $\text{BaPb}_{1-x}\text{Bi}_x\text{O}_3$ See Entry 77111

Superconducting properties and flux pinning in liquid quenched Nb-Ga alloys See Entry 77115

74.20 THEORY

77087 Equations of superconductivity for transition metals in the Wannier representation. G.M.Vujcic, A.L.Kuzemskii, N.M.Plakida (Joint Inst. for Nuclear Res., Dubna, USSR).

Theor. & Math. Phys. (USA), vol.53, no.1, p.1035-40 (Oct. 1982). Translation of: *Theor. & Mat. Fiz. (USSR)*, vol.53, no.1, p.138-45 (Oct. 1982).

In the Wannier representation, a system of equations for superconductivity is obtained for strongly bound electrons in a transition metal, which is described by the Hubbard Hamiltonian. The electron-phonon interaction is written down using the rigid-ion model. A closed system of equations is obtained when the renormalization of the vertex in the mass operator is ignored. (28 refs.)

On theory of the statistical generating functional for the order parameter. III. Effective action formalism for the order parameter See Entry 74366

74.20F BCS theory and its applications

77088 A new semiempirical formula for superconducting transition temperatures of metals and alloys. M.Surma (Inst. of Phys., A. Mickiewicz Univ., Poznan, Poland).

Phys. Status Solidi b (Germany), vol.116, no.2, p.465-74 (1 April 1983).

A new formula describing the superconducting transition temperature is presented. The electron-phonon coupling constant λ and the phonon frequency spectrum parameters of a material are the quantities which define the transition temperature T_c of superconductors. A comparison between the experimental and calculated values of T_c for metals and alloys confirms the validity of the new formula. (25 refs.)

74.30 GENERAL PROPERTIES

77089 Some remarks about surface effects in magnetic superconductors. M.Fusco Girard, F.Mancini (Istituto di Fisica, Univ. di Salerno, Salerno, Italy).

Phys. Lett. A (Netherlands), vol.95A, no.8, p.447-50 (23 May 1983).

A new choice for the boson transformation function is employed for the study of the electromagnetic-field distributions at the interface of vacuum with a magnetic superconductor. The relation with previous approaches is discussed. (8 refs.)

Model calculations of local electron and phonon densities of states in bimetallic superlattices See Entry 76827

74.30C Magnetization curves, Meissner effect, penetration depth

77090 Diamagnetic shielding magnetization in the intermediate state of the organic superconductor ditetramethyltetraselenafulvalenium perchlorate $(\text{TMTSF})_2\text{ClO}_4$. H.Schwenk, K.Andres (Walter-Meissner-Inst. fur Tieftemperaturforschung, Bayerischen Akad. der Wissenschaften, Garching, Germany), F.Wudl.

Phys. Rev. B (USA), vol.27, no.9, p.5846-7 (1 May 1983).

A systematic study of the dependence of both the diamagnetic shielding and Meissner signals on the temperature T_0 , from which they were thermally quenched, reveals that volume superconductivity can almost be eliminated if T_0 is higher than about 27K. (12 refs.)

Superconductivity and magnetism in the pseudoternary system $\text{Dy}(\text{Ru}, \text{Rh}_{1-x})\text{B}_4$ See Entry 77080

Lifetimes of superheated and supercooled phases in tin on transition from a normal to a superconducting state and vice versa See Entry 77113

Mixed states in ferromagnetic superconductors See Entry 77116

Theory of the upper critical field in layered superconductors with magnetic intercalates See Entry 77117

74.30E Thermodynamic properties; thermal conductivity

77091 Specific heat jump for superconducting virtual bound state alloys. Y.Okabe, A.D.S.Nagi (Univ. of Waterloo, Waterloo, Ontario, Canada).

Solid State Commun. (USA), vol.46, no.8, p.639-41 (May 1983).

Using the Anderson model in the non-magnetic limit, the authors have calculated the jump in specific heat at T_c (ΔC), for superconducting virtual bound state alloys. It is found that the normalized (ΔC) vs. normalized T_c curves deviate considerably from the BCS value. A more significant result of the present study is that the initial slope of such a curve has a maximum value of 3.638. It is the highest value reported in literature for the impurity problem and is much larger than obtained even in a large pair breaking situation like the Kondo effect (2.481). (10 refs.)

Low-temperature transport properties of RERh_4B_4 compounds ($\text{RE}=\text{Sm}, \text{Ho}, \text{Er}, \text{Lu}$) See Entry 77078

Effect of a magnetic field on the specific heat jump of a superconducting alloy containing paramagnetic impurities with local states within the gap See Entry 77096

Thermoelectric effects in a superconducting bimetallic loop: superconductors in relative motion: comment on a paper by Ginzburg, Zharkov and Sobyanin See Entry 77103

Specific heat discontinuity of a proximity-effect sandwich system containing Kondo impurities See Entry 77104

74.30G Response to electromagnetic fields, nuclear magnetic resonance, ultrasonic attenuation

77092 Longitudinal ultrasonic attenuation in normal and superconducting lead at low temperatures. S.Sathish, K.Samudravajaya, B.K.Basu (Tata Inst. of Fundamental Res., Bombay, India).

J. Low Temp. Phys. (USA), vol.51, no.3-4, p.423-32 (May 1983).

The authors have measured longitudinal ultrasonic attenuation along the $[110]$ direction in normal and superconducting states in two single crystals of lead, one made from high-purity lead and the other made with high-purity lead doped with 0.1 at.% gold. In both specimens an amplitude-dependent effect in the superconducting state has been observed. The data have been taken in the frequency range from 12 to 108 MHz. In high-purity lead the amplitude-independent ratio α_s/α_n shows the frequency dependence observed

by Randorff and Marshall (1970) whereas in the doped specimen this ratio shows a very small spread with frequency. In both specimens deformation does not change the α_s/α_n ratio appreciably. (10 refs.)

77093 Nonselective effect of electromagnetic radiation on a superconducting film in the resistive state. E.M.Gershenzon, M.E.Gershenzon, G.N.Gol'tsman, A.D.Semenov, A.V.Sergeev (V.I. Lenin Moscow Pedagogical Inst., Inst. of Radio Engng. & Electronics, Acad. of Sci., Moscow, USSR). *JETP Lett. (USA)*, vol.26, no.7, p.296-9 (5 Oct. 1982). Translation of: *Pis'ma v Zh. Eksp. & Teor. Fiz. (USSR)*, vol.36, no.7, p.244-7 (5 Oct. 1982). [received: May 1983]

The quasiparticle-heating effect of electromagnetic radiation on a niobium superconducting film in the resistive state is nonselective over a broad frequency range, from 10^{10} to 10^{13} Hz. The role played by electron-electron collisions in shaping the nonequilibrium quasiparticle distribution function is discussed. (4 refs.)

77094 Far-infrared conductivity and anomalous below-gap absorption in superconducting granular NbN. D.R.Karecki, G.L.Carr, S.Perkowitz (Phys. Dept., Emory Univ., Atlanta, GA, USA), D.U.Gubser, S.A.Wolf. *Phys. Rev. B (USA)*, vol.27, no.9, p.5460-6 (1 May 1983).

The far-infrared ($100\text{--}1000\text{ cm}^{-1}$) complex conductivity of superconducting granular NbN films has been determined from reflection and transmission data. Moderately granular films, with $R_{\square}=150$ and $200\ \Omega/\square$, followed Leplae-modified Bardeen-Cooper-Schrieffer theory predictions with no absorption below the gap frequency ω_g . The derived values of $2\Delta/kT_c$ were 3.8 and 4.0, slightly below the results for homogeneous films. Highly granular films, with $R_{\square}\geq 500\ \Omega/\square$, displayed DC resistive tails and evidence of Josephson coupling. The real part of the far-infrared conductivity was BCS-type for frequencies above ω_g but showed an anomalous absorption below ω_g . This excess absorption may arise from two-dimensional fluctuations in the form of vortices or from normal conducting regions mixed in with the superconducting grains. (25 refs.)

Nature of dislocation hysteresis losses and nonlinear effect in lead at high vibration amplitudes See Entry 76449

74.40 FLUCTUATIONS AND CRITICAL EFFECTS

77095 Fluctuation conductivity of tin films below the superconducting transition temperature. R.S.Parashar, P.N.Dheer (Dept. of Phys. & Astrophys., Univ. of Delhi, Delhi, India).

J. Low Temp. Phys. (USA), vol.51, no.3-4, p.249-55 (May 1983). Measurements have been carried out of the temperature dependence of the fluctuation-induced excess electrical conductivity of thin (thickness much less than the Ginzburg-Landau coherence length) superconducting films of tin below the transition temperature. Two types of specimen were investigated: (a) films deposited on a glass substrate held at 300K and (b) films deposited on a glass substrate at 300 K and then covered by a protective layer of germanium. Special care was taken to ensure sample homogeneity. Analysis of the results shows that the fluctuation parameter, ϵ_0 , is not affected by the germanium layer. Its value is, however, much larger than that predicted by the theory of Kajimura (1971) et al. (17 refs.)

77096 Effect of a magnetic field on the specific heat jump of a superconducting alloy containing paramagnetic impurities with local states within the gap. B.Sihota, A.D.S.Nagi (Univ. of Waterloo, Waterloo, Ontario, Canada). *J. Low Temp. Phys. (USA)*, vol.51, no.3-4, p.347-68 (May 1983).

The effect of a uniform magnetic field on the specific heat jump $\Delta\tilde{C}$ of a superconductor containing paramagnetic impurities has been investigated. The impurities are described by the Shiba-Rusinov model. Taking the normalized position of the bound state within the BCS gap $\epsilon_0=0.8$ and 0.0 and the parameter $\alpha(=\langle S_z^2 \rangle/S^2)=1.0$ and $1/3$ as typical values, the authors find the detailed dependence of $\Delta\tilde{C}$ on the impurity concentration \tilde{c} and the transition temperature T_c . In some cases $\Delta\tilde{C}$ diverges at certain values of \tilde{c} or T_c signaling a change of the normal-superconductor phase transition from second order to first order. (25 refs.)

77097 Quantum fluctuations in quasi-one-dimensional superconductors. H.J.Schulz (Inst. Laue-Langevin, Grenoble, France), C.Bourbonnais. *Phys. Rev. B (USA)*, vol.27, no.9, p.5856-9 (1 May 1983).

A model for the low-temperature properties of quasi-one-dimensional superconductors, including quantum effects is investigated. Both long-range Coulomb effects and scattering by nonmagnetic impurities enhance quantum effects. For strong quantum fluctuations the transition from a fluctuating to a long-range-ordered superconducting state obeys Bardeen-Cooper-Schrieffer-like thermodynamic relations. Application to the tetramethyltetraselenafulvalene-X (TMTSF)_x class of compounds is discussed. The authors' results also apply to other quasi-one-dimensional systems. (23 refs.)

Far-infrared conductivity and anomalous below-gap absorption in superconducting granular NbN See Entry 77094

74.50 PROXIMITY EFFECTS, TUNNELLING PHENOMENA, AND JOSEPHSON EFFECT

77098 Dynamics of accelerated Josephson junctions. P.Russer (Lehrstuhl für Hochfrequenztech., Tech. Univ. München, München, Germany). *Arch. Elektron. & Übertragungstechnik. (Germany)*, vol.37, no.5-6, p.153-9 (May-June 1983).

The generally covariant sine-Gordon equation for arbitrarily shaped large-area Josephson junctions is established. The dynamics of rotating ring-shaped Josephson junctions is investigated. It is shown that solitons have a tendency to conserve their motion with respect to the inertial frame of reference. Possible applications for inertial rotation sensing are discussed. (20 refs.)

77099 Niobium thin-film point-contact Josephson junction. S.Naito, Y.Higashino, M.Ibuka (Yokogawa Electric Works, Tokyo, Japan). *J. Appl. Phys. (USA)*, vol.54, no.5, p.2866-8 (May 1983).

A stable, niobium thin-film point-contact Josephson junction can be fabricated using RF magnetron sputtering and electron beam lithography. Constant-voltage steps based on a AC Josephson effect are observed up to a voltage level of 4 mV at 4.2K when a 9-GHz microwave signal is applied. This voltage level is the highest for any thin-film weak link except for the tunnel junction. (13 refs.)

77100 Odd and even subharmonics and chaos in RF SQUIDS. R.K.Ritala (Res. Inst. for Theoretical Phys., Univ. of Helsinki, Helsinki, Finland), M.M.Salomaa. *J. Phys. C (GB)*, vol.16, no.14, p.L477-84 (20 May 1983).

The authors discuss multistable RF SQUIDS under weak damping, driven by an external flux applied at resonance frequency. Rich subharmonic spectra and several bands of chaotic behaviour are found as functions of the amplitude of the drive. In addition to period-doubling Feigenbaum sequences, they

also encounter an odd subharmonic route to the phase-unlocked regime. The principal chaotic band displays new intrinsic structure, which arises due to an abrupt symmetry break from an orbit with period-5 character to one resembling a period-2 orbit. However, at higher amplitudes of the drive, the symmetry becomes continuously restored. (23 refs.)

77101 The superconductive energy gaps of thin-film AuAl₂ and AuIn₂. D.Van Vechten, L.B.Holdeman, R.J.Soulen, Jr., J.Toots (Center for Absolute Phys. Quantities, NBS, Washington, DC, USA).

J. Low Temp. Phys. (USA), vol.51, no.3-4, p.329-46 (May 1983). Thin films of the intermetallic compounds AuAl₂ and AuIn₂ were prepared and used as electrodes in AuAl₂/oxide/Al, Al/oxide/AuIn₂ or AuAl₂/oxide/AuIn₂ tunnel junctions. The tunnel barriers were produced by RF sputter oxidation. The temperature dependence of the energy gaps of the AuAl₂ and AuIn₂ films was measured and found to agree well with BCS theory. (13 refs.)

77102 High-frequency impedance of superconducting tunnel junctions. D.G.Jablonski (Naval Surface Weapons Center, Silver Spring, MD, USA).

J. Low Temp. Phys. (USA), vol.51, no.3-4, p.433-51 (May 1983). Comparison is made between the high-frequency impedance of a Josephson tunnel junction predicted by the RSJ model and that predicted by the Werthamer theory (1966). Results obtained analytically, numerically, and by electronic simulation illustrate several fundamental differences between the two models. In particular, the small-signal RF resistance of a tunnel junction described by the Werthamer theory exhibits strong variations with temperature and frequency. In addition, the Werthamer theory predicts that a tunnel junction will have a plasma-like resonance in the absence of any electrode capacitance; and that the junction can have a nonzero reactance when current-biased outside of a constant-voltage step. (19 refs.)

77103 Thermoelectric effects in a superconducting bimetallic loop: superconductors in relative motion: comment on a paper by Ginzburg, Zharkov and Sobyenin. G.R.Pickett (Dept. of Phys., Univ. of Lancaster, Lancaster, England).

J. Low Temp. Phys. (USA), vol.51, no.5-6, p.561-8 (June 1983). For paper see V.L. Ginzburg et al., *ibid.*, vol.47, p.427 (1982). The problem of the response of a bimetallic superconducting loop to a normal thermoelectrically generated quasiparticle current in one arm is considered from the point of view of superfluids in relative motion. The recent conclusions of Ginzburg et al. are shown to be invalid. (5 refs.)

77104 Specific heat discontinuity of a proximity-effect sandwich system containing Kondo impurities. S.Yoksan (Dept. of Phys., Srinakharinwirot Univ., Bangkok, Thailand).

J. Low Temp. Phys. (USA), vol.51, no.5-6, p.569-79 (June 1983). The theoretical work of Matsuura et al. (1977) on the Kondo effect in superconductors and McMillan's (1968) tunneling model are applied to a proximity-effect sandwich system containing Kondo impurities. Analytic expressions for the renormalized Green's functions of superconducting and normal-metal electrons are given as functions of the system composition. It is found that as the thicknesses become large, the specific heat discontinuity changes continuously from the Muller-Hartmann-Zittartz (1971) value for the magnetic cases to the Ichinose (1977) value for the nonmagnetic ones. For small values of the layer thickness, and with the films in proximity, the results can be used to calculate the specific heat jump at the transition temperature numerically. (14 refs.)

77105 Switching process between bistable positions of multiquantum flux tubes in a thin-film type I superconductor. J.Parisi, R.P.Huebener, B.Muhlemaier (Phys. Inst. II, Univ. Tübingen, Tübingen, Germany).

J. Low Temp. Phys. (USA), vol.51, no.5-6, p.655-77 (June 1983). A superconducting memory device based on a bistable vortex position represents an interesting storage medium for future Josephson computers. In order to study the operational mode of such a single-flux quantum-memory cell, the authors use a model system multiquantum flux tubes in a thin-film type I superconductor (Pb). By employing high-resolution stroboscopic magnetooptical flux detection, they are able to globally visualize both spatial and temporal behavior of rapidly switching individual flux tubes. All experimental results agree reasonably well with theoretical model considerations of the energy balance during the elementary switching process. (38 refs.)

77106 Tunneling of current carriers in niobium nitride junctions. G.P.Motulevich, D.R.Dzhuraev, E.A.Antonova, V.A.Sukhov (P.N. Lebedev Phys. Inst., Acad. of Sci., Moscow, USSR)

JETP Lett. (USA), vol.36, no.9, p.381-4 (5 Nov. 1982). Translation of: *Pis'ma v Zh. Eksp. & Teor. Fiz. (USSR)*, vol.36, no.9, p.313-16 (5 Nov. 1982). [received: June 1983]

The characteristics $\sigma_c(V)$ and $d\sigma_c(V)/dV$, where σ_c is the even part of the conductivity of a tunnel junction, are investigated for NbN-I-Pb and NbN-I-Ag(I) (I is an Nb oxide) junctions in the voltage range $V-(\Delta_{\text{NbN}}+\Delta_{\text{Pb}})/e=0-30$ meV and $V-\Delta_{\text{NbN}}/e=0-31$ meV, respectively (Δ_{NbN} and Δ_{Pb} are the superconducting energy gaps). The positions of peaks in the electron-phonon interaction (EPI) function are determined in the energy range 0-26 meV. (6 refs.)

77107 Macroscopic quantum tunnelling effects. G.Schon. *Phys. Bl. (Germany)*, vol.39, no.5, p.124-5 (May 1983). In German.

Considers possible quantum mechanical tunnelling in macroscopic systems, where infinite tunnelling times would result. Possible environmental damping is mentioned and reference is made to a Josephson Tunnel Contact which would consist of two superconductors, separated by an oxide layer. The superconductivity current, based on Cooper Pair tunnelling, is compared with normal particle current and displacement current, a barrier potential diagram is shown and masking by noise effects is predicted. (5 refs.) *G.M.E.*

77108 Fluxon propagation and Fiske steps in long Josephson tunnel junctions. S.N.Erne, A.Ferrigno (Phys. Tech. Bundesanstalt, Inst. Berlin, Berlin, Germany), R.D.Parmentier.

Phys. Rev. B (USA), vol.27, no.9, p.5440-6 (1 May 1983).

The dynamical behavior of fluxons propagating in the presence of an applied magnetic field on an overlap-geometry Josephson tunnel junction of length $5\lambda_J$ having a McCumber $\beta_c=5\pi$ is studied by numerical integration of the circuit equations of a 50-section lumped RSJ-type (resistive shunted junction) model. Resonant propagating configurations corresponding to the first and third Fiske steps are found. The fundamental frequencies and power levels of the radiation emitted from one end when the junction is biased on the first and third Fiske steps and on the first zero-field step are comparable, but a magnetic field renders the power spectra at the two ends of the junction different. (18 refs.)

77109 Free vortex-antivortex states in hollow cylindrical Josephson tunnel junction. M.Kuwada, Y.Onodera, Y.Sawada (Res. Inst. of Electrical Communication, Tohoku Univ., Sendai, Japan).

Phys. Rev. B (USA), vol.27, no.9, p.5486-90 (1 May 1983). With the use of a hollow cylindrical Nb-Nb₂-Sn Josephson tunneling junction, dynamic vortex motion was studied by the flux-flow voltage across the junction. The junction voltage versus applied axial magnetic field characteristics

in the presence of the axial trapped flux in the junction showed the first evidence for the free vortex and antivortex trains moving in opposite directions and passing through each other. (10 refs.)

77110 Role of pinning in microbridges made from superconductors with A15 lattice. A.N.Lykov (P.N. Lebedev Phys. Inst., Acad. of Sci., Moscow, USSR).

Sov. Phys.-Solid State (USA), vol.24, no.11, p.1905-9 (Nov. 1982). Translation of: *Fiz. Tverd. Tela (USSR)*, vol.24, no.11, p.3353-60 (Nov. 1982). [received: May 1983]

The pinning effect is used as the basis for analyzing of bridge contacts made from superconductors with the A15 lattice. The occurrence, in microbridges of this type, of phenomena characteristic of Josephson contacts is explained. The temperature dependence of the critical field is also accounted for. Current-voltage characteristics of the bridges in autonomous operation are calculated. Good agreement between the calculated and observed characteristics is found. The theoretical model proposed is applicable to broad microbridges made from any type II superconductors. (18 refs.)

77111 Multiple tunneling in granular three-dimensional $\text{BaPb}_{1-x}\text{Bi}_x\text{O}_3$. N.A.Belous, A.M.Gabovich, I.V.Lezhenko, D.P.Moisev, V.M.Postnikov, S.K.Uvarova (Inst. of Phys., Acad. of Sci., Kiev, Ukrainian SSR).

Sov. Tech. Phys. Lett. (USA), vol.8, no.9, p.463-4 (Sept. 1982). Translation of: *Pis'ma v Zh. Tekh. Fiz. (USSR)*, vol.8, no.17-18, p.1075-8 (Sept. 1982). [received: May 1983]

The authors studied the voltage-current characteristics of samples to the superconducting ceramic $\text{BaPb}_{0.75}\text{Bi}_{0.25}\text{O}_3$, which undergoes a diffuse transition to the superconducting state, and the effect of a microwave field on these characteristics. Samples with dimensions of $5 \times 2 \times 1$ mm and a critical temperature $T_c \approx 10\text{K}$, corresponding to the beginning of the transition, were held at $T = T_c + 4.2\text{K}$ and connected in a current-source circuit. The width of the transition was 2K . (14 refs.)

Effects of energy dependence in the electronic density of states on some superconducting properties See Entry 76826

Voltage-current characteristics of a regular system of weakly coupled superconducting particles See Entry 77112

Theory of the upper critical field in layered superconductors with magnetic intercalates See Entry 77117

74.55 TYPE-I SUPERCONDUCTIVITY

77112 Voltage-current characteristics of a regular system of weakly coupled superconducting particles. V.N.Bogomolov, V.V.Zhuravlev, A.I.Zadorozhnyi, E.V.Kolla, Yu.A.Kumzerov (A.F. Ioffe Physicotech. Inst., Acad. of Sci., Leningrad, USSR).

JETP Lett. (USA), vol.36, no.8, p.365-7 (20 Oct. 1982). Translation of: *Pis'ma v Zh. Eksp. & Teor. Fiz. (USSR)*, vol.36, no.8, p.298-300 (20 Oct. 1982). [received: June 1983]

The voltage-current characteristic of a regular system of identical, weakly coupled superconducting particles has been studied for a sample covered by a metal film. Near T_c , an inverse hysteresis is found, i.e. the current corresponding to the return to the superconducting state is higher than the critical current for the disruption of superconductivity. When samples with clean surfaces are used as both source and detector, they influence each other; i.e. there is a stimulation of superconductivity. (5 refs.)

77113 Lifetimes of superheated and supercooled phases in tin on transition from a normal to a superconducting state and vice versa. G.V.Ermakov, N.L.Sorokin (Div. of Physicotech. Problems in Energetics, Acad. of Sci., Sverdlovsk, USSR).

Sov. Phys.-Solid State (USA), vol.24, no.12, p.2086-9 (Dec. 1983). Translation of: *Fiz. Tverd. Tela (USSR)*, vol.24, no.12, p.3663-9 (Dec. 1983).

A method was developed for measuring the lifetimes of metastable phases appearing in the course of a transition from a normal metal to a type I superconductor. Three tin samples differing in respect of the structure and the cleanliness of the surface finish were investigated. The metastable states (superheating or supercooling) were obtained by a rapid change of the magnetic field intensity at a given temperature. A frequency meter was used to determine the time from the moment of establishment of a field to the transition of a sample to a more stable state, which was deduced from the Meissner-Ochsenfeld effect. The experimental results indicated that the lifetime varied randomly from one experiment to another. There was some deviation from the exponential distribution law. Measurements were made of the average lifetime of superheated and supercooled phases as a function of the magnetic field intensity at temperatures 3.6, 3.2, and 2.8K. The dependence on the magnetic field was nonmonotonic, there was a limit to superheating in a superconducting state corresponding to zero lifetime, but there was no such limit in the case of supercooling. The maximum superheating fields found from the Ginzburg-Landau theory were in good agreement with the experimental results. The theoretical values of the maximum supercooling fields were in the region of one of the minima of the investigated dependence. (28 refs.)

74.60 TYPE-II SUPERCONDUCTIVITY

77114 Scaling law in voltage-current characteristics of hard superconductors. I.Hlasnik, S.Takacs (Electrotech. Inst., Slovak Acad. of Sci., Bratislava, Czechoslovakia).

Cryogenics (GB), vol.23, no.6, p.314-16 (June 1983).

From scaling laws for pinning the authors have suggested scaling laws for voltage-current characteristics of type II superconductors. After linearization of J_c dependence on magnetic field B , temperature T and stress ϵ , they lead to exponential dependence of the voltage E on these parameters. In order to obtain general scaling laws, then the temperature, field and stress dependence of the denominator J_0 in $E = E_0 \exp \{ (J - J_0)/J_0 \}$ should also be determined. The generalization of the instability criterion leads to the conclusion that the prestrain of the superconducting material can enhance or deteriorate the stability of the winding. (22 refs.)

77115 Superconducting properties and flux pinning in liquid quenched Nb-Ga alloys. G.B.Clemente, F.Habbal, J.Bevik (Gordon McKay Lab., Harvard Univ., Cambridge, MA, USA).

Rapidly Solidified Amorphous and Crystalline Alloys. Proceedings of the Materials Research Society Annual Meeting, Boston, MA, USA, Nov. 1981 (New York, USA: North-Holland 1982), p.381-6

$\text{Nb}_{75}\text{-Ga}_{25}$ tapes were prepared by liquid quenching technique in an argon atmosphere. The transition temperature T_c , upper critical field H_{c2} and critical current density J_c were measured in both as-quenched and annealed samples. The values of T_c ranged from 16.5 to 18.0K in the as-quenched samples and increased upon annealing up to 20.0K. Similar increase was also observed in the values of H_{c2} from ~ 190 kOe to values higher than the attainable

field of 220 kOe. For annealed samples near stoichiometric composition, H_{c2} was estimated to be higher than 300 kOe. The critical current densities of these tapes are relatively low compared to other melt-quenched A-15 compounds. Flux pinning force, F_p , does not obey a single scaling law. The existence of two peaks in F_p at low temperatures and of only one peak at 13.4K for $1 \leq x \leq 4$ is discussed in terms of the microstructural characteristics of the samples. (5 refs.)

74.60E Mixed state, H_{c2} , surface sheath

77116 Mixed states in ferromagnetic superconductors. T.Koyama, S.Mae-kawa, M.Tachiki (Res. Inst. for Iron, Steel & Other Metals, Tohoku Univ., Sendai, Japan).

J. Phys. Soc. Jpn. (Japan), vol.52, no.5, p.1750-8 (May 1983).

The magnetization process in the mixed state of ferromagnetic superconductors is theoretically studied. By taking into account the electromagnetic and the s-f exchange interactions between conduction electrons and localized magnetic moments, the Ginzburg-Landau free energy is obtained. The polarization of localized magnetic moments depresses the stability of mixed state and causes a convex curvature in the magnetization versus magnetic field curve near the upper critical field H_{c2} above the ferromagnetic transition temperature. This curvature becomes larger with decreasing temperature, and the magnetization jump occurs at low temperatures. The characteristic features of the magnetization process are in good agreement with those experimentally obtained by Crabtree et al. in single crystals of ErRh_4B_4 .

77117 Theory of the upper critical field in layered superconductors with magnetic intercalates. R.A.Klemm (Exxon Res. & Engng. Co., Linden, NJ, USA).

Solid State Commun. (USA), vol.46, no.9, p.705-8 (June 1983).

The author proposes a model for the layered superconductors with electronically isolated magnetic intercalates in which the electrons propagate freely in the dirty superconducting layers with arbitrarily strong spin-orbit scattering, and spin-flip scatter of the magnetic ions during interlayer tunneling. He calculates the upper critical field H_{c2} including demagnetization effects. In a parallel field below the dimensional-crossover temperature T^* , a new type of spin ordering is predicted. (5 refs.)

Superconductivity and magnetism in the pseudoternary system $\text{Dy}(\text{Ru}, \text{Rh}_{1-x})_2\text{B}_4$ See Entry 77080

Increasing the critical properties of superconducting molybdenum sulfides by hydrogen absorption See Entry 77086

Far-infrared conductivity and anomalous below-gap absorption in superconducting granular NbN See Entry 77094

Role of pinning in microbridges made from superconductors with A15 lattice See Entry 77110

74.60G Flux pinning; fluxon-defect interactions

77118 Low-temperature—irradiation study of flux-line pinning in type-II superconductors. H.R.Kerchner, D.K.Christen, C.E.Klabunde, S.T.Sekula, R.R.Coltman, Jr. (Solid State Div., Oak Ridge Nat. Lab., Oak Ridge, TN, USA).

Phys. Rev. B (USA), vol.27, no.9, p.5467-78 (1 May 1983).

Annealed wires of Nb and Nb-20 at.% Ta were irradiated at liquid-helium temperature in two different modes. In one mode thermal neutrons produced 75% of the damage, while in the other mode fast neutrons produced 85% of the damage. The increase in critical current with fluence was measured in order to determine its dependence on pin type and density and material purity. Damage due to the fast-neutron component of the flux dominated the flux pinning in both modes. The observations were consistent with the collective statistical summation theory and inconsistent with the conventional single-particle theory. The elementary pinning interaction deduced from the data by using the collective statistical theory agreed well with a recent theoretical calculation of the interaction due to the electron scattering mechanism. (18 refs.)

Thermal-relaxation studies of the stability of amorphous structures in zirconium-based superconducting alloys See Entry 77082

Fluxon propagation and Fiske steps in long Josephson tunnel junctions See Entry 77108

Free vortex-antivortex states in hollow cylindrical Josephson tunnel junction See Entry 77109

74.60J Critical currents

77119 Effect of stainless steel reinforcement on the critical current versus strain characteristic of multifilamentary Nb_3Sn superconductors. J.W.Ekin (Electromagnetic Technol. Div., NBS, Boulder, CO, USA), R.Flukiger, W.Specking.

J. Appl. Phys. (USA), vol.54, no.5, p.2869-71 (May 1983).

A series of multifilamentary Nb_3Sn superconductors were fabricated containing from 0% to 52 vol.% stainless steel reinforcement strands as an integral part of the conductor. Critical current versus strain measurements are reported which show that the stainless steel introduces a relatively large compressive prestrain, ϵ_m , into the superconductor, ranging from $\epsilon_m \approx 0.3\%$ for no stainless steel reinforcement to $\epsilon_m = 0.84\%$ for 52 vol.% stainless steel. Accompanying this high compressive prestrain in the reinforced conductors is a large degradation of the conductor's critical current, I_c . The I_c degradation relative to the strain-free value has been measured, for example, to be more than 50% at 13 T for $\epsilon_m = 0.64\%$. Several methods are discussed for reducing the large I_c degradation in A15 superconductors containing internal reinforcement. (11 refs.)

Increasing the critical properties of superconducting molybdenum sulfides by hydrogen absorption See Entry 77086

Role of pinning in microbridges made from superconductors with A15 lattice See Entry 77110

Low-temperature—irradiation study of flux-line pinning in type-II superconductors See Entry 77118

74.70 SUPERCONDUCTING MATERIALS

Superconducting properties of tellurium at high pressure See Entry 77084

Specific heat and NMR spin echo in the superconducting and magnetic region of the Y_2Co_3 compound See Entry 77284

74.70D Material effects on T_c , K , critical currents

(see also 81.40R Electrical properties related to materials treatment)

Switching process between bistable positions of multiquantum flux tubes in a thin-film type I superconductorSee Entry 77105

74.70G Type-I superconductors (non transition metals)

Longitudinal ultrasonic attenuation in normal and superconducting lead at low temperaturesSee Entry 77092

Fluctuation conductivity of tin films below the superconducting transition temperatureSee Entry 77095

Voltage-current characteristics of a regular system of weakly coupled superconducting particlesSee Entry 77112

Lifetimes of superheated and supercooled phases in tin on transition from a normal to a superconducting state and vice versaSee Entry 77113

74.70L Type-II superconductors (transition metals, alloys and compounds)Anomalous linewidths of the crystal electric field excitations in $\text{La}_{0.997}\text{Tm}_{0.003}\text{Al}_2$ below the superconducting transitionSee Entry 76907Low-temperature transport properties of RERh_2B_4 compounds (RE=Sm, Ho, Er, Lu)See Entry 77078Superconductivity and magnetism in the pseudoternary system $\text{Dy}(\text{Ru}_{1-x}\text{Rh}_{1-x})\text{B}_4$ See Entry 77080A new superconducting metal glass $\text{Mo}_{70}\text{Ge}_{20}\text{B}_{10}$ See Entry 77081

Thermal-relaxation studies of the stability of amorphous structures in zirconium-based superconducting alloysSee Entry 77082

Preparation, physical properties, and superconductivity of $\text{La}_{3-x}\text{S}_4$ filmsSee Entry 77085

Increasing the critical properties of superconducting molybdenum sulfides by hydrogen absorptionSee Entry 77086

Diamagnetic shielding magnetization in the intermediate state of the organic superconductor dimerethylenetetrakiselenafulvalenium perchlorate ($\text{TMTSF}_2\text{ClO}_4$)See Entry 77090

Nonselective effect of electromagnetic radiation on a superconducting film in the resistive stateSee Entry 77093

Far-infrared conductivity and anomalous below-gap absorption in superconducting granular NbNSee Entry 77094

Multiple tunneling in granular three-dimensional $\text{BaPb}_{1-x}\text{Bi}_x\text{O}_3$ See Entry 77111

Superconducting properties and flux pinning in liquid quenched Nb-Ga alloysSee Entry 77115

Theory of the upper critical field in layered superconductors with magnetic intercalatesSee Entry 77117

Low-temperature—irradiation study of flux-line pinning in type-II superconductorsSee Entry 77118

Effect of stainless steel reinforcement on the critical current versus strain characteristic of multifilamentary Nb_3Sn superconductorsSee Entry 77119Specific heat and NMR spin echo in the superconducting and magnetic region of the Y_4Co_3 compoundSee Entry 77284**74.70N Dirty superconductors**

Theory of the upper critical field in layered superconductors with magnetic intercalatesSee Entry 77117

75.00 MAGNETIC PROPERTIES AND MATERIALS

(see also 81.40R Magnetic properties related to materials treatment; for galvanomagnetic effects, see 72.15G and 72.20M; for magneto-optical effects, see 78.20L)

75.10 GENERAL THEORY AND MODELS OF MAGNETIC ORDERING

(see also 05.50 Ising problems, 71.25 Nonlocalized single-particle electronic states, 71.70 Level splitting and interactions)

77120 Symmetry analysis of magnetic structures and spin-waves on the basis of a stabilizer concept. Yu.A.Izyumov, O.V.Gurin (Inst. of Metal. Phys., Ural Sci. Center, Sverdlovsk, USSR).

J. Magn. & Magn. Mater. (Netherlands), vol.36, no.3, p.226-36 (April 1983). The common scheme for the group theory analysis of a crystal magnetic structure and a spin wave spectrum is developed. This scheme is based on the representation theory of a crystal space group G (for magnetic structure analysis) and on the co-representation theory of the Shubnikov group M of a magnetically ordered crystal (for spin wave analysis). Unlike the standard calculation, the procedure proposed is based on the conception of the stabilizer, the symmetry group of single atoms, and this considerably simplified the calculation work, reducing it to the work with the elements of the stabilizer and with the representatives of the expansion of the G or M groups with respect to the group of the stabilizer. It is enough to calculate the components of the basic functions only at one atom, as for the other atoms they may be found by the action of the representatives. For the symmetrization of the spin wave Hamiltonian matrix, a new mathematical procedure is used: the expansion of group G over the double coset classes. It lets one easily find the symmetric relations between the different matrix elements. The method is illustrated in the example of the complicated magnetic structure of a garnet, $\text{Dy}_3\text{Al}_2\text{O}_{12}$. The advantages of the new method are especially obvious in the case of structures with a great number of magnetic atoms in a primitive cell. (18 refs.)

Discontinuities of the order parameter in system of mutually interacting single-level particlesSee Entry 77191

75.10D Crystal-field theory and spin Hamiltonians

Exchange interactions between dimers of chromium(III). A cluster approachSee Entry 77169

75.10H Ising and other classical spin models**77121** Monte Carlo simulation of the antiferromagnetic Ising model on the triangular lattice with the first and second neighbour interactions. S.Fujiki, K.Shutoh (Dept. of Appl. Phys., Tohoku Univ., Sendai, Japan), Y.Abe, S.Katsura.

J. Phys. Soc. Jpn. (Japan), vol.52, no.5, p.1531-40 (May 1983). Monte Carlo simulations of the Ising model on the triangular lattice with the antiferromagnetic J and the ferromagnetic nnn interaction J' are carried out. Several physical quantities (magnetizations, energies, susceptibilities, specific heats of sublattices and of the total system) are calculated. A phase which resembles the partially disordered phase proposed by Mekata is observed in the finite temperature region. But it is shown in this region that the sublattice magnetizations vanish at the thermodynamic limit and the Kosterlitz-Thouless phase transition is predicted by the finite size analysis.

77122 Monte Carlo study of a triangular Ising lattice. I. K.Wada (Dept. of Phys., Hokkaido Univ., Sapporo, Japan), T.Ishikawa.

J. Phys. Soc. Jpn. (Japan), vol.52, no.5, p.1774-80 (May 1983). Monte Carlo calculations have been used to study the spin ordering on a triangular Ising lattice with antiferromagnetic nearest neighbor and ferromagnetic next nearest neighbor couplings. It is suggested that a partially disordered antiferromagnetic phase does not occur stably because the sublattices interchange their roles among them due to lattice symmetry.

77123 Free energy of the random Ising model in terms of the magnetizations of sites. T.Morita (Dept. of Engng. Sci., Tohoku Univ., Sendai, Japan). *Physica A (Netherlands)*, vol.119A, no.1-2, p.143-52 (April 1983). The free energy in the pair approximation of the cluster variation method is given in terms of the magnetizations of sites for the random Ising model. For a number of samples of the random-bond Ising model with nearest-neighbour interactions of $+J$ and $-J$, on the square lattice, search is made of the configuration which gives the lowest free energy. It is concluded that the spin-glass state is the state which gives the lowest free energy in the pair approximation for certain values of temperature and probabilities of J and $-J$. (20 refs.)**77124** The linear Ising magnet in a strong time-dependent field. III. Transverse fields rotating at the frequencies $\omega_{\pm 1} = \omega_0 \pm \omega_r$. G.O.Berim, A.R.Kessel (Kazan Phys.-Tech. Inst., Acad. of Sci., Kazan, USSR).

Physica A (Netherlands), vol.119A, no.1-2, p.153-8 (April 1983). For p.t.II see *ibid.*, vol.117A, p.603 (1983). The dynamics of the linear Ising model in the presence of transverse magnetic fields rotating at resonance frequencies not coinciding with the Zeeman frequency is studied. In the resonance approximation the expressions for some time-dependent spin averages are obtained. The property of total destruction of short-range order in the Ising spin-system by a time-dependent field is established. (9 refs.)

77125 Low-temperature renormalization-group study of the random-field model. Mau-chung Chang, E.Abrahams (Serin Phys. Lab., Rutgers Univ., Piscataway, NJ, USA).

Phys. Rev. B (USA), vol.27, no.9, p.5570-5 (1 May 1983). The continuous-spin random-field model is investigated by means of the low-temperature renormalization-group technique with the use of the replica trick. The Wilson-Kogut recursion method is applied. For short-range exchange, the results are in exact agreement with those of the random-axis model studied by Pelcovits. For long-range exchange varying with distance R as $R^{-(d+\alpha)}$, critical exponents are calculated to first order in $d-2\alpha$. They are identical to those in a $d-\sigma$ expansion of the nonrandom model. However, the hyperscaling law becomes $(d+\lambda_T)\nu=2-\alpha$ (λ_T is the eigenvalue associated with the dangerous irrelevant operator T), and, for m -component spins, $-\lambda_T=\sigma+(d-2\alpha)/m$. (18 refs.)

77126 Self-similarity and fractal dimension of the devil's staircase in the one-dimensional Ising model. R.Bruinsma (IBM Thomas J. Watson Res. Center, Yorktown Heights, NY, USA), P.Bak.

Phys. Rev. B (USA), vol.27, no.9, p.5824-5 (1 May 1983). The one-dimensional Ising model with long-range antiferromagnetic interaction in an applied field is known to exhibit a complete devil's staircase in its $T=0$ phase diagram. In this Comment the authors discuss its self-similar properties and determine the fractal dimension. (4 refs.)

Phase transitions for the Ising model on the closed Cayley treeSee Entry 74401

Bond percolation on the square lattice: anisotropic systemsSee Entry 74402

Comment on 'Canonical-ensemble results for the Ising model with random bonds in two dimensions'See Entry 74405

Reply to 'Comment on "Canonical-ensemble results for the Ising model with random bonds in two dimensions"'See Entry 74406

Renormalization groups for two- and three-dimensional kinetic Ising modelsSee Entry 74407

Random-field effect in diluted Ising antiferromagnetsSee Entry 77196

Ising model with magnetic field and the Diophantine moment problemSee Entry 77198

75.10J Heisenberg and other quantized localized spin models**77127** Limit states and potentials of planar Heisenberg dynamics with transverse magnetic field. E.V.Gusev (K.E. Tsiolkovskii Inst. of Aviation Technol., Moscow, USSR).

Theor. & Math. Phys. (USA), vol.53, no.1, p.1018-28 (Oct. 1982). Translation of: *Theor. & Math. Fiz. (USSR)*, vol.53, no.1, p.114-28 (Oct. 1982). It is shown that under the influence of the dynamics determined by the potential of the planar Heisenberg model with transverse magnetic field an initial potential reduces to a first integral of the model and an initial state to a KMS state with respect to a first integral. (11 refs.)

Low-temperature expansion of spin Green's functions and Dyson-Maleev formalismSee Entry 77200

75.10L Band and itinerant models

77128 Magnetic susceptibility of the extended Hubbard model in one-dimensional complexes. S.T.Chui (Bartol Res. Foundation of the Franklin Inst., Univ. of Delaware, Newark, DL, USA). *Solid State Commun. (USA)*, vol.46, no.8, p.657-9 (May 1983). The magnetic susceptibility of a 1-D electron gas with on site and nearest neighbor Coulomb repulsions (U, V) is discussed in terms of antiferromagnetic chain with effective exchange J . For band fillings $\rho \leq 1/4$ $J \sim 4t^4/U^2$; for band fillings $\rho \geq 1/4$ $J \sim 2t^2/U$. This is substantiated by numerical calculations for finite chains with parameters estimated by Hubbard for TCNQ. The author finds that the effective J increases by a factor of ten at $\rho \sim 1/4$ for the TCNQ complexes. (14 refs.)

Influence of long-range order on magnon energy in itinerant electron ferromagnetic alloys See Entry 77165

An itinerant-electron theory of Invar effects See Entry 77234

Magnetovolume effects in the local-band theory of ferromagnetism: pressure dependence of T_c in iron and nickel See Entry 77235

Magnetovolume effects in the Moriya-Kawabata theory of very weak itinerant ferromagnetism See Entry 77236

Electron-phonon interaction model for the relation between magnetic and elastic properties in itinerant electron ferromagnets See Entry 77237

Elastic anomaly in an itinerant-electron antiferromagnet See Entry 77245

75.20 DIAMAGNETISM AND PARAMAGNETISM

Crystal structure and magnetic susceptibility of RCuSn system See Entry 76362

75.20C Nonmetals

77129 Determination of the diamagnetic susceptibility and the electron static polarizability of crystals from X-ray diffraction data. G.A.Ivanov-Smolenskiy, V.G.Tsirel'son, R.P.Ozerov (Mendeleev Inst. of Chem. Technol., Moscow, USSR). *Acta Crystallogr. Sect. A (Denmark)*, vol.A39, pt.3, p.411-15 (1 May 1983).

The relationships associating the structure amplitudes, measured in a diffraction experiment, with the diamagnetic susceptibility and the static electron polarizability of ions for crystals with the NaCl-type structure are obtained. The calculations, carried out for a number of alkali halides and alkaline-earth oxides, have shown a good coincidence with the results of magnetic and optical measurements. The accuracy of the obtained results is analyzed; it is shown that when using accurate diffraction data the diamagnetic susceptibility and the electron polarizability may be determined with an accuracy of about 1%. (26 refs.)

77130 Characteristics of the magnetic susceptibility of films consisting of mixed-valence compounds. M.Sh.Erukhimov (L.V. Kirenski Inst. of Phys., Acad. of Sci., Krasnoyarsk, USSR). *Sov. Phys.-Solid State (USA)*, vol.24, no.11, p.1984-5 (Nov. 1982). Translation of: *Fiz. Tverd. Tela (USSR)*, vol.24, no.11, p.3485-7 (Nov. 1982). [received: May 1983]

The authors calculate the magnetic susceptibility of mixed-valence films employing the simplest model of noninteracting size-quantized systems of conduction electrons and d ions. (3 refs.)

77131 Spin susceptibility of electrons and magnetic hyperfine interactions in a conductor with resonance levels. V.O.Sokolov. *Sov. Phys.-Solid State (USA)*, vol.24, no.11, p.2002-3 (Nov. 1982). Translation of: *Fiz. Tverd. Tela (USSR)*, vol.24, no.11, p.3511-12 (Nov. 1982). [received: May 1983]

Defects in some semiconductors form local levels which are in resonance with conduction electrons, i.e. which lie within the conduction band. The presence of such defects can alter significantly their structure, which in turn affects a number of properties of a crystal containing these defects, including the hyperfine interactions of nuclei. The author considers the spin susceptibility of electrons within the framework of a model employed earlier (1982) and also the influence of defects on the magnetic hyperfine interactions. (4 refs.)

X-ray, crystal data, magnetic susceptibility and electrical conductivity of hydrated trinitric pentasulphide See Entry 76375

Crystalline structure and magnetic properties of the low temperature variation of β -TiFeBr₃ See Entry 76393

Electron transport and magnetic properties of some mixed-valent alkalithiocuprates See Entry 76919

Ternary mixed valence oxygen deficient K₂NiF₄ type copper oxides. Progressive evolution of a semiconducting state from a semimetallic state in La_{2-x}Sr_xCuO_{4-x/2-s} See Entry 76945

Parametric amplification of sound and magnetoacoustic echo in concentrated rare-earth paramagnets of the Van Vleck type See Entry 77009

Influence of Mn ion substitution by Fe on the electrical and magnetic properties of an La_{0.6}Po_{0.4}MnO₃ crystal See Entry 77159

High-pressure growth of polycrystalline molybdenum disulphide See Entry 77591

75.20E Metals and alloys

77132 Magnetic and electrical properties of CrGe and Cr₁₁Ge₈. T.Sato, M.Sakata (Dept. of Instrumentation Engng., Keio Univ., Kanagawa, Japan). *J. Phys. Soc. Jpn. (Japan)*, vol.52, no.5, p.1807-13 (May 1983).

The magnetic susceptibility χ and the electrical resistivity ρ of CrGe and Cr₁₁Ge₈ are investigated at temperatures above 4.2K. The magnetic susceptibility of CrGe exhibits a cusp at about 45K and shows the T^2 dependence with positive coefficient at low temperatures. This behavior of CrGe, together with the behavior of ρ , is explained by the paramagnon theory for a nearly ferromagnetic metal. The reciprocal of χ of Cr₁₁Ge₈ deviates from the Curie-Weiss type relation at low temperatures, and ρ of Cr₁₁Ge₈ shows tendency of saturation at high temperatures. These behaviors of Cr₁₁Ge₈ are explained by the SCR theory for a nearly ferromagnetic metal. The magnetic and electrical properties of CrGe and Cr₁₁Ge₈ indicate that the natures of electron correlations of these compounds locate in the intermediate region between the Pauli paramagnet Cr₅Ge₃ and the ferromagnet Cr₁₁Ge₉. (19 refs.)

77133 Theory of magnetic susceptibility of mixed-valent Ce_{0.76}La_{0.14}Th_{0.1}. J.C.Mohanty, P.K.Misra (Dept. of Phys., Berhampur Univ., Orissa, India). *J. Phys. C (GB)*, vol.16, no.14, p.2779-85 (20 May 1983).

The authors derive an expression for the magnetic susceptibility (χ) of a mixed-valent system in which there is a continuous valence transition to a nearly integral valent phase, taking into account the crystal electric field (CEF) splitting of the localised levels. As an example, they calculate χ of Ce_{0.76}La_{0.14}Th_{0.1} in which CEF excitations have been observed for the first time in a mixed-valent system. There is a good agreement with experimental results. (19 refs.)

77134 Iron above the Curie temperature. D.M.Edwards (Dept. of Math., Imperial Coll., London, England).

J. Magn. & Magn. Mater. (Netherlands), vol.36, no.3, p.213-16 (April 1983). A quantitative discussion is given of recent paramagnetic diffuse neutron scattering data on BCC Fe above T_c . It is found that although the spatial spin correlation function has a weak tail of fairly long range the correlation between nearest neighbour spin directions is very small at 1.24 T_c . It is concluded that the data are inconsistent with the giant short-range order hypothesis of Prange and Korenman (1979), Capellmann (1979) and Sokolov (1975) and another interpretation is given. (14 refs.)

77135 Magnetic susceptibility and electrical resistivity of electrotransport purified scandium single crystals from ≈ 1 to 300K. R.J.Stierman, K.A.Gschneidner, T.-W.E.Tsang, F.A.Schmidt, P.Klavins, R.N.Shelton, J.Queen, S.Legvold (Ames Lab., Iowa State Univ., Ames, IA, USA).

J. Magn. & Magn. Mater. (Netherlands), vol.36, no.3, p.249-54 (April 1983). The magnetic susceptibility of electrotransport purified Sc single crystals was measured from 0.7 to 295K. Both the easy (χ_a) and hard (χ_c) directions were measured using a microcomputer controlled Faraday apparatus. Above 50K the present results agree with earlier work on a less pure sample, but below 50K the present results are lower by as much as 4%. In addition the maximum at ≈ 30 K and the minimum at ≈ 6 K are much more pronounced in the purer material, and the susceptibility increases rapidly as the temperature approaches 0K. Electrical resistivity measurements were made on the same single crystals from 1.6 to 300K. The resistance ratios were 365 for the a -axis crystal and 274 for the c -axis crystal. At 300K, $\rho_a = 2.5 \rho_c$. (17 refs.)

Magnetic field dependence of the electronic specific heat of TiBe₂: an estimate from magnetization data See Entry 76663

Study of the critical behaviour of the magnetization and electrical resistivity in cubic La(Fe, Si)₁₃ compounds See Entry 77155

Localization effect in CrRh alloys See Entry 77172

Magnetization and Mossbauer studies of Y(Fe,Rh)₂ See Entry 77208

Specific heat and NMR spin echo in the superconducting and magnetic region of the Y₆Co₃ compound See Entry 77284

Positron annihilation on pure and carbon-doped α -iron in thermal equilibrium See Entry 77477

75.20H Local moment in dilute alloys; Kondo effect

(see also 72.15Q Electronic conduction)

77136 Kondo effect in disordered two-dimensional systems. F.J.Ohkawa, H.Fukuyama, K.Yosida (Inst. for Solid State Phys., Univ. of Tokyo, Tokyo, Japan).

J. Phys. Soc. Jpn. (Japan), vol.52, no.5, p.1701-9 (May 1983). Interplay between localization and the Kondo effect has been examined for a model two-dimensional system. Various physical quantities associated with localized spins are calculated perturbatively in terms of the exchange coupling constant J and $\lambda = \hbar/2\pi\epsilon_F\tau_0$ where ϵ_F is the Fermi energy and τ_0 is the relaxation time of plane wave states; the susceptibility and the conductivity are shown to have quantum corrections proportional to $\lambda^2 \ln^2(t)$ and $\lambda^2 J^2/t$, respectively, where $t = \hbar/2\pi\tau_0 kT$. It is discussed that the ground states of localized spins are qualitatively the same as in pure systems because the ensemble average of local densities of states defined by $\langle \rho(\epsilon_1, r) \rho(\epsilon_2, r) \dots \rho(\epsilon_n, r) \rangle$ appears to be non zero for any n in the limit of equal energies, $\epsilon_1 = \epsilon_2 = \dots$.

77137 Magnetic-nonmagnetic transition in Ti-Mn alloys. A.S.Shcherbakov, N.V.Volkenshtein, E.G.Valiulin, N.Y.Permiyakov (Inst. of the Phys. of Metals, Acad. of Sci., Ural Sci. Center, USSR).

JETP Lett. (USA), vol.36, no.9, p.390-3 (5 Nov. 1982). Translation of: *Pis'ma v Zh. Eksp. & Teor. Fiz. (USSR)*, vol.36, no.9, p.320-2 (5 Nov. 1982). [received: June 1983]

As the concentration of the magnetic component (Mn) in titanium is increased, the average magnetic moment of the impurity ions decreases, vanishing at ~ 10 at.% Mn. The concentration dependence of the magnetic moment is found. (5 refs.)

77138 Bethe-Ansatz solution of the Anderson model of a magnetic impurity with orbital degeneracy. P.Schlottmann (Inst. fur Festkörperforschung, KFA Julich, Julich, Germany).

Phys. Rev. Lett. (USA), vol.50, no.21, p.1697-700 (23 May 1983). A model for Ce impurities is considered, consisting of the $4f^0$ singlet and a multiplet of total angular momentum j of the $4f^1$ configuration hybridized with conduction states of the metal ($U \rightarrow \infty$ limit of Anderson's model). The model is solved by a Bethe Ansatz and exact expressions for ground-state properties, e.g. valence, spin and charge susceptibilities, and resistivity, are given. (23 refs.)

Magnetic impurities in semiconductors See Entry 76879

On local density of states in Anderson localized systems See Entry 76898

Theory of magnetic susceptibility of mixed-valent Ce_{0.76}La_{0.14}Th_{0.1} See Entry 77133

Fermi-liquid approach to a description of localized magnetic moments in transition metals See Entry 77148

Cluster X_α approach to magnetic interactions and phase transitions in solids See Entry 77173

75.25 SPIN ARRANGEMENTS IN MAGNETICALLY ORDERED MATERIALS (NEUTRON STUDIES, ETC)

77139 Study of frustration effects in two-dimensional triangular lattice antiferromagnets—neutron powder diffraction study of VX₂, X=Cl, Br and I. K.Hirakawa, H.Kadowaki, K.Ubukoshi (Inst. for Solid State Phys., Univ. of Tokyo, Tokyo, Japan).

J. Phys. Soc. Jpn. (Japan), vol.52, no.5, p.1814-24 (May 1983). In order to study the frustration effects, the authors have taken powder diffraction patterns of VX₂ (X=Cl, Br and I) which are thought to be

quasi-two-dimensional triangular lattice antiferromagnets. The spins in VCl_2 , VBr_2 and VI_2 were found to order at 36.0, 29.5 and 16.3 K respectively forming a three sublattice structure in the basal plane. Contrary to expectation, a partially ordered model gives a better fit to the observed diffraction rather than the Neel state with 120° structure though the spins are of Heisenberg symmetry. In VCl_2 and VBr_2 , strong diffuse scattering can be observed not only at $T > T_N$ but also at $T < T_N$. No critical scattering characteristic for 2D could be seen but the temperature variation of sublattice magnetization is rather close to that for the Ising system.

77140 Magnetisation density distribution in $\text{Mn}_{1/4}\text{TaS}_2$: observation of conduction electron spin polarisation. S.S.P.Parkin, E.A.Marseglia (Cavendish Lab., Cambridge Univ., Cambridge, England), P.J.Brown. *J. Phys. C (GB)*, vol.16, no.14, p.2749-64 (20 May 1983).

The authors have determined the magnetisation density distribution in the ferromagnetic layered compound $\text{Mn}_{1/4}\text{TaS}_2$, using the classical polarised neutron technique. These studies show that although the magnetisation is principally localised on the manganese sites, there is a significant spin polarisation of the conduction electrons, extending throughout the unit cell. These measurements thus provide direct evidence of an important interaction between the Ta conduction electrons and the localised moments on the Mn ions, confirming previous speculations based on transport and optical data. Moreover such an interaction suggests an obvious mechanism, the RKKY interaction, for the exchange interaction between the Mn moments. The moment on the Mn sites is depressed, as a result of this interaction, by about 15% compared with that expected for a Mn^{2+} d^5 ion. The Mn ions are surrounded by an antiferromagnetically polarised cloud of electrons and the maximum spin density within the TaS_2 layer is about 3% of the maximum spin density on the Mn site. There is no evidence from these experiments that the S atoms play a role in the magnetic Mn-Mn exchange interactions. (39 refs.)

77141 Magnetic structure of $\text{Co}_{1/3}\text{NbS}_2$ and $\text{Co}_{1/3}\text{TaS}_2$. S.S.P.Parkin, E.A.Marseglia (Cavendish Lab., Cambridge, Univ., Cambridge, England), P.J.Brown.

J. Phys. C (GB), vol.16, no.14, p.2765-78 (20 May 1983). The authors have examined the magnetic structures of the antiferromagnetic layered compounds $\text{Co}_{1/3}\text{NbS}_2$ and $\text{Co}_{1/3}\text{TaS}_2$ using single-crystal neutron photographic and counting methods. The magnetic structure of $\text{Co}_{1/3}\text{NbS}_2$ has been determined in detail, and has an orthorhombic unit cell, containing two Co atoms, arranged on the 'hexagonal ordering of the first kind' scheme. The different symmetries of the crystallographic and magnetic unit cells leads to a complicated domain structure. A large part of the magnetisation in this material is localised on the Co atoms, although the magnetic moment of the Co^{2+} ion is $\sim 10\%$ lower than that of the corresponding spin-only moment. The magnetic structure of the related material, $\text{Co}_{1/3}\text{TaS}_2$, which has the same crystal structure as $\text{Co}_{1/3}\text{NbS}_2$, is very different, and is a triangular antiferromagnetic structure although for this material only the unit cell has been determined. (27 refs.)

77142 Rare earth single-ion anisotropy and the magnetic structures of the RTiO_3 perovskites: $\text{R}=\text{Tb}$, Dy , Ho , Er and Tm . C.W.Turner, J.E.Greedan (Inst. for Materials Res., McMaster Univ., Hamilton, Ontario, Canada). *J. Magn. & Magn. Mater. (Netherlands)*, vol.36, no.3, p.242-8 (April 1983). Attention is drawn to common features in the magnetic structures of the isostructural RMO_3 phases where $\text{R}=\text{Tb}$, Dy , Ho , Er and Tm and $\text{M}=\text{Al}$, Ti , Cr , Fe and Co . The orientation of the rare earth magnetic moment with respect to the orthorhombic c -axis depends only on R. For $\text{R}=\text{Er}$ and Tm the moments are parallel to the c -axis while for $\text{R}=\text{Tb}$, Dy and Ho they lie in the a - b plane. The in-plane moments are canted with respect to the a and b axes with both ferromagnetic and antiferromagnetic components and the canting angles are constant for a given R independent of M. Using symmetry arguments the authors show that the above systematics can be understood in terms of the rare earth single-ion anisotropy. Detailed calculations incorporating a crystal field of C_2 symmetry determined for Er^{3+} in YAlO_3 and an isotropic molecular field of magnitude appropriate to the RTiO_3 compounds produce results in agreement with the experimental observations. Essentially the same results are obtained for the crystal field of D_{4h} symmetry. The $B_0^0 O_0^0$ term in the crystal field Hamiltonian is identified as the factor which determines the orientation of the rare earth moment. (29 refs.)

77143 Canted ferromagnetism in PdMn and PdMnFe alloys. A.Kettshau, J.Boysen, W.D.Brewer (Inst. für Atom und Festkörperphys., Freie Univ. Berlin, Berlin, Germany), I.A.Campbell. *J. Magn. & Magn. Mater. (Netherlands)*, vol.37, no.1, p.L1-6 (May 1983). From nuclear orientation measurements on Pd 3% Mn and Pd 5% Mn 0.35% Fe the authors find that at low temperatures the alloys behave as canted ferromagnets. They can estimate the probability distribution for the individual spin orientations and can observe the reduction in canting in strong applied fields. In the PdMnFe sample the Fe spins are much more highly aligned than the Mn spins. (13 refs.)

77144 Helimagnetism in alloys on the MnAs base. I.F.Gribanov, E.A.Zavadskii (Donetsk Phys.-Tech. Inst., Acad. of Sci., Donetsk, USSR). *J. Magn. & Magn. Mater. (Netherlands)*, vol.37, no.1, p.51-7 (May 1983). Magnetic interactions in pseudobinary alloys on the MnAs base are analyzed using the group theoretical Bertaut method (1968). It is shown that side by side with isotropic exchange the exchange through conduction electrons plays an important part in formation of helimagnetic structure observed. Magnetic behaviour of crystals studied under pressure is discussed. Origin of canted ordering under lattice compression is grounded. (24 refs.)

77145 Antiferromagnetism of the FeNb and FeTa mu-phases. M.S.Ahmed, G.C.Hallam, D.A.Read (Dept. of Phys., Univ. of Leeds, Leeds, England). *J. Magn. & Magn. Mater. (Netherlands)*, vol.37, no.1, p.101-9 (May 1983). The magnetic structure of the antiferromagnetic FeNb and FeTa alloys has been investigated using a variety of techniques including susceptibility, Mossbauer and neutron diffraction measurements. The results indicate a simple structure in which alternate Kagome layers of Fe atoms have their moments oriented in opposite directions, approximately perpendicular to the plane of the layers. Positive Weiss temperatures confirm that the dominant nearest neighbour intra-layer interactions are ferromagnetic. Specific heat and low angle neutron scattering observations suggest extensive short-range order above T_N . The substantial non-magnetic contribution to the Mossbauer spectra is shown to result from $\approx 25\%$ occupation of the high-coordination 'A' sites by Fe atoms with a similar proportion of the low-coordination B2 Kagome sites occupied by Nb. A structural neutron super lattice line too weak to have been observed in earlier work using X-rays suggests that the true μ -phase unit cell may be three times larger in dimensions than previously envisaged. (6 refs.)

77146 A binary ferromagnetic alloy with magnetic moments dependent on local environment. II. Neutron magnetic elastic scattering and hyperfine field distribution. A.V.Zaborov (Dept. of Phys., Ural Polytech. Inst., Sverdlovsk, USSR), M.V.Medvedev.

Phys. Status Solidi b (Germany), vol.116, no.2, p.511-23 (1 April 1983). For Pt I see *ibid.*, vol.116, p.227 (1983). The neutron magnetic elastic scattering and the hyperfine field distribution are calculated for a collinear ferromagnetic alloy with magnetic moments which depend on their local chemical environment in a step-like manner (Jaccarino-Walker model, 1965). The question is analyzed how, using experimental data, one can discern the model under study from a binary magnetic alloy with competitive nearest-neighbour exchange interactions and permanent magnetic moments. In the framework of the Jaccarino-Walker model the concentration dependences of the spontaneous magnetization and Curie temperatures for Ni and Co alloys with elements of the Pt as well as Pd group are considered. (20 refs.)

77147 Neutron diffraction effects of the distorted structure of Ni-67.7 at.% Fe alloy in the magnetic ordered state. S.F.Dubinin, S.G.Teplovchov, S.K.Sidorov (Inst. of Metal Phys., Ural Sci. Centre, Acad. of Sci., Sverdlovsk, USSR).

Physica B & C (Netherlands), vol.119 B+C, no.1-2, p.57-60 (April 1983). (Proceedings of the International Symposium on Magnetoelasticity in Transition Metals and Alloys, Nagoya, Japan, 15-16 Sept. 1982). In a wide temperature range the neutron diffraction patterns of the single crystal Ni-67.7 at.% Fe have been analysed in which long-range ferro- and antiferromagnetic orders are formed in the state with the distorted lattice. Curie and Neel temperatures in this alloy have been estimated to be at the same time the points of the structural transformations indicating additional distortion of the crystal during the transition to the magnetic ordered state. The Invar effect of the Fe-Ni alloy is determined by the magnitude of these distortions. (8 refs.)

Specific heats of $\text{Lu}_6\text{Mn}_{23}$, $\text{Gd}_6\text{Mn}_{23}$, $\text{Dy}_6\text{Mn}_{23}$, and $\text{Er}_6\text{Mn}_{23}$ from 1.7-18K See Entry 77179

Low-temperature scaling for systems with random fields and anisotropies See Entry 77188

Magnetoelastic properties of PrAg See Entry 77229

75.30 MAGNETICALLY ORDERED MATERIALS, OTHER INTRINSIC PROPERTIES

(for critical point effects, see 75.40)

The variation of magnetic properties of Fe-based amorphous alloys along the ribbon length See Entry 77221

75.30C Saturation moments and magnetic susceptibility

77148 Fermi-liquid approach to a description of localized magnetic moments in transition metals. V.N.Gitsovich, A.S.Kondrat'ev, V.M.Uzdin (A.A. Zhdanov State Univ., Leningrad, USSR). *Fiz. Met. & Metalloved. (USSR)*, vol.55, no.4, p.649-54 (April 1983). In Russian. English translation in: *Phys. Met. & Metallogr. (GB)*.

The method of quantum Green functions is used to derive equations in the periodic Anderson model allowing for the correlation interaction between electrons. These relationships correspond to the Fermi-liquid approximation for the description of the electron-electron interaction. A numerical calculation is made of the magnetic moments of α - and γ -modifications of iron corresponding to the ferromagnetic and antiferromagnetic ordering of a crystal. (15 refs.) A.T.

77149 Susceptibility of an isotropic ferromagnet. V.N.Fedosov (Polytech. Inst., Voronezh, USSR).

Fiz. Met. & Metalloved. (USSR), vol.55, no.4, p.660-4 (April 1983). In Russian. English translation in: *Phys. Met. & Metallogr. (GB)*.

A study is made of the distribution of the magnetization in an isotropic ferromagnet in the shape of a rod. The boundaries of opposite domains formed as a result of magnetization switching are shown to have a complex structure which is manifested in the dependence of the magnetic susceptibility on the rod dimensions. (9 refs.) A.T.

77150 Magnetic susceptibility of ordering $\text{Fe}_{1-x}\text{Mn}_x\text{Pd}_3$ alloys. B.V.Cherkashin, Yu.A.Vereshchagin, F.A.Sidorenko, A.A.Kuranov (S.M. Kirov Ural Polytech. Inst., Sverdlovsk, USSR).

Fiz. Met. & Metalloved. (USSR), vol.55, no.4, p.820-2 (April 1983). In Russian. English translation in: *Phys. Met. & Metallogr. (GB)*.

The temperature dependence of the magnetic susceptibility was determined in the range 4.2-1250 K in various magnetic fields. The results were used to identify ferromagnetic and antiferromagnetic interactions in the atomically ordered and disordered states in these alloys. (9 refs.) A.T.

77151 Magnetic properties of amorphous Co and Ni alloys. K.H.J.Buschow (Philips Res. Labs., Eindhoven, Netherlands).

J. Appl. Phys. (USA), vol.54, no.5, p.2578-81 (May 1983).

The magnetic properties of amorphous alloys of the type $\text{Mg}_{1-x}\text{Ni}_x$, $\text{Zr}_{1-x}\text{Ni}_x$, $\text{Hf}_{1-x}\text{Co}_x$, and $\text{Nb}_{1-x}\text{Co}_x$ were studied in the temperature range 4.2-300 K. The saturation moments in these alloys and other Co-base amorphous alloys were analyzed in terms of a model proposed earlier, where account is taken of the size difference of the constituent metal atoms and the presence of compositional short-range ordering. It is shown that an additional moment reduction can be expected in amorphous alloys in which the 3d metal is combined with Ti, Nb, Ta, W, or Mo. (15 refs.)

77152 Magnetic properties and crystal distortion of hexagonal Mn_2Ga . H.Niida, T.Hori (Lab. of Phys., Shibaura Inst. of Technol., Saitama, Japan), Y.Nakagawa.

J. Phys. Soc. Jpn. (Japan), vol.52, no.5, p.1512-14 (May 1983).

Magnetization measurements and X-ray diffraction experiments have been made on $\epsilon\text{-Mn}_2\text{Ga}$ (71.4 at.% Mn) having a triangular spin structure with a weak ferromagnetic component below 460 K. It has been found that the D_{019} -type hexagonal structure is slightly distorted to an orthorhombic structure below 170 K, and that the transition is accompanied by a steep increase of spontaneous magnetization. The crystal distortion may enhance the deviation from the ideal triangular spin configuration.

77153 Random-field effects and magnetic susceptibility in diluted three-dimensional antiferromagnets $\text{Mn}_x\text{Zn}_{1-x}\text{F}_2$. H.Ikeda, K.Kikuta (Dept. of Phys., Ochanomizu Univ., Tokyo, Japan).

J. Phys. C (GB), vol.16, no.14, p.L445-51 (20 May 1983).

Magnetic susceptibility measurements have been made of the effect of applying a field on the critical divergence of the parallel susceptibility of the dilute antiferromagnets $\text{Mn}_x\text{Zn}_{1-x}\text{F}_2$ ($x=0.45$ and 0.6). The diverging susceptibility at the Neel temperature under an extremely weak external field, which originates from the coupling between uniform and staggered fluctuations, is sup-

pressed with increasing magnetic field. This and the appearance of the remnant magnetisation below the Neel temperature suggest that the phase transition in these systems is destroyed by the induced random magnetic fields and the system splits into micro-domains. (12 refs.)

77154 Effects of transition metal substitutions on magnetic properties of Co-based amorphous alloys. K.Hayashi, K.Hotai, M.Hayakawa, Y.Ochiai, H.Matsuda, S.Uedaira, K.Aso (SONY Corp. Res. Center, Yokohama, Japan).

J. Magn. & Magn. Mater. (Netherlands), vol.36, no.3, p.237-41 (April 1983). The effects of dilute concentrations of 3d-, 4d-, and 5d-transition metal solutes on magnetic moment and Curie temperature of Co-based amorphous alloys have been investigated. The changes of magnetic properties with transition metal substitutions are similar to those observed for corresponding crystalline Ni-based dilute alloys except the thermo-magnetic properties. The effects of transition metal substitutions on magnetic moment in Co-based amorphous alloys are well described in terms of the relative position of the Fermi level and the virtual bound state introduced in the 3d-band of the matrix by the transition metal atoms. (20 refs.)

77155 Study of the critical behaviour of the magnetization and electrical resistivity in cubic La(Fe, Si)₁₃ compounds. T.T.M.Palstra, J.A.Mydosh, G.J.Nieuwenhuys (Kamerlingh Onnes Lab., Rijks-Univers., Leiden, Netherlands), A.M.van der Kraan, K.H.J.Buschow.

J. Magn. & Magn. Mater. (Netherlands), vol.36, no.3, p.290-16 (April 1983). The magnetic properties of the cubic NaZn₁₃ type pseudobinary compounds La(T₁Si_{1-x})₁₃ were studied for T=Fe, Co and Ni in the temperature range 4.2-300K. ⁵⁷Fe Mossbauer spectroscopy was performed on LaFe₁₁Si₂ and ⁵⁷Fe-doped LaCo₁₁Si₂. The compounds with T=Fe or Co are ferromagnetic, while the compound LaNi₁₁Si₂ is a Pauli paramagnet. The critical behaviour around the Curie temperature *T_c* was studied in La(Fe_{11-x}Si_x)₁₃ by measuring the temperature dependences of the zero-field susceptibility and the electrical resistivity. The critical exponent γ in the expression $\chi \propto (T-T_c)^{-\gamma}$ was found to be close to 1.38 corresponding to an isotropic Heisenberg ferromagnet. The anomalous critical behaviour shown by electrical resistivity measurements can be explained in terms of lattice softening associated with the Invar effect. (16 refs.)

77156 Note on the magnetic and magneto-optical properties of Ni₂In type 3d transition metal compounds. K.H.J.Buschow, P.G.van Engen (Philips Res. Labs., Eindhoven, Netherlands).

Phys. Status Solidi a (Germany), vol.76, no.2, p.615-20 (16 April 1983). The ternary compounds PtMnGa, PtMnAl, FeMnIn, FeMnIn, FeInGe, FeCoGe, FeMnGe, CoNiSn, FeNiSn, FeCoSn, and MnCoSn are found to crystallize in the hexagonal Ni₂In structure. The lattice constants of these compounds are determined and their magnetic properties studied in the range 4.2 to 300K. It is found that most of these compounds are ferromagnetic. For several of the compounds the complex polar Kerr effect is studied at room temperature in the energy range 0.6 to 4.4 eV. (13 refs.)

77157 Magnetic susceptibility of the canted spin compounds (CH₂)_n(NH₄)₂FeCl₄, n=4, 5, and 7. M.A.Semary, M.F.Mostafa, M.M.Abdel-Kader (Dept. of Phys., Univ. of Cairo, Giza, Egypt). *Phys. Status Solidi a (Germany)*, vol.76, no.2, p.K131-6 (16 April 1983). The authors report results on (CH₂)_n(NH₄)₂FeCl₄ with n=4, 5, and 7. The susceptibility behaviour measured in different values of the magnetic field strength is described. The magnetic susceptibility was measured by the Gouy method, and the diamagnetic correction was carried out. (13 refs.)

77158 Magnetic susceptibility of Fe_{1-x}Co_xSi solid solutions. P.V.Gel'd, A.A.Povzner, L.F.Romasheva (S.M. Kirov Ural Polytech. Inst., Sverdlovsk, USSR).

Sov. Phys.-Dokl. (USA), vol.27, no.8, p.639-40 (Aug. 1982). Translation of: *Dokl. Akad. Nauk SSSR*, vol.265, no.4-6, p.1379-81 (Aug. 1982). [received: May 1983]

Investigates the magnetization and magnetic susceptibility of Fe_{1-x}Co_xSi solid solutions with 0 ≤ x ≤ 0.70 at temperatures from 4.5 to 1000K. The samples were prepared by melting components of high purity. To check that the homogenized alloys were in a single phase, the authors performed metallographic and X-ray structural analyses. These studies have made it clear that the functions $\chi(T)$ for alloys with x < 0.50 display two temperature regions in which the susceptibility obeys a Curie-Weiss law, but with different Curie-Weiss constants and paramagnetic Curie temperatures in each region. In contrast, for x ≥ 0.50 the magnetic susceptibility satisfies a single Curie-Weiss law at all temperatures above *T_c*. (8 refs.)

77159 Influence of Mn ion substitution by Fe on the electrical and magnetic properties of an La_{0.6}Pb_{0.4}MnO₃ crystal. E.P.Svirina, L.P.Shykhina, M.M.Lukina (M.V. Lomonosov State Univ., Moscow, USSR).

Sov. Phys.-Solid State (USA), vol.24, no.11, p.1947-8 (Nov. 1982). Translation of: *Fiz. Tverd. Tela (USSR)*, vol.24, no.11, p.3428-30 (Nov. 1982). [received: May 1983]

The authors obtained new experimental data on the electrical and magnetic properties of La_{0.6}Pb_{0.4}MnO₃ and La_{0.6}Pb_{0.4}Fe_{0.22}Mn_{0.78}O₃ single crystals at temperatures from 80 to 800K. The aim was to determine the influence of partial replacement of Mn with Fe on the electrical and magnetic properties of the manganite crystals. The magnetization was measured with a vibration magnetometer. The spontaneous magnetization σ_s and the Curie temperature *T_c* were found by the method of thermodynamic coefficients. The electrical resistivity ρ and the thermoelectric power were determined using a DC potentiometer. A metal-semiconductor transition occurred in the region of the Curie temperature *T_c* (335K). The results show that the manganites are characterised by an exchange energy which is comparable with the band gap. (11 refs.)

77160 Characteristics of the magnetic microstructure of oxyfluoride ferrites. Sh.Sh.Bashkurov, A.B.Liberman, A.N.Men', A.M.Khasanov (V.I. Ulyanov-Lenin State Univ., Kazan, USSR).

Sov. Phys.-Solid State (USA), vol.24, no.11, p.1959-61 (Nov. 1982). Translation of: *Fiz. Tverd. Tela (USSR)*, vol.24, no.11, p.3448-50 (Nov. 1982). [received: May 1983]

The authors carried out a Mossbauer investigation of oxyfluoride cobalt ferrites Co_{1-x}Fe_xLi_{0.4-x}F_{0.6} (0 ≤ x ≤ 0.7). Values of the lattice parameters, magnetic saturation moments, and Curie temperatures are listed. The Mossbauer measurements were carried out using a gamma resonance spectrometer with constant acceleration. The source of gamma rays was ⁵⁷Co in a palladium matrix. (8 refs.)

Crystal structure and magnetic susceptibility of RCuSn system See Entry 76362

Neutron diffraction study of the Ni₂Mn_{1-x}Cr_xSn system See Entry 76369

X-ray, crystal data, magnetic susceptibility and electrical conductivity of hydrated tririckel pentasulphide See Entry 76375

Preparation and crystal structure of Na₂Mn₂S₃ See Entry 76380

Crystalline structure and magnetic properties of the low temperature variation of β-TlFeBr₃ See Entry 76393

Fluorinated compounds A'BaM₂III₂F₆ (A' = Na, K; M^{III} = Ga, Cr, V, Fe) See Entry 76395

The cation distribution of tin-doped magnetites See Entry 76400

Influence of isotopic substitution on the T=M2 phase transition in V_{1-x}Fe_xO₂ single crystals See Entry 76618

Specific heat of Co(S_{1-x}Se_x)₂ and magnetic properties in weak fields See Entry 76666

The method of thermodynamic perturbation in the intermediate valence problem See Entry 76902

Superconductivity and magnetism in the pseudoternary system Dy(Ru,Rh_{1-x})₂B₄ See Entry 77080

Monte Carlo simulation of the antiferromagnetic Ising model on the triangular lattice with the first and second neighbour interactions See Entry 77121

Magnetic susceptibility of the extended Hubbard model in one-dimensional complexes See Entry 77128

Antiferromagnetism of the FeNb and FeTa mu-phases See Entry 77145

A binary ferromagnetic alloy with magnetic moments dependent on local environment. II. Neutron magnetic elastic scattering and hyperfine field distribution See Entry 77146

Localization effect in CrRh alloys See Entry 77172

Magnetic properties of (Cr_{1-x}Rh_x)₂Te₄ See Entry 77174

Anhyseretic and hysteretic magnetic properties of small Fe₃O₄ particles See Entry 77216

Anomalous thickness dependence of the saturation magnetization in Fe-Ni Invar alloy films See Entry 77220

Thermal expansion and specific heat anomalies in UPt below the ferromagnetic ordering temperature See Entry 77241

The magnetoelectric effect in iron-manganese spinels See Entry 77249

Site distribution in heavily Sc³⁺, Zr⁴⁺, and Hf⁴⁺-substituted yttrium iron garnet See Entry 77310

Spectral studies on new dioxouranium (VI) complexes of tridentate Schiff bases derived from salicylhydrazide and salicylaldehyde or substituted salicylaldehydes See Entry 77372

75.30D Spin waves

(see also 76.50 Spin wave resonance)

77161 Spin waves in ageing ferromagnetic alloys with isostructural precipitates of a new phase. M.V.Medvedev (Inst. of Metal Phys., Acad. of Sci., Sverdlovsk, USSR).

Fiz. Met. & Metalloved. (USSR), vol.55, no.4, p.629-35 (April 1983). In Russian. English translation in: *Phys. Met. & Metallogr. (GB)*

A dilute ageing ferromagnetic alloy with a low concentration of isostructural precipitates of a new phase is considered. It is assumed that the precipitates are distributed at random in the original phase. The Born approximation is used to study the characteristics of the dispersion and damping of long-wavelength spin excitations when they are scattered by the nuclei of the new phase and this is done for the absence of a chemical order and for the case of chemical ordering in the precipitates. (13 refs.) A.T.

77162 Guided magnetostatic surface waves on a metallic strip line. M.Uehara, K.Yashiro, S.Ohkawa (Dept. of Electronic Engng., Chiba Univ., Chiba, Japan).

J. Appl. Phys. (USA), vol.54, no.5, p.2582-7 (May 1983).

This paper gives a theoretical analysis for the geometrical configuration of a metallic strip deposited on ferrite film, which is available for MSSW (magnetostatic surface wave) waveguide. Dispersion curves and magnetic potential distributions are presented when the metallic strip of 100 μm wide is placed on the ferrite film of 10 μm thick. Since MSSW propagates along either the top surface with the strip, or the bottom face with no strip depending on its propagating direction, a strip-guided mode is nonreciprocal in the energy trapping effects, the number of guided modes, and the frequency bands. (6 refs.)

77163 Magnetic excitations in FCC Fe-Ni alloys revealed from detailed magnetization measurements. I.Nakai (Dept. of Phys., Okayama Univ., Okayama, Japan).

J. Phys. Soc. Jpn. (Japan), vol.52, no.5, p.1781-90 (May 1983).

Detailed magnetization measurements for single crystals of Ni-rich Fe-Ni alloys have been carried out between 4.2K and 300K in external magnetic fields up to 16.9 kOe to a relative accuracy of 5 × 10⁻⁵. It is found by iterative least-squares analysis of these observed values that the temperature variation of magnetization consists of two parts: one is due to the spin-wave excitations and the other due to the Stoner-type excitations. The coefficient of the latter part has a considerable value at pure Ni, decreases with addition of Fe atoms to pure Ni, vanishing around 70 at.%Ni, and reappears at about 65 at.%Ni. A simple picture for metallic ferromagnetism at finite temperatures is proposed.

77164 Neutron scattering study of magnetic excitations in quasi-one-dimensional triangular lattice antiferromagnet CsVCl₃. H.Kadowaki, K.Hirakawa, K.Ubukoshi (Inst. for Solid State Phys., Univ. of Tokyo, Tokyo, Japan).

J. Phys. Soc. Jpn. (Japan), vol.52, no.5, p.1799-806 (May 1983).

CsVCl₃ is composed of one-dimensional antiferromagnetic chains which are coupled weakly antiferromagnetically in the basal hexagonal plane. In order to clarify the anomalous properties hitherto observed, an inelastic neutron scattering has been studied. The authors observed good one-dimensionality of $J'/J = 2.7 \times 10^{-4}$. But, although $S = 3/2$, the spin wave dispersion along the chain disagrees with the classical picture. The excitation spectra along the triangular lattice plane are unusual. The excitation is dominated by a dispersionless mode of strong intensity. Compared to this mode, the conventional acoustic spin wave branch seems to be of minor excitation at lower temperatures than the Neel point.

77165 Influence of long-range order on magnon energy in itinerant electron ferromagnetic alloys. S.Lipinski, J.Morkowski (Inst. of Molecular Phys., Polish Acad. of Sci., Poznan, Poland).

Physica B & C (Netherlands), vol.119 B+C, no.1-2, p.37-40 (April 1983).

(Proceedings of the International Symposium on Magnetoelectricity in Transition Metals and Alloys, Nagoya, Japan, 15-16 Sept. 1982). The stoichiometric binary alloys AB₃ of FCC structure are considered. The single-band tight binding Hamiltonian with intraatomic Coulomb interaction is used, the hopping integrals are restricted to nearest neighbouring atomic sites and are assumed independent of the species. The atomic potentials and the Coulomb integrals are assumed different for A and B atoms. The long-

range order parameter p characterizes the occupancies of the 4 s.c. sublattices, in which the FCC lattice is divided. A specific Ansatz is used to simplify the hopping part of the Hamiltonian, complicated in the Bloch basis. The spin wave stiffness constant D is calculated using the CPA method for calculating the average exchange contribution and the perturbation method to find the magnon scattering contribution. The dependence of D on the long-range order parameter p is calculated for Ni_3Fe and compared with the experimental data. (16 refs.)

77166 The problem of summation over physical states in a theory of interacting spin waves. V.G.Bar'yakhtar, V.N.Kirvoruchko, D.A.Yablonsky (Inst. for Theoretical Phys., Acad. of Sci., Kiev, Ukrainian SSR). *Solid State Commun. (USA)*, vol.46, no.8, p.613-18 (May 1983).

A new representation for the spin operators is suggested and on its basis the formalism involving both the rigorously of diagram technique for the spin operators and the simplicity of diagram technique for the Fermi- and Bose-system is developed to calculate the Green's spin functions. This method is a basis for constructing a theory of high-frequency and thermodynamic properties of magnetic ordered crystals and a systematic summation over physical states of interacting magnons at any temperatures. (12 refs.)

77167 Singularities in the spin wave spectra of ferromagnetic metals. A.G.Plyavenev (M.V. Lomonosov State Univ., Moscow, USSR). *Sov. Phys.-Solid State (USA)*, vol.24, no.12, p.2123-4 (Dec. 1983). Translation of: *Fiz. Tverd. Tela (USSR)*, vol.24, no.12, p.3722-4 (Dec. 1983).

The singularities in the magnon dispersion law $\omega=\omega(q)$ of a ferromagnetic metal due to the interaction with conduction electrons characterized by an isotropic electron spectrum manifest themselves for the values $q=p\pm p_+$ of the magnon momentum (p_+ are the limiting electron momenta with opposite spin orientations). The author studies the singularities of $\omega(q)$ and the reciprocal lifetimes of magnons $\Gamma(q)$ for an arbitrary electron spectrum and for magnon momenta $q=p\pm p_+$. (5 refs.)

Observation of dispersion on magnetic polaritons See Entry 76858

Symmetry analysis of magnetic structures and spin-waves on the basis of a stabilizer concept See Entry 77120

Computer simulation of the low-frequency spin dynamics in $\text{EuSr}_{1-x}\text{S}$ See Entry 77186

$O(n)$ spin systems in two dimensions See Entry 77187

Role of T^2 term in temperature dependence of the magnetization for Fe-Ni Invar alloys See Entry 77205

75.30E Exchange and superexchange interactions

(see also 71.70 Level splitting and interactions)

77168 Two-bridge mechanisms of indirect exchange. M.V.Eremin (V.I. Ulyanov-Lenin State Univ., Kazan, USSR).

Sov. Phys.-Solid State (USA), vol.24, no.11, p.1825-8 (Nov. 1982). Translation of: *Fiz. Tverd. Tela (USSR)*, vol.24, no.11, p.3216-22 (Nov. 1982). [received: May 1983]

Two-bridge mechanisms of indirect exchange between paramagnetic ions in insulators are studied. It is shown that they predominate in many cases over the simple additive sum of the contributions due to individual anion bridges and can lead to a strong ferromagnetic coupling. An effective exchange Hamiltonian, accurate up to the fifth order of perturbation theory in the electron hopping energy between an anion and a cation, is obtained and the principal parameters of the present theory are related to the spin densities at anion bridges. (5 refs.)

77169 Exchange interactions between dimers of chromium(III). A cluster approach. U.Hauser, H.U.Gudel (Inst. für Anorganische, Analytische und Phys. Chem., Univ. Bern, Bern, Switzerland).

Theor. Chim. Acta (Germany), vol.62, no.4, p.319-27 (1983).

Exchange interactions in dimers, tetramers and octamers of chromium(III) are treated with an effective Hamiltonian of the Heisenberg-Dirac-van Vleck type. Energies and wave functions of the cluster states are computed. The results of interdimer interactions are: (i) energy splittings and (ii) a contamination of the cluster ground state with excited configurations. The results are used for a qualitative rationalisation of the observed low-temperature properties of $\text{Cs}_3\text{Cr}_2\text{Cl}_9$. (9 refs.)

Changes in the electron structure of Fe-Ni alloys with the FCC lattice as a result of a magnetic phase transition See Entry 76836

Anomalous Hall effect in an antiferromagnetic metal See Entry 76926

Magnetisation density distribution in $\text{Mn}_{1/4}\text{TaS}_2$: observation of conduction electron spin polarisation See Entry 77140

Helimagnetism in alloys on the MnAs base See Entry 77144

Orbital exchange in the rare-earth dialuminides See Entry 77175

Magnetic properties of a disordered magnet with strong fluctuations in the exchange interactions See Entry 77197

Giant intrinsic magnetic hardness: Computer simulations on random moment dilution See Entry 77215

Electron-phonon interaction model for the relation between magnetic and elastic properties in itinerant electron ferromagnets See Entry 77237

Temperature dependences of the sublattice magnetizations in nickel ferrite See Entry 77286

75.30G Anisotropy

77170 The magnetic anisotropy of an aligned MnAlC magnet. U.S.Ram, P.Gaunt (Dept. of Phys., Univ. of Manitoba, Winnipeg, Manitoba, Canada). *J. Appl. Phys. (USA)*, vol.54, no.5, p.2872-4 (May 1983).

The magnetic anisotropy constants K_1 and K_2 have been measured for an aligned MnAlC magnet. The information is extracted from magnetization curves with the magnetic field parallel and perpendicular to the alignment axis. The anisotropy field $H_A=2(K_1-2K_2)/I_s$ (I_s is the saturation magnetization) was determined from a break point in a plot of the perpendicular magnetization against the inverse square of the field. K_1 and K_2 were then found from modified Sucksmith-Thomson plots. The data is used to calculate the 180° wall energies and widths and an estimate of the temperature coefficient of coercive field variation is made and compared with experiment. (8 refs.)

77171 Magnetic anisotropy of ErCo_4Cu single crystals. Z.Drzazga (Inst. of Phys., Silesian Univ., Katowice, Poland).

Phys. Status Solidi a (Germany), vol.76, no.2, p.647-9 (16 April 1983).

Studies of magnetic moment and magnetocrystalline anisotropy of ErCo_4Cu single crystals are presented. ErCo_4Cu can be applied as a permanent magnet changing the sign of the coercive force with temperature. (9 refs.)

Rare earth single-ion anisotropy and the magnetic structures of the RTiO_3 perovskites: $\text{R}=\text{Tb, Dy, Ho, Er}$ and Tm See Entry 77142

Spin-reorientation phase transitions in hexagonal W ferrites in a magnetic field See Entry 77177

Giant intrinsic magnetic hardness: Computer simulations on random moment dilution See Entry 77215

Study of magnetic after-effects in the amorphous alloy $\text{Fe}_{40}\text{Ni}_{40}\text{P}_{14}\text{B}_6$ See Entry 77217

Effect of magnetic field in RF sputtering on the crystal orientation and magnetic properties of Co-Cr perpendicular anisotropy films See Entry 77219

Micromagnetic investigation of stripe domains See Entry 77223

Stabilization of a stripe domain structure in amorphous Co-P films by annealing See Entry 77226

Magnetic hyperfine splitting in Mossbauer spectra of microcrystals See Entry 77303

75.30H Magnetic impurity interactions

77172 Localization effect in CrRh alloys. D.Dadarlat (Inst. of Isotopic & Molecular Technol., Cluj-Napoca, Rumania), T.Petrisor, A.Giurgiu, I.Pop.

Phys. Status Solidi b (Germany), vol.117, no.1, p.155-9 (1 May 1983).

Magnetic susceptibility measurements of CrRh alloys are reported. Below the Neel temperature a temperature independent magnetic susceptibility is observed for the samples containing 10.9 and 14.5 at% Rh. A decrease of the magnetic susceptibility as a function of temperature is observed for samples containing between 5.14 and 14.5 at% Rh in the paramagnetic region. A slight localization, induced by Rh impurities on the host Cr atoms, is proposed in order to explain the peculiar behaviour. The magnetic phase diagram is also given. The Neel point rapidly increases at the beginning, with increasing Rh concentration, and then slowly decreases, giving rise to a large maximum at about 6 at% Rh. (7 refs.)

Magnetic-nonmagnetic transition in Ti-Mn alloys See Entry 77137

Two-bridge mechanisms of indirect exchange See Entry 77168

Electron-spin resonance study of spin dynamics in the one-dimensional magnetic crystal doped with diamagnetic impurities $(\text{CH}_3)_4\text{NMn}^{2+}\text{Cl}_3\cdot\text{Cd}^{2+}$ See Entry 77257

75.30K Magnetic phase boundaries

(inc. magnetic transitions, metamagnetism, etc)

77173 Cluster X_n approach to magnetic interactions and phase transitions in solids. V.A.Gubanov, A.I.Liechtenstein, A.V.Postnikov (Inst. of Chem., Acad. of Sci., Sverdlovsk, USSR).

Int. J. Quantum Chem. (USA), vol.23, no.4, p.1517-28 (April 1983).

A magnetic transition state model is developed for the description of magnetic interactions and magnetic phase transitions in solids. The model is based on the one-electron X_n molecular orbital calculations of clusters embedded in crystal lattice and allows quantitative investigations of magnetic interactions in d and f metals, their alloys, and compounds. The energies of local spin excitations and magnetic transition temperatures are calculated for a series of systems with the electronic states localized to a different extent. The effects of covalent bonding are introduced directly into magnetic parameters calculations and appear to be of crucial importance. Magnetic properties of some disordered alloys are considered basing on the results of X_n cluster calculations performed. In the low concentration limit, the local moment existence problem is being discussed. The dependence of magnetic properties upon concentration is considered. The results of calculations allow to give the reasonable interpretation of the experimental data available and show good possibilities of the cluster model in the description of magnetic effects in solids. (19 refs.)

77174 Magnetic properties of $(\text{Cr}_{1-x}\text{Rh}_x)_2\text{Te}_4$. S.Ohta, A.Fujii, S.Anzai (Keio Univ., Kanagawa, Japan).

J. Phys. Soc. Jpn. (Japan), vol.52, no.5, p.1765-73 (May 1983).

Magnetization and susceptibility are investigated on a solid solution between Cr_2Te_4 [a ferromagnetic (F) and canted ferromagnetic (CF) compound] and Rh_2Te_4 [a Pauli paramagnetic one]. The ferromagnetic Curie temperature T_C decreases with increasing y , while the transition temperature T_1 between CF and F phases increases. In the higher y region, CF phase directly changes to the paramagnetic (P) phase at a transition temperature T_{CF} . The transition temperature T_{CF} decreases with increasing y , and disappears at $y=0.47\pm 0.02$ and $T=55\pm 15\text{K}$. An extra phase (Q) is found beyond CF one. Some characteristics of spin glass or micromagnetic states are observed in Q phase. Between $0.29\pm 0.03\leq y\leq 0.47\pm 0.02$, Q phase changes to CF one as the temperature increases. In the much higher y region, Q phase directly changes to P one. These features, together with the anomalous y -dependence of Weiss constant, are discussed on the competition between the negative and the positive exchange interactions. (16 refs.)

77175 Orbital exchange in the rare-earth dialuminides. B.Barbara, M.F.Rossignol (Lab. Louis Neel, CNRS, Univ. Sci. et Medecale Grenoble, Grenoble, France), E.Belozitzky, P.M.Levy.

Solid State Commun. (USA), vol.46, no.8, p.669-72 (May 1983).

An analysis of recent measurements of the paramagnetic Curie temperatures of the rare-earth dialuminides reveals the presence of an orbital contribution to the exchange interaction. (6 refs.)

77176 Existence of a canted phase in terbium yttrium iron garnets. K.F.Tsitskishvili, A.G.Mandzhavidze, N.G.Bazov, E.A.Biryukova, F.Kh.Akopov, V.M.Fedorov (Inst. of Phys., Acad. of Sci., Tbilisi, Georgian SSR).

Sov. Phys.-Solid State (USA), vol.24, no.11, p.1964-5 (Nov. 1982).

Translation of: *Fiz. Tverd. Tela (USSR)*, vol.24, no.11, p.3456-8 (Nov. 1982).

[received: May 1983]

Spin-reorientation transitions are a new form of magnetic phase transition. In the case of terbium yttrium iron garnets with the formula $\text{Tb}_2\text{Y}_{3-x}\text{Fe}_{10}\text{O}_{12}$ they have been investigated using a Mossbauer spectroscopy in the temperature range 80-300K using a constant-acceleration spectrometer with a $^{56}\text{Co}(\text{Cr})$ source and samples with terbium concentrations $x=0.26$ and 0.40 . In the case of the latter sample there was a spin-reorientation transition near 160K of the same type as the first transition observed at 135K. (12 refs.)

77177 Spin-reorientation phase transitions in hexagonal W ferrites in a magnetic field. Yu.A.Mamalui, V.N.Gorbach (A.M. Gorki State Univ., Kharkov, Ukrainian SSR).

Sov. Phys.-Solid State (USA), vol.24, no.11, p.1990-1 (Nov. 1982).

Translation of: *Fiz. Tverd. Tela (USSR)*, vol.24, no.11, p.3494-6 (Nov. 1982).

[received: May 1983]

The authors construct spin-orientation phase diagrams for uniaxial ferromagnets along two directions of the magnetic field $H=H_x$ and $H=H_z$ and

include sixth-order terms in the expression for the magnetic anisotropy energy. The theoretical conclusions are checked experimentally using samples of the hexagonal ferrite, $\text{BaNi}_{0.5}\text{Co}_{0.5}\text{Fe}_{16}\text{O}_{27}$, which exhibits different types of magnetic anisotropy depending on the temperature. (5 refs.)

Neutron diffraction study of the $\text{Ni}_2\text{Mn}_{1-x}\text{Cr}_x\text{Sn}$ system See Entry 76369
Cation distribution from Curie temperatures in slow cooled and quenched copper ferrite samples See Entry 76376
 Fe_3PO_7 , a case of Fe^{3+} fivefold coordination. Structural and magnetic studies See Entry 76377

Preparation and properties of the systems $\text{Fe}_{2-x}\text{Cr}_x\text{WO}_6$, $\text{Fe}_{2-x}\text{Rh}_x\text{WO}_6$, and $\text{Cr}_{2-x}\text{Rh}_x\text{WO}_6$ See Entry 76379

Crystalline structure and magnetic properties of the low temperature variation of $\beta\text{-TiFeBr}_3$ See Entry 76393

Specific heat of $\text{Co}(\text{S}_{1-x}\text{Se}_x)_2$ and magnetic properties in weak fields See Entry 76666

Thermal expansion of amorphous iron-chromium-boron alloys See Entry 76678

Changes in the electron structure of Fe-Ni alloys with the FCC lattice as a result of a magnetic phase transition See Entry 76836

Low-frequency electrical resistance of iron, cobalt, and nickel in the vicinity of their Curie temperatures See Entry 76924

Characteristics of the electrical resistivity of magnetically ordered Pd-base alloys See Entry 76925

Conductivity and Hall effect in single crystals of CuCr_2Se_4 magnetic spinel See Entry 76978

Superconductivity and magnetism in the pseudoternary system $\text{Dy}(\text{Ru}, \text{Rh}_{1-x})\text{B}_4$ See Entry 77080

Magnetic nonmagnetic transition in Ti-Mn alloys See Entry 77137

A binary ferromagnetic alloy with magnetic moments dependent on local environment. II. Neutron magnetic elastic scattering and hyperfine field distribution See Entry 77146

Neutron diffraction effects of the distorted structure of Ni-67.7 at.% Fe alloy in the magnetic ordered state See Entry 77147

Random-field effects and magnetic susceptibility in diluted three-dimensional antiferromagnets $\text{Mn}_2\text{Zn}_{1-x}\text{F}_2$ See Entry 77153

Effects of transition metal substitutions on magnetic properties of Co-based amorphous alloys See Entry 77154

Magnetic susceptibility of $\text{Fe}_{1-x}\text{Co}_x\text{Si}$ solid solutions See Entry 77158

Influence of Mn ion substitution by Fe on the electrical and magnetic properties of an $\text{La}_{0.6}\text{P}_{0.4}\text{MnO}_3$ crystal See Entry 77159

Characteristics of the magnetic microstructure of oxyfluoride ferrites See Entry 77160

Localization effect in CrRh alloys See Entry 77172

Magnetic properties of a disordered magnet with strong fluctuations in the exchange interactions See Entry 77197

Influence of substitution and addition of calcium on magnetic properties of $\text{Ni}_{0.245}\text{Zn}_{0.755}\text{Fe}_2\text{O}_4$ ferrite See Entry 77210

Magnetoelastic properties of PrAg See Entry 77229

Theoretical aspects of magnetoelasticity in transition metals and alloys See Entry 77233

Magnetovolume effects in the local-band theory of ferromagnetism: pressure dependence of T_c in iron and nickel See Entry 77235

Magnetovolume effects in the Moriya-Kawabata theory of very weak itinerant ferromagnetism See Entry 77236

High-pressure effects on the $2k_F$ and $4k_F$ transitions in the quasi-one-dimensional magnetic conductor $\text{MEM}(\text{TCNQ})_2$ See Entry 77238

Thermal expansion and specific heat anomalies in UPT below the ferromagnetic ordering temperature See Entry 77241

NMR and magnetization study of the mixed systems $(\text{Pd}_{1-x}\text{Cu}_x)_2\text{MnIn}$ and $(\text{Pd}_{1-x}\text{Ni}_x)_2\text{MnIn}$ See Entry 77285

^{57}Fe Mossbauer spectroscopy on FePt Invar alloys See Entry 77312

75.40 CRITICAL-POINT EFFECTS, SPECIFIC HEATS, SHORT-RANGE ORDER

(inc. spin glasses)

77178 Spin glasses. J.Vey. *Ann. Inst. Henri Poincaré Sect. A (France)*, vol.38, no.3, p.255-62 (1983). A cohomological formulation of the frustration model is given for an arbitrary polyhedral complex. (2 refs.)

77179 Specific heats of $\text{Lu}_2\text{Mn}_{23}$, $\text{Gd}_2\text{Mn}_{23}$, $\text{Dy}_2\text{Mn}_{23}$, and $\text{Er}_2\text{Mn}_{23}$ from 1.7-18K. R.J.G.Tompson, H.W.White (Dept. of Phys., Univ. of Missouri, Columbia, MO, USA), K.Hardman, W.J.James. *J. Appl. Phys. (USA)*, vol.54, no.5, p.2838-40 (May 1983).

Specific heat results are reported for the intermetallic rare earth compounds $\text{Lu}_2\text{Mn}_{23}$, $\text{Gd}_2\text{Mn}_{23}$, $\text{Dy}_2\text{Mn}_{23}$, and $\text{Er}_2\text{Mn}_{23}$ in the temperature range 1.7-18K. No evidence was found which indicated changes in magnetic spin structure for $\text{Gd}_2\text{Mn}_{23}$ and $\text{Dy}_2\text{Mn}_{23}$. The origin of a broad bump in the region from 2-8K for $\text{Er}_2\text{Mn}_{23}$ is not understood. The specific heat of the diamagnetic compound $\text{Lu}_2\text{Mn}_{23}$ was well described by the expression, $C = \gamma T + \alpha T^3 + \delta T^5$, where $\gamma = 0.277 \pm 0.005$ and $\delta = 0.00285 \pm 0.00005$ when C is in units of J/mol K. From the value of α , θ_D was calculated to be $270 \pm 2\text{K}$. (5 refs.)

77180 Critical magnetic behavior of uranium monosulphide. A.T.Aldred (Argonne Nat. Lab., Argonne, IL, USA), R.Troc. *J. Magn. & Magn. Mater. (Netherlands)*, vol.36, no.3, p.217-25 (April 1983).

A detailed magnetization study has been made on ferromagnetic US near its Curie temperature. The critical exponent values γ , β and δ have been determined, and are close to those found earlier for UTe. The scaling law and then the homogeneous equation of state are exactly satisfied. The authors also present the tentative results of an analysis of the α exponent, deduced from the heat capacity data of Flotow et al. (1971). The findings are summarized and compared with those previously reported for US and UTe. (34 refs.)

77181 Landau theory of magnetic phase diagrams and first order magnetisation processes. W.I.Khan, D.Melville (Dept. of Phys., Univ. of Southampton, Southampton, England). *J. Magn. & Magn. Mater. (Netherlands)*, vol.36, no.3, p.265-70 (April 1983).

The Landau free energy expansion up to sixth order in the magnetisation has been used to study ferro- and paramagnetic phases in zero and finite applied

magnetic fields. Magnetic phase diagrams are determined in terms of Landau coefficient ratios which indicate first order and metamagnetic phase transitions. In addition the critical magnetic field and specific magnetisations corresponding to first order magnetisation processes are calculated in terms of these coefficients. A method of evaluating Landau coefficients is also demonstrated. (15 refs.)

77182 Calculation of the Green's function for the micromagnetic thin film problem. W.Maass, U.Krey, H.Hofmann (Univ. Regensburg, Regensburg, Germany).

J. Magn. & Magn. Mater. (Netherlands), vol.37, no.1, p.11-29 (May 1983). The spatial dependence of the Green's function of the micromagnetic thin film problem is calculated. Introducing contours of equal function values (coupling areas) the authors discuss the behaviour of the Green's function, which depends crucially on a single constant q resulting from the magnetic and geometric film parameters. In the case of a typical polycrystalline or amorphous film with $q \ll 1$ (i.e. small anisotropy and large magnetization) the contours have a typical long extended shape over a wide range of r -values. This corresponds to Hoffmann's (1964) former linear ripple theory, which supplies a good description of the essential physical features just in this case. On the other hand, in the event of $q \approx 1$ or $q \gg 1$ (i.e. for very thin films with a small magnetization M_s and a large anisotropy) the shape of the coupling areas shows a much stronger dependence on the distance r . This should considerably influence the magnetic properties of such films, e.g., the magnetic ripple spectrum. (17 refs.)

77183 Metastability region in spin-glasses. Z.Gulacsi, M.Crisan, M.Gulacsi, A.Anghel (Dept. of Phys., Cluj Univ., Cluj, Rumania).

J. Magn. & Magn. Mater. (Netherlands), vol.37, no.1, p.58-62 (May 1983). The stability of the Sherrington-Kirkpatrick model (1978) is reconsidered, pointing out that the de Almeida-Thouless line (1978) from the phase diagram does not imply the replica symmetry breaking at the zero magnetic field. (4 refs.)

77184 Spin glasses. I. K.H.Fischer (Inst. für Festkörperforschung, KFA Jülich, Jülich, Germany).

Phys. Status Solidi b (Germany), vol.116, no.2, p.357-414 (1 April 1983). After mentioning in a general way the properties of spin glasses, the author goes on to discuss spin glass models. There are sections on the Edwards-Anderson model, the Sherrington-Kirkpatrick model, ground state properties of spin glasses, frustration and gauge theory, the dynamics of vector spin glasses, the special spin glass system $(\text{EuSr})\text{S}$, random site models and transport properties. The article concludes with a discussion of a few experiments believed to be especially important for the understanding of spin glasses. (214 refs.)

77185 On the Schrodinger spin-exchange ferromagnet. H.A.Brown (Dept. of Phys., Univ. Missouri, Rolla, MO, USA).

Phys. Status Solidi b (Germany), vol.117, no.1, p.177-84 (1 May 1983). The thermodynamic behavior of a ferromagnet whose interactions are described by the Schrodinger spin-exchange operator is investigated. The transition temperatures, magnetization, susceptibility, exchange energy, heat capacity, and entropy are calculated for general spin and lattice coordination number using the constant-coupling approximation. Both first- and second-order phase transitions are found. Comparison with some results of the high-temperature expansion method shows some qualitative agreement. (16 refs.)

77186 Computer simulation of the low-frequency spin dynamics in $\text{Eu}_x\text{Sr}_{1-x}\text{S}$. W.Y.Ching (Dept. of Phys., Univ. of Missouri, Kansas City, MO, USA), D.L.Huber.

Phys. Rev. B (USA), vol.27, no.9, p.5810-12 (1 May 1983). The authors report the results of a computer simulation of the low-frequency harmonic magnon modes in $\text{Eu}_x\text{Sr}_{1-x}\text{S}$ for $x=0.8$ and 0.4. No evidence of hydrodynamic spin-wave modes is found in the spin-glass phase ($x=0.4$) for wave vectors $q \approx \pi a/6$ (where a is the lattice constant), in contrast to the ferromagnetic phase ($x=0.8$) where ferromagnetic spin waves are presented. Comparisons are made with experimental results for the reentrant spin-glass $\text{Fe}_{0.26}\text{Cr}_{0.74}$. (10 refs.)

77187 $O(n)$ spin systems in two dimensions. R.Brout, W.Deans, A.Silov (Faculté des Sci., Univ. Libre de Bruxelles, Bruxelles, Belgium).

Phys. Rev. B (USA), vol.27, no.9, p.5813-14 (1 May 1983). The Monte Carlo data of the two-dimensional $O(3)$ spin system are shown to be interpretable in terms of the simple concepts of reaction field (spherical model), spin waves, and asymptotic freedom. The reaction field is the predominant feature at high temperatures and at low (bare) temperatures and long distances. Spin waves and asymptotic freedom dominate at low temperatures and short distances. (5 refs.)

77188 Low-temperature scaling for systems with random fields and anisotropies. A.Aharony, E.Pytte (IBM Thomas J. Watson Res. Center, Yorktown Heights, NY, USA).

Phys. Rev. B (USA), vol.27, no.9, p.5872-4 (1 May 1983). Random fields (or anisotropies) shift the lower critical dimensionality of spin systems from d_c^0 to d_c . For dimensionalities $d_c^0 < d < d_c$ at low temperatures T , the magnetization has a discontinuity (from zero to m) when Δ (the average square field) approaches zero. The correlation length ξ diverges as $\Delta^{-\nu_2}$. The structure factor is shown to scale as $S(q, \xi) = \xi^{\nu_2} S(q\xi)$. Simple assumptions on scaling near $T=0$ yield $\nu_2 = 1/(d_c - d)$, with $d_c = 4$ for continuous symmetry spins and $d_c = 2$ for Ising spins. (25 refs.)

77189 Dimensional reduction with correlated random fields. A superspace renormalization-group calculation. M.Kardar, B.McClain, C.Taylor (Dept. of Phys., MIT, Cambridge, MA, USA).

Phys. Rev. B (USA), vol.27, no.9, p.5875-8 (1 May 1983). Considers phase transitions in the presence of random magnetic fields, with long-range correlations such that $\langle h(0)h(r) \rangle \sim 1/r^{d-\sigma}$. The upper critical dimension is $6+\sigma$. A superspace renormalization-group calculation is carried out to order ϵ^2 , where $\epsilon = 6+\sigma-d$. To order ϵ , the critical properties are that of a pure system in $d-2-\sigma$ dimensions. This dimensional reduction is also justified by physical arguments concerning the lower critical dimensionality, and the hyperscaling relationship. However, it fails at order ϵ^2 . (17 refs.)

77190 Spin-reorientation phase transition in rare-earth hexagonal ferrites. Yu.A.Mamalui, L.P.Ol'khovik (A.M. Gorki State Univ., Kharkov, Ukrainian SSR).

Sov. Phys.-Solid State (USA), vol.24, no.11, p.1949-50 (Nov. 1982). Translation of: *Fiz. Tverd. Tela (USSR)*, vol.24, no.11, p.3431-3 (Nov. 1982). [received: May 1983]

To explain the low-temperature magnetic behavior, the authors study the spin-reorientation phase transition in a hexagonal ferrite in magnetic fields of different orientations including the sixth-order terms in the anisotropy energy. They discuss in detail the case where the constant $K_2 < 0$, corresponding to the sign of K_2 observed for $\text{La}_{0.5}\text{Na}_{0.5}\text{Fe}_{12}\text{O}_{19}$. (4 refs.)

77191 Discontinuities of the order parameter in system of mutually interacting single-level particles. E.L.Nagaev, A.I.Podel'shchikov. *Sov. Phys.-Solid State (USA)*, vol.24, no.11, p.1951-2 (Nov. 1982). Translation of: *Fiz. Tverd. Tela (USSR)*, vol.24, no.11, p.3434-6 (Nov. 1982). [received: May 1983]

Shows that discontinuities in the order parameter which are not accompanied by any changes in the ordering can occur not only in the obvious case of multilevel particles but also in the case of single-level particles provided their mutual interaction is of special type. As an example, they quote a magnetic system with non-Heisenberg exchange interactions between localized moments of a given length. It has been shown that a first-order order-disorder transition can occur in such a system provided the biquadratic exchange is comparable with the four-spin or biquadratic exchange. However, the possibility of a first-order phase transition of the order type—the same order in non-Heisenberg magnetic materials—has not been discussed. The authors perform a simple molecular-field calculation for a model with the standard two-spin Heisenberg exchange and also with the four-spin and six-spin exchange interactions. (7 refs.)

Magnetic field dependence of the electronic specific heat of TiBe_2 : an estimate from magnetization data See Entry 76663

Specific heat of $\text{Co}(\text{S}_{1-x}\text{Se}_x)_2$ and magnetic properties in weak fields See Entry 76666

Magnetic impurities in semiconductors See Entry 76879

Characteristics of the electrical resistivity of magnetically ordered Pd-base alloys See Entry 76925

Iron above the Curie temperature See Entry 77134

Antiferromagnetism of the FeNb and FeTa mu-phases See Entry 77145

Random-field effects and magnetic susceptibility in diluted three-dimensional antiferromagnets $\text{Mn}_x\text{Zn}_{1-x}\text{F}_2$ See Entry 77153

Magnetic properties of $(\text{Cr}_{1-y}\text{Rh}_y)_2\text{Te}_4$ See Entry 77174

Magnetization and Mossbauer studies of $\text{Y}(\text{Fe,Rh})_2$ See Entry 77208

Thermal expansion and specific heat anomalies in UPt below the ferromagnetic ordering temperature See Entry 77241

Electron-spin resonance study of spin dynamics in the one-dimensional magnetic crystal doped with diamagnetic impurities $(\text{CH}_3)_4\text{NMn}^{2+}\text{Cl}_3\text{Cd}^{2+}$ See Entry 77257

Specific heat and NMR spin echo in the superconducting and magnetic region of the Y_6Co_7 compound See Entry 77284

75.40D Ising and other classical spin models

77192 Renormalisation-group specific heat of the square-lattice Potts ferromagnet. H.O.Martin (Dept. de Física, Univ. Nacional de La Plata, La Plata, Argentina), C.Tsalis.

J. Phys. C (GB), vol.16, no.14, p.2787-95 (20 May 1983). The free and internal energies and specific heat of the q -state Potts ferromagnet are discussed. A real-space renormalisation-group approach is presented, which reproduces a considerable amount of exact particular results for all dimensionalities (hypercubic lattices). The case of the square lattice is investigated in detail using self-dual clusters (which provide the exact critical point for all q). Comparison with Onsager results ($q=2$) is satisfactory; the general tendencies for $q \neq 2$ ($1 \leq q \leq 4$) are exhibited, and the bound percolation limit ($q \rightarrow 1$) is worked out in some detail. (28 refs.)

77193 The existence of a phase transition in classical antiferromagnetic models. F.J.L.C. Calheiros (Centre de Phys. Theorique, CNRS, Marseille, France).

J. Stat. Phys. (USA), vol.31, no.1, p.141-54 (April 1983). For a wide class of antiferromagnetic models the author proves the existence of a phase transition using an extended Peierls argument, taking into account a result of Dobrushin (1968) for an antiferromagnetic Ising model and the results of Malyshev (1975) for ferromagnetic models (such as the anisotropic rotator). In particular the author reviews a result of Fröhlich, Israel, Lieb, and Simon (1980) obtained when reflection positivity holds. (7 refs.)

77194 Critical point estimates for the spin s Ising model from the high temperature series renormalisation group method. K.De Bell, D.D.Betts (Dept. of Phys., Dalhousie Univ., Halifax, Nova Scotia, Canada).

Physica A (Netherlands), vol.119A, no.1-2, p.78-82 (April 1983). By prefacing the high temperature series renormalisation group transformation with a spin restructuring transformation, estimates of the critical point of the spin s Ising model on the square and triangular lattices have been obtained. The systematic nature of the high temperature series method is preserved and the accuracy of the estimates appears to be principally dependent on the accuracy with which the $s=1/2$ critical point is determined. (7 refs.)

77195 Critical temperature for a random-bond Ising model with frustration on a square lattice. T.Horiguchi (Dept. of Engng. Sci., Tohoku Univ., Sendai, Japan).

Physica A (Netherlands), vol.119A, no.1-2, p.83-91 (April 1983). For a random-bond Ising model with frustration on a square lattice in which all the vertical bonds in a column are the same random variable while the horizontal bonds are mutually independent random variables, the author calculates an interface free energy for the ferromagnetic phase by means of the method of Muller-Hartmann and Zittartz. The critical temperature is obtained numerically for the system in which the random bonds take on $J>0$ and $-J$ with respective probabilities p and $1-p$. The interface free energy at zero temperature is obtained in a closed form and the critical concentration is equal to $3/4$. (8 refs.)

77196 Random-field effect in diluted Ising antiferromagnets. M.Fahnle (Max-Planck-Institut für Metallforschung, Inst. für Phys., Stuttgart, Germany).

Phys. Rev. B (USA), vol.27, no.9, p.5821-3 (1 May 1983). It is argued that near the percolation threshold of diluted systems there should be an instability of the long-range order in spatially random fields much smaller than the local molecular fields as a result of the strong ramification of the infinite percolation cluster, in all dimensions. This may give a possible explanation for the experiments of Yoshizawa et al., who find a destruction of the long-range order due to relatively small external magnetic fields in diluted two- and three-dimensional Ising antiferromagnets. (16 refs.)

77197 Magnetic properties of a disordered magnet with strong fluctuations in the exchange interactions. G.A.Petrakovskii, E.V.Kuz'min, S.S.Aplesnin (Inst. of Phys., Acad. of Sci., Krasnoyarsk, USSR).

Sov. Phys.-Solid State (USA), vol.24, no.11, p.1872-6 (Nov. 1982). Translation of: *Fiz. Tverd. Tela (USSR)*, vol.24, no.11, p.3298-304 (Nov. 1982). [received: May 1983]

The Monte Carlo method is applied to an Ising magnet with a random distribution of exchange bonds of different sign and fluctuating strongly in

magnitude. The phase diagram of magnetic states is constructed using the concentration of antiferromagnetic bonds and temperature as the coordinates. The regions of existence of a disordered ferromagnetic state, a spin glass state, a superantiferromagnetic state, and a random antiferromagnetic state are found. Thermodynamic properties of an Ising magnet such as the energy, magnetization, specific heat, and correlation functions are evaluated. The distribution function of local fields is also obtained. (13 refs.)

77198 Ising model with magnetic field and the Diophantine moment problem. V.S.Vladimirov, I.V.Volovich (V.A. Steklov Math. Inst., Acad. of Sci., USSR).

Theor. & Math. Phys. (USA), vol.53, no.1, p.943-52 (Oct. 1982). Translation of: *Theor. & Mat. Fiz. (USSR)*, vol.53, no.1, p.3-15 (Oct. 1982).

The properties of the Lee-Yang measure describing the distribution of the zeros of the partition function for the ferromagnetic Ising model with magnetic field that follow from the condition that its moments be Diophantine are studied. (15 refs.)

Monte Carlo simulation of the antiferromagnetic Ising model on the triangular lattice with the first and second neighbour interactions See Entry 77121

Free energy of the random Ising model in terms of the magnetizations of sites See Entry 77123

Low-temperature renormalization-group study of the random-field model See Entry 77125

Self-similarity and fractal dimension of the devil's staircase in the one-dimensional Ising model See Entry 77126

75.40F Heisenberg and other quantized spin models

77199 Effect of uniaxial long-range exchange interaction on the properties of surface spin waves in a Heisenberg ferromagnet. T.G.Petrova, E.S.Syrkin (Physico-Tech. Inst. of Low Temperatures, Acad. of Sci., Kharkov, Ukrainian SSR).

Phys. Status Solidi b (Germany), vol.116, no.2, p.475-81 (1 April 1983).

The low- and high-frequency surface states in a single-magnon spectrum of the Heisenberg ferromagnet with uniaxial exchange interaction of the long-range type are studied. The energies and damping decrements of surface spin waves and the surface projected spectral densities of magnon states are obtained. It is found that the considered anisotropic interaction results in new formation conditions of the surface spin waves and essentially affects their characteristics. (13 refs.)

77200 Low-temperature expansion of spin Green's functions and Dyson-Maleev formalism. V.G.Baryakhtar, V.N.Krivoruchko, D.A.Yablonskii (Donets Physicotech. Inst., Acad. of Sci., Ukrainian SSR).

Theor. & Math. Phys. (USA), vol.53, no.1, p.1047-50 (Oct. 1982). Translation of: *Theor. & Mat. Fiz. (USSR)*, vol.53, no.1, p.156-60 (Oct. 1982).

A one-to-one correspondence is established in general form between the calculation of the spin Green's functions in the Maleev representation and their calculation in the technique of spin operators. It is shown that the non-Hermiticity of the Maleev representation does not affect the results of the calculations, and the contribution of the unphysical states in the case of a Heisenberg ferromagnet for $T < S_0$ is especially small—of order $\exp(-T^2/T)$, where $T^2 = S(2S+1)J_0$ (S is the spin of the atom, and J_0 is the Fourier component of the exchange integral with zero wave vector). (8 refs.)

Limit states and potentials of planar Heisenberg dynamics with transverse magnetic field See Entry 77127

Magnetovolume effects in the local-band theory of ferromagnetism: pressure dependence of T_c in iron and nickel See Entry 77235

75.50 STUDIES OF SPECIFIC MAGNETIC MATERIALS

(see also 81.40R Magnetic properties related to materials treatment)

75.50B Ferromagnetism of Fe and its alloys

Changes in the electron structure of Fe-Ni alloys with the FCC lattice as a result of a magnetic phase transition See Entry 76836

Thermodynamical and structural properties of amorphous $\text{Fe}_{80}\text{B}_{20}$ and $\text{Fe}_{80}\text{P}_{13}\text{C}_7$ alloys See Entry 76922

Low-frequency electrical resistance of iron, cobalt, and nickel in the vicinity of their Curie temperatures See Entry 76924

Transverse magnetoresistance of amorphous $\text{Fe}_{40-x}\text{Ni}_{40}\text{Cr}_{10}\text{B}_{20}$ alloys in magnetic fields up to 20 T See Entry 76930

Neutron diffraction effects of the distorted structure of Ni-67.7 at.% Fe alloy in the magnetic ordered state See Entry 77147

Fermi-liquid approach to a description of localized magnetic moments in transition metals See Entry 77148

Magnetic susceptibility of ordering $\text{Fe}_{1-x}\text{Mn}_x\text{Pd}_3$ alloys See Entry 77150

Effects of transition metal substitutions on magnetic properties of Co-based amorphous alloys See Entry 77154

Study of the critical behaviour of the magnetization and electrical resistivity in cubic $\text{La}(\text{Fe}, \text{Si})_3$ compounds See Entry 77155

Magnetic susceptibility of $\text{Fe}_{1-x}\text{Co}_x\text{Si}$ solid solutions See Entry 77158

Magnetic excitations in FCC Fe-Ni alloys revealed from detailed magnetization measurements See Entry 77163

Influence of long-range order on magnon energy in itinerant electron ferromagnetic alloys See Entry 77165

Role of T^2 term in temperature dependence of the magnetization for Fe-Ni Invar alloys See Entry 77205

The hysteresis loop of two-phase particulate magnetic composite with nonlinear hard magnetic components See Entry 77207

Preparing conditions and magnetic properties of rapidly quenched high silicon iron ribbons See Entry 77212

Magnetically hard Alnico 5 alloy with a mischmetal addition See Entry 77213

Fe-Cr-Co ductile permanent magnet alloy with $(\text{BH})_{\text{max}} \approx 7.0$ MGOe See Entry 77214

Study of magnetic after-effects in the amorphous alloy $\text{Fe}_{60}\text{Ni}_{40}\text{P}_{14}\text{B}_6$ See Entry 77217

Anomalous thickness dependence of the saturation magnetization in Fe-Ni Invar alloy films See Entry 77220

- The variation of magnetic properties of Fe-based amorphous alloys along the ribbon length See Entry 77221
- Magnetovolume effects in the local-band theory of ferromagnetism: pressure dependence of T_c in iron and nickel See Entry 77235
- Thermal expansion measurements in Fe-base Invar alloys See Entry 77242
- Invar anomalies of Fe-Pd alloys See Entry 77243
- Contribution of the temperature change in the local magnetic moment to the Invar effect See Entry 77244
- Anomalous elastic properties of Fe-Ni (FCC) alloys and their Invar properties See Entry 77246
- Low-temperature elastic-constant anomalies in Fe-Cr-Ni-Mn alloys See Entry 77247
- Magnetoelastic effect in dilute Fe-Co alloys See Entry 77248
- ^{57}Fe Mossbauer study of amorphous $\text{Fe}_{81}\text{B}_{13.5}\text{Si}_{3.5}\text{C}_2$ See Entry 77301
- ^{57}Fe Mossbauer spectroscopy on FePt Invar alloys See Entry 77312
- Positron annihilation on pure and carbon-doped α -iron in thermal equilibrium See Entry 77477
- Comment on 'Spin-polarized Auger spectroscopy from magnetically ordered solids' See Entry 77488
- Spin- and angle-resolved photoemission from ferromagnetic Fe(001) See Entry 77523
- Perpendicularly crystallized ribbons by means of rapid solidifications from melts See Entry 77598
- Thermodynamics of the martensitic transformation in high-nickel iron alloys. Thermal effect See Entry 77640
- Interrelation of the magnetic and mechanical properties with the structural state of hardened and tempered products See Entry 77842

75.50C Ferromagnetism of other metals

- Neutron diffraction study of the $\text{Ni}_2\text{Mn}_{1-x}\text{Cr}_x\text{Sn}$ system See Entry 76369
- Lattice-fringe imaging of precipitation-hardened cobalt rare-earth magnets See Entry 76648
- Low-frequency electrical resistance of iron, cobalt, and nickel in the vicinity of their Curie temperatures See Entry 76924
- Characteristics of the electrical resistivity of magnetically ordered Pd-base alloys See Entry 76925
- Relaxation phenomena in amorphous $\text{Co}_{75-x}\text{Mn}_{25}$ induced by stress annealing See Entry 76929
- Canted ferromagnetism in PdMn and PdMnFe alloys See Entry 77143
- A binary ferromagnetic alloy with magnetic moments dependent on local environment. II. Neutron magnetic elastic scattering and hyperfine field distribution See Entry 77146
- Magnetic properties of amorphous Co and Ni alloys See Entry 77151
- Magnetic properties and crystal distortion of hexagonal Mn_3Ga See Entry 77152
- Study of the critical behaviour of the magnetization and electrical resistivity in cubic $\text{La}(\text{Fe}, \text{Si})_{13}$ compounds See Entry 77155
- Note on the magnetic and magneto-optical properties of Ni_2In type 3d transition metal compounds See Entry 77156
- The magnetic anisotropy of an aligned MnAlC magnet See Entry 77170
- Magnetic anisotropy of ErCo_4Cu single crystals See Entry 77171
- Bloch wall arrangement and Barkhausen noise in steels 22 NiMoCr 3 7 and 15 MnMoNiV 5 3 See Entry 77201
- The hysteresis loop of two-phase particulate magnetic composite with non-linear hard magnetic components See Entry 77207
- Magnetization and ^{161}Dy Mossbauer effect study of DyMn_2 and $\text{Dy}_6\text{Mn}_{23}$ and their ternary hydrides See Entry 77209
- Effect of magnetic field in RF sputtering on the crystal orientation and magnetic properties of Co-Cr perpendicular anisotropy films See Entry 77219
- Stabilization of a stripe domain structure in amorphous Co-P films by annealing See Entry 77226
- Magnetovolume effects in the local-band theory of ferromagnetism: pressure dependence of T_c in iron and nickel See Entry 77235
- Thermal expansion of ZrZn_2 See Entry 77240
- Thermal expansion and specific heat anomalies in UPt below the ferromagnetic ordering temperature See Entry 77241
- NMR and magnetization study of the mixed systems $(\text{Pd}_{1-x}\text{Cu}_x)_2\text{MnIn}$ and $(\text{Pd}_{1-x}\text{Ni}_x)_2\text{MnIn}$ See Entry 77285

75.50D Ferromagnetism of nonmetals

- Specific heat of $\text{Co}(\text{S}_{1-x}\text{Se}_x)_2$ and magnetic properties in weak fields See Entry 76666
- Conductivity and Hall effect in single crystals of CuCr_2Se_4 magnetic spinel See Entry 76978
- Low-temperature transport properties of RERh_4B_4 compounds (RE=Sm, Ho, Er, Lu) See Entry 77078
- Superconductivity and magnetism in the pseudoternary system $\text{Dy}(\text{Ru}, \text{Rh}_{1-x})_4\text{B}_4$ See Entry 77080
- Magnetisation density distribution in $\text{Mn}_{1/4}\text{TaS}_2$: observation of conduction electron spin polarisation See Entry 77140
- Rare earth single-ion anisotropy and the magnetic structures of the RTiO_3 perovskites: R=Tb, Dy, Ho, Er and Tm See Entry 77142
- Helimagnetism in alloys on the MnAs base See Entry 77144
- Magnetic susceptibility of the canted spin compounds $(\text{CH}_2)_n(\text{NH}_3)_2\text{FeCl}_4$; n=4, 5, and 7 See Entry 77157
- Influence of Mn ion substitution by Fe on the electrical and magnetic properties of an $\text{La}_{0.4}\text{P}_{0.4}\text{MnO}_3$ crystal See Entry 77159
- Magnetic properties of $(\text{Cr}_{1-x}\text{Rh}_x)_3\text{Te}_4$ See Entry 77174
- Spin-reorientation phase transitions in hexagonal W ferrites in a magnetic field See Entry 77177
- Critical magnetic behavior of uranium monosulphide See Entry 77180
- Computer simulation of the low-frequency spin dynamics in $\text{EuSr}_{1-x}\text{S}$ See Entry 77186

- Magnetic properties of $\text{Sn}_{1-x}\text{Cr}_x\text{Te}$ crystals See Entry 77206
- Magnetization and ^{161}Dy Mossbauer effect study of DyMn_2 and $\text{Dy}_6\text{Mn}_{23}$ and their ternary hydrides See Entry 77209
- The magnetoelectric effect in iron-manganese spinels See Entry 77249
- Giant hyperfine field on ^{151}Eu in $\text{EuFe}_4\text{P}_{12}$ [Mossbauer study] See Entry 77297

75.50E Antiferromagnetism

- Fe_3PO_7 , a case of Fe^{3+} fivefold coordination. Structural and magnetic studies See Entry 76377
- Preparation and properties of the systems $\text{Fe}_{2-x}\text{Cr}_x\text{WO}_6$, $\text{Fe}_{2-x}\text{Rh}_x\text{WO}_6$, and $\text{Cr}_{2-x}\text{Rh}_x\text{WO}_6$ See Entry 76379
- Preparation and crystal structure of $\text{Na}_2\text{Mn}_2\text{S}_3$ See Entry 76380
- Crystalline structure and magnetic properties of the low temperature variation of β - TiFeBr_3 See Entry 76393
- Fluorinated compounds $\text{A}^{\text{I}}\text{BaM}_2^{\text{III}}\text{F}_4$ ($\text{A}^{\text{I}}=\text{Na}, \text{K}$; $\text{M}^{\text{III}}=\text{Ga}, \text{Cr}, \text{V}, \text{Fe}$) See Entry 76395
- Interacting stereo-irregular chains: a model for conducting polymers See Entry 76828
- Observation of dispersion on magnetic polaritons See Entry 76858
- Anomalous Hall effect in an antiferromagnetic metal See Entry 76926
- Low-temperature transport properties of RERh_4B_4 compounds (RE=Sm, Ho, Er, Lu) See Entry 77078
- Superconductivity and magnetism in the pseudoternary system $\text{Dy}(\text{Ru}, \text{Rh}_{1-x})_4\text{B}_4$ See Entry 77080
- Study of frustration effects in two-dimensional triangular lattice antiferromagnets—neutron powder diffraction study of VX_2 , X=Cl, Br and I See Entry 77139
- Magnetic structure of $\text{Co}_{1/3}\text{NbS}_2$ and $\text{Co}_{1/3}\text{TaS}_2$ See Entry 77141
- Rare earth single-ion anisotropy and the magnetic structures of the RTiO_3 perovskites: R=Tb, Dy, Ho, Er and Tm See Entry 77142
- Helimagnetism in alloys on the MnAs base See Entry 77144
- Antiferromagnetism of the FeNb and FeTa μ -phases See Entry 77145
- Neutron diffraction effects of the distorted structure of Ni-67.7 at.% Fe alloy in the magnetic ordered state See Entry 77147
- Fermi-liquid approach to a description of localized magnetic moments in transition metals See Entry 77148
- Magnetic susceptibility of ordering $\text{Fe}_{1-x}\text{Mn}_x\text{Pd}_3$ alloys See Entry 77150
- Random-field effects and magnetic susceptibility in diluted three-dimensional antiferromagnets $\text{Mn}_x\text{Zn}_{1-x}\text{F}_2$ See Entry 77153
- Magnetic susceptibility of the canted spin compounds $(\text{CH}_2)_n(\text{NH}_3)_2\text{FeCl}_4$; n=4, 5, and 7 See Entry 77157
- Neutron scattering study of magnetic excitations in quasi-one-dimensional triangular lattice antiferromagnet CsVCl_3 See Entry 77164
- Exchange interactions between dimers of chromium(III). A cluster approach See Entry 77169
- Localization effect in CrRh alloys See Entry 77172
- Magnetoelastic properties of PrAg See Entry 77229
- Thermal expansion of Cr and Cr-V alloys See Entry 77239
- Electron-spin resonance study of spin dynamics in the one-dimensional magnetic crystal doped with diamagnetic impurities $(\text{CH}_3)_4\text{NMn}^{2+}\text{Cl}_3\text{Cd}^{2+}$ See Entry 77257
- NMR and magnetization study of the mixed systems $(\text{Pd}_{1-x}\text{Cu}_x)_2\text{MnIn}$ and $(\text{Pd}_{1-x}\text{Ni}_x)_2\text{MnIn}$ See Entry 77285
- Influence of isomer-shift distribution on Mossbauer quadrupole spectra in amorphous magnetic insulators See Entry 77309
- Muon-spin-rotation experiments in orthoferrites See Entry 77315

75.50G Ferrimagnetism

- The cation distribution of tin-doped magnetites See Entry 76400
- Acoustic emission initiated by ion implantation in bubble garnet films See Entry 76567
- Substrates for epitaxial growth of hexaferrite films See Entry 76800
- Symmetry analysis of magnetic structures and spin-waves on the basis of a stabilizer concept See Entry 77120
- Characteristics of the magnetic microstructure of oxyfluoride ferrites See Entry 77160
- Existence of a canted phase in terbium yttrium iron garnets See Entry 77176
- Specific heats of $\text{Lu}_6\text{Mn}_{23}$, $\text{Gd}_6\text{Mn}_{23}$, $\text{Dy}_6\text{Mn}_{23}$, and $\text{Er}_6\text{Mn}_{23}$ from 1.7-18K See Entry 77179
- Spin-reorientation phase transition in rare-earth hexagonal ferrites See Entry 77190
- Magnetization and ^{161}Dy Mossbauer effect study of DyMn_2 and $\text{Dy}_6\text{Mn}_{23}$ and their ternary hydrides See Entry 77209
- Influence of substitution and addition of calcium on magnetic properties of $\text{Ni}_{0.245}\text{Zn}_{0.755}\text{Fe}_2\text{O}_4$ ferrite See Entry 77210
- Anhyseretic and hysteric magnetic properties of small Fe_3O_4 particles See Entry 77216
- Direct observation of domain nucleation in garnet films See Entry 77224
- Problem of the dynamics of nonthrough magnetic bubble domains See Entry 77225
- ΔE effect of a Mn ferrite single crystal at temperatures between 150 and 300K See Entry 77230
- Epitaxial growth and annealing control of EMR properties of thick homogeneous Ga substituted yttrium iron garnet films See Entry 77267
- Temperature dependences of the sublattice magnetizations in nickel ferrite See Entry 77286
- Effect of an electric field on the Mossbauer spectra of the ferrites $\text{BaFe}_{12}\text{O}_{19}$ See Entry 77299
- The hyperfine interaction of gadolinium and holmium in cubic Ho: (Gd, Ce) Fe_2 compounds See Entry 77302
- Influence of isomer-shift distribution on Mossbauer quadrupole spectra in amorphous magnetic insulators See Entry 77309

- Site distribution in heavily Sc^{3+} , Zr^{4+} , and Hf^{4+} -substituted yttrium iron garnet See Entry 77310
- Preparation and magnetic characteristics of garnet films with cylindrical magnetic bubbles in the submicron range See Entry 77563
- Synthesis of gadolinium-gallium garnet See Entry 77603

75.50K Amorphous magnetic materials

- Thermal expansion of amorphous iron-chromium-boron alloys See Entry 76678
- Thermodynamical and structural properties of amorphous $\text{Fe}_{80}\text{B}_{20}$ and $\text{Fe}_{80}\text{P}_{13}\text{C}_7$ alloys See Entry 76922
- Relaxation phenomena in amorphous $\text{Co}_{75-x}\text{Mn}_x\text{B}_{25}$ induced by stress annealing See Entry 76929
- Transverse magnetoresistance of amorphous $\text{Fe}_{40-x}\text{Ni}_{40}\text{Cr}_x\text{B}_{20}$ alloys in magnetic fields up to 20 T See Entry 76930
- Magnetic properties of amorphous Co and Ni alloys See Entry 77151
- Effects of transition metal substitutions on magnetic properties of Co-based amorphous alloys See Entry 77154
- Study of magnetic after-effects in the amorphous alloy $\text{Fe}_{40}\text{Ni}_{40}\text{P}_{14}\text{B}_6$ See Entry 77217
- The variation of magnetic properties of Fe-based amorphous alloys along the ribbon length See Entry 77221
- The effects of ribbon thickness and annealing temperature on the AC magnetic properties of the $\text{Fe}_{81.5}\text{B}_{14.5}\text{Si}_3\text{C}_1$ alloy See Entry 77222
- Stabilization of a stripe domain structure in amorphous Co-P films by annealing See Entry 77226
- ^{57}Fe Mossbauer study of amorphous $\text{Fe}_{81}\text{B}_{13.5}\text{Si}_{3.5}\text{C}_2$ See Entry 77301
- Influence of isomer-shift distribution on Mossbauer quadrupole spectra in amorphous magnetic insulators See Entry 77309
- New magnetic metallic glasses with reduced metalloid content See Entry 77597

75.50M Magnetic liquids

- Dynamics of the shape transition of a magnetic ferrofluid drop See Entry 77250

75.60 DOMAIN EFFECTS, MAGNETIZATION CURVES, AND HYSTERESIS

- The variation of magnetic properties of Fe-based amorphous alloys along the ribbon length See Entry 77221

75.60C Domain walls and domain structure

(for magnetic bubbles, see 75.70K)

- 77201 Bloch wall arrangement and Barkhausen noise in steels 22 NiMoCr 3 7 and 15 MnMoNiV 5 3. P.Deimel, D.Kuppler, K.Herz (Univ. of Stuttgart, Stuttgart, Germany), W.A.Theiner. *J. Magn. & Magn. Mater. (Netherlands)*, vol.36, no.3, p.277-89 (April 1983). The changes of Bloch wall arrangement and of the microstructure (dislocations, precipitates and residual stresses), caused by isothermal tempering were investigated using transmission electron microscopy. For corresponding material conditions the magnetic and acoustic Barkhausen noise was measured using the pick-up technique. It was observed that the Bloch wall arrangement of the 22 NiMoCr 3 7 steel compared with the 15 MnMoNiV 5 3 steel changes distinctly with increasing tempering time. This is also true for the magnetic Barkhausen noise. The different dependence on tempering time for both steels is correlated with the different decrease of the dislocation density with tempering time. Using the microstructural data and the observed Bloch wall arrangements as base, a concept of a model describing the process of remagnetization is discussed. (11 refs.)
- 77202 Domain wall dynamics of rare-earth orthoferrites. Yu.V.Melikhov, O.A.Perekhod. *Ukr. Fiz. Zh. (USSR)*, vol.28, no.5, p.713-16 (May 1983). In Russian. An equation of motion is derived for a hard domain wall in a weak ferromagnet. It is shown that the gyrocoupling force in this type of a domain wall does not appear. Expressions are obtained for velocities of the steady-state motion of the hard domain wall and vertical Bloch line. (16 refs.)
- Susceptibility of an isotropic ferromagnet See Entry 77149
- The magnetic anisotropy of an aligned MnAlC magnet See Entry 77170
- Giant intrinsic magnetic hardness: Computer simulations on random moment dilution See Entry 77215
- Magnetization and structural studies on Cu-ferrite See Entry 77218
- Micromagnetic investigation of stripe domains See Entry 77223
- ΔE effect of a Mn ferrite single crystal at temperatures between 150 and 300K See Entry 77230

75.60E Magnetization curves, hysteresis, Barkhausen and related effects

- 77203 Pulse magnetisation of permanent magnets with a closed-loop assembly of electrical apparatus. V.I.Astapov, V.V.Vasil'ev, V.A.Nesterin. *Izv. VUZ Elektromekh. (USSR)*, no.3, p.87-90 (March 1983). In Russian. Discusses a technique for the magnetisation of permanent magnets, within a closed magnetic circuit of electrical apparatus. The construction of a single-turn magnetising inductor is described, a curve for the magnetic field in the working area is presented and recommendations are made for the choice of the geometrical parameters of the inductor. The procedure envisages the use of a pulse transformer unit, together with the single-turn inductor, for the magnetisation of permanent magnets. (2 refs.) Z.F.V.
- 77204 Hysteresis-free magnetisation in the presence of slowly varying and sinusoidal fields. V.P.Kholodkov. *Izv. VUZ Elektromekh. (USSR)*, no.3, p.91-6 (March 1983). In Russian. Investigates the process of a hysteresis-free magnetisation of ring ferromagnetic cores, in the presence of sinusoidal fields, and fields which vary slowly in an arbitrary manner. Expressions are derived, describing the relationship between the magnetisation of ring cores with a square hysteresis loop and parameters of these fields. (5 refs.) Z.F.V.

- 77205 Role of T^2 term in temperature dependence of the magnetization for Fe-Ni Invar alloys. I.Nakai, F.Ono, O.Yamada (Dept. of Phys., Okayama Univ., Okayama, Japan). *J. Phys. Soc. Jpn. (Japan)*, vol.52, no.5, p.1791-8 (May 1983). Precise measurements of magnetizations for single crystals of FCC Fe-Ni alloys in the Invar region have been made at temperatures from 4.2K to 300K in external applied fields up to 16.9 kOe to a relative accuracy of 5×10^{-3} . In an analysis of these observed results with iterative least-squares method, it is found that there exists a large Stoner-type contribution varying as $T^{2.00 \pm 0.05}$ besides the spin-wave one to the temperature change in magnetization and that the coefficient of the Stoner-type contribution increases rapidly with decreasing Ni concentration, showing a maximum at about 35 at.%Ni, and decreases for the alloys containing less than 35 at.%Ni. It becomes evident that ferromagnetism in FCC Fe-Ni alloys disappears at a critical concentration of about 31 at.%Ni. An anomalous behavior of the magnetization at low temperatures is also shown.
- 77206 Magnetic properties of $\text{Sn}_{1-x}\text{Cr}_x\text{Te}$ crystals. M.Inoue, Y.Takai, K.Fukui, H.Yagi, T.Tatsukawa (Faculty of Engng., Fukui Univ., Fukui, Japan). *J. Magn. & Magn. Mater. (Netherlands)*, vol.36, no.3, p.255-8 (April 1983). Magnetization measurements of magnetic semiconductor $\text{Sn}_{1-x}\text{Cr}_x\text{Te}$ ($x < 5$ at.%) crystals with the Curie temperature $T_c = 150$ -300K were made down to 2K. The magnetic properties are sensitive to isothermal annealing under Zn vapor. The overall magnetizations of the Zn-annealed crystals have paramagnetic and ferro- or antiferromagnetic components. (4 refs.)
- 77207 The hysteresis loop of two-phase particulate magnetic composite with non-linear hard magnetic components. K.-L.Wang, S.-E.Hsu, J.Chen (Nat. Taiwan Univ., Taipei, Taiwan). *J. Magn. & Magn. Mater. (Netherlands)*, vol.37, no.1, p.77-82 (May 1983). The method of calculating the B-H curve of two-phase ferromagnetic composite materials whose components have B-H relations of the form $B = mH + Br$ is extended to include materials whose components have non-linear B-H relations. The functional form of the non-linear B-H curve of the components materials is simulated by hyperbolic tangent functions with adjustable parameters. The results of theoretical calculations are compared to experimental data on Mn-Al-C and Fe-Cr-Co particulate composites. Good agreement is obtained. (9 refs.)
- 77208 Magnetization and Mossbauer studies of $\text{Y}(\text{Fe,Rh})_2$. J.Hrubec, W.Steiner, M.Reissner (Inst. für Angewandte und Tech. Phys., Tech. Univ. Wien, Wien, Austria). *J. Magn. & Magn. Mater. (Netherlands)*, vol.37, no.1, p.93-100 (May 1983). Magnetization as well as ^{57}Fe Mossbauer measurements of the cubic Laves phases $\text{Y}(\text{Fe,Rh})_{1-x}$ ($x \leq 0.3$) are reported. Pauli paramagnetism is observed for YRh_2 . At high temperatures Curie-Weiss behaviour is obtained for $x \geq 0.1$. The effective moments increase with increasing x, indicating that a polarization of the surrounding Rh atoms is caused by the substituted Fe atoms. At low temperatures no long-range magnetic order is observed, however, Mossbauer spectra with magnetic hyperfine splitting are recorded. The field dependence of the magnetization indicates the existence of noninteracting magnetic clusters. Field cooling effects and time dependence of the remanence are also observed. Therefore micromagnetism is suggested for these compounds, although no clear indication for the appearance of a maximum in the temperature dependence of the susceptibility is observed. (27 refs.)
- 77209 Magnetization and ^{161}Dy Mossbauer effect study of DyMn_2 and Dy,Mn_{1-x} and their ternary hydrides. P.C.M.Gubbens, W.Ras, A.M.van der Kraan, K.H.J.Buschow (Interuniv. Reactor Inst., Delft, Netherlands). *Phys. Status Solidi b (Germany)*, vol.117, no.1, p.277-82 (1 May 1983). The compounds DyMn_2 and $\text{Dy}_x\text{Mn}_{2-x}$ and their ternary hydrides are investigated by means of magnetic measurements and ^{161}Dy Mossbauer spectroscopy. In DyMn_2 magnetic ordering disappears after charging with hydrogen gas. In $\text{Dy}_x\text{Mn}_{2-x}$ the absorption of hydrogen gas leads to a strong reduction of the bulk magnetization even though the Dy sublattice remains magnetically ordered at low temperatures, with magnetic moments on the Dy atoms close to the free ion values. (12 refs.)
- 77210 Influence of substitution and addition of calcium on magnetic properties of $\text{Ni}_{0.245}\text{Zn}_{0.755}\text{Fe}_2\text{O}_4$ ferrite. C.Pasnicu, D.Condurache, E.Luca (Phys. Dept., Polytech. Inst. of Iasi, Iasi, Rumania). *Phys. Status Solidi a (Germany)*, vol.76, no.1, p.145-50 (16 March 1983). The influence of both Zn and Ni substitution and Ca addition on the stoichiometry in $\text{Ni}_{0.245}\text{Zn}_{0.755}\text{Fe}_2\text{O}_4$ ferrite on the saturation magnetization, Curie point, and initial permeability is studied. The dependence of these properties on the Ca amount is discussed. The results are interpreted taking into account the solubility of Ca^{2+} ions in the spinel lattice. (14 refs.)
- 77211 Model for a porous magnetized material. A.V.Sandulyak. *Sov. Phys.-Tech. Phys. (USA)*, vol.27, no.11, p.1391-2 (Nov. 1982). Translation of: *Zh. Tekh. Fiz. (USSR)*, vol.52, no.11, p.2267-9 (Nov. 1982). [received: May 1983]
- The theory of how porous materials (consisting of spherical particles) are magnetized is developed further and it is shown that efficient magnetic flux 'channels' are present in such materials. An equation is derived for calculating the magnetic permeability of a quasicontinuous channel and the effective channel radius. (4 refs.)
- 77212 Preparing conditions and magnetic properties of rapidly quenched high silicon iron ribbons. Y.Yoshida, Y.Yamashiro, N.Teshima, K.Narita. *Technol. Rep. Kyushu Univ. (Japan)*, vol.55, no.6, p.627-33 (Dec. 1982). In Japanese. [received: May 1983]
- Preparation conditions and magnetic properties of rapidly quenched high silicon iron ribbons containing 4.5%-6.5%Si have been investigated. The tensile strength and the ductility of high silicon iron ribbons were improved compared with sheet-formed high silicon iron. The specimens were annealed at 1100°C-1200°C for 1 hr in H_2 gas or in vacuum. The maximum permeability μ_m of 17000, and the minimum coercive force H_c of 0.3 Oe were obtained on the specimen of 6.5%Si-Fe with 90 μm thickness. For the 6.5%Si-Fe quenching effect on the coercive force had been investigated, but marked improvement was not observed in the authors' quenching temperature range (400-600°C). (7 refs.)
- Magnetic field dependence of the electronic specific heat of TiBe_2 : an estimate from magnetization data See Entry 76663
- Specific heat of $\text{Co}(\text{S}_{1-x}\text{Se}_x)_2$ and magnetic properties in weak fields See Entry 76666
- Thermodynamical and structural properties of amorphous $\text{Fe}_{80}\text{B}_{20}$ and $\text{Fe}_{80}\text{P}_{13}\text{C}_7$ alloys See Entry 76922
- Susceptibility of an isotropic ferromagnet See Entry 77149
- Magnetic properties of amorphous Co and Ni alloys See Entry 77151
- Random-field effects and magnetic susceptibility in diluted three-dimensional antiferromagnets $\text{Mn}_x\text{Zn}_{1-x}\text{F}_2$ See Entry 77153

Effects of transition metal substitutions on magnetic properties of Co-based amorphous alloys See Entry 77154

Study of the critical behaviour of the magnetization and electrical resistivity in cubic $\text{La}(\text{Fe}, \text{Si})_{13}$ compounds See Entry 77155

Magnetic susceptibility of $\text{Fe}_{1-x}\text{Co}_x\text{Si}$ solid solutions See Entry 77158

Magnetic excitations in FCC Fe-Ni alloys revealed from detailed magnetization measurements See Entry 77163

The magnetic anisotropy of an aligned MnAlC magnet See Entry 77170

Magnetic anisotropy of ErCo_4Cu single crystals See Entry 77171

Magnetic properties of $(\text{Cr}_{1-y}\text{Rh}_y)_2\text{Te}_4$ See Entry 77174

Magnetic properties of a disordered magnet with strong fluctuations in the exchange interactions See Entry 77197

Bloch wall arrangement and Barkhausen noise in steels 22 NiMoCr 3 7 and 15 MnNiV 5 3 See Entry 77201

Fe-Cr-Co ductile permanent magnet alloy with $(\text{BH})_{\text{max}} \approx 7.0$ MGOe See Entry 77214

Anhyseretic and hysateretic magnetic properties of small Fe_3O_4 particles See Entry 77216

Effect of magnetic field in RF sputtering on the crystal orientation and magnetic properties of Co-Cr perpendicular anisotropy films See Entry 77219

Anomalous thickness dependence of the saturation magnetization in Fe-Ni Invar alloy films See Entry 77220

Micromagnetic investigation of stripe domains See Entry 77223

Stabilization of a stripe domain structure in amorphous Co-P films by annealing See Entry 77226

ΔE effect of a Mn ferrite single crystal at temperatures between 150 and 300K See Entry 77230

NMR and magnetization study of the mixed systems $(\text{Pd}_{1-x}\text{Cu}_x)_2\text{MnIn}$ and $(\text{Pd}_{1-x}\text{Ni}_x)_2\text{MnIn}$ See Entry 77285

Perpendicularly crystallized ribbons by means of rapid solidifications from melts See Entry 77598

75.60G High coercivity materials

77213 Magnetically hard Alnico 5 alloy with a mischmetal addition. S.Szymura (Inst. of Phys., Tech. Univ. of Czestochowa, Czestochowa, Poland). *J. Magn. & Magn. Mater. (Netherlands)*, vol.37, no.1, p.69-76 (May 1983). The addition of mischmetal (CeM) to the Alnico 5 alloy of equiaxial grain structure in the amounts of 0.0 to 0.31 wt.% and its effect on the magnetic properties, the crystal structure and on the type of non-metallic inclusions in the alloy has been studied. The addition of CeM in amounts within the examined limits, was found to cause a worsening of all magnetic properties of the Alnico 5 alloy, the greatest changes being observed in the maximum magnetic energy product $(\text{BH})_{\text{max}}$ and the smallest in the coercive force H_c . CeM also causes a considerable reduction in the size of grains. The main types of non-metallic inclusions in the Alnico 5 alloy with CeM addition are: oxide $(\text{CeMM})_2\text{O}_3$, oxysulphides $(\text{CeMM})_2\text{O}_3\text{S}$ and sulphides $(\text{CeMM})_2\text{S}_3$, type, on the edges of which occur titanium or manganese sulphides. For up to 0.16 wt.% of CeM the mean content of non-metallic inclusions in the alloy is decreasing, whereas it is markedly rising with the content of the CeM over 0.16 wt.%. Also the mean size of inclusions is clearly smaller in the alloy with less than 0.16 wt.% of CeM than with higher contents of CeM. A 0.16 wt.% addition of CeM significantly improves the susceptibility of Alnico 5 alloy to surface finishing treatment by grinding. (27 refs.)

77214 Fe-Cr-Co ductile permanent magnet alloy with $(\text{BH})_{\text{max}} \approx 7.0$ MGOe. Li Dongsheng, Peng Huizi, Sun Jinsheng, Zhang Yuquan, Ju Kechang (Tianjin Metall. Res. Inst., China). *Kexue Tongbao (Foreign Lang. Ed.) (China)*, vol.28, no.1, p.45-50 (Jan. 1983). [received: June 1983] The authors present a study of the Fe-Cr-Co alloy with high $(\text{BH})_{\text{max}}$ value. The effects of the addition of Zr, the covering of the Co content and the addition of Si on the magnetic properties B_r , H_c , and $(\text{BH})_{\text{max}}$ are presented. (4 refs.)

77215 Giant intrinsic magnetic hardness: Computer simulations on random moment dilution. M.Fahnlé (Inst. fur Phys., Max Planck Inst. fur Metallforschung, Stuttgart, Germany). *Phys. Rev. B (USA)*, vol.27, no.9, p.5586-91 (1 May 1983). Aspects of the phenomenology of giant intrinsic magnetic hardness in systems such as $\text{R}(\text{Co}_{1-x}\text{M}_x)_2$ (R represents lanthanides; M represents Ni, Cu, Al) are treated theoretically on a topological approach. They encompass the extraordinary strength of the domain-wall pinning at cryogenic temperatures, a chemical regularity concerning the concentration dependence of coercivity $H_c^0(x)$ and the so-called Sm-La paradox which represents the experimental experience that the general curve shape of $H_c^0(x)$ is similar in systems with $R=\text{Sm}$ and $R=\text{La}$ although anisotropy fields are dissimilar (while exchange fields are similar). In particular, the Sm-La paradox leads one to consider topological arrangements within the diluted transition-metal sublattice as an important contribution for intrinsic hardness. A Monte Carlo computer simulation based on single spin-tunneling processes is used to describe the giant intrinsic magnetic hardness. The model relates the onset of the steep increase of the $H_c^0(x)$ curves to the percolation concentration of magnetic Co atoms in the diluted transition-metal sublattice. Because the percolation concentration is totally determined by the topology of the lattice, this gives a natural explanation for the Sm-La paradox. The chemical regularity concerning the curve shapes of $H_c^0(x)$ for different elements M is discussed by taking into account the quenching of Co moments when diluting the transition metal sublattice with various M atoms. (15 refs.)

The magnetic anisotropy of an aligned MnAlC magnet See Entry 77170

Magnetic anisotropy of ErCo_4Cu single crystals See Entry 77171

75.60J Fine-particle systems

77216 Anhyseretic and hyseteretic magnetic properties of small Fe_3O_4 particles. R.Veitch, E.Schmidbauer (Univ. Munchen, Munich, Germany). *J. Magn. & Magn. Mater. (Netherlands)*, vol.37, no.1, p.63-8 (May 1983). The initial anhyseretic susceptibility, initial anhyseretic remanent susceptibility and initial reversible susceptibility have been measured at room temperature on samples of varying concentrations of equidimensional Fe_3O_4 particles in the size range 0.1-0.3 μm as a function of packing factor and sample shape. Hysteresis parameters have been determined on spherical samples with various packing factors. (28 refs.)

The hysteresis loop of two-phase particulate magnetic composite with non-linear hard magnetic components See Entry 77207

Magnetic hyperfine splitting in Mossbauer spectra of microcrystals See Entry 77303

75.60L Magnetic aftereffects

77217 Study of magnetic after-effects in the amorphous alloy $\text{Fe}_{40}\text{Ni}_{40}\text{P}_{14}\text{B}_6$. H.Borner, R.Hohne (Sektion Phys., Karl-Marx-Univ., Leipzig, Germany). *Phys. Status Solidi a (Germany)*, vol.76, no.2, p.499-503 (16 April 1983). The effect is investigated of repeated annealing treatments on the magnetic diffusion after-effect in the amorphous alloy $\text{Fe}_{40}\text{Ni}_{40}\text{P}_{14}\text{B}_6$ using measurements of disaccommodation and induced magnetic anisotropy. The process of varying the magnitude of the disaccommodation maximum due to annealing at various temperatures is repeatable. It is found that evidently the maximum attainable disaccommodation effect decreases with each annealing cycle. Using the damping of free torsional vibrations of the sample in a saturating magnetic field no relaxation effect of induced magnetic anisotropy may be found. There are given two possibilities of interpretation of the observed behaviour. (9 refs.)

Annealing behaviour of dilute FeTi, FeCu, and FeMn alloys in the temperature range above stage III following low-temperature electron irradiation See Entry 77682

75.60N Magnetic annealing and temperature-hysteresis effects

77218 Magnetization and structural studies on Cu-ferrite. S.R.Sawant, R.N.Patil (Dept. of Phys., Shivaji Univ., Kolhapur, India). *Indian J. Pure & Appl. Phys.*, vol.21, no.3, p.145-7 (March 1983). Molecular magnetization, remanent magnetization, remanence ratio and cation distribution are computed for the slow-cooled and quenched samples of CuFe_2O_4 . A-B interactions are strengthened on quenching the samples. The remanence ratio, however, is unaffected by quenching which is explained as due to the impedance to domain-wall motion. All the samples exhibit almost the same hysteresis loss. The quenched samples show higher permeability and less coercivity. Quenched as well as slow-cooled CuFe_2O_4 samples show tetragonal distortion of the lattice which decreases with the increase of the temperature of quenching. This is explained by cation transfer. (11 refs.)

75.70 MAGNETIC FILMS AND PLATES

77219 Effect of magnetic field in RF sputtering on the crystal orientation and magnetic properties of Co-Cr perpendicular anisotropy films. H.Maeda (Tsukuba Labs., Nat. Res. Inst. for Metals, Ibaraki, Japan). *J. Appl. Phys. (USA)*, vol.54, no.5, p.2429-33 (May 1983). Co-23-wt. %Cr alloy films with thicknesses of 0.3 to 2.5 μm were deposited using a conventional RF diode sputtering system when a magnetic field H_s less than 90 Oe is applied during deposition. As H_s increases, the HCP c -axis orientation normal to the film plane develops and the half-angle width of the rocking curve of the (002) line $\Delta\theta_{50}$ reaches to 3.5 deg at H_s more than 40 Oe. The development of the orientation is strongly related to the concentration of O in the films, which is lower in the films deposited in a magnetic field than those in a nonmagnetic field. The magnetic properties such as perpendicular coercive force $H_{c\perp}$ and saturation magnetisation M_s strongly depend on the substrate temperature rather than H_s . (18 refs.)

77220 Anomalous thickness dependence of the saturation magnetization in Fe-Ni Invar alloy films. M.Konno (Dept. of Phys., Metropolitan Coll. of Technol., Tokyo, Japan). *J. Phys. Soc. Jpn. (Japan)*, vol.52, no.5, p.1759-64 (May 1983). Invar alloy films with the FCC structure were prepared using the vacuum evaporation technique. Using the thickness graded film in the alloy compositions of 21%NiFe and 36%NiFe, the thickness dependence of saturation magnetization was studied. As the film thickness decreases from 1000 Å to 200 Å, the saturation magnetization of 36%NiFe decreases monotonically and that of 21%NiFe initially increases down to 350 Å, and finally decreases. The temperature dependence of the saturation magnetization of 21%NiFe shows very flatter one compared with that of the theoretical Brillouin function. These results are supposed to be originated not from the existence of the gradient of the composition but from the appearance of γ_2 phase through the interface interaction between the substrate and film.

77221 The variation of magnetic properties of Fe-based amorphous alloys along the ribbon length. T.Sato, T.Ozawa, T.Yamada, R.Matsumoto (Fundamental Res. Labs., Nippon Steel Corp., Kawasaki, Japan). Rapidly Solidified Amorphous and Crystalline Alloys. Proceedings of the Materials Research Society Annual Meeting, Boston, MA, USA, Nov. 1981 (New York, USA: North-Holland 1982), p.205-9 The variation of AC magnetic properties along the length of melt-spun Fe-based amorphous ribbons was examined in relation to the variations of the roller surface temperature and the ribbon thickness. The results indicated that the lengthwise variation of magnetic properties strongly depends both on the roller surface temperature and the ribbon thickness. The critical cooling rates at which core loss begins to increase were determined from the relationship between core loss and cooling rate. For ribbons cast at lower cooling rate than critical cooling rate, the fine-domain patterns were usually observed on the free surface. From the disappearance of the fine-domain pattern and the remarkable decrease of core loss by removal of the surface layers, it is ascertained that the surface layers deteriorate magnetic properties. (2 refs.)

77222 The effects of ribbon thickness and annealing temperature on the AC magnetic properties of the $\text{Fe}_{81.5}\text{B}_{14.5}\text{Si}_2\text{C}_1$ alloy. S.C.Huang, P.G.Frischmann, F.E.Luborsky, J.D.Livingston, A.Mogro-Campero (General Electric Corporate Res. & Dev., Schenectady, NY, USA). Rapidly Solidified Amorphous and Crystalline Alloys. Proceedings of the Materials Research Society Annual Meeting, Boston, MA, USA, Nov. 1981 (New York, USA: North-Holland 1982), p.211-16 The AC magnetic properties measured at 60 Hz are found to be strongly affected by amorphous ribbon thickness and annealing temperature. These magnetic results are further characterized by observation on magnetic domain structure, crystallization, stress relaxation, and ribbon surface finish. (10 refs.)

Acoustic emission initiated by ion implantation in bubble garnet films See Entry 76567

Calculation of the Green's function for the micromagnetic thin film problem See Entry 77182

The magnetoelectric effect in iron-manganese spinels See Entry 77249

Epitaxial growth and annealing control of EMR properties of thick homogeneous Ga substituted yttrium iron garnet films See Entry 77267
Influence of ion implantation on high-frequency properties of domain walls in thin magnetic films See Entry 77268

75.70K Domain structure (magnetic bubbles)

77223 Micromagnetic investigation of stripe domains. A.S.Zhukarev (M.V. Lomonosov State Univ., Moscow, USSR). *Fiz. Met. & Metalloved. (USSR)*, vol.55, no.4, p.655-9 (April 1983). In Russian. English translation in: *Phys. Met. & Metallogr. (GB)*

A micromagnetic calculation is made of a two-dimensional distribution of the magnetization in a stripe domain structure of the open type observed in plane-parallel plates and films. The period of the structure and the domain wall thickness are found as a function of the plate thickness and anisotropy parameter. The boundary conditions are formulated for the 'surface' of a domain wall. It is found that a domain wall is charged and twisted, and the twist angle depends on two coordinates. (16 refs.) *A.T.*

77224 Direct observation of domain nucleation in garnet films. V.G.Kleparskii, I.Pinter (Central Res. Inst. for Phys., Hungarian Acad. of Sci., Budapest, Hungary).

Phys. Status Solidi a (Germany), vol.76, no.1, p.K1-4 (16 March 1983). Domain nucleation in garnet films is not only of theoretical but also of practical interest especially for magnetic bubble devices in which controlled domain nucleation is used to introduce new information but if uncontrolled can lead to device failure. The authors described direct observation of the domain nucleation process by the high speed photography method (HSP). Experiments were performed using (Y,Yb,Bi,Gd)₃(Fe,Al)₅O₁₂ film grown by the LPE method on (111)-oriented GGG substrate. (4 refs.)

77225 Problem of the dynamics of nonthrough magnetic bubble domains. A.F.Martynov, V.V.Randoshkin, R.V.Telesnin (M.V. Lomonosov State Univ., Moscow, USSR). *Sov. Phys.-Solid State (USA)*, vol.24, no.11, p.1969-70 (Nov. 1982). Translation of: *Fiz. Tverd. Tela (USSR)*, vol.24, no.11, p.3463-5 (Nov. 1982). [received: May 1983]

The authors have used the method of high-speed photography to study the dynamics of translational motion of nonthrough bubble domains under the action of a pulsed gradient field applied to two-layer ferrite garnet films. The pulsed gradient field was created by a pair of conductors located on the surface of a sample and separated by 160 μ m from one another. The pulse duration was selected so as to ensure that the nonthrough bubble domains were displaced by a distance not exceeding one bubble diameter. Before the measurements the domains were brought to the center between the conductors by applying small-amplitude pulses from the side opposite to their subsequent motion. (4 refs.)

77226 Stabilization of a stripe domain structure in amorphous Co-P films by annealing. L.S.Palatnik, A.G.Ravlik, S.T.Roshchenko, V.N.Samofalov, I.G.Shipkova (V.I. Lenin Polytech. Inst., Kharkov, Ukrainian SSR). *Sov. Phys.-Solid State (USA)*, vol.24, no.12, p.2113-14 (Dec. 1983). Translation of: *Fiz. Tverd. Tela (USSR)*, vol.24, no.12, p.3706-8 (Dec. 1983).

The authors have investigated amorphous Co-P films with a stripe domain structure, associated with the so-called transverse anisotropy. The domain structure was revealed by the Akulov-Bitter method. At the same time an induction apparatus was used to observe hysteresis loops from which they deduced the saturation field (H_s) and a rotational anisotropy enabled them to determine—from the torque curves—the anisotropy constant in the plane of the film (K_1) and the saturation magnetization (M_s) amounting to 650.10³ A/m (650 G) for the films under investigation. The transverse anisotropy constant was estimated from $K_{\perp} = \mu_0 M_s^2/2$. The influence of macrostresses in the film was minimized by separating the films from the substrates. (4 refs.)

Preparation and magnetic characteristics of garnet films with cylindrical magnetic bubbles in the submicron range See Entry 77563

75.80 MAGNETOMECHANICAL AND MAGNETOELECTRIC EFFECTS, MAGNETOSTRICTION

77227 Magnetostriction of bismuth and graphite in fields up to 40 Tesla. Y.Iye (Inst. for Solid State Phys., Univ. of Tokyo, Tokyo, Japan), J.Heremans, K.Nakamura, G.Kido, N.Miura, J.-P.Michenaud, S.Tanuma. *J. Phys. Soc. Jpn. (Japan)*, vol.52, no.5, p.1692-700 (May 1983).

Longitudinal magnetostriction has been measured in bismuth along the binary axis and in graphite along the *c*-axis in pulsed magnetic fields up to 40 T. The field dependence of the magnetostriction of bismuth is compared with theoretical calculations based on a model proposed by Vecchi et al. for the lowest quantum number Landau levels. A better correspondence with the experimental result is obtained by using a set of parameter values recently given by Hiruma et al. rather than the original Vecchi et al.'s values. For graphite, a large and field-superlinear magnetostriction has been found.

77228 Giant cobalt-induced anisotropic magnetostriction in GdCo₂. R.Z.Levitin, A.S.Markosyan, V.V.Snegirev (M.V. Lomonosov State Univ., Moscow, USSR).

JETP Lett. (USA), vol.36, no.10, p.445-8 (20 Nov. 1982). Translation of: *Pisma v Zh. Eksp. & Teor. Fiz. (USSR)*, vol.36, no.10, p.367-9 (20 Nov. 1982). [received: June 1983]

An X-ray diffraction analysis of the crystalline structure of the intermetallic compound GdCo₂ was performed in the temperature range 5-500K and giant anisotropic magnetostriction 1×10^{-3} was observed at a temperature 5.5K. From a comparison of X-ray diffraction analyses of the compounds GdAl₂, GdNi₂, and GdFe₂, it is concluded that the anisotropic magnetostriction in GdCo₂ is due to the cobalt. The longitudinal and transverse magnetostriction of GdCo₂ at $T=4.2$ K in pulsed magnetic fields up to 230 kOe is also investigated and the large magnetostriction of the paraprocess, caused by the band nature of the magnetism of cobalt in the compound GdCo₂, is observed. (6 refs.)

77229 Magnetoelastic properties of PrAg. M.Giraud, P.Morin, J.Rouchy, D.Schmitt, E.du Tremolet de Lacheisserie (Lab. Louis Neel, CNRS, Grenoble, France).

J. Magn. & Magn. Mater. (Netherlands), vol.37, no.1, p.83-92 (May 1983). Parastriation and ultrasonic velocity experiments have been performed in order to have a better knowledge of the magnetic and quadrupolar interactions in PrAg, an intermetallic compound (CsCl-type structure) which exhibits puzzling magnetic properties, extensively studied in the recent past. As a first result, the existence of a ferromagnetic transition at $T_c=7.3$ K below the Neel temperature ($T_N=10.5$ K) is confirmed on monocrystalline samples. In all the

ordered range, the magnetic structure is proved to be multiaxial: first the knowledge of the magnetoelastic coefficients allows the authors to rule out the collinear structure, explaining the lack of any spontaneous strain. On the other hand, the quadrupolar interactions, found weakly negative, favour an antiferroquadrupolar arrangement in agreement with a multiaxial spin ordering. The stability of the CsCl-type lattice at low temperature is then discussed in connection with the instability features observed in neighbouring compounds LaAg and CeAg. It appears that in these three compounds many origins may be simultaneously proposed for the instability tendency: an electronic deformation potential coupling, a e_g strain coupling with zone boundary phonon and the magnetoelastic coupling. PrAg appears to be clearly more stable than the other two compounds. (28 refs.)

77230 ΔE effect of a Mn ferrite single crystal at temperatures between 150 and 300K. Y.Kawai, T.Ogawa (Dept. of Phys., Gakushuin Univ., Tokyo, Japan).

Phys. Status Solidi a (Germany), vol.76, no.1, p.375-81 (16 March 1983). The changes of Young's moduli with magnetization (i.e. the ΔE effect) in the [100], [110], and [111] directions of a Mn_{0.87}Fe_{1.13}O₄ single crystal are studied at temperatures between 150 and 300K as a function of the d.c. magnetic field. Two types of ΔE effects in weak magnetic fields are observed. It is found that the effects are closely related to magnetization processes in the specimens. The first type, in which Young's modulus decreases initially and then increases with magnetization, is caused by the displacements of non-180° domain walls, and then is caused by the rotation of magnetization. The second type, in which Young's modulus increases monotonically with magnetization, is caused mainly by the rotation of magnetization. (14 refs.)

77231 Useful relations for highly sensitive sensors based on carrier concentration. A.Chovet, S.Cristoloveanu, Y.Daher (Lab. de Phys. des Composants a Semiconducteurs, Ecole Normale Supérieure d'Electronique et de Radioelectricté, Grenoble, France), V.K.Malyutenko.

Phys. Status Solidi a (Germany), vol.76, no.1, p.K43-8 (16 March 1983). In semiconductor slabs, high current enhancement can be produced by the magnetoconcentration effect when the sensor operates under electric or magnetic fields derive general relations allowing to forecast (according to material properties) the bounds of sensitivity, the optimum slab thickness, the fields to be applied as well as the corresponding carrier concentrations. Moreover it is experimentally evidenced that sensitivities larger than 1500 V/T can be obtained from 100 μ m thick Ge samples. (7 refs.)

77232 Magnetic interactions in plastically deformed Ni₃Mn alloy. S.Takahashi, K.Ikeda (Faculty of Engng., Iwate Univ., Iwate, Japan).

Phys. Status Solidi a (Germany), vol.76, no.1, p.K97-100 (16 March 1983). The modified slip-induced-directional-order model is extended to the magnetic interaction in the cold worked Ni₃Mn alloy. The net magnetisation at 0K versus the dislocation density is estimated. (8 refs.)

77233 Theoretical aspects of magnetoelasticity in transition metals and alloys. M.Shimizu, J.Inoue, Y.Ohta, K.Niwa (Dept. of Appl. Phys., Nagoya Univ., Nagoya, Japan).

Physica B & C (Netherlands), vol.119 B+C, no.1-2, p.3-14 (April 1983). (Proceedings of the International Symposium on Magnetoelasticity in Transition Metals and Alloys, Nagoya, Japan, 15-16 Sept. 1982).

The authors' recent theoretical studies are summarized. The magnetovolume effect in Fe and Ni is discussed and the effects on the volume striction of spin fluctuations are estimated in the paramagnetic state of Fe, Ni, Cr and ZrZn₂. The pressure dependence of the Curie temperature and first-order transition temperature and forced magnetostriction are calculated in a combined model of localized spins and itinerant d-electrons and the observed results for dilute Pd and Pt alloys with Fe, Co and Ni atoms and rare earth-Co₂ compounds are explained. Anisotropic magnetoelastic coupling constants in Fe and deformations of energy levels, Fermi surfaces and density of states due to shear strains in V are calculated in a tight-binding parametrisation scheme. A topological change of the Fermi surfaces due to shear strains is obtained in V. The electronic contribution to elastic shear constants is also calculated. The electronic Grüneisen constant is calculated for Nb and a comparison with experiment is carried out. (53 refs.)

77234 An itinerant-electron theory of Invar effects. H.Hasegawa (Inst. for Solid State Phys., Univ. of Tokyo, Tokyo, Japan).

Physica B & C (Netherlands), vol.119 B+C, no.1-2, p.15-20 (April 1983). (Proceedings of the International Symposium on Magnetoelasticity in Transition Metals and Alloys, Nagoya, Japan, 15-16 Sept. 1982).

The spin fluctuation theory for finite-temperature magnetism developed previously by the present author is applied to discuss anomalously strong magnetovolume effects in Invar alloys. Numerical calculations for NiFe alloys show that a large spontaneous volume magnetostriction in the Invar alloy is attributed to a significant reduction in the amplitude of local magnetic moments, (m^2), in the paramagnetic states compared with the ground-state moment. It is also shown that a large $-\partial T_c/\partial P$ is due to a reduction in (m^2) by an applied pressure P and that a large forced magnetostriction arises from a considerable increase in (m^2) by an applied magnetic field H . It is concluded that Invar anomalies originate from non-rigid local magnetic moments whose amplitude varies easily by changing external parameters such as T , P and H . (20 refs.)

77235 Magnetovolume effects in the local-band theory of ferromagnetism: pressure dependence of T_c in iron and nickel. V.Korenman (Dept. of Phys. & Astron., Univ. of Maryland, College Park, MD, USA).

Physica B & C (Netherlands), vol.119 B+C, no.1-2, p.21-4 (April 1983). (Proceedings of the International Symposium on Magnetoelasticity in Transition Metals and Alloys, Nagoya, Japan, 15-16 Sept. 1982).

In the local-band theory the spontaneous volume magnetostriction and the pressure dependence of T_c are related to one another through their dependence on the volume coefficient of A , the Bloch wall stiffness constant. The available data in iron and nickel are consistent with this relation, and bear a proper relation to the measured energy associated with the phase transition. The author also shows, in the context of a Heisenberg model, that it is short-range order which is mainly responsible for the good agreement. (23 refs.)

77236 Magnetovolume effects in the Moriya-Kawabata theory of very weak itinerant ferromagnetism. D.M.Edwards, C.J.MacDonald (Dept. of Math., Imperial Coll., London, England).

Physica B & C (Netherlands), vol.119 B+C, no.1-2, p.25-9 (April 1983). (Proceedings of the International Symposium on Magnetoelasticity in Transition Metals and Alloys, Nagoya, Japan, 15-16 Sept. 1982).

The Moriya-Kawabata theory is extended to include the effect of pressure and to discuss magnetovolume effects, particularly in the neighbourhood of T_c . It is found that the volume strain $\omega(T)$, relative to the paramagnetic state at $T=0$, satisfies $\omega(T_c)/\omega(0)=\eta(T_c)$ where $\eta(T_c)$ is the ratio of the mean squared local moment at T_c to that at $T=0$. However $\eta(T_c)>1$ so that no negative magnetic contribution to the thermal expansion exists in this theory and the Invar effect frequently observed in very weak itinerant ferromagnets

is not explained: It is found that the pressure dependence of T_c is given by $T_c \propto (1-P/P_c)^{3/4}$. (19 refs.)

77237 Electron-phonon interaction model for the relation between magnetic and elastic properties in itinerant electron ferromagnets. D.J.Kim (Dept. of Phys., Aoyama Gakuin Univ., Tokyo, Japan). *Physica B & C (Netherlands)*, vol.119 B+C, no.1-2, p.30-6 (April 1983). (Proceedings of the International Symposium on Magnetoelasticity in Transition Metals and Alloys, Nagoya, Japan, 15-16 Sept. 1982).
By pursuing the role of the exchange interaction between electrons in the screening of the ion-ion interaction in a metal, the author recently showed how directly the magnetic properties of the metal are reflected on the elastic properties such as phonon frequency and sound velocity. Now he asks the opposite question: Is it necessary to consider the electron-phonon interaction (EPI) in understanding the magnetic properties of a metal? The author finds it essential to consider EPI; by the effect of EPI, in the paramagnetic state of an itinerant electron ferromagnet the spin susceptibility is made Curie-Weiss-like, and in the ferromagnetic state the magnetization can be reduced by as much as $\sim 1 \mu_B$ per atom. These findings offer a comprehensive fundamental viewpoint to discuss the relation between the elastic and magnetic properties in itinerant electron ferromagnets. (10 refs.)

77238 High-pressure effects on the $2k_F$ and $4k_F$ transitions in the quasi-one-dimensional magnetic conductor MEM-(TCNQ)₂. D.Bloch, J.Voiron (Lab. Louis Neel, CNRS, Grenoble, France), C.Vettier, J.W.Bray, S.Oostra. *Physica B & C (Netherlands)*, vol.119 B+C, no.1-2, p.43-50 (April 1983). (Proceedings of the International Symposium on Magnetoelasticity in Transition Metals and Alloys, Nagoya, Japan, 15-16 Sept. 1982).
MEM-(TCNQ)₂ possesses at room pressure both an electronic transition, associated with a $4k_F$ lattice distortion and a magnetic-to-non-magnetic transition associated with a $2k_F$ lattice distortion. The high-pressure phase diagram, determined from neutron scattering, electrical transport, and magnetization experiments, indicates a disappearance of both the $2k_F$ and $4k_F$ distortions above 4 kbar. (28 refs.)

77239 Thermal expansion of Cr and Cr-V alloys. R.B.Roberts, G.K.White (CSIRO Div. of Appl. Phys., Sydney, Australia), E.Fawcett. *Physica B & C (Netherlands)*, vol.119 B+C, no.1-2, p.63-7 (April 1983). (Proceedings of the International Symposium on Magnetoelasticity in Transition Metals and Alloys, Nagoya, Japan, 15-16 Sept. 1982).
At low temperatures, the linear expansion coefficient α of a Cr+0.5% V alloy is similar to that of chromium, i.e. $10^{-6} \alpha = -37 \pm 0.02 \text{ } ^\circ\text{K}^{-1}$ ($T < 30\text{K}$), giving an electronic and/or magnetic Grüneisen parameter $\gamma_{em} \approx -10$. For the non-magnetic alloy Cr+5% V, $10^{-6} \alpha = 11 \pm 0.03 \text{ } ^\circ\text{K}^{-1}$ and $\gamma_{em} \approx 2.0$. At higher temperatures, $\alpha(T)$ for the 5% alloy increases monotonically and is significantly larger than for pure Cr up to 520K; $\alpha(T)$ for the latter shows a negative cusp at 311K with a first-order transition. (22 refs.)

77240 Thermal expansion of ZrZn₂. S.Ogawa (Electrotech. Lab., Ibaraki, Japan). *Physica B & C (Netherlands)*, vol.119 B+C, no.1-2, p.68-71 (April 1983). (Proceedings of the International Symposium on Magnetoelasticity in Transition Metals and Alloys, Nagoya, Japan, 15-16 Sept. 1982).
Thermal expansion of the weak itinerant electron ferromagnet ZrZn₂ has been measured in the temperature range 10 to 260K. An analysis was made to separate a magnetic contribution to thermal expansion. It is concluded that there is a positive magnetic thermal expansion in the paramagnetic state in addition to a negative one in the ferromagnetic state. (13 refs.)

77241 Thermal expansion and specific heat anomalies in UPt below the ferromagnetic ordering temperature. C.F.Kamma, P.H.Frings, J.C.P.Klaasse, J.J.M.Franse (Naturkundig Lab., Univ. van Amsterdam, Amsterdam, Netherlands). *Physica B & C (Netherlands)*, vol.119 B+C, no.1-2, p.72-7 (April 1983). (Proceedings of the International Symposium on Magnetoelasticity in Transition Metals and Alloys, Nagoya, Japan, 15-16 Sept. 1982).
Thermal expansion, AC susceptibility and specific heat measurements in UPt below the ferromagnetic transition temperature ($T_c \approx 27\text{K}$) reveal an additional transition of magnetic origin near 19K, possibly indicating a change in the magnetic spin structure. The coefficient of thermal expansion is negative below 6K and points to a decrease of the intrinsic value of the magnetic moment with increasing temperature. The value for the magnetovolume parameter, derived from forced magnetostriction and magnetization measurements at 4.2K, is close to the results obtained for 3d metals. (13 refs.)

77242 Thermal expansion measurements in Fe-base Invar alloys. F.Ono, T.Kittaka (Coll. of Liberal Arts & Sci., Okayama Univ., Okayama, Japan), H.Maeta. *Physica B & C (Netherlands)*, vol.119 B+C, no.1-2, p.78-83 (April 1983). (Proceedings of the International Symposium on Magnetoelasticity in Transition Metals and Alloys, Nagoya, Japan, 15-16 Sept. 1982).
By using the X-ray bond method, measurements of thermal expansion curves have been made in Fe-Ni and Fe-Pd Invar alloys in the temperature range between 4.2K and room temperatures. A minimum in the thermal expansion curve was observed for each alloy. This anomaly could be explained by considering the magnetovolume coupling term caused by the longitudinal spin fluctuation and the contribution due to the anharmonic terms in the normal lattice vibration energy. In 34.2 at% Pd-Fe alloy an abnormal increase of the linewidth of the (400) X-ray peak was observed with decreasing temperature from room temperature down to 4.2K, while in Fe-Ni and Fe-Pt Invar alloys no such increase in linewidth was observed. (23 refs.)

77243 Invar anomalies of Fe-Pd alloys. M.Matsui, T.Shimizu, K.Adachi (Dept. of Iron & Steel Engng., Nagoya Univ., Nagoya, Japan). *Physica B & C (Netherlands)*, vol.119 B+C, no.1-2, p.84-9 (April 1983). (Proceedings of the International Symposium on Magnetoelasticity in Transition Metals and Alloys, Nagoya, Japan, 15-16 Sept. 1982).
The Mossbauer spectra and the magnetostriction have been observed for Fe_{1-x}Pd_x alloys. The internal field of Fe atoms is $330 \pm 10 \text{ kOe}$ and is almost constant in the Invar region $0.45 \leq x \leq 0.3$. The magnetostriction constants as well as forced magnetostriction ($\partial\omega/\partial H$) increase with decreasing temperature and with decreasing x . Observed large values of magnetostriction constants are related to a lattice instability of the FCC structure, which is confirmed by the measurement of elastic constants. The magnitude of $\partial\omega/\partial H$ is about one-fifth of Fe-Ni Invar. The thermal expansion of Fe_{1-x}Pd_x alloys has also been measured in the whole concentration range. The Invar-like behavior observed in the region $0.28 \leq x > 0$ originates from an annealing effect of the martensite BCC phase. The spontaneous volume magnetostriction in the FCC region increases with decreasing x . The thermal expansion coefficients (α_{exp}) of FCC alloys are analyzed from the Grüneisen equation. The high-temperature anomaly of α_{exp} is discussed. (13 refs.)

77244 Contribution of the temperature change in the local magnetic moment to the Invar effect. O.Yamada (Dept. of Phys., Okayama Univ., Okayama, Japan). *Physica B & C (Netherlands)*, vol.119 B+C, no.1-2, p.90-5 (April 1983). (Proceedings of the International Symposium on Magnetoelasticity in Transition Metals and Alloys, Nagoya, Japan, 15-16 Sept. 1982).
The mean value of the local magnetic moment $M_{loc}(T)$ of Invar alloys at a finite temperature T can be practically expressed by $M_{loc}(T) = M_0(1 - ST^2)$, where M_0 is the magnetization at 0K and S is the coefficient of the T^2 term or the Stoner excitation term. The essential mechanism of the Invar effect is the volume contraction due to the decrease of $M_{loc}(T)$ and not of $M(T)^2$. The magneto-volume coupling constant C has been found to be $1.1\text{--}1.3 \times 10^{-8} \text{ cm}^3/\text{emu}^2$, almost the same value for Fe-base Invar alloys, by experiments on forced volume magnetostriction, thermal expansion coefficients and pressure effects on magnetization. (46 refs.)

77245 Elastic anomaly in an itinerant-electron antiferromagnet. H.Yamada (Dept. of Phys., Gifu Univ., Gifu, Japan). *Physica B & C (Netherlands)*, vol.119 B+C, no.1-2, p.99-108 (April 1983). (Proceedings of the International Symposium on Magnetoelasticity in Transition Metals and Alloys, Nagoya, Japan, 15-16 Sept. 1982).
The anomalous temperature dependence of an elastic constant c_{11} in antiferromagnetic metals, say FCC Mn alloys, is studied. The c_{11} is generally written in terms of a wave-vector dependent electron density susceptibility. This susceptibility in an itinerant-electron antiferromagnet may be calculated by using the extended random phase approximation including the exchange interaction. By numerical calculations in the tight-binding single band approximation, it is shown that c_{11} decreases with increasing energy gap caused by the antiferromagnetic spin ordering both in FCC and BCC lattices. Especially for an FCC antiferromagnet with relatively large e/a ratio, there exists a certain critical value of the energy gap where c_{11} becomes zero as the temperature is reduced from the Neel temperature T_N . For a BCC antiferromagnet, there appears a remarkable gap of c_{11} at T_N . In such an anomalous behaviour of c_{11} the exchange interaction between the itinerant electrons plays a particularly important role. (25 refs.)

77246 Anomalous elastic properties of Fe-Ni (FCC) alloys and their Invar properties. Y.Tanji, Y.Nakagawa, S.Steinemann (Res. Inst. for Iron, Steel & Other Metals, Tohoku Univ., Sendai, Japan). *Physica B & C (Netherlands)*, vol.119 B+C, no.1-2, p.109-14 (April 1983). (Proceedings of the International Symposium on Magnetoelasticity in Transition Metals and Alloys, Nagoya, Japan, 15-16 Sept. 1982).
The authors have measured the elastic properties of Fe-Ni (FCC) alloys over the whole concentration range between 25 and 1150°C, and have found that the concentration dependence shows an anomalous behaviour in the Invar range even at 1000°C. The anomaly suggests the existence of a chemical miscibility gap in the Invar range of the γ phase. The instability of the γ phase is examined based on Cahn's spinodal theory. It is unlikely that the two-phase separation easily takes place by spinodal decomposition. (24 refs.)

77247 Low-temperature elastic-constant anomalies in Fe-Cr-Ni-Mn alloys. H.M.Ledbetter (Fracture & Deformation Div., NBS, Boulder, CO, USA). *Physica B & C (Netherlands)*, vol.119 B+C, no.1-2, p.115-18 (April 1983). (Proceedings of the International Symposium on Magnetoelasticity in Transition Metals and Alloys, Nagoya, Japan, 15-16 Sept. 1982).
By measuring velocities of longitudinal and shear waves the author determined accurately the temperature variation of elastic constants—Young's modulus, shear modulus, bulk modulus, Poisson ratio—of a polycrystalline austenitic steel: Fe-5Cr-26Mn. Versus temperature, near 335K, this alloy exhibits an anomalous elastic-constant transition. In similar alloys, a magnetic-susceptibility cusp occurs at the transition temperature, T_c . The bulk modulus shows a maximum at a higher temperature. Below T_c , the Poisson ratio behaves anomalously, increasing with decreasing temperature. (17 refs.)

77248 Magnetoelastic effect in dilute Fe-Co alloys. S.Ishio, A.Isomura, T.Ikeda, M.Takahashi (Dept. of Appl. Phys., Tohoku Univ., Sendai, Japan), S.Kadowaki. *Physica B & C (Netherlands)*, vol.119 B+C, no.1-2, p.119-24 (April 1983). (Proceedings of the International Symposium on Magnetoelasticity in Transition Metals and Alloys, Nagoya, Japan, 15-16 Sept. 1982).
Elastic constants, c_{11} , c_{33} , c_{55} and c_{66} , of Co, 0.84 at% Fe-Co and 1.37 at% Fe-Co alloys were measured by the pulse-echo-overlap method in magnetic fields up to 20 kOe over the temperature range from room temperature to 400°C. The dependence of elastic constants upon magnetic field orientation and intensity was examined in detail. The results are discussed on the basis of the macroscopic consideration of magnetoelastic energy. (13 refs.)

77249 The magnetoelastic effect in iron-manganese spinels. E.V.Babkin, E.S.Mushalov, V.G.Pyn'ko (L.V. Kirenskiy Phys. Inst., Acad. of Sci., Krasnoyarsk, USSR). *Sov. Phys.-Tech. Phys. (USA)*, vol.27, no.11, p.1403-4 (Nov. 1982). Translation of: *Zh. Tekh. Fiz. (USSR)*, vol.52, no.11, p.2285-6 (Nov. 1982). [received: May 1983]
The authors note that the magnetoelastic effect in a magnetic semiconductor should only be observed for appropriate sample dimensions ($\sim \lambda$, where λ is the Debye screening length) when the external electric field is sufficiently intense. These conditions can be satisfied by placing a thin layer of sample in an electric field produced by bound surface charges on a dielectric. The samples consisted of polycrystalline ferrite-spinel $\text{Mn}_{1-x}\text{Fe}_x\text{O}_4$ films of thickness 1 μm . The magnetic properties were measured in a magnetometer which measured the applied torques. The authors measured the dependence of the saturation magnetization on the potential difference applied to the copper films for a series of samples. The results may be summarized as follows: The existence of a nonzero electric field in the spinel increases the bulk conduction electron density and the magnetization; when the polarity of the electric field is reversed, no increase in the magnetization is observed to within experimental error. The technique is used to observe the magnetoelastic effect in $\text{Mn}_{1-x}\text{Fe}_x\text{O}_4$ when (for the particular sample) a negative voltage is applied. The failure of the magnetization to increase when a positive potential difference is applied is probably due to the absence of space charge in the spinel. (6 refs.)

Proceedings of the International Symposium on Magnetoelasticity in Transition Metals and Alloys See Entry 74217
Magnetostrictive fiber-optic sensor system for detecting DC magnetic fields See Entry 75812
Relaxation phenomena in amorphous $\text{Co}_{75-x}\text{Mn}_{25}$ induced by stress annealing See Entry 76929
Parametric amplification of sound and magnetoacoustic echo in concentrated rare-earth paramagnets of the Van Vleck type See Entry 77009
Neutron diffraction effects of the distorted structure of Ni-67.7 at% Fe alloy in the magnetic ordered state See Entry 77147

- Bulk modulus and martensitic transformation in Mn-Cu alloys See Entry 77642
- Landau theory for a cubic to tetragonal structural phase transformation See Entry 77643

75.90 OTHER TOPICS IN MAGNETIC PROPERTIES AND MATERIALS

77250 Dynamics of the shape transition of a magnetic ferrofluid drop. J.-C. Bacri, D. Salin (Lab. d'Ultrasons, Univ. Pierre et Marie Curie, Paris, France). *J. Phys. Lett. (France)*, vol.44, no.11, p.415-20 (1 June 1983). The prolate ellipsoidal shape of a magnetic fluid drop becomes unstable at a certain magnetic field threshold; the drop jumps from a slightly elongated shape to a much more elongated shape. The authors describe theoretically the dynamics of this first order transition, i.e. the relaxation time of this instability around the critical magnetic threshold. The critical divergence of the characteristic time of this instability, that they have measured in ferrofluid magnetic drops, is in reasonable agreement with the theoretical model. (12 refs.)

76.00 MAGNETIC RESONANCES AND RELAXATION IN CONDENSED MATTER; MOSSBAUER EFFECT

(for measurement techniques, see 07.58)

76.30 ELECTRON PARAMAGNETIC RESONANCE AND RELAXATION

77251 Laser-polarimetric investigations of electron spin resonance and relaxation in glasses. A.A. Antipin, V.S. Zapasskii, S.G. Lunter. *Sov. Phys. Solid State (USA)*, vol.24, no.11, p.1843-6 (Nov. 1982). Translation of: *Fiz. Tverd. Tela (USSR)*, vol.24, no.11, p.3248-54 (Nov. 1982). [received: May 1983]

An optical method for recording ESR was used to investigate glassy matrices activated with paramagnetic ions. Changes in the Faraday rotation angle on saturation of ESR were detected using a highly sensitive polarimeter based on an argon-ion laser. The ESR spectra were determined for all paramagnetic (in the ground state) trivalent rare-earth ions and some ions of the iron group. Preliminary measurements were made of the longitudinal relaxation time of the magnetization of glasses and several features were noted of the relaxation processes of glasses containing paramagnetic impurity centers, compared with the corresponding properties of activated crystals. (11 refs.)

Thermal isomerization and degradation of polyacetylene See Entry 77887

76.30D Ions and impurities: general

77252 Effect of the profile of an inhomogeneously broadened ESR line on the steady-state distribution of the Zeeman temperature under saturation conditions. S.V. Pogrebnyak, E.A. Shadchin (Inst. of Phys., Acad. of Sci., Kiev, Ukrainian SSR).

Sov. Phys. Solid State (USA), vol.24, no.12, p.2114-15 (Dec. 1983). Translation of: *Fiz. Tverd. Tela (USSR)*, vol.24, no.12, p.3708-10 (Dec. 1983). The authors investigate the effect of the profile of an inhomogeneously broadened ESR line on the distribution of the Zeeman temperature in the case of saturation due to a high-frequency field $[H(t) = 2H_1 \cos \omega_0 t]$. (4 refs.)

76.30F Iron group (3d) ions and impurities (Ti-Cu)

77253 EPR study of Cu^{2+} ions in single crystal of strontium formate dihydrate. M. Umar, M.I. Haque, R.J. Singh (Dept. of Phys., Aligarh Muslim Univ., Aligarh, India).

J. Phys. Soc. Jpn. (Japan), vol.52, no.5, p.825-8 (May 1983). Electron paramagnetic resonance of Cu^{2+} ion in $\text{Sr}(\text{HCOO})_2 \cdot 2\text{H}_2\text{O}$ were measured at room temperature. The spectrum was interpreted in terms of the Jahn-Teller effect. Cu^{2+} is found to be incorporated both interstitially and substitutionally. The substitutional Cu^{2+} is found to be in nearly cubic environment and Γ_5 distortion is responsible for Jahn-Teller effect. The interstitial Cu^{2+} finds itself in an octahedral field which undergoes Jahn-Teller splitting due to Γ_3 coupling.

77254 Light-induced ESR centres in single crystal rutile. S.W. Hodgskiss, J.S. Thorp (Dept. of Appl. Phys. & Electronics, Univ. of Durham, Durham, England).

J. Magn. & Magn. Mater. (Netherlands), vol.36, no.3, p.303-9 (April 1983). Electron spin resonance studies have been made on Verneuil-grown rutile single crystals, which were doped with a variety of transition group ions. Measurements were made at 9 GHz, both before and after UV irradiation, at temperatures in the range from 4.2 to 300K. UV irradiation had two effects: (a) to affect the relative intensities of ESR lines due to species already present, (b) to generate new ESR spectra. Both effects are interpreted as representing a redistribution of charge amongst trapping centres. Seven UV generated centres have been identified and characterised in terms of their spin Hamiltonian parameters. Isochronal annealing techniques have been used to determine the ionisation temperatures of the traps. Observation of interactions and charge transfers between centres during isochronal annealing was used to determine the polarity and type of each centre. (15 refs.)

77255 EPR and luminescence of Mn^{2+} in distorted tetrahedral symmetry in CaZnF_4 crystals. M. Heming (Inst. fur Phys. Chem., Westfälischen Wilhelms-Universität Münster, Münster, Germany), G. Lehmann, K. Recker, F. Wallrafen.

Phys. Status Solidi b (Germany), vol.117, no.1, p.271-6 (1 May 1983). Small crystals of CaZnF_4 with scheelite-type structure, doped with about 1% Mn, are obtained from the melt by the Bridgman method with subsequent annealing at 725°C, 50K below a reversible phase transformation detected by DTA. Mn^{2+} exclusively occupies Zn sites as evident from the size of the hyperfine splitting constant. The intrinsic zero field splitting parameter of second order obtained from superposition analysis is in the same range as that for $[\text{MnF}_6]^{4-}$ units. The luminescence spectra do not serve as a critical test for distinction between four- and eightfold coordination. (12 refs.)

77256 EPR study of ordering in stoichiometric β -aluminate. Ph. Colombeau, D. Vivien (Lab. de Chimie Appl. de l'Etat Solide, Ecole Nat. Supérieure de Chimie, Paris, France).

Phys. Status Solidi a (Germany), vol.76, no.2, p.565-74 (16 April 1983). Single crystals of nonstoichiometric ammonium β -aluminate doped with Mn^{2+} ions are investigated by EPR. In the starting material, the nonobservation of the outer fine structure transitions and the existence of forbidden hyperfine lines along the D tensor axis results from disorder in the spinel blocks caused by Frenkel defects at the Al_1 site. The manganese ions lie mainly on the Al_2 'block tetrahedral' site. In stoichiometric oxonium β -aluminate obtained by thermal treatment of the starting material (500°C) exists a partial resolution of the Mn^{2+} fine structure as a consequence of the relaxation of the Frenkel defects and of ordering. There is also evidence of at least three kinds of manganese sites. Treatments at 800°C leads to well-resolved spectra with $D = -0.0253 \text{ cm}^{-1}$ characteristic of manganese in well-ordered spinel blocks. The stacking of these spinel blocks is disordered, and the structure of the material ('3a phase') is related to those of the transition alumina group. This study shows that Mn^{2+} EPR spectroscopy is a sensitive way to investigate the structural transformations of single crystalline solids, and the degree of ordering of the structures. (24 refs.)

77257 Electron-spin resonance study of spin dynamics in the one-dimensional magnetic crystal doped with diamagnetic impurities $(\text{CH}_3)_4\text{NMn}^{2+}\text{Cl}_3\text{Cd}^{2+}$. N. Shah, G. Kemmerer, J.S. Karra (Dept. of Phys., Temple Univ., Philadelphia, PA, USA).

Phys. Rev. B (USA), vol.27, no.9, p.5360-S (1 May 1983). The authors have studied spin dynamics in the impurity-doped $(\text{CH}_3)_4\text{NMn}^{2+}\text{Cl}_3\text{Cd}^{2+}$ using electron-spin resonance. They have measured the room-temperature electron-spin resonance linewidths, lineshapes, dynamic shifts, and fine- and hyperfine-structure constants at X- and Q-band microwave frequencies in several crystals containing different concentrations of Cd^{2+} ion. They have attempted to interpret their data with the aid of the current theories and found that there is only partial agreement between theory and experiment. At very high concentration of Cd^{2+} they have observed fine structure due to single-ion anisotropy and hyperfine structure due to nuclear spin of Mn^{2+} , at $\theta = 0^\circ$, where θ is the angle between the magnetic chain axis (c axis) of the crystal and the constant magnetic field H_0 . The crystal field direction of the single-ion anisotropy was observed to be along the c axis of the crystal. In addition, they have observed hyperfine interaction to be isotropic. They have measured the values of the fine- and hyperfine-interaction constants. (8 refs.)

77258 ESR of Cu^{2+} in the high pressure form of $\text{Ce}_3(\text{PO}_4)_2$. S.S. Romdhane (Lab. de Chimie Minérale, ENIG, Gabes, Tunisia), G. Bacquet.

Solid State Commun. (USA), vol.46, no.8, p.631-2 (May 1983). ESR spectra of polycrystalline Cu^{2+} doped samples of the high pressure phase of $\text{Ce}_3(\text{PO}_4)_2$ were characteristic of the existence of two different paramagnetic centres. The spin-Hamiltonian constants of both defects were determined. Only two of the three possible substitutional cation sites are occupied by copper ions. (6 refs.)

77259 Nonlinear effects in hypersound propagation within the $\text{Ni}^{2+}:\text{Al}_2\text{O}_3$ system. E.M. Gananolskii, D.N. Makovetskii.

Ukr. Fiz. Zh. (USSR), vol.28, no.5, p.722-31 (May 1983). In Russian. The nonlinear spin-phonon interaction in $\text{Ni}^{2+}:\text{Al}_2\text{O}_3$ crystals has been investigated experimentally at liquid helium temperatures both under acoustic paramagnetic resonance (APR) and phaser amplification conditions. An effect of hypersound self-focusing (HS) in the nonlinear APR regime is revealed. Such a type of HS is conditioned by formation of a gradient paramagnetic medium in the $\text{Ni}^{2+}:\text{Al}_2\text{O}_3$ system having a comparatively long spin-lattice relaxation time, $\tau_1 \approx 10^{-2} \text{ s}$. It is shown experimentally that HS exists in an active medium too, but the phase amplification line has a much more complicated structure than the inverted APR line. A model based on analysis of the hypersound resonant dispersion in the phaser is suggested for the HS effect in the active medium. (13 refs.)

The electronic properties of $[\text{CH}(\text{FeCl}_4)_{0.61}]_x$ See Entry 76934

Spectroscopic studies of oxovanadium(IV) complexes of biguanide, diguanides and o-methyl-1-amidinourea See Entry 77373

76.30K Rare-earth ions and impurities

77260 Electric field effect in the case of cubic Gd^{3+} centers in BaF_2 . N. Guskos, I.Kh. Salikhov, S.N. Arkhipov (Tech. Univ., Szczecin, Poland).

Sov. Phys. Solid State (USA), vol.24, no.11, p.1912-14 (Nov. 1982). Translation of: *Fiz. Tverd. Tela (USSR)*, vol.24, no.11, p.3366-9 (Nov. 1982). [received: May 1983]

An investigation was made of the influence of an electric field on the ESR spectra of cubic Gd^{3+} centers in a BaF_2 crystal. The experimental results were interpreted by the appearance of a crystal field harmonic $\Delta V_0^0(E)$ induced by an external electric field. The corresponding parameter of the spin Hamiltonian was $\Delta B_0^0 = (-7.5 \pm 2.5) \times 10^{-7} \text{ cm}^{-1}$ in a field of $E = 355 \text{ kV/cm}$. A calculation carried out using the model of superposition and the experimental data on the uniaxial compression and a calculation made in the approximation of a quasi-molecular model of an impurity center both gave results in agreement with the experimental data. (20 refs.)

76.30L Other ions and impurities

(for colour centres, see 76.30M)

77261 Electron-spin-echo experiments on the one-dimensional conductor $[(\text{fluoranthene})]^{+}[(\text{PF}_6)(\text{SBF}_6))_{1-x}]$ ($x \approx 0.5$). J. Sigg, Th. Priser, K.P. Dinse, H. Brunner, D. Schweitzer, K.H. Hauser (Abteilung für Molekulare Phys., Max-Planck-Inst. für Medizinische Forschung, Heidelberg, Germany).

Phys. Rev. B (USA), vol.27, no.9, p.5366-73 (1 May 1983). The electron-spin-echo decay function was determined for the conducting phase $[(\text{C}_{16}\text{H}_{10})]^{+}\text{X}^{-}$ in the temperature range 183-300K. The decay function exhibited an $\exp[-(\gamma t)^{3/2}]$ dependence, characteristic of one-dimensional spin diffusion. The ratio $5 \times 10^3 \leq D_{\parallel}/D_{\perp} \leq 5 \times 10^8$ for the inner-stack-to-out-of-stack diffusion rates was determined from the characteristic time t_0 , at which the electron-spin-echo decay function changed to the 'conventional' $\exp(-2\gamma t)$ form. The deduced value $2 \times 10^{13} \leq D_{\parallel} \leq 2 \times 10^{16} \text{ rad/s}$ is consistent with the bulk DC conductivity and with recently determined nuclear spin-lattice relaxation rates. The overall assumption of highly mobile electronic spins was confirmed by an Overhauser-type experiment. (22 refs.)

Localized centers in bismuth silicate crystals See Entry 76875

76.30M Colour centres and other defects

77262 Li tunneling effects on spin-lattice relaxation rates of a color center in CaO:Li. D.G.Stinson, H.J.Stapleton (Dept. of Phys., Univ. of Illinois, Urbana, IL, USA). *Phys. Rev. B (USA)*, vol.27, no.9, p.5386-93 (1 May 1983). Low-temperature spin-lattice relaxation rates of the $[F_{Li}]^0$ center in single crystals of CaO:Li at X- and Ku-band microwave frequencies exhibit an anisotropy in the functional form of the temperature dependence: from T in the [100] direction to $cosh(25/T)$ in the [111] direction. A model involving longitudinal and transverse tunneling of a Li ion adjacent to the trapped electron can qualitatively explain this and most of the other characteristics of the relaxation data, with the exception of the hyperfine dependence. (32 refs.)

The effect of annealing on the dislocation dissociation in plastically deformed silicon See Entry 76439

Defect states and donors in thermally annealed or post-hydrogenated chemically vapor-deposited amorphous SiN_x alloy See Entry 76897

76.30P Conduction electrons

77263 Combined effects of exchange and g-value anisotropy in the conduction-electron spin resonance of metals. R.H.Silsbee (Dept. of Phys., Cornell Univ., Ithaca, NY, USA), J.P.Long. *Phys. Rev. B (USA)*, vol.27, no.9, p.5374-85 (1 May 1983). A heuristic model is developed to explore the combined effects of exchange and g-value anisotropy in the conduction-electron spin resonance in polyvalent metals where it may be appropriate to consider the electrons in different Brillouin zones to be partially decoupled from one another. Within the framework of this model the resonance should show structure at low temperature, and the conventional analysis of resonance data, using the theory of Platzman and Wolff (1967) to obtain the exchange parameter B_0 , can be substantially in error if the effects of g-value anisotropy are not properly accounted for. Some features of existing data for aluminum are discussed in the context of this model, and it is noted that spin-resonance results may be able to remove the current ambiguity in the sign of the pseudopotential matrix element V_{111} used in calculations of the band structure of aluminum. (16 refs.)

76.30R Free radicals

Radiation damage in polyacrylonitrile See Entry 76499

A preliminary report on radical yield alternation in even and odd linear alkanes irradiated at 77K: ESR evidence See Entry 77911

76.40 DIAMAGNETIC AND CYCLOTRON RESONANCES

77264 Theory of cyclotron resonance width for electrons inelastically scattered by phonons. T.K.Srinivas, S.Chaudhury, S.Fujita (Dept. of Phys. & Astron., State Univ. of New York, Buffalo, Amherst, NY, USA). *J. Phys. & Chem. Solids (GB)*, vol.44, no.5, p.417-21 (1983). The cyclotron resonance width for a semiconductor under extreme high fields is calculated with the assumptions that electrons are scattered by acoustic phonons inelastically. The numerical results are in very good agreement with the recent experiments on Ge by Miura et al. (1976) ($T \sim 300K$, $B \sim 97$ tesla). The energy-dependent widths arising from the relaxation processes with absorption and emission of a phonon show quite distinctive behaviors at low electron energies. At extreme low temperatures when few phonons are present, the width arising from the zero-point motion of the lattice is finite but very small. The charged-impurity scattering with the density as low as 10^{12} cm^{-3} numerically dominate the width due to the electron-phonon interaction below 10K. The present theory supplements the previous work by Suzuki et al. (1980) where the elastic-scattering and high-temperature approximation were used. (9 refs.)

77265 Cyclotron resonance and the role of polaron effects in surface layers on Hg_{1-x}Cd_xTe. J.Scholz, F.Koch (Phys.-Dept. Tech. Univ. Muenchen, Garching, Germany), J.Ziegler, H.Maier. *Solid State Commun. (USA)*, vol.46, no.8, p.665-8 (May 1983). The authors examine the cyclotron resonance of electrons in surface subbands on Hg_{1-x}Cd_xTe at frequencies in the range of the optical phonon modes. Polaron effects on the surface resonance are shown to be significantly smaller than the polaron shift and broadening of the bulk electron resonance. (21 refs.)

77266 Theory of cyclotron resonance lineshape for electron-phonon systems in two coupling schemes. Sang Don Choi, Ok Hec Chung (Dept. of Phys., Kyungpook Nat. Univ., Taegu, Korea). *Solid State Commun. (USA)*, vol.46, no.9, p.717-20 (June 1983). A theory of cyclotron resonance lineshape due to electron-phonon interactions is presented on the basis of the projection operator method introduced by Argyres and Sigel (1974). In addition to the extremely weak coupling scheme dealt with earlier, the moderately weak coupling scheme is included in the theory. The lineshape functions derived in the two schemes are similar to Lodder-Fujita's formula (1968) and are reduced to Kawabata's formula (1967) in the elastic scattering approximation. (5 refs.)

Two dimensional magnetophonon resonance in GaInAs-InP superlattices See Entry 77037

76.50 FERROMAGNETIC, ANTIFERROMAGNETIC, AND FERRIMAGNETIC RESONANCES; SPIN WAVE RESONANCE (see also 75.30D Spin waves)

77267 Epitaxial growth and annealing control of EMR properties of thick homogeneous Ga substituted yttrium iron garnet films. P.Roschmann, W.Tolksdorf (Philips GmbH Forschungslab., Hamburg, Germany). *Mater. Res. Bull. (USA)*, vol.18, no.4, p.449-59 (April 1983). Homogeneous, 30 μm to 70 μm thick Ga substituted yttrium iron garnet films have been grown on Y or Al substituted gadolinium gallium garnet substrates having lattice parameters matched to that of the films. Resonance field and FMR linewidth measurements as a function of frequency and annealing experiments revealed that the magnetization and cubic anisotropy of the films are identical to data from flux grown bulk single crystals; the FMR losses of the films are only slightly higher. For films grown with supercooling, $\Delta T < 50^\circ\text{C}$, a negative, growth induced, uniaxial anisotropy was found which

could be removed by annealing in air at 1100°C. A compensation of the temperature drift of the FMR frequency can be adjusted in the Ga substituted films by changing the frozen-in Ga-Fe cation distribution by annealing and quenching from different temperatures $> 800^\circ\text{C}$. (24 refs.)

77268 Influence of ion implantation on high-frequency properties of domain walls in thin magnetic films. A.V.Zinovuk, A.F.Kononov, I.A.Mel'nichuk, L.I.Prikhodko, E.I.Filippov, E.F.Khodosov (Physicotech. Inst., Acad. of Sci., Donetsk, Ukrainian SSR). *Sov. Phys.-Solid State (USA)*, vol.24, no.11, p.1967-8 (Nov. 1982). Translation of: *Fiz. Tverd. Tela (USSR)*, vol.24, no.11, p.3461-3 (Nov. 1982). [received: May 1983]

The authors have used the RF method to study the influence of ion implantation on high-frequency properties of domain walls in epitaxial iron garnet systems (Eu, Tm, Y, Ca)₃(Fe,Ge)₅O₁₂ and (Y, Sm, Lu, Ca)₃(Fe, Ge)₅O₁₂ grown on gadolinium gallium garnet substrates cut along a (111) plane. The influence of ion implantation on resonance properties of domain walls was determined by comparing the high-frequency properties of these walls in films of the same composition and the same internal parameters which were either implanted or nonimplanted. (7 refs.)

76.60 NUCLEAR MAGNETIC RESONANCE AND RELAXATION

77269 An ²⁷Al NMR study of complexes between Al³⁺ and imidazolidine-2-one in concentrated aqueous solution. R.Caminiti, A.Lai, G.Saba, G.Crisponi (Univ. di Cagliari, Cagliari, Italy). *Chem. Phys. Lett. (Netherlands)*, vol.97, no.2, p.180-4 (13 May 1983). The complexation between Al³⁺ and imidazolidine-2-one was investigated by ²⁷Al NMR spectroscopy at variable temperature. Several complexes with different stoichiometries were identified. A fitting procedure based on the exchange modified Bloch equations and the Gauss-Newton method furnished the populations and exchange rates. From these the pertinent thermodynamic parameters were found. (19 refs.)

77270 Electron localization on defects and optical nuclear polarization in disordered and semimagnetic semiconductors. N.T.Bagraev (A.F. Ioffe Phys.-Tech. Inst., Acad. of Sci., Leningrad, USSR). *Phys. Status Solidi b (Germany)*, vol.117, no.1, p.367-79 (1 May 1983). Using optical nuclear polarization (ONP) and nuclear magnetic resonance (NMR) techniques silicon single crystal solid solutions containing impurity defects of more than one kind are studied. The application of the ONP techniques to the investigation of nonuniformly doped silicon is demonstrated. The concentration and energy fluctuations of donor levels are determined in silicon doped with elements of III to V and transition groups. Solid solution decay processes are studied by ONP techniques in silicon crystals doped with deep-level impurities. Finally, the ONP technique is applied to the investigations of semimagnetic semiconductors. (21 refs.)

77271 Temperature-dependent nuclear magnetic resonance in CuInX₂ (X=S,Se,Te) chalcopyrite-structure compounds. K.D.Becker (Inst. fur Phys. Chem. und Elektrochem., Univ. Hannover, Hannover, Germany), S.Wagner. *Phys. Rev. B (USA)*, vol.27, no.9, p.5240-9 (1 May 1983). The NMR spectra of ⁶³Cu and ¹¹⁵In in CuInS₂, CuInSe₂, and CuInTe₂ have been measured between room temperature and 550°C. The effects of motional narrowing and of phase transitions on the shape and width of the absorption spectra were evaluated. In all three compounds, the absorption signal of ⁶³Cu shows motional narrowing. For Cu_{1.00}In_{1.00}S_{2.00} the mean jump frequency of the Cu²⁺ ions, $\nu(\text{Cu}^{2+})$, is $2 \times 10^{13} \exp[-(1.25 \pm 0.10 \text{ eV})/kT] \text{ s}^{-1}$. For both CuInSe₂ and CuInTe₂, $\nu(\text{Cu}^{2+})$ is about $3 \times 10^{13} \text{ s}^{-1}$ at 350°C. In copper-deficient Cu_{0.96}In_{1.02}S_{2.00} no motional narrowing of the ⁶³Cu absorption was observed up to 550°C. However, the ⁶³Cu line shape in CuInS₂ depends on the copper-to-indium ratio. A line-shape analysis as a function of composition shows that, at 450°C, CuInS₂ exists in the composition range between Cu_{1.00}In_{1.00}S₂ and Cu_{0.85}In_{1.05}S₂. For specimens with $[\text{Cu}]/[\text{In}] > 1$, Cu₂S contributes to the absorption signal. In a separate study of the ⁶³Cu absorption in Cu₂S, the hexagonal-to-cubic transformation was observed at 440°C. The activation energy for $\nu(\text{Cu}^{2+})$ in cubic Cu₂S is 0.15 eV. The phase-transformation temperatures for the three CuInX₂ compounds (where X is a group-VI element) were determined by differential thermal analysis. A previously unnoticed transformation was found in CuInSe₂ at 665°C. Finally, the quadrupole coupling constant $X_Q(^{63}\text{Cu})$ of a number of Cu₂X₂ compounds (where Z is a group-III element) is shown to be a linear function of the tetragonal distortion parameter $\delta = 2 - c/a$ with $|X_Q| = 1.50 + 90\delta$ MHz. The value for $\delta = 0$ is of the same order of magnitude as the result of a simple model of a point charge on a cubic lattice. (27 refs.)

77272 Amplitude-fluctuation effects on magnetic-resonance line shape and soliton density in incommensurate systems. R.Blinc, P.Prelovsek (Dept. of Phys., J. Stefan Inst., E. Kardelj Univ. of Ljubljana, Ljubljana, Yugoslavia), R.Kind. *Phys. Rev. B (USA)*, vol.27, no.9, p.5404-11 (1 May 1983). The magnetic-resonance line shape in one-dimensionally modulated structurally incommensurate systems has been evaluated for the case of a multisoliton lattice taking into account both phase and amplitude variations in space. Amplitude variations significantly affected the NMR line shape outside the 'plane-wave' regime. A comparison is made between the temperature dependence of the average incommensurate wave vector and the soliton density in the constant-amplitude approximation and in the case when the amplitude variations are taken into account. (10 refs.)

77273 Behavior of the NMR lines coupled by cross relaxation under acoustic saturation conditions. M.M.Shakirzyanov (Physicotech. Inst., Acad. of Sci., Kazan, USSR). *Sov. Phys.-Solid State (USA)*, vol.24, no.12, p.2105-6 (Dec. 1983). Translation of: *Fiz. Tverd. Tela (USSR)*, vol.24, no.12, p.3694-6 (Dec. 1983). The author investigates systematically the effect of cross relaxation on the acoustic saturation of nuclear spin systems with nonequidistant spectra. He concludes that, under certain conditions, the cross relaxation effect has a strong influence on the acoustic saturation of NMR lines. It follows that, when the spin-phonon interaction in crystals is studied by acoustic saturation methods, it is necessary to take into account the possible influence of cross relaxation transitions. (7 refs.)

International Meeting on Lithium Batteries See Entry 74213

Nuclear orientation and NMR/ON of ^{205,207}Po See Entry 74846

Operator and algebraic methods for NMR spectroscopy. I. Generation of NMR spin species See Entry 75408

Operator and algebraic methods for NMR spectroscopy. II. NMR projection operators and spin functions See Entry 75409

Spin coated amorphous chalcogenide films: structural characterization See Entry 76802

Spectral studies on new dioxouranium (VI) complexes of tridentate Schiff bases derived from salicylhydrazide and salicylaldehyde or substituted salicylaldehydes See Entry 77372

Thermal isomerization and degradation of polyacetylene See Entry 77887

Nuclear magnetic resonance of silica polymorphs See Entry 78537

76.60C Chemical and Knight shifts

77274 Solid-state high-resolution ^{29}Si NMR in zunyite. A.-R.Grimmer, F.Von Lampe (Central Inst. of Inorganic Chem., Acad. of Sci., Berlin, Germany), M.Tarmak, E.Lippmaa.

Chem. Phys. Lett. (Netherlands), vol.97, no.2, p.185-7 (13 May 1983). High-resolution ^{29}Si NMR spectra of zunyite $\text{Si}_2\text{Al}_3\text{O}_{20}(\text{OH},\text{F})_8\text{Cl}$ have been studied by magic-angle sample spinning in combination with high-power proton decoupling and polarization transfer. The isotropic ^{29}Si chemical shift depends mainly on the number of Si-O Si bridges and the bond angles in these bridges connecting the different SiO_4 tetrahedra. (14 refs.)

77275 ^1H and ^{13}C NMR of the chloride of tricyclopentadienyluranium IV. Evolution of the contact shift. G.Folcher, G.Langlet, P.Rigny (Dept. de Phys.-Chimie, CENS, Gif-sur-Yvette, France), A.Dormond.

Nouv. J. Chim. (France), vol.7, no.4, p.245-8 (April 1983). In French. The NMR study of $(\eta^5\text{-C}_5\text{H}_4\text{CH}_2\text{C}_6\text{H}_4)_3\text{UCl}$ I allowed the authors, knowing the solid state structure, to analyse the paramagnetic induced shift. The pseudocontact values corresponding to the various atoms of the ligand show that the structure of the solid is maintained in solution not only for I but also for other analogous derivatives $(\eta^5\text{-C}_5\text{H}_4\text{R})_3\text{UCl}$. From the contact term, the hyperfine coupling constants can be calculated and a good order of magnitude of the unpaired spin density delocalised on the ligand is obtained. This result leads the authors to propose a mechanism of spin delocalisation by polarisation of the electrons of the ligand and to assign to these a high covalency at the π bonds. (18 refs.)

77276 ^{23}Na Knight shift of liquid Na-Sn alloys. C.van der Marel, P.C.Stein, W.van der Lugt (Solid State Phys. Lab., Univ. of Groningen, Groningen, Netherlands).

Phys. Lett. A (Netherlands), vol.95A, no.8, p.451-3 (23 May 1983). Measurements of the ^{23}Na Knight shift in liquid Na-Sn alloys provide strong indications for the formation of compounds about the two distinct compositions Na_2Sn and Na_4Sn_3 . (10 refs.)

Chloroacetyltriphenylphosphonium and the corresponding phosphorane. Physical chemistry and conformation study See Entry 75388

Nuclear magnetic resonance study of atomic motions in vanadium See Entry 77277

^{77}Se nuclear magnetic resonance in di-tetramethyltetraselenafulvalene phosphorous hexafluoride $[(\text{TMTSF})_2\text{PF}_6]$ under pressure See Entry 77280

Specific heat and NMR spin echo in the superconducting and magnetic region of the Y_2Co_3 compound See Entry 77284

Spectra and structure of asymmetric carboxylic acid dimers in solution See Entry 77387

Nuclear magnetic resonance of silica polymorphs See Entry 78537

76.60E Relaxation effects

77277 Nuclear magnetic resonance study of atomic motions in vanadium. B.Gunther, O.Kanert (Inst. fur Phys., Univ. Dortmund, Dortmund, Germany). *Acta Metall. (USA)*, vol.31, no.6, p.909-17 (June 1983).

Atomic motions in solid vanadium have been investigated by means of NMR. For that purpose, the Zeeman spin-lattice relaxation time T_1 , the rotating-frame spin-lattice relaxation time $T_{1\rho}$, and the Knight shift K of ^{51}V in polycrystalline vanadium have been measured as a function of temperature in the range between 300 and 2000K. At all temperatures, the relaxation time T_1 is mainly determined by electronic contributions leading to a temperature-dependent expression for the Korringa relation T_1TK^2 . In contrast to the T_1 -data, two pronounced peaks in the relaxation rate $T_{1\rho}^{-1}$ at about 750 and 1600K, respectively, are observed. The peak at 750K arises from fluctuations in the nuclear quadrupolar interaction between vanadium and interstitially migrating oxygen whereas the maximum at 1600K is caused by fluctuations in the nuclear dipole interaction due to atomic self-diffusion. From the low-temperature data, the diffusivity of oxygen is determined to be $D_0 = 3.2 \times 10^{-6} \exp(-0.73 \text{ eV}/kT) \text{ cm}^2/\text{s}$. By comparing the self-diffusion contribution to the relaxation rate with the tracer measurements of Pelleg, the correlation factor f was found to be $f = 0.77 \pm 0.11$ consistent with a monovacancy diffusion mechanism. The uncorrelated self-diffusion coefficient was obtained as $D_{SD} = 0.14 \exp(-3.09 \text{ eV}/kT) \text{ cm}^2/\text{s}$. (30 refs.)

77278 Barriers to rotation of the cyclopentadienyl ligand: spin-lattice relaxation time measurements and atom-atom potential calculations on cyclopentadienyl manganese and rhenium tricarbonyl and vanadium tetracarbonyl complexes. D.F.R.Gilson, G.Gomez, I.S.Butler, P.J.Fitzpatrick (Dept. of Chem., McGill Univ., Montreal, Quebec, Canada).

Can. J. Chem. (Canada), vol.61, no.4, p.737-42 (April 1983). The barriers to cyclopentadienyl ring rotation in the solid phase have been measured by spin-lattice relaxation time methods for the organometallic complexes $\text{CpMn}(\text{CO})_3$ (7.24 kJ mol $^{-1}$), $\text{CpRe}(\text{CO})_3$ (7.15 kJ mol $^{-1}$), and $\text{CpV}(\text{CO})_4$ (7.07 kJ mol $^{-1}$), where $\text{Cp} = \eta^5\text{-C}_5\text{H}_5$. Nonbonded atom-atom potential calculations of the barriers in these complexes and in $\text{BzCr}(\text{CO})_3$ ($\text{Bz} = \eta^5\text{-C}_6\text{H}_5$) show that the molecular conformation of the Mn and Re compounds is determined by crystal packing forces and that concerted ring motions are possible for the cyclopentadienyl complexes, but not for the benzene chromium tricarbonyl. (33 refs.)

77279 The measurements of NMR T_1 and NOE. Wang Jinshan, Xie Dilin (Dept. of Radio Electronics, Beijing Normal Univ., Beijing, China), Chen Liang, Hu Yuxian.

Kexue Tongbao (Foreign Lang. Ed.) (China), vol.28, no.2, p.209-12 (Feb. 1983). In recent years, using of the pulse Fourier transform NMR spectrometer for measuring the nuclear magnetic resonance spin-lattice relaxation time (T_1) has become an important method for the analyses of molecular constructions and the study of molecular dynamics. The authors discuss some problems concerning the techniques for measuring the spin-lattice relaxation time (T_1) and the nuclear Overhauser enhancement factor (NOE) of ^{13}C nuclei, and a few ways of eliminating errors. (4 refs.)

77280 ^{77}Se nuclear magnetic resonance in di-tetramethyltetraselenafulvalene phosphorous hexafluoride $[(\text{TMTSF})_2\text{PF}_6]$ under pressure. L.J.Azevedo, J.E.Schirber (Sandia Nat. Labs., Albuquerque, NM, USA), E.M.Engler.

Phys. Rev. B (USA), vol.27, no.9, p.5842-5 (1 May 1983). The authors report measurements of the Knight shift, spin-lattice relaxation time, linewidth, and absolute susceptibility of ^{77}Se as functions of pressure, field, and temperature in the organic superconductor tetramethyltetraselenafulvalene phosphorous hexafluoride $[(\text{TMTSF})_2\text{PF}_6]$. The results indicate that there is significant p -wave spin density at the Se sites and that the quenching of the spin-density wave (SDW) is a slow function of pressure. That is, there is a significant pressure regime where there is coexistence of a metallic and SDW state. The nature of this coexistence is discussed. (14 refs.)

77281 Nuclear spin-lattice relaxation in doped silicon under optical pumping conditions. N.T.Bagraev, L.S.Vlasenko, I.A.Merkulov (A.F. Ioffe Physico-Inst., Acad. of Sci., Leningrad, USSR).

Sov. Phys.-Solid State (USA), vol.24, no.11, p.1972-3 (Nov. 1982). Translation of: *Fiz. Tverd. Tela (USSR)*, vol.24, no.11, p.3467-70 (Nov. 1982) [received: May 1983]

The authors have investigated the spin-lattice relaxation of ^{29}Si nuclei in silicon subjected to a wide range of magnetic fields and containing donor hydrogen-like centers with different ionization energies. The spin-lattice relaxation of ^{29}Si nuclei in silicon is due to their hyperfine interaction with paramagnetic centers. This hyperfine interaction is most effective for the nearest neighbour ^{29}Si nuclei because its intensity decreases on increase in the distance r from the paramagnetic center. The appearance of a steady state nuclear polarization throughout a crystal is due to a nuclear spin diffusion processes. (9 refs.)

$(\text{Ag}_2\text{O})_x(\text{Li}_2\text{O})_{1-x} \cdot 2\text{B}_2\text{O}_3$ mixed cation glasses See Entry 76694

The melting line for ethylene on graphite See Entry 76787

Relativistic extended Huckel studies of cluster models of solid HgTe, CdTe, and PbTe: densities of states and nuclear spin-spin coupling See Entry 76842

Optical polarization of lattice nuclei in strongly deformed silicon See Entry 77288

76.60G Quadrupole resonance

77282 Nuclear-quadrupole-resonance study of the ground state of praseodymium in lanthanum trifluoride. R.R.Reddy, L.E.Erickson (Nat. Res. Council, Ottawa, Ontario, Canada).

Phys. Rev. B (USA), vol.27, no.9, p.5217-23 (1 May 1983).

A nuclear-quadrupole-resonance study of trivalent praseodymium in a lanthanum trifluoride single crystal is presented. The magnitudes and orientation of the enhanced nuclear Zeeman tensor are obtained for the six magnetically inequivalent sites from measurements in 100-G magnetic fields. By comparing the directions of the site y axis and the crystal a axis, it is concluded that the Pr^{3+} site symmetry is C_2 and not C_{3v} . From a study of the polarization of the optical pump transition for each Pr^{3+} site, it is determined that the $^3\text{H}_4(0 \text{ cm}^{-1}) \rightarrow ^1\text{D}_2(16872 \text{ cm}^{-1})$ optical transition is an electric dipole transition. (29 refs.)

77283 ^{17}O nuclear-quadrupole-resonance measurements in the ferroelectric phase of potassium dihydrogen phosphate: Evidence for proton tunneling. S.D.Goren (Dept. of Phys., Ben Gurion Univ., Beer Sheva, Israel), M.Shporer, Y.Margalit.

Phys. Rev. B (USA), vol.27, no.9, p.5419-23 (1 May 1983). The pure nuclear-quadrupole-resonance spectra of naturally abundant ^{17}O in potassium dihydrogen phosphate (KDP) in the ferroelectric phase was obtained by a double-resonance-sensitive detection method. Fine structure due to dipolar interaction with the protons was resolved. From the best fit between the calculated and experimental spectra it is deduced that proton motion along the hydrogen bond prevails in the ferroelectric phase. The ordering parameter for the proton along the hydrogen bond is estimated. (8 refs.)

Peculiarities of phase transitions and physical properties in $(\text{NH}_4)_2\text{SbF}_6$ See Entry 76613

Measurement of the hyperfine structure of Pr^{3+} YAG by quantum-beat free-induction decay, hole burning, and optically detected nuclear quadrupole resonance See Entry 77291

76.60L Spin echoes

77284 Specific heat and NMR spin echo in the superconducting and magnetic region of the Y_2Co_3 compound. A.Lewicki, Z.Tarnawski, Cz.Kapusta, A.Kolodziejczyk, H.Figiel, J.Chmst (Solid State Phys. Dept., Univ. of Mining & Metall., Cracow, Poland), Z.Lalowicz, L.Sniadower.

J. Magn. & Magn. Mater. (Netherlands), vol.36, no.3, p.297-302 (April 1983). The specific heat and NMR of the magnetic superconductor Y_2Co_3 and other compounds close to this phase were measured. The electronic contribution to the specific heat is mainly caused by Co electrons by the phonon contribution is mainly due to the Y lattice. The coexistence of magnetism and superconductivity was observed through changes of the Knight shift parameter of the NMR spectrum. The most striking result is that the authors found a negative Knight shift for some parts of the h-type Co atoms which might mean that superconductivity originates also from these atoms and not only from the Y band. (22 refs.)

77285 NMR and magnetization study of the mixed systems $(\text{Pd}_{1-x}\text{Cu}_x)_2\text{MnIn}$ and $(\text{Pd}_{1-x}\text{Ni}_x)_2\text{MnIn}$. J.Schaf, I.A.Campbell (Lab. de Phys. des Solides, Univ. Paris-Sud, Orsay, France), K.Le Dang, P.Veillet, A.Hamzik.

J. Magn. & Magn. Mater. (Netherlands), vol.36, no.3, p.310-18 (April 1983). Systematic NMR and magnetization data with concentration show that for decreasing x these systems go from ferromagnetic (F) to antiferromagnetic (AF) order by passing through a mixed phase region where both magnetic orders coexist in different domains. The magnetic phase diagrams for both alloy series are nearly coincident. The NMR spectra show that the Cu or Ni atoms substitute randomly onto Pd sites and the authors find no evidence that the participation of Mn atoms in F or AF domains is at all correlated with their nearest neighbour environments. In the limit where the AF order becomes largely dominant the samples exhibit a magnetic anisotropy after field cooling. (27 refs.)

77286 Temperature dependences of the sublattice magnetizations in nickel ferrite. A.V.Kunevich, G.D.Pavlov, V.V.Filipov.

Sov. Phys.-Solid State (USA), vol.24, no.11, p.1998-9 (Nov. 1982). Translation of: *Fiz. Tverd. Tela (USSR)*, vol.24, no.11, p.3506-8 (Nov. 1982) [received: May 1983]

The authors used the NMR spin echo method to study hyperfine fields at ^{57}Fe and ^{61}Ni nuclei in polycrystalline nickel ferrite $\text{Fe}^{3+}[\text{Ni}^{2+}\text{Fe}^{3+}]_2\text{O}_4$.

with the inverted spinel structure at temperatures $4.2=810\text{K}$ so as to determine the temperature dependences of the nickel and iron sublattice magnetizations, and then calculate the exchange interaction parameters. (7 refs.)

The hyperfine interaction of gadolinium and holmium in cubic Ho: (Gd, Ce)Fe₂ compoundsSee Entry 77302

76.70 MAGNETIC DOUBLE RESONANCES AND CROSS EFFECTS

76.70D Electron-nuclear double resonance (ENDOR)

77287 Electron nuclear double resonance of ¹³C nuclei with natural abundance in trissarcosine calcium chloride doped with Mn²⁺ ions. H.Metz, J.Kuchler, R.Bottcher, W.Windsch (Sektion Phys., Karl-Marx-Univ., Leipzig, Germany).

Chem. Phys. Lett. (Netherlands), vol.97, no.3, p.303-7 (20 May 1983). ¹³C ENDOR measurements were performed at 4.2K on single crystals of trissarcosine calcium chloride doped with Mn²⁺ ions. Hyperfine coupling tensors were measured for six ¹³C nuclei of the carboxyl groups. An attempt is made to interpret the data in terms of electron-transfer and dipole-dipole contributions. (14 refs.)

76.70E Dynamical nuclear polarization

77288 Optical polarization of lattice nuclei in strongly deformed silicon. N.T.Bagraev, L.S.Vlasenko (A.F. Ioffe Physicotech. Inst., Acad. of Sci., Leningrad, USSR).

Sov. Phys.-Solid State (USA), vol.24, no.11, p.1974-5 (Nov. 1982). Translation of: *Fiz. Tverd. Tela (USSR)*, vol.24, no.11, p.3470-2 (Nov. 1982). [received: May 1983]

The authors have investigated processes of optical polarization of nuclei in silicon having a high density of dislocations created by plastic deformation. The strain ϵ created by such deformation in n-type silicon single crystals grown by the floating zone method and containing 10^{13}cm^{-3} of phosphorus was $\epsilon=5\%$, 30% , and $50\text{-}70\%$. (5 refs.)

Electron localization on defects and optical nuclear polarization in disordered and semimagnetic semiconductorsSee Entry 77270

76.70F Double nuclear magnetic resonance (DNMR)

77289 Frequency spectrum of a double nuclear magnetic γ resonance in Ta¹⁸¹. V.K.Voitovetskii, S.M.Chermisin, A.Yu.Dudkin, E.G.Ploskirev (I.V. Kurchatov Inst. of Atomic Energy, Moscow, USSR).

JETP Lett. (USA), vol.36, no.9, p.393-7 (5 Nov. 1982). Translation of: *Pis'ma v Zh. Eksp. & Teor. Fiz. (USSR)*, vol.36, no.9, p.322-5 (5 Nov. 1982). [received: June 1983]

The frequency spectrum of the double nuclear magnetic γ resonance in the excited state of the source nuclei, Ta^{181*}, has been measured. The results are compared with calculations. (7 refs.)

77290 Pulsed double nuclear magnetic resonance in a CaF₂:La³⁺:Na⁺ crystal. D.I.Vainshtein, V.D.Shechepkin, V.A.Safin, V.M.Vinokurov (V.I. Ulyanov-Lenin State Univ., Kazan, USSR).

Sov. Phys.-Solid State (USA), vol.24, no.11, p.1981-2 (Nov. 1982). Translation of: *Fiz. Tverd. Tela (USSR)*, vol.24, no.11, p.3480-3 (Nov. 1982). [received: May 1983]

At 77K the authors applied the DNR method to a CaF₂:La³⁺:Na⁺ crystal grown with an admixture of up to $\sim 0.3\%$ of the appropriate fluoride to the initial charge. The spin-lattice and dipole relaxation times obtained in a magnetic field of the H₀[110] orientation were found to be T₁=28.2 sec and T_{2d}=3.01 sec, respectively. The large difference between the spin-lattice and dipole relaxation times made it possible to record the DNR spectra without recourse to phase detection. (7 refs.)

Solid-state high-resolution ²⁹Si NMR in zunyiteSee Entry 77274

The measurements of NMR T₁ and NOESee Entry 77279

76.70H Optical double magnetic resonance (ODMR)

77291 Measurement of the hyperfine structure of Pr³⁺:YAG by quantum-beat free-induction decay, hole burning, and optically detected nuclear quadrupole resonance. R.M.Shelby, A.C.Tropper, R.T.Harley, R.M.Macfarlane (IBM Res. Lab., San Jose, CA, USA).

Opt. Lett. (USA), vol.8, no.6, p.304-6 (June 1983). The hyperfine splitting of the ground state and the lowest electronic component of the ¹D₂ excited state have been measured for Pr³⁺ in YAG. The authors show that a particularly simple and powerful technique is the production of sublevel coherence by short-pulse (impact) excitation, which is detected by coherent forward scattering of a weak probe beam and Fourier transformation of the resulting quantum-beat signal. This yielded excited-state splittings of 6.49 and 8.29 MHz. The ground state shows large pseudoquadrupole splittings of 33.4 and 41.6 MHz, which were obtained by optically detected nuclear quadrupole resonance. (14 refs.)

77292 ODMR investigation of recombination processes in a-Si_{1-x}C_x:H. S.P.Depinna, B.C.Cavenett (Dept. of Phys., Univ. of Hull, Hull, England), R.Sussmann.

Philos. Mag. B (GB), vol.47, no.5, p.L51-5 (May 1983). An investigation of glow-discharge deposited films of a-Si_{1-x}C_x:H by optically detected magnetic resonance (ODMR) has shown for the first time in group-IV materials a half-field ($g=4.017$) resonance as well as a signal at $g=2.0030$. These quenching signals have been observed for films having low carbon-content ($x>30\%$) and were associated with all but the highest energy emission. Although Fe impurities cannot be ruled out, the ODMR results are consistent with a triplet non-radiative path which competes with highly localized radiative recombination. (16 refs.)

77293 ODMR investigation of recombination in $\mu\text{-Si:H}$. S.P.Depinna, K.Homeewood, B.C.Cavenett (Dept. of Phys., Univ. of Hull, Hull, England), I.G.Austin, T.M.Searle, G.Willeke, S.Kinmond.

Philos. Mag. B (GB), vol.47, no.5, p.L57-62 (May 1983). The luminescence from $\mu\text{-Si:H}$ measured out to 0.54 eV shows a long low-energy tail with a broad maximum near 0.8 eV as well as bands at 0.95 and 1.3 eV. The ODMR shows that the long tail is associated with two enhancing signals with $g=1.999$ and 2.006 implying donor-acceptor recombination in the microcrystallites. A weak quenching ODMR signal at $g=2.005$ is associated with the 1.3 and 0.95 eV emission bands and, in particular, the results for the 1.3 eV band are consistent with it arising in the amorphous intercrystallite

region. The 0.95 eV band is thought to arise from defects similar to those observed in crystalline material. (13 refs.)

77294 Optical detection of cross relaxation between rare-earth ions in lanthanum trichloride crystals. R.Furrer, C.A.Hutchison, Jr. (Dept. of Chem., Univ. of Chicago, Chicago, IL, USA).

Phys. Rev. B (USA), vol.27, no.9, p.5270-8 (1 May 1983). The dynamics of relaxation and interionic energy-transfer processes for Nd³⁺ and Er³⁺ ions, dilutely cosubstituted at La³⁺ sites in LaCl₃ single crystals, have been investigated in a series of optical-magnetic double-resonance experiments. These processes have been studied by measuring the effects of electron-paramagnetic-resonance absorption at microwave frequencies on the fluorescence radiation emitted during continuous Ar-ion-laser irradiation. In cases for which the ratio of the magnetic field energy splitting of the ground Kramers doublet of Er³⁺ to that of Nd³⁺ had values relatively close to 1/2, 1/3, 1/4, or 1/5, the time for regaining steady-state-level populations after termination of microwave irradiation was markedly reduced compared with other ratios and was minimum at those particular values. This observation is interpreted as due to energy-conserving cross-relaxation processes involving several Nd³⁺ and Er³⁺ ions simultaneously. (30 refs.)

Ion implantation in group II-VI compoundsSee Entry 76467

Nuclear-quadrupole-resonance study of the ground state of praseodymium in lanthanum trifluorideSee Entry 77282

76.80 MÖSSBAUER EFFECT; OTHER GAMMA-RAY SPECTROSCOPY

77295 Elastic and inelastic scattering of gamma rays from V₃Si. S.S.Ti, T.R.Finlayson, T.F.Smith, J.D.Cashion, P.E.Clark (Dept. of Phys., Monash Univ., Clayton, Victoria, Australia).

Aust. J. Phys. (Australia), vol.36, no.2, p.185-96 (1983). The elastic and inelastic components of γ -ray scattering from a non-transforming V₃Si single crystal have been measured using a ⁵⁷Co Mossbauer source and resonant absorber. The system places an upper limit of $\pm 4 \times 10^{-8}$ eV on the possible energy transfer which distinguishes inelastic from elastic scattering. The scattering of the (440) Bragg reflection with $q=0$ and $q\sim 0.1\text{ \AA}^{-1}$ has been measured as a function of temperature for two orthogonal orientations of the crystal. Anomalous changes in the inelastic intensities have been observed. It is suggested that these changes are associated respectively with central mode and soft mode aspects of the dynamics of the vanadium atoms. (21 refs.)

77296 Mossbauer spectroscopy of amorphous silicon-tin-hydrogen alloys. D.L.Williamson, S.K.Deb (Solar Energy Res. Inst., Golden, CO, USA).

J. Appl. Phys. (USA), vol.54, no.5, p.2588-92 (May 1983). Amorphous-Si_{1-x}Sn_x:H alloys have been prepared by DC and RF sputtering of composite Si-Sn targets in Ar-H₂ gas mixtures. ¹¹⁹Sn conversion electron Mossbauer spectroscopy and X-ray diffraction reveal the Sn to be incorporated into the films in at least four distinct sites, the relative populations of which depend strongly on preparation conditions. The Mossbauer resonance from the substitutional Sn in the α -Si:H matrix is well characterized by a quadrupole splitting of $0.46\pm 0.05\text{ mm/s}$ independent of x and preparation conditions. Experimental procedures have been found such that samples can be produced which contain only the substitutional Sn site. (14 refs.)

77297 Giant hyperfine field on ¹⁵¹Eu in EuFe₂P₁₂ [Mossbauer study]. A.Gerard, F.Grandjean (Inst. de Phys., Univ. de Liege, Sart-Tilman, Belgium), J.A.Hodges, D.J.Braun, W.Jeitschko.

J. Phys. C (GB), vol.16, no.14, p.2797-801 (20 May 1983). Unusual ¹⁵¹Eu²⁺ hyperfine parameters are observed in EuFe₂P₁₂. The low-temperature saturated hyperfine field ($H= -670\text{ kOe}$) is particularly large and the isomer shift of -6.0 mm s^{-1} (relative to EuF₃) is evidence of a particularly high nuclear s-electron density. In addition, the ferromagnetic ordering temperature is very high (100K) especially in view of the large distance (6.8 Å) between the Eu²⁺ ions and the fact that Fe has no localised magnetic moment. The anomalously high hyperfine field points to the importance of f-d band coupling. (10 refs.)

77298 Evidence for electronic exchange between Fe²⁺ and Fe³⁺ in rhombohedral oxides AFe₂O₄ using ⁵⁷Fe Mossbauer spectroscopy. R.Gerardin, O.Evrard (Lab. de Chimie du Solide Mineral, Univ. de Nancy I, Vandoeuvre les Nancy, France).

J. Phys. & Chem. Solids (GB), vol.44, no.5, p.423-9 (1983). In French. The ABB₂O₄ rhombohedral oxides containing exclusively either Fe²⁺(InFeGe_{0.5}Zn_{0.5}O₄) or Fe³⁺(LuMgFeO₄ and LuMnFeO₄) are investigated with Mossbauer spectroscopy, in their paramagnetic state. A similar study is made on two mixed oxides containing iron under its two oxidation states with the Fe²⁺/Fe³⁺=2 and 1 (InFe_{1.5}Ga_{0.5}O₄ and InFe₂O₄) atomic ratio. Comparing the results, the authors conclude that a fast electronic exchange between Fe²⁺ and Fe³⁺ takes place at room temperature. In this structure, point Fe²⁺ and Fe³⁺ are distributed on the same crystallographic site with the point symmetry C_{3v}. They show that neighbouring effects lower this local symmetry. (14 refs.)

77299 Effect of an electric field on the Mossbauer spectra of the ferrites BaFe₁₂O₁₉. E.G.Rozin, M.N.Shipko, I.S.Zheludev (Inst. of Crystallography, Acad. of Sci., Moscow, USSR).

JETP Lett. (USA), vol.36, no.9, p.385-7 (5 Nov. 1982). Translation of: *Pis'ma v Zh. Eksp. & Teor. Fiz. (USSR)*, vol.36, no.9, p.316-18 (5 Nov. 1982). [received: June 1983] Mossbauer studies of single crystals of hexagonal ferrite BaFe₁₂O₁₉ in an external electric field are performed. An appreciable decrease of the local magnetic field at Fe⁵⁷ nuclei situated in two crystallographic positions: trigonal bipyramid and octahedron, was observed in an electric field for the first time. (7 refs.)

77300 Lattice temperature and hyperfine interactions of Pb_{1-x}Sn_xTe (0.21 $\leq x\leq 0.75$). R.H.Herber (Dept. of Chem., Rutgers State Univ., New Brunswick, NJ, USA), R.Kalish.

J. Solid State Chem. (USA), vol.47, no.3, p.284-92 (May 1983). Thin ($<15\text{ }\mu\text{m}$) samples of lead tin telluride, Pb_{1-x}Sn_xTe ($x=0.21, 0.25, 0.55, \text{ and } 0.75$) have been studied by temperature dependent Mossbauer spectroscopy using the 23.8 keV gamma radiation of ^{119m}Sn. The tin atom occupies a lattice site having cubic symmetry ($Q_S=0\pm 0.020\text{ mm sec}^{-1}$) over the temperature range $78\leq T\leq 240\text{K}$, and there is no evidence for a rhombic (low temperature) to cubic (high temperature) phase transition such as that reported for SnTe in this temperature interval. The lattice temperature as probed by the Sn atom is independent of the compositional parameter x and is similar to that reported for SnTe from Mossbauer studies and for Pb_{0.6}Sn_{0.37}Te from X-ray powder diffraction data. Radiation damage produced by 2-MeV proton irradiation to a total fluence of $\sim 10^{17}\text{ cm}^{-2}$ at liquid nitrogen temperature does not have any effect on the Mossbauer

parameters, possibly because the major damage is annealed at temperatures below 150K. (30 refs.)

77301 ⁵⁷Fe Mossbauer study of amorphous $\text{Fe}_{81}\text{B}_{13.5}\text{Si}_{3.5}\text{C}_2$. R.E.Vandenberghe, D.Gryffroy (Lab. of Magnetism, Univ. of Gent, Gent, Belgium). *J. Magn. & Magn. Mater. (Netherlands)*, vol.36, no.3, p.259-64 (April 1983). The amorphous ferromagnet $\text{Fe}_{81}\text{B}_{13.5}\text{Si}_{3.5}\text{C}_2$ (Metglas 2605SC) has been investigated with Mossbauer spectroscopy. The hyperfine interaction parameters are studied between 80 and 300K from which some characteristic properties are deduced. The behaviour of the amorphous alloy at higher temperatures has been studied by the room temperature spectra of annealed samples. After a structural relaxation process, a two step crystallization transformation is observed leading to Fe-Si alloy and $\text{Fe}_2(\text{B}, \text{C})$. X-ray diffraction of samples annealed at higher temperatures reveals the presence of an orthorhombic Fe-B-Si phase: this structure changes slightly with annealing temperature. (18 refs.)

77302 The hyperfine interaction of gadolinium and holmium in cubic Ho(Gd, Ce) Fe_2 compounds. O.Prakash, M.A.Chaudhry, J.W.Ross, M.A.H.McCausland (Schuster Lab., Univ. of Manchester, Manchester, England).

J. Magn. & Magn. Mater. (Netherlands), vol.36, no.3, p.271-6 (April 1983). The low-temperature hyperfine parameters of the ferrimagnetic C15 intermetallic system $\text{Ho}_{0.93}\text{Ce}_{0.07}\text{Fe}_2$ have been measured at Gd using the 87 γ -ray of ^{155}Gd and at Ho using spin echo NMR of ^{165}Ho . A linear decrease of the hyperfine field B_h with increasing x is observed, the slope being almost the same for both nuclei. The observed slope ($dB_h/dx \approx -37$ T) is nearly three times greater than that found for ^{155}Gd in the analogous $\text{Ho}(\text{Y}, \text{Gd})\text{Fe}_2$ system; this is attributed to the influence of the increased conduction electron density when trivalent lanthanide ions are replaced by Ce^{4+} . (28 refs.)

77303 Magnetic hyperfine splitting in Mossbauer spectra of microcrystals. S.Morup (Lab. of Appl. Phys. II, Tech. Univ. of Denmark, Lyngby, Denmark).

J. Magn. & Magn. Mater. (Netherlands), vol.37, no.1, p.39-50 (May 1983). Below the superparamagnetic blocking temperature of a microcrystal the magnetization direction is in general not fixed, but fluctuates in directions close to an easy direction of magnetization. Such fluctuations (collective magnetic excitations) result in a reduction in the magnetic splitting of the Mossbauer spectrum. A low-temperature approximation for this reduction is derived for microcrystals with arbitrary magnetic energy. Moreover, explicit expressions are presented for particles with special types of magnetic anisotropy and for particles exposed to external magnetic fields. The reduction in the magnetic hyperfine field has its maximum value just below the blocking temperature but does not exceed 5-15% in isolated particles with uniaxial anisotropy in zero applied magnetic field. However, ferro- and ferrimagnetic particles, exposed to external magnetic fields, and particles for which exchange anisotropy is predominant, may exhibit any magnetic hyperfine splitting between zero and the saturation value. It is shown that in special cases an assembly of microcrystals in close contact with each other may behave like a spin-glass. The author discusses how studies of the magnetic hyperfine splitting of Mossbauer spectra of microcrystals give information on the particle size and the prevailing magnetic anisotropies. (47 refs.)

77304 Phase analysis of the oxidation products of plain steels by Mossbauer spectroscopy. O.Dolezel (Ustav Pro Vyzkum Rud, Praha, Czechoslovakia), M.Seberini, M.Vadura, K.Volenik.

Kovove Mater. (Czechoslovakia), vol.21, no.2, p.142-57 (1983). In Czech. The oxide layers produced by high-temperature oxidation of plain steels and separated by the dissolution of steel substrate in an iodine-methanol solution were studied by Mossbauer transmission spectroscopy. The Mossbauer spectra were fitted by an approximative method using a Newlett-Packard calculator and assuming Lorentzian shape of spectral lines. The areas of partial spectra of individual phases were determined. The quantitative phase analysis of the specimens representing binary systems magnetite-hematite and wustite-magnetite was based on calibration curves obtained from the Mossbauer spectra of standard mixtures of synthetic oxides. The same calibration curves were used in the analysis of the ternary system wustite-magnetite-hematite. With the phase analysis results it was possible to calculate the concentration of bivalent iron versus total iron and to compare it with the value determined chemically. This was possible if a sufficient quantity of oxidation products was available, i.e. for thick oxide layers containing wustite. The results show that the systematic errors of phase analysis are considerably smaller than the random ones; the latter can be as large as several per cent. (19 refs.)

77305 A method for fitting complex Mossbauer spectra. Gauss-Newton method with modified factors. Cai Ruiying (Nanjing Inst. of Chem. Technol., China).

Kexue Tongbao (Foreign Lang. Ed.) (China), vol.28, no.3, p.416-22 (March 1983).

Mossbauer spectroscopy is one of the important modern methods for microstructural analysis of substances. For accurate determination of the Mossbauer spectral parameters, namely, the position, intensity, and width of each absorption peak of the spectrum, careful choice of numerical methods and design of applicable computer program for fitting by computer are very important. At present, the most common method used for fitting Mossbauer spectra is the Gauss-Newton method. It is suitable for the simple and good splitting spectrum. But it fails to fit for the slightly split and poorly resolved complex spectrum. In order to overcome these difficulties, a method devised with applicable computer program for fitting complex Mossbauer spectra is introduced and its application illustrated with examples. (4 refs.)

77306 Magnetic order in isoelectronic Co(GaVFe) alloys. G.L.Whittle (Dept. of Solid State Phys., Australian Nat. Univ., Canberra, Australia).

Phys. Status Solidi A (Germany), vol.76, no.1, p.351-6 (16 March 1983). A series of isoelectronic Co-Ga based alloys with V and Fe substituted for Ga is studied by Mossbauer spectroscopy (4.2 to 210K). The alloys are found to have similar bulk magnetic properties, as predicted, despite the wide concentration variation and different microscopic magnetic behaviour. The electron per atom ratio is established to be the controlling parameter for the onset of low temperature ferromagnetism. The data are also consistent with the presence of L_2 order at high V concentrations. (9 refs.)

77307 A Mossbauer study of octahedral site symmetries in systems $\text{Co}_x\text{Mn}_{3-x}\text{Fe}_2\text{O}_4$ and $\text{Ni}_x\text{Mn}_{3-x}\text{Fe}_2\text{O}_4$. V.K.Singh, S.Lokanathan (Dept. of Phys., Univ. of Rajasthan, Jaipur, India).

Pramana (India), vol.20, no.1, p.1-5 (Jan. 1983). [received: May 1983] A Mossbauer study of cation distribution in systems $\text{Co}_x\text{Mn}_{3-x}\text{Fe}_2\text{O}_4$ and $\text{Ni}_x\text{Mn}_{3-x}\text{Fe}_2\text{O}_4$ has been made. It has been found that in both systems all specimens with $y < 0.6$ value exhibit quadrupole doublets corresponding to site symmetries $\text{Fe}^{3+}(\text{I})$ and $\text{Fe}^{3+}(\text{II})$ of octahedral site. As more and more cobalt or nickel is introduced into the matrix the intensity of the inner quadrupole doublet increases while on introducing iron that of the outer quadrupole doublet increases. After a certain concentration of iron the inner doublet starts becoming more intense. It is suggested that this arises possibly from the substitution of cations in the second co-ordination sphere of $\text{Fe}^{3+}(\text{I})$ and

$\text{Fe}^{3+}(\text{II})$ sites. For $y > 0.6$ the Mossbauer spectra show relaxation effects. (11 refs.)

77308 Cation distribution of the system $\text{Zn}_{1-x}\text{Co}_x\text{FeMnO}_4$ by X-ray, electrical conductivity and Mossbauer studies. P.A.Jain, V.S.Dashane (Chem. Dept., Inst. of Sci., Bombay, India).

Pramana (India), vol.20, no.1, p.7-17 (Jan. 1983). [received: May 1983] Structural, electrical and Mossbauer studies were carried out for the system $\text{Zn}_{1-x}\text{Co}_x\text{FeMnO}_4$. It is observed that for $x \leq 0.6$, the ionic configuration of the system is $\text{Zn}_{1-x}^{2+}\text{Mn}_x^{2+}[\text{Co}_x^{3+}\text{Mn}_{1-x}^{3+}\text{Fe}^{3+}]_2\text{O}_4$ and for $x \geq 0.8$ Fe^{3+} ions occupy tetrahedral site also. On the basis of electrical and Mossbauer studies a probable valence distribution of CoMnFeO_4 has been suggested. All the compounds showed positive values of thermoelectric coefficient and electrical conduction takes place by a hopping mechanism. Activation energy and thermoelectric coefficient values decreased with decrease in concentration of Zn^{2+} ions. The compounds possess low mobility values varying between 10^{-10} and 10^{-9} $\text{cm}^2/\text{V sec}$. (30 refs.)

77309 Influence of isomer-shift distribution on Mossbauer quadrupole spectra in amorphous magnetic insulators. M.E.Lines, M.Eibschutz (Bell Labs., Murray Hill, NJ, USA).

Phys. Rev. B (USA), vol.27, no.9, p.5308-12 (1 May 1983). A mechanism is proposed whereby any distribution of isomer shifts in an amorphous material containing Fe^{3+} will broaden the ^{57}Fe paramagnetic Mossbauer doublet lines. The known variance of isomer shift in amorphous $\text{Y}_2\text{Fe}_2\text{O}_7$ is shown to be quite sufficient to account for the observed broadening in this material from that expected for quadrupole energy distribution in a random packed structure. (10 refs.)

77310 Site distribution in heavily Sc^{3+} , Zr^{4+} , and Hf^{4+} -substituted yttrium iron garnet. G.Balestrino (Istituto di Elettronica dello Stato Solido, Consiglio Nazionale delle Ricerche, Roma, Italy), S.Geller.

Phys. Rev. B (USA), vol.27, no.9, p.5807-9 (1 May 1983). Mossbauer spectra of yttrium iron garnet containing large amounts of Sc^{3+} , Zr^{4+} , and Hf^{4+} substituted for Fe^{3+} ions (the last two with electrostatic compensation by Ca^{2+} ions) confirm the conclusions deduced from O-K spontaneous magnetization that the Zr^{4+} and Hf^{4+} ions prefer octahedral sites exclusively. Very small amounts of Sc^{3+} ions enter tetrahedral sites: For a total of one Sc^{3+} ion per formula unit, 0.03 is tetrahedral; for a total of 1.5 Sc^{3+} ions per formula unit, 0.09 is tetrahedral. These results imply that in the region of the ferrimagnetic ground state, i.e., to 0.72 Sc^{3+} ion per formula unit, at most 0.02 is tetrahedral, but it could be that there is none because of the coincidence of the O-K dependence of the spontaneous magnetization on the composition of the Zr^{4+} - and Sc^{3+} -substituted yttrium iron garnets in that region. Thus the model given by Geller et al. for the magnetic behavior of substituted iron garnets is corroborated by these results. (10 refs.)

77311 Mossbauer study of iron hydride formation by low temperature ion implantation. F.Schreyer, G.Frech, G.K.Wolf (Inst. fur Phys. Chem., Univ. Heidelberg, Heidelberg, Germany), F.E.Wagner.

Solid State Commun. (USA), vol.46, no.8, p.647-50 (May 1983). High doses of 18 and 24 keV H_2^+ ions were implanted into α -iron films at liquid nitrogen temperature. Mossbauer spectra reveal the formation of a new phase with a hyperfine field of 30.4 T, a small quadrupole splitting and an isomer shift in the direction of lower electron density at the Fe nuclei. On the basis of its Mossbauer parameters and decomposition behaviour, this component can be identified as the recently described ϵ -phase iron hydride. A comparison with the effects of the low temperature implantation of He^+ ions supports this assignment. (19 refs.)

77312 ^{57}Fe Mossbauer spectroscopy on FePt Invar alloys. J.Hesse, G.Nolle, H.Korner (Inst. fur Metallphys. & Nukleare Festkorperphys., Tech. Univ. Braunschweig, Braunschweig, Germany).

Solid State Commun. (USA), vol.46, no.9, p.721-5 (June 1983). From ^{57}Fe Mossbauer effect investigations on disordered FePt-Invar alloys the authors determined the concentration dependence of both the mean isomer shift and the mean magnetic hyperfine field. Evaluating these changes in terms of charge and spin densities at the nuclei and combining the results with X-ray investigations they find the electronic state of the iron atoms being $3d^4s^1$ in these alloys. They present a 'magnetic' phase diagram and discuss the influence of the martensitic transformation. (18 refs.)

77313 Study of Ti_3Al with a ^{57}Fe impurity by the nuclear gamma resonance method. I.A.Zelenkov, S.N.Pastushenko (Kiev Inst. of Civil Aviation Engrns., Kiev, Ukrainian SSR).

Sov. Powder Metall. & Met. Ceram. (USA), vol.21, no.10, p.813-16 (Oct. 1982). Translation of: *Poroshk. Metall. (USSR)*, vol.21, no.10, p.70-4 (Oct. 1982). [received: May 1983]

A study was made of the ultrafine structure of the Mossbauer nuclear gamma resonance (NGR) absorption spectra of powdered specimens of a $(\text{TiFe})_{50}\text{Al}_{50}$ alloy with the Mg_2Cd order. The spectra were found to contain singlet and doublet components corresponding to the positions of Mossbauer iron atoms in the aluminum and titanium sublattices of Ti_3Al . Deformation of the Ti_3Al alloy after prolonged annealing brought about a substantial broadening of Mossbauer absorption lines. The presence of Al atoms in the near vicinity of the resonant ^{57}Fe atoms led to the filling of the 3d states of the iron atoms through a redistribution of electrons from the nearest aluminum atoms. The nature was determined of the electric field gradients forming on the ^{57}Fe nuclei located on the titanium points of the crystal lattice of ordered Ti_3Al . At lower temperatures the impurity iron atoms in ordered Ti_3Al occupied mainly the aluminum points. (14 refs.)

77314 The isomeric shift anomaly near phase transition temperature. B.Ya.Sukharevskii, V.G.Ksenofontov, A.N.Ulyanov, I.V.Vilkova.

Ukr. Fiz. Zh. (USSR), vol.28, no.5, p.720-2 (May 1983). In Russian. The temperature dependence has been studied for the isomeric shift of the ^{119}Sn Mossbauer resonance line in $\text{CuSnF}_6 \cdot 6\text{H}_2\text{O}$. The isomeric shift is shown to change in a nonmonotonic manner within the temperature range preceding dehydration. (9 refs.)

Fe₃PO₇, a case of Fe³⁺ fivefold coordination. Structural and magnetic studies See Entry 76377

The distribution of Fe³⁺ and Ga³⁺ between octahedral and tetrahedral sites in garnets, Y₃(Fe,Ga)₅O₁₂, at different temperatures See Entry 76402

Cation distributions in (Fe_{1-x}Me₂)₃(PO₄)₂ graftonite-type solid solutions determined by Mossbauer spectroscopy See Entry 76403

Isolation of Fe charge states by ion implantation and their study by Mossbauer spectroscopy See Entry 76468

Observation of impurity-interstitial interaction in irradiated niobium See Entry 76485

Lattice dynamics of isotopic alloys with applications to ⁶⁷Zn Mossbauer spectroscopy See Entry 76573

Diffusion of iron in aluminum studied by Mossbauer spectroscopy See Entry 76705

Changes in the electron structure of Fe-Ni alloys with the FCC lattice as a result of a magnetic phase transition See Entry 76836
Thermodynamic and structural properties of amorphous Fe₈₀B₂₀ and Fe₈₀Fe₁₅C₅ alloys See Entry 76922
Canted ferromagnetism in PdMn and PdMnFe alloys See Entry 77143
Antiferromagnetism of the FeNb and FeTa mu-phases See Entry 77145
Study of the critical behaviour of the magnetization and electrical resistivity in cubic La(Fe, Si)₁₃ compounds See Entry 77155
Characteristics of the magnetic microstructure of oxyfluoride ferrites See Entry 77160
Existence of a canted phase in terbium yttrium iron garnets See Entry 77176
Magnetization and Mossbauer studies of Y(Fe,Rh)₂ See Entry 77208
Magnetization and ¹⁶¹Dy Mossbauer effect study of DyMn₂ and Dy₂Mn₃ and their ternary hydrides See Entry 77209
Invar anomalies of Fe-Pd alloys See Entry 77243
Frequency spectrum of a double nuclear magnetic γ resonance in Ta¹⁸¹ See Entry 77289
Investigation of structural changes during fracture of $\gamma + \epsilon$ steel See Entry 77724
On the fine structure of meteoritical taenite/tetrataenite and its interpretation See Entry 78884

76.90 OTHER TOPICS IN MAGNETIC RESONANCES AND RELAXATION
(inc. muon probe studies)

77315 Muon-spin-rotation experiments in orthoferrites. E.Holzschuh, A.B.Denison, W.Kundig, P.F.Meier, B.D.Patterson (Phys.-Inst., Univ. Zurich, Zurich, Switzerland). *Phys. Rev. B (USA)*, vol.27, no.9, p.5294-307 (1 May 1983).
A systematic study of the behavior of positive muons in orthoferrites RFeO₃ has been performed. Measurements as a function of temperature and applied magnetic field have been made for R=Sm, Eu, Dy, Ho, Y, and Er. Typically several different sites are occupied by the muons at low temperatures, and transitions occur to one stable site with temperature-dependent rate constants. By comparing the measured internal magnetic fields with calculated dipole fields of the iron ions, the position of the stable muon site was found to be on the mirror plane *m* about 1 Å from the nearest oxygen ion, implying the formation of the hydroxyl analog (OH⁻). Muon diffusion was observed for R=Sm with about 10 jumps/ μ s at 296K. (38 refs.)

77.00 DIELECTRIC PROPERTIES AND MATERIALS
(for conductivity phenomena, see 72.20 and 72.80)

77.20 PERMITTIVITY

77316 Strain dependence of the low-frequency dielectric constants of a few alkali halides. G.Balakrishnan, K.Srinivasan, R.Srinivasan (Dept. of Phys., Indian Inst. of Technol., Madras, India). *J. Appl. Phys. (USA)*, vol.54, no.5, p.2875-7 (May 1983).
The variation of the low-frequency dielectric constant of NaCl, KCl, and KBr with stress has been determined by subjecting the crystals to uniaxial compressive stresses. Contrary to expectations, the dielectric constant was found to increase on stressing. On *n* irradiation, the sign of the change in the dielectric constant of the crystals was reversed. This has been attributed to the pinning of the dislocations, whose initial movement under stress might have caused the dielectric constant to increase. (11 refs.)
77317 Order-disorder phase transition and dielectric constant of ice Ic. I.Minagawa (Dept. of Sci., Kokugakuin Univ., Tokyo, Japan). *J. Phys. Soc. Jpn. (Japan)*, vol.52, no.5, p.1641-5 (May 1983).
A theoretical study is made of the order-disorder transition of cubic ice Ic, where interaction energies between water molecules are considered, seven order parameters are used, and Takagi's method is employed. The ordered phase is ferroelectric when the interaction energies between neighbouring molecules are assumed to be the same as that in ice Ih. The transition is of the first order. The Curie-Weiss temperature θ_c is the same as that of Ih in the *c*-axis and the transition temperature is 1.29 θ_c =59K. The phase transition from ice Ic to Ih is discussed. (10 refs.)
77318 Dielectric properties of modified PZT ceramics. Long Wu, Chung-Chuang Wei, Tien-Shou Wu (Res. Inst. of Electronics & Electrical Engng., Nat. Cheng-Kung Univ., Tainan, Taiwan), Chain-Cheau Teng. *J. Phys. C (GB)*, vol.16, no.14, p.2803-12 (20 May 1983).
The dependence of the dielectric constant on the electric field of PZT ceramics can be well explained by the mechanism of domain wall motion. The mobility of the domain wall is increased by the A-site vacancies, due to the reduction of local stress in the domains which undergo domain switching. But O-site vacancies and the grain boundary act as pinning points for domain walls, so the domain wall motion is reduced when O-site vacancies dominate and the grain size is small. As a result, the dielectric constant after poling was larger than that before poling and the coercive field were reduced by the addition of A-site vacancy produce. But the opposite results were obtained, when the O-site vacancy produce was added. (22 refs.)
77319 Instability of the dielectric constant of Cd₂Nb₂O₇. G.A.Smolenskii, N.N.Kolpakova, S.A.Kizhaev (A.F. Ioffe Physicotech. Inst., Acad. of Sci., Leningrad, USSR). *JETP Lett. (USA)*, vol.36, no.8, p.361-4 (20 Oct. 1982). Translation of: *Pis'ma v Zh. Eksp. & Teor. Fiz. (USSR)*, vol.36, no.8, p.295-8 (20 Oct. 1982). [received: June 1983]
An anomalous instability (over time) and an anomalous thermal hysteresis of the dielectric constant have been discovered in Cd₂Nb₂O₇ in the temperature interval 40-80K. The Cd₂Nb₂O₇ may contain an incommensurate phase in the temperature interval 80K= T_3 > T_2 > T_6 =44K. (9 refs.)
77320 Dipole moments of poly(p-chlorostyrene) chains determined in toluene and isopropyl-benzene. F.Blasco, E.Riande (Inst. de Plasticos y Caucho, Madrid, Spain). *J. Polym. Sci. Polym. Phys. Ed. (USA)*, vol.21, no.5, p.835-8 (May 1983).
In order to verify whether solvent effects are apparent in the determination of dipole moments, dielectric constant measurements were conducted in solutions

of poly(p-chlorostyrene) (PPCS) in toluene and isopropyl-benzene, over the temperature ranges 30-70 and 30-90°C, respectively. Values of the dipole moment were calculated. It was concluded that the dipole moments of PPCS chains should have a negligible temperature dependence. (16 refs.)
77321 Temperature dependence of the electron permittivity of IV-VI semiconductors. B.A.Volkov, V.P.Kushnir (P.N. Lebedev Phys. Inst., Acad. of Sci., Moscow, USSR). *Sov. Phys.-Solid State (USA)*, vol.24, no.11, p.1869-72 (Nov. 1982). Translation of: *Fiz. Tverd. Tela (USSR)*, vol.24, no.11, p.3293-7 (Nov. 1982). [received: May 1983]
The effect of optical lattice vibrations on the electron permittivity is studied using a model of the band structure of IV-VI compounds based on atomic p orbitals. It is shown that the permittivity of the centrosymmetric phase should decrease with increasing temperature. The temperature dependence of the permittivity is estimated for the nonsymmetric phase. (6 refs.)
Permittivity measurements of lossy liquids at millimeter-wave frequencies See Entry 74492
Dipole moments of dichlorotoluenes in benzene solution See Entry 75543
Low density properties of a two dimensional dipolar fluid See Entry 76265
2,3-dicyanohydroquinone derivative liquid crystals having strong negative dielectric anisotropy See Entry 76289
New liquid crystal materials; physical properties and performance in displays for automobile, high information density and guest-host applications See Entry 76292
Stable liquid crystals with large negative dielectric anisotropy. II. See Entry 76296
Structural phase transition of layer compound (C₂H₅NH₂)₂FeCl₄ See Entry 76609
Electrical conduction through anodic oxides on InP See Entry 76951
Anomalous photo-emf in a model of a heavily doped and compensated ferroelectric See Entry 77001
Dielectric relaxation and dipole moment measurements of *n*-methylacetamide in benzene and dioxane solutions at different temperatures from microwave absorption studies See Entry 77325
The influence of thermal measurement conditions on the results of dielectric measurements in PLZT ceramic with diffused phase transition See Entry 77327
The theory of nonlinear dielectrics. Polar, polarizable molecules See Entry 77329
Elastic, dielectric, and piezoelectric properties of cancrinite carbonate single crystals See Entry 77332
Applications of piezoferroelectric materials containing niobium oxide See Entry 77333
High-temperature phase transitions in pure and deuterated ammonium dihydrogen phosphate: conductivity and dielectric measurements See Entry 77334
Switching properties of SBN single crystals See Entry 77337
Dielectric properties and ferroelectric phase transitions in mixed Rb_x(NH₄)_{1-x}HSeO₄ crystals See Entry 77338
Temperature coefficient of the phanite refractive index See Entry 77353
Electric birefringence and molecular polarisability of CF₃Cl,CF₃Cl See Entry 77356
Model for optical absorption in transition metals containing d impurities See Entry 77417
A new method for determining relaxation energies by means of AES and XPS and its application to silicon compounds See Entry 77520

77.30 POLARIZATION AND DEPOLARIZATION EFFECTS

77322 Phenomenological theory of shock-induced polarisation. II. Mathematical treatment of the oscillogram. M.De Icaza-Herrera (Inst. de Fisica, Univ. Nacional Autonoma de Mexico, Mexico City, Mexico). *J. Appl. Phys. (USA)*, vol.54, no.5, p.2360-5 (May 1983).
For pt.I see *ibid.*, vol.54, no.5, p.2352 (1983). The mathematical treatment of the theory presented in the preceding paper is detailed. Less than ten distance measurements on the oscillogram are enough to determine the dielectric properties of the shocked medium and the polarisation discontinuity across the shock front. The last one agrees approximately with Allison's mechanical polarisation (1965), but does not depend on the dielectric properties of the shocked medium. The treatment is valid for the dipolar orientation and bond scission models of shock-induced polarisation. Finally, the effect of a changing pressure profile is discussed. (8 refs.)
77323 Investigations of the thermally stimulated change of the surface potential of FEP electrets. W.Stark, R.Danz (Inst. fur Polymerenchem. 'Erich Correns', Akad. der Wissenschaften, Teltow-Seehof, Germany). *Phys. Status Solidi a (Germany)*, vol.76, no.1, p.K101-3 (16 March 1983).
The determination of the thermally stimulated charge decay (TSCD) by changes of the surface potential has proved an efficient tool for characterizing electrets. Numerous investigations have already been performed with negatively charged fluoropolymers PTFE (polytetrafluoroethylene) and FEP (copolymer of tetrafluoroethylene and hexafluoropropylene) because of the high electret stability of these substances. The comparative consideration of the literature data reveals in some measurements an increase of the surface potential preceding its typical decrease at elevated temperatures, while in other measurements the surface potential remains unchanged up to the onset of the decrease. The increase of the surface potential was interpreted by the decrease of a hidden positive charge or heterocharges. The authors suggest that previous authors have misinterpreted measurements of surface charges by neglecting the influence of dimensional changes with temperature. (10 refs.)
Depolarization current in a dielectric with deep trapped charge layers See Entry 76970
Anomalous photo-emf in a model of a heavily doped and compensated ferroelectric See Entry 77001
The theory of nonlinear dielectrics. Polar, polarizable molecules See Entry 77329
Switching properties of SBN single crystals See Entry 77337
Dielectric properties and ferroelectric phase transitions in mixed Rb_x(NH₄)_{1-x}HSeO₄ crystals See Entry 77338

77.40 DIELECTRIC LOSS AND RELAXATION

77324 Dielectric and dynamic-mechanical behaviour of ethylene-vinyl alcohol copolymers. F.P. La Mantia, G. Spadaro (Istituto di Ingegneria Chimica, Univ. of Palermo, Palermo, Italy).

Mater. Chem. & Phys. (Switzerland), vol.8, no.4, p.315-21 (April 1983).

Dynamic-mechanical and dielectric measurements on ethylene-vinyl alcohol copolymers with two different vinyl alcohol contents and, for comparison, on polyvinylalcohol and low density polyethylene have been carried out in order to clarify the nature of the relaxation peak. The relaxation peak observable in the dielectric loss curves of the copolymers has been assigned to the interfacial polarization, MWS type, occurring between hydrogen bonded hydroxyl groups and the apolar polyethylene segments. The shoulder also present in the ϵ'' -T curves of the copolymers seems to correspond to the glass transition peak which is hidden since the dielectric loss curve increases quickly because of the MWS polarization peak. The frequency-temperature map confirms this opinion. (9 refs.)

77325 Dielectric relaxation and dipole moment measurements of *N*-methylacetamide in benzene and dioxane solutions at different temperatures from microwave absorption studies. J.S. Dhull, D.R. Sharma (Dept. of Phys., Himachal Pradesh Univ., Simla, India), D.S. Gill, K.N. Lakshminarayana. *Indian J. Phys. Part B*, vol.56B, no.6, p.334-43 (Dec. 1982). [received: May 1983]

Using standing wave techniques, dielectric constant (ϵ') and dielectric loss (ϵ'') of dilute solutions of *N*-methylacetamide (NMA) in benzene and dioxane have been measured at 9.987 GHz at 25, 35, 45 and 55°C. Following the single frequency concentration variational method, dielectric relaxation time (τ) and the dipole moment (μ) have been evaluated. The results show different types of molecular association of NMA in benzene and dioxane solutions. At low concentrations of NMA in benzene, the association is solute-solvent type which changes into the solute-solute association (dimer formation) at relatively higher concentrations of NMA in benzene. Energy parameters (ΔF^\ddagger , ΔH^\ddagger and ΔS^\ddagger) for the dielectric relaxation of NMA in benzene and dioxane solutions have been calculated from the Eyring's rate equations and compared with corresponding viscosity parameters. A comparison between these two sets of parameters shows that the dielectric relaxation like viscosity, can also be considered as a rate process. (17 refs.)

77326 Structure and dipole relaxation mechanisms in the cyclic alcohols cyclopentanol to cyclo-octanol. M. Shablaikh, L.A. Dissado, R.M. Hill (Chelsea Coll., Univ. of London, London, England).

J. Chem. Soc. Faraday Trans. II (GB), vol.79, pt.3, p.369-417 (March 1983). The phase structure and stability of the solid phases of cyclopentanol, cyclohexanol, cycloheptanol and cyclo-octanol have been investigated by examining the dielectric relaxation mechanisms in these materials. It has been found that a number of the transitions between the stable phases are time-dependent as well as temperature-dependent and these effects have given rise to misconceptions in the phase structure. For the cyclic alcohols examined the stable phases have been characterised and where possible this has been done in terms of dipolar cluster distributions. The results of the dielectric investigation are discussed in terms of the structure of the materials. (38 refs.)

77327 The influence of thermal measurement conditions on the results of dielectric measurements in PLZT ceramic with diffused phase transition. F. Glasse (Inst. of Experimental Phys., Univ. of Wrocław, Wrocław, Poland). *Phys. Status Solidi a (Germany)*, vol.76, no.2, p.K121-3 (16 April 1983).

The author reports on a change of the temperature dependences of the DC and the loss tangent change, when the measurement conditions get nearer to quasi-stationary conditions. For this purpose a PLZT sample was annealed at 300°C during 48 h and then cooled a) with a cooling rate $dT/dt = -0.97$ K/min and b) with $dT/dt = -0.014$ K/min. During cooling the DC and the loss tangent were measured by an automatic capacitance bridge at a frequency of 1 kHz. The AC measuring field had a magnitude of 140 V/cm. (5 refs.)

One-dimensional models of polymer dynamics. I. Dashpot-spring models applied to a single rotor See Entry 76276

One-dimensional models of polymer dynamics. II. A dashpot-spring model See Entry 76277

New liquid crystal materials; physical properties and performance in displays for automobile, high information density and guest-host applications See Entry 76292

CO/N₂ solid solutions: head-tail reorientations See Entry 76330

Instability of the dielectric constant of Cd₂Nb₂O₇ See Entry 77319

77.50 DIELECTRIC BREAKDOWN AND SPACE-CHARGE EFFECTS

Depolarization current in a dielectric with deep trapped charge layers See Entry 76970

Anomalous photo-emf in a model of a heavily doped and compensated ferroelectric See Entry 77001

77.60 PIEZOELECTRICITY AND ELECTROSTRICTION

(for piezo-optical effects, see 78.20H)

77328 Distribution of axisymmetric waves in a piezoceramic planar cylinder. O.Ya. Grigorenko, I.A. Loza, M.O. Shul'ga. *Dopov. Akad. Nauk UKRSR. Ser. A (USSR)*, no.3, p.34-8 (1983). In Ukrainian.

Deals with the problem of propagation of axisymmetric waves in a hollow cylinder and a plane layer of piezoceramic material. Displacements and an electric potential are represented as a radial coordinate power series. A numerical analysis of the obtained dispersion ratios is presented for a long-wave approximation. (7 refs.)

77329 The theory of nonlinear dielectrics. Polar, polarizable molecules. R.L. Fulton (Dublin Inst. for Advanced Studies, School of Theoretical Phys., Dublin, Ireland).

J. Chem. Phys. (USA), vol.78, no.11, p.6877-84 (1 June 1983).

Some aspects of the nonlinear dielectric behavior of a simple fluid composed of polar, polarizable particles having spherical hard cores are discussed. In particular, the connection between the lowest order nonvanishing nonlinear dielectric constant and fluctuations in the polarization and dipole densities is found. By ignoring certain high order fluctuations, the nonlinear dielectric constant is related to two, three, and four body correlation functions. A further approximation involving the neglect of short range angular correlations produces the analog of the Onsager connection for the linear dielectric

constant. The connections given here differ from all previous proposals. Some examples are given to illustrate the relative importance of electrostriction, anisotropic polarizabilities, and permanent dipole moments and the difference with previous proposals. (18 refs.)

77330 Piezoelectric properties of modified PZT ceramics. Long Wu, Chung-Chuang Wei, Tien-Shou Wu (Res. Inst. of Electronics & Electrical Engng., Nat. Cheng-Kung Univ., Tainan, Taiwan), Hsi-Chuan Liu. *J. Phys. C (GB)*, vol.16, no.14, p.2813-21 (20 May 1983).

The influence of impurities on piezoelectric parameters such as the radial coupling factor k_r and mechanical quality factor Q_m have been measured. A mechanism of internal friction is proposed. The effects of the interaction of 90° domain walls with defects introduced by impurities are explained. A-site vacancies reduce the local stress in a domain, making it become remarkably mobile. The easy motion of the domain wall causes the internal friction in the ceramics to increase and thus Q_m to decrease. O-site vacancies act as pinning points for the domain walls, so that domain wall motion is reduced when O-site vacancies are dominant, and Q_m is raised due to the reduced internal friction. The effect of poling conditions is also discussed. (26 refs.)

77331 Longitudinal piezoelectric strain measurements of poly(vinylidene fluoride) films. K. Uchino (Dept. of Phys. Electronics, Tokyo Inst. of Technol., Tokyo, Japan), L.E. Cross.

J. Polym. Sci. Polym. Phys. Ed. (USA), vol.21, no.5, p.765-71 (May 1983). The longitudinal piezoelectric strain of poly(vinylidene fluoride) (PVF₂) films has been measured at room temperature using a high-sensitivity AC capacitance-type dilatometer. The DC bias field dependence of the piezoelectric strain coefficient d_{33} has been determined. The polarization-related electrostrictive coefficient Q_{33} obtained is several hundred times larger than the value in normal piezoelectric oxide crystals and is of opposite sign. (11 refs.)

77332 Elastic, dielectric, and piezoelectric properties of cancrinite carbonate single crystals. I.M. Silvestrova, I.B. Kobayakov, F.A. Belimenko (A.V. Shubnikov Inst. of Crystallography, Acad. of Sci., Moscow, USSR). *Sov. Phys.-Solid State (USSR)*, vol.24, no.11, p.1839-42 (Nov. 1982). Translation of: *Fiz. Tverd. Tela (USSR)*, vol.24, no.11, p.3241-7 (Nov. 1982). [received: May 1983]

The complete set of the elastic, dielectric, and piezoelectric constants was determined for zeolite-like aluminosilicate cancrinite carbonate. The piezoelectric constants were found by a resonance method and the elastic constants by employing ultrasound pulses. The dependences of the elasticity and of the piezoelectric activity on the defect and chemical compositions were observed for the investigated single crystals. The high value of the Poisson ratio $\sigma = 0.45-0.58$ indicated a weak stability of these crystals as a mechanical system, whereas the high value of the piezoelectric modulus $d_{15} = -16.5 \times 10^{-12}$ C/N indicated that cancrinite carbonate was a strong linear piezoelectric. (14 refs.)

77333 Applications of piezoelectric materials containing niobium oxide. E.G. Fesenko, A.Ya. Dantsiger, L.A. Reznichenko, L.A. Shilkina, O.N. Razumovskaya (Sci.-Res. Inst. of Phys., State Univ., Rostov-on-Don, USSR).

Sov. Phys.-Tech. Phys. (USA), vol.27, no.11, p.1389-91 (Nov. 1982). Translation of: *Zh. Tekh. Fiz. (USSR)*, vol.52, no.11, p.2262-6 (Nov. 1982). [received: May 1983]

The selection of materials containing NbO₃ for various applications is studied by examining the relationship between the structural and electrophysical parameters in NaNbO₃-based systems. These relationships are compared with those for PbZrO₃-PbTiO₃ systems, and it is found that they are both more complicated and more ambiguous. It is shown that the main parameters of NaNbO₃ materials (their small dielectric constant, high sound velocity, and low density) cannot be achieved in other solid solution systems. It is concluded that NaNbO₃ materials are best suited for application in bulk and surface wave devices in the HF and UHF ranges. Many compositions with a higher dielectric constant can also be used at lower frequencies. (7 refs.)

Thermal effects in a long rotating cylindrical shaft of piezo-electric material with a concentric circular axial hole See Entry 75896

Switching properties of SBN single crystals See Entry 77337

Preparation and investigation of solid solutions with a perovskite structure See Entry 77604

77.70 PYROELECTRIC AND ELECTROCALORIC EFFECTS

A simple measurement method of pyroelectric coefficient for ferroelectric crystals See Entry 74490

77.80 FERROELECTRICITY AND ANTIFERROELECTRICITY

Degenerate four-wave mixing in semiconductors and ferroelectrics See Entry 75748

The DC resistivity of modified PZT ceramics See Entry 76944

¹⁷O nuclear-quadrupole-resonance measurements in the ferroelectric phase of potassium dihydrogen phosphate: Evidence for proton tunneling See Entry 77283

Electron nuclear double resonance of ¹³C nuclei with natural abundance in trissarcosine calcium chloride doped with Mn²⁺ ions See Entry 77287

Order-disorder phase transition and dielectric constant of ice Ic See Entry 77317

Applications of piezoelectric materials containing niobium oxide See Entry 77333

Indicatrix and the piezooptical properties of diglycine nitrate crystals See Entry 77358

Ferroelectric liquid crystal electro-optics using the surface stabilized structure See Entry 77362

Exoelectron emission from surface states in a ferroelectric See Entry 77538

Preparation and investigation of solid solutions with a perovskite structure See Entry 77604

77.80B Transitions and Curie point

77334 High-temperature phase transitions in pure and deuterated ammonium dihydrogen phosphate: conductivity and dielectric measurements. V.K.Subhadra, U.Syamaprasad, C.P.G.Vallabhan (Dept. of Phys., Univ. of Cochin, Cochin, India).

J. Appl. Phys. (USA), vol.54, no.5, p.2593-6 (May 1983).

Results of axiswise measurements of the electrical conductivity (DC and AC) and dielectric constant of $\text{NH}_4\text{H}_2\text{PO}_4$ confirm the occurrence of the recently suggested high-temperature phase transition in this crystal (at 133°C). The corresponding transition in $\text{ND}_4\text{D}_2\text{PO}_4$ observed here for the first time takes place at 141.5°C . The mechanism involved in these transitions and those associated with the electrical conduction and dielectric anomalies are explained on the basis of the motional effects of the ammonium ions in these crystals. Conductivity values for deuterated crystals give direct evidence for the predominance of protonic conduction throughout the entire range of temperatures studied (30 – 260°C). (23 refs.)

77335 Influence of external electric field on incommensurate-commensurate phase transition in K_2SeO_4 and $(\text{NH}_4)_2\text{BeF}_4$ crystals. I. Static properties. O.Hudak (Inst. of Phys., Czechoslovak Acad. of Sci., Prague, Czechoslovakia).

J. Phys. C (GB), vol.16, no.14, p.2641-58 (20 May 1983).

The author presents a study of the influence of an external electric field on the incommensurate-commensurate phase transition in K_2SeO_4 and $(\text{NH}_4)_2\text{BeF}_4$ -like crystals. Within the constant-amplitude approximation the same type of thermodynamic potential is found in both cases. The phase diagram in the E - T phase plane is found and should exhibit a Lifshitz point. The susceptibility of the incommensurate phase diverges at the transition point while that of the commensurate phase remains finite. (25 refs.)

77336 Influence of external electric field on incommensurate-commensurate phase transition in K_2SeO_4 and $(\text{NH}_4)_2\text{BeF}_4$ crystals. II. Dynamic properties. O.Hudak (Inst. of Phys., Czechoslovak Acad. of Sci., Prague, Czechoslovakia).

J. Phys. C (GB), vol.16, no.14, p.2659-70 (20 May 1983).

For pt.1 see *ibid.*, vol.16, no.14, p.2641 (1983). External electric field influences the fluctuation spectrum of the phase variable in the incommensurate phase of K_2SeO_4 and $(\text{NH}_4)_2\text{BeF}_4$ -like crystals. As well as the usual zero-field branches (phason-like, acoustic-like) a new branch appears for non-zero fields. Analytic description of all these branches is given within the harmonic approximation. (7 refs.)

77337 Switching properties of SBN single crystals. G.Borchardt, J.von Cierninski, G.Schmidt (Sektion Phys., Martin-Luther-Univ. Halle-Wittenberg, Halle, Germany).

Phys. Status Solidi a (Germany), vol.76, no.2, p.K141-5 (16 April 1983).

The authors study the decrease of the switched polarisation observed with increasing number of hysteresis cycles in SBN ($\text{Sr}_x\text{Ba}_{1-x}\text{Nb}_2\text{O}_6$) single crystals. The field dependence of the permittivity and the electromechanical strain were measured by a method described by Schmidt et al. (1982). (14 refs.)

77338 Dielectric properties and ferroelectric phase transitions in mixed $\text{Rb}_x(\text{NH}_4)_{1-x}\text{HSeO}_4$ crystals. Z.Czapla, O.Czupinski, L.Sobczyk (Inst. of Chem., Univ. of Wrocław, Wrocław, Poland), J.Mroz, H.Pykacz.

Phys. Status Solidi a (Germany), vol.76, no.2, p.K155-7 (16 April 1983).

The mixed crystals $\text{Rb}_x(\text{NH}_4)_{1-x}\text{HSeO}_4$ have been grown at 303K from solutions of the total content of 0.2 moles of both salts. The composition has been determined by measuring the density of the mixed crystals. For dielectric studies the samples were cut perpendicularly to the ferroelectric b axis. Measurements are presented of the ferroelectric transition temperature, electric permittivity, spontaneous polarisation and hysteresis. (9 refs.)

77339 Anomalous broadening of phase transitions in lanthanum lead zirconate titanate. V.M.Ishchuk, A.A.Galkin, E.A.Zavadskii, E.M.Morozov.

Sov. Phys.-Solid State (USA), vol.24, no.12, p.2099-101 (Dec. 1983). Translation of: *Fiz. Tverd. Tela (USSR)*, vol.24, no.12, p.3684-8 (Dec. 1983).

An experimental investigation was made of broad phase transitions to the paraelectric state of the lanthanum lead zirconate titanate systems. The broadening of these transitions was found to depend on the position of the composition of a sample in the phase diagram and the strongest broadening was observed for a composition within the hysteresis range separating the ferroelectric and antiferroelectric states. The experimental results were interpreted on the basis of a model allowing for the existence of regions with different types of dipole ordering. (12 refs.)

Rb_xZnCl_4 : three heat-capacity anomalies due to soft-mode and commensurate-incommensurate transitions See Entry 76658

K_2SeO_4 : calorimetric studies of two successive phase transitions See Entry 76660

Instability of the dielectric constant of $\text{Cd}_3\text{Nb}_2\text{O}_7$ See Entry 77319

The influence of thermal measurement conditions on the results of dielectric measurements in PLZT ceramic with diffused phase transition See Entry 77327

Photoelasticity of $\text{Ba}_x\text{Sr}_{1-x}\text{Nb}_2\text{O}_6$ near the ferroelectric phase transition See Entry 77359

Raman scattering by soft plasmon-LO phonon modes in ferroelectric semiconductors See Entry 77380

Integrated scattering of light in lead magnoniobate, which is a ferroelectric with a diffuse phase transition See Entry 77405

77.80D Domain structure and effects; hysteresis

77340 Changes in the domain structure of lead germanate single crystals. V.Ya.Shur, V.V.Letchev, Yu.A.Popov (A.M. Gorki Univ. State Univ., Sverdlovsk, USSR).

Sov. Phys.-Solid State (USA), vol.24, no.11, p.1957-8 (Nov. 1982). Translation of: *Fiz. Tverd. Tela (USSR)*, vol.24, no.11, p.3444-6 (Nov. 1982). [received: May 1983]

It is known that the polarization of freshly grown lead germanate, $\text{Pb}_2\text{Ge}_2\text{O}_7$, single crystals cannot be switched by an electric field and that domains cannot be observed in these crystals. Normal dielectric hysteresis loops and domains penetrating right across a crystal are observed only after 'conditioning' in an external electric field. The characteristics of the domain structure of freshly prepared crystals (the initial domain structure) are usually attributed to the pinning of domain walls by mechanical stresses or space charges. The authors investigated the changes in the initial domain structure occurring in external electric fields. (3 refs.)

Dielectric properties of modified PZT ceramics See Entry 77318

Instability of the dielectric constant of $\text{Cd}_3\text{Nb}_2\text{O}_7$ See Entry 77319

Piezoelectric properties of modified PZT ceramics See Entry 77330

Dielectric properties and ferroelectric phase transitions in mixed $\text{Rb}_x(\text{NH}_4)_{1-x}\text{HSeO}_4$ crystals See Entry 77338

77.85 ELECTRICAL RESONANCES

77341 Paraelectric resonance study of $\text{KCl}:\text{Li}^+$. F.Holuj (Dept. of Phys., Univ. of Windsor, Windsor, Ontario, Canada), F.Bridges.

Phys. Rev. B (USA), vol.27, no.9, p.5286-93 (1 May 1983).

A paraelectric resonance study has been made of $\text{KCl}:\text{Li}^+$ over the frequency range 20 – 150 GHz . The data have been fitted to a (111)-dipole model. The best-fit tunneling parameters (including the estimated systematic errors) are $\eta = -11.34 \pm 0.4$, $\mu = -3.55 \pm 0.4$, and $\nu = 0.21 \pm 0.4$. The electric dipole moment is $5.683 \pm 0.06\text{ D}$. These parameters are compared critically with the existing data on $\text{KCl}:\text{Li}^+$. (18 refs.)

77.90 OTHER TOPICS IN DIELECTRIC PROPERTIES AND MATERIALS

77342 On the theory of nonlinear dielectrics. R.L.Fulton (Lab. for Phys. Chem., Univ. of Amsterdam, Amsterdam, Netherlands).

J. Chem. Phys. (USA), vol.78, no.11, p.6865-76 (1 June 1983).

A simple yet general prescription for finding the connections between phenomenological coefficients and susceptibilities for nonlinear dielectrics is found. In the linear realm the standard connections are recovered. The connections found between the nonlinear susceptibilities and phenomenological coefficients for isotropic polar media are found to differ from previous proposals, all of which rely on extensions of either the procedure of Onsager or of Kirkwood and Fröhlich. Application is made to two simple models; the first that of polar fluids, the second of nonpolar, polarizable fluids. (31 refs.)

77343 Electric susceptibility of mixed cerium/lanthanum ethyl sulfate crystals. R.J.Stubbs, J.P.Harrison (Dept. of Phys., Queen's Univ., Kingston, Ontario, Canada).

J. Low Temp. Phys. (USA), vol.51, no.5-6, p.679-90 (June 1983).

Measurements of the dielectric susceptibility of a series of lanthanum ethyl sulfate/cerium ethyl sulfate crystals (5–100 at.% Ce) have been made over the temperature range 0.05 – 20K . The results confirm the Jahn-Teller distortion in pure cerium ethyl sulfate, demonstrate a distortion for up to 25% La in the mixed crystals, and confirm the inversion of the zero-temperature crystal field splitting at about 40% La. The dipole moment of the cerium ion was found to be $(5.2 \pm 0.4) \times 10^{-31}$ and $(6.7 \pm 0.5) \times 10^{-31}\text{ C m}$ for the applied electric field perpendicular and parallel to the c axis, respectively. (23 refs.)

Excitonic correlations and a first-order phase transition in an excitonic dielectric See Entry 76851

78.00 OPTICAL PROPERTIES AND CONDENSED MATTER SPECTROSCOPY AND OTHER INTERACTIONS OF MATTER WITH PARTICLES AND RADIATION

(for phonon spectra, see 63.)

78.20 OPTICAL PROPERTIES AND MATERIALS

(see also 81.40T Optical properties related to materials treatment; for masers, and lasers see 42.52 and 42.55 respectively)

77344 Effects of semiconducting oxide films on the reflectivity change in a metal on radiation heating. A.V.Burmistrov.

J. Appl. Spectrosc. (USA), vol.37, no.2, p.965-8 (Aug. 1982). Translation of: *Zh. Prikl. Spektrosk. (USSR)*, vol.37, no.2, p.305-9 (Aug. 1982). [received: April 1983]

The reflectivity of a metal heated by radiation in air may change on account of growth of the oxide film and also because of diffusion of oxygen into the metal under the oxide. The author considers another physical factor that governs the energy deposition in the specimen, viz., the increase in the conductivity of the oxide with temperature. It is shown that this factor may prevent the attainment of high absorptivity in the high-temperature stage of the process and slow down or even stop the heating. Another consequence of the temperature dependence of the conductivity relates to the fall in transparency of the coating on heating and the related reduction in the number and amplitude of the interference oscillations in the reflection coefficient, as well as the additional increase in absorption in the low-temperature stage, which accelerates the transition to active oxidation (ignition). (13 refs.)

Time resolved polarization spectroscopy: level kinetics and rotational diffusion See Entry 75552

De-correlation technique for separation of Drude parameters from wavelength modulation spectroscopy data See Entry 76866

78.20B General theory (for pure homogeneous materials)

77345 Prediction of a resonance-enhanced laser-beam displacement at total internal reflection in semiconductors. J.L.Birman, D.N.Pattanayak, A.Puri (Phys. Dept., City Coll., City Univ. of New York, New York, NY, USA).

Phys. Rev. Lett. (USA), vol.50, no.21, p.1664-7 (23 May 1983).

Lateral Goos-Hanchen shifts can be increased by factors of 10 – 100 for laser frequency near an exciton-polariton resonance in semiconductors. A 'negative' shift can occur for laser frequency ω_L in the pseudogap $\omega_0 < \omega_L < \omega_1$. Surface irregularities can be probed with this effect. (10 refs.)

77346 Electromagnetic wave propagation in the uniaxial antiferromagnetic crystals FeF_2 , CoF_2 , MnF_2 . J.Brandmüller (Sektion Phys., Univ. München, München, Germany), A.Lehmeyer, K.M.Haussler, L.Merten.

Phys. Status Solidi b (Germany), vol.117, no.1, p.323-8 (1 May 1983).

In the most general form the matter equations of electrodynamics contain the magneto-electric tensor in addition to the electric and magnetic permeability tensor. By group-theoretical methods, however, it is shown that for crystals belonging to the magnetic point group $4'/\text{mmm}$ the magneto-electric tensor vanishes. Important examples for this point group are the antiferromagnets

FeF_2 , CoF_2 , and MnF_2 . Regarding this essential simplification a generalized Fresnel's equation of the wave normals is derived for these antiferromagnetic crystals. The Fresnel's equation has two solutions describing the magnitudinal and directional dispersion of the refractive index for the two corresponding waves. The limiting cases of these two solutions agree with results already known from literature. Besides, the polarization of both waves is determined. (11 refs.)

78.20D Optical constants and parameters

77347 Infrared optical constants of PtSi. J.M.Pimbley, W.Katz (Corporate Res. & Dev., General Electric Co., Schenectady, NY, USA). *Appl. Phys. Lett.* (USA), vol.42, no.11, p.984-6 (1 June 1983).

Knowledge of the infrared optical constants of PtSi is required for quantum yield calculations of Schottky barrier IR imagers with PtSi electrodes. The authors employ Rutherford backscattering spectrometry to identify the PtSi phase and calculate the infrared optical constants from reflectance data by a Kramers-Kronig analysis technique. Several examples of quantum yield calculations for different imager structures using the calculated optical constants are given. (18 refs.)

77348 Effect of electron-electron interaction on infrared absorption by small metallic particles. B.I.Shklovskii (A.F. Ioffe Physicotech. Inst., Acad. of Sci., Moscow, USSR).

JETP Lett. (USA), vol.36, no.8, p.352-5 (20 Oct. 1982). Translation of: *Pis'ma v Zh. Eksp. & Teor. Fiz.* (USSR), vol.36, no.8, p.287-9 (20 Oct. 1982). [received: June 1983]

It is shown that allowance for electron repulsion at low temperatures, which leads to neutrality of small metallic particles, decreases by unity the exponent a in the power-law dependence of the coefficient of absorption of infrared radiation K on frequency ($K \propto \omega^a$), as compared with existing theories. (5 refs.)

77349 Determination of thermal variation of the refractive index of cubic crystals and measurement of their light absorption coefficient. A.A.Zhilonits, E.K.Maldutis, S.V.Sakalaukas.

J. Appl. Spectrosc. (USA), vol.36, no.5, p.580-5 (May 1982). Translation of: *Zh. Prikl. Spektrosk.* (USSR), vol.36, no.5, p.811-16 (May 1982). [received: Feb. 1983]

Presents an iterative scheme for the calculation of the thermoelastic displacements which arise in cubic crystals upon local heating by laser radiation. The variation of the refractive index and the total temperature coefficient $\Delta n/\Delta T$ is determined with the help of the expressions obtained. The light absorption coefficient of KCl, KBr, KCl, and NaCl crystals is measured at a wavelength $\lambda = 1.06 \mu\text{m}$. (10 refs.)

77350 Refractive index changes of ion-implanted quartz. H.Beez, D.Fasold, H.Karge (Sektion Phys., Friedrich-Schiller-Univ. Jena, Jena, Germany).

Phys. Status Solidi a (Germany), vol.76, no.2, p.K171-4 (16 April 1983).

The authors analyze the thermal stability of the refractive index change with regard to different disorder formation stages. Synthetic α -quartz samples (Z-cut) were implanted with Ar^+ (150 keV) and B^+ (70 keV) ions at room temperature. Measurements of the optical reflectivity were carried out to determine the refractive index of the damaged surface layers. (6 refs.)

77351 Changes in the polarization and diffraction of light at dislocations with screw components in plastically deformed cadmium sulfide. V.Ya.Emelin, N.V.Klassen (Inst. of Solid-State Phys., Acad. of Sci., Chernogolovka, USSR).

Sov. Phys.-Solid State (USA), vol.24, no.11, p.1876-9 (Nov. 1982). Translation of: *Fiz. Tverd. Tela* (USSR), vol.24, no.11, p.3305-10 (Nov. 1982). [received: May 1983]

The propagation of light in plastically deformed cadmium sulfides was studied for large angles between the wave vector and slip bands. A deflected beam with a modified polarization was observed. This was attributed to the effects of elastic fields and of the cores of screw dislocations. Periodic oscillations of the intensity of the deflected beam indicated a periodic distribution of arrays of screw components of dislocations. (13 refs.)

77352 Temperature dependence of the refractive index of amorphous As_2S_3 and As_2Se_3 films near 300K. T.F.Mazets, S.K.Pavlov, E.I.Shifrin (A.F. Ioffe Physicotech. Inst., Acad. of Sci., Leningrad, USSR).

Sov. Tech. Phys. Lett. (USA), vol.8, no.9, p.446 (Sept. 1982). Translation of: *Pis'ma v Zh. Tekh. Fiz.* (USSR), vol.8, no.17-18, p.1036-8 (Sept. 1982). [received: May 1983]

The authors report the first measurements of dn/dT of amorphous As_2S_3 and As_2Se_3 films. At a fixed sample temperature, the differential spectrum of the temperature-modulated transparency is recorded, rather than the ordinary transparency spectrum. The thermal modulation is achieved by a 1-kHz periodic heating of the films. Instead of determining the position of the interference maximum, where the light intensity varies only slightly, they determine the 'null' position of the differential spectrum. The null position can be determined much more accurately, since the minimum measurable modulation depth $\Delta I/I$ is 10^{-6} . (9 refs.)

77353 Temperature coefficient of the phanite refractive index. N.D.Dovga.

Ukr. Fiz. Zh. (USSR), vol.28, no.4, p.605-7 (April 1983). In Russian. The prism method was used to investigate the temperature dependence of the refractive index n , of colourless phanite with composition $0.9 \text{ZrO}_2 \cdot 0.1 \text{Y}_2\text{O}_3$ at $\lambda = 632.8 \text{ nm}$. It is found that n linearly grows in the temperature interval 290 to 820K with coefficient $\beta = \Delta n/\Delta T = 6.075 \times 10^{-6} \text{ K}^{-1}$. The thermo-optical constant of phanite has been determined to be $V = \beta/(n-1) - \alpha = -5.425 \times 10^{-6} \text{ K}^{-1}$. The permittivity was found to be $\epsilon_0 \approx 20$. (6 refs.) V.G.P.

Outlook for the use of the Michelson interferometer for measuring the physical parameters of nonuniform semiconductor structures See Entry 74524

Dipole moments of dichlorotoluenes in benzene solution See Entry 75543

Properties of holographic gratings in silicon crystals under ultrashort light pulse recording. I. Theory See Entry 75606

Dispersion and luminescence measurements of optical waveguides See Entry 75787

Fabrication of optical waveguides in LiNbO_3 and LiTaO_3 crystals by ion irradiation See Entry 75790

Total internal reflection—a method for determining of LC anchoring and orientation on various substrates See Entry 76291

New liquid crystal materials; physical properties and performance in displays for automobile, high information density and guest-host applications See Entry 76292

Some physical properties and point defects in $\text{Bi}_{2-x}\text{In}_x\text{Te}_3$ mixed crystals See Entry 76419

Double doped low dislocation density InP with low optical absorption See Entry 76474

Assessment of damage ranges by measurements of the refractive index in ion implanted LiNbO_3 and LiTaO_3 See Entry 76526

Experimental determination of diffusion coefficients, viscosities, densities and refractive indexes of 11 binary liquid systems See Entry 76679

Optical properties of polaritons in thin crystal films See Entry 76857

Optical conductivity in the impurity band of doped semiconductors See Entry 76993

The electronic structure of GaP (110) and Cu-phthalocyanine overlayers studied by ellipsometry See Entry 77015

Preparation, physical properties, and superconductivity of $\text{La}_{1-x}\text{S}_x$ films See Entry 77085

Electromagnetic wave propagation in the uniaxial antiferromagnetic crystals FeF_2 , CoF_2 , MnF_2 See Entry 77346

The dependence of the trajectory of the extraordinary ray as the crystal rotates on the incident angle See Entry 77354

Electric birefringence and molecular polarisability of $\text{CF}_2\text{ClCF}_2\text{Cl}$ See Entry 77356

Indicatrix and the piezooptical properties of diglycine nitrate crystals See Entry 77358

Vacuum ultraviolet reflectance spectra and band structures of pyrites (FeS_2 , CoS_2 and NiS_2) and NiO measured with synchrotron radiation See Entry 77407

Induced absorption in Icelandic spar crystals under ultraviolet illumination See Entry 77409

Refractive index of GaAs-AlAs superlattice grown by MBE See Entry 77470

Thermal modulation spectrum and electron structure of niobium See Entry 77474

Changes in reflectivity and emissivity of oxide systems subjected to the influence of continuous CO_2 laser radiation See Entry 77920

78.20E Optical rotatory power

Diffraction gyration and reversal of the laser beam wave front in electrooptic crystals See Entry 75750

Temperature dependence of electrogyration in alums See Entry 77364

78.20F Birefringence

(inc. stress birefringence, flow birefringence, etc)

77354 The dependence of the trajectory of the extraordinary ray as the crystal rotates on the incident angle. Zhang Zhixiang, Feng Qingrong (Dept. of Phys., Peking Univ., Peking, China).

Acta Sci. Nat. Univ. Pekin. (China), no.5, p.77-80 (1982). In Chinese. Using data computed for Iceland spar crystal, the authors plotted a series of diagrams showing the dependence of the trajectory of the extraordinary ray as the crystal rotates on the incident angle. (1 ref.)

77355 Birefringence and structural defects in Cu_2O crystals. A.Haydar, R.Labusch (Inst. für Angewandte Phys., Tech. Univ. Clausthal, Clausthal Zellerfeld, Germany), A.Coret.

J. Appl. Phys. (USA), vol.54, no.5, p.2605-10 (May 1983).

The authors have investigated the birefringence in Cu_2O crystals which is induced by internal stress. The observed birefringence near precipitations, called 'teratoides', in as-grown crystals is shown to be related to pile-ups formed in (100) planes. This interpretation is supported by the direct observation of etch pits in the birefringent regions near teratoides and by the observation of the same birefringence in other pile-ups that are not related to teratoides. The analysis of the birefringence using a quarter-wave plate shows that the slow principal axis in the crystal is parallel to Burgers vector of dislocations in pile-ups. Comparison of the birefringence observed in plastically deformed crystals with that near pile-ups in as-grown crystals, indicates the formation of pile-ups by plastic deformation. The pile-ups in this case are perpendicular to the branches of cross shaped birefringent regions. This result is in agreement with the prediction of the excitonic photoconductivity measurements. (20 refs.)

77356 Electric birefringence and molecular polarisability of $\text{CF}_2\text{ClCF}_2\text{Cl}$. A.-M.Benoit-Denis (Lab. de Thermomagnétisme, Univ. de Nancy I, Vandœuvre les Nancy, France).

Mol. Phys. (GB), vol.49, no.1, p.91-101 (May 1983). In French.

Measurements of the refractive index, density, dielectric constant and Kerr constant are reported for liquid $\text{CF}_2\text{ClCF}_2\text{Cl}$ over the temperature range 193-273K, at different wavelengths. Since the compound can exist in the trans (C_{2h}) and gauche form (C_2), the values of the principal molecular polarizabilities of both the isomers are obtained. The Langevin-Born formula is used to express the Kerr constant, since the Lorentz model is correct in the case of a liquid such as $\text{CF}_2\text{ClCF}_2\text{Cl}$ for which the molecular interactions are only dipolar; the author has not included the contributions of the first and second hyperpolarizabilities, (not measured); to know the composition of the equilibrium mixture over the temperature range 193-273K, the Debye formula is used; the principal polarizability, which is orthogonal to the trans form symmetry plane, is calculated from bond polarizability theory. (16 refs.)

77357 Investigation of the photoinduced birefringence in GaP. A.L.Imanova, Ch.O.Kadzhaz, I.A.Mamedbeili, E.Yu.Saleev (Inst. of Phys., Acad. of Sci., Baku, Azerbaïdzhans SSR).

Sov. Phys.-Solid State (USA), vol.24, no.11, p.1955-6 (Nov. 1982). Translation of: *Fiz. Tverd. Tela* (USSR), vol.24, no.11, p.3441-4 (Nov. 1982). [received: May 1983]

A photoinduced birefringence was previously observed in compensated GaAs crystals subjected to an electric field and the magnitude of this effect as well as its sign depended strongly on the region illuminated with additional focused radiation. The authors investigated in a similar manner the electrooptic properties of a GaP crystal subjected to an electric field and strongly absorbed illumination. Measurements of the electrooptic parameters were made at room temperature by the polarization-optical method. (5 refs.)

A quasi-optical nulling method for material birefringence measurements at near-millimeter wavelengths See Entry 74508

Indicatrix and the piezooptical properties of diglycine nitrate crystals See Entry 77358

- Colored and black liquid crystalline mixtures with new anthraquinone dyes See Entry 77360
- Dyes with negative dichroism for liquid crystal displays based on the guest-host effect See Entry 77361

78.20H Piezo-, elasto- and acousto-optical effects

77358 Indicatrix and the piezooptical properties of diglycine nitrate crystals. V.M.Varikash, N.A.Romanyuk, B.G.Myslyk. *J. Appl. Spectrosc. (USA)*, vol.37, no.2, p.977-81 (Aug. 1982). Translation of: *Zh. Prikl. Spektrosk. (USSR)*, vol.37, no.2, p.319-23 (Aug. 1982). [received: April 1983]

The authors have studied the piezooptical properties of diglycine nitrate, established the orientation of the axes of the optical indicatrix as well as the limits of optical frequency, temperature, and mechanical stress for which diglycine nitrate may be utilized. (8 refs.)

77359 Photoelasticity of $\text{Ba}_2\text{Sr}_{1-x}\text{Nb}_2\text{O}_6$ near the ferroelectric phase transition. I.A.Andreev (A.I. Gertsens State Pedagogical Inst., Leningrad, USSR).

Sov. Tech. Phys. Lett. (USA), vol.8, no.9, p.460-1 (Sept. 1982). Translation of: *Pis'ma v Zh. Tekh. Fiz. (USSR)*, vol.8, no.17-18, p.1067-71 (Sept. 1982). [received: May 1983]

The relaxation of the polarization, which is the parameter of the phase transition, governs the thermal anomalies in the dielectric and electromechanical properties of the ferroelectric barium-strontium niobate, $\text{Ba}_2\text{Sr}_{1-x}\text{Nb}_2\text{O}_6$ (BSN). The author reports the first observation of a strong temperature dependence, unusual for ferroelectrics, of the photoelasticity of BSN. The photoelastic constant β_{31}^E of $\text{Ba}_{0.39}\text{Sr}_{0.61}\text{Nb}_2\text{O}_6$ single crystals vanishes at $T_c=80^\circ\text{C}$. (7 refs.)

Effect of pressure on the absorption spectra of solid O_2 See Entry 77412

78.20J Electro-optical effects

77360 Colored and black liquid crystalline mixtures with new anthraquinone dyes. G.Heppke, B.Knippenberg, A.Moller, G.Scherowsky (Liquid Crystals Res. Group, Tech. Univ. of Berlin, Berlin, Germany).

Mol. Cryst. & Liq. Cryst. (GB), vol.94, no.1-2, p.191-204 (1983). Various yellow, red, and blue anthraquinone dyes have been synthesized. The structures of the dyes are presented and their properties are discussed with respect to the dichroic ratios, the color gamut, and the obtainable contrast in black colored liquid crystalline dye mixtures. Dichroic ratios of up to $N=10.2$ in NP 1132 and $N=12.3$ in RO-TN 404 are observed for single dyes. The compositions of achromatic dye mixtures exhibiting effective dichroic ratios of $N_{\text{eff}}=8.3$ in NP 1132 and $N_{\text{eff}}=10.5$ in RO-TN 404 are calculated. The influence of the positions of the absorption bands on the perceived contrast is studied. It is shown that by shifting the absorption bands of the dyes, the effective dichroic ratio can be increased to $N_{\text{eff}}=9.1$ in NP 1132 and $N_{\text{eff}}=11.4$ in RO-TN 404. (18 refs.)

77361 Dyes with negative dichroism for liquid crystal displays based on the guest-host effect. V.G.Rumyantsev, A.V.Ivashchenko, V.M.Muratov, V.T.Lazareva, E.K.Prudnikova, L.M.Blinov (Organic Intermediates & Dyes Inst., Moscow, USSR).

Mol. Cryst. & Liq. Cryst. (GB), vol.94, no.1-2, p.205-12 (1983). The novel approach is proposed to the synthesis of dyes with negative dichroism. The molecular models, which are adequate to the dichroic dyes, are shown. As an example of the approach, the synthesis and dichroic properties of some derivatives of the 2,2'-azoisimidazole are described. The time and contrast characteristics of the displays, based on the guest-host effect, are presented. (12 refs.)

77362 Ferroelectric liquid crystal electro-optics using the surface stabilized structure. N.A.Clark, M.A.Handschi, S.T.Lagerwall (Dept. of Phys., Univ. of Colorado, Boulder, CO, USA).

Mol. Cryst. & Liq. Cryst. (GB), vol.94, no.1-2, p.213-33 (1983). The strong linear coupling of the director \mathbf{n} to electric field \mathbf{E} in ferroelectric liquid crystals can be utilized to perform high-speed electro-optic switching suitable for device applications. The authors summarize the current understanding of the high-speed, bistable, threshold-sensitive electro-optic effects obtained in planar structures using surface interactions to suppress the spontaneous director helix characteristic of the bulk ferroelectric liquid crystal. (12 refs.)

77363 Electroabsorption in single crystal indium phosphide. T.M.McGinnity, G.G.Roberts (Dept. of Appl. Phys. & Electronics, Univ. of Durham, Durham, England).

Solid State Commun. (USA), vol.46, no.8, p.643-5 (May 1983). The electroabsorption properties of InP:Fe and InP:Cr single crystals in the long wavelength region of the fundamental absorption edge have been investigated. By means of several supporting experiments and improved instrumentation the authors have eliminated or compensated for several possible sources of error including photoconductivity and space charge. Using simple one electron theory they have thus obtained accurate values of the reduced effective mass in this important semiconductor. (15 refs.)

77364 Temperature dependence of electrogyration in alums. H.-J.Weber (Inst. fur Kristallographie, Univ. zu Koln, Koln, Germany).

Z. Kristallogr. (Germany), vol.161, no.3-4, p.293-7 (1982). The temperature derivative $\partial s_{123}/\partial T$ of the electrogyration coefficient s_{123} is negative in α - and positive in β -alums. In ammonium and ammonium substituted alums this change of sign is masked by a large positive temperature effect of the ammonium ion. The observed effect at room temperature, essentially of dynamic origin, results in all alums from a partial cancellation of different contributions. (6 refs.)

77365 The linear electro-optical effect in α -quartz: a new determination. L.Bohaty (Inst. fur Kristallographie, Univ. zu Koln, Koln, Germany).

Z. Kristallogr. (Germany), vol.161, no.3-4, p.299-302 (1982). The two independent electro-optic coefficients of α -quartz were redetermined at constant stress employing a sensitive dynamic method of optical interferometry. The results at room temperature and $\lambda=633\text{ nm}$ are: $r_{11}^{\text{eff}}=-0.481(8)$, $r_{231}^{\text{eff}}=-0.235(10)\times 10^{-12}\text{ m/V}$. (11 refs.)

Laser beam critical behaviour and phase conjugation in the semiconductors, resonant media and electrooptic crystals See Entry 75734

Coherent light amplification and optical phase conjugation with photorefractive materials See Entry 75747

Diffraction gyration and reversal of the laser beam wave front in electrooptic crystals See Entry 75750

A fibre optic electric field sensor using the electrooptic effect of $\text{Bi}_2\text{Ge}_2\text{O}_{12}$ See Entry 75829

Low viscous compounds of highly nematic character See Entry 76290

New liquid crystal materials; physical properties and performance in displays for automobile, high information density and guest-host applications See Entry 76292

Relation between TN-cell response time and transition temperatures of liquid crystal materials See Entry 76293

Localized centers in bismuth silicate crystals See Entry 76875

Electric field-induced quenching of luminescence in quantum wells See Entry 77445

Energy position of luminescence (photosensitivity) centres in $\text{CdSe}_{1-x}\text{Te}_x$ solid solutions See Entry 77453

78.20L Magneto-optical effects

77366 Anomalies in the magnetic circular dichroism of benzene in cyclohexane. W.Haberdtz (Sektion Chem., Humboldt-Univ. Berlin, Berlin, Germany), W.Thiemann, U.Jarzak.

Ber. Bunsenges. Phys. Chem. (Germany), vol.87, no.4, p.366-8 (April 1983). The authors have found that by introducing a 20 mm thick iron plate to shield the CD stress modulator from stray magnetic field apparently eliminates the previously reported magneto-optical anomaly. They conclude that the observed phenomenon seems to be an apparatus artefact. (7 refs.)

77367 Measuring the magneto-optic Kerr effect by diffraction. J.Kranz, C.Schrodter (Inst. fur Angewandte Phys., Univ. Dusseldorf, Dusseldorf, Germany).

Appl. Phys. A (Germany), vol.A31, no.2, p.59-63 (June 1983). A method is presented to measure the Magneto-optic Kerr Effect (MOKE) by diffraction. This is accomplished by giving the magnetized surface a magnetization distribution which functions like a linear diffraction grating. It is shown that the first and higher orders of the light diffracted by such a grating are produced by MOKE whereas the zero order approximately represents the reflectivity of the surface (given by the Fresnel formulae assuming zero magnetization). The procedure used here to form a grating is restricted to thin soft magnetic films, and has been demonstrated on evaporated Fe-Ni films. It uses the magnetic field of a pulse-driven meandered stripe-conductor placed in close contact with the film in the presence of a homogeneous external magnetic field. Experimentally determined Kerr intensities were compared with those measured by ellipsometric methods. Good agreement was found in the case of films with uniaxial anisotropy. For films with no anisotropy, the relative dependence of Kerr intensity vs. wavelength, polarisation and angle of incidence could be derived. (8 refs.)

77368 Magnetic gyration studies of mixed crystals of potassium chloride and potassium bromide. M.S.Vijayaraghavan (Technol. Div., Defence Electronics Res. Lab., Chandrayanagutta Lines, Hyderabad, India), V.Sivaramakrishnan.

Opt. Acta (GB), vol.30, no.5, p.653-8 (May 1983). Magneto-optical rotary dispersion studies have been made on mixed crystals of potassium chloride and potassium bromide. The data obtained are explained on the basis of a model which assumes an asymmetric distribution of anions about the cations. (9 refs.)

77369 Magneto-optical study of the fundamental absorption edge in $\text{Cd}_{1-x}\text{Mn}_x\text{Te}$. Nguyen The Khoi, J.Ginter, A.Twardowski (Inst. of Experimental Phys., Univ. of Warsaw, Warsaw, Poland).

Phys. Status Solidi b (Germany), vol.117, no.1, p.67-74 (1 May 1983). The fundamental absorption edge in $\text{Cd}_{1-x}\text{Mn}_x\text{Te}$ for $x=0.01, 0.05, 0.10, 0.20$ in the Faraday configuration, at magnetic fields up to 5 T and in the temperature range 1.8 to 293K is studied. Moreover the exciton spectrum of extremely thin samples (of less than $1\text{ }\mu\text{m}$) is measured. An additional structure on the σ^- edge is found. The appearance of that structure is supposed to be the effect of the mixing of exciton states in the zincblende structure. (8 refs.)

77370 Magneto-optic investigation of crystals containing Fe^{3+} ions by reflection of infrared radiation. G.S.Krinchik, V.E.Zubov, V.A.Lyskov (M.V. Lomonosov State Univ., Moscow, USSR).

Sov. Phys.-Solid State (USA), vol.24, no.12, p.2119-20 (Dec. 1983). Translation of: *Fiz. Tverd. Tela (USSR)*, vol.24, no.12, p.3716-18 (Dec. 1983). Reflection of radiation of photon energy 1-2.2 eV ($1.2-0.55\text{ }\mu$ wavelength range) and a highly sensitive magneto-optic system were used for the first time to determine the spectra of the equatorial Kerr effect (EKE) of single crystals of yttrium orthoferrite (YFeO_3) and yttrium iron garnet ($\text{Y}_3\text{Fe}_5\text{O}_{12}$). The spectral dependences of the EKE revealed singularities associated with the first crystal transitions in the Fe^{3+} ions. (6 refs.)

Anderson transition in the exciton-impurity band in silicon See Entry 76848

Electronic properties of InAs-GaSb superlattices See Entry 77032

Note on the magnetic and magneto-optical properties of Ni_2In type 3d transition metal compounds See Entry 77156

Electron-hole liquid in indium antimonide in a strong magnetic field See Entry 77436

Faraday rotation in the exciton part of the spectrum of CuBr See Entry 77473

78.20N Thermo-optical effects

Temperature coefficient of the phianite refractive index See Entry 77353

Reflectance and thermorefectance spectra and energy band structure of GeSe crystals See Entry 77410

Ge-Al thin films for selective solar absorbers See Entry 78099

78.30 INFRARED AND RAMAN SPECTRA AND SCATTERING

77371 Calculated lifetime and decay mechanism of the 991 cm^{-1} mode in crystalline benzene at 1.6K. R.Righini, P.F.Fracassi, R.G.Della Valle (Istituto di Chimica Fisica, Univ. di Firenze, Florence, Italy).

Chem. Phys. Lett. (Netherlands), vol.97, no.3, p.308-12 (20 May 1983). The lifetime of the 991 cm^{-1} Ag mode in benzene crystal at 1.6K has been calculated in good agreement with the experimental value. The main decay mechanism has been shown to consist of a three-phonon scattering involving the $\nu_{10}\approx 860\text{ cm}^{-1}$ e_{2g} internal vibration and high-frequency lattice modes. (23 refs.)

- 77372 Spectral studies on new dioxouranium (VI) complexes of tridentate Schiff bases derived from salicylhydrazide and salicylaldehyde or substituted salicylaldehydes.** A.Syamal (Dept. of Appl. Sci. & Humanities, Kurukshetra Univ., Kurukshetra, India), D.Kumar. *Indian J. Pure & Appl. Phys.*, vol.21, no.2, p.87-91 (Feb. 1983). New dioxouranium (VI) complexes of the type $\text{UO}_2\text{LCH}_2\text{OH}$ (where LH_2 =Schiff base I) have been synthesized and characterized on the basis of elemental analysis, quantitative determination of ligand, conductance, molecular weight, magnetic susceptibility, IR, NMR and electronic spectra. The reactivity of the complexes towards bidentate ligands has been tested and dioxouranium (VI) heterochelates of the type $\text{UO}_2\text{L}(\text{AA})$ (where AA=bidentate NN donor ligand) have been synthesized. The complexes are non-electrolytes, diamagnetic and monomers. The $\text{UO}_2\text{LCH}_2\text{OH}$ complexes are six-coordinated and the heterochelates are seven-coordinated. (35 refs.)
- 77373 Spectroscopic studies of oxovanadium(IV) complexes of biguanide, dibiguanides and o-methyl-l-aminourea.** A.Syamal (Chem. Dept., Regional Engng. Coll., Kurukshetra, India). *Indian J. Pure & Appl. Phys.*, vol.21, no.2, p.130-2 (Feb. 1983). The ESR (in diamagnetic nickel(II) complex matrix), IR and electronic spectra of oxovanadium(IV) complexes of biguanide; ethylene-, trimethylene-, tetramethylene-, hexamethylene-, piperazine-dibiguanides and of o-methyl-l-aminourea are recorded. The ESR spectra of all these complexes exhibit 8 perpendicular and 8 parallel lines. The ESR parameters exhibit 8 perpendicular and 8 parallel lines. The ESR parameters for a typical complex, viz. $\text{VO}(\text{OH})_2$ (biguanide) $_2$, are determined as $g_{\perp}=1.99$, $A_{\perp}=54$, $g_{\parallel}=1.94$, $A_{\parallel}=154$. The ESR parameters are very similar in the oxovanadium (IV) complexes of biguanide, o-methyl-l-aminourea and dibiguanides indicating the similarity of bonding in these complexes. This fact is further confirmed from the dipolar term $|A_{\perp}-A_{\parallel}|$ which is essentially constant. The observed low values of $\nu(\text{V}=\text{O})$ ($\sim 940\text{ cm}^{-1}$) are consistent with the strong out-of-plane $d\pi-\pi$ bonding. These complexes exhibit three electronic spectral bands due to $d_{xy}-d_{xz}$, d_{yz} , $d_{xy}-d_{xz}-d_{yz}$ and $d_{xy}-d_{yz}$ transitions. (9 refs.)
- 77374 Raman microprobe study of recrystallization in ion-implanted and laser-annealed polycrystalline silicon.** S.Nakashima, Y.Inoue, M.Miyauchi, A.Mitsuihira (Dept. of Appl. Phys., Osaka Univ., Yamadaoka, Japan), T.Nishimura, T.Fukumoto, Y.Akasaka. *J. Appl. Phys. (USA)*, vol.54, no.5, p.2611-17 (May 1983). Implantation-amorphized polycrystalline silicon layers which are directly deposited on single-crystal Si are annealed by a scanning CW laser. The crystallinity of the annealed layers has been examined by a Raman microprobe in combination with polarization measurements. The Raman spectra measured for the specimens annealed at various power levels reveal that the polysilicon layer is regrown liquid epitaxially and is transformed into single crystal at high annealing power levels and that the regrowth at lower power levels is governed by the mixture of solid and liquid epitaxial processes. It is found that for specimens annealed at high power levels the tensile stress in the annealed layer is relaxed to a certain extent, though the weak residual strain still remains. The Raman microprobe spectra from the boundary region between the annealed and amorphous layers are recorded by making the probe laser beam traverse the boundary region. This technique enables the authors to investigate the variation in crystallinity and the regrowth process in the boundary zone which is found to be less than $10\text{ }\mu\text{m}$ width. (20 refs.)
- 77375 Effects of interlamellar forces on longitudinal acoustic modes of n-alkanes.** M.Kobayashi, K.Sakagami, H.Tadokoro (Dept. of Macromolecular Sci., Faculty of Sci., Osaka Univ., Osaka, Japan). *J. Chem. Phys. (USA)*, vol.78, no.11, p.6391-8 (1 June 1983). Effects of the interlamellar interactions in n-alkane crystals on the longitudinal acoustic modes (LAM), including both the fundamental and the higher overtones, were investigated on the basis of the polarized Raman spectra of $n\text{-C}_{28}\text{H}_{58}$, $n\text{-C}_{30}\text{H}_{62}$, $n\text{-C}_{34}\text{H}_{70}$, and $n\text{-C}_{36}\text{H}_{74}$ crystallized in the orthorhombic II form (a double layer polytype of the monoclinic form). The LAM-1 bands of this crystal modification split into a doublet consisting of the (cc) and (bc) polarization components separated by about 6 cm^{-1} . The frequency gaps of the LAM-m bands were found to decrease with m (approximately proportional to m^{-1}). Theoretical considerations on the correlation field splitting and the scattering intensities of the LAM bands led to the conclusion that the observed band splitting was caused by the intermolecular force acting between the successive monomolecular layers. The intrinsic value of the Young modulus of the n-alkane molecules free from the external forces in the crystalline state and the strength of the interlayer force were evaluated from the observed frequencies of the two components of LAM using a simple dynamical model. By comparing the Raman spectra of $n\text{-C}_{28}\text{H}_{58}$ and $n\text{-C}_{30}\text{H}_{62}$ between the triclinic and orthorhombic II modifications, it was concluded that the effect of the lateral force on the LAM was not so significant as that of the longitudinal force. (39 refs.)
- 77376 The far-infrared spectrum of ice Ih in the range 8-25 cm^{-1} . Sound waves and difference bands, with application to Saturn's rings.** O.Mishima, D.D.Klug, E.Whalley (Div. of Chem., Nat. Res. Council, Ottawa, Ontario, Canada). *J. Chem. Phys. (USA)*, vol.78, no.11, p.6399-404 (1 June 1983). The absorption spectrum of single crystals of ice Ih with the light traveling perpendicular or at 5° to the c axis has been measured in the frequency range 8-25 cm^{-1} at 80, 100, 150, and 202K. At high frequencies, the absorptivity is proportional to the fourth power of the frequency, and is caused by fundamental hypersonic waves having wavelengths of about $100\text{ }\text{\AA}$. At low frequencies, it is probably caused by difference bands from the translational lattice vibrations. The theory of the intensity of binary combination bands of ionic crystals has been specialized to the low-frequency difference bands. Ice Ih has been assumed to have the same absorptivity as ice Ic, and ice Ic has been represented by an ordered crystal that resembles spherulite. The model fits the measured absorptivity of ice Ih assuming that the difference bands arise mostly from the strong first-order band centered at $\sim 230\text{ cm}^{-1}$. The acoustic branches do not contribute significantly. The absorptivity, extrapolated to 3.0 cm^{-1} and interpolated to 85K by means of the theory, was used to determine the mean thickness of ice in Saturn's rings from the measured thermal component of the brightness temperature of the rings. If the slab model is used and scattering is neglected, the mean thickness is $30\pm 10\text{ cm}$. (20 refs.)
- 77377 Absorption spectra of cold dilute solid solutions.** R.Holland, W.B.Majer, II, S.M.Freund, W.H.Beattie (Los Alamos Nat. Lab., Univ. of California, Los Alamos, NM, USA). *J. Chem. Phys. (USA)*, vol.78, no.11, p.6405-14 (1 June 1983). Infrared absorption spectra have been obtained for some compounds trapped in crystalline solids by freezing liquid Xe, Kr, Ar, or CH_4 solutions. The optical quality of the solid solutions is good, and they have been cooled to $\sim 80\text{ K}$ in 1.35 cm sample thicknesses to study the absorption in fundamental vibrational bands of the solutes. In the cases discussed, the bands are narrow, with observed full widths at half-maximum absorbance $0.05\text{--}0.30\text{ cm}^{-1}$ greater than the instrumental resolution ($0.18\text{--}0.29\text{ cm}^{-1}$). The spectra appear

- to be free of 'multiple site' and solute aggregate absorptions. Spectra displaying isotropic splitting in bands of natural BCl_3 , SeF_6 , OsO_4 , TiCl_4 , and MoF_6 are presented, and band frequencies are compared with some results obtained in evaporative matrices, in the gas phase, and in liquid solutions. For this comparison the authors have obtained some spectra of SeF_6 and BCl_3 gas. (36 refs.)
- 77378 A structural interpretation of the vibrational spectra of binary fluorohafnate glasses.** R.M.Almeida (Centro de Física Molecular-Complexo I, Inst. Superior Tecnico, Lisboa, Portugal), J.D.Mackenzie. *J. Chem. Phys. (USA)*, vol.78, no.11, p.6502-11 (1 June 1983). Binary glass samples have been prepared in the $\text{HfF}_4\text{-BaF}_2$ system, containing between 62-73 mol.% HfF_4 . Their infrared absorption and polarized Raman spectra have been studied. The glass transition and crystallization temperatures have also been measured. The vibrational modes have been assigned and the results were compared with those previously obtained for $\text{ZrF}_4\text{-BaF}_2$ glasses. The cation isomorphous substitution of Zr by Hf allowed the authors to make a more definite vibrational assignment. The structures of the two glass systems were found to be similar, though not identical. The structural interpretation of the vibrational spectra was consistent with the occurrence of sixfold coordinated Hf atoms, probably forming a network of octahedral chains cross linked by Ba-F ionic bonds, with the degree of bridging increasing with the Hf content of the glasses. Substitution of Ba by Zr did not affect the structure. Due to the large F/Ba ratio of ~ 10 , there is an overlap of neighboring chains that may lead to sharing of a single nonbridging fluorine atom between two Hf atoms belonging to neighboring chains. The existence, on the average, of two such F-atoms for each Hf may raise its effective coordination number from 6 to ~ 8 , when determined from an X-ray radial distribution function analysis, as recent results show. Vibrational spectroscopy, however, appears to be able to effectively distinguish which is the parent Hf atom to which every fluorine is bonded by a predominantly covalent, directional and shorter bond, as part of a highly symmetric octahedral coordination shell. In this respect, vibrational spectroscopy (particularly Raman) appears to be a more sensitive structural tool than X-ray diffraction. (19 refs.)
- 77379 Infrared optical absorption due to one and two phonon processes in black phosphorus.** M.Ikezawa, Y.Kondo (Tohoku Univ., Sendai, Japan), I.Shiratori. *J. Phys. Soc. Jpn. (Japan)*, vol.52, no.5, p.1518-20 (May 1983). Using a single crystal of black phosphorus, anisotropic absorption spectra due to the two-phonon summation process have been found in the wavenumber region from 300 to 900 cm^{-1} . By an oblique incidence method, the dipole moment of an infrared active mode at 470 cm^{-1} has been confirmed to be in the z-direction of the crystal as predicted by Kaneta, Yoshida and Morita. Frequencies of unobserved A_u and B_{1u} modes are estimated to be about 420 and 250 cm^{-1} from the absorption spectra of the two-phonon process.
- 77380 Raman scattering by soft plasmon-LO phonon modes in ferroelectric semiconductors.** S.Katayama (Dept. of Phys., Osaka Univ., Toyonaka, Japan). *J. Phys. Soc. Jpn. (Japan)*, vol.52, no.5, p.1829-37 (May 1983). Presents a theory of Raman scattering by the low-lying soft coupled plasmon-longitudinal optical (LO) phonon modes at low temperatures in semiconducting incipient ferroelectrics. The softening of this mode gives a dynamical intimation of the screened LO phonon instability induced by the dispersive ferroelectric phase transition. The calculations are compared with Raman spectra from $n\text{-KTaO}_3$ observed by Uwe et al. (1980), on the basis of the soft mode-like behavior of the coupled modes as well as of the simple energy band structure. (24 refs.)
- 77381 Infrared and Raman spectra of barium nitrite monohydrate.** O.P.Lamba, H.D.Bist (Dept. of Phys., Indian Inst. of Technol., Kanpur, India). *J. Phys. & Chem. Solids (GB)*, vol.44, no.5, p.445-52 (1983). The low temperature infrared absorption and room temperature laser Raman spectra of polycrystalline $\text{Ba}(\text{NO}_2)_2\cdot\text{H}_2\text{O}$ and its deuterated analogue are studied. The strongly bonded H-atom of the water molecule makes a highly bent H-bond while the weakly bonded H-atom exhibits a slightly bent (or possible bifurcated) bond consistent with recent structural data; the H-bond enthalpies are estimated to be 3.3 and 2.1 Kcal/mole respectively. The wagging, twisting and rocking modes of the water molecule have been assigned using several well known criteria. The force constants of these modes have also been computed. The librational splittings observed at low temperature are consistent with polarization data, and are being attributed to infrared active factor group components. (26 refs.)
- 77382 Infrared absorption spectra of hydrogen complexes in type I diamonds.** G.S.Woods (CSO Valuations Ltd., London, England), A.T.Collins. *J. Phys. & Chem. Solids (GB)*, vol.44, no.5, p.471-5 (1983). The 3107 cm^{-1} peak has been observed in the infrared absorption spectra of all but one of some 50 type I diamonds examined. Evidence is presented which strongly supports the interpretation of this peak as being due to a carbon-hydrogen bond stretching mode. Reasons are given for believing that the hydrogen responsible for this, and the associated 1405 cm^{-1} line, is present as a constituent of the vinylidene group ($>\text{C}=\text{CH}_2$). Several new peaks, of fairly general occurrence, are reported in the wavenumber range 3400 cm^{-1} to 2750 cm^{-1} . Some of these lines, seen only when the specimens exhibit at least partial type Ib character, are almost certainly due to nitrogen-hydrogen bond stretching. Others, found in type Ia and/or partially type Ib specimens may be due to C-H or N-H stretching in different local environments. The observations show that hydrogen is as ubiquitous an impurity in diamond as nitrogen. Possible sites within the crystals for these hydrogenous groups are discussed. (21 refs.)
- 77383 Super-enhanced hyper-Raman scattering from dyes adsorbed on colloidal silver particles.** A.V.Baranov, Ya.S.Bobovich (S.I. Vavilov State Optics Inst., USSR). *JETP Lett. (USA)*, vol.36, no.8, p.339-43 (20 Oct. 1982). Translation of: *Pis'ma v Zh. Eksp. & Teor. Fiz. (USSR)*, vol.36, no.8, p.277-81 (20 Oct. 1982). [received: June 1983] Hyper-Raman-scattering spectra have been measured by the standard technique for the scattering from two rhodamine dyes and a crystalline violet dye adsorbed on silver. The extremely intense spectra found are attributed, in particular, to simultaneous resonances for one- and two-photon transitions. Various mechanisms for the process are discussed. The same effects are observed at the unshifted frequency. (7 refs.)
- 77384 Raman scattering spectra and structural properties of the chalcogenide glasses $\text{Sb}_2\text{As}_{1-x}\text{SI}_x$.** G.S.Svechnikov, M.Ya.Valakh, V.P.Pinzenik. *J. Appl. Spectrosc. (USSR)*, vol.36, no.5, p.566-9 (May 1982). Translation of: *Zh. Prikl. Spektrosk. (USSR)*, vol.36, no.5, p.796-800 (May 1982). [received: Feb. 1983] Presents the results of a study of the Raman scattering spectra of chalcogenide glasses of composition $\text{Sb}_2\text{As}_{1-x}\text{SI}_x$. The studies were carried out using a DFS-24 double spectrometer with a photon counting detection system. The

Raman spectra were excited by the emission of a He-Ne laser (632.8 nm). The spectra were detected in these experiments in the standard right angle geometry. All the measurements were carried out at a temperature $T=300\text{K}$. (12 refs.)

77385 Investigation of the temperature dependence of the dispersion of dielectric characteristics of lithium tantalate by the method of Raman scattering of light. N.S.Abdullov, V.S.Gorelik, B.S.Umarov. *J. Appl. Spectrosc. (USA)*, vol.36, no.5, p.585-9 (May 1982). Translation of: *Zh. Prikl. Spektrosk. (USSR)*, vol.36, no.5, p.817-20 (May 1982). [received: Feb. 1983]

Investigates the temperature dependence of the low-frequency region of the RS spectrum of LiTaO_3 over the 300-928K temperature range. Also obtains the dispersion of the dielectric characteristics of this crystal over a wide temperature range. (7 refs.)

77386 Origin of the absorption bands of crystalline CsI in the CO_2 laser region. A.I.Mitichkin, A.N.Panova, L.V.Udovichenko, K.V.Shakhova.

J. Appl. Spectrosc. (USA), vol.37, no.2, p.893-6 (Aug. 1982). Translation of: *Zh. Prikl. Spektrosk. (USSR)*, vol.37, no.2, p.223-6 (Aug. 1982). [received: April 1983]

The authors have carried out a detailed analysis of the IR spectra obtained on a spectrophotometer at temperatures of 295 and 77K, using CsI crystals specially prepared by the Stockbarger technique with impurity ions CO_3^{2-} , CrO_4^{2-} , and SO_4^{2-} , which exhibit absorption bands near 1000 cm^{-1} . Only in the IR spectra of the $\text{CsI}(\text{CO}_3^{2-})$ crystals do they observe a very weak absorption band in the region of $\sim 940\text{ cm}^{-1}$ which always accompanied several bands which are not attributable to CO_3^{2-} absorption. Heat treatment of the $\text{CsI}(\text{CO}_3^{2-})$ crystals by heating or 30 min at 400°C followed by rapid cooling to room temperature resulted in an increase in the intensity of these bands and the appearance of a series of new absorption bands. (9 refs.)

77387 Spectra and structure of asymmetric carboxylic acid dimers in solution. N.S.Golubev, G.S.Denisov.

J. Appl. Spectrosc. (USA), vol.37, no.2, p.930-6 (Aug. 1982). Translation of: *Zh. Prikl. Spektrosk. (USSR)*, vol.37, no.2, p.265-72 (Aug. 1982). [received: April 1983]

The authors studied the infrared spectra of solutions containing mixtures of trifluoroacetic and trimethylacetic (pivalic) acids as well as several of their isotopically substituted species in pentane and hexadecane at concentrations from 10^{-3} to 10^{-1} mole/litre. The low temperature NMR spectra were recorded in a mixture of freons. The formation of a strong complex (asymmetric cyclic dimer) was noted in every case. The hydrogen bond and proton exchanges were examined. (22 refs.)

77388 Raman spectra and physical structure of cellulose triacetate. S.P.Firsov, R.G.Zhbankov.

J. Appl. Spectrosc. (USA), vol.37, no.2, p.940-7 (Aug. 1982). Translation of: *Zh. Prikl. Spektrosk. (USSR)*, vol.37, no.2, p.276-84 (Aug. 1982). [received: April 1983]

It is shown that the Raman spectra of cellulose acetates possess their own special features in the case of fibres and films and of uniaxially oriented and crystallised films. This reflects the characteristics of their physical structure, caused mainly by the specific ratio of the rotamers of the side groups. (19 refs.)

77389 Study of complexes of hydrogen halides with diethyl ether in aprotic solvents by the method of IR spectroscopy. A.A.Pankov, V.Yu.Borovkov, V.B.Kazanskii.

J. Appl. Spectrosc. (USA), vol.37, no.2, p.953-7 (Aug. 1982). Translation of: *Zh. Prikl. Spektrosk. (USSR)*, vol.37, no.2, p.291-5 (Aug. 1982). [received: April 1983]

The authors previously showed (see Dokl. Akad. Nauk SSSR, vol.258, p.902-6, 1980) that in the interaction of alcohols with hydrogen halides (HCl, HBr) in carbon tetrachloride and methylene chloride, together with complexes with the usual hydrogen bond with a 1:1 composition, complexes of an acid molecule with two alcohol molecules, in which a proton is transferred to the alcohol, are formed. In the present work, complex formation, in aprotic solvents of diethyl ether, which possesses a greater proton affinity than alcohols, with the same hydrogen halides was investigated by the method of IR spectroscopy. (10 refs.)

77390 Study of structure of copolymers of ethylene tetrasulfide and vinyl cyanide. I.T.Mladenov, M.K.Markov, D.D.Todorova.

J. Appl. Spectrosc. (USA), vol.37, no.2, p.957-61 (Aug. 1982). Translation of: *Zh. Prikl. Spektrosk. (USSR)*, vol.37, no.2, p.296-301 (Aug. 1982). [received: April 1983]

The authors studied the structure of the liquid copolymers of ethylene tetrasulfide and vinyl cyanide using infrared spectra. The possibility of vulcanizing these polymers at room temperature is examined. (11 refs.)

77391 Raman spectra and molecular orientation statistics for nematic liquid crystals. S.E.Yakovenko, V.I.Naumenko, A.A.Min'ko, N.M.Ksenofontova.

J. Appl. Spectrosc. (USA), vol.37, no.2, p.962-5 (Aug. 1982). Translation of: *Zh. Prikl. Spektrosk. (USSR)*, vol.37, no.2, p.301-5 (Aug. 1982). [received: April 1983]

Various methods have been described for examining the orientation ordering in liquid crystals (LC). One method that gives the fullest information on the LC ordering is Raman spectroscopy. The authors examine the parameters of the orientation order derived from Raman spectra and birefringence measurements. The results are compared with model concepts on the mesomorphic state. (8 refs.)

77392 The interaction induced spectra of liquid CS_2 . A computer simulation study. P.A.Madden (Dept. of Theoretical Chem., Univ. of Cambridge, Cambridge, England), D.J.Tildesley.

Mol. Phys. (GB), vol.49, no.1, p.193-219 (May 1983). The spectral lineshapes corresponding to the symmetry forbidden spectra of CS_2 (the far infrared spectrum, and the infrared and Raman spectra of the g- and u-symmetry modes, respectively) were calculated from a computer simulation of the liquid at three state points. A multipole expansion was used to obtain the dependence of the interaction induced dipole moments and polarizabilities on the molecular coordinates. The intensities and shapes calculated for the lines are here compared with experimental data, the agreement is found to be good. Intermediate quantities calculated in the simulation are used to test the ideas which have been used in the theoretical description of the spectra, given by Madden and Cox (1981). Their assumptions are generally well supported by the calculations. (29 refs.)

77393 Optical phonons and structure of TlGaS_2 , TlGaSe_2 , and TlInS_2 layer single crystals. N.M.Gasany (Dept. of Phys., Azerbaidzhan State Univ., Baku, Azerbaijan SSR), A.F.Goncharov, N.N.Melnik, A.S.Ragimov, V.I.Tagirov.

Phys. Status Solidi b (Germany), vol.116, no.2, p.427-43 (1 April 1983). The polarization properties of bands in Raman scattering and IR reflection spectra are studied experimentally in TlGaS_2 , TlGaSe_2 , and TlInS_2 layer

single crystals and in solid solutions based on them. Additionally the angular dependence of IR-active modes on the angle between the phonon wave vector and the direction of the optical axis c of single crystals is investigated. It is shown that the observed phonon spectra can be interpreted on the basis of a primitive cell which contains two tetragonal-symmetry layers bonded to each other by an inversion operation. Bands corresponding to cells with a mixed composition are observed in the Raman spectra of the solid solutions. (26 refs.)

77394 Raman scattering from metal smokes. T.Nanba, T.P.Martin (Max-Planck-Inst. fur Festkörperforschung, Stuttgart, Germany).

Phys. Status Solidi a (Germany), vol.76, no.1, p.235-9 (16 March 1983). The effect of enhanced Raman scattering at metal surfaces was used to characterize the impurity layer on Ag and Cu smoke particles. The oxide layer seems to be composed of both MO and MO_2 having a disordered structure. Bands associated with graphitic carbon are also present. (14 refs.)

77395 Quantization of photo-excited carriers in GaAs doping superlattices. C.Zeller, B.Vinter, G.Abstreiter (Phys. Dept., Tech. Univ. München, Garching, Germany), K.Ploog.

Physica B & C (Netherlands), vol.117-118 B+C, pt.2, p.729-31 (March 1983). (Proceedings of the 16th International Conference on the Physics of Semiconductors, Montpellier, France, 6-10 Sept. 1982).

Photo-excited carriers in periodic doping multilayer structures of GaAs are studied using resonant inelastic light scattering techniques. Spin-flip single-particle intersubband excitations clearly demonstrate the quantization of electrons in purely space-charge induced potential wells. With increasing excitation intensity the electric subbands broaden to minibands with considerable dispersion with k perpendicular to the layers. A quasi-three-dimensional behavior is found in both self-consistent calculations and electronic Raman scattering experiments. (6 refs.)

77396 Distinction between 'free' CS_3^{2-} in ionic compounds and coordinated CS_3^{2-} in metallic complexes by the means of IR spectroscopy of solids. J.Roger, J.N.Pons, M.Stern (Univ. Pierre-et-Marie-Curie, Paris, France).

Rev. Chim. Miner. (France), vol.19, no.6, p.663-7 (1982). In French. The vibrations $\nu(\text{C-S})$ and $\nu_2(\text{C-S})$ appear well suited for the purpose. The splitting lies under 50 cm^{-1} with ionic compounds, from 100 to 160 cm^{-1} for Ni(II) or Co(III) trithiocarbonate complexes, near 200 cm^{-1} for covalent compounds like $(\text{C}_2\text{H}_5)_3\text{CS}_3$. (20 refs.)

77397 A comparison of the Raman spectra of ZnGa_2Se_4 and other gallium defect chalcopyrites. P.P.Lottici, C.Razzetti (Istituto di Fisica, Univ. di Parma, Parma, Italy).

Solid State Commun. (USA), vol.46, no.9, p.681-4 (June 1983).

The authors report and comment for the first time the Raman spectrum of ZnGa_2Se_4 . Looking for family trends they compare the present results with those obtained in other gallium defect chalcopyrites. The proportionality law between the frequencies of corresponding phonons in different compounds is verified for all the modes with the exception of the lowest energy polar modes. Evidence of the peculiarity of these modes is obtained, confirming that reported for $\text{Zn}_x\text{Cd}_{1-x}\text{Ga}_2\text{S}_4$ pseudoternary compounds. (8 refs.)

77398 Reflection of light from a two-phase metal-insulator system. I.A.Vasserman, V.V.Ganin, Yu.G.Zaretskii, A.D.Kurbatov, A.D.Fistul', A.Ya.Shik, Yu.V.Shmartshev (A.F. Ioffe Physicotechn. Inst., Acad. of Sci., Leningrad, USSR).

Sov. Phys.-Solid State (USA), vol.24, no.11, p.1919-21 (Nov. 1982). Translation of: *Fiz. Tverd. Tela (USSR)*, vol.24, no.11, p.3377-80 (Nov. 1982). [received: May 1983]

An investigation was made of the reflection spectra of finely dispersed W+LiInO_3 mixtures with different proportions of the components. It was found that when the concentration of W was between 20 and 80 vol.%, the samples exhibited a metallic conduction, but the reflection spectrum was typical of an insulator. The effect is explained using the percolation theory. (10 refs.)

77399 Raman light scattering in semiconductors containing dislocations. V.I.Belyavskii, V.V.Sviridov (Polytech. Inst. Voronezh, USSR).

Sov. Phys.-Solid State (USA), vol.24, no.11, p.1987-8 (Nov. 1982). Translation of: *Fiz. Tverd. Tela (USSR)*, vol.24, no.11, p.3490-2 (Nov. 1982). [received: May 1983]

Raman scattering is one of the most direct methods for investigating the electron-phonon interaction which may play an important role in the formation of the dislocation energy bands. The authors calculate the Raman spectrum using a general theory of the secondary radiation emitted by semiconductors developed for the Raman scattering case allowing for the presence of bulk excitons and longitudinal optical phonons. The interaction of dislocation excitons with light can be considered in the dipole approximation, i.e. the wave vectors of phonons can be ignored compared with the quasimomenta K of dislocation excitations. (9 refs.)

77400 Nonequilibrium phonons in ZnSe single crystals. V.A.Korneichuk (Inst. of Semiconductors, Acad. of Sci., Kiev, Ukrainian SSR).

Sov. Phys.-Solid State (USA), vol.24, no.11, p.1992-3 (Nov. 1982). Translation of: *Fiz. Tverd. Tela (USSR)*, vol.24, no.11, p.3496-9 (Nov. 1982). [received: May 1983]

Reports an investigation of the Raman scattering spectra of ZnSe at high rates of two-photon excitation. The results are used to extract the effective temperature of both TO phonons and LO phonons. It is shown that in the case of polar semiconductors with a parabolic conduction band, the main mechanism of hot carrier thermalisation is scattering by LO phonons. (7 refs.)

77401 The Brownian rotational motion and shape of IR-absorption lines. E.N.Ivanov, E.N.Shermatov.

Ukr. Fiz. Zh. (USSR), vol.28, no.5, p.667-71 (May 1983). In Russian. The model of Brownian inertial rotation, earlier suggested by one of the authors, has been used to develop the theory of shape and width for IR molecule absorption lines in condensed media. The line width is discussed as a function of parameters characteristic of the Brownian rotation. (13 refs.)

77402 Raman spectroscopy for characterization of annealing of ion-implanted InP. D.R.Myers, P.L.Gourley (Sandia Nat. Labs., Albuquerque, NM, USA), K.V.Vaidyanathan, H.L.Dunlap.

Gallium Arsenide and Related Compounds, 1982. Tenth International Symposium on Gallium Arsenide and Related Compounds, Albuquerque, NM, USA, 19-22 Sept. 1982 (Bristol, England: IOP 1983), p.635-40. Raman spectroscopy has been used as a noncontacting, nondestructive tool to evaluate the properties of Si^{3+} - and Be^{2+} -implanted InP samples annealed at temperatures ranging from 600 to 750°C using phosphosilicate glass (PSG) as the encapsulant. Carrier activation, carrier mobility and recovery of damage as a function of anneal temperature obtained from analysis of Raman data agree very well with independent electrical measurements. (11 refs.)

- Vibrational studies on conformational equilibrium in dimethylmethylphosphonate and methylmethylphosphonate See Entry 75385
- Chloroacetyltriphenylphosphonium and the corresponding phosphorane. Physical chemistry and conformation study See Entry 75388
- Surface enhanced Raman scattering (SERS) from pyridine on silver-UHV interfaces: excitation spectra See Entry 75393
- Vibrational and conformational studies of cyclopropylcarbonyl chloride See Entry 75394
- Synthesis and structural study of *N*-ethylnortropane-3-spiro-5'-oxazolidine-2,4'-dione and its hydrochloride See Entry 75395
- Picosecond time-resolved CARS in isotopically mixed crystals of benzene See Entry 75719
- Structure of liquid hydrogen fluoride studied by infrared and Raman spectroscopy See Entry 76272
- 'Nonclassical' temperature dependence of the order parameter of nematic liquid crystals See Entry 76302
- The structural analysis of $\text{Li}_2\text{O} \cdot 2\text{SiO}_2$ glass and melt by Raman spectroscopy See Entry 76311
- Neutron diffraction study of 2 $\text{TeO}_2 \cdot \text{V}_2\text{O}_5$ glass See Entry 76314
- On the problem of cross links in trans-polyacetylene: normal-coordinate calculations See Entry 76322
- The distribution of Fe^{3+} and Ga^{3+} between octahedral and tetrahedral sites in garnets, $\text{Y}_3(\text{Fe,Ga})_5\text{O}_{12}$, at different temperatures See Entry 76402
- Optical transmission at 3.39 μm during pulsed laser annealing of silicon See Entry 76489
- Incorporation of oxygen atoms into As^+ implanted silicon during CW CO_2 laser annealing in O_2 See Entry 76490
- Radiation effects in CaWO_4 crystals See Entry 76498
- Influence of electron relaxation on the damping of long-wavelength optical phonons in metals heavily doped semiconductors See Entry 76575
- Dynamical behaviour of interstitials in elemental semiconductors See Entry 76576
- A study on the orientation of imidazoles on copper as corrosion inhibitor and possible adhesion promoter for electric devices See Entry 76775
- Raman scattering by optically absorbing molecules adsorbed on 'smooth' Ag and Au surfaces: crystal violet See Entry 76784
- Spin coated amorphous chalcogenide films: structural characterization See Entry 76802
- Observation of dispersion on magnetic polaritons See Entry 76858
- Localized centers in bismuth silicate crystals See Entry 76875
- Residual donors and acceptors in high-purity GaAs and InP grown by hydride VPE See Entry 76883
- Magnetic-field dependence of the Hall factor of gallium arsenide See Entry 76980
- Self quenching of extrinsic photoconductivity in GaAs:Cr See Entry 76990
- Electrical and Raman study of lithium borotungstate and boromolybdate glasses See Entry 77011
- Electronic properties of InAs-GaSb superlattices See Entry 77032
- Infrared optical constants of PtSi See Entry 77347
- Fluorescence of molecular crystals at high levels of optical pumping See Entry 77415
- Photoinduced absorption spectra of ZnS:Fe crystals See Entry 77416
- Polarized light absorption of the magnetic semiconductor CdCr_2Se_4 See Entry 77472
- Production methods and properties of diamond-like carbon films See Entry 77566
- The fining of glass. A Raman-spectrometric investigation into the action of arsenic oxides See Entry 77615
- Electrical conductivity and infrared absorption spectrometry study of hematite precipitation from defective ferrites See Entry 77647
- Thermal isomerization and degradation of polyacetylene See Entry 77887
- Raman spectroscopic studies of the structure of electrolytes used in the Li/SOCl_2 battery See Entry 77978
- Ge-Al thin films for selective solar absorbers See Entry 78099

78.35 BRILLOUIN AND RAYLEIGH SCATTERING

- 77403 Determination of the ratios K_{11}/K_{22} and γ_1/K_{11} in nematic liquid crystals by correlation spectroscopy. S.A.Ivanov, V.Yu.Vetrov. *J. Appl. Spectrosc. (USA)*, vol.37, no.2, p.975-7 (Aug. 1982). Translation of: *Zh. Prikl. Spektrosk. (USSR)*, vol.37, no.2, p.316-19 (Aug. 1982). [received: April 1983]
- The authors have demonstrated the use of correlation spectroscopy for the determination of the ratios of elastic constants K_{11}/K_{22} and the viscoelastic ratios η_1/K_{11} and γ_1/K_{11} . The simplicity and precision of the determination of these ratios suggests that this method is promising for the study of the viscosity and elastic properties of nematic liquid crystals. (7 refs.)
- 77404 Acoustic phonon absorption and dispersion in hydroxyl-doped KCl crystals at low temperatures [Brillouin scattering]. J.F.Berret, J.Pelous, R.Vacher (Lab. de Spectrometrie Rayleigh-Brillouin, Univ. des Sci. et Tech. du Languedoc, Montpellier, France). *J. Phys. Lett. (France)*, vol.44, no.11, p.433-41 (1 June 1983).
- The acoustic properties of hydroxyl-doped KCl crystals have been measured by Brillouin scattering in the temperature range 1 to 50K. For samples with OH^- content higher than 200 ppm, two features dominate the temperature dependence of the attenuation, namely an absorption peak around 20K and a strong increase of the damping with decreasing temperature below 5K. The results bear some similarities to the behaviour observed in glasses and have been accounted for by assuming relaxational and resonant phonon absorption processes. (24 refs.)
- 77405 Integrated scattering of light in lead magnoniobate, which is a ferroelectric with a diffuse phase transition. N.N.Krainik, V.A.Trepakov (A.F.Ioffe Physicotech. Inst., Acad. of Sci., Leningrad, USSR). *Sov. Phys-Solid State (USA)*, vol.24, no.11, p.1942-5 (Nov. 1982). Translation of: *Fiz. Tverd. Tela (USSR)*, vol.24, no.11, p.3419-25 (Nov. 1982). [received: May 1983]
- Above the average Curie temperature there were no significant changes in the size of the scatterers responsible for the temperature-dependent component of the integrated scattering of light observed right up to 360°C. There were

slight anomalies in the scattering at temperatures $\sim 100\text{-}160^\circ\text{C}$ and the maximum of the depolarized components in the region of $\sim 80^\circ\text{C}$. The results obtained were analyzed on the assumption of fluctuations of the composition with a partial ordering of the octahedral ions. (30 refs.)

Time-resolved study of the subpicosecond dynamics of molecular rotations in liquids See Entry 75327

Oriental fluctuations of a lyotropic nematic liquid crystal measured by quasielastic light scattering See Entry 76297

The effect of particle size on the haze of polymer films See Entry 77469

78.40 VISIBLE AND ULTRAVIOLET SPECTRA

- 77406 Fundamental optical absorption and valence bands in alkali silver halide crystals. K.Edamatsu, M.Ikezawa, K.Sato, S.Kono, T.Sagawa (Dept. of Phys., Tohoku Univ., Sendai, Japan). *J. Phys. Soc. Jpn. (Japan)*, vol.52, no.5, p.1521-4 (May 1983).
- Anisotropic fundamental optical absorption bands have been found at 4.4 eV in K_2AgI and Rb_2AgI , and at 4.9 eV in Rb_2AgBr_3 . The X-ray photoelectron spectrum of Rb_2AgI indicates that the uppermost valence band is the p-band of halogen. Optical absorption spectra are interpreted in terms of transitions of the charge transfer type from the halogen to the silver ion. The photo-excitation in the fundamental absorption region have been observed to induce luminescence and a radiation damage effect at low temperature.
- 77407 Vacuum ultraviolet reflectance spectra and band structures of pyrites (FeS_2 , CoS_2 and NiS_2) and NiO measured with synchrotron radiation. S.Suga, K.Inoue, M.Taniguchi, S.Shin, M.Seki (Inst. for Solid State Phys., Univ. of Tokyo, Tokyo, Japan), K.Sato, T.Teranishi. *J. Phys. Soc. Jpn. (Japan)*, vol.52, no.5, p.1848-56 (May 1983).
- Reflectance spectra of FeS_2 , CoS_2 , and NiS_2 pyrites have been measured in the photon energy region from 4 to 30 eV with synchrotron radiation and compared with the results of NiO and related compounds. Dielectric constants, optical constants, effective electron numbers as well as energy-loss functions are evaluated by means of the Kramers-Kronig analysis. Fine structures of the reflectance spectra are qualitatively interpreted providing information on band structures. Characteristic features of band structures related to the 3d electrons in the low-spin state are experimentally elucidated.
- 77408 Temperature dependence of optical absorption near the order-disorder phase transition of sodium nitrate. R.Kawashima, K.Suzuki (Dept. of Appl. Material Sci., Muroran Inst. of Technol., Muroran, Japan). *J. Phys. Soc. Jpn. (Japan)*, vol.52, no.5, p.1857-65 (May 1983).
- The optical absorption spectrum of sodium nitrate, NaNO_3 , has been measured for the wavelength range from 6000 Å to 2000 Å at temperatures between 49.5°C and 298.6°C. The optical absorption of the two absorption bands shows anomalous temperature dependence near the order-disorder phase transition of NaNO_3 . The phenomenological relation between the energy gaps and the heat capacity has been confirmed. Low energy tails of the two absorption bands have shifted to lower energy side with increasing temperature, and they have been found to obey the Urbach rule within experimental error. (26 refs.)
- 77409 Induced absorption in Icelandic spar crystals under ultraviolet illumination. E.V.Kas'yanenko, O.P.Matveeva, A.V.Skropyshev. *J. Appl. Spectrosc. (USA)*, vol.36, no.5, p.572-4 (May 1982). Translation of: *Zh. Prikl. Spektrosk. (USSR)*, vol.36, no.5, p.803-5 (May 1982). [received: Feb. 1983]
- Studies the peculiarities of the variation in the optical properties of rose Icelandic spar when it is exposed to UV illumination. The measurements were carried out on single crystals of $\text{CaCO}_3 \cdot \text{Pb}^{2+}$ containing lead concentrations in the range 0.01-0.2%. The absorption and excitation spectra were recorded on a Beckman spectrophotometer over the wavelength range 200-800 nm, while the emission spectra were recorded on a CDL-1 spectrometer. (7 refs.)
- 77410 Reflectance and thermorefectance spectra and energy band structure of GeSe crystals. G.Valiukonis (Inst. of Semiconductor Phys., Acad. of Sci., Vilnius, Lithuanian SSR), F.M.Gashimzade, D.A.Guseinova, G.Krivaite, A.M.Kulibekov, G.S.Orudzhev, A.Sileika. *Phys. Status Solidi b (Germany)*, vol.117, no.1, p.81-92 (1 May 1983).
- The reflectance spectra of orthorhombic GeSe crystals are studied in the region 0.5 to 12 eV in polarized light with $\text{E}||\text{a}$ and $\text{E}||\text{b}$ at 290K and a Kramers-Kronig analysis is performed. The thermorefectance spectra are investigated in the region 1 to 5 eV for $\text{E}||\text{a}$ and $\text{E}||\text{b}$ at 300 and 90K. The energy band structure calculations of GeSe are carried out using the pseudopotential method, and the spectra of the imaginary part of the dielectric constant are calculated by the $\mathbf{k} \cdot \mathbf{p}$ method. A classification and interpretation of main structures of optical spectra of GeSe by direct interband transitions at critical points Γ , U, T and high symmetry lines B' , V, A is presented on the basis of calculated band structure and selection rules for optical dipole transitions of orthorhombic $\text{A}''\text{B}^0$ crystals. (25 refs.)
- 77411 Infrared photomodulation of the band edge transmission in semi-insulating GaAs. J.Bonnafant, M.de Murcia, M.Castagne, J.P.Fillard (Centre d'Electronique de Montpellier, Univ. des Sci. et Tech. du Languedoc, Montpellier, France). *Phys. Status Solidi a (Germany)*, vol.76, no.2, p.K147-50 (16 April 1983).
- The authors describe the observation of a photo-induced modulation effect in the band edge transmission in GaAs and its possible explanations. The transmission spectrum is measured with a low intensity monochromatic light beam. Infrared illumination is provided by a chopped YAG:Nd CW laser (400 mW) and an optical guide. (5 refs.)
- 77412 Effect of pressure on the absorption spectra of solid O_2 . A.F.Prikhot'ko, Yu.G.Pikus, A.I.Shanskii. *Ukr. Fiz. Zh. (USSR)*, vol.28, no.4, p.615-717 (April 1983). In Russian.
- Spectral methods were used to investigate the dependence of the $\beta \rightarrow \alpha$ transformation in solid O_2 crystals on pressure. It is shown that the observed phenomenon is mainly characterised by the strengthening of the exchange interactions during the compression of O_2 . (9 refs.) V.G.P.
- 77413 Reflectivity spectra of Sb_2S_3 , Sb_2Se_3 , Bi_2S_3 . V.V.Sobolev, V.M.Kramar', E.F.Zagaynov. *Ukr. Fiz. Zh. (USSR)*, vol.28, no.5, p.783-4 (May 1983). In Russian.
- Investigates the reflectivity spectra of cleaved Sb_2S_3 , Sb_2Se_3 and Bi_2S_3 monocrystals in polarized light $\text{E}||\text{c}$, $\text{E}||\text{a}$ at 80 and 293K in the region 1 to 4.8 eV. Each spectrum was found to contain 13-18 maxima. The electronic structures and transition polarisations have been calculated. (5 refs.) V.G.P.
- The distribution of Fe^{3+} and Ca^{3+} between octahedral and tetrahedral sites in garnets, $\text{Y}_3(\text{Fe,Ga})_5\text{O}_{12}$, at different temperatures See Entry 76402
- Neutron induced colour and luminescence centres in yttrium-aluminium garnet single crystals See Entry 76422
- On production of Z_1 centres in NaCl:Sm^{2+} crystals See Entry 76423

Photo-chemical reaction and photo-induced polarization studies in sulphur-doped potassium bromide See Entry 76482

Radiation effects in CaWO_4 crystals See Entry 76498

Two-photon transitions to exciton polaritons See Entry 76856

Localized centers in bismuth silicate crystals See Entry 76875

Self quenching of extrinsic photoconductivity in GaAs:Cr See Entry 76990

Photoconductivity of Y_2O_3 crystals with self-localized excitons See Entry 77003

Electrical and optical properties of SnO_2 thin layers received using the method of oxidation of thermally vapoured Sn layers See Entry 77073

Colored and black liquid crystalline mixtures with new anthraquinone dyes See Entry 77360

Reflection of light from a two-phase metal-insulator system See Entry 77398

Photoinduced absorption spectra of ZnS:Fe crystals See Entry 77416

Optical properties of the $\text{Tl}^0(1)$ center in KCl See Entry 77419

Spectroscopic properties of $\text{TbP}_5\text{O}_{14}$, $\text{TbLiP}_4\text{O}_{12}$, and $\text{TbAl}_3(\text{BO}_3)_4$ See Entry 77426

Thermoluminescence and optical absorption studies. Rubidium bromide doped with barium See Entry 77463

Polarized light absorption of the magnetic semiconductor CdCr_2Se_4 See Entry 77472

Thermal modulation spectrum and electron structure of niobium See Entry 77474

Structural and optical properties of sprayed CuInSe_2 films See Entry 77564

78.45 STIMULATED EMISSION

(see also 42.65C in nonlinear optics)

77414 Radiation generation by collective phenomena in semiconductors. E.Gornik, R.A.Hopfel (Inst. für Experimentalphys., Univ. Innsbruck, Innsbruck, Austria). *Arch. Elektron. & Übertragungstechn. (Germany)*, vol.37, no.5-6, p.213-16 (May-June 1983).
The properties of two-dimensional plasma oscillations at present in surface inversion layers are discussed. The excitation spectrum is calculated using Bose-Einstein statistics. The mechanism of the coupling between the nonradiative plasma waves and the radiation field via a periodic grating in the nearfield of the inversion layer is described. Possibilities for generating coherent light in a semiconductor with this principle are discussed. (9 refs.)

77415 Fluorescence of molecular crystals at high levels of optical pumping. V.Kh.Brikenshtein (Inst. of Biological Testing of Chem. Compounds, Acad. of Sci., Chernogolovka, USSR), V.A.Benderskii, P.G.Filippov. *Phys. Status Solidi b (Germany)*, vol.117, no.1, p.9-39 (1 May 1983).
The authors cover the published data on phenomena occurring in molecular crystals under conditions of high-power optical pumping. Some of them, e.g. stimulated emission and nonlinear fluorescence quenching (NFQ) have been studied extensively and utilized for scientific purposes in the study of other effects in molecular crystals. Thus, the stimulated emission of impurities have been used as a method for the determination of vibronic relaxation times in the ground state. NFQ proves to be a common phenomenon for all molecular crystals and solutions. An understanding of this phenomenon enables calculations to be made of rate constants and their temperature dependence for the recombination and energy transfer processes. Research into other related processes is at the beginning. (131 refs.)

Superradiation of extended systems See Entry 75610

Crystalline $\text{Kd}(\text{WO}_4)_2$ laser with a semiconductor pump system See Entry 75645

Spectrum studies on a GaAs-AlGaAs multi-quantum-well laser diode grown by molecular beam epitaxy See Entry 75690

Stimulated emission by charged particles in natural hollow crystalline channels See Entry 76541

Theoretical calculations of fluorescent branching ratios for $\text{YAlO}_3:\text{Er}^{3+}$ from the complete Judd-Ofelt theory See Entry 77427

78.50 IMPURITY AND DEFECT ABSORPTION IN SOLIDS

77416 Photoinduced absorption spectra of ZnS:Fe crystals. H.Zimmermann, R.Boyn, N.Nagel (Sektion Phys., Humboldt-Univ. zu Berlin, Berlin, Germany). *Phys. Status Solidi b (Germany)*, vol.117, no.1, p.229-39 (1 May 1983).
Photoinduced absorption (PA) spectra of ZnS:Fe crystals are measured between 0.3 and 3.6 eV by means of a modulation technique. Transitions related to the charge states Fe^{3+} and Fe^{2+} , which have been detected by EPR a long time ago, are believed to be seen in these spectra. In particular, the processes $\text{Fe}^{3+} \rightarrow \text{Fe}^{2+} + h$ and $\text{Fe}^{2+} \rightarrow \text{Fe}^{3+} + e$ are identified, the latter manifesting itself most clearly in the excitation spectrum of the PA band due to the former transition. The shapes of the photoneutralization and photoionization spectra are discussed, and the position of the Fe^{2+} ground state in the forbidden gap is estimated. (23 refs.)

77417 Model for optical absorption in transition metals containing d impurities. J.C.Parlebans (Lab. de Magnetisme et de Structure Electronique des Solides, Univ. Louis Pasteur, Strasbourg, France). *Phys. Status Solidi b (Germany)*, vol.117, no.1, p.255-9 (1 May 1983).
The effect of a 'd' impurity is investigated on the contribution to the optical absorption in a transition metal from electronic intra- and interband transitions. Within a tight-binding approximation a previous calculation of the imaginary part $\epsilon_2(\omega)$ of the dielectric constant in simple models is extended to realistic multiband dilute alloys. The possibility is shown of exploring critical points in nickel host band structure, for example by wave-vector non-conserving transitions induced by impurities, in relation with recent experimental data. (11 refs.)

77418 Fluctuations in light transmission of zinc sulphide. J.M.Noras (Dept. of Phys., Univ. of Bradford, Bradford, England). *Phys. Status Solidi b (Germany)*, vol.76, no.1, p.K53-6 (16 March 1983).
Samples of melt-grown polycrystalline ZnS have been studied by optical absorption. At temperatures near 6K, under steady illumination by white light the authors have observed a quasi-periodic fluctuation in the intensity of transmitted light. The modulation was of the order of 10% of the maximum transmission and the period some 30 min. (4 refs.)

77419 Optical properties of the $\text{Tl}^0(1)$ center in KCl . L.F.Mollenauer, N.D.Vieira, L.Szeto (Bell Telephone Lab., Holmdel, NJ, USA). *Phys. Rev. B (USA)*, vol.27, no.9, p.5332-46 (1 May 1983).
The authors report both experimental and theoretical studies of the $\text{Tl}^0(1)$ center in KCl , a center consisting of a neutral Tl atom perturbed by the field of an adjacent anion vacancy. Absorption bands peaking at 1040, 720, 550, and 340 nm were all shown to belong to the $\text{Tl}^0(1)$ center. The relatively weak ($f \approx 0.01$) bands at 1040 and 720 nm correspond to absorptions terminating on the crystal-field-split components of the $6^2P_{3/2}$ level, while the stronger band at 550 nm corresponds to transition to a state derived largely from $7^2S_{1/2}$. The sole luminescence band is the laser-active band having 1.6- μsec decay time and peaking at 1520 nm. The model presented here can account for the transition energies of the 6p manifold, including the Stokes shift between absorption (at 1040 nm) and luminescence, as well as the polarization properties and relative oscillator strengths of the 1040-, 720-, and 550-nm bands. (11 refs.)

77420 Valence-band splitting of SrTiO_3 . K.W.Blazey, M.Aguilar, J.G.Bednorz, K.A.Muller (IBM Zurich Res. Lab., Ruschlikon, Switzerland). *Phys. Rev. B (USA)*, vol.27, no.9, p.5836-8 (1 May 1983).
Optical charge-transfer transitions from the oxygen valence bands to Fe^{5+} and V^{5+} impurity states at Ti^{4+} sites in SrTiO_3 reveal a 0.42-eV valence-band splitting. Since these transitions are observed with conventional optical-absorption spectroscopy, their resolution is far better than previously obtained by photoelectron spectroscopy. (9 refs.)

Neutron induced colour and luminescence centres in yttrium-aluminium garnet single crystals See Entry 76422

On production of Zr_1 centres in NaCl:Sm^{2+} crystals See Entry 76423

Chemical effects of carbon ion implantation into alkali halides See Entry 76470

Incorporation of oxygen atoms into As^+ implanted silicon during CW CO_2 laser annealing in O_2 See Entry 76490

Radiation damage in polyacrylonitrile See Entry 76499

Dynamical behaviour of interstitials in elemental semiconductors See Entry 76576

AgCl intrinsic properties modifications by ion implantation See Entry 76640

Residual donors and acceptors in high-purity GaAs and InP grown by hydride VPE See Entry 76883

Energy level diagrams for d^2-d^8 configurations in a cubic field See Entry 76905

Self quenching of extrinsic photoconductivity in GaAs:Cr See Entry 76990

Formation of lattice defects in CdS crystals by nitrogen laser radiation See Entry 77450

78.55 PHOTOLUMINESCENCE

77421 Luminescent properties of terbium-activated lanthanum oxysulfide. Guo Fengyu, Huang Zhupo (Dept. of Chem., Peking Univ., Peking, China). *Acta Sci. Nat. Univ. Pekin. (China)*, no.5, p.81-5 (1982). In Chinese.
Lanthanum oxysulfide samples activated by terbium (with the mole ratio of Tb to La $\sim 5 \times 10^{-3}$ - 7×10^{-2}) were prepared by sulphidizing the mixed oxides of lanthanum and terbium at high temperature. The luminescent properties of these samples under the excitation of UV light, cathode-ray and X-ray were investigated. In all three cases, the phosphor's brightness increases with the terbium concentration, and comes up to a maximum at the terbium content about 5×10^{-3} . The cathode-ray luminescence efficiency of $\text{La}_2\text{O}_3\text{:Tb}$ (4×10^{-3}) may reach 62.8 Lumen/Watt. The emission spectra of UV-, CR- and X-ray-excited luminescence of all $\text{La}_2\text{O}_3\text{:Tb}$ samples are quite similar. The peaks of 489, 545, 587 and 620 nm stem from $^3\text{D}_4 \rightarrow ^3\text{F}_6$, $^3\text{D}_4 \rightarrow ^3\text{F}_5$, $^3\text{D}_4 \rightarrow ^3\text{F}_4$ and $^3\text{D}_4 \rightarrow ^3\text{F}_3$ transitions of Tb^{3+} ion respectively. The relative intensities of these 4 peaks remain unchanged within the concentration range of terbium studied. Therefore the values of colour indices of all these samples are about the same. (4 refs.)

77422 Quantum fluctuations and their role in applied roentgenoluminescence. A.M.Gurvich (Moscow Sci. Res. Roentgenoradiological Inst., Moscow, USSR). *Bull. Acad. Sci. USSR, Phys. Ser. (USA)*, vol.46, no.5, p.128-33 (1982). Translation of: *Izv. Akad. Nauk SSSR Ser. Fiz.*, vol.46, no.5, p.964-9 (1982). [received: May 1983] (Proceedings of the All-Union Conference on Luminescence Commemorating the Ninetieth Anniversary of the Birth of the Academician S.I. Vavilov, Leningrad, USSR, 21-24 April 1981).
The results of measurements of granularity performed by R.V. Katomina on photographs obtained from screens made of CaWO_4 luminophor of two types are given. As the luminophor load decreases and a corresponding growth occurs in the contrast transmission factor K , the granularity of the image characterized by the negative logarithm of the threshold brightness B_{tr} (at which this granularity on the photograph becomes noticeable) also increases. In order to express the dependence of the noise on the FCC (frequency contrast characteristic), the concept of the effective width of the spatial pass-band is introduced. It is set equal to the space frequency ν_{ex} at which K decreases by a factor of e. Since $\delta_s \sim 1/\sqrt{\Omega}$, (Ω is the area of the considered image element), it follows that assuming $\Omega = (1/2\nu_{ex})^2$, the authors find $\delta_s \sim \nu_{ex}/\sqrt{\eta K}$. The quantity $\nu_{ex}/\sqrt{\eta K}$ may be called the screen index of the quantum granularity. In roentgenoscopy (visual observation of the image on the screen) the noise level is in addition proportional to $\sqrt{\nu_{el}}$, where ν_{el} is the temporal frequency at which K decreases by a factor of e. (22 refs.)

77423 Intensities of $f-f$ transitions in the luminescence of ionic crystals activated by rare-earth elements. A.A.Kaminskii, B.Z.Malkin, L.A.Bumagina (V.I. Lenin Kazan State Univ., Kazan, USSR). *Bull. Acad. Sci. USSR, Phys. Ser. (USA)*, vol.46, no.5, p.144-9 (1982). Translation of: *Izv. Akad. Nauk SSSR Ser. Fiz.*, vol.46, no.5, p.979-84 (1982). [received: May 1983] (Proceedings of the All-Union Conference on Luminescence Commemorating the Ninetieth Anniversary of the Birth of the Academician S.I. Vavilov, Leningrad, USSR, 21-24 April 1981).
The electric dipole moments between the energy levels of the $4f^n$ -shell of free rare-earth (RE) ions are parity-forbidden. In a crystal this forbiddenness may be removed if the point symmetry group of the RE-ion does not contain the inversion operation. Two principal mechanisms which are responsible for the intense radiative $f-f$ transitions in dielectric matrices may be isolated: the Judd-Ofelt mechanism, within the framework of which the electric dipole transitions become allowed as a consequence of the mixing of different-parity states of the odd component of the crystal field (CF), and the dynamic-polarization mechanism in which $f-f$ transitions are stimulated by the variable component of the even CF modulated by the radiation field. In both cases the problem of analyzing the intensities of the transitions can be reduced to calculating the CF parameters and the structure of the local high-frequency electric field induced by the electromagnetic wave at the location of the

luminescence center. The authors have solved this problem for yttrium-aluminum garnet activated by Nd^{3+} ions. (8 refs.)

77424 Low-temperature luminescence in Eu^{3+} -doped tunstates of the perovskite stacking-variant type. G.Blasse (Phys. Lab., Utrecht Univ., Utrecht, Netherlands), S.Kemmler-Sack.
Ber. Bunsenges. Phys. Chem. (Germany), vol.87, no.4, p.352-5 (April 1983).
The photoluminescence at low temperatures of Eu^{3+} -activated tungstates of the perovskite stacking-variant type are reported. The main examples were $\text{Ba}_2\text{La}_{1-x}\text{Eu}_x\text{W}_2\text{O}_{12}$ (12 layer) and $\text{Ba}_2\text{Y}_{1-x}\text{Eu}_x\text{W}_2\text{O}_{18}$ (18 layer). The luminescence of 12 and 18 layer compounds were strikingly different. Not only were the emission and absorption spectra of the Eu^{3+} ions different, but also the energy transfer processes were not the same. (22 refs.)

77425 Phosphorescent lifetime and quantum yield measurements of $\text{K}_4\text{Pt}_2(\text{H}_2\text{P}_2\text{O}_5)_4$ from 1.6 to 300K. J.T.Markert, D.P.Clements, M.R.Corsen, J.K.Nagle (Bowdoin Coll., Brunswick, ME, USA).
Chem. Phys. Lett. (Netherlands), vol.97, no.2, p.175-9 (13 May 1983).
Phosphorescent lifetime measurements were performed on $\text{K}_4\text{Pt}_2(\text{H}_2\text{P}_2\text{O}_5)_4$ in 2/1 ethylene glycol/water solution, as well as on green and brown crystalline forms, from 1.6 to 300K. Quantum yield measurements on $\text{K}_4\text{Pt}_2(\text{H}_2\text{P}_2\text{O}_5)_4$ in solution were performed over the same temperature range. Data for the dissolved sample were fit to yield a 41.8 cm^{-1} energy splitting of the assumed $^3A_{2u}$ excited term into E_u ($\tau=4.2 \mu\text{s}$) and A_{1u} ($\tau=6.06 \text{ ms}$) components. The quantum yield for this sample varied from 0.13 at 4.2K to 0.43 at 77K. The green and brown crystalline forms showed similar behavior, with somewhat shorter lifetimes. A purple crystalline form showed no detectable luminescence from 1.6 to 300K. (12 refs.)

77426 Spectroscopic properties of $\text{TbP}_2\text{O}_{14}$, $\text{TbLiP}_2\text{O}_{12}$, and $\text{TbAl}_3(\text{BO}_3)_4$. W.K.Zwicker, S.Colak, J.Khurgin (Philips Labs., Briarcliff Manor, NY, USA), J.M.Robertson.
Proc. SPIE Int. Soc. Opt. Eng. (USA), vol.335, p.5-9 (1982). [received: May 1983] (Advanced Laser Technology and Applications, Arlington, VA, USA, 6-7 May 1982).
Stoichiometric crystals of $\text{TbP}_2\text{O}_{14}$, $\text{TbLiP}_2\text{O}_{12}$, and $\text{TbAl}_3(\text{BO}_3)_4$ were obtained by fluxed growth techniques. The emission spectra of various transitions of Tb^{3+} in these crystals were obtained at different temperatures. The fluorescence lifetimes of 3D_4 states were measured at various temperatures. The emission cross sections of $^3D_4 \rightarrow ^7F_5$ transition are reported. (19 refs.)

77427 Theoretical calculations of fluorescent branching ratios for $\text{YAlO}_3:\text{Er}^{3+}$ from the complete Judd-Ofelt theory. K.K.Deb (US Army Night Vision & Electro-Optics Lab., Fort Belvoir, VA, USA).
Proc. SPIE Int. Soc. Opt. Eng. (USA), vol.335, p.31-5 (1982). [received: May 1983] (Advanced Laser Technology and Applications, Arlington, VA, USA, 6-7 May 1982).
The optical properties of the Er^{3+} ion in yttrium orthoaluminate (YAlO_3) are analyzed with a crystal-field Hamiltonian of C_3 symmetry. Starting with the best-fit crystal field parameters, B_{eff} , the crystal field splitting schemes, the Judd-Ofelt intensity parameters, and multiplet-to-multiplet and line-to-line fluorescence branching ratios for Er^{3+} in YAlO_3 have been predicted. The calculated energy levels and the Judd-Ofelt intensity parameters compare reasonably well with available experimental data. It is suggested that the present theory predicts the correct order of line-to-line intensities for the laser transitions emanating from the $^3S_{3/2}$ manifold to 1I_1 channels of Er^{3+} in YAlO_3 . (24 refs.)

77428 Spectroscopic properties of triplet excited polyvinylcarbazoles and vinylcarbazole copolymers. A.Kal'nitskii, O.M.Faidish, O.V.Mavrenik.
Dopov. Akad. Nauk UkrSR. Ser. A (USSR), no.1, p.55-8 (1983). In Ukrainian.
A difference is found between a temperature dependence of phosphorescence for homopolymer polyvinylcarbazole and that for 9-vinylcarbazole copolymers with methylmethacrylate. In copolymers the transition from 4.2K to 77K does not influence phosphorescence very much whereas in the homopolymer such a transition causes a marked decrease in the intensity and appearance of an almost structureless band. The observed phenomena are due to detrapping of excitations from traps, migration and annihilation of unidimensional excitons as well as to triplet excimer formation. (9 refs.)

77429 Temperature dependence of the relaxation decay time and the integrated intensity of the photoluminescence from the magnetic semiconductor CdCr_2Se_4 . S.S.Yao, R.R.Alfano (Dept. of Phys., City Coll. of New York, New York, NY, USA), W.J.Miniscalco.
IEEE J. Quantum Electron. (USA), vol.QE-19, no.4, p.111-13 (April 1983).
The photoluminescence relaxation decay time of the band-to-band transition in CdCr_2Se_4 was measured from 4 to 250K. The decay time was measured to be $\sim 45 \text{ ps}$ at 4K, which monotonically decreased to $< 10 \text{ ps}$ at 250K. The integrated intensity of the steady-state photoluminescence from CdCr_2Se_4 was measured from 15 to 220K. The steady-state intensity increased as the temperature decreased, and increased quadratically with the excitation intensity. The temperature dependence of the relaxation decay time is theoretically fitted to the temperature dependence of the steady-state integrated intensity. (5 refs.)

77430 Quantum efficiency of alexandrite. M.L.Shand (Corporate Res. & Dev., Allied Corp., Morristown, NJ, USA).
J. Appl. Phys. (USA), vol.54, no.5, p.2602-4 (May 1983).
The first measurement of the radiative quantum efficiency (QE) of alexandrite has been determined using a photoacoustic (PA) technique which depends on the phase of the PA signal as a function of chopping frequency. The measured QE = 0.95 ± 0.05 . (7 refs.)

77431 Photoluminescence of molecular beam epitaxially grown Ge-doped GaAs. M.Baffleur, A.Munoz-Yague (Lab. d'Automatique et d'Analyse des Systemes, CNRS, Toulouse, France), J.L.Castano, J.Piqueras.
J. Appl. Phys. (USA), vol.54, no.5, p.2630-4 (May 1983).
The role played by molecular beam epitaxial growth conditions in Ge-doped GaAs and the introduction of deep levels inside the forbidden gap were investigated by means of photoluminescence. Firstly, a qualitative correlation was established between the compensation ratio obtained from Hall measurements and the ratio between the integrated intensity of the conduction band-acceptor transition to that of the donor-valence band. Secondly, two peaks at 1.41 and 1.45 eV, very similar to those introduced by another amphoteric impurity (Si) and systematically found in nearly all the samples, were studied in order to clarify their origin. Ge_{As} appears to be involved in both cases. The intensity of the 1.45 eV line increases with growth temperature which agrees with the assignment to a $\text{Ge}_{\text{As}}-\text{V}_{\text{As}}$ complex already suggested elsewhere. Conversely, the emission intensity at 1.41 eV decreases strongly with increasing growth temperature and the presence of $\text{Ge}_{\text{As}}-\text{As}_i$ and/or $\text{Ge}_{\text{As}}-\text{As}_{\text{Ga}}$ complexes is suggested to explain this result. (15 refs.)

77432 Photoluminescent and electrical properties of InGaPAs mixed crystals liquid-phase-epitaxially grown on (100) GaAs. S.Mukai (Electrotech. Lab., Ibaraki, Japan).
J. Appl. Phys. (USA), vol.54, no.5, p.2635-45 (May 1983).
The liquid-phase-epitaxial growth of InGaPAs layers on (100) GaAs is described for growth temperatures of 785 and 815°C. Photoluminescence (PL) spectra and electron Hall mobility of the layers are investigated as a function of crystal composition. The width of PL spectra measured at 300K is 40 meV, approximately the same value as that of GaAs, when the energy gap E_g of the layers is 1.9 eV or lower than 1.6 eV. The spectral width is around 80 meV when the energy gap of the layers is around 1.75 eV. The increase in the spectral width is attributed to variation of the local energy gap from analysis of dependence of the PL spectra on temperature and on excitation intensity. The indication that local energy gap varies in layers with E_g around 1.75 eV is consistent with the composition dependence of electron mobility. The mobility shows a sharp dip down to $1000 \text{ cm}^2/\text{Vs}$ around this composition, while it depends on composition only slightly for layers with E_g lower than 1.6 eV. The dip in composition dependence is attributed to space-charge scattering from analysis of temperature dependence of mobility. X-ray diffraction spectrum and surface morphology are also reported. The width of X-ray diffraction spectra is large for layers with E_g around 1.75 eV. This indicates that the local lattice constant varies significantly. Thick and uniform layers are particularly difficult to grow for such composition. These composition dependences of PL spectra, X-ray diffraction, and surface morphology are more significant in layers grown at 785°C than in layers grown at 815°C. The local variation of energy gap and lattice constant is attributed to variation of local composition caused by immiscibility of InGaPAs. (31 refs.)

77433 Time characteristics of secondary emissions in ZnTe under band-to-band excitation. T.Kushida, S.Kinoshita, F.Ueno, T.Ohtsuki (Dept. of Phys., Osaka Univ., Osaka, Japan).
J. Phys. Soc. Jpn. (Japan), vol.52, no.5, p.1838-47 (May 1983).
Transient behavior of secondary emission intensity has been measured near the fundamental absorption edge of ZnTe by means of a time-correlated single photon counting method under the excitation by subnanosecond light pulses from a CW mode-locked Ar^{+} ion laser. The obtained time responses of bound-exciton luminescence lines, exciton-polariton luminescence bands and a Raman-like $2LO$ line are analyzed. The dynamics of excitonic polaritons derived from the result are compared with a theoretical calculation, and the mechanisms of the appearance of the Raman-like LO lines and the polariton luminescence bands are discussed. (28 refs.)

77434 Time resolved stimulated fluorescence spectrum of the uranyl ion in the mineral metaautunite. L.V.Haley, J.A.Koningsstein (Ottawa-Carleton Inst. for Res. & Graduate Studies in Chem., Carleton Univ., Ottawa, Ontario, Canada).
J. Phys. & Chem. Solids (GB), vol.44, no.5, p.431-3 (1983).
The time resolved stimulated emission spectrum of the uranyl ion of the mineral metaautunite $\text{Ca}(\text{UO}_2)_2(\text{PO}_4)_2 \cdot 8\text{H}_2\text{O}$ is reported. The rise and decay time of this fluorescence is interpreted in terms of a simple model, proposed earlier by Lessing et al. (1970) and Flemming et al. (1977). (6 refs.)

77435 Ultrafast vibrational relaxation and hot luminescence of Ti^{+} centers in KI. G.S.Zavt, V.G.Plekhanov, V.V.Khizhnyakov, V.V.Shepelev (Inst. of Phys., Acad. of Sci., Tartu, Estonian SSR).
JETP Lett. (USA), vol.36, no.7, p.288-91 (5 Oct. 1982). Translation of: *Pis'ma v Zh. Eksp. & Teor. Fiz. (USSR)*, vol.36, no.7, p.235-8 (5 Oct. 1982). [received: May 1983]
Hot luminescence bands are observed in KI-Ti crystals. These bands are interpreted as emission from the first classical turning point in the process relaxation of the configurational coordinate, which represents a complex non-Markovian process with scale time $\sim 0.5 \text{ ps}$. (8 refs.)

77436 Electron-hole liquid in indium antimonide in a strong magnetic field. I.V.Kavetskaya, Ya.Ya.Kost', N.N.Sibeldin, V.A.Tsvetkov (P.N. Lebedev Phys. Inst., Acad. of Sci., Moscow, USSR).
JETP Lett. (USA), vol.36, no.7, p.311-14 (5 Oct. 1982). Translation of: *Pis'ma v Zh. Eksp. & Teor. Fiz. (USSR)*, vol.36, no.7, p.254-6 (5 Oct. 1982). [received: May 1983]
A new emission band which is related to decomposition of the electron-hole liquid (EHL) stabilized by a magnetic field, is observed in the magnetophotoluminescence spectra of pure indium antimonide crystals at high levels of excitation. (4 refs.)

77437 Luminescence in gadoliniumchlorotungstate (GdWO_4Cl). G.Blasse (Phys. Lab., State Univ., Utrecht, Netherlands), L.H.Brixner.
J. Solid State Chem. (USA), vol.47, no.3, p.368-72 (May 1983).
The luminescence of GdWO_4Cl , EuWO_4Cl , and $\text{GdWO}_4\text{Cl}:\text{Eu}^{3+}$ is reported. The tetrahedral tungstate group in these compounds luminesces similarly to those in other host lattices. The Gd^{3+} ions form a luminescent system which is not connected to the tungstate groups. The Gd^{3+} system transfers the greater part of its energy to defective tungstate groups in GdWO_4Cl and to Eu^{3+} in $\text{GdWO}_4\text{Cl}:\text{Eu}^{3+}$. (11 refs.)

77438 Physicochemical and spectral luminescence properties of a glass based on the $\text{SiO}_2-\text{Al}_2\text{O}_3-\text{La}_2\text{O}_3-\text{Nd}_2\text{O}_3$ system. G.E.Malashkevich, V.N.Tadeush, V.V.Kuznetsova, Kh.A.Charches, N.I.Bliznyuk, V.G.Mikhalevich, M.B.Rzhevskii.
J. Appl. Spectrosc. (USA), vol.37, no.2, p.926-9 (Aug. 1982). Translation of: *Zh. Prikl. Spektrosk. (USSR)*, vol.37, no.2, p.261-5 (Aug. 1982). [received: April 1983]

The results of work on the synthesis and investigation of certain physicochemical and spectral luminescence properties of a glass with a high concentration of rare earth ions are presented. The physicochemical properties studied were density, Young's modulus, Poisson coefficient, shear modulus, thermal conductivity, microhardness, linear thermal expansion coefficient and X-ray phase analysis. The concentration dependence of the luminescence quantum yield for Nd^{3+} ions when La^{3+} ions are replaced by them was examined. (5 refs.)

77439 A theoretical study of the effects of inhomogeneous level broadening on the spectral kinetic characteristics of the delayed emission from solid polar solutions of complex compounds. S.K.Gorbatsevich, I.M.Gulis, A.I.Komyak.
J. Appl. Spectrosc. (USA), vol.37, no.2, p.968-74 (Aug. 1982). Translation of: *Zh. Prikl. Spektrosk. (USSR)*, vol.37, no.2, p.309-16 (Aug. 1982). [received: April 1983]
The present study is a theoretical continuation of the authors previous work (see *ibid.*, vol.37, no.1, p.92, 1982) in which it was shown by experiment that under conditions of inhomogeneous broadening there is a considerable dependence on the excitation frequency for the spectral and kinetic characteristics of the delayed fluorescence and phosphorescence, and this applies also to the emission spectrum in pulse excitation. (10 refs.)

- 77440 Enhanced excitation transfer during vibrational relaxation after pumping and generalized Forster's formula.** H.Sumi (Inst. of Materials Sci., Univ. of Tsukuba, Sakura-mura, Ibaraki, Japan). *Phys. Rev. Lett. (USA)*, vol.50, no.21, p.1709-12 (23 May 1983). Electron or excitation transfer can be enhanced during vibrational relaxation after optical excitation of a donor. When it occurs after vibrational relaxation with a thermal activation energy E_A , enhanced transfer during vibrational relaxation is also governed by an activation energy E_H which, however, is smaller than E_A or even vanishes. The decrement $E_A - E_H$ depends on the total energy of vibrations triggered by optical excitation, and also on their average direction relative to that of the activation barrier for transfer in the phonon-coordinate space. (11 refs.)
- 77441 Low-frequency secondary radiation in polar semiconductors at finite temperatures.** F.Comas, C.Trallero Giner (Dept. of Theoretical Phys., Havana Univ., Havana, Cuba). *Phys. Status Solidi b (Germany)*, vol.116, no.2, p.445-53 (1 April 1983). Secondary radiation in polar direct-gap semiconductors is considered for finite, but not too large, temperatures. For sufficiently pure and perfect samples, photoexcited electrons (holes) relax via phonon scattering. Assuming an infinite recombination time, the differential cross-section for photon emission is calculated in the low-frequency region of the spectra. Rather intense secondary radiation is predicted for high temperatures. The general shape of emission and excitation spectra is discussed in detail. (11 refs.)
- 77442 Decay behaviour of high-excitation luminescence in GaP:N. I. Model for the decay of two coexisting phases.** H.Weinert (Sektion Phys., Karl-Marx-Univ. Leipzig, Leipzig, Germany). *Phys. Status Solidi b (Germany)*, vol.116, no.2, p.525-32 (1 April 1983). The time behaviour of the radiative recombination of nitrogen-doped GaP is investigated at pulsed intense optical excitations and low temperatures ($T=2$ and 27 K). The decay behaviour of the luminescence intensities corresponding to the electron-hole liquid (EHL) and the coexisting low-density phase (LDP) is found for all nitrogen concentrations ($n_N=2 \times 10^{17}$ to $2.9 \times 10^{18} \text{ cm}^{-3}$) to be nonexponential. It is interpreted as a consequence of interactions between both coexisting phases. A model is introduced where the EHL is fed by the LDP continuously. It describes the observed decay of the luminescence very well, even for different nitrogen concentrations and different excitation intensities. (20 refs.)
- 77443 Decay behaviour of high-excitation luminescence in GaP:N. II. Experimental results on the densities of the coexisting phases and the relevant recombination processes.** H.Weinert, R.Bindemann, K.Kreher (Sektion Phys., Karl-Marx-Univ. Leipzig, Leipzig, Germany). *Phys. Status Solidi b (Germany)*, vol.117, no.1, p.247-53 (1 May 1983). For pt.1 see *ibid.*, vol.116, p.525 (1983). The radiative recombination of isoelectronic nitrogen-doped GaP is investigated under high optical excitation at several temperatures ($T=2$, 4.2 , 27 , and 77 K). A previously reported phase separation is confirmed. The parameters of the electron-hole liquid and the coexisting low-density phase are determined both from luminescence spectra and decay measurements. The dominating recombination processes for the carrier system are found to be phonon-assisted band-to-band Auger recombination, phononless radiative recombination with participation of the nitrogen impurities, and phononless Auger recombination with participation of the nitrogen impurities. The respective rate coefficients are determined. (11 refs.)
- 77444 Radiative recombination in γ -La₂S₃ single crystals.** A.N.Georgobiani, M.V.Glushkov, E.S.Logozinskaya, Zh.A.Pukhlii, I.M.Tiginyanu, A.A.Scherbakov (P.N. Lebedev Phys. Inst., Acad. of Sci., Moscow, USSR). *Phys. Status Solidi a (Germany)*, vol.76, no.1, p.311-17 (16 March 1983). The photoluminescent properties of specially undoped γ -La₂S₃ single crystals are investigated. An interpretation of the complicated behaviour of the emission band under various excitation conditions is given, based on the concept of donor-acceptor pairs. A scheme of the deep levels and the electron transitions in γ -La₂S₃ single crystals is presented. (22 refs.)
- 77445 Electric field-induced quenching of luminescence in quantum wells.** E.E.Mendez, G.Bastard, L.L.Chang, L.Esaki (IBM Thomas J. Watson Res. Center, Yorktown Heights, NY, USA), H.Morkoc, R.Fischer. *Physica B & C (Netherlands)*, vol.117-118 B+C, pt.2, p.711-13 (March 1983). (Proceedings of the 16th International Conference on the Physics of Semiconductors, Montpellier, France, 6-10 Sept. 1982). Photoluminescence measurements have been performed on GaAs quantum wells under an electric field perpendicular to them. With an increasing field, the intensity decreases and becomes completely quenched at an average field of a few tens of kV/cm. This is accomplished by a shift to lower energies of the peak positions. The results are interpreted as caused by the field, which induces a separation of electrons and holes and modifies the energies of the quantum states. (8 refs.)
- 77446 Extrinsic photoluminescence from GaAs quantum wells.** R.C.Miller, A.C.Gossard, W.T.Tsang (Bell Labs, Murray Hill, NJ, USA). *Physica B & C (Netherlands)*, vol.117-118 B+C, pt.2, p.714-16 (March 1983). (Proceedings of the 16th International Conference on the Physics of Semiconductors, Montpellier, France, 6-10 Sept. 1982). Extrinsic photoluminescence has been studied from both undoped and p-type doped single and multiquantum well (MOW) GaAs-Al_xGa_{1-x}As heterostructures grown by molecular beam epitaxy. For undoped MOW samples this luminescence is attributed to $n=1$ electrons recombining with shallow neutral acceptors (probably carbon) near the well center whereas for single well samples the acceptors (probably carbon) are frequently concentrated in a thin GaAs layer at the first grown heterointerface. Ionization energies obtained from these data are in reasonable agreement with the calculations of Bastard. With Be-doped samples one can also see luminescence due to ground state heavy hole excitons bound to Be neutral acceptors. These data provide estimates of the dissociation energy of the heavy hole exciton neutral acceptor complex. (10 refs.)
- 77447 Impurity photoluminescence in GaAs/Ga_{1-x}Al_xAs multiple quantum wells.** B.Lambert, B.Deveaud, A.Regreny, G.Talalaieff (CNET, Lannion, France). *Physica B & C (Netherlands)*, vol.117-118 B+C, pt.2, p.717-19 (March 1983). (Proceedings of the 16th International Conference on the Physics of Semiconductors, Montpellier, France, 6-10 Sept. 1982). Luminescence experiments have been performed on multiple quantum wells structures with well thicknesses varying between 100 \AA and 1000 \AA . Varying the laser excitation density between 10 mW cm^{-2} and 5 kW cm^{-2} allows the authors to separate different bands related to hydrogenic impurities. The position of these bands are compared to the results of theoretical calculations on the binding energy of the impurity and on subband position. (9 refs.)
- 77448 Time resolved luminescence in n-i-p-i doping superlattices.** W.Rehm, H.Kunzel, G.H.Dohler, K.Ploog, P.Ruden (Max-Planck-Inst. fur Festkörperforschung, Stuttgart, Germany). *Physica B & C (Netherlands)*, vol.117-118 B+C, pt.2, p.732-4 (March 1983). (Proceedings of the 16th International Conference on the Physics of Semiconductors, Montpellier, France, 6-10 Sept. 1982). The luminescence spectrum of n-i-p-i doping superlattices shows a strong, excitation dependent red shift. Time resolved measurements of the decay of the luminescence provide a valuable tool for the determination of both radiative and non-radiative lifetimes. Results obtained from GaAs n-i-p-i crystals, grown by molecular beam epitaxy, reconfirm that recombination across the indirect gap in real space is the mechanism responsible for the luminescence. The radiative lifetime increases by more than five orders of magnitude during detectable decay, in agreement with the theoretically expected behavior. (8 refs.)
- 77449 Selective site excitation of europium-doped monoclinic Gd₂O₃.** J.G.Daly, J.A.Schmidt (Dept. of Phys., North Dakota State Univ., Fargo, ND, USA), J.B.Gruber. *Phys. Rev. B (USA)*, vol.27, no.9, p.5250-6 (1 May 1983). Monoclinic crystals of Eu³⁺:Gd₂O₃ were studied at 80K with the use of fluorescence spectra to interpret the energy levels. A tunable dye laser was used to selectively excite levels of the ³D_{0,1,2} manifolds. Three distinct crystallographic sites for Eu³⁺ ions were identified for a majority of the Stark levels of the ⁷F_{0,1,2,3,4} and ³D_{0,1} multiplets. Comparisons of the fluorescence spectra from different sites were used in this energy-level assignment. Several fluorescence-lifetime measurements were also recorded. (6 refs.)
- 77450 Formation of lattice defects in CdS crystals by nitrogen laser radiation.** N.E.Korsunskaya, I.V.Markevich, M.D.Moin, M.A.Tanatar, I.Yu.Shablii (Inst. of Semiconductors, Acad. of Sci., Kiev, Ukrainian SSR). *Sov. Phys.-Solid State (USA)*, vol.24, no.11, p.1829-32 (Nov. 1982). Translation of: *Fiz. Tverd. Tela (USSR)*, vol.24, no.11, p.3223-8 (Nov. 1982). [received: May 1983] A study was made of the influence of nitrogen laser radiation on the electrical, photoelectric, luminescence, and optical properties of CdS crystals. It was found that point defects of two types—shallow donors $E_d = E_c - 0.045 \text{ eV}$ and acceptors $E_a = E_v + 0.18 \text{ eV}$ —were formed in the surface layer of a crystal. These defects were sulfur vacancies V_s and interstitial sulfur atoms S_i , or complexes containing them. Irradiation generated a layer in which the exciton transition frequencies differed from those in the bulk of a crystal. This difference was attributed to the influence of electric fields and mechanical stresses generated in this layer by laser irradiation. (13 refs.)
- 77451 Influence of external agencies on nonradiative deactivation of the electron excitation energy in dysprosium-doped neodymium pentaphosphate crystals.** A.V.Krutikov, S.N.Perepetchko, V.P.Sakun, V.A.Smirnov, I.A.Scherbakov (P.N. Lebedev Phys. Inst., Acad. of Sci., Moscow, USSR). *Sov. Phys.-Solid State (USA)*, vol.24, no.11, p.1835-8 (Nov. 1982). Translation of: *Fiz. Tverd. Tela (USSR)*, vol.24, no.11, p.3234-40 (Nov. 1982). [received: May 1983] An analysis of the time evolution of the population of the ⁴F_{3/2} metastable states of Nd³⁺ in lanthanum neodymium dysprosium pentaphosphate was made on the basis of an investigation of the transfer of the electron excitation energy in a condensed medium. Changes in temperature and the application of a magnetic field altered the ratio of the interaction microparameters C_{DA} and C_{DD} and this provided an opportunity to study various models of migration-accelerated relaxation and the ranges of validity of these models. A general approach to the calculation of the rate of migration-limited relaxation W was developed and this made it possible to analyze the experimental results and thus show quantitatively the validity of the hopping model of energy degradation. It was found that an external magnetic field accelerated the rate of energy migration in space. (13 refs.)
- 77452 The superficial nature of subthreshold thermostructural alterations in ZnSe under continuous radiation.** P.V.Vodolazskii, B.R.Kiyak, M.G.Mat-sko, V.B.Nosov, G.T.Petrovskii, A.V.Shatilov. *Ukr. Fiz. Zh. (USSR)*, vol.28, no.4, p.625-7 (April 1983). In Russian. Investigates the low-temperature photoluminescence spectra of ZnSe single crystals at $T=4.2 \text{ K}$ up to and after the action of subthreshold continuous radiation with $\lambda=10.6 \text{ \mu m}$. It is shown that the temperature changes which appear have a surface character. (4 refs.) V.G.P.
- 77453 Energy position of luminescence (photosensitivity) centres in CdSe_{1-x}Te_x solid solutions.** I.B.Ermolovich, M.K.Sheinkman. *Ukr. Fiz. Zh. (USSR)*, vol.28, no.4, p.627-9 (April 1983). In Russian. Presents the results of investigating the photoconductivity electroabsorption and luminescence of single crystals and layers of CdSe_{1-x}Te_x, obtained by evaporation in vacuum. All data on the energy absorption of luminescing centres (photosensitivity) agree between $x=0$ and $x=1$. It is shown that the main photosensitivity centres in CdSe_{1-x}Te_x ($x=0$ to 1) are luminescence centres corresponding to the bands $\lambda_{\text{max}}=0.95 \text{ \mu m}$ and $\lambda_{\text{max}}=1.19 \text{ \mu m}$ in CdSe spectra. (12 refs.) V.G.P.
- 77454 Luminescence kinetics of lead compounds.** M.U.Belyi, N.G.Musienko, B.A.Okrimenko. *Ukr. Fiz. Zh. (USSR)*, vol.28, no.5, p.672-5 (May 1983). In Russian. Luminescence kinetics of complex Pb compounds has been investigated over a 90-200K temperature range. The luminescence spectrum is found to be not simple. This spectrum is divided into elementary parts. Four excited electron states are found for the Pb²⁺ ion, two of which are metastable. Depths of the metastable levels are estimated. (13 refs.)
- 77455 Colour centre luminescence of α -Al₂O₃.** V.A.Grigorov, E.F.Martynovich, A.G.Tokarev. *Ukr. Fiz. Zh. (USSR)*, vol.28, no.5, p.784-5 (May 1983). In Russian. Investigates the colour centre absorption and photoluminescence spectra of α -Al₂O₃ monocrystals irradiated with reactor neutrons. A new radiation band with a maximum of 3.82 eV has been found, which coincides with the F⁺-centre band but which is excited beyond the absorption boundary of F⁺-centres. (4 refs.) V.G.P.
- 77456 Deep acceptor photoluminescence in GaAs.** T.Nishino, Y.Fujiwara, Y.Hamakawa (Faculty of Engng. Sci., Osaka Univ., Osaka, Japan). Gallium Arsenide and Related Compounds, 1982. Tenth International Symposium on Gallium Arsenide and Related Compounds, Albuquerque, NM, USA, 19-22 Sept. 1982 (Bristol, England: IOP 1983), p.71-8. Low-temperature photoluminescence of deep acceptors associated with 3d transition metals in GaAs has been studied, with particular emphasis on the near-infrared luminescence in Ni-diffused GaAs. It has been found that the intracenter luminescence due to Ni deep acceptors depends in a complicated way upon the substrate crystals into which Ni is diffused. These results are compared with the well-known intracenter luminescence in GaAs:Cr. (10 refs.)

77457 Photoluminescence of oxygen-induced states in GaAs_{1-x}P_x. D.J.Wolford (IBM Thomas J. Watson Res. Center, Yorktown Heights, NY, USA), S.Modesti, B.G.Streetman. Gallium Arsenide and Related Compounds, 1982. Tenth International Symposium on Gallium Arsenide and Related Compounds, Albuquerque, NM, USA, 19-22 Sept. 1982 (Bristol, England: IOP 1983), p.501-8. Reports the photoluminescence (PL) of O-doped GaAs_{1-x}P_x. O-induced gap states are formed by implantation and unambiguously identified from their O-dependence and known origins in GaP. Prominent PL is attributable to formation of ZnO near neighbor (isoelectronic trap) complexes and more distant O-donor-Zn-acceptor pairs. Resulting ZnO trap and O-donor levels behave as deep electron states, varying linearly in x with slopes of -5.45 and -7.1 meV/% GaAs, respectively. Extensions to x=0 identify 0.64 eV PL in GaAsO as O_{As}-related DA pair recombination. The authors predict O_{As} induces in GaAs a deep donor near E_c-0.79 eV and acceptor-O_{As} isoelectronic complexes just below the conduction band edge. (41 refs.)

Time resolved polarization spectroscopy: level kinetics and rotational diffusion See Entry 75552

Luminescence of laser crystals See Entry 75642

Transition rates of Tb³⁺ in TbP₃O₁₄, TbLiP₃O₁₂, and TbAl₃(BO₃)₄: an evaluation for laser applications See Entry 75643

Spectrum studies on a GaAs-AlGaAs multi-quantum-well laser diode grown by molecular beam epitaxy See Entry 75690

Nonphotochemical hole burning in a hydrogen bonding glass: dependence on deuteration See Entry 75709

Dispersion and luminescence measurements of optical waveguides See Entry 75787

Neutron induced colour and luminescence centres in yttrium-aluminium garnet single crystals See Entry 76422

Incorporation of amphoteric impurities in high purity GaAs See Entry 76475

Radiation effects in CaWO₄ crystals See Entry 76498

Radiation damage in polyacrylonitrile See Entry 76499

Schottky anomaly and phase transition in the specific heat and in the spectra of K₂(MoO₄)₂ See Entry 76664

Anderson transition in the exciton-impurity band in silicon See Entry 76848

Emission of free and bound excitons in layered GaSe crystals See Entry 76850

Optical properties of polaritons in thin crystal films See Entry 76857

Residual donors and acceptors in high-purity GaAs and InP grown by hydride VPE See Entry 76883

Electronic structure of thallous centres and Ti⁴⁺-V_k recombination in KCl crystal See Entry 76888

Re-examination of the mid-gap electron trap (EL2) in different GaAs wafers by photocapacitance, DLTS and photoluminescence spectra See Entry 76892

Deep levels in InP grown by SSD method See Entry 76895

Photoelectric fatigue of photoresistors based on polycrystalline CdS:Cu:Cl films See Entry 77075

EPR and luminescence of Mn²⁺ in distorted tetrahedral symmetry in CaZnF₄ crystals See Entry 77255

ODMR investigation of recombination processes in a-Si₃C_{1-x}-x:H See Entry 77292

ODMR investigation of recombination in μc-Si:H See Entry 77293

Fluorescence of molecular crystals at high levels of optical pumping See Entry 77415

Optical properties of the Ti⁰(1) center in KCl See Entry 77419

Zero-phonon lines in electroluminescence and photoluminescence of ZnS:Mn thin films grown by atomic layer epitaxy See Entry 77459

MOCVD growth and characterization of high luminescence efficiency Al_xGa_{1-x}As See Entry 77583

Investigation of capless heat treatment of MBE n-GaAs See Entry 77686

Passivation of GaAs surfaces See Entry 77780

Solute-solvent exciplex versus twisted intramolecular charge-transfer state in anomalous fluorescence of 4-NN-dimethylaminobenzonitrile See Entry 77902

Photophysics of derivatives of all-trans-1,6-diphenyl-1,3,5-hexatriene (DPH). I. Model involving fluorescence from S₂ and S₁ excited states See Entry 77903

78.60 OTHER LUMINESCENCE SPECTRA AND RADIATIVE RECOMBINATION

(for photoconduction and photovoltaic effects, see 72.40; for photoluminescence, see 78.55)

78.60F Electroluminescence

77458 Electrolumiphors on the basis of ZnS:Sn. S.Pakeva, R.Dafinova (Sofia Univ., Sofia, Bulgaria). *Phys. Status Solidi a (Germany)*, vol.76, no.1, p.K77-80 (16 March 1983). The electroluminescence properties of ZnS:Sn are studied in a dismountable cell. The active layer consisted of electroluminescent powder mixed with castor oil. The width of the so prepared electroluminescent cell can easily be changed and adjusted with a precision of 20 μm. The brightness is not very strong, but separate small spots glow especially brightly. In a qualitative aspect the characteristics of the ZnS:Sn electrolumiphors do not differ from the corresponding characteristics of the ZnS:Cu electrolumiphors. (11 refs.)

77459 Zero-phonon lines in electroluminescence and photoluminescence of ZnS:Mn thin films grown by atomic layer epitaxy. W.Busse (Inst. fur Festkörperfys., Tech. Univ. Berlin, Berlin, Germany), H.-E.Gumlich, R.O.Tornqvist, V.-P.Tanninen. *Phys. Status Solidi a (Germany)*, vol.76, no.2, p.553-8 (16 April 1983). The energy of the zero-phonon-lines of the transition ⁶A₁→⁶E, ⁶A₁→⁴T₂ and ⁴T₁→⁶A₁ within the 3d-shell of Mn²⁺ in thin films of ZnS:Mn grown by atomic layer epitaxy (ALE) are determined by luminescence spectroscopy. A comparison of these values with the energies obtained with polymorphic ZnS:Mn single crystals indicates a predominantly hexagonal structure in the thin films in fair agreement with the data obtained by X-ray analysis. The zero-phonon-lines in both photoluminescence and high field electroluminescence of thin films are compared. (13 refs.)

78.60H Cathodoluminescence, ionoluminescence

77460 Effects of Cd-vapor and Te-vapor heat treatments on the luminescence of vapor-phase-grown CdTe. C.B.Norris (Sandia Nat. Labs., Albuquerque, NM, USA), L.R.Shiozawa. *J. Electron. Mater.* (USA), vol.12, no.2, p.267-87 (March 1983). From cathodoluminescence measurements at 80-300K, the authors report the first studies of the effects of Cd-vapor and Te-vapor heat treatments on the injection level dependence, temperature dependence, and frequency response of the luminescence in vapor-phase-grown (VPG) CdTe. At 80K, the as-grown material shows edge emission near 1.57 eV together with an extrinsic band near 1.4 eV and a weak extrinsic band near 1.2 eV. Following heat treatment in Cd-vapor, both the 1.4 eV and 1.2 eV bands are enhanced and the 1.2 eV band is joined by an overlapping band centered near 1.1 eV. Moderate heat treatments in Te-vapor weaken the 1.4 eV and 1.2 eV bands but enhance a band near 1.54 eV that is noticeable as a weak shoulder on the low energy side of the edge emission in as-grown material. (10 refs.)

77461 Effect of ionization density on the time dependence of luminescence from liquid argon and xenon. A.Hitachi, T.Takahashi (Inst. of Phys. & Chem. Res., Saitama, Japan), N.Funayama, K.Masuda, J.Kikuchi, T.Doke. *Phys. Rev. B (USA)*, vol.27, no.9, p.5279-85 (1 May 1983).

The time dependence of luminescence in liquid argon and xenon has been studied for electron, α-particle, and fission-fragment excitation. The lifetimes of low excited molecular states (¹Σ_g⁺ and ³Σ_g⁺) do not depend on the density of excited species while the intensity ratio of ¹Σ_g⁺ to ³Σ_g⁺ is found to be larger at higher deposited energy density. The lifetimes obtained for the ¹Σ_g⁺ and ³Σ_g⁺ states are 7.0±1.0 nsec and 1.6±0.1 μsec, respectively, in liquid argon, and 4.3±0.6 and 22.0±2.9 nsec, respectively, in liquid xenon. The mechanism of quenching of luminescence at high density of excited species in liquid argon and xenon is discussed. (34 refs.)

77462 Localization of electronic states and cathodoluminescence of bound exciton complexes in ZnSe crystals. V.S.Vavilov, Vu Zoon Mien, G.N.Ivanov, D.D.Nedoglo, A.V.Simashkevich, M.V.Chukichev (V.I. Lenin State Univ., Kishinev, USSR).

Sov. Phys.-Solid State (USA), vol.24, no.12, p.2091-4 (Dec. 1983). Translation of: *Fiz. Tverd. Tela (USSR)*, vol.24, no.12, p.3670-5 (Dec. 1983). The cathodoluminescence spectra of ZnSe crystals doped with a shallow donor impurity were investigated in the temperature range 4.2-300K. It was established that the form of the edge luminescence spectra depended on the impurity concentration. At low temperatures when the donor concentration was N_d=1×10¹⁶ cm⁻³, electrons were fully localized at impurities. The conduction process in the crystals was then of a hopping nature and the luminescence spectrum exhibited a fine structure of the lines due to the luminescence emitted by bound exciton complexes. An increase in the impurity concentration above 10¹⁶ cm⁻³ resulted in delocalization of electrons from impurities, formation of an impurity energy band, and dissociation of exciton-impurity complexes. (10 refs.)

Evaluation of misfit dislocations in planar, zinc-diffused In_{0.53}Ga_{0.47}As PIN photodiodes See Entry 76434

Radiation effects in CaWO₄ crystals See Entry 76498

Light-induced recombination centers during pulse radiolysis of an electrolyte-semiconductor system See Entry 77046

Luminescent properties of terbium-activated lanthanum oxyfluoride See Entry 77421

78.60K Thermoluminescence

77463 Thermoluminescence and optical absorption studies. Rubidium bromide doped with barium. S.B.S.Sastry, S.Nagarajan (Dept. of Phys., Indian Inst. of Technol., Madras, India). *Phys. Status Solidi b (Germany)*, vol.117, no.1, p.171-5 (1 May 1983). Thermoluminescence (TL) and optical absorption studies are made on RbBr:Ba²⁺. An absorption band due to Z₁-centres appears at 1.58 eV on F-light bleaching subsequent to γ-irradiation. A TL glow peak attributable to Z₁-centres is identified. TL emission under the main glow peak shows a broad emission at 2.65 eV with a shoulder at 1.95 eV. This 1.95 eV emission is attributed to V₃^M-centres which give rise to an absorption band around 4.1 eV. A tentative energy band scheme is suggested explaining the various TL processes. (15 refs.)

77464 On the mechanisms of thermoluminescence and deformation luminescence in gamma-irradiated KCl. R.Mayer, A.Winnacker (Phys. Inst., Univ. Heidelberg, Heidelberg, Germany). *Radiat. Eff. (GB)*, vol.64, no.1-4, p.135-41 (1982). [received: May 1983]. (Proceedings of the First International Conference on 'Radiation Effects in Insulators', Arco, Largo di Garda, Italy, 1981). Thermoluminescence (TL) and deformation luminescence (DL) studies in KCl γ-irradiated at room temperature are reported. The roles that F-centres and their higher conglomerates on the one hand, and V₂- and V₃-centres as recombination centres on the other hand, play in these processes are specified. Two peaks at 2.5 eV and 3 eV are observed in the emission spectra of both TL and DL. The close relationship between TL and DL is confirmed. (9 refs.)

77465 I. The emission spectra of TL produced by ion implanted CaF₂. U.Bangert, K.Thiel (Inst. fur Kernchemie, Univ. Koln, Koln, Germany), K.Ahmed, P.D.Townsend.

Radiat. Eff. (GB), vol.64, no.1-4, p.143-51 (1982). [received: May 1983]. (Proceedings of the First International Conference on 'Radiation Effects in Insulators', Arco, Largo di Garda, Italy, 1981). Rare earth doping of CaF₂ produces material which gives strong thermoluminescence signals. In an attempt to separate the influence of impurity and intrinsic defects CaF₂ has been implanted with ions of Ce, Dy, Mn, Ca and F. Comparisons are made with chemically doped samples and the effect of thermal treatments have been made in all cases. The cerium and dysprosium ions influence both the shallow charge trapping levels, which determine the temperature of the glow peaks, and the recombination sites which control the photon spectra. After implantation the strong TL signals show emission at wavelengths near 360 nm for Ce, 480 nm for Dy and for Mn. Re-excitation of the trapping levels reveals selective emission for some defects, restructuring of less stable defects and major changes in defect concentrations with thermal treatment. The effects of impurity and intrinsic defects on the spectra are discussed. One major observation is that addition of cerium to 'pure' samples does not enhance the TL sensitivity, whereas Dy and Mn both show new glow peaks. In the case of Dy it is thought that the charge trap and the luminescent site are directly linked within one complex defect. (13 refs.)

77466 II. Thermally induced changes in the TL of ion implanted CaF_2 . U.Bangert, K.Thiel (Inst. fur Kernchemie, Univ. Koln, Koln, Germany), K.Ahmed, P.D.Townsendm. *Radiat. Eff. (GB)*, vol.64, no.1-4, p.153-60 (1982). [received: May 1983] (Proceedings of the First International Conference on 'Radiation Effects in Insulators', Arco, Largo di Garda, Italy, 1981).
For pt.1 see *ibid.*, vol.64, p.143 (1982). Thermal treatment of CaF_2 has a significant influence on the number and intensity of the peaks seen by thermoluminescence. A combination of ion implants and anneal cycles leads to the conclusion that the 90°C glow peak is derived from a defect of a substitutional impurity (e.g. Ce^{+3}) linked to an interstitial fluorine ion. Perturbations of this centre by other defects modify the centre and the glow peak temperature is raised to 110°C. The peaks at 180, 220 and 350°C all involve intrinsic defect clusters. The building of models for the different glow peaks was helped by a comparison of impurity and self ion implantations. (15 refs.)
A new phosphor $\text{Li}_3\text{B}_2\text{O}_7\text{:Cu}$ for TLD See Entry 75198
On production of Zr^{3+} centres in NaCl:Sm^{2+} crystals See Entry 76423
Radiation damage in polyacrylonitrile See Entry 76499

78.60M Sonoluminescence, triboluminescence

On the mechanisms of thermoluminescence and deformation luminescence in gamma-irradiated KCl See Entry 77464

78.65 OPTICAL PROPERTIES OF THIN FILMS

77467 Selective properties of overcoated copper granular films. S.Damas-kinos, F.E.Girouard, Vo-Van Truong (Dept. of Phys., Univ. de Moncton, Moncton, New Brunswick, Canada). *Can. J. Phys. (Canada)*, vol.61, no.5, p.709-13 (May 1983).
Granular copper films were formed by thermal evaporation of copper onto glass substrates maintained at 300°C. They were subsequently overcoated at room temperature with a thick layer of aluminium having a thickness of ~100 nm. The optical properties of the overcoated films have been studied in the spectral region from 0.3 to 1.0 μm . Results indicated that the granular films preserved their aggregate structure even after overcoating. Successive annealings showed a considerable lowering of reflectivity over this spectral range and suggested the potential use of such a system of overcoated granular films for solar energy collection. (16 refs.)
77468 Electron-hole drops in vanadium dioxide. A.A.Bugaev, V.V.Gudyalis, B.P.Zakharichyena, F.A.Chudnovskii (A.F. Ioffe Physicotech. Inst., Acad. of Sci., Moscow, USSR). *JETP Lett. (USA)*, vol.36, no.10, p.440-2 (20 Nov. 1982). Translation of: *Pis'ma v Zh. Eksp. & Teor. Fiz. (USSR)*, vol.36, no.10, p.363-5 (20 Nov. 1982). [received: June 1983].
The detection of anisotropy in the coefficient of reflection, induced by picosecond excitation of a vanadium dioxide film with quantum energy 1.17 eV, is reported. The phenomenon is related to the formation of electron-hole drops. (4 refs.)
77469 The effect of particle size on the haze of polymer films. R.J.Tabar, C.T.Murray, R.S.Stein (Polymer Res. Inst., Univ. of Massachusetts, Amherst, MA, USA). *J. Polym. Sci. Polym. Phys. Ed. (USA)*, vol.21, no.5, p.831-3 (May 1983).
Haze in thin polymer films is discussed in terms of the scattering of unpolarized monochromatic light by a medium containing isotropic random inhomogeneities. It is shown that haze is not necessarily reduced by reducing the size of the inhomogeneities in the polymer film but that there is a critical size when the haze is at a maximum. (7 refs.)
77470 Refractive index of GaAs-AlAs superlattice grown by MBE. Y.Suzuki, H.Okamoto (Musashino Electrical Communication Lab., Nippon Telegraph & Telephone Public Corp., Musashino-shi, Tokyo, Japan). *J. Electron. Mater.* (USA), vol.12, no.2, p.397-411 (March 1983).
Refractive index \bar{n} of GaAs-AlAs superlattices grown by MBE is measured in the spectral range 1.2-1.8 eV at 300K. Results show that for superlattices with $L_B \leq 40-50 \text{ \AA}$, \bar{n} is determined by the averaged AlAs mole fraction, but that for superlattices with $L_B \geq 40-50 \text{ \AA}$, \bar{n} is determined by energy separation of confined electrons and holes (E_c - e - h). (10 refs.)
77471 Picosecond reflectivity measurements on glow discharge a-Si:H. H.Bergner (Sektion Phys., Friedrich-Schiller-Univ. Jena, Jena, Germany), V.Bruckner, D.Dietrich, F.Kerstn, W.Nowick. *Phys. Status Solidi b (Germany)*, vol.117, no.1, p.197-202 (1 May 1983).
The temporal behaviour of photoinduced charge carriers in amorphous hydrogenated silicon films is studied by means of time-resolved reflectivity measurements using a Nd:YAG laser. The investigated a-Si:H films, deposited by the glow discharge technique under systematic variation of the silane-hydrogen pressure, show different structures and defects. The temporal behaviour of the non-equilibrium charge carriers of all samples is determined by a two-step relaxation process. In accordance with the model the photoexcited carriers relax from the conduction band to an intermediate state in the mobility gap and then to the ground state. The characteristic times of these relaxation processes are 30 to 85 ps and 0.75 to 2.5 ns, respectively. The influence of the structure of the a-Si:H films on the relaxation times is discussed. (11 refs.)
77472 Polarized light absorption of the magnetic semiconductor CdCr_2Se_4 . I.S.Edelman, G.Dustmuradov, V.P.Kononov (L.V. Kirenski Inst. of Phys., Acad. of Sci., Krasnoyarsk, USSR). *Phys. Status Solidi b (Germany)*, vol.117, no.1, p.351-4 (1 May 1983).
The absorption of polarized light in CdCr_2Se_4 thin films in the spectral region 10000 to 22000 cm^{-1} at different temperatures is investigated. Through the whole spectral region the absorption intensity differs for right-handed and left-handed circularly polarized light or for parallel and perpendicular linearly polarized light. The character of the temperature and polarization dependence of the absorption intensity is different for different parts of the spectrum. The observed absorption is considered as a sum of the interband transitions and the transitions between localized states. (12 refs.)
77473 Faraday rotation in the exciton part of the spectrum of CuBr. Vo Hoang Thai, V.K.Miloslavskii, V.V.Mussil (A.M. Gorki State Univ., Kharkov, Ukrainian SSR). *Sov. Phys.-Solid State (USA)*, vol.24, no.11, p.1859-60 (Nov. 1982). Translation of: *Fiz. Tverd. Tela (USSR)*, vol.24, no.11, p.3276-8 (Nov. 1982). [received: May 1983].
Thin epitaxial CuBr films grown on NaCl crystalline substrates with the $100\text{NaCl}||100\text{CuBr}$ orientation were used in a study of the absorption spectra and of the Faraday rotation. The difference between the thermal expansion coefficients of NaCl and CuBr (39×10^{-6} and $19 \times 10^{-6} \text{ K}^{-1}$) and the temperatures at which the samples were prepared (420K) and measured (90K) gave rise to thermal stresses in the CuBr film

and these split at low-frequency exciton peak $z_{1,2}$ ($\Gamma_8 \times \Gamma_6$, 1s exciton) into two components: $z_1(\Gamma_6 \times \Gamma_6$, 1s, wave vector group D_{2d}) and $z_2(\Gamma_7 \times \Gamma_6$, 1s). A comparison and analysis of the experimental data on the spectral dependences of the angle of rotation of the plane of polarization in a magnetic field $H=2 \text{ T}$ and of the optical density $D(E)$ with the exciton bands approximated by Lorentzian profiles was used to determine the g factors of the z_1 , z_2 , and z_3 peaks, which were $g_1=-0.34 \pm 0.05$, $g_2=1.14 \pm 0.1$, and $g_3=1.02 \pm 0.11$, as well as their oscillator strengths (2.08×10^{-2} , 1.02×10^{-2} , and 1.34×10^{-2} per unit cell). The method of invariants was used to show that, under the simultaneous action of a magnetic field and thermal stresses, the g factors g_1 and g_2 were related to the electron g factor g_e and to the hole factor $2\bar{x}$ by $g_1=-g_e-6\bar{x}$ and $g_2=g_e-2\bar{x}$ subject to the condition $\Delta \gg \Delta_{\text{exch}}$, where Δ is the energy of splitting due to thermal stresses and Δ_{exch} is the exchange interaction energy. The values of the band g factors were found to be $g_e=0.94 \pm 0.08$ and $\bar{x}=-0.1 \pm 0.02$. (6 refs.)
77474 Thermal modulation spectrum and electron structure of niobium. A.I.Golovashkin, A.L.Shelekhov (P.N. Lebedev Phys. Inst., Acad. of Sci., Moscow, USSR). *Sov. Phys.-Solid State (USA)*, vol.24, no.11, p.1897-9 (Nov. 1982). Translation of: *Fiz. Tverd. Tela (USSR)*, vol.24, no.11, p.3339-43 (Nov. 1982). [received: May 1983].
Spectra of the thermal modulation of the reflection coefficient $\beta=d(\ln R)/dT$ of niobium were recorded in the range 0.5-3.1 eV. The method of least squares was applied to the thermal modulation spectra and this yielded the most important electronic characteristics of Nb: the Fourier components of the pseudopotential, the collision frequencies and densities of electrons participating in interband transitions, as well as the densities and collision frequencies of conduction electrons. The observed changes in the thermal modulation spectra of Nb due to a deterioration of the quality of the samples were attributed to the broadening of a peak of the density of electron states near the Fermi energy on a reduction in the mean free path of electrons. (12 refs.)
Spectrum studies on a GaAs-AlGaAs multi-quantum-well laser diode grown by molecular beam epitaxy See Entry 75690
Residual donors and acceptors in high-purity GaAs and InP grown by hydride VPE See Entry 76883
Electrical and optical properties of SnO_2 thin layers received using the method of oxidation of thermally vapoured Sn layers See Entry 77073
Photoelectric fatigue of photoresistors based on polycrystalline CdS:Cu:Cl films See Entry 77075
Preparation, physical properties, and superconductivity of $\text{La}_{1-x}\text{S}_4$ films See Entry 77085
ODMR investigation of recombination processes in a-Si $_x\text{C}_{1-x}\text{H}$ See Entry 77292
Temperature dependence of the refractive index of amorphous As_2S_3 and As_2Se_3 films near 300K See Entry 77352
Measuring the magnetooptic Kerr effect by diffraction See Entry 77367
Raman microprobe study of recrystallization in ion-implanted and laser-annealed polycrystalline silicon See Entry 77374
Raman spectra and physical structure of cellulose triacetate See Entry 77388
Quantization of photo-excited carriers in GaAs doping superlattices See Entry 77395
Photoluminescence of molecular beam epitaxially grown Ge-doped GaAs See Entry 77431
Photoluminescent and electrical properties of InGaPAs mixed crystals liquid-phase-epitaxially grown on (100) GaAs See Entry 77432
Electric field-induced quenching of luminescence in quantum wells See Entry 77445
Extrinsic photoluminescence from GaAs quantum wells See Entry 77446
Impurity photoluminescence in GaAs/ $\text{Ga}_{1-x}\text{Al}_x$ As multiple quantum wells See Entry 77447
Time resolved luminescence in n-i-p-i doping superlattices See Entry 77448
Zero-phonon lines in electroluminescence and photoluminescence of ZnS:Mn thin films grown by atomic layer epitaxy See Entry 77459
Structural and optical properties of sprayed CuInSe_2 films See Entry 77564
Production methods and properties of diamond-like carbon films See Entry 77566
MOCVD growth and characterization of high luminescence efficiency $\text{Al}_x\text{Ga}_{1-x}\text{As}$ See Entry 77583
Hydrogen pretreatment of CdS films and properties of CdS/NaOH/Pt cells See Entry 78089
Ge-Al thin films for selective solar absorbers See Entry 78099

78.70 OTHER INTERACTIONS OF MATTER WITH PARTICLES AND RADIATION

77475 Comments on the bremsstrahlung cross section formula using exact electron-distorted wave functions. J.Asai (Accelerator Lab., Univ. of Saskatchewan, Saskatoon, Saskatchewan, Canada), H.Ogata. *Z. Phys. A (Germany)*, vol.311, no.4, p.281-2 (1983).
Rozics and Johnson's formula is examined and its inconsistency is pointed out. (5 refs.)
The influence of the planar potential form on the channelling radiation spectrum See Entry 76529
Electromagnetic radiation of quasicchannelling positrons See Entry 76530
Undulator radiation of relativistic electrons in a polydomain ferromagnetic See Entry 76531
Molecular-type channeling of relativistic electrons in crystals See Entry 76535

78.70B Positron annihilation
(see also 71.65 Positron states)

77476 Study of positron lifetimes in α , β and γ cerium at high pressures. A.M.Boring, C.-Y.Huang (Los Alamos Nat. Lab., Los Alamos, NM, USA), K.A.Gschneidner, Jr., J.D.McGervey, M.Panigrahi, S.G.Umar. *J. Magn. & Magn. Mater. (Netherlands)*, vol.37, no.1, p.L7-10 (May 1983).
The positron lifetimes in the α , β and γ phases of Ce have been measured by applying hydrostatic pressure (up to 1.4 GPa) and by reducing the temperature (to 80K). Two-component fitting programs showed that the main com-

ponent ($\approx 90\%$) had virtually the same mean lifetime (≈ 233 ps) in all three phases. The uncertainty in each lifetime was ± 2 ps. With this high precision, the results are in agreement with those of band calculations which give the same number of 4f electrons (≈ 1.2) in all phases. (26 refs.)

77477 Positron annihilation on pure and carbon-doped α -iron in thermal equilibrium. L. De Schepper (Materials Phys. Group, Limburgs Univ. Centrum, Diepenbeek, Belgium), D. Segers, L. Dorikens-Vanpraet, M. Dorikens, G. Knuyt, L. M. Stals, P. Moser.

Phys. Rev. B (USA), vol. 27, no. 9, p. 5257-69 (1 May 1983).

Positron-annihilation S-parameter measurements in thermal equilibrium on pure and carbon-doped (50 and 750 at. ppm) α -iron are presented. It is shown that trapping of positrons on both monovacancies and carbon-vacancy pairs occurs, even far above the dissociation temperature of the vacancy pairs. Therefore, a three-state trapping model is used in the analysis of the measured S curves. The vacancy-formation enthalpy in both the paramagnetic and ferromagnetic state is deduced: It is found to be 1.79 ± 0.10 eV in the paramagnetic state and 2.0 ± 0.2 eV in the ferromagnetic state. These values are larger than those published so far. The activation enthalpy for vacancy migration obtained by combining the values cited above with recently published self-diffusion enthalpy values confirms the applicability of the one-interstitial model in α -iron. (47 refs.)

The inhomogeneity effect in the vacancy-dislocation interaction for α -iron See Entry 76483

Positron-annihilation measurements of the Fermi surface of copper-base solid solutions with gallium, germanium, and nickel See Entry 76833

Temperature effects on positronium formation and inhibition: a contribution to the elucidation of early spur processes. IV. Methanol and ethanol solutions See Entry 77913

78.70C X-ray scattering

Intensity of X-rays scattered by layered structures with short-range order factors $S \geq 1$, $G \geq 1$ See Entry 76246

78.70D X-ray absorption and absorption edges

77478 X-ray spectroscopic study of ternary chalcopyrite semiconductors of the type CuMS_2 ($M = \text{Al, Ga, In, Tl}$). A. P. Deshpande, V. B. Sapre, C. Mande (Dept. of Phys., Nagpur Univ. Campus, Nagpur, India).

J. Phys. C (GB), vol. 16, no. 13, p. L433-5 (10 May 1983).

The chemical shifts of the K absorption discontinuity of copper have been studied in the ternary chalcopyrite compounds CuMS_2 ($M = \text{Al, Ga, In, Tl}$). It is observed that there exists a linear relationship between the chemical shift ΔE and the band gap E_g in the systems. This relationship has been used to estimate the band gap in the compound CuTiS_2 , which comes out to be about 1.39 eV. (11 refs.)

77479 Amorphous problem in EXAFS data analysis. A. L. Ageev, Yu. A. Babanov, V. V. Vasin, N. V. Ershov, A. V. Serikov (Ural Sci. Centre, Acad. of Sci., Sverdlovsk, USSR).

Phys. Status Solidi b (Germany), vol. 117, no. 1, p. 345-50 (1 May 1983).

It is shown that the radial atomic distribution function for disordered systems can, in principle, be determined from the oscillating extended fine structure of X-ray absorption spectra using the regular algorithms of solution of incorrect problems. The radial atomic distribution function for $\text{Fe}_{50}\text{B}_{50}$, obtained from experimental EXAFS data and corresponding to the results of diffraction studies, is presented. (14 refs.)

77480 X-ray K-absorption fine structure study of $\text{Cu}_x\text{Zn}_{1-x}\text{Fe}_2\text{O}_4$ ($x = 0.2, 0.4, 0.6$ and 0.8). V. Sahasrabudhe (Dept. of Phys., Shivaji Univ., Kolhapur, India).

Solid State Commun. (USA), vol. 46, no. 9, p. 697-703 (June 1983).

For $\text{Cu}_x\text{Zn}_{1-x}\text{Fe}_2\text{O}_4$ spinel ferrites ($x = 0.2, 0.4, 0.6$ and 0.8), EXAFS of Cu and Fe K-absorption edges have been studied employing LSS theory. With change in copper content, in the spinel system, the basic dependence of cation distribution on degree of inversion has been reported by plotting variation of bond distance 'd' with EXAFS parameter 'a'. This is further substantiated by plotting chemical shifts (ΔE) with EXAFS parameter 'a'. The necessity of the determination of final state wavefunction for the knowledge of distribution of charge is stressed. (20 refs.)

77481 Absorption of unsupported photo resist films using synchrotron radiation in the region from 4.5 nm to 30 nm. R. J. Howe, D. M. Shinozaki, J. W. McGowan (Univ. of Western Ontario, London, Ontario, Canada).

Fifteenth Annual Synchrotron Radiation Users Group Conference (papers in summary form only received), Stoughton, WI, USA, 18-19 Oct. 1982 (Stoughton, WI, USA: Synchrotron Radiat. Center 1982), p. 26

The linear absorption coefficients for resist materials polymethyl-methacrylate (PMMA), poly(butene-1-sulfone) (PBS), phenylvinyl ketone (PVK), poly(methyl isopropenyl ketone) (PMIPK), tert butyl vinyl ketone (TBVK) and Kodak negative resist K747 have been calculated from measured $\mu \times$ graphs. Graphs obtained are collected from information of the incident intensity and transmitted intensity through each sample using a well collimated photon beam produced from the 'Tantalus' storage ring. Irradiation damage was also performed on several samples and produced differences in the $\mu \times$ graphs demonstrating various damage modes. For example, some of the samples show discrete mass loss behavior while others demonstrate absorption changes with mass loss. (no refs.)

X-ray L_{III} absorption spectroscopy of europium in intermetallics of the EuM_2Si_2 type See Entry 76903

78.70E X-ray emission threshold and fluorescence

77482 Soft X-ray emission spectra of aluminium in β -phase Cu-Ni-Al and Cu-Mn-Al alloys. K. Tanaka, T. Saito, M. Yasuda (Dept. of Metall. Engng., Nagoya Inst. of Technol., Nagoya, Japan).

J. Phys. Soc. Jpn. (Japan), vol. 52, no. 5, p. 1718-24 (May 1983).

Electronic states associated with aluminium atoms in ternary Cu-Ni-Al and Cu-Mn-Al alloys with B2 and L2₁ order structures, respectively, were investigated by measuring Al K β emission spectra. The spectra generally consisted of three peaks which changed in strength and in energy (Cu-Mn-Al) systematically with compositions. The lower two peaks were assigned to bonding states of aluminium 3p electrons hybridizing with the 3d states of copper and nickel or manganese atoms. These assignments were consistent with a CPA model calculation on the K emission spectra of transition-transition and transition-simple metal alloys by Kudrnovsky et al.

Local partial DOS and experimental Al K spectra of transition metal aluminides. Charge transfer trend See Entry 76870

The relative importance of multiple inelastic scattering in the quantification of EELS See Entry 77490

78.70G Microwave and radiofrequency interactions (exc. resonances)

Dielectric relaxation and dipole moment measurements of *n*-methylacetamide in benzene and dioxane solutions at different temperatures from microwave absorption studies See Entry 77325

78.90 OTHER TOPICS IN OPTICAL PROPERTIES OF CONDENSED MATTER AND OTHER INTERACTIONS OF MATTER WITH PARTICLES AND RADIATION

77483 Channeling of light in a medium with a periodically varying refractive index. O. V. Konstantinov, I. A. Shmulevich (A. F. Ioffe Physicotech. Inst., Acad. of Sci., Leningrad, USSR).

Sov. Phys-Solid State (USA), vol. 24, no. 11, p. 1817-21 (Nov. 1982). Translation of: *Fiz. Tverd. Tela (USSR)*, vol. 24, no. 11, p. 3201-9 (Nov. 1982). [received: May 1983]

It is shown that in the propagation of light along the layers of a three-dimensional phase grating the optical field becomes localized in regions having a high refractive index. This effect is analogous to the channeling of fast electrons in single crystals. The localization is analyzed both numerically and by means of an approximate analytical solution of the wave equation that is a generalization of the well known Raman-Nath solution, the latter does not predict any localization. The effect occurs only when the light wavelength λ is much less than the lattice period $d \propto \sqrt{u_1/2}$, where u_1 is the amplitude of sinusoidal modulation of the refractive index. In that case, it can be regarded as the result of light focusing by a converging lens with a distributed variation of the refractive index. The occurrence of strong focusing at a distance $f = d/4\sqrt{u_1}$ is predicted. Ordinary channeling occurs at distances exceeding f . (19 refs.)

79.00 ELECTRON AND ION EMISSION BY LIQUIDS AND SOLIDS; IMPACT PHENOMENA

79.20 IMPACT PHENOMENA

(inc. electron spectra and sputtering)

77484 Angular distribution of particles escaping at low angles to the surface of a medium as a function of the depth of location of the plane source within the material. V. S. Remizovich (Engng.-Phys. Inst., Moscow, USSR).

Sov. Phys-Dokl. (USA), vol. 27, no. 8, p. 621-3 (Aug. 1982). Translation of: *Dokl. Akad. Nauk SSSR*, vol. 265, no. 4-6, p. 863-7 (Aug. 1982). [received: May 1983]

The problem of calculating the angular and energy distributions of particles reflected in 'glancing' incidence is a particular case of the more general problem of calculating the spectrum of particles escaping from a medium when a plane source emitting particles at a low angle to its plane is present with the material. An analytical expression is obtained for the angular spectrum of escaping particles in the case of purely elastic scattering when a plane source is present within the material. (8 refs.)

79.20D Laser-light impact phenomena

77485 Comments on 'Laser excitation of surface electronic states for a one-dimensional semiconductor' by W. C. Murphy and T. F. George. G. W. Bryant (McDonnell Douglas Res. Labs., St. Louis, MO, USA).

Surf. Sci. (Netherlands), vol. 127, no. 3, p. L149-55 (May 1983).

For original paper see ibid., vol. 114, p. 189 (1982). Murphy and George calculated the optical absorption cross section for the transfer of electrons from valence states to localized surface states in a semiconductor modeled by a finite one-dimensional chain. They suggested that by using a laser to excite electrons to or from the surface states, one can control the surface charge and the electrostatic force between the surface and an adsorbed species. The present author corrects several important errors in their presentation and indicate how their conclusions must be modified. (4 refs.)

77486 Reply to comments on 'Laser excitation of surface electronic states for a one-dimensional semiconductor' by G. W. Bryant. W. C. Murphy, K. T. Lee, T. F. George (Dept. of Chem., Univ. of Rochester, Rochester, NY, USA).

Surf. Sci. (Netherlands), vol. 127, no. 3, p. L156-8 (May 1983).

For original paper see ibid., vol. 114, p. 189 (1982). For comments see ibid., vol. 127, p. L149 (1983). A semiconductor modeled by a finite one-dimensional chain is shown to have either a continuous or discrete number of surface states. The exact number is determined by the choice of phase factors. Laser-induced charge transfer of electrons from the bulk to these surface states is also shown to be a maximum at the band edge. (5 refs.)

77487 Laser formation of a 'cold liquid'. A. B. Gerasimov, I. A. Gogoladze, A. A. Tsertsvadze.

Sov. Tech. Phys. Lett. (USA), vol. 8, no. 9, p. 444-5 (Sept. 1982). Translation of: *Pis'ma v Zh. Tekh. Fiz. (USSR)*, vol. 8, no. 17-18, p. 1032-5 (Sept. 1982). [received: May 1983]

The authors examine the thermodynamics of the formation of a cold liquid. They consider the melting of a sample as it absorbs a laser beam. They assume that the photon energy satisfies $\epsilon_0 \approx \Delta E$, where ΔE is the energy gap of the amorphous substance; in other words, an electron is transferred from the valence band to the bottom of the conduction band. This process is accompanied by an increase in the potential energy of the solid phase. (4 refs.)

Periodic structure formed during the action of high-power coherent radiation on a semiconductor surface See Entry 76495

Observation of superstructure formation on Rh(001) by laser-pulse assisted field evaporation See Entry 76761

- Synthesis of cellular amorphous films on the surfaces of alloys with a periodic-pulse CO₂ laser See Entry 76762
- Effect of a static field on the parameters of a superlattice created in a semiconductor by a standing laser wave See Entry 77041
- Formation of lattice defects in CdS crystals by nitrogen laser radiation See Entry 77450

79.20F Electron impact: Auger emission

- 77488** Comment on 'Spin-polarized Auger spectroscopy from magnetically ordered solids'. G.Zajac, J.Zak, S.D.Bader (Argonne Nat. Lab., Argonne, IL, USA). *Phys. Rev. Lett. (USA)*, vol.50, no.21, p.1713 (23 May 1983). For original paper see M. Landolt and D. Mauri, *ibid.*, vol.49, p.1783 (1982). Landolt and Mauri have demonstrated the importance of spin-polarized Auger spectroscopy in opening up new perspectives in the study of magnetic solids. They detected a strongly polarized satellite of unknown origin, above the Fe $M_{2,3}VV$ transition, that had no visible counterpart in the intensity spectrum. The present authors identify this satellite as being due to autoionization emission corresponding to the resonant 3p-to-3d transition, and report its observation in the unpolarized intensity spectrum of polycrystalline Fe. Since this process is the electron-stimulated analog of resonant photoemission, it is of interest in providing new insights also into the role of many-body effects in electron spectroscopies. (7 refs.)
- Matrix effect and surface oxidation in depth profiling of Al_{1-x}Ga_xAs by secondary ion mass spectrometry using O₂⁺ primary ions See Entry 76479
- Measuring the density distribution of a charged impurity in thin silicon films by electron reflection See Entry 76480
- Electron and ion beam effects in Auger electron spectrometry See Entry 76514
- The formation of a surface iodide on Ni[100] and adsorption of I₂ at low temperatures See Entry 76789
- The temperature dependence of the interaction of oxygen with Pd(111); a study by photoemission and Auger spectroscopy See Entry 76790
- A LEED-AES study of the structure of sulfur monolayers on the Mo(100) crystal face See Entry 76791
- The role of sulfur in oxygen adsorption on niobium See Entry 76792
- Auger and AC impedance studies of the RF sputter deposited Fe₂O₃ films See Entry 76810
- A new method for determining relaxation energies by means of AES and XPS and its application to silicon compounds See Entry 77520

79.20H Electron impact: secondary emission

- 77489** Electron backscattering at various angles of incidence. H. J. Fitting, R. Technow (Sektion Phys., Wilhelm-Pieck-Univ. Rostock, Rostock, Germany). *Phys. Status Solidi a (Germany)*, vol.76, no.2, p.K151-4 (16 April 1983). The authors have tried to find a simple empirical expression including as the only parameter the integral backscattering ratio η_0 at normal incidence. Similarly they were successful in describing the electron penetration, the energy depth transfer, and the energy distribution of backscattering and transmitted electrons. (14 refs.)

79.20K Other electron impact phenomena

- 77490** The relative importance of multiple inelastic scattering in the quantification of EELS. A.J.Bourdillon, D.J.Hall, C.J.Morrison, W.M.Stobbs (Dept. of Metall. & Materials Sci., Cambridge Univ., Cambridge, England). *J. Microsc. (GB)*, vol.130, pt.2, p.177-86 (May 1983). (MICRO 82: High Resolution Electron Microscopy, London, England, 12-16 July 1982). A comparison is given of energy loss results obtained for the L and K edges of aluminium as a function of specimen thickness, crystallographic orientation and collection angle. It is demonstrated that as the thickness is increased post-loss elastic scattering is generally important in reducing the fraction of electrons collected. The implications for the quantification of EELS data are discussed while a comparison of the Fe/C ratio in cementite demonstrates the improved consistency which can be obtained when comparing K and L losses at lower energy separation than are the losses for aluminium. (19 refs.)
- 77491** Retrieval of single-loss profiles from energy-loss spectra. A new approach. P.Schattschneider (Inst. of Appl. & Tech. Phys., Tech. Univ. Vienna, Vienna, Austria). *Philos. Mag. B (GB)*, vol.47, no.5, p.555-60 (May 1983). A new method to recover the single-loss probability p_1 from an electron-energy loss spectrum, taken in transmission, is presented. Previously used methods are either limited to specimens not exceeding a thickness of one mean free path length, or afford data-sampling over much more of an extended energy interval than one is interested in. The new method exhibits neither of these shortcomings. Assuming that no energy-gain processes take place, all spectra involved are redefined in terms of triangular matrices. Based upon the Poisson distribution for multiple scattering, a series expansion for the matrix corresponding to p_1 is then derived. The series is shown to converge for any finite thickness of the specimen. (11 refs.)
- 77492** Inelastic electron scattering from small metal spheres. P.C.Das, J.I.Gersten (Dept. of Phys., City Coll., City Univ. of New York, New York, NY, USA). *Phys. Rev. B (USA)*, vol.27, no.9, p.5412-18 (1 May 1983). Inelastic electron scattering from isolated metal spheres is considered. Expressions for the scattering cross section and for radiative scattering are derived. The only energy-loss mechanism studied here is due to local plasma-oscillation excitation. (4 refs.)
- 77493** Multiplet effects and breakdown of dipole selection rules in the 3d-4f core-electron-energy-loss spectra of La, Ce, and Gd. J.A.D.Matthew (Dept. of Phys., Univ. of York, Heslington, England), G.Strasser, F.P.Netzer. *Phys. Rev. B (USA)*, vol.27, no.9, p.5839-41 (1 May 1983). Electron-energy-loss spectra of La, Ce, and Gd in the region of the 3d¹⁰4fⁿ-3d⁹4fⁿ⁺¹ excitations show doublet structures associated with each spin-orbit component. The relative intensities of the structures vary systematically with excitation energy, the lower-energy component being emphasized at lower primary energies. The effects are interpreted in terms of the multiplet structure of the final state coupled to progressive breakdown of optical selection rules with decreasing energy of the exciting beam. (10 refs.)

- 77494** Variation of the characteristic electron energy loss spectra of molybdenum, doped with Ba⁺ ions. B.Ye.Umirzakov, M.T.Normuradov, A.Kh.Kasymov. *Radio Eng. & Electron. Phys. (USA)*, vol.27, no.6, p.151-3 (June 1982). Translation of: *Radiotekh. & Elektron. (USSR)*, vol.27, no.6, p.1237-9 (June 1982). [received: May 1983] Presents the results of a study of the variation of the electron energy loss spectra (EELS) of Mo for the cases of doping with Ba⁺ ions and adsorption of Ba atoms. (9 refs.)
- 77495** A new scattering mechanism for EELS. W.L.Schaich (Phys. Dept., Indiana Univ., Bloomington, IN, USA). *Surf. Sci. (Netherlands)*, vol.127, no.3, p.L145-8 (May 1983). Estimates the efficiency of a new mechanism for the scattering of slow electrons by vibrations at a metal surface. The coupling is long ranged but its scattering characteristics resemble more those of impact rather than those of dipole scattering. This similarity applies to both angular dependence and overall strength. (9 refs.)
- 77496** Multiple scattering of relativistic particles in crystals. N.F.Shul'ga, V.I.Truten', S.P.Fomin (Physicotech. Inst., Acad. of Sci., Kharkov, Ukrainian SSR). *Sov. Phys.-Tech. Phys. (USA)*, vol.27, no.11, p.1399-400 (Nov. 1982). Translation of: *Zh. Tekh. Fiz. (USSR)*, vol.52, no.11, p.2279-80 (Nov. 1982). [received: May 1983] The authors address a new and important feature of fast particle scattering in crystals, i.e. in crystals without channeling the mean square of the scattering angle of a relativistic particle may greatly exceed the mean square scattering angle in amorphous materials. This difference is a result of correlations between successive collisions of the particles with atoms in the lattice and is strongly dependent on the angle between the crystallographic axes and the momentum vector of the incoming particles, the particle energy, and the crystal thickness. (9 refs.)
- 77497** Energy loss measurements on Co₅Sm thin films. P.Schattschneider, J.Fidler, V.Chopov (Inst. für Angewandte und Tech. Phys., Tech. Univ. Wien, Wien, Germany). *Vak.-Tech. (Germany)*, vol.32, no.3, p.75-80 (April 1983). In German. Energy loss measurements on Co₅Sm thin films performed in a transmission setup reveal a broad, atypical plasmon at 15 eV and faint structure at about 5 eV. The latter is shown to disappear with decreasing grain size and is assumed to correspond to a transition in which (s,d)-hybridized states are involved. Wave number resolved measurements demonstrate that the plasmon peak disperses negatively, in contrast to the usual NFE plasmon behaviour. In order to explain this anomaly it is tentatively proposed that there exists a near lying interband transition, into which the plasmon is hybridized. (18 refs.)
- Measuring the density distribution of a charged impurity in thin silicon films by electron reflection See Entry 76480
- Experimental energy-loss function, $\text{Im}[-1/\epsilon(q,\omega)]$, for aluminium See Entry 76537
- Vibrational interaction between hydrogen atoms adsorbed on Pd(100) See Entry 76766
- Determination of the molecular symmetry of acetylene on Ni(001) by electron-impact scattering See Entry 76782
- ## 79.20N Atom, molecule, and ion impact
- 77498** Scattering and surface recoiling TOF spectra of neutrals and ions from rare gas bombardment of Ge, GeO₂, and H₂O adsorbed on Ge. R.Kumar, J.A.Schultz, J.W.Rabalais (Dept. of Chem., Univ. of Houston, Houston, TX, USA). *Chem. Phys. Lett. (Netherlands)*, vol.97, no.3, p.256-60 (20 May 1983). TOF spectra of scattered primary and surface recoiled neutrals and ions for He⁺, Ne⁺, and Ar⁺ bombardment of Ge, GeO₂, and H₂O adsorbed on Ge are presented. Ion fractions are determined for scattered and recoiled particles and the role of scattering cross sections and surface charging effects on detection of recoiling hydrogen are considered. (18 refs.)
- 77499** Charge state-dependent effects in electronic sputtering by fast ions. N.E.B.Corn (Nuclear Phys. Div., AERE Harwell, Didcot, England). *Radiat. Eff. Lett. Sect. (GB)*, vol.76, no.1-2, p.1-6 (1983). Reported yields of ejecta sputtered from dielectric and organic materials by MeV/amu O and F ions show a strong dependence on the incident ion charge state. These observations are consistent with a (dE/dx)²-dependence of sputtering yield, provided that proper account is taken of the charge-state equilibration process as the ion beam enters the solid. From a knowledge of this process, an effective interaction depth for the coupling of electronic excitation to prompt sputtering is inferred to be ≤ 6 nm for the case of 1.24 MeV/amu O incident on glycylglycine. A somewhat smaller depth is inferred for uranium sputtered by 1 MeV/amu F incident on UF₄. (12 refs.)
- 77500** Computer simulation of the self-sputtering of uranium. M.T.Robinson (Solid State Div., Oak Ridge Nat. Lab., Oak Ridge, TN, USA). *J. Appl. Phys. (USA)*, vol.54, no.5, p.2650-9 (May 1983). The sputtering of polycrystalline α -uranium by uranium ions of energies below 10 keV has been studied in the binary collision approximation using the computer simulation program MARLOWE. Satisfactory agreement of the computed sputtering yields with the small amount of available experimental data was achieved using the Moliere interatomic potential, a semilocal inelastic loss function, and a planar surface binding barrier, all with conventional parameters. The model is used to discuss low energy sputtering processes and the energy and angular distributions of the reflected primaries and the sputtered target particles. (27 refs.)
- 77501** Energy dependence of the sputtering yield of silicon bombarded with neon, argon, krypton, and xenon ions. P.C.Zalm (Philips Res. Labs., Eindhoven, Netherlands). *J. Appl. Phys. (USA)*, vol.54, no.5, p.2660-6 (May 1983). Sputtering yields of Si were determined for bombardment with Ne, Ar, Kr, and Xe ions at normal incidence in the energy range 0.2-20 keV under ultrahigh vacuum conditions ($<10^{-7}$ Pa). Mass selection was employed and the energy spread was limited to a few electron volts. High fluences in excess of 10^{18} cm⁻² were used to obtain stationary state yields. A special method was adopted for the yield determination, involving accurate current integration and eroded crater volume measurement with a micromechanical stylus. As a spinoff of the adopted technique, relative sputtering yields for Mo could also be determined. The data agree with the sparse other recent experimental results. Discrepancies with older data sets are sizeable but can be attributed to improved beam definition and better surface conditions. The measured yields are, even quantitatively, in surprisingly good agreement with predictions from Sigmund's (1969) linear cascade theory in the low and intermediate energy range. At higher energy the yields fall off more rapidly than the

theory predicts, the deviations increasing with decreasing projectile mass. This behavior cannot be explained entirely in terms of the parameters and assumptions entering the Sigmund model. Various proposed empirical modifications and alternatives for Sigmund's theory are critically examined and a new quite useful simplification of the latter is derived. (24 refs.)

77502 Ion knock-on broadening effects in Auger sputter profiling studies of ultra-thin SiO_2 layers on Si. M.A.Taubenblatt, C.R.Helms (Dept. of Electrical Engng., Stanford Univ., Stanford, CA, USA).

J. Appl. Phys. (USA), vol.54, no.5, p.2667-71 (May 1983).
Ultrathin layers of SiO_2 on Si (less than ~ 100 to 200 \AA) show a reduction in the measured width of the Si- SiO_2 interface when profiled using ion sputtering. Although previously attributed to the intrinsic properties of thin oxides or surface roughening due to ion-beam etching, this effect is predominantly caused by ion knock-on broadening or knock-on enhanced diffusion. It is important to realize that this effect is an artifact of the sputtering process, and not a property of the system under study. A model is developed based on the spatial distribution of the energy deposited by the sputtering ions to explain the observed reduction in measured interface width. This model is compared with interface widths obtained using Auger electron spectroscopy from identically grown thermal SiO_2 samples which have been thinned by chemical etching to eliminate oxidation kinetic effects. (13 refs.)

77503 Energy redistribution among internal states of nitric oxide molecules upon scattering from Pt(111) crystal surface. M.Asscher, W.L.Guthrie, T.-H.Lin, G.A.Somorjai (Dept. of Chem., Univ. of California, Berkeley, CA, USA).

J. Chem. Phys. (USA), vol.78, no.11, p.6992-7004 (1 June 1983).
The internal states distributions rotation and vibration of nitric oxide molecules scattered from the Pt(111) crystal surface are reported. These distributions were measured as a function of crystal temperature (T_s) and scattering angles. The extent of equilibration of the three degrees of freedom, e.g. translation, rotation, and vibration with the metal surface is discussed in terms of the energy accommodation coefficients γ . It was found that $\gamma_{\text{trans}} > \gamma_{\text{vib}} < \gamma_{\text{rot}}$. A model is suggested to account for the cold rotational distribution of molecules scattered via a trapping desorption mechanism. The vibrational distributions are determined by kinetic effects and by the competition between vibrational excitation of the adsorbed molecules and their desorption. (31 refs.)

77504 Energy distribution of sputtered metastable Ca atoms. W.Husinsky, G.Betz, I.Girgis (Inst. für Allgemeine Phys., Tech. Univ. Wien, Wien, Austria).

Phys. Rev. Lett. (USA), vol.50, no.21, p.1689-92 (23 May 1983).
The energy distribution of sputtered metastable Ca atoms in the 3P_2 sublevel of the lowest-lying triplet state has been measured by Doppler-shift laser-fluorescence spectroscopy. The energy distribution was found to peak at values higher than known for sputtered ground-state atoms. No threshold energy has been found. With increasing oxygen partial pressure the flux of sputtered metastable atoms increased by an order of magnitude; however, the shape of the energy distribution remained unchanged. (26 refs.)

77505 Fundamental problems of the interaction of ions with insulators.

U.Littmark, K.Rössler (Inst. für Grenzflächenforschung und Vakuumphys., KFA Jülich GmbH, Jülich, Germany).
Radiat. Eff. (GB), vol.64, no.1-4, p.49 (1982). [received: May 1983]
(Proceedings of the First International Conference on 'Radiation Effects in Insulators', Arco, Largo di Garda, Italy, 1981).
Summary form only given, as follows. The special situation of insulators necessitates a discussion as to whether the classical collision theory which had mainly been developed for metallic systems still holds in ionic or covalently bound solids. Special problems which should be treated are: (a) changes in the interaction potentials due to the localization of electrons of the target atoms, (b) the influence of charge states of the projectiles, which due to slower neutralization processes, might be higher on the average in insulators than in metals, (c) the effect of specific structure, multielemental composition on the trajectories ('focusing'), (d) the importance of covalent binding of the molecular units, and (e) the energy loss via chemical interactions by formation of stable bonds at low kinetic energies and transient ones at higher energies ('chemical stopping'). These problems are treated by a comparison of experimental results with theory and computer simulation of collision cascades. (no refs.)

77506 Chemical sputtering, a discussion of mechanisms. H.F.Winters (IBM Res. Lab., San Jose, CA, USA).

Radiat. Eff. (GB), vol.64, no.1-4, p.79 (1982). [received: May 1983]
(Proceedings of the First International Conference on 'Radiation Effects in Insulators', Arco, Largo di Garda, Italy, 1981).
Summary form only given. The authors review the evidence for chemical sputtering and discuss mechanisms based on experimental information obtained for the chemical sputtering of silicon and SiO_2 under argon ion bombardment in the presence of a molecular beam of XeF_2 . Under these conditions, 25 or more silicon atoms can leave the surface per incident argon ion. About 75% of the silicon is emitted as SiF_4 (gas) and the rest leaves as silicon atoms or SiF_3 radicals. The total yield (silicon plus fluorine) is greater than 100 atoms/ion. The measured yields are a strong function of XeF_2 flux and a much weaker function of ion energy in the range 500-5000 eV. The chemical-sputtering yield for SiO_2 is smaller than that of silicon by about an order of magnitude, but it is still larger than the physical-sputtering yield. Moreover, SiO_2 is also sputtered by electrons. These results indicate that the incident radiation induces a chemical reaction between silicon and absorbed fluorine which produces SiF_4 , and the SiF_3 is subsequently desorbed into the gas phase. This process is defined as chemical sputtering. The large yields are probably a consequence of weak binding between the surface and the SiF_4 molecule. (no refs.)

77507 Sputtering of condensed noble gases by keV ions. R.Pedrys, R.A.Haring, A.Haring, F.W.Saris, A.E.de Vries (FOM Inst. for Atomic & Molecular Phys., Kruislaan, Amsterdam, Netherlands).

Radiat. Eff. (GB), vol.64, no.1-4, p.81 (1982). [received: May 1983]
(Proceedings of the First International Conference on 'Radiation Effects in Insulators', Arco, Largo di Garda, Italy, 1981).
Summary form only given, as follows. Layers of Kr and Xe condensed at $\sim 15\text{K}$ and 35K have been bombarded by $3\text{-}6 \text{ keV Ar}^+$, Kr^+ and Xe^+ ions. The sputtered neutrals were detected after a 1.43 m flight path by means of a mass spectrometer. Among the sputtered particles are considerable numbers of Van der Waals molecules, Kr_2 , Kr_3 , Xe_2 , XeKr and XeKr_2 . The energy distribution of the sputtered particles give clues to the sputtering mechanisms involved. (no refs.)

77508 Ion sputtering of minerals and glasses: a first step to the simulation of solar wind erosion. K.Thiel, U.Sassmannshausen, H.Kulzer, W.Herr (Inst. für Kernchemie, Univ. Köln, Köln, Germany).

Radiat. Eff. (GB), vol.64, no.1-4, p.83-8 (1982). [received: May 1983]
(Proceedings of the First International Conference on 'Radiation Effects in Insulators', Arco, Largo di Garda, Italy, 1981).
Selected rockforming minerals (plagioclase, augite, olivine, ilmenite, silicate and metal phases of the meteorite 'Brenham') as well as silicate and phosphate glasses were irradiated with heavy ion ($^4\text{He}^+$, $^{14}\text{N}^+$, $^{20}\text{Ne}^+$, $^{40}\text{Ar}^+$, $^{56}\text{Fe}^+$, Xe^+) in the energy range of 50-130 keV in order to study ion-induced sputtering. Sputtering yields were measured independently by means of multiple beam interferometry and particle track autoradiography. The theory of sputtering by Sigmund (1969) modified by Smith (1978), was used to convert experimental heavy ion sputtering yields to H^+ and He^+ -sputtering yields of the same target. Taking into account solar wind irradiation conditions at the lunar surface, an estimate of lunar erosion rates due to solar wind sputtering is given for the targets studied. (18 refs.)

77509 Catastrophic sputtering of sulfur by helium. D.Fink, J.P.Biersack (Hahn-Meitner-Inst. für Kernforschung Berlin, Berlin, Germany).

Radiat. Eff. (GB), vol.64, no.1-4, p.89-95 (1982). [received: May 1983]
(Proceedings of the First International Conference on 'Radiation Effects in Insulators', Arco, Largo di Garda, Italy, 1981).
The sputtering yield of sulfur by $30\text{-}300 \text{ keV He}^+$ at 20°C was found to be of the order of 10^{10} sulfur atoms per incident ^4He , dependent on the energy and total implanted fluence, and independent of the ion flux onto the target. This effect may be explained by a weakening of the van der Waals binding between the S_8 rings due to Coulomb repulsion in the homogeneously charged volume, after a sufficient charge has accumulated in the highly insulating sample. Sulphur emission continues even for some time after the beam is switched off, and emission of sulfur atoms is also observed from non-irradiated areas adjacent to the irradiated spot, even from the rear side of 2-mm thick sulfur targets. (11 refs.)

77510 Sodium halide sputtering by H^+ , He^+ , Ar^+ ions. J.P.Biersack, E.Santner (Hahn-Meitner-Inst. für Kernforschung Berlin GmbH, Berlin, Germany).

Radiat. Eff. (GB), vol.64, no.1-4, p.97 (1982). [received: May 1983]
(Proceedings of the First International Conference on 'Radiation Effects in Insulators', Arco, Largo di Garda, Italy, 1981).
Summary form only given, as follows. Sputtering experiments were performed with 70 to 300 keV H^+ , He^+ and Ar^+ ions impinging on KCl, KBr and KI [sic]. The alkali halide samples are prepared as polycrystalline layers of about 2500 \AA thickness, deposited on carbon-aluminum backings. During the ion bombardment the targets are kept at elevated temperatures between 50 and 300°C , in order to study the temperature dependence of sputtering. During the irradiation the removal of halogen and sodium is simultaneously observed by Rutherford backscattering. The results indicate (i) preferential sputtering of the halogen atoms, (ii) temperature dependent sputtering yields with 0.2 eV activation energy, (iii) sputtering yields proportional to the electronic stopping power rather than the nuclear stopping power, and (iv) sputtering yields orders of magnitude higher than estimated by elastic collision cascade theories. These findings can be interpreted by a Pooley process with subsequent migration of the interstitial halogen atom to the surface. (no refs.)

77511 Ion-beam depth-profiling studies of leached glasses. C.A.Houser, I.S.Tsong, W.B.White (Materials Res. Lab., Pennsylvania State Univ., University Park, PA, USA), A.L.Wintenberg, P.D.Miller, C.D.Moak.

Radiat. Eff. (GB), vol.64, no.1-4, p.103-8 (1982). [received: May 1983]
(Proceedings of the First International Conference on 'Radiation Effects in Insulators', Arco, Largo di Garda, Italy, 1981).
Ion-beam depth-profiling was carried out on three different glasses leached (or hydrated) in deionized water using the $^{19}\text{F}(\text{p},\gamma)^{18}\text{O}$ nuclear reaction, secondary ion mass spectrometry (SIMS), and ^{18}O -induced photon spectrometry (SIPS) techniques. The depth-profiles show an interdiffusion mechanism in which the sodium ions in the glass are depleted and replaced by hydrogen (H^+) or hydronium (H_3O^+) ions from the solution. The leaching behavior does not show significant difference whether the glass surface is fractured or polished. Problems of mobile ion migration caused by ion bombardment and loss of hydrogen during analysis are discussed. (17 refs.)

77512 Sputtering of Al_2O_3 and LiNbO_3 in the electronic stopping region. Qiu.Yuanxun, J.E.Griffith, Tombrello. T.A. (W.K. Kellogg Radiation Lab., California Inst. of Technol., Pasadena, CA, USA).

Radiat. Eff. (GB), vol.64, no.1-4, p.111-16 (1982). [received: May 1983]
(Proceedings of the First International Conference on 'Radiation Effects in Insulators', Arco, Largo di Garda, Italy, 1981).
Because of recent interest in the role played by the thermal properties of materials that exhibit high energy sputtering, the authors have sputtered Al_2O_3 and LiNbO_3 with chlorine ions at energies between 3 MeV and 25 MeV . To detect the sputtered Al and Nb they employ thin carbon catcher foils, which are analyzed with Rutherford scattering in the forward direction. Al surface densities of $10^{14}/\text{cm}^2$ and Nb surface densities of $10^{13}/\text{cm}^2$ are easily measured. The sputtering yields for both Al_2O_3 and LiNbO_3 increase rapidly with increasing chlorine energy, and the Al and Nb yields are both approximately 0.2 at 20 MeV . Tests for dose, beam current, and contamination effects will be discussed. (10 refs.)

77513 Angular distributions of Au and Cu atoms sputtered from Au-Cu alloys by keV Ar^+ ion bombardment. H.J.Kang, Y.Matsuda, R.Shimizu (Dept. of Appl. Phys., Osaka Univ., Osaka, Japan).

Surf. Sci. (Netherlands), vol.127, no.3, p.179-85 (May 1983).
Angular distributions of Au and Cu atoms sputtered from Au-Cu alloys under 3 keV Ar^+ ion bombardment were measured to understand the preferential sputtering. The surface composition of sputter-deposited Au-Cu films on substrates mounted at different ejection angles was analyzed by Auger electron spectroscopy and electron probe microanalysis. Although the result indicated that the proportion of sputtered Cu atoms to the Au atoms in the Au-Cu alloy depends on the ejection angle, marked enhancement of the lighter component in the direction normal to the surface has not been observed in spite of the larger mass ratio of the constituent atoms of the Au-Cu alloy. (14 refs.)

77514 Computer simulations of ion scattering spectra for 2.4 keV Ne^+ incident on Ni(001). J.A.Yarmoff, R.S.Williams (Dept. of Chem. & Biochem., Univ. of California, Los Angeles, CA, USA).

Surf. Sci. (Netherlands), vol.127, no.3, p.461-86 (May 1983).
Monte-Carlo computer simulations of Buck's (1979, 1980) time-of-flight ion scattering spectroscopy data collected for 2.4 keV Ne^+ incident on a Ni (001) surface were used to examine the importance of various input parameters in the computational model. The binary collision approximation was found to yield satisfactory results for this particular projectile, energy, and target. The calculated energy spectra were quite sensitive to the screening length of the Moliere potential used for calculating the binary collision interactions and to the magnitude of the mean square vibrational amplitudes chosen for the Ni

atoms in the lattice. The agreement between the calculated and experimental spectra was good, but the calculations probably could have been improved a little further by fine tuning the parameters in the simulation. The simulations show that the ISS spectra for 2.4 keV Ne⁺ ion beam incidence directions along the [100] azimuth of Ni(001) were dominated by multiple scattering events and that the second layer of the surface contributed most to the backscattering because of the focusing effect of the first layer atoms. (36 refs.)

77515 Excitations in charge-transfer atom scattering. J.E.Inglesfield (Daresbury Lab., Sci. & Engng. Res. Council, Warrington, England). *Surf. Sci. (Netherlands)*, vol.127, no.3, p.555-68 (May 1983). The electronic excitations are calculated for a tight-binding model of 25-1000 eV Na atoms scattering off W, assuming a classical trajectory for the Na atoms which interact with a single half-filled band on the substrate. The excitation spectrum consists of substrate electron-hole pairs at low energies, with a jump at the ionization threshold due to electron transfer from the Na to the W. If the Na ionization level crosses the Fermi energy beyond the range of hopping between the Na and the W substrate, the ionization probability is high. As the Na kinetic energy is reduced the ionization probability decreases, but the substrate electron-hole excitations increase in importance, and this is discussed in semi-classical terms. (14 refs.)

77516 Band structure effects in high energy ion beam surface interaction at grazing incidence. H.Winter, R.Zimny, A.Schirmacher, B.Becker, H.J.Andra (Inst. für Kernphys., Univ. Münster, Münster, Germany), R.Frohling. *Z. Phys. A (Germany)*, vol.311, no.4, p.267-80 (1983).

The analysis of charge state distributions after the interaction of fast Li- and N-ions with a surface at grazing incidence at energies between 50 and 350 keV yields for Li a strongly suppressed and for N an enhanced fraction of neutrals in comparison to the beam-foil interaction. These findings are supported by corresponding alkali-spectra which are dominated by lines from transitions in singly ionized atoms. The experiments are consistently interpreted in terms of a two step model: (1) collisional excitation in the close vicinity of the surface and (2) modification of this population by resonant electron transfer from (to) nonlocalized states in the conduction (valence) band to (from) the ion. The model is also applied to interpret recent beam-foil experiments where preferential populations of Rydberg levels in highly ionized atoms were found. (32 refs.)

Theoretical aspects of cluster formation by keV bombardment of rare-gas solids See Entry 75563

Fabrication of optical waveguides in LiNbO₃ and LiTaO₃ crystals by ion irradiation See Entry 75790

Study of ytterbium implanted calcia stabilized zirconia thin films and yttria stabilized zirconia single crystals See Entry 76472

Matrix effect and surface oxidation in depth profiling of Al_xGa_{1-x}As by secondary ion mass spectrometry using O₂⁺ primary ions See Entry 76479

Radiation damage in ion-implanted quartz crystals. Part I: Nuclear and electronic energy deposition See Entry 76523

79.20R Atomic and molecular beam interactions

Energy redistribution among internal states of nitric oxide molecules upon scattering from Pt(111) crystal surface See Entry 77503

Chemical sputtering, a discussion of mechanisms See Entry 77506

79.40 THERMIONIC EMISSION

77517 General quantitative expression of the positive ionization efficiency in dissociative self-surface ionization of ionic crystals. H.Kawano (Dept. of Chem., Faculty of Sci., Ehime Univ., Matsuyama, Japan). *J. Chem. Phys. (USA)*, vol.78, no.11, p.7012-13 (1 June 1983). Positive ion emission occurs when thick polycrystalline layers of MX deposited on a metal surface are heated in vacuum. In various research fields, this phenomenon has been utilized as a simple method to generate ion beams from ionic crystals. Recent study has concluded that (1) the ion emission originates from 'dissociative self-surface ionization (DSSI)', (2) the layer surface is inhomogeneous with respect to work function, (3) the real surface area for the ion emission is much smaller than that for the neutral molecular evaporation, and also (4) the ionization efficiency is usually less than 10⁻⁴ thereby indicating that the degree of dissociation is smaller than unity. DSSI is investigated theoretically. (9 refs.)

79.60 PHOTOEMISSION AND PHOTOELECTRON SPECTRA

77518 Photoelectron emission from a platinum electrode into liquid ammonia solutions. F.A.Urbe, T.Sawada, A.J.Bard (Dept. of Chem., Univ. of Texas, Austin, TX, USA).

Chem. Phys. Lett. (Netherlands), vol.97, no.2, p.243-6 (13 May 1983). Photoelectron emission from a Pt electrode into liquid NH₃ under Ar-ion laser illumination at wavelengths corresponding to 2.41, 2.54, 2.71 and 3.41 eV is described. Plots of photocurrent (*i*) versus electrode potential (*V*) in the 'five-halves law' (*i*^{0.4} versus *V*) form show 'two-slope' plots that yield threshold potentials and electron injection levels. Based on these, an energy level diagram involving injection of electrons at energies 0.13-0.97 eV above the solvated electron level (which is -1.3 eV versus vacuum) is proposed. (16 refs.)

77519 Reply to 'Comment on 'X-ray photoelectron spectroscopic studies of oxygen chemisorption on thick films of photoconducting cadmium sulphide'. D.P.Amalnerkar, S.Badrinarayanan, S.K.Date, A.P.B.Sinha (Phys. Chem. Div., Nat. Chem. Lab., Pune, India). *J. Appl. Phys. (USA)*, vol.54, no.5, p.2881-2 (May 1983). For original paper see D.P. Amalnerkar et al., *Appl. Phys. Lett.*, vol.41, p.270 (1982). For comment see M. Lichtensteiger and C. Webb, *J. Appl. Phys.*, vol.54, p.2129 (1983). A thorough examination of the authors' experimental data revealed that the two additional photopeaks in question do not originate from indeterminate stray AlK_α radiation as suggested by Lichtensteiger and Webb, but are due to sulphur-oxygen species formed on the surface of CdS thick films. (8 refs.)

77520 A new method for determining relaxation energies by means of AES and XPS and its application to silicon compounds. F.Bechstedt, R.Enderlein (Sektion Phys., Humboldt-Univ. zu Berlin, Berlin, Germany), R.Fellenberg, P.Streubel, A.Meisel.

J. Electron Spectrosc.: & Relat. Phenom. (Netherlands), vol.31, no.2, p.131-43 (May 1983).

A new method is presented for the determination of the absolute dynamic relaxation energy *R_D* from experimental Auger parameters, the static dielectric constant and the plasmon energy of the solids. The relaxation energies of the Si 1s and 2p core levels in Si, SiC, SiO₂, Si₃N₄ and Na₂SiF₆ are investigated by comparing the experimental values with theoretical results from a semiempirical dielectric theory. Both the experimental and theoretical results are valid only for the least-bound Si 2p state. The calculated relaxation shifts $\Delta R_D^{(1s)}$ and $\Delta R_D^{(2p)}$ are in reasonable agreement with the experimental values, and describe the extraatomic polarization effect well also for a deep level. (31 refs.)

77521 Resonant photoemission from Si. K.L.I.Kobayashi (Central Res. Lab., Hitachi Ltd., Kokubunji, Tokyo, Japan), H.Daimon, Y.Murata.

Phys. Rev. Lett. (USA), vol.50, no.21, p.1701-4 (23 May 1983). Anomalous evolution of the silicon valence-band photoemission spectra is observed in the photon energy region from the 2p core-excitation threshold to about 3 eV above the threshold. The 3p-like topmost emission band shows a Fano-type resonance, and stronger intensity enhancement is observed in the deeper binding-energy region around 7.6 eV. The present results show the existence of a decaying localized core exciton at the 2p core-excitation threshold. (10 refs.)

77522 Far ultraviolet photoelectric study of thin SnSe evaporated films.

A.Bennouna (Lab. de Spectroscopie, CNRS, Univ. de Rennes 1, Rennes, France), P.Y.Tessier, M.Priol, Q.Dang Tran, S.Robin.

Phys. Status Solidi b (Germany), vol.117, no.1, p.51-6 (1 May 1983). Energy distribution curves of photoemitted electrons are obtained for SnSe thin polycrystalline films in the 10 to 40 eV energy range. The method of preparation of the sample under ultrahigh vacuum conditions is described and the synthesis of the initial material. The quality of the sample is checked by Auger analysis which reveals a weak reactivity of the material. The EDCs show structures appearing at 0.9, 2.1 to 2.7, 3.9, 7.4 eV below the top of the valence band. The Sn 4d levels are also investigated. The 4d(5/2) is found at 24.3 eV and the 4d(3/2) at 25.3 eV below the top of the valence band. Structures in the EDCs are compared with those of existing similar works and are interpreted by means of a theoretical bands scheme. (26 refs.)

77523 Spin- and angle-resolved photoemission from ferromagnetic Fe(001). R.Feder, W.Gudat, E.Kisker, A.Rodriguez, K.Schroder (Inst. für Festkörperforschung KFA Jülich, Jülich, Germany).

Solid State Commun. (USA), vol.46, no.8, p.619-23 (May 1983). For near-normal photoemission from ferromagnetic Fe(001) excited by linearly polarized synchrotron radiation, energy-resolved spin polarization and intensity distribution have been measured at 60 eV photon energy. Calculations using a one-step theory of photoemission consistently reproduce the present spin-resolved data as well as earlier spin-averaged measurements. The quasi-particle exchange splitting deduced from the data is 2 eV. The agreement with band structure calculations is suggested to be coincidental due to a compensation of real and imaginary self-energy corrections. (25 refs.)

77524 Photoemission of Xe and Kr adsorbed on the W(110) plane.

R.Opila, R.Gomer (Dept. of Chem., Univ. of Chicago, Chicago, IL, USA). *Surf. Sci. (Netherlands)*, vol.127, no.3, p.569-97 (May 1983). The UPS and XPS spectra of Xe adsorbed on clean, O, CO, and Xe covered W(110) surfaces and the UPS spectrum for Kr on clean and O covered W(110) surfaces have been investigated. On clean W, Xe and Kr show a splitting of the 5p_{3/2} and 4p_{3/2} hole states respectively. For Xe the coverage dependence of this splitting was investigated in detail; neither the positions nor the intensity ratio of the substates are coverage dependent for $\theta \geq 0.04$, suggesting that splitting is due to differences in the image interaction of the $m_j = \pm 3/2$ and $m_j = \pm 1/2$ components. For Xe equal shifts, relative to vacuum, of ~1.0 eV were observed for 5p, 4d, and 3d levels suggesting that initial state effects are small. Image interaction for Xe and Kr on clean W could best be fitted by assuming an increase, rather than a decrease in the effective hole-image separation from the nominal value, suggesting that the image plane is moved back into the metal by a screening length. For Xe adsorbed on Xe/W(110) or on virgin-CO/W(110), polarization of the intermediate layers was found to contribute significantly to relaxation. Coadsorbed oxygen broadened Xe 5p and Kr 4p peaks. There was an almost linear relation. Coadsorbed oxygen broadened Xe 5p and Kr 4p peaks. There was an almost linear relation between O 2p UPS intensity at the energies of the various peaks and the amounts of broadening, suggesting that the latter results from resonance neutralization by electrons from the O 2p states. (33 refs.)

77525 Resonant photoemission and f-band dispersion in UIr₃. A.J.Arko, D.D.Koelling (Argonne Nat. Lab., Argonne, IL, USA), B.Reihl.

Fifteenth Annual Synchrotron Radiation Users Group Conference (papers in summary form only received), Stoughton, WI, USA, 18-19 Oct. 1982 (Stoughton, WI, USA: Synchrotron Radiat. Center 1982), p.1-2. Angle-resolved and resonant photoemission techniques have been used to determine both the f-band dispersions and partial f-electron density in UIr₃. The results are compared to a self-consistent APW band structure calculation where the potential was included in the warped muffin-tin approximation. The photoemission measurements were performed with a two-dimensional display-type analyzer in both the angle-integrated ($\Delta\theta = 86^\circ$) and angle-resolved ($\Delta\theta = 6^\circ$) mode. (2 refs.)

77526 \tilde{A}, \tilde{P} effects in polar angle dependence of photoemission from Cu(001). R.L.Benbow, M.R.Thuler, Z.Hurych (Phys. Dept., Northern Illinois Univ., DeKalb, IL, USA), N.V.Smith, P.D.Johnson.

Fifteenth Annual Synchrotron Radiation Users Group Conference (papers in summary form only received), Stoughton, WI, USA, 18-19 Oct. 1982 (Stoughton, WI, USA: Synchrotron Radiat. Center 1982), p.4-5. Angle-resolved photoelectron spectra were collected in the plane of incidence for p-polarized light with angle of incidence $\sim 70^\circ$ from normal. The comparison of spectra obtained at equal angles from normal in the plane of incidence shows that the spectra may differ radically. In particular, the Cu conduction band is usually strong at polar angles $\theta \leq 25^\circ$ from normal on the side of normal toward which the light is reflected. At the same angle, but in the opposite sense from normal, the conduction band is generally seen to diminish and for certain polar angles and photon energies may disappear altogether. (3 refs.)

77527 Optical 4d excitation in a monolayer of Xe on Au. W.Eberhardt, A.Zangwill (Brookhaven Nat. Lab., Upton, NY, USA). Fifteenth Annual Synchrotron Radiation Users Group Conference (papers in summary form only received), Stoughton, WI, USA, 18-19 Oct. 1982 (Stoughton, WI, USA: Synchrotron Radiat. Center 1982), p.15-16. The authors measure the strength of the 4d core level Rydberg transitions in a monolayer of Xe adsorbed onto Au by monitoring the intensity of the Auger electron emission following the decay of the 4d hole created in the primary excitation. The data show that the oscillator strength in the Rydberg transition region is nearly identical to the equivalent transitions in gaseous or solid Xe and does not vanish as it was observed for the 5p-6s transition in the same system. (2 refs.)

77528 Photoemission does not measure the energies of orbitals (or: Configurational model of adsorbate structure and excitations). C.P.Flynn, J.E.Cunningham (Dept. of Phys. & Materials Res., Univ. of Illinois, Urbana, IL, USA). Fifteenth Annual Synchrotron Radiation Users Group Conference (papers in summary form only received), Stoughton, WI, USA, 18-19 Oct. 1982 (Stoughton, WI, USA: Synchrotron Radiat. Center 1982), p.17. The structure and excitation spectra of atoms adsorbed on metal surfaces are discussed with particular emphasis on the way the metal substrate influences ionic behavior. The authors present a configurational model which is useful for discussing photoexcitation of and photoemission from molecular adsorbates. The model accounts in a satisfactory way for the excited state configurational switching observed in synchrotron radiation investigations of the excitation spectra of rare gas atoms adsorbed on metal surfaces. By means of this model they also identify an unfortunately widespread misunderstanding of the way a metallic substrate influences the energies for photoemission from adsorbates. The model shows how molecular adsorbates develop dipole moments and strong bonding as the excited state switch condition is passed, as is observed experimentally. The emergence of these ground state properties may, however, be significantly less sharp than the excited state switching, owing to the influence of higher excited levels. (3 refs.)

77529 The bandstructure of CO on Cu(111); breakdown of the single particle picture. H.-J.Freund, W.Eberhardt (Brookhaven Nat. Lab., Upton, NY, USA), D.Heskett, E.W.Plummer. Fifteenth Annual Synchrotron Radiation Users Group Conference (papers in summary form only received), Stoughton, WI, USA, 18-19 Oct. 1982 (Stoughton, WI, USA: Synchrotron Radiat. Center 1982), p.19-20. Many body effects are known to cause shifts of core level photoemission lines to an apparently lower binding energy than calculated by a standard, single particle calculation. Actually, a sum rule exists that correlates the calculated value of the core binding energy with the intensity weighted average of the energy of all photoemission lines corresponding to ionization of the same core level. Therefore the larger the satellite intensities, the lower is the apparent binding energy of the main line. This sum rule has been verified experimentally by now for several molecular systems. The authors have used the system of CO chemisorbed on Cu(111) to study the effect of many body excitations on bandstructure measurements by angle resolved photoemission. In this adsorbate system the bands are strictly two dimensional therefore no ambiguity exists about the determination of the normal momentum component required in bulk bandstructure measurements. (2 refs.)

77530 The electronic structure of the Na_xWO_3 bronzes: a photoemission study. G.Hollinger, F.J.Himpel, N.Martensson, B.Reihl (IBM Thomas J. Watson Res. Center, Yorktown Heights, NY, USA), P.Pertosa, J.P.Doumerc. Fifteenth Annual Synchrotron Radiation Users Group Conference (papers in summary form only received), Stoughton, WI, USA, 18-19 Oct. 1982 (Stoughton, WI, USA: Synchrotron Radiat. Center 1982), p.21. W4f, Na2p core-level spectra and valence band spectra are presented for a series of metallic Na_xWO_3 ($0.4 < x < 0.85$) bronzes, in the 20-130 eV photon energy range. From a comparison of experimental and theoretical conduction band densities of states, it is found that in the measured composition range the trends of the Rigid Band Model behavior are respected. Fano-type resonances in the 5d conduction band intensity have been observed at the $5p_{1/2}$ and $5p_{3/2}$ photoabsorption threshold for Na_xWO_3 as well as for ReO_3 , WO_2 , and W. The Na_xWO_3 bronze spectra exhibit a characteristic double resonance structure different from the simple resonance peaks measured for ReO_3 , WO_2 , and W. In contrast, the photoemission W4f spectra for the high x Na_xWO_3 and ReO_3 are apparently similar. The results could be related to a mixed valence character for the metallic bronzes revealed in the final state of the photoemission process. (no refs.)

77531 Photoemission studies of silicon surfaces, Si-metal interfaces, Si hydrogenation and Si oxidation. G.Hollinger, F.J.Himpel, R.J.Purtell, G.W.Rubloff, R.A.Pollak, P.S.Ho (IBM Thomas J. Watson Res. Center, Yorktown Heights, NY, USA). Fifteenth Annual Synchrotron Radiation Users Group Conference (papers in summary form only received), Stoughton, WI, USA, 18-19 Oct. 1982 (Stoughton, WI, USA: Synchrotron Radiat. Center 1982), p.22-3. Angle-integrated photoemission measurements have been performed on Si(111)-(2×1), Si(111)-(7×7), and Si(100)-(2×1) surfaces in the 20-120 eV photon energy range. Core-level binding energies and valence bands have been measured with high resolution (0.1-0.3 eV) and high accuracy on clean surfaces and metal (Pt, Pd, Ni), hydrogen- and oxygen-covered surfaces. By tuning the photon energy and, therefore, the electron escape depth, both chemical shifts and band bending effects have been observed. (no refs.)

77532 The transition from linear to spiked X-ray edge. D.Gibbs, T.H.Chui, J.E.Cunningham, C.P.Flynn (Dept. of Phys. & Materials Res., Univ. of Illinois, Urbana, IL, USA). Fifteenth Annual Synchrotron Radiation Users Group Conference (papers in summary form only received), Stoughton, WI, USA, 18-19 Oct. 1982 (Stoughton, WI, USA: Synchrotron Radiat. Center 1982), p.24-5. The authors have discovered a phenomenon which, they believe, has extremely important consequences for the understanding of the response of a Fermi liquid to a localized shock. It is well known that the alkali metals Na, K, Rb and Cs have outer core $np^6 \rightarrow np^5(n+1)s$ excitation spectra which start abruptly at threshold with a sharp edge. This is the 'X-ray edge' which has been related to the Fermi liquid response. There is a small overshoot or spike on each of these threshold shoulders. They have discovered that when one of these alkalis is alloyed into a second alkali as a dilute impurity, the spectrum takes this form only in certain cases. In other cases the core excitation spectrum increases linearly from zero at threshold, with no sign of a sharp edge. (no refs.)

77533 Synchrotron radiation photoemission as a probe for overlayers on compound semiconductor surfaces: GeGaAs(110). G.J.Lapeyre, P.Zurcher, J.Anderson, F.Cerrina, G.R.Williams, D.Frankel, J.C.Hermanson (Dept. of Phys., Montana State Univ., Bozeman, MT, USA). Fifteenth Annual Synchrotron Radiation Users Group Conference (papers in summary form only received), Stoughton, WI, USA, 18-19 Oct. 1982 (Stoughton, WI, USA: Synchrotron Radiat. Center 1982), p.33-4. The problem of determining the effects of overlayers on compound semiconductor surfaces has been approached by performing electronic structure studies with polarization-dependent angle-resolved photoemission (PARPES). The results indicate that the principal effect is shifts in the energies of the interband transitions associated with the substrate emission. The above is to be contrasted with the typical PES chemisorption study where one finds the principal effect to be new emission features derived from the orbitals of the chemisorbed species. In order to perform such studies one needs to first characterize the substrate emission by identifying the interband transitions. (no refs.)

77534 Angle-resolved photoemission study of the GaAs(100) surface and the Ge-GaAs(100) interface. L.G.Salmon, T.N.Rhodin (School of Appl. & Engng. Phys., Cornell Univ., Ithaca, NY, USA). Fifteenth Annual Synchrotron Radiation Users Group Conference (papers in summary form only received), Stoughton, WI, USA, 18-19 Oct. 1982 (Stoughton, WI, USA: Synchrotron Radiat. Center 1982), p.47-8. Heterojunction properties cannot be described adequately by traditional models based on bulk parameters. A more effective model must incorporate characteristics of the heterojunction interface. Important to the development of such a model is a study of the formation of a simple lattice-matched heterojunction interface, such as Ge-GaAs(100). The numerous reconstructions obtainable on GaAs(100) permit a controlled study of the effects of substrate surface structure on the interface. The formation of the Ge-GaAs(100) interface is studied from initial stages to an established heterojunction. Heterojunctions are formed on GaAs(100) surfaces which had been grown by molecular beam epitaxy. The epitaxial Ge layers were grown by MBE under UHV conditions at a substrate temperature at 350°C to obtain clean abrupt interfaces. The interfaces were studied in situ by angle-resolved photoelectron spectroscopy (ARPES) to determine electronic states, by LEED to indicate crystal structure, and by Auger spectroscopy to verify cleanliness and surface stoichiometry. (no refs.)

Fifteenth Annual Synchrotron Radiation Users Group Conference (papers in summary form only received) See Entry 74225

Data acquisition and analysis in X-ray photoelectron spectroscopy using an Apple II microcomputer See Entry 74570

Photoelectron spectra of adsorbed carbonates See Entry 75440

X-ray and UV photoelectron-spectroscopic studies of pyridine adsorbed on evaporated nickel and palladium in the temperature range 140-385K See Entry 75441

An X-ray photoelectron spectroscopy study of the surface segregation of LaNi₅ heated in H₂-atmosphere See Entry 76756

Strongly bound chemisorption state for benzene on silicon (111) See Entry 76768

The temperature dependence of the interaction of oxygen with Pd(111); a study by photoemission and Auger spectroscopy See Entry 76790

Recent investigations on the electronic structure of the fourth and fifth group transition metal monocarbides, mononitrides, and monoxides See Entry 76840

Si-transition metal interface formation and bulk electronic structure of 3d metal disilicides See Entry 77053

Fundamental optical absorption and valence bands in alkali silver halide crystals See Entry 77406

79.70 FIELD EMISSION AND FIELD IONIZATION

77535 Field emission fluctuation phenomena of potassium microcrystals on tungsten. I. Spectral density functions and flip-flop. T.Biernat (Inst. of Experimental Phys., Univ. of Wrocław, Wrocław, Poland), Ch.Kleint, R.Mclewski.

Surf. Sci. (Netherlands), vol.127, no.3, p.487-97 (May 1983). The field emission flicker noise technique has been applied to study dynamical properties of epitaxial potassium microcrystals on tungsten. Spectral density functions of the (111) region for temperatures between 78 and about 230K were obtained. Some preliminary observations of flip-flop behaviour of potassium crystals are presented and discussed. (26 refs.)

77536 Field emission fluctuation phenomena of potassium microcrystals on tungsten. II. Temperature dependence and simulation of noise properties. T.Biernat (Inst. of Experimental Phys., Univ. of Wrocław, Wrocław, Poland), Ch.Kleint.

Surf. Sci. (Netherlands), vol.127, no.3, p.498-512 (May 1983). For pt.I see *ibid.*, vol.127, p.487 (1983). The temperature dependence of the flicker noise of potassium microcrystals is described in terms of spectral densities, exponents of spectral density functions, knee frequencies, and noise activation energies. The results of a simulation procedure of the spectral properties and their temperature dependence by different Lorentzian functions are presented and discussed together with some autocorrelation functions obtained by Wiener-Khinchine transformation of the simulated spectra. The observed noise is thought to be due to fluctuations in shape of the crystal in the built-up state, changes in cluster size and premelting phenomena. (21 refs.)

77537 Multiphonon effects in field electron emission. M.Yu.Sumetskii (M.A. bonch-Bruевич Electrical Engng. Inst. of Communications, Leningrad, USSR).

Sov. Phys.-Solid State (USA), vol.24, no.11, p.2003-4 (Nov. 1982). Translation of: *Fiz. Tverd. Tela (USSR)*, vol.24, no.11, p.3513-15 (Nov. 1982). [received: May 1983]

It is known that in weak fields characterized by slowness of electron tunneling the dynamic coupling of an electron with lattice vibrations is very strong. Therefore, vibrations of surface atoms in field electron emission in sufficiently weak electric fields may result in multiphonon excitation of electrons and in a deviation of the current-voltage characteristic from the Fowler-Nordheim curve. The author determines under which conditions the current in question can be observed. (4 refs.)

Observation of superstructure formation on Rh(001) by laser-pulse assisted field evaporation See Entry 76761

79.75 EXOELECTRON EMISSION

77538 Exoelectron emission from surface states in a ferroelectric. A.M.Kostsov, A.S.Sidorkin, V.S.Zal'tsberg, S.P.Gribkov (Lenin Konsomol State Univ., Voronezh, USSR). *Sov. Phys.-Solid State (USA)*, vol.24, no.11, p.1952-3 (Nov. 1982). Translation of: *Fiz. Tverd. Tela (USSR)*, vol.24, no.11, p.3436-8 (Nov. 1982). [received: May 1983]
The authors used a high-sensitivity method for detection of electrons with an open-type secondary electron multiplier and data-conversion apparatus to investigate thermally stimulated exoelectron emission in a 10^{-5} torr vacuum from cut surfaces of ferroelectric triglycine sulfate (TGS) single crystals in the temperature range 20-70°C. Electron emission was observed under conditions of linear heating and spontaneous cooling. The dependence of the emission current j_{em} from the surface of a TGS crystal on the temperature of the crystal when the heating rate was $v=0.01^{\circ}\text{C}/\text{sec}$ is shown; the results are given for two different samples. The thermally stimulated exoelectron emission appeared only during heating. It was not observed when the samples were cooled. A second heating at the same rate produced the effect only after intermediate exposure to air for ~ 200 h. Some sensitivity of the emission to contact with the atmosphere indicated that the surface electron states dominated the emission process. (4 refs.)

80.00 CROSS-DISCIPLINARY PHYSICS AND RELATED AREAS OF SCIENCE AND TECHNOLOGY

81.00 MATERIALS SCIENCE

77539 Correspondence analysis for describing the morphology of powders. Application to a commercial alumina powder. M.Deletter, F.Cambier, C.Lebud, M.R.Anseau (Centre de Recherches, Industrie Belge de la Ceramique, Mons, Belgium). *Acta Metall. (USA)*, vol.31, no.6, p.893-902 (June 1983).
The authors define a method which allows the shape of a whole set of different objects to be studied. The Fourier series allows the shape of each object to be quantified by a set of parameters. This information is gathered by 'correspondence analysis'. It allows points relative to the harmonics of the Fourier series and points relative to the objects that are taken into consideration, to be represented in the same space simultaneously. The projection of this set onto plans containing the maximum of information allows it to be visualized and maps to be obtained which are the shape pictures of the set of objects. As an example, the mathematical treatment is applied to a commercial alumina powder and the shape maps thus obtained are discussed. (10 refs.)
77540 Highlights of US Air Force metallurgical research programs. A.H.Rosenstein (Air Force Office of Sci. Res., Boiling Air Force Base, Washington, DC, USA). *J. Met. (USA)*, vol.35, no.3, p.64-73 (March 1983).
Presents highlights of current research programs sponsored by the US Air Force. These programs are aimed at better understanding of the basic metallurgical factors which affect strength, toughness, high-temperature performance and resistance to aggressive environments of materials required to operate near the limit of their capacities in aerospace applications. Results of these studies are presented in three areas: materials synthesis, processing science, and materials behaviour. (1 refs.)
77541 An introduction to silane project in ROC. C.S.Liu, H.L.Hwang (Nat. Sci. Council, Taipei, Taiwan).
Conference Record of the Sixteenth IEEE Photovoltaic Specialists Conference - 1982, San Diego, CA, USA, 27-30 Sept. 1982 (New York, USA: IEEE 1982), p.137-9
A National Silane Project managed by National Science Council (NSC) with an aim towards developing its own silicon technologies has been initiated since 1981. NSC of ROC coordinates the Industrial Technology Research Institute, Institute of Nuclear Energy Research and Universities in a joint effort to develop technologies from mining survey to low cost silicon production. The paper described the scope of this project and briefly reviews the first year programme. (1 ref.)
Conference Record of the Sixteenth IEEE Photovoltaic Specialists Conference - 1982 See Entry 74219

81.10 METHODS OF CRYSTAL GROWTH AND PURIFICATION
(for physics of crystal growth, see 61.50C; for epitaxial growth methods, see 81.15)

77542 Preparation and properties of Fe-1.65 wt.%Cr single crystals. A.Gabasova, S.Kadeckova (Fyzikalni Ustav CSAV, Praha, Czechoslovakia). *Kovove Mater. (Czechoslovakia)*, vol.21, no.2, p.197-205 (1983). In Czech.
The results of a study of growth conditions of Fe-1.65 wt.%Cr oriented single crystals and defects in the as-grown crystals are presented. It has been found that oxygen content of 100 to 170 wt.ppm has a pronounced effect on preparation of crystals with uniform grain size which is necessary for single crystal growth. The main defects in as-grown crystals are twin grains and dislocations. The average dislocation density is $\geq 10^7 \text{ m}^{-2}$. The stress-strain curves of Fe-1.65 wt.%Cr single crystals oriented in the middle of the unit triangle and tested in tension at room temperature are similar to those of pure iron, only the critical resolved shear stress being a little higher for the alloy. (16 refs.)
77543 Automatic system for regulation of radius of crystals. V.S.Leibovich, V.A.Sukharev, V.M.Shushkov. *Prib. & Sist. Upr. (USSR)*, no.3, p.17-18 (1983). In Russian. English translation in: *Sov. J. Instrum. & Control (GB)*
The system is used to regulate the characteristic dimension of a crystal within boundaries of phase changes (from crystalline to fluid or gaseous). It is based

on determination of crystal growth parameters. The dynamical model is described and the structure of regulator is illustrated. (3 refs.) J.K.S.

77544 Flat-plate solar array progress and plans. W.T.Callaghan (Jet Propulsion Lab., California Inst. of Technol., Pasadena, CA, USA).
Conference Record of the Sixteenth IEEE Photovoltaic Specialists Conference - 1982, San Diego, CA, USA, 27-30 Sept. 1982 (New York, USA: IEEE 1982), p.115-18
Technical progress in the areas of silicon feedstock refinement; large-area sheet formation; flat-plate module process sequence development, and engineering and environmental testing are discussed, in the context of a revised thrust developed by the US Department of Energy. The new thrust of FSA is directed toward higher-risk, longer-term-payoff work that emphasizes the assumption of those technological risks that industrial firms are not likely to finance in the effort to develop reliable, low-cost photovoltaic modules. (1 ref.)
Gallium Arsenide and Related Compounds, 1982. Tenth International Symposium on Gallium Arsenide and Related Compounds See Entry 74226
Sunshine Project Solar Photovoltaic Programme and recent activities in Japan See Entry 77989
Guidelines and methodology for design and analysis of advanced PV technology systems See Entry 78039

81.10B Growth from vapour

77545 Vapour phase growth of some II-VI compounds. D.W.G.Ballentyne (Electrical Engng. Dept., Imperial Coll., London, England). *Prog. Cryst. Growth & Charact. (GB)*, vol.6, no.2, p.163-89 (1983).
The state of the art of the growth of II-VI compounds from the vapour phase is reviewed. It is shown that the conditions of growth can now be predicted from theoretical considerations. The limitations of the method are discussed and the factors which must be taken into account to refine the theory are outlined. (30 refs.)
Ice crystal morphology and growth rates at low supersaturations and high temperatures See Entry 76331
Chemical transport of MnS and MnSe using HCl as a transporting agent See Entry 77883

81.10D Growth from solutions

77546 Hydrogen uranyl arsenate hydrate single crystals: $\text{H}_2(\text{UO}_2)_2(\text{AsO}_4)_2 \cdot 8\text{H}_2\text{O}$: gel growth and characterization. E.Manghi, G.Polla (Dept. de Fisica, CNEA, Buenos Aires, Argentina). *J. Cryst. Growth (Netherlands)*, vol.61, no.3, p.606-14 (April-May 1983).
Single crystals of hydrogen uranyl arsenate hydrate (HUAsH) were grown in tetramethoxysilane gels at different temperatures, below and above the paracelsite-ferroelastic transition temperature, T_0 . The crystals were characterized by X-ray diffraction, chemical etching, scanning electron microscopy and optical microscopy. The habit of the gel grown crystals allowed the three-dimensional features of the domain structure to be studied for the first time. A correlation was made between crystal perfection, domain structure and growth history. (14 refs.)
77547 Reconstruction by multidirectional holographic interferometry of the concentration field in a supersaturated solution near a growing NaClO_3 crystal. F.Bedarida, L.Zefiro, P.Boccacci (Istituto di Mineralogia, Genova Univ., Genova, Italy), C.Pontiggia. *J. Cryst. Growth (Netherlands)*, vol.61, no.3, p.641-4 (April-May 1983).
A real three-dimensional map of the concentration changes in a supersaturated solution around a growing crystal has been obtained by multidirectional holographic interferometry. This technique is a sort of optical tomography, since it gives the concentration field at different levels in the solution. (4 refs.)
77548 Growth of single crystals of hexagonal boron nitride. T.Ishii, T.Sato (Nat. Inst. for Res. in Inorganic Materials, Ibaraki, Japan). *J. Cryst. Growth (Netherlands)*, vol.61, no.3, p.689-90 (April-May 1983).
Single crystals of hexagonal boron nitride were prepared with Si flux. A mixture of Si and B powders was heated above 1850°C in a crucible made of hexagonal boron nitride under a N_2 atmosphere for 2 h. The largest crystals were about 2 mm in plane dimension and 20 μm in thickness. The large plane of the crystals was perpendicular to the c-axis. (6 refs.)
77549 Growth of single crystals from solutions using semi-permeable membranes. A.J.Varkey, C.E.Okeke (Dept. of Phys. & Astron., Univ. of Nigeria, Nsukka, Nigeria). *J. Cryst. Growth (Netherlands)*, vol.61, no.3, p.701-4 (April-May 1983).
Using this technique single crystals of copper sulphate, potassium bromide and ammonium dihydrogen phosphate have been successfully grown. Advantages of this technique over other methods are discussed. (10 refs.)
77550 Characterization of flux-grown $\text{Ca}(\text{WO}_4)_x(\text{MoO}_4)_{1-x}$ crystals. S.K.Arora, R.S.Godbole, G.S.Trivikrama Rao (Dept. of Phys., Sardar Patel Univ., Gujarat, India). *J. Am. Ceram. Soc. (USA)*, vol.66, no.5, p.321-3 (May 1983).
Crystals of $\text{Ca}(\text{WO}_4)_x(\text{MoO}_4)_{1-x}$, in the range $x=0.072$ to 0.86 were successfully grown by the flux technique. Neither the densities of the mixed crystals nor the cell parameters vary linearly. The dislocation density of the mixed crystals, determined by the etching technique, is greater than that of the end partners. The variation in microhardness of the mixed configurations is found to be linear and has no correlation with their dislocation content. (11 refs.)
Spectroscopic properties of TbP_2O_7 , TbLiP_2O_7 , and $\text{TbAl}_2(\text{BO}_3)_4$ See Entry 77426

81.10F Growth from melts

77551 Temperature profile and thermal stress calculations in GaAs crystals growing from the melt. M.Duseaux (Lab. d'Electronique et de Phys. Appl., Limeil-Brevannes, France). *J. Cryst. Growth (Netherlands)*, vol.61, no.3, p.576-90 (April-May 1983).
Temperature and thermal stress distributions are analyzed here for two kinds of crystal growth techniques: the LEC (Liquid Encapsulated Czochralski) method, and the LEK (Liquid Encapsulated Kyropoulos) method. The influence of the crystal diameter has especially been studied. The stress values reach 4 kg mm^{-2} near the B_2O_3 -argon interface in 50 mm diameter Czochralski crystals and 1-2 kg mm^{-2} in 15 mm crystals. In the case of the LEK procedure, the stress level is lower, especially in long and flat top crystals. It is shown that this level is not affected by the crystal diameter. (25 refs.)

77552 Effect of variable thermal conductivity on isotherms in Bridgman growth. R.J.Naumann, S.L.Lehoczky (Space Sci. Lab., NASA/Marshall Space Flight Center, Huntsville, AL, USA).

J. Cryst. Growth (Netherlands), vol.61, no.3, p.707-10 (April-May 1983). A change in thermal conductivity associated with melting or solidification can have a profound influence on the isotherms near the solidification interface if the material is being directionally solidified in an ampoule whose walls carry a substantial portion of the heat. This analysis was prompted by a recent discovery that the thermal conductivity of $Hg_{1-x}Cd_xTe$ increased dramatically as the material is heated above the solidus curve. An illustrative example is shown in which the sample is approximated as an infinite cylinder with constant but different thermal properties in the solid and melt. The boundary conditions are fixed on the surface by a conductive ampoule in a two-zone Bridgman furnace with an adiabatic region separating the two zones. The effect of the adiabatic zone in this case is to intensify the curvature of the interface rather than to lessen it. (10 refs.)

77553 Crystal growth of solid solutions $La_{1-x}Ba_xF_{3-x}$. A.Roos (Solid State Dept., Utrecht Univ., Utrecht, Netherlands). *Mater. Res. Bull. (USA)*, vol.18, no.4, p.405-9 (April 1983). Single crystals of solid solutions $La_{1-x}Ba_xF_{3-x}$ ($0 < x \leq 0.104$) have been grown by means of a modified Stockbarger method using RF heating. All crystals appeared to be single phase with the $LaF_3(P3c1)$ structure. The quality of the crystals depends strongly on the growth rate. The crystals are transparent from 11 μm to 0.33 μm . (9 refs.)

77554 Directional solidification of silicon in carbon crucibles by an Oscillating Crucible Technique. T.Daud (Jet Propulsion Lab., California Inst. of Technol., Pasadena, CA, USA), K.A.Dumas, G.H.Schwuttke, P.Smetana, K.M.Kim.

Conference Record of the Sixteenth IEEE Photovoltaic Specialists Conference - 1982, San Diego, CA, USA, 27-30 Sept. 1982 (New York, USA: IEEE 1982), p.63-7

To increase quality of cast silicon ingots a new method of directional solidification called the oscillating crucible technique (OCT) is developed. During growth, a carbon crucible is oscillated to provide for effective stirring of the melt. This growth technique (seeded growth only), along with material characterization and solar-cell fabrication and testing, is described. Solar-cell efficiencies of up to 13% at 100 mW/cm² are obtained in the single crystalline areas. Minority-carrier diffusion lengths exceeding 100 μm are measured even in the polycrystalline areas of the wafers. Limitations of the present setup and possible future improvements are discussed. (13 refs.)

77555 Advanced crystallization techniques of 'solar grade' silicon. M.Gasparini (Heliosil SpA, Milano, Italy), C.Calligaris, P.Rava, L.Sardi, M.Alessandri, F.Redaeli, S.Pizzini.

Conference Record of the Sixteenth IEEE Photovoltaic Specialists Conference - 1982, San Diego, CA, USA, 27-30 Sept. 1982 (New York, USA: IEEE 1982), p.74-9

Microstructural, electrical and photovoltaic characteristics of polycrystalline silicon solar cells fabricated with silicon ingots containing 5, 100 and 500 ppmw iron are reported and discussed. All silicon ingots were grown by the directional solidification technique in graphite or special quartz moulds and doped intentionally with iron, in order to evaluate the potentiality of the DS technique when employed with solar silicon feedstocks. Results indicate that structural breakdown limits the amount of the ingot which is usable for solar cells fabrication, but also that efficiencies in excess of 10% are obtained using the 'good' region of the ingot. (7 refs.)

77556 Progress in growth of silicon ribbon by a low angle, high rate process. D.N.Jewett, H.E.Bates, J.W.Locher (Energy Materials Corp., Lancaster, MA, USA).

Conference Record of the Sixteenth IEEE Photovoltaic Specialists Conference - 1982, San Diego, CA, USA, 27-30 Sept. 1982 (New York, USA: IEEE 1982), p.86-9

Substantial progress has been achieved in the development of the Low Angle Silicon Sheet (LASS) crystal growth technique since its inception in mid 1979. Continuously grown ribbons of 10 to 30 meters are produced routinely at growth rates of 10 to 80 cm/min. Ribbon widths are 4 to 15 cm and thickness varies from 0.3 to 0.6 mm with 0.5 mm typical. At an average growth speed of 30 cm/min and a width of 15 cm, productivity of 450 cm²/min of ribbon has been demonstrated. (3 refs.)

77557 Large area silicon sheet produced by the spinning method. Y.Maeda, T.Yokoyama, I.Hide (Res. Labs., Hoxan Corp., Sapporo, Japan).

Conference Record of the Sixteenth IEEE Photovoltaic Specialists Conference - 1982, San Diego, CA, USA, 27-30 Sept. 1982 (New York, USA: IEEE 1982), p.133-6

Polycrystalline silicon sheets having a 6-in., 4-in. dia. or 100 mm×100 mm with a thickness of 0.3-0.4 mm have been obtained directly by spinning the silicon melt dropped on a plate. Production time of sheet formation from the melt is about one second per sheet. The crystallites of the sheet have columnar structures. Material loss in the production process is little or none because of a clean recovery of the surplus silicon. Using this sheet, p-n junction solar cells with an AMI efficiency of 6.1% have been made experimentally. (5 refs.)

77558 In situ purification growth of undoped semi-insulating GaAs single crystals. T.Fukuda, K.Terashima, H.Nakajima (Optoelectronics Joint Res. Lab., Kawasaki, Japan).

Gallium Arsenide and Related Compounds, 1982. Tenth International Symposium on Gallium Arsenide and Related Compounds, Albuquerque, NM, USA, 19-22 Sept. 1982 (Bristol, England: IOP 1983), p.23-9

A new in situ melt purification growth technique to obtain undoped semi-insulating GaAs single crystals, with high reproducibility, has been developed. Undoped semi-insulating <100> crystals were grown by a computer controlled LEC technique linked with a new technique, in which melt purification was carried out by a special distillation process and the degree of purity was analysed by measurement of the electrical conductivity of the melt. Highly homogeneous undoped semi-insulating crystals, 2 inches in diameter, of resistivity 2×10^8 ohm cm, and low EPD, 8×10^7 /cm² were grown. (8 refs.)

Interface shape studies for silicon ribbon growth by the EFG technique. I. Transport phenomena modeling See Entry 76333

Interface shape studies for silicon ribbon growth by the EFG technique. II. Effect of die asymmetry See Entry 76334

Crystal growth and temperature variation of the lattice parameters in LaF_3 , CeF_3 , PrF_3 and NdF_3 See Entry 76335

Mathematical model for corundum single crystal growth by Verneuil method See Entry 76336

Segregation during directional melting and its implications on seeded crystal growth: a theoretical analysis See Entry 76337

LEC growth of $InP(Mn)$ for p-type and semi-insulating materials See Entry 76341

Reproducibility and uniformity considerations in LEC growth of undoped, semi-insulating GaAs for large-area, direct implantation technology See Entry 76342

X-ray investigation of crystal defects in Czochralski grown InP single crystals See Entry 76435

Double doped low dislocation density InP with low optical absorption See Entry 76474

A direct comparison of LEC GaAs grown using low- and high-pressure techniques See Entry 76942

Interaction between cast silicon properties and solar cell performance See Entry 77592

Variation of optical inhomogeneity of ruby crystals See Entry 77771

Achievement and properties of self-supporting polysilicon solar cells made from RAD ribbons See Entry 78022

81.10H Zone melting and zone refining

77559 Zone-melting recrystallization of polycrystalline silicon films on fused silica substrates using RF heated carbon susceptor. Y.Kobayashi, A.Fukami, T.Suzuki (Hitachi Res. Lab., Hitachi Ltd, Ibaraki, Japan). *IEEE Electron Device Lett. (USA)*, vol.EDL-4, no.5, p.132-4 (May 1983).

High-quality recrystallized silicon films on fused silica substrates have been produced with a new micro-zone-melting method using an RF heated carbon susceptor. In this method, the fused silica substrate, on which a 0.5 to 1.0- μm -thick polycrystalline silicon film encapsulated with a 1.2- μm -thick CVD SiO_2 layer has been deposited, is moved across the carbon susceptor surface, which has a narrow-strip high-temperature zone. Recrystallized silicon films with (100) texture and elongated grains several tens times several hundreds of microns in size have been obtained. n-channel MOSFETs fabricated with these films exhibit surface electron mobilities as high as 700 to 1000 cm²/Vs. (10 refs.)

77560 A new method for the growth of circular nickel crystals by zone melting. S.Hayashi, S.Ono, H.Komatsu (Res. Inst. for Iron, Steel & Other Metals, Tohoku Univ., Sendai, Japan).

J. Cryst. Growth (Netherlands), vol.61, no.3, p.698-700 (April-May 1983).

A new method has been established for the growth of circular nickel crystals by floating-zone melting. The as-grown crystals were single crystalline and their growth direction rotated continuously with the mechanical rotation. It was found from these results that the nickel grows equally along all crystallographic directions. (6 refs.)

77561 Preparation of bulk alloys of III-V compounds. E.M.Swiggard, R.L.Henry, H.Lessoff (Naval Res. Lab., Washington, DC, USA).

Gallium Arsenide and Related Compounds, 1982. Tenth International Symposium on Gallium Arsenide and Related Compounds, Albuquerque, NM, USA, 19-22 Sept. 1982 (Bristol, England: IOP 1983), p.1-5

A crystal growth technique for preparing radially and longitudinally homogeneous bulk crystals of III-V alloys has been developed. The technique is a zone leveling procedure with special features that make it possible to prepare homogeneous alloys of materials that have high vapor pressures at their melting point. The equipment is a horizontal pressure vessel capable of being operated at pressures up to 50 atmospheres. The growth technique is a liquid encapsulated procedure using boric oxide with provision for in-situ removal of the boric oxide before cooling. (1 ref.)

81.10J Growth from solid phases

(inc. multiphase diffusion and recrystallisation)

An analysis of the process of recrystallization of silicon thin films with either a scanning laser or strip heater See Entry 76801

81.15 METHODS OF THIN FILM DEPOSITION

(inc. epitaxial growth methods; see also 68.55 Thin film growth, structure, and epitaxy)

77562 Solid-phase lateral epitaxy of chemical-vapor-deposited amorphous silicon by furnace annealing. Y.Kunii, M.Tabe, K.Kajiyama (Electrical Communication Labs., Nippon Telegraph & Telephone Public Corp., Tokyo, Japan).

J. Appl. Phys. (USA), vol.54, no.5, p.2847-9 (May 1983).

A single-crystalline silicon-on-insulator structure has been fabricated with solid-phase lateral epitaxy. Chemical-vapor-deposited amorphous silicon (CVD a-Si) deposited on a SiO_2 stripe is crystallized by furnace annealing. A new CVD technique (clean CVD) has met the conditions required for solid-phase epitaxy; clean interface and reduction of impurities and microcrystallites in the a-Si film. In the case of a 4- μm -wide SiO_2 stripe parallel to the (100) direction, the entire deposited layer grows epitaxially by low-temperature furnace annealing (550~650°C). In the case of a 10- μm -wide SiO_2 stripe, the whole surface region also grows epitaxially, although the deep region partially becomes polycrystalline in areas distant from the open substrate surface. The grown-layer crystallinity is improved by subsequent high-temperature annealing. (7 refs.)

77563 Preparation and magnetic characteristics of garnet films with cylindrical magnetic bubbles in the submicron range. V.M.Dmitruk, A.M.Zyuzin, A.M.Prokhorov, V.V.Randoshkin, V.I.Smokin, Yu.V.Starostin, M.I.Timoshchuk (P.N. Lebedev Phys. Inst., Acad. of Sci., Moscow, USSR). *Sov. Phys.-Dokl. (USSR)*, vol.27, no.7, p.573-4 (July 1982). Translation of: *Dokl. Akad. Nauk SSSR*, vol.265, no.1-3, p.63-5 (July 1982). [received: April 1983]

The purpose of this work was to develop apparatus for growing high-quality crystals of neodymium-gallium garnet, producing uniform epitaxial films of ferrite-garnets with submicron cylindrical magnetic bubbles, and optimizing their parameters. (5 refs.)

77564 Structural and optical properties of sprayed $CuInSe_2$ films. O.P.Agnihotri, P.Raja Ram, R.Thangaraj, A.K.Sharma, Atul Raturi (Phys. Dept., Indian Inst. of Technol., New Delhi, India).

Thin Solid Films (Switzerland), vol.102, no.4, p.291-7 (29 April 1983).

p-CuInSe₂ thin films with the chalcopyrite structure were prepared by spray pyrolysis. The films were characterized by X-ray diffraction, optical transmission, transmission and scanning electron microscopy and electrical measurements. They were found to have a preferred orientation with (112) parallel to the substrate. The resistivity of these films was varied from 0.1 to about 100 Ω cm by varying the Cu:In ratio from 1.2 to unity. (24 refs.)

77565 Thin-film epitaxial solar cells on substrates made from MG silicon by the HEM process. C.P.Khattak, F.Schmid (Crystal Systems Inc., Salem, MA, USA), P.H.Robinson, R.V.D'Aiello. Conference Record of the Sixteenth IEEE Photovoltaic Specialists Conference - 1982, San Diego, CA, USA, 27-30 Sept. 1982 (New York, USA: IEEE 1982), p.128-32

Describes progress made in applying the Heat Exchanger Method (HEM) in the direct solidification of commercially available metallurgical grade (MG) silicon for the fabrication of substrates suitable for the epitaxial growth of solar-cell structures. Attention is focused on the problem of SiC particle formation, its relationship to the starting MG feedstock, the characteristics of particle distribution in the ingots, and the effects of potential solar-cell yield. Methods are described for significantly reducing particles including proper selection of commercial MG feedstock, modifications and in-situ purifications added to the basic HEM process. After the introduction of these changes, quantitative estimates of ingot utilization and epitaxial solar-cell performance are given. Best solar-cell results were 12% on 4 cm², and 10.7% on 10 cm² area cells. (12 refs.)

Gallium Arsenide and Related Compounds, 1982. Tenth International Symposium on Gallium Arsenide and Related Compounds See Entry 74226

Application of a continuous monitoring technique for the deposition of multilayer dielectric films with reproducible characteristics over a wide spectral region See Entry 75775

Formation of semiconductor epitaxial films by pulse heating crystallization or regrowth See Entry 76811

Structural investigations of detonation-deposited tungsten carbide-cobalt coatings See Entry 77611

Formation of a nickel-clad titanium carbide coating and effect of spraying conditions on its structure and properties See Entry 77612

Sunshine Project Solar Photovoltaic Programme and recent activities in Japan See Entry 77989

Evaporation of CuCl and CuCl₂ for the fabrication of Cu₂S/CdS thin film solar cells See Entry 78011

Realisation et caracterisation de cellules solaires Cu₂S-CdZnS (Realisation and characterisation of Cu₂S-CdZnS solar cells) See Entry 78013

Thin film polycrystalline silicon solar cell See Entry 78025

Guidelines and methodology for design and analysis of advanced PV technology systems See Entry 78039

81.15C Deposition by cathodic sputtering

77566 Production methods and properties of diamond-like carbon films. A.V.Balakov, E.A.Konshina.

Sov. J. Opt. Technol. (USA), vol.49, no.9, p.591-9 (Sept. 1982). Translation of: *Opt.-Mekh. Prom-st. (USSR)*, vol.49, no.9, p.52-9 (Sept. 1982).

Methods of obtaining carbon films having diamond-like properties, based on ion-plasma techniques, are reviewed. There are two main development trends that can be identified: ion sputtering of graphite and hydrocarbon destruction. The effect of the deposition conditions on the structure and phase composition of the films is analyzed. The microscopic and macroscopic properties of the carbon films and some of their technical applications are examined. (49 refs.)

77567 Microstructure trends in metal/aluminum, copper, indium, lead, tin-metal oxide thin films prepared by reactive ion beam sputter deposition. S.Nakahara, A.F.Hebard (Bell Labs., Murray Hill, NJ, USA).

Thin Solid Films (Switzerland), vol.102, no.4, p.345-60 (29 April 1983).

Transmission electron microscopy has been used to study the microstructural trends of thin film composites prepared by sputtering of a metal (aluminum, copper, indium, lead or tin) target with argon ions in the presence of a reactive gas (oxygen). Results of these studies reveal that there is a general progression in the metal component microstructure which correlates with an increasing metal oxide component in the films and can be classified as belonging to an agglomerated-columnar-granular-amorphous sequence. These structural trends and the concomitant effect on film properties, such as resistivity, adhesion and mechanical stability, are a direct consequence of the metal-metal oxide interaction and the inhibiting effect which the native metal oxides have on metal atom diffusion during film formation. (30 refs.)

77568 Thin film field effect transistors incorporating hydrogenated amorphous silicon produced by r.f. magnetron sputtering. M.C.Abdulrida, J.Allison (Dept. of Electronic & Electrical Engng., Univ. of Sheffield, Sheffield, England).

Thin Solid Films (Switzerland), vol.102, no.4, p.L43-6 (29 April 1983).

The authors report on thin film FETs incorporating a-Si:H prepared by r.f. magnetron sputtering, which have an ON-OFF current ratio of better than 10⁴ with applied gate voltages V_g of around 10 V. The midgap density of states in the a-Si:H is less than 10¹⁷ eV⁻¹ cm⁻³, as derived from field effect data following Spear and LeComber (1972). These results and other measured characteristics of the magnetron-sputtered a-Si:H, together with the performance of the related FETs, particularly the transfer and drain characteristics, are similar to those for glow discharge material and associated devices. (12 refs.)

Metal/Insulator/Si structures with low interface state density fabricated by combined ion beam sputtering and atomic hydrogen beam treatment See Entry 77061

Effect of magnetic field in RF sputtering on the crystal orientation and magnetic properties of Co-Cr perpendicular anisotropy films See Entry 77219

Fabrication of ZrN coatings See Entry 77774

Copper sulfide/cadmium sulfide heterojunction cell research by sputter deposition See Entry 78088

81.15G Vacuum deposition

77569 Crystallization of amorphous mercury selenide films. K.N.Sharma, K.Barua (Dept. of Phys., Dibrugarh Univ., Dibrugarh, India).

Indian J. Pure & Appl. Phys., vol.21, no.2, p.116-18 (Feb. 1983).

The crystallization of amorphous mercury selenide (a-HgSe) films has been studied as a function of annealing temperature (343K<T<365K). The crystallization process was found to be gradual, which took place at any finite temperature and was thermally activated with an activation energy of 0.963 eV. The characteristic time associated with the microscopic reaction between the neighbouring atoms was 1.273×10⁻¹⁰ s. (10 refs.)

77570 Incorporation rates of gallium and aluminum on GaAs during molecular beam epitaxy at high substrate temperatures. R.Fischer, J.Klem, T.J.Drummond, R.E.Thorne, W.Kopp, H.Morkoc, A.Y.Cho (Dept. of Electrical Engng., Univ. of Illinois, Urbana, IL, USA).

J. Appl. Phys. (USA), vol.54, no.5, p.2508-10 (May 1983).

Gallium arsenide, aluminum arsenide, and aluminum gallium arsenide epitaxial layers were grown by molecular beam epitaxy in the substrate temperature range 590-720°C. The incorporation rates of Ga and Al in this temperature range were studied by means of thickness measurements. The growth rates of GaAs and Al_{0.3}Ga_{0.7}As were observed to be dependent on growth temperature above 640°C while the AlAs growth rate was observed to be independent of growth temperature in the range investigated. The reduction of the GaAs growth rate at a growth temperature above 640°C was found to be lessened by the presence of minute amounts of Al and excess As. For the fixed Ga flux and a growth temperature of 700°C the GaAs growth rate and the Ga contribution to the growth rate of Al_{0.3}Ga_{0.7}As were 0.50 and 0.89 times their low temperature values, respectively, while at 680°C these values were 0.88 and 0.99, respectively. (7 refs.)

77571 Growth of high quality Ge MBE film. Y.Ota (Bell Labs., Reading, PA, USA).

J. Cryst. Growth (Netherlands), vol.61, no.3, p.431-8 (April-May 1983).

Germanium single crystal films were grown on a germanium substrate by MBE technique in an ultra-high vacuum. The epitaxial growth was carried out on a p⁺ (ρ≤0.002 Ω cm), (100) or (111) Ge substrate at a growth temperature ranging from 600 to 920°C. The X-ray diffraction pattern and dislocation etching revealed that the epitaxial films were high-quality single crystal with low density of crystalline defects if the growth was carried out under proper conditions. The films had a bulk-like electrical property and a p-n junction mesa diode fabricated showed an excellent diode characteristic. (28 refs.)

Interface states and current threshold of GaAs/Al_{0.3}Ga_{0.7}As double-heterostructure lasers grown by molecular beam epitaxy See Entry 75640

Spectrum studies on a GaAs-AlGaAs multi-quantum-well laser diode grown by molecular beam epitaxy See Entry 75690

Antistatic and abrasion-resistant coating on polymer optical components having a complicated surface profile See Entry 75776

Modulation doping structures in silicon by molecular beam epitaxy and off-line ion implantation See Entry 76461

Influences of substrate surface structures and water vapor on the nucleation, epitaxy and graphoeptitaxy of tin thin films grown on potassium chloride substrates See Entry 76806

The heterojunction ZnSe-(Zn_{1-x}Cd_x)Te_{1-y}(In₂Te₃)_y having high sensitivity in the visible light range and its applications See Entry 77024

Angle-lapping and staining observations of Si doping superlattice structures See Entry 77025

Preparation, physical properties, and superconductivity of La_{3-x}S₄ films See Entry 77085

Far ultraviolet photoelectric study of thin SnSe evaporated films See Entry 77522

Photovoltaic and electrical properties of n-CdS/p-Si heterojunction solar cells See Entry 78003

81.15H Chemical vapour deposition

77572 Fabrication of GaAs-Mo-Si structures by metalorganic chemical vapor deposition and laser annealing. K.Okamoto, T.Imai (Univ. of Electro-Communications, Tokyo, Japan).

Appl. Phys. Lett. (USA), vol.42, no.11, p.972-4 (1-June 1983).

Undoped-polycrystalline GaAs layers were deposited on Mo layers by metalorganic chemical vapor deposition and annealed by pulse laser irradiation. The laser used here was a Q-switched ruby laser and the annealing was done by immersing the samples in SnCl₄-dissolved methanol. Then, recrystallization and doping of the GaAs layers were successfully done. The Schottky characteristics were observed between the top GaAs layer and the Mo layer underneath; the barrier height was 0.53 eV. (7 refs.)

77573 A comparison between InP films growth by the hydride and chloride techniques. K.A.Jones (Electrical Engng. Dept., Colorado State Univ., Fort Collins, CO, USA).

J. Cryst. Growth (Netherlands), vol.61, no.3, p.525-34 (April-May 1983).

The differences and similarities in the properties of InP films growth by the hydride and chloride techniques are attributed to thermodynamics or kinetic effects. The primary difference in the source zone is that an InP⁺ crust is formed in the chloride system. It is suggested that the crust does not completely cover the liquid indium, and that the change in the background carrier concentration when the PCl₃ flow rate is altered is due to transient behavior between two steady state conditions. The larger background carrier concentration in the hydride grown films is partially attributed to a lower HCl concentration; the growth of p-type films in the chloride system by introducing PCl₃ downstream cannot be explained thermodynamically and the larger growth rates in the hydride system must be due to kinetic factors such as the slow decomposition of PH₃. (20 refs.)

77574 Reactive pulse plasma crystallization of TiN layers on substrates at 500K. A.Michalski, Z.Romanowski (Inst. of Materials Sci. & Engng., Warsaw Tech. Univ., Warsaw, Poland).

J. Cryst. Growth (Netherlands), vol.61, no.3, p.675-80 (April-May 1983).

Compact, up to a few tenths of micrometers thick TiN_{0.9} layers having a Vickers microhardness of μHV₂₀=1600 and which showed protective antiwear properties for abrasive tools were deposited on steel at 500K. TEM observations of the first crystallization stages showed the nucleation of nearly monodisperse, small (d≈15 nm) TiN_x particles in the plasma as well as their migration on carbon substrate films even at 500K. The TEM observations may explain the mechanism of material crystallization of high melting layers from a pulse plasma. (11 refs.)

77575 The growth of epitaxial InP by the chloride process in nitrogen and in the presence of phosphine. P.L.Giles, P.Davies, N.B.Hasdell (Allen Clark Res. Centre, Plessey Res. (Caswell), Caswell Ltd., England).

J. Cryst. Growth (Netherlands), vol.61, no.3, p.695-7 (April-May 1983).

Following the growth of epitaxial GaAs in the Ga/AsCl₃N₂ system, the authors have demonstrated that the growth of epitaxial InP in the equivalent In/PCl₃/N₂ system, under similar conditions, is not possible and possible thermodynamic reasons for this are suggested. With the addition of small amounts of phosphine, InP growth is possible in nitrogen and similar phosphine additions to the In/PCl₃/H₂ system produce dramatically increased growth rates. (12 refs.)

77576 Modelling of GaAs growth in the low pressure halide transport system. E.Veuhoff, N.Putz, J.Korec, M.Heyen, P.Balk (Inst. of Semiconductor Electronics, Aachen, Germany).

J. Electron. Mater. (USA), vol.12, no.2, p.235-46 (March 1983).

The authors discuss the application of an earlier proposed model to GaAs growth in the HCl-Ga-AsH₃-H₂ system at hydrogen pressures in the range 10⁻²-10³ Pa. The model takes into account the kinetic steps of gas phase diffusion, adsorption of the various species from the gas phase on the crystal surface and the chemical reaction itself, which produces the material to be deposited. A good quantitative description of the dependence of growth rate on hydrogen pressure, growth temperature, and input pressures of HCl and AsH₃ is obtained. The model leads to a better understanding of the growth mechanism and allows proper choice of the deposition parameters in order to obtain optimum material characteristics. (15 refs.)

77577 Low pressure metalorganic chemical vapor deposition on InP and related compounds. M.Razeghi, M.A.Poisson, J.P.Larivain, J.P.Duchemin (Thomson-CSF, Domaine de Corbeville, Orsay, France).

J. Electron. Mater. (USA), vol.12, no.2, p.371-95 (March 1983).

The low pressure metalorganic chemical vapor deposition epitaxial growth and characterization of InP, Ga_{0.47}In_{0.53}As and Ga_{0.47}In_{0.53}P_{1-y} lattice-matched to InP substrate are described. The layers were found to have the same etch pit density (EPD) as the substrate. The best mobility obtained for InP was 5300 cm² V⁻¹ S⁻¹ at 300K and 58900 cm² V⁻¹ S⁻¹ at 77K and for GaInAs was 11900 cm² V⁻¹ S⁻¹ at 300K, 54600 cm² V⁻¹ S⁻¹ at 77K and 90000 cm² V⁻¹ S⁻¹ 2K. The authors report the first successful growth of a GaInAs-InP superlattice and the enhanced mobility of a two dimensional electron gas at a GaInAs/InP heterojunction grown by LP-MO CVD. LP MO CVD material has been used for GaInAsP-InP, DH lasers emitting at 1.3 μm and 1.5 μm. These devices exhibit a low threshold current, a slightly higher than liquid phase epitaxy devices and a high differential quantum efficiency. (29 refs.)

77578 The production of high quality polysilicon film in the semiconductor devices and its detecting method. Wei Xiwen, Ma Lingzhi, Niu Defang (Dalian Inst. of Technol., Dalian, China).

J. Dalian Inst. Technol. (Dalian Gongxueyuan Xuebao) (China), vol.21, no.4, p.181-5 (Dec. 1982). In Chinese. [received: June 1983]

Introduces how to produce high quality polysilicon film in semiconductor devices and how to monitor the deposition temperature at the same time as the film grows. With the help of a high-precision semiconductor flowmeter the reaction gas and carrier gas flow are measured. (4 refs.)

77579 Effect of deposition parameters on the microstructure of chemically vapour-deposited SnO₂ films. N.Srinivasa Murty, S.R.Jawalekar (Dept. of Electrical Engng., Indian Inst. of Technol., Bombay, India).

Thin Solid Films (Switzerland), vol.102, no.4, p.283-9 (29 April 1983).

Transparent electrically conducting tin oxide films were deposited onto Pyrex glass substrates by oxidation of SnCl₂. The deposition temperature was in the range 400-500°C and oxygen with a flow rate of 1.35-2.50 l min⁻¹ was used as both the carrier gas and the oxidizing agent. Scanning electron microscope studies of these films indicate that the mean grain size varies from 0.083 to 0.303 μm. It was found that the film uniformity and the mean grain size increase with increasing deposition temperature and decreasing oxygen flow rate. This behaviour is explained in terms of the deposition rate, surface mobility and grain growth rate. SnO₂ films deposited at a high temperature (500°C) with a low oxygen flow rate (1.35 l min⁻¹) are uniform with a large mean grain size (0.303 μm). Doping SnO₂ films with antimony to 4 mol.% does not affect the film microstructure. (11 refs.)

77580 Investigation of crystallographic properties of thin germanium crystals grown on silicon substrates by chemical vapor deposition. H.Aharoni (Dept. of Electrical Engng., Ben Gurion Univ. of the Negev, Beer-Sheva, Israel), D.Durembergova.

Thin Solid Films (Switzerland), vol.102, no.4, p.327-43 (29 April 1983).

The quality of germanium crystals deposited from the gas phase by chemical vapor deposition using pyrolytic decomposition of GeH₄ in a helium atmosphere at various growth temperatures on silicon substrates was determined. X-ray diffraction and rocking curve measurements proved to be very useful in determining the degree of preferred orientation of the germanium deposit, since they distinguish clearly between the reflections of the thin germanium deposited layer and those of the thick silicon substrate. Therefore they permit fairly accurate calculations. Laue measurements, in this case, proved to be unsatisfactory because of inadequately low resolution. The results show that a preferred orientation of germanium crystallites in the layer of up to 99.9% was reached. (14 refs.)

77581 Efficiency of the SiH₄ oxidation reaction in chemical vapour deposition of SiO₂ films at low temperature. C.Cobianu, C.Pavelescu (Microelectronica, Bucharest, Rumania).

Thin Solid Films (Switzerland), vol.102, no.4, p.361-6 (29 April 1983).

Evaluates the efficiency of the SiH₄ oxidation reaction in the heterogeneous low temperature chemical vapour deposition (CVD) of SiO₂ films onto wafers at atmospheric pressure in SiH₄-O₂-N₂ systems as a function of the CVD conditions. The authors obtained an increase-maximum-decrease type of dependence of the reaction efficiency on the [O₂]/[SiH₄] mole ratio with temperature as a parameter, in the temperature range 200-400°C. At a given [O₂]/[SiH₄] mole ratio the reaction efficiency increases with temperature. These results are qualitatively explained in terms of the bimolecular surface reaction theory and of the dependence of the film density on the CVD conditions. A reactor figure of merit is defined to compare the reaction efficiency on wafers for different CVD reactors. (16 refs.)

77582 A low-cost polysilicon process based on the synthesis and decomposition of dichlorosilane. J.R.McCormick, F.Plahutnik, D.Sawyer, A.Arvidson, S.Goldfarb (Hemlock Semiconductor Corp., Hemlock, MI, USA).

Conference Record of the Sixteenth IEEE Photovoltaic Specialists Conference - 1982, San Diego, CA, USA, 27-30 Sept. 1982 (New York, USA: IEEE 1982), p.57-62.

Major process steps of a dichlorosilane based chemical vapor deposition (CVD) process for the production of polycrystalline silicon have been evaluated. While an economic analysis of the process indicates that it is not capable of meeting JPL/DOE price objectives (\$14.00/kg in 1980 dollars), product price in the \$19.00/kg to \$25.00/kg range may be achieved. Product quality has been evaluated and ascertained to be comparable to semiconductor-grade polycrystalline silicon. Solar cells fabricated from the material are also equivalent to those fabricated from semiconductor-grade polycrystalline silicon. (11 refs.)

77583 MOCVD growth and characterization of high luminescence efficiency AlGa_{1-x}As. D.Kasemset, C.S.Hong, N.B.Patel, P.D.Dapkus (Rockwell Internat., Thousand Oaks, CA, USA), K.Mohammed, J.L.Merz.

Gallium Arsenide and Related Compounds, 1982. Tenth International Symposium on Gallium Arsenide and Related Compounds, Albuquerque, NM, USA, 19-22 Sept. 1982 (Bristol, England; IOP 1983), p.79-84.

Electrical and optical characteristics of AlGa_{1-x}As grown by atmospheric MOCVD without graphite baffles are described. It was found that the material properties of AlGaAs grown by this technique are sensitive to reactor conditions, especially after prolonged shutdown. Nevertheless, materials with good electrical and optical properties have been obtained using this technique. Comparison between the AlGa_{1-x}As visible lasers grown by LPE and MOCVD techniques indicates that the MOCVD technique can produce materials with essentially the same luminescence efficiencies as LPE. (16 refs.)

Development of fabrication technology and measurement systems for multi-mode, single-mode and polarization maintaining optical fibers See Entry 75796

Morphology of organometallic CVD grown GaAs epitaxial layers See Entry 76804

Interface reactions and grain growth processes in poly-GaAs deposited on molybdenum substrates by the organometallic process See Entry 76805

Mechanism of graphite baffle gettering in organometallic vapor phase epitaxy; adsorption of trimethylaluminum on graphite See Entry 76809

Defect states and donors in thermally annealed or post-hydrogenated chemically vapour-deposited amorphous SiN_x alloy See Entry 76897

The variation of the p/n junction position in GaAs/GaAlAs double heterostructures grown by low pressure MO VPE See Entry 77027

Solid-phase lateral epitaxy of chemical-vapour-deposited amorphous silicon by furnace annealing See Entry 77562

Superlattice cascade solar cell See Entry 78067

Recent developments for the AlGaAsSb cell See Entry 78077

81.15J Ion plating and other vapour deposition

Selective properties of overcoated copper granular films See Entry 77467

Review of oxidation processes in plasmas See Entry 77778

81.15L Deposition from liquid phases (melts and solutions)

77584 LPE growth of InP/InGaAs/InP DH wafers on (100) InP substrates. N.S.Takahashi, T.Sasaki, A.Fukushima, S.Kurita (Dept. of Electrical Engng., Keio Univ., Yokohama, Japan).

Electron. Lett. (GB), vol.19, no.11, p.402-3 (26 May 1983).

An InP/InGaAs/InP double heterostructure wafer is grown directly on a (100) InP substrate using very low temperature LPE growth. This crystal exhibits a thin transition layer at a InP-InGaAs interface because of dissolution of the ternary layer. (13 refs.)

77585 Direct liquid phase epitaxial growth of high-quality InP on (111)A oriented In_{0.53}Ga_{0.47}As. K.Nakajima, S.Yamazaki, K.Akita (Semiconductor Materials Lab., Fujitsu Lab. Ltd., Kawasaki, Japan).

J. Cryst. Growth (Netherlands), vol.61, no.3, p.535-45 (April-May 1983).

The liquid phase epitaxial (LPE) growth conditions for lattice-matched In_{0.53}Ga_{0.47}As on (111)A oriented InP, the growth rate of (111)A In_{1-x}Ga_xAs, and the surface morphology of InP and In_{1-x}Ga_xAs were investigated in detail. It was found that the distribution coefficients of Ga and As on the (111)A face are quite similar to those on the (100) face, but are different from those on the (111)B face. Suitable LPE growth conditions needed to obtain (111)A oriented high-quality InP/In_{0.53}Ga_{0.47}As/InP double heterostructures were determined. These conditions were found by investigating the effects of the cooling rate, the degree of supercooling and the growth temperature on the dissolution of In_{0.53}Ga_{0.47}As in InP solution. The surface of InP grown on (111)A In_{0.53}Ga_{0.47}As was found to be smooth enough for use in optical devices. The InP/In_{0.53}Ga_{0.47}As interfaces were found to be quite sharp by SIMS depth profiling measurements. (24 refs.)

77586 Growth of polysilicon sheets on a carbon shaper by the RAD process. C.Belouet, C.Texier-Hervo, M.Mautref (Lab. de Marcoussis, Centre de Recherches de la CGE, Marcoussis, France), C.Belin, J.Paulin, J.Schneider.

J. Cryst. Growth (Netherlands), vol.61, no.3, p.615-28 (April-May 1983).

The basic aspects of the RAD process, a sheet melt-growth process, and the characteristics of the continuous carbon shaper are described. It is shown that layers 5 cm in width and 100 μm in thickness can be grown at pulling rates of 10 cm/min with a crystallinity similar to that of self-supporting silicon ribbons. The present solar cells made from this material, using the carbon shaper as a back-contact, have an air-mass-one (AM1) conversion efficiency of nearly 10%. (26 refs.)

77587 The role played by the anions in cadmium electroplating from some acidic baths. A.M.Abd el-Halim, M.I.Sobahi, A.O.Baghlaf (Dept. of Chem., King Abdulaziz Univ., Jeddah, Saudi Arabia).

Surf. Technol. (Switzerland), vol.18, no.3, p.225-32 (March 1983).

The electrodeposition of cadmium from four selected baths with nearly the same composition except for the anion was examined. These baths were based mainly on acidic aqueous solutions of cadmium sulphate, cadmium chloride, cadmium bromide and cadmium iodide. It was found that the nature of the anion influenced to some extent the cathodic polarization and the throwing power of the cadmium electroplating from each bath; it also influenced the growth morphology and microhardness of the cadmium plates. (18 refs.)

77588 The effect of AC superimposed on DC in the electrodeposition of metals. M.D.Maksimovic, D.C.Totovski, A.P.Ivic (Univ. of Belgrade, Belgrade, Yugoslavia).

Surf. Technol. (Switzerland), vol.18, no.3, p.233-41 (March 1983).

The effect of the amplitude of AC superimposed on DC on the morphology of metal deposits is discussed, and the procedure for determination of the maximum amplitude of AC at which smooth deposits are obtained is given. A good agreement is obtained between the theory, experiments and literature data. (18 refs.)

- 77589 Gradient-free isothermal liquid-phase heteroepitaxy of $A^{III}B^V$ compounds.** Yu.B.Bolkhovityanov, V.I.Yudaev. *Sov. Tech. Phys. Lett. (USA)*, vol.8, no.9, p.466-7 (Sept. 1982). Translation of: *Pis'ma v Zh. Tekh. Fiz. (USSR)*, vol.8, no.17-18, p.1081-5 (Sept. 1982). [received: May 1983]
The authors describe controllable isothermal film growth in systems in which the difference between the lattice constants of the substrate and the source is such that continuous dissolution of the source can be arranged, with a corresponding continuous growth of the film on the substrate in the absence of a temperature gradient. As objects of study, they chose the heterosystems In-Ga-As, Ga-As-Sb, In-As-P, and Ga-As-P. (6 refs.)
- Electromagnetic bearing for an epitaxy centrifuge in high vacuum** See Entry 74488
- High-output room-temperature pulsed operation for broad contact InP/In_{0.53}Ga_{0.47}As/InP lasers grown by molecular beam epitaxy** See Entry 75636
- Spin coated amorphous chalcogenide films: structural characterization** See Entry 76802
- Growth kinetics of LPE Ga_{0.83}Al_{0.17}Sb layers grown from supercooled solutions** See Entry 76807
- Electroepitaxy from a limited solution volume: growth kinetics calculations** See Entry 76808
- A possibility to obtain microdiscontinuous chromium coatings by cathodic treatment in acidic media** See Entry 77805
- Some possibilities for the use of stressed cathodically hydrogenated electrolytic nickel coatings for the deposition of microporous and microcracked chromium plates** See Entry 77806

81.20 OTHER METHODS OF PREPARATION OF MATERIALS

- 77590 Developments in research on the theory of metal forming.** Cheng Ru-xin, Xu Jian-ou, Deng Li-xin, Zhang Shu-gang (Chongqing Univ., China). *Acta Mech. Solida Sin. (China)*, no.1, p.137-45 (1982). In Chinese.
Presents the developments in research in recent years on the theory of metal forming with respect to basic laws, methods for solving problems in mechanics of forming, friction, the model experimental technique in the forming process, etc. (75 refs.)
- 77591 High-pressure growth of polycrystalline molybdenum disulphide.** S.K.Srivastava, B.N.Avasthi (Dept. of Chem., Indian Inst. of Technol., Kharagpur, India), B.Das, S.Basu. *Mater. Lett. (Netherlands)*, vol.1, no.5-6, p.178-80 (April 1983).
Polycrystalline molybdenum disulphide was prepared by high-pressure (56 kg/cm²) reduction of molybdenum trisulphide at 200°C. The stoichiometry was tested by chemical analysis and the crystallinity by X-ray diffraction studies. The room-temperature AC conductivity measurement showed a value of $1 \times 10^{-4} \Omega^{-1} \text{cm}^{-1}$. The material was diamagnetic with $\chi_L = 0.05 \times 10^{-6}$ emu. A band gap of 1.18 eV was obtained and n-type conductivity found. SEM studies showed 10-20 μm grain size. Temperature effect on the grain size was also studied. (11 refs.)
- 77592 Interaction between cast silicon properties and solar cell performance.** S.Hyland (Jet Propulsion Lab., Pasadena, CA, USA), P.Iles, D.Leung, G.Schwutke, J.A.A.Engelbrecht.
Conference Record of the Sixteenth IEEE Photovoltaic Specialists Conference - 1982, San Diego, CA, USA, 27-30 Sept. 1982 (New York, USA: IEEE 1982), p.68-73
Three types of cast silicon, Silso (Wacker), HEM (heat-exchanger method-crystal systems) and UCP (ubiquitous crystallization process-semix) were studied for their use as solar cells. Optical microscopy after etching revealed a high density of uniform dislocations (approaching $10^5/\text{cm}^2$), lines of dislocations indicating stress during crystal growth, and precipitates, some of which generate dislocations. Solar cells were fabricated by three processes. Results of solar cell processing revealed that these materials produce cells of lower efficiency than Czochralski control cells, and that the efficiencies of the three materials were quite close. Diffusion length and spectral response data are shown. Certain structural features are correlated with solar cell efficiency, diffusion length, and spectral response. Electron-beam induced current (EBIC) and light spot scanning are used to back up other measurements. (11 refs.)
- 77593 Silicon electrorefining using a semipermeable Cu₂Si:Si anode.** J.M.Olson, K.Carleton, A.Kibbler (Solar Energy Res. Inst., Golden, CO, USA).
Conference Record of the Sixteenth IEEE Photovoltaic Specialists Conference - 1982, San Diego, CA, USA, 27-30 Sept. 1982 (New York, USA: IEEE 1982), p.123-7
The authors have recently developed a silicon permeable anode material that significantly enhanced the effectiveness of the molten salt silicon electrorefining process and permits the low temperature fabrication of 'silicon' anode plates, a prerequisite for the operation of an efficient, multiplate electrorefining process. Using metallurgical grade silicon (Si) as feedstock, this hybrid process has yielded 99.996+% pure silicon in a stable, poly- or single-crystalline form and is particularly effective at removing boron, phosphorus, aluminum, and iron. This one-step electrorefining process is described. (7 refs.)
- Thin-film epitaxial solar cells on substrates made from MG silicon by the HEM process** See Entry 77565
- Sunshine Project Solar Photovoltaic Programme and recent activities in Japan** See Entry 77899
- Guidelines and methodology for design and analysis of advanced PV technology systems** See Entry 78039

81.20E Powder techniques, compaction and sintering

- 77594 On the analytic description of the process of electric-discharge sintering of metal powders.** V.A.Belyi, V.V.Meshkov, N.K.Myshkin, A.I.Sviridenok (Inst. of Mech. of Metal-Polymer Systems, Acad. of Sci., Gomel, Belorussian SSR).
Sov. Phys.-Dokl. (USA), vol.27, no.8, p.642-4 (Aug. 1982). Translation of: *Dokl. Akad. Nauk SSSR*, vol.265, no.4-6, p.1121-4 (Aug. 1982). [received: May 1983]
Develops methods of calculating the main characteristics of pressure sintering of a powder system. The approach used is based on the decisive role of the generalized contact conductivity of the system in the process of its formation under the combined action of the thermal energy supplied to the contact of

powder particles and the mechanical stresses from the pressing force. (13 refs.)

- 77595 Crystal structure and electrical resistivity of MoS₂-NbS₂ alloys produced by self-propagating high-temperature synthesis.** V.L.Kalikhman, A.A.Golubnichaya, E.P.Gladchenko, V.K.Prokudina, L.P.Shechipinova (All-Union Sci.-Res. Inst. of Electromech., Acad. of Sci., Chernogolovka, USSR). *Sov. Powder Metall. & Met. Ceram. (USA)*, vol.21, no.10, p.801-3 (Oct. 1982). Translation of: *Poroshk. Metall. (USSR)*, vol.21, no.10, p.56-9 (Oct. 1982). [received: May 1983]
Presents results of an investigation of sulfide alloys produced by self-propagating high temperature synthesis (SHS). Replacing Mo by Nb atoms in MoS₂ brings about a sharp fall in the latter's electrical resistivity because Nb is an acceptor impurity for MoS₂. The substitution of 5%Nb lowers ρ to $(1-2) \cdot 10^{-3} \Omega \cdot \text{cm}$, i.e., to the electrical resistivity level of graphite. The SHS method enables substituted Mo_{1-x}Nb_xS₂ compounds (solid solutions) to be obtained directly from a mixture of the elements (without the need to prepare Mo-Nb alloys), which results in higher productivity and lower power consumption. Admixture of a substituted compound as a means of lowering the reaction temperature makes it possible to obtain a product whose electrical resistivity is fairly evenly distributed over the ingot (cake) cross section and, in addition, is appreciably lower than that obtained with the admixture of MoS₂. The formation of solid solutions during SHS occurs mainly in those places where the charge melts, i.e. at distances from the reaction cake surface greater than 5-7 mm. (4 refs.)
- Lithium doping of candidate fusion reactor alloys to simulate simultaneous helium and damage production** See Entry 75177
- The DC resistivity of modified PZT ceramics** See Entry 76944
- Correspondence analysis for describing the morphology of powders. Application to a commercial alumina powder** See Entry 77539
- Volume changes experienced by Al-Zn compacts during liquid-phase sintering** See Entry 77596
- Raney type nickel catalysts from RSR atomization of Al-Ni powders** See Entry 77599
- Fabrication and characterization of TiC_{1-x}N_x (0 ≤ x ≤ 1) and MoB_{2-x}C_x (x = 0, 1.0, 2.0) by high-pressure hot-pressing** See Entry 77602
- Synthesis of gadolinium-gallium garnet** See Entry 77603
- Some characteristics of the cold densification of wurtzite boron nitride powders under conditions of high pressures** See Entry 77605
- Sintering kinetics of tantalum carbide** See Entry 77606
- Recrystallization of silicon nitride powders during hot pressing** See Entry 77607
- Effect of physicochemical transformations occurring in compacts during heating on the properties of manganese-zinc ferrites** See Entry 77608
- Characterization of spray pyrolysed spinel powders** See Entry 77609
- Control over the structure of hard metals and other heterophase materials produced by liquid-phase sintering. II. Principles of optimum design of hard metals** See Entry 77610
- Structural investigations of detonation-deposited tungsten carbide-cobalt coatings** See Entry 77611
- Formation of a nickel-clad titanium carbide coating and effect of spraying conditions on its structure and properties** See Entry 77612
- FCC and BCC solidification products in a rapidly solidified austenitic steel** See Entry 77628
- Analysis of a rapidly solidified high-phosphorus austenitic steel containing an amorphous phase** See Entry 77660
- Structure/property relationships and applications of rapidly solidified aluminum alloys** See Entry 77661
- Characteristics of recrystallization of ultrafine powders during sintering** See Entry 77669
- Effect of heat treatment on the distribution of elements in the phase components of a W-Ni-Fe alloy** See Entry 77684
- Effect of a CaF₂ addition on the oxidation of hot-pressed silicon nitride-base materials** See Entry 77783
- Surface reinforcement of iron-base materials** See Entry 77804
- 81.20G Specific metals and alloys (compacts, pseudoalloys)**
- 77596 Volume changes experienced by Al-Zn compacts during liquid-phase sintering.** A.P.Savitskii, N.N.Burtsev, L.S.Martunova (Physicotech. Inst., Acad. of Sci., USSR).
Sov. Powder Metall. & Met. Ceram. (USA), vol.21, no.10, p.760-4 (Oct. 1982). Translation of: *Poroshk. Metall. (USSR)*, vol.21, no.10, p.11-16 (Oct. 1982). [received: May 1983]
The sintering of compacts from aluminum powders with zinc additions in the presence of a liquid phase is accompanied by their volume growth and a corresponding increase in their porosity. The volume growth of compacts from Al-Zn powder mixtures during liquid-phase sintering is mainly due to the Kirkendall effect, which manifests itself during the formation of a solid solution on the aluminum particles as a result of the diffusion of zinc atoms from the melt to the particles preceding their dissolution in the liquid phase. When the zinc content of a compact does not exceed its limit of solid-phase solubility in aluminum at the sintering temperature, the process of dissolution of aluminum in the melt may be ignored. The extent to which the volume of compacts from an Al-Zn powder mixture grows during sintering increases with increasing mean aluminum powder particle size. (6 refs.)
- 77597 New magnetic metallic glasses with reduced metalloïd content.** R.C.O'Handley, N.J.Grant (MIT, Cambridge, MA, USA).
Rapidly Solidified Amorphous and Crystalline Alloys. Proceedings of the Materials Research Society Annual Meeting, Boston, MA, USA, Nov. 1981 (New York, USA: North-Holland 1982), p.217-23
Several new magnetic amorphous alloys containing early transition metals and having reduced metalloïd content have been melt spun. Some properties of three examples of this new class, Co₅₀Nb₁₄B₆, Co₅₄Nb₁₀B₆, and Fe₈₁Nb₅B₁₄, are presented. The dominant late transition metal content assures an appreciable magnetic moment while the presence of an early transition metal significantly enhances the stability against crystallization. Crystallization temperatures are 742K, 698K, and 762K for the three alloys, respectively. X-ray diffraction patterns show the materials to be amorphous and to exhibit a large- r correlation length that is shorter than is typically observed in TL₉₀M₁₀ glasses containing more than one transition metal species. The coercivities of the glass compositions range from 30 to 70 mOe. (16 refs.)

77598 Perpendicularly crystallized ribbons by means of rapid solidifications from melts. N.Tsuya, K.I.Arai, K.Ohmori (Res. Inst. of Electrical Communication, Tohoku Univ., Sendai, Japan). *Rapidly Solidified Amorphous and Crystalline Alloys*, Proceedings of the Materials Research Society Annual Meeting, Boston, MA, USA, Nov. 1981 (New York, USA: North-Holland 1982), p.331-42.
Silicon-iron alloy ribbons containing around 6 wt.% silicon and Sendust alloy ribbons in the crystalline state were prepared by a rapidly quenching roll method. In the as-prepared ribbons, columnar grains were observed to grow from the surface to the middle part of the ribbon thickness. For the high silicon-iron ribbons annealed at 1200°C for 30 minutes, the grain size was more than 1 mm and the texture was highly oriented to (100)[0 k] cube-on-face. The coercive force was 55 mOe for the 6.6 Si-93.4 Fe ribbons annealed at 1180°C for 60 minutes in vacuum, and the average magnetic iron loss of the ribbons was measured. For Sendust ribbons, the lowest coercive force was 8 mOe when the ribbons were annealed at 1040°C for 30 minutes and then cooled at the rate of 60 deg/hour down to 550°C in vacuum. The recording heads made of laminated Sendust ribbons exhibit much better recording characteristics than ferrite heads, while frequency response remains flat. (21 refs.)

77599 Raney type nickel catalysts from RSR atomization of Al-Ni powders. C.S.Brooks, F.D.Lemkey, G.S.Golden (United Technol. Res. Center, East Hartford, CT, USA). *Rapidly Solidified Amorphous and Crystalline Alloys*, Proceedings of the Materials Research Society Annual Meeting, Boston, MA, USA, Nov. 1981 (New York, USA: North-Holland 1982), p.397-407.
The synthesis and catalytic properties of hydrogenation catalysts of the Raney type derived from aluminum-nickel and aluminum-molybdenum-nickel rapid solidification rate (RSR) alloy powders have been evaluated. Activated Al-Ni alloy powder produced by RSR with 28.5 w/o nickel provides superior hydrogenation rates over bulk cast RaneyTM nickel catalyst for several selected, diverse organic functional groups. Rapid solidification, followed by heat treatment at 850°C in a fluidized bed of Al-Ni alloy powders with about 42 w/o nickel, appears to offer an alternate enrichment path for Al₃Ni and subsequently an enhanced catalytically active nickel. Rapid atomization synthesis of Al-Ni alloy powders by procedures such as RSR offers a promising new route for preparation of improved nickel hydrogenation catalysts of the skeletal Raney type. (10 refs.)

77600 Hot consolidation/devitrification metallic glasses—novel multiphase crystalline alloys in bulk shapes with technological potentials. R.Ray (Marko Materials Inc., N.Billerica, MA, USA). *Rapidly Solidified Amorphous and Crystalline Alloys*, Proceedings of the Materials Research Society Annual Meeting, Boston, MA, USA, Nov. 1981 (New York, USA: North-Holland 1982), p.435-40.
Iron, nickel and/or cobalt base metallic glasses with low contents of metal-oids, predominantly boron, upon heat treatment at temperatures well above the crystallization temperature of the glassy phase, transform into ultra-fine-grained (microcrystalline) alloys containing finely dispersed boride phases. Microcrystalline alloys devitrified from glassy phase are characterized by high strength, excellent thermal stability and superior corrosion/oxidation resistance. Mechanical properties of bulk microcrystalline alloys hot consolidated-devitrified from selected low metalloid metallic glass alloys are reported. (6 refs.)

Lithium doping of candidate fusion reactor alloys to simulate simultaneous helium and damage production See Entry 75177

Preparation and study of the structure development of amorphous Pb-Sb alloys See Entry 76308

On the analytic description of the process of electric-discharge sintering of metal powders See Entry 77594

Control over the structure of hard metals and other heterophase materials produced by liquid-phase sintering. II. Principles of optimum design of hard metals See Entry 77610

FCC and BCC solidification products in a rapidly solidified austenitic steel See Entry 77628

Analysis of a rapidly solidified high-phosphorus austenitic steel containing an amorphous phase See Entry 77660

Structure/property relationships and applications of rapidly solidified aluminum alloys See Entry 77661

Effect of heat treatment on the distribution of elements in the phase components of a W-Ni-Fe alloy See Entry 77684

Surface reinforcement of iron-base materials See Entry 77804

81.20J Dispersion-, fibre-, and platelet-reinforced metal-based composites

77601 Composite materials: some recent developments. K.K.Chawla (Post Graduate Div., Inst. Militar de Engenharia, Rio de Janeiro, Brazil). *J. Met. (USA)*, vol.35, no.3, p.82-7 (March 1983).

A state-of-the-art review of the current situation in composite materials is presented. The review is based on papers presented at the Fourth International Conference on Composite Materials, Tokyo, October 1982, and on the author's discussions with colleagues and composite manufacturers. Special emphasis is given to the Japanese work in this field. Among the so-called advanced fibers, carbon fiber today represents a fairly standard and acceptable engineering materials, and Japanese manufacturers dominate the fiber market worldwide. Kevlar fiber continues to make further inroads in aircraft and other industries while boron fiber continues to be a very expensive fiber. Among the ceramic fibers, continuous Al₂O₃ and SiC fibers appear to be very promising for metal matrix reinforcement. This is especially so now in view of the revolutionary processes (from organometallic compounds by heat treatment) for the manufacture of these continuous fibers developed in Japan. (11 refs.)

81.20L Ceramics and refractories

77602 Fabrication and characterization of TiC_{1-x}N_x (0 ≤ x ≤ 1) and Mo₂B_{2-x}C_x (x = 0, 1.0, 2.0) by high-pressure hot-pressing. M.Shimada, T.Suzuki, M.Koizumi (Inst. of Sci. & Industrial Res., Osaka Univ., Osaka, Japan).

Mater. Lett. (Netherlands), vol.1, no.5-6, p.175-7 (April 1983).
High-pressure reaction sinterings of TiN-TiC and MoC-MoB systems were carried out at 3.0 GPa and 1600°C for 30 min. The temperature dependences of Vickers microhardness and thermal conductivity were examined. (5 refs.)

77603 Synthesis of gadolinium-gallium garnet. O.V.Gorshkova, E.S.Lukin (D.I. Mendeleev Inst. of Chem. Technol., Moscow, USSR). *Glass & Ceram. (USA)*, vol.39, no.5-6, p.299-301 (May-June 1982). Translation of: *Steklo & Keram. (USSR)*, vol.39, no.6, p.23-4 (June 1982). [received: March 1983]

The purpose of the authors' investigation was to determine the possibility of producing a highly homogeneous powder of gadolinium-gallium garnet, active to sintering, by low-temperature synthesis from hydroxides prepared by the method of joint precipitation from concentrated chloride salt solutions. The effect of precipitation conditions (different combinations of the temperature of the precipitating agent and salt solution of the initial components) on such properties of the hydroxide powders as dispersion, filterability, and also on the microstructure and phase composition of synthesized gadolinium-gallium garnet powders was investigated. (2 refs.)

77604 Preparation and investigation of solid solutions with a perovskite structure. I.N.Belyaev, L.N.Aver'yanova, B.S.Medvedev, S.S.Lopatin (Rostov State Univ., Rostov-on-Don, USSR).

Inorg. Mater. (USA), vol.18, no.7, p.1007-10 (July 1982). Translation of: *Izv. Akad. Nauk SSSR Neorg. Mater.*, vol.18, no.7, p.1194-8 (July 1982). [received: Feb. 1983]

It was proved that no PbAl_{1-x}Nb_xTi_{1-x/2}O₃ solid solutions are formed on direct reactions of the components PbTiO₃(PbZrO₃) and Pb₂AlNbO₆ up to a temperature of 1000°C. These solid solutions can be obtained only by gradual introduction of the component parts into them. Isomorphic substitution of titanium by aluminum and niobium in PbTiO₃ reduces the electrical conductivity and tan δ by 1-2 orders and makes it possible to obtain highly dense ceramics susceptible to polarization and suitable for use as piezoelectric materials. Favorable conditions for the appearance of the ferroelectric state develop on similar substitution of zirconium in PbZrO₃. (10 refs.)

77605 Some characteristics of the cold densification of wurtzite boron nitride powders under conditions of high pressures. S.S.Dzhamarov, N.P.Pavlenko, A.V.Bochko, P.A.Kornienko (Inst. of Materials Sci., Acad. of Sci., Ukrainian SSR).

Sov. Powder Metall. & Met. Ceram. (USA), vol.21, no.10, p.755-9 (Oct. 1982). Translation of: *Poroshk. Metall. (USSR)*, vol.21, no.10, p.6-10 (Oct. 1982). [received: May 1983]

Determinations were made, using mercury porosimetry methods, of the specific surfaces and mean particle sizes of the main fractions of wurtzite boron nitride powders and compacts. It was found that in pressing in the pressure range 1.0-10.0 GPa densification was accompanied by intense comminution of BN_w particles. The re-pressing of BN_w powders granulated after being pressed under a pressure of 4.3 GPa was satisfactorily described by Bal'shin's equation. (16 refs.)

77606 Sintering kinetics of tantalum carbide. P.S.Kislyi, S.A.Shvab, F.F.Egorov (Inst. of Materials Sci., Acad. of Sci., Ukrainian SSR).

Sov. Powder Metall. & Met. Ceram. (USA), vol.21, no.10, p.765-7 (Oct. 1982). Translation of: *Poroshk. Metall. (USSR)*, vol.21, no.10, p.16-19 (Oct. 1982). [received: May 1983]

A study was made of the influence exerted by one of the more effective methods of activating the sintering process, powder comminution, on the densification kinetics of TaC compacts. It was found that tantalum carbide sintered at a temperature above 2500°C. Decreasing the powder particle size activated the sintering process, but even with a powder of 0.17-μm particle size specimens sintered at 2700°C had a porosity of 11%. Coarse powders (>7-8 μm) sintered without densification, at 2000-2200°C by a surface self-diffusion mechanism. Fine powders (<7-8 μm) under densification at temperatures above 1400°C by a diffusion-viscous flow and a volume self-diffusion mechanism during long holding periods and also probably by an activated grain-boundary sliding mechanism in the initial stage of sintering after rapid heating. (9 refs.)

77607 Recrystallization of silicon nitride powders during hot pressing. I.I.Osipova, D.A.Pogorelova, V.N.Paderni, G.M.Kheidemane, T.A.Shapoval (Inst. of Materials Sci., Acad. of Sci., Ukrainian SSR).

Sov. Powder Metall. & Met. Ceram. (USA), vol.21, no.10, p.789-92 (Oct. 1982). Translation of: *Poroshk. Metall. (USSR)*, vol.21, no.10, p.43-7 (Oct. 1982). [received: May 1983]

To study the recrystallization processes accompanying the hot pressing of silicon nitride, several grades of silicon nitride powders were subjected to particle size and chemical composition determinations. The hot pressing of comminuted silicon nitride powders enables a uniform fine-grained structure of one and the same mean grain size to be obtained irrespective of the type of starting Si₃N₄ powder. At milling times of more than 100 h no significant decrease in particle size is observed. The recrystallization of milled silicon nitride powders during hot pressing takes place chiefly in the fine fractions appearing during milling. The degree of recrystallization attained is higher with ultrafine active silicon nitride powders (PCS) than with comminuted powders. (8 refs.)

77608 Effect of physicochemical transformations occurring in compacts during heating on the properties of manganese-zinc ferrites. A.V.Kopayev, V.P.Pashchenko, V.V.Ganin, T.S.Fedoseeva (Ivano-Frankovsk State Pedagogical Inst., USSR).

Sov. Powder Metall. & Met. Ceram. (USA), vol.21, no.10, p.806-9 (Oct. 1982). Translation of: *Poroshk. Metall. (USSR)*, vol.21, no.10, p.62-6 (Oct. 1982). [received: May 1983]

A study was made of the physicochemical transformations occurring during the heating of specimens pressed from manganese-zinc ferrite powders. The effect of method of preparation of ferrite powders on the character of processes taking place in compacts during heating is demonstrated. The degree of decomposition of the spinel at a given rate of heating is lower in powders produced by the carbonate coprecipitation method than in powders obtained from an oxide mixture. The reason for this is that the structure of carbonate-grade powders has comparatively few defects. Lowering the rate of heating of specimens in the temperature range 550-650°C increases the degree of decomposition of the spinel, ensures a better reproducibility of properties, and improves the quality of ferrite parts. (11 refs.)

77609 Characterization of spray pyrolysed spinel powders. S.Kanzaki (Government Industrial Res. Inst., Nagoya, Japan), K.Hirao, N.Otsuka, K.Saito, Z.Nakagawa, K.Hamano.

Yogyo-Kyokai-Shi (Japan), vol.91, no.2, p.81-6 (1983). In Japanese.
Stoichiometric MgAl₂O₄ spinel powders have been synthesized from magnesium and aluminum nitrates solution by spray pyrolysis method. The obtained powders were characterized by means of X-ray diffraction, measurements of specific surface area, grain-size and pore-size distribution and scanning electron microscopy. The powders synthesized above 800°C consisted of spinel phase. The synthesized spinel powder consisted of agglomerated hollow spherical particles. The particle size in the agglomerates ranged from submicron to 20 μm in diameter. Further, each hollow spherical particle was formed by very fine primary particles (100 to 800 Å in diameter) among which much smaller pores (10 to 100 Å in diameter) were included. Diameter of the

agglomerates increased as the concentration of the solution and/or the water content in the solvent was increased. The specific surface area and the pore volume of the powders depended on the ratio of water/methanol content in the solvent, but they were not affected by solution concentration. (11 refs.)

Calculating the temperature coefficient of linear expansion of glazes and calcined ceramic masses See Entry 76674

The DC resistivity of modified PZT ceramics See Entry 76944

Correspondence analysis for describing the morphology of powders. Application to a commercial alumina powder See Entry 77539

Microstructure and mechanical strength of aluminum titanate ceramic prepared from mixture of alumina and titania See Entry 77758

Effect of a CaF_2 addition on the oxidation of hot-pressed silicon nitride-base materials See Entry 77783

81.20N Cermets, ceramic and refractory composites

77610 Control over the structure of hard metals and other heterophase materials produced by liquid-phase sintering. II. Principles of optimum design of hard metals. O.P.Kolchin (All-Union Sci.-Res. & Design Inst. of Refractory Metals & Hard Alloys, USSR).

Sov. Powder Metall. & Met. Ceram. (USA), vol.21, no.10, p.768-71 (Oct. 1982). Translation of: *Poroshk. Metall. (USSR)*, vol.21, no.10, p.19-23 (Oct. 1982). [received: May 1983]

For pt.1 see Poroshk. Metall., no.9, p.14-8 (1982). Considers some hitherto little investigated problems common to materials produced by LPS. Suggestions are made, the implantation of which necessitate a critical assessment of methods of manufacture of hard metals and alloys. (3 refs.)

77611 Structural investigations of detonation-deposited tungsten carbide-cobalt coatings. R.A.Alfintseva, V.Kh.Kadyrov, V.K.Fedorenko, A.Z.Sharypov (Inst. of Materials Sci., Acad. of Sci., Ukrainian SSR).

Sov. Powder Metall. & Met. Ceram. (USA), vol.21, no.10, p.772-6 (Oct. 1982). Translation of: *Poroshk. Metall. (USSR)*, vol.21, no.10, p.24-9 (Oct. 1982). [received: May 1983]

A study was made of the character of structure formation in the detonation deposition of VK20 hard-metal mixtures and of the mechanism of disintegration of the coating material under the action of vibratory contact loading and fretting corrosion. The phase composition of detonation-deposited VK type coatings was found to differ from that of the starting mixtures. A deposited layer contains about 40-50% of the tungsten carbide WC present in the starting mixture, metallic tungsten and cobalt, the intermetallic compounds Co_3W_6 and Co_3W , traces of W_2C , and a small amount of complex carbides. The amount and particle size of the tungsten carbide in a coating are determined by the particle size distribution of the powder being deposited and detonation process parameters. The investigations have shown that the optimum powder particle size range for the process of detonation deposition of hard-metal mixtures may be taken to be 5-40 μm . During detonation deposition under the conditions investigated the usual hard-metal structure and composition are not obtained. Most of the starting tungsten carbide decomposes with the formation of tungsten and cobalt intermetallic compounds. (13 refs.)

77612 Formation of a nickel-clad titanium carbide coating and effect of spraying conditions on its structure and properties. F.I.Kitaev, A.S.Namychkin, A.G.Bakanov, L.M.Ryabich, I.I.Timofeeva, N.P.Tel'nikova (Kuibyshev Aviation Inst., Kuibyshev, USSR).

Sov. Powder Metall. & Met. Ceram. (USA), vol.21, no.10, p.776-80 (Oct. 1982). Translation of: *Poroshk. Metall. (USSR)*, vol.21, no.10, p.29-33 (Oct. 1982). [received: May 1983]

Use of nickel-clad titanium carbide in plasma spraying leads to the formation of a wear-resistant coating composed of TiC grains which are fairly evenly distributed in a matrix containing reaction products of the starting components. To study the behavior of particles in the plasma jet and the character of coating formation, experiments were carried out in which composite materials (CMs) with nickel contents of 25, 35, and 50 wt.% (KTP-25N, KTP-35N, and KTP-50N) were sprayed into water and onto glass. The investigation showed that the metallic shells on the CM particles were generally preserved during the latter's flight to the substrate. In CMs spray-deposited onto glass no sizable regions were found of metal without carbide cores. In microsections of particles sprayed into water there were no sharp boundaries between the cladding layers and carbide grains. The microhardness of the outer layers varied in the range (2-8) $\cdot 10^3$ MPa. (1 ref.)

Interfacial conduction in lithium iodide containing inert oxides See Entry 76693

81.20P Glasses

77613 Variation of lighting engineering characteristics of selenium-cadmium glass during hardening. E.B.Sevryuk, A.I.Neich, V.A.Khvostova. *Glass & Ceram. (USA)*, vol.39, no.5-6, p.231-4 (May-June 1982). Translation of: *Steklo & Keram. (USSR)*, vol.39, no.5, p.12-14 (May 1982). [received: March 1983]

Articles of this glass are subjected to liquid hardening to increase the heat resistance in the range of 250-400°C. It is known that hardening of red selenium-cadmium glass results in a shift of the spectral transmission curve. Investigations of the effect of different production factors on the nature and extent of variation of the lighting engineering characteristics (color tone λ , saturation P, and integral light transmission τ) during hardening of glass colored with cadmium sulfoselenide are presented. Heat-resistant glass of the $\text{SiO}_2\text{-Al}_2\text{O}_3\text{-B}_2\text{O}_3\text{-ZnO-Na}_2\text{O}$ system was investigated. Se, CdS, and CdCO_3 were introduced as the coloring materials. (4 refs.)

77614 Melt processing and properties of barium-Sialon glasses. W.K.Tredway, S.H.Risbud (Dept. of Ceramic Engng., Univ. of Illinois, Urbana, IL, USA).

J. Am. Ceram. Soc. (USA), vol.66, no.5, p.324-7 (May 1983). Bulk oxynitride glasses in the system Ba-Sialon were prepared by cooling homogenized melts from $\approx 1740^\circ\text{C}$ at $\approx 50^\circ\text{C}/\text{min}$. The microchemistry, microstructure, and properties of these materials were studied by DTA, dilatometry, electron microscopy, and energy dispersive X-ray analysis. Up to ≈ 7 at.% nitrogen was retained in the glasses by the conventional glass-processing techniques used. Microscopically homogeneous glasses were obtained despite macroscopic segregation of millimeter-sized metallic spheres consisting of Si and Fe. Incorporation of nitrogen in the glass network led to decreasing thermal expansion coefficients, higher glass-transition temperatures, and greater values of indentation hardness with increasing nitrogen content. (19 refs.)

77615 The fining of glass. A Raman-spectrometric investigation into the action of arsenic oxides. H.Verweij (Philips Res. Labs., Eindhoven, Netherlands).

Philips Tech. Rev. (Netherlands), vol.40, no.10, p.310-15 (1982).

A study has been made of the fining action of arsenic oxides in glass formation. Specimens composed of 30 mol.% K_2CO_3 , 70 mol.% SiO_2 , and 1 mol.% As_2O_3 were exposed for an hour to temperatures of 700, 800, 850, 900, 1000 or 1100°C . After cooling the specimens rapidly to room temperature, spectra were recorded with a laser-Raman spectrometer. Above 900°C there is reduction from pentavalent to trivalent arsenic, accompanied by the release of oxygen. This oxygen has a fining action, either by causing the CO_2 bubbles produced earlier in the melt to expand, or by displacing the CO_2 . Any oxygen bubbles still remaining dissolve again in the melt on cooling. The Raman spectra also suggest that the reduction of As^{5+} to As^{3+} is chemically induced, by a reduction of the potassium content in the liquid glass phase during the glass-forming process. (3 refs.)

Installation to determine the index of the heterogeneity of glass See Entry 74540

Thermal expansion of high-silica glass See Entry 76673

Calculating the temperature coefficient of linear expansion of glazes and calcined ceramic masses See Entry 76674

New magnetic metallic glasses with reduced metalloidal content See Entry 77597

81.30 PHASE DIAGRAMS AND MICROSTRUCTURES DEVELOPED BY SOLIDIFICATION AND SOLID-SOLID PHASE TRANSFORMATIONS

(see also 61. Structure of liquids and solids 64.70 Phase equilibria, phase transitions, and critical points)

Solid+liquid equilibrium diagram of acetanilide+phenacetin mixtures determined by differential scanning calorimetry See Entry 76585

Large area silicon sheet produced by the spinning method See Entry 77557

81.30B Phase diagrams of metals and alloys

77616 Thermodynamic properties of liquid silver-thallium alloys. K.Kameda, Y.Yoshida, S.Sakairi (Dept. of Metall., Iwate Univ., Morioka, Japan).

J. Jpn. Inst. Met. (Japan), vol.47, no.5, p.406-12 (1983). In Japanese.

The EMF of a galvanic cell involving fused salt electrolytes has been measured, in order to obtain thermodynamic data of the liquid Ag-Tl system for $N_{\text{Tl}}=0.231\text{-}0.850$ in the temperature range from 938 to 1131°C . The concentration dependence of activities of both thallium and silver shows a positive moderate deviation from the Raoult's law. The order of magnitude of both activities and heats of mixing of IB metals (Cu, Ag and Au)-thallium binary alloys in the intermediate composition range is the same as that in the Periodic Table (i.e. Cu, Ag and Au). The activities and the heats of mixing of the liquid Cu-Tl and Ag-Tl alloys are respectively quite different from those of the liquid Au-Tl system, in which the activities show negative moderate deviations and the heats of mixing are slightly exothermic in the whole concentration range, owing to the larger electronegativity factor in the gold alloys. Furthermore, results of both activities and heats of mixing measurements in the liquid binary alloys composed of IB metals and thallium, lead, bismuth and those composed of IB metals and other normal metals (i.e. Zn, Cd, Al, Ga, In, Sn and Sb) have been compared and discussed in connection with the electronic structure of the elements and with the alloy theory by Engel concerning the phase stability of solid solution between IB metals and normal metals. (38 refs.)

77617 Determination of thermodynamic activities of components in the sections $x_{\text{Cr}}=0.11$ and $x_{\text{Cr}}=0.33$ of γ -solid solution Cr-Fe-Ni at 1500K. J.Vrestal (CSAV, Brno, Czechoslovakia), A.Rek.

Kovove Mater. (Czechoslovakia), vol.21, no.2, p.97-104 (1983). In Czech.

Thermodynamic activities of components in the γ -solid solution Cr-Fe-Ni were measured by the effusion method together with the analysis of the ratio of components in the condensed layer by an electron probe microanalyser. The sections $x_{\text{Cr}}=0.11$ and $x_{\text{Cr}}=0.33$ were studied at 1500K. The pure FCC-metals (Fe,Ni) and BCC-chromium were chosen as standard states. The measured values were optimised by a procedure securing the consistency with previous results. The Gibbs-Duhem equation and the thermodynamic condition of solution stability are satisfied for the concentration dependence of the activity of components at 1500K. The interaction coefficients characterizing the influence of the third component concentration on the activity of binary system components for $x_{\text{Fe}} \rightarrow 0$ and $x_{\text{Ni}} \rightarrow 0$ are calculated for both sections. (13 refs.)

77618 Bi-In system. D.S.Evans, A.Prince (General Electric Co. plc, Hirst Res. Centre, Wembley, England).

Met. Sci. (GB), vol.17, no.3, p.117-21 (March 1983).

The Bi-In system has been redetermined mainly using thermal analysis but supplemented as appropriate by metallographic and X-ray examination. It is confirmed that the system contains four compounds BiIn , Bi_2In_3 , BiIn_2 and an ϵ phase at approximately 90 at.%In. Bi and BiIn form a eutectic at 46.8 at.%In and 109.7°C . The compound Bi_2In_3 is generated in a peritectic reaction at 88.9°C and forms a eutectic with BiIn₂ at approximately 64.6 at.%In and 88.7°C . The ϵ phase is also generated in a peritectic reaction, at a temperature of 93.5°C , and forms a eutectic with BiIn₂ at 78.5 at.%In and 72.7°C . The probable accuracy of the results is ± 0.5 at.%In and $\pm 0.5\text{K}$. The ϵ phase decomposes eutectoidally at $49 \pm 1^\circ\text{C}$. Equations representing the main liquidus boundaries and the α -In solidus boundary are given. (12 refs.)

77619 Decomposition of sigma phase in a Ni-Cr-W system. M.Kikuchi, M.Kajihara, Y.Kadoya, R.Tanaka (Dept. of Metall. Engng., Tokyo Inst. of Technol., Tokyo, Japan).

Ser. Metall. (USA), vol.17, no.4, p.475-8 (April 1983).

Presents a preliminary observation of the decomposition of σ phase at the temperatures lower than 1000°C . The distribution of phases in the aged specimens was examined by optical as well as back scattered electron metallography. Phase identification was carried out by means of powder X-ray diffraction method. It was shown that no σ phase exists as an equilibrium phase in the Ni-Cr-W system below 950°C . The alloys without σ phase above 950°C are not prone to σ phase formation below 950°C . (23 refs.)

Intermediate phases of vanadium-rhenium system See Entry 76361

Phase diagram of ZrV_2 See Entry 76589

- Potentiometric study of the thermodynamic properties of intermetallic compounds Ca_2Ni_7 . Structural interpretation See Entry 76667
- On the formation of Fe-carbides in Cu-Fe and Cu-Au-Fe alloys See Entry 77652
- Effect of heat treatment on the distribution of elements in the phase components of a W-Ni-Fe alloy See Entry 77684
- Application of neutron diffraction to a study of phases in Type 316 stainless steel weld metals See Entry 77685

81.30D Phase diagrams of other materials

- 77620 Multicomponent glasses of GeO_2 and Sb_2O_3 with Bi_2O_3 , Ti_2O_3 , and/or PbO . K.Nassau, D.L.Chadwick (Bell Labs., Murray Hill, NJ, USA). *J. Am. Ceram. Soc. (USA)*, vol.66, no.5, p.332-7 (May 1983). Previous studies on glass formation involving GeO_2 with Bi_2O_3 , Ti_2O_3 , and PbO were extended by the use of Sb_2O_3 . Wide areas of glass formation occur in the systems GeO_2 - PbO - Sb_2O_3 and GeO_2 - Bi_2O_3 - Sb_2O_3 at all but the lowest GeO_2 contents; the region of single-phase glasses in the system GeO_2 - Ti_2O_3 - Sb_2O_3 is severely restricted. Glasses were examined by powder X-ray diffraction, differential thermal analysis, thermomechanical analysis, and Archimedes' technique to obtain glass transition and crystallization exotherm temperatures, thermal expansion coefficients, and densities; these properties are presented in diagrams for the GeO_2 - Sb_2O_3 binary and for two ternary systems. Based on calculated values of λ_0 , the wavelength for zero material dispersion, and $dM/d\lambda$, the material dispersion slope at λ_0 , compositions in these systems may be useful for the construction of ultralow-loss optical waveguides in the 3 to 4 μm region. (13 refs.)
- Thermodynamics on UO_2 - ZrO_2 - LaO_{2-x} solid solutions See Entry 76586
- Study of the solid-liquid equilibria of pseudo-binary systems MPO_3 - $\text{Ce(PO}_3)_3$ ($\text{M} = \text{Rb, Cs}$) See Entry 76590
- Vaporization study on the niobium-oxygen solid solution by mass-spectrometric method See Entry 76602
- Mass spectrometric study on the vaporization of ternary compounds PuM_2 ($\text{M} = \text{Fe, Co, Ni}$) See Entry 76603
- Liquid immiscibility in the systems $\text{X}_2\text{O-MO-B}_2\text{O}_3\text{-SiO}_2$ ($\text{X} = \text{Na, K; M} = \text{Mg, Ca, Ba}$) and $\text{Na}_2\text{O-MgO-BaO-B}_2\text{O}_3\text{-SiO}_2$ See Entry 76634

81.30F Solidification

(see also 64.70D Solid-liquid transitions)

- 77621 Oscillatory crystallization of a stratifying alloy. M.B.Geilikman, D.E.Temkin (Inst. of Experimental Mineralogy, Acad. of Sci., Moscow, USSR). *JETP Lett. (USA)*, vol.36, no.7, p.292-5 (5 Oct. 1982). Translation of: *Pis'ma v Zh. Eksp. i Teor. Fiz. (USSR)*, vol.36, no.7, p.238-41 (5 Oct. 1982). [received: May 1983]
- It is shown that in a certain range of parameters, an oscillatory process leading to the formation of a layered structure arises. The position of the kinetic transition line from this regime to the stationary regime, which leads to the formation of a solid phase with homogeneous composition, is indicated. (4 refs.)
- 77622 Direct observation of the coarsening of solidification structure in Sn-Pb alloy. K.Kusabiraki (Dept. of Metall. Engng., Toyama Univ., Takakoka, Japan), K.Imai. *J. Jpn. Inst. Met. (Japan)*, vol.47, no.5, p.450-6 (1983). In Japanese.
- In order to elucidate the coarsening process of the dendrite structure during isothermal holding in the liquid-solid region, in situ observation was carried out. It was found that it is possible to estimate a dendrite structure in a bulk from that on a surface, because both the dendrite arm spacings are almost similar. It was confirmed by the direct observation that the coarsening occurred due to the disappearance of smaller arms and the melting off of arms in a necked region. In the case of a small cylindrical arm, the coarsening of dendrite structure is explained by Model I proposed by Kattamis et al. In the case of melting off of dendrite arm in the necked region, the coarsening of dendrite structure is not explained by Model II proposed by Kattamis et al. A new model based on the kinetics of sintering of powder was proposed for this case. (14 refs.)
- 77623 Simplified determination of cooling conditions of aluminium-silicon alloys. H.E.Exner, J.Paul (Max-Planck-Inst. fur Metallforschung, Inst. fur Werkstoffwissenschaften, Stuttgart, Germany). *Met. Sci. (GB)*, vol.17, no.3, p.141-3 (March 1983).
- A method is described for estimating the velocities of the solidification front from the cooling rates immediately after solidification which can easily be determined from cooling curves by means of thermocouples. The equations have been tested by means of experiments carried out with a eutectic aluminium-silicon alloy and satisfactory agreement has been obtained. Possible practical applications are nondestructive determination of local microstructural parameters and, in turn, local properties, or local cooling conditions from simple counting measurements from metallographic samples. (13 refs.)
- 77624 Ferrite morphology in rapidly solidified ferritic Fe-Cr-C steels. P.A.Molian (Dept. of Mech. Engng., Iowa State Univ., Ames, IA, USA), W.E.Wood. *Scri. Metall. (USA)*, vol.17, no.4, p.431-4 (April 1983).
- Laser surface alloying of chromium into electrolytically pure iron and carbon steels was carried out to produce high chromium ferritic steels. The morphology of the ferrite was then investigated as a function of carbon and chromium contents of the alloys. It is proposed that during laser processing, the ferritic Fe-Cr and Fe-Cr-C alloys do not experience sufficient undercooling ahead of the solid-liquid interface to cause nucleation and therefore the growth mechanism is essentially epitaxial. When the carbon content is increased from 0.2 to 0.5% greater constitutional undercooling is developed, promoting a transition from grain to cell morphology. (1 ref.)
- 77625 Structure of Fe-40 at.%Al obtained by rapid quenching from melt. N.Junqua, J.Grilhe (Lab. de Metall. Phys., Faculte des Sci., Poitiers, France). *Scri. Metall. (USA)*, vol.17, no.4, p.441-4 (April 1983). In French.
- Using ultrafast quenching from the melt, the authors observed the existence of antiphase domains and a new phase not seen on the equilibrium diagram. This L10 phase is found to have a grain structure consisting of 'needles' and 'platelets'. Electron microscopic evidence is presented which supports these findings. (3 refs.) U.M.G.
- 77626 Behavior of rod macrocoolers in the reinforcement of ingots and castings. A.B.I.Medovar, V.Ya.Saenko, V.I.Us, L.B.Medovar (E.O. Paton Inst. of Electric Welding, Acad. of Sci., Ukrainian SSR). *Sov. Phys.-Dokl. (USA)*, vol.27, no.7, p.581 (July 1982). Translation of: *Dokl. Akad. Nauk SSSR*, vol.265, no.1-3, p.330-1 (July 1982). [received: April 1983]
- When the material used for sectional macrocoolers is a metal with a melting point below the solidification point of the melt, shrinkage cavities typical of an ordinary casting are formed in them during crystallization. If the melting point of the rod is higher than the solidification point of the melt, i.e. if relatively refractory metal rods are used, they remain unmelted in the ingot (casting). But if the melting point of the rod is below the solidification temperature of the melt, the rod—having been immersed in liquid metal—first causes crystals to grow in the adjoining volume of this melt and becomes thicker, as it were, and then, as in the case of a sphere, melts partially or completely. The rate of melting and solidification of the reinforcing rod is determined by the relative speed of the melt and the rod (when the rod is immersed in the melt, or when the melt is raised into the space in which the rod has been set up). (1 ref.)
- 77627 Rapid solidification of steels. B.Cantor (Dept. of Metall. & Sci. of Materials, Univ. of Oxford, Oxford, England).
- Rapidly Solidified Amorphous and Crystalline Alloys. Proceedings of the Materials Research Society Annual Meeting, Boston, MA, USA, Nov. 1981 (New York, USA: North-Holland 1982), p.317-30
- Reviews some fundamental aspects of the rapid solidification of iron-based alloys and commercial steels, concentrating on heat flow during cooling, the thermodynamics and kinetics of solidification, post-solidification solid state phase transformations, and the effect of these processes on the resulting steel microstructures. (58 refs.)
- 77628 FCC and BCC solidification products in a rapidly solidified austenitic steel. T.F.Kelly, J.B.Vander Sande, M.Cohen (Dept. of Materials Sci. & Engng., MIT, Cambridge, MA, USA).
- Rapidly Solidified Amorphous and Crystalline Alloys. Proceedings of the Materials Research Society Annual Meeting, Boston, MA, USA, Nov. 1981 (New York, USA: North-Holland 1982), p.349-54
- The microstructures and local composition variations in centrifugally atomized high-sulfur stainless steel powder are investigated. Both FCC and BCC are found to be primary solidification phases in the as-solidified powder, where the smaller powder particles tend to be BCC. Cellular solidification structures, with sulfide precipitates at the cell walls, are observed in both FCC and BCC particles. A noncellular BCC structure is also observed with small sulfide precipitates throughout the entire structure. Analysis of the nucleation process for solidification indicates that a transition from FCC nucleation to BCC nucleation occurs with increasing wetting angle in heterogeneous nucleation. Thus BCC should nucleate in the smaller droplets of a liquid dispersion where catalytic surfaces of low potency tend to be the only heterogeneous nucleants available. (5 refs.)
- 77629 Microstructure of a rapidly solidified Al-Fe-Co-Ni alloy. T.H.Sanders, Jr. (Purdue Univ., West Lafayette, IN, USA), H.G.Paris, J.W.Mullins.
- Rapidly Solidified Amorphous and Crystalline Alloys. Proceedings of the Materials Research Society Annual Meeting, Boston, MA, USA, Nov. 1981 (New York, USA: North-Holland 1982), p.369-74
- Observations made on different consolidated and wrought microstructures suggested that in addition to the simple variations in size and size distributions there were also differences in shape. Furthermore, clusters of oriented precipitates were often observed. The different particle morphologies were related to solidification rate effects. The authors describe the changes in microstructure which occur during the heating of rapidly solidified Al-3.3Fe-4.6Co-2.31Ni splat. (7 refs.)
- 77630 Rapidly solidified long range ordered alloys. E.H.Lee, C.C.Koch, C.T.Liu (Metals & Ceramics Div., Oak Ridge Nat. Lab., Oak Ridge, TN, USA).
- Rapidly Solidified Amorphous and Crystalline Alloys. Proceedings of the Materials Research Society Annual Meeting, Boston, MA, USA, Nov. 1981 (New York, USA: North-Holland 1982), p.375-9
- The influence of rapid solidification processing on the microstructure of long-range-ordered alloys in the (Fe,Co,Ni)₃V system has been studied by transmission electron microscopy. The main microstructural feature of the as-quenched alloys was a fine cell structure (~300 nm diameter) decorated with carbide particles. This structure was maintained after annealing treatments which develop the ordered crystal structure. Other features of the microstructures both before and after annealing are presented and discussed. (10 refs.)
- Oscillatory morphological instabilities due to non-equilibrium segregation See Entry 76592
- Microstructures of rapidly solidified Fe-Al-Zr alloys See Entry 76649
- Transmission electron microscopy of RSP Fe/Cr/Mn/Mo/C alloy See Entry 76653
- Directional solidification of silicon in carbon crucibles by an Oscillating Crucible Technique See Entry 77554
- Thin-film epitaxial solar cells on substrates made from MG silicon by the HEM process See Entry 77565
- Interaction between cast silicon properties and solar cell performance See Entry 77592
- Perpendicularly crystallized ribbons by means of rapid solidifications from melts See Entry 77598
- Grain-coarsening resistance and the stability of second-phase dispersions in rapidly solidified steels See Entry 77654
- Analysis of a rapidly solidified high-phosphorus austenitic steel containing an amorphous phase See Entry 77660
- Effect of two-phase solidification on fracture toughness of aluminium alloys See Entry 77726
- Thin film polycrystalline silicon solar cell See Entry 78025

81.30H Constant-composition solid-solid phase transformations: polymorphic, massive, and order-disorder
(see also 64.70K Solid-solid transitions)

77631 Diffusionless omega transformations in quenched and pressurized Zr-Mo alloys. O.Botstein (Dept. of Materials Sci. & Engng., Technion Israel Inst. of Technol., Haifa, Israel), M.Talianker, A.Rabinkin. *Acta Metall. (USA)*, vol.31, no.6, p.947-53 (June 1983). Metastable structures formed in Zr-Mo alloys on quenching and following high pressure application were studied by transmission electron microscopy and X-ray phase analysis. New structures consisting of a mixture of α -phase and ω phase originating in α [i.e. $\omega(\alpha)$] were observed. Complex structures form in quenched Zr alloys with 1.5-2.5 at.% Mo which contain α , β and ω originating in both α and β . The maximum possible number of the ω particle orientations (ω -variants) in a sample is seven: three for $\omega(\alpha)$ and four for $\omega(\beta)$. High pressure application to the quenched structures gives rise to the α - $\omega(\alpha)$ and β - $\omega(\beta)$ transformation. Pressure induced ω phase can be retained at atmosphere pressure upon unloading. The genesis of various metastable structures is proposed by consideration of metastable phase equilibria existing in the Zr-Mo system. (20 refs.)

77632 Order-disorder transformation study in 25-35 at.% Cd-Mg alloys by energy dispersive X-ray diffraction (EDXD). E.S.U.Laine, I.T.Lahteenmaki (Dept. of Phys. Sci., Univ. of Turku, Turku, Finland). *Mater. Lett. (Netherlands)*, vol.1, no.5-6, p.166-70 (April 1983). It is shown that the energy dispersive X-ray diffraction (EDXD) method is in some cases a very applicable tool to study the order-disorder transformation. (12 refs.)

77633 Influence of the crystallography of the grain boundary/grain system on the α - γ phase shift in Fe-4%Ni alloys. N.Benfetima, C.Haut, S.Lartigue, D.Bouchet, L.Priester (Lab. de Metall. Phys., Univ. Paris-Sud, Orsay, France). *Mem. & Etud. Sci. Rev. Metall. (France)*, vol.80, no.3, p.149-55 (March 1983). In French. Work was carried out on an Fe-4%Ni alloy containing 150.10⁻⁶ wt.% carbon. The preparation of transparent cuts by the double-jet technique. Results are presented and interpreted. (18 refs.)

77634 TTT curves for the formation of austenite. U.R.Lenel (Fulmer Res. Inst., Slough, England). *Ser. Metall. (USA)*, vol.17, no.4, p.471-4 (April 1983). Describes the main features of time-temperature-transformation (TTT) diagrams which have been determined for re-austenitisation of two contrasting low carbon steels, one containing 10% Cr, the other 1% Mn. (5 refs.)

77635 Phase transformation studies of laser-processed Fe-0.2%C-Cr surface alloys. P.A.Molian, P.J.Wang (Materials Sci. Dept., Oregon Graduate Center, Beaverton, OR, USA), K.H.Khan, W.E.Wood. Rapidly Solidified Amorphous and Crystalline Alloys. Proceedings of the Materials Research Society Annual Meeting, Boston, MA, USA, Nov. 1981 (New York, USA: North-Holland 1982), p.511-15. Phase transformations in laser-processed Fe-0.2%C-Cr surface alloys with 5%, 10%, 20%, and 30% Cr were studied by light and electron microscopy. Alloys containing 5% and 10% Cr were found to be fully martensitic with a dislocated lath type substructure. Thin films of retained austenite and a homogeneous dispersion of fine carbides were observed at the lath boundaries and prior austenite grain boundaries. The alloy with a 20%Cr content showed a unique microstructure of twinned austenite needles in a dislocated ferrite matrix while the alloy containing 30% Cr exhibited a dislocated ferrite structure with M₂₃C₆ carbides. (3 refs.)

Short-range ordering in nickel-chromium thermocouple alloys See Entry 76367

Irradiation induced order-disorder in Ni₃Al and NiAl See Entry 76504

Structural changes of a piezoelectric crystal BaZnGeO₄ on thermal phase transition See Entry 76621

The β - α transition in rapidly quenched Sn-Ge alloys See Entry 76622

Microstructure and properties of fine grained supersaturated Fe-C alloys See Entry 76650

Nonlinear resonance in Cu₃Au See Entry 77691

81.30K Martensitic transformations
(see also 64.70K Solid-solid transitions)

77636 On the change in the austenite lattice parameter due to the martensitic transformation in an Fe-32Ni alloy. M.Hayakawa, M.Oka (Dept. of Mech. Engng., Tottori Univ., Tottori, Japan). *Acta Metall. (USA)*, vol.31, no.6, p.955-9 (June 1983). For the purpose of clarifying the mechanism of the often reported reduction in the austenite lattice parameter due to the martensitic transformation, the lattice parameters of an Fe-32Ni alloy prepared by different cooling rates from the austenitization temperature have been measured in the states before and after the martensitic transformation. From the measurement made, the stress levels have also been calculated for both states. In the slowly cooled stress-free specimen no significant change in the lattice parameter was found after the martensitic transformation, which is in agreement with the theoretical prediction, whereas in the quenched specimens, in which quenching stress is present, an appreciable reduction in the parameter was found. The latter is accounted for by stress relaxation due to the martensitic transformation. (16 refs.)

77637 Influence of a high pressure on the kinetics of formation of lath (packet) martensite. V.I.Izotov, A.V.Omel'chenko, L.S.Pankratova, V.I.Soshnikov (Inst. of Metall. & Phys. of Metals, Moscow, USSR). *Fiz. Met. & Metalloved. (USSR)*, vol.55, no.4, p.711-16 (April 1983). In Russian. English translation in: *Phys. Met. & Metallogr. (GB)*. A magnetometric method was used to study the kinetics of a martensitic transformation occurring at pressures up to 8000 atm in an alloy of the Fe-8.5 Cr-1 Ni composition, in which lath (packet) martensite was formed. The transformation was isothermal. A complex pressure dependence was observed for the temperatures of initiation and termination of the martensitic transformation. An estimate was obtained of the kinetic parameters of the isothermal martensitic transformation, which agreed with the parameters of the plastic deformation process. It was concluded that the nucleation of martensite was associated with thermally activated motion of dislocations. (20 refs.) A.T.

77638 Martensitic transformations in low-carbon nickel-molybdenum steels. V.M.Schastlivtsev, I.L.Barmina, I.L.Yakovleva, S.E.Karzunov, D.A.Mirzaev, O.P.Morozov, Yu.L.Legostae, T.G.Semicheva (Inst. of Metal Phys., Acad. of Sci., Sverdlovsk, USSR). *Fiz. Met. & Metalloved. (USSR)*, vol.55, no.4, p.724-32 (April 1983). In Russian. English translation in: *Phys. Met. & Metallogr. (GB)*. Magnetometric, electron-microscopic, and durometric methods were used to study the kinetics of transformation of austenite in low-carbon 10N5MF and 12KhN4MF steels during cooling at various rates (from 10 to 3×10⁵°C/sec). It was found that, depending on the rate of cooling, one could expect bainitic and martensitic transformations of two types (isothermal and athermal) with the martensitic points 340-310 and 215°C, respectively. A reduction in the cooling rate resulted in a continuous change from the isothermal martensitic transformation to the bainitic. The structure and microhardness of the products of the martensitic transformations were determined. (13 refs.) A.T.

77639 Influence of the composition of the particles contained in austenite on the characteristics of the γ - α transformation. L.P.Gun'ko, V.M.Ermakov, Yu.N.Koval', L.E.Kozlova, V.V.Kokorin (Inst. of Metal Phys., Acad. of Sci., Kiev, Ukrainian SSR). *Fiz. Met. & Metalloved. (USSR)*, vol.55, no.4, p.739-43 (April 1983). In Russian. English translation in: *Phys. Met. & Metallogr. (GB)*. An analysis was made of the influence of composition of coherent particles formed in austenite on the characteristics of the γ - α transformation. The example of Fe-Ni-Cu alloys (with the precipitates in the form of solid solutions based on Cu) and Fe-Ni-Co-Ti alloys (with the precipitates in the form of particles of the γ' phase) showed that those particles which had high values of the Young modulus tended to exhibit features typical of thermoelastic martensitic transformations. (10 refs.) A.T.

77640 Thermodynamics of the martensitic transformation in high-nickel iron alloys. Thermal effect. D.A.Mirzaev (Lenin Komsomol Polytech. Inst., Chelyabinsk, USSR). *Fiz. Met. & Metalloved. (USSR)*, vol.55, no.4, p.774-80 (April 1983). In Russian. English translation in: *Phys. Met. & Metallogr. (GB)*. It was found that allowance for the ferromagnetism of the γ phase of Fe-Ni alloys made it possible to reduce strongly the discrepancy between the theoretical and experimental values of the heat of martensitic transformation Q when calculations were made of the difference between the enthalpies of the α - and γ -phases. The composition dependence of Q was accounted for and an estimate was made of the energy stored in α -martensite. (21 refs.) A.T.

77641 Structure mechanics connected with the martensitic transformation of steels. Consequences for industry. L.Hyspecka (Acad. des Sci., Usine Vitkovice, Ostrava, Czechoslovakia). *Mem. & Etud. Sci. Rev. Metall. (France)*, vol.80, no.3, p.157-69 (March 1983). In French. A study is presented of the morphology problems of martensite with regard to mechanical properties. Effects of the structure condition on the mechanical properties are investigated for high-alloy steels type 13%Cr-6%Ni (Mo) and 9%Ni (Mo), and for low-alloy steels with 0.3%C (Mn, Si, Mo) and with 0.4%C (Mn, Si, Cr, Ni, Mg). (37 refs.)

77642 Bulk modulus and martensitic transformation in Mn-Cu alloys. Y.Tsunoda, N.Oishi, N.Kunitomi (Faculty of Sci., Osaka Univ., Osaka, Japan). *Physica B & C (Netherlands)*, vol.119 B+C, no.1-2, p.51-5 (April 1983). (Proceedings of the International Symposium on Magnetoelasticity in Transition Metals and Alloys, Nagoya, Japan, 15-16 Sept. 1982). The concentration dependence of elastic moduli has been measured over a wide concentration range of Mn-Cu alloys by means of neutron inelastic scattering and ultrasonic measurements. The elastic constant C₁₁ markedly decreases with the increase of Mn content and attains its minimum value near the composition Mn₅₂Cu₄₈ at which the martensitic transformation takes place at room temperature. However, a direct trigger of the phase transition is attributed to the vanishing of the shear modulus, contrary to the authors' previous results of neutron inelastic scattering. An anomalous volume effect is discussed in connection with the small bulk modulus near the martensitic transformation in γ -MnCu alloys. The possibilities of d-electron Coulomb correlation and the formation of the local magnetic moment are discussed as origins of the martensitic transformation in Mn-rich Mn-Cu alloys. (7 refs.)

77643 Landau theory for a cubic to tetragonal structural phase transformation. T.C.Choy, W.Young (Queen Mary Coll., Univ. of London, London, England), R.D.Lowe. *Physica B & C (Netherlands)*, vol.119 B+C, no.1-2, p.56 (April 1983). (Proceedings of the International Symposium on Magnetoelasticity in Transition Metals and Alloys, Nagoya, Japan, 15-16 Sept. 1982). Summary form only given, as follows. The authors present a new phenomenological description of a cubic to tetragonal martensitic phase transformation. The essential feature of the martensitic transition in which the transition takes a substantial temperature interval to complete is incorporated by starting from a free energy that contains the fractional volume of converted material as an additional order parameter. This model is remarkable in having a co-existing first- and second-order phase transition at the same critical temperature T_M. The c-axis order parameter has a jump, while the a-axis and fractional conversion x remain continuous at T_M. The authors have found it necessary to impose a generalised constraint condition related to the internal pressure on the system. They discuss the origin of this constraint and relate it to the magnetoelastic coupling which drives the phase transformation. Application of this theory to experiments on the alloy Mn₈₅Ni₁₅C₆ in its antiferromagnetic state (T_M<T_N) is discussed. (no refs.)

On the stability of surface martensite in β -phase Cu-Zn alloys See Entry 76758

⁵⁷Fe Mossbauer spectroscopy on FePt Invar alloys See Entry 77312

Carbon content of retained austenite in quenched steels See Entry 77666

Elasticity and anelasticity of a 304 stainless steel at below room temperature See Entry 77692

High-temperature shape memory in titanium nickelide See Entry 77702

81.30M Precipitation
(inc. segregation; see also 64.75 Solubility, segregation and mixing)

77644 Precipitation studies in lead-tin alloys. P.A.Varkey, A.R.K.L.Padmini (Appl. Phys. Dept., M.S. Univ. of Baroda, Baroda, India). *Acustica (Germany)*, vol.52, no.5, p.290-5 (April 1983). Investigation of cellular precipitation process in Pb rich, Pb-Sn alloys containing 6.1 and 12.1 wt percentage of Sn has been carried out using the composite oscillator technique. From the measured longitudinal and shear ultrasonic velocities a set of elastic moduli and related parameters are estimated. The internal friction is also measured. The elastic parameters and the internal friction are found to exhibit interesting variations during the precipitation

process. The results are interpreted on the basis of the theory of kinetics of cellular precipitation proposed by Turnbull. (19 refs.)

77645 The formation of discrete precipitate dispersions on mobile interphase boundaries in iron-base alloys. R.A.Ricks, P.R.Howell (Dept. of Metall. & Materials Sci., Univ. of Cambridge, Cambridge, England). *Acta Metall. (USA)*, vol.31, no.6, p.853-61 (June 1983). Concerns the formation of particulate carbide precipitates on high-energy interphase boundaries in alloy steels. Specifically it is shown that such boundaries may act as nucleation sites for the precipitation of alloy carbides, despite their high mobility, and that the precipitation may influence the growth mechanisms of the boundary. In addition the crystallography of the reaction is discussed with respect to the adoption of a unique orientation relationship between the ferrite and carbide phases of two distinctly different types of alloy carbides. (31 refs.)

77646 A TEM investigation of the structure of nitrogen-implanted Ti-6Al-4V. R.Hutchings (Brown Boveri Res. Center, Baden, Switzerland). *Mater. Lett. (Netherlands)*, vol.1, no.5-6, p.137-40 (April 1983). The microstructure of nitrogen-implanted Ti-6Al-4V has been investigated by transmission electron microscopy. Implantation conditions were typical of those used in metallurgical applications. The major effects of implantation are a considerable decrease in grain size and copious precipitation of TiN with a recognizable orientation relationship to the hexagonal matrix. (8 refs.)

77647 Electrical conductivity and infrared absorption spectrometry study of hematite precipitation from defective ferrites. B.Gillot, R.M.Benloucif, F.Jemali (Lab. de Recherches sur la Reactivite des Solides, Faculte des Sci. Mirande, Dijon, France). *Mater. Chem. & Phys. (Switzerland)*, vol.8, no.4, p.349-63 (April 1983). In French.

The hematite precipitation from zinc or cobalt-substituted defective spinels of type $(M_{1-x}^{2+}Fe^{3+})_{(8-2x)/3}[O_{(1-x)/2}]O_4$ has been investigated using electrical conductivity and infrared spectrometry. The experimental data show that the temperature and kinetics of hematite precipitation depend of substitution extent x and might be closely associated with the cation vacancy in the spinel lattice. Stabilization of spinel solid solution by the cation is more pronounced for zinc than for cobalt and the effect of the cation is interpreted in terms of cation distribution in the spinel lattice. (27 refs.)

77648 On the precipitation of Laves phase in 12 Cr-Mo-V-W steel heated for a long time. M.Nakahashi, S.Komatsu, S.Nakamura (Res. & Dev. Center, Toshiba Corp., Kawasaki, Japan), M.Yamada. *J. Jpn. Inst. Met. (Japan)*, vol.47, no.5, p.426-31 (1983). In Japanese. Studies on 12 Cr-Mo-V-W steel for steam turbine blade show that the Fe_3Mo intermetallic compound, so called Laves phase, is precipitated at grain boundaries after long time heating. The composition of the Laves phase in this steel having internal lattice defects is expressed by the formula $(Fe_{23}Cr_7)(Mo_{20}W_{12})$ and is unchanged after long time heating. The $M_{23}C_6$ -Laves phase transformation appeared to occur in situ, and the growth rate for the Laves phase during heating was larger than that for $M_{23}C_6$. The Laves phase area fraction was directly proportional to the Larson-Miller parameter ($P=T(C+\log t) \times 0.001$) in the 23-23.5 range. (10 refs.)

77649 The investigation of dissolution and precipitation kinetics of secondary phases in a Cr15Ni70W10MoAlTiB alloy. K.Hrbacek (Prvni Brnenska Strojirna k.p., Brno, Czechoslovakia), J.Kudrman, J.Hakl, R.Pech. *Kovove Mater. (Czechoslovakia)*, vol.21, no.2, p.115-130 (1983). In Czech. The dissolution kinetics of γ' phase and carbides during heating as well as their precipitation kinetics was studied. The results show the γ' phase dissolution above 900°C and the instability of carbides occurring at grain boundaries above 1050°C. The MC precipitates are also stable in this temperature region. The strengthening kinetics was investigated at six different temperatures between 780-910°C. The measured values seem to be in a good agreement with theoretical models. (23 refs.)

77650 VC coarsening in 0.5Cr-0.5Mo-0.25V steel. J.M.Silcock (CEGB, Central Electricity Res Labs., Leatherhead, England). *Met. Sci. (GB)*, vol.17, no.3, p.101-6 (March 1983). Observations of VC particles in 0.5Cr-0.5Mo-0.25V steels show that the coarsening rate is generally very low. Insufficient data are available to determine the time dependence exactly so that coefficients have been calculated using a cube relationship to enable comparison with some relevant published data. The wide range of particle sizes in as-heat treated materials is emphasized. Interphase particles appear to coarsen less readily than dislocation nucleated particles. (6 refs.)

77651 Carbide transformations in microstructurally unstable low alloy ferritic steel. R.B.Carruthers, M.J.Collins (Sci. Services Dept., CEGB, Harrogate, England). *Met. Sci. (GB)*, vol.17, no.3, p.107-10 (March 1983). The changes in carbide size and chemical composition accompanying prolonged exposure at elevated temperature have been studied on a number of casts of a low alloy ferritic steel. It is shown that the reactions occurring are more complex than originally believed and that particle size measurements cannot yet be used as an aid to estimating the remanent creep life of plant components. (8 refs.)

77652 On the formation of Fe-carbides in Cu-Fe and Cu-Au-Fe alloys. O.Schneeweiss, U.Gonser, H.-G.Wagner (Fachbereich Werkstoffwissenschaften, Univ. des Saarlandes, Saarbrücken, Germany). *Scr. Metall. (USA)*, vol.17, no.4, p.463-6 (April 1983). The authors have observed that carburisation of the alloys only takes place after remelting in a graphite crucible in a H_2 atmosphere. The precipitation of Fe-C particles and subsequent changes in morphology were in agreement with the phase diagram. (5 refs.)

77653 Deceleration of relaxation in a Cu-Si alloy. A.Coujou, P.Coulomb (Microscopie et Structure des Materiaux, Univ. Paul Sabatier, Toulouse, France). *Scr. Metall. (USA)*, vol.17, no.4, p.485-90 (April 1983). The authors take advantage of the specific shape of relaxation curves in a Cu-4.5 at.% Si alloy at moderate temperatures ($T \sim 0.4 T_m$) in order to obtain further data on solute pinning of dislocations. It was observed that segregation occurs during the waiting time of dislocations in front of obstacles, that is of 'forest trees'. This concept agrees with recent models of the Portevin-Le Chatelier effect slowing down of the relaxation is a precursor of this effect. Pinning corresponds to a slight change in the obstacles: 50% spreading with a few % increase in height. If segregation is due to the Suzuki effect as expected from static ageing studies, diffusion of a few solute atoms is sufficient to achieve this obstacle change; this type of interaction might also explain segregation speed. (17 refs.)

77654 Grain-coarsening resistance and the stability of second-phase dispersions in rapidly solidified steels. G.B.Olson, H.C.Ling, J.S.Montgomery, J.B.Vander Sande, M.Cohen (MIT Cambridge, MA, USA). *Rapidly Solidified Amorphous and Crystalline Alloys*, Proceedings of the Materials Research Society Annual Meeting, Boston, MA, USA, Nov. 1981 (New York, USA: North-Holland 1982), p.355-62. Control of alloy composition and processing to achieve grain coarsening resistance in rapidly solidified alloys is examined via the theory of grain boundary pinning and particle coarsening. The principles are illustrated for the case of manganese sulfides in steels. A thermodynamic survey of potential stable dispersed phases identifies TiN and rare-earth sulfides as particularly promising for alloy development via rapid solidification. (24 refs.)

Vacancy pump as a mechanism of growth of precipitates during precipitation of solid solutions See Entry 76630

Investigation of the precipitation of supersaturated solid solutions in alloys of magnesium with dysprosium See Entry 76632

Thermal evolution of precipitated phases in Au implanted MgO single crystal See Entry 76641

On the nature of the phases formed when metals are implanted with oxygen or nitrogen See Entry 76643

Microstructures of rapidly solidified Fe-Al-Zr alloys See Entry 76649

Microstructural study of devitrified amorphous alloys See Entry 76651

Investigation of redistribution of the alloying elements during diffusion annealing of titanium alloys See Entry 76687

Anomalous elastic properties of Fe-Ni (FCC) alloys and their Invar properties See Entry 77246

FCC and BCC solidification products in a rapidly solidified austenitic steel See Entry 77628

Analysis of a rapidly solidified high-phosphorus austenitic steel containing an amorphous phase See Entry 77660

Effects of the quenching conditions on the growth of GP zones in Al-Zn alloys See Entry 77664

Electron magnetic spectrometer investigation of fracture surfaces formed in vacuum and in air See Entry 77725

Intergranular creep embrittlement by non-soluble impurity: Pb in precipitation hardened Al-Mg-Si alloys See Entry 77746

The oxidation behaviour of hot pressed aluminium nitride See Entry 77781

Effects of segregated phosphorus on stress corrosion cracking susceptibility of 3Cr-0.5Mo steel See Entry 77799

81.40 TREATMENT OF MATERIALS AND ITS EFFECTS ON MICROSTRUCTURES AND PROPERTIES

77655 Studies of epoxy resin systems. I. A study of the origins of the secondary relaxations of epoxy resins by thermally stimulated depolarization. T.D.Chang, S.H.Carr, J.O.Brittain (Dept. of Materials Sci. & Engng., Northwestern Univ., Evanston, IL, USA).

Polym. Eng. & Sci. (USA), vol.22, no.18, p.1205-12 (Dec. 1982). The relaxation behavior of several epoxy resin systems, which have systematic structural differences, has been studied by the thermally stimulated discharge (TSD) technique. Two TSD peaks centered at about 115K (γ peak) and 185K (β peak) were found for epoxy resins cured with a diamine. Structural change, either in the epoxy resin molecule or the amine molecule, did not seem to affect these two peaks. The TSD thermogram of the DGEBA (diglycidyl ether of bisphenol A) epoxy resin part only showed a small new peak at 160K instead of the β peak at 185K. This result, together with the fact that postcuring increased β peak height, leads to the conclusion that the β peak is most likely due to the newly-created molecular segment during the curing reaction. The peak at 160K was assigned to the epoxy group. This assignment was based on the fact that the 160K peak of an epoxy homopolymer, which has fewer epoxy groups, was smaller than that of the parent DGEBA. The β and γ peaks were found to be of distributed characteristics, and the distribution of activation energy was studied by the partial heating method. (24 refs.)

77656 Studies of epoxy resin systems. II. Effect of crosslinking on the physical properties of an epoxy resin. T.D.Chang, S.H.Carr, J.O.Brittain (Dept. of Materials Sci. & Engng., Northwestern Univ., Evanston, IL, USA). *Polym. Eng. & Sci. (USA)*, vol.22, no.18, p.1213-20 (Dec. 1982). For pt.I see *ibid.*, vol.22, p.1205 (1982). An epoxy system consisting of diglycidyl ether of butanediol, DGEBA, cured with 4,4'-diaminodiphenyl sulfone, DDS, has been used for a study of the effect of crosslinking density on the properties of the epoxy resin. Because of the low curing rate at room temperature and the low glass-transition temperature this system was amenable to a wide range of controlled crosslinking density. The crosslinking density was monitored by FTIR (Fourier transform infrared spectroscopy), which followed the change in concentration of the epoxy groups during the curing reaction. The bulk density was found to increase linearly with the crosslinking density. The modulus, the upper yield point, the lower yield point, and the degree of retraction of a deformed sample all increased with the degree of crosslinking. The thermally stimulated depolarization (TSD) β -peak was found to vary with crosslinking density, but the γ -peak was not changed. The TSD α -peak was found to decrease in strength, but increased in temperature as the crosslinking density increased. This observation suggests that TSD measurements are a good monitor of crosslinking density of epoxy resins, particularly near the final stage of the crosslinking reaction. (24 refs.)

77657 Studies of epoxy resin systems. III. Effect of sub- T_g aging on the physical properties of a fully cured epoxy resin. T.D.Chang, J.O.Brittain (Dept. of Materials Sci. & Engng., Northwestern Univ., Evanston, IL, USA). *Polym. Eng. & Sci. (USA)*, vol.22, no.18, p.1221-7 (Dec. 1982). For pt.II see *ibid.*, vol.22, p.1213 (1982). The effect of sub- T_g aging on the properties of an epoxy resin system, diglycidyl ether butanediol, DGEBA, cured with 4,4'-diaminodiphenyl sulfone, DDS, has been studied. Aging was found to increase the DSC (differential scanning calorimetric) endothermic peak, the density, and the upper yield point. In contrast, the lower yield point was relatively unchanged. This result, together with the observation of the elimination of the DSC endothermic peak by deformation and the absence of a yield point after deformation, suggested that the aging effect was eliminated by deformation. The thermally stimulated depolarization (TSD) α -peak was found to decrease in strength with aging time. All of the observations were best rationalized on the basis of the free-volume concept. (26 refs.)

77658 Studies of epoxy resin systems. IV. Fracture toughness of an epoxy resin: a study of the effect of crosslinking and sub- T_g aging. T.D.Chang, J.O.Brittain (Dept. of Materials Sci. & Engng., Northwestern Univ., Evanston, IL, USA).

Polym. Eng. & Sci. (USA), vol.22, no.18, p.1228-37 (Dec. 1982). For pt.III see *ibid.*, vol.22, p.1221 (1982). The fracture toughness of an epoxy resin system, diglycidyl ether butanediol, DGEb, cured with 4,4'-diaminodiphenyl sulphone, DDS, has been studied by varying the crosslinking density and state of aging. A stable, but rough, crack propagation was observed with specimens that were 99 percent cured and quenched. When the extent of curing was less than 99 percent or the material was aged for more than 20 min at 62°C, crack propagation was of the unstable stick-slip nature. Aging was found to decrease the initiation fracture toughness dramatically, but the arrest fracture toughness was almost unchanged. This result was associated with a change of relaxation strength of the primary, α , transition with aging. An increase of crosslinking density was found initially to reduce the fracture toughness of this epoxy resin, but the fracture toughness increased after 87 percent of curing. The initial decrease of the fracture toughness was attributed to a decrease of relaxation strength of the primary transition (i.e. the area under the α -relaxation peak), while the increase of the fracture toughness after 87 percent curing was explained by the onset of the stable-rough crack propagation. Micrographs taken by scanning electron microscopy showed possible existence of blunting during crack propagation and a decrease of blunting with the extent of aging. (20 refs.)

77659 Algorithms for constructing spline regression polynomial models [material science data]. B.Ya.Oleksiv, B.A.Popov (G.V. Karpenko Physico-mech. Inst., Acad. of Sci., Lvov, Ukrainian SSR). *Sov. Mater. Sci. (USA)*, vol.18, no.4, p.366-70 (July-Aug. 1982). Translation of: *Fiz.-Khim. Mekh. Mater. (USSR)*, vol.18, no.4, p.85-90 (July-Aug. 1982). [received: May 1983]

Proposes an adaptive algorithm for the construction of spline regression polynomial models for the computer. The selection of the nodes of the spline was done based on the condition of adequateness of the polynomial models with maximum lengths of the members of the spline. The adequateness (correspondence to experimental results) of the models is checked based on the Fisher F-criterion, the nature of which includes comparison of the dispersion of the two normal samples. (16 refs.)

77660 Analysis of a rapidly solidified high-phosphorus austenitic steel containing an amorphous phase. T.F.Kelly, G.B.Olson, J.B.Vander Sande (MIT, Cambridge, MA, USA).

Rapidly Solidified Amorphous and Crystalline Alloys. Proceedings of the Materials Research Society Annual Meeting, Boston, MA, USA, Nov. 1981 (New York, USA: North-Holland 1982), p.343-7.

Rapid solidification of a high-phosphorus austenitic steel produces a fine cellular solidification structure containing an amorphous phase at the cell walls. The amorphous phase, which is stable to $\sim 500^\circ\text{C}$, is enriched in phosphorus and chromium, but contains significantly less phosphorus than conventional glass-forming alloys. Hot consolidation of powders produces a chemically-uniform metastable austenite which can be effectively precipitation hardened by phospho-carbides. (8 refs.)

77661 Structure/property relationships and applications of rapidly solidified aluminum alloys. C.M.Adam (Government Products Div., Pratt & Whitney Aircraft, West Palm Beach, FL, USA).

Rapidly Solidified Amorphous and Crystalline Alloys. Proceedings of the Materials Research Society Annual Meeting, Boston, MA, USA, Nov. 1981 (New York, USA: North-Holland 1982), p.411-22.

Pratt & Whitney Aircraft has developed rapid solidification powder metallurgy and consolidation techniques to produce advanced aluminum alloys. A centrifugal rotary atomization device with forced high velocity helium convective cooling has been developed to pilot-plant stage, to produce aluminum alloys of novel compositions for advanced gas turbine engine applications. Rapidly solidified aluminum alloys solidify as spherical droplets up to 100 μm diameter with cooling rates of 10^3 - 10^4K/sec , and demonstrate new microstructural features which have been exploited to develop elevated temperature mechanical properties. Alloys have been developed for 400-500°F fan and compressor applications that have traditionally used titanium alloys, and the author reviews the microstructural evolution of rapidly solidified structures during thermomechanical processing. (32 refs.)

Temperature fields and thermal stress fields in radiation shieldings See Entry 75202

Characterization and properties of laser quenched aluminum bronzes See Entry 76497

81.40C Solid solution hardening, precipitation hardening, dispersion hardening

77662 Strengthening mechanisms in hot-rolled magnesium and magnesium alloys. G.Sambasiva Rao, Y.V.R.K.Prasad (Dept. of Metall., Indian Inst. of Sci., Bangalore, India).

Mater. Lett. (Netherlands), vol.1, no.5-6, p.171-4 (April 1983). The relative contributions of various strengthening mechanisms such as grain-boundary strengthening, texture strengthening and solid-solution strengthening in hot-rolled Mg, Mg-12.5Li, Mg-5Ti and Mg-12.7Cd (at.%) are investigated. Grain-boundary strengthening and texture strengthening are found to be significant in magnesium, whereas in Mg-5Ti the former is more important and in Mg-12.7Cd the latter. The addition of Li, Ti or Cd causes solid-solution strengthening primarily due to differences in atomic size. (14 refs.)

77663 Toughening by monoclinic zirconia. H.Ruf, A.G.Evans (Dept. of Materials Sci. & Mineral Engng., Univ. of California, Berkeley, CA, USA). *J. Am. Ceram. Soc. (USA)*, vol.66, no.5, p.328-32 (May 1983). The toughening induced by monoclinic ZrO_2 in the absence of microcracking was investigated, using ZnO as the host material. Toughness levels K_{IC} in excess of the host toughness K_{IC}^M were achieved, attaining a peak toughness $K_{IC}/K_{IC}^M \approx 1.7$, at monoclinic ZrO_2 volume concentrations ≥ 0.2 . This toughening is attributed to crack/particle interactions, associated with the deflection and bowing of the crack by the residual strain field around the monoclinic ZrO_2 particles. (20 refs.)

77664 Effects of the quenching conditions on the growth of GP zones in Al-Zn alloys. M.Ohta (School of Engng., Okayama Univ., Okayama, Japan), T.Kanadani, A.Sakakibara.

J. Jpn. Inst. Met. (Japan), vol.47, no.5, p.375-81 (1983). In Japanese. Dilute Al-Zn alloys (4 wt.%) quenched under various conditions were studied by measurement of electrical resistivity. In order to compare the results for different quenching conditions correctly, the same specimen was used repeatedly throughout the experiments for the same aging temperature. Intensities of SAXS were also measured. When the aging temperature was fixed,

the quasi-equilibrium resistivity, ρ_E , increased with the quenching temperature, T_Q . Guinier radius, R_G , became smaller as ρ_E became larger when $T_Q \leq 773\text{K}$, while the integrated intensity remained constant. For $T_Q \geq 823\text{K}$, R_G at the state of ρ_E was about 1.15 nm irrespective of the aging and quenching temperature and was a little larger than that at the stage of maximum resistivity. When ρ_E was plotted against ρ_0 (as-quenched resistivity) for a fixed aging temperature, instead of plotting against T_Q , ρ_E relates to ρ_0 regularly. ρ_E depends on ρ_0 linearly with large slope in the region of lower ρ_0 (lower T_Q), on the other hand, with small slope in the region of higher ρ_0 (higher T_Q). In the case of $T_Q \geq 673\text{K}$, ρ_0 increased with increasing quenching speed and ρ_E increased with ρ_0 , that is, with increasing quenching speed. On the other hand, when $T_Q \geq 773\text{K}$, ρ_0 increased with decreasing quenching speed, while ρ_E increased with ρ_0 . ρ_E values corrected for the contribution of secondary defects were almost independent of ρ_0 when aged at 263K, but when aged at 233K, ρ_E depends upon ρ_0 even at higher T_Q . (12 refs.)

77665 Strengthening mechanisms in Inconel 718 superalloy. M.C.Chaturvedi, Ya-fang Han (Dept. of Mech. Engng., Univ. of Manitoba, Winnipeg, Canada).

Met. Sci. (GB), vol.17, no.3, p.145-9 (March 1983). The yielding behaviour of underaged Inconel alloy 718, which is precipitation hardened by coherent ordered BCT γ'' and ordered FCC γ' phases, has been studied. It was found that the yielding of the underaged specimens occurs by the shearing of the precipitate particles by the glide dislocations which move in pairs. During this stage the yield strength of materials can be adequately accounted for mainly by the coherency hardening mechanism. (22 refs.)

77666 Carbon content of retained austenite in quenched steels. H.K.D.H.Bhadeshia (Dept. of Metall. & Materials Sci., Univ. of Cambridge, Cambridge, England).

Met. Sci. (GB), vol.17, no.3, p.151-2 (March 1983). Much effort has recently been directed towards the determination of the carbon content of retained austenite in directly quenched, or quenched and tempered low alloy steels. The results indicate that it may be significantly higher than the average carbon content of the alloy concerned. The author's analysis is concerned with the possibility that some redistribution of carbon may occur during the transformation of austenite to what is generally referred to as 'lath martensite' in low alloy steels. It is shown that the experimental results on martensite may only be claimed to be consistent (without proving) with carbon diffusion during growth if, and only if, some factor other than carbon redistribution, e.g. mechanical stabilization, prevents the residual austenite from undergoing displacive transformation. (4 refs.)

Crystallization behavior and properties of rapidly solidified Ni-Mo-B alloys See Entry 76320

Effect of neutron irradiation on the deformation of copper and internally oxidized copper-aluminium alloy See Entry 76519

Microstructure and mechanical properties of laser-processed Ni-Al-Mo base alloys See Entry 76652

Thermal expansivity measurements below 300K on a copper-beryllium alloy See Entry 76676

Determination of threshold stress intensity for crack growth at high temperature in silicon carbide ceramics See Entry 77731

81.40E Cold working, work hardening; annealing, recovery and recrystallisation; textures

77667 Investigation of the structure and phase composition of a stainless steel wire after electroplastic drawing. O.A.Troitskii, Yu.V.Baldokhin, N.E.Kir'yanchev, V.G.Ryzhkov, V.D.Kalugin, N.V.Sokolov, A.A.Klekovkin, S.A.Klevtsur (Inst. of Phys. Chem., Acad. of Sci., Moscow, USSR).

Fiz. Met. & Metalloved. (USSR), vol.55, no.4, p.744-8 (April 1983). In Russian. English translation in: *Phys. Met. & Metallogr. (GB)*

A confirmation is reported of an earlier observation by the present authors that electroplastic drawing (during which a constant current of high density amounting to 250 A/mm² passed through the deformation zone) of a wire made of metastable austenitic stainless steel reduced strongly the content of the martensite formed as a result of deformation of the α phase. The distribution of the residual α -phase over the wire cross section was determined. The results indicated that this residual α -phase was concentrated mainly on the surface and was present in the form of disperse inclusions. (7 refs.) A.T.

77668 Influence of the temperature and rate of deformation on the dynamic recrystallization of KhN77TiYr alloy single crystals. N.D.Bakhteeva, V.I.Levit (Inst. of Metal Phys., Acad. of Sci., Sverdlovsk, USSR).

Fiz. Met. & Metalloved. (USSR), vol.55, no.4, p.761-7 (April 1983). In Russian. English translation in: *Phys. Met. & Metallogr. (GB)*

The investigated single crystals were oriented to ensure easy slip and elongation tests were made at temperatures 1273-1473K at shear deformation rates from 10^{-3} to 10^{-1}sec^{-1} . Softening in accordance with the dynamic recovery mechanism was observed under all stretching conditions. Dynamic recrystallizations occurred only at 1373 and 1473K and the degree of such recrystallization in single crystals increased on increase in the temperature and on reduction in the deformation rate. (14 refs.) A.T.

77669 Characteristics of recrystallization of ultrafine powders during sintering. Ya.E.Geguzin, L.N.Parititskaya, V.V.Bogdanov, V.I.Novikov (A.M. Gorki State Univ., Kharkov, USSR).

Fiz. Met. & Metalloved. (USSR), vol.55, no.4, p.768-73 (April 1983). In Russian. English translation in: *Phys. Met. & Metallogr. (GB)*

During the initial stage of sintering of ultrafine Cu and Ni powders with a linear grain size $l \approx 5 \times 10^{-8}\text{m}$ it was found that low-temperature recrystallization occurred at $T \geq 200^\circ\text{C}$. This process produced spherical (radius $\sim 10^{-5}\text{m}$) single-crystal inclusions, i.e. inclusions consisting of $\sim 10^9$ powder grains. A model was proposed for this process: according to this model the recrystallization motion of the boundaries is hindered by the detachment of atoms from one wall of a boundary and the attachment to the other. The kinetics of this process can be described by a specific boundary flux of particles. (3 refs.) A.T.

77670 Calculations from texture of earing in deep drawing for FCC metal sheets. N.Kanetake, Y.Tozawa, T.Otani (Dept. of Iron & Steel Engng., Nagoya Univ., Nagoya, Japan).

Int. J. Mech. Sci. (GB), vol.25, no.5, p.337-45 (1983).

The present study aims to calculate the height at each peripheral position of a cup drawn from polycrystalline sheet using texture data. In the analytical treatment the polycrystalline sheet is simplified to an aggregation of many single crystals with various orientations, and the texture is represented by a three-dimensional crystallite orientation distribution function. The ear is calculated crystallographically using the orientation distribution function as a volume fraction of a certain oriented crystal. In the experiment aluminium, Al-Mg alloy and copper sheets which are treated under various conditions of cold rolling and heat treatment are used. The average textures over the

thicknesses of the sheets are measured by the Schulz reflection method. The calculated ears based on the measured textures are compared with the experimental ears for each material. The results show that all the principal features of the ears of drawn cups are predicted satisfactorily by the calculation. (22 refs.)

77671 Austenitising process of steels and effect of plastic deformation on the process. I.Tamura (Faculty of Engng., Kyoto Univ., Kyoto, Japan). *J. Soc. Mater. Sci. Jpn. (Japan)*, vol.32, no.352, p.1-5 (Jan. 1983). In Japanese.

Dual phase steel, having both ferritic and martensite structures, has achieved commercial importance in the manufacture of automobiles. It is low in yield point and high in tensile strength, uniform elongation percentage and work hardening—good workability. When cold-rolled steel is heated and then rapidly cooled, the steel changes over from austenite into martensite, and the final steel contains ferrite and martensite crystals. In this phase transformation the austenitising process plays an important role. Austenite is a solid solution of ferrite and cementite in each other. It forms when the metal solidifies, and remains a solution until it cools to a red heat. But manganese, nickel or carbon contained in the steel will preserve austenite to a temperature below -195°C . The paper describes the austenitising process. (6 refs.) K.B.

77672 Structural dependence of microscopic residual shear stress at worked surface. T.Hanabusa, H.Fujiwara (Faculty of Engng., Tokushima Univ., Tokushima, Japan).

J. Soc. Mater. Sci. Jpn. (Japan), vol.32, no.354, p.245-50 (March 1983). In Japanese.

Describes the structural dependence of ψ -splitting behavior observed in the X-ray stress measurement of worked surfaces. In order to investigate at first the effect of the cementite phase on the X-ray residual strain distribution, the lattice spacings at many orientations (ϕ, ψ) were measured for the ground or orthogonally planned surfaces of annealed S55C and pure iron. The variation of measured interplanar spacing against $\sin^2\psi$ for S55C was closely approximated by the following fundamental triaxial stress-strain relation: $\epsilon_{\psi\psi} = \frac{1}{2} s_1^2 [\sigma_1 \cos^2\phi + \sigma_2 \sin^2\phi + \sigma_{22} \sin^2\psi - \sigma_{33} \sin^2\psi + \frac{1}{2} s_2 s_3 + s_1 [\sigma_{11} + \sigma_{22} + \sigma_{33}] + \frac{1}{2} s_2 [\sigma_1 \cos^2\phi + \sigma_2 \sin^2\phi] \sin^2\psi]$. However, the values for pure iron showed remarkable deviations from the elliptical distribution in the $\sin^2\psi$ diagram because of sharp preferred orientations produced by hard mechanical working. Secondly, the effect of morphology of the cementite phase on the $\sin^2\psi$ diagram was investigated for SK 3 specimens which were prepared by four different heat treatments in order to include the spheroidized structure and the pearlite structure. (19 refs.)

77673 Properties of γ/γ' - δ eutectic composite material. K.Kovacova (Ustav Materialov a Mechaniky Strojov SAV, Bratislava, Czechoslovakia), J.Ivan, S.Kubo.

Kovove Mater. (Czechoslovakia), vol.21, no.2, p.189-96 (1983). In Slovak.

The minimum interphase free energy is one of the basic features of morphological stability conditioning the formation of a certain preferred orientation relation among the coexisting phases in the eutectic composite material. In the Ni-Ni₃Al-Ni₃Nb ternary eutectic material prepared by the unidirectionally controlled solidification the mutual crystallographic orientation of phases was determined and relative solubility of elements in the phases was assessed. In Ni-Nb 22.5-Al 2.5 wt% monovariant ternary alloy in the interval of directional solidification rates from 1.44×10^{-6} to $5.56 \times 10^{-6} \text{ m.s}^{-1}$ the following generally valid orientation relation exists: lamellar interphase $\{111\}_\gamma, \{101\}_\delta$ growth direction $\parallel [110]_\gamma, \parallel [100]_\delta$, which is not a function of the growth rate. In the Ni-Ni₃Al-Ni₃Nb eutectic composite material the solubility of nickel in the matrix is by 20% higher when compared to its solubility in the reinforcing lamella of δ -phase. Solubility of niobium in γ intermetallic phase is twofold when compared to its solubility in the matrix. (10 refs.)

77674 Recrystallization of a nickel-base superalloy: kinetics and microstructural development. A.J.Porter, B.Ralph (Dept. of Metall. & Materials Sci., Univ. of Cambridge, Cambridge, England).

Mater. Sci. & Eng. (Switzerland), vol.59, no.1, p.69-78 (May 1983).

The primary recrystallization of a commercial nickel-base superalloy, Nimonic 115, has been investigated. The migration kinetics of the recrystallization interface have been examined by light optical microscopy and hardness testing; the reasons for a high apparent value of activation energy so obtained are discussed. The grain refinement resulting from recrystallization has been studied by transmission electron microscopy. A mechanism, based on enhanced recovery near to the recrystallization interface leading to repeated nucleation of recrystallization, is proposed. (25 refs.)

77675 Relative work hardening rates. R.Rawlings (Dept. of Metall. & Materials Sci., Univ. Coll., Cardiff, Wales).

Met. Sci. (GB), vol.17, no.3, p.150 (March 1983).

The author has collected some results to illustrate the relationship $d\sigma/d\epsilon = TS(1 + e_\sigma)$ where σ and ϵ are the true stress and true strain respectively, TS is the tensile strength and e_σ is the maximum uniform strain. The results are for various materials including high density polyethylene and nylon which show a maximum in the force-extension curve. It can be seen that neither the work hardening nor the relative work hardening ratios at a constant strain are any guide to the maximum uniform strain. (3 refs.)

77676 Static and dynamic strain aging in a Ni(C) solid solution. G.H.van Haastert, A.van den Beukel (Lab. of Metall., Delft Univ. of Technol., Delft, Netherlands).

Phys. Status Solidi A (Germany), vol.76, no.2, p.609-14 (16 April 1983).

Static and dynamic strain aging experiments are performed on the interstitial solid solution Ni(0.55% C) to discriminate between two models recently proposed in the literature, the 'dislocation-solute interaction' (DSI) and the 'dislocation-dislocation interaction' (DDI) model. The results can, for the major part, be described in terms of the first model and in some respects clearly disagree with the second. (12 refs.)

77677 The growth of helium bubbles in stainless steel at high temperatures. J.Rothaut, H.Schroeder, H.Ullmaier (KFA Jülich, Jülich, Germany). *Philos. Mag. A (GB)*, vol.47, no.5, p.781-95 (May 1983).

The influence of annealing time (1-1000 hours), applied tensile stress (0-130 MPa), temperature (973-1073 K) and helium content (10-300 a.p.p.m.) on the size distribution and density of helium bubbles within the grains of AISI Type 316 stainless steel has been studied by TEM of α -implanted foil specimens. The results are compared with theoretical predictions assuming different growth mechanisms. The experimental data are best described by assuming that (1) the bubble coarsening is due to Ostwald ripening and (2) the helium in the bubbles obeys a highly non ideal equation of state. From such a comparison an activation energy for helium permeation through the lattice of 3.5 eV can be deduced, which is comparable with theoretical estimates. It was further observed that tensile stresses can lead to bimodal size distributions, which are attributed to the presence of two mobile and supersaturated components (helium and vacancies) during the nucleation stage. The subsequent growth of matrix bubbles seems to be rather insensitive to stress, in contrast to the behaviour of grain boundary bubbles. It could be shown that, within

the covered parameter range, the implanted helium is entirely precipitated into bubbles with diameters $\geq 1.5 \text{ nm}$ that are detectable by TEM. (13 refs.)

77678 Influence of aging on secondary recrystallization and mechanical properties of polycrystalline NaCl samples prepared by hot pressing. S.N.Val'kovskii, M.F.Imaev (Inst. of Solid-State Phys., Acad. of Sci., Chernogolovka, USSR).

Sov. Phys.-Solid State (USA), vol.24, no.11, p.1832-4 (Nov. 1982). Translation of: *Fiz. Tverd. Tela (USSR)*, vol.24, no.11, p.3229-33 (Nov. 1982). [received: May 1983]

A study was made of the influence of room-temperature aging on the yield stress and on the parameters of secondary recrystallization of polycrystalline samples formed by hot pressing. After aging for nearly a year a considerable reduction (by over an order of magnitude) was observed in the activation energy of motion of grain boundaries and of the yield stress. The reduction was by a factor of ~ 3 . Crystals with different grain sized obeyed the Hall-Petch relationship in which the constant was $K = 0.82 \text{ MPa.cm}^{1/2}$. (15 refs.)

77679 Preferred orientation in splat-quenched materials. N.W.Blake, F.A.Hames, R.W.Smith (Dept. of Metall. Engng., Queen's Univ., Kingston, Ontario, Canada).

Rapidly Solidified Amorphous and Crystalline Alloys. Proceedings of the Materials Research Society Annual Meeting, Boston, MA, USA, Nov. 1981 (New York, USA: North-Holland 1982), p.363-7

High purity, splat-quenched metal ribbons, produced by the melt spinning technique, were examined for preferred orientation using X-ray diffraction. Of the materials tested (Zn, Cd, Ag, Bi, Pb, Sb, Mg, Sn), all except Sn exhibited some degree of preferred orientation in the plane of the metal ribbon. The HCP metals Zn and Cd showed an extreme degree of preferred orientation with the 002 plane being closely parallel to the ribbon plane. The Zn ribbon was analysed more closely with a view to its use as a crystal monochromator for X-ray diffraction. The high purity Zn was found to have some instability of preferred orientation with increase in time and temperature. The orientation was found to be effectively stabilized by the intentional addition of impurities, or by the use of lower purity Zn. In this form, the Zn ribbon could be used as a crystal analyser for X-ray diffraction with both intensity and resolution comparable to that of the 1011 plane in quartz. (5 refs.)

Furnace annealing of ion implanted polycrystalline silicon See Entry 76473

Swelling in cold-deformed Okh16N15M3B steel on irradiation in a high-voltage electron microscope See Entry 76517

Effect of neutron irradiation on the deformation of copper and internally oxidized copper-aluminium alloy See Entry 76519

Analysis on plasticity in materials with strain hardening and strain-rate sensitivity under uniaxial tension See Entry 76548

Internal friction in cold-worked nickel-carbon See Entry 76563

Microstructural study of devitrified amorphous alloys See Entry 76651

Interface reactions and grain growth processes in poly-GaAs deposited on molybdenum substrates by the organometallic process See Entry 76805

Epitaxial growth and annealing control of EMR properties of thick homogeneous Ga substituted yttrium iron garnet films See Entry 77267

Strengthening mechanisms in hot-rolled magnesium and magnesium alloys See Entry 77662

Influence of plastic deformation on the properties of chromium bronze See Entry 77703

Cold deformation of a nickel-base superalloy See Entry 77714

High-temperature transgranular fracture in an austenitic stainless steel See Entry 77754

Ion nitriding behavior of several low alloy steels See Entry 77798

Interrelation of the magnetic and mechanical properties with the structural state of hardened and tempered products See Entry 77842

Achievement and properties of self-supporting polysilicon solar cells made from RAD ribbons See Entry 78022

81.40G Other heat and thermomechanical treatments

77680 Influence of heat treatment on the structure and long-term strength of γ/γ' -MeC nickel eutectic. Length memory effect. S.T.Kishin, I.L.Svetlov, L.P.Sorokina, S.G.Morozova, E.R.Golubovskii, F.V.Yushakova (All-Union Sci.-Res. Inst. of Aviation Materials, Moscow, USSR).

Fiz. Met. & Metalloved. (USSR), vol.55, no.4, p.754-60 (April 1983). In Russian. English translation in: *Phys. Met. & Metallogr. (GB)*

A study was made of the effects of heat treatment on the structure, phase composition and long-term strength (measured at $900-1100^{\circ}\text{C}$) of a nickel-based eutectic with a directional γ/γ' -MeC structure. It was found that quenching from the temperature of complete dissolution of the γ' -phase and ageing at 900°C for 30 h ensured the optimal size and morphology of the γ' -phase. This increased the long-term strength measured at 900 and 1000°C . Repeated heat treatment after tests of certain durations restored the initial structure, mechanical properties, and dimensions of the samples. (8 refs.) A.T.

77681 Characteristics of formation of the structure during deformation of low-alloy chromium by rolling at temperatures 1400-1450K. V.I.Trefilov, N.A.Storchak, V.N.Minakov, V.A.Manilov, L.S.Igolkina, Yu.E.Zubets (Inst. of Problems in Materials Sci., Acad. of Sci., Kiev, Ukrainian SSR).

Fiz. Met. & Metalloved. (USSR), vol.55, no.4, p.781-7 (April 1983). In Russian. English translation in: *Phys. Met. & Metallogr. (GB)*

The methods of X-ray structure investigations and electron transmission spectroscopy were used to study the formation of the structure in polycrystalline samples of low-alloy chromium as a result of a change of the degree of single plastic deformation by rolling at $1400-1450\text{K}$. It was found that when the degree of plastic deformation was in excess of 30% per rolling, the process could be described by the following scheme: initial structure—cellular structure—fragmented+cellular structure. (20 refs.) A.T.

77682 Annealing behaviour of dilute FeTi, FeCu, and FeMn alloys in the temperature range above stage III following low-temperature electron irradiation. F.Walz (Inst. fur Phys., Max-Planck-Inst. fur Metall., Stuttgart, Germany), H.J.Blythe, F.Dworschak.

Phys. Status Solidi A (Germany), vol.76, no.1, p.267-76 (16 March 1983).

The annealing behaviour of the dilute iron-based alloys FeCu, FeTi, and FeMn following low-temperature (44K) irradiation with 3 MeV electrons is investigated in the temperature range above stage III (200K) by means of magnetic after-effect measurements. The development of higher temperature ($T > 200\text{K}$) relaxation processes upon annealing is interpreted in terms of a two-interstitial model assuming interstitial clustering. This model is further supported by the occurrence of low-temperature ($T < 20\text{K}$) orientation-type processes in FeTi, FeNi, and FeSi which, following a detailed analysis, are

attributed to trapping reactions between mobile impurity interstitials and immobile vacancies resulting in the formation of anisotropic impurity interstitial-vacancy complexes. (16 refs.)

77683 Heating of a thin wire by a constant current with density sufficient for the appearance of thermoplasticity. O.A.Troitskii (Inst. of Phys. Chem., Acad. of Sci., Moscow, USSR). *Sov. Phys.-Dokl. (USA)*, vol.27, no.8, p.648-9 (Aug. 1982). Translation of: *Dokl. Akad. Nauk SSSR*, vol.265, no.4-6, p.1131-3 (Aug. 1982). [received: May 1983]

The transport of heat within a wire is described by Fick's heat-conduction equations. At the metal-water interface the heat-conduction flux is coupled with the flux through the surface on account of heat transfer into the liquid. The author constructs a formula which relates the rate of plastic deformation of a wire, heated by a current, to experimentally measurable quantities—the average stress $\bar{\sigma}$, the current density (in terms of T), and the constants of the metal. With the use of this formula it is not difficult to calculate the rates of deformation of the wire for various current densities and at the average temperature estimated from formula. The main effect in these expressions for the temperature and stress is the heat transfer from the surface where the jump in the temperature is localized. (1 ref.)

77684 Effect of heat treatment on the distribution of elements in the phase components of a W-Ni-Fe alloy. V.G.Bukato, V.M.Romashov, Yu.V.Gostev (All-Union Sci.-Res. & Design Inst. of Refractory Metals & Hard Alloys, USSR).

Sov. Powder Metall. & Met. Ceram. (USA), vol.21, no.10, p.785-8 (Oct. 1982). Translation of: *Poroshk. Metall. (USSR)*, vol.21, no.10, p.38-41 (Oct. 1982). [received: May 1983]

A study was made of the effect of various heat treatments on the distribution of elements between the tungsten phase and matrix grains in specimens of W-Ni-Fe. Unetched microsections of alloy specimens were examined using an electron probe microanalyzer. The observed redistribution of elements in the alloy investigated was apparently due not only to the temperature dependence of the solubilities of the components in the phases but also to the fact that an equilibrium had not been attained in its structural constituents during sintering and heat treatment.

77685 Application of neutron diffraction to a study of phases in Type 316 stainless steel weld metals. G.F.Slattey, C.G.Windsor. Report ND-R-880(R), UKAEA, Risley, Lancs, England (Jan. 1983), 33 pp. Neutron diffraction techniques have been utilised to study the phases in Type 316 austenitic stainless steel weld metal both in the as-welded condition and after stress-relieving and ageing heat treatments. The amounts of the principal crystallographic phases present in bulk specimens have been measured. Two compositions of weld metal were selected to provide a 'low' (6%) and 'high' (16%) initial ferrite level and the subsequent volume fractions of transformation products were measured after heat treatment. Some retained ferrite was observed in all the heat treated specimens, ranging from 4% for specimens of both initial ferrite levels treated at 625°C for 1000 hours, to around 1% for the specimens treated at 850°C for 6 hours. The high initial ferrite specimen produced 0.9% of sigma phase after the 850°C treatment and 0.2% sigma after the 625°C treatment. The low initial ferrite specimen produced 1.5% $M_{23}C_6$ carbide after both heat treatments. The results compare well with previous findings on similar samples of weld metal using optical and electron microscopy. (35 refs.)

77686 Investigation of capless heat treatment of MBE n-GaAs. S.H.Xin, W.J.Schaff, C.E.C.Wood, L.F.Eastman (School of Electrical Engng., Cornell Univ., Ithaca, NY, USA).

Gallium Arsenide and Related Compounds, 1982. Tenth International Symposium on Gallium Arsenide and Related Compounds, Albuquerque, NM, USA, 19-22 Sept. 1982 (Bristol, England: IOP 1983), p.613-18

Both capless and Si_3N_4 capped annealing of molecular beam epitaxial n-GaAs were investigated by photoluminescence and computerized deep-level spectroscopy. The 1.507 eV emission bands (defect excitation) and the 1.4934 eV (carbon) and the 0.83 eV (EL2) electron trap are greatly enhanced after Si_3N_4 encapsulated annealing at 700°C. These features were not observed in capless annealed material. It is concluded that capless annealing using an InAs ambient can avoid surface-impurity drive-in and stress effects in the MBE film. In addition Si_3N_4 capping causes surface topographic degradation on annealing whereas capless annealing does not. (15 refs.)

Crystallization behavior and properties of rapidly solidified Ni-Mo-B alloys See Entry 76320

Theory of annealing of vacancy pores in thin metal foils See Entry 76418

Implantation annealing in GaAs by incoherent light See Entry 76477

Microhardness of glassy chalcogenides in the $(As_2Se_3)_x(Bi_2Se_3)_{1-x}$ system See Entry 76553

The β - α transition in rapidly quenched Sn-Ge alloys See Entry 76622

Microstructures of rapidly solidified Fe-Al-Zr alloys See Entry 76649

Microstructural study of devitrified amorphous alloys See Entry 76651

Investigation of redistribution of the alloying elements during diffusion annealing of titanium alloys See Entry 76687

Effect of heat treatment on the conduction and structure of Ge-Se-Te amorphous alloys See Entry 76950

Superconducting properties and flux pinning in liquid quenched Nb-Ga alloys .. See Entry 77115

Block wall arrangement and Barkhausen noise in steels 22 NiMoCr 3 7 and 15 MnNiMoN 5 3 See Entry 77201

The effects of ribbon thickness and annealing temperature on the AC magnetic properties of the $Fe_{81.5}B_{14.5}Si_2C_1$ alloy See Entry 77222

Epitaxial growth and annealing control of EMR properties of thick homogeneous Ga substituted yttrium iron garnet films See Entry 77267

Raman spectroscopy for characterization of annealing of ion-implanted InP See Entry 77402

Perpendicularly crystallized ribbons by means of rapid solidifications from melts See Entry 77598

Raney type nickel catalysts from RSR atomization of Al-Ni powders See Entry 77599

Recrystallization of silicon nitride powders during hot pressing See Entry 77607

Microstructure of a rapidly solidified Al-Fe-Co-Ni alloy See Entry 77629

Rapidly solidified long range ordered alloys See Entry 77630

Carbide transformations in microstructurally unstable low alloy ferritic steel .. See Entry 77651

Studies of epoxy resin systems. III. Effect of sub- T_g aging on the physical properties of a fully cured epoxy resin See Entry 77657

Studies of epoxy resin systems. IV. Fracture toughness of an epoxy resin: a study of the effect of crosslinking and sub- T_g aging See Entry 77658

Strengthening mechanisms in hot-rolled magnesium and magnesium alloys See Entry 77662

Effects of the quenching conditions on the growth of GP zones in Al-Zn alloys See Entry 77664

Austenitising process of steels and effect of plastic deformation on the process See Entry 77671

Preferred orientation in splat-quenched materials See Entry 77679

X-ray stress measurement of high manganese austenitic steels See Entry 77687

Pseudo-elastic behaviour in rapidly-quenched dilute tin alloys See Entry 77695

High-temperature creep and dislocation structure of vanadium See Entry 77700

Influence of plastic deformation on the properties of chromium bronze See Entry 77703

Influence of thermal decomposition on the mechanical properties of magnesia-stabilized cubic zirconia See Entry 77732

The mechanical properties and tensile fracture characteristics of partially annealed low carbon mild steel sheet See Entry 77743

Mechanical properties of $(Fe_{100-x}Mn_x)_{83}B_{17}$ metallic glasses See Entry 77760

Surface alloying of iron alloys by laser beam melting See Entry 77807

Property enhancement in rapidly quenched alloy surfaces See Entry 77811

Interrelation of the magnetic and mechanical properties with the structural state of hardened and tempered products See Entry 77842

Evaluation of electrode shape and nondestructive evaluation method for welded solar cell interconnects See Entry 77858

Density change of glassy $Pd_{77}Si_{16.2}Cu_{6.5}$ alloy during cold drawing See Entry 77860

81.40J Elasticity and anelasticity

(see also 62.20D Elastic constants, 62.40 Anelasticity, internal friction, and mechanical resonances)

77687 X-ray stress measurement of high manganese austenitic steels. H.Miyagawa, S.Oyama, A.Oda (Ariake Tech. Coll., Omuta, Japan).

J. Soc. Mater. Sci. Jpn. (Japan), vol.32, no.354, p.240-4 (March 1983). In Japanese.

By using the ψ , oscillation method with $CrK\beta$ γ (311) diffraction, the X-ray stress measurement was made on five specimens, which were obtained by water toughening and various plastic working treatments (tensile pre-strain, hammered and explosive hardening) from Hadfield's high manganese austenitic steel, and their mechanical elastic constants, X-ray elastic constants and the accuracy of measurement were examined. The mechanical elastic constant for 13% Mn austenitic steel after water toughening was 18900 kg/mm². This value gradually decreased with increasing tensile pre-strain. The K -value ($K_X = -37.26$ kg/mm²/deg) of austenitic steel adopted in the standard method of X-ray stress measurement is considered suitable for the X-ray stress measurement of 13% Mn austenitic steel which has not been subjects to severe plastic deformation. (14 refs.)

77688 X-ray stress measurement of coarse grained 18-8 stainless steel by complex oscillation technique. H.Miyagawa, S.Oyama, A.Oda (Ariake Tech. Coll., Omuta, Japan).

J. Soc. Mater. Sci. Jpn. (Japan), vol.32, no.354, p.292-7 (March 1983). In Japanese.

With the $CrK\beta$ γ (311) diffraction plane, the X-ray stress measurements on coarse grained 18Cr-8Ni austenitic stainless steel was carried out by the complex oscillation technique using the $\phi\theta$ oscillation and specimen oscillation at the same time, and the accuracy of the measurements and the X-ray elastic constant were examined. Using the complex oscillation technique, the stress of 18-8 stainless steel having an average grain size 155 μ m can be measured with the error less than ± 1 kg/mm², if the limit of confidence is set at 95 per cent. The X-ray elastic constant for the material having the average grain size 93 μ m is almost the same as those for the fine grained specimens. But the value of the one with a grain size of 155 μ m is different from these values. (14 refs.)

77689 The elastic constants of ultradrawn polypropylene. W.P.Leung, C.L.Choy (Dept. of Phys., Chinese Univ. of Hong Kong, Hong Kong).

J. Polym. Sci. Polym. Phys. Ed. (USA), vol.21, no.5, p.725-52 (May 1983).

The five independent elastic constants C_{11} , C_{12} , C_{13} , C_{33} , and C_{44} for uniaxially drawn polypropylene with draw ratios $1 < \lambda \leq 20$ have been measured from -40 to 130°C by an ultrasonic method (2.5 MHz). The crystalline and amorphous orientation functions f_c and f_a were also determined from wide-angle X-ray diffraction and birefringence; f_c increases sharply at low λ and becomes saturated above $\lambda=8$, but f_a increases monotonically up to $\lambda=20$. Below the glass transition temperature (ca. 60°C at 2.5 MHz) only the axial longitudinal and tensile moduli, C_{33} and E_{\parallel} , show large increase. At 110°C, however, all the moduli increase with λ ; E_{\parallel} , E_{\perp} (transverse tensile modulus), C_{44} (axial shear modulus), and C_{66} (transverse shear modulus) increase 30, 3, 5, and 2.5 times, respectively, as λ increases from 1 to 20. The improvement in the mechanical properties can be attributed to the increase in the fraction of taut tie molecules which was monitored by f_a . The results were analyzed in terms of the two-phase models of Takayanagi (1966) and Seferis et al. (1976). The effects of porosity were also studied. (41 refs.)

77690 Effect of porosity on the mechanical properties of nitrogen ceramics. J.C.Glandu, P.Boch (Ecole Nat. Supérieure de Ceramique Industrielle, Limoges, France).

Rev. Chim. Miner. (France), vol.20, no.1, p.9-19 (1983). In French.

The porosity dependence of the most important mechanical properties (elastic moduli, strength) of three nitrogen ceramics is studied and the results are discussed in the frame of the usual behaviour laws of the literature. The well-known decrease in mechanical properties when the porosity increases is observed, but it is shown that the amount of porosity is not the single one parameter to take into account because of the importance of other terms (i.e. morphology and nature of pores) dealing with these effects. (27 refs.)

77691 Nonlinear resonance in Cu_3Au . K.Miura, M.Wuttig, T.Yokoyama (Dept. of Mech. Engng., Yokohama Nat. Univ., Yokohama, Japan).

Ser. Metall. (USA), vol.17, no.4, p.427-9 (April 1983).

Presents first measurements of resonance curves in the vicinity of the order-disorder transformation in Cu_3Au and show how they can be understood formally in terms of the nonlinear theory. (21 refs.)

- 77692 Elasticity and anelasticity of a 304 stainless steel at below room temperature.** D.Boothman, L.Verdini (Istituto di Fisica, Univ. di Perugia, Perugia, Italy). *Scr. Metall. (USA)*, vol.17, no.4, p.445-50 (April 1983). A dynamic non-destructive technique developed for and primarily used in the analysis of pure or binary component metals is extended to the case of a complex alloy in order to study the onset of phase transformations and magnetic reorderings. The alloy chosen was a specimen of the well-known commercial 304 stainless steel, containing 18% Cr and 9% Ni. It has been shown that, by exciting flexural vibrations in a steel disc, it is possible to identify the martensitic transformation temperature if the sample has not already been subjected to temperature cycling sufficient to produce a metastable equilibrium concentration of b.c.c. material. (22 refs.)
- 77693 Elastic moduli, hardness and thermal expansion of some metaphosphate glasses.** M.Ashizuka, T.Sakai, A.Iwata (Kyushu Inst. of Technol., Kitakyushu-shi, Japan). *Yogyo-Kyokai-Shi (Japan)*, vol.91, no.2, p.87-94 (1983). In Japanese. Density, elastic moduli, Vickers hardness and thermal expansion coefficients for some metaphosphate glasses have been studied. Two linear relationships existed between mean molar volume and the cube of radii of modifier cation in glasses $(r_{M^{2+}})^3$ for Ca, Sr, Ba, Mg and Zn, and $3(r_{M^{+}})^3$ for Li and Na). One corresponds to normal type glasses (Ca, Sr, Ba, Li and Na groups) and the other corresponds to anomalous type glasses (Mg and Zn groups) proposed by Kordes. It is estimated that anomalous type glasses have more vacant space than normal ones by comparison of these linear lines. There were constant relationships between elastic moduli (bulk modulus K , Young's modulus E , shear modulus G and Poisson's ratio ν) and mean atomic volume V . Two linear relationships existed between Vickers hardness and cation-oxygen attraction $(2Z/d^4)$. (33 refs.)
- 77694 Elastic properties of alkali silicate glasses.** K.Takahashi, A.Osaka (Dept. of Industrial Chem., School of Engng., Okayama Univ., Okayama-shi, Japan). *Yogyo-Kyokai-Shi (Japan)*, vol.91, no.3, p.116-20 (1983). In Japanese. The longitudinal and transverse ultrasonic wave velocities have been measured for the glasses in the systems R_2O-SiO_2 ($R=Li, Na, K$, and Cs) by the pulse transmission method. The velocities and densities measured by the Archimedes method provided the elastic constants of the glasses; the shear modulus G , the bulk modulus K and Young's modulus E . The log-log plot of the bulk modulus vs. the mean atom-pair volumes can be approximated by a line of slope $-4/3$ throughout the glasses investigated. The results are different from those of the glasses in the systems $MO-SiO_2$ reported by Soga et al. (*J. Non-Cryst. Solids*, vol.22, p.67-76, 1976). Based on the previous models of the alkali silicate glasses (Osaka and Takahashi, *Yogyo-Kyokai-Shi*, vol.90, p.703-09, 1982) the relations between the bulk moduli and the volumes have been explained qualitatively in terms of the packing effects of the alkali ions and of the formation of the non-bridging oxygens. The former results in increasing elastic constants and the latter the inverse effect. (13 refs.)
- 77695 Pseudo-elastic behaviour in rapidly-quenched dilute tin alloys.** W.M.Gallerneault, R.W.Smith (Dept. of Metall. Engng., Queen's Univ., Kingston, Ontario, Canada). *Rapidly Solidified Amorphous and Crystalline Alloys. Proceedings of the Materials Research Society Annual Meeting, Boston, MA, USA, Nov. 1981* (New York, USA: North-Holland 1982), p.429-32. Ribbons of pure tin (99.9999%) and dilute Sn-Ge alloys, prepared by melt spinning using a 4" diameter copper cylinder, were strained in tension. Reversible strains of a few percent were recorded in the dilute alloys but not in the pure tin. X-ray diffraction examination suggests that this pseudo-elasticity is due to twinning rather than a martensitic transformation. (4 refs.)
- Modified two-phase model for the mechanical properties of the semicrystalline polymer—polyethylene** See Entry 76323
- Gamma radiation effects on the strength of a borosilicate glass** See Entry 76502
- Measurement of elastic moduli of small specimen by means of rectangular parallel piped resonance method** See Entry 76547
- Internal friction in cold-worked nickel-carbon** See Entry 76563
- Mechanism of high ionic conductivity in elastomeric networks** See Entry 76696
- Piezoelectric properties of modified PZT ceramics** See Entry 77330
- Precipitation studies in lead-tin alloys** See Entry 77644
- Deceleration of relaxation in a Cu-Si alloy** See Entry 77653
- Studies of epoxy resin systems. I. A study of the origins of the secondary relaxations of epoxy resins by thermally stimulated depolarization** See Entry 77655
- Studies of epoxy resin systems. II. Effect of crosslinking on the physical properties of an epoxy resin** See Entry 77656
- Damping capacity and pitting corrosion resistance of Fe-Mo-Cr alloys** See Entry 77793
- X-ray investigation of stress measurement of heat resisting materials (on the X-ray elastic constants and the residual stresses of nickel base alloy)** See Entry 77817
- Investigation of internal friction in fused quartz, steel, Plexiglass, and Westerly granite from 0.01 to 1.00 Hertz at 10^{-8} to 10^{-7} strain amplitude** See Entry 77833

81.40L Deformation, plasticity and creep

(see also 62.20F Deformation and plasticity, 62.20H Creep)

- 77696 Diffusive intergranular cavity growth in creep in tension and torsion.** S.E.Stanzl, A.S.Argon, E.K.Tschoeg (MIT, Cambridge, MA, USA). *Acta Metall. (USA)*, vol.31, no.6, p.833-43 (June 1983). Creep experiments were performed at 500°C in tension and torsion on high conductivity copper tubes with a uniform initial coverage of implanted water vapor bubbles on all grain boundaries. The results indicate that the cavities grow in a crack-like mode but at one tenth the rate predicted from the theoretical model of Pharr and Nix. This difference is attributed partly to load shedding from boundaries normal to the maximum principal tensile stress to slanted boundaries, and partly to a lack of knowledge about the surface diffusion constant. The results indicate further that the contribution to intergranular cavity growth by power-law creep is negligible in comparison to the contribution by diffusional flow. Complementary tension and torsion experiments performed in initially uncavitated samples result in shorter creep lives in torsion than in tension due to more effective cavity nucleation in the former. The times of fracture in both of these cases obey Monkman and Grant's law, indicating the presence of constraints on growth by the lagging

deformations by power-law creep in the surroundings of the cavitating isolated grain facets. (32 refs.)

- 77697 A study of intergranular cavity growth controlled by the coupling of diffusion and power law creep.** J.S.Wang, L.Martinez, W.D.Nix (Dept. of Materials Sci. & Engng., Stanford Univ., Stanford, CA, USA). *Acta Metall. (USA)*, vol.31, no.6, p.873-81 (June 1983). A technique based on pre-creeping and sintering is used to create large, widely spaced cavities at grain boundaries in copper. The size and spacing of the cavities is such that cavity growth is expected to be controlled by the coupling of diffusion and power law creep. The rupture properties of these pre-cavitated samples are studied over a range of stresses and temperatures and the results are compared with the predictions of various theoretical treatments of cavity growth. The stress and temperature dependence of rupture can be described using an analysis of the type suggested by Chen and Argon, provided that the diffusional length is based on the ligament stress rather than the applied stress. (13 refs.)
- 77698 Modified method for determination of energy stored in metal during its deformation.** S.P.Gadaj, E.Galkowska, J.Kaczmarek, W.Olifcruk (Acad. Polonaise des Sci., Warsaw, Poland). *Bull. Acad. Pol. Sci. Ser. Sci. Tech. (Poland)*, vol.30, no.1-2, p.37-46 (1982). Presents a modified method for the determination of stored energy. This energy is found as the difference of the mechanical energy supplied to the tensioned metal sample and the heat released during its deformation. The modification consists in the fact that the heating process due to increasing extensile stress is simulated by electrical energy supplied in a controlled way. Thus, it is possible to determine the amount of heat released by the sample without introducing any coefficients of heat exchange with the surrounding. Advantages and disadvantages of this modified method are discussed and compared to calorimetric methods. Stored energy is determined as a function of deformation of tensioned 1KH18N9T steel. The analysis of errors is performed for the results obtained. (1 ref.)
- 77699 Tensile strength of ultra high modulus linear polyethylene filaments.** D.L.M.Cansfield, I.M.Ward, D.W.Woods (Dept. of Phys., Univ. of Leeds, Leeds, England), A.Buckley, J.M.Pierce, J.L.Wesley. *Polym. Commun. (GB)*, vol.24, no.5, p.130-1 (May 1983). The tensile stress-strain behaviour of ultra high modulus linear polyethylene has been shown to be very dependent on strain rate. At room temperature, a transition from ductile to brittle behaviour was observed at $\sim 10^3$ s, and the tensile strengths of the comparatively low molecular weight material examined increased to 1.4 GPa at high strain rates at -10°C . (3 refs.)
- 77700 High-temperature creep and dislocation structure of vanadium.** V.M.Alyab'ev, O.V.Antonova, L.N.Lebeleva, V.A.Pavlov, V.I.Shalaev (Inst. of Metal Phys., Acad. of Sci., Sverdlovsk, USSR). *Fiz. Met. & Metalloved. (USSR)*, vol.55, no.4, p.798-804 (April 1983). In Russian. English translation in: *Phys. Met. & Metallogr. (GB)*. A study was made of the creep of vanadium in annealed and hardened (by a mechanothermal treatment) states. The processes of formation of a dislocation structure during this mechanothermal treatment were investigated and changes in the structure during creep were observed. The mechanisms of creep were analysed and the factors responsible for an improvement in the refractory properties as a result of the treatment were considered. (21 refs.) A.T.
- 77701 Nature of the anomalous spontaneous deformation of iron in the presence of hydrogen.** V.I.Shapovalov, V.Yu.Karpov (Metall. Inst., Dnepropetrovsk, USSR). *Fiz. Met. & Metalloved. (USSR)*, vol.55, no.4, p.805-10 (April 1983). In Russian. English translation in: *Phys. Met. & Metallogr. (GB)*. It has been established that an anomalous spontaneous deformation due to a polymorphic transformation in the presence of H is not exhibited by metals forming hydrides. This effect appears in iron and its alloys, and also in manganese. A mechanism is proposed for this effect: when a polymorphic transformation occurs in the presence of hydrogen, a layer appears at the boundary between the growing and disappearing phases and this layer is strongly supersaturated with hydrogen. Experimental data (derived from microstructure investigations and cooling curves) and theoretical arguments are given in support of the proposed explanation. (10 refs.) A.T.
- 77702 High-temperature shape memory in titanium nickelide.** V.A.Likha-chev, M.V.Masterova (A.A. Zhdanov State Univ., Leningrad, USSR). *Fiz. Met. & Metalloved. (USSR)*, vol.55, no.4, p.814-16 (April 1983). In Russian. English translation in: *Phys. Met. & Metallogr. (GB)*. Titanium nickelide (TiNi) was alloyed with iron in order to reduce the martensitic transformation temperature. It was found that the high-temperature shape memory effect was due to certain reactions and particularly due to a transition from one form of the nickelide to another. All the experiments were carried out in the torsion regime. (4 refs.) A.T.
- 77703 Influence of plastic deformation on the properties of chromium bronze.** Yu.D.Koryagin, N.T.Kareva, M.A.Smirnov (Lenin Komsomol Polytech. Inst., Chelyabinsk, USSR). *Fiz. Met. & Metalloved. (USSR)*, vol.55, no.4, p.823-6 (April 1983). In Russian. English translation in: *Phys. Met. & Metallogr. (GB)*. Mechanical properties were investigated of an alloy based on Cu and containing 0.38%Cr and 0.1% each of Ni and Fe. The alloy was subjected to plastic deformation at temperatures 20-600°C. Changes in the lattice constant and in the mechanical properties were determined. It was found that hardening resulted from rolling at 20 and 500°C involving compression by 70%. Plastic deformation affected also the nature of fracture. (4 refs.) A.T.
- 77704 A viscous shell formulation for the analysis of thin sheet metal forming.** E.Onate (ETS Ing. de Caminos, Univ. Politecnica de Barcelona, Barcelona, Spain), O.C.Zienkiewicz. *Int. J. Mech. Sci. (GB)*, vol.25, no.5, p.305-35 (1983). A finite element method to analyse large plastic deformations of thin sheets of metal is presented. The formulation is based on an extension of the general viscoplastic flow theory for continuum problems to deal with thin shells. Axisymmetric situations are considered first and here the simple two noded reduced integration element is used. Numerical results for the stretch forming and deep drawing of circular sheets are presented and comparisons with experimental results are made. The second part of the paper deals with the deformation of sheets of arbitrary shape. The general viscous shell element is derived from the standard reduced integration, 'thick shell' element. Numerical results for simple 3-D sheet forming problems are given. (63 refs.)
- 77705 Measuring temperature dependence of secondary forming behavior of cellular polystyrene sheets.** K.Ito, O.Yatabe, M.Tsutsui (Coll. of Engng., Hosei Univ., Tokyo, Japan), H.Fujiaki. *Int. J. Polym. Mater. (GB)*, vol.10, no.1, p.39-52 (1983). A modified Erichen testing apparatus with heating chamber was used for evaluating the temperature dependence of the post-forming ability of foamed polystyrene sheet. Circular sheets (90 mm diameter) of thickness (1.5 mm-2.4 mm) were used as test specimens. The fracture of sheet specimens at a

hemi-spherical punch corner was observed through an upper glass plate during the punch penetration travel. (16 refs.)

77706 Spall studies of differently treated 2024A1 specimens. Z.Rosenberg, G.Luttwak, Y.Yeshurun, Y.Partom. *J. Appl. Phys. (USA)*, vol.54, no.5, p.2147-52 (May 1983). Commercial manganin stress gauges are used in planar impact experiments to determine spall strengths of variously heat-treated 2024A1 specimens. A one-dimensional Lagrangian code is used to find the best fit of calculated versus experimental stress histories by varying the spall strength in the code and using a simple threshold criterion. The authors found values in the range of 1.2-1.75 GPa for spall strengths of the differently treated specimens. These values are in good agreement with published data obtained by other methods. They also confirmed the spall strength values by a series of low-stress experiments resulting in only incipient spalls. A specimen of 2024T351 which was shocked perpendicular to the rolling direction has a lower spall strength (by about 0.3 GPa) than a specimen shocked along the rolling direction. This difference is very close to that predicted earlier. (16 refs.)

77707 The analysis of dislocation networks formed in Zircaloy-4 during high temperature creep. I.Armas, M.Boeck (Inst. für Material- und Festkörperforschung II, Kernforschungszentrum Karlsruhe, Karlsruhe, Germany). *J. Nucl. Mater. (Netherlands)*, vol.115, no.2-3, p.263-70 (April 1983). A TEM analysis of the Burgers vectors of hexagonal network dislocations in Zircaloy-4 crept at 800°C has shown that these networks are formed by parallel sets of predominantly screw dislocations with an $\langle a \rangle$ type Burgers vector. These dislocations lie in intersecting {1010} prism planes, however, the networks themselves form by interaction in the basal plane. The main glide system in Zircaloy-4 at 800°C is the prism system $\{10\bar{1}0\}$; $1/3\langle 1120 \rangle$ which is also the operative system at low temperatures. Hence the networks formed in the {0001} plane are obviously non-glide in this plane. Especially at higher temperatures however the networks can easily leave the basal plane. Mechanisms are proposed to explain the lack of edge dislocations in the crept specimens. (7 refs.)

77708 Thermal stress measurements of tungsten fiber-copper composites. Y.Ikeuchi (Niihama Tech. Coll., Niihama, Japan), H.Fujiwara. *J. Soc. Mater. Sci. Jpn. (Japan)*, vol.32, no.354, p.271-6 (March 1983). In Japanese. Thermal stress behaviors of tungsten fiber-copper composites have been studied in situ by means of an X-ray diffraction technique. The composites with 50 vol.% and 100 μ m diameter tungsten wires were fabricated by a liquid infiltration technique followed by hot rolling. The X-ray diffraction technique was found to be an effective method to analyze the thermal stress of the composites, and both the matrix and the fiber stresses which were generated due to thermal expansion mismatch of the components could be measured in situ. Both the matrix and the fibers deformed so as to accommodate thermal expansion mismatch when the composites experienced a temperature change. On thermal cyclic of 282K-503K, the matrix deformed plastically and a steady state of the thermal stress-temperature hysteresis loop was achieved after only a few cycles. (13 refs.)

77709 Rectangular tubular steel columns loaded biaxially. Z.Razzaq (Dept. of Civil Engng., Old Dominion Univ., Norfolk, VA, USA), W.W.McVinnie. *J. Struct. Mech. (USA)*, vol.10, no.4, p.475-93 (1982-1983). An inelastic analysis of rectangular tubular steel columns subjected to a constant axial load and a gradually increasing biaxial end moment is presented. Analytical thrust-moment-curvature relationships are given for the cross section with bilinear material stress-strain characteristics. An iterative procedure based on column deflection curves is used to predict moment-deflection curves up to collapse, and numerical examples are given for square and rectangular tubular steel columns. The interaction of biaxial moments, as well as the effect of strain-hardening, is explained for the nonproportional loading considered. The technique can be modified for beam-columns with other types of end moments. (9 refs.)

77710 Creep of 0.6Cr-0.6Mo-0.3V steel at low stresses. V.Foldyna (Vyzkumne Ustavy, Koncern Vitkovice, Ostrava, Czechoslovakia), A.Jakobova, J.Fiala, V.Sklenicka, J.Novotny, J.Cadek. *Kovove Mater. (Czechoslovakia)*, vol.21, no.2, p.158-68 (1983). In Czech. In the temperature and applied stress region typical for the exploitation of the contemporary power plants the diffusion creep of low alloy CrMoV steel was observed to take place, characterized by the applied stress exponent $m \approx 1$ and the activation energy $Q = 176.5 \text{ kJ mol}^{-1}$. This value of Q is close to the activation enthalpy of grain boundary diffusion $\Delta H_B = -1.675 \text{ kJ mol}^{-1}$. Assuming the known diffusion creep mechanisms that could operate the theoretically calculated Coble diffusion creep rates were found an order of magnitude higher than those determined experimentally. The value of activation energy of creep Q , as well as the comparison mentioned above, suggests that Coble mechanism operates under the conditions given, though-because the mean effective grain diameter dependence of creep rate could not be determined—the Nabarro-Herring mechanism or the parallel operation of the Coble and Nabarro-Herring mechanisms cannot be excluded. The threshold stress σ_0 was found proportional to the reciprocal of temperature. In the comparable temperature intervals it is by a factor of 2 to 3 higher than that for alpha iron. (30 refs.)

77711 Mechanical properties and structural stability of alloys. V.Paidar (CSAV, Praha, Czechoslovakia). *Kovove Mater. (Czechoslovakia)*, vol.21, no.2, p.169-179 (1983). In Czech. Mechanical properties of metals and alloys, for example the flow stress in homogeneous phases, are controlled by the dislocation core structure which is essential for the dislocation mobility in the crystal lattice. It is shown how a useful information on changes in the dislocation core can be deduced from the phase stability and structural data and how the alloying effect on mechanical properties can be predicted. (15 refs.)

77712 The activation area and the activation enthalpy of cadmium single crystals determined during creep. M.Hamersky (Přirodovedecká Fakulta, Univ. J.E. Parkyne, Brno, Czechoslovakia), P.Lukac. *Kovove Mater. (Czechoslovakia)*, vol.21, no.2, p.180-8 (1983). In Czech. The creep behaviour of cadmium single crystals tested at temperatures between 78K and 383K have been investigated. The influence of the resolved shear stress τ on the activation area can be described by the following relationship $A = C\tau^{-r}$. The temperature dependences of C and r are given where the values of C and r for $T < 78K$ are also included. In the temperature range from 78K to 383K except of 204K the values of C and r can be assumed to be independent of temperature. The temperature dependence of the activation enthalpy is nearly quadratic and can be expressed in the form $\Delta H \sim T^{2.1 \pm 0.2}$. The stress dependence of the activation area can be explained under the assumption that the nonconservative jog motion is the rate controlling mechanism in creep of cadmium single crystals. (14 refs.)

77713 Thermal activation analysis by stress relaxation in some FCC metals. K.K.Ray, A.K.Mallik (Dept. of Metall. Engng., Indian Inst. of Technol., Bombay, India). *Mater. Sci. & Eng. (Switzerland)*, vol.59, no.1, p.59-67 (May 1983). An analysis was made to evaluate the values of the activation volume for the forward flow of dislocations in aluminium, copper and nickel from stress relaxation experiments using the equation proposed by Feltham (1961). It was found that the value of the activation volume varies with the chosen time span of the relaxation profile. This variation is explained in terms of the effect of variation in the mobile dislocation density, the effect of a possible variation in the activation volume with effective stress, the influence of backward dislocation flow and the occurrence of dislocation flow by more than one mechanism. A method to determine the activation volume for the forward flow of dislocation accurately is suggested. The results indicate that two rate-controlling energy barriers should be considered in general for the plastic flow in these FCC metals at low temperatures. (31 refs.)

77714 Cold deformation of a nickel-base superalloy. C.Y.Barlow, B.Ralph (Dept. of Metall. & Materials Sci., Univ. of Cambridge, Cambridge, England). *Mater. Sci. & Eng. (Switzerland)*, vol.59, no.1, p.115-26 (May 1983). An analysis of the low deformation level (less than 5% strain) characteristics of polycrystalline samples of an engineering alloy is presented. The material used was a wrought nickel-base superalloy, Nimonic 80A, the microstructure of which had been modified in a controlled way to give a related series of phase distributions. This allowed the roles of the various microstructural constituents to be assessed. Selected mechanical property data were correlated with the deformation microstructures as determined by transmission electron microscopy. The presence of carbide particles on the grain boundaries was found to affect both the observed deformation patterns and the work-hardening rate. However, although the majority of the dislocation nucleation events occurred at the grain boundaries, the stress-strain characteristics were more sensitive to intragranular than to intergranular microstructures. (33 refs.)

77715 Composition and processing effects on the properties of one-component polyurethanes. S.A.Iobst, H.W.Cox (Polymers Dept., General Motors Res. Labs., Warren, MI, USA). *Polym. Eng. & Sci. (USA)*, vol.22, no.18, p.1177-83 (Dec. 1982). A polyurethane consisting of a poly(propylene oxide) soft segment and a diphenylmethane diisocyanate-hydroquinone di-(β -hydroxyethyl) ether (HQEE) hard block has been characterized over the composition range of 30 to 60 percent hard block. The flexural modulus varied from 60 to 900 MPa over this composition range. The elongation was approximately 250 percent at the lower hard block contents but fell below 100 percent at 60 percent hard block. Differential scanning calorimetric measurements showed that the crystallinity associated with the hard phase increased with increasing hard block content but decreased with increasing cure temperature. The heat sag was found to decrease with increasing hardblock and increase with increasing cure temperature. A material with properties comparable to current fascia materials had a significantly better heat sag resistance than a current RIM (reaction injection molding) polyurethane. The combination of the solid chain extender, HQEE, and a solid catalyst, zinc stearate, yields a resin having a pot life of greater than 8 h at 20°C allowing it to be processed as a one-component resin in standard injection molding machines. (8 refs.)

77716 A recommended procedure for determining the strain rate sensitivity in superplasticity. T.G.Langdon, P.Yavari (Dept. of Materials Sci., Univ. of Southern California, Los Angeles, CA, USA). *Ser. Metall. (USA)*, vol.17, no.4, p.435-40 (April 1983). Reviews two procedures for the determination of the strain rate sensitivity m . The preferred procedure is by using a number of specimens, each tested at a different strain rate under conditions where there is negligible grain growth, and logarithmically plotting the steady-state stress, σ , versus the strain rate, $\dot{\epsilon}$. The strain rate cycling procedure, often employed in superplasticity, leads to an accurate and consistent value for m only if grain growth is negligible and the material exhibits a true steady-state condition. The individual datum points obtained from these procedures may be logarithmically plotted either as σ versus $\dot{\epsilon}$ or as $\dot{\epsilon}$ versus σ . For both types of plot, it is convenient to divide the results into linear portions to provide experimental values for m (or n) in the various regions of flow. (25 refs.)

77717 Tensile strength of hot-pressed $\text{ZrO}_2\text{-Y}_2\text{O}_3$ at high temperature. K.Matsusue, Y.Fujisawa, K.Takahara (Nat. Aerospace Lab., Chofu, Japan). *Yogyo-Kyokai-Shi (Japan)*, vol.91, no.1, p.49-51 (1983). Uniaxial tensile strength tests of hot-pressed zirconia containing the metastable tetragonal phase were carried out at a temperature range from room temperature to 1600°C in air. The tensile strength rapidly decreased with increasing temperature, being at 500°C, 60% of that at room temperature, and above 1000°C was below 10%. (3 refs.)

Tensile properties of 1.4970 austenitic stainless steel after corrosion caused by uranium dioxide and simulated fission products See Entry 75100

Pinning of dislocations on the departure side of strengthening dispersoids See Entry 76447

Effects of triaxial stressing on creep cavitation of grain boundaries See Entry 76451

Swelling in cold-deformed Okh16N15M3B steel on irradiation in a high-voltage electron microscope See Entry 76517

Effect of neutron irradiation on the deformation of copper and internally oxidized copper-aluminum alloy See Entry 76519

The effect of implanted helium on the high temperature mechanical properties of a model austenitic Fe-17% Cr-17% Ni alloy See Entry 76521

Analysis on plasticity in materials with strain hardening and strain-rate sensitivity under uniaxial tension See Entry 76548

Microstructure and properties of fine grained supersaturated Fe-C alloys See Entry 76650

Microstructural study of devitrified amorphous alloys See Entry 76651

Evidence of the formation of twins by deformation and 'growth-accidents' in evaporated thin films of gold See Entry 76815

The Lorenz function for aluminium of different chemical purity, neutron irradiated or plastically deformed See Entry 76928

Preparing conditions and magnetic properties of rapidly quenched high silicon iron ribbons See Entry 77212

Preparation and properties of Fe-1.65 wt.% Cr single crystals See Entry 77542

Deceleration of relaxation in a Cu-Si alloy See Entry 77653

Studies of epoxy resin systems. II. Effect of crosslinking on the physical properties of an epoxy resin See Entry 77656

- Studies of epoxy resin systems. III. Effect of sub- T_g aging on the physical properties of a fully cured epoxy resin See Entry 77657
- Studies of epoxy resin systems. IV. Fracture toughness of an epoxy resin: a study of the effect of crosslinking and sub- T_g aging See Entry 77658
- Strengthening mechanisms in Inconel 718 superalloy See Entry 77665
- Influence of the temperature and rate of deformation on the dynamic recrystallization of KhN77TYuR alloy single crystals See Entry 77668
- Austenitising process of steels and effect of plastic deformation on the process See Entry 77671
- Structural dependence of microscopic residual shear stress at worked surface See Entry 77672
- Relative work hardening rates See Entry 77675
- Influence of heat treatment on the structure and long-term strength of γ/γ' -MeC nickel eutectic. Length memory effect See Entry 77680
- Characteristics of formation of the structure during deformation of low-alloy chromium by rolling at temperatures 1400-1450K See Entry 77681
- Heating of a thin wire by a constant current with density sufficient for the appearance of thermoplasticity See Entry 77683
- X-ray stress measurement of high manganese austenitic steels See Entry 77687
- Effect of porosity on the mechanical properties of nitrogen ceramics See Entry 77690
- Laws connecting viscous fracture with the flow limit See Entry 77720
- Life time calculations for LCF loading combined with tensional hold periods. Applications to Zircaloy-4 and AISI 304 See Entry 77728
- Thermal stability in microstructure and rupture strength of directionally solidified Ni-Al-Ti eutectic alloys See Entry 77736
- The mechanical properties and tensile fracture characteristics of partially annealed low carbon mild steel sheet See Entry 77743
- Intergranular creep embrittlement by non-soluble impurity: Pb in precipitation hardened Al-Mg-Si alloys See Entry 77746
- Effect of prior deformation on the cleavage of zinc single crystals See Entry 77747
- Fractography of polyethylene glycol dimethacrylate doped with polymethyl methacrylate See Entry 77748
- Strain localization and hydrogen embrittlement See Entry 77749
- Ion implantation effect on fatigue crack initiation in Ti-24V See Entry 77750
- The effect of pre-existing epsilon martensite on the hydrogen induced fracture of austenitic stainless steel See Entry 77752
- A brittle to ductile transition in NiAl of a critical grain size See Entry 77753
- Deformation induced dilatations and new observations on fracture in compression in metallic glasses at low temperatures See Entry 77761
- On the yield loads of plates with array of holes See Entry 77823
- Density change of glassy $\text{Pd}_{77}\text{Si}_{16.5}\text{Cu}_{6.5}$ alloy during cold drawing See Entry 77860

81.40N Fatigue, embrittlement, and fracture

(inc. hardness; see also 62.20M Fatigue, brittleness, fracture and cracks)

- 77718 Cyclic grain boundary migration during high temperature fatigue. I. Microstructural observations. T.G.Langdon (Dept. of Materials Sci. & Mech. Engng., Univ. of Southern California, Los Angeles, CA, USA), R.C.Gifkins. *Acta Metall. (USA)*, vol.31, no.6, p.927-38 (June 1983). Experiments were conducted on high purity lead at room temperature using reverse bending and torsion fatigue at low cyclic frequencies (≤ 1.50 Hz). Metallographic observations after testing show that there is a one-to-one correspondence between the markings from grain boundary migration and the number and pattern of cyclic loading, and this correspondence is maintained up to >100 cycles. Grain boundary sliding occurs in each cycle in addition to the migration, and this leads to the development of broad triple point folds. If the strain amplitude is maintained constant, it is shown that the average distance migrated in each cycle increases as the imposed frequency is decreased. The distance migrated is often exceptionally large in the first cycle of testing, and there is often a similar large initial displacement if the test is interrupted for periods of time from 1 to 24 h and then continued. For large grain sizes (≥ 2000 μm), the migration markings may lead to a zig-zag pattern where the individual segments lie fairly close to 45° to the stress axis. A model is described which accounts for the one-to-one correspondence and which is consistent with a fine structure observed within the migration markings. (36 refs.)
- 77719 Cyclic grain boundary migration during high temperature fatigue. II. Measurements of grain boundary sliding. T.G.Langdon (Dept. of Materials Sci. & Mech. Engng., Univ. of Southern California, Los Angeles, CA, USA), D.Simpson, R.C.Gifkins. *Acta Metall. (USA)*, vol.31, no.6, p.939-36 (June 1983). For pt. I see *ibid.*, vol.31, p.927-38 (1983). Experiments were conducted to measure the extent of grain boundary sliding in high purity lead subjected to fatigue testing at room temperature. It is shown that the average sliding offset perpendicular to the surface, \bar{u} , increases rapidly during the initial ~ 25 cycles of testing, increases at a reduced rate thereafter, and ultimately stabilizes after ~ 300 cycles. The value of \bar{u} at any selected number of testing cycles decreases with decreasing strain amplitude at constant frequency but is independent of frequency at constant strain amplitude within the limited range of frequencies examined experimentally (0.17-0.50 Hz). The value of \bar{u} also increases with an increase in grain size at constant frequency and strain amplitude. In fatigue tests conducted at zero mean strain, there is an essentially equal contribution from positive and negative sliding offsets, so that the net displacement is zero. Slide hardening is not important in fatigue at low cycles in the presence of extensive grain boundary migration. The average rates of sliding in fatigue are comparable to the average sliding rates in the very early stages of creep. (31 refs.)
- 77720 Laws connecting viscous fracture with the flow limit. T.M.Golovinskiĭ, A.A.Kaminskiĭ. *Dopov. Akad. Nauk UkrSR. Ser. A (USSR)*, no.1, p.35-8 (1983). In Ukrainian. A pattern of yield-point-dependent changes in crack resistance was studied for a number of structural alloy steels from positions of fracture mechanics. It is shown that for high-strength unstable structural steels the dependence of fracture toughness K_{IC} on the yield point $\sigma_{0.2}$ is of a complex and nonuniversal nature. With instability lost, the steel $K_{IC} = f(\sigma_{0.2})$ dependence becomes an inversely proportional exponential. (8 refs.)

- 77721 Theoretical prediction of the cracking stress of three-dimensional randomly distributed steel fibre reinforced concrete. I.A.Pathan, M.A.Qureshi (Mehran Univ. of Engng. & Technol., Jamshoro, Pakistan). *Mehran Univ. Res. J. Eng. & Technol. (Pakistan)*, vol.1, no.3, p.17-27 (July 1982). [received: April 1983] A short method based on the crack arrest concept has previously been proposed for the prediction of the cracking stress of continuous wire reinforced concrete. The comparison of the theoretical and experimental results has demonstrated the validity of this method. In this paper the method is further extended to the case of the cracking stress of three dimensional randomly distributed steel fibre reinforced concrete. The effective spacing of short fibres is determined by considering their directional efficiency and length efficiency in restraining the crack propagation. The theoretical cracking stresses for various volume fractions of steel fibres are determined and compared with experimental results. (21 refs.)
- 77722 Polymer-filler interaction in polystyrene filled with coated glass spheres. I. Interfacial adhesion control. G.F.Abate, D.Heikens (Eindhoven Univ. of Technol., Lab. of Polymer Technol., Eindhoven, Netherlands). *Polym. Commun. (GB)*, vol.24, no.5, p.137-40 (May 1983). In gaining a better understanding of some aspects of the mechanism by which fillers may reinforce polymers, a system containing glass spheres in a polystyrene matrix with adhesive interlayers of varying strength was realized. The strength increase is achieved by compatibilization arising from interaction between the interlayer bound to the filler and the matrix. The results are shown by scanning electron microscopy, SEM. (17 refs.)
- 77723 Helium embrittlement of iron-chromium alloys. K.Suganuma (Inst. of Sci. & Industrial Res., Osaka Univ., Suita, Japan), H.Sakairi, H.Kayano. *Radiat. Eff. Lett. Sect. (GB)*, vol.76, no.3, p.83-5 (1983). The helium embrittlement of Fe-(0-15)wt.%Cr alloys was examined with high temperature tensile testing. Helium injection was performed partly by using a cyclotron and partly by thermal neutron irradiation with boron alloying. The helium embrittlement was more severe in lower chromium alloys. Helium bubbles were observed in Fe but not in Fe-15Cr, both of which contained 24 atppm helium tested at 1023K. (6 refs.)
- 77724 Investigation of structural changes during fracture of $\gamma + \epsilon$ steel. G.N.Belozerskiĭ, V.N.Gittsovich, E.M.Sosenushkin, O.G.Sokolov, A.S.Chekashova (A.A. Zhdanov State Univ., Leningrad, USSR). *Fiz. Met. & Metallogr. (USSR)*, vol.55, no.4, p.788-91 (April 1983). In Russian. English translation in: *Phys. Met. & Metallogr. (GB)* The nuclear gamma resonance (Mossbauer) method was used in the backscattering geometry to study structural changes occurring in $\gamma + \epsilon$ steels as a result of fracture. The phase composition of a steel was determined directly on a fracture surface and it was established that the fracture occurred in zones whose structure was very different from the original one. It was found that the fracture was preceded by the formation of the gamma phase and the amount of the latter in the zone where defects were concentrated amounted to 90% and was determined by the loading conditions. (6 refs.) A.T.
- 77725 Electron magnetic spectrometer investigation of fracture surfaces formed in vacuum and in air. V.G.Bragin, I.N.Shabanova, O.A.Kulyabina, V.A.Trapeznikov (Inst. of Metal Phys., Acad. of Sci., Izhevsk, USSR). *Fiz. Met. & Metallogr. (USSR)*, vol.55, no.4, p.829-32 (April 1983). In Russian. English translation in: *Phys. Met. & Metallogr. (GB)* X-ray electron spectroscopy was used to study fracture surfaces obtained in vacuum and in air for samples of the same steel 37KhN3A. A comparison of the data obtained in vacuum and in air indicated that the results of a quantitative analysis were in good agreement in respect of the segregating element (phosphorus), but in the case of fracture surfaces formed in air the information on oxygen segregation was lost. (10 refs.) A.T.
- 77726 Effect of two-phase solidification on fracture toughness of aluminum alloys. N.K.Das, R.K.Mahanti, C.S.Sivaramakrishnan, R.Kumar (Nat. Metall. Lab., Jamshedpur, India). *Indian J. Technol.*, vol.20, no.11, p.434-7 (Nov. 1982). [received: May 1983] It is concluded that fracture toughness (K_{IC}) of high strength Al-Cu and Al-Zn-Mg containing Li and a dispersion of graphite particles is influenced by solidification and grain size. Whilst solidification from the two-phase region (TPS) improved K_{IC} , grain size up to a certain level lowered K_{IC} and thereafter improved it. (9 refs.)
- 77727 Welding of polymers of nonuniform molecular weight. S.Prager (Dept. of Chem., Univ. of Minnesota, Minneapolis, MN, USA), D.Adolf, M.Tirrell. *J. Chem. Phys. (USA)*, vol.78, no.11, p.7015-16 (1 June 1983). The chain dynamics responsible for the welding or healing process which occurs when two pieces of the same polymer are brought together have recently received considerable attention, motivated by the publication of reliable experimental results on crack healer. The authors have extended the treatment of their previous paper (*ibid.*, vol.75, p.5194, 1981) to allow for polydispersity. A potential complication introduced by polydispersity is the possible segregation of low molecular weight species at the annealed surfaces of the polymer samples before contact. The authors therefore assume the bulk composition of the polymer to extend right up to the junction surface and concern themselves only with the consequences of configurational relaxation. (7 refs.)
- 77728 Life time calculations for LCF loading combined with tensional hold periods. Applications to Zircaloy-4 and AISI 304. M.Bocek, A.Armas, D.Piel (Inst. fur Material- und Festkörperforschung, Kernforschungszentrum Karlsruhe, Karlsruhe, Germany). *J. Nucl. Mater. (Netherlands)*, vol.115, no.2-3, p.159-68 (April 1983). The life time in high amplitude strain cycling with tensional hold periods is analysed presuming that creep failure damage is life determining. The life fraction rule (LFR) is used to calculate the life time consumed during the dwell period in strain controlled tests as well as during tensional hold time stress cycles. It follows that stress relaxation occurring during the strain hold periods plays the dominant influence upon the relationship between life and dwell time. For strong stress relaxation (e.g. high temperature) less damage is accumulated as compared to suppressed relaxation (low temperature). The damage in stress relaxation is calculated by means of the LFR and the results are compared to experiments conducted on Zircaloy-4 and the austenitic stainless steel Type AISI 304. (20 refs.)
- 77729 The effect of radiation and cryogenic temperature on the fatigue resistance of G-11 CR glass-cloth/epoxy laminates. B.Korukonda, J.C.Conway, Jr., R.A.Queney (Pennsylvania State Univ., University Park, PA, USA), W.S.Diehorn. *J. Nucl. Mater. (Netherlands)*, vol.115, no.2-3, p.197-202 (April 1983). Tension-tension fatigue tests were performed on unirradiated and irradiated G-11 CR notched fatigue specimens at 295 and 77K. Fatigue failure was based on the initiation and propagation of fatigue cracks from the notch roots to a selected length. Results indicate an increase in fatigue resistance at

cryogenic temperature, a moderate radiation effect at both test temperatures and substantially different failure modes at 295 and 77K. (5 refs.)

77730 Effects of sodium and lithium environments on mechanical properties of ferrous alloys. O.K.Chopra (Materials Sci. & Technol. Div., Argonne Nat. Lab., Argonne, IL, USA).

J. Nucl. Mater. (Netherlands), vol.115, no.2-3, p.223-38 (April 1983).

A review of the current status of work on the mechanical properties of structural materials in liquid sodium and lithium environments is presented. The influence of the environment as well as the effects of the microstructural and compositional changes that occur in austenitic and ferritic steels during long-term exposure are discussed. Requirements for additional data on mechanical properties are identified. (44 refs.)

77731 Determination of threshold stress intensity for crack growth at high temperature in silicon carbide ceramics. E.J.Minford, R.E.Tressler (Dept. of Materials Sci. & Engng., Pennsylvania State Univ., University Park, PA, USA).

J. Am. Ceram. Soc. (USA), vol.66, no.5, p.338-40 (May 1983).

A method for estimating the threshold stress intensity for crack growth is presented. The technique requires prior knowledge of the flaw population of a material and uses applied static loads followed by a fast fracture to assess the effect of initial applied stress intensity on flaw behaviour. The technique was applied to a hot-pressed SiC at 1200° and 1400°C in a non-oxidizing atmosphere. At 1400°C with a static load time of 4 h, the threshold stress intensity was determined to be $\approx 1.75 \text{ MPa}\cdot\text{m}^{1/2}$ with a slight tendency toward higher fracture stress with increasing initial stress intensity below the threshold. At 1200°C for a static load time of 4 h, apparent strengthening was observed below a threshold stress intensity of $\approx 2.25 \text{ MPa}\cdot\text{m}^{1/2}$. This strengthening effect appears to result from stress relaxation in the crack-tip region, probably by plastic deformation which involves the oxide grain-boundary phase. (8 refs.)

77732 Influence of thermal decomposition on the mechanical properties of magnesia-stabilized cubic zirconia. M.V.Swain, R.C.Garvie, R.H.J.Hannink (CSIRO Div. of Materials Sci., Advanced Materials Lab., Melbourne, Victoria, Australia).

J. Am. Ceram. Soc. (USA), vol.66, no.5, p.358-62 (May 1983).

Cubic magnesia-stabilized zirconia was decomposed by isothermal heat treatment at 1100°C. The mechanical properties, including strength, fracture toughness, and hardness, were measured at various stages during the decomposition process. The strength initially decreased with aging but then recovered almost to its initial value. This strength decrease was associated with cracking of islands of the cubic phase in the matrix of monoclinic zirconia. The fracture toughness followed the strength although it was found that the monoclinic phase exhibited stable crack growth during notched beam fracture experiments or R-curve behavior. Measurements of the hardness indicated that the cubic phase was much harder than the monoclinic phase. In addition, X-ray diffraction, optical, and transmission electron microscopy studies were made of the decomposition process. (24 refs.)

77733 Fracture toughness of unidirectional glass/carbon hybrid composites. H.T.Thorat, S.C.Lakkad (Dept. of Aeronautical Engng., Indian Inst. of Technol., Bombay, India).

J. Compos. Mater. (USA), vol.17, no.1, p.1-14 (Jan. 1983). [received: June 1983]

The results of fracture toughness of the glass/carbon fibre reinforced epoxy hybrid composites, as expressed by K_{IC} and G_{IC} —the critical stress intensity factor and the critical strain energy release rate respectively, in the crack opening mode—are presented. The tests have been conducted in the 3-point bending configuration for the specimens having a total reinforcement content of about 55%. The K_{IC} has been evaluated from the G_{IC} and also from the standard expressions normally used for isotropic materials. Similarly, the G_{IC} and K_{IC} have been evaluated by using both P_{max} , the maximum load, and P_0 , the point of intersection on the load displacement curve with a line having 5% less slope than the slope of the curve at the origin. The trend of the results obtained by these two methods is considerably different particularly with increasing glass content in the hybrids. (14 refs.)

77734 Enhancement of strength in composites reinforced with previously stressed fibers. P.W.Manders, T.-W.Chou (Dept. of Mech. & Aerospace Engng., Univ. of Delaware, Newark, DE, USA).

J. Compos. Mater. (USA), vol.17, no.1, p.26-44 (Jan. 1983). [received: June 1983]

Failure of a fiber in an aligned composite causes a stress wave to propagate outwards placing a dynamic overstress on the neighboring fibers. This is generally greater than the static stress concentration factor which prevails after the system has settled, and increases the probability that adjacent fibers also fail, weakening the composite. This analysis shows how weak fibers may be pre-fractured to eliminate the dynamic overstress thereby increasing the strength of the composite. This strength enhancement is discussed with reference to the level of pre-stress, fiber variability, stress concentration factors, and size of the composite. (13 refs.)

77735 Distributions of fatigue life and fatigue strength in notched specimens of a carbon eight-harness-satin laminate. T.Shimokawa, Y.Hamaguchi (Second Airframe Div., Nat. Aerospace Lab., Tokyo, Japan).

J. Compos. Mater. (USA), vol.17, no.1, p.64-76 (Jan. 1983). [received: June 1983]

Investigates the distribution properties of fatigue life and fatigue strength in sharply notched specimens of a carbon fabric laminate, which was made of three layers of eight-harness-satin/epoxy prepreg sheets. Fatigue life distributions were obtained at six stress levels by carefully designed fatigue tests of four point plane bending under a constant temperature and humidity condition. Sample sizes were 30 for the three high stress levels and 12 for the three low stress levels. The amount of scatter and distributional form of fatigue life and fatigue strength are discussed from the test results. It is found that fatigue strength distributions are practically normal and their standard deviations are constant regardless of fatigue life. (9 refs.)

77736 Thermal stability in microstructure and rupture strength of directionally solidified Ni-Al-Ti eutectic alloys. Rong Wu Zhang (Inst. of Aeronaut. Materials, Beijing, China), J.Echigoya, H.Suto.

J. Jpn. Inst. Met. (Japan), vol.47, no.5, p.432-8 (1983). In Japanese.

Thermal stability in microstructure as well as static and creep rupture strengths of directionally solidified Ni-Al-Ti eutectic alloys for high temperature use were investigated; the dislocation substructure in ruptured specimens was observed by means of transmission electron microscopy. The oriented structure of γ and γ' phases, so-called 'DS' structure was fairly stable in the temperature range below 1273K, but it was disintegrated at higher temperatures. The more the γ content was, the more stable the DS structure was. DS structure was disintegrated rapidly by thermal cycling. Static tensile strength showed a maximum value at temperatures ranging between 973K and 1173K, and decreased rapidly at higher temperatures. γ fibres were broken by tension at temperatures below 1173K, but they were elongated with matrix at 1373K. DS structure disintegrated during creep at higher temperatures than 1273K.

It was considered from the above-mentioned results that the temperature range for use of these alloys was limited below 1273K, but the rupture strength of the present alloy (L:80.Sat.%Ni-1.0at.%Al-8.Sat.%Ti) was superior to that of a Jackson's alloy. Characteristic dislocation substructures in specimens subjected to creep were observed. (18 refs.)

77737 Effects of thickness and compressive residual stress of boronized layer on bending fatigue strength properties of boronized steels. T.Endoh, M.Kawakami (Dept. of Metall. Engng., Tokai Univ., Tokyo, Japan).

J. Soc. Mater. Sci. Jpn. (Japan), vol.32, no.354, p.251-7 (March 1983). In Japanese.

Plane and rotating bending fatigue tests of boronized steels with various thickness of boronized layers were conducted. The effects of thickness and compressive residual stress of the boronized layer on the fatigue strength were investigated. Furthermore, the X-ray method was successfully applied to measure the changes in residual stress and half-value breadth during plane bending fatigue. Fatigue crack initiation occurred both in the boronized surface layer and at the boundary between the boronized layer and the matrix. The surface compressive residual stress hardly changed during fatigue, but the half-value breadth increased. The compressive residual stress is effective for increasing the fatigue strength when crack initiation occurs at the surface. (8 refs.)

77738 X-ray fractography on fatigue fractured surface. Y.Sekita (Mitsubishi Heavy Industries Ltd., Sagami-hara, Japan), S.Kodama, H.Misawa.

J. Soc. Mater. Sci. Jpn. (Japan), vol.32, no.354, p.258-63 (March 1983). In Japanese.

As a basic study of X-ray fractography, the relation between the residual stress on the fatigue fractured surface and some parameters of the fracture mechanics were investigated. The materials used were Ni-Cr-Mo-steel, 0.5%C steel and high strength steel (UTS>588 MPa). The test pieces were CT-specimens with $W=51 \text{ mm}$ and $B=12 \text{ mm}$. The fatigue tests were carried out under constant load and constant range of stress intensity factor. On the fatigue fractured surface the residual stress along the crack propagation direction, was measured by a parallel beam X-ray stress measurement system, and the half value breadths of the diffraction profile were also measured. In the linear crack propagation stage of conventional constant load fatigue tests the residual stress on the fracture surface increased at first, and then decreased with increasing ΔK after about $\Delta K=30 \text{ MPa}\cdot\text{m}^{1/2}$. For Ni-Cr-Mo-steel and 0.5%C steel, the residual stress could be expressed as a function of ΔK and was affected only slightly by the stress ratio. (4 refs.)

77739 X-ray fractographic study on fatigue fracture surface of SM50A steel. K.Ogura, Y.Miyoshi (Faculty of Engng. Sci., Osaka Univ., Toyonaka, Japan), M.Kayama, M.Tsuiji.

J. Soc. Mater. Sci. Jpn. (Japan), vol.32, no.354, p.264-70 (March 1983). In Japanese.

The residual stress and breadth of the diffraction intensity curve were measured at and beneath the fracture surface. The analysis of residual stress on the fatigue fracture surface was also conducted by using the finite element method. A emphasis was made on finding the correlation between the residual stress or the plastic zone size determined from the X-ray measurements and the applied stress intensity factor. Both the distribution of residual stress and half-value breadth were found to be useful for the prediction of monotonic plastic zone size or K_{max} , although it still remained in question for the possibility of estimating cyclic plastic zone size. The correlation between the surface values of residual stress and the applied stress intensity factor was not clear. The effect of fatigue crack closure on the residual stress of the fracture surface was found to be relatively small and limited to the very thin layer near the fracture surface. (15 refs.)

77740 Effect of specimen size and configuration of fatigue crack growth behavior of mild steel butt welded joints. Y.Kitsunai (Res. Inst. of Industrial Safety, Kyose, Japan).

J. Soc. Mater. Sci. Jpn. (Japan), vol.32, no.354, p.304-9 (March 1983). In Japanese.

A study was made to determine the effects of specimen size, configuration and crack orientation to the weld axis on the fatigue crack growth rate of mild steel butt welded joints. Two types of welded specimens, the compact type (CT) specimens with three different sizes and the center-cracked-tension (CCT) specimens were used. Residual stress distributions in CT specimens were examined by means of the strain gauge method. In the case of welded specimens, the fatigue crack growth rates of CT specimens having widths of 100 and 260 mm were roughly the same regardless of crack orientations to the weld axis, while the crack growth rates in specimens with width less than 100 mm were faster than those of the larger width specimens. In the case of base metal specimens, the specimen size had no appreciable effect on crack growth rates. The crack growth rates of welded CT specimens were markedly reduced as compared with those of CCT specimens. (16 refs.)

77741 Impact fracture mechanisms in polymer blends: rubber-toughened nylon. Souheng Wu (Central Res. & Dev. Dept., E.I. du Pont de Nemours & Co., Wilmington, DE, USA).

J. Polym. Sci. Polym. Phys. Ed. (USA), vol.21, no.5, p.699-716 (May 1983).

The impact fracture mechanisms of rubber-toughened nylon are analyzed by measuring the energy dissipated in several different processes during notched fracture. An energy balance is thus established for the impact fracture. The stress-whitened zone is shown to be the energy dissipation zone, having an energy dissipation density of 5.30 cal/g . About 25% (i.e. 1.44 cal/g) of the impact energy is dissipated by matrix crazing. About 75% (i.e. 3.86 cal/g) is dissipated as heat by matrix yielding, causing a temperature rise of 9.1°C in the energy dissipation zone. Surface energy storage on the fracture surfaces is negligible (i.e. $1.45 \times 10^{-5} \text{ cal/g}$). During matrix yielding, about 12% of α -tricalcic nylon crystals is transformed into pseudohexagonal crystals. (29 refs.)

77742 The ductile fracture of metals: a microstructural viewpoint. H.G.F.Wilsdorf (Dept. of Materials Sci., Univ. of Virginia, Charlottesville, VA, USA).

Mater. Sci. & Eng. (Switzerland), vol.59, no.1, p.1-39 (May 1983).

A review of the literature on the ductile fracture of metals and alloys reveals almost immediately that the majority of investigations approach the topic from a fracture mechanics point of view and that papers based entirely on microstructural research are rare. Some aspects of continuum theory and the atomic approach to fracture are discussed. The microstructural regime covers the broad area between these two concepts. Since ductile fracture depends on the history of plastic deformation in the specimen, an outline of a successful theory of work hardening has been included. The experimental tools for microstructural investigations are briefly reviewed. Rupture is discussed. The most common mode, fibrous fracture, is reviewed. A variety of topics which have a bearing on a more comprehensive understanding of ductile fracture (such a delamination and cleavage fractures, the role of voids in microcrack initiation, the energy of dislocation cell walls, and the thickness of microtensile specimens and the rate of straining in situ experiments) are emphasized and discussed critically. (166 refs.)

- 77743 The mechanical properties and tensile fracture characteristics of partially annealed low carbon mild steel sheet.** M.S.Devgun, A.J.Carrillo, T.A.Roosen (Dept. de Mecanica, Univ. Simon Bolivar, Caracas, Venezuela). *Mater. Sci. & Eng. (Switzerland)*, vol.59, no.1, p.49-57 (May 1983). The tensile mechanical properties and static fracture characteristics of partially annealed low carbon mild steel are reported. Partially annealed samples were prepared by annealing the previously cold-rolled (0%, 28% and 50% cold reduction) steel sheet at 610°C in a salt bath for 0, 60 and 300 s. These samples were subjected to tensile tests to determine their mechanical properties and the Charpy impact tests and Kahn-type tear tests to measure their tensile fracture properties. It was concluded that the crack initiation and crack propagation energies are linearly related to the corresponding tensile mechanical properties. Furthermore, a transition in the behaviour of partially annealed steel occurs at an energy level of 40 J and at the following mechanical properties: ultimate tensile strength, 6.2×10^2 MPa; yield stress, 6.1×10^2 MPa; Charpy impact energy, 2.5×10^3 J m⁻²; total elongation, 12%. Below this point the material is more resistant to crack propagation than to crack initiation. (23 refs.)
- 77744 Low cycle fatigue of aluminum at elevated temperatures.** J.C.Tsou, D.J.Quesnel (Mech. Engrg. Dept., Univ. of Rochester, Rochester, NY, USA). *Mater. Sci. & Eng. (Switzerland)*, vol.59, no.1, p.99-113 (May 1983). High temperature low cycle fatigue data are reported for polycrystalline aluminum of 99.988% purity. Experiments were carried out at a constant strain rate over a range of temperatures from ambient temperature to 400°C. Strain rate change tests were employed to determine the rate-sensitive behavior. Cyclic hardening curves and saturated hysteresis loops undergo a gradual transition in their characteristic shapes with increasing temperature, suggesting a change in the mechanisms controlling deformation. These changes in behavior are not reflected in the cyclic stress-strain curve which shows a gradual decrease in work-hardening rate with increasing temperature. The temperature dependence of the cyclic saturation stress appears to be linear but does not exhibit a region of rapid stress drop. The discussion focuses on the role of vacancies in determining the high temperature deformation behavior of a cellular microstructure. (37 refs.)
- 77745 The influence of the static I load and R ratio on mode III fatigue crack growth behaviour in mild steel.** E.K.Tschegg (Inst. of Appl. & Tech. Phys., Tech. Univ. Vienna, Vienna, Austria). *Mater. Sci. & Eng. (Switzerland)*, vol.59, no.1, p.127-37 (May 1983). The influence of a superimposed static mode I load and of different mode III mean torques on mode III fatigue crack growth (antiplane shear mode) in cylindrical circumferentially notched AISI C1018 steel specimens has been studied. Increasing the static mode I crack opening by an axial load reduces the sliding crack closure influence (friction, abrasion and mutual support between the fracture surfaces). At high torsional stress levels it is possible to suppress the sliding crack closure almost completely in specimens with shallow cracks by applying an axial load; this is not the case for low torsional stresses. The crack growth rate may be correlated with an effective stress level from which the crack closure effect has been subtracted; this value is found by an extrapolation procedure. The crack growth rate is not influenced by small axial loads (a resulting K_I value of 0.3 MPa m^{1/2}). However, if the axial load K_I is increased to 4.9 MPa m^{1/2}, the mode III crack growth rate increases. (16 refs.)
- 77746 Intergranular creep embrittlement by non-soluble impurity: Pb in precipitation hardened Al-Mg-Si alloys.** M.Guttman, B.Quantin, P.Dumoulin (Centre des Matériaux, Ecole des Mines, Evry, France). *Met. Sci. (GB)*, vol.17, no.3, p.123-40 (March 1983). Minute amounts of Pb induce intergranular embrittlement of precipitation hardened Al-Mg-Si alloys in creep conditions but not in tension and toughness tests. Auger and Rutherford backscattering analyses of impact-fracture surfaces revealed the presence of submonolayer Pb coverages which were first attributed to a segregation of Pb to grain boundaries. However, in view of the contradictions which arose from the two types of results, further experiments using scanning Auger and X-ray microanalysis revealed that in fact Pb was essentially in precipitated form, its solubility being much smaller than expected, and that it spread on the surface by diffusion immediately after fracture. The preferential association between Pb globules and large AlFeSi inclusions favours this process since the latter particles initiate transgranular dimples. The surface analysis results are discussed on the basis of a semi-quantitative description of the possible distribution of globules on fracture surfaces. The surface diffusion process and the Pb-(AlFeSi) association are also responsible for the mechanism of embrittlement of Pb in creep conditions. (41 refs.)
- 77747 Effect of prior deformation on the cleavage of zinc single crystals.** C.Messmer (Harris Semiconductor, Melbourne, FL, USA), D.Dew-Hughes, J.C.Biello. *Philos. Mag. A (GB)*, vol.47, no.5, p.635-56 (May 1983). The critical stress intensity factor, K_{Ic} , for basal cleavage at 77K has been measured on a number of zinc single crystals, either as-grown or pre-deformed by tension or by torsional fatigue. The dislocation distribution and the extent of the plastic zone associated with cleavage were studied by chemical etching and by X-ray topography. K_{Ic} is found to decrease with prior deformations, and with increasing density of non-basal 'forest' dislocations. This result is consistent with the forest dislocations limiting the extent of plastic deformation which accompanies cleavage, even at 77K. This is confirmed by the X-ray topography studies of plastic zone size. However, effective fracture surface energies are found to be considerably less than the thermodynamic surface energy for the basal plane of zinc. (23 refs.)
- 77748 Fractography of polyethylene glycol dimethacrylate doped with polymethyl methacrylate.** M.Atsuta, D.T.Turner (Dental Res. Center, Univ. of North Carolina, Chapel Hill, NC, USA). *Polym. Eng. & Sci. (USA)*, vol.22, no.18, p.1199-204 (Dec. 1982). The presence of polymethyl methacrylate (PMMA) can greatly affect the properties of materials made by polymerization of ethylene glycol dimethacrylate (EGDM). Fracture surfaces, examined by scanning electron microscopy, show a much wider range of morphologies in mist regions than observed in previous work on PEGDM alone. These morphologies are attributed to the modernization of brittle fracture by localized plastic deformation. It is suggested that the effect of PMMA is due to its segregation around clusters of highly cross-linked particles of PEGDM that, as a result, become more discrete and, hence, more susceptible to interparticle displacements during fracture. In agreement with this suggestion, the mist regions usually exhibit a particulate microstructure. (17 refs.)
- 77749 Strain localization and hydrogen embrittlement.** M.R.Louthan, Jr. (Dept. of Materials Engrg., Virginia Polytech. Inst. & State Univ., Blacksburg, VA, USA). *Scr. Metall. (USA)*, vol.17, no.4, p.451-4 (April 1983). Irreversible thermodynamic considerations and the observation of dislocation transport of hydrogen during plastic deformation provide a justification for hydrogen enhanced strain localization in metals and alloys. This justification

is based on the symmetry of the Onsager coefficients and the fact that entropy production is positive during plastic deformation. This justification therefore provides support for the argument that one mechanism of hydrogen embrittlement is hydrogen enhanced strain localization. (18 refs.)

- 77750 Ion implantation effect on fatigue crack initiation in Ti-24V.** K.V.Jata, J.Han (Fracture & Fatigue Res. Lab., Georgia Inst. of Technol., Atlanta, GA, USA), E.A.Starke, Jr., K.O.Legg. *Scr. Metall. (USA)*, vol.17, no.4, p.479-83 (April 1983). The results of a study of aluminum implanted Ti-24V (β -Ti alloy) are reported. It was found that implantation slightly improves the fatigue life in plastic strain controlled tests. The maximum improvement is observed to be about 40% at a plastic strain amplitude of 1.5×10^{-3} . The replica study in plastic strain controlled tests suggests that the surface deformation in the non-implanted Ti-24V occurs in coarse slip bands, while in the implanted Ti-24V slip is accommodated in more than one slip plane and the slip lines remain finer (as compared to the non-implanted condition) with continued cycling. The replica study also indicates that the fatigue crack initiation occurs on the surface, at slip bands for non-implanted samples and at grain boundaries for implanted samples. A considerable improvement in high cycle fatigue life is observed with aluminum implantation. The improvement is approximately two orders of magnitude at a stress level corresponding to 50% of the yield stress. This improvement is mainly due to the compressive residual stresses arising from aluminum implantation. (5 refs.)
- 77751 Effect of multiple crack propagation on the high temperature low cycle fatigue of a cast nickel-base alloy.** M.Y.Nazmy (Brown Boveri Res. Center, Baden, Switzerland). *Scr. Metall. (USA)*, vol.17, no.4, p.491-4 (April 1983). A preliminary investigation was carried out to study the effect of multiple crack propagation on the high temperature low cycle fatigue life (HTLCF) behaviour of IN 738 superalloy. The longer HTLCF lives of specimens tested under cycles with hold time compared to that of specimens tested under continuous cycling were explained on the basis of the effect of multiple cracks on crack growth rate. A multiple notched specimen, used as a model to clarify this effect, showed a longer life than the normal smooth specimens tested under the cycles with hold times. (16 refs.)
- 77752 The effect of pre-existing epsilon martensite on the hydrogen induced fracture of austenitic stainless steel.** S.-P.Hannula (Dept. of Mining & Metall., Helsinki Univ. of Technol., Espoo, Finland). *Scr. Metall. (USA)*, vol.17, no.4, p.509-13 (April 1983). Demonstrates the effect of pre-existing ϵ -martensite on hydrogen induced fracture by using a technique where deformation-induced phases are first revealed in a controlled dissolution sequence. It was concluded that in a slightly deformed matrix hydrogen induced fracture propagates mainly along $\{111\}$ planes and primarily along the ϵ/γ -interface. In regions between the active slip planes, the fracture propagates in a steplike manner and only a part of these steps is on the $\{111\}$ -planes. (20 refs.)
- 77753 A brittle to ductile transition in NiAl of a critical grain size.** E.M.Schulson, D.R.Barker (Thayer School of Engrg., Dartmouth Coll., Hanover, NH, USA). *Scr. Metall. (USA)*, vol.17, no.4, p.519-22 (April 1983). Tensile experiments have been carried out on the strongly ordered B2 aluminate, NiAl. It was established that the ductility is very low and essentially independent of grain size for aggregates of grains larger than about 20 μ m; for finer-grained aggregates the ductility increases sharply with decreasing grain size. NiAl thus exhibits a critical grain size below which polycrystalline aggregates are ductile in tension. The yield strength obeys the Hall-Petch equation $\sigma_y = \sigma_0 + k_y d^{-1/2}$ where $\sigma_0 = 152$ MPa and $k_y = 0.16$ MPa m^{1/2} under the conditions noted. For all grain sizes, fracture occurs in a brittle manner through a combination of intergranular decohesion and transgranular cleavage. (9 refs.)
- 77754 High-temperature transgranular fracture in an austenitic stainless steel.** T.Hasegawa, B.Ilschner (Inst. fur Werkstoffwissenschaften I, Univ. Erlangen-Nurnberg, Erlangen, Germany). *Scr. Metall. (USA)*, vol.17, no.4, p.523-7 (April 1983). Attempts to clarify the cause of transgranular fracture in Incoloy 800 H, an austenitic stainless steel. It is concluded that cold-rolling, a common manufacturing process to form Incoloy 800 H into a final sheet product, tends to break hard second-phase particles (probably Ti(C,N)) present randomly in this alloy. The fissures introduced into the particles may act as nuclei for the formation of internal microcracks during high-temperature straining and, thus, may cause accelerated creep rupture in a transgranular mode. (7 refs.)
- 77755 Crack resistance of pearlitic eutectoid steels. I. Fracture of steels in short-term loading.** O.N.Romaniv, E.A.Shur, A.N.Tkach, T.N.Kiseleva, V.N.Simin'kovich (G.V. Karpenko Physicomech. Inst., Acad. of Sci., Lvov, Ukrainian SSR). *Sov. Mater. Sci. (USA)*, vol.18, no.4, p.325-31 (July-Aug. 1982). Translation of: *Fiz.-Khim. Mekh. Mater. (USSR)*, vol.18, no.4, p.42-8 (July-Aug. 1982). [received: May 1983]. An investigation is made of the influence of the form and size of the cementite particles and also of the effective austenitic grain size on the resistance to brittle fracture of eutectoid steels with a structure of lamellar and granular pearlite. (17 refs.)
- 77756 Influence of vacuum and low temperature on fatigue crack growth rate in magnesium alloy sheets.** N.M.Grinberg, V.A.Serdyuk, T.I.Malinkina, A.S.Kamyshkov (Physicotech. Inst. of Low Temperatures, Acad. of Sci., Kharkov, Ukrainian SSR). *Sov. Mater. Sci. (USA)*, vol.18, no.4, p.331-6 (July-Aug. 1982). Translation of: *Fiz.-Khim. Mekh. Mater. (USSR)*, vol.18, no.4, p.48-54 (July-Aug. 1982). [received: May 1983]. An investigation was made of the growth rate of through and blind fatigue cracks in magnesium alloys differing in composition and heat treatment in a wide range of change in stress intensity factor in vacuum and at low temperature. A reduction in temperature influences the fatigue crack growth rate ambiguously. With low values of K_{max} it decreases at low temperature in comparison with the crack rate at room temperature in all of the alloys. With high values of K_{max} crack growth may either become slower or intensify depending upon the composition of the alloys and their structural condition. With a decrease in temperature the level of K_{th} increases, while the value of K_{Ic} is predetermined by the microstructure of the alloys. The fracture micromechanisms and their change under the influence of the medium and temperature correlate with the macroscopic parameters of fatigue crack growth. (8 refs.)

77757 Cyclic strength of magnesium-base reinforced composites. D.M.Karpinos, A.I.Gordienko, V.K.Samarin, V.Kh.Kadyrov, A.F.Voitenko (Inst. of Materials Sci., Acad. of Sci., Ukrainian SSR). *Sov. Powder Metall. & Met. Ceram. (USA)*, vol.21, no.10, p.810-12 (Oct. 1982). Translation of: *Poroshk. Metall. (USSR)*, vol.21, no.10, p.66-70 (Oct. 1982). [received: May 1983]

The results of an investigation into the cyclic strength of composite materials (CMs) based on magnesium reinforced with boron and steel fibers show that such CMs possess good resistance to fatigue fracture. High-strength fibers in a ductile matrix act as barriers on the path of propagation of a crack during cyclic loading, as a result of which a material of high fatigue strength is obtained. Under these conditions, the ductile steel fibers, whose modulus is higher than that of the matrix material, inhibit the propagation of a crack. A crack meeting a fiber may cease to grow, and subsequent fracture of such a magnesium-base CM will occur through the formation of new fatigue cracks in the matrix. In materials with the brittle boron fibers fatigue cracks may form and propagate both in the fibers (because of the statistical character of their strength) and directly in the matrix. The propagation of a main fatigue crack may be impeded by the fiber/matrix interfaces. Discontinuities at an interface result in local blunting of the crack, which lowers the stress concentration at its tip and arrests its growth. The method described for investigating the cyclic strength of magnesium-base CMs, in which allowance is made for changes in rigidity experienced in the course of cyclic deformation, is suitable also for studying the fatigue of CMs with other matrices. (7 refs.)

77758 Microstructure and mechanical strength of aluminum titanate ceramic prepared from mixture of alumina and titania. K.Hamano, Y.Ohya, Z.Nakagawa (Res. Lab. of Engng. Materials, Tokyo Inst. of Technol., Yokohama-shi, Japan).

Yogyo-Kyokai-Shi (Japan), vol.91, no.2, p.94-101 (1983). In Japanese. To improve mechanical strength of aluminum titanate ceramic, relations between microstructure and mechanical strength of the fired specimens were investigated. Specimens were prepared from stoichiometric mixtures of calcined aluminum hydroxide at 700°-1200°C for 2 h or fine corundum and anatase or rutile. During heating, alumina and titania of all specimens were converted into corundum and rutile, and aluminum titanate formation started from then at about 1300°C and completed at 1450°C. The specimens were fired at 1350°C, 1400°C, 1450°C and 1500°C each for 4 h. The density of any specimen was less than 80% of the theoretical density, and showed minimum for the specimens fired at 1400°C, which caused by volume expansion accompanied with formation of aluminum titanate from alumina and rutile. Size of aluminum titanate grains of fired bodies was 3-4 µm. Many grains agglomerated each other and formed large aggregates of 100-200 µm. Under the crossed nicols figure of polarization microscope, each aluminum titanate grain in one large aggregate showed simultaneous extinction, which means that the aluminum titanate grains in each aggregate oriented strongly. (11 refs.)

77759 Prediction of intergranular failure in Ni-Cr based alloys in low cycle fatigue at high temperatures - UK16. M.F.Day, G.B.Thomas. Report NPL-DMA(A)62, Nat. Phys. Lab., Teddington, England (1983), 55 pp. The fractional life approach was successful in correlating the results of LCF tests using a wide range of cyclic conditions. Metallographic measurements of fracture damage in IN597 generally supported the assumptions implicit in the fractional life approach. Failure mechanisms in both IN597 and IN738 LC were generally consistent with assumptions made to modify and extend the applicability of the fractional life approach. Strain range partitioning could not be successfully applied to either material. In the case of IN597 a marked stress dependence of the CP lifetime relationship has been found. For IN738 LC several negative values were obtained for CP, PC and CC lifetimes. When the compression part of a cycle with a tensile dwell period was carried out at a lower temperature the intergranular damage in specimens of IN597 was increased and life was reduced compared with an isothermal test in otherwise similar conditions. (14 refs.)

77760 Mechanical properties of $(\text{Fe}_{100-x}\text{M}_x\text{B}_{17})$ metallic glasses. G.Hunger, B.L.Mordike (Inst. für Werkstoffkunde und Werkstofftech., Tech. Univ. Clausthal, Clausthal, Germany).

Rapidly Solidified Amorphous and Crystalline Alloys. Proceedings of the Materials Research Society Annual Meeting, Boston, MA, USA, Nov. 1981 (New York, USA: North-Holland 1982), p.277-81. The mechanical properties hardness, tensile strength and fracture toughness of $(\text{Fe}_{100-x}\text{M}_x\text{B}_{17})$ glasses were measured for different alloying contents and heat treatments. If the as-quenched state the hardness is influenced mainly by changes in the metal-metalloid bonding. The fracture toughness is dependent on the alloying elements as well as the actual state of the glass. Heat treatment of the glass thus hardly influences the hardness whereas the toughness decreases strongly and significant changes in the fracture surface occur. Calorimetric observations suggest that structural relaxation is the primary reason for this behaviour although some effect of annealing out of internal stresses must be present. (16 refs.)

77761 Deformation induced dilatations and new observations on fracture in compression in metallic glasses at low temperatures. J.Megusar, A.S.Argon, N.J.Grant (MIT, Cambridge, MA, USA). Rapidly Solidified Amorphous and Crystalline Alloys. Proceedings of the Materials Research Society Annual Meeting, Boston, MA, USA, Nov. 1981 (New York, USA: North-Holland 1982), p.283-7. Deformation induced dilatations were measured on a Pd-Cu-Si glass by a differential dilatometric method during crystallization. At large pre-strains, these dilatations are large and of the order of 20%. Fracture surfaces of specimens in compression show either the characteristic features of tensile separation or evidence for repeated nucleation of fracture. Rubbing was observed only in a small fraction of a fracture surface. (9 refs.)

77762 The effect of hydrogen on an iron based amorphous alloy. H.Shahani, H.Soderhjelm (Dept. of Casting of Metals, Royal Inst. of Technol., Stockholm, Sweden).

Rapidly Solidified Amorphous and Crystalline Alloys. Proceedings of the Materials Research Society Annual Meeting, Boston, MA, USA, Nov. 1981 (New York, USA: North-Holland 1982), p.289-93. Systematically studies the brittleness and the atomic structure in an Fe(SiBC) alloy. Different amounts of hydrogen have been dissolved in the alloy. It has then been studied at different cooling rates. Hydrogen gas of different partial pressures was dissolved into the melt. The alloy was then rapidly quenched by a chill block melt spinning method. The cooling rates were changed by changing the velocity on the chilling roll. The brittleness and the atomic structure were examined by bending tests and X-ray diffraction. X-ray diffraction showed that the ribbons were amorphous when the cooling rate was sufficient. Amorphous ribbons without any hydrogen were ductile, crystalline ribbons of this alloy were brittle. The ribbons with dissolved hydrogen and amorphous structure were brittle even at small amounts of hydrogen. At the highest cooling rates the ribbons with low hydrogen content were ductile. There seems to be a connection between the hydrogen content and the amorphous ribbons

ductility. The hydrogen content only has a slight influence to amorphous structure. (7 refs.)

77763 Environmental cracking of amorphous alloys. S.Ashok, T.P.Slavin, N.S.Stoloff, M.E.Glicksman (Rensselaer Polytech. Inst., Troy, NY, USA). Rapidly Solidified Amorphous and Crystalline Alloys. Proceedings of the Materials Research Society Annual Meeting, Boston, MA, USA, Nov. 1981 (New York, USA: North-Holland 1982), p.309-13. Six amorphous metals have been tested in liquid metal environments or while charging with hydrogen. Differences in sensitivity to each environment are correlated with fractographic features. Evidence in support of enhanced shear as the mechanism of environmental cracking is presented. (6 refs.)

An assessment of acoustic emission for nuclear pressure vessel monitoring See Entry 75099

Fracture mechanics tests in static and cyclic loading conditions on structure graphite for high temperature reactor plants See Entry 75110

Distribution of pressure necessary to produce Griffith cracks of prescribed shape in an orthotropic medium See Entry 75957

Fatigue and fracture mechanics See Entry 75960

Crystallization behavior and properties of rapidly solidified Ni-Mo-B alloys See Entry 76320

Gamma radiation effects on the strength of a borosilicate glass See Entry 76502

Effect of 5.5-MeV electron bombardment on the high-temperature mechanical properties of nickel See Entry 76516

The effect of implanted helium on the high temperature mechanical properties of a model austenitic Fe-17% Cr-17% Ni alloy See Entry 76521

The effect of He-irradiation on the fracture toughness of ThO_2 See Entry 76522

Microhardness of glassy chalcogenides in the $(\text{As}_2\text{Se}_3)_x(\text{Bi}_2\text{Se}_3)_{1-x}$ system See Entry 76553

Theory of fatigue for brittle flaws originating from residual stress concentrations See Entry 76555

A quantitative approach to the cell shuttling model See Entry 76557

On the contrast between mode I and mode III fatigue crack propagation under variable-amplitude loading conditions See Entry 76558

Mechanism of fatigue crack propagation in metallic materials See Entry 76561

Microstructure and properties of fine grained supersaturated Fe-C alloys See Entry 76650

Microstructure and mechanical properties of laser-processed Ni-Al-Mo base alloys See Entry 76652

Transmission electron microscopy of RSP Fe/Cr/Mn/Mo/C alloy See Entry 76653

Characterization of flux-grown $\text{Ca}(\text{WO}_4)_x(\text{MoO}_4)_{1-x}$ crystals See Entry 77550

Formation of a nickel-clad titanium carbide coating and effect of spraying conditions on its structure and properties See Entry 77612

Melt processing and properties of barium-Sialon glasses See Entry 77614

Martensitic transformations in low-carbon nickel-molybdenum steels See Entry 77638

Studies of epoxy resin systems. IV. Fracture toughness of an epoxy resin: a study of the effect of crosslinking and sub- T_g aging See Entry 77658

Toughening by monoclinic zirconia See Entry 77663

Influence of aging on secondary recrystallization and mechanical properties of polycrystalline NaCl samples prepared by hot pressing See Entry 77678

Influence of heat treatment on the structure and long-term strength of γ/γ' -MeC nickel eutectic. Length memory effect See Entry 77680

Elastic moduli, hardness and thermal expansion of some metaphosphate glasses See Entry 77693

Tensile strength of ultra high modulus linear polyethylene filaments See Entry 77699

Influence of plastic deformation on the properties of chromium bronze See Entry 77703

Measuring temperature dependence of secondary forming behavior of cellular polystyrene sheets See Entry 77705

Mechanisms of material removal during erosion of a stainless steel See Entry 77764

The effect of molybdenum addition on the mechanical metallurgy and corrosion properties of the 13%Cr4%Ni steel See Entry 77797

Surface melting of cast iron with a high power laser beam See Entry 77810

Property enhancement in rapidly quenched alloy surfaces See Entry 77811

Technique to predict specimen failure in cyclic fatigue tests See Entry 77812

Assessment of critical temperature of embrittlement and transverse widening of the test piece in impact bend test See Entry 77826

81.40P Friction, lubrication, and wear (see also 62.20P Tribology)

77764 Mechanisms of material removal during erosion of a stainless steel. S.Soderberg, S.Hogmark, H.Swahn (Uppsala Univ. Inst. of Technol., Uppsala, Sweden).

ASLE Trans. (USA), vol.26, no.2, p.161-72 (April 1983). Solid particle erosion of an austenitic stainless steel was studied utilizing various metallographic techniques. Examination of single impacts on a polished surface resulted in a semiquantitative crater classification. It was, however, found that material removal generally involves the interactive effect of several cumulative impacts. Consequently, topography and internal structure of the target surface layer after multiple impacts was investigated. In particular, preeroded targets were reexamined after additional single impacts. The strength of the surface layer was estimated by a simple tape experiment, which also supplied information of the size and morphology of presumptive wear debris. Two major erosion mechanisms were distinguished: cutting erosion—detachment of crater lips by cutting action of one or several impacts; and deformation erosion—detachment of material by surface fragmentation due to multiple cumulative impacts. Surface layer hardness and ductility are the most important material properties for cutting and deformation erosion resistance respectively. (30 refs.)

77765 Geometrical aspects of the tribological properties of graphite fiber reinforced polyimide composites. R.L.Fusaro (NASA, Lewis Res. Center, Cleveland, OH, USA).

ASLE Trans. (USA), vol.26, no.2, p.209-21 (April 1983).

A Latin-square statistical experimental test design was used to evaluate the effect of temperature, load, and sliding speed on the tribological properties of graphite fiber reinforced polyimide (GFRPI) composite specimens. Hemispherically tipped composite riders were slid against 440C HT stainless steel disks. Comparisons were made to previous studies in which hemispherically tipped 400C HT stainless steel riders were slid against GFRPI composite disks and to studies in which GFRPI was used as a liner in plain spherical bearings. The results indicate that sliding surface geometry is especially important, in that different geometries can give completely different friction and wear results. Load, temperature, and sliding distance were found to influence the friction and wear results but sliding speed was found to have little effect. Experiments on GFRPI riders with 10 weight percent additions of graphite fluoride showed that this addition had no effect on friction and wear. (24 refs.)

77766 Scuffing under cyclic loading—unexpected effect of frequency. A.G.D.Smith, A.Cameron (Imperial Coll., London, England).

ASLE Trans. (USA), vol.26, no.2, p.236-42 (April 1983).

Using the hydrostatic 'disk' (or ring) machine developed in the authors' laboratory, a fluctuating load of ± 5 percent was superimposed on a steady load. At about 15 Hz the load-carrying capacity dropped by 40 percent compared with the steady value. It returned to its original value at about 60 Hz. The friction (and surface temperature) rose as the load-carrying capacity dropped. In one set of tests, the pitting life dropped from 13 hours to 30 minutes. The drop did not seem to depend on waveform and no sign of a machine resonance was found despite a careful search. The most likely explanation of the effect was thought to be a modification of the film shape due to the squeeze-film component. (13 refs.)

77767 Wear analysis. D.Scott.

Phys. Technol. (GB), vol.14, no.3, p.133-9 (May 1983).

The implications of wear cause considerable concern in industry. The problems associated with wear are outlined and techniques of wear detection, measurement and analysis are discussed. (7 refs.)

77768 Nitrogen migration during wear in an implanted steel. S.Fayeulle, D.Treheux, P.Guiraldeau (Dept. Metall. Phys.-Materiaux, Ecole Centrale de Lyon, Ecully, France), T.Barnavon, J.Tousset, M.Robelet.

Ser. Metall. (USA), vol.17, no.4, p.459-62 (April 1983).

Nitrogen migration during wear, though assumed for several years, is still not well understood and few studies have been able to clearly show it. The authors present results of a study on this migration using Z 200 C13 steel (13% Cr, 2% C). Previous studies have shown that the nitrogen penetration passes through a maximum as a function of fluence. The present authors have found that the maximum occurred near $2 \times 10^{19} \text{ }^{15}\text{N}^+ \text{ cm}^{-2}$. (10 refs.)

77769 Fretting of amorphous alloys. R.Becker, G.Sepold (Bremer Inst. für Angewandte Strahltech., Bremen, Germany).

Rapidly Solidified Amorphous and Crystalline Alloys. Proceedings of the Materials Research Society Annual Meeting, Boston, MA, USA, Nov. 1981 (New York, USA: North-Holland 1982), p.295-9.

Amorphous surface layers produced by bonding Metglas ribbons on to steel specimens were tested for their resistance to fretting. Friction and weight loss were determined and the worn surfaces were examined optically. There was no general tendency towards a better wear resistance of the tested amorphous metals as compared to crystallized metals or to a simple structural steel. The results are discussed. (7 refs.)

77770 Wear of transition metal rich glassy alloys. S.H.Whang, B.C.Giesen (Materials Sci. Div., Northeastern Univ., Boston, MA, USA).

Rapidly Solidified Amorphous and Crystalline Alloys. Proceedings of the Materials Research Society Annual Meeting, Boston, MA, USA, Nov. 1981 (New York, USA: North-Holland 1982), p.301-8.

Reviews the results of a systematic investigation of the wear behavior of several types of glassy alloys rich in transition metals, focussing on the coefficient of friction, wear rate, surface morphology and wear mechanism. (10 refs.)

Transmission electron microscopy of RSP Fe/Cr/Mn/Mo/C alloy

See Entry 76653

Determining the frictional properties of thin films of lubricants

See Entry 76817

Ion nitriding behavior of several low alloy steels

See Entry 77798

81.40R Electrical and magnetic properties (related to treatment conditions)

(see also 72.80 Conductivity of specific semiconductors and insulators, 74.70 Superconducting materials, 75.50 Studies of specific magnetic materials)

Furnace annealing of ion implanted polycrystalline silicon

See Entry 76473

Relaxation phenomena in amorphous $\text{Co}_{75-x}\text{Mn}_{25}$ induced by stress annealing

See Entry 76929

Superconducting properties and flux pinning in liquid quenched Nb-Ga alloys

See Entry 77115

The effects of ribbon thickness and annealing temperature on the AC magnetic properties of the $\text{Fe}_{81.5}\text{B}_{14.5}\text{Si}_3\text{C}_1$ alloy

See Entry 77222

New magnetic metallic glasses with reduced metalloid content

See Entry 77597

Perpendicularly crystallized ribbons by means of rapid solidifications from melts

See Entry 77598

Interrelation of the magnetic and mechanical properties with the structural state of hardened and tempered products

See Entry 77842

81.40T Optical properties (related to treatment conditions)

(see also 78.20 Optical properties and materials)

77771 Variation of optical inhomogeneity of ruby crystals. V.S.Konevskii, E.V.Krivososov, L.A.Litvinov.

Sov. J. Opt. Technol. (USSR), vol.49, no.9, p.574-6 (Sept. 1982). Translation of: *Opt.-Mekh. Prom.-st. (USSR)*, vol.49, no.9, p.35-7 (Sept. 1982).

The optical inhomogeneity of ruby, grown by the Verneuil method under diverse conditions (for a convex, concave-convex and plane growth isotherm), has been investigated. The optical inhomogeneity of these crystals has been

studied as a function of the annealing conditions at a temperature near the melting point ($T_{\text{ann}} = T_{\text{melt}} - 10^\circ\text{C}$). (8 refs.)

81.60 CORROSION, OXIDATION AND SURFACE TREATMENTS

77772 Changes of the surface composition of glass during reactive and argon ion etching. C.Jech, Z.Bastl (J. Heyrovsky Inst. of Phys. Chem. & Electrochem., Czechoslovak Acad. of Sci., Praha, Czechoslovakia).

Radiat. Eff. Lett. Sect. (GB), vol.76, no.1-2, p.25-8 (1983).

Removal of a radioactive implant (^{212}Pb + ^{212}Bi) from a glass surface was measured during reactive CF_4 and argon ion etching and accompanying changes in the surface composition were determined using ESCA. During reactive etching in CF_4 the formation of fluoride (Na,Ca,Mg) surface layers was observed. The high etching rate at low pressure of CH_4 can be explained by the combined action of the reactive etch of the silica component and RF sputtering of the residual nonvolatile fluorides. (3 refs.)

77773 Determining the maximum permissible operating temperatures for ceramics in aggressive media. M.I.Kushel', Yu.Ya.Eiduk, B.M.Shabrov, V.V.Kovalenko (Riga Polytech. Inst., Riga, USSR).

Glass & Ceram. (USA), vol.39, no.5-6, p.296-8 (May-June 1982). Translation of: *Steklo & Keram. (USSR)*, vol.39, no.6, p.21-3 (June 1982). [received: March 1983]

It is shown that, in order to establish the maximum permissible operating temperature for a ceramic material exposed to an active reagent, it is sufficient to determine experimentally two values of the corrosion rate at high temperatures (above 100°C). (7 refs.)

77774 Fabrication of ZrN coatings. J.J.Cuomo, P.A.Leary, D.S.Yee (IBM Corp., Armonk, NY, USA).

IBM Tech. Disclosure Bull. (USA), vol.25, no.11A, p.5506 (April 1983).

Describes a reactive sputtering process for the fabrication of ZrN coatings which are used in decorative applications to produce articles that are gold colored, conductive, and wear resistant. (no refs.)

77775 Real-time etch plasma monitor system. H.A.Khoury (IBM Corp., Armonk, NY, USA).

IBM Tech. Disclosure Bull. (USA), vol.25, no.11A, p.5721-3 (April 1983).

The monitor features an optical grating for dispersing the plasma radiation into specific wavelengths, a photodiode array for sensing the intensities of the various wavelengths and data processing means for digitizing the diode array signals and analyzing them so as to identify a plasma signature which may be used to analyze the plasma. (no refs.)

77776 Pre-clean treatment for prevention of nodular electroless nickel plating. G.R.Firth, M.A.Fury, J.M.Harvilchuck, R.L.Weisman (IBM Corp., Armonk, NY, USA).

IBM Tech. Disclosure Bull. (USA), vol.25, no.11A, p.5724 (April 1983).

An improved process is described for effectively cleaning NOVACULITE (grit) deposits on substrate surfaces prior to plating. (no refs.)

77777 Characterization of mechanochemically polished (111) surface of silicon crystal by diffuse X-ray scattering. N.Kashiwagura, J.Harada (Dept. of Appl. Phys., Nagoya Univ., Nagoya, Japan), M.Ogino.

J. Appl. Phys. (USA), vol.54, no.5, p.2706-10 (May 1983).

Diffuse X-ray scattering technique was applied to characterize the surface of a (111) silicon wafer polished mechanochemically. Extra diffuse scattering, which is considered to be attributable to localized strain fields was detected. The localized lattice distortions were of similar characteristics to those found in a (111) surface lapped with white aluminum (No. 2000) and etched by 30–60 μm [S. Yasuami and J. Harada, *J. Appl. Phys.*, 52, 3989 (1981)]. The thickness of the damaged layer induced by mechanochemical polishing was only about 15 μm , however, which is much smaller than that obtained by lapping (about 100 μm). This is the first observation of the damage in a mechanochemically polished (111) silicon surface. (6 refs.)

77778 Review of oxidation processes in plasmas. P.Friedel, S.Gourrier (Lab. d'Electronique et de Phys. Appl., Limeil Brevannes, France).

J. Phys. & Chem. Solids (GB), vol.44, no.5, p.353-64 (1983).

The authors review some of the major properties of oxygen plasma sources and describe some experimental set-ups. In a second part, they study the physical processes occurring in some specific cases of plasma oxidation and finally present some applications (Si MOS devices, Al_2O_3 capacitors, formation of the tunneling barrier of Josephson junctions). (46 refs.)

77779 Delayed fracture characteristics of soda-lime-silica glass in water. Y.Kimura, T.Yagasaki (Dept. of Chem. Engng., Kogakuin Univ., Tokyo, Japan), T.Kunio.

J. Soc. Mater. Sci. Jpn. (Japan), vol.32, no.354, p.315-21 (March 1983). In Japanese.

Four points bending delayed fracture tests in deionized water were conducted by using the soda-lime-silica glass plate specimens with the initial crack and indentation pit by Vickers diamond indentation. The results show that the lateral crack morphology is a governing factor for the delayed fracture characteristics of the specimens. This fact is brought about by the crack propagation behavior. The initiated crack (radial crack) propagates around the lateral crack. (23 refs.)

77780 Passivation of GaAs surfaces. J.I.Pankove, J.E.Berkeyheiser, S.J.Kilpatrick, C.W.Magee (RCA Labs., Princeton, NJ, USA).

J. Electron. Mater. (USA), vol.12, no.2, p.359-70 (March 1983).

Exposure to atomic hydrogen lowers the decomposition temperature of GaAs. Simultaneous exposure of GaAs to atomic hydrogen and atomic nitrogen above 500°C results in a layer rich in GaN. The degree of passivation was monitored by photoluminescence. A fourfold improvement in luminescence efficiency was obtained by nitridization, while a factor-of-ten improvement can be obtained with the more complicated technique of generating an (AlGa)As skin. (11 refs.)

77781 The oxidation behaviour of hot pressed aluminium nitride. M.Billy, J.Jarrige, J.P.Lecomte, J.Mexmain, S.Yefsah (Univ. de Limoges, Limoges, France).

Rev. Chim. Miner. (France), vol.19, no.6, p.673-83 (1982). In French.

The oxidation behaviour of AlN in static air was investigated in the temperature range $1200\text{--}1700^\circ\text{C}$ on dense hot-pressed specimens prepared without additives or by using oxides (MgO , CaO , Y_2O_3) for densification. The oxidation resistance is found to be good up to 1300°C . At higher temperatures, however, this resistance is lowered in the presence of additives, except for CaO . In this case, the outward migration of Ca and its precipitation (Ca_6) at the top of the oxidation scale do not really modify the protective character of the bulk. This phenomena suggests the existence of a new nitrogen vitreous phase in the CaAlON system. (5 refs.)

77782 High-temperature adsorption of atmospheric oxygen on silicon nitride powders. V.A.Lavrenko, E.A.Pugach, P.P.Pikuza (Kiev Polytech. Inst., Acad. of Sci., Ukrainian SSR). *Sov. Powder Metall. & Met. Ceram. (USA)*, vol.21, no.10, p.793-7 (Oct. 1982). Translation of: *Poroshk. Metall. (USSR)*, vol.21, no.10, p.47-52 (Oct. 1982). [received: May 1983]
The high-temperature adsorption of atmospheric oxygen on silicon nitride powders produced by various methods and containing different amounts of impurities was studied by the derivatographic method. Experiments were carried out at 20-1000°C in air at 1.10³ Pa under nonisothermal conditions; the rate of temperature variation was 20 deg C/min. The characteristics of each system was assessed by the results of a differential thermal analysis (DTA curve) and a thermogravimetric study. (TG and DTG curves). The sensitivity of the method in all experiments was the same. Air adsorption was found to have a specific individual character for each powder. It reflected the conditions of preparation of the powder by each process, its purification and treatment with reagents, and also the state of its surface. (15 refs.)

77783 Effect of a CaF₂ addition on the oxidation of hot-pressed silicon nitride-base materials. G.I.Postogvard, I.T.Ostapenko, V.A.Zelenskaya (Kharkov Physicotech. Inst., Kharkov, Ukrainian SSR). *Sov. Powder Metall. & Met. Ceram. (USA)*, vol.21, no.10, p.798-800 (Oct. 1982). Translation of: *Poroshk. Metall. (USSR)*, vol.21, no.10, p.53-6 (Oct. 1982). [received: May 1983]
A study was made of the oxidation of a hot-pressed Si₃N₄-10% MgO material containing 1-20% CaF₂ as an antiriction lubricant, at 1100-1250°C. As starting material a grade 1 silicon nitride powder was used containing, in addition to combined silicon and nitrogen, 1.5% free silicon and the following impurities: more than 3% carbon, 0.3% each iron and calcium, 0.1% aluminum, 0.2% titanium, and not more than 0.1% total chromium, nickel, magnesium, copper, lead, tin, zinc, and manganese. Hot-pressed Si₃N₄-10% MgO material possessed good oxidation resistance in air at temperatures in the range 1100-1200°C. When such a material contains an antiriction lubricant (1-20% CaF₂), raising the latter's concentration increases its rate of oxidation by decreasing the viscosity of the oxide layer, which facilitates access of oxygen to the specimen surface. At CaF₂ contents of more than 5% the material lacks mechanical strength owing to the formation of a thick oxide layer and appearance of cracks. (10 refs.)

77784 Study by electron spectroscopy for chemical analysis of silicon, SiO₂ and Si₃N₄ surfaces treated with various CF₄-containing plasmas. A.Licciardello, S.Pignataro (Istituto Dipartimentale di Chimica e Chimica Industriale, Univ. di Catania, Catania, Italy), M.Panczel. *Surf. Technol. (Switzerland)*, vol.18, no.3, p.189-99 (March 1983).
Silicon, SiO₂ and Si₃N₄ surfaces were treated with three different types of commercial plasma containing CF₄. The spectra obtained in electron spectroscopy for chemical analysis of these surfaces showed relatively low carbon and fluorine contamination. The latter contaminant was found on SiO₂ or Si₃N₄ surfaces but was no longer present on the silicon-like surfaces after treatment. The results are interpreted in terms of known mechanisms of plasma etching. (15 refs.)

Some aspects and results of the electrochemical etching of a thin-foil track detectorSee Entry 75233

Development of a new EPL-free etchant for soda-glass nuclear track detectorsSee Entry 75234

A new track etchant for plastic detectorsSee Entry 75237

On the nature of point defects and the effect of oxidation on substitutional dopant diffusion in siliconSee Entry 76416

Orientation dependence of oxidation stacking fault density in siliconSee Entry 76457

Matrix effect and surface oxidation in depth profiling of Al₂Ga_{1-x}As by secondary ion mass spectrometry using O₂⁺ primary ionsSee Entry 76479

Critical factors in laser and electron beam glazing of materialsSee Entry 76496

Electrochemical study of the thermal treatment effects on Cu₂S thin filmsSee Entry 76987

Structural investigations of detonation-deposited tungsten carbide-coalt coatingsSee Entry 77611

Formation of a nickel-clad titanium carbide coating and effect of spraying conditions on its structure and propertiesSee Entry 77612

Impact fracture mechanisms in polymer blends: rubber-toughened nylonSee Entry 77471

81.60B Metals and alloys
(inc. stress corrosion cracking; anticorrosion)

77785 Investigation on the corrosion of Ti-Al alloy in sulphuric acid. M.V.Susic (Inst. of Phys. Chem., Belgrade, Yugoslavia). *Mater. Chem. & Phys. (Switzerland)*, vol.8, no.3, p.193-202 (March 1983).
By means of chronocyclic electrochemical methods the investigation of the corrosion, i.e. the passivation of titanium and aluminium (3% Al, 0.25% Cr, 0.25% Fe, 0.25% Si) alloy was carried out. The values essential for the assessment of corrosion stability of the samples tested were determined and discussed. It was shown that by means of chronocyclic electrochemical methods reliable characteristics of corrosive behaviour of the material of this type can be determined. Differential thermal and thermogravimetric analyses showed the behaviour of the material when being heated up to 1100°C in air. (9 refs.)

77786 Electrochemical and morphological characterization of prefilmed aluminium brass. G.Brunoro (Istituto Chimico, Univ. di Ferrara, Ferrara, Italy), P.Spinelli. *Mater. Chem. & Phys. (Switzerland)*, vol.8, no.4, p.337-48 (April 1983).
Electrochemical and morphological characterization of aluminium brass prefilmed with benzimidazole-2-thiol (BIE) was made in 0.1 N sodium chloride solutions of various pHs. The prefilming treatment produces a surface layer with very good protective properties. The effect of the prefilming temperature is to increase the protectivity of the film. It was shown that the film resistance depends on the pH of the test solution. Upon prolonged immersion in the sodium chloride solution, a uniform removal of the surface film occurs, never giving rise to localized attack. An interaction between the inhibitor and the metal seems to be responsible for a marked limitation of the cathodic current density for oxygen reduction. A stabilization of the oxide layer as a consequence of the inhibitor interaction is suggested. (8 refs.)

77787 The UO₂-Zircaloy chemical interaction. D.R.Olander (Dept. of Nuclear Engng., Univ. of California, Berkeley, CA, USA). *J. Nucl. Mater. (Netherlands)*, vol.115, no.2-3, p.271-85 (April 1983).
Existing experimental data on the interaction of uranium dioxide and Zircaloy are analyzed with a model that accounts for the formation and growth of three corrosion layers between the oxide and the metal. The kinetics of the process are governed by diffusion of oxygen and uranium in the five-zone system with chemical equilibrium at four interfaces. Three of the zones consist of two elements and are treated by conventional scaling theory. Transport of all three elements (Zr, U, and O) occurs in the remaining two zones, one of which consists of two coexisting phases. Modeling of the system results in product layer growth rates which are in good agreement with the experimental results at 1500°C, which is the only temperature that both kinetic and thermodynamic information is available for application of the theoretical model. (24 refs.)

77788 Relative critical potentials for pitting corrosion of 304 stainless steel, Incoloy 800 and Inconel 600 in alkaline high-temperature aqueous solutions. W.F.Bogaerts, A.A.Van Haute, M.J.Brabers (Electrochem. & Corrosion Lab., Univ. of Leuven, Heverlee, Belgium). *J. Nucl. Mater. (Netherlands)*, vol.115, no.2-3, p.339-42 (April 1983).
Describes electrochemical corrosion tests conducted on Inconel 600 at temperatures up to 300°C and pressures up to 100 bar (10 MPa) in neutral and alkaline chloride solutions. The major objective of the tests was to determine the influence of solution temperature and composition (e.g. pH, Cl⁻ concentration) and of the alloy composition (Fe, Cr and Ni content) on the pitting corrosion behaviour of these austenitic materials. (9 refs.)

77789 Behaviour of alloying elements in high-temperature (1600°C-1800°C) transient oxidation of Zircaloy-4 LWR cladding tubes. M.Cambini, P.Bottelier, G.Buscaglia, C.Miglierina (Joint Res. Centre, Ispra Establ., Ispra, Italy). *J. Nucl. Mater. (Netherlands)*, vol.115, no.2-3, p.343-6 (April 1983).
Oxidation tests were performed on LWR Zircaloy-4 pipe segments. The results indicated that, under oxidising conditions at high temperature, the great majority of the alloying elements are transported in liquid form to the inner zone of the tubes. Since the thermodynamic activity of Zr in this liquid enriched in the alloying elements is lower than that of α-Zr(O), the oxidation of this latter phase is preferred. (10 refs.)

77790 The role of the electrode potential control in corrosion research of stress corrosion crack growth propagation in austenite stainless steels for nuclear reactor components. B.Eremias (Statni Vyzkumny Ustav Ochraný Materialu G.V. Akimova, Praha, Czechoslovakia). *Jad. Energ. (Czechoslovakia)*, vol.29, no.5, p.180-2 (May 1983). In Czech.
The role of the electrode potential control in stress corrosion crack growth propagation process is briefly discussed. Special attention is paid to the application of potentiostatic method in study of stress corrosion cracking of austenitic stainless steels for nuclear reactor components in high temperature water. (3 refs.)

77791 High temperature oxidation of vanadium-chromium alloys by low pressure oxygen. M.Yamawaki, T.Yoneoka, M.Kanno (Faculty of Engng., Univ. of Tokyo, Tokyo, Japan). *J. Jpn. Inst. Met. (Japan)*, vol.47, no.5, p.389-97 (1983). In Japanese.
Oxidation behaviour of vanadium-chromium alloys containing 5 and 10 at.% chromium has been investigated at temperatures ranging from 800 to 993K and at oxygen pressures at 1.33 and 133 Pa by means of a thermobalance, an X-ray diffractometer, an electron probe microanalyzer, a microhardness tester as well as metallographic techniques. Whereas mass gain due to oxidation initially followed the parabolic rate law, it then turned into very slow linear kinetics. Consequently, the oxidation resistance of vanadium was highly improved, especially at lower temperatures, lower oxygen pressures and higher chromium concentrations. Both alloys exhibited similar oxidation kinetics and scale structures. The oxide scale consisted mostly of a monolayer of VO₂ of low chromium content (≤0.65 mol.% Cr₂O₃) except for the oxidation at 993K and 133 Pa. A very thin chromium-concentrated layer (≤0.2 μm) was formed at the oxide scale-alloy substrate interface, to which could be attributed the retarded diffusion of vanadium into the oxide scale as well as that of oxygen into the substrate. (23 refs.)

77792 The selective dissolution of SUS04 and SUS16 austenitic stainless steels in a hydrochloric acid solution. R.Nishimura, M.Araki, K.Kudo (Corrosion Engng. Div., Government Industrial Res. Inst. of Chugoku, Kure, Japan). *J. Jpn. Inst. Met. (Japan)*, vol.47, no.5, p.413-19 (1983). In Japanese.
The anodic behavior and selective dissolution of SUS304 and SUS316 austenitic stainless steels were investigated as a function of potential in a 1 kmol.m⁻³ HCl solution by using electrochemical technique and inductively coupled plasma emission spectrometry (ICP). On the basis of the comparison between the amount of total anodic charge passed and that of electric charge obtained from dissolution, it was found that the anodic polarization curves of SUS304 and SUS316 were divided into three regions, the active dissolution, the film formation, and the film destruction. The compositions of metal ions dissolved in the solution revealed that the preferential dissolution of Fe took place on both steels in the active dissolution region and led to the enrichment of Cr on SUS304 surface and that of Cr, Ni and Mo on SUS316 surface. In the region of the film formation, it was found that a film formed on SUS304 was enriched with Cr because of the preferential dissolution of Fe. In the case of SUS316, it was suggested in terms of the preferential dissolution of Ni and Mo that a film changed from Cr, Ni, Mo-rich layer into Cr-rich layer during anodic oxidation. It was, furthermore, deduced that Mo lowered the activity or density of active centers such as MnS on SUS316 surface in the process of active dissolution and consequently contributed to the formation of a uniform film free from defects. (15 refs.)

77793 Damping capacity and pitting corrosion resistance of Fe-Mo-Cr alloys. H.Masumoto, S.Sawaya, M.Hinai (Res. Inst. of Electric & Magnetic Alloys, Sendai, Japan). *J. Jpn. Inst. Met. (Japan)*, vol.47, no.5, p.439-45 (1983). In Japanese.
The damping capacity and the anodic polarization behaviour in a 3%NaCl solution were studied on Fe-Mo-Cr alloys containing 1-16%Mo and 2-35%Cr after various heat-treatments. Measurement of the internal friction Q⁻¹ was carried out by the inverted torsion pendulum method at a frequency of 1 Hz. The tensile strength σ_t and the pitting potential E_p were measured using an Instron-type testing machine and a potentiostat, respectively. In the state of furnace-cooling, the Q⁻¹ value of the Fe-Mo-Cr alloys with small amounts of Mo and Cr is considerably high, while the alloys with large amounts of Mo and Cr are low in Q⁻¹ because the intermetallic compounds precipitate in the ferromagnetic α phase matrix. On the other hand, the numerous alloys subjected to water-quenching are fairly high in Q⁻¹ because of the single phase α solid solution. The σ_t in both the state increases considerably with increasing Mo and Cr contents. The increment in σ_t upon furnace-cooling is more than that in the case of water-quenching. The E_p value of the furnace-cooled

alloys is generally low, while the numerous alloys become higher in E_p by water-quenching where high Q^{-1} value appears. (19 refs.)

77794 Improvement of corrosion fatigue strength of notched high strength steel by partial unloading method. M.Kido (Hiroshima Inst. of Technol., Hiroshima, Japan), K.Nakasa, H.Takei. *J. Soc. Mater. Sci. Jpn. (Japan)*, vol.32, no.354, p.310-14 (March 1983). In Japanese.

The effect of partial unloading on the corrosion fatigue strength in water was investigated on the notched specimens of SNCM439 steel quenched and tempered at 473K. The corrosion fatigue strength was markedly increased by the partial unloading method. This fact may be explained by the decrease of tensile stress at the notch root surface which suppresses the destruction of the protective film due to repeating slips in the material and prevent the corrosion reaction. (8 refs.)

77795 The application of high resolution electron microscopy to the study of oxidation. S.B.Newcomb (Dept. of Metall. & Materials Sci., Univ. of Cambridge, Cambridge, England), D.J.Smith, W.M.Stobbs. *J. Microsc. (GB)*, vol.130, pt.2, p.137-46 (May 1983). (MICRO 82: High Resolution Electron Microscopy, London, England, 12-16 July 1982). High resolution electron microscopy has been used to examine both the similarities and differences in the growth morphologies of Fe_2O_3 , Cr_2O_3 as formed on iron alloys, and MgO as formed by burning Mg in moist air. A general discussion is also given of the relative advantages and disadvantages of a variety of TEM techniques as applicable to the study of oxidation phenomena. (20 refs.)

77796 The transmission electron microscopy of oxide scale formation on Fe-Ni-Cr alloys. S.B.Newcomb, W.M.Stobbs (Dept. of Metall. & Materials Sci., Univ. of Cambridge, Cambridge, England). *J. Microsc. (GB)*, vol.130, pt.2, p.233-48 (May 1983). (MICRO 82: High Resolution Electron Microscopy, London, England, 12-16 July 1982). The oxidation behaviour of 10 Cr and 20 Cr iron alloys, with nickel contents from 0 to 34 wt.% both in air and in CO/CO_2 , is summarized with particular emphasis on the form and chemistry of the different scales as they were observed using transmission electron microscopy. The various modes of inward oxidation are for example characterized with 'internal' and 'inner' oxidation taking place under different circumstances. The role of carbon during oxidation in a CO/CO_2 atmosphere is also discussed as is the way in which a given alloy can show either chemical or mechanical passivation failure in different environments. (25 refs.)

77797 The effect of molybdenum addition on the mechanical metallurgy and corrosion properties of the 13Cr4%Ni steel. J.Hubackova (CSAV, Ostrava-Poruba, Czechoslovakia), V.Cihal, K.Mazanec. *Kovove Mater. (Czechoslovakia)*, vol.21, no.2, p.131-41 (1983). In Czech. The susceptibility to the temper embrittlement of the 13Cr4%Ni steel (occurring to a limited extent) has been completely eliminated by the addition approximately of 0.5% molybdenum. This addition leads to the improvement of corrosion resistance; the susceptibility to the intergranular corrosion has been reduced only partially. By addition of 1.48% Mo the toughness has not been improved, but the corrosion resistance has been considerably increased and the susceptibility to the intergranular corrosion of 13Cr4%Ni steel eliminated. The evaluation of the corrosion resistance, susceptibility to the intergranular corrosion and the extent of re-austenitization during the tempering at intercritical temperatures can be carried out by means of the modified potential polarization method, based on the measurements of the electrochemical parameters particularly after the reactivation from the complete or incomplete passivation region. (10 refs.)

77798 Ion nitriding behavior of several low alloy steels. C.V.Robino, O.T.Inal (Dept. of Metall. & Materials Engng., New Mexico Inst. of Mining & Technol., Socorro, NM, USA). *Mater. Sci. & Eng. (Switzerland)*, vol.59, no.1, p.79-90 (May 1983).

The ion nitriding behavior of several low alloy steels, US Steel T1 type A, AISI 4140, AISI 6150 and Nitralloy 135M, has been examined under varying process conditions using microhardness-depth correlations, friction and wear measurements, optical microscopy and transmission electron microscopy. The process variables included time (2-48 h) and temperature (400-600°C). All four steels exhibited a diffusion layer case growth rate which was dependent on the square root of the exposure time. The highest nitrided hardnesses and lowest case depths were observed in the Nitralloy 135M steel while the lowest hardnesses and highest case depths were seen in the T1 steel. In general the behaviors of the T1, AISI 4140 and AISI 6150 steels were similar. The white layer thickness was independent of the material and increased with increasing treatment time. Both the case depth and the white layer thickness were found to increase strongly with temperature while the hardness decreased. (26 refs.)

77799 Effects of segregated phosphorus on stress corrosion cracking susceptibility of 3Cr-0.5Mo steel. G.T.Burstein, J.Woodward (Dept. of Metall. & Materials Sci., Univ. of Cambridge, Cambridge, England). *Met. Sci. (GB)*, vol.17, no.3, p.111-16 (March 1983). An examination has been made of the rate of intergranular stress corrosion cracking (SCC) of 3Cr-0.5Mo steel in hot 8 M NaOH solution as a function of the heat treatment of the alloy. The results show that the rate of SCC is extremely sensitive to the concentration of segregated phosphorus in the grain boundaries. Analysis of the segregation levels of trace elements after the steel had been heat treated at 823K for different times is presented. (22 refs.)

77800 Fatigue corrosion behaviour of various metallic materials in chloride environment. M.Truchon (Inst. de Recherches de la Siderurgie Francaise, Saint-Germain-en-Laye, France), P.Rabbe. *Mem. & Etud. Sci. Rev. Metall. (France)*, vol.80, no.3, p.117-30 (March 1983). In French.

Results of fatigue corrosion tests carried out in synthetic sea water A3 for three stainless steels, a structural steel and an aluminium alloy are presented. Their resistance at the initial and the propagation stage is evaluated. (26 refs.)

77801 Oxidation kinetics of Cu-Zn-Al alloys. D.Farkas, G.Nunez (Dept. Metalurgia, Fac. Univ. Nacional Autonoma de Mexico, Mexico City, Mexico). *Ser. Metall. (USA)*, vol.17, no.4, p.505-8 (April 1983).

The influence of composition on the oxidation kinetics of Cu-Zn-Al alloys has been studied. The results indicate that for lower Zn contents the Al content needs to be as high as 4% to ensure protective properties of the scale. (8 refs.)

77802 Mathematical model of corrosion fatigue. F.F.Azhogin, Yu.S.Goryachko, Yu.G.Ozhiganov. *Sov. Mater. Sci. (USA)*, vol.18, no.4, p.350-5 (July-Aug. 1982). Translation of: *Fiz.-Khim. Mekh. Mater. (USSR)*, vol.18, no.4, p.69-75 (July-Aug. 1982). [received: May 1983]

From the concepts developed of the mechanism of fatigue and corrosion fatigue failure the following conclusions are drawn: there exists a physical corrosion fatigue limit; the relationship of the number of cycles until failure

N to the level of tensile stresses σ is described by the equation $(\sigma - A)\sqrt{N} = K_{\sigma}$; in the presence of a strengthened layer with large amplitudes of oscillations a break is formed on the corrosion fatigue curve in σ vs. $1/\sqrt{N}$ coordinates. The treatment of experimental data on the corrosion fatigue of carbon, low-alloy, high-chrome, and chrome-nickel steels presented in many works of many authors show that these data satisfy the derived equation of the corrosion fatigue curve. (45 refs.)

77803 Temperature stresses in a plate in friction hardening. Yu.M.Kolyano, Yu.I.Babei, V.Z.Didyk, B.M.Korduba (Inst. of Appl. Problems of Mech. & Math., Acad. of Sci., Lvov, Ukrainian SSR). *Sov. Mater. Sci. (USA)*, vol.18, no.4, p.356-62 (July-Aug. 1982). Translation of: *Fiz.-Khim. Mekh. Mater. (USSR)*, vol.18, no.4, p.75-81 (July-Aug. 1982). [received: May 1983]

The authors have determined the temperature fields and the thermally stressed condition of a metal plate occurring in friction hardening and have investigated the influence of heat transfer out of the heating area on the temperature stresses. (6 refs.)

77804 Surface reinforcement of iron-base materials. B.S.Mitin, V.K.Narva, N.T.Salibaev (Moscow Inst. of Steel & Alloys, Moscow, USSR). *Sov. Powder Metall. & Met. Ceram. (USA)*, vol.21, no.10, p.780-4 (Oct. 1982). Translation of: *Poroshk. Metall. (USSR)*, vol.21, no.10, p.33-8 (Oct. 1982). [received: May 1983]

A study was made of the application of a wear-resistant TiC-Kh12M steel layer to type 45 steel by methods consisting in simultaneous pressing and sintering and in the sinter-bonding of a pressed or sintered layer to a sintered base. It has been established that the alloying of the basis material with 1% of Cu substantially increases its density and adhesion to the coating. It is shown that a layer can be applied to a sintered base with or without a substrate. It has been found that the highest bond strength, $(10-14) \times 10^7$ Pa, is attained when a layer and a base containing 1% of Cu are simultaneously pressed under a pressure of 3.10^8 Pa and then simultaneously sintered at 1673K. (5 refs.)

77805 A possibility to obtain microdiscontinuous chromium coatings by cathodic treatment in acidic media. S.Rashkov, M.Monev, N.Atanassov (Inst. of Phys. Chem., Bulgarian Acad. of Sci., Sofia, Bulgaria). *Surf. Technol. (Switzerland)*, vol.18, no.3, p.201-7 (March 1983).

A possibility is described for obtaining microdiscontinuous chromium coatings by cathodic treatment of conventional chromium electroplates in sulphuric acid solutions in the presence of selenite ions. The relationships are determined between the microdiscontinuities formed in the chromium coatings and the cathodic treatment conditions (duration, selenite ion concentration and pH of the medium) and the thickness of the chromium layer. The microporous and microcracked chromium coatings formed by this method substantially improve the corrosion resistance of the Ni/Cr system. (10 refs.)

77806 Some possibilities for the use of stressed cathodically hydrogenated electrolytic nickel coatings for the deposition of microporous and microcracked chromium plates. S.Rashkov, M.Monev, N.Atanassov (Inst. of Phys. Chem., Bulgarian Acad. of Sci., Sofia, Bulgaria). *Surf. Technol. (Switzerland)*, vol.18, no.3, p.217-23 (March 1983).

It has been established that hydrogenated bright nickel coatings containing nickel hydride as the surface phase, owing to the properties of the latter (disintegration into molecular hydrogen creating high internal stresses), can be used for the plating of microporous and microcracked chromium coatings, depending on their thickness. Similar chromium coatings improve the corrosion resistance of the Ni-Cr system. It is proposed that the formation of microcracked chromium coatings on bright nickel during direct deposition from electrolytes containing selenite ions is related to the formation of a stressed nickel layer as a result of the appearance and disintegration of nickel hydride formed during the initial stages of chromium plating. (20 refs.)

77807 Surface alloying of iron alloys by laser beam melting. B.L.Mordike, H.W.Bergmann (Inst. fur Werkstoffkunde und Werkstofftech., Univ. of Clausthal, Clausthal, Germany).

Rapidly Solidified Amorphous and Crystalline Alloys. Proceedings of the Materials Research Society Annual Meeting, Boston, MA, USA, Nov. 1981 (New York, USA: North-Holland 1982), p.463-83. The surface heat treatment of iron alloys using high power lasers is reported. The essential features, e.g. epitaxial growth, homogeneity, etc., are discussed. The results are tabulated for the technically important alloys. The possibilities of laser hardening are demonstrated by four examples. (10 refs.)

77808 Production and properties of amorphous layers on metal substrates by laser and electron beam melting. H.W.Bergmann, B.L.Mordike (Inst. fur Werkstoffkunde und Werkstofftech., Tech. Univ. Clausthal, Clausthal, Germany).

Rapidly Solidified Amorphous and Crystalline Alloys. Proceedings of the Materials Research Society Annual Meeting, Boston, MA, USA, Nov. 1981 (New York, USA: North-Holland 1982), p.497-503. Various techniques of laser glazing are presented. Rules are given for the choice of systems which are suitable for producing amorphous surface layers. Methods of demonstrating the existence of a truly amorphous layer are discussed. Two examples are given: (1) electron beam glazing of Ni-Nb coated single crystals, (2) laser beam glazing of Fe-B coated Fe-Cr-C cold working steel. (5 refs.)

77809 Laser surface treatment of aerospace steels. G.Christodoulou, P.Henry, W.M.Steen, D.R.F.West (Dept. of Metall. & Materials Sci., Imperial Coll., London, England).

Rapidly Solidified Amorphous and Crystalline Alloys. Proceedings of the Materials Research Society Annual Meeting, Boston, MA, USA, Nov. 1981 (New York, USA: North-Holland 1982), p.505-10.

An investigation is reported of the laser surface melting of four alloy steels with carbon contents ranging up to 1 wt%. Studies were made of the profiles, microstructures and hardnesses of zone produced using a laser power of 1.7 kW and a range of traverse speeds and beam diameters. The observed zone profiles were correlated with calculations from a three-dimensional, moving source, heat transfer model. In the high carbon steels, the shallow laser melted zones contained substantial amounts of retained austenite. (7 refs.)

77810 Surface melting of cast iron with a high power laser beam. Y.Nilsen (Dept. of Casting Metals, Royal Inst. of Technol., Stockholm, Sweden). Rapidly Solidified Amorphous and Crystalline Alloys. Proceedings of the Materials Research Society Annual Meeting, Boston, MA, USA, Nov. 1981 (New York, USA: North-Holland 1982), p.517-21.

An investigation is done on partial surface hardening and alloying on cast iron by means of a high power laser beam. Samples of cast iron have been covered with alloying material, i.e. Ti, Cr, Si, V and Nb respectively. The samples were irradiated with a 2.5 kW laser beam. A partial melting of the surface occurred and the alloys were dissolved. The carbide structure in the resolidified part was governed by the alloy addition. The carbide structure was metallographically analysed. The effect of different parameters as beam

diameter, scanning rate, power and alloy content have been investigated and the crack frequency has been evaluated. (2 refs.)

77811 Property enhancement in rapidly quenched alloy surfaces. M.Tuli (Pilgrim Materials Corp., South Windsor, CT, USA), P.R.Strutt. Rapidly Solidified Amorphous and Crystalline Alloys. Proceedings of the Materials Research Society Annual Meeting, Boston, MA, USA, Nov. 1981 (New York, USA: North-Holland 1982), p.535-9. Electron beam glazed surfaces on a circular bar are of sufficiently good quality either for direct use or after light mechanical grinding. The technique may be applied for reconstituting plasma deposited layers thereby eliminating porosity and obtaining a highly homogeneous refined microstructure. By this treatment it was found that the microhardness of a plasma deposited layer of chromium carbide in molybdenum binder increased from 525 VHN to 750 VHN. (5 refs.)

Current understanding of pitting and crevice corrosion and its application to test methods for determining the corrosion susceptibility of nuclear waste metallic containers See Entry 75091

Tensile properties of 1.4970 austenitic stainless steel after corrosion caused by uranium dioxide and simulated fission products See Entry 75100

Study of the deactivation mechanisms for some constructional steels by secondary-ion mass spectrometry See Entry 75107

Microstructure and mechanical properties of laser-processed Ni-Al-Mo base alloys See Entry 76652

Rapidly solidified microstructure in surface layers of laser-alloyed Mo on Fe-C substrates See Entry 76763

A study on the orientation of imidazoles on copper as corrosion inhibitor and possible adhesion promoter for electric devices See Entry 76775

The temperature dependence of the interaction of oxygen with Pd(111): a study by photoemission and Auger spectroscopy See Entry 76790

Phase analysis of the oxidation products of plain steels by Mossbauer spectroscopy See Entry 77304

Effects of semiconducting oxide films on the reflectivity change in a metal on radiation heating See Entry 77344

Reactive pulse plasma crystallization of TiN layers on substrates at 500K See Entry 77574

The role played by the anions in cadmium electroplating from some acidic baths See Entry 77587

The effect of AC superimposed on DC in the electrodeposition of metals See Entry 77588

Phase transformation studies of laser-processed Fe-0.2% C-Cr surface alloys See Entry 77635

Effects of thickness and compressive residual stress of boronized layer on bending fatigue strength properties of boronized steels See Entry 77737

Effect of prior deformation on the cleavage of zinc single crystals See Entry 77747

Environmental cracking of amorphous alloys See Entry 77763

A simple method for the determination of the coating thickness of galvanized steel See Entry 77847

Potentiostatic etching of carburized steels See Entry 77857

On the processes responsible for the degradation of the aluminium-lithium electrode used as anode material in lithium aprotic electrolyte batteries See Entry 77892

Oxidized rare earth-iron compounds in photoassisted electrolysis of water See Entry 77896

Polarization of the lithium electrode in sulfonyl chloride solutions See Entry 77970

Li/SOCl₂ cells for high temperature applications See Entry 77971

Surface films on lithium in acetonitrile-sulphur dioxide solutions See Entry 77979

81.70 MATERIALS TESTING

(inc. sample preparation for examination, metallographic techniques, ion and electron microprobe techniques, Auger and photoelectron techniques, defectoscopy; for measurement in the mechanics of solids and rheology, see 46.30R)

77812 Technique to predict specimen failure in cyclic fatigue tests. N.Tamada, Y.Iwasa (Francis Bitter Nat. Magnet Lab., MIT, Cambridge, MA, USA).

Appl. Phys. Lett. (USA), vol.42, no.9, p.799-800 (1 May 1983). The authors report a technique with which to predict specimen failure from cyclic fatigue tests. The technique observes one of the resonant frequencies of the specimen. A definite shift in the resonant frequency has been seen to occur preceding failure; this shift may be used to predict specimen failure. (4 refs.)

77813 Study on surface crack opening displacement and its applications in pressurized vessels and pipings. Yang Fangyu, Wang Yanyan, Qin Hong, Li Huirong, Gao Guilan (Dalian Inst. of Technol., China).

Acta Mech. Sin. (China), no.1, p.34-44 (1983). In Chinese. Presents a simple method to estimate the surface crack opening displacement (SCOD) of tension specimens and pressurized vessels. To date, the only procedure for estimating SCOD is introduced by A.S. Kobayashi (1976). In order to examine the proposed method experiments have been performed on crack growth and fracture in plate specimens and cylinders. Good agreement between predicted and experimental results has been obtained as shown by curves of normalized SCOD versus normalized depth of crack. One of the applications of SCOD equation is to evaluate the depth of surface crack in plates or vessels. A procedure for estimating crack depth is presented. SCOD equation can be also be used to monitor crack growth in pressurized vessels and pipings. A new experimental procedure for evaluating crack growth d/dN and ΔK_I without any mechanical or thermal moving on the tip of crack has been developed. The measuring technique of SCOD in flawed tension plates and cylinders is explained in detail. (10 refs.)

77814 Method of testing glass for strength with constant loading rate. D.L.Orlov, E.A.Abramyan, A.A.Perova, R.Leieritis. *Glass & Ceram. (USA)*, vol.39, no.5-6, p.277-9 (May-June 1982). Translation of: *Steklo & Keram. (USSR)*, vol.39, no.6, p.12-13 (June 1982). [received: March 1983]

A method is described which permits one to use ordinary tensile testing machines without electronic regulation of the loading rate to test glass at constant loading rate. (2 refs.)

77815 Advances in instrumentation for materials characterization. R.M.Fisher (Corporate Res., US Steel Res., Monroeville, PA, USA).

J. Met. (USA), vol.35, no.3, p.42-5 (March 1983). Most of what is known about the complexities of the effects of microstructure on the properties of alloys has resulted from scientific studies of metal structures. Since the phases and features that most strongly affect metal properties are of the size range 10^{-1} to 10^{-7} mm, sophisticated instruments are required to observe, identify, and characterize them. Recent developments and trends in this type of instrumentation as applied to metals and metallic phases are summarized. (11 refs.)

77816 Present status and problem of high temperature corrosion testing methods. Y.Harada (Takasago Tech. Inst., Mitsubishi Heavy Industries Ltd., Takasago, Japan).

J. Soc. Mater. Sci. Jpn. (Japan), vol.31, no.349, p.999-1011 (Oct. 1982). In Japanese. [received: April 1983]

Methods and considerations for the corrosion test and assessment of engineering components and structures for high-temperature applications are described. High-temperature corrosion tests provide significant data for assessing the applicability of a corrosion protection technique of interest. A brief outline is given of the methods: (1) burning tests using experimental burning equipment; (2) heating tests for a test piece coated with or immersed in corrosion activator; (3) measurements of the quantity of oxygen consumed for the corrosion reaction of a test piece in a furnace; and (4) electrochemical tests. In addition, test conditions and environment control are summarized. (52 refs.) K.B.

77817 X-ray investigation of stress measurement of heat resisting materials (on the X-ray elastic constants and the residual stresses of nickel base alloy). J.Arima, Y.Iwai (Nara Tech. Coll., Nara, Japan).

J. Soc. Mater. Sci. Jpn. (Japan), vol.32, no.354, p.277-83 (March 1983). In Japanese.

The elastic constants of a nickel base alloy at high temperatures were studied by the X-ray method with a new apparatus consisting of a horizontal type tensile testing machine and a vacuum furnace. Residual stresses due to precipitation hardening were also studied. The microstructure of the material was observed at various temperatures. After the heat treatment for precipitation hardening, all the plate specimens of Inconel X were finished and then electropolished before being exposed to X-rays. The strain was determined by measuring the diffraction from the (311) atomic plane by means of the conventional $\sin^2\psi$ diagrams using a counter technique. The elastic constants of Inconel X obtained by the X-ray technique are in good agreement with those measured mechanically within the experimental errors. The lattice spacings or lattice constants changed about 5.2 degree in 2θ from room temperature at 923K. (18 refs.)

77818 Fractographic examination in the scanning electron microscope as a tool in evaluating through-thickness tension test results. M.M.McDonald, D.C.Ludwigson (Res. Lab., United States Steel Corp., Monroeville, PA, USA).

J. Test. & Eval. (USA), vol.11, no.3, p.165-73 (May 1983). The through-thickness tension tests is used to assess resistance to lamellar tearing. Observed through-thickness reduction-of-area (TTRA) values are usually well above the 20% minimum specification level in steels produced for lamellar-tearing-resistant applications. Low TTRA values, when encountered, indicate susceptibility to lamellar tearing but provide little indication of the source of premature fracture. Fractographic examination, especially with the scanning electron microscope, provides information about the origins of low ductility. Sources of premature fracture discussed herein are indigenous inclusions, exogenous inclusions, occluded hydrogen, undissolved alloy additions, and solidification microvoids. (15 refs.)

77819 Numerical analysis of ductile fracture experiments using single-edge notched tension specimens. T.Hollstein (Fraunhofer-Inst. fur Werkstoffmech., Freiburg, Germany), W.Schmitt, J.G.Blaue.

J. Test. & Eval. (USA), vol.11, no.3, p.174-81 (May 1983).

The elastic compliance C and the J -integral are investigated for single-edge notched tension specimens. The parameters are discussed with respect to crack length, thickness of specimen; load level, stress state, and loading system. Test results for a structural steel St E 460 (nickel-vanadium) at room temperature are presented together with two- and three-dimensional finite element calculations for some of these specimens. The overall specimen behavior including J for the 10-mm-thick specimens is reproduced by a plane stress model. Even the 40-mm-thick specimens are better modelled in plane stress than in plane strain. The strong influence of the angular stiffness of the loading system on the specimen behavior is demonstrated. For the experimental arrangement used in this study a single-specimen estimation procedure is developed to calculate J from the work done on the specimen. (18 refs.)

77820 Stressing for test purposes of materials in tubular form using elastomeric inserts—practical testing procedures. K.Mosley (Dept. of Sci. & Industrial Res., Lower Hutt, New Zealand).

J. Test. & Eval. (USA), vol.11, no.3, p.182-92 (May 1983).

Describes mainly the practical aspects of a simple and rapid method of elastic hoop stressing materials in tubular form using elastomeric inserts. The method can be used for stressing to required limits, for testing to fracture, or for obtaining yield loads. It is extremely suitable for the testing of brittle materials. Stress equations and insert specimen coefficients of friction are given in the appendixes. (3 refs.)

77821 An improved method for threshold fatigue crack propagation testing on an electromagnetic resonance type machine. S.Nishijima, S.Matsuoka, S.Ohtsubo (Nat. Res. Inst. for Metals, Tokyo, Japan).

J. Test. & Eval. (USA), vol.11, no.3, p.193-201 (May 1983).

An improved technique for fatigue crack propagation testing is proposed for the determination of threshold stress intensity range ΔK_{th} using an electromagnetic resonance type testing system. A special device is used to compensate for the change of specimen compliance during the test. It is composed of a set of transverse mutually hinged at one end between which an elastic body and a specimen are mounted in parallel, respectively, at predetermined distances from the hinge, so that the resultant composite compliance of the device is designed to be practically insensitive to the change of specimen compliance. A series of ΔK_{th} measurements was performed at various load ratios of six steels of various strength levels, using small compact type (CT) specimens of 25 mm width and 5 mm thickness, under combined control modes of the applied load and the backface strain of the specimen. The use of the compliance stabilizing device improved markedly the controlling stability of the testing machine and facilitated the determination of ΔK_{th} value under auto-decreasing ΔK conditions at high load ratios. The obtained ΔK_{th} values from the experiments were in excellent agreement with those found in the literature. (10 refs.)

- 77822 A new transducer to monitor fatigue crack propagation.** P.K. Liaw (Westinghouse Electric Corp., Res. & Dev. Center, Pittsburgh, PA, USA), H.-R. Hartmann, W.A. Logsdon. *J. Test. & Eval. (USA)*, vol.11, no.3, p.202-7 (May 1983).
A sputter deposition technique has been successfully used to fuse automatically a high-temperature DC transducer, in the form of a thin film Krak-Gage, directly onto a test specimen for developing fatigue crack propagation rate data. The rates of fatigue crack growth measured by this technique are in good agreement with those measured by the compliance method at 288 and 427°C (550 and 800°F). The data acquisition and analysis are automated by interfacing with a computer which saves costly labor associated with fatigue crack growth tests. This new development, based on thin film sputtering technology, is expected to enable researchers to conduct fatigue and fracture mechanics testing in various adverse high-temperature environments. (10 refs.)
- 77823 On the yield loads of plates with array of holes.** U.C. Jindal, M.L. Mandal (Mech. Engng. Dept., Delhi Coll. of Engng., Delhi, India). *J. Test. & Eval. (USA)*, vol.11, no.3, p.208-16 (May 1983).
Yield loads of mild steel plates with one, three, five, and nine holes in different combinations and orientations have been determined experimentally using an Instron universal testing machine. The yield loads of these specimens were very close to the yield loads of the specimens without holes. It was further observed that for up to a 30% reduction in area in the critical section (along which final fracture takes place), the yield load remains the same. Specimens with a single hole were also studied under moderately dynamic strains, up to a strain rate of 0.42/min. It was observed that yield load and yield point elongation increased with increasing strain rate. This showed that a hole in the specimen has negligible effect on these properties of the specimen. (12 refs.)
- 77824 J_{Ic} measurement point determination for HY130, CMS-9, and Inconel Alloy 718.** J.R. Matthews (Defence Res. Estab. Pacific, Victoria, BC, Canada), G.D. West. *J. Test. & Eval. (USA)*, vol.11, no.3, p.217-24 (May 1983).
Determination of the elastic-plastic fracture toughness for three medium strength materials of varying ductility has been carried out. The materials in order of decreasing ductility are HY130 steel, CMS-9 steel, and Inconel Alloy 718. A survey of measurement-point techniques for J_{Ic} has been incorporated in the study to evaluate the effect of ductility of the determination of the elastic-plastic fracture parameter and subsequent estimation of the elastic fracture toughness K_{Ic} . (14 refs.)
- 77825 Development and applications of tester with twin bar for alloy solidification.** Jr. Chen Guangjun Zhao (Dept. of Mech., Dalian Inst. of Technol., Dalian, China). *J. Dalian Inst. Technol. (Dalian Gongxueyuan Xuebao) (China)*, vol.21, no.4, p.133-9 (Dec. 1982). In Chinese. [received: June 1983]
In order to study the alloy factor effect in connection with casting defects causing hot tearing, cold tearing, flexure, deformation and residual stress, the author has designed and developed a twin bar tester for alloy solidification contraction. (8 refs.)
- 77826 Assessment of critical temperature of embrittlement and transverse widening of the test piece in impact bend test.** J. Wozniak, M. Jakob (Vitkovice Zelezarny a Strojirny Klementa Gottwalda, Koncernovy Podnik, Ostrava-Vitkovice, Czechoslovakia). *Kovove Mater. (Czechoslovakia)*, vol.21, no.2, p.206-12 (1983). In Czech.
The authors summarize the experimentally determined values of lateral expansion and the percentage of ductile fracture with a given type of steel. From the comparison of the results obtained it was found that the method of lateral expansion evaluation is more exact than the method of ductile fracture measurement. It is not possible to apply lateral expansion criteria of ASME Code for the testing equipment used in our laboratories. It is necessary to compile a larger amount of experimental material from various laboratories to be able to fix the limit value of lateral expansion replacing the up-to-now used limit of 50 percent ductile fracture. (11 refs.)
- 77827 Measurement of crack profile of semi-elliptical surface cracks using the AC potential technique.** A.A. Aboutorabi, M.J. Cowling (Dept. of Mech. Engng., Univ. of Glasgow, Glasgow, Scotland). *NDT Int. (GB)*, vol.16, no.3, p.139-43 (June 1983).
The growth of semi-elliptical surface cracks by fatigue was monitored by the AC potential technique. Detailed marking of the fracture surface during crack growth allowed correlation of crack profile and potential measurements. A series of modification factors has been produced to allow accurate sizing of such defects from a simple NDT technique. (11 refs.)
- 77828 Stress-shadow magnetic inspection technique for far-side anomalies in steel pipe.** D.L. Atherton (Dept. of Phys., Queen's Univ., Kingston, Canada). *NDT Int. (GB)*, vol.16, no.3, p.145-9 (June 1983).
A two-step process for obtaining strong magnetic leakage flux signals from far-side anomalies in steel pipe is described. The pipe is magnetized by a magnetic pig while it is stressed by line pressure. Anomalous local stresses on the near side of the steel caused by far-side corrosion produce anomalies in the residual magnetization. These near-side residual field anomalies due to the stress shadows from exterior corrosion are then readily detectable. Initial laboratory tests are described. (1 ref.)
- 77829 Some results on the resolution of small inclusions in ultrasonic immersion testing of steel with focused probes.** G. Canella, F. Monti, L. Pedicelli, A.L. Erede (Centro Sperimentale Metall., Roma, Italy). *NDT Int. (GB)*, vol.16, no.3, p.151-3 (June 1983).
Results are presented for an analysis of ultrasonic signals reflected from small flaws (≤ 1 mm) in steel samples during immersion testing with 10 MHz and 15 MHz focused probes. A technique is introduced for setting up the working parameters in ultrasonic testing of flat specimens to take account of the position of inclusions relative to the focal zone, according to the thickness of the layer to be examined and the resolution required. (10 refs.)
- 77830 Fracture toughness (K_{Ic}) testing with a mini-compact tension (CT) specimen.** C.Y.-C. Lee, W.B. Jones Jr. (Materials Lab., Air Force Wright Aeronautical Labs., Wright-Patterson AFB, OH, USA). *Polym. Eng. & Sci. (USA)*, vol.22, no.18, p.1190-8 (Dec. 1982).
A testing method using the rheometrics mechanical spectrometer as the loading instrument to measure the fracture toughness K_{Ic} , which is related to a specific sample geometry and dimensions (half-inch compact tension) is reported. The small sample size requirement makes it attractive to do fracture toughness testing on newly synthesized material for preliminary material study and comparison purposes. Commercially available epoxy resins were used to check the procedure at different temperatures (-150° to 250° C). An empirical crack length averaging method was used that appears to give constant K_{Ic} values independent of the a/W ratio values. The fracture surfaces were studied using scanning electron microscopy. (13 refs.)
- 77831 Infrared measurement of specimen temperature profiles during fatigue crack propagation tests.** M.T. Hahn, R.W. Hertzberg, J.A. Manson (Materials Res. Center, Cox Lab., Lehigh Univ., Bethlehem, PA, USA). *Rev. Sci. Instrum. (USA)*, vol.54, no.5, p.604-6 (May 1983).
Hysteretic heating of the crack tip often occurs during tests of fatigue crack propagation. If hysteretic heating occurs to a significant extent at and ahead of the crack tip in a notched polymer specimen, fatigue crack propagation behavior may be altered in a complex way. It is, therefore, important to monitor the temperature at crack tips during testing. Methods of temperature measurement are reviewed, and a semiautomated apparatus incorporating an infrared microscope for measuring temperature profiles during fatigue tests is described. (12 refs.)
- 77832 Optical measurement of crack length for the fatigue crack propagation test.** S. Ueda, T. Kanamaru (Kawasaki Heavy Industries Ltd., Akashi, Japan). *Syst. & Control (Japan)*, vol.27, no.2, p.130-7 (1983). In Japanese.
In the fatigue crack propagation test, which is a fatigue test of materials, length of crack caused by cyclic loading should be measured with high accuracy. The authors have developed an equipment to measure the crack length by means of microcomputer and line sensor camera which can be mechanically operated in X, Y and Z axis. They describe a method to extract crack and to measure crack length. Images of scratches on the specimen are eliminated through the comparison of pictures before and after propagation of crack. Crack length is measured by subtracting x-coordinate of the starting point of crack from that of the ending point of crack. The picture processing time is reduced by defining the region of interest. (5 refs.)
- 77833 Evaluation of acoustic properties of 'thin' laminations and one-line nonmetallic inclusions in steel sheets.** K.E. Abbakumov, A.S. Golubev (V.I. Ulyanov Leningrad Inst. of Electrical Engng., Leningrad, USSR). *Sov. J. Nondestr. Test. (USA)*, vol.18, no.9, p.685-7 (Sept. 1982). Translation of: *Defektoskopiya (USSR)*, vol.18, no.9, p.22-4 (Sept. 1982).
A study was made of reflection and acoustic-transmittance coefficients for discontinuities calculated in accord with a suggested impedance model and checked experimentally, with a satisfactory agreement of the results. The model can be recommended for the solution of a number of practical problems that involve the actual inspection sensitivity for steel sheets. (4 refs.)
- 77834 Samples for determining the point of exit and the angle of entry of the ultrasonic beam in pipe inspection.** Ya.F. Grebenyuk. *Sov. J. Nondestr. Test. (USA)*, vol.18, no.9, p.688-9 (Sept. 1982). Translation of: *Defektoskopiya (USSR)*, vol.18, no.9, p.25-6 (Sept. 1982).
To determine the angle of beam entry for transducers with a curved working surface, the authors propose using a sample in the shape of a semicylinder (or a quarter-cylinder), on which a scale is drawn. The radius of the semicircle must correspond to the radius R_p of the testpiece. The sample is made from a metal with acoustical properties similar to those of the testpiece. Since transducers with a definite angle of incidence of $30-40^\circ$ are used for the ultrasonic inspection of pipe, a combination sample can be made to determine the point of exit and the angle of entry of the beam. (4 refs.)
- 77835 Maximum attainable sensitivity of inspection by 'multiple shadows' method.** V.E. Artemov, S.K. Pavros (V.I. Ulyanov Leningrad Inst. of Electrical Engng., Leningrad, USSR). *Sov. J. Nondestr. Test. (USA)*, vol.18, no.9, p.691-3 (Sept. 1982). Translation of: *Defektoskopiya (USSR)*, vol.18, no.9, p.28-9 (Sept. 1982).
Ultrasonic defectoscopy of product samples with rough surfaces by the shadow method has an important disadvantage—its sensitivity is low. This can be explained by fluctuations of the transmitted signal due to instability of the acoustic contact and due to scattering of sound by surface asperities. The sensitivity can be improved by the 'multiple shadows' technique, in which presence of a defect is recorded by the N-th ($N > 1$) pulse passing through the sample. The probability density distribution of amplitudes of signals passing through a product sample with rough surfaces is derived. Relations are presented which yield expressions for the defectoscope triggering threshold for a given inspection reliability. Equating these expressions to one another yields an estimate of the maximum attainable sensitivity. (4 refs.)
- 77836 Use of oblique wide-beam probe for inspection of strips with normal waves.** V.A. Pilui. *Sov. J. Nondestr. Test. (USA)*, vol.18, no.9, p.694-5 (Sept. 1982). Translation of: *Defektoskopiya (USSR)*, vol.18, no.9, p.30-1 (Sept. 1982).
For ultrasonic inspection of strips with normal waves, one uses oblique transducers which cover a large inspection zone during a single pass, up to 1.5-m wide with a 24×35 -mm large piezoelectric transducer. The sensitivity and the nonuniformity of such an inspection, depending on the distance of a defect as well as on other factors, is determined by the linear dimensions of the piezoelectric transducer. For a more reliable inspection, it is necessary that the piezoelectric transducer be elongated in the direction of its movement. Then the lengthening of the near zone in its longitudinal plane will reduce the nonuniformity of its sensitivity within the inspection zone, while widening the beam of ultrasonic waves will increase the inspection reliability. Experiments were performed on strips of aluminum alloys with ultrasonic waves incident at angles of 36 and 57° , respectively, and with a drilled through-hole 1 mm in diameter as control reflector. (2 refs.)
- 77837 Interpretation of the results of thermal inspection with changes in the emitting capacity of the surface of objects of inspection.** N.A. Bekeshko (Sci.-Res. Inst. of Introscopy, Moscow, USSR). *Sov. J. Nondestr. Test. (USA)*, vol.18, no.9, p.696-8 (Sept. 1982). Translation of: *Defektoskopiya (USSR)*, vol.18, no.9, p.32-4 (Sept. 1982).
A method and the equipment making it possible to take into consideration a change in the emitting capacity of objects of inspection and to eliminate errors in revealing defects related to this are described. (3 refs.)
- 77838 A universal heat source for active thermal inspection.** N.A. Bekeshko, I.D. Voronin, P.V. Sokolov. *Sov. J. Nondestr. Test. (USA)*, vol.18, no.9, p.698-9 (Sept. 1982). Translation of: *Defektoskopiya (USSR)*, vol.18, no.9, p.34-6 (Sept. 1982).
Describes the type IN-1 universal heat source, which is designed for heating a broad range of parts and materials (both metallic and nonmetallic) from room temperature to 300° C with a controllable heating time in active thermal inspection. The basis of its operation is the principle of heating a portion of the surface of the object of inspection with a directed flow of radiant energy created by a series of infrared lamps located in parallel in a special reflector. The amount of radiant energy flow depends upon the distance between the heater and the heated surface. The source of radiation is a system consisting of two groups of type KG220-1000 infrared quartz-halogen lamps (power of each lamp 1000 W). The direct flow of radiation and also that reflected from the surface of the reflector, occurring with supply of a voltage to the lamps, are directed to the object and, absorbed by the surface, heat it. (1 ref.)

77839 Distribution of magnetic induction in ferromagnetic product samples magnetized by pole method. A.S.Shleenkov (Inst. of Metal Phys., Acad. of Sci., USSR).

Sov. J. Nondestr. Test. (USA), vol.18, no.9, p.713-17 (Sept. 1982). Translation of: *Defektoskopiya (USSR)*, vol.18, no.9, p.52-6 (Sept. 1982). An approximate method is proposed for calculating the magnetic induction inside ferromagnetic product samples having dimensions comparable with those of the electromagnet and having a nonuniform magnetic flux distribution. Results of experimental verification are also presented. (2 refs.)

77840 A method of reducing the effect of the gap in eddy-current measurements of conductivity. D.I.Kosovskii, A.I.Nikitin, Yu.M.Shkarlet (All-Union Sci. Res. Tech. Inst., Dnepropetrovsk, USSR).

Sov. J. Nondestr. Test. (USA), vol.18, no.9, p.717-22 (Sept. 1982). Translation of: *Defektoskopiya (USSR)*, vol.18, no.9, p.56-62 (Sept. 1982). A method of reducing the effect of a change in the distance between the superimposed transducer and the plane article under test on the reading of eddy-current amplitude-phase and phase instruments for measuring the electrical conductivity of the material of the article is described. The basic idea of the method is undercompensation by a certain amount of the open-circuit voltage (impedance) of the superimposed transducers and the use of the change in the sign of the curvature of the hodograph characterizing the dependence of the voltage introduced by the superimposed transformer transducer on the increase in the distance between them and the plane article being monitored. (8 refs.)

77841 IMPOK-1 pulse magnetic flow-line controller. M.A.Mel'gui, V.F.Matyuk (Inst. of Appl. Phys., Acad. of Sci., Belorussian SSR).

Sov. J. Nondestr. Test. (USA), vol.18, no.9, p.722-5 (Sept. 1982). Translation of: *Defektoskopiya (USSR)*, vol.18, no.9, p.62-6 (Sept. 1982). A description is given of the flow chart and technical data of the IMPOK-1 installation for checking the mechanical properties of mild steels in flow-production systems. (5 refs.)

77842 Interrelation of the magnetic and mechanical properties with the structural state of hardened and tempered products. M.N.Mikheev, E.S.Gorkunov, V.M.Somova, A.B.Kut'kin (Inst. of Metal Phys., Acad. of Sci., USSR).

Sov. J. Nondestr. Test. (USA), vol.18, no.9, p.725-32 (Sept. 1982). Translation of: *Defektoskopiya (USSR)*, vol.18, no.9, p.66-75 (Sept. 1982). Studies the effect of hardening and various tempering regimes on the physical properties of the structural steels SP-28, 30KhGSA, and 40Kh. It discusses the possibility of using the investigated magnetic characteristics as parameters of the nondestructive inspection of the mechanical properties of products made of the mentioned steels after hardening and tempering. (14 refs.)

77843 Approximate calculation of three-dimensional models in the theory of eddy current inspection with attached transducers. Yu.K.Fedosenko (Sci.-Res. Inst. of Introspect, Moscow, USSR).

Sov. J. Nondestr. Test. (USA), vol.18, no.9, p.732-9 (Sept. 1982). Translation of: *Defektoskopiya (USSR)*, vol.18, no.9, p.75-83 (Sept. 1982). The theory of eddy current inspection is examined with special reference to the conditions in which the defect field depends on all three coordinates. Approximate equations are derived for the introduced voltage for rectangular and square transducers taking into account the dimensions of their windings. Signals from defects are measured and compared with the calculated values. The results do not differ by more than 30-35%. (5 refs.)

77844 Determination of the thickness of the information-carrying layer in the examination of the structure by the Barkhausen noise method. V.I.Vengrinovich (Inst. of Appl. Phys., Acad. of Sci., Belorussian SSR).

Sov. J. Nondestr. Test. (USA), vol.18, no.9, p.739-42 (Sept. 1982). Translation of: *Defektoskopiya (USSR)*, vol.18, no.9, p.83-7 (Sept. 1982). The thickness of the information-carrying layer x_i in structure examination by the Barkhausen noise method refers to the depth of the thin layer, the signal from which attenuates e times. A calculation-experimental method of determining this thickness is substantiated. The method is based on the asymptotic expansion of the integral $\int_0^{\infty} V_0(\delta) e^{-z/\delta} dz$ in power x_i , where z is the coordinate of the layer; $V_0(\delta)$, normalized intensity of Barkhausen noise after removing a layer with thickness δ (determined by means of experiments). It is shown that the resonance Barkhausen noise method can be used to control the depth of the information-carrying-layer in the region from 40 to 300-400 μm . (7 refs.)

77845 A device with improved selective sensitivity for structure examination by the Barkhausen noise method. V.I.Vengrinovich, V.N.Bus'ko, V.I.Tsukerman (Inst. of Appl. Phys., Acad. of Sci., Belorussian SSR).

Sov. J. Nondestr. Test. (USA), vol.18, no.9, p.742-4 (Sept. 1982). Translation of: *Defektoskopiya (USSR)*, vol.18, no.9, p.87-9 (Sept. 1982). A new method of increasing the selective sensitivity of structure examination is used in a digital Barkhausen noise analyzer. The device can be set with respect to the controllable parameter and tuned away from the interfering factors. The analyzer can work in automatic or manual regime. It is shown that the analyzer can be used for reliable sorting of pipes on the basis of grades of steels. The analyzer can be used for the magnetic phase analysis of steels, for inspecting the carbon and nickel content of steels, and for the sorting of steel into grades. (7 refs.)

77846 Oscillators of short high-power electric pulses for the electromagnetic-acoustic excitation of ultrasound. M.S.Boiko, Yu.V.Petrov (Chelyabinsk Polytech. Inst., Chelyabinsk, USSR).

Sov. J. Nondestr. Test. (USA), vol.18, no.9, p.748-9 (Sept. 1982). Translation of: *Defektoskopiya (USSR)*, vol.18, no.9, p.92-3 (Sept. 1982). The introduction of the electromagnetic-acoustic (EMA) method of the excitation and registration of ultrasound into the practice of nondestructive testing is restricted by the low sensitivity in comparison with the piezoelectric method. The sensitivity of the method is expressed by the useful signal-noise ratio. One of the methods of increasing the sensitivity of the EMA method is to increase the output power of the oscillators of probing pulses of the EMA flaw detection device. Investigators at the Chelyabinsk Polytechnical Institute developed and constructed a magnetohyristor oscillator of probing pulses. (4 refs.)

77847 A simple method for the determination of the coating thickness of galvanized steel. R.M.Saleh, F.M.Abel Wahab, M.M.Badran, A.A.El Hosary (Lab. of Electrochem. & Corrosion, Nat. Res. Centre, Cairo, Egypt). *Surf. Technol. (Switzerland)*, vol.18, no.3, p.283-90 (March 1983). The dissolution of galvanized steel in acid solutions was followed by the thermometric, potential-time and weight loss techniques. Only the zinc coat is attached in HCl and H_2SO_4 , whereas in HNO_3 curves representing the stepwise dissolution of the coating layer and the steel base are obtained. Comparable values of the time t required for complete dissolution of the zinc coat were obtained by the three techniques. The dissolution in 2 N H_2SO_4 of steel pieces with various coating thicknesses was examined by the thermometric method. Starting from the initial temperature T_i , the temperature of the system rose to attain a maximum value T_m after a time t and then decreased.

For a coating thickness of up to 6 g dm^{-2} , both $\Delta T = T_m - T_i$ and t varied linearly with coating thickness. The results suggest that the thermometric method is suitable for the determination of the coating thickness of galvanized steel. (11 refs.)

77848 Quality control through non-destructive testing. E.Burgisser.

Schweiz. Tech. Z. (Switzerland), vol.80, no.10, p.6-9 (18 May 1983). In German.

To secure good quality of final steel products the semi-finished steel must be thoroughly inspected and the present, well established, method of inspection of surface integrity consists of spreading a fine magnetic powder and generating a magnetic field through the tested material. This method shows the 'skin effect'. A drawing shows the scatter of flux caused by a surface crack. A sketch of the test facility is given and the test procedure is described in detail. By altering the grain size of the magnetic powder and the strength of the magnetic field it is possible to discriminate serious defects from small ones that can be tolerated. (no refs.) G.R.S.

77849 Know your welding NDT-radiographic testing. C.R.Weymueller.

Weld. Des. & Fabr. (USA), vol.56, no.3, p.49-59 (March 1983). Reviews radiographic testing, by X-ray and gamma ray, which locates and depicts defects in welds and weldments, thin to thick. (no refs.)

77850 Magnetic flux leakage inspection of wire rope. M.J.Bergander.

In book: *International advances in nondestructive testing. Vol.9*, W.J.McGonagle [Ed.], p.113-23. New York, USA: Gordon & Breach (1983), 363 pp. [0 677 16440 8]

The most important types of damage in steel wire ropes are listed. The technique and apparatus for magnetic flux leakage inspection are briefly outlined. The applications of the testing procedures and ways of interpreting the test results are discussed. (18 refs.)

77851 An inverse problem formulation of electromagnetic rope testing.

R.Sezenc (Lab. Central des Ponts et Chaussées, Bouguenais, France). In book: *International advances in nondestructive testing. Vol.9*, W.J.McGonagle [Ed.], p.125-58. New York, USA: Gordon & Breach (1983), 363 pp. [0 677 16440 8]

An analysis is presented for the frequency response of an encircling solenoid to the internal structure of a sample. A numerical procedure allows the extraction of the spatial variations of the core electrical conductivity and magnetic permeability from the frequency response of the sensor. The method is illustrated both with numerical examples and model experiments. (16 refs.)

77852 The Seebeck effect as used for the nondestructive evaluation of metals. C.M.Stuart (Technicorp., Wayne, NJ, USA).

In book: *International advances in nondestructive testing. Vol.9*, W.J.McGonagle [Ed.], p.177-91. New York, USA: Gordon & Breach (1983), 363 pp. [0 677 16440 8]

The principle of the Seebeck effect in measuring the EMF (electromotive force) created at the heated junction of dissimilar metals is being employed as a technique for nondestructively sorting metals and alloys. (2 refs.)

77853 An electrostatic charge decay technique for nondestructive evaluation of nonmetallic materials. Ming-Kai Tse, N.P.Suh (Lab. for Mfg. & Productivity, MIT, Cambridge, MA, USA).

In book: *International advances in nondestructive testing. Vol.9*, W.J.McGonagle [Ed.], p.193-226. New York, USA: Gordon & Breach (1983), 363 pp. [0 677 16440 8]

A novel nondestructive evaluation technique based on electrostatic charge decay (ECD) in nonmetallic materials is introduced. The basic concepts and the feasibility studies are reviewed. Recent experimental results on thin non-metallic coatings are presented. Finally, the key practical considerations in applying this technique are also examined. (11 refs.)

77854 Digital nondestructive evaluation of composite materials [ultrasonic inspection]. R.A.Blake (Center for Composite Materials, Univ. of Delaware, Newark, DE, USA).

In book: *International advances in nondestructive testing. Vol.9*, W.J.McGonagle [Ed.], p.227-48. New York, USA: Gordon & Breach (1983), 363 pp. [0 677 16440 8]

The versatility and computational abilities associated with digital systems are applied to the ultrasonic evaluation of composite materials. A digital approach offers flexibility regarding the form of the output from ultrasonic inspections and facilitates data interpretation. The introduction of A/D converters operating above 20 MHz has allowed for the development of a digital analyzer which can adapt to the requirements of nondestructively evaluating the complex structures of composites. Computer graphics and digital imaging are incorporated to produce a totally digital system which demonstrates superior performance and provides the quantitative base necessary for the implementation of more sophisticated signal and image processing techniques. (7 refs.)

77855 Multi-dimensional eddy current coils. R.A.Nance, A.J.Caffarel, W.H.Hartley (Westinghouse Bettis Atomic Power Lab., Mifflin, PA, USA).

In book: *International advances in nondestructive testing. Vol.9*, W.J.McGonagle [Ed.], p.249-56. New York, USA: Gordon & Breach (1983), 363 pp. [0 677 16440 8]

One of the major problems associated with the eddy current inspection of tubing by either an internal bobbin coil probe or an external encircling coil is the inability of such sensors to reliably detect transverse oriented cracks. A dual winding eddy current test coil system is described which can be used either as an internal probe or as an external encircling coil to inspect tubing for transverse cracking as well as cracks in other orientations. Further, this coil system provides approximately equal peak-to-peak response for a specific size crack no matter what its orientation (from transverse to axial). (no refs.)

77856 Evaluation of microencapsulated penetrant inspection. J.M.Portaz

(Aircraft Engine Group, General Electric Co., Cincinnati, OH, USA). In book: *International advances in nondestructive testing. Vol.9*, W.J.McGonagle [Ed.], p.283-363. New York, USA: Gordon & Breach (1983), 363 pp. [0 677 16440 8]

The results are presented of a program to evaluate the merits and shortcomings of microencapsulated penetrants for use in fluorescent penetrant inspection to evaluate capsule and spray parameters to effectively use microencapsulated penetrants, and to compare the sensitivity of such a system to a conventional MIL-I-25135 Group VI liquid fluorescent penetrant inspection system. The program was divided into four phases which encompassed selection of materials for encapsulation, evaluation of capsule and spray variables, investigation of removal and developer techniques, measurement of sensitivity, and a process demonstration including environmental and economic analysis. The work culminated with the successful demonstration that microencapsulated penetrants could be applied in such a way to achieve equivalent sensitivity with a MIL-I-25135 Group VI liquid penetrant system. The microencapsulated penetrant system as now developed uses only nonaqueous wet developers which are more costly than dry or aqueous wet developers. (no refs.)

77857 Potentiostatic etching of carburized steels. P.Helbach, E.Bullock. Report EUR 8138 EN, Comm. European Communities, Luxembourg (1982), 29 pp.

Traditional etching techniques have proved inadequate for the accurate estimation of carbides in carburized steels by optical imaging. The requirement for etch uniformity precludes the use of alkaline etchants and the necessity for sharp edges prohibits acid etching of the surrounding austenite. In response to this shortfall, a new technique has been developed for the controlled deposition of layers, by potentiostatic anodisation of polished alloy surfaces. This process provides much greater contrast between carbide and matrix than that obtainable from vapour-deposited or reaction-sputtered interference films, while retaining the very accurate edge definition and the phase identification capability of these techniques. In order to demonstrate the advantages of the new process, the investigation includes a comparison with several currently available carbide contrasting techniques as applied to a series of typically carburised steels. (2 refs.)

77858 Evaluation of electrode shape and nondestructive evaluation method for welded solar cell interconnects. C.R.Baraona, S.J.Klima, T.J.Moore, W.E.Frey, A.F.Forestieri (Lewis Res. Center, NASA, Cleveland, OH, USA). Conference Record of the Sixteenth IEEE Photovoltaic Specialists Conference - 1982, San Diego, CA, USA, 27-30 Sept. 1982 (New York, USA: IEEE 1982), p.90-5

Resistance welds of solar cell interconnect tabs were evaluated. Both copper-silver and silver-silver welds were made with various heat inputs and weld durations. Parallel gap and annular gap weld electrode designs were used. The welds were analyzed by light microscope, electron microprobe and scanning laser acoustic microscope. These analyses showed the size and shape of the weld, the relationship between the acoustic micrographs, the visible electrode footprint, and the effect of electrode misalignment. The effect of weld heat input on weld microstructure was also shown. (6 refs.)

77859 Nondestructive testing of interconnect welds using the Scanning Laser Acoustic Microscope (SLAM). C.L.Vorres, D.E.Yuhas, J.Semmens, M.G.Oravecz (Sonoscan Inc., Bensenville, IL, USA). Conference Record of the Sixteenth IEEE Photovoltaic Specialists Conference - 1982, San Diego, CA, USA, 27-30 Sept. 1982 (New York, USA: IEEE 1982), p.102-7

Three recent studies involving the evaluation of resistance welds between interconnects and silicon solar cells using the SLAM are described. Using this technique, nondestructive testing of the bond between the tap and cell can be made rapidly and with high resolution. Different configurations and compositions of interconnectors as well as cells with and without coverglasses were tested. Degradation in the bonding of the coverglass was also observed. Metallographic sections were made following the third study. Excellent correlation was found between SLAM results and areas found bonded after sectioning. (2 refs.)

International advances in nondestructive testing. Vol.9 See Entry 74231

Operating experience with the type UT-80B electromagnetic-acoustic thickness gauge See Entry 74440

A device for measuring the residual electrical conductivity of single crystals See Entry 74494

An assessment of acoustic emission for nuclear pressure vessel monitoring See Entry 75099

Testing of radiation shielding concrete walls with portable betatrons See Entry 75204

Some aspects and results of the electrochemical etching of a thin-foil track detector See Entry 75233

Development of a new EPL-free etchant for soda-glass nuclear track detectors See Entry 75234

A new track etchant for plastic detectors See Entry 75237

A review of holographic nondestruction evaluation at Lawrence Livermore National Laboratory See Entry 75607

Holographic nondestructive evaluation: status and future See Entry 75608

A piezoelectric displacement transducer for use in a pulse-shape based analysis of acoustic emission See Entry 75889

A method for automatic measurement of Brinell hardness using a microcomputer See Entry 75969

The relative accuracy of axial and non-axial methods for the measurement of lattice spacings See Entry 76262

Measurement of elastic moduli of small specimen by means of rectangular parallel piped resonance method See Entry 76547

Longitudinal piezoelectric strain measurements of poly(vinylidene fluoride) films See Entry 77331

Application of neutron diffraction to a study of phases in Type 316 stainless steel weld metals See Entry 77685

X-ray stress measurement of high manganese austenitic steels See Entry 77687

X-ray stress measurement of coarse grained 18-8 stainless steel by complex oscillation technique See Entry 77688

Thermal stress measurements of tungsten fiber-copper composites See Entry 77708

A recommended procedure for determining the strain rate sensitivity in superplasticity See Entry 77716

X-ray fractography on fatigue fractured surface See Entry 77738

The application of high resolution electron microscopy to the study of oxidation See Entry 77795

The transmission electron microscopy of oxide scale formation on Fe-Ni-Cr alloys See Entry 77796

Designing an analytical microscopy laboratory See Entry 77935

Atomic scale analysis with the atom probe See Entry 77936

Protection in industrial radioscopes in the radiographic examination of objects in nonstationary conditions See Entry 78362

81.90 OTHER TOPICS IN MATERIALS SCIENCE

77860 Density change of glassy $\text{Pd}_{77}\text{Si}_{16.5}\text{Cu}_{6.5}$ alloy during cold drawing. Deguo Deng, Banghong Lu (Inst. of Precious Metals, Kunming, Yunnan, China).

Ser. Metall. (USA), vol.17, no.4, p.515-18 (April 1983).

Reports the results of density change experiments using thick $\text{Pd}_{77}\text{Si}_{16.5}\text{Cu}_{6.5}$ glassy wires, and compares them with various theories and experiments. The general trend of the results is consistent with those of Megusar et al. (1981). (9 refs.)

77861 Current research in adhesiveless bonding of cover glasses to solar cells. D.W.Egelkrut, A.C.Day, W.E.Horne (Boeing Aerospace Co., Seattle, WA, USA).

Conference Record of the Sixteenth IEEE Photovoltaic Specialists Conference - 1982, San Diego, CA, USA, 27-30 Sept. 1982 (New York, USA: IEEE 1982), p.108-14

Reviews recent research on electrostatic bonding of cover glasses to newly developed high temperature solar cells. Although high temperature solar cells were developed to withstand temperature excursions up to 700°C for about 1 to 15 minutes, a newly discovered damage mechanism causes severe degradation of these cells during the ESB process at temperatures of only 550°C in 4 to 6 minutes. The damage was found to be the result of a synergistic effect of the electric fields and temperatures used in the ESB process. The theory for this process is presented and a solution is proposed and partially demonstrated. Also, a process called field assisted laser bonding has been investigated. The process utilizes rapid heating of cover glasses by 10.6 μm laser energy in combination with electric fields to produce bonding. The use of a potential grid to distribute the electric field is described and a reaction observed between the grid and glass is discussed. (17 refs.)

Anodic bonding of imperfect surfaces See Entry 76797

82.00 PHYSICAL CHEMISTRY

International Symposium on Theoretical Organic Chemistry See Entry 74216

82.20 CHEMICAL KINETICS

77862 Quantum chemical and statistical-thermodynamic studies of equilibria and rates. R.Zahradnik (J. Heyrovsky Inst. of Phys. Chem. & Electrochem., Acad. of Sci., Prague, Czechoslovakia). *Pure & Appl. Chem. (GB)*, vol.55, no.2, p.391-400 (Feb. 1983). (International Symposium on Theoretical Organic Chemistry, Dubrovnik, Croatia, Yugoslavia, 30 Aug.-3 Sept. 1982).

A review of the main results from the author's laboratory for the period 1969-1982 is presented. In the introductory part, allowed and forbidden processes are discussed from the point of view of constants of motion. Specific suggestions are presented as to how to make forbidden processes allowed. In addition to energy forbiddenness, entropy forbiddenness is also mentioned. In the section on equilibria attempts to locate minima of potential energy surfaces (PES), and statistical-thermodynamic calculations of equilibrium constants for common and van der Waals molecules, are summarized. Then information follows on the location of saddle points on PES, reaction coordinates and statistical-thermodynamic calculations of rate constants of elementary reactions. The final section deals with studies of catalytic reactions. (69 refs.)

77863 A comparison of various MO methods for predicting regioselectivity in Diels-Alder reactions. Chen Zhixing (Chem. Dept., Zhongshan Univ., Guangzhou, China). *Theor. Chim. Acta (Germany)*, vol.62, no.4, p.293-9 (1983).

Various semiempirical MO methods for predicting regioselectivity in Diels-Alder reactions are compared in order to examine their reliability. They are the frontier molecular orbital method using CNDO/2, HMO and MNDO molecular orbitals and the HMO approach on pericyclic reactions presented by A. Tang (1975). (14 refs.)

Correlation analysis in organic chemistry: retrospect See Entry 74248

An automatic microcomputer-based system for measuring reaction rates by UV spectroscopy See Entry 74543

A theoretical study of the structure, charge distribution and gas-phase basicity of 1H-indazole and its N-methyl derivatives See Entry 75293

Understanding the middle atmosphere via the laboratory: ion cluster investigations See Entry 75664

Decomposition kinetics of iodine monochloride in shock waves See Entry 77866

The mechanism of carbonyl reduction by LiBH_4 : an ab initio investigation with inclusion of solvent effects See Entry 77867

Catalytic effect on the selectivity of the Diels-Alder reaction See Entry 77869

Mechanistic studies of oxene reactions with organic substrates: reaction paths on MINDO enthalpy surfaces—models for cytochrome P450 oxidations See Entry 77871

Sequential isomerism of activated complexes: interfering versus noninterfering intermediate See Entry 77872

Topological determinants in organic chemistry See Entry 77873

Transient kinetics of chemical reactions with bounded diffusion perpendicular to the reaction coordinate: intermolecular processes with slow conformational changes See Entry 77879

Chemical effects of nuclear transformations in mixed potassium hexahalogeno-metallates (IV), $\text{K}_2\text{MX}_6\text{V}_{6-n}$. I. Chemical effects of the $^{81}\text{Br}(n,\gamma)^{82}\text{Br}$ nuclear process in mixed potassium hexabromochloro-osmates (IV), $\text{K}_2\text{OsBr}_n\text{Cl}_{6-n}$ See Entry 77912

Model cluster study of the acid-base properties of zeolite catalysts See Entry 77914

Structure-activity relationship and the mechanism of analgesia of the analgesic drug 3-methyl-fentanyl and its analogs See Entry 78134

82.20K Potential energy surfaces for chemical reactions

(see also 31.70F -in atomic and molecular physics, 34.20 Intermolecular forces, 34.50L Atomic and molecular beam studies)

77864 Topography of potential energy surfaces. M.V.Basilevsky (Karpov Inst. of Phys. Chem., Moscow, USSR). *Pure & Appl. Chem. (GB)*, vol.55, no.2, p.207-12 (Feb. 1983). (International Symposium on Theoretical Organic Chemistry, Dubrovnik, Croatia, Yugoslavia, 30 Aug.-3 Sept. 1982).

The curves on a multi-dimensional potential energy surface (PES) linking the reactant and the transition state configurations are constructed. They are generally distinct from usual reaction path curves and a special term 'optimum ascent path' (OAP) is accepted for them. A local criterion is formulated allowing one to distinguish the points located on an OAP among other points in its vicinity. A mathematical analysis of singular points of a PES, where its

valleys or ridges emerge, dissipate or bifurcate, is presented. These points are specified as different branching points of OAPs. (11 refs.)

On the reaction $Mg + N_2O \rightarrow MgO + N_2$ See Entry 77877

Potential surfaces for simple rearrangements See Entry 77885

82.20R Energy distribution and transfer, relaxation

(see also 31.70H Time-dependent phenomena in atomic and molecular physics)

77865 Effects of diffusion on long-range electron transfer. A.M.Kuznetsov (Inst. of Electrochem., Acad. of Sci., Moscow, USSR), J.Ulstrup. *Chem. Phys. Lett. (Netherlands)*, vol.97, no.3, p.285-91 (20 May 1983). The competition between diffusive hops and direct tunnelling of solvated electrons to scavenger molecules in solid glasses has been discussed in the literature. The authors have considered these two reaction paths in terms of stationary kinetic diffusion equations and multiphonon electron-transfer rate theory, and for coupling of the solvated electron to a broad continuum of nuclear modes. Diffusion can only be expected to be important for less polar glasses. (34 refs.)

Dynamics of $O(^1D_2)$ reactions with bifunctional substrates: alcohols and thiols See Entry 77875

82.30 SPECIFIC CHEMICAL REACTIONS; REACTION MECHANISMS

77866 Decomposition kinetics of iodine monochloride in shock waves. Zhang Rongyao, Sha Guohe, Han Denglong, Wang Yimin, Zhang Cunhao. *Acta Mech. Sin. (China)*, no.2, p.203-5 (1983). In Chinese. The decomposition kinetics of ICl in Ar mixture have been studied in a shock tube over the temperature range 1000 to 2000K. Dual absorption spectrophotometry is used to follow the course of the reaction. A rate constant correlation given by $k_1 = 1.21 \times 10^{12} \exp(-35.8 \times 10^3/RT)$ cm³/mole. sec is obtained to fit the measured data. The heteroatom recombination $I+Cl+Ar \rightarrow ICl+Ar$ is about a factor of 10 faster than the homoatom recombination $I+I+Ar \rightarrow I_2+Ar$ with a larger negative temperature coefficient. Both facts can be reasonably interpreted in terms of a plausible pathway proceeding via the Cl-Ar complex. (8 refs.)

77867 The mechanism of carbonyl reduction by $LiBH_4$: an ab initio investigation with inclusion of solvent effects. R.Bonaccorsi (Istituto di Chimica Quantistica ed Energetica Molecolare, CNR, Pisa, Italy), R.Cimiraglia, J.Tomasi, S.Miertus. *THEOCHEM (Netherlands)*, vol.11, no.1-2, p.11-23 (June 1983). The mechanism of the reaction $H_2CO+LiBH_4 \rightarrow$ products has been investigated by using SCF calculations in a modified formalism which includes solvent effects. The effects of the solvent are represented by a one-electron operator added to the Fock Hamiltonian of the molecular system. The influence of the solvent on the reaction energy profile, on the geometry of the transition state, intermediate species, reagents and products is brought out by comparing the results with similar ones referring to the same reaction in vacuo (J. Mol. Struct., *Theochem*, 87 (1982) 181). Attention is paid to alternative mechanisms involving ionic dissociation of the reactant. (36 refs.)

77868 Molecular topology and chemical reactivity: interaction of a chemical bond with simple cubic, body centered cubic and face centered cubic alkali metal lattices. J.Pancir, R.Zahradnik (J. Heyrovsky Inst. of Phys. Chem. & Electrochem., Acad. of Sci., Prague, Czechoslovakia). *THEOCHEM (Netherlands)*, vol.11, no.1-2, p.23-35 (June 1983). The simplest version of a topological method is used to study the interaction between a chemical bond (parametrized as a hydrogen molecule) and metal crystals parametrized as sodium. Planes with Miller indices of (100), (110), (111), and (112) are considered for simple cubic (SC), body centered cubic (BCC) and face centered cubic (FCC) lattices. Throughout the calculation, all electronic repulsion integrals are neglected and uniform metal-metal bond strengths assumed. Interaction energies are calculated by the second order perturbation theory. All the planes of the SC and BCC lattices have uniform charge distribution because only even-membered rings are present. Of all the interactions studied, the bonding of one atom of the interacting diatomic molecule with two neighbouring metal atoms is preferred. If such a type of interaction is impossible for steric reasons, interaction of the chemical bond with two nearest non-neighbouring metal atoms is most advantageous. Interaction energies with SC and BCC lattices are smaller than those for isolated atoms but the opposite is true for the FCC lattice. Simple selection rules are suggested which control interaction between a chemical bond and the σ part of any metal cluster. (9 refs.)

77869 Catalytic effect on the selectivity of the Diels-Alder reaction. V.Branchadell, A.Oliva, J.Bertran (Dept. de Quimica Fisica, Univ. Autònoma de Barcelona, Barcelona, Spain). *Chem. Phys. Lett. (Netherlands)*, vol.97, no.4-5, p.378-80 (27 May 1983). Using the MINDO/3 method, variation of the potential barrier for the Diels-Alder reaction between 1-hydroxybutadiene and acrolein, catalyzed by BF_3 and NH_4^+ , has been studied. An interpretation of the experimental facts about the increase of regioselectivity and stereoselectivity for Diels-Alder reactions catalyzed by Lewis acids is given. (27 refs.)

77870 The evaluation of synthetic strategies for oligonucleotides of defined sequence. I. Computer programs in nucleic acid synthesis. S.Lombardi, H.Seidell, J.Hachmann (Oligonucleotides Section, Genex Corp., Rockville, MD, USA). *Comput. Programs Biomed. (Netherlands)*, vol.16, no.1-2, p.71-6 (Feb.-April 1983). Describes a computer program to aid in the evaluation of strategies for the synthesis of oligodeoxyribonucleotides of defined sequence. The program reduces the time required for the development of the most cost-effective strategy from several hours to a few minutes. The chemist supplies the program with the order of internucleotide bond formation, the final amount of material desired and the data giving anticipated reaction yields and molar ratios of reactants. The M_n and amount required for each intermediate in the proposed synthetic approach is then calculated. All of these data can be stored, edited or printed. By changing various input parameters (e.g. order of internucleotide bond formation, expected reaction yield), the chemist can utilize this program to analyze multiple synthetic approaches rapidly. The synthetic approach that will minimize the amounts of the expensive starting materials needed to complete the synthesis of the desired DNA can thus be quickly identified. (25 refs.)

77871 Mechanistic studies of oxene reactions with organic substrates: reaction paths on MINDO enthalpy surfaces—models for cytochrome P450 oxidations. A.T.Pudzianowski, G.H.Loew (Life Sci. Div., SRI Internat., Menlo Park, CA, USA). *Int. J. Quantum Chem. (USA)*, vol.23, no.4, p.1257-68 (April 1983). In a systematic study, the characteristics of triplet oxene models for alkane, alkene, chloroalkane, and aryl oxidations by the cytochrome P450s have been examined using the semiempirical molecular orbital method MNDO and the formalism of statistical mechanics. Specific model substrates chosen were: methane, ethylene, propene, carbon tetrachloride, chloroform, and toluene. It was found that transition state geometries and activation entropies were reliably predicted, but that an empirical factor was necessary to correct overestimation of activation enthalpies. It was determined that both hydroxylations and epoxidation initiated by a $O(^1P)$ atom are nonconcerted; and that oxidations of C-Cl bonds (halosylations) occur by a two-step mechanism similar to hydroxylation. It is shown that the radical mechanisms derived from these studies are consistent with a range of observed properties of cytochrome P450 reactions and provide reasonable explanations for secondary deuterium isotope effect and substituent effects in cytochrome P450 epoxidation of styrenes, suicide inactivation of a P450 enzyme by ethylene, and the characteristics of aerobic CCl_4 and $CHCl_3$ metabolism. A triplet oxene mechanism for the initial steps of aromatic epoxidation and hydroxylation is also discussed. (36 refs.)

77872 Sequential isomerism of activated complexes: interfering versus noninterfering intermediate. Z.Slanina (J. Heyrovsky Inst. of Phys. Chem. & Electrochem., Acad. of Sci., Prague, Czechoslovakia). *Int. J. Quantum Chem. (USA)*, vol.23, no.4, p.1553-61 (April 1983). A unimolecular process is considered that was treated experimentally as a concerted one; however, subsequent quantum-chemical analysis has proved that the process is realized via an intermediate (double sequential isomerism of activated complexes). The intermediate is supposed to contribute directly to values of the primary observed data (e.g., spectral absorbances). Within this approach of interfering intermediate any degree of this interference is allowed including the limit case of noninterfering intermediate serving as a reference standard. A technique a suggested enabling correct comparison of the quantum-chemical outputs with the experimental overall values for rate constants and activation enthalpy and entropy. The technique employs mere amount of information currently obtainable from quantum-chemical study of a rate process (i.e. representation of potential energy hypersurface by its stationary points and activated-complex theory). Properties of the derived formulae are illustrated with model examples. The results are important for meaningful comparison of experimental and theoretical data in the case of processes with sequential isomerism of activated complexes disclosed only theoretically. (28 refs.)

77873 Topological determinants in organic chemistry. P.G.Seybold (Dept. of Chem., Wright State Univ., Dayton, OH, USA). *Int. J. Quantum Chem. (USA)*, vol.23, no.4, p.1683 (April 1983). Summary form only given. It is well recognized that molecular topology determines or strongly influences many molecular properties, but a more precise description has remained elusive. A graph-theoretical technique is introduced to analyze topological features of conjugated and aromatic networks. An atomic structural index, related to the molecular Wiener index, can be used as a measure of the connectedness of an atom to other atoms of a network. Thus it is recognized that some positions are strongly connected, and others weakly connected, to the conjugated system. Substitutions or replacements as strongly connected positions have a greater effect on molecular properties than those at weakly connected positions. Two fundamental features of the carcinogenic activity of polycyclic aromatic hydrocarbons (PAHs) serve as illustrations. Using graph-theoretical analysis, it can be shown that the 'bay region' geometry, believed important for the carcinogenic activity of many PAHs, allows carbonium ion formation to occur at strongly connected positions, thereby yielding more stable carbonium ions. Furthermore, many features of the effects of substituents on carcinogenic activity can be understood on simple topological grounds. Applications to a variety of topics in organic chemistry are in progress. (no refs.)

77874 Solvent effects in organic chemistry studied by correlation analysis. N.B.Chapman (Dept. of Chem., Univ. of Hull, Hull, England). *Indian J. Phys. Part B*, vol.56B, no.6, p.9-14 (Dec. 1982). [received: May 1983] The author studies the effect of a change of solvent on the kinetics of organic reactions. He presents some recent work done by his own group by selecting a range of pure liquids as solvents to avoid 'solvent-sorting'. They make much use of the reactions between carboxylic acids (mainly aromatic) and diazodiphenylmethane (DDM) which are readily followed by visible spectroscopy. Moreover such reactions are facile with otherwise unreactive acids and the mechanism, which involves a rate-limiting proton transfer, is well-established. (10 refs.)

77875 Dynamics of $O(^1D_2)$ reactions with bifunctional substrates: alcohols and thiols. N.Goldstein, J.R.Wiesenfeld (Dept. of Chem., Cornell Univ., Ithaca, NY, USA). *J. Chem. Phys. (USA)*, vol.78, no.11, p.6725-31 (1 June 1983). The OH and OD product ratios and vibrational distributions following the reactions of $O(^1D_2)$ with isotopically labeled alcohols and several thiols were characterized using laser induced fluorescence. The primary site of $O(^1D_2)$ attack upon the alcohols is the O-H bond, attack upon the C-H bond also being observed. Both reactions occur via an insertion/elimination mechanism. Product vibrational distributions for each pathway are similar to those observed following reaction with the corresponding monofunctional substrate. (33 refs.)

77876 Determination of product population and alignment using laser-induced fluorescence. C.H.Greene (Dept. of Phys. & Astron., Louisiana State Univ., Baton Rouge, LA, USA), R.N.Zare. *J. Chem. Phys. (USA)*, vol.78, no.11, p.6741-53 (1 June 1983). For collision systems having axial symmetry, the anisotropy of the laser-induced fluorescence is given explicitly in terms of the zeroth, second, and fourth rank moments of the angular momentum distribution, which, respectively, are proportional to the population, the quadrupole alignment, and hexadecapole alignment of the product internal state under study. Expressions are presented for determining these three quantities from the dependence of the fluorescence intensity on the polarizations of the absorbed and detected photons. Results are presented for an arbitrary excitation-detection geometry which is then specialized to the commonly occurring cases where the direction of fluorescence detection is at right angles to the axis of cylindrical symmetry and the direction of the incoming light beam is either along the axis of cylindrical symmetry or at right angles to it and to the fluorescence detection direction. The approach of these expressions to the high- J limit is considered. The effect of nuclear spin on the fluorescence intensity is analyzed and the extent of depolarization is shown to be unimportant for large J . The use of

angular momentum recoupling algebra permits the geometrical and dynamical aspects of this problem to be completely disentangled. (23 refs.)

77877 On the reaction $\text{Mg} + \text{N}_2\text{O} \rightarrow \text{MgO} + \text{N}_2$. D.R.Yarkony (Dept. of Chem., Johns Hopkins Univ., Baltimore, MD, USA). *J. Chem. Phys. (USA)*, vol.78, no.11, p.6763-72 (1 June 1983). The lowest singlet ($^1A'$) and triplet ($^3A'$) potential energy surfaces of the reaction $\text{Mg} + \text{N}_2\text{O}(\Sigma^+)=\text{MgO} + \text{N}_2(\Sigma^+)$ are investigated using ab initio SCF, two configuration MCGSCF and CI wave functions. The reactivity of $\text{Mg}(^1S)$ and $\text{Mg}(^3P)$ is contrasted. These surfaces can be qualitatively partitioned into three contiguous, nonadjacent regions characterized by distinct values of an approximate reaction coordinate (ξ): a reactant region in which $\xi \approx \xi_1 \approx R(\text{Mg}-\text{O})$, a bending region in which $\xi \approx \xi_2 \approx \angle \text{NNO}$, and a product region in which $\xi \approx \xi_3 \approx (N-O)$. Evolution into region 3 requires Mg to N_2O charge transfer which facilitates, and is facilitated by, bending of N_2O . On the $^1A'$ surface which correlates with $\text{MgO}(^1\Pi)$, this process is largely downhill and involves an orbital reorganization in the N_2O moiety for $\xi \approx \xi_3$. A small barrier to vertical charge transfer is predicted at the CI level. On the $^3A'$ surface, which correlates with $\text{MgO}(^3\Sigma^+)$ approach is uphill for $\xi \approx \xi_1$. Possible explanations for the profound differences in the reactivity of calcium and magnesium with N_2O are suggested. (50 refs.)

77878 Vibrational excitation of the allene-fluorine reaction in cryogenic matrices: possible mode selectivity. A.K.Knudsen, G.C.Pimentel (Chem. Dept., Univ. of California, Berkeley, CA, USA). *J. Chem. Phys. (USA)*, vol.78, no.11, p.6780-92 (1 June 1983). The infrared induced reaction of allene (C_3H_4) and fluorine in N_2 , Ar, Kr, and Xe matrices at 12 K has been studied. The reaction is promoted by the selective vibrational excitation of $\text{C}_3\text{H}_4\text{F}_2$ reactive pairs and the course of the reaction followed by infrared spectroscopy. Four products are detected, consistent with the concerted addition of F_2 across the C-C double bond to form vibrationally excited cis- and gauche- $\text{CH}_2\text{CFCH}_2\text{F}$ which may then eliminate HF to yield either $\text{CH}\equiv\text{CH}_2\text{FHF}$ or $\text{CH}_2=\text{C}=\text{CHFHF}$ pairs. The relative abundance of each product depends markedly upon the matrix. Selective vibrational photoisomerization of $\text{CH}_2=\text{CFCH}_2\text{F}$ was used to distinguish and assign spectral features due to the cis- and gauche-rotamers as well as to provide evidence about the torsional barrier in the matrix. In a particular matrix, the allene-fluorine reaction product distribution is independent of the exciting frequency, with measurements at 1679, 1953, 1999, and 3076 cm^{-1} . However, the relative quantum yield at 3076 cm^{-1} is three orders of magnitude higher than observed at the lower frequencies. Furthermore, the quantum yields at 1680, 1953, and 1999 cm^{-1} show differences that implicate mode selectivity in the allene-fluorine reaction. The CH_2 rocking overtone $2\nu_9$ at 1999 cm^{-1} and perhaps as well the CH_2 bending overtone $2\nu_{10}$ at 1679 cm^{-1} show a higher reaction propensity than that of the asymmetric skeletal stretching vibration ν_6 at 1953 cm^{-1} . (31 refs.)

77879 Transient kinetics of chemical reactions with bounded diffusion perpendicular to the reaction coordinate: intermolecular processes with slow conformational changes. N.Agmon, J.J.Hopfield (Div. of Chem. & Biology, California Inst. of Technol., Pasadena, CA, USA). *J. Chem. Phys. (USA)*, vol.78, no.11, p.6947-59 (1 June 1983). Intramolecular reactions inside macromolecules (e.g., binding of ligands to iron inside heme proteins) may often be coupled to slow random fluctuations in the reaction center geometry. This motion is 'perpendicular' to the reaction coordinate. It can be described as bounded diffusion in the presence of a binding potential field and an intramolecular rate constant which depends on the perpendicular degree of freedom. The diffusion equation is solved under the appropriate reflective boundary conditions. The transient decay of the total population is multiexponential (power law) for small diffusivity, changing to monoexponential kinetics for large diffusivity. For large times or large diffusivity, direct integration is very tedious, but an eigenvalue expansion converges rapidly. It also allows the calculation of the 'average survival time' (an extension of the 'first passage time') a natural candidate for replacing the reciprocal rate constant in multiexponential kinetics. An example is given for electron transfer between two loosely bound sites in a macromolecule. The average survival time shows a non-Kramers dependence on diffusivity, of the found in the binding kinetics in heme proteins. (26 refs.)

77880 Comparison of chemical reactions in liquid lithium with those in liquid sodium. R.J.Pulham, P.Hubberstey (Chem. Dept., Univ. of Nottingham, Nottingham, England). *J. Nucl. Mater. (Netherlands)*, vol.115, no.2-3, p.239-50 (April 1983). A comparison is made of the chemical properties of liquid lithium and of liquid sodium which are relevant to the use of the liquid metals in fusion and fission reactors. The liquids dissolve both metals and non-metals: the solubility of transition metals is enhanced by the presence of dissolved non-metals, e.g. nitrogen and oxygen, and this is most obvious in the case of lithium contaminated with nitrogen where the enhanced solubility is accompanied by the existence of stable ternary nitrides, e.g. Li_3FeN_2 . The solubilities of selected non-metals, hydrogen, carbon, nitrogen and oxygen, in the liquid metals are compared, and the fate of salts with polyatomic anions, e.g. NaOH , Li_2CO_3 , is discussed. Chemical reactions are followed in the laboratory, often by pressure and electrical resistivity techniques, and more recently by electrochemical cells. The reactions can be divided arbitrarily into non-metal with non-metal, non-metal with dissolved metal, and non-metal with solid transition metal. (32 refs.)

77881 Ternary ion exchange. IV. Activity corrections for the solution phase. P.Fletcher, R.P.Townsend (Dept. of Chem., City Univ., London, England). *J. Chem. Soc. Faraday Trans. II (GB)*, vol.79, pt.3, p.419-32 (March 1983). For pt.III see ibid., vol.77, p.2077 (1981). A previously developed model for the evaluation of activity coefficient ratios in mixed dilute solution is employed with particular respect to ternary cation exchange in zeolites in the presence of up to three different coanions in solution. Potential errors arising from ignoring either completely or partially the non-ideality correction for the solution phase are evaluated and discussed. Exchanges involving counter-ions of the same valency, or involving ions of different valencies, are both considered. It is shown that when all the counter-ions have the same valency, the magnitude of the non-ideality correction is independent of the selectivity of the exchanger. When the valencies of the counter-ions are different it is essential to apply the mixed-salt activity correction for any accurate studies of ternary ion-exchange equilibria. (18 refs.)

77882 Proton phototransfer and nonradiative deactivation in hydrogen-bonded complexes of 2-anthrol. L.M.Rubekov, B.M.Uzhinov. *J. Appl. Spectrosc. (USA)*, vol.36, no.5, p.562-5 (May 1982). Translation of: *Zh. Prikl. Spektrosk. (USSR)*, vol.36, no.5, p.792-6 (May 1982). [received: Feb. 1983]. Studies the energy decay processes of electron excitation concurrent with intra-complex transfer of a proton in excited complexes of 2-anthrol, as well as energy decay in which ion pairs are formed. (9 refs.)

77883 Chemical transport of MnS and MnSe using HCl as a transporting agent. A.Pajczkowska (Inst. of Phys., Polish Acad. of Sci., Warsaw, Poland). *Mater. Res. Bull. (USA)*, vol.18, no.4, p.397-403 (April 1983). The preparation of MnS and MnSe single crystals by chemical transport in a closed system with HCl as a transporting agent has been studied. The reaction of NH_4Cl and Cl_2 serves as a source of dry HCl. The results of thermodynamic calculations and experiments are discussed. MnS crystals grow with two types of platelet shapes in the low temperature region, and as octahedra at temperatures above 1100 K . MnSe crystals grow only in the octahedral form. The transport rate for MnS is higher than that for MnSe for ΔT greater than 50 K . Single crystals of MnS and MnSe in the form of octahedra with a maximum edge length of 4 mm were obtained. (9 refs.)

77884 Diffusional-drift-influenced chemical reactions at all gas densities. M.R.Flannery (School of Phys., Georgia Inst. of Technol., Atlanta, GA, USA). *Phys. Rev. Lett. (USA)*, vol.50, no.21, p.1656-9 (23 May 1983). In chemical reactions between species A and B, which interact within a background gas at high density N via a non-Coulomb attraction, it is shown that the key sequence of physical mechanisms for transport is diffusion at asymptotic (A-B) separations R , diffusional drift at intermediate R , and pure diffusion at the reaction sink. Reduction in gas density N causes the onset at the sink of pure inward drift. For pure Coulomb species in a gas, the corresponding sequence is asymptotic drift, diffusional drift, and pure diffusion at high N , and diffusional drift at lower N . (7 refs.)

77885 Potential surfaces for simple rearrangements. J.A.Pople (Dept. of Chem., Carnegie-Mellon Univ., Pittsburgh, PA, USA). *Pure & Appl. Chem. (GB)*, vol.55, no.2, p.343-6 (Feb. 1983). (International Symposium on Theoretical Organic Chemistry, Dubrovnik, Croatia, Yugoslavia, 30 Aug.-3 Sept. 1982). Quantum mechanical methods for the location and characterization of rearrangement transition structures are reviewed. Activation barriers are shown to be sensitive to the inclusion of polarization basis functions and electron correlation. Applications to vinylidene-acetylene rearrangements are described. The parent species, H_2CC , rearranges to HCCH without a significant activation barrier. However, significant barriers are found for certain substituted vinylidenes. (14 refs.)

An economical transfer vessel with detachable reactor for XPS studies See Entry 74571

Theoretical investigations of the interaction of but-2-ene with a sodium ion See Entry 75292

N-H... π hydrogen bonding: infrared study of *N*-cyclohexylformamide-aromatic donor systems See Entry 75383

Symmetric charge exchange between negative ions and atoms See Entry 75497

An electron-diffraction investigation of the molecular structure and thermal dissociation of gaseous PCl_5 at 90°C See Entry 75512

Theoretical aspects of cluster formation by keV bombardment of rare-gas solids See Entry 75563

Understanding the middle atmosphere via the laboratory: ion cluster investigations See Entry 75564

Local partial DOS and experimental Al K spectra of transition metal aluminides. Charge transfer trend See Entry 76870

Dielectric relaxation and dipole moment measurements of *n*-methylacetamide in benzene and dioxane solutions at different temperatures from microwave absorption studies See Entry 77325

Spectral studies on new dioxouranium (VI) complexes of tridentate Schiff bases derived from salicylhydrazide and salicylaldehyde or substituted salicylaldehydes See Entry 77372

Spectra and structure of asymmetric carboxylic acid dimers in solution See Entry 77387

Study of complexes of hydrogen halides with diethyl ether in aprotic solvents by the method of IR spectroscopy See Entry 77389

Effects of diffusion on long-range electron transfer See Entry 77865

Thermal isomerization and degradation of polyacetylene See Entry 77887

A study in real and reciprocal space of the electron-beam-induced decomposition of sodium aluminum hydride single crystals See Entry 77898

Hydrogen production with visible light by using dye-sensitized TiO_2 powder See Entry 77904

Adsorption-complex isomerism and quantum-chemical studies in heterogeneous catalysis See Entry 77916

The adsorption and dissociation of methyl isocyanide on $\text{Rh}(111)$ See Entry 77918

The mechanism of the CO_2 formation on $\text{Pt}(111)$ and polycrystalline surfaces at low temperatures See Entry 77921

Direct current and complex plane polarographic behaviour of copper(II)-EDTA complexes See Entry 77932

Polarographic studies of cobalt (III) complexes with biguanide and substituted biguanides See Entry 77933

Transfer and storage of chemical and radiation potential See Entry 78091

82.35 POLYMER REACTIONS AND POLYMERIZATION

77886 Gelation in finite polycondensation systems. J.F.Yan (Weyerhaeuser Technol. Center, Weyerhaeuser Co., Tacoma, WA, USA). *J. Chem. Phys. (USA)*, vol.78, no.11, p.6893-6 (1 June 1983). Flory's theory of gelation is modified with the consideration of the conservation of both polymers and monomers. This result is an implicitly renormalized truncated weight distribution applicable to the entire system. Weight-average degree of polymerization is obtained by using the cascade theory with a finite number of generations. The dispersity of the weight distribution reaches a maximum at the gel point. In the post-gel region, a new relation for calculating the extinction probability is obtained. Results on weight-average DP and the gel fraction are in excellent agreement with those obtained by Donoghue and Gibbs (1979) and Ziff and Stell (1980). (8 refs.)

77887 Thermal isomerization and degradation of polyacetylene. P.Bernier (Groupe de Dynamique des Phases Condensées, Montpellier, France), S.Lefrant, M.Rolland, M.Aldissi, M.Galtier, A.Montaner, C.Linaya, F.Schue. *J. Electron. Mater. (USA)*, vol.12, no.2, p.289-322 (March 1983). Presents an experimental study of the isomerization from cis to trans (CH), induced by a thermal treatment of the film. Infrared, Raman, EPR and

NMR spectroscopies have been used, in addition to DC conductivity measurements, in order to characterize the kinetics of the isomerization process. All the spectroscopic methods show that the isomerization is thermally activated with an activation energy of ~18 kcal/mole. It is also shown that degradation processes are also involved and an activation energy close to 30 kcal/mole is derived from EPR data. Optimal conditions to perform a thermal isomerization of cis-(CH)_x, with respect to the extent of conjugation, are suggested. (28 refs.)

77888 Biceritricity in the polymerization of chains and rings. J.C.Wheeler, R.G.Petschek (Chem. Dept., Univ. of California, San Diego, La Jolla, CA, USA), P.Pleuty.

Phys. Rev. Lett. (USA), vol.50, no.21, p.1633-6 (23 May 1983). The equilibrium polymerization of chains and rings can be viewed as a biceritric point in a suitably augmented parameter space. The polymerization of chains in equilibrium with rings is described by the cross-over exponent, ϕ , for quadratic anisotropy in the $O(n)$ vector model with $n \rightarrow 1$. While the total mass fraction of polymerized material is described by the Ising exponent α , the mass fraction of chains separately (and therefore also of rings) is described by the exponent $\alpha_c = \phi - 1 + \alpha$. (16 refs.)

Statistical theory of the degree of polymerizationSee Entry 74392

82.40 CHEMICAL KINETICS AND REACTIONS: SPECIAL REGIMES

77889 A nonlinear problem arising from combustion theory: Linan's problem. S.P.Hastings (Dept. of Math., State Univ. of New York, Buffalo, NY, USA), A.B.Poore.

SIAM J. Math. Anal. (USA), vol.14, no.3, p.425-30 (May 1983). The differential equation $y'' = y \exp(\alpha x - y)$, $\lim_{x \rightarrow \infty} dy/dx = -\theta$ and $\lim_{x \rightarrow \infty} dy/dx = 0$ for $\theta > 0$ governs the thin reaction diffusion zone in many diverse problem in combustion theory. This problem with $\theta = 1$ is known as Linan's problem and continues to arise through the use of large activation energy asymptotics in the study of various combustion phenomena. The main issues for this problem are those of existence and uniqueness which are established for each positive α and θ . (11 refs.)

77890 Instabilities, pattern formation, and turbulence in flames. G.I.Sivashinsky (Dept. of Math., Univ. of California, Berkeley, CA, USA). In book: *Annual review of fluid mechanics. Vol.15*, M.Van Dyke, J.V.Wehausen, J.L.Lumley [Ed.], p.179-99. Palo Alto, CA, USA: Annual Reviews (1983), 534 pp. [0 8243 0715 1]

Considerable progress has recently been achieved in the understanding of the nature and character of spontaneous instabilities in premixed flames. The paper is devoted to the latest theoretical results in this area, which have disclosed a deep affinity between flames and other nonequilibrium physical systems capable of generating regular and intrinsically chaotic structures. (67 refs.)

10-Hz coherence anti-Stokes Raman spectroscopy apparatus for turbulent combustion studiesSee Entry 74542

Vibrational energy transfer in $A^2\Sigma^+ OH$ in flamesSee Entry 75482

Thermal structure of a flat plate turbulent boundary layer diffusion flameSee Entry 76125

A study of the steady-state reaction-zone structure of a homogeneous and a heterogeneous explosiveSee Entry 76126

Fiber-optic absorption/fluorescence probes for combustion measurementsSee Entry 77927

82.40T Chemiluminescence and chemical laser kinetics
(see also 42.55K Chemical lasers, 78.60P Chemiluminescence)

77891 Singlet molecular oxygen pumping of IF $B^2\Pi(O^+)$. P.D.Whitefield, R.F.Shea, S.J.Davis (New Laser Concepts Branch, Air Force Weapons Lab., Kirtland AFB, NM, USA).

J. Chem. Phys. (USA), vol.78, no.11, p.6793-801 (1 June 1983). Chemiluminescence from the reactions: $I_2 + F_2$; $I_2 + F_2 + O_2(^1\Delta)$; and $I_2 + F + O_2(^1\Delta)$ has been studied. All three reactions produced emission from the $B^2\Pi(O^+) \rightarrow X^1\Sigma^+$ system of IF. The two reactions utilizing $O_2(^1\Delta)$ produced much higher chemiluminescent intensities than did the $I_2 + F_2$ reaction. The photon yield of the $I_2 + F + O_2(^1\Delta)$ reaction was measured to be 0.3%. Rotational and vibrational temperatures in IF(B) were determined. Rotational temperatures were approximately 300K while nonthermal vibrational distributions were observed. Possible mechanisms of IF(B) production are discussed. (30 refs.)

Determination of product population and alignment using laser-induced fluorescenceSee Entry 77876

82.45 ELECTROCHEMISTRY AND ELECTROPHORESIS

(see also 66.10 Ionic conduction in liquids; for electro-osmosis, see 82.65)

77892 On the processes responsible for the degradation of the aluminium-lithium electrode used as anode material in lithium aprotic electrolyte batteries. M.Garreau, J.Thevenin, M.Fekir (CNRS Phys. des Liquides et Electrochimie, Paris, France).

J. Power Sources (Switzerland), vol.9, no.3-4, p.235-8 (April-May 1983). (International Meeting on Lithium Batteries, Rome, Italy, 27-29 April 1982). A study has been carried out of the different processes, chemical corrosion, solid state diffusion and mechanical disintegration, affecting aluminium-lithium electrodes formed either by an electrochemical or a pyrometallurgical process. Cycling operations present similar limitations with aprotic electrolytes using dioxolane and propylene carbonate as solvents, and $LiClO_4$ and $LiAsF_6$ as solutes. Preliminary tests conducted with compressed LiAl powder electrodes show the existence of other processes responsible for the degradation of these electrodes during cycling. (4 refs.)

77893 Mechanistic studies of oxide electrodes reversibly incorporating Li^+ ions. G.Pistoia (Centro di Studio per la Electrochimica e la Chimica Fisica, CNR, Rome, Italy).

J. Power Sources (Switzerland), vol.9, no.3-4, p.307-20 (April-May 1983). (International Meeting on Lithium Batteries, Rome, Italy, 27-29 April 1982). Transition metal oxides capable of reversibly incorporating Li^+ ions are examined with particular emphasis on their structural features. The thermodynamic, kinetic, and electrochemical aspects of the insertion processes are also discussed. (47 refs.)

77894 Introduction to the scaling properties in electrochemistry: from the 'TEISI' model to the lithium fractal ordering in $Li_0.5FeS_2$ layered structure. A.Le Mehaute, A.Dugast (Lab. de Marcoussis, Centre de Recherches de la CGE, Marcoussis, France).

J. Power Sources (Switzerland), vol.9, no.3-4, p.359-64 (April-May 1983). (International Meeting on Lithium Batteries, Rome, Italy, 27-29 April 1982). Attention is drawn to the generalisation to the fractal geometry of the relations which control the interfacial energy and mass exchange in the linear approximation. From this kinetic analysis the solid state motion of lithium in $Li_0.5FeS_2$ is shown to be related to the fractal ordering of this ion in the lattice. Scaling phase transitions are pointed out. (19 refs.)

77895 A reversible graphite-lithium negative electrode for electrochemical generators. R.Yazami, P.Touzain (Lab. d'Adsorption et Reaction de Gaz sur Solides, Domaine Univ., Saint Martin d'Heres, France).

J. Power Sources (Switzerland), vol.9, no.3-4, p.365-71 (April-May 1983). (International Meeting on Lithium Batteries, Rome, Italy, 27-29 April 1982). Lithium intercalation compounds in graphite have been obtained by electrochemical methods using a solid organic electrolyte (polyethylene oxide with lithium perchlorate). Intermittent electrochemical techniques have enabled the kinetic (diffusion coefficient) and thermodynamic (enthalpy) values to be calculated. Some secondary battery cycling tests using lithium-graphite as a negative electrode are reported. (10 refs.)

77896 Oxidized rare earth-iron compounds in photoassisted electrolysis of water. A.Shamsi, W.E.Wallace (Dept. of Chem., Univ. of Pittsburgh, Pittsburgh, PA, USA).

Mater. Res. Bull. (USA), vol.18, no.4, p.389-95 (April 1983). Anodes for use in a photoelectrolysis cell can be prepared by heating rare earth (R) iron compounds (RF_2 , RF_3 , R_2Fe_{17} and R_6Fe_{23}) in air using the flame of a Fisher burner. For comparison, iron oxide and titanium oxide were also prepared by heating iron and titanium metal in air. The current-voltage (I-V) properties of these materials were measured in an aqueous solution of 1 M NaOH. The flatband potentials (V_{fb}) were determined with respect to a fixed potential (SCE) by extrapolating the I-V curves to zero current. Anodic photocurrents were generated by light with energy exceeding the band gap of the photoanode material. Photoelectrolysis of water occurred, as evidenced by the evolution of oxygen from the $RFeO_4$ electrodes and hydrogen from the Pt electrode. Most of these electrodes were found to be stable under experimental conditions. (17 refs.)

77897 A conductance equation for binary liquid systems consisting of an electrolyte component and an indifferent solvent. Yu.Ya.Fialkov, N.I.Kulinich, V.L.Chumak (Kiev Polytech. Inst., Kiev, Ukrainian SSR). *Sov. Electrochem. (USA)*, vol.18, no.8, p.910-12 (Aug. 1982). Translation of: *Elektrokhimiya (USSR)*, vol.18, no.8, p.1024-7 (Aug. 1982). [received: May 1983]

A nonempirical conductance equation for binary liquid systems consisting of an electrolyte component and an indifferent solvent has been derived and analyzed; it links specific conductance to the electrolyte's viscosity, dielectric permittivity, and concentration. (8 refs.)

International Meeting on Lithium BatteriesSee Entry 74213

Convective diffusion toward rotating polar spherical electrodeSee Entry 76027

Lithium insertion into manganese spinelsSee Entry 76391

Mechanism of ion conduction in alkali metal-polymer complexesSee Entry 76695

Auger and AC impedance studies of the RF sputter deposited Fe_2O_3 filmsSee Entry 76810

The role played by the anions in cadmium electroplating from some acidic bathsSee Entry 77587

Silicon electrorefining using a semipermeable $Cu_3Si:Si$ anodeSee Entry 77593
A possibility to obtain microdiscontinuous chromium coatings by cathodic treatment in acidic mediaSee Entry 77805

Some possibilities for the use of stressed cathodically hydrogenated electrolytic nickel coatings for the deposition of microporous and microcracked chromium platesSee Entry 77806

Lithium-cupric sulfide cellsSee Entry 77968

Electrochemistry of a nonaqueous lithium/sulfur cellSee Entry 77969

Polarization of the lithium electrode in sulfonyl chloride solutionsSee Entry 77970

Li/SOCl₂ cells for high temperature applicationsSee Entry 77971

Li-AgBi(CrO₄)₂: a new highly reliable lithium battery for long service life applicationsSee Entry 77972

A pre-testable low temperature lithium thermal batterySee Entry 77973

The use of the reactive ether, tetrahydrofuran (THF), in rechargeable lithium cellsSee Entry 77975

The reactivity of organic electrolytes with lithium: mechanistic aspectsSee Entry 77976

Film forming reaction at the lithium/electrolyte interfaceSee Entry 77977

Raman spectroscopic studies of the structure of electrolytes used in the Li/SOCl₂ batterySee Entry 77978

Surface films on lithium in acetonitrile-sulphur dioxide solutionsSee Entry 77979

Electrochemical method for studying the reversibility of the lithium intercalation in secondary batteriesSee Entry 77980

Chromium oxides as cathodes for lithium cellsSee Entry 77981

Behaviour of various cathode materials for non-aqueous lithium cellsSee Entry 77982

Mechanistic studies of reversible layer-type electrodesSee Entry 77984

Characterization of the chemistry at the anode and cathode in the Li/SO₂ battery systemSee Entry 77985

Development and evaluation of the Texas Instruments Solar Energy SystemSee Entry 78090

82.50 PHOTOCHEMISTRY AND RADIATION CHEMISTRY

(see also 33.50 Fluorescence, phosphorescence; radiationless transitions)

77898 A study in real and reciprocal space of the electron-beam-induced decomposition of sodium aluminum hydride single crystals. P.J.Herley (Dept. of Materials Sci. & Engng., State Univ. of New York, Stony Brook, NY, USA), W.Jones.

Mater. Lett. (Netherlands), vol.1, no.5-6, p.131-6 (April 1983). Decomposition induced by the electron beam has been studied using transmission electron microscopy in sodium aluminum hydride, NaAlH_4 , single crystals. Results show rapid formation of small diffuse nuclei. These nuclei do not increase in size appreciably but grow in number as the reaction proceeds. No evidence for cracking was observed at the hydride/product interface: the final product is a finely-divided aggregate of metallic particles. (6 refs.)

77899 The mechanism of the photochemical oxidation of water to oxygen with silver chloride colloids. K.Chandrasekaran, J.K.Thomas (Dept. of Chem., Univ. of Notre Dame, Notre Dame, IN, USA).

Chem. Phys. Lett. (Netherlands), vol.97, no.4-5, p.357-60 (27 May 1983). Photoexcitation of silver chloride colloids in the presence of excess silver ions leads to the decomposition of water. Hydroxyl radicals were found to be intermediates in the decomposition process. Irradiation leads to hydroxyl radicals, which recombine to give hydrogen peroxide, on the colloidal particle surface. Subsequent decomposition of H_2O_2 to give O_2 is catalyzed by silver ions. Addition of alcohols such as methanol and isopropanol reduce the oxygen yield, as they react with OH radicals and reduce the H_2O_2 yield. (10 refs.)

77900 Photoreduction of carbon dioxide to formic acid, formaldehyde, methanol, acetaldehyde and ethanol using aqueous suspensions of strontium titanate with transition metal additives. M.Ulman (Isotope Dept., Weizmann Inst. of Sci., Rehovot, Israel), A.H.A.Tinnemans, A.Mackor, B.Aurian-Blajeni, M.Halmann.

Int. J. Sol. Energy (Switzerland), vol.1, no.3, p.213-22 (1982). The photoassisted reduction of aqueous carbon dioxide was carried out in the presence of suspensions of powdered strontium titanate, surface treated with various transition metal oxide additives, using either high-pressure mercury lamps or sunlight as the energy source. The organic products observed included formic acid, formaldehyde, methanol, acetaldehyde and ethanol. (10 refs.)

77901 Connecting a chemical fast reactor to an AIM 65 microcomputer. G.R.Heal (Dept. of Chem. & Appl. Chem., Univ. of Salford, Salford, England).

Lab. Microcomput. (GB), vol.1, no.2, p.14-26 (Summer 1982). Describes how to record data from a flash photolysis unit on Rockwell AIM 65 microcomputer, via an analogue-digital converter (ADC). Details are given of how to wire the ADC and of machine code subroutines that set up the interface and run the ADC. The assembly program and the main control program (the latter in BASIC) are listed. (3 refs.)

77902 Solute-solvent exciplex versus twisted intramolecular charge-transfer state in anomalous fluorescence of 4-NN-dimethylaminobenzonitrile. R.J.Visser, C.A.G.O.Varma, J.Konijnenberg, P.Bergwerf (Dept. of Chem., State Univ., Leyden, Netherlands).

J. Chem. Soc. Faraday Trans. II (GB), vol.79, pt.3, p.347-67 (March 1983). The authors pay attention to four topics concerning the effects of solute-solvent interactions on the behaviour of electronically excited 4-NN-dimethylaminobenzonitrile, namely the influence of solvent deuteration on anomalous fluorescence yield, the Stokes shift of the fluorescence in a polar glassy solution, photoinduced electrical conductivity and a quantum chemical analysis of the implications of the exciplex model. (27 refs.)

77903 Photophysics of derivatives of all-trans-1,6-diphenyl-1,3,5-hexatriene (DPH). I. Model involving fluorescence from S_2 and S_1 excited states. P.C.Alford, T.F.Palmer (Chem. Dept., Univ. of Nottingham, Nottingham, England).

J. Chem. Soc. Faraday Trans. II (GB), vol.79, pt.3, p.433-47 (March 1983). Absorption, fluorescence excitation and emission spectra have been measured for several derivatives of all-trans-1,6-diphenyl-1,3,5-hexatriene (DPH) in several non-polar solvents over a range of temperatures. Emission is shown to occur from the low-lying $^1A_g^*$ state (S_1) and the $^1B_u^*$ state (S_2) which is at slightly higher energy. A model is proposed in which thermal repopulation of S_2 from S_1 proceeds at a rate which is comparable to radiative and non-radiative decay from S_1 . (27 refs.)

77904 Hydrogen production with visible light by using dye-sensitized TiO_2 powder. K.Hashimoto, T.Kawai, T.Sakata (Inst. for Molecular Sci., Okazaki, Japan).

Nouv. J. Chim. (France), vol.7, no.4, p.249-53 (April 1983). Hydrogen was produced from water by exciting various organic dyes on TiO_2 or Pt/TiO_2 with visible light in the presence of a reducing agent. The quantum efficiency of hydrogen production was estimated to be in the order of 10^{-1} for $\text{Ru}(\text{bipy})_2^{2+}$ with EDTA as the reducing agent. It is postulated that hydrogen is produced by the reduction of water through a dye-sensitized process. (29 refs.)

77905 Direct observation of the local-field-enhanced surface photochemical reactions. C.J.Chen, R.M.Osgood (Dept. of Electrical Engng., Columbia Univ., New York, NY, USA).

Phys. Rev. Lett. (USA), vol.50, no.21, p.1705-8 (23 May 1983). The enhancement of photochemical reactions on surface-supported metallic particles is reported. The result is obtained by UV photodissociation of organometallic molecules adsorbed on the supporting surface. Transmission electron-microscope micrographs of the resulting photodeposited film reveal enhanced deposition on and near the metal particles, and a clear interference pattern resulting from the mixing of the incident and reradiated light. The importance of the particle plasma resonance is described. (10 refs.)

77906 Formation of metal images by a new peel-apart system. S.Honma, E.Inoue (Imaging Sci. & Engng. Lab., Tokyo Inst. of Technol., Yokohama, Japan).

Photogr. Sci. & Eng. (USA), vol.27, no.2, p.47-50 (March-April 1983). The imaging photosensor is made of a photosensitive polymer layer, comprising a polymer and a photosensitive material such as a diazo compound, which is coated on a metal layer deposited over a base film, and a cover film is then laminated on the photosensitive layer. After imagewise exposure through the cover film, peeling off the cover film from the base followed by heating at 50 to 100°C for a few minutes forms metal images on these films. The photographic properties depend both on the polymers and photosensitive materials which constitute the photosensitive layer. For example, a positive metal image of the original is formed on the base film by the use of polyvinyl chloride (PVC) and 2,6-di-(4'-azidobenzal)-4-methylcyclohexane, whereas a negative

one is obtained by the use of 2,5-dibutoxy-4-morpholino-benzediazonium tetrafluoroborate as the photosensitive material. This imaging system gives a high contrast image ($\gamma > 10$), with a resolving power of 25 lps/mm. The total range of the image can be controlled from high to low gamma depending on the concentration of the photosensitive materials or variation of heating periods. (10 refs.)

77907 Gelatin-substituted cyanine dyes as spectral sensitizers for silver halide emulsions. R.Steiger (CIBA-Geigy Photochem. Ltd., Fribourg, Switzerland), J.F.Reber.

Photogr. Sci. & Eng. (USA), vol.27, no.2, p.59-65 (March-April 1983). Cyanine dyes which react with gelatin without significant cross-linking of the gelatin have been synthesized. Their reaction product, cyanine dyes chemically bonded to gelatin (gelatin-substituted cyanines), can be used to spectrally sensitize silver halide emulsion crystals. Some physical-chemical properties of gelatin-substituted cyanines in solution and adsorbed to silver halides are described. It is shown that only a small fraction of all bonded dye molecules present in the adsorbed gelatin layer are able to approach the AgHal crystal surface closely enough to enable direct charge transfer between the excited dye and the silver halide. Since only this fraction of the cyanine molecules was shown to spectrally sensitize, the contribution of Forster energy transfer must be negligible with respect to electron transfer in photographic emulsions, in agreement with previous experiments on evaporated AgHal layers. By using a gelatin-substituted cyanine as an energy donor and an appropriate cyanine acceptor directly adsorbed at the grain surface, concerted energy-electron transfer may occur. (11 refs.)

77908 Kinetics of silver cluster formation and trapped hole neutralization in silver halide emulsion grains digested with cadmium salts. C.Rippon, B.Levy (Polaroid Corp., Cambridge, MA, USA).

Photogr. Sci. & Eng. (USA), vol.27, no.2, p.65-74 (March-April 1983). Digestion of a monodisperse octahedral AgBr emulsion in the presence of CdCl_2 lowers the ionic conductivity of the emulsion grains, reduces the rate of photocharge decay, and increases the photographic sensitivity. $\text{Cd}(\text{NO}_3)_2$ digestion, KCl digestion and pAg adjustments with AgNO_3 and KBr yield much smaller changes in the parameters measured than are obtained with CdCl_2 digestion. The kinetics of photocharge decay are described by concurrent first- and second-order rate processes. CdCl_2 digestion reduces the rate of the first-order decay to a much greater extent than the second order decay. This corresponds to a shift of the order of the major reaction leading to silver cluster formation from first order to second order. Similarly, the photogenerated silver ion vacancy adjacent to a trapped hole is shown to be responsible for neutralization of the trapped photohole. The introduction of Cd^{2+} may promote the increase in photographic sensitivity for a number of reasons. The shift of the mechanism for silver cluster formation from first-order kinetics to second-order is considered to be an important factor contributing to the improved photographic response. The simultaneous increase in lifetime of the photocharge decay process allows time for an enhancement of the concentration of interstitial silver ions at fewer centers within a grain, thereby increasing the efficiency of photographic development. The combined effect of these processes is frequently an increase in photographic speed, fog stability, and improved high-intensity reciprocity characteristics. (42 refs.)

77909 A study of properties of clusters of photographic interest by means of a redox buffer solution. T.Tani (Res. Lab., Fuji Photo Film Co., Kanagawa, Japan).

Photogr. Sci. & Eng. (USA), vol.27, no.2, p.75-80 (March-April 1983). Properties of clusters of photographic interest were studied by oxidizing and reducing them in a redox buffer solution. The oxidation potential of latent images, formed in sulfur-plus-gold-sensitized emulsions was much more positive than those of latent images in unsensitized, sulfur-sensitized, reduction-sensitized, and-iridium-sensitized emulsions. The oxidation potential of latent images became more negative as the degree of the speed increase by each chemical sensitization increased. The oxidation potential of fog centers with excessive sulfur sensitization was much more positive (by more than 0.6 eV) than that of fog centers with excessive reduction sensitization. Latent sub-images as revealed by gold-latensification were reduced to form development centers by a buffer solution with a relatively negative redox potential. On the other hand, the oxidation potential of sub-images was more positive than that of latent images. Based on the above-stated results, conclusions are made on the mechanism of photographic sensitivity. (16 refs.)

77910 Image formation processes in concentric shell emulsions. J.W.Mitchell (Dept. of Phys., Univ. of Virginia, Charlottesville, VA, USA).

Photogr. Sci. & Eng. (USA), vol.27, no.2, p.81-94 (March-April 1983). The relevant aspects of the concentration theory are applied to image formation processes in direct positive and reversal emulsions. The production of these predominantly internal image emulsions with the introduction of controlled levels of physical lattice imperfection and internal chemical structural imperfection is discussed. Image formation processes in direct positive emulsions with surface-fogged grains are analyzed with emphasis on the variables responsible for sensitivity and contrast. Image formation during exposure and reversal processing of unfogged concentric shell and core-shell emulsions is then considered. Finally, the concentric shell internal image systems with reversal processing are compared with the usual negative surface image systems. (191 refs.)

77911 A preliminary report on radical yield alternation in even and odd linear alkanes irradiated at 77K: ESR evidence. M.Fukaya, K.Toriyama, M.Iwasaki (Government Industrial Res. Inst., Nagoya, Japan), T.Ichikawa, N.Ohta.

Radiat. Phys. & Chem. (GB), vol.21, no.5, p.463-5 (1983). It has been found that the yields of trapped alkyl radicals in linear alkanes irradiated at 77K exhibit an alternation depending upon whether the carbon number is even or odd. The alternation becomes more prominent in a series of higher alkanes starting from $n\text{-C}_{11}\text{H}_{24}$ to $n\text{-C}_{19}\text{H}_{40}$, for which the crystal structures as well as the ESR spectral features are known to exhibit a regular alternation. The results suggest that the radiation chemical events are affected by the molecular packing, that is the crystal structures at the chain end and/or the interchain structures. (7 refs.)

Physico-Chemical Behaviour of Atmospheric Pollutants. Proceedings of the Second European Conference See Entry 74233

Lifetime, triplet-triplet absorption spectrum and relaxation energy of an acyclic conjugated triene triplet: a pulse radiolysis study See Entry 75321

On avoided crossing between molecular excited states; photochemical implications See Entry 75324

Peculiarities of dip (hole) burning in the spectra of organic molecules in vitreous matrices See Entry 75364

Photophysics of aryl substituted 1,3,4-oxadiazoles: the triplet state of 2,5-diphenyl-1,3,4-oxadiazole See Entry 75365

Twisted intramolecular charge transfer (TICT) excited states: energy and molecular structure See Entry 75433

- Thermal broadening of optical homogeneous linewidths in organic glasses and polymers studied via photochemical hole-burning See Entry 75448
- Generation of electromagnetic waves during photochemical reactions See Entry 75613
- Photo-chemical reaction and photo-induced polarization studies in sulphur-doped potassium bromide See Entry 76482
- Light-induced recombination centers during pulse radiolysis of an electrolyte-semiconductor system See Entry 77046
- Proton phototransfer and nonradiative deactivation in hydrogen-bonded complexes of 2-anthrol See Entry 77882
- Oxidized rare earth-iron compounds in photoassisted electrolysis of water See Entry 77896
- Photoreactions on finely divided semiconductors See Entry 77915
- Transfer and storage of chemical and radiation potential See Entry 78091

82.55 RADIOCHEMISTRY

- 77912 Chemical effects of nuclear transformations in mixed potassium hexahaloeno-metallates (IV), $K_2MX_6Y_{6-n}$. I. Chemical effects of the $^{81}Br(n,\gamma)^{82}Br$ nuclear process in mixed potassium hexabromochloro-osmates (IV), $K_2OsBr_4Cl_{2-n}$. H.Muller, P.Bekk (Inst. für Anorganische Chem., Univ. Freiburg, Freiburg, Germany). *Radiat. Eff. (GB)*, vol.64, no.1-4, p.183-8 (1982). [received: May 1983] (Proceedings of the First International Conference on 'Radiation Effects in Insulators', Arco, Largo di Garda, Italy, 1981). The chemical fate of ^{82}Br recoil atoms with a mean recoil energy of 100 eV from the nuclear reaction $^{81}Br(n,\gamma)^{82}Br$ has been investigated in mixed potassium hexabromochloro-osmates(IV). The experimental results can be explained by the following reaction paths: $12 \pm 3\%$ primary retention, $9 \pm 1\%$ free bromide yield, $61 \pm 3\%$ billiard ball reaction, and $16 \pm 5\%$ products resulting from large disorder. $2 \pm 2\%$ of the ^{82}Br appear as hydrolysis products with unknown origin. The experiments have shown that the fate of ^{82}Br recoil atoms is equal for impacts with Br and Cl atoms. (19 refs.)
- 77913 Temperature effects on positronium formation and inhibition: a contribution to the elucidation of early spur processes. IV. Methanol and ethanol solutions. J.Talamoni, J.Ch.Abbe, G.Duplatre, A.Haessler (Div. de Chimie et Phys. des Rayonnements, Univ. Louis Pasteur, Strasbourg, France). *Radiat. Phys. & Chem. (GB)*, vol.21, no.5, p.431-8 (1983). Temperature effects between 173 and 348K on the inhibition of positronium formation by NO_3^- and Cl^- in methanol and in ethanol solutions have been investigated. Whilst the inhibition promoted by NO_3^- , a total inhibitor, is temperature independent, this is not the case for Cl^- , a limited inhibitor. However, different effects are observed in the two solvents and the role of the solvation states of the e^- (and of the e^+) is discussed. (24 refs.)
- Chemical effects of carbon ion implantation into alkali halides See Entry 76470

82.60 CHEMICAL THERMODYNAMICS

(see also 05.70 Thermodynamics)

- 10-Hz coherence anti-Stokes Raman spectroscopy apparatus for turbulent conduction studies See Entry 74542
- N-H... π hydrogen bonding: infrared study of N-cyclohexylformamide-aromatic donor systems See Entry 75383
- Excess enthalpies of liquid (copper-tellurium) alloys See Entry 76283
- Heat capacity and thermodynamic properties of molybdenum from 5 to 302K See Entry 76657
- Rb₂ZnCl₄: three heat-capacity anomalies due to soft-mode and commensurate-incommensurate transitions See Entry 76658
- Quantum chemical and statistical-thermodynamic studies of equilibria and rates See Entry 77862
- Solvent effects in organic chemistry studied by correlation analysis See Entry 77874
- Comparison of theoretical and thermodynamic values of interconstituent interactions in DNA See Entry 78121

82.65 SURFACE PROCESSES

- 77914 Model cluster study of the acid-base properties of zeolite catalysts. R.Vetrivel, B.Viswanathan (Dept. of Chem., Indian Inst. of Technol., Madras, India). *THEOCHEM (Netherlands)*, vol.11, no.1-2, p.187-92 (June 1983). The remarkable catalytic properties of aluminosilicates are usually associated with their surface acid-base properties. These properties depend on various factors such as the nature of the metal ion which neutralises the negative charge created by $[AlO_4]^-$ units, the extent of metal ions exchange, the electrostatic field produced by such ions and the number of oxygen vacancies present at the surface. Several attempts have been made to evaluate the acid-base properties of these systems by a number of experimental procedures using probe molecules and also to correlate them with the observed specific catalytic activity. The authors devise theoretical procedures for estimating acid-base properties of solid catalysts and rationalise the observed catalytic properties on the basis of these estimated acid-base properties. (11 refs.)
- 77915 Photoreactions on finely divided semiconductors. O.Peshev (Inst. of General & Inorganic Chem., Acad. of Sci., Sofia, Bulgaria). *Int. J. Quantum Chem. (USA)*, vol.23, no.4, p.1529-33 (April 1983). Photoreactions on finely divided semiconductors are discussed. Experimental results on photo-oxidation of CO, isobutane, and NH₃ over UV-irradiated n-TiO₂ (anatase) particles of different size are discussed. The possibility of using size-quantized films for spectroscopy of absorbates is also considered. (6 refs.)
- 77916 Adsorption-complex isomerism and quantum-chemical studies in heterogeneous catalysis. Z.Slanina (J. Heyrovsky Inst. of Phys. Chem. & Electrochem., Acad. of Sci., Prague, Czechoslovakia). *Int. J. Quantum Chem. (USA)*, vol.23, no.4, p.1563-70 (April 1983). The present quantum-chemical studies of the interaction of gases with solid surfaces indicate frequently the existence of several different structures of the model cluster complex with the adsorbed system. The usual approach to this adsorption-complex isomerism consists of selection of the potential energy-lowest member of the set of isomers. A weighting treatment is presented within which all the isomeric structures (or the part of them that is active in the respective experimental technique) can contribute to the values of observables. The treatment suggested requires information amount which corre-

sponds to the usual capabilities of today's numerical quantum chemistry, i.e. concept of localized adsorption is employed. In this way correct theoretical equivalents of experimental data can be obtained. Two types of the isomerism are considered, viz. site-caused isomerism and adsorbate-caused isomerism. It is shown that the treatment in the latter case can, under acceptable assumptions, be reduced to the recently described technique for the site-caused isomerism. An illustrative example is presented based on the literature data about the water-silica interaction. The results are important for correct comparison of theoretical and observed data in the field of heterogeneous catalysis and sorption. (17 refs.)

- 77917 Radiation damage enhancement of the penetration of water into silica glass. C.Burman, W.A.Lanford (Dept. of Phys., State Univ. of New York, Albany, NY, USA). *J. Appl. Phys. (USA)*, vol.54, no.5, p.2312-15 (May 1983). A dramatic increase in the rate of penetration of water into silica glass as a result of ion implantation with noble gas ions is reported. The damage caused by the implantation leads to the rapid uptake of water to a saturation concentration of hydrogen of approximately 10^{22} atoms/cm³. The effects of ion implant dose and ion mass are investigated. The results indicate that the mechanism responsible for this enhanced penetration is the creation of chemically reactive defects which greatly enhance the reaction between the water and the silica network. (10 refs.)
- 77918 The adsorption and dissociation of methyl isocyanide on Rh(111). S.Semancik, G.L.Haller, J.T.Yates Jr. (Surface Sci. Div., NBS, Washington, DC, USA). *J. Chem. Phys. (USA)*, vol.78, no.11, p.6970-81 (1 June 1983). The coordination chemistry of methyl isocyanide (CH₃NC), and CO are similar in a number of transition metal complexes, and it is therefore of interest to consider the surface chemistry of these molecules. The authors have used high resolution electron energy loss spectroscopy (EELS), temperature programmed desorption (TPD), and Auger electron spectroscopy (AES) to characterize the interaction of CH₃NC with Rh(111). At 120K, EELS measurements indicate that CH₃NC adsorbed nondissociatively as a bridged species. As the coverage is increased, vibrational loss features attributable to singly coordinated bonding occur, and multilayers of CH₃NC eventually develop. In contrast, CO bonds initially to Rh in atop sites, with a bridged form occurring only at higher coverages. Thermally induced changes in the adsorbed CH₃NC have also been monitored; TPD shows that H₂, HCN, and N₂ are liberated from the surface between 350 and 850K, and EELS have been used to follow the vibrational mode changes that accompany decomposition. Additional insight was provided by adsorbing CH₃NC onto surfaces preadsorbed with O₂ or CO, both of which produced some site blocking. Other interactional effects include CO and perhaps carbonate formation when CH₃NC reacts with oxygen, and rapid removal of the intensity of the EELS modes associated with CO when CH₃NC is adsorbed onto preadsorbed CO. Comparisons are made with previous results for CH₃NC adsorption on Ni(111), Ag(311), and alumina-supported Rh clusters. (23 refs.)
- 77919 D₂O product angular and translational energy distributions from the oxidation of deuterium on Pt(111). S.T.Ceyer, W.L.Guthrie, T.-H.Lin, G.A.Somorjai (Dept. of Chem., Univ. of California, Berkeley, CA, USA). *J. Chem. Phys. (USA)*, vol.78, no.11, p.6982-91 (1 June 1983). The angular and translational energy distributions of D₂O produced from the oxidation of deuterium on the (111) crystal face of platinum have been measured over the surface temperature range of 440-913K. Although the angular distributions are described by a cosine function, the translational energy distributions deviate from the corresponding Maxwell-Boltzmann distributions. At the normal angle, the D₂O mean translational energy $\langle E \rangle / 2k$ varies from 220 to 400K over the temperature range investigated. Two mechanisms for the production of translationally cold product molecules are discussed. (38 refs.)
- 77920 Changes in reflectivity and emissivity of oxide systems subjected to the influence of continuous CO₂ laser radiation. P.A.Skiba. *J. Appl. Spectrosc. (USA)*, vol.37, no.2, p.909-13 (Aug. 1982). Translation of: *Zh. Prikl. Spektrosk. (USSR)*, vol.37, no.2, p.242-7 (Aug. 1982). [received: April 1983] Investigations of the thermochemical processes which occur under the influence of laser radiation are of great interest for obtaining selective changes of the properties of surface layers of solids and, in particular, of oxide materials. The accumulation of reaction products (metal) during the reduction of oxides sharply increases the reflectivity of the material. At the same time the temperature of the surface layer and, accordingly, the reaction rate are reduced. Therefore, in order to optimize the energy consumption in the laser-induced reduction of oxide materials and in order to obtain the required degree of surface layer conversion, the time t_i of the thermochemical instability of the oxide must be determined, i.e., the time in which a strong correlation exists between overheating and absorption; similarly, the time t_m at which the metal phase in the irradiated zone develops must be determined. It is possible to determine t_i and t_m by establishing the relation between the degree to which a thin surface layer of an oxide sample is reduced and the reflectivity or emissivity of the sample. Samples (sheets with a size of $6 \times 10 \times 3$ mm) of copper oxide (CuO), iron oxide (Fe₂O₃), and nickel oxide (NiO) and samples of a M 400 NN nickel-zinc ferrite were employed. (8 refs.)
- 77921 The mechanism of the CO₂ formation on Pt(111) and polycrystalline surfaces at low temperatures. T.Matsushima (Res. Inst. for Catalysis, Hokkaido Univ., Sapporo, Japan). *Surf. Sci. (Netherlands)*, vol.127, no.3, p.403-23 (May 1983). The mechanism of the reaction of oxygen with CO on Pt(111) and polycrystalline surfaces was studied at low temperatures, with reactive thermal desorption and isotope tracer techniques. Two CO₂ formation processes were observed. The first is the interaction between CO and oxygen adatoms, which takes place below 200K. The second is the reaction of CO adatoms with oxygen adatoms. The desorption flux of the product CO₂ of both processes shows a very sharp angular distribution along the surface normal. (29 refs.)
- 77922 Studies on a palladium hydrogen window. N.Mitsuishi, T.Yuki, I.Ichihara. *Technol. Rep. Kyushu Univ. (Japan)*, vol.55, no.6, p.537-43 (Dec. 1982). In Japanese. [received: May 1983] Studies have been conducted on the permeation characteristics of hydrogen-inert gas mixtures through a palladium alloy tube wall as a hydrogen window. The palladium alloy tube used was Pd-20%Ag-5%Au, 1.44 mm ID and 100 mm in length. Permeabilities of hydrogen and deuterium were measured at 400°C under atmospheric pressure using H₂-Ar and D₂-Ar mixtures. The same permeation experiment was performed with an H₂-D₂-Ar mixture. The permeation data of the mixture agreed with the theoretical estimation for the H₂, D₂ and Ar mixture using the values of the permeability obtained by the H₂-Ar, and D₂-Ar experiments. The permeation rates of the hydrogen isotope mixtures in the hydrogen window may be estimated by the authors' equations. (9 refs.)

77923 Catalytic hydrogenation with amorphous and crystalline $\text{Pd}_{80}\text{Si}_{20}$. B.C.Giessen, S.S.Mahmoud, D.A.Forsyth, M.Hediger (Materials Sci. Div., Inst. of Chem. Analysis, Boston, MA, USA). *Rapidly Solidified Amorphous and Crystalline Alloys*. Proceedings of the Materials Research Society Annual Meeting, Boston, MA, USA, Nov. 1981 (New York, USA: North-Holland 1982), p.255-8.
Several metallic glasses in the form of ribbons were screened for activity as hydrogenation catalysts. $\text{Pd}_{80}\text{Si}_{20}$ and $(\text{Ni}_{10}\text{Fe}_{90})_{80}\text{B}_{20}$ showed activity in reducing cyclohexene. $\text{Pd}_{80}\text{Si}_{20}$ was further examined for differences between the glassy and crystalline phases in the selectivity shown during hydrogenation reactions of *n*-hexenes, phenylethyne, α -pinene, and cyclododecene. No significant differences were found for catalytic selectivity in regard to cis-trans isomerization, double bond migration, and stereochemistry of addition under the reaction conditions used. Minor differences were observed in hydrogen-deuterium exchange. (5 refs.)

UHV-compatible reaction cell for combined high- and low-pressure studies of surface reactions See Entry 74487

Analysis of precision in determination of diffusion coefficients by the isotope exchange technique See Entry 74579

Photoelectron spectra of adsorbed carbonates See Entry 75440

X-ray and UV photoelectron-spectroscopic studies of pyridine adsorbed on evaporated nickel and palladium in the temperature range 140-385K See Entry 75441

The concentration of surface V=O species on oxidized vanadium oxide catalysts See Entry 76755

A MINDO/3 approach to the chemisorption of hydrogen on graphite See Entry 76769

A MINDO/3 approach to the chemisorption on graphite of electrophilic adsorbates See Entry 76770

Rates of molecular desorption from solid surfaces: adsorption site dependence for CO on Ni(100) See Entry 76771

Quasiclassical trajectories study on the two-dimensional model of the dissociative chemisorption of H_2 on a lithium cluster surface See Entry 76772

The adsorption of ammonia on an Fe(110) single-crystal surface studied by high-resolution electron energy-loss spectroscopy (EELS) See Entry 76777

Quantum chemical studies of chemisorption at anion or cation sites of the GaP (110) surface. Coverage dependence of adsorption energy and equilibrium in cases of positive and negative partial charge injection See Entry 76778

A LEED-AES study of the structure of sulfur monolayers on the Mo(100) crystal face See Entry 76791

The role of sulfur in oxygen adsorption on niobium See Entry 76792

Sorption of hydrogen and deuterium in a glassy Pd-Si alloy by a bending-cantilever method See Entry 76795

Raney type nickel catalysts from RSR atomization of Al-Ni powders See Entry 77599

Mechanistic studies of oxene reactions with organic substrates: reaction paths on MINDO enthalpy surfaces—models for cytochrome P450 oxidations See Entry 77871

Photoreduction of carbon dioxide to formic acid, formaldehyde, methanol, acetaldehyde and ethanol using aqueous suspensions of strontium titanate with transition metal additives See Entry 77900

Direct observation of the local-field-enhanced surface photochemical reactions See Entry 77905

Hydrogen pretreatment of CdS films and properties of CdS/NaOH/Pt cells See Entry 78089

82.70 DISPERSE SYSTEMS

(for flow behaviour, see 47.55K)

77924 On the structure of random tissues or froths, and their evolution. N.Rivier (Blackett Lab., Imperial Coll., London, England).

Philos. Mag. B (GB), vol.47, no.5, p.L45-9 (May 1983).

Von Neumann's law (1952), governing the evolution of two-dimensional soap bubble froths is shown to be a direct consequence of the structural law of Lewis (1928), and both express mathematically the most probable filling of space. Von Neumann's and Lewis's laws can therefore be generalised to a considerable variety of froths, tissues, metallurgical aggregates, etc., in two and three dimensions. Moreover, a hitherto arbitrary parameter in Lewis's law measures ageing of the structure. (10 refs.)

77925 Dust concentration measurement probe using beta attenuation. S.E.Slezak, R.O.Buckley (Dept. of Mech. & Industrial Engng., Univ. of Illinois, Urbana, IL, USA).

Rev. Sci. Instrum. (USA), vol.54, no.5, p.618-25 (May 1983).

A small probe utilizing the attenuation of the beta emissions from promethium-147 has been constructed and calibrated for measuring the suspension concentration of dusts in the range of 0.1 to 2.0 kg/m³. The absorption of beta particles (negatively charged electrons) is related to the amount of matter through which the particles pass. The probe discussed here measures the beta absorption through a 5.1-cm path length at sample rates up to 20 samples per second. The small size of the probe (16 cm overall) allows real-time in situ local measurements of the suspension of a dust. The basic theory of operation and details of the probe operation are presented. Data from the probe for use in dust flammability experiments are also presented. (17 refs.)

Dynamic particle sizing in suspension by laser anemometry technique See Entry 76130

Orientalational fluctuations of a lyotropic nematic liquid crystal measured by quasielastic light scattering See Entry 76297

Raman scattering from metal smokes See Entry 77394

Gelation in finite polycondensation systems See Entry 77886

The mechanism of the photochemical oxidation of water to oxygen with silver chloride colloids See Entry 77899

Gelatin-substituted cyanine dyes as spectral sensitizers for silver halide emulsions See Entry 77907

Kinetics of silver cluster formation and trapped hole neutralization in silver halide emulsion grains digested with cadmium salts See Entry 77908

A study of properties of clusters of photographic interest by means of a redox buffer solution See Entry 77909

Image formation processes in concentric shell emulsions See Entry 77910

82.80 CHEMICAL ANALYSIS AND RELATED PHYSICAL METHODS OF ANALYSIS

77926 RECLAS: resonant-enhanced CARS from C_2 produced by laser ablation of soot particles. D.A.Greenhalgh (Engng. Sci. Div., AERE, Harwell, England).

Appl. Opt. (USA), vol.22, no.8, p.1128-30 (15 April 1983).

Reports the use of both CARS and resonant-enhanced CARS for simultaneous soot particle detection and gas phase temperature measurement. The technique uses a standard broadband single-pulse CARS spectrometer to simultaneously detect soot particles and determine their surrounding gas temperature and composition. (21 refs.)

77927 Fiber-optic absorption/fluorescence probes for combustion measurements. G.Kychakoff, M.A.Kimball-Linne, R.K.Hanson (Dept. of Mech. Engng., Stanford Univ., Stanford, CT, USA).

Appl. Opt. (USA), vol.22, no.10, p.1426-8 (15 May 1983).

Describes the use of fiber-optic probes to measure the concentrations of chemical species in combustion gases. The authors have been interested primarily in measuring the concentrations of minor species, including radicals such as OH, CH, CN, C₂, CH₂, NO, NH, and NH₂, which often serve as important reaction intermediates in combustion processes. Experimental measurements of the concentrations of these radicals are helpful in the development of fundamental combustion and chemical kinetics models. The techniques proposed could also be applied to pollution monitoring, control of industrial processes, or the development and testing of full scale devices such as gas turbine combustors. (8 refs.)

77928 The study of Cr-Mn-Ni-Si-N (20, 10, 4, 3 wt.%) stainless steel by ESCA and AES. Yu Chih-chung (Shanghai Inst. of Testing Technol., Shanghai, China).

Chin. J. Sci. Instrum. (China), vol.4, no.1, p.49-56 (Feb. 1983). In Chinese.
The in-depth composition profile of Cr-Mn-Ni-Si-N (20, 10, 4, 3 wt.%) stainless steel was obtained by ESCA and AES with argon ion sputter etching, and the chemical states of Si, Mn, Ni, Cr, Fe, O, C of surface composition elements were described. Mn appeared in its oxide state in a great depth. The reduction of the density of valence electron for Cr of the surface layer and the double-peak of the Cr LMM Auger spectra were observed. The variation of the valence electron orbit of Cr led to the drop of the anti-oxidizing capability. The addition of Mo and Si would make the thickness of surface oxygen enriched layer smaller and that would lead to an increase of its anti-oxidizing capability. (12 refs.)

77929 Automatic identification of maxima in X-ray fluorescence spectrum. J.H.Jordanov (Higher Chem.-Tech. Inst., Sofia, Bulgaria), T.V.Tsanov, R.Stefanov, N.Jordanov.

C.R. Acad. Bulg. Sci. (Bulgaria), vol.36, no.3, p.349-52 (1983).

The process of automatic identification can be divided into three stages: 1) initial identification of the found maxima with X-ray lines of the different elements within the identification interval; 2) drawing up a list of the chemical symbols of the elements whose lines were found in the sample and juxtaposition to every chemical symbol of a certain sum of weights of its lines; and 3) evaluation of the presence of an element in the sample in accordance with the sum of weights of its X-ray lines. (5 refs.)

77930 X-ray attenuation coefficients of carbon in the energy range 5 to 20 keV. L.Gerward (Lab. of Appl. Phys. III, Tech. Univ. of Denmark, Lyngby, Denmark).

Acta Crystallogr. Sect. A (Denmark), vol.A39, pt.3, p.322-5 (1 May 1983).

Mass attenuation coefficients for pyrolytic graphite have been determined by an X-ray energy-dispersive method with a relative experimental error of about 0.5%. Results are given for the Fe, Co, Cu and Mo α_1 and α_2 lines. (28 refs.)

77931 A programmable tristate voltage scan generator. S.Birlasekaran, H.N.Venkoba Rao (Central Electrochem. Res. Inst., Karaikudi, India).

Indian J. Technol., vol.20, no.11, p.457-60 (Nov. 1982). [received: May 1983]

A low cost single triangle function generator circuit for selected voltage excursion in a ramp or triangle wave is described. Initial potential, final potential and peak of the triangular pulse can be programmed along with the slope rate. Apart from single triangle function, discrete multiple number of triangles and continuously repetitive triangular waves can also be obtained. By suitably programming one can get ramp, square and rectangular pulses. (6 refs.)

77932 Direct current and complex plane polarographic behaviour of copper(II)-EDTA complexes. P.Sridhar, R.S.Subrahmanya (Dept. of Inorganic & Phys. Chem., Indian Inst. of Sci., Bangalore, India).

Indian J. Chem. A, vol.21A, no.10, p.953-7 (Oct. 1982). [received: April 1983]

The DC and complex plane polarographic behaviour of copper-EDTA system has been studied under conditions where pure (CuY^{2-}) and mixed hydroxy (CuYOH^{3-}) complexes are present. The reduction process is quasi-reversible by DC polarography while complex plane polarography reveals the process to be pretty irreversible. The interpretation of the charge transfer resistance (R_θ) value is given on the basis of the theoretical θ versus $E-E_0$ and q versus $E-E_0$ curves. The value of β (anodic transfer coefficient) needed for these calculations is obtained from the DC polarogram. The rate constants have also been calculated. (9 refs.)

77933 Polarographic studies of cobalt (III) complexes with biguanide and substituted biguanides. B.Datta, K.Singh, D.Sen (Dept. of Chem., Indian Inst. of Technol., Kharagpur, India).

Indian J. Chem. A, vol.21A, no.10, p.958-60 (Oct. 1982). [received: April 1983]

The polarographic reduction of Co(III) chloride complexes with biguanide and substituted biguanides has been studied in aqueous 0.1 M KCl and 0.01% gelatin. The complexes are reduced in two steps (one-electron and two-electron respectively) at the d.m.e. The process is irreversible for all the complexes except for the simple biguanide complex. The $E_{1/2}$ values, overall rate constants and activation energies of the electrode processes etc., have been found to be related to the average Dq values of the complexes. Variation of these parameters with the size and nature of the substituent on the parent ligand has also been studied. (12 refs.)

77934 HPLCs 'artificial intelligence' gives quality separations. R.Lehrer (DuPont Co., Wilmington, DE, USA).

Ind. Res./Dev. (USA), vol.25, no.4, p.116-19 (April 1983).

The four-solvent system in HPLC lets the researcher determine optimum composition for the mobile phase for any given separation in only seven experiments. New software operates the system and 'learns' to improve quality and to speed HPLC analyses. (4 refs.)

77935 Designing an analytical microscopy laboratory. R.Kossowsky (Westinghouse R&D Center, Pittsburgh, PA, USA).

J. Met. (USA), vol.35, no.3, p.47-53 (March 1983).
Contemporary materials characterization requires sophisticated electron microscopes with chemical analysis capabilities. Such instrumentation has progressed rapidly over the past decade and continues to improve. The author discusses the considerations involved in the major updating of the materials characterization laboratory of a large international corporation with a wide range of materials characterization requirements. The general capabilities, merits, and limitations of the most important analytical instruments are described, and the trial specimens and procedures used to evaluate the final candidate instrumentation are discussed. (12 refs.)

77936 Atomic scale analysis with the atom probe. S.S.Brenner, M.K.Miller (US Steel Res. Lab., Monroeville, PA, USA).

J. Met. (USA), vol.35, no.3, p.54-63 (March 1983).
The atom probe is a unique instrument, quite distinct from the electron-optical instruments more commonly used in microanalytical studies. It is conceptually very simple and yet its microstructural and microchemical resolution are still unsurpassed, in that it can show and analyse individual atoms. Recent instrumental advances, especially in computer control of data collection and processing, have greatly increased the versatility of the atom probe as an analytical tool for material science. The instrument has been successfully applied to a broad range of studies including phase transformations and interface segregation. The authors discuss the basic concepts and general operating characteristics of the atom probe, and demonstrate its applications in precipitation strengthening of HSLA steels, segregation in irradiated material and heat-treated alloys, and phase transformations. (19 refs.)

77937 Electron trajectory-linked phenomena in thin foil X-ray microanalysis. I.P.Jones, A.W.Nicholls (Dept. of Metall. & Materials, Univ. of Birmingham, Birmingham, England).

J. Microsc. (GB), vol.130, pt.2, p.155-64 (May 1983). (MICRO 82: High Resolution Electron Microscopy, London, England, 12-16 July 1982).
The methods of calculating electron trajectories are reviewed. Approximate methods may be necessary because of computing time problems on small computers. The various situations in microanalysis where electron trajectories are important are discussed in turn. It appears that the single scattering theory of Goldstein et al. (1977) is useful for situations dominated by high scattering angle events whereas the Gaussian theory of Doig et al. (1981a) may be appropriate to multiple low angle scattering. This type of calculation might turn out to be unnecessary if coincident counting techniques are exploited. (23 refs.)

77938 Prospects for improvement in EDX microanalysis. P.J.Statham (Link Systems Ltd., High Wycombe, England).

J. Microsc. (GB), vol.130, pt.2, p.165-76 (May 1983). (MICRO 82: High Resolution Electron Microscopy, London, England, 12-16 July 1982).
There is still considerable room for improvement in the EDX (energy-dispersive X-ray) technique, particularly for the analysis of thin samples in transmission electron microscopes. Further research is required to characterize changes which are introduced during specimen preparation and a technique for mass thickness determination has to be established which is both accurate and convenient to implement. Since detector efficiency is difficult to predict at low energies, a suitable standard sample needs to be found which produces X-ray peaks suitable for establishing fixed points on the detector efficiency curve. With current technology, there are several instrumental improvements which can be realized, most of which centre around the use of time-variant pulse-processing circuitry and reduction of electronic noise. Problems of overload with high-voltage microscopes can be minimized, resolution improved and pile-up rejection made more effective so that higher data rates can be accommodated. With the beryllium vacuum window removed, detection of boron is possible provided the influence of electronic noise is minimized; but further investigation is still required into the physics of interactions in the first 100 nm layer of the detector. (28 refs.)

77939 Condenser aperture misalignment and solute profile asymmetries in STEM X-ray microanalysis. G.Cliff (Dept. of Metall., Univ. of Manchester Inst. of Sci. & Technol., Manchester, England).

J. Microsc. (GB), vol.130, pt.2, p.RP3-4 (May 1983). (MICRO 82: High Resolution Electron Microscopy, London, England, 12-16 July 1982).
Large condenser apertures, used to increase the incident beam current and hence the X-ray counting statistics in STEM X-ray microanalysis, can increase beam convergence angles to the point where the effect of spherical aberration in the probe-forming lens will dominate and the electron probe will exhibit extensive non-Gaussian tails. These can be shown to contain a significant fraction of the incident beam current (Cliff and Kenway, 1982). More-over misalignment of an aperture which is larger than that required to limit the analysis probe may produce an asymmetry in the shape of the tails surrounding the probe. A typical electron distribution asymmetry is shown by the densitometer trace from the major axis of a STEM probe. Condenser aperture misalignment may have only a limited effect on bright field STEM image quality but it can introduce significant asymmetries into solute profiles measured by X-ray microanalysis at phase boundaries. (2 refs.)

77940 Determination of trace aluminum and calcium impurities by intracavity spectroscopy. V.S.Burakov, V.N.Verenik, V.A.Malashonok, P.A.Naumenkov, S.V.Nechayev, R.A.Puko.

J. Appl. Spectrosc. (USA), vol.37, no.2, p.869-71 (Aug. 1982). Translation of: *Zh. Prikl. Spektrosk. (USSR)*, vol.37, no.2, p.197-200 (Aug. 1982). [received: April 1983]

The high sensitivity of intracavity spectroscopy enables one to use it efficiently to determine low concentrations of various elements. However, attainment of the maximum possible sensitivity of the method in each specific case requires the refinement of a series of steps in the analysis process: selection of the type of laser, atomizer, conditions for recording the spectral absorption lines, preparation of the samples for analysis, etc. The authors elucidate a set of these conditions for the case of determination of low concentrations of aluminum and calcium by atomic-absorption intracavity spectroscopy, and establish the maximum possibilities of the method. Monitoring of the trace content of selected elements is important in a number of technological processes of the semiconductor industry. (8 refs.)

77941 Fundamental parameter of the optimum excitation conditions in the analytical emission spectroscopy. The difference in ionization potential between the matrix and the analysis elements in the plasma. Chen Meifang (Inst. of Precious Metals, Ministry of Metall. Industry of PRC, Kunming, China).

Kexue Tongbao (Foreign Lang. Ed.) (China), vol.28, no.2, p.178-83 (Feb. 1983).

The DC carbon arc source is one of the fundamental sources used in analytical emission spectroscopy. Though during the past two decades many other new sources have been developed, the carbon arc source, due to its simplicity, suitability and sensitivity, is still being commonly used in numerous fields. By using this source in the analysis of various materials, the study of the dependence of spectral line intensity on the composition of the samples is a subject

in which all workers in analytical emission spectroscopy are interested. The aim of the present work is to study the dependence of spectral line intensity on different compositions of materials. (7 refs.)

77942 Microcolumns for more efficient LPC [liquid phase chromatography].

Mes. Regul. Autom. (France), vol.48, no.5, p.53-5 (5 April 1983). In French.
The Hewlett-Packard HP1090 low-dispersion chromatograph is described with an introductory review of microcolumn theory and estimates of savings from reduction of column diameter and length. The rate of flow is reduced fivefold, requiring a pump with 1 ml/min resolution. Chromatograms and graphs show the effects of column diameter, number of theoretical plates, and grain size, and contrast the detail obtainable from the same 100×2.1 mm microcolumn on the new product and on a standard apparatus. (no refs.) M.B.D.

77943 On the measurement of binding energies in liquid ESCA and the relation to electrochemical half-cell EMFs. H.Siegbahn, M.Lundholm, M.Arbram, S.Holmberg (Inst. of Phys., Uppsala Univ., Uppsala, Sweden).

Phys. Scr. (Sweden), vol.27, no.4, p.241-4 (April 1983).
The question of the reference level of the binding energy scale in liquid ESCA is discussed. The experimental conditions for liquid ESCA are equivalent to those for an electrochemical half-cell, which means that measured gas-liquid shifts can be related to differences in redox potentials. On this basis, liquid ESCA spectra can be referenced to the vacuum level by means of separately measured electrochemical data. (14 refs.)

77944 Determining distribution and concentration of certain elements with the aid of a charged-particle beam. I.G.Berzina, E.B.Gusev, A.V.Drushchits, V.S.Kulikasaus, A.F.Tulinov.

Sov. At. Energy (USA), vol.53, no.3, p.648-52 (Sept. 1982). Translation of: *At. Energ. (USSR)*, vol.53, no.3, p.178-81 (Sept. 1982). [received: May 1983]
The methods used in practice to determine the elements of which a substance is composed usually require destruction of the object to be examined and do not allow a selective simultaneous determination of both the distribution and the concentration of several elements. The authors use a method of elementary analysis which can be used for the selective simultaneous determination of the local concentrations of lithium, boron, oxygen, nitrogen, and fluorine with the aid of the (p,α) reaction and, besides that, with the (α, n) reaction for determining beryllium in micro- or macrosections of multicomponent objects. (4 refs.)

77945 X-ray fluorescence analysis for the detection of heavy metals in plant matter. H.Rethfeld (Agricultural Experimental & Res. Establ., Munster, Germany), L.Beitz.

Siemens Power Eng. (Germany), vol.5, no.2, p.55-7 (March-April 1983).
When plant matter is chemically monitored, a full analysis can be made with the X-ray fluorescence method in approximately 10 minutes. The specimens are easily prepared. For all plant matrices, evaluation of the measurements is carried out with only one calibration function per element. In the case of the heavy metals examined, i.e. chromium, manganese, iron, nickel, copper, zinc and lead, the limit of statistical proof was between 0.5 and 1 ppm. The analysis accuracy in the concentration range of 20 to 1000 ppm was approximately 2% relative. (6 refs.)

77946 Rapid chemical methods for identification and study of short-lived nuclides. G.Herrmann (Inst. für Kernchem., Univ. Mainz, Mainz, Germany), N.Trautmann.

In book: *Annual review of nuclear and particle science. Vol.32*, J.D.Jackson, H.E.Gove, R.F.Schwitters [Ed.], p.117-47. Palo Alto, CA, USA: Annual Reviews (1982), 595 pp. [0 8243 1532 4]

The authors outline recent trends in the design of rapid chemical separations, including some perspectives for future developments. They emphasize techniques that allow the isolation of individual elements from complex mixtures on a time scale of a few seconds with direct detection of their isotopes. They also include somewhat slower techniques in cases where very similar elements have to be separated. Since they wish to show how rapid separations can be performed technically, the article is organized according to the principal chemical step, not according to elements. They discuss first separations from and in aqueous solutions and then separations via gaseous phases. In solution chemistry one takes advantage of the broad experience accumulated over long times in radio-chemical separations; gas phase chemistry is less developed but very attractive for rapid work because of the short separation times involved. (100 refs.)

77947 Limitations of a single optical fibre fluorimeter system due to back-ground fluorescence. J.P.Gakin, A.J.King (Plessey Electronic Systems Res. Ltd., Havant, England).

First International Conference on Optical Fibre Sensors, London, England, 26-28 April 1983 (London, England: IEE 1983), p.195-9
Discusses the relative importance of fibre fluorescence in remote fibre fluorimetry in relation to experimental results and a likely mechanism has been found to explain the results obtained. (4 refs.)

The compensated reciprocating pump model BHB-1 for HPLC See Entry 74447

Characteristics of semiconductor gas sensors. I. Steady state gas response See Entry 74450

The design of an amperometric detector for FIA See Entry 74453

Highly sensitive polarimetric techniques (review) See Entry 74514

Pressure pulse in an infrared pneumatic detector: theory based on the Einstein coefficient for induced absorption See Entry 74536

10-Hz coherence anti-Stokes Raman spectroscopy apparatus for turbulent combustion studies See Entry 74542

Automation of a gas analyser by personal computer See Entry 74554

AES investigation of silicon nitride film See Entry 74559

A modified bias-method for the determination of spectrometer functions See Entry 74560

Automatic electron probe microanalyser based on double measurement of dose See Entry 74564

Data acquisition and analysis in X-ray photoelectron spectroscopy using an Apple II microcomputer See Entry 74570

Simple quasi-two-crystal X-ray spectrometer See Entry 74573

Installation and commissioning of a Siemens SRS200 sequential X-ray fluorescence spectrometer See Entry 74577

Study of the deactivation mechanisms for some constructional steels by secondary-ion mass spectrometry See Entry 75107

Neutron spectrum determination by multiple foil activation method See Entry 75159

Photoelectron spectra of adsorbed carbonates See Entry 75440

Density of uranium ions in the $^4I_{9/2}^0$ ground state in a hollow-cathode type discharge See Entry 76223

- ALCHEMI: a new technique for locating atoms in small crystals** See Entry 76261
- Structural aspect of a $Zn_{0.25}Mn_{0.12}Fe_{0.13}S_{0.5}$ crystal** See Entry 76385
- Matrix effect and surface oxidation in depth profiling of $Al_xGa_{1-x}As$ by secondary ion mass spectrometry using O_2^+ primary ions** See Entry 76479
- Sputtering of condensed noble gases by keV ions** See Entry 77507
- An introduction to silane project in ROC** See Entry 77541
- Changes of the surface composition of glass during reactive and argon ion etching** See Entry 77772
- Study by electron spectroscopy for chemical analysis of silicon, SiO_2 and Si_3N_4 surfaces treated with various CF_4 -containing plasmas** See Entry 77784
- Advances in instrumentation for materials characterization** See Entry 77815
- Evaluation of electrode shape and nondestructive evaluation method for welded solar cell interconnects** See Entry 77858
- Behaviour of various cathode materials for non-aqueous lithium cells** See Entry 77982
- Characterization of the chemistry at the anode and cathode in the Li/SO_2 battery system** See Entry 77985
- Detection and identification of emission sources on the basis of the trace element composition of aerosols** See Entry 78116
- SO_2 -measurement with the new UV-BINOS** See Entry 78119
- Determination of radium-226 in urine** See Entry 78405
- Determination of phosphorus in natural waters by long-capillary-cell absorption spectrometry** See Entry 78654
- Sources of background current in the ECC ozonesonde: implications for total ozone measurements** See Entry 78697
- On the fine structure of meteoritical taenite/tetrataenite and its interpretation** See Entry 78884

86.00 ENERGY RESEARCH AND ENVIRONMENTAL SCIENCE

86.10 ENERGY RESOURCES AND THEIR UTILISATION

(inc. economic aspects; for nuclear engineering and nuclear power studies, see 28.00)

77948 Home energy use in nine OECD countries, 1960-1980. L.Schipper, A.Ketoff (Lawrence Berkeley Lab., Univ. of California, Berkeley, CA, USA). *Energy Policy (GB)*, vol.11, no.2, p.131-47 (June 1983). Government institutions and individuals have responded to fluctuations in energy supply and price with the implementation of policies and the initiation of conservation. While these activities have resulted in noticeable conservation of energy, primarily through behavioural actions, further savings could be achieved through the exchange of information regarding promising policies and technologies. Toward this end, data on residential sector energy use for nine OECD countries (Canada, Denmark, France, West Germany, Italy, Japan, Sweden, the UK and the USA) have been collected over the period 1960-1980 and have been analysed using both indicators of energy-use intensity and econometric methods. (21 refs.)

77949 Energy conservation in US buildings: solving the high potential/low adoption paradox from a behavioural perspective. A.Shama (Solar Energy Res. Inst., Golden, CO, USA). *Energy Policy (GB)*, vol.11, no.2, p.148-67 (June 1983). The engineering, economic and behavioural perspectives are discussed, and the importance of integration is emphasized. The framework for diffusion of innovations is shown to be useful in an understanding of how demand for energy conservation forms and spreads. Specific recommendations to speed the adoption of energy conservation are outlined. (23 refs.)

77950 UK energy policy—issues and priorities. J.Cheshire (Sci. Policy Res. Unit, Sussex Univ., Brighton, England). Colloquium on 'Resource Conservation for the Electrical Engineer', London, England, 19 April 1983 (London, England: IEE 1983), p.1/1-6. Compared with its major international competitors, the UK is well-endowed with three fossil fuels and nuclear construction and operating experience. However, complacency is to be avoided at all costs. This is because the lead times involved in RD&D and in conservation and fuel substitution investment are relatively long. The decade of the 1980s is unlikely to provide a fair reflection of the emergence of supply difficulties in the 1990s. Hence the need for carefully considered interventions by Government to underpin market forces. As far as the electricity sector is concerned, it is likely that a modest programme of thermal reactors will be launched but that the level of support for the breeder will be reduced in real terms and conducted more fully on an international, collaborative basis. Demand side electrical technologies, however, such as homeostatic controls and heat pumps, may well reach maturity and witness considerable increases in market penetration. (no refs.)

77951 Industrial energy usage. R.C.Bending (Cavendish Lab., Univ. of Cambridge, Cambridge, England). Colloquium on 'Resource Conservation for the Electrical Engineer', London, England, 19 April 1983 (London, England: IEE 1983), p.2/1-3. Discusses energy conservation and the role electrical engineers have to play in improving the efficiency of electrical energy in its familiar uses for motive power and lighting. Electricity may also have a growing role as a heat fuel in industry, and here the challenge to the electrical engineer is to ensure that the sophisticated techniques available are used, within the production process as a whole, in ways that are both cost-effective and energy-efficient. (no refs.)

VDE-Kongress '82 (VDE-Congress '82) See Entry 74218

Proceedings of the Fifth Power Plant Dynamics, Control and Testing Symposium See Entry 74224

86.10B Fossil and other fuels

77952 Alternative energy options. K.F.Bennett. *S. Afr. Mech. Eng. (S. Africa)*, vol.33, no.3, p.60-5 (March 1983). 'South Africa is going to be heavily reliant on coal as its prime energy source for the remainder of this century. None of the alternatives under investigation has the potential to alter this trend.' This in the conclusion the author arrived

at after examining all the alternative energy options available to South Africa. (28 refs.)

77953 Technical and economic analysis of the viability of heating equipment. J.M.Martins dos Santos. *Electr. Energ.-Electron. (Portugal)*, no.185, p.112-14 (March 1983). In Portuguese.

The author analyses the economic feasibility of heating equipment and establishes a procedure for decision making. (no refs.)

77954 Possibility for application of high CO_2 content gases to generate electric energy. G.Veres, S.Baliko (Budapesti Muzskai Egyetem, Budapest, Hungary). *Energ. & Atomtech. (Hungary)*, vol.36, no.1, p.30-7 (Jan. 1983). In Hungarian.

The authors discuss the possibility of using less combustible natural gases containing 40 to 80 vol. percent CO_2 occurring in large quantities in Hungary by means of the gas turbine conversion cycle. The influence of CO_2 upon the output and efficiency of the gas turbine are investigated, and various flow diagrams for increasing efficiency are analysed. (15 refs.)

77955 The potential supply of synthetic fuels from Alaskan hydroelectric power and coal. M.Steinberg, J.R.Powell (Dept. of Energy & Environment, Brookhaven Nat. Lab., Upton, NY, USA). *Int. J. Hydrogen Energy (GB)*, vol.8, no.5, p.355-62 (1983).

It is proposed to develop and utilize the large potential hydroelectric power resources in Alaska to produce hydrogen by the electrolytic decomposition of water and to combine the hydrogen with the large Alaskan coal reserves to produce synthetic liquid and gaseous fuels. It is estimated that in this manner, as much as 1.8 million bbls/day of gasoline or 6.2 billion SCF/day of substitute natural gas can be produced. The existing and projected Alaskan pipelines would provide the means of transporting the fuels to energy consuming load centers in the US. This development would move the US a considerable way towards energy independence as well as employing the natural resources in Alaska in an efficient manner. (10 refs.)

77956 Hydrogen for dual fuel engine operation. B.Haragopala Rao, K.N.Shrivastava, H.N.Bhakta (Dept. of Mech. Engng., Banaras Hindu Univ., Varanasi, India). *Int. J. Hydrogen Energy (GB)*, vol.8, no.5, p.381-4 (1983).

In the investigation, an attempt was made to burn hydrogen in compression ignition engines that were operated on a dual fuel principle. Hydrogen was supplied along with intake air in small proportions and ignition was initiated by injecting diesel fuel in the conventional manner. A single cylinder compression ignition engine was operated throughout its load range inducing small proportions of hydrogen in intake air. Such an operation resulted in an increase of thermal efficiency at full load, a reduction in exhaust temperature and an increase in maximum pressure. Nitrogen oxides in the exhaust were observed to increase though the hydrocarbon emissions reduced as expected. Closed vessel explosions were conducted to study the effect of adding a hydrocarbon to a hydrogen-air mixture on the flame propagation velocities. The effect of increasing the proportion of hydrogen in the hydrogen-hydrocarbon-air mixture was observed to increase the flame propagation velocity. (5 refs.)

77957 Safety's impact on an alternative energy source—coal. D.K.Denton (Coll. of Engng. & Technol., Southern Illinois Univ., Carbondale, IL, USA). *Occup. Health & Saf. (USA)*, vol.52, no.1, p.12-16 (Jan. 1983). [received: June 1983]

The ability to make underground mines a safe place to work will be a major concern to those seeking to use coal as an energy source. Increased production will stimulate a heightened concern for making mining a more effective energy resource. This effectiveness means that unless safe performance is achieved, the cost of poor safety, such as loss of lives and costly delays due to breakdowns and other failures, will greatly reduce productivity of underground mining operations. As such, coal companies and miners must be prepared to safely manage their operation before underground mining makes a significant effect on energy independence. (7 refs.)

77958 Modelling a peat power plant for development of new control strategies. K.Lehtomaki (Control Engng. Lab., Tampere Univ. of Technol., Tampere, Finland), U.Kortela.

Proceedings of the Fifth Power Plant Dynamics, Control and Testing Symposium, Knoxville, TN, USA, 21-23 March 1983 (Knoxville, TN, USA: Univ. Knoxville 1983), p.8/01-11 vol.1

Peat is a domestic fuel that today is used in several power plants in Finland. The inhomogeneity of peat causes extra difficulties in the operation and control of peat power plants compared with plants burning better fuels. The main purpose of the modelling work described is to build a model suitable for simulation and testing of different control strategies for peat power plants. The plant consists of many interconnected subprocesses. Because a fairly exact and covering model for the entire plant would include a great number of states and parameters, lots of restrictive assumptions have been made in the course of modelling. (5 refs.)

A solar-hydrogen economy for USA See Entry 78107

The radiation dose from coal burning: a review of pathways and data See Entry 78341

86.10D Wind energy

77959 Investigation and analysis concerning the atmospheric environment for wind turbine generator. H.Iwamura, T.Shimada. *Ishikawajima-Harima Eng. Rev. (Japan)*, vol.22, no.6, p.402-6 (Nov. 1982). In Japanese.

In 1981, a project for developing a 100 kW-class wind turbine generator was started, known as the 'Sunshine' national project. IHI started the research in 1979 to design a wind turbine generator. Wind observations have been conducted at Miyake Island since 1980. A summary of site measurement in the last two years are presented. (4 refs.)

77960 Wind power plant modelling and simulation. S.Bergman (Sydkraft AB, Malmo, Sweden), S.E.Mattsson.

Proceedings of the Fifth Power Plant Dynamics, Control and Testing Symposium, Knoxville, TN, USA, 21-23 March 1983 (Knoxville, TN, USA: Univ. Knoxville 1983), p.7/01-25 vol.1

A mathematical simulation model for a large horizontal axis wind turbine system is presented. Examples of performed simulations are also given. The model is intended for simulation of the synchronization of the wind turbine generator against the utility grid and the operation of the wind turbine system under different wind conditions and with different control algorithms. Particular attention has been given to the modularization. The model is divided into subsystems to make it easy to modify the model and adapt it to systems of similar type. The interactive simulation package SIMNON which allows

good structuring and programming in a high level language has been used. (12 refs.)

86.10K Solar energy

77961 Calculating internal radiation in greenhouses in the Evora region. A.M.Almeida E Silva, M.J.Petrolino Carvalho. *Electr. Eng.-Electron. (Portugal)*, no.185, p.122-6 (March 1983). In Portuguese.

Taking the hourly hemispherical radiation values in different inclined surfaces, the hourly beam radiation in a surface normal to the sun rays and the hourly diffuse radiation in a horizontal surface, given by Luis Aparicio da Mata of the INMG, the authors have calculated the hourly hemispherical radiation inside greenhouses, on the surface soil. The results obtained are one of the main components of the radiative balance and they are valid in any other greenhouse with different shapes. Although all the results cannot be presented here, the authors say that comparing the results of the different greenhouses, with other variables defining the radiative and heat balance, they can obtain the optimized model in a particular place with its climatic conditions. (4 refs.)

77962 Static concentrators theory for non-homogeneous extended sources. J.C.Minano, A.Luque (Univ. Politecnica de Madrid, Madrid, Spain). *Sol. Cells (Switzerland)*, vol.8, no.4, p.297-315 (May 1983).

Solar concentrators, in particular static solar concentrators, see the Sun as a sky-extended time-averaged non-homogeneous source. The rules for increasing the energy cast on the concentrator's collector are derived and figures of merit are proposed for concentrators working under these conditions. The preceding ideas are applied to several specific static concentrators illuminated by the time-averaged sky radiance of Madrid. The present paper generalizes from a previous paper on homogeneous extended sources but, in contrast with the conclusions which were reached for homogeneous sources, it was found that no upper limit exists for the power that can be cast in the collector. (8 refs.)

77963 Luminescent solar concentrators as bifacial captors. G.Lifante, F.Cusso, F.Meseguer, F.Jaque (Dept. de Optica y Estructura de la Materia, Univ. Autonoma de Madrid, Madrid, Spain). *Sol. Cells (Switzerland)*, vol.8, no.4, p.355-60 (May 1983).

The behaviour of luminescent solar concentrators (LSCs) as bifacial captors was considered. When these concentrators were coupled to a static diffusing reflector the overall efficiency was increased by 80%, regardless of the solar time. The effect of various geometries, LSC materials and diffusing surfaces was also studied. (9 refs.)

77964 Design and fabrication of the BDM southwest photovoltaic residence prototype. T.J.Lambarski, D.L.Forrester, C.G.Hoover (BDM Corp., Albuquerque, NM, USA).

Conference Record of the Sixteenth IEEE Photovoltaic Specialists Conference - 1982, San Diego, CA, USA, 27-30 Sept. 1982 (New York, USA: IEEE 1982), p.205-10

The paper first presents an overview of the PV residence design including the residential energy features and the energy efficiency predictions, followed by a discussion of the PV array design with emphasis on the module bypass diode design, the series string selection, and array layout. Next the power conditioning design for the residence is presented. The paper concludes with a discussion of the experience gained from the prototype construction and operation. (4 refs.)

77965 Design and development of a point focus concentrated PV module operating above 100 suns. S.Olah, F.Ho, S.Khemthong (Appl. Solar Energy Corp., City of Industry, CA, USA).

Conference Record of the Sixteenth IEEE Photovoltaic Specialists Conference - 1982, San Diego, CA, USA, 27-30 Sept. 1982 (New York, USA: IEEE 1982), p.590-4

Describes the design, development fabrication and performance test of a highly efficient and cost effective concentrated photovoltaic module which can operate above 100 suns concentration and which can be mass produced and is reliable, with minimum maintenance. (no refs.)

77966 The design and development of a high concentration and high efficiency photovoltaic concentrator utilizing a curved Fresnel lens. A.L.Moffat, R.S.Scharlack (Thermo Electron Corp., Waltham, MA, USA).

Conference Record of the Sixteenth IEEE Photovoltaic Specialists Conference - 1982, San Diego, CA, USA, 27-30 Sept. 1982 (New York, USA: IEEE 1982), p.601-6

The design and development of an innovative photovoltaic concentrator which utilizes a low cost molded Fresnel lens is described. The lens design and fabrication are discussed, as well as the design of the collector module and tracking structure. A description of instrumentation developed to aid in the testing of lenses and solar cells is presented, and includes the test results. (no refs.)

77967 Design, processing, and assembly of large area concentrator cells and subassemblies. S.P.Tobin, M.J.Nowlan, G.A.Landis (Spire Corp., Patriots Park, Bedford, MA, USA).

Conference Record of the Sixteenth IEEE Photovoltaic Specialists Conference - 1982, San Diego, CA, USA, 27-30 Sept. 1982 (New York, USA: IEEE 1982), p.607-10

Describes the development of silicon concentrator cells for use in state-of-the-art linear focus Fresnel lens systems with average sunlight concentration of 30-50 suns. Primary goals were high cell efficiency and a simple, producible, low cost process. In the design phase, a collecting grid pattern optimized for the nonuniform intensity profile of the Fresnel lens was developed. A simple baseline cell process was defined. The most noticeable differences were the silicon resistivity (0.3 ohm-cm), texture etched surfaces to improve current collection, and the grid pattern. Initial cell results measured by Sandia were quite good, with efficiency exceeding 18% at 50 suns. Nine-cell strings interconnected and bonded to glass were delivered to the concentrator system manufacturer and passed all electrical and environmental tests. Several efficiency-enhancing options to the baseline process are also described. These include improved junction anneal schedules, oxide surface passivation, multi-layer antireflection coatings, and a planar process to reduce leakage currents. (5 refs.)

Conference Record of the Sixteenth IEEE Photovoltaic Specialists Conference - 1982 See Entry 74219

Design and performance trades for a miniaturized photovoltaic concentrator array See Entry 78020

Engineering design for a photovoltaic central station power plant using tracking concentrator photovoltaic arrays See Entry 78030

Guidelines and methodology for design and analysis of advanced PV technology systems See Entry 78039

Dispersive concentrating (DISCO) systems based on transmission phase holograms for solar applications See Entry 78045

F-chart method applied to large-scale solar collector systems subject to a shadow effect of adjacent collectors See Entry 78093

Radiation heat exchange in a solar cavity-type receiver at various times See Entry 78094

A simplified theory for a matrix solar collector See Entry 78096

Performance of *n* forced circulation water heating systems in series See Entry 78097

Seasonal thermal inventory See Entry 78105

Theoretical and experimental aspects of a two-step short cycle, based on ZnO and CdO intended for storage of solar energy See Entry 78106

A solar-hydrogen economy for USA See Entry 78107

86.10N Nuclear energy

Uranium estimation in Mussoorie phosphorites using solid state nuclear track detector See Entry 78483

Uranium enrichment in Archaean crustal basement associated with overthrusting See Entry 78494

86.30 ENERGY CONVERSION

Conference Record of the Sixteenth IEEE Photovoltaic Specialists Conference - 1982 See Entry 74219

86.30D Electrochemical conversion: general (for superionic conductors, see 66.30H)

77968 Lithium-cupric sulfide cells. L.Werblan, J.Lesinski, A.Suzdorf, J.Lyzdorek, R.Drachal (Dept. of Chem., Univ. of Warsaw, Warsaw, Poland). *J. Power Sources (Switzerland)*, vol.9, no.3-4, p.409-16 (April-May 1983).

(International Meeting on Lithium Batteries, Rome, Italy, 27-29 April 1982). Results for the preparation and properties of cupric sulfide electrodes prepared by two different methods are given. Details concerning the chemical composition, the porosity, and the structure of the sulfide electrode are presented. Problems related to the selection of appropriate organic solvents and electrolyte solutions in order to determine those which would be compatible with the electrode materials (Li/CuS), and would also secure the best conditions for transport of charge and mass through the solution, are presented. The following solvents and their mixtures were tested: gamma-butyrolactone (gBL), tetrahydrofuran (THF), 1,2-dimethoxyethane (1,2-DME), 1,1-dimethoxyethane (1,1-DME), and two component mixtures of gBL with 1,2-DME and gBL with 1,1-DME. Transport phenomena—the electrical conductivity and viscosity of lithium perchlorate solutions in these solvents were measured. A laboratory technology for the construction of a Li/CuS cell has been developed. (12 refs.)

International Meeting on Lithium Batteries See Entry 74213

Mechanism of ion conduction in alkali metal-polymer complexes See Entry 76695

Mechanistic studies of oxide electrodes reversibly incorporating Li⁺ ions See Entry 77893

86.30E Primary cells

77969 Electrochemistry of a nonaqueous lithium/sulfur cell. H.Yamin, E.Peled (Dept. of Chem., Tel-Aviv Univ., Tel Aviv, Israel).

J. Power Sources (Switzerland), vol.9, no.3-4, p.281-7 (April-May 1983). (International Meeting on Lithium Batteries, Rome, Italy, 27-29 April 1982).

The development and the electrochemistry of low-rate laboratory prototype Li/S button cells is described. The cell consists of a lithium anode, a porous catalytic current collector which is loaded with sulfur, and an organic solvent containing lithium polysulfide. The case of the cell was made from stainless steel and sealing was accomplished by the use of a combination of organic elastomer and cement (with no crimp). After 3 weeks storage at 60°C, the button cells lost only about 1 mg of weight. The lithium polysulfide reacts with the Li anode to form a passivating layer which acts as a solid electrolyte interphase (SEI). The EMF of the cells changes from 2.38 to 2.15 V depending on the composition of the solutions. Cells exhibit flat discharge curves at low drains. The energy density of the cells is 730 W h/kg or 900 W h/l at room temperature and 950 W h/kg or 1200 W h/l at 60°C (calculated on the basis of all cell components, excluding the case). Storage and discharge tests at 60°C show a capacity loss of 2-5% per month depending on solution composition. This indicates a shelf life of at least 10 years at room temperature. (9 refs.)

77970 Polarization of the lithium electrode in sulfolyl chloride solutions. F.Alessandrini, B.Scrosati (Istituto di Chimica Fisica, Univ. of Rome, Rome, Italy), F.Croce, M.Lazzari, F.Bonino.

J. Power Sources (Switzerland), vol.9, no.3-4, p.289-94 (April-May 1983). (International Meeting on Lithium Batteries, Rome, Italy, 27-29 April 1982).

The growth of the passivating film on a lithium electrode in contact with sulfolyl chloride solutions has been examined by micropolarization and complex impedance measurements. The results tend to confirm the hypothesis of a two-layer film, where probably the first layer is thin and compact and the second layer is porous and defective. (7 refs.)

77971 Li/SOCl₂ cells for high temperature applications. M.Babai, J.Binech (Lithium Battery Plant, Tadiran, Israel).

J. Power Sources (Switzerland), vol.9, no.3-4, p.295-305 (April-May 1983). (International Meeting on Lithium Batteries, Rome, Italy, 27-29 April 1982).

The capacity of Li/SOCl₂ cells operating at temperatures as high as 150°C has been measured at discharge rates up to 5 mA/cm². The results indicate the unique chemical and electrochemical stability of the system, manifested by its ability to be discharged continuously at 150°C for more than 2 months while obtaining 70% of the cell nominal capacity. The capacity-temperature plot shows a maximum at 50°C. Above 50°C the capacity decreases as a result of the increase in the self-discharge current at higher temperature. An anomalous capacity increase is found at temperatures above 100°C. Above this temperature it has been shown that thermal decomposition products may increase the cathodic reaction rate and modify the structure of the passivation layer on the anode surface. Over the 100-150°C temperature range the lithium chloride film morphology, as analysed by SEM, tends to be of a smaller crystal size the higher the temperature. This trend is in opposition to that found at the lower temperature range, e.g. -40 to 70°C. In addition,

the decomposition product, e.g. SO_2 , improves the transport properties of the electrolyte and thus increases the carbon cathode efficiency. (12 refs.)

77972 Li-AgBi(CrO₄)₂ a new highly reliable lithium battery for long service life applications. M.Broussely, J.P.Rivault, J.P.Gabano (Saft-Gipelec, Poitiers, France).

J. Power Sources (Switzerland), vol.9, no.3-4, p.339-44 (April-May 1983). (International Meeting on Lithium Batteries, Rome, Italy, 27-29 April 1982). The Li/AgBi(CrO₄)₂ battery system was patented in 1977. It has been studied for several years to obtain a better knowledge of the electrochemical reactions as well as of the discharge characteristics of a prototype cell. An exceptionally low level of self discharge and the use of a very well-known stable electrolyte such as propylene carbonate 1M Li/ClO₄ satisfy the necessary requirements for long service life application: high efficiency was obtained on long time discharges even at high temperature, e.g. 70°C at the two years rate. Performances over a wide range of current drains and temperatures are presented as well as projected results at a very low drain. (5 refs.)

77973 A pre-testable low temperature lithium thermal battery. Hai-De Song, Wen-Rong Lu (Tianjin Inst. of Power Sources, Tianjin, China). *J. Power Sources (Switzerland)*, vol.9, no.3-4, p.417-25 (April-May 1983). (International Meeting on Lithium Batteries, Rome, Italy, 27-29 April 1982). The operating temperature of the LiAl/NaAlCl₄/CuCl₂ thermal battery is about 200°C, and it can work in an ambient temperature range of -40 to +50°C. When discharged through a constant resistance of 700 Ω at room temperature, it can operate effectively for 10 min. Prior to use, the battery can be pretested to see whether it is properly assembled and to ensure its performance and reliability. Batteries after pretesting can still be activated without substantially reduced performance. (7 refs.)

77974 A characteristic of separators used in the primary and secondary cells with alkaline electrolyte. J.Dobryszky (Centralnym Lab. Akumulatorow i Ogniwi, Poznan, Poland). *Wiad. Elektrotech. (Poland)*, vol.50, no.13-14, p.408-10 (Nov.-Dec. 1982). In Polish. [received: April 1983]

The role of the separator in primary and secondary cells with alkaline electrolyte, range of separation materials used in alkaline systems, and their characteristic properties are all examined. (5 refs.)

Film forming reaction at the lithium/electrolyte interface See Entry 77977
Raman spectroscopic studies of the structure of electrolytes used in the Li/SOCl₂ battery See Entry 77978

Surface films on lithium in acetonitrile-sulphur dioxide solutions See Entry 77979

86.30F Secondary cells

77975 The use of the reactive ether, tetrahydrofuran (THF), in rechargeable lithium cells. K.M.Abraham, J.L.Goldman (EIC Labs. Inc., Newton, MA, USA).

J. Power Sources (Switzerland), vol.9, no.3-4, p.239-45 (April-May 1983). (International Meeting on Lithium Batteries, Rome, Italy, 27-29 April 1982). The usefulness of tetrahydrofuran (THF) as a cosolvent with 2-methyl-tetrahydrofuran (2-Me-THF)/LiAsF₆ for improving the low temperature rate capability of rechargeable Li cells has been explored. Lithium-titanium disulphide cells utilizing 2-Me-THF/LiAsF₆ blended with 15-50 vol.% THF have shown substantially improved rate characteristics at 0 and -10°C. In addition, the Li electrode in such cells has exhibited practically useful cycling efficiencies. (12 refs.)

77976 The reactivity of organic electrolytes with lithium: mechanistic aspects. V.R.Koch (Covalent Associates Inc., Framingham, MA, USA).

J. Power Sources (Switzerland), vol.9, no.3-4, p.247-51 (April-May 1983). (International Meeting on Lithium Batteries, Rome, Italy, 27-29 April 1982). The overall rate of Li-organic electrolyte reactivity is governed by heterogeneous redox chemistry at the Li electrode surface and by homogeneous acid-base chemistry in the bulk. While the former mode of reactivity may lead to protective films, the latter mode invariably results in rapid electrolyte degradation with time and must be considered the most serious source of poor cycling life in rechargeable cells. (18 refs.)

77977 Film forming reaction at the lithium/electrolyte interface. E.Peled (Dept. of Chem., Tel-Aviv Univ., Tel Aviv, Israel).

J. Power Sources (Switzerland), vol.9, no.3-4, p.253-66 (April-May 1983). (International Meeting on Lithium Batteries, Rome, Italy, 27-29 April 1982). Active metal nonaqueous systems can be divided into three groups: (a) solid electrolyte interphase (SEI)-free, aqueous-like, active-metal nonaqueous systems, such as aluminium plating baths; (b) metal solvent blue solutions, or solvated electron systems; (c) SEI battery systems. It is concluded that the only type of system that can be applied in primary and secondary lithium batteries is the SEI electrolyte system. The following are presented and discussed: The deposition-dissolution mechanism and the kinetics of SEI electrodes, the effect of several parameters on the resistivity of the SEI, the growth rate of the SEI, the morphology of the overall passivating layer and the voltage delay problem. (33 refs.)

77978 Raman spectroscopic studies of the structure of electrolytes used in the Li/SOCl₂ battery. Y.Bedier, J.Corset (Lab. de Spectrochimie Infrarouge et Raman, CNRS Section de Thiais, Thiais, France), M.C.Dhamelincourt, F.Wallart, P.Barbier.

J. Power Sources (Switzerland), vol.9, no.3-4, p.267-72 (April-May 1983). (International Meeting on Lithium Batteries, Rome, Italy, 27-29 April 1982). The importance of the Li/SOCl₂ cell using thionyl chloride as a liquid cathode has given rise to studies of the structure of the electrolytes used in this lithium cell. The electrolytes are made from LiAlCl₄ dissolved in SOCl₂ in which SO₂ is formed during the discharge process. The paper deals with a structural study, using Raman spectroscopy, of solutions of LiAlCl₄ in pure SOCl₂ and SO₂, and in mixtures of both solvents. The complexes [Li(SOCl₂)₂]⁺[AlCl₄]⁻ and [Li(SO₂)₃]⁺[AlCl₄]⁻ were characterized at room temperature in the pure solvents SOCl₂ and SO₂, respectively. In the ternary system LiAlCl₄-SOCl₂-SO₂ the existence of [Li(SO₂, SOCl₂)₂]⁺[AlCl₄]⁻ was established. (4 refs.)

77979 Surface films on lithium in acetonitrile-sulphur dioxide solutions. Y.Geronov, B.Puresheva, R.V.Mosheev (Central Lab. of Electrochem. Power Sources, Acad. of Sci., Sofia, Bulgaria).

J. Power Sources (Switzerland), vol.9, no.3-4, p.273-9 (April-May 1983). (International Meeting on Lithium Batteries, Rome, Italy, 27-29 April 1982). The growth of the passive film on Li in acetonitrile-sulphur dioxide solutions of LiBr, LiAsF₆, LiAlCl₄ and LiClO₄ with time has been followed by galvanostatic pulse measurements and SEM observations. It was found that the specific conductivity of the primary film on Li in AN-SO₂-LiBr solutions ($k=4 \times 10^{-9} \text{ ohm}^{-1} \text{ cm}^{-1}$) is practically insensitive to changes in concentration of SO₂ and LiBr. The substitution of Br⁻ by AsF₆⁻ anions in AN-SO₂

electrolytes significantly changes the properties of the film; the rate of growth and the 'steady state' value of the polarization resistance are much higher as compared with those of films obtained on Li in Br⁻-containing electrolytes. Water contamination above 1000 ppm enhances the growth of the passive film as compared with that in 'dry' electrolytes. (6 refs.)

77980 Electrochemical method for studying the reversibility of the lithium intercalation in secondary batteries. F.Dalard, D.Deroo (Lab. d'Energetique Electrochimique, Domaine Univ., Saint Martin d'Heres, France), R.Mauger. *J. Power Sources (Switzerland)*, vol.9, no.3-4, p.321-4 (April-May 1983). (International Meeting on Lithium Batteries, Rome, Italy, 27-29 April 1982). In studies of the rechargeability of intercalation material there is no clear demonstration of performance, mainly because experimental data conditions differ between authors. These data depend on material structure, grain size, preparation mode and also cycling procedure. In this article, we present a theoretical study of intercalation during galvanostatic cycling. Experimental results on the intercalation of lithium in MoO₃ are in good agreement with theory. The chemical diffusion coefficient of Li in MoO₃ has been calculated: $D=4 \times 10^{-11} \text{ cm}^2 \text{ s}^{-1}$ at 25°C. (5 refs.)

77981 Chromium oxides as cathodes for lithium cells. Y.Takeda, R.Kanno, Y.Tsuiji, O.Yamamoto (Dept. of Chem., Mie Univ., Tsu, Japan), H.Taguchi.

J. Power Sources (Switzerland), vol.9, no.3-4, p.325-8 (April-May 1983). (International Meeting on Lithium Batteries, Rome, Italy, 27-29 April 1982). The performances of organic electrolyte lithium cells with the chromium oxides, Cr₂O₃, CrO₃, Cr₂O₁₂, Cr₂O₅, Cr₆O₁₅, and Cr₃O₈, as cathodes, have been examined. The discharge behaviors of the couples Li/Cr₂O₃, Li/Cr₆O₁₅, and Li/Cr₃O₈ gave satisfactory results, especially in terms of energy density. The highest calculated energy density, based on the weights of the chromium oxides and to a 2.0 V cutoff at 0.5 mA/cm², was 1210 W h/kg for the Li/Cr₃O₈ couple. Further, the performance of a coin-type cell with a Cr₃O₈ cathode was demonstrated, and it was found that the cell exhibited good rechargeability. (5 refs.)

77982 Behaviour of various cathode materials for non-aqueous lithium cells. H.Ikeda, S.Narukawa (Sanyo Electric Co. Ltd., Kobe-shi, Japan).

J. Power Sources (Switzerland), vol.9, no.3-4, p.329-34 (April-May 1983). (International Meeting on Lithium Batteries, Rome, Italy, 27-29 April 1982). The reaction mechanisms with Li of various metal oxides, sulfides and a selenide in nonaqueous electrolyte have been studied by the galvanostatic method, X-ray diffraction analysis, and ion-microanalysis. As a result, cell reactions were classified into 3 types. (1) The directly reduced type: cathode materials are reduced directly to metal; CuO, etc. (2) The 2 step reaction type: reaction proceeds through intermediate products: FeS₂. (3) The solid diffusion type, based on the so-called intercalation reaction; MnO₂, LiS₂. These reaction mechanisms are discussed. (9 refs.)

77983 Some critical considerations in the design of multicell lithium-manganese dioxide batteries. K.L.Hampartumian, A.Momchilov, N.Ichev, V.Maney (Central Lab. of Electrochem. Power Sources, Acad. of Sci., Sofia, Bulgaria).

J. Power Sources (Switzerland), vol.9, no.3-4, p.335-8 (April-May 1983). (International Meeting on Lithium Batteries, Rome, Italy, 27-29 April 1982). A Li-MnO₂ counterpart of the standard 6F22 Leclanche battery was designed in 3 different versions—paper lined, spiral wound, and layer stacked. The performance of all 3 types was tested according to the IEC discharge conditions, and the results were juxtaposed with Leclanche and zinc-air batteries of identical size and voltage. The merits and shortcomings in terms of capacity, polarization, ability to withstand continuous discharge, and technological back up are discussed. Although all 3 designs displayed superior characteristics as compared with the Leclanche batteries, optimum performance can be achieved by observing several critical requirements concerning the design, materials, and technology. (5 refs.)

77984 Mechanistic studies of reversible layer-type electrodes. J.Rouxel, P.Molinie, L.H.Top (Lab. de Chimie des Solides, Nantes, France).

J. Power Sources (Switzerland), vol.9, no.3-4, p.345-57 (April-May 1983). (International Meeting on Lithium Batteries, Rome, Italy, 27-29 April 1982). In layered type intercalation electrodes ions are stored reversibly during the functioning of secondary batteries. The behaviour of the system depends on geometrical and electronic factors. The geometrical factors are concerned with the localization of the ions in the host structure; they deal with average structure determinations and local ordering problems. The diffusion properties of the intercalated ions depend on the site geometry, the population of the Van Der Waals gap, the ionicity of the bonds in the host, the stoichiometry of the host, and the mechanical properties of its slabs. Electrons have to be accommodated by the host. The band structure of the host plays an important role in respect of the ability to intercalate, the phase limit, and the stability of the products. Metal-insulator transition may be induced. Other possible factors such as Jahn-Teller effects have also to be considered. (23 refs.)

77985 Characterization of the chemistry at the anode and cathode in the Li/SO₂ battery system. W.P.Kilroy, C.R.Anderson (Naval Surface Weapons Center, Silver Springs, MD, USA).

J. Power Sources (Switzerland), vol.9, no.3-4, p.397-407 (April-May 1983). (International Meeting on Lithium Batteries, Rome, Italy, 27-29 April 1982). The discharge product of Li/SO₂ cells discharged at 25°C at 1-2 mA/cm² was quantitatively analyzed for sulfite, thiosulfate, and dithionite. Analysis of the lithium anodes of commercial Li/SO₂ batteries by XPS, SAM, SEM, and mass spectroscopy techniques determined the passive film chemistry to be complex, but generally dominated by lithium sulfite and sulfate formation. The anode microstructure and chemistry is inhomogeneous and sensitively dependent upon the state of discharge and the discharge temperature. (8 refs.)

77986 Morphology of the positive active power of the lead-acid accumulator. J.D.Milewski.

Wiad. Elektrotech. (Poland), vol.50, no.13-14, p.406-8 (Nov.-Dec. 1982). In Polish. [received: April 1983]
The morphology of the positive active power of the lead-acid accumulator is discussed. Possibilities of improving the attachment to the cathode in 'calcium' accumulators are also considered. (12 refs.)

On the processes responsible for the degradation of the aluminium-lithium electrode used as anode material in lithium aprotic electrolyte batteries See Entry 77992

A reversible graphite-lithium negative electrode for electrochemical generators See Entry 77995

A characteristic of separators used in the primary and secondary cells with alkaline electrolyte See Entry 77974

Estimation of battery charge in photovoltaic systems See Entry 78054

86.30G Fuel cells

Development and evaluation of the Texas Instruments Solar Energy System See Entry 78090

86.30J Photoelectric conversion: solar cells and arrays

77987 Optically enhanced amorphous silicon solar cells. H.W.Deckman, C.R.Wronski, H.Witzke, E.Yablonovitch (Exxon Res. & Engng. Co., Linden, NJ, USA).

Appl. Phys. Lett. (USA), vol.42, no.11, p.968-70 (1 June 1983). The authors describe the first application of optical enhancement to thin-film (~0.75 μ m thick) amorphous silicon solar cells and define cell geometries which maximize enhancement effects. They observed that due to the improved infrared absorption the external AM1 short circuit current increases by 3.0 mA/cm² in cells constructed in accordance with the principles of optical enhancement. (7 refs.)

77988 Polycrystalline X-ray topography (PXT) of a cast silicon photovoltaic cell. R.G.Rosemeier, K.C.Yoo (Univ. of Maryland, College Park, MD, USA), S.M.Johnson.

Mater. Lett. (Netherlands), vol.1, no.5-6, p.194-6 (April 1983). Contiguous (404), and (440)₂ polycrystalline X-ray topographs (PXT) have been obtained simultaneously within a single image for two grains of a cast polycrystalline silicon solar cell. A special two-step twinning orientation relationship between the adjacent grains gives a condition of only faint diffraction contrast being observed at the boundary interface. Stereographic projection analysis was employed to identify simultaneous reflection conditions, and a portable image X-ray intensifier was routinely used to align X-ray images in real time. (7 refs.)

77989 Sunshine Project Solar Photovoltaic Programme and recent activities in Japan. M.Kamimoto, H.Hayashi (Agency of Industrial Sci. & Technol., Ministry of Internat. Trade & Industry, Tokyo, Japan).

Int. J. Sol. Energy (Switzerland), vol.1, no.3, p.185-95 (1982). The Japanese solar photovoltaic program milestone, technological development plans, and their structures in the 'sunshine project' are introduced. Also described is the present status of the solar photovoltaic research and development projects. (no refs.)

77990 Determination of minority carrier lifetime and effective back surface recombination velocity in BSF silicon solar cells from transient measurements. S.C.Jain, S.K.Agarwal, U.C.Ray (Solidstate Phys. Lab., Delhi, India).

Electron. Lett. (GB), vol.19, no.10, p.365-7 (12 May 1983). The method of determining the base lifetime τ_B and the effective surface recombination velocity S_{eff} in a BSF solar cell from the transient decay of open-circuit voltage and short-circuit current is extended to include emitter recombinations. If the emitter recombinations in modern Si solar cells are neglected in interpreting the experimental data, the experimental value of S_{eff} is found to be in large error. (11 refs.)

77991 Solar cells. Present state and development. D.Teodorescu.

Elektr. Masch. (Germany), vol.62, no.4, p.105-12 (April 1983). In German. The limiting factor in solar installations is still the very high cost of solar cells. However, this is anticipated to come down significantly in the coming years. Present development trends are to put to terrestrial use astronautics experience in the production of solar generators which could make a greater contribution to the energy balance. But this entails cost reductions in the production of solar cells, improving their efficiency and life span. This also raises problems of energy storage, of improving technological processes for the production of active materials for solar cells, and of integrating such technologies into conventional ones to bring down production costs, giving great scope for CdS and similar low cost solar cells. Solar and thermo-electric solar installations are described and diagrammatically illustrated. (21 refs.) P.F.K.

77992 A new type of monolithic double junction solar cell. C.Flores.

Electron. Oggi (Italy), no.3, p.227-32 (March 1983). In Italian. A new type of monolithic solar cell (TTC2) is described highlighting technology and performance. The new cell consists of one p-n GaAs junction (1.4 eV) coupled to a second n-p junction of GaAlAs (1.7 eV). The zones are interconnected through a n-layer but are electrically independent forming a 3-terminal device similar to a p-n-p transistor. Resultant efficiency is 20.5% at a solar concentration of 80 decreasing to 16.2% at 500 concentration. Technology performance and application details are included. (8 refs.) T.H.

77993 The influence of hydrogen ion bombardment on the photovoltaic properties of Cu/Cu₂O Schottky barrier solar cells. R.J.Iwanowski, D.Trivich (Dept. of Chem., Wayne State Univ., Detroit, MI, USA).

Radiat. Eff. Lett. Sect. (GB), vol.76, no.3, p.87-92 (1983). The influence of hydrogen ion bombardment on the photovoltaic properties of Cu/Cu₂O Schottky barrier solar cells was investigated. Two main cases of junction formation process were considered depending on the sequence of applied procedures: thermal evaporation of thin Cu layer and irradiation of the substrate by H⁺ ion beam. (5 refs.)

77994 A three-dimensional double junction GaAs/GaAlAs cascade solar cell. C.Flores (CISE SpA, Milano, Italy).

IEEE Electron Device Lett. (USA), vol.EDL-4, no.4, p.96-9 (April 1983). Describes the fabrication process and performances of a new type of monolithic solar cell with two junctions and bandgaps of 1.4 eV (GaAs) and 1.69 eV (GaAlAs) respectively, with the novel feature of only four epitaxial layers. The structure is a three-terminal device similar to a p-n-p transistor with a thick base. For the first prototypes, an overall conversion efficiency of 20.5 percent has been measured at 80 suns. It is expected that further optimization steps can lead to a conversion efficiency of 25 percent AM 1.5 for this structure. (8 refs.)

77995 Physics of BSF solar cells at high levels of illumination. S.R.Dhariwal, R.Gadre, R.K.Mathur (Dept. of Phys., Government Coll., Ajmer, India).

IEEE Electron Device Lett. (USA), vol.EDL-4, no.4, p.105-7 (April 1983). The theory of BSF solar cells by Fossum et al. (see IEEE Trans. Electron Devices, vol.ED-27, no.4, p.785-91, 1980) is extended to high levels of injection. For such intensities, more general J_{sc} - V_{oc} relationships are derived which show deviation from the ideal exp (qV/kT) relationship. (5 refs.)

77996 Use of tin oxide as an inexpensive antireflection coating for p on n polycrystalline silicon solar cells. B.C.Chakravarty, S.N.Singh, B.K.Das (Div. of Materials, Nat. Phys. Lab., New Delhi, India).

IEEE Electron Device Lett. (USA), vol.EDL-4, no.5, p.138-9 (May 1983). The potential of tin oxide as an inexpensive antireflection (AR) coating for polycrystalline silicon solar cells has been investigated. Undoped tin oxide films of a desired thickness were deposited over p-n polycrystalline silicon solar cells by spray pyrolysis of an alcoholic solution of hydrated stannic chloride at 500°C. Evaluation of cell performance before and after this AR

coating showed that the AR coating is highly compatible with the polycrystalline silicon solar cells. About 40-50 percent improvement in the short-circuit current of p-n polycrystalline cells has been measured. The coating may be highly suited to large-scale production of low-cost polycrystalline silicon solar cells for terrestrial application. (7 refs.)

77997 Computer simulation of amorphous silicon based alloy p-i-n solar cells. M.Hack (Energy Conservation Devices Inc., Troy, MI, USA), M.Shur.

IEEE Electron Device Lett. (USA), vol.EDL-4, no.5, p.140-3 (May 1983). The authors report on the results of a computer simulation of amorphous silicon-based alloy p-i-n solar cells based on the complete set of transport equations. The model takes into account the spatial and energy variations of the localized state spectrum, nonuniform doping profiles, and nonuniform optical excitation. The computed dark and light current-voltage characteristics are in good agreement with experimental data. The results suggest that carrier back diffusion is not a significant effect in optimized p-i-n devices and that the open circuit voltage is determined by the recombination current. Also shown is the importance of residual boron doping in the intrinsic layer for cells illuminated through the n⁺-layer, and that hole transport limits device performance. (18 refs.)

77998 Efficiency of the a-Si:H solar cell and grain size of SnO₂ transparent conductive film. H.Ida, N.Shiba, T.Mishuku, H.Karasawa, A.Ito (Tech. Lab., Taiyo Yuden Co. Ltd., Gumma, Japan), M.Yamanaka, Y.Hayashi.

IEEE Electron Device Lett. (USA), vol.EDL-4, no.5, p.157-9 (May 1983). The relationship between average grain size on the surface of SnO₂ transparent conductive film and conversion efficiency of the a-Si:H solar cell was investigated. a-Si:H solar cells were fabricated on SnO₂/glass substrates with various grain sizes. The cell structure was glass/p(SiC)-i-n/Al and the effective cell area was 4x10⁻² cm². The reflectivity from the glass substrate was reduced to about 7 percent with increasing the grain size from 0.1 to 0.8 μ m, and the short-circuit current was increased from 12 to 14 mA/cm². A 7.9 percent of conversion efficiency was achieved using milky SnO₂ film of 0.4- μ m average grain size at AM-100 mW/cm². (2 refs.)

77999 The spectral response of BSF silicon solar cells fabricated through masked ion implantation. A.Silard (Dept. of Electronics, Polytech. Inst., Bucharest, Romania), R.Marinescu, M.Tazlauanu.

IEEE Electron Device Lett. (USA), vol.EDL-4, no.6, p.164-6 (June 1983). Presents the main peculiarities of the spectral response of back-surface-field (BSF) silicon solar cells fabricated through masked ion implantation of the n⁺-p junction. The emphasis is on the shift of maximum responsivity toward the visible spectrum and on the large bandwidth of these n⁺-p-p⁺ optical sensors. The dependence of these parameters on technological parameters are outlined in the communication. (4 refs.)

78000 Flash-lamp annealing of ion-implanted silicon and its application to solar cells. A.Usami, N.Yoshida, Y.Inoue (Dept. of Electronics, Nagoya Inst. of Technol., Nagoya, Japan).

IEEE Electron Device Lett. (USA), vol.EDL-4, no.6, p.166-8 (June 1983). Xe-lamps were used to anneal p⁺-implanted silicon. The redistribution of implanted dopants does not occur by flash annealing. The substrate-orientation dependence of electrical activity of implanted dopants between (100) and (111) silicon is found. Solar cells fabricated by p⁺-implantation at 25 keV and annealing by the lamp energy density of 28 J/cm² show an efficiency of about 10.4 percent (AM 2) without AR coating and BSF structures. (5 refs.)

78001 Interfacial stability of SnO₂/n-Si and In₂O₃/Sn/n-Si heterojunction solar cells. H.P.Maruska, A.K.Ghosh, D.J.Eustace, T.Feng (Corporate Res. Lab., Exxon Res. & Engng. Co., Linden, NJ, USA).

J. Appl. Phys. (USA), vol.54, no.5, p.2489-94 (May 1983). High efficiency SnO₂/n-Si and In₂O₃/Sn/n-Si solar cells have been fabricated which when encapsulated in EVA (ethylene vinyl acetate copolymers) and kept at temperatures below 200°C exhibit long-term stability. However, in the absence of proper encapsulation or at high temperatures, it is possible for the properties of heterojunction SnO₂/n-Si and In₂O₃/Sn/n-Si solar cells to suffer degradation through two distinct mechanisms, one optical and the other thermal in nature. In either case, losses in V_{oc} can be correlated with changes in the dark current-voltage characteristics: light stress increases the dark saturation current J_0 , while heat stress decreases the diode quality factor n . Both degradation mechanisms are related to changes in the stored charges in the SiO_x interphase region between the conducting oxide and the silicon. The thermal process is only relevant for temperatures above 300°C, while the optical process is only evidenced if ultraviolet light is incident on the cell. Thus, cells kept at $T < 200^\circ\text{C}$ behind a suitable UV-absorbing filter remain stable indefinitely. (17 refs.)

78002 High efficiency in 'semithermal' solar energy converters. R.T.Ross (Dept. of Biochem., Ohio State Univ., Columbus, OH, USA).

J. Appl. Phys. (USA), vol.54, no.5, p.2883-4 (May 1983). A photonic device in which the excited carriers thermally equilibrate both among themselves and with the lattice, but maintain distinct chemical potentials in the ground and excited bands, has the same high ideal efficiency as a converter in which only the carriers are hot. Because the hot carriers need only be removed from the absorber faster than band-to-band transitions, such a 'semithermal' device should be more practical than devices in which carriers may not equilibrate with the lattice. (6 refs.)

78003 Photovoltaic and electrical properties of n-CdS/p-Si heterojunction solar cells. T.Suda, A.Kuroyanagi (Dept. of Electronics, Inst. of Vocational Training, Kanagawa, Japan), S.Kurita.

J. Cryst. Growth (Netherlands), vol.61, no.3, p.494-8 (April-May 1983). Heterojunction solar cells of CdS/In/Si have been fabricated by electron-beam evaporation of CdS, and their electrical and photovoltaic properties are studied. The forward I-V characteristics of these cells are in good agreement with the tunneling model. To obtain an optimum condition for cell fabrication several parameters have been varied; such as substrate temperature, amount of In doping in CdS, and annealing temperature in various ambients (H₂, N₂ and S vapor). The CdS/In/p⁺-Si cell shows no degradation at room temperature in air over 30 months, whereas the CdS/In,Ag/p⁺-Si cell shows rapid degradation after 3 months. From the DLTS measurements using a computer controlled digital system five electron traps have been measured in an evaporated CdS/In/p⁺-Si cell. (18 refs.)

78004 Research on polycrystalline thin-film photovoltaic devices. A.M.Hermann, L.Fabick (Solar Energy Res. Inst., Golden, CO, USA).

J. Cryst. Growth (Netherlands), vol.61, no.3, p.658-64 (April-May 1983). The United States Department of Energy Polycrystalline Thin-Film Photovoltaic Device Program encompasses materials and device research on a variety of compound semiconductors with emphasis on II-VI compounds and II-VI ternary analogs. The preparation (emphasizing thin-film deposition) and characterization of semiconducting materials such as Cu₂-S, Cu₂-Se, CdTe and CuInSe₂ are covered. Photovoltaic device characteristics of these absorbers with heterojunction partners such as CdS are discussed. Excitement in the

program has been generated by recent progress in the (Cd,Zn/S)/CuInSe₂ device area. Unencapsulated (Cd,Zn)/S/CuInSe₂ cells have been subjected to more than 6000 h of accelerated stability testing with no measurable degradation in photovoltaic performance. Other program highlights include fabrication of a hybrid CdS/Cu₂S device (evaporated CdS, sputtered Cu₂S) all-sputtered CdS/Cu₂S cell. Preliminary data are presented on the achievement of intrinsically stable high-efficiency (>9%) wet-processed CdS/Cu₂S cells. A 5.3% (AM1) CVD Au/n-CdTe Schottky barrier cell is described. (41 refs.)

78005 Efficient pAl_{0.5}Ga_{1.5}As-pGaAs:Si-nGaAs photocells for use in intense sunlight. A.M.Allakhverdiev, B.V.Egorov, V.M.Lantratov, S.I.Troshkov (A.F. Ioffe Physicotech. Inst., Acad. of Sci., Leningrad, USSR). *Sov. Phys.-Tech. Phys. (USA)*, vol.27, no.11, p.1425-6 (Nov. 1982). Translation of: *Zh. Tekh. Fiz. (USSR)*, vol.52, no.11, p.2312-14 (Nov. 1982). [received: May 1983]

The authors report findings from a study of highly efficient solar photocells based on nGaAs-pGaAs-pAl_{0.5}Ga_{1.5}As heterostructures. The authors were able to increase the thickness of the p-type GaAs layer without increasing the recombination losses by preparing the layer from a silicon-doped melt (solution). (6 refs.)

78006 Variable minority carrier transport model for amorphous silicon solar cells. H.Okamoto, H.Kida, S.Nonomura, Y.Hamakawa (Faculty of Engng. Sci., Osaka Univ., Osaka, Japan). *Sol. Cells (Switzerland)*, vol.8, no.4, p.317-36 (May 1983).

A new carrier transport model describing the photovoltaic characteristics of amorphous silicon (a-Si) p-i-n junction (where i denotes intrinsic material) solar cells is proposed. In the model, the operative i layer is divided into two regions at a variable boundary; in each region, either electrons or holes are assumed to act just like the minority carriers dominating the carrier recombination rate. Based on this variable minority carrier transport model, comprehensive interpretations of the carrier collection efficiency spectra and dark and illuminated current density-voltage characteristics are given in terms of several basic parameters responsible for them, i.e. mobility-lifetime products, effective surface recombination velocities and conductivities at the p-i and i-n interfaces. The model presented can be used not only for explaining and predicting the photovoltaic properties but also for evaluating these parameters in actual a-Si solar cells. Furthermore, an identification of the relevant properties in various types of a-Si solar cell enables us to make clear how to design and fabricate the cells in order to attain higher photovoltaic performances. (25 refs.)

78007 Importance of the emitter in thin back-surface field solar cells. S.K.Mehta, S.C.Jain (Solid State Phys. Lab., Delhi, India). *Sol. Cells (Switzerland)*, vol.8, no.4, p.337-53 (May 1983).

The variation in the short-circuit current density J_{sc} , the open-circuit voltage V_{oc} and the efficiency η with the base thickness of an n⁺-p-p⁺ back-surface field (BSF) solar cell with a resistivity of 10 Ω cm is reported for 1 sun air mass 0 illumination. The effects of different emitter dark saturation current densities J_{E0} and different base diffusion lengths L_B on the variation in V_{oc} with the change in base thickness were calculated. The effective surface recombination velocity S_{eff} at the edge of the low-high junction is calculated as a function of the thickness w_H of the high region for various values of the recombination velocity S_r at the back contact. The temperature degradation coefficient of V_{oc} for a BSF cell was calculated with the band gap narrowing in both the emitter and the high region taken into account. (32 refs.)

78008 Analysis of the effects of the lateral resistance of the superficial zone on the current voltage characteristics of linear gridded solar cells. D.Lincot, M.Barbe, G.Cohen-Solal, F.Bailly (Lab. de Phys. des Solides, Meudon Bellevue, France). *Sol. Cells (Switzerland)*, vol.8, no.4, p.361-9 (May 1983). In French.

The paper analyses the influence of sheet series resistances on the terminal current-voltage characteristics of linear gridded solar cells. Analytical relations are established, in particular for the case of significant losses due to sheet resistances under illumination. These relations permit solar cell behaviour to be described quantitatively and allow their characteristics to be optimized. (10 refs.)

78009 Model calculations for silicon inversion layer solar cells. M.A.Miller, L.C.Olsen (Joint Center for Graduate Study, Richland, WA, USA). *Sol. Cells (Switzerland)*, vol.8, no.4, p.371-95 (May 1983).

Theoretical models for the current versus voltage characteristics of inversion layer (IL) solar cells are developed and used in modelling calculations. Two-dimensional carrier transport from the base region to the inversion layer and collector grid is taken into account by modelling the cell as a series of infinitesimally thin slices which supply current to the inversion layer and by solution of the two-dimensional diffusion equation for minority carriers. Significant device parameters are identified and model calculations are carried out over a range covering most physically realizable values for these parameters for p-type silicon-based devices. Conditions necessary for good device performance are identified and the results of poor device parameters discussed. Finally, modelling calculations of IL solar cells carried out by others are discussed and compared with those presented here. (39 refs.)

78010 Barrier height enhancement in semiconductor-insulator-semiconductor solar cells due to surface states and insulator charges. N.R.Saha, D.Roychoudhuri, P.K.Basu (Inst. of Radio Phys. & Electronics, Calcutta, India). *Sol. Cells (Switzerland)*, vol.8, no.4, p.397-401 (May 1983).

Studies of the changes in the barrier heights in both sputtered and sprayed n-ITO-SiO₂-pSi cells with changes in the positive fixed charges Q_{fix}^+ , in the substrate doping level N_A and in the thickness δ of the interfacial layer, and identifies values of these parameters which will increase the barrier height. In addition, the voltage drop across the insulator is studied with various control parameters. (9 refs.)

78011 Evaporation of CuCl and CuCl₂ for the fabrication of Cu₂S/CdS thin film solar cells. M.Burgelman, A.De Vos (Lab. voor Elektronika en Meettech., Rijksunivers. te Gent, Ghent, Belgium). *Thin Solid Films (Switzerland)*, vol.102, no.4, p.367-74 (29 April 1983).

The so-called dry method for the fabrication of Cu₂S/CdS thin film solar cells uses a thin CuCl film, in order to convert the surface layer of the CdS film into Cu₂S. Usually, the CuCl film is deposited by evaporation of freshly prepared CuCl powder. The authors investigate the influence of contamination of this evaporation material by CuCl₂ and by CuCl₂·2H₂O. The experiments show that about 99% of these contaminants decompose into CuCl during the evaporation process. (20 refs.)

78012 Amelioration des performances de la pile solaire au silicium de grand diametre (Amelioration of the performance of a large diameter silicon solar pile). D.Diguet.

Report EUR 8145 FR, Comm. European Communities, Luxembourg (1982), 48 pp. In French. Contract 426-78-3 ESF.

Presents an interim report on a long term project, expected to last until 1990. The introduction describes the various phases which are planned followed by a description of the actual way in which various parts of the work will actually be carried out. The results obtained to date are reported including analysis methods, comparative analysis, and a simplified method of preparing substrates. Serialised contacts are studied as is the subject of connection welding. Some analyses of results are given, together with thoughts on the production of the electrical equipment. The final section is on cell interconnections.

78013 Realisation et caracterisation de cellules solaires Cu₂S-CdZnS (Realisation and characterisation of Cu₂S-CdZnS solar cells). M.Cadene.

Report EUR 8153 FR, Comm. European Communities, Luxembourg (1982), 46 pp. In French. Contract 431-78 ESF.

The preparation, by different evaporative methods, of Cd_{1-x}Zn_xS films with values of x between 0.04 and 0.2 is described. Their intrinsic and extrinsic properties (crystallisation, carrier density, mobility, trap levels etc.) as a function of Zn content are studied by independent optical, electrical and optoelectronic methods. The process of topotaxial growth of Cu₂S film is studied and the photocurrents and photovoltages of backwall CdZnS-Cu₂S cells made from these films are measured. The spectral responses of pure CdS, Cd_{0.98}Zn_{0.02}S and Cd_{0.95}Zn_{0.05}S cells formed by double-crucible evaporation, and of a Cd_{0.92}Zn_{0.08}S cell evaporated from the solid solution, are plotted and discussed. (15 refs.)

78014 New directions in solar array development. J.Scott-Monck (Jet Propulsion Lab., California Inst. of Technol., Pasadena, CA, USA).

Conference Record of the Sixteenth IEEE Photovoltaic Specialists Conference - 1982, San Diego, CA, USA, 27-30 Sept. 1982 (New York, USA: IEEE 1982), p.7-12

This paper presents a broad overview of current and near term solar array technology that would be suitable for space use in the event that NASA, commercial and US defense planners decide to aggressively pursue and exploit the advantages of space photovoltaics. (16 refs.)

78015 Technology components of solar arrays for space platforms. K.Bogus (European Space Res. & Technol. Centre, ESA, Noordwijk, Netherlands).

Conference Record of the Sixteenth IEEE Photovoltaic Specialists Conference - 1982, San Diego, CA, USA, 27-30 Sept. 1982 (New York, USA: IEEE 1982), p.13-20

Space platform concepts are categorised in the frame of the European space programme into four classes containing near-term missions and follow-up generations. Common and distinguishing requirements on the solar array subsystem in each of the four classes are identified leading to a definition of photovoltaic technology development requirements. Current space photovoltaic technology activities in Europe which respond to these requirements are described and activities for future space platform applications are assessed. (19 refs.)

78016 Status of AlGaAs/GaAs heteroface solar cell technology. W.P.Rahilly (Air Force Wright Aeronautical Labs., Wright-Patterson Air Force Base, OH, USA), B.Ansbaugh.

Conference Record of the Sixteenth IEEE Photovoltaic Specialists Conference - 1982, San Diego, CA, USA, 27-30 Sept. 1982 (New York, USA: IEEE 1982), p.21-4

The paper reviews the various GaAs solar cell programs that have been and are now ongoing which are directed at bringing this particular technology to fruition. The discussion emphasizes space application—both concentrator and flat plate. The rationale for pursuing GaAs cell technology is given along with the different cell types (concentrator, flat plate), approaches to fabricate the devices, the hybrid cells under investigation and approaches to reduce cell mass are summarized. The outlook for the use of GaAs cell technology is given within the context for space application. (10 refs.)

78017 Solar array shuttle flight experiment—hardware development and testing. R.V.Elms (Lockheed Missiles & Space Co. Inc., Palo Alto, CA, USA).

Conference Record of the Sixteenth IEEE Photovoltaic Specialists Conference - 1982, San Diego, CA, USA, 27-30 Sept. 1982 (New York, USA: IEEE 1982), p.25-30

The paper reports on the fabrication and ground testing of (a) a large area, light-weight, flexible substrate developmental solar array wing that has been built for NASA-MSFC (Contract NAS8-31352) and of (b) the supporting structure and data acquisition system (DAS) which, with the wing will be flown in the shuttle as an experiment in 1984. The experiment will verify the dynamics, thermodynamic, and electrical performance predictions of the array wing and will demonstrate the structural capability of the array wing for Orbiter launch and re-entry environments. The accommodation of the Shuttle payload requirements has resulted in several array wing and operation modifications since the ground demonstration of the array wing in the technology development program. The experiment hardware verification program was designed to minimize costs and risk of experiment performance degradation while maintaining shuttle and crew safety. (2 refs.)

78018 Technical aspects of the INTELSAT V solar array. H.E.Pollard, W.R.Baron (Ford Aerospace & Communications Corp., Palo Alto, CA, USA).

Conference Record of the Sixteenth IEEE Photovoltaic Specialists Conference - 1982, San Diego, CA, USA, 27-30 Sept. 1982 (New York, USA: IEEE 1982), p.31-5

The INTELSAT V solar array is the largest rigid solar array used for a commercial communication satellite. The paper describes salient technology applications of the electrical design, development and manufacture of the INTELSAT V solar array. The circuits including cells, interconnects and wiring are being assembled using solderless welding techniques; the first solar array of this size to do so. Special welding process controls are described including monitor of electrical pulse, resistance and head pressure which provide the quality control to assure satisfactory welds. With the extensive use of solderless cells, various techniques were employed to ensure humidity resistance. The use of the Scanning Auger Microprobe as well as X-ray fluorescence for Palladium measurements are summarized. The electrical and environmental test program for the project is reviewed. (3 refs.)

78019 New component development for multi-100 kW low-cost solar array applications. G.J.Pack, J.A.Mann (Lockheed Missiles & Space Co. Inc., Sunnyvale, CA, USA).
Conference Record of the Sixteenth IEEE Photovoltaic Specialists Conference - 1982, San Diego, CA, USA, 27-30 Sept. 1982 (New York, USA: IEEE 1982), p.36-8
Studies of the costs and performance of flexible arrays have shown that the most dramatic reductions in the \$/Watt figure of merit are achieved by increasing performance. An examination of those properties that contribute to array performance indicated areas where radical changes in current design practice and philosophy would result in significant cost and performance impacts. To take advantage of the predicted cost reductions, modules were fabricated and tested that had ultra-thin superstrates as a load carrying member and large area dielectric wraparound (DWA), gridded back surface and copper contacted solar cells. (no refs.)

78020 Design and performance trades for a miniaturized photovoltaic concentrator array. R.E.Patterson, H.S.Rauschenbach, M.D.Cannady (TRW Space & Technol. Group, Redondo Beach, CA, USA).
Conference Record of the Sixteenth IEEE Photovoltaic Specialists Conference - 1982, San Diego, CA, USA, 27-30 Sept. 1982 (New York, USA: IEEE 1982), p.39-44
A miniaturized Cassegrainian concentrator module for space applications has been designed, assembled, and tested. Results to date support technical feasibility. Trade studies have shown that the performance of an earlier selected base-line design using silver coated, 0.25 mm electroformed nickel optics with circular elements arranged in a hexagonal close packed configuration can be improved. Specific power values of 27.3 W/kg BOL and 25.0 W/kg after 5 years in LEO have been projected at the 4 kW array level. At the 500 kW level, 20 W/kg BOL had been predicted earlier for the same cell efficiency. (8 refs.)

78021 Advances in solar cell welding technology. L.G.Chidester, D.R.Lott (Lockhead Missiles & Space Co. Inc., Sunnyvale, CA, USA).
Conference Record of the Sixteenth IEEE Photovoltaic Specialists Conference - 1982, San Diego, CA, USA, 27-30 Sept. 1982 (New York, USA: IEEE 1982), p.51-6
In addition to developing the rigid substrate welded conventional cell panels for an earlier US flight program, LMSC recently demonstrated a welded lightweight array system using both 2x4 and 5.9x5.9 cm wraparound solar cells. This weld system uses infrared sensing of weld joint temperature at the cell contact metallization interface to precisely control weld energy on each joint. Modules fabricated using this weld control system survived low-earth-orbit simulated 5-year tests (over 30000 cycles) without joint failure. The data from these specifically configured modules, printed circuit substrate with copper interconnect and dielectric wraparound solar cells, can be used as a basis for developing weld schedules for additional cell array panel types. (2 refs.)

78022 Achievement and properties of self-supporting polysilicon solar cells made from RAD ribbons. C.Belouet, C.Hervo, M.Mautref, C.Fages, J.Hervo (Centre de Recherches, Compagnie Generale d'Electricite, Marcoussis, France).
Conference Record of the Sixteenth IEEE Photovoltaic Specialists Conference - 1982, San Diego, CA, USA, 27-30 Sept. 1982 (New York, USA: IEEE 1982), p.80-5
The paper reports on the general status of the RAD growth process. The growth achievements and the consequences of the burn-off of the carbon ribbon after growth are briefly discussed. Emphasis is placed on the characteristics of the solar cells made from the self-supported layers obtained from the burn-off step; it is shown that i) these characteristics are impaired mainly by trapping effects and ii) low-temperature annealings at 430°C considerably reduce the activity of traps. It is concluded on the basis of a comprehensive study that AM₁ conversion efficiencies in the 11 to 13% range, should be obtained provided the trapping effect by obviated. (11 refs.)

78023 Solar array system for solar maximum mission. R.A.Meese, L.J.Goldhammer (Hughes Aircraft Co., Space and Communications Group, Los Angeles, CA, USA), D.K.McCarthy.
Conference Record of the Sixteenth IEEE Photovoltaic Specialists Conference - 1982, San Diego, CA, USA, 27-30 Sept. 1982 (New York, USA: IEEE 1982), p.96-101
On 14 February 1980, NASA's Goddard's Solar Maximum Mission (SMM) observatory was launched from the Eastern Test Range, Florida. Approximately 70 minutes after launch, having reached its planned circular orbit of 315 n.m., 28.5° inclination, the Solar Array System (SAS) was successfully deployed. The system, has provided all electrical power required during the observatory's two-year mission which was directed toward scientific exploration of the sun's activity. The SAS is the first solar array to be fully compatible with the power module of NASA's multimission modular spacecraft (MMS) and is the first array to employ solar cells whose covers are bonded by means of FEP Teflon. This paper describes the SAS design, its unique features, and the results of its successful in-orbit operation. (1 ref.)

78024 Research on polycrystalline silicon solar cells: goals and accomplishments. J.B.Milstein, R.W.Hardy, Y.S.Tsuo (Solar Electric Conversion Res. Div., Solar Energy Res. Inst., Golden, CO, USA).
Conference Record of the Sixteenth IEEE Photovoltaic Specialists Conference - 1982, San Diego, CA, USA, 27-30 Sept. 1982 (New York, USA: IEEE 1982), p.119-22
Reviews the results obtained in the polycrystalline silicon solar cell task area at the Solar Energy Research Institute (SERI) since the last IEEE Photovoltaic Specialists Conference, and presents a description of the goals which are expected to be achieved in the next year and beyond. Some of the future program elements are presented in general terms, in view of Requests for Proposals that are presently in process. (16 refs.)

78025 Thin film polycrystalline silicon solar cell. A.Z.Lin, Z.Q.Fan, H.Y.Sheng, X.W.Zhao (General Res. Inst. of Non-Ferrous Metals, Beijing, China).
Conference Record of the Sixteenth IEEE Photovoltaic Specialists Conference - 1982, San Diego, CA, USA, 27-30 Sept. 1982 (New York, USA: IEEE 1982), p.140-5
Epitaxial solar cells of different types are studied by taking the refined metallurgical grade silicon as original material, including the unidirectionally recrystallized silicon on the graphite substrate and then deposition of a thin silicon film to form the p-n junction. Also included are the horizontally and unidirectionally solidifying polycrystalline ingots in a graphite crucible and Czochralski-grown ingots, which were cut into wafers and then a silicon film deposited to form the p-n junction. Some electrical characteristics of these different types of solar cell are described. The impurity situations of the cells were analyzed, including the measurements of DLTS. (11 refs.)

78026 Large area, low cost space solar cells. J.Kukulka, P.A.Iles (Applied Solar Energy Corp., City of Industry, CA, USA).
Conference Record of the Sixteenth IEEE Photovoltaic Specialists Conference - 1982, San Diego, CA, USA, 27-30 Sept. 1982 (New York, USA: IEEE 1982), p.146-9
Describes cost effective production-ready space solar cells which can meet the requirements for use on the space shuttle and other large space missions. Actual yield and performance data for these cells, as well as cost comparisons between these and standard space cells are included. (3 refs.)

78027 Large area space solar cell assemblies. M.J.Nowlan, M.B.Spitzer (Spire Corp., Bedford, MA, USA).
Conference Record of the Sixteenth IEEE Photovoltaic Specialists Conference - 1982, San Diego, CA, USA, 27-30 Sept. 1982 (New York, USA: IEEE 1982), p.150-5
Results of the development of a 34.3 cm² space solar cell and integral glass cover are presented. Average AM0 cell efficiency is 14%. The cell design includes a high performance back surface reflector yielding a thermal alpha of approximately 0.66. A novel process is described which integrates cell fabrication and encapsulation thereby achieving a reduction of encapsulation cost. Test results indicate the potential of this new technology. (6 refs.)

78028 Recent advances in thin silicon solar cells. F.Ho, P.A.Iles (Applied Solar Energy Corp., City of Industry, CA, USA), H.Curtis, C.Baraona.
Conference Record of the Sixteenth IEEE Photovoltaic Specialists Conference - 1982, San Diego, CA, USA, 27-30 Sept. 1982 (New York, USA: IEEE 1982), p.156-9
Reviews recent progress in thin (2-4 mils, 50-100 μm) silicon solar cells, in three areas: preparation for production processing, coplanar back contact, and formation of cells with very low solar absorptance (α_s < 0.66). (13 refs.)

78029 Mechanical wraparound contacted cell for low cost space arrays. N.Mardesch, D.Joslin, D.Michaels (Spectrolab, Inc., Sylmar, CA, USA).
Conference Record of the Sixteenth IEEE Photovoltaic Specialists Conference - 1982, San Diego, CA, USA, 27-30 Sept. 1982 (New York, USA: IEEE 1982), p.160-3
Presents the advantages, performance, reliability and cost of a mechanical wraparound contact on a large area solar cell. The wraparound contact consists of a silver ribbon laminated to the metallisation of the back of a solar cell with an insulating acrylic-Kapton-acrylic sandwich and wrapped around the edge to the N⁺ metallisation and welded. The wraparound contact can increase the cell cost by approximately 20%, which must be offset by the panel assembly savings. (1 ref.)

78030 Engineering design for a photovoltaic central station power plant using tracking concentrator photovoltaic arrays. E.J.Simburger (Aerospace Corp., El Segundo, CA, USA).
Conference Record of the Sixteenth IEEE Photovoltaic Specialists Conference - 1982, San Diego, CA, USA, 27-30 Sept. 1982 (New York, USA: IEEE 1982), p.164-9
A preliminary engineering design has been developed for a photovoltaic central station power plant that utilizes tracking concentrator photovoltaic (PV) arrays. In previous work in this programme power plant design using flat plate photovoltaic technology was developed. The principles developed in the earlier work have now been applied to the design that uses tracking concentrator photovoltaic arrays. The approach taken was to use electric utility design practices wherever possible and to provide sufficient definition of equipment to permit subsequent preparation of engineering cost estimates. (9 refs.)

78031 An advanced photovoltaic system simulator to demonstrate the performance of advanced photovoltaic cells and devices. L.Mrig, R.DeBlasio (Solar Energy Res. Inst., Golden, CO, USA), G.A.O'Sullivan, R.P.Tomko.
Conference Record of the Sixteenth IEEE Photovoltaic Specialists Conference - 1982, San Diego, CA, USA, 27-30 Sept. 1982 (New York, USA: IEEE 1982), p.199-204
Describes a photovoltaic system simulator for characterizing and evaluating the performance of advanced photovoltaic cells, modules, and arrays as well as for simulating the operation of advanced conceptual photovoltaic systems. The system simulator is capable of extrapolating the performance from a single laboratory cell, or of a module to power levels up to 10 kW. The major subsystems comprising the system simulator are (1) Solar Array Simulator, (2) Power Conditioning Unit, (3) Load Controller and Resistive Load Unit, (4) Data Acquisition and Control Unit, and (5) Cell Test Bed. (1 ref.)

78032 Deep level defects and annealing studies in one-MeV electron irradiated (AlGa)As-GaAs solar cells. Sheng S. Li (Univ. of Florida, Gainesville, FL, USA), W.L.Wang, R.Y.Loo, W.P.Rahilly.
Conference Record of the Sixteenth IEEE Photovoltaic Specialists Conference - 1982, San Diego, CA, USA, 27-30 Sept. 1982 (New York, USA: IEEE 1982), p.211-15
Investigates the deep-level defects induced by one-MeV electron irradiation in the (AlGa)As-GaAs solar cells subject to different irradiation and annealing conditions. Both undoped and Sn-doped GaAs cells are fabricated. For Sn-doped GaAs cells, electron irradiation is performed for fluences of 1x10¹⁴, 1x10¹⁵, and 2x10¹⁶ e/cm², and subsequently annealed at 230°C for 10, 20, 30 and 60 minutes. In addition, irradiation is also made on Sn-doped cells with flux rates of 4x10¹⁰ and 2x10¹¹ e/cm²-s and at cell temperatures of 150 and 200°C. For undoped cells, irradiation is made at 200°C for two fluences (1x10¹⁴ and 1x10¹⁵ e/cm²). DLTS and C-V measurements are performed on these cells to determine the defect and recombination parameters. Details of the results are presented. (9 refs.)

78033 Radiation damage in front and back illuminated high resistivity silicon solar cells. I.Weinberg, C.Goradia, C.K.Swartz, H.W.Brandhorst, Jr. (NASA, Lewis Res. Center, Cleveland, OH, USA).
Conference Record of the Sixteenth IEEE Photovoltaic Specialists Conference - 1982, San Diego, CA, USA, 27-30 Sept. 1982 (New York, USA: IEEE 1982), p.216-21
Radiation induced degradation, in front and back illuminated 84 and 1250 ohm-cm n⁺pp⁺ silicon solar cells, was determined and cell performance interpreted using calculated optically injected charge distributions and cell voltage components. The 84 ohm-cm cell degraded less when illuminated from the front or n⁺ side compared to that when illuminated from the back or p⁺ side. On the other hand, the 1250 ohm-cm cell degraded less when back illuminated. It was concluded that, in addition to the usual mechanisms leading to decreased collection efficiencies, loss of conductivity modulation is a major cause of radiation damage in high resistivity silicon solar cells. These results suggest that radiation damage to high resistivity n⁺pp⁺ cells can be decreased by increasing cell collection efficiency and illuminating the cells from the p⁺ side. (4 refs.)

78034 Comparative values of advanced space solar cells. L.W.Slifer, Jr. (Goddard Space Flight Center, Greenbelt, MD, USA).

Conference Record of the Sixteenth IEEE Photovoltaic Specialists Conference - 1982, San Diego, CA, USA, 27-30 Sept. 1982 (New York, USA: IEEE 1982), p.222-7.

This methodology for deriving a first order dollar value estimate for advanced solar cells consists of defining scenarios for solar array production and launch to orbit and the associated costs for typical spacecraft, determining that portion affected by cell design and performance and determining the attributable cost differences. Break-even values are calculated for a variety of cells; confirming that efficiency and related effects of radiation resistance and temperature coefficient are major factors; array tare mass, packaging and packing factor are important; but cell mass is of lesser significance. Associated dollar values provide a means of comparison. (10 refs.)

78035 The metal interconnected cascade solar cell. R.A.LaRue, G.P.Borden, M.J.Ludowise, P.E.Gregory, W.T.Dietze (Varian Associates Inc., Palo Alto, CA, USA).

Conference Record of the Sixteenth IEEE Photovoltaic Specialists Conference - 1982, San Diego, CA, USA, 27-30 Sept. 1982 (New York, USA: IEEE 1982), p.228-30.

A cascade cell employing a new type of interconnect is described. It uses a groove etch and metallisation process to connect the base of the top cell to the emitter of the bottom cell. The best cell yielded 21.3% efficiency under conditions of AM3, 130 suns, 50°C, with the result not corrected for grid coverage. Other features include a 1.2-micron thick 1.82-Ev AlGaAs top cell with a BSF under the base and an n/p heteroface GaAs bottom cell that is stable during top cell growth. (7 refs.)

78036 Effects of indirect bandgap top cells in a monolithic cascade cell structure. H.B.Curtis, M.P.Godlewski (NASA, Lewis Research Center, Cleveland, OH, USA).

Conference Record of the Sixteenth IEEE Photovoltaic Specialists Conference - 1982, San Diego, CA, USA, 27-30 Sept. 1982 (New York, USA: IEEE 1982), p.231-5.

The effect of having a slightly indirect top cell in a three junction cascade monolithic stack is calculated. The minority carrier continuity equations are utilized to calculate individual junction performance. Absorption coefficient curves for general III-V compounds are calculated for a variety of direct and indirect gap materials. The results indicate that for a small excursion into the indirect region, (about 0.1 eV), the loss of efficiency is acceptably small (<2.5 percent) and considerably less than attempting to make the top junction a smaller direct bandgap. (11 refs.)

78037 End-of-life aspects of BSF technology for thin silicon solar cells.

K.-E.Rasch, K.Roy, K.-H.Tentscher (AEG-Telefunken, Heilbronn, Germany).

Conference Record of the Sixteenth IEEE Photovoltaic Specialists Conference - 1982, San Diego, CA, USA, 27-30 Sept. 1982 (New York, USA: IEEE 1982), p.236-9.

A matrix of solar cells (100 and 200 microns, 10 ohm-cm crucible grown) was fabricated to identify BSF technology with highest effectiveness under BOL and EOL conditions. The BSF structure was formed by boron diffusion, boron ion implantation, evaporated aluminium alloying and screen printed aluminium firing. The BOL and EOL characteristics after electron irradiation at fluences up to 1×10^{15} e/cm² are presented. (3 refs.)

78038 An alternate approach for low cost space cells. P.M.Stellar, T.F.Miyahira (Jet Propulsion Lab., California Inst. of Technol., Pasadena, CA, USA).

Conference Record of the Sixteenth IEEE Photovoltaic Specialists Conference - 1982, San Diego, CA, USA, 27-30 Sept. 1982 (New York, USA: IEEE 1982), p.240-5.

Silicon solar cells manufactured for the terrestrial market are examined as a potential low cost option for low earth orbit space flight use. The results of simulated space environmental testing of representative samples are reported and discussed. It is shown that although the terrestrial cells are compatible with most space use requirements significant deficiencies still exist. Cell modifications are discussed which would enhance the space applicability of the various cells examined. In most cases these are expected to be of minimal cost impact. Concern for contact/interconnector designs capable of surviving 30000 thermal cycles (corresponding to five years in LEO) however, needs to be resolved for the large area terrestrial devices. (4 refs.)

78039 Guidelines and methodology for design and analysis of advanced PV technology systems. T.J.Lambarski, C.A.Irby, M.G.Semmens (BDM Corp., Albuquerque, NM, USA), L.Mrig, R.DeBlasio.

Conference Record of the Sixteenth IEEE Photovoltaic Specialists Conference - 1982, San Diego, CA, USA, 27-30 Sept. 1982 (New York, USA: IEEE 1982), p.289-94.

The paper presents the technologies chosen for conceptual design development, the methodology used, results of the system design and analysis, and conclusions and guidelines based on the results. (9 refs.)

78040 The intensity dependence of surface recombination in high concentration solar cells with charge induced passivation. J.L.Gray, R.J.Schwartz, M.S.Lundstrom (School of Electrical Engng., Purdue Univ., West Lafayette, IN, USA), R.D.Nasby.

Conference Record of the Sixteenth IEEE Photovoltaic Specialists Conference - 1982, San Diego, CA, USA, 27-30 Sept. 1982 (New York, USA: IEEE 1982), p.437-41.

High intensity solar cells which are designed to minimize series resistance and shadowing losses, frequently employ an illuminated surface which is relatively far removed from the collecting junctions. This requires that the surface be well passivated to minimize surface recombination. One technique frequently employed to minimize surface recombination is to incorporate a fixed charge in the passivating oxide. The authors show that at sufficiently high intensities the surface recombination can increase dramatically. This results in a reduction in the high intensity collection efficiency. A comparison of the collection efficiency of interdigitated back contact cells and etched multiple vertical junction cells is given which shows that EMVJ cells are less sensitive to this effect than IBC cells. (4 refs.)

78041 Technology for highly efficient silicon cells for operation above 100 suns. S.Khemthong, F.Ho, P.A.Iles (Applied Solar Energy Corp., City of Industry, CA, USA).

Conference Record of the Sixteenth IEEE Photovoltaic Specialists Conference - 1982, San Diego, CA, USA, 27-30 Sept. 1982 (New York, USA: IEEE 1982), p.442-7.

In the past year, the efficiency of silicon solar cells has been increased for concentration levels up to 300-suns. Cells with efficiency over 20% at 100-suns, have retained efficiency above 19.5% at 200-suns, and 19% at 300-suns. The design principles and results are presented. (4 refs.)

78042 Some advanced testing techniques for concentrator photovoltaic cells and lenses. J.J.Wiczor, R.J.Chaffin, R.E.Hibray (Sandia Nat. Labs., Albuquerque, NM, USA).

Conference Record of the Sixteenth IEEE Photovoltaic Specialists Conference - 1982, San Diego, CA, USA, 27-30 Sept. 1982 (New York, USA: IEEE 1982), p.448-53.

For convenient characterization of concentrator solar cells, the authors have developed a method for measuring the entire illuminated I-V curve of a photovoltaic cell with a single flash of intense simulated sunlight. This method reduces the heat input to the cell and the time required to test a cell, thus making possible quick indoor measurements of photovoltaic conversion efficiency at concentrated illumination levels without the use of elaborate cell mounting fixtures or heat sink attachments. The other test method that they have developed provides a technique to analyze the spatially dependent, spectral distribution of intense sunlight collected and focused by lenses designed for use in photovoltaic concentrator systems. This information is important in the design of multijunction photovoltaic receivers, secondary concentrators, and in optimizing the performance of conventional silicon cell concentrator systems. (6 refs.)

78043 Measurement of concentrator solar cell short-circuit current linearity. R.W.Sanderson, C.E.Backus, J.Birkeland (Coll. of Engng. & Appl. Sci., Arizona State Univ., Tempe, AZ, USA).

Conference Record of the Sixteenth IEEE Photovoltaic Specialists Conference - 1982, San Diego, CA, USA, 27-30 Sept. 1982 (New York, USA: IEEE 1982), p.454-8.

The linearity of silicon solar cell short-circuit current with irradiance is investigated using two separate measurement approaches. The first approach involves the measurement of spectral response under concentrated irradiance. The second approach uses neutral density filters to provide a known attenuation to concentrated sunlight, allowing direct measurement of the effect of concentrated sunlight on solar cell short-circuit current. Results indicate a superlinear trend in cell short-circuit current with irradiance, with the greatest deviation from linearity seen for the highest base resistivity cells tested. (5 refs.)

78044 Manufacturing cost analysis of 1980 vintage photovoltaic arrays. T.S.Chan, R.C.Hodge (Advanced Energy Programs Dept., General Electric Co., King of Prussia, PA, USA).

Conference Record of the Sixteenth IEEE Photovoltaic Specialists Conference - 1982, San Diego, CA, USA, 27-30 Sept. 1982 (New York, USA: IEEE 1982), p.459-62.

Within DOE the photovoltaic concentrator technology project has a technology readiness milestone of substantiating a factory array price of \$2.80/peak watt in a 1980 timeframe. For this timeframe the three most promising concentrator PV approaches are linear focus Fresnel and trough and a point focus Fresnel. Using actual module test data to project annual energy collection potential and detailed manufacturing and installation cost estimates \$/annualized peak watt projections of \$3.50 to \$4.78/watt have been projected. This paper summarizes the work performed to arrive at these cost projections. (5 refs.)

78045 Dispersive concentrating (DISCO) systems based on transmission phase holograms for solar applications. W.H.Bloss, M.Griesinger, E.R.Reinhardt (Inst. fuer Phys. Elektronik, Univ. Stuttgart, Stuttgart, Germany).

Conference Record of the Sixteenth IEEE Photovoltaic Specialists Conference - 1982, San Diego, CA, USA, 27-30 Sept. 1982 (New York, USA: IEEE 1982), p.463-8.

The efficiency of photovoltaic generators based on different semiconductor materials with optimized band gaps can achieve considerably higher values than those obtained with single junction solar cells. A new type of a concentrating system is presented which allows high concentration and simultaneously splitting of the spectral region. This dispersive and concentrating (DISCO) system is based on volume phase transmission holograms which exhibit minimum absorption, high diffraction efficiency and adjustable dispersion. The spectral imaging properties of volume phase transmission holograms can be optimized with respect to the requirements for solar applications. An essential tool for this optimization process is the theoretical and numerical description of volume phase holograms. (12 refs.)

78046 Experimental demonstration of the efficacy of global versus direct beam use in performance prediction of flat plate photovoltaic modules. R.D.Whitaker, G.A.Zerlaut, A.W.Purnell (DSET Labs. Inc., Phoenix, AZ, USA).

Conference Record of the Sixteenth IEEE Photovoltaic Specialists Conference - 1982, San Diego, CA, USA, 27-30 Sept. 1982 (New York, USA: IEEE 1982), p.469-74.

Accuracy in prediction of module output in the installed configuration is critical to growth of the terrestrial photovoltaics market. Due to momentum from the space application, the United States has tended to retain reliance upon the 'better known' reference spectrum, used in the prediction of photovoltaic output, from the direct beam component at Air Mass 1.5. However, flat plate modules view a hemispherical or global spectrum. Differences have resulted which require resolution. Experiments were performed which show the differences in reference cell calibration constant due solely to the difference in spectrum under which the calibrations were performed. Analysis and experiments demonstrate the ultimate effect of that difference upon I-V curve normalization and resulting power determination. (5 refs.)

78047 Experimental nonidealities in light response and quality factor of photovoltaic diodes. R.R.Potter, J.R.Sites (Dept. of Phys., Colorado State Univ., Fort Collins, CO, USA).

Conference Record of the Sixteenth IEEE Photovoltaic Specialists Conference - 1982, San Diego, CA, USA, 27-30 Sept. 1982 (New York, USA: IEEE 1982), p.475-9.

A comparative study has been made of the nature of nonideal behavior in photovoltaic diodes. Several types of solar cells obey the current superposition principle, except for series resistance effects, over a wide temperature range. Other cells, notably lattice mismatched heterojunction cells, show a lack of superposition, interpreted here as an illumination induced reduction in barrier height. All the cells show a large diode quality factor at sufficiently low current densities and generally a fairly sudden transition to a value near one at higher densities. In the better cells this transition occurs many decades below the operating current range; in poorer ones it occurs in or above the operating range directly degrading performance. (4 refs.)

78048 Diffusion length and solar cell efficiency. D.Huber, R.Wahlich, A.Bachmaier (Wacker-Chemitronic, Burghausen, Germany).

Conference Record of the Sixteenth IEEE Photovoltaic Specialists Conference - 1982, San Diego, CA, USA, 27-30 Sept. 1982 (New York, USA: IEEE 1982), p.480-4.

The diffusion length of the minority carriers of a solar cell defines the appropriate technology which should be applied for the solar cell fabrication. Back surface techniques only pay off if the diffusion length is long enough. Monocrystalline material with different lifetime killing defects was investi-

gated and an experimental correlation between the diffusion length measured on the unprocessed wafer and the efficiency of the finished cell could be established. (6 refs.)

78049 The flux method applied to excess carrier transport in solar cells. A.M.Buonocristiani, J.Thomchick (Dept. of Phys., Christopher Newport Coll., Newport News, VA, USA). Conference Record of the Sixteenth IEEE Photovoltaic Specialists Conference - 1982, San Diego, CA, USA, 27-30 Sept. 1982 (New York, USA: IEEE 1982), p.485-9

Describes an alternative theoretical treatment of the transport of excess charge carriers in a solar cell. This analysis avoids the limitations due to the relatively large transport distances inherent in the usual macroscopic device theory. It describes the macroscopic current in terms of microscopic parameters of the semiconductor, for example carrier mobility; the space-charge field effects are treated directly. The results of numerical calculations of the quantum efficiency of a solar cell obtained with this treatment are discussed. (7 refs.)

78050 Generalised boundary conditions for the minority carrier diffusion equation in solar cells. P.T.Landsberg, M.S.Abrahams (Math. Dept., Univ. of Southampton, Southampton, England).

Conference Record of the Sixteenth IEEE Photovoltaic Specialists Conference - 1982, San Diego, CA, USA, 27-30 Sept. 1982 (New York, USA: IEEE 1982), p.490-4

For lifetime determinations by photovoltage decay the minority carrier diffusion equation has to be solved. Some results are given of a treatment by Sturm-Liouville transform for the excess minority carrier concentration for decay from a steady state and for the response to a short square light pulse. Carrier profiles and decay data are shown for fairly general time-independent boundary conditions. (6 refs.)

78051 Determination of silicon cell model parameters using a least-squares-fit to experimental spectral response and the V-I curve. G.W.Masden (School of Engng., Walla Walla Coll., College Place, WA, USA).

Conference Record of the Sixteenth IEEE Photovoltaic Specialists Conference - 1982, San Diego, CA, USA, 27-30 Sept. 1982 (New York, USA: IEEE 1982), p.495-500

An algorithm for the determination of photovoltaic cell parameters and absolute spectral response from terminal V-I measurements is presented. Input consists of V-I curve data measured with the cell operating under full-test illumination, the short circuit current response to superimposed quasi-monochromatic illumination and the spectral distribution of the quasi-monochromatic illumination. The algorithm yields internal spectral response and approximate values for cell model parameters such as minority carrier lifetimes, doping densities, junction depth, recombination velocities, and/or others provided the sensitivity of the cell response to changes in the parameter allows a satisfactory resolution of the parameter. Effects of measurement errors on the computed spectral response and parameters are presented. (3 refs.)

78052 Intensity enhancement in textured optical sheets for solar cells. E.Yablonovitch (Exxon Res. & Engng. Co., Linden, NJ, USA).

Conference Record of the Sixteenth IEEE Photovoltaic Specialists Conference - 1982, San Diego, CA, USA, 27-30 Sept. 1982 (New York, USA: IEEE 1982), p.501-6

Describes a statistical mechanical approach for the optics of textured and inhomogeneous optical sheets. As a general rule, the local light intensity in such a medium will tend to be $2n^2(x)$ times greater than the externally incident light intensity, where $n(x)$ is the local index of refraction in the sheet. This enhancement can contribute toward a $4n^2(x)$ increase in the effective absorption of indirect-gap semiconductors like crystalline silicon. Also it may lead to a voltage increase equal to $KT/q 4n^2$. (no refs.)

78053 Maximum power point tracker for photovoltaic power plants. V.Arcidiacono, S.Corsi, L.Lambri (Res. & Dev. Dept., Italian Electricity Board, ENEL, Automatica Res. Center, Milan, Italy).

Conference Record of the Sixteenth IEEE Photovoltaic Specialists Conference - 1982, San Diego, CA, USA, 27-30 Sept. 1982 (New York, USA: IEEE 1982), p.507-12

Describes two different closed-loop control criteria for the maximum power point tracking of the voltage-current characteristic of a photovoltaic generator. The two criteria are discussed and compared, inter alia, with regard to the setting-up problems that they pose. Although a detailed analysis is not embarked upon, the paper also provides some quantitative information on the energy advantages obtained by using electronic maximum power point tracking systems, as compared with the situation in which the point of operation of the photovoltaic generator is not controlled at all. Lastly, two high-efficiency MPPT converters for experimental photovoltaic plants of the stand-alone and the grid-interconnected type are presented. (7 refs.)

78054 Estimation of battery charge in photovoltaic systems. J.Appelbaum (Dept. of Electrical Engng., Univ. of Colorado, Boulder, CO, USA), R.Weiss.

Conference Record of the Sixteenth IEEE Photovoltaic Specialists Conference - 1982, San Diego, CA, USA, 27-30 Sept. 1982 (New York, USA: IEEE 1982), p.513-18

The ability to estimate the battery state of charge in an operating system, at any time, is very important from system design point of view. The authors introduce a new on-line method of lead acid battery state of charge determination in a working photovoltaic system. The proposed method is based on the extension of the known open-circuit voltage-charge relation to operating battery voltage-charge relation, combining it with the ampere-hour accounting method for finite periods of time, and averaging out random measurement errors. The method uses electrical measurement of voltage and current at sampling times. The new method was compared experimentally with charge determination methods for a battery at rest (off line methods) and shows good agreement at the control points. The method was developed and validated experimentally for operating conditions which prevail in autonomous photovoltaic systems. (8 refs.)

78055 Inverter characteristics/problems encountered at the Southwest Residential Experiment Station. G.E.Hocking, M.A.Lieberman (New Mexico Solar Energy Inst., Las Cruces, NM, USA).

Conference Record of the Sixteenth IEEE Photovoltaic Specialists Conference - 1982, San Diego, CA, USA, 27-30 Sept. 1982 (New York, USA: IEEE 1982), p.519-24

This paper briefly discusses the Southwest Residential Experiment Station (SW RES) experiences with residential-sized, utility-interactive inverters during its first 18 months of operation. The SW RES, operated by the New Mexico Solar Energy Institute (NMSEI) at New Mexico State University, is a test facility established under the National Photovoltaic Program. The experiences with multiple utility-interactive, photovoltaic-powered inverters are summarized, with a specific detailed time line that describes operating versus inactive time. Inverter comparisons encompass DC filters, transformers, night switches, failure mechanisms, and protective features. A discussion of array

configuration and their impact on diagnostics and servicing is included. (no refs.)

78056 The effect of operating-point-control strategy on the annual energy production of degraded photovoltaic arrays. H.M.Branz (Lincoln Lab., MIT, Lexington, MA, USA).

Conference Record of the Sixteenth IEEE Photovoltaic Specialists Conference - 1982, San Diego, CA, USA, 27-30 Sept. 1982 (New York, USA: IEEE 1982), p.525-31

A new computer simulation of the annual operation of degraded flat-plate photovoltaic (PV) arrays is used to evaluate the need for maximum-power-point tracking in real PV systems. The simulations are based on single-glitch I-V curve shapes rather than particular array degradations, making the data reported applicable to any system whose likely failure modes are predictable and result in single-glitch I-V curves. The simulations show that with a reasonable array wiring strategy, effective maintenance, periodic I-V curve tracing, and avoidance of frequent and serious array shadowing, there is no reason that considerations of degradation should force the adoption of maximum-power-point-tracking power conditioning on a PV system that would otherwise operate economically at fixed voltage. (5 refs.)

78057 A new method of impurity gettering in polycrystalline solar cells. V.Schlosser, F.Kuchar, K.Seeger (Ludwig Boltzmanninst. fur Festkorperphys., Univ. Wien, Wien, Austria).

Conference Record of the Sixteenth IEEE Photovoltaic Specialists Conference - 1982, San Diego, CA, USA, 27-30 Sept. 1982 (New York, USA: IEEE 1982), p.532-6

Impurity gettering is a widely used process to improve properties of semiconductor devices. A new method applying a-Si for the gettering in solar cells is reported. Solar cells made on either single crystal or cast polycrystalline substrates, some of them doped with gold were used to show the effect of a-Si as a getter for impurities in the silicon substrate. The a-Si layer is removed by either wet or gas phase etching after the gettering process. As an impurity Au was chosen because it is commonly used for lifetime control in silicon devices. The solar cells are characterized by their minority carrier diffusion lengths L_n and L_p respectively which strongly depend on the number of recombination centers. The diffusion length is determined from spectral response measurements. The spectral response data are fitted to a physical model by means of a least square fit. The results are interpreted as a gettering process of gold impurities by an applied a-Si layer. (6 refs.)

78058 Improved efficiencies of semiconductor and metallurgical grade cast silicon solar cells by hydrogen plasma treatment. W.Schmidt, K.-D.Rasch, K.Roy (AEG-Telefunken, Heilbronn, Germany).

Conference Record of the Sixteenth IEEE Photovoltaic Specialists Conference - 1982, San Diego, CA, USA, 27-30 Sept. 1982 (New York, USA: IEEE 1982), p.537-42

Hydrogenation of grain boundaries in multicrystalline silicon solar cells is a promising passivation technique against recombination losses presently under intensified investigation. The improvement of the photovoltaic parameters of hydrogen plasma treated solar cells from large-grain multicrystalline silicon ingots with semiconductor grade (SG) and metallurgical grade (MG) starting silicon is discussed. The change of the photovoltaic parameters distribution, the influence of base resistivity, dopant type, impurity concentration and crystallization technique are analysed. Relative efficiency improvements up to 40% for SG and 85% for upgraded MG solar cells were achieved. (4 refs.)

78059 Grain boundary effects and Li passivation in polycrystalline silicon. F.Kai, G.Rajewaran, M.A.Jackson, V.J.Rao, W.A.Anderson (Dept. of Electrical & Computer Engng., State Univ. of New York, Buffalo, NY, USA).

Conference Record of the Sixteenth IEEE Photovoltaic Specialists Conference - 1982, San Diego, CA, USA, 27-30 Sept. 1982 (New York, USA: IEEE 1982), p.543-7

A relatively new technique for Li passivation has been used to reduce the active grain boundary effects in poly-Si. The Li passivated cells have generally shown better photovoltaic data, higher spectral response and smaller ideality factor in dark and light I-V than both etched and annealed cells. The interface state density of the passivated cell is lower than for the non-passivated cells. Ion probe data shows Li to diffuse three orders more rapidly in the grain boundary than in the solid silicon. (15 refs.)

78060 The measurement of variations in minority carrier lifetime due to microstructural defects in large area polysilicon wafers. S.M.Johnson, J.S.Culik (Solarex Corp., Rockville, MD, USA).

Conference Record of the Sixteenth IEEE Photovoltaic Specialists Conference - 1982, San Diego, CA, USA, 27-30 Sept. 1982 (New York, USA: IEEE 1982), p.548-53

Describes the measurement and analysis of minority carrier lifetime inhomogeneities in large area polysilicon wafers used to fabricate solar cells. Variations in free carrier lifetime are measured using a contactless microwave technique. The use of a subsequent Secco etch enables structurally related minority carrier lifetime degradation mechanisms to be distinguished from impurity related lifetime decreases. (19 refs.)

78061 Enhanced diffusion of phosphorus at grain boundaries [Si solar cells]. L.J.Cheng, C.M.Shyu, K.M.Stika, T.Daud, G.T.Crotty (Jet Propulsion Lab., California Inst. of Technol., Pasadena, CA, USA).

Conference Record of the Sixteenth IEEE Photovoltaic Specialists Conference - 1982, San Diego, CA, USA, 27-30 Sept. 1982 (New York, USA: IEEE 1982), p.554-8

Enhanced diffusion of phosphorus at grain boundaries in cast polycrystalline photovoltaic materials (Wacker, HEM, and Semix) was studied. It was found that the enhancements for the three materials were the same, indicating that the properties of boundaries are similar, even though they were grown by different techniques. In addition, it was observed that grain boundaries capable of enhancing the diffusion always have strong recombination activities. Both phenomena could be related to dangling bonds existing at the boundaries. The present study gives the first evidence that incoherent second order twins of {111}/{111} type are diffusion-active. (9 refs.)

78062 Bifacial cells of p^+in^+ structure. G.L.Araujo (Inst. de Energia Solar, Univ. Politecnica de Madrid, Madrid, Spain), A.Luque, E.Sanchez, M.J.Calleja, S.Lopez Romero, J.Castano.

Conference Record of the Sixteenth IEEE Photovoltaic Specialists Conference - 1982, San Diego, CA, USA, 27-30 Sept. 1982 (New York, USA: IEEE 1982), p.559-64

Bifacial cells of p^+in^+ structure are intrinsically very symmetric as shown both, theoretically and experimentally. Their bifacial behaviour is analyzed and compared to that of p^+nn^+ cells in low injection for low values of the diffusion length. Cells of p^+in^+ structure are anticipated to present better bifacial behaviour for all the ranges of L. An approximate two-exponential formula is given to account for the behaviour of p^+in^+ cells and the values of the parameters in this formula are measured in typical cases. The validity of superposition is studied, leading to the conclusion that it is not theoretically satisfied. The results of a pilot fabrication of p^+in^+ bifacial cells are given and compared to those of low injection bifacial cells. (8 refs.)

78063 On the effective minority carrier diffusion length of polycrystalline silicon solar cells. S.Kumari, S.K.Jain, B.K.Das, G.C.Jain (Nat. Phys. Lab., New Delhi, India).

Conference Record of the Sixteenth IEEE Photovoltaic Specialists Conference - 1982, San Diego, CA, USA, 27-30 Sept. 1982 (New York, USA: IEEE 1982), p.565-8

Polycrystalline substrates can be characterized in terms of an 'effective' minority carrier diffusion length, L_e . Based on a generalised expression, L_e has been computed for polycrystalline Si solar cells in terms of the intragrain diffusion length L_g , grain size d and the distance λ to which the grain boundary has an influence βL_g , in accordance with a model suggested by Koliwad and Daud (1980). They have demonstrated $\beta=1$. These theoretical computations have been compared with the experimental results of diffusion length measurements on solar cells fabricated out of solar grade polysilicon. The value of β has been found to vary randomly between 1.3 to 1.7 assuming uniform L_g in all the grains. This is thought to be due to impurity induced effects. Non uniform grain boundary enrichment of impurities like Fe, Cr, Ni and Cu has been observed using SAM and SIMS techniques. (6 refs.)

78064 Fabrication process and performances of a new type of GaAs-GaAlAs cascade solar cell. C.Flores (CISE SpA, Milano, Italy).

Conference Record of the Sixteenth IEEE Photovoltaic Specialists Conference - 1982, San Diego, CA, USA, 27-30 Sept. 1982 (New York, USA: IEEE 1982), p.569-73

A novel cascade solar cell with two junctions and three terminals, has been fabricated. The cell consists of a GaAs P-N junction covered with a $Ga_{0.8}Al_{0.2}As$ N-P junction. This structure has been realized using a process that involves a minimum number of epitaxial layers and an easy fabrication process. The cell has been tested at different sun concentrations. The conversion efficiency is 20.5% at 80 suns and decreases to 16.2% at 500 suns. (7 refs.)

78065 The V-groove silicon solar cell. P.G.Borden, R.Walsh (Varian Associates, Palo Alto, CA, USA), R.D.Nasby.

Conference Record of the Sixteenth IEEE Photovoltaic Specialists Conference - 1982, San Diego, CA, USA, 27-30 Sept. 1982 (New York, USA: IEEE 1982), p.574-7

The V-groove silicon solar cell is designed to achieve high efficiency at high concentration. It uses a V-groove front surface to obtain minimal grid shadowing losses, while allowing high fractional grid coverage. The serrated structure and front surface refraction minimizes the photon penetration depth, reducing the required diffusion length and allowing use of epitaxial layers on highly doped substrates. This minimizes base resistance. Cells have achieved 17.4% AM1 efficiency at 200 suns, 24°C, with 25% front grid coverage. (10 refs.)

78066 Reduction of open circuit voltage in solar cells at very high illumination intensity. J.E.Parrott, H.R.A.Beddie (Dept. of Phys., Electronics & Electrical Engng., Univ. of Wales Inst. of Sci. & Technol., Cardiff, Wales).

Conference Record of the Sixteenth IEEE Photovoltaic Specialists Conference - 1982, San Diego, CA, USA, 27-30 Sept. 1982 (New York, USA: IEEE 1982), p.578-83

Examines the behaviour of GaAs and Si solar cells over a range of illumination intensities up to about 10^5 W/cm². Photovoltage saturation as described by Parrott and others (1974, 1976) was apparently not observed due to the appearance of an effect causing a voltage decrease at the higher illumination levels. Experimental results for a few cells are shown and the various possible mechanisms for this effect are discussed. (7 refs.)

78067 Superlattice cascade solar cell. M.W.Wanlass, A.E.Blakeslee (Solar Energy Res. Inst., Golden, CO, USA).

Conference Record of the Sixteenth IEEE Photovoltaic Specialists Conference - 1982, San Diego, CA, USA, 27-30 Sept. 1982 (New York, USA: IEEE 1982), p.584-9

Reports progress toward realization of a new cascade solar cell structure whose chief advantages over other present concepts are: use of silicon for the substrate and low bandgap cell; avoidance of the necessity of lattice matching; and incorporation of a GaAs/GaP superlattice to enhance efficiency and provide a low-resistance connecting junction. Details of the design and operation of an OMCVD system from growing this structure are presented. Results of experiments to optimize layer thickness, compositional uniformity, and surface morphology are described. (17 refs.)

78068 A four-cell photovoltaic system based on InP and GaAs. B.Beaumont, G.Nataf, F.Raymond, C.Verie (Lab. Phys. du Solide et Energie Solaire, Valbonne, France).

Conference Record of the Sixteenth IEEE Photovoltaic Specialists Conference - 1982, San Diego, CA, USA, 27-30 Sept. 1982 (New York, USA: IEEE 1982), p.595-600

A four-bandgap photovoltaic system is proposed. It combines two monolithic stacked two-bandgap solar cells coupled through a dichroic mirror. Detailed modelling studies together with a discussion on the choice of semiconductor materials for the photovoltaic cells are described. The projected operating efficiency is shown to be above 35%, reaching a value as high as 42% in the case of the four-cell converter. Experiments are under progress. (11 refs.)

78069 Grain boundary structure and properties in polycrystalline silicon. Y.S.Tsuo, R.W.Hardy, J.B.Milstein (Solar Electric Conversion Res. Div., Solar Energy Res. Inst., Golden, CO, USA).

Conference Record of the Sixteenth IEEE Photovoltaic Specialists Conference - 1982, San Diego, CA, USA, 27-30 Sept. 1982 (New York, USA: IEEE 1982), p.610-21

Reviews recent advances in studying the grain boundary properties of polycrystalline silicon solar cell materials are reviewed. Of particular importance are the recent improvements in hydrogen grain boundary passivation techniques that have not only shortened the required passivation treatment time to only a few minutes but also demonstrated the ability to significantly increase polycrystalline silicon solar cell efficiencies for both large-grained and small-grained materials. (36 refs.)

78070 Grain boundaries in silicon solar cells. L.L.Kazmerski, P.E.Russell, P.J.Ireland, C.R.Herrington, J.R.Dick, R.J.Matson, K.M.Jones (Solar Energy Res. Inst., Golden, CO, USA).

Conference Record of the Sixteenth IEEE Photovoltaic Specialists Conference - 1982, San Diego, CA, USA, 27-30 Sept. 1982 (New York, USA: IEEE 1982), p.622-6

The correlations between the electrical and compositional properties of grain boundaries in polycrystalline Si are examined in detail. High-resolution surface analysis techniques (AES, SIMS, XPS, EELS) and microelectrical (SAM, EBIC, minority-carrier lifetime) characterization methods are used. The direct evidence for impurity segregation to the intergrain regions is presented. Effect of illumination on the grain boundary electrical characteristics are correlated with impurity compositions. Finally, the interrelationships among heat-treatment, oxygen segregation and grain boundary electrical activity are discussed. (24 refs.)

78071 Evaluation of EBIC images at grain boundaries. J.Marek (Max-Planck-Inst. fur Festkörperforschung, Stuttgart, Germany).

Conference Record of the Sixteenth IEEE Photovoltaic Specialists Conference - 1982, San Diego, CA, USA, 27-30 Sept. 1982 (New York, USA: IEEE 1982), p.627-32

A physically appropriate model for EBIC images in polycrystalline semiconductors is developed. EBIC signals are calculated for a set of parameters ranging from 1 to 200 μ m for the diffusion length of the grain and 5 to 60 keV for the electron beam energy. Experiments on large-grain Si solar cells are performed and compared with theory. The experimental and calculated profiles agree within 2%. The analysis of the profile allows determination of the diffusion length in the grain and of the grain boundary recombination velocity. (13 refs.)

78072 Carrier transport at grain boundaries in silicon. H.C.Card, J.G.Shaw, G.C.McGonigal, D.J.Thomson, A.W.de Groot, K.C.Kao (Dept. of Electrical Engng., Univ. of Manitoba, Winnipeg, Manitoba, Canada).

Conference Record of the Sixteenth IEEE Photovoltaic Specialists Conference - 1982, San Diego, CA, USA, 27-30 Sept. 1982 (New York, USA: IEEE 1982), p.633-9

A series of experimental measurements is presented of electron and hole transport at grain boundaries (and dislocations) in cast silicon. These experiments include four-probe measurements on individual grain boundaries, the effects of grain-boundary proximity on Schottky barrier characteristics and spectral/photovoltaic behaviour of 1 cm² grating solar cells (both minMIS and majority-carrier types). In addition, the results of theoretical studies are described, which employ numerical finite-element methods with the Newton-Raphson-Kantorovich algorithms. In these calculations, the quasi-Fermi potentials and the electrostatic potential across the grain boundary are solved self-consistently, without the need for a priori assumptions of particular carrier transport mechanisms. (24 refs.)

78073 Grain boundary effects in polycrystalline silicon solar cells. N.C.Halder (Dept. of Phys., Univ. of South Florida, Tampa, FL, USA).

Conference Record of the Sixteenth IEEE Photovoltaic Specialists Conference - 1982, San Diego, CA, USA, 27-30 Sept. 1982 (New York, USA: IEEE 1982), p.640-3

By solving the three-dimensional diffusion equation by Green's function method, the I-V characteristics of polycrystalline Si solar cells with vertical grain boundaries and n-p junctions have been investigated. The procedure includes the effects of grain size, thickness of the cell and the recombination velocity of the minority carriers at the grain boundary. The results of this study suggest that an efficiency as high as 15% may be achieved with samples of grain size 100 μ m, thickness 100 μ m, and velocity 100 m/sec when other loss mechanisms are negligibly small or absent. (8 refs.)

78074 Design principles for high efficiency small-grain polysilicon solar cells, with supporting experimental studies. F.A.Lindholm (Univ. of Florida, Gainesville, FL, USA), A.Neugroschel, C.T.Sah.

Conference Record of the Sixteenth IEEE Photovoltaic Specialists Conference - 1982, San Diego, CA, USA, 27-30 Sept. 1982 (New York, USA: IEEE 1982), p.644-7

Design principles suggested here aim toward high conversion efficiency (>15%) in polysilicon cells. The principles seek to increase the liabilities of both intragrain and grain-boundary-surface defects. The advantages of a phosphorus atom concentration gradient in a thin (≤ 50 μ m) base of a $p^+/n(x)/n^+$ drift-field solar cell, which produces favorable gradients in chemical potential, minority-carrier mobility and diffusivity, and recombination lifetime (via phosphorus gettering). The degrading effects of grain boundaries are reduced by these three gradients and by substituting atoms (P, H, F or Li) for vacancies on the grain-boundary surface. From recent experiments comes support for the benefits of P diffusion down grain boundaries and for quasi-grain-boundary-free and related structures. New analytic solutions for the $n(x)$ -base include the effect of a power-law dependence between P concentration and lifetime. These provide an upper-bound estimate on the open-circuit voltage. Finite-difference numerical solutions of the Shockley equations furnish complete information about all solar-cell parameters and add insight concerning design. (25 refs.)

78075 Theoretical and experimental studies of tandem or cascade solar cells: a review. J.J.Loferski (Brown Univ., Providence, RI, USA).

Conference Record of the Sixteenth IEEE Photovoltaic Specialists Conference - 1982, San Diego, CA, USA, 27-30 Sept. 1982 (New York, USA: IEEE 1982), p.648-54

Discusses the principles underlying the fabrication of high efficiency solar cells of the tandem or cascade type. Such a PV cell system consists of a number of individual cells in which the photovoltaically active semiconductors (PVAS) have different bandgaps selected in accordance with certain rules. The author describes the 'unit cell' for such a cascade system; the unit cell incorporates minority carrier mirrors to optimize its performance. Identification of semiconductors having energy gaps in the range 1.0 eV to 2.0 eV for the cascade cells is discussed. It is shown that semiconductor alloys must be used for the PVAS. A few potential alloy systems are examined and it is shown that satisfying all the requirements for PVAS in cascade systems results in a very limited number of suitable systems. A brief discussion of the status of experimental work aimed at realization of these PVAS and tandem cells is also included. (15 refs.)

78076 Ternary III-V solar cells for multicolor applications. L.M.Fraas, B.K.Shin, J.A.Cape, R.A.Ransom, D.E.Sawyer (Chevron Res. Co., Richmond, CA, USA).

Conference Record of the Sixteenth IEEE Photovoltaic Specialists Conference - 1982, San Diego, CA, USA, 27-30 Sept. 1982 (New York, USA: IEEE 1982), p.655-62

High efficiency, shallow-junction GaAs(1-x)P(x) and GaAs(1-y)Sb(y) ternary III-V solar cells are reported for the first time. The authors report a GaAs(0.82)P(0.18) cell with a band gap of 1.65 eV and an energy conversion efficiency of 14.8% at 7.4 suns and a GaAs(0.88)Sb(0.12) cell with a band gap of 1.2 eV and a conversion efficiency of 15.6% at 18 suns. Both cells were fabricated on GaAs substrates. These cells were then used as the building blocks for multicolor solar cells. Both two-dimensional and three-terminal, two-color cells were fabricated. The two-terminal devices used a p^+/n GaAs-shorting junction to series connect a GaAs(1-x)P(x) n^+/p visible light-sensing junction to a GaAs(1-y)Sb(y) n^+/p infrared-sensing junction. The expected voltage addition was demonstrated. The three-terminal devices were transistor-like devices in which an n^+/p GaAs(1-x)P(x) cell was grown on a p^+/n GaAs(1-y)Sb(y) cell. The third terminal was attached via etched-in grooves to the GaAs(1-x)P(x) p-layer. The three-terminal device allows independent testing of both active junctions in a monolithic two-color stack. Both junctions in these three terminal devices performed qualitatively as expected. (11 refs.)

78077 Recent developments for the AlGaAsSb cell. M.L.Timmons (Research Triangle Inst., Research Triangle Park, NC, USA), S.M.Bedair, R.J.Markunas, J.A.Hutchby. Conference Record of the Sixteenth IEEE Photovoltaic Specialists Conference - 1982, San Diego, CA, USA, 27-30 Sept. 1982 (New York, USA: IEEE 1982), p.663-8

Improvements in open circuit voltage of the individual components of two junction, monolithic solar cells in the Al-Ga-As-Sb material system are reported. These improvements have accompanied reductions in dislocation densities which have been obtained since changing from (111)A- to (100)-oriented GaAs as the growth substrate. Limits of defect reduction by conventional LPE are being approached, and therefore, further significant device improvements seem unlikely. Hybrid growth using both OMCDV and LPE and growth of superlattice structures are described. These approaches probably have the best chance of solving the remaining defect problem and permitting evaluation of the AlGaAsSb cell's ability to attain the voltages of the cascade model. (10 refs.)

78078 Test data analysis and results for concentrating photovoltaic modules. M.W.Edenburn, H.J.Gerwin, C.J.Chiang (Sandia Nat. Labs., Albuquerque, NM, USA). Conference Record of the Sixteenth IEEE Photovoltaic Specialists Conference - 1982, San Diego, CA, USA, 27-30 Sept. 1982 (New York, USA: IEEE 1982), p.669-74

Presents an expression for efficiency that is a linear function of cell temperature and illumination. This expression is used to correlate test data for concentrating photovoltaic modules. The linear form of the equation is justified by showing that it derives from a cell model that considers the cell to be a parallel current source and diode in series with a resistance. The linear expression has been used to correlate test results for a variety of concentrating modules. Results for those modules that are currently the most promising and interesting to the photovoltaic community are presented in the paper. (4 refs.)

78079 A passive cooled 1000X GaAs module with secondary optics. N.Kaminar, P.Borden, M.Grounner, P.Gregory, R.LaRue (Varian Associates Inc., Palo Alto, CA, USA).

Conference Record of the Sixteenth IEEE Photovoltaic Specialists Conference - 1982, San Diego, CA, USA, 27-30 Sept. 1982 (New York, USA: IEEE 1982), p.675-8
Describes a new module design using 36 GaAs cells running at 1000:1 concentration ratio with passive cooling. The unique optical system uses flat Fresnel lenses and solid glass secondary concentrators to improve on- and off-track performance. Over 18% module efficiency and $\pm 0.8^\circ$ allowable tracking error have been obtained in tests of this optical system. (no refs.)

78080 Design parameters of high efficiency a-SiC:H/a-Si:H heterojunction solar cells. Y.Hamakawa (Faculty of Engng. Sci., Osaka Univ., Osaka, Japan), Y.Tawada, K.Nishimura, K.Tsuge, M.Kondo, K.Fujimoto, S.Nonomura, H.Okamoto.

Conference Record of the Sixteenth IEEE Photovoltaic Specialists Conference - 1982, San Diego, CA, USA, 27-30 Sept. 1982 (New York, USA: IEEE 1982), p.679-84
Design concept and a series of technical data on the a-SiC:H/a-Si:H heterojunction solar cell having conversion efficiency of 8.8% are demonstrated. The cell has a wide band gap window heterojunction layer made of hydrogenated amorphous silicon carbide (a-SiC:H) with a proper valency control. A series of basic properties of the hydrogenated a-SiC:H films are presented. Device physics considerations and optimizations of design parameters for heterojunction solar cells with this new material are demonstrated. Remarkable improvements in cell performances have been attained employing the a-SiC:H window junction. A brief discussion is given on the realistic limit of the conversion efficiency in this type cell. (29 refs.)

78081 Prospects of II-VI based solar cells. S.Wagner (Dept. of Electrical Engng. & Computer Sci., Princeton Univ., Princeton, NJ, USA).

Conference Record of the Sixteenth IEEE Photovoltaic Specialists Conference - 1982, San Diego, CA, USA, 27-30 Sept. 1982 (New York, USA: IEEE 1982), p.685-91
Three out of the four thin film cells that have reached an efficiency of 10% are based on II-VI semiconductors. Does this success in the laboratory forebode a commercial II-VI technology? In an attempt to answer this question the author reviews the applications which the II-VIs have found as windows and as absorbers. He concludes with a discussion of the principal cells, $\text{Cu}_2\text{S}/(\text{Zn,Cd})\text{S}$, $\text{CuInSe}_2/(\text{Zn,Cd})\text{S}$ and CdTe/CdS in the light of a list of empirical criteria for a large scale technology. (21 refs.)

78082 Optimal design of high-efficiency tandem cells. J.C.C.Fan, B.-Y.Tsaur, B.J.Palm (Lincoln Lab., MIT, Lexington, MA, USA).

Conference Record of the Sixteenth IEEE Photovoltaic Specialists Conference - 1982, San Diego, CA, USA, 27-30 Sept. 1982 (New York, USA: IEEE 1982), p.692-701
Computer analysis indicates that a substantial increase in solar cell conversion efficiencies can be achieved by using two-cell, multibandgap tandem structures instead of single-junction cells. Practical AM1 efficiencies of about 30% at one sun and over 30% at multiple suns are to be expected. The further increases in efficiency calculated for a three-cell tandem structure are much smaller and may not justify the added complexity. For inexpensive two-cell tandem modules, Si is preferred for the bottom cell, and the top-cell material should have a bandgap of 1.75 to 1.80 eV. The GaAs-AlAs and GaAs-GaP systems are very attractive candidates for the top cell. Significant advances have been achieved in growing GaAs on Ge-coated Si substrates (for the two-terminal, two-cell structure) and in growing free-standing ultrathin GaAs layers (for the two-terminal or four-terminal structures). These advances should be transferable to the GaAs-AlAs and GaAs-GaP systems. (22 refs.)

78083 Photovoltaic concentrator progress. E.C.Boes (Sandia Nat. Labs., Albuquerque, NM, USA).

Conference Record of the Sixteenth IEEE Photovoltaic Specialists Conference - 1982, San Diego, CA, USA, 27-30 Sept. 1982 (New York, USA: IEEE 1982), p.702-12
Gives a brief but comprehensive summary of the status of photovoltaic concentrator technology. It includes a discussion of various concentrator concepts; a report on the experiences of 6 experimental PV concentrator array fields; test results on more recent PV concentrator module designs; a discussion of data analysis tools; new results on concentrator component development; a discussion of the solar resource differences for flat plate and concentrating collectors; and a discussion of cost analyses and price targets for this technology. (19 refs.)

78084 Final results on the development of high efficient, stable Cu_2S -CdS thin film solar cells. G.H.Hewig, F.Pfisterer, H.W.Schock, W.Arndt, W.H.Bloss (Inst. fuer Phys. Elektronik, Univ. Stuttgart, Stuttgart, Germany).

Conference Record of the Sixteenth IEEE Photovoltaic Specialists Conference - 1982, San Diego, CA, USA, 27-30 Sept. 1982 (New York, USA: IEEE 1982), p.713-18
A procedure for the production of stable Cu_2S -CdS thin film solar cells and modules is described. Diagnostic methods applied in order to optimize the production parameters and the respective material properties of high efficiency cells are summarized. Possible degradation mechanisms are outlined and ways to avoid them are discussed. Large area cells (42 cm^2) show efficiencies up to 8% at AM 1.5. Results of outdoor tests are reported indicating no measurable degradation after more than three years operation with maximum power load. (8 refs.)

78085 Stability of thin-film Cu_2S -based solar cells at V_{oc} under continuous illumination. J.E.Phillips, R.W.Birkmire, P.G.Lasswell (Inst. of Energy Conversion, Univ. of Delaware, Newark, DE, USA).

Conference Record of the Sixteenth IEEE Photovoltaic Specialists Conference - 1982, San Diego, CA, USA, 27-30 Sept. 1982 (New York, USA: IEEE 1982), p.719-22
Thin-film Cu_2S -based solar cells have been developed which are free of the shunting defects that cause the electrochemical decomposition of the Cu_2S . These cells have been held at open-circuit voltage under continuous illumination in an inert or reducing atmosphere for over 500 hours with no degradation in efficiency, short-circuit current, or open-circuit voltage. Laser scanning techniques have been developed as a tool for detecting cell defects and recently, these techniques have been used to locate shunting defects in ungridded Cu_2S -based cells. By using the laser scanner, it has been possible to detect and eliminate defects that cause electrochemical decomposition of the Cu_2S . (11 refs.)

78086 A study of the stability of cadmium sulfide/copper sulfide solar cells. G.T.Noel, G.B.Gaines, N.A.Richard (Battelle Columbus Labs., Columbus, OH, USA).

Conference Record of the Sixteenth IEEE Photovoltaic Specialists Conference - 1982, San Diego, CA, USA, 27-30 Sept. 1982 (New York, USA: IEEE 1982), p.723-30

The results of an experimental study of the intrinsic degradation mechanisms in cadmium sulfide/copper sulfide solar cells are reported. Behavior during degradation of both voltage and current is described. No major trend of fill factor degradation was observed for the primary cells used in this study, although significant degradation of this parameter has been observed in other cell types. The voltage degradation can be recovered by 'resting' or reverse biasing the cells, while recovery of the degradation of the light generated current requires reirradiation. Statistical summaries of degradation data, including degradation rates, for cell groups exposed to combinations of stresses (temperature, load, illumination, roof-top ambient) are presented. These indicate that open-circuit is the most stressful load condition. Possible mechanisms and causative factors for the observed degradation modes are discussed. Preliminary results of a study of the stability of cadmium sulfide/copper-indium selenide photovoltaic devices are also presented. (14 refs.)

78087 Development of spectral response ratios as a diagnostic tool for $\text{Cu}_2\text{S}/\text{CdS}$ thin film cells. L.A.Brickman, J.A.Bragagnolo, H.R.Zwicker (Thin Film Div., Solvovolt Internat., Newark, DE, USA).

Conference Record of the Sixteenth IEEE Photovoltaic Specialists Conference - 1982, San Diego, CA, USA, 27-30 Sept. 1982 (New York, USA: IEEE 1982), p.731-6

Ratios of pairs of spectral response curves for $\text{Cu}_2\text{S}/\text{CdS}$ thin-film solar cells are shown to exhibit highly sensitive spectral shapes which are characteristic of certain process variations or degradation modes. These shapes can be related to variations in specific parameters in a theoretical quantum efficiency model which describes both photon and electron losses in the device. This 'ratio technique' is used as a non-destructive diagnostic tool for light-generated current losses in $\text{Cu}_2\text{S}/\text{CdS}$ cells. (11 refs.)

78088 Copper sulfide/cadmium sulfide heterojunction cell research by sputter deposition. J.A.Thornton (Telic Co., Santa Monica, CA, USA), D.G.Cornog, W.W.Anderson, R.B.Hall, J.E.Phillips.

Conference Record of the Sixteenth IEEE Photovoltaic Specialists Conference - 1982, San Diego, CA, USA, 27-30 Sept. 1982 (New York, USA: IEEE 1982), p.737-42

Reports on an investigation concerning the use of magnetron reactive sputtering for fabricating $\text{Cu}_2\text{S}/\text{CdS}$ solar cells. Hybrid cells have been fabricated which combine reactive sputtered Cu_2S with evaporated CdS and (CdZn)S layers. A $\text{Cu}_2\text{S}/(\text{CdZn})\text{S}$ (14 at.% Zn) cell of this type, with an evaporated Ta_2O_5 antireflection layer, has yielded: $J_{sc}=18.5 \text{ mA/cm}^2$, $V_{oc}=0.53 \text{ V}$, $\text{FF}=0.72$ and $\eta=7.20\%$. All-sputtered planar thin film $\text{Cu}_2\text{S}/\text{CdS}$ cells have been deposited onto glass substrates, without breaking vacuum, using a multi-source deposition apparatus. A cell of this type without an antireflection coating has yielded: $J_{sc}=12.2 \text{ mA/cm}^2$, $V_{oc}=0.53 \text{ V}$, $\text{FF}=0.62$ and $\eta=3.94\%$. (17 refs.)

Some maximal thermodynamic efficiencies for the conversion of blackbody radiation See Entry 74419

Thermal performance of radiative cooling panels See Entry 75908

Photovoltaic measurement of bandgap narrowing in moderately doped silicon See Entry 77000

An introduction to silane project in ROC See Entry 77541

Flat-plate solar array progress and plans See Entry 77544

Directional solidification of silicon in carbon crucibles by an Oscillating Crucible Technique See Entry 77554

Advanced crystallization techniques of 'solar grade' silicon See Entry 77555

Progress in growth of silicon ribbon by a low angle, high rate process See Entry 77556

Large area silicon sheet produced by the spinning method See Entry 77557

Thin-film epitaxial solar cells on substrates made from MG silicon by the HEM process See Entry 77565

A low-cost polysilicon process based on the synthesis and decomposition of dichlorosilane See Entry 77582

Growth of polysilicon sheets on a carbon shaper by the RAD process See Entry 77586

Interaction between cast silicon properties and solar cell performance See Entry 77592

Evaluation of electrode shape and nondestructive evaluation method for welded solar cell interconnects See Entry 77588

Nondestructive testing of interconnect welds using the Scanning Laser Acoustic Microscope (SLAM) See Entry 77589

- Current research in adhesiveness bonding of cover glasses to solar cells See Entry 77861
- Luminescent solar concentrators as bifacial captors See Entry 77963
- Hydrogen pretreatment of CdS films and properties of CdS/NaOH/Pt cells See Entry 78089
- Development and evaluation of the Texas Instruments Solar Energy System See Entry 78090

86.30K Photoelectrochemical conversion

78089 Hydrogen pretreatment of CdS films and properties of CdS/NaOH/Pt cells. C.D.Lokhande, M.D.Uplane, S.H.Pawar (Dept. of Phys., Shivaji Univ., Kolhapur, India). *Indian J. Pure & Appl. Phys.*, vol.21, no.2, p.78-81 (Feb. 1983). Cadmium sulphide films have been deposited on both glass and stainless steel substrates by chemical bath deposition technique. The post-preparation heat treatment in hydrogen atmosphere is given to the films and CdS/NaOH/Pt cells are formed. The influence of hydrogen treatment to CdS film electrode on the electrical and optical properties of these cells is studied. The variation of I_{sc} and V_{oc} is explained as due to the diffusion of sulphur vacancies and due to the increase in crystallinity in the CdS film both being caused by the heat treatment. (17 refs.)

78090 Development and evaluation of the Texas Instruments Solar Energy System. W.R.McKee, K.R.Carson, J.D.Levine (Texas Instruments Inc., Dallas, TX, USA).

Conference Record of the Sixteenth IEEE Photovoltaic Specialists Conference - 1982, San Diego, CA, USA, 27-30 Sept. 1982 (New York, USA: IEEE 1982), p.257-62

The Texas Instruments Solar Energy System (TISES) is a unique solar energy conversion and storage system with many potential cost advantages over other approaches now being considered. The individual photovoltaic elements are tiny silicon spheres which are packed into thin glass sheets and then immersed in an HBr electrolyte where they perform an electrolysis function. The system provides for storage of the reaction products and then recombination in a fuel cell to produce an electrical output. The development status of the various system components are presented. Plans for outdoor testing of a complete, functional prototype unit are discussed. (5 refs.)

86.30Q Chemical energy conversion

(for electrochemical conversion, see 86.30D; for photoelectrochemical conversion, see 86.30K)

78091 Transfer and storage of chemical and radiation potential. G.Porter (Davy Faraday Res. Lab., Royal Inst., London, England). *J. Chem. Soc. Faraday Trans. II (GB)*, vol.79, pt.3, p.473-82 (March 1983). The change in potential which accompanies any spontaneous process is given by $RT \ln[1 - (j/J)]$, where j is the net forward flux and J is the forward flux at the same reactant potential but in the absence of products. This equation is applied to thermal and photochemical reactions. For the latter, the author introduces and evaluates the quantities 'radiation potential' and 'scattered radiation potential' in analogy with 'chemical potential'. 'Storage' of energy is defined and shown to be a two-stage process. Thermodynamic losses are relatively small provided the rather stringent requirements of geometry and transport kinetics can be met. The influences of these several factors on the efficiency of solar-energy collection and storage are evaluated. (12 refs.)

86.30S Photothermal conversion

78092 Flow distribution in parallel connected manifolds for evacuated tubular solar collectors. R.C.McPhedran, D.J.M.Mackey, D.R.McKenzie, R.E.Collins (School of Phys., Univ. of Sydney, Sydney, NSW, Australia). *Aust. J. Phys. (Australia)*, vol.36, no.2, p.197-219 (1983).

A model is presented for predicting the flow distribution in solar collector manifolds in which risers are connected in parallel between headers. Both frictional and Bernoulli effects are considered. The distributions resulting from flow in the manifold in which header streams are parallel and opposed are calculated and compared with experiment. Parallel flow gives a more uniform distribution. The outlet header is found to be more critical in balancing the flow distribution than the inlet header. Conditions under which thermosiphon effects are important and flow reversal in risers may occur are discussed with reference to experiment. (10 refs.)

78093 F-chart method applied to large-scale solar collector systems subject to a shadow effect of adjacent collectors. M.Schroeder (Vereinigte Deutsche Metallwerke AG, Frankfurt, Germany). *Int. J. Sol. Energy (Switzerland)*, vol.1, no.3, p.169-84 (1982).

The specific example of a 400-bed hotel is investigated to determine how the shadow effect due to adjacent collectors, arising through a limited roof area, is reflected in the behaviour of the annual f as a function of the collector surface. The study is performed for two different locations of the hotel, Almeria, Spain, and Freiburg, Germany, which reveals the dependence of the latitude on the shadow effect. It is illustrated that the effect of shading is substantially affected by the monthly distribution of the occupation of the hotel. The optimal collector surface in the presence of the shadow effect is then determined from economic aspects by seeking the surface yielding the maximum life-cycle savings. (8 refs.)

78094 Radiation heat exchange in a solar cavity-type receiver at various times. K.Spindler, U.Gross, E.Hahne (Inst. fur Thermodynamik und Warmetech., Univ. Stuttgart, Stuttgart, Germany). *Int. J. Sol. Energy (Switzerland)*, vol.1, no.3, p.197-212 (1982).

Steady-state solar and infrared radiation heat exchange in the cavity receiver of a solar tower is presented in the form of a mathematical model. The inside cavity walls consist partly of tubes containing air as a heat carrier. The distribution of tube wall temperatures, air temperature, and the heat flux density along the tubes are calculated at different times of day for different seasons. The efficiency of solar and infrared radiation exchange in the cavity is determined, as well as cosine losses of the heliostate field. The receiver layout is based on maximum gain on 21 June, 12 o'clock noon. (3 refs.)

78095 Present state and development of solar techniques. D.Teodorescu. *Elektr. Masch. (Germany)*, vol.62, no.2, p.43-8 (Feb. 1983). In German. Discusses the production of temperatures above 300°C by solar energy devices for power production. Several solar heat absorbers capable of meeting such power requirements are described. Heat transfer is up by a flow of liquid or gas. Particular attention is paid to the lagging. A revolving sun ray collector incorporating focusing mirrors is described. Other developments and applications dealt with are Stirling cycle solar motors and solar cells. (31 refs.) G.R.S.

78096 A simplified theory for a matrix solar collector. D.Singh, N.K.Bansal (Indian Inst. of Technol., Hauz Khas, New Delhi, India). *Int. J. Energy Res. (GB)*, vol.7, no.2, p.173-7 (April-June 1983).

Presents a simple generalized analysis for a matrix collector and obtains closed form solutions for the equations. Numerical calculations are performed corresponding to the experimental data of Chau and Henderson. (3 refs.)

78097 Performance of n forced circulation water heating systems in series. M.S.Sodha, V.S.V.Bapeshwara Rao, G.N.Tiwari (Indian Inst. of Technol., New Delhi, India). *Int. J. Energy Res. (GB)*, vol.7, no.2, p.179-86 (April-June 1983).

Presents an analytical investigation of the thermal performance of a forced circulation solar water heating system in which n water heating systems are connected in series. Numerical calculations have been made for a typical cold day (26 January 1980) in Delhi, India, and some interesting conclusions have been presented. (15 refs.)

78098 A dynamic simulation of a flat-plate collector system. A.Annino (Istituto di Fisica, Facolta di Ingegneria, Catania, Italy). *Nuovo Cimento B (Italy)*, vol.74B, ser.2, no.2, p.139-50 (11 April 1983).

Starting with the energy balance analysis of a solar flat-plate collector, a model has been developed to simulate the system's behaviour. The model uses the state equation formalism which permits an easy simulation by minicomputer (Olivetti P6060). The experimental tests performed show that the model describes well the energy output, the spatial distribution and the time dependence of temperature in various elements. (12 refs.)

78099 Ge-Al thin films for selective solar absorbers. F.R.Kessler, K.Dettmer, E.-W.Ritters (Inst. fur Halbleiterphys. und Optik, Tech. Univ. Braunschweig, Braunschweig, Germany). *Phys. Status Solidi A (Germany)*, vol.76, no.2, p.533-41 (16 April 1983).

Ge-Al thin films prepared by simultaneous evaporation in high vacuum show plasma resonance adjustable between 1 and 3 μm . The relatively sharp change from high reflectivity at $\lambda < \lambda_r$ to low reflectivity in connection with negligible transparency at $\lambda < \lambda_r$ make them suitable for selective solar absorbers especially at high working temperatures between 50 and 250°C. The selectivity is about 25. Under AM 1 illumination and thermal isolation a stationary steady-state temperature of 280°C is reached. This value is valid in the case of an additive antireflection coating adjusted for $\lambda = 0.55 \mu\text{m}$. The static and dynamic characteristics are given. The very high degree of degeneracy of the p-type overdoped germanium thin films is characterised by the position of the Fermi level inside the valence band down to 0.7 eV. The resulting optical properties of the thin films are discussed. Thermoreflection measurements especially indicate the failure of the E_0' and $E_0' + \Delta_0$ interband transitions near 3.2 eV. (9 refs.)

78100 Effects of a solar reflecting film on the reduction of solar heat gain through fenestration. Y.Urano, A.Hoyano, Y.Shiotsuki, S.Chirifu, Y.Kumagawa. *Technol. Rep. Kyushu Univ. (Japan)*, vol.55, no.6, p.657-65 (Dec. 1982). In Japanese. [received: May 1983]

Control of solar heat gain through fenestration has been considered to be of increasing importance as a result of the great use of glass in buildings. The effects of a solar reflecting film attached on the inner surface of window panes on the thermal environment of a room were investigated. The measurements were carried out in an existing building in which 75% of the facade area was covered with glass and which had no concavities. The components of solar heat gain were calculated and the solar heat gain factors of the reflecting film were obtained. The use of the reflecting film with 17% solar transmittance reduces the solar heat gain by 25 to 55% as compared with the conditions without the film, and the use of it improves the thermal environment at the perimeter zone of the room. (7 refs.)

78101 Entwicklung von autarken Solarkuhlanlagen mit konzentrierenden Kollektoren (Development of self-sufficient solar cooling devices with concentrating collectors). H.Simon. *Report EUR 8165 DE*, Comm. European Communities, Luxembourg (1982), 35 pp. In German. Contract ESA/C/043/D.

Tests are reported on an ammonia-water-absorption cooling machine of about 10 kW capacity (with electrical collector simulation) to observe its performance and efficiency. Two modes of coupling of the collector and the absorption cooling unit were tried out and compared; the direct coupling enabled good system control. The achieved efficiency of the system was about 20% below the predicted one. By reducing the air heat exchanger rating to half the system could be successfully used for air conditioning. Data of the two systems are tabulated and results of tests carried out in summer and winter in various geographical locations are shown.

78102 Weathering performance of cover materials for flat plate solar collectors. E.J.Clark, W.E.Roberts. *Report NBS-TN-1170*, Nat. Bur. Stand., Washington, DC, USA (Nov. 1982), x+69 pp.

Weathering studies were performed to obtain data on the performance and durability of cover plate materials for flat plate solar collectors used in solar heating and cooling systems. Ten materials were evaluated to assess their durability after natural weathering and artificial weathering with a xenon arc light. The materials were weathered for four years on small minicollectors in Arizona, Florida, and Maryland after which the solar energy transmittance and the effect of dirt on the transmittance were measured. The tensile properties of selected film materials were also assessed after weathering. The effects of the natural weathering are compared: (1) for materials exposed as inner and outer cover plates for each weathering site; (2) for the three weathering sites; and (3) with materials artificially weathered with a xenon arc light. (19 refs.)

78103 Design and construction of a hybrid photovoltaic (3 kW_{th})-thermal solar energy system for a residential/commercial building. J.J.Loferski, C.Case, G.Doodesack, B.Roessler, R.Dobbins, T.Russell, J.Beall, J.Krikorian (Div. of Engng., Brown Univ., Providence, RI, USA).

Conference Record of the Sixteenth IEEE Photovoltaic Specialists Conference - 1982, San Diego, CA, USA, 27-30 Sept. 1982 (New York, USA: IEEE 1982), p.188-93

Describes the planning, design and construction of a flat plate hybrid photovoltaic/thermal system with an electric heat pump intended for on-site generation of heat and electricity for a dwelling or commercial building. The twenty PV/T collectors have 3'x6' absorber surfaces and incorporate approximately 3000 four inch diameter silicon cells bonded to glass with a high-temperature-tolerant, UV-degradation-resistant silicone bonding cement. Extensive computer modelling of the system has shown that about 65% of the total annual energy needs (heating, cooling, hot water, distributed electric load) will be provided by the PV/T system. Half of this energy will be electrical; half, thermal. Coupling with the utility is through a synchronous inverter. The system can store thermal energy for space heating in a rock bin storage box. Results of an economic analysis are also included. (4 refs.)

| | |
|--|-----------------|
| Static concentrators theory for non-homogeneous extended sources | See Entry 77962 |
| Design and fabrication of the BDM southwest photovoltaic residence prototype | See Entry 77964 |
| The design and development of a high concentration and high efficiency photovoltaic concentrator utilizing a curved Fresnel lens | See Entry 77966 |

86.30Z Other topics

| |
|---|
| 78104 The importance of biomass peak power plants in power industry. M.Vronsky. <i>Energetika (Czechoslovakia)</i> , vol.33, no.3, p.114-16 (1983). In Slovak. The concept of biomass conversion based on a dry fermenting process is described. It is pointed out that investment costs for power plants based on this process are relatively low and that even small plants which can be situated near the sources of biological waste materials can become feasible. Drive motors suitable for biomass converting plants are briefly dealt with. It is pointed out that costs savings can be achieved by using some by-products of the conversion process (fertilizers). The potential of the conversion process in Czechoslovakia is assessed. (4 refs.) E.D. |
|---|

86.40 ENERGY STORAGE (SECONDARY ENERGY)

86.40F Storage in thermal energy

| | |
|--|-----------------|
| 78105 Seasonal thermal inventory. C.I.Staicu, C.Bilegan, A.Mihaila, A.Predica. <i>Energetica (Romania)</i> , vol.31, no.1, p.35-9 (Jan. 1983). In Rumanian. The present all-over seasonal thermal inventory stage is presented and the solutions applied for the heat storage are described briefly. Technical data for practical seasonal thermal inventories are given. Referring to the theoretical study of the thermal storage it is shown that the equations describing hydrodynamic and transfer processes are solved by the method of finite elements by computer. Finally, the main problems which determine the seasonal thermal storage are outlined. (7 refs.) | |
| Design and fabrication of the BDM southwest photovoltaic residence prototype | See Entry 77964 |
| Design and construction of a hybrid photovoltaic (3 KW _p)-thermal solar energy system for a residential/commercial building | See Entry 78103 |

86.40H Storage in chemical energy

| | |
|---|-----------------|
| Development and evaluation of the Texas Instruments Solar Energy System | See Entry 78090 |
| Theoretical and experimental aspects of a two-step short cycle, based on ZnO and CdO intended for storage of solar energy | See Entry 78106 |

86.40K Hydrogen storage and technology

| | |
|--|-----------------|
| 78106 Theoretical and experimental aspects of a two-step short cycle, based on ZnO and CdO intended for storage of solar energy. M.Comtat (Lab. de Chimie-Phys. et d'Electrochimie, Univ Paul-Sabatier, Toulouse, France), M.Ducarroir, F.Sibieude, G.Crozat, B.Spinner. <i>Int. J. Energy Res. (GB)</i> , vol.7, no.2, p.137-53 (April-June 1983). Chemical and energetical considerations about hybrid thermal electrochemical cycles based on zinc and cadmium oxides are developed. Intermediate reactions have been taken into account. Numerical data obtained from decomposition experiments of the oxides in a solar furnace and from electrolysis experiments with Zn and Cd metals (or metal-oxide mixtures) used as an anode, are discussed. The energy balance for the hydrogen production using the mentioned cycles is compared with a direct electrolytic water-splitting process working with thermopiles or photopiles solar plants as electricity source. (23 refs.) | |
| 78107 A solar-hydrogen economy for USA. J.O'M.Bockris, T.N.Vezirloglu (Texas A&M Univ., Coll. Station, TX, USA). <i>Int. J. Hydrogen-Energy (GB)</i> , vol.8, no.5, p.323-40 (1983). For the post-fossil fuel era, there are two main options. One is well known: a fusion hydrogen combination, in which fusion is the primary energy source and hydrogen is the energy carrier. The other option, the solar-hydrogen alternative, is less widely discussed, though it is far more likely to succeed in a reasonable time-scale. It is envisaged that the solar energy will be collected in the highly insulated regions, where it will be used to produce hydrogen from water. Hydrogen would then be transported to consumption centres to meet the energy requirements. There are many ways through which hydrogen can be used in homes and buildings, in cars, in airplanes, in industry, in chemistry and metallurgy, in synthetic food production and in military, more efficiently than any other known fuel. Economically it would not be feasible to replace the fossil-based energy structure all at once, but it would be prudent to start phasing in the solar-hydrogen system by limiting the change to new energy conversion plants. Such a change would be most cost-effective and could be completed in ca 40-60 years—the average life span for energy conversion and distribution systems. To achieve this conversion, a National Energy Resources Executive is recommended. (55 refs.) | |
| Sorption of hydrogen and deuterium in a glassy Pd-Si alloy by a bending-cantilever method | See Entry 76795 |
| Hydrogen production with visible light by using dye-sensitized TiO ₂ powder | See Entry 77904 |
| Catalytic hydrogenation with amorphous and crystalline Pd ₄₀ Si ₆₀ | See Entry 77923 |
| The potential supply of synthetic fuels from Alaskan hydroelectric power and coal | See Entry 77955 |
| Development and evaluation of the Texas Instruments Solar Energy System | See Entry 78090 |

86.70 ENVIRONMENTAL SCIENCE

(see also 87.60R Radioactive pollution; for oceanographic aspects, see 92.10; for hydrological aspects see 92.40; for meteorological aspects see 92.60)

86.70C Soil

| |
|--|
| 78108 An evaluation of soil sampling for ¹³⁷ Cs using various field-sampling volumes. J.W.Nyhan, G.C.White, T.G.Schofield, G.Trujillo (Los Alamos Nat. Lab., Los Alamos, NM, USA). <i>Health Phys. (GB)</i> , vol.44, no.5, p.541-52 (May 1983). The sediments from a liquid effluent receiving area at the Los Alamos National Laboratory and soils from an intensive study area in the fallout pathway of Trinity were sampled for ¹³⁷ Cs using 25-, 500-, 2500- and 12500-cm ³ field sampling volumes. A highly replicated sampling program was used to determine mean concentrations and inventories of ¹³⁷ Cs at each site, as well as estimates of spatial, aliquoting, and counting variance components of the radionuclide data. The sampling methods were also analyzed as a function of soil size fractions collected in each field sampling volume and of the total cost of the program for a given variation in the radionuclide survey results. Coefficients of variation (CV) of ¹³⁷ Cs inventory estimates ranged from 0.063 to 0.14 for Mortandad Canyon sediments, whereas CV values for Trinity soils were observed from 0.38 to 0.57. (20 refs.) |
|--|

86.70E Water

| | |
|--|-----------------|
| 78109 The actual ³ H content of the hydrosphere in Central Europe (1980). D.Rank, V.Rajner (Geotech. Inst. der Bundesversuchs- und Forschungsanstalt Arsenal, Wien, Austria). <i>Acta Phys. Acad. Sci. Hung. (Hungary)</i> , vol.52, no.3-4, p.435-41 (1982). In German. [received: May 1983] (Proceedings of the Hungarian-Austrian Health Physicists' Meeting, Gyor, Hungary, 28 Sept.-1 Oct. 1981). Explains that the ³ H content of the hydrosphere is (due to nuclear weapon tests) 5 to 10 times the normal level (due to natural radiation). The ³ H content of precipitation and lakes is gradually dropping (to 4.8 Bq/kg in 1980). The radiation dose, per head of population in the public water supply of Vienna, was 70 nSv per annum, in 1980. Maps, graphs and tables show details of measurements. (5 refs.) J.S. | |
| 78110 Finite element analysis of transport of radionuclides in porous media. F.Havlicek (Statni Vyzkumny Ustav Pro Stavbu Stroj, Praha, Czechoslovakia). <i>Jad. Energ. (Czechoslovakia)</i> , vol.29, no.5, p.176-9 (May 1983). In Czech. Outlines the mathematical description of transport of radionuclides in geosphere, and the corresponding finite element analysis. The method allows to solve a fluid flow and associated transport of radionuclides in a porous media of general shapes and under general conditions. (9 refs.) | |
| Fourth International Ocean Disposal Symposium | See Entry 74222 |
| Problems in modelling the transport of material from deep-sea dumpsites | See Entry 75111 |
| The effects of radiation exposure on aquatic organisms | See Entry 75112 |
| Studies of the radiosensitivity of deep-sea bacteria | See Entry 75113 |
| Effect of radiation on sister chromatid exchanges and chromosomal deletions in the benthic worm <i>Neanthes arenaceodentata</i> | See Entry 75114 |
| Radioactive contamination of the marine environment, uptake and distribution of tritium and technetium in <i>Acetabularia</i> and other marine algae | See Entry 75115 |
| The role of biogenic debris in the vertical transport of transuranic wastes in the sea | See Entry 75116 |
| Comparative behavior of plutonium and americium in the Equatorial Pacific | See Entry 75117 |
| The influence of diagenetic redox reactions on the distribution of ^{239,240} Pu, ¹³⁷ Cs, ²⁴¹ Am and ⁵⁵ Fe in sediments of the US continental margin | See Entry 75118 |
| Behavior of long-lived nuclides associated with radioactive wastes in the deep-sea | See Entry 75119 |
| Development of an ocean model for use in radiological assessments of sea disposal of solid radioactive wastes | See Entry 75120 |
| Equipment for 3-dimensional measurements of natural and artificial tracers in the sea | See Entry 75121 |
| Relationship between the distribution of radionuclides and the seimentological and mineralogical traits of the coastal marine sediments (Gaeta, Latina, La Spezia, Italy) | See Entry 75122 |
| The NEA research and environmental surveillance program related to sea disposal of radioactive waste | See Entry 75123 |
| Surface water considerations in facility design and operation | See Entry 75128 |
| Predictability of solute transport in diffusion-controlled hydrogeologic regimes | See Entry 75145 |
| Estimation of per caput dose and collective dose from the use of Danube water | See Entry 78340 |
| Radioactive contamination of filamentous green algae in the Hungarian reach of the River Danube | See Entry 78363 |
| Radioactivity of fish in the Hungarian reach of the River Danube | See Entry 78364 |
| Transport and deposition of plutonium in the ocean: evidence from Gulf of Mexico sediments | See Entry 78557 |
| Preliminary observations on californium-252 behaviour in sea water, sediments and zooplankton | See Entry 78558 |
| On the radiocarbon record in banded corals: exchange parameters and net transport of ¹⁴ CO ₂ between atmosphere and surface ocean | See Entry 78559 |
| Large particle transport of plutonium and other fallout radionuclides to the deep ocean | See Entry 78561 |
| Determination of phosphorus in natural waters by long-capillary-cell absorption spectrometry | See Entry 78654 |

86.70G Atmosphere

78111 Examination of a hot particle from a recent atmospheric test. I.Maschek, T.Csepregi ('Frederic Joliot-Curie' Nat. Res. Inst. for Radiobiology & Radiohygiene, Budapest, Hungary). *Acta Phys. Acad. Sci. Hung. (Hungary)*, vol.52, no.3-4, p.405-11 (1982). [received: May 1983] (Proceedings of the Hungarian-Austrian Health Physicists' Meeting, Gyor, Hungary, 28 Sept.-1 Oct. 1981). Changes in airborne activity concentration can usually be observed by determining the radioactivity of collected aerosol. A hot particle was found on an aerosol sample. The hot particle contained fission nuclides like ^{95}Zr and ^{95}Nb , it was solely present on the sample, it originated in the atmospheric nuclear test of 16 October 1980, it was captured a few days before reaching the maximum activity of ^{95}Nb induced directly by ^{95}Zr , and finally its size was about one micrometer. (4 refs.)

78112 Parametrization of air pollution in the surface layer of a complex of transforming and interacting admixtures. K.G.Ganev, D.L.Yordanov (Geophys. Inst., Bulgarian Acad. of Sci., Sofia, Bulgaria). *C.R. Acad. Bulg. Sci. (Bulgaria)*, vol.36, no.1, p.69-72 (1983). A method for the parametrization of pollution is generalized in the case of surface layer pollution by a number of different weightless admixtures which interact and turn into one another. The approximation of stationary turbulent diffusion of admixtures from an infinite flat horizontal homogeneous source in a stationary and horizontal homogeneous surface layer is included. (2 refs.)

78113 An exact solution to the Gaussian cloud approximation for γ absorbed dose due to a ground-level release. T.J.Overcamp, R.A.Feld (Environmental Systems Engng., Clemson Univ., Clemson, SC, USA). *Health Phys. (GB)*, vol.44, no.4, p.367-72 (April 1983). An exact solution is presented for the classical Gaussian cloud approximation for long-term averaged estimates of γ adsorbed dose due to a ground-level release of radioactive gases and particles. The solution is in the form of relatively simple functions and is much easier to implement than the traditional solution. Also, it is shown that the Gaussian cloud approximation predicts lower absorbed dose than the uniform cloud approximation. The difference is significant when the product of γ attenuation coefficient and vertical dispersion coefficient is small. Since the Gaussian cloud approximation is based on a more realistic concentration distribution than the uniform cloud approximation, the calculations using the former should give more accurate estimates of the long-term averaged dose for the sector-averaged plume. (6 refs.)

78114 Uncertainties of predictions of future atmospheric CO_2 concentrations. H.Oeschger, M.Heimann (Phys. Inst., Univ. of Bern, Bern, Switzerland). *J. Geophys. Res. (USA)*, vol.88, no.C2, p.1258-62 (20 Feb. 1983). (Symposium on the Rise in Atmospheric Carbon Dioxide, Bern, Switzerland, 14-18 Sept. 1981). Linear carbon cycle models, tuned to reproduce the CO_2 increase observed at Mauna Loa, independently of their individual assumptions, predict almost identical CO_2 concentration trends for fossil energy scenarios assuming a slightly increasing production in the next few decades. The basic information for such prognoses therefore is the airborne fraction observed over the last 20 years. Uncertainties in this quantity are due to possible errors in the estimate of fossil fuel consumption and the corresponding CO_2 emission, possible natural fluctuations in the baseline CO_2 level, and uncertainties regarding the biospheric CO_2 input and uptake as a result of deforestation and reforestation and land management. Depending on different assumptions the effective airborne fraction, defined as the ratio of CO_2 increase due to fossil fuel CO_2 alone to the integrated CO_2 production, might be as low as 0.38 or as high as 0.72, compared to the apparent airborne fraction of 0.55. (16 refs.)

78115 Distribution of and changes in industrial carbon dioxide production. R.M.Rotty (Inst. for Energy Analysis, Oak Ridge Assoc. Univ., Oak Ridge, TN, USA). *J. Geophys. Res. (USA)*, vol.88, no.C2, p.1301-8 (20 Feb. 1983). (Symposium on the Rise in Atmospheric Carbon Dioxide, Bern, Switzerland, 14-18 Sept. 1981). The burning of fossil fuels is believed to be the major source responsible for an observed increase in the concentration of carbon dioxide in the atmosphere. This paper revises earlier published data on the annual amounts of carbon released to the atmosphere during the period 1950-1978 and updates the record through 1980. A latitudinal distribution of the fossil fuel source is presented as an aid in explaining the differences in the observed CO_2 concentrations at several stations. The latitudinal distribution of the fossil fuel production of CO_2 should be an important aid in carbon-cycle analysis. (17 refs.)

78116 Detection and identification of emission sources on the basis of the trace element composition of aerosols. J.Berzi, G.Koomley, Zs.Molnar, T.Varkonyi (Nuclear Training Reactor, Tech. Univ. of Budapest, Budapest, Hungary). *Period. Polytech. Electr. Eng. (Hungary)*, vol.26, no.1-2, p.123-37 (1982). In the course of these investigations, a method to accurately determine the main and trace elements of aerosols in the atmosphere has been developed. In the basis of the results of chemical analysis, two methods, different in principle, to identify the emission sources are discussed. These methods were used to prove the doubtless relation between environmental samples and samples obtained from the flue of the power plant in different points and at different times on the basis of an analysis of emission and environmental samples resulting from the Komlo Power Plant and its environment. The analytical and computation method developed is considered to be suited for handling more complex environmental problems where more emission sources have to be identified, and their contribution to the combination of the environment has to be determined exactly. (16 refs.)

Symposium on the Rise in Atmospheric Carbon Dioxide See Entry 74212
Physico-Chemical Behaviour of Atmospheric Pollutants. Proceedings of the Second European Conference See Entry 74233

Fiber-optic absorption/fluorescence probes for combustion measurements See Entry 77927

Repetitive scanning type self-modulation spectroscopy applied to a monitor of ambient air pollution See Entry 78118

SO_2 -measurement with the new UV-BINOS See Entry 78119

Analysis of tritium in tree rings See Entry 78365

Feedback mechanisms in the climate system affecting future levels of carbon dioxide See Entry 78602

Exponential growth and atmospheric carbon dioxide See Entry 78604

The sources of sulfate in precipitation. I. Parameterization scheme and physical sensitivities See Entry 78612

The sources of sulfate in precipitation. II. Sensitivities to chemical variables See Entry 78613

On the relationship between the greenhouse effect, atmospheric photochemistry, and species distribution See Entry 78615

Chlorocarbon emission scenarios: potential impact on stratospheric ozone See Entry 78616

Effect of coupled anthropogenic perturbations on stratospheric ozone See Entry 78617

The seasonal variation of the atmospheric SO_2 to SO_4^{2-} conversion rate See Entry 78623

86.70J Noise

(see also 43.50 Noise, its effects and control)

78117 Physical parameters at the valuation of the annoyance of industrial noises. W.Brennecke, H.Remmers (Fachbereich Phys., Univ. Oldenburg, Oldenburg, Germany). *Acustica (Germany)*, vol.52, no.5, p.279-89 (April 1983). In German. 25 representative industrial noises are presented to 80 subjects for the evaluation of annoyance by pair-comparison. The evaluation of the subjective estimation is made by the process of the principle components analysis. Relevant acoustic parameters, whose measuring methods are presented and discussed, are taken for correlation with these results. In addition to the loudness it is especially the sharpness of the noises which delivers significant correlations with the subjectively perceived annoyance. After equalization of the sound level of the noises to a medium level-value, it is also the roughness and tonality which show significant correlations with the factors from the preference analysis. (28 refs.)

86.70L Measurement techniques in environmental science

78118 Repetitive scanning type self-modulation spectroscopy applied to a monitor of ambient air pollution. T.Izumi, N.Takeda. *Anritsu Tech. Bull. (Japan)*, no.44, p.57-67 (March 1983). In Japanese. Design principles of the self-modulation spectroscopy (SELMOD) are discussed and in particular an improved SELMOD system to which a wavelength scanning and a moving average technique are introduced. In this improved method, the average of the second derivative spectra is obtained by repetitive wavelength scanning, and both the sensitivity and stability are remarkably improved. Experimental results show the lower detection limit of the instantaneous reading of the concentration for NO_2 and both SO_2 and NO is 2-3 ppb and 5-6 ppb respectively, even if the ambient temperature fluctuates between 0-40°C. (8 refs.)

78119 SO_2 -measurement with the new UV-BINOS. G.Wiegleb, A.Radow, R.Ross (Leybold Heraeus GmbH, Hanau, Germany). *Tech. Mess. tm (Germany)*, vol.50, no.4, p.143-50 (April 1983). In German. Sulphur dioxide (SO_2) is one of the most important industrial gases. The present SO_2 -measuring technique in process control and exhaust-monitoring is based on the IR-absorption principle. This principle has some disadvantages such as water vapour interference and resolution limitation. An absorption measurement in the UV-range around 285 nm with the BINOS-system doesn't have these disadvantages, so that it is possible to measure SO_2 -concentrations up to 100 ppm and a resolution of 0.1 ppm without water vapour interference. (4 refs.)

Proceedings of the Hungarian-Austrian Health Physicists' Meeting See Entry 74198

Proceedings of the Symposium on Low-Level Waste Disposal. Vol.3. Facility Design, Construction, and Operating Practices (NUREG/CP-0028) See Entry 74223

Equipment for 3-dimensional measurements of natural and artificial tracers in the sea See Entry 75121

Environmental monitoring considerations for low-level waste disposal sites See Entry 75131

Environmental monitoring system at the Paks Nuclear Power Station See Entry 75188

Telemetric and data acquisition system for environmental monitoring at the Paks Nuclear Power Station See Entry 75189

Gamma spectrometric measuring system for environmental sample analysis See Entry 75190

Monitoring external radiation in the environment: instruments and results of measurements See Entry 75193

Fiber-optic absorption/fluorescence probes for combustion measurements See Entry 77927

Detection and identification of emission sources on the basis of the trace element composition of aerosols See Entry 78116

Acoustic remote sensing of the boundary layer See Entry 78707

86.70Z Other topics

Deposition and retention of ^{141}Ce and ^{134}Cs aerosols on cool desert vegetation See Entry 78367

87.00 BIOPHYSICS, MEDICAL PHYSICS, AND BIOMEDICAL ENGINEERING

87.10 GENERAL, THEORETICAL, AND MATHEMATICAL BIOPHYSICS

(inc. logic of biosystems, quantum biology, and relevant aspects of thermodynamics, information theory, cybernetics, and bionics)

Markov analysis of alpha-helical, beta-sheet and random coil regions of proteins See Entry 78137

Pointwise bounds for the solution of a nonlinear problem in cell membrane theory See Entry 78161

Establishment of an oscillatory regime in a dissipative biological system See Entry 78165

- Analysis of limit-cycle conditions in intercoupled relay oscillators with reference to gastrointestinal modelling See Entry 78169
- Micromotion in smooth muscle related to circulation control: a hypothesis See Entry 78216
- Constructing a mathematical model for myocardial infarction See Entry 78223
- A mathematical model of the effects of light on the eclosion rhythm of the fruit fly *Drosophila pseudoobscura* See Entry 78235
- Statistical characterisation of a critical group See Entry 78342

87.15 MOLECULAR BIOPHYSICS

(see also 36.20 Macromolecules and polymer molecules)

- 78120** Intermolecular interactions for phosphatidyl choline and phosphatidyl ethanolamine. R.Flaim, S.E.Friberg (Chem. Dept., Univ. of Missouri-Rolla, Rolla, MI, USA), P.L.M.Plummer. *Colloids & Surf. (Netherlands)*, vol.6, no.4, p.395-404 (May 1983). Intermolecular interaction between pairs of methylphosphocholine (MPC) and methylphosphoethanolamine were calculated using an extended CNDO/2 program. Experimentally determined conformations were used for the ethanolamine and chlorine groups. In the methylphosphocholine the major interaction was intramolecular, involving the phosphate ester-choline groups, while in the ethanolamine the maximum attraction was intermolecular between the ethanolamine and the phosphate ester of a neighboring molecule(s). (21 refs.)
- 78121** Comparison of theoretical and thermodynamic values of interconstituent interactions in DNA. M.Shibata, T.Kieber-Emmons, R.Rein (Dept. of Experimental Pathology & Biophys., Roswell Park Memorial Inst., Buffalo, NY, USA). *Int. J. Quantum Chem. (USA)*, vol.23, no.4, p.1283-93 (April 1983). Experimental base stacking and hydrogen bonding enthalpies, as determined from double standard DNA melting studies, are compared with theoretical calculations of interactions between the respective DNA interconstituent components. Comparisons are made in relation to the differences in magnitudes, sequence dependent spreads, and trends. It is shown that the use of an effective dielectric constant reconciles the differences between the experimental and theoretical values. Suggestions are made for calibration of potential functions suitable for nucleic acid conformational analysis. (31 refs.)
- 78122** β -lactam ring stability and antibacterial potency: a novel eigenvalue problem. R.H.Davies, T.R.Morris (ICI plc, Macclesfield, England). *Int. J. Quantum Chem. (USA)*, vol.23, no.4, p.1385-405 (April 1983). Low inoculum potency data in vitro for 16 clinical β -lactam antibiotics have been analyzed, and a physical model for interpreting the results of a number of bacterial strains has been derived. An analytic criterion for performing a unitary transformation on the potency data is developed following the identification of a physical vector present within the data which is attributable to an activation energy required for the transport of the β -lactam into a biological membrane. This vector has inverse slope relations in Gram positive and Gram negative bacteria and provides the basis for the analytic criterion for the unitary transformation. Compounds with similar potency spectra which differ only in the absolute magnitude of their effect will possess similar transport properties. It is shown that a slow rate of membrane entry for the β -lactam has overriding consequences on differences in fast rates of binding to the target enzymes and to β -lactamases, and a second primary vector is established directly from the biological data related to the case of β -lactam ring opening. This vector offers precise evidence for testing the solvational and theoretical requirements for predicting the biological stability of novel β -lactam ring compounds. (21 refs.)
- 78123** Evidence for coherent excitation in biological systems. H.Frohlich (Dept. of Phys., Univ. of Liverpool, Liverpool, England). *Int. J. Quantum Chem. (USA)*, vol.23, no.4, p.1589-95 (April 1983). From theoretical considerations, three types of coherent excitations of biological systems have been suggested: (i) vibrations of membranes and of proteins with frequencies above 10^9 Hz; (ii) near static excitation of a highly polar metastable state; and (iii) low frequency periodic enzyme reactions. Recent experimental evidence is discussed. (32 refs.)
- 78124** Energy transfer in B-DNA: mechanism and effects. P.Beaconsfield, E.Balanovski (Bedford Coll. Univ. of London, London, England). *Phys. Lett. A (Netherlands)*, vol.95A, no.8, p.454-6 (23 May 1983). Calculations are presented of effective soliton mass, coupling constant between intermolecular excitation and chain displacement, and energy transfer in B-DNA. (7 refs.)
- Molecular electrostatic potential of a triple stranded helix: poly(dT).poly(dA).poly(dT) See Entry 78465
- The evaluation of synthetic strategies for oligonucleotides of defined sequence. I. Computer programs in nucleic acid synthesis See Entry 77870
- The metal centers of cytochrome c oxidase: structures and interactions See Entry 78129
- Quantum chemical study of the molecular patterns of MAO inhibitors and substrates See Entry 78135
- Molecular dynamics of a bilayer membrane See Entry 78153
- Radiation sensitivity of DNA-metal complexes: a pulse radiolysis study See Entry 78267

87.15B Structure, configuration, conformation, and active sites at the biomolecular level

- 78125** The structure of ribosomal proteins. I.N.Serdyuk (Inst. of Protein Res., Acad. of Sci., Poustchino, USSR). *Comments Mol. & Cell. Biophys. Comments Mod. Biol. Part A (GB)*, vol.2, no.1, p.17-39 (April 1983). This review is to give a description of the results of physical experiments undertaken at the author's institute on the small subparticle of *E. coli* ribosomes. As a result of these experiments it is concluded that the greatest part of ribosomal proteins can be described as globular compact molecules both in solution and within the ribosome. (45 refs.)
- 78126** The structure of bovine rhodopsin. P.A.Hargrave (Dept. of Medical Biochem., School of Medicine, Southern Illinois Univ., Carbondale, IL, USA), J.H.McDowell, D.R.Curtis, J.K.Wang, E.Juszczak, Shao-Ling Fong, J.K.Mohana Rao, P.Argos. *Biophys. Struct. & Mech. (Germany)*, vol.9, no.4, p.235-44 (1983). The authors have isolated 16 peptides from a cyanogen bromide digest of rhodopsin. These cyanogen bromide peptides account for the complete composition of the protein. Methionine-containing peptides from other chemical and enzymatic digests of rhodopsin have allowed the authors to place the

cyanogen bromide peptides in order, yielding the sequence of the protein. They have completed the sequence of most of the cyanogen bromide peptides. This information, in conjunction with that from other laboratories, forms the basis for their prediction of the secondary structure of the protein and how it may be arranged in the disk membrane. (17 refs.)

78127 The structure of Panulirus interruptus hemocyanin at 4.0 Å resolution and a preliminary description of the copper-containing oxygen binding site. W.P.J.Gaykema, E.J.M.van Schaick, W.G.Schutter, W.G.J.Hol (Dept. of Chem., Univ. of Groningen, Groningen, Netherlands). *Chem. Scr. (Sweden)*, vol.21, no.1-5, p.19-23 (1983). The hemocyanin from the spiny lobster *Panulirus interruptus*, a hexamer with a molecular weight of approximately 540000, was crystallized with the complete molecule in the asymmetric unit. X-ray diffraction data to 4 Å resolution were collected by the oscillation method for the native crystals and two isomorphous derivatives. The K_2PtCl_4 derivative contained 36 heavy atom sites and the *o*-mercury phenol derivative 70 sites. From the heavy atom positions the 32 point group symmetry of the hemocyanin molecule could be deduced, and the molecular centre accurately established. Multiple isomorphous phases were used for the calculation of an electron density distribution from which the molecular envelope could be obtained. A few cycles of density averaging and phase improvement procedures yielded a much better quality map. Due to the low pH of the crystallization medium, the structure observed is presumably deoxy hemocyanin. (32 refs.)

78128 Three-dimensional structure of membrane-bound cytochrome c oxidase. J.F.Deatherage, R.Henderson, R.A.Capaldi (MRC Lab. of Molecular Biology, Cambridge, England). *Chem. Scr. (Sweden)*, vol.21, no.1-5, p.35-9 (1983). The authors have determined the three-dimensional structure of cytochrome c oxidase in the membrane to a resolution of 20 Å by electron microscopy of two-dimensional vesicle crystals. They investigated the three-dimensional structure of the enzyme by analysis of electron micrographs of tilted, negatively-stained specimens. The resulting map showed the shape of the part of the cytochrome c oxidase molecule which protrudes from the lipid bilayer. The projected structure of the parts of the molecule which are buried in the phospholipid bilayer was determined by electron microscopy of glucose-embedded vesicle crystals. The authors then determined the relative locations of the protruding (solvent-exposed) and buried (membrane-bound) domains of the molecule by varying the density of the embedding medium in electron microscopy. By combining information from these studies, they derived the full connected three-dimensional structure and its relationship to the bilayer. (15 refs.)

78129 The metal centers of cytochrome c oxidase: structures and interactions. D.F.Blair, C.T.Martin, J.Gelles, Hsin Wang, G.W.Brudvig, T.H.Stevens, S.I.Chan (A.Noyes Lab. of Chem. Phys., California Inst. of Technol., Pasadena, CA, USA). *Chem. Scr. (Sweden)*, vol.21, no.1-5, p.43-53 (1983). Studies directed toward the elucidation of the structures of the metal centers in cytochrome c oxidase are reviewed. Progress towards an understanding of the interactions between these centers and their spatial distributions within the protein is also presented. The authors' studies are based primarily on optical and low-temperature electron paramagnetic resonance (EPR) spectroscopy. They have employed nitric oxide (NO), as well as other exogenous ligands, to probe the O_2 reduction site of the enzyme. In addition, they have isolated auxotrophs of *Saccharomyces cerevisiae* in order to metabolically incorporate isotopically substituted amino acids into the yeast protein. Low-temperature EPR and electron nuclear double resonance (ENDOR) spectroscopic studies of these isotopically substituted derivatives have provided unambiguous information on the structure of two of the four metal centers. The degree to which metal centers within the protein interact with one another has been assessed by examining the extent to which redox changes of one metal center modulate changes in the EPR and optical characteristics of the other centers. Conceptions about the overall spatial distribution of the metal centers within the protein emerge from these data. The implications of the authors' results with respect to the mechanisms of dioxygen reduction and energy conservation in cytochrome c oxidase are discussed. (54 refs.)

78130 Structural studies of a bacteriochlorophyll-containing protein. M.F.Schmid, D.E.Tröndrud, B.W.Matthews (Dept. of Phys., Univ. of Oregon, Eugene, OR, USA). *Chem. Scr. (Sweden)*, vol.21, no.1-5, p.67-9 (1983). The bacteriochlorophyll *a*-protein from the green photosynthetic bacterium *Prosthechloris aestuarii* consists of three identical subunits, each of which has a core of seven bacteriochlorophyll *a* molecules enclosed within a 'bag' of protein. The bacteriochlorophylls are arranged in an irregular manner, suggesting that this may be the case in other bacteriochlorophyll-protein complexes. The arrangement of the phytol chains may serve as a model for lipid-protein interactions. In the bacteriochlorophyll protein, the phytol tails have irregular conformations but are not disordered, the bends occur at substituted positions, and the chains have predominantly parallel interactions. Each of the seven magnesiums appear to be five-coordinate; in five cases the presumed ligand is a histidine side-chain, in one case a polypeptide carbonyl oxygen and in the other case a water molecule. Diffraction data to a resolution of 1.9 Å have been collected by oscillation photography, and the refinement of the structure is nearing completion (crystallographic residual $R=20.4\%$). (12 refs.)

78131 Theoretical studies of the electrostatic stability of A, B, C, and Z-DNA conformers as a function of monovalent ion concentration and ion type. B.J.Klein, G.R.Pack (Dept. of Biomedical Sci., Univ. of Illinois Coll. of Medicine, Rockford, IL, USA). *J. Biol. Phys. (USA)*, vol.11, no.1, p.23-5 (1983). Theoretical calculations using a two-state model of counterion-phosphate interactions have been performed in order to determine the electrostatic stability of DNA in various ionic environments. Comparison of the stabilities of different conformations leads to results consistent with the B \rightarrow Z transitions observed in high-salt environments and suggest that a very low ionic strengths the left-handed Z(II) form is an electrostatically preferred conformation. An ion-type dependence of the high-salt B \rightarrow Z transition midpoint is predicted. Calculations of the energies of the A and C conformations are also discussed in relation to experimentally observed transitions. (28 refs.)

78132 Possible incorporation of the purine-purine mispairs in the DNA helix and the interpretation of the transversion-type point mutations. V.Kothekar, G.Bolis, R.Rein (Dept. of Experimental Pathology, Roswell Park Memorial Inst., Buffalo, NY, USA). *Int. J. Quantum Chem. (USA)*, vol.23, no.4, p.1295-303 (April 1983). The stereochemical and energetic compatibility of incorporation of the non-Watson-Crick hydrogen bonded purine-purine base pairs of normal tautomers in the helical structure of B-DNA is studied. The hydrogen bonding positions of the possible 'mispairs' of the bases GA, GG, and AA are optimized first in the base plane by translational and rotational movement along the hydrogen bonds and then introduced at an appropriate position in the

DNA structure. The optimum backbone geometries which can accommodate the 'mispairs' are obtained by force field computations. The stereochemical and energetic aspects of the various mispairs are discussed in light of their possible incorporation in DNA and as mutational intermediates for the 'transversion'-type point mutations. (32 refs.)

78133 Theory of living state. VII. Bose-Einstein-like ordering in temperature and time domain. R.K.Mishra, K.Bhowmik (Dept. of Biophys., All-India Inst. of Medical Sci., New Delhi, India). *Int. J. Quantum Chem. (USA)*, vol.23, no.4, p.1579-87 (April 1983). The Bose-Einstein-like ordering was earlier proposed as an important mechanism of energy handling in the living systems. In this regard two questions arise at once: (1) is such ordering feasible at body temperature and (2) what is the time that may be taken for establishing coherence? The authors answer and satisfy these two questions. (9 refs.)

78134 Structure-activity relationship and the mechanism of analgesia of the analgesic drug 3-methyl-fentanyl and its analogs. Chen Changying, Li Leming (Dept. of Chem., Peking Univ., Beijing, China). *Int. J. Quantum Chem. (USA)*, vol.23, no.4, p.1597-608 (April 1983). The semiempirical self-consistent field MO (CNDO/2) calculations have been undertaken for 13 compounds involving 3-methyl-fentanyl and its analogs. Various quantum chemical indices were obtained. The relationships between the biological activity and quantum chemical indices of molecules of these compounds were investigated and it was found that there are remarkable relationships between the activity and some important quantum chemical indices such as the π -electron density of β substituent and the electron density of piperidyl nitrogen. The nature of interaction between the analgesics' molecule and the receptor was discussed on the basis of the relationships between the activity and quantum chemical indices and it was proposed that the β -substituent functions not only as a hydrophobic group, but also its electronic property has important effect on the activity. It may act as an electron acceptor and form acceptor-donor complex with receptor through the charge transfer process. The piperidyl nitrogen interacts with receptor forming quaternary ammonium ion and acting as positive charge center, and its electron density also has an important effect on the activity. The amide oxygen and nitrogen may be other active centers which function as donors when they interact with the receptor. The influence on activity through introduction of the hydroxyl group to the β -position of the 1-substituent of the piperidyl ring has also been discussed. (32 refs.)

78135 Quantum chemical study of the molecular patterns of MAO inhibitors and substrates. M.Martin, F.Sanz, M.Campillo, L.Pardo, J.Perez, J.Turmo (Dept. of Bioestadística, Univ. Autònoma de Barcelona, Barcelona, Spain). *Int. J. Quantum Chem. (USA)*, vol.23, no.4, p.1627-41 (April 1983). Similarities and differences between mitochondrial monoamine oxidase (MAO) substrates and inhibitors (both A and B types) are considered, studying quantitatively two molecular electrostatic potential (MEP). The following molecules are considered: substrates: PHEA, BZA, tele-N-methyl-histamine, phenylethanolamine, phenylpropylamine, tryptamine, dopamine, phenoxylethylamine, noradrenaline, serotonin, and *p*-nitro-phenylethanolamine; inhibitors: Deprenil, Clorgyline, and Lilly 51641 (only the moiety involved in the A-B differentiation is considered). The wave functions needed to calculate the analyzed properties are of ab initio quality, and have been calculated in analogous conformations, all near the energetic minima. Electron densities distributions are qualitatively compared by means of a correlation coefficient defined over the whole space. Otherwise, patterns of the possible zones of electrostatic interactions are described by means of the distances and angles between minima, in order to differentiate MAO-A and MAO-B substrates. The results reproduce efficiently the experimental classification and enable one to predict the type of enzymatic action of molecules not yet experimentally classified. (14 refs.)

78136 Small-angle X-ray scattering of chain molecules in a hydrodynamic field. The internal rigidity of double-stranded DNA. B.Sjöberg, R.Österberg (Dept. of Medical Biochem., Univ. of Göteborg, Göteborg, Sweden). *J. Appl. Crystallogr. (Denmark)*, vol.16, pt.3, p.349-53 (1 June 1983). Small-angle X-ray scattering data from flowing solutions of double-stranded calf thymus DNA, in phosphate buffer of pH 6.91 and 0.2 mol dm^{-3} ionic strength, have been recorded over a velocity-gradient range from zero up to a maximum value of 15300 s^{-1} . In comparison with small-angle X-ray measurements performed on stationary solutions, the method of flowing the solution through a capillary tube provides information regarding the internal flexibility of the macromolecule in solution. All the X-ray data recorded in this work can be explained by a slightly modified bead-spring chain model of DNA, which consists of linear segments filled with touching beads. The segments are joined together at the ends to form a long array with complete flexibility at each joint. The lengths of the segments follow a Gaussian distribution with a root-mean-square length equal to 100 nm. The diameter of each bead is equal to 3.0 nm. (22 refs.)

78137 Markov analysis of alpha-helical, beta-sheet and random coil regions of proteins. M.Macchiato (Istituto di Fisica Sperimentale, Napoli, Italy), A.Tramontano. *Lett. Nuovo Cimento (Italy)*, vol.37, ser.2, no.3, p.89-94 (21 May 1983). The rules up to now used to predict the spatial configuration of proteins from their primary structure are mostly based on the recurrence analysis of some doublets, triplets and so on of contiguous amino acids, but they do not take into account the correlation characteristics of the whole amino acid sequence. The authors have carried out a statistical analysis of amino acid sequences for the alpha-helical, beta-sheet and random coil regions of about twenty proteins with known secondary structure by considering correlation effects. The results demonstrate that these sequences are at least a second-order Markov chain i.e. they appear as if they were generated by a source that remembers at least the two aminoacids before the one being generated and that these two previous symbols influence the present choice. (10 refs.)

78138 Polyoma virus 'hexamer' tubes consist of paired pentamers. T.S.Baker, D.L.D.Caspar (Rosentel Basic Medical Sci. Res. Center, Brandeis Univ., Waltham, MA, USA), W.T.Murakami. *Nature (GB)*, vol.303, no.5916, p.446-8 (2 June 1983). The authors examination of negatively-stained polyoma virus tubes by digital image processing of low-irradiation electron micrographs shows that all tubes are assemblies of paired pentameric capsomeres. They report that the packing arrangement of the pentamers in the hexamer tubes is simply related to the pentagonal tessellation representing the packing in the narrow pentamer tubes. In all the tube structures examined, at least one pairwise contact between neighbouring pentamers closely resembles the contact between the pentavalent and hexavalent capsomeres in the icosahedral capsid. (8 refs.)

Quantum chemical structure-activity relationships on β -carbolines as natural monoamine oxidase inhibitors See Entry 75275

Conformational studies of the $\beta(1\rightarrow3)$ linked disaccharide component of the immunologically active pentasaccharide of the Forssman antigen See Entry 75297

Quantum chemical studies on the conformational structure of bacterial peptidoglycan. V. PCIO calculations on $\beta(1\rightarrow4)$ linked disaccharide of N-acetyl-glucosamine and N-acetyl muramic acid See Entry 75298

Electronic structure of model chlorophyll systems See Entry 75397

Transient kinetics of chemical reactions with bounded diffusion perpendicular to the reaction coordinate: intermolecular processes with slow conformational changes See Entry 7779

The thermotropic properties of coenzyme Q_{10} and its lower homologues See Entry 78143

Structural and functional evidence for multiple channel complexes in the outer membrane of *Neurospora crassa* mitochondria See Entry 78154

A fast method for arranging DNA sequence fragments See Entry 78390

Peak-shape analysis for protein neutron crystallography with position-sensitive detectors See Entry 78401

87.15M Interactions with radiations at the biomolecular level

78139 Fluorescence of blowfly metarhodopsin. D.G.Stavenga (Dept. of Biophys., Rijksuniv. Groningen, Groningen, Netherlands). *Biophys. Struct. & Mech. (Germany)*, vol.9, no.4, p.309-17 (1983). The visual pigment of blowfly peripheral photoreceptors displays a marked red fluorescence when the pigment is in the metarhodopsin state as demonstrated in vivo by simultaneous measurements of transmission and fluorescence. The rhodopsin state is non-fluorescent. It is argued that fluorescence offers a unique means to study visual pigment properties in completely intact living animals and, furthermore, provides the opportunity for studying the photoreceptor optics of visual waveguides. As an example the action of the pupil mechanism of blowfly visual sense cells on the fluorescence signal is demonstrated. (28 refs.)

78140 Thermally stimulated luminescence studies of X-irradiated L-alanine:Cr³⁺ single crystals. D.W.Cooke, M.S.Jahan (Dept. of Phys., Memphis State Univ., Memphis, TN, USA). *J. Chem. Phys. (USA)*, vol.78, no.11, p.6477-83 (1 June 1983). Thermally stimulated luminescence studies of X-irradiated L-alanine:Cr³⁺ have been conducted in the interval 10-300K. Glow peaks were observed at 42, 60, 72, 148, and 208K. The 148K peak has been previously reported, while the one at 208K was of insufficient intensity to study. Also, the 60K peak was difficult to analyze due to overlap with the neighboring peaks. Detailed analyses of the 42 and 72K peaks yielded, respectively, the following parameters: $E=24 \text{ meV}$, $s=5.3 \text{ s}^{-1}$, and $l=1$; $E=180 \text{ meV}$, $s=2.4 \times 10^{10} \text{ s}^{-1}$, and $l=2.8$, where l is the kinetics order. Identical emission was observed from each peak, characterized by a maximum at 445 nm with FWHM equal to 0.605 eV. A tentative model is presented to explain these results in terms of detrapping and deexcitation via the excited singlet and triplet states. (43 refs.)

78141 Long-wavelength-absorbing forms of bacteriochlorophyll *a* in solutions of Triton X-100. J.Gottstein, H.Scheer (Botanisches Inst., Univ. München, München, Germany). *Proc. Natl. Acad. Sci. USA*, vol.80, no.8, p.2231-4 (April 1983). At least three forms of Triton X-100-solubilized bacteriochlorophyll *a* (Bchl *a*) have been characterized by UV/visible/near-IR absorption and CD spectra. One, absorbing at 770 nm, is similar to a monomeric solution in methanol. The two others have strongly red-shifted absorption peaks (860 nm and 930, 835 nm) and intense and complex CD bands in this region, indicative of strong interaction of at least two and three molecules of Bchl *a*, respectively. (53 refs.)

78142 Nanosecond absorption spectroscopy of hemoglobin: elementary processes in kinetic cooperativity. J.Hofrichter, J.H.Sommer, E.R.Henry, W.A.Eaton (Lab. of Chem. Phys., Nat. Inst. of Health, Bethesda, MD, USA).

Proc. Natl. Acad. Sci. USA, vol.80, no.8, p.2235-9 (April 1983). A nanosecond absorption spectrometer has been used to measure the optical spectra of hemoglobin between 3 ns and 100 ms after photolysis of the CO complex. The data from a single experiment comprise a surface, defined by the time-ordered set of 50-100 spectra. Singular value decomposition is used to represent the observed spectra in terms of a minimal set of basis spectra and the time course of their amplitudes. Both CO rebinding and conformational changes are found to be multiphasic. Prior to the quaternary structural change, two relaxations are observed that are assigned to germinate recombination followed by a tertiary structural change. These relaxations are interpreted in terms of a kinetic model that points out their potential role in kinetic cooperativity. The rapid escape of CO from the heme pocket compared with the rate of rebinding observed for both *R* and *T* quaternary states shows that the quaternary structure controls the overall dissociation rate by changing the rate at which the Fe-CO bond is broken. A comparable description of the control of the overall association rates must await a more complete experimental description of the kinetics of the quaternary *T* state. (28 refs.)

Application of photoelectron spectroscopy to biologically active molecules and their constituent parts. IX. 1,4-benzodiazepin-2-ones See Entry 75438

The structure of *Panulirus interruptus* hemocyanin at 4.0 Å resolution and a preliminary description of the copper-containing oxygen binding site See Entry 78127

Destruction of gelatin irradiated in its aqueous solutions at low temperatures See Entry 78252

Effect of α -particles on bacteriophage T4 See Entry 78253

Comparison of neutron- and γ -radiation-induced transformations of 2-deoxy-D-ribose in aqueous solutions See Entry 78254

Influence of dose-rate on the formation of double-strand DNA breaks See Entry 78255

Radiation sensitivity of DNA-metal complexes: a pulse radiolysis study See Entry 78267

Immunoelectrophoretic study of the effect of radiation on protein mixtures See Entry 78268

Peak-shape analysis for protein neutron crystallography with position-sensitive detectors See Entry 78401

87.16 BIOTHERMICS

78143 The thermotropic properties of coenzyme Q₁₀ and its lower homologues. H.Katsikas, P.J.Quinn.

J. Bioenerg. & Biomembranes (USA), vol.15, no.2, p.67-79 (April 1983). The thermotropic properties of coenzymes Q₁₀, Q₉, Q₈, and Q₇ have been examined by differential scanning calorimetry and wide-angle X-ray diffraction. Typical scanning calorimetry cooling curves of coenzyme Q from the liquid state exhibit a single exothermic phase transition into a crystalline state at a temperature that decreases as the length of the polyisoprenoid side-chain substituent decreases. Upon subsequent heating, the molecules undergo a series of thermal events which precede the main crystalline-to-liquid endothermic phase transition. The temperature of these transitions increases with increasing chain length. The crystallization phase transition temperature depends markedly on the rate at which the sample is cooled and increases with decreasing scan rate; the temperature of the melting endotherm is not markedly affected by the scan rate. Detailed calorimetric studies of coenzyme Q₁₀ indicate that two crystalline states are formed, one at relatively high cooling rates to low temperatures and the other when preparation area cooled slowly from the liquid state to relatively high temperatures. Heating the crystalline phase formed by rapid cooling causes its transformation into the phase observed by cooling slowly. X-ray diffraction analysis confirmed the existence of these two crystal phases in coenzymes Q₉ and Q₁₀ and the transformation from the rapidly crystallized form to the more ordered form associated with slower cooling rates. At body temperature (310K) under equilibrium conditions coenzyme Q₁₀ exists in an ordered crystalline phase; the implications of the thermotropic behavior of coenzyme Q₁₀ on mitochondrial function in vitro and in vivo are discussed. (22 refs.)

78144 Giant squids may die when exposed to warm water currents. O.Brix (Zoological Lab., Univ. of Bergen, Bergen, Norway).

Nature (GB), vol.303, no.5916, p.422-3 (2 June 1983). Stranding of giant squids in Newfoundland waters has been correlated with the in flow of warm water, suggesting that increased temperature may be causing their death. Squids have also been carried to the Norwegian coast with the warm North Atlantic current and on 23 August 1982 a live specimen was caught off Røddøy near Bergen, Norway. This catch gave an unprecedented opportunity to study the effects of temperature on the oxygen binding properties of blood from the giant squid. The present finding of an excess of a fourfold decrease in O₂ affinity when temperature is increased from 6.4 to 15°C strongly suggests that giant squids may suffocate from arterial desaturation when increased ambient temperatures are experienced. (11 refs.)

78145 Growth of 'black smoker' bacteria at temperatures of at least 250°C. J.A.Baross (School of Oceanography, Oregon State Univ., Corvallis, OR, USA), J.W.Deming.

Nature (GB), vol.303, no.5916, p.423-6 (2 June 1983). Reports that a bacterial community originally cultured from 206°C water is capable of chemolithotrophic growth in a titanium growth chamber under in situ vent pressure of 265 atm and at temperatures of at least 250°C. (At 265 atm, seawater remains liquid at temperatures of at least 460°C.) Transmission electron microscopy of thin sections of bacteria cultured at 250°C has revealed the presence of at least two morphologically distinct organisms. (24 refs.)

Comparison of theoretical and thermodynamic values of interconstrictions in DNA See Entry 78121

Inhibition of repair of radiation-induced strand breaks by hyperthermia, and its relationship to cell survival after hyperthermia alone See Entry 78159

Effects of hyperthermia on the repair of X-ray-induced DNA double strand breaks in mouse L cells See Entry 78160

Effects of microwaves and hyperthermia on capping of antigen-antibody complexes on the surface of normal mouse B lymphocytes See Entry 78231

Experimental studies of laser thermal retinal injury See Entry 78240

Feasibility of ultrasound hyperthermia in the treatment of malignant brain tumors See Entry 78277

Cardio-surgical thermography See Entry 78291

Infrared radiation in therapeutic hyperthermia See Entry 78293

Portable processing thermometer See Entry 78378

87.20 MEMBRANE BIOPHYSICS

78146 Ion distributions in inhomogeneous regions [biomembranes]. V.S.Vaidyanathan (Dept. of Biophys., Cary Hall School of Medicine, State Univ. of New York, Buffalo, NY, USA).

Colloids & Surf. (Netherlands), vol.6, no.4, p.291-306 (May 1983). Based on the premise that ion-ion interaction energy term contributions to the chemical potential of an ionic species in the inhomogeneous region cannot be neglected, the basic nonlinear differential equations relating the electric potential profile, dielectric profile and concentration profiles are formulated. Analytical expressions for solutions of these differential equations are obtained. It is shown that the magnitudes of the inhomogeneous region and electric potential difference are determined by the system in a self-consistent manner. Certain interesting conclusions, in contradiction with classic Gouy-Chapman theory, are obtained. (15 refs.)

78147 Exchange currents across the electrolyte/membrane interface in frog skin. Ming De Li, J.T.Tarvin, M.Ali, D.Bernard, M.A.Dinno (Dept. of Phys. & Astron., Univ. of Mississippi, University, MS, USA).

Colloids & Surf. (Netherlands), vol.6, no.4, p.307-14 (May 1983). Using bipolar current pulses of 1-100 μ A amplitude and 1-50 s duration, the current-over-potential behavior of the frog skin (*Rana pipiens*) has been determined in a bicarbonate-containing Ringer's solution. This behavior is analyzed using a model based on rate theory. In this manner, it is possible to measure both the open-circuit exchange current and the contribution of the membrane potential to the energy barrier representing ionic movement across the frog skin. In a double-exponential least-squares fit of the data, the exchange current was found to be independent of pulse duration, suggesting that the system is already in a steady state by 1s. The experimentally measured current-over-potential curves were asymmetric for hyperpolarization vs. depolarization. This asymmetry is predicted by the authors' model, and suggests that Na⁺ and Cl⁻ do not contribute equally to the exchange current. (9 refs.)

78148 Mass action kinetics of vesicle aggregation and fusion. J.Bentz (Dept. of Pharmacy & Pharmaceutical Chem., Univ. of California, San Francisco, CA, USA), S.Nir, J.Wilschut.

Colloids & Surf. (Netherlands), vol.6, no.4, p.333-63 (May 1983). The kinetics of Ca²⁺-induced fusion of both large and small phosphatidylserine vesicles has been examined theoretically and experimentally. With the

Tb/DPA assay for mixing of vesicle contents, the kinetics of vesicle aggregation can be separated from the kinetics of vesicle fusion by varying the initial concentration of vesicles. Both the rate constant for vesicle dimerization and the rate constant for the actual membrane fusion can be determined by this analysis. The kinetics of release of vesicle contents during and following the fusion event have also been examined. The theoretical analysis can be easily adapted to other fusion assays and, as such, provides a unique opportunity for a quantitative evaluation of the factors which affect the fusion of vesicles such as temperature, cations bound to the lipids, and the membrane composition. The effect of aggregation reversibility on the kinetics of the overall fusion process is considered in detail. Analysis of the initial kinetics of the Ca²⁺-induced fusion of phosphatidylserine vesicles shows that the fusion step itself can be very rapid (of the order of ms-s) and the initial leakage associated with the fusion event, per se, is essentially zero for the large vesicles and quite small for the small vesicles.

78149 Permeability characteristics of the basement membrane (basal lamella) of the intestine of *Ascaris* suum. M.J.Donahue, C.G.Beames, Jr., K.S.Bost (Dept. of Physiological Sci., Oklahoma State Univ., Stillwater, OK, USA).

J. Biol. Phys. (USA), vol.11, no.1, p.11-13 (1983). Permeability characteristics have been determined for isolated ribbons of the basement membrane of the intestine of *Ascaris suum*. The solute permeability coefficient (P_s) was measured for a series of hydrophobic, nonionic molecules of graded molecular size. The geometric pore area per unit path length (A_g/Δx) was estimated to be 24.0 cm from the diffusion rates for the various solute molecules. A filtration coefficient (L_p) of 18.1 × 10⁻¹² cm³/dyne-sec was determined by a method that employs osmotic pressure. The preceding values were used to calculate an average pore radius of 24.0 Å for the membrane. The unstirred layer was estimated to be 30 μ m thick from measurements of the change in the rate of diffusion of water across the membrane with change in the rate of perfusion. The preceding values were used to calculate a reflection coefficient (σ), effective permeability coefficient (ω), and a permeability coefficient (ω). The results support the view that this basement membrane functions as a filter and selective barrier to diffusion of constituents of the worm's body fluid. (19 refs.)

78150 Further comments on negative solvent pressure in osmosis. H.R.Hirsch (Dept. of Physiology & Biophys., Univ. of Kentucky, Lexington, KY, USA).

J. Biol. Phys. (USA), vol.11, no.1, p.26 (1983).

A previously proposed gedanken experiment (see H.R. Hirsch, *ibid.*, vol.8, p.11, 1980) on osmotic pressure and low flow is supplemented to illustrate the circumstances in which equilibrium is achieved. The concept that solvent pressure can be negative and can be described as a partial pressure is thus given additional credence. (2 refs.)

78151 Dual-mode potential oscillations on an immobilized acetylcholinesterase membrane system. T.R.Chay (Dept. of Biological Sci., Univ. of Pittsburgh, Pittsburgh, PA, USA), N.J.Zabusky.

J. Biol. Phys. (USA), vol.11, no.1, p.27-31 (1983).

The authors have studied by numerical simulations the effects of varying external salt concentration on a multibarrier kinetic model of a synthetic membrane system bearing AChE and BSA. For certain parameters, they find a 'spiky' high frequency modulation imposed on a 'bursting' low frequency carrier. In the absence of added salt, oscillations with only one mode arise, consistent with the experimental result of Friboulet and Thomas (1982). From this study, the authors suggest how periodic ionic permeability changes of ions may arise in excitable membranes. (11 refs.)

78152 Electrostatics and gating of excitable membranes. I.Lundstrom, C.Nylander (Dept. of Phys. & Measurement Technol., Linköping, Inst. of Technol., Linköping, Sweden).

Int. J. Quantum Chem. (USA), vol.23, no.4, p.1269-82 (April 1983).

Two electrostatic models for ion permeability of membranes are considered. In the first model ions pass hydrated through the membrane and in the second model ions pass unhydrated through a channel lined with polar groups. In both cases it is found that it is not necessary to assume a high macroscopic dielectric constant of the membrane or channel to provide a low enough potential energy of the ion in the membrane. Gating of excitable membranes is considered a special case of electrostatic interaction in membranes. A simple physical model which fits with Hodgkin and Huxley's empirical relation is derived. Finally, the authors have speculated upon other membrane bound biological phenomena were electrostatic effects may be important. (19 refs.)

78153 Molecular dynamics of a bilayer membrane. P.van der Ploeg, H.J.C.Berendsen (Lab. of Phys. Chem., Univ. of Groningen, Groningen, Netherlands).

Mol. Phys. (GB), vol.49, no.1, p.233-48 (May 1983).

A molecular dynamics simulation was carried out for a bilayer of 2 × 64 decane molecules as a model for a biological membrane. Two dimensional periodic conditions were used and head groups were subjected to a simple mean force interaction. Four runs at two different temperatures and head group densities were executed, each over 80 ps. Molecular order parameters were analysed and compared with experiment. A fluctuating tilt of the molecules occurs with respect to the bilayer normal with a spatial correlation of about 1 nm and a temporal correlation of 8 ps. The molecules do not rotate isotropically around their long axes, and a different behaviour of odd and even numbered bonds is apparent. The density profile shows a dip near the middle of the bilayer and the lateral pressure profile shows a negative region near the head groups compensated by a positive region near the tails. Translational diffusion is inhibited by a long negative tail of the velocity autocorrelation functions, but still exceeds experimental values. The results are discussed in terms of implications for membrane structure. Results confirm earlier simulations on a smaller model (J. Chem. Phys., 76, 3271, 1982), except for the cooperativity of molecular tilt. (27 refs.)

78154 Structural and functional evidence for multiple channel complexes in the outer membrane of *Neurospora crassa* mitochondria. C.A.Mannella (Center for Labs. & Res., New York State Dept. of Health, Albany, NY, USA), N.C.Colombini, J.Frank.

Proc. Natl. Acad. Sci. USA, vol.80, no.8, p.2243-7 (April 1983).

The outer membrane of mitochondria contains proteins that form channels called VDAC (voltage-dependent anion-selective channels). Two independent lines of evidence suggest that these channels occur in specific complexes in the outer membrane of *Neurospora crassa* mitochondria. Electron microscopic images of these outer membranes reveal polymorphic crystalline arrays of putative pores. These arrays can be shown to be interrelated by movement in the membrane plane of a particular rigid channel triplet or of regular aggregates of this triplet. Detergent extracts of the same outer membranes induce single- and multiple-step conductances in planar phospholipid membranes, with a marked preference for the insertion of triplets and multiples of triplets. The tendency of the mitochondrial channels, to occur as extended arrays,

apparently built up from triplets, may have important functional and evolutionary implications. (29 refs.)

78155 Aggregation and fusion of phospholipid vesicles. S.Nir (Seagram Centre for Soil & Water Sci., Hebrew Univ. of Jerusalem, Rehovot, Israel), J.Bentz, J.Wilschut, N.Duzgunes. *Prog. Surf. Sci. (GB)*, vol.13, no.1, p.1-124 (1983). Membrane fusion and aggregation of phospholipid vesicles are reviewed and discussed. The fusion process is viewed as consisting of several stages: aggregation and close apposition of the particles, destabilization, and finally, merging of the bilayers. A procedure is presented which yields both the rate constant of the dimerization (C_{11}) and the rate constant for fusion of the dimers (f_{11}), which is a direct measure of the probability that two apposed vesicles will fuse. Experimental methods used in the study of membrane fusion are reviewed, primarily with respect to their capacity to monitor the kinetics of vesicle fusion. A few kinetic studies on the mixing of aqueous contents, leakage and increase in size of fusing vesicles are presented in detail. Factors affecting fusion such as cations, temperature, membrane composition vesicle concentration and size are reviewed and analyzed. Di- or trivalent cations induce fusion of acidic phospholipid vesicles (except for phosphatidylinositol) in either pure or mixed form. Among the neutral phospholipids, phosphatidylcholine (PC) inhibits but phosphatidylethanolamine (PE) sustains or enhances the fusion capacity of acidic phospholipid vesicles. Monovalent cations induce reversible aggregation of negatively charged vesicles, but they inhibit the fusion induced by divalent cations such as Ca^{2+} or Mg^{2+} . (303 refs.)

Intermolecular interactions for phosphatidyl choline and phosphatidyl ethanolamine See Entry 78120

Evidence for coherent excitation in biological systems See Entry 78123

Three-dimensional structure of membrane-bound cytochrome c oxidase See Entry 78128

Pointwise bounds for the solution of a nonlinear problem in cell membrane theory See Entry 78161

Processing of noisy high resolution electron micrographs of crystalline biological membranes See Entry 78392

87.25 CELLULAR BIOPHYSICS

78156 Contractils: quantum mechanical fibrils. S.Rowlands, C.P.Eisenberg, L.S.Sewchand (Faculty of Medicine, Univ. of Calgary, Calgary, Alberta, Canada).

J. Biol. Phys. (USA), vol.11, no.1, p.1-4 (1983). When an erythrocyte rouleau is pulled apart by micromanipulation the cells remain attached to each other by long fibrils which may reach lengths of over 100 μm . The tension and length of the fibrils are drastically reduced when the cellular membrane potential is abolished or when the cells are depleted of ATP. It is inferred that the fibrils consist of macromolecules and that the tension is largely derived from a quantum mechanical long-range interaction which accords with the theory of Frohlich. (20 refs.)

78157 Dielectric measurements on live biological materials under magnetic resonance conditions. A.H.Jafary-Asl, S.N.Solanki, E.Aarholt, C.W.Smith (Dept. of Electronic & Electrical Engng., Univ. of Salford, Salford, England).

J. Biol. Phys. (USA), vol.11, no.1, p.15-22 (1983). In the course of work on the interactions of electric and magnetic fields with both living and dead biological materials, it was noticed that certain published dielectrophoretic yield curves for biological cells showed unexplained deviations in the region of 2 kHz. Dielectrophoretic measurements made at frequencies and magnetic fields which satisfied the nuclear magnetic resonance conditions showed sharply resonant features. Dielectric measurements showed small, but sharp, resonances most easily seen in the dielectric loss curves which had a bandwidth of the order of one Hertz and presented at the frequencies which satisfied the magnetic resonance conditions for the ambient magnetic field. Resonances were found corresponding to the frequencies for electron spin resonance and nuclear magnetic resonance for ^1H , ^{31}P , ^{23}Na , ^{37}Cl and ^{39}K . The onset of these resonances occurs at the value of the steady magnetic field strength so that one quantum of magnetic flux (2.07×10^{-15} wb) would link a single biological cell or pair of cells, approximately 1 G (100 μT) in the case of a 5- μm yeast cell. The effects of these magnetic resonance conditions on the mean generation time of *E. coli* and on the reaction of the enzyme lysozyme with the substrate *m. lysodeikticus* cells are also shown. (9 refs.)

78158 Understanding blood cell motion. M.D.Levine (Dept. of Electrical Engng., McGill Univ., Montreal, Quebec, Canada), P.B.Noble, Y.M.Youssef. *Comput. Vision, Graphics & Image Process. (USA)*, vol.21, no.1, p.58-84 (Jan. 1983).

The main function of the surface of a blood cell is to receive information from the environment. Experiments have indicated that the cell membrane plays a vital role in the life, development, and regulation of cells. There is, however, no existing method to quantify the observable changes in membrane shape that occur in locomotion. This paper describes research to develop an image interpretation system capable of analyzing the structural changes in the morphology of cells from a sequence of pictures, using automatic techniques of image processing. A model for a general dynamic scene analysis system is described. It consists of three basic entities: dynamic data, static data, and a collection of analysis processes. Based on this model, a rule-based image interpretation system for moving cells has been implemented. The system consists of different cooperating computational processes, which interact with two common memories, a short term memory (STM) and a long term memory (LTM). The STM contains a dynamic record of the instantaneous cell motion, shape, and structural changes, as well as the current global description of the cell behavior. The LTM data are static, and are implemented as rules. These describe the general model of the morphology of the cells under analysis, as well as control information pertinent to the computational processes. (17 refs.)

78159 Inhibition of repair of radiation-induced strand breaks by hyperthermia, and its relationship to cell survival after hyperthermia alone. J.B.M.Jorritsma, A.W.T.Konings (Dept. of Radiopathology, Univ. of Groningen, Groningen, Netherlands).

Int. J. Radiat. Biol. (GB), vol.43, no.5, p.505-16 (May 1983). Ehrlich ascites cells growing in vitro have been used to investigate the influence of hyperthermia on the formation and repair of DNA strand breaks after X-irradiation. Different heat pretreatments were given immediately prior to a dose of 6 Gy of X-rays. When a temperature of 42°C was used, up to 4 hours of pretreatment had only a slight inhibitory effect on the repair of DNA strand breaks induced by radiation. At a temperature of 43°C progressively more inhibition was observed with longer treatment times. This was also the case for temperatures of 44°C and 45°C. When the treatment times of 43-45°C were longer, strand breaks in DNA were induced by the hyper-

thermic treatment alone. Under these conditions almost no repair was found of strand breaks induced by a subsequent radiation dose. The data obtained strongly suggest a correlation between the effect of the hyperthermic treatment alone on cell survival and the kinetics of repair of strand breaks in DNA as induced by radiation. (24 refs.)

78160 Effects of hyperthermia on the repair of X-ray-induced DNA double strand breaks in mouse L cells. I.R.Radford (Biological Res. Unit, Cancer Inst., Melbourne, Victoria, Australia).

Int. J. Radiat. Biol. (GB), vol.43, no.5, p.551-7 (May 1983). Presents the following observations: (1) X-ray induced DNA double strand break repair can be markedly inhibited by prior hyperthermic treatment. (2) Hyperthermic treatment can enhance the level of DNA double strand breakage produced by subsequent X-irradiation. (3) DNA double strand breakage is detectable in cells given a lethal hyperthermic treatment, following subsequent incubation at 37°C. (16 refs.)

Electronic structure of model chlorophyll systems See Entry 75397

The structure of ribosomal proteins See Entry 78125

Structural studies of a bacteriochlorophyll-containing protein See Entry 78130

Long-wavelength-absorbing forms of bacteriochlorophyll *a* in solutions of Triton X-100 See Entry 78141

Growth of 'black smoker' bacteria at temperatures of at least 250°C See Entry 78145

Structural and functional evidence for multiple channel complexes in the outer membrane of *Neurospora crassa* mitochondria See Entry 78154

On the effect of the concentration profile of red cells on blood flow in the artery with stenosis See Entry 78217

Dose-effect relationship for 14.5 MeV (d+T) neutron-induced chromosome aberrations in human lymphocytes irradiated in a man phantom See Entry 78228

DNA replication and repair in human cells exposed to thermal neutrons See Entry 78229

Effects of microwaves and hyperthermia on capping of antigen-antibody complexes on the surface of normal mouse B lymphocytes See Entry 78231

Effects of microwave exposure on the hamster immune system. I. Natural killer cell activity See Entry 78232

Effects of microwave exposure on the hamster immune system. II. Peritoneal macrophage function See Entry 78233

Immunological effects of amplitude-modulated radio frequency radiation: B lymphocyte capping See Entry 78234

Laser induced visual pigment conversions in fly photoreceptors measured in vivo See Entry 78236

Mechanism of chromatin degradation in thymocytes of irradiated rats. VI. Postirradiation changes in poly (ADP-ribose) polymerase activity See Entry 78241

Cell spheroids as the object for radiobiological research See Entry 78242

Changes in the chromosome pattern of mouse lymphosarcoma cells during long-term continuous irradiation See Entry 78243

Comparative study of radiosensitivity of normal and regenerating tissues. I. Interphase cell death and aplasia of the regenerating and normal bone marrow and spleen of C57B1 mice See Entry 78244

Dynamics of early postirradiation changes in capillary endothelium (quantitative electron-microscopic analysis) See Entry 78247

The role of changes in the oxygen concentration upon modification of the reproductive death of cells in vitro. II. Modification of radiosensitivity with the varying rate of oxygen consumption in cells See Entry 78248

Response of lymph and blood coagulative systems to exposure to γ -radiation at high altitudes See Entry 78256

Migration of lymphocytes in conditions of internal irradiation. II. Disturbance of the microenvironment of lymphocytes in mouse organs See Entry 78257

The induction of chromosome aberrations in human lymphocytes by exposure to tritiated water in vitro See Entry 78262

Studies into certain specificities of gamma-ray mutants and the parent strain *Humicola lutea* 72, producing acid protease See Entry 78263

Induction and repair of DNA strand breaks in CHO-cells irradiated in various phases of the cycle See Entry 78266

Kinetics of double strand break repair in the DNA of X-irradiated synchronized mammalian cells See Entry 78269

Comparison of type and frequency of chromosome aberrations by conventional and G-staining methods in Hiroshima atomic bomb survivors See Entry 78271

Changes in radiosensitivity of the in vitro fertilized mouse ova during zygotic stage from fertilization to first cleavage See Entry 78272

Mucosal structure and radon in head carcinoma dosimetry See Entry 78350

Characterization of the solid components of biological tissues by cross-polarization, magic angle NMR spectrometry See Entry 78402

87.25D Biological transport; cellular and subcellular transmembrane physics

78161 Pointwise bounds for the solution of a nonlinear problem in cell membrane theory. A.M.Arthurs (Dept. of Maths., Univ. of York, York, England), W.M.Arthurs.

Bull. Math. Biol. (GB), vol.45, no.2, p.155-68 (1983).

Pointwise upper and lower bounds for the solution of a class of nonlinear problems arising in the steady-state finite cable model of cell membranes are presented. Simple analytical bounding curves are obtained for an illustrative example in the theory of nerve membranes. (6 refs.)

78162 Effects of alternating electric fields on material transport in heterogeneous media. M.M.Breuer, H.Van Der Lee (Gillette Res. Inst., Rockville, MD, USA).

Colloids & Surf. (Netherlands), vol.6, no.4, p.315-31 (May 1983).

Whenever alternating electric fields act on systems in which gradients of dielectric constants or conductivities exist, charge accumulations occur. As a consequence of these interactions, provided the conductive mode is ionic, material transport will also ensue. The phenomenon is known as dielectric diffusion. The authors derived phenomenological equations expressing the magnitude of this effect under various conditions. Using these equations, they computed material fluxes for a system consisting of fibers immersed into a liquid containing a diffusing material. The results of these calculations suggested that dielectric diffusion could change the rate of material transport into fibers. Using hair fibers immersed in solutions of dyes and other com-

pounds, the authors measured the magnitude of the effects that alternating electric fields of various frequencies and intensities have on the transport of dissolved materials into the fibers. The results indicated that the magnitude and the direction of the effect depended on both the experimental conditions and the nature of the diffusing material. Both enhancement and retardation of material transport could be observed as a result of superimposed alternating electric fields. (12 refs.)

78163 Erythrocytes sedimentation profiles under gravitational field as determined by He-Ne laser. VI. Effect of various hematocrits. K.P.Joseph, Megha Singh (Biomedical Engng. Div., Indian Inst. of Technol., Madras, India). *J. Math. & Phys. Sci. (India)*, vol.16, no.5, p.489-97 (Oct. 1982). [received: May 1983]

Erythrocytes sedimentation profiles, under a gravitational field, for blood samples of different hematocrit are determined. It is observed that the sedimentation profiles, depending on the hematocrit of the sample, differ significantly. This enables one to find the location of any percentage of cells after any specified interval of time. (8 refs.)

78164 Voltage-gated Ca^{2+} channel in mouse myeloma cells. Y.Fukushima, S.Hagiwara (Dept. of Physiology, Univ. of California, Los Angeles, CA, USA).

Proc. Natl. Acad. Sci. USA, vol.80, no.8, p.2240-2 (April 1983). Electrical properties of the cell membrane were studied in the neoplastic lymphocyte, mouse myeloma cell line S194, by using the whole-cell patch clamp technique. Inward Ca^{2+} currents due to voltage-gated Ca^{2+} channels were found. The current, which decayed exponentially after reaching a peak, was first activated at about -50 mV and attained its maximum peak amplitude at about -20 mV in a 10 mM Ca^{2+} solution. Outward current was negligible for the potential range more negative than $+30$ mV. The channel was permeable to Sr^{2+} and Ba^{2+} in addition to Ca^{2+} . Among these species, Sr^{2+} carried the greatest current. The time constants of the decay of the current depended neither on the species nor on the concentration of charge carrier. The steady-state inactivation was observed at potentials more negative than those at which the inward Ca^{2+} current was activated. Thus, it was concluded that the inactivation of the channel was mainly voltage dependent. For reasons that are not yet understood, the amplitude of the Ca^{2+} current varied greatly among cells. (19 refs.)

78165 Establishment of an oscillatory regime in a dissipative biological system. A.M.Kosevich, I.L.Kruglikov (Inst. for Low Temperature Phys. & Engng., Acad. of Sci., Kharkov, Ukrainian SSR). *Phys. Scr. (Sweden)*, vol.27, no.5, p.380-4 (May 1983).

A distributed cell system which exchanges substance with the surrounding medium is considered. The state of the system is described by the cell size distribution function, $f(R,t)$, and the concentration of the nutrient, c , in the solution, which obey a pair of nonlinear equations. The system is characterized by a definite temporal period, connected with the life cycle of an individual cell, and by the average frequency of cell death. It is shown that at constant feeding of substance to the system a stationary regime will be necessarily established in it due time. As a rule, in the stationary regime the function $f(R,t)$ and the concentration c do not depend on time. However, sometimes in the system an oscillatory regime can appear. The sufficient conditions of appearing of such a regime are obtained, and the corresponding oscillations are described. (11 refs.)

β -lactam ring stability and antibacterial potency: a novel eigenvalue problem See Entry 78122

Electrostatics and gating of excitable membranes See Entry 78152

Structural and functional evidence for multiple channel complexes in the outer membrane of *Neurospora crassa* mitochondria See Entry 78154

Light activated electrogenic $\text{Na}^{+}\text{-Ca}^{2+}$ -exchange in fly photoreceptors: modulation by $\text{Na}^{+}/\text{K}^{+}$ -pump activity See Entry 78184

87.30 BIOPHYSICS OF NEUROPHYSIOLOGICAL PROCESSES

(exc. perception processes and speech)

78166 EMG activity of the vastus medialis oblique and the vastus lateralis in their role in patellar alignment. L.Reynolds (Dept. of Phys. Therapy, Kaiser Permanente Medical Center, Hayward, CA, USA), T.A.Levin, J.M.Medeiros, N.S.Adler, A.Hallum.

Am. J. Phys. Med. (USA), vol.62, no.2, p.61-70 (April 1983). Using intramuscular electrodes the integrated electromyographic activity of the vastus medialis oblique and the vastus lateralis was examined in twenty normal females. The activity was recorded during the last thirty degrees of distal segment stabilized knee extension, when patellar subluxation commonly occurs. The electromyographic activity was normalized and expressed as a percentage of a maximal isometric contraction. Both muscles exhibited low levels of activity with no significant differences between the two. This study provides a quantitative method to assess whether muscular imbalance is present in patients with patellar subluxation. (33 refs.)

78167 The study of exercise and the relation to Q-T interval. D.E.Biddlecombe, M.J.English (Graduate Div. of Biomedical Engng., Univ. of Sussex, Brighton, England), R.Vincent, D.J.Woolons. *Automedica (GB)*, vol.4, no.4, p.209-16 (1983).

The experimental results reported show that: (1) Q-T interval response lags behind changes in heart rate. (2) More than one value of Q-T interval is possible at any single heart rate. (3) The plot of Q-T interval against heart rate for increasing rates is different to that for decreasing rates (hysteresis). (4) The general appearance and length of a Q-T trace provides an indication of possible cardiac disease. In addition, this method of presentation of the data may be more readily amenable to interpretation than by present means. (2 refs.)

78168 A transfer function model for AV conduction in the human heart. I.Van Der Tweel, J.N.Herbschleb, F.L.Meijler (Dept. of Cardiology, Univ. Hospital, Utrecht, Netherlands). *Automedica (GB)*, vol.4, no.4, p.251-5 (1983).

An effort to explain the conduction through the AV node during random stimulation by fitting a transfer function model to the S-S and S-R intervals is described. Data from 3 patients are analysed. (3 refs.)

78169 Analysis of limit-cycle conditions in intercoupled relay oscillators with reference to gastrointestinal modelling. D.P.Atherton (School of Engng. & Appl. Sci., Univ. of Sussex, Brighton, England), D.A.Linkens. *Bull. Math. Biol. (GB)*, vol.45, no.2, p.239-57 (1983).

Presents an exact analysis of a mutually coupled relay oscillator based on a method originated by Y.Z. Tsytkin (1955). Limit-cycle frequencies and phases can be determined exactly using this method, unlike other approximate methods based on describing functions and harmonic balance techniques. A

new method of exact determination of limit-cycle stability is also shown to give excellent agreement with simulation studies. Different types of intercoupling are shown to give different stability conditions, and these are discussed in relation to gastrointestinal (GI) smooth muscle modelling. GI tract electrical activity has previously been modelled using bidirectionally coupled nonlinear oscillators, and the results of the present analysis of relay oscillators is compared with other studies using Van der Pol dynamics. (32 refs.)

78170 Kinetic theory of neural systems: analysis of the activity of the two-dimensional model. F.Ventriglia (Istituto di Cibernetica, CNR, Napoli, Italy).

Biol. Cybern. (Germany), vol.46, no.2, p.93-9 (1983).

The behaviour of some two-dimensional neural systems is studied by a numerical solution of the associated kinetic equations. The ability of the model to sustain the propagation of informational waves and rhythmic activities as well as memory effects has been demonstrated. (10 refs.)

78171 Evaluation of neuronal coupling dynamics. J.Schneider, R.Eckhorn, H.Reitbock (Philipps-Univ. Marburg, Marburg, Germany).

Biol. Cybern. (Germany), vol.46, no.2, p.129-34 (1983).

Temporary correlated activity of neuron assemblies is believed to play a substantial role for the brain's pattern recognition ability. To study the underlying principles of such mechanisms, a method is proposed for the characterization of the interneuronal and stimulus-response coupling changes of two periodically driven and simultaneously recorded units. The coupling measure is derived from the cross correlation function by calculating the actual correlation contributions without performing the subsequent time-average (which would give the cross correlation function). Examples are given for simultaneously recorded spike trains from visual cortical units, but the method can be applied equally well to evoked potentials or intracellular recordings. (10 refs.)

78172 Bioelectric considerations in the design of high-voltage power lines.

M.Reichmann, A.A.Marino (Dept. of Orthopaedic Surgery, Louisiana State Univ. Medical Center, Shreveport, LA, USA).

J. Bioelectr. (USA), vol.1, no.3, p.329-38 (1982).

Public-health considerations require that all practical steps be taken to minimize the environmental electric and magnetic fields of high-voltage power lines. These fields are influenced not only by the line's operating voltage, but also by various design features including line configuration, phase-spacing, line height, and cable diameter. The largest effect is associated with line configuration. Beyond about 50 meters, the fields of a horizontal line are less than that of the equivalent vertical line; they become progressively more so with increasing distance. As a consequence, for a line having a given energy-carrying capacity, the horizontal configuration minimizes the ground-level fields at points beyond the right-of-way. None of the other design features considered had a significant effect on the fields. (10 refs.)

78173 Electromyographic study of the bulbo-cavernosus muscle in women according to parity and during labor. V.Gallai, C.Firenze, G.Mazzotta, L.Agostini (Inst. of Clinical Neurology, Univ. of Perugia, Perugia, Italy). *Electromyography & Clin. Neurophysiol. (Belgium)*, vol.23, no.3, p.195-201 (March-April 1983).

The bulbo-cavernosus muscle was electromyographically examined in 30 non-pregnant females; and also in 30 females during the expulsion stage of labor, divided into 3 groups according to parity. In the non-pregnant females the action potentials had a duration of amplitude respectively of 4.6 ± 0.7 msec and $303.3 - 20.4$ μ V for the nulliparae; 4.5 ± 0.9 msec and 299.7 ± 28.4 μ V for the uniparae; 4.4 ± 0.8 msec and 281.4 ± 25.6 μ V for the multiparae. In the females during labor the action potentials had a duration and an amplitude respectively of 5.8 ± 0.6 msec and 430.7 ± 28.6 μ V for the uniparae; 5.7 ± 0.5 msec and 413.5 ± 22.5 μ V for the biparae; and 5.1 ± 0.4 msec and 362.5 ± 17.4 μ V for the multiparae. In addition, the bulbo-cavernosus muscle and the external sphincter of the anus in non-pregnant females were examined simultaneously; as was the bulbo-cavernosus muscle and the uterine muscles of pregnant females during the expulsion stage. The authors conclude that the cloaca derived musculature has a synchronous and simultaneous activity, and that the coordination between the uterine muscle activity and that of the perineal diminishes with repeated pregnancies. (7 refs.)

78174 EMG parameters changes in the effort pattern at various loads in diseased muscle. I.Petrusewicz, J.Kocep (Dept. of Neurology, Medical School, Warsaw, Poland). *Electromyography & Clin. Neurophysiol. (Belgium)*, vol.23, no.3, p.213-28 (March-April 1983).

Mechanical and electrical activity in m. biceps brachii during contractions of 10, 30, 50, 70 and 100% of maximal force of the given subject were examined. The investigations were done in a control group of 11 healthy subjects, in 14 cases of myopathy and 11 cases of neurogenic atrophy. The electrical activity was analyzed using a computerized method developed in the authors' institute. The dynamics of increasing density and amplitude and recruitment of motor units up to maximal effort seems to be different in various pathological states of muscle. The authors have also proved the possibility of evaluating the single potential during submaximal effort. (18 refs.)

Ion distributions in inhomogeneous regions [biomembranes] See Entry 78146

Exchange currents across the electrolyte/membrane interface in frog skin See Entry 78147

Dual-mode potential oscillations on an immobilized acetylcholinesterase membrane system See Entry 78151

Electrostatics and gating of excitable membranes See Entry 78152

Dielectric measurements on live biological materials under magnetic resonance conditions See Entry 78157

Voltage-gated Ca^{2+} channel in mouse myeloma cells See Entry 78164

Magnetic measurements and modelling for the investigation of the human-heart conduction system See Entry 78204

First magnetic measurements of action currents in isolated cardiac Purkinje fibers See Entry 78207

Inferences concerning anatomy and physiology of the human brain based on its magnetic field See Entry 78208

Control of muscle contractile force through indirect high-frequency stimulation See Entry 78213

Motor reaction time and stereotyped pattern of the EMG activities in ballistic elbow extension See Entry 78220

Changes in the electric activity of rat stomach directly affected by X-radiation See Entry 78259

Neuromagnetic measurements at hospital: instrumentation and preliminary tests See Entry 78280

High-resolution magnetic measurements of human cardiac electrophysiological events See Entry 78281

- High-resolution magnetocardiographic recordings of the ST segment in patients with electrical late potentials. See Entry 78285
- Precordial electrocardiographic map using the IBM-Bonner program See Entry 78373
- The mapping of the measured cardiac electric potential and magnetic-field distribution See Entry 78374
- Interference electromyogram processing. I. Influence of the motor unit action potential shape on the interference electromyogram spectra See Entry 78375
- Automated analysis of abnormal electroencephalograms See Entry 78376
- An implantable, externally powered radiotelemetric system for long-term ECG and heart-rate monitoring See Entry 78388
- On-line analysis of neuromuscular bioelectric potentials See Entry 78389
- The use of time domain dielectric spectroscopy to characterize the progress of wound repair See Entry 78400
- Multichannel microelectrode for recording neural activity See Entry 78403

87.32 PHYSIOLOGICAL OPTICS, VISION

- Experimental studies of laser thermal retinal injury See Entry 78240

87.32C Anatomy and optics of the eye

- Mechanical model of the insect eye See Entry 78391

87.32E Physiology of the eye; nerve structure and function

- 78175 The spectral analysis of the visual evoked potentials of normal and congenital dull children (Down's disease). Xie Zhongjie (Dept. of Maths., Peking Univ., Peking, China). *Acta Sci. Nat. Univ. Pekin. (China)*, no.6, p.91-6 (1982). In Chinese. The statistical analysis shows that the spectral estimates of dull children (near 3 1/3 Hz and 10 Hz) are obviously different from that of normal children. The Bayesian discriminant function clearly divides the sample pairs of two populations into two regions on the plane. (8 refs.)
- 78176 An analogue model of the luminosity-channel in the vertebrate cone retina. I. Hardware and responses to square wave voltages. R.Siminoff (Inst. fur Physiologie, Freien Univ. Berlin, Berlin, Germany). *Biol. Cybern. (Germany)*, vol.46, no.2, p.101-10 (1983). Deals with a description of the hardware for an analogue simulation of the generalized vertebrate cone retina using Eckmiller's (1971) model as a starting point, but modified to be compatible with the author's model. A number of simplifications were made, such as limiting the cone mosaic to only one spectral type of cone, limiting the unit hexagon to only 7 cones and omitting stray light effects and electrical coupling between like-cones. Nevertheless, the model is a realistic representation for a number of simple parameters of the luminosity-channel of the vertebrate cone retina. The feasibility of the model was established by a study of response characteristics to stationary stimuli and noting physiological correlates. The roles of negative feedback from the horizontal cell (HC) to the cones, electrical coupling of HCs and center-surround interactions were elucidated and shown to be important for the organization of the retina. (32 refs.)
- 78177 Lateral inhibition shapes the oscillatory responses of the horseshoe crab's compound eye. G.H.Renninger (Dept. of Phys., Univ. of Guelph, Guelph, Ontario, Canada). *Biol. Cybern. (Germany)*, vol.46, no.2, p.119-27 (1983). The synchronized response of the compound eye of the horseshoe crab to uniform illumination arises from the integration of excitation with the strong lateral inhibition present in many specimens. At the higher levels of excitation, the steady production of nerve impulses by individual eccentric cells is often replaced by periodically recurring volleys of impulses. This behavior is shown to be the result of the temporal behavior of the post-synaptic potentials responsible for lateral inhibition. For a broad class of inhibitory potentials, a simple condition is established which separates potentials which permit volleys at high excitation levels from those which support only the steady production of impulses throughout the physiological range of excitations. (16 refs.)
- 78178 Retinotopic map on the visual cortex for eccentrically placed patterns: first noninvasive measurement. E.MacIin, Y.C.Okada, L.Kaufman, S.J.Williamson (Dept. of Psychology & Phys., New York Univ., New York, NY, USA). *Nuovo Cimento D (Italy)*, vol.2D, ser.1, no.2, p.410-19 (March-April 1983). (Proceedings of the Fourth International Workshop on Biomagnetism, Rome, Italy, 14-16 Sept. 1982). The observed cortical magnetic field evoked by a stimulus presented at various eccentricities in the visual field was interpreted as arising from current dipoles along the longitudinal fissure. The depth of the source increased as the eccentricity was increased, in agreement with the classical retinotopic map. (16 refs.)
- 78179 Visual processing in the leech central nervous system. E.L.Peterson (Dept. of Biology, McGill Univ., Montreal, Quebec, Canada). *Nature (GB)*, vol.303, no.5914, p.240-2 (19 May 1983). In animals with complex visual systems spatial contrast is enhanced by mutual inhibition between retinal neurones monitoring different fields. By analogy, if animals like leeches and some caterpillars, that have several simple (nonimage-forming) eyes aimed in different directions, are capable of rudimentary form detection, one might predict mutual antagonism between eyes monitoring different fields. In support of this prediction the author reports a paired interneurone in the central nervous system (CNS) of the leech which is stimulated by eyes on one side of the animal and inhibited by eyes on the other. There are striking parallels between these neurones and other integrating neurones, in particular those processing bilateral auditory input in crickets, suggesting that the visual system of the leech may be representative of a general class of sensory processing systems. (17 refs.)
- Bump latency distribution and bump adaptation of Limulus ventral nerve photoreceptor in varied extracellular calcium concentrations See Entry 78182
- Chromatic induction: responses of neurophysiological double opponent units? See Entry 78185
- Neuromagnetic localization of two components of the transient visual evoked response to patterned stimulation See Entry 78209
- The effects of some recording variables on the visual evoked response. I. A comparison of surface and needle electrode recording of the visual evoked response See Entry 78369

- The effects of some recording variables on the visual evoked response. II. The effects of system bandpass on the recording of the visual evoked response See Entry 78370

- Visual evoked potentials in the newborn: awake and asleep See Entry 78371

87.32L Light detection; adaptation and discrimination

- 78180 Progress in phototransduction. D.G.Stavenga, W.J.de Grip (Dept. of Biophys., Univ. of Groningen, Groningen, Netherlands). *Biophys. Struct. & Mech. (Germany)*, vol.9, no.4, p.225-30 (1983). Various aspects of the phototransduction mechanism have been highlighted during the Vth International Congress of Eye Research, held in Veldhoven, the Netherlands (from 5-8 October 1982). The correspondences and differences of phototransduction in both vertebrate and invertebrate photoreceptor cells were extensively discussed. The authors briefly review the present views. (48 refs.)
- 78181 Sensitizing pigment in the fly. K.Vogt, K.Kirschfeld (Max-Planck-Inst. fur Biologische Kybernetik, Tubingen, Germany). *Biophys. Struct. & Mech. (Germany)*, vol.9, no.4, p.319-28 (1983). The sensitizing pigment hypothesis for the high UV sensitivity in fly photoreceptors (R1-6) is further substantiated by measurements of the polarisation sensitivity in the UV. The quantum yield of the energy transfer from sensitizing pigment to rhodopsin was estimated by electrophysiological measurements of the UV sensitivity and the rhodomeric absorbance (at 490 nm) in individual receptor cells. The transfer efficiency is ≥ 0.75 in receptors with an absorbance in the rhodomer of 0.55-0.05. This result suggests that the sensitizing pigment is bound in some way to the rhodopsin. A ratio of two molecules of sensitizing pigment per one rhodopsin is proposed. (30 refs.)
- 78182 Bump latency distribution and bump adaptation of Limulus ventral nerve photoreceptor in varied extracellular calcium concentrations. H.Stieve, M.Bruns (Inst. fur Neurobiologie, KFA Julich GmbH, Julich, Germany). *Biophys. Struct. & Mech. (Germany)*, vol.9, no.4, p.329-39 (1983). Bumps were recorded as voltage signals following dim flashes of light. Bump amplitude and width did not much depend upon external Ca^{2+} -concentration. However, the distribution of bump latencies was strongly shifted to longer latencies and broadened more than two-fold when the external Ca^{2+} -concentration was lowered from 10 mmol/l to 0.25 mmol/l. Raising the external Ca^{2+} -concentration to 40 mmol/l had the opposite effect. A preadapting light flash caused shortening the narrowing of bump latency distribution similar to the effect of raised external Ca^{2+} -concentration. The bump amplitude was not correlated with the length of the latent period of the bump, indicating that the amplification processes determining the bump size are distinctly from those which determine the latent period. (21 refs.)
- 78183 Variations in the voltage response to single quanta of light in the photoreceptors of *Locusta migratoria*. J.Howard (Dept. of Neurobiology, Res. School of Biological Sci., Canberra, Australia). *Biophys. Struct. & Mech. (Germany)*, vol.9, no.4, p.341-8 (1983). Brief, dim flashes of light that produced on average only one response per three to six flashes were presented to dark-adapted locust photoreceptors. The amplitude, latency, and half-duration of the discrete voltage responses showed substantial variation. However all frequency distribution curves were single peaked, indicating that there is only one class of discrete voltage responses in the locust. Correlations between these parameters are low (accounting for less than 7% of the variance) but statistically significant. The low correlations suggest that different processes underlie the generation of amplitude, latency and duration of the bumps. (14 refs.)
- 78184 Light activated electrogenic Na^{+} - Ca^{2+} -exchange in fly photoreceptors: modulation by $\text{Na}^{+}/\text{K}^{+}$ -pump activity. E.Armon, B.Minke (Dept. of Physiology, Hebrew Univ.-Hadassah Medical School, Jerusalem, Israel). *Biophys. Struct. & Mech. (Germany)*, vol.9, no.4, p.349-57 (1983). The authors found recently that illumination of white-eyed *Musca* photoreceptors following application of ruthenium red (RR), (a known inhibitor of Ca^{2+} -uptake into intracellular organelles) induced a transient post-illumination-after depolarization (TA). They found that the TA depended strongly on Na^{+} and Ca^{2+} -gradients across the cell membrane suggesting that it arose from activation of electrogenic Na^{+} - Ca^{2+} -exchange. Since the magnitude of the TA was dependent on the Na^{+} -gradient, in this work the authors studied the effects of the $\text{Na}^{+}/\text{K}^{+}$ -pump, which controls the Na^{+} -gradient, on the TA. Increasing extracellular K^{+} -concentration which largely increased pump activity also increased the TA. Application of 100 μM ouabain, for a short time, depressed the TA considerably without causing any noticeable effect on the resting or the receptor potential. Only after longer exposure to ouabain, when the TA was totally depressed, where the resting and receptor potentials abolished by only a few strong light flashes. Trains of strong light pulses either facilitated or inhibited the TA depending on the degree of increase in internal Ca^{2+} -ions by light and on the activity of the $\text{Na}^{+}/\text{K}^{+}$ -pump. (12 refs.)
- Fluorescence of blowfly metarhodopsin See Entry 78139
- Laser induced visual pigment conversions in fly photoreceptors measured in vivo See Entry 78236

87.32N Colour detection; adaptation and discrimination

- 78185 Chromatic induction: responses of neurophysiological double opponent units?. A.Valberg, T.Seim (Dept. of Biophys., Univ. of Oslo, Oslo, Norway). *Biol. Cybern. (Germany)*, vol.46, no.2, p.149-58 (1983). Equations have been derived that improve the quantification of sensory equidistant colour and lightness differences. This has been achieved by a physiological approach involving nonlinear responses of cone mechanisms and two subsequent stages of linear opponent transformation to describe the Munsell System (Seim and Valberg, 1980). Using the formulation for the first opponent stage, colours induced into an achromatic center field, by a chromatic surround varying in purity, are shown to follow the same power function of the opponent coordinates for all hues. By analogy, a physiological model for colour coding and colour induction is offered. Double opponent neurones with spatially antagonistic, spectrally opponent and symmetric receptive fields constitute the units of the model. Colour induction is related to lateral excitation and colour differences to response differences of these units. (39 refs.)

87.32S Psychophysics of vision, visual perception, binocular vision

78186 Human performance engineering. Looking through the user's eyes. R.W.Bailey. *Computerworld (USA)*, vol.17, no.18, p.ID1-6 (2 May 1983). Gives an introduction to visual perception as it relates to human performance engineering, for example in CRT or keyboard design. The importance of schema, or format, is emphasised. (no refs.)

78187 Perception of movement, the correlation model and the landing reaction of the flesh fly (Calliphoridae). L.Beghi (Seminario Matematico, Padova, Italy), N.Saviolo, E.Xausa, M.Zanforline. *Biol. Cybern. (Germany)*, vol.46, no.2, p.81-91 (1983). An analysis is made of the variations in sensitivity to movement in flesh flies (Calliphoridae) when placed in front of various fixed screens structured with black and white stripes. Two vertical bands moving from the centre to the periphery were projected onto these screens. The threshold of sensitivity to these bands was measured using the landing reaction. The results are compared with maximal values of theoretically predicted responses to movement, obtained using the model of nonlinear (2nd order) interaction between two pairs of neighbouring ommatidia (Reichardt, 1969) and taking into account the lateral inhibitory interaction between moving stripes and the background (4th order, *p*-order 2), as proposed by Reichardt and Poggio (1976). Experimental and theoretical results matched reasonably well except for screens with fixed alternate black and white stripes whose angular frequency ranged from 0.5 to 0.8 rad⁻¹, and for two screens of greatly reduced luminosity. (13 refs.)

Visual perception of a phonemic code for a tactile hearing aid See Entry 78385

87.34 AUDITION

78188 Studies of auditory evoked magnetic and electric responses: modality specificity and modelling. T.Tuomisto, R.Hari, T.Katila, T.Poutanen, T.Varpula (Dept. of Tech. Phys., Helsinki Univ. of Technol., Espoo, Finland). *Nuovo Cimento D (Italy)*, vol.2D, ser.1, no.2, p.471-83 (March-April 1983). (Proceedings of the Fourth International Workshop on Biomagnetism, Rome, Italy, 14-16 Sept. 1982). The sources of auditory evoked electric and magnetic responses were modelled with multiple current dipoles. The activity at the auditory cortices 2.6 cm beneath the skull, explains the observed *N*100m field distribution. An additional current source near the vertex is needed to explain the corresponding potential distributions. The locations of the current sources of *N*100m did not show any systematic dependence on the tonal frequency. (14 refs.)

78189 Determination of the normal threshold of hearing by bone conduction using different types of bone vibrators. I. K.Brinkmann, U.Richter. *Audiol. Akust. (Germany)*, vol.22, no.3, p.62-85 (May-June 1983). In German, English. In the frequency range from 125 Hz to 8000 Hz, on a large number of otologically normal persons, the bone-conduction hearing threshold was determined for three different types of bone vibrators. The mastoid and the forehead served as placement sites. The vibrotactile threshold which represents an upper level limit for an exact measurement of the bone-conduction hearing threshold, was also measured. The results show that for all bone vibrators which are in compliance with IEC specifications, the hearing threshold on the mastoid can be described by a single series of equivalent threshold force levels. Another series of values is valid for the hearing threshold on the forehead. At 125 Hz, the level range utilizable for measuring the bone conduction hearing threshold amounts only to about 14 dB (mastoid coupling) but increases towards higher frequencies. The differences between the thresholds of hearing by air and bone conduction of otologically normal persons show an approximately normal distribution with regard to the 0 dB value, differences exceeding ± 7.5 dB being still found in about 20% of the cases. (38 refs.)

78190 Music perception and elementary auditory sensations. II. E.Terhardt. *Audiol. Akust. (Germany)*, vol.22, no.3, p.86-96 (May-June 1983). In German, English. Between the essential features of music perception and the elementary hearing characteristics, interrelationships exist which in part prove to be surprisingly simple and clear. Such interrelationships have been found, among other things, to be of importance for the evaluation of the consequences of functional hearing disorders in the perception of music. The interrelationships applying to normally hearing persons are described, as far as they relate to the melodic and harmonic aspects of music. It is demonstrated that the sense of harmony is based on the psycho-acoustical fundamental principles of pitch perception and that the general pleasantness of sound (called sensory consonance) can be traced back to the three hearing attributes: roughness, sharpness and timbre. The interaction between harmony and pleasantness of sound results in the phenomenon of musical consonance and permits an adequate hearing-related description of many musical phenomena. (19 refs.)

78191 Speech competition effects on synthetic stop-vowel perception by normal and hearing-impaired listeners. S.M.Gordon-Salant (Dept. of Hearing & Speech Sci., Univ. of Maryland, College Park, MD, USA), F.L.Wightman. *J. Acoust. Soc. Am. (USA)*, vol.73, no.5, p.1756-65 (May 1983). A triadic comparisons task and an identification task were used to evaluate normally hearing listeners' and hearing-impaired listeners' perceptions of synthetic CV stimuli in the presence of competition. The competing signals included multitalker babble, continuous speech spectrum noise, a CV masker, and a brief noise masker shaped to resemble the onset spectrum of the CV masker. All signals and maskers were presented monotonically. Interference by competition was assessed by comparing multidimensional scaling solutions derived from each masking condition to that derived from the baseline (quiet) condition. Analysis of the effects of continuous maskers revealed that multitalker babble and continuous noise caused the same amount of change in performance, as compared to the baseline condition, for all listeners. CV masking changed performance significantly more than did brief noise masking, and the hearing-impaired listeners experienced more degradation in performance than normals. Finally, the velar CV maskers (g and k) caused significantly greater masking effects than the bilabial CV maskers (b and p), and were most resistant to masking by other competing stimuli. The results suggest that speech intelligibility difficulties in the presence of competing segments of speech are primarily attributable to phonetic interference rather than to spectral masking. Individual differences in hearing-impaired listeners' performances are also discussed. (21 refs.)

78192 Perception of static and dynamic acoustic cues to place of articulation in initial stop consonants. D.Kewley-Port, D.B.Pisoni (Dept. of Psychology, Indiana Univ., Bloomington, IN, USA), M.Studdert-Kennedy. *J. Acoust. Soc. Am. (USA)*, vol.73, no.5, p.1779-93 (May 1983). Two recent accounts of the acoustic cues which specify place of articulation in syllable-initial stop consonants claim that they are located in the initial portions of the CV waveform and are context-free. Stevens and Blumstein [ibid., vol.64, p.1358-1368 (1978)] have described perceptually relevant spectral properties of these cues as dynamic. Three perceptual experiments were conducted to test predictions derived from these accounts. Experiment 1 confirmed that acoustic cues for place of articulation are located in the initial 20-40 ms of natural stop-vowel syllables. Next, short synthetic CVs modeled after natural syllables were generated using either a digital, parallel-resonance synthesizer in experiment 2 or linear prediction synthesis in experiment 3. One set of synthetic stimuli preserved the static spectral properties proposed by Stevens and Blumstein. Another set of synthetic stimuli preserved the dynamic properties suggested by Kewley-Port. Listeners in both experiments identified place of articulation significantly better from stimuli which preserved dynamic acoustic properties than from those based on static onset spectra. Evidently, the dynamic structure of the initial stop-vowel articulatory gesture can be preserved in context-free acoustic cues which listeners use to identify place of articulation. (33 refs.)

78193 Reply to 'Comments on "Ear dominance and sequential interactions"' by E. William Yund. D.Deutsch (Center for Human Information Processing, Univ. of California, San Diego, La Jolla, CA, USA). *J. Acoust. Soc. Am. (USA)*, vol.73, no.5, p.1865-7 (May 1983). The author replies to comments by Yund (see ibid., vol.71, p.1287, 1982) on her original work (see ibid., vol.67, p.220, 1980), pointing out that the pitch assignment is in the octave corresponding to the frequency delivered to the dominant ear, that there is no valid basis for Yund's objection to the use of the 2AFC method, and that other arguments of his are erroneous. (7 refs.)

78194 Perceptual identification and discrimination of phase distortions. P.J.Bloom (Div. of Engng., Polytech. of Central London, London, England), D.Preis. Proceedings of ICASSP 83. IEEE International Conference on Acoustics, Speech and Signal Processing, Boston, MA, USA, 14-16 April 1983 (New York, USA: IEEE 1983), p.1396-9 vol.3 Experimental results on the audibility of phase distortion produced by minimum-phase 4kHz and 15 kHz anti-alias filters are reported. Numerous impulse response pairs with identical spectral magnitudes but linear-phase and minimum-phase responses were compared by five test subjects who listened dichotically on earphones. Group-delay distortion was doubled, progressively, until at least 67% mean correct discrimination was attained. At 4kHz, the phase distortion introduced by a cascade of two eighth-order Butterworth filter pairs was audible as was that from only a single pair of seventh-order elliptic filters. At 15kHz, the cascade of up to 4 pairs of seventh-order elliptic filters introduced no perceptible effects. Experimental details and several representative filter frequency and transient responses are included. (2 refs.)

78195 Development of a technique for high frequency audiometry. M.A.Krasner, K.N.Stevens, D.M.Green, S.H.Blumenthal (Bolt Beranek & Newman Inc., Cambridge, MA, USA). Proceedings of ICASSP 83. IEEE International Conference on Acoustics, Speech and Signal Processing, Boston, MA, USA, 14-16 April 1983 (New York, USA: IEEE 1983), p.1400-3 vol.3 Describes the development of a new technique for the assessment of hearing thresholds in the range 8-20 kHz. The authors describe a model that circumvents some major difficulties encountered by present audiometric methods at high frequencies and present measurements that validate that model. A technique that can provide accurate and reliable measurements is described and evaluated. (5 refs.)

Some tentative model considerations based on experimental neuromagnetic data See Entry 78211

Auditory evoked magnetic fields: a replication, with comments on the magnetic P50 analog See Entry 78212

Effects of digital filtering on the waveform and peak parameters of the auditory brainstem response See Entry 78377

87.36 SPEECH

(see also 43.70 Speech communication)

78196 The influence of inter- and intra-speaker tempo on fundamental frequency and palatalization. W.E.Cooper, C.Soaes, A.Ham, K.Damon (Dept. of Psychology, Harvard Univ., Cambridge, MA, USA). *J. Acoust. Soc. Am. (USA)*, vol.73, no.5, p.1723-30 (May 1983). A study was conducted to examine the influence of speaking rate and emphatic stress on patterns of fundamental frequency (*F*₀) and palatalization across word boundaries. Two groups of speakers, exhibiting characteristically fast versus slow speech, uttered preselected sentences at normal, fast, and slow rates. Acoustic analysis of *F*₀ showed somewhat higher *F*₀ peaks for characteristically fast speakers and for fast rates of speech. Emphatic stress was accompanied by a typical heightening of *F*₀ on the emphasised word and by a lowering of *F*₀ on a neighboring word. Palatalization across word boundaries was more frequent among characteristically fast speakers and at fast rates of speech. In addition, palatalization was more frequent in the absence of emphatic stress at the key site. The results for *F*₀ were discussed in terms of the influence vocal fold tension, while the results for palatalization were discussed in terms of the incompatibility of phonological processes of lengthening versus shortening as well as possible look-ahead restrictions. (15 refs.)

78197 Declination of fundamental frequency in speakers' production of parenthetical and main clauses. E.J.Kutik, W.E.Cooper (Harvard Univ., Cambridge, MA, USA), S.Boyce. *J. Acoust. Soc. Am. (USA)*, vol.73, no.5, p.1731-8 (May 1983). An experimental study was conducted to investigate fundamental frequency (*F*₀) contours in sentences with and without parenthetical clauses. Sentences consisted of a systematically lengthened parenthetical clause inserted between the subject noun phrase and the verb phrase of the main clause. The middle portion of the parenthetical was lengthened incrementally in each sentence to test the effects of sentence length on fundamental frequency contours of seven test sentences. Computer-aided measurements were made for: *F*₀ peaks of key stressed segments; duration of the main clause, parenthetical clause, and clause-final syllables within each; and pauses immediately preceding and following the parenthetical. Mean results demonstrate: (1) a drop in *F*₀ for the parenthetical clause, well below the main clause declination and forming a separate contour of declination; (2) a sharp rise in *F*₀ on return to the main clause; (3) no effect of longer parenthetical length on final segment durations of either the parenthetical or the main clause; and (4) no effect of increased parenthetical length on main clause duration or pause length. These results

suggest that parenthetical clauses are mentally programmed as independent constituents, but are subject to some of the same general declination constraints as main clauses. (23 refs.)

78198 Further evidence of acoustic invariance in speech production: the stop-glide contrast. M.Mack, S.E.Blumstein (Brown Univ., Providence, RI, USA).

J. Acoust. Soc. Am. (USA), vol.73, no.5, p.1739-50 (May 1983).

The authors have conducted a detailed comparative acoustic analysis of the labial stop and glide, [b] and [w], and they have attempted to identify an invariant acoustic property which can accurately distinguish stops and glides. To this end, they conducted three experiments. In experiment I, they undertook computer analysis of the labial stop [b] and the labial glide [w] as produced in five vowel contexts by two speakers. Results indicated that transition durations and formant frequencies often differed considerably in these two classes of sounds—and to a much greater extent than suggested in previous perception experiments. In experiment II the authors examined a measure of amplitude—unit energy. They calculated the degree of relative amplitude change occurring in the vicinity of the stop and glide release and found reliably larger changes in energy associated with the stop release than the glide release across vowel contexts and speakers. These changes seemed to provide an invariant property characterizing the stop-glide contrast. In experiment III the authors tested the generality of their claims by examining a new set of data consisting of the stops [d] and [g] and the glide [y]. Results of this experiment further supported their hypothesis. They have related their findings to a general theory of acoustic invariance in speech. (25 refs.)

78199 Some effects of speaking rate on the production of /b/ and /w/. J.L.Miller (Dept. of Psychology, Northeastern Univ., Boston, MA, USA), T.Baer.

J. Acoust. Soc. Am. (USA), vol.73, no.5, p.1751-5 (May 1983).

One of the acoustic properties distinguishing the syllable-initial stop consonant /b/ from the semivowel /w/ is the duration of the initial formant transitions; syllables beginning with /b/ have shorter transitions than those beginning with /w/. This experiment investigated the way in which the transition durations of /b/ and /w/ change as a function of speaking rate by examining tokens of /ba/ and /wa/ produced by four male speakers. At any given speaking rate the /wa/ transitions were, on average, longer than the /ba/ transitions, although pooled across rates, the distributions of transition duration for /ba/ and /wa/ were overlapping. In addition, the magnitude of the difference between average /ba/ and /wa/ transition durations increased with decreases in speaking rate. This is because as rate of speech decreased so that syllable duration increased, there was little change in the initial transition duration of /ba/, but a considerable increase in the initial transition duration of /wa/. Given the overall pattern of results, the transition duration that could optimally distinguish /ba/ from /wa/ was not constant, but increased with syllable duration. This is in accord with Miller and Liberman's (1979) finding that when listeners identify /ba/ and /wa/ on the basis of transition duration, they do so in relation to the duration of the syllable. (15 refs.)

78200 A preliminary model of subjective voice quality. G.J.Boggs (GTE Labs., Waltham, MA, USA).

Proceedings of ICASSP 83. IEEE International Conference on Acoustics, Speech and Signal Processing, Boston, MA, USA, 14-16 April 1983 (New York, USA: IEEE 1983), p.1404-6 vol.3

Psychophysical scaling is a popular methodology for subjective speech quality assessment. Unfortunately, scaling techniques are not bias-free measurements. A conceptual model is developed, based on the theory of signal detectability and the internal-noise model. The implications of the conceptual model for speech quality assessment are discussed. (9 refs.)

Perception of static and dynamic acoustic cues to place of articulation in initial stop consonants See Entry 78192

87.38 MECHANICAL AND CHEMIO-CEPTIONS

(inc. biosonic generation, detection and guidance)

78201 Vibrotactile identification of vowels. B.G.Green, J.C.Craig, A.M.Wilson, D.B.Pisoni, R.P.Rhodes (Dept. of Psychology, Indiana Univ., Bloomington, IN, USA).

J. Acoust. Soc. Am. (USA), vol.73, no.5, p.1766-78 (May 1983).

The ability of subjects to identify vowels in vibrotactile transformations of consonant-vowel syllables was measured for two types of displays: a spectral display (frequency by intensity), and a vocal tract area function display (vocal tract location by cross-sectional area). Both displays were presented to the fingertip via the tactile display of the Optacon transducer. In the first experiments the spectral display was effective for identifying vowels in /b-V/ context when as many as 24 or as few as eight spectral channels were presented to the skin. However, performance fell when the 12- and 18-channel displays were reduced in size to occupy 1/2 or 1/3 of the 24-row tactile matrix. The effect of reducing the size of the display was greater when the spectrum was represented as a solid histogram ('filled' patterns) than when it was represented as a simple spectral contour ('unfilled' patterns). Spatial masking within the filled pattern was postulated as the cause for this decline in performance. Another experiment measured the utility of the spectral display when the syllables were produced by multiple speakers. The resulting increase in response confusions was primarily attributable to variations in the tactile patterns caused by differences in vocal tract resonances among the speakers. The final experiment found an area function display to be inferior to the spectral display for identification of vowels. The results demonstrate that a two-dimensional spectral display is worthy of further development as a basic vibrotactile display for speech. (40 refs.)

Somatosensory evoked magnetic fields: mappings and the influence of the stimulus repetition rate See Entry 78210

Visual perception of a phonemic code for a tactile hearing aid See Entry 78385

87.40 BIOMAGNETISM

(inc. magnetocardiography)

78202 The magnetic field produced by the conduction system of the human heart. J.L.Patrick, D.W.Hess, H.J.Tripp, D.E.Farrell (Dept. of Phys., Case Western Reserve Univ., Cleveland, OH, USA).

Nuovo Cimento D (Italy), vol.2D, ser.1, no.2, p.255-65 (March-April 1983). (Proceedings of the Fourth International Workshop on Biomagnetism, Rome, Italy, 14-16 Sept. 1982).

The authors have exploited the spatial resolution of the magnetic sensor to provide numerical estimates of the atrial contribution to magnetic fields recorded just prior to ventricular depolarisation. The contribution is found to be small, strengthening the authors' original interpretation that such fields originate mostly in the conduction system of the heart. (17 refs.)

78203 Atrial activity during the PR segment of the MCG. M.Leifer (Dept. of Phys., Stanford Univ., Stanford, CA, USA), N.Capos, J.Griffin, J.Wikswa, Jr.

Nuovo Cimento D (Italy), vol.2D, ser.1, no.2, p.266-79 (March-April 1983). (Proceedings of the Fourth International Workshop on Biomagnetism, Rome, Italy, 14-16 Sept. 1982).

Sloping signals were observed in the PR segment of normal magnetocardiograms recorded from five dogs. Larger ramps were observed after first-degree AV nodal blockade was induced pharmacologically, and complete atrial repolarisation was observed following isolated atrial contractions in two animals with second-degree block. These ramps, ranging up to 6.7 pT in size and arising from the atria, may complicate magnetic detection of His-Purkinje activity. (10 refs.)

78204 Magnetic measurements and modelling for the investigation of the human-heart conduction system. R.R.Fenici (Unita Biomagnetica, Univ. Cattolica, Roma, Italy), G.L.Romani, R.Leoni.

Nuovo Cimento D (Italy), vol.2D, ser.1, no.2, p.280-90 (March-April 1983). (Proceedings of the Fourth International Workshop on Biomagnetism, Rome, Italy, 14-16 Sept. 1982).

Since 1980, systematic investigations of the activity of the His-Purkinje system (HPS) by the biomagnetic method have been reported on both normal subjects and patients affected by different kinds of conduction disturbances. A first attempt to interpret the experimental results by means of a theoretical model satisfactorily accounted for the measured 'ramp' patterns. Moreover, a good temporal coincidence was observed between magnetic signals and invasively recorded His bundle electrograms. An alternative explanation of the 'ramp' pattern, in terms of atrial repolarisation, has been recently proposed on the basis of animal experimental investigation. In order to try to solve this problem, the authors have carried out a twofold approach: a new second-order gradiometer, specifically designed for HPS activity investigation has been successfully set up and tested; it provides a sensitivity of 20 fT/√Hz in the band width of interest ((0.5-300) Hz). Second, a new model based on a closer correspondence to anatomical features of the HPS has been developed. This model provides well-defined patterns which are in quite good agreement with experimental results. (15 refs.)

78205 The influence of inhomogeneities on the cardiac-magnetic-field distribution. M.J.Peters, M.J.M.Swennenhuis, A.van Oosterom, J.J.Wevers-Henke (Dept. of Tech. Phys., Twente Univ. of Technol., Enschede, Netherlands).

Nuovo Cimento D (Italy), vol.2D, ser.1, no.2, p.324-39 (March-April 1983). (Proceedings of the Fourth International Workshop on Biomagnetism, Rome, Italy, 14-16 Sept. 1982).

Numerical computations were performed on the magnetic field generated by the heart during ventricular depolarization. The purpose of this study was to investigate the contribution of inhomogeneities in the volume conductor to the total field and to establish the influence of gradiometers as used in experimental recordings. (22 refs.)

78206 On the influence of the volume conductor in magnetocardiography: an experimental approach. I.R.Eghrari, E.Costa Monteiro, P.Costa Ribeiro, J.P.von der Weid (Dept. de Fisica, Pontificia Univ. Catolica do Rio de Janeiro, Rio de Janeiro, Brazil).

Nuovo Cimento D (Italy), vol.2D, ser.1, no.2, p.346-55 (March-April 1983). (Proceedings of the Fourth International Workshop on Biomagnetism, Rome, Italy, 14-16 Sept. 1982).

To study the effect of the volume conductor geometry on the MCG, experiments using isolated rabbit hearts were done. An increase of the magnetic signal when increasing the volume conductor's size was observed. The results are discussed in terms of using a fixed-origin current dipole and a voltage source model for the heart. (6 refs.)

78207 First magnetic measurements of action currents in isolated cardiac Purkinje fibers. J.P.Wikswa, J.P.Barach, S.C.Gundersen (Dept. of Phys. & Astron., Vanderbilt Univ., Nashville, TN, USA).

Nuovo Cimento D (Italy), vol.2D, ser.1, no.2, p.368-78 (March-April 1983). (Proceedings of the Fourth International Workshop on Biomagnetism, Rome, Italy, 14-16 Sept. 1982).

Presents the first measurements of the magnetic field associated with the action potential in a bundle of isolated cardiac Purkinje fibers. These findings demonstrate the feasibility of using magnetic techniques to measure the axial current in a bundle of spontaneously active cardiac cells. (10 refs.)

78208 Inferences concerning anatomy and physiology of the human brain based on its magnetic field. Y.C.Okada (Dept. of Psychology, New York Univ., New York, NY, USA).

Nuovo Cimento D (Italy), vol.2D, ser.1, no.2, p.379-409 (March-April 1983). (Proceedings of the Fourth International Workshop on Biomagnetism, Rome, Italy, 14-16 Sept. 1982).

Research in the evoked magnetic field reported in the last two years is reviewed. The studies have shown that the magnetic technique may be used (1) to reveal complementary aspects of the current sources common to evoked potential, (2) to identify the organization of the cerebral cortex and subcortical areas of the brain, and (3) to measure functional properties of the active neural areas whose locations are identified. (58 refs.)

78209 Neuromagnetic localization of two components of the transient visual evoked response to patterned stimulation. F.Richer, D.S.Barth, J.Beatty (Dept. of Psychology, Univ. of California, Los Angeles, CA, USA).

Nuovo Cimento D (Italy), vol.2D, ser.1, no.2, p.420-8 (March-April 1983). (Proceedings of the Fourth International Workshop on Biomagnetism, Rome, Italy, 14-16 Sept. 1982).

Corresponding electrical and magnetic components of the brain's visual evoked response peaking at 120 and 180 ms poststimulus are examined. Results show that both magnetic components are localized in the superficial occipital cortex tangential to the scalp. The distribution of M120 suggests that the generators for the electrical and magnetic components are related, but the electrical field record is an elaborate modification of that produced by the source. (8 refs.)

78210 Somatosensory evoked magnetic fields: mappings and the influence of the stimulus repetition rate. D.Teszner, R.Hari, P.Nicholas, T.Varpula (Hopital Ambroise Pare, Boulogne, France).

Nuovo Cimento D (Italy), vol.2D, ser.1, no.2, p.429-37 (March-April 1983). (Proceedings of the Fourth International Workshop on Biomagnetism, Rome, Italy, 14-16 Sept. 1982).

Somatosensory evoked magnetic fields were compared with corresponding electric scalp potentials in order to study their neural sources. Mappings of the magnetic responses showed activity at the primary and secondary somatosensory cortices. Additional sources besides these areas seem to be involved in the generation of the somatosensory vertex scalp potentials. (15 refs.)

78211
Some tentative model considerations based on experimental neuro-magnetic data.
K.Saermark (Phys. Lab. I, Tech. Univ. of Denmark, Lyngby, Denmark).
Nuovo Cimento D (Italy), vol.2D, ser.1, no.2, p.438-59 (March-April 1983).
(Proceedings of the Fourth International Workshop on Biomagnetism, Rome, Italy, 14-16 Sept. 1982).

Presents some tentative model considerations, based on the concept of an equivalent current dipole to account for observed auditory evoked responses, with the aim of attempting a comparison of variations in amplitude and latency with calculations based on Rall's (1962) greatly simplified nerve model. A phenomenological analysis of experimental data on the late, auditory evoked magnetic field from the human auditory cortex is presented. The emphasis is placed on relations between signal properties (e.g. amplitude and latency) and between signal properties and stimulus properties (e.g. amplitude/latency and relative frequency glide $\Delta f/f$ for a frequency glide stimulus) rather than on questions related to the location of the equivalent current dipole, e.g. the tonotopic organization discussed by Eiberling et al. (1982) and by Romani et al.(1982). Some results of a numerical calculation based on a linear-cable model are presented and compared with experimental results. (50 refs.)

78212
Auditory evoked magnetic fields: a replication, with comments on the magnetic P50 analog.
J.T.Zimmerman, M.Reite (School of Medicine, Univ. of Colorado, Denver, CO, USA), J.E.Zimmerman, J.Edrich.
Nuovo Cimento D (Italy), vol.2D, ser.1, no.2, p.460-70 (March-April 1983).
(Proceedings of the Fourth International Workshop on Biomagnetism, Rome, Italy, 14-16 Sept. 1982).

Auditory evoked magnetic fields (AEFs) and EEG auditory evoked potentials (AEPs) were recorded from left and right auditory cortical regions of 12 normal adult subjects. The magnetic sensor was a figure-eight SQUID gradiometer with a 4 cm baseline oriented so as to be maximally sensitive to a current dipole oriented normal to the Sylvian fissure. Stimuli were 100 ms long 1 kHz tone pips with a modal interstimulus interval of 700 ms delivered at sound pressure levels of 40, 60, 80 and 100 dB. AEF amplitude was found to be related to stimulus intensity in a quadratic fashion, AEP amplitude in a linear fashion. AEFs were of larger amplitude in response to contralateral as compared to ipsilateral stimulation. AEPs did not exhibit such a relationship. In a second experiment right-hemisphere AEFs and AEPs in response to contralateral ear tone stimulation in these 12 subjects were combined with similar previous data from 24 subjects, providing a total of 36 subjects, to examine the comparability of the AEP P50 wave form and the AEF P50 analog. The latency of the P50 was found to decrease as a function of increasing stimulus intensity for both AEFs and AEPs, and the P50 latency was consistently shorter in magnetic compared to potential recordings. (14 refs.)

Proceedings of the Fourth International Workshop on Biomagnetism See Entry 74209

Magnetic sensors with good signal-to-interference discrimination [biomagnetism application] See Entry 74497

Optimisation of the second-order gradiometer base length that has been designed for the measurement of weak inhomogeneous magnetic fields [biomagnetism application] See Entry 74498

Dielectric measurements on live biological materials under magnetic resonance conditions See Entry 78157

Retinotopic map on the visual cortex for eccentrically place patterns: first noninvasive measurement See Entry 78178

Studies of auditory evoked magnetic and electric responses: modality specificity and modelling See Entry 78188

A symmetric third order gradiometer without external balancing for magneto-cardiography See Entry 78279

Neuromagnetic measurements at hospital: instrumentation and preliminary tests See Entry 78280

High-resolution magnetic measurements of human cardiac electrophysiological events See Entry 78281

High-resolution recordings of the PR segment in magnetocardiography See Entry 78282

High-resolution isofield mapping on magnetocardiography See Entry 78283

Comparison between measured and simulated magnetocardiograms in a case of anterolateral myocardial infarction See Entry 78284

High-resolution magnetocardiographic recordings of the ST segment in patients with electrical late potentials. See Entry 78285

Optimizing vector magnetocardiographic lead fields by using a physical torso model See Entry 78286

The mapping of the measured cardiac electric potential and magnetic-field distribution See Entry 78374

Instrumentation for biomagnetism See Entry 78393

First-gradient balancing of higher-order gradiometers [biomagnetism application] See Entry 78394

Measurement of biomagnetic fields using multichannel superconducting-magnetometer techniques See Entry 78395

An eddy-current-shielded room with a partially closed entrance [for biomagnetic measurements] See Entry 78396

Adaptive noise cancellation in neuromagnetic measurement systems See Entry 78397

Alternatives to the SQUID magnetometer for some biomagnetic measurements See Entry 78398

A portable biomagnetic measuring system See Entry 78399

Characterization of the solid components of biological tissues by cross-polarization, magic angle NMR spectrometry See Entry 78402

87.45 BIOMECHANICS, BIORHEOLOGY, BIOLOGICAL FLUID DYNAMICS

78213
Control of muscle contractile force through indirect high-frequency stimulation.
M.Solomonow (Dept. of Engng. Systems, Univ. of California, Los Angeles, CA, USA), E.Eldred, J.Lyman, J.Foster.
Am. J. Phys. Med. (USA), vol.62, no.2, p.71-82 (April 1983).

With a view to possible application in an orthotic device, study was made of the attenuation of background, indirectly induced muscle tetanus produced by superimposing high-frequency electrical stimulation of the muscle nerve. The effects of varying duration, current and frequency of pulses of the stimulus were outlined, and it was concluded that optimal application might be obtained using a stimulus frequency of 500 Hz, a pulse duration of 50 μ sec, and varying the frequency to grade the effect. (14 refs.)

78214
Heart rate variability and blood pressure oscillations in diabetics with autonomic neuropathy.
T.J.Van Den Akker, A.S.M.Koelman (Dept. of Medical Phys., Free Univ., Amsterdam, Netherlands), L.A.H.Hogenhuis, O.Rompelman.
Automedica (GB), vol.4, no.4, p.201-8 (1983).

The frequency of the spontaneous narrow band blood pressure oscillations in both groups of diabetics with autonomic neuropathy and healthy persons was compared using the power spectrum of the heart rate variability signal. The shift in the centre frequency of the narrow band oscillation might provide a method of assessing early sympathetic nervous disorders in diabetics. (34 refs.)

78215
Beat-to-beat variability of heart interval and blood pressure.
R.W.De Boer, J.M.Karemaker, J.Strackee (Univ. of Amsterdam, Amsterdam, Netherlands).
Automedica (GB), vol.4, no.4, p.217-21 (1983).

A set of three mathematical equations is proposed to model the beat-to-beat properties of the fast blood pressure regulation system. The equations are based on the following physiological considerations: (1) The length of the RR-interval is dependent on the systolic pressure (baroreflex). (2) The pulse pressure is dependent on the length of the preceding interval (due to the restitution properties of the myocardium and to Starling's law). (3) During diastole the pressure decay can be described by a Windkessel equation. As preliminary results the authors found that blood pressure data from hypertensive patients which showed respiratory sinus arrhythmia agreed well with Eqs. (1) and (3), and that data from a patient with atrial fibrillation agreed with Eqs. (2) and (3). (12 refs.)

78216
Micromotion in smooth muscle related to circulation control: a hypothesis.
W.A.Van Duyl (Dept. of Biological & Medical Phys., Erasmus Univ. Rotterdam, Rotterdam, Netherlands).
Automedica (GB), vol.4, no.4, p.233-9 (1983).

The so-called 10-second-rhythm in blood pressure is considered. At the moment the prevailing explanation of this rhythm is that it comes from the overall blood pressure control, i.e. it is generated by an oscillator of the global type. By taking into account features of smooth muscle the author presents an alternative view concerning the origin of this rhythm, in which oscillatory phenomena of the local type are involved. (18 refs.)

78217
On the effect of the concentration profile of red cells on blood flow in the artery with stenosis.
J.Perkkio (Dept. of Medical Phys., Univ. of Helsinki, Helsinki, Finland), R.Keskinen.
Bull. Math. Biol. (GB), vol.45, no.2, p.259-67 (1983).

The effects of the viscosity-concentration dependence and of the concentration profile on blood flow through a vessel with stenosis have been studied. The flow resistance and the wall shear stress have been found to be smaller than in the two-fluid model with constant viscosities (Shukla et al., 1980). (14 refs.)

78218
The information transmitted at final position in visually triggered forearm movements.
B.Sakitt, F.Lestienne, T.A.Zeffiro (Dept. of Psychology, MIT, Cambridge, MA, USA).
Biol. Cybern. (Germany), vol.46, no.2, p.111-18 (1983).

Visually triggered forearm movements are analyzed by an information theory approach. Human subjects made smooth movements which were characterized by moderate speeds, ranging about 100 degrees per second, by continuity in the position and velocity traces, and attainment of final average EMG levels before completion of the movement. The authors calculate the information transmitted by final position, biceps EMG, triceps EMG, and the ratio of the EMGs. (18 refs.)

78219
Physical principles for economies of skilled movements.
W.L.Nelson (Bell Labs., Murray Hill, NJ, USA).
Biol. Cybern. (Germany), vol.46, no.2, p.135-47 (1983).

Presents some elementary principles regarding constraints on movements, which may be useful in modeling and interpreting motor control strategies for skilled movements. Movements which are optimum with respect to various objectives, or 'costs', are analyzed and compared. The specific costs considered are related to movement time, distance, peak velocity, energy, peak acceleration, and rate of change of acceleration (jerk). The velocity patterns for the various minimum cost movements are compared with each other and with some skilled movement patterns. The concept of performance trade-offs between competing objectives is used to interpret the distance-time relationships observed in skilled movements. Examples of arm movements during violin bowing and jaw movements during speech are used to show how skilled movements are influenced by considerations of physical economy, or 'ease', of movement. (16 refs.)

78220
Motor reaction time and stereotyped pattern of the EMG activities in ballistic elbow extension.
H.Nagasaki, N.Irie, R.Nakamura (Inst. of Rehabilitation Medicine, Tohoku Univ., Sendai, Japan).
Electromyography & Clin. Neurophysiol. (Belgium), vol.23, no.3, p.167-81 (March-April 1983).

Motor reaction time (MT) of the triceps brachii, an interval from the initiation of the EMG activities to the overt motor response, was examined for a ballistic elbow extension in a horizontal plane under conditions of different initial joint angles of the elbow and external loads. MT was independent of joint angles over a range from 120° to 30° flexion and increased linearly from 35 to 70 msec with the external load from 0 to 2.5 kg. The rectified and the added EMG activities exhibited a stereotyped pattern during first 70 msec, which was not affected by the change of initial joint angle or external load. The pattern was also independent from the timing of the initiation of the actual movement. These results were interpreted as follows: (1) MT represents a time necessary to develop muscular tension for the movement initiation, and the rate of the tension development is controlled to be constant over a wide range of joint angles, (2) under loading, the rate still remains unchanged, but MT increases because greater tension is required for the movement initiation against the load, (3) the stereotyped EMG pattern gives evidence that an early stage of ballistic movement is centrally preprogrammed and it follows that the timing of the movement initiation is also under control of the motor centre. (20 refs.)

78221
A theoretical model of absorption of gases by the bronchial wall.
M.R.Davidson (Appl. Maths. & Computing Div., Australian Atomic Energy Comm. Res. Establ., Lucas Heights, Sutherland, Australia), R.C.Schroter.
J. Fluid Mech. (GB), vol.129, p.313-35 (April 1983).

The pattern of dispersion and uptake of an inhaled slug of tissue-soluble gas is examined within a branching model of the bronchial airways of the human lung, considered as an assembly of segments from infinitely long, straight rigid tubes with absorbing walls of finite thickness. The model is based on the first three (time-dependent) spatial moments of the solute distribution in such tubes, determined by the Aris method of moments. Poiseuille flow in each airway is assumed, and the solute distribution is taken to be initially zero in the tissue and radially uniform in the gas. First, the time dependence of axial velocity and mixing coefficient of the advancing solute in infinitely long tubes is shown and the mechanisms responsible are discussed. Transit times, uptake,

uptake efficiency and mixing coefficient predicted from the model are then shown for different flow rates and solubilities, as functions of the generation of branching. As is expected, greater penetration is found for lower-solubility gases. (21 refs.)

78222 A hydrodynamic study of vascular lesion. M.Kawaguti, A.Hamano (Dept. of Phys., Keio Univ., Yokohama, Japan). *Proc. Indian Acad. Sci. Eng. Sci.*, vol.5, pt.2, p.85-105 (July 1982). [received: April 1983]

In order to search for the origin of vascular lesion from the hydrodynamic point of view, the viscous flows in a constricted channel and in a channel with a branch are studied numerically. The results obtained show the importance of the temporal variation of shearing stress on the wall. (13 refs.)

78223 Constructing a mathematical model for myocardial infarction. F.I.Obratsov, G.G.Avtandilov, A.S.Vol'mir (Central Inst. for Improvement of Physicians, USSR).

Sov. Phys.-Dokl. (USA), vol.27, no.8, p.655-7 (Aug. 1982). Translation of: *Dokl. Akad. Nauk SSSR*, vol.265, no.4-6, p.1090-3 (Aug. 1982). [received: May 1983]

Considers myocardial infarction as resulting from a catastrophe in the cardiovascular system, accompanied by abrupt changes in the blood supply to the heart; this study makes use of the general mathematical theory of catastrophes and is correlated with studies on the stability of the vascular membranes. The article is devoted to consideration of the most important mechanical effects associated with changes in the coronary blood flow in the period preceding the development of the myocardial infarct. (15 refs.)

78224 Modeling systolic mitral valve motion: a tool for clarifying mitral valve prolapse. J.F.Hunter (Dept. of Veterinary Physiology & Pharmacology, Texas A&M Univ., College Station, TX, USA), D.P.Seaton, W.M.Lively, G.E.Miller, D.L.Stoner.

Texas J. Sci. (USA), vol.35, no.1, p.5-36 (March 1983). A dynamic model of the human heart's mitral valve motion during systole is presented. This model includes a description of the geometrical interrelationships between components of the mitral apparatus, namely mitral valve leaflets, annulus, chordae tendineae, papillary muscles, and left ventricle. The biomechanical properties of the mitral valve leaflets and chordae tendineae and the contractile nature of the annulus, papillary muscles and left ventricle are considered. Mitral valve profile/position is described for selected properties of model components. (85 refs.)

78225 Fluid mechanics of green plants. R.H.Rand (Dept. of Theoretical & Appl. Mech., Cornell Univ., Ithaca, NY, USA).

In book: *Annual review of fluid mechanics*. Vol.15, M.Van Dyke, J.V.Wehausen, J.L.Lumley [Ed.], p.29-45. Palo Alto, CA, USA: Annual Reviews (1983), 534 pp. [0 8243 0715 1]

Studies of each of the parts of a plant have involved special fluid mechanics problems based on the particular physiological function and geometry. The article introduces the reader to the concepts and problems that are unique to the fluid mechanics of plants and reviews the mathematical literature on this subject. (56 refs.)

Annual review of fluid mechanics. Vol.15See Entry 74234

Annular arrays for quantitative pulsed Doppler ultrasonic flowmetersSee Entry 76138

EMG parameters changes in the effort pattern at various loads in diseased muscleSee Entry 78174

Velocity detection of Korotkoff soundsSee Entry 78276

Superimposition of krypton-81 m single photon emission CT and X-ray CT images for cerebral blood flow evaluationSee Entry 78294

An improved method of estimating the portal venous fraction of total hepatic blood flow from computerized radionuclide angiographySee Entry 78329

Initial results of noninvasive measurement of finger blood pressure according to PenazSee Entry 78372

Contribution of measurement system artifacts to systolic spikesSee Entry 78379

A simple means for recording foot contact sequence during gaitSee Entry 78380

87.50 BIOLOGICAL EFFECTS OF RADIATIONS

(inc. effects of fields)

78226 Relationship between field strength and arousal response in mice exposed to 60-Hz electric fields. R.S.Rosenberg, P.H.Duffy, G.A.Sacher, C.F.Ehret (Div. of Biological & Medical Res., Argonne National Lab., Argonne, IL, USA).

Bioelectromagnetics (USA), vol.4, no.2, p.181-91 (1983). White-footed mice, *Peromyscus leucopus*, were exposed to 60-Hz electric fields to study the relationship between field strength and three measures of the transient arousal response previously reported to occur with exposures at 100 kV/m (see R.S. Rosenberg et al., ibid., vol.2, p.291-303, 1981). Five groups of 12 mice each were given a series of four 1-h exposures, separated by an hour, with each group exposed at one of the following field strengths: 75, 50, 35, 25, and 10 kV/m; 8 additional mice were sham-exposed with no voltage applied to the field generator. The first exposure produced immediate increases in arousal measures, but subsequent exposures had no significant effect on any measure. These arousal responses were defined by significant increases of gross motor activity, carbon dioxide production, and oxygen consumption, and were frequently recorded with field strengths of 50 kV/m or higher. The results show that the amplitude of the transient arousal response is related to the strength of the electric field, but different measures of arousal may have different relationships to field strength. (17 refs.)

78227 Effects of high-intensity 60 Hz fields of bone growth. C.F.Walker (Dept. of Biomed. Engng., Tulane Univ., New Orleans, LA, USA), D.L.Seitelman, J.H.McElhaney, S.P.Mullen, B.Hagadorn, Yeb Jo Seto.

J. Bioelectr. (USA), vol.1, no.3, p.339-49 (1982). As part of an ongoing investigation of physiologic effects of high-voltage power frequency electric fields, femora from 55 adult rats which had been conceived, born, and raised in an 80 kV/m, 60 Hz unperturbed field were excised and studied. Specimens from 49 sham-exposed animals were also characterized in this double-blind study. Parameters evaluated were body weight, wet and dry bone weights, bone length, specific gravity, and various ratios of these parameters. Results from a statistical analysis indicated that chronic field exposure enhanced growth in the long bones, causing increased length and mass. (21 refs.)

78228 Dose-effect relationship for 14.5 MeV (d+T) neutron-induced chromosome aberrations in human lymphocytes irradiated in a man phantom. M.Bauchinger (Abteilung für Strahlenbiologie, Cyto genetics, Neuberger, Germany), H.Kuhn, J.Dresp, E.Schmid, S.Streng.

Int. J. Radiat. Biol. (GB), vol.43, no.5, p.571-8 (May 1983). Human lymphocytes were irradiated with 14.5 MeV (d+T) neutrons at the positions sternal, retrosternal, liver and gonads of a waterfilled Plexiglas man phantom of 37°C. After BUDR treatment of lymphocyte cultures and FPG-staining of metaphases, exclusively first post-irradiation divisions (M_1 -cells) were analysed. A regression analysis was carried out by means of a weighted least-squares method. Dose-effect relations of dicentric and acentric could be fitted by the linear-quadratic model. A comparison of the dose-effect curves established with either conventional or FPG-staining techniques revealed statistically significant differences. The M_1 -evaluation yielded about 46 per cent more dicentrics and about 37 per cent more acentrics. The consequences of these results are discussed in relation to the application of chromosome analysis in 'biological dosimetry'. (24 refs.)

78229 DNA replication and repair in human cells exposed to thermal neutrons. M.D.Ford (Dept. of Biochem., Univ. of Queensland, Brisbane, Australia), M.F.Lavin, D.Wilson.

J. Radiat. Res. (Japan), vol.23, no.4, p.423-30 (Dec. 1982). [received: May 1983]

The degree of inhibition of DNA replication and the level of DNA repair synthesis induced by thermal neutron irradiation was determined in human lymphoblastoid cell lines. Dose response experiments revealed that, when compared with equivalent doses of ^{60}Co - γ -irradiation, thermal neutrons gave rise to similar levels of inhibition of DNA replication but induced relatively low levels of DNA repair synthesis. The amount of repair synthesis after exposure of cells to thermal neutrons, was about ten-fold lower than that observed after γ -radiation. Reasons for this difference are discussed in terms of the type and incidence of damage induced by thermal neutrons. (17 refs.)

The effects of radiation exposure on aquatic organismsSee Entry 75112

Effect of radiation on sister chromatid exchanges and chromosomal deletions in the benthic worm *Neanthes arenaceodentata*See Entry 75114

Effects of alternating electric fields on material transport in heterogeneous mediaSee Entry 78162

Effects of high and superhigh doses of ^{60}Co - γ -quanta and fission neutrons on ratsSee Entry 78245

87.50B Interactions of biosystems with radiations

On stochastic models of light absorptionSee Entry 75584

87.50E Bio-optics (effects of microwaves, light, laser and other electromagnetic waves)

78230 Testicular function of rats following exposure to microwave radiation. R.M.Lebowitz, L.Johnson (Univ. of Texas Health Sci. Center, Dallas, TX, USA).

Bioelectromagnetics (USA), vol.4, no.2, p.107-14 (1983).

Male Sprague-Dawley rats were exposed for 6 h per day for nine days to pulse-modulated microwave radiation (1.3 GHz, at 1- μs pulse width, 600 pulses per second). Exposures were carried out in cylindrical waveguide sections at a mean dose rate of 6.3 mW/g; sham controls were treated similarly and received no irradiation. At time periods corresponding to 0.5, 1.0, 2.0, and 4.0 cycles of the seminiferous epithelium, groups of four sham-irradiation and four irradiated rats were killed and the testes removed for analysis. Net mass of the testes, epididymides, and seminal vesicles; daily sperm production (DSP) per testis and per gram of testis; sperm morphology; and the number of epididymal sperm were determined. There were no statistically significant differences between the sham-irradiated and irradiated groups with respect to any measured variable. In a group of seven surrogate animals of similar body mass, the dose rate of 6.3 mW/g caused a net change in body temperature (via rectal probe) of 1.5°C. (20 refs.)

78231 Effects of microwaves and hyperthermia on capping of antigen-antibody complexes on the surface of normal mouse B lymphocytes. M.F.Sultan, C.A.Cain (Dept. of Electrical Engng., Univ. of Illinois, Urbana, IL, USA), W.A.F.Tompkins.

Bioelectromagnetics (USA), vol.4, no.2, p.115-22 (1983).

Normal mouse B lymphocytes were tested for the ability to cap plasma membrane antigen-antibody complexes following exposure to 2.45-GHz continuous wave microwaves at power densities up to 100 mW/cm² (45 W/kg specific absorption rate), at 37, 41, and 42.5°C. After a 30-minute treatment, the irradiated cells and the nonirradiated controls were tested for capping by the direct immunofluorescence technique. First, the cells were incubated for nine minutes at 37°C with fluorescein isothiocyanate-conjugated goat anti-mouse immunoglobulin. After fixing and washing, the percentage of capped cells was determined under a fluorescence microscope. The results show that for the nonirradiated controls, capping is reduced from 90% at 37°C, to 52% at 41°C, to less than 5% for cells that were pretreated at 42.5°C. There was no significant difference between the microwave-treated cells and the controls when both were maintained at the same temperature. In another experiment, there was no significant difference in the percentage of capping between controls and cells that were exposed to microwave radiation during capping, when the temperature in both preparations was kept at 38.5°C. The results demonstrate that B-lymphocyte capping is sensitive to temperature in the range that is proposed for use in tumor therapy. (26 refs.)

78232 Effects of microwave exposure on the hamster immune system. I. Natural killer cell activity. H.K.Yang (Dept. of Pathobiology, Univ. of Illinois, Urbana, IL, USA), C.A.Cain, J.Lockwood, W.A.F.Tompkins.

Bioelectromagnetics (USA), vol.4, no.2, p.123-39 (1983).

Hamsters were exposed to repeated or single doses of microwave energy and monitored for changes in core body temperature, circulating leukocyte profiles, serum corticosteroid levels, and natural killer (NK) cell activity in various tissues. NK cytotoxicity was measured in a ^{51}Cr -release assay employing baby hamster kidney (BHK) targets or BHK infected with herpes simplex virus. Repeated exposure of hamsters at 15 mW/cm² for 60 min/day had no significant effect on natural levels of spleen-cell NK activity against BHK targets. Similarly, repeated exposure at 15 mW/cm² over a 5-day period had no demonstrable effect on the induction of spleen NK activity by vaccinia virus immunization, that is, comparable levels of NK were induced in untreated and microwave-treated animals. In contrast, treatment of hamsters with a single 60-min microwave exposure at 25 mW/cm² caused a significant suppression in induced spleen NK activity. A similar but less marked decrease in spleen NK activity was observed in sham-exposed animals. (33 refs.)

78233 Effects of microwave exposure on the hamster immune system. II. Peritoneal macrophage function. G.Rama Rao, C.A.Cain, J.Lockwood, W.A.F.Tompkins (Dept. of Electrical Engng., Univ. of Illinois, Urbana, IL, USA).

Bioelectromagnetics (USA), vol.4, no.2, p.141-55 (1983). For pt.1 see *ibid.*, vol.4, p.123-39 (1983). Acute exposure of hamsters to microwave energy (2.45 GHz; 25 mW/cm² for 60 min) resulted in activation of peritoneal macrophages that were significantly more viricidal to vaccinia virus as compared to sham-exposed or normal (minimum-handling) controls. Macrophages from microwave-exposed hamsters became activated as early as 6 h after exposure and remained activated for up to 12 days. The activation of macrophages by microwave exposure paralleled the macrophage activation after vaccinia virus immunization. Activated macrophages from vaccinia-immunized hamsters did not differ in their viricidal activity when the hamsters were microwave or sham-exposed. Exposure for 60 min at 15 mW/cm² did not activate the macrophages while 40 mW/cm² exposure was harmful to some hamsters. Average maximum core temperatures in the exposed (25 mW/cm²) and sham groups were 40.5°C (± 0.35 SD) and 38.4°C (± 0.5 SD), respectively. In vitro heating of macrophages to 40.5°C was not as effective as in vivo microwave exposure in activating macrophages to the viricidal state. (22 refs.)

78234 Immunological effects of amplitude-modulated radio frequency radiation: B lymphocyte capping. M.F.Sultan, C.A.Cain (Dept. of Electrical Engng., Univ. of Illinois, Urbana, IL, USA), W.A.F.Tompkins. *Bioelectromagnetics (USA)*, vol.4, no.2, p.157-65 (1983).

B lymphocytes collected from normal ICR Swiss mouse spleens were exposed in vitro in a Crawford cell to 147-MHz radiofrequency (RF) radiation, amplitude modulated by a 9-, 16-, or 60-Hz sine wave. The power densities ranged between 0.11 and 48 mW/cm². The irradiated samples and the controls were maintained at 37°C or 42°C, with temperature variations less than 0.1°C. Immediately after a 30-minute exposure, the distribution of antigen-antibody (Ag-Ab) complexes on the cell surface was evaluated at 37°C by immunofluorescence. Under normal conditions (37°C, no RF), Ag-Ab complexes are regrouped into a polar cap by an energy-dependent process. The results demonstrate that the irradiated cells and the nonirradiated controls capped Ag-Ab complexes equally well after exposure at 37°C. Capping was equally inhibited at 42°C in both the controls and irradiated cells. No statistically significant differences in capping were observed between the RF-exposed and control samples at any of the modulation frequencies and power densities employed as long as both preparations were maintained at the same temperature. (17 refs.)

78235 A mathematical model of the effects of light on the eclosion rhythm of the fruit fly *Drosophila pseudoobscura*. R.J.Schilling (ECE Dept., Clarkson Coll., Potsdam, NY, USA). *Bull. Math. Biol. (GB)*, vol.45, no.2, p.169-92 (1983).

A mathematical formulation useful in characterizing the effects of light on the pupal eclosion rhythm of the fruit fly *Drosophila pseudoobscura* is presented. It is based upon the premise that the underlying pacemaker oscillator behaves in a manner analogous to a customized version of a phase-locked loop circuit. Theoretical analyses supplemented with numerical simulations reveal that this phase-locked loop approach yields a concise mathematical characterization which is quite comprehensive in its scope, yet surprisingly accurate in the detail with which it can be used to successfully predict observed experimental results. (30 refs.)

78236 Laser induced visual pigment conversions in fly photoreceptors measured in vivo. B.Kruizinga, R.L.Kamman, D.G.Stavenga (Dept. of Biophys., Rijksunivers. Groningen, Groningen, Netherlands). *Biophys. Struct. & Mech. (Germany)*, vol.9, no.4, p.299-307 (1983).

The photochemical cycle of fly visual pigment was studied in vivo with laser methods. Two pulsed dye lasers were used, one delivering the visual pigment converting flash and the other testing the pigment state after a variable interval. Transmission through the rhabdomeres was measured in the eye of blowfly *Calliphora erythrocephala*. It followed that rhodopsin R490 converts into metarhodopsin M580 via two intermediates, with time constants of 700 ns and 80 μ s respectively. In the reverse pathway, i.e. the photoconversion of metarhodopsin into rhodopsin, an intermediate decaying with a time constant of 4 μ s was found. (19 refs.)

78237 A test of the dopamine hypothesis of microwave energy effects. A.H.Frey, L.S.Wesler (Randomline Inc., Huntingdon Valley, PA, USA). *J. Bioelectr. (USA)*, vol.1, no.3, p.305-12 (1982).

Exposure to low intensity microwave energy has been found to alter the behavior of test animals. Frey and Spector (URSI Annual Meeting, Amherst, USA, p.93, 1976) hypothesized that the dopamine systems of the brain may be involved in the mediation of these and other effects of the energy. The dopamine system has been implicated in the regulation of tail pressure behaviors. Thus, microwave energy exposure should modify tail pressure behaviors. This prediction was tested and it was found that microwave energy exposure does affect this set of behaviors. The pressure used as well as odor cues influences the effect. (20 refs.)

78238 Microwaves and the blood-brain barrier: a review. A.S.Segal, R.L.Magin (Dept. of Electrical Engng., Univ. of Illinois, Urbana, IL, USA). *J. Bioelectr. (USA)*, vol.1, no.3, p.351-98 (1982).

The research conducted during the past decade on the interaction of microwaves with the blood-brain barrier (BBB) is reviewed. The structure and function of the BBB is briefly described, the major results of experimental studies are summarized, and directions for future research are suggested. (42 refs.)

78239 Microwaves and neoplasia in mice: analysis of a reported risk. N.J.Roberts, Jr., S.M.Michaelson (Dept. of Medicine, Univ. of Rochester, Rochester, NY, USA).

Health Phys. (GB), vol.44, no.4, p.430-3 (April 1983). In IRE Trans. Biomed. Electron., vol.9, p.104-8, 1962, Prausnitz and Susskind reported the results of experiments designed to examine the effects of chronic exposure of mice to microwaves. They found that 'neoplasms of the white blood cells' were more prevalent in the irradiated group than in control mice, but 'longevity of the mice did not appear to be affected under the prevailing conditions'. The authors describe an analysis of Prausnitz and Susskind's experiments and discuss the original observations with regard to known effects of temperature variation on leukocyte functions. They submit that the Prausnitz and Susskind report does not support a link between exposure to microwave radiation and the development of neoplasia. (18 refs.)

78240 Experimental studies of laser thermal retinal injury. R.Birngruber, V.-P.Gabel, F.Hillenkamp (Augenklinik, Univ. Muenchen, Muenchen, Germany).

Health Phys. (GB), vol.44, no.5, p.519-31 (May 1983). In damage tests conducted on rabbit and monkey eyes, the threshold values for retinal damage resulting from different laser radiation were determined. The reproduction of the 'worst-case' situation was ensured by the test apparatus. All physical parameters, such as power/energy, exposure time, and retinal spot, were carefully controlled. Probit analysis showed a very precise determination of the threshold values based on ophthalmoscopic visibility. The attempt of a simple physical interpretation of the thresholds leads to contradictions in major points, so a detailed calculation of damage functions and thermal model calculations are necessary. (46 refs.)

Investigations on microwave radiation exposure See Entry 78356

87.50G Ionizing radiations (u.v., X-ray, gamma-ray; particle radiation effects)

78241 Mechanism of chromatin degradation in thymocytes of irradiated rats. VI. Postirradiation changes in poly (ADP-ribose)polymerase activity. N.Zotovar, S.R.Umanski, V.I.Tokarskaya (Inst. of Biological Phys., Acad. of Sci., Pushchino, USSR).

Radiobiologiya (USSR), vol.23, no.2, p.152-6 (1983). In Russian. For pt.V see *ibid.*, vol.23, no.1, p.31, 1983. A biphasic change in poly (ADP-ribose) polymerase activity of the thymocyte chromatin was observed after 10 Gy irradiation of rats: during the first minutes the incorporation of ¹⁴C-NAD increased by 40% then started decreasing to give 110, 60 and 35% after 1, 2 and 3 h, respectively. Irradiation of rat thymus chromatin in vitro sharply decreased poly (ADP-ribose) polymerase activity. The possible role of changes in the poly (ADP-ribose) synthesis in the activation of nuclear Ca/Mg-dependent endonuclease and in the postirradiation degradation of the thymocyte chromatin is discussed. (16 refs.)

78242 Cell spheroids as the object for radiobiological research. E.Kopp, G.Erntgraber, Kh.Abel' (Central Inst. of Molecular Biology, Berlin, Germany).

Radiobiologiya (USSR), vol.23, no.2, p.161-71 (1983). In Russian. Cell spheroids are conglomerates of closely arranged cells with reciprocal effects among them. Spheroids are histologically similar to nodular tumours. Cells constituting these spheroids are heterogenous in their sensitivity to X-rays and fast neutrons. The radiosensitivity of cells in a small spheroid is lower than that of similar cells grown in a monolayer. (33 refs.)

78243 Changes in the chromosome pattern of mouse lymphosarcoma cells during long-term continuous irradiation. V.Yurashkova (Inst. of Biophys., Czechoslovak Acad. of Sci., Brno, Czechoslovakia), V.Kliment, R.Tuscany, V.Drshil.

Radiobiologiya (USSR), vol.23, no.2, p.172-6 (1983). In Russian. In experiments of lymphosarcoma cells LS/BL, a study was made of changes in the chromosome pattern after long-term continuous irradiation at a low dose rate (35.8 $\times 10^{-3}$ mC.kg⁻¹.s⁻¹). To ensure reliable detection of changes in the chromosome length the method of automated computer analysis of the chromosome pattern with subsequent statistical evaluation was used. The radiation effect was manifested by a higher frequency of shape abnormalities in continuously exposed cells. (23 refs.)

78244 Comparative study of radiosensitivity of normal and regenerating tissues. I. Interphase cell death and aplasia of the regenerating and normal bone marrow and spleen of C57B1 mice. N.S.Samokhvalova, M.F.Popova (A.N. Severtsov Inst. of Evolutionary Morphology & Ecology of Animals, Acad. of Sci., Moscow, USSR).

Radiobiologiya (USSR), vol.23, no.2, p.177-81 (1983). In Russian. A comparative study of the radiosensitivity of cells of normal and regenerating tissues of bone marrow and spleen has demonstrated that a single exposure to X-rays produces a lesser damaging effect on regenerating tissues than on normal ones. The data obtained indicate that the increase in radioresistance of the organism during active regeneration of the haemopoietic organs is due not merely to the increase in the dividing cell pool of these organs but also to qualitative changes in their functional state. (15 refs.)

78245 Effects of high and superhigh doses of ⁶⁰Co- γ -quanta and fission neutrons on rats. G.A.Lavrova, L.N.Postnikov, A.G.Silina, S.N.Valter, T.V.Pushkareva, A.G.Sverdlov (B.P. Konstantinov Leningrad Inst. of Nuclear Phys., Acad. of Sci., Leningrad, USSR).

Radiobiologiya (USSR), vol.23, no.2, p.187-91 (1983). In Russian. A transient form of acute radiation sickness could be distinguished in Wistar rats after total-body exposure to ⁶⁰Co- γ -rays in high doses (150-200 Gy). With local exposure of the head, in addition to the direct damaging effect on the nervous system, the organismic factors play an important role in the development of the CNS syndrome. Effects of fractionation of superhigh doses of γ -quanta and fission neutrons were not observed. The RBE of neutrons should constitute 1.8 for the transient form of radiation sickness to develop. This value is much less than that needed for the development of haemopoietic and intestinal lesions. PAPP, 'gammaphos' and the combination of these agents do not influence the effect on rats of high doses of γ -quanta. (20 refs.)

78246 Possible influence of natural radiation background on the development of mammals. A.M.Kuzin, L.V.Slozenikina, L.A.Fialkovskaya, V.N.Primak-Mirolyubov (Inst. of Biological Phys., Acad. of Sci., Pushchino, USSR).

Radiobiologiya (USSR), vol.23, no.2, p.192-4 (1983). In Russian. The deceleration of the development of young rats during the postnatal ontogenesis under conditions of a low-background chamber (a 10-fold decrease in the natural radiation background) was detected using the criterion of individual growth of body weight for 10 days of observation. The administration, to the low-background chamber, of uranium salts, which restored the natural background (all other experimental conditions being retained) removed the effect observed. (7 refs.)

78247 Dynamics of early postirradiation changes in capillary endothelium (quantitative electron-microscopic analysis). R.P.Stepanov, V.F.Dubrovskaya. *Radiobiologiya (USSR)*, vol.23, no.2, p.196-9 (1983). In Russian.

Oedema, breakage and fragmentation of plasmalemma and mitochondrial damages developed in rats 1-48 h following total-body X-irradiation (4.5 Gy). These changes were most pronounced 2-6 h after exposure, when they spread over 20-30% of the population, and were accompanied by the appearance of wide gaps in the endothelial layer and maximal accretion of free lipids in the endotheliocyte cytoplasm. Changes in the sizes and number of mitochondria were responsible for the tendency toward the increase in their relative total volume which was most pronounced after 12 h. (15 refs.)

78248 The role of changes in the oxygen concentration upon modification of the reproductive death of cells in vitro. II. Modification of radiosensitivity with the varying rate of oxygen consumption in cells. Yu.N.Korystov (Inst. of Biological Phys., Acad. of Sci., Pushchino, USSR).

Radiobiologiya (USSR), vol.23, no.2, p.200-4 (1983). In Russian. For pt.1 see *ibid.*, vol.23, no.1, p.39, 1983. A study was made of the role of changes in the concentration of oxygen occurring upon modification of radiosensitivity of cells in vitro using temperature (0-37°C), uncoupling agents and respiration inhibitors, and also upon stimulation of the oxygen consumption by microsomes. When cells were irradiated in suspension, monolayer, spheroid and roots of plants a change in the rate of the oxygen consumption

by cells and a corresponding change in their oxygenation can contribute considerably to a radiomodifying effect. (16 refs.)

78249 Seasonal radiosensitivity of rats and dogs. S.A.Rogacheva, O.V.Luzanova, E.N.Kirillova, L.D.Murzina, T.I.Uryadnitskaya (Inst. of Biophys., USSR Ministry of Health, Moscow, USSR). *Radiobiologiya (USSR)*, vol.23, no.2, p.205-9 (1983). In Russian. Data are submitted obtained from 10.5 thousand Wistar rats and 350 mongrel dogs exposed to γ -radiation (LD_{50} - LD_{100}) in different seasons. The radiosensitivity of both animal species was highest in autumn (August and September) and lowest in winter (February and January). The seasonal DMF for rats and dogs with LD_{16} , LD_{50} and LD_{84} was 1.24 and 1.31, 1.13 and 1.17, and 1.04 and 1.07, respectively. The curves for seasonal radiosensitivity of dogs with LD_{84} , LD_{50} and LD_{16} exhibited a single-phase character throughout a year. For rats, the seasonal radiosensitivity curves with LD_{84} were single-phase, and the curve with LD_{50} , and particularly LD_{16} , exhibited the second peak of radioresistance in June. The increase in radioresistance of rats and dogs correlated with the increase in the number of leukocytes in the peripheral blood of the animals. (17 refs.)

78250 Recovery of rats from ^{252}Cf -induced damages. E.S.Zhorova, S.V.Stepanov, G.A.Zalikin (Inst. of Biophys., USSR Ministry of Health, Moscow, USSR). *Radiobiologiya (USSR)*, vol.23, no.2, p.210-15 (1983). In Russian. The types of recovery processes were demonstrated in experiments on albino rats damaged with ^{252}Cf . The frequency and the degree of manifestation of both pathological and recovery processes were functions of both the radiation dose and the time since the processes initiation. The results obtained indicate that changes induced by the incorporation of ^{252}Cf , within a wide range of doses, are compensated incompletely to be manifested later by sclerotic, hyperplastic and neoplastic processes. (8 refs.)

78251 Radiation-induced and postirradiation changes in the forest biogeocenosis after acute γ -irradiation. I. Comparison of seasonal radiosensitivity of pine-and-birch stand after acute γ -irradiation. N.N.Mishenkov, D.A.Spirin, R.M.Aleksakhin, R.T.Karaban, E.A.Fedorov, G.N.Romanov. *Radiobiologiya (USSR)*, vol.23, no.2, p.220-3 (1983). In Russian. In order to describe the state of the upper-tree layer of a pine-and-birch stand exposed at the stage of active growth (in spring) and at the resting stage (in autumn) the following parameters were determined: (a) the increase in the growth of annual shoots, (b) the loss of needles and wood biomass, (c) changes in the primary productivity, and (d) lethal doses for pine stands. According to these indices seasonal radiosensitivity of the pine stand was shown to be 2-3 times higher in spring than in autumn. (11 refs.)

78252 Destruction of gelatin irradiated in its aqueous solutions at low temperatures. N.V.Zakatova, E.O.Svanidze, V.A.Sharpatyi (Inst. of Chem. Phys., Acad. of Sci., Moscow, USSR). *Radiobiologiya (USSR)*, vol.23, no.2, p.227-30 (1983). In Russian. The methods of electrophoresis and ESR were used to determine the radiochemical yield of breaks in polypeptide chains of gelatin fractions and the formation of primary anion-macroradicals in irradiated, at 77K, 5 and 10% gelatine solutions. The obtained values gave $G(\text{breaks})=G(R_p)=0.03$. This excludes the contributions of anion-macroradicals in which free valence was localized on the fragment $-C-O^{\cdot}$ of proline and hydroxyproline residues: their isomerization leads to a change in the conformation of the macromolecule rather than to the destruction thereof. (6 refs.)

78253 Effect of α -particles on bacteriophage T4. G.A.Leont'eva, A.E.Grigor'ev, I.G.Akoev, I.M.Dmitrievskii (Inst. of Biological Phys., Acad. of Sci., Pushchino, USSR). *Radiobiologiya (USSR)*, vol.23, no.2, p.230-3 (1983). In Russian. Exponential survival curves were obtained for a dry film culture of bacteriophage T4 Br⁺ after exposure to both α -particles and γ -quanta. The relative biological effectiveness of α -particles was 4.68 with respect to survival. The mutation spectrum after α -irradiation slightly differed from that produced by γ -radiation. (3 refs.)

78254 Comparison of neutron- and γ -radiation-induced transformations of 2-deoxy-D-ribose in aqueous solutions. N.P.Krushinskaya, A.E.Serebryanyi (Inst. of Biophys., Ministry of Health, Moscow, USSR). *Radiobiologiya (USSR)*, vol.23, no.2, p.235-7 (1983). In Russian. The effectiveness of neutron radiation (1 MeV) was nearly twice as low as that of electrons and γ -quanta with regard to the formation of products of radiolysis of 2-deoxy-D-ribose in aqueous solutions. A change in the dose-rate of sparsely ionizing radiation by the order of 5-6, and variation in the concentration of 2-deoxy-D-ribose from 1 to 5 mM, did not substantially influence the G products of radiolysis. (6 refs.)

78255 Influence of dose-rate on the formation of double-strand DNA breaks. N.V.Kondakova, V.V.Sakharova (Sci. Res. Lab. of Biological Structures, Ministry of Health, Moscow, USSR). *Radiobiologiya (USSR)*, vol.23, no.2, p.243-6 (1983). In Russian. It has been shown that sparsely ionizing radiation produces double-strand DNA breaks in solution more readily at high dose-rates (20 Gy/min) than at low ones (0.03-0.06 Gy/min). Possible mechanisms of the effect observed are discussed. (14 refs.)

78256 Response of lymph and blood coagulative systems to exposure to γ -radiation at high altitudes. S.B.Daniyarov, V.V.Pukhov (Kirgiz State Medical Inst., Frunze, USSR). *Radiobiologiya (USSR)*, vol.23, no.2, p.247-50 (1983). In Russian. A study was made of coagulation and cellularity of blood and lymph of thoracic duct of dogs exposed to 2.5 Gy radiation at the altitudes of 760 m and 3200 m above sea level after one-month adaptation. Irrespective of the irradiation conditions coagulation of blood decreased and that of lymph increased. Radiation-induced changes in the cellularity of both blood and lymph were less pronounced in conditions of natural hypoxia than at the altitude of 760 m. (13 refs.)

78257 Migration of lymphocytes in conditions of internal irradiation. II. Disturbance of the microenvironment of lymphocytes in mouse organs. Yu.N.Anokhin, T.A.Norets, A.A.Yarilin (Sci. Res. Inst. of Medical Radiology, Acad. of Medical Sci., Obninsk, USSR). *Radiobiologiya (USSR)*, vol.23, no.2, p.256-9 (1983). In Russian. At later times after the injection of selenium-75-selenium methionine to CBA mice a long lasting inhibition of migration of intravenously injected normal ^{51}Cr lymphocytes to the lymph nodes and liver was found. On the contrary, no changes in the normal lymphocyte migration within the animal body were observed after total-body γ -irradiation with a dose of 4 Gy. The data obtained are indicative of a radiation-induced disturbance of the microenvironment factors, which affect migration of lymphocytes within the body, during the long-term exposure to radiation emitted by the incorporated source. (13 refs.)

78258 Regularities of postirradiation recovery of the organism in conditions of external nonuniform irradiation. VII. Postirradiation radiosensitivity of rats as function of the preirradiation dose with an oral form of radiation sickness. G.M.Avetisov, R.N.Zaitseva, M.V.Sergeeva (Inst. of Biophys., USSR Ministry of Health, Moscow, USSR). *Radiobiologiya (USSR)*, vol.23, no.2, p.263-7 (1983). In Russian. Radiosensitivity of rats was studied after double X-irradiation of the head, first with doses of 15 and 13 Gy, then with 8-21 Gy. (8 refs.)

78259 Changes in the electric activity of rat stomach directly affected by X-radiation. K.P.Balitskii, A.V.Syromyatnikov, L.P.Voitenko (R.E. Kavetsky Inst. of Oncology Problems, Acad. of Sci., Kiev, Ukrainian SSR). *Radiobiologiya (USSR)*, vol.23, no.2, p.267-71 (1983). In Russian. In experiments on rats inhibition of the electric activity of X-irradiated stomach was discovered. The disturbance of the nervous regulation of the exposed stomach was manifested mainly by inhibition of the transmission of exciting stimuli via choline- and serotonin-reactive structures of the vegetative nervous system. The administration of serotonin and phentolamine normalized the stomach activity. (16 refs.)

78260 Affection of dogs estimated by some integral indices after the combined effect of external γ -irradiation and inhalation of ^{239}Pu submicron dioxide. Z.I.Kalmykova, A.P.Nifatov (Inst. of Biophys., USSR Ministry of Health, Moscow, USSR). *Radiobiologiya (USSR)*, vol.23, no.2, p.271-4 (1983). In Russian. The possibility of quantitation of the organism affection by the combined effect of external γ -irradiation (103.2 and 51.6 mC/kg) and succeeding inhalation of different amounts of ^{239}Pu submicron dioxide was shown on 55 mongrel dogs using the following criteria: the rate of extracellular fluid accretion and the body weight loss. (14 refs.)

78261 Combined effect of ^{239}Pu and external γ -radiation on pregnant and lactating rats. E.P.Ovcharenko, T.P.Fomina (Inst. of Biophys., Ministry of Health, Moscow, USSR). *Radiobiologiya (USSR)*, vol.23, no.2, p.275-7 (1983). In Russian. Exposure of pregnant and lactating rats to external γ -radiation (12.9-103.2 mC/kg) caused ^{239}Pu redistribution within their bodies. The increase in the transfer of ^{239}Pu to the progeny was maximum after γ -irradiation of pregnant rats with a dose of 25.8 mC/kg. The decrease in the intake of ^{239}Pu by the progeny was maximum after γ -irradiation of lactating rats with a dose of 12.9 mC/kg. Comparing the combined effect of γ - and α -radiation, γ -radiation was shown to play the major role in the embryos death. (7 refs.)

78262 The induction of chromosome aberrations in human lymphocytes by exposure to tritiated water in vitro. J.S.Prosser, D.C.Lloyd, A.A.Edwards, J.W.Stather (Nat. Radiological Protection Board, Didcot, England). *Radiat. Prot. Dosim. (GB)*, vol.4, no.1, p.21-6 (1983). An in vitro dose response has been obtained from chromosome aberration induction in human lymphocytes exposed for 24 hours to tritiated water in whole blood. An RBE at low doses of 1.13 ± 0.18 has been calculated by comparison with 250 kVp X-rays. The application of these results in cases of accidental exposure to tritiated water is discussed. (24 refs.)

78263 Studies into certain specificities of gamma-ray mutants and the parent strain *Humicola lutea* 72, producing acid protease. P.P.Aleksieva, A.A.Djerova, I.V.Grigorov, P.D.Sheremetska (Inst. of Microbiology, Bulgarian Acad. of Sci., Sofia, Bulgaria). *C.R. Acad. Bulg. Sci. (Bulgaria)*, vol.36, no.3, p.361-64 (1983). Gamma-ray exposure can be used as a mutagenic factor for obtaining mutants from a fungi strain of *Humicola lutea* 72, producing acid protease. The aim of the authors' work was to undertake a comparative morphological and physiological study of the most active mutants and the parent strain. (8 refs.)

78264 Life-table factors for use in estimating the cancer risk of radiation exposure to workers. H.D.Maillie (Dept. of Radiation Biology & Biophys., Univ. of Rochester School of Medicine & Dentistry, Rochester, NY, USA). *Health Phys. (GB)*, vol.44, no.4, p.317-27 (April 1983). Recent publications have discussed the use of life-tables in estimating the risks of radiation-induced cancer (B. Bunker et al., *ibid.*, vol.40, p.439, 1981; N.H. Harley and B.S. Pasternack, *ibid.*, vol.40, p.307, 1981). These studies have been useful in estimating the hazards to groups of individuals exposed to radiation. However, they are not always presented in a way which is useful to health physicists. Life-table factors are presented here which may be of use in calculating such risks to individuals or groups. (12 refs.)

78265 Problems with the linear-quadratic dose-response relationship. P.R.J.Burch (Dept. of Medical Phys., Univ. of Leeds, Leeds, England). *Health Phys. (GB)*, vol.44, no.4, p.411-13 (April 1983). The BEIR-III Report (*ibid.*, vol.41, p.769-74, 1981) assumes that the total risk (R) of cancer, after an absorbed dose D of low-LET radiation, is given by: $R = \alpha_0 + \alpha_1 D + \alpha_2 D^2$, where α_0 is the risk in the absence of radiation exposure and the constants α_1 and α_2 , valid over a limited dose range, are derived from observations on irradiated populations. The author feels that although this equation may sometimes offer an acceptable approximation to dose-response relations at low D, the values of α_1 and α_2 will usually have to be derived from observations at relatively high D where it will seldom be legitimate to ignore the complications outlined here, particularly those relating to repair mechanisms. (9 refs.)

78266 Induction and repair of DNA strand breaks in CHO-cells irradiated in various phases of the cycle. S.Graubmann, E.Dikomey (Inst. of Biophys. & Radiobiology, Univ. of Hamburg, Hamburg, Germany). *Int. J. Radiat. Biol. (GB)*, vol.43, no.5, p.475-83 (May 1983). Induction and repair of DNA strand breaks was investigated in synchronized CHO cells by using the alkaline DNA-unwinding technique followed by chromatography on hydroxyapatite. The velocity of DNA denaturation in an alkaline solution (pH 12.1) was found to be independent of the position in the cycle. In unirradiated cells the number of DNA strand breaks per 3.6×10^{12} dalton was found to vary with age in cell cycle amounting to about 250 breaks per cell for G₁, 400 for S, and 500 for G₂+M cells. The number of induced DNA strand breaks per unit dose was found to be the same in all phases; an average of 340 strand breaks were induced per Gy and per 3.6×10^{12} dalton. Within the first hour after irradiation about 90 per cent of all radiation-induced strand breaks are rejoined. (27 refs.)

78267 Radiation sensitivity of DNA-metal complexes: a pulse radiolysis study. P.C.Beaumont, E.L.Powers (Patterson Labs., Univ. of Texas, Austin, TX, USA). *Int. J. Radiat. Biol. (GB)*, vol.43, no.5, p.485-94 (May 1983). The effect of silver(I) and mercury(II) complexing upon the rate of reaction of both the hydrated electron and the OH radical with DNA has been investigated using the technique of pulse radiolysis. The results presented do not support the hypothesis that the mechanism of radiation sensitivity by these metals is mediated through increased rate of free radical attack upon DNA. Also, there is evidence presented that neither metal, when complexed with DNA, reacts at a significant rate with the free radical species e_{aq}^{\cdot} and OH.

The technique of pulse radiolysis was also used to study the complexation of both silver(I) and mercury(II) with DNA (calf-thymus, 40 per cent GC). Scatchard plots, derived from the experimental data, gave association constants of $1.85 \times 10^5 \text{ dm}^3 \text{ mol}^{-1}$ and $9.9 \times 10^4 \text{ dm}^3 \text{ mol}^{-1}$ and n values (number of complexing sites per nucleotide) of 0.71 and 0.31 for silver(I) and mercury(II) respectively. (27 refs.)

78268 Immuno-electrophoretic study of the effect of radiation on protein mixtures. J.Maffei, M.Soszynski, T.C.Bog-Hansen (Protein Lab., Univ. of Copenhagen, Copenhagen, Denmark). *Int. J. Radiat. Biol. (GB)*, vol.43, no.5, p.541-50 (May 1983). Demonstrates the suitability of immuno-electrophoretic methods in studies of radiation effects on protein mixtures. Single serum proteins (IgG, albumin, transferrin), albumin-transferrin mixtures and human serum were irradiated with doses of 3-52 kGy. The irradiated proteins were analysed using rocket-, crossed-, crossed-with-intermediate-gel, and fused-rocket immuno-electrophoretic methods. Using crossed immuno-electrophoresis with intermediate gel, complex formation between albumin and transferrin was observed. Gel filtration monitored by fused-rocket immuno-electrophoresis was demonstrated to be a most promising method for studying protein degradation and hybrid formation. (15 refs.)

78269 Kinetics of double strand break repair in the DNA of X-irradiated synchronized mammalian cells. D.Blocher, M.Nusse, P.Bryant (GSF-Abteilung für Biophys. Strahlenforschung, Frankfurt am Main, Germany). *Int. J. Radiat. Biol. (GB)*, vol.43, no.5, p.579-84 (May 1983). Reports on experiments in which the kinetics of repair of DNA double strand breaks (DSB) in Ehrlich ascites tumour cells was measured in G1-, G1/S-, late S- and G2-phases. Measurements have been made using both the neutral sucrose gradient centrifugation, and the unwinding method (Bryant and Blocher 1980). It is concluded that the repair of DSB in the DNA of X-irradiated cells proceeds at approximately the same rate in all the major phases of the cell cycle, and that the cell cycle dependent variation in radiosensitivity observed in mammalian cells cannot be attributed to deficiencies in the ability of cells to repair DSB at certain cycle stages. (24 refs.)

78270 How to assess natural risks. M.Sakka (Tohoku Radiological Sci. Center, Sendai-shi, Japan). *J. Radiat. Res. (Japan)*, vol.23, no.4, p.411-22 (Dec. 1982). [received: May 1983] The low dose considered here is about 2R in 40 years which corresponds to the difference in the highest and the lowest background radiations in several prefectures in Japan. Examples of risk are cancer of adults (40-79 years old) and of childhood (0-9 years old) and childhood vital statistics. The quantity of risk is expressed in 10^{-5} Y^{-1} for cancers and in 10^{-3} Y^{-1} for childhood vital statistics with a standard deviation which gives the estimates uncertainty. Risk factors of the ICRP are given in terms of $10^{-2} \sim 10^{-5} \text{ Sv}^{-1}$. The risk factors provide convenient measures for point assessment of lifetime detriment after the relevant population is expired. But the risk factor is not satisfactory for public health purposes because it does not give annual rate nor statistical variation of the total detriment. The purpose of this report is to supplement some insufficiency of risk estimation. (9 refs.)

78271 Comparison of type and frequency of chromosome aberrations by conventional and G-staining methods in Hiroshima atomic bomb survivors. K.Ohtaki (Dept. of Clinical Labs., Radiation Effects Res. Found., Hiroshima, Japan), H.Shimba, A.A.Awa, T.Sofuni. *J. Radiat. Res. (Japan)*, vol.23, no.4, p.441-9 (Dec. 1982). [received: May 1983]

Somatic chromosomes derived from lymphocytes of 23 Hiroshima A-bomb survivors were analyzed to determine the type and frequency of radiation-induced chromosome aberrations, using both the ordinary staining method (O-method) and the trypsin G-banding method (G-method). Of 896 cells examined, 342 had aberrations, including 31 unidentifiable cells even by the G-method. The number of aberrations detected was 376 in 31P-cells. The majority of them were intra- or inter-chromosomal symmetric exchanges, while only 24 were found to be asymmetric exchanges (dicentric, rings and interstitial deletions). Further, 28 aberrations included acentric fragments and terminal deletions, and the remaining 36 were complex intra- and inter-chromosomal exchanges showing insertions and double translocations. An analysis of the same metaphases examined by sequential O- and G-methods was carried out independently on 361 aberrations. It was found that 78 were detectable only by the G-method; among these were 14 paracentric inversions, 48 reciprocal interchanges of chromosome segments with either equal or unequal length, 14 minor deletions and 2 complex rearrangements, all of which were judged as the normal variation by the O-method. In contrast, 25 aberrations detected by the O-method were found to show normal banding patterns by the G-method. (12 refs.)

78272 Changes in radiosensitivity of the in vitro fertilized mouse ova during zygotic stage from fertilization to first cleavage. T.Yamada, O.Yukawa, Y.Matsuda, A.Ohkawa (Div. of Biology, Nat. Inst. of Radiological Sci., Chiba, Japan). *J. Radiat. Res. (Japan)*, vol.23, no.4, p.450-6 (Dec. 1982). [received: May 1983]

The radio sensitivity of mouse zygotes fertilized in vitro (BC3F₁ ovum × ICR sperm) to X-rays has been measured as a function of time from fertilization to first cleavage. The dose of X-rays (LD₅₀) required to prevent development of 50% of the zygotes to the blastocyst stage in vitro varied markedly depending on the time of irradiation from about 40 to 400 R. Sensitivity is relatively low shortly after sperm entry and becomes extremely high (LD₅₀, 40 R) at the stage just before pronuclear formation (4 to 6 hr after insemination). In the later pronuclear stage (12 hr of fertilization) the sensitivity becomes low (LD₅₀, about 400 R), and it increases again just before first cleavage. (12 refs.)

Studies of the radiosensitivity of deep-sea bacteria See Entry 75113

Inhibition of repair of radiation-induced strand breaks by hyperthermia, and its relationship to cell survival after hyperthermia alone See Entry 78159

Effects of hyperthermia on the repair of X-ray-induced DNA double strand breaks in mouse L cells See Entry 78160

Radiation exposure and associated cancer risk due to radon and decay products See Entry 78333

Mucosal structure and radon in head carcinoma dosimetry See Entry 78350

87.60 MEDICAL AND BIOMEDICAL USES OF FIELDS, RADIATIONS, AND RADIOACTIVITY

(see also 28.80 Nuclear radiation technology, including shielding)

78273 Modeling three-dimensional computer reconstructions from surface contours for diagnostic imaging. L.T.Cook, P.N.Cook, S.J.Dwyer, S.Batnitsky, Kyo Rak Lee, H.I.Price (Dept. of Diagnostic Radiology, Univ. of Kansas Coll. of Health Sci., Kansas City, KS, USA). *Proc. SPIE Int. Soc. Opt. Eng. (USA)*, vol.359, p.152-5 (1983). (Applications of Digital Image Processing IV, San Diego, CA, USA, 24-27 Aug. 1982). Digital medical imaging modalities construct and display images as cross-sections of anatomy. The technologies of these digital systems are moving towards thinner cross-section thicknesses, higher spatial resolutions, and larger dynamic ranges. These imaging modalities provide cross-sectional displays in which there is no superimposing of organs. This provides relatively precise two-dimensional geometric information. Information regarding the general three-dimensional (3-D) space relationships among a number of anatomic structures is difficult to acquire from a large number of thin serial sections. Clinicians are required to visualize such information by mentally stacking these serial sections to obtain the complete structure. A number of 3-D surface reconstruction algorithms have been developed for displaying 3-D anatomic structures on raster graphic displays. The authors present a comparison among these reconstruction algorithms for: (1) computation time; (2) algorithm complexity; (3) computer storage requirements; and (4) clinical efficacy. The authors will report on a three-year study of the clinical utilization of 3-D display algorithms using raster graphic display systems. (19 refs.)

78274 Physical constraints in the optimization of medical imaging filters for maximum signal-to-noise ratio. P.R.Moran (Depts. of Radiology, Phys. & Medical Phys., Univ. of Wisconsin, Madison, WI, USA). *IEEE Trans. Med. Imaging (USA)*, vol.MI-1, no.3, p.197-204 (Nov. 1982). [received: May 1983]

To filter an image by an aperture function $A(r)$, or in Fourier space by it transform $A(f)$, requires that $A(r)$ and $A(f)$ are physically realizable and mathematically exist as transform pairs. This constrains both functions to being square-integrable to guarantee their uniform convergence both in spatial and frequency domains. This paper presents a general method for deriving filter forms which maximize image SNR and also satisfy the existence constraints. The author shows that asymptotic limiting forms of the constrained filters reduce to the 'ideal observer' result, but demonstrates that the 'ideal' filter form has a divergent square integral in some simple cases important in medical imaging. The author applies these properly constrained filter forms to radiographic image and CT image models, and derives the range of arguable signal-to-noise advantage, which 'more' optimum filters may exhibit with respect to the simple 'matched' filter limit. (7 refs.)

87.60B Sonic and ultrasonic radiation

78275 Biological signals processing: an application to ultrasonic echo signals sounding. P.Larizza, B.Castagnolo (Univ. di Bari, Bari, Italy). *Electron. Oggi (Italy)*, no.3, p.97-106 (March 1983). In Italian. Ultrasonic echo signals processing in medical diagnostics and biological research is discussed. Relevant computer programs are reviewed including selected hardware. Signal filtering methods are detailed analysing inverse filtering, LMS, LMSA, FFT CLS and homomorphic filtering techniques. Computer processing methods are compared with a conclusion that FFT (Fast Fourier Transforms) algorithms are most expedient. (4 refs.) T.H.

78276 Velocity detection of Korotkoff sounds. A.E.Sibley, T.Winsor, D.A.Grigsby, E.Pischel. *Med. Instrum. (USA)*, vol.17, no.2, p.159-62 (March-April 1983). High-speed oscillograms were made showing the time relationships between the ECG and arterial pressure waves detected by three microphones successively placed beneath a standard blood pressure cuff along the brachial artery. As the cuff was deflated through the systolic/diastolic range, the indicated propagation velocity of the Korotkoff waves changed from approximately 1 m/sec near systolic pressure to about 2.5 m/sec near diastolic pressure. Non-Korotkoff waves (noise artifacts), on the other hand, were observed to propagate at much higher velocities, on the order of 5-10 m/sec. This phenomenon can be utilized to identify Korotkoff waves in the presence of other disturbances, particularly in exercise situations, and to determine diastolic pressure in the presence of arterially conducted valve and turbulence noise. (24 refs.)

78277 Feasibility of ultrasound hyperthermia in the treatment of malignant brain tumors. R.H.Britt, B.E.Lyons, D.W.Pounds, S.D.Pronas. *Med. Instrum. (USA)*, vol.17, no.2, p.172-7 (March-April 1983). In order to test the biological feasibility of using ultrasound-generated hyperthermia for the treatment of brain tumors, damage threshold studies and thermal dosimetry studies as a function of temperature were performed in 44 acute experiments in cats. Bilateral craniotomies were performed to expose the dural surface. Ultrasonic radiation was applied for 50 minutes at different intensities to generate temperatures up to 48°C. Thermal fields were mapped using an electrode array to three triple-junction thermocouple probes. The results of this study are important in two respects. First, it demonstrates that ultrasound can effectively heat the brain in an extremely controlled and precise manner. Second, the brain can withstand temperatures to 42°C without showing histological evidence of damage, which is the temperature range at which neoplastic cells begin to show cytotoxic effects. (35 refs.)

78278 Algorithms and experimental results in acoustic tomography using Rytov's approximation. M.Soumekh, M.Kaveh, R.K.Mueller (Dept. of Electrical Engng., Univ. of Minnesota, Minneapolis, MN, USA). Proceedings of ICASSP 83, IEEE International Conference on Acoustics, Speech and Signal Processing, Boston, MA, USA, 14-16 April 1983 (New York, USA: IEEE 1983), p.135-8 vol.1. Theoretical, algorithmic and experimental results on the use of Rytov's approximation in acoustic tomography are presented. The approximation error is related to the disturbance size and magnitude. A method of phase unwrapping which is based on a combination of profile to profile phase comparison coupled with some well-known phase unwrapping algorithms used in signal processing is introduced. Frequency and spatial domain reconstructions are compared with respect to computational efficiency and accuracy of interpolation. (6 refs.)

Lateral inverse filtering of ultrasonic B-scan images See Entry 75866

A new wire phantom for accurate measurement of acoustic resolution See Entry 75887

Annular arrays for quantitative pulsed Doppler ultrasonic flowmeters See Entry 76138

- Breast tissue classification using diagnostic ultrasound and pattern recognition techniques. I. Methods of pattern recognition See Entry 78382
- Breast tissue classification using diagnostic ultrasound and pattern recognition techniques. II. Experimental results See Entry 78383

87.60D Electric and magnetic fields (d.c. and pulsed)

- 78279** A symmetric third order gradiometer without external balancing for magnetocardiography. A.C.Bruno, P.Costa Ribeiro (Dept. de Fisica, Pontificia Univ. Catolica de Rio de Janeiro, Rio de Janeiro, Brazil). *Cryogenics (GB)*, vol.23, no.6, p.324-6 (June 1983).
A feasibility study is being carried out on the operation of a SQUID gradiometer without any balancing techniques in a non-shielded environment. The paper compares empirically the performances of second and third order gradiometers; it also presents a general procedure for the design of third order gradiometers, taking into account the measured spatial dependence of the magnetic field of the human heart. The performance of a third order gradiometer is very promising for a noisy environment; it has a better low frequency noise rejection than the second order gradiometers tested, and needs no external balancing. (10 refs.)
- 78280** Neuromagnetic measurements at hospital: instrumentation and preliminary tests. P.Nicolas (INSERM, Paris, France), D.Duret, D.Teszner, T.Tuomisto. *Nuovo Cimento D (Italy)*, vol.2D, ser.1, no.2, p.184-94 (March-April 1983). (Proceedings of the Fourth International Workshop on Biomagnetism, Rome, Italy, 14-16 Sept. 1982).
A SQUID system was specially built in a Parisian hospital, allowing neuromagnetic measurements in clinical investigations. A second-order symmetrical gradiometer operates inside an eddy current shield. This was designed for optimising the cost and the efficiency of the system. Its performances were tested with data from patients and normal subjects. (13 refs.)
- 78281** High-resolution magnetic measurements of human cardiac electrophysiological events. R.R.Fenici (Unita di Biomagnetismo Cardiovascolare, Univ. Cattolica, Roma, Italy), G.L.Romani, S.N.Erne. *Nuovo Cimento D (Italy)*, vol.2D, ser.1, no.2, p.231-47 (March-April 1983). (Proceedings of the Fourth International Workshop on Biomagnetism, Rome, Italy, 14-16 Sept. 1982).
The fundamental motivation for investigating cardiac electrophysiological phenomena by means of the biomagnetic method has been that this technique should have added spatial resolution and provided complementary information as opposed to electric recordings only. So far the interest of experimentalists has been concentrated on two different kinds of cardiac phenomena: (1) the study of the activity of the cardiac conduction system and (2) of abnormally delayed ventricular depolarisation (late potentials). The clinical interest for the noninvasive investigation of the His-Purkinje system is well known. Noninvasive clinical recording of late potentials is particularly desirable as they seem to be precious markers for risk of sudden death. A review of the state of research in both fields is presented. (37 refs.)
- 78282** High-resolution recordings of the PR segment in magnetocardiography. S.N.Erne, R.R.Fenici, H.D.Hahlbohm, M.Masselli, H.P.Lehmann, Z.Trontelj (Phys.-Tech. Bundesanstalt, Inst. Berlin, Berlin, Germany). *Nuovo Cimento D (Italy)*, vol.2D, ser.1, no.2, p.248-54 (March-April 1983). (Proceedings of the Fourth International Workshop on Biomagnetism, Rome, Italy, 14-16 Sept. 1982).
The PR interval of magnetocardiograms has been measured with a SQUID sensor in the Berlin magnetically shielded room. In addition to previously reported ramps with isolated superimposed signals in several cases a structured morphology has been found. (8 refs.)
- 78283** High-resolution isofield mapping ion magnetocardiography. S.N.Erne, R.R.Fenici, H.D.Hahlbohm, W.Jaszczuk, H.P.Lehmann, M.Masselli (Phys.-Tech. Bundesanstalt, Inst. Berlin, Berlin, Germany). *Nuovo Cimento D (Italy)*, vol.2D, ser.1, no.2, p.291-300 (March-April 1983). (Proceedings of the Fourth International Workshop on Biomagnetism, Rome, Italy, 14-16 Sept. 1982).
A possible clinical application of a high-resolution magnetic isofield contour mapping technique in cardiography is discussed. Preliminary results are presented in applying this technique to patients with recent myocardial infarction. The patients could be divided into two classes; one of them contained patients with late electrical potentials as a subclass. (9 refs.)
- 78284** Comparison between measured and simulated magnetocardiograms in a case of anterolateral myocardial infarction. P.Siltanen (Cardiovascular Lab., Helsinki Univ. Central Hospital, Helsinki, Finland), T.Poutanen, T.Katila, M.Seppanen, T.Varpula. *Nuovo Cimento D (Italy)*, vol.2D, ser.1, no.2, p.301-10 (March-April 1983). (Proceedings of the Fourth International Workshop on Biomagnetism, Rome, Italy, 14-16 Sept. 1982).
The MCGs measured in a case of an anterolateral myocardial infarction were compared with the corresponding simulated MCGs. The most distinctive changes in the measured MCGs were observed in the upper and lower parts of the thorax as predicted by the simulation. (13 refs.)
- 78285** High-resolution magnetocardiographic recordings of the ST segment in patients with electrical late potentials. S.N.Erne, R.R.Fenici, H.D.Hahlbohm, W.Jaszczuk, H.P.Lehmann, M.Masselli (Phys.-Tech. Bundesanstalt, Inst. Berlin, Berlin, Germany). *Nuovo Cimento D (Italy)*, vol.2D, ser.1, no.2, p.340-5 (March-April 1983). (Proceedings of the Fourth International Workshop on Biomagnetism, Rome, Italy, 14-16 Sept. 1982).
High-resolution magnetocardiograms of patients with recent myocardial infarction have been recorded. In three cases, signals have been found in the ST segment that are time correlated with simultaneously recorded late electric potentials. (5 refs.)
- 78286** Optimizing vector magnetocardiographic lead fields by using a physical torso model. H.Eskola, J.Malmivuo (Electronics Lab., Tampere Univ. of Technol., Tampere, Finland). *Nuovo Cimento D (Italy)*, vol.2D, ser.1, no.2, p.356-67 (March-April 1983). (Proceedings of the Fourth International Workshop on Biomagnetism, Rome, Italy, 14-16 Sept. 1982).
The ideality and sensitivity of several vector magnetocardiographic leads were tested by using an inhomogeneous, physical torso model. The postero-anterior component of the heart's magnetic vector was found easiest to detect. New, more ideal leads for the other two components are suggested. However, these have lower sensitivity. The differences from the results of former investigators can be explained by the differences of the models. (13 refs.)
- The mapping of the measured cardiac electric potential and magnetic-field distribution See Entry 78374

87.60G Laser beams, microwaves, and other electromagnetic waves

(inc. NMR; for X-rays and gamma-rays, see 87.60J)

- 78287** A lamp for cancer phototherapy. F.Jacka (Mawson Inst. for Antarctic Res., Univ. of Adelaide, Adelaide, Australia), A.J.Blake. *Aust. J. Phys. (Australia)*, vol.36, no.2, p.221-6 (1983).
A lamp described comprises a 1000 W incandescent filament source, long- and short-wave pass filters, and a non-imaging reflector system. The output of 24 W in the 620-720 nm band is delivered through a 53 mm diameter aperture with a maximum divergence half-angle of 60°. Refracting components may be fitted to modify the output angular or intensity distribution. This lamp has been used to irradiate several different types of malignant tumour in human patients, following intravenous injection of the photoactive drug haematoporphyrin derivative, causing selective necrosis of the malignant tissue. The clinical results are regarded as encouraging. (7 refs.)
- 78288** Three-dimensional display of nuclear magnetic resonance (NMR) cardiovascular images. L.Axel, G.T.Herman, J.K.Udupa (Dept. of Radiology, Univ. of Pennsylvania, Philadelphia, PA, USA), P.A.Bottomley, W.A.Edelstein. *J. Comput. Assisted Tomogr. (USA)*, vol.7, no.1, p.172-4 (Feb. 1983).
A set of contiguous nuclear magnetic resonance images of the thorax of a living dog was used to create various types of three-dimensional display of the myocardium and great vessels. These structures can be displayed separately or together as transparent or opaque surfaces and can be shown as rotating three-dimensional figures. (11 refs.)
- 78289** Medical laser equipment for continuous operation. G.F.Fedotkin, G.A.Skorubskii (All-Union Sci. Res. Inst. of Medical Instrument Manufacture, Moscow, USSR). *Biomed. Eng. (USA)*, vol.16, no.4, p.133-6 (July-Aug. 1982). Translation of: *Med. Tekh. (USSR)*, vol.16, no.4, p.39-43 (July-Aug. 1982). [received: April 1983]
When designing medical laser equipment special attention is paid to the development of the systems for transmitting radiation to the irradiated object, to visual guidance systems for the infrared radiation, and to systems for controlling the exposure dosage and density of the laser radiation. The authors consider basic diagrams that provide solutions for these problems when using laser radiation in surgery and therapy. (9 refs.)
- 78290** Technique and method of bronchography. R.M.Mamlyayev, I.P.Nalimov, V.M.Antonov, A.Kh.Shakirov (N.A.Semashko Moscow Medical Stomatologic Inst., Moscow, USSR). *Biomed. Eng. (USA)*, vol.16, no.4, p.137-8 (July-Aug. 1982). Translation of: *Med. Tekh. (USSR)*, vol.16, no.4, p.43-5 (July-Aug. 1982). [received: April 1983]
Preliminary data suggest that bronchography creates new prospects for investigation of the bronchi under normal and pathological conditions, enables the depth of the bronchi, their mutual arrangement, and location of the blood vessels to be determined, and the direction, course and angles of branching of the bronchi to be established. (2 refs.)
- 78291** Cardio-surgical thermography. A.R.Fiorini, R.Fumero, R.Marchesi (Dipartimento di Energetica, Politecnico di Milano, Milano, Italy). *Proc. SPIE Int. Soc. Opt. Eng. (USA)*, vol.359, p.249-56 (1983). (Applications of Digital Image Processing IV, San Diego, CA, USA, 24-27 Aug. 1982).
Extracorporeal circulation allows direct access inside the chest: it may be used to carry out physiological research. The thermo-chemical protection of myocardium during heart surgery, called cardioplexy, is one of the latest outstanding techniques in patient safety. Thermocardiography monitoring during the infusion of the cardioplegic solution allows continuous assessment of rapid temperature distribution changes and shows exactly the extent of myocardium involved. Using a peculiar pseudocolor digital image enhancement, it is possible to emphasize involved areas coronary flow and to model the thermofluid-dynamical actions of inspected heart. (5 refs.)
- 78292** Study of RF, gradient pulse and magnet instability effect in NMR tomography. C.H.Oh, H.S.Kim, H.W.Park, W.S.Kim, S.W.Lee, Z.H.Cho (Korea Advanced Inst. of Sci., Seoul, Korea). *IEEE Trans. Nucl. Sci. (USA)*, vol.30, no.3, p.1899-904 (June 1983).
Newly emerged NMR imaging requires careful studies of RF pulse shapes and sequencing for the selection of the region, gradient pulsing for the 2- or 3-D spatial coding, and suitable signal handling technique for the compensation of the inherent instability of the system, especially fluctuation of the static magnetic field. The above subjects are discussed in detail and a new method for the line integral projection reconstruction is proposed. The method could equally be applied to other 3-D NMR imaging techniques such as KWE (Kumar-Welt-Ernst) direct Fourier reconstruction or planar integral projection type reconstruction. (10 refs.)
- 78293** Infrared radiation in therapeutic hyperthermia. J.Dutreix (Faculte de Medecine, Alexandrie, Egypt), E.Damia, A.Salama, P.Janoray, J.-M.Cosset. *J. Biophys. & Med. Nucl. (France)*, vol.7, no.1, p.25-35 (1983). In French.
Infrared radiation provides a convenient way for heating superficial tumours. Geometrical and spectral distributions have been studied for a commercial radiator (Philips). The attenuation of the radiation has been measured in phantom and biological media with a diode. The thermal distribution has been studied with thermocouple in phantoms and in living tissues. The temperature distribution has been theoretically computed as a function of the applied radiation intensity and superficial cooling by air blowing. Measurements and computations show that reasonably uniform heating can be achieved throughout a thickness approaching 1 cm. Therapeutic results for 25 patients are reported. (13 refs.)
- 87.60J Corpuscular radiation and radioisotopes**
(inc. X-rays and gamma-rays)
- 78294** Superimposition of krypton-81 m single photon emission CT and X-ray CT images for cerebral blood flow evaluation. T.Higa, S.Tanada, W.Taki, H.Fukuyama, Y.Ishii, T.Fujita, Y.Yonekawa, T.Odori, T.Mukai, H.Handa, M.Kameyama, R.Morita, K.Torizuka (Kyoto Univ. Hospital, Kyoto, Japan). *J. Comput. Assisted Tomogr. (USA)*, vol.7, no.1, p.37-41 (Feb. 1983).
Selective arteriographic infusion of krypton-81 m was used to obtain cerebral single photon emission computed tomograms. These were then superimposed on X-ray computed tomograms to assess topographically the perfusion of the entire brain. This method enhances the detecting capability for abnormal perfusion areas and has been used in 21 patients with various brain diseases. (7 refs.)

- 78295 Correction for scattered radiation in a ring detector positron camera by integral transformation of the projections.** M.Bergstrom (Dept. of Neuro-radiology, Karolinska Hospital, Stockholm, Sweden), L.Eriksson, C.Bohm, G.Blomqvist, J.Litton.
J. Comput. Assisted Tomogr. (USA), vol.7, no.1, p.42-50 (Feb. 1983).
A 'deconvolution' algorithm for the determination of the scatter contribution in positron emission tomography is described. The projected distributions of scattered radiation measured with a line source at different positions in water phantoms are described analytically. It is shown that an integral transformation of the observed projections with a slightly modified analytical function gives an adequate description of the scattered radiation. The scatter distribution from any composite object can thus be calculated and subsequently subtracted. The algorithm is tested on different objects. The result shows that the level of scattered radiation can be reduced from 25 to 1% of the total count rate in the center of the projection from a homogeneous phantom. (19 refs.)
- 78296 Element-sensitive computed tomography with fast neutrons.** J.C.Overly (Dept. of Phys., Univ. of Oregon, Eugene, OR, USA).
J. Comput. Assisted Tomogr. (USA), vol.7, no.1, p.117-25 (Feb. 1983).
Neutrons and X-rays are mathematically equivalent as probes in computed tomography. However, structure in the energy dependence of neutron total cross sections and the feasibility of using time-of-flight techniques for energy sensitivity in neutron detection suggest that spatial distributions of specific substances can be determined from neutron transmission data. It is demonstrated that this is possible by tomographically reconstructing from such data a phantom containing several different structural materials. (10 refs.)
- 78297 Organ and lesion volume measurements with computed tomography.** M.H.Reid (Dept. of Radiology, Univ. of California Davis Medical Center, Sacramento, CA, USA).
J. Comput. Assisted Tomogr. (USA), vol.7, no.2, p.268-73 (April 1983).
Useful clinical information will often result from determinations of organ and lesion tissue volumes from measurements of computed tomographic (CT) cross sections. This paper discusses simple applications of stereology to volume estimations of organs and disease processes. The method is applied to CT sections and, for equivalent accuracy, is less time consuming than planimeter or CT scanner region of interest outlining and measurements. (7 refs.)
- 78298 A Monte Carlo simulation of Compton scattering in positron emission tomography.** J.Logan, H.J.Bernstein (Dept. of Chem., Brookhaven Nat. Lab., Upton, NY, USA).
J. Comput. Assisted Tomogr. (USA), vol.7, no.2, p.316-20 (April 1983).
A Monte Carlo technique was used to simulate some of the important physical processes involved in the coincidence detection of gamma rays by a positron emission tomograph. The major effect considered here is the detection of Compton scattered gamma rays as coincidence counts. The Compton scattering of gamma rays in a H_2O filled phantom was simulated using the Klein-Nishina cross section. Results obtained in the form of profiles of activity were compared to a model which represents scatter as the convolution of the true signal with an exponential. (12 refs.)
- 78299 Computer technique for monitoring time dependent changes from sequential CT images.** R.F.Mattrey, S.A.Long (Dept. of Radiology, Univ. of California, San Diego, CA, USA), S.W.Erickson, C.B.Higgins.
J. Comput. Assisted Tomogr. (USA), vol.7, no.2, p.379-82 (April 1983).
The sequential computed tomography (CT) images used in this manuscript are electrocardiogram-gated images of the same cross section of the heart (10 in this study) depicting one cardiac cycle from end-diastole to the next end-diastole. Each of these 10 reconstructions corresponds to 10% intervals extending from one R wave to the next R wave. When each image of the series of 10 images is assigned a consecutive table position, using the program for sagittal reconstructions a chronogram along any line through the X-Y plane of the left ventricular (LV) wall can be produced. The chronograms display changes in wall thickness and wall motion in relation to time throughout the cardiac cycle at a preselected site in the LV and can be used to demonstrate the LV myocardial response to perturbations. This technique adds the dimension of time to spatial information in the CT images and can be used to monitor cardiac physiology in a quantitative fashion. (5 refs.)
- 78300 Development prospects for power supplies for diagnostic X-ray sets.** V.V.Klyuev, G.I.Dmitriev, V.P.Kurozav, V.A.Bakushev, L.V.Vladimirov, N.P.Kolesnikov, K.A.Pimenov, P.G.Smetanin, V.Yu.Khlebtsevich, A.Z.Shvartsman (Spektr Production Cooperative, Moscow, USSR).
Biomed. Eng. (USA), vol.16, no.4, p.99-104 (July-Aug. 1982). Translation of: *Med. Tekh. (USSR)*, vol.16, no.4, p.3-9 (July-Aug. 1982). [received: April 1983] (6 refs.)
- 78301 Basic quality parameters of X-ray diagnostic equipments.** A.M.Gurvich, N.N.Blinov (Moscow X-Radiological Res. Inst., Min. of Health, Moscow, USSR).
Biomed. Eng. (USA), vol.16, no.4, p.105-11 (July-Aug. 1982). Translation of: *Med. Tekh. (USSR)*, vol.16, no.4, p.10-18 (July-Aug. 1982). [received: April 1983]
The quality parameters of X-ray diagnostic facilities (X-ray sets, tubes, and detectors) play an important part in obtaining the maximum diagnostic information with a minimum radiation exposure, since they control the optimum conditions for obtaining an X-ray picture. Recent advances in research on the factors controlling image quality go with advances in image intensification and transformation to make it necessary to reconsider the parameters of X-ray diagnostic systems. The present authors consider mainly what needs to be measured and standardized, not how to do it. (19 refs.)
- 78302 Effects of X-ray hardness on fluorogram informativeness.** G.A.Chuiko, V.M.Tsvetkov (Flaw-Detection Res. Inst., Moscow, USSR).
Biomed. Eng. (USA), vol.16, no.4, p.117-19 (July-Aug. 1982). Translation of: *Med. Tekh. (USSR)*, vol.16, no.4, p.23-6 (July-Aug. 1982). [received: April 1983]
It is possible to replace X-radiography by fluorography using image intensifiers II only if the two methods are equivalent in informativeness. The informativeness of a fluorogram is dependent not only on the constraints arising from the method and from the parameters of the II but also on the working conditions, which are related to the mode of operation of the power supply. As an example, the authors consider a fluorograph that includes the URPF power supply, which employs a single-phase source with a full-wave rectification circuit. The URPF makes it possible to perform fluorography with photographic monitoring and automatically selects the voltage on the anode in relation to the density of the object. (1 ref.)

- 78303 Photographic recording conditions in a diagnostic X-ray system with an image intensifier.** A.M.Yakobson, G.A.Chuiko, V.A.Marko (Flaw-Detection Res. Inst., Moscow, USSR).
Biomed. Eng. (USA), vol.16, no.4, p.120-4 (July-Aug. 1982). Translation of: *Med. Tekh. (USSR)*, vol.16, no.4, p.27-31 (July-Aug. 1982). [received: April 1983]
The authors consider the interaction between the factors that determine the informativeness of a fluorogram, and also determine the compatibility of the requirements laid down in the technical specifications for X-ray diagnostic sets as regards photographic recording. (1 ref.)
- 78304 Transmission of scattered radiation by X-ray grids.** O.B.Sokolov (Special Designs Office for Diagnostic Apparatus, Kiev, Ukrainian SSR).
Biomed. Eng. (USA), vol.16, no.4, p.125-7 (July-Aug. 1982). Translation of: *Med. Tekh. (USSR)*, vol.16, no.4, p.31-4 (July-Aug. 1982). [received: April 1983]
A cutoff grid of linear type is a basic means of preventing interference from scattered radiation in X-ray diagnosis. The author examines briefly the limiting performance of a linear grid and defines the optimum structure for a grid, which should be used in future designs. (no refs.)
- 78305 Determination of the basic parameters of PER2-3-P xeroradiographic plate.** P.D.Baltrushaitis, R.A.Kavalyauskas, V.V.Mamontov, B.K.Rakauskene (Electrography Res. Inst. & Oncology Res. Inst., Min. of Health, Vilnius, Lithuanian SSR).
Biomed. Eng. (USA), vol.16, no.4, p.128-32 (July-Aug. 1982). Translation of: *Med. Tekh. (USSR)*, vol.16, no.4, p.34-9 (July-Aug. 1982). [received: April 1983]
The authors have determined the range of working potentials for the xeroradiographic layer under practical conditions, along with the sensitivity, the relative fall in the potential in darkness, and the fatigue and they have evaluated the significance of these parameters under clinical conditions. The stability of the charging conditions has also been examined. (5 refs.)
- 78306 The GPR-1 longitudinal radioisotope gamma tomograph.** E.Yu.El'kind, V.P.Chernobrovkin, K.D.Kalantarov, Yu.M.Sidorov, V.G.Tyurin, A.L.Kangun (All-Union Res. Inst. of Medical Instrumental, Moscow, USSR).
Biomed. Eng. (USA), vol.16, no.4, p.139-42 (July-Aug. 1982). Translation of: *Med. Tekh. (USSR)*, vol.16, no.4, p.45-9 (July-Aug. 1982). [received: April 1983]
The principle of action, construction, and technical characteristics of the GPR-1 longitudinal radioisotope gamma tomograph, with analog picture formation, are described. The GPR-1 gamma tomograph is designed to obtain four longitudinal gamma tomograms and two standard gamma tomograms during each cycle of investigation. (no refs.)
- 78307 Production of a new modified type of applicator type 'Simon' with cobalt-60.** M.I.Mihajlov, T.Petkov, K.J.Mutafchiev.
Yad. Energ. (Bulgaria), no.18, p.89-93 (1983).
Cancer of the uterus is treated for some indications basically with intercavity radium therapy. A new, modified type of applicator, type 'Simon' with Cobalt-60 is proposed by the authors. The technology of production together with its advantages is given. A protective container designed and developed specially for the transportation and operation of these applicators, is described as well. (9 refs.)
- 78308 A computer program for compression of dynamic studies.** J.Verdenet, J.C.Cardot, M.Baud, A.C.Bidet (Service de Medecine Nucleaire, Lab. Biophys., CHU Besancon, France), J.Duvernoy, R.Bazin, R.Bidet.
Comput. Programs Biomed. (Netherlands), vol.16, no.1-2, p.77-82 (Feb.-April 1983).
The program described applies the well known Karhunen-Loeve transformation to the compression of the information carried by scintigraphic sequences. As a result it releases a few principal images which are associated with the dominant temporal behaviour in the sequences. The program is illustrated, and validated in the case of gated cardiac blood pool studies, mathematical and mechanical models. (8 refs.)
- 78309 A system for computer analysis of panorex radiographs.** S.D.Cook, K.A.Thomas (Dept. of Orthopaedic Surgery, Tulane Univ. Medical School, New Orleans, LA, USA), J.N.Kent.
Comput. Programs Biomed. (Netherlands), vol.16, no.1-2, p.97-104 (Feb.-April 1983).
A computer system developed for rapid analysis of panorex (panoramic) radiographs is described. Features of the system include capabilities to compare nonstandardized radiographs, and the ability to superimpose plots of a series of X-ray films. Measurements of alveolar ridge heights and comparisons at intervals in a clinical series are also performed. Simple statistics calculations can also be computed. (5 refs.)
- 78310 Cone beam convolution formula.** B.D.Smith (Radiology Dept., Hospital of the Univ. of Pennsylvania, Philadelphia, PA, USA).
Comput. Biol. & Med. (GB), vol.13, no.2, p.81-7 (1983).
Presents a three-dimensional convolution formula for a general set of cone beam data. This formula is illustrated by examining at length the formula for a particular set of cone beam data—the set of cone beam data from source points which are located along a straight line. How the three-dimensional formula could be implemented for a general set of cone data is discussed. (5 refs.)
- 78311 Rapid and accurate determination of total lung capacity (TLC) from routine chest radiograms using a programmable hand-held calculator.** R.P.C.Rodgers (Faculte de Medecine, Univ. Catholique de Louvain, Bruxelles, Belgium), R.Tannen.
Comput. Biol. & Med. (GB), vol.13, no.2, p.125-40 (1983).
Since its appearance in 1960, the method of Barnhard and associates for the determination of total lung capacity (TLC) from routine chest radiograms has been widely studied in normal and diseased subjects. The method appears to be as accurate as the current definitive procedure, total body plethysmography. The method is in routine use in major medical institutions where the procedure has been automated, but the method does not seem to have gained the wide use it deserves. This is likely due to the tedium of the technique when performed manually—a single determination can require 30 minutes. This paper presents implementation of the Barnhard method for the HP41-C hand-held programmable calculator. In conjunction with the use of a transparent reticle used for obtaining the required measurements, the program allows a single measurement to be made in under 12 minutes. (14 refs.)
- 78312 Array processors in medical imaging.** P.Alexander (Numerix Corp., Newton, MA, USA).
Computer (USA), vol.16, no.6, p.17-30 (June 1983).
Medical image processing has historically included the use of general-purpose array processors and related special-purpose high-speed computational devices. Current imaging modalities include nuclear medical imaging, computed tomography scanners, ultrasound techniques, positron emission tomography, digital radiography, and nuclear magnetic resonance. This article focuses on just

three: computed tomography, digital radiography, and nuclear magnetic resonance. These modalities represent the three techniques where the use of APs is most easily justified. (9 refs.)

78313 Filters—what metal do I use? R.F.Fleay (Dept. of Medical Phys., Royal Perth Hospital, Perth, Australia). *Radiographer (Australia)*, vol.30, no.1, p.24-6 (March 1983). The use of a heavy metal foil, namely the element erbium, is described to show that entrance skin doses to a patient can be reduced dramatically without overloading the X-ray tube. K absorption filtration techniques have a specific application and cannot be used over a wide range of kilovoltages. The selection criteria and application of erbium is described. (5 refs.)

78314 Reconstruction from sparsely sampled data by ART with interpolated rays. K.Kouris (Dept. of Phys., Univ. of Surrey, Guildford, England), H.Tuy, A.Lent, G.T.Herman, R.M.Lewitt. *IEEE Trans. Med. Imaging (USA)*, vol.MI-1, no.3, p.161-7 (Nov. 1982). [received: May 1983]

After a brief discussion of the algebraic reconstruction techniques (ART), the authors introduce the attenuation problem in positron emission tomography (PET). They anticipate that a generalization of ART, the so-called cyclic subgradient projection (CSP) method, may be useful for solving this problem. This, however, has not been successfully realized, due to the fact that data collected by the authors' proposed stationary PET detector ring are too sparsely sampled. That this is, in fact, a major problem is demonstrated by showing that ordinary ART produces reconstructions with unacceptably strong artifacts even on perfect (no attenuation) data collected according to the PET geometry. The authors demonstrate that the source of this artifact is the sparse sampling, and they propose the use of interpolated rays to overcome the problem. This approach is successful, as is illustrated by showing reconstructions from sparsely sampled data by ART with interpolated rays. (12 refs.)

78315 Undersampling errors in region-of-interest tomography. P.V.Sankar (School of Engng., Univ. of California, Irvine, CA, USA), O.Nalciglu, J.Sklansky. *IEEE Trans. Med. Imaging (USA)*, vol.MI-1, no.3, p.168-73 (Nov. 1982). [received: May 1983]

A detailed error analysis for the dual-sampling region-of-interest X-ray tomography is presented. Simulation studies are used along with a range of sampling rates to quantitate the amount of sampling errors within the region of interest. It is shown that as the rate of sampling outside the region of interest becomes sparse the amount of sampling errors within the region of interest increases considerably. (8 refs.)

78316 Streak preventive image reconstruction with ART and adaptive filtering. R.M.Rangayyan (Dept. of Electrical Engng., Univ. of Manitoba, Winnipeg, Manitoba, Canada). *IEEE Trans. Med. Imaging (USA)*, vol.MI-1, no.3, p.173-8 (Nov. 1982). [received: May 1983]

Streaks arise in computed tomograms for a variety of reasons, such as presence of high-contrast edges and objects, aliasing errors, patient movement, and use of very few views. The problem appears to be an inherent difficulty with all reconstruction methods, including backprojection (with convolution) and the algebraic reconstruction technique (ART). This paper presents the derivation and results of an ART-like algorithm (SPARTAF) oriented towards prevention of streaks via optimization of a cost function based on features of streaks, subject to the constraints of the given projection data. The object-dependent method employs pattern recognition of streaks and adaptive filtering during iterative reconstruction by ART. Results of experiments with a test pattern and of application of the method to reconstructive tomography from radiographic films are presented and the convergence properties demonstrated. (27 refs.)

78317 Super PETT I: a positron emission tomograph utilizing photon time-of-flight information. M.M.Ter-Pogossian, D.C.Ficke (Edward Mallinckrodt Inst. of Radiology, Washington Univ. School of Medicine, St. Louis, MO, USA), M.Yamamoto, J.T.Hood, Sr. *IEEE Trans. Med. Imaging (USA)*, vol.MI-1, no.3, p.179-87 (Nov. 1982). [received: May 1983]

The physical characteristics and some imaging capabilities of Super PETT I, a positron emission tomograph utilizing time-of-flight (TOF) in its image reconstruction process, were assessed experimentally by means of measurements carried out in phantoms and clinical imaging studies. The performance characteristics assessed included sensitivity, spatial resolution, image improvements resulting from time-of-flight information utilization, system dead time, and linearity. The clinical examples included imaging of the brain, the heart, the liver, and a demonstration of Super PETT I's capability of achieving cardiac gating. (14 refs.)

78318 Experimental assessment of the gain achieved by the utilization of time-of-flight information in a positron emission tomograph (Super PETT I). M.Yamamoto (Edward Mallinckrodt Inst. of Radiology, Washington Univ. School of Medicine, St. Louis, MO, USA), D.C.Ficke, M.M.Ter-Pogossian. *IEEE Trans. Med. Imaging (USA)*, vol.MI-1, no.3, p.187-92 (Nov. 1982). [received: May 1983]

The gain achieved in image quality by utilizing, in the image forming process, the time-of-flight information (TOF) of positron annihilation photons between their inception and detection was measured experimentally by means of a positron emission tomograph (PET)-Super PETT I. The measurements were carried out by imaging a 35 cm cylindrical uniform phantom containing different positron activity concentrations. The gain achieved through the incorporation of TOF information, defined as the ratio of variances in images reconstructed with and without TOF information, was found to be approximately 3 at the lowest activity concentration and 5-8 in the activity concentration range typically encountered in clinical studies, especially in fast or dynamic studies. This increase in gain with activity was interpreted as resulting from the reduction of random coincidences when TOF information is used. Further image improvement is yielded by incorporating TOF information into the PET attenuation correction provided by the measurement of transmission of annihilation photons in the object imaged. (17 refs.)

78319 An improved algorithm for reprojecting rays through pixel images. P.M.Joseph (Dept. of Diagnostic Radiology, Univ. of Maryland, Baltimore, MD, USA). *IEEE Trans. Med. Imaging (USA)*, vol.MI-1, no.3, p.192-6 (Nov. 1982). [received: May 1983]

It is often desired to calculate line integrals through a field of reconstructed CT density pixels for the purpose of improving CT image quality. Two algorithms widely published and discussed in the past are known to either degrade spatial resolution or generate errors in the results due to the discontinuous 'square pixel' modeling of the reconstructed image. An algorithm is described, based on linear interpolation between pixels, which provides superior accuracy without unnecessary loss of resolution. It was tested on simulated data for a head section and on a narrow Gaussian density distribution. The experimental results demonstrated improved performance. The

method is expected to prove useful for many types of post-reconstruction processing, including beam hardening, missing data, and noise suppression algorithms. (26 refs.)

78320 Errors in isocenter of Picker C-9000 teletherapeutic unit. F.J.Bova, L.T.Fitzgerald (Univ. of Florida Coll. of Medicine, Gainesville, FL, USA).

Health Phys. (GB), vol.44, no.5, p.553-4 (May 1983). In routine maintenance of the authors' Picker C-9000 ⁶⁰Co teletherapy unit, the isocentric stability was checked by mapping the movement of the front pointer, light field projection, and radiation field as the unit rotated about its isocenter. The original specifications for the unit upon installation (1966) set the limit of the deviations from isocenter to plus or minus 2 mm. It has recently become evident that the isocentricity of the unit does not meet this tolerance. The errors described are clinically significant and have forced the authors to use the unit for nonisocentric techniques only. It is recommended that whenever these units are checked for isocentric stability, that points significantly above or below isocenter be examined for coincidence of not only the mechanical and light field, but also the radiation field, to ensure that compensating errors are not inadvertently overlooked. (1 ref.)

78321 Image reconstruction from list-mode data in an emission tomography system having time-of-flight measurements. D.L.Snyder, D.G.Politte (Washington Univ., St. Louis, MO, USA).

IEEE Trans. Nucl. Sci. (USA), vol.ns-30, no.3, p.1843-9 (June 1983). List-mode data collected in a positron-emission tomography system having time-of-flight measurements are three dimensional, but all algorithms which have been published to date operate on two-dimensional data derived from these three-dimensional data. The authors argue that additional information present in 3-D data is useful for reconstruction of images. (13 refs.)

78322 Reconstruction from limited angular projection data using constrained optimization. H.Katsulai, N.Arimizu (Dept. of Radiology, Faculty of Medicine, Chiba Univ., Chiba, Japan). *IEEE Trans. Nucl. Sci. (USA)*, vol.ns-30, no.3, p.1870-9 (June 1983).

A new type of pixel decomposition is introduced to suppress modeling noise and then an algebraic method is developed for reconstruction from limited angular projection data. The basic idea with this method is to directly control the tradeoff between resolution and noise, taking into account the uncertainty of the discrepancy criterion generally used in an algebraic method for reconstruction. The results of a simulation using a simple mathematical phantom are also presented, demonstrating the effectiveness of this method. (8 refs.)

78323 Experimental results of the dichotomic sampling in circular ring positron emission tomograph. Z.H.Cho, S.K.Hilal, J.B.Ra, K.S.Hong, H.S.Lee (Korea Advanced Inst., of Sci., Seoul, Korea), R.E.Bigler. *IEEE Trans. Nucl. Sci. (USA)*, vol.ns-30, no.3, p.1892-8 (June 1983).

Experimental verification of the new dichotomic sampling scheme was attempted and applied to a circular ring PET system. Two different types of aperture collimators were adopted for high resolution (HR) and very high resolution (VHFR) imaging. In HR mode, a resolution of 6.5 mm FWHM was obtained without appreciable degradation in overall sensitivity. In phantom studies with HR mode a sensitivity of 4500 counts/sec/μCi/cc was obtained for a 20 cm diameter uniform phantom filled with water. (25 refs.)

78324 Enhancement of nodular lesions in CT liver scans. R.L.Webber, A.Dwyer, H.Cramer, M.Putterman. *J. Clin. Eng. (USA)*, vol.8, no.1, p.69-79 (Jan.-March 1983).

The impact of selected image-processing schemes on diagnostic performance obtainable from computer-processed CT scans containing simulated nodular lesions was determined from controlled radiological observations. Normal CT scans of the upper abdomen were processed by a computer to simulate the presence of a randomly-located, disk shaped, low-contrast, nodule within the liver stroma. Results for selected enhancement techniques were tallied using a balanced experimental design. The data indicate that suitably processed displays significantly improved diagnostic performance expressed in terms of diagnostic errors, information transfer, and the implied noise relative signal strength, d'. The same mode of display significantly reduces the time required in making diagnostic decisions relative to the status quo. (11 refs.)

78325 Cardiac blood pool emission tomography. R.Itti, L.Philippe, J.M.Lorgeron, B.Charbonnier, P.Raynaud, M.Brochier (Services de Médecine Nucleaire et de Cardiologie, CHU Trousseau, Tours, France). *J. Biophys. & Med. Nucl. (France)*, vol.7, no.1, p.7-10 (1983). In French.

After blood pool labeling using technetium-99 m, a series of cardiac pictures is acquired during the rotation of a gamma-camera about the patient. Computer processing leads to reconstruction of various tomographic slices from the original planar projections. Electrocardiographic gating selects the different phases of the cardiac cycle. Individual slices through the left ventricular region are added in order to provide 'thick' slices on which global and regional parameters of the left ventricular function can be determined. Due to the proportionality existing between count rates and labeled blood volumes, any geometrical model can be avoided. The delineation of regions of interest for count integration is made easier due to the absence of superimposition of structures; no correction for background is necessary. Tomography thus appears to be more consistent and more accurate than the classical methods using planar projections. In addition, right ventricular morphological and kinetic studies can be performed in the same conditions as for the left ventricle. (4 refs.)

78326 Lung exploration by SPECT current status and perspectives. D.J.Macey, R.Marshall (Dept. of Radiation Phys. & Chest Diseases, Churchill Hospital, Oxford, England). *J. Biophys. & Med. Nucl. (France)*, vol.7, no.1, p.11-19 (1983).

If SPECT of the lung is to be introduced as a routine clinical procedure the additional information provided must justify the complexity of the test. The transverse section images must depict adequately the relative distribution of a radiopharmaceutical in the lungs. For the thorax in particular, where there is a comparatively large spread of attenuation coefficients from lung to bone density, the use of a single mean attenuation coefficient must be validated. A rotating gamma camera system for SPECT of the lung uses standard doses and radiopharmaceuticals and only requires a modest addition to the capital cost of a computerised gamma camera facility. The present SPECT systems improve the depth resolution with some degradation of the conventional X and Y resolution but in view of the movement of the heart and lungs with respiration the spatial resolution is about 2 cm FWHM in three dimensions. The authors have used a transmission-emission method to check the accuracy of SPECT images of the lung perfusion scan. The correct total number of counts in the transverse slices can be determined by the transmission-emission method and the resultant images are the best description of the distribution of activity in the lungs. With SPECT of the lung transverse section images can be obtained which are qualitative on a relative and absolute scale. (16 refs.)

78327 Performance and quality control of scintillation cameras. J.L.Moret, D.Iachetti (Lab. de Biophys. Experimentale, CHU, Henri-Mondor, Creteil, France), J.F.Brandon, G.Pascal, E.Sachot, J.Legrand, A.Lansari, L.Guerin, A.Desgrez, G.Meyniel, B.Mensch, J.Mensch, F.Therain, F.Soussaline, D.Barre, G.Taunay.

J. Biophys. & Med. Nucl. (France), vol.7, no.1, p.43-57 (1983). In French. Acceptance testing, quality and control assurance of gamma-cameras are a part of diagnostic quality in clinical practice. Several parameters are required to achieve a good diagnostic reliability: intrinsic spatial resolution, spatial linearity, uniformities, energy resolution, count-rate characteristics, multiple window spatial analysis. Each parameter was measured and also estimated by a test easy to implement in routine practice. The instrumentation required was a 4028 multichannel analyzer linked to a microcomputer, minicomputers and a set of phantoms. Several tests proposed by NEMA and WHO have to be improved concerning too punctual spatial determinations during distortion measurement with a multiple window. Contrast control of image needs to be monitored with a high counting rate. This study shows the need to avoid punctual determinations and the value of giving sets of values of the same parameter for the whole field and to report mean values with their standard variation. (48 refs.)

78328 Geometric determination of left ventricular volume from gated blood-pool studies using a slant-hole collimator. R.F.Uren, H.N.Newman, B.F.Hutton, J.Cormack, L.Bernstein, L.Allen, I.Dyer (Dept. of Nuclear Medicine, Royal Prince Alfred Hospital, Camperdown, NSW, Australia).

Radiology (USA), vol.147, no.2, p.541-5 (May 1983). A geometric method of measuring absolute left ventricular volumes from gated blood-pool studies obtained in a single-plane modified left anterior oblique view was evaluated prospectively in 30 patients who also underwent single-plane contrast ventriculography. The gated studies used a 30° straight-bore slant-hole collimator with the holes slanted caudally. Left ventricular end-diastolic volume was calculated using the area-length method, with semiautomatic definition of the left ventricular region of interest and the maximum length of the left ventricle. Ejection fraction was determined from the left ventricular time activity curve. The left ventricular end-systolic volume was derived using the end-diastolic volume and ejection fraction. Correlation coefficients between the two methods were 0.93 for end-diastolic volume, 0.95 for end-systolic volume, and 0.91 for ejection fraction. This method provided accurate and highly reproducible measurements of actual left ventricular volumes and was easily applicable in routine clinical studies. (17 refs.)

78329 An improved method of estimating the portal venous fraction of total hepatic blood flow from computerized radionuclide angiography. R.Sarper, Y.A.Tarcan (Dept. of Radiology, Emory Univ. School of Medicine, Atlanta, GA, USA).

Radiology (USA), vol.147, no.2, p.559-62 (May 1983). The measurement of portal venous flow of the liver is important in the evaluation of patients for shunt surgery. A previous report (see R. Sarper et al., *ibid.*, vol.141, p.179-84, 1981) described a method using slope analysis of hepatic radionuclide angiograms to generate an index of relative portal flow, which correlated well with angiographic grades of portal perfusion. The present report describes a refinement in bolus administration and a modification in technique that appear to reflect true portal venous flow more accurately. A total of 109 studies was performed, including seven normal and 80 cirrhotic patients. The method was reproducible ($r=0.998$) and showed good correlation with the angiographic grades of perfusion ($r=-0.906$). (4 refs.)

78330 Physical and clinical evaluation of new high-strip-density radiographic grids. K.Doi, P.H.Frank, Heang-Ping Chan, C.J.Vyborny, S.Makino, N.Iida, M.Carlin (Dept. of Radiology, Univ. of Chicago, Chicago, IL, USA).

Radiology (USA), vol.147, no.2, p.575-82 (May 1983). The imaging performance of new high-strip-density (HSD) grids having 57 lines/cm was compared with that of conventional low-strip-density (LSD) grids having 33 or 40 lines/cm. The unique advantage of HSD grids is that, under most standard radiographic conditions, the grid lines are not noticeable on the final image, even if the grid is stationary. This is due to the combined effect of the high fundamental spatial frequency of HSD grids, the modulation transfer function of screen-film systems and of the human visual system, and scattered radiation. Monte Carlo simulation studies, phantom images, and clinical evaluation indicate that HSD grids can provide contrast improvement factors and Bucky factors that are comparable with or slightly better than those obtained with LSD grids. Therefore, it may now be possible to eliminate moving Bucky trays from radiographic tables and fluoroscopic devices. (7 refs.)

78331 Materials and method of certification of standard specimens for checking computerized X-ray tomographs. E.I.Vainberg, I.A.Kazak, V.P.Kurozaev, G.Z.Plotkina (Sci.-Res. Inst. of Introscopy, Moscow, USSR). *Sov. J. Nondestr. Test. (USA)*, vol.18, no.9, p.672-7 (Sept. 1982). Translation of: *Defektoskopiya (USSR)*, vol.18, no.9, p.7-14 (Sept. 1982). Groups of organic materials of a standardized elemental composition and method of certifying standard specimens for checking computerized X-ray tomographs with a certain mass density by a standardized method are recommended. (13 refs.)

XX National Congress of the Italian Society for Nuclear Biology and Medicine held in association with the VI Annual Meeting of the Nuclear Medicine Section of the Italian Association for Radiology and Nuclear Medicine

Technique and method of bronchography See Entry 78290

Quantitative profile scanning, a means for internal dose assessment See Entry 78335

Time-dose-fractionation See Entry 78345

Diagnostic X-ray shielding design based on an empirical model of photon attenuation See Entry 78360

Shielding device for brachytherapy sources See Entry 78361

Image restoration in CT by the method of projection onto convex sets See Entry 78384

Biomedical applications of MWPC's for digital imaging of soft β emitters See Entry 78406

87.60M Radiation dosimetry

78332 Hungarian-Austrian co-operation in radiation dosimetry. K.Zsanzs (Nat. Office of Measures, Budapest, Hungary), K.E.Dufschmid. *Acta Phys. Acad. Sci. Hung. (Hungary)*, vol.52, no.3-4, p.265-74 (1982). [received: May 1983] (Proceedings of the Hungarian-Austrian Health Physicists' Meeting, Gyor, Hungary, 28 Sept.-1 Oct. 1981). Since 1974 a close and fruitful co-operation has been in progress between the Hungarian National Office of Measures (OMH) and the Austrian Research

Center Seibersdorf in the field of radiation dosimetry. The work began with intercomparison measurements and calibration of dose meters at OMH. The practical experiences gained at OMH have been applied in the design of the new Austrian dosimetry laboratory established between 1975 and 1977. Since 1976 the cooperation of the two Institutions has been included in the Hungarian-Austrian inter-governmental agreement on technical-scientific co-operation as a joint priority dosimetry standard and the calibration facilities in both countries. (7 refs.)

78333 Radiation exposure and associated cancer risk due to radon and decay products. E.Pohl, F.Steinhauser, W.Hofmann, J.Pohl-Ruling (Div. of Biophys., Univ. of Salzburg, Salzburg, Austria). *Acta Phys. Acad. Sci. Hung. (Hungary)*, vol.52, no.3-4, p.291-6 (1982). [received: May 1983] (Proceedings of the Hungarian-Austrian Health Physicists' Meeting, Gyor, Hungary, 28 Sept.-1 Oct. 1981).

The atmospheric content of radon and its decay products, especially in buildings, represents a significant contribution to the radiation exposure of a man even in a normal environment. A study in Salzburg-City/Austria over several years was carried out in over 1000 working-, living- and bedrooms. Dose calculations were performed on 729 test persons, considering individual differences in age, sex and life-style and atmospheric nuclide concentration at different sites. Induction of lung cancer caused by inhalation of radon and its decay products was correlated with cumulative exposure based on experience with lung cancer incidence amongst uranium miners. It was shown for Salzburg City that 15 to 35% of the observed number of lung cancer cases may be induced by radon and its decay products, although Salzburg is an area with a 'normal' natural radioactive environment. (12 refs.)

78334 Stochastic aspects of lung dosimetry for radon decay products at low dose levels. W.Hofmann (Div. of Biophys., Univ. of Salzburg, Salzburg, Austria).

Acta Phys. Acad. Sci. Hung. (Hungary), vol.52, no.3-4, p.297-302 (1982). [received: May 1983] (Proceedings of the Hungarian-Austrian Health Physicists' Meeting, Gyor, Hungary, 28 Sept.-1 Oct. 1981).

The determination of upper limits for the amount of inhaled radon decay products needs detailed information on the resulting radiation dose in different organs and tissues, particularly in the respiratory tract. The common procedure of theoretical lung dosimetry is characterized by applying simple analytical techniques to a data base consisting of mean values for all anatomical and physiological parameters involved. However, it is well known that great inter- as well as intra-subject variabilities of lung dimensions and clearance processes could be observed, questioning, therefore, the applicability of simplified anatomical and clearance models. Substituting the mean values by probability distributions and applying Monte Carlo techniques a dosimetric method for determining lung doses is presented, taking into consideration these variabilities. A second source of fluctuations in lung dosimetry is caused by the randomness of nuclide distributions, lung tissue structure and stochastic energy absorption in lung cells. (5 refs.)

78335 Quantitative profile scanning, a means for internal dose assessment. A.Andrasi, E.Beleznay (Health Phys. Dept., Central Res. Inst. for Phys., Budapest, Hungary).

Acta Phys. Acad. Sci. Hung. (Hungary), vol.52, no.3-4, p.303-10 (1982). [received: May 1983] (Proceedings of the Hungarian-Austrian Health Physicists' Meeting, Gyor, Hungary, 28 Sept.-1 Oct. 1981).

A combined measuring and computing method is given by means of which the Committed Effective Dose Equivalent can be estimated. A sensitive detector equipped with a suitable collimator moving along the length of a person being investigated, enables the count rate profile to be obtained from which organ activities can be deduced. With repeated measurements the activity time variations and their time integrals can be derived, the latter being proportional to the organ doses. The general description of the methods and its implementation in the radiation protection practice of the Central Research Institute for Physics is given. Test experiments show the method to be suitable for internal dose assessment when the activity exceeds 0.5 kBq per organ. (8 refs.)

78336 Retrospective evaluation of occupational annual doses received by workers producing radioactive sources. I.Bojtor ('Frederic Joliot-Curie' Nat. Res. Inst. for Radiobiology & Radiohygiene, Budapest, Hungary), F.Golder, M.Osavy, E.Bobok.

Acta Phys. Acad. Sci. Hung. (Hungary), vol.52, no.3-4, p.311-16 (1982). [received: May 1983] (Proceedings of the Hungarian-Austrian Health Physicists' Meeting, Gyor, Hungary, 28 Sept.-1 Oct. 1981).

Personal dosimetric data from external radiation recorded during a 19-year period at the Institute of Isotopes were subjected to extensive computer analysis to examine the applications of the relevant ICRP dose limitation system by following the trend of radiation exposures and estimating the risk levels for various occupational fields. Based on the values of the average annual dose equivalents and Ω obtained from the whole observation period, even the most exposed group of maintenance, packaging and transportation workers can be classified as belonging to working category 'B' of UNSCEAR, thereby permitting the conclusion that working conditions at the Institute are satisfactory. The average annual dose equivalents in time intervals of employment were found to decrease with increased time spent doing the same work. The risk levels were estimated from 25-year-lifetime doses by using 'time-related' average annual doses. The risk for the highest exposed group (workers in maintenance, packaging and transportation) was assessed to be $1.2 \cdot 10^{-3}$ fatalities per working lifetime. It may be concluded that in each occupational group of the Institute the mortality risk of radiation-induced cancer is lower than the hazards in non-radiation occupations having high standards of safety. (11 refs.)

78337 Determination of the energy response of dosimeters with a Bragg-monochromatized beam. N.Vana, H.Aiginger (Atomic Inst. of Austrian Univs., Vienna, Austria).

Acta Phys. Acad. Sci. Hung. (Hungary), vol.52, no.3-4, p.333-9 (1982). [received: May 1983] (Proceedings of the Hungarian-Austrian Health Physicists' Meeting, Gyor, Hungary, 28 Sept.-1 Oct. 1981).

In the energy region below 50 keV the energy response of dosimeters is usually determined by means of filtered Bremsstrahlung radiation. The 'monochromatic' radiation produced by filtering the continuous X-ray spectrum of an X-ray tube shows a broad energy distribution for the maximum of the intensity and a considerable 'tail' to low energies. To avoid this disadvantage a Bragg monochromator is used for the energy region between 10 keV and 50 keV. The Bragg monochromator, a commercially available X-ray spectrometer, reflects selectively monochromatic X-rays from a continuous bremspectrum of a tungsten X-ray tube. The angle of reflection and the energy are determined by the Bragg condition. The energy resolution obtained was 2%. The photon flux density at the place of the dosimeter was measured with an efficiency calibrated Ge(Li) semiconductor detector. From this photon flux density the actual exposure of the dosimeter under examination can be calculated. (4 refs.)

- 78338 Measurement of the energy response of LiF, CaF₂ and CaSO₄ TL-dosimeters.** N.Vana, H.Aiginger, W.Erath, T.Michev (Atomic Inst., Austrian Univs., Vienna, Austria). *Acta Phys. Acad. Sci. Hung. (Hungary)*, vol.52, no.3-4, p.341-5 (1982). [received: May 1983] (Proceedings of the Hungarian-Austrian Health Physicists' Meeting, Gyor, Hungary, 28 Sept.-1 Oct. 1981). The most important materials used in thermoluminescence dosimetry (TLD) are LiF, CaF₂ and CaSO₄ with various dopants. LiF:Mg, Ti is almost tissue equivalent and therefore the most applied TLD-material in personnel and medical dosimetry. CaF₂:Dy offers the highest sensitivity of the above mentioned materials and is used in environmental and low-dose dosimetry. CaSO₄:Dy can easily be labor made and is the cheapest phosphor. As the effective atomic numbers of CaF₂ and CaSO₄ differ markedly from that of tissue material the response curve of both materials must be carefully determined in the energy range dominated by the photoeffect. The energy responses of these three listed phosphors were determined by means of a Bragg monochromator, filtered radiation from a gold target bombarded by electrons from a Van de Graaff accelerator, the radiation of a ¹³⁷Cs-source (662 keV) and a ⁶⁰Co-source (1.17, 1.33 MeV). The response-energy dependence of the three dosimeters shows maxima at 35 keV (LiF and CaF₂) and 40 keV (CaSO₄). (4 refs.)
- 78339 Lithium drifted beryllium oxide high sensitivity thermoluminescent dosimeter.** S.Makra (Nat. Oncological Inst., Budapest, Hungary). *Acta Phys. Acad. Sci. Hung. (Hungary)*, vol.52, no.3-4, p.353-6 (1982). [received: May 1983] (Proceedings of the Hungarian-Austrian Health Physicists' Meeting, Gyor, Hungary, 28 Sept.-1 Oct. 1981). A new BeO:Li detector sensitized by a novel method is described. The glow curve of the detectors shows two peaks, the ratio of peak heights depends on dose. The light output per unit dose slightly exceeds that of lithium fluorides. Reproducibility is $\pm 2\%$ for doses higher than 3 mGy, detection limit is 50 μ Gy, exceeding by two-three order of magnitude the values obtained for commercial BeO detectors. Response shows less than $\pm 15\%$ change with photon energy. Fading is lower than 2% per months. (8 refs.)
- 78340 Estimation of per caput dose and collective dose from the use of Danube water.** M.Tschurlovits (Atomic Inst., Austrian Univs., Vienna, Austria). *Acta Phys. Acad. Sci. Hung. (Hungary)*, vol.52, no.3-4, p.413-17 (1982). [received: May 1983] (Proceedings of the Hungarian-Austrian Health Physicists' Meeting, Gyor, Hungary, 28 Sept.-1 Oct. 1981). Deals with methods for assessment of both per caput and collective dose resulting from the use of the water of the Danube river, where drinking water and fish consumption pathways are considered. Results of previous measurements are used as basis for the estimation. It was found that the dose from natural radionuclides considerably exceeds the dose from artificial radionuclides. (7 refs.)
- 78341 The radiation dose from coal burning: a review of pathways and data.** J.O.Corbett (Berkeley Nuclear Labs., CEGB, Berkeley, England). *Radiat. Prot. Dosim. (GB)*, vol.4, no.1, p.5-19 (1983). All stages of the coal fuel-cycle, including mining, combustion and utilisation or disposal of the ash, cause minor perturbations of the natural radiation environment. Many radiological assessments of this effect have already been made, often for comparison with nuclear power, though few have considered the cycle as a whole. This review is an attempt to cover as broadly as possible the various environmental pathways leading to radiation dose in man, and to identify and summarise the sources of relevant data. Although local variations may be very significant, the resulting doses are normally only a small fraction of the natural background. Collective doses to the population arise primarily through inhalation of radioactivity in ash emitted from chimneys and through ingestion in food after deposition on crops and pasture or in the sea. On a global scale, there is a comparable reduction in collective dose due to the dilution of atmospheric carbon-14 by stable carbon dioxide emission. Two less familiar effects, the occupational dose to miners and the population dose from the use of ash in building materials, should also be taken into account, but their proper assessment depends on what alternative occupation or material is chosen for comparison; the net effects can be either positive or negative. Although the nuclear fuel cycle is briefly discussed, it is argued that comparisons between radiation doses from coal burning and nuclear power are of limited value. (103 refs.)
- 78342 Statistical characterisation of a critical group.** M.Tschurlovits (Atominst. of Austrian Univs., Wien, Austria), D.Beninson. *Radiat. Prot. Dosim. (GB)*, vol.4, no.1, p.27-31 (1983). A proposal is made to separate a possible critical group from the remaining exposed group. The basic assumption is that the distribution of doses, both in the general exposed group and in the critical group, can be described by statistical distribution functions. It is proposed that when no clear identification of the critical group is feasible, the 5% higher end of the dose distribution in the candidate exposed population group is selected as the critical subgroup, and that the average dose in that 'tail' can be used for limitation purposes. The actual dose distribution or parts of it must be determined by appropriate monitoring or modelling procedures. (10 refs.)
- 78343 Specific activity estimation of minerals and other materials containing natural radionuclides.** W.A.Kolb (Phys.-Tech. Bundesanstalt, Braunschweig, Germany). *Radiat. Prot. Dosim. (GB)*, vol.4, no.1, p.33-6 (1983). Most radiation protection regulations and codes define limits on gross specific activity below which radiation protection measures are not required. The question arises as to which radionuclides contained in a sample have to be taken into account in calculating the gross activity. This paper considers natural radionuclides according to their radiotoxicity and relative dose contributions and suggests criteria against which radiological relevance can be judged. Several examples of naturally occurring materials are discussed. (11 refs.)
- 78344 The use of solid-state nuclear track detectors in radiation dosimetry, medicine and biology.** S.A.Durrani (Dept. of Phys., Univ. of Birmingham, Birmingham, England). *Nucl. Tracks & Radiat. Meas. (GB)*, vol.6, no.4, p.209-28 (1982). The author briefly surveys the applications in radiation protection and life sciences. The major emphasis is on the use of plastic track detectors for the dosimetry of neutrons, both thermal and fast. Alpha particle dosimetry is also considered, with special emphasis on radon measurements in houses. Both active and passive dosimeters are briefly considered. A few typical and representative examples of the application of SSNTDs in the medical and radiobiological fields are next presented. These encompass the filtration of malignant cells in blood, the measurement of α -emitters in the environment, and the distribution of lead in teeth and bones. Finally a very brief review of some automatic and semi-automatic methods of scanning normal or electrochemical etching of the plastic detectors, is given. (43 refs.)

- 78345 Time-dose-fractionation.** P.Drake. *Radiographer (Australia)*, vol.30, no.1, p.5-9 (March 1983). The time-dose-fractionation (TDF) system has been researched, used and evaluated in the authors' clinic since May 1981. Since August 1981 it has been used routinely in all dosage calculations. There has only been a limited amount of iso-effect planning, due, mainly, to a lack of time to plan in dual modes. This paper is the synthesis of that research, use and evaluation. It has been demonstrated that the TDF method overcomes most of the obstacles currently faces. It is a consistent, reliable technique which lends itself to future analysis. If the method was widely accepted and used there would exist a legitimate means of intercomparison. This could lead, ultimately, to a far better understanding of radiobiology and its clinical implications. (25 refs.)
- 78346 Estimation of shallow-dose equivalent using a two-element dosimeter.** V.P.Gupta (EG&G Idaho Inc., Idaho Nat. Engng. Lab., Idaho Falls, ID, USA). *Health Phys. (GB)*, vol.44, no.4, p.373-8 (April 1983). Estimation of shallow-dose equivalent using a two-element dosimeter is described under the guidelines of a standard adopted by the Health Physics Society Standards Committee and the dosimetry practices followed by most dosimeter processors. This standard is to be used in a future mandatory testing program in the US. A mathematical formulation, correlating dosimeter response and 'shallow-dose equivalent factors' at different energies, is presented. A thermoluminescent dosimeter (TLD), currently used at the author's institute, is examined for determining shallow-dose equivalent response and the results are discussed for beta as well as photon responses. (16 refs.)
- 78347 Depth-dose curves for ⁹⁰Sr and natural and depleted uranium in Mylar.** R.L.Coleman, C.G.Hudson, P.A.Plato (Tennessee Valley Authority, Health Phys. Services, Muscle Shoals, AL, USA). *Health Phys. (GB)*, vol.44, no.4, p.395-402 (April 1983). Describes the generation of accurate depth-dose curves in Mylar for ⁹⁰Sr and slabs of natural and depleted uranium from 0 to 1000 mg/cm², utilizing an extrapolation chamber. The absorbed dose rate produced by natural uranium was found to decrease from 235 mrad/hr at a depth of 7 mg/cm² to 43 mrad/hr at 300 mg/cm² to 4.8 mrad/hr at 1000 mg/cm². The dose rate produced by depleted uranium was found to decrease from 205 mrad/hr at 7 mg/cm² to 34 mrad/hr at 300 mg/cm² to 2.3 mrad/hr at 1000 mg/cm². A 1-mCi extended area ⁹⁰Sr source (encapsulated in 50 mg/cm² Ag) was found to produce an absorbed dose rate of 16997 mrad/hr at 57 mg/cm², 5000 mrad/hr at 300 mg/cm², and 27.1 mrad/hr at 1050 mg/cm². Doses to deep organs determined historically at depths ranging from 300 to 1000 mg/cm². The results of this study show that ⁹⁰Sr and uranium produce significant absorbed dose rates at a depth of 300 mg/cm². Thus, if doses for deep depths are determined at 300 mg/cm² for mixed β - γ exposures, the dose will be overestimated due to the presence of the β component. (13 refs.)
- 78348 Biologically and physically recorded doses after an accidental exposure to ⁶⁰Co- γ rays.** G.Stephen, W.Hadnagy, C.Hammermaier, U.Imhof (Inst. fur Strahlenhygiene des Bundesgesundheitsamtes, Neuberberg, Germany). *Health Phys. (GB)*, vol.44, no.4, p.409-11 (April 1983). Reports an accidental exposure of two individuals who received fairly homogeneous whole-body doses of ⁶⁰Co- γ rays. Chromosome analyses were performed 103 days after the accident in the other. From time correction factors, biological doses were estimated and compared with physically calculated doses and those recorded from the film badges. (11 refs.)
- 78349 RADOK: an integrating, passive radon monitor.** M.Annanmaki, H.Koskela, M.Koponen, O.Parvainen (Inst. of Radiation Protection, Helsinki, Finland). *Health Phys. (GB)*, vol.44, no.4, p.413-16 (April 1983). A passive, integrating radon monitor with characteristics suitable for mine surroundings has been constructed. This monitor is based on the principle of electrostatic collection of radon daughters. The detection system has been adapted from the Alphameter-400. (2 refs.)
- 78350 Mucosal structure and radon in head carcinoma dosimetry.** R.A.Schlenker (Centre for Human Radiobiology, Argonne Nat. Lab., Argonne, IL, USA). *Health Phys. (GB)*, vol.44, no.5, p.556-62 (May 1983). The investigation reported shows that: (1) The location of the epithelial cells implied by ICRP Publication 26 is incorrect. It leads to dose rates from bone and to dose rate ratios which are much too high. (2) Epithelial thickness has little effect on the ratio of dose rates. (3) The dose rate ratio is strongly dependent on the thickness of the lamina propria and would depend strongly on the thickness of the cytoplasm layer if direct nuclear hits were required for cell transformation. (4) Based on the limited data available for lamina propria and epithelial thicknesses, the air-spaces would probably be the dominant source of dose in the mastoid air cells if the ratio of radioactivity levels in bone and airspace were no more than 1.1/g. This would be true whether targets were spread throughout the whole cell or confined to the nucleus alone. (9 refs.)
- 78351 A virtual-nuclides method for whole-body counting and quality control.** Mao-Hsiung Chen (Inst. of Electronics, Nat. Chiao-Tung Univ., Hsinchu, Taiwan), Pao-Shan Weng. *Health Phys. (GB)*, vol.44, no.5, p.562-6 (May 1983). Whole-body counting using NaI(Tl) detectors is discussed. A radionuclide analysis method based on the matrix method is described. Minimum detectable activities are considered. (9 refs.)
- 78352 Neutronspektrum es dozisoszlas vizsgalatok szamitassal es mersel elliptikus fantomban ²⁵²Cf es nehezvizvel moderalt ²⁵²Cf neutron forrasokra** (Neutron spectra and dose distribution calculations and measurements for a filled elliptical phantom using bare and heavy-water moderated ²⁵²Cf neutron sources). J.Palfalvi. Report KFKI-1983-47, Hungarian Acad. Sci., Budapest (1983), 18 pp. In Hungarian. Calculations and measurements for the dose distribution in a water-filled elliptical phantom when irradiated with neutrons of a bare and a heavy water moderated californium neutron sources are presented. The calculations were performed by a Monte Carlo code, and different nuclear track detectors were used for the measurements. (11 refs.)
- Proceedings of the Hungarian-Austrian Health Physicists' Meeting See Entry 74198
- Health physics monitoring practices at commercial low-level waste disposal sites in light of 10 CFR 61 requirements See Entry 75132
- Neutron sensitivity of SSNTD See Entry 75187
- Comparison of field dose rate measurements and Monte Carlo calculations See Entry 75191
- Comparison between two thermoluminescence dosimeter materials See Entry 75194

Large volume electret dosimeter for measurement of low level radiationSee Entry 75195

Calculation of the activation energies for single TLD-900 glow-curve componentsSee Entry 75196

A new phosphor $\text{Li}_2\text{B}_4\text{O}_7\text{:Cu}$ for TLDSee Entry 75198

Multi-element dosimeters for radiation protection measurementsSee Entry 75199

New health physics perspectives affecting instrumentation technologySee Entry 75200

A LiF as a CaSO_4 thermoluminescens detektorok neutronrezekenysegenek vizsgálata (Thermal neutron sensitivity of LiF and CaSO_4 thermoluminescent detectors)See Entry 75208

An exact solution to the Gaussian cloud approximation for γ absorbed dose due to a ground-level releaseSee Entry 78113

Problems with the linear-quadratic dose-response relationshipSee Entry 78265

A secondary standard dosimetry system for calibration of radiation protection instrumentsSee Entry 78353

TLD measurements with LiF and $\text{CaSO}_4\text{:Tm}$ See Entry 78355

Retention and dosimetry of ^{106}Ru inhaled along with inert particles by Fischer-344 ratsSee Entry 78366

Determination of radium-226 in urineSee Entry 78405

87.60P Radiation protection
(inc. radiation monitoring)

78353 A secondary standard dosimetry system for calibration of radiation protection instruments. K.E.Duftschmid (Austrian Res. Center Seibersdorf, Seibersdorf, Austria), J.Hizo. *Acta Phys. Acad. Sci. Hung. (Hungary)*, vol.52, no.3-4, p.275-82 (1982). [received: May 1983] (Proceedings of the Hungarian-Austrian Health Physicists' Meeting, Gyor, Hungary, 28 Sept.-1 Oct. 1981). In view of the increasing need and accuracy requirements for the calibration of radiation protection dosimeters, a novel secondary standard system consisting of a low level ionization chamber with 10^4 cm^3 sensitive volume operating at ambient atmospheric pressure and an automated digital current integrator with dose/dose rate calculation has been designed. The spherical ionization chamber of 27 cm diameter and 3 mm wall thickness is made from high pressure extruded polyacetal resins (CH_2O), providing a rugged structure of excellent long term stability of sensitive volume combined with extremely flat energy response. The wall thickness of the chamber is sufficient for secondary electron equilibrium up to several MeV of photon radiation without additional build-up-caps, etc. (3 refs.)

78354 The role of radioactivity standard reference materials in Hungarian health physics practice. A.Szorenyi (Nat. Office of Measures, Budapest, Hungary). *Acta Phys. Acad. Sci. Hung. (Hungary)*, vol.52, no.3-4, p.283-9 (1982). [received: May 1983] (Proceedings of the Hungarian-Austrian Health Physicists' Meeting, Gyor, Hungary, 28 Sept.-1 Oct. 1981). Radioactivity Standard Reference Materials (RSRMs) have been issued by the National Office of Measures (OMH) for more than ten years. At the present time OMH offers various solutions and solid standards for over 50 radionuclides. The interest in RSRMs has especially increased since 1976 after the issue of the Government Decree of Measures. The author shows the role of RSRMs by several examples in radiation protection of nuclear power plants and in nuclear medicine. Suitable absolute and relative methods and equipment have been developed for the activity determination of RSRMs of very different forms. The equipment and their most important parameters are briefly reviewed. (6 refs.)

78355 TLD measurements with LiF and $\text{CaSO}_4\text{:Tm}$. P.P.Szabo (Central Res. Inst. for Phys., Budapest, Hungary). *Acta Phys. Acad. Sci. Hung. (Hungary)*, vol.52, no.3-4, p.323-31 (1982). [received: May 1983] (Proceedings of the Hungarian-Austrian Health Physicists' Meeting, Gyor, Hungary, 28 Sept.-1 Oct. 1981). LiF chips of Polish origin used for personnel monitoring at the author's Institute are planned to be used at the Paks Nuclear Power Station, (Hungary). The thermal and intermediary neutron sensitivities of the LiF chips were established. In environmental monitoring, Hungarian $\text{CaSO}_4\text{:Tm}$ TLDs are used in tandem: one being heavily, the other being slightly filtered. In this way not only the dose but also the low energy contribution of terrestrial radiation can be established. The system was tested in International Intercomparisons. Certain other dose rate dependence measurements of $\text{CaSO}_4\text{:Tm}$ in the literature are questionable, leading to the conclusions of TLD reader instability. (34 refs.)

78356 Investigations on microwave radiation exposure. T.Predmerszky, L.Ballay, E.Boloni, L.D.Szabo, L.Vamos ('Frederic Joliot-Curie' Nat. Res. Inst. for Radiobiology & Radiohygiene, Budapest, Hungary). *Acta Phys. Acad. Sci. Hung. (Hungary)*, vol.52, no.3-4, p.479-86 (1982). [received: May 1983] (Proceedings of the Hungarian-Austrian Health Physicists' Meeting, Gyor, Hungary, 28 Sept.-1 Oct. 1981). The extensive use of microwave devices calls for the radiation control of equipment, work places and environment also in Hungary. Because of the lack of comprehensive knowledge about the biological effects of microwaves there exist no internationally accepted safety standards. The power density values measured at work places seldom exceed the level of $100\text{ }\mu\text{W}/\text{cm}^2$ recommended in Hungary. Investigations were made with humans and animals. Several persons working in telecommunication for more than five years complained of headache, fatigue, irritability and some vegetative symptoms, but no expressed health damage was observed. Experiments on animals supplied new data about the thermal effects of microwaves on embryos, including effects on liver and brain. To solve the problems of microwave radiation protection Hungarian researchers have started interdisciplinary cooperation. (6 refs.)

78357 Development of protection against radiation in Austria during the past decade. J.K.Hohenberg (Bundesmin. fur Soziale Verwaltung, Wien, Austria). *Acta Phys. Acad. Sci. Hung. (Hungary)*, vol.52, no.3-4, p.317-21 (1982). In German. [received: May 1983] (Proceedings of the Hungarian-Austrian Health Physicists' Meeting, Gyor, Hungary, 28 Sept.-1 Oct. 1981). Describes the work of Austrian authorities concerned with protection against radiation including the annual checks of equipment and of exposed personnel. Tables show the numbers of medically examined employees found unsuitable for exposure to radiation (28 out of 7100 in 1979) and the number of persons reported to be injured by radiation (2 per year from 1976 to 1979). (no refs.) J.S.

78358 Building designs permitted according to the Austrian Radiation Protection Act. J.K.Hohenberg (Bundesmin. fur Soziale Verwaltung, Wien, Austria). *Acta Phys. Acad. Sci. Hung. (Hungary)*, vol.52, no.3-4, p.475-37 (1982). In German. [received: May 1983] (Proceedings of the Hungarian-Austrian Health Physicists' Meeting, Gyor, Hungary, 28 Sept.-1 Oct. 1981). Explains that the dose output of enclosed radioactive materials must not exceed 10^{-6} Sv/h at a distance of 10 cm, according to Austrian law, unless a special permit has been issued (e.g. equipment used in dentistry, materials for non-destructive testing, smoke detector, thickness measuring instruments, level gauges). (no refs.) J.S.

78359 Radiation monitors measure potential health hazards. J.Browne. *Microwaves & RF (USA)*, vol.22, no.3, p.121-8, 154 (March 1983). Like many other phenomena once dismissed as harmless, nonionizing radiation is now considered a potential health hazard at certain power levels. The author describes radiation monitors, which were once extremely narrow-band devices intended expressly for leak detection in microwave ovens, and which have blossomed into extremely sensitive, broadband devices capable of measuring near-and far-field nonionizing radiation at frequencies as high as 40 GHz. Most modern radiation monitors are similar in appearance and consist of a diode-based detection probe connected directly or via coaxial cable to a measurement meter. (3 refs.)

78360 Diagnostic X-ray shielding design based on an empirical model of photon attenuation. B.R.Archer, J.L.Thornby, S.C.Bushong (Baylor Coll. of Medicine, Houston, TX, USA). *Health Phys. (GB)*, vol.44, no.5, p.507-17 (May 1983). A series of nomograms that simplify determination of diagnostic X-ray shielding requirements with lead are presented. All recommendations of the NCRP, except that to 'add one half value layer (HVL)' in determining secondary barriers, were followed in the production of these curves. For secondary barriers, the shielding required to reduce the weekly exposure to the applicable maximum permissible dose has been determined. This eliminates the over-shielding inherent in the 'add one HVL' approximation and allows a variety of more cost effective materials to be considered for secondary barriers. (15 refs.)

78361 Shielding device for brachytherapy sources. A.J.Schneider, H.S.Clarke (Dept. of Radiology, Medical Coll. of Ohio, Toledo, OH, USA). *Health Phys. (GB)*, vol.44, no.5, p.554-5 (May 1983). The greatest exposure to radiation therapy personnel occurs during brachytherapy procedures. The authors have designed and constructed a shielded loading device which significantly reduces the exposure to the hands and forearms. The device is intended to be used with the Nuclear Associates improved Fletcher-Suit-Delchos applicator system (model 67-980). (no refs.)

78362 Protection in industrial radioscopes in the radiographic examination of objects in nonstationary conditions. L.V.Vladimirov, E.A.Gusev, B.I.Leonov (Sci.-Res. Inst. of Introsocopy, Moscow, USSR). *Sov. J. Nondestr. Test. (USA)*, vol.18, no.9, p.678-81 (Sept. 1982). Translation of: *Defektoskopiya (USSR)*, vol.18, no.9, p.15-19 (Sept. 1982). The principles of the rational construction of biological protection of radioscopes used in nonstationary conditions in industrial production are examined. Models of technical realization of shielding for typical problems of nondestructive inspection are given. (12 refs.)

2nd Annual Meeting of the Canadian Radiation Protection Association (papers in summary form only received)See Entry 74210

Health physics monitoring practices at commercial low-level waste disposal sites in light of 10 CFR 61 requirementsSee Entry 75132

Environmental monitoring system at the Paks Nuclear Power StationSee Entry 75188

Telemetric and data acquisition system for environmental monitoring at the Paks Nuclear Power StationSee Entry 75189

Monitoring external radiation in the environment: instruments and results of measurementsSee Entry 75193

SPICER: a sensitive radiation survey instrumentSee Entry 75197

Multi-element dosimeters for radiation protection measurementsSee Entry 75199

New health physics perspectives affecting instrumentation technologySee Entry 75200

1.73 μm eyesafe laser rangefinderSee Entry 75677

Quantitative profile scanning, a means for internal dose assessmentSee Entry 78335

The use of solid-state nuclear track detectors in radiation dosimetry, medicine and biologySee Entry 78344

87.60R Radioactive pollution
(see also 86.70 Environmental science)

78363 Radioactive contamination of filamentous green algae in the Hungarian reach of the River Danube. E.Holland, B.Sztanyik, L.Vanicsek ('Frederic Joliot-Curie' Nat. Res. Inst. for Radiobiology & Radiohygiene, Budapest, Hungary). *Acta Phys. Acad. Sci. Hung. (Hungary)*, vol.52, no.3-4, p.419-23 (1982). [received: May 1983] (Proceedings of the Hungarian-Austrian Health Physicists' Meeting, Gyor, Hungary, 28 Sept.-1 Oct. 1981). In connection with the national nuclear power station programme a series of measurements was initiated to detect radionuclides in the River Danube. Examinations started in Spring 1978 at six sampling points along the Hungarian reach of the Danube. From among algae of various species of the Danube the localized and well-propagating filamentous green algae (*Cladophora* sp., *Vaucheria* sp.) were investigated. The activity concentration of gamma-radiating nuclides absorbed by algae was determined with a Canberra 8100 type Ge(Li)-spectrometer. This apparatus facilitated radioactivity measurements on wet samples or samples subjected to simple physical preparation. The metabolic character and accumulative abilities of filamentous green algae showed them to be suitable indicators of radionuclide contamination of the water ecosystem. Results are ^{131}I nuclide at min. 72.5 mBq/g to max, 5440.0 mBq/g and other fission products from 55 mBq/g to 929 mBq/g . (7 refs.)

78364 Radioactivity of fish in the Hungarian reach of the River Danube. E.Kurtacs ('Frederic Joliot-Curie' Nat. Res. Inst. for Radiobiology & Radiohygiene, Budapest, Hungary). *Acta Phys. Acad. Sci. Hung. (Hungary)*, vol.52, no.3-4, p.425-7 (1982). [received: May 1983] (Proceedings of the Hungarian-Austrian Health Physicists' Meeting, Gyor, Hungary, 28 Sept.-1 Oct. 1981). In connection with the national nuclear power programme a series of measurements was initiated to detect radionuclides in fish of the Danube

river. Since spring 1978 a number of species of fish have been investigated at two sampling points near the nuclear station region. The beta activity of samples was counted with anticoincidence shielded low background Tesla NZ-602 type apparatus. The radioactivity of samples was measured after simple physical or radiochemical preparation. The results show no significant difference according either to sampling place or season. Activity concentrations of ^{90}Sr and ^{137}Cs of natural or global fallout origin are low and hardly differ from values obtained earlier by other researchers. (2 refs.)

78365 Analysis of tritium in tree rings. K.Kozak (Inst. of Isotopes, Budapest, Hungary).

Acta Phys. Acad. Sci. Hung. (Hungary), vol.52, no.3-4, p.429-34 (1982). [received: May 1983] (Proceedings of the Hungarian-Austrian Health Physicists' Meeting, Gyor, Hungary, 28 Sept.-1 Oct. 1981).

Tritium in the cellulose content of the growth rings of two trees was analysed. The two trees were separated by a distance of 5 km; one of them grew just beside the building of the Institute of Isotopes, Budapest. The distribution of tritium concentration in the sequence of the rings of the latter tree showed good agreement with the environmental background concentrations for the years 1957-63. Excess tritium was found in the rings of subsequent years. This was due to the activity of the Institute and indicated the elevated level of the local environment. The tritium content of a few rings of the other tree reflected the environmental background level of the past years and showed no contamination due to the Institute. (8 refs.)

78366 Retention and dosimetry of ^{106}Ru inhaled along with inert particles by Fischer-344 rats. M.B.Snipes, G.M.Kanapilly (Inhalation Toxicology Res. Inst., Lovelace Biomedical & Environmental Res. Inst., Albuquerque, NM, USA).

Health Phys. (GB), vol.44, no.4, p.335-48 (April 1983).

This study was done to provide data useful for predicting the deposition, retention and radiation dose patterns for humans who might be exposed to an aerosol containing $^{106}\text{RuO}_4$ and respirable particles. Ruthenium-106 tetroxide was introduced into air containing inert particles. In addition to condensation of $^{106}\text{RuO}_4$ on pre-existing particles, self-nucleation occurred, presumably resulting from the formation of RuO_3 . It appears there was a significant amount of $^{106}\text{RuO}_4$ present in the inhalation exposure system. When a group of Fischer-344 rats inhaled this exposure atmosphere, approx. 12% of the initial body burden reached the pulmonary region of the respiratory tract. The distribution of the remaining 88% of the initial burden is described. Relative radiation doses accumulated to 100 days after inhalation exposure, normalized to a lung dose of 1.0 are given. Comparable results are predicted for man inhaling a similar exposure atmosphere, which could be encountered under certain circumstances in nuclear industry operations. (22 refs.)

78367 Deposition and retention of ^{141}Ce and ^{134}Cs aerosols on cool desert vegetation. G.C.Millard, L.Fraley, Jr. (Dept. of Radiology & Radiation Biology, Colorado State Univ., Fort Collins, CO, USA), O.D.Markham.

Health Phys. (GB), vol.44, no.4, p.349-57 (April 1983).

Deposition velocities and retention times were obtained for submicron aerosols of ^{141}Ce and ^{134}Cs deposited on two cool desert plant species, big sagebrush (*Artemisia tridentata*) and bottlebrush grass (*Sitanion hystrix*). Mean deposition velocities for sagebrush were 0.18 cm/s (^{141}Ce) and 0.13 cm/s (^{134}Cs). Mean deposition velocities for grass were 0.022 (^{141}Ce) and 0.023 cm/s (^{134}Cs). Species differences were significant ($p < 0.05$), however, nuclide differences were not significant. The loss of activity on the vegetation consisted of two components. A rapid initial loss was found with effective half-times of approx. 1 d (1-8 d for ^{141}Ce and 0.6 d for ^{134}Cs) on sagebrush and approx. 2 d (2.8 d for ^{141}Ce and 2.3 d for ^{134}Cs) on grass. This was followed by a slower, long-term loss with effective half-times ranging from 11 d for ^{141}Ce and 15 d for ^{134}Cs on sagebrush to 9 d for ^{141}Ce and 11 d for ^{134}Cs on grass. (17 refs.)

78368 Effects of recent neptunium studies on high-level waste hazard assessments. B.L.Cohen (Dept. of Phys. & Astron., Univ. of Pittsburgh, Pittsburgh, PA, USA).

Health Phys. (GB), vol.44, no.5, p.567-9 (May 1983).

It has recently been pointed out that alterations in metabolic data given in ICRP Publication 30 (1979) have brought about large changes in hazard assessments of radioactive waste (see B.L. Cohen, *ibid.*, vol.42, p.133, 1982). The most important of these alterations was for ^{237}Np , causing that radionuclide to dominate the long term hazard. The author points out that new studies of neptunium metabolism (see M.F. Sullivan et al., *Radiation Res.*, vol.94, no.1, p.199, 1983; R.C. Thompson, *Radiation Res.*, vol.90, no.1, p.1, 1982) have produced information that largely reverses that alteration, greatly reducing the importance of neptunium in hazard assessment and thereby substantially reducing the total long term hazard. (7 refs.)

Proceedings of the Hungarian-Austrian Health Physicists' Meeting

See Entry 74198

Finite element analysis of transport of radionuclides in porous media

See Entry 78110

Radiation exposure and associated cancer risk due to radon and decay products

See Entry 78333

Estimation of per caput dose and collective dose from the use of Danube water

See Entry 78340

A virtual-nuclides method for whole-body counting and quality control

See Entry 78351

Preliminary observations on californium-252 behaviour in sea water, sediments and zooplankton

See Entry 78558

87.70 BIOMEDICAL ENGINEERING

78369 The effects of some recording variables on the visual evoked response. I. A comparison of surface and needle electrode recording of the visual evoked response. C.Yiannikas, J.C.Walsh (Dept. of Clinical Neurophysiology, Royal Prince Alfred Hospital, Camperdown, Sydney, Australia).

Am. J. EEG Technol. (USA), vol.23, no.1, p.3-7 (March 1983).

Stainless steel needle and silver/silver chloride surface electrodes are compared with respect to their recording fidelity for visual evoked response. Stainless steel electrodes behave as biological capacitors and at low frequencies have a high impedance and greater electrode offset potential. In the frequency range of the major components of the VER obtained using an amplification system with a high input impedance there is no significant difference in the recordings obtained from the two electrode types. Furthermore, the speed and efficiency of application of subdermal needle electrodes establishes a place for their use in routine evoked potential recording. (13 refs.)

78370 The effects of some recording variables on the visual evoked response. II. The effects of system bandpass on the recording of the visual evoked response. C.Yiannikas, J.C.Walsh (Dept. of Clinical Neurophysiology, Royal Prince Alfred Hospital, Camperdown, Sydney, Australia).

Am. J. EEG Technol. (USA), vol.23, no.1, p.9-14 (March 1983).

For pt.1 see *ibid.*, vol.23, no.1, p.3-7, 1983. The effect of five filter conditions with cutoff ranging from 3.2 kHz to 80 Hz with a 12 db/octave rolloff were studied when averaging the pattern generated visual evoked response. Distortions of the P100 latencies were observed for lowpass filtering below 320 Hz. It is emphasized that the system bandpass should extend at least to 320 Hz when studying the VER components and when estimating the peak latency of the P100 component. Precise information about the system bandpass, including the rolloff and averager sampling rate, should be included in published reports. (8 refs.)

78371 Visual evoked potentials in the newborn: awake and asleep. A.DeGuire, D.G.Glaze, J.D.Frost, Jr. (Dept. of Neurology, Baylor Coll. of Medicine, Houston, TX, USA).

Am. J. EEG Technol. (USA), vol.23, no.1, p.15-23 (March 1983).

Describes the technique of recording the visual evoked potential (VEP) in the newborn during a study conducted to determine the influence of awake-sleep status on evoked potential parameters. It has been established in adults that the VEP waveform characteristics are dependent on the behavioral state, but only limited data have been presented for the infant. The study showed that there is no significant difference between the flash VEP waveforms during waking and sleep in the neonate. It is suggested that the test be performed during sleep so as to minimize artifacts and patient distress. (16 refs.)

78372 Initial results of noninvasive measurement of finger blood pressure according to Penaz. P.G.Molhoek (Dept. of Cardiology, Leiden Univ. Hospital, Leiden, Netherlands), K.H.Wesseling, A.C.Arntzenius, J.J.M.Settels, E.Van Vollenhoven, H.W.H.Weeda, B.De Wit.

Automedica (GB), vol.4, no.4, p.241-6 (1983).

Comparison of simultaneous measurements of intra-arterial pressure in the brachial artery and finger blood pressures (measured noninvasively according to the technique of J. Penaz, see Digest 10th Int. Conf. Med. Biol. Engng., Dresden, p.104, 1973) was performed in 33 patients suspected of having hypertension. In 12 patients evaluation of the technique could not be carried out due to technical failures or highly distorted blood pressure wave forms. Results of the remaining 21 patients showed underestimation of intra-arterial blood pressure by finger cuff blood pressure of 0.8 kPa regarding mean values both for systolic and diastolic measurement, with scatter ranges from 1.9 to -3.5 kPa for systolic, and 0.1 to -2.5 kPa for diastolic values. (6 refs.)

78373 Precordial electrocardiographic map using the IBM-Bonner program. O.Nakagaki, Y.Nose, H.Yano, M.Nakamura (Cardiovascular Clinic, Kyushu Univ. Hospital, Fukuoka, Japan).

Comput. Programs Biomed. (Netherlands), vol.16, no.1-2, p.91-5 (Feb.-April 1983).

The precordial electrocardiographic map may be useful for noninvasive assessment of the extent of the acutely infarcted myocardium. Rapid and serial precordial electrocardiographic maps also may be useful to evaluate the effects of interventions of drugs and efforts on the ischemic myocardium. In this study, the IBM-Bonner program was applied to produce a system for the precordial electrocardiographic map. Six electrodes at one intercostal space were moved in parallel from the second to the seventh intercostal space. Twelve electrocardiograms (ECGs) could be recorded from 36 precordial sites, 6x6 matrix, and analyzed using the IBM-Bonner program. The measured values of the ECG waveform make feasible the automatic procurement of the precordial electrocardiographic map. The authors' mapping program can be used readily and anywhere the IBM-Bonner program is in use. (15 refs.)

78374 The mapping of the measured cardiac electric potential and magnetic-field distribution. M.J.Peters, Z.Dunajski, A.Heringa, R.T.van Dam (Dept. of Tech. Phys., Twente Univ. of Technol., Enschede, Netherlands).

Nuovo Cimento D (Italy), vol.2D, ser.1, no.2, p.311-23 (March-April 1983). (Proceedings of the Fourth International Workshop on Biomagnetism, Rome, Italy, 14-16 Sept. 1982).

The distribution of both the cardiac electric potential on the body surface and the cardiac magnetic field near the chest and back was recorded at fixed time instants of the heart cycle. The general features of both types of maps are simple and reproducible, moreover they both reveal different information. (9 refs.)

78375 Interference electromyogram processing. I. Influence of the motor unit action potential shape on the interference electromyogram spectra. J.L.Coatrieux (Lab. de Traitement du Signal, Univ. de Rennes I, Rennes, France).

Electromyography & Clin. Neurophysiol. (Belgium), vol.23, no.3, p.229-42 (March-April 1983).

Reports a study on the influence of the motor unit action potential (MUAP) morphology on the electromyogram (EMG) by means of a simulation model and spectral analysis. This work applies to surface and needle EMG signals and suggests signal processing and data analysis methods to discriminate between different pathologies. The author shows: (1) The relation between the interference EMG spectra and the single MUAP mean spectra in the high frequency domain. (2) The influence of higher and lower amplitude MUAPs and linked potentials spectra. (3) The evolution of spectrum shape applied to interference EMG involving a heterogeneous MU population, both diseased and healthy. The analysis is limited to the moderate and unfatigued case where the steady discharge of motoneurons do not show any dependence between intervals of successive nerve impulses. (13 refs.)

78376 Automated analysis of abnormal electroencephalograms. P.Y.Ktonas (Dept. of Electrical Engng., Univ. of Houston, Houston, TX, USA).

CRC Crit. Rev. Biomed. Eng. (USA), vol.9, no.1, p.39-97 (1983).

Presents a critical review of various attempts at computerized analysis of abnormal electroencephalograms (EEGs). A description of normal and abnormal EEGs from the viewpoint of the clinician is presented, along with guidelines used in the visual detection and quantification of EEG abnormalities. A brief review of some important computerized methodologies for clinical EEG analysis is given. Automated detection and quantification of epileptogenic EEG transients and seizures are reviewed, and digital computer (software) as well as hardwired systems are presented. Computerized techniques for the quantification of abnormal EEGs in cerebrovascular disorders and coma, metabolic disorders, and for the localization of brain lesions and tumors are presented. Future directions and the general problem of man-machine agreement are elaborated upon. (169 refs.)

78377 Effects of digital filtering on the waveform and peak parameters of the auditory brainstem response. J.R.Boston (Dept. of Anesthesiology/CCM, School of Medicine, Univ. of Pittsburgh, Pittsburgh, PA, USA).

J. Clin. Eng. (USA), vol.8, no.1, p.79-84 (Jan.-March 1983).

Since the auditory brainstem response (ABR) has a narrower bandwidth than the spontaneous EEG, filtering can be used to improve the signal-to-noise ratio (SNR) prior to averaging. The author compared the effects of different

digital filters. Filters evaluated included lowpass (40-1600 Hz), bandpass (200-1600 Hz), and time invariant a posteriori Wiener filters. All filters were digitally implemented and had zero phase-shift. The filters were digitally implemented and had zero phase-shift. The filters were applied to averaged auditory brainstem responses based on different numbers of individual responses (128 to 1024). The effects of the filters on both room-mean-square (RMS) error and on Jewett wave parameters (peak latency and amplitude) were considered. The lowpass filter did not affect the RMS error or wave amplitude; it did reduce the wave latency variability, but it did not affect the mean latency value. It greatly facilitated wave identification by removing high frequency noise. The bandpass filter behaved similarly, except that a slow wave activity in the response was removed also, resulting in an increased RMS error. The performance of the Wiener filters was essentially the same as the lowpass filters except for a tendency to attenuate the waveform mean square error and wave latency and amplitude variability should be considered. (18 refs.)

78378 Portable processing thermometer. G.Mallet (Lab. de Biophys., Univ. de Nice, Nice, France), D.Maillard.
J. Biophys. & Med. Nucl. (France), vol.7, no.1, p.37-41 (1983). In French. Describes a portable and autonomous instrument allowing on one hand to measure and record, in less than 1 minute, the temperature of 32 samples, and on the other hand, to follow during more than 24 hours tiny temperature variations, with a precision as good as 0.01°C. The recorded data can be transferred to a punch-tape for computer processing. (2 refs.)

78379 Contribution of measurement system artifacts to systolic spikes. Z.Ladin, E.Trautman, R.Teplick.
Med. Instrum. (USA), vol.17, no.2, p.110-12 (March-April 1983). A clinical study was conducted to determine if the systolic spike often observed in an invasive blood pressure display originates in the measurement system. The clinical system consisted of a catheter, stopcocks, 4 ft of tubing, an amplifier (containing a 12-Hz low-pass filter), and a continuous flush device. A second transducer was connected directly to the patient's catheter, in parallel with the clinical system. Its output was conditioned by an amplifier modified to exclude the low-pass filter. Simultaneous measurements were taken from both transducers, recorded, and later analyzed. A comparison of the traces in the time domain, as well as an analysis of the signals in the frequency domain, suggests that the systolic spike did not originate in the pressure tubing or in the amplifier system. (6 refs.)

78380 A simple means for recording foot contact sequence during gait. G.F.Harris, R.E.Halbach.
Med. Instrum. (USA), vol.17, no.2, p.119-20 (March-April 1983). A simple circuit has been developed that can be used in conjunction with standard gait analysis foot switches to decrease the number of channels needed for recording. (3 refs.)

78381 A microprocessor-based arrhythmia monitor/recorder for the operating and recovery rooms. A.V.Sahakian, W.J.Tompkins, B.M.Tompkins, J.F.Kreul.
Med. Instrum. (USA), vol.17, no.2, p.131-4 (March-April 1983). A microprocessor-based cardiac arrhythmia monitor/recorder was designed to detect and document arrhythmias that occur during general anesthesia. A Holter tape recorder controlled by the monitor records arrhythmias and associated annotation. These condensed records are later manually scanned for final classification. The project was undertaken to build a database of arrhythmias correlated with various inhalation anesthetic agents, while simultaneously evaluating real-time rhythm analysis algorithms. (6 refs.)

Biomedical Engineering Society Symposia (papers in summary form only received) See Entry 74202

Velocity detection of Korotkoff sounds See Entry 78276

A symmetric third order gradiometer without external balancing for magneto-cardiography See Entry 78279

Neuromagnetic measurements at hospital: instrumentation and preliminary tests See Entry 78280

High-resolution magnetic measurements of human cardiac electrophysiological events See Entry 78281

High-resolution recordings of the PR segment in magnetocardiography See Entry 78282

High-resolution isofield mapping ion magnetocardiography See Entry 78283

Comparison between measured and simulated magnetocardiograms in a case of anterolateral myocardial infarction See Entry 78284

High-resolution magnetocardiographic recordings of the ST segment in patients with electrical late potentials. See Entry 78285

Optimizing vector magnetocardiographic lead fields by using a physical torso model See Entry 78286

87.70E Diagnostic methods and instrumentation
(see also 87.60 Medical and biomedical uses of fields, radiations and radioactivity)

78382 Breast tissue classification using diagnostic ultrasound and pattern recognition techniques. I. Methods of pattern recognition. S.Finette, A.Bleier, W.Swindell (Dept. of Radiology, Univ. of Arizona, Tucson, AZ, USA).
Ultrasound Imaging (USA), vol.5, no.1, p.55-70 (Jan. 1983). Discusses the application of statistical pattern recognition techniques to problems in diagnostic ultrasound. Using their own system as an example, the authors describe the concepts and specific methods that they have applied to a problem involving the computer-aided classification of breast tissue in vivo. Topics include feature generation, feature selection and classification, as well as a method which estimates the probability of error on classifying future data. (27 refs.)

78383 Breast tissue classification using diagnostic ultrasound and pattern recognition techniques. II. Experimental results. S.Finette, A.R.Bleier, W.Swindell, K.Haber (Univ. of Arizona, Tucson, AZ, USA).
Ultrasound Imaging (USA), vol.5, no.1, p.71-86 (Jan. 1983). For pt.1 see ibid., vol.5, no.1, p.55 (1983). The methods of statistical pattern recognition have been applied to the problem of in vivo ultrasonic characterization of breast disease in humans. Backscattered A-mode signals obtained from a commercial pulse imaging system were used to generate a large set of potentially useful features. Using statistical tests, a small subset of discriminatory features was selected to design a Bayes decision rule for each of two tissue classification schemes: malignant disease vs. benign disease, and malignant disease vs. (benign disease+normal tissue). Classification results obtained by the rotation method included sensitivities of 88 percent and 76 percent for the two schemes, based on data obtained from 32 women. These results are encouraging, though a definitive statement concerning the extrap-

olation of these numbers to the general population should only be made after obtaining results with a large data base. (26 refs.)

78384 Image restoration in CT by the method of projection onto convex sets. M.I.Sezan, H.Stark (Dept. of Electrical, Computer & Systems Engng., Rensselaer Polytech. Inst., Troy, NY, USA).
Proceedings of ICASSP 83. IEEE International Conference on Acoustics, Speech and Signal Processing, Boston, MA, USA, 14-16 April 1983 (New York, USA: IEEE 1983), p.139-42 vol.1

In many foreseeable applications of computerized tomography (CT) it may not be possible (e.g., because of obstructions) to obtain 360 degree view-data and reconstruction from partial view data may be unsatisfactory. In this paper the authors describe the method of projections onto convex sets (POCS) by which the missing data can be restored from partial viewdata and a priori known properties of the original image. POCS performs significantly better than the conventional Gerchberg-Papoulis (GP) method. (10 refs.)

XX National Congress of the Italian Society for Nuclear Biology and Medicine held in association with the VI Annual Meeting of the Nuclear Medicine Section of the Italian Association for Radiology and Nuclear Medicine See Entry 74203

Modeling three-dimensional computer reconstructions from surface contours for diagnostic imaging See Entry 78273

Physical constraints in the optimization of medical imaging filters for maximum signal-to-noise ratio See Entry 78274

Biological signals processing: an application to ultrasonic echo signals sounding See Entry 78275

Algorithms and experimental results in acoustic tomography using Rytov's approximation See Entry 78278

Three-dimensional display of nuclear magnetic resonance (NMR) cardiovascular images See Entry 78288

Technique and method of bronchology See Entry 78290

Study of RF, gradient pulse and magnet instability effect in NMR tomography See Entry 78292

Superimposition of krypton-81 m single photon emission CT and X-ray CT images for cerebral blood flow evaluation See Entry 78294

Correction for scattered radiation in a ring detector positron camera by integral transformation of the projections See Entry 78295

Element-sensitive computed tomography with fast neutrons See Entry 78296

Organ and lesion volume measurements with computed tomography See Entry 78297

A Monte Carlo simulation of Compton scattering in positron emission tomography See Entry 78298

Computer technique for monitoring time dependent changes from sequential CT images See Entry 78299

Development prospects for power supplies for diagnostic X-ray sets See Entry 78300

Basic quality parameters of X-ray diagnostic equipments See Entry 78301

Effects of X-ray hardness on fluorogram informativeness See Entry 78302

Photographic recording conditions in a diagnostic X-ray system with an image intensifier See Entry 78303

Transmission of scattered radiation by X-ray grids See Entry 78304

Determination of the basic parameters of PER2-3-P xeroradiographic plate See Entry 78305

The GPR-1 longitudinal radioisotope gamma tomograph See Entry 78306

A system for computer analysis of panorex radiographs See Entry 78309

Cone beam convolution formula See Entry 78310

Array processors in medical imaging See Entry 78312

Filters—what metal do I use? See Entry 78313

Reconstruction from sparsely sampled data by ART with interpolated rays See Entry 78314

Undersampling errors in region-of-interest tomography See Entry 78315

Streak preventive image reconstruction with ART and adaptive filtering See Entry 78316

Super PETT I: a positron emission tomograph utilizing photon time-of-flight information See Entry 78317

Experimental assessment of the gain achieved by the utilization of time-of-flight information in a positron emission tomograph (Super PETT I) See Entry 78318

An improved algorithm for reprojecting rays through pixel images See Entry 78319

Image reconstruction from list-mode data in an emission tomography system having time-of-flight measurements See Entry 78321

Reconstruction from limited angular projection data using constrained optimization See Entry 78322

Experimental results of the dichotomic sampling in circular ring positron emission tomograph See Entry 78323

Enhancement of nodular lesions in CT liver scans See Entry 78324

Cardiac blood pool emission tomography See Entry 78325

Lung exploration by SPECT current status and perspectives See Entry 78326

Performance and quality control of scintillation cameras See Entry 78327

Geometric determination of left ventricular volume from gated blood-pool studies using a slant-hole collimator See Entry 78328

An improved method of estimating the portal venous fraction of total hepatic blood flow from computerized radionuclide angiography See Entry 78329

Physical and clinical evaluation of new high-strip-density radiographic grids See Entry 78330

Materials and method of certification of standard specimens for checking computerized X-ray tomographs See Entry 78331

Diagnostic X-ray shielding design based on an empirical model of photon attenuation See Entry 78360

Biomedical applications of MWPC's for digital imaging of soft β emitters See Entry 78406

87.70G Patient care and treatment

Feasibility of ultrasound hyperthermia in the treatment of malignant brain tumors See Entry 78277

A lamp for cancer phototherapy See Entry 78287

- Medical laser equipment for continuous operation See Entry 78289
 Cardio-surgical thermography See Entry 78291
 Infrared radiation in therapeutic hyperthermia See Entry 78293
 Production of a new modified type of applicator type 'Simon' with cobalt-60 See Entry 78307
 Errors in isocenter of Picker C-9000 teletherapeutic unit See Entry 78320
 Shielding device for brachytherapy sources See Entry 78361

87.70J Prosthetics and other practical applications

- 78385 Visual perception of a phonemic code for a tactile hearing aid.** Hoi-Young Chan, E.M.O'Brien (Clemson Univ., Clemson, SC, USA). IEEE SOUTHEASTCON '83 Conference Proceedings, Orlando, FL, USA, 11-14 April 1983 (New York, USA: IEEE 1983), p.376-9.
 A new type of tactile hearing aid is considered which will present only phonemic information to the tactile senses of totally deaf people. This will relay on a speed-to-phoneme convertor which is still not a reality but will be someday. A phonemic code has been evaluated visually. The code consists of a 2x4 array of on-off stimulators to represent the 41 phonemes of English. Single phonemes through five phoneme words were evaluated by seven subjects. The percent correctly perceived were as follows: single phonemes, 98%; two phoneme through five phoneme words, 90, 82, 78 and 74% respectively. The phonemes were presented at a rate of about one per second which is well below normal speed for spoken English. However, the results are encouraging given the brief exposure of the subjects to the code. The next step is a tactile evaluation of the code. (3 refs.)

87.80 BIOPHYSICAL INSTRUMENTATION AND TECHNIQUES

- 78386 Inhalation chambers for air ion research.** J.M.Charry, P.A.Cerniglia, J.M.Weiss (Rockefeller Univ., New York, NY, USA), T.J.Michel, R.F.Finger. *Bioelectromagnetics (USA)*, vol.4, no.2, p.167-80 (1983).
 Many previous problems in establishing the nature of biological and behavioural effects of small air ions have been due to poor control over the ion-inhalation and microclimate, resulting in nonuniform electrical fields and highly uneven concentrations of small air ions. The authors have developed a corona discharge air ion-inhalation system for use with animals that incorporates rigorous control over the microclimate and produces highly uniform concentrations of small air ions throughout the exposure area. (15 refs.)
- 78387 Application of interferometry to the monitoring of sheep and cattle behaviour in arid zone paddocks.** B.R.Davis (Dept. of Electrical Engng., Univ. of Adelaide, Adelaide, S Australia), M.C.Willcocks. *Bioelectm. & Patient Monit. (Switzerland)*, vol.9, no.4, p.185-204 (1982).
 Reviews methods of monitoring animal movement and behaviour in response to environmental changes. The method based on radio interferometry is discussed in some detail, including consideration of the criteria which determine the choice of system parameters such as operating frequency and transmitter power. A prototype system based on radio interferometry and applied to the study of sheep behaviour in arid zones is described and some preliminary results presented. Suggestions for improvement and realization as a full automated data acquisition system are included. (23 refs.)
- 78388 An implantable, externally powered radiotelemetric system for long-term ECG and heart-rate monitoring.** B.Hansen (Finsen Lab., Copenhagen, Denmark), K.Aabo, J.Bojsen. *Bioelectm. & Patient Monit. (Switzerland)*, vol.9, no.4, p.227-37 (1982).
 An externally inductive powered implantable ECG radiotelemetry unit has been developed for continuous long-term measurements of cardiophysiological changes following administration of cardiotoxic drugs. The power density distribution (320 kHz) inside the cage has been measured to be 3-11 mW/cm². The implantable unit has a volume of 38x22x8 mm and a mass of 9 g, and has been tolerated by the animal (guinea pig) during a continuous registration period of 6 months. (7 refs.)
- 78389 On-line analysis of neuromuscular bioelectric potentials.** S.R.Quint (Dept. of Neurology, Univ. of North Carolina School of Medicine, Chapel Hill, NC, USA), J.F.Howard, Jr., L.Antoni. *Comput. Programs Biomed. (Netherlands)*, vol.16, no.1-2, p.3-12 (Feb.-April 1983).
 A computer system is presented which provides for on-line data capture and analysis of evoked end-plate potentials and action potentials, and on-line data capture with off-line analysis of spontaneously occurring miniature end-plate potentials at the end-plate region of the neuromuscular junction. Sampling of evoked waveforms begins after an adjustable delay following the stimulus. Spontaneously occurring waveforms are captured by 'freezing' the contents of a circular buffer. The software provides MENU selectable support functions including storage and retrieval of data and calculated parameters, analog and digital display of waveforms, data calibration and gain modification, data editing, file management, and hardcopy output. Calculated parameters of the waveform are optionally placed in a data base file by the analysis programs. The data base may be used for editing, arithmetic operations, and subsetting of variables as well as statistical analysis and plotting of any selected variables. (14 refs.)
- 78390 A fast method for arranging DNA sequence fragments.** G.Osterburg, K.H.Glatting, J.Buchert (German Cancer Res. Center, Inst. of Documentation, Information & Statistics, Heidelberg, Germany), J.Wolters. *Comput. Programs Biomed. (Netherlands)*, vol.16, no.1-2, p.61-9 (Feb.-April 1983).
 A method is described which allows efficient arrangement of DNA sequence fragments and, based on this arrangement, reconstruction of a complete DNA sequence. The concepts and algorithms used are based on the mathematical theory of graphs. The amount of human interaction required is considerably reduced compared to existing methods. An experiment with a set of 168 fragments yields a DNA sequence of about 5800 bases almost automatically. (4 refs.)
- 78391 Mechanical model of the insect eye.** R.T.Schneider (Dept. of Nuclear Engng. Sci., Univ. of Florida, Gainesville, FL, USA), J.F.Long. *Proc. SPIE Int. Soc. Opt. Eng. (USA)*, vol.359, p.139-49 (1983). (Applications of Digital Image Processing IV, San Diego, CA, USA, 24-27 Aug. 1982).
 Most optical instruments in use are modeled after the human eye. The design of insect eyes is fundamentally different and is governed by the laws of multiaperture optics. It can be shown that for certain applications, instruments using multiaperture optics are superior to single aperture instruments. For study of multiaperture optics and function of the insect eye a mechanical model resembling an insect eye was constructed. An individual eyelet of the

- mechanical model consists of a lens system and a detection system. The diameter of the front lens is 2 mm (7 mm f1), the aperture of the back lens is 1 mm (2 mm f1). Each eyelet has seven optical fibers which transport the incident light to individual detectors. The model has a total of 100 eyelets (700 detectors). Each detector is sequentially read by a multiplexer which is interfaced with a microcomputer, which displays the output on a video terminal. (10 refs.)
- 78392 Processing of noisy high resolution electron micrographs of crystalline biological membranes.** S.B.Luscher (Inst. für Kommunikationstechn., Zurich, Switzerland). *Proc. SPIE Int. Soc. Opt. Eng. (USA)*, vol.359, p.233-41 (1983). (Applications of Digital Image Processing IV, San Diego, CA, USA, 24-27 Aug. 1982).
 The problems associated with the interpretation of structure preserving low-dose electron micrographs have been solved for crystalline biological specimens by using specialized image processing routines. Fourier domain techniques are used to extract the periodic signal component. Hardly visible in the noisy unprocessed micrograph, the periodic structure becomes manifest by the discrete reflexions in the power spectrum. The different filtering methods and symmetrisation procedures have been applied to noisy, low contrast electron micrographs of crystalline sheets of various biological specimens. The increase in interpretability and reliability of structure determination is demonstrated at the different stages of processing. (7 refs.)
- 78393 Instrumentation for biomagnetism.** D.Duret (LETI, CEA, Grenoble, France), P.Karp. *Nuovo Cimento D (Italy)*, vol.2D, ser.1, no.2, p.123-41 (March-April 1983). (Proceedings of the Fourth International Workshop on Biomagnetism, Rome, Italy, 14-16 Sept. 1982).
 The instrumentation suitable for the acquisition of biomagnetic signals is reviewed. The basic magnetometer components, i.e. SQUIDs, flux transformers and dewars, are studied separately. Possible improvements to the present instrumentation as well as complete set-ups including ferromagnetic or eddy current shields are discussed and their efficiency evaluated. (57 refs.)
- 78394 First-gradient balancing of higher-order gradiometers [biomagnetism application].** J.Vrba, J.McCubbin (CTF Systems Inc., Port Coquitlam, BC, Canada). *Nuovo Cimento D (Italy)*, vol.2D, ser.1, no.2, p.142-52 (March-April 1983). (Proceedings of the Fourth International Workshop on Biomagnetism, Rome, Italy, 14-16 Sept. 1982).
 A formalism for the vector and tensor description of a balancing procedure is developed and a first-gradient and field-balancing method is outlined. The experimental apparatus and measurements of the first-gradient common-mode vector, C_{G1} , are discussed. (11 refs.)
- 78395 Measurement of biomagnetic fields using multichannel superconducting-magnetometer techniques.** M.Seppanen, T.Katila, T.Tuomisto, T.Varpula (Dept. of Tech. Phys., Helsinki Univ. of Technol., Espoo, Finland), D.Duret, P.Karp. *Nuovo Cimento D (Italy)*, vol.2D, ser.1, no.2, p.166-74 (March-April 1983). (Proceedings of the Fourth International Workshop on Biomagnetism, Rome, Italy, 14-16 Sept. 1982).
 The authors have constructed a three-channel differential SQUID magnetometer for the simultaneous measurement of the three orthogonal components of the magnetic field in the same location. The structure of the device is described and MCG data measured are shown. Interference effects between the channels are discussed. (10 refs.)
- 78396 An eddy-current-shielded room with a partially closed entrance [for biomagnetic measurements].** G.Stroink, C.Purcell, F.Brauer, B.Blackford (Dept. of Phys., Dalhousie Univ., Halifax, NS, Canada). *Nuovo Cimento D (Italy)*, vol.2D, ser.1, no.2, p.195-202 (March-April 1983). (Proceedings of the Fourth International Workshop on Biomagnetism, Rome, Italy, 14-16 Sept. 1982).
 It is shown that substantial improvements can be obtained in the shielding properties of an eddy-current-shielded room by covering the doorway with conductive plates. Results suggest that it is unnecessary to install a conductive door and show that it is worthwhile covering a small part of the doorway permanently. (6 refs.)
- 78397 Adaptive noise cancellation in neuromagnetic measurement systems.** J.S.Hansen, D.Bowser, H.Ko (Appl. Phys. Lab., Johns Hopkins Univ., Laurel, MD, USA), D.Brenner, F.Richer, J.Beatty. *Nuovo Cimento D (Italy)*, vol.2D, ser.1, no.2, p.203-13 (March-April 1983). (Proceedings of the Fourth International Workshop on Biomagnetism, Rome, Italy, 14-16 Sept. 1982).
 The noise spectrum of a superconducting second-derivative gradiometer has been investigated in an urban environment. Data have been acquired from the gradiometer with three orthogonal accelerometers and a triaxial fluxgate magnetometer attached to the dewar. These data have been analysed by using signal processing techniques, primarily an adaptive noise canceller, to reduce noise in the gradiometer data. Results shown here indicate that the environmental noise and/or the dewar motion noise can be reduced as much as 40 dB in noise power. It is also shown, in the case of poor signal-to-noise ratio ($S/N \sim 1$), that a 10 Hz sine wave can be extracted. This technique not only shows promise for noise reduction, but also aids in the identification of noise signals which might be misconstrued as part of the evoked response. Analysis of data containing evoked responses is now underway. (4 refs.)
- 78398 Alternatives to the SQUID magnetometer for some biomagnetic measurements.** Z.Trontelj, J.Luznik, J.Pirnart (Dept. of Phys., Univ. E. Kardeelj of Ljubljana, Ljubljana, Yugoslavia). *Nuovo Cimento D (Italy)*, vol.2D, ser.1, no.2, p.214-23 (March-April 1983). (Proceedings of the Fourth International Workshop on Biomagnetism, Rome, Italy, 14-16 Sept. 1982).
 Flux gate and resonance type of magnetometers (free precession, optically pumped), which can in some cases replace the SQUID magnetometer, are discussed. The principles of operation, sensitivity, dynamical range and frequency response are described. The application of these magnetometers for biomagnetic measurements is mentioned. (19 refs.)
- 78399 A portable biomagnetic measuring system.** V.L.Vvedensky, S.P.Naurzakov, V.I.Ozhogin, S.Yu.Shabanov (Kurchatov Inst. of Atomic Energy, Moscow, USSR). *Nuovo Cimento D (Italy)*, vol.2D, ser.1, no.2, p.224-30 (March-April 1983). (Proceedings of the Fourth International Workshop on Biomagnetism, Rome, Italy, 14-16 Sept. 1982).
 The instrumentation for biomagnetic applications is described. The small size and weight of the SQUID gradiometer permit easy transport and positioning of the instrument, thus making biomagnetic measurements possible in any noise-free location. The equipment is provided with a battery power supply, and, when filled with 60 cm³ of liquid helium, will operate continuously for 6 h. The device is suitable for magnetocardiography. (3 refs.)

78400 The use of time domain dielectric spectroscopy to characterize the progress of wound repair. F.X.Hart (Dept. of Phys., Univ. of the South, Sewanee, TN, USA). *J. Bioelectr. (USA)*, vol.1, no.3, p.313-28 (1982).
The electrical properties of wounded plant tissue are observed to change during the course of healing. Such changes could serve as an objective measure of the progress of repair. Time domain dielectric spectroscopy is used to rapidly measure these properties. Under microprocessor control a voltage step is applied to a stem and the resulting current-time characteristic sampled. Fourier Transformation yields the variation of stem conductance and capacitance with frequency. (5 refs.)

78401 Peak-shape analysis for protein neutron crystallography with position-sensitive detectors. B.P.Schoenborn (Biology Dept., Brookhaven Nat. Lab., Upton, Long Island, NY, USA). *Acta Crystallogr. Sect. A (Denmark)*, vol.A39, pt.3, p.315-21 (1 May 1983).
In neutron protein crystallography, the use of position-sensitive detectors controlled by a modern data acquisition system permits new approaches to data collection strategies. Instead of dealing with conventional scans, like the θ - 2θ scan, that provide an integrated intensity as a function of a rotational parameter, the computer-linked counter can be used to produce a three-dimensional reflection profile. As the crystal steps ($\Delta\omega$) through a reflection, the observed data for each step are stored in an external memory as a function of extent in 2θ and height (y) of a reflection. In this space, the reflection will be a three-dimensional distribution with dimensions determined by such basic geometrical conditions as $\Delta\lambda$, crystal size, mosaic spread, counter-resolution, and beam-collimation parameters. Knowledge of the interaction of these basic parameters will allow the design of optimal beam optics and will permit the delineation of the reflection from the background and permit, therefore, an accurate intensity determination. (21 refs.)

78402 Characterization of the solid components of biological tissues by cross-polarization, magic angle NMR spectrometry. C.E.Brown (Dept. of Biochem., Medical Coll. of Wisconsin, Milwaukee, WI, USA), C.A.Wilkie. *CRC Crit. Rev. Biomed. Eng. (USA)*, vol.9, no.1, p.1-38 (1983).
A biological tissue is composed of cytosol, which can be investigated by high resolution nuclear magnetic resonance (NMR) spectroscopy, and membrane and particulate components, which yield NMR spectra similar to those of solids. In this review, the theoretical and technical requirements of recording NMR spectra of solids with cross polarization and magic angle sample spinning techniques are compared with the physical characteristics of the solid components of biological tissues. Current applications of cross-polarization, magic angle NMR spectroscopy to the investigation of membranes, mineral deposits and biosynthetic pathways are presented and discussed in terms of the biomedical questions to which this technique might be applied. (277 refs.)

78403 Multichannel microelectrode for recording neural activity. J.J.Cuomo, W.W.Molzen, J.L.Speidel (IBM Corp., Armonk, NY, USA). *IBM Tech. Disclosure Bull. (USA)*, vol.25, no.11A, p.5588-97 (April 1983).
Relates generally to apparatus for recording electrophysiological data and more particularly to a multichannel microelectrode for recording neural activity. The microelectrode contains an array of recording sites connected via transmission lines to output pad circuits. (no refs.)

78404 Combining accurate defocus with low-dose imaging in high resolution electron microscopy of biological material. N.G.Wrigley, E.Brown, R.K.Chillingworth (Nat. Inst. for Medical Res., London, England). *J. Microsc. (GB)*, vol.130, pt.2, p.225-32 (May 1983). (MICRO 82: High Resolution Electron Microscopy, London, England, 12-16 July 1982).
High resolution (<2 nm) electron microscopy of biological specimens requires three exacting conditions to be met simultaneously: (a) fine specimen detail must be protected from destruction by the electron beam (low dose), (b) the electron optics must be adjusted to be capable of imaging that detail interpretably (accurate defocus), and (c) a suitable field of interest must be identified. The authors describe a method encompassing all three with an 80% success rate using only minor modifications to a transmission electron microscope, and no expensive on-line computing. (17 refs.)

78405 Determination of radium-226 in urine. G.H.Kramer, P.C.Beaulieu. *Report AECL-7979*, Atomic Energy Canada Ltd., Chalk River, Ont. (March 1983), 14 pp.
The method for determining radium-226 in urine that is currently being used by the Bioassay Laboratory has been tested and documented. Radium-226 is coprecipitated from urine by alkaline calcium phosphate. This precipitate is redissolved in hydrochloric acid and the radium purified by cation exchange. Radium is collected by a barium sulphate coprecipitation and then estimated by alpha counting. The method has been tested using radium-226 and cross-contamination studies were performed using Am-241, Pu-239, Np-237, Th-Nat and U-233. With the exception of Am-241, cross-contaminations were found to be negligible. The method gives an overall chemical recovery of $80 \pm 5\%$ and the detection limit is estimated to be 0.39 mBq-counting time, 71 h; background, 0.05 counts per minute (cpm). (22 refs.)

78406 Biomedical applications of MWPC's for digital imaging of soft β emitters. R.Bellazzini, A.Del Guerra, M.M.Massai, G.Spandre. *Report INFN/TC-83/6*, Ist. Naz. Fis. Nucl., Pisa, Italy (24 Feb. 1983), 6 pp.
The authors have built an experimental facility equipped with MultiWire Proportional Chambers (MWPC) and a PDP 11/23 mini-computer for the digital imaging of two-dimensional ^3H distributions in biological and medical applications. A spatial resolution of ~ 1.5 mm (FWHM), a sensitivity of 10^{-1} Bq/cm 2 , and an efficiency of $\sim 10\%$ with a uniformity of 4% have been measured with a MWPC working at atmospheric pressure with 2 mm anode pitch and cathode coupled delay line read-out. A second chamber with 1 mm anode pitch at 45° with respect to the cathode wires has been operated at 2 atm. In this case a spatial resolution of ~ 800 μm (FWHM) for ^3H sources has been measured along both directions. The authors present images for the identification of human clones with defective repair of UV-induced damage, and for the study of regional carbohydrate consumption in myocardial tissue. (6 refs.)

78407 Contact microscopy of biological specimens using synchrotron radiation. P.C.Cheng (Dept. of Anatomy, Univ. of Illinois, Medical Center, Chicago, IL, USA), R.J.Howe, J.W.McGowan, D.M.Shinozaki. *Fifteenth Annual Synchrotron Radiation Users Group Conference* (papers in summary form only received), Stoughton, WI, USA, 18-19 Oct. 1982 (Stoughton, WI, USA: Synchrotron Radiat. Center 1982), p.12
Attempts were made to produce contact microscopic images of biological specimens on PMMA X-ray resist with synchrotron radiation. *Xenopus laevis* embryo cells were cultured in Formvar coated (1500 Å) gold grid grids, fixed in 1% glutaraldehyde; dehydrated in ethanol and critical point dried in CO $_2$. The grids are then placed in intimate contact with PMMA (polymethylmethacrylate; 0.6 μm or 2 μm) resist (either supported by a Si $_3$ N $_4$ window or a silicon wafer). Exposures are made on Tantalus either with an Al filter 0-72 eV, below or above the phosphorous edge or with 130 eV (95.4 Å) and 140 eV (88.5 Å) monochromatic light. The exposures with Al filtered light are

15-60 minutes while the exposure with monochromatic light requires approximately 8 hours. Detailed biological structures such as nucleus, nucleolus, stress fiber, yolk granulus, mitochondria can be clearly visible. Microchemical analysis of phosphorus is in progress. (no refs.)

78408 A fiber optics fluorimeter for algae detection and mapping. T.Lund. *First International Conference on Optical Fibre Sensors*, London, England, 26-28 April 1983 (London, England: IEE 1983), p.190-4
Optical fiber bundles provide a very versatile means for in situ fluorescence studies of natural water. The technique is also applicable to other in situ natural targets, like vegetation, and it may further prove useful in a variety of general industrial measurement tasks. The completely passive sensor head can, with proper choice of optical fibers, withstand excessive pressures and temperatures. Furthermore, monitoring of elastic scattering, attenuation and environmental light should require only minor modifications to the sensor head. The fiber bundle approach also allows for use of a number of source/receiver combinations. In particular, use of a low power HeNe laser to monitor blue-green algae, which is of increasing importance in lake eutrophication, seems a promising example. (7 refs.)

Magnetic sensors with good signal-to-interference discrimination [biomagnetism application] See Entry 74497

Optimisation of the second-order gradiometer base length that has been designed for the measurement of weak inhomogeneous magnetic fields [biomagnetism application] See Entry 74498

Lateral inverse filtering of ultrasonic B-scan images See Entry 75866

A new wire phantom for accurate measurement of acoustic resolution See Entry 75887

Annular arrays for quantitative pulsed Doppler ultrasonic flowmeters See Entry 76138

Immunoelectrophoretic study of the effect of radiation on protein mixtures See Entry 78268

Biological signals processing: an application to ultrasonic echo signals sounding See Entry 78275

87.90 OTHER TOPICS IN BIOPHYSICS, MEDICAL PHYSICS, AND BIOMEDICAL ENGINEERING

78409 Health risks from electricity generation. B.L.Cohen (Univ. of Pittsburgh, Pittsburgh, PA, USA). *Comments Mol. & Cell. Biophys. Comments Mod. Biol. Part A (GB)*, vol.2, no.1, p.1-15 (April 1983).
According to the author's analysis, nuclear electricity has far milder health effects than coal burning or photovoltaic technologies. On a short term basis, the 25 deaths/GWe-yr from coal burning greatly exceeds the 0.12 from nuclear, or even the 2.5 claimed by antinuclear activists. For photovoltaics, the 3% of coal burning predicts 0.8 deaths/GWe-yr, still many times larger than the government estimates for nuclear. On a long term basis, the deaths from both coal and photovoltaics greatly exceed those from nuclear high level waste, not to mention the very large life saving contribution from mining uranium, 3000 times the effects of high level waste. (20 refs.)

90.00 GEOPHYSICS, ASTRONOMY AND ASTROPHYSICS

91.00 SOLID EARTH GEOPHYSICS

78410 Evolution of the Earth-Moon system. B.Czapiewska, M.Bielicki (Obs. Astron., Uniwersytetu Warszawskiego, Warsaw, Poland). *Postępy Astron. (Poland)*, vol.30, no.3-4, p.239-58 (July-Dec. 1982). In Polish. [received: April 1983]
Observations concerning the time-scale of the orbital evolution of the Earth-Moon system are presented. The results obtained with different methods are compared. The most probable value characterizing this evolution—the Moon's acceleration—is $16''/\text{century}^2$, which corresponds to increasing the Moon's distance at 2.3 cm/year. It is shown that the results obtained from archaic corals are reliable. (9 refs.)

Transits of Earth as seen from Mars See Entry 78797

91.10 GEODESY AND GRAVITY
(for relations of gravity observations to tectonics and isostasy, see 91.45 Physics of plate tectonics)

78411 A numerical study of the divergence of spherical harmonic series of the gravity and height anomalies at the Earth's surface. C.Jekeli (Air Force Geophys. Lab., Hanscom AFB, Bedford, MA, USA). *Bull. Geod. (France)*, vol.57, no.1, p.10-28 (1983).
The problem of the divergence of the geopotential spherical harmonic series at the Earth's surface is investigated from a numerical, rather than a theoretical, approach. A representative model of the Earth's potential is devised on the basis of a density layer, which, in the spherical approximation, generates a gravity field whose harmonic constituents decay according to an accepted degree variance model. This field, expanded to degree 300, and a topographic surface specified to a corresponding resolution of 67 km are used to compute the differences between truncated inner and outer series of the gravity and height anomalies at the surface of the Earth model. (18 refs.)

78412 Effects of adopting new precession, nutation and equinox corrections on the terrestrial reference frame. S.-Y.Zhu, I.I.Mueller (Dept. of Geodetic Sci. & Surveying, Ohio State Univ., Columbus, OH, USA). *Bull. Geod. (France)*, vol.57, no.1, p.29-42 (1983).
The effect on polar motion is a diurnal periodic term with an amplitude increasing linearly in time; on UT1 it is a linear term. The effects of small rotations (such as precession, nutation or equinox corrections) of the frame of a Conventional Inertial Reference System (CIS) on the frame of the Conventional Terrestrial Reference System (CTS) are given. Seven CTS options are

presented, one of which is necessary to accommodate such rotations (corrections). The last of these options requiring no changes in the origin of terrestrial longitudes and in UT1 is advocated; this option would be maintained by eventually referencing the Greenwich Mean Sidereal Time to a fixed point on the equator, instead of to the mean equinox of data, the current practice. Accommodating possible future changes in the astronomical nutation is discussed. The Appendix deals with the effects of differences which may exist between the various CTSs and CISs (inherent in the various observational techniques) on Earth rotation parameters (ERP) and how these differences can be determined. (10 refs.)

78413 Sparse matrix algorithms applied to DEM generation. W.Stark (Univ. Stuttgart, Stuttgart, Germany), F.Steidler. *Bull. Geod. (France)*, vol.57, no.1, p.43-61 (1983). A method for generating a digital elevation model (DEM) was suggested by Ebner (1979). The heights of grid points are interpolated from arbitrarily distributed reference points using the finite element method. The requested grid heights of the DEM are defined as unknowns and estimated from the available reference points and a general curvature minimization of the interpolation surface with filtering at the reference points. This problem can be interpreted as an adjustment of indirect observations and can be solved using the least squares method. This leads to a banded structured system of normal equations in case of numbering the unknowns in a row-wise order. This ordering may not be the best strategy for the solution of the normal equations, because the band contains many zero elements. Therefore algorithms which exploit the nonzero/zero structure to better advantage have been applied in combination with the pivot strategies of 'Nested Dissection' and 'Minimum Degree Ordering' (OPTORD). The operational characteristics of these algorithms are compared with those of the band-algorithm for several DEM problems that vary in size to over 4000 unknowns. (16 refs.)

78414 Gravity anomalies, seismic structure and geothermal history of the central Alps. E.Kissling, St.Mueller, D.Werner (Inst. fur Geophys., ETH-Honggerberg, Zurich, Switzerland). *Ann. Geophys. (France)*, vol.1, no.1, p.37-46 (Jan.-Feb. 1983). A new interpretation of the gravity anomalies in the Swiss Alps from the geothermal point of view is presented. The regional gravity distribution is partly caused by the topography of the crust-mantle boundary. Taking 0.5 g/cm^3 as the average density contrast between crust and mantle the Bouguer map of Switzerland contains a residual field which indicates a density anomaly in the mantle. This finding, results from seismic surface-wave investigations, and P -wave travel time observations can be interpreted as a consequence of the genesis of the Alps. A kinematic model of the Alps is constructed simulating the mass displacements during the last 40 m.y. In this two-dimensional model the subsidence of cold mantle material is taken into consideration forming a 'lithospheric roof'. Based on this kinematic model the temperature distribution in the moving medium can be calculated, taking into account the radiogenic heat sources. From the calculated temperature field at present time the thermally induced density deviation can be determined. (34 refs.)

78415 Tidal friction in historical time and in the remote past. B.Jeffreys (Girton Coll., Cambridge, England). *Geophys. J. R. Astron. Soc. (GB)*, vol.73, no.3, p.765-8 (June 1983). Comments on Jeffreys's (1982) extension of his treatment of tidal friction in historical time. Amendments are presented of the theory given in *The Earth* (Jeffreys, 1970, 1976) concerning the Moon's orbit and the Earth's rotation in the remote past. (11 refs.)

78416 Stokes's theorem for the case of many isolated bodies. M.A.Aleksidze (Inst. of Geophys., Acad. of Sci., Georgian SSR). *Izv. Acad. Sci. USSR. Phys. Solid Earth (USA)*, vol.18, no.2 (1982). Translation of: *Izv. Akad. Nauk SSSR Fiz. Zemli*, vol.18, no.2, p.111-18 (1982). Examines problems of the determination of the external potential for many isolated bodies when the total masses of the bodies and, with an accuracy up to arbitrary terms, the potential on the closed surfaces, are given rather than the density distribution within the bodies. (9 refs.)

78417 Solution of inverse gravimetric problems for several contact surfaces. V.I.Starostenko, A.N.Zavorot'ko (S.I. Subbotin Inst. of Geophys., Acad. of Sci., Ukrainian SSR). *Izv. Acad. Sci. USSR. Phys. Solid Earth (USA)*, vol.18, no.3, p.196-206 (1982). Translation of: *Izv. Akad. Nauk SSSR Fiz. Zemli*, vol.18, no.3 (1982).

Statements of inverse linear and nonlinear gravimetric problems are given for a number of contact surfaces. In the solution of linear problems, excessive densities of layers situated between known contact surfaces are determined. The solution of nonlinear problems makes it possible to reconstruct the position of several contacts if the layer densities are known, as well as the position of the upper (or lower) contact. Algorithms by Tikhonov (1979) for refining the solution are presented, with particular attention given to the nonlinear case. The efficiency of the methods of solution used are illustrated by examples. (20 refs.)

78418 Direct integration of Stokes' undulation and Vening Meinesz's deflection equations for geographically defined gravity anomaly blocks. G.Obenson (Univ. of Lagos, Lagos, Nigeria). *J. Geophys. Res. (USA)*, vol.88, no.B1, p.665-8 (10 Jan. 1983). [received: May 1983]

Gives a direct solution of this problem by converting, in an indirect way, the relevant integral equations over each block to their equivalent line integrals taken along and around the boundary curves of the block. Results of sample computations given clearly demonstrate the convergence and stability of these line integrals. Geoidal parameters due to a $30^\circ \times 30^\circ$ inner zone alone at 71 grid locations in Cameroon are calculated using $1^\circ \times 1^\circ$ anomalies and integration steps of 30° for the four innermost blocks and 180° for the rest of the blocks and compared these with equivalent values from the midpoint method. (5 refs.)

78419 Global postseismic deformation in a stratified viscoelastic Earth: effects on Chandler wobble excitation. M.Dragoni, D.A.Yuen (Dept. of Geology, Arizona State Univ., Tempe, AZ, USA), E.Boschi. *J. Geophys. Res. (USA)*, vol.88, no.B3, p.2240-50 (10 March 1983). The principle purpose of this paper is to examine whether movement of matter in a stratified viscoelastic Earth can enhance the excitation of the Chandler wobble. A two-layer model consisting of an elastic lithosphere overlying a Maxwell viscoelastic mantle is constructed in order to calculate explicitly the temporal evolution of the inertia tensor from earthquake faulting. It is found that the ability of the viscoelastic flows to produce an additional increment of the inertia tensor depends critically on R , the ratio of the inner radius to the outer radius. Only for $R \geq 0.7$ is there a substantial increase. For the Earth ($R \approx 0.98$) an amplification of between four and six is obtained from the models considered. However, the time scales over which this enhancement of the moment of inertia takes place is about 10 Maxwell times, thus making this model unlikely to excite the Chandler wobble for values of the mantle viscosity derived from postglacial uplifts. (28 refs.)

78420 Tidal gravity parameters at Brussels reconfirmed by a superconducting gravity meter. B.Ducarme (Obs. Royal de Belgique, Brussels, Belgium). *Phys. Earth & Planet. Inter. (Netherlands)*, vol.32, no.1, p.2-3 (April 1983). The results of the Trans World tidal gravity profiles (67 stations established in Asia, South Pacific and East Africa) are based upon instrumental constants determined at Brussels as the fundamental station. A superconducting gravimeter operating at Brussels for only two months fully reconfirms the instrumental constants related to the instrumental phase lags. (6 refs.)

Hotspot-spin axis motion or magnetic far-sided effect? See Entry 78436

Thermal parameters of the oceanic lithosphere estimated from geoid height data See Entry 78491

The relationship between surface topography, gravity anomalies, and temperature structure of convection See Entry 78509

Tectonophysical zoning of the juncture of the Aldan Shield and the Stanovoi Highlands according to geodesic measurements See Entry 78514

Applications of an orbiting gravity gradiometer See Entry 78655

A technique for reducing low-frequency, time-dependent errors present in network-type surveys See Entry 78692

Optical tracking of synchronous Earth's satellites for geophysical purposes See Entry 78693

Use of residual gravity anomalies to estimate the scale of ore fields See Entry 78712

Anomalous bulk viscosity of two-phase fluids and implications for planetary interiors See Entry 78834

91.25 GEOMAGNETISM AND PALAEOMAGNETISM; GEOELECTRICITY

78421 Existence and interpretation of an electrically conducting zone within the plateau basalts of Kerguelen Islands (TAAF). R.Ballestracci (UER Sci. et Tech., Univ. Toulon, La Garde, France), J.Nougier, Y.Benderitter. *C.R. Seances Acad. Sci. Ser. II (France)*, vol.296, no.11, p.833-8 (21 March 1983). In French.

A reconnaissance field-trip by audiomagnetotelluric profiles has been carried out on Kerguelen Islands (Terres australes et antarctiques francaises) where historic eruptions and hydrothermal post-volcanic phenomena are recorded. Data processing of profiles made over the plateau basalts pillings are specified. They show a conducting level parallel to the topographic surface and located between 500 and 700 m deep with a thickness over 300 m. Critical analysis of this anomaly favors a hydrothermic system of convection type. The upper conducting limit should be the highly ionised interface between downward meteoritic waters and thermic gradients, the temperature being relatively low. The example of hot springs is analysed as characteristic of a system drained by an open fracture and a fast water transit. (14 refs.)

78422 Difference in autocorrelation functions of AA-indices for the northern and southern hemispheres. E.M.Apostolov (Geophys. Inst., Bulgarian Acad. of Sci., Sofia, Bulgaria). *C.R. Acad. Bulg. Sci. (Bulgaria)*, vol.36, no.1, p.77-9 (1983).

The average monthly values of the aa-indices for the series N and S for the 1968-1979 period were used to analyse the degree of dependence between the values of each time series and then to compare them. (1 ref.)

78423 A palaeomagnetic reconnaissance of Kashmir, northwestern Himalaya, India. C.T.Klootwijk (Res. School of Earth Sci., Australian Nat. Univ., Canberra, Australia), S.K.Shah, J.Gergan, M.Lal Sharma, B.Tirkey, B.K.Gupta. *Earth & Planet. Sci. Lett. (Netherlands)*, vol.63, no.2, p.305-24 (May 1983).

Thermal demagnetization studies of 800 Palaeozoic and Lower Mesozoic samples, mainly carbonates, from 14 localities in Kashmir, showed four magnetic components: (A) A recent field component of normal polarity and large intensity. (B) A Middle to Late Tertiary secondary component of large intensity and of reversed and normal polarity, which indicates clockwise tectonic rotation of central and eastern Kashmir. (C) Primary magnetic components of Triassic, Late Permian, Early Carboniferous, Siluro-Ordovician and Middle to Early Ordovician age. The Triassic and Late Permian components show a $20\text{--}30^\circ$ cumulative counterclockwise offset with respect to the Indo-Pakistan apparent polar wander path. (D) A component of low inclination and predominantly east-west declination, which is observed only in rocks of pre-Panjal Traps age. A secondary origin associated with extrusion of the Panjal Traps flows is surmised. The Triassic and Late Permian primary component directions are predominantly of normal polarity. This suggests a pre-Punjabian (Late Permian) upper age limit for the Permo-Carboniferous (Kiaman) reversed polarity interval. (44 refs.)

78424 Palaeomagnetism of red beds of Early Devonian age from Central Iran. H.Wensink (Dept. of Structural Geology, Utrecht State Univ., Utrecht, Netherlands).

Earth & Planet. Sci. Lett. (Netherlands), vol.63, no.2, p.325-34 (May 1983). Palaeomagnetic results are reported from 13 sites of red beds of Early Devonian age from Central Iran. Detailed palaeomagnetic analyses were carried out. Two types of partial progressive demagnetization were applied, one using alternating magnetic fields, the other heating. These procedures resulted in the detection of the characteristic remanences with a mean direction with $D=24.2^\circ$, $I=1.3^\circ$ ($\alpha_{95}=10.1^\circ$). The palaeomagnetic pole is located at 51.3°N , 163.7°W . If one shifts the Iranian landmass to its most likely position in the Gondwana configuration, then the position of the palaeomagnetic pole coincides with the alternative polar wander path which crossed South America in early Middle Paleozoic times. (23 refs.)

78425 Geomagnetic field analysis. I. Stochastic inversion. D.Gubbins (Bullard Labs., Univ. of Cambridge, Cambridge, England).

Geophys. J. R. Astron. Soc. (GB), vol.73, no.3, p.641-52 (June 1983). Most of the Earth's magnetic field and its secular change originate in the core. Provided the mantle can be treated as an electric insulator, stochastic inversion enables surface observations to be analysed for the core field. A priori information about the variation of the field at the core boundary leads to very stringent conditions at the Earth's surface. The field models are identical with those derived from the method of harmonic splines (Shure, Parker and Backus, 1982) provided the a priori information is specified appropriately. The method is applied to secular variation data from 106 magnetic observatories. The hypothesis that magnetic fields are frozen to the core fluid implies that certain integrals of the secular variation vanish. This idea is tested by computing the integrals and their standard and maximum errors. (18 refs.)

78426 The spatial scale of correlation of the day-to-day variability of S_q . D.M.Schlapp, R.J.Mann (Phys. Dept., Univ. of Exeter, Exeter, England). *Geophys. J. R. Astron. Soc. (GB)*, vol.73, no.3, p.671-3 (June 1983). It is confirmed that even when disturbance variations are taken into account, the spatial scale of day-to-day variability of S_q is local, that is, of the order of one or two thousand kilometres, rather than globally correlated. (5 refs.)

78427 Use of the frozen flux approximation in the interpretation of archaeomagnetic and palaeomagnetic data. D.Gubbins (Bullard Labs., Univ. of Cambridge, Cambridge, England), N.Roberts. *Geophys. J. R. Astron. Soc. (GB)*, vol.73, no.3, p.675-87 (June 1983). The frozen flux approximation of Roberts and Scott (1965) is a constraint on the core field that can be used to aid interpretation of the very sparse datasets that palaeomagnetism and archaeomagnetism provide. It gives bounds on the size of the components of the magnetic field at a point of the Gauss coefficients, and, if valid over such long time periods, limits the shape of the field during transitions between normal and reversed polarities. The maximum intensity at a point consistent with the present flux is 281 μT or 4 times the maximum field observed today. The present dipole is about 50 per cent of its upper bound. Polarity reversal is impossible if the transition field is purely axisymmetric. None of the measurements considered violate the frozen flux approximation. (23 refs.)

78428 Lower Jurassic magnetostratigraphy at the Breggia Gorge (Ticino, Switzerland) and Alpe Turati (Como, Italy). F.Horner, F.Heller (Inst. fur Geophys., ETH-Honggerberg, Zurich, Switzerland). *Geophys. J. R. Astron. Soc. (GB)*, vol.73, no.3, p.705-18 (June 1983). The Breggia gorge (Ticino, Switzerland) provides a continuous outcrop of Mesozoic limestones covering the time between the Lower Jurassic and Upper Cretaceous. The Jurassic section from the Lower Pliensbachian to Aalenian is well dated by ammonites. The limestones of these stages are a good quality recorder of the polarity of the geomagnetic field during this time interval. More than 500 cores have been drilled along a 120 m thick section with a median distance between cores of about 20 cm. Detailed thermal and AF demagnetization and further rock magnetic studies are used to determine the characteristic NRM direction for each sample. Initial NRM intensities and low field susceptibilities reflect variations in oxidation potential and sedimentation rate during carbonate deposition. (36 refs.)

78429 Distorting effects during electromagnetic sounding of horizontally non-uniform media using an artificial field source. A.N.Kuznetsov (All Union Sci. Res. Inst. of Geophys. Methods of Exploration, USSR). *Izv. Acad. Sci. USSR. Phys. Solid Earth (USA)*, vol.18, no.2 (1982). Translation of: *Izv. Akad. Nauk SSSR Fiz. Zemli*, vol.18, no.2, p.130-7 (1982). Specific behavior of different field components of an electrosounding instrument in a horizontally non-uniform medium is studied. Distortions of the electromagnetic field are classified. (5 refs.)

78430 Late Precambrian Keweenaw asymmetric polarities as analyzed by axial offset dipole geomagnetic models. H.Nevanlinna (Dept. of Geophys., Univ. of Helsinki, Helsinki, Finland), L.J.Pesonen. *J. Geophys. Res. (USA)*, vol.88, no.B1, p.645-58 (10 Jan. 1983). [received: May 1983] The Great Logan Paleomagnetic Loop has been interpreted to be a paleomagnetic signature of the North American plate motion during the Keweenaw igneous activity (1200-1000 Ma). However, the presence of three successive asymmetric polarities, along with new geochemical data from the Mamaine Point area, makes this interpretation untenable. A new interpretation is presented according to which the asymmetric polarities represent long-term zonal nondipole geomagnetic field components. Wilson's single-dipole offset model can in general explain the inclination asymmetries, but it yields intensity ratios (reversed/normal) significantly lower than those observed. A coaxial two-dipole model is proposed that better takes into account the observed intensity data. This model consists of a geocentric dipole and an offset dipole located at the core-mantle boundary. A new interpretation for the evolution of the Logan Loop is described according to which at least 50% of the hairpin-shaped loop is produced by oscillation of the dipole strength ratio. Apparent polar wander (APW) is still evident, but the shape of the loop and the APW speed along the loop is reduced. (44 refs.)

78431 Geomagnetic spherical harmonic analyses. I. Techniques. D.R.Schmitz (Colorado School of Mines, Golden, CO, USA), J.C.Cain. *J. Geophys. Res. (USA)*, vol.88, no.B2, p.1222-8 (10 Feb. 1983). Improved techniques for direct least squares analysis of the main geomagnetic field are introduced and tested with simulated data. One improvement involves adding secular change data to the least squares analysis (as well as the usual spatial data). As a result, the secular variation (SV), as observed at fixed magnetic observatories and repeat stations, directly adjusts the SV terms of the spherical harmonic coefficients, while spatial data adjust both the spatial and SV terms. Simulations show that SV errors can be reduced by factors of 2 or 3 by introducing SV as data. The second refinement involved obtaining uncorrelated spherical harmonic coefficient sets through employment of a uniform distribution of data by area or by a compromise of an area-weighting scheme. The latter was shown to reduce high cross correlations between spherical harmonic coefficients by up to a factor of 3 in simulated tests. (14 refs.)

78432 Core and crustal geomagnetic fields. L.R.Aldredge (US Geological Survey, Denver, CO, USA). *J. Geophys. Res. (USA)*, vol.88, no.B2, p.1229-34 (10 Feb. 1983). The spherical harmonic content of fields from core sources and that from extended crustal sources overlap so much that very long wavelength anomalies obtained by subtracting a core field model up to only degree 10 from the observations will be distorted so badly that interpretation in terms of geological sources will be difficult. (10 refs.)

78433 Statistical averaging of marine magnetic anomalies and the aging of oceanic crust. R.J.Blakely (US Geological Survey, Menlo Park, CA, USA). *J. Geophys. Res. (USA)*, vol.88, no.B3, p.2289-96 (10 March 1983). Visual comparison of Mesozoic and Cenozoic magnetic anomalies in the North Pacific suggests that older anomalies contain less short-wavelength information than younger anomalies in this area. To test this observation, magnetic profiles from the North Pacific are examined from crust of three ages: 0-2.1, 29.3-33.1, and 64.9-70.3 my BP. The results are interpreted using a multilayer model for marine magnetic anomalies in which the upper layer, corresponding to pillow basalt of seismic layer 2A, acts as a source of noise to the magnetic anomalies. As the ocean crust ages, this noisy contribution by the pillow basalts becomes less significant to the anomalies. Consequently, magnetic sources below layer 2A must be faithful recorders of geomagnetic reversals. (36 refs.)

78434 High paleointensities of the geomagnetic field from thermomagnetic studies on rift valley pillow basalts from the Mid-Atlantic Ridge. M.Prevot, E.A.Mankinen, S.Gromme (US Geological Survey, Menlo Park, CA, USA), A.Lecailla. *J. Geophys. Res. (USA)*, vol.88, no.B3, p.2316-26 (10 March 1983). Nineteen pillow basalts dredged within the rift valley of the Mid-Atlantic Ridge at 36.8°N were studied by the Thellier stepwise heating method in order to determine the paleointensity of the geomagnetic field when they erupted on to the sea floor. Previously reported fission track ages are 2000 to 6000 years for the youngest rocks (mainly olivine basalts) and 10000 to 100000 years for the others (mainly plagioclase basalts and pyroxene basalts). The accuracy and validity of this method of paleointensity determination is discussed. The palaeo intensity results suggest that the latest eruptions on the inner floor of the Rift Valley at 36.8°N occurred 1500 \pm 1000 years ago. (55 refs.)

78435 Paleomagnetism of Carboniferous intrusions in North Carolina. C.Barton, L.Brown (Dept. of Geology & Geography, Univ. of Massachusetts, Amherst, MA, USA). *J. Geophys. Res. (USA)*, vol.88, no.B3, p.2327-35 (10 March 1983). Paleomagnetic samples of two late Paleozoic plutons were collected from the eastern Piedmont Province in North Carolina. Results from the early Carboniferous (326 \pm 27 m.y.) Lilesville pluton, located in the Carolina Slate Belt, indicate a pole position similar to that of the stable North American craton for the lower Carboniferous. The late Carboniferous Churchland pluton, located in the Charlotte Belt, gives a pole of 34°N, 126°E which correlates well with other North American poles for the late Carboniferous. Observations made by Kent and Opdyke (1978) on rocks from the eastern edge of the northern Appalachians suggest gross lateral displacement between the mid-Devonian and late Carboniferous in the late Paleozoic. This paleomagnetic information from the eastern Piedmont regions implies that the area of the Carolina Slate Belt and Charlotte Belt was associated with the North American platform for the entire Carboniferous period. (42 refs.)

78436 Hotspot-spin axis motion or magnetic far-sided effect? D.Epp, W.W.Sager, F.Theyer (Hawaii Inst. of Geophys., Univ. of Hawaii, Honolulu, HI, USA), S.R.Hammond. *Nature (GB)*, vol.303, no.5915, p.318-20 (26 May 1983). Paleomagnetic data from central Pacific sediments and from the Hawaiian-Emperor volcanic chain indicate that, during the Tertiary, either the derived magnetic pole was located alternately on the far and near side of the geographical pole, or that the hotspot coordinate systems (thought to be fixed relative to the Earth's mantle) oscillated relative to the Earth's spin axis. (23 refs.)

78437 Local contributions to the M_2 lunar geomagnetic variations in the south-west of England. A.M.Hart, C.D.Honebon, W.G.V.Rosser (Phys. Dept., Exeter Univ., Exeter, England). *Phys. Earth & Planet. Inter. (Netherlands)*, vol.32, no.1, p.60-4 (April 1983). By comparing the M_2 lunar geomagnetic variations of 12.42 h period at Sidmouth and Exeter, it is shown that local concentrations of the electric currents, induced by sea tides in the seas and oceans around the UK, can give a significant contribution to the M_2 variations at the two observatories. (4 refs.)

78438 Analogue model study of electromagnetic induction in the Newfoundland region. D.Hebert, H.W.Dosso, W.Nienaber (Dept. of Phys., Univ. of Victoria, Victoria, Canada), J.A.Wright. *Phys. Earth & Planet. Inter. (Netherlands)*, vol.32, no.1, p.65-84 (April 1983). The behaviour of magnetic field variations over the Newfoundland, Canada region is studied using a scaled laboratory analogue model. The model source frequencies used simulate periods of 100 s, 300 s, 900 s, and 1800 s. Large anomalous in-phase and quadrature model magnetic fields are observed over the Strait of Belle Isle and Cabot Strait. The 'cape effect', that is, the large field enhancements due to deflection of induced current at capes, is observed for all four periods. The magnitudes and directions of inter-station induction arrows and single station induction arrows are studied. The coastal effects would not produce serious perturbations to the field measured over crustal anomalies within the central regions of Newfoundland. (23 refs.)

78439 Paleomagnetism of some Precambrian rocks in south-east Greenland. G.E.J.Beckmann (School of Phys., Newcastle upon Tyne Univ., Newcastle upon Tyne, England). *Phys. Earth & Planet. Inter. (Netherlands)*, vol.32, no.1, p.85-99 (April 1983). A palaeomagnetic pole is established at 25.1°N 273.9°E ($dp=10.6^\circ$, $dm=14.3^\circ$) from the norite-charnockite complex at Angmagssalik, emplaced at 1800 Ma. A somewhat older palaeomagnetic pole at 4.2°S 246.7°E ($dp=4.2^\circ$, $dm=8.3^\circ$) is obtained from Archaean gneisses close to the northern boundary of the Nagssugtoqidian mobile belt where reversals of magnetization are present. Both magnetizations were imposed during slow cooling following the Nagssugtoqidian metamorphism. (28 refs.)

78440 The electromagnetic field of S_q variations. V.V.Aksenov (Sci. Res. Inst. of Systems, Novosibirsk, USSR). *Sov. Geol. & Geophys. (USA)*, vol.23, no.3, p.80-4 (1982). Translation of: *Geol. & Geofiz. (USSR)*, vol.23, no.3, p.90-6 (1982). Discusses the problem of the structure and composition of the electromagnetic field of S_q variations. It is shown that it consists of two types of fields: magnetic and electrical. Their tensions in magnetic components are comparable, but in the electrical components the electrical field is significantly greater. (9 refs.)

Electromagnetic field of an oscillating point dipole in the presence of spherical interfaces See Entry 75565

Model heat flow and [magnetotellurics] for the San Andreas and oceanic transform faults See Entry 78478

A detailed study of the Cobb Offset of the Juan de Fuca Ridge: evolution of a propagating rift See Entry 78512

TRM, ARM and Isr of two natural magnetites of MD and PSD grain size See Entry 78524

Microcrack connectivity in rocks: a renormalization group approach to the critical phenomena of conduction and failure in crystalline rocks See Entry 78528

Electrical conductivity of molten basalt and andesite to 25 kilobars pressure: geophysical significance and implications for charge transport and melt structure See Entry 78535

A comparison of time and frequency domain geomagnetic sounding See Entry 78688

Dielectric logging with downhole invasion effects See Entry 78689

Magnetic polarity stratigraphy: stochastic properties of data, sampling problems, and the evaluation of interpretations See Entry 78694

- Direct inversion of one-dimensional magnetotelluric data See Entry 78695
 Radial characteristics of focusing probes of magnetoelectric logging See Entry 78711
 On the theory of the three-element probe in electromagnetic wave logging See Entry 78715
 Circumvention of Parker's bound on galactic magnetic monopoles See Entry 78807

91.30 SEISMOLOGY

- 78441 High frequency radiation from dynamic earthquake fault models.** R. Madariaga (Dept. de Sci. de la Terre, Univ. Paris VII, Paris, France). *Ann. Geophys. (France)*, vol.1, no.1, p.17-23 (Jan.-Feb. 1983).
 Studies the radiation of high frequency waves from a simple antiplane model of an earthquake source. In this model only antiplane waves are generated so that the mathematics is relatively simple, but the physics is the same as in the more complex plane of three dimensional models where P and S waves are radiated. An exact solution is found for the problem of an arbitrarily moving semi-infinite crack in the presence of a general dynamic stress drop. In the case when friction is independent of time, an algebraic expression is obtained for particle velocity. This result is exploited to understand the origin of high frequency waves, and the role of rupture velocity and stress intensity on the radiation. The author shows that barriers and asperities dominate the radiation, but that they are indistinguishable from a high frequency point of view. (16 refs.)
- 78442 An aftershock study of the El Asnam (Algeria) earthquake of 1980 October 10.** M. Oued (Lab. de Geophys. Interne, Univ. Sci. et Médicale de Grenoble, Grenoble, France), G. Yielding, D. Hatzfeld, G. C. P. King. *Geophys. J. R. Astron. Soc. (GB)*, vol.73, no.3, p.605-39 (June 1983).
 An array of 28 portable seismic stations was operated in the region of El Asnam following the magnitude 7.3 (M_s) thrust earthquake of 1980 October 10. Locations of 494 events are presented and provide an indication of the overall form of the aftershock distribution. Tests to establish location accuracy (particularly depth) reduce this set to 277 events which, it is argued, are well constrained. P-waves alone are used in this study as a consequence of a debate about the reliability of reading S-phases. From the reduced set of 277 events, 81 events provide well-constrained focal mechanisms. The locations are presented in the form of maps and cross-sections, and discussed in relation to information already derived from field mapping of surface breaks and teleseismic studies of the waveforms of the main event. (32 refs.)
- 78443 Spatial distribution of microearthquakes beneath the Japan Trench from ocean bottom seismographic observations.** N. Hirata, T. Yamada (Geophys. Inst., Univ. of Tokyo, Tokyo, Japan), H. Shimamura, H. Inatani, K. Suyehiro. *Geophys. J. R. Astron. Soc. (GB)*, vol.73, no.3, p.653-69 (June 1983).
 The area of the Japan Trench, about 40°N off the Tohoku District of north-eastern Honshu, Japan, was for the first time extensively covered by an ocean bottom seismograph (OBS) array. Hypocentres are calculated by using a generalized inversion technique. Sixty-five events, mostly with magnitudes from 1.5 to 3.0, which were not located by a land network, were determined to be within or near the area covered by the OBS array. The OBS array enabled the authors to determine the focal depth of microearthquake activity with better resolution than was previously possible. The authors report the first direct observations to clarify the spatial distribution of microearthquakes associated with the bending and/or subducting of the oceanic plate just beneath the Japan Trench axis. (46 refs.)
- 78444 Source mechanism and surface wave excitation for two earthquakes in northern Baja California, Mexico.** F. A. Nava (Univ. Nacional Autónoma de México, México City, México), J. N. Brune. *Geophys. J. R. Astron. Soc. (GB)*, vol.73, no.3, p.739-63 (June 1983).
 Two earthquakes of comparable local magnitude from different regions of northern Baja California (the 1975 July 17 Pino Solo earthquake, $M_L=5.1$, from the Peninsular Ranges region, and the 1976 December 7 Mesa de Andrade earthquake, $M_L=5.3$, from the Colorado River Delta region) are studied in detail to determine possible causes for the observed stronger excitation of surface waves by earthquakes from the Delta region relative to earthquakes of comparable local magnitude in the Peninsular Ranges region. Data from distant stations are complemented with data from aftershock studies using local arrays and, for the Mesa de Andrade earthquake, with data from two strong motion stations. (36 refs.)
- 78445 Group velocity distribution of surface waves in the North Atlantic.** T. B. Yanovskaya (Faculty of Phys., Leningrad State Univ., Leningrad, USSR). *Izv. Acad. Sci. USSR, Phys. Solid Earth (USA)*, vol.18, no.2 (1982). Translation of: *Izv. Akad. Nauk SSSR Fiz. Zemli*, vol.18, no.2, p.83-9 (1982).
 A smoothed velocity distribution of Rayleigh waves with periods of 20, 30, 40, 50 and 60 sec in the North Atlantic is obtained by the Backus-Gilbert (1968) method. At depths corresponding to the penetration of waves with periods of 20 to 30 sec a sharp asymmetry of the lithosphere structure manifests itself to the west and to the east of the mid-oceanic ridge. At greater periods a rift zone is revealed as a region of low surface wave velocities. (8 refs.)
- 78446 Elastic-wave radiation during a camouflaged explosion.** S. Z. Dunin, O. V. Nagornov, Ye. A. Popov (Moscow Engng. & Phys. Inst., Moscow, USSR). *Izv. Acad. Sci. USSR, Phys. Solid Earth (USA)*, vol.18, no.2 (1982). Translation of: *Izv. Akad. Nauk SSSR Fiz. Zemli*, vol.18, no.2, p.98-103 (1982).
 The problem of elastic-wave radiation during an explosion in a porous medium is considered with allowance for the dilatancy effect. The character of the elastic-energy radiation at various moments of time is investigated. An analysis is made of the spectral composition of the radiated seismic signal, and of the effect of the strength parameters of this medium, the porosity and the dilatancy coefficient on the magnitude of the elastic energy radiated during an explosion. (14 refs.)
- 78447 New characteristics of the focal extent of near earthquakes.** I. V. Gorbunova, Z. A. Kal'met'eva (O.Yu. Schmidt Inst. of Earth Phys., Acad. of Sci., USSR). *Izv. Acad. Sci. USSR, Phys. Solid Earth (USA)*, vol.18, no.3, p.188-95 (1982). Translation of: *Izv. Akad. Nauk SSSR Fiz. Zemli*, vol.18, no.3 (1982).
 A new approach to interpretation of P and S waves from near earthquakes, based on a theoretical concept and models of the development of the failure process in the focus, and data on studies of faults during earthquakes, are discussed. Only direct waves at distances of up to 180 km are investigated, since secondary (exchange or reflected) waves do not yet appear on this segment of the path. Short-period equipment with table-type amplitude-frequency response for periods from 0.3 to 1 sec is used. Besides interpretation of the first arrivals of P-waves, which correspond to the incipient rupture

at the earthquake focus, the P_{\max} wave, which is emitted by the focus at the maximum destruction time, is interpreted. (18 refs.)

- 78448 Anelastic response of the Earth to a dip slip earthquake.** H. J. Melosh, A. Raefsky (Earth & Space Sci. Dept., State Univ. of New York, Stony Brook, NY, USA). *J. Geophys. Res. (USA)*, vol.88, no.B1, p.515-26 (10 Jan. 1983). [received: May 1983]
 The deformation of the Earth's surface immediately following an earthquake is well modeled by a dislocation in an elastic half space. Some time after the event, however, the elastic stresses begin to relax due to flow in the more fluid regions of the upper mantle (the asthenosphere). This relaxation causes further slow displacements observable at the Earth's surface. This paper examines the pattern and timing of these postseismic motions for a vertical dip slip fault and a 30° dip thrust fault. A variety of rheological models are studied. These models encompass variations in asthenosphere thickness, mesosphere viscosity, fault depth, and, most important, power law flow. (43 refs.)
- 78449 Regionalization of crustal coda Q in the continental United States.** S. Singh, R. B. Herrmann (Dept. of Earth & Atmospheric Sci., Saint Louis Univ., Saint Louis, MO, USA). *J. Geophys. Res. (USA)*, vol.88, no.B1, p.527-38 (10 Jan. 1983). [received: May 1983]
 A contour map of crustal Q_0 values for the entire United States is presented based on a scattering model to explain the coda waves of local and near regional earthquakes. These coda Q_0 values are in good agreement with Q of Lg waves. Data are obtained from over 250 local earthquakes, with most magnitudes between 3.0 and 5.0, recorded by 25 WWSSN and 27 LRSM stations throughout the continental United States. These two sets of data provide a range of frequencies from 0.5 to 3.5 Hz. A frequency dependence of Q is observed in the range of frequencies considered. A power law dependence of the form $Q = Q_0(f/f_0)^n$ is assumed. The value of frequency dependence is found to be maximum in the tectonically active western United States and least in the stable regions of the central and south central United States. The lowest Q_0 values are obtained in the western United States. (46 refs.)
- 78450 Strain dependent attenuation: observations and a proposed mechanism.** R. R. Stewart, M. N. Toksoz (Dept. of Earth & Planetary Sci., MIT, Cambridge, MA, USA), A. Timur. *J. Geophys. Res. (USA)*, vol.88, no.B1, p.546-54 (10 Jan. 1983). [received: May 1983]
 The measured attenuation (Q^{-1}) of a rock is a function of a number of parameters, one of those being the applied strain amplitude. Near source (large strain) wave propagation may behave highly non-linearly, and the strain amplitude dependence can provide insight into the attenuation mechanism. A physical model based on the contact friction between crack surfaces in the rock has been developed to describe rock deformation and dissipation under large applied strain. The three-dimensional crack surfaces are characterized by a statistical distribution of asperity heights. The sliding contact of these spherically-tipped asperities dissipates frictional energy. The results of ultrasonic pulse transmission experiments on sandstone and lucite are compared with the model's prediction. (33 refs.)
- 78451 Focal depths and fault plane solutions of earthquakes under the Tibetan Plateau.** P. Molnar (Dept. of Earth & Planetary Sci., MIT, Cambridge, MA, USA), Wang-Ping Chen. *J. Geophys. Res. (USA)*, vol.88, no.B2, p.1180-96 (10 Feb. 1983).
 Compares synthetic and recorded P waveforms to place constraints on the focal depths and fault plane solutions of 16 crustal earthquakes beneath the highest parts (>4000 m) of the Tibetan Plateau. Fault plane solutions for all 16 events show combinations of normal and strike slip faulting with T axes oriented approximately east-west. None of these solutions show thrust faulting. Thus the data corroborate previous inferences that the active tectonics are dominated by east-west extension. Focal depths for all 16 events are less than 15 km and appear to be between 5 and 10 km. This style of deformation and these depths of faulting are similar to those in the Basin and Range province of the western United States. Two intermediate depth events below the crust of southern Tibet occurred in the mantle beneath a thick, aseismic lower crust. Their occurrence suggests that brittle deformation occurs there in response to a stress field similar to that operating at shallow depths beneath Tibet. (29 refs.)
- 78452 Some statistical properties of a sequence of historical Calabro-Peloritan earthquakes.** A. Bottari, G. Neri (Istituto Geofisico e Geodetico, Univ. di Messina, Messina, Italy). *J. Geophys. Res. (USA)*, vol.88, no.B2, p.1209-12 (10 Feb. 1983).
 A statistical analysis is applied to the sequence of earthquakes, with epicentral intensity $I_0 \geq VIII$ MSK, which occurred in the Calabro-Peloritan Arc region (southern Italy) during the period 1600-1974. The study reveals, by the application of the Poisson test, an evident level of interdependence of the shocks which appear grouped in temporal clusters satisfying the simple Poisson process. In fact, the equations which characterize the generalized Poisson process give a good fit of the observed data, the distribution of the events in the clusters being of the Pareto type (discrete). The values 0.90 and 2.8 have been found for k' and E parameters, which are the average number of clusters occurring in unit time and the parameter of the Pareto distribution, respectively. A subsequent elaboration of these results makes the calculation of some quantities, like the clustering length, possible. (17 refs.)
- 78453 Assigning probability gain for precursors of four large Chinese earthquakes.** T. Cao, K. Aki (Dept. of Earth & Planetary Sci., MIT, Cambridge, MA, USA). *J. Geophys. Res. (USA)*, vol.88, no.B3, p.2185-90 (10 March 1983).
 The concept of probability gain associated with a precursor (Aki, 1981) is extended to a set of precursors which may be mutually dependent. Making use of a new formula, the authors derive a criterion for selecting precursors from a given data set in order to calculate the probability gain. The probabilities per unit time immediately before four large Chinese earthquakes are calculated. They are approximately 0.09, 0.09, 0.07 and 0.08 per day for 1975 Haicheng ($M=7.3$), 1976 Tangshan ($M=7.8$), 1976 Longling ($M=7.6$), and Songpan ($M=7.2$) earthquakes, respectively. These results are encouraging because they suggest that the investigated precursory phenomena may have included the complete information for earthquake prediction, at least for the above earthquakes. With this method, the step-by-step approach to prediction used in China may be quantified in terms of the possibility of earthquake occurrence. (31 refs.)
- 78454 Source times and scaling relations of large earthquakes.** M. Furumoto (Dept. of Earth Sci., Nagoya Univ., Nagoya, Japan). *J. Geophys. Res. (USA)*, vol.88, no.B3, p.2191-8 (10 March 1983).
 Source time is a kinetic fault parameter corresponding to the duration of seismic source time functions and is accurately determined from phase spectra of long-period surface waves. Source times are determined for 36 large earthquakes during the last three decades. Scaling relations among source times, seismic moments, and fault dimensions are derived. Seismic moment is pro-

portional to the cube of source time, and fault dimension is proportional to source time. Source times for low-angle thrust earthquakes along deep-sea trenches are found to be longer than those of other types, such as intraplate shocks and deep shocks. They are also significantly longer than the rupture times expected from a Haskell model, suggesting that, generally, there exists an introductory stage of faulting that precedes the main stage of the rupture propagation. (35 refs.)

78455 A teleseismic analysis of the New Brunswick earthquake of January 9, 1982. G.L.Choy (US Geological Survey, Denver, CO, USA), J.Boatwright, J.W.Dewey, S.A.Sipkin. *J. Geophys. Res. (USA)*, vol.88, no.B3, p.2199-212 (10 March 1983).

The analysis of the $m_{5.7}$ New Brunswick earthquake of January 9, 1982, has important implications for the evaluation of seismic hazards in eastern North America. Source characteristics of this earthquake have been determined from analysis of data that were digitally recorded by the Global Digital Seismograph Network. From broadband displacement and velocity records of P waves, a dynamic description of the rupture process as well as conventional static properties of the source have been determined. The depth of the hypocenter is estimated to be 9 km from depth phases. The focal mechanism determined from the broadband data corresponds to predominantly thrust faulting. From the variation in the waveforms the direction of slip is inferred to be up-dip on a west dipping NNE striking fault plane. The steep dip of the inferred fault plane suggests that the earthquake occurred on a preexisting fault that was at one time a normal fault. The estimated rupture length is 5.5 km. (40 refs.)

78456 Seismicity near Palmdale, California, and its relation to strain changes. J.Sauber, K.M.Nally, J.C.Pechmann, H.Kanamori (Seismological Lab., California Inst. of Technol., Pasadena, CA, USA).

J. Geophys. Res. (USA), vol.88, no.B3, p.2213-19 (10 March 1983). Evaluates the relationships between the spatio-temporal patterns and faulting mechanisms of small earthquakes and the recent temporal changes in horizontal strain observed along the 'big bend' portion of the San Andreas fault near Palmdale, California. Microearthquake activity along the entire big bend of the San Andreas fault increased in November 1976 concurrent with the initiation of an earthquake swarm at Juniper Hills. This activity then decreased abruptly to the northwest and southeast of Juniper Hills during the beginning of 1979. This drop in seismic activity occurred around the time that crustal dilatation was observed on the US Geological Survey Palmdale trilateration network. Focal mechanisms from the study region are predominantly thrust. There are two time periods when the mechanisms are closer to strike slip than to thrust. The first period corresponds to the beginning of the Juniper Hills swarm. The second period approximately coincides with a change in trend of the strain data from uniaxial N-S compression to dilatation. (14 refs.)

78457 Three-dimensional crust and upper mantle structure at the Nevada Test Site. S.R.Taylor (Lawrence Livermore Nat. Lab., Livermore, CA, USA).

J. Geophys. Res. (USA), vol.88, no.B3, p.2220-32 (10 March 1983). The three-dimensional crust and upper mantle structure at the Nevada Test Site (NTS) is derived by combining teleseismic P wave travel time residuals with P_n source time terms. The NTS time terms and relative teleseismic residuals are calculated by treating the explosions at a network of 'receivers' which record 'shots' located at the surrounding stations. Average relative teleseismic P wave residuals show a consistent progression of positive (late arrivals) to negative residuals from east to west across the NTS. However, P_n time terms beneath Rainier Mesa are at least 0.3 and 0.5 s less than those beneath Pahute Mesa and Yucca flat, respectively, indicating the Pahute Mesa are surprisingly uniform, and the largest time terms and residuals are observed in the northwest and southern parts of Yucca Flat. (52 refs.)

78458 Rayleigh waves excited by the discontinuous advance of a rupture front. J.G.Harris (Theoretical & Appl. Mech., Univ. of Illinois, Urbana, IL, USA), J.D.Achenbach, A.N.Norris.

J. Geophys. Res. (USA), vol.88, no.B3, p.2233-9 (10 March 1983). Analytical results are presented for Rayleigh waves excited by a sudden change in the rate of growth of a subsurface zone of rupture. The curved rupture front advances across an inclined plane. The rupture can be brittle or cohesive tractions can act at its front. The analysis consists of two parts: First, ray theory is used to calculate wavefront approximations to the waves emitted when the rupture front speed suddenly changes. Secondly, a representation integral for the Rayleigh wave, where the integration is performed over a surface enclosing the rupture front, is constructed by using the emitted waves in combination with an appropriate Green's tensor. This integral is evaluated asymptotically. Synthetic accelerographs are constructed which illustrate how the rupture process, and the geometry of the rupture front and the fault plane affect the excitation of Rayleigh waves. (9 refs.)

78459 Viscoelastic stress relaxation on deep fault sections as a possible source of very long period elastic waves. M.Bonafede, E.Boschi (Istituto di Geofisica, Univ. di Bologna, Bologna, Italy), M.Dragoni.

J. Geophys. Res. (USA), vol.88, no.B3, p.2251-60 (10 March 1983). Observations of very long elastic waves are attributed to 'silent' earthquakes, events which are presumed to occur at depth in a nonbrittle regime. The fault at depth is modeled as a thin viscoelastic gouge layer embedded in an elastic medium. The source of silent earthquakes is envisaged as a prolonged, slow slippage of the fault faces, which yields a radiation spectrum strongly depleted in the high-frequency components and dominated by the near-field term. The results of the model are compared with the dominant frequencies, mean duration, and amplitude of a long-period perturbation recorded at Trieste in the years preceding the 1976 Friuli (Italy) earthquake. The role that silent earthquakes may play in the overall earthquake mechanism (in particular, as precursory phenomena) is discussed. (73 refs.)

78460 Three-dimensional crust and upper mantle structure of the Eurasian continent. C.-C.Feng, T.-L.Teng (Dept. of Geological Sci., Univ. of Southern California, Los Angeles, CA, USA).

J. Geophys. Res. (USA), vol.88, no.B3, p.2261-72 (10 March 1983). Group velocities of fundamental mode Rayleigh waves of 109 wave paths within Eurasia have been measured by an improved frequency-time analysis technique. Stochastic inversion theory is applied to the mixed-path measurements to extract pure path group velocities of $10^\circ \times 10^\circ$ grid elements that form the subdivisions of Eurasia. Then a three-dimensional crust and upper mantle structure of the Eurasian continent to a depth of 300 km is constructed. The average crustal thickness of Eurasia is found to be about 40 km. Abnormally thick crust from 50 to 65 km is obtained in areas of Tien Shan, the Altai mountains, Afghanistan, Pamir, Tibet, and Burma. (25 refs.)

78461 The geoid, small-scale convection, and differential travel time anomalies of shear waves in the central Indian Ocean. M.Stark, D.W.Forsyth (Dept. of Geological Sci., Brown Univ., Providence, RI, USA).

J. Geophys. Res. (USA), vol.88, no.B3, p.2273-88 (10 March 1983). 37 differential travel times have been measured for the phase pairs SS-S, sSS-sS, ScS2-ScS, ScS2-S, sScS2-sScS, and sScS2-sS. Each pair included a surface bounce point in the central Indian Ocean between 4°N and 21°S and

69° and 85°E . Residuals were calculated relative to both the J-B travel time tables and the PEM-C Earth model and were corrected for the elevation of the bounce points. The mean J-B residual associated with bounce points in the Central Indian Basin is -2.8 ± 0.7 s (fast). This is similar to the -4.0 s found for old continental nuclei. After correcting for known differences between continental and oceanic crustal structure and for differences in measurement technique, it was found that travel times in the mantle beneath the Central Indian Basin are midway in character between those beneath pre-Cambrian shields and those beneath the western Pacific ocean basin. The fastest differential travel times occur along a line passing close to the center of the large Indian Ocean geoidal low. There is a clear increase in travel time with distance from the center of the geoid low. The Chagos-Laccadive Ridge seems to coincide with a transition from the fast differential travel times of the Central Indian Basin to slower differential travel times associated with bounce points beneath young seafloor near active spreading centers. (45 refs.)

78462 Velocity and attenuation anisotropy in deep-sea carbonate sediments. D.-C.Kim, K.W.Katahara, M.H.Manghani, S.O.Schlanger (Hawaii Inst. of Geophys., Univ. of Hawaii, Honolulu, HI, USA).

J. Geophys. Res. (USA), vol.88, no.B3, p.237-43 (10 March 1983). Laboratory studies have been carried out to determine the causes of velocity and attenuation anisotropy in pelagic carbonate sediments from Deep Sea Drilling Project site 288 on the Ontong-Java Plateau. Compressional velocity V_p was measured under independently controlled pore pressure and confining pressure. Velocity anisotropy for compressional waves (horizontal velocity $>$ vertical velocity) is found to decrease with increasing effective pressure, i.e. with closure of pores. The present results indicate that preferred horizontal orientation of grain contacts and flat pores is also a significant cause of the observed anisotropy for many samples. Significant anisotropy in ultrasonic attenuation for compressional (Q_p^{-1}) and shear (Q_s^{-1}) waves is observed such that the losses are greatest for propagation modes that can generate relative motion across horizontal grain contacts or flat horizontal pores. The results are discussed in terms of the possible mechanisms of dissipation. (26 refs.)

78463 In situ studies of velocity in fractured crystalline rocks. D.Moos (Dept. of Geophys., Stanford Univ., Stanford, CA, USA), M.D.Zoback.

J. Geophys. Res. (USA), vol.88, no.B3, p.2345-58 (10 March 1983). A study of the effects of macroscopic fractures on P and S wave velocities has been conducted in four wells drilled in granitic rock to depths between 0.6 and 1.2 km. The effect of macroscopic fractures is to decrease both V_p and V_s and increase V_p/V_s . In wells with a relatively low density of macroscopic fractures, the in situ velocity is similar to that of saturated core samples under confining pressure in the laboratory, and there is a clear correlation between zones with macroscopic fractures and anomalously low velocities. In wells with numerous macroscopic fractures, the in situ velocity is lower than that of intact samples under pressure, and there is a correlation between the rate at which in situ velocity increases with depth and the rate at which the velocity of laboratory samples increase with pressure. Differences in in situ P wave velocity between wells cannot be explained solely by differences in the degree of macroscopic fracturing, thus emphasizing the importance of composition and microcracks on velocity. Chemical alteration of rock adjacent to macroscopic fractures appears to play an important role in reducing in situ velocities. (33 refs.)

78464 Scattering of Rayleigh waves by a rectangular rough surface.

T.Momoi (Earthquake Res. Inst., Univ. of Tokyo, Tokyo, Japan). *J. Phys. Earth (Japan)*, vol.30, no.4, p.295-319 (1982).

A theoretical study is made on the scattering of Rayleigh waves which are incident to a rectangular rough surface. The partition of the energy flux of the waves scattered by a mountain is obtained. It is then revealed that resonant standing Rayleigh waves occurring along the top surface of the rectangular mountain enhance the transmissivity of incident Rayleigh waves when the mountain is low ($L/B \leq 0.7$) while suppressing the transmissivity when the mountain is high ($L/B \geq 0.8$), where L and B are the height and half-width of the mountain. When the mountain is high, resonant standing Rayleigh waves occur along the vertical cliff in the case of $kB < 1$ (k : wave number of S waves). The generation of these standing waves remarkably suppresses the transmissivity of incident Rayleigh waves through the mountain. As for the directivity of the scattered body waves (case of $L/B = 0.5$), they are transmitted away, mainly by S waves, vertically downwards when $kB \leq 1$ and toward the leeward quarter space when $kB > 1$. (18 refs.)

78465 Magnitude, seismic moment and apparent stress for major deep earthquakes. K.Abe (Dept. of Geophys., Hokkaido Univ., Sapporo, Japan).

J. Phys. Earth (Japan), vol.30, no.4, p.321-30 (1982). On the basis of an extensive data-set of major deep and intermediate-depth earthquakes, the relation between body-wave magnitude m_B and seismic moment M_0 is discussed in terms of apparent stress. m_B is determined from amplitudes and periods of P , PP and S waves recorded by broad-band instruments, and is therefore suitable for measuring the overall size of major earthquakes. The relation between m_B and $\log M_0$ is approximately linear for the data set of m_B greater than 6. This indicates that the apparent stress is, on the average, nearly constant. A gross average of 60 bar is obtained for the earthquakes over a large depth range. For a simple fault model, one has $E_s = (7.10^{-3}) M_0$, where E_s is the radiated seismic energy. The constant apparent stress implies a decrease of seismic efficiency with an increase of depth. A very similar relation between m_B and $\log M_0$ is applicable to large shallow earthquakes. (31 refs.)

78466 Effect of Poisson's ratio on elastic wave radiation in a semi-infinite medium. I.Onda (Faculty of Engng., Gunma Univ., Gunma, Japan).

J. Phys. Earth (Japan), vol.30, no.4, p.349-66 (1982). Radiation patterns of elastic waves due to a normal and a horizontal traction applied on a free surface of a semi-infinite medium are discussed in relation to the Poisson's ratio ν . The field is derived by means of the method of steepest descent. The P radiation is much less than the S radiation, and is reduced as ν becomes large. The Rayleigh wave generation diminishes with increasing of ν . The S -radiation factor is complex at the colatitudinal angle θ larger than θ_c , where $\theta_c = \sin^{-1}(S \text{ velocity}/P \text{ velocity})$. The S energy due to a normal traction is mostly radiated at angles larger than θ_c , particularly, if ν is close to 0.5. The S radiation due to a horizontal one has a maximum at an angle θ_1 larger than 45° and vanishes at 45° . (8 refs.)

78467 On the correlation between the syzygies and great earthquakes in Hebei of China. Ren Zhenqiu (Acad. of Meteorological Sci., Central Meteorological Bur. of China, Beijing, China).

Kexue Tongbao (Foreign Lang. Ed.) (China), vol.28, no.1, p.74-9 (Jan. 1983). [received: June 1983]

The author examines the great earthquake ($M_s \geq 6$) record of Hebei Province in China, in conjunction with the lunar phases. Hence the correlation between earthquakes and syzygies in this area is determined. (4 refs.)

78468 Seismicity of Yemen. N.N.Ambraseys, C.P.Melville (Dept. of Civil Engng., Imperial Coll., London, England). *Nature (GB)*, vol.303, no.5915, p.321-3 (26 May 1983). Shows that historical sources of local information describe a fairly continuous occurrence of medium magnitude, damaging shocks over the past 12 centuries, including a destructive event in 1941 that in many respects resembles the earthquake of December 1982. The common presumption that the Arabian Peninsula has a very low seismicity is incorrect. (19 refs.)

78469 Evidence for dyke intrusion earthquake mechanisms near Long Valley caldera, California. B.R.Julian (US Geological Survey, Menlo Park, CA, USA). *Nature (GB)*, vol.303, no.5915, p.323-5 (26 May 1983). A re-analysis of the magnitude 6 earthquakes that occurred near Long Valley caldera in eastern California on 25 and 27 May 1980, suggests that at least two of them, including the largest, were probably caused by fluid injection along nearly vertical surfaces and not by slip on faults. Several investigators have reported difficulty in explaining both the long-period surface-wave amplitudes and phases and the locally recorded shorter-period body-wave first motions from these events, using conventional double-couple (shear fault) source models. It is shown that the data agree well with the predictions for a compensated linear-vector dipole equivalent-force system, with its principal extensional axis, horizontal and trending N 55-65° E. Such a mechanism is what would be expected for fluid injection into dykes striking N 25-35° W, which is the approximate strike of numerous normal faults in the area. (10 refs.)

78470 Phase and group velocities and Q of mantle Love and Rayleigh waves of the first two modes and their azimuthal dependences for the 1963 Kurile Islands earthquake. Y.Fukao, M.Kobayashi (Dept. of Earth Sci., Nagoya Univ., Nagoya, Japan). *Phys. Earth & Planet. Inter. (Netherlands)*, vol.32, no.1, p.4-35 (April 1983). Analyzes phase and group velocities and Q of mantle Love and Rayleigh waves from the 1963 Kurile Islands earthquake ($M_w=8.5$), for both the fundamental and the first higher modes. The period ranges are from 100-500 s for the fundamental modes and from 100-275 s for the first higher modes. Love and Rayleigh waves were extracted from 24 stations. (64 refs.)

78471 Determination of magnitude for large shallow earthquakes 1898-1917. K.Abe (Dept. of Geophys., Faculty of Sci., Hokkaido Univ., Sapporo, Japan). *Phys. Earth & Planet. Inter. (Netherlands)*, vol.32, no.1, p.45-59 (April 1983). In order to arrive at a uniform basis for a study of the global seismicity, the surface-wave magnitude M_s of shallow earthquakes for 1898-1917 is determined by using maximum amplitudes of surface waves recorded by undamped Milne and Omori seismographs. The effective gain of these instruments needs to be calibrated with great care, because of the lack of a damping device. The calibration of Milne instruments is based on a comparison of amplitudes measured by Milne instruments with those by more modern, damped instruments. M_s is determined for a large number of earthquakes between 1898 and 1917. To supplement the data for 1913-1917, records of undamped Omori seismographs are used. For the entire period from 1898 to 1917, 308 shallow earthquakes with $M \geq 7.0$ are listed. Both this list and the previous catalogue of Abe (1981) for 1918-1960 provide a catalogue of large shallow earthquakes much more uniform than any previously established. (23 refs.)

78472 On the localization of seismic events. M.Dragoni (Istituto di Geofisica, Univ. di Bologna, Bologna, Italy). *M.Gasperini. Riv. Nuovo Cimento (Italy)*, vol.5, ser.3, no.11, p.1-28 (1982). The authors re-propose the method of hypocentre localization based on the evaluation of the azimuth and the angle of emergence of seismic waves. This method is intended to be employed mainly in local networks of seismic stations, where seismicity is studied with greater detail and more accurate determination of earthquake foci are required. Its principal characteristics are analysed and compared with those of currently used methods, based on time measurements only. The basic mathematical theory which is implied is briefly reviewed. Some historical articles and books on the subject are also referenced in the course of the paper. (39 refs.)

78473 Estimating the kinematic parameters of seismic waves by the focusing method. S.V.Gol'din (Inst. of Geology & Geophys., Novosibirsk, USSR). *Sov. Geol. & Geophys. (USA)*, vol.23, no.4, p.65-75 (1982). Translation of: *Geol. & Geofiz. (USSR)*, vol.23, no.4, p.71-80 (1982). If a reversed continuation of the seismic wave field is constructed, with various values of the velocity v_0 in the lower half-space, for certain values of $v_0 = v_{ex}$ the waves identifiable as representing the geometry of the reflecting objects will have the maximum amplitude. In the general case, the extreme velocity v_{ex} is not the same as the true (or effective) velocity in the medium. Formulae are derived relating the extreme velocity to the derivatives of the eikonal of the reflected wave and also to the parameters of the medium. These formulae can be used in solving the reverse kinematic problems. (7 refs.)

78474 Focusing properties of seismological transformations. L.D.Gik (Inst. of Geology & Geophys., Novosibirsk, USSR). *Sov. Geol. & Geophys. (USA)*, vol.23, no.4, p.76-83 (1982). Translation of: *Geol. & Geofiz. (USSR)*, vol.23, no.4, p.81-9 (1982). Conditions of maximum image brightness for an object with a cylindrical reflection surface are investigated for D-transformation and M-transformation, RDR, and according to CDP summation. An expression for the apparent value of seismic velocity when the maximum is present is obtained. In particular, with D-transformations, the apparent value of velocity coincides with the real value only for a point object, while for a flat object it is $\sqrt{2}$ times higher. It has been shown that for the above mentioned types of transformations there is a possibility of false images if the interval of the receiver array exceeds $\lambda/2$ for a CRP observation system, and $\lambda/4$ in central rays. (9 refs.)

78475 On the results of measurements of vibroseismic signals and noise levels in vibro-DSS. V.I.Yushin (Inst. of Geology & Geophys., Novosibirsk, USSR). *Sov. Geol. & Geophys. (USA)*, vol.23, no.4, p.84-8 (1982). Translation of: *Geol. & Geofiz. (USSR)*, vol.23, no.4, p.89-94 (1982). Presents results of absolute measurements of amplitudes of vibroseismic vibrations, generated by a powerful vibration source, at different ranges over a distance of up to 300 km. Also presented are results concerning the level of microseismic noise and the real coefficients of noise stability which were obtained by a correlation method of signal accumulation and signal condensing. Limits of the vibro-DSS method are predicted. (10 refs.)

78476 Algorithm of quick transformation of frequency seismograms into pulse seismograms. G.P.Evchatov (Sci.-Res. Inst. of Geology, Geophys. & Raw Materials, Novosibirsk, USSR). *Sov. Geol. & Geophys. (USA)*, vol.23, no.4, p.97-9 (1982). Translation of: *Geol. & Geofiz. (USSR)*, vol.23, no.4, p.103-6 (1982). An efficient algorithm for the transformation of the phase-distorted frequency response of a geologic medium into a pulse reaction is described. The algorithm is due to a Fourier quick transformation and is intended to be used in the processing of vibroseismic information obtained by the frequency method. (6 refs.)

Analysis of run up height of surface waves in a liquid body excited by the seismological effect See Entry 76050

Gravity anomalies, seismic structure and geothermal history of the central Alps See Entry 78414

The West-African craton margin in eastern Senegal: a seismological study See Entry 78477

Mathematical modeling in the solution of a two-dimensional inverse problem according to deep seismic sounding data See Entry 78484

A seismic model of a partially molten inner core See Entry 78492

A seismological constraint on the depth of basalt-eclogite transition in a subducting oceanic crust See Entry 78496

Temporal variation of the different parameters of the seismo-tectonic process See Entry 78505

A detailed study of the Cobb Offset of the Juan de Fuca Ridge: evolution of a propagating rift See Entry 78512

Elastic anisotropy in marine sedimentary rocks See Entry 78527

Investigation of internal friction in fused quartz, steel, Plexiglass, and Westerly granite from 0.01 to 1.00 Hertz at 10^{-8} to 10^{-7} strain amplitude See Entry 78533

A filtering procedure for great circle data See Entry 78684

Recovery of reflector series by determining the beginning position of estimated wavelets using short-time homomorphic analysis See Entry 78685

Seismic transducers: noise suppression and prevention in the piezoelectric transduction systems See Entry 78686

Seismic transducers: calibration systems See Entry 78687

Prediction of sites of occurrence of strong earthquakes in large seismogenic zones of Tadzhikistan See Entry 78690

Seismic velocity anisotropy in a medium containing oriented cracks—transversely isotropic case See Entry 78701

Estimation of source function and medium response function by autoregressive method See Entry 78706

A method of studying the Earth's crust by refracted P- and S-waves See Entry 78713

Approximate analogs of Dix formulas for a stratified medium with curvilinear boundaries and variable bed velocities See Entry 78714

The determination of stratal velocities in horizontally layered media by the hyperboloid approximation of hodographs See Entry 78716

Primitive extraction for a syntactic pattern recognizer of features in seismic signals See Entry 78719

The wavelet reconstructed with phase-only and a study of its uniqueness See Entry 78720

Seismic velocity estimators See Entry 78721

Deconvolution of band-limited signals See Entry 78722

A model reduction algorithm by spline approximation in the deconvolution of seismic signals See Entry 78723

Anomalous bulk viscosity of two-phase fluids and implications for planetary interiors See Entry 78834

91.35 EARTH'S INTERIOR STRUCTURE AND PROPERTIES

78477 The West-African craton margin in eastern Senegal: a seismological study. C.Dorbat (Office de la Recherche Sci. et Tech. Outre-Mer, Paris, France), L.Dorbat, A.Le Page, R.Gaulon.

Ann. Geophys. (France), vol.1, no.1, p.25-36 (Jan.-Feb. 1983).

A vertical short period seismological survey was operated for six months in eastern Senegal. Large P-wave travel-time anomalies are in fairly good relation with the gravity and geological features. Two-dimensional inversion of the data shows the existence of a major vertical discontinuity extending from the surface to 150-200 km depth. The other heterogeneities are mainly located in the crust and related to specific segments of the regional geology: craton, Mauritanides and Senegalo-Mauritanian basin. The main discontinuity dipping to the east is interpreted. The authors propose the following geodynamical process to explain the formation of the Mauritanides orogenic belt: continental collision after opening of a back-arc marginal basin in Late Precambrian and its closure until the Devonian. (43 refs.)

78478 Model heat flow and [magnetotellurics] for the San Andreas and oceanic transform faults. Y.Ricard, C.Froidevaux (Lab. de Geophys. et Geodynamique Interne, Univ. de Paris-Sud, Orsay, France), J.F.Hernance.

Ann. Geophys. (France), vol.1, no.1, p.47-52 (Jan.-Feb. 1983).

Two-dimensional temperature structures are computed for a lithospheric shear zone in order to predict the geometry of the hot anomalous region caused by shear heating. The results are compatible with earlier one-dimensional models. The comparison with the heat flow data from California is quite satisfactory. It requires to take into account the geometrical constraints corresponding to the migration of the Medocino triple point (Furlong, 1982). This is obtained by solving the time dependent heat equation. The possibility to probe the existence of a sub-Moho hot window by magnetotelluric sounding is then examined. A drop in apparent resistivity by a factor 2 to 4 is predicted. However, the presence of conductive sedimentary basins at the surface may hide this effect in California. (18 refs.)

78479 A Nd isotope investigation of sediments related to crustal development in the British Isles. R.K.O'Nions, P.J.Hamilton, P.J.Hooker (Dept. of Earth Sci., Cambridge Univ., Cambridge, England).

Earth & Planet. Sci. Lett. (Netherlands), vol.63, no.2, p.229-40 (May 1983).

The times of original fractionation of the Sm and Nd component of clastic sediments from a mantle source (=crustal residence age) have been estimated from Sm-Nd model ages calculated relative to a depleted mantle evolution. In this way the provenance and evolution of selected Precambrian and Phanerozoic sediments and metasediments from the British Isles have been examined. Whereas some Archaean and early Proterozoic sediments have Sm-Nd model

ages that are close to their stratigraphic age, the Phanerozoic sediments analysed have model ages as much as 2.0 Ga in excess of their stratigraphic age. A more detailed study of Lower Palaeozoic sediments deposited on the northern margin of the Iapetus Ocean provides evidence for a marked change of provenance in the Ordovician after the deposition of the Dalradian Supergroup. A component with comparatively high $^{143}\text{Nd}/^{144}\text{Nd}$ and Sm/Nd ratio (presumably basaltic) is present in the sediments throughout the accretionary prism. Crustal residence age estimates average about 1.5 Ga for both these Lower Palaeozoic sediments, and modern pelagic clays, and collectively fail to provide any evidence for significant continental growth during the Phanerozoic. (72 refs.)

78480 Isotopic and trace element constraints on the genesis of the Faeroe lava pile. C.Gariépy, J.Ludden, C.Brooks (Dept. de Géologie, Univ. de Montréal, Montréal, Québec, Canada). *Earth & Planet. Sci. Lett. (Netherlands)*, vol.63, no.2, p.257-72 (May 1983). Basaltic lavas from the Faeroe Islands form three stratigraphic series which define two geochemical groups. Both the lower and middle series are LREE enriched and are characterized by convex LREE profiles; in contrast, the upper series comprises both depleted and enriched lavas. This twofold geochemical division is also evident from the incompatible trace elements such as Zr, Nb, Hf and Ta and the compatible trace elements Cr, Ni, Sr and Y. Nd-Sr-Pb isotopic measurements show that the basalts are contaminated by crustal materials, implying the presence of Precambrian sialic basement underneath the Faeroes block, a conclusion supported by geophysical data. The uncontaminated end-members, for the LREE-depleted basalts and for the LREE-enriched basalts require two different mantle source regions thus posing serious problems for petrogenetic models. The authors interpret the LREE-depleted basalts as partial melts of the oceanic asthenosphere whilst the LREE-enriched basalts may result either from the partial melting of deep mantle blobs or of the subcontinental lithosphere during upwelling of the asthenosphere. (48 refs.)

78481 Sr isotope and trace element evidence for the role of continental crust in calc-alkaline volcanism on Santorini and Milos, Aegean Sea, Greece. M.Barton, V.J.M.Salters, J.P.P.Huijsmans (Dept. of Geochem., State Univ. of Utrecht, Utrecht, Netherlands). *Earth & Planet. Sci. Lett. (Netherlands)*, vol.63, no.2, p.273-91 (May 1983). $^{87}\text{Sr}/^{86}\text{Sr}$, major and trace element data are presented for calc-alkaline lavas from Santorini and Milos islands in the Aegean Sea, Greece. $^{87}\text{Sr}/^{86}\text{Sr}$ ratios of fresh lavas from Santorini range from 0.70472 to 0.70509 whereas those of fresh lavas from Milos lie in the range 0.70540-0.70620. Altered lavas from both islands have higher $^{87}\text{Sr}/^{86}\text{Sr}$ ratios. The range of $^{87}\text{Sr}/^{86}\text{Sr}$ ratios of fresh lavas from Santorini is only just greater than the maximum analytical uncertainty and is thus considered to reflect that of the parental magmas from which the lava series was derived. For the analysed Milos lavas (dacite-rhyolite) there is no correlation between $^{87}\text{Sr}/^{86}\text{Sr}$ and any major or trace element concentration. The relatively high $^{87}\text{Sr}/^{86}\text{Sr}$ ratios of the Santorini and Milos parental magmas indicate that terrigenous material has played a role in their genesis. This could be either via the subduction process or by assimilation of lower crustal material during ascent of mantle-derived magmas. (58 refs.)

78482 Age determinations in the Precambrian basement of the Wadi Araba area, southwest Jordan. G.Jarrar (Dept. of Geology & Mineralogy, Univ. of Jordan, Amman, Jordan), A.Baumann, H.Wachendorf. *Earth & Planet. Sci. Lett. (Netherlands)*, vol.63, no.2, p.292-304 (May 1983). The Precambrian basement of Jordan belongs to the northern margin of the Arabian-Nubian Shield. Age determinations by U-Pb isotopic analyses on sized and magnetic zircon fractions, a monazite and an apatite sample and by Rb-Sr isotopic studies on whole-rocks and minerals of metasedimentary rocks, granodiorites, granites and dykes have elucidated the following events: (1) A major regional high-grade metamorphism accompanied by migmatization and synkinematic plutonism occurred at about 800 Ma. (2) During a postkinematic plutonic event between 615 and 600 Ma extensive masses of granodiorite to granitic composition and dykes were emplaced. (3) A younger plutonic event produced diorites and dykes at about 570 Ma. The plutonic events are related to the Pan-African orogenic phase. The low initial $^{87}\text{Sr}/^{86}\text{Sr}$ ratios of the plutonic rocks correspond to values reported from equivalent rocks throughout the Arabian-Nubian Shield and suggest that no significant portions of ancient sialic crustal material contributed to the generation of the granitic to granodioritic magmas. (33 refs.)

78483 Uranium estimation in Mussoorie phosphorites using solid state nuclear track detector. Surinder Singh, H.S.Virk (Dept. of Phys., Guru Nanak Dev Univ., Amritsar, India). *Indian J. Pure & Appl. Phys.*, vol.21, no.2, p.125-6 (Feb. 1983). A fission track analysis has been used to estimate the uranium concentration in phosphorite deposits of Mussoorie syncline in the lesser Himalayan region of Uttar Pradesh. The uranium content in these deposits has been found to vary from 0.01 to 0.06%. (8 refs.)

78484 Mathematical modeling in the solution of a two-dimensional inverse problem according to deep seismic sounding data. N.I.Pavlenkova, I.Psencik (O.Yu. Schmidt Earth Phys. Inst., Acad. of Sci., USSR). *Izv. Akad. Sci. USSR, Phys. Solid Earth (USA)*, vol.18, no.2 (1982). Translation of: *Izv. Akad. Nauk SSSR Fiz. Zemli*, vol.18, no.2, p.90-7 (1982). The possibilities of mathematical modeling for constructing velocity cross sections of the Earth's crust on the basis of deep seismic sounding data are considered. A brief description is given of the RATLIM program developed for calculating the times and amplitudes of reflected and refracted waves in horizontally inhomogeneous media. In the case of one of the seismic profiles it is shown that mathematical modeling enables one to broaden the class of investigated media and to determine the nature of the main components of the wave field. (28 refs.)

78485 On the thermal effects of groundwater flow. I. Regional scale systems. L.Smith (Dept. of Geological Sci., Univ. of British Columbia, Vancouver, Canada), D.S.Chapman. *J. Geophys. Res. (USA)*, vol.88, no.B1, p.593-608 (10 Jan. 1983). [received: May 1983] Numerical solutions of the equations of fluid flow and heat transport are used to quantify the effects of groundwater flow on the subsurface thermal regime. Simulations are carried out for a vertical section through a basin with a distance of 40 km separating the regional topographic high and low. Emphasis is placed on understanding the conditions under which advective effects significantly perturb the thermal field. The transition from conduction-dominated to advection-dominated thermal regimes is sharp and depends primarily on the topographic configuration of the water table, the magnitude and spatial distribution of permeability, hydraulic anisotropy, and the depth of active flow. Deviations of surface heat flow from the background heat flux are a measurable effect of groundwater flow and depend on the same factors. The results show that from 0% to almost 100% of the section may have surface heat flow significantly different from background heat flow, depending upon the nature of the hydrogeologic environment. (60 refs.)

78486 Heat transfer through the sediments of the mounds hydrothermal area, Galapagos Spreading Center at 86°W. K.Becker (Marine Phys. Lab., Univ. of California, La Jolla, CA, USA), R.P.Von Herzen. *J. Geophys. Res. (USA)*, vol.88, no.B2, p.995-1008 (10 Feb. 1983). Heat transfer processes at the mounds area of the Galapagos Spreading Center at 86°W are revealed by temperatures measured at $\approx 10\text{-m}$ intervals in the 30 $\pm 10\text{ m}$ sediment at each of 12 holes at DSDP Leg 70 Sites 506-509 and by temperatures of up to five thermistors on eleven 8-12 m long piston cores. The 325 needle-probe values show a significant linear increase of thermal conductivity with depth in each core. About half of the temperature-thermal resistance profiles are nonlinear and are fit to a steady state, vertical pore water advection model. Results indicate high and variable total heat flow and localized hydrothermal discharge at $\approx 10^{-8}\text{ m/s}$, associated with individual mounds. Recharge is indicated at similar rates in the low heat flow belt $\approx 5\text{ km}$ south of the mounds and is suggested at slower rates in the intermediate heat flow belt surrounding the mounds heat flow high. Possible slow entrained recharge within $\approx 100\text{ m}$ of discharging mounds is suggested. Also suggested is strong local discharge along the major fault bounding the mounds crustal block to the north. (37 refs.)

78487 Heat transfer and intraplate deformation in the Central Indian Ocean. C.A.Geller, J.K.Weissel, R.N.Anderson (Lamont-Doherty Geological Obs., Columbia Univ., Palisades, NY, USA). *J. Geophys. Res. (USA)*, vol.88, no.B2, p.1018-32 (10 Feb. 1983). Nineteen new heat flow measurements made across deformed oceanic lithosphere in the Central Indian Ocean and previously published data show that heat flow is significantly higher than predicted by models for cooling oceanic lithosphere over much of the region. Many of the temperature-depth profiles are nonlinear. Upward convection of water is the most likely explanation for the curvature of the temperature profiles. This interpretation requires water velocities of the order of $7 \times 10^{-8}\text{ m/s}$, which is unusual because the lithosphere is relatively old (72-82 m.y.) and a thick sedimentary cover (1-2.5 km) is present. These observations suggest that the processes causing deformation of the plate have increased the heat flux through the sediment-water interface. Extra heat is being generated at shallow depths (perhaps less than 35 km) in the plate. (53 refs.)

78488 Numerical models for the hydrothermal field at the Galapagos Spreading Center. U.Fehn (Dept. of Geological Sci., Univ. of Rochester, Rochester, NY, USA), K.E.Green, R.P.Von Herzen, L.M.Cathles. *J. Geophys. Res. (USA)*, vol.88, no.B2, p.1033-48 (10 Feb. 1983). The heat flow distribution at the Galapagos Spreading Center is compared to results of two-dimensional numerical models for the hydrothermal convection through oceanic crust. The model calculations are based on the equations for fluid flow through porous media adapted for the situation at spreading oceanic ridges. The temperature and pressure-dependent thermodynamic characteristics of water were used in the fluid flow equations. Models with average permeabilities of approximately $5 \times 10^{-15}\text{ m}^2$ and penetration depths between 2 and 5 km produce heat flow distributions compatible with the observations at the Galapagos Spreading Center. Because of the convective heat loss, temperatures within the hydrothermal layer are significantly lower than for conductively cooling crust. Two different types of convection cells develop. (41 refs.)

78489 Heat flow on the western flank of the East Pacific Rise at 21°N. K.Becker (Marine Phys. Labs., Univ. of California, San Diego, La Jolla, CA, USA), R.P.Von Herzen. *J. Geophys. Res. (USA)*, vol.88, no.B2, p.1057-66 (10 Feb. 1983). Reports 48 new heat flow measurements on the western flank of the East Pacific Rise at 21°N. The stations were taken in 1 to 30 m of sediment on 0.4 to 1.4 m.y. old crust. The low average measured value of $\approx 173\text{ mW/m}^2$ (including 12 tilted minimum values) is about 1/3 the mean heat flow predicted for crust of this age range by cooling plate theory. This may be partly due to a bias of measurement locations in sediment ponds. Nevertheless, 4-km running averages of measured heat flows, projected normally to the axis, display an oscillatory trend suggestive of cellular hydrothermal circulation in the basement. (47 refs.)

78490 Anomalous heat flow in the northwest Atlantic: a case for continued hydrothermal circulation in 80-m.y. crust. R.W.Embley (Nat. Ocean Survey/NOAA, Rockville, MD, USA), M.A.Hobart, R.N.Anderson, D.Abbott. *J. Geophys. Res. (USA)*, vol.88, no.B2, p.1067-74 (10 Feb. 1983). A detailed study of a $60 \times 150\text{ km}$ area at 60°W, 24°N at the eastern end of the Nares Abyssal Plain indicates that hydrothermal circulation is still active in the 80 m.y. B.P. oceanic crust. The 58 heat flow measurements made at five stations in the area have revealed (1) constant heat flow over the abyssal plain (56 mW m^{-2}), (2) a cyclic heat flow over the abyssal hills (mean of 77 mW m^{-2}), and (3) a large anomaly of 710 mW m^{-2} over one of several small domes which protrude from the abyssal plain. The domes are 0.5-1.0 km in diameter near the top and rise 50 m above the level of the abyssal plain. These features are probably small volcanoes. Overall, the results from the Nares survey vividly show the age independent muting effect of sediment on the surface manifestation of crustal convection. In this survey area the mode of heat transfer varies from purely conductive in the more thickly sedimented abyssal plain areas ($\sim 300\text{ m}$ sediment cover) to moderate amplitude convection pattern beneath the abyssal hills ($\sim 75\text{ m}$ sediment cover) to a very large thermal anomaly over the small dome or 'chimneylike' structure ($\sim 10\text{ m}$ sediment cover). (36 refs.)

78491 Thermal parameters of the oceanic lithosphere estimated from geoid height data. A.Cazenze, B.Lago, K.Dominh (Groupe de Recherche de Géodésie Spatiale, Centre Nat. d'Etudes Spatiales, Toulouse, France). *J. Geophys. Res. (USA)*, vol.88, no.B2, p.1105-18 (10 Feb. 1983). Geoid height anomalies derived from SEASAT altimeter data have been analyzed across fracture zones and over ocean ridges in two limited regions of the South Pacific (Eltanin fracture zone system; East Pacific Rise) and southeast Indian Ocean. Observed geoid height-age and geoid height derivative (with respect to age)-age relationships have been established. Comparison with theoretical relationships computed for the plate model of lithospheric cooling permits an estimation of the thermal parameters entering into the model. Two quantities can be derived: the product $\alpha k T_m$ (α , thermal diffusivity; k , volume coefficient of thermal expansion; T_m , bottom boundary temperature) and the thickness H of the plate. (28 refs.)

78492 A seismic model of a partially molten inner core. D.E.Loper (Geophys. Fluid Dynamics Inst., Florida State Univ., Tallahassee, FL, USA), D.R.Fearn. *J. Geophys. Res. (USA)*, vol.88, no.B2, p.1235-42 (10 Feb. 1983). Fearn et al. (1981) recently proposed a mechanism whereby the inner core contains a significant fraction of liquid. The authors construct a model of a partially molten inner core compatible with seismic observations. Specifically, an improved model of bulk anelasticity is developed including the effect of thermal and material diffusion. It is shown that it is quantitatively capable of explaining the observed anelasticity. Also, studies of the reflection of seismic

waves from the inner-core boundary are used to estimate the mass fraction of liquid in the inner core. (50 refs.)

78493 Isotope geochemistry of Cenozoic volcanic rocks reveals mantle heterogeneity below western USA. M.A.Menzies (Dept. of Earth Sci., Open Univ., Milton Keynes, England), W.P.Leeman, C.J.Hawkesworth. *Nature (GB)*, vol.303, no.5914, p.205-9 (19 May 1983).
Isotope geochemistry of Cenozoic volcanic rocks from the western USA demonstrates considerable mantle heterogeneity in the source regions. The Basin and Range volcanic rocks have tapped a source similar to mid-oceanic ridge basalts and the Hawaiian islands, while the magmas erupted in the Sierran Province formed in enriched grossly heterogeneous garnet bearing mantle. Within the bimodal rhyolite-basalt province of the Snake River Plain and Yellowstone National Park, there exist olivine tholeiites that have retained the primary isotopic characteristics of their mantle source area. (38 refs.)

78494 Uranium enrichment in Archean crustal basement associated with overthrusting. L.M.Lobato, J.M.A.Forman (Nuclebras, Rio de Janeiro, Brazil), W.S.Fyfe, R.Kerrick, R.L.Barnett. *Nature (GB)*, vol.303, no.5914, p.235-7 (19 May 1983).
Uranium deposits cumulatively in the 100000 tonne U_3O_8 range occur within ductile shear zones transecting Archean basement gneisses at Lagoa Real, north-east of Caetite, State of Bahia, Brazil. The authors describe the detailed geology of these deposits and discuss their origin. Limited U-Pb dating of the deposits indicates that U-mineralization occurred at ~820 Myr, involving removal of Si and K coupled with Na addition in oxidizing conditions. V, Pb and light rare-earth elements were introduced along with uranium, from hypersaline CO_2 -hydrocarbon-rich fluids, with $\delta^{18}O-4$ at temperatures of ~540°C, depths of ~15 km, and $P_{fluid} > P_{load}$. It is shown that the geological constraints are consistent with release, through hydrofracturing, of ~1000 km³ of over-pressurized-metamorphic water-recharged formation brines in the Proterozoic sediments up through the hot overlying gneisses. (33 refs.)

78495 Redox state of Earth's upper mantle from kimberlitic ilmenites. S.E.Haggerty, L.A.Tompkins (Dept. of Geology, Univ. of Massachusetts, Amherst, MA, USA). *Nature (GB)*, vol.303, no.5915, p.295-300 (26 May 1983).
Temperatures and oxygen fugacities are reported on discrete ilmenite nodules in kimberlites from West Africa which demonstrate that the source region in the upper mantle is moderately oxidized, consistent with other nodule suites in kimberlites from southern Africa and the United States. A model is presented for a variety of tectonic settings, proposing that the upper mantle is profiled in redox potential, oxidized in the fertile asthenosphere but reduced in the depleted lithosphere. (54 refs.)

78496 A seismological constraint on the depth of basalt-eclogite transition in a subducting oceanic crust. Y.Fukao, S.Hori (Dept. of Earth Sci., Nagoya Univ., Nagoya, Japan), M.Ukawa. *Nature (GB)*, vol.303, no.5916, p.413-15 (2 June 1983).
The oceanic crust primarily has a basaltic composition which must transform into eclogite on subduction of the oceanic crust beneath continents. There has been a considerable debate about the role of the basalt-eclogite transformation in driving lithospheric plate motion and in the thermal regime of subducting plates. How important this transformation is in tectonics critically depends on the depth of transformation, which is affected by factors such as temperature, bulk rock chemical composition, water content and, perhaps, stress environment. Because it would be practically impossible to evaluate all these factors correctly, the authors attempt to constrain the transformation depth by a more direct seismological method. (18 refs.)

78497 Age of the Dashkinskii Formation of the Yenisei Ridge. V.Yu.Shenfil, A.N.Didenko, V.G.Pyatiletov (Inst. of Geology & Geophysics, Acad. of Sci., Novosibirsk, USSR). *Sov. Geol. & Geophys. (USA)*, vol.23, no.3, p.37-45 (1982). Translation of: *Geol. & Geofiz. (USSR)*, vol.23, no.3, p.44-52 (1982).
A complete stratigraphic description of the deposits of the Dashkinskii Formation along the Uderey River is given. Based on finds of plant microfossils, the authors establish its Late Riphean age. The justification for identifying the lower boundary of the Bedomian, or Kudash, according to microfossils is debated. (30 refs.)

78498 The tectonic complex of Baikalian age in the Yakut ASSR. A.K.Basharin, G.S.Gusev, F.F.Tretyakov (Inst. of Geology & Geophysics, Novosibirsk, USSR). *Sov. Geol. & Geophys. (USA)*, vol.23, no.4, p.15-19 (1982). Translation of: *Geol. & Geofiz. (USSR)*, vol.23, no.4, p.19-24 (1982).
Sets forth a basic scheme for the structure of the Baikalian (Lower Proterozoic (?) to Riphean) complex that developed in the east of the Siberian platform and within the Verkhoyan-Kolyma folded region. It is stated that the separation of the Verkhoyan-Kolyma region from the platform did not occur until Middle and Late Riphean time, and that the plate complex within the platform as well as the geosynclinal complex in the Northeastern USSR were formed in the Caledonian stage of tectonic development. (18 refs.)

Gravity anomalies, seismic structure and geothermal history of the central Alps See Entry 78414

Geomagnetic field analysis. I. Stochastic inversion See Entry 78425

Group velocity distribution of surface waves in the North Atlantic See Entry 78445

Regionalization of crustal coda Q in the continental United States See Entry 78449

Three-dimensional crust and upper mantle structure at the Nevada Test Site See Entry 78457

Three-dimensional crust and upper mantle structure of the Eurasian continent See Entry 78460

The geoid, small-scale convection, and differential travel time anomalies of shear waves in the central Indian Ocean See Entry 78461

The isotopic and chemical evolution of Mount St. Helens See Entry 78500

Structure of the extremal velocity field of advective tectonic movements See Entry 78504

Temporal variation of the different parameters of the seismo-tectonic process See Entry 78505

Nucleation and growth of strike slip faults in granite See Entry 78506

Large-scale Quaternary detachments in Ventura basin, southern California See Entry 78507

Episodic rifting and volcanism at Krafla in north Iceland: growth of large ground fissures along the plate boundary See Entry 78508

The relationship between surface topography, gravity anomalies, and temperature structure of convection See Entry 78509

Mechanics of fold-and-thrust belts and accretionary wedges See Entry 78511

A detailed study of the Cobb Offset of the Juan de Fuca Ridge: evolution of a propagating rift See Entry 78512

Kerguelen hotspot source for Rajmahal Traps and Ninetyeast Ridge? See Entry 78513

Tectonophysical zoning of the juncture of the Aldan Shield and the Stanovoi Highlands according to geodesic measurements See Entry 78514

Convection under a rapidly moving plate and its appearance in the tectonics of platform areas See Entry 78515

Pore water chemistry of the mounds hydrothermal field, Galapagos Spreading Center: results from Glomar Challenger piston coring See Entry 78517

Glacial-Holocene transition in deep-sea sediments: manganese-spike in the east-equatorial Pacific See Entry 78520

Elastic anisotropy in marine sedimentary rocks See Entry 78527

Isotope composition of lead ore of some fields of the Sayan-Baikal region See Entry 78543

Porosity and hydraulic properties of sediments from the Galapagos Spreading Center and their relation to hydrothermal circulation in the oceanic crust See Entry 78566

On the terrestrial heat flow and physical limnology of Crater Lake, Oregon See Entry 78567

Thermal fading of fission tracks at variable temperature: applications to geochronology See Entry 78682

A new method for measuring radon exhalation See Entry 78700

A method of studying the Earth's crust by refracted P- and S-waves See Entry 78713

The determination of stratal velocities in horizontally layered media by the hyperboloid approximation of hodographs See Entry 78716

Anomalous bulk viscosity of two-phase fluids and implications for planetary interiors See Entry 78834

91.40 VOLCANOLOGY

78499 About the existence of two volcanic cycles within the initial volcanism of Virunga (Northern Kivu, Zaire). A.B.Kampunzu (Lab. de Petrologie, Univ. d'Aix-Marseille, Marseille, France), R.T.Lubala, J.P.H.Caron, P.-J.Vellutini. *C.R. Seances Acad. Sci. Ser. II (France)*, vol.296, no.11, p.839-44 (21 March 1983). In French.
Basalts belonging to the olivine tholeiitic series were observed underlaying the alkaline lavas of the initial stage of the Virunga volcanism in the African rift. The different terms of the alkaline series (ankaraites, basanites, hawaïites, mugearites and benmoreites) can be interpreted as the result of a fractional crystallization process. The tholeiitic and sodic alkaline lavas (first and second volcanic cycle) are related to normal faults of the rift and marks the initial fracture stage in this region. They are capped by the potassic and perpotassic alkaline lavas clearly associated with transverse faults of the rift. (19 refs.)

78500 The isotopic and chemical evolution of Mount St. Helens. A.N.Halliday, A.E.Fallick, A.P.Dickin, A.B.Mackenzie (Scottish Univs. Res. & Reactor Centre, Glasgow, Scotland), W.E.Stephens, W.Hildreth. *Earth & Planet. Sci. Lett. (Netherlands)*, vol.63, no.2, p.241-56 (May 1983).
Isotopic and major and trace element analysis of nine samples of eruptive products spanning the history of the Mount St. Helens volcano suggest three different episodes: (1) 40000-25000 years ago: eruptions of dacite with $\epsilon_{Nd} = +5$, $\epsilon_{Sr} = -10$, variable $\delta^{18}O$, $^{206}Pb/^{204}Pb \sim 18.76$, $Ca/Sr \sim 60$, $Rb/Ba \sim 0.1$, $La/Yb \sim 18$, (2) 2500-1000 years ago: eruptions of basalt, andesite and dacite with $\epsilon_{Nd} = +4$ to $+8$, $\epsilon_{Sr} = -7$ to -22 , variable $\delta^{18}O$, $^{206}Pb/^{204}Pb = 18.81-18.87$, variable Ca/Sr , Rb/Ba , La/Yb and high Zr, (3) 1000 years ago to present day: eruptions of andesite and dacite with $\epsilon_{Nd} = +6$, $\epsilon_{Sr} = -13$, $\delta^{18}O \sim 6$ per mille, variable $^{206}Pb/^{204}Pb$, $Ca/Sr \sim 77$, $Rb/Ba \sim 0.1$, $La/Yb \sim 11$. None of the products exhibits Eu anomalies and all are LREE enriched. There is a strong correlation between $^{87}Sr/^{86}Sr$ and differentiation indices. These data are interpreted in terms of a mantle heat source melting young crust bearing zircon and garnet, but not feldspar, followed by intrusion of this crustal reservoir by mantle-derived magma which caused further crustal melting and contaminated the crustal magma system with mafic components. (33 refs.)

Episodic rifting and volcanism at Krafla in north Iceland: growth of large ground fissures along the plate boundary See Entry 78508

91.45 PHYSICS OF PLATE TECTONICS

78501 Hercynian ductile deformation of granites within the Marche fault (French Central Massif): evidence for sinistral transcurrent shearing. P.Choukroune, D.Gapais, P.Matte (Univ. de Rennes, Rennes, France). *C.R. Seances Acad. Sci. Ser. II (France)*, vol.296, no.11, p.859-62 (21 March 1983). In French.

Along the Marche fault, structures and quartz fabric patterns within Hercynian syntectonic granites give evidence of large ductile transcurrent sinistral shearing. On a larger scale, the general geometry of fault pattern reflects a large rotation of bulk principal strain axes along the Hercynian belt between the Armorican Massif and the Central Massif. (13 refs.)

78502 West-American Cordillera structures, east of the Sierra Nevada: geodynamic implications. R.Blanchet, H.de La Tour du Pin, M.Le Vo (GIS Oceanologie et Geodynamique, Brest, France), F.Roure, M.Tardy, A.Villien. *C.R. Seances Acad. Sci. Ser. II (France)*, vol.296, no.11, p.863-8 (21 March 1983). In French.
From the Rocky Mountains foreland to the Sierra Nevada, the structural framework of the West-American Cordillera is hyper-allochthonous. The actual superposition of continental realms formerly severed by marine basins with unknown substratum, originated with eastward shearings, generated by Laramian and Oregonian compressive phases. The 'metamorphic core complexes' are located below the thrusting of Beltia. (12 refs.)

78503 The Kanna Thrust (IZU collision zone, central Japan): evolution of the stress regime at the Eurasian-Philippine Sea plates boundary. P.Huchon (Univ. Pierre et Marie Curie, Paris, France). *C.R. Seances Acad. Sci. Ser. II (France)*, vol.296, no.11, p.869-72 (21 March 1983). In French.
Field analysis of brittle deformation shows that two compressive events occurred during the Quaternary. The first event (NW-SE compression) is related to folding and closing of a deep trough (a subduction trench); the second event (NNE-SSW compression) corresponds to present deformation. Using stratigraphic data, these results show that the collision of Izu with

Central Japan, as a drastic change in the tectonic stress regime, occurred some 300000 years ago. (14 refs.)

78504 Structure of the extremal velocity field of advective tectonic movements. V.L.Novikov (Moscow Power Inst., Moscow, USSR). *Izv. Acad. Sci. USSR. Phys. Solid Earth (USA)*, vol.18, no.3, p.167-71 (1982). Translation of: *Izv. Akad. Nauk SSSR Fiz. Zemli*, vol.18, no.3 (1982).

The instability of a two-layer Newtonian viscous incompressible fluid under density inversion conditions is considered. On the basis of a variational principle of advection, the dependence of the structure of the extremal velocity field on the parameters of the problem is obtained. With allowance for this dependence, an attempt is made to formulate a rule for determining the shape of a moving density discontinuity surface from the known values of the mechanical and geometrical parameters of the problem. (5 refs.)

78505 Temporal variation of the different parameters of the seismotectonic process. A.A.Lukk, I.L.Nersesov (O.Yu. Schmidt Inst. of Phys. of Earth, Acad. of Sci., USSR).

Izv. Acad. Sci. USSR. Phys. Solid Earth (USA), vol.18, no.3, p.172-83 (1982). Translation of: *Izv. Akad. Nauk SSSR Fiz. Zemli*, vol.18, no.3 (1982).

Investigates the temporal variations of the elastic-wave velocities v_p , v_s and v_p/v_s , the ratio v_p/v_s , the mean depth of the earthquake foci in the interval 0-10 km, the number N_d of the earthquakes at depths of 13-40 km and the seismotectonic deformation (strain) parameters μ_M and κ , which govern the stress state and the magnitude of the intensity of the mean mechanism tensor, for the Central Garm region, from 1973 to June 1979. The authors perform a correlation analysis of the time series of the above-listed parameters and stress the need for a review of the existing concepts on the parameters v_p/v_s as an independent source of information, for purposes of elucidating the temporal variations in the development of the seismotectonic process. In comparable time series the authors identify the regular variation, which is common for all the parameters in question. There is a definite regularity in the phase shifts of this variation in the time series of the different parameters. This result is interpreted. (42 refs.)

78506 Nucleation and growth of strike slip faults in granite. P.Segall, D.D.Pollard (US Geological Survey, Menlo Park, CA, USA).

J. Geophys. Res. (USA), vol.88, no.B1, p.555-68 (10 Jan. 1983). [received: May 1983]

Fractures within granodiorite of the central Sierra Nevada, California, were studied to elucidate the mechanics of faulting in crystalline rocks, with emphasis on the nucleation of new fault surfaces and their subsequent propagation and growth. Within the study area the fractures form a single, subparallel array which strikes N50°-70°E and dips steeply to the south. Some of these fractures are identified as joints because displacements across the fracture surfaces exhibit dilation but no slip. The joints are filled with undeformed minerals, including epidote and chlorite. Other fractures are identified as small faults because they display left-lateral strike slip separations of up to 2 m. Slickensides, developed on fault surfaces, plunge 0°-20° to the east. The faults occur parallel to, and in the same outcrop with, the joints. The faults are filled with epidote, chlorite, and quartz, which exhibit textural evidence of shear deformation. These observations indicate that the strike slip faults nucleated on earlier formed, mineral-filled joints. Secondary, dilatational fractures propagated from near the ends of some small faults contemporaneously with the left-lateral slip on the faults. Other features of the faulting process are described. (30 refs.)

78507 Large-scale Quaternary detachments in Ventura basin, southern California. R.S.Yeats (Dept. of Geology, Oregon State Univ., Corvallis, OR, USA).

J. Geophys. Res. (USA), vol.88, no.B1, p.569-83 (10 Jan. 1983). [received: May 1983]

The Ventura basin is an east-north-east trending trough in the California Transverse Ranges which records major Quaternary detachment faulting at three levels. The earliest thrusting occurred along weak siltstone interbeds in a sequence dominated by competent basin-plain turbidite sandstone. Because sedimentation continued during thrusting, the age, rate, and direction of thrusting can be worked out. Faulting began 1.3 m.y. ago and ceased 0.65 m.y. ago. The fault set moved up a 45° ramp and ended as a blind thrust. The ramp had topographic expression on the seafloor affecting marine sedimentation. Following the end of deposition 0.2 m.y. ago, the competent basin-plain turbidites underwent flexural slip folding over an incompetent Miocene sequence dominated by shale. The south flank of the Ventura Avenue anticline tilted at 3.4 $\mu\text{rad/yr}$, the anticlinal crest rose at a rate of 15-16 mm/yr decelerating to 4.3-5.2 mm/yr, and the anticline and an adjacent syncline shortened at a rate of 20 mm/yr. The high rate of folding in the Ventura Avenue oil field is described. Further tectonic aspects of this area are described. (37 refs.)

78508 Episodic rifting and volcanism at Krafla in north Iceland: growth of large ground fissures along the plate boundary. E.Hauksson (Lamont-Doherty Geological Obs., Columbia Univ., Palisades, NY, USA).

J. Geophys. Res. (USA), vol.88, no.B1, p.625-36 (10 Jan. 1983). [received: May 1983]

The rifting of the plate boundary in north Iceland forms new ground fissures and reactivates old ones. Continuous growth of fissures is observed in the crust above a magma chamber beneath the Krafla caldera as it responds to changes in subterranean magma pressure. Rapid episodes of fissure formation and reactivation are observed in conjunction with magma intrusions at depth along the rift zone that constitutes the plate boundary between the North American and Eurasian plates. The Krafla caldera contains several fissures that open during periods of uplift lasting 100 to 300 days and that close incompletely in subsidence episodes lasting several hours to 3 weeks. The author describes further aspects of the rifting and describes in detail events that occurred in AD 1977 and 1980. (23 refs.)

78509 The relationship between surface topography, gravity anomalies, and temperature structure of convection. B.Parsons (Dept. of Earth & Planetary Sci., MIT, Cambridge, MA, USA), S.Daly.

J. Geophys. Res. (USA), vol.88, no.B2, p.1129-44 (10 Feb. 1983).

Normal stresses associated with convection in a fluid layer, whose boundaries can deform, produce topography on those boundaries. When the equations of the motion are linear, integral relations between topography on the boundaries and the temperature structure can be found as a function of wavelength. Expressions of this kind have been derived for the case of convection in a constant viscosity fluid when inertial effects are negligible. The total gravity anomaly is the sum of contributions due to the topography on the two boundaries and to temperature variations within the fluid, and similar integral relations between gravity and the temperature structure can also be derived. At wavelengths large compared to the depth the shape of the kernels in the integrals, particularly that for gravity, is sensitive to the boundary conditions used. The transfer function between gravity and topography is also characteristic of the boundary conditions at long wavelengths. In all the cases con-

sidered, there is a transition between short-and long-wavelength behavior which occurs at wavelengths proportional to the layer depth. If the bottom boundary can deform as well as the upper boundary, the gravity anomaly tends to zero-at long wavelengths as the gravity kernel tends to zero everywhere. (32 refs.)

78510 Constraints on extension of continental lithosphere. P.England (Dept. of Geological Sci., Harvard Univ., Cambridge, MA, USA).

J. Geophys. Res. (USA), vol.88, no.B2, p.1145-52 (10 Feb. 1983).

The extension of the continental lithosphere is considered in terms of the deformation of a thin viscous sheet with a temperature-dependent rheology which is governed primarily by the strength of the upper mantle. The lithosphere is subjected either to a constant strain rate or to a strain rate decreasing with time, corresponding to the stretching of a region of fixed volume with a constant velocity boundary condition. The progress of the extension is influenced by the decrease in strength of the lithosphere, owing to its attenuation, and by an increase in strength resulting from cooling. The relative importance of these two effects is studied. (20 refs.)

78511 Mechanics of fold-and-thrust belts and accretionary wedges. D.Davis (Dept. of Earth & Planetary Sci., MIT, Cambridge, MA, USA), J.Suppe, F.A.Dahlen.

J. Geophys. Res. (USA), vol.88, no.B2, p.1153-72 (10 Feb. 1983).

The overall mechanics of fold-and-thrust belts and accretionary wedges along compressive plate boundaries is considered to be analogous to that of a wedge of soil or snow in front of a moving bulldozer. The material within the wedge deforms until a critical taper is attained, after which it slides stably, continuing to grow at constant taper as additional material is encountered at the toe. The critical taper is the shape for which the wedge is on the verge of failure under horizontal compression everywhere, including the basal décollement. A wedge of less than critical taper will not slide when pushed but will deform internally, steepening its surface slope until the critical taper is attained. Common silicate sediments and rocks in the upper 10-15 km of the crust have pressure-dependent brittle compressive strengths which can be approximately represented by the empirical Coulomb failure criterion, modified to account for the weakening effects of pore fluid pressure. A simple analytical theory that predicts the critical tapers of subaerial and submarine Coulomb wedges is developed and tested. (49 refs.)

78512 A detailed study of the Cobb Offset of the Juan de Fuca Ridge: evolution of a propagating rift. H.P.Johnson, J.L.Karsten, J.R.Delaney (School of Oceanography, Univ. of Washington, Seattle, WA, USA), E.E.Davis, R.G.Currie, R.L.Chase.

J. Geophys. Res. (USA), vol.88, no.B3, p.2297-315 (10 March 1983).

The Cobb Offset on the northern portion of the Juan de Fuca Ridge has been identified as the tip of a northward propagating rift. Map compilations of magnetic and seismic data from four new cruises define the present locus of spreading and volcanism on the two ridge segments abutting the Offset and permit detailed modeling of the recent evolution within this transform zone. (27 refs.)

78513 Kerguelen hotspot source for Rajmahal Traps and Ninetyeast Ridge?. J.J.Mahoney, J.D.MacDougall, G.W.Lugmair (Scripps Instn. of Oceanography, La Jolla, CA, USA), K.Gopalan.

Nature (GB), vol.303, no.5916, p.385-9 (2 June 1982).

The hypothesis that hotspots are the sources of many continental flood basalts is evaluated geochemically for the proposed Rajmahal Traps—Ninetyeast Ridge—Kerguelen hotspot system. It appears that the Kerguelen hotspot did not directly feed Rajmahal magmas, although it may have provided a source of heat for Rajmahal activity. (35 refs.)

78514 Tectonophysical zoning of the juncture of the Aldan Shield and the Stanovoi Highlands according to geodesic measurements. E.E.Fotiadi, N.N.Eisikov, G.V.Bocharov, E.P.Chuprina, D.Ya.Yurenas (Inst. of Geology & Geophysics, Acad. of Sci., Novosibirsk, USSR).

Sov. Geol. & Geophys. (USA), vol.23, no.3, p.1-10 (1982). Translation of: *Geol. & Geofiz. (USSR)*, vol.23, no.3, p.3-15 (1982).

A major plan for tectonophysical zoning is developed which uses geodesic data on horizontal movements of the crust. Based on duplicate measurements of the geodesic network in the juncture zone of the southern Aldan Shield and the Stanovoi Range (1954-1979), zoning was accomplished according to the type of deformation, nature of dilation, and intensity of the variation in form with the establishment of the orientation of the major horizontal deformation axes and directions of maximal displacements. (34 refs.)

78515 Convection under a rapidly moving plate and its appearance in the tectonics of platform areas. S.A.Tychkov (Inst. of Geology & Geophys., Acad. of Sci., Novosibirsk, USSR).

Sov. Geol. & Geophys. (USA), vol.23, no.3, p.11-16 (1982). Translation of: *Geol. & Geofiz. (USSR)*, vol.23, no.3, p.15-23 (1982).

Presents some features of the tectonic development of platform areas in the Phanerozoic which could have formed due to the effects of small-scale thermal convection in the upper mantle on the lithosphere of Africa and Eurasia in the period of extensive movement of these plates. (10 refs.)

A palaeomagnetic reconnaissance of Kashmir, northwestern Himalaya, India ... See Entry 78423

Anelastic response of the Earth to a dip slip earthquake See Entry 78448

Focal depths and fault plane solutions of earthquakes under the Tibetan Plateau See Entry 78451

Seismicity near Palmdale, California, and its relation to strain changes See Entry 78456

The geoid, small-scale convection, and differential travel time anomalies of shear waves in the central Indian Ocean See Entry 78461

The West-African craton margin in eastern Senegal: a seismological study See Entry 78477

Model heat flow and [magnetotellurics] for the San Andreas and oceanic transform faults See Entry 78478

Heat transfer and intraplate deformation in the Central Indian Ocean See Entry 78487

A seismological constraint on the depth of basalt-eclogite transition in a subducting oceanic crust See Entry 78496

The tectonic complex of Baikalian age in the Yakut ASSR ... See Entry 78498

91.50 MARINE GEOLOGY AND GEOPHYSICS

78516 Neogene sedimentation and erosion in the Amirante Passage, western Indian Ocean. D.A. Johnson (Dept. of Geology & Geophys., Woods Hole Oceanographic Instn., Woods Hole, MA, USA), M.T. Ledbetter, J.E. Damuth.

Deep-Sea Res. Part A (GB), vol.30, no.2A, p.195-219 (Feb. 1983). Twenty piston cores from the northern Mascarene Basin and Amirante Passage reflect the effects of the Deep Western Boundary Current (DWBC) upon the lithologic and stratigraphic record of the Late Cenozoic. The cores span a depth interval of 3350 to 5200 m, representing the transition zone between modern Northern Atlantic Deep Water (NADW)-Circumpolar Water (CPW) and the underlying Antarctic Bottom Water (AABW). Fluctuations in the intensity of circumpolar flow rather than in the rate of production of NADW may have been the major controlling factor in the Late Tertiary erosional history of the Amirante Passage. (59 refs.)

78517 Pore water chemistry of the mounds hydrothermal field, Galapagos Spreading Center: results from Glomar Challenger piston coring. M.L. Bender (Graduate School of Oceanography, Univ. of Rhode Island, Kingston, RI, USA).

J. Geophys. Res. (USA), vol.88, no.B2, p.1049-56 (10 Feb. 1983). On DSDP Leg 70, Glomar Challenger piston coring hydrothermal MnO₂-encrusted nontronite mounds and adjacent pelagic sediments through to basement. Pore waters were collected by centrifuging, squeezing, and in situ sampling; analyses are presented here for Ca, Mg, Si, NH₃, Mn, and Fe. The results confirm Maris and Bender's (1982) conclusions that hydrothermal solutions enriched in Ca by 1-2 mM and depleted in Mg by ~2 mM are upwelling through the mounds and the surrounding pelagic sediments. Si, NH₃, and Mn²⁺ concentrations generally increase upcore, reflecting addition of products of metabolic reactions to upwelling hydrothermal solutions. Pore water iron concentrations decrease upcore, probably as a result of oxidation and precipitation of upwelling hydrothermal iron. The formation of nontronite involves oxidation of dissolved Fe²⁺. (45 refs.)

78518 Constraints upon water advection in sediments of the Mariana Trough. D.H. Abbott, W. Menke (Dept. of Geological Sci., Columbia Univ., Palisades, NY, USA), R. Morin.

J. Geophys. Res. (USA), vol.88, no.B2, p.1075-93 (10 Feb. 1983). Thermal gradient measurements, consolidation tests, and pore water compositions from the Mariana Trough imply that water is moving through the sediments in areas with less than about 100 m of sediment cover. The maximum advection rates implied by the thermal measurements and consolidation tests may be as high as 10⁻⁵ cm s⁻¹ but are most commonly in the range of 1 to 5 × 10⁻⁶ cm s⁻¹. Theoretical calculations of the effect of the highest advection rates upon carbonate dissolution indicate that dissolution may be impeded or enhanced (depending upon the direction of flow) by a factor of 2 to 5 times the rate for diffusion alone. (35 refs.)

78519 Longshore motion generated on beaches by obliquely incident bores. S.C. Ryrie (School of Maths., Univ. of Bristol, Bristol, England).

J. Fluid Mech. (GB), vol.129, p.193-212 (April 1983). Numerical solutions of the two-dimensional shallow-water equations are found for motion on a sloping beach generated by a single bore and by a periodic succession of bores, both incident at small angles. For the latter, periodic longshore motion can always be found if bottom friction (described by the Chezy law) is included. The timescale of the development of longshore motion is also considered. (21 refs.)

78520 Glacial-Holocene transition in deep-sea sediments: manganese-spike in the east-equatorial Pacific. W.H. Berger, R.C. Finkel, J.S. Killingley (Scripps Instn. of Oceanography, Univ. of California, San Diego, La Jolla, CA, USA), V. Marchig.

Nature (GB), vol.303, no.5914, p.231-3 (19 May 1983). Over large areas of the tropical Pacific, calcareous sediments show one or more dark-coloured manganese-rich layers within the uppermost 40 cm of the record. In the east-equatorial Pacific two layers are strongly developed, with the upper one appearing as a double layer in places. The authors report that the lower layer is centred on the glacial-Holocene boundary. Evidence is presented that shows its origin is tied to a pronounced drop in fertility of the ocean. Such a fertility decrease is implicit in a weakening of east-equatorial upwelling systems. If real, it has important ramifications for the history of oceanic (and atmospheric) chemistry. (39 refs.)

78521 Iron-manganese concretions on the ocean bed. E.S. Bazilevskaya. *Priroda (USSR)*, no.3, p.88-93 (1983). In Russian.

The results obtained from the 28-month voyage of the 'Dmitrii Mendeleev' scientific research vessel in the equatorial zone of the Pacific Ocean to study the iron-manganese concretions are discussed. Particular reference is made to the problem of determining the valence state of the manganese in the concretions and the underlying sediments as well as the problem of determining the mobility or the chemical reactions involving Fe, Cu, Ni, Zn and Co. The mechanism by which the iron-manganese concretions are formed is considered. (1 ref.) L.M.H.

Velocity and attenuation anisotropy in deep-sea carbonate sediments See Entry 78462

Heat transfer through the sediments of the mounds hydrothermal area, Galapagos Spreading Center at 86°W See Entry 78486

Numerical models for the hydrothermal field at the Galapagos Spreading Center See Entry 78488

Heat flow on the western flank of the East Pacific Rise at 21°N See Entry 78489

Anomalous heat flow in the northwest Atlantic: a case for continued hydrothermal circulation in 80-m.y. crust See Entry 78490

Diagenesis of magnetic minerals in Recent haemipelagic sediments See Entry 78539

Large particle transport of plutonium and other fallout radionuclides to the deep ocean See Entry 78561

Porosity and hydraulic properties of sediments from the Galapagos Spreading Center and their relation to hydrothermal circulation in the oceanic crust See Entry 78566

Relation between the changes of clay mineralogy in the cores of marine deposits and the paleoclimatic vicissitudes See Entry 78642

Measurement of ⁵³Mn in deep-sea iron and stony spherules See Entry 78883

91.60 PHYSICAL PROPERTIES OF ROCKS AND MINERALS

78522 Discussion and supplement to 'The stress state of rock and lining in viscoelastic-plastic rock media'. Wang Tsejun (Station of Water Resources & Electric Power, China), Zhu Weishen.

Acta Mech. Sin. (China), no.1, p.95-101 (1983). In Chinese. This is a discussion of a previous paper, 'The stress state of rock and lining in viscoelastic-plastic rock media' (ref. unobtainable). Formulae are revised to include considerations of the existence of deteriorated plastic region in the rock. The authors provide a method to calculate the proper lining time by taking into account the relative action of rock and lining. It is considered that when the lining rigidity is smaller or when its thickness is very thin, there can be a deteriorated plastic region in the rock. This case can also be calculated. Meanwhile some mistakes are corrected in the original paper. (no refs.)

78523 A computerized database for the mechanical properties of coal. M. Costantino (Lawrence Livermore Nat. Lab., Livermore, CA, USA).

Comput. & Geosci. (GB), vol.9, no.1, p.53-8 (1983). (First Annual Conference on 'The Management, Analysis, and Display of Geoscience Data', Golden, CO, USA, 27-29 Jan. 1982). A relational database containing experimental data for the mechanical properties of US and foreign coals is described. Data on the failure curve (compressive strength), hydrostat, Young's modulus, shear modulus, Poisson's ratio, bulk modulus and compressional and shear wave speeds are included, along with references to the original publications. The database contains approximately 50 references and 5000 data entries. (29 refs.)

78524 TRM, ARM and Isr of two natural magnetites of MD and PSD grain size. R.L. Hartstra (Palaeomagnetic Lab., Utrecht, Netherlands).

Geophys. J. R. Astron. Soc. (GB), vol.73, no.3, p.719-37 (June 1983). TRM, ARM and Isr stabilities with respect to alternating fields and high- and low-temperature treatment are compared for a set of artificial rock specimens. The specimens contain grain-size fractions of a homogeneous natural magnetite and a natural magnetite showing exsolution lamellae. The grain-size fractions are in the PSD-MD range and vary between <5 and 250 μm. The use of ARM instead of TRM to determine palaeointensities is discussed in relation to the results obtained. The results of the study are discussed in terms of a remanence composed of PSD surface moments and MD and PSD bulk moments. (43 refs.)

78525 Piezoelectric fabrics of quartz-bearing rocks and their symmetry properties. A.N. Nikitin, E.I. Parkhomenko (O.Yu. Schmidt Inst. of Phys. of Earth, USSR).

Izv. Acad. Sci. USSR. Phys. Solid Earth (USA), vol.18, no.2 (1982). Translation of: *Izv. Akad. Nauk SSSR Fiz. Zemli*, vol.18, no.2, p.104-10 (1982). It was proved experimentally on specimens of vein quartz that the most reliable determination of the type of symmetry of a piezoelectric fabric of a rock is that based on the property of the nature of the symmetry of the fabric being reflected in the structure of the electric field arising in piezoelectric polarization of a rock specimen. The conditions necessary for determining the order of the axes of symmetry of the piezoelectric fabrics of rocks were found experimentally. Criteria are formulated for the unambiguous determination of the type of symmetry of the piezoelectric fabric of a rock. (9 refs.)

78526 Use of magnetic susceptibility tensor for solving problems in structural geology. V.N. Zavoyskiy (S.I. Subbotin Inst. of Geophys., Acad. of Sci., Ukrainian SSR).

Izv. Acad. Sci. USSR. Phys. Solid Earth (USA), vol.18, no.3, p.217-23 (1982). Translation of: *Izv. Akad. Nauk SSSR Fiz. Zemli*, vol.18, no.3 (1982). Analyzes the relationship between the character of plastic deformation in natural rock outcrops and the eigendirections of the tensor of irreversible magnetic susceptibility, determined on oriented rock samples. It is found that the orientation of the eigendirection corresponding to the maximum eigenvalue of the susceptibility tensor is governed by shearing deformation of the rock. The author gives examples to illustrate the use of measurements of magnetic susceptibility tensor for solving problems concerning the structural geology of different kinds of rocks of the Ukrainian shield. (10 refs.)

78527 Elastic anisotropy in marine sedimentary rocks. R.T. Bachman (Naval Ocean Systems Center, San Diego, CA, USA).

J. Geophys. Res. (USA), vol.88, no.B1, p.539-45 (10 Jan. 1983). [received: May 1983]

Measurements of four of the five elastic stiffnesses of marine calcareous rocks and estimates of the fifth, c_{13} , allow more detailed discussion of elastic wave propagation in these rocks than previously possible. The constant c_{13} , which is seldom measured and was not measured in the rocks of this study, was derived by equating the Gassmann and Hashin-Shtrikman estimates of the bulk moduli of chalk and limestone and then solving for the single unknown c_{13} . On the basis of these measurements and estimates, the effect of elastic anisotropy on seismic reflection determinations of vertical compressional wave speed in calcareous rocks below the Earth's surface is small ($\pm 6\%$), whereas similar determinations of vertically polarized shear wave speeds may be unreliable. Relationships are provided to convert seismic refraction measurements of horizontal compressional wave velocity to vertical velocity. (46 refs.)

78528 Microcrack connectivity in rocks: a renormalization group approach to the critical phenomena of conduction and failure in crystalline rocks. T.R. Madden (Dept. of Earth & Planetary Sci., MIT, Cambridge, MA, USA).

J. Geophys. Res. (USA), vol.88, no.B1, p.585-92 (10 Jan. 1983). [received: May 1983]

A study is made of the critical phenomena associated with the onset of electrical conductivity and the onset of failure in a rock with a random distribution of microcracks using a renormalization group theory approach. The interaction between different length scales is an important element in the theory, which is a departure from the results of equivalent media theory. The crack parameter that determines if the rock can conduct or is to fail is the crack count per unit area times the square of the crack length. The parameter space is divided up into regions or phases. These phases are those of no conduction and no failure, conduction and no failure, and conduction and failure. The predictions of the model agree well with SEM data on the microcrack populations of stressed and unstressed rock samples. The crack densities seen in unstressed Westerly granite fall in the range that predicts conduction but no failure. (17 refs.)

78529 Study of ¹⁸O diffusion in magnesium orthosilicate by nuclear microanalysis. O. Jaoul, B. Houlier (Lab. de Geophys. et Geodynamique Interne, Univ. Paris-Sud, Orsay, France), F. Abel.

J. Geophys. Res. (USA), vol.88, no.B1, p.613-24 (10 Jan. 1983). [received: May 1983] The self-diffusion of ¹⁸O-enriched oxygen in forsterite was determined by measuring the bulk concentration using the nuclear reaction ¹⁸O(p,α)¹⁵N. Important technical improvements led to a more precise determination of the

¹⁸O diffusion profiles. These results indicate that the self-diffusion coefficient D^* is independent of the annealing duration and the oxygen partial pressure. In addition, the D^* values are found to be lower by nearly 1 order of magnitude than those previously published (preexponential factor $D_0 \sim 2.3 \times 10^{-6} \text{ cm}^2/\text{s}$, activation energy, $\sim 70 \text{ kcal/mole}$). (33 refs.)

78530 Domain wall resonance and stability in magnetite. G.M. Smith, R.T. Merrill (Geophys. Program, Univ. of Washington, Seattle, WA, USA). *J. Geophys. Res. (USA)*, vol.88, no.B1, p.637-44 (10 Jan. 1983). [received: May 1983]

An understanding of the factors governing domain wall stability is crucial to any attempt to model remanence in multidomain materials. This paper introduces a technique to the study of multidomain remanence which has not previously seen application in rock magnetism: domain wall resonance (DWR). It is shown that the variation of the DWR spectra with different RF power levels gives useful, and hitherto unavailable, information about the nature of the potentials which govern domain wall motion. In particular, the authors demonstrate that these potentials must rise less rapidly than a harmonic potential, contrary to previous models. The possible mechanisms for domain wall pinning are discussed and it is concluded that the likeliest candidates for pinning sites in the authors' samples, at least, are large nonuniform dislocation arrays. Finally, a possible method for selectively demagnetizing multidomain grains based on DWR techniques is described. (37 refs.)

78531 On the stability of shear cracks and the calculation of compressive strength. J.K. Dienes (Los Alamos Nat. Lab., Los Alamos, NM, USA). *J. Geophys. Res. (USA)*, vol.88, no.B2, p.1173-9 (10 Feb. 1983).

Griffith's 1921 theory of crack stability is extended to account for the frictional energy dissipation associated with interfacial sliding when the crack faces are in contact. This global energy balance approach is essentially different from Griffith's 1924 local theory of compression cracks, which assumes that instability occurs when the stress at any point exceeds the intrinsic strength of the material. An explicit expression for critical crack size in compression is obtained. On the basis of this expression the authors find the most critical crack orientation and define theoretical strength as the critical stress for that orientation. This uniaxial compression strength significantly exceeds the tensile strength. For example, when the coefficient of friction is unity, the ratio of compressive to tensile strength is 8.7, and the crack plane lies at 13° to the loading direction. Following this, the heating due to interfacial sliding is found by a one-dimensional thermoelastic analysis. It is concluded that under normal conditions the stress field acting on the crack faces is only slightly affected by frictional heating, though the temperature rise may be very high, and melting may occur within microseconds. (15 refs.)

78532 The dependence of fracture mechanical and fluid flow properties on fracture roughness and sample size. Y.W. Tsang, P.A. Witherspoon (Lawrence Berkeley Lab., Univ. of California, Berkeley, CA, USA).

J. Geophys. Res. (USA), vol.88, no.B3, p.2359-66 (10 March 1983). A parameter study has been carried out to investigate the interdependence of mechanical and fluid flow properties of fractures with fracture roughness and sample size. A rough fracture can be defined mathematically in terms of its aperture density distribution. Correlations were found between the shapes of the aperture density distribution function and the specific fractures of the stress-strain behavior and fluid flow characteristics. Well-matched fractures had peaked aperture distributions that resulted in very nonlinear stress-strain behaviour. With an increasing degree of mismatching between the top and bottom of a fracture, the aperture density distribution broadened and the nonlinearity of the stress-strain behavior became less accentuated. The different aperture density distributions also gave rise to qualitatively different fluid flow behavior. Findings from this investigation make it possible to estimate the stress-strain and fluid flow behavior when the roughness characteristics of the fracture are known. (7 refs.)

78533 Investigation of internal friction in fused quartz, steel, Plexiglass, and Westerly granite from 0.01 to 1.00 Hertz at 10^{-8} to 10^{-7} strain amplitude. H.-P. Liu, L. Peselnick (US Geological Survey, Menlo Park, CA, USA).

J. Geophys. Res. (USA), vol.88, no.B3, p.2367-79 (10 March 1983). A detailed evaluation on the method of internal friction measurement by the stress-strain hysteresis loop method from 0.01 to 1 Hz at 10^{-8} to 10^{-7} strain amplitude and 23.9°C is presented. The values of Q_s^{-1} (internal friction under uniaxial compression) determined from the relative phase measurements are $|Q_s^{-1} - Q_s^{-1}| < 2.8 \times 10^{-3}$ for the tool steel sample and $|Q_s^{-1} - Q_s^{-1}| < 2.2 \times 10^{-3}$ for the Westerly granite sample, where Q_s^{-1} is the internal friction of the fused quartz stress sensor under uniaxial compression. These values are consistent with those inferred from the relative modulus dispersion data also presented in this paper. The polymethyl methacrylate (PMM, trade name Plexiglass) sample shows high values of internal friction ($Q_s^{-1} \approx 5 \times 10^{-2}$) with strong frequency dependence and with a maximum in Q_s^{-1} at $\approx 0.4 \text{ Hz}$. (23 refs.)

78534 Deformation of single-crystal clinopyroxenes. II. Dislocation-controlled flow processes in Hedenbergite. J.J. Kolle, J.D. Blacic (Los Alamos Sci. Lab., Los Alamos, NM, USA).

J. Geophys. Res. (USA), vol.88, no.B3, p.2381-93 (10 March 1983). For pt.1 see *ibid.*, vol.87, no.B5, p.4019-34 (1982). Laboratory deformation experiments were carried out on two single-crystal clinopyroxenes: chrome diopside and hedenbergite. The tests were made in a Griggs solid-medium, triaxial, and creep tester. A confining pressure of 1000 MPa was applied in all the experiments. The crystals were deformed at strain rates from 10^{-4} s^{-1} to 10^{-8} s^{-1} and at temperatures from 400°C to 1200°C . Two orientations of the crystals with respect to the maximum principal compressive stress were tested. The authors present results of experiments on (mainly) hedenbergite oriented such that twinning is not possible and deformation occurs by a dislocation-controlled flow process. Empirical flow laws for hedenbergite are presented and contrasted with the twinning results. (18 refs.)

78535 Electrical conductivity of molten basalt and andesite to 25 kilobars pressure: geophysical significance and implications for charge transport and melt structure. J.A. Tyburczy, H.S. Waff (Dept. of Geology, Univ. of Oregon, Eugene, OR, USA).

J. Geophys. Res. (USA), vol.88, no.B3, p.2413-30 (10 March 1983). Electrical conductivities of molten Hawaiian tholeiite and Crater Lake andesite were measured between 1200°C and 1400°C at atmospheric pressure and at pressures up to 17 and 25 kbar, respectively. Isobaric plots of $\log \sigma$ versus $1/T$ (σ is electrical conductivity) are linear, with the exception of the zero pressure tholeiite melt data. Conductivities decrease with increasing pressure in both melts, with the andesitic melt exhibiting a greater pressure dependence. Between 5 and 10 kbar, abrupt decreases in the slopes of isothermal $\log \sigma$ versus P plots (i.e. decreases in activation volume) are observed for both rock melts. This discontinuity probably reflects changes in melt structure, as opposed to changes in conduction mechanism. A qualitative model involving depolymerization of the melt with increased pressure leading to increased efficiency of packing can explain the observed discontinuity in activation volume as well as the observed pressure dependences of other melt physical properties such as viscosity and density. (89 refs.)

78536 Shock temperatures of SiO_2 and their geophysical implications. G.A. Lyzenga, T.J. Ahrens (Seismological Lab., California Inst. of Technol., Pasadena, CA, USA), A.C. Mitchell.

J. Geophys. Res. (USA), vol.88, no.B3, p.2431-44 (10 March 1983). The temperature of SiO_2 in high-pressure shock states has been measured for samples of single-crystal α -quartz and fused quartz. Pressures between 60 and 140 GPa have been studied using projectile impact and optical pyrometry techniques. Both data sets indicate the occurrence of a shock-induced phase transformation at ~ 70 and $\sim 50 \text{ GPa}$ along the α - and fused quartz Hugoniot, respectively. The suggested identification of this transformation is the melting of shock-synthesized stishovite, with the onset of melting delayed by metastable superheating of the crystalline phase. Some evidence for this transition in conventional shock wave equation of state data is given, and when these data are combined with the shock temperature data, it is possible to construct the stishovite-liquid phase boundaries. The melting temperature of stishovite near 70 GPa pressure is found to be 4500K . (29 refs.)

78537 Nuclear magnetic resonance of silica polymorphs. J.V. Smith (Dept. of the Geophys. Sci., Univ. of Chicago, Chicago, IL, USA), C. Scott Blackwell.

Nature (GB), vol.303, no.5914, p.223-5 (19 May 1983). The chemical bonding in silica polymorphs and silicates can be studied by both experimental and theoretical methods. Spinning at the octahedral (magic) angle yields sharp peaks in the NMR patterns for ^{29}Si and ^{27}Al . The authors report magic angle spinning (MAS) spectra for seven polymorphs of silica and interpret the chemical shifts empirically in terms of interatomic distances and angles determined by X-ray diffraction. The conclusions provide a partial basis for quantitative interpretation of spectra for framework aluminosilicates, especially zeolite molecular sieves; additional effects from aluminium substitution and nonframework atoms will need to be evaluated. (29 refs.)

78538 Olivine to spinel transformation in Mg_2SiO_4 via faulted structures. J.N. Boland (Inst. of Earth Sci., State Univ. of Utrecht, Utrecht, Netherlands), Lin-gun Liu.

Nature (GB), vol.303, no.5914, p.233-5 (19 May 1983). The authors report the results of transmission electron microscopy of the $\alpha \rightarrow \gamma$ high-pressure transformation in the pure end-member olivine, forsterite (Mg_2SiO_4). Not only is there a special orientation relationship between the two phases during the transformation, that is, $(100)_{\text{OI}}$ is parallel to $(111)_{\text{SP}}$ and $[001]_{\text{OI}}$ parallel to $[110]_{\text{SP}}$, but some of the residual olivine grains have an extremely high density of stacking faults in $(100)_{\text{OI}}$ as well as a high dislocation density. (14 refs.)

78539 Diagenesis of magnetic minerals in Recent hemipelagic sediments. R. Karlin, S. Levi (School of Oceanography, Oregon State Univ., Corvallis, OR, USA).

Nature (GB), vol.303, no.5915, p.327-30 (26 May 1983). Rapidly deposited sediments from marine and lake environments are being used increasingly to study decadal to millennial fluctuations in the Earth's magnetic field. The objectives are to gain more fundamental understanding of the geodynamo and to establish a new dating technique for sediments. The authors report downcore magnetic profiles from undisturbed Kasten cores taken in rapidly deposited laminated sediments from the Gulf of California and in bioturbated hemipelagic muds on the Oregon continental slope which give apparently reliable directions, but show dramatic decreases in the intensities of natural and artificial remanences with depth. (16 refs.)

78540 Thermal behavior of fine-grained soils. L.A. Salomone, W.D. Kovacs, H. Wechsler.

Report NBS-BSS-149, Nat. Bur. Stand., Washington, DC, USA (Nov. 1982), xii+91 pp.

Laboratory thermal probe tests performed on an AASHTO standard reference material (a silty clay) showed that thermal resistivity ($^\circ\text{C}\cdot\text{cm}/\text{watt}$) varies with soil moisture content and dry density. The tests were performed to correlate soil thermal behavior with the limit states of fine-grained soils. Over 80 thermal resistivity measurements were made on specimens compacted to various densities and moisture contents. (27 refs.)

Heat capacity, relative enthalpy, and calorimetric entropy of silicate minerals: an empirical method of prediction See Entry 76655

Strain dependent attenuation: observations and a proposed mechanism See Entry 78450

In situ studies of velocity in fractured crystalline rocks See Entry 78463

Nucleation and growth of strike slip faults in granite See Entry 78506

Thermophysical properties of the basic varieties of rocks in the Irkutsk amphitheater See Entry 78544

The dynamic tensile strength of ice and ice-silicate mixtures .. See Entry 78833

91.65 GEOPHYSICAL ASPECTS OF GEOLOGY, MINERALOGY AND PETROLOGY

78541 Microwave emissions from soils with rough surfaces. L. Tsang (Electrical Engng. Dept., Texas A&M Univ., College Station, TX, USA), R.W. Newton.

J. Geophys. Res. (USA), vol.87, no.C11, p.9017-24 (20 Oct. 1982). [received: May 1983]

The effect of surface roughness on the thermal microwave emission of soils has been studied with the Kirchhoff approach. A model is presented that includes both the coherent and incoherent reflectivities of the rough surface. It is demonstrated that both the coherent and incoherent terms must be included in order for theoretical computations to provide good agreement with the experimental data, especially for wet soil, where surface roughness causes a dramatic increase in brightness temperature. In addition, the model including both the coherent and incoherent terms allows one to use the physically measured surface height deviations of the rough surface in the model. Previous models have required that an effective height, not equal to the actual surface height measurements, be used in order for theoretical computations to match measurements. (25 refs.)

78542 Dual nature of ignimbrites. N.V. Koronovskii.

Priroda (USSR), no.3, p.12-18 (1983). In Russian. The special characteristics of ignimbrites, acidic volcanic rocks consisting of volcanic glass and mineral phenocrysts such as quartz, feldspar and pyroxenes, are examined, in particular their dual nature as lavas and brecciated (pyroclastic) volcanogenic rocks. The history of the study of ignimbrites is traced. The acidic volcanic rocks are analysed and divided into two groups—those characterised by extremely small volumes and comprising short lava flows, extruded domes and subvolcanic massifs and those characterised by striation and elongated lens-shaped inhomogeneities. The nature and origins of inhomogeneities in the glass of ignimbrites are discussed as well as the viscosity of acidic ignimbrite melts. From the analysis of the nature of ignim-

brites, a mechanism is postulated for the formation of the lava ignimbrites. (3 refs.) L.M.H.

78543 Isotope composition of lead ore of some fields of the Sayan-Baikal region. N.V.Vilor, N.N.Fefelov, V.N.Solodiyankina, S.B.Brandt (Inst. of Earth's Crust, Acad. of Sci., Irkutsk, USSR). *Sov. Geol. & Geophys. (USA)*, vol.23, no.3, p.57-61 (1982). Translation of: *Geol. & Geofiz. (USSR)*, vol.23, no.3, p.65-70 (1982). Discusses lead isotope studies of lead ore in some gold ore and polymetal fields of the folded framework of the Siberian Platform. Interpretation of isotope data is proposed in terms of a two-stage model, according to which the formation of the ore field in the Sayan-Baikal folded belt could be connected with two major tectonic-magmatic cycles: Middle Proterozoic (1750 ± 75 million years) and Caledonian (460 million years). (19 refs.)

78544 Thermophysical properties of the basic varieties of rocks in the Irkutsk amphitheater. R.P.Dorofeeva (Inst. of Earth's Crust, Irkutsk, USSR). *Sov. Geol. & Geophys. (USA)*, vol.23, no.4, p.103-5 (1982). Translation of: *Geol. & Geofiz. (USSR)*, vol.23, no.4, p.113-15 (1982). Results of an experimental determination of thermal parameters of rocks in the sedimentary cover and the crystalline basement of the Irkutsk amphitheater are discussed. Histograms of the distribution of the coefficients of thermal and temperature conductivity and rock density are constructed. (2 refs.)

Lower Jurassic magnetostratigraphy at the Breggia Gorge (Ticino, Switzerland) and Alpe Turati (Como, Italy) See Entry 78428

Velocity and attenuation anisotropy in deep-sea carbonate sediments See Entry 78462

Age of the Dashkinskii Formation of the Yenisei Ridge See Entry 78497

Use of magnetic susceptibility tensor for solving problems in structural geology See Entry 78526

Nuclear magnetic resonance of silica polymorphs See Entry 78537

91.90 OTHER TOPICS IN SOLID EARTH GEOPHYSICS

78545 Modelling of flow phenomena in porous media. L.Balla (Petroleum Engng. Res. Lab., Hungarian Acad. of Sci., Budapest, Hungary). *Acta Geod. Geophys. & Montan. (Hungary)*, vol.17, no.3-4, p.317-28 (1982). The modelling of flow phenomena in porous media is dealt with. Based on mathematical correlations of the flow, the scaling criteria are described and their suitability for practical use is analyzed. The scaling criteria derived require that the porous structure of the model and that of the prototype should be the same. Further investigations are, however, needed to reproduce the porous structure of the prototype in the model because the parameters characterizing the porous structure are theoretically not yet defined unambiguously and there is no exact measurement method available. Further investigations are required to decide whether the permeability and exponent of the capillary pressure function can unambiguously characterize the porous structure from the point of view of fluid mechanics, or some further parameters have to be defined. If the parameters characterizing the porous structure are unambiguously defined, the next task is to analyse the effect of these parameters on the relative permeability and the wettability, and to express mathematically these relationships. Knowing the parameters characterizing the porous structure and their effect on other parameters influencing the flow, the mathematical model of the flow can be modified. (12 refs.)

78546 Vibration effect and its influence on exogenous geological processes. B.P.Agaonov (Inst. of Earth's Crust, Irkutsk, USSR). *Sov. Geol. & Geophys. (USA)*, vol.23, no.4, p.89-96 (1982). Translation of: *Geol. & Geofiz. (USSR)*, vol.23, no.4, p.95-103 (1982). Reveals some perspectives on the study of exogenous geological processes from the point of view of the influence of natural and technogenic vibration sources on the development of these processes. The influence of vibration sources manifests itself both in slow, imperceptible microshifts of soils and in local stripping movements. Four morphological varieties of stripping are distinguished. Torrents and avalanches are regarded as factors of their own vibration generation, and therefore, of their own self-development. Questions are broached which concern the creation of rock slides and the separation of particles of heavy minerals under the influence of vibration forces. (15 refs.)

78547 Lightning craters. S.Campbell. *Weather (GB)*, vol.38, no.4, p.106-9 (April 1983). Discusses the origin of several craters found at Monynut Edge (1963, July), East Lotherian. The author discusses various possibilities and concludes that they were formed due to lightning. (9 refs.)

Topical Meeting on Optical Techniques for Remote Probing of the Atmosphere. Technical Digest See Entry 74221

Elastic-wave radiation during a camouflaged explosion See Entry 78446

Microwave emissions from soils with rough surfaces See Entry 78541

Threshold friction velocities and rupture moduli for crusted desert soils for the input of soil particles into the air See Entry 78601

Climatic influence of background and volcanic stratosphere aerosol models See Entry 78640

Different atmospheric effects in remote sensing of uniform and nonuniform surfaces See Entry 78649

Frost mapping in southern Victoria: an assessment of HCMM thermal imagery See Entry 78656

Radial characteristics of focusing probes of magnetoelectric logging See Entry 78711

Crater ejecta scaling laws: fundamental forms based on dimensional analysis See Entry 78835

92.00 HYDROSPHERIC AND ATMOSPHERIC GEOPHYSICS

(for marine geology and geophysics, see 91.50)

92.10 PHYSICS OF THE OCEANS

(see also 43.30 Underwater sound)

78548 The kinematics of a stochastic field of internal waves modified by a mean shear current. H.Peters (Inst. für Meereskunde, Kiel, Germany). *Deep-Sea Res. Part A (GB)*, vol.30, no.2A, p.119-48 (Feb. 1983). Modes and dispersion curves of high-frequency internal waves are calculated from observed profiles of the Brunt-Vaisala frequency and of the mean shear current. Cases treated are from the tropical Atlantic (GATE) and from the North Atlantic (JASIN). The dispersion characteristics are anisotropic. The feature increases in importance with increasing frequency, wavenumber, and mode number. The mean shear strongly deforms the eigenfunctions for modes 2 and higher at upstream wave directions, and separated wave guides occur at different depths. The higher the mode number, the more effective is the critical-layer absorption. By means of the stochastic superposition of shear modes a model of the kinematics of a field of free, linear internal waves is constructed for the GATE situation. (21 refs.)

78549 The translation of isolated cold eddies on a sloping bottom. D.Nof (Dept. of Oceanography, Florida State Univ., Tallahassee, FL, USA). *Deep-Sea Res. Part A (GB)*, vol.30, no.2A, p.171-82 (Feb. 1983). A two-layer analytical model is considered to examine the dynamics of cold isolated patches on the ocean floor. Such patches have been observed in the North Atlantic Ocean and are characterized by a bounding interface that intersects the bottom along a closed curve. They correspond, therefore, to isolated anticyclonic eddies with a lens-like cross section. The model incorporates steady movements resulting from the swirl velocity within the eddy and a topographically-induced translation. For steady motions, analytical solutions are obtained using the full equations of motion in a coordinate system moving with the eddy itself. (18 refs.)

78550 Upwelling along the 60-m isobath from Cape Canaveral to Cape Hatteras and its relationship to fish distribution. L.P.Atkinson, T.E.Targett (Skidaway Inst. of Oceanography, Savannah, GA, USA). *Deep-Sea Res. Part A (GB)*, vol.30, no.2A, p.221-6 (Feb. 1983). During a cruise north in the Gulf Stream from Cape Canaveral to Cape Hatteras several zones of upwelling were observed. Acoustic measurements suggested that fish aggregations were associated with areas of upwelling. Surface salinity and alongshore velocity observations suggest an offshore flow of shelf water in the 32 to 33°N area. (26 refs.)

78551 On perturbations of harmonic constants in the Thames Estuary. M.Amin (Inst. of Oceanographic Sci., Bidston Obs., Birkenhead, England). *Geophys. J. R. Astron. Soc. (GB)*, vol.73, no.3, p.587-603 (June 1983). A long series of South-east sea-level observations (1929-79) is analysed using the harmonic method of tidal analysis. This method introduces a systematic error in tidal analysis and prediction. It is observed that small secular trends are present in amplitudes and phase lags of some principal tidal constituents. The influence of these secular trends in amplitudes is to increase the tidal range and extreme levels. A comparison of old records with tides synthesized by modern constituents for London Bridge suggests that the phase of the tide was almost stable there from 1683 to 1835; then a large change occurred after 1835. Similar changes are noted in the tidal range. The nature of these changes is discussed. (16 refs.)

78552 Experiments on solitary internal Kelvin waves. T.Maxworthy (Dept. of Mech. & Aerospace Engng., Univ. of Southern California, Los Angeles, CA, USA).

J. Fluid Mech. (GB), vol.129, p.365-83 (April 1983). Elementary calculations indicate that the effect of the Earth's rotation is likely to be important in the dynamics of most internal waves in oceans, lakes and the atmosphere. The author presents measurements of the structure and properties of one class of such waves, namely solitary internal Kelvin waves, in which the Coriolis force generated by wave motion in a stratified fluid is opposed by a pressure gradient and hence change in wave amplitude along its crest. The author confirms that the wave speed is independent of the rate at which the system rotates and depends only on the stratification and maximum wave amplitude. However, rotation is shown to have a large effect on both the rate at which the amplitude varies with time and the 'cross-stream' structure of the wave. In accordance with well-established theory, the amplitude transverse to the direction of propagation varies exponentially. This results in a decreasing wave speed with increasing distance from the wall, which in turn requires the wave front to be curved backwards in order for the wave as a whole to propagate at a speed given by its maximum amplitude. Such a front curvature is not contained within the available theories. (29 refs.)

78553 Barge motions in random seas—a comparison of theory and experiment. D.T.Brown, R.Eatock Taylor, M.H.Patel (Dept. of Mech. Engng., London Centre for Marine Technol., Univ. Coll. London, London, England). *J. Fluid Mech. (GB)*, vol.129, p.385-407 (April 1983).

Describes a comparison of experimental data and theoretical results for the motions in waves of large flat-bottomed barges having zero forward speed. The experimental data are derived from model tests at two scales (1:36 and 1:108). These consist of measurements of motions in surge, sway, heave, roll, pitch and yaw to long-crested seas approaching the barge models at two orientation angles (head and beam seas). The experimental data are compared with results computed from linearized potential-flow theory, which accounts for the diffraction and radiation of gravity waves around the barge. The boundary-integral scheme employed to solve this potential-flow problem is briefly reviewed. The experimental data at two scales and the theoretical results show that potential-flow theory is in reasonable agreement with experimental data for all motions except roll near resonance. These roll-motion discrepancies, due to vortex shedding from bilge-keel edges, are discussed. Some of the observable effects of scale in the model tests are highlighted. (11 refs.)

78554 An advective solution of a zonally uniform thermocline regime. P.F.Hodnett (Dept. of Appl. Math., Nat. Inst. for Higher Education, Limerick, Ireland). *Proc. R. Ir. Acad. Sect. A (Ireland)*, vol.82A, no.2, p.187-99 (Dec. 1982). [received: May 1983]

The thermocline region of a large ocean is driven by a surface wind stress and a surface temperature which are independent of longitude. An advective solution is derived where motion takes place under geostrophic and hydrostatic balance and heat is transferred by convection only. Proper account is taken of the Earth's spherical geometry. It is found that the advective solution can satisfy all the boundary conditions, i.e. (i) the bottom velocity condition, (ii) the surface velocity condition and (iii) the surface temperature

condition, contrary to the conclusions of Needer (1971), when considering thermocline models with arbitrary barotropic flow. (10 refs.)

78555 Breaking waves on beaches. D.H.Peregrine (School of Math., Univ. of Bristol, Bristol, England).

In book: *Annual review of fluid mechanics. Vol.15*, M.Van Dyke, J.V.Wehausen, J.L.Lumley [Ed.], p.149-78. Palo Alto, CA, USA: Annual Reviews (1983), 534 pp. [0 8243 0715 1]

Visitors to any coastline exposed to open water can see the dramatic transformation of surface waves that occurs as they advance onto a beach. The waves offshore have a relatively smooth water surface, whereas the waves arriving at the shoreline have rough white fronts of spray and bubbles. The transition between these two types of waves is the subject of this review: the term 'wave breaking' is used to describe the transition from a smooth wave to the quasi-steady state with a white-water front rather than to any particular instant within the transition. (110 refs.)

78556 The form and dynamics of Langmuir circulations. S.Leibovich (Sibley School of Mech. & Aerospace Engng., Cornell Univ., Ithaca, NY, USA).

In book: *Annual review of fluid mechanics. Vol.15*, M.Van Dyke, J.V.Wehausen, J.L.Lumley [Ed.], p.391-427. Palo Alto, CA, USA: Annual Reviews (1983), 534 pp. [0 8243 0715 1]

Many mechanisms for Langmuir circulations have been proposed since Langmuir first reported his observations. Most of these easily can be shown to be nonessential to the phenomenon, and have therefore been dismissed. These early ideas are briefly mentioned, followed by theories not so easily discounted, although serious objections can also be raised about some members of this latter group. Before reviewing the theories, the author gives a sketch of the phenomenon these theories must explain. (81 refs.)

Annual review of fluid mechanics. Vol.15 See Entry 74234

Circulation in the coastal ocean See Entry 74236

Modal dispersion effects on coherent signal processing parameters See Entry 75867

Neogene sedimentation and erosion in the Amirante Passage, western Indian Ocean See Entry 75816

Longshore motion generated on beaches by obliquely incident bores See Entry 78519

On the radiocarbon record in banded corals: exchange parameters and net transport of $^{14}\text{C}_2$ between atmosphere and surface ocean See Entry 78559

Trace metal fronts in European shelf waters See Entry 78560

Large particle transport of plutonium and other fallout radionuclides to the deep ocean See Entry 78561

Mid-latitude model analysis of solar radiation, the upper layers of the sea, and seasonal climate See Entry 78641

High resolution spectral analysis and the acoustic remote sensing of ocean current velocity See Entry 78717

Lower bounds on pulsed-Doppler current profiler accuracy See Entry 78718

92.20 INTERDISCIPLINARY ASPECTS OF OCEANOGRAPHY

78557 Transport and deposition of plutonium in the ocean: evidence from Gulf of Mexico sediments. M.R.Scott, P.F.Salter (Dept. of Oceanography, Texas A&M Univ., College Station, TX, USA), J.E.Halverson.

Earth & Planet. Sci. Lett. (Netherlands), vol.63, no.2, p.202-22 (May 1983).

A study of sediments in the Gulf of Mexico shows dramatic gradients in Pu content and isotope ratios from the continental shelf to the Sigsbee Abyssal Plain. In terms of predicted direct fallout inventory of Pu, one shelf core contains 745% of the predicted inventory, while abyssal plain sediments contain only 15-20% of the predicted value. Absolute Pu concentrations of shelf sediments are also conspicuously high, up to 110 dpm/kg, compared to 13.5 dpm/kg in Mississippi River suspended sediment. There is no evidence of Pu remobilization in Gulf of Mexico shelf sediments, based on comparison of Pu profiles with Mn/Al and Fe/Al profiles. Horizontal transport of fallout nuclides from the open ocean to removal sites in ocean margin sediments is concluded to be the source of both the high concentrations and high inventories of Pu reported here. (60 refs.)

78558 Preliminary observations on californium-252 behaviour in sea water, sediments and zooplankton. S.R.Aston, S.W.Fowler (Internat. Lab. of Marine Radioactivity, Musee Oceanographique, MC, Monaco).

Health Phys. (GB), vol.44, no.4, p.359-65 (April 1983).

Reports radiotracer experiments on the behaviour of ^{252}Cf in the marine environment. The particulate fraction of californium in sea water approached 45% after four days. Californium rapidly adsorbed onto marine coastal and deep-sea sediments with Kd values from 1.4×10^4 to $\geq 1 \times 10^5$. The concentration of ^{252}Cf in euphausiids reached near-equilibrium factors of 3×10^2 in water after one week; in contrast, the assimilation from food was very low. Excreted pellet pellets, molts and zooplankton carcasses are potentially important vectors for californium re-distribution in the oceans. (15 refs.)

78559 On the radiocarbon record in banded corals: exchange parameters and net transport of $^{14}\text{C}_2$ between atmosphere and surface ocean. E.M.Druffel (Chem. Dept., Woods Hole Oceanographic Inst., Woods Hole, MA, USA), H.E.Suess.

J. Geophys. Res. (USA), vol.88, no.C2, p.1271-80 (20 Feb. 1983). (Symposium on the Rise in Atmospheric Carbon Dioxide, Bern, Switzerland, 14-18 Sept. 1981).

Radiocarbon measurements of banded hermatypic corals from Florida, Belize, and the Galapagos Islands have been made. Interpretation is presented here of these previously reported results. These measurements represent the $^{14}\text{C}/^{12}\text{C}$ ratios in dissolved inorganic carbon (DIOC) in the surface ocean waters of the Gulf Stream and the Peru Current at the time of coral ring formation. A depletion in radiocarbon concentration was observed in corals that grew from A.D. 1900-1952. It was caused by dilution of existing ^{14}C levels with dead CO_2 from fossil fuel burning (the Suess effect, or S_{eff}). The observed depletion of radiocarbon was greater in corals from the Gulf Stream (-11%) than in corals from the Peru Current (-6%). A similar trend was observed in the distribution of bomb-produced ^{14}C in corals that had grown during the years following A.D. 1952. The authors discuss the implications these observations have on vertical mixing and circulation in the ocean. (40 refs.)

78560 Trace metal fronts in European shelf waters. K.Kremling (Inst. für Meereskunde, Kiel, Germany).

Nature (GB), vol.303, no.5914, p.225-7 (19 May 1983).

The Hebrides shelf edge area is characterized by strong horizontal salinity gradients (fronts) which mark the boundary between Scottish coastal and oceanic waters. The results presented here, obtained in summer 1981 on a

transect between the open North Atlantic and the German Bight, confirm that the hydrographical front is accompanied by dramatic increases in inorganic nutrients (phosphate, silicate) and dissolved trace elements such as Cd, Cu, Mn, and ^{226}Ra . These data (together with measurements from North Sea regions) suggest that the trace metals are mobilized from partly reduced (organic-rich) sediments and vertically mixed into the surface waters. The regional variations evident from the transect are interpreted as being the result of the hydrography prevailing in waters around the British Isles. (22 refs.)

78561 Large particle transport of plutonium and other fallout radionuclides to the deep ocean. H.D.Livingston, R.F.Anderson (Dept. of Chem., Woods Hole Oceanographic Inst., Woods Hole, MA, USA).

Nature (GB), vol.303, no.5914, p.228-31 (19 May 1983).

Artificial radionuclides introduced to the atmosphere as a consequence of atmospheric nuclear weapons tests have been detected in deep sediments of the Atlantic and Pacific Oceans. The nuclides which have been found in these sediments have half lives long enough to be detectable 10 or more years after their introduction to the ocean and biogeochemistries which permit particle association and transport. They include such nuclides as $^{239,240}\text{Pu}$, ^{238}Pu , ^{241}Am , ^{59}Fe and ^{137}Cs . For fallout nuclides to have been transported to the deep ocean in the two to three decades since they were delivered to the sea surface, relatively rapid transport through the water column is required. The authors describe the results of radiochemical analyses of Pu and other fallout nuclides in three series of sediment trap samples collected as part of the PARFLUX program. The data are used to consider the role that large particles have in processes which transfer particle reactive artificial radionuclides through oceanic water columns. (33 refs.)

78562 Salinity of sea water. O.I.Mamaev.

Priroda (USSR), no.3, p.19-23 (1983). In Russian.

The problem of determining an absolute value for the salinity of the sea is considered and an attempt is made to find an indirect method of determining salinity rapidly. Previously devised formulae and methods of determining salinity are examined and progress to date in the search for the absolute expression is traced. A new scale is described which yields a value designated as the 'practical' salinity. (3 refs.) L.M.H.

Fourth International Ocean Disposal Symposium See Entry 74222

Problems in modelling the transport of material from deep-sea dumpsites See Entry 75111

The effects of radiation exposure on aquatic organisms See Entry 75112

Studies of the radiosensitivity of deep-sea bacteria See Entry 75113

Effect of radiation on sister chromatic exchanges and chromosomal deletions in the benthic worm *Neanthes arenaceodentata* See Entry 75114

Radioactive contamination of the marine environment, uptake and distribution of tritium and technetium in *Acetabularia* and other marine algae See Entry 75115

The role of biogenic debris in the vertical transport of transuranic wastes in the sea See Entry 75116

Comparative behavior of plutonium and americium in the Equatorial Pacific See Entry 75117

The influence of diagenetic redox reactions on the distribution of $^{239,240}\text{Pu}$, ^{137}Cs , ^{241}Am and ^{59}Fe in sediments of the US continental margin See Entry 75118

Behavior of long-lived nuclides associated with radioactive wastes in the deep-sea See Entry 75119

Development of an ocean model for use in radiological assessments of sea disposal of solid radioactive wastes See Entry 75120

Equipment for 3-dimensional measurements of natural and artificial tracers in the sea See Entry 75121

Relationship between the distribution of radionuclides and the sedimentological and mineralogical traits of the coastal marine sediments (Gaeta, Latina, La Spezia, Italy) See Entry 75122

The NEA research and environmental surveillance program related to sea disposal of radioactive waste See Entry 75123

Pore water chemistry of the mounds hydrothermal field, Galapagos Spreading Center: results from Glomar Challenger piston coring See Entry 78517

Glacial-Holocene transition in deep-sea sediments: manganese-spike in the east-equatorial Pacific See Entry 78520

Determination of phosphorus in natural waters by long-capillary-cell absorption spectrometry See Entry 78654

Measurement of ^{53}Mn in deep-sea iron and stony spherules See Entry 78883

92.40 HYDROLOGY AND GLACIOLOGY

78563 The transient flow in naturally fractured reservoirs with three-porosity systems. Wu Yushu (Sci. Res. Inst. of Petroleum Exploration & Dev., China), Ge Jiali.

Acta Mech. Sin. (China), no.1, p.81-5 (1983). In Chinese.

Presents analytical solutions for the three-porosity model of naturally fractured reservoirs in both infinite and finite systems by using the Laplace transform and the finite Hankel transform, and discusses the general behaviour of this model. In addition, the pressure-drawdown and buildup equations are given for engineering applications. (5 refs.)

78564 Alluvions washing experiment and other difficulties at the hydro-power plants intakes on the Olt river during the May 1981 floodings. S.Cerchez.

Energetica (Romania), vol.30, no.12, p.582-6 (Dec. 1982). In Rumanian.

[received: May 1983]

An experiment for washing away alluvions for a storage lake on the Olt river during a 1500 m³/s flood and the energetic and economic aspects of this operation are presented. The difficulties of fighting the effects of river alluvions during flooding periods are referred to and the components of the relationship of erosion-deposits-energetic effects are appreciated. (7 refs.)

78565 Aero-diffusion method of estimating evaporation in a non-stratified atmosphere. H.S.Takhar, M.W.Liddament (Simon Engng. Labs., Univ. of Manchester, Manchester, England).

Indian J. Pure & Appl. Math., vol.14, no.3, p.412-25 (March 1983).

Experimental observations from four sites are used to verify the aero-diffusion approach (Takhar 1972) to evaporation estimation. Climatological and evaporation data from two of the sites were taken from the published results of Rowher (1931) and the Lake Hefner Base Data Report (1954). The remaining experiments were performed at the Stocks Reservoir, Yorkshire, where meteorological data recorded from an automatic recording station positioned over the water surface were used to compare evaporation estimates given by the aero-diffusion method with those given by the Penman (1948) method,

and at a site near Arley, Cheshire, where the aero-diffusion estimates were compared with the direct measurements from a nine metre diameter, water tight evaporation pool. The results of these experimental studies showed that there was generally good agreement between the water budget estimates and the aero-diffusion estimation of evaporation. (10 refs.)

78566 Porosity and hydraulic properties of sediments from the Galapagos Spreading Center and their relation to hydrothermal circulation in the oceanic crust. S.Karato (Ocean Res. Inst., Univ. of Tokyo, Tokyo, Japan), K.Becker. *J. Geophys. Res. (USA)*, vol.88, no.B2, p.1009-17 (10 Feb. 1983). Density and porosity of sediments were measured on DSDP legs 69 and 70 samples from the Galapagos spreading center. Permeability and the hydraulic impedance of each sediment layer were estimated from measured values of porosity. The gradients of porosity and density with depth where sediment layers are thin (≤ 50 m thick) are anomalously high compared with those of other areas and with the upper part of thicker sediment layers in this area. A good correlation was found between the anomalous porosity and density gradients and the present-day heat flow. These observations suggest that these high gradients may be due to active hydrothermal circulation through a thin sediment cover, which is inhibited by a thicker sediment layer, and that the pattern of hydrothermal circulation may be essentially fixed with the moving plate. Hydraulic impedance of the sediment layer was estimated from the observed depth variation of porosity and was shown to increase rapidly with its thickness. (26 refs.)

78567 On the terrestrial heat flow and physical limnology of Crater Lake, Oregon. D.L.Williams (US Geological Survey, Denver, CO, USA), R.P.Von Herzen.

J. Geophys. Res. (USA), vol.88, no.B2, p.1094-104 (10 Feb. 1983). The heat flow into 7000-year-old Crater Lake caldera is dominated by hydrothermal processes. The average of the conducted heat flow value is 138 ± 121 mW/m² (3.3 ± 2.9 HFU). The total heat flow is estimated to be between 669 and 1381 mW/m² (16 and 33 HFU). Hydrothermal fluids penetrate into the lake floor to a depth of at least 1.5 to 2.0 km and possibly much deeper. Two thermal spring areas were discovered on the deep lake floor. These springs, and probably others as yet undiscovered, have a dramatic effect on the water temperature, circulation, and stratification of the lake. Dense thermal waters pond in the southwest basin. The deep waters of the east and northwest basin are warmed to the point that they convect, causing the lake to be vertically mixed. (40 refs.)

78568 Transport of radon in flowing boreholes at Stripa, Sweden. P.H.Nelson, R.Rachiele, A.Smith (Lawrence Berkeley Lab., Berkeley, CA, USA).

J. Geophys. Res. (USA), vol.88, no.B3, p.2395-405 (10 March 1983). Granitic rock in an underground experimental waste storage site at Stripa, Sweden, is unusually high in natural radioelements (~40 ppm uranium), with higher concentrations occurring locally in thin chloritic zones and fractures. Consequently, groundwater seeping through fractures into open boreholes is highly anomalous in its radon content, with activity as high as 1 μ Ci/l. When total count gamma-ray logs are run in boreholes where groundwater inflow is appreciable, the result is quite unusual: the radon daughter activity in the water adds considerably to the gamma contribution from the rock, and in fact often dominates the log. The total gamma activity increases where radon-charged groundwater enters a borehole and decays as the water flows along the hole in response to the hydraulic gradient. (17 refs.)

78569 A branch grain theory of temperature gradient metamorphism in snow. R.A.Sommerfeld (USDA Forest Service, Rocky Mountain Forest & Range Experiment Station, Fort Collins, CO, USA).

J. Geophys. Res. (USA), vol.88, no.C2, p.1484-94 (20 Feb. 1983). Temperature gradient metamorphism in snow results in the development of branch grains at the expense of other types of grains. At constant density, the development of branch grains decreases the strength, thermal conductivity, and crystal number density while increasing the mean crystal size. A theory is developed that uses the following major assumptions: (1) at growth sites the thermal gradient is a function of crystal separation and (2) vapor flux is a function of local thermal gradient. A computer model based on the theory is compared with stereological measurements of snow from a carefully controlled experiment. (26 refs.)

78570 Erosional process of fine cohesive sediments. T.Kusuda, T.Umita, Y.Awaya (Dept. of Civil Engng. Hydraulics, Kyushu Univ., Fukuoka, Japan). *Mem. Fac. Eng. Kyushu Univ. (Japan)*, vol.42, no.4, p.317-33 (Dec. 1982). [received: May 1983]

A series of erosion tests on fine cohesive sediment by use of an annular flume was performed to investigate the characteristics of the erosional process. The critical shear stress defined as a stress above which deposit is slightly eroded is shown to depend on the solid fraction of deposit. The initial rate of erosion is given as an exponential function of shear stress. The erosional process at a constant shear stress is divided into two phases. One is a relatively rapid erosion phase. Another is a slow erosion phase in which rheopexy and the armoring effect appear in the uneroded deposit, and they make deposit resistant on erosion. In the erosional process at a stepwise changed shear stress, the most important factor to estimate the rate of erosion for fine cohesive sediments is found to be shear stress history due to rheopexy. (12 refs.)

78571 Comparison of CO₂ measurements by two laboratories on air from bubbles in polar ice. J.M.Barnola, D.Raynaud (Lab. de Glaciologie et de Geophys. de l'Environnement, Grenoble, France), A.Neffel, H.Oeschger. *Nature (GB)*, vol.303, no.5916, p.410-13 (2 June 1983).

The CO₂ content of air enclosed in bubbles in polar ice has previously been reported by our two laboratories (in Grenoble and Bern) to be representative of the atmospheric CO₂ concentration at the time the ice was formed. Both laboratories are currently measuring various ice cores in order to determine the pre AD 1850 CO₂ level in the atmosphere, which relates to the partitioning of anthropogenic CO₂ among the atmospheric, biospheric and oceanic reservoirs. The two laboratories use different ice cores and different analytical procedures and need to know to what extent the measurements are quantitatively comparable. The authors present the results of a comparison between the two laboratories based on measurements from the same ice core sections, which indicate that the measurements can be compared with great confidence. (9 refs.)

78572 Computer simulation in flood forecasting. E.Thro. *Simulation (USA)*, vol.40, no.3, p.105-6 (March 1983). Describes FLUVIAL, a model based on several principles of river dynamics. In its virgin state a river balances the power it expends along its length to find a state of equilibrium. Human activities, such as mining or bridge building, distort the natural balance and cause the river to seek a new equilibrium. According to the theory of minimum power, a river adjusts its width to minimize power expenditure. The current molds the channel so that each segment does equal work. When a river expends power equally along its channel, it uses the minimum power over its reach (length). This principle is used to simulate river changes. Using FORTRAN, FLUVIAL calculates three kinds of river changes: bed elevation, channel width, and lateral migra-

tion (the sideways movement of the bed within the floodplain). Several measurements are used in FLUVIAL simulation: water routing, sediment routing and stream width and profile. (no refs.)

78573 Detection of abrupt changes occurring in a rainfall sequence represented by a periodic function. T.Ueda, K.Jinno, A.Kawamura, S.Takayoshi.

Technol. Rep. Kyushu Univ. (Japan), vol.55, no.6, p.585-91 (Dec. 1982). In Japanese. [received: May 1983]

By assuming that a rainfall sequence is represented by a periodic function, the adaptive Kalman filtering theory coupled with a generalized likelihood ratio test satisfactorily detects the presence of abrupt changes of a system occurring in the sequence and estimates their magnitudes and time of occurrence. Whereas the ordinary Kalman filter cannot be employed even in the detection of the abrupt changes, this adaptive Kalman filtering theory also accurately achieves the compensation of the forecast values. Simplification of this theory shortens CPU time and decreases the use of a large number of memory storages. (10 refs.)

78574 Snow avalanche motion and related phenomena. E.J.Hopfinger (Inst. de Mecanique, Univ. de Grenoble, Grenoble, France).

In book: *Annual review of fluid mechanics. Vol.15*, M.Van Dyke, J.V.Wehausen, J.L.Lumley [Ed.], p.47-76. Palo Alto, CA, USA: Annual Reviews (1983), 534 pp. [0 8243 0715 1]

Different types of avalanches are classified morphologically. Snow release mechanisms are discussed. The flow characteristics of avalanches are considered. Impact forces and airborne powder avalanches are also considered. (82 refs.)

Surface water considerations in facility design and operation. See Entry 75128

Predictability of solute transport in diffusion-controlled hydrogeologic regimes. See Entry 75145

Ice crystal morphology and growth rates at low supersaturations and high temperatures. See Entry 76331

The actual ³H content of the hydrosphere in Central Europe (1980). See Entry 78109

Finite element analysis of transport of radionuclides in porous media. See Entry 78110

Estimation of per caput dose and collective dose from the use of Danube water. See Entry 78340

Radioactive contamination of filamentous green algae in the Hungarian reach of the River Danube. See Entry 78363

Radioactivity of fish in the Hungarian reach of the River Danube. See Entry 78364

On the thermal effects of groundwater flow. I. Regional scale systems. See Entry 78485

Heat transfer through the sediments of the mounds hydrothermal area, Galapagos Spreading Center at 86°W. See Entry 78486

Heat transfer and intraplate deformation in the Central Indian Ocean. See Entry 78487

Numerical models for the hydrothermal field at the Galapagos Spreading Center. See Entry 78488

Heat flow on the western flank of the East Pacific Rise at 21°N. See Entry 78489

Anomalous heat flow in the northwest Atlantic: a case for continued hydrothermal circulation in 80-m.y. crust. See Entry 78490

Pore water chemistry of the mounds hydrothermal field, Galapagos Spreading Center: results from Glomar Challenger piston coring. See Entry 78517

Constraints upon water advection in sediments of the Mariana Trough. See Entry 78518

The dependence of fracture mechanical and fluid flow properties on fracture roughness and sample size. See Entry 78532

Persistence of wet and dry spells at Uccle (Belgium). See Entry 78637

Determination of phosphorus in natural waters by long-capillary-cell absorption spectrometry. See Entry 78654

Frost mapping in southern Victoria: an assessment of HCMM thermal imagery. See Entry 78656

The dynamic tensile strength of ice and ice-silicate mixtures. See Entry 78833

92.60 METEOROLOGY

(see also 43.28 Aeroacoustics and atmospheric sound)

78575 Investigation of the medium temperature at 11.7 GHz [microwave attenuation estimation]. W.Riedler, R.Lang (Inst. fur Nachrichtentech. und Wellenausbreitung, Tech. Univ. Graz, Graz, Austria).

Arch. Elektron. & Uebertragungstechnik (Germany), vol.37, no.5-6, p.199-202 (May-June 1983).

The temperature of the propagating medium is an important parameter for investigations of the attenuation characteristics of satellite paths. Using experimental results from the satellite OTS as well as from radiometers it is shown in the paper, that in many cases the widely used value of 270K leads to a severe underestimation of the expected attenuation and that a value of ca. 235K is more adequate. (5 refs.)

78576 On the calculation of total solar radiation. II. Huang Runben, Deng Hanzeng, Liu Senyuan.

Acta Sci. Nat. Univ. Sunyatseni (Zhongshandaxue Xuebao) (China), no.4, p.117-21 (1982). In Chinese.

Some parameters used to calculate the total solar radiation in the Averkiev formula are given a further treatment. Besides, some numeric data of calculating the total solar radiation appropriate to South China are given. (9 refs.)

78577 Rain day frequency and mean daily rainfall intensity as determinants of total rainfall over the eastern Orange Free State. M.S.J.Harrison (Climatology Res. Group, Univ. of the Witwatersrand, Johannesburg, S Africa).

J. Climatol. (GB), vol.3, no.1, p.35-45 (Jan.-March 1983).

Summer rainfall totals over the eastern Orange Free State are described in terms of number of days of rain and of mean rainfall per rain day. Variations in rainfall may be considered to result from frequency changes in an objectively-chosen subset of significant rain days. It is demonstrated that increases in mean rainfall per rain day result from an increased number of, and increased intensity of, rain on, the heaviest rain days. Some implications of these findings for studies of atmospheric circulation changes and for weather modification are discussed. (39 refs.)

78578 Numerical experiments on airflow patterns around a cone-shaped island. S.Ishijima (Junior Coll. Div., General Education Univ. of the Ryukyus, Okinawa, Japan).

Bull. Coll. Sci. Univ. Ryukyus (Japan), no.35, p.81-106 (March 1983).

Airflow patterns revealed as perturbations in the large scale prevailing airflow due to the topographical effect are studied with the aid of the mixed layer integrated numerical model. The author discusses the Froude Number, the Coriolis force, the frictional force, the heat and moisture vertically transported from the Earth surface, and the precipitation. (12 refs.)

78579 Aerosols within the World Climate Research Programme. D.Spankuch (Main Meteorological Obs., Potsdam, Germany).

Adv. Space Res. (GB), vol.2, no.5, p.1-2 (1982). [received: April 1983] (Proceedings of the Topical Meeting of the COSPAR Interdisciplinary Scientific Commission A (Meetings A1 and A2) of the COSPAR Twenty-Fourth Plenary Meeting, Ottawa, Canada, 16 May-2 June 1982).

Based on the findings of the meeting of Joint Scientific Committee experts on 'Aerosol and Climate' (Geneva, 27-31 October 1980) the general research strategy consisting of three phases presented. Phase I: sensitivity tests with available models. Phase II: improvement of climate models and data bases. Phase III: development of advanced climate models with internal aerosol generation and regulation processes. COSPAR's role within this research strategy is outlined. (3 refs.)

78580 The effect of aerosols on climate and aerosol climatology on the basis of observations from space. K.Ya.Kondratyev, A.A.Grigoryev, O.M.Pokrovsky (Main Geophysics Obs., State Committee for Hydrometeorology & Control of the Natural Environment, Moscow, USSR).

Adv. Space Res. (GB), vol.2, no.5, p.3-10 (1982). [received: April 1983] (Proceedings of the Topical Meeting of the COSPAR Interdisciplinary Scientific Commission A (Meetings A1 and A2) of the COSPAR Twenty-Fourth Plenary Meeting, Ottawa, Canada, 16 May-2 June 1982).

Principal aspects of the effect of aerosols on climate are discussed and the possibilities of obtaining a climatic data set of global aerosols are analyzed. Based on the analysis of space images, new data are obtained on gigantic dust outbreaks in various regions of the Earth. It is shown that dust outbreaks can propagate over hundreds and sometimes thousands of kilometers. (29 refs.)

78581 The role of aerosols in the climate system: results of numerical experiments in climate models. R.A.Reck (Phys. Dept., General Motors Res. Labs., Warren, MI, USA).

Adv. Space Res. (GB), vol.2, no.5, p.11-18 (1982). [received: April 1983] (Proceedings of the Topical Meeting of the COSPAR Interdisciplinary Scientific Commission A (Meetings A1 and A2) of the COSPAR Twenty-Fourth Plenary Meeting, Ottawa, Canada, 16 May-2 June 1982).

Three principal questions are recurrent with the consideration of an aerosol related climatic effect: (1) do aerosols heat or cool the atmosphere, (2) are aerosol climatic effects significant and (3) can numerical models be validated by predicting a climatic change associated with a measured aerosol-event? Each of these questions is addressed from a historical perspective. In addition, aerosol-related modeling is discussed as well as recommendations for future research. (57 refs.)

78582 Aerosol observations from Nimbus-7 CZCS along the South African west coast. N.M.Walters, O.G.Malan, D.C.Neethling (Nat. Phys. Res. Lab., CSIR, Pretoria, S Africa).

Adv. Space Res. (GB), vol.2, no.5, p.105-7 (1982). [received: April 1983] (Proceedings of the Topical Meeting of the COSPAR Interdisciplinary Scientific Commission A (Meetings A1 and A2) of the COSPAR Twenty-Fourth Plenary Meeting, Ottawa, Canada, 16 May-2 June 1982).

In the course of the South African participation in the Nimbus-7 coastal zone colour scanner project, a fair amount of cloud-free data were collected along the South African west coast, mainly to study upwelling phenomena. Examples of aerosol radiance maps produced during analysis of these data, including some anomalous results, are discussed. (9 refs.)

78583 Satellite measurements of tropospheric aerosols. M.Griggs (Electronic Vision & Systems Div., Sci. Applications, Inc., San Diego, CA, USA).

Adv. Space Res. (GB), vol.2, no.5, p.109-18 (1982). [received: April 1983] (Proceedings of the Topical Meeting of the COSPAR Interdisciplinary Scientific Commission A (Meetings A1 and A2) of the COSPAR Twenty-Fourth Plenary Meeting, Ottawa, Canada, 16 May-2 June 1982).

A global-scale ground-truth experiment was conducted in 1980 with the AVHRR on NOAA-6 to determine the relationship between the upwelling visible radiance and the aerosol optical thickness at ten ocean sites around the globe. The data for four sites have been analyzed, and the aerosol contents measured by the AVHRR and by sunphotometers are compared. A preliminary analysis of AVHRR Channel 1 (0.65 μm) and Channel 2 (0.85 μm) radiances suggest that useful information on the aerosol size distribution may also be obtained from satellite observations. (9 refs.)

78584 Monitoring of Saharan dust over the Atlantic using Meteosat-VIS-data. M.Kastner, P.Kopke, H.Quenzel (Meteorologisches Inst., Univ. Munchen, Munchen, Germany).

Adv. Space Res. (GB), vol.2, no.5, p.119-21 (1982). [received: April 1983] (Proceedings of the Topical Meeting of the COSPAR Interdisciplinary Scientific Commission A (Meetings A1 and A2) of the COSPAR Twenty-Fourth Plenary Meeting, Ottawa, Canada, 16 May-2 June 1982).

The optical depth of Saharan dustclouds (a component of the radiation budget), which can be clearly seen in satellite images taken over the Atlantic, can be determined from the Meteosat VIS-data. 'Favourable angles' between Sun, observed point and satellite are chosen so that the optical depth is determined with an accuracy of only about 20%. Several clouds, their change over time, and some of their other interesting features are presented. The results are discussed. (6 refs.)

78585 Can turbidity measurements be used for the estimation of aerosol parameters? D.Spankuch (Meteorological Service of Germany, Main Meteorological Obs., Potsdam, Germany), W.von Hoyningen-Huene.

Adv. Space Res. (GB), vol.2, no.5, p.131-4 (1982). [received: April 1983] (Proceedings of the Topical Meeting of the COSPAR Interdisciplinary Scientific Commission A (Meetings A1 and A2) of the COSPAR Twenty-Fourth Plenary Meeting, Ottawa, Canada, 16 May-2 June 1982).

In a previous paper (Zeitschrift fur Meteorologie, vol.29, p.146, 1979) the authors showed that the aerosol size distribution can be estimated with reasonable accuracy from spectral extinction measurements in a limited spectral region ($\lambda \leq 1 \mu\text{m}$) only. Using the same method they discuss whether the anticipated WMO turbidity network with four spectral channels has the potential of estimating the aerosol size distribution. (17 refs.)

78586 Rocket studies of atmospheric scattering and the aerosol size distribution in the troposphere and lower stratosphere over Thumba. B.H.Subbaraya, A.Jayaraman (Phys. Res. Lab., Ahmedabad, India).

Adv. Space Res. (GB), vol.2, no.5, p.135-8 (1982). [received: April 1983] (Proceedings of the Topical Meeting of the COSPAR Interdisciplinary Scientific Commission A (Meetings A1 and A2) of the COSPAR Twenty-Fourth Plenary Meeting, Ottawa, Canada, 16 May-2 June 1982).

Measurements have been made of the atmospheric scattering in the ultraviolet ($\lambda < 0.31 \mu\text{m}$) during the 16 February 1980 solar eclipse rocket campaign. The amplitude of the scattered fluxes as well as the angular distribution could be measured from ground up to an altitude of about 24 km. The Rayleigh scattering component was estimated using standard atmospheric models and the observations have been used to study the scattering due to aerosols at tropospheric and lower stratospheric altitudes. (7 refs.)

78587 On the quasi-biennial oscillation in equatorial stratospheric temperatures and total ozone. C.S.Zerefos (Phys. Dept., Univ. of Thessaloniki, Thessaloniki, Greece).

Adv. Space Res. (GB), vol.2, no.5, p.177-81 (1982). [received: April 1983] (Proceedings of the Topical Meeting of the COSPAR Interdisciplinary Scientific Commission A (Meetings A1 and A2) of the COSPAR Twenty-Fourth Plenary Meeting, Ottawa, Canada, 16 May-2 June 1982).

The results of a cross-spectral analysis between monthly mean temperatures at 100 mb, 50 mb and 30 mb over the equator and the corresponding monthly mean UV total ozone at different latitude zones are presented for the period 1970-1977. Significant squared coherences between total ozone and 50 mb equatorial temperatures at 26 months are only found between 5 degrees on each side of the equator, between 45 deg N and 55 deg N and at 45 deg S. At latitudes where the QBO in stratospheric temperature diminishes so does the QBO in total ozone. Over subtropical latitudes there is a tendency towards a more biennial oscillation in total ozone and at 65 deg N and 65 deg S total ozone oscillates at periods greater than the equatorial QBO. (14 refs.)

78588 Global pictures of the ozone field, from high altitudes, from DE-I. G.M.Keating (NASA Langley Res. Center, Hampton, VA, USA), L.Frank, J.Craven, M.Shapiro, D.Young, P.Bhartia.

Adv. Space Res. (GB), vol.2, no.5, p.183-8 (1982). [received: April 1983] (Proceedings of the Topical Meeting of the COSPAR Interdisciplinary Scientific Commission A (Meetings A1 and A2) of the COSPAR Twenty-Fourth Plenary Meeting, Ottawa, Canada, 16 May-2 June 1982).

Using the imaging instrumentation aboard the Dynamics Explorer spacecraft (DE-I), total column ozone densities are obtained in the sunlit hemisphere by measuring the intensities of backscattered solar ultraviolet radiation. The high apogee altitude (23000 km) of the eccentric polar orbit allows high resolution global-scale images of the terrestrial ozone field to be obtained within 12 minutes. Previous ozone-monitoring spacecraft have required much longer time periods for comparable spatial coverage because of their lower altitudes ($< 1200 \text{ km}$). The much higher altitude of DE-I also provides hours of continuous imaging of features compared to minutes or seconds with previous spacecraft. Near perigee, high resolution images can be gained with pixel size as small as 3 km to view mesoscale atmospheric variations. The effects of planetary-scale, synoptic-scale, and mesoscale dynamical processes, which control the distribution of ozone near the tropopause, can be studied. (16 refs.)

78589 Measurements of atmospheric ozone from aircraft and from balloons. W.A.Matthews (Max-Planck-Inst. fur Aeronomie, Katlenburg-Lindau, Germany).

Adv. Space Res. (GB), vol.2, no.5, p.189-95 (1982). [received: April 1983] (Proceedings of the Topical Meeting of the COSPAR Interdisciplinary Scientific Commission A (Meetings A1 and A2) of the COSPAR Twenty-Fourth Plenary Meeting, Ottawa, Canada, 16 May-2 June 1982).

The first ozone data from the Northern Hemisphere meridional flight 'SIMOC' are presented. The flight was made in May of 1981 from Germany up to 82°N and then down to the Equator and back with the Falcon 20E German research aircraft. These data include those obtained using a differential solar absorption spectrometer developed and built at the Max-Planck-Institut fur Aeronomie in Lindau. Ozone profiles obtained from an intensive series of balloon flights launched in northern Sweden over a two-week period are also presented and discussed in terms of the variability in ozone concentration that they demonstrate in the middle atmosphere. (3 refs.)

78590 A mesospheric ozone profile at sunset. H.Yamamoto, H.Sekiguchi, T.Makino (Dept. of Phys., Rikkyo Univ., Tokyo, Japan), T.Watanabe, K.S.Zalpur, T.Ogawa.

Adv. Space Res. (GB), vol.2, no.5, p.197-9 (1982). [received: April 1983] (Proceedings of the Topical Meeting of the COSPAR Interdisciplinary Scientific Commission A (Meetings A1 and A2) of the COSPAR Twenty-Fourth Plenary Meeting, Ottawa, Canada, 16 May-2 June 1982).

An altitude profile of the ozone concentration from 55 to 95 km was measured at sunset in January by simultaneous measurements of the 1.27 μm radiation and the solar UV radiation using rocket-borne radiometers at Uchinoura, Japan (31°N). The ozone profiles deduced by two different methods agree with each other at approximately 70 km. The profile was consistent with previous results obtained at the same station in September, and with the sunset profile obtained at Wallops Island (38°N) during the WMO/FAA/NASA international ozone rocketsonde intercomparison. The data show no seasonal variation of ozone in the 55-95 km region at Uchinoura. (9 refs.)

78591 Periodic and aperiodic ozone variations in the middle and upper stratosphere. J.London (Dept. of Astro-Geophysics, Univ. of Colorado, Boulder, CO, USA).

Adv. Space Res. (GB), vol.2, no.5, p.201-4 (1982). [received: April 1983] (Proceedings of the Topical Meeting of the COSPAR Interdisciplinary Scientific Commission A (Meetings A1 and A2) of the COSPAR Twenty-Fourth Plenary Meeting, Ottawa, Canada, 16 May-2 June 1982).

Umkehr, ozonesonde and satellite observations are used to determine the height/latitude distribution of the amplitude and phase of the periodic components of the variation of the ozone mixing ratio in the middle and upper stratosphere. The amplitude of the first (annual) harmonic is small in the subtropics and increases to a maximum at polar latitudes. It also increases with height in the mid and upper stratosphere to an apparent maximum just below the stratopause. The second (semi-annual) harmonic has an amplitude that is largest in tropical regions and in subpolar regions at a level of about 40 km. The phase of the first harmonic shows a marked transition from a winter/spring maximum below 30 km to a summer maximum at 30 km, changing rapidly to a maximum in winter in both hemispheres. (8 refs.)

78592 Solar eclipse induced variations in mesospheric ozone concentrations. S.Lal, B.H.Subbaraya (Phys. Res. Lab., Ahmedabad, India).

Adv. Space Res. (GB), vol.2, no.5, p.205-8 (1982). [received: April 1983] (Proceedings of the Topical Meeting of the COSPAR Interdisciplinary Scientific Commission A (Meetings A1 and A2) of the COSPAR Twenty-Fourth Plenary Meeting, Ottawa, Canada, 16 May-2 June 1982).

A model study of the solar eclipse induced variations in mesospheric ozone concentrations was undertaken. This study includes, in addition to the Chapman reactions, the chemistry involving hydrogen species (H , OH and HO_2) which are found to be important in the destruction of odd oxygen in this altitude region. Coupled time dependent continuity equations are solved for the eclipse duration. The results from the present study are compared with earlier theoretical model and the experimental observations during the 16 February 1980 solar eclipse as well as the results obtained during earlier solar eclipses. (18 refs.)

78593 Solar UV and ozone balloon measurements. D.J.McEwen, P.Chakrabarty (Inst. of Space & Atmospheric Studies, Univ. of Saskatchewan, Saskatoon, Saskatchewan, Canada).

Adv. Space Res. (GB), vol.2, no.5, p.209-12 (1982). [received: April 1983] (Proceedings of the Topical Meeting of the COSPAR Interdisciplinary Scientific Commission A (Meetings A1 and A2) of the COSPAR Twenty-Fourth Plenary Meeting, Ottawa, Canada, 16 May-2 June 1982).

Absolute solar UV spectra were obtained with a $1/4$ m spectrometer on a balloon flight from Palestine, Texas, on September 23, 1981. This balloon reached a float altitude of 39 km at solar noon. The ozone density profiles derived from these spectra are discussed. The measurements are compared with data obtained from the same calibrated instrument flown in 1976 at solar minimum. (6 refs.)

78594 Modelling of the ion composition of the middle atmosphere. L.Thomas (Dept. of Phys., Univ. Coll. of Wales, Aberystwyth, Wales).

Ann. Geophys. (France), vol.1, no.1, p.61-73 (Jan.-Feb. 1983).

Discusses the nature of the primary ions produced during the ionization processes and information on ion composition. Model studies of the composition at D and E regions, which have attracted considerable attention over the past decade, are reviewed in some detail. For stratospheric heights, the treatment is restricted to a consideration of reaction schemes describing the chemistry which produce the positive and negative ions which have recently been identified. (101 refs.)

78595 Comparison of the bistatic cross-section and reflectivities of spherical and spheroidal raindrops at microwave frequencies. D.G.Charlton, A.R.Holt, B.G.Evans (Univ. of Essex, Colchester, England).

IEE Proc. F (GB), vol.130, no.4, p.317-24 (June 1983).

Investigates one aspect of the validity of models currently used to calculate rain-scatter interference in radio and satellite communication systems. Exact bistatic scattering cross-sections from spheroidal shaped raindrops are compared with those obtained from spheroids in the Rayleigh approximation and from spheres using the Mie theory at 11.7, 20 and 30 GHz. Comparisons are also made between bistatic radar reflectivities for rain populations at these frequencies. It is found that both the Rayleigh and Mie (sphere) approximations to the spheroidal raindrop yield errors in the bistatic scattering reflectivities. These errors can be significant in the case of the Rayleigh theory, but the Mie theory, in general, yields much closer results to the exact. (23 refs.)

78596 The optical and radiation field signatures produced by lightning return strokes. Changming Guo, E.P.Krider (Inst. of Atmospheric Phys., Univ. of Arizona, Tucson, AZ, USA).

J. Geophys. Res. (USA), vol.87, no.C11, p.9813-22 (20 Oct. 1982). [received: May 1983]

The optical signals radiated by Florida lightning in the 0.4- to 1.1- μ m wavelength interval have been recorded in correlation with wide-band electric field signatures. The initial light signal from a return stroke tends to be linear for about 15 μ s and then rises more slowly to a peak that is delayed about 60 μ s from the electric field peak. The transition between the fast linear portion and the slower rise may be due to the return stroke entering the cloud base. A small percentage of the records indicate that two different branches of the same stepped leader can initiate separate return strokes. The light pulses from cloud discharges tend to be smaller and more slowly varying than those from return strokes. The total optical power radiated by first strokes in the 5- to 35-km range has a mean and standard deviation of $2.3 \pm 1.8 \times 10^9$ W at peak. (56 refs.)

78597 Parameterization of IR cooling in a middle atmosphere dynamics model. I. Effects on the zonally averaged circulation. J.P.Apruzese, M.R.Schoeberl, D.F.Strobel (Plasma Phys. Div., Naval Res. Lab., Washington, DC, USA).

J. Geophys. Res. (USA), vol.87, no.C11, p.8951-66 (20 Oct. 1982). [received: May 1983]

A computationally efficient two-stream parameterization of IR cooling is developed for a middle atmosphere dynamics model. The parameterization combines the monochromatic feature of an emissivity formulation with the computational simplicity of a single spatial integral to evaluate the monochromatic transfer equation. The calculations show strong radiative control of the mesopause region (radiative relaxation rate $> [5 \text{ days}]^{-1}$) and the need for substantial deceleration of the mean zonal winds ($\sim 40 \text{ m s}^{-1} \text{ day}^{-1}$). Calculated temperatures show good agreement in the summer hemisphere where planetary wave activity is negligible, but in the polar night of the winter hemisphere they are ~ 30 K too cold which suggests planetary wave heating must make up the deficit. With observed ozone densities the globally averaged radiative equilibrium temperatures in the 65-75 km region are too cold and an additional heat source $\sim 1 \text{ K day}^{-1}$ is required. (42 refs.)

78598 Nitric acid column densities over Antarctica. W.J.Williams, J.J.Kosters, D.G.Murcray (Dept. of Phys., Univ. of Denver, Denver, CO, USA).

J. Geophys. Res. (USA), vol.87, no.C11, p.8976-80 (20 Oct. 1982). [received: May 1983]

Nitric acid column densities derived from atmospheric infrared spectral emission data measured from the NSF USARP C130 research aircraft in the Spring of 1978 are presented, summarized by latitude. An increase of the column density with latitude is noted, along with a longitudinal asymmetry in the latitudinal dependence. Column densities range in values from $1.2 \pm 0.2 \times 10^{20}$ molecules m^{-2} at 53° S latitude to $3.4 \pm 0.7 \times 10^{20}$ molecules m^{-2} at 89° S latitude. Also, the liquid helium cooled spectral radiometer used to obtain the data and the associated calibration procedures are described. (13 refs.)

78599 The quasi-biennial oscillation in atmospheric ozone. S.J.Oltmans (NOAA, Boulder, CO, USA), J.London.

J. Geophys. Res. (USA), vol.87, no.C11, p.8981-9 (20 Oct. 1982). [received: May 1983]

Analysis of various characteristics of the statistical spectra of total ozone covering a 15 year period (1964-78), and of ozone in the stratosphere over a period of about 7 years, indicates that the strong QBO in the zonal winds of

the tropical stratosphere is associated with a detectable, although often weak, signal in total ozone and the ozone concentration in the lower and middle stratosphere. The region of strongest relationship between tropical stratospheric zonal winds and total ozone (e.g. maximum ozone associated with strong west winds) is in the tropics, mid-latitudes of the southern hemisphere, and, apparently, at high latitudes of the northern hemisphere. (34 refs.)

78600 The Saudi Arabian heat low: aerosol distributions and thermodynamic structure. S.A.Ackerman, S.K.Cox (Dept. of Atmospheric Sci., Colorado State Univ., Fort Collins, CO, USA).

J. Geophys. Res. (USA), vol.87, no.C11, p.8991-9002 (20 Oct. 1982). [received: May 1983]

Radiation and microphysical data are employed to deduce the bulk radiative and microphysical characteristics of the aerosol layer over the Saudi Arabian Peninsula and the adjacent Arabian Sea. Observed particle size distributions, total mass loadings, and vertical distributions of the dust are presented for five analysis periods. There is a large daily variability of the dust mass loading over the desert. The broadband radiative characteristics of the dust are inferred by comparing calculations for a dust free atmosphere with in situ broadband radiative measurements. The dust had no detectable effect on the longwave radiation fluxes, while it approximately doubled the clear sky shortwave absorption. (19 refs.)

78601 Threshold friction velocities and rupture moduli for crusted desert soils for the input of soil particles into the air. D.A.Gillette (Air Resources Lab., NOAA, Boulder, CO, USA).

J. Geophys. Res. (USA), vol.87, no.C11, p.9003-15 (20 Oct. 1982). [received: May 1983]

Desert soils having clay crusts, mostly from the Mojave Desert, were tested for threshold friction velocity (the friction velocity at which soil erosion begins) with the open-bottomed wind tunnel. The soils were also tested for content of clay, water-soluble material, calcium carbonate, organic material, mineralogy of clay and of salts, soil moisture, modulus of rupture, and crust thickness. If no loose material existed on the soil surface, crusts having modulus of rupture greater than 0.7 bar and crust thickness of 0.7 cm to 0.3 cm were effective in protecting against wind erosion. Disturbed clay crusts having modulus of rupture before disturbance greater than 2 bar with thickness less than 1.9 cm did not experience significant wind erosion. Modulus of rupture was related to composition of soil but was shown to depend mostly on clay content. (20 refs.)

78602 Feedback mechanisms in the climate system affecting future levels of carbon dioxide. W.W.Kellogg (Nat. Center for Atmospheric Res., Boulder, CO, USA).

J. Geophys. Res. (USA), vol.88, no.C2, p.1263-9 (20 Feb. 1983). (Symposium on the Rise in Atmospheric Carbon Dioxide, Bern, Switzerland, 14-18 Sept. 1981).

The rate of increase of concentration of atmospheric carbon dioxide depends on the consumption of fossil fuels (the major source of 'new' carbon dioxide) and the natural sinks for this trace constituent, primarily the oceans and the biosphere. The rate of operation of these sinks depends on several factors determined by the state of the climate system, and they will therefore presumably change as the greenhouse effect of increasing carbon dioxide warms the earth. Five specific feedback loops are discussed, two of which are positive (amplifying the rate of increase), two are weakly negative and one is undetermined but probably positive. It is concluded that it would be well to be prepared for the possibility that carbon dioxide may increase faster than predicted by models on the current or past state of the climate system. (26 refs.)

78603 Three-dimensional tracer model study of atmospheric CO₂ response to seasonal exchanges with the terrestrial biosphere. I.Fung, K.Prentice, E.Matthews, J.Lerner, G.Russell (Inst. for Space Studies, NASA/Goddard Space Flight Center, New York, NY, USA).

J. Geophys. Res. (USA), vol.88, no.C2, p.1281-94 (20 Feb. 1983). (Symposium on the Rise in Atmospheric Carbon Dioxide, Bern, Switzerland, 14-18 Sept. 1981).

A three-dimensional tracer transport model is used to investigate the annual cycle of atmospheric CO₂ concentration produced by seasonal exchanges with the terrestrial biosphere. The tracer model uses winds generated by a global general circulation model to advect and convect CO₂; no explicit diffusion coefficients are employed. A biospheric exchange function constructed from a map of net primary productivity, and Azevedo's (1982) seasonality of CO₂ uptake and release closely simulates the annual cycles at coastal stations. The results show that zonal homogeneity in surface CO₂ concentrations can never be achieved at mid-latitudes where the time scale for zonal mixing is longer than the time scale for biospheric exchange. Analysis of the zonal mean balance in the lower troposphere reveals that atmospheric transport processes may alter the CO₂ response to local biospheric exchanges by 50% or more. (23 refs.)

78604 Exponential growth and atmospheric carbon dioxide. J.A.Laumann (Gas Res. Inst., Chicago, IL, USA), R.M.Rotty.

J. Geophys. Res. (USA), vol.88, no.C2, p.1295-9 (20 Feb. 1983). (Symposium on the Rise in Atmospheric Carbon Dioxide, Bern, Switzerland, 14-18 Sept. 1981).

The adequacy of assumptions required to project atmospheric CO₂ concentrations in time frames of practical importance is reviewed. Relevant issues concern the form assumed for future fossil fuel release, carbon cycle approximations, and the implications of revisions in fossil fuel patterns required to maintain atmospheric CO₂ levels below a chosen threshold. In general, it was found that with a judiciously selected exponential fossil fuel release rate, and with a constant airborne fraction, it is possible to estimate atmospheric CO₂ growth over the next 50 years based on essentially surprise free scenarios. Resource depletion effects must be included for projections beyond about 50 years, and on this time frame the constant airborne fraction approximation has to be questioned. (13 refs.)

78605 CO₂ and radon 222 as tracers for atmospheric transport. H.Dorr, B.Kromer, I.Levin, K.M.Unnich, H.-J.Volpp (Inst. für Umweltphys., Univ. of Heidelberg, Heidelberg, Germany).

J. Geophys. Res. (USA), vol.88, no.C2, p.1309-13 (20 Feb. 1983). (Symposium on the Rise in Atmospheric Carbon Dioxide, Bern, Switzerland, 14-18 Sept. 1981).

Time variations of the CO₂ concentration and the radon 222 daughter activity in the atmosphere are observed 16 m above the ground in the outskirts of Heidelberg (Germany), situated in the rather densely populated and intensively cultivated upper Rhine valley. These parallel recorded data series are used to estimate the CO₂ respiration rate from the soil and from plant leaves. Atmospheric concentration variations of both gases appear to be merely due to variations in atmospheric mixing. From direct measurements of concentration profiles in the soil air the authors deduce the ²²²Rn exhalation rate, which is nearly constant with time and about 4000 dpm $\text{m}^{-2} \text{ h}^{-1}$. This flux is consistent with the one derived from observed pileup of the ²²²Rn activity of an air mass during passage over the continent. (16 refs.)

- 78606 Preliminary study of CO₂ variations at Amsterdam Island (Territoire des Terres Australes et Antarctiques Françaises).** A.Gaudry, J.M.Ascencio, G.Lambert (Centre des Faibles Radioactivités, CNRS, Gif sur Yvette, France). *J. Geophys. Res. (USA)*, vol.88, no.C2, p.1323-9 (20 Feb. 1983). (Symposium on the Rise in Atmospheric Carbon Dioxide, Bern, Switzerland, 14-18 Sept. 1981).
- The preliminary measurements of atmospheric CO₂ concentrations performed at Amsterdam Island between April and the end of 1980 showed two kinds of short-term variations. The first one, attributed to local effects of the photosynthesis of the island vegetation, does not seem considerably to affect the monthly mean CO₂ concentrations. The second one has been attributed to long range transport phenomena. That corresponds to large scale meteorological perturbations and generally is correlated with variations of the atmospheric radon concentrations. Therefore, the existence of regional CO₂ sources and sinks in the southern hemisphere can be felt at a very large distance. (13 refs.)
- 78607 Interpretation of atmospheric CO₂ measurements at Mt. Cimone (Italy) related to wind data.** L.Ciattaglia (Vigna di Valle Obs., Rome, Italy). *J. Geophys. Res. (USA)*, vol.88, no.C2, p.1331-8 (20 Feb. 1983). (Symposium on the Rise in Atmospheric Carbon Dioxide, Bern, Switzerland, 14-18 Sept. 1981).
- Technical details on the apparatus and the CO₂ program at Mt. Cimone are reported, together with information on the sampling site and on the wind regime. Hourly values of atmospheric CO₂ are examined, and a preliminary interpretation is given, taking into account simultaneous observations of wind direction and wind speed at Mt. Cimone. In particular, a seasonal CO₂ trend is clearly identified along with a CO₂ dependence on synoptic situations, especially wind speed and direction. (6 refs.)
- 78608 Concentration of atmospheric carbon dioxide over Japan.** M.Tanaka, T.Nakazawa, S.Aoki (Upper Atmosphere Res. Lab., Tohoku Univ., Sendai, Japan). *J. Geophys. Res. (USA)*, vol.88, no.C2, p.1339-44 (20 Feb. 1983). (Symposium on the Rise in Atmospheric Carbon Dioxide, Bern, Switzerland, 14-18 Sept. 1981).
- Aircraft measurements of atmospheric CO₂ concentration over Japan have been initiated in January 1979 at the Upper Atmosphere Research Laboratory of the Tohoku University. An average annual increase of CO₂ concentration during a period from the beginning to April 1981 is estimated to be 1.5 ppmv/year. Yearly average values for the concentration decrease rapidly with increasing height above ground, in the lowest layer of the troposphere, and decrease slightly in the layer above it, showing that the ground acts as a CO₂ source. The amplitude of the seasonal variation decreases markedly with elevation. The maximum occurs early in May and the minimum early in August at low levels. (17 refs.)
- 78609 Sampling strategy to obtain data used in models of global annual CO₂ increase and global carbon cycle.** D.A.Gillette (Air Resources Labs., Boulder, CO, USA), K.J.Hanson. *J. Geophys. Res. (USA)*, vol.88, no.C2, p.1345-8 (20 Feb. 1983). (Symposium on the Rise in Atmospheric Carbon Dioxide, Bern, Switzerland, 14-18 Sept. 1981).
- Simple models were constructed to assess with somewhat limited CO₂ data the effects of both frequency of sampling and spatial distribution of sampling locations on the variance of estimates of interest to the global carbon cycle. The CO₂ data for use in these models were obtained from seven air flask sampling locations, globally distributed in latitude but restricted to the longitude sector 80°W to 170°W, during the period 1977-1979. The results of analysis with these models show (1) that locations north of 30°N are quite important in possibly providing information on carbon cycle exchange processes and that (2) improved sampling techniques including greater sampling frequency would be desirable for sampling locations in the southern hemisphere. (7 refs.)
- 78610 Selection of CO₂ concentration data from whole-air sampling at three locations between 1968 and 1974.** D.A.Gillette (Air Resources Labs., NOAA, Boulder, CO, USA), A.T.Steele. *J. Geophys. Res. (USA)*, vol.88, no.C2, p.1349-59 (20 Feb. 1983). (Symposium on the Rise in Atmospheric Carbon Dioxide, Bern, Switzerland, 14-18 Sept. 1981).
- Three methods for rejection of CO₂ data were used to obtain CO₂ concentration versus time for 1968-1973 for Station Charlie (a ship in the North Atlantic), Niwot Ridge near Nederland, Colorado, and Key Biscayne near Miami, Florida. From examination of the results it was concluded that short-term variation and error were not large for the Station Charlie data. There was a suggestion of occasional contamination at Key Biscayne and evidence of more frequent contamination at Niwot Ridge, after 1970. Values obtained for annual CO₂ increases were 1.3 and 1.2 ppm (1959 SIO index) for Station Charlie and Niwot Ridge. Annual amplitudes were 5, 11 and 9.7 ppm for Station Charlie, Niwot Ridge, and Key Biscayne, respectively. (10 refs.)
- 78611 Tropospheric NO_x and O₃ budgets in the equatorial Pacific.** S.C.Liu, M.McFarland, D.Kley (NOAA, Aeronomy Lab., Boulder, CO, USA), O.Zafriou, B.Huebert. *J. Geophys. Res. (USA)*, vol.88, no.C2, p.1360-8 (20 Feb. 1983).
- By combining the results of model calculations and simultaneous measurements of O₃, NO, HNO₃, particulate NO₃⁻, and meteorological parameters in the mid-Pacific, the authors have investigated the budget and photochemistry of near surface atmospheric ozone and odd nitrogen. The observed decrease of O₃ toward the Intertropical Convergence Zone is consistent with the transport of O₃ from higher latitude and a photochemical sink for O₃ by the reaction between H₂O and O(¹D). The total deposition flux of odd nitrogen deduced from the data is about $1.3 \times 10^9 \text{ cm}^{-2} \text{ s}^{-1}$ deposition flux is due to HNO₃ and particulate NO₃⁻. Since the residence time of odd nitrogen in the lower troposphere is short, a widely distributed, diffuse source of odd nitrogen is required to balance the deposition flux. It seems that the NO formed by cloud lightning is the most likely source. (73 refs.)
- 78612 The sources of sulfate in precipitation. I. Parameterization scheme and physical sensitivities.** D.A.Hegg (Atmospheric Sci. Dept., Univ. of Washington, Seattle, WA, USA). *J. Geophys. Res. (USA)*, vol.88, no.C2, p.1369-74 (20 Feb. 1983).
- The parameterization scheme for sulfate washout derived by Scott see J. Appl. Meteorol., vol.17, p.1375-89 (1978) is modified to allow estimation of the relative contributions of nucleation scavenging, in-solution production, and below-cloud scavenging to the sulfate content of precipitation. The parameterization scheme predicts changes in precipitation sulfate concentration by up to a factor of 6 for large variations in key cloud physics parameters. The results suggest in-solution sulfate production can be a substantial contributor to the sulfate content of precipitation. (24 refs.)

- 78613 The sources of sulfate in precipitation. II. Sensitivities to chemical variables.** R.J.Charlson, R.Vong, D.A.Hegg (Dept. of Civil Engng., Univ. of Washington, Seattle, WA, USA). *J. Geophys. Res. (USA)*, vol.88, no.C2, p.1375-7 (20 Feb. 1983).
- For pt.1 see ibid., vol.88, no.C2, p.1369-74 (1983). A convective cloud model used to examine the relative contribution to sulfate in rain of nucleation scavenging (NS) below-cloud scavenging (BCS) and in cloud production of sulfates (SP) shows that considerable variation may be expected due to change in the amounts of input sulfur species. The case of high input of both SO₂ and SO₄²⁻ bearing aerosol (industrial case) shows SP to be dominant while low inputs yield results ranging from NS and SP being roughly equal to dominance by NS. For the conditions chosen, BCS is low. The sensitivities of the partitioning between these three pathways to changes in SO₂, SO₄²⁻ aerosol, and pH are briefly surveyed. (3 refs.)
- 78614 A numerical model of the zonally averaged dynamical and chemical structure of the middle atmosphere.** R.R.Garcia (Nat. Center for Atmospheric Res., Boulder, CO, USA), S.Solomon. *J. Geophys. Res. (USA)*, vol.88, no.C2, p.1379-400 (20 Feb. 1983).
- A two-dimensional, time-dependent model has been constructed to study the zonally averaged structure of the middle atmosphere (16-116 km) allowing interaction among dynamics, radiation and photochemistry. The zonally averaged dynamics are governed by a stream function equation for the residual Eulerian meridional circulation wherein the effects of wave transience and dissipation have been neglected. The resulting circulation is thus driven by diabatic heating and cooling, with Rayleigh friction introduced to balance the momentum budget. The temperature structure is computed from the zonal mean thermodynamic equation, while the appropriate continuity equations are solved to determine the distribution of the various chemical species and families. In the chemical continuity equations, two types of eddy transport processes are present in addition to the transport by the residual Eulerian circulation. (101 refs.)
- 78615 On the relationship between the greenhouse effect, atmospheric photochemistry, and species distribution.** L.B.Callis (NASA Langley Res. Center, Hampton, VA, USA), M.Natarajan, R.E.Boughner. *J. Geophys. Res. (USA)*, vol.88, no.C2, p.1401-26 (20 Feb. 1983).
- A radiative-convective-photochemical model that extends from 0 to 53 km is used to examine the effect on atmospheric constituents and thermal structure of changes in the atmospheric levels of CO₂, CFMs, CO, N₂O and combinations of these species. Calculations were carried out for two reference atmospheres, one with high (HINOX) and one with low (LONOX) levels of NO_x. The HINOX troposphere provides a net photochemical source of O₃ and is not greatly sensitive to downward transport of O₃ from the stratosphere. The LONOX troposphere is a photochemical sink for O₃ and, as a result, is sensitive to such variations in downward transport. Results of this study suggest that (1) infrared opacity changes due to CO₂ and CFM increases can cause significant changes in tropospheric O₃, OH, CH₃, CO, and other species through changes in tropospheric water vapor; (2) perturbation or sensitivity studies conducted with tropospheric photochemical models may be subject to significant errors due to the absence of modulating effects provided by the stratosphere. Some other findings of this model are described. (120 refs.)
- 78616 Chlorocarbon emission scenarios: potential impact on stratospheric ozone.** D.J.Wuebbles (Lawrence Livermore Nat. Lab., Univ. of California, Livermore, CA, USA). *J. Geophys. Res. (USA)*, vol.88, no.C2, p.1433-43 (20 Feb. 1983).
- Prior analyses of chlorocarbons and their effects on stratospheric ozone have primarily concentrated on examining potential perturbations from two chlorofluorocarbons, CFCl₃ (CFC-11) and CF₂Cl₂ (CFC-12). The purpose of this study is to provide an updated theoretical analysis of the potential effect on ozone due to past and future chlorocarbon emissions. To assess the overall impact from chlorinated emissions on the ozone layer, all chlorocarbons presently thought to be of likely concern are examined. A broad spectrum of scenarios is evaluated in order to provide an envelope including conceivable changes in future chlorocarbon emissions. Results indicate that CFCl₃, CF₂Cl₂ (CFC-113), CH₂Cl₂, and CCl₄ could contribute significantly to predicted changes in total ozone based on their current emission rates. (46 refs.)
- 78617 Effect of coupled anthropogenic perturbations on stratospheric ozone.** D.J.Wuebbles, F.M.Luther, J.E.Penner (Lawrence Livermore Nat. Lab., Univ. of California, Livermore, CA, USA). *J. Geophys. Res. (USA)*, vol.88, no.C2, p.1444-56 (20 Feb. 1983).
- In order to compare theoretical calculations of ozone levels with recent measurements of ozone and to project expected changes over the next few decades, one must consider the effect from perturbations other than from chlorofluorocarbons. In this paper, the coupling between several possible anthropogenic atmospheric perturbations is considered. The effects of past and possible future increases of chlorocarbons, CO₂, N₂O, and NO_x are examined. The focus of these calculations is on the potential changes in ozone due to chlorocarbon emissions, how other anthropogenic perturbations may have influenced the actual change in ozone over the last decade, and how these perturbations may influence future changes in ozone. There is very little change predicted in total ozone over the coming decades when other anthropogenic sources are included. Increasing CO₂ concentrations have the largest offsetting effect on the change in total ozone due to chlorocarbons. (67 refs.)
- 78618 Stratospheric sulfuric acid vapor: new and updated measurements.** A.A.Viggiano, F.Arnold (Max-Planck-Inst. für Kernphys., Heidelberg, Germany). *J. Geophys. Res. (USA)*, vol.88, no.C2, p.1457-62 (20 Feb. 1983).
- The measurements of gas phase H₂SO₄ in the stratosphere have been continued. It has been realized that the measurements may include other sulfur-containing species such as HSO₃ and HSO₅. The technique has been improved through the use of a mass spectrometer with a larger mass range and better measurements of the parameters involved in the derivation of the H₂SO₄ concentration. The results from the first two flights of this new instrument are reported, and the older data have been revised in accordance with the new measurements of the parameters. In addition, the lower height range has been extended to 15 km. (35 refs.)
- 78619 Simultaneous measurements of vertical distributions of stratospheric NO₃ and O₃ at different periods of the night.** P.Rigaud (Station Sci. du Val Jouvey, Villepreux, France), J.P.Naudet, D.Huguenin. *J. Geophys. Res. (USA)*, vol.88, no.C2, p.1463-7 (20 Feb. 1983).
- Simultaneous measurements of NO₃ and O₃ were performed at different periods of the night from stratospheric balloons launched from the CNES balloon station at Aire-sur-l'Adour in September 1980 and September 1981. The experimental NO₃ vertical profiles compare favorably with those predicted by the photochemical theory. Differences can be explained by the dependence of the recombination rate of NO₂ and O₃ upon altitude. The O₃ concentrations above 30 km measured by spectrophotometry around λ=660 nm present a remarkable stability. Measurements obtained by means of this technique could be used as a reference for the detection of long-term variations of O₃. (21 refs.)

78620 UV rocket spectroscopy measurement of the nighttime ozone distribution. J.L. Lean (Dept. of Phys., Univ. of Adelaide, Adelaide, Australia). *J. Geophys. Res. (USA)*, vol.88, no.C2, p.1468-74 (20 Feb. 1983). Nocturnal ozone densities between 32 and 72 km have been derived from observations of the full Moon, made by three optical ozone detectors, each comprising three ultraviolet photometers. The three similar detectors were carried on a single spinning rocket, launched at Wallops Island on November 4, 1979. The mean of the three measured ozone profiles is consistent with other nighttime ozone profiles obtained from the LRIR satellite experiment and also from ground based millimeter wave observations. The relative standard error in the mean ozone profile is approximately 5%. At 70 km the ozone concentration of $1.5 \times 10^{19} \text{ cm}^{-3}$ is a factor of three greater than the US Standard Atmosphere, 1976 mid latitude daytime model. (29 refs.)

78621 A preliminary global oceanic cloud climatology from satellite albedo observations. N.A. Hughes (Dept. of Geography, Univ. of Liverpool, Liverpool, England), A. Henderson-Sellers. *J. Geophys. Res. (USA)*, vol.88, no.C2, p.1475-83 (20 Feb. 1983). A pilot study has lead to the establishment of a preliminary predictive relationship for cloud amount as a function of satellite observed system albedo. The United States Air Force 3D-nephanalysis cloud archive is used as the source of cloud data and is compared with monthly mean system albedo values calculated by NOAA/NESS from the NOAA satellite scanning radiometer data at a resolution of 2.5° by 2.5° . The predictive relationship is applied to ocean areas to produce new global oceanic cloud climatologies. (20 refs.)

78622 Lightning propagation and flash density in squall lines as determined with radar. V. Mazur (Cooperative Inst. for Mesoscale Meteorological Studies, Univ. of Oklahoma, Norman, OK, USA), W.D. Rust. *J. Geophys. Res. (USA)*, vol.88, no.C2, p.1495-502 (20 Feb. 1983). The propagation of lightning has been studied using radar techniques. The rise time of radar echoes is explained by ionized channel propagation through the radar beam. The calculated values agree well with those obtained experimentally. Measurements of the radial velocity of streamer propagation (along the antenna beam) show speeds of at least $2.5 \times 10^5 \text{ m/s}$. The time-range variations in lightning echoes are indicative of (1) new ionization as streamers develop into different parts of the cloud, (2) channel decay during which adequate ionization exists for radar detection, or (3) continuing current. Lightning flash density has been determined for two squall lines, one in the USSR and the other in the United States. The maximum lightning density tends to be near the leading edge of the precipitation cores in developing cells. As a cell in the squall line develops and the total lightning density increases, long discharges are produced, but shorter ones predominate. In contrast, as the cell dissipates, short flashes diminish or cease, and the long flashes dominate. (18 refs.)

78623 The seasonal variation of the atmospheric SO_2 to SO_4^{2-} conversion rate. J.F. Meagher, E.M. Bailey (Air Resources Program, Tennessee Valley Authority, Muscle Shoals, AL, USA), M. Luria. *J. Geophys. Res. (USA)*, vol.88, no.C2, p.1525-7 (20 Feb. 1983). Data collected during eight separate field studies conducted at four coal-fired power plants were combined to investigate the dependence of the nonaqueous phase SO_2 oxidation rate on various meteorological parameters. The data exhibited a strong seasonal trend with average morning SO_2 oxidation rates varying from a winter low of $1.5 \times 10^{-3} \text{ h}^{-1}$ to a summer high of $1.3 \times 10^{-2} \text{ h}^{-1}$. (11 refs.)

78624 Atmospheric gravity wave production for the total eclipse of 11 June 1983. G.L. Goodwin (School of Phys., South Australia Inst. of Technol., Ingle Farm, S. Australia). *J. Atmos. & Terr. Phys. (GB)*, vol.45, no.4, p.273-4 (April 1983). Internal atmospheric gravity bow waves generated by the eclipse of 11 June 1983 will focus over central Australia. (6 refs.)

78625 The wave properties in the process of nocturnal radiation inversion. Zhou Mingyu, Zhang Yi (Acad. Sinica, Beijing, China). *Kexue Tongbao (Foreign Lang. Ed.) (China)*, vol.28, no.2, p.216-20 (Feb. 1983). It is difficult to maintain the steady state of the stable atmospheric boundary layer, in which the meteorological elements often change. Therefore a study of the characteristics of the nocturnal atmospheric boundary layer, especially of the characteristics and development regularity of the radiation inversion process, has important significance for theoretical research of the atmospheric boundary layer and such practical problems as the transport and diffusion of atmospheric pollutants. (6 refs.)

78626 On the initialization in numerical weather prediction in the tropics. Zhou Jiabin, Wu Peizhen (Inst. of Atmospheric Phys., Acad. Sinica, Beijing, China). *Kexue Tongbao (Foreign Lang. Ed.) (China)*, vol.28, no.1, p.69-73 (Jan. 1983). [received: June 1983] Due to the undesirable sensitivity to initial values and small-scale disturbances of the primitive equation used for weather prediction in the tropics, nine initialization schemes are evaluated. These variously take into account the distinct characteristics for different latitudes, the linkage between levels in the vertical, and divergence in the initial field. They are assessed in a series of tests using a four-level primitive equation model. (8 refs.)

78627 Stratospheric NO_2 and upper limits of CH_3Cl and C_2H_6 from measurements at 3.4 μm . D.J.W. Kendall (Herzberg Inst. of Astrophys., Nat. Res. Council of Canada, Ottawa, Ontario, Canada), H.L. Buijs. *Nature (GB)*, vol.303, no.5914, p.221-2 (19 May 1983). Reports high resolution absorption spectra that have been obtained from a balloon-borne platform in the 3.4 μm spectral region, a region which contains bands due to several atmospheric constituent gas species including methane (CH_4), hydrochloric acid (HCl), nitrogen dioxide (NO_2), methyl chloride (CH_3Cl) and ethane (C_2H_6). From analysis of the atmospheric spectra obtained during sunset, mixing ratio versus altitude profiles have been obtained for HCl (which will be reported elsewhere) and NO_2 , and upper limits have been obtained for the lower stratospheric mixing ratios of CH_3Cl and C_2H_6 . (29 refs.)

78628 In situ aircraft measurements of enhanced levels of N_2O associated with thunderstorm lightning. J.S. Levine (Atmospheric Sci. Div., NASA Langley Res. Center, Hampton, VA, USA), E.F. Shaw, Jr. *Nature (GB)*, vol.303, no.5915, p.312-14 (26 May 1983). Reports the first series of measurements of enhanced levels of atmospheric N_2O associated with thunderstorm lightning. N_2O is an environmentally significant species since its reaction with excited oxygen (O^1D) in the stratosphere produces NO which through the catalytic NO_x cycle is responsible for about 65% of the total global destruction of ozone (O_3) in the stratosphere. In addition, due to its absorption at 7.8 μm in the atmospheric window, N_2O absorbs and then re-emits Earth-emitted IR radiation which leads to an enhancement of the surface temperature, and hence, has important implications for climate considerations. (21 refs.)

78629 Positive ion composition measurements and acetonitrile in the upper stratosphere. E.A. Jijds, D. Nevejan, J. Ingels (Belgian Inst. for Space Aeronomy, Brussels, Belgium). *Nature (GB)*, vol.303, no.5915, p.314-16 (26 May 1983). Reports the first positive ion composition data obtained using a balloon-borne instrument between 42 and 46 km altitude. These data extend the density profile of molecule X and give supplementary indications about its identity. The data were obtained with a mass spectrometer that was flown on 23 September 1982 on a stratospheric balloon from the CNES launching base of Aire-sur-l'Adour (44°N). (27 refs.)

78630 The role of radar in weather forecasting. K.A. Browning (Radar Res. Lab., Royal Radar Estab., Malvern, England). *Phys. Technol. (GB)*, vol.14, no.3, p.140-5 (May 1983). Radar is a versatile observational tool in meteorology. The author discusses the use of networks of weather radars for tracking rain areas and thunderstorms. Doppler radars can detect the hazardous winds sometimes associated with such storms. (3 refs.)

78631 The global distribution of thunderstorm activity observed by the ionosphere sounding satellite (ISS-b). M. Kotaki, I. Kuriki, C. Katoh, H. Sugiuchi. *Rev. Radio Res. Lab. (Japan)*, vol.28, no.146, p.369-86 (June 1982). In Japanese. Observation of the global distribution of atmospheres, especially lightning discharges, has been made by means of four channel HF receivers on board the Ionosphere Sounding Satellite-b. The operational frequencies of the receivers are set in the guard band of the standard frequency transmission at 2.5, 5, 10 and 25 MHz so as to avoid interference from terrestrial radio transmitters. The count of lightning discharges which were observed was accumulated in each geographic bin ($10^\circ \times 10^\circ$ in both longitude and latitude) and normalized by the observation time for the area. Based on the data obtained during the period from June, 1978 to May, 1980, the active regions of lightning were mapped out in the form of global distribution divided into every four hours in universal time, 22-02, 02-06, 06-10, 10-14, 14-18, and 18-22 hr of a day for the four seasons. The authors estimate the global lightning frequency to be 64 sec^{-1} for the northern spring, 55 sec^{-1} for the summer, 80 sec^{-1} for the fall, and 54 sec^{-1} for the winter. The peak lightning frequency occurs at $10^\circ\text{-}20^\circ\text{S}$ during the northern winter and at $10^\circ\text{-}20^\circ\text{N}$ during the summer. The diurnal variation of global lightning frequency has a peak at 12 hr UT. (15 refs.)

78632 Global distribution of atmospheric radio noise derived from the global distribution of lightning activity. M. Kotaki, C. Katoh. *Rev. Radio Res. Lab. (Japan)*, vol.28, no.146, p.411-33 (June 1982). In Japanese. Based on global maps of thunderstorm activity measured by the Ionosphere Sounding Satellite-b the atmospheric radio noise levels over the world were calculated. Global distribution maps of atmospheric radio noise were made for frequencies of 2.5, 5, 10 and 20 MHz, for every four hours in universal time during autumn. The calculated results agree better with world-wide measurements than those given by CCIR report no.322, and, moreover, some characteristics of the atmospheric radio noise can be well explained by the present method. (15 refs.)

78633 The seasonal variation of wind speed in the United Kingdom. S.G. Smith (Meteorological Office, Bracknell, England). *Weather (GB)*, vol.38, no.4, p.98-103 (April 1983). Within the meteorological office a statistical model is being developed for simulating sequences of hourly mean wind speeds for different locations in the United Kingdom (UK). To achieve this it is necessary to describe the seasonal variation of wind speed and fit it to a mathematical function. Spatial differences in the seasonal variation are studied by using a common 15-year period of data for 20 stations. The long-term (100 years) seasonal variation is considered by recourse to monthly speeds obtained from surface pressure gradients. (4 refs.)

78634 Large falls of rain in Wales—a simple statistical case study. I.T. Jolliffe (Math. Inst., Univ. of Kent, Canterbury, England). *Weather (GB)*, vol.38, no.4, p.103-5 (April 1983). Perry and Howells (1982) presented data from various stations in South Wales in an attempt to answer the question 'Are large falls of rain in Wales becoming more frequent?' The tables and figures in that paper suggested persuasively that the answer is 'Yes' to the more specific question 'Are large falls...more frequent in the years 1926-1980 than before 1925?' However, the analysis of the data was purely descriptive, and no attempt was made to use statistical techniques to assess whether the differences between the two time periods could have arisen by chance. The author's note remedies this omission by presenting some relatively simple statistical analyses of the data. In doing so it illustrates the use in practice of three well-known probability distributions. (1 ref.)

78635 North-African cyclonic systems and springtime temperatures in Israel. M. Druryan (Dept. of Geography, Bar Ilan Univ., Ramat Gan, Israel). *Weather (GB)*, vol.38, no.4, p.110-11 (April 1983). Considers the fate of low pressure regions found over north-west Africa during the months March, April and May, as depicted by the Synoptic Weather Maps (of the Northern Hemisphere). Daily Series (1953-1968) and operational weather charts of the Israel Meteorological Service (1966-1967, 1970-1977). It is of primary interest to establish whether or not a particular cyclonic system eventually triggered a sharav (heat wave), and how the consequences were related to synoptic developments. Sharav was taken as having occurred on a day when the maximum temperature at Bet Dagan (about 10 km south-east of Tel Aviv) as recorded in Israel's Monthly Weather Summary (1953-63) was more than 5 deg C greater than its long-term mean (interpolated to each day from the monthly normals of daily maximum temperature). (5 refs.)

78636 Observations of abnormal microwave propagation phenomena during melting layer conditions. M. Kharadly (Univ. of British Columbia, Vancouver, BC, Canada), N. Owen, J. Van der Star, D. Michelson, T. Engren. Third International Conference on Antennas and Propagation ICAP '83, Norwich, England, 12-15 April 1983 (London, England: IEE 1983), p.214-18 part 2. Many investigators, including Watson (1976), Oomari and Aoyagi (1971), Austin (1964), and Van der Star and Kharadly (1981), have reported that the presence of a melting layer in a propagation channel increased the channel attenuation above that which could be attributed to rain. This paper presents, in addition to observations depicting severe cases of this phenomenon, other anomalous fading phenomena that were associated with the presence of the melting layer. These observations were made on a microwave slant path in British Columbia approximately 200 km inland from the Pacific Ocean. (8 refs.)

- Proceedings of the Topical Meeting of the COSPAR Interdisciplinary Scientific Commission A (Meetings A1 and A2) of the COSPAR Twenty-Fourth Plenary Meeting See Entry 74204
- Symposium on the Rise in Atmospheric Carbon Dioxide See Entry 74212
- Cloud Dynamics. Proceedings of a Symposium held at the Third General Assembly of IAMAP See Entry 74227
- Analysis of dust rain in the historic times of China See Entry 74245
- Absolute band strengths of halocarbons F-11 and F-12 in the 8-to 16- μ m region See Entry 75381
- Understanding the middle atmosphere via the laboratory: ion cluster investigations See Entry 75564
- Calculating internal radiation in greenhouses in the Evora region See Entry 77961
- Examination of a hot particle from a recent atmospheric test See Entry 78111
- Uncertainties of predictions of future atmospheric CO₂ concentrations See Entry 78114
- Distribution of and changes in industrial carbon dioxide production See Entry 78115
- Analysis of tritium in tree rings See Entry 78365
- Microwave emissions from soils with rough surfaces See Entry 78541
- Lightning craters See Entry 78547
- Experiments on solitary internal Kelvin waves See Entry 78552
- The form and dynamics of Langmuir circulations See Entry 78556
- On the radiocarbon record in banded corals: exchange parameters and net transport of ¹⁴CO₂ between atmosphere and surface ocean See Entry 78559
- Aero-diffusion method of estimating evaporation in a non-stratified atmosphere See Entry 78565
- Comparison of CO₂ measurements by two laboratories on air from bubbles in polar ice See Entry 78571
- Detection of abrupt changes occurring in a rainfall sequence represented by a periodic function See Entry 78573
- Persistence of wet and dry spells at Uccle (Belgium) See Entry 78637
- Climatic clusters of the Indian region See Entry 78638
- Modelling climate and the nature of climate models: a review See Entry 78639
- Climatic influence of background and volcanic stratosphere aerosol models See Entry 78640
- Mid-latitude model analysis of solar radiation, the upper layers of the sea, and seasonal climate See Entry 78641
- On the influence of rough water surfaces on polarimetric investigations of aerosols from space See Entry 78644
- Aerosol measurements from Earth orbiting spacecraft See Entry 78646
- Remote monitoring of aerosols from space See Entry 78647
- The characterization of atmospheric spread functions affecting satellite remote sensing of the Earth's surface See Entry 78650
- A method for estimating cross radiance See Entry 78651
- O₂ absorption cross sections (187-225 nm) from stratospheric solar flux measurements See Entry 78652
- Modelling the isotope composition of oxygen in the ancient atmosphere of the Earth See Entry 78653
- Passive remote sensing of aerosols from space now and in the future See Entry 78657
- Most suitable conditions for aerosol monitoring from space See Entry 78658
- Laser sounding of aerosols using airborne and space facilities See Entry 78659
- Retrieval of aerosol characteristics from scattering and extinction measurements See Entry 78661
- Validation of aerosol measurements by the satellite sensors SAM II and SAGE See Entry 78662
- Retrieval of aerosol size distribution from extinction measurements and verification with observations at a tropical station See Entry 78663
- Determination of aerosol optical depth from ground measurements See Entry 78664
- Condensation sampling of soluble atmospheric trace gases See Entry 78696
- Sources of background current in the ECC ozonesonde: implications for total ozone measurements See Entry 78697
- Semiautomatic nondispersive infrared analyzer apparatus for CO₂ air sample analyses See Entry 78698
- Registration of thunderstorm centers by automatic atmospheric stations See Entry 78699
- A new method for measuring radon exhalation See Entry 78700
- Ultraviolet hygrometer for measuring fluctuations in α atmospheric humidity See Entry 78705
- Acoustic remote sensing of the boundary layer See Entry 78707
- Airflow resistivity instrument for in situ measurement on the Earth's ground surface See Entry 78708

92.60S Climatology

- 78637 Persistence of wet and dry spells at Uccle (Belgium). A.Berger, C.Goossens (Inst. of Astron. & Geophys., Catholic Univ. of Louvain-la-Neuve, Louvain, Belgium). *J. Climatol. (GB)*, vol.3, no.1, p.21-34 (Jan.-March 1983). The rainfall persistence at Uccle (Belgium) is examined statistically using 75 years of daily observations. Different kinds of distributions expressing this persistence have been fitted to the sequences of dry and wet days: the geometric series, the logarithmic series, the Eggenberger-Polya distribution, the simple Markov Chain and the Markov Chain of order higher than one. Wet and dry spells are best described by a Markov Chain model of order four. Nevertheless, for wet days, the Eggenberger-Polya distribution provides a good fit to the observed data. For Uccle, the rainfall persistence seems to remain constant after four consecutive days of precipitation. (27 refs.)

- 78638 Climatic clusters of the Indian region. S.Gadgil, N.V.Joshi (Centre for Theoretical Studies, Indian Inst. of Sci., Bangalore, India). *J. Climatol. (GB)*, vol.3, no.1, p.47-63 (Jan.-March 1983). Derives climatic clusters of the Indian region using monthly mean profiles of the precipitation, the moisture index and the minimum temperature. The delineation of regions over which the profile patterns of important climatic factors are similar is necessary for the determination of meteorological zones over which prediction can be made as well as for understanding the distribution of vegetation cover. The latter has been the major aim of the studies of climatic classification. The variation of the climatic patterns over the Indian region is analysed to obtain climatic clusters, which represent natural grouping of the patterns and hence of the meteorological stations at which they occur, as well as the climatic boundaries separating these clusters. This analysis is facilitated by an initial reduction of the mean monthly profiles of the moisture index are obtained. (24 refs.)

- 78639 Modelling climate and the nature of climate models: a review. K.P.Shine, A.Henderson-Sellers (Dept. of Geography, Univ. of Liverpool, Liverpool, England). *J. Climatol. (GB)*, vol.3, no.1, p.81-94 (Jan.-March 1983). A new structural framework for climate models is presented. Four basic types are discussed: general circulation models, energy balance models, one dimensional radiative convective models and two dimensional zonally averaged dynamical models. The fundamental importance of three primary processes in the climate system-radiation, dynamics and surface processes—is underlined and the degree to which each of these mechanisms is incorporated in each model is highlighted. (80 refs.)

- 78640 Climatic influence of background and volcanic stratosphere aerosol models. P.Y.Deschamps, M.Herman, J.Lenoble, D.Tanre (Lab. d'Optique Atmospherique, Univ. des Sci. et Tech. de Lille, Villeneuve d'Ascq, France). *Adv. Space Res. (GB)*, vol.2, no.5, p.171-6 (1982). [received: April 1983] (Proceedings of the Topical Meeting of the COSPAR Interdisciplinary Scientific Commission A (Meetings A1 and A2) of the COSPAR Twenty-Fourth Plenary Meeting, Ottawa, Canada, 16 May-2 June 1982).

- A simple modelization of the Earth atmosphere system including tropospheric and stratospheric aerosols is derived and tested. Analytical expressions are obtained for the albedo variation due to a thin stratospheric aerosol layer. Also outlined are the physical procedure and the respective influence of the main parameters: aerosol optical thickness, single scattering albedo and asymmetry factor, and sublayer albedo. The method is applied to compute the variation of the zonal and planetary albedos due to a stratospheric layer of background H₂SO₄ particles and of volcanic ash. (6 refs.)

- 78641 Mid-latitude model analysis of solar radiation, the upper layers of the sea, and seasonal climate. T.P.Charlock (Nat. Center for Atmospheric Res., Boulder, CO, USA). *J. Geophys. Res. (USA)*, vol.87, no.C11, p.8923-30 (20 Oct. 1982). [received: May 1983]

- A simplified, time-dependent energy balance climate model is run at the latitude belt 40°-50°N. The model solves for the temperatures of the land, air, and 12 vertical oceanic layers, and it includes a wind stirred mixed layer. Because the attenuation of solar radiation in the model ocean varies significantly with wavelength in the visible, fine wavelength resolution radiative transfer for Rayleigh scattering and ozone absorption is used between 340 and 720 nm. The optical properties of the model clouds are functions of the cloud liquid water contents. A change in model ocean optical turbidity from relatively clear (Jerlov I) to particle rich (Jerlov III) conditions decreases the effective thickness of the oceanic layer in which heat is stored seasonally and increases the seasonal variation of sea surface temperature by 2°-3°C. (45 refs.)

- 78642 Relation between the changes of clay mineralogy in the cores of marine deposits and the paleoclimatic vicissitudes. He Liangbiao (First Inst. of Oceanography, Nat. Bur. of Oceanography, Qingdao, China). *Kexue Tongbao (Foreign Lang. Ed.) (China)*, vol.28, no.2, p.232-6 (Feb. 1983).

- With respect to the relation between the changes of clay mineralogy in the cores of marine deposits and the paleoclimatic vicissitudes, two completely different viewpoints prevail in the international circles today. One holds that paleoclimatic vicissitudes might be indicated by the changes of clay mineralogy in the cores. The other holds that it has nothing to do with the changes of clay mineralogy. Based on the comprehensive qualitative and quantitative analyses on clay minerals in two cores from the Pacific and in eight cores from the Huanghai Sea, and the data obtained by his colleagues from corresponding cores, the author deems that the changes of clay minerals in the cores, especially those of dominant clay minerals, exhibit a close relationship with the paleoclimatic vicissitudes. This fact gives a strong support to the first viewpoint. (4 refs.)

- Analysis of dust rain in the historic times of China See Entry 74245

- Aerosols within the World Climate Research Programme See Entry 78579

- The effect of aerosols on climate and aerosol climatology on the basis of observations from space See Entry 78580

- The role of aerosols in the climate system: results of numerical experiments in climate models See Entry 78581

- Feedback mechanisms in the climate system affecting future levels of carbon dioxide See Entry 78602

- The seasonal variation of wind speed in the United Kingdom See Entry 78633

- Large falls of rain in Wales—a simple statistical case study See Entry 78634

92.65 ATMOSPHERIC OPTICS

(see also 42.00 Optics)

- 78643 Instantaneous integrated Raman scattering. S.Egert, A.Cohen (Hebrew Univ. of Jerusalem, Jerusalem, Israel), M.Kleiman, N.Ben-Yosef. *Appl. Opt. (USA)*, vol.22, no.10, p.1592-7 (15 May 1983). Lidar detection of atmospheric molecules using a Raman scattering technique being usually limited by low signals is enhanced by integration of the forward Raman scattered light over a large atmospheric volume. This integral can be measured instantaneously in the presence of a reflector at one edge of the optical path, increasing the SNR by a factor of 100 in the case of a perfect reflector and a beam path of ~2 km. Natural reflectors such as clouds leading to the same effect are also discussed. (12 refs.)

78644 On the influence of rough water surfaces on polarimetric investigations of aerosols from space. T.Prosch, D.Hennings, E.Raschke (Inst. für Geophys. und Meteorologie, Univ. zu Köln, Köln, Germany). *Adv. Space Res. (GB)*, vol.2, no.5, p.33-8 (1982). [received: April 1983] (Proceedings of the Topical Meeting of the COSPAR Interdisciplinary Scientific Commission A (Meetings A1 and A2) of the COSPAR Twenty-Fourth Plenary Meeting, Ottawa, Canada, 16 May-2 June 1982). The equation of radiative transfer is solved for the complete Stokes's vector in order to study the polarization of solar radiation on top of a turbid atmosphere. Results of surface model calculations are compared with polarimeter measurements. (7 refs.)

78645 Retrieval of aerosol optical characteristics from polarization measurements of reflected solar radiation above the oceans. R.Santer, M.Herman, J.Lenoble (Lab. d'Optique Atmosphérique, Univ. des Sci. et Tech. de Lille, Villeneuve d'Ascq., France). *Adv. Space Res. (GB)*, vol.2, no.5, p.65-70 (1982). [received: April 1983] (Proceedings of the Topical Meeting of the COSPAR Interdisciplinary Scientific Commission A (Meetings A1 and A2) of the COSPAR Twenty-Fourth Plenary Meeting, Ottawa, Canada, 16 May-2 June 1982). The reflected near infrared solar radiation observed from space above the oceans is due mainly to atmosphere scattering, as the ocean surface is nearly black. The molecular Rayleigh contribution is also minimized at infrared wavelengths and can be evaluated. It is shown that the degree of polarization is much more sensitive to the aerosol properties than the radiance. Measurements of polarization at two wavelengths and with angular scanning are simulated and an inversion algorithm is proposed. An 'equivalent aerosol model' reproduces the optical thickness and the asymmetry factor of the actual aerosol at all wavelengths in the solar spectrum. (9 refs.)

78646 Aerosol measurements from Earth orbiting spacecraft. M.P.McCormick (Atmospheric Sci. Div., NASA Langley Res. Center, Hampton, VA, USA). *Adv. Space Res. (GB)*, vol.2, no.5, p.73-86 (1982). [received: April 1983] (Proceedings of the Topical Meeting of the COSPAR Interdisciplinary Scientific Commission A (Meetings A1 and A2) of the COSPAR Twenty-Fourth Plenary Meeting, Ottawa, Canada, 16 May-2 June 1982). Since the fall of 1978, two Earth-orbiting spacecraft sensors, SAM II (Stratospheric Aerosol Measurement II) and SAGE (Stratospheric Aerosol and Gas Experiment), have been monitoring the global stratospheric aerosol. These experiments use the Sun as a source to make Earth-limb extinction measurements during each spacecraft sunrise and sunset. This paper describes the global aerosol data base that is evolving. Seasonal and hemispheric variations such as the springtime layer expansion with warming temperatures and the local wintertime polar stratospheric clouds are described. The detection and tracking of a number of volcanoes whose effluents penetrated the tropopause are also described. (10 refs.)

78647 Remote monitoring of aerosols from space. O.A.Avaste, S.H.Keevallik (Inst. of Astrophys. & Atmospheric Phys., Acad. of Sci., Tartu, Estonian SSR). *Adv. Space Res. (GB)*, vol.2, no.5, p.87-93 (1982). [received: April 1983] (Proceedings of the Topical Meeting of the COSPAR Interdisciplinary Scientific Commission A (Meetings A1 and A2) of the COSPAR Twenty-Fourth Plenary Meeting, Ottawa, Canada, 16 May-2 June 1982). Using the four-channel tele-radiometer 'Micron' aboard Salyut-4 and Salyut-6 the brightness profiles were determined in the near-infrared spectral region up to a height of 60 km (noctilucent clouds up to 80-85 km). Information on the global and vertical distributions of atmospheric aerosol, water vapour concentration and the optical properties of the noctilucent clouds has been obtained. (12 refs.)

78648 Investigation of the atmospheric aerosols by the visible and IR channels of the AVHRR radiometer on NOAA-6. T.Takashima, Y.Takayama (Meteorological Res. Inst., Tsukuba, Japan). *Adv. Space Res. (GB)*, vol.2, no.5, p.95-104 (1982). [received: April 1983] (Proceedings of the Topical Meeting of the COSPAR Interdisciplinary Scientific Commission A (Meetings A1 and A2) of the COSPAR Twenty-Fourth Plenary Meeting, Ottawa, Canada, 16 May-2 June 1982). The diffusely reflected radiation in the daytime and diffusely transmitted radiation at night from an inhomogeneous, plane parallel planetary atmosphere bounded by the ocean surface are calculated for the visible and IR region. In the daytime the effect of the solar radiation from the top is taken into account. The present study deals with the problem of no cloud contamination in data. Water vapor, molecular nitrogen, nitrous oxide, carbon dioxide and methane are taken as absorbent constituents and aerosols as the scattering constituent. (3 refs.)

78649 Different atmospheric effects in remote sensing of uniform and nonuniform surfaces. Y.J.Kaufman, R.S.Fraser (Goddard Lab. for Atmospheric Sci., NASA/Goddard Space Flight Center, Greenbelt, MD, USA). *Adv. Space Res. (GB)*, vol.2, no.5, p.157-55 (1982). [received: April 1983] (Proceedings of the Topical Meeting of the COSPAR Interdisciplinary Scientific Commission A (Meetings A1 and A2) of the COSPAR Twenty-Fourth Plenary Meeting, Ottawa, Canada, 16 May-2 June 1982). The atmospheric effect on the radiance of sunlight scattered from the Earth-atmosphere system is greatly dependent on the surface reflectance pattern, the contrast between adjacent fields, and the optical properties of the atmosphere. In addition, the atmospheric effect is described by the range and magnitude of the adjacency effects, the atmospheric modulation transfer function and the apparent spatial resolution of remotely sensed imagery. This paper discusses the atmospheric effect on classification of surface features and shows that surface nonuniformity can be used for developing procedures to remove the atmospheric effect from the satellite imagery. (23 refs.)

78650 The characterization of atmospheric spread functions affecting satellite remote sensing of the Earth's surface. R.W.L.Thomas (EG&G Washington Analytical Services Center Inc., Riverdale, MD, USA). *Adv. Space Res. (GB)*, vol.2, no.5, p.157-66 (1982). [received: April 1983] (Proceedings of the Topical Meeting of the COSPAR Interdisciplinary Scientific Commission A (Meetings A1 and A2) of the COSPAR Twenty-Fourth Plenary Meeting, Ottawa, Canada, 16 May-2 June 1982). A Monte Carlo simulation program has been used to compute the signal contribution of surface elements outside the field of view of a satellite borne sensor in both the visible and infrared spectra for realistic atmospheric models. For azimuthally symmetric reflection the effect of an arbitrary surface albedo pattern can be represented by two spread functions, namely, the ground-satellite spread function, and the ground-ground spread function. Examples of computed spread functions are shown together with their Fourier correspondents, the modulation transfer functions. It has been shown that the central portions of the line spread functions behave as the inverse distance while the point spread functions always possess a region behaving as the inverse square of the radial distance. (15 refs.)

78651 A method for estimating cross radiance. D.Spankuch (Meteorological Service of Germany, Meteorological Main Obs., Potsdam, Germany), I.Laszlo.

Adv. Space Res. (GB), vol.2, no.5, p.167-70 (1982). [received: April 1983] (Proceedings of the Topical Meeting of the COSPAR Interdisciplinary Scientific Commission A (Meetings A1 and A2) of the COSPAR Twenty-Fourth Plenary Meeting, Ottawa, Canada, 16 May-2 June 1982). When imaging the surface from satellites or aircraft, 'cross radiance' diminishes the information content of the pictures. A simple method is presented to estimate the value of cross radiance. This method includes a height-dependent aerosol size distribution model and the calculations refer to the single scattering approximation. The height variation of aerosol size distribution has significant effect on the value of cross radiance, while the areal distribution does not change much in comparison with that of the height-independent aerosol model. (4 refs.)

78652 O₂ absorption cross sections (187-225 nm) from stratospheric solar flux measurements. J.R.Herman, J.E.Mentall (NASA/Goddard Space Flight Center, Greenbelt, MD, USA). *J. Geophys. Res. (USA)*, vol.87, no.C11, p.8967-75 (20 Oct. 1982). [received: May 1983]

The absorption cross sections of molecular oxygen are calculated in the wavelength range from 187 to 230 nm from solar flux measurements obtained within the stratosphere. Within the Hertzberg continuum wavelength region the molecular oxygen cross sections are found to be about 30% smaller than the laboratory results of Shardanand and Rao (1977) from 200 to 210 nm and about 50% smaller than those of Hasson and Nicholls (1971). The effective absorption cross sections of O₂ in the Schumann-Runge band region from 187 to 200 nm are calculated and compared to the empirical fit given by Allen and Frederick (1982). The calculated cross sections indicate that the transmissivity of the atmosphere may be underestimated by the use of the Allen and Frederick cross sections between 195 and 200 nm. (14 refs.)

Proceedings of the Topical Meeting of the COSPAR Interdisciplinary Scientific Commission A (Meetings A1 and A2) of the COSPAR Twenty-Fourth Plenary Meeting See Entry 74204

Topical Meeting on Meteorological Optics. Technical Digest See Entry 74220

Absolute band strengths of halocarbons F-11 and F-12 in the 8-to 16-μm region See Entry 75381

Satellite measurements of tropospheric aerosols See Entry 78583

Monitoring of Saharan dust over the Atlantic using Meteosat-VIS-data See Entry 78584

Can turbidity measurements be used for the estimation of aerosol parameters? See Entry 78585

Rocket studies of atmospheric scattering and the aerosol size distribution in the troposphere and lower stratosphere over Thumba See Entry 78586

Global pictures of the ozone field, from high altitudes, from DE-I See Entry 78588

A mesospheric ozone profile at sunset See Entry 78590

Solar UV and ozone balloon measurements See Entry 78593

The optical and radiation field signatures produced by lightning return strokes See Entry 78596

Parameterization of IR cooling in a middle atmosphere dynamics model. I. Effects on the zonally averaged circulation See Entry 78597

The Saudi Arabian heat low: aerosol distributions and thermodynamic structure See Entry 78600

On the relationship between the greenhouse effect, atmospheric photochemistry, and species distribution See Entry 78615

Climatic influence of background and volcanic stratosphere aerosol models See Entry 78640

Passive remote sensing of aerosols from space now and in the future See Entry 78657

Most suitable conditions for aerosol monitoring from space See Entry 78658

Laser sounding of aerosols using airborne and space facilities See Entry 78659

Spaceborne lidar measurement accuracy: simulation of aerosol, cloud, molecular density, and temperature retrievals See Entry 78660

Retrieval of aerosol characteristics from scattering and extinction measurements See Entry 78661

Retrieval of aerosol size distribution from extinction measurements and verification with observations at a tropical station See Entry 78663

Determination of aerosol optical depth from ground measurements See Entry 78664

Research note: 13-color photometry, San Pedro Martir, 1973-79 See Entry 78826

92.90 OTHER TOPICS IN HYDROSPHERIC AND ATMOSPHERIC GEOPHYSICS

78653 Modeling the isotope composition of oxygen in the ancient atmosphere of the Earth. V.N.Melenevskii (Sci. Res. Inst. of Geology, Geophysics, & Mineral Raw Materials, Novosibirsk, USSR).

Sov. Geol. & Geophys. (USA), vol.23, no.3, p.17-23 (1982). Translation of: *Geol. & Geophys. (USSR)*, vol.23, no.3, p.23-9 (1982). From data on fractionation of oxygen isotopes and theories of the intensity of photosynthesis on the continents and in the World Ocean, a quantitative estimate is made of the balance of oxygen isotopes for the modern biosphere. The authors discuss the major factors which could have influenced the oxygen isotope composition of the Earth's ancient atmosphere. (42 refs.)

Symposium on the Rise in Atmospheric Carbon Dioxide See Entry 74212

93.00 GEOPHYSICAL OBSERVATIONS, INSTRUMENTATION, AND TECHNIQUES

93.30 INFORMATION RELATED TO GEOGRAPHICAL REGIONS

- Analysis of dust rain in the historic times of China See Entry 74245
- Comparative behavior of plutonium and americium in the Equatorial Pacific See Entry 75117
- The influence of diagenetic redox reactions on the distribution of $^{239,240}\text{Pu}$, ^{137}Cs , ^{241}Am and ^{55}Fe in sediments of the US continental margin See Entry 75118
- Relationship between the distribution of radionuclides and the sedimentological and mineralogical traits of the coastal marine sediments (Gaeta, Latina, La Spezia, Italy) See Entry 75122
- The actual ^3H content of the hydrosphere in Central Europe (1980) See Entry 78109
- Estimation of per caput dose and collective dose from the use of Danube water See Entry 78340
- Radioactive contamination of filamentous green algae in the Hungarian reach of the River Danube See Entry 78363
- Radioactivity of fish in the Hungarian reach of the River Danube See Entry 78364
- Analysis of tritium in tree rings See Entry 78365
- Gravity anomalies, seismic structure and geothermal history of the central Alps See Entry 78414
- Direct integration of Stokes' undulation and Vening Meinesz's deflection equations for geographically defined gravity anomaly blocks See Entry 78418
- Tidal gravity parameters at Brussels reconfirmed by a superconducting gravity meter See Entry 78420
- Existence and interpretation of an electrically conducting zone within the plateau basalts of Kerguelen Islands (TAAF) See Entry 78421
- A palaeomagnetic reconnaissance of Kashmir, northwestern Himalaya, India See Entry 78423
- Paleomagnetism of red beds of Early Devonian age from Central Iran See Entry 78424
- Lower Jurassic magnetostratigraphy at the Breggia Gorge (Ticino, Switzerland) and Alpe Turati (Como, Italy) See Entry 78428
- Late Precambrian Keweenaw asymmetric polarities as analyzed by axial offset dipole geomagnetic models See Entry 78430
- Statistical averaging of marine magnetic anomalies and the aging of oceanic crust See Entry 78433
- High paleointensities of the geomagnetic field from thermomagnetic studies on rift valley pillow basalts from the Mid-Atlantic Ridge See Entry 78434
- Paleomagnetism of Carboniferous intrusions in North Carolina See Entry 78435
- Local contributions to the M_2 lunar geomagnetic variations in the south-west of England See Entry 78437
- Analogue model study of electromagnetic induction in the Newfoundland region See Entry 78438
- Palaeomagnetism of some Precambrian rocks in south-east Greenland See Entry 78439
- An aftershock study of the El Asnam (Algeria) earthquake of 1980 October 10 See Entry 78442
- Spatial distribution of microearthquakes beneath the Japan Trench from ocean bottom seismographic observations See Entry 78443
- Source mechanism and surface wave excitation for two earthquakes in northern Baja California, Mexico See Entry 78444
- Group velocity distribution of surface waves in the North Atlantic See Entry 78445
- Regionalization of crustal coda Q in the continental United States See Entry 78449
- Focal depths and fault plane solutions of earthquakes under the Tibetan Plateau See Entry 78451
- Some statistical properties of a sequence of historical Calabro-Peloritan earthquakes See Entry 78452
- Assigning probability gain for precursors of four large Chinese earthquakes See Entry 78453
- A teleseismic analysis of the New Brunswick earthquake of January 9, 1982 See Entry 78455
- Seismicity near Palmdale, California, and its relation to strain changes See Entry 78456
- Three-dimensional crust and upper mantle structure at the Nevada Test Site See Entry 78457
- Viscoelastic stress relaxation on deep fault sections as a possible source of very long period elastic waves See Entry 78459
- Three-dimensional crust and upper mantle structure of the Eurasian continent See Entry 78460
- The geoid, small-scale convection, and differential travel time anomalies of shear waves in the central Indian Ocean See Entry 78461
- On the correlation between the syzygies and great earthquakes in Hebei of China See Entry 78467
- Seismicity of Yemen See Entry 78468
- Evidence for dyke intrusion earthquake mechanisms near Long Valley caldera, California See Entry 78469
- The West-African craton margin in eastern Senegal: a seismological study See Entry 78477
- Model heat flow and [magnetotellurics] for the San Andreas and oceanic transform faults See Entry 78478
- A Nd isotope investigation of sediments related to crustal development in the British Isles See Entry 78479
- Isotopic and trace element constraints on the genesis of the Faeroe lava pile See Entry 78480

- Sr isotope and trace element evidence for the role of continental crust in calc-alkaline volcanism on Santorini and Milos, Aegean Sea, Greece See Entry 78481
- Age determinations in the Precambrian basement of the Wadi Araba area, southwest Jordan See Entry 78482
- Uranium estimation in Mussoorie phosphorites using solid state nuclear track detector See Entry 78483
- Heat transfer through the sediments of the mounds hydrothermal area, Galapagos Spreading Center at 86°W See Entry 78486
- Heat transfer and intraplate deformation in the Central Indian Ocean See Entry 78487
- Numerical models for the hydrothermal field at the Galapagos Spreading Center See Entry 78488
- Heat flow on the western flank of the East Pacific Rise at 21°N See Entry 78489
- Anomalous heat flow in the northwest Atlantic: a case for continued hydrothermal circulation in 80-m.y. crust See Entry 78490
- Thermal parameters of the oceanic lithosphere estimated from geoid height data See Entry 78491
- Isotope geochemistry of Cenozoic volcanic rocks reveals mantle heterogeneity below western USA See Entry 78493
- Uranium enrichment in Archaean crustal basement associated with overthrusting See Entry 78494
- Age of the Dashkinskii Formation of the Yenisei Ridge See Entry 78497
- The tectonic complex of Baikalian age in the Yakut ASSR See Entry 78498
- About the existence of two volcanic cycles within the initial volcanism of Virunga (Northern Kivu, Zaire) See Entry 78499
- The isotopic and chemical evolution of Mount St. Helens See Entry 78500
- Hercynian ductile deformation of granites within the Marche fault (French Central Massif): evidence for sinistral transcurrent shearing See Entry 78501
- West-American Cordillera structures, east of the Sierra Nevada: geodynamic implications See Entry 78502
- The Kannawa Thrust (IZU collision zone, central Japan): evolution of the stress regime at the Eurasian-Philippine Sea plates boundary See Entry 78503
- Temporal variation of the different parameters of the seismo-tectonic process See Entry 78505
- Nucleation and growth of strike slip faults in granite See Entry 78506
- Large-scale Quaternary detachments in Ventura basin, southern California See Entry 78507
- Episodic rifting and volcanism at Krafla in north Iceland: growth of large ground fissures along the plate boundary See Entry 78508
- A detailed study of the Cobb Offset of the Juan de Fuca Ridge: evolution of a propagating rift See Entry 78512
- Kerguelen hotspot source for Rajmahal Traps and Ninetyeast Ridge? See Entry 78513
- Tectonophysical zoning of the juncture of the Aldan Shield and the Stanovoi Highlands according to geodesic measurements See Entry 78514
- Convection under a rapidly moving plate and its appearance in the tectonics of platform areas See Entry 78515
- Neogene sedimentation and erosion in the Amirante Passage, western Indian Ocean See Entry 78516
- Pore water chemistry of the mounds hydrothermal field, Galapagos Spreading Center: results from Glomar Challenger piston coring See Entry 78517
- Constraints upon water advection in sediments of the Mariana Trough See Entry 78518
- Glacial-Holocene transition in deep-sea sediments: manganese-spike in the east-equatorial Pacific See Entry 78520
- Isotope composition of lead ore of some fields of the Sayan-Baikal region See Entry 78543
- Thermophysical properties of the basic varieties of rocks in the Irkutsk amphitheater See Entry 78544
- Lightning craters See Entry 78547
- The kinematics of a stochastic field of internal waves modified by a mean shear current See Entry 78548
- Upwelling along the 60-m isobath from Cape Canaveral to Cape Hatteras and its relationship to fish distribution See Entry 78550
- On perturbations of harmonic constants in the Thames Estuary See Entry 78551
- Transport and deposition of plutonium in the ocean: evidence from Gulf of Mexico sediments See Entry 78557
- On the radiocarbon record in banded corals: exchange parameters and net transport of $^{14}\text{CO}_2$ between atmosphere and surface ocean See Entry 78559
- Trace metal fronts in European shelf waters See Entry 78560
- Large particle transport of plutonium and other fallout radionuclides to the deep ocean See Entry 78561
- Aero-diffusion method of estimating evaporation in a non-stratified atmosphere See Entry 78565
- Porosity and hydraulic properties of sediments from the Galapagos Spreading Center and their relation to hydrothermal circulation in the oceanic crust See Entry 78566
- On the terrestrial heat flow and physical limnology of Crater Lake, Oregon See Entry 78567
- Transport of radon in flowing boreholes at Stripa, Sweden See Entry 78568
- On the calculation of total solar radiation. II See Entry 78576
- Rain day frequency and mean daily rainfall intensity as determinants of total rainfall over the eastern Orange Free State See Entry 78577
- Aerosol observations from Nimbus-7 CZCS along the South African west coast See Entry 78582
- Rocket studies of atmospheric scattering and the aerosol size distribution in the troposphere and lower stratosphere over Thumba See Entry 78586
- The optical and radiation field signatures produced by lightning return strokes See Entry 78596
- Nitric acid column densities over Antarctica See Entry 78598
- The Saudi Arabian heat low: aerosol distributions and thermodynamic structure See Entry 78600

- Threshold friction velocities and rupture moduli for crusted desert soils for the input of soil particles into the air See Entry 78601
- CO₂ and radon 222 as tracers for atmospheric transport See Entry 78605
- Preliminary study of CO₂ variations at Amsterdam Island (Territoire des Terres Australes et Antarctiques Françaises) See Entry 78606
- Interpretation of atmospheric CO₂ measurements at Mt. Cimone (Italy) related to wind data See Entry 78607
- Concentration of atmospheric carbon dioxide over Japan See Entry 78608
- Selection of CO₂ concentration data from whole-air sampling at three locations between 1968 and 1974 See Entry 78610
- Tropospheric NO_x and O₃ budgets in the equatorial Pacific See Entry 78611
- Lightning propagation and flash density in squall lines as determined with radar See Entry 78622
- Atmospheric gravity wave production for the total eclipse of 11 June 1983 See Entry 78624
- The seasonal variation of wind speed in the United Kingdom See Entry 78633
- Large falls of rain in Wales—a simple statistical case study See Entry 78634
- North-African cyclonic systems and springtime temperatures in Israel See Entry 78635
- Observations of abnormal microwave propagation phenomena during melting layer conditions See Entry 78636
- Persistence of wet and dry spells at Uccle (Belgium) See Entry 78637
- Climatic clusters of the Indian region See Entry 78638
- Relation between the changes of clay mineralogy in the cores of marine deposits and the paleoclimatic vicissitudes See Entry 78642
- Frost mapping in southern Victoria: an assessment of HCMM thermal imagery See Entry 78656
- Retrieval of aerosol size distribution from extinction measurements and verification with observations at a tropical station See Entry 78663
- A comparison of time and frequency domain geomagnetic sounding See Entry 78688
- Condensation sampling of soluble atmospheric trace gases See Entry 78696

93.55 INTERNATIONAL ORGANIZATIONS, NATIONAL AND INTERNATIONAL PROGRAMS

- Aerosols within the World Climate Research Programme See Entry 78579

93.85 INSTRUMENTATION AND TECHNIQUES FOR GEOPHYSICAL RESEARCH

- 78654** Determination of phosphorus in natural waters by long-capillary-cell absorption spectrometry. Wei Lei, K.Fujiwara, K.Fuwa (Dept. of Chem., Univ. of Tokyo, Tokyo, Japan). *Anal. Chem. (USA)*, vol.55, no.6, p.951-5 (May 1983).
Use of a long capillary cell (LCC) effectively enhances the detection power of ordinary colorimetry. The minimum necessary volume of sample is about 1-3 mL. By application of this method to molybdenum-blue colorimetry, 5 pg/mL of phosphorus is detectable. Phosphorus concentrations less than 1 ng/mL in seawater and lake water are successfully determined by using LCC. The advantages of LCC are low cost of construction, simple manipulation, and high stability of obtained signal. Theoretical and experimental aspects of LCC are discussed. (13 refs.)
- 78655** Applications of an orbiting gravity gradiometer. O.L.Colombo (Inst. for Phys. Geodesy, Tech. Univ. of Darmstadt, Darmstadt, Germany), A.Kleusberg. *Bull. Geod. (France)*, vol.57, no.1, p.83-101 (1983).
Considering present attempts to develop a gradiometer with an accuracy between 10^{-3} E and 10^{-6} (1E, or Eotvos unit is 10^{-9} s⁻²), two applications for such a device have been studied: (a) mapping the gravitational field of the Earth and (b) estimating the geocentric distance of a satellite carrying the instrument. A simulation study based on numerical orbit integrations suggests that a simple adjustment of the initial conditions based on gradiometer data could produce orbits where the geocentric distance is accurate to 10 cm or better, provided the orbits are 2000 km high and some improvement in the gravity field up to degree 30 is first achieved. (14 refs.)
- 78656** Frost mapping in southern Victoria: an assessment of HCMM thermal imagery. J.D.Kalma, G.F.Byrne, M.E.Johnson (Inst. of Biological Resources, CSIRO, Canberra, Australia), G.P.Laughlin. *J. Climatol. (GB)*, vol.3, no.1, p.1-19 (Jan.-March 1983).
HCMM satellite thermal imagery is used in a detailed frost assessment in an important horticultural area near Melbourne, Australia. Good general agreement is found to exist between plots based on night-time HCMM data which show surface temperature differences across the study area and frost risk maps based on terrain and land cover. However, it is concluded that the HCMM data have insufficient spatial resolution for use in local frost mapping in the study area. Improved thermal resolution will make thermal imagery from future satellites an increasingly important tool in topoclimatology. Without such improvements local frost mapping will, in the absence of climatic network data or mobile topoclimatological surveys, continue to depend on data from thermal scanners in aircraft and on detailed assessment of terrain and land cover. (30 refs.)
- 78657** Passive remote sensing of aerosols from space now and in the future. H.Quenzel (Meteorologisches Inst., Univ. Munchen, Munchen, Germany). *Adv. Space Res. (GB)*, vol.2, no.5, p.19-28 (1982). [received: April 1983]
(Proceedings of the Topical Meeting of the COSPAR Interdisciplinary Scientific Commission A (Meetings A1 and A2) of the COSPAR Twenty-Fourth Plenary Meeting, Ottawa, Canada, 16 May-2 June 1982).
Aerosols modify scattered solar radiation leaving the atmosphere and this fact can be exploited to determine the aerosol optical depth. The interaction processes between solar radiation and aerosol particles are outlined. A quasi-linear relationship ('conversion curves') between the radiance at the satellite, L_{sat} , and the aerosol optical depth, $a_{p\lambda}$, is found from both numerical and empirical studies. Because L_{sat} is not only controlled by a p_{λ} , but also by a series of other atmospheric parameters (perturbing quantities), the concept of 'favourable viewing conditions' is presented, where the effects of the perturbing quantities are minimal. The paper ends with some lines of thought on a concept for a turbidity satellite. (16 refs.)

- 78658** Most suitable conditions for aerosol monitoring from space. P.Kopke, H.Quenzel (Meteorological Inst., Univ. of Munich, Munich, Germany). *Adv. Space Res. (GB)*, vol.2, no.5, p.29-32 (1982). [received: April 1983]
(Proceedings of the Topical Meeting of the COSPAR Interdisciplinary Scientific Commission A (Meetings A1 and A2) of the COSPAR Twenty-Fourth Plenary Meeting, Ottawa, Canada, 16 May-2 June 1982).
Favorable zenith angles of the satellite and favorable wavelengths are presented for an atmosphere with maritime aerosols with and without Saharan dust. (8 refs.)
- 78659** Laser sounding of aerosols using airborne and space facilities. V.E.Zuev (Inst. of Atmospheric Optics, Acad. of Sci., Tomsk, USSR). *Adv. Space Res. (GB)*, vol.2, no.5, p.39-47 (1982). [received: April 1983]
(Proceedings of the Topical Meeting of the COSPAR Interdisciplinary Scientific Commission A (Meetings A1 and A2) of the COSPAR Twenty-Fourth Plenary Meeting, Ottawa, Canada, 16 May-2 June 1982).
Presents the results of sounding of water droplet crystal and mixed clouds carried out using an airborne lidar. A new method of determining the phase state of a cloud is described. The results are given on numerical experiments of laser sounding of various clouds using a polarization lidar. Numerical simulation of laser sounding of aerosols from space for different lidar parameters and geometrical schemes of sounding is carried out using new models of aerosol vertical profiles. (11 refs.)
- 78660** Spaceborne lidar measurement accuracy: simulation of aerosol, cloud, molecular density, and temperature retrievals. P.B.Russell, B.M.Morley (SRI Internat., Menlo Park, CA, USA), E.V.Browell. *Adv. Space Res. (GB)*, vol.2, no.5, p.49-53 (1982). [received: April 1983]
(Proceedings of the Topical Meeting of the COSPAR Interdisciplinary Scientific Commission A (Meetings A1 and A2) of the COSPAR Twenty-Fourth Plenary Meeting, Ottawa, Canada, 16 May-2 June 1982).
Spaceborne lidar measurements and retrievals are simulated using realistic errors in signal, conventional density information, atmospheric transmission, and lidar calibration. To reduce molecular-density uncertainties and also to provide density and temperature profiles, a procedure that combines returns at 0.35 and 1.06 μ m is developed. This technique significantly improves UT/NVS aerosol retrieval accuracy and also yields useful density and temperature profiles. Strong particulate contamination limits the technique to the cloud-free upper troposphere and above. (5 refs.)
- 78661** Retrieval of aerosol characteristics from scattering and extinction measurements. A.Deepak, P.-H.Wang (Inst. for Atmospheric Optics & Remote Sensing, Hampton, VA, USA). *Adv. Space Res. (GB)*, vol.2, no.5, p.55-64 (1982). [received: April 1983]
(Proceedings of the Topical Meeting of the COSPAR Interdisciplinary Scientific Commission A (Meetings A1 and A2) of the COSPAR Twenty-Fourth Plenary Meeting, Ottawa, Canada, 16 May-2 June 1982).
A versatile inversion code has been developed which is capable of retrieving profiles of aerosol size distribution and concentration from multi-wavelength measurements of either the scattered radiance from the Earth's sunlit atmosphere in both the limb-viewing mode and downward-viewing mode, or the extinction of direct solar radiation by the Earth's atmosphere. The inversion code in its present form is a composite of three sub-codes corresponding to the three measurement modes. A description of these codes is given and results of retrievals are discussed. (5 refs.)
- 78662** Validation of aerosol measurements by the satellite sensors SAM II and SAGE. P.B.Russell (SRI Internat., Menlo Park, CA, USA), M.P.McCormick, T.J.Swisher. *Adv. Space Res. (GB)*, vol.2, no.5, p.123-6 (1982). [received: April 1983]
(Proceedings of the Topical Meeting of the COSPAR Interdisciplinary Scientific Commission A (Meetings A1 and A2) of the COSPAR Twenty-Fourth Plenary Meeting, Ottawa, Canada, 16 May-2 June 1982).
The satellite sensors SAM II and SAGE have been developing a global data base on stratospheric aerosols since they were launched in October 1978 and February 1979, respectively. The validity of this data base is tested by numerous comparisons with other measurements made by lidars, balloon-borne particle counters, and aircraft-borne impactors and filters. Because the satellite sensors measure extinction and the correlative sensors measure other properties, special techniques are required to convert each measured property to other properties and to quantify conversion uncertainties and measurement uncertainties. Use of these techniques in two major comparative experiments shows that the SAM II and SAGE extinction measurements agree with each other and with values derived from dustsonde, lidar, and filter measurements. (6 refs.)
- 78663** Retrieval of aerosol size distribution from extinction measurements and verification with observations at a tropical station. P.Sikka, R.Vijayakumar, A.M.Selvan, Bh.V.R.Murty (Indian Inst. of Tropical Meteorology, Pune, India). *Adv. Space Res. (GB)*, vol.2, no.5, p.127-9 (1982). [received: April 1983]
(Proceedings of the Topical Meeting of the COSPAR Interdisciplinary Scientific Commission A (Meetings A1 and A2) of the COSPAR Twenty-Fourth Plenary Meeting, Ottawa, Canada, 16 May-2 June 1982).
Aerosol size distributions are retrieved by computing aerosol extinction parameters using extensive measurements of direct solar radiation made in the 0.4 and 0.6 μ m wavelengths at Pune with a Volz type sunphotometer during winter (November-February), pre-monsoon (March-May), monsoon (June-August) and post-monsoon (September-October) seasons of 1980-81. The computed aerosol size distributions are compared with the direct measurements made using Anderson eight-stage cascade impactor. The retrieval method is simple and useful for intensive aerosol measurement programmes. (3 refs.)
- 78664** Determination of aerosol optical depth from ground measurements. C.Frohlich (Phys.-Meteorologisches Obs., World Radiation Center, Davos, Switzerland). *Adv. Space Res. (GB)*, vol.2, no.5, p.139-45 (1982). [received: April 1983]
(Proceedings of the Topical Meeting of the COSPAR Interdisciplinary Scientific Commission A (Meetings A1 and A2) of the COSPAR Twenty-Fourth Plenary Meeting, Ottawa, Canada, 16 May-2 June 1982).
The methods used to determine the aerosol optical depth as a function of wavelength are briefly described and discussed. Some results from the operational network of the World Meteorological Organization and other, more research oriented studies, are reviewed and critically analysed to assess the reliability and accuracy of such determinations and their value as ground truth measurements for space applications. (13 refs.)
- 78665** Recent developments in ion mass spectrometers in the energy range below 100 keV. H.Balsiger (Phys. Inst., Univ. of Bern, Bern, Switzerland). *Adv. Space Res. (GB)*, vol.2, no.7, p.3-11 (1982).
The recognition that heavy ions often have similar or higher abundance than protons in space plasmas and the fact that ions with masses and/or charges larger than unity are ideally suited to test theories on origin, transport, acceleration, and loss of these plasmas led to the development of new and

more sophisticated mass spectrometers during the last decade. The characteristics of several state-of-the-art instruments which have been flown or selected for missions are discussed and aims for future developments given. (19 refs.)

78666 Some recent advances in energetic ion mass spectrometry. B.A. Whalen (Herzberg Inst. of Astrophys., Nat. Res. Council of Canada, Ottawa, Ontario, Canada).

Adv. Space Res. (GB), vol.2, no.7, p.13-20 (1982).
New techniques are being developed which will extend the capability of spacecraft-borne ion mass spectrometers into previously unexplored momentum regimes. These instruments include time-of-flight mass spectrometers and large laboratory class spectrometers suitable for spacelab applications. Their characteristics, strengths and weaknesses are reviewed. (6 refs.)

78667 Spherical ion traps for 'INTERCOSMOS-BULGARIA-1300'. T.N.Ivanova (Central Lab. for Space Res., Bulgarian Acad. of Sci., Sofia, Bulgaria), T.D.Samardjiev, S.M.Halova, P.T.Kostov, G.S.Karamishev, I.S.Kutiev, G.L.Gdalevich.

Adv. Space Res. (GB), vol.2, no.7, p.21-5 (1982).
Describes the P6-IT device for investigating the ion composition of the ionospheric plasma. The device is necessary for the study of the complex dynamic behaviour of the plasma, the interaction of the ionosphere and the magnetosphere, and the global distribution of charged particles. The P6-IT is composed of two spherical sensors and an electronic unit. This paper discusses the working characteristics of the instrument and gives, as a sample, the ion distribution along orbit number 175. (7 refs.)

78668 The ion energy and mass analyzer on board the 'INTERCOSMOS-BULGARIA-1300' satellite. P.Nenovski, Y.Semkova, R.Koleva, S.Chapkunov, N.Kanchev, N.Tabov, A.Kanchev, O.Valsberg, V.Smirnov, G.Zastenker, A.Leibov (Central Lab. for Space Res., Bulgarian Acad. of Sci., Sofia, Bulgaria).

Adv. Space Res. (GB), vol.2, no.7, p.27-30 (1982).
An original instrument for ion energy distribution measurement in ionospheric plasma above the F-layer was designed and launched on board the INTERCOSMOS-BULGARIA-1300 satellite. The instrument performs differential energy analysis of ion species within the two energy ranges of 1-27 eV/q and 0.2-8 keV/q. (5 refs.)

78669 An instrument for DC electric field and AC electric and magnetic field measurements aboard 'INTERCOSMOS-BULGARIA-1300' satellite. G.Stanev, M.Petrunova, D.Teodosiev, I.Kutiev, K.Serafimov, S.Chapkunov, V.Chmyrev, N.Isaev, P.Puschae, I.Pimenov, S.Bilichanko (Central Lab. for Space Res., Bulgarian Acad. of Sci., Sofia, Bulgaria).

Adv. Space Res. (GB), vol.2, no.7, p.43-7 (1982).
The instrument IESP-IPMP represents a complex unit measuring the vector of the DC electric field, the vectors of the electric and magnetic field in the frequency range of 0.2-6.5 Hz (wave form), autocorrelation functions of waves with frequencies of 0.1-5 kHz, and wave amplitudes in eight bandpass channels. Some results are shown and compared in the various frequency ranges. (9 refs.)

78670 Field and wave measurements aboard the Aureol-3 spacecraft. J.J.Berthelier (LGE, CNRS, St. Maur, France), A.Berthelier, Yu.I.Galperin, V.A.Gladyshev, F.Lefevre, N.I.Massevitch, M.Mogilevsky, O.A.Molchanov.

Adv. Space Res. (GB), vol.2, no.7, p.49-52 (1982).
In the Soviet-French Arcad-3 project, 3 experiments TBF-ONCH, TRAC and ISOPROBE are carried out on board the Aureol-3 satellite to measure the AC and DC electric and magnetic fields and waves. Several modes of telemetry, real time and memory regimes are available for data transmission. Examples of inflight measurements from the above instruments and their presentation on microfiches are shown. Some new phenomena are emphasized and briefly discussed. (12 refs.)

78671 The resonance cone technique for exciting electron acoustic waves in equatorial ionosphere. S.P.Gupta (Phys. Res. Lab., Ahmedabad, India).

Adv. Space Res. (GB), vol.2, no.7, p.87-8 (1982).
A rocketborne radio frequency resonance cone technique is discussed. The technique is ideal over the geomagnetic equator where the Earth's magnetic field is horizontal. The radio frequency exciter is fixed along the axis of the rocket. By measuring the semi-angle of this cone various plasma parameters can be derived, such as electron density and temperature. (3 refs.)

78672 A retarding potential analyser for rocket experiments. B.Kirov (Central Lab. for Space Res., Bulgarian Acad. of Sci., Sofia, Bulgaria), K.Georgieva, E.Apostolov, M.Gusheva, I.Kutiev, S.Chapkunov, Yu.Simeonova.

Adv. Space Res. (GB), vol.2, no.7, p.89-92 (1982).
A retarding potential analyzer is designed using a micro-channel plate in front of the collector as a flow amplifier, which makes it possible to detect ion species with very low concentration ($<0.5 \text{ cm}^{-3}$). A technique is described for using the micro-channel plate at abnormally high pressure ($>0.01 \text{ N/m}^2$). This allows the precise determination of the mass composition of the low ionosphere. An adaptive retarding potential consisting of 2048 steps is used to increase the sensitivity. The sensor is hermetically sealed and opens on command. (4 refs.)

78673 Measurements of the energy spectra of charged particles within the VERTICAL-10 rocket experiment. I.Ivanov, Ts.Dachev, Yu.Matviichuk, D.Krezhova, D.Gochev, I.Rumchev (Central Lab. for Space Res., Bulgarian Acad. of Sci., Sofia, Bulgaria).

Adv. Space Res. (GB), vol.2, no.7, p.93-5 (1982).
The 21 December 1981 'VERTICAL-10' payload included a low-energy two-channel spectrometer for measuring the differential flows of electrons and the protons within the energy range 0.1 to 10 keV, covered by 15 exponentially distributed energy levels. The device was installed so as to measure the electron flows in the direction of movement of the scientific payload container and to determine proton flows perpendicular to it. (no refs.)

78674 Digital processing of Spacelab imagery. P.Muralikrishna, S.Prakash, B.H.Subbaraya (Phys. Res. Lab., Ahmedabad, India).

Adv. Space Res. (GB), vol.2, no.7, p.107-10 (1982).
A digital technique for processing and analyzing OH-cloud photographs to be retrieved from the ISRO-CNES collaborative experiment on the first Spacelab is presented and discussed. The method adopted for processing the photographs incorporates the following major steps (i) digitising the OH photographs, (ii) applying corrections for vignetting, geometric distortions and brightness variations and (iii) superimposing the geographical coordinates on the linearised OH photograph. (2 refs.)

78675 WAMDIH—a wide angle Michelson Doppler imaging interferometer for Spacelab. W.A.Gault, G.G.Shepherd (Centre for Res. in Experimental Space Sci., York Univ., Toronto, Ontario, Canada).

Adv. Space Res. (GB), vol.2, no.7, p.111-14 (1982).
A CCD imaging device has been designed which combines a spatial resolution of $0.1''$ with a spectral resolving power of 10^5 , sufficient to measure doppler shifts and line widths of individual atmospheric emission lines. It will be

flown aboard Spacelab and will be used to study neutral winds and temperatures as functions of height, latitude and time of day. (6 refs.)

78676 Airglow atmospheric imager on board the 'IK-BULGARIA-1300' satellite. M.Gogoshev (Central Lab. for Space Res., Bulgarian Acad. of Sci., Sofia, Bulgaria), N.Petkov, A.Kuzmin, Ts.Gogosheva, St.Spassov, Iv.Kostadinov.

Adv. Space Res. (GB), vol.2, no.7, p.115-20 (1982).
Shows the possibilities of the optical scanning imager for investigation of the structure of the auroral, SAR and tropical arcs and in this way to study the particle precipitation, neutral winds across the magnetic equator, drifts, electric fields and the current systems in the ionosphere. (15 refs.)

78677 Measurement of electric fields in the ionosphere by incoherent scatter radar techniques. T.Hagfors (EISCAT Sci. Assoc., Kiruna, Sweden), J.Silen.

Adv. Space Res. (GB), vol.2, no.7, p.121-9 (1982).
Various methods for the extraction of electric fields from incoherent scatter radar observations are discussed. The random errors in electric field determinations are derived and it is shown that under typical conditions observations such as EISCAT should measure electric fields with an r.m.s. error of about 1 mV/m with one minute integration time. Some preliminary EISCAT results are shown and compared with other observations. (4 refs.)

78678 BARS—a dual bistatic auroral radar system for the study of electric fields in the Canadian sector of the auroral zone. A.G.McNamara (Nat. Res. Council, Ottawa, Ontario, Canada), D.R.McDiarmid, G.J.Sofko, J.A.Koehler, P.A.Forsyth, D.R.Moorcroft.

Adv. Space Res. (GB), vol.2, no.7, p.145-8 (1982).
One instrument of the Canadian Auroral Network for the Open Program Unified Study (CANOPUS) is a pulsed dual bistatic auroral radar system (BARS) for the mapping of ionospheric electric fields, using the STARE technique. The Canadian system is presently in the specification and design phases, with the objective of being operational by mid-1984. This paper describes the geometry of the BARS system, the design considerations, and the planned data and control network. (17 refs.)

78679 Interactive analysis of magnetic field data. C.T.Russell (Inst. of Geophys. & Planetary Phys., Univ. of California, Los Angeles, CA, USA).

Adv. Space Res. (GB), vol.2, no.7, p.173-6 (1982).
A pair of programs, entitled BANAL and TANAL, have been created in the UCLA Space Sciences Group for the interactive analysis of magnetic field data. These programs reduce the time from the inception of an idea to its testing, and thereby enhance both the productivity and creativity of the user. They accomplish this through menu-driven procedures for the display and analysis of time series data, including Fourier analysis. Cursor selection of subsections of the data for entry into the analysis procedures as well as automatic scaling minimize the required keyboard input from the user. (3 refs.)

78680 Ionospheric plasma parameters measurement instrument for satellite experiment with SIT. T.N.Ivanova, S.M.Halova, P.T.Kostov, G.S.Karamishev (Central Lab. for Space Res., Bulgarian Acad. of Sci., Sofia, Bulgaria).

C.R. Acad. Bulg. Sci. (Bulgaria), vol.36, no.1, p.81-4 (1983).
Describes the measurement of the ionic plasma parameters (concentration of ions N_i , temperature T_i , mass composition M_i and energy distribution E_i), as well as of the electron concentration, temperature and energy, by means of a complex scientific apparatus mounted on the Interkosmos Bulgaria-1300 satellite, which makes it possible to analyse a number of physical parameters connected with the heat balance and the dynamic processes in the ionosphere. The P6-SIT instrument was designed for the measurement of the above ion parameters by means of three- and four-electrode spherical ion traps (SIT). (6 refs.)

78681 Statistical techniques using NURE airborne geophysical data and NURE geochemical data. K.Campbell (Los Alamos Nat. Lab., Los Alamos, NM, USA).

Comput. & Geosci. (GB), vol.9, no.1, p.17-21 (1983). (First Annual Conference on 'The Management, Analysis, and Display of Geoscience Data', Golden, CO, USA, 27-29 Jan. 1982).
Some standard techniques in multivariate analysis are used to describe the relationships among remotely sensed observations (Landsat and airborne geophysical data) and between these variables and hydrogeochemical and stream sediment analyses. Gray-level pictures of such factors make the analytic results more accessible and easier to interpret. (no refs.)

78682 Thermal fading of fission tracks at variable temperature: applications to geochronology. Y.Cantelaube (Lab. de Mineralogie, Museum d'Histoire Naturelle, Paris, France).

Nucl. Tracks & Radiat. Meas. (GB), vol.6, no.4, p.143-60 (1982).
The Arrhenius law is extended to the case when the fading temperature varies over time. The proposed equation is induced from the Arrhenius equation, independently of any representative function of some track-fading parameter, and without taking into account any of the usual track-annealing models. The author uses r_i -diagrams to plot plateau-age curves. A simple method is deduced to discriminate between previously affected and unaffected fossil-track populations, by using track-density data of the plateau-age technique. The onset of the last fission-track storage and the end of the last partial track-fading, and therefore the average track-fading rate corresponding to this time interval, can thus be determined. Values of affected and unaffected fossil-track populations are compared with those which have been obtained by other methods. (9 refs.)

78683 A new etching technique for developing fission tracks in epidote. A.B.Chakranarayan, K.B.Powar (Dept. of Geology, Univ. of Poona, Pune, India).

Nucl. Tracks & Radiat. Meas. (GB), vol.6, no.4, p.193-5 (1982).
The authors present the results of etching epidotes from skarn rocks from Belka Pahar, Rajasthan, India. They were etched in both NaOH and HF under varying conditions of temperature, time, and etchant concentration, but tracks were only revealed by etching with 25N NaOH for 1 to 2 hours at 15°C and then with 45% HF for 15 minutes at room temperature. (7 refs.)

78684 A filtering procedure for great circle data. A.Souriau, M.Souriau (Centre Nat. d'Etudes Spatiales, Groupe de Recherches de Geodesie Spatiale, Toulouse, France).

Ann. Geophys. (France), vol.1, no.1, p.7-10 (Jan.-Feb. 1983).
Proposes a filtering method which applies to great circle data, i.e. to data which represent the integral, along great circles, of a function defined at each point of the sphere. This filter is based on the vanishing of the odd harmonics in the global spherical harmonic expansion of great circle values. This filter also enables to obtain a lower estimate of the S/N ratio in the data using a comparison with synthetic data. The authors present two examples relevant to seismological data. (3 refs.)

78685 Recovery of reflector series by determining the beginning position of estimated wavelets using short-time homomorphic analysis. J.Y. Kim, J. Behrens (Inst. für Angewandte Geophys., Petrologie und Lagerstättenforschung, Tech. Univ. Berlin, Berlin, Germany).

Ann. Geophys. (France), vol.1, no.1, p.11-15 (Jan.-Feb. 1983).
The use of cepstral gating to estimate the reflector series directly has led sometimes to erroneous results, especially in the fine structure investigations. In addition, it should be noted that the estimated sequences are in general uniformly time-delayed. It is mainly due to cepstral disturbances caused by mixed-delay reflector series, time-varying character of source signal and additive noise. The author discusses recovering the reflector series by determining the beginning position of the estimated wavelets. The paper is based on the short-time homomorphic analysis comprising a number of windows. This technique is illustrated by means of both synthetic and real data. (10 refs.)

78686 Seismic transducers: noise suppression and prevention in the piezoelectric transduction systems. C. Parmigiani.

Elettrom. Oggi (Italy), no.2, p.173-80 (Feb. 1983). In Italian.
Noise generation mechanisms in seismic instrumentation are analysed. Suppression and prevention methods are suggested. Capacitive and electromagnetic couplings are discussed detailing isolating amplifier connection modes and circuit arrangements. Piezoelectric transducer connection circuitry configurations are shown comparing various systems operations. The main recommendations include usage of low noise coaxial cables, single point earth connection, isolation of adjacent cables, amplification and instrument selection. (no refs.) T.H.

78687 Seismic transducers: calibration systems. C. Parmigiani.

Elettrom. Oggi (Italy), no.3, p.209-20 (March 1983). In Italian.
Seismic transducer calibration system and standards are reviewed. Reciprocity calibration method (Bouche-Levy) is analysed highlighting accuracy grades and test procedures. Reference standards are discussed detailing frequency response calibration. Frequency responses under various conditions are considered quoting numerous response curves. Shock response tests are detailed showing test procedures and an error analysis method. (4 refs.) T.H.

78688 A comparison of time and frequency domain geomagnetic sounding. D. Beamish (Inst. of Geological Sci., Edinburgh, Scotland).

Geophys. J. R. Astron. Soc. (GB), vol.73, no.3, p.689-704 (June 1983).
A three-site geomagnetic data set from the Borders region of southern Scotland is used to examine the empirical relationships established by differential geomagnetic sounding experiments. A time domain analysis of such relationships reveals time domain transfer functions which appear to be almost independent of time. A frequency domain analysis is then used to illustrate both a significant phase rotation and a significant dependence on period of the equivalent frequency domain response functions. The formalism of conventional geomagnetic sounding is re-examined. It is found that difference fields are not required to establish the appropriate horizontal field relationships. (17 refs.)

78689 Dielectric logging with downhole invasion effects. J.S. Yu (Sandia Nat. Labs., Albuquerque, NM, USA), P.C. Reardon, P.C. Lyne.

IEEE Trans. Antennas & Propag. (USA), vol.AP-31, no.3, p.397-405 (May 1983).
The transfer impedance between conducting coils is evaluated to estimate the downhole dielectric properties that can contribute to more effective exploration and production of gas/oil reservoirs. The earth formation with a borehole-mud filtrate invasion is simulated by concentric zones of variable dielectric properties to account for rocks saturated by different fluids. The authors have imposed analytical restrictions to allow only magnetic-dipole coupling between logging coils and to limit logging source frequencies from 10 to 30 MHz for typical coil spacings. Depending on the depth of invasion front, guided waves may exist in the invaded formation. When guided waves do not exist, rapidly converging branchcut integrations are used to evaluate the transfer impedance. When the invasion front begins to support guided waves the numerical convergence becomes somewhat slower using spatial-band-limited integrations. Both types of integration are used to produce inversion charts from which dielectric properties and invasion-front radii can be estimated from downhole-measurable transfer impedances. Ambiguity in parameter inversion is also demonstrated to provide insight for developing a future inverse process based on array processing of adequately sampled data. (21 refs.)

78690 Prediction of sites of occurrence of strong earthquakes in large seismicogenic zones of Tadzhikistan. A.S. Malamud, V.K. Kulagin (Inst. of Earthquake Resistant Construction & Seismology, Acad. of Sci., Tadzhik SSR).

Izv. Akad. Sci. USSR, Phys. Solid Earth (USA), vol.18, no.3, p.184-7 (1982). Translation of: *Izv. Akad. Nauk SSSR Fiz. Zemli*, vol.18, no.3 (1982).
A method is described for predicting the sites of occurrence of strong ($M \geq 5.5$) earthquakes by constructing spatiotemporal graphs reflecting the sequence of liberation of seismic energy along large seismicogenic zones. The results obtained confirm a hypothesis that sections which remain vacant a long time are the most likely sites of occurrence of strong earthquakes. A prediction map of such sites on the territory of Tadzhikistan and contiguous regions is constructed. (12 refs.)

78691 Method of quenching functions and its application for determining the singular points of geophysical fields satisfying three-dimensional equations of Laplace and Helmholtz. G.M. Voskoboynikov, A.F. Shestakov (Inst. of Geophys., Acad. of Sci., USSR).

Izv. Akad. Sci. USSR, Phys. Solid Earth (USA), vol.18, no.3, p.207-16 (1982). Translation of: *Izv. Akad. Nauk SSSR Fiz. Zemli*, vol.18, no.3 (1982).

The method of determining the singular points of geophysical field satisfying the equations of Laplace and Helmholtz is discussed with the aid of the quenching function of real variables. The physical and mathematical bases of this method and the principles of constructing computation schemes for determining the coordinates, type, and orientation of the characteristics of the field, are explained. The techniques of compiling initial data for the problem and the prospects for applying the method to the interpretation of basic geophysical fields are discussed. (12 refs.)

78692 A technique for reducing low-frequency, time-dependent errors present in network-type surveys. J.R. Cloutier (US Naval Oceanographic Office, NSTL Station, Bay St. Louis, MS, USA).

J. Geophys. Res. (USA), vol.88, no.B1, p.659-63 (10 Jan. 1983). [received: May 1983]

At each node of a network-type survey, two surveyed values are obtained. In the absence of errors, these two values should be equal, providing that the quantity being surveyed is, for all practical purposes, time independent. When a low-frequency, time-dependent error enters the system, it can be indirectly observed in the form of surveyed-value differences occurring at the network nodes. This paper describes a technique for reducing such an error. The method consists of using a conjugate gradient projection algorithm to find the unbiased, discrete function of minimum weighted variation which produces

the observed nodal differences. After inspecting the discrete solution, a suitably chosen continuous function can be fitted to the discrete data and used to reduce the time-dependent error. This technique has been successfully used to reduce the radial ephemeris error present in SEASAT geoid height data (Cloutier, 1981). (5 refs.)

78693 Optical tracking of synchronous Earth's satellites for geophysical purposes. S. Catalano (Istituto di Astronomia, Univ. di Catania, Catania, Italy), R. McCrosky, A. Milani, A.M. Nobili.

J. Geophys. Res. (USA), vol.88, no.B1, p.669-76 (10 Jan. 1983). [received: May 1983]

Tracking data from synchronous Earth's satellites can be analyzed to provide the resonant geopotential coefficients, mainly C_{22} and S_{22} which represent the ellipticity of the Earth's equator. Geosynchronous satellites currently used for telecommunication purposes can be easily tracked with moderate size large field telescopes measuring the satellite angular coordinates with respect to some catalogue field stars. The accuracy is at least 2 arc sec (≈ 400 m). Optical tracking does not need any onboard device and is easily accomplished. It is concluded that the organization of a worldwide optical tracking campaign would allow an improvement in the knowledge of the long-wavelength geoid by at least one order of magnitude. (24 refs.)

78694 Magnetic polarity stratigraphy: stochastic properties of data, sampling problems, and the evaluation of interpretations. N.M. Johnson, V.E. McGee (Dartmouth Coll., Hanover, NH, USA).

J. Geophys. Res. (USA), vol.88, no.B2, p.1213-21 (10 Feb. 1983).

A statistical model has been derived which can be used either to test the interpretation of a given magnetic stratigraphy or to make time estimates from the paleomagnetic data. The model is based on the presently accepted statistical properties of the Earth's magnetic field and the stochastic nature of the paleomagnetic sampling process. Given knowledge of the number of paleomagnetic sites, the distribution of the sites, an estimate of the geologic time span sampled, and the mean length of the magnetic polarity zones, the expected success of the sampling program can be calculated and compared with its actual performance. The mean time span for polarity intervals in the late Neogene has been established from existing data at 120000 years. Once the mean timespan for polarity intervals has been established, estimates for stratigraphic timespan can be made by means of the statistical model. (17 refs.)

78695 Direct inversion of one-dimensional magnetotelluric data. S. Coen, F. Quercia, M. Mackiewicz (Dept. of Materials Sci. & Mineral Engng., Univ. of California, Berkeley, CA, USA).

J. Geophys. Res. (USA), vol.88, no.B3, p.2407-12 (10 March 1983).

It is shown that the conductivity profile of a layered Earth can be obtained directly (noniteratively) from one-dimensional magnetotelluric observations. The approach used is based on the Born approximation to the electric field integral equation. The inversion algorithm is applied to two data sets. The first one is analytic, and it is possible to show analytically all the steps in the inversion algorithm. The resulting conductivity profile is an adequate approximation to the actual profile. The second data set contains the apparent resistivities from a particular field site at 21 frequencies, and the resulting conductivity profile compares adequately with well log measurements. The results obtained are promising enough to consider the direct inversion of two-dimensional data. (10 refs.)

78696 Condensation sampling of soluble atmospheric trace gases. J.C. Farmer, G.A. Dawson (Inst. of Atmospheric Phys., Univ. of Arizona, Tucson, AZ, USA).

J. Geophys. Res. (USA), vol.87, no.C11, p.8931-42 (20 Oct. 1982). [received: May 1983]

The condensation of water vapor onto a cooled surface can be used as a method of sampling atmospheric components; the method is investigated theoretically and experimentally. From solutions to the heat and mass flow within the convective boundary layer, it is shown that the method has greatest collection efficiency for highly soluble gases. Discrimination against particles and relatively insoluble gases should be excellent. The method is illustrated by some measurements of NH_3 , HNO_3 , HNO_2 , SO_2 , HCl , H_2O , HCHO , HCOOH , and CH_3COOH in the vicinity of Tucson, Arizona. Concentrations are in the part-per-billion range or below. Diurnal variations in these concentrations are discussed. (20 refs.)

78697 Sources of background current in the ECC ozonesonde: implications for total ozone measurements. D.C. Thornton, Nagla Niaz (Dept. of Chem., Drexel Univ., Philadelphia, PA, USA).

J. Geophys. Res. (USA), vol.87, no.C11, p.8943-50 (20 Oct. 1982). [received: May 1983]

The source of the background current in the usual operation of the electrochemical concentration cell ozonesonde is the reduction of tri-iodide (iodine) normally present in the cathode solution. The authors can explain the time variations in the background current by the slow rates of solution mass transport and of heterogeneous electron transfer for tri-iodide. Oxygen does not contribute to the background current through reaction with iodide to produce tri-iodide. Direct reduction of oxygen at the cathode is negligible once the electrodes have been exposed to iodide for 24 hours. The present background current correction is altitude-dependent, since it is based on an assumed sensitivity of the electrochemical concentration cell to oxygen. (13 refs.)

78698 Semiautomatic nondispersive infrared analyzer apparatus for CO_2 air sample analyses. W.D. Komhyr, L.S. Waterman (Air Resources Labs., NOAA, Boulder, CO, USA), W.R. Taylor.

J. Geophys. Res. (USA), vol.88, no.C2, p.1315-22 (20 Feb. 1983). (Symposium on the Rise in Atmospheric Carbon Dioxide, Bern, Switzerland, 14-18 Sept. 1981).

A semiautomatic nondispersive infrared analyzer apparatus has been developed for analysis of up to 50 CO_2 air samples per day. The samples are collected in 500-ml glass flasks and are transferred to the analyzer with a novel, free-floating piston pump. Sample and calibration gas transfer operations are controlled by a microprocessor, and data are recorded, analyzed, and output by a Hewlett-Packard 9845A/S desktop computer. The apparatus is described, including operating and test modes, and performance characteristics determined from 2 years of operation are given. (7 refs.)

78699 Registration of thunderstorm centers by automatic atmospheric stations. H. Volland, J. Schafer, P. Ingmann (Radioastronomisches Inst., Univ. Bonn, Bonn, Germany), W. Harth, G. Heydt, A. J. Eriksson, A. Manes.

J. Geophys. Res. (USA), vol.88, no.C2, p.1503-18 (20 Feb. 1983).

A new generation of VLF-atmospheric receivers and analyzers is presented that operates completely automatically and allows the realtime identification of thunderstorm activity centers. The mean azimuth and angular spread of each thunderstorm center within the detection range as well as the mean statistical properties of three measured spectral parameters of the atmospherics originating at that center are determined within each measuring period (20 min) by a desktop computer. Using a suitable statistical procedure for determining the mean angular and spectral parameters and applying a new extended model for VLF-propagation as function of the solar zenith

angle and of the magnetic field component along the propagation path, the operation program determines in real time the distances and strengths (atmospheres/min) of the activity centers so that all data can be immediately printed out and stored on the internal magnetic tape cartridge. Additionally, an external plotter is used for marketing the thunderstorm centers on a map. (19 refs.)

78700 A new method for measuring radon exhalation. P.Fernandez, L.S.Quindos, J.Soto, E.Villar, D.Guedalia (Dept. of Fundamental Phys., Univ. of Santander, Santander, Spain).

J. Geophys. Res. (USA), vol.88, no.C2, p.1519-24 (20 Feb. 1983).

A method for measuring radon exhalation based on the determination of radon profile into the soil by gamma spectrometry using an ^{137}Cs detector is developed. Detection efficiency is determined by employing Monte Carlo method. Experimental results are described, and they show the workability of the method. (20 refs.)

78701 Seismic velocity anisotropy in a medium containing oriented cracks—transversely isotropic case. O.Nishizawa (Geological Survey of Japan, Ibaraki, Japan).

J. Phys. Earth (Japan), vol.30, no.4, p.331-47 (1982).

A new method is developed for calculating effective elastic parameters of a medium containing oblate spheroidal cracks having parallel planes. This new method is free from the restrictions of isotropic matrix material and low crack density. Velocity anisotropy is calculated for the case of oriented cracks filled with fluid. Effects of crack aspect ratio, fluid bulk modulus, and crack volume on velocity anisotropy are investigated. The present results show smaller anisotropy than that given by Anderson et al. (1974) for a medium containing oriented spheroidal cracks. The relation between velocity and crack density parameter using these results. (25 refs.)

78702 Development trends in hygrometry. M.A.Berliner.

Meas. Tech. (USA), vol.25, no.9, p.754-8 (Sept. 1982). Translation of: *Izmer. Tekh. (USSR)*, vol.25, no.9, p.44-6 (Sept. 1982). [received: May 1983]

Advances in hygrometry methods and facilities are discussed, particular attention being paid to the influence of microcircuit technology. Advances in processing and displaying data are also discussed and the role of microprocessors is emphasised. A method of choosing the optimal design of a hygrometer with regard to metrological characteristics, working characteristics, economic parameters, ergonomics and metrological support is presented. (7 refs.)

78703 Development prospects for dewpoint hygrometers. V.P.Petukhov.

Meas. Tech. (USA), vol.25, no.10, p.847-50 (Oct. 1982). Translation of: *Izmer. Tekh. (USSR)*, vol.25, no.10, p.46-8 (Oct. 1982).

Discusses the general trends in the development of dewpoint hygrometers. These include implementation of microelectronic and microprocessor devices which provide a basis for control systems for measuring the humidity over a wide dewpoint range. Such systems can provide stabilisation of the condensate film and can include self-monitoring and fault-diagnosis systems. The general structure of an automatic flow hygrometer with a wide dewpoint range is described. (13 refs.)

78704 Field differential hygrometer. V.A.Glushikin, S.I.Krechmer.

Meas. Tech. (USA), vol.25, no.10, p.850-2 (Oct. 1982). Translation of: *Izmer. Tekh. (USSR)*, vol.25, no.10, p.48-50 (Oct. 1982).

Discusses the development of a field meter for the humidity profile, which in essence consists of two identical dewpoint hygrometers. The measuring systems can measure and record the absolute humidity (dewpoint temperature) and the difference in humidity at two points of measurement simultaneously. The hygrometer consists of two blocks: a stationary one and a head unit, which are connected by a cable. In gradient measurements with two hygrometers, the thermocouples enable one to duplicate the dewpoint-difference measurements and to measure the difference in air temperature. Field measurement conditions differ from laboratory ones mainly in three factors: it is necessary to place the transducer at a large distance from the stationary unit, there is a wind that alters the temperature equilibrium in a random fashion, and the solar radiation affects the automatic-control system. (1 ref.)

78705 Ultraviolet hygrometer for measuring fluctuations in α atmospheric humidity. S.I.Kreshmer, S.A.Sitnov, V.V.Kudryavtsev.

Meas. Tech. (USA), vol.25, no.10, p.859-62 (Oct. 1982). Translation of: *Izmer. Tekh. (USSR)*, vol.25, no.10, p.56-8 (Oct. 1982).

Advantages of a UV hygrometer, particularly for field measurements, are that the mass and size are comparatively small, the baseline is short (only 15-20 mm), and the design is simple. Operation of the UV hygrometer is described and its development in the Soviet Union is discussed. An advanced version of the UV hygrometer is described which operates in the range 103 to 4×10^3 Pa with an overall error 6Pa is described. Examples of fluctuation curves obtained with this hygrometer on the Black Sea expedition are presented. (16 refs.)

78706 Estimation of source function and medium response function by autoregressive method. G.J.Nair (Bhabha Atomic Res. Centre, Bombay, India).

Phys. Earth & Planet. Inter. (Netherlands), vol.32, no.1, p.36-44 (April 1983).

By modelling seismograms as 'low' and 'high' order autoregressive (AR) processes, the source function and the medium response function are separated from a single channel seismogram. Akaike's final prediction error is used to select the appropriate 'low' and 'high' AR order of the process. Case studies of synthetic data show that the recovered source and reflectivity functions compare very well with the input functions. Using this method, arrivals of the surface reflected P phases of five explosions from the Soviet region and of two earthquakes from Kamchatka, recorded at Gauribidanur, India, are identified. Certain features of the source and source region of these events are also inferred. (15 refs.)

78707 Acoustic remote sensing of the boundary layer. S.P.Singal, B.S.Gera (Nat. Phys. Lab., New Delhi, India).

Proc. Indian Acad. Sci. Eng. Sci., vol.5, pt.2, p.131-57 (July 1982). [received: April 1983]

An acoustic echo sounder (called sodar) has been developed, designed and fabricated. This equipment has been operating successfully for several years and has been shown to have important applications in the areas of air pollution control, studies, microwave and millimetre wave radio communication including troposcatter, aviation and micrometeorology. Work on the development of the sodar was taken up at the Indian National Physical Laboratory (NPL) in 1972. At that time, this was one of the few equipment of its kind in the world. It has been designed in the laboratory and has been built with indigenous components. The equipment currently probes the thermal structure of the atmosphere upto a height of 700 m but can be extended to a kilometre. Two sodars are in operation—one at the National Physical Laboratory, Delhi and the other at the Micrometeorological Laboratory, Tarapur in collaboration with BARC, Bombay. The design criteria of the NPL sodar and experiments with it are described in this paper. (36 refs.)

78708 Airflow resistivity instrument for in situ measurement on the Earth's ground surface. A.J.Zuckerwar (NASA-Langley Res. Center, Hampton, VA, USA).

Rev. Sci. Instrum. (USA), vol.54, no.5, p.597-9 (May 1983).

An airflow resistivity instrument features a novel specimen holder, especially designed for in situ measurement on the Earth's ground surface. This capability eliminates the disadvantages of prior intrusive instruments, which necessitate the removal of a test specimen from the ground. A prototype instrument can measure airflow resistivities in the range 10-5000 cgs rayl/cm, at specimen depths up to 15.24 cm (6 in.), and at differential pressures up to 2490.8 dyn/cm² (1 in. H₂O) across the specimen. Because of the close relationship between flow resistivity and acoustic impedance, this instrument should prove useful in acoustical studies of the Earth's ground surface. Results of airflow resistivity measurements on an uncultivated grass field for varying values of moisture content are presented. (6 refs.)

78709 Estimation of f_oF_2 from interferences appearing on AGC data of ISS-b topside sounder. S.Igi, N.Matsumura.

Rev. Radio Res. Lab. (Japan), vol.28, no.146, p.333-43 (June 1982). In Japanese.

Concerns a method for estimation of f_oF_2 from the lowest frequency of the interferences appearing on automatic gain control (AGC) data of the topside sounder on-board ISS-b. For frequencies below f_oF_2 , the AGC output is mainly caused by the background noises from cosmic origin revealing a monotonous frequency distribution, while for frequencies above f_oF_2 , the AGC output is mainly caused by the interferences from the ground radio origin exhibiting rather complex frequency structures with high intensity levels. Such a change in the frequency distribution of the sounder AGC data provides a possibility for estimation of f_oF_2 values by detecting the lowest frequency of the interferences, f_i . In order to investigate validity of the method for f_oF_2 estimation, a statistical comparison was made with respect to about 47000 ionograms from ISS-b between the f_oF_2 values scaled from the echo traces on the topside ionograms and the f_i values determined from the sounder AGC data with the aid of computer processing. The results show that the value of f_i provides a fairly accurate estimation of f_oF_2 value over the regions where the intensity of man-made noises is high, while the accuracy is influenced by the D-region absorption of the ground noises during daytime and by existence of the ionospheric irregularities. (7 refs.)

78710 Measurement of total electron content by simultaneous reception of ISS-b telemetry signals. K.Aikyo, T.Marukaya, M.Kotaki.

Rev. Radio Res. Lab. (Japan), vol.28, no.146, p.479-89 (June 1982). In Japanese.

The ISS-b carries two telemetry transmitters with frequencies in VHF (136.810 Hz) and UHF (400.900 MHz) bands. Both telemetry signals are PCM-modulated by the identical data with a bit rate of 26.624 kbps for the dump-mode and 1.024 kbps for the realtime-mode. The measurement of the differential time-delay between two signals by time comparison of the decoded waveforms enables measurement of the total electron content (TEC) of the ionosphere along the ray path between the spacecraft and the ground station. The authors deal with the principle, the measuring implement, evaluation of the errors in the measured time delay and the method of calibration. A comparison is also made between the TEC measured above Kashima and the first order mid-latitude TEC model derived by Klobuchar and Allen (1970). Consequently, it is confirmed that this method gives columnar TEC data in good accuracy even for oblique propagation except in case of the large horizontal gradient in electron density. (20 refs.)

78711 Radial characteristics of focusing probes of magnetoelectric logging. L.A.Taborovskii, Yu.A.Dashevskii (Inst. of Geology & Geophys., Acad. of Sci., Novosibirsk, USSR).

Sov. Geol. & Geophys. (USA), vol.23, no.3, p.71-9 (1982). Translation of: *Geol. & Geofiz. (USSR)*, vol.23, no.3, p.81-90 (1982).

Continues studying the geophysical possibilities of the method of magnetoelectric logging (MEL) of boreholes. A method is proposed for geometric focusing at a constant current, which permits elimination of the influence of the borehole and the penetration zone from the measurement results. The parameters of the MEL focusing systems are calculated, and their radial characteristics studied. The authors investigate the problems which have a direction relationship to the technical implementation of the method: influence of the insulating base of the probe and calibration of the equipment which records the magnetic field. (2 refs.)

78712 Use of residual gravity anomalies to estimate the scale of ore fields. V.I.Andreev, M.G.Stuskin (Inst. of Mineral Resources, Dnepropetrovsk, USSR).

Sov. Geol. & Geophys. (USA), vol.23, no.3, p.96-8 (1982). Translation of: *Geol. & Geofiz. (USSR)*, vol.23, no.3, p.108-10 (1982).

Proposes a new noise-resistant method of determining anomalous mass (ore reserves) and dimensions of isolated or compactly grouped sources, whose shape is close to isometric. The method is integral with respect to content; the authors use a transformant which is calculated as the ratio of the difference in the values of gravity, averaged for the vicinities of two radii, to the difference of these radii, which does not depend on the regional (constant and linear) constituents. The authors use sources of the gravity field situated in a certain depth interval. (4 refs.)

78713 A method of studying the Earth's crust by refracted P- and S-waves. A.L.Aleynikov, S.N.Golod, A.M.Tuinova (Inst. of Geophys., Sverdlovsk, USSR).

Sov. Geol. & Geophys. (USA), vol.23, no.3, p.109-15 (1982). Translation of: *Geol. & Geofiz. (USSR)*, vol.23, no.3, p.120-7 (1982).

A method is proposed for reproducing the velocity cross section by travel-time curves of first waves with a random law of variation of velocity with depth (even in the presence of a waveguide). The method finds application in engineering seismics, seismic exploration, and deep seismic sounding. Its use for interpretation of P- and S-waves permitted the development of a method to estimate the density and composition of deep rocks with considerably greater reliability than before. (21 refs.)

78714 Approximate analogs of Dix formulas for a stratified medium with curvilinear boundaries and variable bed velocities. E.A.Biyas (Inst. of Geology & Dev. of Mineral Fuels, Acad. of Sci., Kuibyshev, USSR).

Sov. Geol. & Geophys. (USA), vol.23, no.3, p.116-22 (1982). Translation of: *Geol. & Geofiz. (USSR)*, vol.23, no.3, p.128-35 (1982).

A method is proposed for approximate solution of the kinematic problem for a stratified medium with curvilinear boundaries and variable bed velocities, based on the approximate reverse of the formulae obtained previously for solving the direct problem. (3 refs.)

78715 On the theory of the three-element probe in electromagnetic wave logging. Yu.N.Antonov, V.G.Burkov (Inst. of Geology & Geophys., Novosibirsk, USSR).

Sov. Geol. & Geophys. (USA), vol.23, no.4, p.50-7 (1982). Translation of: *Geol. & Geofiz. (USSR)*, vol.23, no.4, p.58-65 (1982).

The relative characteristics of electromagnetic wave logging (EMWL) are classified according to the sensitivity to dielectric permeability and the specific electrical resistivity of the rocks. The authors describe a synthesis of the original characteristics of the field, whose measurement makes it possible to determine the dielectric permeability of high- and low-resistivity, oil-, gas-, and water-bearing strata. (12 refs.)

78716 The determination of stratal velocities in horizontally layered media by the hyperboloid approximation of hodographs. E.A.Blyas.

Sov. Geol. & Geophys. (USA), vol.23, no.4, p.58-64 (1982). Translation of: *Geol. & Geofiz. (USSR)*, vol.23, no.4, p.66-71 (1982).

The new method of determining the strata velocities in horizontally layered media proposed does not require finding the limiting effective parameters (the first two terms in the expansion of the reflected-wave hodographs), but uses the parameters of hyperbolas approximating real hodographs. An example illustrating the effectiveness of the method is given. (6 refs.)

78717 High resolution spectral analysis and the acoustic remote sensing of ocean current velocity. W.S.Hodgkiss, D.S.Hansen (Marine Phys. Lab., Scripps Inst. of Oceanography, San Diego, CA, USA).

Proceedings of ICASSP 83. IEEE International Conference on Acoustics, Speech and Signal Processing, Boston, MA, USA, 14-16 April 1983 (New York, USA: IEEE 1983), p.961-4 vol.3.

Doppler sonars use the perceived shift in carrier frequency between the outgoing pulse and returning echo to estimate scatterer radial velocity at several ranges of interest. Scatterers suspended neutrally buoyant in the water column are used as tracers for the remote sensing of water mass motion. The application of pth-order autoregressive time series analysis models to estimation of the time-evolving Doppler sonar reverberation power spectrum is reported. With the aid of a reverberation model, it is shown that the spatial transfer function characteristics of a transducer have a significant influence on the time-evolving shape of the reverberation power spectrum. Thus, it is suggested that the use of first-order models for the purpose of Doppler shift estimation simply is inadequate. The results of an exploratory analysis of pings from a 67 kHz Doppler sonar appear to confirm this caution. (11 refs.)

78718 Lower bounds on pulsed-Doppler current profiler accuracy. K.B.Theriault (Bolt Beranek & Newman Inc., Cambridge, MA, USA).

Proceedings of ICASSP 83. IEEE International Conference on Acoustics, Speech and Signal Processing, Boston, MA, USA, 14-16 April 1983 (New York, USA: IEEE 1983), p.985-8 vol.3.

Lower bounds on performance (velocity and shear estimate variance) are computed for a four-beam pulsed Doppler shear profiler system. It is shown that performance is asymptotic to a constant as SNR increases; this is evidently due to the assumed incoherent scattering properties of the medium. Curves and expressions are presented which define the tradeoffs between resolution and accuracy for an operational system. (6 refs.)

78719 Primitive extraction for a syntactic pattern recognizer of features in seismic signals. J.E.Gaby (Engng. Experiment Station, Georgia Inst. of Technol., Atlanta, GA, USA), K.R.Anderson.

Proceedings of ICASSP 83. IEEE International Conference on Acoustics, Speech and Signal Processing, Boston, MA, USA, 14-16 April 1983 (New York, USA: IEEE 1983), p.993-6 vol.3.

Describes research into the morphological structure of regional seismic signals. This study is designed to aid in the development of a syntactic pattern recognition system to automate the analysis of seismic signals. (4 refs.)

78720 The wavelet reconstructed with phase-only and a study of its uniqueness. Tong Chang, Yenta Li, Zhongze Wu (Dept. of Automation, Qinghua Univ., Beijing, China).

Proceedings of ICASSP 83. IEEE International Conference on Acoustics, Speech and Signal Processing, Boston, MA, USA, 14-16 April 1983 (New York, USA: IEEE 1983), p.997-1000 vol.3.

The concept of waveform uniqueness in deconvolution of seismic traces is discussed. Under this conception, mixed-phase wavelets can be classified into three types. Based on the theorem of uniqueness of a sequence with a phase function by M.H. Hayes et al. (1981) and with some extensions, two types of wavelets have been reconstructed using a zero-perturbation relaxed iterative algorithm. A new criterion function which judges the convergence of iteration and a new criterion of classification are also presented. Several examples of mixed-phase wavelet reconstruction are provided. (3 refs.)

78721 Seismic velocity estimators. R.L.Kirlin, L.A.Dewey (Electrical Engng. Dept., Laramie, WY, USA).

Proceedings of ICASSP 83. IEEE International Conference on Acoustics, Speech and Signal Processing, Boston, MA, USA, 14-16 April 1983 (New York, USA: IEEE 1983), p.1001-4 vol.3.

The layered subsurface geologic model leads to an approximate hyperbolic curve of delay vs. sensor offset distance for seismic signals. Four 'optimum' estimators for the RMS seismic velocity are given and analyzed by simulation for RMS error. Parameters varied include center-point depth (time), a priori velocity variance and mean, delay-estimate variance and inter-delay-estimate correlation. The maximum likelihood estimator is shown to be best when a priori information is relatively good, but a least mean square estimator is best otherwise. (4 refs.)

78722 Deconvolution of band-limited signals. D.R.Martinez, S.H.Bickel (ARCO Oil & Gas Co., Dallas, TX, USA).

Proceedings of ICASSP 83. IEEE International Conference on Acoustics, Speech and Signal Processing, Boston, MA, USA, 14-16 April 1983 (New York, USA: IEEE 1983), p.1009-12 vol.3.

The inverse filter to a minimum-phase wavelet with infinite bandwidth is often calculated from its autocorrelation by applying the Wiener-Levinson algorithm. Physical limitations of seismic data require the wavelet to have a finite bandwidth which violates the minimum-phase condition. An unstable filter results when the Wiener-Levinson algorithm is applied to band-limited data. Although 'processing noise' is often added to stabilize the algorithm, this procedure can obscure problems associated with the data instability from the seismic interpreter. This paper presents an approach to the deconvolution of band-limited data by mapping the frequency response to span the full spectrum based on a set of sampling rate changes according to the lower and upper frequency cutoffs. (6 refs.)

78723 A model reduction algorithm by spline approximation in the deconvolution of seismic signals. S.D.Kollias, C.C.Halkias (Dept. of Electronics, Nat. Tech. Univ. of Athens, Athens, Greece).

Proceedings of ICASSP 83. IEEE International Conference on Acoustics, Speech and Signal Processing, Boston, MA, USA, 14-16 April 1983 (New York, USA: IEEE 1983), p.1013-16 vol.3.

A new method for obtaining approximate low-order recursive (ARMA) realizations of convolution models is based upon optimum piecewise linear or cubic spline approximation of the convolution kernel. The basic seismic wavelet is approximated by splines and a fixed-lag smoothing state-space representation, equivalent to the resulting ARMA model, is derived. Use of Kalman filtering gives fixed-lag smoothed estimates of the so-called reflection coefficient sequence. Adaptive estimation is used when the seismic wavelet is not known a priori. Simulation results using a Ricker wavelet illustrate the performance of the proposed method. (10 refs.)

78724 EISCAT—the facility, the technique, and representative early results. M.J.Baron, K.Folkestad.

Third International Conference on Antennas and Propagation ICAP 83, Norwich, England, 12-15 April 1983 (London, England: IEE 1983), p.169-75 part 2.

The EISCAT Scientific Association was created as an educational and scientific organization to conduct high latitude upper atmosphere research, using the incoherent scatter radar technique. For this purpose, two high-power radar systems were designed for installation and operation in northern Scandinavia. The tri-static UHF system began operations in the summer of 1981. The monostatic VHF is scheduled for completion in 1983. This paper first reviews the incoherent scatter technique. Then, the EISCAT facility itself is described. Finally, some representative results are shown. (9 refs.)

Proceedings of the Topical Meeting of the COSPAR Interdisciplinary Scientific Commission A (Meetings A1 and A2) of the COSPAR Twenty-Fourth Plenary Meeting See Entry 74204

Topical Meeting on Optical Techniques for Remote Probing of the Atmosphere. Technical Digest See Entry 74221

Hygrometer classification and standardization models for static and dynamic characteristics See Entry 74474

Standard humid-air generator for checking high-temperature hygrometer See Entry 74475

Standard hygrometer facilities at the Promenergoremont cooperative See Entry 74479

Standard facilities for measuring microconcentration of water in gases See Entry 74480

Remote interferometric sensors using frequency modulated laser sources See Entry 74528

Electromagnetic field of an oscillating point dipole in the presence of spherical interfaces See Entry 75565

A detector for acoustic directionality See Entry 75858

Estimating the kinematic parameters of seismic waves by the focusing method See Entry 78473

Domain wall resonance and stability in magnetite See Entry 78530

Can turbidity measurements be used for the estimation of aerosol parameters? See Entry 78585

Measurements of atmospheric ozone from aircraft and from balloons See Entry 78589

Nitric acid column densities over Antarctica See Entry 78598

Interpretation of atmospheric CO₂ measurements at Mt. Cimone (Italy) related to wind data See Entry 78607

Sampling strategy to obtain data used in models of global annual CO₂ increase and global carbon cycle See Entry 78609

Stratospheric sulfuric acid vapor: new and updated measurements See Entry 78618

Simultaneous measurements of vertical distributions of stratospheric NO₃ and O₃ at different periods of the night See Entry 78619

The role of radar in weather forecasting See Entry 78630

Instantaneous integrated Raman scattering See Entry 78643

On the influence of rough water surfaces on polarimetric investigations of aerosols from space See Entry 78644

Different atmospheric effects in remote sensing of uniform and nonuniform surfaces See Entry 78649

The characterization of atmospheric spread functions affecting satellite remote sensing of the Earth's surface See Entry 78650

A method for estimating cross radiance See Entry 78651

Observations of the thermal plasma in the topside ionosphere by RPT mission of ISS-b: electron density, temperature and mean ion mass See Entry 78748

A payload for the study of electric fields and electron density in the equatorial region See Entry 78773

High resolution thermal plasma measurements aboard the Aureol 3 spacecraft See Entry 78774

An instrument for total ion drift velocity measurements aboard the 'INTER-COSMOS-BULGARIA-1300' satellite See Entry 78776

Advances in auroral imaging from space See Entry 78779

Application of numerical Fourier transformation on measurements made on board rotating spacecraft See Entry 78780

Sond-R, an instrument for vertical probing of ionospheric plasma by means of CLP on board of a geophysical rocket See Entry 78781

Operation and experimental results of ionosphere sounding satellite-b (ISS-b, UME-2). I. Outline of ISS-b project See Entry 78784

Topside sounder onboard ISS-b See Entry 78785

Characteristics of the radio noise receiving equipment See Entry 78786

The ISS-b retarding potential analyzer See Entry 78787

Ion mass spectrometer on ionosphere sounding satellite (ISS-b) See Entry 78788

Operation of primary processing and data analysis system for ISS See Entry 78793

94.00 AERONOMY AND SPACE PHYSICS

94.10 PHYSICS OF THE NEUTRAL ATMOSPHERE

(for planets, see 96.30)

78725 An incoherent scatter study of short- and long-term temperature and atomic oxygen variations in the thermosphere. J.Fontanari (CESR, Univ. Paul Sabatier, Toulouse, France), D.Alcayde, P.Bauer. *Ann. Geophys. (France)*, vol.1, no.1, p.81-9 (Jan.-Feb. 1983). Diurnal distributions of exospheric temperature and atomic oxygen concentration at 200 km, deduced from incoherent scatter observations during the period 1974-1977, are fitted by a function including a mean value and diurnal and semi-diurnal oscillations. The characteristics of each component are combined with similar values obtained in the same way during high solar activity (1969-1972). All the data are then analyzed in order to evidence long-term variations (seasonal, annual, and as a function of geomagnetic activity indices), over a large range of solar activity (70 to 170×10^{22} Jansky). The results of the analysis of the diurnal temperature profiles from 120 to 200 km are compared to those obtained from independent data gathered in the upper thermosphere. (25 refs.)

78726 The diurnal and semidiurnal oscillations in meteor winds over Atlanta. M.I.Ahmed, R.G.Roper (School of Geophys. Sci., Georgia Inst. of Technol., Atlanta, GA, USA).

J. Atmos. & Terr. Phys. (GB), vol.45, no.4, p.181-92 (April 1983).

The wind data collected over Atlanta during the period August 1974-February 1978 using the Georgia Tech. Radio Meteor Wind Facility, is analyzed to yield an average picture of the seasonal behavior of its diurnal tides. Both the zonal and meridional components are studied. The vertical structures of these oscillations over Atlanta are compared with similar studies over Garchy, Urbana and Adelaide. (16 refs.)

78727 The dissipation of a sodium cloud. V.W.J.H.Kirchhoff, B.R.Clemesha (INPE Conselho Nacional de Desenvolvimento Científico e Tecnológico, Sao Paulo, Brazil).

Planet. & Space Sci. (GB), vol.31, no.4, p.369-72 (April 1983).

Occasional observations of strong increases in the atmospheric sodium densities and/or Na nightglow intensities suggest that the cause is the deposition of a sodium cloud in addition to the local equilibrium sodium layer. This situation is simulated to investigate the response of the atmospheric sodium layer to variations of the source influx rate. The settlement of the sodium to the equilibrium layer after the deposition of a sodium cloud is shown to be a long lived event in which the excess sodium is transported downwards, to the sink, by eddy diffusion. The possibility of a modulated source influx rate is also investigated showing a tendency for a strong attenuation of this modulation below the source. (15 refs.)

Modelling of the ion composition of the middle atmosphere See Entry 78594

A numerical model of the zonally averaged dynamical and chemical structure of the middle atmosphere See Entry 78614

Digital processing of Spacelab imagery See Entry 78674

Measurements of the structure and drift velocities of airglow ($\lambda=557.7$ nm) irregularities: Saskatoon (52°N , 107°W), Canada See Entry 78729

Lunar modulation of the equatorial electrojet See Entry 78738

The effects of neutral air winds on the electron content of the mid-latitude ionosphere and protonosphere in summer See Entry 78741

Collisional vibrational quenching of $\text{O}_2^+(\nu)$ and other molecular ions in planetary atmospheres See Entry 78809

Magneto-atmospheric waves See Entry 78810

94.10Q Airglow and nightglow

78728 Night intensity of oxygen triplet about $\lambda 1304 \text{ \AA}$ in upper atmosphere. K.B.Serafimov (Central Lab. for Space Res., Bulgarian Acad. of Sci., Sofia, Bulgaria).

C.R. Acad. Bulg. Sci. (Bulgaria), vol.36, no.3, p.337-40 (1983). (13 refs.)

78729 Measurements of the structure and drift velocities of airglow ($\lambda=557.7$ nm) irregularities: Saskatoon (52°N , 107°W), Canada. C.E.Meek, A.H.Manson (Inst. of Space & Atmospheric Studies, Univ. of Saskatchewan, Saskatoon, Canada).

J. Atmos. & Terr. Phys. (GB), vol.45, no.4, p.203-12 (April 1983).

A scanning photometer is used in conjunction with moving pattern analysis, to measure the horizontal motion of fluctuations in the airglow (557.7 nm) intensity: a modified full correlation analysis, and spatial correlation function analysis are used. The directions of these drifts often differ by $\geq 90^\circ$ from winds measured simultaneously by a medium frequency radar system. Temporal fluctuations of the airglow intensity, and the spectra of these, are interpreted in terms of internal gravity waves ($\sim 10 > \tau > 90$ min) and the semi-diurnal tide. (28 refs.)

78730 Intensity variations and ratios of (9-4) and (7-3) hydroxyl bands in nightglow at Poona. S.R.Gogawale, A.D.Tillu (Dept. of Phys., Poona Univ., Pune, India).

Planet. & Space Sci. (GB), vol.31, no.4, p.423-33 (April 1983).

The observed types of nocturnal intensity variations for the OH (9-4) and OH (7-3) bands during IQSY at this station, are further analysed using the theoretical band intensity distribution of Evans and Llewellyn (1972). A considerable agreement is noticed between observed and theoretical intensity ratios, $I(9-4)/I(7-3)$, for a major portion of the data ($\sim 70\%$) which has a 'continuous decrease' type of nocturnal intensity variation. For the remaining portion of the data ($\sim 30\%$), which has an 'increase followed by decrease' type of intensity variation and higher intensities, the observed ratios are also systematically higher than the above. A satisfactory explanation is offered, by postulating a second layer of emission. (60 refs.)

Particle and optical measurements aboard the AUREOL 3 spacecraft (ARCAD 3 project). A—The particle experiments. B—Optical measurements See Entry 78778

94.10S Aurora

78731 Radar auroral observations and ionospheric electric fields. E.Nielsen (Max-Planck-Inst. für Aeronomie, Katlenburg-Lindau, Germany), J.D.Whitehead.

Adv. Space Res. (GB), vol.2, no.7, p.131-44 (1982).

The ground-based systems STARE and SABRE utilize radar auroral phenomena to estimate ionospheric electric fields. Some of the assumptions

underlying these systems have been tested and general agreement with expectations have been found. However, as the results have been analysed in detail, it has become clear that the error in the irregularity drift velocity can at times amount to 100 ms^{-1} . Direct comparisons with other E-field measurements, as well as assessments of the results of applications of the STARE data clearly demonstrate that the electric field, calculated on the basis of the irregularity drift velocity, is a useful estimate of the actual horizontal electric field in the ionosphere and is sufficiently accurate for a great variety of geophysical studies. (34 refs.)

Radio aurora magnetic and streaming aspect sensitivities on 6 simultaneous links at 50 MHz See Entry 78732

Particle and optical measurements aboard the AUREOL 3 spacecraft (ARCAD 3 project). A—The particle experiments. B—Optical measurements See Entry 78778

Advances in auroral imaging from space See Entry 78779

94.20 PHYSICS OF THE IONOSPHERE

(for planets, see 96.30)

78732 Radio aurora magnetic and streaming aspect sensitivities on 6 simultaneous links at 50 MHz. G.J.Sofko (Inst. of Space & Atmospheric Studies, Univ. of Saskatchewan, Saskatoon, Saskatchewan, Canada), J.A.Koehler, J.Gilmer, A.G.McNamara, D.R.McDiarmid.

Adv. Space Res. (GB), vol.2, no.7, p.149-52 (1982).

During August 1981, a 50 MHz c.w. radar system was operated in central Canada to measure auroral scatter amplitudes and Doppler spectra from a scattering region centered near 66° magnetic invariant latitude ($L \approx 6.0$). Narrow beams from 3 transmitters, differing in frequency by 1 KHz, were directed to cover a common volume of the ionosphere over a ground location at 56.3°N , 103.5°W . The scattered signals were received on narrow beam antennas at two receiving sites, and recorded in analog form on magnetic tape under the control of an AIM65 microcomputer. The analog tapes were digitized later and FFT-processed to obtain Doppler spectra and amplitudes. Preliminary results are reported. (9 refs.)

78733 Some modifications of Jaeger's formula [ionospheric absorption]. R.Misra (Contai P.K. Coll., Midnapur, West Bengal, India), B.Chakravarty.

Indian J. Theor. Phys., vol.29, no.3, p.261-9 (Sept. 1981).

The drawbacks in the application of Jaeger's formula to absorption calculations have been discussed. Some modified forms of this formula have been presented which are suitable for application under various conditions. The values of absorption have been calculated with the modified form of Jaeger's formula taking ν and f_i into consideration. It has been shown that the values of absorption calculated with Jaeger's formula on replacing f_o/f by F_o/F agree with those from magneto-ionic theory. (13 refs.)

78734 Simple M-factor algorithm for improved estimation of the basic maximum usable frequency of radio waves reflected from the ionospheric F-region. M.Lockwood (Rutherford Appleton Lab., Chilton, Didcot, England).

IEE Proc. F (GB), vol.130, no.4, p.296-302 (June 1983).

The equations of Milsom are evaluated, giving the ground range and group delay of radio waves propagated via the horizontally stratified model ionosphere proposed by Bradley and Dudeney. Expressions for the ground range which allow for the effects of the underlying E- and F1-regions are used to evaluate the basic maximum usable frequency or M-factors for single F-layer hops. An algorithm for the rapid calculation of the M-factor at a given range is developed, and shown to be accurate to within 5%. The results reveal that the M(3000)F2-factor scaled from vertical-incidence ionograms using the standard URSI procedure can be up to 7.5% in error. A simple addition to the algorithm effects a correction to ionogram values to make these accurate to 0.5%. (14 refs.)

78735 Autumn and winter anomalies in ionospheric absorption as measured by riometers. H.Ranta, A.Ranta, T.J.Rosenberg, D.L.Detrick (Inst. for Phys. Sci. & Technol., Univ. of Maryland, College Park, MD, USA).

J. Atmos. & Terr. Phys. (GB), vol.45, no.4, p.193-202 (April 1983).

Seasonal variation of ionospheric absorption has been studied on the basis of riometer (A2) measurements obtained over a wide latitude range. Equinoctial maxima of approximately equal amplitude are observed in the auroral zone and near the equator. At mid-latitudes riometer absorption maximizes during the fall. The autumn maximum or autumn anomaly, in riometer absorption is observed at much higher geographic latitude in the southern than in the northern hemisphere but at comparable geomagnetic latitudes in both hemispheres. The different methods to determine a quiet-day curve are discussed. (23 refs.)

78736 Refractive index surfaces. G.F.Stott (Cavendish Lab., Univ. of Cambridge, Cambridge, England).

J. Atmos. & Terr. Phys. (GB), vol.45, no.4, p.219-29 (April 1983).

The refractive index surface is a very powerful concept which has been widely used for describing electromagnetic wave propagation in the plasmas of the Earth's ionosphere and magnetosphere. Because of the simple analytic form of the cold plasma dispersion relation it is possible to examine in some detail the properties of these refractive index surfaces. The purpose of this paper is to review briefly the properties that are widely known and present some features which have not been previously discussed. (25 refs.)

78737 Loss cone fluxes and pitch angle diffusion at the equatorial plane during auroral radio absorption events. P.N.Collis, J.K.Hargreaves (Dept. of Environmental Sci., Univ. of Lancaster, Lancaster, England), A.Korth.

J. Atmos. & Terr. Phys. (GB), vol.45, no.4, p.231-43 (April 1983).

The flux and pitch angle distribution of energetic electrons near the loss cone have been investigated over the energy range 15-300 keV, using measurements on the geosynchronous satellite GEOS-2 at the times of auroral radio absorption events detected by riometers in Scandinavia. It is shown that conditions of strong pitch angle diffusion apply only during the most intense absorption events ($\geq 6 \text{ dB}$ at 30 MHz) which are relatively infrequent. During most events the loss cone is partially depleted, with the degree of depletion increasing as the absorption becomes weaker. The variation of the pitch angle diffusion coefficient with the observed radio absorption is estimated. An empirical law is derived which enables the computation of radio absorption consistent with measurements. D-region recombination laws are discussed and limits are set on the height profile of the effective recombination coefficient. (41 refs.)

78738 Lunar modulation of the equatorial electrojet. K.Maeda.

J. Atmos. & Terr. Phys. (GB), vol.45, no.4, p.245-54 (April 1983).

An attempt has been made to reproduce the counter electrojet (CE) in the equatorial dynamo by considering neutral winds with solar (1-2), (2,4), (2,2) and lunar (2,2) tidal modes as well as a constant electrostatic field (E_e). The daily variation of conductivity (σ) is assumed to consist of steady (average), diurnal and semi-diurnal components. An equation governing the relationship between j_y (jet current), E_e , σ and wind is given, and this equation is then used to describe diurnal, semi-and ter-diurnal variations of j_y separately. The

seasonal characteristics and the solar activity dependence of CE are demonstrated to be predictable. (33 refs.)

78739 Travelling ionospheric disturbances detected by UHF angle-of-arrival measurements. J.V.Evans (MIT Lincoln Lab., Lexington, MA, USA), R.H.Wand.

J. Atmos. & Terr. Phys. (GB), vol.45, no.4, p.255-65 (April 1983).

From January 1971 to March 1973, the Millstone Hill L-band satellite tracking radar was employed in a study of ionospheric refraction. Satellites of the Navy Navigation Series were tracked smoothly by radar (at 1295 MHz) by commanding the 84-ft diameter antenna to follow the predicted path of the satellite across the sky, and allowing any measured angular errors slowly to close out the offsets. Simultaneously, the apparent position of the satellite was sensed passively by receiving (on the same antenna) the UHF beacon signals. Ionospheric refraction manifested itself during the rising and setting portions of the path as a displacement between the UHF and L-band apparent positions. In addition, quasi-sinusoidal fluctuations in the displacement were seen at intervals along the path that are believed to be caused by travelling ionospheric disturbances. These TIDs appear to be confined largely to the lower thermosphere and manifest themselves in tilting the lower surface of the ionosphere where the density gradients are largest. (41 refs.)

78740 Collision frequencies in the high-latitude D-region. M.Friedrich (Dept. of Communications & Wave Propagation, Tech. Univ. Graz, Graz, Austria), K.M.Torkar.

J. Atmos. & Terr. Phys. (GB), vol.45, no.4, p.267-71 (April 1983).

D-region collision frequencies derived from rocket flights are subjected to a harmonic seasonal analysis. The proportionality between collision frequency and pressure has been derived and found to be in excellent agreement with laboratory data. Some implications of the results are discussed. (15 refs.)

78741 The effects of neutral air winds on the electron content of the mid-latitude ionosphere and protonosphere in summer. G.C.Sethia (Dept. of Environmental Sci., Univ. of Lancaster, Lancaster, England), G.J.Bailey, R.J.Moffett, J.K.Hargreaves.

Planet. & Space Sci. (GB), vol.31, no.4, p.377-87 (April 1983).

The effects of neutral air winds on the electron content and other parameters of the mid-latitude ionosphere are modelled by means of mathematical solutions of the time-dependent continuity and momentum equations for oxygen and hydrogen ions. The geometry is chosen to represent a propagation path between a geosynchronous satellite and a ground station, and the computations are compared with results from slant path observations of the ATS-6 radio beacon made at Lancaster (UK) and Boulder, Colorado (USA). (15 refs.)

78742 Plasmaspheric hiss observed in the topside ionosphere at mid-and low-latitudes. T.Ondoh, Y.Nakamura, S.Watanabe, K.Aikey, T.Murakami (Radio Res. Labs., Tokyo, Japan).

Planet. & Space Sci. (GB), vol.31, no.4, p.411-22 (April 1983).

Latitudinal characteristics of ELF hiss in mid- and low-latitudes are statistically studied by using ELF/VLF electric field spectra (50 Hz-30 kHz) from ISIS-1 and -2 received at Kashima station, Japan, from 1973 to 1977. The ELF hiss is classified into the steady ELF hiss whose upper frequency limit is approximately constant with latitude and the ELF hiss whose upper frequency limit increases with latitude. Spectral shape and bandwidth of ELF hiss in the topside ionosphere and the occurrence rate are discussed. ELF hiss events correlation with geomagnetic activity are discussed. Ray tracing results suggest that waves of ELF hiss generated in the equatorial outer plasmasphere propagate down in the electrostatic whistler mode towards the equatorial ionosphere, bouncing between the LHR reflection points in both the plasmaspheric hemispheres. (16 refs.)

78743 Global distribution of the ionospheric F-layer critical frequency f_oF_2 . N.Matuura, K.Aikey, R.Nishizaki, T.Ogata, S.Igi, T.Maryuma, H.Yabuuma, M.Yamanishi, T.Ide.

Rev. Radio Res. Lab. (Japan), vol.28, no.146, p.315-31 (June 1982). In Japanese.

The critical frequency of the ionospheric F-layer f_oF_2 , one of the basic parameters of the ionosphere, was derived from the topside sounding data obtained by the digital type swept-frequency sounder on-board the ISS-b. The measurements of f_oF_2 were carried out on a routine basis with three or four observational revolutions operated in a day, where the values of f_oF_2 at about 100 data points were obtained from each revolution. Global mapping analysis was performed with respect to each data group of the world-wide f_oF_2 data collected from those observed within each four-months period between August 1978 and June 1979 and also within the time interval of ± 1 hr around each hour of UT. The mapping analysis was carried out in the manner as determining the coefficients of the functional form of the spherical surface harmonic expansion to make it best fit to the global data of the observed f_oF_2 . The authors describe the global observation by ISS-b, the global mapping analysis of f_oF_2 , the comparison of the results with those from ground based observations including the CCIR model, and some characteristics of the global distribution of f_oF_2 . (13 refs.)

78744 Global distribution of topside spread F. T.Maryuma, N.Matuura.

Rev. Radio Res. Lab. (Japan), vol.28, no.146, p.345-55 (June 1982). In Japanese.

The global distribution of the occurrence probability of topside spread F is investigated through the analysis of topside ionograms recorded by the ISS-b satellite for the period from April 1978 to June 1980. The latitudinal distribution of the spread F shows two distinct high occurrence regions, mid to higher latitudes and equatorial latitudes, with relatively low occurrence regions at around 30° in magnetic latitude between the two in both the northern and southern hemispheres. Spread F at the equatorial latitudes (ESF), which is a night-time phenomenon, exhibits clear longitudinal-seasonal variation in the occurrence; for the northern winter and for the northern summer seasons high occurrence of ESF observed at the Atlantic longitudes and at the Pacific longitudes, respectively. Spread F at mid to higher latitudes appears throughout all the local time, and the occurrence probability of that increases with latitudes. Longitudinal dependence of the spread F occurrence in the night-time is also found at mid latitudes in the winter hemisphere. (25 refs.)

78745 Long-distance HF propagation modes deduced from the simultaneous observation by chirp sounder and ISS-b. M.Ichinose, S.Fujii, K.Nozaki, S.Igi.

Rev. Radio Res. Lab. (Japan), vol.28, no.146, p.357-63 (June 1982). In Japanese.

The propagation modes on 9200 km circuit from Federal Republic of Germany to Japan were identified based on the chirp oblique sounding data and also the ionospheric data along the circuit which were obtained by Ionosphere Sounding Satellite-b (ISS-b). The oblique sounding ionograms for the circuit were obtained every hour during the period from November 1978 to May 1979 by the chirp-sounder operated with the swept frequency range from 4 to 30 MHz. The ionospheric condition along the circuit was observed by ISS-b of which orbital path could be fairly close to the circuit on some

occasions. The propagation time on the circuit were calculated for every frequency steps by substituting the ionospheric factor of the control points to the analytical formulas which were introduced for the parabolic model of the F2 layer. The traces for the oblique ionogram were simulated by plotting these calculated propagation time against the frequency. The simulated traces for 3- to 5-hop propagation modes were compared with those obtained from observations. The results show that the MOF is greater than the theoretical MUF by about 1 MHz. (7 refs.)

78746 Short-term prediction of HF propagation. Y.Takenoshita, S.Ito, R.Maeda, T.Koizumi.

Rev. Radio Res. Lab. (Japan), vol.28, no.146, p.365-7 (June 1982). In Japanese.

Global maps of the MUF variability were made from the F-layer critical frequencies observed with the Ionosphere Sounding Satellite-b from October 1978 to March 1979. The maps were used weekly in a trial to correct the monthly MUF of HF circuits predicted in advance of three months by the Radio Research Laboratories. The correction was carried out as a weekly prediction with consideration of temporal and spatial characteristics found in the CCIR MUF maps. An adequacy of the trial was examined, taking into account of HF circuit data obtained at Hiraio Branch. The trial with the most reliable data succeeded 55 times, failed 6 times and missed 39 times in correction. (no refs.)

78747 The effects of the ionosphere on the extent of the radio horizon at high frequency band. M.Kotaki, I.Kuriki, C.Kato, H.Suguchi.

Rev. Radio Res. Lab. (Japan), vol.28, no.146, p.399-409 (June 1982). In Japanese.

In order to estimate the size of the radio window viewed from the satellite with high frequency radio waves, the computational study of three dimensional ray trajectories in anisotropic and inhomogeneous ionospheres has been made. The size of the radio window changes with frequency of emitted radio waves and the properties of the ionosphere such as the electron density, the thickness and gradient of the layer. The authors clarify the relations between the size of the radio window and the characteristics of the ionized media. The calculated results are supported experimentally by observations of the Ionosphere Sounding Satellite (ISS-b). (2 refs.)

78748 Observations of the thermal plasma in the topside ionosphere by RPT mission of ISS-b: electron density, temperature and mean ion mass. E.Sagawa, S.Miyazaki, H.Mori, T.Ogawa.

Rev. Radio Res. Lab. (Japan), vol.28, no.146, p.435-47 (June 1982). In Japanese.

Procedures and results of analysis of the electron data (Langmuir curves) obtained by RPT mission of ISS-b are presented. The electron density (N_e), electron temperature (T_e), and mean ion mass (M_i) are deduced from a Langmuir curve of the RPT data by means of a technique of nonlinear least squares fit. Latitudinal and local time dependences of these quantities are in good agreement with previous observations by other satellites. Their long term variations are examined from the data obtained from August 1978 to November 1979. Annual variation of T_e at the middle latitude is consistent with that by the incoherent scattering observations, but there is an asymmetry between the northern and southern hemispheres. The results also indicate that the annual variation has comparable amplitude to that of the semiannual variation around the magnetic equator. Global maps of observed quantities are depicted by using the spherical surface harmonic expansion method. Longitudinal dependences of these quantities in addition to latitudinal ones are evident in these maps. The distributions of T_e and M_i in low latitudes are related to each other, and they can be interpreted by the effects of the field-aligned interhemispheric plasma flows caused by atmospheric winds. (34 refs.)

78749 Observational results of the nighttime ion temperatures in the topside ionosphere by ISS-b. S.Miyazaki, E.Sagawa, H.Mori, T.Ogawa.

Rev. Radio Res. Lab. (Japan), vol.28, no.146, p.449-55 (June 1982). In Japanese.

Global distributions of the nighttime ion temperatures in the topside ionosphere were obtained from Ionosphere Sounding Satellite (ISS-b) during August to December 1978. First, a computer processing method for analysis of the ion temperature from ion current of the retarding potential analyzer is described, secondly the observational results of the ion temperatures are described. The results indicate that ion temperatures at low latitudes are lower than that at high latitudes in general, but these latitudinal dependencies vary with longitude. The ion temperatures near the equator are high over the Pacific region compared with other regions. The nighttime ion temperatures in the low latitudes are gradually decreasing with time. (13 refs.)

78750 Observation of the ion composition by ionosphere sounding satellite. I.Iwamoto, E.Sagawa, T.Suiz.

Rev. Radio Res. Lab. (Japan), vol.28, no.146, p.457-70 (June 1982). In Japanese.

Fairly complete latitudinal, diurnal and seasonal variations of the ion composition have been obtained from the observation by a Bennett ion mass spectrometer aboard the Ionosphere Sounding Satellite (ISS-b). The data used in this study were taken during the periods Aug. 1978 and Dec. 1979, which correspond to a solar maximum condition. The latitudinal profiles of the light ions, H^+ and He^+ , almost always show the mid-latitude trough structure. The trough is deeper in the nighttime than in the daytime. The distributions of He^+ have a marked depression at the geomagnetic equator. The equatorial depression of He^+ is also deeper in the nighttime. The seasonal variations of He^+ clearly show the winter bulge structure in the daytime but it disappears in the nighttime. The cause of the disappearance is attributed to the increased loss of He^+ in the winter night. Dependence of the mid-latitude trough position on K_p -index has been derived statistically from the invariant-latitudinal profiles of He^+ . (35 refs.)

78751 Characteristics of seasonal variations of O^+ ion density troughs in the nighttime topside ionosphere. S.Miyazaki, I.Iwamoto, H.Mori, E.Sagawa, T.Suiz, T.Ogawa.

Rev. Radio Res. Lab. (Japan), vol.28, no.146, p.471-7 (June 1982). In Japanese.

Proton, helium ion and oxygen ion densities at about 1100 km in the topside ionosphere were observed by the Bennett type ion mass spectrometer on ISS-b during the maximum solar activity period from August 1978 to November 1979. Their global characteristics for seasonal and local time variations were studied by using the spherical surface harmonic expansion method. The results show that there exist distinguished O^+ ion density trough regions, and that the centers of main trough are located around the longitudes $0^\circ E$ and $180^\circ E$ respectively in northern summer and in northern winter, and around the latitudes $35^\circ \sim 70^\circ$ in the winter hemisphere. The main trough region changes its location with respect to the seasons by almost 180° in longitude and by moving toward the opposite hemisphere in winter, during rather short term around equinox conditions. The regions of relatively high and low O^+ ion density show good correlation with the regions of the eastward and westward declination of the earth's magnetic field in connection with the seasons.

A theoretical interpretation is examined such that the O^+ ion density trough is enhanced by the field-aligned plasma flow induced from neutral air wind pattern coupled with the Earth's magnetic field. The seasonal variation of O^+ ion density can be explained by the changes in the direction of the vertical plasma flow depending on the seasonal changes in the neutral air wind system. (14 refs.)

78752 HF radar Doppler studies of the effects of ionospheric motions on radio waves propagating in different modes. P.A.Bradley, A.J.Gibson, J.W.King (Rutherford Appleton Lab., Chilton, England). Third International Conference on Antennas and Propagation ICAP 83, Norwich, England, 12-15 April 1983 (London, England: IEE 1983), p.191-5 part 2

The magnitudes of the Doppler shifts and spreads imparted to HF sky-waves reflected from different ionospheric layers are indicated and it is shown that the correlation between the Doppler shifts imparted in different locations can be used to yield estimates of the speed and direction of movement of travelling ionospheric disturbances. The magnitude and periodicity of the Doppler shifts may also be used to infer the vertical magnitude and wavelength of the ionospheric corrugation associated with the disturbances. (2 refs.)

78753 Ionospheric aspect effect in the caustic zone. S.A.Namazov (Inst. of Radioengng. & Electronics, Acad. of Sci., USSR).

Third International Conference on Antennas and Propagation ICAP 83, Norwich, England, 12-15 April 1983 (London, England: IEE 1983), p.196-8 part 2

Investigations of ionospheric irregularities especially those using high power radio waves show that irregularities are field-aligned and have an anisotropic form. Radiowave scattering on these anisotropic irregularities has an aspect sensitivity and in the illuminated region (far from the caustic) takes place near the cone of the scattered radiation. Investigation of such field-aligned scattering (FAS) is of practical interest. In this report the results of Born approximation analysis are presented taking into account scattering intensity as a function of magnetic inclination, incident wave azimuth and Airy-function oscillations. (1 ref.)

78754 The determination of the propagation characteristics of very low frequency radio waves. K.E.Mowforth, T.B.Jones (Univ. of Leicester, Leicester, England).

Third International Conference on Antennas and Propagation ICAP 83, Norwich, England, 12-15 April 1983 (London, England: IEE 1983), p.199-203 part 2

A number of analytical techniques are available that enable the phase and amplitude of a propagating Very Low Frequency (VLF) wave to be determined as a function of distance for a given D-region model. Renewed interest in the prediction of VLF propagation characteristics has been stimulated by the development of the Omega radio navigation system, in which phase stability over great distances is an essential feature. The principal theoretical approaches currently employed are discussed. Propagation under a variety of conditions is considered and results from different techniques compared. Finally, one method is applied in a prediction of dawn phase changes over a long path at 10.2 kHz. (13 refs.)

Spherical ion traps for 'INTERCOSMOS-BULGARIA-1300' .See Entry 78667

The ion energy and mass analyzer on board the 'INTERCOSMOS-BULGARIA-1300' satelliteSee Entry 78668

An instrument for DC electric field and AC electric and magnetic field measurements aboard 'INTERCOSMOS-BULGARIA-1300' satelliteSee Entry 78669

Field and wave measurements aboard the Aureol-3 spacecraftSee Entry 78670

The resonance cone technique for exciting electron acoustic waves in equatorial ionosphereSee Entry 78671

A retarding potential analyser for rocket experimentsSee Entry 78672

Measurements of the energy spectra of charged particles within the VERTIC-10 rocket experimentSee Entry 78673

Measurement of electric fields in the ionosphere by incoherent scatter radar techniquesSee Entry 78677

BARS—a dual bistatic auroral radar system for the study of electric fields in the Canadian sector of the auroral zoneSee Entry 78678

Ionospheric plasma parameters measurement instrument for satellite experiment with SITSee Entry 78680

Estimation of f_oF_2 from interferences appearing on AGC data of ISS-b topside sounderSee Entry 78709

Measurement of total electron content by simultaneous reception of ISS-b telemetry signalsSee Entry 78710

EISCAT—the facility, the technique, and representative early resultsSee Entry 78724

Radar auroral observations and ionospheric electric fieldsSee Entry 78731

Field-aligned current density versus electrical potential characteristics for magnetosphere flux tubesSee Entry 78757

Terrestrial magnetic stormsSee Entry 78759

Polarisation characteristics of Pi 2 pulsations and implications for their source mechanisms: influence of the westward travelling surgeSee Entry 78762

The MAGION sub-satellite experimentSee Entry 78772

A payload for the study of electric fields and electron density in the equatorial regionSee Entry 78773

High resolution thermal plasma measurements aboard the Aureol 3 spacecraftSee Entry 78774

An instrument for total ion drift velocity measurements aboard the 'INTERCOSMOS-BULGARIA-1300' satelliteSee Entry 78776

Particle and optical measurements aboard the AUREOL 3 spacecraft (ARCAD 3 project). A—The particle experiments. B—Optical measurementsSee Entry 78778

Sond-R, an instrument for vertical probing of ionospheric plasma by means of CLP on board of a geophysical rocketSee Entry 78781

Operation and experimental results of ionosphere sounding satellite-b (ISS-b, UME-2). I. Outline of ISS-b projectSee Entry 78784

Topside sounder onboard ISS-bSee Entry 78785

The ISS-b retarding potential analyzerSee Entry 78787

Ion mass spectrometer on ionosphere sounding satellite (ISS-b)See Entry 78788

Operation of primary processing and data analysis system for ISSSee Entry 78793

On the application of housekeeping data to ISS-b operations ..See Entry 78794

Automation of satellite control system and its effectiveness in actual operationSee Entry 78795

94.30 PHYSICS OF THE MAGNETOSPHERE (for planets, see 96.30)

78755 Estimation of wave vector characteristics. S.D.Shawhan (Dept. of Phys. & Astron., Univ. of Iowa, Iowa City, IA, USA). *Adv. Space Res. (GB)*, vol.2, no.7, p.31-41 (1982).

In the realistic case of multiple electromagnetic plasma wave sources and multiple propagation paths, auto-correlation and cross-correlation products of the six wave components can be utilized to fit model parameters for the wave normal vector and Poynting vector distribution functions. With the complete wave vector characteristics, the wave mode can be identified, the index of refraction derived and the wave ray traced back towards the wave source region. Plasma wave instrumentation suitable for estimating some wave vector characteristics has been carried on satellites starting with FR-1 in 1964 and has evolved in various configurations on OGO-5, Injun-5, GEOS, Voyager, ISEE, Dynamics Explorer and the proposed OPEN spacecraft. Plasma wave research developments are considered. (24 refs.)

78756 Computer constructed imagery of distant plasma interaction boundaries. E.W.Greenstadt, H.D.Schurr, R.K.Tsugawa (TRW Space & Technol. Group, Advanced Products Lab., Appl. Technol. Div., One Space Park, Redondo Beach, CA, USA). *Adv. Space Res. (GB)*, vol.2, no.7, p.163-8 (1982).

Computer constructed sketches of plasma boundaries arising from the interaction between the solar wind and the magnetosphere can serve as both didactic and research tools. In particular, the structure of the Earth's bow shock can be represented as a nonuniform surface according to the instantaneous orientation of the IMF, and temporal changes in structural distribution can be modeled as a sequence of sketches based on observed sequences of spacecraft-based measurements. Viewed rapidly, such a sequence of sketches can be the basis for representation of plasma processes by computer animation. (5 refs.)

78757 Field-aligned current density versus electrical potential characteristics for magnetosphere flux tubes. J.Lemaire, M.Scherer (Inst. for Space Aeronomy, Brussels, Belgium). *Ann. Geophys. (France)*, vol.1, no.1, p.91-6 (Jan.-Feb. 1983).

The field-aligned current density (J_{tot}) is a non-linear function of the applied potential difference (ϕ) between the ionosphere and the magnetosphere. This non-linear function is calculated for plasma boundary conditions typical in a dayside cusp magnetic flux tube. The J -characteristic of such a flux tube changes when the temperatures of the warm magnetospheric electrons and of the cold ionospheric electrons are modified; it changes also when the relative density of the warm plasma is modified; the presence of trapped secondary electrons changes also the J -characteristic. The partial currents contributed by the warm and cold electrons, and by warm and cold ions are illustrated. (9 refs.)

78758 Electrostatic waves in the magnetosphere. D.C.Agarwal, D.C.Pande (J.K. Inst. of Appl. Phys. & Technol., Univ. of Allahabad, Allahabad, India).

Indian J. Theor. Phys., vol.29, no.3, p.247-60 (Sept. 1981).

Electromagnetic waves have been observed in the magnetosphere both with the OGO 5 and the topside sounder Alouette 2. These waves were detected during VLF electric field observations, as half harmonic waves. The authors present a critical examination of the results. There are a wide variety of instabilities in a collisionless plasma which could provide a turbulent wave spectrum in the magnetosphere. Such electrostatic instabilities responsible for the generation of electrostatic waves in the magnetosphere are reviewed; the triggering and saturation mechanisms of such waves are also studied. (27 refs.)

78759 Terrestrial magnetic storms. J.Untiedt (Westfälischen Wilhelms-Universität, Münster, Germany).

Phys. Bl. (Germany), vol.39, no.5, p.111-16 (May 1983). In German.

Gives explanations for magnetic variations, also known as magnetic storms, and defines the parameters of such storms as SD variations (solar and disturbed), AE effects (auroral aerolets), DST variations (disturbed and storm time) in terms of ionospheric electric currents. Describes measurements by MAGSAT and by the Bear Island Observatory and proposes models for magnetic storm systems, based on currents to produce equivalent magnetic fields. Finally, effects of solar wind are quantified. (14 refs.) G.M.E.

78760 Does IMF B_z induce the cusp field-aligned currents? F.Primdahl, F.Spangshov (Danish Space Res. Inst., Lyngby, Denmark). *Planet. & Space Sci. (GB)*, vol.31, no.4, p.363-7 (April 1983).

A well established correlation exists between the IMF B_z component and the cusp field-aligned and horizontal currents (Wilhelm et al., 1978). The northern and southern cusp currents may be parts of one large scale current system (D'Angelo, 1980) flowing mainly at the magnetopause and driven by the z -component of the solar wind electric field. Primdahl and Spangshov (1981) suggested that the large scale current system seems to shield out the IMF B_z from the interior of the magnetosphere. The authors propose that the currents are induced by the change in sign of B_z at the IMF sector boundary crossings, and argues that the time constant for the decay of the currents may be one week or larger. Experimental tests are proposed to demonstrate the feasibility of and possibly distinguish between the mechanisms. (10 refs.)

78761 The effect of a meridional $E \times B$ drift on the thermal plasma at $L=1.4$. G.J.Bailey (Dept. of Appl. & Computational Maths., Univ. of Sheffield, Sheffield, England).

Planet. & Space Sci. (GB), vol.31, no.4, p.389-409 (April 1983).

A fully time dependent mathematical model of the thermal plasma at $L=1.4$ is described. In the mathematical model account is taken of a quiet-time $E \times B$ drift in the meridional plane. Atmospheric conditions appropriate to the equinox at sunspot minimum and at sunspot maximum are considered. Results of the model calculations are presented. Emphasis is placed on the effects on the thermal plasma of a quiet-time $E \times B$ drift in the meridional plane. A comparison of the model calculations which include an $E \times B$ drift with those in which there is no $E \times B$ drift shows that an $E \times B$ drift significantly affects the plasma concentration and temperature distributions during the day at both sunspot minimum and sunspot maximum; the effects at night are very small. (41 refs.)

78762 Polarisation characteristics of Pi 2 pulsations and implications for their source mechanisms: influence of the westward travelling surge. J.C. Samson, G. Rostoker (Dept. of Phys., Univ. of Alberta, Edmonton, Alberta, Canada).

Planet. & Space Sci. (GB), vol.31, no.4, p.435-58 (April 1983).

Expands the results of Rostoker and Samson (1981), who noted that there are two latitudinal areas of Pi 2 localisation near the high latitude, substorm enhanced electrojets. The detailed study presented outlines the morphology of the polarisations of the Pi 2's in and near the westward travelling surge. There are two latitudinal areas of Pi 2 localisation. A poleward Pi 2 predominates within the surge and to the East, whereas an equatorward Pi 2 predominates equatorward and West of the surge. These Pi 2 localisations appear to correlate with the substorm enhanced westward and eastward electrojets respectively. The elliptical polarisation of the Pi 2's is most likely caused by azimuthal (longitudinal) expansion of the field-aligned currents in the surge, in association with reflection of the field-aligned current pulses from northern and southern high latitude ionospheres. (30 refs.)

78763 Local time asymmetry in the characteristics of Pc 5 magnetic pulsations. K. Yumoto, T. Saito (Onagawa Magnetic Obs., Tohoku Univ., Sendai, Japan), T. Sakurai.

Planet. & Space Sci. (GB), vol.31, no.4, p.459-71 (April 1983).

The wave characteristics of Pc 5 magnetic pulsations are analysed with data ofOGO-5, ISEE-1 and -2 satellites. The toroidal modes of Pc 5 pulsations are observed at a higher magnetic latitude in the dawnside outer magnetosphere. The compressional and poloidal modes of Pc 5 pulsations are mostly observed near the magnetic equator in the duskside outer magnetosphere. This LT asymmetry in the occurrence of dominant modes of Pc 5's in space is explained as is the asymmetric behaviour of Pc 5 pulsation activity on the ground across the noon meridian. (65 refs.)

78764 Propagation properties of hydromagnetic waves in a hot plasma and right-hand polarised PC 1 and PC 5. T. Namikawa, H. Hamabata, Y. Hosoya (Dept. of Phys., Osaka City Univ., Osaka, Japan).

Planet. & Space Sci. (GB), vol.31, no.4, p.473-81 (April 1983).

Propagation characteristics of hydromagnetic waves in a hot plasma are investigated and the results are used for the interpretation of Pc 1 and Pc 5 with right-hand polarisation guided along the geomagnetic field line. (33 refs.)

78765 Three-dimensional ray tracing of low frequency electromagnetic waves in the Earth's magnetosphere. V.I. Aksenov, A.V. Moshkov (Inst. of Radioengng. & Electronics, Acad. of Sci., Moscow, USSR).

Third International Conference on Antennas and Propagation ICAP 83, Norwich, England, 12-15 April 1983 (London, England: IEE 1983), p.204-8 part 2

In the present work a procedure of numerical integration of a set of differential equations describing three-dimensional ray tracing of LF electromagnetic waves in a spherically inhomogeneous multicomponent magnetospheric plasma is proposed. The developed procedure is used to investigate an influence of ray deflection of a magnetic meridian plane on such basic characteristics of LF signal as group delay time, arrival latitude and longitude. A possibility of propagation of LF signals in three-dimensional geomagnetic ducts (enhancements of ionization which are geomagnetic field aligned) is also analysed, an influence of wave normal declination of a magnetic meridian plane and duct characteristics on path pattern and conditions of wave trapping into duct being considered. (19 refs.)

Magnetospheric plasma physics See Entry 74230

Field and wave measurements aboard the Aureol-3 spacecraft See Entry 78670

Refractive index surfaces See Entry 78736

The effects of neutral air winds on the electron content of the mid-latitude ionosphere and protonosphere in summer See Entry 78741

Plasmaspheric hiss observed in the topside ionosphere at mid-and low-latitudes See Entry 78742

The MAGION sub-satellite experiment See Entry 78772

High resolution thermal plasma measurements aboard the Aureol 3 spacecraft See Entry 78774

94.40 COSMIC RAYS

Workshop on Science Underground See Entry 74199

Circumvention of Parker's bound on galactic magnetic monopoles See Entry 78807

94.40C Origin and propagation outside the solar system

Detection of 2×10^{15} to 2×10^{16} eV gamma-rays from Cygnus X-3 See Entry 78944

94.40H Energetic solar particles and photons

78766 Isotopic anomalies among solar energetic particles: contribution of preacceleration in collapsing magnetic neutral sheets. D.J. Mullan (Bartol Res. Found., Univ. of Delaware, Newark, DE, USA).

Astrophys. J. (USA), vol.268, no.1, pt.1, p.385-95 (1 May 1983).

Anomalous abundances of elements among solar flare particles have previously been interpreted in terms of a contribution from preacceleration in collapsing magnetic neutral sheets. The isotopic anomalies which are predicted by this preacceleration mechanism are examined. Enhancements of neutron-rich isotopes are found but the enhancements are not a monotonic function of the mass ratio. Thus, enhancement of $^{22}\text{Ne}/^{20}\text{Ne}$ need not be accompanied by any significant enhancements in, say, $^{18}\text{O}/^{16}\text{O}$ or $^{26}\text{Mg}/^{24}\text{Mg}$. High temperatures (such as those in flares) favor enhancement of $^{22}\text{Ne}/^{20}\text{Ne}$ as the dominant isotopic anomaly. These results may help to account for some of the observed isotopic anomalies among solar energetic particles. (29 refs.)

Direct evidence of type III electron streams propagating in coronal streamers See Entry 78894

94.40K Solar modulation and geophysical effects

Ground albedo neutrons produced by cosmic radiations See Entry 78767

94.40L Composition and energy spectra

78767 Ground albedo neutrons produced by cosmic radiations. M. Kodama

(Yamanashi Medical Coll., Yamanashi, Japan).

J. Phys. Soc. Jpn. (Japan), vol.52, no.5, p.1503-4 (May 1983).

Day-to-day variations of cosmic-ray-produced neutron fluxes near the Earth's ground surface are measured by using three sets of paraffin-moderated BF₃ counters, which are installed in different locations: 3 m above ground, ground level and 20 cm under ground, respectively. Neutron flux decreases observed by these counters when snowcover exists show that there are upward-moving neutrons, that is, ground albedo neutrons near the ground surface. The amount of albedo neutrons is estimated to be about 40% of total neutron flux in the energy range $1-10^6$ eV. (6 refs.)

Comment on the cosmic ray energy spectrum in the light of results from atmospheric Cerenkov studies See Entry 78768

94.40N Extensive air showers

78768 Comment on the cosmic ray energy spectrum in the light of results from atmospheric Cerenkov studies. R.W. Clay, A.G. Gregory, P.R. Gerhardt, G.J. Thornton (Phys. Dept., Univ. of Adelaide, Adelaide, Australia).

Aust. J. Phys. (Australia), vol.36, no.2, p.227-33 (1983).

New information has become available on the development of cosmic ray showers in the atmosphere. This information is used to show that the energy spectrum of cosmic rays must exhibit more pronounced structure than previously thought at energies of about 10^{16} eV. Possible interpretations of this structure are discussed. (19 refs.)

The Fly's Eye See Entry 78817

Detection of 2×10^{15} to 2×10^{16} eV gamma-rays from Cygnus X-3 See Entry 78944

94.40R High-energy interactions

High-energy hadrons produced by cosmic-ray muons in the earth as a source of background in proton-decay experiments See Entry 74823

Physics with underground leptons of atmospheric origin See Entry 78769

94.40T Muons and neutrinos

78769 Physics with underground leptons of atmospheric origin. T.K. Gaisser (Bartol Res. Found. Univ. of Delaware, Newark, DE, USA).

AIP Conf. Proc. (USA), no.96, p.203-13 (1982). [received: May 1983]

(Workshop on Science Underground, Los Alamos, CA, USA, 1982). Muons of great energy and neutrinos of all energies produced in the atmosphere by cosmic rays can penetrate to deep underground detectors. With existing and proposed proton decay detectors in mind, the authors review the physics accessible to underground cosmic ray experiments. Primary emphasis is on use of multiple coincident muons to study composition of primary cosmic rays at energies inaccessible to direct experiment. (26 refs.)

78770 Signatures for underground neutrinos. M. Crouch (Case Western Reserve Univ., Cleveland, OH, USA).

AIP Conf. Proc. (USA), no.96, p.225-35 (1982). [received: May 1983]

(Workshop on Science Underground, Los Alamos, CA, USA, 1982). Careful attention to the concept of the signature is especially important in neutrino experiments where the background usually predominates strongly over the signal. Examples are given of signature techniques that have been successful, as well as cases where signatures have proved to have shortcomings. (10 refs.)

Particle physics below the Earth's surface, an overview of possibilities See Entry 74243

High-energy hadrons produced by cosmic-ray muons in the earth as a source of background in proton-decay experiments See Entry 74823

The Gallium Solar Neutrino Detector See Entry 78816

Detection of gravitational collapse See Entry 78818

Underground science at Homestake [solar neutrino experiment] See Entry 78888

The analysis of solar models—neutrinos and oscillations See Entry 78889

The case of the missing solar neutrinos See Entry 78890

A radiochemical solar neutrino experiment using $^{81}\text{Br}/^{78}\text{Kr}$ See Entry 78891

A proposed geological solar neutrino measurement See Entry 78892

Could ^7Be be destroyed by neutron absorption in the Sun? A note on the solar neutrino puzzle See Entry 78897

94.40V Cosmic-ray effects in meteorites and terrestrial matter

Measurement of ^{53}Mn in deep-sea iron and stony spherules See Entry 78883

A proposed geological solar neutrino measurement See Entry 78892

94.60 INTERPLANETARY SPACE

(see also 96.60 Solar physics)

78771 A numerical method based on the Fourier-Fourier transform approach for modeling 1-D electron plasma evolution. A.J. Klimas (Lab. for Extraterrestrial Phys., NASA/Goddard Space Flight Center, Greenbelt, MD, USA).

J. Comput. Phys. (USA), vol.50, no.2, p.270-306 (May 1983).

A numerical method for studying one-dimensional electron plasma evolution under typical interplanetary conditions is presented. The method uses the Fourier-Fourier transform approach to a plasma model which is a generalization of the electrostatic Vlasov-Poisson system of equations. Conservation laws which are modified to include the plasma model generalization and also the boundary effects of nonperiodic solutions are given. A new conservation law for entropy in the transformed space is introduced. These conservation laws are used to check the accuracy of the numerical solutions. A discretization error analysis is given. Two numerical instabilities and the methods used for their suppression are discussed. Several solution examples are presented. Two of these are comparisons with earlier independent results; the comparison is favorable. A third example is also discussed which uses an interplanetary observation of a bump-on-tail unstable velocity distribution as initial data. It

is shown that in interplanetary plasma conditions the bump-on-tail instability leads to significant excitation of plasma oscillations at the Bohm-Gross frequency and its second harmonic. An explanation of the second harmonic excitation in terms of wave-wave coupling during the growth phase of the instability is given. (26 refs.)

Magnetospheric plasma physics See Entry 74230

Ion sputtering of minerals and glasses: a first step to the simulation of solar wind erosion See Entry 77508

Computer constructed imagery of distant plasma interaction boundaries See Entry 78756

Does IMF B_z induce the cusp field-aligned currents? See Entry 78760

Instrumentation and data systems for high-time resolution study of space plasma shocks See Entry 78777

A correlation interferometer for interplanetary scintillation observations See Entry 78814

Dynamic stabilization of hydromagnetic surface waves: applications to cometary plasma tails See Entry 78866

94.80 AEROSPACE FACILITIES AND TECHNIQUES; SPACE RESEARCH

(see also 87.65 Aerospace biophysics and medical physics)

78772 The MAGION sub-satellite experiment. P.Triska, F.Jiricek, J.Vojta, A.Czapek (Geophys. Inst., Czechoslovak Acad. Sci., Prague, Czechoslovakia). *Adv. Space Res. (GB)*, vol.2, no.7, p.53-6 (1982).
MAGION (1978-099C) was launched as a part of the Interkosmos 18 satellite and separated from this parent spacecraft on 14 November 1978, with the aim of studying the spatial structure of ELF-VLF phenomena using simultaneous measurements of the two near-spaced satellites. The MAGION experiment went on for almost three years, till the decay date of September 10, 1981. A description of the experiment is given and some new aspects of the satellite-subsatellite experimental technique for near-space research are indicated. (9 refs.)

78773 A payload for the study of electric fields and electron density in the equatorial region. S.Pal, S.Prakash, Y.B.Acharya, R.N.Misra (Phys. Res. Lab., Ahmedabad, India). *Adv. Space Res. (GB)*, vol.2, no.7, p.57-9 (1982).
A rocket borne payload for simultaneous measurement of the electric field along and perpendicular to the rocket spin axis and the electron density in the medium was developed and flown from Thumba ($8^\circ 31'N$, $0^\circ 47'S$ dip) onboard two Centaure rockets for the study of plasma dynamics in the equatorial E-region. The arrangement of sensors in this payload allows near continuous measurements of some of these parameters to be made. (3 refs.)

78774 High resolution thermal plasma measurements aboard the Aureol 3 spacecraft. C.Beghin (CRPE, CNRS, Orleans, France), J.J.Berthelot, R.Debrie, Yu.I.Galperin, V.A.Gladyshev, N.I.Massevitch, D.Roux. *Adv. Space Res. (GB)*, vol.2, no.7, p.61-6 (1982).
Two instruments using different techniques have been designed for making thermal electron and ion measurements performed aboard the AUREOL 3 satellite with the Soviet-French project ARCAD 3. The ISOPROBE gives precise measurements of electron density and temperature and their fluctuations with a high time resolution by using the mutual impedance technique. The ion mass-spectrometer DYCION performs measurements of number density, temperature and three-component velocity vector of the three major ionospheric thermal ions H^+ , He^+ and O^+ . After a brief description of the instruments, a few preliminary results are given. (15 refs.)

78775 An instrument for rapidly measuring plasma distribution functions with high resolution. C.W.Carlson (Space Sci. Lab., Univ. of California, Berkeley, CA, USA), D.W.Curtis, G.Paschmann, W.Michael. *Adv. Space Res. (GB)*, vol.2, no.7, p.67-70 (1982).
A new instrument which can rapidly measure plasma particle distribution functions has been developed based upon innovations in electrostatic analyzer design and position sensitive particle detection. The new analyzer uses a quadrupole geometry, but has a completely uniform 360° fan-shaped field of view. The polar angular distribution of entering particles is spatially imaged onto a position sensitive detector at the annular exit aperture after a deflection through 90° . Several methods of position sensitive detection have been successfully used in conjunction with this analyzer. The simplest is individual channel multipliers spaced around the annular exit. Microchannel plate electron multipliers permit greater position resolution to be obtained, and a detector using microchannel plates followed by a resistive anode image converter obtains angular resolution of about one degree, 360 individual angle pixels. Instruments of this type were flown on a sounding rocket in early 1982 and will be included on the Giotto comet mission and the AMPTE ion release module. (4 refs.)

78776 An instrument for total ion drift velocity measurements aboard the 'INTERCOSMOS-BULGARIA-1300' satellite. L.G.Bankov (Central Lab. for Space Res., Bulgarian Acad. of Sci., Sofia, Bulgaria), M.N.Gousheva, B.B.Kirov, N.G.Bankov, Yu.Shulchishin, K.Greshnev, N.Nikolaeva. *Adv. Space Res. (GB)*, vol.2, no.7, p.71-4 (1982).
The ion driftmeter, ID-1, aboard this satellite was intended to measure ion density irregularities, the ion drift velocity and photoelectron fluxes. The purpose of this paper is to present a brief description of the ID-1 instrumentation and to show the first results obtained from the flight instrument. (2 refs.)

78777 Instrumentation and data systems for high-time resolution study of space plasma shocks. V.M.Balebanov (Space Res. Inst., Acad. of Sci., Moscow, USSR), O.L.Vaisberg, E.M.Vasiliev, G.N.Zastenko, V.P.Evdokimov, E.G.Eroshenko, L.V.Pesotski, V.F.Babkin, S.Fisher, Z.Nemechek, Ya.Shafrankova. *Adv. Space Res. (GB)*, vol.2, no.7, p.75-9 (1982).
Deals with the principal methods of achieving high-time resolution measurements for the study of fine structure of shocks and other discontinuities in space plasmas. In the measurements of ion energy spectra, time resolution of about 1 s has been obtained. The Soviet-Czechoslovak INTERSHOCK project will obtain temporal resolution better than 0.1 s in the measurement of plasma parameters. (10 refs.)

78778 Particle and optical measurements aboard the AUREOL 3 spacecraft (ARCAD 3 project). A—The particle experiments. B—Optical measurements. J.M.Bosquet (CESR, CNRS, Toulouse Univ., Toulouse, France), Yu.I.Galperin, R.A.Kovrazhkin, Yu.N.Ponomarev, H.Reme, J.A.Sauvaud, F.K.Shuiskaya. *Adv. Space Res. (GB)*, vol.2, no.7, p.81-5 (1982).
CESR Toulouse-1K1 Moscow particles instrument package aboard the Aureol-3 satellite which consists of a complete set of charge particle spectrometers which measure electron and ion fluxes from 15 eV to 25 keV in 128 steps and in 11 directions. In addition, 4 channel spectrometers (2 electron and 2 ion channels in parallel) allow high time resolution measurements (up to 10 msec) with onboard calculation of auto and cross correlation functions. For higher energies (40-280 keV), solid-state spectrometers are used to measure electron and proton fluxes in 4 channels in parallel. Two Geiger counters are used for the determination of the trapping boundaries. Two mass-energy ion spectrometers (1 to 32 AMU, 0.02-15 keV) are placed with viewing angles which allow a distinction between nearly isotropic auroral proton precipitation and conical beams accelerated in the auroral ionosphere. Auroral and airglow photometry is performed aboard the AUREOL-3 satellite by a set of 3 parallel directed photometers with tiltable interference filters. Examples of data from inflight measurements using the instruments are presented and briefly discussed. (9 refs.)

78779 Advances in auroral imaging from space. C.D.Anger (Dept. of Phys., Univ. of Calgary, Calgary, Alberta, Canada). *Adv. Space Res. (GB)*, vol.2, no.7, p.97-105 (1982).
A new type of imaging instrument being built in Canada for the Swedish Viking satellite will employ a two-dimensional CCD array detector which is fibre-optically coupled to a microchannel plate intensifier. It will produce images of low level auroral emissions at the rate of one image per spin of the satellite (20 seconds). The instrument operates in the vacuum ultraviolet and uses a fast inverse Cassegrain optical system. Charge is shifted in the CCD imaging array in synchronism with the moving image so that exposure times of approximately one second will be achieved. (27 refs.)

78780 Application of numerical Fourier transformation on measurements made on board rotating spacecraft. R.Grabowski, B.Bosch, H.Wolf (Fraunhofer-Inst. fur Phys. Messtech., Freiburg, Germany). *Adv. Space Res. (GB)*, vol.2, no.7, p.169-72 (1982).
Signals obtained on board rocket payloads or satellites are often 'spin modulated'. The relevant information is then found within the envelope and the phase of the signal. The most efficient method of extracting this information is the numerical Fourier analysis. The efficiency and the accuracy of this technique are demonstrated. (5 refs.)

78781 Sond-R, an instrument for vertical probing of ionospheric plasma by means of CLP on board of a geophysical rocket. T.N.Ivanova, S.M.Halova (Central Lab. for Space Res., Bulgarian Acad. of Sci., Sofia, Bulgaria). *C.R. Acad. Bulg. Sci. (Bulgaria)*, vol.36, no.3, p.345-8 (1983).
The Sond-R instrument measured the local parameters of the space plasma near the irretrievable container of the geophysical rocket Vertical 10 (fired on December 21, 1981) at a height of 1505 km: electron density (N_e), temperature of electrons (T_e), function of their distribution, and, in particular, potential of body (V_0), as well as ion density (N_i) and ion mass composition (M_i). The sensitive element (sensor) is a onesidedly protected cylindrical Langmuir probe (CLP) with a 120-mm long collector and a 2-mm diameter, let out on a rod outside the container. The sawtooth voltage of the sweep (U) produced in the instrument is directly transmitted to the probe's protected electrode or to the common rim of the DC amplifier (DCA) insulated from the body. The dependence of the DCA-recorded probe current (I) on U gives the probe volt-amp characteristic ($I(U)$), from which the parameters of the ionospheric plasma are determined by mathematical processing (on board and ground). (2 refs.)

78782 The microgravity payload for the first Eureka mission. G.Seibert (Space Transportation Systems, Paris, France), K.Fuhrmann. *ESA Bull. (France)*, no.34, p.6-12 (May 1983).
From a user viewpoint, a gap exists between the short-duration research opportunities offered by Spacelab and the permanent space stations planned for the 1990s. It is shown how this gap can be filled by exploiting the deployment and retrieval capability of the Space Shuttle, Eureka, a retrievable autonomous platform. (no refs.)

78783 IRAS, the Infrared Astronomical Satellite. *Nature (GB)*, vol.303, no.5915, p.287-91 (26 May 1983).
The Infrared Astronomical Satellite, launched on 26 January 1983, is providing the first map of the entire IR sky. This article describes the operation and preliminary results of the IRAS mission. (no refs.)

78784 Operation and experimental results of ionosphere sounding satellite-b (ISS-b, UME-2). I. Outline of ISS-b project. Y.Hakura. *Rev. Radio Res. Lab. (Japan)*, vol.28, no.146, p.149-54 (June 1982). In Japanese.

The project of ISS (Ionosphere Sounding Satellite) has been promoted under the cooperation of the Radio Research Laboratories (RRL), Ministry of Posts and Telecommunications, and the National Space Development Agency of Japan (NASDA). The main objective of the satellite is to carry out observations of the worldwide distributions of ionospheric parameters and radio noises in conjunction with the global survey of radio environment necessary for improvement of efficiency on radio communications. The spacecraft installs the following four mission apparatus, (1) a digital swept frequency sounder for sounding of the topside ionosphere (TOP), (2) narrow band HF receivers for radio noise measurement (RAN), (3) a retarding potential trap for plasma measurement (RPT), and (4) the Bennett type ion-mass spectrometers for detecting positive ion composition (PIC). In observation modes, the four missions are executed sequentially in every 64 sec. The regular stage of ISS-b observation has been carried out by the RRL since April 24, 1978. With the routine observation performed for almost three years, a great deal of data over the entire global regions have been accumulated. The author summarizes the operational status and the experimental results of this most successful environmental monitoring satellite. (no refs.)

78785 Topside sounder onboard ISS-b. R.Nishizaki, N.Matsuura, A.Takahira. *Rev. Radio Res. Lab. (Japan)*, vol.28, no.146, p.155-65 (June 1982). In Japanese.

The ISS-b carries a HF pulse radar system so called a digital topside sounder for the execution of the TOP mission. The basic functions of the system are to transmit the pulsed radio wave of swept frequency and to receive echoes returned to the satellite after reflection in the ionosphere and at the ground. In the TOP mission there are two modes provided: TOP-A and TOP-B, of which are allocated times of 8 and 16 seconds, respectively, among 64 seconds of the time for an observational sequence. For TOP-A observation, the lowest frequency of the interference signals from the ground, f_u and the ionospheric critical frequency, f_c are determined automatically by the onboard preprogrammed logic circuit. Unfortunately, the operational test conducted after the

launch confirmed the malfunction of this logic circuit. The detailed examination revealed that the malfunction arises from misidentification of the internally produced signal at around 0.5 MHz of the frequency as if it is the interference from the ground. Furthermore, the obliquely propagating interference below the critical frequency and the intense noise frequently observed in the polar region also makes it difficult to make the TOP-A observation. The authors describe the characteristics of the antenna system, the transmitter and the receiver, and discusses the problems of the sounder system. (9 refs.)

78786 Characteristics of the radio noise receiving equipment. C.Kato, H.Kuriki, M.Kotaki, H.Suguchi.
Rev. Radio Res. Lab. (Japan), vol.28, no.146, p.167-74 (June 1982). In Japanese.

Describes the characteristics of the radio noise measurement equipment on-board the Ionosphere Sounding Satellite, ISS-b, which was launched on February 16, 1978 into a near-circular orbit at an altitude of about 1100 km. The radio measurement equipment is composed of four HF receivers of which center frequencies are, in order to avoid interferences, fixed in the guard bands of the standard frequency transmission of 2.5, 5, 10, and 25 MHz, respectively. Each receiver adopted a straight type amplifier, instead of conventional frequency conversion type, so as to exclude non-linear distortion. The band width of the receiver is limited to about 1 kHz by using the monolithic crystal filter. The overall dynamic range of the receiver covers more than 60 dB and it can respond to the violent change of field strength of radio waves radiated from lightning discharges. (4 refs.)

78787 The ISS-b retarding potential analyzer. H.Mori, S.Miyazaki, E.Sagawa, T.Ogawa.
Rev. Radio Res. Lab. (Japan), vol.28, no.146, p.175-82 (June 1982). In Japanese.

A retarding potential analyzer with spherical electrodes is mounted on the ISS-b. The primary objective is to measure the electron and ion densities and the electron and ion temperatures in the ionosphere. The authors give a description of the retarding potential analyzer. (3 refs.)

78788 Ion mass spectrometer on ionosphere sounding satellite (ISS-b). I.Iwamoto, N.Fugono, T.Suitz.
Rev. Radio Res. Lab. (Japan), vol.28, no.146, p.183-95 (June 1982). In Japanese.

An ion mass spectrometer was flown on the Ionosphere Sounding Satellite (ISS-b), which was put into a nearly circular orbit with an inclination of 70 degrees and an altitude of about 1100 km. The observations of global distribution of the positive ions are assured by two identical Bennett spectrometer tubes which are mounted at the top- and bottom-covers of the spacecraft. The Bennett tube is constructed from fifteen planar grids and works as a RF linear accelerator. The mass scan range is 1 to 20 AMU and major positive ions such as H^+ , O^+ and He^+ can be observed. The absolute densities of the positive ions are deduced by in-flight calibration method. In addition to detailed description of the instrument, brief accounts of the observational results are also given. (12 refs.)

78789 On the structure and functions of the ISS-b satellite control systems. K.Muranaga, M.Uratsuka, M.Shikatanai.
Rev. Radio Res. Lab. (Japan), vol.28, no.146, p.197-203 (June 1982). In Japanese.

The construction of Satellite Control Systems and Center building for ISS-b at Kashima Branch RRL, started in July 1970 and was completed in July 1975. All the sub-systems in the Satellite Control Center are controlled by the computer and so they conduct automatically relevant operation like satellite tracking, telemetry data reception and command transmission according to operational pass schedule. As a result of this computer system CSSC, Computer System for Satellite Control, it could be realized to obtain accurately and efficiently the observational data from ISS-b and also to reduce manpower to some extent. The outline of the structure and functions of ISS-b Satellite Control System at Kashima station is described, especially in the facilities based on the process computer control systems. (3 refs.)

78790 Scheduling of ISS-b operations. T.Ide, K.Aikey.
Rev. Radio Res. Lab. (Japan), vol.28, no.146, p.205-18 (June 1982). In Japanese.

The ISS-b spacecraft is capable of storing the observed data with the aid of an on-board tape recorder with a maximum recording time slightly longer than the satellite orbital period. In addition to this recording capability, the delay command function controlling the start time of data recording enables choice of satellite passes so that the observational points are distributed over the Earth as uniformly as possible, successfully achieving worldwide observations of the ionospheric parameters and radio noises. The stored data are telemetered to a ground station through a fast playback mode at the speed of 26 times faster than the recording speed. The authors describe the operational scheduling for ISS-b and the computer algorithm used for actual operations at Kashima and Ottawa ground stations. The basic policy of the scheduling, in general, can be applied to the mapping purposes with the limited number of satellites and TT&C (Telemetry, Tracking and Command) stations. (5 refs.)

78791 Operations of ISS-b at Kashima station and their result. M.Uratsuka, T.Yanagiya, E.Kawai, S.Iguchi.
Rev. Radio Res. Lab. (Japan), vol.28, no.146, p.219-38 (June 1982). In Japanese.

The most active period of ISS-b at Kashima station RRL as regards obtaining the experimental data was the first two years since the beginning of the regular stage operation in April 1978. The authors state some operation modes and processes to control the ISS-b, e.g. the tracking, telemetry and command. Also they discuss the matters and characteristic variations encountered in the operations, e.g. solar cell's electric power, battery voltage, Sun spin angle, temperature of equipment on board, etc. (7 refs.)

78792 Orbit and attitude of ISS-b. S.Yamamoto, F.Sawada.
Rev. Radio Res. Lab. (Japan), vol.28, no.146, p.239-47 (June 1982). In Japanese.

Accurate determination of the position and the attitude of ISS-b is necessary for the operation and analysis of the data obtained. Attempts to determine the orbit and the attitude of ISS-b were successfully made at Kashima Station. The attitude determination algorithm has been used on a routine basis. The authors outline the methods. Some features of long-term variations in the orbit and attitude determined by the methods are also discussed. (6 refs.)

78793 Operation of primary processing and data analysis system for ISS. M.Nagayama, S.Igi, M.Yamanishi.
Rev. Radio Res. Lab. (Japan), vol.28, no.146, p.249-90 (June 1982). In Japanese.

Satellite Operation Planning and Data Analysis System (SODAS) completed in 1976 has been utilized favorably for the operation of ISS-b and for the subsequent data processing and analysis. The authors describe the four sub-systems included in SODAS prepared for the purposes of carrying out the primary processing and analysis of the ISS-b data. The subsystems include

the data communication system for the satellite data transmission in real time basis and for exchanging information via 7 GHz microwave link between the headquarters of RRL and the earth station at Kashima. Discusses also the satellite data monitoring system for acquiring information of the four missions and the condition of the electric power and the attitude immediately, the satellite data processing system to make digital data tapes for experimenters' effectual utilization, and the online ionogram analysis system to scale critical frequency (f_oF_2) and resonance frequencies, and to get $N(h)$ profiles from the satellite data. (5 refs.)

78794 On the application of housekeeping data to ISS-b operations. R.Nishizaki, A.Takahira, T.Ide.
Rev. Radio Res. Lab. (Japan), vol.28, no.146, p.291-308 (June 1982). In Japanese.

Since the attitude of the ISS-b is solely governed by spin stabilization, the satellite conditions such as thermal structure and power supply vary in a complicated manner. Hence, predictions of the satellite conditions are necessary so as to make the satellite operations under optimum scheduling. By using the HK data acquired after injection into the orbit, the empirical equations were obtained for expressing the long term variations of the Sun-spin angle, the ecliptic ratio, the generated power and the temperatures of various parts of the spacecraft equipments including the battery and the magnetic tape recorder as functions of the revolution number or the date. These equations have been used to predict the satellite conditions which must be taken into consideration in the scheduling of the satellite operations. (no refs.)

78795 Automation of satellite control system and its effectiveness in actual operation. T.Iida, M.Uratsuka, K.Sawaji.
Rev. Radio Res. Lab. (Japan), vol.28, no.146, p.309-13 (June 1982). In Japanese.

Describes purposes and outlines the fully automated system for Ionosphere Sounding Satellite ISS-b control, and shows that the automation increases the successful pass rate from 88% to 97% and that it can reduce the number of operators from two to one, compared with the semiautomated system. (1 ref.)

Global pictures of the ozone field, from high altitudes, from DE-1 See Entry 78588

Global distribution of atmospheric radio noise derived from the global distribution of lightning activity See Entry 78632

Spherical ion traps for 'INTERCOSMOS-BULGARIA-1300' See Entry 78667

The ion energy and mass analyzer on board the 'INTERCOSMOS-BULGARIA-1300' satellite See Entry 78668

An instrument for DC electric field and AC electric and magnetic field measurements aboard 'INTERCOSMOS-BULGARIA-1300' satellite See Entry 78669

Field and wave measurements aboard the Aureol-3 spacecraft See Entry 78670

WAMDI— a wide angle Michelson Doppler imaging interferometer for Space-lab See Entry 78675

Airglow atmospheric imager on board the 'IK-BULGARIA-1300' satellite See Entry 78676

Ionospheric plasma parameters measurement instrument for satellite experiment with SIT See Entry 78680

Estimation of f_oF_2 from interferences appearing on AGC data of ISS-b topside sounder See Entry 78709

Measurement of total electron content by simultaneous reception of ISS-b telemetry signals See Entry 78710

EISCAT—the facility, the technique, and representative early results See Entry 78724

Observations of the thermal plasma in the topside ionosphere by RPT mission of ISS-b: electron density, temperature and mean ion mass See Entry 78748

Periodic motion of a satellite under the gravitational attraction of a rotating rigid body See Entry 78799

Microcomputer applications in space-borne instruments See Entry 78819

95.00 FUNDAMENTAL ASTRONOMY AND ASTROPHYSICS, INSTRUMENTATION AND TECHNIQUES AND ASTRONOMICAL OBSERVATIONS

95.10 FUNDAMENTAL ASTRONOMY

78796 Meridian circle observations of FK4 radio stars. G.Carrasco, E.Costa, P.Loyola (Dept. de Astron., Univ. de Chile, Santiago, Chile).
Astron. & Astrophys. Suppl. Ser. (France), vol.52, no.2, p.279-80 (May 1983).

Meridian circle observations of 8 FK4 radio stars, south of $\delta \sim +40^\circ$, are presented. For 6 of the sources α and δ have been determined, for the remaining 2 sources only α has been obtained at present. The results are given in the FK4 system. (8 refs.)

78797 Transits of Earth as seen from Mars. J.Meeus, E.Goffin.
J. Br. Astron. Assoc. (GB), vol.93, no.3, p.120-3 (April 1983).

On 1984 May 11, as seen from the planet Mars there will be a transit of the Earth across the Sun's disk. Because this event is both rare and fascinating, a detailed article on the subject seems appropriate, even when such a transit cannot be seen from the Earth. (7 refs.)

Solar eclipse induced variations in mesospheric ozone concentrations See Entry 78592

Asteroid occultations: a 1981 status report See Entry 78842

Jupiter's satellites J VI and J VII. Ephemerides for the years 1981 to 1990. ... See Entry 78844

Occultation of Hyd - 22°58794 by Neptune on 1983 June 15 See Entry 78863

Comet IRAS (1983f) See Entry 78869

Periodic Comet Du Toit-Neujmin-Delporte (1983g) See Entry 78870

Comet Sugano-Saigusa-Fujikawa (1983e) See Entry 78871

Comet IRAS (1983f) See Entry 78874

Comet Sugano-Saigusa-Fujikawa (1983e) See Entry 78876

- Comet Sugano-Saigusa-Fujikawa (1983e) See Entry 78877
 Observations of the Sun with the CERGA astrolabe in 1981 .. See Entry 78895
 Photographic observations of visual double stars See Entry 78946

95.10C Celestial mechanics

(for dynamics and kinematics of stellar systems, see 98.10)

78798 Gravitational three-body problem in 120 deg axial coordinates. W.E. Bleick (Naval Postgraduate School, Monterey, CA, USA). *J. Guid. Control & Dyn. (USA)*, vol.6, no.2, p.124-8 (March-April 1983). Recently (1982) the author introduced a symmetrical system of distance coordinates for studying the planar motion of a three-body system of point masses in its internal degrees of freedom. This work, devoted largely to the small vibration problem, is expanded to give the details of a complete numerical solution of the gravitation problem, including the three angular degrees of freedom. The three coordinate axes pass through the masses with the positive halves intersecting at angles of 120 deg with each other at a moving origin. The distance coordinates are taken as the signed distances of the masses from the moving origin. If the angular orientation of the coordinate axes is defined by the Euler angles, an attempt to determine these angles by integrating their time rates of change fails because of singularities. It is shown that such singularities are avoided by the use of Rodrigues' orthogonal matrix to specify the angular orientation. The Lagrange equations are solved for the appropriate time derivatives, separating the distance variables from themselves and the angular velocities, thus making possible a simple computer numerical solution. (4 refs.)

78799 Periodic motion of a satellite under the gravitational attraction of a rotating rigid body. A.H. Borham. *Vestn. Mosk. Univ. Ser. I (USSR)*, no.2, p.74-8 (March-April 1983). In Russian.

Proves the existence of a family of periodic solutions for the problem of particle motion under the gravitational action of a homogeneous three-axial ellipsoid close to a sphere of the same volume and rotating uniformly about the smallest axis. (5 refs.)

Inverse Feigenbaum bifurcations in Hamiltonian systems See Entry 74260

Irreducible tensors and their application in problems of the motion of a solid body in strong fields See Entry 74269

Evolution of the Earth-Moon system See Entry 78410

Tidal friction in historical time and in the remote past See Entry 78415

On the stability of the Solar System See Entry 78830

Binary-single star scattering. I. Numerical experiments for equal masses See Entry 78961

Binary-single star scattering. II. Analytic approximations for high velocity See Entry 78962

95.30 FUNDAMENTAL ASPECTS OF ASTROPHYSICS

78800 The equilibria of rotating, isothermal clouds. I. Method of solution. S.W. Stahler (Center for Radiophys. & Space Res., Cornell Univ., Ithaca, NY, USA).

Astrophys. J. (USA), vol.268, no.1, pt.1, p.155-64 (1 May 1983).

In an effort to resolve the current controversy in dynamical models of rotating protostellar collapse, a detailed study has been made of the axisymmetric equilibrium configurations for differentially rotating, isothermal clouds. The physical assumptions underlying the calculation are stated and the numerical technique outlined. The clouds are assumed to have the angular momentum distribution or rigidly rotating, uniform-density spheres of the same mass. Magnetic and viscous effects are neglected. The computational method is designed to handle highly flattened structures, should they arise, and to yield numerical values of the density. (30 refs.)

78801 The equilibria of rotating, isothermal clouds. II. Structure and dynamical stability. S.W. Stahler (Center for Radiophys. and Space Res., Cornell Univ., Ithaca, NY, USA).

Astrophys. J. (USA), vol.268, no.1, pt.1, p.165-84 (1 May 1983).

For pt.1 see ibid., vol.268, no.1, p.155-64 (1983). Numerical results are presented for the structure of differentially rotating, isothermal clouds. The equilibria can be characterized by two parameters: a dimensionless mass M and the rotational parameter β ($0 \leq \beta \leq 1/2$). At any fixed β , there exists a critical mass $M^*(\beta)$ which is marginally dynamically unstable to axisymmetric perturbations. Stability is diagnosed by investigating the change in M as a function of density contrast at fixed β . This 'static method' is proved rigorously for the present case. The structure of unstable equilibria with $M < M^*(\beta)$ is displayed. The marginally unstable normal modes of oscillation at the critical masses are obtained numerically over the full range of β . Similar cases of instability in the fundamental mode are shown to exist in nonrotating polytropes bounded by a finite external pressure. Finally, a comparison of the stability results for isothermal clouds with the dynamical collapse calculations suggests a simple interpretation for the latter. Ringlike collapses or other runaway situations are obtained with initial conditions such that $M > M^*(\beta)$. Stable, disklike configurations are obtained for subcritical masses. (34 refs.)

78802 Nonlinear propagation of hydromagnetic waves in high-beta plasmas. P.K. Shukla (Inst. für Theoretische Phys., Ruhr-Univ. Bochum, Bochum, Germany).

Astrophys. J. (USA), vol.268, no.1, pt.1, p.396-7 (1 May 1983).

Nonlinear interaction of hydromagnetic waves with slow plasma motion is considered in high- β plasmas. The possibility of modulational instability is investigated. Relevance to the propagation of cosmic rays in the interstellar medium is discussed. (11 refs.)

78803 Effect of screening due to free mobile charges on the binding energy of an H^- ion. D.E. Phelps (Air Force Wright Aeronautical Labs., Wright Patterson AFB, OH, USA), K.K. Bajaj.

Astrophys. J. (USA), vol.268, no.1, pt.1, p.447-50 (1 May 1983).

A calculation of the binding energy of a negative hydrogen ion (H^-), defined as the energy required to remove one of the two electrons from the H^- ion to infinity in the presence of other free mobile charges, is reported. The effective interactions between the constituent particles of the H^- ion are assumed to be described by Dingle-Mansfield potentials. This potential is valid for a Fermion gas of an arbitrary degeneracy. The variation of the binding energy of an H^- ion as a function of the screening parameter δ is calculated, using a variational approach. It is shown that the binding energy of an H^- ion goes to zero for $a\delta = 0.87$, where a is the Bohr radius. The binding energy of a hydrogen atom itself in the presence of free mobile charges goes to zero for $a\delta = 1.2$. The relative significance of these two values is discussed. (14 refs.)

78804 Simulation models for the evolution of cloud systems. I. Introduction and preliminary simulations. W.A. Pumphrey, J.M. Scalo (Dept. of Astron., Univ. of Texas, Austin, TX, USA).

Astrophys. J. (USA), vol.269, no.2, pt.1, p.531-59 (15 June 1983).

The evolution of systems of interacting gas clouds is investigated, with application to protogalaxies in galaxy clusters, proto-globular clusters in galaxies, and protostellar fragments in interstellar clouds. The evolution of these systems can be parameterized in terms of three dimensionless quantities: the number of clouds, the volume filling factor of clouds, and the fraction of the mass of the system in clouds. The authors discuss the range of parameter space in which direct cloud collisions, tidal encounters, interactions of clouds with ambient gas, cloud collapse, cloud orbital motion due to the gravitational acceleration of the rest of the system, and cumulative long-range gravitational scatterings are important. The only practical approach to quantitative study of cloud systems is statistical modeling, whose chief limitation is the restricted availability of realistic interaction cross sections, which must come from external hydrodynamic calculations. A general kinetic equation representing the deterministic evolution of the joint distribution function for the cloud properties—position, velocity, size, and mass—is presented. The generalized coalescence equation is a moment form of this kinetic equation. A few comparisons of simulation results with known analytic solutions of restricted forms of the kinetic equation are made. A number of simplified problems involving pure coalescence with no ambient gas or external forces are then simulated in order to investigate the dependence of the final cloud mass spectrum on the adopted initial mass distribution, coalescence cross section, and initial velocity distribution. (118 refs.)

78805 The Jeans problem for a thin galaxy in steady state. R. Whitley (Univ. of California, Irvine, CA, USA).

J. Astrophys. & Astron. (India), vol.3, no.2, p.111-23 (June 1982). [received: June 1983]

Given the potential, the equation of continuity and Poisson's equation are solved for the variation perpendicular to the Galactic plane for a thin galaxy in a steady state. Simple expressions are obtained for the joint density function for the mass density and velocity, and for the distribution function for the velocity and its moments. These results are applied using a potential suggested by Woolley and Stewart (1967) and Whitley (1977), which is Camm's (1950) potential due to an isothermal gas stratified in parallel layers, plus the potential due to the galactic centre. A formula, valid under conditions more general than usual, is found for the total mass density in the neighbourhood of the Sun. (18 refs.)

78806 The massive neutrino and clustering phenomena in the Universe. Lu Tan, Zhu Peichen (Dept. of Astron., Nanjing Univ., Nanjing, China).

Kexue Tongbao [Foreign Lang. Ed.] (China), vol.28, no.1, p.63-8 (Jan. 1983). [received: June 1983]

The formation mechanisms of galaxies and clusters of galaxies are studied without the dust approximation, and the effect of the speed of sound is discussed. (9 refs.)

78807 Circumvention of Parker's bound on galactic magnetic monopoles. D.A. Dicus (Center for Particle Theory, Univ. of Texas, Austin, TX, USA), V.L. Teplitz.

Nature (GB), vol.303, no.5916, p.408-9 (2 June 1983).

There is a possibility that a magnetic monopole has been observed by Cabrera (1982). The monopole density implied by the observation appears to violate bounds on the density of such particles derived from the total mass density of the Universe and from the existence of galactic magnetic fields. The authors show that the observation is not inconsistent with these bounds if the monopoles and antimonopoles are bound into positronium like states with principal quantum n high enough so that the Earth's magnetic field will break them apart, but small enough so that the weaker galactic magnetic field will not. The authors determine a range of values for n and show that lifetimes for such bound states are longer than the current age of the Universe. (16 refs.)

78808 Gravitational waves. B. Muchotrzeb (Centrum Astron. im. M. Kopernika, Warszawa, Poland).

Postępy Astron. (Poland), vol.30, no.3-4, p.293-305 (July-Dec. 1982). In Polish. [received: April 1983]

Discusses the theoretical background of the phenomenon of gravitational waves. Simplifications are introduced to avoid applying the full general relativity formalism. (no refs.)

78809 Collisional vibrational quenching of $O_2^+(v)$ and other molecular ions in planetary atmospheres. B. Bohringer, M. Durup-Ferguson, E.E. Ferguson, D.W. Fahey (Aeronomy Lab., NOAA, Boulder, CO, USA).

Planet. & Space Sci. (GB), vol.31, no.4, p.483-7 (April 1983).

New experimental techniques have yielded several thermal energy vibrational quenching rate constants for $O_2^+(v)$. Rates for quenching of $O_2^+(v=1)$ by O_2 , N_2 , Ar, CO_2 , H_2 , and CH_4 are 3(-10), 2(-12), 1(-12), 1(-10), 2.5(-12), and 6(-10) $cm^3 s^{-1}$ at 300K. The quenching is somewhat faster for $O_2^+(v=2)$. The triatomic ions CO_3^+ , NO_2^+ , N_2O^+ , SO_2^+ , and H_2O^+ are all vibrationally deactivated with an efficiency greater than 10^{-3} in Ar or Ne collisions. A theoretical rationalisation of the experimental results leads to the prediction that vibrational quenching in planetary atmospheres will generally be efficient, $k > 1(-12) cm^3 s^{-1}$ for almost all ion and neutral gas pairs. (19 refs.)

78810 Magneto-atmospheric waves. J.H. Thomas (Dept. of Mech. Engng., Univ. of Rochester, Rochester, NY, USA).

In book: *Annual review of fluid mechanics. Vol.15*, M. Van Dyke, J.V. Wehausen, J.L. Lumley [Ed.], p.321-43. Palo Alto, CA, USA: Annual Reviews (1983), 534 pp. [0 8243 0715 1]

Magneto-atmospheric waves, or magneto-acoustic-gravity waves as they are also known, occur in a compressible, stratified, electrically conducting atmosphere under gravity, permeated by a magnetic field. These waves are supported by the combined restoring forces due to compression, buoyancy, and distortion of the magnetic field. They may be thought of as acoustic-gravity waves modified by the magnetic field or as magneto-acoustic waves modified by the stratification and buoyancy. The author considers the cases where all three restoring forces contribute to the wave motion. (66 refs.)

78811 Gamma-ray astronomy. R. Ramaty (Lab. for High-Energy Astrophys., NASA/Goddard Space Flight Center, Greenbelt, MD, USA), R.E. Linfenfelter.

In book: *Annual review of nuclear and particle science. Vol.32*, J.D. Jackson, H.E. Gove, R.F. Schwitters [Ed.], p.235-69. Palo Alto, CA, USA: Annual Reviews (1982), 595 pp. [0 8243 1532 4]

The authors describe gamma-ray observations from the solar system, from rapid nonsolar transients, from quasi-steady galactic sources and from extragalactic sites. They consider the most reliable and statistically significant observations; gamma-ray observations, in some cases, are still limited by counting statistics that can lead to questionable results. They particularly emphasize the physical processes responsible for astrophysical gamma-ray production. These involve processes of atomic physics (positronium formation and annihilation), of low-energy nuclear physics (deexcitation lines), of medium-

energy particle physics (π^0 meson production), of electromagnetism and magnetohydrodynamics (electron-positron pair production, confinement, and annihilation), as well as the more exotic processes in and around neutron stars, close to black holes, and possibly even in the early universe. (226 refs.)

78812 Dyon black hole in the Tomimatsu-Sato-Yamazaki space-time. M.Kasuya (Inst. for Nuclear Study, Univ. of Tokyo, Tokyo, Japan). Gauge Theory and Gravitation. Proceedings of the International Symposium, Nara, Japan, 20-24 Aug. 1982 (Berlin, Germany: Springer-Verlag 1983), p.41-4.

The symmetry between electric and magnetic charge which is inherent in Maxwell's equations does not seem to be realized in nature. Dirac pointed out, however, that quantum mechanics does not preclude the existence of magnetic monopoles. The author presents an exact stationary rotating dyon solution in the Tomimatsu-Sato-Yamazaki space-time. (13 refs.)

Tachyonium, an action-at-a-distance model See Entry 74274

Post-Newtonian gravitational radiation of a binary system of relatively extended bodies in the field theory of gravitation See Entry 74339

The geometrical hierarchy model and $N=1$ supergravity See Entry 74355

Gravitational waves and their detection See Entry 74362

Grand unification—a review See Entry 74467

Hot, dense matter in the bulk equilibrium approximation. II. Adiabats and alpha-particle effects See Entry 74888

The configurations $3s^2 3p^3 3d$ and $3s 3p^4 3d$ in Mn VIII and Fe IX See Entry 75340

The microwave and far-infrared spectra of the CH radical See Entry 75371

HOC^+ : laboratory observation of a proposed interstellar species See Entry 75550

Isotopic anomalies among solar energetic particles: contribution of preacceleration in collapsing magnetic neutral sheets See Entry 78766

A numerical method based on the Fourier-Fourier transform approach for modeling 1-D electron plasma evolution See Entry 78771

The Gallium Solar Neutrino Detector See Entry 78816

Detection of gravitational collapse See Entry 78818

The dynamic tensile strength of ice and ice-silicate mixtures See Entry 78833

Dynamic stabilization of hydromagnetic surface waves: applications to cometary plasma tails See Entry 78866

Magnetohydrostatic model of solar faculae See Entry 78887

The analysis of solar models—neutrinos and oscillations See Entry 78889

The case of the missing solar neutrinos See Entry 78890

Could ^7Be be destroyed by neutron absorption in the Sun? A note on the solar neutrino puzzle See Entry 78897

Enhancement of thermonuclear reaction rate due to screening by relativistic degenerate electrons See Entry 78903

Structure and stability of rotating fluid disks around massive objects. II. General relativistic formulation See Entry 78940

On the possibly low H_2 formation rate in dense clouds See Entry 78979

The stability of a magnetically confined radio jet See Entry 78997

Global stability of disk-bulge systems: spiral structure of disk galaxies See Entry 79005

X-ray nebular models See Entry 79025

Counterpart of the Kasner model in Brans-Dicke theory See Entry 79031

Antiproton interactions with light elements as a test of GUT cosmology See Entry 79040

95.55 ASTRONOMICAL INSTRUMENTS

78813 The Clark Lake Teepee-Tee telescope. W.C.Erickson, M.J.Mahoney, K.Erb (Clark Lake Radio Obs., Univ. of Maryland, College Park, MD, USA). *Astrophys. J. Suppl. Ser. (USA)*, vol.50, no.3, p.403-19 (Nov. 1982). [received: May 1983]

A new, fully steerable, decametric array for radio astronomy has been built at the Clark Lake Radio Observatory near Borrego Springs, California. This array is a "T" of 720 conical spiral antennas (teepee-shaped antennas), 3.0 km by 1.8 km. It is capable of operating between 15 and 125 MHz but has best sensitivity in the 25 to 75 MHz range. Both its operating frequency and beam position are adjustable in ~ 1 ms. A 1024 channel digital correlator has been built and attached to the array. This permits the simultaneous measurement of the complex visibility functions on 512 interferometer baselines between various portions of the array. After Fourier transformation these visibility data yield a 32×32 resolution element picture of the area of sky under observation, with frequency-dependent angular resolution ranging from $20'$ to $2.7'$ and a sensitivity of 1 Jy per beam. The system is described, and some initial observations are presented. (5 refs.)

78814 A correlation interferometer for interplanetary scintillation observations. S.K.Alurkar, R.V.Bhonsle, R.Sharma, A.D.Bobra, Sohan Lal, N.S.Nirman, P.Venat, G.Sethia (Phys. Res. Lab., Ahmedabad, India). *J. Inst. Electron. & Telecommun. Eng. (India)*, vol.28, no.11, p.577-82 (Nov. 1982). [received: April 1983]

A correlation interferometer of the phase-switching type operating at a frequency of 103 MHz, developed for interplanetary scintillation (IPS) observation, is described. Two outputs, sin and cos, of the correlation receiver give rapidly changing voltage fluctuations produced by a compact scintillating radio source. A scintillometer output, proportional to the square of the scintillating flux, enables measurement of scintillation index. More than 100 strong and weak scintillating sources have been observed. This is the first of the three IPS radio telescopes being developed in India for studying the interplanetary medium. (14 refs.)

78815 Parameters of the radio telescope RT-3. M.Szymczak, A.Kus, G.Gawronska (Katedra Radioastron., Uniwersytet Mikołaja Kopernika, Toruń, Poland). *Postępy Astron. (Poland)*, vol.30, no.3-4, p.307-14 (July-Dec. 1982). In Polish. [received: April 1983]

Presents technical parameters of the 15-meter radio telescope and electrical characteristics. Special attention is paid to the pointing calibration. The antenna pattern, effective aperture and sensitivity are given. (18 refs.)

Fabrication of a grid on a non-flat substrate by e-beam lithography [telescope lens fabrication] See Entry 75841

Recent developments in ion mass spectrometers in the energy range below 100 keV See Entry 78665

95.70 OTHER INSTRUMENTATION AND TECHNIQUES

(inc. clocks, frequency standards)

78816 The Gallium Solar Neutrino Detector. W.Hampel (Max-Planck-Inst. für Kernphys., Heidelberg, Germany), R.Davis, Jr., B.T.Cleveland, G.Friedlander, S.Katcoff, L.P.Remser, J.K.Rowley, J.Weneser, T.Kirsten, W.Hampel, G.Heusser, M.Hubner, J.Kiko, E.Pernicka, R.Schlotz, R.Wunderlich, I.Dostrovsky, J.N.Bahcall, K.Lande, R.I.Steinberg. *AIP Conf. Proc. (USA)*, no.96, p.88-95 (1982). [received: May 1983] (Workshop on Science Underground, Los Alamos, CA, USA, 1982).

The author presents the status of the Gallium Solar Neutrino Experiment. The scientific goals of the experiment and the general experimental approach are described with details of the chemical procedure, the counting technique and the influence of background effects. (12 refs.)

78817 The Fly's Eye. R.Cady, G.L.Cassiday, J.Elbert, E.Loh, Y.Mizumoto, P.Sokolsky, D.Steck, M.Ye (Univ. of Utah, Salt Lake City, UT, USA). *AIP Conf. Proc. (USA)*, no.96, p.191-202 (1982). [received: May 1983] (Workshop on Science Underground, Los Alamos, CA, USA, 1982).

The authors describe a high energy physics observatory, the Fly's Eye, designed to measure extensive air showers in the energy range 10^{17} - 10^{21} eV via atmospheric fluorescence. Preliminary results are presented for the following measurements: (1) the high energy cosmic ray spectrum at 10^{17} - 10^{19} eV, (2) the total proton cross section σ_{pp} , (3) limits on the extra-galactic neutrino flux at 10^{20} eV. (7 refs.)

78818 Detection of gravitational collapse. J.C.Wheeler, J.A.Wheeler (Univ. of Texas, Austin, TX, USA). *AIP Conf. Proc. (USA)*, no.96, p.214-24 (1982). [received: May 1983] (Workshop on Science Underground, Los Alamos, CA, USA, 1982).

At least one kind of supernova is expected to emit a large flux of neutrinos and gravitational radiation because of the collapse of a core to form a neutron star. Such collapse events may in addition occur in the absence of any optical display. The corresponding neutrino bursts can be detected via Cerenkov events in the same water used in proton decay experiments. Dedicated equipment is under construction to detect the gravitational radiation. Events throughout the Galaxy could be detectable, but are expected only at intervals exceeding a decade. Nevertheless, the next event could come tomorrow, so every attempt should be made to make the monitoring for such events routine. (16 refs.)

78819 Microcomputer applications in space-borne instruments. W.C.Gibson (Dept. of Space Sci., Southwest Res. Inst., San Antonio, TX, USA). *Adv. Space Res. (GB)*, vol.2, no.7, p.153-62 (1982).

The recent applications of microprocessors to space experiments at Southwest Research Institute are presented. Some of the lessons learned from these applications are discussed. (no refs.)

78820 Method of calculating the expected background luminance from the Moon for planning astronomical observations. S.I.Vereshchagin, S.A.Likhomanov. *Sov. J. Opt. Technol. (USA)*, vol.49, no.9, p.551-3 (Sept. 1982). Translation of: *Opt.-Mekh. Prom-st. (USSR)*, vol.49, no.9, p.15-17 (Sept. 1982).

A calculation method is described for the a priori estimation of the background luminance from the Moon in a given region of the sky, based on the results of a statistical analysis of experimental data. The method has been implemented in the form of a library of computer programs, which permits a rapid consideration of the astrolimatic conditions of an observation point and to simulate the background luminance distribution in a given region of the sky when preparing to carry out observations of different classes of astronomical objects. (10 refs.)

Workshop on Science Underground See Entry 74199

Particle physics below the Earth's surface, an overview of possibilities See Entry 74243

A proton decay and solar neutrino experiment with a liquid argon Time Projection Chamber See Entry 75230

Physics with underground leptons of atmospheric origin See Entry 78769

Signatures for underground neutrinos See Entry 78770

Underground science at Homestake [solar neutrino experiment] See Entry 78888

A radiochemical solar neutrino experiment using $^{81}\text{Br}(\nu_e)^{-81}\text{Kr}$ See Entry 78891

95.75 TECHNIQUES OF OBSERVATION AND REDUCTION

78821 The ages of the disks of S0 galaxies. N.Caldwell (Yale Univ. Obs., New Haven, CT, USA).

Astrophys. J. (USA), vol.268, no.1, pt.1, p.90-101 (1 May 1983). A photometric system using a broad-band color combined with a line strength index is employed to distinguish age differences from metallicity differences between the bulges and disks of S0 galaxies. A color difference independent of metallicity changes of about $\Delta(U-V)=0.10$ is found for the sample of galaxies observed. Several S0 galaxies have absorption line strengths that indicate the disks are as metal rich as the most luminous elliptical galaxies. It is concluded that the disks of S0 galaxies are probably younger than the bulges, but the distinction between a younger turnoff and residual star formation cannot be made. (45 refs.)

78822 The brightest stars as extragalactic distance indicators. R.M.Humphreys (Univ. of Minnesota, Minneapolis, MN, USA). *Astrophys. J. (USA)*, vol.269, no.2, pt.1, p.335-51 (15 June 1983).

The luminosities of the brightest blue and red supergiants are calibrated by spectra and photometry of such stars in six Local Group galaxies. The visually brightest blue supergiants are all A type supergiants. Their luminosities depend strongly on the luminosity of the parent galaxy. The same relationship also occurs for the most luminous (bolometric) stars in the galaxies. There is a tight upper limit to the visual luminosities of the M supergiants at $M_{\text{bol}} = -8.0 \pm 0.2$ mag in spiral and irregular type galaxies covering nearly 6 mag of galactic luminosity from $M_{\text{bol}} = -20.5$ to -14.8 mag. The brightest M supergiant in each galaxy averages $M_{\text{bol}}(1) = -8.1 \pm 0.06$ mag with a σ of 0.14 mag, and the first three brightest M star luminosities in each of these six galaxies average $M_{\text{bol}}(3) = -7.9 \pm 0.07$ mag with a σ of 0.18 mag. The brightest M supergiants should be excellent extragalactic distance indicators for a wide range of galaxy types and luminosities. (45 refs.)

78823 A revised and extended calibration for the Spinrad-Taylor scanner system. B.J.Taylor (Dept. of Phys. & Astron., ESC, Brigham Young Univ., Provo, UT, USA).

Astrophys. J. Suppl. Ser. (USA), vol.50, no.3, p.391-401 (Nov. 1982). [received: May 1983]

New spectrophotometric data are presented for the standards of the Spinrad-Taylor scanner photometric system. The new data are in the 4040-6180 Å wavelength range and are used to construct a calibration of Spinrad-Taylor data to absolute units in this range. In addition, a previously published calibration for $\lambda > 6100$ Å is revised and extended through use of data in the literature. The calibrations—fused into a single whole—and the Spinrad-Taylor data themselves are tested for systematic error, partly through use of further new spectrophotometry at $\lambda > 6100$ Å; those tests which can currently be made yield generally satisfactory results. (39 refs.)

78824 Computational astrophysics on the array processor. R.T.Farouki, S.L.Shapiro, S.A.Teukolsky (Center for Radiophys. & Space Res., Cornell Univ., Ithaca, NY, USA).

Computer (USA), vol.16, no.6, p.73-83 (June 1983).

Modeling the dynamics of the universe is no small-scale problem and usually requires costly, off-site mainframes. Astrophysicists at Cornell, however, have found an economical, in-house alternative. Soon after an early model of the floating point systems AP-1901, array processor arrived at Cornell in 1978, theoretical astrophysicists and researchers joined physical scientists at the university who, together with Cornell Computer Services, were planning to finance and use the AP for large-scale scientific computing. They needed a means to tackle several large-scale, nonlinear problems in computational astrophysics and general relativity and had a rather limited computing budget to work with. They have used the AP to solve diverse problems in theoretical astrophysics and general relativity—problems that encompass many different physical regimes and, naturally, require a variety of solutions. The problems examined thus far deal either with the dynamical structure and evolution of self-gravitating, large N -body systems or with the spherical collapse of stars to black holes. These experiences are related. (33 refs.)

78825 The effectiveness of astronomical speckle transfer function reweighting algorithms. R.Barakat, P.Nisenson (Harvard Univ. Cambridge, MA, USA).

Opt. Commun. (Netherlands), vol.45, no.5, p.311-16 (1 May 1983).

Two methods for reweighting the astronomical speckle transfer function are compared using a combination of analysis and numerical computation. One method, long exposure subtraction is shown to perform well only for very short wavefront correlation lengths (shorter than the correlation length expected from a real atmosphere). The other method, reference star division is demonstrated to be effective and accurate, even when the wavefront statistics for the reference star data are substantially changed from the object data statistics. An experimental result using real telescope data is included which substantiates the analysis. (10 refs.)

78826 Research note: 13-color photometry, San Pedro Martir, 1973-79. W.J.Schuster (Inst. de Astron., Univ. Nacional Autonoma de Mexico, Mexico City, Mexico).

Rev. Mex. Astron. & Astrofis. (Mexico), vol.5, no.3, p.149-60 (July 1982). [received: April 1983]

Atmospheric extinction data, probable errors of observation, standard star lists, observing procedures, reduction equations, and other miscellaneous data are given and discussed for 225 nights of 13-color photometry observed at the San Pedro Martir Observatory in Baja California. In addition a partial bibliography for the 13-color and Borgman photometric systems and for the uses of such intermediate-band photometry is presented. (49 refs.)

78827 A simple method of photographic photometry data reduction. J.M.Garcia-Pelayo, E.J.Alfaro (Inst. de Astrofísica de Andalucía, Granada, Spain).

Rev. Mex. Astron. & Astrofis. (Mexico), vol.5, no.3, p.167-72 (July 1982). [received: April 1983]

Presents a variant of the standard methods in photographic photometry data reduction. The compact and fast least squares fitting with orthogonal polynomials has been combined with the analysis of variance, in order to obtain calibration curves corrected for magnitude and color effects. An example of application to four R plates (Becker's-RGL system) is also included. (10 refs.)

The equilibria of rotating, isothermal clouds. I. Method of solution See Entry 78800

The Clark Lake Teepee-Tee telescope See Entry 78813

Micron-sized particles detected near Saturn by the Voyager plasma wave instrument See Entry 78850

95.80 ASTRONOMICAL OBSERVATIONS (LISTED BY TECHNIQUES OF OBSERVATION)

95.80D Radio and radar

Comet IRAS-Araki-Alcock (1983d) See Entry 78872

A coronal transient associated with a high-speed type II burst See Entry 78886

Direct evidence of type III electron streams propagating in coronal streamers .. See Entry 78894

Time structure of solar decametre type III radio bursts See Entry 78896

An attempt to resolve pulsar magnetospheres using interstellar scintillations See Entry 78933

A radio pulsar in the Large Magellanic Cloud See Entry 78936

VLBI observations of a radio flare of Circinus X-1 See Entry 78945

An energetic, bisymmetrically expanding H I remnant See Entry 78966

An extensive galactic search for conformer H I glycine See Entry 78967

A rotating protocluster in W58:HCO⁺ aperture synthesis maps See Entry 78972

Observations of the supernova remnants HB 9 and IC 443 at 34.5 MHz See Entry 78981

A multifrequency study of star formation in the blue compact dwarf galaxy I Zw 36 See Entry 78995

Radio continuum observations of the bar of NGC 1097 See Entry 79002

A statistical VLBI study of milli-arcsecond cores in extragalactic radio sources See Entry 79014

Measurement of unambiguous rotation measures of extragalactic sources See Entry 79016

VLA observations of hot spots in high luminosity radio sources See Entry 79017

Extragalactic 1 millimeter sources: simultaneous observations at centimeter, millimeter, and visual wavelengths See Entry 79019

The incidence of 21 centimeter absorption in QSO redshift systems selected for Mg II absorption: evidence for a two-phase nature of the absorbing gas See Entry 79020

Neutral hydrogen absorption in the quasar 3C 268.4: possible evidence for galactic halo clouds See Entry 79022

The optical identification content of the Einstein Observatory deep X-ray survey of a region in Pavo See Entry 79024

Cosmic noise observations at high radio frequencies See Entry 79028

95.80G Far infrared (bolometric, photoconductive)

Spectrophotometry of Saturn and its rings from 60 to 180 microns See Entry 78856

Comet IRAS (1983f) See Entry 78868

Comet IRAS (1983f) See Entry 78869

Solar emission lines near 12 microns See Entry 78893

Stellar diameter measurements by two-aperture interferometry in the infrared .. See Entry 78911

Infrared photometry and mass loss rates for Of-type stars See Entry 78921

Infrared observations of OB star formation in NGC 6334 See Entry 78974

Observation of ice mantles toward HD 29647 See Entry 78978

Interstellar ice grains in the Taurus molecular clouds See Entry 78982

A multifrequency study of star formation in the blue compact dwarf galaxy I Zw 36 See Entry 78995

The variation of dust temperatures in Maffei 2 See Entry 78999

The identification of CTA 21 See Entry 79018

95.80J Photographic region (near infrared, visible, and normal ultraviolet)

Meridian circle observations of FK4 radio stars See Entry 78796

The ages of the disks of S0 galaxies See Entry 78821

A revised and extended calibration for the Spinrad-Taylor scanner system See Entry 78823

Interpretation of whole-disk photometry of Phobos and Deimos See Entry 78840

UBV photometry of the minor planets 86 Semele, 521 Brixia, 53 Kalyppo and 113 Amalthea See Entry 78841

Observed departure of the IO plasma torus from rigid corotation with Jupiter .. See Entry 78843

Theoretical interpretation of the ground-based photometry of Saturn's B ring ... See Entry 78846

Spatially resolved methane band photometry of Saturn. II. Cloud structure models at four latitudes See Entry 78855

Eight-colour photometry of Hyperion, Iapetus, and Phoebe See Entry 78859

High-resolution spectra of C₂ Swan bands from Comet West 1976 VI [sic] See Entry 78867

Comet IRAS (1983f) See Entry 78868

Periodic Comet Du Toit-Neujmin-Delporte (1983g) See Entry 78870

Comet Sugano-Saigusa-Fujikawa (1983e) See Entry 78871

Comet IRAS-Araki-Alcock (1983d) See Entry 78872

Periodic Comet Tempel 2 (1982d) See Entry 78873

Comet IRAS (1983f) See Entry 78874

Periodic Comet Kopff (1982k) See Entry 78875

Comet Sugano-Saigusa-Fujikawa (1983e) See Entry 78876

A coronal transient associated with a high-speed type II burst See Entry 78886

Observations of the Sun with the CERGA astrolabe in 1981 .. See Entry 78895

Survey of H α emission in globular cluster red giants See Entry 78907

A photometric atlas of the spectrum of γ Tauri $\lambda\lambda$ 5186-8700 Å See Entry 78913

Observational studies of the symbiotic stars. II. Emission-line relative intensity variations in CI Cygni, BF Cygni, AX Persei, and V1016 Cygni See Entry 78916

The binary nature of the barium stars. II. Velocities, binary frequency, and preliminary orbits See Entry 78917

A spectroscopic study of four late-type galactic WN stars: the question of duplicity See Entry 78919

Photometry of the post T Tauri star HD 36705 See Entry 78923

HD 87072: a new, bright, very small amplitude, short period Cepheid See Entry 78927

Thirteen-color photometry of sixteen variable Be stars. I. Photometry See Entry 78930

Supernova in NGC 4753 See Entry 78931

Supernova in NGC 3106 See Entry 78932

Spectroscopy of V711 Tauri (=HR 1099): fundamental properties and evidence for starspots See Entry 78941

Photographic observations of visual double stars See Entry 78946

TV Cassiopeiae in the Utrecht Photometric System See Entry 78947

Contribution to the study of F, G, K, M type binaries. I. Orbital elements of the double lined spectroscopic binaries HD 47415 and HD 210763 See Entry 78948

Four-colour photometry of eclipsing binaries. XV B. Light curves of V Puppis See Entry 78950

On the period of EG Cephei See Entry 78954

Radial velocity measurements of α Pyx and ζ Cma See Entry 78955

New eclipsing supergiant 22 Vul See Entry 78957

XY Leo and the star BD+18°2304 See Entry 78958

- V-photometry of bright stars in central region of globular cluster M5 See Entry 78965
- Optical studies of Cassiopeia A VI. Observations during the period 1976-80 See Entry 78968
- Ring ejection in Type II supernovae: 1E 0102.2-7219 in the Small Magellanic Cloud See Entry 78976
- Observation of ice mantles toward HD 29647 See Entry 78978
- Spectrophotometric observations of a peculiar nitrogen-rich planetary nebula NGC 2440 See Entry 78980
- Optical emission from the SNRs G126.2+1.6, G206.9+2.3 and CTB 13 See Entry 78983
- Internal motions in H II regions. X. Are there optical H II regions associated with the Origen Loop? See Entry 78984
- Internal motions in H II regions. XI. The emission nebula Sharpless 206 See Entry 78985
- The filamentary nebula S 188 See Entry 78986
- Spatially extended narrow emission-line gas in the Seyfert galaxy NGC 4151 See Entry 78987
- Mrk 744 and Mrk 1066: two Seyfert galaxies with strong absorption-line spectra See Entry 78991
- The transitory nature of the filaments in NGC 5128 (Centaurus A) See Entry 78994
- A multifrequency study of star formation in the blue compact dwarf galaxy I Zw 36 See Entry 78995
- Spectroscopic evidence for activity in the nuclei of normal spiral galaxies See Entry 78996
- Double galaxy investigations. I. Observations See Entry 79004
- Direct evidence for a massive galactic halo See Entry 79009
- The variability of the optical counterparts of four extragalactic radio sources See Entry 79015
- Extragalactic 1 millimeter sources: simultaneous observations at centimeter, millimeter, and visual wavelengths See Entry 79019
- The optical identification content of the Einstein Observatory deep X-ray survey of a region in Pavo See Entry 79024

95.80M Space ultraviolet

- Tentative confirmation of an aurora on Uranus See Entry 78864
- Infall and outflow of S^{+3} ions in 15 Monocerotis, tau Canis Majoris, and iota Orionis See Entry 79000
- Simultaneous X-ray and ultraviolet observations of ϵ Orionis and κ Orionis See Entry 78908
- Observations of ultraviolet carbon lines in the spectra of three DC white dwarfs See Entry 78910
- Observational studies of the symbiotic stars. II. Emission-line relative intensity variations in CI Cygni, BF Cygni, AX Persei, and V1016 Cygni See Entry 78916
- The binary central star of the planetary nebula LT-5 See Entry 78973
- Ring ejection in Type II supernovae: 1E 0102.2-7219 in the Small Magellanic Cloud See Entry 78976
- Ultraviolet continuum and H_2 fluorescent emission in Herbig-Haro objects 43 and 47 See Entry 78977
- A multifrequency study of star formation in the blue compact dwarf galaxy I Zw 36 See Entry 78995

95.80N X-ray

- Simultaneous X-ray and ultraviolet observations of ϵ Orionis and κ Orionis See Entry 78908
- High-velocity, asymmetric Doppler shifts of the X-ray emission lines of Cassiopeia A See Entry 78969
- Extended soft X-ray emission from NGC 4151 See Entry 78988
- X-ray observations of 20 3CR radio galaxies and their environs See Entry 78990
- 2-165 keV observations of active galaxies and the diffuse background See Entry 78992
- Rapid X-ray variability from the Seyfert I galaxy NGC 4051 See Entry 79000
- X-ray studies of quasars with the Einstein Observatory. III. The 3CR sample See Entry 79023
- The optical identification content of the Einstein Observatory deep X-ray survey of a region in Pavo See Entry 79024

95.80Q gamma-ray and elementary particle

- Measurement of the 0.511 MeV γ -ray line from the galactic center See Entry 79010

95.80S Other (inc. gravitational radiation, magnetograms, etc)

- Venus gravity anomalies and their correlations with topography See Entry 78838
- Direct observational upper limit to gravitational radiation from millisecond pulsar PSR 1937+214 See Entry 78935

95.85 CATALOGUES, ATLASES ETC

- 78828 Catalog of luminous stars in the southern Coal-Sack zone. H.G. Marraco (Steward Obs., Univ. of Arizona, Tucson, AZ, USA), A.M. Orsatti, *Rev. Mex. Astron. & Astrofis. (Mexico)*, vol.5, no.3, p.183-208 (July 1982). [received: April 1983]
- A catalog including all the luminous stars in the zone $300^\circ \leq l \leq 308^\circ$, $-10^\circ \leq b \leq 10^\circ$ was compiled and is presented. A search in the literature was also made for MK spectral types, *UBV* photometry, beta indices, radial velocities, and polarimetry for these stars and is presented. (105 refs.)

- A photometric atlas of the spectrum of γ Tauri $\lambda\lambda$ 5186-8700 Å See Entry 78913

95.90 OTHER TOPICS IN ASTRONOMY AND ASTROPHYSICS

- J.E. Keeler's discovery of a gap in the outer part of the A ring See Entry 78845

96.00 SOLAR SYSTEM

96.10 GENERAL, SOLAR NEBULA, AND COSMOGONY

- 78829 Extinct radioactivities: a three-phase mixing model. D.D. Clayton (Dept. of Space Phys. & Astron., Rice University, Houston, TX, USA), *Astrophys. J. (USA)*, vol.268, no.1, pt.1, p.381-4 (1 May 1983).
- A new class of models is advanced for interpreting the relationship of radioactive abundances in the early solar system to their average concentration in the interstellar medium. The model assumes that fresh radioactivities are ejected from supernovae into the hot interstellar medium, and that the time scales for changes of phase into molecular clouds determine how much survives for solar system formation. A more realistic and physically motivated understanding of the low observed concentrations of ^{129}I , ^{244}Pu , and ^{107}Pd may result. (18 refs.)
- 78830 On the stability of the Solar System. S.Kasperczuk (Zaklad Fizyki Politech. Swietokrzyskiej, Kielcach, Poland), *Postepy Astron. (Poland)*, vol.30, no.3-4, p.259-68 (July-Dec. 1982). In Polish. [received: April 1983]
- The problem of Solar System stability defined by Laplace and Lagrange in the second half of the 18th century, in celestial mechanics appears as Lagrange's theorem. The author presents data concerning Solar System stability. (22 refs.)

96.20 MOON

- 78831 Seismic velocity structure of the lunar mantle. Y. Nakamura (Inst. for Geophys., Univ. of Texas, Galveston, TX, USA), *J. Geophys. Res. (USA)*, vol.88, no.B1, p.677-86 (10 Jan. 1983). [received: May 1983]
- The recently completed set of seismic arrival times from the Apollo lunar seismic network have been inverted to estimate the average seismic velocities in three sections of the lunar mantle: two for the upper mantle and one for the middle mantle. The method used is a variation of the linearized least squares inversion where the inversion is accomplished in steps. The higher velocities of the middle mantle may suggest initial melting of the Moon down to at least 1000-km depth. (23 refs.)
- Ion sputtering of minerals and glasses: a first step to the simulation of solar wind erosion See Entry 77508
- Evolution of the Earth-Moon system See Entry 78410
- Tidal friction in historical time and in the remote past See Entry 78415
- Crater ejecta scaling laws: fundamental forms based on dimensional analysis See Entry 78835
- Tectonic evolution of Mercury: comparison with the Moon See Entry 78837

96.30 PLANETS AND SATELLITES

(exc. the Moon; for celestial mechanics, see 95.10; for Earth as an astronomical body, see 91. Geophysics)

- 78832 The role of dissipation in shepherding of ring particles. R.Greenberg (Planetary Sci. Inst., Tucson, AZ, USA), *Icarus (USA)*, vol.53, no.2, p.207-18 (Feb. 1983). (Saturn Conference, Tucson, AZ, USA, 11-15 May 1982).
- In the absence of any damping mechanism, a shepherd satellite would force oscillations in the motion of a ring particle (relative to circular motion) that are symmetrical with respect to the encounter geometry. No net torque would be exerted by the satellite on the rings. Only in the presence of some damping mechanism can a particle's response lag so as to provide the asymmetry that permits a torque. The standard formula for the confining torque exerted by a shepherd satellite seems to be independent of damping. Moreover, many heuristic derivations of the formula tend to obscure the role of damping. (9 refs.)
- 78833 The dynamic tensile strength of ice and ice-silicate mixtures. M.A. Lange, T.J. Ahrens (Seismological Lab., California Inst. of Technol., Pasadena, CA, USA), *J. Geophys. Res. (USA)*, vol.88, no.B2, p.1197-208 (10 Feb. 1983).
- The dynamic tensile strength of ice and ice-silicate mixtures at strain rates of $\sim 10^4 \text{ s}^{-1}$ was determined. At these strain rates, ice has a tensile strength of $\sim 17 \text{ MPa}$, and ice-silicate mixtures with 5 and 30 wt.% sand content have strengths of ~ 20 and 22 MPa , respectively. These values lie significantly above tensile strengths of $\sim 1.6 \text{ MPa}$ for ice and of $\sim 5-6 \text{ MPa}$ for frozen silt, measured at strain rates of $\sim 10^{-2}$ to 10^0 s^{-1} , but markedly below values found for a variety of rocks at comparable strain rates. Results of the present experiments are used to derive parameters for continuum fracturing models in icy media, which are used to determine relations between tensile strength and strain rate, and to predict stress and damage histories as well as size frequency distributions for ice and ice-silicate fragments. (22 refs.)
- 78834 Anomalous bulk viscosity of two-phase fluids and implications for planetary interiors. D.J. Stevenson (Div. of Geological & Planetary Sci., California Inst. of Technol., Pasadena, CA, USA), *J. Geophys. Res. (USA)*, vol.88, no.B3, p.2445-55 (10 March 1983).
- A calculation is presented for the irreversible entropy production that accompanies the imposition of a pressure perturbation on a two-phase medium consisting of a dilute suspension of one phase in another (liquid) phase of significantly different composition. No metastability is allowed, and the relaxation process is then dominated by the finite diffusivity of solute. The fluid medium behaves as though it has a very large bulk viscosity (typical value $\sim 10^{12} \text{ P}$ in the low-frequency limit). The minimum quality factor Q for acoustic or tidal pressure oscillations is found to be typically $\sim 10^2-10^3$. The model is applied to helium rain clouds in the deep interiors of giant planets

and is found to be capable in principle of providing a tidal $Q \sim 10^5$, needed to explain the volcanism of Io and resurfacing of Enceladus. The model is also applied to the Earth's outer core and found to be marginally capable of explaining the attenuation of radial modes and potentially capable of providing significant attenuation of Earth tides. (40 refs.)

78835 Crater ejecta scaling laws: fundamental forms based on dimensional analysis. K.R.Housen, R.M.Schmidt (Shock Phys. & Appl. Mech., Boeing Aerospace Co., Seattle, WA, USA), K.A.Holsapple. *J. Geophys. Res. (USA)*, vol.88, no.B3, p.2485-99 (10 March 1983).

A model of crater ejecta is constructed using dimensional analysis and a recently developed theory of energy and momentum coupling in cratering events. General relations are derived that provide a rationale for scaling laboratory measurements of ejecta to larger events. Specific expressions are presented for ejection velocities and ejecta blanket profiles in two limiting regimes of crater formation: the so-called gravity and strength regimes. In the gravity regime, ejecta velocities at geometrically similar launch points within craters vary as the square root of the product of crater radius and gravity. In the strength regime, ejecta velocities are independent of crater size. (39 refs.)

78836 Planetary magnetic fields. D.J.Stevenson (Div. of Geological & Planetary Sci., California Inst. of Technol., Pasadena, CA, USA). *Rep. Prog. Phys. (GB)*, vol.46, no.5, p.555-620 (May 1983).

As a consequence of the smallness of the electronic fine structure constant, the characteristic time scale for the free diffusive decay of a magnetic field in a planetary core is much less than the age of the Solar System, but the characteristic time scale for thermal diffusion is greater than the age of the Solar System. Consequently, primordial fields and permanent magnetism are small and the only means of providing a substantial planetary magnetic field is the dynamo process. This requires a large region which is fluid, electrically conducting and maintained in a non-uniform motion that includes a substantial RMS vertical component. The attributes of fluidity and conductivity are readily provided in the deep interiors of all planets and most satellites, either in the form of an Fe alloy with a low eutectic temperature (e.g. Fe-S-O in terrestrial bodies and satellites) or by the occupation of conduction states in fluid hydrogen or 'ice' ($H_2O-NH_3-CH_4$) in giant planets. It is argued that planetary dynamos are almost certainly maintained by convection (compositional and/or thermal). (184 refs.)

Periodic motion of a satellite under the gravitational attraction of a rotating rigid body See Entry 78799

Collisional vibrational quenching of $O_2^+(v)$ and other molecular ions in planetary atmospheres See Entry 78809

96.30D Mercury

78837 Tectonic evolution of Mercury: comparison with the Moon. P.G.Thomas, P.Masson (Lab. de Geologie Dynamique Interne, Univ. Paris-Sud, Orsay, France).

Ann. Geophys. (France), vol.1, no.1, p.53-8 (Jan.-Feb. 1983). With regard to the Earth or to Mars, the Moon and Mercury look like tectonically planetary bodies, and the prominent morphologies of these two planets are due to impact and volcanic processes. Despite these morphologies, several types of tectonic activities may be shown. Statistical studies of lineaments direction indicate that Mercury, as well as the Moon, have a planet wide lineament pattern, known as a 'grid'. Statistical studies of Mercury scarps and the Moon grabens indicate an interaction between planetary lithospheric evolution and large impact basins. Detailed studies of the largest basins indicate specific tectonic motions directly related to impacts. These three tectonic types are compared on each planet. (26 refs.)

96.30E Venus

78838 Venus gravity anomalies and their correlations with topography. W.L.Sjogren, B.G.Bills, P.W.Birkeland, P.B.Esposito, A.R.Konopliv, N.A.Mottinger, S.J.Ritke (Jet Propulsion Lab., Pasadena, CA, USA), R.J.Phillips.

J. Geophys. Res. (USA), vol.88, no.B2, p.1119-28 (10 Feb. 1983). This report provides a summary of the high-resolution gravity data obtained from the Pioneer Venus Orbiter radio tracking data. Gravity maps, covering a 70° latitude band through 360° of longitude, are displayed as line-of-sight and vertical gravity. Topography converted to gravity and Bouguer gravity maps are also shown in both systems. Topography to gravity ratios are made over several regions of the planet. There are markedly different ratios for the Aphrodite area as compared to the Beta and Atla areas. (10 refs.)

96.30G Mars

78839 The stability of ground ice in the equatorial region of Mars. S.M.Clifford (Dept. of Phys. & Astron., Univ. of Massachusetts, Amherst, MA, USA), D.Hillel.

J. Geophys. Res. (USA), vol.88, no.B3, p.2456-74 (10 March 1983). Consideration of the partial pressure of H_2O in the Martian atmosphere and the range of mean annual temperatures at the Martian surface suggests that the occurrence of ground ice in equilibrium with the atmosphere is restricted to latitudes poleward of $\pm 40^\circ$. However, there is a growing body of morphologic evidence that indicates that substantial quantities of ground ice may have been present in the equatorial regolith throughout Martian geologic time. The accepted explanation for this apparent contradiction has been that the H_2O found near the equator is a relic, emplaced very early in Martian geologic history and under substantially different climatic conditions. It is generally believed that this fossil ground ice layer has been preserved to the present day by the diffusion-limiting properties of a relatively shallow layer (≤ 10 m) of fine-grained regolith. To evaluate this hypothesis, the lifetime of a 200-m layer of ground ice, buried below 100 m of ice-free regolith, has been examined for the latitudes between $\pm 30^\circ$ on Mars. Twelve model pore size distributions, representative of silt and clay-type soils found on Earth, were selected to simulate the pore structure of the Martian regolith. The parallel pore model of gaseous diffusion was then used to calculate the flux of escaping H_2O molecules from the buried ground ice layer. Important factors affecting the stability of equatorial ground ice appear to be (1) soil structure, (2) the magnitude of the geothermal gradient, and (3) the climatic desorption of CO_2 from the regolith. We conclude that while the conditions necessary for the long-term survival of ground ice may exist in isolated regions within the equatorial regolith, on the global scale it appears unlikely that a fossil ground ice layer has been preserved throughout Martian geologic history. If massive ground ice does presently exist in the equatorial regolith, then its presence may imply the existence of some continuous or periodic process of replenishment. (130 refs.)

78840 Interpretation of whole-disk photometry of Phobos and Deimos. K.D.Pang, J.W.Rhoads, G.A.Hanover (Jet Propulsion Lab., California Inst. of Technol., Pasadena, CA, USA), K.Lumme, E.Bowell.

J. Geophys. Res. (USA), vol.88, no.B3, p.2475-84 (10 March 1983). The phase curves (whole-disk brightness vs. solar phase angle) of the Martian satellites were compiled out to 125° phase angle from ground-based and spacecraft photometric observations. The data were modeled with the Lumme-Bowell theory. Accurate phase integrals, zero-phase geometric albedos and Bond albedos were obtained from the best fit theoretical curves. The microstructural and particulate surface properties of Phobos differ little from those of Deimos. The satellites' very similar whole-body densities and geochemical and microphysical makeup suggest a common origin. However, having spent a considerable portion of their lifetimes in proximity to Mars probably did modify their surface characteristics. The value of the surface roughness, the debris mantle on Deimos and the grooves on Phobos are probably evidence of such modifications. (41 refs.)

Transits of Earth as seen from Mars See Entry 78797

96.30H Asteroids

78841 UBV photometry of the minor planets 86 Semele, 521 Brixia, 53 Kalypso and 113 Amalthea. J.Surdej, A.Surdej, B.Louis (Inst. d'Astrophys. Univ. de Liege, Ougree-Liege, Belgium).

Astron. & Astrophys. Suppl. Ser. (France), vol.52, no.2, p.203-11 (May 1983).

Asteroids 86 Semele, 521 Brixia and 53 Kalypso, 113 Amalthea were observed photometrically during the 1980 and 1981 oppositions, respectively. Synodic rotation periods, color indices and light variations are determined. The $B-V$ and $U-B$ color indices of these four minor planets do not present any variation exceeding the mean scatter over the observed rotation cycles. (10 refs.)

78842 Asteroid occultations: a 1981 status report. P.D.Maley (Ford Aerospace & Communications Corp., NASA Johnson Space Center, Houston, TX, USA).

Rev. Mex. Astron. & Astrofis. (Mexico), vol.5, no.3, p.213-16 (July 1982). [received: April 1983]

A summation is presented of the historical observations, methods of prediction, and results of the known Earth-based sightings of occultations of stars by minor planets through the end of 1981. Techniques are outlined to encourage uniformity in site positioning, data recording, and observer training. (27 refs.)

96.30K Jupiter

78843 Observed departure of the IO plasma torus from rigid corotation with Jupiter. R.A.Brown (Space Telescope Sci. Inst., Baltimore, MD, USA).

Astrophys. J. Lett. Ed. (USA), vol.268, no.1, pt.2, p.L47-50 (1 May 1983). A study of [S II] red doublet spectra indicates that the Io plasma torus at $5.9 R_J$ does not corotate rigidly with Jupiter. The lag is found to be $6\% \pm 4\%$, where the variability range, not the uncertainty, is indicated. Comparison with existing models indicates the lag may be due primarily to ion creation in the Io torus. (16 refs.)

78844 Jupiter's satellites J VI and J VII. Ephemerides for the years 1981 to 1990. P.Rocher (Service de Mecanique Celeste du Bureau des Longitudes, Paris, France).

Astron. & Astrophys. Suppl. Ser. (France), vol.52, no.2, p.333-72 (May 1983).

The proposed ephemerides come from a numerical integration of G.B.S. type (Gragg-Bulirsch-Stoer). The numerical constants of integration are given. The observational data are analogous to those used by Bordoovystina and Bykova (1978). Mean values and standard deviations in the O-C s are listed. The published quantities are equatorial astrometric coordinates: right ascension, declination and true distance Jupiter-satellite. (2 refs.)

Anomalous bulk viscosity of two-phase fluids and implications for planetary interiors See Entry 78834

96.30M Saturn

78845 J.E. Keeler's discovery of a gap in the outer part of the A ring. D.E.Osterbrock (Lick Obs., Board of Studies in Astron. & Astrophys., Univ. of California, Santa Cruz, CA, USA), D.P.Cruikshank.

Icarus (USA), vol.53, no.2, p.165-73 (Feb. 1983). (Saturn Conference, Tucson, AZ, USA, 11-15 May 1982).

In early January 1888, James E. Keeler was one of the first astronomers to work with the very new Lick Observatory 36-in refractor. On January 7 while observing Saturn visually on a night of very fine seeing, he discovered a narrow, dark 'division' in the outer part of the A-ring. Neither Keeler nor any of the other Lick observers saw this gap again until over a year later on March 2, 1889. On that occasion not only Keeler, but also E.S. Holden, J.M. Schaeberle, and E.E. Barnard, all observed 'Mr. Keeler's division', as Barnard called it. The outer edge of the Encke division is where Keeler placed his gap, although he did not see the low-contrast structure in the Encke division. The images obtained from the Pioneer and Voyager space probes confirm the narrow Keeler feature as a true gap in the outer part of the A-ring. (24 refs.)

78846 Theoretical interpretation of the ground-based photometry of Saturn's B ring. K.Lumme, W.M.Irvine (Dept. of Phys. & Astron., Univ. of Massachusetts, Amherst, MA, USA), L.W.Esposito.

Icarus (USA), vol.53, no.2, p.174-84 (Feb. 1983). (Saturn Conference, Tucson, AZ, USA, 11-15 May 1982).

New photographic photometry at small tilt angles during the 1979 and 1981 apparitions is combined with earlier data to yield several physical parameters for Saturn's B-ring in red and blue colours. Phase curves are obtained for a mean tilt angle $B \approx 6^\circ$. The value of the volume density is discussed. The results and the derived amount of multiple scattering as a function of tilt angle constrain the particle phase function in the red to be moderately back-scattering. No indication was found that the particle photometric properties might depend on the vertical distance from the central plane. The results show that the ground-based photometry is entirely consistent with the classical, many-particle-thick ring model. (24 refs.)

78847 Bending waves in Saturn's rings. F.H.Shu, J.N.Cuzzi, J.J.Lissauer (Astron. Dept., Univ. of California, Berkeley, CA, USA).

Icarus (USA), vol.53, no.2, p.185-206 (Feb. 1983). (Saturn Conference, Tucson, AZ, USA, 11-15 May 1982).

Investigates certain brightness variations seen in Saturn's A-ring. The authors find them to be due to vertical corrugations of the local ring plane caused by a spiral bending wave. This wave is resonantly excited by Mimas and propagates

ates inward via the collective gravity of the ring particles. Smith et al. (1981) had previously associated vertical relief with this feature due to its observed azimuthal variations and its proximity to an inclination resonance with Mimas. The authors develop the theory of forced bending waves, some aspects of which have been treated in the galactic context by Hunter and Toomre (1969) and by Bertin and Mark (1980). The presence of these bending waves may resolve the conflict between ground-based estimates of 1-2 km for the global ring thickness, e.g. Brahic and Sicardy (1981) and Voyager stellar occultation measurements of <200 m for the local ring thickness (Lane et al., 1982; Marouf and Tyler, 1982). (23 refs.)

78848 A model for the formation of spokes in Saturn's ring. C.K.Goertz, G.Morfill (Max-Planck-Inst. für Aeronomie, Katlenburg-Lindau, Germany). *Icarus (USA)*, vol.53, no.2, p.219-29 (Feb. 1983). (Saturn Conference, Tucson, AZ, USA, 11-15 May 1982). Suggests that spokes consist of charged micron-sized dust particles elevated from the rings by radially moving dense plasma columns created by meteoroid impacts on the ring. Dense plasma causes electrostatic wall-sheaths at the ring and charging of the ring with electric fields strong enough to overcome the gravitational force on small dust particles. Under 'ordinary' conditions only very few dust particles will be elevated as the probability of a dust particle having at least one excess electronic charge is very low. Dense plasma raises this probability significantly. The radial motion of the plasma column is due to an azimuthal polarisation electric field built up by the relative motion between the corotating plasma and the negatively charged dust particles which move with a Keplerian speed. (26 refs.)

78849 On the evolution of Saturn's 'spokes': theory. G.E.Morfill (Max-Planck-Inst. für Extraterrestrische Phys., Garching, Germany), F.Grun, C.K.Goertz, T.V.Johnson. *Icarus (USA)*, vol.53, no.2, p.230-5 (Feb. 1983). (Saturn Conference, Tucson, AZ, USA, 11-15 May 1982). Starting with the assumption that negatively charged micron-sized dust grains may be elevated above Saturn's ring plane by plasma interactions, the subsequent evolution of the system is discussed. The discharge of the fine dust by solar UV radiation produces a cloud of electrons which moves adiabatically in Saturn's dipolar magnetic field. The electron cloud is absorbed by the ring after one bounce, alters the local ring potential significantly, and reduces the local Debye length. As a result, more micron-sized dust particles may be elevated above the ring plane and the spoke grows. This process continues until the electron cloud has dissipated. (11 refs.)

78850 Micron-sized particles detected near Saturn by the Voyager plasma wave instrument. D.A.Gurnett, E.Grun, D.Gallagher, W.S.Kurth, F.L.Scarf (Dept. of Phys. & Astron., Univ. of Iowa, Iowa City, IA, USA). *Icarus (USA)*, vol.53, no.2, p.236-54 (Feb. 1983). (Saturn Conference, Tucson, AZ, USA, 11-15 May 1982). During the Voyager 2 Saturn encounter the plasma wave instrument detected a region of intense impulsive noise centred on the ring plane at a distance of 2.88 Saturn radii, slightly outside of the G-ring. The noise has been attributed to small micron-sized particles hitting the spacecraft. Investigation of various coupling mechanisms suggested that the noise was produced by impact ionisation of particles striking the spacecraft body, thereby releasing a cloud of charged particles, some of which were collected by the plasma wave antenna. A method was developed to determine the mass and size distribution of the particles from the RMS voltage of the induced noise and the impulse rate. The results obtained show that the mass distribution varies as m^{-3} , and that most of the particles detected had radii in the range from 0.3 to 3 μm . The effective north-south thickness of the particle distribution is 106 km. (19 refs.)

78851 A search for Saturn electrostatic discharges in the Voyager plasma wave data. W.S.Kurth, D.A.Gurnett, F.L.Scarf (Dept. of Phys. & Astron., Univ. of Iowa, Iowa City, IA, USA). *Icarus (USA)*, vol.53, no.2, p.255-61 (Feb. 1983). Voyager plasma wave data are searched for evidence of Saturn electrostatic discharges which have previously been reported by the planetary radio astronomy team following the Voyager 1 and 2 encounters with Saturn. On the basis of the radio astronomy observations, the discharges should have been observable by the plasma wave experiment on Voyager; however, there is no evidence in the plasma wave data for the phenomenon. The authors analyse the statistical significance and comment on the ramifications of this null result and entertain various explanations of the lack of plasma wave observations of electrostatic discharges, including the possibility that many events are of a much shorter duration than previously reported or that there could possibly be a nonlinear distortion in the radio astronomy receiver which could artificially broaden the spectrum of the discharges. (9 refs.)

78852 Albedo, internal heat flux, and energy balance of Saturn. R.A.Hanel, B.J.Conrath, V.G.Kunde, J.C.Pearl, J.A.Pirraglia (Lab. for Extraterrestrial Phys., NASA/Goddard Space Flight Center, Greenbelt, MD, USA). *Icarus (USA)*, vol.53, no.2, p.262-85 (Feb. 1983). (Saturn Conference, Tucson, AZ, USA, 11-15 May 1982). Full-disk and high-resolution measurements recorded during the Voyager 1 flyby of Saturn by the radiometer of the infrared instrument, IRIS, indicate a geometric albedo which is lower than previous estimates. Combining this measurement with the Pioneer-derived phase integral yields a Bond albedo. Infrared spectra recorded at the same time by the Michelson interferometer, along with a model extrapolation to wavenumbers not covered by the instrument, yield an effective temperature. The rings of Saturn significantly affect both the short- and long-wavelength fluxes. From these measurements the internal heat flux and the energy balance are determined. (51 refs.)

78853 Thermal structure of Saturn from Voyager infrared measurements: implications for atmospheric dynamics. B.J.Conrath, J.A.Pirraglia (Lab. for Extraterrestrial Phys., Goddard Space Flight Center, Greenbelt, MD, USA). *Icarus (USA)*, vol.53, no.2, p.286-92 (Feb. 1983). Saturn atmospheric temperatures at the 150-mbar level retrieved from Voyager IRIS measurements indicate the presence of small-scale meridional gradients which are approximately symmetric with respect to the equator, but are superposed on a large-scale hemispheric thermal asymmetry. Under the assumption that the retrieved values at this atmospheric level represent kinetic temperatures on a constant pressure surface, it is suggested that the small-scale structure is produced by a meridional circulation associated with the dissipative decay of the zonal winds with height, while the hemispheric asymmetry represents a thermal response to the seasonally varying insolation. The small-scale gradients are correlated with zonal winds derived from Voyager images at mid and high latitudes through the thermal wind relation. (16 refs.)

78854 Thermal infrared constraints on ammonia ice particles as candidates for clouds in the atmosphere of Saturn. G.S.Orton (Jet Propulsion Lab., Earth & Space Sci. Div., California Inst. of Technol., Pasadena, CA, USA). *Icarus (USA)*, vol.53, no.2, p.293-300 (Feb. 1983). (Saturn Conference, Tucson, AZ, USA, 11-15 May 1982).

It is possible for large particles of NH_3 ice to explain two phenomena associated with observations of thermal infrared emission from the atmosphere of Saturn: (1) the depression of thermal brightness near the equator, which is coincident with a visibly bright zone-like region, and (2) some disagreements between infrared and radio occultation results. Particles of NH_3 ice can provide the requisite opacity to explain the contrast between the equatorial region and the brighter area near 15°S for Pioneer Saturn Infrared Radiometer $45\text{-}\mu\text{m}$ channel data. NH_3 ice particle clouds can also reconcile the $45\text{-}\mu\text{m}$ brightness of both regions (near the equator and near 15°S) with the mean temperature structure of the Voyager 2 radio occultation results. A cloud model with ice particles distributed in equal ratio with gas particles up to the 100-mbar pressure level best fits the equatorial data; a thinner cloud or one which does not extend higher than the 400-mbar limit of the convective region best matches data for the 15°S region. (29 refs.)

78855 Spatially resolved methane band photometry of Saturn. II. Cloud structure models at four latitudes. R.A.West (Dept. of Astro-Geophys., Univ. of Colorado, Boulder, CO, USA). *Icarus (USA)*, vol.53, no.2, p.301-9 (Feb. 1983). (Saturn Conference, Tucson, AZ, USA, 11-15 May 1982).

For pt.I see *ibid.*, vol.51, no.1, p.51-64 (1982). Spatially resolved measurements of Saturn's reflectivity in the 6190-, 7250-, and 8996-Å methane bands are analysed to determine cloud vertical structures in the Equatorial Zone, South Equatorial Belt, and North and South Temperate Regions near latitudes $\pm 30^\circ$. Radiative transfer models are computed for a simple two-parameter structure. The parameters are the methane column abundance in an aerosol-free layer at the top of the atmosphere, and the specific abundance of methane in a semi-infinite homogeneous gas and cloud mixture deep in the atmosphere. Some suggestions are proposed to explain differences between model parameters derived using different absorption bands. (18 refs.)

78856 Spectrophotometry of Saturn and its rings from 60 to 180 microns. G.Melnick, R.W.Russell, T.R.Gosnell, M.Harwit (Centre for Radiophys. & Space Res., Cornell Univ., Ithaca, NY, USA).

Icarus (USA), vol.53, no.2, p.310-18 (Feb. 1983). (Saturn Conference, Tucson, AZ, USA, 11-15 May 1982). Observes Saturn at far-infrared and submillimeter wavelengths during the Earth's March 1980 passage through the plane of Saturn's rings. Comparison with earlier spectroscopic observations by Ward (1977), obtained at a time when the tilt angle of the rings was 21.8° , permits separation of the disk and ring contributions to the flux observed in this wavelength range. The observed emission of the disk between 60 and 180 μm corresponds to a brightness temperature of $104 \pm 2\text{K}$, and the brightness temperature of the ring drops approximately 20K between 60 and 80 μm . The data, in conjunction with the data obtained by other observers between 1 μm and 1 mm, permit the authors to derive an improved estimate for the total Saturnian surface brightness effective temperature ratio of radiated to incident power and intrinsic luminosity. (37 refs.)

78857 The evolution of Enceladus. S.W.Squyres, R.T.Reynolds, P.M.Cassen (NASA Ames Res. Centre, Moffett Field, CA, USA), S.J.Peale. *Icarus (USA)*, vol.53, no.2, p.319-31 (Feb. 1983). (Saturn Conference, Tucson, AZ, USA, 11-15 May 1982).

Describes the tectonic features of Enceladus and presents a preliminary analysis of the relation between internal geophysical processes and the formation of these features. The authors conclude that H_2O or $\text{H}_2\text{O-NH}_3$ vulcanism was responsible for resurfacing portions of the satellite, and that global expansion played a role in the formation of grooves. It is clear that some heat source has been active for an extended period of Enceladus' history. Theoretical calculations suggest that tidal heating is the most likely possibility, but only if Enceladus' orbit has evolved markedly in the last few billion years. Evidence that the satellite is currently being significantly heated is discussed. (31 refs.)

78858 The control networks of Mimas and Enceladus. M.E.Davies, F.Y.Katayama (Rand Corp., Santa Monica, CA, USA).

Icarus (USA), vol.53, no.2, p.332-40 (Feb. 1983). Control networks for Mimas and Enceladus are computed using a bundle-type analytical triangulation program. The Mimas network encircles the satellite with 110 points measured on 32 Voyager 1 pictures. The adjustment contained 1356 observation equations and 316 normal equations, and gives a standard error of measurement of 13.43 μm . The Enceladus network does not completely encircle the satellite; it contains 71 points measured on 22 Voyager 2 pictures. The adjustment contains 994 observation equations and 208 normal equations, and gives a standard error of measurement of 19.19 μm . Many of the control points are identified on illustrations and by name and their coordinates are given in tables. The analytical triangulation program is used to solve for the mean radii and the three principal axes of best-fit ellipsoids. (9 refs.)

78859 Eight-colour photometry of Hyperion, Iapetus, and Phoebe. D.J.Tholen, B.Zellner (Lunar & Planetary Lab., Univ. of Arizona, Tucson, AZ, USA).

Icarus (USA), vol.53, no.2, p.341-7 (Feb. 1983). (Saturn Conference, Tucson, AZ, USA, 11-15 May 1982).

Eight-colour spectrophotometry was obtained of Phoebe, Hyperion, and the dark side of Iapetus. The V magnitudes and Voyager-derived diameters yield geometric albedos for Iapetus, Phoebe, and Hyperion. Hyperion and Iapetus have quite reddish spectra similar to each other and the spectra of D-type asteroids. Hyperion, however, has a much higher albedo than the dark side of Iapetus or any D-type asteroid measured to date. The mean spectrum of Phoebe is much flatter, with a broad absorption feature near 1 μm . Therefore the surface materials of Phoebe and the dark side of Iapetus are optically quite different, a result that constrains the possible modes of interaction between Phoebe and the other two satellites. (24 refs.)

78860 The atmosphere of Titan: an analysis of the Voyager 1 radio occultation measurements. G.F.Lindal, G.E.Wood, H.B.Hotz, D.N.Sweetnam (Jet Propulsion Lab., California Inst. of Technol., Pasadena, CA, USA), V.R.Eshleman, G.L.Tyler.

Icarus (USA), vol.53, no.2, p.348-63 (Feb. 1983). (Saturn Conference, Tucson, AZ, USA, 11-15 May 1982). Two coherently related radio signals transmitted from Voyager 1 at wavelengths of 13 cm (S-band) and 3.6 cm (X-band) were used to probe the equatorial atmosphere of Titan. The measurements were conducted during the occultation of the spacecraft by the satellite on November 12 1980. An analysis of the differential dispersive frequency measurements did not reveal any ionisation layers in the upper atmosphere of Titan. Abrupt signal changes observed at ingress and egress indicate a surface radius which leads to a mean density for the satellite. The non-dispersive data are used to derive profiles in height of the gas refractivity data, which extend from the surface

to about 200 km altitude, is interpreted. Arguments concerning the temperature lapse rates computed from the radio measurements appear to favour models in which methane forms at most a limited haze layer high in the troposphere. (28 refs.)

78861 Radiative equilibrium model of Titan's atmosphere. R.E.Samuelson (Lab. for Extraterrestrial Phys., NASA/Goddard Space Flight Centre, Greenbelt, MD, USA).

Icarus (USA), vol.53, no.2, p.364-87 (Feb. 1983). (Saturn Conference, Tucson, AZ, USA, 11-15 May 1982).

A simple global radiative equilibrium model is developed for Titan. It is restricted to the two-stream approximation, is vertically homogeneous in its scattering properties, and is spectrally divided into one thermal and two solar channels. A partially absorbing 'violet' channel is responsible for heating in the stratosphere, while a conservatively scattering 'red' channel permits heating at the surface. The spectrally integrated mass absorption coefficient at thermal wavelengths is approximately constant throughout the stratosphere and roughly linear with pressure in the troposphere. This in turn implies the presence of a uniformly mixed aerosol in the stratosphere, and suggests pressure-induced absorption by gaseous N_2 - CH_4 - H_2 in the troposphere. In addition there appear to be two regions of enhanced opacity near 30 and 500 mbar which may be due to C_2H_2 - C_2H_6 - C_3H_8 and CH_4 condensation clouds, respectively. (33 refs.)

78862 Voyager to Jupiter and Saturn: the journey of a lifetime. II. G.E.Hunt (Imperial Coll., London, England).

J. Br. Astron. Assoc. (GB), vol.93, no.3, p.105-10 (April 1983).

For pt.1 see *ibid.*, vol.93, no.2, p.62-9 (1983). Discusses the satellites of Jupiter and the rings. (2 refs.)

Saturn Conference See Entry 74211

The far-infrared spectrum of ice Ih in the range 8-25 cm^{-1} . Sound waves and difference bands, with application to Saturn's rings See Entry 77376

Anomalous bulk viscosity of two-phase fluids and implications for planetary interiors See Entry 78834

Tentative confirmation of an aurora on Uranus See Entry 78864

96.30T Other planets

78863 Occultation of Hyd -22°58794 by Neptune on 1983 June 15. D.Mink.

I.A.U. Circ. (USA), no.3818, 1 pp. (1 June 1983).

Presents improved predictions for this event indicating that the centre of Neptune's shadow will pass near the Earth's south pole. Possible ring occultations are mentioned. (1 ref.)

78864 Tentative confirmation of an aurora on Uranus. J.Caldwell, R.Wagener, T.Owen (Dept. of Earth & Space Sci., State Univ. of New York, Stony Brook, NY, USA), M.Combes, T.Encrenaz.

Nature (GB), vol.303, no.5915, p.310-12 (26 May 1983).

Reports the detection of emission features due to molecular hydrogen, H_2 , near 1,600 Å. This detection is near the limit of the IUE sensitivity. If it is real, the detection of H_2 emission strongly supports the conclusion that Uranus has an aurora comparable in strength with those of the inner two giant planets, Jupiter and Saturn. The first published IUE spectra of the Saturn aurora are also presented. (7 refs.)

96.50 OTHER OBJECTS IN THE PLANETARY SYSTEM

96.50D Interplanetary matter, magnetic and electric fields

(inc. gegenschein and zodiacal light; see also 94.60 Interplanetary space)

78865 The integral equation approach to the study of interplanetary dust.

J.Buitrago, R.Gomez, F.Sanchez (Inst. de Astrofisica de Canarias, Univ. de La Laguna, La Laguna, Canary Islands, Spain).

Planet. & Space Sci. (GB), vol.31, no.4, p.373-6 (April 1983).

Some considerations about the zodiacal light (ZL) brightness integral from the standpoint of the theory of integral equations are made. It is shown that for observation directions confined to a plane perpendicular to the ecliptic and passing through the Sun, the ZL brightness integral can be formally considered as a first kind integral equation of Volterra type (VIE). In a second step, this equation is transformed into a VIE of the second kind, from which, and under certain assumptions, the spatial distribution of dust out of the ecliptic is obtained. (13 refs.)

96.50G Comets

78866 Dynamic stabilization of hydromagnetic surface waves: applications to cometary plasma tails. B.Buti (Phys. Res. Lab., Ahmedabad, India).

Astrophys. J. (USA), vol.268, no.1, pt.1, p.420-7 (1 May 1983).

Hydromagnetic waves, at the interface of two superposed magnetofluids, are studied in the presence of electrostatic coherent waves propagating parallel to the surface of discontinuity. Due to nonlinear interaction with the electrostatic waves, hydromagnetic waves, which may be unstable otherwise, can be stabilized. The model developed is applied to study the interaction of the solar wind with the cometary plasma tails. (10 refs.)

78867 High-resolution spectra of C_2 Swan bands from Comet West 1976 VI [sic]. D.L.Lambert (Dept. of Astron., Univ. of Texas, Austin, TX, USA), A.C.Danks.

Astrophys. J. (USA), vol.268, no.1, pt.1, p.428-46 (1 May 1983).

A 0.3 Å resolution spectrum of the $\Delta v = +1$ sequence in the C_2 Swan system from Comet West 1976 VI at a heliocentric distance $r_H = 0.78$ AU is found to correspond to a vibrational and rotational temperature of $T_{ex} = 3500 \pm 400$ K for the upper $d''\Pi_g$ state. If intercombination transitions are neglected, the predicted temperature for C_2 excited by fluorescence in sunlight is considerably hotter than the observed temperature. The triplet C_2 states may be cooled by intercombination transitions linking the triplet and singlet states. The electronic transition moment of the $d''\Pi_g - A''\Sigma_g^+$ transition is estimated. On high-resolution spectra of selected lines in the Swan 0-0 band, several $^{12}C^{13}C$ lines are identified. The 0-0 band is probably superior to the 1-0 $^{12}C^{13}C$ 4745 Å band head for $^{12}C/^{13}C$ ratio determinations. (47 refs.)

78868 Comet IRAS (1983f). J.Davies, K.S.Russell.

I.A.U. Circ. (USA), no.3814, 1 pp. (20 May 1983).

It is reported that the Infrared Astronomical Satellite has discovered a 17th-magnitude comet in Hydra. Two approximate positions are reported for the epoch 1983 May 13, and two semi-accurate positions for 1983 May 18. (no refs.)

78869 Comet IRAS (1983f). J.Davies, B.G.Marsden.

I.A.U. Circ. (USA), no.3815, 1 pp. (24 May 1983).

Reports additional observations with the IRAS on 1983 May 23, parabolic orbital elements and an ephemeris for the period 1983 February 15-July 5 at 10-day intervals. (no refs.)

78870 Periodic Comet Du Toit-Neujmin-Delporte (1983g). J.Gibson.

I.A.U. Circ. (USA), no.3816, 1 pp. (1 June 1983).

Reports the recovery on 1.2 m Palomar Schmidt plates, precise positions on 1983 May 20 and 21, a description of the objects appearance and the ephemeris correction. (1 ref.)

78871 Comet Sugano-Saigusa-Fujikawa (1983e). Y.Takatsuki, T.Seki, K.Suzuki, J.Gibson, E.Everhart, R.E.McCrosky, B.G.Marsden.

I.A.U. Circ. (USA), no.3816, 1 pp. (1 June 1983).

Reports precise positions for the period 1983 May 10-22 and presents parabolic orbital elements determined from 22 observations from 1983 May 9-21. (2 refs.)

78872 Comet IRAS-Araki-Alcock (1983d). G.Richter, W.Altenhoff, W.Batrla, W.Huchtmeier, J.Schmidt, P.Stumpff, M.Walmsley, R.Nolthenius, J.D.Drummond, V.F.de Assis Neto.

I.A.U. Circ. (USA), no.3817, 1 pp. (1 June 1983).

Reports a 1983 April 17 prediscovery position, 13 mm wavelength observations of a pointlike continuum source, NH_3 and H_2O line detections, brightness temperature determinations on May 11 and 12, visual observations of an occultation of SAO 98040 on May 12, a minor meteor shower, and total visual magnitude estimates for the period May 11-18. (2 refs.)

78873 Periodic Comet Tempel 2 (1982d). J.Bortle.

I.A.U. Circ. (USA), no.3817, 1 pp. (1 June 1983).

Reports total visual magnitude estimates for 1983 May 14 and 18.

78874 Comet IRAS (1983f). J.Gibson.

I.A.U. Circ. (USA), no.3818, 1 pp. (1 June 1983).

Presents precise positions for 1983 May 18 and 20 and an approximate position for May 31.

78875 Periodic Comet Kopff (1982k). J.E.Bortle, C.E.Spratt, J.D.Shanklin, J.-C.Merlin.

I.A.U. Circ. (USA), no.3818, 1 pp. (1 June 1983).

Presents total visual magnitude estimates for the period 1983 May 5-17.

78876 Comet Sugano-Saigusa-Fujikawa (1983e). J.D.Shanklin, J.E.Bortle, C.S.Morris, J.-C.Merlin, Y.Sheffer, N.Ishiyama, E.Everhart, R.E.McCrosky, C.-Y.Shao, B.G.Marsden.

I.A.U. Circ. (USA), no.3819, 1 pp. (1 June 1983).

Reports total visual magnitude estimates for 1983 May 12-24, precise positions for May 9-29, improved parabolic orbital elements based on 27 observations (May 9-29), and an ephemeris for the period 1983 June 3-8 at daily intervals.

78877 Comet Sugano-Saigusa-Fujikawa (1983e). B.G.Marsden.

I.A.U. Circ. (USA), no.3820, 1 pp. (1 June 1983).

Continues the ephemeris given on IAU Circ no.3819 for the period 1983 June 8-17 at 6-hourly intervals. (1 ref.)

96.50K Meteors, showers and meteoroids

78878 Fireball of 1981 May 25. H.Miles (Dept. of Math., Coventry Polytech., Coventry, England).

J. Br. Astron. Assoc. (GB), vol.93, no.3, p.111-13 (April 1983).

On 1981 May 25, at 2217 UT, a brilliant fireball was observed to cross southern England and South Wales. Observations were received from an area covering the whole of southern England, the Midlands and as far north as Lancashire and Yorkshire, together with a large number from South Wales. The fireball travelled on a heading of 311° passing directly over Christchurch (Hants) and Cardiff. It descended at an angle of 15° . When first observed it was at a height of about 100 km and extinction took place just west of Llandeilo (Dyfed) at a height of 12 km. (no refs.)

Comet IRAS-Araki-Alcock (1983d) See Entry 78872

96.50M Meteorites, micrometeorites

78879 U-Th-Pb in chondrites—evidence of elemental mobilities and the singularity of primordial Pb. F.Tera (Dept. of Terrestrial Magnetism, Carnegie Instn. of Washington, Washington, DC, USA).

Earth & Planet. Sci. Lett. (Netherlands), vol.63, no.2, p.147-66 (May 1983).

A unified graphical approach that emphasizes the strict corollarity in the U-Th-Pb systematics and projects subtle diagnostic deviations from it has been adopted for the evaluation of the existing data base. It has been revealed that: (1) Excess radiogenic Pb in chondrites is largely an artifact stemming from Pb contamination of some samples and apparent recent U loss from other samples. (2) Taken at face value, the data indicate that recent U-Th mobility on the chondrule-scale is pervasive in Allende. (3) Allende carries the isotopic imprints of recent multiple disturbances in which elemental mobilities were effected but not isotopic homogenization of Pb. (4) For Allende, the Pb isotope pattern of the matrix samples suggests terrestrial contamination. If this is the case, the systematics indicates for the matrix recent U gain as well. The U-rich chondrules and inclusions, whose discordance is often consistent with U loss, are the probable source. (5) Canyon Diablo primitive Pb appears to represent the primordial composition from which chondritic Pb evolved. (35 refs.)

78880 Nickel isotopic studies in meteorites. P.Morand, C.J.Allegre (Dept. des Sci. de la Terre, Univ. de Paris VI et VII, Paris, France).

Earth & Planet. Sci. Lett. (Netherlands), vol.63, no.2, p.167-76 (May 1983).

The nickel isotopic composition of meteoritic materials were analysed by high-precision mass spectrometry. The samples analyzed include almost all meteorite types for which large isotopic anomalies have been reported for oxygen, silver, magnesium and titanium. These samples are C_1 , C_3 , L, LL, H and E chondrites, IVB irons, Eagle Station pallasite and inclusion, matrix and 'whole rock' samples of the Allende meteorite. The result is that isotope anomalies were not found for nickel within the experimental accuracy. (43 refs.)

78881 Ni isotopic compositions in Allende and other meteorites. T.Shimamura, G.W.Lugmair (Dept. of Chem., Univ. of California, San Diego, La Jolla, CA, USA).

Earth & Planet. Sci. Lett. (Netherlands), vol.63, no.2, p.177-88 (May 1983). A new technique for high-precision isotopic analyses of Ni was developed and applied to terrestrial samples, Allende inclusions and materials from other meteorites. The Ni isotopic abundances are indistinguishable from normal within presently obtainable precision with only one possible exception. The latter inclusion has to contain a significantly fractionated magnesium isotopic pattern of 9 per mille/amu. A normal Ni isotopic pattern has also been observed for the chromite/carbon fraction of an Allende acid residue. All other meteoritic samples analysed (Kohar matrix and chondrules, Murray matrix, a Tieschitz chondrule and an Orgueil magnetic fraction) all show normal isotopic compositions of Ni; no evidence for effects from now extinct ^{60}Fe could be detected. (40 refs.)

78882 Cooling history of pyroxene chondrules in the Yamato-74191 chondrite (L3)—an electron microscopic study. M.Kitamura, M.Yasuda, S.Watanabe, N.Morimoto (Dept. of Geology & Mineralogy, Kyoto Univ., Sakyo, Japan).

Earth & Planet. Sci. Lett. (Netherlands), vol.63, no.2, p.189-201 (May 1983). Fine textures of clinopyroxene in an extroradial pyroxene chondrule (EPC) and a comb-like pyroxene chondrule (CPC) in the Yamato-74191 chondrite (L3) have been studied by analytical electron microscopy. Both pyroxenes consist of three regions different in composition and texture; core, mantle and marginal regions, though the pyroxenes of the CPC are more Fe-rich than those of the EPC. The core region is the most Mg-rich with no Ca component and commonly shows polysynthetic (100) twins. The polysynthetic twins, cracks and subgrain boundaries in the core in the EPC and CPC must have formed during the transition from proto-type to clino-type pyroxenes. The exsolution textures in the mantle and marginal regions indicate initial crystallization of pigeonite-C followed by decomposition into pigeonite-P and augite. The periodicity of 15-20 nm in the spinodal decomposition textures indicates that the cooling rate of the pyroxenes, when passing through about 1000°C, was of the order of a few tens to several degrees centigrade per hour. The cooling history of the chondrules has been explained by a monotonous cooling controlled by the cooling rate of the surrounding medium. (29 refs.)

78883 Measurement of ^{53}Mn in deep-sea iron and stony spherules. K.Nishizumi (Dept. of Chem., Univ. of California, San Diego, CA, USA). *Earth & Planet. Sci. Lett. (Netherlands)*, vol.63, no.2, p.223-8 (May 1983). Cosmic-ray-produced ^{53}Mn ($t_{1/2}=3.7 \times 10^6$ years) was measured in individual and groups of deep-sea iron and stony spherules by highly sensitive neutron activation analysis. The activities found were less than 20 dpm $^{53}\text{Mn}/\text{kg Fe}$ (10^{-5} – 10^{-6} dpm $^{53}\text{Mn}/\text{sample}$) in iron spherules except one iron spherule whose activity was 241 ± 73 dpm $^{53}\text{Mn}/\text{kg Fe}$. These low activities may indicate evaporative loss of ^{53}Mn due to heating in the Earth's atmosphere. On the other hand, all stony spherules contained 200-260 dpm $^{53}\text{Mn}/\text{kg Fe}$ which is similar to chondritic values. These spherules may be ablation debris from large objects. (22 refs.)

78884 On the fine structure of meteoritic taenite/tetrataenite and its interpretation. J.F.Albertsen (Phys. Lab. I, H.C. Orsted Institute, Copenhagen, Denmark), H.P.Nielsen, V.F.Buchwald.

Phys. Scr. (Sweden), vol.27, no.4, p.314-20 (April 1983). Taenite fields from several meteorites have been investigated by TEM, electron microprobe and Mossbauer spectroscopy. The investigations have disclosed a delicate pattern of antiphase domains in the tetrataenite and the presence of low-Ni taenite at the antiphase boundaries, in what was hitherto believed to be pure tetrataenite. The observations indicate that the 'cloudy taenite' (cloudy zone II) was formed by a magnetically induced spinodal decomposition of the metastable taenite during slow cooling below 400°C. As recently demonstrated such a decomposition is likely to occur when the Curie-temperature of the alloy changes rapidly with composition, as it does in f.c.c. iron-nickel alloys containing approximately 28-43% Ni. (All compositions in weight %). The large contribution to Gibbs free energy from magnetic ordering gives rise to inflections in the Gibbs free energy curve, making the alloy unstable towards decomposition, here into a magnetically and atomically ordered Ni-rich alloy plus a magnetically and atomically disordered Ni-poor alloy. The model accounts apparently well for the structure and composition of the two phases in the cloudy taenite, and also for the peculiar response of f.c.c. iron-nickel alloys to irradiation with energetic neutrons or electrons at temperatures below 400°C. (23 refs.)

The dissipation of a sodium cloud See Entry 78727

96.60 SOLAR PHYSICS

78885 Structure and spectrum of quiescent prominences IV. The ultraviolet ionization continua of hydrogen and helium. J.N.Heasley, R.W.Milkey (Inst. for Astron., Univ. of Hawaii, Honolulu, HI, USA).

Astrophys. J. (USA), vol.268, no.1, pt.1, p.398-402 (1 May 1983). For pt.III see *ibid.*, vol.221, no.2, pt.1, p.677-88 (1978). Examines the formation of the ground-state ionization continua of hydrogen (A912) and helium (A504) and the information about the physical state of the prominence which can be obtained from observation of these features. (10 refs.)

78886 A coronal transient associated with a high-speed type II burst. T.E.Gergely, M.R.Kundu (Clark Lake Radio Obs., Univ. of Maryland, College Park, MD, USA), E.Hildner.

Astrophys. J. (USA), vol.268, no.1, pt.1, p.403-11 (1 May 1983). Discusses several characteristics of a white light transient observed by the ATM Coronagraph experiment aboard Skylab. The transient was associated with a very high speed type II radio burst. Based on the relative speeds of the transient and the radio burst, the type II disturbance must have propagated in a still undisturbed corona, at an $\sim 35^\circ$ angle to the preexisting streamer and along an essentially open field configuration. The electron density gradients derived from the radio and the white light observations are compared. The assumption that the type II was a weak MHD shock leads to large values for the coronal magnetic field. The type II radiation may have originated in a strong shock, of magnetic Mach number $M > 2$. (24 refs.)

78887 Magnetohydrostatic model of solar faculae. V.A.Osherovich (Environmental Res. Lab., NOAA, Boulder, CO, USA), T.Fla, G.A.Chapman.

Astrophys. J. (USA), vol.268, no.1, pt.1, p.412-19 (1 May 1983). A self-similar magnetohydrostatic model of solar faculae is presented. The model is based on the Schluter-Temesvary equation, originally derived for sunspots. Magnetic tension and twisted magnetic field are taken into account. The exact magnetohydrostatic solution obtained from an observability derived pressure deficit basically Chapman's semiempirical facular model without tension. The difference between a facula and a sunspot and the thermodynamic consequences of a twisted magnetic field are discussed. Pressure and temperature profiles at different heights are presented. (15 refs.)

78888 Underground science at Homestake [solar neutrino experiment]. R.Davis, Jr., B.T.Cleveland, J.K.Rowley (Brookhaven Nat. Lab., Upton, NY, USA).

AIP Conf. Proc. (USA), no.96, p.2-15 (1982). [received: May 1983] (Workshop on Science Underground, Los Alamos, CA, USA, 1982).

A brief overview is given of some of the scientific work that has been done in the Homestake mine. The problems and advantages of working in active mines are discussed. Some details on the construction of the chlorine solar neutrino experiment are presented and the current results of this experiment are given. The report concludes with a discussion of the importance and feasibility of a much larger chlorine experiment. (15 refs.)

78889 The analysis of solar models—neutrinos and oscillations. R.K.Ulrich (Univ. of California, Los Angeles, CA, USA), E.J.Rhodes, Jr., S.Tomeczek, P.J.Dumont, W.M.Brunish.

AIP Conf. Proc. (USA), no.96, p.66-79 (1982). [received: May 1983] (Workshop on Science Underground, Los Alamos, CA, USA, 1982).

The theory of stellar structure and evolution is used to calculate the properties of a variety of objects from red giants and supernova precursors to white dwarfs and neutron stars. Accurate tests of the theory in the context of these applications are generally not available. The Sun as the nearest star provides a unique example of a star which can be subjected to a variety of precise tests not possible with remote stars. The authors concentrate on two of these tests, solar neutrinos and solar oscillations, which currently indicate that there is something seriously wrong with our standard solar model. (20 refs.)

78890 The case of the missing solar neutrinos. W.A.Fowler (Will Keith Kellogg Radiation Lab., California Inst. of Technol., Pasadena, CA, USA).

AIP Conf. Proc. (USA), no.96, p.80-7 (1982). [received: May 1983] (Workshop on Science Underground, Los Alamos, CA, USA, 1982).

Observations employing the Cl-Ar technique find only one-fourth the neutrino flux from the Sun at the Earth expected on the basis of standard solar models and the rates of the nuclear reactions which fuse hydrogen into helium as measured in terrestrial laboratories. The current situation concerning nuclear reaction rates is discussed. It is concluded that the Ga-Ge technique which will detect the model and reaction rate independent flux of pp-neutrinos from the Sun should be put into full-scale operation as soon as possible. Other techniques which will probably require a National Underground Science Facility are discussed briefly. (15 refs.)

78891 A radiochemical solar neutrino experiment using $^{81}\text{Br}(\nu_e)^{81}\text{Kr}$. G.S.Hurst, C.H.Chen, S.D.Kramer, M.G.Payne (Health & Safety Res. Div., Oak Ridge Nat. Lab., Oak Ridge, TN, USA), R.D.Willis.

AIP Conf. Proc. (USA), no.96, p.96-104 (1982). [received: May 1983] (Workshop on Science Underground, Los Alamos, CA, USA, 1982).

Both geochemical and radiochemical experiments based on the interaction $^{81}\text{Br}(\nu_e)^{81}\text{Kr}$ to detect ^8Be solar neutrinos have been suggested as a logical extension of the ^{37}Cl experiment of Davis et al. The ^{81}Br experiment, however, requires the development of a direct counter for the slowly decaying ^{81}Kr . Progress toward such a detector based on resonance ionization spectroscopy (RIS) is discussed. (24 refs.)

78892 A proposed geological solar neutrino measurement. G.A.Cowan, W.C.Haxton (Los Alamos Nat. Lab., Los Alamos, NM, USA).

AIP Conf. Proc. (USA), no.96, p.105-8 (1982). [received: May 1983] (Workshop on Science Underground, Los Alamos, CA, USA, 1982).

It may be possible to measure the boron-8 solar neutrino flux, averaged over the past several million years, from the concentration of technetium-98 in molybdenum-rich ore. This geochemical experiment could provide the first test of nonstandard solar models that suggest a relation between the chlorine-37 solar neutrino puzzle and the most recent glacial epoch. The necessary conditions for achieving a meaningful measurement are identified and discussed. (7 refs.)

78893 Solar emission lines near 12 microns. J.Brault (Kitt Peak Nat. Obs., Tucson, AZ, USA), R.Noyes.

Astrophys. J. Lett. Ed. (USA), vol.269, no.2, pt.2, p.L61-6 (15 June 1983).

The newly discovered 12 μm emission lines in the solar spectrum are found to vary strongly with position on the solar disk. The two strongest lines strengthen greatly toward the limb and disappear in spot umbrae. They show pronounced splitting in spot penumbrae and plages, characteristic of simple Zeeman triplets with $g \sim 1$. Their narrow line profiles suggest a chromospheric rather than coronal origin, but the lines remain unidentified. Forty-one additional unidentified far-infrared solar emission lines are reported. Potential uses of the lines for astrophysical investigations are noted. (5 refs.)

78894 Direct evidence of type III electron streams propagating in coronal streamers. M.R.Kundu, T.E.Gergely, P.J.Turner (Astron. Program, Clark Lane Radio Obs., Univ. of Maryland, College Park, MD, USA), R.A.Howard.

Astrophys. J. Lett. Ed. (USA), vol.269, no.2, pt.2, p.L67-71 (15 June 1983).

Using two-dimensional solar images at 73.8 MHz, obtained with the Clark Lake Multifrequency Radioheliograph. The authors present direct evidence that type III electron streams propagate in dense coronal streamers. This evidence is substantiated by the excellent coincidence that the authors find in position angle between the densest parts of streamers observed with the Solwind coronagraph on the P78-1 satellite and the maximum brightness of type III burst sources. (15 refs.)

78895 Observations of the Sun with the CERGA astrolabe in 1981. F.Laclare, M.Glentzlin (Centre d'Etudes et de Recherches Géodynamiques et Astron., Grasse, France).

Astron. & Astrophys. Suppl. Ser. (France), vol.52, no.2, p.265-7 (May 1983). In French.

The results of a new campaign of solar position observations are reported. For computation procedures the authors use latitudes and times published by the B.I.H. The accuracy obtained for one measurement is $0.020''$ for $\Delta\alpha$ and $0.18''$ for $\Delta\delta$. (4 refs.)

78896 Time structure of solar decametric type III radio bursts. G.Thejappa, C.V.Sastry (Indian Inst. of Astrophys., Bangalore, India).

J. Astrophys. & Astron. (India), vol.3, no.2, p.151-9 (June 1982). [received: June 1983]

The time structure of solar radio decametric type III bursts occurring during the periods of enhanced emission is investigated. It is found that the time profiles can take a variety of forms of which three distinct types are the following: (1) profiles where the intensity rises to a small but steady value before the onset of the main burst, (2) the intensity of the main burst reduces to a finite level and remains steady before it decays to the base level, (3) the steady state is present during the rise as well as the decay phase of the main burst. It is shown that these profiles are not due to random superposition of bursts with varying amplitudes. They are also probably not manifestations of fundamental-harmonic pairs. (15 refs.)

78897 Could ${}^7\text{Be}$ be destroyed by neutron absorption in the Sun? A note on the solar neutrino puzzle. Huang Zu-qia (Low Energy Nuclear Phys. Inst., Beijing Normal Univ., Beijing, China).

Commun. Theor. Phys. (China), vol.1, no.4, p.527-30 (1982).

A comparison is made between the rate of the ${}^7\text{Be}(\text{p},\gamma){}^8\text{B}$ reaction and the rate of the neutron absorption reaction ${}^7\text{Be}(\text{n,p}){}^7\text{Li}$ which might have been important in destroying ${}^7\text{Be}$ in the solar interior. (5 refs.)

78898 Computer reduction of solar whole disk drawings. L.M.Dougherty, F.Dyson, M.D.Fickling (Ravenstone Obs., Percival Whitley Coll., Halifax, England).

J. Br. Astron. Assoc. (GB), vol.93, no.3, p.117-19 (April 1983).

The work-load and the boredom of reducing the large number of solar whole disk drawings within the Solar Section are outlined. The authors report the earlier practice and draw attention to its shortcomings. After reporting the investigation to seek alternative techniques the authors present the current computer reduction program as suitable for use by individual observers with stand-alone microcomputers such as those commonly available in the high street shops. (17 refs.)

78899 Evidence for a distorted solar core rotating with a 12.4-day period.

R.H.Dicke (Phys. Dept., Princeton Univ., Princeton, NJ, USA).

Nature (GB), vol.303, no.5915, p.292-5 (26 May 1983).

The periodicity discovered in the solar Doppler velocity may be due to an Eddington-Sweet current driven in the photosphere by a distorted gravitational potential rotating rigidly with a synodic period of 12.81 ± 0.10 days (12.4 days sidereal). (14 refs.)

Workshop on Science Underground See Entry 74199

A proton decay and solar neutrino experiment with a liquid argon Time Protection Chamber See Entry 75230

Isotopic anomalies among solar energetic particles: contribution of preacceleration in collapsing magnetic neutral sheets See Entry 78766

The Gallium Solar Neutrino Detector See Entry 78816

Physical processes determining stellar chromospheres structure. II See Entry 78904

97.00 STARS

97.10 STELLAR CHARACTERISTICS

78900 Infall and outflow of S^{+3} ions in 15 Monocerotis, tau Canis Majoris, and iota Orionis. D.C.Morton (Anglo-Australian Obs., Epping, NSW, Australia).

Astrophys. J. (USA), vol.268, no.1, pt.1, p.217-24 (1 May 1983).

High-resolution Copernicus scans (0.051 Å FWHM) in 1980 from 1061.8 to 1064.6 Å and 1072.1 to 1074.9 Å along with short scans in 1972 or 1973 from 1062.4 to 1063.0 Å are used to check the report by Snow and Morton (1976) of infalling S IV ions in 15 Mon (O7 V), τ CMa (O9 II), and ι Ori (O9 III). The original lower resolution data are found to be misleading. Nevertheless, a shift of about $+50 \text{ km s}^{-1}$ in 1972 is confirmed in ι Ori, and a possible shift of about $+15 \text{ km s}^{-1}$ in 1973 is suspected in τ CMa. However, by 1980 the S IV in both stars had changed to outflow velocities somewhere between -30 and -140 km s^{-1} . On both occasions, 15 Mon showed no evidence of shifts. New data also have been obtained on the interstellar absorption of S IV, C II, and Fe II toward these stars. (28 refs.)

78901 Differential rotation in F stars: a comparison between theory and observation. G.Belvedere (Istituto di Astron., Univ. di Catania, Catania, Italy), L.Paterno.

Astrophys. J. (USA), vol.268, no.1, pt.1, p.246-9 (1 May 1983).

Gray (1982) recently observed seven stars on or slightly above the main sequence in the spectral region between F2 and F8, looking at the Fourier transforms of their line profiles. His observations show no or very small differential rotation in the examined stars, contradicting the theoretical predictions of Belvedere et al. (1980). However, in the spectral range examined by Gray, only an F5 V model was computed, adopting for it the standard equatorial velocity of 30 km s^{-1} , thus guessing the differential rotation behavior of main-sequence stars between F5 and G2 (Sun) by simply connecting these two models with a convenient curve. The authors compute models for each star Gray observed, using the same differential rotation computer code as in Belvedere et al. and the observed rotational velocities given by Gray. The results are explained and discussed on the basis of interaction of rotation with convection and also in the framework of the very recent observations by Wohl (1983). (5 refs.)

78902 The luminosity-core mass relation: why and how. Tuchman Y., A.Glasner, Z.Barkat (Racah Inst. of Phys., Hebrew Univ. of Jerusalem, Jerusalem, Israel).

Astrophys. J. (USA), vol.268, no.1, pt.1, p.356-60 (1 May 1983).

Shows how relevant stellar structure parameters establish the luminosity-core mass relation. (15 refs.)

78903 Enhancement of thermonuclear reaction rate due to screening by relativistic degenerate electrons. S.Ichmaru, K.Utsumi (Dept. of Phys., Univ. of Tokyo, Tokyo, Japan).

Astrophys. J. Lett. Ed. (USA), vol.269, no.2, pt.2, p.L51-5 (15 June 1983).

Contrary to the prevailing view based on a qualitative argument, it is shown through quantitative analyses that the screening effect of the relativistic degenerate electrons does produce a significantly large contribution to the enhancement factor of the thermonuclear reaction rate in the dense stellar matter. Physically, this feature stems from the fact that the relativistic effect acts to enhance the screening by 'softening' the electrons against compression. The computed results for the enhancement factor are parameterized in a form of analytic formulae to facilitate practical uses in the calculations of stellar evolution. (13 refs.)

78904 Physical processes determining stellar chromospheres structure. II. Z.Musielak (Inst. Fizyki Teoretycznej i Astrofizyki Uniwersytetu Gdanskiego, Gdansk, Poland).

Postępy Astron. (Poland), vol.30, no.3-4, p.269-92 (July-Dec. 1982). In Polish. [received: April 1983]

Observational data and some correlations between chromospheric and other atmospheric parameters are discussed. The construction of models of solar and stellar chromospheres is described. These theoretical models are based on the energy balance between radiative losses and the amount of dissipated mechanical energy. Some problems of inhomogeneity of the theoretical models as well as evolutionary effects are discussed. (47 refs.)

78905 Thirteen-color photometry of O stars. W.J.Schuster (Inst. de Astron., Univ. Nacional Autónoma de Mexico, Mexico City, Mexico).

Rev. Mex. Astron. & Astrofis. (Mexico), vol.5, no.3, p.137-48 (July 1982). [received: April 1983]

Thirteen-color photometry for O stars (spectral types B2 and earlier) are presented. Partial data (8C or 6RC) for 27 stars and complete 13-C data for 33 stars are included. (16 refs.)

78906 On the intensity and shape of radio recombination lines from ionized stellar winds. L.F.Rodriguez (Inst. de Astron., Univ. Nacional Autónoma de Mexico, Mexico City, Mexico).

Rev. Mex. Astron. & Astrofis. (Mexico), vol.5, no.3, p.179-82 (July 1982). [received: April 1983]

The ionized wind of early-type stars emit continuum (free-free) radiation that has been detected in the radio frequencies for an appreciable number of stars. The measurement of this continuum emission allows a reliable determination of the ratio of mass-loss rate to wind terminal velocity: \dot{M}/V_∞ . These winds should also emit very weak and wide radio recombination lines. The detection of these lines would allow a determination of V_∞ and \dot{M} separately. The author calculates the expected intensity and shape of these lines. For typical winds the lines are too weak and wide to be detected with presently available instruments. However, stellar winds with peculiarly low terminal velocities may have detectable radio recombination line emission. In particular, lines have been detected recently in MWC 349. The author discusses the line characteristics of this source. (11 refs.)

The equilibria of rotating, isothermal clouds. I. Method of solution See Entry 78800

The equilibria of rotating, isothermal clouds. II. Structure and dynamical stability See Entry 78801

Simulation models for the evolution of cloud systems. I. Introduction and preliminary simulations See Entry 78804

The brightest stars as extragalactic distance indicators See Entry 78822

A revised and extended calibration for the Spinrad-Taylor scanner system See Entry 78823

Research note: 13-color photometry, San Pedro Martir, 1973-79 See Entry 78826

The analysis of solar models—neutrinos and oscillations See Entry 78889

Survey of H α emission in globular cluster red giants See Entry 78907

Simultaneous X-ray and ultraviolet observations of ϵ Orionis and κ Orionis See Entry 78908

On the nature of upsilon Sagittarii See Entry 78909

Observations of ultraviolet carbon lines in the spectra of three DC white dwarfs See Entry 78910

Stellar diameter measurements by two-aperture interferometry in the infrared .. See Entry 78911

The pulsation properties of DB white dwarfs: a preliminary analysis See Entry 78912

A photometric atlas of the spectrum of γ Tauri $\lambda\lambda$ 5186-8700 Å See Entry 78913

A survey of spectral morphology and rotational velocities among the helium-rich stars See Entry 78914

The spectra of Wolf-Rayet stars. I. Optical line strengths and the hydrogen-to-helium ratios in WN type stars See Entry 78915

Observational studies of the symbiotic stars. II. Emission-line relative intensity variations in CI Cygni, BF Cygni, AX Persei, and V1016 Cygni See Entry 78916

The binary nature of the barium stars. II. Velocities, binary frequency, and preliminary orbits See Entry 78917

Angular momentum loss and the evolution of cataclysmic binaries See Entry 78918

A spectroscopic study of four late-type galactic WN stars: the question of duplicity See Entry 78919

Narrow-band photometric periods in SS 433 See Entry 78920

Infrared photometry and mass loss rates for Of-type stars See Entry 78921

The discovery of nonradial instability strips for hot, evolved stars See Entry 78922

Photometry of the post T Tauri star HD 36705 See Entry 78923

New optical positions and proper motions of late type stars associated with SiO masers See Entry 78924

HD 87072: a new, bright, very small amplitude, short period Cepheid See Entry 78927

Additional historical brightenings of VY Aquarii? See Entry 78928

On the changes in the light curves of long period variables See Entry 78929

Thirteen-color photometry of sixteen variable Be stars. I. Photometry See Entry 78930

Supernova in NGC 4753 See Entry 78931

Supernova in NGC 3106 See Entry 78932

Oblateness effects on the spindown of fast pulsars See Entry 78937

Abnormal neutron stars with abnormal protons. III. Metastable stars and phase transition See Entry 78938

Some characteristics of a rapidly rotating magnetized neutron star See Entry 78939

Spectroscopy of V711 Tauri (=HR 1099): fundamental properties and evidence for starspots See Entry 78941

X-ray spectra and light curves of accreting magnetic degenerate dwarfs See Entry 78942

Approximations to the radii of Roche lobes See Entry 78943

Detection of 2×10^{15} to 2×10^{16} eV gamma-rays from Cygnus X-3 See Entry 78944

VLBI observations of a radio flare of Circinus X-1 See Entry 78945

TV Cassiopeiae in the Utrecht Photometric System See Entry 78947

Contribution to the study of F, G, K, M type binaries. I. Orbital elements of the double lined spectroscopic binaries HD 47415 and HD 210763 See Entry 78948

Lightcurve synthesis of the semi-detached binaries LT Her, WX Eri, AW Cam See Entry 78949

Four-colour photometry of eclipsing binaries. XV B. Light curves of V Puppis See Entry 78950

- Analysis of the UVB light curves of TT Hydrae by Kopal's frequency domain method See Entry 78951
- Spectroscopic binaries near the North Galactic Pole. IV. HD 120803 See Entry 78952
- Spectroscopic binaries near the North Galactic Pole. V. HD 117064 See Entry 78953
- On the period of EG Cephei See Entry 78954
- Radial velocity measurements of α Pyx and ζ CMA See Entry 78955
- Infrared variability of HR 7275 See Entry 78956
- New eclipsing supergiant 22 Vul See Entry 78957
- XY Leo and the star BD+18°2304 See Entry 78958
- On radial velocity and the motion of spectroscopic binary stellar systems See Entry 78959
- The orbit of visual binary ADS 4396=A 2657 See Entry 78960
- Spectroscopy analysis of dwarf and subgiant stars in 47 Tucanae See Entry 78964
- V-photometry of bright stars in central region of globular cluster M5 See Entry 78965
- The effects of mass and metallicity upon planetary nebula formation See Entry 78970
- A rotating protocluster in W58:HCO⁺ aperture synthesis maps See Entry 78972
- The binary central star of the planetary nebula LT-5 See Entry 78973
- Infrared observations of OB star formation in NGC 6334 See Entry 78974
- Ring ejection in Type II supernovae: 1E 0102.2-7219 in the Small Magellanic Cloud See Entry 78976
- Ultraviolet continuum and H₂ fluorescent emission in Herbig-Haro objects 43 and 47 See Entry 78977
- Observation of ice mantles toward HD 29647 See Entry 78978
- A multifrequency study of star formation in the blue compact dwarf galaxy I Zw 36 See Entry 78995
- Direct evidence for a massive galactic halo See Entry 79009
- X-ray nebular models See Entry 79025

97.20 NORMAL STARS (BY CLASS): GENERAL OR INDIVIDUAL

- 78907 Survey of H α emission in globular cluster red giants. C.Cacciari (Astron. Div., ESTEC, Villafranca, Spain), K.C.Freeman. *Astrophys. J. (USA)*, vol.268, no.1, pt.1, p.185-94 (1 May 1983). From a spectroscopic survey (resolution 0.67 Å) of 143 red giants of 12 globular clusters and three open clusters, direct evidence of H α emission was found for about one-third of the stars brighter than log (L/L_{\odot})=2.9. There is no clear dependence of H α emission (or mass loss rate) on metallicity. A few stars were observed many times over an interval of about 1 year, and there is clear evidence that the H α emission is variable. From the distribution of stars in the log H α - M_{bol} plane (H_0 is the corrected FWHM for the apparent H α absorption feature), the authors suggest that weak H α emission (i.e. a lower rate of mass loss) may be present in most globular cluster giants with log (L/L_{\odot}) between 2.9 and 2.3 and perhaps even fainter. The authors argue that this H α emission is associated with the main part of the pre-horizontal-branch mass loss. (65 refs.)
- 78908 Simultaneous X-ray and ultraviolet observations of ϵ Orionis and κ Orionis. J.P.Cassinelli (Washburn Obs., Univ. of Wisconsin, Madison, WI, USA), L.Hartmann, W.T.Sanders, A.K.Dupree, R.V.Myers. *Astrophys. J. (USA)*, vol.268, no.1, pt.1, p.205-16 (1 May 1983). Simultaneous observations were made with the Einstein Observatory, the International Ultraviolet Explorer, and the Copernicus satellite of the supergiant stars ϵ Ori (B0 Ia) and κ Ori (B0.5 Ia). No variations were detected in the X-ray flux or spectrum or in the ultraviolet line profiles of Auger enhanced ionization states. For ϵ Ori, the X-ray count rate was the same as it was during an observation 11 months earlier, while for κ Ori, the X-ray count rate was 46% larger than it was 11 months earlier. This change could be explained by an increase in the source temperature from 10^6 K to $10^{6.4}$ K, or by an increase in the source emission measure of 46%, or by a decrease in the column density of the intervening matter of several times 10^{20} cm⁻². The ultraviolet line profiles are found to be insensitive to changes of X-ray flux which are less than 50%. Various constraints imposed on current models for the X-ray production in early-type stars are discussed. (43 refs.)
- 78909 On the nature of upsilon Sagittarii. D.Schonberger, I.S.Drilling (Louisiana State Univ. Obs., Baton Rouge, LA, USA). *Astrophys. J. (USA)*, vol.268, no.1, pt.1, p.225-7 (1 May 1983). Presents a new explanation for the nature and evolution of the extremely hydrogen-deficient binary ν Sgr which is consistent with all observational and theoretical facts. First, the system goes through a case B mass exchange in which most of the hydrogen-rich envelope of a massive primary (5-14 M_{\odot}) is lost. The remaining envelope still contains ~50% hydrogen (by number), but is now of negligible mass, so that the star will evolve like a pure helium star. If its mass is between 1 and 2 M_{\odot} , the star will reach low surface temperatures and become a supergiant before the onset of carbon burning. This star (the original primary) will then fill its Roche lobe a second time, spilling its now helium-rich envelope over onto the secondary (case BB mass exchange). The authors argue that ν Sgr is in this state at the present time, and that the visible star is an evolved helium star of ~1 M_{\odot} with a degenerate carbon-oxygen core and a helium-burning shell which provides the high luminosity. (24 refs.)
- 78910 Observations of ultraviolet carbon lines in the spectra of three DC white dwarfs. G.Wegner (Dept. of Astron., Pennsylvania State Univ., University Park, PA, USA). *Astrophys. J. (USA)*, vol.268, no.1, pt.1, p.282-90 (1 May 1983). Ultraviolet spectra of three DC white dwarfs have been obtained using the International Ultraviolet Explorer satellite (IUE). These objects are LDS 275A (=EG 66=0935-37), G187-15 (=LTT 16151=EG 262=2059+31), and L 791-40 (=LTT 9491=EG 264=2317-17). All three show the strong ultraviolet lines of neutral carbon recently found in the spectra of a number of other DC stars. Published observations of LDS 275B and G187-15 establish that they have continuous visual spectra, while recent scans of L791-40 and G187-15 show weak $\lambda\lambda 4472$ and 5876 lines of neutral helium and possibly the (0, 0) Swan band of C₂, respectively. These new objects enlarge the sample of degenerates already known to have atmospheres containing carbon, either from visual or ultraviolet observations. When this type of white dwarf is plotted along with the other spectral classes in the Stromgren two-color diagram, it appears that white dwarfs observed having

carbon occupy a restricted region, and no C₂ white dwarfs occur that are cooler than $T_{\text{eff}} \approx 6800$ K. (37 refs.)

- 78911 Stellar diameter measurements by two-aperture interferometry in the infrared. G.P.di Benedetto, G.Conti (Istituto di Fisica Cosmica, CNR, Milano, Italy). *Astrophys. J. (USA)*, vol.268, no.1, pt.1, p.309-18 (1 May 1983). Angular diameters of the giant stars α Boo, α Tau, γ Dra, β And, and μ Gem are measured at 2.2 μ m wavelength by the Michelson method. Near the first null, the percentage of visibility is determined to within an accuracy of a few hundredths. It follows that angular dimensions can be derived with a relative error of few percent, even with a poor point source calibration. For the bright α Tau a clear secondary maximum is also found in the visibility function. Effective temperatures are also derived for the observed stars. A new temperature of $T_{\text{eff}} = 4240 \pm 118$ K is determined for the important star α Boo, and implications on the existing models are then discussed. (47 refs.)
- 78912 The pulsation properties of DB white dwarfs: a preliminary analysis. D.E.Winget (McDonald Obs. & Dept. of Astron., Univ. of Texas, Austin, TX, USA), H.M.Van Horn, M.Tassoul, C.J.Hansen, G.Fontaine. *Astrophys. J. Lett. Ed. (USA)*, vol.268, no.1, pt.2, p.L33-6 (1 May 1983). Reports preliminary results of a numerical investigation of the nonradial g-mode pulsation properties of evolutionary DB white dwarf models. The authors solve the fully nonadiabatic equations for modes corresponding to spherical harmonic index $l=1$ through 3. For each of the sequences of models examined ($M_{\text{He}} = 0.6 M_{\odot}$; and helium layer masses of $10^{-6} M_{\text{He}}$ and $10^{-4} M_{\text{He}}$), the authors find a nonradial g-mode instability strip about 3000K wide. For models with standard ML1 convection, this strip lies in the effective temperature range 19000 K $\geq T_{\text{eff}} \geq 16000$ K. The boundaries of the instability strip are extremely sensitive to the assumed efficiency of convection, however, and for sequences with more efficient (ML3) convection, the authors find the instability strip to be in the range 29000K $\geq T_{\text{eff}} \geq 26000$ K. Extrapolation of the calculations to 0.4 M_{\odot} and 0.9 M_{\odot} indicates that the instability strip boundaries are insensitive to uncertainties in the total stellar mass. The most unstable modes have e-folding times of the order of days. (15 refs.)
- 78913 A photometric atlas of the spectrum of γ Tauri $\lambda\lambda$ 5186-8700 Å. L.Appelquist (Copenhagen Univ. Obs., Copenhagen, Denmark), J.Andersen, W.A.Fisher, J.M.Fletcher, P.Kjaergaard. *Astron. & Astrophys. Suppl. Ser. (France)*, vol.52, no.2, p.237-63 (May 1983). A photometric atlas has been prepared of the spectrum of the K giant γ Tau, covering the wavelength range 5186-8700 Å and thus supplementing that for the blue-green region by Gratton et al. (1975). Based on spectrograms of dispersion 4.9 Å/mm obtained with the 1.2 m telescope and coude spectrograph of the Dominion Astrophysical Observatory, the atlas is the first in a set of four comprising also α Boo, ρ Boo, and δ Boo A, that will illustrate separately the effects upon the spectrum of variations in temperature and metal abundance. The region 7000-8685 Å is shown in extenso. The full atlas is available on magnetic tape from the Stellar Data Center at Strasbourg. (19 refs.)
- The brightest stars as extragalactic distance indicators See Entry 78922
- Infall and outflow of S⁺ ions in 15 Monocerotis, tau Canis Majoris, and iota Orionis See Entry 78900
- Differential rotation in F stars: a comparison between theory and observation See Entry 78901
- Observational studies of the symbiotic stars. II. Emission-line relative intensity variations in CI Cygni, BF Cygni, AX Persei, and V1016 Cygni See Entry 78916
- The binary nature of the barium stars. II. Velocities, binary frequency, and preliminary orbits See Entry 78917
- New optical positions and proper motions of late type stars associated with SIQ masers See Entry 78924
- The period variations of UX Dra See Entry 78926
- X-ray spectra and light curves of accreting magnetic degenerate dwarfs See Entry 78942
- Analysis of the UVB light curves of TT Hydrae by Kopal's frequency domain method See Entry 78951
- Spectroscopic binaries near the North Galactic Pole. IV. HD 120803 See Entry 78952
- Spectroscopic binaries near the North Galactic Pole. V. HD 117064 See Entry 78953
- Radial velocity measurements of α Pyx and ζ CMA See Entry 78955
- New eclipsing supergiant 22 Vul See Entry 78957
- Spectroscopy analysis of dwarf and subgiant stars in 47 Tucanae See Entry 78964
- The binary central star of the planetary nebula LT-5 See Entry 78973
- Ultraviolet continuum and H₂ fluorescent emission in Herbig-Haro objects 43 and 47 See Entry 78977
- Direct evidence for a massive galactic halo See Entry 79009

97.30 VARIABLE AND PECULIAR STARS (inc. novae)

- 78914 A survey of spectral morphology and rotational velocities among the helium-rich stars. N.R.Walborn (Lab. for Astron. & Solar Phys., Goddard Space Flight Center, Greenbelt, MD, USA). *Astrophys. J. (USA)*, vol.268, no.1, pt.1, p.195-204 (1 May 1983). A morphologically homogeneous list of the helium-rich B stars is given: according to the present criteria, 20 members of this category brighter than 10th magnitude are known, all but one of which have been newly observed. Three 11th magnitude helium-rich stars are also noted; other objects previously associated with the helium-rich category which do not meet the present criteria are listed separately. Equivalent widths of hydrogen, helium, and metal lines in the spectra of the helium-rich and comparison stars are given. Uniform determinations of the projected rotational velocities are also made for the helium-rich stars. The distribution of their rotational velocities, and in particular the often noted 'predominance' of slow rotators, is found to be indistinguishable from that of normal early B dwarfs, except for a possible excess of rapid ($v \sin i \sim 160$ km s⁻¹) rotators which, however, depends upon only two or three stars. Two questions are critically discussed. (1) Are there any metal abundance anomalies in the helium-rich spectra or not? (2) Are the helium-rich stars massive ($\sim 10 M_{\odot}$) Population I objects with normal main-sequence cores and surface helium enhancements, or are they low-mass ($1-4 M_{\odot}$), highly evolved objects with processed cores? (44 refs.)

- 78915 The spectra of Wolf-Rayet stars. I. Optical line strengths and the hydrogen-to-helium ratios in WN type stars.** P.S.Conti, E.M.Eeep, D.N.Perry (Joint Inst. for Lab. Astrophys., Univ. of Colorado, Boulder, CO, USA). *Astrophys. J. (USA)*, vol.268, no.1, pt.1, p.228-45 (1 May 1983). Studies spectra of Wolf-Rayet stars by examining the optical line strengths of WN stars in the Galaxy and the Large Magellanic Cloud to see what similarities and differences exist among them. Tables of equivalent widths extracted from spectra are presented and some conclusions are drawn. There is a wide dispersion in line strengths for all ions even among stars of the same subtype, with WN 7 stars weaker overall than surrounding types. Nitrogen line ratios indicate that the WN subtypes represent an ionization sequence, but one with considerable overlap: the classification scheme is not single valued; other physical parameters must play a role. The Balmer-Pickering decrement is used to estimate the H/He ratio for most of the WN stars with available spectra. The abundance of H probably relates to structural differences in the winds that, in part, give rise to a dispersion in observed line strengths. The authors estimate the C/N ratio. In most cases the observations suggest that the C/N ratio is consistent with 'evolved' models for WN stars. (42 refs.)
- 78916 Observational studies of the symbiotic stars. II. Emission-line relative intensity variations in CI Cygni, BF Cygni, AX Persei, and V1016 Cygni.** N.A.Oliver, C.M.Anderson (Washburn Obs., Univ. of Wisconsin, Madison, WI, USA). *Astrophys. J. (USA)*, vol.268, no.1, pt.1, p.250-63 (1 May 1983). For pt.1 see ibid. vol.242, no.1, p.188-94 (1980). Low-resolution spectra ($\lambda\lambda 3800-5900$) are presented of the symbiotic stars CI Cygni, BF Cygni, AX Persei, and V1016 Cygni, which were obtained with the Washburn Observatory Boller and Chivens Cassegrain spectrograph and intensified Reticon. The nebular electron temperature and density are derived from the [O III] $\lambda 5007$ and $\lambda 4363$ emission lines and the UV intercombination lines of $\lambda 1661$ and $\lambda 1667$. Relative emission-line intensity variations were observed in all four stars. The relative emission line changes correlated with photometric minima for CI Cyg, AX Per, and possibly BF Cyg. These changes are interpreted as due to a red giant eclipsing a nebula surrounding the exciting source. A decline in the intensity ratios of [Ne III] $\lambda 3869$ to [O III] and He I $\lambda 5876$ to [O III] $\lambda 5007$ were also observed during the 1980 minimum of CI Cyg. (37 refs.)
- 78917 The binary nature of the barium stars. II. Velocities, binary frequency, and preliminary orbits.** R.D.McClure (Dominion Astrophys. Obs., Herzberg Inst. of Astrophys., Victoria, BC, Canada). *Astrophys. J. (USA)*, vol.268, no.1, pt.1, p.264-73 (1 May 1983). For pt.1 see *Astrophys. J. Lett. Ed. (USA)*, vol.238, no.1, p.L35-8 (1980). A series of radial velocity observations has been obtained over the last 3 years of a sample of 20 Ba II stars. Seventeen of these (85%) are found to show long-term velocity variations ranging in amplitude from a few to tens of km s⁻¹. Thus it seems likely that all Ba II stars are binary systems. An additional Ba II star in the open cluster NGC 2420 is also found to have a variable velocity. Orbits for seven Ba II stars indicate low-mass companions, compatible with their being white dwarfs. Separations are large, about 2 AU on average. The peculiar abundances are not explained, but the fact remains that multiplicity must bear a causal relationship to these peculiarities. (36 refs.)
- 78918 Angular momentum loss and the evolution of cataclysmic binaries.** R.E.Taam (Dept. of Phys. & Astron., Northwestern Univ., Evanston, IL, USA). *Astrophys. J. (USA)*, vol.268, no.1, pt.1, p.361-7 (1 May 1983). Considers the influence of angular momentum losses on the evolution of low-mass binary systems with collapsed companions; specifically losses due to magnetically coupled stellar winds, to mass ejection associated with nova explosions, and to gravitational radiation. All evolutionary sequences are found to evolve ultimately to shorter orbital periods since angular momentum losses are effective in outweighing the effects of mass transfer from the less massive to the more massive component. Typical mass transfer rates, induced by the loss of angular momentum associated with magnetically coupled winds, are $\geq 10^{-5} M_{\odot} \text{ yr}^{-1}$. If the empirical braking law for cool main-sequence stars can be applied to the entire lower main sequence, it is found that angular momentum loss via winds dominates gravitational radiation losses in promoting mass transfer in a binary for secondaries $\geq 0.1 M_{\odot}$. (27 refs.)
- 78919 A spectroscopic study of four late-type galactic WN stars: the question of duplicity.** R.L.Lamontagne, A.F.J.Moffat (Dept. de Phys., Univ. de Montreal, Montreal, Quebec, Canada), W.Seggewiss. *Astrophys. J. (USA)*, vol.269, no.2, pt.1, p.596-604 (15 June 1983). Spectroscopic observations of four late-type galactic WN stars (WNL) indicate that MR 122, MR 119, and HDE 313846 are probably single stars and that HD 177230 may be a binary system with a low-mass, probably compact companion. The study adds strong support to the hypothesis that, at least among the WNL stars, the duplicity rate of Wolf-Rayet stars is like that of normal stars. Stellar wind is therefore probably the main mechanism that removes the outer layers of an O star as it evolves of a luminous WN star. (26 refs.)
- 78920 Narrow-band photometric periods in SS 433.** S.F.Anderson, B.Margon (Astron. Dept., Univ. of Washington, Seattle, WA, USA), S.A.Grandi. *Astrophys. J. (USA)*, vol.269, no.2, pt.1, p.605-12 (15 June 1983). Analyzes the variation of the ratio of the rest-wavelength ('stationary') H α emission-line flux to continuum strength in SS 433 on 200 spectra obtained during a four-year interval from 1978 to 1982. Fourier and least-squares analyses reveal four highly significant periods: at 162 ± 1 , 81 ± 1 , 13.090 ± 0.007 , and 6.545 ± 0.007 days. The authors argue that these observed narrow-band periods are, at least partly, manifestations of broad-band variations reported by other observers; however, several lines of evidence suggest that the line flux also varies periodically. The 13.1 and 6.5 day variations are doubtless eclipse-related analogues of the 13.1 day radial velocity variations which are ascribed to the binary orbital period of the system. The observation of the 162 and 81 day variations are the first highly significant detections of photometric analogues to the large amplitude spectroscopic variations of the relativistic jet in SS 433. The data provide support models where the direction of the ejected jets is directly controlled by the orientation of an accretion disk. Further, the analysis strongly confirms the suggestion of Crampton and Hutchings (1981) that it is the radial velocity curve of the stationary He II $\lambda 4686$ emission (and not that of the stationary Balmer emission) which reflects the true binary orbital motion, and hence that the binary components have rather different masses. The data constrain the mass-loss through the jets. (31 refs.)
- 78921 Infrared photometry and mass loss rates for Of-type stars.** P.Persi, M.Ferrari-Toniolo (Istituto Astrofisica Spaziale, CNR, Frascati, Italy), G.L.Grasdalen. *Astrophys. J. (USA)*, vol.269, no.2, pt.1, p.625-33 (15 June 1983). Using infrared photometry from 2.3 μm up to 10 μm , numerical relations between 10 μm free-free and bound-free emission flux models, and the ratio M/\dot{m}_{∞} developed for different semiempirical wind velocity laws, the authors obtain mass loss rates for 15 Of-type stars, including 10 Of, three O(f) and two O((f)) stars in the spectral type range O4-O8.5. Independent of the spectral type and luminosity, the authors detected a group of stars including HD 108, HD 14947, HD 47129, HD 16691, and Cyg OB2 No.5 with a strong IR excess already present at 2.3 μm . The derived mass loss rates are very similar to the M values obtained for WR stars indicate that radiation pressure alone is sufficient to drive the stellar wind in these Of stars. Three of the most luminous Of stars in the Cyg OB2 association, known to be radio sources, were included in the program stars. (31 refs.)
- 78922 The discovery of nonradial instability strips for hot, evolved stars.** S.G.Starrfield, A.N.Cox (Theoretical Div., Los Alamos Nat. Lab., Los Alamos, NM, USA), S.W.Hodson, W.D.Pennell. *Astrophys. J. Lett. Ed. (USA)*, vol.268, no.1, pt.2, p.L27-32 (1 May 1983). Performs radial and nonradial, linear, nonadiabatic pulsation analyses of model stellar envelopes in the effective temperature range from $8 \times 10^4 \text{ K}$ to $1.5 \times 10^5 \text{ K}$. These models have total masses of $0.6 M_{\odot}$ and radii chosen so that they line up along a pre-white dwarf cooling curve computed by Schonberger (1979). The authors use three different interior compositions: (1) 100% carbon; (2) 50% ^{12}C and 50% ^{16}O (by mass); and (3) 10% ^{12}C and 90% ^{16}O (by mass). The authors find nonradial and radial instability strips for each composition caused by the partial ionization of carbon or oxygen or both. The objective is to find the cause of the observed pulsations of PG 1159-035, a hot, evolved star with $T_{\text{eff}} \geq 10^5 \text{ K}$. While this star may be too hot to lie within any of our new instability strips, the closest agreement comes from models with significant amounts of ^{16}O near the stellar surface. If correct, this result implies that helium burning in evolved stars produces much more ^{16}O than heretofore believed. (20 refs.)
- 78923 Photometry of the post T Tauri star HD 36705.** S.M.Rucinski (Max-Planck-Institut für Astrophysik, München, Germany). *Astron. & Astrophys. Suppl. Ser. (France)*, vol.52, no.2, p.281-7 (May 1983). Two series of observations in the *uvby* and *UBVRI* systems separated by 3 months are presented. The short rotational period of 0.514 days is confirmed, the light curves show high level of variability on time scales ranging from a few days to months. The mean values of the (*b-y*) or (*B-V*) colours are consistent with a K1 spectrum but other indices suggest a flatter spectral distribution than in normal stars. Variations in photometric indices correlate poorly with those in brightness suggesting that in addition to spots the chromospheric sources might contribute significantly to the observed variability. The young age inferred from the short period and the presence of lithium in the atmosphere indicate a possible similarity to the fast rotating K-type stars in the Pleiades cluster. (19 refs.)
- 78924 New optical positions and proper motions of late type stars associated with SiO masers.** G.Soulie, A.Baudry (Obs., Univ. de Bordeaux, Floirac, France). *Astron. & Astrophys. Suppl. Ser. (France)*, vol.52, no.2, p.299-309 (May 1983). The 33 cm astrophotograph of the Bordeaux Observatory has been used to derive with respect to AGK3 reference stars, accurate positions of late type variable stars associated with strong SiO maser emission. It is suggested that selected maser stars can be used to link the HIPPARCOS system and the VLBI extragalactic reference frame. The proper motions of the program (SiO) and reference stars are derived and, for the program stars, are compared to the McCormick catalog of proper motions. (28 refs.)
- 78925 Additional variable stars in the SRS catalogue.** C.Lopez (Obs. Felix Aguilar, San Juan, Argentina). *Inf. Bull. Variable Stars (Hungary)*, no.2328, 1 pp. (6 May 1983). A new cross index between 29 known variables and Southern Reference Stars is presented. (1 ref.)
- 78926 The period variations of UX Dra.** M.Vetevnik (Dept. of Astron., Brno Univ., Brno, Czechoslovakia). *Inf. Bull. Variable Stars (Hungary)*, no.2329, 2 pp. (6 May 1983). New times of minimum light of the carbon star UX Dra are derived from the three colour photoelectric observations made at Brno Observatory and from the observations made by Dzervitis et al. (1973). The lengthening of the period is discussed. (2 refs.)
- 78927 HD 87072: a new, bright, very small amplitude, short period Cepheid.** O.J.Eggen (Cerro Tololo Inter-American Obs., La Serena, Chile). *Inf. Bull. Variable Stars (Hungary)*, no.2331, 3 pp. (9 May 1983). HD 87072 is classified F8 Ib/II by Houk and Cowley (1975) and was included in a program of intermediate band and H β observations of F-type supergiants. Single, one-per-night, observations over a two-year span are listed. The light elements, $\text{Max} = \text{JD } 2445033.630 + 2.063515^d$ best satisfy these results and the resulting light and colour curves are shown. An alternative period of 0.6737^d doubles the dispersion of the individual observations. (1 ref.)
- 78928 Additional historical brightenings of VY Aquarii?.** G.A.Richter (Akad. der Wissenschaften, Sonneberg, Germany). *Inf. Bull. Variable Stars (Hungary)*, no.2332, 3 pp. (11 May 1983). Reports the results of examining more than 1000 plates of the Sonneberg sky patrol. Further investigation by authors having access to other plate archives is invited. (3 refs.)
- 78929 On the changes in the light curves of long period variables.** J.Mergentaler (Inst. Astron. Uniwersytetu Wrocławskiego, Wrocław, Poland). *Postępy Astron. (Poland)*, vol.30, no.3-4, p.315-19 (July-Dec. 1982). In Polish. [received: April 1983] Shape differences between even and odd light curves of long period variables are discussed. The distribution of occurrence of the effect is discussed. Deviations from the mean of the light increase time for RW Sgr and X Gem are given. (2 refs.)
- 78930 Thirteen-color photometry of sixteen variable Be stars. I. Photometry.** M.Alvarez, W.J.Schuster (Inst. de Astron., Univ. Nacional Autonoma de Mexico, Mexico City, Mexico). *Rev. Mex. Astron. & Astrofis. (Mexico)*, vol.5, no.3, p.173-8 (July 1982). [received: April 1983] Presents thirteen-color photometry of 16 variable Be stars observed at the Observatorio Astronomico Nacional in San Pedro Martir in Baja California. The data cover the years 1977 to 1979, and the authors include earlier measurements of Johnson and Mitchell from 1965 to 1968 that have been corrected in order to have a homogeneous set of data. (24 refs.)
- Spectroscopy of V711 Tauri (=HR 1099): fundamental properties and evidence for starspots** See Entry 78941
- X-ray spectra and light curves of accreting magnetic degenerate dwarfs** See Entry 78942
- Radial velocity measurements of α Pyx and ζ CMa** See Entry 78955
- Infrared variability of HR 7275** See Entry 78956
- Direct evidence for a massive galactic halo** See Entry 79009

97.60 LATE STAGES OF STELLAR EVOLUTION

(inc. black holes)

Hot, dense matter in the bulk equilibrium approximation. II. Adiabats and alpha-particle effects See Entry 74888

97.60B Supernovae

78931 Supernova in NGC 4753. C.J.Peterson, R.Evans. *I.A.U. Circ. (USA)*, no.3814, 1 pp. (20 May 1983).

Reports UVB photometry of the supernova in NGC 4753 on 1983 April 10 to 11 and April 17 to 19. The data suggest photometric behaviour typical of a Type I supernova. It is also reported that visual observations suggest that the supernova was 0.2 mag. brighter on April 10 than on April 6 and 9. (1 ref.)

78932 Supernova in NGC 3106. Yu.V.Terebizh.

I.A.U. Circ. (USA), no.3815, 1 pp. (24 May 1983).

Reports the discovery of a supernova 11" east and 12" south of the nucleus. The photographic magnitude was 16.0 on 1983 April 8. (no refs.)

Detection of gravitational collapse See Entry 78818

Ring ejection in Type II supernovae: IE 0102.2-7219 in the Small Magellanic Cloud See Entry 78976

97.60G Pulsars

78933 An attempt to resolve pulsar magnetospheres using interstellar scintillations. J.M.Cordes (Cornell Univ., Ithaca, NY, USA), J.M.Weisberg, V.Boriakoff.

Astrophys. J. (USA), vol.268, no.1, pt.1, p.370-80 (1 May 1983).

Interstellar scintillations of separate pulse components were measured as a test for whether the corresponding emission regions are spatially separated when radiation toward an observer. Pulse components scintillate identically within the errors, implying that the emission regions have transverse separations $\leq 10^3$ km. In polar cap models, such separations correspond to a limit on emission altitude of 6% of the light-cylinder radius for PSR 0525+21. In light cylinder models, the limits require that nonazimuthal velocities of the emission regions must be identified to within $\Delta v/v \leq 0.06$ and must be within 3° of the radial direction. (26 refs.)

78934 Is the millisecond pulsar formed from coalescence of a close neutron-star binary? H.F.Henrichs, E.P.J.van den Heuvel (Astron. Inst., Univ. of Amsterdam, Amsterdam, Netherlands).

Nature (GB), vol.303, no.5914, p.213-16 (19 May 1983).

The combination of short pulse period and abnormally weak surface dipole magnetic-field strength of PSR 1937+214 has led to the suggestion that it is an old neutron star that was spun up by accretion in a binary system. In this article the authors point out the difficulties with such a model: massive binaries are unlikely to live sufficiently long to allow the required amount of spin-up matter ($\geq 0.1 M_\odot$) to be accreted; in low-mass binaries the companion star is still expected to be present. It is argued that a likely alternative is: formation by coalescence of two neutron stars that formed a close binary such as PSR1913+16. These (inevitable) events may occur in the galaxy at a rate $\sim 10^{-4} \text{ yr}^{-1}$, and provide a natural explanation of the millisecond rotation period. (39 refs.)

78935 Direct observational upper limit to gravitational radiation from millisecond pulsar PSR 1937+214. J.Hough (Dept. of Natural Philosophy, Glasgow Univ., Glasgow, Scotland), R.W.P.Drever, H.Ward, A.J.Munley, G.P.Newton, B.J.Meers, S.Hoggan, G.A.Kerr.

Nature (GB), vol.303, no.5914, p.216-17 (19 May 1983).

The millisecond pulsar PSR 1937+214 has such a high rotational rate, 642 Hz, that any significant quadrupole moment not aligned with the spin axis could lead to a large flux of gravitational radiation. Although recently reported slowdown rates suggest an energy loss corresponding to a currently unobservable level of gravitational radiation, existing evidence may not completely rule out all possibilities for production of detectable gravitational waves. For example, continuing accretion might provide additional energy for gravitational radiation: the authors describe a search that has set an upper limit to gravitational wave amplitude at twice the pulsar rotation frequency. (6 refs.)

78936 A radio pulsar in the Large Magellanic Cloud. P.M.McCulloch, P.A.Hamilton (Dept. of Phys., Univ. of Tasmania, Hobart, Tasmania, Australia), J.G.Ables, A.J.Hunt.

Nature (GB), vol.303, no.5915, p.307-8 (26 May 1983).

A high-sensitivity search for pulsars in the Large Magellanic Cloud is in progress using the 64-m radio telescope at Parkes, New South Wales. About 7 square degrees have yielded the first extragalactic radio pulsar, PSR 0529-66, and several promising but weaker candidates which require further observations. The new pulsar has a period of 0.9757141 s, a dispersion measure of $125 \text{ cm}^{-3} \text{ pc}$, and a mean flux density of 1.4 mJy at 645 MHz. Its position is RA=05 h 29 min 30 \pm 1 s, dec=-66 $^\circ$ 57' \pm 8' (1950.0). (4 refs.)

78937 Oblateness effects on the spin-down of fast pulsars. R.Cowsik, P.Ghosh, M.A.Melvin (Tata Inst. of Fundamental Res., Bombay, India).

Nature (GB), vol.303, no.5915, p.308-10 (26 May 1983).

Assuming that the very rapidly rotating pulsar PSR 1937+214 is a fast-rotating superdense fluid, it is shown that the increase in the moment of inertia and in the gravitational self-energy of the spheroid due to its oblateness lead to substantial differences in the time evolution of the pulsar from that predicted by the standard models. Careful observations of its \dot{P} , \ddot{P} and its spectrum can put constraints on the properties of neutron star matter. Even with the existing observation of $\dot{P}=1.56 \text{ ms}$, considerations of dynamical stability of the rapidly rotating neutron star yield a lower limit $\dot{P} > 1.7 \times 10^{-14} \text{ g cm}^{-3}$ for the mean stellar density. (12 refs.)

Tachyonium, an action-at-a-distance model See Entry 74274

Some characteristics of a rapidly rotating magnetized neutron star See Entry 78939

The differential rotation of The Galaxy and the change of pulsar period See Entry 79007

97.60J Neutron stars

78938 Abnormal neutron stars with abnormal protons. III. Metastable stars and phase transition. Qu Qin-yue, Wang Zhen-ru (Astron. Dept., Nanjing Univ., Nanjing, China).

Commun. Theor. Phys. (China), vol.1, no.4, p.531-4 (1982).

For pt.II see ibid., vol.1, no.3, p.371-7 (1982). The abnormal neutron stars containing abnormal protons are compared with the normal neutron stars in

order to determine which of them are metastable and the phase transition between metastable and stable stars is discussed. (5 refs.)

78939 Some characteristics of a rapidly rotating magnetized neutron star.

A.Ray, S.M.Chitre (Tata Inst. of Fundamental Res., Bombay, India).

Nature (GB), vol.303, no.5916, p.409-10 (2 June 1983).

The 1.5-ms pulsed radio source PSR 1937+214 could be close to the onset of rotational instabilities if it is envisaged to be a rotating neutron star which gives interesting lower limits for neutron star masses. The authors examine the implications of polar gap models for such a rapidly rotating magnetic neutron star. It appears, on the basis of such models, that a higher fraction of high-frequency microwave radiation compared with the Crab pulsar is an expected result. On the other hand, the outer gap discharge models invoked for longer period pulsars yield a large amount of high-energy radiation which is not observed. The high-energy cutoff in the γ -ray region evaluated from assumed values of the magnetic field inside the light cylinder will be around 1000 GeV. (18 refs.)

Is the millisecond pulsar formed from coalescence of a close neutron-star binary? See Entry 78934

Direct observational upper limit to gravitational radiation from millisecond pulsar PSR 1937+214 See Entry 78935

Quantized synchrotron radiation as a cause of γ -ray bursts See Entry 79026

97.60L Black holes

78940 Structure and stability of rotating fluid disks around massive objects. II. General relativistic formulation. D.K.Chakraborty, A.R.Prasanna (Phys. Res. Lab., Ahmedabad, India).

J. Astrophys. & Astron. (India), vol.3, no.2, p.193-206 (June 1982). [received: June 1983]

For pt.I see ibid., vol.2, no.4, p.421-37 (1982). Considers the structure of a thick perfect fluid disk of constant density rotating around a Schwarzschild black hole and its stability under axisymmetric perturbation. The inner edge of such disk cannot lie within 4 m . The critical γ_c for neutral stability is found to be much less than $4/3$ indicating that the disks are generally stable. (11 refs.)

Dyon black hole in the Tomimatsu-Sato-Yamazaki space-time See Entry 78812

Antiproton interactions with light elements as a test of GUT cosmology See Entry 79040

97.80 BINARY AND MULTIPLE STARS

(inc. extrasolar planetary systems)

78941 Spectroscopy of V711 Tauri (=HR 1099): fundamental properties and evidence for starspots. F.C.Fekel, Jr. (Lab. for Astron. & Solar Phys., Goddard Space Flight Center, Greenbelt, MD, USA).

Astrophys. J. (USA), vol.268, no.1, pt.1, p.274-81 (1 May 1983).

As a result of continued spectroscopic observations, new orbital elements are determined for the bright RS CVn-type system V711 Tau (=HR 1099). The spectroscopic period is refined to $2.83774^d \pm 0.00001^d$. From the estimated age of the system and evolutionary considerations, the inclination of the system is $33^\circ \pm 2^\circ$. This inclination, combined with the orbital elements and the $v \sin i$ for each component, results in the masses, radii, and equatorial rotational velocities for Aa and Ab. Evolutionary models suggest that mass transfer may begin in $7-8 \times 10^7$ yr. High signal-to-noise Reticon observations at red wavelengths show substantial differences in rotational velocity and line strength between the two components, as well as asymmetries in all absorption lines of Aa, the more massive, active, cooler star. These asymmetries are correlated with the photometric variations and move across the line profiles with time. They are the result of starspot regions rotating in and out of view. The detection of such asymmetries at times of low photometric amplitude in 1981 is evidence for a redistribution of spots rather than a substantial change in activity level. (56 refs.)

78942 X-ray spectra and light curves of accreting magnetic degenerate dwarfs. J.Imamura (Dept. of Astron., Univ. of Virginia, Charlottesville, VA, USA), R.H.Durisen.

Astrophys. J. (USA), vol.268, no.1, pt.1, p.291-308 (1 May 1983).

Reports detailed calculations of the X-ray spectra and X-ray light curves of accreting magnetic $1 M_\odot$ degenerate dwarfs. The authors use accretion funnel models in which plasma flows toward the dwarf along dipole magnetic field lines and accretes onto a small cap at the dwarf's magnetic pole of area $4\pi R_*^2 f$, where R_* is the stellar radius and $f \leq 1$. The X-ray spectra of weakly magnetic degenerate dwarfs are qualitatively similar to the spectra of non-magnetic dwarfs. The majority of the X-rays escape in directions perpendicular to the field lines. This has two effects: (1) For magnetic and nonmagnetic models with equivalent accretion rates per square centimeter, the emergent photons in the magnetic case suffer fewer scatterings than those in the nonmagnetic case and thus show less energy degradation. The shapes of the light curves are sensitive to f and L_* to the inclination of the magnetic field axis to the dwarf's rotation axis, and to the viewing angle of the dwarf. Thus, observed X-ray light curves can be used to constrain the physical characteristics and geometry of the accreting degenerate dwarf. (32 refs.)

78943 Approximations to the radii of Roche lobes. P.P.Eggleton (Inst. of Astron., Univ. of Cambridge, Cambridge, England).

Astrophys. J. (USA), vol.268, no.1, pt.1, p.368-9 (1 May 1983).

Effective radii of Roche lobes are computed and compared with the results of Kopal (1959) and Pacynski (1971). A convenient approximation is given, whose derivative is smooth and fairly accurate. (2 refs.)

78944 Detection of 2×10^{15} to 2×10^{16} eV gamma-rays from Cygnus X-3. M.Samorski, W.Stamm (Inst. für Reine und Angewandte Kernphys., Univ. of Kiel, Kiel, Germany).

Astrophys. J. Lett. Ed. (USA), vol.268, no.1, pt.1, p.L17-21 (1 May 1983).

The experimental data of the extensive air shower experiment at Kiel have been analyzed with respect to showers from Cyg X-3. The measurements have been performed from 1976 March 18 to 1980 January 7 with an angular resolution of 1° . The effective on-source observation time was 3838 hr at a sensitive area of 2.800 m^2 . The time-averaged analysis gives a 4.4σ excess of showers from the direction $\delta = 40.9^\circ \pm 1.5^\circ$ and $\alpha = 307.8^\circ \pm 2.0^\circ$. In addition, the excess showers show the typical 4.8 hr modulation, with a signal-to-noise ratio of 9 in the phase maximum. The time-averaged integral γ -ray flux is derived. It corresponds to a luminosity of $6 \times 10^{36} \text{ ergs s}^{-1}$ in the energy region $2 \times 10^{15} \text{ eV}$ to $2 \times 10^{16} \text{ eV}$. This is the first experimental evidence for a clearly identified γ -ray point source emitting at energies greater than 10^{15} eV . (19 refs.)

78945 VLBI observations of a radio flare of Circinus X-1. R.A.Preston, D.D.Morabito, A.E.Wehrle (Jet Propulsion Lab., California Inst. of Technol., Pasadena, CA, USA), D.L.Jauncey, M.J.Batty, R.F.Haynes, A.E.Wright, G.D.Nicolson.

Astrophys. J. Lett. Ed. (USA), vol.268, no.1, pt.2, p.L23-6 (1 May 1983). A strong (~ 1.2 Jy) radio flare of the binary star system Circinus X-1 was observed with VLBI at three southern hemisphere observatories. The 2.3 GHz observations were made from 1980 April 22 to 28 and commenced 1 day prior to the flare outburst. Throughout the observation period, the flaring component of the radio source had an angular size, θ , in the range of $0.0015'' \leq \theta \leq 0.015''$. This is equivalent to a linear size of 15-150 AU at the 10 kpc distance of Circinus X-1. The quiescent component of the radio source observed prior to the flare was found to have an angular size of $\geq 0.2''$. This is equivalent to a linear size of ≥ 2000 AU at 10 kpc. Hence, the quiescent radio emission comes from a region much larger than that proposed in recent models for Circinus X-1. The quiescent component appears to be variable on a time scale of years and is probably fueled by the Circinus X-1 binary system. (15 refs.)

78946 Photographic observations of visual double stars. E.van Albada-van Dien (Astron. Inst., Univ. of Amsterdam, Amsterdam, Netherlands).

Astron. & Astrophys. Suppl. Ser. (France), vol.52, no.2, p.193-202 (May 1983). Presents the results of photographic observations of 199 visual double stars, obtained at the Bosscha Observatory at Lembang, Indonesia, in the years 1958-1975 (with one 1953 plate). The material comprises 708 plates with an average of 37 images measured per plate. (3 refs.)

78947 TV Cassiopeiae in the Utrecht Photometric System. A.C.de Landt-sheer (Astron. Inst., Rijksuniv. Utrecht, Utrecht, Netherlands).

Astron. & Astrophys. Suppl. Ser. (France), vol.52, no.2, p.213-36 (May 1983).

Four UPS light curves of TV Cas are presented. An instantaneous period analysis of these curves and previously published data reveals erratic relative period changes of over $10E-6$ a year. The secondary minimum appears to be at phase 0.502. Light curve analysis indicates that the cool component fills its Roche lobe and is of spectral type G5-G9IV. Roche lobe overflow is not sufficient to explain the observed secular decrease of the period. Other mechanisms may be found in the chromospheric activity of the cool component. This activity is suggested by the observed small variations in the light curves with a characteristic period of about a year. (55 refs.)

78948 Contribution to the study of F, G, K, M type binaries. I. Orbital elements of the double lined spectroscopic binaries HD 47415 and HD 210763. R.Nadal, J.M.Carquillat, A.Pedoussaut, N.Ginestet (Obs. de Pic-du-Midi et de Toulouse, Toulouse, France).

Astron. & Astrophys. Suppl. Ser. (France), vol.52, no.2, p.293-7 (May 1983). In French.

The spectroscopic binaries HD 47415 and HD 210763 were observed at the Observatoire de Haute-Provence in order to determine their spectrographic orbits. The orbital elements obtained are presented. For these two binaries, the mass-ratio near 0.8 and the primary spectral type (F8 IV and F5 IV respectively) indicates a main sequence F-type secondary. The two systems appear to be detached and eclipses are possible for HD 210763. (11 refs.)

78949 Lightcurve synthesis of the semi-detached binaries LT Her, WX Eri, AW Cam. G.Russo, L.Milano (Capodimonte Astron. Obs., Napoli, Italy).

Astron. & Astrophys. Suppl. Ser. (France), vol.52, no.2, p.311-16 (May 1983).

Analyzes, by means of a Roche-model-based method for lightcurve synthesis, the photometric observations of the eclipsing binaries LT Her, WX Eri, AW Cam. All systems are found to be semi-detached, with a main sequence primary and a lobe filling evolved secondary. (21 refs.)

78950 Four-colour photometry of eclipsing binaries. XV B. Light curves of V Puppis. J.V.Clausen, B.Nordstrom, B.Reipurth (Copenhagen Univ. Obs., Tollose, Denmark).

Astron. & Astrophys. Suppl. Ser. (France), vol.52, no.2, p.323-31 (May 1983).

UBV light curves of the semi-detached early B-type eclipsing binary V Puppis are presented. (2 refs.)

78951 Analysis of the UVB light curves of TT Hydrae by Kopal's frequency domain method. J.Koul, K.D.Abhyanekar (Centre of Advanced Study in Astron., Osmania Univ., Hyderabad, India).

J. Astrophys. & Astron. (India), vol.3, no.2, p.93-9 (June 1982). [received: June 1983]

The light curves of the totally eclipsing system TT Hya in UVB colours observed by Kulkarni and Abhyankar (1981) during 1973-77 are analysed by Kopal's (1979) frequency domain method with slight modification. The authors find r_p (primary) = 0.104 ± 0.005 , r_s (secondary) = 0.215 ± 0.008 and $i = 89^\circ \pm 1^\circ$. The value of r_s obtained is smaller than that determined earlier by Kulkarni and Abhyankar by the method of Russell and Merrill; this confirms the undersized nature of the secondary component. The ultraviolet colour excess of the secondary is also confirmed. (9 refs.)

78952 Spectroscopic binaries near the North Galactic Pole. IV. HD 120803. R.F.Griffin (Obs., Cambridge Univ., Cambridge, England).

J. Astrophys. & Astron. (India), vol.3, no.2, p.101-5 (June 1982). [received: June 1983]

For pt.III see *ibid.*, vol.3, no.1, p.1-4 (1982). Photoelectric radial-velocity measurements show that HD 120803 is a spectroscopic binary with a rather eccentric orbit and a period of 700 days. Early DDO photographic observations, published individually by the author for the first time, fit the orbit well. (7 refs.)

78953 Spectroscopic binaries near the North Galactic Pole. V. HD 117064. R.F.Griffin (Obs., Cambridge Univ., Cambridge, England).

J. Astrophys. & Astron. (India), vol.3, no.2, p.107-9 (June 1982). [received: June 1983]

For pt.IV see *ibid.*, vol.3, no.2, p.101-5 (1982). Photoelectric radial-velocity measurements, which in 1971 showed HD 117064 to be a spectroscopic binary, have been continued and now permit the derivation of an eccentric orbit with a period of 6.08 years. (7 refs.)

78954 On the period of EG Cephei. U.Hopp (Inst. fur Astron., Technische Univ., Berlin, Germany), E.H.Geyer, F.T.Lentes.

Inf. Bull. Variable Stars (Hungary), no.2327, 4 pp. (4 May 1983).

The authors have reobserved this β Lyrae-type eclipsing binary in the nights of Sept. 1/2, 2/3, 3/4, 1980 with a double beam photometer attached at the Nasmyth focus of the 106 cm Cassegrain telescope of Hoher List Observatory. A total of 307 U, 614 B and 614 V-observations were obtained. One time instant for the primary and two time instants for the secondary minima are derived by the Pogson method. A period of 0.54462159^d is indicated and shown to be constant during 1959-80 to within 9×10^{-5} day. (8 refs.)

78955 Radial velocity measurements of α Pyx and ζ Cma. C.Sterken, D.Vander Linden (Astrophys. Inst., Vrije Univ., Brussels, Belgium).

Inf. Bull. Variable Stars (Hungary), no.2330, 4 pp. (9 May 1983). In 1980 a spectroscopic monitoring of bright southern B stars using the 90 cm telescope of Manuel Foster Observatory, Santiago de Chile, was started. The programme consists of systematic observations of southern early-type B stars which are too bright to be observed photometrically. During the first months of operation a one-prism spectrograph with a dispersion of 36 \AA/mm at H γ was used. ζ Canis Majoris (HR 2282) was monitored during 4 nights in December 1980 and January 1981 and α Pyxidis (HR 3468) during 5 nights in December 1980 and March 1981. (4 refs.)

78956 Infrared variability of HR 7275. M.Zeilik, R.Elston, G.Henson, P.Smith (Dept. of Phys. & Astron., Univ. of New Mexico, Albuquerque, NM, USA).

Inf. Bull. Variable Stars (Hungary), no.2333, 4 pp. (13 May 1983).

Reports infrared photometry of the long-period, non-eclipsing system HR 7275 that clearly shows phase-dependent infrared light curves. All observations were carried out with the 1.3-meter telescope at Kitt Peak National Observatory during the day. The observations spanned December 1980 to February 1981; most were clustered in January 1981. (4 refs.)

78957 New eclipsing supergiant 22 Vul. S.B.Parsons (Lab. for Astron. & Solar Phys., Goddard Space Flight Center, Greenbelt, MD, USA), T.B.Ake.

Inf. Bull. Variable Stars (Hungary), no.2334, 1 pp. (13 May 1983).

An eclipse of 22 Vul (HD 192713, V=5.15), spectral type G3 Ib-II, was observed on 17 April 1983 during IUE observations from 18^h to 21^h UT. The star is a single-lined spectroscopic binary with period 249.1 days. (no refs.)

78958 XY Leo and the star BD+18°2304. D.R.Faulkner, D.H.Grossoehme (Astron. Dept., Indiana Univ., Bloomington, IN, USA).

Inf. Bull. Variable Stars (Hungary), no.2335, 2 pp. (16 May 1983).

De Carlo and Sabatini (1967) may have observed XY Leo (BD+18°2307) and misidentified it as BD+18°2304. To test this hypothesis both XY Leo and BD+18°2304 were observed on five nights during the spring of 1983 using the 41 cm reflector of the Morgan-Monroe Station of the Goethe Link Observatory. Johnson UVB filters were used with a 1P21 photomultiplier tube cooled with dry ice. The comparison star used was BD+18°2306. The complete light curve of XY Leo was observed, thus if BD+18°2304 is a variable having a similar period, variations in its brightness should have been apparent. However, the magnitude of BD+18°2304 as determined with each filter remained constant within 0.05^m . It is concluded that BD+18°2304 is not an eclipsing binary and that De Carlo and Sabatini unknowingly observed XY Leo. (3 refs.)

78959 On radial velocity and the motion of spectroscopic binary stellar systems. V.G.Shkodrov, B.Z.Kovachev (Astron. Obs., Bulgarian Acad. of Sci., Sofia, Bulgaria).

C.R. Acad. Bulg. Sci. (Bulgaria), vol.36, no.1, p.11-13 (1983).

When the components of a close binary stellar system move in a plan tangential to the celestial sphere τ , the radial velocity γ is considered to be zero. On the other hand, in celestial mechanics it is well known that, when two bodies move around their mass centre, oscillations are observed in the inclination of the orbital plane. These are caused by the non-uniform distribution of the matter in the two components. Consequently the oscillations, if they do exist, must be the cause of the non-zero radial velocities. The effect of the oscillation of the orbital plane around τ on the radial velocity γ is formulated theoretically. (6 refs.)

78960 The orbit of visual binary ADS 4396=A 2657. R.R.de Freitas Mourao, O.C.Tavares, M.R.Nunes (Obs. Nacional, Rio de Janeiro, Brazil).

Rev. Mex. Astron. & Astrofis. (Mexico), vol.5, no.3, p.135-6 (July 1982). [received: April 1983]

The physical and orbital elements of the binary star ADS 4396=A 2657 are determined. The reductions were performed on the IBM 370/145 computer at the LCC-Laboratorio de Computacao Cientifica do CNPq (Conselho Nacional de Desenvolvimento Cientifico e Tecnologico). (2 refs.)

Post-Newtonian gravitational radiation of a binary system of relatively extended bodies in the field theory of gravitation See Entry 74339

On the nature of epsilon Sagittarii See Entry 78909

Observational studies of the symbiotic stars. II. Emission-line relative intensity variations in CI Cygni, BF Cygni, AX Persei, and V1016 Cygni See Entry 78916

The binary nature of the barium stars. II. Velocities, binary frequency, and preliminary orbits See Entry 78917

Angular momentum loss and the evolution of cataclysmic binaries See Entry 78918

A spectroscopic study of four late-type galactic WN stars: the question of duplicity See Entry 78919

Narrow-band photometric periods in SS 433 See Entry 78920

Additional historical brightenings of VY Aquarii? See Entry 78928

Is the millisecond pulsar formed from coalescence of a close neutron-star binary? See Entry 78934

The binary central star of the planetary nebula LT-5 See Entry 78973

X-ray nebular models See Entry 79025

97.90 OTHER TOPICS IN STELLAR ASTRONOMY

Meridian circle observations of FK4 radio stars See Entry 78796

Catalog of luminous stars in the southern Coal-Sack zone See Entry 78828

98.00 STELLAR SYSTEMS; GALACTIC AND EXTRAGALACTIC OBJECTS AND SYSTEMS; THE UNIVERSE

98.10 STELLAR DYNAMICS

78961 Binary-single star scattering. I. Numerical experiments for equal masses. P.Hut, J.N.Bahcall (Inst. for Advanced Study, Princeton, NJ, USA).

Astrophys. J. (USA), vol.268, no.1, pt.1, p.319-41 (1 May 1983).

More than a million numerical orbit calculations have been carried out for binary-single star gravitational scattering in the case of equal masses. For the first time a Monte Carlo sampling has been possible over the full dimen-

sionalities of phase space without having to make any assumptions about dependence on orientation, phase angles, or impact parameter. Total cross sections are obtained for ionization, exchange, and resonance scattering and their detailed dependence on incoming velocity is plotted for initial binary orbits of zero, moderate, and extreme eccentricity. (26 refs.)

78962 Binary-single star scattering. II. Analytic approximations for high velocity. P.Hut (Inst. for Advanced Study, Princeton, NJ, USA). *Astrophys. J. (USA)*, vol.268, no.1, pt.1, p.342-55 (1 May 1983).

For pt.1 see *ibid.*, vol.268, no.1, pt.1, p.319-41 (1983). Differential cross sections are derived for binary-single star gravitational scattering at high incoming velocity as a function of the amount of energy exchange, in the impulsive approximation. The full dependence of the differential cross sections on the initial orbital eccentricity of the binary is given for flyby and exchange scattering. Total cross sections for ionization and exchange scattering are presented and shown to be independent of binary eccentricity. The results are compared with detailed balance relations, previous analytic approximations by Heggie (1975), and numerical calculations by Hut and Bahcall (1983). (4 refs.)

78963 Analysis of box orbits in a triaxial galaxy. M.Vietri, M.Schwarzschild (Princeton Univ. Obs., Princeton, NJ, USA).

Astrophys. J. (USA), vol.269, no.2, pt.1, p.487-99 (15 June 1983). Binney and Spergel (1982) have pointed out that in a triaxial potential, box orbits—indeed all regular orbits—are quasi-periodic. This strong feature of regular orbits is exploited to derive a short development for box orbits in the equatorial plane of a triaxial potential. For the zero order terms the closed orbit was chosen which lies along the long (X) axis in the stationary case (no figure rotation) or near this axis in the case with figure rotation. The period of this orbit provides the first frequency. The first order terms were taken to be the linear perturbation of this closed orbit, which through the corresponding Floquet equations provide the second frequency. On the second order terms only those which directly improve the reproduction of the shape of the orbit have been retained; those providing corrections to the frequencies have been ignored. In the resulting development each term is a product of one factor periodic in the first frequency and another factor harmonic in the second frequency. This development to incomplete second order was applied to a number of box orbits with a radial extent of about 10 core radii. (6 refs.)

98.20 STELLAR CLUSTERS AND ASSOCIATIONS

78964 Spectroscopic analysis of dwarf and subgiant stars in 47 Tucanae. R.A.Bell (Nat. Sci. Foundation, Washington, DC, USA), J.E.Hesser, R.D.Cannon.

Astrophys. J. (USA), vol.269, no.2, pt.1, p.580-91 (15 June 1983). Spectra have been obtained for 11 dwarfs ($B - 18.2$ mag) and five brighter stars ($B - 16$ mag) in NGC 104 (47 Tuc, C 0021-723). A range of CN strengths is observed among subgiant and dwarf stars of otherwise very similar spectra. The spectroscopic results are combined with photometric data to argue that some, if not all, of the dwarfs have the same temperature. Spectrum synthesis calculations are then used to infer that the observed range of CN strengths could be produced by a star-to-star range of nitrogen abundances of ~ 5 . This result is in accord with a previous analysis based upon much lower resolution data. The range inferred is similar to that required to explain observations of high evolved stars in 47 Tuc. (31 refs.)

78965 V-photometry of bright stars in central region of globular cluster M5. N.M.Spassova (Astron. Obs., Bulgarian Acad. of Sci., Sofia, Bulgaria). *C.R. Acad. Bulg. Sci. (Bulgaria)*, vol.36, no.1, p.15-18 (1983).

The results are presented of photometry of the nucleus of globular cluster M5. The V-magnitudes of the bright red stars in the cluster's central part were obtained on three plates taken with the 65-cm Pulkovsky refractor. The V-system was realized by means of Kodak OaD plates + filter JS 16, while the cluster's central part was divided by 3-min and 4-min exposures. With the given scale (19.81" per mm) and the available photomaterial, reliable photometry in the central part could be obtained only for stars brighter than $V = 13.21$. The plates were measured on an iris microphotometer in the Pulkovsky observatory. (10 refs.)

Simulation models for the evolution of cloud systems. I. Introduction and preliminary simulations See Entry 78804

Survey of H α emission in globular cluster red giants See Entry 78907

A rotating protocluster in W58:HCO $^+$ aperture synthesis maps See Entry 78972

98.40 INTERSTELLAR MATTER; AND NEBULAE

78966 An energetic, bisymmetrically expanding H I remnant. F.J.Lockman, B.L.Ganzel (Nat. Radio Astron. Obs., Charlottesville, VA, USA).

Astrophys. J. (USA), vol.268, no.1, pt.1, p.117-22 (1 May 1983). There is a unique H I system in Monoceros that contains two arcs of gas, expanding bisymmetrically at 26 km s $^{-1}$, apparently moving through the interstellar medium like solid bodies. One of them is interacting with a large H I cloud. The total mass in moving atomic gas is $2.4 \times 10^5 M_{\odot}$, with a kinetic energy of 1.6×10^{50} ergs. The arcs are ~ 5 kpc from the Sun and overlap to form a ring with a projected diameter of ~ 200 pc. The kinetic temperature in some parts of the moving features is less than 350K. The singular morphology and kinematics of this system makes it unlikely that it resulted from a spherical or circularly symmetric explosion. There are also problems in accounting for the energy and momentum of the moving gas, the details of the geometry, and the density ratio between the moving gas and the cloud into which it is apparently moving. (23 refs.)

78967 An extensive galactic search for conformer II glycine. L.E.Snyder (Univ. of Illinois, Urbana, IL, USA), J.M.Hollis, R.D.Suenram, F.J.Lovas, L.W.Brown, D.Buhl.

Astrophys. J. (USA), vol.268, no.1, pt.1, p.123-8 (1 May 1983). Conducts the most extensive galactic search reported to date for conformer II glycine, a higher energy form of the simplest amino acid. The search utilized four glycine transitions at centimeter wavelengths and 21 at millimeter wavelengths to observe 18 galactic molecular sources and one comet. No conformer II glycine lines were detected and measurements of representative sources were used to compute upper limits on total column densities. Several unidentified lines were detected and are reported with some suggested possible identifications. (19 refs.)

78968 Optical studies of Cassiopeia A VI. Observations during the period 1976-80. S.van den Bergh (Dominion Astrophys. Obs., Herzberg Inst. of Astrophys., Victoria, BC, Canada), K.W.Kamper.

Astrophys. J. (USA), vol.268, no.1, pt.1, p.129-33 (1 May 1983). For pt.V see *Astrophys. J. Suppl. Ser.*, vol.32, no.2, p.351-66 (1976). Previously published observations of the fast moving knots in Cas A obtained between 1951 and 1975 have been supplemented by eight new Hale 5 m

prime focus plates taken in 1976, 1977, and 1980. Combining new observations of 46 long-lived knots with previously published data yields an explosion date $T_0 = 1658 \pm 3$. No significant deceleration was detected in 36 knots that have been observed for at least 20 years. New proper motions are also given for three quasi-stationary flocculi. Attention is drawn to a cluster of exceedingly faint flocculi located outside the Cas A radio shell. One of these objects became visible almost simultaneously at optical and at radio wavelengths. (10 refs.)

78969 High-velocity, asymmetric Doppler shifts of the X-ray emission lines of Cassiopeia A. T.H.Markert, C.R.Canizares, G.W.Clark (Dept. of Phys., MIT, Cambridge, MA, USA), P.F.Winkler.

Astrophys. J. (USA), vol.268, no.1, pt.1, p.134-44 (1 May 1983). Performs high spectral resolution measurements of several X-ray emission lines from the young supernova remnant Cassiopeia A. The spectrum of the X-ray emitting gas in the northwest half of Cas A is redshifted with respect to that in the southeast. The authors interpret this phenomenon. The measurements demonstrate directly that the bulk of the gas making up Cas A is moving at high velocities. The authors construct a simple geometric model consistent with the general features of the X-ray spectrum and image of Cas A. The data require an expansion velocity in excess of 2000 km s $^{-1}$. The high velocities required for the X-ray matter imply that the relatively cool X-ray emitting material observed is most probably supernova ejecta which has been heated by a reverse shock wave. The X-ray and optical data are most compatible with the view that Cas A is still in its free-expansion stage. The authors find the X-ray emitting mass and the kinetic energy. (41 refs.)

78970 The effects of mass and metallicity upon planetary nebula formation. K.A.Papp (Dept. of Phys., Univ. of Waterloo, Waterloo, Ontario, Canada), C.R.Purton, S.Kwok.

Astrophys. J. (USA), vol.268, no.1, pt.1, p.145-54 (1 May 1983). Constructs a parameterized function which describes the possible dependence of planetary nebula formation upon metal abundance and stellar mass. Data on galaxies in the Local Group compared with predictions made from the parameterized function indicate that heavy element abundance is the principal agent influencing the formation of planetary nebulae; stars which are rich in heavy elements are the progenitors of planetary nebulae. The analysis, when compared with the observations, argues for a modest degree of pre-enrichment in a few of the sample galaxies. The heavy elements dependence of planetary nebula formation also accounts for the deficit of planetary nebulae in the nuclei of NGC 221 and NGC 224, and in the bulge of our Galaxy. (70 refs.)

78971 X-ray sources in molecular clouds. S.Lepp, R.McCray (Joint Inst. for Lab. Astrophys., Univ. of Colorado, Boulder, CO, USA).

Astrophys. J. (USA), vol.269, no.2, pt.1, p.560-7 (15 June 1983). Models are calculated for the structure and infrared line emission from a dense interstellar gas cloud containing a compact X-ray source. For constant gas pressure models, the resulting structure consists of nested spherical shells containing, respectively, coronal gas at $T > 10^6$ K, and H II region with $T \sim 10^4$ K, an H I region with $T \sim 8000$ K, and finally an H $_2$ region with $T < 5000$ K. Scaling laws are given for the locations of the transitions. Approximately 10% of the X-ray luminosity absorbed in the H $_2$ region is converted into infrared emission lines that may be observable. Line ratios are presented. (51 refs.)

78972 A rotating protocluster in W58:HCO $^+$ aperture synthesis maps. S.N.Vogel, W.J.Welch (Radio Astron. Lab., Univ. of California, Berkeley, CA, USA).

Astrophys. J. (USA), vol.269, no.2, pt.1, p.568-79 (15 June 1983). Maps 89.2 GHz HCO $^+$ ($J = 1-0$) emission from a molecular cloud near K3-50. The cloud, which the authors call W58 (HCO $^+$), has $T > 40$ K, $n(\text{H}_2) > 10^5$ cm $^{-3}$, and $M \approx 2000 M_{\odot}$. The maps show a systematic velocity gradient of 8 km s $^{-1}$ pc $^{-1}$ extending over more than 1 pc. The velocity gradient is best fitted by rotation of the cloud with velocity increasing outwards and is consistent with solid body rotation. A plausible history is discussed. In all likelihood W58 (HCO $^+$) is the precursor to an open cluster or association, and fragments within the cloud are now forming stars. The cloud rotates significantly faster than open clusters and is much denser. However, the authors find that the eventual expansion of the cluster leads to a rotational velocity and mass density in accord with observations of open clusters. The effect of expansion on rotation of open clusters is considered. (35 refs.)

78973 The binary central star of the planetary nebula LT-5. W.A.Feibelman (Lab. for Astron. & Solar Phys., NASA Goddard Space Flight Center, Greenbelt, MD, USA), J.B.Kaler.

Astrophys. J. (USA), vol.269, no.2, pt.1, p.592-5 (15 June 1983). The authors found with the IUE that the true central star of the giant planetary Longmore-Tritton 5 ($339 + 88^\circ 1$) is a binary companion to the G5 star SAO 82570. The slope of the energy distribution curve indicates that the star may be one of the hottest known. The Mg II doublet associated with the G star is very strong, consistent with the existence of a close binary companion. (13 refs.)

78974 Infrared observations of OB star formation in NGC 6334. P.M.Harvey, I.Gatley (Astron. Dept., Univ. of Texas, Austin, TX, USA), I.Gatley.

Astrophys. J. (USA), vol.269, no.2, pt.1, p.613-24 (15 June 1983). Infrared photometry and maps from 2 to 100 μ m are presented for three of the principal far-infrared sources in NGC 6334. Each region is powered by two or more very young stars. The distribution of dust and ionized gas is probably strongly affected by the presence of the embedded stars; one of the sources is a blister H II region, another has a bipolar structure, and the third exhibits asymmetric temperature structure. Spherically symmetric models are clearly not applicable to any of the clouds around these objects. The presence of protostellar objects throughout the region suggests that star formation has occurred nearly simultaneously in the whole molecular cloud rather than having been triggered sequentially from within. (31 refs.)

78975 Why high-latitude clouds in our Galaxy and the highly redshifted clouds observed in front of OSOs do not belong to the same parent population. A.M.Wolfe (Univ. of Pittsburgh, Pittsburgh, PA, USA).

Astrophys. J. Lett. Ed. (USA), vol.268, no.1, pt.2, p.L1-5 (1 May 1983). International Ultraviolet Explorer observations of high-latitude gas in our Galaxy reveal the presence of both C II and C IV absorption in the spectra of stars with $z > 2$ kpc. On the other hand, C II is generally absent from unbiased samples of QSO redshift systems with C IV absorption. Comparison between the equivalent-width distributions of the QSO sample and of the galactic sample (which is suitably corrected for contamination by disk absorption) shows that the probability that the two samples are drawn from the same parent population is less than 1% for C II and less than 10% for C IV. Thus it is highly unlikely that gaseous halos comprised of material with properties of the high-latitude gas are responsible for the bulk of known QSO redshift systems. (18 refs.)

78976 Ring ejection in Type II supernovae: 1E 0102.2-7219 in the Small Magellanic Cloud. I.R.Tuohy, M.A.Dopita (Mount Stromlo & Siding Spring Obs., Australian Nat. Univ., Woden, Australia).

Astrophys. J. Lett. Ed. (USA), vol.268, no.1, pt.2, p.L11-15 (1 May 1983). Presents a velocity map of the young oxygen-rich supernova remnant (1E 0102.2-7219) in the Small Magellanic Cloud, obtained with the Anglo-Australian Telescope. The velocity structure is complex and implies a high degree of asymmetry during the Type II supernova explosion. The velocity data can be modeled in terms of a severely distorted ring of ejecta. This result, together with the evidence for expanding rings in similar remnants, suggests nonspherical ejection to be an intrinsic characteristic of Type II supernovae. The authors have also obtained two-dimensional spectroscopy of the diffuse halo of emission which partially surrounds 1E 0102.2-7219. The halo emits in the He II $\lambda 4686$ line and is either a fossil H II region created by a UV flash accompanying the supernova, or alternatively, is being excited by intense UV radiation from the remnant itself. It is the first clear association of a high-excitation region with a supernova remnant. (26 refs.)

78977 Ultraviolet continuum and H₂ fluorescent emission in Herbig-Haro objects 43 and 47. R.D.Schwartz (Phys. Dept., Univ. of Missouri, St. Louis, MO, USA).

Astrophys. J. Lett. Ed. (USA), vol.268, no.1, pt.2, p.L37-40 (1 May 1983). The results of International Ultraviolet Explorer (IUE) short-wavelength spectra of the low-excitation Herbig-Haro objects HH 43 and HH 47 are reported. In HH 43 a number of emission lines in the Lyman band of H₂ from the excited state $1s_n^+ \nu=1, J=4$ are observed. The lines are produced by fluorescence from the H Ly α line which pumps the lower state $1s_n^+, \nu=2, J'=5$ which in turn is excited by a low-velocity shock wave. No evidence of emission from highly ionized gas is present in the UV spectra. Both objects exhibit a UV continuum which peaks in the vicinity of 1500 Å and which is probably caused by hydrogen two-photon emission enhanced by collisional excitation in a low-velocity shock. (23 refs.)

78978 Observation of ice mantles toward HD 29647. J.H.Goebel (NASA Ames Res. Center, Moffett Field, CA, USA).

Astrophys. J. Lett. Ed. (USA), vol.268, no.1, pt.2, p.L41-5 (1 May 1983). The water ice absorption band at 3.1 μ m has been observed in HD 29647, which is a late B-type star with an anomalous ultraviolet extinction curve. The interpretation is that ice mantles are present on the dust grains in the intervening cloud and that these mantles are responsible for suppressing the 2200 Å interstellar absorption feature. This is the first observation of both the 2200 Å region and the 3.1 μ m interstellar absorption feature toward the same star. A comparison of recent UV laboratory data of water ice with the UV spectrum of HD 29647 further supports the presence of water ice mantles in the same column density as that observed in the infrared. The diffuse interstellar features have been reported to be weakened in this star, consistent with their origin being on grain core surfaces, rather than in mantles or gaseous molecules. (30 refs.)

78979 On the possibly low H₂ formation rate in dense clouds. T.P.Snow (Dept. of Astrophysics, Univ. of Colorado, Boulder, CO, USA).

Astrophys. J. Lett. Ed. (USA), vol.269, no.2, pt.2, p.L57-9 (15 June 1983). It has been found for the ρ Ophiuchi cloud, and suggested for diffuse cloud cores in general, that H₂ has a lower formation rate than normally expected in diffuse clouds. It is proposed that this may be due to a reduction in grain surface area per unit volume, if the grains in these regions are enlarged due to coagulation. For the ρ Oph cloud, there is independent evidence that grain coagulation has occurred, so this hypothesis regarding H₂ formation has a more substantial basis than for other clouds, where the evidence for suppressed H₂ formation is less certain, and for which there is little information on grain sizes. (16 refs.)

78980 Spectrophotometric observations of a peculiar nitrogen-rich planetary nebula NGC 2440. R.Louise (Obs. de Marseille, Marseille, France).

J. Astrophys. & Astron. (India), vol.3, no.2, p.145-50 (June 1982). [received: June 1983] By using the Boller and Chivens spectrograph with a moderate dispersion (59 Å mm⁻¹) in the red spectral region, the author obtained 65 spectra covering the whole surface of the planetary nebula NGC 2440. Intensities of H α , [N II] λ 6548-6584 and [S II] λ 6717-6731 lines are derived. The nebula is known to be a nitrogen-rich nebula (Peimbert 1978) surrounded by secondary structures (Minkowski 1964). The unusual high value of the [N II]/H α in the central core (~ 3.0) is certainly due to the nitrogen overabundance occurring in that part of the nebula. Its variations from the centre to the outer regions are interpreted as a consequence of small-scale ionization structure (Capiotti, Cromwell and Williams 1971). (22 refs.)

78981 Observations of the supernova remnants HB 9 and IC 443 at 34.5 MHz. K.S.Dwarakanath, R.K.Shevgaonkar, C.V.Sastry (Raman Res. Inst., Bangalore, India).

J. Astrophys. & Astron. (India), vol.3, no.2, p.207-16 (June 1982). [received: June 1983] Observes the extended supernova remnants HB 9 (G160.5+2.8) and IC 443 (G189.1+2.9) at 34.5 MHz. A map of HB 9 is presented. The integrated flux density of HB 9 at 34.5 MHz is 750 \pm 150 Jy. The spectral index in the frequency range from 34.5 MHz to 2700 MHz is found to be constant (-0.58 ± 0.06) without any spectral break such as was reported earlier by Willis (1973). There is no significant variation of the spectral index across the remnant. The integrated flux density of IC 443 at 34.5 MHz is 440 \pm 88 Jy. The spectral index in the frequency range from 20 MHz to 10700 MHz is -0.36 ± 0.04 . The reduction in flux at very low frequencies (10 MHz) is attributable to free-free absorption in the interstellar medium and/or in the H II region S 249. (33 refs.)

78982 Interstellar ice grains in the Taurus molecular clouds. D.C.B.Whittet (Div. of Phys. & Astron., Preston Polytech., Preston, England), M.F.Bode, A.J.Longmore, D.W.T.Baines, A.Evans.

Nature (GB), vol.303, no.5914, p.218-21 (19 May 1983). Reports observations made in November 1981 using the United Kingdom Infrared Telescope (UKIRT) at Mauna Kea of the 3 μ m ice absorption feature in the spectra of several obscured stars in the Taurus interstellar clouds. The feature correlated in strength with extinction at visual wavelengths (A_V), and is present in stars with A_V as low as 4-6 mag, a remarkable result when compared with other regions of The Galaxy. Ice may be widespread in the Taurus clouds, vindicating previous ideas on grain composition and growth. (31 refs.)

78983 Optical emission from the SNRs G126.2+1.6, G206.9+2.3 and CTB 13. M.Rosado (Inst. de Astron., Univ. Nacional Autonoma de Mexico, Mexico City, Mexico).

Rev. Mex. Astron. & Astrofis. (Mexico), vol.5, no.3, p.127-9 (July 1982). [received: April 1983]

Obtains narrow-band interference filter photographs in the light of H α , [S II] and [O III] of the SNRs G126.2+1.6 and G206.2.3 whose optical emission has been recently discovered, as well as that of the SNR CTB 13 which has been identified with some filaments on the PSS results. The first two SNRs

show high [S II]/H α and [O III]/H α line-ratios. The photograph of CTB 13 obtained in [O III] shows a spur coincident with the filaments visible on the PSS. A discussion of these individual SNRs is given. (15 refs.)

78984 Internal motions in H II regions. X. Are there optical H II regions associated with the Origen Loop? P.Pismis, I.Hasse (Inst. de Astron., Univ. Nacional Autonoma de Mexico, Mexico City, Mexico).

Rev. Mex. Astron. & Astrofis. (Mexico), vol.5, no.3, p.161-5 (July 1982). [received: April 1983]

For pt.IX see *ibid.*, vol.5, no.2, p.79-85 (1981). The proposition that the emission nebulae Sharpless 254, 255, 257, 261 and 269 are physically related to the old SNR—the Origen Loop—is examined. Optical radial velocities obtained by the Fabry Perot method are given over the regions S261 and S269 while those of S254, 255 and 257 are published earlier. The kinematic distances of the H II regions as well as the photometric distances of their ionizing stars are discussed. On the basis of these distances it is concluded that of these five H II regions only S261 may belong to the Origen Loop. (20 refs.)

78985 Internal motions in H II regions. XI. The emission nebula Sharpless 206. P.Pismis, I.Hasse (Inst. de Astron., Univ. Nacional Autonoma de Mexico, Mexico City, Mexico).

Rev. Mex. Astron. & Astrofis. (Mexico), vol.5, no.3, p.209-12 (July 1982). [received: April 1983]

For pt.X see *ibid.*, vol.5, no.3, p.161-5 (1982). Radial velocities at 142 points are obtained on the H II region S 206 by photographic Fabry-Perot interferometry using the reflectors with apertures of 2.1 meters at San Pedro Martir and 1-m at Tonantzintla. The overall velocity agrees with previous determinations. The velocities cover the western faint extensions of the nebula not studied hitherto. The velocity field is consistent with a directional expansion of S 206. (14 refs.)

78986 The filamentary nebula S 188. M.Rosado (Inst de Astron., Univ. Nacional Autonoma de Mexico, Mexico City, Mexico), K.B.Kwitter.

Rev. Mex. Astron. & Astrofis. (Mexico), vol.5, no.3, p.217-22 (July 1982). [received: April 1983]

The crescent shaped nebula Sharpless 188 is identified as a planetary nebula (PN) of Peimbert's (1981) Type I on the basis of its observed nebular spectrum. New FP interferometric work allows one to determine the motion of this nebula. The derived kinematical distance exceeds Cudworth's (1974) distance estimate supporting the idea that Peimbert's Type I PNs have larger ejected masses than typical PNs. A discussion about the origin of its non-spherical shape is also given. (19 refs.)

HOC⁺: laboratory observation of a proposed interstellar species See Entry 75550

The equilibria of rotating, isothermal clouds. I. Method of solution See Entry 78800

The equilibria of rotating, isothermal clouds. II. Structure and dynamical stability See Entry 78801

Circumvention of Parker's bound on galactic magnetic monopoles See Entry 78807

Catalog of luminous stars in the southern Coal-Sack zone See Entry 78828

An attempt to resolve pulsar magnetospheres using interstellar scintillations See Entry 78933

Spatially extended narrow emission-line gas in the Seyfert galaxy NGC 4151 See Entry 78987

Extended soft X-ray emission from NGC 4151 See Entry 78988

Mrk 744 and Mrk 1066: two Seyfert galaxies with strong absorption-line spectra See Entry 78991

The transitory nature of the filaments in NGC 5128 (Centaurus A) See Entry 78994

A multifrequency study of star formation in the blue compact dwarf galaxy I Zw 36 See Entry 78995

The variation of dust temperatures in Maffei 2 See Entry 78999

Radio continuum observations of the bar of NGC 1097 See Entry 79002

The incidence of 21 centimeter absorption in QSO redshift systems selected for Mg II absorption: evidence for a two-phase nature of the absorbing gas See Entry 79020

Neutral hydrogen absorption in the quasar 3C 268.4: possible evidence for galactic halo clouds See Entry 79022

X-ray nebular models See Entry 79025

98.50 THE GALAXY, EXTRAGALACTIC OBJECTS AND SYSTEMS

78987 Spatially extended narrow emission-line gas in the Seyfert galaxy NGC 4151. T.M.Heckman (Astron. Program, Univ. of Maryland, College Park, MD, USA), B.Balick.

Astrophys. J. (USA), vol.268, no.1, pt.1, p.102-4 (1 May 1983). Presents narrow-band images of the emission-line gas in the type I Seyfert galaxy NGC 4151. These data are compared with optical spectroscopic data, radio continuum maps, and (especially) with new X-ray imaging data (Elvis, Briel, and Henry, 1982). Both the emission-line gas and X-ray gas are asymmetrically extended to the SW of the nucleus. The quiescent kinematics of the emission-line clouds would seem to preclude models in which the clouds themselves are accelerated out of the nucleus, subsequently collide with the ambient medium, and so produce X-rays. The authors argue that the extended emission-line region is ambient interstellar material which is photoionized by X-rays emitted from an adjacent region of shocked interstellar gas. The narrow, elongated morphology of the extended emission-line region would then suggest that the nucleus supplies energy to its environs in a collimated fashion. (17 refs.)

78988 Extended soft X-ray emission from NGC 4151. M.Elvis (Harvard-Smithsonian Center for Astrophysics, Cambridge, MA, USA), U.G.Briel, J.P.Henry.

Astrophys. J. (USA), vol.268, no.1, pt.1, p.105-10 (1 May 1983).

An Einstein HRI exposure of ~ 8000 s shows evidence for an extended emission region centered $\sim 5''$ to the SW of the nucleus of NGC 4151. This emission accounts for $\sim 15\%$ of the total HRI flux and is equivalent to a luminosity of $\sim 5 \times 10^{40}$ ergs s⁻¹. The X-rays do not appear to come from the radio jet and are more likely to be associated with the large forbidden emission line region. The authors consider three possible sources: a hot thermal plasma in pressure equilibrium with the optical line emitting clouds and confining them; shock heating of outflowing forbidden line clouds as they impact on the normal interstellar medium of the galaxy; enhanced star formation, stimulated by shocks originating from outflowing emission line clouds leading to an unusual concentration of SNR and massive X-ray binaries. (32 refs.)

78989 The galactic gamma-ray source population. C.P.Godfrey (Iowa State Univ., Ames, IA, USA).

Astrophys. J. (USA), vol.268, no.1, pt.1, p.111-16 (1 May 1983).
The galactic gamma-ray source population as a whole is studied under the assumption that the discrete source are distributed in the same manner as the total galactic gamma-ray emissivity. The total emissivity distribution of high energy gamma rays (70 MeV < E < 5 GeV) as seen by the COS B satellite is derived via the geometrical unfolding technique. The assumption of proportionality between the discrete source component and the total emissivity at each point of the galactic disk then allows the relative distribution of the COS B-like sources to be found. This, together with the properties of the COS B catalog of sources, i.e. the total number of sources observed and the limiting flux sensitivity for source detection as a function of galactic longitude, can be used to derive parameters which describe the source population. (49 refs.)

78990 X-ray observations of 20 3CR radio galaxies and their environs. E.D.Feigelson, C.J.Berg (Dept. of Phys., MIT, Cambridge, MA, USA).

Astrophys. J. (USA), vol.269, no.2, pt.1, p.400-15 (15 June 1983).
Reports X-ray observations of a sample of 3CR radio galaxies using the Imaging Proportional Counter on the Einstein satellite. Possible relationships between X-ray emission and a variety of optical and radio properties are sought, partly to help determine whether the X-rays are produced predominantly in the active nucleus or in a gaseous intracuster medium. X-ray luminosity is statistically correlated with the radio power of the core, with the lobe radio power and with the steepness of the lobe radio spectrum at high frequencies. The complex interrelations between X-ray luminosities and radio core, radio lobe, optical nuclei, and galaxy clustering are discussed in detail. The data also provide constraints on synchrotron and inverse Compton production of X-rays in radio lobes and on mechanisms of lobe confinement. The authors discuss how correlations between X-ray and radio luminosities can be derived from flux-limited samples. (85 refs.)

78991 Mrk 744 and Mrk 1066: two Seyfert galaxies with strong absorption-line spectra. R.W.Goodrich, D.E.Osterbrock (Univ. of California, Santa Cruz, CA, USA).

Astrophys. J. (USA), vol.269, no.2, pt.1, p.416-22 (15 June 1983).
Spectrophotometric observations of the nuclei of two Seyfert galaxies, Mrk 744 and Mrk 1066, are reported. Both these objects have strong absorption-line spectra due to the underlying galaxies. A least squares fitting procedure is used to decompose the spectra into the galaxy contribution, the power-law featureless continuum, and the emission-line spectrum. Equivalent widths of the G, b, and E₂ absorption features are measured and the corresponding values of the fraction of power-law contribution at 4800 Å calculated and compared to the least squares results. It is suggested that Seyfert 1.8 galaxies like Mrk 744, and Seyfert 1.9 galaxies as well, may be objects in which the broad-line emitting region is seen nearly edge-on, so that the effects of extinction by dust are unusually large. (16 refs.)

78992 2-165 keV observations of active galaxies and the diffuse background. R.E.Rothschild (Univ. of California, San Diego, CA, USA), R.F.Mushotzky, W.A.Baity, D.E.Gruber, J.L.Matteson, L.E.Peterson.

Astrophys. J. (USA), vol.269, no.2, pt.1, p.423-37 (15 June 1983).
The HEAO 1 spectral observations of 12 active galaxies are presented in the 12-165 keV and 2-50 keV ranges. The mean spectrum of these galaxies is assumed to be representative of active galaxies in general. Then comparison of the mean active galaxy spectrum to the diffuse X-ray spectrum constrains the contribution of active galaxies to the diffuse flux, and gives upper limits to break energies in active galaxies. The data constrain the degree of number density evolution of active galaxies and point out the occurrence of nearly identical spectral indices, and dispersion in spectral index, from cores of active galaxies (as deduced from our measurements), 3CR radio sources, flat-spectrum radio sources, jets from active galaxies, and disks of spiral galaxies. This may indicate that the X-ray emission from the cores of active galaxies is also due to relativistic particles, as is believed to be the case for the radio sources. (60 refs.)

78993 Morphology of optical forms of N galaxies. W.W.Morgan, R.D.Dreier (Yerkes Obs., Williams Bay, WI, USA).

Astrophys. J. (USA), vol.269, no.2, pt.1, p.438-9 (15 June 1983).
Follows Weedman's (1977) suggestion of a spectroscopic definition for Seyfert galaxies, to present a simple four-box classification of the forms of N galaxies. The complete types for these galaxies must include a spectroscopic parameter that would show which of the Ns are also Seyferts—and the type of the Seyfert spectra in each case. (11 refs.)

78994 The transitory nature of the filaments in NGC 5128 (Centaurus A). J.A.Graham (Cerro Tololo Inter-American Obs., La Serena, Chile).

Astrophys. J. (USA), vol.269, no.2, pt.1, p.440-3 (15 June 1983).
New optical observations demonstrate differential velocities of at least 800 km s⁻¹ within a group of gaseous filaments near the middle NE radio lobe of the galaxy NGC 5128. These optical fragments are at a projected distance of 30 kpc from the main body of the galaxy and are associated with an extended source of soft X-rays. Compared with reasonable values for the average space velocity of the gas, the internal velocity spread is too high for it to have traveled in its present turbulent state over the full distance from the nucleus. The gaseous filaments, as observed, are evidently only temporary and will disperse over a time of the order of 10⁶-10⁷ years. (5 refs.)

78995 A multifrequency study of star formation in the blue compact dwarf galaxy I Zw 36. F.Viallefond (Obs. de Paris-Meudon, Paris, France), T.X.Thuan.

Astrophys. J. (USA), vol.269, no.2, pt.1, p.444-65 (15 June 1983).
Presents radio, near-infrared, optical, and ultraviolet observations of the blue compact dwarf galaxy I Zw 36 ≡ Mrk 209 ≡ Haro 29. The visible star formation region is associated with the core but is slightly shifted with respect to the H I peak column density. I Zw 36 has about a tenth of the solar metallicity. Its dust-to-oxygen abundance ratio by mass is discussed. The near-infrared observations indicate the presence of an old stellar population of G and K giants. Star formation models with an initial mass function of slope 1.5 (the Salpeter value is 1.35) and a burst age or duration of a few million years fit well the optical spectrophotometric measurements. To account for the metallicity, one previous burst of very short duration with a strength comparable to the present one is needed. Alternatively, no previous massive star formation is needed if there has been continuous star formation at a constant rate for the last 7 million years. The old stellar population can account for the virial mass only if it is spatially much more extended than the young population. In that case, low-mass stars must have formed in the past independently from the burst producing the massive stars. (46 refs.)

78996 Spectroscopic evidence for activity in the nuclei of normal spiral galaxies. W.C.Keel (Lick Obs., Univ. of California, Santa Cruz, CA, USA).

Astrophys. J. (USA), vol.269, no.2, pt.1, p.466-86 (15 June 1983).
The emission spectra of 29 spiral galaxies with low-ionization emission are studied in detail, using synthetic galaxy spectra to correct the observed spectra for the contribution of starlight. The resulting emission-line intensities and

ratios are compared to published models of shock-heated and power-law photoionized plasmas. The observed spectra are best described by models in which a weak flat-spectrum (power-law) radiation field photoionizes the gas; this nonthermal continuum is generally too weak to be seen directly in the optical. Broad H α emission extending over a total velocity range as great as 400 km s⁻¹, is identified in several 'normal' nuclei with strong low-ionization emission. The inferred nonthermal continuum and observed broad permitted lines indicate the presence of low-luminosity active nuclei in most, if not all, spiral galaxies. (80 refs.)

78997 The stability of a magnetically confined radio jet. H.Cohn (Dept. of Phys., Univ. of Illinois, Urbana, IL, USA).

Astrophys. J. (USA), vol.269, no.2, pt.1, p.500-12 (15 June 1983).
The linear stability against pinching modes of a model for a magnetically confined extragalactic radio jet is investigated. An analytic dispersion relation for these modes is obtained and then solved numerically. For comparison the dispersion relation for the Kelvin-Helmholtz pinching modes of a pressure confined jet is also solved numerically. The behavior of the modes is found to be fairly independent of the confinement mechanism. Subsonic and Mach 1 jets are found to be unstable to a single pinching mode at every wavenumber. In addition to this fundamental mode, supersonic jets have an infinite set of higher order ('reflection') pinching modes that enter at points of marginal stability. When the jet velocity is less than hypersonic, these reflection modes have large spatial growth rates and thus may be responsible for the observed knot structure of radio jets. (37 refs.)

78998 Can secondary infall produce flat rotation curves? C.Pryor, M.Lecar (Harvard-Smithsonian Center for Astrophysics, Cambridge, MA, USA).

Astrophys. J. (USA), vol.269, no.2, pt.1, p.513-30 (15 June 1983).
Performs a series of numerical experiments to simulate the formation of galactic halos by dissipationless secondary infall. The purpose is to test Gunn's (1977) suggestion that density profiles as shallow as r^{-2} could be produced when a surrounding region with greater than critical density falls in on a $\sim 10^{11} M_{\odot}$ galaxy which had formed earlier. As predicted, the maximum expansion density profiles were as shallow as r^{-2} , but these shallow profiles were not preserved in the subsequent infall. One reason for this was that the initial conditions which yielded shallow profiles at maximum expansion also enhanced the collective relaxation during the collapse, which steepened the final profiles. Another reason was that the infall adiabatically compressed the material in the outer halo less than that in the inner regions. This effect steepened the profile of the outer half of the mass and, like the collective relaxation, was more pronounced for shallow maximum expansion profiles. Both effects combined to prevent the formation of profiles shallow enough to explain the observed flat rotation curves of galaxies. (25 refs.)

78999 The variation of dust temperatures in Maffei 2. L.J.Rickard (Dept. of Phys. & Astron., Howard Univ., Washington, DC, USA), P.M.Harvey.

Astrophys. J. Lett. Ed. (USA), vol.268, no.1, pt.2, p.L7-9 (1 May 1983).
Reports far-infrared photometry for the central regions of Maffei 2. The fitted dust temperatures show a definite decline away from the nucleus. This supports the hypothesis that the molecular clouds close to the nucleus represent a different population from the disk clouds. Extragalactic studies that assume constant temperatures to convert CO integrated intensity to molecular hydrogen surface mass density may be in serious error. (20 refs.)

79000 Rapid X-ray variability from the Seyfert 1 galaxy NGC 4051. F.E.Marshall, S.S.Holt, R.F.Mushotzky (Lab. for High Energy Astrophysics, NASA Goddard Space Flight Center, Greenbelt, MD, USA), R.H.Becker.

Astrophys. J. Lett. Ed. (USA), vol.269, no.2, pt.2, p.L31-5 (15 June 1983).
Strong variable X-ray emission from the nearby low-luminosity Seyfert 1 galaxy NGC 4051 has been discovered during observations with the imaging proportional counter (IPC) of the Einstein Observatory. During one 2304 s observation, the X-ray flux more than doubled in an approximately linear fashion, and a 70% increase for 150 s was seen during another 968 s observation. The authors present evidence that the X-ray spectrum of NGC 4051 is unusually soft compared with Seyfert 1 galaxies or QSOs. The emission mechanism is probably not synchrotron or synchrotron self-Compton, but the emission can be plausibly explained by various black hole accretion models. (25 refs.)

79001 Low-ionization active galactic nuclei: X-ray or shock heated? J.P.Halpern (Harvard-Smithsonian Center for Astrophysics, Cambridge, MA, USA), J.E.Steiner.

Astrophys. J. Lett. Ed. (USA), vol.269, no.2, pt.2, p.L37-41 (15 June 1983).
Evaluates narrow-line ratios for a wide variety of active galactic nuclei, including those claimed to be shock heated. In the context of a Seyfert photoionization model, the entire range of observed narrow-line excitation conditions can be accounted for by varying a single parameter related to the photon flux. The characteristic [O II]:[O I]:[O III] line ratios which define Heckman's (1980) 'Liners' are reproduced, obviating the need to invoke shock heating for these low-ionization nuclei. X-ray data on a number of Liners provide preliminary evidence for an ionizing continuum. The Seyfert 1.8 and 1.9 galaxies (weak, broad wings) appear to be transition cases between Seyferts and Liners. The authors conclude that Liners are low-luminosity or obscured Seyfert nuclei, or both. The photoionization model also explains the large [N II]/H α ratio often seen in the nuclei of galaxies. (37 refs.)

79002 Radio continuum observations of the bar of NGC 1097. M.P.Ondrechen, J.M.Van Der Hulst (Dept. of Astron., Univ. of Minnesota, Minneapolis, MN, USA).

Astrophys. J. Lett. Ed. (USA), vol.269, no.2, pt.2, p.L47-50 (15 June 1983).
Radio continuum observations of NGC 1097 at 1465 MHz with the VLA reveal emission coincident with the straight, narrow dust lanes in the bar. The authors believe this is nonthermal emission produced by the shock compression of the gas, dust, and magnetic field in the bar. This shock compression is a common feature of models dealing with the gas flow in barred spiral galaxies. The results thus provide strong evidence that the predicted shock fronts to indeed exist. (36 refs.)

79003 Density gradients for disc- and halo-stars in the direction of the globular cluster NGC 7006. W.Becker, S.Karaali (Astron. Inst., Univ. of Basle, Binningen, Switzerland).

Astron. & Astrophys. Suppl. Ser. (France), vol.52, no.2, p.269-77 (May 1983).

A photographic RGU-photometry of 1810 stars down to the limiting magnitude $G=19^m$ has been carried out in a field of 0.29 square degrees near the globular cluster NGC 7006 ($\alpha=64^{\circ}$, $\delta=-19^{\circ}$). The possibilities of identifying main-sequence stars and late-type giants of both populations by means of the two-colour diagrams are discussed. No interstellar absorption could be detected in this direction. Density functions have been determined for main-sequence stars and late-type giants of Population I and for main-sequence stars of Population II. The Population I functions are compared with the ones valid for the solar neighbourhood reduced to the galactic latitude of the field ($D/\sin b$). The luminosity function for main-sequence stars of Population I within 400 to 800 pc has been determined and compared to the ones valid for

the solar neighbourhood and for $z=200$ pc. Finally the colour-magnitude diagrams of both populations are discussed. (9 refs.)

79004 Double galaxy investigations. I. Observations. W.G.Tift (Steward Obs., Univ. of Arizona, Tucson, AZ, USA). *Astrophys. J. Suppl. Ser. (USA)*, vol.50, no.3, p.319-89 (Nov. 1982). [received: May 1983]

Redshift information from 240 Å mm⁻¹ spectrograms is presented for 370 double galaxy systems from Karachensev (1972) including all pairs in that catalog with separation less than 80". An extensive error discussion utilizing internal and external (21 cm) comparisons provides calibration of systematic error and determines the uncertainty for a typical high weight optical redshift to be ± 65 km s⁻¹. Internal differential redshifts within single spectra using common lines achieve accuracies of 18-30 km s⁻¹, depending upon separation, and are available for ~200 pairs. Extensive information on emission and other properties is also provided. (20 refs.)

79005 Global stability of disk-bulge systems: spiral structure of disk galaxies. A.Ambastha, R.K.Varma (Phys. Res. Lab., Ahmedabad, India). *J. Astrophys. & Astron. (India)*, vol.3, no.2, p.125-44 (June 1982). [received: June 1983]

The spiral arms of disk galaxies are very sensitive to various morphological properties. The stability of self-gravitating annular disks surrounding the central rigid bulge component is studied in order to explain the transition from the tight spiral arms in Sa galaxies to rather open patterns in Sc galaxies as the central amorphous component diminishes. When the disk-to-bulge mass ratio is small, a tight pattern results restricted to the inner regions of the disk. This pattern opens up and occupies larger disk areas as the disk component becomes comparable to the bulge. It is found that unstable modes of the annular disk can be suppressed by increasing the thermal pressure sufficiently. (28 refs.)

79006 Compact radio cores and the relation between the radio and optical axes of elliptical galaxies. V.K.Kapahi, D.J.Saikia (Radio Astron. Centre, Tata Inst. of Fundamental Res., Bangalore, India). *J. Astrophys. & Astron. (India)*, vol.3, no.2, p.161-71 (June 1982). [received: June 1983]

Investigates the reported tendency for the extended radio structures associated with bright elliptical galaxies to be oriented preferentially along the optical minor axes. It is found that such a tendency exists only for those galaxies in which the compact radio cores coincident with their nuclei are quite prominent. If the galaxies are divided into two groups according to whether their cores account for less than or greater than 10 per cent of the total flux density at 2.7 GHz, the angle ϕ (between the radio axis and the optical minor axis) appears to be uniformly distributed between 0° and 90° for the former, but is nearly always <30° for the latter group. One possible explanation is that the radio emission from compact cores suffers thermal absorption by ionized gas that is distributed differently in the two groups. (38 refs.)

79007 The differential rotation of The Galaxy and the change of pulsar period. Rong Jianxiang, Xia Yifei (Dept. of Astron., Nanjing Univ., China). *Kexue Tongbao (Foreign Lang. Ed.) (China)*, vol.28, no.3, p.352-6 (March 1983).

The rate of periodical change, \dot{P} , is one of the most important parameters for pulsars, for it provides a lot of valuable information for studying the physical processes of them. At present, the intrinsic mechanisms of pulsar radiation responsible for the change of radio pulse period are being discussed heatedly on a world scale, but research into the external causes that are independent of the intrinsic mechanisms that affect the change has been neglected. Among the external causes, the effect of differential rotation of the Galaxy on the change of pulsar period is a subject the authors have studied. Owing to the presence of differential rotation of the Galaxy, for each pulsar there exists a factor affecting the rate of periodical change of the pulsar. Therefore this effect is of universal significance. (7 refs.)

79008 Inversion symmetry of radio lobes in extragalactic sources. Gopal-Krishna, S.M.Chitre (Radio Astron. Centre, Tata Inst. of Fundamental Res., Bangalore, India). *Nature (GB)*, vol.303, no.5914, p.217-18 (19 May 1983).

The collimated beams of relativistic particles ejected from the central engines of extragalactic radio sources are traced out by means of the jet-like features of nonthermal radio emission which are observed to extend up to a few hundred kiloparsecs. These jets exhibit departures from linearity in a variety of ways. In some less luminous large radio galaxies, the jets show structures with a distinctive S-shaped bending (inversion symmetry) at distances of the order of 100 kpc from the galactic nucleus. The authors propose that such a sharp bending can result from the interaction of the relativistic beam fluid with faint, rotating shells similar to those seen around some nearby galaxies. The possible implications of this hypothesis are discussed. (40 refs.)

79009 Direct evidence for a massive galactic halo. M.R.S.Hawkins (Royal Obs., Edinburgh, Scotland). *Nature (GB)*, vol.303, no.5916, p.406-8 (2 June 1983).

Reports the discovery of a very distant galactic RR Lyrae star, R15. Spectroscopic observations of the object show that it has a high negative radial velocity, implying a lower limit to the mass of the Galaxy of $1.4 \times 10^{12} M_{\odot}$. (10 refs.)

79010 Measurement of the 0.511 MeV γ -ray line from the galactic center. J.O.D.Jardim, J.L.Benson, M.V.A.Jardim, I.M.Martin (Inst. de Pesquisas Espaciais, Rio de Janeiro, Brazil). *Rev. Mex. Astron. & Astrofis. (Mexico)*, vol.5, no.3, p.131-3 (July 1982). [received: April 1983]

The detection of the 0.511 MeV electron-positron annihilation line coming from the galactic center can provide the means to estimate the rate of positron production and to test some theoretical sources of positrons. The authors present the result of the measurements of the 0.511 MeV line flux made in a gamma-ray experiment on board a stratospheric balloon. (12 refs.)

Inverse Feigenbaum bifurcations in Hamiltonian systemsSee Entry 74260

Viscous fluid in static spherically symmetric space-timeSee Entry 74330

Simulation models for the evolution of cloud systems. I. Introduction and preliminary simulationsSee Entry 78804

The Jeans problem for a thin galaxy in steady stateSee Entry 78805

Dyon black hole in the Tomimatsu-Sato-Yamazaki space-timeSee Entry 78812

The ages of the disks of S0 galaxiesSee Entry 78821

The brightest stars as extragalactic distance indicatorsSee Entry 78822

Supernova in NGC 4753See Entry 78931

Supernova in NGC 3106See Entry 78932

A radio pulsar in the Large Magellanic CloudSee Entry 78936

Structure and stability of rotating fluid disks around massive objects. II. General relativistic formulationSee Entry 78940

Why high-latitude clouds in our Galaxy and the highly redshifted clouds observed in front of OSOs do not belong to the same parent populationSee Entry 78975

The evolution of clusters of galaxies. I. Very rich clustersSee Entry 79011

The Cancer Cluster: an unbound collection of groupsSee Entry 79012

Redshift quantization in compact groups of galaxiesSee Entry 79013

A statistical VLBI study of milli-arcsecond cores in extragalactic radio sourcesSee Entry 79014

Extragalactic 1 millimeter sources: simultaneous observations at centimeter, millimeter, and visual wavelengthsSee Entry 79019

X-ray nebular modelsSee Entry 79025

Can graininess in the early Universe make galaxies?See Entry 79029

Cosmological self-similar shock waves and galaxy formationSee Entry 79030

98.50K Groups, clusters, superclusters

79011 The evolution of clusters of galaxies. I. Very rich clusters. D.O.Richstone, E.M.Malumuth (Dept. of Astron., Univ. of Michigan, Ann Arbor, MI, USA). *Astrophys. J. (USA)*, vol.268, no.1, pt.1, p.30-46 (1 May 1983).

A multiple one-body Monte Carlo code is developed which follows the evolution of galaxies in a steady cluster potential under the influence of dynamical friction, two-body relaxation, tidal stripping, and galaxy mergers. The authors show that the formation of a very massive cluster galaxy depends critically on the number of galaxies, the initial division of cluster material between galaxies and a smooth intracluster medium (ICM), the mass spectrum of the galaxies, and luck. Using a Schechter mass spectrum with no initial intra-cluster medium, the authors find that 30% of the simulations produce a very massive galaxy at the cluster center. This fraction can be altered by changing the mass spectrum or the ICM fraction. The mass, location, and low velocity relative to the cluster center of this very massive object, when it is produced, are consistent with identifying it as a cD galaxy. By the end of all simulations, less than half of the mass in the central region of the cluster is bound to galaxies. (50 refs.)

79012 The Cancer Cluster: an unbound collection of groups. G.D.Bothun, M.J.Geller, T.C.Beers, J.P.Huchra (Harvard-Smithsonian Center for Astrophys., Cambridge, MA, USA). *Astrophys. J. (USA)*, vol.268, no.1, pt.1, p.47-55 (1 May 1983).

Presents a surface density contour map of the Cancer Cluster derived from galaxy counts in the Zwicky catalog. The contour map shows that the galaxy distribution is clumpy. When this spatial distribution is combined with nearly complete velocity information, the clumps stand out more clearly; there are significant differences in the mean velocities of the clumps which exceed their internal velocity dispersions. The Cancer Cluster is not a proper 'cluster' but is a collection of discrete groups, each with a velocity dispersion $\sigma_v \approx 300$ km s⁻¹, separating from one another with the cosmological flow. The mass-to-light ratio for galaxies in the main concentration is discussed. (26 refs.)

79013 Redshift quantization in compact groups of galaxies. W.J.Cocke, W.G.Tift (Steward Obs., Univ. of Arizona, Tucson, AZ, USA). *Astrophys. J. (USA)*, vol.268, no.1, pt.1, p.56-9 (1 May 1983).

Radio data (21 cm) on the redshifts of galaxies in small groups are analyzed for the previously 72 km s⁻¹ quantization. The redshift differentials definitely clump about multiples of 72 km s⁻¹, at a confidence level of 99.5%. The detailed deviations of the data from exact quantization are discussed in terms of the superposition of redshift states. (13 refs.)

The massive neutrino and clustering phenomena in the UniverseSee Entry 78806

X-ray observations of 20 3CR radio galaxies and their environsSee Entry 78990

The irregular distribution of galaxies and the anisotropies in the microwave background photonsSee Entry 79027

98.70 OTHER OBJECTS AND BACKGROUND RADIATIONS OF UNKNOWN ORIGIN AND DISTANCES

(for pulsars, see 97.60G)

98.70D Discrete radio sources

79014 A statistical VLBI study of milli-arcsecond cores in extragalactic radio sources. R.A.Preston, D.D.Morabito (Jet Propulsion Lab., California Inst. of Technol., Pasadena, CA, USA), D.L.Jauncey. *Astrophys. J. (USA)*, vol.269, no.2, pt.1, p.387-99 (15 June 1983).

VLBI observations at 2.3 GHz have been performed with a baseline of $\sim 8 \times 10^7$ wavelengths on a complete sample of 103 sources from the Parkes $\pm 4^\circ$ catalog. Compact milli-arcsecond cores were found in 35% of all sources: 80% of quasars, only 10% of galaxies, and 20% of empty field sources. Virtually all of the sources appear to be at least partially resolved. For quasars, the percentage of the source flux density found to be coming from milli-arcsecond cores increased with increasing radio spectral index, radio variability and optical redness. Quasars with extended radio structure ($\geq 10''$) seem more likely to possess a detectable milli-arcsecond core than do extended radio galaxies. The absence of a strong correlation between quasar milli-arcsecond structure and redshift is evidence for a lack of strong physical evolution in quasars, a hypothesis which is in agreement with previous studies of the size evolution of both quasar large-scale radio structure and radio lobe hot spots. (35 refs.)

79015 The variability of the optical counterparts of four extragalactic radio sources. H.R.Miller (Dept. of Phys. & Astron., Georgia State Univ., Atlanta, GA, USA). *Astron. & Astrophys. Suppl. Ser. (France)*, vol.52, no.2, p.289-91 (May 1983).

Theoretical variability of four extragalactic radio sources has been studied using the archival plates at the Harvard College Observatory. Three of these sources, PKS 1123+264, B2 1132+303, and 4C 18.36, were conclusively found to exhibit significant optical variability. No conclusive evidence was found for optical variability for B2 1128+315 with a range $\Delta m < 0.3$ magnitude, based on a limited number of plates. (16 refs.)

79016 Measurement of unambiguous rotation measures of extragalactic sources. L.Rudnick (Dept. of Astron., Univ. of Minnesota, Minneapolis, MN, USA), E.Zukowski, P.P.Kronberg. *Astron. & Astrophys. Suppl. Ser. (France)*, vol.52, no.2, p.317-21 (May 1983).

Reports the results of polarization measurements conducted specifically to check for the existence of very high Faraday rotation measures, which might otherwise have been undetected. Polarization measurements are presented for 24 extragalactic radio sources at 4 contiguous bands around λ 9 cm, from observations at the NRAO 300' telescope. These measurements can be used to derive rotation measures (and limits) which are free from π phase ambiguities around λ 9 cm. Data cannot be made consistent with arbitrarily large rotation measures. Revised rotation measures and initial position angles are presented for the observed sources. (5 refs.)

79017 VLA observations of hot spots in high luminosity radio sources. R.T.Schilizzi (Netherlands Foundation for Radio Astron., Dwingeloo, Netherlands), V.K.Kapahi, S.G.Neff. *J. Astrophys. & Astron. (India)*, vol.3, no.2, p.173-87 (June 1982). [received: June 1983]

VLA observations at 6 cm have been made of 16 distant luminous 3C sources that appeared to be unresolved or slightly resolved in Cambridge maps but which were known from VLBI observations to contain significant fine structure on the scale of about 1 kpc in their lobes. The general morphology of these sources is very similar to that of their nearby powerful counterparts; most of the lobes contain low brightness tails which are often directed from the hot spots towards the associated optical object. The hot spots are generally unresolved by the VLA observations; in 3C 254, 3C 268.4 and 3C 352, one of the lobes contains two hot spots. (20 refs.)

79018 The identification of CTA 21. D.A.Allen (Anglo-Australian Obs., Epping, NSW, Australia), A.E.Wright, J.G.Ables. *J. Astrophys. & Astron. (India)*, vol.3, no.2, p.189-92 (June 1982). [received: June 1983]

CTA 21 has long been the outstanding example of a strong, compact radio source lacking an optical identification. The authors report the discovery at infrared wavelengths of the counterpart of CTA 21, and show that its spectral shape is unusual. (9 refs.)

A correlation interferometer for interplanetary scintillation observations See Entry 78814

Observational studies of the symbiotic stars. II. Emission-line relative intensity variations in CI Cygni, BF Cygni, AX Persei, and V1016 Cygni See Entry 78916

Narrow-band photometric periods in SS 433 See Entry 78920

New optical positions and proper motions of late type stars associated with SiO masers See Entry 78924

Spectroscopy of V711 Tauri (=HR 1099): fundamental properties and evidence for starspots See Entry 78941

Optical studies of Cassiopeia A VI. Observations during the period 1976-80 See Entry 78968

High-velocity, asymmetric Doppler shifts of the X-ray emission lines of Cassiopeia A See Entry 78969

A rotating protocluster in W58:HCO⁺ aperture synthesis maps See Entry 78972

Observations of the supernova remnants HB 9 and IC 443 at 34.5 MHz See Entry 78981

Optical emission from the SNRs G126.2+1.6, G206.9+2.3 and CTB 13 See Entry 78983

The filamentary nebula S 188 See Entry 78986

X-ray observations of 20 3CR radio galaxies and their environs See Entry 78990

The transitory nature of the filaments in NGC 5128 (Centaurus A) See Entry 78994

The stability of a magnetically confined radio jet See Entry 78997

Radio continuum observations of the bar of NGC 1097 See Entry 79002

Compact radio cores and the relation between the radio and optical axes of elliptical galaxies See Entry 79006

Neutral hydrogen absorption in the quasar 3C 268.4: possible evidence for galactic halo clouds See Entry 79022

98.70J Quasars

79019 Extragalactic 1 millimeter sources: simultaneous observations at centimeter, millimeter, and visual wavelengths. R.Landau, T.W.Jones (Astron. Dept., Univ. of Minnesota, Minneapolis, MN, USA), E.E.Epstein, G.Neugebauer, B.T.Soffer, M.W.Werner, J.J.Puschell, T.J.Balonek. *Astrophys. J. (USA)*, vol.268, no.1, pt.1, p.68-75 (1 May 1983).

Observations simultaneously made at visual (B, V, and R) wavelengths, at 1, 1.4, and 3.4 mm and at 1.3, 2, 6, and 20 cm of 9 QSOs and BL Lac objects are reported. The range of the millimeter-visual spectral index may indicate that the electrons radiating synchrotron emission in this portion of the spectrum are not subjected to large radiative losses, and therefore relative bulk motion with Doppler factors ~ 10 are required. The visual spectral index is much more broadly distributed. The spectral energy distributions have not changed much in the last 2-5 years except for 2251+15 and perhaps 0235+164. Only 1749+09 shows a sharp spectral break shortward of 1 mm. (39 refs.)

79020 The incidence of 21 centimeter absorption in QSO redshift systems selected for Mg II absorption: evidence for a two-phase nature of the absorbing gas. F.H.Briggs, A.M.Wolfe (Dept. of Phys. & Astron., Univ. of Pittsburgh, Pittsburgh, PA, USA).

Astrophys. J. (USA), vol.268, no.1, pt.1, p.76-89 (1 May 1983).

A search for 21 cm absorption in the continua of 15 radio-bright QSOs reveals that 21 cm absorption occurs in two out of 18 redshifted clouds selected for Mg II absorption. There is no evidence that optical properties such as Mg II equivalent width, Mg II double ratio, or Mg I equivalent width are correlated with 21 cm optical depth. The lack of correlation between optical and radio absorption properties is related to the multi-component nature of the absorbing gas. While most of the narrow velocity components detected in this gas may not contain enough H I to produce 21 cm absorption, they still dominate saturated equivalent widths of UV resonance lines owing to the large internal velocity interval which they span. Occasionally, most of the H I is in one or more narrow components which produce detectable 21 cm absorption, but which make negligible contribution to optical equivalent widths. Lower limits are placed on the spin temperature of three Mg II systems, which rule out galactic disks as the absorption sites. A two-

phase model is suggested to unify the entire sample of Mg II systems. (57 refs.)

79021 Quasar evolution derived from the Palomar Bright Quasar Survey and other complete quasar surveys. M.Schmidt (Palomar Obs., California Inst. of Technol., Pasadena, CA, USA), R.F.Green.

Astrophys. J. (USA), vol.269, no.2, pt.1, p.352-74 (15 June 1983).

Presents the Bright Quasar Survey (BQS) consisting of 114 objects to an average limiting magnitude $B=16.16$ over an area of 10714 deg². There are 92 quasars with $M_B < -23$ in the sample. The authors use the BQS and complete samples from published surveys to derive models of the statistical evolution of quasars. The increase of space density with redshift depends strongly on absolute luminosity, being close to zero for low-luminosity quasars. Detailed predictions are given for the distribution of redshifts and magnitudes and for the total counts based on the evolution models. (65 refs.)

79022 Neutral hydrogen absorption in the quasar 3C 268.4: possible evidence for galactic halo clouds. A.D.Haschick (Haystack Obs., Westford, MA, USA), P.C.Crane, W.A.Baan.

Astrophys. J. Lett. Ed. (USA), vol.269, no.2, pt.2, p.L43-6 (15 June 1983).

Detects neutral hydrogen absorption at 21 cm wavelengths in the quasar-galaxy pair 3C 268.4/NGC 4138. The absorption spectrum exhibits two features which are separated by 65 and ~ 120 km s⁻¹, respectively, from the center velocity of 880 km s⁻¹ of the neutral hydrogen emission profile from NGC 4138. The line of sight to the quasar 3C 268.4 is separated by ~ 14 kpc (2.9') from NGC 4138 and lies very close ($< 5^\circ$) to the minor axis of the galaxy where the radial component of its rotation velocity is small. This leads to the suggestion that, in view of the large relative velocities of the neutral hydrogen clouds producing the observed absorption features, they are situated in the halo region rather than in the disk of the galaxy. The detection of this second example of absorption in a close quasar-galaxy pair further weakens the argument for association of the quasar with the galaxy. (22 refs.)

Why high-latitude clouds in our Galaxy and the highly redshifted clouds observed in front of OSOs do not belong to the same parent population See Entry 78975

A statistical VLBI study of milli-arcsecond cores in extragalactic radio sources See Entry 79014

VLA observations of hot spots in high luminosity radio sources See Entry 79017

X-ray studies of quasars with the Einstein Observatory. III. The 3CR sample See Entry 79023

X-ray nebular models See Entry 79025

98.70L IR sources

(see also 98.40 in nebulae)

Observational studies of the symbiotic stars. II. Emission-line relative intensity variations in CI Cygni, BF Cygni, AX Persei, and V1016 Cygni See Entry 78916

New optical positions and proper motions of late type stars associated with SiO masers See Entry 78924

The identification of CTA 21 See Entry 79018

98.70Q X-ray and gamma-ray sources

79023 X-ray studies of quasars with the Einstein Observatory. III. The 3CR sample. H.Tananbaum, J.F.C.Wardle, G.Zamorani, Y.Avni (Harvard-Smithsonian Center for Astrophysics, Cambridge, MA, USA).

Astrophys. J. (USA), vol.268, no.1, pt.1, p.60-7 (1 May 1983).

For pt.II see ibid., vol.245, no.2, p.357-74 (1981). Using the Einstein Observatory, the authors have detected X-ray emission from each of the 33 3CR quasars in Schmidt's complete sample. The authors observe a rather narrow distribution of X-ray luminosity compared to the distributions of radio and optical luminosity. The X-ray (2 keV) luminosity is strongly correlated with optical (2500 Å) luminosity, while there is no evidence within the sample for a dependence of X-ray luminosity on redshift or on total radio (5 GHz) luminosity. The authors derive an estimate of the X-ray luminosity distribution function for 3CR quasars and discuss the cosmological evolution of the X-ray luminosity function. For 3CR quasars which have a 'triple' radio structure the authors find a correlation between X-ray luminosity and radio luminosity of the central radio component. (34 refs.)

79024 The optical identification content of the Einstein Observatory deep X-ray survey of a region in Pavo. R.E.Griffiths, S.S.Murray, R.Giacconi, J.Bechtold (Harvard-Smithsonian Center for Astrophysics, Cambridge, MA, USA), P.Murdin, M.Smith, H.T.MacGillivray, M.Ward, J.Danziger, J.Lub, B.A.Peterson, A.E.Wright, M.J.Batty, D.L.Jauncey, D.F.Malin.

Astrophys. J. (USA), vol.269, no.2, pt.1, p.375-86 (15 June 1983).

Results are presented from the Einstein deep X-ray survey in Pavo, with correlated optical and radio observations of a complete sample of candidate identifications. There are 16 X-ray sources detected with positional accuracy better than 10", of which five are identified, with a further seven (and a maximum nine) probable identifications. Of the identified sources, four are QSOs with J -magnitude ~ 20 (one is an inverted spectrum radio source) and one is associated with extended emission from a pair or cluster of galaxies. Of the probable identifications, one is a galaxy and the rest are a subset of a yellow stellar object population which may also be QSOs. Identifications with QSOs and QSO candidates with $J < 24$ account for 60-80% of the detected sources. (34 refs.)

79025 X-ray nebular models. T.R.Kallman, R.McCray (Joint Inst. for Lab. Astrophys., Univ. of Colorado, Boulder, CO, USA).

Astrophys. J. Suppl. Ser. (USA), vol.50, no.3, p.263-318 (Nov. 1982).

[received: May 1983]

Theoretical models are presented for the temperature and ionization structure of spherically symmetric, constant density, gaseous nebulae surrounding compact X-ray sources and for the optical, UV, and X-ray spectra emerging from the nebulae. The structure is determined by assuming a local balance between heating and cooling in the gas, and the radiation field is found by solving a simplified equation of transfer. The calculations include an accurate and comprehensive treatment of the atomic processes affecting the state of the gas and the radiation field. The destruction of line radiation during resonance scattering causes models to be significantly hotter and more highly ionized than previous models of the same type. Model results are presented for a wide variety of gas densities and X-ray source spectra, scaling laws which allow these results to be generalized to a wide variety of astrophysical solutions are discussed, and column densities of multiply charged species are tabulated. (92 refs.)

- 79026** Quantized synchrotron radiation as a cause of γ -ray bursts. T.L.Chow (Dept. of Phys., California State Coll., Turlock, CA, USA). *Lett. Nuovo Cimento (Italy)*, vol.37, ser.2, no.4, p.142-4 (28 May 1983). The author considers gamma-ray bursts, quantised magnetic bremsstrahlung radiation in intense magnetic fields from the surface layers of neutron stars is investigated as a possible burst mechanism. (8 refs.)
- Gamma-ray astronomy** See Entry 78811
- Observational studies of the symbiotic stars. II. Emission-line relative intensity variations in CI Cygni, BF Cygni, AX Persei, and V1016 Cygni** See Entry 78916
- Spectroscopy of V711 Tauri (=HR 1099): fundamental properties and evidence for starspots** See Entry 78941
- Detection of 2×10^{15} to 2×10^{16} eV gamma-rays from Cygnus X-3** See Entry 78944
- Optical studies of Cassiopeia A VI. Observations during the peroid 1976-80** See Entry 78968
- High-velocity, asymmetric Doppler shifts of the X-ray emission lines of Cassiopeia A** See Entry 78969
- X-ray sources in molecular clouds** See Entry 78971
- Ring ejection in Type II supernovae: 1E 0102.2-7219 in the Small Magellanic Cloud** See Entry 78976
- Observations of the supernova remnants HB 9 and IC 443 at 34.5 MHz** See Entry 78981
- Spatially extended narrow emission-line gas in the Seyfert galaxy NGC 4151** See Entry 78987
- Extended soft X-ray emission from NGC 4151** See Entry 78988
- The galactic gamma-ray source population** See Entry 78989
- 2-165 keV observations of active galaxies and the diffuse background** See Entry 78992
- The transitory nature of the filaments in NGC 5128 (Centaurus A)** See Entry 78994
- Rapid X-ray variability from the Seyfert 1 galaxy NGC 4051** See Entry 79000
- Low-ionization active galactic nuclei: X-ray or shock heated?** See Entry 79001

98.70V Background radiations

- 79027** The irregular distribution of galaxies and the anisotropies in the microwave background photons. C.Ceccarelli, F.Melchiorri, L.Pietranera (Istituto di Fisica, Univ. di Roma, Roma, Italy), G.Dall'Oglio, B.O.Melchiorri. *Astrophys. J. Lett. Ed. (USA)*, vol.269, no.2, pt.2, p.L27-9 (15 June 1983). An infrared search for the Sunyaev-Zeldovich effect toward the intergalactic 'void' discovered by Kirshner et al. (1981) has given a null result within 1×10^{-4} K at 1 standard deviation. The result implies that the change of the Comptonization parameter toward the hole is less than 2×10^{-2} . From the hypothesis that the hot gas is absent in the hole, the authors obtain an upper limit 0.5 for the normalized density of the extragalactic gas. (12 refs.)
- 79028** Cosmic noise observations at high radio frequencies. M.Kotaki, I.Kuriki, C.Katoh, H.Sugiuchi. *Rev. Radio Res. Lab. (Japan)*, vol.28, no.146, p.387-97 (June 1982). In Japanese. Using the equipments on-board ISS-b, the average galactic radio noise has been obtained at the frequencies of 5, 10 and 25 MHz, and the noise powers from the galactic centre and anti-centre at 2.5, 5, 10 and 25 MHz. Generally, the antenna used for receiving on space vehicles has so wide an aperture in most cases, it becomes difficult to distinguish the direction of coming radio waves. Since ISS-b has the circular orbit of about 1100 km altitude, the strength of the galactic noise from the centre and anti-centre can be distinguished by the reason that the galactic centre is occulted by the Earth at a certain position on an orbit. The average temperatures of the galactic radio noise at the frequencies of 5, 10 and 25 MHz have the values of $(1.71 \pm 0.48) \times 10^6$ K, $(4.15 \pm 1.05) \times 10^6$ K, and $(3.47 \pm 1.07) \times 10^6$ K, respectively. The radiated power coming from the direction of the galactic centre is higher than that of the anticentre by 2.2-3.5 dB at high frequency range. (10 refs.)
- 2-165 keV observations of active galaxies and the diffuse background** See Entry 78992

98.80 COSMOLOGY

(for observational cosmology, see 98.70V; for origin and evolution of galaxy, see 98.50)

- 79029** Can graininess in the early Universe make galaxies?. B.J.Carr (Inst. of Astron., Univ. of Cambridge, Cambridge, England). *Astrophys. J. (USA)*, vol.268, no.1, pt.1, p.1-16 (1 May 1983). Examines whether the density fluctuations required to explain galaxies and their clustering could have arisen spontaneously in an initially Friedmann Universe as a result of statistical effects associated with the Universe developing nonlinear lumps. Such graininess could be produced whenever the Universe underwent a phase transition, and the associated fluctuations would arise either from an intrinsic randomness in the grain formation process or from the grains developing small-scale motions. In both cases the fluctuations would have the same distinctive form at their inception, and the authors show how they would evolve thereafter. Even if the grain-induced fluctuations cannot produce galaxies directly, they may still be able to produce objects smaller than galaxies. Since astrophysical processes associated with these objects could themselves produce large-scale density fluctuations, it may be possible to generate galaxies and the observed correlation function from the grain effect indirectly. (78 refs.)
- 79030** Cosmological self-similar shock waves and galaxy formation. E.Bertschinger (Princeton Univ. Obs., Princeton, NJ, USA). *Astrophys. J. (USA)*, vol.268, no.1, pt.1, p.17-29 (1 May 1983). A new family of similarity solutions is found for a point blast in a $\Omega=1$ Friedmann cosmology (Einstein-de Sitter Universe). The given solutions are valid several Hubble times after an explosion. Initially the shock wave formed satisfies the Sedov solution for adiabatic evolution in a constant medium, but it is modified by the cosmological expansion to form a self-similar thin dense shell which cools by adiabatic expansion and is unstable to gravitational fragmentation and collapse. The shock solution is applied to the explosive amplification model of galaxy formation of Ostriker and Cowie (1981). (34 refs.)

- 79031** Counterpart of the Kasner model in Brans-Dicke theory. V.B.Johri (Dept. of Math., Indian Inst. of Technol., Madras, India), G.K.Goswami. *Aust. J. Phys. (Australia)*, vol.36, no.2, p.235-7 (1983). The authors present a simple and elegant generalization of the Kasner model in Brans-Dicke (BD) theory by solving the BD field equations corresponding to the Bianchi type I metric. (2 refs.)
- 79032** Particle physics and the new cosmology. P.J.Steinhardt (Univ. of Pennsylvania, Philadelphia, PA, USA). *AIP Conf. Proc. (USA)*, no.98, p.343-57 (1982). [received: May 1983] (Conference on Particles and Fields - 1982, College Park, MD, USA, 28-30 Oct. 1982). During the past year, astounding progress has been made in the development of a radically new theory of the evolution of the early Universe. The new theory derives from the possibility that the Universe underwent a symmetry breaking phase transition in its early history that was strongly first order. During such a transition, the Universe can supercool into a metastable phase with a large vacuum energy density which results in a period of exponential expansion. It has recently been shown that in special types of first order transitions the Universe can escape from the metastable phase to a stable phase. Without a vacuum energy density contribution to the total energy density, the Universe returns to the expansion rate found in the hot big bang model. The existence of an epoch of exponential growth leads to a natural explanation of the cosmological homogeneity, isotropy, flatness, monopole and domain wall problems that plague the standard hot big bang model. The new cosmology has also been shown to lead to a (nearly) scale invariant spectrum of density perturbations in the early Universe, just the spectrum many cosmologists believe is necessary to explain the evolution of galaxies and clusters in our Universe. (26 refs.)
- 79033** Larger numbers hypothesis. II. Electromagnetic radiation. P.J.Adams (Phys. Dept., Univ. of Puget Sound, Tacoma, WA, USA). *Int. J. Theor. Phys. (USA)*, vol.22, no.5, p.421-36 (May 1983). For pt.I see *ibid.*, vol.21, p.607 (1982). The author develops the theory of electromagnetic radiation in the units covariant formalism incorporating Dirac's large numbers hypothesis (LNH). A direct field-to-particle technique is used to obtain the photon propagation equation which explicitly involves the photon replication rate. This replication rate is fixed uniquely by requiring that the form of a free-photon distribution function be preserved, as required by the 2.7K cosmic radiation. One finds that with this particular photon replication rate the units covariant formalism developed in part I actually predicts that the ratio of photon number to proton number in the Universe varies as $t^{1/4}$ precisely in accord with LNH. The cosmological red-shift law is also derived and it is shown to differ considerably from the standard form of $\nu R = \text{const.}$ (11 refs.)
- 79034** Large numbers hypothesis. IV. The cosmological constant and quantum physics. P.J.Adams (Phys. Dept., Univ. of Puget Sound, Tacoma, WA, USA). *Int. J. Theor. Phys. (USA)*, vol.22, no.5, p.461-7 (May 1983). For pt.III see *ibid.*, vol.22, no.5, p.437 (1983). In standard physics quantum field theory is based on a flat vacuum space-time. This quantum field theory predicts a nonzero cosmological constant. Hence the gravitational field equations do not admit a flat vacuum space-time. This dilemma is resolved using the units covariant gravitational field equations. The author shows that the field equations admit a flat vacuum space-time with nonzero cosmological constant if and only if the canonical LNH is valid. This allows an interpretation of the LNH phenomena in terms of a time-dependent vacuum state. If this is correct then the cosmological constant must be positive. (16 refs.)
- 79035** The influence of neutrino rest mass on Dirac cosmology. Su Rukung (Dept. of Phys., Fudan Univ., Shanghai, China), Zhang Shiwei. *Kexue Tongbao (Foreign Lang. Ed.) (China)*, vol.28, no.3, p.325-7 (March 1983). Under the framework of unified Dirac cosmology, the influences of neutrino rest mass on Dirac cosmology are investigated. (4 refs.)
- 79036** A special law of variation for Hubble's parameter. M.S.Berman (Dept. de Fisica, Inst. Tecnológico de Aeronautica, Sao Paulo, Brazil). *Nuovo Cimento B (Italy)*, vol.74B, ser.2, no.2, p.182-6 (11 April 1983). A law of variation for Hubble's parameter in evolutionary models, that yields a constant value for the deceleration parameter, is presented. It leads naturally to the exclusion of open universes. (2 refs.)
- 79037** Generalised cosmological Friedmann equations and the de Sitter solution. A.V.Minkevich (Dept. of Phys., Byelorussian State Univ., Minsk, Byelorussian SSR). *Phys. Lett. A (Netherlands)*, vol.95A, no.8, p.422-4 (23 May 1983). It is shown that the generalised cosmological Friedmann equations in the gauge theory of gravitation obtained earlier have solutions with the de Sitter metric and vanishing as well as nonvanishing torsion. (20 refs.)
- 79038** Dynamical reduction of internal dimensions in the early Universe. T.Dereli (Dept. of Phys., Middle East Tech. Univ., Ankara, Turkey), R.W.Tucker. *Phys. Lett. B (Netherlands)*, vol.125B, no.2-3, p.133-5 (26 May 1983). An $(n+4)$ dimensional de Sitter model is constructed in which the metric scale factor for space-time expands exponentially in cosmic time while the internal space scale factor contracts exponentially. (7 refs.)
- 79039** Do we live inside a domain wall?. V.A.Rubakov, M.E.Shaposhnikov (Inst. for Nuclear Res., Acad. of Sci., Moscow, USSR). *Phys. Lett. B (Netherlands)*, vol.125B, no.2-3, p.136-8 (26 May 1983). The authors discuss the possibility that space-time has $(3+N)+1$ dimensions, but ordinary (light) particles are confined in a potential well which is narrow along N spatial directions and flat along three others. A five-dimensional model is considered in which this picture arises naturally. In a Universe of this type, processes looking like $e^+e^- \rightarrow$ nothing are possible at high energies. (7 refs.)
- 79040** Antiproton interactions with light elements as a test of GUT cosmology. V.M.Chechetkin, M.Yu.Khlopov (Inst. of Appl. Math. M.V. Keldysh, Moscow, USSR), M.G.Sapozhnikov. *Riv. Nuovo Cimento (Italy)*, vol.5, ser.3, no.10, p.1-79 (1982). The review starts with a brief description of the modern views on the evolution of the Universe. After that the authors discuss the problem of the existence of antimatter in the Universe and its possible astrophysical observational effects. They show that unique information on the possible presence of antimatter at the stage of radiation domination in the Universe ($t < 10^{13}$ s) may be obtained from the study of $p^0\text{He}$ annihilation. The difficulties of early attempts to include antimatter in cosmological considerations are described. The sources of antimatter, predicted by some GUTs, are discussed. They consider the physics of primordial black holes (their formation and evaporation), the formation and annihilation of antimatter domains, the relationship between these sources of antimatter and the phase transitions in the early Universe as well as heavy metastable particles predicted by GUTs. Some aspects of the theory of galaxy formation are in close touch with these prob-

lems. The observed abundances of light elements and their possible changes due to annihilation are discussed. In conclusion the necessary measurements and the restrictions on the parameters of GUT models which may be obtained from these measurements are considered. (94 refs.)

79041 Quantization of a homogeneous isotropic cosmological model in five-dimensional field theory. Yu.S.Vladimirov, V.V.Kislov (Moscow State Univ., Moscow, USSR).

Theor. & Math. Phys. (USA), vol.53, no.1, p.970-8 (Oct. 1982). Translation of: *Teor. & Mat. Fiz. (USSR)*, vol.53, no.1, p.43-54 (Oct. 1982).

A homogeneous isotropic cosmological model is quantized in the framework of five-dimensional field theory (unified theory of gravitation, electromagnetism, and a scalar field). A two-dimensional equation of DeWitt type with signature $(+ -)$ is obtained, which ensures the dynamics in the quantum variant of the theory. It is shown that the evolution of the quantum cosmological model is due to processes of redistribution of the matter in the Universe between its different forms. (12 refs.)

Conference on Particles and Fields - 1982 See Entry 74201

Absence of particle creation as an equilibrium condition See Entry 74340

Vanishing of the cosmological constant in non-Abelian Kaluza-Klein theories ..
..... See Entry 74344

Extra space-time dimensions: towards a solution to the cosmological constant problem See Entry 74346

Why is the cosmological constant small? See Entry 74348

The geometrical hierarchy model and $N=1$ supergravity See Entry 74355

Large numbers hypothesis. III. Kinetic theory, statistical physics, and thermodynamics See Entry 74418

Light spinor monopole See Entry 74606

Early unification and the Weinberg angle in the $SU(4)^4$ grand unified model
..... See Entry 74673

Cosmological phase transition in microcanonical gravity See Entry 74689

The massive neutrino and clustering phenomena in the Universe
..... See Entry 78806

Circumvention of Parker's bound on galactic magnetic monopoles
..... See Entry 78807

Quasar evolution derived from the Palomar Bright Quasar Survey and other complete quasar surveys See Entry 79021

The irregular distribution of galaxies and the anisotropies in the microwave background photons See Entry 79027

Author index

| | | | | | | | | | |
|------------------------|-------|---------------------------------|-------|----------------------------|-------|------------------------|-------|-------------------------|-------|
| +Aabo, K. | 78388 | +Ahlers, M. | 76758 | Alford, P.C. + | 77903 | Andrews, L. + | 75378 | +Arellano G., J. | 75084 |
| +Aarholt, E. | 78157 | +Ahlert, J. | 74918 | +Ali, M. | 78147 | Andrews, L. + | 75379 | Arends, J. + | 74962 |
| +Aarson, J. | 75005 | +Ahlrichs, R. | 76273 | Aliev, M.I. + | 76665 | +Andronov, Yu.F. | 74901 | +Argon, A.S. | 77761 |
| Aashamar, K. + | 75314 | +Ahmad, A. | 75053 | +Aliyev, V.A. | 76988 | Andzelm, J. + | 75257 | +Argon, A.S. | 77696 |
| +Abascal, J.L.F. | 76275 | Ahmad, I. + | 74917 | +Allaberdin, M.L. | 74809 | Angelis, A.De | | +Argos, P. | 78126 |
| Abate, G.F. + | 77722 | Ahmad, S. | 75053 | Allain, C. + | 74378 | see De Angelis, A. | | Ariguib, N.Kbir | |
| Abbakumov, K.E. + | 77833 | Ahmedi Goodarz | | Allakhverdiev, A.M. + | | Angelotti, S. + | 74428 | see Kbir Ariguib, N. | |
| +Abbe, J.Ch. | 77913 | see Goodarz Ahmedi | | | 78005 | Angelov, B.M. | 76906 | Arijis, E. + | 78629 |
| +Abbott, D. | 78490 | +Ahmed, K. | 77465 | +Allan, M. | 74544 | Angelskii, O.V. + | 75605 | +Arima, A. | 75024 |
| Abbott, D.H. + | 78518 | +Ahmed, K. | 77466 | Aldredge, L.R. | 78432 | Anger, C.D. | 78779 | Arima, J. + | 77817 |
| Abbott, M. | 75180 | Ahmed, M.D.Iqbal. see Iqbal | | Allegre, G. + | 76328 | +Anghel, A. | 77183 | +Arimizu, N. | 78322 |
| Abd el-Halim, A.M. + | | Ahmed, M.D. | | +Allegre, G. | 76239 | Anikina, M.Kh. + | 75011 | +Arinkina, E.L. | 76400 |
| | 77587 | Ahmed, M.I. + | 78726 | +Allegre, C.J. | 78880 | +Anisimova, L.I. | 76687 | Aristov, V.V. + | 76439 |
| Abd-Elkhalek, F.A.E. + | | Ahmed, M.S. + | 77145 | Allen, D.A. + | 79018 | Annamalai, A. + | 75311 | +Arjona, F. | 76987 |
| | 76035 | Ahn, R.M.C. + | 76747 | Allen, E.J.Van. | | Annamalai, A. + | 75356 | +Arkhipov, S.N. | 7724 |
| +Abdel Wahab, F.M. | | +Ahopelto, J. | 75352 | see Van Allen, E.J. | | Annamaki, M. + | 78349 | Arkhipov, V.V. + | 74546 |
| | 77847 | +Ahrar, H. | 75053 | +Allen, L. | 75787 | Annino, A. | 78098 | Arko, A.J. + | 77525 |
| +Abdel-Kader, M.M. | 77157 | +Ahrens, T.J. | 78833 | +Allen, L. | 78328 | Anokhin, S.B. + | 76854 | +Arlinghaus, R.T. | 75378 |
| Abdel-Malik, T.G. | 76961 | +Ahrens, T.J. | 78536 | +Allen, S.L. | 76214 | Anokhin, Yu.N. + | 78257 | +Arlinghaus, R.T. | 75379 |
| Abdullaeva, S.G. + | 76988 | Ai Chi-fong. see Chi-fong Ai | | Allen-Booth, D. + | 75863 | +Anokhina, N.P. | 75776 | +Armas, A. | 77728 |
| Abdulloev, N.S. + | 77385 | Aielli, W.A. + | 75970 | Allen-Booth, D. | 75864 | +Ansari, M.A. | 76015 | Armas, I. + | 77707 |
| Abdulrida, M.C. + | 77568 | +Aiginger, H. | 78337 | Allias, P. | 75791 | +Anseau, M.R. | 77539 | Armon, E. + | 78184 |
| +Abe, H. | 76293 | +Aiginger, H. | 78338 | Alliluev, S.P. + | 74321 | +Anspaug, B. | 78016 | +Armour, D.G. | 75490 |
| Abe, K. | 78465 | +Aikawa, Y. | 77045 | Allinger, N.L. + | 75282 | Anthony, T.R. | 76797 | +Armstrong, J. | 76704 |
| Abe, K. + | 78471 | Aikiyo, K. + | 78710 | +Allison, J. | 77568 | Antipenko, A.P. + | 75220 | Armstrong, R.A. + | 76200 |
| +Abe, K. | 74669 | +Aikiyo, K. | 78790 | Allison, J.N. + | 76771 | Antipin, A.A. + | 77251 | +Arndt, W. | 78084 |
| +Abe, Y. | 77121 | +Aikiyo, K. | 78743 | Almeida, R.M. + | 77378 | Antipov, S.A. + | 76448 | +Arnold, F. | 78618 |
| +Abe, F. | 78529 | +Aikiyo, K. | 78742 | Almeida E Silva, A. M. + | | +Antolkovic, B. | 74923 | +Arnold, G.B. | 76827 |
| Abel, Kh. | 78242 | Aindow, J.D. + | 75882 | | 77961 | Antonchenko, V.Ya. + | | +Arnold, N. | 76708 |
| +Abhyankar, K.D. | 78951 | Akama, K. | 74335 | +Alonso, E.V. | 75490 | | 76751 | Arnowitz, R. + | 74358 |
| +Abievov, V.K. | 74699 | +Akap'ev, G.N. | 75162 | +Alonso, J.A. | 76869 | +Antoni, L. | 78389 | +Arnowitz, R. | 74670 |
| +Ables, J.G. | 79018 | +Akasaka, Y. | 77374 | Alston, S. | 75503 | +Antonia, R.A. | 75992 | +Arntzenius, A.C. | 78372 |
| +Ables, J.G. | 78936 | Akdeniz, K.G. + | 74357 | Altarelli, M. | 77035 | +Antonia Valerdi, M. | | Aroney, M.J. + | 75416 |
| +Abouaf-Marguin, L. | | +Ake, T.B. | 78957 | +Altenhoff, W. | 78872 | | 76585 | Arora, S.K. + | 77550 |
| | 75382 | +Akhermerov, R.V. | 74963 | Altshuler, P.D. + | 76848 | +Antoniadis, D.A. | 76796 | Arora, V.K. + | 76916 |
| Abouchacra, G. + | 76641 | +Aki, K. | 78453 | Alurkar, S.K. + | 78814 | Antonietta Macip, M. + | | Artemov, V.E. + | 77835 |
| Aboutorabi, A.A. + | 77827 | Akimov, A.I. + | 75631 | Alvarez, G.A. + | 75972 | | 76585 | Arthurs, A.M. + | 78161 |
| Abraham, K.M. + | 77975 | +Akita, K. | 77585 | Alvarez, M. | 78930 | Antonishin, N.V. + | 76105 | +Arthurs, W.M. | 78161 |
| +Abrahams, E. | 77125 | Akker, T.J.Van Den. see Van Den | | +Aly, M.N. | 75085 | +Antonov, N.A. | 75073 | Artisimovich, V.L. + | 75758 |
| +Abrahams, M.S. | 78050 | Den Akker, T | | Alyab'ev, V.M. + | 77700 | +Antonov, N.A. | 75074 | +Aurldaus, G. | 75375 |
| Abramov, V.N. + | 77003 | +Akoev, I.G. | 78253 | Amalnerkar, D.P. + | 77519 | +Antonov, N.A. | 75151 | Arutyan, Yu.V. + | 74481 |
| +Abramyan, E.A. | 76673 | +Akopov, F.Kh. | 77176 | Amaral, N.C. + | 76844 | +Antonov, N.A. | 75152 | Arutyunyan, G.M. + | 76030 |
| +Abramyan, E.A. | 77814 | Aksenov, V.I. + | 78765 | Amastha, A. + | 79005 | Antonov, V.A. + | 75699 | +Arutyunyan, S.G. | 74595 |
| Abrikosov, A.A., Jr. | 74728 | Aksenov, V.P. + | 76495 | Ambrion, J. + | 74580 | Antonov, V.L. + | 75207 | +Arvidson, A. | 77582 |
| +Abrikwah, J.K. | 76883 | Aksenov, V.V. | 78440 | Ambrion, J. + | 74696 | +Antonov, V.M. | 78290 | Arvis, J.F. | 74745 |
| +Abstreiter, G. | 77395 | Aksenova, E.Yu. + | 76400 | Ambraseys, N.N. + | 78468 | Antonov, Yu.N. + | 78715 | Asai, J. + | 77475 |
| +Abu-Shady, Y. | 75085 | Akul'shin, A.M. + | 75346 | +Amelinckx, S. | 76368 | +Antonova, E.A. | 77106 | +Asai, T. (ed.) | 74227 |
| +Acevedo, R. | 75264 | +Al-Adl, A.I. | 76950 | Amey, W. + | 75861 | +Antonova, O.V. | 77700 | +Asaka, S. | 75715 |
| +Acharya, Y.B. | 78773 | Al-Chalabi, S.A. + | 74527 | Amin, M. | 78551 | +Anzai, H. | 76932 | +Asawa, C.K. | 75819 |
| Achasov, N.N. + | 74732 | Al-Ismail, S.A.Y. + | 77068 | +Ammar, A.A. | 76950 | +Anzai, H. | 76863 | +Ascencio, J.M. | 78606 |
| +Achenbach, J.D. | 78458 | Alamo, J.A.Del. | | Ammosov, V.V. + | 74771 | +Anzai, S. | 77174 | Ashalata, N. + | 75039 |
| +Aciorno, D. | 75977 | see Del Alamo, J.A. | | +Amos, K. | 74964 | Aoki, K. + | 75915 | +Ashcroft, D.W. | 77083 |
| Acker, F. + | 76663 | Albada-van Dien, E.van | | Amthauer, G. + | 76402 | +Aoki, S. | 78608 | Ashenford, D.E. + | 76358 |
| Ackerman, S.A. + | 78600 | see van Albada-van Dien, | | An, H. | 75969 | +Aoyama, K. | 75814 | Ashizuka, M. + | 77693 |
| +Adachi, K. | 77243 | E. | | An Dao Khac. see Dao Khac | | +Apel', P.Yu. | 75162 | Ashok, S. + | 77763 |
| Adam, C.M. | 77661 | Alberigi Quaranta, A. + | | An | | +Apel, W.D. | 74783 | +Ashuri, K. | 75927 |
| +Adam, J.A. | 75144 | | 75239 | An Ying + | 74598 | +Aplesnin, S.S. | 76666 | +Aso, K. | 77154 |
| Adam, J.C. + | 76192 | Albertsen, J.F. + | 78884 | Anantaraman, N. + | 74898 | +Aplesnin, S.S. | 77197 | +Asplund, L. | 75353 |
| Adamashvili, G.T. | 75852 | Albeverio, S. + | 74296 | Anastasovski, P. | 75545 | +Apostolov, E. | 78672 | Asscher, M. + | 77503 |
| Adams, P.J. | 74418 | +Alcayde, D. | 78725 | Anbang Dai. see Dai Anbang | | Apostolov, E.M. | 78422 | Assis Neto, V.F.de | |
| Adams, P.J. | 79033 | Aldezabal, G. + | 74698 | +Andersen, J. | 78913 | Appel, F. + | 76443 | see de Assis Neto, V.F. | |
| Adams, P.J. | 79034 | +Alidissi, M. | 77887 | +Anderson, A.C. | 74473 | Appelbaum, J. + | 78054 | Astapov, V.I. + | 77203 |
| +Adamski, J. | 75651 | Aldred, A.T. | 76371 | +Anderson, B. | 75095 | Appelquist, H. + | 75121 | Aston, S.R. + | 75119 |
| +Adelberger, E.G. | 74904 | Aldred, A.T. + | 77180 | +Anderson, C.M. | 78916 | Appelquist, L. + | 78913 | Aston, S.R. + | 78558 |
| +Adler, G. | 76778 | Aleinikov, A.L. + | 78713 | +Anderson, C.R. | 77985 | +Appleton, B.R. | 76463 | Astratov, V.N. + | 75597 |
| +Adler, L. | 75845 | +Aleksakhin, R.M. | 78251 | +Anderson, J. | 77533 | Apreuzes, J.P. + | 78597 | Atake, T. + | 76658 |
| Adler, M.S. | 76838 | +Aleksan, R. | 74783 | +Anderson, K.R. | 78719 | Aptekar', I.L. + | 76612 | Atake, T. + | 76660 |
| +Adler, N.S. | 78166 | Aleksandrov, A.A. + | 75244 | +Anderson, R.F. | 78561 | +Apukhtina, N.P. | 75561 | Atanassov, N. + | 76453 |
| Adler, S.L. | 74352 | Aleksandrov, G.A. + | 75776 | +Anderson, R.N. | 78490 | +Arai, K.I. | 77598 | +Atanassov, N. | 77805 |
| Adler, S.L. | 74645 | Aleksandrov, I.V. + | 76581 | +Anderson, S.F. + | 78920 | +Arai, T. | 76444 | +Atanassov, N. | 77806 |
| Adliene, D. + | 76567 | Aleksandrov, L.N. | 76811 | +Anderson, W.A. | 78059 | +Arai, Y. | 75148 | Atherton, D.L. | 77828 |
| +Adloff, J.C. | 75034 | Aleksandrov, L.N. + | 76812 | +Anderson, W.W. | 78088 | +Arai, Y. | 76603 | Atherton, D.P. + | 78169 |
| +Adolf, D. | 77727 | +Aleksenko, V.I. | 76566 | +Anderson, B. | 74738 | +Arakawa, R. | 74870 | Atkinson, L.P. + | 78550 |
| Afanasyev, A.A. + | 75630 | +Alekscev, V.A. | 76762 | Andersson, B. | 74738 | +Arakelian, S.M. | 75711 | Atsuta, M. + | 77748 |
| Agafonov, B.P. | 78546 | Alekseev, V.I. | 75426 | Andlauer, G. | 75215 | Arakelyan, S.M. + | 76307 | +Atul Raturi | 77564 |
| Agarwal, D.C. + | 78758 | Alekseevskii, N.E. + | 77086 | Ando, K. + | 76690 | +Araki, K. | 76503 | +Au, C.K. | 74610 |
| +Agarwal, S.K. | 77990 | Aleksidze, M.A. | 78416 | +Ando, K. | 74579 | +Araki, M. | 77792 | +Aucoin, R.J. | 77056 |
| Agee, E.M. (ed.) | 74227 | Aleksieva, P.P. + | 78263 | Ando, T. | 76864 | Aranchuk, L.E. + | 76193 | +Aullo, J.M. | 75275 |
| Ageev, A.L. + | 77479 | +Alessandri, M. | 77555 | +Andra, H.J. | 77516 | Arapis, G. + | 75115 | +Aurian-Blajeni, B. | 77900 |
| Agmon, N. + | 77879 | Alessandrini, F. + | 77970 | Andrasi, A. + | 78335 | Aras, N.K. + | 74913 | Auriault, J.L. | 75897 |
| Agnihotri, O.P. + | 77564 | Alexander, J. + | 75250 | Andrasi, A. + | 75190 | +Aras, N.K. | 75056 | Aurivillius, B. | 76372 |
| +Agostini, L. | 78173 | Alexander, M.H. + | 75470 | +Andrasi, A. | 75188 | +Arasly, D.G. | 76665 | Auslender, M.I. + | 76873 |
| +Agrawal, D.K. | 75092 | Alexander, P. | 78312 | +Andrasi, A. | 75191 | Araujo, G.L. + | 78062 | Austern, N. | 74938 |
| Agrawal, G.P. | 75746 | +Alexandrov, G. | 75153 | +Andrasi, J. | 76146 | +Arbman, M. | 77943 | +Austern, N. | 75050 |
| Agrawal, H.L. + | 76021 | +Alfaro, R.R. | 77429 | +Andrasi, J. | 75308 | Arbuzov, V.L. + | 76516 | +Austin, I.G. | 77293 |
| +Aguiar, M. | 77420 | +Alfaro, E.J. | 78827 | Andreev, A.V. + | 75610 | Archer, B.R. + | 78360 | +Auvert, G. | 76492 |
| Aharoni, H. + | 75780 | Alfaro, J. + | 74627 | Andreev, I.A. | 77359 | Arcidiacono, V. + | 78053 | Avakyan, A.R. + | 74595 |
| Aharoni, S.M. + | 76270 | Alfaro, V.de | | Andreev, V.A. + | 76532 | Arditty, H.J. + | 75825 | Avaldi, L. + | 75488 |
| Aharonov, Y. + | 74610 | see de Alfaro, V. | | Andreev, V.I. + | 78712 | +Arduoin, D. | 75035 | Avaste, O.A. + | 78647 |
| Aharonov, Y. | 77188 | Alfintseva, R.A. + | 77611 | +Andres, K. | 77090 | Aref, H. | 76048 | +Avasthi, B.N. | 77759 |

- Aver'yanov, E.M. + 76302
 Aver'yanov, V.K. + 75901
 + Aver'yanova, L.N. 77604
 Avestov, G.M. + 78258
 Aveltskii, S.K. + 75728
 Avkhutsii, L.M. + 76613
 + Avni, Y. 79023
 + Avouris, Ph. 76782
 Avramenko, A.S. + 75779
 + Avtandilov, G.G. 78223
 + Awa, A.A. 78271
 Awasthi, R.C. + 75979
 + Awaya, Y. 78570
 + Awes, T. 75036
 Awwad, A.M. + 76570
 Axel, L. + 78288
 + Aydinli, A. 76494
 Aymerich-Humet, X. + 76820
 Ayupov, Sh.A. 74250
 Azam, M. + 74617
 Azevedo, L.J. + 77280
 Azhugin, F.F. + 77802
 Azimov, S.A. + 74809
 Azizur Rahman, B.M. 75794
 + Azumi, M. 76164

 + Baan, W.A. 79022
 + Baazov, N.G. 77176
 + Baba, H. 74870
 Babai, M. + 77971
 Babakov, A.V. 76088
 + Babanov, Yu.A. 77479
 + Babei, Yu.I. 77803
 Babenko, V.I. + 75917
 + Babenko, V.V. 75981
 Babkin, E.V. + 77249
 + Babkin, V.F. 78777
 Babolat, C. 75774
 + Babu, V.H. 76423
 Babu, V.Hari. see Hari Babu, V.
 Bacci, C. + 75196
 + Bachmaier, A. 78048
 Bachman, R.T. 78527
 + Bachmann, R. 76257
 Bachrach, R.Z. + 75221
 Back, B.B. + 75029
 + Back, B.B. 75035
 + Backus, C.E. 78043
 + Bacquet, G. 77258
 Baeri, J.-C. + 77250
 + Badatiya, R.C. 74798
 + Bader, S.D. 77488
 Badr, H.M. 75982
 + Badran, M.M. 77847
 + Badrinarayana, S. 75719
 Bae Lee Chun. see Chun Bae Lee
 Baekler, P. + 74624
 Baer, M. + 75615
 + Baer, T. 78199
 + Baert, F. 75388
 Baeleuf, M. + 77431
 + Baghlaif, A.O. 77587
 + Bagley, M. 76734
 Bagraev, N.T. 77270
 Bagraev, N.T. + 77288
 Bagraev, N.T. + 77281
 + Bagus, P. 75310
 Bahouth, S. + 75194
 + Bahcall, J.N. 78816
 + Bahcall, J.N. 78961
 Bai-lin Hao. see Hao Bai-lin
 + Baidokha, L.N. 77075
 Baier, R. + 74717
 + Bailey, E.M. 78623
 Bailey, G.J. 78761
 + Bailey, G.J. 78741
 Bailey, R.W. 78186
 + Bailly, F. 78008
 Bain, A.J. + 76142
 + Baines, D.W.T. 78982
 + Baiocchi, E. 76310
 + Baisden, P.A. 75035
 + Baity, W.A. 78992
 + Bajaj, K.K. 78803
 Bajpai, R.P. + 74758
 + Bak, P. 77126
 + Bak, P. 76583
 + Bakanov, A.G. 77612
 Bakanov, D.G. + 75620
 Baker, J.M. + 77050
 Baker, T.S. + 78138
 + Bakshii, P.S. 76353
 + Bakshii, P.S. 75360
 + Bakshii, P.S. 75361
 Bakhiteeva, N.D. + 77668
 Bakirov, M.Ya. + 77038
 Bakos, J.S. + 76202
 + Bakushev, V.A. 78300
 Balaban, A.T. 75256
 Balabanyan, G.O. 75618
 + Baladron, C. 76869
 Balaes, A.M.E. + 74577
 Balagurov, B.Ya. 77069
 Balakov, A.V. + 77566
 Balakrishnan, G. + 77316
 Balankin, A.S. 76545
 Balankin, A.S. 76589
 + Balanovski, E. 78124
 + Balanzat, E. + 76415
 Balasubramanian, K. 75408
 Balasubramanian, K. 75409
 Balazs, N. 74931
 Baldauf, W. + 76679
 Baldis, H.A. + 76184
 + Baldo-Ceolin, M. 74756
 + Baldokhin, Yu.V. 77667
 + Baldy, M. 77027
 Balebanov, V.M. + 78777
 Balestrino, G. + 77310
 Balibar, F. + 76240
 + Balibar, S. 76723
 + Balic-Zunic, T. 76401
 + Balick, B. 78987
 + Baliko, S. 77954
 Balitskii, K.P. + 78259
 + Balk, P. 77576
 Ball, R.C. + 74759
 Balla, L. 78545
 Ballard, R.E. + 75442
 Ballard, R.E. + 75436
 Ballard, R.E. + 75437
 + Ballay, L. 78356
 Ballentyne, D.W.G. 77545
 Ballestracci, R. + 78421
 Ballman, A.A. + 76474
 + Ballman, A.A. 76964
 + Ballman, A.A. 76341
 Ballone, P. + 76159
 + Balonek, T.J. 79019
 Balsiger, H. 78665
 Baltushaitis, P.D. + 78305
 Bamberger, A. + 74290
 + Banaev, Yu.N. 74699
 + Bandopadhyay, B.K. 74807
 + Banerjee, D. 75046
 + Banerjee, D. 75047
 Banerjee, H. + 74799
 + Banerjee, R. 74801
 Banerjee, S. + 74814
 Banerjee, S. + 74794
 + Banerjee, S. 74783
 Banerjee, S.N. + 74743
 Banerjee, S.N. + 74750
 Bangert, D. + 75030
 Bangert, U. + 77465
 Bangert, U. + 77466
 + Banghong Lu 77860
 Bankov, L.G. + 78776
 + Bankov, N.G. 78776
 + Banks, B. 77055
 Banks, T. 74688
 + Banovets, I. 75170
 + Bansal, N.K. 78096
 + Bao Zong-ming 74491
 Bao-Ping Liu see Liu Bao-Ping
 + Bapeshwara Rao, V.S.V. + 78097
 + Barach, J.P. 78207
 Barakat, R. + 78825
 Baran, S.A. 74345
 Baran, V.M. + 75494
 Baranov, A.V. + 77383
 + Baranov, A.V. 76666
 + Baranov, V.Yu. 76762
 + Baraona, C. 78028
 Baraona, C.R. + 77858
 Barbara, B. + 77175
 + Barbe, M. 78008
 Barber, M.N. 74408
 + Barbier, P. 77978
 Barbini, R. + 75648
 Barcielli, A. 74318
 + Barclay, J.A. 74897
 + Bard, A.J. 77518
 Bardeen, W.A. + 74650
 Bardsley, J.N. 75496
 Barengchi, C.F. + 74429
 Barger, V. + 74762
 Barger, V. + 74811
 Barger, V. + 74828
 + Barkat, Z. 78902
 + Barker, D.R. 77753
 + Barker, J.R. 75483
 + Barlea, M. 75638
 Barlow, A.J. + 75827
 Barlow, C.Y. + 77714
 + Barmina, I.L. 77638
 + Barnavon, T. 77768
 Barnes, A.J. + 75387
 + Barnes, A.J. 75385
 + Barnes, D.C. 76174
 + Barnett, G. 76887
 + Barnett, R.L. 78494
 Barnola, J.M. + 78571
 Baron, M.J. + 78724
 + Baron, R. 76894
 + Baron, W.R. 78018
 Barone, V. + 76752
 Baross, J.A. + 78145
 + Barranco, M. 74864
 + Barranco, M. 74888
 + Barre, D. 78327
 Bartal, Y. + 75081
 Barteau, M.A. + 75440
 Barteaux, G.M. + 76325
 + Barth, D.S. 78209
 + Barth, P.F. 74401
 + Barthelat, J.C. 75562
 Bartke, J. 74812
 + Bartlett, R.J. 75268
 Barton, C. + 78435
 Barton, M. + 78481
 + Baritschat, K. 75509
 + Barua, K. 77569
 Bar'yakhtar, V.G. + 77166
 Bar'yakhtar, V.G. + 77200
 Baryshevskii, V.G. + 76915
 Barz, H.W. + 75020
 Basch, E.E. + 75591
 Basdevant, C. 75988
 + Baseyan, G.Z. 74595
 Basharin, A.K. + 78498
 + Bashilov, S.M. 75107
 Bashkirov, Sh.Sh. + 77160
 Basile, M. + 74821
 Basilevsky, M.V. 77864
 Baskakov, A.P. + 76104
 Basov, N.G. + 76168
 + Bastard, G. 77445
 + Bastl, Z. 77772
 + Basu, A.N. 76323
 + Basu, B.K. 77092
 + Basu, D.N. 74868
 + Basu, M. 74801
 + Basu, M. 75047
 + Basu, P.K. 78010
 + Basu, S. 75367
 + Basu, S. 77591
 + Basu Chowdhury, K. 74800
 + Basu Chowdhury, K. 74801
 Basyk, A.I. + 76971
 + Bates, H.E. 77556
 Bates, P.A. 74244
 + Batnitsky, S. 78273
 + Batozskii, Yu.V. 75911
 + Batrla, W. 78872
 Batson, P.E. + 76537
 Battaglin, G. + 76513
 Battistoni, G. + 74766
 Battistoni, G. + 75225
 + Battly, M.J. 79024
 + Battly, M.J. 78924
 Baturin, V.N. + 74983
 + Batyrev, V.A. 75630
 Bau, H.H. + 76008
 + Baublis, V.V. 76532
 Bauchinger, M. + 78228
 + Baud, M. 78308
 Bauder, A. + 75368
 + Baudry, A. 78924
 Bauer, G.V. + 74482
 + Bauer, P. 78725
 + Bauer, W. 76214
 + Bauskus, J.P. 76894
 + Baumann, A. 78482
 Bauror, Yu.A. + 74699
 Bauschlicher, C.W., Jr. 75305
 + Bauschlicher, C.W., Jr. 75330
 + Bauser, E. 74488
 Bayer-Helms, F. 75695
 Bazela-Wrobel, W. + 76369
 Bazilevskaya, E.S. 78521
 + Bazin, C. 75650
 + Bazin, R. 78308
 Bazylev, V.A. + 76528
 + Bdziel, J.B. 76126
 Beaconsfield, P. + 78124
 Beale, P.D. 74404
 + Beale, P.D. 76917
 + Beall, J. 78103
 + Beames, C.G., Jr. 78149
 Beamish, D. 78688
 Beamish, J.R. + 76732
 + Beattie, W.H. 77377
 + Beatty, J. 78397
 + Beatty, J. 78209
 + Beaulieu, P.C. 78405
 Beaumont, B. + 78068
 Beaumont, P.C. + 78267
 Beavis, D. + 75017
 + Becchetti, F.D. 74889
 Bechstedt, F. + 77520
 Bechstedt, F. + 76867
 + Bechtold, J. 79024
 + Beck, C. 74832
 Beck, H.P. 76383
 + Becker, B. 77516
 Becker, K. + 78486
 Becker, K. + 78489
 + Becker, K. 78566
 Becker, K.D. + 77271
 + Becker, P.J. 75313
 Becker, R. + 77769
 + Becker, R.H. 79000
 Becker, U. + 75476
 Becker, W. + 79003
 Becker, W. + 75669
 Beckmann, G.E.J. 78439
 + Bedair, S.M. 78077
 Bedarida, F. + 77547
 Bedlier, Y. + 77978
 Bedilov, M.R. + 75646
 + Bednorz, J.G. 77420
 + Beedie, H.R.A. 78066
 Beeley, P.A. + 75005
 + Beers, T.C. 79012
 Beet, S.W. + 75874
 Beez, H. + 77350
 + Begemann, M.H. 74545
 Beghi, L. + 78187
 Beghin, C. + 78774
 + Behera, B. 75957
 Behere, D.V. + 75407
 Behrend, H.J. + 74783
 + Behrens, J. 78685
 Beijeren, H.van see van Beijeren, H.
 + Beijerinck, H.C.W. 75347
 + Beisembayeva, Kh.B. 75646
 + Beitz, L. 77945
 Bejan, A. 76012
 + Bejan, A. 76107
 Bek, V.V. + 74389
 Bekeshko, N.A. 77837
 Bekeshko, N.A. + 77838
 + Bekk, P. 77912
 Bekki, N. 76190
 Beklemishev, A.I. + 74454
 + Belery, P. 75006
 + Belczyn, E. 78335
 Belfrage, C. + 75349
 + Belimenko, F.A. 77332
 + Belin, C. 77586
 Bell, K.W. + 74797
 Bell, R.A. + 78964
 Bellazzini, R. + 78406
 + Bellotti, E. 74766
 + Bellotti, E. 75225
 Belonozhko, V.M. + 74475
 + Belorizky, E. 77175
 Beloshitskii, A.P. + 74480
 + Beloshitskii, A.P. 74477
 Beloshitsky, V.V. + 76530
 Belouet, C. + 78022
 Belouet, C. + 77586
 Belous, N.A. + 77111
 + Belousov, Yu.A. 74480
 + Belov, N.V. 76349
 + Belov, N.V. 76346
 + Belov, N.V. 76412
 + Belov, N.V. 76398
 + Belov, N.V. 76347
 + Belov, N.V. 76348
 + Belov, N.V. 76350
 + Belov, N.V. 76399
 Belova, N.E. + 76243
 Belozerskii, G.N. + 77724
 Beltracchi, L. 75076
 Beltran, F.Gomez. see Gomez Beltran, F.
 Bel'tyukova, S.V. + 75451
 Belvedere, G. + 78901
 Belyaev, I.N. + 77604
 Belyaev, Yu.N. + 76244
 Belyayeva, A.I. + 74472
 Belyavskii, V.I. + 77399
 + Belyavskii, V.I. 76448
 Belyi, M.U. + 77454
 Belyi, V.A. + 77594
 Belz, J. + 76524
 Bemer, B. + 75097
 + Ben-Yosef, N. 78643
 Benade, A.H. + 75876
 Benbow, R.L. + 76794
 Benbow, R.L. + 77526
 Bender, M.L. 78517
 + Benderitter, Y. 78421
 + Benderskii, V.A. 77415
 Bending, R.C. 77951
 Bendi, P. + 76822
 Benedetto, G.P.di see di Benedetto, G.P.
 Benhao Sa see Sa Benhao
 + Beninson, D. 78342
 + Benloucif, R.M. 77647
 Bennett, K.F. 77952
 Bennouna, A. + 77522
 Benoit-Denis, A.-M. 77356
 + Benson, J.L. 79010
 Benson, S. + 75672
 Bentz, J. + 78148
 + Bentz, J. 78155
 + Bera, R.K. 76470
 + Berard, D. 75825
 Bercozi, J. + 78116
 Berdahl, P. + 75908
 Berekhnitskii, L.T. + 75926
 + Berendsen, H.J.C. 78153
 Berenstein, C.A. + 75593
 Berezhevskii, A.M. + 76913
 + Berezhnitskii, L.T. 75963
 + Berg, C.J. 78990
 + Berg, J.C. 76119
 Berg, R.Van Den see Van Den Berg, R.
 Bergander, M.J. 77850
 + Berge, J.P. 74771
 Berger, A. 78637
 Berger, E.L. 74716
 Berger, S.A. + 76116
 Berger, W.H. + 78520
 + Berggren, K.-F. 76877
 + Berggren, R.G. 75101
 + Bergh, R.A. 75822
 Bergh, S.van den see van den Bergh, S.
 Bergh, G.vanden see Vanden Bergh, G.
 + Bergher, M. 75650
 Bergman, S. + 77960
 Bergmann, E.E. 75778
 Bergmann, H.W. + 76319
 Bergmann, H.W. + 76318
 Bergmann, H.W. + 77808
 + Bergmann, H.W. 76678
 + Bergmann, H.W. 76650
 + Bergmann, H.W. 77807
 Bergner, H. + 74741
 + Bergnes, C. 75475
 Bergou, J. + 74664
 Bergstrom, M. + 78295
 + Bergwerf, P. 77902
 + Beri, S.B. 75045
 Berim, G.O. + 77124
 Beringhelli, T. + 76351
 + Berkekyteiser, J.E. 77780
 Berlepsch, H.von see von Berlepsch, H.
 Berliner, M.A. 78702
 + Berman, B.L. 74959
 + Berman, M. 75434
 Berman, M.S. 79036
 Bermudez, A. + 76677
 + Bernabei, R. 75196
 + Bernard, D. 78147
 Bernardes, L.S.De see De Bernardes, L.S.
 Bernier, P. + 77887
 Bernier, R.N. + 76132
 + Bernstein, H.J. 78298
 + Bernstein, I. 75657
 + Bernstein, L. 78328
 Berret, J.F. + 77404
 + Berrier-Ronsin, G. 74847
 Berry, A.J. + 75725
 Berry, B.S. + 76795
 Berry, H.G. + 75554
 + Bert, J. 76640
 Bertel, I.M. + 75453
 + Berthelier, A. 78670
 Berthelier, J.J. + 78670
 + Berthelier, J.J. 78774
 + Berthollet, R. 75040
 + Berti, M. 76472
 + Bertran, J. 77869
 + Bertrand, L. 76675
 + Bertsch, H.H. 74835
 Bertschinger, E. 79030
 Berzina, I.G. + 77944
 + Besagni, T. 76800
 + Beskos, J. 75592
 Bessmann, T.M. 76669
 Beshaposhnikov, A.A. + 76229
 Beterov, I.M. + 75335
 Betterman, P. + 76394
 + Bettinelli, M. 76310
 + Bettini, J.P. 75825
 + Betts, D.D. 77194
 + Betts, R. 75035
 + Betts, R.R. 75029
 + Betz, G. 77504
 Beukel, A.van den see van den Beukel, A.
 + Beurskens, P.T. 76249
 + Bevk, J. 77115
 + Beyreleier, A.L. 76680
 Bezid'ko, S.N. 75770
 + Bezudnyaya, T.M. 75779
 Bezerra, V.B. 74622
 + Bezruchko, V.M. 75699
 Bezzerides, B. + 76183
 Bhadesha, H.K.D.H. 77666
 Bhadra, K. + 74403
 + Bhaduri, R.K. 74763
 Bhaduri, S. + 75950
 + Bhakta, H.N. 77956
 + Bhalla, K.B. 75045
 Bhamathi, G. 74896
 + Bhamathi, G. 74895
 Bhanja, R. + 75044
 + Bhanja, R. 75039
 + Bhanja, R. 75045
 + Bharti, A. 75045
 + Bhartia, P. 78588
 Bhat, A.M. + 75903
 Bhat, A.M. + 76013

- + Bhatia, A.K. 75621
 + Bhatia, V.S. 75045
 + Bhattacharjee, B. 76299
 + Bhattacharya, P.K. 76893
 + Bhattacharya, S. 74833
 + Bhattacharyya, A. 74801
 + Bhattacharyya, P. 76736
 + Bhonsle, R.V. 78814
 + Bhoraskar, S.V. 76969
 + Bhosmik, K. 78133
 + Bhutra, M.P. 75449
 + Bibichev, B.A. + 75068
 + Bibikov, Sh.K. 76144
 + Bickel, S.H. 78722
 + Biddlecombe, D.E. + 78167
 + Bidet, A.C. 78308
 + Bidet, R. 78308
 + Bielicki, M. 78410
 + Biering, H. + 74537
 + Biernat, T. + 77536
 + Biernat, T. + 77535
 + Biersack, J.P. + 77510
 + Biersack, J.P. + 76525
 + Biersack, J.P. 77509
 + Bigio, I. 75735
 + Bigler, R.E. 78323
 Bij, J.J. van der
 + see van der Bij, J.J.
 + Bilegan, C. 78105
 + Bilello, J.C. 77747
 + Bilichanko, S. 78669
 + Bilicki, Z. + 76094
 + Billardon, M. + 75650
 + Billing, G.D. 75462
 + Billmann, J. 75393
 + Billotet-Hoffmann, C. + 75595
 + Bills, B.G. 78838
 + Billy, M. + 77781
 + Bimberg, D. 76479
 + Bindal, V.N. + 76131
 + Bindemann, R. 77443
 + Binder, H. 75089
 + Binder, K. + 74405
 + Binder, M. 74830
 + Bineth, J. 77971
 + Bingham, D. 74897
 Bingxin Yang
 + see Yang Bingxin
 + Bionta, R.M. + 75226
 + Birkeland, J. 78043
 + Birkeland, P.W. 78838
 + Birkmire, R.W. 78085
 + Birlasekaran, S. + 77931
 + Birman, J.L. + 77345
 + Birnbaum, G. + 75608
 + Birngruber, R. + 78240
 + Biro, T.S. 75020
 + Biryukova, E.A. 77176
 + Bisi, H.D. 75394
 + Bist, H.D. 77381
 + Bist, H.D. 77381
 + Biswas, A. + 74785
 + Biswas, P.K. + 76323
 + Bizzarri, U. + 75670
 + Bjorken, J.D. 74724
 + Blacknig, R. + 76283
 + Blacic, J.D. 78534
 + Blackford, B. 78396
 + Blackwell, C. Scott.
 + see Scott Blackwell, C.
 + Blaha, P. + 76841
 + Blair, D.F. + 78129
 + Blake, A.J. 78287
 + Blake, N.W. + 77679
 + Blake, R.A. 77854
 + Blakely, R.J. 78433
 + Blakemore, J.S. 75636
 + Blakers, A.W. 76798
 + Blakeslee, A.E. 78067
 + Blamey, P.J. + 74897
 + Blanc, R. 74371
 + Blanchet, R. + 78502
 + Blanchet, R. 77061
 + Blanche, H. 76316
 + Blann, M. 75000
 + Blasco, F. + 77320
 + Blasse, G. + 77437
 + Blasse, G. + 77424
 + Blau, W. 76870
 + Blaue, J.G. 77819
 + Blazey, K.W. + 77420
 + Blazhenova-Mikulich, L.Yu. + 74343
 + Bleick, W.E. 78798
 + Bleier, A. 78382
 + Bleier, A.R. 78383
 + Bleuler, H. 74488
 + Blewitt, G. 75226
 + Blinc, R. + 77272
 + Blinov, L.M. 77361
 + Blinov, N.N. 78301
 + Bliznet, J.A. 74797
 + Bliznyuk, N.I. 77438
 + Bloch, D. + 75744
 + Bloch, D. + 77238
 + Blocher, D. + 78269
 + Blokhin, V.I. 76229
 + Blomqvist, G. 78295
 + Bloom, E.D. 74711
 + Bloom, P.J. + 78194
 + Bloss, W.H. + 78045
 + Bloss, W.H. 78084
 + Blumenthal, S.H. 78195
 + Blumstein, S.E. 78198
 + Blyas, E.A. 78714
 + Blyas, E.A. 78716
 + Blythe, H.J. 77682
 + Blythe, P.A. + 76006
 + Boatwright, J. 78455
 + Bobashev, S.V. 76168
 + Bobel, G. + 76374
 + Bobenko, A.I. + 74322
 + Bobisut, F. 74756
 + Bobok, E. 78336
 + Bobovich, Ya.S. 77383
 + Bobra, A.D. 78814
 + Bobrov, Yu.G. + 75107
 + Bobrovski, D.M. 75153
 + Boccacci, P. 77547
 + Bocek, M. + 77728
 + Bocek, M. 77707
 + Boch, P. 77690
 + Bocharov, G.V. 78514
 + Bocho, A.V. 77605
 + Bochkova, R.I. 76412
 + Bockris, J.O.M. + 78107
 + Bode, M.F. 78982
 + Bodenkamp, J. 74783
 + Bodizs, D. 75204
 + Bodot, H. 75382
 + Bodtker, E. + 74518
 + Boehmer, H.E. 75655
 + Boer, F.W.N. de. see de Boer, F.W.N.
 + Boer, R.W. De.
 + see De Boer, R.W.
 + Boer, W. De.
 + see De Boer, W.
 + Boes, E.C. 78083
 + Bog-Hansen, T.C. 78268
 + Bogaerts, W.F. + 77788
 + Bogdanov, V.V. 77669
 + Bogdanova, E.V. 76115
 + Bogert, D. 74771
 + Bogess, T.F. 75708
 + Bogess, T.F. 75753
 + Boggs, G.J. 78200
 + Bogolyubov, N.N., Jr. + 74365
 + Bogomolov, V.N. + 77112
 + Bogus, K. 78015
 + Bohaty, L. 77365
 + Bohm, C. 78295
 + Bohm, M.C. 76830
 + Bohm, M.C. 76831
 + Bohm, M.C. 76832
 + Bohr, T. 76583
 + Bohringer, H. + 78809
 + Boiarski, A.A. + 76141
 + Boiko, M.S. + 77846
 + Boiko, V.A. + 74549
 + Boivin, A. 75781
 + Boivin, R. + 75781
 + Bojens, J. 78388
 + Bojtor, I. + 78336
 + Boland, J.N. + 78538
 + Boldyreva, A.L. 75270
 + Boilev, C.D. 75175
 + Boilis, G. 78132
 + Bolikhovityanov, Yu.B. + 77589
 + Bolter, H. + 76389
 + Bolmont, D. 76785
 + Bologna, G. 74766
 + Bologna, G. 75225
 + Boloni, E. 78356
 + Bolotin, H.H. + 74844
 + Bol'shov, L.A. 76363
 + Bonaccorsi, A. + 77867
 + Bonacic-Koutecky, V. 75324
 + Bonacic-Koutecky, V. 75391
 + Bonafede, M. + 78459
 + Bondeson, A. 76179
 + Bondybeg, V.E. + 75419
 + Bone, M.C. + 75824
 + Bonek, E. + 75147
 + Boni, R. 75648
 + Bonino, F. 77970
 + Bonnafe, J. + 77411
 + Bonner, W.A. 76882
 + Bonotto, S. 75115
 + Boodaghians, R.B. + 75423
 + Bookin, D. 75469
 + Boone, T. 76434
 + Boothman, D. + 77692
 + Boozar, A. 76207
 + Booser, A.H. 76206
 + Borchardt, G. + 77337
 + Borden, P. 78079
 + Borden, P.G. + 78065
 + Borden, P.G. 78035
 + Bordenave-Montesquieu, D. + 75475
 + Borderie, B. 75033
 + Borham, A.H. 78799
 + Boriakoff, V. 78933
 + Borie, B. + 76248
 + Boring, A.M. + 77476
 + Boris, A.Yu. 76058
 + Borisenko, O.M. 76028
 + Borisevich, N.A. + 75625
 + Borner, H. + 77217
 + Borovkov, V.Yu. 77389
 + Borrass, K. + 75174
 + Borrell, P. 75423
 + Borrell, P.M. 75423
 + Borshch, A. 75734
 + Bortle, J. 78873
 + Bortle, J.E. + 78875
 + Bortle, J.E. 78876
 + Bosacchi, B. + 75716
 + Bosch, B. 78780
 + Bosch, F. 75502
 + Boschi, E. 78459
 + Boschi, E. 78419
 + Bosetti, P.C. 75231
 + Bosquet, J.M. + 78778
 + Bossus, A. 75115
 + Bost, K.S. 78149
 + Bostanjoglo, O. 76814
 + Bostick, J.M. 75412
 + Boston, J.R. 78377
 + Boswarva, I.M. 76554
 + Bothun, G.D. + 79012
 + Botstein, O. + 77631
 + Bottari, A. + 78452
 + Bottcher, C. 75518
 + Bottcher, C. 75521
 + Bottcher, P. 76380
 + Bottcher, R. 77287
 + Bottelier, P. 77789
 + Bottomley, P.A. 78288
 + Botvinkin, O.K. 76673
 + Bouchard, P. 76223
 + Bouchaud, P. 75594
 + Bouchet, D. 77633
 + Bouchez, J. 74783
 + Bougnier, R.E. 78615
 + Bougnot, G. 76807
 + Boulnois, J.L. 75745
 + Bourbin, J. 75825
 + Bourbonnais, C. 77097
 + Bourdillon, A.J. + 77490
 + Bourgoign, J.C. 76878
 + Bourret, E.D. + 76337
 + Boutonnet, A. 75475
 + Bouzou, C. + 75420
 + Bova, F.J. + 78320
 + Bowell, E. 78840
 + Bowser, D. 78397
 + Boxtel, R. Van.
 + see Van Boxtel, R.
 + Boyanovsky, D. + 74370
 + Boyce, S. 78197
 + Boyd, D.M. 75607
 + Boyd, I.W. 76490
 + Boyer, K. + 75653
 + Boyn, R. 77416
 + Boysen, J. 77143
 + Braaten, E. + 74619
 + Brabers, M.J. 77788
 + Bradley, P.A. + 78752
 + Bradlow, H.S. 75019
 + Bradt, R.C. 76502
 + Brady, M.J. + 75809
 + Brady, M.J. + 75807
 + Bragagnolo, J.A. 78087
 + Bragin, V.G. + 77725
 + Brakman, C.M. 76255
 + Branchadell, V. + 77869
 + Brand, H. 76106
 + Brandhorst, H.W., Jr. 78033
 + Brandmuller, J. + 77346
 + Brandmuller, J. 76858
 + Brandon, J.F. 78327
 + Brandt, S. 74905
 + Brandt, S.B. 78543
 + Branz, H.M. 78056
 + Braski, D.N. 76521
 + Bratton, C.B. 75226
 + Brau, C.A. 75653
 + Brauer, E. + 76700
 + Brauer, F. 78396
 + Brault, J. + 78893
 + Braun, D.J. 77297
 + Braun, O.M. + 76935
 + Brauning, D. 75209
 + Braunstein, R. 76866
 + Bray, J.W. 77238
 + Bray, M. 74328
 + Brazuk, A. 75498
 + Brehmer, L. 77019
 + Breitenstein, M. + 75528
 + Brenner, R. 76783
 + Brengle, T.A. + 75176
 + Brennan, K.F. 76960
 + Brennecke, W. + 78117
 + Brennen, C.E. 76132
 + Brenner, D. 78397
 + Brenner, M. + 74901
 + Brenner, S.S. 77936
 + Brentano, P. von.
 + see von Brentano, P.
 + Breuer, H. 74988
 + Breuer, H. 74977
 + Breuer, M.M. + 78162
 + Brewer, W.D. 77143
 + Brezini, A. + 76900
 + Brice, D.K. 75490
 + Brickman, L.A. + 78087
 + Bridges, F. 77341
 + Briel, U.G. 78988
 + Briggs, F.H. + 79020
 + Brightwell, J.W. + 76952
 + Brikenshtein, V.Kh. + 77415
 + Brincourt, G. 76146
 + Bringer, A. 75493
 + Brink, D.M. + 74298
 + Brinkmann, K. + 78189
 + Britt, H.C. 75036
 + Britt, R.H. + 78277
 + Brittain, J.O. 77655
 + Brittain, J.O. 77656
 + Brittain, J.O. 77658
 + Brittain, J.O. 77657
 + Brix, O. 78144
 + Brixner, L.H. 77437
 + Broadwater, R.P. + 75165
 + Brochier, M. 78325
 + Brockway, G.S. + 75795
 + Brodimas, G. 74316
 + Brodin, M. 75734
 + Brodsky, S.J. 74702
 + Brokmeier, U. 76319
 + Brondi, A. + 75122
 + Bronger, W. 76380
 + Brooks, C.A. + 76550
 + Brooks, C. 78480
 + Brooks, C.S. + 77599
 + Broome, T.A. + 74981
 + Broome, T.A. 74797
 + Brouckere, G. De.
 + see De Brouckere, G.
 + Broude, C. + 74835
 + Broughton, J.Q. + 76767
 + Broussell, M. + 77972
 + Brout, R. + 77187
 + Brower, H. 74463
 + Brovov, V.A. 76442
 + Browell, E.V. 78660
 + Brown, B.A. 74904
 + Brown, C.E. + 78402
 + Brown, D.T. + 78553
 + Brown, E. 78404
 + Brown, G.E. 74856
 + Brown, G.R. 76627
 + Brown, H. 76474
 + Brown, H. 76341
 + Brown, H.A. 77185
 + Brown, J.M. + 75371
 + Brown, L. 78435
 + Brown, L.W. 78967
 + Brown, P.J. 77140
 + Brown, P.J. 77141
 + Brown, R. + 76218
 + Brown, R.A. 78843
 + Browne, J. 78359
 + Browne, L.W.B. + 75992
 + Browning, K.A. 78630
 + Bruce, P.G. 76391
 + Brucker, G.J. 76506
 + Brucker, J. 76007
 + Bruckner, H.-P. 76618
 + Bruckner, S. + 76239
 + Bruckner, V. 77471
 + Bruckner, W. 76618
 + Brudvig, G.W. 78129
 + Bruinsma, R. + 77126
 + Brummell, M.A. + 77037
 + Bruna, P.J. 75312
 + Brune, J.N. 78444
 + Brunish, W.M. 78889
 + Brunner, H. 77261
 + Bruno, A.C. + 78279
 + Brunoro, G. + 77786
 + Bruns, M. 78182
 + Bryant, F.J. 76467
 + Bryant, G.W. 77485
 + Bryant, P. 78269
 + Bryngdahl, O. 75595
 + Bryukhanov, O.N. + 74505
 + Brzic, A.N. 75383
 + Bubnov, V.A. 76715
 + Buccella, F. 74662
 + Buccella, F. 74692
 + Buchert, J. 78390
 + Buchholz, F.J. 76722
 + Buchwald, V.F. 78884
 + Buckius, R.O. 77925
 + Buckley, A. 77699
 + Buckley, C.N. 76952
 + Bucurescu, D. + 74874
 + Budden, K.G. 76170
 + Budina, N.E. + 75783
 + Buemi, G. + 75398
 + Buenerd, M. 75040
 + Buener, R.J. 75312
 + Bugaev, A.A. + 77468
 + Bugg, D.V. 74792
 + Buhl, D. 78967
 + Buijs, H.L. 78627
 + Buitrago, J. + 78865
 + Bukatov, V.G. + 77684
 + Bukhalenkov, V.V. 76836
 + Bukshpan, S. 76468
 + Bulanen, V.I. + 75069
 + Bulat, L.P. + 76718
 + Bulloch, C. + 76957
 + Bullock, E. 77857
 + Bulman, G.E. + 76960
 + Bumagina, L.A. 77423
 + Bunakov, V.E. + 74982
 + Bunakov, V.E. + 74986
 + Bunkin, F.V. + 75853
 + Buoncrisiani, A.M. + 78049
 + Burakov, V.S. + 76217
 + Burakov, V.S. + 77940
 + Burch, P.R.J. 78265
 + Burd, M. 76866
 + Burden, C.J. + 74726
 + Burelman, M. + 78011
 + Burger, W.J. 74804
 + Burgers, P.C. + 75550
 + Burgisser, E. 77848
 + Burke, P.G. 75509
 + Burkov, S.E. + 76933
 + Burkov, V.G. 78715
 + Burman, C. + 77917
 + Burmistrov, A.S. + 75693
 + Burmistrov, A.V. 77344
 + Burnham, R.D. + 75689
 + Burnk, J.L. 75117
 + Burns, G. 76784
 + Burshtein, Z. 75240
 + Burstein, E. + 76784
 + Burstein, G.T. + 77799
 + Burstell, C.B. 75809
 + Burt, P.B. 74602
 + Burtsev, N.N. 77596
 + Buscaglia, G. 77789
 + Busch, F. 75030
 + Buschhorn, G. 74783
 + Buschow, K.H.J. 77151
 + Buschow, K.H.J. + 77156
 + Buschow, K.H.J. 77209
 + Buschow, K.H.J. 77155
 + Bushong, S.C. 78360
 + Busing, W.R. 76408
 + Buso, K. V.N. 77845
 + Bussac, M.N. 76172
 + Busse, W. + 77459
 + Buti, B. 78866
 + Butler, I.S. 77278
 + Butler, S.E. 75505
 + Byer, R.L. 75678
 + Bykov, S.I. 75901
 + Bykovsky, Yu.A. 76530
 + Byrd, R.C. 74999
 + Byrne, G.F. 78656
 + Byteva, I.M. + 75421
 + Cacciari, C. + 78907
 + Caccia, I. + 75351
 + Cadek, J. 77710
 + Cadene, M. 78013
 + Cady, R. + 78817
 + Caffarel, A.J. 77855
 + Cahill, K. 74827
 + Cahn, F. 75868
 + Cai Ruying 77305
 + Cain, C.A. 78233
 + Cain, C.A. 78231
 + Cain, C.A. 78234
 + Cain, C.A. 78232
 + Cain, J.C. 78431
 + Cairns, R.A. + 76198
 + Calarco, J.R. + 74959
 + Calderbank, K.E. 75416
 + Caldwell, J. + 78864
 + Caldwell, N. 78821
 + Calkins, D. 77034
 + Calheiros, F.J.L.C. 77193
 + Calkins, M. 76745
 + Callaghan, W.T. 77544
 + Callan, C.G., Jr. 74668
 + Calleja, M.J. 78062
 + Calligaris, C. 77555
 + Callis, L.B. + 78615
 + Camarero, E. Garcia.
 + see Garcia Camarero, E.
 + Cambiaggio, M.C. + 74871
 + Cambier, F. 77539
 + Cambini, M. + 77789
 + Cameron, A. 77766
 + Caminiti, R. + 77269
 + Campana, C.F. 76382
 + Campana, P. 74766
 + Campana, P. 75225
 + Campbell, A.B. 76634
 + Campbell, E.J. + 75417
 + Campbell, E.J. 75544
 + Campbell, I.A. 77143
 + Campbell, I.A. 77285
 + Campbell, K. 78681
 + Campbell, P. 74303
 + Campbell, S. 78547
 + Campillo, M. 75275

- +Campillo, M. 78135
 Campos, C. + 76238
 +Camps, R.A. 74561
 +Camras, M.D. 75689
 Canadell, E. + 75294
 +Canali, C. 76128
 +Candeia, R.M. 75638
 +Candela, D. 76573
 Candelas, P. 74633
 Canella, G. + 78729
 +Canestaro, C. 74363
 +Canetti, M. 76326
 +Canaizares, C.R. 78969
 +Cannady, M.D. 78020
 Cannington, P.H. + 75443
 +Cannon, R.D. 78964
 Cansfield, D.L.M. + 77699
 Cantelaupe, Y. 76882
 Canteloup, J. + 74554
 Cantor, B. 77627
 +Cantow, H.-J. 75972
 Cao, T. + 78453
 +Capaldi, R.A. 78128
 +Cape, J.A. 78076
 +Capel, H.W. 74253
 Capella, A. + 74810
 Capkova, P. + 76579
 Capodanno, P. 76051
 Capodanno, P. 76100
 +Caponi, M.Z. 75655
 +Capos, N. 78203
 Capri, A.Z. + 74581
 Capurso, M. 75934
 +Cara Romeo, C. 74821
 Caramana, E.J. + 76209
 Carasco, F. + 76972
 +Carbonara, R. 76651
 +Carbotte, J.P. 76825
 +Carbotte, J.P. 76826
 Card, H.C. + 78072
 Cardimona, D.A. + 76588
 +Cardoso, L.P. 76238
 +Cardot, J.C. 78308
 +Cardy, J.L. 74370
 Carey, V.P. 76018
 +Carles, M. 75382
 +Carleton, K. 77593
 Carley, A.F. 74570
 +Carlin, M. 78330
 Carlson, C.W. + 78775
 +Carlson, F.M. 76333
 Carlson, J. + 74861
 Carlson, P. (ed.) 74228
 Carlson, T.A. + 75446
 +Carnes, H.A. 75591
 +Carnesecchi, G. 74783
 +Caro, R.G. 75736
 +Caron, J.P.H. 78499
 Carpenter, R.N. + 75857
 +Carquilat, J.M. 78948
 Carr, B.J. 79029
 +Carr, G.L. 77094
 +Carr, S.H. 77655
 +Carr, S.H. 77656
 Carrasco, G. + 78796
 +Caravatta, V. 75351
 +Carroll, A.J. 77743
 +Carroll, J.E. 74509
 Caruthers, R.B. + 77651
 +Carson, K.R. 78090
 Carstens, D.H.W. + 75178
 +Carton, J.P. 74371
 Carton, J.-P. + 74384
 +Cartwright, K. 75141
 Carvalho, M.J. Petrolino
 see Petrolino Carvalho, M.J.
 Casagrande, C. + 76295
 Casarosa, C. + 76020
 +Casas-Vazquez, J. 74383
 +Case, C. 78103
 +Cashion, J.D. 74897
 +Cashion, J.D. 77295
 +Caspar, D.L.D. 78138
 +Casper, T.A. 76214
 Caspers, W.J. + 74369
 Casperson, L.W. 75629
 +Cassen, P.M. 78857
 +Cassiday, G.L. 78817
 +Cassidy, K. 75029
 Cassinelli, J.P. + 78908
 Cassing, W. + 74924
 +Cassing, W. 74879
 +Cassing, W. 74929
 +Cassing, W. 74930
 +Castagne, M. 77411
 +Castagnoli, C. 74766
 +Castagnoli, C. 75225
 +Castagnoli, B. 78275
 +Castano, J. 78062
 +Castano, J.L. 77431
 Castellano, J.A. 76288
 +Castellano, M. 75648
 +Casten, R.F. 74908
 Castiglione, S. + 75425
 +Castleman, A.W., Jr. 75564
 +Castoldi, C. 74759
 +Castro, E.A. 75271
 +Cata, G. 74874
 Catalan, J. + 75293
 Catalano, S. + 78693
 Catellani, A. + 76128
 +Catellani, A. 75239
 +Cathles, L.M. 78488
 +Caticha-Ellis, S. 76238
 Catnu, A.M. + 75402
 +Catto, P.J. 76205
 +Cattoni, A. 75648
 +Cavallio, N. 75648
 +Cavenett, B.C. 77292
 +Cavenett, B.C. 77293
 Cazenave, A. + 78491
 Cebece, T. + 75999
 Ceccarelli, C. + 79027
 +Cederbaum, L.S. 75434
 +Celotti, G. 76711
 +Center, R.E. 75651
 Cerchez, S. 78564
 +Cercignani, C. 75915
 +Cerniglia, P.A. 78386
 +Cernobrovkin, V.V. 75170
 Cerrina, F. 75773
 +Cerrina, F. 77533
 +Cerrina, F. 76768
 +Cerven, I. 76309
 Cesnák, L. + 74489
 Ceulemans, A. 75374
 +Cevenini, F. 75648
 Ceyer, S.T. + 77919
 Cha, C.Y. + 75560
 Cha, D. 74881
 +Chadwick, D.L. 77620
 +Chaffin, R.J. 78042
 +Chain-Cheng Teng 77318
 Chakrabarti, C.G. 74424
 +Chakrabarti, S. 74814
 +Chakrabarty, P. 78593
 +Chakrabarty, A. 74743
 Chakraborty, D.B. + 78940
 Chakravarthy, A.K. + 78683
 +Chakravarty, B. 78733
 Chakravarty, B.C. + 77996
 Chalapaty, V. Venkata
 see Venkata Chalapaty, V.
 Chambers, F.W. + 75983
 +Chamseddine, A.H. 74358
 +Chamseddine, A.H. 74670
 Chan, C.F. + 76074
 +Chan, S.I. 78129
 Chan, T.S. + 78044
 Chan Heang-Ping
 see Heang-Ping Chan
 Chan Hoi-Young
 see Hoi-Young Chan
 Chandna, O.P. + 76122
 Chandra, S. 75738
 Chandra Mukesh
 see Mukesh Chandra
 Chandramohan, T. 74779
 Chandrasekaran, K. + 77899
 Chandrasekhar, K. + 76411
 +Chang, J.S. 76095
 +Chang, L.L. 77445
 +Chang, L.L. 77033
 Chang, L.S. + 76119
 Chang, T.D. + 77658
 Chang, T.D. + 77655
 Chang, T.D. + 77656
 Chang, T.-D. + 77657
 Chang Chi-Yang
 see Chi-Yang Chang
 Chang Chin-An. see Chin-An
 Chang
 Chang Mau-chung
 see Mau-chung Chang
 Chang Tong
 see Tong Chang
 Chang Yu-liang 74452
 Chang-de Gong
 see Gong Chang-de
 Changlin Guo
 see Guo Changlin
 Changming Guo + 78596
 Changying Chen
 see Chen Changying
 +Chanowitz, M. 74669
 Chant, N.S. 74852
 Chao, K.A. + 76877
 +Chao, K.A. 76828
 Chao, T.H. + 75587
 +Chao Pau-In 74502
 Chaoguo Wang
 see Wang Chaoguo
 +Chapkunov, S. 78672
 +Chapkunov, S. 78668
 +Chapkunov, S. 78669
 +Chaplya, M.E. 75963
 +Chapman, D.S. 78485
 +Chapman, G.A. 78887
 Chapman, N.B. 74248
 Chapman, N.B. 77874
 +Charbonnier, B. 78325
 +Charity, R.J. 75032
 +Charkin, O.P. 75270
 Charlock, T.P. 78641
 Charlson, R.J. + 78613
 Charlton, D.G. + 78595
 Charry, J.M. + 78386
 +Chasse, R.L. 78512
 +Chassagne, G. 76641
 +Chatterjee, L. 74800
 +Chatterjee, L. 74801
 +Chatterjee, M. 74911
 Chattopadhyay, T.K. + 76661
 Chaturvedi, M. + 74394
 Chaturvedi, M.C. + 77665
 Chatzidimitriou-Dreismann, C.A. 75429
 Chau, F.T. 75354
 Chau Ling-Lie
 see Ling-Lie Chau
 +Chauba Singh, S. 76721
 +Chaudhary, M. 75045
 +Chaudhry, M.A. 77302
 +Chaudhuri, B.K. 76658
 +Chaudhuri, B.K. 76660
 +Chaudhury, M. 76919
 +Chaudhury, S. 77264
 Chauhan, M. + 76685
 Chawla, K.K. 77601
 Chay, T.R. + 78151
 +Chebotarev, V.P. 75335
 Chechekin, V.M. + 79040
 +Chekashova, S.A. 77724
 +Chen, C. 74783
 +Chen, C.H. 78891
 Chen, C.J. + 77905
 Chen, H.C. 75568
 Chen, H.H. + 75230
 +Chen, J. 77207
 Chen, P. + 76785
 Chen, T.R. + 76719
 Chen, X.S. + 74864
 +Chen, Y.H. 76489
 Chen, Y.M. + 74287
 Chen Changying + 78134
 Chen Er-ting
 see Er-ting Chen
 Chen Guangjun Zhao, Jr. 77825
 Chen Hsiang-chen + 74557
 +Chen Liang 77279
 Chen Mao-Hsiung
 see Mao-Hsiung Chen
 Chen Mao Hsiung
 see Mao Hsiung Chen
 Chen Meifang 77941
 +Chen Shi 74598
 Chen Shi-gang 76002
 Chen Shu-chi Fang + 74470
 Chen Wang-Ping
 see Wang-Ping Chen
 Chen Yi-zhou + 75955
 +Chen Zheng-xiong 74301
 Chen Zhixing 77863
 Cheng, L.J. + 78061
 Cheng, P.C. + 78407
 Cheng Ru-xin + 77590
 Chenghe Xu
 see Xu Chenghe
 +Chenskii, E.V. 77001
 +Chenpenko, V.G. 74548
 Cheradame, H. + 76696
 +Cherches, Kh.A. 77438
 +Cheremisin, S.M. 77289
 +Cherkasui, R. 77500
 Cherkashin, B.V. + 77150
 +Chermette, H. 75289
 Chern, G.C. + 76802
 Chern, R.T. + 76702
 +Chernobrod, B.M. 75721
 +Chernobrovkin, V.P. 78306
 +Chernov, S.F. 76645
 +Chernyak, A.A. 74512
 Chernyshenko, S.I. 76031
 +Chernysheva, G.I. 76673
 +Cherry, J.A. 75145
 +Chesnulavichyus, I. 75681
 Chesshire, J. 77950
 +Cheung, F.B. 76098
 +Cheung, M.M. 75711
 +Chevaganov, B.A. 76542
 +Chevriev, J. 77006
 +Cheynis, B. 75026
 Chhi-Chong Wu + 77007
 Chi Po-chun 75890
 Chi Sheng
 see Sheng Chi
 Chi-chia Liu
 see Liu Chi-chia
 +Chi-fong Ai + 76761
 Chi-Yang Chang + 76712
 +Chianelli, R. 78079
 +Chiang, C.J. 76781
 Chiang, C.-L. + 76964
 +Chiang, F.P. 74434
 +Chiarella, V. 74766
 +Chiarella, V. 75225
 Chiari, J.A. + 74459
 +Chicklis, E. 75677
 +Chicklis, E. 75682
 Chidester, L.G. + 78021
 Chieh, C. 76345
 Chien Chung + 75055
 Chien Shih-nan 74432
 Chih-chung Yu
 see Yu Chih-chung
 +Chihara, H. 76658
 +Chihara, H. 76660
 +Chikamura, T. 77024
 Child, M.S. + 75467
 +Childress, S. 74759
 +Chilingaryan, Yu.S. 76286
 +Chillingaryan, Yu.S. 76307
 +Chillingworth, R.K. 78404
 Chin, A.K. + 76434
 +Chin, L.-Y. 76333
 +Chin-An Chang 77033
 Ching, W.Y. + 77186
 Ching Shen. see Shen Ching
 Ching-an Meng
 see Meng Ching-an
 Chinlon Lin 75720
 +Chiodelli, G. 76694
 +Chirifu, S. 78100
 +Chitre, S.M. 79008
 +Chitre, S.M. 78939
 +Chiu, L.C. 76719
 +Chiu, T.H. 77532
 +Chivers, R.C. 75882
 Chizhov, A.V. + 74658
 +Chizhov, M.V. 74658
 +Chizov, J. 77284
 +Chmyrev, V. 78669
 +Cho, A.Y. 77570
 Cho, Z.H. + 78323
 +Cho, Z.H. 78292
 +Choi, C.H. 76934
 Choi Sang Don
 see Sang Don Choi
 +Choma, I. 76773
 Chong-Cheng Fu + 76138
 +Chopov, V. 77497
 Chopra, O.K. 77730
 +Chou, T.-W. 77734
 Chou Zuwei 75996
 Choukroune, P. + 78501
 +Chourasia, N.C. 77070
 Chovet, A. + 77231
 Chow, T.L. 79026
 +Chow, W.W. 75627
 Chowdhury, A. Roy
 see Roy Chowdhury, A.
 Chowdhury, K. + 75904
 Chowdhury, K. Basu
 see Basu Chowdhury, K.
 Chowdhury, K. Roy
 see Roy Chowdhury, K.
 +Choy, C.L. 77689
 Choy, G.L. + 78455
 Choy, T.C. + 77643
 +Chrien, R.E. 74913
 Chrisp, M.P. 74568
 Chrisp, M.P. 75601
 +Christen, D.K. 77118
 Christenson, H.K. 76274
 +Christiansen, P.A. 75279
 Christodoulou, G. + 77809
 Christophorou, L.N. + 76884
 +Christou, N. 77048
 +Chrobacek, D. 74783
 +Chrusicielewski, W. 75233
 +Chu, S.Y. 75017
 Chu Juehui + 76939
 +Chuang, L.S. 75004
 +Chubachi, N. 75850
 +Chubachi, N. 76764
 +Chubinsky, O.V. 74901
 +Chubukov, A.V. 76620
 +Chudakovskii, F.A. 77468
 Chueng Keng-tong + 75938
 Chui, S.T. 77128
 Chuiko, G.A. + 78302
 +Chuiko, G.A. 78303
 +Chukhovskii, F.N. 76240
 +Chukichev, M.V. 77462
 Chuljian, D.T. + 75309
 +Chumak, V.L. 77897
 +Chun Bae Lee 75436
 +Chun Bae Lee 75437
 +Chung, C. 74913
 Chung, C.H. + 76895
 +Chung, Y. 77055
 Chung Chien
 see Chien Chung
 Chung Ok Hec
 see Ok Hec Chung
 +Chung-Chuang Wei 76944
 +Chung-Chuang Wei 77318
 +Chung-Chuang Wei 77330
 +Chung-liang Ku 74470
 Chunzhang Zhang. see Zhang
 Chunzhang
 +Chuprina, E.P. 78514
 Chuprunov, E.V. + 76349
 +Churakov, V.V. 75453
 +Churchill, T.L. 75651
 Churnetski, B.V. 75090
 +Chutskii, N.A. 76500
 Ciangaru, G. 74976
 Ciarkowski, A. 75567
 Ciattaglia, L. 78607
 Cicotti, G. + 76615
 Cieminski, J. von
 see von Cieminski, J.
 +Cifarelli, L. 74821
 +Cihal, V. 77797
 +Cimiraglia, R. 77867
 +Ciocci, F. 75670
 Ciok, Z. 76222
 Ciqun Liu. see Liu Ciqun
 Civitarese, O. + 74873
 Claassen, H.A. + 76163
 +Claeys, E.G. 75386
 Clark, B.C. + 74941
 Clark, B.C. + 74987
 Clark, E.J. + 78102
 +Clark, G.W. 78969
 Clark, N.A. + 77362
 +Clark, P.E. 77295
 +Clark, S. 76436
 +Clarke, H.S. 78361
 +Clauser, A.H. 76649
 +Clauser, A.H. 76763
 +Claus, R.O. 75894
 Clausen, J.V. + 78950
 +Clausner, J.F. 76214
 Claverie, P. 75466
 Clay, R.W. + 78768
 +Clayton, C.R. 76497
 Clayton, D.D. 78829
 Clegg, W. + 76406
 Clemente, G.B. + 77115
 +Clemente, E. 75310
 +Clements, D.P. 77425
 +Clemesha, B.R. 78727
 Clerc, J.P. + 74371
 +Cleveland, B.T. 78888
 +Cleveland, B.T. 78816
 Cliff, G. 77939
 Clifford, P.K. + 74450
 Clifford, P.K. + 74451
 Clifford, S.M. + 78839
 Cline, D.B. 74770
 Cline, D.B. 75227
 Cline, H.E. 76801
 +Cline, J.F. 75140
 Cloutier, J.R. 78692
 +Clower, C.A. 76214
 Coatrieux, J.L. 78375
 Cobianu, C. + 77581
 Cocke, W.J. + 79013
 Coen, S. + 78695
 +Coensgen, F.H. 76214
 Coffey, W.T. + 74413
 +Coffin, C.T. 74759
 +Coffin, J.P. 75031
 +Coffin, J.P. 75065
 Cogan, D.de
 see de Cogan, D.
 +Cogneau, M. 75115
 +Cohen, A. 78643
 +Cohen, B.I. 75176
 Cohen, B.L. 78368
 Cohen, B.L. 78409
 Cohen, C. + 76472
 Cohen, J. 75049
 +Cohen, J.B. 76253
 +Cohen, M. 77628
 +Cohen, M. 77654
 +Cohen, M.M. 75870
 +Cohen-Solal, G. 78008
 Cohn, H. 78997
 Coisson, R. + 75659
 Colak, S. + 75643
 +Colak, S. 77426
 +Colas, P. 74783
 Colbeck, S.C. 76331
 +Cole, A.J. 75040
 Coleman, R.L. + 78347
 Colgan, E.G. + 77071
 +Collard, J. 75115
 +Colle, R. 74427
 +Collins, A.T. 77382
 +Collins, M.J. 77651
 +Collins, R.E. 78092
 Collis, P.N. + 78737
 Collocott, S.J. 74433
 Colomban, Ph. + 77256
 +Colombini, J.Y. 75825
 +Colombini, M. 78154
 Colombo, O.L. + 78655
 Colson, W.B. + 75649
 +Coltman, R.R., Jr. 77118
 +Coluzza, C. 74449
 Comas, F. + 77441
 Comber, P.G. Le
 see Le Comber, P.G.
 +Combes, M. 78864
 +Comer, J.J. 76477
 +Comerford, L.D. 75807
 +Comerford, L.D. 75809
 +Comfort, J.R. 74853
 +Compaan, A. 76494
 +Comrie, C. 76710
 Comtat, M. + 78106
 +Comtet, A. 74827
 +Condurache, D. 77210
 +Conforto, G. 74759
 Conklin, J.C. 75167

- + Conn, R.W. 75173
 Connerade, J.P. 75322
 +Conradi, M.S. 76330
 Conrath, B.J. + 78853
 +Conrath, B.J. 78852
 +Constantinescu, G. 74874
 +Conti, G. 78911
 Conti, P.S. + 78915
 +Contin, A. 74821
 Contopoulos, G. 74260
 +Contreras, R.H. 75403
 +Conversi, M. 74241
 +Conway, J.C., Jr. 77729
 Conway, J.H. + 74400
 +Conzett, H.E. 74972
 Cook, L.T. + 78273
 +Cook, P.N. 78273
 +Cook, R.F. 76555
 Cook, S.D. + 78309
 Cooke, D.W. + 78140
 +Cool, R. 74669
 Cooman, B.C. De
 see De Cooman, B.C.
 +Cooney, P.J. 74555
 Cooper, R.K. + 75663
 Cooper, S. 74829
 Cooper, W.E. + 78196
 +Cooper, W.E. 78197
 Coppa, G. + 75804
 +Coppens, P. 76250
 Corbett, J.O. 78341
 +Corbin, M.H. 75130
 Corbin, S. + 75465
 Cordes, J.M. + 78933
 +Cordier, A. 74783
 +Coret, A. 77355
 Coriell, S.R. + 76592
 +Corke, M. 76140
 +Cormack, J. 78328
 Cormier, T.M. 75021
 +Cornet, E. 76182
 +Cornog, D.G. 78088
 +Correll, D.L. 76214
 +Correra, L. 76486
 +Corset, J. 77978
 +Corisi, S. 78053
 +Corson, M.R. 77425
 +Cortez, B.G. 75226
 +Cortona, P. 76374
 +Cosby, P.C. 75456
 +Cosset, J.-M. 78293
 Cost, J.R. 74446
 +Costa, E. 78796
 +Costa Monteiro, E. 78206
 +Costa Ribeiro, P. 78279
 +Costa Ribeiro, P. 78206
 Costantini, D. + 74368
 Costantino, M. 78523
 Cotrim Vasconcellos, J.I. 75754
 +Cotter, R.J. 74553
 Coufal, H. + 75879
 Coujou, A. + 77653
 +Coulomb, P. 77653
 Coulthard, J. 76133
 Courbage, M. + 74423
 +Courtois, A. 76377
 +Coussement, R. 76468
 +Couzi, M. 77011
 Cowan, G.A. + 78892
 Cowern, N.E.B. 77499
 +Cowley, R.A. 76741
 +Cowling, M.J. 77827
 Cowisk, R. + 78937
 +Cox, A.N. 78922
 Cox, E.R. + 75820
 +Cox, H.W. 77715
 Cox, I.J. + 74531
 +Cox, S.K. 78600
 +Coxon, J.A. 74539
 +Cozzika, G. 74783
 +Craig, J.C. 78201
 +Cramer, H. 78324
 +Crandall, D.H. 75522
 +Crane, P.C. 79022
 +Crasemann, B. 75504
 +Craven, J. 78588
 +Crawley, G.M. 74898
 +Cremers, R.M.M. 75345
 +Crisan, M. 77183
 +Crisler, M.B. 74759
 +Crisponi, G. 77269
 +Cristoforeanu, S. 77231
 +Croce, F. 77970
 Crochet, M.J. + 76079
 Crooks, M.J. + 76727
 +Croset, M. 76472
 +Crosley, D.R. 75482
 Cross, A.J. + 75552
 +Cross, L.E. 77331
 +Crotty, G.T. 78061
 +Crouch, M. 78770
 Crow, J.D. 75808
 +Crozat, G. 78106
 +Cruikshank, D.P. 78845
 Cruz, S.A. + 75490
 Csanady, G.T. 74236
 Cseh, J. 74946
 +Csépregi, T. 78111
 +Csizmadia, I.G. 75329
 +Csizmadia, I.G. 75267
 Csom, Gy. + 75158
 +Csom, Gy. 75201
 Csorna, S.E. 74760
 +Cujec, B. 75010
 +Culik, J.S. 78060
 +Culshaw, B. 74527
 +Culshaw, B. 75826
 +Culshaw, B. 74528
 Cumming, J.B. 74951
 +Cummins, W.F. 76214
 +Cundy, D.C. 74766
 +Cundy, D.C. 75225
 Cunhao Zhang
 see Zhang Cunhao
 +Cunningham, J.E. 77528
 +Cunningham, J.E. 77532
 Cunxian Sha
 see Sha Cunxian
 Cuomo, F.W. 75892
 Cuomo, J.J. + 77774
 Cuomo, J.J. + 78403
 +Currie, R.G. 78512
 +Curry, T.J. 75857
 Curtin, M.W. + 74892
 +Curtis, D.R. 78126
 +Curtis, D.W. 78775
 +Curtis, H. 78028
 Curtis, H.B. + 78036
 Curto, D. + 75977
 +Curtright, T. 74619
 +Curro, F. 77963
 +Cusson, R.Y. 74933
 +Cutoiu, D. 74874
 +Cutolo, A. 75648
 +Cuzzilla, J.N. 78847
 +Czapack, M. 75239
 +Czapiek, A. 78772
 Czapiewski, B. + 78410
 Czaplak, Z. + 77338
 Czarnecki, P. + 76930
 +Czupinski, P. 77338
 +Da Hsuan Feng 74875
 +Dachev, Ts. 78673
 +Dacol, F.H. 76784
 Dadarlat, D. + 75638
 Dadarlat, D. + 77172
 +D'Adda, A. + 74649
 +Dafinova, R. 77458
 +Dagnac, R. 75475
 +D'Agostini, G. 74783
 +Dagotto, E. 74698
 +Daher, Y. 77231
 +Dahlen, F.A. 78511
 Dahlie, W.E. + 77065
 +Dai, N.X. 75025
 +Dai Anbang 76386
 Dai Dao-xuan + 74559
 +Dai Yao 75952
 Daichik, M.L. + 74455
 +D'Aiello, R.V. 77565
 +Daimon, H. 77521
 +Dakowski, M. 75034
 Dalard, F. + 77980
 +Daley, H.M. 74797
 +Dalgaro, A. 75505
 +D'Ali, G. 74821
 Daling Luo see Luo Daling
 +Dall'Oglio, G. 79027
 Daly, J.G. + 77449
 +Daly, S. 78509
 +Daly, S.F. 76025
 Dam, R.T. van see van Dam, R.T.
 Damaskinos, S. + 77467
 +Damaskinski, E.A. 76532
 +Damia, E. 78293
 D'Amico, A. + 74449
 D'Amico, A. + 77013
 Damien, D. + 76689
 +Damm, C.C. 76214
 +Damon, K. 78196
 +Damuth, J.E. 78516
 Damzen, M.J. + 75727
 Dan Hsi see Hsi Dan
 +Dandridge, A. 74529
 Dang, C. + 75619
 Dang, K.L. see Le Dang, K.
 +Dang Tran, Q. 77522
 +d'Angelo, S. 75196
 +Daniel, H. 75558
 Danielewicz, P. 74955
 +Daniels, P.G. 76006
 +Daniels, R.R. 77042
 +Danilchenko, V.E. 76366
 Danilenko, V.A. + 76066
 +Danilov, S.E. 76516
 Danilyuk, I.I. 75902
 Danyarov, S.B. + 78256
 +Danks, A.C. 78867
 +Dantsiger, A.Ya. 77333
 +Danz, R. 77323
 +Danziger, J. 79024
 Dao Khac An + 76703
 Dao-xuan Dai
 see Dai Dao-xuan
 +Dapkus, P.D. 77583
 Darachyunas, R.I. + 74548
 +Darmawan, J. 76893
 Das, A.K. + 75957
 Das, B. 77591
 +Das, B.K. 77996
 +Das, B.K. 78063
 +Das, G. 74804
 Das, N.K. + 77726
 +Das, P. 76478
 Das, P.C. + 77492
 +Dasgupta, K. 74734
 +Dasgupta, P. 74734
 +Dashane, V.S. 77308
 +Dashevskii, Yu.A. 78711
 Dasmahapatra, B. + 75010
 +Date, S.K. 77519
 Datta, B. + 77933
 Dattoi, D.P. + 74736
 +Dattoli, G. 75656
 +Dattoli, G. 75670
 Daud, T. + 77554
 +Daud, T. 78061
 +Dautet, H. 74911
 Davari, B. + 76478
 +David, W.F. 76391
 +David, W.R. 75178
 +Davidovich, R.L. 76613
 +Davidovics, G. + 75382
 +Davidovsky, F. 74835
 +Davidson, F.M. 77067
 +Davidson, H. 75856
 Davidson, M.R. + 78221
 +Davier, M. 74783
 Davies, D.E. + 76477
 +Davies, D.E.N. 74527
 +Davies, D.E.N. 75826
 +Davies, D.E.N. 74528
 +Davies, G.A. 76081
 Davies, J. + 78869
 Davies, J. + 78868
 Davies, M.E. + 78858
 +Davies, P. 77575
 Davies, P.B. + 75336
 Davies, R.H. + 78122
 Davis, A.C. + 74611
 +Davis, A.C. 74649
 Davis, B.R. + 78387
 Davis, C.M. + 75821
 Davis, D. + 78511
 +Davis, E.E. 78512
 +Davis, H.A. 76182
 +Davis, H.T. 74374
 Davis, R. Jr. + 78888
 +Davis, R. Jr. 78816
 Davis, S.H. + 76114
 +Davis, S.J. 77891
 +Davis, S.L. 75470
 Davni, E. + 74835
 Daware, A.L. + 77074
 +Dawber, P.G. 76526
 Dawidowicz, A.L. + 76773
 Dawson, D.A. 74314
 +Dawson, G.A. 78696
 +Day, A.C. 77861
 Day, M.F. + 77759
 Dayu Yang see Yang Dayu
 +De, B.R. 75301
 De, K.S. + 76946
 +De, T. 74799
 +De, T. 74785
 +De Alfaro, V. 74336
 +De Angelis, A. 75670
 +De Assis Neto, V.F. 78872
 +De Bernardez, L.S. 76758
 +De Boer, F.W.N. 74834
 De Boer, R.W. + 78215
 +De Boer, W. 74783
 De Brucker, G. 75276
 +De Cogan, D. 76951
 +De Cooman, B.C. 76793
 De Filippis, S. + 74294
 de Freitas Mourao, R.R. + 78960
 de Graaff, H.C. + 77012
 +de Grip, W.J. 78180
 +de Groot, A.W. 78072
 +de Heer, F.J. 75498
 De Icaza-Herrera, M. 77322
 +de Jeu, W.H. 76301
 De Jong, T. + 76461
 De Kam, J. + 75557
 De Keijser, Th.H. + 76254
 +de Kowalewski, D.G. 75403
 de Kozak, A. + 76395
 de la Selva, S.M.T. + 74363
 +de La Tour du Pin, H. 78502
 de Lacheisserie, E. du Tremolet
 see du Tremolet de Lacheisserie, E.
 de Lardshier, A.C. 78947
 De Li Ming see Ming De Li
 +de Marchi, G. 76513
 +De Martini, F. 75659
 de Masi, A. + 74391
 +de Meyer, H.E. 74647
 +de Murcia, M. 77411
 +De Paoli, A.L. 74873
 +De Pinho, A.C. 75492
 de Ritis, R. + 74341
 de Schepper, L. + 76413
 De Schepper, L. + 77477
 +de Schepper, L. 76483
 +De Simone, S. 75648
 +de Urries, F.J. 74586
 +de Vargas, L. 75974
 +De Vos, A. 78011
 de Vos, A.M. + 75540
 +de Vries, A.E. 77507
 De Vries, O. 76060
 De Weijer, P. van
 see van de Weijer, P.
 +De Wit, B. 78372
 +de Witt, H. 74756
 De-xin Wang
 see Wang De-xin
 +Deacon, D.A.G. 75672
 +Deacon, D.A.G. 75650
 Deak, P. 76839
 +Deans, W. 77187
 Deatherage, J.F. + 78128
 Deb, K.K. 77427
 Deb, N.C. + 75524
 +Deb, S.K. 77296
 +Deb Roy, M. 76940
 Debeauvais, M. + 75236
 DeBell, K. + 77194
 Debiez, T.P. + 74571
 +DeBlasio, R. 78039
 +DeBlasio, R. 78031
 +Debrrie, R. 78774
 Deckman, H.W. + 77987
 +Dederichs, P.H. 76835
 Dedkov, G.V. + 76536
 Deepak, A. + 78661
 De'er Zhang
 see Zhang De'er
 Defang Niu see Niu Defang
 DeFreez, R.K. + 75636
 +Dega-Szafran, Z. 75384
 DeGuire, A. + 78371
 Deguo Deng + 77860
 +Dehalle, J. 75308
 +DeHoff, R.T. 76713
 Deimel, P. + 77201
 +Deiters, U. 76266
 Dejonckere, P.H. + 75872
 +Dekhtyar, I.Ya. 76922
 Del Alamo, J.A. + 77000
 +Del Guerra, A. 78406
 +Del Re, G. 76752
 +Delagebeaudeuf, D. 77006
 +Delaney, J.R. 78512
 Delbar, T. + 74923
 Delbar, T. + 75006
 Delbar, T. + 74848
 +Delescluse, P. 77006
 Deletter, M. + 77539
 +Della Mea, G. 76513
 +Della Valle, R.G. 77371
 +Delle, W. 75110
 Deller, J.R., Jr. 75873
 +Demare, G.R. 75267
 +Demas, N.G. 75165
 Deme, S. + 75189
 +Deme, S. 75188
 Demikhovskii, V.Ya. + 77008
 Demin, N.A. + 76418
 +Deming, J.W. 78145
 +Demura, A.V. 76528
 +Demuth, J.E. 76782
 Den Akker, T.J. Van see Van Den Akker, T.J.
 Den Berg, R. Van
 see Van Den Berg, R.
 den Bergh, S. van
 see van den Bergh, S.
 den Beukel, A. van
 see van den Beukel, A.
 den Heuvel, E.P.J. van
 see van den Heuvel, E.P.J.
 +DeNatale, J.F. 76540
 Deng Deguo
 see Deguo Deng
 +Deng Hanzeng 78576
 +Deng Li-xin 77590
 Denglong Han
 see Han Denglong
 +Denison, A.B. 77315
 Denison, A.A. + 75160
 +Denison, A.G. 74771
 +Denison, G.S. 77387
 +Denison, Yu.P. 76687
 Denisyuk, G.V. + 75596
 +Denisyuk, I.T. 75926
 +Denschlag, H.O. 75057
 Denton, D.K. 77957
 Depinna, S.P. + 77292
 Depinna, S.P. + 77293
 DePoorter, G.L. 75129
 der Bij, J.J. van
 see van der Bij, J.J.
 Der Hulst, J.M. Van see Van Der Hulst, J.M.
 der Jeugt, J. Van
 see Van der Jeugt, J.
 Der Kelen, G.P. Van see Van Der Kelen, G.P.
 der Kraan, A.M. van see van der Kraan, A.M.
 Der Lee, H. Van
 see Van Der Lee, H.
 der Linden, J. van
 see van der Linden, J.
 der Lugt, W. van see van der Lugt, W.
 der Marel, C. van
 see van der Marel, C.
 der Meer, S. van
 see van der Meer, S.
 der Merwe, P. du T. van
 see van der Merwe, P. du T.
 der Ploeg, P. van see van der Ploeg, P.
 der Star, J. Van
 see Van der Star, J.
 Der Tweel, I. van
 see Van Der Tweel, I.
 Der Veken, B.J. Van see Van Der Veken, B.J.
 der Velde, G. van see van der Velde, G.
 der Velde, J.C. van
 see van der Velde, J.C.
 Der Wal, R. Van
 see Van Der Wal, R.
 der Weid, J.P. von
 see von der Weid, J.P.
 der Woude, A. van
 see van der Woude, A.
 Dereli, T. + 79038
 Derem, A. 75846
 Derenbach, H. + 75454
 Derfel, G. 76625
 +Derkach, L.G. 76303
 +Deroo, D. 77980
 +Derrick, M. 74669
 Derzhanski, A.I. + 76291
 +Desai, H.S. 75508
 +Desai, M. 75075
 Desbat, B. + 76272
 Deschamps, P.Y. + 78640
 +Desgrez, A. 78327
 Deshpande, A.P. + 77478
 Desi, S. 75205
 +Detraz, C. 74915
 +Detrick, D.L. 78735
 +Dettmer, K. 78099
 +D'Ettore Piazzoli, B. 75225
 +D'Ettore Piazzoli, B. 74766
 +Deuchars, W.M. 76218
 Deutsch, D. 78193
 +Devdariani, O.A. 75534
 +Deveaud, B. 77447
 Devgun, M.S. + 77743
 Devi, N. Ashalata
 see Ashalata Devi, N.
 +Devi, N.A.L. 75044
 +Devyanin, S.A. 74732
 +Dew-Hughes, D. 77747
 +Dewey, J.W. 78455
 +Dewey, L.A. 78721
 DeWitt, B.S. 74351
 DeWitt-Morette, C. 74642
 +Deyst, J. 75075
 +Dhamelincourt, M.C. 77978
 +Dhar Ojha, I. 75039
 Dhariwal, S.R. + 77995
 +Dheer, P.N. 77095
 Dhull, J.S. + 77325
 di Benedetto, G.P. + 78911
 di Marzio, F. + 74964
 di Nardo, M. + 74949
 +Di Rocco, H.O. 75337
 +Di Sipio, L. 76310
 +di Toro, M. 74949
 +di Vecchia, P. 74649
 +Di Vita, P. 75804
 +Diane, Ch. 76640
 +Diana, B.J. 74834
 Diberder, F. Le
 see Le Diberder, F.
 Dick, B. + 75458
 +Dick, B. 75461
 +Dick, J.R. 78070
 Dicke, R.H. 78899
 +Dickin, A.P. 78500
 +Dickman, R. 74363
 Dicus, D.A. + 78807
 +Didenko, A.N. 78497
 +Didyk, V.Z. 77803
 Diebold, R. 75213

- Dien, E. van Albada-van.....
see van Albada-van Dien, E.
 Dienes, J.K. 78531
 + Diethorn, W.S. 77729
 + Dietrich, D. 77471
 Dietrich, F.S. + 74967
 + Dietrich, F.S. 74972
 + Dietrich, K. 74931
 + Dietz, A.S. 75113
 + Dietze, W.T. 78035
 + Dietzsch, O. 75019
 + Dietzsch, O. 74849
 Diguett, D. 78012
 Dijkkamp, D. + 75498
 Dikhta, V.V. 75844
 + Dikomey, E. 78266
 Dilin Xie, *see* Xie Dilin
 + Dillen, J. 75511
 Diller, D.E. 76149
 DiNardo, N.J. + 76782
 Ding, E.-J. 74385
 Ding-kun Li, *see* Li Ding-kun
 + Dinno, M.A. 78147
 + Dinse, K.P. 77261
 + Dissard, D. 75034
 + Dissado, L.A. 77326
 Ditze, K. + 75098
 + Divakaruni, P.P. 74617
 + Divakaruni, S.M. 75164
 + DiVincenzo, D.P. 75272
 + Dix, C. 75840
 + Dix, C. 75688
 + Dixit, N.S. 74464
 Dixon, M. 76280
 Dixon, M. 76281
 + Djalali, C. 74898
 + Djeroova, A.A. 78263
 + Djeu, N. 75737
 D'Leon, R. Tascon
see Tascon D'Leon, R.
 + Dmitriev, G.I. 78300
 + Dmitrievskii, I.M. 78253
 Dmritruk, V.M. + 77563
 Dnestrovskii, Yu.N. + 76227
 + Dobbins, R. 78103
 + Dobes, J. 74838
 + Dobkowski, J. 75433
 Dobryszewski, J. 77974
 + Doe, P.J. 75230
 Doesburg, H.M. + 76249
 + Dogadushkin, V.Yu. 76561
 + Dohi, K. 76311
 + Dohler, G.H. 77448
 Doi, K. + 78330
 Doi, M. 75973
 + Duke, T. 77461
 Dolezel, O. + 77304
 + Dolgov, A.N. 74576
 + Domanski, T. 75233
 + Domcke, W. 75434
 + Dominh, K. 78491
 Don Choi Sang
see Sang Don Choi
 Donahue, M.J. + 78149
 Donald, A.M. 76300
 + Dondes, P.A. 74569
 Dong Rui-qi
see Rui-qi Dong
 + Dong Xi-wei 74559
 Dongsheng Li
see Li Dongsheng
 + Donnelly, R.J. 74429
 + Donnelly, R.J. 76040
 + Donnelly, S.E. 76753
 + Donnelly, T.W. 74959
 + Donnelly, W.H. 75210
 Donofrio, R.L. + 74511
 + Doodlesack, G. 78103
 + Doorn, S. 76461
 + Dopita, M.A. 78976
 Doraiswamy, S. + 75291
 Dorbath, C. + 78477
 + Dorbath, L. 78477
 Dorfan, J. 74789
 Dorfman, A.L. 76096
 + Dorikens, M. 77477
 + Dorikens-Vanpraet, L. 77477
 + Doring, J. 74903
 + Dormond, A. 77275
 Dorofeeva, R.P. 78544
 Dorokhov, O.N. 76872
 Dorokhov, O.N. 76899
 Dorr, H. + 78605
 dos Santos, J.M. Martins
see Martins dos Santos, J.M.
 + Dosso, H.W. 78438
 + Dostrovsky, I. 78816
 Dougal, R.A. + 75341
 Dougherty, L.M. + 78898
 + Douglas, J.C. 74551
 + Douma, W.A.S. 76461
 + Doumer, J.P. 77530
 + Dover, C.B. 74895
 + Dovesi, R. 76885
 Dovga, N.D. 77353
 + Dow, J.D. 76843
 + Downing, J.W. 75391
 + Doyle, P.A. 75845
 Draayer, J.P. + 74876
 + Drachal, R. 77968
 Dragoni, M. + 78472
 Dragoni, M. + 78419
 + Dragoni, M. 78459
 Drake, M.D. + 75835
 Drake, P. 78345
 + Drake, T.E. 74842
 Draper, C.W. + 76497
 + Drashil, V. 78243
 + Dreiser, R.D. 78993
 + Dremin, A.N. 76559
 + Drentje, A.G. 75498
 + Drentje, A.G. 74948
 + Dresp, J. 78228
 Dressler, R.E. 74544
 + Drevai, V.E. 75971
 + Drever, R.W.P. 78935
 Drew, D.A. 76097
 + Drickamer, H.G. 77044
 + Drigo, A.V. 76472
 + Drilling, I.S. 78909
 Driscoll, R.J. + 75993
 + Dritis, V.A. 76245
 + Dritis, V.A. 76246
 Drouffe, J.M. 74585
 + Drozdova, L.P. 75207
 Drozhbin, Yu.A. + 75702
 + Drozhzhin, A.I. 76448
 Druffel, E.M. + 78559
 Drummond, I.T. 76191
 + Drummond, J.D. 78872
 + Drummond, T.J. 77570
 + Druschbits, A.V. 77944
 Druyan, M. 78635
 + Dryanov, A.N. 74483
 Drzazga, Z. 77171
 Du, P. + 74315
 Du Jiaji + 75953
 du Pin, H. de La Tour, *see* de La Tour du Pin, H.
 Du Qing-hua + 75924
 + du Tremolet de Lacheis-
 serie, E. 77229
 + Du Yongchang 76876
 + Dua, S.K. 75195
 Duarte-Ramos, H. 76225
 Dube, G. 75676
 Dube, R.S. 75919
 Dubetskii, B.Ya. 75334
 Dubinin, S.F. + 77147
 + Dubinskii, A.A. 74506
 + Dubkova, V.I. 76566
 + Dubler, F. 76779
 + Dubois-Violette, E. 74384
 Duboshinskii, D.B. + 75570
 + Duboshinskii, Ya.B. 75570
 + Dubov, B.S. 74454
 + Dubrovskaya, V.F. 78247
 + Duc, D. 74981
 Ducarme, B. 78420
 + Ducarroir, M. 78106
 + Duchemin, J.P. 77027
 + Duchemin, J.P. 77577
 + Ducloy, M. 75744
 + Ducros, Y. 74783
 Dudarev, E.F. + 76442
 Dudchik, Yu.I. + 76529
 + Dudkin, A.Yu. 77289
 Dudkin, V.A. + 75362
 + Dudnik, E.M. 76904
 Dudnikova, V.B. + 76638
 Duff, J.L. *see* Le Duff, J.
 Duff, B.R. 76110
 + Duffy, M.E. 74759
 + Duffy, P.H. 78226
 Duffy, W. + 74707
 Duftschmid, K.E. + 78353
 + Duftschmid, K.E. 78332
 + Dugast, A. 77894
 Duggan, T.V. 75960
 Duhaaj, P. + 76315
 Duinjeveldt, F.B. van *see* van Duinjeveldt, F.B.
 Duinker, P. 74755
 Dul'nev, G.N. + 75913
 + Dumas, K.A. 77554
 + Dumont, P.J. 78889
 + Dumoulin, P. 77746
 Dunaevskii, S.M. 76460
 + Dunajski, Z. 78374
 Duncan, W.M. + 76942
 Dunin, S.Z. + 78446
 + Dunlap, B.D. 76662
 + Dunlap, H.L. 77402
 Dunn, A.G. + 76659
 Dunn, M.H. 75724
 Dunn, R.W. + 75627
 Duo, R. + 76987
 + Duplatre, G. 77913
 + Dupon, R. 76695
 Dupont, Y. 74681
 + Dupree, A.K. 78908
 + Dupuy, C. 76471
 + Dupuy, J. 76640
 Durbec, N. + 76438
 Durbin, S.D. + 75711
 + Durebergova, D. 77580
 Duret, D. + 78393
 + Duret, D. 78280
 + Duret, D. 78395
 + Durham, B. 74444
 Durig, J.R. + 75394
 + Durisen, R.H. 78942
 + Durovich, E.Yu. 75779
 Durrani, S.A. 78344
 + Durup-Ferguson, M. 78809
 Duseaux, M. 77551
 Dussel, G.G. + 74902
 + Dustmuradov, G. 77472
 Dutreix, J. + 78293
 + Dutt, B.V. 76434
 + Dutta, A.K. 76981
 Duval, P. + 76264
 + Duvergier, C. 76568
 + Duvergier, C. 76569
 + Duvernoy, J. 78308
 Duyl, W.A. van *see* Van Duyl, W.A.
 + Duzgunes, N. 78155
 + Dvurechenskii, S.V. 76229
 Dwarakanath, K.S. + 78981
 + Dwight, K. 76379
 + Dwight, K. 76947
 + Dworschak, F. 77682
 + Dwyer, A. 78324
 + Dwyer, S.J. 78273
 D'yachenko, N.G. + 77005
 + Dye, M.S. 75827
 + Dyer, I. 78328
 Dyke, J.M. + 75444
 Dyke, M. Van. *see* Van Dyke, M.
 Dykman, I.M. + 77041
 + Dysko, A.L. 75614
 + Dyson, F. 78898
 + Dyumaev, K.M. 74549
 + Dzhabrailov, T.G. 76665
 Dzhammarov, S.S. + 77605
 + Dzhabova, T.D. 75011
 + Dzhrubav, D.R. 77106
 E Silva, A.M. Almeida
see Almeida E Silva, A.M.
 + Eagle, R.J. 75117
 + Easler, T.E. 76502
 + Eastman, L.F. 77686
 + Eatock Taylor, R. 78553
 + Eaton, W.A. 78142
 Ebel, H. + 74560
 + Ebel, M.F. 74560
 Eberhardt, W. + 75447
 Eberhardt, W. + 77527
 + Eberhardt, W. 77529
 Ebina, K. + 76868
 + Ebisawa, K. 75185
 + Echigoya, J. 77736
 + Eckhorn, R. 78171
 + Eckstein, J.N. 75672
 Eda, K. 77043
 Edamatsu, K. + 77406
 + Edelen, D.G.B. 74237
 + Edelman, F.L. 76812
 Edelman, I.S. + 77472
 + Edel'shtein, Yu.G. 75832
 + Edelstein, W.A. 78288
 Edenburn, M.W. + 78078
 Edery, D. + 76172
 + Edgworth, S.O. 74809
 + Edighoffer, J.A. 75655
 + Edrich, J. 78212
 + Edwards, A. 78262
 Edwards, D.M. 77134
 Edwards, D.M. + 77236
 + Edwards, D.O. 76723
 Edwards, T.J. 74461
 Edwards, W.D. + 75397
 + Edzhuibay, Z.F. 74484
 + Eenshuistra, P.J. 75347
 + EerNisse, E.P. 74439
 + Efendiev, T.Sh. 75681
 + Efremenko, V.I. 74771
 + Efremova, N.N. 76904
 Eftekhari, G. + 76951
 Egelkrut, D.W. + 77861
 + Eger, D. 76983
 Eger, S. + 78643
 Eggen, O.J. 78927
 Eggleston, J.M. + 75678
 Eggleston, P.P. 78943
 Eghrari, I.R. + 78206
 + Egorov, B.V. 78005
 + Egorov, F.F. 77606
 Eguchi, T. + 74637
 + Ehlitzky, F. 74664
 + Ehret, C.F. 78226
 Ehrhart, A. + 76929
 Ehrhart, P. + 75558
 Ehst, D.A. + 75175
 + Eibschutz, M. 77309
 + Eicher, C. 75787
 + Eichhorn, F. 76243
 Eidenschink, R. 76290
 + Eiduk, Yu.Ya. 77773
 + Eijnde, J.P.H.W. 76747
 + Eimerl, D. 75172
 + Eisenberg, C.P. 78156
 Eisenhart, C. + 74427
 Eisenmann, B. + 76387
 + Eisler, W.J., Jr. 76258
 Eitelberg, G. 76046
 Ekin, J.W. + 77119
 + Eknayan, O. 76943
 Ekpo Eno, E. + 76498
 + El Hosary, A.A. 77847
 El Nadi, A.M. + 76211
 + El Shehawey, El S.F. 76120
 el-Halim, A.M. Abd. *see* Abd el-Halim, A.M.
 + el-Sayed, M. 77064
 + Elayoubi, M. 76224
 + Elbaum, C. 76732
 + Elbert, J. 78817
 + Eldred, E. 78213
 + Eldridge, G.W. 76342
 Elenin, G.G. + 76032
 Elfinov, V.S. 74272
 Eliel, E.R. + 75280
 Eliseev, Yu.N. + 76189
 + Elitzur, S. 74650
 El'kind, E.Yu. + 78306
 + Elkins, J.W. 75381
 Elleaume, P. 75671
 + Elleaume, P. 75650
 Elliott, C.J. 75668
 + Elliott, C.R. 76436
 + Elliott, R.A. 75636
 Ellis, H.B., Jr. + 75439
 Ellis, J. + 74701
 Ellis, J. + 74356
 Ellis, J.L. 75143
 + Ellison, G.B. 75439
 Elms, R.V. 78017
 + Elston, R. 78956
 Elton, R.C. 75622
 Elvis, M. + 78988
 + Emanuelson, R.M. 75691
 Embley, R.W. + 78490
 Emch, G.G. 74313
 Emelin, V.Ya. + 77351
 + Emel'yanov, D.A. 76631
 + Encenaz, T. 78864
 + Enderlein, R. 76867
 + Enderlein, R. 77520
 + Enderl, H. 76168
 + Endesfelder, A. 75528
 + Endo, H. 75086
 + Endo, J. 74639
 + Endo, Y. 75369
 Endoh, T. + 77737
 + Endort, R. 74771
 + Engren, T. 78636
 + Eng, R.S. 75705
 Engel, P. + 76401
 + Engelbrecht, J.A.A. 77592
 Engelke, R. + 76126
 + Engelstein, P. 75031
 + Engelstein, P. 75065
 Engen, P.G. van *see* van Engen, P.G.
 England, P. 78510
 + Engler, C. 76778
 + Engler, E.M. 77280
 + Engler, J. 74783
 + English, J.H. 75419
 + English, M.J. 78167
 Eno, E. Ekpo
see Ekpo Eno, E.
 + Entin, R.I. 76647
 Enz, U. 74620
 + Epherre, M. 74915
 Epitotis, N.D. 75303
 Epp, D. + 78436
 + Epstein, E.E. 79019
 Epstein, M. + 76098
 + Er-ting Chen 75302
 Eramzhyan, R.A. + 74958
 + Erasmus, S.J. 74562
 + Erath, W. 78338
 + Erb, K. 78813
 + Ercolani, M. 75670
 Eremenko, V.N. + 76361
 Eremias, B. 77790
 Eremim, M.V. 77168
 Eremko, A.A. + 76860
 + Erickson, E.G. 75685
 + Erickson, G.F. + 74574
 + Erickson, L.E. 77282
 + Erickson, S.W. 78299
 Erickson, W.C. + 78813
 + Ericsson, T. 76403
 + Eriksson, A.J. 78699
 + Eriksson, L. 78295
 Erland, J. 74550
 Erley, W. + 76777
 Ermakov, G.V. + 77113
 Ermakov, M.G. + 76875
 + Ermakov, V.M. 77639
 Erman, P. + 75457
 Ermolaev, V.A. + 76605
 Ermolenko, I.N. + 76566
 Ermolovich, I.B. + 77453
 Erne, S.N. + 78283
 Erne, S.N. + 78285
 Erne, S.N. + 78282
 Erne, S.N. + 77108
 + Erne, S.N. 78281
 Ernewin, J. 75229
 + Eroshenko, E.G. 78777
 + Errede, S. 75226
 + Ershov, N.V. 77479
 Ershova, T.Ya. 75937
 + Erten, H.N. 75056
 + Ertsgraeber, G. 78242
 Erukhimov, M.Sh. 77130
 + Esaki, L. 77445
 + Esaki, L. 77033
 + Esaulov, A.S. 74963
 Escudier, M.P. 76134
 + Eshleman, V.R. 78860
 + Esikov, N.N. 78514
 Eska, G. + 76740
 Eskola, H. + 78286
 + Eskola, K. 74906
 + Esposito, B. 74821
 + Esposito, L.W. 78846
 + Esposito, P.B. 78838
 Essemilali, M. + 75797
 + Essen, H. 75467
 + Esterlund, R.A. 74928
 Estrada, H. 75434
 + Estrin, Yu.Z. 76443
 + Eterashvili, T.V. 76647
 + Etienne, B. 76973
 Etim, E. 74353
 Etim, E. 74739
 + Etioh, S. 77049
 + Eustace, D.J. 78001
 + Evans, A. 78982
 + Evans, A.G. 77663
 + Evans, B.G. 78595
 Evans, D.S. + 77618
 + Evans, E.H. 76407
 Evans, J.V. + 78739
 + Evans, K., Jr. 75175
 + Evans, M.L. 75387
 + Evans, R. 78931
 + Evans, R. 76749
 Evchatov, G.P. 78476
 Evdokimenko, Yu.I. + 75675
 + Evdokimov, V.P. 78777
 + Evenson, K.M. 75371
 + Everhart, E. 78876
 + Everhart, E. 78871
 + Eversheim, D. 74972
 + Eyraud, O. 77298
 + Eysev, O.A. 75767
 + Ewen, D.A. 76731
 Exner, H.E. + 77623
 Extance, P. + 75818
 + Eyrych, W. 75007
 + Ezhevskaya, T.B. 74546
 + Fabick, L. 78004
 Fabjan, C.W. + 75249
 Facelli, J.C. + 75403
 + Faenov, A.Ya. 74549
 Faessler, A. + 74865
 + Faessler, A. 74863
 + Fages, C. 78022
 + Fahney, D.W. 78809
 + Fahli, A. 75031
 Fahline, M. 77196
 Fahline, M. 77215
 Fahrman, K. + 75096
 + Fahrman, K. 75097
 + Fahrman, K. 75098
 Fai, G. + 74956
 + Faishid, O.M. 77428
 Faik, A. + 75787
 Faik, A. + 76526
 + Faini, S. 75648
 + Fairbank, W.M., Jr. 75548
 Faisner, H. + 74756
 Falck, N.K. + 74613
 + Falconer, K.L. 75124
 + Fallover, S. 74913
 + Fallick, A.E. 78500
 + Faltsen, A. 75663
 + Fam Le Kien 74365
 Fan, J.C.C. + 78082
 + Fan, Z.Q. 78025
 Fand, R.M. + 76007
 Fang Chen Shu-chi
see Chen Shu-chi Fang
 Fang Shouxian + 75216

- Fangyu Yang +Filip, V.A. 76043
 + see Yang Fangyu
 + Fanourakis, G.K. 74759
 Fantoni, S. + 74886
 Farid, M. + 75234
 + Faris, J.L. 75370
 Farkas, D. + 77801
 Farmer, J.C. + 78696
 Farouki, R.T. + 78824
 + Farrell, D.E. 78202
 + Fasold, D. 77350
 Fasoli, U. + 74992
 + Fatas, E. 76987
 + Fateev, N.V. 75335
 Faulkner, D.R. + 78958
 + Faulkner, L.R. 77044
 + Favier, J.J. 76337
 + Fawcett, E. 77239
 Fayet, P. + 74657
 Fayulle, S. + 77768
 Fearey, B.L. + 75709
 + Fearn, D.R. 78492
 Fedders, P.A. 76481
 Feder, R. + 77523
 + Fedorchenko, A.M. 74291
 + Fedorenko, V.K. 77611
 + Fedorov, E.A. 78251
 + Fedorov, G.V. 76925
 Fedorov, M.V. 75673
 + Fedorov, V.M. 77176
 + Fedoseev, A.I. 75620
 + Fedoseeva, T.S. 77608
 Fedosenko, Yu.K. 77843
 Fedosov, V.N. 77149
 Fedotkin, G.F. + 78289
 + Fedotov, A.V. 74771
 + Fedotov, P.I. 75068
 + Fedotov, S.I. 76168
 + Fefelov, N.N. 78543
 Fehér, I. + 75188
 + Fehér, I. 75189
 Fehn, U. + 78488
 Feibelman, W.A. + 78973
 Feigelson, E.D. + 78990
 Feile, R. + 76907
 Feinberg, M. + 74416
 Feit, M.D. 75817
 Fekel, F.C., Jr. 78941
 + Fekir, M. 77892
 + Felderhof, B.U. 74382
 + Felderhof, B.U. 74422
 Feldman, B.J. + 75735
 Feldman, U. + 75621
 + Fellenberg, R. 77520
 Feng, C.-C. + 78460
 + Feng, M. 76476
 + Feng, T. 78001
 Feng Da Hsuan
 + see Da Hsuan Feng
 + Feng Qingrong 77354
 + Feng Shuijing 75886
 Feng Yuan-ping + 74590
 Fengyu Guo
 + see Guo Fengyu
 Fengzhen Lu
 + see Lu Fengzhen
 Fenici, R.R. + 78281
 Fenici, R.R. + 78204
 + Fenici, R.R. 78282
 + Fenici, R.R. 78283
 + Fenici, R.R. 78285
 + Fenner, H. 74783
 + Fenselau, C. 74553
 Feraday, M.A. 75146
 Feranchuk, I.D. + 76542
 + Ferdinand, K.V. 77074
 + Ferey, G. 76395
 + Ferguson, E.E. 78809
 + Ferguson, R.L. 75026
 Ferguson, T.A. 74769
 + Ferla, G. 76711
 + Fernandez, F.M. 75271
 + Fernandez, J.C. 74621
 Fernandez, P. + 74406
 Fernandez, P. + 78700
 + Ferrari-Toniolo, M. 78921
 + Ferretti, O. 75122
 + Ferrier, J.L. 75742
 Ferriere, R. + 75590
 Ferriue, F. + 76492
 + Ferrigno, A. 77108
 + Ferron, J. 76758
 Fesenko, E.G. + 77333
 + Fiala, J. 77710
 Fialkov, Yu. Ya. + 77897
 + Fialkovskaya, L.A. 78246
 + Fick, H.A. 76381
 + Ficke, D.C. 78317
 + Ficke, D.C. 78318
 + Fickling, M.D. 78898
 Fidler, J. 76648
 + Fidler, J. 77497
 Fiedeldey, H. + 74927
 + Field, J.E. 76070
 + Field, J.H. 74783
 Fields, C.A. + 74834
 + Figiel, H. 77284
 + Filatova, I.V. 76362
 + Filimonov, Yu.M. 76535
 + Filippov, E.I. 77268
 + Filippov, P.G. 77415
 + Filippov, V.V. 77286
 + Filippovskii, N.F. 76104
 Filla, M. + 76103
 + Fillard, J.P. 77411
 + Filyanov, E.M. 76560
 Finette, S. + 78382
 Finette, S. + 78383
 Finetti, M. + 77047
 + Finetti, M. 77071
 + Finger, L.W. 76604
 + Finger, R.F. 78386
 Fink, D. + 77509
 + Finkel, R.C. 78520
 + Finkelmann, H. 76295
 + Finkel'shtein, L.D. 76904
 + Finkel'shtein, L.D. 76903
 + Finlayson, T.R. 77295
 Finocchiaro, R.S. + 76672
 + Finster, J. 76757
 + Finsterholz, H. 76858
 + Fintz, P. 75031
 + Fiorentino, E. 75670
 Fiorini, A.R. + 78291
 + Fiorini, E. 75225
 + Firenze, C. 78173
 Firsov, S.P. + 77388
 Firth, G.R. + 77776
 Fischer, B. 75741
 Fischer, H. + 76465
 Fischer, H. + 76523
 + Fischer, H.-P. 76833
 Fischer, K.H. 77184
 Fischer, R. + 77570
 + Fischer, R. 77445
 Fischler, W. + 74612
 + Fiser, J. 76772
 Fisher, N.S. + 75116
 + Fisher, R.A. 75735
 Fisher, R.M. 77815
 + Fisher, S. 78777
 + Fisher, W.A. 78913
 Fishman, G. + 77034
 Fisk, H.E. + 74757
 + Fistul', A.D. 77398
 Fitch, W.L. + 75526
 Fitting, H.-J. + 77489
 + Fitzgerald, L.T. 78320
 + Fitzpatrick, P.J. 77278
 + Fiurorini, E. 74766
 + Fjeld, R.A. 78113
 Fjeldberg, T. + 75510
 + Fla, T. 78887
 Flaim, R. + 78120
 Flamm, D. + 76780
 + Flammer, M. 76214
 Flannery, M.R. 77884
 Flavin, P.G. + 75840
 Fleay, R.F. 78313
 Fleckinger, R. + 75348
 Fleet, M.E. 76593
 + Fleischmann, P. 76568
 + Fleischmann, P. 76569
 Fleming, G.N. 74767
 + Fleming, G.R. 75552
 Flerov, G.N. + 75162
 + Fletcher, J.M. 78913
 Fletcher, P. + 77881
 Flint, C.D. 75366
 + Florencio, F. 75395
 Flores, C. 77992
 Flores, C. 77994
 Flores, C. 78064
 + Floss, N. 74962
 Flowers, K.D. 75867
 + Flugge, G. 74783
 + Flukiger, R. 77119
 Flynn, C.P. + 77528
 + Flynn, C.P. 77532
 Focht, M.W. + 76937
 Foglio, M.E. 76902
 Folcher, G. + 77275
 + Foldes, I.B. 76202
 Foldyna, V. + 77710
 + Folkestad, K. 78724
 + Fomin, S.P. 77496
 + Fomina, T.P. 78261
 Fong Man
 + see Man Fong
 Fong Shao-Ling
 + see Shao-Ling Fong
 + Fontaine, G. 78912
 + Fontaine, J. 75797
 Fontanari, J. + 78725
 + Foote, J.H. 76214
 + Forcella, P. 74428
 Ford, M.D. + 78229
 + Forrester, A.F. 77858
 + Forman, J.M.A. 78494
 + Fornaca, S. 75655
 + Forrester, D.L. 77964
 + Forrester, P.J. + 76156
 + Forsten, K. 74906
 + Forster, E. 76168
 + Forsyth, D.A. 77923
 + Forsyth, D.W. 78461
 + Forsyth, P.A. 78678
 + Fortenberry, R. 75726
 Fortes, M.A. 76236
 Fortes, M.A. 76329
 + Fortunato, G. 74449
 + Fossan, D.B. 74840
 + Foster, G.W. 75226
 + Foster, J. 78213
 + Foster, S.C. 74539
 Foster, V. 74457
 Fotiadis, E.E. + 78514
 + Foulon, M. 75388
 + Fournier, D. 74783
 + Fowler, M.M. 75036
 + Fowler, S.W. 75119
 + Fowler, S.W. 78558
 + Fowler, S.W. 75116
 Fowler, W.A. 78890
 Fowler, W.B. 76425
 Fraas, L.M. + 78076
 + Fracassi, P.F. 77371
 Fradkin, E.S. + 74361
 Fradkin, E.S. + 74748
 + Fraenkel, Z. 75036
 Fraga, S. 76268
 + Fraley, L., Jr. 78367
 Franciosi, A. + 77053
 + Franciosi, A. 76768
 + Francis, R.W. 76989
 + Frank, J. 78154
 + Frank, L. 78588
 + Frank, P.H. 78330
 Franke, H.-G. + 76321
 + Frankel, D. 77533
 + Franse, J.J.M. 77241
 + Frantsevich, I.N. 76616
 + Franzen, D.L. 75801
 Franzosi, P. + 76435
 + Fraser, R.S. 78649
 Frauendorf, S. + 74837
 + Frech, G. 77311
 + Freddi, G. 75425
 Freed, C. 75701
 + Freeman, K.C. 78907
 + Freeman, L.A. 74561
 + Freeman, R.M. + 74832
 + Freitag, K. 74846
 Freitas Mourao, R.R. de
 + see de Freitas Mourao, R.R.
 French, J.B. + 74872
 + Frenzel, E. 74756
 Frere, J.-M. + 74653
 Freund, H.-J. + 77529
 + Freund, H.-J. 75447
 Freund, P.G.O. 74360
 + Freund, S.M. 77377
 Frey, A.H. + 78237
 + Frey, M. 76172
 + Frey, W.E. 77858
 Friar, J.L. 74855
 Friar, J.L. 74866
 + Friberg, S.E. 78120
 + Frick, B. 76907
 Frick, H. 76004
 + Fricke, B. 75284
 Friedel, J. + 76819
 Friedel, P. + 77778
 Friedlander, E.M. + 75016
 + Friedlander, G. 78816
 + Friedman, J. 74669
 Friedrich, M. + 78740
 + Fries, D.C. 74783
 + Friman, B.L. 74886
 + Frings, P.H. 77241
 Fripiat, J.G. + 75308
 + Frischmann, P.G. 77222
 + Frishman, Y. 74650
 Fritsch, G. + 76921
 + Fritsch, H.U. 76318
 + Fritsch, L. 76642
 + Fritzkowski, G. 76930
 Frohlich, C. 78664
 Frohlich, H. 78123
 + Frohlich, K.I. 75170
 + Frohling, R. 77516
 + Froidevaux, C. 78478
 + Frolov, V.V. 75069
 + Frolova, G.I. 76664
 Fromling, G. 76165
 + Frost, J.D., Jr. 78371
 Fu Chong-Cheng
 + see Chong-Cheng Fu
 Fu Jia
 + see Jia Fu
 Fuda, M.G. 74926
 Fuentetaja, P. + 75263
 + Fues, W. 74783
 + Fugono, N. 78788
 + Fuhrmann, K. 78782
 + Fuji, K. 76635
 + Fujii, A. 77174
 + Fujii, S. 78745
 Fujii, Y. 74691
 + Fujii, Y. 75290
 Fujiki, S. + 77121
 + Fujimoto, K. 78080
 Fujimoto, T. + 75946
 + Fujimura, T. 76609
 Fujimura, Y. + 75460
 + Fujisaki, H. 77705
 + Fujisawa, N. 75184
 + Fujisawa, N. 75185
 + Fujisawa, Y. 77717
 + Fujita, S. 76897
 + Fujita, S. 77264
 + Fujita, T. 78294
 Fujiwara, H. + 76608
 + Fujiwara, H. 77672
 + Fujiwara, H. 77708
 + Fujiwara, H. 74639
 + Fujiwara, K. 78654
 Fujiwara, S. + 77024
 + Fujiwara, Y. 77456
 + Fukai, M. 77024
 + Fukami, A. 77559
 Fukao, Y. + 78496
 Fukao, Y. + 78470
 Fukaya, M. + 77911
 Fukuchi, S. + 76879
 + Fukuchi, Y. 75025
 Fukuda, R. 74713
 Fukuda, T. + 75013
 Fukuda, T. + 74630
 Fukuda, T. + 77558
 Fukuda, Y. + 75538
 + Fukuhara, A. 74639
 + Fukui, K. 77206
 + Fukumoto, T. 77374
 + Fukushima, A. 77584
 Fukushima, Y. + 78164
 + Fukuyama, A. 75185
 + Fukuyama, H. 78294
 + Fukuyama, H. 77136
 Fukuyu, A. 75987
 Fuller, E.R. + 76555
 Fulling, S.A. 74632
 Fulton, R.L. 77329
 Fulton, R.L. 77342
 + Fumero, R. 78291
 + Fumi, F.G. 76374
 + Funahashi, S. 75070
 + Funayama, N. 77461
 Fung, I. + 78603
 + Fung, S.Y. 75017
 + Funke, L. 74903
 + Furetta, C. 75196
 + Furetta, C. 75194
 Furrer, R. + 77294
 + Furukawa, K. 76289
 + Furukawa, K. 76279
 Furumoto, M. 78454
 + Furuno, K. 75025
 + Furuno, K. 75004
 + Furuse, T. 75687
 + Fury, M.A. 77776
 Fusaro, R.L. 77765
 Fusco Girard, M. + 77089
 Fusheng Jin
 + see Jin Fusheng
 + Fussen, D. 75477
 + Fuwa, K. 78654
 Fuyun Xi
 + see Xi Fuyun
 + Fyfe, W.S. 78494
 G., J. Arellano
 + see J. Arellano
 + Gabano, J.P. 77972
 Gabasova, A. + 77542
 + Gabel, V.-P. 78240
 Gabovich, A.M. + 77079
 + Gabovich, A.M. 77111
 Gabrielse, G. 76215
 Gaby, J.E. + 78719
 + Gachechiladze, R.G. 74481
 + Gachechiladze, T.A. 74481
 Gadaj, S.P. + 77698
 Gadgil, S. + 78638
 + Gadajkov, V.I. 75072
 + Gadre, R. 77995
 Gaebell, H.-C. + 76388
 Gaebler, W. + 75209
 Gaggioli, N.G. + 75594
 + Gagne, J.M. 76223
 + Gagola, A. 75787
 + Gaidot, A. 74783
 Gaidukov, G.N. + 76429
 + Gaillard, M.K. 74701
 + Gaines, G.B. 78086
 Gaisser, T.K. 78769
 + Gajewski, W. 75226
 Gakin, J.P. + 77947
 Galakhov, M.A. + 75984
 + Galashin, A.E. 76612
 + Galavotti, M.C. 74368
 + Galchenkov, D.V. 77026
 + Gal'chinskii, A.V. 77004
 + Galeazzi, G. 74992
 + Galgani, L. 75910
 Galiev, G.V. + 76480
 + Galkin, A.A. 77339
 Galkin, S.L. + 75645
 + Galkowska, E. 77698
 + Gallagher, D. 78850
 Gallai, V. + 78173
 + Galliano, G.P. 75670
 Gallerneault, W.M. + 76622
 Gallerneault, W.M. + 77695
 Galli, R. + 76326
 + Galonsky, A. 74898
 + Galperin, Yu.I. 78774
 + Galperin, Yu.I. 78670
 + Galperin, Yu.I. 78778
 + Galster, W. 75023
 + Galtier, M. 77887
 Galvez, E. + 75395
 Gamayunov, N.I. + 76123
 + Gamedinger, K. 74783
 + Gamp, A. 75040
 Ganapol'skii, E.M. + 77259
 Ganas, P.S. + 75515
 + Gandini, A. 76696
 Ganev, K.G. + 78112
 Gang, L.-A. 74558
 Gang Hu
 + see Hu Gang
 + Ganguli, S.N. 74794
 + Ganguli, S.N. 74814
 + Ganguly, N.K. 74868
 + Ganiev, D.K. 76684
 + Ganin, V.V. 77608
 + Ganin, V.V. 77398
 + Ganzel, B.L. 78966
 + Gao Guilan 77813
 + Gao Zhimin 75886
 + Gapais, D. 78501
 + Gapenko, G.S. 74771
 + Gapenko, V.A. 74771
 Garbaczewski, P. 74587
 Garcia, N. 75580
 Garcia, N. + 75579
 Garcia, R.D.M. + 75067
 Garcia, R.R. + 78614
 + Garcia Camarero, E. 76987
 + Garcia-Blanco, S. 75395
 Garcia-Pelayo, J.M. + 78827
 + Gardes, D. 75033
 + Gariyban, O.V. 76307
 Gariel, J. 74275
 Garriep, C. + 78480
 Garreau, M. + 77892
 Garrigues, M. + 77061
 Garrison, B.J. + 75563
 Garrside, B.K. + 74535
 + Garrside, B.K. 75619
 + Garvie, R.C. 77732
 Gasanly, N.M. + 77393
 Gashenko, I.N. + 74263
 + Gashimzade, F.M. 77410
 Gashtol'd, L.P. 76072
 Gasparini, M. + 77555
 + Gasparini, M. 78472
 Gasser, J. + 74708
 Gasser, J. + 74721
 + Gatley, L.P. 75515
 + Gathér, B. 76283
 + Gatley, I. 78974
 + Gatley, I. 78974
 + Gatos, H.C. 77060
 + Gatos, H.C. 76689
 Gaudry, A. + 78606
 + Gaulon, R. 78477
 Gault, W.A. + 78675
 + Gaunt, P. 77170
 Gaupp, A. 75658
 + Gauthier-Roy, B. 75382
 + Gauvin, H. 75033
 + Gavezzotti, A. 76351
 + Gavron, A. 75036
 Gavronskaya, E.A. + 75628
 Gawedzki, K. + 74390
 + Gawronska, G. 78815
 Gay, R. + 76734
 Gaykema, W.P.J. + 78127
 Gazanhes, C. + 75842
 + Gazdzinskii, M. 75011
 + Gazengel, J. 75742
 + Gdalevich, G.L. 78667
 + Ge Jiali 78563
 + Ge Mo-lin 74590
 Gea-Banacloche, J. + 74827
 Gedney, C.J. 75985
 Geguzin, Ya.E. + 76765
 Geguzin, Ya.E. + 77669
 Geigenmüller, U. + 74382
 Geigenmüller, U. + 74422
 + Geiger, A. 76273
 Geilikman, M.B. + 77621
 + Geise, H.J. 75511
 + Gelberg, A. 74906
 + Gelbke, C.K. 75035
 Gel'd, P.V. + 77158
 + Gelius, U. 75353
 Geller, C.A. + 78487
 + Geller, M.A. 76105
 + Geller, M.J. 79012
 + Geller, S. 77310
 + Gelles, J. 78129
 + Gellert, W. 74908
 Gel'mont, B.L. 76881

- +Gemmell, D.S. 74555
 Gence, J.N. 75995
 Genkin, G.M. + 76531
 Genpei Li. *see* Li Genpei
 +George, E.V. 75172
 +George, R. 74783
 +George, T.F. 77486
 Georgiev, M.N. + 76561
 +Georgieva, K. 78672
 Georgobiani, A.N. + 77444
 +Gera, B.S. 78707
 Geracids, J. + 75372
 Geramb, H.V. von
see von Geramb, H.V.
 Gerard, A. + 77297
 +Gerard, J.-M. 74653
 Gerardin, R. + 77298
 +Gerardin, R. 76377
 Gerasimov, A.B. + 77487
 +Gerasimov, V.B. 76494
 +Gerassimova, I. 76314
 +Gerber, G. 75115
 +Gerber, P.R. 76292
 +Gergan, J. 78423
 Gergely, T.E. + 78886
 +Gergely, T.E. 78894
 +Gerhardy, P.R. 78768
 Geronov, Y. + 77979
 Gerschel, C. + 75027
 Gershenzon, E.M. + 77093
 +Gershenzon, M.E. 77093
 Gershkovich, E.A. + 74478
 +Gershun, V.D. 74661
 Gershuni, G.Z. + 76029
 +Gersten, J.I. 77492
 Gerward, L. 77930
 +Gerwin, H.J. 78078
 +Gerzberg, L. 76138
 +Geszties, F. 74296
 +Getmanets, V.F. 75911
 +Geyer, E.H. 78954
 +Ghandhi, S.K. 76804
 +Ghandhi, S.K. 76805
 +Ghandour, G. 74619
 +Ghatge, N.D. 76969
 +Ghezzi, C. 76435
 +Ghose, J. 76946
 Ghose, P. 74675
 Ghose, P. 74676
 +Ghosh, A.K. 78001
 +Ghosh, A.K. 76989
 Ghosh, B.P. + 76919
 Ghosh, D. + 74800
 Ghosh, D. + 74801
 Ghosh, D. + 75047
 Ghosh, D. + 75046
 Ghosh, G.C. + 74807
 +Ghosh, P. 78937
 +Ghosh, U.S. 76544
 +Giacconi, R. 79024
 +Giansiracusa, G. 74949
 Gibbons, G.W. + 74354
 Gibbs, D. + 77532
 Gibbs, H.M. + 75714
 +Gibbs, H.M. 75707
 +Gibbs, J.H. 74420
 +Gibson, A.J. 78752
 Gibson, B.F. + 74895
 Gibson, J. 78870
 Gibson, J. 78874
 +Gibson, J. 78871
 Gibson, W.C. 78819
 Gibson, W.G. 76720
 Giessen, B.C. + 77923
 +Giessen, B.C. 76672
 +Giessen, B.C. 77770
 +Gifkins, R.C. 77718
 +Gifkins, R.C. 77719
 Gik, L.D. 78474
 Gil, J. Gomez
see Gomez Gil, J.
 Gilbert, R.S. 75156
 Gilchristie, M.G.D. 74712
 +Gilchrist, R.L. 75132
 +Gile, I.P. 74528
 Giles, I.P. + 75826
 Giles, P.L. + 77575
 +Gill, D.S. 77325
 +Gill, R.L. 74913
 Gillette, D.A. 78601
 Gillette, D.A. + 78609
 Gillette, D.A. + 78610
 Gillham, R.W. + 75145
 Gillet, B. + 77647
 Gillet, B. + 76955
 +Gilmer, G.H. 76767
 +Gilmer, J. 78732
 Gilmore, R. + 74875
 Gilson, D.F.R. + 77278
 Gimbutis, G.I. 75912
 Gindler, J.E. + 75061
 +Gindler, J.E. 74917
 +Gindler, J.E. 75029
 Giner, C. Trallero
see Trallero Giner, C.
 +Ginestet, N. 78948
 +Ginter, J. 77369
 Giordano, N. 76728
 Giordano, R. + 75022
 Giorgini, M.G. 75546
 Girard, M. Fusco
see Fusco Girard, M.
 +Girardi, G. 74701
 +Giraud, G. 74371
 Giraud, M. + 77229
 +Girgis, I. 77504
 Girod, M. + 74882
 Girotti, H.O. + 74603
 +Girouard, F.E. 77467
 Gisclon, J. + 76640
 +Gitis, N.V. 76817
 +Gitomer, S.J. 76183
 Gitsu, D.V. + 76995
 +Gittelman, B. 74669
 Gittsovich, V.N. + 77148
 +Gittsovich, V.N. 77724
 Giuliano, C.R. + 75740
 Giulietti, D. + 75910
 +Giurgiu, A. 77172
 +Giusti, P. 74821
 +Glachenko, E.P. 77595
 Gladkov, S.M. + 75396
 +Gladyshev, V.A. 78774
 +Glagola, B.G. 75029
 Glagoleva, O.N. + 75401
 Glandus, J.C. + 77690
 +Glas, F. 76646
 +Glasner, A. 78902
 +Glas, A.M. 76474
 Glasse, F. 77327
 +Glasser, M.L. 74401
 Glasser Leme, D. + 76691
 +Glatting, K.H. 78390
 +Glaze, D.G. 78371
 Glazkov, Yu.V. + 75613
 +Gleitzer, C. 76377
 +Glendenin, L.E. 75029
 +Glendenin, L.E. 75061
 +Glentzin, M. 78895
 +Glicksman, M.E. 77763
 +Glisson, T.H. 76959
 +Glockner, P.G. 75943
 Glushikhin, V.A. + 78704
 +Glushkov, M.V. 77444
 +Gmelin, E. 76661
 +Gmitro, M. 74958
 Gnatenko, Yu.P. + 76850
 Goascoz, V. Le
see Le Goascoz, V.
 +Gobbi, A. 75034
 +Gochev, D. 78673
 +Goda, M. 76829
 +Godbole, R.S. 77550
 +Goddard, W.A., III. 76771
 Godfrey, C.P. 78989
 +Godlewski, M.P. 78036
 +Godovants', O.I. 76360
 Godoy, S.V. 74396
 Goebel, J.H. 78978
 +Goedghebuur, J.P. 75590
 Goeke, K. + 74883
 Goertz, C.K. + 78848
 +Goertz, C.K. 78849
 +Goffin, E. 78797
 Gogawale, S.R. + 78730
 +Gogoladze, I.A. 77487
 Gogoshev, M. + 78676
 +Gogosheva, Ts. 78676
 +Gokmen, A. 74988
 +Gokmen, A. 74977
 +Golant, K.M. 76978
 +Goldberg, M. 74783
 +Goldberg, M. 74669
 +Golden, G.S. 77599
 +Golder, F. 78336
 +Goldfarb, S. 77582
 +Goldhaber, M. 75226
 +Goldhammer, L.J. 78023
 Gold'in, S.V. 78473
 +Goldman, J.L. 77975
 +Goldring, G. 74835
 Goldsmid, H.J. + 76717
 Goldstein, M.E. + 76111
 Goldstein, N. + 77875
 Goldstein, R.J. + 76023
 Golikov, E.G. + 74961
 +Golod, S.N. 78713
 +Golokhvastov, A.I. 75011
 +Golomb, O.L. 75421
 Golosovskii, M.A. + 76441
 Golovashkin, A.I. + 77474
 Golovchan, V.T. + 75898
 Golovins'ka, T.M. + 77720
 +Golovinski, L.P. 76681
 +Gol'tsman, G.N. 77093
 +Golubev, A.S. 77833
 Golubev, B.G. + 77002
 Golubev, N.S. + 77387
 +Golubnichaya, A.A. 77595
 +Golubovskii, E.R. 77680
 +Golusko, V.V. 75170
 +Gomer, R. 77524
 +Gomes, F. 75835
 +Gomes, L.C. 75214
 +Gomez, G. 77278
 +Gomez, L.S. 75113
 +Gomez, R. 78865
 +Gomez Beltran, F. 76911
 Gomez Gil, J. + 74254
 Gomez-Santos, G. 76821
 +Goncharov, A.F. 77393
 +Goncz, A.R. 75884
 +Gong Chang-de 74417
 +Gonser, U. 76929
 +Gonser, U. 77652
 +Gonzalez-Arroyo, A. 74698
 Goodarz Ahmadi. 76121
 +Gooden, D.K. 76093
 +Goodenough, J.B. 76391
 +Goodman, J.W. 75799
 +Goodman, R.K. 76214
 Goodrich, R.W. + 78991
 Goodwin, G.L. 78624
 +Goodyear, C.C. 75874
 +Goossens, C. 78637
 +Gopal, S. 75399
 Gopal-Krishna + 79008
 +Gopala, K. 74914
 Gopala Rao, R.V. + 76271
 +Gopala Rao, R.V. 76282
 +Gopalan, K. 78513
 Gopalswamy, N. + 76186
 Gopalsamy, K. 74259
 +Goradia, C. 78033
 +Gorbach, V.N. 77177
 Gorbatshev, S.K. + 77439
 +Gorbunov, L.M. 75758
 Gorbunov, V.A. 75730
 Gorbunova, I.V. + 78447
 Gordeev, V.F. + 76596
 +Gordienko, A.I. 77757
 +Gordienko, P.S. 76613
 Gordon, H. + 74669
 Gordon-Salant, S.M. + 78191
 Gordov, E.P. + 75468
 +Gorelik, L.Yu. 76871
 +Gorelik, V.S. 77385
 +Gorelik, V.V. 75767
 Goren, S.D. + 77283
 Gorev, G.V. + 74479
 Gorev, N.B. + 76147
 +Gorev, V.V. 76193
 +Gorichev, P.A. 74771
 +Gorina, I.I. 76446
 +Gorkunov, E.S. 77842
 Gorman, A.A. + 75321
 +Gorn, I.A. 76875
 +Gorn, W. 75017
 Gornik, E. + 77414
 Gorkhovskii, A.A. + 75364
 Gorokhova, O.V. + 77603
 +Gorshokov, A.M. 76536
 Gortyshov, Yu.F. + 76026
 +Goryachko, Yu.S. 77802
 +Gosele, U. 76416
 +Gosnell, T.R. 78856
 Goss, L.P. + 74542
 +Gossard, A.C. 75714
 +Gossard, A.C. 75707
 +Gossard, A.C. 77446
 +Gostev, Yu.V. 77684
 +Goswami, D. 74329
 +Goswami, G.K. 79031
 +Goswami, K.N. 76409
 +Goto, K.S. 76692
 Goto, T. + 76547
 +Goto, T. 76609
 Gotoh, T. + 75157
 +Gotow, K. 74804
 +Gotsulyak, E.A. 75927
 +Gottfried, K. 74669
 Gottstein, J. + 78141
 +Gotz, G. 76465
 +Gotz, G. 76523
 +Gotz, K. 76168
 Gough, T.E. + 75373
 +Gouin, F.L. 74535
 +Gourley, P.L. 77402
 +Gourrier, S. 77778
 Goursot, A. + 75289
 +Gousheva, M.N. 78776
 +Gove, H.E. *ed.* 74232
 Govindarajan, T.R. + 74596
 Gower, M.C. + 75736
 +Goyal, P.K. 76948
 Graaff, H.C. de
see de Graaff, H.C.
 Grabowski, R. + 78780
 Grabowski, Z.R. + 75433
 Grace, R. 74893
 Grade, M. + 75527
 +Graftstrom, P. 75349
 Graham, J.A. 78994
 +Graindorge, Ph. 75825
 +Grammaticos, B. 74882
 Grammatin, A.P. + 75771
 +Granatstein, V.L. 75680
 +Grandi, S.A. 78920
 +Grandjean, F. 77297
 Grange, P. + 75062
 +Grannis, P. 74669
 +Grant, N.J. 75177
 +Grant, N.J. 77761
 +Grant, N.J. 77597
 Gras-Marti, A. 74666
 +Grasdalen, G.L. 78921
 Grasse, D. + 76520
 +Grasser, R. 76498
 Grau, G. 75833
 Graubmann, S. + 78266
 +Graves, R.S. 75101
 +Graveson, R.T. 75197
 Gray, J.L. + 78040
 Gray, J.W. + 75894
 Greben, J.M. + 74984
 +Grebinkina, V.G. 76984
 Grebenyuk, Ya.F. 77834
 +Greedan, J.E. 77142
 Green, B.G. + 78201
 +Green, D.M. 78195
 +Green, H.S. 74741
 +Green, K.E. 78488
 Green, M.A. + 76798
 Green, M.B. + 74744
 +Green, P.W. 74975
 +Green, R.B. 74444
 +Green, R.F. 79021
 +Greenberg, J. 75226
 Greenberg, R. 78832
 Greene, C.H. + 77876
 Greenhalgh, D.A. 77926
 Greenstadt, E.W. + 78756
 Greenwood, L.R. 76518
 +Gregoire, G. 74848
 +Gregoire, G. 74923
 +Gregoire, G. 75006
 +Gregory, A.G. 78768
 Gregory, D.C. + 75522
 +Gregory, P. 78079
 +Gregory, P.E. 78035
 +Greiner, W. 75037
 +Grehk, E.P. 74477
 +Greshnev, K. 78776
 +Grewal, B.S. 74900
 +Grey, A.E. 75124
 Gribanov, I.F. + 77144
 +Gribkov, S.P. 77538
 Gridnev, A.S. + 74476
 +Gridnev, A.S. 74475
 Gridnev, K.A. + 75009
 +Griesinger, M. 78045
 +Griffin, D.C. 75518
 +Griffin, D.C. 75521
 +Griffin, J. 78203
 Griffin, R.F. 78952
 Griffin, R.F. 78953
 Griffith, G.A. 75684
 +Griffith, J.E. 77512
 Griffiths, M. + 76509
 Griffiths, M. + 76510
 Griffiths, R.E. + 79024
 Griffiths, S.K. + 76080
 +Grigas, J. 76613
 Griggs, M. 78583
 +Grigolini, P. 74413
 Grigorenko, O.Ya. + 77328
 Grigorenko, Ya.M. + 75927
 Grigorenko, Ya.M. + 75918
 +Grigor'ev, A.E. 78253
 +Grigor'ev, V.P. 74389
 +Grigorov, I.V. 78263
 Grigorov, T.J. + 75243
 Grigorov, V.A. + 77455
 +Grigor'yan, A.A. 76516
 +Grigoryan, A.A. 78580
 +Grigsby, D.A. 78276
 +Grilhe, J. 77625
 +Grimm, F.A. 75446
 +Grimm, M. 74756
 Grimmer, A.R. + 77274
 Grinshaw, J.M. + 76459
 +Grin', Yu.M. 76360
 Grinberg, N.M. + 77756
 +Grinberg, O.Ya. 74506
 +Grincheshin, I.N. 76995
 Grinchishin, Ya.T. + 74753
 +Grindhammer, G. 74783
 Grinevich, G.P. + 76681
 Griniv, I.A. + 76360
 Grip, W.J. de
see de Grip, W.J.
 +Grivaz, J.F. 74783
 +Grodenkskii, I.M. 77026
 Groenendaal, A. van
see van Groenendaal, A.
 Rognard, R.J.-M. 76194
 Groh, W. + 75500
 +Groh, W. 75519
 +Gromme, S. 78434
 +Gromyko, S.N. 76616
 Groot, A.W. de. *see* de Groot, A.W.
 Gross, E.P. 74364
 +Gross, U. 78094
 +Grosse-Wiesmann, P. 74783
 +Grossetete, B. 74783
 Grossman, B. 75810
 +Grossoehme, D.H. 78958
 Grosswig, S. + 76340
 +Gronner, M. 78079
 +Grubb, D.P. 76214
 Grube, G.J. 74936
 Grube, G.J. + 74935
 +Gruber, D.E. 78992
 +Gruber, J.B. 77449
 +Grubl, G. 74581
 Grudnitskii, V.G. + 76059
 +Griebler, W. 75004
 +Grun, E. 78850
 +Grun, F. 78849
 +Grun, N. 75476
 +Gruner, R. 76700
 +Gruzdev, A.A. 75207
 Gruzintsev, E.N. + 75059
 +Gryffroy, D. 77301
 Gryko, J. 76993
 Grzymkowski, R. + 76336
 +Gschneider, K.A. 77135
 +Gschneider, K.A., Jr. 77476
 +Guan Yintong. 76386
 +Guan Zhong-xin. 75955
 Guang-jiong Ni
see Ni Guang-jiong
 Guang-xian Xu
see Xu Guang-xian
 Guang-zhao Zhou
see Zhou Guang-zhao
 Guangjun Zhao, Jr. Chen. *see* Chen Guangjun Zhao, Jr.
 Gubanov, V.A. + 77173
 Gubbens, P.C.M. + 77209
 Gubbins, D. 78425
 Gubbins, D. + 78427
 +Gubser, D.U. 77094
 Guchhait, R.K. + 74833
 +Gudat, W. 77523
 +Gudel, H.U. 77169
 Gudeman, C.S. + 74545
 +Gudkov, V.P. 74982
 +Gudkov, V.P. 74986
 +Gudyalis, V.V. 77468
 +Guedalia, D. 78700
 +Guen, L. 76393
 +Guenzburger, D. 76844
 Guerch, G. + 75541
 +Guerin, L. 78327
 Guermazi, M. + 76471
 Guerra, A. Del
see Del Guerra, A.
 +Guet, C. 75040
 +Guiducci, S. 75648
 Guilan Gao. *see* Gao Guilan
 Guilbeault, B.D. 75133
 Guillaume, G. + 75031
 +Guillaume, G. 75065
 +Guillemaud-Mueller, D. 74915
 Guillou, D. + 76294
 +Guillope, M. 76615
 Guillery, J. + 75674
 Guillou, J.C. Le
see Le Guillou, J.C.
 +Guiraldenq, P. 77768
 +Gulacsi, M. 77183
 Gulacsi, Z. + 77183
 Gulati, P.S. + 74273
 +Gulati, S. 74273
 +Gulbasin, V. 75752
 Guldner, Y. 77032
 Gulino, D.A. + 77044
 +Gulis, I.M. 77439
 +Gulyaev, V.I. 75927
 Gumerov, N.A. 75986
 +Gumlich, H.-E. 77459
 +Gunasekaran, S. 75357
 +Gundersen, S.C. 78207
 +Gundersen, B. 74783
 Gundu Rao, K.S. + 74914
 Gun'ko, L.P. + 77639
 +Gunsom, R. 75864
 Gunten, O. Van
see Van Gunten, O.
 Gunter, P. 75747
 Gunther, B. + 77277
 +Gunzler, V. 76402
 +Guo, S.C. 76178
 Guo Changlin + 76242
 Guo Changming
see Changming Guo
 Guo Fengyu + 77421
 Guo Han-ying + 74591
 +Guo Hanyang. 74598
 +Guo Zhiyuan. 75216
 Guobing Zhang
see Zhang Guobing
 Guohe Sha. *see* Sha Guohe
 +Gupta, B.K. 78423
 Gupta, J.P. + 74536
 Gupta, M. + 74774
 Gupta, M. + 76090
 +Gupta, M. 74780
 +Gupta, M. 74737
 Gupta, P.C. + 75195
 Gupta, P.C. + 76101
 Gupta, R.K. + 76353
 Gupta, S.D. 75766
 Gupta, S.K. + 75932
 Gupta, S.P. 78671
 +Gupta, V.K. 75045
 Gupta, V.P. 78346

- Gupta Raj K. 76734
 see Raj K. Gupta
 +Gura, L.A. 76028
 +Guralnik, G. 74707
 Gurbutt, P. + 75123
 +Gurbutt, P.A. 75120
 Gurevich, M.E. + 76493
 Gurgenci, H. + 76091
 +Gurgenidze, R.Sh. 74481
 +Gurin, O.V. 77120
 +Gurinovich, G.P. 75421
 Gurnett, D.A. + 78850
 +Gurnett, D.A. 78851
 +Gurtu, A. 74794
 +Gurtu, A. 74814
 Gurvich, A.M. 77422
 Gurvich, A.M. + 78301
 +Gur'yanov, G.M. 75107
 +Gusciovna, D.A. 77410
 Gusev, E.A. + 74575
 +Gusev, E.A. 78362
 +Gusev, E.B. 77944
 Gusev, E.V. 77127
 +Gusev, G.S. 78498
 +Gusheva, M. 78672
 Guskos, N. + 77260
 Gussoni, M. + 75380
 +Gustafson, H.R. 74759
 +Gustafsson, O. 75457
 +Gusten, H. 75445
 +Guthrie, W.L. 77503
 +Guthrie, W.L. 77919
 Gutman, I. 75281
 Gutman, I. + 75252
 Gutowski, M. + 76914
 Guttman, M. + 77746
 Guy, A.G. 76671
 Guyader, J. + 76397
 +Guyon, E. 74371
 +Guyot, P. 76415
 +Guzhva, N.P. 74477
 +Gyarmati, E. 75245
 Gzyl, H. 74320
- +Hall, H.E. 76734
 +Hall, R.B. 78088
 +Hallam, G.C. 77145
 +Hallam, H.E. 75387
 +Haller, G.L. 77918
 Halliday, A.N. + 78500
 +Hallock, R.B. 76730
 +Hallock, R.B. 76731
 +Hallum, A. 78166
 +Halmann, M. 77900
 +Halova, S.M. 78667
 +Halova, S.M. 78681
 +Halova, S.M. 78780
 +Halpern, A. 75415
 Halpern, J.B. + 75422
 Halpern, J.P. + 79001
 Halpern, L. 74333
 Halprin, A. + 74916
 +Halverson, J.E. 78557
 +Ham, A. 78196
 +Ham, N.S. 75443
 +Hama, S. 74941
 +Hama, S. 74987
 +Hamabata, H. 78764
 +Hamaguchi, Y. 77735
 Hamakawa, Y. + 78080
 +Hamakawa, Y. 77456
 +Hamakawa, Y. 78006
 Hamaker, H.C. + 78022
 +Hamano, A. 77758
 Hamano, K. + 77609
 Hamasaki, S. + 76197
 +Hamblett, I. 75321
 Hamer, C.J. 74397
 Hamer, C.J. 74398
 Hamersky, M. + 77712
 +Hames, F.A. 76769
 +Hamilton, P.A. 78936
 +Hamilton, P.J. 78479
 +Hammermaier, C. 78348
 +Hammond, S.R. 78436
 +Hamon, O. 74783
 Hampartzumian, K.L. + 77983
 Hampel, W. + 78816
 +Hampel, W. 78816
 +Hamrick, D.K. 74466
 +Hamrick, D.K. 75598
 +Hamzik, A. 77285
 +Han, J. 77750
 +Han, W. 76934
 +Han, Wenglong 77866
 Han Ya-fang *see* Ya-fang Han
 Han-ying Guo *see* Guo Han-ying
 Hanabusa, T. + 77672
 +Hanappe, F. 75033
 +Handa, H. 78294
 Handrich, K. 76716
 +Handschy, M.A. 77362
 +Handy, N.C. 75435
 Hanel, R.A. + 78852
 +Hanft, R. 74771
 +Hanic, F. 76315
 +Hanna, D.C. 75725
 Hanna, J. + 76997
 +Hannink, R.H.J. 77732
 Hannula, S.P. 77752
 +Hanover, G.A. 78840
 Hansen, B. + 78388
 +Hansen, C.J. 78912
 +Hansen, D.S. 78717
 +Hansen, F.Y. 76783
 Hansen, G. + 74553
 Hansen, J.E. + 75337
 Hansen, J.S. + 78397
 +Hansen, L.F. 75000
 +Hansen, O. 75036
 Hansen, R.G. + 75108
 +Hansl-Kozanecka, T. 74756
 +Hanson, K.J. 78609
 +Hanson, R.K. 77927
 Hanxin He. *see* He Hanxin
 Hanying Guo *see* Guo Hanying
 Hanzheng Deng *see* Deng Hanzheng
 +Hao Bai-lin 74366
 Haoqing Ni. *see* Ni Haoqing
 +Haque, M.I. 77253
 +Hara, E.H. 75834
 Hara, O. 74677
 +Harada, J. 77777
 Harada, M. 76607
 Harada, Y. 77816
 Haragopala Rao, B. + 77956
 +Harakeh, M.N. 74948
 Harder, C. + 75696
 Hardie, D.J.W. + 75499
 Harding, S.E. 75559
 +Hardman, K. 77179
 +Hardy, R.W. 78024
 +Hardy, R.W. 78069
 Hargrave, P.A. + 78126
 +Hargreaves, J.K. 78737
 +Hargreaves, J.K. 78741
- +Hari, R. 78210
 +Hari, R. 78188
 +Hari Babu, V. 76975
 +Hari Babu, V. 76697
 Hariharan, P.C. + 75299
 +Haring, A. 77507
 +Haring, R.A. 77507
 +Harley, R.T. 77291
 +Harling, O.K. 75177
 Harminder. 76682
 Harned, D.S. 76210
 Harper, P.G. + 75858
 +Harris, C.E. 75705
 Harris, F.E. 75273
 Harris, G.F. + 78380
 Harris, J.G. + 78458
 Harrison, F.L. + 75114
 +Harrison, H.B. 76473
 +Harrison, J.P. 77343
 Harrison, M.S.J. 78577
 Harrison, R.J. + 75435
 +Harrod, J.F. 75549
 Hart, A.M. S. 78437
 +Hart, D.G. 76436
 Hart, F.X. 78400
 +Hart, J.C. 74797
 Harten, A. + 74421
 +Harth, W. 78699
 +Hartley, W.H. 77855
 Hartman, P. 76357
 +Hartmann, F.J. 75558
 +Hartmann, H.-R. 77822
 +Hartmann, L. 78908
 +Hartstein, A. 77059
 Hartstra, R.L. 78524
 +Hartwig, J. 76340
 Harvey, J.R. + 75238
 Harvey, P.M. + 78974
 +Harvey, P.M. 78999
 +Harvilchuk, J.M. 77776
 +Harwit, M. 78856
 +Hasan, M.M. 76010
 Haschick, A.D. + 79022
 +Hassell, N.B. 77575
 Hasegawa, A. + 75082
 +Hasegawa, A. 75815
 Hasegawa, E. + 76001
 Hasegawa, H. 77234
 Hasegawa, T. + 77754
 Hasenfratz, P. + 74706
 +Hashi, T. 75538
 Hashimoto, K. + 77904
 +Hass, M. 75554
 +Hass, M. 74835
 Hassan, A.R. 76856
 +Hasse, I. 78984
 +Hasse, I. 78985
 +Hasson, A. 76719
 Hasted, J.B. 74206
 Hastings, D.E. 76491
 Hastings, S.P. + 77889
 +Hata, K. 74870
 +Hata, T. 76743
 +Hatanaka, K. 75003
 +Hatta, Y. 76176
 +Hattori, A. 76755
 +Hatfield, D. 78442
 Haubold, H.J. + 75041
 Hauksson, E. 78508
 +Hauser, J.R. 76959
 Hauser, U. + 77169
 +Hauser, K.H. 77261
 Haussler, K.M. + 76858
 +Haussler, K.M. 77346
 +Haut, C. 77633
 Hautala, M. 76533
 Haute, A.A. Van *see* Van Haute, A.A.
 Havlicek, F. 78110
 +Hawkesworth, C.J. 78493
 Hawkins, E.F. 75135
 Hawkins, M.R.S. 79009
 +Hawrynski, M. 75233
 +Haxton, W.C. 78892
 Hayakawa, M. + 77636
 +Hayakawa, M. 77154
 Hayakawa, T. + 75637
 +Hayashi, H. 75637
 +Hayashi, H. 77989
 Hayashi, K. + 77154
 +Hayashi, M. 75959
 Hayashi, S. + 77560
 +Hayashi, Y. 77998
 +Hayashi, Y. 74765
 +Hayashi, Y. 77020
 Hayday, A. + 77355
 +Hayes, J.M. 75709
 +Haynes, R.F. 78945
 Hays, T.R. + 75428
 Hazeltine, R.D. + 76205
 Hazen, R.M. + 76604
 He Hanxin + 74859
 He Liangbiao 78642
 Heal, G.R. 77901
 +Heang-Ping Chan 78330
 Heasley, J.N. + 78885
 +Hebard, A.F. 76799
 +Hebard, A.F. 77567
 Hebert, D. + 78438
- Hec Chung Ok *see* Ok Hec Chung
 Hecht, G. + 76600
 Hecht, H.G. 75585
 +Hecht, M.H. 75221
 +Heckman, H.H. 75016
 Heckman, T.M. + 78987
 +Hedberg, K. 75512
 +Hedberg, L. 75512
 +Hedderich, D. 75098
 +Hediger, M. 77923
 +Hedman, S. 75353
 +Hedstrom, J.H. 75432
 Heer, F.J.de *see* de Heer, F.J.
 Heerden, I.J.van *see* van Heerden, I.J.
 Heeringa, W. + 74993
 +Heftel, E.F. 75009
 Hegarty, D. + 75259
 +Hegerath, A. 74962
 Hegg, D.A. 78612
 +Hegg, D.A. 78613
 +Hehl, F.W. 74624
 +Heidemann, K.F. 76524
 +Heikens, D. 77722
 +Heil, R. 75519
 Heil, T.G. + 75505
 +Heimann, M. 78114
 +Heinemann, K. 76806
 Heintz, A. + 76599
 Heinze, D. 74474
 Helbach, P. + 77857
 Helenclund, K. + 75353
 +Heller, D. 74553
 +Heller, D.F. 75686
 +Heller, F. 78428
 Helm, H. + 75456
 +Helmbrecht, U. 76726
 Helmer, R.G. + 74907
 +Helms, C.R. 77502
 Heming, M. + 77255
 Henderson, B. 76424
 +Henderson, D.J. 75061
 +Henderson, R. 78128
 +Henderson-Sellers, A. 78621
 +Henderson-Sellers, A. 78639
 +Hendow, S.T. 75627
 Henghui Sun *see* Sun Henghui
 Henichart, J.P. + 75388
 +Henke, W.E. 75428
 +Hennings, D. 78644
 Henrichs, H.F. + 78934
 +Henry, E.A. 74905
 +Henry, E.R. 78142
 +Henry, J.P. 78988
 +Henry, L. 76264
 +Henry, P. 77809
 +Henry, R.L. 77561
 +Hensel, E. 76757
 +Henson, G. 78956
 Heppke, G. + 77360
 +Herault, J.P. 75842
 Herber, R.H. + 77300
 +Herbschleb, J.N. 78168
 +Herbster, G.A. 75691
 +Heremans, J. 77227
 +Heringa, A. 78374
 Herley, P.J. + 77898
 +Herman, G.T. 78288
 +Herman, G.T. 78314
 Herman, J.R. + 78652
 +Herman, M. 78640
 +Herman, M. 78645
 +Herman, M.A. 75385
 Herman, Z.S. + 76887
 +Hernance, J.F. 78478
 Hermann, A.M. + 78004
 Hermann, H. 76313
 Hermann, K.H. + 76996
 +Hermanson, J.C. 77533
 Hernandez, E.S. + 74319
 +Herr, W. 77508
 +Herrington, C.R. 78070
 +Herrington, W.N. 75132
 Herrmann, G. + 77946
 +Herrmann, R. 76454
 +Herrmann, R.B. 78449
 Hersee, S.D. + 77027
 +Hertz, J. 76667
 +Hertzberg, R.W. 77831
 +Hervo, C. 78022
 +Hervo, J. 78022
 +Herz, K. 77201
 Herzen, R.P. Von *see* Von Herzen, R.P.
 Herzig, P. 76356
 +Herzog, B.L. 75141
 Herzog, P. + 74846
 Herzog, U. 75617
 +Heskett, D. 77529
 +Hess, D.W. 78202
 Hess, K. 77031
 +Hess, K. 76960
 +Hess, K. 75689
 +Hesse, D. 76639
- Hesse, J. + 77312
 Hesse, K.-F. + 76405
 Hesselink, L. + 76127
 +Hesser, J.E. 78964
 +Hetherington, W.M., III. 75726
 +Hetrick, D. 75084
 +Heuer, A.H. 76611
 Heully, J.-L. + 75319
 Heusch, B. + 75065
 +Heusch, B. 75030
 +Heusch, B. 75031
 +Heusser, G. 78816
 Heuvel, E.P.J.van den *see* van den Heuvel, E.P.J.
 Hewett, D.W. + 76208
 +Hewett, D.W. 76174
 Hewig, G.H. + 78084
 +Heydt, G. 78699
 +Heyen, M. 77576
 +Hibray, R.E. 78042
 Hicks, H.G. + 74905
 +Hida, H. 77030
 +Hide, I. 77557
 Hide, R. 76118
 Higa, T. + 78294
 Higashi, I. 76384
 +Higashino, Y. 77099
 +Higgins, C.B. 78299
 Higgy, H.R. 76519
 +Higuchi, H. 75634
 +Hiikata, T. 75637
 +Hikata, A. 76732
 +Hilal, S.K. 78323
 +Hildebrand, H. 74846
 +Hildebrand, O. 76708
 +Hildenbrand, K.D. 75030
 +Hildner, E. 78886
 +Hildreth, W. 78500
 +Hill, M.D. 75120
 +Hill, R. 74561
 +Hill, R.M. 77326
 +Hill, W.J. 75166
 +Hillairiet, J. 76415
 +Hillel, D. 78839
 +Hillenkamp, F. 78240
 +Hillman, J.J. 75370
 +Hills, R.N. 74429
 +Himpel, F.J. 77530
 +Himpel, F.J. 77531
 +Himai, M. 77793
 +Hinchcliffe, I. 74669
 Hinde, D.J. + 75032
 +Hines, J. 74917
 +Hino, T. 75175
 +Hinov, H.P. 76291
 Hippe, D. + 74840
 Hippler, H. + 75484
 Hippler, H.J. + 75485
 Hirakawa, K. + 77139
 +Hirakawa, K. 77164
 +Hirano, R. 75634
 +Hirano, Y. 75949
 Hirao, K. + 76317
 +Hirao, K. 77609
 Hirata, N. + 78443
 +Hirayama, Y. 75632
 +Hirota, E. 75369
 Hirsch, C. + 75997
 Hirsch, H.R. 78150
 Hirschfeld, P. + 76735
 +Hirschwald, W. 75527
 +Hirshfeld, A.C. 74613
 Hirvonen, M.T. 75565
 Hitachi, A. + 77461
 +Hiyamizu, S. 77030
 +Hizo, J. 78353
 +Hjalmarson, H.P. 76843
 Hlasnik, I. + 77114
 Hloušek, L. + 75548
 Ho, F. + 78028
 Ho, F. + 75719
 +Ho, F. 78041
 +Ho, F. 77965
 +Ho, P.S. 77531
 Ho Yu-ping 75572
 Ho Yu-ping + 74301
 Hoang Mai Le *see* Le Hoang Mai
 Hoang Thai Vo *see* Vo Hoang Thai
 +Hobart, M.A. 78490
 +Hobgood, H.M. 76342
 +Hochstrasser, R.M. 75719
 Hocking, G.E. + 78055
 +Hodge, R.C. 78044
 +Hodges, J.A. 77297
 Hodgkiss, W.S. + 78717
 Hodgskiss, S.W. + 77254
 Hodnett, P.F. 78554
 +Hodoscek, M. 75295
 +Hodson, S.W. 78922
 +Hoegh-Krohn, R. 74296
 +Hoffmann, D. 74756
 +Hoffmann, G.W. 74997
 +Hoffmann, G.W. 74998
 +Hoffmann, R. 77182
 +Hoffmann, R. 75502
 +Hofmann, A. 75007

- Hofmann, H.M. + 75223
+ Hofmann, P. 75100
Hofmann, W. 78334
+ Hofmann, W. 78333
Hofrichter, J. 78142
+ Hofman, J.S. 74759
+ Hogan, J.J. 75005
+ Hogan, J.J. 75055
Hogan, S.J. 76056
+ Hough, C.A. 77068
+ Hogenhuis, L.A.H. 78214
Hogervorst, W. 75332
+ Hogervorst, W. 75280
+ Hoggins, S. 78935
Hoggins, J.T. + 76378
+ Hoggund, A. 74487
+ Hogmark, S. 77764
Hoheisel, C. + 76266
Hohenberg, J.K. 78357
Hohenberg, J.K. 78358
Hohlneicher, G. + 75461
+ Hohlneicher, G. 75458
+ Hohne, R. 77217
Hoi Pham see Pham Hoi
Hoi-Young Chan + 78385
+ Hol, W.G.J. 78127
+ Holdeman, L.B. 77101
Holden, A.J. + 75893
Holladay, A. + 76250
+ Holland, B.W. 76759
Holland, E. + 78363
Holland, O.W. + 76463
Holland, R. + 77377
Hollinger, G. + 77530
Hollinger, G. + 77531
+ Hollis, J.M. 78967
Hollstein, T. + 77819
+ Holmberg, S. 77943
+ Holmes, J.L. 75550
+ Holonyak, N., Jr. 75689
+ Holsapple, K.A. 78835
+ Holt, A.G.J. 75856
+ Holt, A.R. 78595
+ Holt, S.S. 79000
Holten, J.W. van see van Holten, J.W.
Holtz, R.L. + 76676
Holuj, F. + 77341
Holzrichter, J.F. + 75172
Holzschuh, E. + 77515
Holzwarth, N.A.W. + 75272
+ Homewood, K. 77293
+ Honda, T. 74437
+ Honebon, C.D. 78437
Hong, C.S. + 75640
+ Hong, C.S. 77583
+ Hong, K.S. 78323
Hong Qin see Qin Hong
Hong Shon Nguyen see Nguyen Hong Shon
Honma, S. + 77906
Hood, G.M. + 76704
+ Hood, J.T., Sr. 78317
+ Hook, J.R. 76734
+ Hooker, C.D. 75132
+ Hooker, P.J. 78479
+ Hooper, E.B. 76214
+ Hooper, R.M. 76550
+ Hooper, C.G. 77964
Hopf, F. 75616
Hopf, F.A. 75713
+ Hopfen, R.A. 77414
+ Hopfenberg, H.B. 76702
+ Hopfield, J.J. 77879
Hopfinger, E.J. 78574
+ Hopkins, D.B. 75660
+ Hopp, G. 74783
Hopp, U. + 78954
+ Hoppe, R. 76388
+ Horak, J. 76419
Horenstein, M.N. 74493
+ Hori, S. 78496
+ Hori, T. 77152
Horibe, M. + 74634
Horiguchi, T. 77195
+ Hori, K. 75850
+ Hori, K. 76764
+ Horikoshi, Y. 75960
Horn, H.M. van see Van Horn, H.M.
+ Horn, K. 76786
+ Hornady, R.S. 76214
+ Horne, W.E. 77861
Horne, F. + 78428
Horowitz, C.J. 74887
Horowitz, C.J. + 74890
Horvath, C. + 76390
Horwitz, G. 74689
Hosary, A.A. El see El Hosary, A.A.
+ Hoshino, K. 76829
+ Hosoya, A. 74634
Hosoya, H. + 75290
Hosoya, M. 76327
+ Hosoya, Y. 78764
+ Hotai, K. 77154
Hotokka, M. + 76842
+ Hotz, H.B. 78860
Hou Jing-ya 75644
Hough, J. 74362
Hough, J. + 78935
+ Houlter, B. 78529
+ Housley, G.T. 76108
Housen, K.R. + 78835
Houser, C.A. + 77511
+ Houssein, R. 75388
Hove, M.A. Van see Van Hove, M.A.
Howard, J. 78183
+ Howard, J.F., Jr. 78389
+ Howard, R.A. 78894
Howe, R.J. + 77481
+ Howe, R.J. 78407
+ Howell, C.R. 74999
+ Howell, P.R. 77645
Howitt, D.G. + 76540
+ Howson, J. 75250
+ Hoyano, A. 78100
Hoyningen-Huene, W. von see von Hoyningen-Huene, W.
Hoyos, J. + 74586
Hrbacek, K. + 77649
Hrubec, J. + 77208
Hsi Dan + 74502
+ Hsi-Chuan Liu 76944
+ Hsi-Chuan Liu 77330
+ Hsiang-Yan-yu 74591
Hsiang-chen Chen see Chen Hsiang-chen
Hsieh, C.K. + 74468
+ Hsin Wang 78129
+ Hsin-Yang Yeh 75343
+ Hsin-Yang Yeh 75452
Hsiung Chen Mau see Mau Hsiung Chen
+ Hsu, S.-E. 77207
+ Hsu, W.L. 76214
Hsuan Feng Da see Da Hsuan Feng
Hsueh-wen Wu see Wu Hsueh-wen
Hu Gang + 76756
+ Hu xi-wen 74301
+ Hu Yuxian 77279
+ Hua Zhonglu 76876
+ Huang, C.-Y. 77476
Huang, S.C. + 77222
Huang Hui-Li see Hui-Li Huang
Huang Ming-ke see Ming-ke
Huang 78576
Huang Runben + 78576
Huang Si-xun 74252
Huang Xun-Cheng 74288
+ Huang Zhupo 77421
Huang Zu-qia 78897
Hubackova, J. + 77797
Hubbard, C.R. 76251
+ Hubbard, C.R. 76407
+ Hubbard, C.R. 76252
+ Hubberstey, P. 77880
Huber, D. + 78048
+ Huber, D.L. 77186
+ Huber, M.G. 75066
+ Huber, T.E. 76746
Hubner, H. 75480
+ Hubner, M. 78816
Huchon, P. 78503
+ Huchra, J.P. 79012
+ Huchtmeier, W. 78872
Huck, P.M. + 75095
Hudak, O. 77335
Hudak, O. 77336
+ Hudson, C.G. 78347
+ Hudson, J.L. 76038
+ Huebener, R.P. 77105
+ Huebert, B. 78611
+ Hui-Li Huang 76712
+ Huestis, D.L. 75456
Hufner, J. + 74994
Hughes, B. + 76891
+ Hughes, B.D. 74374
Hughes, N.A. + 78621
+ Huguenin, D. 78619
+ Huguenin, R. 76663
Hui-chang Yen Ma see Ma Hui-chang Yen
Hui-fang Wu see Wu Hui-fang
+ Hui-yu 74453
+ Huie, A. 75017
Huifang Liu see Liu Huifang
Huignard, J.P. 75733
+ Huijsmans, J.P.P. 78481
Huirong Li see Li Huirong
Huizi Peng see Peng Huizi
+ Hull, C.M. 74354
Hull, R. + 76414
Hulst, J.M. Van Der see Van Der Hulst, J.M.
+ Hum, R.H. 75834
Hummel, R.E. + 76713
+ Humphreys, C.J. 76414
Humphreys, R.M. 78822
Hung, C.Y. 75093
+ Hung Lei 76890
Hunger, G. + 76678
Hunger, G. + 77760
+ Hunt, A.J. 78936
+ Hunt, A.L. 76214
Hunt, G.E. 78862
+ Hunt, J.C.R. 75990
+ Hunt, J.T. 75172
Hunter, A.T. + 76894
Hunter, J.F. + 78224
+ Huang, P.V. 76272
Hurle, D.T.J. 76332
Hurst, G.S. + 78891
+ Hurych, Z. 76794
+ Hurych, Z. 77526
Husinsky, W. + 77504
Hut, P. + 78962
+ Hutchby, J.A. 78077
+ Hutchison, D.A. 74975
+ Hutchings, B.J. 76086
Hutchings, R. 77646
+ Hutchinson, M.H.R. 75727
+ Hutchison, C.A., Jr. 77294
+ Huttel, G. 75098
+ Huttel, G. 75096
+ Hutton, B.F. 78328
+ Huybers, M.T.M. 77012
+ Huynh-ba, T. 76296
+ Huzita, H. 74756
+ Hwang, H.L. 77541
Hwang Kehchih + 75952
Hyland, S. + 77592
+ Hyman, J.M. 74421
+ Hynes, M.V. 74968
Hyspecka, L. 77641
+ Iachello, F. + 75359
+ Iachetti, D. 78327
+ Iannuzzi, G. 76711
+ Iarocci, E. 74766
+ Iarocci, E. 75225
+ Ibach, H. 76777
Ibanez, L.E. 74674
+ Ibragimov, Sh.Sh. 76485
+ Ibuka, M. 77099
Icaza-Herrera, M. De see De Icaza-Herrera, M.
+ Ichihara, I. 77922
+ Ichihara, T. 75222
+ Ichihara, T. 74966
Ichikawa, K. + 76743
+ Ichikawa, T. 77911
Ichimaru, S. + 76161
Ichimaru, S. + 78903
Ichimaru, M. 74950
Ichinose, M. + 78745
Ichinose, S. + 74643
+ Ichinose, T. 76135
Ichinyanagi, M. 74375
Ichien, N.M. 75155
Ida, H. + 77998
Ide, T. + 78790
+ Ide, T. 78743
+ Ide, T. 78794
Ieki, K. 75018
+ Igarashi, K. 76279
Igi, S. + 78709
+ Igi, S. 78745
+ Igi, S. 78743
+ Igi, S. 78793
+ Ignacz, P.N. 76202
+ Ignat'ev, M.B. 76188
Ignatiev, A.Yu. + 74673
Ignatov, A.A. 76918
+ Igolkina, L.S. 77681
+ Iguchi, S. 78791
Ihle, D. + 76847
+ Iida, N. 78330
Iida, T. + 78795
Iijima, K. + 76621
Iizuka, S. + 76176
Iizumi, M. + 75070
+ Ikai, S. 76125
+ Ikawa, K. 75103
Ikeda, H. + 77153
Ikeda, H. + 77982
Ikeda, K. 75712
+ Ikeda, K. 77232
+ Ikeda, S. 75441
+ Ikeda, T. 77248
Ikouchi, Y. + 77708
Ikezawa, M. + 77379
+ Ikezawa, M. 77406
+ Ikoma, T. 76892
+ Ikossi, P.G. 74904
+ Ikui, T. 76035
+ Ikushima, A.J. 74462
+ Ilchev, N. 77983
+ Iles, P. 77592
+ Iles, P.A. 78028
+ Iles, P.A. 78041
+ Iles, P.A. 78026
+ Ilieva, K.D. 75072
+ Il'in, V.V. 76751
Il'ina, M.A. 77084
+ Il'inski, A.V. 75597
+ Il'inski, Yu.A. 75610
Illas, F. + 76769
Illas, F. + 76770
+ Ilischer, B. 77754
+ Ilyukhin, V.V. 76347
+ Ilyukhin, V.V. 76348
+ Ilzyer, D. 76983
+ Imaev, M.F. 77678
+ Imai, K. 77622
+ Imai, M. 75811
+ Imai, M. 76484
+ Imai, T. 75185
+ Imai, T. 77572
+ Imaichi, K. + 76041
+ Imamura, J. + 78942
+ Imanova, A.L. + 77357
+ Imhof, U. 78348
+ Imoto, S. 76635
+ Imry, Y. 77010
+ Imura, T. 76445
+ Inagaki, K. 77063
+ Inai, O.T. 77798
+ Inatani, H. 78443
+ Inayama, M. 77030
+ Ingels, J. 78629
Ingelstam, E. 75574
+ Inger, G.R. 76064
Inglesfield, J.E. 77515
+ Ingmann, P. 78699
+ Iniguez, M.P. + 76869
+ Inogamov, Sh.V. 74809
+ Inopin, E.V. 74963
+ Inoue, E. 76997
+ Inoue, E. 77906
+ Inoue, H. 76289
+ Inoue, J. 77233
Inoue, K. + 74686
+ Inoue, K. 77407
Inoue, M. + 77030
Inoue, M. + 77206
+ Inoue, M. 76035
+ Inoue, M. 75013
Inoue, Y. + 75441
+ Inoue, Y. 77374
+ Inoue, Y. 78000
+ Inuishi, Y. 77030
Inukai, T. + 76289
+ Invernizzi, M. 75077
+ Iobst, S.A. + 77715
+ Ioffe, I.V. + 76305
+ Ioltukhovskii, A.G. 76517
+ Ionov, S.P. 76874
+ Ipatova, I.P. + 76617
+ Ipatova, I.P. + 76575
+ Iqbal Ahmed, M.D. 76423
+ Irby, C.A. 78039
+ Ireland, P.J. 78070
+ Irfan, M. 75053
+ Irie, N. 78220
+ Irons, G.A. + 76095
+ Irtuganov, Sh.Sh. 75767
+ Irvine, W.M. 78846
Isacker, P. Van see Van Isacker, P.
+ Isaev, N. 78669
+ Isaev, N.I. + 75816
+ Isakov, A.I. 74576
+ Ishchuk, V.M. + 77339
+ Ishida, H. 76775
+ Ishiguro, T. + 76932
+ Ishihara, M. 75013
+ Ishii, T. + 77548
+ Ishii, Y. 78294
+ Ishijima, S. 78578
+ Ishikawa, M. 75004
+ Ishikawa, T. 77122
+ Ishio, S. + 77248
+ Ishioka, S. 76686
+ Ishiyama, N. 78876
+ Ishizaki, K. + 76503
+ Ishwar, N.B. + 75547
+ Isida, M. + 75964
+ Isomura, A. 77248
+ Isokaki, T. 75169
+ Itkis, M.G. 75059
+ Ito, A. 77998
+ Ito, H. 75715
+ Ito, K. + 77705
+ Ito, N. 74765
+ Ito, S. 78746
+ Itoh, N. 76421
+ Itoyama, H. + 74727
+ Itti, R. + 78325
+ Ivan, J. 77673
+ Ivano, M. + 75431
+ Ivanenkov, G.V. 76216
+ Ivanov, A.V. 76848
+ Ivanov, E.N. + 77401
+ Ivanov, I. + 78673
+ Ivanov, M.V. 76854
+ Ivanov, S.A. + 77403
+ Ivanov-Omskii, V.I. 77002
+ Ivanov-Smolenskii, G.A. + 77129
+ Ivanova, G.N. 77462
+ Ivanova, T.N. + 78781
+ Ivanova, T.N. + 78680
+ Ivanova, T.N. + 78667
+ Ivanyutenko, V.I. 76105
+ Ivascu, M. 74874
+ Ivashchenko, A.V. 77361
+ Ivashchenko, V.E. 74483
+ Ivic, A.P. 77588
Ivonchik, N.P. + 74291
+ Iwai, T. 76701
+ Iwai, Y. 77817
+ Iwamoto, I. + 78788
+ Iwamoto, I. + 78750
+ Iwamoto, I. 78751
+ Iwamoto, K. 75103
+ Iwamoto, N. + 76311
+ Iwamura, H. + 75690
+ Iwamura, H. + 77959
+ Iwan, M. 76786
+ Iwanaga, H. + 76338
+ Iwanizewski, J. 74387
+ Iwanowski, R.J. + 77993
+ Iwasa, Y. 77812
+ Iwasaki, M. 77911
+ Iwasaki, Y. + 74615
+ Iwasaki, Y. + 74616
+ Iwasaki, Y. + 74638
+ Iwata, A. 77693
Iye, Y. + 77227
+ Iyer, S.B. 77062
+ Iyetomi, H. 76161
Izotov, V.I. + 77637
Izumi, T. + 78118
+ Izydorek, J. 77968
Izyumov, Yu.A. + 77120
Jablonski, D.G. 77102
Jacak, B.V. + 74952
Jacks, F. + 78287
Jaciwi, R. 74626
+ Jackowska, I. 75350
+ Jackson, D.A. 76140
+ Jackson, J. 74669
Jackson, J.D. (ed.) 74232
+ Jackson, M.A. 78059
+ Jacob, M. 74816
+ Jacobs, J.J. 74577
+ Jacoby, M.H. + 74569
+ Jadach, S. 74783
Jafari-Asl, A.H. + 78157
Jaffe, J. + 77083
Jafiolia, R. + 74911
+ Jagadish, C. 77074
+ Jahan, M.S. 78140
+ Jahns, J. 74522
Jain, A. + 75531
+ Jain, G.C. 78063
+ Jain, J.K. 75464
+ Jain, P.A. + 77308
+ Jain, P.C. + 75360
+ Jain, P.K. + 77072
+ Jain, P.K. + 75164
+ Jain, R.K. 75748
+ Jain, R.K. 76092
+ Jain, S.C. + 77990
+ Jain, S.C. 78007
+ Jain, S.K. 78063
+ Jakob, M. 77826
+ Jakobova, A. 77710
+ James, A.N. 74975
+ James, R.B. 75751
+ James, W.J. 77179
+ Jameson, A.K. 75432
+ Jamnion, M. 74978
+ Jamolkowski, A. 74311
+ Jancovici, B. 76156
+ Janeczek, J. + 74889
+ Janewa, N.B. 75150
+ Janicjevic, L. 75575
+ Jankowski, K. 75278
+ Jannussis, A. 74316
+ Janoray, P. 78293
+ Janssen, P.A.E.M. + 76180
+ Janssens, P. 75997
+ Janszky, J. + 76539
+ Janszky, J. 76999
+ Jaoul, O. + 78529
+ Jaque, F. 77963
+ Jardim, J.O.D. + 79010
+ Jardim, M.V.A. 79010
+ Jardine, S.I. 75858
+ Jaros, M. 76880
+ Jarrar, G. + 78482
+ Jarrije, J. 77781
+ Jarvis, P.D. + 74741
+ Jarzak, U. 77366
+ Jaszczuk, W. 78283
+ Jaszczuk, W. 78285
+ Jata, K.V. + 77750
+ Jauncey, D.L. 79024
+ Jauncey, D.L. 78945
+ Jauncey, D.L. 79014

- +Jawalekar, S.R. 77579
 +Jawdosiuik, M. 75391
 Jayaram, B. + 75905
 +Jayarama Reddy, P. 77076
 +Jayaraman, A. 75886
 +Jean, Y.C. 75556
 Jech, C. + 77772
 Jeffreys, B. 78415
 +Jeitschko, W. 77297
 Jekeli, C. 78411
 Jellison, G. + 76173
 +Jemmali, F. 76955
 +Jemmali, F. 77647
 Jenkins, D.A. + 74995
 Jenni, P. 74818
 +Jensen Tsai, 77007
 Jensen, L.G. + 76742
 Jensen, M.H. + 76583
 +Jericevic, Z. 75553
 Jeu, W.H.de
 see de Jeu, W.H.
 Jeugt, J.Van der
 see Van der Jeugt, J.
 Jeulin, D. 74563
 Jeung, G.H. + 75562
 Jewell, J.L. + 75707
 +Jewell, J.L. 75714
 +Jewess, M. 76659
 Jewett, D.N. + 77556
 Jha, B. + 76299
 +Jha, B.L. 75547
 Ji-tao Wang
 see Wang Ji-tao
 +Jia Fu 76037
 +Jia Youquan 75953
 Jiabin Zhou *see* Zhou Jiabin
 Jiayi Du
 see Du Jiayi
 Jiali Ge
 see Ge Jiali
 Jian-Guo Yu
 see Yu Jian-Guo
 Jian-min Liu
 see Liu Jian-min
 Jian-ou Xu
 see Xu Jian-ou
 Jian-ping Shen
 see Shen Jian-ping
 Jianjun Xu
 see Xu Jianjun
 Jianshe Lian
 see Lian Jianshe
 Jianxiang Rong
 see Rong Jianxiang
 Jianzu Zhang
 see Zhang Jianzu
 Jicheng Zhou
 see Zhou Jicheng
 Jifeng Lu
 see Lu Jifeng
 Jin Fusheng 74278
 Jindal, U.C. + 77823
 Jing-ong Ren
 see Ren Jing-ong
 Jing-ya Hou
 see Hou Jing-ya
 Jingde Lee
 see Lee Jingde
 Jingtang Ye *see* Ye Jingtang
 +Jinno, K. 78573
 Jinshan Wang
 see Wang Jinshan
 Jinsheg Sun
 see Sun Jinsheg
 Jinzaki, Y. + 74462
 +Jiricek, F. 78772
 Jiuhan Shao
 see Shao Jiuhan
 Jo Seto Yeb
 see Yeb Jo Seto
 Joachain, C.J. + 74205
 Joardner, R.N. + 76282
 +Jog, J.P. 76969
 +John, R.W. 75041
 Johnson, C.H. + 74990
 Johnson, C.H.J. 76462
 Johnson, D.A. + 78516
 +Johnson, G.L. 75378
 +Johnson, G.L. 75379
 Johnson, H.P. + 78512
 +Johnson, L. 78230
 +Johnson, M.E. 78656
 Johnson, N.M. 76896
 Johnson, N.M. + 78694
 +Johnson, P.D. 77526
 Johnson, S.M. + 78060
 +Johnson, S.M. 77988
 Johnson, T.M. + 75141
 +Johnson, T.V. 78849
 Johnston, S. + 75762
 Johri, V.B. + 79031
 +Jokela, T.A. 75117
 Jolliffe, I.T. 78634
 +Jona, P. 75380
 Jones, B.E. + 75830
 +Jones, B.E. 75820
 Jones, E. 75823
 Jones, G.J.R. + 76759
 Jones, I.P. + 77937
 +Jones, J. 75436
 +Jones, J. 75437
 +Jones, J. 75442
 Jones, J.D.C. + 76140
 Jones, K.A. 77573
 +Jones, K.M. 78070
 +Jones, L.W. 74759
 +Jones, M.E. 75840
 Jones, R. 75179
 Jones, R. + 76359
 Jones, R. + 76837
 +Jones, R.E. 75812
 Jones, R.G. + 76789
 +Jones, T.B. 78754
 +Jones, T.W. 75226
 +Jones, T.W. 79019
 +Jones, W. 77898
 +Jones, W.B., Jr. 77830
 Jong, T.De. *see* De Jong, T.
 Jonkman, H.T. + 75424
 +Jordan, T.M. 76506
 Jordanov, J.D. + 75073
 Jordanov, J.D. + 75074
 Jordanov, J.D. + 75151
 Jordanov, J.D. + 75152
 Jordanov, J.H. + 77929
 +Jordanov, N. 77929
 Jorritsma, J.B.M. + 78159
 Joseph, K.P. + 78163
 Joseph, P.M. 78319
 Joseph, R.R. + 75045
 +Joseph, R.R. 75039
 +Joseph, R.R. 75044
 Joshi, N.K. + 76167
 +Joshi, N.V. 78638
 Joshi, S.G. + 76969
 +Joshi, Y.N. 75402
 Joslin, C.G. 76265
 +Joslin, D. 78029
 +Jouhier, B. 74378
 Jouini, N. + 76393
 +Joullie, A. 76807
 +Jourdain, J.-C. 74898
 +Journé, V. 74783
 +Jouty, R. 76308
 +Jouvet, C. 75420
 Jovanovic, D. 76185
 +Ju Kechang 77214
 Juehui Chu *see* Chu Juehui
 Julian, B.R. 78469
 Jun-Qing Li *see* Li Jun-Qing
 Jung Jungchung
 see Jungchung Jung
 +Jungchung Jung 75175
 Jungerman, R.L. + 75883
 Junqua, N. + 77625
 +Jury, J.W. 74960
 +Justiniano, E. 75502
 +Juszczak, E. 78126
 +Kalifa, J. 74847
 Kalikhman, V.L. + 77595
 Kalinchuk, I.N. 75789
 Kalinowski, M.W. 74344
 +Kalish, R. 77300
 Kallman, T.R. + 79025
 Kalma, J.D. + 78656
 Kalman, Z.H. + 76241
 +Kal'met'eva, Z.A. 78447
 Kalmykova, Z.I. + 78260
 Kalnay, A.J. 74310
 Kalnay, A.J. 74652
 Kal'nits'kii, A. + 77428
 +Kalomiris, V.E. 75835
 +Kalugin, V.D. 77667
 Kam, J.De. *see* De Kam, J.
 Kamal, M. + 76308
 +Kamalov, S.S. 74958
 +Kamarinos, G. 77064
 +Kambe, T. 76044
 Kameda, K. + 77616
 Kamegashira, N. + 76614
 +Kamei, H. 74532
 +Kameyama, M. 78294
 +Kamezawa, N. 76293
 Kamimoto, M. + 77989
 Kaminar, N. + 78079
 +Kaminska, M. 76889
 Kaminskii, A.A. + 77423
 +Kaminskii, A.A. 77720
 Kaminskii, V.A. + 75534
 Kaminskii, V.E. + 74524
 Kamma, C.F. + 77241
 +Kampan, R.L. 78236
 +Kamper, K.W. 78968
 Kampunzu, A.B. + 78499
 Kamrakov, A.S. + 76169
 +Kamyshev, A.S. 77756
 +Kamzeeva, E.E. 76762
 Kanada, T. + 75814
 +Kanadani, T. 77664
 +Kanamaru, T. 77832
 +Kanamori, C. 76743
 +Kanamori, H. 78456
 +Kanapilly, G.M. 78366
 Kanber, H. + 76476
 +Kanchev, A. 78668
 +Kanchev, N. 78668
 +Kane, T. 75678
 +Kane, W.R. 74908
 +Kaneke, Y. 75472
 +Kaneri, O. 77277
 Kanetake, N. + 77670
 Kang, H.J. + 77513
 Kang Zhen-Chuan
 see Zhen-Chuan Kang
 +Kangun, A.L. 78306
 +Kanno, M. 77791
 +Kanno, R. 77981
 +Kano, T. 76816
 +Kanpur, I.I.T. 74777
 Kanrar, A. + 76544
 +Kanter, E.P. 74555
 Kantor, M.M. + 76517
 Kantrowitz, F. + 75173
 +Kantsyrev, V.L. 74576
 Kanzaki, S. + 77609
 +Kao, K.C. 78072
 Kao, Y.C. + 76943
 +Kapaev, V.V. 76480
 Kapahi, V.K. + 79006
 +Kapahi, V.K. 79017
 +Kappert, H.F. 76524
 Kapshai, V.N. + 74623
 Kapur, A.K. + 75464
 +Kapusta, C. 77284
 +Kavasta, F. 74783
 Kapusta, J. 75014
 +Karaali, S. 79003
 +Karaban, R.T. 78251
 +Karagullef, C. 75725
 +Karaki, T. 76433
 +Karamishev, G.S. 78667
 +Karamishev, G.S. 78680
 +Karant, Y.J. 75016
 +Karasawa, H. 77998
 Karasev, V.P. + 75611
 Karato, S. + 78566
 Karavanov, V.B. + 74513
 +Karayan, A.S. 76307
 +Karbovskii, A.V. 76855
 Kardar, M. + 77189
 Karecki, D.R. + 77094
 +Karemaker, J.M. 78215
 +Kareva, N.T. 77703
 +Karge, H. 77350
 +Karge, H. 76465
 +Karge, H. 76523
 +Karimov, M.G. 75396
 Karlin, R. + 78539
 +Karmohapatro, S.B. 75497
 Karol, P.J. 74980
 +Karol, P.J. 74912
 +Karp, P. 78393
 +Karp, P. 78395
 Karpeta, C. + 75149
 Karpinos, D.M. + 77757
 +Karpov, V.V. 75421
 +Karpov, V.Yu. 77071
 Karpushin, A.G. + 76144
 Karpushin, V.A. + 74512
 +Karra, J.S. 77257
 +Karsch, F. 74706
 +Karsten, J.L. 78512
 Kartushinskii, A.I. + 76084
 +Karzunov, S.E. 77638
 +Kasahara, Y. 76503
 +Kasai, S. 75184
 +Kasemo, B. 74487
 Kasemset, D. + 77583
 Kashimura, S. + 75103
 +Kashiwagi, H. 75288
 +Kashiwagi, H. 75277
 Kashiwagura, N. + 77777
 Kashlev, Yu.A. 74415
 +Kasilov, V.I. 75220
 +Kaspar, F. 75315
 Kasperczuk, S. 78830
 Kastrhuri, K. + 76102
 Kastner, M. + 78584
 Kasuya, M. 78812
 Kas'yanenko, E.V. + 77409
 +Kasyanik, V.N. 74263
 +Kas'yanov, Yu.S. 75758
 +Kasyarum, O.P. 76707
 +Kasymov, A.Kh. 77494
 +Katahara, K.W. 78462
 +Katanov, L.M. 74455
 +Katayama, F.Y. 78858
 Katayama, S. 77380
 +Katcoff, S. 78816
 +Katila, T. 78395
 +Katila, T. 78284
 +Katila, T. 78188
 Katnani, A.D. + 77042
 Katnani, A.D. + 77023
 +Kato, K. 76932
 +Kato, N. 76234
 +Kato, R. 75169
 +Kato, S. 75003
 +Kato, T. 76597
 Katoh, C. + 78786
 +Katoh, C. 78631
 +Katoh, C. 78632
 +Katoh, C. 78747
 +Katoh, C. 79028
 Katoh, K. 75248
 +Katona, T. 75163
 +Katori, K. 75013
 Katriel, J. + 75253
 Katriel, J. + 74367
 Katsikas, H. + 78143
 Katsnel son, A.A. + 76762
 +Katsnel'son, M.I. 76873
 Katsulai, H. + 78322
 +Katsura, S. 77121
 Katsuta, H. + 76701
 Katsyuba, S.A. + 75363
 +Katz, W. 77347
 Kauder, L.R. + 76571
 +Kaufman, J.J. 75299
 +Kaufman, L. 78178
 Kaufman, S.A. + 74467
 Kaufman, Y.J. + 78649
 +Kaul, G.L. 75045
 +Kaul, R.K. 74596
 +Kaup, U. 74840
 +Kaup, U. 74906
 +Kaur, A.J. 76353
 +Kaur, A.J. 75360
 +Kaur, A.J. 75361
 +Kaur, G. 75045
 +Kaur, M. 75045
 +Kaur, N. 74774
 +Kavalayauskas, R.A. 78305
 +Kaveh, H. 78278
 Kavetskaya, I.V. + 77436
 Kawaguti, M. + 78222
 +Kawai, E. 78791
 +Kawai, H. 74637
 +Kawai, T. 77904
 Kawai, Y. + 77230
 +Kawaji, S. 77063
 +Kawakami, M. 77737
 +Kawakami, S. 74765
 +Kawamura, A. 78573
 Kawamura, T. + 76234
 +Kawamura, Y. 75602
 +Kawana, T. 76806
 Kawano, H. 77517
 +Kawano, H. 75687
 Kawasaki, K. 76725
 Kawashima, R. + 77408
 +Kawawa, S. 75764
 +Kayama, M. 77739
 +Kayano, H. 77723
 +Kayanuma, Y. 76879
 +Kayushkii, V.A. 76553
 +Kazak, I.A. 78331
 Kazanskii, A.G. + 76994
 +Kazanskii, V.B. 77389
 Kazantsev, A.P. 76792
 +Kazarian, E.M. 75728
 +Kazawa, Y. 75157
 Kazior, T.E. + 77060
 Kazmerski, L.L. + 78070
 +Kaznacheev, A.V. 76306
 +Kbala, M. 77011
 +Kbir Ariguib, N. 76590
 Ke Wu
 see Wu Ke
 +Keane, D. 75017
 +Kear, B.H. 76496
 Keating, G.M. + 78588
 Kechang Ju. *see* Ju Kechang
 Keck, K.-E. + 74487
 Keefe, D. 75181
 +Keefe, D. 75663
 Keefe, D.H. 75877
 Keel, W.C. 78996
 Keesee, R.G. + 75564
 +Keevallik, S.H. 78647
 Keguang Tang
 see Tang Keguang
 Kehchih Hwang
 see Hwang Kehchih
 Kehlenbeck, G. + 74918
 Keijser, Th.H.de
 see De Keijser, Th.H.
 Kelen, G.P.Van Der *see* Van Der Kelen
 +Keller, G.L. 75999
 Kellin Wang
 see Wang Kellin
 Kellogg, W.W. 78602
 Kelly, J.J. 74970
 Kelly, R. 76643
 Kelly, T.F. + 77660
 Kelly, T.F. + 77628
 Kemblovskii, Z. + 75976
 +Kemmerer, G. 77257
 +Kemmler-Sack, S. 77424
 Kemnitz, P. + 74903
 Kendall, D.J.W. + 78627
 Keng tong Chueng
 see Chueng Keng tong
 +Kennedy, J.K. 76883
 +Kennedy, L.A. 75993
 Kenney-Wallace, G.A. +
 75731
 +Kent, J.N. 78309
 +Keomley, G. 78116
 Kerchner, H.R. + 77118
 +Kerlin, T.W. 75088
 +Kern, R. 76929
 Kerner, B.S. + 76986
 +Kerr, G.A. 78935
 +Kerr, R.G. 76214
 +Kerrich, R. 78494
 +Kersey, A.D. 76140
 +Kershaw, R. 76379
 +Kershaw, R. 76947
 +Kerstian, F. 77471
 +Keshavamurthy, R.S.
 75052
 +Keshavamurthy, R.S.
 75054
 +Keski-Rahkonen, O. 75525
 +Keskinen, R. 78217
 +Kessel, A.R. 77124
 Kessler, F.R. + 78099
 Kestin, J. + 76148
 +Kestin, J. 76094
 +Ketoff, A. 77948
 Kettischau, A. + 77143
 Kewley-Port, D. + 78192
 Kezun Xu
 see Xu Kezun
 +Khabibullaev, P.K. 75646
 Khac An Dao *see* Dao Khac An
 +Khadiakar, S.B. 74865
 +Khakhali, S.Ya. 74549
 +Khal'chukov, F.F. 74823
 +Khalepp, B.P. 75363
 +Khalilov, S.N. 77001
 +Khalimovna, I.N. 75699
 +Khalilullina, N.Z. 75776
 Khan, A.A. + 77055
 +Khan, A.R. 75053
 +Khan, K.H. 77635
 Khan, W.I. + 77181
 Khanna, F.C. + 74910
 +Khanna, F.C. 74899
 Khanna, K.M. + 76721
 +Khanna, M.P. 74780
 +Khanna, M.P. 74737
 Kharadly, M. + 78636
 Khare, A. + 74700
 +Kharkova, A.M. 76361
 Kharkyanen, V.N. 75355
 +Kharkyanen, V.N. 76884
 Kharlamov, A.P. + 74264
 +Kharlamov, A.P. 74267
 Kharlamov, M.P. 74266
 Kharlamov, M.P. 74270
 Kharlamov, P.V. + 74256
 Kharlamova, E.I. + 74268
 +Kharlamova, T.Yu. 74482
 +Khasanov, A.M. 77160
 +Khatanova, N.A. 76762
 Khattak, C.P. + 77565
 +Kheidemane, G.M. 77607
 Khemthong, S. + 78041
 +Khemthong, S. 77965
 +Khil'manovich, L.A.
 75613
 Khin Maung Maung +
 74937

- +Khitrun, M.K. 75625
 +Khizhnyak, A.I. 75606
 +Khizhnyakov, V.V. 77435
 +Khlebtsevich, V.Yu. 78300
 +Khoplov, M.Yu. 79040
 Khodel, V.A. 75247
 +Khodinski, A.N. 75679
 +Kholdos, I.I. 76439
 +Kholdosov, E.F. 77268
 Khoi Nguyen The
 see Nguyen The Khoi
 Kholdokov, V.P. 77204
 +Khomich, A.V. 76875
 Khon, Yu.A. 76364
 +Khorozov, S.A. 75011
 Khoury, H.A. 77775
 Khrilovich, L.M. + 76657
 +Khurgin, J. 77426
 +Khuri-Yakub, B.T. 75883
 +Khusainov, E.K. 75011
 +Khusid, B.M. 76325
 +Khvostova, V.A. 77613
 Kiang Yuan-sun
 see Yuan-sun Kiang
 +Kibbler, A. 77593
 +Kida, H. 78006
 +Kidd, D.E. 76218
 Kido, G. + 76974
 +Kido, G. 77227
 Kido, M. + 77794
 +Kieber-Emmons, T. 78121
 Kiebas, A. 76000
 +Kielczewski, D. 75526
 +Kielich, S. 75757
 Kien Fam Le
 see Fam Le Kien
 +Kiesling, C. 74783
 +Kikas, Ya.V. 75364
 Kikineshi, A.A. + 75760
 +Kiko, J. 78816
 +Kikuchi, J. 77461
 Kikuchi, M. + 77619
 +Kikuta, K. 77153
 Killingbeck, J.P. 74235
 +Killingley, J.S. 78520
 +Killis, A. 76696
 +Killworth, P. 75120
 +Kilpatrick, S.J. 77780
 Kilroy, W.P. + 77985
 Kim, B.Y. + 75822
 +Kim, C.K. 76895
 Kim, D.-C. + 78462
 Kim, D.J. 77237
 Kim, E.M. + 75801
 +Kim, H.S. 78292
 Kim, J.Y. + 78685
 +Kim, K.M. 77554
 +Kim, W.S. 78292
 +Kimball-Linne, M.A. 77927
 +Kimura, H. 75185
 +Kimura, H. 76623
 Kimura, Y. + 77779
 Kin, C.C. + 74434
 +Kind, R. 77272
 +Kindl, D. 77028
 King, A.H. 76815
 +King, A.J. 77947
 +King, G.C.P. 78442
 +King, J.W. 78752
 +King, T. 76359
 +King, T. 76837
 Kingsley, S.A. 74530
 +Kingsley, S.A. 76141
 Kingston, H.M. + 75094
 +Kinmond, S. 77293
 +Kino, G.S. 75883
 +Kinoshita, J. 75632
 +Kinoshita, J. 77063
 +Kinoshita, S. 77433
 Kinzel, W. 76781
 +Kirby, C. 75444
 Kirchhoff, V.W.J.H. + 78727
 +Kirchmann, R. 75115
 +Kireeva, S.A. 74549
 +Kirillova, E.N. 78249
 +Kirkin, A.S. 75692
 Kirlin, R.L. + 78721
 Kirov, B. + 78672
 +Kirov, B.B. 78776
 +Kirschfeld, K. 78181
 +Kirsten, T. 78816
 +Kirvoruchko, V.N. 77166
 +Kir'yanchev, N.E. 77667
 +Kiselev, V.F. 76994
 +Kiselev, T.N. 77755
 +Kishi, K. 75441
 +Kishimoto, H. 76164
 Kishkin, S.T. + 77680
 Kisker, D.W. + 76809
 +Kisker, E. 77523
 +Kislov, V.V. 79041
 Kislukha, N.I. + 76855
 Kislyi, P.S. + 77606
 Kissling, E. + 78414
 Kitaev, F.I. + 77612
 +Kitaev, Yu.E. 76617
 +Kitaji, S. 75474
 +Kitamura, J. 76135
 Kitamura, M. + 78882
 Kitamura, T. 76572
 +Kitamura, T. 76293
 Kitching, P. + 74975
 Kitsunai, Y. 77740
 +Kittaka, T. 77242
 +Kiyak, B.R. 77452
 Kiyashko, V.A. + 75729
 +Kizhaev, S.A. 77319
 +Kjaergaard, P. 78913
 +Kjems, J.K. 76907
 +Klaasse, J.C.P. 77241
 Klaassen, K.B. + 74431
 +Klabunde, C.E. 77118
 +Klapisch, M. 75338
 +Klar, A. 74871
 +Klarsfeld, A. 74783
 Klascinc, L. + 75445
 Klascinc, L. + 75438
 +Klassen, N.V. 77351
 +Klavins, P. 77135
 +Kleiman, M. 78643
 Klein, B.J. + 78131
 Klein, D.J. 75304
 Klein, M.B. + 75748
 +Klein, M.L. 76606
 +Kleint, Ch. 77535
 +Kleint, Ch. 77536
 +Klekovkin, A.A. 77667
 +Klem, J. 77570
 Klemm, R.A. 77117
 Klemarski, V.G. + 77224
 Klepp, K. + 76380
 +Klepp, K. 76389
 +Kleusberg, A. 78655
 +Klevtsur, S.A. 77667
 +Kley, D. 78611
 +Klier, E. 77028
 Klima, M. 75786
 +Klima, S.J. 77858
 Klimas, A.J. 78771
 +Klimenko, A.G. 76666
 +Kliment, V. 78243
 Klinkhamer, F.R. 74584
 +Klobukowski, M. 75257
 +Klokova, N.P. 74454
 Klootwijk, C.T. + 78423
 Klos, A. + 77073
 +Klotsman, S.M. 76516
 +Klug, D.D. 77376
 Klyuev, V.V. + 78300
 Klyuev, V.V. + 74440
 +Klyukhin, V.I. 74771
 +Knapp, G.S. 76662
 +Knapp, H. 76679
 +Kneissl, U. 75519
 +Knight, D.G. 75373
 Knight, L.B. Jr. + 75412
 Knights, M. + 75677
 +Knights, M.G. 75682
 +Knippenberg, B. 77360
 +Knop, J.V. 75553
 +Knorr, K. 76907
 +Knott, K. 75147
 Knudsen, A.K. + 77878
 +Knudson, A.R. 76506
 Knuyt, F. + 75066
 +Knuyt, G. 76483
 +Knuyt, G. 76413
 +Knuyt, G. 77477
 +Knuyt, G. 76505
 Ko, C. + 76668
 +Ko, H. 78397
 Kobayashi, F. + 76816
 +Kobayashi, H. 75690
 Kobayashi, K. + 77045
 Kobayashi, K.L.I. + 77521
 Kobayashi, M. + 77375
 +Kobayashi, M. 78470
 Kobayashi, N. + 75472
 +Kobayashi, N. 75185
 +Kobayashi, S. 75222
 +Kobayashi, S. 74966
 +Kobayashi, S. 75003
 +Kobayashi, S. 74532
 +Kobayashi, T. 76934
 Kobayashi, Y. + 77559
 +Kobes, R. 74581
 +Kobilarov, N.L. 75383
 Kobling, L. + 75191
 +Kobaykov, I.B. 77332
 +Kocar, O. 76520
 +Koch, C.C. 77630
 +Koch, F. 77265
 Koch, V.R. 77976
 Kojan, D. + 75295
 +Kocis, E. 75158
 Kodama, M. 78767
 +Kodama, S. 77738
 +Kodama, T. 76743
 Kodama, Y. + 75815
 +Kodato, S. 76938
 +Koehler, J.A. 78678
 +Koehler, J.A. 78732
 +Koeleman, A.S.M. 78214
 +Koelling, D.D. 77525
 Koene, B. 74803
 Koepf, G.A. 75718
 Koezuka, H. + 77049
 Kogan, S.H. + 77014
 +Kohanty, U. 74381
 Kohl, K.-H. 75487
 +Kohler, E. 75558
 +Kohlmeier, B. 75030
 +Koike, Y. 75004
 Koima, M. + 76686
 +Koizumi, M. 77602
 +Koizumi, T. 75966
 +Koizumi, T. 78746
 +Koizumi, T. 76001
 Kojumdzieva, N.T. + 75150
 +Kokhanovskii, S.A. 75218
 +Kokin, A.A. 74524
 +Kokkas, K. 75005
 +Kokorin, V.V. 77639
 Kolb, W.A. 78343
 Kolchin, O.P. 77610
 +Kolesnikov, N.P. 78300
 +Kolesnikov, V.E. 75832
 +Koleva, R. 78668
 +Kolla, E.V. 77112
 Kolle, J.J. + 78534
 Kollias, S.D. + 78723
 +Kolodziejczyk, A. 77284
 +Kolomenskii, A.A. 76216
 +Kolotinskii, V.N. 76517
 +Kolpakov, A.V. 76244
 +Kolpakova, N.N. 77319
 +Kol'shev, N.D. 74478
 Kolyano, Yu.M. + 77803
 +Komarov, F.F. 76529
 Komarovs'ka, L.P. + 76362
 +Komatsu, H. 77560
 +Komatsu, H. 74686
 +Komatsu, S. 77648
 Komatsu, T. + 76136
 Komesker, H. + 74547
 Komhyr, W.D. + 78698
 Komitov, L. + 76298
 +Komyak, A.I. 77439
 +Konagai, M. 76938
 Konar, A. + 75405
 +Konarik, M. 75170
 Kondakova, N.V. + 78255
 +Kondo, K. 75538
 +Kondo, M. 78080
 +Kondo, Y. 77379
 +Kondrat'ev, A.S. 77148
 +Kondrat'ev, V.I. 75170
 Kondrat'ko, M.Ya. + 75063
 Kondratyev, K.Ya. + 78580
 Kondevskii, V.S. + 77771
 +Konijnenberg, J. 77902
 +Konings, A.W.T. 78159
 +Koningsstein, J.A. 77434
 Konno, M. 77220
 +Kono, S. 77406
 +Kononchev, Yu.V. 76418
 +Kononchuk, G.L. 75494
 +Kononenko, V.G. 76765
 +Kononov, V.A. 75679
 +Kononov, V.P. 77472
 +Konopliv, A.R. 78838
 +Konovalov, A.F. 77268
 Konovalova, E.S. + 76904
 +Konshina, E.A. 77566
 Konstantinov, O.V. + 77483
 Koo, K.P. + 74529
 Kopaev, A.V. + 77608
 +Kopeck, J. 78174
 Kopke, P. + 78658
 +Kopke, P. 78584
 +Koponen, M. 78349
 Kopp, E. + 78242
 +Kopp, V. 77570
 +Korablev, V.A. 75913
 Korczak, W. + 76335
 +Korduba, B.M. 77803
 +Korec, J. 77576
 Koren, G. 75459
 +Koren, U. 76719
 Korenman, V. 77235
 Korepin, V.E. 74323
 +Koreshev, V.I. 74771
 +Korneev, V.I. 75596
 Korneichuk, V.A. 77400
 +Korner, H. 77312
 +Kornienko, L.S. 75620
 +Kornienko, P.A. 77605
 +Korobkin, V.V. 75758
 +Korobov, V.I. 75981
 +Koroknay, P. 74488
 +Korolev, V.D. 76193
 +Korol'kov, M.V. 75630
 Koronovskii, N.V. 78542
 +Koros, W.J. 76702
 +Koroteev, N.I. 75396
 +Korpel, A. 75588
 Korsunskaya, N.E. + 77450
 +Kortela, U. 77958
 +Korth, A. 78737
 Korukonda, B. + 77729
 +Korving, J. 75495
 Koryagin, Yu.D. + 77703
 Korystov, Yu.N. 78248
 Korzhuev, M.A. 76845
 +Kosawada, T. 75949
 Kosevich, A.M. + 78165
 +Koskela, H. 78349
 +Koski, W.S. 75299
 +Kosonovskii, E.A. 74809
 Kosov, L.I. 74456
 +Kosov, L.I. 74454
 Kosovskii, D.I. + 77840
 Kosowsky, R. 77935
 +Kost', Ya.Ya. 77436
 +Kostadinov, Iv. 78676
 Koster, U. + 76316
 +Koster, U. 76321
 +Kosters, J.J. 78598
 +Kostiuk, T. 75370
 +Kostov, P.T. 78667
 +Kostov, P.T. 78680
 Kostov, A.M. + 77538
 Kostyshin, M.T. + 76707
 Kosvintsev, Yu.Yu. + 75217
 +Kota, V.K.B. 74872
 Kotaki, M. + 78632
 Kotaki, M. + 78631
 Kotaki, M. + 78747
 Kotaki, M. + 79028
 +Kotaki, M. 78710
 +Kotaki, M. 78786
 Kote, F. Van
 see Van Kote, F.
 Kotegawa, H. 75517
 Kothari, A. + 75449
 Kothekar, V. + 78132
 Kotomin, E. + 76888
 +Kotrappa, P. 75195
 +Kotthaus, R. 74783
 +Kotlyuk, A.F. 75703
 +Koudelka, L. 76419
 Koul, J. + 78951
 Kouris, K. + 78314
 +Kourtakis, K. 76947
 +Kovac, B. 75445
 +Kovachev, B.Z. 78959
 +Kovacic, P. 75391
 Kovacova, K. + 77673
 +Kovacs, F. 74783
 +Kovacs, W.D. 78540
 +Koval', Yu.N. 77639
 Kovalenko, A.P. 76574
 +Kovalenko, V.F. 76971
 +Kovalenko, V.V. 77773
 +Kovalev, V.P. 75984
 +Kovalyuk, Z.D. 76850
 +Kovarskii, A.P. 75107
 +Kovazhkin, R.A. 78778
 +Kovayzin, Yu.A. 74961
 Kowalewski, D.G. de
 see de Kowalewski, D.G.
 +Kowalewski, V.J. 75403
 +Kowalski, S. 74842
 Kox, S. + 75040
 Koyama, T. + 77116
 Kozak, A. de
 see de Kozak, A.
 Kozak, K. 78365
 +Kozich, V.P. 74541
 +Kozimirov, N.G. 74673
 Kozlov, G.I. + 76201
 Kozlov, L.P. + 75981
 +Kozlov, N.P. 76169
 +Kozlov, S.K. 75207
 +Kozlova, L.E. 77639
 Kraan, A.M. van der
 see van der Kraan, A.M.
 +Krabendam, H. 76343
 +Kraevs'ka, L.V. 76553
 Kragel'skii, I.V. + 76817
 Krainik, N.N. + 77405
 +Krall, N.A. 76197
 +Kramer, V.M. 77413
 Kramarenko, N.L. + 76303
 Kramchenko, O.A. + 76500
 Kramer, G.H. + 78405
 +Kramer, S.D. 78891
 Kramer, U. 76440
 +Krammer, P. 75889
 Kranz, J. + 77367
 Krasavin, A.Yu. + 75520
 +Krascheninnikov, I.S. 75160
 Krasil'shchikova, E.A. 75849
 Krasner, M.A. + 78195
 Krasnikov, N.V. + 74718
 +Krasnogolovets, V.V. 76699
 +Krasnova, G.F. 76457
 +Krasovskii, E.I. 75779
 +Kratky, S. 76404
 +Krause, M.O. 75446
 +Kravchenko, L.K. 75931
 +Kravchenko, T.B. 75451
 +Kravchuk, D.N. 74264
 +Krechner, S.I. 78704
 +Kreher, J. 77443
 +Kreissig, U. 76757
 Krell, M. + 75048
 Kremling, K. 78560
 +Kreps, I.B. 74475
 Kreshner, S.I. + 78705
 +Kreul, J.F. 78381
 +Krey, U. 77182
 +Krezhova, D. 78673
 +Krieger, E.P. 78596
 +Kriegsmann, G.A. 76114
 +Krikorian, J. 78103
 Krinchik, G.S. + 77370
 Krinsky, S. + 75654
 Krichan, J. + 75089
 Krichner, H. + 76404
 +Krichner, H. 76406
 +Krischan, S. 76186
 +Krishna Murthy, E. 75358
 Krishna Sastry, D.V. + 77076
 Krishnamurty, G. + 75399
 Krishnaswamy, M.R. + 74765
 +Krivaite, G. 77410
 +Krivaneck, O.L. 76798
 +Krivonozov, E.V. 77771
 +Krivoruchko, V.N. 77200
 +Krivshich, A.G. 76532
 Krizan, J.E. + 74401
 +Krokhin, O.N. 74576
 Kroll, N.M. + 75652
 +Kroll, S. 75349
 +Kromer, B. 78605
 +Kronberg, P.P. 79016
 +Kroon, J. 75540
 +Kroon, J.P.C. 75347
 +Kropotov, G.I. 77002
 +Kropp, W.R. 75226
 Krori, K.D. + 74329
 Krowne, C.M. 77057
 Krowne, C.M. 77058
 +Krushchin, S.P. 74771
 +Kruger, G.B. 75087
 Kruger, J. + 75091
 +Kruglikov, I.L. 78165
 Kruijzing, B. + 78236
 +Kruise, H. 74836
 +Kruise, U. 74783
 Krushinskaya, N.P. + 78254
 Krutikov, A.V. + 77451
 +Kruzelecky, R.V. 77072
 +Krylovich, V.I. 76566
 +Ksenofontov, V.G. 77314
 +Ksenofontova, N.M. 77391
 Ktonas, P.Y. 78376
 +Ku, H.H. 74427
 Ku Chung-liang
 see Chung-liang Ku
 Kuang Zhen-bang 75954
 +Kubach, C. 75477
 +Kubantsev, M.A. 74771
 +Kubo, J. 74613
 +Kubo, S. 77673
 +Kucha, V.V. 76875
 +Kuchar, F. 76992
 +Kuchar, F. 78057
 +Kuchenev, A.N. 75520
 +Kuchler, Ya.R. 76596
 +Kucherov, J. 77287
 +Kudin, L.G. 76532
 +Kudinov, V.M. 76066
 +Kudo, K. 77792
 +Kudrman, J. 77649
 +Kudryavtsev, A.A. 76707
 +Kudryavtsev, V.V. 78705
 Kuebart, W. + 76708
 +Kuffel, E. 76153
 +Kuhn, H. 78228
 +Kuhn, K. 75678
 +Kuhrt, E. 76534
 +Kuihs, W.F. 76257
 Kuiken, H.K. 76003
 Kuktarev, N. + 75734
 Kuktarev, N.V. 75750
 +Kukulich, S.G. 75410
 Kukuika, J. + 78026
 +Kulagin, V.K. 78690
 +Kulibekov, A.M. 77410
 +Kulikauskas, V.S. 77944
 +Kulinich, N.I. 77897
 +Kulyabina, O.A. 77725
 +Kulzer, H. 77508
 +Kumagawa, Y. 78100
 Kumar, B.V.K. Vijaya
 see Vijaya Kumar, B.V.K.
 +Kumar, D. 77372
 +Kumar, P. 77074
 Kumar, R. + 77498
 +Kumar, R. 77726
 Kumar, S. + 76297
 +Kumar, S. 75045
 Kumar, S. Raj
 see Raj Kumar, S.
 Kumar, V. + 77062
 +Kumar, V. 75045
 Kumari, S. + 78063
 +Kumekhov, M.H. 76530
 Kummer, W. 74720
 +Kumpulainen, J. 74839
 +Kumzerov, Yu.A. 77112
 +Kunde, V.G. 78852
 +Kundeleva, N.E. 75771
 +Kundig, W. 77315
 Kundu, K.K. 75896
 Kundu, M.R. + 78894

| | | | | | | | | | |
|-------------------------|-------|------------------------------|--------------------|---------------------|------------------|-------------------|-----------------|------------------------|-----------------|
| +Kundu, M.R. | 78886 | +Labarre, J.-F. | 75541 | +Lasswell, P.G. | 78085 | +Lehmann, G. | 77255 | Li Xinzhou+ | 74606 |
| Kundu, S. + | 75497 | Labonte, G. | 74604 | +Last, I. | 75615 | +Lehmann, H.P. | 78282 | Li Yenta | see Yenta Li |
| Kunevich, A.V. + | 77286 | +Labusch, R. | 77355 | +Laszlo, I. | 78651 | +Lehmann, H.P. | 78283 | Li Yucheng | 76055 |
| Kunii, Y. + | 77562 | Lach, J. + | 76016 | Latner, N. + | 75197 | +Lehmann, H.P. | 78285 | Li-xin Deng | see Deng Li-xin |
| +Kunio, T. | 77779 | Lacheisserie, E. du Tremolet | | +Latrofa, E. | 76020 | +Lehmeyer, A. | 77346 | Lian Jiansheng | 76548 |
| +Kunitomi, N. | 77642 | de | see du Tremolet de | +Lau, K.-S. | 76023 | +Lehmeyer, A. | 76858 | Liang Chen | see Chen Liang |
| +Kunsch, B. | 76284 | Lacheisserie, E. | | +Lau, K.Y. | 75696 | +Lelochky, S.L. | 77552 | Liangbiao He | |
| Kunz, H. + | 76846 | Lachlare, F. + | 78895 | +Laughlin, G.P. | 78656 | Lehrer, R. | 77934 | see He Liangbiao | |
| +Kunzel, H. | 77448 | Lacy, M. | 75328 | +Lauks, I. | 76802 | Lehtomaki, K. + | 77958 | Liansheng Li | |
| +Kuo, T.T.S. | 74863 | Ladha, G.S. | 76102 | Lau, H.M. | 75975 | Lei Hung | see Hung Lei | Liao Liu | see Liu Liao |
| +Kupainen, A. | 74390 | Ladin, Z. + | 78379 | Lauder, B.E. + | 75991 | Leib, Wei. | see Wei Lei | Liaw, P.K. + | 77822 |
| Kupka, J. | 74380 | Lagasse, P.E. | 75793 | Lauder, B.E. + | 76085 | Leibovich, S. | 78556 | +Liberman, A.A. | 74467 |
| +Kuppenheimer, J. | 75677 | +Lagerwall, S.T. | 77362 | Launois, H. + | 76646 | Leibovich, V.S. + | 77543 | +Liberman, A.B. | 77160 |
| +Kuppler, D. | 77201 | +Lago, B. | 78491 | +Laurence, R.L. | 76114 | +Leichter, P. | 75147 | Liberman, I. + | 75623 |
| +Kuranov, A.A. | 77150 | Lagowski, J. + | 76889 | +Laurent, Y. | 76397 | Leifer, M. + | 78203 | Libove, C. | 75941 |
| Kurashige, M. | 75940 | +Lagowski, J. | 77060 | +Laurent, Y. | 76396 | +Leigh, J.R. | 75032 | Licci, F. + | 76800 |
| +Kurbatov, A.D. | 77398 | +Lagunsov, N.I. | 75533 | Laurenzi, B.J. + | 75542 | +Leino, M.E. | 74906 | Liacciardello, A. + | 77784 |
| Kurdyumov, A.V. + | 76616 | +Lahana, R. | 75541 | Laurmann, J.A. + | 78604 | +Leissa, A.W. | 75951 | +Lichtenberg, A.J. | 76111 |
| +Kurdyumov, S.P. | 76032 | +Lahlou, F. | 75010 | +Laursen, C.L. | 75920 | +Leiteris, R. | 77814 | +Liddament, M.W. | 78505 |
| Kurdyumov, V.G. | 76431 | +Lahteenmaki, I.T. | 77632 | +Lavagne, Y. | 74783 | Leiva, H. + | 76379 | +Liebau, F. | 76394 |
| Kurihara, R. + | 75169 | Lahtinen, J. + | 75525 | +Laval, G. | 76192 | +Leiva, H. | 76947 | Lieberman, A.G. | 75583 |
| Kurik, M.V. + | 75761 | +Lai, A. | 77269 | +Lavery, R. | 75465 | +Lejus, A.M. | 76556 | +Lieberman, M.A. | 78055 |
| +Kuriki, I. | 78786 | Lai, S.K. | 77016 | +Lavin, M.F. | 78229 | Lemaire, J. + | 78757 | Lieberman, M.A. | 76157 |
| +Kuriki, I. | 78631 | Laidig, W.D. + | 75268 | +Lavine, R. | 74416 | +Lembrikov, B.I. | 76305 | +Lieberman, J.F. | 75266 |
| +Kuriki, I. | 78747 | Laine, E.S.U. + | 77632 | +Lavorn, M. | 77006 | Leme, D.Glasser | see Glasser | Liebowitz, D. + | 74830 |
| +Kurita, S. | 78003 | +Lakkad, S.C. | 77733 | +Lavorgna, M. | 74341 | Leme, D. | | +Lichtenstein, A.I. | 77173 |
| +Kurita, S. | 77584 | +Lakshman, S.V.K. | 76905 | Lavrenko, V.A. + | 77782 | Lemin Li | see Li Leming | +Lierl, H. | 74783 |
| Kurki, J.A. | 75796 | Lakshman Pandey + | 75404 | Lavrova, G.A. + | 78245 | Lemke, H. | 76886 | +Liesegang, G.W. | 74445 |
| Kurochkin, V.D. | 76226 | +Lakshmi | 76375 | +Lawn, B.R. | 76555 | +Lemkey, F.D. | 77599 | +Lietoila, A. | 77000 |
| +Kurokawa, Y. | 76690 | +Lakshminarayana, G. | | Lawson, R.D. | 74845 | Lenel, U.R. | 77634 | Lifante, G. + | 77963 |
| +Kuroyanagi, A. | 78003 | | 75399 | +Lazareva, V.T. | 77361 | +Lenoble, J. | 78640 | Likhachev, V.A. + | 77702 |
| +Kurozaev, V.P. | 78300 | +Lakshminarayan, K.N. | | +Lazzari, M. | 77970 | +Lenoble, J. | 78645 | +Likhachev, V.A. | 76605 |
| +Kurozaev, V.P. | 78331 | | 77325 | Lazzizzera, I. + | 74556 | +Lent, A. | 78314 | +Likhomanov, S.A. | 78820 |
| Kurtas, E. | 78364 | Lal, S. + | 78592 | +Le Comber, P.G. | 77022 | +Lentes, F.T. | 78954 | +Lim, E.C. | 75432 |
| Kurten, K.E. + | 76729 | +Lal Sharma, M. | 78423 | +Le Dang, K. | 77285 | Leon, J.P.P. + | 74621 | +Lim, H. | 76878 |
| Kurth, W.S. + | 78851 | Li Sohan | see Sohan Li | +Le Diberder, F. | 74783 | +Leoni, R. | 78204 | +Limanova, V.F. | 74549 |
| +Kurth, W.S. | 78850 | +Lalita Sarkar, K. | 75404 | Le Duff, J. | 75665 | Leonov, A.I. + | 76077 | Lin, A.Z. + | 78025 |
| +Kus, A. | 78815 | +Lalowitz, Z. | 77284 | +Le Goscoz, V. | 77064 | +Leonov, B.I. | 74575 | +Lin, J.F. | 76489 |
| Kusabiraki, K. + | 77622 | +Lam, N.Q. | 76508 | Le Guillois, J.C. + | 75251 | +Leonov, B.I. | 78362 | +Lin, S.H. | 75460 |
| Kusalik, P.N. + | 76587 | +Lam, S.T. | 75879 | +Le Hoang Mai. | 76703 | Leonov, M.Ya. + | 75935 | +Lin, T.-H. | 77503 |
| +Kushch, V.I. | 75898 | Lamba, O.P. + | 77381 | Le Kien Fam | | +Leonov, S.N. | 75628 | +Lin, T.-H. | 77919 |
| Kushel, M.I. + | 77773 | Lambarski, T.J. + | 77964 | see Fam Le Kien | | +Leonov, V.A. | 76084 | Lin Chin-lon | see Chinlon Lin |
| Kushibiki, J. + | 75850 | Lambarski, T.J. + | 78039 | Le Mehaute, A. + | 77894 | Leont'eva, G.A. + | 78253 | Lin Yan-tian | 75929 |
| Kushibiki, J. + | 76764 | Lambert, A.J.D. | 76158 | +Le Nest, J.F. | 76696 | +Leontovich, A.M. | 75692 | +Lin-gun Liu | 78538 |
| Kushida, T. + | 77433 | Lambert, B. + | 77447 | +Le Page, A. | 78477 | Lepage, P. | 74669 | +Linaya, C. | 77887 |
| +Kushnir, O.B. | 77004 | Lambert, C.J. + | 76917 | +Le Roy, R.J. | 75467 | +Lepoutre, F. | 76675 | Lincot, D. + | 78008 |
| +Kushnir, V.P. | 77321 | Lambert, D.L. + | 78867 | +Le Rot, M. | 78502 | Lepp, S. + | 78971 | +Lind, R.C. | 75740 |
| Kusno, D. + | 74869 | +Lambert, G. | 78606 | Le-min Li | see Li Le-min | +L'Erede, A. | 77829 | Lindal, G.F. + | 78860 |
| +Kuster, H. | 74783 | +Lambert, W.A. | 76550 | Lean, J.L. | 78620 | +Lerner, J. | 78603 | +Lindau, I. | 75221 |
| Kusuda, T. + | 78570 | +Lambri, L. | 78053 | +Leandre, J. | 75842 | +Lesina, M.Yu. | 74256 | +Lindau, I. | 76790 |
| +Kuten, S.A. | 76915 | Laumontagne, R.L. + | 78919 | Learned, J.G. | 74243 | +Lesinski, J. | 77968 | +Lindberg, W.R. | 76087 |
| Kuti, J. | 74703 | Lamouroux, B.F. + | 74516 | +Learned, J.G. | 75226 | +Leslie, S.G. | 75623 | Linden, D.Vander | |
| +Kutiev, I. | 78672 | Lampe, F.Von | | +Leary, P.A. | 77774 | +Lesnick, M. | 75835 | see Vander Linden, D. | |
| +Kutiev, I. | 78669 | see Von Lampe, F. | | Leavitt, R.P. + | 75647 | Lesser, M.B. + | 76070 | Linden, J.van der | |
| +Kutiev, I.S. | 78667 | +Lancelot, J.P. | 74464 | +Lebacqz, J. | 75872 | +Lesser, P.M.S. | 74835 | see van der Linden, J. | |
| Kutik, E.J. + | 78197 | Landau, A.I. | 76428 | Lebedev, N.A. + | 75838 | +Lessoff, H. | 77561 | Lindenbaum, S.J. | 74695 |
| +Kut'kin, A.B. | 77842 | Landau, R. + | 79019 | Lebedev, V.A. + | 76412 | +Lestienne, F. | 78218 | Lindenbaum, S.J. | 74714 |
| Kutnyakova, N.I. | 75772 | Landau, R.H. | 74867 | Lebedev, V.A. + | 76346 | +Letardi, T. | 75670 | Lindenbaum, S.J. | 74796 |
| Kutsenko, N.I. + | 75769 | Landau, R.H. | 75555 | +Lebedev, Ya.S. | 74506 | +Letchev, V.S. | 77340 | Lindenberg, K. + | 74381 |
| Kuwada, M. + | 77109 | +Landau, R.H. | 74969 | +Lebedeva, L.N. | 77700 | Letelier, P.V. | 74342 | +Linderberg, J. | 75255 |
| +Kuwahara, K. | 76067 | +Lande, K. | 78816 | +Leblanc, M. | 76395 | +Leung, D. | 77592 | Lindholm, F.A. + | 78074 |
| +Kuwaya, Y. | 76034 | +Landis, G.A. | 77967 | +Leblond, J.B. | 75420 | +Leung, P. | 76250 | +Lindstrom, R. | 76698 |
| +Kuzel, R. | 76579 | +Landrum, J.H. | 74905 | +Leblud, C. | 77539 | Leung, W.P. + | 77689 | Lindstrom, R.-L. + | 76698 |
| +Kuzemskii, A.L. | 77087 | Landsberg, P.T. | 74419 | Lebovitz, R.M. + | 78230 | +Leutwyler, H. | 74708 | Lines, M.E. + | 77309 |
| Kuzin, A.M. + | 78246 | Landsberg, P.T. + | 78050 | +Lecaille, A. | 78434 | +Leutwyler, H. | 74721 | +Ling, H.C. | 77654 |
| Kuzmichev, V.E. | 74942 | Landtsheer, A.C.de | | +Lecar, M. | 78998 | Lev, F.M. | 74302 | +Ling, T.Y. | 74759 |
| +Kuzmin, A. | 78676 | see de Landtsheer, A.C. | | +Lecompte, J.P. | 77781 | Levai, F. | 75104 | +Ling-Rong-fu. | 74559 |
| +Kuz'min, A.E. | 76350 | Landuyt, J.van | | Ledbetter, H.M. | 77247 | Levasseur, A. + | 77011 | +Ling-hui. | 74470 |
| +Kuz'min, E.A. | 76346 | see van Landuyt, J. | | +Ledbetter, M.T. | 78516 | Levelut, A. | 75851 | Ling-Lie Chau | 74646 |
| +Kuz'min, E.A. | 76412 | +Lanford, W.A. | 77917 | Lee, C.Y.-C. + | 77830 | Levi, A. + | 75240 | Ling-Lie Chau | 74820 |
| +Kuz'min, E.V. | 77197 | Lang, A.R. | 76458 | Lee, D.M. | 76733 | +Levi, S. | 78539 | +Lingenfelter, R.E. | 78811 |
| +Kuz'min, R.N. | 76541 | +Lang, R. | 78575 | Lee, E.H. + | 77630 | +Levin, E.M. | 76903 | Lingzhi Ma | see Ma Lingzhi |
| +Kuzmin, A. | 74673 | Langacker, P. | 74666 | +Lee, H.S. | 78323 | Levin, E.V. + | 75533 | +Linke, N.T. | 77006 |
| Kuz'min, V.L. | 76267 | Langdon, T.G. + | 77718 | Lee, H.Van Der | | +Levin, I. | 78605 | +Link, R.A. | 75635 |
| +Kuznetsov, A.I. | 77003 | Langdon, T.G. + | 77719 | see Van Der Lee, H. | | +Levin, T.A. | 78166 | +Linkens, D.A. | 78169 |
| Kuznetsov, A.M. + | 77865 | Langdon, T.G. + | 77716 | +Lee, I.-Y. | 75026 | +Levine, J.D. | 78090 | Linkevich, A.D. + | 74772 |
| +Kuznetsov, V.A. | 76201 | Lange, M.A. + | 78833 | Lee, J.K. + | 75951 | Levine, J.S. + | 78628 | +Lintern, A.L. | 74797 |
| +Kuznetsov, V.I. | 75162 | +Lange, W. | 75717 | +Lee, J.K.P. | 74911 | Levine, M.D. + | 78158 | +Lipin, V.D. | 74809 |
| Kuznetsov, Yu.A. + | 75079 | Langevin, M. + | 74915 | +Lee, K.T. | 77486 | +Levine, R.D. | 75359 | Lipinski, S. + | 77165 |
| +Kuznetsova, E.S. | 75011 | +Langhammer, H.T. | 76936 | Lee, M.C. + | 76494 | +Levine, R.D. | 75463 | Lipkin, H.J. | 74694 |
| +Kuznetsova, V.V. | 77438 | +Langlet, G. | 77275 | +Lee, S.H. | 75762 | Levinson, M. | 77054 | Lipkin, H.J. | 74740 |
| Kuznetsov, A.N. | 78429 | Lanham, T.E. | 74458 | Lee, S.L. | 76130 | Levinson, M. + | 76882 | Lipkin, H.J. | 74764 |
| +Kuzubova, L.F. | 76412 | Lanham, T.E. | 75880 | Lee, S.M. + | 75023 | +Levit, V.I. | 77668 | +Lipovchenko, A.N. | 76857 |
| Kvach, V.V. + | 74541 | Lanham, T.E. | 75881 | +Lee, S.M. | 75024 | Levitin, R.Z. + | 77228 | +Lippmaa, E. | 77274 |
| +Kveder, V.V. | 76439 | +Lansiaart, A. | 78327 | +Lee, S.M. | 75025 | +Levshin, L.V. | 75631 | Lipscomb, G.F. + | 75819 |
| Kvitsinskii, A.A. | 74922 | +Lantratos, V.M. | 78005 | +Lee, S.W. | 78292 | +Levy, B. | 77908 | Lisetskii, L.N. | 76304 |
| Kwiatkowski, K. + | 75064 | Lapeyre, G.J. + | 77533 | Lee Chun Bac | see Chun Bac Lee | +Levy, P.M. | 77175 | +Lisetskii, L.N. | 76303 |
| Kwiatkowski, K. + | 74988 | +Lapin, N.I. | 75220 | Lee | | +Lewenstein, M. | 74407 | +Lisgarten, N.D. | 76358 |
| +Kwiatkowski, K. | 74977 | +Lapin, O.G. | 76687 | Lee Jingde | 74392 | Lewerenz, M. + | 75312 | +Lisienko, V.G. | 75899 |
| +Kwiter, K.B. | 78986 | +Laplanché, F. | 74783 | Lee Kyo Rak | | Lewicki, A. | 77284 | Lissaman, P.B.S. | 76061 |
| +Kwok, S. | 78970 | +Lappert, M.F. | 75510 | see Kyo Rak Lee | | +Lewis, B.G. | 76496 | +Lissauer, J.J. | 78847 |
| Kychakoff, G. + | 77927 | +Lapshov, O.B. | 75207 | Leeb, W.R. | 75777 | Lewis, B.R. | 75872 | +Lisy, V. | 74386 |
| +Kyo Rak Lee | 78273 | +Lapunova, R.V. | 76360 | +Leeman, W.P. | 78493 | +Lewitt, R.M. | 78314 | Litai Ma | see Ma Litai |
| +Kyoh, B. | 76635 | Larese, J.Z. + | 76787 | +Leep, E.M. | 78915 | +Lexow, J. | 76394 | +Litovitz, T.A. | 75821 |
| | | +Larikov, L.N. | 76493 | +Lefeuve, F. | 78670 | +Lezhnenko, I.V. | 77111 | Litovskii, R.N. | 76979 |
| | | +Larivain, J.P. | 75757 | +Lefevre, H.C. | 75825 | Lezhu Zhou | see Zhou Lezhu | +Litovskii, R.N. | 77066 |
| | | Larizza, P. + | 78275 | +Lefevre, H.C. | 75822 | +Li, C. | 76891 | +Litster, J.D. | 76297 |
| | | Larsen, A.Nylandsted | | +Lefrant, S. | 77887 | Li, J.C.M. | 76551 | +Little, J.A. | 76818 |
| | | see Nylandsted Larsen, A. | | +Legg, K.O. | 77750 | Li Ding-kun | | +Little, T.S. | 75394 |
| | | +Larson, N.M. | 74990 | +Legostaev, Yu.L. | 77638 | Li Dongsheng + | 77214 | +Little, W.A. | 75970 |
| | | +Larson, T.H. | 75141 | +Legrand, J. | 78327 | Li Genpei + | 76386 | +Littlejohn, M.A. | 76959 |
| | | +Larsson, M. | 75457 | +Legvold, S. | 77135 | +Li Hui-rong | 77813 | Littmark, U. + | 77505 |
| | | +Lartigue, S. | 77633 | +Leheny, R.F. | 76973 | Li Jun-Qing | 75062 | +Litto, C. | 75542 |
| | | +LaRue, R. | 78079 | +Lehman, D.R. | 74895 | +Li Le-min + | 75296 | +Litton, J. | 78295 |
| | | LaRuc, R.A. + | 78035 | +Lehmann, E. | 75097 | +Li Lemin | 78134 | +Litvin, S.E. | 76922 |
| | | +Lashmore-Davies, C.N. | | +Lehmann, E. | 75226 | +Li Liansheng | 76890 | Litvinov, A.M. | 74485 |
| | | | 76198 | +Lehmann, E. | 75098 | Li Ming De | see Ming De Li | +Litvinov, A.M. | 74486 |
| | | Laskowski, B.C. + | 75279 | +Lehmann, E. | 75096 | Li Sheng S. | see Sheng S. Li | +Litvinov, A.M. | 74486 |
| La Mantia, F.P. + | 77324 | | | | | | | | |
| +La Mantia, F.P. | 75977 | | | | | | | | |
| La Selva, S.M.T.de | | | | | | | | | |
| see de la Selva, S.M.T. | | | | | | | | | |
| La Tour du Pin, H.de | | | | | | | | | |
| La Tour du Pin, H. | | | | | | | | | |
| +Laaksonen, L. | 76842 | | | | | | | | |

- +Litvinov, O.A. 75511
+Litvinov, V.P. 75405
Liu, C.S.+ 77541
+Liu, C.T. 77630
Liu, H.C.+ 76504
+Liu, H.C. 74742
Liu, H.-P.+ 78533
+Liu, J.Q. 74287
Liu, S.C.+ 78611
Liu Bao-Ping+ 74285
Liu Chi-chia+ 74447
Liu Ciquan 76099
Liu Hsi-Chuan
 see Hsi-Chuan Liu
+Liu Huifang 75390
Liu Jian-min+ 74417
Liu Liao+ 74337
Liu Lin-gun, see Lin-gun Liu
Liu Ruo-Zhuang+ 75300
+Liu Senyuan 78576
Liu Shang-Bin
 see Shang-Bin Liu
Liu Xi-li 75916
Liu Yinian+ 76037
+Liu Yuan 74985
Liu Zhiyi+ 77081
+Liukenon, R.A. 75628
+Lively, W.M. 78224
Livingston, H.D.+ 78561
+Livingston, H.D. 75118
+Livingston, J.D. 77222
+Llavona, J.G. 74254
Llewellyn Smith, C.H. 74684
+Lloyd, D.C. 78262
+Lo, H.W. 76494
+Lobashev, V.M. 75218
Lobato, L.M.+ 78494
+Locatelli, M. 76459
+Locatelli, M. 74496
+Locher, J.W. 77556
Lochmann, R.+ 75292
Lockman, F.J.+ 78966
+Lockwood, J. 78233
+Lockwood, J. 78232
Lockwood, M. 78734
Lodge, A.S.+ 75974
+Loe, R.S. 74569
+Loew, G.H. 77771
+Loewenhaupt, M. 76907
Loferski, J.J. 78075
Loferski, J.J.+ 78103
Logan, J. 78298
+Logan, J.A. 76278
+Logan, R.A. 75635
+Logozinskaya, E.S. 77444
+Logsdon, W.A. 77822
+Logvinovich, P.N. 76566
+Loh, E. 78817
Loh Rong+ 75765
Lohmann, A.W.+ 75577
+Lohmann, A.W. 74522
+Lokanathan, S. 75045
+Lokanathan, S. 77307
Lokhande, C.D.+ 78089
+Lokshin, M.M. 77066
Lomakin, V.V.+ 76449
Lombardi, S.+ 77870
+Lombardo, U. 74949
Lomon, E.L. 74850
+London, G. 74783
London, J. 78591
+London, J. 78599
+Long, J.F. 78391
+Long, J.P. 77263
+Long, S.A. 78299
Long Wu+ 77138
Long Wu+ 77330
Long Wu+ 76944
+Long Yongxing. 76177
Longa, L.+ 76301
+Longueue, N. 75040
+Longmore, A.J. 78982
+Longo, M.J. 74759
Lonnroth, T.+ 74839
+Loo, R.Y. 78032
+Lopatini, S.S. 77604
Loper, D.E.+ 78492
Lopez, C. 78925
+Lopez, M.V. 75395
+Lopez Romero, S. 78062
+Lorenz, B. 76847
Lorenz, W.+ 76778
Lorenzen, C.-J.+ 75333
+Loretto, M. 74756
+Loretto, M.H. 76509
+Loretto, M.H. 76510
+Lorgeron, J.-M. 78325
+LoSecco, J.M. 75226
Lostak, P.+ 76419
+Lott, D.R. 78021
Lottici, P.P.+ 77397
+Louis, B. 78841
Louise, R. 78980
Louthan, M.R., Jr. 77749
+Lovas, F.J. 78967
Love, W.G.+ 74853
+Love, W.G. 74973
+Lovelace, R.V. 76213
+Loveland, W. 74952
+Loveless, R.J. 74759
Lovey, F.C.+ 76758
Low, T.S.+ 76475
+Low, T.S. 76883
+Lowde, R.D. 77643
+Loyola, P. 78796
+Loza, I.A. 77328
+Lozovoi, V.I. 76681
+Lu, J.J. 75017
Lu Banghong
 see Banghong Lu
+Lu Fengzheng. 76890
Lu Jifeng+ 74985
Lu Tan+ 78806
Lu Wen-Rong
 see Wen-Rong Lu
Lu Yu
 see Yu Lu
+Lub, J. 79024
+Lubala, R.T. 78499
+Luborsky, F.E. 77222
+Luca, E. 77210
+Lucas, A.A. 76753
+Lucas, K. 76266
Lucas, P.G.J.+ 76040
+Lucchesi, M. 75910
+Luccio, A. 75654
+Lucht, R.A. 76200
+Ludden, J. 78480
Ludeking, L.D.+ 74991
+Ludlam, T. 75249
+Ludwiese, M.J. 78035
+Ludwiese, M.J. 76893
+Ludwigson, D.C. 77818
+Luers, D. 74783
+Luger, P. 75297
+Luginbuhl, H.W. 75841
+Lugmair, G.W. 78513
+Lugmair, G.W. 78881
Lugovoi, V.N. 75697
Lugovoi, V.N.+ 75614
Lugt, H.J. 76047
Lugt, W.van der. see van der
 Lugt, W.
 +Lukac, P. 77712
 +Lukacs, B. 75020
 Lukasiak, A.+ 74879
 Lukasiak, A.+ 74929
 Lukasiak, A.+ 74930
 Lukasiewicz, S.+ 75943
 Lukaszewski, M.+ 75350
 +Luke, T.M. 75314
 +Lukin, E.S. 77603
 +Lukin, K.A. 75675
 +Lukin, S.N. 76912
 +Lukina, M.M. 77159
Lukk, A.A.+ 78505
+Lukstyn'sh, Yu. 75011
+Lumley, J.L. (ed.) 74234
Lumme, K.+ 78846
+Lumme, K. 78840
Lund, T. 78408
+Lundholm, M. 77943
+Lundstrom, T. 76904
Lundstrom, I.+ 78152
+Lundström, M.S. 78040
+Lunter, S.G. 77251
+Luo, L.F. 74742
+Luo Daling. 75246
+Luo Xing-hua. 74559
+Lupashko, E.A. 75775
+Lupinski, M.M. 74455
+Luque, A. 78062
+Luque, A. 77962
+Luria, M. 78623
+Luscher, E. 76921
Luscher, S.B. 78392
+Lushchik, T.I. 75769
Lust, D. 74683
+Luth, H. 77015
+Luther, F.M. 78617
+Lutpallaev, S.L. 74809
Lutts, A. 76259
+Luttwak, G. 77706
+Lutz, G.J. 75094
+Luzanova, O.V. 78249
+Luznik, J. 78398
+Luzzi, G. 77013
L'vov, G.I. 75967
+Lyakhov, G.A. 75853
Lykov, A.N. 77110
+Lyman, J. 78213
+Lynch, W.G. 75035
+Lynen, U. 75034
Lynn, J.E. 75060
Lyon, S.A.+ 76489
+Lyons, B.E. 78277
Lysak, L.I.+ 76366
Lysenko, V.S.+ 77066
+Lyskov, V.A. 77370
+Lyskovich, A.B.+ 77004
+Lyskovich, A.B. 78689
+Lyubliner, I.P. 76566
Lyul'ka, V.A. 74768
Lyzenka, G.A.+ 78536
Ma Hui-chang Yen+ 74453
+Ma Lingzhi. 77578
+Ma Litai. 76242
Ma Ning-Yuan Richard
 see Ning-Yuan Richard Ma
Ma Shang-keng
 see Shang-keng Ma
Ma Tengcai+ 76177
+Ma Yuanle. 76063
Ma Zhongqi. 74599
Maaref, S.+ 76392
Maass, W.+ 77182
McAdams, R.+ 74533
McAdoo, J.H.+ 75680
+McCaffery, A.J. 76142
+McCall, J. 76651
+McCall, S.L. 75714
+McCarroll, R. 75501
+McCarthy, D.K. 78023
McCarthy, J.C.+ 75682
+McCausland, M.A.H. 77302
Macchiato, M.+ 78137
+McClain, B. 77189
McClelland, B.W.+ 75512
McClure, R.D. 78917
+McConville, C.F. 76789
McCorkle, R.A. 75573
McCormick, J.R.+ 77582
McCormick, M.P. 78646
+McCormick, M.P. 78662
+McCray, J.G. 75142
+McCray, R. 79025
+McCray, R. 78971
+McCrosky, R. 78693
+McCrosky, R.E. 78876
+McCrosky, R.E. 78871
+McCubbin, J. 78394
McCubbin, P.A. 74802
McCulloch, N.M.+ 78936
McCurdy, C.W.+ 75529
+McDiarmid, D.R. 78678
+McDiarmid, D.R. 78732
+Macdonald, B.G. 74542
+Macdonald, C.J. 77236
McDonald, M.M.+ 77818
Macdonald, R.I.+ 75834
+McDonald, W.J. 74975
+Macdougall, J.D. 78513
+McDowell, J.H. 78126
+Mace, P.N. 74574
+Macedo, P.B. 75821
+McElhany, J.H. 78227
McEwen, D.J.+ 78593
Macey, D.J.+ 78326
+McFarland, M. 78611
+McFarlane, A.J. 74611
+McFarlane, R.M. 77291
+McFee, J.H. 75636
+McGaughy, P.L. 74952
+McGee, V.E. 78694
+McGervey, J.D. 77476
+McGillivray, H.T. 79024
McGinnity, T.M.+ 77363
+McGonigal, G.C. 78072
McGonnagle, W.J. (ed.) 74231
+McGowan, J.W. 78407
+McGowan, J.W. 77481
McGurn, A.R. 74402
+Mach, R. 74958
McHarris, W.C.+ 74932
+McHedlidze, L.D. 74478
Machin, E.S.+ 76355
+McIntosh, C.B.G. 74331
Macip, M.Antonietti
 see Antonietti Macip, M.
+McIver, J.K. 75669
Mack, M.+ 78198
McKee, W.R.+ 78090
+McKellar, A.R.W. 75413
+Mackenzie, A.B. 78500
+McKenzie, D.R. 78092
+Mackenzie, J.D. 77378
+Mackey, D.J.M. 78092
McKibbin, R.+ 76009
+Mackiewicz, M. 78695
+Mackor, A. 77900
McLachlan, D.S. 74499
+McLellan, R.B. 76668
MacIn, E.+ 78178
+McMahan, M.A. 75035
+McMahon, D.H. 75828
McMahon, D.R.A. 74409
+McMurdie, H.F. 76407
+McNally, K. 78456
+McNally, P.J. 76477
McNamara, A.G.+ 78678
+McNamara, A.G. 78732
McNeil, J.A.+ 74996
McNulty, G.J.+ 75864
+McNulty, R.J. 75863
McPhedran, G.C.+ 78092
+McVinnie, W.W. 77709
McVoy, K.W.+ 74957
+Madar, R. 76392
Madariaga, R. 78441
+Madtov, R.S. 77038
+Madden, M. 74995
Madden, P.A.+ 77392
Madden, T.R. 78528
Madey, J.M.J. 75661
+Madey, J.M.J. 75672
+Madey, J.M.J. 75650
Madhusudan Singh+ 76578
+Madix, R.J. 75440
Madsen, P.A.+ 75989
Maeda, H. 77219
Maeda, K. 78738
+Maeda, R. 78746
Maeda, Y.+ 77557
+Maekawa, S. 77116
+Maeno, M. 75184
+Maenpaa, M. 77071
+Maeta, H. 77242
Maewal, A. 75921
Maffei, J.+ 78268
+Maffeo, B. 76844
+Magee, C.W. 77780
+Magerl, G. 75147
Magerlein, J.H. 77051
+Magerlein, J.H. 77050
+Maggiore, G.M. 75306
+Magain, R.L. 78238
Magistris, A.+ 76694
+Magnus, W. 74369
+Magnusson, C.E. 75339
Maguire, C.F.+ 75026
+Mahanti, R.K. 77726
+Maharana, J. 74665
Mahaux, C. 74884
+Mahaux, C. 74990
Maheshwar, K.P.+ 76985
+Mahler, H.-J. 75230
+Mahmoud, S.S. 77923
+Mahne, G. 75866
Mahoney, J.J.+ 78513
+Mahoney, M.J. 78813
Mai Le Hoang
 see Le Hoang Mai
+Maier, H. 77265
+Maier, H.E. 76404
+Maier, M. 76479
+Maier, W.B., II. 77377
+Mailard, D. 78378
Maille, H.D. 78264
+Main, C. 76957
+Main, C. 76998
+Maiorov, V.P. 75068
+Mairty, C. 76415
+Maiti, M.M. 76324
+Maiti, S. 76324
Maiti, S.R. 74330
+Majumdar, C.K. 74403
Makara, V.A.+ 76450
+Makarenko, I.N. 76581
+Makarov, M.M. 74983
+Makh, V. 75170
Makhan'kov, V.G.+ 74325
+Makhlin, A.R. 74389
+Makhlyueva, I.V. 74771
+Makino, S. 78330
+Makino, T. 78590
+Makovetskii, D.N. 77259
+Makov'skii, M.M. 76751
Makra, S. 78339
Maksic, Z.B.+ 75320
+Maksimov, S.K. 76429
+Maksimova, G.M. 77008
Maksimov, M.D.+ 77588
Makumbi, S. 74442
Malakhov, Yu.I.+ 75551
+Malaman, B. 76377
Malamad, A.S.+ 78690
+Malan, O.G. 78582
Malashkevich, G.E.+ 77438
+Malashonok, V.A. 77940
+Malautent, J.-C. 76264
+Maldutis, E.K. 77349
Maley, P.D. 78842
Mal'gin, A.S.+ 74823
+Malgrange, C. 76240
+Malhaire, J.-M. 76397
+Malhotra, P.K. 74794
+Malhotra, P.K. 74814
Malikov, Yu.K.+ 75899
+Malin, D.F. 79024
+Malinkina, T.I. 77756
+Malink, B.Z. 77423
+Maliko, J. 74771
Mallet, G.+ 78378
+Mallik, A.K. 77713
+Mallik, B. 76776
+Mallik, U. 74783
+Malmivuo, J. 78286
+Malmuth, E.M. 79011
+Malykhin, V.A. 75767
+Malysh, V.I. 75752
+Malyutenko, V.K. 77231
Mamaev, O.I. 78562
Mamalui, Yu.A.+ 77177
+Mamalui, Yu.A. 77190
+Mamaluyi, Yu.A. 76400
+Mamedbeili, I. 77357
Mamiliyaev, R.M.+ 78290
+Mamonova, T.I. 75162
+Mamontov, V.V. 78305
+Man Fong. 76074
Manakova, L.A.+ 76874
+Mancini, F. 77089
+Mandal, M.L. 77823
+Mande, C. 77478
Mandel, T.+ 76786
+Mandelbaum, P. 75338
Manders, P.W.+ 77734
+Mandrakhlebov, V.F. 74475
+Mandrakhlebov, V.F. 74476
+Mandrakhlebov, V.F. 74484
+Mandzhavidze, A.G. 77176
+Manes, A. 78699
+Manev, V. 77983
Manghi, E.+ 77546
+Manghnani, M.H. 78462
+Mangotra, L.K. 75045
Mani, S.A. 75667
+Manilov, V.A. 77681
+Mankinen, E.A. 78434
Mann, A.K. 74240
+Mann, J.A. 78019
Mann, J.E. 75584
+Mann, R.J. 78426
Mannella, C.A.+ 78154
Mannheim, P.D. 74682
+Manning, D.R. 75875
+Mannocchi, G. 74766
+Mannocchi, G. 74766
+Mannocchi, G. 75225
Manogaran, S.+ 75411
Manoukian, E.B. 74593
Mansfield, M.L. 76276
Mansfield, M.L. 76277
+Manson, A.H. 78729
+Manson, J.A. 77831
Mansuripur, M. 76628
Mantia, F.P. La
 see La Mantia, F.P.
Mantl, S.+ 76705
+Mao, S.Z. 75587
Mao-Hsiung Chen+ 78351
Maouxan Yan
 see Yan Maouxan
+Maple, M.B. 77080
+Maple, M.B. 77078
+Maple, M.B. 76924
Maps, J.+ 76730
+Maradudin, A.A. 75579
Maras, A.M.+ 75856
Marchand, R.+ 76396
+Marchenko, V.V. 76532
Marchesi, M. 76269
+Marchesi, R. 78291
Marchi, G.de. see de Marchi,
 G.
+Marchig, V. 78520
+Marciano, W. 74669
+Marcos, S. 74888
Mardesich, N.+ 78029
Marek, J. 78071
Marel, C.van der
 see van der Marel, C.
+Marest, G. 76642
+Margalit, S. 76719
+Margalit, Y. 77283
+Margaritondo, G. 77023
+Margaritondo, G. 77042
+Margaritondo, G. 76768
+Margaret, F.J. 74871
+Margon, B. 78920
Margulis, W.+ 74534
+Mariani, C. 76786
+Marin, P. 74413
+Marinescu, R. 77999
+Maringer, R. 76651
+Marino, A. 75670
+Marino, A.A. 78172
Marion, C.+ 74564
Maris, H.J.+ 76746
+Marisova, S.V. 76857
+Mark, H. 75504
+Mark, J. 74518
Markert, J.T.+ 77425
Markert, T.H.+ 78969
+Markovich, I.V. 77450
+Markham, O.D. 78367
+Markhonov, V.M. 75645
+Markie, W. 74552
+Marko, V.A. 78303
+Markosyan, A.S. 77228
+Markov, M.K. 77390
Markova, L.A.+ 75768
Marks, L.D. 76452
Marks, L.D.+ 76263
Marks, L.D.+ 76456
Marks, R.F.+ 75759
+Markunas, R.J. 78077
+Marmo, G. 74294
Marraco, H.G.+ 78828
Marro, J.+ 76637
Marsden, B.G. 78877
+Marsden, B.G. 78869
+Marsden, B.G. 78876
+Marsden, B.G. 78871
+Marsaglia, E. 77140

- + Marsegli, E.A. 77141
+ Marsh, O.J. 76894
Marshall, R.G. + 77067
Marshall, F.E. + 79000
Marshall, J.M. + 76998
+ Marshall, J.M. 76957
+ Marshall, R. 78326
+ Marten, H.W. 76708
+ Martensson, N. 77530
+ Martensson-Pendrill, A.M. 75319
+ Martin, A.D. 74762
+ Martin, A.D. 74811
+ Martin, A.D. 74828
+ Martin, C.T. 78129
Martin, H. 75418
Martin, H.O. + 77192
+ Martin, I.M. 79010
Martin, M. + 75275
Martin, M. + 78135
+ Martin, M. 75908
+ Martin, M. 76833
+ Martin, R.J. 75636
+ Martin, T.P. 77394
Martinelli, M. 75798
Martinez, D.R. + 78722
+ Martinez, L. 77697
+ Martinez, M. 75395
Martini, F.De
see De Martini, F.
Martins dos Santos, J.M. 77953
+ Martisunova, L.S. 77596
+ Marty, N. 74898
+ Martynenko, O.G. 74239
Martynov, A.F. + 77225
+ Martynovich, E.F. 77455
+ Marukaya, T. 78710
+ Marumo, F. 76621
Maruska, H.P. + 78001
Maruyama, T. + 78744
+ Maruyama, T. 78743
Marynick, D.S. + 75266
Marziani, M.F. 74317
Marzio, F.di
see di Marzio, F.
+ Masalov, A.V. 75752
Maschek, I. + 78111
Masden, G.W. 78051
Mashanov, V.I. + 76754
+ Masharov, S.I. 76926
Maskho, V.V. 74515
+ Maskhovskii, A.A. 75389
Masi, A.de.
see de Masi, A.
Maskill, H. + 74543
Maslov, A.Yu. + 76852
Mason, E. + 76381
+ Massai, M.M. 78406
+ Massam, T. 74821
Massaro, D.W. + 75870
+ Masselli, M. 78282
+ Masselli, M. 78283
+ Masselli, M. 78285
Massen, R. 74443
+ Massevitch, N.I. 78774
+ Massevitch, N.I. 78670
+ Massimilla, L. 76103
+ Masson, P. 78837
+ Masterova, M.V. 77702
+ Mastuygin, L.I. 75839
+ Masuda, K. 77461
+ Masuda, M. 74430
+ Masullo, M.R. 75648
Masumoto, H. + 77793
Masut, R. + 76990
Matal, O. + 75170
Mateev, E. + 76175
+ Mathews, G.J. 74988
+ Mathews, G.J. 74977
+ Mathot, P. 75115
Mathur, P.C. + 76948
+ Mathur, P.C. 77074
+ Mathur, R.K. 77995
Matsov, B.G. 75537
Matkovskii, A.O. + 76553
+ Matsko, M.G. 77452
Matskovskaya, Yu.Z. + 75832
+ Matson, R.J. 78070
+ Matsuda, H. 74630
+ Matsuda, H. 77154
Matsuda, K. 76155
+ Matsuda, T. 76195
+ Matsuda, T. 74639
+ Matsuda, Y. 77513
+ Matsuda, Y. 78272
Matsui, M. + 77243
Matsui, T. + 76622
+ Matsumoto, H. 75185
Matsumoto, K. + 74376
+ Matsumoto, R. 77221
Matsumoto, T. + 76893
Matsumura, H. 76011
+ Matsumura, S. 76543
Matsunaga, S. + 76920
+ Matsuo Kagaya, H. 76594
+ Matsuoka, M. 75715
+ Matsuoka, N. 75003
+ Matsuoka, N. 77821
Matsue, T. + 75024
Matsushima, T. 77921
+ Matsushita, Y. 76796
Matsusue, K. + 77717
Matsuzawa, K. + 75474
+ Matsuzawa, M. 75491
+ Matte, P. 78501
+ Matteson, J.L. 78992
Matthew, J.A.D. + 77493
+ Matthews, B.W. 78130
+ Matthews, E. 78603
Matthews, J.R. + 77824
Matthews, W.A. 78589
Mattrey, R.F. + 78299
+ Matsui-Goto, S. 76713
+ Mattsson, S.E. 77960
+ Matushko, G.K. 75001
Matuura, N. + 78743
+ Matuura, N. 78709
+ Matuura, N. 78744
+ Matuura, N. 78785
+ Matveev, A.V. 75838
Matveev, V.A. + 76925
+ Matveev, V.B. 74322
+ Matveev, V.V. 75207
+ Matveev, V.V. 75160
+ Matveeva, O.P. 77409
+ Matvienko, E.N. 76399
+ Matviachuk, Yu. 78673
+ Matsyuk, S. 75925
+ Matyuk, V.F. 77841
Matz, W. + 76284
Matzke, H. + 76522
Matzke, H. 76488
+ Matzke, H. 76691
Mau Hsiung Chen + 75504
Mau-chung Chang + 77125
+ Mauersberger, H. 75170
+ Mauger, R. 77980
+ Maulik, M.Yu. 75769
Maung Khin Maung
see Khin Maung Maung
Maung Maung Khin
see Khin Maung Maung
+ Mautref, M. 77586
+ Mautref, M. 78022
+ Mavrenik, O.V. 77428
Mavroyannis, C. 75722
Maxworthy, T. 78552
+ May, F.R. 74837
+ Maybury, R. 74797
Mayer, I. 75285
+ Mayer, R. + 77464
+ Mayr, K. + 74567
+ Mazanec, K. 77797
Mazets, T.F. + 77352
Mazo, R.M. + 76145
+ Mazot, P. 76562
+ Mazumdar, D. 74801
Mazur, V. + 78622
+ Mazzurkiewicz, M. 75109
+ Mazzoldi, P. 76513
+ Mazzoni, M. 75402
+ Mazzotta, G. 78173
Mea, G.Della
see Della Mea, G.
+ Meadows, J.W. 75061
Meagher, J.F. + 78623
Mebariki, M. + 76807
+ Mecking, B. 74962
+ Meclowski, R. 77535
+ Medeiros, J.M. 78166
Medovar, A.B.I. + 77626
+ Medovar, L.B. 77626
Medvezky, L. 75187
+ Medvedev, B.S. 77604
Medvedev, M.V. 77161
+ Medvedev, M.V. 77146
+ Medvid', A.P. 76979
Meek, C.E. + 78729
Meer, S.van der
see van der Meer, S.
+ Meers, B.J. 78935
Meese, R.A. + 78023
Meess, J. + 78797
+ Megierdicheva, I.A. 74540
+ Megha Singh 78163
Megusar, J. + 77761
Megusar, J. + 75177
Mehaute, A.Le
see Le Mehaute, A.
Mehta, S.K. + 78007
+ Meier, P.F. 77315
Meifang Chen
see Chen Meifang
+ Meijer, F.G. 75337
+ Meijer, H.C. 74463
+ Meijer, F.L. 78168
+ Meiler, W. 75292
Meiron, D.I. + 76053
+ Meisel, A. 77520
Meisels, R. + 76992
Meixler, H.-H. + 75057
Mekjian, A. 74733
+ Melchiorri, B.O. 79027
+ Melchiorri, F. 79027
+ Melde, C. 75232
Melenevskii, V.N. 78653
Mel'gui, M.A. + 77841
Melikhov, Yu.V. + 77202
+ Melikian, A.O. 75728
+ Melikulov, A.S. 76595
Melikyan, A.O. + 75706
Melikyan, R.A. 77052
+ Melissinos, A. 74669
Mello-Grand, S. 75836
+ Mel' nichuk, L.S. 75962
+ Mel' nichuk, I.A. 77268
Melnick, G. + 78856
+ Melnik, N.N. 77393
+ Mel'nikov, N.M. 74507
Mel'nikova, L.V. + 77085
Melosh, H.J. + 78448
+ Melville, C.P. 78468
+ Melville, D. 77181
+ Melvin, M.A. 78937
+ Men, A.N. 77160
Mendes, P.Souza
see Souza Mendes, P.
Mendez, E.E. + 77445
+ Mendez, E.E. 77033
Mendez, J.A. + 75592
+ Menet, J. 75040
Meng Ching-an 74501
Mengyu Shen
see Shen Mengyu
+ Menke, W. 78518
Menon, M. + 76827
+ Menon, M.G.K. 74765
+ Mensch, B. 78327
+ Mensch, J. 78327
+ Mentall, J.E. 78652
Mentzoni, M. 76220
Menzies, M.A. + 78493
+ Mercer, R.L. 74941
+ Mercer, R.L. 74987
Mergentaler, J. 78929
+ Merkulov, I.A. 77281
+ Merlin, J.-C. 78875
+ Merlin, J.-C. 78876
Mermaz, M.C. 75008
+ Merrill, R.T. 78530
+ Mertelmeier, T. 75223
+ Merten, L. 77346
+ Merten, L. 76858
Mertig, I. + 76835
Mertz, L. 74520
Mertz, L. 74521
Meruane, T. + 75264
Merwe, P. du T.van der
see van der Merwe, P. du T.
+ Merz, J.L. 77583
+ Meseguer, F. 77963
+ Meshcherkin, A.P. 76168
+ Meshkov, V.V. 77594
Mesko, L. + 75163
Messerschmidt, U. + 76445
+ Messerschmidt, U. 76443
+ Messina, G. 75670
Messmer, C. + 77747
+ Mesyats, G.A. 76962
Metry, A.A. + 75130
Metz, H. + 77287
+ Metzler, S.P. 75998
Meubus, P. + 76224
+ Mexmain, J. 77781
Meyer, A.Y. 75539
Meyer, C. + 76479
+ Meyer, G. 76388
+ Meyer, H. 75528
+ Meyer, H. 76744
+ Meyer, H. 76745
Meyer, H.E.De
see De Meyer, H.E.
+ Meyer, R.A. + 75236
+ Meyer, R.A. 74906
+ Meyer, R.A. 75087
+ Meyer, R.A. 74905
+ Meynell, G. 78327
+ Meyrueis, P. 75797
+ Mezhevov, A.A. 76762
+ Mezhova, N.Ya. 76561
+ Michael, W. 78775
+ Michaelian, K. 74975
+ Michaels, D. 78029
+ Michaelson, S.M. 78239
Michalski, A. + 77574
+ Michel, T.J. 78386
+ Michelson, D. 78636
+ Michenaud, J.-P. 77227
+ Michev, T. 78338
Michl, J. + 75391
+ Middelmann, H.U. 76786
Mien Vu Zoan.
see Vu Zoan Mien
+ Miertus, S. 77867
+ Migliorina, C. 77789
+ Mignerey, A.C. 74988
+ Mignerey, A.C. 74977
+ Mihaila, A. 78105
Mihajlov, M.I. + 78307
Mihalj, K. 75206
+ Mikhailov, Yu.A. 76168
Mikhailovskii, I.Y. 76455
Mikhailchenko, R.S. + 75911
+ Mikhailevich, V.G. 77438
Mikheev, M.N. + 77842
+ Mikheev, V.P. 75768
Mikhonov, S.A. + 75679
Miki, N. + 75930
Mikkola, E. + 75352
+ Mikla, V.I. 75760
+ Mikolajczak, P. 76335
+ Mikulas, K. 75009
Mikulski, A.T. + 75153
+ Mikumo, T. 75025
+ Milani, A. 78693
+ Milano, L. 78949
+ Milazzo, M. 75488
Miles, H. 78878
Milewski, J.D. 77986
Miley, G.H. + 75624
+ Milkey, R.W. 78885
+ Millan, J. 76820
Millard, G.C. + 78367
+ Miller, A. 75708
+ Miller, B.I. 75636
+ Miller, C.A. 74975
+ Miller, G.A. 74857
+ Miller, G.E. 78224
+ Miller, H.R. 79015
+ Miller, J.L. + 78199
+ Miller, K. 75197
+ Miller, K.M. 76437
+ Miller, L.S. 76952
+ Miller, M.A. + 78009
+ Miller, M.D. 76788
+ Miller, M.K. 77936
+ Miller, P.D. 77511
+ Miller, R.C. + 77446
+ Miller, R.D. 75391
+ Miller, R.D.C. 74597
+ Millie, P. 75420
Milonni, P.W. 74697
+ Miloslavskii, V.K. 77473
Milstein, J.B. + 78024
+ Milstein, J.B. 78069
+ Milton, S.V. 75419
+ Min, K.W. 75560
+ Minaev, V.N. 76561
Minagawa, I. 77317
+ Minakov, V.N. 77681
Minakuchi, Y. + 75966
Minano, J.C. + 77962
+ Minari, F. 76438
+ Minasian, H.R. 75428
+ Minehart, R.C. 74804
Minford, E.J. + 77731
Ming De Li + 78147
Ming-Kai Tse + 77853
Ming-ke Huang + 76064
Mingyu Zhou
see Zhou Mingyu
+ Miniscalco, W.J. 77429
Mink, D. 78863
+ Minke, B. 78184
Minkevich, A.V. 79037
+ Min'ko, A.A. 77391
Minot, C. + 77018
Minowa, H. 74379
Mirmov, N.I. + 75907
Mironov, A.I. + 76043
Mironova, M.L. + 76673
+ Mirzaa, M.C. 75581
Mirzaev, D.A. 77640
+ Mirzaev, D.A. 77638
+ Mirzoyan, R.G. 75692
+ Misawa, H. 77738
Mishenkov, N.N. + 78251
Mishima, O. + 77376
Mishra, B.C. + 75481
Mishra, J.P. + 76375
Mishra, R.K. + 78133
+ Mishuk, T. 77998
Misiorek, H. + 76928
+ Misra, P.K. 77133
Misra, R. + 78733
+ Misra, R. 76685
+ Misra, R.N. 78773
+ Misra, S.N. 75449
Misra, S.P. 74813
Misra, S.P. + 74723
+ Misra, T.N. 76776
+ Mitchell, A.C. 78536
+ Mitchell, G.R. 76285
+ Mitchell, I.V. 75488
+ Mitchell, J.W. 77910
+ Mitchell, T.E. 76504
+ Mitichkin, A.I. + 77386
+ Mitin, A.V. 77086
Mitin, B.S. + 77804
+ Mitkin, R.B. 74512
Mitra, N. 74704
+ Mitra, S. 75407
Mitra, S.K. 76629
Mitra, S.K. + 74292
Mitrovic, B. + 76825
Mitrovic, B. + 76826
Mitschke, F. + 75717
+ Mitsushige, G.Yu. 77374
Mitsuishi, N. + 77922
+ Mitsyavichyus, G.Yu. 74548
+ Mittal, R. 74900
Mittelbrunn, J.Ramirez
see Ramirez Mittelbrunn, J.
Mittelstaedt, P. 74308
+ Mittemeijer, E.J. 76254
+ Mittra, I.S. 75045
Mitus', A.Ya. + 76584
+ Miura, I. 75013
Miura, K. + 77691
+ Miura, N. 77227
+ Miura, N. 76974
Miyagawa, H. + 77687
Miyagawa, H. + 77688
+ Miyahira, T.F. 78038
+ Miyake, S. 74765
Miyamoto, A. + 76755
Miyamoto, K. + 75185
Miyamoto, K. + 75184
+ Miyachi, M. 77374
+ Miyachi, N. 75637
Miyayama, M. + 76982
+ Miyazaki, N. 75169
Miyazaki, S. + 78751
+ Miyazaki, S. + 78749
+ Miyazaki, S. 78787
+ Miyazaki, S. 78748
+ Miyazaki, Y. 76614
+ Miyazono, S. 75169
Miyoshi, E. + 75288
Miyoshi, E. + 75286
+ Miyoshi, Y. 77739
+ Mizomoto, M. 76125
+ Mizrahi, S.S. 74319
Mizurukhin, L.V. + 75606
Mizubayashi, H. + 76444
+ Mizumoto, Y. 78817
Mladenov, I.T. + 77390
+ Mlynec, J. 75717
+ Mo, O. 75293
+ Mo Peigen 76890
Mo-lin Ge.
see Ge Mo-lin
+ Moak, C.D. 77511
Mobbs, S.F. + 75120
+ Moccia, R. 75351
+ Mochinaga, J. 76279
+ Mochizuki, K. 76338
+ Mochnicki, B. 76336
Modaresi, A. + 76377
+ Modesti, S. 77457
+ Moffat, A.F.J. 78919
Moffat, A.L. + 77966
Moffatt, H.K. 75994
+ Moffett, R.J. 78741
Mogilevich, V.N. 75788
+ Mogilevsky, M. 78670
+ Mogro-Campero, A. 77222
+ Mohamed, A. 76950
Mohamed, A. el M.A. + 76120
+ Mohammed, K. 77583
Mohan, S. + 75357
+ Mohana Rao, J.K. 78126
Mohanty, J.C. + 77133
Mohanty, S. + 74795
Mohapatra, J.K. + 74665
+ Mohapatra, J.K. 74795
Mohapatra, R.B. + 75958
+ Mojn, M.D. 77450
+ Moiseev, D.P. 77111
+ Moiseev, D.P. 77085
+ Mokerov, V.G. 76480
Mokichev, N.N. + 76432
+ Mokler, P.H. 75502
+ Mokrousov, V.A. 75244
+ Molchanov, O.A. 78670
Molhoek, P.G. + 78372
Molian, P.A. + 77635
Molian, P.A. + 77624
+ Molinie, P. 77984
Mollenauer, L.F. + 77419
+ Moller, A. 77360
+ Mollmann, K.-P. 76996
Molnar, P. + 78451
+ Molnar, Zs. 78116
Molodets, A.M. + 76559
+ Moloney, J.V. 75714
+ Molvik, A.W. 76214
+ Molzen, W.W. 78403
+ Momchilov, A. 77983
Momo, T. 78464
+ Monahan, E. 74438
+ Mondal, N.K. 74765
+ Mondal, S. 74801
+ Monev, M. 77805
+ Monev, M. 77806
Montagnani, R. + 75326
+ Montaner, A. 77887
Montanet, L. 74725
Monteiro, E.Costa.
see Costa Monteiro, E.
Montenegro, E.C. + 75492
Montenaro, A. 76310
+ Montgomery, J.S. 77654
+ Monti, F. 77829
+ Moorcroft, D.R. 78678
+ Moore, B.N. 76182
+ Moore, R.S. 74804
+ Moore, T.J. 77858
Moos, D. + 78463
+ Morabito, D.D. 78945
+ Morabito, D.D. 79014

- + Morales, P. 75425
 Moran, P.R. 78274
 Morand, P. + 78880
 + Moravcsik, M.J. 74869
 Mordike, B.L. + 76650
 Mordike, B.L. + 77807
 + Mordike, B.L. 77808
 + Mordike, B.L. 76678
 + Mordike, B.L. 77760
 + Morehead, F.F. 76416
 Moreno, C. + 74295
 Moretti, J.L. + 78327
 + Morfill, G. 78848
 Morfill, G.E. + 78849
 Morgan, W.W. + 78993
 + Morgante, C.G. 75432
 + Morgenstern, I. 74405
 + Mori, E. 75891
 Mori, H. + 78787
 + Mori, H. 78749
 + Mori, H. 78751
 + Mori, H. 78748
 + Morii, Y. 76743
 + Morimoto, N. 78882
 + Morin, P. 77229
 + Morin, R. 78518
 Morishita, K. 75805
 + Morita, R. 78294
 Morita, T. 77123
 + Morioka, J. 77063
 + Morkoc, H. 77570
 + Morkoc, H. 77445
 + Morkowski, J. 77165
 + Morlet, M. 74898
 + Morley, B.M. 78660
 + Morosini, M.B.Z. 75639
 Moroz, B.Z. 74309
 Morozov, E.M. + 75961
 + Morozov, E.M. 77339
 + Morozov, O.P. 77638
 + Morozov, V.F. 76532
 + Morozov, V.I. 75217
 + Morozova, S.G. 77680
 + Morris, A. 75444
 + Morris, C.S. 78876
 Morris, M.C. + 76407
 + Morris, T.R. 78122
 + Morrison, C.J. 77490
 + Morrison, F.A., Jr. 76080
 + Morrison, I. 74844
 + Morrissey, D.J. 74952
 + Morten, F.D. 74459
 Morton, D.C. 78900
 + Morton, P.L. 75663
 Morup, S. 77303
 + Moser, P. 76413
 + Moser, P. 77477
 + Moscoso, A.V. 75063
 + Moshkov, A.V. 78765
 + Moshkrefzadeh, R. 75726
 + Moshkev, R.V. 77979
 Mosley, K. 77820
 Moss, J.M. 74979
 + Moss, S.C. 76520
 + Moss, S.C. 76373
 + Mostafa, M.F. 77157
 + Motobayashi, T. 75025
 + Mottinger, N.A. 78838
 Motulevich, G.P. + 77106
 Mourao, R.R. de Freitas, R.R.
 see de Freitas Mourao, R.R.
 Mowforth, K.E. + 78754
 Moy, D. + 74473
 Mozalevskaia, G.V. 74262
 + Mozalevskaia, G.V. 74268
 + Mozharovskiy, A.M. 75692
 Mrig, L. + 78031
 + Mrig, L. 78039
 + Mrosan, E. 76835
 + Mroz, J. 77338
 Muchotrzeb, B. 78808
 + Mueller, A.C. 74915
 + Mueller, A.H. 74727
 + Mueller, I.I. 78412
 + Mueller, R.K. 78278
 + Mueller, St. 78414
 Muhlberg, M. + 76639
 + Muhleimeier, B. 77105
 + Mujica, F.V. 75084
 Mukai, S. 77432
 + Mukai, T. 78294
 + Mukai, T. 75641
 + Mukherjee, B. 74736
 + Mukherjee, D.C. 75301
 Mukoh, A. + 76293
 Mukoyama, T. + 75316
 + Mulder, J.J.C. 74367
 + Mulgi, A.S. 76084
 Mullan, D.J. 78766
 + Mullen, S.P. 78227
 Muller, A. + 75519
 + Muller, A. 75500
 Muller, C. + 76870
 Muller, F. 74822
 Muller, H. + 77912
 + Muller, H. 74783
 + Muller, H.H. 75055
 Muller, H.J. + 76626
 + Muller, J. 76321
 + Muller, J. 75906
 + Muller, K.A. 77420
 Muller, L. 74860
 + Muller, W. 75034
 + Muller, W.R. 75553
 + Mullins, J.W. 77629
 + Mumma, M.J. 75370
 Munakata, T. 76582
 + Munch, J. 75655
 + Munchow, L. 74891
 + Munger, R.H. 76214
 + Muning, H.F. 75243
 + Munley, A.J. 78935
 + Munnich, K.O. 78605
 + Munoz-Yague, A. 77431
 Munson, B.R. + 76045
 Munster, G. 74583
 Murahara, M. + 75602
 + Murakami, T. 78742
 + Murakami, W.T. 78138
 + Murakami, Y. 76755
 Muralikrishna, P. + 78674
 Muranaga, K. + 78789
 Murata, H. 75792
 Murata, I. 75325
 + Murata, K. 76932
 + Murata, Y. 77521
 + Muratov, V.M. 77361
 Murcia, M.de
 see de Murcia, M.
 + Murray, D.G. 78598
 + Murdin, P. 79024
 + Murphy, N.S. 76270
 Murphy, T. + 74651
 Murphy, W.C. + 77486
 + Murray, C.T. 77469
 Murray, R.T. 74441
 + Murray, S.S. 79024
 + Murtas, G.O. 75225
 + Murtas, G.P. 74766
 + Murtas, G.P. 74766
 Murthy, E.Krishna
 see Krishna Murthy, E.
 + Murthy, K.S.R.C. 76946
 + Murthy, P.V. 76499
 Murthy, P.V.Ramana
 see Ramana Murthy, P.V.
 + Murtsovkin, V.A. 76123
 + Murty, Bh.V.R. 78663
 Murty, N.Srinivasa
 see Srinivasa Murty, N.
 + Murtycheva, L.E. 74482
 + Murzina, L.D. 78249
 + Mushailov, E.S. 77249
 + Mushotzky, R.F. 79000
 + Mushotzky, R.F. 78992
 Musielak, Z. 78904
 + Musienko, N.G. 77454
 + Mussil, V.V. 74773
 Mustafaev, R.A. + 76684
 + Mustafayev, Yu.M. 77038
 + Mutafiev, K.J. 78307
 + Muther, H. 74863
 + Muzhitski, V.F. 74440
 Mya Oou + 76044
 Myasnikov, V.N. + 76857
 + Mydosh, J.A. 77155
 Myers, D.R. + 77402
 + Myers, R.V. 78908
 Myers, W.D. + 74877
 + Myerson, A.S. 76410
 + Myshkin, N.K. 77594
 + Myslin, V.A. 76229
 + Mytsyk, B.G. 77358
 + Naha, S. 74801
 + Naha, S. 75046
 + Naha, S. 75047
 + Nahan, S. 74800
 Nahory, R.E. + 76341
 + Nahory, R.E. 76474
 + Nahory, R.E. 76973
 + Naik, S. 74723
 + Naiman, M.L. 77056
 Nair, G.P. 78706
 Nair, V.P. + 74667
 + Naito, K. 76602
 Naito, S. + 77099
 Najmabadi, F. + 76157
 Nakagaki, O. + 78373
 + Nakagawa, T. 75023
 + Nakagawa, Y. 75025
 + Nakagawa, Y. 77152
 + Nakagawa, Y. 77246
 + Nakagawa, Z. 77609
 + Nakagiri, N. 76608
 Nakahara, S. + 76799
 Nakahara, S. + 77567
 Nakahashi, M. + 77648
 + Nakai, H. 75942
 Nakai, I. 77163
 Nakai, I. + 77205
 + Nakajima, H. 77558
 Nakajima, K. + 77585
 + Nakajima, I. 76034
 + Nakamura, K. 77227
 Nakamura, M. + 75222
 + Nakamura, M. 78373
 + Nakamura, M. 74966
 + Nakamura, M. 75003
 + Nakamura, R. 78220
 + Nakamura, S. 77648
 + Nakamura, T. 76868
 + Nakamura, T. 75472
 + Nakamura, T. 75286
 + Nakamura, T. 75182
 Nakamura, Y. 76069
 Nakamura, Y. 78831
 + Nakamura, Y. 78742
 Nakanishi, N. 74349
 + Nakasa, K. 77794
 Nakashima, N. + 75427
 Nakashima, S. + 77374
 Nakatsuka, H. + 75715
 + Nakayama, S. 75013
 Nakazaki, S. 75516
 + Nakazawa, T. 78608
 Nakwaski, W. 75633
 + Nalcioglu, O. 78315
 + Nalimov, I.P. 78290
 Namazov, S.A. 78753
 + Namba, M. 76062
 + Namba, S. 75602
 Namikawa, T. + 78764
 + Namninov, V.L. 76962
 Namiot, V.A. 76152
 + Namizaki, H. 75634
 + Namyckin, A.S. 77612
 Nan Yang Shin
 see Shin Nan Yang
 Nanba, M. + 74579
 Nanba, T. + 77394
 Nanbu, K. 75980
 + Nanbu, K. 77030
 Nance, R.A. + 77855
 + Nandi, P.K. 74504
 Nandy, A. 74749
 + Nandy, S. 74801
 + Nania, R. 74821
 + Nanopoulos, D.V. 74356
 + Nanstad, R.K. 75101
 + Naoumidis, A. 76586
 + Narasimham, V.S. 74765
 Narayan, D.S. 75002
 Narayan, J. + 76598
 + Narayan, J. 76463
 Narayana, P.A. + 75854
 Narayana, P.A. + 75855
 Nardo, M.di
 see di Nardo, M.
 Nardone, V.C. + 76447
 + Narducci, L.M. 75716
 + Narimanidze, N.I. 74481
 Narison, S. + 74719
 + Narita, K. 77212
 + Narita, T. 75082
 Naroska, B. 74787
 + Narukawa, S. 77982
 + Narumi, H. 74989
 + Narva, V.K. 77804
 + Nasby, R.D. 78065
 + Nasby, R.D. 78040
 Nassau, K. + 77620
 + Nasu, H. 76312
 + Nataf, G. 78068
 + Nataf, H.-C. 76025
 + Nataraian, M. 78615
 Natesan, K. 75102
 Nath, A. + 75415
 Nath, P. + 74670
 Nath, P. + 74780
 + Nath, P. 74358
 + Natsik, V.D. 76446
 Naude, W.J. + 75019
 + Naudet, J.P. 78619
 Naumann, R.J. + 77552
 + Naumenko, V.I. 77391
 + Naumenkov, P.A. 77940
 + Naumov, A.S. 76245
 + Naumov, A.S. 76246
 Naumov, V.A. + 75511
 + Naurzakov, S.P. 78399
 Nava, F. + 76711
 Nava, F.A. + 78444
 Nayeab-Hashemi, H. + 76558
 + Nazarenko, N.A. 75451
 Nazmy, M.Y. 77751
 + Nebel, R.A. 76209
 + Nebel, R.A. 76204
 + Nechaev, S.V. 77940
 + Neehwaal, A. 76778
 Neckel, A. 76840
 + Nedderman, R.M. 76108
 + Nedoglo, D.D. 77462
 Nedospasov, A.V. 76166
 + Needelman, A. 76451
 Needler, G.T. 75111
 + Neethling, D.C. 78582
 + Nefedov, S.N. 76624
 + Neff, S.G. 79017
 + Neftali, A. 78571
 + Negele, J.W. 74878
 Neghabian, A.R. 75318
 + Negri, P. 74766
 + Negri, P. 74766
 + Negri, P. 75225
 + Neich, A.I. 77613
 + Neil, G.R. 75655
 Neild, D.W. 74578
 + Neilson, G.C. 74975
 Neister, S.E. 75683
 + Nekrasov, V.V. 75767
 + Nekunde, A.P. 74576
 + Nelson, A.W. 75688
 + Nel'son, K.V. 75561
 + Nelson, L.V. 75651
 Nelson, P.H. + 78568
 Nelson, W.L. 78219
 + Nelyubin, V.V. 76532
 + Nelyubin, V.V. 74983
 + Nembach, E. 76833
 + Nemecek, Z. 78777
 + Nemes, M.C. 74298
 + Nemeth, I. 75191
 + Nemtsev, G.Z. 76457
 Nenovski, P. + 78668
 + Neoh, C.L. 76473
 Neov, S. + 76314
 + Neri, G. 78452
 + Nersesov, I.L. 78505
 + Nersesyan, G.A. 74484
 Nersisyan, S.R. + 76286
 Nest, J.F. Le
 see Le Nest, J.F.
 + Nesterin, V.A. 77203
 Nesterov, S.V. + 76124
 Neto, V.F. de Assis
 see de Assis Neto, V.F.
 Netrebko, A.V. 75947
 + Netzer, F.P. 77493
 + Neugebauer, G. 79019
 + Neugebrosch, A. 78074
 + Neuhaus, L. 74544
 + Neumaier, K. 76740
 Nevanlinna, H. + 78430
 + Nevejan, D. 78629
 Newcomb, S.B. + 77795
 Newcomb, S.B. + 77796
 Newcomb, S.B. + 76818
 + Newman, H.N. 78328
 + Newman, B.E. 75653
 + Newton, G.P. 78935
 + Newton, J.O. 75032
 + Newton, R.W. 78541
 + Nexsen, W.E. 76214
 + Nezavdal, G. 74567
 + Nezhrick, F.A. 74771
 Ng, B.W. + 75556
 Ng, Y.J. + 74679
 Nghi Nguyen Thanh
 see Nghi Nguyen Thanh Nghi
 + Ngo, C. 74864
 + Ngo, H. 74864
 Nguyen, An + 76454
 Nguyen, N. + 76945
 + Nguyen Hong Shon. 76976
 + Nguyen Thanh Nghi
 76339
 Nguyen Thi Khoi + 77369
 Nguyen Van Trong 76862
 + Ni Guang-jiong 74589
 Ni Haoqing 76050
 + Niarchos, D.G. 76662
 Niazzy Nagla
 see Nagla Niazzy
 + Nicholas, P. 78210
 + Nicholas, R.J. 77037
 + Nicholls, A.W. 77937
 + Nicholson, W.L. 76237
 + Nickel, H. 76586
 + Nickel, H. 75109
 + Nickel, H. 75110
 + Nicolaides, C.A. 75344
 Nicolas, P. + 78280
 + Nicolet, M.-A. 77071
 + Nicolet, M.-A. 77047
 + Nicoletti, G. 74766
 + Nicoletti, G. 75225
 + Nicolson, G.D. 78945
 Nielsen, B. 74608
 + Nielsen, C.J. 74518
 Nielsen, E. + 78731
 + Nielsen, H.P. 78884
 + Nielsen, P.B. 75121
 + Niemax, K. 75333
 + Niemeskern, A. 74832
 + Nienaber, W. 78438
 + Nieuwenhuis, G.J. 77155
 Niewisch, J. + 75889
 + Nifatov, A.P. 78260
 Niida, H. + 77152
 Nijhoff, F.W. + 74253
 + Nikishkov, G.P. 75961
 + Nikitin, A.I. 77840
 Nikitin, A.N. + 78525
 + Nikitin, B.G. 76922
 Nikitin, L.P. + 76853
 + Nikitin, V.V. 75346
 + Nikolaev, V.M. 75645
 + Nikolaeva, N. 78776
 Nikolich, A.D. + 75383
 Nilsson, Y. 77810
 Ning-Yuan Richard Ma +
 76680
 Nir, S. 78155
 + Nir, S. 78148
 + Nirmann, N.S. 78814
 + Nisensohn, P. 78825
 + Nishenko, M.M. 76922
 + Nishi, S. 77029
 Nishida, A. (ed.) 74230
 Nishizumi, K. 78883
 Nishijima, K. 74640
 Nishijima, S. + 77821
 + Nishimura, K. 78080
 Nishimura, R. + 77792
 + Nishimura, T. 77374
 Nishino, H. 74359
 Nishino, T. + 77456
 + Nishino, Y. 76445
 Nishioka, M. 74605
 Nishizaki, R. + 78785
 Nishizaki, R. + 78794
 + Nishizaki, R. 78743
 Nishizawa, O. 78701
 + Niu Defang 77578
 + Niu Zhenan 76033
 + Niwa, K. 77233
 + Ni, W.D. 77697
 + Nixon, W.C. 74561
 + Nobili, A.M. 78693
 + Nobili, C. 76711
 Noble, J.V. 74851
 + Noble, P.B. 78158
 + Nobuhara, S. 76196
 Noel, G.T. + 78086
 Nof, D. 78549
 + Noguchi, S. 78471
 + Noguera, C. 76819
 + Noh, S.K. 76895
 Nojima, S. 76953
 + Nojima, T. 76806
 + Noldeke, G. 74962
 Nolle, A.W. 75878
 + Nolle, G. 77312
 + Nolthenius, R. 78872
 + Nomi, T. 75942
 + Nomoto, K. 76658
 + Nomoto, K. 76660
 + Nomura, A. 76816
 + Nomura, M. 76608
 + Nomomura, S. 78080
 + Nomomura, S. 78006
 Noras, J.M. 77418
 Nord, A.G. + 76403
 + Nordstrom, B. 78950
 + Norenberg, W. 74879
 + Norenberg, W. 74929
 + Norenberg, W. 74930
 + Norets, T.A. 78257
 + Normundaradov, M.T. 77494
 + Noro, T. 74966
 + Noro, T. 75003
 + Norris, A.N. 78458
 Norris, C.B. + 74439
 Norris, C.B. + 77460
 + North, A.M. 76570
 Nose, S. + 76606
 + Nose, Y. 78373
 Noshkin, V.E. + 75117
 + Nosov, V.B. 77452
 Notin, M. + 76667
 + Nougier, J. 78421
 Novaro, O. 75287
 + Novikov, I.I. 76517
 + Novikov, P.A. + 75900
 + Novikov, V.I. 77669
 + Novikov, V.L. 78504
 + Novikov, V.P. 76619
 + Novitskii, F.N. 74575

- +Novitskii, V.G. 76493
 Novopashin, A.A. + 76674
 +Novotny, J. 77710
 +Novotny, R. 75026
 +Nowacki, W. 76401
 Nowatzki, E.A. + 75142
 +Nowick, W. 77471
 Nowlan, M.J. + 78027
 +Nowlan, M.J. 77967
 +Noyes, R. 78893
 +Nozaki, K. 78745
 +Nunes, M.R. 78960
 +Nunez, G. 77801
 +Nurgozhin, N.N. 75011
 +Nurso, M. 78269
 +Nuyts, G. 75115
 Nyberg, C. + 76766
 +Nyberg, J. 74901
 Nyhan, J.W. + 78108
 +Nylander, C. 78152
 Nylandsted Larsen, A. + 76486
- +Obara, S. 75288
 Obayashi, S. + 76067
 +Obenshain, F.E. 75026
 Obenson, G. 78418
 Oberacker, V.E. + 75037
 Oberlack, H. 74788
 +Oberlack, H. 74783
 +Oberle, L. 75236
 Obermeier, F. 76068
 Obraztsov, F.I. + 78223
 +O'Brien, E.M. 78385
 +Ochiai, Y. 77154
 Ockendon, H. 76430
 +O'Connor, D.J. 76526
 +Oda, A. 77687
 +Oda, A. 77688
 +Odajima, K. 75185
 Odinkov, S.E. + 75389
 +Odintsov, A.I. 75620
 Odintsov, V.I. + 75732
 Odoni, W. + 77078
 +Odori, T. 78294
 Oeschger, H. + 78114
 +Oeschger, H. 78571
 +Oganesyan, V.O. 76286
 +Ogata, H. 77475
 +Ogata, H. 75013
 +Ogata, H. 74471
 +Ogata, T. 78743
 +Ogawa, H. 75222
 +Ogawa, H. 74966
 +Ogawa, H. 75003
 Ogawa, S. 77240
 +Ogawa, T. 77230
 +Ogawa, T. 78749
 +Ogawa, T. 78751
 +Ogawa, T. 78787
 +Ogawa, T. 78748
 +Ogawa, T. 78590
 +Ogawa, Y. 75154
 +Ogi, S. 76982
 +Ogino, M. 77777
 +Ogiobly, V.I. 76681
 Ogura, K. + 77739
 +Ogura, K. 75930
 Oh, C.H. + 78292
 +Oh, S. 75164
 +O'Halloran, T. 74669
 +O'Handley, R.C. + 77597
 O'Hara, J.G. 74249
 +Ohji, K. 75930
 +Ohkawa, A. 78272
 Ohkawa, F.J. 76898
 Ohkawa, F.J. + 77136
 +Ohkawa, S. 77162
 +Ohmi, K. 76041
 +Ohmichi, T. 76603
 +Ohmori, J. 75185
 +Ohmori, K. 77598
 Ohno, H. + 76279
 +Ohno, H. 76701
 +Ohno, H. 77029
 +Ohno, K. 75288
 +Ohno, T. 75185
 Ohring, S. 74282
 Ohrn, Y. + 75255
 Ohshima, K.-I. + 76373
 Ohta, M. + 77664
 Ohta, N. 74687
 +Ohta, N. 77911
 Ohta, S. + 77174
 +Ohta, Y. 77233
 Ohtaki, K. + 78271
 +Ohtani, F. 74966
 +Ohtsubo, S. 77821
 +Ohtsuka, Y. 75811
 +Ohtsuki, T. 77433
 +Ohya, Y. 77758
 +Oishi, N. 77642
 +Oishi, Y. 76690
- +Oishi, Y. 74579
 +Oishi, Y. 74286
 +Ojeda-Castaneda, J. 75577
 +Ojha, I.D. 75044
 Ojha, I.Dhar. *see* Dhar Ojha, I.
 Ojima, I. 74641
 +Ok Hec Chung 77266
 +Oka, M. 77636
 +Oka, M. 76954
 Okabe, Y. + 77091
 Okada, K. + 74437
 Okada, Y.C. 78208
 +Okada, Y.C. 78178
 Okamoto, H. + 78006
 +Okamoto, H. 78080
 +Okamoto, H. 76743
 +Okamoto, H. 77470
 Okamoto, K. + 75752
 +Okamoto, M. 75184
 +Okamoto, M. 75185
 +Okeke, C.E. 77549
 +Okhrimenko, B.A. 77454
 +Okhrimenko, V.A. 76366
 +Okolovich, V.N. 75059
 +Okonov, E.O. 75011
 Okuda, H. + 75632
 +Okuda, S. 76444
 +Okuda, Y. 74462
 Olah, S. + 77965
 Olander, D.R. 77787
 +Oleinik, G.S. 76616
 Oleksiv, B.Ya. + 77659
 +Oliferuk, W. 77698
 Olinik, O.Ya. + 74280
 +Olimov, K. 74809
 +Oliva, A. 77869
 +Olive, J.P. 75869
 Oliversen, N.A. + 78916
 +Oliver, G. 76900
 +Oliver, P.D. 75586
 +Ol'khovik, L.P. 77190
 Olmer, C. 74971
 +Olmi, A. 75034
 +Olson, L.C. 78009
 +Olson, W.C. 74975
 +Ol'shanetskii, B.Z. 76754
 Olson, G.B. + 77654
 +Olson, G.B. 77660
 Olson, J.M. + 77593
 +Olson, R.E. 75499
 +Olson, S. 74669
 +Olsson, N.A. 75635
 Olaszewski, J. + 75233
 Olmats, S.J. + 78599
 +O'Meara, T.R. 75740
 +Omeltchenko, A.V. 77637
 +Omote, M. 74643
 Onate, E. + 77704
 Onda, I. 78466
 Ondhof, T. + 78742
 Ondrechen, M.P. + 79002
 +O'Neill, D.G. 77053
 O'Nions, R.K. + 78479
 Ono, F. + 77242
 +Ono, F. 77205
 +Ono, S. 77560
 +Onodera, Y. 77109
 Onuki, A. 76724
 Oomura, E. + 75634
 Oosterom, A. *van* 77777
see van Oosterom, A.
 +Oostro, S. 77238
 Oou Mya. *see* Mya Oou
 +Ophir, J. 75854
 +Ophir, J. 75855
 +Ophir, J. 75854
 Opila, R. + 77524
 Opitz, C. + 76779
 +Oppermann, H. 76618
 Opradolce, L. + 75501
 +O'Riagain, T. 74651
 +Orava, R. 74771
 +Oravec, M.G. 77859
 Oreshkina, L.N. + 74267
 +Oreshnikova, N.G. 76673
 +Orishchin, E.M. 76532
 Oristaglio, M.L. 75865
 +Orlov, A.N. 76630
 Orlov, D.L. + 77814
 Orlov, V.G. 76644
 +Orlov, V.K. 75694
 +Orlovich, V.A. 74541
 Orlovskii, A.A. 75571
 +Oron, M. 76966
 +Orsatti, A.M. 78828
 +Ortega, J.M. 75650
 +Ortega-Navarro, P. 74295
 Ortnier, H. + 75007
 Orton, G.S. 78854
 +Orudzhev, G.S. 77410
 +Orzechowski, T.J. 76214
 +Osaka, A. 77694
 Osaka, H. + 76034
 Osaka, T. + 76806
 +Osakabe, N. 74639
 Osche, G.R. + 75705
 Osetskii, A.I. 76427
 +Osgood, R.M. 77905
 +O'Shea, S.F. 76587
- Osheroich, V.A. + 78887
 +Oshima, S. 76113
 +Osiko, V.V. 75642
 +Osinskii, M.E. 76922
 Osipova, I.I. + 77607
 +Osipova, N.E. 74479
 +Osipyan, Yu.A. 76439
 Osman, A. 74953
 Osman, M.A. + 76296
 +Osnes, E. 74863
 +Ostanevich, T.G. 75011
 +Ostapenko, I.T. 77783
 +Osterberg, R. 78136
 +Osterberg, U. 76228
 Osterbrock, D.E. + 78845
 +Osterbrock, D.E. 78991
 Osterburg, G. + 78390
 +Ostrovskaya, N.F. 76616
 +O'Sullivan, G.A. 78031
 +Osvay, M. 78336
 Ota, R. + 76597
 +Ota, R. 76312
 Ota, Y. 76803
 Ota, Y. 77571
 Otake, S. + 75764
 +Otani, T. 77670
 Otozaki, K. + 74870
 Otroshchenko, L.P. + 76398
 Otsuka, M. + 76195
 +Otsuka, N. 77609
 +Ott, H. (ed.) 74233
 +Ott, H.R. 77078
 +Ottavi, H. 74371
 +Otto, A. 75393
 Oudar, J.-L. 75755
 Ouilion, R. + 75486
 +Outred, M. 75337
 Ouyed, M. + 78442
 Ovadyahu, Z. + 77010
 Ovcharenko, A.P. + 75775
 Ovcharenko, E.P. + 78261
 +Ovchinnikov, A.A. 76913
 Overcamp, T.J. + 78113
 Overley, J.C. 78296
 +Ovrt, B.A. + 74355
 +Ovrt, B.A. 74679
 +Ovseyan, S.T. 76030
 +Owen, D.G. 76634
 Owen, D.L. 74806
 +Owen, N. 78636
 +Owen, T. 78864
 +Oyama, S. 77687
 +Oyama, S. 77688
 +Oyama, Y. 75182
 +Ozawa, T. 77221
 +Ozernoi, A.P. 76485
 +Ozerov, R.N. 77129
 +Ozhigianov, Yu.G. 77802
 +Ozhogin, V.I. 78399
 +Ozisik, M.N. 75909
 Oztunali, O.I. 75125
 +Ozzello, T. 74843
- +Paar, V. 74905
 Pack, G.J. + 78019
 +Pack, G.R. 78131
 +Paderno, V.N. 77607
 +Paderno, Yu.B. 76904
 +Padmini, A.R.K.L. 77644
 Paez, M.J. + 74969
 Page, A.L. *see* Le Page, A.
 Pagliarini, G. + 75860
 +Paic, G. 74848
 +Paic, G. 74923
 +Paic, G. 75006
 Paidar, V. 77711
 +Paige, F. 74669
 Pajackowska, A. 77883
 Pakeva, S. + 77458
 +Pakhlov, V.B. 76286
 +Pakhomov, L.G. 76432
 Pal, A. + 76736
 +Pal, B.R. 75950
 Pal, P. + 74734
 Pal, S. + 78773
 +Pal'-Val', L.N. 76449
 Palatnik, L.S. + 77226
 +Palchadhuri, S. 76282
 +Paldus, J. 75278
 +Palfavi, J. 75235
 +Palfavi, J. 75242
 +Palfavi, J. 78352
 +Palfavi, J. 75208
 Paliwal, K.K. + 75871
 Pallas, N.R. + 76750
 +Palm, B.J. 78082
 +Pal'm, V.V. 75364
 +Palmer, T.F. 77903
 +Palmonari, F. 74821
 Palstra, T.T.M. + 77155
 Palumbo, F. 74600
 +Pamela, J. 74783
 +Pan, E.-T.-S. 77047
- Pan, V.M. + 76922
 Pananakakis, G. + 77064
 Panasyuk, V.V. + 75963
 Pancer, J. + 77868
 +Pancel, M. 77784
 +Panda, A.R. 74723
 +Pande, D.C. 78758
 Pande, P. + 76565
 +Pandey, B.P. 76565
 Pandey Lakshman. *see* Lakshman Pandey
 Pandharipande, V.R. + 76726
 +Pandharipande, V.R. 74861
 +Pandharipande, V.R. 74861
 +Pandya, N.C. 74886
 +Pandya, N.C. 77070
 Panferov, Yu.F. + 74506
 Pang, K.D. + 78840
 +Panigrahi, M. 77476
 Pankov, A.A. + 77389
 Pankove, J.I. + 77780
 +Pankratova, L.S. 75917
 +Pankratova, N.D. 76538
 +Panova, A.N. 77386
 +Pansart, J.P. 74783
 +Pantelev, Ts.Ts. 75243
 +Pao, C.V. 74285
 +Pao-Shan Weng. 78351
 Paoli, A.L. *De* *see* De Paoli, A.L.
 +Papadopoulos, K. 76178
 +Papalouas, L. 74316
 Papanicolaou, N.A. + 77048
 Papp, K.A. + 78970
 +Papucci, C. 75122
 +Papuchon, M. 75825
 Parashar, R.S. + 77095
 +Pardo, L. 75275
 +Pardo, L. 78135
 +Paretzkin, B. 76407
 +Parga, N. 74698
 +Parham, A.G. 74797
 +Parhi, H. 75958
 +Parjia, I. 75015
 +Paris, H.G. 77629
 Parisi, J. + 77105
 +Paritskaya, L.N. 77669
 +Park, H. 75226
 +Park, H.W. 78292
 +Park, J.Y. 74935
 +Park, J.Y. 74934
 +Park, S.C. 76895
 Park, Y.W. + 76934
 Parker, D.J. 75392
 +Parker, H.S. 76407
 +Parker, J.W. 75824
 Parker, L. 74340
 Parker, L. 74631
 +Parkheta, R.G. 76706
 +Parkhomenko, E.I. 78525
 +Parkhomov, L.G. 76348
 Parkin, S.S.P. + 77140
 Parkin, S.S.P. + 77141
 Parlebas, J.D. 77417
 +Parli, J.C. 74444
 +Parmentier, R.D. 77108
 Parmigiani, C. 78686
 Parmigiani, C. 78686
 Parrott, J.E. + 78066
 +Parsey, J.M. 76889
 +Parsons, A.D. 75893
 Parsons, B. + 78509
 +Parsons, C.R. 76173
 Parsons, S.B. + 78957
 +Partom, Y. 77706
 Partridge, H. + 75330
 +Parvainen, O. 78349
 +Paschal, G. 78327
 +Paschmann, G. 78775
 Pasco, R.W. + 76714
 +Pasemann, M. 76453
 +Pashaev, O.K. 74325
 +Pashchenko, V.P. 77608
 +Pashitskii, E.A. 76935
 +Pashkin, S.V. 76229
 +Pashkovskii, M.V. 76500
 Pasnicu, C. + 77210
 +Passner, A. 75714
 +Passner, A. 75707
 +Pastushenko, S.N. 77313
 +Pastuzak, R. 76396
 +Patangi, S.B. 75052
 +Patangi, S.B. 75054
 +Patashinskii, A.Z. 76584
 Patel, A.N. + 76649
 Patel, A.R. + 77070
 +Patel, M.H. 78553
 Patel, N.B. + 75639
 +Patel, N.B. 77583
 +Paterno, L. 78901
 Pathan, I.A. + 77721
 +Patil, R.N. 77218
 Patil, S.A. 76376
 Patiletyov, Yu.S. + 76552
 +Patki, B.A. 76564
 +Patnaik, P.K. 74798
- Pato, M. Porto. *see* Porto Pato, M.
 Patorski, K. 75578
 Patrick, J.L. + 78202
 +Pattabhi, V. 76411
 +Pattanayak, D.N. 77345
 +Patteri, P. 75648
 +Patterson, B.D. 77315
 Patterson, R.E. + 78020
 +Pattyn, H. 76468
 +Patzelt, P. 74928
 Pau-In Chao. *see* Chao Pau-In
 Paukov, I.E. + 76664
 +Paukov, I.E. 76657
 +Paul, A.C. 75660
 +Paul, G.L. 76717
 Paul, J. + 76774
 +Paul, J. 77623
 +Paul, R. 76299
 +Paul, S. 76299
 +Paulin, J. 77586
 +Pauz, R. 74367
 +Pavan, P. 74992
 +Pavelescu, C. 77581
 +Pavlenko, N.P. 77605
 Pavlenkova, N.I. + 78484
 +Pavlin, I. 74420
 +Pavlov, G.D. 77286
 +Pavlov, S.K. 77352
 +Pavlov, V.A. 77700
 +Pavlyuk, A.A. 75645
 +Pavros, S.K. 77835
 +Pawar, S.H. 78089
 +Payne, B.T. 74797
 +Payne, M.G. 78891
 Payne, S.H. + 76908
 Payne, S.H. + 76909
 Payne, S.H. + 76910
 Paz, O. 76963
 P.B. Macedo. *see* Macedo, P.B.
 Peace, A.J. + 76042
 +Peale, S.J. 78857
 +Pearl, J.C. 78852
 +Pearson, D. 75857
 Pearson, H.J. + 75990
 +Pease, D.C. 75341
 +Pech, R. 77649
 +Pechmann, J.C. 78456
 Peck, C.W. 74790
 Pedersen, K.S. + 76741
 +Pedersen, O.Z. 74537
 Pedersen, P. + 75920
 +Pedicelli, L. 77829
 +Pedoussaut, A. 78948
 +Pedromi, R.S. 74999
 Pedrys, R. + 77507
 Peck, J.M. 75523
 Peichen Zhu. *see* Zhu Peichen
 Peigen Mo. *see* Mo Peigen
 Peizhen Wu. *see* Wu Peizhen
 +Peka, G.P. 76971
 Pekarev, A.I. + 76457
 Peled, E. 77977
 +Peled, E. 77969
 +Pelissier, M. 75562
 +Pellat, R. 76172
 +Pellegriani, C. 75654
 Pelletier, E. + 75549
 Pelis, G.P. 76512
 +Pelous, J. 77404
 +Pelte, D. 75026
 +Penchina, C.M. 76990
 Pendrill, L.R. 75323
 Pendrill, L.R. + 76228
 +Peng, K.S. 75744
 +Peng Huizi. 77214
 +Peng Qing-quan. 74954
 +Penigault, E. 75289
 +Penner, J.E. 78617
 Peppen, J.C.L. *van* 77136
see van Peppen, J.C.L.
 +Perazzo, R.P.J. 74902
 Perchak, D. + 74395
 Peregrine, D.H. 78555
 +Pereshko, O.A. 77202
 +Perezhaler, E. 76257
 +Perepechko, S.N. 77451
 Peres, A. 74594
 +Pereverzev, G.V. 76227
 Perez, A. + 76642
 +Perez, J. 75275
 +Perez, J. 78135
 +Perez, J.M. 75084
 +Perez, P. 75293
 Perez-Madrid, A. + 74383
 Perez-y-Jorba, J. 74791
 Perko, J. + 78217
 +Perkowitz, S. 77094
 +Permyakov, N.Y. 77137
 +Pernicka, E. 78816
 +Perov, P.I. 76875
 +Perova, A.A. 77814
 +Perrin, C. 75040
 +Perrin, N. 75027
 +Perry, D.N. 78915
 +Perry, D.R. 74981

- +Perryman, G.P. 75708
 +Pershin, A.V. 75106
 +Pershin, N.P. 75911
 Persi, P. + 78921
 +Persson, W. 75337
 +Pertosa, P. 77530
 Peschanskaya, N.N. + 76560
 +Pesselnick, L. 78533
 Peshev, O. 77915
 +Peshko, I.I. 75606
 +Pessnell, W.D. 78922
 +Pesonen, L.J. 78430
 +Pesotski, L.V. 78777
 +Petcov, S.T. 74916
 +Peter, J. 75033
 Peters, H. 78548
 Peters, M.J. + 78374
 Peters, M.J. + 78205
 +Peterson, B.A. 79024
 Peterson, C.J. + 78931
 Peterson, E.L. 78179
 +Peterson, L.E. 78992
 Peterson, M.R. + 75329
 +Peterson, R.S. 75506
 +Pethica, B.A. 76750
 +Pethrick, R.A. 76570
 Petke, J.D. + 75306
 +Petkov, N. 78676
 +Petkov, T. 78307
 Petrakovskii, G.A. + 76666
 Petrakovskii, G.A. + 77197
 +Petrisor, T. 77172
 +Petrucco, G. 74449
 +Petrucco, G. 77013
 +Petroff, Y. 75650
 +Petrolino Carvalho, M.J. 77961
 +Petrow, A.G. 76298
 +Petrow, G.E. 76532
 Petrow, Yu.V. 77846
 +Petrow, Yu.V. 77199
 Petrova, T.G. + 75252
 +Petrovic, S. 74967
 +Petrovich, F. 75645
 +Petrovskii, G.T. 77452
 +Petrun'kin, V.Yu. 75645
 +Petrunova, M. 78669
 Petrusiewicz, I. + 78174
 +Petry, W. 76705
 +Petrzhak, K.A. 75063
 +Petrazilka, M. 76292
 +Petecheck, R.G. 77888
 +Petterson, M. 76228
 +Petukhov, B.V. 76450
 +Petukhov, V.O. 75453
 Petukhov, V.P. 78703
 +Peyerimhoff, S.D. 75312
 +Peyre, H. 76264
 +Pfaff, J. 75454
 +Pfeuty, P. 77888
 +Pfisterer, F. 78084
 Pfizterer, M. + 76738
 +Pfothenauer, J.M. 76040
 +Pham Hoi 76703
 Phan-Thien, N. 76076
 Phan-Thien, N. + 76075
 Phelps, A.K. + 75127
 Phelps, D.E. + 78803
 +Philippe, L. 78325
 +Phillips, D. 75427
 Phillips, J.E. + 78085
 +Phillips, J.E. 78088
 +Phillips, R.J. 78838
 +Phillips, R.J.N. 74762
 +Phillips, R.J.N. 74811
 +Phillips, R.J.N. 74828
 Phipps, J.B. + 76693
 +Phu Xuan, N. 75742
 Pi, M. + 74888
 Pianarosa, P. + 76223
 Piancastelli, M.N. + 76768
 Piazzoli, B.D'Ettore
 see D'Ettore Piazzoli, B.
 Piazzoli, B.D'Ettore
 see D'Ettore Piazzoli, B.
 +Picchi, P. 74766
 +Picchi, P. 75225
 +Pichaud, B. 76438
 Piche, M. 75700
 Pickett, G.R. 77103
 +Pickles, W.L. 76214
 Picklesimer, A. 74925
 +Picklesimer, A. 74968
 +Pidzhimyan, P.A. 74482
 +Pieczka, W. 76016
 +Piegaia, R.N. 75403
 +Piel, D. 77728
 +Piela, L. 76914
 Pieper, R.J. + 75588
 +Pieper, S.C. 76726
 +Pierce, J.M. 77699
 +Pieri, J.C. 76308
 +Pierre, F. 74783
 +Piesl, J. 76520
 +Pietronera, L. 79027
 Pietronero, L. 74388
 Pignataro, M. + 75944
 +Pignataro, M. 75945
 +Pignataro, S. 77784
 Pignatelli, G. + 76514
 +Pikus, Yu.G. 77412
 +Pikuz, S.P. 76216
 +Pikuz, S.P. 77782
 Pilat, J.F. + 75210
 +Pilipenko, V.I. 76487
 Pilipetskii, N.F. + 75604
 +Pili, A.A. 75019
 Pilui, V.A. 77836
 +Pilyankevich, A.N. 76616
 Pimbley, J.M. + 77347
 +Pimenov, I. 78669
 +Pimenov, L.A. 78300
 +Pimentel, G.C. 77878
 Pimia, M. 74817
 Pin, H. de La Tour du see de La Tour du Pin, H.
 Pindzola, M.S. + 75518
 Pindzola, M.S. + 75521
 Pinho, A.C. De see De Pinho, A.C.
 Pinkston, W.T. 75038
 +Pinston, J. 75040
 +Pinter, I. 77224
 +Pinzenik, V.P. 77384
 +Pipkin, F. 74669
 +Piqueras, J. 77431
 +Pirnat, J. 78398
 Pirogov, Y.F. 74659
 +Pirraglia, J.A. 78853
 +Pirraglia, J.A. 78852
 Pisani, C. + 76885
 +Pischel, E. 78276
 Pismis, P. + 78984
 Pismis, P. + 78985
 +Pisoni, D.B. 78201
 +Pisoni, D.B. 78192
 Pistoia, G. 77893
 +Pitt, C.W. 75787
 +Pitt, G.D. 75818
 +Pitukhin, P.V. 74771
 +Piven, B.T. 75761
 +Privorov, A.A. 74718
 +Pizzala, L. 75382
 +Pizzini, S. 77555
 +Pladzwicz, J.R. 75483
 +Pladutin, F. 77582
 +Plakida, N.M. 77087
 +Plasil, F. 75026
 +Plasil, F. 75036
 +Plastino, A. 74871
 +Plastino, A. 74873
 +Platania, G. 74341
 +Platkov, V.Ya. 76449
 +Plato, P.A. 78347
 Plekhanov, A.I. + 75721
 +Plekhanov, V.G. 77435
 Plicht, J. vander
 see vander Plicht, J.
 Ploeg, P. van der see van der Ploeg, P.
 +Ploog, K. 77448
 +Ploog, K. 77395
 +Ploskirev, E.G. 77289
 +Plotkina, G.Z. 78331
 +Plotnikov, E.P. 75971
 +Plummer, E.W. 77529
 +Plummer, P.L.M. 78120
 Plyavenek, A.G. 77167
 Po-chun Chi
 see Chi Po-chun
 Pochi Yeh 74523
 Pockrand, I. + 75393
 +Podel'shchikov, A.I. 77191
 +Podrezov, A.A. 76429
 +Poe, R.T. 75017
 +Poeti, G. 76294
 +Poggioli, L. 74783
 +Pogorelov, A.E. 76493
 +Pogorelov, D.A. 77607
 Pogosyan, T.I. 74261
 Pogrebnyak, S.V. + 77252
 +Pohl, B.A. 75000
 Pohl, E. + 78333
 +Pohl-Ruling, J. 78333
 Poiree, B. 76057
 Poirier, R.A. + 75267
 +Poisson, M.A. 77037
 +Poisson, M.A. 77577
 Pokhmurskii, V.I. + 76706
 Poklonski, N.A. + 76949
 +Pokrovsky, O.M. 78580
 +Pokrovsky, V.L. 76933
 +Pokryvailo, N.A. 76027
 +Pol, Y.S. 75011
 Polchinski, J. + 74663
 +Politzhaev, V.V. 75776
 +Pollette, D.G. 78321
 Politzer, P. + 75254
 Polla, D.L. 76965
 +Polla, G. 77546
 +Pollack, E. 75506
 +Pollak, R.A. 77531
 +Pollak, R.A. 75759
 +Pollard, D.D. 78506
 Pollard, H.E. 78018
 Pollock, D.D. 76367
 Polls, A. + 74863
 Pols, L.C.W. + 75869
 +Poluektov, N.S. 75451
 Polvado, R.O. 74826
 Polyakovskii, V.M. + 76976
 +Pombo, J.L. 75806
 +Pominov, I.S. 75363
 +Pompoli, R. 75860
 +Ponomarenko, V.I. 76855
 +Ponomarev, Yu.N. 78778
 +Pons, J.N. 77396
 Pontenagel, W.M.G.F. + 76343
 +Pontiggia, C. 77547
 +Pontikis, V. 76615
 Poole, M.W. + 75662
 Poon, S.J. 77082
 +Poore, A.B. 77889
 +Pop, I. 77172
 Pople, J.A. 77885
 Popov, A.A. + 76687
 +Popov, A.I. 75693
 +Popov, A.K. 75729
 Popov, A.P. 76861
 +Popov, A.Yu. 77005
 +Popov, B.A. 77659
 +Popov, V.S. 74321
 Popov, V.V. + 76631
 +Popov, Ye.A. 78446
 +Popov, Yu.A. 77340
 +Popova, M.F. 78244
 +Popovich, N.S. 76995
 Poppe, C.H. + 74972
 Poppe, W. 75843
 +Porey, P.D. 76083
 +Portal, J.C. 77037
 Portaz, J.M. 77856
 Porter, A.J. + 77674
 Porter, G. 78091
 Porter, W.A. + 75586
 +Porto, F. 75022
 Porto Pato, M. + 75214
 +Post, D.E. 74205
 Postma, H. + 74463
 +Postma, H. 74993
 +Postnikov, A.V. 77173
 +Postnikov, L.N. 78245
 +Postnikov, V.M. 77111
 +Postnikov, V.M. 77085
 Postogard, G.I. + 77783
 Potapenko, P.T. 75080
 Potapenko, P.T. 75161
 +Potepun, L.I. 75561
 Potter, R.R. + 78047
 +Pouget, J.P. 76863
 Poulikakos, D. + 76107
 +Poulsen, P. 76214
 +Pounds, D.W. 78277
 +Pourcin, J. 75382
 +Poutanen, T. 78284
 +Poutanen, T. 78188
 Povedallo, V.A. 75626
 +Powzner, A.B. 77158
 +Powar, K.B. 78683
 +Powell, J.R. 77955
 +Powers, E.L. 78267
 Powles, J.G. + 76275
 Prabha, S. + 76092
 +Prade, B.S. 74516
 +Pradhan, T. 74700
 +Pradhan, T. 75481
 Prager, S. + 77727
 Prakash, C. 74399
 Prakash, J. 76482
 Prakash, J. + 75543
 Prakash, O. + 77302
 +Prakash, R. 75903
 +Prakash, R. 76013
 Prakash, S. 76591
 +Prakash, S. 78674
 +Prakash, S. 78773
 +Prakash, Y. 75045
 +Pranevicius, L. 76567
 +Prasad, M. 76916
 +Prasad, M. 75377
 +Prasad, Y.V.R.K. 77662
 +Prasanna, A.R. 78940
 +Prata, A.T. 76015
 +Predica, A. 78105
 Predmetsky, T. + 78356
 +Preece, C.M. 76497
 +Preedom, B.M. 74804
 +Preger, M. 75648
 +Preis, D. 78194
 +Prekul, A.F. 76931
 +Prelovsek, P. 77272
 +Prentice, K. 78603
 Prescott, C.Y. 74715
 Prescott, C.Y. 74825
 +Preskill, J. 74612
 Preston, R.A. + 79014
 Preston, R.A. + 78945
 +Presutti, E. 74391
 +Pretorius, R. 76710
 +Preuss, H. 75263
 Prevot, M. + 78434
 +Prewitt, C.T. 76370
 +Price, H.I. 78273
 Price, L.E. 75228
 +Price, M. 74766
 +Price, M. 75225
 Price, P.J. 77036
 Price, P.J. 77040
 +Pridehl, E. 75170
 +Priester, L. 77633
 +Priestogine, I. 74423
 +Prikhod'ko, L.I. 77268
 Prikhot, A.F. + 77412
 Primak, W. + 74438
 +Primak-Mirolyubov, V.N. 78246
 Primdahl, F. + 78760
 +Prince, A. 77618
 Prince, E. + 76237
 Prins, J.F. 76941
 +Priol, M. 77522
 +Prionas, S.D. 78277
 +Prisner, Th. 77261
 +Pritchett, W.C. 76795
 +Privalov, Yu.V. 75170
 +Prokhorov, A.M. 75763
 +Prokhorov, A.M. 75767
 +Prokopenko, V.E. 75702
 Proksch, P. 75566
 +Prokudina, V.K. 75795
 +Prokunin, A.N. 76077
 Prosch, T. + 78644
 Prosnitz, D. + 75660
 Prosser, J.S. + 78262
 +Prost, J. 74384
 +Protasov, Yu.S. 76169
 +Protsenko, N.A. 76699
 Proudfoot, J. 74784
 +Prudnikov, E.K. 77361
 Pryor, C. + 78998
 +Psenic, I. 78484
 +Pshenichnaya, G.N. 76487
 Pudziaonowski, A.T. + 77871
 +Pueyo, L. 76911
 +Pugach, E.A. 77782
 +Puglierin, G. 74756
 +Puglisi, O. 76513
 +Pugolovok, M.M. 75917
 +Puhlhofer, F. 75030
 +Pukhlili, Zh.A. 77444
 +Pukhov, V.V. 78256
 +Puko, R.A. 77940
 Pulham, R.J. + 77880
 +Pullia, A. 74766
 +Pullia, A. 75225
 +Pullman, B. 75465
 Pumphrey, W.A. + 78804
 +Purandar, K. 76905
 +Purcell, C. 78396
 +Purdy, G.R. 76709
 +Puresheva, B. 77979
 +Puri, A. 77345
 +Puri, M.L. 74292
 Purkayastha, A.K. + 75367
 +Purnell, A.W. 78046
 Purniah, B. + 76563
 +Purtell, R.J. 77531
 +Purton, C.R. 78970
 +Purvish, G.D., III. 75268
 +Puschae, P. 78669
 +Puschell, J.J. 79019
 +Pushkareva, T.V. 78245
 +Pushkin, V.V. 75207
 +Pustogarov, A.V. 76596
 +Putterman, M. 78324
 +Puttock, J.S. 75990
 Putvinski, S.V. 76203
 +Putz, N. 77576
 +Pyatiletov, V.G. 78497
 +Pyatkov, Yu.V. 75244
 +Pykacz, H. 77338
 +Pyn'ko, V.G. 77249
 +Pyrrros, N.P. + 76252
 +Pyrrros, N.P. 76407
 +Pytte, E. 77188
 +Pyykko, P. 76842
 Qianer, Z. 75274
 +Qin Hong. 77813
 Qin-yue Qu see Qu Yin-yue
 Qing Sun see Sun Qing
 Qing-hua Du see Du Qing-hua
 Qing-quan Peng see Peng Qing-quan
 Qinggui, W. 74255
 Qingrong Feng see Feng Qingrong
 Qiu, Y. + 76153
 Qu Yin-yue + 78938
 +Quantin, B. 77746
 Quaranta, A. Alberigi see Alberigi Quaranta, A.
 +Quazi, A.H. 75859
 +Queen, J. 77135
 +Queeney, R.A. 77729
 +Queirolo, G. 76711
 +Queirolo, G. 76514
 Quenzel, H. 78657
 +Quenzel, H. 78584
 +Quenzel, H. 78658
 +Querchia, F. 78695
 Quesnel, D.J. + 76557
 +Quesnel, D.J. 77744
 +Quillec, M. 76646
 +Quimby, D.C. 75651
 +Quindos, L.S. 78700
 +Quinn, A.J. 75858
 +Quinn, P.J. 78143
 Quint, S.R. + 78389
 +Quiros, M. 74586
 +Quisapel, G.R.W. 74253
 +Qureshi, M.A. 77721
 +Ra, J.B. 78323
 +Rabalais, J.W. 77498
 +Rabbe, P. 77800
 +Rabii, S. 75272
 +Rabinkin, A. 77631
 +Rabinovici, E. 74650
 +Raby, S. 74355
 +Rachiele, R. 78568
 +Racz, S. 76999
 +Radautsan, S.I. 76978
 +Radermacher, E. 74756
 Radford, I.R. 78160
 +Radhakrishna, S. 76499
 Radkevich, E.V. + 76595
 Radousky, H.B. + 76662
 +Radow, A. 78119
 +Radzio-Andzelm, E. 75257
 +Radziszewski, G.J. 75391
 +Rae, W.D.M. 75019
 +Rae, A. 78448
 +Rafalowicz, J. 76928
 Rafat, M. + 74777
 +Ragazzi, S. 74766
 +Ragazzi, S. 75225
 +Raghavan, R. 74794
 +Raghavan, R. 74814
 +Ragimov, A.S. 77393
 Rahilly, W.P. + 78016
 +Rahilly, W.P. 78032
 Rahman, B.M. Azizur see Azizur Rahman, B.M.
 Rahnamai, H. + 76129
 +Rahul 75543
 Rai, A.K. + 75400
 +Rai, B. 75543
 +Rai, D.K. 75400
 +Rai, S.B. 75400
 +Raj, R.K. 75744
 Raj K. Gupta + 75361
 Raj Kumar, S. + 74710
 +Raja Ram, P. 77564
 +Rajagopalan, S. 75992
 Rajeev, S.G. 74348
 +Rajeswaran, G. 78059
 +Rajner, V. 78109
 +Rajput, B.S. 74710
 Rak Lee Kyo see Kyo Rak Lee
 +Rakauskene, B.K. 78305
 +Rakhlin, M.Ya. 77075
 +Rakhmenkulov, F.S. 76666
 Rakov, A.F. 76422
 +Ralarosy, J. 75236
 +Ralph, B. 77714
 +Ralph, B. 77674
 +Ram, P.C. 76021
 Ram, P. Raja see Raja Ram, P.
 Ram, S.N. + 74735
 Ram, U.S. + 77170
 Rama Rao, G. + 78233
 Ramachandran, G. + 75052
 Ramachandran, G. + 75054
 +Ramachandran, R. 74777
 +Ramakrishna Rao, T.V. 75331
 +Ramakrishna Reddy, R. 75331
 Ramaley, L. + 74539
 +Ramana Murthy, P.V. 75226
 Ramana Rao, G. + 75307
 +Ramana Rao, G. 75358
 Ramaty, R. + 78811
 +Rami, F. 75031
 +Rami, F. 75065
 +Ramirez Mittelbrunn, J. 74586
 Ramsey, N.F. 74773
 Ramulu, K. Sree see Sree Ramulu, K.
 +Rana, V.D. 75932
 Rand, R.H. 78225
 Randic, M. 75283

- Randic, M. 74506
 +Randall, H. 74783
 +Randoshkin, V.V. 77563
 +Randoshkin, V.V. 77225
 +Randrup, J. 74956
 +Ranganathan, R. 76563
 Rangayyan, R.M. 78316
 Range, K.-J. + 76636
 Rank, D. + 78109
 +Ransom, R.A. 78076
 +Ranta, A. 78735
 Ranta, H. + 78735
 Rao, B. Haragopala
 see Haragopala Rao, B.
 Rao, G. Rama
 see Rama Rao, G.
 Rao, G. Ramana
 see Ramana Rao, G.
 Rao, G. Sambasiva
 see Sambasiva Rao, G.
 Rao, G.S. Trivikrama
 see Trivikrama Rao, G.S.
 Rao, H.N. Venkoba
 see Venkoba Rao, H.N.
 Rao, J.K. Mohana
 see Mohana Rao, J.K.
 Rao, K.S. Gundu
 see Gundu Rao, K.S.
 +Rao, N.K. 75045
 Rao, N.S. + 75508
 Rao, P. Sambasiva
 see Sambasiva Rao, P.
 +Rao, P.V.S. 75871
 Rao, R.V. Gopala
 see Gopala Rao, R.V.
 Rao, T.V. Ramakrishna
 see Ramakrishna Rao, T.V.
 +Rao, V.J. 78059
 Rao, V.S.V. Bapeshwara
 see Bapeshwara Rao, V.S.V.
 Rapaport, J. 74831
 Rapley, C.W. + 74460
 +Rapoport, V.I. 76915
 +Ras, W. 77209
 +Rasch, K.-D. 78058
 +Rasch, K.-E. + 78037
 +Raschke, E. 78644
 +Rashid, K. + 75284
 +Rashkov, S. + 77805
 +Rashkov, S. + 77806
 +Rashleigh, S.C. 74517
 +Rashleigh, S.C. 75813
 +Rasmussen, A.L. 75704
 +Rasmussen, J.J. 76180
 +Rasmussen, J.O. 74932
 +Ratishvili, I.G. 76365
 Raturi Atul
 see Atul Raturi
 +Rau, T.F. 76347
 Rau, V.G. + 76348
 Rau, V.G. + 76347
 +Rauch, F. 76700
 +Rauch, V. 75034
 +Rauschenbach, H.S. 78020
 Rauth, D. + 76409
 +Rautian, S.G. 75721
 +Rava, P. 77555
 +Raveau, B. 76945
 +Ravikumar, K.G. 75357
 +Ravishankar, V. 75052
 +Ravishankar, V. 75054
 +Ravlik, A.G. 77226
 Rawitscher, G. 74940
 Rawlings, R. 77675
 +Rawlins, W.T. 76200
 Rawson, E.G. + 77939
 Ray, A. + 75075
 Ray, A. + 76324
 +Ray, A.K. 76571
 +Ray, B. 76952
 +Ray, B. 76420
 Ray, K.K. + 77713
 Ray, L. 74939
 Ray, L. + 74997
 Ray, L. + 74998
 +Ray, L. 74987
 Ray, L. 74996
 Ray, R. 77600
 +Ray, U.C. 77990
 +Rayment, J.J. + 76653
 +Raymond, F. 78068
 +Raynaud, D. 78571
 +Raynaud, P. 78325
 Raza, S.H. 74393
 Razavy, M. 74304
 +Razdobarin, G.T. 76217
 Razeghi, M. + 77577
 +Razeghi, M. 77037
 +Razumovskaya, O.N. 77333
 Razzag, Z. + 77709
 +Razzetti, C. 77397
 Re, G. Del
 see Del Re, G.
 +Read, D. 77145
 Read, W.G. + 75544
 +Read, W.G. 75417
 +Ream, S.L. 76763
 +Reardon, P.C. 78689
 +Rebane, L.A. 75364
 +Reber, J.F. 77907
 +Rebhan, U. 75342
 +Rebolledo, M.A. 75609
 +Rebrin, Yu.I. 74494
 +Rebrov, A.V. 75767
 Reck, R.A. 78581
 +Recker, K. 77255
 +Redaeli, F. 77555
 +Reddy, C.P.K. 75404
 Reddy, K.N. + 76423
 +Reddy, K.P.J. 75698
 +Reddy, K.V. 76689
 Reddy, P. Jayarama
 see Jayarama Reddy, P.
 Reddy, R.R. + 77282
 Reddy, R. Ramakrishna
 see Ramakrishna Reddy, R.
 Redfield, D. 77021
 +Redondo, A. 76771
 Reed, E.D. + 75685
 +Reeder, D.D. 74759
 Reeder, P.L. 75058
 Reep, D.H. + 76804
 Regel, L.L. + 76339
 +Regel, V.R. 76446
 +Regnault, J.C. 76436
 Regnier, P.G. + 76508
 +Regreny, A. 77447
 Rehm, W. + 77448
 +Reich, C.W. 74907
 +Reich, S.L. 74902
 +Reichardt, D. 76867
 +Reiche, C. 75096
 +Reichelt, W. 76618
 Reichenbach, H. 74247
 Reichmanis, M. + 78172
 +Reid, J. 75619
 Reid, J.L. + 74602
 Reid, M.H. 78297
 +Reihl, B. 77525
 +Reihl, B. 77530
 Reik, H.G. + 75315
 Reiman, A. + 76207
 Reiman, A.H. 76181
 +Rein, D. 74756
 +Rein, R. 78132
 +Rein, R. 78121
 +Reineker, P. 76849
 +Reinen, D. 76402
 +Reines, F. 75226
 +Reinhardt, E.R. 78045
 +Reinhardt, P.-G. 74933
 +Reinisch, G. 74621
 Reintjes, J. + 75737
 +Reipurth, B. 78950
 +Reissner, M. 77208
 +Reitbock, H. 78171
 +Reite, M. 78212
 +Reiterov, V.M. 75783
 +Reithler, H. 74756
 +Rek, A. 77617
 +Rekalo, M.P. 74753
 +Reme, H. 78778
 Remizovich, V.S. 77484
 +Remmers, H. 78117
 +Remsberg, L.P. 78816
 +Ren Jing-ong 75296
 Ren Zhenqiu 78467
 Rendon-Diazmiron, L.E. + 76382
 +Renier, M. 76753
 +Renieri, A. 75670
 +Renieri, A. 75649
 +Renieri, A. 75656
 Renninger, G.H. 78177
 +Rensink, M.E. 76214
 Rentergem, M. Van
 see Van Rentergem, M.
 +Rentzepis, P.M. 75419
 +Repp, H. 76163
 Reshetin, O.D. 75914
 Rethfeld, H. + 77945
 +Reuss, J. 75372
 +Reva, M.G. 75401
 +Revin, I.D. 75675
 Revina, A.A. 77046
 Revuz, D. 74372
 Reynolds, L. + 78166
 +Reynolds, R.T. 78857
 +Reynolds, W.C. 75991
 +Reznichenko, L.A. 77333
 +Reznik, L.E. 76664
 +Reznikov, S.N. 75597
 Rho, M. 74854
 Rhoades-Brown, M.J. + 74933
 +Rhoades-Brown, M.J. 75037
 +Rhoads, J.W. 78840
 +Rhodes, E.J., Jr. 78889
 +Rhodes, R.P. 78201
 +Rhodin, T.N. 77534
 Rhung-tai Wang
 see Wang Rhung-tai
 +Rhynke, K. 75091
 Riah, N. 76024
 +Riande, E. 77320
 +Riani, P. 75326
 Ribeiro, P. Costa
 see Costa Ribeiro, P.
 Ricard, Y. + 78478
 +Rice, D.W. 75114
 +Richard, N.A. 78086
 Richard Ma Ning-Yuan
 see Ning-Yuan Richard Ma
 +Richards, W.B. 75876
 Richardson, S.M. 76078
 Richer, F. + 78209
 +Richer, F. 78397
 +Richert, J. 75031
 Richstone, D.O. + 79011
 Richter, F.M. + 76025
 Richter, G. + 78872
 Richter, G.A. 78928
 Richter, J. + 76927
 +Richter, U. 78189
 Rickard, L.J. + 78999
 +Rickard, W.H. 75140
 Ricker, D.W. 75885
 Ricks, R.A. + 77645
 Riedler, W. + 78575
 +Rienstra, W.W. 76182
 Rigaud, P. + 78619
 Righini, R. + 77371
 +Rigny, P. 77275
 +Riklund, R. 76828
 +Rikus, L. 74865
 +Riley, N. 76042
 +Rinaldi, S. 76800
 +Ring, E.J. 75108
 +Rinzivillo, R. 75648
 +Rioux, C. 74972
 +Ripper, J.E. 75639
 Rippon, C. + 77908
 +Risbud, S.H. 77614
 +Riss, U. 74547
 +Ristig, M.L. 76729
 Ritala, R.K. + 77100
 Ritchie, B.G. + 74804
 +Ritchie, R.O. 76558
 Ritis, R. de
 see de Ritis, R.
 +Ritke, S.J. 78838
 +Ritters, E.-W. 78099
 Ritz, A. + 77015
 +Rivalet, J.P. 77972
 Rivet, M.F. + 75033
 Rivier, N. 77924
 +Riviere, D. 76291
 +Riviere, M. 74783
 Rivoire, G. + 75742
 +Rizaev, Kh.A. 74809
 Rizz, N. + 75945
 +Rizzi, N. 75944
 +Robbins, V.M. 76960
 +Robelet, M. 77768
 +Roberge, P.C. 75365
 +Robert, G. 77363
 +Robert, N. 78427
 Roberts, N.J., Jr. + 78239
 Roberts, P.H. 75569
 Roberts, R.B. + 77239
 +Roberts, T.J. 74759
 +Roberts, W.E. 78102
 +Robertson, J.M. 77426
 +Robin, S. 77522
 Robino, C.V. + 77798
 +Robinson, B.J. 76727
 Robinson, E.R. + 75859
 Robinson, G.R., Jr. + 76655
 +Robinson, K. 75672
 +Robinson, K.E. 75650
 Robinson, M.T. 75627
 Robinson, M.T. 77500
 +Robinson, P.H. 77565
 +Robinson, R.L. 75026
 Roby, A.R. 75078
 Rocco, H.O. Di
 see Di Rocco, H.O.
 Rocher, P. 78844
 Rochette, J.F. + 77006
 Rockmore, R.M. 75051
 +Rode, A.V. 76168
 Rode, D.L. + 76980
 Rodgers, J. 74435
 Rodgers, R.P.C. + 78311
 +Rodi, W. 76085
 Rodigin, V.N. 74448
 Rodrigues, W.A., Jr. 74276
 +Rodriguez, A. 77523
 Rodriguez, L.F. 78906
 +Roe, B.P. 74759
 +Roessler, B. 78103
 +Rogachev, A.A. 76848
 +Rogacheva, L.F. 75732
 Rogacheva, S.A. + 78249
 Roger, A. 75576
 Roger, J. + 77396
 Rogers, V.C. + 75144
 +Rogl, P. 76390
 +Rohatgi, V.K. 76167
 +Rohatgi, V.K. 74464
 +Rohrecker, L. 75147
 Rokhlin, L.L. 76632
 +Rolland, M. 77887
 +Rolfsson, R.J. 76787
 +Rollier, M. 74766
 +Rollier, M. 75225
 +Romani, G.L. 78204
 +Romani, G.L. 78281
 +Romanichev, M.K. 75207
 +Romanis, M. 77073
 Romaniv, O.N. + 77755
 +Romanov, G.N. 78251
 +Romanov, V.A. 74494
 +Romanowski, T.A. 74759
 +Romanowski, Z. 77574
 +Romanyuk, D.A. 76674
 +Romanuk, N.A. 77358
 +Romashova, L.F. 77158
 +Romashov, A.P. 75703
 +Romashov, V.M. 77684
 Romdhan, S.S. + 77258
 Romeo, C. Cara
 see Cara Romeo, C.
 +Romeo, G. 75398
 Romero, S. Lopez
 see Lopez Romero, S.
 +Rompelman, O. 78214
 Rong Jianxiang + 79007
 Rong Loh
 see Loh Rong
 Rong Wu Zhang + 77736
 Rong-fu Ling
 see Ling Rong-fu
 Rongyao Zhang
 see Zhang Rongyao
 Roos, A. 77553
 Roos, O. von
 see von Roos, O.
 +Roosen, T.A. 77743
 Root, J.W. + 75469
 +Roper, R.G. 78726
 +Ropke, G. 74891
 +Roques, R. 75541
 +Rosa, R. 74368
 Rosado, M. 78983
 Rosado, M. + 78986
 Rosander, S. 75666
 Roschmann, P. + 77267
 Rose, J. + 76834
 +Rose, J.W. 76601
 Rosemeier, R.G. + 77988
 +Rosen, A. 76774
 +Rosen, D.C. 75266
 Rosen, N. + 74347
 +Rosen, S.P. 74916
 Rosenberg, R.S. + 78226
 +Rosenberg, T.J. 78735
 Rosenberg, Z. + 77706
 +Rosenblat, S. 76114
 +Rosenbluth, M.N. 75652
 +Rosensteel, G. 74876
 Rosenstein, A.H. 77540
 +Roshchenko, A.T. 77226
 +Roshchupkin, S.M. 76449
 +Rosinger, W. 75527
 Ross, J.N. 74519
 +Ross, J.W. 77302
 +Ross, R. 78119
 Ross, R.T. 78002
 +Rossbach, D. 74827
 +Rosser, W.G.V. 78437
 Rossi, H.H. 75199
 Rossi, M.J. + 75483
 +Rossignol, M.F. 77175
 Rossler, K. + 76470
 +Rossler, K. 77505
 +Rossler, K. 76538
 Rossum, M. van
 see van Rossum, M.
 +Rostoker, G. 78762
 Rotbard, G. + 74847
 +Roth, T.J. 76883
 Rothaut, J. + 77677
 +Rothe, H.J. 74603
 Rothschild, R.E. + 78992
 Rotter, I. 74919
 Rotter, I. 74943
 Rotty, R.M. 78115
 +Rotty, R.M. 78604
 +Roubal, S. 75149
 Rouby, D. + 76568
 Rouby, D. + 76569
 +Rouchy, J. 77229
 Rouhani, S.Z. + 76089
 Roulet, M.E. + 75841
 +Roult, G. 76396
 +Roure, F. 78502
 Rousseau, M. 75847
 Rousseau, M. 75848
 +Rousseng, J. 74371
 Rousset, G. + 76675
 +Routbot, J.L. 76522
 +Roux, D. 78774
 Rouxel, J. + 77984
 +Rovid, M. 75189
 +Rowe, D.J. 74947
 +Rowlands, J. 75136
 Rowlands, S. + 78156
 +Rowley, D. 74972
 +Rowley, J.K. 78888
 +Rowley, J.K. 78816
 +Rox, A. 74928
 +Roy, A.K. 74504
 +Roy, J. 74800
 +Roy, J. 74801
 +Roy, J. 75046
 +Roy, J. 75047
 +Roy, K. 78037
 +Roy, K. 78058
 Roy, M. Deb
 see Deb Roy, M.
 Roy, R.J. Le
 see Le Roy, R.J.
 Roy, S.K. + 76627
 +Roy, T. 74801
 +Roy Chowdhury, A. 74801
 +Roy Chowdhury, K. 74801
 +Roychaudhuri, D. 78010
 +Royen, P. 75418
 +Rozaendal, H.C.F. 76254
 Rozin, E.G. + 77299
 +Rozov, B.S. 75768
 Ru-xin Cheng
 see Cheng Ru-xin
 Rubakov, V.A. + 74672
 Rubakov, V.A. + 74346
 Rubakov, V.A. + 79039
 Rubeko, L.M. + 77882
 +Rubi, J.M. 74383
 Rubinov, A.N. + 75681
 Rubinshtein, V.M. + 75703
 +Rubloff, G.W. 77531
 Ruchti, C.B. + 76213
 +Ruchti, R. 74669
 Rucinski, S.M. 78923
 +Ruckl, R. 74717
 +Rudakov, L.I. 76193
 +Rudakov, T.N. 74505
 +Rudchenko, V.V. 76442
 +Ruden, P. 77448
 Rudnick, L. + 79016
 Rudolf, G. + 75034
 +Rudykh, I.A. 74483
 +Ruegger, B. 75123
 Ruf, H. + 77663
 +Ruhl, F. 75803
 Rui-gi Dong + 75845
 Ruiying Cai
 see Cai Ruiying
 Rukung Su
 see Su Rukung
 Rukhlinski, V.V. + 76028
 Rulin Wang
 see Wang Rulin
 Rulliere, C. + 75365
 +Rumchev, I. 78673
 Rummyantsev, V.G. + 77361
 Runben Huang
 see Huang Runben
 Ruo-Zhuang Liu
 see Liu Ruo-Zhuang
 +Ruolene, Yu.I. 76302
 +Rupnik, K. 75320
 +Rusanov, A. Ya. 75059
 +Rusanov, I.B. 76853
 +Ruscic, B. 75438
 Rushton, E. + 76081
 Rusinko, K.N. 75936
 Russell, C.T. 78679
 +Russell, G. 78603
 +Russell, K.S. 78868
 Russell, P.B. + 78662
 Russell, P.B. + 78660
 +Russell, P.E. 78070
 +Russell, R.W. 78856
 +Russell, T. 78103
 Russer, P. 77098
 Russo, G. + 78949
 +Russo, G. 74949
 +Rust, W.D. 78622
 Rvachov, V.L. + 75931
 +Ryabich, L.M. 77612
 +Ryabov, G.A. 76532
 Ryabov, Yu.V. + 75001
 +Ryban, C.G. 74844
 +Ryban, J.D. 74511
 +Ryban, T.G. 76477
 +Rybsnyj, V.G. 74823
 +Ryazhskaya, O.G. 74823
 +Rybalko, A.F. 76926
 +Rychkov, B.A. 75935
 +Rygalin, V.N. 76059
 Rykalin, N.N. + 76188
 +Ryrie, S.C. 78519
 +Rysakov, O.M. 75597
 +Ryzhikov, V.D. 75401
 +Ryzhkov, V.G. 77667
 +Ryzhov, N.V. 75160
 Rzaigui, M. + 76590
 +Rzhevskii, M.B. 77438

- +Sabljić, A. 75438
 +Sachdev, R.N. 74536
 +Sacher, G.A. 78226
 +Sachot, E. 78327
 +Sadana, D.K. 76507
 +Sadocco, P. 76326
 +Sacki, K. 76176
 +Saenki, V.Ya. 77626
 Saermark, K. 74609
 Saermark, K. 78211
 +Saffman, P.G. 76053
 +Safin, V.A. 77290
 +Safonov, V.P. 75721
 +Sagalovich, A.Ya. 75694
 +Sagalovskaya, O.V. 74576
 Sagawa, E. + 78748
 +Sagawa, E. 78750
 +Sagawa, E. 78749
 +Sagawa, E. 78751
 +Sagawa, E. 78787
 +Sagawa, T. 77406
 Sagayama, Y. + 75086
 +Sager, W.W. 78436
 +Sah, C.T. 78074
 Sah, C.-T. + 77017
 Saha, N. 75513
 Saha, N.R. + 78010
 Sahakian, A.V. + 78381
 Sahasrabudhe, V. 77480
 Sahimi, M. + 74374
 +Sahota, H.S. 74900
 +Saidov, R.P. 75646
 Saikans, S. 75743
 +Saikia, D.J. 79006
 +Saini, D.R. 75978
 +Saini, J.S. 75903
 +Saini, J.S. 76013
 +Saini, S. 75035
 +St.-Pierre, L.E. 76627
 +Saint-Dizier, J.P. 76223
 +Saito, G. 76932
 +Saito, K. 77609
 +Saito, K. 75169
 +Saito, R. 76344
 Saito, S. + 75369
 +Saito, T. 74870
 +Saito, T. 77482
 +Saito, T. 78763
 +Saka, H. 76445
 +Sakagami, K. 77375
 Sakaguchi, H. + 74966
 +Sakaguchi, H. 75222
 +Sakaguchi, H. 75003
 Sakai, E. 75241
 Sakai, N. 74685
 Sakai, S. 74601
 +Sakai, T. 77693
 +Sakairi, H. 77723
 +Sakairi, S. 77616
 Sakaki, H. + 77029
 +Sakakibara, A. 77664
 +Sakakibara, Y. 75634
 +Sakalauska, S.V. 77349
 Sakamoto, H. + 75003
 +Sakamoto, H. 75222
 +Sakamoto, H. 74966
 Sakamoto, T. 75763
 Sakamoto, T. 77025
 +Sakanishi, K. 75103
 +Sakata, M. 77132
 Sakata, S. + 75959
 +Sakata, T. 77904
 Sakharov, B.A. + 76245
 +Sakharov, B.A. + 76246
 +Sakharova, V.V. 78255
 +Sakhnovskii, M.Yu. 74513
 Sakimoto, K. 75471
 +Sakita, B. 74627
 Sakitt, B. + 78218
 Sakka, M. 78270
 +Sakkal, F. 75908
 +Sakomoto, J. 74634
 +Saku, T. 75690
 +Sakuma, I. 75687
 +Sakuma, S. 75891
 +Sakun, V.P. 77451
 Sakunthalamma, Y. + 76905
 Sakurai, J.J. 74693
 +Sakurai, T. 78763
 +Salama, A. 78293
 Saleem, S.S. + 75375
 +Saleev, E.Yu. 77357
 Saleh, R.M. + 77847
 +Salehpour, A. 76017
 +Salerno, M. 74294
 Sales, B.C. + 76924
 +Saletskii, A.M. 75631
 +Salibaev, N.T. 77804
 +Salikhov, I.Kh. 77260
 +Salin, D. 77250
 +Sall, M.A. 74322
 Salmeron, M. + 76791
 Salmon, L.G. + 77534
 +Salomaa, M.M. 77100
 Salomone, L.A. + 78540
 +Salsac, P. 76807
 +Salsano, A. 77013
 +Salter, P.F. 78557
 +Salters, V.J.M. 78481
 +Salveti, O. 75326
 +Salzborn, E. 75500
 +Salzborn, E. 75519
 +Samardjiev, T.D. 78667
 +Samarin, V.K. 77757
 +Samariskii, A.A. 76032
 Sambasiva Rao, G. + 77662
 Sambasiva Rao, P. + 75331
 +Sambataro, S. 75022
 Samelson, H. + 75686
 +Samm, U. 74756
 +Samofalov, V.N. 77226
 +Samoilova, L.I. 75162
 +Samokhin, A.I. 76216
 Samokhvalova, N.S. + 78244
 Samorski, M. + 78494
 +Samouel, M. 76395
 +Sampaio, F.C. 74849
 +Sams, R.L. 75381
 Samson, J.C. + 78762
 Samsonidze, G.E. + 76630
 +Samsonov, L.G. 76532
 +Samsonov, V.M. 76532
 Samsonova, N.D. + 76903
 +Samudravajaya, K. 77092
 +Samuel, M. 74669
 Samuelson, R.E. 78861
 +Sanada, J. 75004
 +Sanchez, E. 78062
 +Sanchez, F. 78865
 Sande, J.B.Vander. 75362
 +Sander, A.A. + 75704
 Sanders, T.H., Jr. + 77629
 +Sanders, W.T. 78908
 Sanderson, M.L. 76139
 Sanderson, R.W. + 78043
 +Sandiford, D.J. 76734
 Sandomirskii, V.B. + 77001
 Sandomvskii, V.A. + 74494
 Sandulyak, A.V. 77211
 +Sanelli, C. 75648
 Sang Don Choi + 77266
 +Sanjeeviah, H. 74914
 Sankar, P.V. + 78315
 +Sankhayadhar, S. 75045
 +Sann, H. 75034
 Sannigrahi, A.B. + 75301
 +Sannikov, S.P. 75362
 Sano, O. + 74465
 +Santana, M.R. 75795
 Santer, R. + 78645
 Santilli, R.M. 74238
 +Santner, E. 77510
 Santos, J.M. Martins dos. 75362
 +Santos, J.M. Martins dos. 75362
 Sanyal, S. + 74504
 +Sanz, F. 76769
 +Sanz, F. 76770
 +Sanz, F. 75275
 +Sanz, F. 78135
 +Sanz, J. 76111
 Sanz, J.J. + 75609
 +Sanz, M. 77011
 +Sapozhnikov, M.G. 79040
 Sapozhnikov, M.N. + 75426
 +Sapre, V.B. 77478
 +Saracoglu, A.I. 76406
 Saradzhev, A.M. + 74484
 +Sarasa, J.P. 75294
 +Sarawathy, P. 75399
 +Sardi, L. 77555
 +Sargent, C.P. 74842
 +Saris, F.W. 76461
 +Saris, F.W. 77507
 Sarkar, K. Lalita. 74504
 +Sarker, A.K. 74750
 +Sarmah, J.C. 74329
 Sarper, R. + 78329
 +Sartorelli, G. 74821
 +Sasaki, A. 76897
 Sasaki, G. + 76897
 Sasaki, R. 74625
 +Sasaki, T. 77584
 +Sasamoto, N. 75182
 Sasano, K. + 75491
 +Sasayama, T. 75148
 +Sasayama, T. 76603
 Saska, M. + 76410
 +Sassmannshausen, U. 77508
 +Sastru, C.V. 78981
 +Sastru, C.V. 78896
 Sastry, D.V. Krishna. 7463
 +Sastry, S.B.S. + 77463
 Sathish, S. + 77092
 +Sathyanarayana, D.N. 75411
 +Sato, K. 77406
 +Sato, K. 77407
 Sato, M. 74628
 +Sato, N. 76176
 Sato, T. + 77221
 Sato, T. + 77132
 +Sato, T. 77548
 +Sato, Y. 75491
 +Satoh, J. 76594
 +Satoh, K. 76196
 +Satoh, M. 76293
 +Satpathy, B.M. 76271
 +Sattii, S. 75045
 +Satyamurthy, P. 74464
 +Saty, T.A. 74477
 Sauber, J. + 78456
 Sauer, J. 75269
 +Sauer, C. 75415
 +Sauer, P.U. 74841
 +Sautenkov, V.V. 75346
 +Sauter, A.D. 75526
 +Sautkin, V.E. 77008
 +Sauvaud, J.A. 78778
 Savage, C.M. + 75723
 Savage, S.B. + 76108
 +Savel'ev, A.V. 75767
 +Savenchuk, N.A. 75832
 +Saviolo, N. 78187
 Savitri, C. + 74798
 Savitskii, A.P. + 77596
 +Savits'kii, I.V. 76553
 Savkun, L.Z. + 74483
 +Savkun, L.Z. 74480
 +Savostin, P.I. 75768
 +Savrodin, J. 76772
 +Savrin, V.I. 74772
 Savukynas, A.J. 75317
 Savvides, N. 76633
 +Sawa, T. 75966
 +Sawada, F. 78792
 Sawada, M. + 75004
 Sawada, R. + 76433
 +Sawada, T. 77518
 +Sawada, Y. 77109
 +Sawada, Y. 75185
 +Sawaji, K. 78795
 Sawant, S.R. + 77218
 +Sawaya, S. 77793
 +Sawyer, D.E. 78076
 Saxena, A.P. + 76187
 +Saxena, M.C. 76685
 Saxon, D.H. 74752
 +Saxon, D.H. 74797
 Saxton, W.O. + 74562
 +Saykally, R.J. 74545
 Sayles, F.L. + 75118
 Scacco, A. + 76501
 Scaglia, A. 75012
 +Scaglia, A. 75022
 +Scalo, J.M. 78804
 +Scarf, F.L. 78850
 +Scarf, F.L. 78851
 +Scavnicar, S. 76401
 +Schacht, P. 74783
 +Schachter, M.J. 74783
 Schadt, M. + 76292
 +Schadt, W. 75502
 Schaeffelt, J.A., Jr. 74525
 Schaeffelt, J.A., Jr. 74526
 Schaeffelt, J.A., Jr. 75888
 Schaf, J. + 77285
 Schafer, E. + 74538
 +Schaefer, H.E. 76387
 +Schaefer, J. 78699
 Schaefer, L. + 75100
 +Schaff, W.J. 77686
 Schaich, W.L. 77495
 Schaich, E.J.M. van. 77495
 +see van Schaick, E.J.M.
 Schamberger, R.D., Jr. 74782
 +Scharlack, R.S. 77966
 +Scharmann, A. 76498
 Schastlivtsev, V.M. + 77638
 Schattschneider, P. 77491
 Schattschneider, P. + 77497
 Schattschneider, P. + 76247
 +Schatzman, M. 74290
 +Scheer, H. 78141
 +Scheib, U. 75007
 +Scheibling, F. 75034
 +Scheid, W. 75476
 +Scheid, W. 74934
 +Schellenberger, U. 76340
 Schepper, L. de. 77495
 +see de Schepper, L.
 Schepper, L. de. 77495
 +see De Schepper, L.
 +Scherer, M. 78757
 +Scherowsky, G. 77360
 +Schieber, M.C. 75240
 +Schieve, W.C. 74363
 Schilizzi, R.T. + 79017
 Schilling, R.J. 78235
 +Schimizu, J. 75025
 +Schimizu, J. 75004
 +Schindewolf, U. 76688
 +Schink, H. 76921
 Schipper, L. + 77948
 +Schirber, J.E. 77280
 +Schirmacher, A. 77516
 +Schlachter, A.S. 75500
 +Schlag, E.W. 75428
 +Schlanger, S.O. 78462
 Schlapp, D.M. + 78426
 Schleifer, F. + 76586
 Schlenker, R.A. 78350
 Schlosberg, W.H. + 76253
 +Schlosser, K. 74846
 Schlosser, V. + 78057
 Schlottmann, P. 77138
 +Schlotz, R. 78816
 +Schmelting, T. 76748
 Schmid, B.J. + 76849
 +Schmid, E. 78228
 +Schmid, F. 77565
 Schmid, H.G. 76426
 Schmid, M.F. + 78130
 +Schmidbauer, E. 77216
 +Schmidt, C. 74489
 +Schmidt, F.A. 77135
 +Schmidt, G. 74783
 +Schmidt, G. 77337
 +Schmidt, J. 78872
 +Schmidt, J.A. 77449
 Schmidt, M. + 79021
 +Schmidt, M. 74891
 +Schmidt, R.M. 78835
 +Schmidt, V. 75454
 Schmidt, W. + 78058
 +Schmidt-Bocking, H. 75502
 +Schmitt, D. 77229
 +Schmitt, W. 77819
 Schmitz, D.R. + 78431
 +Schneck, D.D. 76209
 Schneeweiss, O. + 77652
 Schneider, A.J. + 78361
 +Schneider, H. 74783
 Schneider, J. + 78171
 +Schneider, J. 77586
 Schneider, P.E.M. 76049
 Schneider, R.T. + 78391
 +Schneider, W.F.W. 75030
 Schnering, H.G. von. 77793
 +see von Schnering, H.G.
 Schober, H.R. 76417
 +Schock, H.W. 78084
 +Schoeberl, M.R. 78597
 Schoenborn, B.P. 78401
 Schoenlein, L.H. + 76611
 +Schoepe, W. 76740
 Schofield, D. + 75875
 +Schofield, T.G. 78108
 Scholten, O. + 74836
 Scholten, O. + 74843
 Scholtz, A.L. 75784
 Scholz, J. + 77265
 Schomberg, H. + 75866
 Schon, G. 77107
 Schonberger, D. + 78909
 +Schonfeldt, W.A. 75502
 +Schrrall, D.M. 74571
 Schreiber, D.L. 75128
 +Schreurs, A.M.M. 75540
 Schreyer, F. + 77311
 +Schroder, K. 77523
 +Schroder, V. 74783
 +Schroder, C. 77367
 Schroeder, H. + 76521
 +Schroeder, H. 77677
 +Schroeder, H.-W. 76321
 +Schroeder, K. 76705
 Schroeder, M. 78093
 +Schroter, R.C. 78221
 Schryvers, D. + 76368
 +Schubert, F. 75110
 +Schubert, G. 76927
 Schuch, R. + 75502
 +Schuchardt, R. 76834
 Schudder, D.W. 76212
 +Schue, F. 77887
 +Schuh, H.W. 74840
 +Schull, D. 75030
 Schulson, E.M. + 77753
 +Schultz, J. 75226
 +Schultz, J.A. 77498
 +Schultz, R.J. 76704
 Schulz, H. + 74891
 +Schulz, H. 74890
 +Schulz, H. 76257
 Schulz, H.J. + 77097
 Schulze, D. + 76757
 +Schumacher, M. 74918
 +Schumann, D.L. 74759
 +Schurmann, B. 74931
 +Schurr, H.D. 78756
 Schuster, W.J. 78826
 Schuster, W.J. 78905
 +Schuster, W.J. 78930
 +Schutter, W.G. 78127
 Schwandt, P. 74965
 +Schwartz, B. 76937
 Schwartz, R.D. 78977
 +Schwartz, R.J. 78040
 +Schwarz, J.A. 76714
 +Schwarz, J.H. 74744
 +Schwarz, K. 76841
 Schwarzblat, K. M. + 75084
 Schwarzmeier, J.L. + 76174
 +Schwarzschild, M. 78963
 +Schweig, A. 75528
 +Schweitzer, D. 77261
 Schweitzer, D.G. 75137
 +Schweitzer, N. 75338
 Schweitzer, V.G. + 74488
 Schwenk, H. + 77090
 +Schwerdtfeger, P. 75263
 +Schwerer, H. 76387
 +Schwitters, R.F. (ed.) 74232
 +Schwob, J.-L. 75338
 +Schwutke, G. 77592
 +Schwutke, G.H. 77554
 +Scifres, D.R. 75689
 +Sciulli, F. 74757
 Scoebel, W. + 75000
 +Scoles, G. 75373
 Scott, A. + 74973
 +Scott, B.J. 75818
 Scott, D. 77767
 +Scott, D.K. 74892
 Scott, M.R. + 78557
 Scott, N.S. + 75509
 +Scott Blackwell, C. 78537
 Scott-Monck, J. 78014
 Scovell, P.D. + 76464
 Seranton, D.R. + 76087
 +Scriven, L.E. 74374
 +Scrosati, B. 77970
 Scruby, C.B. + 75099
 +Seaborg, G.T. 74952
 +Searle, T.M. 77293
 Sears, T.J. + 75413
 +Seaton, D.P. 78224
 +Sebenne, C.A. 76785
 +Seberini, M. 77304
 +Sedivy, J. 76579
 Sedlet, J. 75131
 +Seeger, K. 78057
 Seetharaman, M. 74326
 Segal, A.S. + 78238
 Segall, P. + 78506
 Segar, A.M. 74805
 +Segers, D. 77477
 +Seggewiss, W. 78919
 Segre, E.R.A. 75478
 +Seghal, L.M. 74576
 +Seghal, N.K. 77077
 Seibert, G. + 78782
 Seibert, J. + 75261
 +Seidel, G.M. 76746
 +Seidell, H. 77870
 +Seifert, F. 76394
 +Seim, T. 78185
 +Seip, R. 75510
 +Seitelman, D.L. 78227
 +Sekerka, R.F. 76592
 +Sekerzh-Zen'kovich, S.Ya. 76124
 +Seki, M. 77407
 +Seki, S. 75004
 +Seki, T. 78871
 +Seki, Y. 74630
 +Sekigawa, T. 77020
 +Sekiguchi, H. 78590
 +Sekii, H. 76344
 +Sekine, T. 74870
 Sekita, Y. + 77738
 +Sekula, S.T. 77118
 +Self, P.G. 76262
 +Selsyan, R.P. 76853
 Selva, S.M.T. de la. 76124
 +see de la Selva, S.M.T.
 +Selvam, A.M. 78663
 +Selzle, H.L. 75428
 +Semak, D.G. 75760
 Semancik, S. + 77918
 Semary, M.A. + 77157
 +Semenets, T. 75734
 +Semenov, A.D. 77093
 +Semenov, A.M. 76169
 Semenov, A.N. + 76620
 Semenov, E.P. 75831
 +Semenov, O.G. 74576
 +Semenov, V.B. 75702
 +Semicheva, T.G. 77638
 +Semjonov, V.M. 75009
 +Semkova, Y. 78668
 +Semmens, J. 77859
 +Semmens, M.G. 78039
 +Sen, D. 77933
 +Sen, S. 74833
 Sen-Yu Yin. see Yin Sen-Yu
 +Senator, G. 76159
 +Sengoku, S. 75184
 +Sengupta, K. 74800
 +Sengupta, K. 74801
 +Sengupta, K. 75046
 +Sengupta, K. 75047
 +Sengupta, S. 76323
 Senior, J.E. 74246
 +Senkov, N.V. 75346
 +Senturia, S.D. 77056
 Senyuan liu. see liu Senyuan
 +Sepold, G. 77769
 Seppala, N.K. + 76737
 Seppanen, M. + 78395
 +Seppanen, M. 78284
 +Serafimov, K. 78669
 Serafimov, K.B. 78728

| | | | | | | | | | |
|-----------------------|------------------|-----------------------|-------|------------------------|------------------------|-------------------------------|--------------------|---------------------------|------------------|
| Serdaryk, I.N. | 78125 | + Sharma, R.G. | 76101 | + Shilkina, L. | 77333 | + Sibgatullin, N.R. | 74343 | + Sipe, J.E. | 75726 |
| + Serdyuk, V.A. | 77756 | + Sharma, R.P. | 76948 | + Shiloh, M. | 76983 | + Sibiede, F. | 78106 | + Sipio, L.Di. | see Di Sipio, L. |
| + Serebryakov, M.S. | 74672 | + Sharma, S.C. + | 75530 | + Shilshstein, S.Sh. | 76243 | + Sibille, A. | 76515 | + Sipkin, S.A. | 78455 |
| + Serebryanyi, A.E. | 78254 | + Sharma, S.D. | 75291 | + Shimada, M. + | 77602 | + Sibley, A.E. + | 78276 | + Sircar, A. + | 76776 |
| + Sergeev, A.V. | 77093 | + Sharma, V.D. + | 76065 | + Shimada, T. | 77959 | + Sibrán, C. | 77061 | + Sirotenko, V.I. | 74771 |
| Sergeev, E.K. | 74265 | + Sharpatiy, V.A. | 78252 | + Shimamoto, Y. | 74430 | + Sidel'nikov, Yu.V. | 76231 | + Sites, J.R. | 78047 |
| Sergeeva, A.I. | 75837 | + Sharpe, R.W. | 75329 | + Shimamura, H. | 78443 | + Sidel'nikov, Yu.V. | 74576 | + Sitnov, S.A. | 78705 |
| + Sergeeva, M.V. | 78258 | + Sharutin, V.V. | 76412 | + Shimamura, T. + | 78881 | + Sidis, V. + | 75477 | + Sivaramakrishnan, C.S. | 77726 |
| + Sergienko, A.I. | 76860 | + Sharypov, A.Z. | 77611 | + Shimba, H. | 78271 | + Sidorak, I.I. | 76706 | + Sivaramakrishnan, V. | 77368 |
| + Sergiescu, V. | 75486 | + Shashkov, V.V. | 75079 | + Shimer, J.A. | 77065 | + Sidorenko, F.A. | 77150 | + Sivashinsky, G.I. | 77890 |
| + Serikov, A.V. | 77479 | + Shastry, C.S. + | 75015 | + Shimizu, M. + | 77233 | + Sidorenko, V.D. | 75068 | + Sivers, D. | 74722 |
| + Serio, M. | 75648 | + Shastry, S.K. + | 76805 | + Shimizu, R. | 77513 | + Sidorin, A.S. | 75758 | + Sizova, N.L. + | 76446 |
| Serizawa, A. | 76019 | + Shatilov, A.V. | 77452 | + Shimizu, Z. | 77243 | + Sidorov, S.K. | 77147 | + Sjoberg, B. + | 78136 |
| Serot, B.D. | 74921 | + Shavokhina, N.S. | 74277 | + Shimizu, T. | 75959 | + Sidorov, Yu.M. | 78306 | + Sjoberg, P. | 75254 |
| + Serot, B.D. | 74987 | + Shaw, E.D. + | 75691 | + Shimoda, T. | 75013 | + Sieber, K. + | 76947 | + Sjogren, W.L. + | 78838 |
| Serr, F.E. + | 74878 | + Shaw, E.F., Jr. | 78628 | + Shimokawa, T. + | 77735 | + Siebhan, R. + | 75109 | + Skachkov, N.B. | 74624 |
| + Serra, T.J.B. | 75639 | + Shaw, H.J. | 75822 | + Shin, B.K. | 78076 | + Siebahn, H. + | 77943 | + Skachkov, N.B. | 74771 |
| + Serra-Mestres, F. | 76820 | + Shaw, G.G. | 78072 | + Shin, S. | 77407 | + Siebahn, P. | 75310 | + Skatkin, V.M. | 75160 |
| + Serughetti, J. | 76641 | + Shaw, W.C. + | 74551 | + Shin Nan Yang | 74858 | + Siebahn, P.E.M. | 75330 | + Skiba, P.A. | 77920 |
| + Serveniene, A.G. | 76192 | + Shawhan, S.D. | 78755 | + Shinagawa, K. | 74639 | + Siegmán, A. + | 75739 | + Sklansky, J. | 78315 |
| + Seshadri, V. | 74381 | + Shchegel'skii, V.A. | 76532 | + Shinaishin, M.A. + | 75085 | + Siejka, J. | 76472 | + Sklenicka, V. | 77710 |
| + Sessarego, J.P. | 75842 | + Shchegolev, V.A. | 75162 | + Shine, K.P. + | 78639 | + Siemann, H. | 74669 | + Sklizkov, G.V. | 76168 |
| + Sessler, A.M. | 75660 | + Shchepinova, L.P. | 77595 | + Shinozaki, D.M. | 78407 | + Siemens, P.J. | 74892 | + Skobolev, I.Yu. | 74549 |
| + Sethia, G. | 78814 | + Shchepkin, V.D. | 77290 | + Shinozaki, D.M. | 77481 | + Siemoff, H. | 76549 | + Skolnick, J. | 74395 |
| Sethia, G.C. + | 78741 | + Shcherback, S.F. | 75220 | + Shinsky, K. | 74669 | + Siethoff, H. | 76549 | + Skolozdra, R.V. | 76362 |
| + Setlow, R.B. | 75112 | + Shcherbakov, A.A. | 77444 | + Shiotani, K. | 76823 | + Siewert, C.E. | 75067 | + Skorubskii, G.A. | 78289 |
| Seto Yeb Jo | see Yeb Jo Seto | + Shcherbakov, A.S. + | 76931 | + Shiotani, Y. | 78100 | + Sigg, J. + | 77261 | + Skorupa, W. | 76757 |
| + Settels, J.J.M. | 78372 | + Shcherbakov, A.S. + | 77137 | + Shiozawa, L.R. | 77460 | + Siklossy, P. | 75168 | + Skromme, B.J. + | 76883 |
| + Sevast'yanov, B.N. | 75535 | + Shcherbakov, I.A. | 77451 | + Shiozo, M.N. | 77299 | + Sil, N.C. | 75524 | + Skromme, B.J. | 76475 |
| + Seves, A. | 76326 | + Shcherbakov, I.A. | 75642 | + Shipkova, I.G. | 77226 | + Silaev, A.A. | 76994 | + Skropyshev, A.V. | 77409 |
| + Sevryuk, E.B. + | 77613 | + Shcherbakova, M.F. | 77066 | + Shiplyak, M.M. | 75760 | + Silaev, E.A. | 74472 | + Skrynsek, R. | 75139 |
| + Sewchand, L.S. | 78156 | + Shchukin, V.A. | 76575 | + Shirafuji, T. | 74332 | + Silaev, V.I. | 74472 | + Skrynnyk, B.K. | 75675 |
| Seybold, P.G. | 77873 | + Shchukin, V.K. | 76043 | + Shirakawa, H. | 76934 | + Silaev, V.P. | 74455 | + Skubenko, P.A. | 76850 |
| + Seyler, C.E. | 76174 | + Shear, R.F. | 77891 | + Shirkova, I.A. | 75816 | + Silcox, J. | 76537 | + Sladen, F.M.E. | 75800 |
| Sezan, M.I. + | 78384 | + Shechter, H. | 76783 | + Shirohani, I. | 77379 | + Silen, J. | 78677 | + Slanina, Z. | 77872 |
| Seznez, R. | 77851 | + Sheffer, Y. | 78876 | + Shishatskaya, L.P. | 75783 | + Silina, A.G. | 78245 | + Slanina, Z. | 77916 |
| + Sha Cunxian | 75765 | + Shehawy, El S.F.El. | 77876 | + Shvakumar, G.K. | 77070 | + Silov, A. | 77187 | + Slastnikov, V.N. | 75001 |
| + Sha Guohue | 77866 | + Sheinkman, M.K. | 77453 | + Shiwei Zhang | see Zhang Shiwei | + Silsbee, R.H. + | 77263 | + Slater, J.M. + | 75651 |
| + Shabanov, S.Yu. | 78399 | + Shek, M.L. | 76790 | + Shizhu Wen | see Wen Shizhu | + Siltanen, P. + | 78284 | + Slattinen, P. | 75735 |
| + Shabanov, V.F. | 76302 | + Shchekyuan, V.I. | 74771 | + Shkadarevich, A.P. | 75645 | + Silva, A.M.Almeida E. | 77685 | + Slattery, G.F. + | 77685 |
| + Shabanova, I.N. | 77725 | + Shchekyan, V.I. | 74771 | + Shkarlet, Yu.M. | 77840 | see Almeida E Silva, A.M. | 77663 | + Slavin, T.P. | 77763 |
| + Shablakh, M. + | 77326 | + Sheldrick, G.M. | 76406 | + Shklovskii, B.I. | 77348 | + Silver, M. | 75050 | + Slezak, S.E. + | 77925 |
| + Shablii, I.Yu. | 77450 | + Shelle, A.U. + | 76619 | + Shkoldov, V.G. + | 78959 | + Sil'vestrova, I.M. + | 77332 | + Slifer, L.W., Jr. | 78034 |
| + Shabrov, B.M. | 77773 | + Shcheklov, A.L. | 77474 | + Shkunov, V.V. | 75604 | + Simashevich, A.V. | 77462 | + Sloane, N.J.A. | 74400 |
| + Shadchin, E.A. | 77252 | + Shelenin, L.A. | 75611 | + Shleenkov, A.S. | 77839 | + Simburger, E.J. | 78030 | + Slobodkin, L.S. | 76487 |
| + Shafi, M. | 75053 | + Shelginski, A. | 76020 | + Shluger, A. | 76888 | + Simeonova, Yu. | 78672 | + Slobodyuk, E.A. | 74771 |
| + Shafrankova, Ya. | 78777 | + Shelton, R.N. | 77135 | + Shlyakhina, L.P. | 77159 | + Simin'kovich, V.N. | 77755 | + Slovenas, Yu. | 75681 |
| Shah, J. + | 76973 | + Shelyubskii, V.I. + | 74540 | + Shmartsev, Yu.V. | 77398 | + Siminoff, R. | 78176 | + Sluzhenkina, L.V. | 78246 |
| + Shah, N. + | 77257 | + Shen, B.C. | 75017 | + Shmid, M. | 74913 | + Simmons, W.W. | 75172 | + Sluckin, T.J. | 76287 |
| + Shah, S.K. | 78423 | + Shen, Y.R. | 75711 | + Shmulevich, I.A. | 77483 | + Simon, B. | 74297 | + Slutskin, A.A. + | 76871 |
| + Shabani, H. + | 77762 | + Shen Ching. | 76071 | + Shobu, M. | 75290 | + Simon, H. | 78101 | + Slyusarenko, Yu.V. | 74284 |
| + Shabar, A. + | 76966 | + Shen Jian-ping. | 74894 | + Shokanov, A.K. | 76485 | + Simon, J.P. | 76415 | + Smailagic, A. | 74654 |
| + Shail, R. + | 76093 | + Shen Mengyu + | 76063 | + Shon Nguyen Hong | 76473 | + Simone, S.De | 76415 | + Small, G.J. | 75709 |
| + Shakhova, K.V. | 77386 | + Shen Zhiye + | 75390 | see Nguyen Hong Shon | 76258 | see De Simone, S. | 76214 | + Small, J.G. | 75627 |
| + Shakin, C.M. | 74880 | + Shenfeng, Y.Yu. + | 78497 | + Short, M.T. + | 76258 | + Simonen, T.C. + | 76214 | + Smallman, R.E. | 76509 |
| + Shakir, S.A. + | 75581 | + Sheng Chi | 76890 | + Shouman, S.M. + | 75909 | + Simonetta, M. | 76351 | + Smallman, R.E. | 76510 |
| + Shakirov, A.Kh. | 78290 | + Sheng S. Li + | 78032 | + Shouxian Fang | see Fang Shouxian | + Simons, G.J. | 74508 | + Smelov, E.M. | 74963 |
| + Shakirzyanov, M.M. | 77273 | + Sheng Shao-shan | 77700 | see Fang Shouxian | 75613 | + Simonov, M.A. | 76399 | + Smend, F. | 74918 |
| + Shakked, Z. | 76232 | see Shao-shan Sheng | 77700 | + Shipen'kov, G.P. | 75613 | + Simonov, V.I. | 76398 | + Smetana, P. | 77554 |
| + Shalaev, V.I. | 77700 | + Shenoy, A.V. + | 75978 | + Shipigel, A.S. | 77079 | + Simons, B. | 76405 | + Smetanin, P.G. | 78300 |
| + Sham, T.-L. + | 76451 | + Shepard, J.R. | 74920 | + Shporer, M. | 77283 | + Simons, J. | 75309 | + Smilga, A.V. + | 74660 |
| + Shama, A. | 77949 | + Shepelev, V.V. | 77435 | + Shpotyuk, O.I. | 76553 | + Simpkins, P.G. | 76006 | + Smirenl, G.N. | 75059 |
| + Shamsi, A. + | 77896 | + Shepherd, G.G. | 78675 | + Shrivastava, K.N. | 77956 | + Simpson, D. | 77719 | + Smirl, A.L. + | 75708 |
| + Shand, M.L. | 77430 | + Shepherd, J.G. | 75120 | + Shriver, D.F. + | 76695 | + Simulic, M.D. | 74480 | + Smirl, A.L. + | 75753 |
| + Shang-Bin Liu + | 76330 | + Sheppard, C.J.R. | 74531 | + Shrock, R. | 74669 | + Sinclair, D. | 75226 | + Smirnov, V. | 78668 |
| + Shang-keng Ma. | 74411 | + Sheppard, D.M. | 74975 | + Shteingart, L.M. | 75790 | + Sinclair, D. | 75019 | + Smirnov, V.A. | 77451 |
| + Shank, C.V. | 75710 | + Sher, A. + | 76983 | + Shu, F.H. + | 78847 | + Sindt, H. | 74783 | + Smirnov, V.P. | 76193 |
| + Shanker, J. | 76353 | + Sherepetska, P.D. | 78263 | + Shu-ch'i Fang Chen | see Chen Shu-ch'i Fang | + Sinekop, M.S. | 75931 | + Smirnov, Yu.M. | 75520 |
| + Shanker, J. | 75360 | + Sherer, J.B. | 76942 | see Chen Shu-ch'i Fang | 75909 | + Sinel'nikova, V.S. + | 76984 | + Smith, A. | 78568 |
| + Shanker, J. | 75361 | + Shermakov, A.E. | 75207 | + Shu-gang Zhang | see Zhang Shu-gang | + Singal, L.C. + | 76022 | + Smith, A.G.D. + | 77766 |
| + Shanklin, J.D. + | 78876 | + Shermatov, E.N. | 77401 | + Shubav, S.N. | 74440 | + Singal, S.P. + | 78707 | + Smith, B.D. | 78310 |
| + Shanskii, A.I. | 77412 | + Shesler, A.T. | 75083 | + Shuiskaya, F.K. | 78778 | + Singh, A. | 76685 | + Smith, C.H.Llewellyn | 77700 |
| + Shao, C.-Y. | 76355 | + Shestakov, A.F. | 78691 | + Shujing Feng | see Feng Shujing | + Singh, C.P. | 74735 | see Llewellyn Smith, C.H. | 75998 |
| + Shao Juan. | 76890 | + Shestakov, A.I. | 76174 | + Shukla, A.P. | 76948 | + Singh, D. + | 78096 | + Smith, C.R. + | 78157 |
| + Shao Shi-ping. | 74490 | + Shestakov, G.N. | 74732 | + Shukla, J.P. | 76685 | + Singh, J.B. | 74815 | + Smith, C.W. | 74561 |
| + Shao-Ling Feng. | 78126 | + Shestopalov, A.V.P. | 75675 | + Shukla, P.K. | 78802 | + Singh, K. + | 74900 | + Smith, D.J. + | 76414 |
| + Shao-shan Sheng. | 74470 | + Sheveleva, A.S. | 77005 | + Shulchishin, Yu. | 78776 | + Singh, K. | 77993 | + Smith, D.J. | 76263 |
| + Shaohuo, C. | 75785 | + Shevgaonkar, R.K. | 78981 | + Shul'ga, M.O. | 77328 | + Singh, R.J. | 77253 | + Smith, D.J. | 77795 |
| Shaomin Wang | see Wang Shaomin | + Shi Chen Shi | 77429 | + Shul'man, Z.P. | 76325 | + Singh, R.N. | 75376 | + Smith, D.J. | 74562 |
| + Shapiro, M. | 78588 | + Shi-Chune Yao | 76014 | + Shuman, O.B. | 75853 | + Singh, S. + | 78449 | + Smith, D.J. | 75226 |
| + Shapiro, S.L. | 78824 | + Shi-Chune Yao + | 76017 | + Shumard, E. | 75226 | + Singh, S. | 75311 | + Smith, D.W. | 76156 |
| + Shapochkin, M.B. | 75551 | + Shi-gang Chen | 77700 | + Shumovskii, A.S. | 74365 | + Singh, S. | 75237 | + Smith, E.R. | 74759 |
| + Shaposhnikov, M.E. | 74346 | see Chen Shi-gang | 77700 | + Shur, E.A. | 77755 | + Singh, S.Chauha. see Chauha | 75376 | + Smith, G.M. + | 75482 |
| + Shaposhnikov, M.E. | 79039 | + Shi-Jin Zheng. | 77700 | + Shur, M. | 77997 | + Singh, S. | 75376 | + Smith, G.P. + | 75482 |
| + Shapoval, T.A. | 77607 | see Zheng Shi-Jin | 77700 | + Shur, V.Ya. + | 77340 | + Singh, S.K. + | 74257 | + Smith, J.A.Smoother | 76663 |
| + Shapovalov, V.I. + | 77701 | + Shi-ping Shao. | 77700 | + Shushkov, V.M. | 77543 | + Singh, S.N. + | 76010 | see Smoother Smith, J.A. | 77998 |
| + Shapovalov, V.P. | 77039 | see Shao Shi-ping | 77700 | + Shutoh, K. | 77121 | + Singh, S.N. | 77996 | + Smith, J.S. | 75696 |
| + Sharafutdinov, A.B. | 75699 | + Shiba, K. + | 76135 | + Shuxiang Wu | see Wu Shuxiang | + Singh, S.N. | 77996 | + Smith, J.V. + | 78537 |
| + Sharafutdinov, F.I. | 76043 | + Shiba, N. | 77998 | + Shvab, S.A. | 77066 | + Singh, T. + | 75237 | + Smith, K.C.A. | 74561 |
| + Sharaf, W. | 75431 | + Shibata, K. | 75829 | + Shvartsman, A.Z. | 78300 | + Singh, V.K. + | 77307 | + Smith, L. + | 78485 |
| + Sharkov, A.V. | 75913 | + Shibata, M. + | 78121 | + Shvets, V.T. | 76923 | see Madhusudan Singh | 77307 | + Smith, M. | 79024 |
| + Sharma, A. + | 74737 | + Shibata, S. + | 74912 | + Shyam, M. | 75039 | + Singh Megha | see Megha Singh | + Smith, N.V. | 77526 |
| + Sharma, A.K. | 77564 | + Shibata, T. + | 75942 | + Shyam, M. | 75044 | see Megha Singh | 77526 | + Smith, P.D. + | 74445 |
| + Sharma, A.P. | 75234 | + Shibata, T. | 76136 | + Shyam, M. | 75045 | + Singh Surinder | see Surinder Singh | + Smith, R. | 76082 |
| + Sharma, B.K. | 76654 | + Shida, S. | 75959 | + Shyam, R. | 76065 | + Singh Surjit | see Surjit Singh | + Smith, R. | 76054 |
| + Sharma, C.P. | 76022 | + Shiffrin, E.I. | 77352 | + Shyn, T.W. | 75532 | + Sinha, A.P.B. | 77519 | + Smith, R.W. | 77679 |
| + Sharma, D.R. | 77325 | + Shigemitsu, J. | 74636 | + Shyu, C.M. | 78061 | + Sinha, C. | 74944 | + Smith, R.W. | 76622 |
| + Sharma, H.S. | 76090 | + Shigi, T. | 76743 | + Si-xun Huang | see Huang Si-xun | + Sinha, O.P. | 75524 | + Smith, R.W. | 77695 |
| + Sharma, K.N. + | 77569 | + Shih, C. + | 75655 | + Siafarikas, P. + | 74316 | + Sinkevich, V.F. | 76986 | + Smith, S.D. | 75665 |
| + Sharma, L.K. | 74305 | + Shih-nan Chien | 77700 | + Sibbett, W. | 74534 | + Sipe, J.E. | 75726 | + Sipio, L.Di. | see Di Sipio, L. |
| + Sharma, L.K. | 74730 | see Chien Shih-nan | 77700 | + Sibel'din, N.N. | 77436 | + Sipkin, S.A. | 78455 | + Sircar, A. + | 76776 |
| + Sharma, M.Lal. | 76354 | + Shik, A.Ya. | 77398 | + Shikung Wu | see Shikung Wu | + Sirotenko, V.I. | 74771 | + Sites, J.R. | 78047 |
| see Lal Sharma, M. | 78814 | see Wu Shikang | 77398 | + Shikun Wu | see Shikun Wu | + Sitnov, S.A. | 78705 | + Sivaramakrishnan, C.S. | 77726 |
| + Sharma, R. | 78814 | + Shikatan, M. | 78789 | + Shikun Wu | see Shikun Wu | + Sivaramakrishnan, V. | 77368 | + Sivashinsky, G.I. | 77890 |

- Smith, S.G. 78633
 Smith, S.P. 74655
 +Smith, T.F. 77295
 +Smith, T.I. 75672
 +Smith-Verdier, P. 75395
 Smitt, R. + 75340
 +Smokin, V.I. 77563
 Smolenskii, G.A. + 77319
 +Smoother Smith, J.A. 75394
 +Snegirev, V.V. 77228
 +Snadower, L. 77284
 +Snighireva, I.I. 76439
 Snipes, M.B. + 78366
 Snover, K.A. + 74904
 Snow, D.B. 76652
 Snow, T.P. 78979
 Snyder, A.W. + 75803
 Snyder, D.L. + 78321
 Snyder, L.E. + 78967
 Snyderman, N.J. 74746
 +Soares, C. 78196
 +Sobahi, M.I. 77587
 +Sobczyk, L. 77338
 +Sobel, H. 75226
 +Sobie, R.J. 74842
 Sobolev, V.V. + 77413
 +Sobolevskii, N.M. 75218
 +Sofko, T.I. 75170
 +Sokol, P.M. 76111
 +Soda, K.J. 76477
 Soderberg, S. + 77764
 +Soderhjelm, H. 77762
 Sodha, M.S. + 78097
 Sodosoli, H. 76970
 +Sofia, H.M. 74902
 +Sofianos, S.A. 74927
 Sofko, G.J. + 78732
 +Sofko, G.J. 78678
 +Sofuni, T. 78271
 Soga, N. + 76312
 +Soga, N. 76547
 +Soga, N. 76317
 +Soga, N. 76597
 +Sohal, M.S. 76089
 +Sohan Lal. 78814
 +Soifer, B.T. 79019
 +Soifer, Ya.M. 76441
 Soileau, M.J. + 75756
 +Sokolov, N.A. 76229
 +Sokolov, N.V. 77667
 Sokolov, O.B. 78304
 +Sokolov, O.G. 77724
 +Sokolov, P.V. 77838
 Sokolov, V.O. 77131
 +Sokolovskii, A.I. 76147
 +Sokolovsky, P. 78817
 Sokov, I.A. + 74477
 +Solanki, S.N. 78157
 Soldatov, E.A. + 76350
 +Soldatov, E.A. 76346
 +Solimeno, S. 75648
 +Soll, M. 75174
 Sollogub, V.S. 74436
 +Solmajer, T. 75295
 +Solodukhin, A.S. 75453
 +Solodyankina, V.N. 78543
 +Solomatini, I.I. 75692
 +Solomon, S. 78614
 Solomonow, M. + 78213
 Soloukhin, R.I. + 74239
 +Solymar, L. 75599
 +Som, J.N. 76131
 Soma, T. + 76594
 Somaiah, K. + 76697
 +Somenkov, V.A. 76243
 +Somma, F. 76501
 +Sommer, J.H. 78142
 Sommerfeld, R.A. 78569
 +Sommermann, H.M. 74994
 +Sommers, C. 76374
 +Somon, J.P. 76172
 +Somorjai, G.A. 77503
 +Somorjai, G.A. 77919
 +Somorjai, G.A. 77018
 +Somorjai, G.A. 76791
 +Somova, V.M. 77842
 Song Hai-De
 see Hai-De Song
 +Sonin, A.S. 76306
 Sonntag, D. 76151
 +Sorba, P. 74701
 Sordo, J.A. + 76911
 +Sorlei, Z. 76202
 +Sorokin, N.L. 77113
 +Sorokina, L.P. 77680
 +Sosenshkin, E.M. 77724
 +Sosnikov, V.I. 77637
 +Soskin, M.S. 75606
 +Soszynski, M. 78268
 +Sotgiu, A. 76310
 +Sotnikova, E.N. 75561
 +Soto, J. 78700
 Souheng Wu 77741
 +Souillard, B. 76846
 +Soukup, J. 74975
 +Soule, J.L. 76172
 +Soulen, R.J., Jr. 77101
 +Soulet, Y. 75348
 Soulie, G. + 78924
 Soumekh, M. + 78278
 Souriau, A. + 78684
 +Souriau, M. 78684
 +Sournies, F. 75541
 +Soussaline, F. 78327
 +Souza Mendes, P. 76015
 +Spadaro, G. 77324
 +Spalek, K. 74567
 +Spandreg, G. 78406
 +Spangis, F. 78760
 Spankuch, D. 78579
 Spankuch, D. + 78651
 Spankuch, D. + 78585
 Sparrow, E.M. + 76015
 +Spasov, St. 78676
 Spassova, N.M. 78964
 +Spataro, B. 75648
 Spear, W.E. + 76958
 +Spear, W.E. 76972
 +Spear, W.E. 77022
 +Specking, W. 77119
 +Speidell, J.L. 78403
 Spektor, A.A. 75968
 Spence, J.C.H. + 76261
 +Spencer, R.L. 76208
 +Spencer, R.L. 76174
 +Spiering, J.L. 76197
 Speth, J. 74945
 +Speth, J. 74883
 +Spicer, W.E. 75221
 +Spicer, W.E. 76790
 Spillman, W.B., Jr. + 75828
 Spindler, K. + 78094
 +Spinelli, P. 77786
 +Spinner, B. 78106
 +Spirdenkov, E.M. 76532
 +Spirin, D.A. 78251
 +Spitzer, M.B. 78027
 +Spooncer, R.C. 75830
 Sprangle, P. + 75657
 +Spratt, C.E. 78875
 Sprinks, T. + 76054
 +Spurgin, E.J. 76464
 Squire, P.T. 76109
 Squires, S.W. + 78857
 Sree Ramulu, K. + 75358
 +Sreekantan, B.V. 74765
 Sridhar, P. + 77932
 Srinivas, T.K. + 77264
 Srinivasa Murty, N. + 77579
 +Srinivasan, K. 77316
 +Srinivasan, R. 77316
 Srinivasan, S.K. + 74377
 Srivastava, A.C. 76143
 Srivastava, D.K. + 74868
 Srivastava, G.P. + 77077
 Srivastava, G.P. 74607
 +Srivastava, S.B. 76683
 Srivastava, S.K. + 77591
 +Srivastava, S.K. 74533
 Srivastava, S.L. + 75377
 +Srivastava, V. 74394
 +Sroelov, V.S. 75170
 +Stacchiotti, R. 76128
 +Stachura, Z. 75502
 +Stadele, M. 76525
 +Stadlbauer, J.M. 75556
 Staes, K. + 74552
 Stafstrom, S. + 76828
 Stahler, S.W. 78800
 Stahler, S.W. 78801
 Staicu, C.I. + 78105
 +Stainer, M. 76695
 +Stallard, B.W. 76214
 +Stals, L.M. 76413
 +Stals, L.M. 77477
 +Stals, L.M. 76483
 +Stals, L.M. 76505
 +Stamm, W. 78944
 Stanev, G. + 78669
 +Stannett, V.T. 76702
 Stanzl, S.E. + 77696
 +Stapleton, G.B. 74981
 +Stapleton, H.J. 77262
 Star, J. Van der
 see Van der Star, J.
 +Stark, H. 78384
 Stark, M. + 78461
 Stark, W. + 77323
 Stark, W. + 78413
 +Starke, E.A., Jr. 77750
 Starke, T.P. + 76182
 Starostenko, V.I. + 78417
 +Starostin, K.V. 77026
 +Starostin, Yu.V. 75563
 Starrfield, S.G. + 78922
 Stassinopoulos, E.G. + 76506
 Statham, P.J. 77938
 +Stather, J.W. 78262
 +Stauffer, D. 74371
 +Stauffer, L. 75841
 +Staveley, L.A.K. 76659
 Stavenga, D.G. 78139
 Stavenga, D.G. + 78180
 +Stavenga, D.G. 78236
 +Steadman, J. 75412
 +Stearns, R. 76866
 +Steck, D. 78817
 +Stedman, G.E. 76908
 +Stedman, G.E. 76909
 +Stedman, G.E. 76910
 Steeds, J.W. + 76260
 +Steele, A.T. 78610
 Steemers, H. + 77022
 +Steemers, H. 76958
 +Steen, W.M. 77809
 Steenbergen, A. van
 see van Steenbergen, A.
 +Stefan, P.M. 76790
 +Stefanov, R. 77929
 Stegeman, G.I. + 75726
 +Steidler, F. 78413
 Steiger, A. 74731
 Steiger, R. + 77907
 +Stein, D.L. 76735
 +Stein, P.C. 77276
 +Stein, R.S. 77469
 +Stein, W.E. 75653
 Steinberg, M. + 77955
 +Steinberg, R.I. 78816
 +Steinberg, V. 76106
 Steinberger, J. 74778
 +Steinemann, S. 77246
 +Steiner, J.E. 79001
 +Steiner, W. 77208
 +Steinfink, H. 76378
 +Steinfink, H. 76382
 Steinhart, P.J. 79032
 +Steinhart, P.J. 76742
 +Steinhausler, F. 78333
 Steinmetz, K.-H. + 76833
 Stella, P.M. + 78038
 +Stelmakh, V.F. 76949
 +Stelmakhov, Yu.N. 74472
 +Stenz, R. 74962
 +Stepanov, K.N. 76189
 Stepanov, R.P. + 78247
 +Stepanov, S.V. 78250
 +Stepanov, V.A. 76560
 +Stepanov, V.A. 76546
 +Stepanova, Z.A. 75536
 Stephan, P. 74274
 Stephens, G. + 78348
 Stephens, M.E. + 75313
 +Stephens, W.E. 78500
 Sterken, C. + 78955
 +Stern, D.P. 75336
 +Stern, M. 77396
 Sterzhanov, N.I. + 76487
 +Stetsenko, Yu.E. 74472
 +Stevens, F.J. 76258
 Stevens, J. + 75506
 +Stevens, K.N. 78195
 +Stevens, T.H. 78129
 +Stevenson, D.A. 76809
 Stevenson, D.J. 78834
 Stevenson, D.J. 78836
 +Stewart, G.R. 76663
 +Stewart, M.E. 75176
 +Stewart, R.R. + 78450
 +Stewartson, K. 75999
 +Sticker, H. 74669
 Stierman, R.J. + 77135
 Stieve, H. + 78182
 +Stika, K.M. 78061
 +Stillman, G.E. 76960
 +Stillman, G.E. 76475
 +Stillman, G.E. 76980
 +Stillman, G.E. 76883
 Stillman, G.E. (ed.) 74226
 +Stingl, M. 74924
 Stinson, D.G. + 77262
 +Stinson, G.M. 74975
 Stirland, D.J. + 76436
 Stishov, S.M. + 76624
 +Stishov, S.M. 76581
 +Stiskin, M.G. 78712
 +Stobbs, W.M. 77490
 +Stobbs, W.M. 76262
 +Stobbs, W.M. 76818
 +Stobbs, W.M. 77795
 +Stobbs, W.M. 77796
 +Stochino, G. 77013
 +Stoll, H. 75263
 +Stoloff, N.S. 77763
 +Stolte, S. 75372
 +Stone, C.A. 74913
 +Stone, J.L. 75226
 +Stoner, D.L. 78224
 +Stootman, H.J. 75416
 +Storchak, N.A. 77681
 Stordeur, M. + 76936
 Storey, J.R. 74497
 Storey, L.R.O. 76160
 +Stornaiolo, C. 74341
 Stott, G.F. 78736
 +Stout, R.P. 75709
 +Stover, G.D. 75660
 +Strackee, J. 78215
 +Strasser, G. 77493
 Strauss, H.R. 76171
 +Streetman, B.G. 77457
 +Streett, W.B. 76599
 +Streifer, W. 75689
 +Streit, L. 74296
 +Streng, S. 78228
 Streubel, G. + 75232
 +Streubel, P. 77520
 Strey, R. + 76748
 Strickland, R.N. 75589
 +Strieder, W. 75905
 +Strizhevskii, V.L. 75699
 +Strobel, D.F. 78597
 +Stroher, H. 75519
 Stroink, G. + 78396
 +Strok, L.P. 76561
 Strominger, A. 74350
 +Stroud, C.R., Jr. 76588
 +Struve, W. 74841
 Strutt, P.R. + 76496
 +Strutt, P.R. 77811
 Struve, W.S. + 75432
 Stryland, E.W. Van
 see Van Stryland, E.W.
 Stuart, C.M. 77852
 Stubbs, R.J. + 77343
 +Stuchbery, A.E. 74844
 +Studdert-Kennedy, M. 78192
 +Studer, F. 76945
 +Stumpff, P. 78872
 Stupakov, G.V. 76154
 +Sturges, L.D. 76045
 Stylianou, S.A. + 76601
 +Styskal, G.W. 75835
 Su, S.F. + 74466
 Su, S.F. + 75598
 Su Rukeng + 79035
 +Su Zhao-bin 74366
 +Subashiev, A.V. 76575
 +Subashiev, A.V. 76617
 Subbaraya, B.H. + 78586
 +Subbaraya, B.H. 78592
 +Subbaraya, B.H. 78674
 +Subbotin, V.B. 75009
 Subhadra, V.K. + 77334
 +Subrahmanya, R.S. 77932
 +Subrahmanian, A. 74794
 +Subrahmanian, A. 74814
 Subrahmanian, K. + 76083
 +Suchy, J. 76336
 +Suckewer, S. 75621
 Suda, T. + 78003
 +Sudarkin, A.N. 75604
 +Sudhakar, K. 74814
 +Sudhakar, K. 74794
 Sudo, K. + 76113
 +Sudoh, G. 76503
 +Suenram, R.D. 78967
 +Suess, H.E. 78559
 Suga, S. + 77407
 Suganuma, K. + 77723
 Sugarwara, H. 74690
 +Sugihara, M. 75184
 +Sugihara, M. 75185
 +Sugita, Y. 74639
 +Suguchi, H. 78786
 +Suguchi, H. 78631
 +Suguchi, H. 78747
 +Suguchi, H. 79028
 Sugiura, I. + 76938
 +Sugiyama, T. 75004
 +Suh, N.P. 77853
 Suhai, S. 76865
 +Suito, T. 78750
 +Suito, T. 78788
 +Suito, T. 78751
 Sukhanov, L.P. + 75270
 +Sukharev, A.A. 77543
 Sukharevskii, B.Ya. + 77314
 +Sukhatme, U.P. 74810
 +Sukhinin, V.A. 76596
 +Sukhov, V.A. 77106
 +Sukigara, M. 77045
 +Sulaberidze, G.A. 75534
 +Sulaberidze, G.A. 75533
 Sulaberidze, V.Sh. + 75106
 +Sulak, L.R. 75226
 +Sulimenov, B.S. 75011
 +Sulimov, V.V. 76532
 +Sulimov, V.V. 74983
 +Sulka, A.P. 75775
 +Sulkes, M. 75420
 Sultan, M.F. + 78231
 Sultan, M.F. + 78234
 Sultanov, N.V. + 75105
 +Sumbaev, O.I. 76532
 Sumetskii, M.Yu. 77537
 Sumi, H. 77440
 +Sumi, S. 75946
 Sumino, K. + 76484
 +Summers, H.P. 76218
 Summers, W.M. 75224
 +Sun, J.Y.-C. 77017
 +Sun Henghui 76890
 +Sun Jinseng 77214
 +Sun Qing 76890
 +Suni, I. 77047
 +Suppe, J. 78511
 +Sural, D. 74801
 +Surdej, A. 78841
 +Suresh, S. 76558
 Surinder Singh + 78483
 +Surjit Singh 75356
 Surma, M. 77088
 +Suryanarayana, N.S. 76187
 +Susaki, W. 75634
 Susic, M.V. 77785
 Suski, J. + 76878
 +Suslina, L.G. 76852
 +Sussmann, R. 77292
 +Sutherland, E. 75436
 +Sutherland, E. 75437
 +Sutherland, E. 75442
 Sutherland, R.I. 74312
 +Suto, H. 77736
 +Sutton, R.A. 74960
 Suura, H. 74747
 +Suyehiro, K. 78443
 +Suzanne, J. 76783
 +Suzdorf, A. 77968
 Suzuki, A. + 74763
 Suzuki, K. + 75949
 +Suzuki, K. 77408
 +Suzuki, K. 78871
 +Suzuki, N. 75184
 +Suzuki, R. 74639
 Suzuki, T. + 74989
 Suzuki, T. + 76609
 +Suzuki, T. 77559
 +Suzuki, T. 77602
 Suzuki, Y. + 76603
 Suzuki, Y. + 75148
 Suzuki, Y. + 77470
 +Suzuoki, A. 75157
 +Svanberg, S. 75349
 +Svanidze, E.O. 78252
 Svechnikov, G.S. + 77384
 Svidenkov, N. + 75339
 +Svendsen, I.A. 75989
 +Svensson, L.A. 75340
 +Sverdlow, A.G. 78245
 +Svetlov, I.L. 77680
 +Sviderskaya, O.M. 76230
 +Sviridenok, A.I. 77594
 +Sviridov, V.V. 77399
 Svirina, E.P. + 77159
 +Svoboda, R. 75226
 +Swahn, H. 77764
 Swain, M.V. + 77732
 +Swaminathan, S. 76411
 Swanson, D.K. + 76370
 +Swanson, R.M. 77000
 +Swartz, C.K. 78033
 +Swartz, L.E. 75221
 +Sweetnam, D.N. 78860
 +Swennenhuis, M.J.M. 78205
 +Swenson, C.A. 76676
 +Swiatecki, W.J. 74877
 +Swicker, W.K. 75643
 Swiggard, E.M. + 77561
 +Swindell, W. 78382
 +Swindell, W. 78383
 +Swineea, J.S. 76378
 +Swissler, T.J. 78662
 +Switzer, G.L. 74542
 Swyngenhoven, H. van. see van Swyngenhoven, H.
 +Syam, D. 74799
 Syamal, A. 77373
 Syamal, A. + 77372
 +Syamaprasad, U. 77334
 +Sydzhimov, B. 76314
 Syms, R.R.A. + 75599
 +Syrykin, E.S. 77199
 +Syromyatnikov, A.V. 78259
 +Syrus, V. 75752
 +Szabo, L.D. 78356
 Szabo, P.P. 78355
 Szabo, P.P. + 75208
 Szafraan, M. + 75384
 Szapiel, S. 75582
 Szentpaly, L. von
 see von Szentpaly, L.
 Szepessy, B. 74572
 +Szeto, L. 77419
 Szondi, E.J. 75202
 Szondi, E.J. 75203
 +Szondi, E.J. 75158
 +Szondi, E.J. 75159
 +Szondi, E.J. 75201
 Szorenyi, A. 78354
 +Sztyaniy, B. 78363
 +Szucs, I. 75158
 +Szymanski, K. 75553
 Szymczak, M. + 78815
 Szymura, S. 77213
 +Szytula, A. 76369
 Ta, L.B. + 76342

- Taam, R.E. 78918
 Tabar, R.J. + 77469
 Tabarovskii, L.A. + 78711
 +Tabe, M. 77562
 +Taber, R. 75672
 Tabhane, V.A. + 76564
 +Tabiryian, N.V. 76286
 +Tabov, N. 78668
 +Tuchiki, M. 77116
 Tack, L.M. + 75410
 Taddeucci, T.N. 74974
 +Tadeush, V.N. 77438
 +Tadokoro, H. 77375
 +Taft, J. 76261
 +Tagger, M. 76172
 +Tagirov, V.I. 77393
 +Tagishi, Y. 75004
 +Taguchi, H. 77981
 Taguchi, T. + 76420
 Tah-hui Wang.
 see Wang Tah-hui
 +Tai, K. 75714
 +Takacs, S. 77114
 +Takada, T. 75288
 +Takagi, R. 76279
 Takagui, E.M. + 74849
 +Takahara, K. 77717
 Takahashi, K. + 77694
 +Takahashi, K. 76938
 +Takahashi, M. 77248
 +Takahashi, M. 76609
 +Takahashi, N.S. + 77584
 +Takahashi, S. + 77232
 +Takahashi, S. 75949
 +Takahashi, T. 77461
 +Takahira, A. 78785
 +Takahira, A. 78794
 +Takai, Y. 77206
 +Takaki, R. 74465
 +Takano, K. 75290
 Takaoaka, H. + 77033
 Takashima, T. + 78648
 +Takasugi, K. 75764
 Takatsuki, Y. + 78871
 +Takayama, Y. 78648
 +Takayoshi, S. 78573
 +Takeda, N. 78118
 Takeda, Y. + 77981
 +Takai, H. 76621
 +Takai, H. 77794
 Takenaga, M. + 75198
 Takenoshita, Y. + 78746
 +Takeshita, S. 74686
 +Takeuchi, J. 76954
 +Takeuchi, S. 76338
 Takhar, H.S. + 78565
 +Taki, W. 78294
 +Takizuka, T. 76164
 +Talaiaeff, G. 77447
 Talamoni, J. + 77913
 +Talbot, L. 76116
 +Tale, I. 76888
 +Talianker, M. 77631
 +Talmán, J.D. 75314
 Talwar, D.N. 76576
 +Tam, A.C. 75879
 Tamada, N. + 77812
 +Tamin, B. 75033
 +Tamaki, S. 76920
 +Tamisier, R. 74847
 Tamor, S. 76199
 Tamura, I. 77671
 +Tamura, T. 75028
 +Tamvakis, K. 74356
 Tan, T.Y. + 76416
 Tan Lu.
 see Lu Tan
 +Tanabe, J.T. 75660
 +Tanada, S. 78294
 Tanaka, K. + 77482
 +Tanaka, K. 76823
 Tanaka, M. + 78608
 Tanaka, M. + 76344
 +Tanaka, M. 75013
 +Tanaka, R. 77619
 Tanaka, S. + 75182
 Tanaka, Y. + 74430
 Tananbaum, H. + 79023
 Tanas, R. + 75757
 +Tanatar, M.A. 77450
 +Tanchou, A. 75864
 Tandon, J.L. + 76473
 +Tandy, P.C. 74937
 +Tandy, P.C. 74968
 +Tang, C.L. 75327
 +Tang, C.M. 75657
 Tang, D. + 76038
 +Tang, X.T. 74957
 Tang Keguang + 75886
 +Tang Wenxia. 76386
 Tang Xiao.
 see Xiao Tang
 +Tang Youqi. 76386
 Tani, K. + 76164
 +Tani, K. 75184
 Tani, T. 77909
 +Tanigawa, M. 75538
 Taniguchi, K. 74573
 Taniguchi, K. + 76796
 Taniguchi, M. + 76892
 +Taniguchi, M. 77407
 +Taniguchi, Y. 75004
 +Tanji, M. 75086
 Tanji, Y. + 77246
 +Tannen, R. 78311
 +Tannenbaum, M. 74669
 +Tanner, R.I. 76075
 +Tanninen, V.-P. 77459
 +Tanre, D. 78640
 +Tanuma, S. 77227
 +Taran, G.G. 75011
 +Tarankova, Z.A. 75389
 +Tarasov, G.A. 74548
 +Tarasova, T.P. 74809
 +Taratin, A.M. 76535
 Tarazona, P. + 76749
 +Tarcán, Y.A. 78329
 +Tardy, M. 78502
 +Tarey, G. 76985
 +Targett, T.E. 78550
 +Targan, I. 76999
 +Tarkhova, T.N. 76349
 +Tarmak, M. 77274
 +Tarnawski, Z. 77284
 +Targ, S.S. 75714
 +Taroni, A. 76128
 +Tarrach, R. 74719
 +Tarshish, R.L. 74479
 +Tarvin, J.T. 78147
 +Tascon D'Leon, R. 75486
 Tashiro, K. + 76709
 +Tassie, L.J. 74726
 +Tassoul, M. 78912
 +Tatar, R.C. 75272
 +Tatarskii, V.I. 74289
 +Tatewaki, H. 75286
 T.A. Tombrello.
 see Tombrello, T.A.
 +Tatsukawa, T. 77206
 +Taub, H. 76783
 Taubenblatt, M.A. + 77502
 +Taubert, G.E. 74347
 +Taunay, G. 78327
 +Tavanov, E.G. 76962
 +Tavares, O.C. 78960
 +Tavkhelidze, N.N. 74718
 +Tawada, Y. 78080
 +Taylor, B.A. 75593
 Taylor, B.J. 78823
 +Taylor, C. 77189
 +Taylor, F. 74669
 Taylor, P. + 76634
 Taylor, R. Eatock.
 see Eatock Taylor
 Taylor, R.
 see Taylor, R.
 Taylor, S.R. 78457
 Taylor, T.R. 74614
 Taylor, T.R. + 74705
 Taylor, W.J. 75260
 +Taylor, W.R. 78698
 +Tazlauanu, M. 77999
 +Tazzari, S. 75648
 +Tazzoli, F. 75648
 Tcheremissine, F.G. 76073
 +Te Kaat, E. 76524
 +Te Xian Zhao. 77042
 +Technow, R. 77489
 +Tekel, P. 74498
 +Telesnin, R.V. 77225
 +Tel'nikova, N.P. 77612
 Temkin, A.G. 74410
 +Temkin, D.E. 77621
 +Temkin, H. 76882
 +Templeton, W. 75123
 +Temps, F. 75336
 Tendeloo, G. van
 see van Tendeloo, G.
 +Teng, T.-L. 78460
 Teng Chain-Cheau.
 see Chain-Cheau Teng
 Tengcai Ma.
 see Ma Tengcai
 +Tengstal, C.G. 76766
 +Tentscher, K.-H. 78037
 Teodorescu, D. 77991
 Teodorescu, D. 78095
 +Teodorovich, O.A. 75063
 +Teodosiev, D. 78669
 +Teplitz, R. 78379
 +Teplitz, V.L. 78807
 +Teplovichov, S.G. 77147
 +Ter-Mikaelyan, M.L. 75706
 Ter-Pogossian, M.M. +
 see Ter-Pogossian, M.M.
 Tera, F. 78879
 Teramae, H. + 76823
 +Teranishi, T. 77407
 +Terashima, K. 77558
 +Terashima, K. 76289
 Terebizh, Yu.V. 78932
 +Terckhov, G.I. 75217
 +Terent'ev, F.M. 76620
 Terhardt, E. 78190
 +Terhune, R.W. 75414
 +Terhune, R.W. 75450
 Terry, F.L., Jr. + 77056
 Terychyni, S.I. + 74338
 Terukov, E.I. + 76618
 +Teshima, N. 77212
 +Tessier, P.Y. 77522
 Testard, O.A. + 74496
 Teszner, D. + 78210
 +Teszner, D. 78280
 +Teukolsky, S.A. 78824
 +Tevezadze, G.A. 75534
 +Texier-Hervo, C. 77586
 +Tezlevan, V.E. 76978
 Thackeray, M.M. + 76391
 Thai Vo Hoang.
 see Vo Hoang Thai
 Thakurta, S.R.G. + 76981
 +Thaler, R.M. 74968
 +Thangaraj, R. 77564
 Thanh Nghi Nguyen.
 see Nguyen Thanh Nghi
 Thanh Van Tran.
 see Tran Thanh Van
 The Khoi Nguyen.
 see Nguyen The Khoi
 +Theiner, W.A. 77201
 Thejappa, G. + 78896
 +Therain, F. 78327
 Theriault, K.B. 78718
 Thery, J. + 76556
 Thevenard, P. 76469
 +Thevenard, P. 76471
 +Thevenin, J. 77892
 +Theyer, F. 78436
 +Thibault, C. 74915
 Thiel, K. + 77508
 +Thiel, K. 77465
 +Thiel, K. 77466
 Thiel, W. 75455
 Thiele, W. + 75110
 +Thiemann, W. 77366
 Thijssen, H.P.H. + 75448
 Tholen, D.J. + 78859
 +Thomas, A.S.W. 75983
 +Thomas, A.W. 75048
 +Thomas, G. 76653
 +Thomas, G.B. 77759
 Thomas, J.H. 78810
 +Thomas, J.K. 77899
 +Thomas, K.A. 78309
 Thomas, L. 78594
 Thomas, P.G. + 78837
 +Thomas, R.N. 76342
 Thomas, R.W.L. 78650
 Thomas, V.G. + 76683
 +Thomchick, J. 78049
 +Thompson, D.G. 75531
 +Thompson, J.T. 74543
 +Thompson, M.N. 74960
 +Thomson, D.J. 78072
 Thorat, H.T. + 77733
 +Thorn, C. 74619
 +Thorn, C. 75036
 +Thornby, J.I. 78360
 +Thorne, A. 75510
 +Thorne, R.E. 77570
 Thornley, F.R. 76235
 Thornton, D.C. + 78697
 +Thornton, G.J. 78768
 Thornton, J.A. + 78088
 +Thorp, J.S. 77254
 +Thorpe, M.F. 76917
 Thro, E. 78572
 +Thuan, T.X. 78995
 +Thuler, M.R. 76794
 +Thuler, M.R. 77526
 Thyss, K.-E. 75473
 Ti, S.Y., T.S. 77295
 Tianyi Zhang.
 see Zhang Tianyi
 Tiedje, T. + 76989
 +Tien, J.K. 76447
 +Tien-Shou Wu. 76944
 +Tien-Shou Wu. 77318
 +Tien-Shou Wu. 77330
 Tift, W.G. 79004
 +Tift, W.G. 79013
 +Tiginyanu, I.M. 77444
 Tigner, M. 75212
 Tikhedeev, S.G. 74327
 Tiktopoulos, G. 75489
 +Tikviki, M. 75861
 +Tildesley, D.J. 77392
 Tillieu, J. + 74306
 Tillieu, J. + 74307
 +Tillu, A.D. 78730
 Timmons, M.L. + 78077
 +Timofeev, V.P. 75729
 +Timofeeva, I.I. 77612
 +Timoshchkin, M.I. 77563
 +Timoshenko, I.I. 76546
 +Timur, A. 78450
 Ting, S.C.C. 74754
 +Ting, T.C.T. 75922
 +Tinnemans, A.H.A. 77900
 +Tiraspol'skaya, R. Ya.
 see R. Ya. Tiraspol'skaya
 +Tirkey, B. 78423
 +Tirrell, M. 77727
 +Tischer, H. 75479
 Titov, Yu.I. + 74963
 +Titulaer, U.M. 74382
 +Titulaer, U.M. 74422
 +Tiwari, G.N. 78097
 Tiwary, S.N. 75514
 Tiwary, S.N. + 75344
 Tjong, S.C. 76810
 +Tkach, A.N. 77755
 +Tkach, V.I. 74661
 +Tkach, V.V. 75605
 +Tkailich, V.S. 74280
 Tobin, S.P. + 77967
 +Todorov, N. 75153
 +Todorova, D.D. 77390
 +Toews, H. 76122
 +Tokarev, A.G. 77455
 +Tokarskaya, V.I. 78241
 +Toki, H. 74892
 +Toksoz, M.N. 78450
 +Tokumoto, H. 76932
 +Tokumoto, M. 76932
 Tolf, G. 75933
 +Tolkachev, V.A. 75625
 +Tolksdorf, W. 77267
 Tolokonnikov, G.K. 74324
 +Tolpadi, S. 76578
 +Tolstikov, V.N. 75059
 +Tomasi, E. 74864
 +Tomasi, J. 77867
 +Tombrello, T.A. 77512
 Tomchuk, P.M. + 76699
 +Tomchuk, P.M. 77041
 +Tomczyk, S. 78889
 Tomeno, I. + 76543
 Tomimatsu, A. 74334
 +Tomko, R.P. 78031
 +Tompkins, B.M. 78381
 +Tompkins, L.A. 78495
 +Tompkins, W.A.F. 78233
 +Tompkins, W.A.F. 78231
 +Tompkins, W.A.F. 78234
 +Tompkins, W.A.F. 78232
 +Tompkins, W.J. 78381
 Tompson, R.J.G. + 77179
 Tong Chang + 78720
 Tonin, M. 74588
 +Tonio, D. 74992
 Tonomura, A. + 74639
 +Toots, J. 77101
 +Top, L.H. 77984
 +Topchii, V.N. 76487
 Toppare, L. + 75056
 Torchinskaya, T.B. + 77075
 +Toriyama, K. 77911
 +Torizuka, K. 78294
 +Torkar, K.M. 78740
 Tornow, W. + 74999
 +Tornqvist, R.O. 77459
 Toro, M. di
 see di Toro, M.
 +Torok, I. 75245
 +Torrance, K.E. 76008
 +Torzecki, J. 75976
 +Tosi, M.P. 76159
 +Tosic, M.M. 76472
 +Totovski, D.C. 77588
 Touati, A. 74373
 +Touchard, F. 74915
 Tour du Pin, H. de La.
 see de La Tour du Pin, H.
 +Tournoux, M. 76393
 +Tousek, J. 77028
 Tousekova, J. + 77028
 +Tousset, J. 77768
 +Touzain, P. 77895
 Towner, I.S. + 74899
 +Towner, I.S. 74910
 +Townsend, P.D. 77465
 +Townsend, P.D. 75787
 +Townsend, P.D. 76526
 +Townsend, P.K. 74644
 +Townsend, R.P. 77881
 +Townsendm, P.D. 77466
 +Toyoda, K. 75602
 Toyoda, T. 74582
 +Tozawa, Y. 77670
 Tozeren, H. 76039
 +Trachsel, C.A. 75175
 Trainor, K.S. 76580
 +Trallero Giner, C. 77441
 +Tramer, A. 75420
 +Tramontano, A. 78137
 Tran, Q. Dang
 see Dang Tran, Q.
 +Tran Thanh Van. 74810
 +Trapeznikov, V.A. 77725
 +Trapp, K.D. 76434
 +Trasatti, L. 74766
 +Trasatti, L. 75225
 +Trask, T.O. 74444
 +Trautman, E. 78379
 +Trautmann, N. 77946
 +Traxler, A. 74488
 +Trayner, B.T. 75827
 +Treacy, M.J. 76646
 Tredway, W.K. + 77614
 Treffers, M.A. + 75495
 Trefilov, V.I. + 77681
 +Treherne, D.M. 75858
 +Treheux, D. 77768
 +Treilleux, M. 76642
 Tremolet de Lacheisserie, E. du
 see du Tremolet de Lacheisserie, E.
 +Trenholme, J.B. 75172
 +Trepakov, V.A. 77405
 +Tressler, R.E. 77731
 +Tret'yakov, F.F. 78498
 +Tricks, G. 76292
 +Trickey, S.B. 76571
 +Tricoire, H. 75027
 +Trigo, G.G. 75395
 +Trillo, S. 75648
 +Trimmer, W.S. 76434
 +Trimmer, W.S.N. + 75887
 Trinaistic, N. + 75553
 +Trinaistic, N. 75438
 +Trinaistic, N. 75261
 +Tripathi, K.N. 77077
 +Tripier, J. 75236
 +Tripp, H.J. 78202
 Triska, P. + 78772
 +Trivia, G. 75488
 +Trivich, D. 77993
 +Trivikrama Rao, G.S.
 see Rao, G.S.
 +Troc, R. 77180
 +Troce, J. 75484
 +Troee, J. 75485
 Troitskii, O.A. 77683
 Troitskii, O.A. + 77667
 +Tromborg, B. 74518
 Trong Nguyen Van.
 see Nguyen Van Trong
 +Tronrud, D.E. 78130
 Trontelj, Z. + 78398
 +Trontelj, Z. 78282
 +Tropper, A.C. 77291
 Troshin, S.M. + 74793
 +Troshkov, S.I. 78005
 Trostel, R. 74592
 +Trott, G.J. 76494
 +Trout, J. 75719
 +Trower, W.P. (ed.) 74228
 Truchon, M. + 77800
 +Trujillo, G. 78108
 Trukhanov, E.M. 76813
 +Trump, D.D. 74542
 Truong Vo-Van.
 see Vo-Van Truong
 +Trushin, E.V. 75767
 +Trushin, S.A. 75453
 +Trushin, Yu.V. 76630
 Trushnikovskii, L.M. 74425
 Truszkowski, K. + 76760
 +Truten', V.I. 77496
 +Tsai, C.L. 76672
 +Tsai, S.T. 76178
 Tsai Jansen.
 see Jansen Tsai
 +Tsallisi, T. 77192
 Tsang, L. + 78541
 Tsang, M.B. + 75035
 +Tsang, T.-W.E. 77135
 Tsang, W.T. + 75635
 +Tsang, W.T. 77446
 Tsang, Y.W. + 78532
 +Tsanov, T.V. 77929
 Tsarevskii, S.L. 77009
 +Tsaar, B.-Y. 78082
 +Tsai, W.-S. 75719
 Tschege, E.K. 77745
 +Tschege, E.K. 77696
 Tschirf, E. + 75193
 Tschurlovits, M. 78340
 Tschurlovits, M. + 78342
 Tse Ming-Kai.
 see Ming-Kai Tse
 Tseitlin, M.Yu. 74426
 Tsejun Wang.
 see Wang Tsejun
 +Tsender, E.M. 75069
 +Tsertsvadze, A.A. 77487
 +Tseytlin, A.A. 74361
 +Tseytlin, A.A. 74748
 +Tsintsadze, G.A. 76912
 +Tsirel'son, V.G. 77129
 Tsitskishvili, K.F. + 77176
 +Tsong, I.S.T. 77511
 +Tsong, T.T. 76761
 Tsou, J.C. + 77744
 +Tsou, J.C. 76557
 +Tsuda, I. 74376
 +Tsugawa, R.K. 78756
 +Tsugba, A.R. 74455
 +Tsuge, K. 78080
 Tsui, M. + 75154
 +Tsui, Y. 77739
 +Tsui, Y. 77981
 +Tsujichi, J. 74437
 +Tsukerman, V.L. 77445
 Tsunoda, Y. + 77642
 Tsuo, Y.S. + 78069
 +Tsuo, Y.S. 78024
 Tsurkan, V.V. + 76978
 +Tsuru, H. 75964
 +Tsutsui, M. 77705
 Tsuya, N. + 77598
 +Tsvetkov, V.A. 77436
 +Tsvetkov, V.M. 78302

- Tuchman Y. + 78902
 +Tuschscherer, H. 74756
 +Tuck, B. 76951
 Tucker, P.G. 75126
 +Tucker, R.W. 79038
 Tucker, T.R. + 76763
 +Tuda, T. 75184
 +Tugushev, V.V. 76851
 +Tuimova, A.M. 78713
 +Tulach, V.Ya. 75625
 Tuli, M. + 77811
 +Tuli, S.K. 75039
 +Tuli, S.K. 75044
 +Tuli, S.K. 75045
 +Tulinov, A.F. 77944
 +Tuma, D.T. 74450
 +Tuma, D.T. 74451
 Tumakaev, G.K. + 75536
 Tung-sheng Wang. *see* Wang
 Tung-sheng
 Tuohy, I.R. + 78976
 +Tuokko, C. 74839
 Tuomisto, T. + 78188
 +Tuomisto, T. 78280
 +Tuomisto, T. 78395
 +Tuponogov, V.G. 76104
 Turchanyi, G. + 76999
 +Turdaliev, K.T. 74809
 +Turmo, J. 75275
 +Turmo, J. 78135
 +Turner, C.W. + 77142
 +Turner, D.T. 77748
 +Turner, J.L. 75529
 +Turner, P.J. 78894
 +Turner, W.C. 76214
 +Tuscany, R. 78243
 +Tuts, M. 74669
 +Tuy, H. 78314
 +Tuzun, U. 76108
 +Tveten, A.B. 74529
 +Tvorogov, S.D. 75468
 +Twardowski, A. 77369
 Tweel, I. *van Der*
 +Van Der Tweel, I.
 Tyagi, M.S. 76968
 Tyburczy, J.A. + 78535
 Tychkov, S.A. 78515
 Tye, C. + 75166
 +Tye, H. 74669
 +Tyler, G.L. 78860
 +Tyupkina, O.G. 76552
 +Tyurin, A.V. 77005
 +Tyurin, N.E. 74793
 +Tyurin, V.G. 78306
 +Tyvand, P.A. 76009
 +Tzanakos, G. 74669
 +Tzou, J.J.-T. 77017
 Untiedt, J. 78759
 Upadhyaya, B.R. (*ed.*)
 74224
 +Uplane, M.D. 78089
 +Ura, M. 76136
 Urano, Y. + 78100
 Uratsuka, M. + 78791
 +Uratsuka, M. 78795
 +Uratsuka, M. 78789
 Uray, I. + 75245
 +Urban, K. 76511
 +Urbonavicius, V. 76613
 Uren, R.F. + 78328
 Uribe, F.A. + 77518
 Urman, Yu.M. 74269
 Urries, F.J.de
 *see de* Urries, F.J.
 +Urusov, V.S. 76638
 +Urusov, L.I. 76193
 +Uryadnitskaya, T.I. 78249
 +Us, V.I. 77626
 Usacev, L.N. 75071
 Usami, A. + 78000
 +Ushenko, A.G. 75605
 +Usmar, S.G. 77476
 +Usubov, Z.U. 74771
 +Utemisov, K. 76243
 Uteviski, L.M. + 76647
 +Utsumi, K. 78903
 Uttam, D. + 74528
 +Uvarov, L.N. 74983
 +Uvarova, S.K. 77111
 +Uzzidin, V.M. 77148
 +Uzhinov, B.M. 77882
 +Vaccaro, S. 76103
 +Vacccher, C. 75388
 +Vacher, R. 77404
 +Vadura, M. 77304
 +Vager, Z. 74555
 Vaidhyanathan, V.S. 78146
 +Vaidyanathan, K.V. 77402
 Vain, O. + 76027
 Vainberg, E.I. + 78331
 +Vainberg, V.M. 74321
 +Vainer, A.Ya. 74549
 Vainshtein, D.I. + 77290
 +Vaisala, S. 74906
 +Vaisberg, O. 78668
 +Vaisberg, O.L. 78777
 Vaisburd, D.I. + 76962
 +Vakul'chik, P.A. 76487
 +Valakh, M.Ya. 77384
 Valberg, A. + 78185
 +Valenti, G. 74821
 +Valentin, L. 75027
 Valerdi, M. Antonia
 *see* Antonia Valerdi, M.
 Valin, P. 74808
 +Valiron, P. 75501
 +Valiukonis, G. + 77410
 +Valiulin, E.G. 77137
 Val'kovskii, S.N. + 77678
 +Vallabhan, C.P.G. 77334
 Vallario, E.J. 75200
 Valle, R.G. Della
 *see* Della Valle, R.G.
 +Valles, J.L. 76637
 +Valley, G.C. 75740
 +Valley, G.C. 75748
 +Valter, S.N. 78245
 +Vamos, L. 78356
 van Albada-van Dien, E.
 78946
 +Van Allen, E.J. 75600
 +Van Beijeren, H. 76145
 +Van Bostel, R. 75113
 +van Dam, R.T. 78374
 van de Weijer, P. + 75345
 Van Den Akker, T.J. +
 78214
 +Van Den Berg, R. 75448
 van den Bergh, S. + 78968
 +van den Beukel, A. 76776
 +van den Heuvel, E.P.J.
 78934
 van der Bij, J.J. + 74656
 +Van Der Hulst, J.M.
 79002
 Van der Jeugt, J. + 74647
 +Van Der Kelen, G.P.
 75386
 +van der Kraan, A.M.
 77209
 +van der Kraan, A.M.
 77155
 +Van Der Lee, H. 78162
 +van der Linden, J. 74253
 +van der Lugt, W. 77276
 van der Marel, C. + 77276
 van der Meer, S. 75219
 +van der Merwe, P. du T.
 74315
 van der Ploeg, P. + 78153
 +Van der Star, J. 78636
 Van Der Tweel, I. + 78168
 Van Der Veken, B.J. +
 75385
 +van der Velde, G. 75259
 +van der Velde, J.C. 75226
 Van Der Wal, R. + 76352
 +van der Woude, A. 74948
 +van Duijneveldt, F.B.
 75540
 Van Duyl, W.A. 78216
 Van Dyke, M. (*ed.*) 74234
 +van Engen, P.G. 77156
 +van Groenendaal, A.
 74306
 +van Groenendaal, A.
 74307
 +Van Gunten, O. 76506
 van Haastert, G.H. + 77676
 +Van Haute, A.A. 77788
 +van Heerden, I.J. 74975
 +van Holten, J.W. 74611
 +Van Horn, H.M. 78912
 +Van Hove, M.A. 77018
 Van Isacker, P. 74909
 Van Kote, F. 75134
 +van Landuyt, J. 76368
 +van Oosterom, A. 78205
 +van Peppen, J.C.L. 74431
 Van Rentergem, M. + 75386
 van Rossum, M. + 76468
 +van Schaick, E.J.M.
 78127
 +van Steenberg, A.
 75654
 +Van Strijland, E.W. 75756
 van Swygenhoven, H. +
 76505
 +van Swygenhoven, H.
 76483
 +van Tendeloo, G. 76368
 Van Tran Thanh
 *see* Tran Thanh Van
 Van Trong Nguyen
 *see* Nguyen Van Trong
 Van Vechten, D. + 77101
 +Van Vollenhoven, E.
 78372
 +Van Wyck, N.E. 75726
 Vana, N. + 78337
 Vana, N. + 78338
 +Vana, N. 75193
 Vance, E.R. + 75092
 +VanDalen, G. 75017
 +Vanden Bergh, G. 74647
 +Vandenbergh, J.M. 76497
 Vandenbergh, R.E. + 77301
 +Vander Linden, D. 78955
 vander Plicht, J. + 75036
 +Vander Sande, J.B. 77628
 +Vander Sande, J.B. 77660
 +Vander Sande, J.B. 77654
 +Vanicek, L. 78363
 Vankar, V.D. + 76793
 +Vannier, M. 74564
 Vanyurkin, A.I. + 74510
 +Vardenga, G.L. 75011
 +Varela, M.E. 75114
 +Varfolomeev, I.M. 76026
 Vargas, L.de
 *see de* Vargas, L.
 +Vargas-Aburto, C. 75490
 +Vargin, E.P. 75207
 Varikash, V.M. + 77358
 Varkey, A.J. + 77549
 Varkey, P.A. + 77644
 Varkhalev, Yu.P. 74271
 +Varkonyi, T. 78116
 +Varma, C.A.G.O. 77902
 +Varma, H.K. 76022
 +Varma, M.P. 75547
 +Varma, R.K. 79005
 Varnavsky, O.P. + 75692
 +Varpula, T. 78395
 +Varpula, T. 78284
 +Varpula, T. 78210
 +Varpula, T. 78188
 +Varvarovski, F. 75170
 +Vary, J.P. 74871
 +Vary, J.P. 74991
 Vasconcellos, J.I. Cotrim
 *see* Cotrim Vasconcellos, J.I.
 +Vasilenko, A.T. 75918
 Vasil'ev, A.B. + 76645
 +Vasil'ev, V.K. 76517
 +Vasil'ev, V.V. 77203
 Vasil'eva, M.A. + 75752
 Vasilenskaya, A.S. + 76306
 +Vasiliev, E.M. 78777
 +Vasin, V.V. 77479
 +Vasnin, G.M. 74961
 Vassamillet, L. + 76651
 +Vassamillet, L.F. 76649
 Vassanji, M.G. + 74947
 Vasserman, I.A. + 77398
 +Vassilakis, J.P. 74554
 Vasu, R.M. + 75698
 +Vasudeva, K. 75979
 Vasyukov, V.N. + 76912
 +Vatoux, S. 75825
 +Vautherin, D. 74298
 Vavilov, V.S. + 77462
 +Vavilov, V.S. 76994
 Vecchia, P. di. *see* di Vecchia, P.
 Vechten, D. Van
 *see* Van Vechten, D.
 Vedel, F. + 76146
 +Vedel, M. 76146
 +Veillet, J.J. 74783
 +Veillet, P. 77285
 Veitch, R. + 77216
 Veken, B.J. Van Der. *see* Van
 Der Veken, B.J.
 Velde, G. van der. *see* van der
 Velde, G.
 Velde, J.C. van der. *see* van der
 Velde, J.C.
 Veldkamp, W.B. + 75600
 +Velghe, M. 75650
 +Velichanskii, V.L. 75346
 +Velikanova, T.Ya. 76361
 Velisek, J. 76670
 +Vellutini, P.-J. 78499
 +Velsko, S. 75719
 +Velyakova, I.G. 75907
 +Vemuri, S.B. 76005
 +Venat, P. 78814
 +Veneziano, G. 74705
 Vengrinovich, V.L. 77844
 Vengrinovich, V.L. + 77845
 +Venkata Chalapathi, V.
 75307
 +Venkataramaiah, P. 74914
 Venkataramani, N. + 74464
 +Venkoba Rao, H.N. 77931
 Ventriglia, F. 78170
 +Verbiest, E. 76468
 +Verbruggen, A. 75210
 Verdenet, J. + 78308
 +Verdini, L. 77692
 +Verenik, V.N. 77940
 Veres, G. + 77954
 Vereshchagin, S.I. + 78820
 +Vereshchagin, Yu.A.
 77150
 Veretennikov, V.A. + 74576
 Vergados, J.D. 74648
 +Vergnes, M. 74847
 +Verhaar, B.J. 76747
 Verheijen, M.J. + 75347
 +Verie, C. 78068
 Verma, R.C. 74775
 +Vernotte, J. 74847
 +Verrells, M.V. 75818
 Versino, B. (*ed.*) 74233
 +Verster, N.F. 75347
 Verweij, H. 77615
 +Vescovi, M. 75648
 +Veselago, V.G. 76978
 +Vest, C.M. 75608
 Vetesnik, M. 78926
 Vetrivel, R. + 77914
 +Vetrov, V.Yu. 77403
 +Vetsko, V.M. 75534
 Vetterling, W.T. + 76573
 +Vettier, C. 77238
 Veuhoff, E. + 77576
 Vey, J. 77178
 +Veyssie, M. 76295
 +Veziroglu, T.N. 78107
 +Veziroglu, T.N. 76091
 Viallefond, F. + 78995
 Viallet, C.M. 74635
 +Viano, J.B. 75040
 +Viano, J.M. 76677
 +Vichniac, G. 74878
 +Vicini, I. 76326
 Vickers, G.H. + 74444
 +Vieira, N.D. 77419
 Vietri, M. + 78963
 Vigak, V.M. 75895
 Vigfusson, J.O. 74412
 Viggiano, A.A. + 78618
 +Vignal, L. 76640
 +Vignati, A. 75670
 +Vignola, G. 75648
 Vijaya Kumar, B.V.K.
 75780
 +Vijayakumar, R. 78663
 +Vijayalakshmi, B. 74596
 Vijayaraghavan, M.S. +
 77368
 +Vikharev, V.D. 76193
 +Vikhrov, V.V. 74983
 +Viktorovitch, P. 77061
 +Vilasi, G. 74294
 +Vilkomerson, D. 75887
 +Vilkova, I.V. 77314
 +Villa, M. 76694
 +Villalobos, A. 75084
 +Villar, E. 78700
 Villar, H.O. + 75271
 +Villien, A. 78502
 +Villiger, A. 76292
 Vilor, N.V. + 78543
 +Vinas, X. 74864
 +Vincent, R. 78167
 +Vincent, R. 76260
 Viney, C. + 76285
 +Vinitskii, A.L. 76687
 +Vinogradov, G.V. 75971
 Vinokur, M. 74281
 +Vinokurov, V.M. 77290
 +Vinter, B. 77395
 +Viola, V.E. Jr. 74988
 +Viola, V.E. Jr. 75064
 +Viola, V.E. Jr. 74977
 Viragh, E. 75192
 Virasoro, M.A. 74680
 +Virgili, J. 76769
 +Virgili, J. 76770
 +Virk, H.S. 75237
 +Virk, H.S. 78483
 Virnik, Ya.Z. + 75694
 +Vischaskas, J. 75752
 Visser, R.J. + 77902
 +Viste, A. 76842
 +Viswanathan, B. 77914
 Vita, P. Di. *see* Di Vita, P.
 Vitrchenko, E.A. + 75767
 +Vivien, D. 77256
 Vladimirov, L.V. + 78362
 +Vladimirov, L.V. 78300
 +Vladimirov, V.S. + 77198
 +Vladimirov, Yu.S. + 79041
 +Vlasenko, L.S. 77281
 +Vlasenko, L.S. 77288
 +Vlasov, A.A. 74339
 Vo Hoang Thai + 77473
 +Vo-Van Truong
 77467
 Vodolazskii, P.V. + 77452
 +Vogel, H. 74669
 Vogel, S.N. + 78972
 +Vogl, G. 76705
 Vogl, P. + 76843
 Vogt, K. + 78181
 +Vohra, K.G. 74536
 +Voiron, J. 77238
 +Voitenko, A.F. 77757
 +Voitenko, L.P. 78259
 Voitoevskii, V.K. + 77289
 +Voita, J. 78772
 Voitik, J. + 76772
 +Volenik, K. 77304
 +Volk, J.T. 74759
 +Volkenstein, N.V. 76925
 +Volkenstein, N.V. 76931
 +Volkenstein, N.V. 77137
 +Volker, S. 75448
 Volkov, B.A. + 77321
 Volkov, B.A. + 76851
 Volkov, D.V. + 74661
 +Volkov, V. 75734
 Volkov, V.A. + 77026
 Volkov, V.A. + 76926
 Volkov, V.P. + 75561
 +Volkov, V.V. 75899
 Volland, H. + 78699
 Vollenhoven, E. Van. *see* Van
 Vollenhoven, E.
 Vollhardt, D. 76739
 +Vollman, W. 75866
 +Vol' mir, A.S. 78223
 +Volovich, I.V. 77198
 +Volovik, G.E. 76737
 +Volpp, H.-J. 78605
 von Berlepsch, H. + 77019
 +von Brentano, P. 74840
 +von Cierninski, J. 77337
 +von der Weid, J.P. 78206
 von Geramb, H.V. 74885
 +von Geramb, H.V. 74973
 +von Herzen, R.P. 78486
 +von Herzen, R.P. 78489
 +von Herzen, R.P. 78488
 +von Herzen, R.P. 78567
 +von Hoyningen-Huene, W.
 78585
 +von Lampe, F. 77274
 von Roos, O. 76967
 +von Schnering, H.G.
 76661
 +von Szepenty, L. 75263
 +Vong, R. 78613
 +Vook, R.W. 76793
 +Vorob'ev, E.D. 75162
 +Vorobiev, S.A. 76535
 +Voronin, I.D. 77838
 +Voronin, V.B. 76229
 +Voronko, M.P. 76922
 Voron'ko, Yu.K. + 75642
 Vorontsova, N.M. + 75839
 +Vorris, C.L. + 77859
 Vos, A. De. *see* De Vos, A.
 Vos, A.M. de
 *see* de Vos, A.M.
 Voskobonnikov, G.M. +
 78691
 +Vot, M. Le. *see* Le Vot, M.
 +Votava, C. + 76273
 +Votinov, S.N. 76716
 +Vovk, Ya.N. 76366
 Voykov, G.K. + 75072
 +Vrabcek, P. 74498

- Vrba, J. + 78394
 Vrestal, J. + 77617
 Vries, A.E.de
 see de Vries, A.E.
 Vries, O.De. *see* De Vries, O.
 Vronsky, M. 78104
 + Vu Zhan Mien 77462
 Vujicic, G.M. + 77087
 Vvedensky, V.L. + 78399
 Vyatkin, E.G. + 76535
 + Vyborny, C.J. 78330
 Vysotskii, V.I. + 76541
 + Vysotsky, M.I. 74660

 + Wachendorf, H. 78482
 Wada, K. + 77122
 + Wadley, H.N.G. 75099
 + Waff, H.S. 78535
 + Wagendristel, A. 76247
 + Wager, R. 78864
 Wagner, A. 74781
 + Wagner, F.E. 77311
 + Wagner, H.G. 75336
 + Wagner, H.-G. 77652
 Wagner, K.-G. 74469
 + Wagner, P. 75031
 Wagner, S. 78081
 + Wagner, S. 77271
 + Wagner, S. 76964
 Wagner, S.G. + 75083
 Wahab, F.M.Abdel
 see Abdel Wahab, F.M.
 + Wahlich, R. 78048
 + Wakeham, W.A. 76148
 Wal, R.Van der
 see Van Der Wal, R.
 Walborn, N.R. 78914
 + Walsh, S.P. 75279
 + Waldeck, D.H. 75552
 + Wali, K.C. 74667
 + Walitzki, H. 74846
 Walker, C.F. + 78227
 + Walker, D.C. 75556
 + Walker, T.G. 74797
 + Wallace, S.C. 75431
 + Wallace, S.C. 75731
 + Wallace, S.J. 74996
 + Wallace, W.E. 77896
 + Wallart, F. 77978
 + Walling, J.C. 75686
 Wallis, G.B. + 76086
 Wallis, R.H. 76956
 + Wallrahen, F. 77255
 + Walls, D.F. 75723
 + Walsley, M. 78872
 + Walsh, C.J. 76184
 + Walsh, J.C. 78369
 + Walsh, J.C. 78370
 + Walsh, J.L. 75737
 + Walsh, R. 78065
 + Walter, M. 76600
 + Walter, R.L. 74999
 + Walters, C.T. 76763
 + Walters, K. 76079
 Walters, N.M. + 78582
 + Walters, W.B. 74913
 + Walukiewicz, W. 76889
 Walz, F. + 77682
 + Walzade, S.J. 76969
 Wan, C.C. 76320
 + Wand, R.H. 78739
 + Wang, A.J. 75951
 + Wang, E. 74759
 + Wang, J.K. 78126
 + Wang, J.S. + 77697
 + Wang, K.-L. + 77207
 + Wang, P.-H. 78661
 + Wang, P.J. 77635
 + Wang, R. + 76783
 + Wang, W.I. 75640
 + Wang, W.L. 78032
 + Wang Chaoguo 77081
 + Wang De-xin 74559
 Wang Hsin *see Hsin Wang*
 + Wang Ji-tao 74559
 Wang Jinshan + 77279
 + Wang Kellin 74606
 + Wang Rung-tai + 74589
 + Wang Rulin 74985
 + Wang Shaomin 75749
 + Wang Tai-hui 74502
 + Wang Tsejun + 78522
 + Wang Tung-sheng + 74503
 + Wang Xiu-zhen 75296
 + Wang Yanyan 77813
 + Wang Yimin 77866
 + Wang Yun-jian 75948
 + Wang Zhen-rui 78938
 + Wang Zong-xin + 74491
 + Wang-Ping Chen 78451
 Wanlass, M.W. + 78067
 Wanxie Zhong
 see Zhong Wanxie
 Warble, C.E. 74565
 Ward, D.R. 74819
 + Ward, H. 78935
 + Ward, I.M. 77699
 + Ward, M. 79024
 + Ward, T.E. 74988
 + Ward, T.E. 74977
 + Wardle, J.F.C. 79023
 Warner, D.D. + 74908
 + Warner, N.P. 74354
 + Warren, R.W. 75653
 Washburn, J. + 76507
 + Washburn, S. 76744
 + Washburn, S. 76745
 + Watanabe, J. 76433
 + Watanabe, S. 78882
 + Watanabe, S. 78742
 + Watanabe, T. 78590
 Watanabe, Y. + 75277
 Watanabe, Y. + 76954
 + Waterman, L.S. 78698
 + Watnick, S. 75197
 Watson, A. 74678
 Watt, R.G. + 76204
 Weaver, H.A. + 75370
 + Weaver, J.H. 77053
 + Weaver, J.H. 76768
 + Webb, A.I.C. 74460
 Webber, R.L. + 78324
 + Weber, E.-H. 76780
 Weber, H.-J. 77364
 Weber, W.H. + 75414
 Weber, W.H. + 75450
 + Wechsler, H. 78540
 + Wedell, R. 76534
 + Weeda, H.W.H. 78372
 + Weeks, A.R. 75238
 Wegner, G. 78910
 + Wegner, H.E. 75036
 + Wehausen, J.V. (ed.)
 74234
 + Wehrle, A.E. 78945
 Wei Chung-Chuang
 see Chung-Chuang Wei
 Wei Lei + 78654
 Wei Xiwen + 77578
 Wei Zhonglei + 76033
 Weid, J.P.von der
 see von der Weid, J.P.
 + Weidenmuller, H.A. 75062
 + Weidenmuller, H.A.
 75223
 + Weigmann, W. 75714
 + Weiguny, A. 74924
 Weijer, P.van de
 see van de Weijer, P.
 + Weill, C. 76295
 Weinberg, I. + 78033
 Weinberg, S. 74618
 Weinberg, Z.A. + 77059
 Weinberger, B.R. 76991
 + Weinberger, D.A. 75714
 Weinert, H. 77442
 Weinert, H. + 77443
 + Weingarten, D. 74707
 Weinstein, R. 74751
 Weis, J. + 76309
 + Weisberg, J.M. 78933
 Weishen Zhu
 see Zhu Weishen
 + Weisman, R.L. 77776
 + Weiss, J.M. 78386
 + Weiss, R. 78054
 + Weissel, J.K. 78487
 Weissman-Wenocur, D.L. +
 76790
 + Weissmann, S. 76241
 + Welch, W.J. 78972
 + Weller, Th. 75292
 Wen Shizhu 75956
 + Wen-Rong Lu 77973
 + Wendelken, H.J. 75484
 + Wendelken, H.J. 75485
 + Wendler, L. 76859
 + Weneser, J. 78816
 Weng Pao-Shan
 see Pao-Shan Weng
 Wensink, H. 78424
 Wenxia Tang
 see Tang Wenxia
 Werblan, L. + 77968
 + Werner, D. 78414
 + Werner, M.W. 79019
 + Wesler, L.S. 78237
 + Wesley, J.L. 77699
 + Wesseling, K.H. 78372
 + West, D.R.F. 77809
 + West, G.D. 77824
 West, R.A. 78855
 Westbrook, L.D. + 75688
 Westhaus, P. 75262
 + Westmacott, K.H. 76508
 Westmeier, W. + 74928
 Westmeier, W. + 76538
 + Westphal, G.H. 76942
 Westrum, E.F., Jr. 76656
 + Wevers-Henke, J.J. 78205
 + Wexler, B.L. 75737
 Weymueller, C.R. 77849
 Whalen, B.A. 78666
 + Whalley, E. 77376
 Whang, S.H. + 77770
 + Wheeler, J.A. 78818
 Wheeler, J.C. + 77888
 Wheeler, J.C. + 78818
 + Whelan, J.M. 76476
 + Wherrett, B.S. 75708
 + Wherrett, B.S. 75753
 Whitaker, R.D. + 78046
 + White, B.S. 76127
 + White, C.W. 76598
 + White, D. 74669
 + White, G.C. 78108
 + White, G.K. 77239
 + White, H.W. 77179
 White, I.H. + 74509
 White, L.W. 75138
 + White, M.G. 75127
 + White, W.B. 77511
 Whitefield, P.D. + 77891
 + Whitehead, J.D. 78731
 Whitehead, M.A. + 75258
 Whitley, R. 78805
 + Whitley, T.A. 75446
 Whitlow, H.J. + 76753
 + Whitmore, D.H. 76693
 + Whitson, J.C. 76211
 + Whittaker, J.B. 74797
 Whittet, D.C.B. + 78982
 Whittle, G.L. 77306
 Wiczor, J.J. + 78042
 Wiechert, H. + 76722
 Wiedemann, H. 75664
 + Wiedemann, W. 76740
 Wiegart, N.J. + 75342
 Wiegand, G. 78119
 + Wiegmann, W. 75707
 + Wienecke, J. 75527
 + Wiersma, D.A. 75424
 + Wiesenfeld, J.R. 77875
 + Wieser, E. 76284
 + Wightman, F.L. 78191
 + Wikswo, J., Jr. 78203
 Wikswo, J.P. + 78207
 Wilczek, F. 74709
 + Wild, J.F. 74906
 + Wildermuth, A. 76921
 + Wilhelmsson, H. 75674
 + Wilhelmly, J.B. 75036
 + Wilkie, C.A. 78402
 + Wilkins, B.D. 75029
 + Will, E. 74903
 + Willcocks, M.C. 78387
 Wille, R. 75965
 + Willeke, G. 77293
 + Willer, J. 76921
 + Williams, C.K. + 76959
 + Williams, D.L. + 78567
 + Williams, G.R. 77533
 + Williams, H.D. + 75124
 + Williams, H.H. 74669
 + Williams, J.S. 76473
 + Williams, P.F. 75341
 + Williams, R.K. + 75101
 + Williams, R.S. 77514
 + Williams, W.E. 75756
 + Williams, W.J. + 78598
 + Williamson, C.F. 74842
 + Williamson, D.L. + 77296
 + Williamson, S.J. 78178
 + Willis, A. 74898
 + Willis, R.D. 78891
 Wilson, J.P. + 75812
 + Wilschut, J. 78148
 + Wilschut, J. 78155
 Wildorf, H.G.F. 77742
 + Wilson, A.E.J. 75893
 + Wilson, A.J.C. 76328
 + Wilson, A.M. 78201
 Wilson, A.R. 76233
 + Wilson, D. 78229
 + Wilson, M.R. 76341
 + Wilson, P.B. 75663
 + Wilson, R. 74669
 Wilson, S. + 75278
 + Windle, A.H. 76285
 + Windsch, W. 77287
 + Windsor, C.G. 77685
 Winget, D.E. + 78912
 Winkler, D.M. 75862
 Winkler, P. 75507
 + Winkler, P.F. 78969
 + Winnacker, A. 77464
 + Winnewisser, M. 74538
 + Winograd, N. 75563
 + Winske, D. 76178
 + Winsor, T. 78276
 + Winston, J.G. 75653
 + Wintenberg, A.L. 77511
 + Winter, G. 74903
 Winter, H. + 77516
 + Winter, H. 75498
 Winters, H.F. 77506
 + Winters, R.R. 74990
 Wirlinga, R.B. 74862
 + Wirlinga, R.B. 74861
 + Wirlinga, R.B. 76726
 Wirth, F.W. + 76731
 + Wise, M.B. 74663
 + Wisman, J.A. 74444
 + Wiss, J. 74669
 Wit, B.De. *see* De Wit, B.
 + Witherspoon, P.A. 78532
 + Witt, A.F. 76337
 Witt, H.de. *see* de Witt, H.
 Witte, W. 76137
 + Witzke, H. 77987
 + Woigard, J. 76562
 + Wold, A. 76379
 + Wold, A. 76947
 + Wolf, F. 74918
 + Wolf, G.K. 77311
 + Wolf, H. 78780
 + Wolf, M. 76618
 Wolf, P.E. + 76723
 + Wolf, S.A. 77094
 Wolfe, A.M. 78975
 + Wolfe, A.M. 79020
 + Wolfe, C.M. 76980
 + Wolfe, C.R. 75970
 Wolfe, D.H. + 74968
 Wolfel, E.R. 76256
 + Wolfenstein, L. 74671
 + Wolfe, P. 76738
 Wolford, D.J. + 77457
 + Wolfram, S. 74580
 + Wolfram, S. 74696
 + Wolfsberg, K. 75057
 + Woloshyn, R.M. 74984
 + Wolschin, G. 75557
 + Wolters, J. 78390
 + Wouthuis, A. 76470
 + Wong, C. 75000
 + Wong, H.V. 76182
 + Wong, K.M. 75117
 Wong, M.K.F. + 75343
 Wong, M.K.F. + 75452
 + Woo, J.C. 76934
 + Wood, C.E.C. 77686
 + Wood, G.E. 78860
 Wood, G.V. 74251
 + Wood, L. 76218
 + Wood, W.E. 77624
 + Wood, W.E. 77635
 Woodhead, A.D. + 75112
 + Woodruff, D.P. 76789
 + Woods, D.W. 77699
 Woods, G.S. + 77382
 + Woodward, J. 77799
 + Woodward, R.W. 75412
 Woodworth, M.R. 76219
 + Woollam, J.A. 77055
 + Woollons, D.J. 78167
 + Worm, G. 76454
 + Worswick, R.D. 76659
 + Wortman, D.E. 75647
 Woude, A.van der
 see van der Woude, A.
 Wozniak, J. + 77826
 + Wright, A.E. 79018
 + Wright, A.E. 79024
 + Wright, A.E. 78945
 + Wright, J.A. 78438
 Wrigley, N.G. + 78404
 + Wronski, C.R. 77987
 Wu, C.S. + 76178
 Wu Chhi-Chong
 see Chhi-Chong Wu
 + Wu Hsueh-wen 74503
 Wu Hui-fang + 74894
 + Wu Ke 74591
 Wu Long *see Long Wu*
 + Wu Peizhen 78626
 + Wu Shikang 75886
 Wu Shuxiang + 76876
 Wu Souheng
 see Souheng Wu
 Wu Tien-Shou
 see Tien-Shou Wu
 + Wu Xi-zhen 74954
 Wu Xianghui 74299
 + Wu Yingzhi 75216
 + Wu Yue 76756
 Wu Yushu + 78563
 Wu Zhang Rong
 see Rong Wu Zhang
 Wu Zhongze
 see Zhongze Wu
 + Wudl, F. 77090
 Wuebbles, D.J. 78616
 Wuebbles, D.J. + 78617
 + Wuest, C. 75226
 Wulfman, C.E. + 75463
 + Wunderlich, R. 78816
 + Wurtele, J.S. 75660
 + Wuttig, M. 77691
 Wyart, J.-F. + 75338
 Wyatt, P.W. 75171
 + Wyatt, P.W. 77056
 Wyck, N.E.Van
 see Van Wyck, N.E.
 Wyler, D. + 74671
 + Xausa, E. 78187
 + Xi Fuyun 74293
 Xi-li Liu *see Liu Xi-li*
 Xi-wei Dong *see Dong Xi-wei*
 xi-wei Hu *see Hu xi-wei*
 Xi-zhen Wu *see Wu Xi-zhen*
 + Xia Yifei 79007
 Xianghui Wu
 see Wu Xianghui
 + Xiao Tang 75422
 + Xie Dilin 77279
 Xie Zhongjie 78175
 Xin, S.H. + 77686
 Xing-hua Luo
 see Luo Xing-hua
 Xinzhou Li *see Li Xinzhou*
 Xiong Yaoli 75923
 Xiu-zhen Wang
 see Wang Xiu-zhen
 Xiwen Wei *see Wei Xiwen*
 + Xu, Z. 75035
 + Xu Chenghe 75612
 + Xu Guang-xian 75296
 + Xu Jian-ou 77590
 Xu Jianjun 76036
 + Xu Kezun 74293
 Xuan, N.Phu. *see* Phu Xuan,
 N.
 Xuehua Zhou
 see Zhou Xuehua
 Xuequan, E. 76117
 Xun-Cheng Huang
 see Huang Xun-Cheng
 + Ya-fang Han 77665
 Yablonoitch, E. 78052
 + Yablonoitch, E. 77987
 + Yablonskii, D.A. 77200
 + Yablonsky, D.A. 77166
 + Yabuuma, H. 78743
 + Yacamán, M.J. 76760
 Yadav, J.S. 75298
 Yadav, J.S. + 75297
 + Yagasaki, T. 77779
 + Yagi, H. 77206
 Yahagi, M. + 76692
 + Yakel, H.L. 76248
 Yakobson, A.M. + 78303
 Yakovenko, S.E. + 77391
 + Yakovleva, I.L. 77638
 + Yakovleva, O.I. 74467
 Yakubovich, O.V. + 76399
 + Yakunov, A.V. 75494
 + Yalovets, V.S. 75900
 + Yamabe, T. 76823
 Yamada, H. 77245
 + Yamada, H. 76034
 + Yamada, M. 77648
 Yamada, O. 77244
 + Yamada, O. 77205
 Yamada, T. + 78272
 + Yamada, T. 78443
 + Yamada, T. 78438
 + Yamagata, M. 75157
 + Yamaguchi, T. 75949
 + Yamakami, T. 76609
 Yamamoto, H. + 78590
 Yamamoto, M. + 78318
 + Yamamoto, M. 78317
 + Yamamoto, O. 77981
 + Yamamoto, O. 75198
 Yamamoto, S. + 78792
 + Yamamoto, S. 75637
 + Yamamoto, S. 75184
 + Yamamoto, T. 75185
 Yamamoto, Y. + 75641
 + Yamamoto, Y. 76035
 + Yamanaka, M. 77998
 + Yamanishi, M. 78743
 + Yamanishi, M. 78793
 + Yamanouchi, C. 77063
 + Yamanouchi, M. 75025
 + Yamasaki, N. + 76062
 + Yamashiro, Y. 77212
 Yamashita, M. + 76623
 + Yamashita, T. 75198
 + Yamachi, M. 75185
 Yamawaki, M. + 77791
 + Yamazaki, S. 77585
 Yamadagni, N. 74824
 Yamin, H. + 77969
 Yan, J.F. 77886
 + Yan Maolin 76876
 Yan-tian Lin
 see Lin Yan-tian
 Yan-yu Hsiang
 see Hsiang Yan-yu
 + Yanagida, H. 76982
 + Yanagiya, T. 78791
 + Yanez, M. 75293
 Yang, A.J. + 74420
 Yang, G.C. + 74742

- Yang, H.K. + 78232
 + Yang, S.L. 74468
 + Yang Bingxin 74293
 + Yang Dayu 77081
 Yang Fangyu + 77813
 Yang Shin Nan
 see Shin Nan Yang
 Yang Ying-hui + 74954
 + Yang Yongyuan 75886
 + Yankielowicz, S. 74705
 + Yano, H. 78373
 + Yano, S. 75637
 Yanovskaya, T.B. 78445
 Yanyan Wang
 see Wang Yanyan
 + Yao, L.-S. 76116
 + Yao, S.K. 75819
 Yao, S.S. + 77429
 Yao Dai *see* Dai Yao
 Yao Shi-Chune
 see Shi-Chune Yao
 Yao York-Peng
 see York-Peng Yao
 + Yao Zhen-han 75924
 Yaoxi Xiong
 see Xiong Yaoxi
 Yarema, S. Ya. + 75962
 + Yarinin, A.A. 78257
 + Yaris, R. 74395
 + Yariv, A. 76719
 + Yariv, A. 75696
 Yarkony, D.R. 77877
 Yarmoff, J.A. + 77514
 + Yarmolyuk, Ya.P. 76360
 + Yarzhevskovskii, V.D.
 75645
 + Yashiro, K. 77162
 + Yashkir, Yu.N. 75699
 + Yasuda, M. 78882
 + Yasuda, M. 77482
 Yasumoto, K. + 74286
 + Yatabe, O. 77705
 + Yates, J.T., Jr. 77918
 + Yates, K. 75267
 + Yatsenko, V.V. 75605
 + Yatsui, K. 76196
 Yatsuzuka, M. + 76196
 + Yatsuyuk, V.G. 76718
 + Yavari, P. 77716
 Yayanos, A.A. + 75113
 Yazami, R. 77895
 + Yazeva, T.V. 76853
 + Ye, M. 78817
 Ye Jingtang 74279
 Yeats, R.S. 78507
 + Yeb Jo Seto. 78227
 + Yee, D.S. 77774
 + Yefsa, S. 77781
 Yeh, P. 75603
 Yeh Hsin-Yang
 see Hsin-Yang Yeh
 Yeh Pochi *see* Pochi Yeh
 Yen, S. + 74842
 Yen Ma Hui-chang
 see Ma Hui-chang Yen
 Yen-ching Yu
 see Yu Yen-ching
 + Yenta Li 78720
 Yeo, M.R. 74495
 + Yergey, J. 74553
 + Yeshurun, Y. 77706
 + Yger, A. 75593
 Yi Zhang *see* Zhang Yi
 Yi-jin Shi *see* Shi Yi-jin
 Yi-zhou Chen
 see Chen Yi-zhou
 Yianni[†] as, C. + 78369
 Yiannikas, C. + 78370
 + Yielding, G. 78442
 Yifei Xia *see* Xia Yifei
 + Yiftah, S. 75081
 Yimin Wang
 see Wang Yimin
 + Yin Sen-Yu 74557
 Ying An *see* An Ying
 Ying-hui Yang
 see Yang Ying-hui
 Yingzhi Wu *see* Wu Yingzhi
 Yinian Liu *see* Liu Yinian
 Yintong Guan
 see Guan Yintong
 Yizhong Zhuo
 see Zhuo Yizhong
 + Yogesh 74758
 + Yokota, W. 75025
 Yokoyama, H. + 74532
 + Yokoyama, K. 74630
 + Yokoyama, M. 76196
 + Yokoyama, T. 77557
 + Yokoyama, T. 77691
 Yoksan, S. 77104
 Yomosa, S. 76577
 + Yonekawa, Y. 78294
 + Yoneoka, T. 77791
 Yoneya, T. 74629
 Yongchang Du
 see Du Yongchang
 Yongxing Long
 see Long Yongxing
 Yongyuan Yang
 see Yang Yongyuan
 + Yoo, K.C. 77988
 + Yoo, K.H. 76934
 + Yordanov, D.L. 78112
 + York-Peng Yao 74656
 + Yoshida, N. 78000
 Yoshida, S. + 76775
 Yoshida, Y. + 77212
 + Yoshida, Y. 76716
 + Yoshie, T. 74615
 + Yoshie, T. 74616
 + Yoshie, T. 74638
 Yoshihiro, K. + 77063
 + Yoshiie, T. 76338
 Yoshikawa, S. 76221
 + Yoshimine, K. 75966
 + Yoshino, J. 77029
 Yoshino, S. + 76829
 + Yoshizawa, M. 76609
 + Yosida, K. 77136
 + Yosoi, M. 75222
 + Yosoi, M. 74966
 You-wen Yu
 see Yu You-wen
 + Young, D. 78588
 + Young, G.R. 75026
 + Young, G.R. 75036
 + Young, L.M. 75653
 + Young, M.H. 76894
 + Young, W. 77643
 Youqi Tang *see* Tang Youqi
 Youquan Jia
 see Jia Youquan
 + Yousef, Y.M. 78158
 Yuchuan, *see* Tuchman Y.
 + Yu, F.T.S. 75587
 Yu, I. + 76745
 Yu, I. + 76744
 Yu, J.S. + 78689
 + Yu, K.H. 76719
 + Yu, L.H. 75634
 + Yu, L.H. 76901
 + Yu, L.J. 76297
 Yu, S.H. + 76901
 + Yu, T.H.-chung 76214
 Yu Chih-chung 77928
 + Yu Jian-Guo 75300
 + Yu Lu 74366
 + Yu Yen-ching 74447
 + Yu You-wen 74894
 Yu-liang Chang
 see Chang Yu-liang
 Yu-ping Ho *see* Ho Yu-ping
 Yuan Liu *see* Liu Yuan
 Yuan-ping Feng
 see Feng Yuan-ping
 Yuan-sun Kiang + 75302
 Yuanle Ma *see* Ma Yuanle
 Yuanxi Zou *see* Zou Yuanxi
 Yuanxun, Qiu + 77512
 Yucheng Li *see* Li Yucheng
 + Yudaev, V.I. 77589
 + Yudovin, Z.M. 75900
 Yue Wu *see* Wu Yue
 + Yuen, D.A. 78419
 Yufeng Zhang
 see Zhang Yufeng
 + Yuh, Y.H. 75282
 + Yuhas, D.E. 77859
 + Yukawa, O. 78272
 Yukhimchuk, S.A. + 76230
 + Yuki, T. 77922
 + Yuldashev, A.A. 74809
 + Yuldashev, B.S. 74809
 Yumoto, K. + 78763
 Yun-jian Wang
 see Wang Yun-jian
 Yuquan Zhang
 see Zhang Yuquan
 Yurashkova, V. + 78243
 + Yurenas, D. Ya. 78514
 + Yurin, I.M. 76978
 + Yurkin, E.K. 75346
 + Yurov, G.V. 75729
 + Yushakova, F.V. 77680
 Yushin, V.I. 78475
 + Yushin, Yu. Ya. 76539
 Yushu Wu *see* Wu Yushu
 + Yusuf, N.A. 75581
 Yuxian Hu *see* Hu Yuxian
 + Yuzhakov, V.I. 75631
 + Zabolitzky, J.G. 76726
 Zaborov, A.V. + 77146
 Zabransky, B.J. + 74555
 Zabugina, M.P. + 75971
 + Zabusky, N.J. 78151
 Zachariades, A.E. + 76278
 + Zadorozhni, A.I. 77112
 + Zaets, V.G. 74771
 + Zafar, M. 75053
 + Zafiriou, O. 78611
 Zag, W. + 76511
 + Zagajnow, E.F. 77413
 + Zago, G. 74992
 Zahradnik, R. 77862
 + Zahradnik, R. 77868
 + Zaitsev, I.I. 74510
 + Zaitseva, R.N. 78258
 Zajac, G. + 77488
 + Zak, J. 77488
 Zakatova, N.V. + 78252
 + Zakeim, A.L. 75645
 + Zakharchenya, B.P. 77468
 + Zakharov, M.V. 75694
 Zakharov, S.M. + 76216
 + Zakharov, S.V. 76193
 + Zakrzewski, T. 76928
 + Zaleski, E. 77073
 + Zalikin, G.A. 78250
 Zalm, P.C. 77501
 + Zalpur, K.S. 78590
 + Zal'tsberg, V.S. 77538
 + Zamfir, N.V. 74874
 + Zamorani, G. 79023
 + Zamarini, G. 75239
 Zanolforie, L. 74492
 + Zanolforie, M. 78187
 + Zangwill, A. 77527
 Zannoni, G. + 76322
 + Zannoni, R. 74992
 + Zanotti, L. 74766
 + Zanotti, L. 75225
 Zapasskii, V.S. 74514
 + Zapasskii, V.S. 77251
 + Zare, R.N. 77876
 + Zarek, H. 74842
 + Zaretskii, Yu.G. 77398
 + Zarek, A. 75033
 Zarka, A. 76610
 + Zastenker, G. 78668
 + Zastenker, G.N. 78777
 Zatonvsky, A.V. + 74386
 + Zavadskii, E.A. 77144
 + Zavadskii, E.A. 77339
 + Zavorot'ko, A.N. 78417
 Zavorotnyi, V.U. + 74289
 Zavoyskiy, V.N. 78526
 Zavt, G.S. + 77435
 Zav'yalov, Yu.G. + 74486
 + Zav'yalova, N.Yu. 76517
 Zdaniewski, W.A. + 76502
 + Zecca, A. 74556
 + Zediker, M.S. 75624
 + Zeffiro, T.A. 78218
 + Zeffiro, L. 77547
 Zeilik, M. + 78956
 + Zeiri, Y. 76771
 + Zeiss, G.D. 75258
 Zelenko, I.A. + 77313
 + Zelenskaya, V.A. 77783
 Zelenski, A.N. + 75218
 Zelev, S.F. 74566
 + Zelinski, T. 75153
 + Zell, K.O. 74840
 Zeller, C. + 77395
 + Zeller, R. 76835
 + Zellner, B. 78859
 Zemel, A. + 74838
 + Zemel, J.N. 76129
 + Zemnukhova, L.A. 76613
 + Zerbi, G. 75380
 + Zerbi, G. 76322
 Zerefos, C.S. 78587
 + Zerlaut, G.A. 78046
 + Zerner, M.C. 75397
 + Zetterberg, P.O. 75339
 + Zhandarov, S.F. 76193
 Zhang Chunzhang + 75246
 + Zhang Chunhao 77866
 Zhang De'er 74245
 + Zhang Guobing 76939
 + Zhang Jianzu 74606
 Zhang Rong Wu
 see Rong Wu Zhang
 Zhang Rongyao + 77866
 + Zhang Shiwei 79035
 + Zhang Shu-gang 77590
 + Zhang Tianyi 76939
 + Zhang Yi 78625
 + Zhang Yufeng 76876
 + Zhang Yuquan 77214
 Zhang Zhixiang + 77354
 Zhang Ziping + 74293
 + Zhang Zong-ye 74894
 Zhao, Jr. Chen Guangjun *see*
 Chen Guangjun Zhao, Jr.
 + Zhao, X.W. 78025
 Zhao Te-Xiu
 see Te-Xiu Zhao
 + Zhao Zheng 74337
 + Zhao Zhongxian 77081
 Zhao-bin Su
 see Su Zhao-bin
 + Zharovskii, L.F. 77075
 + Zhabnikov, R.G. 77388
 + Zheludev, I.S. 77299
 + Zhelyazkov, I. 76175
 Zhen-bang Kuang
 see Kuang Zhen-bang
 Zhen-Chuan Kang 76385
 Zhen-han Yao
 see Yao Zhen-han
 Zhen-ru Wang
 see Wang Zhen-ru
 + Zheng, Z. 75033
 + Zheng Shi-Jin 75300
 Zheng Zhao
 see Zhao Zheng
 Zheng-xiong Chen
 see Chen Zheng-xiong
 Zhennan Niu
 see Niu Zhennan
 Zhenqiu Ren
 see Ren Zhenqiu
 + Zhernov, V.S. 75207
 + Zhernov, V.S. 75160
 Zhernovoi, A.I. + 74507
 Zhetbaev, A.K. + 76485
 + Zhilinskii, A.A. 74477
 Zhilions, A.A. + 77349
 Zhimin Gao *see* Gao Zhimin
 + Zhirko, Yu.I. 76850
 Zhiwei, L. + 75088
 Zhixiang Zhang
 see Zhang Zhixiang
 Zhixing Chen
 see Chen Zhixing
 Zhiye Shen *see* Shen Zhiye
 Zhiyi Liu *see* Liu Zhiyi
 Zhiyuan Guo
 see Guo Zhiyuan
 + Zhokina, I.A. 75105
 + Zhong Wanxie 75938
 Zhong-xin Guan
 see Guan Zhong-xin
 Zhongjie Xie
 see Xie Zhongjie
 Zhonglei Wei
 see Wei Zhonglei
 Zhonglu Hua
 see Hua Zhonglu
 Zhongqi Ma
 see Ma Zhongqi
 Zhongxian Zhao
 see Zhao Zhongxian
 + Zhongze Wu 78720
 Zhorova, E.S. + 78250
 + Zhou, S.H. 74988
 Zhou, S.H. + 74977
 + Zhou, Y.M. 76178
 Zhou Guang-zhao + 74366
 Zhou Jiabin + 78626
 + Zhou Jicheng 76890
 Zhou Lezhu + 75612
 Zhou Mingyu + 78625
 Zhou Xuehua 76150
 Zhou Zhulin 75939
 Zhu, S.-Y. + 78412
 + Zhu Peichen 78806
 + Zhu Weishen 78522
 + Zhuang, S.L. 75587
 + Zhuikov, V.A. 76302
 Zhukarev, A.S. 77223
 + Zhukhovitskii, E.M. 76029
 Zhulin Zhou
 see Zhou Zhulin
 + Zhuo Yizhong 74859
 Zhuo Huang
 see Huang Zhuo
 + Zhuravlev, A.F. 76493
 + Zhuravlev, V.V. 77112
 + Zhurkin, B.G. 76495
 + Zhytnikov, V.V. 74338
 + Zibrov, A.S. 75346
 Zichichi, A. 74242
 + Zichichi, A. 74821
 Zichichi, A. (ed.) 74229
 + Ziegler, L. 74918
 + Ziegler, J. 77265
 + Zienkiewicz, O.C. 77704
 + Zieske, P. 76835
 + Ziesche, P. 76870
 + Zil'berberg, V.V. 75311
 Zil'berman, L.A. 76824
 + Zimanyi, J. 75020
 + Zimmer, W.D. 76340
 + Zimmermann, J.E. 78212
 + Zimmermann, J.T. + 78212
 + Zimmermann, D. 76214
 + Zimmermann, H. + 77416
 + Zimny, R. 75156
 + Zinchenko, M.I. 75628
 Zingu, E.C. + 76710
 Zinn-Justin, J. 74300
 + Zinn-Justin, J. 75251
 Zinovuk, A.V. + 77268
 + Zintl, R. 76636
 + Zioc, H.J. 74804
 + Zioc, K.O.H. 74830
 Ziping Zhang
 see Zhang Ziping
 + Zisman, A.N. 76624
 + Zittlau, W. 75528
 Zivkovic, T.P. 75265
 Zoan Mien Vu *see* Vu Zoan
 Mien
 + Zoback, M.D. 78463
 + Zolotukhin, M.N. 76439
 + Zombori, P. 75190
 + Zombori, P. 75191
 Zong-ming Bao
 see Bao Zong-ming
 Zong-xin Wang
 see Wang Zong-xin
 Zong-ye Zhang
 see Zhang Zong-ye
 Zotovar, N. + 78241
 Zou Yuanxi + 76890
 Zrubec, V. + 74498
 Zsdanszky, K. + 78332
 Zsolnay, E.M. + 75201
 Zsolnay, E.M. + 75159
 + Zsolnay, E.M. 75158
 Zu-qia Huang
 see Huang Zu-qia
 + Zuba, G. 74560
 Zubanov, D. + 74960
 Zubarev, D.N. 74414
 + Zubauskas, G. 76567
 + Zuber, J.R. 76434
 + Zubets, Yu.E. 77681
 + Zubov, V.E. 77370
 + Zuccarello, F. 75398
 Zucker, U.H. + 76257
 Zuckerwar, A.J. 78708
 Zuev, V.E. 78659
 + Zukotynski, S. 77072
 + Zukowski, E. 79016
 + Zunger, A. 76822
 + Zurcher, P. 77533
 + Zussman, A. 76966
 Zuwei Chou
 see Chou Zuwei
 Zwarts, F. + 74948
 + Zwicker, H.R. 78087
 Zwicker, W.K. + 77426
 Zwiers, R.I. + 75922
 + Zyrjanov, V. Ya. 76302
 Zytikiewicz, Z.R. 76808
 + Zyuzin, A.M. 77563

BIBLIOGRAPHY INDEX

| | |
|--|-------|
| ⁴ He photodisintegration, (53 refs.)..... | 74959 |
| Antiproton interactions with light elements as a test of GUT cosmology, (94 refs.)..... | 79040 |
| Applicability of non-degenerate many-body perturbation theory to quasidegenerate electronic states: a model study, (56 refs.)..... | 75278 |
| Auditory evoked magnetic responses, (50 refs.)..... | 78211 |
| Automated analysis of abnormal electroencephalograms, (169 refs.)..... | 78376 |
| Autoturbation in fluid dynamics, (64 refs.)..... | 76047 |
| Beam-foil spectroscopy, (132 refs.)..... | 75554 |
| Biological tissues solid components characterisation by NMR spectrometry, (277 refs.)..... | 78402 |
| Breaking waves on beaches, (110 refs.)..... | 78555 |
| Calorimetry in high-energy physics, (146 refs.)..... | 75249 |
| Charged-current neutrino interactions, (174 refs.)..... | 74757 |
| Charmed particles, production and properties, (88 refs.)..... | 74822 |
| Chemical equilibria and rate constant studies, (69 refs.)..... | 77862 |
| Climate models, (80 refs.)..... | 78639 |
| Climate effects of aerosols, (57 refs.)..... | 78581 |
| CNDO/S parameters of C, O, and Si for solid state calculations, (63 refs.)..... | 76839 |
| Coal Sack southern zone star catalogue, (105 refs.)..... | 78828 |
| Compressible liquid impact, (94 refs.)..... | 76070 |
| Computer generation of isomeric structures, (69 refs.)..... | 75553 |
| Coxeter-Todd lattice, Mitchell group and related sphere packings, (61 refs.)..... | 74400 |
| Detailed analysis of the scope of the modified Firsov model, (53 refs.)..... | 75490 |
| Ductile fracture of metals, (166 refs.)..... | 77742 |
| E ⁺ e ⁻ physics at PETRA, (118 refs.)..... | 74755 |
| Earth upper mantle redox state, (54 refs.)..... | 78495 |
| Effective interactions at low and intermediate energy, (85 refs.)..... | 74884 |
| Electric-dipole moments of particles, (118 refs.)..... | 74773 |
| Electron excitation induced defect creation in alkali halides, (61 refs.)..... | 76421 |
| Electron-positron physics, (148 refs.)..... | 74752 |
| Electronic density of states, energy depend. effects on normal props., (55 refs.)..... | 76825 |
| Electronic density of states, energy depend. effects on supercond. props., (57 refs.)..... | 76826 |
| Electronic structure of fourth and fifth group transition metal monocarbides, mononitrides and monoxides, (100 refs.)..... | 74640 |
| Electroweak physics of the 80s, (93 refs.)..... | 74693 |
| Energy-dependent energy transfer: deactivation of azulene (S ₀ , E _{vib}) by 17 collider gases, (50 refs.)..... | 75483 |
| Finite element method in fracture mechanics, (80 refs.)..... | 75961 |
| Flames, instabilities and turbulence, (67 refs.)..... | 77890 |
| Flow in curved pipes, (168 refs.)..... | 76116 |
| Fluid flow freezing-melting interfaces, (82 refs.)..... | 76098 |
| Fluid mechanics of green plants, (56 refs.)..... | 78225 |
| Fluorescence of molecular crystals, (131 refs.)..... | 77415 |
| Galaxy formation in early Universe, (78 refs.)..... | 79029 |
| Gamma-ray astronomy, (226 refs.)..... | 78811 |
| Geometric quantisation theory and applications, (59 refs.)..... | 74303 |
| Heat and mass transfer bibliography—Soviet works, (380 refs.)..... | 74239 |
| High power pulsed lasers for inertial fusion, (83 refs.)..... | 75172 |
| High temperature corrosion testing methods, (52 refs.)..... | 77816 |
| Hybridization and surface relaxation in diamond-like crystals, (53 refs.)..... | 76752 |
| Inferences concerning anatomy and physiology of the human brain based on its magnetic field, (58 refs.)..... | 78208 |
| Instrumentation for biomagnetism, (57 refs.)..... | 78393 |
| Interacting cosmic gas clouds, (118 refs.)..... | 78804 |
| Intermediate vector bosons, (88 refs.)..... | 74701 |
| Ion implantation in group II-VI compounds, (100 refs.)..... | 76467 |

| | |
|---|-------|
| Ionic-covalent problem in the H ⁺ +H ⁻ ⇌H*+H collisional system, (57 refs.)..... | 75477 |
| Langmuir circulations, (81 refs.)..... | 78556 |
| Long-wavelength-absorbing forms of bacteriochlorophyll <i>a</i> in solutions of Triton X-100, (53 refs.)..... | 78141 |
| Magneto-atmospheric waves, (66 refs.)..... | 78810 |
| Magnetoelasticity in transition metals and alloys, (53 refs.)..... | 77233 |
| Metal centres of cytochrome c oxidase, (54 refs.)..... | 78129 |
| Metal forming theory research developments, (75 refs.)..... | 77590 |
| Metal phase formation by ion implantation, (119 refs.)..... | 76643 |
| Middle atmosphere ion composition, (101 refs.)..... | 78594 |
| Molecular mechanics of organic halides, (70 refs.)..... | 75539 |
| Multimode and single-mode polarisation maintaining fibre fabrication technology and measurement system development, (79 refs.)..... | 75796 |
| Non-Newtonian fluid mechanics, (89 refs.)..... | 76079 |
| Nuclear masses and deformations, macroscopic approaches, (126 refs.)..... | 74877 |
| Nuclear pressure vessel monitoring, (57 refs.)..... | 75099 |
| Nuclear statistical spectroscopy, (56 refs.)..... | 74872 |
| Optical fibre amplification by stimulated Raman scattering, (57 refs.)..... | 75718 |
| Percolation, (159 refs.)..... | 74371 |
| Phospholipid vesicles aggregation and fusion, (303 refs.)..... | 78155 |
| Photoelectron spectroscopy of NHO ⁻ and DNO ⁻ , (62 refs.)..... | 75439 |
| Planar volume phase holograms formed in bleached photographic emulsions, (50 refs.)..... | 75599 |
| Planetary magnetic fields, (184 refs.)..... | 78836 |
| Planetary nebulae formation, (70 refs.)..... | 78970 |
| Point defects in II-VI compounds, (195 refs.)..... | 76420 |
| Polycrystalline thin-film photovoltaic devices, (41 refs.)..... | 78004 |
| Positive hole pressures and negative exit pressures generated by molten polyethylene flowing through a slit die, (66 refs.)..... | 75974 |
| Proton capture to excited states of ¹⁶ O, (66 refs.)..... | 74904 |
| QCD phenomenology, unified approach, (69 refs.)..... | 74702 |
| Quantum chromodynamics, (108 refs.)..... | 74709 |
| Radiation damage in insulators, (181 refs.)..... | 76488 |
| Radiation dose from coal burning, (103 refs.)..... | 78341 |
| Radwaste metallic containers corrosion susceptibility test methods, (108 refs.)..... | 75091 |
| Rapid chemical methods for identification and study of short-lived nuclides, (100 refs.)..... | 77946 |
| Rapid solidification of steels, (58 refs.)..... | 77627 |
| Reaction Mg+N ₂ O→MgO+N ₂ , (50 refs.)..... | 77877 |
| Rotationally inelastic collisions, M dependence in cell experiments for molecules in ² state, (62 refs.)..... | 75470 |
| Saturn, energy characteristics, (51 refs.)..... | 78852 |
| Semiconductor epitaxial film crystallisation, (51 refs.)..... | 76811 |
| Snow avalanches, (82 refs.)..... | 78574 |
| Solar hydrogen economy for USA, recommendations, (55 refs.)..... | 78107 |
| Spin glasses, (214 refs.)..... | 77184 |
| Stochastic transport in disordered systems, (73 refs.)..... | 74374 |
| Systolic mitral valve motion modelling, (85 refs.)..... | 78224 |
| Theory of giant resonances, (184 refs.)..... | 74883 |
| Thirteen colour photometry at San Pedro Martir, (49 refs.)..... | 78826 |
| Transition metal oxide electrodes reversibly incorporating Li ⁺ ions, (47 refs.)..... | 77893 |
| Turbulent wall jet, (69 refs.)..... | 76085 |
| Two-phase flow modelling, (71 refs.)..... | 76097 |
| Two-phase flow patterns, (69 refs.)..... | 76089 |
| Valence bond theory for conjugated hydrocarbons, (69 refs.)..... | 75304 |
| Vortex dynamics, (204 refs.)..... | 76048 |
| W and Z bosons and gauge theories, (53 refs.)..... | 74684 |
| X-ray nebular models, (92 refs.)..... | 79025 |

BOOK INDEX

| |
|--|
| Annual review of fluid mechanics. Vol.15; M.Van Dyke, J.V.Wehausen, J.L.Lumley (editor/s), [Palo Alto, CA, USA: Annual Reviews 1983] 74234 (introductory abstract), 74247, 75995, 76047-8, 76060-1, 76070, 76079, 76085, 76097-8, 76116, 77890, 78225, 78555-6, 78574, 78810 |
| Annual review of nuclear and particle science. Vol.32; J.D.Jackson, H.E.Gove, R.F.Schwitters (editor/s), [Palo Alto, CA, USA: Annual Reviews 1982] 74232 (introductory abstract), 74701, 74709, 74722, 74757, 74773, 74872, 74877, 74883, 75021, 75181, 75249, 75554, 77946, 78811 |
| Circulation in the coastal ocean; G.T.Csanady, [Dordrecht, Netherlands: Reidel 1982] 74236 |
| Foundations of theoretical mechanics. II. Birkhoffian generalization of Hamiltonian mechanics; R.M.Santilli, [Berlin, Germany: Springer-Verlag 1983] 74238 |

| |
|--|
| Gauge theory of dislocations and disclinations; A.Kadic, D.G.B.Edelen, [Berlin, Germany: Springer-Verlag 1983] 74237 |
| International advances in nondestructive testing. Vol.9; W.J.McGonagale (editor/s), [New York, USA: Gordon & Breach 1983] 74231 (introductory abstract), 74525-6, 75607-8, 75817, 75888, 77850-6 |
| Magnetospheric plasma physics; A.Nishida (editor/s), [Dordrecht, Netherlands: Reidel 1982] 74230 |
| Microcomputer quantum mechanics; J.P.Killingbeck, [Bristol, England: Adam Hilger 1983] 74235 |

CONFERENCE INDEX

| |
|--|
| Acoustics, speech and signal processing; Boston, MA, USA, 14-16 April 1983, [IEEE] [New York, USA: IEEE 1983] 75857-9, 75867-8, 78194-5, 78200, 78278, 78384, 78717-23 |
| Advanced laser technology and applications; Arlington, VA, USA, 6-7 May 1982, [1982] 74207 (introductory abstract), 74434, 75623-4, 75676-8, 75682-6, 75701, 75705, 76901, 77426-7 |
| Antennas and propagation; Norwich, England, 12-15 April 1983, [London, England: IEE 1983] 78636, 78724, 78752-4, 78765 |
| Atmospheric aerosols and ozone space observations; Ottawa, Canada, 16 May-2 June 1982, [1982] 74204 (introductory abstract), 78579-93, 78640, 78644-51, 78657-64 |
| Biomagnetism; Rome, Italy, 14-16 Sept. 1982, [March-April 1983] 74209 (introductory abstract), 74497-8, 78178, 78188, 78202-12, 78280-6, 78374, 78393-9 |
| Biomedical Engineering Society Symposia; Chicago, IL, USA, 11-15 April 1983, [1983] 74202 (introductory abstract), |

| |
|--|
| Canadian radiation protection; Ottawa, Canada, 5-6 May 1981, [April 1983] 74210 (introductory abstract), |
| Cloud dynamics; Hamburg, Germany, 17-28 Aug. 1981, E.M.Agee, T.Asai (editor/s), [Dordrecht, Netherlands: Reidel 1982] 74227 (introductory abstract), |
| Digital image processing IV; San Diego, CA, USA, 24-27 Aug. 1982, [1983] 74569, 78273, 78291, 78391-2 |
| Fiber optics, 1982; San Diego, CA, USA, 24-25 Aug. 1982, [1982] 74208 (introductory abstract), 74535, 75591, 75720, 75797-801, 75834-5 |
| Free electron lasers; Bendor, France, 26 Sept.-1 Oct. 1982, [CNRS; CENS; et al] [Feb. 1983] 74214 (introductory abstract), 74500, 75616, 75648-72, 75691 |
| GaAs and related compounds; Albuquerque, NM, USA, 19-22 Sept. 1982, [Air Force Office Sci. Res] G.E.Stillman (editor/s), [Bristol, England: IOP 1983] 74226 (introductory abstract), 75640-1, 76341-2, 76474-7, 76481, 76646, 76708, 76889-95, 76973, 76980, 77006, 77402, 77456-7, 77558, 77561, 77583, 77686 |

- Gauge theory and gravitation;** Nara, Japan, 20-24 Aug. 1982, *K.Kikkawa, N.Nakanishi, H.Nariai (editor/s)*, [Berlin, Germany: Springer-Verlag 1983] 74332-5, 74340, 74347, 74349-51, 74358-61, 74624-44, 74685-91, 74713, 74747-8, 78812
- Grain boundaries in semiconductors;** Boston, MA, USA, Nov. 1981, *H.J.Leamy, G.E.Pike, C.H.Seager (editor/s)*, [New York, USA: North-Holland 1982] 76473, 77043, 77054
- High energy limit;** Erice, Italy, 31 July-11 Aug. 1980, *A.Zichichi (editor/s)*, [New York, USA: Plenum 1983] 74229 (introductory abstract), 74336, 74352-3, 74645-6, 74662, 74692-5, 74714-15, 74739-40, 74754-5, 74764, 74770, 74778, 74790-1, 74820-2, 74825
- High energy physics, 1982;** Mysore, India, 6-11 Dec. 1982, [Bombay, India: Dept. Atomic Energy 1982] 74326, 74665, 74700, 74710, 74723, 74734-7, 74749, 74758, 74774-5, 74777, 74779-80, 7485-6, 74794-5, 74798-801, 74813-15, 74896, 75002, 75042-7, 75054, 75481
- High resolution electron microscopy;** London, England, 12-16 July 1982, [May 1983] 74561-2, 76261-2, 76414, 76456, 77490, 77795-6, 77937-9, 78404
- Hungarian-Austrian Health Physics;** Gyor, Hungary, 28 Sept.-1 Oct. 1981, [1982] 74198 (introductory abstract), 74567, 75089, 75187-93, 75245, 78109, 78111, 78332-40, 78353-8, 78363-5
- Interaction between medium energy nucleons in nuclei;** Bloomington, IN, USA, 28-30 Oct. 1982, [NSF: DOE: Indiana Univ] [1982] 74200 (introductory abstract), 74792, 74831, 74841, 74850-7, 74880, 74884-7, 74893, 74898-9, 74910, 74920-1, 74937-41, 74945, 74950, 74965-79, 75003, 75222, 75555
- Lithium batteries;** Rome, Italy, 27-29 April 1982, [April-May 1983] 74213 (introductory abstract), 76693-6, 77892-5, 77968-73, 77975-85
- Low-level waste disposal, facility design, construction, and operating practices;** Washington, DC, USA, 29-30 Sept. 1982, [Office Nucl. Mater. Safety & Safeguards; U.S. Nucl. Regul. Comm.; Oak Ridge Nat. Lab] [Oak Ridge, TN, USA: Oak Ridge Nat. Lab 1982] 74223 (introductory abstract), 75124-46
- Luminescence, Leningrad;** Leningrad, USSR, 21-24 April 1981, [1982] 75334, 75364, 75610-11, 75642, 75706, 76217, 77422-3
- Magnetoelasticity in transition metals and alloys;** Nagoya, Japan, 15-16 Sept. 1982, [April 1983] 74217 (introductory abstract), 77147, 77165, 77233-48, 77642-3
- Management, analysis, and display of geoscience data;** Golden, CO, USA, 27-29 Jan. 1982, [Math. Geol. United States] [1983] 78523, 78681
- Meteorological optics;** Incline Village, NV, USA, 12-14 Jan. 1983, [Opt. Soc. America; Air Force Office Sci. Res] [Washington, DC, USA: Opt. Soc. America 1983] 74220 (introductory abstract)
- Microlithography;** Grenoble, France, 5-8 Oct. 1982, [Ministere de la Recherche et de l'Industrie] [Grenoble, France: Comité du Colloque International sur la Microlithographie 1982] 75774, 75840-1
- Microwave circuit CAD techniques;** London, England, 18 April 1983, [London, England: IEE 1983] 74495
- Non-invasive on-line measurement in industry;** London, England, 13 April 1983, [London, England: IEE 1983] 74578, 76139
- Nucleus-nucleus collisions;** East Lansing, MI, USA, 26 Sept.-1 Oct. 1982, [U.S. Dept. Energy; NSF: IUPAC; et al] [East Lansing, MI, USA: Michigan State Univ. 1982] 74733, 74878-9, 74890-2, 74928-36, 74943-4, 74955-7, 75022-41, 75064-6, 75215
- Ocean disposal;** Plymouth, Devon, England, 11-15 April 1983, [Plymouth, Devon, England: Plymouth Polytechnic 1983] 74222 (introductory abstract), 75111-23
- Optical fibre sensors, 1983;** London, England, 26-28 April 1983, [London, England: IEE 1983] 74441, 74517, 74519, 74527-30, 75209, 75818-30, 76140-1, 77947, 78408
- Optical phase conjugation and instabilities;** Cargese, Corsica, France, 20-24 Sept. 1982, [CNRS] [March 1983] 74215 (introductory abstract), 75327, 75710-15, 75733-48, 75753, 75851, 76192
- Optical techniques for remote probing of the atmosphere;** Incline Village, NV, USA, 10-12 Jan. 1983, [Opt. Soc. America; Air Force Office Sci. Res] [Washington, DC, USA: Opt. Soc. America 1983] 74221 (introductory abstract)
- Particles and fields, 1982;** College Park, MD, USA, 28-30 Oct. 1982, [1982] 74201 (introductory abstract), 74667-70, 74702-3, 74716, 74751, 74759-60, 74766, 74776, 74781-2, 74796, 74805-6, 74826, 75212-13, 79032
- Photovoltaic specialists conference;** San Diego, CA, USA, 27-30 Sept. 1982, [New York, USA: IEEE 1982] 74219 (introductory abstract), 77541, 77544, 77554-7, 77565, 77582, 77592-3, 77858-9, 77861, 77964-7, 78014-88, 78090, 78103
- Physico-chemical behaviour of atmospheric pollutants;** Varese, Italy, 29 Sept.-1 Oct. 1981, *B.Versino, H.Ott (editor/s)*, [Dordrecht, Netherlands: Reidel 1982] 74233 (introductory abstract)
- Physics in collision;** Stockholm, Sweden, 2-4 June 1982, *P.Carlson, W.P.Trower (editor/s)*, [New York, USA: Plenum 1983] 74228 (introductory abstract), 74684, 74711-12, 74724-5, 74738, 74747, 74787-9, 74802-3, 74816-19, 74824, 74829
- Physics of semiconductors;** Montpellier, France, 6-10 Sept. 1982, [IUPAP: Societe Francaise de Physique; European Phys. Soc] [March 1983] 76956, 77029-37, 77063, 77395, 77445-8
- Power plant dynamics, control and testing;** Knoxville, TN, USA, 21-23 March 1983, [Univ. Tennessee; IEEE; EPRI; et al] *B.R.Upadhyaya (editor/s)*, [Knoxville, TN, USA: Univ. Knoxville 1983] 74224 (introductory abstract), 75083-8, 75164-7, 75171, 77958, 77960
- Radiation effects in insulators;** Arco, Largo di Garda, Italy, 1981, [1982] 76421, 76424-5, 76459, 76468-72, 76488, 76512-14, 76520, 76525-6, 76538-9, 76640-3, 76999, 77464-6, 77505-12, 77912
- Rapidly solidified amorphous and crystalline alloys;** Boston, MA, USA, Nov. 1981, *B.H.Kear, B.C.Giessen, M.Cohen (editor/s)*, [New York, USA: North-Holland 1982] 76318-21, 76496-7, 76551, 76598, 76622, 76649-53, 76672, 76678, 76763, 76795, 77115, 77221-2, 77597-600, 77627-30, 77635, 77654, 77660-1, 77679, 77695, 77760-3, 77769-70, 77807-11, 77923
- Recent developments in high frequency electromagnetic field analysis in finite element methods;** London, England, 16 May 1983, [London, England: IEE 1983] 75793-4
- Resource conservation for the electrical engineer;** London, England, 19 April 1983, [London, England: IEE 1983] 77950-1
- Rise in atmospheric carbon dioxide;** Bern, Switzerland, 14-18 Sept. 1981, [20 Feb. 1983] 74212 (introductory abstract), 78114-15, 78559, 78602-10, 78698
- Saturn, its rings, and satellites;** Tucson, AZ, USA, 11-15 May 1982, [Feb. 1983] 74211 (introductory abstract), 78832, 78845-50, 78852, 78854-7, 78859-61
- Science underground;** Los Alamos, CA, USA, 1982, [1982] 74199 (introductory abstract), 74240-3, 74666, 74765, 75225-31, 78769-70, 78816-18, 78888-92
- SOUTHEASTCON '83;** Orlando, FL, USA, 11-14 April 1983, [New York, USA: IEEE 1983] 74466, 75598, 75894, 78385
- Synchrotron radiation users group conference, 1982;** Stoughton, WI, USA, 18-19 Oct. 1982, [Stoughton, WI, USA: Synchrotron Radiat. Center 1982] 74225 (introductory abstract), 75221, 75446-7, 75773, 76794, 77042, 77053, 77481, 77525-34, 78407
- System simulation and scientific computation;** Montreal, Canada, 8-13 Aug. 1982, [IMACS; Int. Assoc. Math. Modelling; Int. Soc. Comput. Methods Eng.; et al] [New Brunswick, NJ, USA: IMACS 1982] 75863-4
- Theoretical organic chemistry;** Dubrovnik, Croatia, Yugoslavia, 30 Aug.-3 Sept. 1982, [Feb. 1983] 74216 (introductory abstract), 75256, 75282-3, 75290, 75302-4, 75324-5, 75391, 75433, 75445, 75461, 75553, 77862, 77864, 77885
- VDE-Congress '82;** Dusseldorf, Germany, 4-6 Oct. 1982, [1982] 74218 (introductory abstract)
- XX National Congress of the Italian Society for Nuclear Biology and Medicine;** Porto Cervo, Italy, 4-7 May 1983, [April-June 1983] 74203 (introductory abstract)

CORPORATE AUTHOR INDEX

Atomic Energy Canada Ltd., Chalk River, Ont.

Determination of radium-226 in urine, AECL-7979, 78405

Comm. European Communities, Luxembourg

Amelioration des performances de la pile solaire au silicium de grand diametre (Amelioration of the performance of a large diameter silicon solar pile), EUR 8145 FR, 78012

Entwicklung von autarken Solarkuhlanlagen mit konzentrierenden Kollektoren (Development of self-sufficient solar cooling devices with concentrating collectors), EUR 8165 DE, 78101

Potentiostatic etching of carburized steels, EUR 8138 EN, 77857

Realisation et caracterisation de cellules solaires Cu₂S-CdZnS (Realisation and characterisation of Cu₂S-CdZnS solar cells), EUR 8103 FR, 78013

Council for Miner. Technol., Randburg, S. Africa

Installation and commissioning of a Siemens SRS200 sequential X-ray fluorescence spectrometer, M80, 74577

Preparation and certification of a uranium reference material, M84, 75108

Hungarian Acad. Sci., Budapest

A LiF es a CaSO₄ termolumineszenz detektorok neutronerzekenysegenek vizsgalata (Thermal neutron sensitivity of LiF and CaSO₄ thermoluminescent detectors), KFKI-1983-45, 75208

(Neutron, alpha) magreakcion alapulo szilardtest nyomdozimeter hatasfokanak elemlesi es kiserleti vizsgalata (Neutron, alpha) nuclear reaction solid track detector efficiency: Theoretical and experimental studies), KFKI-1983-46, 75242

Neutronspektrum es doziseszloszas vizsgalatok szamitással es meressel elliptikus fantomban ²⁵²Cf es nehezvizzel moderalt ²⁵²Cf neutron forrasokra (Neutron spectra and dose distribution calculations and measurements for a filled elliptical phantom using bare and heavy-water moderated ²⁵²Cf neutron sources), KFKI-1983-47, 78352

Self-focusing of laser beam crossing a laser plasma, KFKI-1983-12, 76202

Theoretische Beschreibung des Reaktorrauschens in einem stark gekoppelten reaktorphysikalisch-thermohydraulischen System (Theoretical determination of the reactor noise in a strongly coupled reactor kinetic-thermohydraulic system), KFKI-1983-36, 75163

Israel Atomic Energy Comm., Yavne

WIMSCORE - A code for producing group constants for TDB, TRITON and CITATION codes from WIMS output, IA-1380, 75081

Ist. Naz. Fis. Nucl., Pisa, Italy

Biomedical applications of MWPC's for digital imaging of soft β emitters, INFN/TC-83/6, 78406

Japan Atomic Energy Res. Inst., Tokai, Ibaraki

Annual report of the division of high temperature engineering (April 1, 1981-March 31, 1982), JAERI-M-82-133, 75211

Annual report of the Fusion Research and Development Center for the period of April 1, 1981 to March 31, 1982, JAERI-M-82-154, 75186

Benchmark experiment on D-T neutrons and secondary gamma rays streaming through a concrete bent duct, JAERI-M-82-130, 75182

BIRTH: A beam deposition code for non-circular tokamak plasmas, JAERI-M-82-129, 76195

Comparisons of energy dependent point-wise cross-section generation codes: RESEND, RESEND, RECENT, JAERI-M-82-128, 75082

Japanese contributions to IAEA INTOR Workshop, Phase IIA. Chapters I, II, III: Summary and INTOR concept, JAERI-M-82-170, 75183

Japanese contributions to IAEA INTOR Workshop, Phase IIA. Chapter IV: Plasma confinement and control, JAERI-M-82-171, 75184

Japanese contributions to IAEA INTOR Workshop, Phase IIA. Chapter V: RF heating and current drive, JAERI-M-82-172, 75185

Research proposal for advanced diffractometer (US-Japan collaborative research in neutron scattering), JAERI-M-82-157, 75070

Kernforschungsanlage, Jülich, Germany

Fracture mechanics tests in static and cyclic loading conditions on structure graphite for high temperature reactor plants, JUL-1831, 75110

Investigation of inhomogeneity in ceramic reactor-materials using laser-localized emission spectroscopy, JUL-1834, 75109

Max-Planck-Inst. Stromungsforschung, Göttingen, Germany

FO₂ radical and LMR spectra in reactions of fluorine atoms, 19/1982, 75336

- Messung feinstrukturaufgeloster differentieller Streuquerschnitte für Stöße von Kalium an Quecksilber mittels teilchen-Photon-Koinzidenz (Measurement of fine structure perturbed differential scattering cross-sections for the collision of potassium and mercury by particle-photon coincidence), 15/1982. 75480
- Stöße laserangeregter Atome zur Potentialbestimmung für die Systeme K (4S²O²P)-Ne, Ar, Kr, Xe (Laser-stimulated atomic collisions for potential determination for the system K (4S²O²P)-Ne, Ar, Kr, Xe), 16/1982. 75479
- Streuquerschnitte für die Rotationsanregung von N₂, O₂ und CH₄ durch Stöße mit He-Atomen (Scattering cross-section for the rotational excitation of N₂, O₂ and CH₄ by collisions with the atoms), 17/1982. 75487
- Structure and behavior of a turbulent ring vortex, 12/1982. 76049
- Nat. Bur. Stand., Washington, DC, USA**
- Electromagnetic formulation for treating optical reflections from graded-material surfaces, NBS-TN-1171. 75583
- Expression of the uncertainties of final measurement results: Reprints, NBS-SP-644. 74427
- Standard X-ray diffraction powder patterns. Section 19 - Data for 51 substances, NBS-MN-25-19. 76407
- System for measuring energy and peak power of low-level 1.064 μ m laser pulses, NBS-TN-1058. 75704
- Thermal behavior of fine-grained soils, NBS-BSS-149. 78540
- Weathering performance of cover materials for flat plate solar collectors, NBS-TN-1170. 78102
- Nat. Phys. Lab., Teddington, England**
- Prediction of intergranular failure in Ni-Cr based alloys in low cycle fatigue at high temperatures - UK16, NPL-DMA(A)62. 77759
- Theoretical model for the Speech Input Device SID3. 1. Filters, NPL-DITC-20/83. 75875
- Phys.-Tech. Bundesanstalt, Braunschweig, Germany**
- Derivation of the coupling coefficients for the eigenfunctions of a spherical, optical resonator in the case of mismatching and misalignment of the incident wave, PTB-Me-43. 75695
- Rutherford Appleton Lab., Chilton, Oxon., England**
- Detecting t-quark pairs at pp colliders using transverse dilepton masses and jets, RL-83-025. 74762
- Hadronic final states in e⁺ e⁻ annihilation. Recent results from TASSO, RL-83-031. 74784
- Spin-rotation measurements in $\pi^-p \rightarrow K^0\Lambda$, RL-83-005. 74797
- UKAEA, Risley, Lancs., England**
- Application of neutron diffraction to a study of phases in Type 316 stainless steel weld metals, ND-R-880(R). 77685

The economic use of electric road vehicles in a changing environment

PPL Conference Publication 15

This volume contains the papers presented at the 2nd International Electric Vehicle Development Group conference, held in Sheffield, England, 23rd & 24th May 1978, to examine the factors involved in the implementation of large numbers of high performance vehicles and to draw upon the experience of those now operating delivery and public passenger electric road vehicles.

The conference was organised by the Electric Vehicle Development Group, with the support of the National Freight Corporation, the National Bus Company, the International Union of Public Transport, the Electrical Research Association, the Lead Development Association, the Chartered Institute of Transport, the International Road Transport Union, the South Yorkshire Passenger Transport Executive, the Greater Manchester Passenger Transport Executive, the Greater London Council, and Electronics & Power.

The rising cost of fuels and projected shortages will encourage a diversification of transport into systems which are less energy intensive and not dependent on hydrocarbon fuels. Patterns of land use will alter and people will tend to move back into towns, where they

will require both higher economic standards and an improved quality of life. The electric vehicle is the only form of transport which can provide the level of transport required by an active urban centre and at the same time make towns attractive places to live in. The authors of papers presented at the conference represent international research organisations, government departments, manufacturers and transport operators.

October 1978, 13 papers, 110pp., 297 x 210mm, photolitho, soft covers, ISBN 0 906048 08 7, price £11.50 UK, \$23.95 in the USA and Canada, £13.50 Elsewhere

Inquiries and orders with remittances, should be sent to.

Peter Peregrinus Ltd.,
PO Box 26 Hitchin, Herts, SG5 1SA,
England.

Orders for the USA and Canada should be sent to:

The Society of Automotive Engineers,
Inc., 400 Commonwealth Drive, Warrendale,
PA.15096, USA.



Gas discharges

IEE Conference Publication 165

The papers presented at the 5th international conference on gas discharges have now been published as number 165 in the IEE Conference Publication series. The conference held in Liverpool, England in September 1978 was sponsored by the IEE Science, Education and Management Division in association with the IEEE, the IoP, the IERE, and the Welding Institute.

Topics covered include gas blast switchgear, plasma radiation and diagnostics, corona discharges, long sparks, arcs, and high voltage technology. Fuses, radio-frequency

and glow discharges, pre-breakdown phenomena, vacuum switches and electrode phenomena, and high pressure sparks are also covered.

91 papers, 345 pp., 297 x 210 mm, photolitho, ISBN 0 85296 192 8, September 1978, soft covers, price £16.00 UK, £19.00 Overseas

Inquiries, and orders with remittances should be sent to:

Publication Sales Department,
IEE,
PO Box 26, Hitchin,
Herts. SG5 1SA, England



COMPUTER & CONTROL ABSTRACTS

A Complete Information Service in Computer Science and Control Engineering

● Coverage

Over 30,000 references are included each year. These are selected by scanning about 2,800 journals and the proceedings of over 500 conferences. In addition coverage is given of books, reports and dissertations.

● What Information is Included?

Each reference in CCA includes the following information:

Title of paper

All author's names and affiliation of first author

Source of paper (eg name of journal, volume and issue number, page numbers and date of publication)

100-150 word abstract of the reference.

● Ease of use

Careful classifying and indexing of entries puts information at your fingertips. References are classified under 250 headings, allowing you to go straight to the information of most interest to you. (A summary of the classification appears in every issue).

These six separate indexes are included in each issue:

Subject guide

Author index

Bibliography index

Book index

Conference index

Corporate author index

The above indexes are cumulated at six-monthly intervals. The author and subject indexes are also cumulated at four-yearly intervals*.

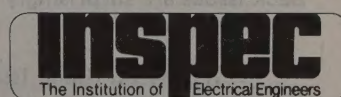
● Do You Have Access to This Important Journal?

Does your library or information service provide you with access to this important journal? If not, ask your librarian to contact INSPEC for a free sample and subscription details or write to us direct.

(* four year cumulative indexes not included in annual subscription price)

INSPEC Marketing Department
IEE
Station House
Nightingale Road
Hitchin
Herts SG5 1RJ England
Tel: (0462) 53331
Telex: 825962

INSPEC
IEEE Service Center
445 Hoes Lane
Piscataway
NJ 08854
USA
Tel: 201 981 0060
Telex: 833233



Developments in distribution switchgear

The papers presented at the international conference on developments in distribution switchgear have now been published as number 168 in the IEE Conference Publication series. The Conference, held in London in November 1978, was sponsored by the IEE Power Division in association with the Institute of Electrical and Electronics Engineers and the Institute of Mathematics and its Applications.

Topics covered include arc interruption media, insulation materials and design, and switchgear design for industrial applications. Substation design and operational aspects, switch and fusegear arrangements, and testing approval and service experience are also covered.

28 papers, 120 pp., 297 x 210mm, photolitho, ISBN 0 85296 194 4, November 1978, soft covers, £8.50 UK, \$20.00 Americas, £10.00 Elsewhere.

Inquiries, and orders with remittances should be sent to:

Publication Sales Department,
Institution of Electrical Engineers,
PO Box 26, Hitchin,
Herts. SG5 1SA, England.

Orders for the Americas should be sent to:

The Institution of Electrical Engineers,
IEEE Service Center,
445 Hoes Lane,
Piscataway, NJ 08854, USA.



MISSING ISSUES? NEW SUBSCRIPTION?

Why not dramatically increase the effectiveness of your information resources by holding previous years copies of INSPEC Abstracts Journals?

Do you find that your collection of INSPEC Abstracts Journals has gaps — a missing index perhaps? Then why not fill those gaps with the appropriate back issues?

Back issues are surprisingly inexpensive and available from:-

Wm Dawson (Back Issues) Ltd
Cannon House
Folkestone
Kent

No space for back volumes? Why not convert your holdings to microfilm? We can give you a quote without any obligation on your part, just contact

INSPEC, Marketing Department
The Institution of Electrical Engineers
Station House
Nightingale Road
Hitchin, Herts
SG5 1RJ

inspec
The Institution of Electrical Engineers

ABSTRACTS AND CURRENT PAPERS JOURNALS
SUBSCRIPTION PRICES 1983

| | USA \$ | UK £ | ROW £ | JAPAN ¥ |
|---|-----------|---------|----------|------------|
| PHYSICS ABSTRACTS (PA) | 1350 | 540 | 690 | 462,300 |
| 2nd and subsequent copies | 560 | 300 | 300 | 201,000 |
| ELECTRICAL & ELECTRONICS ABSTRACTS (EEA) | 1000 | 460 | 560 | 375,200 |
| COMPUTER & CONTROL ABSTRACTS (CCA) | 610 | 285 | 350 | 234,500 |
| PA/EEA/CCA COMBINED SUBSCRIPTION | 2650 | 1120 | 1430 | 958,100 |
| EEA/CCA COMBINED SUBSCRIPTION | 1460 | 650 | 830 | 556,100 |
| CURRENT PAPERS IN PHYSICS | | | | |
| Member rate | 78 | 38 | 38 | — |
| Non-Member rate | 170 | 98 | 98 | 65,000 |
| CURRENT PAPERS IN ELECTRICAL & ELECTRONICS ENGINEERING | | | | |
| Member rate | 78 | 38 | 38 | — |
| Non-Member rate | 145 | 80 | 80 | 53,600 |
| CURRENT PAPERS ON COMPUTERS & CONTROL | | | | |
| Member rate | 78 | 38 | 38 | — |
| Non-Member rate | 145 | 80 | 80 | 53,600 |
| KEY ABSTRACTS | | | | |
| Member rate* | 38 | 19 | 19 | — |
| Non-Member rate | 80 | 36 | 36 | 24,100 |
| KEY ABSTRACTS | | | | |
| EMI/PMI COMBINED | — | 60 | 60 | 40,200 |
| All Key Abstracts combined | | | | |
| Member rate | 250 | 125 | 125 | — |
| Non-Member rate | 580 | 275 | 275 | 184,200 |

*The Key Abstracts Member rate is available to Members of the IEE and IEEE only.

CUMULATIVE INDEXES

Cumulative indexes are available for *Physics Abstracts*, *Electrical & Electronics Abstracts* and *Computer & Control Abstracts*, for both

authors and subjects. These cumulations generally cover a period of four years, with the exception of *Computer & Control Abstracts*

where the initial volume covered the period 1966-68. The table below shows the prices and periods for the two types of cumulative index.

| | PHYSICS ABSTRACTS | | ELECTRICAL & ELECTRONICS ABSTRACTS | | COMPUTER & CONTROL ABSTRACTS | |
|---------|-------------------|--------|------------------------------------|--------|------------------------------|--------|
| | Subject | Author | Subject | Author | Subject | Author |
| | £ | £ | £ | £ | £ | £ |
| 1955-59 | 20 | 20 | 15 | 20 | — | — |
| 1960-64 | 40 | 17 | 20 | 12 | — | — |
| 1965-68 | 60 | 25 | 35 | 20 | — | — |
| 1969-72 | — | — | 72 | 64 | 48 | 30 |
| 1973-76 | 600 | 300 | 250 | 150 | 150 | 75 |
| 1977-80 | 770 | 450 | 380 | 250 | 250 | 120 |
| 1966-68 | — | — | — | — | 15 | |

For US\$ and Yen prices please contact the appropriate address below

ORDERING PROCEDURE

THE AMERICAS

North (including Canada), Central and South

All orders from the above areas, and orders from members of Institute of Electrical and Electronics Engineers Inc. anywhere in the world, should be sent to Fulfillment Manager, Institute of Electrical & Electronics Engineers Inc., 445 Hoes Lane, Piscataway, N.J. 08854, USA. Telephone (201) 981 0060

日本のお客様にご案内申し上げます

日本国内に於けるINSPECの購入価格はすべて円建てとなっております。また刊行物はすべて航空便で配達されます。INSPEC刊行物の価格、その他についてのお問い合わせは最寄の支店取扱専門店または輸入総代理店様ユー・エス・エンジニアテック カンパニー 〒105東京都港区新橋1-13-12、TEL 03 (502) 6471 までご連絡ください。

REMAINDER OF THE WORLD

All remaining subscriptions should be sent to INSPEC Marketing Department, P.O. Box 26, Hitchin, Herts SG5 7RS, England. Telephone Hitchin 53331, Telex 825962, Telegrams IEE G.

OTHER INSPEC SERVICES

SDI

(Selective Dissemination of Information.) This is a service individually tailored to the requirements and interests of the engineer or research worker. Details of information relevant to the interest profile of the individual subscriber are selected from the data being processed for the INSPEC database. Information is dispatched weekly on 150 mm x 100 mm (6" x 4") cards.

TOPICS

This is an SDI service based on standard profiles. There are over 70 subjects covering high-activity areas of research and development. This is an inexpensive card service designed to alert engineers and researchers to the availability of literature within their subject area.

MAGNETIC TAPES

Tapes containing all the information included in the INSPEC publications are issued twice monthly. They enable the larger research and development organisations to produce their own internal information and current-awareness services.

Physics Abstracts

15th August 1981

Summary Classification

The full classification and contents are given at the front of the journal, followed by an **Alphabetical Index** to the subjects covered

00.00 General

- 01.00 Communication, Education, History and Philosophy
- 02.00 Mathematical Methods in Physics
- 03.00 Classical and Quantum Physics; Mechanics and Fields
- 04.00 Relativity and Gravitation
- 05.00 Statistical Physics and Thermodynamics
- 06.00 Measurement Science, General Laboratory Techniques, and Instrumentation Systems
- 07.00 Specific Instrumentation and Techniques of General Use in Physics

10.00 The Physics of Elementary Particles and Fields

- 11.00 General Theory of Fields and Particles
- 12.00 Specific Theories and Interaction Models; Particle Systematics
- 13.00 Specific Reactions and Phenomenology
- 14.00 Properties of Specific Particles and Resonances

20.00 Nuclear Physics

- 21.00 Nuclear Structure
- 23.00 Radioactivity and Electromagnetic Transitions
- 24.00 Nuclear Reactions and Scattering: General
- 25.00 Nuclear Reactions and Scattering: Specific Reactions
- 27.00 Properties of Specific Nuclei listed by Mass Ranges
- 28.00 Nuclear Engineering and Nuclear Power Studies
- 29.00 Experimental Methods and Instrumentation for Elementary-Particle and Nuclear Physics

30.00 Atomic and Molecular Physics

- 31.00 Theory of Atoms and Molecules
- 32.00 Atomic Spectra and Interactions with Photons
- 33.00 Molecular Spectra and Interactions with Photons
- 34.00 Atomic and Molecular Collision Processes and Interactions
- 35.00 Properties of Atoms and Molecules; Instruments and Techniques
- 36.00 Studies of Special Atoms and Molecules

40.00 Classical Areas of Phenomenology

- 41.00 Electricity and Magnetism; Fields and Charged Particles
- 42.00 Optics
- 43.00 Acoustics
- 44.00 Heat Flow, Thermal and Thermodynamic Processes
- 46.00 Mechanics, Elasticity, Rheology
- 47.00 Fluid Dynamics

50.00 Fluids, Plasmas and Electric Discharges

- 51.00 Kinetic and Transport Theory of Fluids; Physical Properties of Gases
- 52.00 The Physics of Plasmas and Electric Discharges

60.00 Condensed Matter: Structure, Thermal and Mechanical Properties

- 61.00 Structure of Liquids and Solids; Crystallography
- 62.00 Mechanical and Acoustic Properties of Condensed Matter
- 63.00 Lattice Dynamics and Crystal Statistics
- 64.00 Equations of State, Phase Equilibria, and Phase Transitions
- 65.00 Thermal Properties of Condensed Matter
- 66.00 Transport Properties of Condensed Matter (Nonelectronic)
- 67.00 Quantum Fluids and Solids; Liquid and Solid Helium
- 68.00 Surfaces and Interfaces; Thin Films and Whiskers

70.00 Condensed Matter: Electronic Structure, Electrical, Magnetic, and Optical Properties

- 71.00 Electron States
- 72.00 Electronic Transport in Condensed Matter
- 73.00 Electronic Structure and Electrical Properties of Surfaces, Interfaces, and Thin Films
- 74.00 Superconductivity
- 75.00 Magnetic Properties and Materials
- 76.00 Magnetic Resonances and Relaxation in Condensed Matter; Mossbauer Effect
- 77.00 Dielectric Properties and Materials
- 78.00 Optical Properties and Condensed Matter Spectroscopy and other Interactions of Matter with Particles and Radiation
- 79.00 Electron and Ion Emission by Liquids and Solids; Impact Phenomena

80.00 Cross-Disciplinary Physics and Related Areas of Science and Technology

- 81.00 Materials Science
- 82.00 Physical Chemistry
- 86.00 Energy Research and Environmental Science
- 87.00 Biophysics, Medical Physics, and Biomedical Engineering

90.00 Geophysics, Astronomy and Astrophysics

- 91.00 Solid Earth Geophysics
- 92.00 Hydrospheric and Atmospheric Geophysics
- 93.00 Geophysical Observations, Instrumentation, and Techniques
- 94.00 Aeronomy and Space Physics
- 95.00 Fundamental Astronomy and Astrophysics, Instrumentation and Techniques and Astronomical Observations
- 96.00 Solar System
- 97.00 Stars
- 98.00 Stellar Systems; Galactic and Extragalactic Objects and Systems; The Universe